REVUE ROUMAINE
DE
CHIMIE

ORSZÁGOS MŰSZAKI KÖNYVTÁR * BUDAPEST

Tome 20, N° 2 Février 1975

D. I. MARCHIDAN and M. CIOPEC, Enthalpy of non-stoichiometric uranium oxides and sapphire to 1500 K by drop calorimetry 143–158

S. STERNBERG and VALERIA PETRESCU, Overvoltage in chlorine discharge on graphite electrode in AgCl – KCl molten mixture at various temperatures (400 – 700°) 159–168

LAURA VASU, On the electrical conductivity of molten alkali halides . . . . . 169–175 R

D. R. ARMSTRONG, P. G. PERKINS and J. J. P. STEWART, The electronic structure and spectra of titanium tetrachloride and the methyltitanium chlorides 177–194

C. BENDIC and D. OANCEA, Reactivity of benzyl halides in S_N2 reactions 195–201

C. I. GHIRVU, A rotational study of *o*-chloronitrobenzene and *o*-dinitrobenzene 203–208

MARIA MAVRODIN-TĂRĂBÎC, IOANA ONACA et I. SOLACOLU, L'influence de la température et de la concentration de l'électrolyte sur les performances d'une pile à combustible hydrogène-oxygène . . . . 209–216 R

I. UDREA and D. CRIȘAN, The catalytic system $ZnO-Al_2O_3$. I. The influence of chemical composition and crystalline structure upon the formation of the active phases in the decomposition reaction of isopropyl alcohol 217–225

ALEXANDRU T. BALABAN, Chemical Graphs. XXV. Isomers of the porphyrins – an exercise using Pólya's counting theorem 227–232

F. IORDACHE, F. CHIRALEU and MARGARETA AVRAM, Bicyclo[2.2.2] octane derivatives. I. Stereoisomeric 5,6,7,8-tetracarbomethoxy-bicyclo [2.2.2]oct-2-enes 233–240

S. H. DOSS, Sultam-steroide. I. Die Synthese von Estern einiger Sterine mit Sultamyl-N-phenylcarbonsäuren 241–244

P. BUCHWALD and A. KÖVENDI, Cyanoethylation of ketoximes. I. Cyanoethylation of *para*-substituted acetophenone oximes 245–250

A. ARSENE et M. GERMAIN, Étude du partage de l'acide formique, de l'uranium (VI) et du plutonium (IV) dans le système tributylphosphate – dodécane – acide nitrique – acide formique – eau 251–258

D. C. CÖRMÖȘ, IOVANCA HAIDUC and P. STEȚIU, Synthetic single crystal lead sulphide electrode. I. Direct potentiometric titration of lead with Na_2 EDTA 259–265

MARIA PLENICEANU et OLIMPIA RUSU, Étude spectrophotométrique de la réaction du wolfram (VI) avec le solochrome violet RS . . . 267–273

I. M. ISSA, A. M. ISLAM, R. M. ISSA and A. K. ABDELKADER, Spectrophotometric studies of some derivatives of phenindione 275–282

ILEANA DRĂGUȚAN, C. DRĂGHICI and ECATERINA CIORĂNESCU, Carbonium ion reactions. XII. Benzobicyclononene derivatives through double bond participation 283–295

Rev. Roumaine Chim. **20**, *2*, 141–296 (1975), Bucarest

Revue Roumaine de Chimie, **20**, *2*, 143–158 (1975)

ENTHALPY OF NON-STOICHIOMETRIC URANIUM OXIDES AND SAPPHIRE TO 1500 K BY DROP CALORIMETRY

D. I. MARCHIDAN and M. CIOPEC
Centre of Physical Chemistry, str Galați 31, P. O. Box 2103
Bucharest, Romania

Received June 17, 1974

A precision drop calorimetric system has been used to measure the enthalpy of $UO_{2.19}$, $UO_{2.34}$ and N.B.S. sapphire in the temperature range of 400 to 1500 K, relative to 298.15 K. All the temperatures are based on IPTS–68. Results of non-stoichiometric uranium oxides can be represented by the empirical equations which produce the best fit. A transition with an associated enthalpy increment of (1000 ± 65) J mol^{-1} occurs in the temperature range 855 to 865 K for $UO_{2.19}$ and two transitions with an associated enthalpy increment of (1500 ± 75) J mol^{-1} and (2800 ± 95) J mol^{-1} occur in the temperature range 860 to 870 K and respectively 1335 to 1355 K for $UO_{2.34}$. Values of $H^0(T) - H^0(298.15\ K)$, C_p, $S^0(T) - S^0(298.15\ K)$ and $S^0(T) - \{G^0(T) - H^0(298.15\ K)\}/T$ are tabulated. The sapphire results are used for determination of the calibration factor of the calorimetric block in comparison with the "electrical" calibration factor.

1. INTRODUCTION

The importance of non-stoichiometric uranium oxides in the atomic energy program has resulted in intense studies of these materials. Their thermodynamic properties, especially enthalpy and heat capacity, are important from both the chemical and reactor view point. Uranium oxide constitute the main component of ceramic fuels for power reactors. The need for heat content or specific heat data of fuel materials has become evident in areas of growing interest.

High temperature enthalpy and heat capacity of uranium dioxide and triuranium octaoxide have mostly derived from drop calorimetric experiments.[1–9] One recent paper studies heat capacity of $UO_{2.017}$ and

---

[1] G. E. MOORE and K. K. KELLEY, *J. Amer. Chem. Soc.*, **69**, 2105 (1947).

[2] J. B. CONWAY and R. A. HEIN, *J. Nuclear Mater.*, **15**, 149 (1965).

[3] A. E. OGARD and J. A. LEARY, in "Thermodynamics of Nuclear Materials", 1967, Proceedings of a Symposium, Vienna, 4–8 september 1967, IAEA, Vienna, 1968, STI/PUB/162, p. 651.

[4] R. A. HEIN, L. H. SJODAHL and R. SZWARC, *J. Nuclear Mater.*, **25**, 99 (1968).

[5] C. AFFORTIT, *High Temp.–High Press.*, **1**, 27 (1969).

[6] L. LEIBOWITZ, L. W. MISHLER and M. G. CHASANOV, *J. Nuclear Mater.*, **29**, 356 (1969).

[7] D. R. FREDRICKSON and M. G. CHASANOV, *J. Chem. Thermodynamics*, **2**, 623 (1970).

[8] R. A. HEIN, P. N. FLAGELLA and J. B. CONWAY, *J. Amer. Ceramic Soc.*, **51**, 291 (1968).

[9] K. MAGLIC and R. HERAK, *Rev. Internat. Hautes Temper. et Refract.*, **7**, 247 (1970).

$UO_{2.254}$ by adiabatic calorimetry[10] and other papers study high temperature enthalpy of $UO_{2.25}$ by drop calorimetry.[11] For UO_2 and U_3O_8 heat capacity data are available from adiabatic calorimetry.[12]

Measurements on samples with intermediate composition between UO_2 and U_3O_8 were performed by drop calorimetry over a temperature range of 300 to 1300 K.[13-16] Following our earlier investigations of thermodynamic properties of non-stoichiometric uranium-oxygen compounds, we have measured the high temperature enthalpies of $UO_{2.19}$ and $UO_{2.34}$.

2. EXPERIMENTAL

MATERIALS

To prepare uranium oxides $UO_{2.19}$ and $UO_{2.34}$ we started from uranyl nitrate. The obtained powder was pressed and sinterized in nitrogen atmosphere and the O/U ratio was determined by oxidation to U_3O_8 in the air.

A 5.7661 g sample of $UO_{2.19}$ and a 5.9722 g sample of $UO_{2.34}$ were each introduced in a platinum container of tronconical shape in which the top is connected to a narrow neck welded to a Jena glass ground joint. After filling it with uranium oxide, the container was attached to a vacuum equipment. After a number of vacuumings and fillings with purified argon (free of oxygen) and after evacuation at $0.3 - 0.7\ \mathrm{Nm}^{-2}$ the glass tube was cut off and closed with a gas-oxygen torch close to the body of the container, retaining the vacuum inside. The platinum neck may be pinched shut near the top and sealed by gas-oxygen welding. After each run the container was weighed and no weight loss was observed after 30 runs for $UO_{2.19}$ and 42 runs for $UO_{2.34}$. There was, therefore, no leakage from the containers and no change in the composition of the samples as a result of the thermal cycling to which the samples were subjected.

Another concern of this study was the investigation of synthetic sapphire (Al_2O_3) prepared by the National Bureau of Standards for the Calorimetry Conference in March 1949, as calorimetric standards. A 8.9915 g sample of the synthetic sapphire crystals (NBS Standard Reference Material 720) was similarly loaded into the platinum container (8.2229 g) and subjected to dropping experiments to 1500 K.

APPARATUS

High temperature enthalpies were determined in a precision drop calorimeter operating with isothermal jacket at 298.15 K.[14] The container and the specimen, mass about 18 g, were suspended by a 6 mm diameter of cronix alloy (Ø = 0,1 mm) ring clamped between two solid kanthal electrodes. The container, suspended from the dropping mechanism, was held in the constant temperature-controlled zone of the furnace for at least one hour before each dropping. It was then dropped rapidly into the copper-block calorimeter of known heat capacity, due to the strong electrical current passed through the suspension wire causing it to vaporize rapidly. The temperature rise (corrected for the heat exchange between the calorimeter block and the isothermal jacket) of the calorimeter thus obtained was a measure of the change in the enthalpy $\{H^0(T) - H^0(T')\}$ of the sample caused by its cooling from the furnace temperature T to the final calorimeter temperature T'. The final calorimeter temperature was always slightly above the reference temperature of 298.15 K and small corrections were required to obtain the function $\{H^0(T) - H^0(298.15\text{ K})\}$.

---

[10] F. Grønvold, N. J. Kveseth, A. Sveen and J. Tichy, *J. Chem. Thermodynamics*, **2**, 665 (1970).

[11] A. C. Macleod, *J. Chem. Thermodynamics*, 4, 699 (1972).

[12] M. M. Popov, G. L. Gal'cenko and M. D. Senin, *Zhur. neorg. Khim.*, **3**, 1734 (1958).

[13] D. I. Marchidan and M. Ciopec, *Rev. Roumaine Chim.*, **15**, 1287 (1970).

[14] D. I. Marchidan and M. Ciopec, *Rev. Roumaine Chim.*, **16**, 1145 (1971).

[15] D. I. Marchidan and M. Ciopec, *Rev. Roumaine Chim.*, **17**, 1657 (1972).

[16] D. I. Marchidan and M. Ciopec, in "Third Conference on Chemical Thermodynamics" jointly with the "Symposium on Physico-Chemical Techniques at High Temperatures (1000—4000 K)", 3—7 September, 1973, Baden near Vienna, Austria, vol. VI, Report 9/11a, p. 117.

After completion of the series of measurements on the container with specimen a similar series was carried out for the empty capsule at exactly the same experimental temperatures as before. The differences between the two sets of measurements were the values of $\{H^0(\mathrm{T}) - H^0(298.15\text{ K})\}$ for each specimen, being assumed that the heat lost by the capsule was the same whether empty or full.

3. RESULTS

CALIBRATION

The calibration factor of the calorimeter block was determined by supplying a known amount of electrical energy to the calibration heater and observing the temperature change of the block which is corrected for heat losses to the isothermal surrounding. The potential drop V and I across the heater were measured with high precision at 30 s intervals.

The calibration factor of the calorimeter is given by

$$W = Q/\Delta\theta \qquad J\mathrm{K}^{-1} \tag{1}$$

where Q is the heat liberated in the calorimeter and $\Delta\theta$ is the observed temperature change of the block corrected for its heat exchange with the isothermal surrounding. A series of nineteen runs with temperature increase from 0.08 to 1.8 degrees gave a calibration factor

$$\overline{W} = 3988.2 \pm 3.6\ J\mathrm{K}^{-1}$$

with a percentage standard deviation of ($\pm$ 0.1) per cent (table 1).

Another set of determinations for the calibration factor was made with synthetic sapphire. The enthalpy of this standard substance was determined with high accuracy by Furukawa,[17] Macleod,[18] Ginnings,[19] Chekhovskoi[20] and Fredrickson[21] using the drop method. A complete review of the experimental data on the specific heat of aluminum oxide was made by Buyco.[22]

Fredrickson's experimental enthalpies data for sapphire over the temperature range 450 to 1400 K are given by the following equation

---

[17] G. T. Furukawa, T. B. Douglas, R. E. Mc Coskey and D. C. Ginnings, *J. Res. Nat. Bur. Stand.*, **57**, 67 (1965).

[18] A. C. Macleod, *Trans. Faraday Soc.*, **63**, 300 (1967).

[19] D. C. Ginnings, *J. Phys. Chem.*, **67**, 1917 (1963).

[20] V. Ya. Chekhovskoi, *Teplofiz. Vysok. Temp.*, **2**, 296 (1964).

[21] D. R. Frerickson and M. G. Chasanov, *J. Chem. Thermodynamics*, **2**, 623 (1970).

[22] E. H. Buyco, in "Proceedings Fourth Symposium on Thermophysical Properties", Univ. of Maryland, College Park, Maryland, p. 161.

Table 1

Experimental values for calibration factor W (electrical measurements)

Run N°	$\frac{\Delta\theta}{K}$	$\frac{W_i}{JK^{-1}}$	Deviations $\frac{\overline{W}-W_i}{J\,K^{-1}}$	 $\frac{\overline{W}-W_i}{\overline{W}}\times 100$ percent
1	0.086	3983.5	4.7	0.12
2	0.184	3985.7	2.5	0.06
3	0.313	3984.7	3.5	0.09
4	0.537	3985.9	2.3	0.06
5	0.605	3988.5	−0.3	−0.01
6	0.629	3988.4	−1.2	−0.03
7	0.674	3994.4	−5.2	−0.15
8	0.810	3982.9	5.3	0.13
9	0.874	3987.8	0.4	0.01
10	0.916	3991.8	−3.6	−0.09
11	0.952	3984.4	3.8	0.10
12	0.969	3989.6	−1.4	−0.04
13	1.073	3986.8	1.4	0.04
14	1.109	3987.6	0.6	0.01
15	1.152	3993.7	−5.5	−0.14
16	1.308	3995.8	−7.6	−0.19
17	1.560	3985.8	2.4	0.06
18	1.768	3990.8	−2.6	−0.07
19	1.865	3986.7	1.5	0.04

with the constants determined by the method of least squares[21] (standard deviation is 146.4 J mol^{-1}).

$$H^0(T) - H^0(298.15\ \text{K}) = \{115.4792(T/\text{K}) + 6.7527\times 10^{-3}(T/\text{K})^2 + 40.4106\times 10^5(T/\text{K})^{-1} - 48343.23\}\ \text{J mol}^{-1} \qquad (2)$$

A series of fourteen runs made before and after uranium oxides measurements in which the heat content of Al_2O_3 was calculated with equation (2), gave a calibration factor

$$\overline{W} = 3988.0 \pm 11.9\ JK^{-1}$$

with a percentage standard deviation of (± 0.28) percent (table 2).

This procedure was performed in the range 400 to 1400 K so that all measurements confirm that the apparatus was functioning properly both before and after studies on uranium oxides.

URANIUM OXIDES

Enthalpy determinations on $UO_{2.19}$ and $UO_{2.34}$ are listed in column two of table 3 and in column two of table 4, respectively and plotted in figure 1 and figure 2, respectively. It is evident that the transitions occur in the range of 860 K for $UO_{2.19}$ and in the range of 850 K and 1340 K for $UO_{2.34}$.

The enthalpy values of $UO_{2.19}$ and $UO_{2.34}$ were subjected to the least square analysis in order to obtain a mathematical relationship between enthalpy and temperature. The computer program TERMOX[23] was used to test four empirical equations for the best fit of the experimental data; these fitting schemes have been proposed for the enthalpy function of solid substances.[10,24] From the smoothed equations (table 5 and table 6) we chose those for which the standard deviation was minimum and calculated $H^0(T) - H(298.15\ \mathrm{K})$ for $T = 298.15$ K was around zero.

Table 2

Experimental values for calibration factor *W* from NBS Standard Reference Materials N° 720 enthalpy measurements

Run N°	T/K	$\Delta\theta$/K	$H^0(T)-H^0$ (298.15 K) J mol^{-1} (calculated eq. (2))	Q/J	W_i/JK^{-1}	Deviations: $\overline{W}-W_i$ / JK^{-1}	Deviations: $\frac{\overline{W}-W_i}{\overline{W}}\times 100$ percent
1	433.1	0.272	12268.0	1081.8	3977.4	10.6	0.26
2	479.7	0.378	17030.1	1501.8	3973.1	14.9	0.37
3	485.6	0.390	17647.6	1556.3	3990.4	− 2.3	−0.06
4	621.1	0.718	32492.1	2865.3	3990.7	− 2.6	−0.06
5	651.8	0.798	35994.8	3174.2	3977.7	10.4	0.26
6	724.2	0.984	44408.4	3916.2	3979.8	8.3	0.21
7	724.7	0.988	44467.2	3921.4	3970.0	18.1	0.45
8	826.7	1.250	56626.6	4993.6	3994.9	− 6.8	−0.17
9	876.2	1.385	62635.9	5523.6	3988.1	− 0.1	−0.00
10	1240.4	2.389	108544.7	9572.1	4006.7	−18.6	−0.47
11	1268.2	2.470	112154.5	9890.4	4004.2	−16.1	−0.40
12	1289.3	2.542	114903.4	10132.8	3986.1	1.9	0.05
13	1311.5	2.599	117803.9	10388.6	3997.1	− 9.0	−0.23
14	1353.9	2.722	123366.8	10879.2	3996.7	− 8.6	−0.22

For $UO_{2.19}$ in the temperature range:

300 to 860 K

$$H^0(T) - H^0(298.15\ \mathrm{K}) = \{56.495\,(T/\mathrm{K}) + 8.088 \times 10^{-3}\,(T/\mathrm{K})^2 + 14.932 \times 10^{-6}\,(T/\mathrm{K})^3 - 17940.5\}\ \mathrm{J\,mol^{-1}} \qquad (3)$$

860 to 1500 K

$$H^0(T) - H^0\,(298.15\ \mathrm{K}) = \{122.227\,(T/\mathrm{K}) - 47.63 \times 10^{-3}\,(T/\mathrm{K})^2 + 21.028 \times 10^{-6}\,(T/\mathrm{K})^3 - 37715\}\ \mathrm{J\,mol^{-1}} \qquad (4)$$

---

[23] M. Ciopec and D. I. Marchidan, *Rev. Roumaine Chim.*, **17**, 1139 (1972).

[24] E. H. Buyco and F. F. Davis, *J. Chem. and Eng. Data*, **15**, 518 (1970).

Table 3

Experimental enthalpy data of $UO_{2.19}$ (mol. wt. = 273.07)

$\frac{T}{K}$	$H^0(T) - H^0(298.15\ K)$ J mol^{-1}		Deviation (calc. − obs.)	
	observed	calculated eq. (3)	J mol^{-1}	percent
399.90	6923.699	6900.328	23.371	0.3
435.00	9355.699	9394.516	− 38.816	−0.4
436.85	9543.500	9527.813	15.688	0.2
503.38	14405.797	14452.164	− 46.367	−0.3
504.41	14595.398	14530.469	64.930	0.4
551.91	18148.500	18213.789	− 65.289	−0.4
553.26	18148.898	18320.574	−171.676	−0.9
619.93	23950.098	23748.539	201.559	0.8
648.52	26383.500	26172.297	211.203	0.8
661.87	27319.398	27324.742	− 5.244	−0.0
731.17	33494.098	33527.996	− 33.898	−0.1
782.03	37984.000	38328.535	−344.535	−0.9
823.03	42473.797	42360.277	113.520	0.3
		calculated eq. (4)		
873.33	47714.797	47513.633	201.164	0.4
878.22	47901.199	48027.199	− 126.000	−0.3
946.03	52578.199	53091.441	− 513.242	−1.0
1014.11	59875.199	59183.539	691.660	1.2
1075.62	65300.898	64816.934	483.965	0.7
1075.92	65677.375	64844.777	832.598	1.3
1124.63	69793.875	69413.625	380.250	0.5
1132.10	70167.688	70123.750	43.938	0.1
1135.34	70353.188	70432.563	− 79.375	−0.1
1180.26	74281.875	74767.813	− 485.938	−0.7
1180.43	74658.188	74784.438	− 126.250	−0.2
1241.57	80271.500	80861.875	− 590.375	−0.7
1275.98	83264.063	84381.313	−1117.250	−1.3
1339.89	91498.750	91128.500	370.250	0.4
1373.00	95054.563	94740.500	314.063	0.3
1431.90	102724.500	101380.125	1344.375	1.3
1469.29	106653.750	105747.063	906.688	0.9

For $UO_{2.34}$ in the temperature range:

300 to 865 K

$$H^0(T) - H^0(298.15\ \mathrm{K}) = \{-43.573\,(T/\mathrm{K}) + 87.11 \times 10^{-3}\,(T/\mathrm{K})^2 - \\ - 7.037 \times 10^{6}\,(T/\mathrm{K})^{-1} + 29136.2\}\ \mathrm{J\ mol^{-1}} \qquad (5)$$

865 to 1350 K

$$H^0(T) - H^0(298.15\ \mathrm{K}) = \{-9.729\,(T/\mathrm{K}) + 68.51 \times 10^{-3}\,(T/\mathrm{K})^2 - \\ - 14.707 \times 10^{-6}\,(T/\mathrm{K})^3 + 15583.4\}\ \mathrm{J\ mol^{-1}} \qquad (6)$$

Fig. 1. — Enthalpy increments $\{H^0(T) - H^0(298.15\text{K})\}$ of $UO_{2.19}$. ●, present results obtained by drop calorimetry experiments; full curve, calculated enthalpy data with equations (3) and (4).

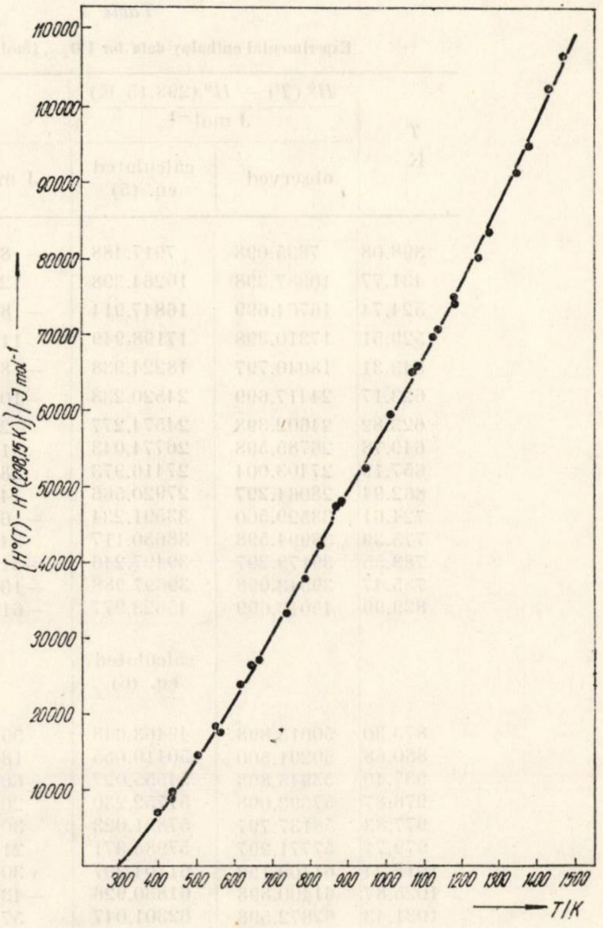

1350 to 1500 K

$$H^0(T) - H^0(298.15\ \text{K}) = \{1303.5\ (T/\text{K}) + 450.89 \times 10^{-3}\ (T/\text{K})^2 - 40.743 \times 10^{-5}\ (T/\text{K})^3 - 1489403\}\ \text{J mol}^{-1} \qquad (7)$$

After completion of enthalpy experiments, uranium oxides were removed from the full containers and their U/O ratio was redetermined. The results indicate that no significant change in the O/U ratio had taken place in the course of these studies. Platinum containers were examined visually; no indications on the interaction of the samples with the containers were observed.

The second order transitions occur over ranges about 10 K, as shown in figure 1 and figure 2. The values for the enthalpies changes associat-

Table 4

Experimental enthalpy data for $UO_{2.34}$ (mol. wt. = 275.47)

$\frac{T}{K}$	$H^0(T) - H^0(298.15\ K)$ J mol^{-1}		Deviation (calc. − obs.)	
	observed	calculated eq. (5)	J mol^{-1}	percent
398.08	7835.098	7917.488	− 82.391	−1.1
431.77	10387.398	10264.398	123.000	1.2
524.74	16764.699	16847.914	− 83.215	−0.5
529.51	17310.398	17198.949	111.449	0.6
543.31	18040.797	18224.938	−184.141	−1.0
623.17	24417.699	24520.238	−102.539	−0.4
623.82	24602.398	24574.277	28.121	0.1
649.78	26785.598	26774.043	11.555	0.0
657.19	27403.004	27416.973	283.527	1.0
662.94	28064.297	27920.566	143.730	0.5
724.61	33529.500	33591.234	− 61.734	−0.2
775.39	38994.598	38650.117	344.480	0.9
783.55	39179.297	39497.246	−317.949	−0.8
785.47	39543.098	39697.988	−154.891	−0.4
839.99	45013.699	45623.977	−610.277	−1.4
		calculated eq. (6)		
873.30	50015.898	49463.648	552.250	1.1
880.68	50291.500	50110.055	181.445	0.4
937.40	53945.898	54555.027	−609.129	−1.1
976.87	57593.098	57752.230	200.867	0.3
977.83	58137.797	57831.023	306.773	0.5
979.71	57771.297	57985.371	−214.074	−0.4
1017.24	61409.199	61104.207	304.992	0.5
1025.87	61400.898	61830.926	−430.027	−0.7
1031.43	62872.598	62301.047	571.551	0.9
1076.33	66144.000	66147.875	− 3.875	−0.0
1076.87	66152.250	66194.625	− 42.375	−0.1
1124.80	70341.188	70395.438	− 54.250	−0.1
1131.14	70699.688	70957.813	−258.125	−0.4
1131.25	70887.063	70967.625	− 80.563	−0.1
1176.05	75067.750	74983.063	84.688	0.1
1178.03	74896.875	75162.125	−265.250	−0.4
1180.22	75260.750	75360.313	− 99.563	−0.1
1241.14	80732.180	80933.875	−201.688	−0.2
1241.20	81457.063	80939.438	517.625	0.6
1242.08	81278.000	81020.750	257.250	0.3
1276.83	84190.250	84247.813	− 57.563	−0.1
1326.47	88929.688	88907.875	21.813	0.0
		calculated eq. (7)		
1353.11	91300.250	91429.750	−129.500	−0.1
1371.67	96036.688	95443.000	593.688	0.6
1402.37	101323.188	101668.000	−344.813	−0.3
1430.72	104420.750	105302.000	−881.250	−0.8
1469.52	107517.875	106886.000	631.875	0.6

Fig. 2. —Enthalpy increments $\{H^0(T) - H^0(298 \cdot 15\mathrm{K})\}$ of $UO_{2.34}$.

●, present results obtained by drop calorimetry experiments; full curve, calculated enthalpy data with equations (5), (6) and (7).

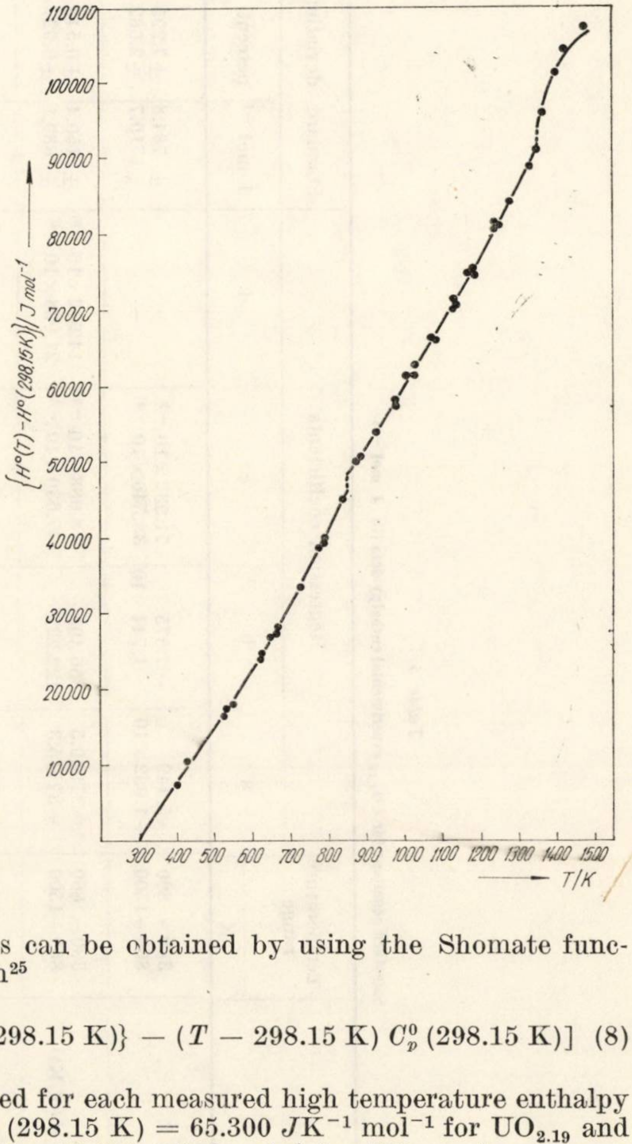

ed with these transitions can be obtained by using the Shomate function Ø, given by relation[25]

$$Ø = T[\{H^0(T) - H^0\,(298.15\ \mathrm{K})\} - (T - 298.15\ \mathrm{K})\, C_p^0\,(298.15\ \mathrm{K})] \quad (8)$$

The function Ø is evaluated for each measured high temperature enthalpy value using a value of C_p^0 (298.15 K) = 65.300 $J\mathrm{K}^{-1}\ \mathrm{mol}^{-1}$ for $UO_{2.19}$ and a value of C_p^0 (298.15 K) = 67.740 $\mathrm{JK}^{-1}\ \mathrm{mol}^{-1}$ for $UO_{2.34}$. An approximate value λ for the enthalpy of transition is obtained by inspection of the enthalpy curve and the function

$$\psi = \{Ø - T\,(\lambda + y)\,(T - 298.15\ \mathrm{K})^{-2}\} \quad (9)$$

---

[25] T. B. DOUGLAS and E. G. KING, in "Experimental Thermodynamics", vol. 1, ed. J. P. McCullough and D. W. Scott, Butterworths, London, 1968, p. 327.

Table 5

Smoothed equations for $UO_{2.19}$ experimental enthalpy data (in J mol $^{-1}$)

Smoothed equation	Temperature range	Regression coefficients				Standard deviation	
	K	a	b	c	d	J mol $^{-1}$	percent
$H^0(T) - H^0(298.15\text{K})$ $= a + b\,(T/\text{K}) + c(T/\text{K})^2$	300 – 860	-5.449	-7.575	71.932×10^{-3}	—	± 784.8	±7.295
	860 – 1500	-1.032×10	1.744×10	38.540×10^{-3}	—	±1710.7	±2.682
$H^0(T) - H^0(298.15\text{ K})$ $= a + b\,(T/\text{K}) + c\,(T/\text{K})^2 + d\,(T/\text{K})^3$	300 – 860	-17940.5	56.495	8.088×10^{-3}	14.932×10^{-6}	± 150.4	±0.543
	860 – 1500	-37715.3	122.227	-47.630×10^{-3}	21.028×10^{-6}	± 689.1	±0.927
$H^0(T) - H^0(298.15\text{ K})$ $= a + b\,(T/\text{K}) + c\,(T/\text{K})^2 + d\,(T/\text{K})^{-1}$	300 – 860	-1831.6	18.186	45.585×10^{-3}	-2.472×10^6	± 153.3	±0.591
	860 – 1500	-11959.1	56.279	16.709×10^{-3}	-3.039×10^6	± 993.8	±1.323
$H^0(T) - H^0(298.15\text{ K})$ $= a + b\,(T/\text{K}) + c\,(T/\text{K})^2 + d\,(T/\text{K})^{-2}$	300 – 860	-252.3	44.424	-2.192×10^{-3}	100.9×10^6	±7615.3	±62.7
	860 – 1500	-120.1	60.986	-6.326×10^{-4}	96.4×10^6	±8161.1	±8.979

Table 6

Smoothed equations for $UO_{2.34}$ experimental enthalpy data (in J mol $^{-1}$)

Smoothed equation	Temperature range K	Regression coefficients				Standard deviation	
		a	b	c	d	J mol^{-1}	percent
$H^0(T) - H^0(298.15\ \mathrm{K}) = a + b\,(T/\mathrm{K}) + c\,(T/\mathrm{K})^2$	300–865	-2.165	-62.599×10^{-1}	72.437×10^{-3}	—	± 468.8	±4.077
	865–1350	-8.751×10^{-2}	37.003	22.694×10^{-3}	—	±299.1	±0.469
	1350–1500	-3.313×10^{-1}	29.407	30.099×10^{-3}	—	± 945.5	±0.935
$H^0(T) - H^0(298.15\ \mathrm{K}) = a + b\,(T/\mathrm{K}) + c\,(T/\mathrm{K})^2 + d\,(T/\mathrm{K})^3$	300–865	−29.094.97	127.97	-126.87×10^{-3}	95.790×10^{-6}	±269.3	±0.946
	865–1350	15 583.45	− 9.729	68.51×10^{-3}	-14.707×10^{-6}	±288.6	±0.458
	1350–1500	-14894.03×10^{2}	130.35×10^{1}	450.89×10^{-3}	-40.743×10^{-5}	±740.9	±0.720
$H^0(T) - H^0(298.15\ \mathrm{K}) = a + b(T/\mathrm{K}) + c\,(T/\mathrm{K})^2 + d(T/\mathrm{K})^{-1}$	300–865	29136.2	−43.573	87.11×10^{-3}	-7.037×10^{6}	±272.3	±0.832
	865–1350	−10827.4	51.483	17.00×10^{-3}	2.030×10^{6}	±292.1	±0.463
	1350–1500	63987.5×10^{2}	-24.881×10^{2}	154.68×10^{-3}	-4.364×10^{9}	±841.7	±0.818
$H^0(T) - H^0(293.15\ \mathrm{K}) = a + b(T/\mathrm{K}) + c\,(T/\mathrm{K})^2 + d\,(T/\mathrm{K}^{-2})$	300–865	−301.1	45.688	-294.61×10^{-5}	109.434×10^{6}	±8197.4	±79.4
	865–1350	−34.849	63.115	-86.292×10^{-6}	43.74×10^{6}	±332.9	±5.079
	1350–1500	−26.553	72.217	-39.967×10^{-6}	53.104×10^{6}	±2024.4	±2.050

is the plotted against T for various values of y until a value is found which permits a smooth curve to be drawn through the region of the anomaly.[26] If this is not possible the correct value of y will be that value which causes the intersect at the temperature of the anomaly. The results obtained from this analysis are the following:

For $UO_{2.19}$: Transition temperature (860 ± 5) K
Enthalpy of transition (1000 ± 65) J mol^{-1}

For $UO_{2.34}$:

$$\text{I}\begin{cases}\text{Transition temperature } (865 \pm 5)\text{ K}\\ \text{Enthalpy of transition } (1500 \pm 75)\text{ J mol}^{-1}\end{cases}$$

$$\text{II}\begin{cases}\text{Transition temperature } (1345 \pm 10)\text{ K}\\ \text{Enthalpy of transition } (2800 \pm 95)\text{ J mol}^{-1}\end{cases}$$

4. DISCUSSION

The results of our $UO_{2.19}$ and $UO_{2.34}$ enthalpy experiments are compared with other enthalpy data for $UO_{2.21}$ and $UO_{2.366}$ obtained in similar conditions[15] and with other literature data for the UO_2, U_4O_9 and U_3O_8 obtained by high temperature drop calorimetry [11,21,27] (table 7). The diferences between enthalpy of each non-stoichiometric oxide and stoichiometric uranium dioxide *vs.* temperature are plotted in figure 3. This *excess enthalpy* can be assigned to the enthalpy of the excess oxygen which was accepted by the UO_2 lattice. To verify this supposition the contribution of non-stoichiometric excess oxygen to the *excess enthalpy* was

Table 7

Comparison of enthalpy values for $UO_{2.19}$ and $UO_{2.34}$ from equations (3) – (7) with enthalpies of $UO_{2.21}$ and $UO_{2.366}$ [15] and with otherliterature data for UO_2 [21], U_4O_9 [11] and U_3O_8 [27]

T/K	$\{H^\circ(T) - H^\circ(298.15\text{ K})\}/\text{J mol}^{-1}$						
	UO_2 from reference ([21])	$UO_{2.19}$ present work	$UO_{2.21}$ from reference ([15])	$UO_{2.25}$ from reference([11])	$UO_{2.34}$ present work	$UO_{2.366}$ from reference([15])	$UO_{2.666}$ from refer.[27]
400	6937	6907	7920	7702	8052	8302	8597
500	14315	14195	15724	15593	15053	16402	18990
600	22014	22093	23748	23752	22624	24526	28170
700	29925	30691	31994	32166	31267	32673	37368
800	38025	40077	40460	40814	41234	44688	46633
900	46256	49038	49147	49702	51603	53251	55990
1000	54610	57909	58054	58814	59663	62185	65455
1100	63079	67090	67182	68157	68210	71494	
1200	71653	76709	76531	77726	77157	81174	
1300	80328	86883	86101	87520	86416	91227	
1400	89101	97749		100834	101271		
1500	97969	109427		110993	106587		

---

[26] C. H. Shomate, *J. Phys. Chem.*, **58**, 368 (1954).

[27] K. Maglic and R. Hérak, *Rev. Int. Hautes Tempér. et Réfract.*, **7**, 247 (1970).

calculated using JANAF Thermochemical Tables data for the enthalpy of monoatomic oxygen,[28] and plotted *vs*. temperature (full curves figure 3).

The agreement between calculated and experimental *excess enthalpy* is obtained only at 620 K for $UO_{2.366}$ and at 800 K for $UO_{2.19}$, $UO_{2.25}$ and $UO_{2.34}$. For $UO_{2.21}$ we observed a slighter discrepancy between 700 and 900 K whereas for $UO_{2.666}$ this discrepancy is very significant within the

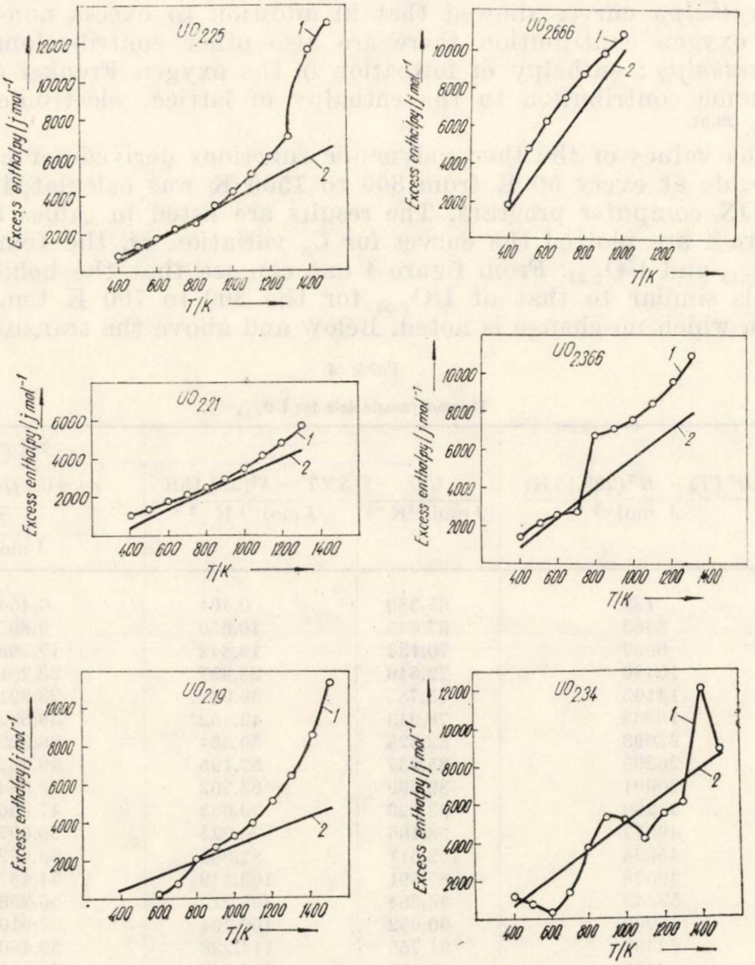

Fig. 3. — The differences between enthalpy of non-stoichiometric uranium oxide and stoichiometric uranium dioxide.

1, experimental difference; *2*, calculated differences.

---

[28] "JANAF Thermochemical Tables", ed. D. R. STULL, Dow Chemical Company, Midland, Mich., 1965, N=PB 168–370.

whole range of temperature. Figure 3 very clearly shows that before transition temperatures, experimental *excess enthalpy* is diminished and after these temperatures it is very strongly increased. These variations are probably in connection with disorder — disproportionate transitions which occur over a range of about 20 K. The shape of experimental *excess enthalpy* curves showed that in addition to excess non-stoichiometric oxygen contribution there are also other contributions to the *excess enthalpy* : enthalpy of formation of the oxygen Frenkel defects,[29] anharmonic contribution to the enthalpy of lattice, electronic contributions.[30,31]

The values of the thermodynamic functions derived for each uranium oxide at every 50 K from 300 to 1500 K was calculated by the TERMOX computer program. The results are listed in tables 8 and 9. In figure 4 are plotted the curves for C_p variation *vs.* the temperature for $UO_{2.19}$ and $UO_{2.34}$. From figure 4 one can see that the behaviour of $UO_{2.19}$ is similar to that of $UO_{2.34}$ for the 300 to 700 K temperature range in which no change is noted. Below and above the transition tem-

Table 8

Thermodynamic data for $UO_{2.19}$

$\frac{T}{\mathrm{K}}$	$\frac{H^0(T) - H^0(298.15\,\mathrm{K})}{\mathrm{J\,mol^{-1}}}$	$\frac{C_p^0}{\mathrm{J\,mol^{-1}K^{-1}}}$	$\frac{S^0(T) - S^0(298.15\mathrm{K})}{\mathrm{J\,mol^{-1}\,K^{-1}}}$	$S^0(T) + \frac{G^0(T) - H^0(298.15\,\mathrm{K})}{T}$ $\mathrm{J\,mol^{-1}\,K^{-1}}$
300	139	65.380	0.404	0.464
350	3463	67.645	10.650	9.897
400	6907	70.133	19.842	17.268
450	10480	72.846	28.257	23.291
500	14195	75.783	36.082	28.391
550	18062	78.943	43.452	38.842
600	22093	82.328	50.464	36.823
650	26299	85.937	57.195	40.461
700	30691	89.769	63.702	43.844
750	35280	93.826	70.033	47.040
800	40077	98.106	76.224	50.097
850	45094	102.611	82.305	53.052
900	49038	87.591	100.449	54.487
950	53443	88.664	105.212	56.256
1000	57909	90.052	109.794	57.910
1050	62453	91.755	114.228	59.480
1100	67090	93.773	118.542	60.991
1150	71836	96.107	122.760	62.466
1200	76706	98.757	126.905	63.922
1250	81717	101.722	130.996	65.374
1300	86883	105.002	135.048	66.834
1350	92222	108.598	139.078	68.313
1400	97749	112.509	143.097	69.821
1450	103478	116.735	147.118	71.365
1500	109427	121.277	151.151	72.952

---

[29] R. Szwarc, *J. Phys. Chem. Solids*, **30**, 705 (1969).

[30] C. R. Brooks and R. E. Bingham, *J. Phys. Chem. Solids*, **29**, 1553 (1968).

[31] C. R. Brooks, W. E. Norem, D. E. Hendrix, J. W. Wright and W. G. Northcutt, *J. Phys. Chem. Solids*, **29**, 565 (1968).

Table 9

Thermodynamic data for $UO_{2.34}$

$\frac{T}{K}$	$\frac{H^0(T) - H^0(298.15\ K)}{J\ mol^{-1}}$	$\frac{C_p^0}{J\ mol^{-1}K^{-1}}$	$\frac{S^0(T) - S^0(298.15K)}{J\ mol^{-1}\ K^{-1}}$	$S^0(T) + \frac{G^0(T) - H^0(298.15K)}{T}$ $J\ mol^{-1}\ K^{-1}$
300	447	67.820	0.540	1.490
350	4450	68.683	12.907	12.716
400	8052	69.582	22.532	20.130
450	11530	70.101	30.726	25.624
500	15053	71.690	38.148	30.108
550	18728	75.516	45.150	34.051
600	22624	80.512	51.928	37.708
650	26793	86.332	58.597	41.220
700	31267	92.749	65.227	44.668
750	36075	99.609	71.858	48.100
800	41234	106.806	78.514	51.543
850	46760	114.261	85.212	55.012
900	51603	77.862	55.816	57.337
950	55566	80.632	60.101	58.491
1000	59663	83.182	64.302	59.663
1050	63881	85.512	68.418	60.839
1100	68210	87.620	72.446	62.009
1150	72639	89.508	76.383	63.265
1200	77157	91.176	80.228	64.298
1250	81753	92.623	83.981	65.403
1300	86416	93.849	87.638	66.474
1350	91134	94.855	91.199	67.507
1400	101271	170.337	1866.162	70.196
1450	105294	93.251	1869.042	72.336
1500	106587	41.251	1869.906	73.508

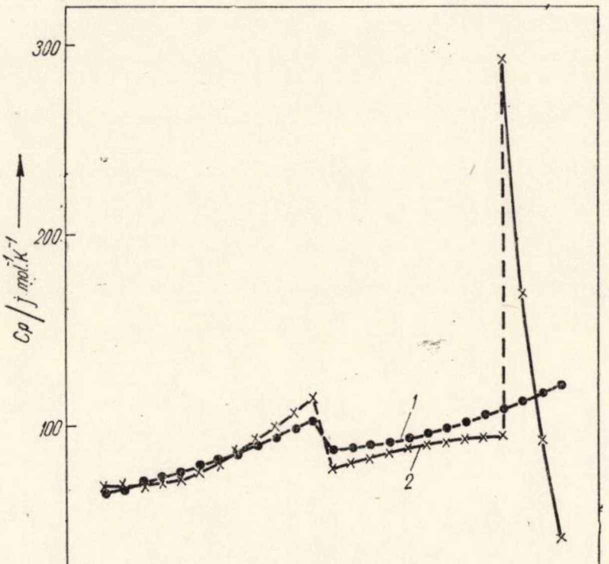

Fig. 4. — Heat capacity of studied uranium oxides.
1, $UO_{2.19}$; *2*, $UO_{2.34}$.

perature the discrepancy between heat capacities is more significant and becomes drastic for $UO_{2.34}$ in the region of the second transition temperature. In this connexion it is worth emphasizing, as already pointed out by Kelley, [32] that enthalpies are more fundamental to thermodynamic calculations than are heat capacities; the conversion of enthalpies to heat capacities is almost always unnecessary. On the other hand, for any quantitative assessment of the lattice dynamics of UO_{2+x} phase the directly measured heat capacity by high temperature adiabatic calorimetry should be more reliable than the values obtained by the differentiation of enthalpy equations resulted from drop calorimetry determinations.

Acknowledgements. We wish to express our deep gratitude to Professor I. G. Murgulescu for his interest in our work. Thanks are due to C. Volcovici for his technical assistance.

---

[32] K. K. Kelley, *U. S. Bur. Mines*, **Bull. 584.** 1960.

Revue Roumaine de Chimie, **20**, *2*, 159–168 (1975)

OVERVOLTAGE IN CHLORINE DISCHARGE ON GRAPHITE ELECTRODE IN AgCl – KCl MOLTEN MIXTURE AT VARIOUS TEMPERATURES (400–700°)

S. STERNBERG and VALERIA PETRESCU
Polytechnic Institute, Str. Polizu 1, Bucharest, Romania

Received May 13, 1974

Chlorine discharge on spectral carbon is studied in the eutectic mixture AgCl–KCl at various temperatures (400–700°). The stationary state galvanostatic method was used in order to collect current density/overvoltage curves. The ohmic drop correction was made by determining the resistance by means of the method of galvanostatic pulses. Tafel slopes corresponding to the theoretical one RT/2F were obtained at all studied temperatures for decrease current densities, proving that in this range of intensities (below 1 A/cm^2) it is the heterogeneous combination reaction which is the rate determining step. Similarly, larger Tafel slopes than the previous ones were found at all studied temperatures, for relatively high current densities (over 1 A/cm^2). The possible mechanisms of slope modifications discussed.

The chlorine discharge reaction on a graphite electrode has been investigated by a number of authors both by the stationary state method[1–3] and by the transitional state method.[4–8]

Shams el Din[1] interpreted overvoltage as being induced by an ohmic drop of tension in a surface layer. Murgulescu and Sternberg[6–8] and also Fondanaiche and Kikindai[2,3] have studied depolarization occurring at low current densities and have described it as being a nonequilibrium state of the adsorption-desorption reaction taking place on the electrode.

The chlorine adsorption phenomenon on the graphite electrode has also been studied by some authors.[2,3,9–14]

---

[1] A. M. Shams El Din, *Electrochim. Acta*, **4**, 242 (1961).

[2] J. C. Fondanaiche and T. Kikindai, *Compt. rend.*, **260**, 2801 (1965).

[3] J. C. Fondanaiche and T. Kikindai, *Compt. rend.*, **260**, 5517 (1965).

[4] P. Drossbach, *Z. Elektrochem.*, **60**, 387 (1956).

[5] R. Piontelli, O. Sternheim and F. Fumagalli, *Ricerca Sci.*, **28**, 160 (1958).

[6] S. Sternberg and D. I. Marchidan, *Z. Phys. Chem. (Frankfurt)*, **218**, 250 (1961).

[7] I. G. Murgulescu, S. Sternberg, L. Medinţev and C. Mustaţă, *Electrochim. Acta*, **8**, 65 (1963).

[8] I. G. Murgulescu, S. Sternberg and L. Medinţev, *Electrochim. Acta*, **9**, 219 (1964).

[9] J. C. Fondanaiche and T. Kikindai, *Bull. Soc. chim. France*, **5**, 1914 (1968).

[10] J. C. Fondanaiche and T. Kikindai, *Bull. Soc. chim. France*, **5**, 1921 (1968).

[11] I. G. Murgulescu, S. Sternberg and L. Bejan, *Rev. Roumaine Chim.*, **11**, 447 (1966).

[12] S. Sternberg and I. Galasiu, *Rev. Roumaine Chim.*, **13**, 991 (1968).

[13] S. Sternberg and I. Galasiu, *Rev. Roumaine Chim.*, **15**, 1169 (1970).

[14] S. Sternberg and V. Petrescu, *Rev. Roumaine Chim.*, **19** (1), (1974).

The study of overvoltage in chlorine discharge on the graphite electrode was resumed by several authors. Recently, Tunold[15] has carried out such studies for the molten system AgCl—NaCl at 600°. In order to develop a systematic study of overvoltage in chlorine discharge on a spectral graphite electrode, taking into account the variation with temperature, we used the molten mixture AgCl—KCl.

1. EXPERIMENTAL

Fig. 1. illustrates the working cell.

Electrode Ag/AgCl (a 2 mm diameter Ag rod) is highly reproducibile and reversible. This fact prompted us to use it both as a cathode and as a reference electrode.

Experiments were also made using two silver electrodes, one as a cathode and the other as a reference electrode. The results obtained were similar.

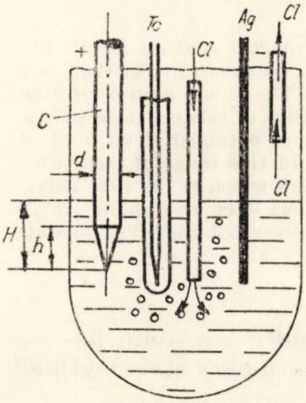

Fig. 1. — Scheme of the cell.

We used as a working electrode a 6 mm diameter rod of spectral carbon conically turned at the top and introduced into the melt with height H so as to have an approx. 1 cm² contact surface with salt. The cell (fig. 1) contains, in addition to the two electrodes, the T_c thermocouple protected by a quartz sheath and two tubes supposed to introduce and evacuate gaseous chlorine into the system.

The electrical circuit used consists of two parts, i.e. one circuit intended for the galvanostatic anodic polarization of the chlorine-carbon electrode and a second circuit devised for the measurement of the ohmic resistance of the cell (fig. 2). A third auxiliary circuit (switch K_1 in position B) serves for the "formation" of the graphite electrode.

It has been found that the equilibrium potential in the graphite electrode can be more readily achieved if conducting a few anodic polarization followed by cathodic polarizations with a 100—200 mA current for a couple of hours. This process which we have identified as being the "formation" of the working electrode facilitates attainment of the equilibrium potential of the chlorine electrode obtained by bubbling chlorine through the melt.

For each temperature we determined several sets of readings obtained both with the intensity increase and with its stepwise decrease. After each intensity change (switch K_1 in position A and variation of resistance R_1), 5—10 minutes are allowed to pass before the potential read on the electronic voltmeter VE remains constant (or at high intensity it oscillates around a constant mean value). The chlorine current through the cell was maintained throughout these measurements. After each reading, the value of the potential "at rest" was checked and recorded before beginning a set of determinations the internal cell resistance being determined at the end by the method of galvanostatic pulses. An extremely slight increase of cell resistance was found in the case of a measurement performed after anodic polarization of the electrode. Since this variation was insignificant we worked for each set of determinations with a mean resistance value between the onset value and the last value of the set.

The effective determination of cell resistance by means of the method of galvanostatic pulses involved the following procedure. The circuit intended for this measurement consists of the rectangular puls generator GI, a standard resistance R_e a switch K_2 which assures the use of the same oscilloscope OS for measuring both the potential drop on the cell (position A) and on the standard resistance R_e (position B). As a standard resistance we used $R_0 = 1\,\Omega - 10\,\Omega$.

The rectangular pulse generator was of an "Orion — Void Range frequency generator" type which enabled a possible frequence variation from 1 Hz to 500 kHz for a 0.1 V to 30 V out put terminal voltage.

---

[15] R. Tunold, H. M. Bo, K. A. Paulsen and J. O Yttredal, *Electrochim. Acta* **16**, 2101 (1971).

The following approach is made for the determination of cell resistance. The connection between the cell and the circuit intended for resistance measurement is provided by switches I_1 and I_2. It is necessary to cut off the connection with the other circuit for reasons relating to the removal of all additional impedances from the circuit, in order to diminish as much as possible signal distorsion. The pulse generator is turned on. Switch K_2 is fixed in position A — the oscilloscope is coupled to the cell. We wait the signal obtained on the oscilloscope to stabilize. A slight evolution of the signal image is found and it stabilizes relatively fast (within a few minutes).

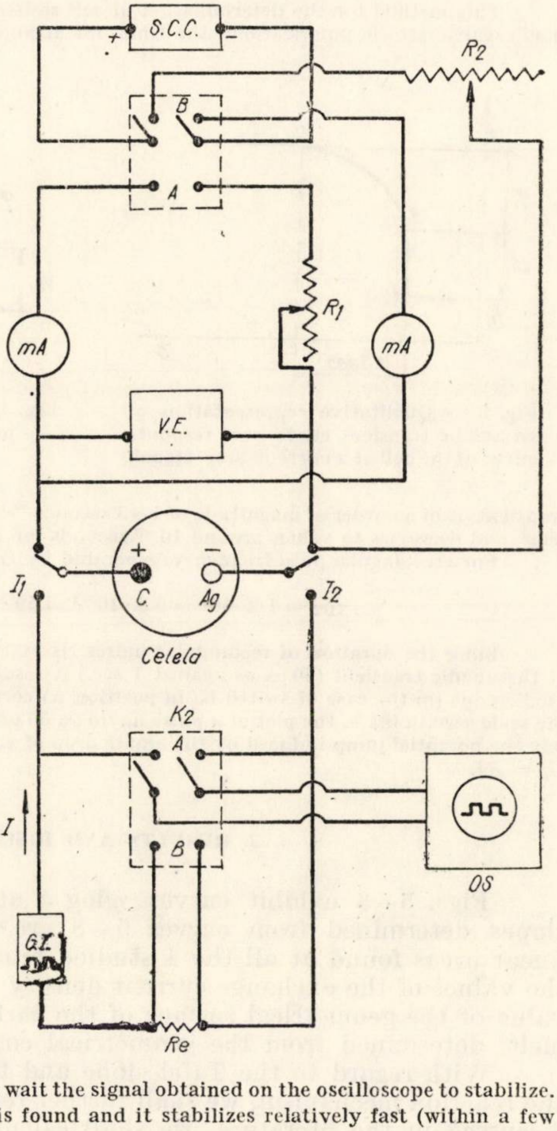

Fig. 2. — Scheme of the installation for the determination of overvoltage.

Noting by R the cell resistance to be determined; I — the current passing through the circuit Generator — Standard Resistance — Cell; U_{R_e} — the voltage drop on the standard resistance measured on the oscilloscope; U_c — the voltage drop on the cell being measured on the oscilloscope, by applying Ohm's law for the cell and the standard resistance, we find cell resistance :

$$R = \frac{U_c}{U_{R_e}} \cdot R_e \tag{1}$$

This method for the determination of cell resistance relies on the fact that, in case of anodic galvanostatic polarization, the time for attaining the stationary potential (anodic

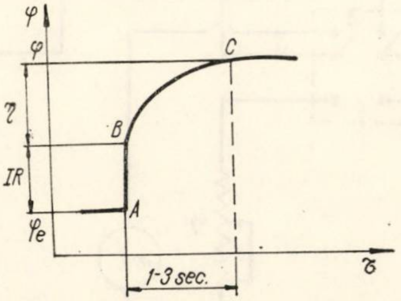

Fig. 3. — Qualitative representation of an anodic transient curve—the response curve of the cell at a current step signal.

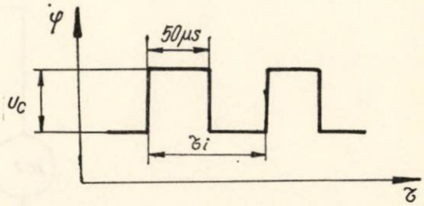

Fig. 4. — Rectangular pulses obtained on an oscilloscope as a cell response.

transient) is of an order of magnitude of 1—3 seconds [16,17] for a current intensity around 50 mA/ /cm^2 and decreases to values around 10^{-3} seconds for $I \simeq 1200$ mA/cm^2.

For a rectangular pulse frequency (generated by GI) of 10kHz, the duration of a pulse is :

$$\tau_{1/2} = 1/2 \cdot 10^4 = 0.5 \cdot 10^{-4} = 50 \cdot 10^{-6} \text{ sec} = 50 \ \mu\text{s}$$

Since the duration of rectangular pulses is extremely short compared to the duration of the anodic transient (50 μs as against 1 sec.) it results that U_c in fig. 4 measured on the oscilloscope (in the case of switch K_2 in position A) corresponds to IR in fig. 3. Evidently in the scale seen in fig. 3, the plot of a pulse having a 50 μs duration overlaps line Ab, i.e. precisely the potential jump induced by the ohmic drop of voltage of the cell.This justifies relation $U_c = RI$.

2. RESULTS AND DISCUSSION

Figs. 5—8 exhibit curves η/log i at various temperatures. Tafel slopes determined from curves 5—8 are indicated in table 1 for both linear areas found at all the 4 studied temperatures. Table 1 also shows the values of the exchange current density i_0. To calculate i_0 we used the value of the geometrical surface of the carbon found in contact with the melt, determined from the geometrical conditions resulting from fig. 9.

With regard to the Tafel slope and the information it provides on the reaction mechanism, we shall further refer to the possible mechanisms discussed in the literature, we shall calculate their corresponding theoretical slopes and we shall compare them to the experimental ones in order to identify the most plausible mechanisms.

---

[16] J. THONSTAD, *Electrochim. Acta*, **15**, 1569 (1970).

[17] W. E. TRIACA, C. SOLOMONS and J. O'M, BOCKRIS, *Electrochim. Acta*, **13**, 1949 (1968).

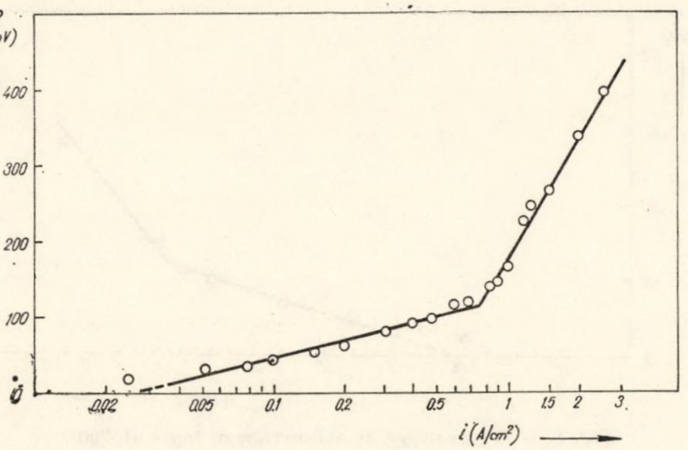

Fig. 5. — Overvoltage as a function of log *i* at 400°.

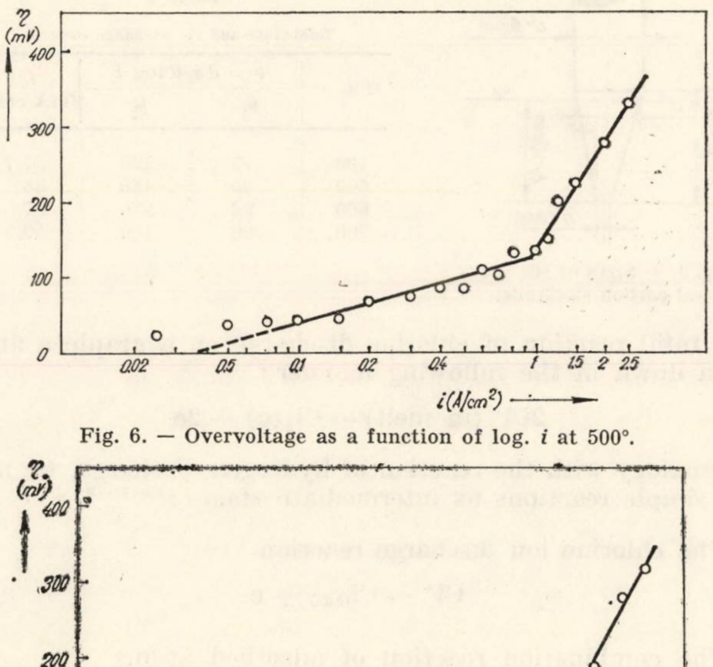

Fig. 6. — Overvoltage as a function of log. *i* at 500°.

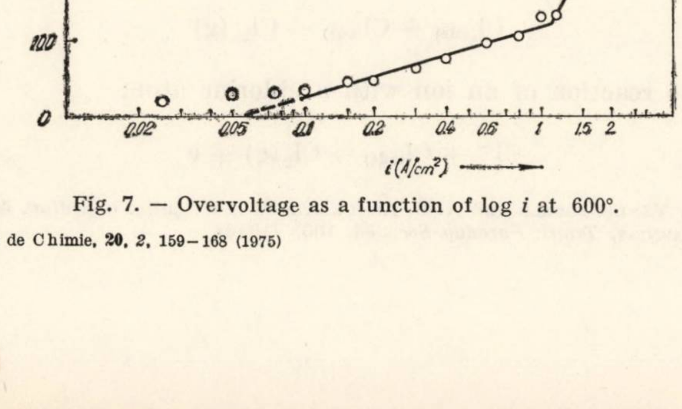

Fig. 7. — Overvoltage as a function of log *i* at 600°.

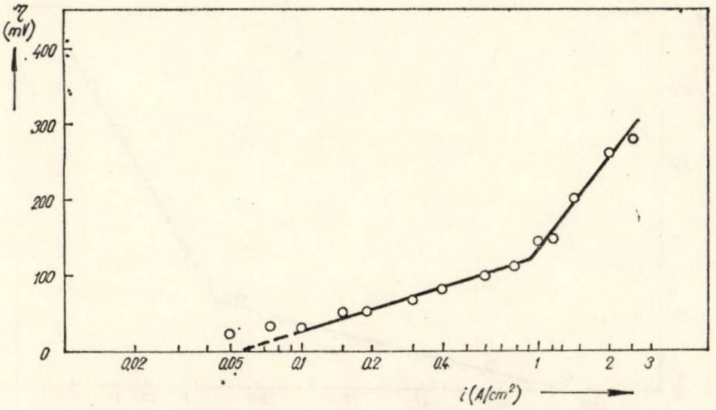

Fig. 8. — Overvoltage as a function of log i at 700°.

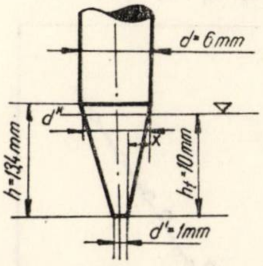

Fig. 9. — Sizes of the spectral carbon electrode.

Table 1

Tafel slope and the exchange current

T°C	$b = d\,\eta/d \log i$		i_0 (mA/cm²)
	b_1	b_2	
400	75	525	27.7
500	80	480	36
600	92	550	57.5
700	96	400	59.5

The total reaction of chlorine discharge on a graphite anode may be written down in the following manner:

$$2Cl^- \text{(in melt)} \rightarrow Cl_2(g) + 2e \tag{2}$$

By analogy with the reaction of hydrogen discharge, we may assume three simple reactions as intermediate stages: [15,17–19]

1. The chlorine ion discharge reaction

$$Cl^- \rightarrow Cl_{(ads)} + e \tag{3}$$

2. The combination reaction of adsorbed atoms

$$Cl_{(ads)} + Cl_{(ads)} \rightarrow Cl_2\ (g) \tag{4}$$

3. The reaction of an ion with a chlorine atom

$$Cl^- + Cl_{(ads)} \rightarrow Cl_2(g) + e \tag{5}$$

---

[18] H. J. Vandenbroele and A. J. Arvia. *Anales Asoc. quim. argentina*, **55**, 21 (1967).
[19] R. Parsons, *Trans. Faraday Soc.*, **54**, 1053 (1958).

These three reactions may be combined by two possible mechanisms having as a global effect reaction (2), i.e. :

A : Reaction 1 followed by reaction 2

B : Reaction 1 followed by reaction 3

Equations giving the reaction rate depend on the type of the adsorption isotherm observed by the adsorbed intermediates i.e. it may be a simple Langmuir isotherm or a Temkin — type isotherm.[20,21] In the latter case the adsorption heat is a function of the coverage degree. This adsorption may be of two types, inactivated or activated. By writing the equations of reaction rates in the three hypotheses referring to the adsorption isotherms (Langmuir, Temkin — inactivated Temkin — activated) which are possible for the three simple reactions (3, 4, 5), Tunold et al.[15] have determined according to Parsons[22] the expressions of theoretical Tafel slopes for the possible reaction mechanisms. Using these expressions we calculated the values of theoretical slopes for the 4 temperatures involved (400—700°) which we present in table 2. A comparison between the values of experimentally determined Tafel slopes (table 1) and the theoretical ones (table 2) shows, concerning the first Tafel slope, i.e. b_1, that the experimental values 75—96 mV/log unity correspond to expression RT/2F (with theoretical values 67—96 mV). According to table 2, the only possible reaction that may lead to such slopes is the combination reaction 2 under the conditions of the Langmuir adsorption isotherm or of the inactivated Temkin isotherm. Vandenbroele and Arvia,[18] Triaca et al.[17] and Tunold et al.[15] found the same slope RT/2F for other chlorides and other temperatures. Since for a stationary state anodic process it os very unlikely that $\theta \to 0$ and it is much more likely that $0.2 < \theta < 0.8$ it results that tfe anodic process of chlorine discharge at current densities up to 1 A/cm^2 is controlled by a combination reaction developed under the conditions of the Temkin adsorption isotherm.

For large current densities (over 1 A/cm^2) the Tafel slopes experimentally obtained (table 1) compared to the theoretical ones (table 2) lead to various reaction development mechanisms as a function of temperature. For $T = 400°$ the experimental Tafel slope is considerable larger than the largest theoretical slope (experimental 525 mV as against theoretical 400 mV). This would correspond to the coupled mechanism 1 + 2 following the activated Temkin adsorption isotherm. For the other temperatures, experimental values are closer to theoretical values. Thus at 500°, slope $b_2 = 480$ mV is relatively close to the theoretical slope 458 mV/log. unit. which corresponds to the coupled mechanism 1 + 2, with the activated Temkin adsorption isotherm. Similarly, at 600° the experimental slope $b_2 = 550$ mV corresponds to a theoretical slope of 517 mV/log. unit., also for a coupled mechanism 1 + 2, with the activated Temkin isotherm. At 700° the situation changes, obtaining relatively smaller experimental slope for b_2 than at the other temperatures, namely

---

[20] E. Gileadi, B. E. Conway, in "Modern Aspects of Electrochemistry" vol. 3, ed. JO'M. Bockris and B. E. Conway, Butterworths, London, 1964.

[21] J. G. N. Thomas, *Trans Faraday Soc.*, **57**, 1603 (1961).

[22] R. Parsons, *J. Chim. phys.*, **49**, C 82 (1952).

Table 2

Theoretical Tafel slopes for various possible reaction mechanisms

Mechanism		A, Reaction 1 + 2				Mechanism	B, Reaction 1 + 3			
Ads. isotherm / Rate controlling step		Langmuir		Temkin		Ads. isotherm / Rate controlling step	Langmuir		Temkin	
		$\theta \to 0$	$\theta \to 1$	$\theta \approx 0.5$			$\theta \to 0$	$\theta \to 1$	$\theta \approx 0.5$	
				inact.	activated				inact.	activated
Single mechanism, reaction 2 rate-controlling, η small		$\frac{RT}{2F}$	$\to \infty$	$\frac{RT}{2F}$	$\frac{RT}{2\alpha_2 F}$	Single mechanism reaction 3 rate-controlling, η small	$\frac{RT}{(1+\alpha_3)F}$	$\frac{RT}{\alpha_3 F}$	$\frac{RT}{(1+\alpha_3)F}$	$\frac{RT}{2\alpha_3 F}$
$\alpha_1 = \alpha_2 = \alpha_3 = 0.5$	400°C	67		67	133		89	266	89	133
	500°C	77		77	153		102	306	102	153
	600°C	86		86	173		115	344	115	173
	700°C	96		96	193		128	396	128	193
Coupled mechanism, η large		$\frac{RT}{\alpha_1 F}$	$\to \infty$	$\frac{(2+\alpha_1)RT}{2\alpha_1 F}$	$\frac{(2\alpha_2+\alpha_1)RT}{2\alpha_1, \alpha_2 F}$	Coupled mechanism, η large	$\frac{RT}{\alpha_1 F}$	$\frac{RT}{\alpha_3 F}$	$\frac{(1+\alpha_1)RT}{\alpha_1(1+\alpha_3)F}$	$\frac{(\alpha_3+\alpha_1)RT}{2\alpha_1\alpha_3 F}$
$\alpha_1 = \alpha_2 = \alpha_3 = 0.5$	400°C	266		333	400		266	266	266	266
	500°C	306		382	458		306	306	306	306
	600°C	344		430	517		344	344	344	344
	700°C	396		482	578		396	396	396	396

400 mV/log. unit., which is fairly close to the theoretical slope 396 mV/log. unit. met in several possible mechanisms : reaction 3 with the Langmuir isotherm at $\theta \to 1$ or a coupled mechanisms 1 + 3 any of the 3 variants referring to the adsorption isotherm. Slope $b = 396$ mV/log. unit. (at 700°) actually corresponds to relation $b = RT/0.5F$, that is to say, to the discharge reaction (3).

In table 3 we have synthesized this comparison between experimental and theoretical results, also indicating the possible mechanisms suggested by this information.

The following conclusions may be reached from the above results. For a rather large interval of current densities (up to about 1000 mA/cm^2) the process is controlled by the recombination reaction (2) all along the investigated temperature interval. In this case, the Tafel slope increases proportional to the absolute temperature according to relation $b = RT/2F$ and overvoltage depends on the coverage degree θ which is higher than the coverage degree at a reversible potential.

In a series of previous papers, Sternberg and Galasiu[23,24] have shown that for the activated carbon — halogn electrode, both the coverage degree and the desorption rate show relatively slight variation with temperature. The same fact is likely to happen also with the spectral carbon, which accounts for the relative small increase of the exchange current with temperature (table 1).

Table 3

Possible mechanisms for various values of the Tafel slopes

T°C	b_{exp}	$b_{theoret}$	Possible mechanisms
400	75	67	Reaction 2, activated Temkin isotherm
500	525	400	Coupled mechanism 1 + 2, activated Temkin
	80	77	Reaction 2, inactivated Temkin isotherm
600	480	458	Coupled mechanism 1 + 2, activated Temkin
	92	86	Reaction 2, inactivated Temkin
700	550	517	Coupled mechanism, 1 + 2 activated Temkin
	96	96	Reaction 2, inactivated Temkin
	400	396	Reaction 3, Langmuir isotherm or reaction 1 + 3 (any isotherm)

---

[23] S. Sternberg and I. Galasiu, *Electrochim. Acta*, in press.

[24] S. Sternberg and I. Galasiu, *Rev. Roumaine Chim.*, in press.

With larger current densities (above 1000 mA/cm^2) Tafel slopes are much larger and decrease with temperature. In this case we obviously deal with a coupled mechanism, very likely following reaction (1) and (2). In the case of the coupled mechanism, theoretical calculations [19,21,22] show that b >RT/0.5 F. The coverage degree is very likely to be higher than 0.5 and for this reason, experimental slopes are larger than the calculated ones. With the temperature increase it may be assumed that the recombination reaction rate (2) increases very much and becomes at a certain moment higher than the reaction rate (1). This explains the decrease of constant b with temperature in the domain of large current densities. At 700°, constant b equals RT/0.5 F, the electrode process being probably controlled by reaction (1).

It was shown that at relatively low current densities, the overvoltage is slowly established in approx. 1—3 seconds. For instance, at 50 mA/cm^2 the overvoltage is of about 30 mV and the anodic transient is of 1 — 3 seconds. An apparent electrode capacity is obtained :

$$\bar{C} = \frac{\Delta Q \cdot 10^6}{\eta} = \frac{(1-3)\cdot 0.050}{0.030} \approx (1.5 - 4.5)\cdot 10^6 \mu\mathrm{F} \qquad (6)$$

In the domain of large overvoltage, for instance at $i = 1250$ A/cm^2 when $\tau = 10^{-3}$ seconds one obtains :

$$\bar{C} = \frac{10^{-3}\cdot 1.250 \cdot 10^6}{0.225} \approx 5\cdot 10^3 \mu\mathrm{F} \qquad (7)$$

The capacity of the double layer of solid electrodes [25,26] in molten salts is of approx. 100 μF/cm^2.

One obtains a ratio $S_{\mathrm{real}}/S_{\mathrm{geometrical}} \approx 50$, which is in agreement with other observations. Therefore, in the domain of high overvoltages, transient τ may be attributed to the double layer charging.

The apparent capacity obtained by relation (6) is of about 10^3 times larger than that found by relation (7) and cannot be explained by the double layer charging. This behaviour may be explained if we admit that the amount of electricity $i\tau$ is consumed for covering the carbon electrode by adsorbed chlorine. The authors have made a systematic study of chlorine electrochemical adsorption on activated carbon on which an apparent capacity of about $60 \cdot 10^6$ μF/cm^2 has been obtained.

Considering that this carbon has a much larger real surface than the spectral one, we may say that the order of magnitude is observed.

---

[25] E. A. Ukshe, *Elektrokhimya*, 4, 1116 (1968).

[26] S. Sternberg and T. Vişan, *Rev. Roumaine Chim.*, **18**, 221 (1973).

Revue Roumaine de Chimie, **20**, *2*, 169–175 (1975)

ON THE ELECTRICAL CONDUCTIVITY OF MOLTEN ALKALI HALIDES

LAURA VASU
Centre of Physical Chemistry
Str. Galaţi 31, Bucharest, Romania

Received December 21, 1973

In this paper, the temperature dependence of the electrical conductivity of molten alkali halides is explained on the basis of a lattice model with vacancies, describing the transport as an activated process. It is found that the experimental activation energy for electrical conductivity is mainly the jump energy of the ions into vacancies.

It is a well established experimental fact that the temperature dependence of the equivalent electrical conductivity of molten alkali halides is almost perfect exponential, expressed by an Arrhenius relation :

$$\lambda = A_e^{-B/RT} \tag{1}$$

(A, B are constants), which is suggesting for an activated process.

As well known, a very good framework for describing activated processes is given by the theory of rate processes, on condition that structural details of the substance be known or guessed. We emphasize that the theory of rate processes should be a suitable tool for describing transport processes in molten alkali halides. This theory implicitly assumes an amount of local order. In molten alkali halides a local order due to the coulombian forces is expected.

Recently, it has been theoretically proved[1] that molten alkali halides, at the melting point, have a quasi-crystalline local structure, well expressed in terms of a cellular hole model (a lattice vacancy model).

Consequently, we shall start from a cellular model with holes, corresponding to a quasi-crystalline lattice with vacant sites.

Considering the ionic transport through the melt by the displacement of vacancies, we have the basic equation for the diffusion[2] of i-type holes :

$$D_i = k_0^i \frac{n_i}{N} d^2 \tag{2}$$

---

[1] I. G. Murgulescu and G. Vasu, *Rev. Roumaine Chim.*, **11**, 681 (1966).

[2] D. K. Majumdar, *Z. phys. Chem.* (*Leipzig*), **233**, 374 (1966).

where D_i is the diffusion coefficient, k_0^i — the jump frequency, $\frac{n_i}{N}$ — the hole ratio (all referred to i-type holes), and d — the distance of jump, i.e. the path of the diffusing ion.

If we write the jump of the ions in the melt as an activated process, the jump frequency of the i ion is :

$$k_0^i = \frac{kT}{h}\frac{Z_i^*}{Z_i}\exp(-e_0^i/kT) = \left(\frac{kT}{2\pi m_i}\right)^{1/2}\frac{\exp(-e_0^i/kT)}{v_f^{1/3}} \tag{3}$$

where Z_i^*, Z_i are partition functions for an i ion in the activated and inactivated state; v_f — free volume/particle, m_i — mass of i—type ion, and e_i^0 — activation energy for jump of i—type ion.

Now, taking into account the fact that the displacement of a hole is associated to a charge transport and using the Nernst-Einstein equation

$$\lambda_i = \frac{F^2}{RT}D_i \tag{4}$$

from (2), (3) and (4) we obtain for the equivalent electrical conductivity λ_i associated to the motion of i—type holes :

$$\lambda_i = \frac{1.118\times10^9}{T}\frac{\mathrm{d}^2}{v_f^{1/3}}\left(\frac{kT}{2\pi m_i}\right)^{1/2}\frac{n_i}{N}\exp(-e_0^i/kT)\ \mathrm{ohm}^{-1}\,\mathrm{cm}^2 \tag{5}$$

The values : v_f, $\frac{n_i}{N}$, $e_0{}^i$ and d are to be defined in the particular case of molten alkali halides.

Free volume. We shall use McLellan's approximation,[3] i.e. linear dependence of the free volume on the number of neighbouring holes. McLellan defines an y parameter as the ratio : number of occupied positions/total number of positions, and by minimizing the free energy, shows that for reduced temperatures below 10, y may be well approximated by the occupation degree θ defined as $\theta = V_S/V_L$, i.e the ratio of the solid (extrapolated) volume V_S to the liquid volume V_L.

For molten alkali halides, it was shown[1] that y is indeed well approximated by θ.

Therefore, we use McLellan's approximation in the form :

$$v_f = (1-\theta)W = (1-\theta)\frac{V\theta}{2N} \tag{6}$$

where

$$\theta = V_S/V_L \tag{7}$$

---

[3] A. G. Mc.Lellan, *J. Chem. Phys.*, **40**, 567 (1964).

Hole ratio. It was verified, in a theoretical work,[1] that the number of holes in the melt — as a function of temperature — is not given by an exponential equation, but may be expressed in terms of the occupation degree θ.

If the conductivity process has no restriction (jumps by pairs, for instance), the effective hole ratio to be taken into account is $\frac{1-\theta}{\theta}$. But the jumps of two neighbouring opposite charge ions in the same direction — jumps by pairs — which may interfere with smaller probability, can be ineffective for electrical conduction. The difference between the jump frequency of an ion in a hole and in a pair of holes is in part due to the difference between the jumps energies. We proceed to a comparison with the crystalline state. In solid alkali halides, the jump energy of positive ions in a pair of vacancies is close to or slightly higher than that of a jump in a vacancy.[4,5] In the melt, differences between jump energies can be even smaller and, therefore, we suppose that the same energy of jump may be used.

Therefore, the probability to have a pair of holes being $\left(\frac{1-\theta}{\theta}\right)^2$, the effective single hole fraction is :

$$\frac{n}{N} \approx \left[\frac{1-\theta}{\theta} - Z\alpha\left(\frac{1-\theta}{\theta}\right)^2\right] \tag{8}$$

where Z is the number of the next neighbours from the hypothetical structure of the solid ($Z = 6$) and α is a parameter <1.

From all hole pairs in the melt, only those pairs which have the dipole axes in the same direction with the electric field are ineffective and of these a small fraction is associated in "effective" groups of three holes. That means that the parameter α must be somewhat smaller than $\frac{1}{3}$; we have chosen for α the value $\frac{1}{4}$.

Jump distance, d, is difficult to estimate. We can approximate it in terms of the molar volume as :

$$d \approx \left(\frac{V\theta}{N}\right)^{1/3} \tag{9}$$

We have now all the parameters in eq. (5) well defined.

---

[4] K. Thamarlingam and A. B. Lidiard, *Phil. Mag.*, **69**, 1157 (1961).

[5] N. Laurance, *Phys. Rev.*, **120**, 57 (1960).

The formula for the equivalent electrical conductivity of a MX alkali halide is then :

$$\lambda_{MX} = 1.118 \times 10^{9} \left(\frac{V\theta}{N}\right)^{2/3} \frac{2^{1/3}N^{1/3}}{V^{1/3}\theta^{1/3}} \left\{ \frac{\dfrac{1-\theta}{\theta} - \dfrac{3}{2}\left(\dfrac{1-\theta}{\theta}\right)^{2}}{(1-\theta)^{1/3}T^{1/2}} \right\} \left(\frac{k}{2\pi}\right)^{1/2} \times$$

$$\times \left[\frac{\exp(-e_0^{+}/kT)}{m_{+}^{1/2}} + \frac{\exp(-e_0^{-}/kT)}{m_{-}^{1/2}} \right] \tag{10}$$

which for ions of nearly equal masses, where $e_0^{+} \approx e_0^{-} = e_0$, becomes :

$$\lambda_{MX} = 6.043 \times 10^{4}\, V^{1/3}\theta^{1/3} \left\{ \left[\frac{1-\theta}{\theta} - \frac{3}{2}\left(\frac{1-\theta}{\theta}\right)^{2} \right] \Big/ (1-\theta)^{1/3}T^{1/2} \right\} \times$$

$$\times \left(\frac{1}{M_{+}^{1/2}} + \frac{1}{M_{-}^{1/2}} \right) \exp(-E_0/RT) \tag{11}$$

or

$$\lambda_{MX} = A_T \exp(-E_0/RT), \tag{12}$$

A_T is a preexponential factor, temperature dependent, and E_0 is the mean jump energy of the ions pro mol.

In the particular case of some molten alkali halides, the calculated A_T values (by introducing the experimental value of θ) are nearly constant for a wide range of temperature (table 1).

The calculated values of the preexponential factor are comparable with the experimental ones (taking into account the difference between the reported experimental values) and are almost similar with the experimental preexponential factors for salts with ions of nearly equal sizes and masses (see KCl).

This means that the experimental exponential factor B has the same significance as E_0, supporting the idea that temperature differences of the various factors from A_T cancel out each other. This conclusion is in agreement with an earlier paper[6] in which we have proceeded to a comparison with crystals and have found that the experimental activation energy for electrical conductivity in molten alkali halides is mainly the energy of motion of the ions into vacancies (see table 1).

Supposing the existence of a Stokes-Einstein relation, if the free volume and the hole ratio are correctly estimated, an "ideal" ionic conductivity of i-type ions, without restrictions due to pairs, i.e. for which

---

[6] I. G. Murgulescu and L. Vasu, *Rev. Roumaine Chim.*, **15**, 837 (1970).

Table 1

Electrical conductivity of some molten alkali halides

Salt	T, K	*) A_T calcd. ohm^{-1}cm^2	$A_{\text{exp.}}$ ohm^{-1}cm^2	E^e_m calcd. kcal/mol	$B_{\text{exp.}}$ kcal/mol
NaCl	1073	576	441^7, 544^8	2.7	2.5^7, 3.0^8
	1173	559			
KCl	1043	514	535^7, 548^8	3.3	3.4^7, 3.4^8
	1173	523			
RbCl	995	478	546^0, 754^8	4.5	4.0^9, 4.4^8
	1073	470			
NaBr	1020	351	406^7, 623^8	2.8	2.4^7, 3.2^8
	1123	361			
KBr	1007	451	581^7, 591^8	3.5	3.7^7, 3.75^8
	1073	451			
NaI	935	415	447^7, 694^8		
	1023	417			

*) the values for V and θ are taken from the references: [1], [7], [8], [9], [10]

the effective hole ratio is $\frac{1-\theta}{\theta}$, is related to the viscosity of the fused salt by:

$$\eta = \frac{k \times 1.118 \times 10^9}{A\pi r_i \lambda_0^i} \tag{13}$$

where r_i = radius of i—type ions and $A = 4$.

Let us have an "ideal" ionic conductivity $\lambda_0^i = \frac{\lambda_0}{2}$ given by:

$$\lambda_0^i = \frac{6.043 \times 10^4}{2} V^{1/3}\theta^{1/3}\left\{\left(\frac{1-\theta}{\theta}\right)\bigg| (1-\theta)^{1/3} T^{1/2}\right\} \times$$

$$\times \left(\frac{1}{M_+^{1/2}} + \frac{1}{M_-^{1/2}}\right)\exp(-E_0/RT) \tag{14}$$

---

[7] Şt. Zuca and L. Ionescu-Vasu, *Rev. Roumaine Chim.*, **12**, 1285 (1967).

[8] G. J. Janz "Molten Salts Handbook", Academic Press, New York, 1967, p. 45, 47, 288, 289.

[9] Şt. Zuca and M. Olteanu, *Rev. Roumaine Chim.*, **13**, 1567 (1968).

[10] C. J. West "International Critical Tables", McGraw-Hill, New York, London, 1933, part 1, p. 150, 153 and part. 3 p. 43, 44.

and take λ experimental/2 as an effective mean ionic conductivity; then the "ideal" experimental ionic conductivity would be:

$$\lambda_0^i \exp = \frac{\lambda \exp}{2}\left\{\left(\frac{1-\theta}{\theta}\right)\Big/\left[\left(\frac{1-\theta}{\theta}\right)-\frac{3}{2}\left(\frac{1-\theta}{\theta}\right)^2\right]\right\} \tag{15}$$

and the viscosity of the melt:

$$\eta = \frac{2k \times 1.118 \times 10^9}{4\pi r_m \cdot \lambda_0^i \exp} \tag{16}$$

where

$$r_m = \frac{r_+ + r_-}{2}$$

Evidently, this oversimplified treatment is valid only for salts with cations and anions of similar size and mass. The best test is the computation of η and its temperature dependence for an adequate salt – KCl – (see table 2).

Table 2

Viscosity of some molten alkali chlorides

Salt	T K	η calcd. C.P.	η exp C.P.
KCl	1043	1.11	1.20[11]
	1173	0.87	0.85
KBr	1007	1.24	1.19 [12]
	1073	1.06	1.04
RbCl	995	1.46	1.38 [11]
	1073	1.21	1.07

The correlations already reported refer to temperature dependence of the electrical conductivity of molten alkali halides at constant pressure (λ_p); it is interesting to see if the same model can also explain the temperature dependence of conductivity at constant density (λ_V). The experimental values of λ_V are obtained from constant temperature and constant pressure measurements, using the equation[13]:

$$(\partial \ln \lambda/\partial T)_V = (\partial \ln \lambda/\partial T)_p (\partial P/\partial T)_V \tag{17}$$

The experimental activation energy at constant pressure, – in fact Gibbs free energy[14] is related to that at constant volume through the thermodynamic relation:

$$E_P = E_V + PV \tag{18}$$

---

[11] I. G. Murgulescu and St. Zuca, *Z. phys. Chem (Leipzig)*, **222**, 360 (1963).

[12] I. G. Murgulescu and St. Zuca, *Z. phys. Chem. (Leipzig)*, **218**, 379 (1961).

[13] B. Cleaver, S. I. Smedley and P. N. Spencer, *J. Chem. Soc. Faraday Trans I*, **9**, 1720 (1972).

[14] A. B. Lidiard "Ionic Conductivity" in "Handbuch der Physik" S. Flügge ed. Band XX, Springer Verlag, Berlin, 1957, p. 277.

so that:

$$E_V \approx E_P - RT \tag{19}$$

If we use the already established formula:

$$\lambda_V \sim \frac{d^2}{v_f^{1/3}\, T^{1/2}} \frac{n}{N} \exp\left(-E_0/RT\right)$$

to calculate constant volume value λ_V, a slight change in the temperature dependence of the preexponential factor can interfere.

At $V =$ constant, the distance of jump $d \approx$ constant and also $\frac{n}{N} =$ $=$ constant so that:

$$\lambda_V \sim T^{-1/2}\, v_f^{-1/3} - \exp\left(-E_V/RT\right) \tag{20}$$

but, as the two temperature factors, $T^{-1/2}$ and $v_f^{-1/3}$ change in opposite directions, the preexponential factor is almost constant. It results:

$$\lambda_V = A_V \exp\left(-E_V/RT\right) \tag{21}$$

with E_V taken as the mean jump energy at constant volume.

The experimental measurements at constant density[13] give an Arrhenius dependence of λ_V on temperature.

Table 3

Comparison between calculated and experimental values of E_V

Salt	$E_V$calcd. kcal/ mol	E_V exp.[13]. kcal/mol
KCl	1.4	1.7
RbCl	2.0	1.9
CsCl	1.9−2.1	2.0
KBr	1.7	2.0
RbBr	1.7−1.2	1.9

The correspondence between the experimental constant volume activation energy and calculated E_V is satisfactory, taking into account the combined incertitude due to approximations and experiment.

CONCLUSIONS

This oversimplified picture introduces many approximations, but the conclusions we can reach are not affected by these approximations:

— McLellan's approximation of the free volume is sufficiently good for molten alkali halides with opposite charged ions of nearly equal masses and sizes.

— The experimental activation energy for electrical conductivity is mainly the energy of jump of ions into vacancies.

— A Stokes-Einstein relation is verified only by taking into account that jumps by pairs (which may be the main effective jumps in the process of viscous flow,[15]) are not effective in the process of electrical mobility.

---

[15] GH. VASU, *Rev. Roumaine Chim.*, **14**, 167 (1969).

Revue Roumaine de Chimie, **20**, *2*, 169−175 (1975)

Revue Roumaine de Chimie, 20, 2, 177–194 (1975)

THE ELECTRONIC STRUCTURE AND SPECTRA OF TITANIUM TETRACHLORIDE AND THE METHYLTITANIUM CHLORIDES

D. R. ARMSTRONG, P. G. PERKINS, and
J. J. P. STEWART

Dept. of Pure and Applied Chemistry
University of Stratholyde
Glasgow, C. 1, Scotland

Received February 13, 1974

The electronic structure and spectra of the series of methyltitanium chlorides of general formula $Me_{11}TiCl_{4-n}(n = 0 - 4)$ are calculated by the all-valence-electron self-consistent molecular orbital method. In $TiCl_4$ the highest filled orbitals fall in the energy sequence $1t_1 > 3t_2 > 1e > 2t_2 > 2a$; and their energies are in good agreement with data obtained from the photoelectron spectrum of the compound. The energies calculated for the lower electronic excited states are in accordance with the observed electronic spectrum. The methyl compounds are built up electronically from essentially separate contributions from titanium, chlorine, and the methyl groups. The orbitals governing the titanium methyl σ bond lie at high energies and the low-lying excited states of the compounds involve excitations from these orbitals to those antibonding across the same link. The excited states fit satisfactorily to the observed electronic spectra where these are known and explain the photolytic lability of the compounds. The formal charge on the titanium atom decreases continuously across the series from $TiCl_4$ to Me_4Ti.

1. INTRODUCTION

The electronic structure and spectrum of $TiCl_4$ has been previously calculated by various authors. Early calculations on the system were performed using the simple Wolfsberg-Helmholtz approximation[1,2] and by means of qualitative ligand field theory.[3,4] Later calculations were more sophisticated : Fenske[5] obtained atomic charges, eigenvalues and bond orders but the method used has been criticised on the grounds of inconsistency.[6] There have been three calculations on $TiCl_4$ by a CNDO MO SCF scheme. Dahl and his co-workers have obtained ground-state properties, first by preliminary[7] and then from a thorough calculation on

---

[1] (*a*) A. Viste and H. B. Gray, *Inorg. Chem.*, **3**, 1113 (1964);
(*b*) H. Basch, A. Viste and H. B. Gray, *Theor. Chim. Acta*, **3**, 459 (1965).

[2] L. Oleari, G. DeMichelis, and L. Di Sipio, *Molecular Physics*, **10**, 111 (1966).

[3] C. Dijkgraaf, *Spectrochim. Acta*, **21**, 769 (1965).

[4] C. Dijkgraaf and J.P.G. Rousseau, *Spectrochim. Acta*, **24**, 1212 (1968).

[5] R. F. Fenske and D. D. Radtke, *Inorg. Chem.*, **7**, 479 (1968).

[6] J. P. Dahl and C. J. Ballhausen, *Adv. In Quantum Chem.*, **4**, 170 (1967).

[7] J. P. Dahl and H. Johansen, *Theor. Chim. Acta*, **1**, 8 (1968).

$TiCl_4$.[8] In the latter work the minimum energy of the molecule was obtained by optimisation of the valence orbitals. Although this approach is most elegant, the eigenvectors reported in ref.[8] lead to the ground-state electronic configuration: Ti, $4s^{1.73}\ 4p^{3.07}\ 3d^{2.26}$, Cl, $3s^{1.82}\ 3p^{4.42}$. If the overlap charge partitioning is neglected, the configuration affords a negative charge on the titanium atom of 3.06, whilst each chlorine atom shows an electron deficit of 0.76. These results do not seem in accord with chemical intuition, especially the large electron population of the titanium $4p$ orbital.

The third previous investigation of $TiCl_4$ was concerned solely with its electronic absorption spectrum.[9] In this particular work, the electronic bands were assigned on the basis of orbital-orbital excitation only. Assignments of this type suffer from the severe approximation that the exchange integral K_{ik} is neglected in the expression for the singlet configuration energy

$$\varepsilon_{i\rightarrow k} = \varepsilon_k - \varepsilon_i - J_{ik} + 2K_{ik}$$

This means that only one energy band is predicted per interorbital gap, even when the levels involved are highly degenerate. Hence, error occurs when the experimental bands are correlated with energy gaps. We have therefore recalculated the energies of these lower excited states of $TiCl_4$, including all electronic interaction terms, and have further improved the state energies by extensive second-order configuration interaction.

Titanium also forms the series of organometallic compounds $Me_n TiCl_{4-n} (n = 1 - 4)$. All are photosensitive and coloured; on cooling, $MeTiCl_3$ yields a yellow liquid which freezes to a purple, crystalline solid,[10] whilst Me_2TiCl_2 affords a black, crystalline solid[11] at $-80°C$ but spontaneously decomposes in the dark at room temperature, with a half-life of ~ 2 hours.[10] Further, Me_3TiCl has been prepared but not fully characterised, whilst Me_4Ti is yellow, volatile, and decomposes at temperatures $> -10°C$.[12] Because of the sensitivity of these compounds to light, coupled with their intrinsic thermodynamic instability, little detailed information is available about their optical spectra in the visible and ultraviolet regions.

Interest in these compounds stems mainly from the intriguing nature of the metal-carbon bond. The strengths of such transition-metal-carbon σ bonds are demonstrably low and many such compounds containing them are highly labile. Many, like $MeTiCl_3$, are light-sensitive, undergoing fission of the bond in question and producing free radicals. Moreover, reactions involving this bond are of great technical importance — for example, the Ziegler-Natta catalyst.[13] The compound $MeTiCl_3$ has been examined previously by Dijkgraaf and Rousseau[14] and these authors have also discussed its electronic structure and spectrum.

---

[8] C. A. L. Becker and J. P. Dahl, *Theor. Chim. Acta*, **14**, 26 (1969).

[9] C. A. L. Becker, C. J. Ballhausen, and I. Trabjerg, *Theor. Chim. Acta*, **13**, 355 (1969).

[10] A. P. Gray, A. B. Callear, and F. H. C. Edgecombe, *Canad. J. Chem.*, **41**, 1502 (1963).

[11] C. Beerman and H. Bestian, *Angew. Chem.*, **71**, 618 (1959).

[12] K. Clauss and C. Beerman, *Angew. Chem.*, **71**, 617 (1959).

[13] J. Boor, *Makromol. Revs.*, 2, 115 (1967).

In the latter work, on account of the photosensitive nature of the material, considerable difficulty was encountered in obtaining a reliable spectrum but absorptions at 25,000 and 43,000 cm^{-1} were reported. These two bands were assigned, on the basis of symmetry arguments, to $^1A_1 \rightarrow {}^1A_2$ and $^1A_1 \rightarrow {}^1E$ state excitations, respectively. The authors also constructed a simple energy-level diagram and put forward the limited ground-state configuration of the compound as $(1a_1)^2\,(1e)^4(2a_1)^2(3a_1)^2(2e)^4(1a_2)^2$. Although useful, this theoretical scheme is only qualitative and hence, in order to throw light on (i) the nature and stability of the metal-carbon bond, (ii) the reasons for the photosensitivity of the compound, and (iii) the electronic spectra of these compounds, we also performed a series of calculations of the electronic structures of the ground and excited states of these molecules.

2. CALCULATIONAL METHODS

The method of calculation used was a modified version[15] of the CNDO MO SCF procedure.[16] In constructing the Fock matrix elements we propose a somewhat different and improved approach to that which has hitherto been employed. Thus, the diagonal element of the Fock matrix (**1**) becomes (**2**) under zero differential overlap.

$$F_{\mu\mu} = H_{\mu\mu} + \sum_{\lambda\sigma} P_{\lambda\sigma}\left[<\mu\mu\,|\,\lambda\sigma> - \frac{1}{2}<\mu\lambda\,|\,\mu\sigma>\right] \tag{1}$$

$$F_{\mu\mu} = H_{\mu\mu} + \sum_{\lambda} P_{\lambda\lambda}<\mu\mu\,|\,\lambda\lambda> - \frac{1}{2} P_{\mu\mu}<\mu\mu\,|\mu\mu> \tag{2}$$

When all the atoms are completely separated, relation (3) is given, *i.e.*, the occupancy of orbital λ in the isolated

$$P_{\lambda\sigma} = 0,\ P_{\lambda\lambda} = P^{q}_{\lambda\lambda} \tag{3}$$

atom, and $F_{\mu\mu}$ is then the self-consistent energy of an electron in orbital μ. Now, for an atom of configuration ns^p, np^q, nd^r, we have expression (4) for the energy of an electron in any orbital, λ, where $U^{0}_{\lambda\lambda}$ and $U^{-1}_{\lambda\lambda}$ are the valence-state ionisation potentials of the same orbital in the neutral atom

$$E_{\lambda} = \frac{1}{2} P^{q}_{\lambda\lambda}\,(U^{0}_{\lambda\lambda}) + \left(1 - \frac{1}{2} P^{q}_{\lambda\lambda}\right)(U^{-1}_{\lambda\lambda}) \tag{4}$$

---

[14] C. Dijkgraaf and J. P. G. Rousseau, *Spectrochim Acta*, **25**A, 1455 (1969).

[15] (*a*) D. H. Brown, P. G. Perkins, and J. J. P. Stewart, *J. Chem. Soc.*, 1972, 1105. (*b*) D. R. Armstrong, P. G. Perkins, and J. J. P. Stewart, *J. Chem. Soc.*, **1971**, 3674.

[16] J. A. Pople, D. P. Santry, and G. A. Segal, *J. Chem. Phys.*, **43**, S129 (1965).

and negative ion, respectively. This expression has the correct behaviour at values of $P^q_{\lambda\lambda}$ of 0, 1, and 2 and we assume that the E_λ obtained by interpolating non-integral values of $P^q_{\lambda\lambda}$ are physically sensible.

If we now write equation (5), we can then obtain equation

$$\gamma_{\lambda\lambda} = U^{-1}_{\lambda\lambda} - U^0_{\lambda\lambda} \tag{5}$$

(6) and thus (7) and (8).

$$E_\lambda = \frac{1}{2} P^q_{\lambda\lambda} \, (U^0_{\lambda\lambda}) + \left(1 - \frac{1}{2} P^q_{\lambda\lambda}\right) (U^0_{\lambda\lambda} + \gamma_{\lambda\lambda}) \tag{6}$$

$$F_{\mu\mu} = U^0_{\mu\mu} + \gamma_{\mu\mu}\left(1 - \frac{1}{2} P^q_{\mu\mu}\right) \tag{7}$$

$$= H_{\mu\mu} + \sum_\lambda P^q_{\mu\mu}\gamma_{\lambda\mu} - \frac{1}{2} P_{\mu\mu}\,\gamma_{\mu\mu} \tag{8}$$

If the atoms are now considered to be at positions where there is significant interaction, then the orbital occupancy $P^q_{\lambda\lambda}$ will deviate from that of the ground state of the atom (*i.e.*, an integral number). Thus we have equation (9) and this is the form of Fock diagonal which is employed in the

$$\begin{aligned} F_{\mu\mu} &= U^0_{\mu\mu} - \sum_\lambda P^q_{\lambda\lambda}\,\gamma_{\lambda\mu} + \gamma_{\mu\mu} + \sum_\lambda P_{\lambda\lambda}\,\gamma_{\lambda\mu} - \frac{1}{2} P_{\mu\mu}\,\gamma_{\mu\mu} \\ \textit{i.e.,}\ F_{\mu\mu} &= U_{\mu\mu} + \sum_\lambda (P_{\lambda\lambda} - P^q_{\lambda\lambda})\,\gamma_{\lambda\mu} + \left(1 - \frac{1}{2} P_{\mu\mu}\right)\gamma_{\mu\mu} \end{aligned} \tag{9}$$

present series of calculations. If equation (9) is rewritten using the Pople-type 'atomic' repulsion integrals, then we obtain equation (10).

$$F_{\mu\mu} = U^0_{\mu\mu} + \sum_\lambda (P_{\lambda\lambda} - P^q_{\lambda\lambda})\,\gamma_{AB} + \left(1 - \frac{1}{2} P_{\mu\mu}\right)\gamma_{AA} \tag{10}$$

The middle term becomes :

$$\begin{aligned} \sum_\lambda (P_{\lambda\lambda} - P^q_{\mu\mu})\,\gamma_{AB} &= \sum_B \sum_\lambda^{B} (P_{\lambda\lambda} - P^q_{\lambda\lambda})\,\gamma_{AB} \\ &= \sum_B (P_{BB} - P^q_{BB})\,\gamma_{AB} \\ &= \sum_B (P_{BB} - Z_{BB})\,\gamma_{BB} \\ &= \sum_{B\neq A} (P_{BB} - Z_B)\gamma_{AB} + (P_{AA} - Z_A)\,\gamma_{AA} \end{aligned}$$

The final term is :

$$\left(1 - \frac{1}{2} P_{\mu\mu}\right)\gamma_{AA}$$

so, taken together, we have equation (11) which reduces

$$F_{\mu\mu} = U^{0}_{\mu\mu} + \sum_{B \neq A}(P_{BB} - Z_{B})\gamma_{AB} + \left(P_{AA} - \frac{1}{2} P_{\mu\mu} + 1 - Z_{A}\right)\gamma_{AA} \qquad (11)$$

to the Pople-Segal-Santry equation.

One-centre, two-electron repulsion integrals for titanium $<4s\ 4s/4s\ 4s>$, $<4p\ 4p/4p\ 4p>$ and $<3d\ 3d/3d\ 3d>$are needed and these were accorded the single value 9.0 eV. This was obtained as an average of the exactly computed individual values. Ref.[17] recommends the adoption of a scaling procedure for the off-diagonal elements of the electron repulsion matrix but a minor change in the method of carrying this out for the excited-state calculation is here proposed. This arises from the fact that when very diffuse orbitals are involved, *e.g.*, the $3d$ set on chlorine, the usual method of scaling to evaluate the two-electron two-centre integrals (the Mataga[18] and Ohno[19] methods) are less appropriate. In ground-state calculations, diffuse atomic orbitals are usually less important and the loss in accuracy resulting from using Mataga-based approximations is insignificant. However, excited-state calculations involve virtual orbitals which frequently incorporate large contributions from diffuse orbitals and so the above approximations must be re-examined. By analogy with the Ballhausen[20] modification of the M–W–H approximation[21] for one-electron matrix elements, we propose that the off-diagonals of the electron repulsion matrix be calculated from the equation

$$\gamma_{ij} = \frac{14.397}{\left(\dfrac{14.397^{2}}{\gamma_{ii} \times \gamma_{jj}} + r^{2}\right)^{\frac{1}{2}}}$$

The difference brought about by this new approximation is very slight in all cases where normal 'contracted' valence orbitals are in use. The remaining input parameters for the calculation are given in table 1. Bond orders, valencies, and anisotropies are defined in ref.[22]

Titanium tetrachloride is regularly tetrahedral with Ti–Cl bond length of 0.217 nm.[23] None of the shapes of the four organometallic compounds is known : however, Me_4Ti is almost certainly similar to $TiCl_4$. It seems unlikely that significant error will ensue from assuming that the intermediates can be derived from $TiCl_4$ and Me_4Ti. Their symmetries are, therefore, $MeTiCl_3$, C_{3v}; Me_2TiCl_2, C_{2v} and Me_3TiCl, C_{3v}.

---

[17] K. A. Levison and P. G. Perkins, *Theor. Chim. Acta*, **14**, 206 (1969).

[18] N. Mataga and K. Nishimoto, *Z. Phys. Chem. (Frankfurt)*, **13**, 140 (1957).

[19] K. Ohno, *Theor. Chim. Acta*, **2**, 219 (1964).

[20] C. J. Ballhausen and H. B. Gray, *Inorg. Chem.*, **1**, 111 (1967).

[21] M. Wolfsberg and L. Helmholtz, *J. Chem. Phys.*, **20**, 837 (1952).

[22] D. R. Armstrong, P. G. Perkins, and J. J. P. Stewart, *J. Chem. Soc.*, 1973, 838.

[23] H. Uehara and Y. Morino, *J. Chem. Phys.*, **45**, 4543 (1966).

The bond length of Ti – C in tetrabenzyl titanium has been determined by X-ray analysis[24] and lies between 0.213 and 0.215 nm. In all the compounds studied here, the Ti – C bond length is given the value 0.215 nm. The Ti – Cl bond length was taken as 0.2183 nm[23] and the C – H bond length as 0.11 nm. Tetrahedral angles were assumed throughout.

Table 1

Input data

	VSIP's (eV)			Two-electron integrals (eV)			Orbital Exponents		
	s	*p*	*d*	*s*	*p*	*d*	*s*	*p*	*d*
Ti^c	6.07	3.35	5.58		⟵ 9.00 ⟶		1.075	0.725	2.28
Cl^a	25.29	13.99	2.20	15.33	13.20	7.52	2.183	1.733	1.000
H^b	13.06	—	—	17.00	—	—	1.000	—	—
C^b	19.44	10.67	—	15.60	14.37	—	1.550	1.325	—

a. ref. 17

b. ref. 15*b*

c. ref. 1*b*

In order to separate the states generated from transitions between degenerate molecular orbitals, a first-order configuration interaction treatment is necessary. This is particularly relevant to $TiCl_4$ and $TiMe_4$. Moreover, to improve the states still further, a second-order treatment is valuable. In the present work the calculations were performed on configurations generated from all possible transitions from the six highest filled to the nine lowest vacant molecular orbitals. In such a large configuration interaction calculation a difficulty arises in discussing the nature of a molecular electronic state in terms which are helpful and illuminating. The difficulty may be alleviated to some extent by constructing a density matrix representation of the configurations which contribute to the overall state.

Let the ith electronic state be composed of a linear combination of configurations formed by an excitation of an electron from molecular orbital *j* to molecular orbital *l* : *i.e.*,

$$\Phi^i = \sum_{jl} a_{jl} \Psi^l_j$$

Then the density matrix element of the occupied (${}^{i0}P_{\lambda\sigma}$) and the empty (${}^{ie}P_{\lambda\sigma}$) 'state orbital' is given by

$$ {}^{i0}P_{\lambda\sigma} = \sum_l \sum_j C_{j\lambda}\, C_{j\sigma}\, a^2_{jl} $$

$$ {}^{ie}P_{\lambda\sigma} = \sum_l \sum_j C_{l\lambda}\, C_{l\sigma}\, a^2_{jl} $$

where $C_{j\lambda}$ is the eigenvector of atomic orbital λ in the jth molecular orbital.

---

[24] I. W. Bassi, G. Allegra, R. Scordamaglia, and G. Chioccoola, *J. Amer. Chem. Soc.*, **93**, 3787 (1971).

3. RESULTS AND DISCUSSION

In presenting and discussing the results, it is convenient to deal with $TiCl_4$ first and then with the organometallics as an integral group.

3.1. MOLECULAR ORBITAL LEVELS OF $TiCl_4$

The calculated eigenvalues are presented in table 2. The ordering for the ground-state levels disagrees slightly with that of Fenske[5] and of Dahl[8] in that their ordering for the first four levels is $\mathbf{1}t_2<\mathbf{1}a_1<2t_2<2a_1$: our results invert levels **1** and 2 and levels 3 and 4. For the virtual orbitals the agreement with the Fenske order ($2e<4t_2<5t_2<3e$) is reasonable, whereas the results of Dahl (order : $3a_1<4t_2<2e<5t_2$) are totally dissimilar.

The results of a recent determination of the photoelectron spectrum of $TiCl_4$[25,26] are also presented in table 2. On the usual assumption that Koopman's theorem[27] holds and, hence, that the calculated and observed energy levels are directly comparable, the agreement between these is good. Furthermore, the energy level assignments derived from the photoelectron spectrum are in accord with our computed orbital symmetries.

Table 2

Calculated orbital energies for titanium tetrachloride (eV)

Orbital			Orbital energy (eV)	
11	Unfilled	$5t_2$	1.59	
10		$3a_1$	1.46	
9		$4t_2$	−1.39	
8		$2e$	− 1.65	
7	Filled	$1t_1$	−11.82	−11.78[a]
6		$3t_2$	−11.93	−12.78[a]
5		$1e$	−13.26	−13.23[a]
4		$2t_2$	−13.68	
3		$2a_1$	−14.24	−13.97[a]
2		$1t_2$	−24.77	
1		$1a_1$	−28.00	

[a] energies abstracted from the photoelectron spectrum; refs. [26,27]

Orbital 1 is a combination of the *s* orbitals of the titanium and of the four chlorine atoms. The second orbital ($1t_2$) is almost exclusively formed from the 3*s* orbitals of chlorine. The remaining five occupied orbitals form a band of energy levels from −11.82 eV to −14.24 eV. The third orbital ($2a_1$) is composed of 3*s* and 3*p* orbitals of chlorine and the *s* orbital of the titanium, whilst the $2t_2$ orbitals are largely composed of the 3*p* orbitals of the chlorines. The major components of the fifth orbital (1*e*) are the 3*p* orbitals on the chlorines combined with a minor amount (6%) of the 3*d* orbitals on titanium. Orbital levels 6, the $3t_2$, are also predominantly composed of 3*p* orbitals on the chlorine together with moderate titanium 3*d* orbital participation (16%). Finally, the highest filled molecular orbitals ($1t_1$) are again composed of the 3*p* orbitals of the chlorine atoms.

---

[25] P. A. Cox, S. Evans, A. Hammett and A. F. Orchard, *Chem. Phys. Letters*, **7**, 414 (1970).

[26] J. C. Green, M. L. H. Green, P. J. Joachim, A. F. Orchard, and D. W. Turner, *Phil. Trans.*, **A268**, 111 (1970).

[27] T. A. Koopmans, *Physica*, **1**, 104 (1933).

The first and second sets of lowest vacant orbitals are largely composed of the *3d* orbitals of titanium with 94% and 80% participation, respectively. The ordering of these two sets of levels is gratifyingly consistent with the $e<t_2$ order predicted by simple application of a tetrahedral crystal field in a Ti^{n+} ion. However, in addition, our calculation reveals the antibonding nature of these orbitals. Orbital 10 ($3a_1$) is composed of the titanium *4s* orbital (80%) and the *3s* orbitals of the chlorine atoms (12%), whilst the $5t_2$ orbital is chiefly built from the *4p* orbital of titanium.

3.2. ELECTRONIC SPECTRUM OF TiCl_4

Two separate calculations on the excited states of the TiCl_4 molecule were performed. The first considered 54 configurations stemming from transitions from the six highest filled to the nine lowest empty orbitals, whilst the second dealt with the excited states of T_2 symmetry only, arising from transitions from the twelve highest filled to the nine lowest vacant orbitals. The object of this second series of calculations was to apply extended configuration interaction to the calculation of those excited states to which transitions are allowed by symmetry. The calculated electronic states and the experimental spectrum of TiCl_4 are presented together in table 3. Inclusion of the extra t_2 configurations induces only a small change in the energies of the lower electronic states but for higher-energy states the effect is significant. Agreement between the calculated and experimental data over the seven observed bands is fairly good and, hence, our calculation gives a satisfying account of the electronic spectrum. It is a feature of the results that the calculated states occur in groups which are associated with 'single' experimental bands. However, the energy separations between the calculated states is small within each group and natural line widths will tend to blur the experimental states together. This is a feature which could be investigated more closely experimentally, however, and until that time our assignments must necessarily retain a degree of inexactitude. The intensities are helpful and, although they are not correlatable on an absolute basis, there is a generally satisfactory differential order here over the whole spectrum.

The nature of the excited states is revealed by the density matrix elements governing the contribution of the excited configurations to the overall state. These are given in table 4. In general, the excitations possess charge-transfer character involving electron transfer from the *3p* orbitals on chlorine to empty orbitals centred essentially on the titanium atom. For convenience, the *3d* orbitals on titanium are divided into the subsets $3d(e)$ and $3d(t_2)$. For the first twelve transitions the excitation is to the *3d* orbitals on the titanium, with the $d(e)$ component being the more important in the first, second and fifth transitions. The remaining states (12 –22) involve excitations to the *4p* orbitals on the titanium.

Table 3

Calculated excited states for Ti Cl_4

	Calculation 1			Calculation 2			Experimental spectrum [a]	
Symmetry	Energy (eV)	Oscillator strength	Principal configuration	Energy (eV)	Oscillator strength	Principal configuration	Every (eV)	Relative intensity
T_1	3.92		$3t_2 \rightarrow 2e$					
T_2	3.93	0.001	$3t_2 \rightarrow 2e$	3.92	0.001	$3t_2 \rightarrow 2e$	4.0	sh.
T_2	4.16	0.005	$1t_1 \rightarrow 2e$	4.11	0.000	$1t_1 \rightarrow 4t_2$		
E	4.35		$1t_1 \rightarrow 4t_2$					
T_1	4.39		$1t_1 \rightarrow 2e$					
T_2	4.46	0.0002	$1t_1 \rightarrow 2e$	4.25	0.002	$1t_1 \rightarrow 2e$	4.43	0.9
E	4.50		$3t_2 \rightarrow 4t_2$					
T_1	4.50		$3t_2 \rightarrow 4t_2$					
T_1	4.71		$1t_1 \rightarrow 4t_2$					
A_2	4.89		$1t_1 \rightarrow 4t_2$					
T_2	5.47	0.266	$3t_2 \rightarrow 4t_2$	4.86	0.060	$1t_1 \rightarrow 2e$	5.38	1.0
A_1	6.69		$3t_2 \rightarrow 4t_2$					
T_2	7.04	0.021	$3t_2 \rightarrow 5t_2$	6.10	0.001	$2t_2 \rightarrow 2e$	7.07	2.2
E	7.23		$3t_2 \rightarrow 5t_2$	6.14	0.026	$1e \rightarrow 4t_2$		
T_1	7.24		$3t_2 \rightarrow 5t_2$	6.65	0.123	$2t_2 \rightarrow 4t_2$		
T_1	7.37		$1t_1 \rightarrow 3a_1$					
A_1	7.40		$3t_2 \rightarrow 5t_2$					
T_2	7.42	0.008	$3t_2 \rightarrow 3a_1$	7.09	0.039	$3t_2 \rightarrow 5t_2$	7.39	4.2.
E	7.60		$1t_1 \rightarrow 5t_2$	7.25	0.033	$1a_1 \rightarrow 4t_2$		
A_2	7.66		$1t_1 \rightarrow 5t_2$	7.40	0.013	$3t_2 \rightarrow 3a_1$		
T_1	7.71		$1t_1 \rightarrow 5t_2$	8.13	0.203	$1e \rightarrow 5t_2$		
T_2	8.58	0.752	$1t_1 \rightarrow 5t_2$					
				9.14	0.056	$1e \rightarrow 5t_2$	9.35	1.9
				9.23	0.013	$2t_2 \rightarrow 3a_1$		
				9.84	0.075	$2a_1 \rightarrow 5t_2$	10.04	4.1
				10.42	1.069	$2a_1 \rightarrow 5t_2$		

[a] ref [9]

Table 4

The density matrix elements for the occupied and empty 'state orbitals' for the electronic transitions of titanium tetrachloride *

State	Occupied orbital					Empty orbital						
	Titanium	Chlorine				Titanium				Chlorine		
	$s, p, d(e)$,	$d(t_2)$	s	p	d		s p	$d(e)$	$d(t_2)$	s	p	d
1 T_1	all elements zero to the second significant figure	0.17	all elements zero to the second significant figure	0.83	all elements zero to the second significant figure		elements zero to the seconde significant figure	0.89	0.04	0.00	0.07	0.00
2 T_2		0.17		0.83				0.88	0.05	0.00	0.07	0.00
3 T_2		0.08		0.92				0.35	0.50	0.01	0.14	0.01
4 E		0.02		0.98				0.00	0.80	0.01	0.18	0.01
5 T_1		0.00		1.00				0.91	0.02	0.00	0.06	0.00
6 T_2		0.00		1.00				0.40	0.46	0.00	0.13	0.01
7 E		0.15		0.85				0.00	0.80	0.01	0.18	0.01
8 T_1		0.17		0.83				0.06	0.75	0.01	0.18	0.01
9 T_1		0.00		1.00				0.02	0.78	0.01	0.18	0.01
10 A_2		0.00		1.00				0.00	0.80	0.01	0.18	0.01
11 T_2		0.09		0.91		0.03	0.07	0.23	0.52	0.01	0.14	0.01
12 A_1		0.17		0.83		0.00	0.32	0.00	0.51	0.02	0.14	0.01
13 T_2		0.16		0.84		0.22	0.63	0.00	0.01	0.05	0.07	0.93
14 E		0.17		0.83		0.00	0.89	0.00	0.01	0.03	0.06	0.96
15 T_1		0.17		0.83		0.02	0.87	0.00	0.01	0.03	0.06	0.96
16 T_1		0.00		1.00		0.60	0.20	0.00	0.02	0.08	0.08	0.00
17 A_1		0.17		0.83		0.00	0.57	0.00	0.29	0.02	0.10	0.87
18 T_2		0.14		0.86		0.38	0.46	0.00	0.00	0.06	0.07	0.91
19 E		0.00		1.00		0.00	0.89	0.00	0.01	0.03	0.06	0.96
20 A_2		0.00		1.00		0.00	0.89	0.00	0.01	0.03	0.06	0.96
21 T_1		0.00		1.00		0.16	0.70	0.00	0.01	0.05	0.06	0.93
22 T_2		0.04		0.96		0.15	0.62	0.02	0.08	0.04	0.07	0.00

* data taken from calculation *1*.

3.3. VALENCE ELECTRON DISTRIBUTION IN $TiCl_4$

The valence electron populations in $TiCl_4$ are listed in table 5. The fact that titanium bears a large positive charge (+1.59) is in keeping with

Table 5

Electronic charge distribution in the series of compounds $Ti\ Cl_n\ Me_{4-n}$ ($n = 0 - 4$)

		$TiCl_4$	$TiCl_3Me$	$TiCl_2Me_2$	$TiClMe_3$	$TiMe_4$
Ti	$4s$	0.47	0.49	0.50	0.51	0.51
	$4p_x$ $4p_y$ $4p_z$	0.28	0.26	0.24	0.22	0.21
$3d_{x^2-y^2}$ $3d_{z^2}$		0.11	0.09	0.07	0.05	0.03
$3d_{xz}$ $3d_{xy}$ $3d_{yz}$		0.35	0.44	0.53 0.49 0.53	0.58	0.65
Nett charge on Ti		+1.40	+1.23	+1.09	+0.96	+0.85
Nett charge on Cl		−0.35	−0.37	−0.40	−0.41	—
Nett charge on C		—	−0.37	−0.38	−0.38	−0.39
Average Nett charge on H		—	+0.09	+0.08	+0.07	+0.06

chemical intuition based on the relative electronegativities of chlorine and titanium. The occupation of the titanium $4p$ orbitals (0.60) is much smaller than that calculated by Becker and Dahl (3.07).[8] The 'extra' charge on the chlorine resides mainly in the $3p$ orbitals.

3.4. THE METHYLTITANIUMHALIDES, ORBITAL ENERGIES

The first results of interest, because they should throw light on the reactivity and lability of the molecules, are the sequences of orbital energies. These results for all the compounds are shown in tables 6−9 and figures 1−4.

Table 6

Orbital energies for Me Ti Cl_3 (eV)

Symmetry	Energy	Orbital Character
$9a_1$	11.41	$C-H\sigma^*$
$9e$	9.78	$C-H\sigma^*$
$8a_1$	4.52	Ti $s+p$
$7a_1$	4.28	Ti $p+s$
$8e$	4.23	Ti P
$7e$	0.25	Ti d
$6a_1$	0.18	$Ti-C\sigma^*$
$6e$	−0.13	Ti d
$5a_1$	−9.81	$Ti-C\sigma$ bond
$1a_2$	−11.05	Cl p
$5e$	−11.27	Cl p
$4e$	−11.36	Cl p
$3e$	−12.57	Cl p
$4a_1$	−12.90	Cl p
$3a_1$	−13.18	Cl p
$2e$	−13.86	C−H
$1e$	−24.99	Cls−Ti p
$2a_1$	−27.48	Cls−Tis
$1a_1$	−37.73	C−H

Table 7

Orbital energies for Me_2 Ti Cl_2 (eV)

Symmetry	Energy	Orbital Character
$8b_1$	12.09	$C-H\ \sigma^*$
$12a_1$	11.99	
$4a_2$	10.44	
$7b_1$	10.41	
$7b_2$	10.38	
$11a_1$	10.36	
$10a_1$	5.30	$s+p$ on Ti
$6b_1$	5.17	p on Ti
$9a_1$	5.00	$p+s$ on Ti
$6b_2$	4.98	p on Ti
$5b_2$	0.97	d on Ti
$8a_1$	0.94	
$5b_1$	0.87	$Ti-C\ \sigma^*$
$3a_2$	0.60	d on Ti
$7a_1$	0.59	
$4b_1$	−8.92	$Ti-C\ \sigma$ bonds
$6a_1$	−9.50	
$4b_2$	−10.69	p on Cl
$3b_2$	−10.70	p on Cl
$2a_2$	−10.88	p on Cl
$3b_1$	−11.26	p on Cl
$5a_1$	−12.03	p on Cl
$4a_1$	−12.46	p on Cl
$1a_2$	−12.80	C−H
$2b_1$	−12.94	C−H
$2b_2$	−13.46	C−H
$3a_1$	−13.55	C−H
$1b_2$	−24.43	Cls−Ti
$2a_1$	−25.99	Cls−Ti
$1b_1$	−36.03	C−H
$1a_1$	−38.05	C−H

The SCF results for $MeTiCl_3$ (figure 1, table 6) show clearly that it can be described electronically in terms of the sum of three distinct entities, *i.e.*, a methyl group, a set of three Ti$-$Cl σ bonds and a non-bonding set of nine molecular orbitals derived from the $3p$ orbitals on chlorine.

Although some mixing of these does occur, a good general basis for a description of the electronic structure of $MeTiCl_3$ can be obtained by assuming no mixing whatsoever. Accordingly, it is possible to set up a correlation diagram showing how these moieties are placed in the energy scale.

Table 8

Orbital energies for Me_3 Ti Cl (eV)

Symmetry	Energy	Orbital Character
$11e$	12.63	C$-$H σ^*
$10a_1$	12.48	C$-$H σ^*
$10e$	10.96	C$-$H σ^*
$2a_2$	10.96	C$-$H σ^*
$9e$	10.87	C$-$H σ^*
$9a_1$	10.87	C$-$H σ^*
$8a_1$	5.95	*s* on Ti
$8e$	5.80	*P* on Ti
$7a_1$	5.61	*P* on Ti
$6a_1$	1.55	*d* on Ti+ +Ti$-$C σ^*
$7e$	1.47	Ti$-$C σ^*
$6e$	1.20	*d* on Ti
$5e$	$-$ 8.35	Ti$-$Cσ
$5a_1$	$-$ 9.47	Cl *p*+Ti+C
$4e$	$-$10.56	Cl *p*
$1a_2$	$-$11.30	Ti$-$C σ
$4a_1$	$-$11.77	Cl *p*+Ti+C
$3e$	$-$12.30	C$-$H
$2e$	$-$13.02	C$-$H
$3a_1$	$-$13.16	*s* on Cl
$2a_1$	$-$24.71	
$1e$	$-$35.53	C$-$H
$1a_1$	$-$38.37	C$-$H

Table 9

Orbital energies for Ti Me_4 (eV)

Symmetry	Energy	Orbital Character
$7t_2$	13.08	C$-$H σ^*
$4a_1$	12.88	C$-$H σ^*
$2t_1$	11.41	C$-$H σ^*
$3e$	11.36	C$-$H σ^*
$6t_2$	11.30	C$-$H σ^*
$3a_1$	6.50	*s* on Ti
$5t_2$	6.34	*P* on Ti
$4t_2$	1.98	Ti$-$C σ^*
$2e$	1.72	*d* on Ti
$3t_2$	$-$ 7.88	Ti$-$C σ
$1t_1$	$-$10.83	C$-$H pure
$2a_1$	$-$10.96	Ti$-$C+C$-$ $-$H
$1e$	$-$12.24	C$-$H
$2t_2$	$-$12.76	C$-$H
$1t_2$	$-$35.11	C$-$H
$1a_1$	$-$38.69	C$-$H

The orbital which figures mainly in the titanium-carbon σ bond is of high energy and separated by $\sim$1 eV from the essentially non-bonding molecular orbitals derived from chlorine. The accidental degeneracy expected for the non-bonding M.O.'s is slightly lifted by Cl$-$Cl and Cl$-$Ti interactions and hence a band of energies, $\sim$2 eV wide, is generated. Of the virtual orbitals, the σ^* titanium-carbon antibonding orbital is almost degenerate, with two sets of π M.O.'s derived from the $3d$ orbitals on Ti. In the higher energy levels the $4s$ and $4p$ orbitals on Ti figure largely, followed at $\sim$10 eV by the methyl C$-$H antibonding group.

As we pass from $MeTiCl_3$ through Me_2TiCl_2 to Me_3TiCl, generally corresponding orbital levels shift to progressively higher energies (figures 2 and 3). This is due principally to the change in electronegativity on passing from chlorine to the methyl group as substituent. Chlorine binds electrons more closely than methyl, and this effect is carried over into compounds in which it participates. The overall positive charge on tita-

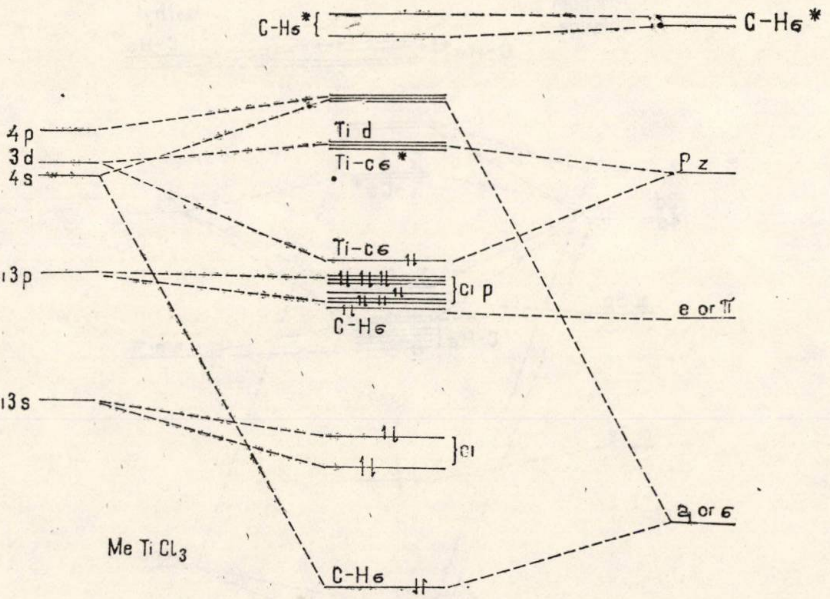
C-Hσ*
C-Hσ*
4p
3d
4s
Ti d
Ti-cσ*
Pz
Ti-cσ
cl 3p
cl p
C-Hσ
e or π
cl 3s
cl
a1 or σ
Me Ti Cl3
C-Hσ

Fig. 1. — Correlation diagram for $MeTiCl_3$.

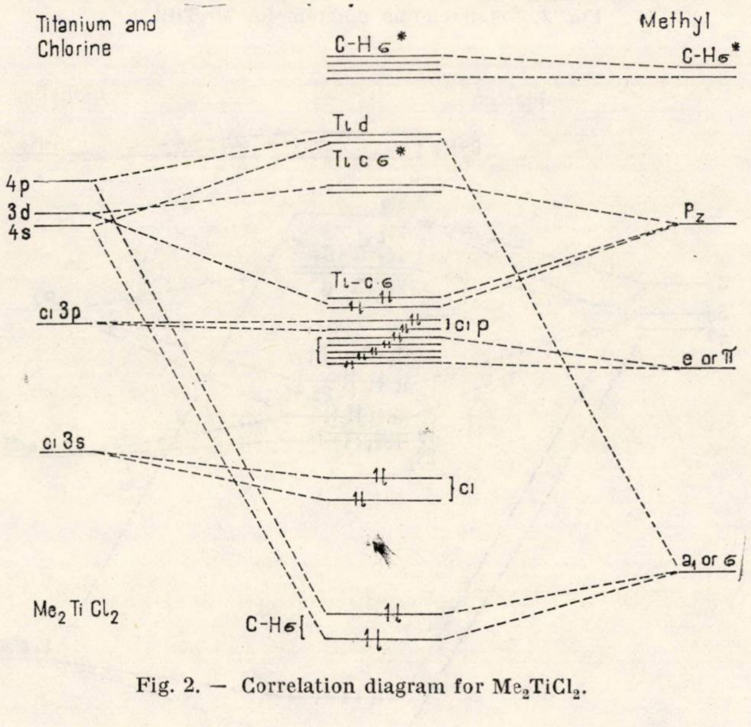
Titanium and
Chlorine
Methyl
C-Hσ*
C-Hσ*
Ti d
Ti cσ*
4p
3d
4s
Pz
Ti-cσ
cl 3p
cl p
e or π
cl 3s
cl
a1 or σ
Me2 Ti Cl2
C-Hσ

Fig. 2. — Correlation diagram for Me_2TiCl_2.

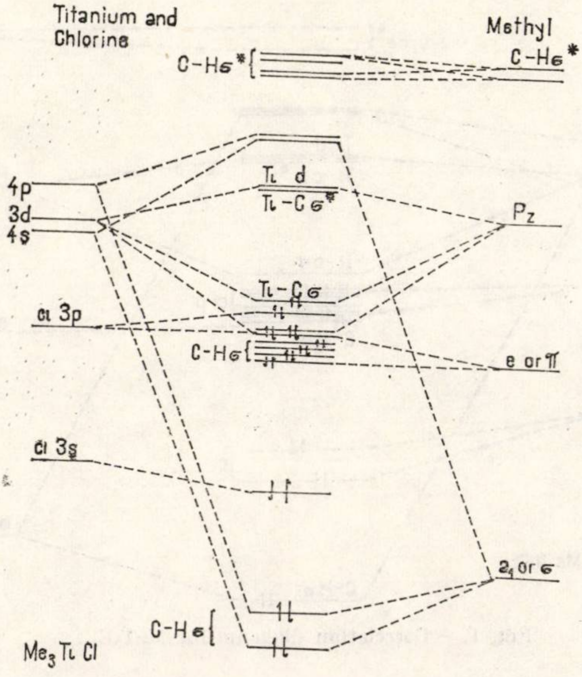
Titanium and Chlorine
Methyl
C-Hσ*
C-Hσ*
4p
3d
4s
Ti d
Ti-C σ*
Pz
Ti-C σ
Cl 3p
C-Hσ
e or π
Cl 3s
a₁ or σ
C-Hσ
Me₃ Ti Cl

Fig. 3. – Correlation diagram for Me_3TiCl.

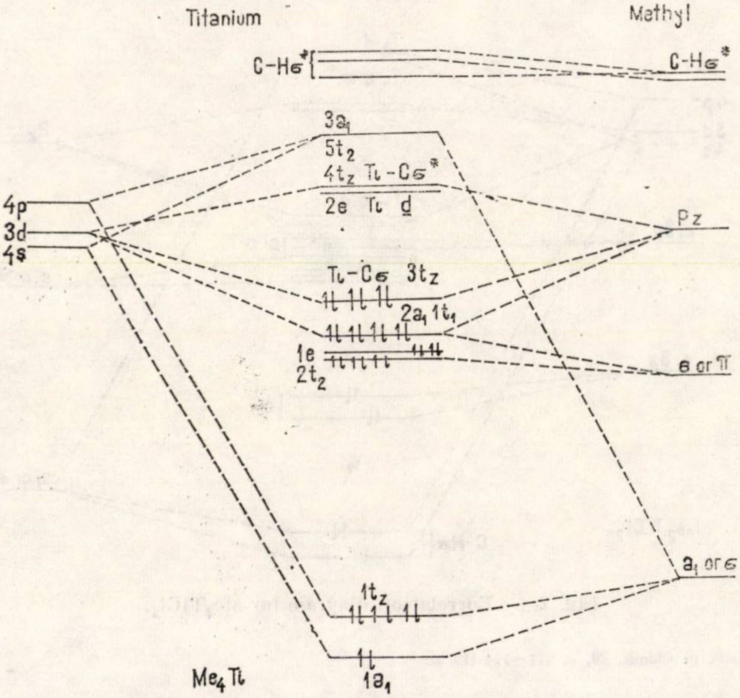
Titanium
Methyl
C-Hσ*
C-Hσ*
3a₁
5t₂
4t₂ Ti-Cσ*
2e Ti d
4p
3d
4s
Pz
Ti-Cσ 3t₂
2a₁ 1t₁
1e
2t₂
e or π
a₁ or σ
1t₂
1a₁
Me₄ Ti

Fig. 4. – Correlation diagram for Me_4Ti.

nium steadily decreases as the number of methyl groups increases (table 5) and, as a result, electron-electron repulsion on titanium increases. This effect manifests itself in the steady rise in energy of the virtual orbitals over the series, since these are dominated in character by the σ^*s, p and d orbitals on titanium.

It might be expected that, in all these compounds, the filled Ti$-$C σ bonding orbital would lie at the highest energy and this is indeed the case. In Me_4Ti, however, the second highest filled molecular orbital is not a Ti$-$C a_1 bonding M.O. but is of t_1 symmetry and is completely localised on the methyl groups. This t_1 orbital is only slightly higher in energy than the lower of the two sets of Ti$-$C σ bonding molecular orbitals. In fact, in *overall average* energy, the Ti$-$C bonding molecular orbitals are, as expected, those of highest energy.

It is helpful, in the context of the Ti$-$C bonding, to study the energy levels of CH_4 and the $CH_3^{\cdot}$ radical. These are given in table 10. It is seen that the C$-$H bonding orbitals split into two sets, a non-degenerate molecular orbital and a doubly or triply degenerate set of higher energy. If Me_4Ti is viewed in terms of four methyl groups joined by their carbons to the titanium, then the energy levels of Me_4Ti should reflect the bonding in an isolated $CH_3^{\cdot}$ or CH_4 species. This is indeed the case : the four accidentally degenerate molecular orbitals of the four methyls separate into t_2 and a_1 molecular orbitals, both of which are very similar in energy to those of free $CH_3^{\cdot}$ or CH_4, whilst their degenerate levels split into t_1, t_2, and e molecular orbitals, again similar in energy to those of the free group. In tetramethyltitanium the $4s$ contribution from titanium is important. Under T_d symmetry, the four σ orbitals on the methyl group transform as a_1 and t_2, whilst the atomic orbitals on titanium transform as $4s$; a_1 $4p$, $3d$; t_2 and $3d$; e. The a_1 molecular orbital from the methyls can only interact with $4s$ on Ti. The other triply degenerate molecular orbital arising from the methyl groups can interact with the $4p$ and $3d$ titanium orbitals. Hence, in terms of hybridisation theory, we can refer to Ti as being '$sp^3 + sd^3$' hybridised. This reasoning is also applicable to all the intermediates, and includes $TiCl_4$.

Table 10

Orbital energies for $CH_3^{\cdot}$ and CH_4 and (eV)

$CH_3^{\cdot}$		CH_4	
Symmetry	Energy	Symmetry	Energy
$2e'$	11.15	$2a_1$	11.42
$2a_1'$	10.64	$2t_2$	10.98
$1a_2''$	$-$ 2.12	$1t_2$	-14.04
$1e'$	-14.71	$1a_1$	-37.00
$1a_1'$	-32.26		

In crystal field terms, when bonding to Ti (IV), both methyl and chlorine act as 'covalent' ligands. Thus, the d-orbital splitting is almost independent of the number of methyls and chlorines attached to the titanium. The methyl group, however, is a more strongly directively polarising ligand than chlorine. Whereas chlorine can both σ and $\pi-$bond to the central atom, only the first interaction is significant for methyl (hyper-conjugation is almost nonexistent). Of the d orbitals, the t_2 set can σ bond to the ligands, whilst the e set can take part in π bonding. If the latter is limited, then clearly the occupancy of the $d(e)$ set

Table 11

Calculated excited states (eV) for methyl titanium chlorides

	1Γ				3Γ		
Me_4T	Symmetry	Energy	F	Major contributing configurations	Symmetry	Energy	Major contributing configurations
	T_1	2.84	0	$3t_2 \rightarrow 2e$	A_2	2.14	$3t_2 \rightarrow 4t_2$
	T_2	2.84	0.00	$3t_2 \rightarrow 2e$	T_2	2.68	$3t_2 \rightarrow 4t_2$
	E	3.75	0	$3t_2 \rightarrow 4t_2$	T_1	2.84	$3t_2 \rightarrow 2e$
	T_1	3.75	0	$3t_2 \rightarrow 4t_2$	T_2	2.84	$3t_2 \rightarrow 2e$
	T_2	4.73	0.41	$3t_2 \rightarrow 4t_2$	E	3.74	$3t_2 \rightarrow 4t_2$
	E	6.96	0	$1t_1 \rightarrow 4t_2$	T_1	3.75	$3t_2 \rightarrow 4t_2$
	T_2	7.09	0.06	$1t_1 \rightarrow 4t_2$	T_2	6.94	$1t_1 \rightarrow 4t_2$
	T_1	7.28	0	$1t_1 \rightarrow 2e$			
	A_1	7.29	0	$3t_2 \rightarrow 4t_2$			
	T_2	7.41	0.15	$1t_1 \rightarrow 2e$			
	T_1	7.67	0	$1t_1 \rightarrow 4t_2$			
	A_1	8.00	0	$1t_1 \rightarrow 4t_2$			
$TiClMe_3$	A_2	2.72	0	$5e \rightarrow 6e$	A_1	2.16	$5e \rightarrow 7e$
	E	2.72	0.00	$5e - 6e$	E	2.56	$5e \rightarrow 7e$
	A_1	2.73	0.00	$5e \rightarrow 6e$	A_2	2.71	$5e \rightarrow 6e$
	E	3.43	0.00	$5e \rightarrow 6a_1$	A_1	2.73	$5e \rightarrow 6e$
	A_2	3.71	0	$5e \rightarrow 7e$	E	2.73	$5e \rightarrow 6e$
	E	4.24	0.12	$5e \rightarrow 7e$	E	3.45	$5e \rightarrow 6a_1$
	E	4.36	0.00	$5a \rightarrow_1 6e$	A_2	3.71	$5e \rightarrow 7e$
	A_1	4.84	0.09	$5a_1 \rightarrow 6a_1$	E	4.35	$5a_1 \rightarrow 6e$
	E	5.78	0.24	$5a_1 \rightarrow 7e$	A_1	4.65	$5a_1 \rightarrow 6a_1$
	E	6.05	0.00	$4e \rightarrow 6a_1$	E	4.95	$5a_1 \rightarrow 7e$
	A_2	6.10	0	$4e \rightarrow 6e$	E	6.02	$4e \rightarrow 6a_1$
	E	6.22	0.19	$4e \rightarrow 6a_1$			
	A_1	6.23	0.04	$4e \rightarrow 6e$			
	E	6.62	0.07	$4e \rightarrow 7e$			
	A_2	6.83	0	$4e \rightarrow 7e$			
	A_1	7.01	0.36	$4e \rightarrow 7e$			
	E	7.18	0.05	$1a_3 \rightarrow 7e$			
	E	7.34	0.16	$1a_2 \rightarrow 7e$			
	A_2	7.64	0	$1a_2 \rightarrow 6a_1$			
	A_1	7.69	0.06	$5a_1 \rightarrow 6a_1$			
$TiCl_2Me_2$	B_1	2.59	0.00	$7b_1 \rightarrow 7a_1$	A_1	2.22	$4b_1 \rightarrow 5b_1$
	A_1	2.61	0.00	$7b_1 \rightarrow 3a_2$	B_1	2.52	$4b_1 \rightarrow 8a_1$
	A_2	3.22	0.00	$7b_1 \rightarrow 5b_2$	B_1	2.57	$4b_1 \rightarrow 7a_1$
	B_2	3.56	0.00	$6a_1 \rightarrow 7a_1$	B_2	2.61	$4b_1 \rightarrow 3a_2$
	A_2	3.57	0.00	$6a_1 \rightarrow 3a_2$	A_2	3.22	$4b_1 \rightarrow 5b_1$
	B_1	3.63	0.03	$4b_1 \rightarrow 8a_1$	A_1	3.56	$6a_1 \rightarrow 7a_1$
	A_1	4.12	0.02	$6a_1 \rightarrow 8a_1$	A_2	3.57	$6a_1 \rightarrow 3a_2$
	B_2	4.25	0.03	$6a_1 \rightarrow 5b_2$	B_1	3.98	$6a_1 \rightarrow 5b_1$
	B_1	5.16	0.00	$4b_2 \rightarrow 3a_2$	B_2	4.06	$6a_1 \rightarrow 5b_2$
	B_2	5.18	0.00	$4b_2 \rightarrow 7a_1$	A_1	4.14	$6a_1 \rightarrow 8a_1$
	A_1	5.50	0.08	$4b_2 \rightarrow 5b_2$	B_1	5.16	$4b_2 \rightarrow 3a_2$
	B_1	5.57	0.00	$3b_2 \rightarrow 3a_2$			
	A_1	5.67	0.00	$3b_2 \rightarrow 5b_2$			
	B_2	5.70	0.00	$3b_2 \rightarrow 7a_1$			
	B_2	5.72	0.03	$4b_2 \rightarrow 8a_1$			
	A_2	5.77	0.00	$2a_2 \rightarrow 7a_1$			
	B_1	5.82	0.78	$6a_2 \rightarrow 5b_1$			
	B_1	5.87	0.01	$2a_2 \rightarrow 5b_2$			
	A_1	6.04	0.22	$2a_2 \rightarrow 3a_2$			

Table 11 (*continued*)

	1Γ				3Γ		
Me_4 Ti	Symmetry	Energy	F	Major contributing configurations	Symmetry	Energy	Major contributing configurations
$TiCl_3Me$	A_2	6.06	0.00	$2a_2 \rightarrow 8a_1$			
	E	2.88	0.00	$5a_1 \rightarrow 6e$	A_1	2.13	$5a_1 \rightarrow 6a_1$
	E	3.53	0.00	$5a_1 \rightarrow 7e$	E	2.87	$5a_1 \rightarrow 6e$
	A_1	4.94	0.02	$5e \rightarrow 6e$	E	3.49	$5a_1 \rightarrow 7e$
	E	4.96	0.00	$5e \rightarrow 6e$	A_1	4.85	$5e \rightarrow 7e$
	A_2	4.97	0	$5e \rightarrow 6e$			
	A_1	5.12	0.15	$5a_1 \rightarrow 6a_1$			
	E	5.16	0.00	$1a_2 \rightarrow 6e$			
	E	5.21	0.00	$1a_2 \rightarrow 7e$			
	A_1	5.38	0.03	$4e \rightarrow 7e$			
	E	5.40	0.01	$4e \rightarrow 6a_1$			
	E	5.52	0.00	$4e \rightarrow 7e$			
	A_2	5.54	0	$4e \rightarrow 6e$			
	A_2	5.56	0	$5e \rightarrow 7e$			
	A_1	5.59	0.15	$5a_1 \rightarrow 6a_1$			
	E	5.75	0.00	$5e \rightarrow 6a_1$			
	A_2	5.84	0	$1a_2 \rightarrow 6a_1$			
	E	5.92	0.03	$5e \rightarrow 6a_1$			
	A_1	6.05	0.00	$5e \rightarrow 7e$			
	A_2	6.06	0	$4e \rightarrow 7e$			
	E	6.18	0.03	$4e \rightarrow 6a_1$			
	A_2	6.52	0	$3e \rightarrow 7e$			

will be small. Clearly, it will diminish with an increasing number of methyl groups around titanium.

With regard to the distribution of charge (table 5), it is interesting that the charge on the carbon atom remains almost constant over the whole series, whilst that of the titanium changes quite markedly. In fact, the extra electrons transferred to titanium are almost completely accommodated in the titanium d_{xy}, d_{xz}, d_{yz} set of atomic orbitals. This must reflect on the chemical properties of organotitanium compounds in general.

3.5. SPECTRA AND MODE OF DECOMPOSITION

Only for $MeTiCl_3$ has the optical spectrum been determined; two peaks exist, one at 25,000 and one at 43,000 cm^{-1}. The other three compounds are coloured, hence they must absorb in the range 300 to 700 mμ, unless the colour is caused by impurity formed on decomposition. Excitation would be expected to occur from the Ti–C σ-bonding molecular orbitals and the non-bonding chlorine molecular orbitals to the Ti–C σ* antibonding group and the *s*, *p*, and *d* on titanium. Strong configurational mixing precludes complete definition of a transition as involving any particular configurational change, but most excitations involve generally 95% or more of one configuration. This configuration is given, along with state energies and symmetries, in table 11. A very distinct trend appears : in $MeTiCl_3$ the first four transitions are Ti – C σ to d on Ti with the $\sigma - \sigma^*$ transition at a slightly higher energy, while in Me_2TiCl_2 the first five transitions are $\sigma - \sigma^*$. Me_3TiCl and Me_4Ti are similar. In the triplet states the lowest-lying states are exclusively $\sigma - \sigma^*$, followed by those of $n - \pi^*$ type.

In all the species, on photo-excitation, the Ti – C σ bond loses an electron, which enters either a d orbital or the Ti – C σ^* antibonding orbital. In both cases the ultimate result would be the same, in that scission of the Ti – C bond would be facilitated and free methyl radicals would result. The calculations show that, for $MeTiCl_3$, there should be two weak bands near 3 eV and these correlate with that observed at 3.1. eV. [14] Since the latter is a shoulder on a larger peak, it is not possible to differentiate the two components, although the low-energy side of this peak is not of gaussian form. This experimental transition will involve a $Ti - C(\sigma) \rightarrow \rightarrow Ti - C(\sigma^*)$ excitation and is almost certainly the absorption which causes photolysis. At higher energy there are several calculated absorptions in the range 5.12 – 5.59 eV and all stem from $n - \pi_4$ transitions. The experimental spectrum shows a rapid rise in absorption near 3 eV and a levelling off near 5 eV. The measurements were not carried further, hence the number of peaks in this region is not known. In the absence of further information, we assign the three calculated absorptions between 5.00 and 5.25 eV to this band.

We thank the S.R.C. for a Maintenance Grant (to J.J.P.S)

Revue Roumaine de Chimie, **20**, *2*, 195–201 (1975)

REACTIVITY OF BENZYL HALIDES IN SN_2 REACTIONS

C. BENDIC and D. OANCEA

Physical Chemistry Department, University of Bucharest,
Bd. Republicii 13, Romania

Received December 19, 1973

The reactivity of benzyl halides in SN_2 reactions is discussed in terms of the charge densities on α carbon. The calculated charge densities are supported by the good agreement between experimental and calculated dipole moments, as well as by the chemical shifts of methylene protons. The activation energies of the reactions between benzyl halides and sodium alkoxides are also discussed. The presence of a minimum for benzyl bromide can be qualitatively accounted for in view of the combined action of the different components of the activation energy.

INTRODUCTION

The reactivity of benzyl halides in SN_2 reactions was a subject often examined. There are many papers dealing with different aspects of the matter, such as the solvent[1] or salt[2] effects, the effects of the halogen[3] or nucleophile,[4] the influence of the substitution on the aromatic ring,[5] etc. The increase in the reactivity of benzyl halides as compared to alkyl halides without double bonds in α position was assigned to a stabilization of the transition state arising from the conjugation of the reaction orbital with aromatic ring.[6]

In the present paper, an attempt is made to explain the influence of the halogen atom on the reactivity of benzyl halides in their reactions with sodium alkoxides resulted from primary unbranched alcohols

$$RO^- + PhCH_2X \longrightarrow PhCH_2OR + X^- \qquad (1)$$

where $R = CH_3,\ C_2H_5,\ nC_3H_7,\ nC_4H_9,\ nC_5H_{11},\ nC_6H_{13}$

$X = Cl,\ Br,\ I$

This influence is correlated with the charge density on the α carbon, calculated by HMO–LCAO method. The activation energies of these reactions cannot be correlated with charge densities on the α carbon and, consequently, they are discussed in terms of different structural and solvent contributions.

---

[1] E. Tommila, *Ann. Acad. Sci. Fennicae*, **139 A**, 1 (1967).
[2] S. D. Bowers Jr. and J. M. Sturtevant, *J. Amer. Chem. Soc.*, **77**, 4903 (1955).
[3] M. Conrad and C. Brückner, *Z. phys. Chem.*, **4**, 631 (1889).
[4] J. F. Bunnett and J. D. Reinheimer, *J. Amer. Chem. Soc.*, **84**, 3284 (1962).
[5] E. T. McBee, I. Serfaty and T. Hodgins, *J. Amer. Chem. Soc.*, **93**, 5711 (1971).
[6] A. Streitwieser Jr., *Chem. Revs.*, **56**, 571 (1956).

EXPERIMENTAL

Riedel benzyl chloride and Schuchardt benzyl bromide were redistilled under low pressure, obtaining colourless liquids having the following physical constants : $PhCH_2Cl - n_D^{20} = 1.5415$, $d^{20} = 1.1026$ g/cc ; $PhCH_2Br - n_D^{22} = 1.5755$. $d^{22} = 1.4380$ g/cc. Benzyl iodide was prepared by the reaction of benzyl chloride with sodium iodide in acetone solution.[7] After three recrystallizations from ethanol a crystalline and colourless product was obtained (m.p. = 27—28°, $n_D^{40} = 1.6248$; $d^{40} = 1.7146$ g/cc).

The dipole moments of benzyl halides were determined by Guggenheim's method[8], consisting in dielectric constant and refraction index measurements of benzyl halide solution in *n* heptane. The measurements were carried out for five solutions of each benzyl halide within the range $0.07 < C \times 10^3$ (mol/cc) < 1, at 20°, using a DK 600 RL Oehme dielcometer and an Abbé refractometer. The NMR spectra of benzyl halides were recorded for the solutions in carbon tetrachloride using TMS as internal reference.

RESULTS

The experimental results are given in table 1.

Table 1

Physical properties of benzyl halides

Compound	n_D	d(g/cc)	$\alpha_0 \times 10^{23}$ (cc)*	τ_{CH_2}(ppm)	μ_{exp} (D)
$PhCH_2Cl$	1.5415^{20}	1.1026^{20}	1.43	5.53	1.85
$PhCH_2Br$	1.5755^{22}	2.4380^{22}	1.56	5.61	1.78
$PhCH_2I$	1.6248^{40}	1.7146^{40}	1.78	5.65	1.59

* α_0 polarisability from molar refraction.

The dipole moments were calculated from the equation

$$\mu^2 = \frac{9kT}{4\pi N} \cdot \frac{3}{(D_1' + 2)(n_1^2 + 2)} \cdot \left(\frac{\Delta}{m}\right)_0 \qquad (2)$$

where D_1' and n_1 are the dielectric constant and refraction index of pure *n* heptane, respectively, and Δ is given by

$$\Delta = (D' - n^2) - (D_1' - n_1^2) \qquad (3)$$

where D' and n are the dielectric constant and refraction index of the different solutions of concentration m (mol/cc), respectively, $(\Delta/m)_0$ is the slope of the plot Δ against *m*, when $m \to 0$. The plots Δ against *m* are given in figure 1. The kinetic data referring to these reactions were taken from three previous papers[9-11] and given in table 2.

---

[7] G. H. Coleman and C. R. Hauser, *J. Amer. Chem. Soc.*, **50**, 1196 (1928).

[8] E. A. Guggenheim, *Trans. Faraday Soc.*, **45**, 714 (1949).

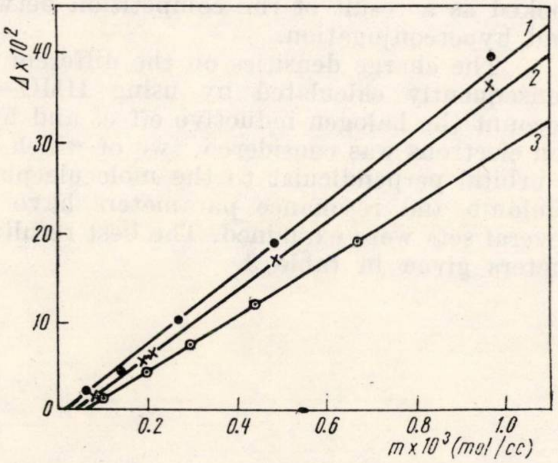

Fig. — 1. Plots of function Δ vs. solvent concentration (mole cc^{-1}); *1*, benzyl chloride; *2*, benzyl bromide; *3*, benzyl iodide.

Table 2

Activation parameters of the reactions $PhCH_2X + RO^- \to PhCH_2OR + X^-$ (ref.[9-11])

RO^-		CH_3O^-	$nC_2H_5O^-$	$nC_3H_7O^-$	$nC_4H_9O^-$	$nC_5H_{11}O^-$	$nC_6H_{13}O^-$
k^{50}_{rel}	$PhCH_2Cl$	0.026	0.018	0,021	0.024	0.027	0.025
	$PhCH_2Br$	0.777	0.651	0.740	0.747	0.710	0.743
	$PhCH_2I$	1.000	1.000	1,000	1.000	1.000	1.000
E_A (Kcal·mol^{-1})	$PhCH_2Cl$	20.32	20.93	18.87	18.05	17.70	17.69
	$PhCH_2Br$	17.88	17.12	16.63	16.43	16.19	15.97
	$PhCH_2I$	18.65	19.31	18.35	17.46	18.12	17.66
log A*	$PhCH_2Cl$	13.48	13.93	12.50	11.87	11.53	11.40
	$PhCH_2Br$	13.29	12.92	12.51	12.24	11.92	11.69
	$PhCH_2I$	13.99	14.61	13.85	13.11	13.42	13.02

* *A* in cc mol.$^{-1}$ sec.$^{-1}$

DISCUSSION

An analysis of the UV absorption spectra of α halogenated toluenes has indicated that the substitution of a side chain hydrogen through a halogen gave rise to a decrease in hyperconjugation, through which the

---

[9] I. G. Murgulescu, D. Oancea and G. Mincu, *Rev. Roumaine Chim.*, **14**, 3 (1969).
[10] I. G. Murgulescu and D. Oancea, *Idem*, **15**, 299 (1970).
[11] *Idem*, **15**, 1635 (1970).

methyl group can bring electrons into aromatic ring.[12] The examination of NMR spectra of α halogenated toluenes and related compounds[13] has also indicated that the chemical shifts of the side chain protons as well as of the benzene ring protons could be easily understood if they were looked as a result of the competition between halogen inductive effect and hyperconjugation.

The charge densities on the different atoms of benzyl halides were consequently calculated by using HMO–LCAO method, taking into account the halogen inductive effect and hyperconjugation. A system of ten electrons was considered, two of which have resulted from a halogen *p* orbital perpendicular to the molecule plane. Since different values of coulomb and resonance parameters have been used in literature[14–15], several sets were examined. The best results were obtained for the parameters given in table 3.

Table 3

Coulomb and resonance parameters for benzyl halides (ref.[14,15])

Compound	h_{H_2}	h_{C_2}	h_X	k_{CH_2}	k_{CX}
$PhCH_2Cl$	−0.5	0.56	1.7	2	0.6
$PhCH_2Br$	−0.5	0.36	1.4	2	0.4
$PhCH_2I$	−0.5	0.20	1.2	2	0.1

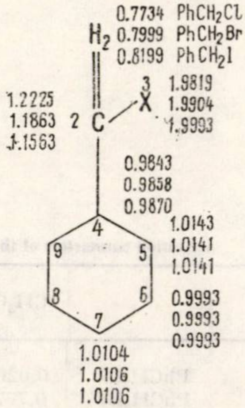

Fig. 2.— Molecular diagrams of benzyl halides.

Th resulting charge densities are given in fig. 2.

These results are, on the one hand, supported by the satisfactory agreement between the experimental and calculated dipole moments and, on the other hand, by the charge density changes on the methylene protons which are consistent with the corresponding chemical shift in NMR spectra of these compounds. The experimental dipole moments, the σ dipole moments of C – X bonds (for the other bonds these components were neglected), the π dipole moments, calculated from the charge distributions, the angles θ between σ and π components and the overall dipole moments are given in table 4.

The deviation between calculated and experimental values does not exceed 10%, which is a fairly good result. At the same time, it can be seen from fig. 2, that the charge density on the methylene protons increases on going from benzyl chloride to benzyl iodide, giving rise to a gradual shielding of the respective protons in good agreement with τ values given in table 1.

---

[12] W. F. Hamner and F. A. Matsen, *J. Amer. Chem. Soc.*, **70**, 2482 (1948).

[13] P. L. Corio and B. P. Dailey, *J. Amer. Chem. Soc.*, **78**, 3043 (1956).

[14] A. Streitwieser Jr., "Molecular Orbital Theory for Organic Chemists", Wiley, New York, 1961, p. 135.

[15] W. P. Purcell and J. A. Singer, *J. Chem. and Eng. Data*, **12**, 235 (1967).

Table 4

Experimental and calculated dipole moments of benzyl halides

Compound	$\mu_\sigma(D)^{16}$	$\mu_\pi(D)$	θ	$\mu_{calc.}(D)$	$\mu_{exp.}$
$PhCH_2Cl$	1.57	1.63	109.5	1.85	1.85
$PhCH_2Br$	1.48	1.26	109.5	1.59	1.78
$PhCH_2I$	1.29	1.32	109.5	1.50	1.59

The charge density on the saturated carbon of benzyl halides decreases from chloride to iodide (fig. 2) leading to a corresponding increase of the SN_2 reaction rate constants.

Although the agreement between the charge density on the substitution center and the rate constant is fairly good, however, there is no correlation between the charge density and the activation energy (table 2). Such a behaviour has been long ago ascertained and assigned to the so-called compensation effect,[17–18] whose origin is not yet completely clarified.[19]

The activation energy of the reactions between sodium alkoxides and benzyl halides exhibits a minimum for benzyl bromide irrespective of the alcohol nature (table 2). Because of the lack of a rigorous theoretical method for the calculation of the activation energy of the reactions in solution, four different components have been recognized, which, in a first approximation, have been assumed to be independent of each other and additive,[20] namely : 1) the stretching of bonds in the reacting molecules and the incipient formation of new bonds ; 2) repulsion between unbonded atoms on close approach ; 3) electrostatic interaction between the reactants, modified by the solvent ; 4) reorganization of the solvent molecules, first to allow the reactants to come together, and then to form the solvated transition state. Each of these components will be successively discussed.

1) As for all these reactions only C–O bond is formed, the contribution of the first component arises only from the differences brought about by the breaking energy of carbon-halogen bond. However, both carbon-halogen bond energies and enthalpies of heterolytic dissociation $PhCH_2X \rightarrow$

---

[16] C. P. Smith, "Dielectric Behaviour and Structure", Mc Graw-Hill, New York, 1955.

[17] M. Polanyi and M. G. Evans, *Trans. Faraday Soc.*, **32**, 1333 (1936).

[18] a) J. E. Leffler, *J. Org. Chem.*, **20**, 1202 (1955) ; **31**, 533 (1966).
b) G. I. Lihtenstein, *Zhur. fiz. Khim.*, **44**, 1908 (1970).

[19] O. Exner, *Ind. chim. belge*, **33**, 343 (1968).

[20] E. F. Caldin, *J. Chem. Soc.*, 1959, 3345.

$PhCH_2^+ + X^-$ in the gas phase (table 5) decrease from chloride to iodide, while the activation energy exhibits a minimum for benzyl bromide. At the same time, the reactions between sodium alkoxides and benzyl halides occur to a great extent because of the great difference between carbon and oxygen electronegativity as compared to the less difference between carbon and halogen electronegativity (table 5).

Table 5

Some physical properties of the reactants correlated with the activation energy

X	Cl	Br	I	O−R
$E_{bond}(C-X)$ $(kcal \cdot mol^{-1})$[21]	67	54	45	70
$\Delta H(PhCH_2X \rightarrow PhCH_2^+ + X^-$ $(kcal \cdot mol^{-1})$[6]	152	141	137	–
$\Delta\varkappa\ (= \varkappa_C - \varkappa_X)$[21]	−0.5	−0.3	0.0	−1.0
r_{X^-} (Å)[22]	0.99	1.14	1.33	–
$\alpha_0 \times 10^{23}$ $(PhCH_2X)$ (cc)	1.43	1.56	1.78	–
$\Delta H_{solv}(X^-)$ in CH_3OH $(Kcal\ mol^{-1})$[23]	−89	−79	−70	–
$E_A(CH_3O^- + PhCH_2X)$ $(kcal \cdot mol^{-1})$	20.32	17.88	18.65	–

These differences favour to a greater extent the reactions of benzyl iodide and to a decreasing extent the reactions of benzyl bromide and chloride, respectively. The opposite action of these two effects – bond energy and electronegativity difference – would account qualitatively for the experimental values of activation energy.

2) A steric hindrance will generally be expected in SN_2 reactions since the transition state is more crowded than the initial state, especially when the coordinated groups are more bulky.[24] The repulsive energy which, in this case, will give rise to an increase in the activation energy will consequently decrease from iodide to chloride because of the decreasing in halogen radius (table 5). Over this short range repulsive energy, the electrostatic interaction energy between nucleophile RO^- and methylene hydrogen atoms whose negative charge increases from chloride to

[21] A. JULG, "Chimie cuantică", translated from French, Editura ştiinţifică, Bucharest, 1971.

[22] L. PAULING, "The Nature of Chemical Bond", Cornell Univ. Press. New York, 1948, p. 346.

[23] B. E. CONWAY and J. O'M. BOCKRIS, in "Modern Aspects of Electrochemistry", edited by J. O'M. Bockris, vol. 1, Butterworths London, 1954, p. 47.

[24] C. K. INGOLD, "Structure and Mechanism in Organic Chemistry", Cornell Univ. Press, New York, 1953, chap. 7.

iodide (fig. 2) is also superposed to the same effect. On the other hand, in the transition state of an ion — dipole reaction occurring through an SN_2 mechanism, electrostatic interaction between the nucleophile and leaving group exists[25] since the negative charge is shared between them. When the leaving group (in this case the halogen) is easily polarisable, its charge can be shifted outwards, resulting in a stabilization of the transition state because of the decreasing of the electrostatic repulsion, and hence, in an increasing of the rate constant. As the polarisability decreases from iodide to chloride (table 5) this interaction acts in opposite direction with short range repulsion.

3) The ion-dipole electrostatic interaction energy, altered by the dielectric properties of the solvent, decreases from benzyl chloride to benzyl iodide. The activation energy corrected for the ion-dipole interaction by using different electrostatic models exhibits also a minimum for benzyl bromide.[26]

4) The energy needed for the reorganization of the solvent molecules during the formation of the transition state of the ion-dipole reactions arises to a great extent from the energy of the partial dissolution of the reactant ion, which is the same for all these reactions occurring in the same alcohol. In addition, the partial solvation, in the transition state, of the leaving group must be taken into account. Assuming the solvation energy of the leaving group in the transition state to be proportional to the solvation enthalpy of the halide ion (table 5), and taking into account that the leaving group solvation produces a lowering of the activation energy[27], it can be concluded that the solvent reorganization energy favours to a greater extent the reaction of benzyl chloride and to a lesser extent the reaction of benzyl iodide.

As some components cause an increase and others a decrease of the activation energy, their combined action would qualitatively explain the presence of a minimum of the experimental activation energy.

---

[25] K. B. Wiberg, "Physical Organic Chemistry", Wiley, New York, 1964, p. 425.

[26] D. Oancea, Thesis, Bucharest, 1972.

[27] C. G. Swain and R. W. Eddy, *J. Amer. Chem. Soc.*, **70**, 2989 (1948).

Revue Roumaine de Chimie, **20**, *2*, 203–208 (1975)

A ROTATIONAL STUDY OF *O*-CHLORONITROBENZENE AND *O*-DINITROBENZENE

C. I. GHIRVU*

The "Al. I. Cuza" University, Physical Chemistry Laboratory, Calea 23 August
11, Jassy, Romania

Received December 10, 1973

The influence of the internal rotation of the nitro groups about the C–N bond on the electronic transitions and on some ground state properties of *o*-chloronitrobenzene and *o*-dinitrobenzene has been investigated by using a modified Pariser-Parr-Pople method.

INTRODUCTION

In a previous paper[1] the electronic properties of the molecules of *o*-chloronitrobenzene and *o*-dinitrobenzene have been studied. Both of them were considered to be planar. But as is well known the steric effects may be of large magnitude in molecules of this kind. Therefore, it would be of some interest to study the influence of internal rotation of the nitro groups on the electronic properties. The most probable equilibrium conformation and the barriers to internal rotation of the nitro groups about the C–N bond have also been investigated. [2]

In this paper we have studied the effects of the internal rotation of the nitro groups on the electronic properties by performing calculations within a modified Pariser-Parr-Pople (PPP) approximation for the π-electrons.[3]

CALCULATION METHOD

As stated above, the method used in the present investigation is a modified PPP method developed for pure hydrocarbons,[3] and extended later to many other groups of compounds.[4–12] The features of the method are briefly outlined below.

---

* Present address: Polytechnic Institute of Jassy, Faculty of Chemistry and Chemical Engineering, Physical Chemistry Laboratory, Splaiul Bahlui 71, Jassy, Romania

[1] C. I. Ghirvu and O. Gropen, *Acta Chem. Scand.*, **25**, 1011 (1971).

[2] C. I. Ghirvu, O. Gropen and P. N. Skancke, *Acta Chem. Scand.*, **25**, 2023 (1971).

[3] B. Roos, *Acta. Chem. Scand.*, **21**, 233 (1967).

[4] B. Roos, *Acta. Chem. Scand.*, **21**, 2318 (1967).

[5] I. Fischer-Hjalmars and M. Sundbon, *Acta. Chem. Scand.*, **22**, 607 (1968).

[6] B. Grabe, *Acta. Chem. Scand.*, **22**, 2237 (1968).

[7] H. Jensen and P. N. Skancke, *Acta. Chem. Scand.*, **22**, 2899 (1968).

[8] G. Højer, *Acta. Chem. Scand.*, **23**, 2589 (1969).

[9] O. Gropen and P. N. Skancke, *Acta. Chem. Scand.*, **23**, 2685 (1969).

[10] A. Skancke and P. N. Skancke, *Acta Chem. Scand.*, **24**, 23 (1970).

[11] P. G. Seybold and I. Fischer-Hjalmars, *Acta Chem. Scand.*, **24**, 1373 (1970).

[12] O. Gropen and P. N. Skancke, *Acta Chem. Scand.*, **24**, 1768 (1970).

The one-electron parameter W_μ is made dependent on the surroundings to atom μ through the relation

$$W_\mu = W_\mu^0 + \sum_\nu \Delta W_\mu(\nu) \tag{1}$$

where the symbols have the same meaning as in the original paper.[3] In Eq. (1) $\Delta W_\mu(\nu)$ varies with the nature of the neighbouring atom ν and also with the bond distance $R_{\mu\nu}$ through an assumed linear relation

$$\Delta W_\mu(\nu) = \Delta W_\mu^0(\nu) + \delta_{\mu\nu}^W (R_{\mu\nu} - R_{\mu\nu}^0) \tag{2}$$

The core resonance integrals and the two-electron two-center Coulomb repulsion integrals between nearest neighbours are expressed by linear distance dependent relations

$$\beta_{\mu\nu} = \beta_{\mu\nu}^0 + \delta_{\mu\nu}^\beta (R_{\mu\nu} - R_{\mu\nu}^0) \tag{3}$$

$$\gamma_{\mu\nu} = \gamma_{\mu\nu}^0 + \delta_{\mu\nu}^\gamma (R_{\mu\nu} - R_{\mu\nu}^0) \tag{4}$$

RESULTS AND DISSCUSIONS

For practical calculations, numerical values of the parameters mentioned above were obtained from different sources.[3,6,9] The two-electron two-center repulsion integrals for non-nearest neighbours have been determined by a modified version of the uniformly charged sphere approximation,[13] valid for non-parallel *p*-orbitals.[14] For the one-center two-electron integrals we have adopted values previously determined by Skancke.[15]

The core-resonance integral between nitrogen and the neighbouring carbon atom has been made dependent upon the rotation angle through the following relation

$$\beta_{\mathrm{CN}}(\varphi) = \beta_{\mathrm{CN}}(0)\,|\cos\varphi| \tag{5}$$

where φ is the angle of twist. The corresponding two-electron repulsion integral has been treated as in a previous paper.[2] The following expression was used

$$(\mathrm{NN}\,|\,\mathrm{CC})_\varphi = \cos^2\varphi\,(\mathrm{N}_x\mathrm{N}_x\,|\,\mathrm{C}_x\mathrm{C}_x) + \sin^2\varphi\,(\mathrm{N}_x\mathrm{N}_x\,|\,\mathrm{C}_y\mathrm{C}_y) \tag{6}$$

For Slater type orbitals the following expression is valid

$$(\mathrm{N}_x\mathrm{N}_x\,|\,\mathrm{C}_y\mathrm{C}_y) = (\mathrm{N}_x\mathrm{N}_x\,|\,\mathrm{C}_x\mathrm{C}_x) - 2(\mathrm{N}_x\mathrm{N}_y\,|\,\mathrm{C}_x\mathrm{C}_y) \tag{7}$$

---

[13] R. Pariser and R. G. Parr, *J. Chem. Phys.*, **21**, 466, 467 (1953).

[14] H. Jensen and P. N. Skancke, *Acta Chem. Scand.*, **24**, 3766 (1970).

[15] P. N. Skancke, *Arkiv Fysik*. **30**, 573 (1965).

The first integral on the right side of Eq. (7) has been estimated by the procedure described in the parametrization scheme.[3] For the integral $(N_xN_y|C_xC_x)$, which is very small at the actual internuclear distances, we have adopted a theoretical value based on the orbital exponents of Duncanson and Coulson.[16]

For practical calculations we used the notation of the atoms and rotational angles as given in figure 1. During rotation all bond distances and valence angles were kept unchanged. The structure parameters for *o*-chloronitrobenzene were chosen to correspond to the geometry of nitrobenzene[17] and to the C—Cl bond in chlorobenzene.[18] For the dinitrobenzene the benzene structure of the ring together with the nitro group geometry from the nitrobenzene were assumed to be adequate.

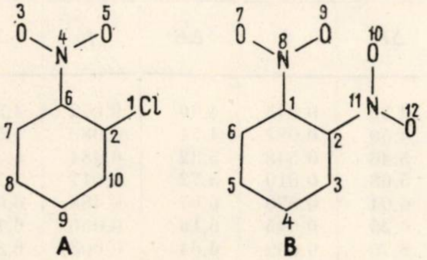

Fig. 1. — Notation of the atoms and rotational angles.
A. *o*-chloronitrobenzene
B. *o*-dinitrobenzene.

The calculation results concerning the effect of the rotation angles on the electronic spectra of *o*-chloronitrobenzene and *o*-dinitrobenzene are given in tables 1 and 2.

The experimental results quoted in these tables were taken from different sources.[19-21]

Table 1

Effect of the rotation angle on the electronic spectra of orthochloronitrobenzene (ΔE in eV)

Calculated										Observed	
$\alpha = 0°$		$\alpha = 30°$		$\alpha = 45°$		$\alpha = 60°$		$\alpha = 90°$			
ΔE	f	ΔE	f	ΔE	f	ΔE	f	ΔE	f	ΔE	f (log ε)
4.47	0.005	4.54	0.0014	4.63	0.001	4.73	0.003	4.89	0.06	4.19[a]	3.041
4.92	0.164	4.95	0.141	4.98	0.109	5.01	0.064	5.03	0.00	5.06	3.602
5.59	0.188	5.56	0.174	5.50	0.144	5.42	0.096	5.27	0.00	5.54	3.954
6.12	0.468	6.12	0.421	6.10	0.354	6.08	0.265	6.04	0.172		
6.51	0.137	6.55	0.146	6.61	0.195	6.68	0.289	6.80	0.458		
6.85	0.134	6.99	0.144	7.13	0.337	7.16	0.771	7.08	1.123		
7.33	1.184	7.33	0.647	7.25	1.151	7.19	1.210	7.11	0.887		
7.36	0.441	7.91	0.095	7.30	0.412	7.39	0.019	7.59	0.000		
7.84	0.137	8.44	0.005	7.96	0.065	8.02	0.047	8.06	0.034		
8.35	0.005	8.62	0.044	8.52	0.028	8.52	0.045	8.48	0.047		

[a]. Ref. [19].

[16] W. E. DUNCANSON and C. A. COULSON, *Proc. Roy. Soc. Edinburgh*, **A62**, 37 (1943/49)
[17] J. TROTTER, *Acta Cryst.*, **12**, 884 (1959).
[18] T. G. STRAND, *Acta Chem. Scand.*, **21**, 2111 (1967).
[19] W. F. FORBES, *Canad. J. Chem.*, **38**, 1104 (1960).
[20] A. I. KISS and G. HORVÁTH, *Acta Chim. Acad. Sci. Hung.*, **39**, 39 (1963).
[21] M. GODFREY and J. N. MURRELL, *Proc. Roy. Soc.*, **A278**, 71 (1964).

Table 2

Calculated and observed spectra of orthodinitrobenzene (ΔE in eV)

CALCULATED VALUES

$\alpha = 30^\circ ; \beta = 0^\circ$		$\alpha = 0^\circ ; \beta = 30^\circ$		$\alpha = 0^\circ ; \beta = 45^\circ$		$\alpha = 0^\circ ; \beta = 60^\circ$		$\alpha = 0^\circ ; \beta = 90^\circ$	
ΔE	f	ΔE	f	ΔE	f	ΔE	f	ΔE	f
4.36	0.045	4.36	0.072	4.33	0.125	4.29	0.184	4.22	0.249
4.50	0.082	4.51	0.083	4.54	0.064	4.60	0.044	4.77	0.129
5.40	0.548	5.32	0.484	5.23	0.392	5.10	0.267	4.86	0.000
5.68	0.019	5.72	0.017	5.74	0.040	5.72	0.051	5.63	0.126
6.04	0.570	6.07	0.488	6.04	0.078	5.94	0.091	5.89	0.000
6.25	0.045	6.16	0.056	6.14	0.380	6.27	0.287	6.35	0.082
6.70	0.002	6.64	0.003	6.88	0.267	6.48	0.033	6.48	0.188
7.21	0.387	6.91	0.253	7.26	1.185	6.82	0.320	6.73	0.477
7.41	0.074	7.27	0.894	7.40	0.829	7.21	1.224	7.16	1.546
7.45	0.825	7.42	0.577	7.54	0.084	7.37	0.935	7.34	1.106

$\alpha = 30^\circ ; \beta = 30^\circ$		$\alpha = 30^\circ ; \beta = 45^\circ$		$\alpha = 30^\circ ; \beta = 60^\circ$		$\alpha = 30^\circ ; \beta = 90^\circ$		$\alpha = 45^\circ ; \beta = 45^\circ$	
ΔE	f	ΔE	f	ΔE	f	ΔE	f	ΔE	f
4.37	0.068	4.34	0.117	4.27	0.175	4.19	0.242	4.34	0.085
4.45	0.093	4.45	0.065	4.49	0.034	4.62	0.0000	4.36	0.108
5.23	0.416	5.11	0.317	4.96	0.196	4.71	0.055	4.98	0.214
5.68	0.012	5.64	0.036	5.59	0.048	5.53	0.130	5.55	0.041
6.03	0.073	5.91	0.093	5.78	0.097	5.67	0.0000	5.78	0.108
6.57	0.006	6.06	0.219	6.17	0.133	6.31	0.055	6.42	0.007
6.95	0.311	6.49	0.010	6.41	0.025	6.43	0.087	6.94	0.437
7.25	1.149	6.94	0.366	6.90	0.045	6.76	0.559	7.17	1.297
7.38	0.791	7.21	1.256	7.17	1.244	7.12	1.193	7.32	1.016
7.53	0.133	7.35	0.933	7.32	1.030	7.29	1.093	7.75	0.011

Calculated values										Observed values	
$\alpha=45^\circ ; \beta=60^\circ$		$\alpha=45^\circ ; \beta=90^\circ$		$\alpha=60^\circ ; \beta=60^\circ$		$\alpha=60^\circ ; \beta=90^\circ$		$\alpha=90^\circ ; \beta=90^\circ$			
ΔE	f	ΔE	f	ΔE	f	ΔE	f	ΔE	f	ΔE	f ($\log \varepsilon$)
4.24	0.127	4.13	0.203	4.14	0.054	4.01	0.117	3.82	0.000	4.41[a]	3.14
4.37	0.084	4.37	0.000	4.26	0.144	4.10	0.000	3.82	0.000	5.15	3.90
4.83	0.099	4.66	0.007	4.72	0.016	4.65	0.006	4.75	0.085	5.83	0.4[b] ; 4.19
5.45	0.036	5.40	0.119	5.29	0.021	5.18	0.000	4.92	0.000		
5.63	0.108	5.43	0.000	5.46	0.105	5.22	0.090	4.92	0.000		
6.17	0.062	6.26	0.031	6.21	0.019	6.20	0.009	6.14	0.000		
6.35	0.011	6.40	0.029	6.28	0.006	6.39	0.006	6.40	0.000		
6.92	0.545	6.80	0.647	6.92	0.661	6.83	0.772	6.93	1.037		
7.12	1.276	7.09	1.230	7.07	1.276	7.04	1.259	6.95	1.171		
7.29	1.086	7.24	1.137	7.23	1.118	7.18	1.132	7.12	1.080		

a. The assignment of bands is doubtful, these appearing as shoulders – Ref. [20]

b. Ref. [21].

The calculated π-components of the dipole moments and the ionization potentials for different rotational angles of the nitro groups are given in tables 3 and 4, where, for comparison, we have again collected available experimental data.[22-25]

As is well known[26] the twisting of a substituent group relative to the benzene ring will give rise to a decrease of the conjugation. This decre-

Table 3

The π-dipole moments and ionization potentials for o-chloronitrobenzene

Angle of twist α (degrees)	π-Dipole moment (D)		Ionization potential	
	Calculated	Observed *	Calculated (eV)	Observed
0	3.92	3.65[a]; 4.41[b]	10.02	
30	3.763	4.36[c]; 4.9[d]	10.05	
45	3.614		10.09	
60	3.463		10.12	
90	3.312		10.15	

* Total dipole moment for the equilibrium configuration

[a] Ref. 22; [b] Ref. 23; [c] Ref. 24; [d] Ref. 25;

Table 4

The π-dipole moments and ionization potentials for o-dinitrobenzene

Angles of twist (degrees)		π-Dipole moment (D)		Ionization potential (eV)	
α	β	Calculated	Observed *	Calculated	Observed
0	0	6.19		10.30	
0	30		6.9[a]	10.28	
0	45			10.27	
0	60			10.25	
0	90			10.23	
30	30			10.25	
30	45			10.22	
30	60			10.19	
30	90			10.18	
45	45			10.18	
45	60			10.14	
45	90			10.11	
60	60			10.09	
60	90			10.04	
90	90			9.96	

* Total dipole moment for the equilibrium conformation

[a] Ref. [25].

---

[22] S. I. Ahmed and K. C. Lal, *Ind. J. Pure Appl. Phys.*, **1**, 104 (1963).

[23] H. Goetz, F. Nerdel and K. Rehse, *Liebigs Ann. Chem.*, **681**, 1 (1961).

[24] L. Tiganic, *Z. phys. chem. (Leipzig)*, **13B**, 425 (1931).

[25] W. Kemula and J. Geisler, *Roczniki Chem.*, **38**, 1961 (1967).

[26] P. P. Shorygin and Z. F. Il'icheva, *Izvest. Acad. Nauk, S.S.S.R., Otdel. fiz. Nauk.*, **22**, 1058 (1958).

ase of the conjugation will produce a blue shift of the band, together with a decrease in the band intensity.

Shorygin and Il'icheva[26] have found that the twisting angle in *o*-chloronitrobenzene is approximately 60°. They pointed out that the second absorption band in the uv spectra suffered a significant decrease in intensity by going from nitrobenzene to *o*-chloronitrobenzene. From the experimental data quoted in table 1 we can see that this band has an intensity smaller than that corresponding to both *meta*- and *para*-compounds (see also ref.[1]). From the intensity point of view this effect is observable in the theoretical values given in the same table. The position of the band, however, is in the reverse order. This means that in the case of *o*-compounds one of the groups or even both are rotated out of the plane. The influence of the rotation angle on the position and intensity of the bands of *o*-cloronitrobenzene is given in table 1. From table 1 we see that there are two kinds of bands, namely those which have an increase in the wavelength of the band and those which have a decrease. It is normal to correlate the decrease in the wavelength of the band with the decrease of the conjugation, and as the table shows, this is the case for the first two absorption bands. The discussion is almost the same in the case of dinitrobenzenes. Yet in this case we have two equivalent groups and both can be rotated out of the plane. So we calculated the transition energies and the oscillator strengths in all possible cases which are presented in table 2.

For the dipole moments and ionization potentials we did obtain but temperate variations. These are given in tables 3 and 4. In these tables we can see that for *o*-chloronitrobenzene the dipole moment decreases from 3.9 D for $\alpha = 0°$ to 3.31 D for $\alpha = 90°$, while the ionization potential increases from 10.02 to 10.15 eV. The dipole moment of *o*-dinitrobenzene has the smallest value, 4.3 D, for $\alpha = 90°$, $\beta = 90°$ and the greatest one, 6.33 D, for $\alpha = 0°$, $\beta = 0°$. The ionization potentials varied between 9.96 eV ($\alpha = 90°, \beta = 90°$) and 10.30 eV ($\alpha = 0°, \beta = 0°$).

Revue Roumaine, de Chimie, 20, 2, 209–216 (1975)

L'INFLUENCE DE LA TEMPÉRATURE ET DE LA CONCENTRATION DE L'ÉLECTROLYTE SUR LES PERFORMANCES D'UNE PILE À COMBUSTIBLE HYDROGÈNE-OXYGÈNE

MARIA MAVRODIN-TĂRĂBÎC, IOANA ONACA et I. SOLACOLU
Centre de Chimie Physique, Bucarest, 31, str. Galaţi

Reçu le 26 décembre 1973

On a étudié l'influence de la température et de la concentration de l'électrolyte sur les caractéristiques électriques d'une pile à combustible hydrogène-oxygène avec anode en nickel et cathode en argent, réalisée dans notre laboratoire. Les températures ont été variées entre 25 et 75° et les concentrations de l'électrolyte KOH entre 2N et 8N. On a déterminé les courbes de décharge sur résistance variable $E-i$ et la méthode d'interprétation de ces courbes nous a permis le calcul des pertes par polarisation et des rendements réalisés par la pile étudiée. On a calculé aussi les caractéristiques électriques de la pile, dans les conditions d'une puissance maximale débitée dans le circuit extérieur.

Parmi les sources modernes d'énergie électrique, les piles à combustible se distinguent par les rendements réalisés dans la conversion de l'énergie chimique du combustible, rendements nettement supérieurs à ceux réalisés par les procédés conventionnels. Il est évident que le développement des recherches dans ce domaine est justifié aussi par les problèmes actuels de la valorisation supérieure des combustibles naturels.

Le rendement de conversion de l'énergie dépend tant du rendement thermodynamique de la réaction chimique qui est à la base de l'obtention du courant électrique dans les conditions de fonctionnement de la pile, que du rendement électrique, dont la valeur varie selon la grandeur des pertes énergétiques irréversibles (polarisation de transfert de charge, de concentration et de résistance ohmique, pertes électriques dans les contacts et dans les conducteurs, etc.).[1]

Etant donné le prix relativement élevé de l'énergie électrique obtenue dans la pile à combustible du type hydrogène-oxygène, les études concernant la détermination des valeurs optimales des paramètres de fonctionnement qui conduisent à la réalisation des rendements maximaux présentent un intérêt considérable.

Le prix de revient de l'énergie électrique obtenue est influencé par le prix de l'installation et surtout par le prix des électrocatalyseurs utilisés pour l'activation des réactions. Etant donné que pour les systèmes qui utilisent comme électrolyte des solutions alcalines concentrées il n'y a que le prix de l'électrocatalyseur anodique qui soit déterminant (des études récentes[2-6] ont établi que l'argent ou le charbon activé sont des électrocatalyseurs efficients pour l'électroréduction de l'oxygène), les recherches actuelles sont orientées dans la direction du remplacement des catalyseurs chers à base de métaux platiniques ; parmi ces catalyseurs moins chers on mentionne le nickel caractérisé par des performances électrochimiques supérieures et aussi par de bonnes propriétés mécaniques et de résistance à la corrosion dans les conditions de travail.[7-9]

---

[1] M. MAVRODIN-TĂRĂBÎC, I. ONACA et I. SOLACOLU, *Studii şi Cercetări Chim. Acad. Bucureşti*, **21**, 335 (1973).

Dans nos travaux antérieurs nous avons étudié les performances électrochimiques des électrodes à gaz en nickel dans la réaction d'oxydation de l'hydrogène[10,11] et des électrodes à gaz en argent dans la réaction de réduction de l'oxygène.[12] Ces études nous ont permis de déterminer les valeurs optimales des paramètres d'obtention des électrodes qui conduisent à des caractéristiques supérieures de fonctionnement.

Dans ce travail nous nous sommes proposé d'étudier l'influence de la température et de la concentration de l'électrolyte sur les caractéristiques électriques et sur les rendements de conversion réalisés par une pile à combustible du type hydrogène-oxygène avec anode en nickel et cathode en argent, réalisée dans notre laboratoire.

1. PARTIE EXPÉRIMENTALE

1.1. RÉALISATION DE LA PILE HYDROGÈNE-OXYGÈNE

On a réalisé une source chimique de courant du type

$$(-)\ H_2\,(Ni)/KOH/(Ag)O_2\ (+)$$

Dans ce but on a utilisé :

— *une anode* — électrode à gaz en nickel (A_1) du type DSK (« Doppel Skelet Katalyst »), obtenue en comprimant, dans des matrices en acier, à une pression de $4{,}6.10^8$ N/m², un mélange homogène qui contient 25 % nickel ex nickel carbonyle, 50 % carbonate de nickel et 25 % acide oxalique, les dimensions des particules étant les suivantes : au-dessous de 3 microns (pour le nickel carbonyle), jusqu'à 5 microns (pour le carbonate de nickel) et d'environ 40—60 microns (pour l'acide oxalique). Les électrodes obtenues, de forme cylindrique, à un diamètre de 10 mm et une épaisseur de 3 mm, ont été frittées à 700°, pendant 30 minutes, en atmosphère d'hydrogène. L'électrode (A_2) a été obtenue dans les mêmes conditions, mais comprimée à une pression de $5{,}4.\ 10^8$N/m².

---

[2] J. Jausta, *Coll. Czech. Chem. Comm.*, **33**, 160 (1968).
[3] I. Lindholm, *J. Electrochem. Soc.*, **116**, 1150 (1969).
[4] J. Mrha et J. Jindra, *Coll. Czech. Chem. Comm.*, **34**, 2465 (1969).
[5] J. Jausta et K. Micka, *Coll. Czech. Chem. Comm.*, **35**, 1650 (1970).
[6] J. Marcos, *J. Electroanalyt. Chem.*, **20**, 479 (1969).
[7] V. A. Tracy et N. J. Williams, *Electrochem. Technol.*, **3**, 17 (1965).
[8] V. A. Tracy, *Powder Met.*, **8**, 241 (1965).
[9] R. J. Jasinski, *Electrochem. Technol.*, **3**, 40 (1965).
[10] Mavrodin-Tărăbîc, I. Onaca et I. Solacolu, *Rev. Roumaine Chim.*, **18**, 1121 (1973).
[11] M. Mavrodin-Tărăbîc, I. Onaca et I. Solacolu, *Rev. Roumaine Chim.* (sous presse).
[12] O. Radovici, M. Mavrodin-Tărăbîc, I. Onaca et I. Solacolu, *Rev. Romaine Chim.*, **17**, 1153 (1972).

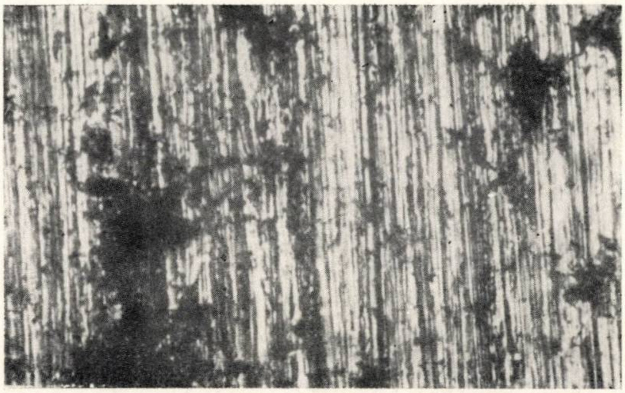

Fig. 1. — Structure de l'électrode A_1 avec une porosité totale de 59, 2 %. Microphotographie, 500 ×.

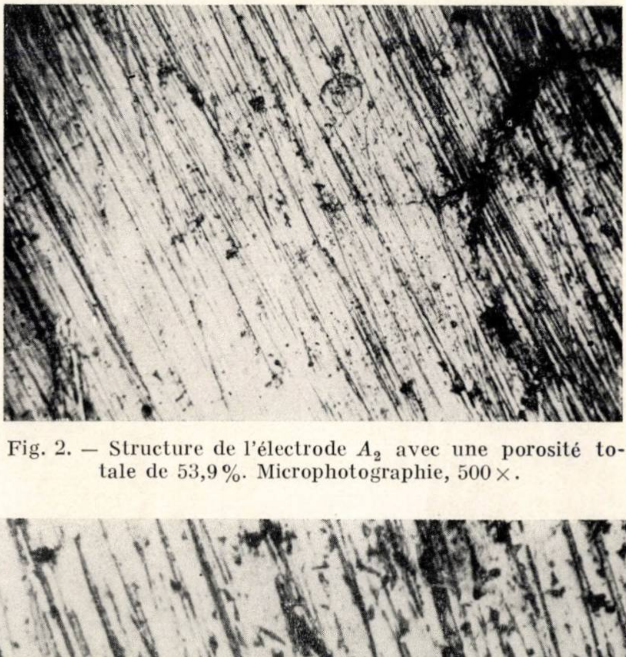

Fig. 2. — Structure de l'électrode A_2 avec une porosité totale de 53,9 %. Microphotographie, 500 ×.

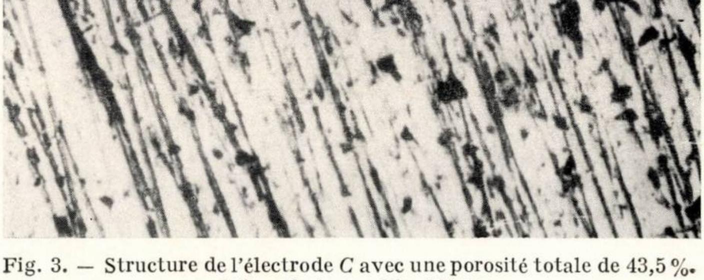

Fig. 3. — Structure de l'électrode C avec une porosité totale de 43,5 %. Microphotographie, 500 ×.

— *une cathode* — électrode à gaz en argent (C) du type DSK, obtenue en comprimant, à une pression de 2,8. 10^8 N/m^2, un mélange homogène qui contient 81,25 % carbonate d'argent et 18,75 % bicarbonate d'ammonium, les dimensions des particules étant les suivantes : jusqu'à 5 microns et, respectivement, 40 — 60 microns. Les électrodes, à un diamètre de 10 mm et à une épaisseur de 3 mm, ont été frittées, pendant 15 minutes, à 375°, en atmosphère d'hydrogène,

— *électrolyte* — solution de KOH.

On a utilisé des substances de pureté *p.a.*

La cellule de travail (120 × 72 × 56 mm) a été confectionnée en polystyrène.

L'alimentation de l'anode avec de l'hydrogène, à la surpression de 200 mm Hg, et de la cathode avec de l'oxygène, à la surpression de 600 mm Hg, a été réalisée à l'aide d'une installation présentée dans un travail antérieur.[13]

La température de travail a été variée entre 25 et 70° ; pour obtenir une température constante (précision de ±0,1°) on a utilisé un thermostat de type U—10.

La concentration de l'électrolyte a été variée entre 2 et 8N.

1.2. DÉTERMINATIONS DE LA STRUCTURE ET DE LA POROSITÉ

Les électrodes ont été caractérisées du point de vue structural par :

— l'étude de la répartition des pores, par un examen microscopique à l'aide d'un microscope métallographique de réflexion du type MIM—7 ;

— des déterminations de la porosité totale, en pesant les électrodes avant et après l'imprégnation avec du toluène.

L'examen microscopique a démontré que les pores, petits et grands, caractéristiques de la structure du type DSK, sont uniformément répartis dans la masse de l'électrode (fig. 1—3).

De l'examen comparatif des microphotographies présentées dans les figures 1 et 2 et des valeurs des porosités totales, il résulte que l'augmentation de la pression, à partir de 4,6.10^8 N/m^2 (A_1) jusqu'à 5,4.10^8 N/m^2 (A_2), conduit à l'obtention des électrodes caractérisées par un degré de frittage plus avancé et une porosité totale moins grande (53,9 % en comparaison de 59,2 %).

1.3. DÉTERMINATION DES CARACTÉRISTIQUES ÉLECTRIQUES

En vue de déterminer les courbes de décharge $E-i$ de la pile à combustible, à différentes températures et concentrations de l'électrolyte, la pile réalisée a été déchargée, tout en variant la résistance (on a utilisé une boîte à résistance caractérisée par une précision de ±0,1 ohm), dans un montage décrit dans un travail antérieur.[13]

Les valeurs des courants ont été mesurées à l'aide d'un milliampèremètre de classe 0,5 et les tensions électriques à l'aide d'un millivoltmètre électronique Radiometer 22 (précision ± ±1 mV).

2. RÉSULTATS ET DISCUSSIONS

2.1. L'INFLUENCE DE LA TEMPÉRATURE DE L'ÉLECTROLYTE

En vue d'établir l'effet de la température de l'électrolyte sur les performances électriques de la pile hydrogène-oxygène, réalisée dans notre laboratoire, on a déterminé les courbes de décharge $E-i$, à différentes températures, comprises entre 25 et 65° pour la pile avec anode A_1 et entre 40 et 70° pour la pile avec anode A_2.

---

[13] O. Radovici, M. Mavrodin-Tărăbîc, I. Onaca et I. Solacolu, *Rev. Roumaine Chim.*, **18**, 767 (1973).

Les courbes de décharge $E-i$ offrent une image des phénomènes qui ont lieu pendant le fonctionnement de la pile, l'analyse de ces courbes permettant la détermination des caractéristiques électriques et du rendement de conversion de l'énergie chimique du combustible en énergie électrique. La méthode d'interprétation des courbes a été décrite en détail dans un travail antérieur.[13]

Les courbes de décharge, à différentes températures, caractéristiques à la pile avec anode A_1 sont présentées dans la figure 4.

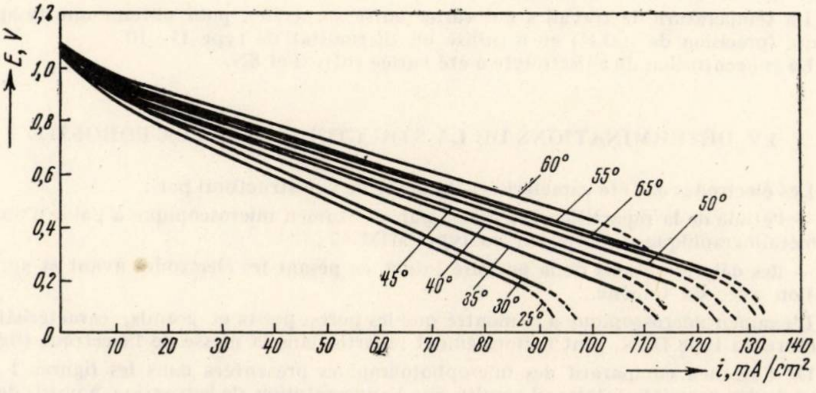

Fig. 4. — Courbes de décharge $E-i$, caractéristiques à la pile à combustible avec anode A_1, à différentes températures de l'électrolyte. $\Delta P_{H_2} = 200$ mm Hg $\Delta P_{O_2} = 600$ mm Hg. Electrolyte, KOH 5N.

Les caractéristiques électriques et les valeurs des rendements de conversion, calculées à l'aide des courbes de décharge, sont présentées dans le tableau 1.

De l'examen des données présentées dans le tableau 1, il résulte que la variation de la température de l'électrolyte dans l'intervalle 25—65° a un effet favorable sur les caractéristiques électriques (dans les conditions d'une puissance maximale débitée dans le circuit extérieur) et sur les rendements réalisés, jusqu'à la température de 60°.

L'augmentation de la température de l'électrolyte produit, d'une part, une diminution de la solubilité de l'hydrogène et de l'oxygène (effet défavorable sur les performances des électrodes) et, d'autre part, une augmentation de la vitesse de diffusion des espèces réactives et des produits de réaction (effet favorable) ; il est évident que les performances des électrodes dépendent de ces deux phénomènes.

Des études récentes concernant l'influence de la température de l'électrolyte sur le comportement des électrodes à gaz dans la réaction d'oxydation de l'hydrogène[11,14] et de réduction de l'oxygène[14] ont démontré que, dans le premier cas, entre —20 et 80°, les performances des électrodes s'améliorent continuellement, tandis que dans le cas de l'électrode à oxygène, dans l'intervalle considéré, les performances présentent un maximum à 60°.

---

[14] D. B. Lucesoli, Thèse, Univ. Paris, 1971.

De l'examen des données présentées dans le tableau 1 il résulte que la pile à combustible, avec anode A_1, présente des caractéristiques électriques élevées et réalise le meilleur rendement de conversion à la température de 60° ($E = 500$ mV, $i = 84{,}74$ mA/cm², $P = 42{,}367$ mW//cm², $\varepsilon_{\max} = 0{,}8334$, $\varepsilon_{\text{moyen}} = 0{,}4167$, $\eta_{\max} = 0{,}6771$ et $\eta_{\text{réel}} = 0{,}3386$.

Les courbes de décharge, à différentes températures, caractéristiques à la pile avec anode A_2, sont représentées dans la figure 5.

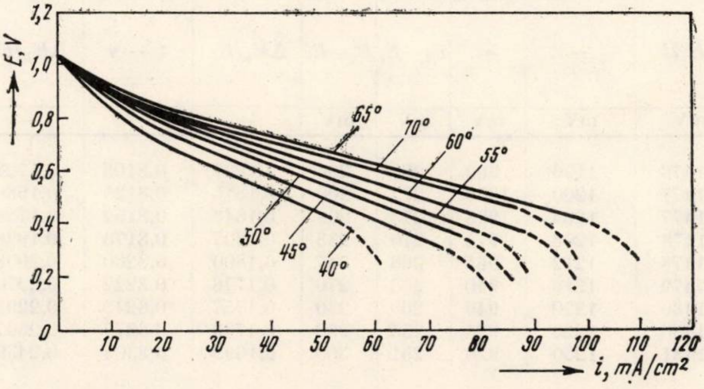

Fig. 5. — Courbes de décharge $E-i$, caractéristiques à la pile à combustible avec anode A_2, à différentes températures de l'électrolyte. $\Delta P_{H_2} = 200$ mm Hg. $\Delta P_{O_2} = 600$ mm Hg. Electrolyte, KOH 5N.

A l'aide de ces courbes on a calculé les caractéristiques électriques et les rendements réalisés (tabl. 2).

Les données du tableau 2 confirment l'existence d'un domaine optimal de température (60° à 65°), domaine dans lequel les performances sont élevées. Les valeurs maximales sont : à 65°, $i = 87{,}96$ mA/cm², et $P = 41{,}78$ mW/cm² et à 60°, $E = 500$ mV, $\varepsilon_{\max} = 0{,}8334$, $\varepsilon_{\text{moyen}} = 0{,}4167$, $\eta_{\max} = 0{,}6771$ et $\eta_{\text{réel}} = 0{,}3386$.

Les valeurs relativement plus élevées du domaine optimal de température, dans le cas de la pile avec anode A_2, peuvent être expliquées par le fait que, le frittage de l'anode étant plus avancé et donc les pores ayant des diamètres comparativement moins grands, l'étape de diffusion influence davantage le développement des processus anodiques.

2.2. INFLUENCE DE LA CONCENTRATION DE L'ÉLECTROLYTE

Pour établir l'effet de la concentration de l'électrolyte sur les performances électriques de la pile hydrogène-oxygène avec anode A_1, on a déterminé les courbes de décharge $E-i$, à différentes concentrations de l'électrolyte comprises entre 2N et 8N (fig. 6).

A l'aide des courbes représentées dans la figure 6 on a calculé les caractéristiques électriques et les rendements de conversion réalisés (le tableau 3).

Tableau

Caractéristiques électriques et rendements de conversion réalisés par la pile avec

Température de l'électrolyte	Tension électrique totale	Tension électrique idéale	Tension électrique réelle	Perte thermodynamique	Perte électrique	Facteur thermodynamique	Rendement thermodynamique	Facteur de polarisation	Rendement électrique maximal
	E_t	E_i	E_r	ΔE_u	ΔE_p	ν	η_T	μ	$\varepsilon_{\max}$
	$\Delta H/zF$	—	—	$E_t - E_i$	$E_i - E_r$	$\Delta E_u/E_t$	$1 - \nu$	$\Delta E_p/E_i$	$1 - \mu$
°C	mV	mV	mV	mV	mV	—	—	—	—
65	1476	1196	990	280	206	0,1897	0,8103	0,1722	0,8278
60	1477	1200	1000	277	200	0,1875	0,8125	0,1666	0,8334
55	1477	1204	995	273	209	0,1848	0,8152	0,1736	0,8264
50	1478	1208	975	270	233	0,1827	0,8173	0,1928	0,8072
45	1478	1212	965	266	247	0,1800	0,8200	0,2038	0,7962
40	1479	1216	940	263	276	0,1778	0,8222	0,2270	0,7730
35	1480	1220	940	260	280	0,1757	0,8243	0,2295	0,7705
30	1480	1225	935	255	290	0,1723	0,8277	0,2367	0,7633
25	1481	1230	930	251	300	0,1695	0,8305	0,2439	0,7561

Tableau

Caractéristiques électriques et rendements de conversion réalisés par la pile avec

Température de l'électrolyte	E_t	E_i	E_r	ΔE_u	ΔE_p	ν	η_T	μ	$\varepsilon_{\max}$
°C	mV	mV	mV	mV	mV	—	—	—	—
70	1476	1192	945	284	247	0,1924	0,8076	0,2072	0,7928
65	1476	1196	950	280	246	0,1897	0,8103	0,2057	0,7943
60	1477	1200	1000	277	200	0,1875	0,8125	0,1666	0,8334
55	1477	1204	980	273	224	0,1848	0,8152	0,1860	0,8140
50	1478	1208	965	270	243	0,1827	0,8173	0,2011	0,7989
45	1478	1212	940	266	272	0,1800	0,8200	0,2244	0,7756
40	1479	1216	880	263	336	0,1778	0,8222	0,2763	0,7237

Tableau

Caractéristiques électriques et rendements de conversion réalisés par la pile

Concentration de l'électrolyte	E_t	E_i	E_r	ΔE_u	ΔE_p	ν	η_T	μ	$\varepsilon_{\max}$
équiv. cm^{-3}	mv	mV	mV	mV	mV	—	—	—	—
8	1481	1230	825	251	405	0,1695	0,8305	0,3292	0,6708
7	1481	1230	830	251	400	0,1695	0,8305	0,3252	0,6748
6	1481	1230	870	251	360	0,1695	0,8305	0,2926	0,7074
5	1481	1230	860	251	370	0,1695	0,8305	0,3008	0,6992
4	1481	1230	850	251	380	0,1695	0,8305	0,3089	0,6911
3	1481	1230	835	251	395	0,1695	0,8305	0,3211	0,6789
2	1481	1230	830	251	400	0,1695	0,8305	0,3252	0,6748

1

anode A_1 à différentes températures de l'électrolyte (KOH 5N)

Rendement électrique moyen	La pente de la zone des courants moyens	Densité de courant maximale	Densité de courant moyenne	Puissance électrique maximale	Tension électrique en conditions de puissance maximale	Coefficient de pertes par polarisation	Rendement de conversion maximal	Rendement de conversion réel
ε_{moyen}	R	i_{max}	$i_{moyenne}$	P_{max}	E	σ	η_{max}	$\eta_{réel}$
$\frac{1}{2}\ \varepsilon_{max}$	—	$(1-\mu)E_i/R$	$\frac{1}{2}\ i_{max}$	$i^2_{moyenne}\ R$	$E_t - \Delta E_u - \Delta E_p - R i_{moyenne}$	$\Delta E_p/E_t$	$1-\nu-\sigma$	$1-\nu-\sigma-\frac{R_{i\,moyenne}}{E_t}$
—	ohm	mA/cm²	mA/cm²	mW/cm²	mV	—	—	—
0,4139	6,0	164,99	82,50	40,838	495	0,1395	0,6708	0,3354
0,4167	5,9	169,48	84,74	42,367	500	0,1354	0,6771	0,3386
0,4132	5,96	166,94	83,47	41,525	498	0,1415	0,6737	0,3368
0,4036	6,0	162,50	81,25	39,609	488	0,1576	0,6597	0,3299
0,3981	6,2	155,64	77,82	37,547	483	0,1671	0,6529	0,3265
0,3865	6,3	149,20	74,60	35,061	470	0,1866	0,6356	0,3178
0,3853	7,1	132,39	66,20	31,115	470	0,1891	0,6352	0,3176
0,3817	8,8	106,25	53,13	24,841	468	0,1959	0,6318	0,3159
0,3781	9,0	103,34	51,67	24,028	464	0,2025	0,6280	0,3140

2

anode A_2 à différentes températures de l'électrolyte (KOH 5N)

ε_{moyen}	R	i_{max}	$i_{moyenne}$	P_{max}	E	σ	η_{max}	$\eta_{réel}$
—	ohm	mA/cm²	mA/cm²	mW/cm²	mV	—	—	—
0,3964	5,5	171,81	85,90	40,583	472	0,1673	0,6403	0,3202
0,3972	5,4	175,93	87,96	41,780	475	0,1616	0,6437	0,3219
0,4167	7,7	129,87	64,93	32,467	500	0,1354	0,6771	0,3386
0,4070	7,7	127,27	63,63	31,176	490	0,1516	0,6636	0,3318
0,3995	8,2	117,68	58,84	28,390	471	0,1644	0,6529	0,3265
0,3888	8,8	106,81	53,40	25,094	470	0,1840	0,6360	0,3180
0,3619	8,9	98,88	49,44	21,754	440	0,2272	0,5950	0,2975

3

avec anode A_1 à différentes concentrations de l'électrolyte (température, 25°)

ε_{moyen}	R	i_{max}	$i_{moyenne}$	P_{max}	E	σ	η_{max}	$\eta_{réel}$
—	ohm	mA/cm²	mA/cm²	mW/cm²	mV	—	—	—
0,3354	5,9	139,82	69,91	28,836	402	0,2734	0,5571	0,2786
0,3374	5,9	140,68	70,34	29,192	415	0,2700	0,5605	0,2803
0,3537	5,8	150,00	75,00	32,630	434	0,2430	0,5875	0,2938
0,3496	5,3	162,27	81,13	34,885	430	0,2498	0,5807	0,2904
0,3456	5,1	166,66	83,33	35,414	425	0,2565	0,5704	0,2852
0,3395	5,8	143,95	71,94	30,171	418	0,2665	0,5640	0,2820
0,3374	7,1	116,90	58,45	24,256	415	0,2700	0,5605	0,2803

Des données présentées dans le tableau 3 il résulte que le domaine optimal de concentration de l'électrolyte est compris entre 4N et 6N. Les performances de la pile à combustible sont : à 4N, $i = 83{,}33$ mA/cm², $P = 35{,}414$ mW/cm² et, à 6N, $E = 434$ mV, $\varepsilon_{\max} = 0{,}7074$, $\varepsilon_{\text{moyen}} = 0{,}3537$, $\eta_{\max} = 0{,}5875$ et $\eta_{\text{réel}} = 0{,}2938$, en concordance avec les données de la littérature concernant l'effet de la concentration de l'électrolyte sur les performances des électrodes.

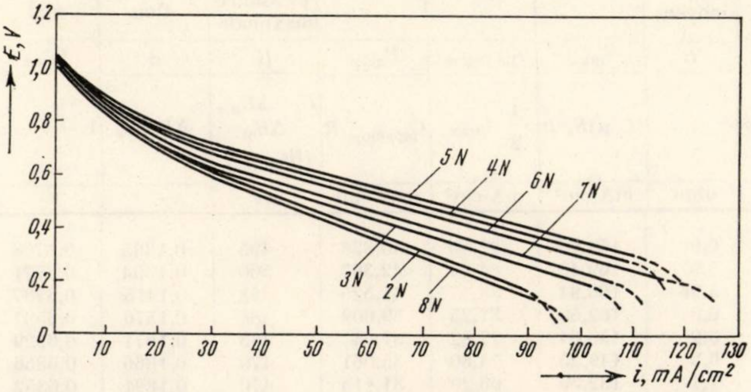

Fig. 6. — Courbes de décharge $E - i$, caractéristiques à la pile à combustible avec anode A_1, à différentes concentrations de l'électrolyte. $\Delta P_{H_2} = 200$ mm Hg. $\Delta P_{O_2} = 600$ mm Hg. Température, 25°.

3. CONCLUSIONS

1. L'augmentation de la température de l'électrolyte jusqu'à 60° présente un effet favorable sur les caractéristiques électriques et sur les rendements réalisés par la pile hydrogène-oxygène avec anode (A_1) en nickel et cathode (C) en argent.

2. Les performances de la pile, dans les conditions d'une puissance maximale débitée dans le circuit extérieur, à 60°, sont : $E = 500$ mV, $i = 84{,}74$ mA/cm², $P = 42{,}367$ mW/cm², $\varepsilon_{\max} = 0{,}8334$, $\varepsilon_{\text{moyen}} = 0{,}4167$, $\eta_{\max} = 0{,}6771$ et $\eta_{\text{réel}} = 0{,}3386$.

3. Dans le cas de la pile avec anode A_2, qui présente un degré de frittage plus avancé, le domaine optimal de température est compris entre 60 et 65°. Les performances sont : $E = 500$ mV (60°), $i = 87{,}96$ mA/cm² (65°), $P = 41{,}78$ mW/cm² (65°), $\varepsilon_{\max} = 0{,}8334$ (60°), $\varepsilon_{\text{moyen}} = 0{,}4167$ (60°), $\eta_{\max} = 0{,}6771$ (60°) et $\eta_{\text{réel}} = 0{,}3386$ (60°).

4. La variation de la concentration de l'électrolyte entre 2N et 6N a démontré l'existence d'un domaine optimal de concentration, compris entre 4N et 6N, à la température de 25°.

5. Dans ces conditions les performances sont : $E = 434$ mV (6N), $i = 83{,}33$ mA/cm² (4N), $P = 35{,}414$ mW/cm² (4N), $\varepsilon_{\max} = 0{,}7074$ (6N), $\varepsilon_{\text{moyen}} = 0{,}3537$ (6N), $\eta_{\max} = 0{,}5875$ et $\eta_{\text{réel}} = 0{,}2938$ (6N).

Revue Roumaine de Chimie, 20, 2, 217–225 (1975)

THE CATALYTIC SYSTEM $ZnO-Al_2O_3$. I

THE INFLUENCE OF CHEMICAL COMPOSITION AND CRYSTALLINE STRUCTURE UPON THE FORMATION OF THE ACTIVE PHASES IN THE DECOMPOSITION REACTION OF ISOPROPYL ALCOHOL

I. UDREA * and D. CRIŞAN **

*Faculty of Chemistry, Splaiul Independenţei 87, Bucharest,

** Institute of Physical Chemistry, Dumbrava Roşie 23, Bucharest, Romania

Received April 2, 1974

The catalytic system $ZnO-Al_2O_3$ with different chemical compositions was submittedto thermal treatment at 500, 700 and 900°. The samples were tested in the reaction of *i*-PrOH decomposition. At lower concentrations of ZnO the studied system exhibits only a dehydrating activity. The dehydrogenating activity is observed only in the vicinity of stoichiometrical composition. Increase of ZnO content beyond the stoichiometrical one induces an important increase in the dehydrogenation activity. Experimental data based on differential thermal analysis and X-ray diffraction allowed us to assume that dehydration activity observed in samples with $ZnO/Al_2O_3 \leqslant 1$ molar ratios is due to the defective spinelic structure whereas the activity of dehydrogenation prevailing in the samples with molar ratios > 1 may be assigned to the interface between ZnO and $ZnAl_2O_4$.

INTRODUCTION

ZnO is known to be a catalyst which presents dehydrogenation properties. In the presence of different metallic oxides in binary or ternary systems these properties are more accentuated.[1-3]

The system created by ZnO together with Al_2O_3 displays a series of particularities. This system which is formed by oxides with quite different catalytic properties in respect with the preparation method and with the mixture composition, may present varied catalytic properties, starting from a strong dehydration up to a significant dehydrogenation activity, even more enhanced than that of a pure ZnO. The activity of the system is often assigned to structural modifications which arise during the thermal treatment.

---

[1] J. E. Germain, B. Gras and J. P. Beaufils, "Coloquio sobre Quimica Fisica de procesos en superficies solidas" (XXV Aniversario del C.S.I.C., octubre 1964), Cientifica Medinaceli, Madrid, 1965.

[2] J. F. Garcia de la Banda, *J. Catalysis*, **1**, 136 (1962).

[3] J. Burzyk, J. Haber and J. Nowotny, *Bull. Acad. polon. Sci., Ser. Sci. Chim.*, **17**, 543 (1969).

It has been proved that simultaneously with the increase of calcination temperature, both oxides interact with each other eventually forming zinc spinel. Intermediate phases preceding spinel formation are characterized by a disturbed crystalline structure with active catalytic properties.[4]

If the presence of Al^{3+} ions with tetrahedral coordination explains the dehydration activity of the system, the literature still provides many conflicting data concerning the active phase responsible for dehydrogenation activity. For instance, some authors[4,5] connect the dehydrogenation activity with the apperance of the zinc spinel. In contrast, Alsop and Dowden[6] found that stoichiometric spinel is without activity and dehydrogenation activity appears only in the presence of traces of free ZnO. Also, Bhattacharyya[7] and co-workers suggested that the dehydrogenation activity may be connected to the ZnO dispersion on the Al_2O_3 surface. Finally, Uma and Kuriacose[8] hypothesized that a new species is formed due to the interaction between ZnO and Al_2O_3, undetectable by X-ray, which is responsible for the dehydrogenation activity. According to the authors, this species may be a spinel or a "precursor" of the spinel.

In the present study we revealed, by means of a ZnO/Al_2O_3 molar ratio modification, the active phases which arise in the system during the thermal treatment, using DTA and X-ray determination. At the same time some considerations have been made, concerning the nature of the phases having a determining role in the dehydration/dehydrogenation activity of this system.

EXPERIMENTAL DATA

$ZnO-Al_2O_3$ samples with a different chemical composition and with molar ratios shown in the table below were prepared from their nitrates and ammonium carbonate by means of a mixing method.[9] After drying, the samples were calcined at 500, 700 and 900° for two hours. The following molar ratios have been chosen :

Samples	ZA_1	ZA_2	ZA_3	ZA_4	ZA_5
$ZnO : Al_2O_3$ molar ratio	1 : 0.1	1 : 0.5	1 : 1	0.5 : 1	0.1 : 1

The DTA of the catalyst was followed by means of a F. Paulik, J. Paulik and L. Erdey derivatograph. The heating rate was 10°/min., sensitivity 1/5, in the air using $\alpha-Al_2O_3$ as reference.

---

[4] Von A. Simon, Chr. Oehme and K. Pohl, *Z.anorg. Chem.*, **323**, 160 (1963).

[5] Von A. Simon, Chr. Oehme and K. Pohl, *Z.anorg. Chem.*, **317**, 230 (1962).

[6] B. C. Alsop and D. A. Dowden, *J. Chim. phys.*, **51**, 678 (1954).

[7] S. K. Bhattacharyya, K. S. De, S. N. Pandao and G. V. Chandrashekhar, "Proc Intern. Congr. Catalysis 3 rd, Amsterdam 1964 "(North-Holland Publ. Co. 1965), vol. 1, p. 474.

[8] R. Uma and J. C. Kuriacose, *Indian J. Chem.*, **9**, 322 (1971).

[9] I. V. Nicolescu, A. Popescu, A. Szabo, C. Făgărăşanu, S. Şerban, V. Levinţa and. A. Marcu, Brevet R.S.R. 61889/17 December 1969.

X-ray measurements were carried out on a TUR-M 61 equipment fitted with HZG–3 diffractometer, using CuKα as radiation source and a nickel filter. The pulse range was of 60×10^3 pulses/min and 18×10^3 pulses/min (for the samples marked in the figures with *).

Specific surface areas were determined by applying the BET method to the adsorption isotherms of nitrogen at −196°, obtained by a Carlo Erba Sorptomatic.

The activity patterns were established in a flow-type reactor at atmospheric pressure. The reactions were carried out at 340° and 0.6 space velocity.

RESULTS AND DISCUSSION

The phase transformations which take place in the $ZnO-Al_2O_3$ system of different chemical composition are shown in figure 1.

The DTA outlines a process of physically-adsorbed water elimination due to the presence of endothermal peaks recorded in the range of 120–150°. The actual subsequent process of already selected molar ratios has a specific course depending on the mixture composition. Thus, this process was found to be delayed due to increase of ZnO amount in the catalyst composition, since the corresponding endothermic peaks are displaced from 150° to 310°, a fact that has already been reported by other authors.[10]

The decomposition process may be considered as completed at 500°. Beyond this temperature exothermic effects appear on the DTA curves as a consequence of the interaction between the two components, ZnO and Al_2O_3. Due to low contents of ZnO in the samples ZA_1 and ZA_2, the above interactions could not be revealed under our experimental conditions. Conversely, for the same conditions, one observes the appearance of a clear exothermic effect starting with ZA_3 sample, due to spinel formation whose maximum is displaced towards higher temperatures as the ZnO/Al_2O_3 ratio increases.

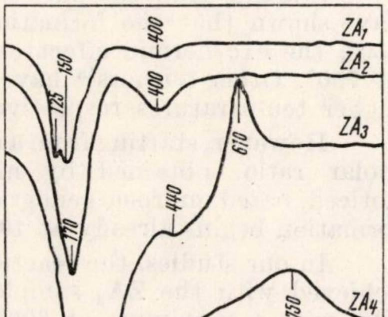

Fig. 1. – DTA curves of ZA samples and pure ZnO.

It is well known that, as a result of the solid state reaction between ZnO and Al_2O_3, a new combination with a proper crystalline lattice—zinc spinel—arises:

---

[10] S. K. Bhattacharyya, G. Srinivasan and N. D. Ganguly, *J. Indian Chem. Soc.* **41**, 4 (1964).

$$ZnO + Al_2O_3 = ZnAl_2O_4$$

According to Hauffe,[11] the spinel formation from oxide mixtures takes place by means of mobile component (ZnO) migration towards the more stable thermic components (Al_2O_3). Thus, ZnO, which has already become mobile at 400°, penetrates in the defective Al_2O_3 spinel lattice. Al^{3+} ions are forced to penetrate in the octahedral holes and Zn^{2+} ions fill the tetrahedral positions.[12] Obviously, this process takes place easier as the contact between the two components is closer.

Starting from the pure oxide mixture von Simon and co-workers[5] have shown that the formation of the spinel begins at approximately 550°, the exothermic effect on the DTA curves presenting a maximum at 750°. Other authors[13] have found that zinc spinel is formed at still higher temperatures respectively at 860°.

However, starting from a double zinc aluminium hydroxide with 1:1 molar ratio, obtained by nitrates precipitation, the authors[4] have noticed, based on roentgenographical structure studies, that the spinel formation begins already at 400° and ends between 500 and 600°.

In our studies, the reaction for the spinel formation is more rapidly achieved with the ZA_3 sample (1 : 1 molar ratio); it starts even under 500° with a maximum at 600° and the process is entirely completed at 700°. In the samples ZA_4 and ZA_5 this process is displaced towards higher temperatures, 750° and 850°, respectively, the peaks becoming broader and broader and less defined, due to the excess of ZnO which probably delays the process of the spinel formation.

In order to highlight the influence of the structural modifications taking place with temperature, conditioned by the ZnO/Al_2O_3 molar ratio, upon the catalytic activity, we have selected the following calcination temperatures, based on data provided by DTA : 500° — when the spinel is scarcely formed; 700° — when most of the spinel is formed and 900° — when the process of the spinel formation is completed.

From X-ray determinations (fig. 2, 3, 4 and table 1) carried upon these samples it has been found that, excepting ZA_1, all the samples exhibit the $ZnAl_2O_4$ spectrum whose content increases with the increase in ZnO content reaching a maximum when the molar ratio is 1 : 1.

It should be mentioned that although the Al_2O_3 spectrum fails to appear on the X-ray plot of ZA_3—500 sample it still exists, probably in an amorphous state. This statement is based on the fact that as the calcination temperature increases, the free ZnO content decreases in favour of $ZnAl_2O_4$ so that ZA_3—900 contains only spinel.

---

[11] K. Hauffe, "Reaktionen in und an festen Stoffen", Springer Verlag, Berlin, 1955, p. 590.

[12] E. S. W. Verwey, B. P. Braun, E. W. Gorter, F. C. Romeyn and J. H. van Santan, *Z. phys. Chem. (Leipzig)*, **198**, 6 (1951).

[13] G. F. Hüttig, H. Wörl and H. H. Weitzer, *Z. anorg. Chem.*, **283**, 207 (1956).

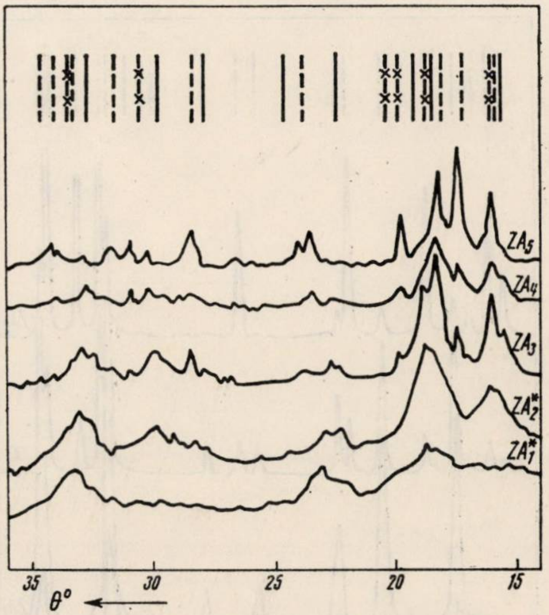

Fig. 2. — X-ray spectra of the samples calcined at 500°.

— — — ZnO
— × — × — η-Al_2O_3
——— Zn Al_2O_4

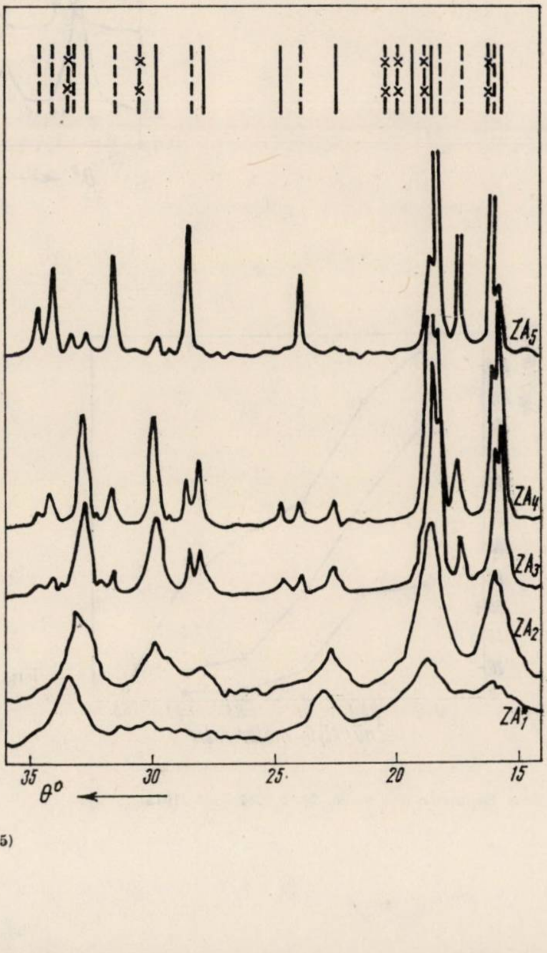

Fig. 3. — X-ray spectra of the samples calcined at 700°.

Fig. 4. — X-ray spectra of the samples calcined at 900°.

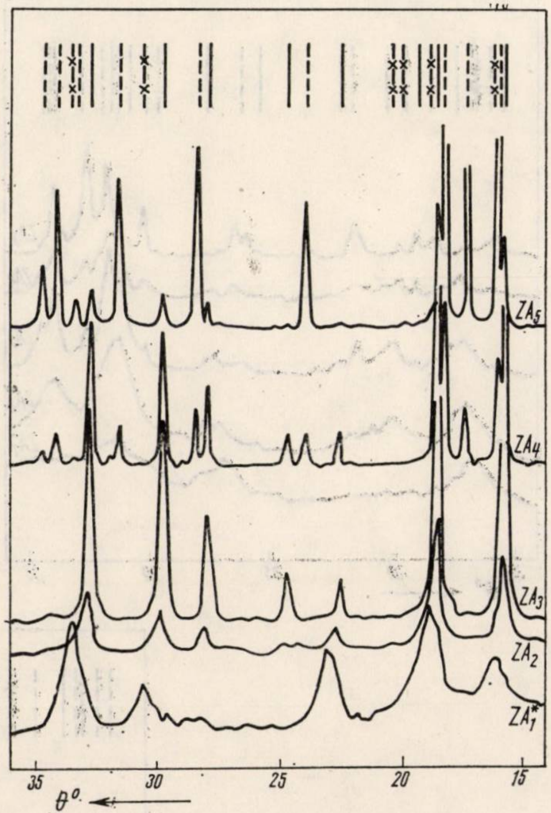

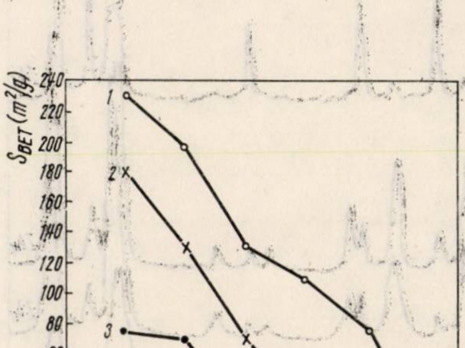

Fig. 5. — Specific surface areas in ZA-series.
1, ZA – 500; *2*, ZA – 700; *3*, ZA – 900.

Generally speaking, the rise in the calcination temperature induces an increase of crystallinity as a consequence of particles size growth. It is worth noticing that also at 900° alumina has a spinelic structure in the samples ZA_1 and ZA_2, its X-ray spectrum being very close to the $\eta-Al_2O_3$. The interplanar spacings are slightly larger than those of the $\eta-Al_2O_3$, probably due to the presence of some small amounts of $ZnAl_2O_4$ which seem to hinder the transformation of $\eta-Al_2O_3$ towards superior transition phases. Therefore, one may state that $ZnAl_2O_4$ plays an important part as stabilizer of the spinelic structure of $\eta-Al_2O_3$.

Table 1

Phases determined by Y-ray diffraction

Sample	Phases determined by X-ray diffraction		
	500°	700°	900°
ZA_1	$\eta-Al_2O_3$ + amorphous phase	$\eta-Al_2O_3$ + amorphous phase	$\eta-Al_2O_3$ + amorphous phase
ZA_2	$\eta-Al_2O_3$ + $(ZnAl_2O_4)$	$\eta-Al_2O_3$ + $(ZnAl_2O_4)$	$\eta-Al_2O_3$ + $(ZnAl_2O_4)$
ZA_3	$ZnAl_2O_4$ + (ZnO)	$ZnAl_2O_4$ + (ZnO)	$ZnAl_2O_4$
ZA_4	ZnO + $(ZnAl_2O_4)$	ZnO + $ZnAl_2O_4$	ZnO + $ZnAl_2O_4$
ZA_5	ZnO + + $(ZnAl_2O_4)$	ZnO + $(ZnAl_2O_4)$	ZnO + $(ZnAl_2O_4)$

At the same time, the increase of ZnO content as well as of the calcination temperature produces a continuous decrease of specific surface areas as seen in figure 5.

The specific activity of the samples studied in the decomposition of isopropyl alcohol is shown in figs. 6, 7 and 8.

For the molar ratio $ZnO/Al_2O_3 \leqslant 1$ it has been found that the dehydration activity is prevalent (fig. 6) and it passes through a maximum for the samples calcined at 700°.

The absence of dehydrogenation properties of samples with $ZnO/Al_2O_3 \leqslant 1$ molar ratio may be assigned to the existence of some intermediate phases which are characterized by a disordered crystalline structure.[4] The explanation consists in the fact that in a lattice with such a structure there still is a percentage of Al^{3+} ions with tetrahedral coordination. As these are insufficiently coordinated in respect with octahedric aluminium ions they aim towards saturation by means of anion-trapping from the reaction medium, especially OH groups from water. In this

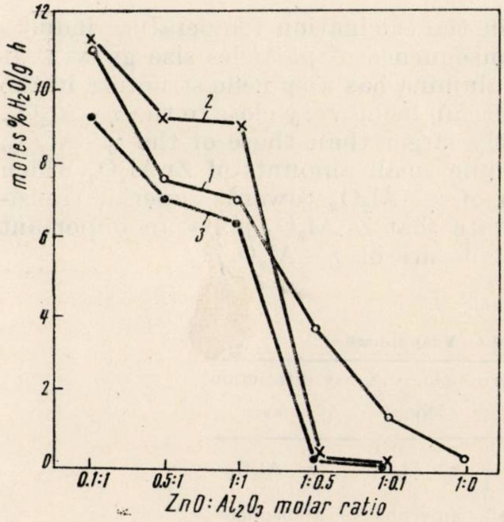

Fig. 6. — Variation of dehydration activity with chemical composition and thermal treatment in ZA-samples.

1, ZA – 500 ; *2*, ZA – 700 ; *3*, ZA – 900. The reaction temperature = 340°, space velocity = 0,6.

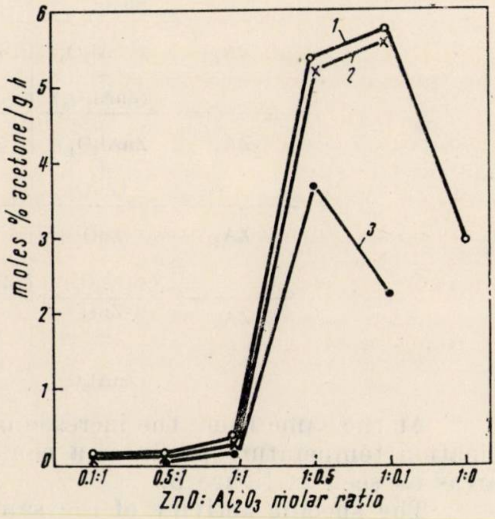

Fig. 7. — Variation of dehydrogenation activity with chemical composition and thermal treatment in ZA-samples.

1, ZA – 500 ; *2*, ZA – 700 ; *3*, ZA – 900.

The reaction temperature = 340°, space velocity = 0,6.

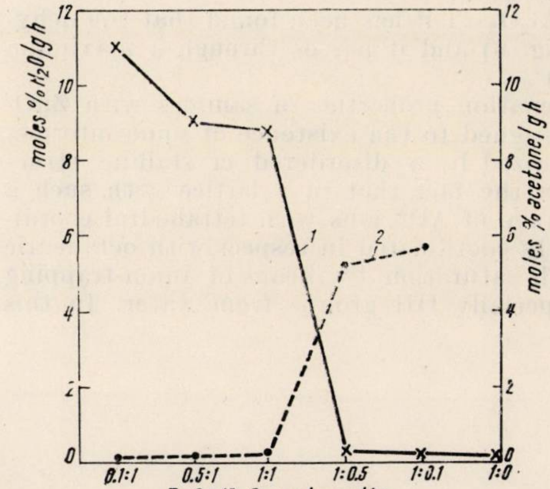

Fig. 8. — Variation of dehydration (1) and dehydrogenation (2) activities with composition in the samples calcined at 700°.

The reaction temperature = 340°, space velocity = 0.6.

way protons occur, which migrate on the catalyst surface influencing the catalytic process toward dehydration.

The decrease of dehydration activity for the sample calcined at a temperature higher than 700° is due to the process of rearrangement of crystalline lattice by the migration of Al^{3+} ions from tetrahedric sites to octahedral sites.

The increase of ZnO content beyond the stoichiometrical composition ($ZnO/Al_2O_3 > 1$ molar ratio) entails a very pronounced diminution of the dehydration activity simultaneously with a very important increase of the dehydrogenation activity. This activity decreases together with the increase of the calcination temperature of the samples when the sintering process takes place, which leads to a continuous decrease of the specific surface area (fig. 5).

If $ZnAl_2O_4$ were responsible for the dehydrogenation activity then, in the case of ZA_3 samples with spinelic composition, an enhanced dehydrogenation activity should exist which would increase with calcination temperature, as a rearrangement of a lattice occurs. But it has been found that all ZA_3 samples, inclusively ZA_3-900, which contains **100%** spinel, exhibit a very lowered dehydrogenation activity. Moreover, these samples present a pronounced dehydrating character, a fact which disagrees with the findings of other authors.[14]

According to X-ray data, the samples with $ZnO/Al_2O_3 > 1$ molar ratio which are characterized by a higher dehydrogenation activity than that of the spinel and also that of the pure ZnO, contain only ZnO and $ZnAl_2O_4$. Therefore, ZnO dehydrogenation activity is enhanced by the presence of $ZnAl_2O_4$. In consequence, we can assume that the activity sites in the dehydrogenation activity of i-PrOH are placed at the ZnO – $ZnAl_2O_4$ interface.

Acknowledgement. The authors wish to thank hereby Mr. G. Nedelcu from the Faculty of Chemistry for DTA determination.

---

[14] G. M. SCHWAB and E. SCHWAB-AGALLIDES, *J. Amer. Chem. Soc.*, **71**, 1809 (1949).

way products occur, which [illegible] in the catalyst surface influencing the catalytic process toward dehydration.

The decrease of dehydration activity for the sample calcined at a temperature higher than 750° is due to the process of rearrangement of crystalline lattice by the migration of Al^{3+} ions from tetrahedral sites to octahedral sites.

The increase of ZnO content beyond the stoichiometrical composition (ZnO:Al_2O_3 1:1 molar ratio) entails a very pronounced diminution of the dehydration activity simultaneously with a very important increase of the dehydrogenation activity. This activity decreases together with the increase of the calcination temperature of the samples when the sintering process takes place, which leads to a continuous decrease of the specific surface area (Fig. 3).

If $ZnAl_2O_4$ were responsible for the dehydrogenation activity shown in the case of ZA samples with spinels composition, an enhanced dehydrogenation activity should exist which would increase with calcination temperature, as a rearrangement of a lattice occurs. But it has been found that all ZA samples, inclusively ZA_1 – 950, which contains 100% spinel, exhibit a very lowered dehydrogenation activity. Moreover, these samples present a pronounced dehydrating character, a fact which disagrees with the findings of other authors.[8]

According to X-ray data, the samples with ZnO : Al_2O_3 > 1 molar ratio which are characterized by a higher dehydrogenation activity than that of the spinel and also that of the pure ZnO, contain only ZnO and $ZnAl_2O_4$. Therefore, ZnO dehydrogenation activity is enhanced by the presence of $ZnAl_2O_4$. In consequence, we can assume that the activity sites for the dehydrogenation activity of [illegible] should be placed at the ZnO – $ZnAl_2O_4$ interface.

Acknowledgment. The authors wish to thank [illegible] from the [illegible] of Chemistry for BET determination.

---

[8] G. M. Schwab and [illegible], J. Amer. Chem. Soc. 71, [illegible] (1949).

Revue Roumaine de Chimie, **20**, *2*, 227 – 232 (1975)

CHEMICAL GRAPHS. XXV *

ISOMERS OF THE PORPHYRINS—AN EXERCISE USING PÓLYA'S COUNTING THEOREM

ALEXANDRU T. BALABAN
Chair of Organic Chemistry, The Polytechnic of Bucharest, Romania

Received August 7, 1974

By means of a rigorous mathematical method, the numbers of substituted porphyrin isomers are calculated in order to correct an error in the literature (ref.[1a]).

The column "Textbook Errors" of *Journal of Chemical Education* featured a paper by D. Blackman entitled "Isomers of the Porphyrins".[1a] After mentioning that several textbooks incorrectly give the numbers of possible isomers of the etioporphyrins or coproporphyrins (substitution type A_4B_4) as four, and of the mesoporphyrins or protoporphyrins (type $A_4B_2C_2$) as fifteen, Blackman noted that the eight pyrrolic sites of the delocalized porphin skeleton (I), numbered 1 through 8, may be represented simply by means of a tic-tac-toe diagram (II). He then proceeded to derive empirically the possible isomers finding incorrectly eight A_4B_4 and thirty-three $A_4B_2C_2$ isomers.**

By using a rigorous mathematical approach, we will show that the correct numbers of isomers are thirteen for A_4B_4 and sixty for $A_4B_2C_2$; at the same time we present in detail how this general approach is applied in the present case, in order to make it available to chemists who are interested in similar problems.

Isomer counting in acyclic organic or coordinative chemistry is usually done empirically because the algorithms are fairly simple. However, graph theory[2] does provide a sound mathematical basis for a theoretical solution of the problem. Constitutional isomers correspond to graphs, whose points represent atoms, and whose lines represent covalent bonds. Hydrogen atoms in organic compounds may be ignored in the first approximation, leaving a "reduced constitutional graph" of the molecule.

Thus there exist two and only two isomers for C_4H_{10} because graph theory proves that there are only two "trees" with four points. Similarly, only two isomers are possible for C_2H_6O because there can exist only two chains C – C – O and C – O – C. Recently, a computer program was developed for enumerating all chemically reasonable isomers with a given molecular formula, obtained from a high-resolution mass spectrum, provided that no cycles were involved.[3] Cyclic compounds, however, pose more difficult problems.[4,5]

---

* Preceding part in the series : A. Barabas and A. T. Balaban, *Rev. Roumaine Chim.* **19**, 1927 (1974).

** These numbers of isomers would apply to a delocalized [8]annulene. [1b]

[1a] D. Blackman, *J. Chem. Educ.* **50**, 258 (1973).

[1b] A. T. Balaban, D. Fărcaşiu and F. Harary, *J. Labelled Comp.* **6**, 211 (1970).

[2] F. Harary, "Graph Theory", Addison-Wesley, Reading, Mass., 1969.

Two rigorous mathematical treatments of the isomer counting problem are available, both for cyclic and acyclic compounds : the first one is based on Pólya's counting theorem,[6–8] the more recent one, due to Ruch, is based on double cosets.[9] We will use the former treatment, whose relative simplicity makes it useful in many similar problems.

CYCLE INDEX

Pólya's theorem makes use of the *cycle index* Z(A) of the molecule having permutation group A. The cycle index is an expression of all symmetry operations involving axes of rotation, and has the form of a polynomial :

$$Z(A) = \frac{1}{A} \sum_{\alpha \in A} \prod_{k=1}^{d} y_k^{j_k(\alpha)} \tag{1}$$

For a permutation α, expressed as a product of disjoint cycles, $j_k(\alpha)$ denotes the number of cycles of length k; the numbers $j_k(\alpha)$ constitute a partition of the integer d, the degree of the permutation group A. This may look confusing, but the practical application is quite straightforward.

Both molecule I and scheme II have one C_{4v} axis of rotation (OP in III), and five C_2 axes : one C_{2v} (OP) and four C_{2h} axes (OQ, OR, OS, OT). Thus, the following three types of symmetry operations may be performed on I – III, expressed as operations on permutation groups.[10] The numbers in the upper row indicate the atoms before the symmetry operation, those in the lower row, after the operation. The same permutation may be represented more briefly using brackets, as disjoint cycles (where each number is only specified once), writing alternatively corresponding numbers from the upper and lower rows until the cycle closes. This disjoint-cycle representation of the symmetry operation is translated as a product of y_k terms, where each y_k corresponds to a cycle of length k, i. e. with k numbers.

---

[3] J. Lederberg, G. L. Sutherland, B. G. Buchanan, E. A. Feigenbaum, A. V. Robertson, A. M. Duffield and C. Djerassi, *J, Amer. Chem. Soc.* **91**, 2973 (1969).

[4a] A. T. Balaban, *Rev. Roumaine Chim.* **18**, 635 (1973).

[4b] Idem, chapter 5 in "Chemical Applications of Graph Theory" (A. T. Balaban, editor), Academic Press, London, 1975 (to appear).

[5] L. Masinter, N. S. Sridharan, J. Lederberg and D. H. Smith, Stanford Artificial Intelligence Laboratory Memo AIM – 216 (1973).

[6] G. Pólya, *Acta Math.* **68**, 145 (1937).

[7] F. Harary, E. M. Palmer, R. C. Read and R. W. Robinson, chapter 3 in ref.[4b]

[8] F. Harary and E. M. Palmer, "Graphical Enumeration", Academic Press, New York, 1973, p. 41.

[9] E. Ruch, W. Hasselbarth and B. Richter, *Theoret. Chim. Acta* (*Berlin*), **19**, 228 (1970).

[10] M. Hall Jr., "The Theory of Groups", Macmillan, New York, 1959, chapter 5.

1. Identity :

$$\begin{array}{cccccccc} 1 & 2 & 3 & 4 & 5 & 6 & 7 & 8 \\ 1 & 2 & 3 & 4 & 5 & 6 & 7 & 8 \\ \hline (1) & (2) & (3) & (4) & (5) & (6) & (7) & (8) = y_1^8 \end{array}$$

2. Rotations with 90° (C_4 axis, OP in III) :

$$\begin{array}{cccccccc} 1 & 2 & 3 & 4 & 5 & 6 & 7 & 8 \\ 7 & 8 & 1 & 2 & 3 & 4 & 5 & 6 \\ \hline (1, & 7, & 5, & 3) & (2, & 8, & 6, & 4) = y_4^2 \end{array} \qquad \begin{array}{cccccccc} 1 & 2 & 3 & 4 & 5 & 6 & 7 & 8 \\ 3 & 4 & 5 & 6 & 7 & 8 & 1 & 2 \\ \hline (1, & 3, & 5, & 7) & (2, & 4, & 6, & 8) = y_4^2 \end{array}$$

3. Rotations with 180° (C_2 axes) :

$$(OP):\begin{array}{cccccccc} 1 & 2 & 3 & 4 & 5 & 6 & 7 & 8 \\ 5 & 6 & 7 & 8 & 1 & 2 & 3 & 4 \\ \hline \multicolumn{8}{c}{(1, 5)\,(2, 6)\,(3, 7)\,(4, 8) = y_2^4} \end{array} \qquad (OQ):\begin{array}{cccccccc} 1 & 2 & 3 & 4 & 5 & 6 & 7 & 8 \\ 2 & 1 & 8 & 7 & 6 & 5 & 4 & 3 \\ \hline \multicolumn{8}{c}{(1, 2)\,(3, 8)\,(4, 7)\,(5, 6) = y_2^4} \end{array}$$

$$(OR):\begin{array}{cccccccc} 1 & 2 & 3 & 4 & 5 & 6 & 7 & 8 \\ 8 & 7 & 6 & 5 & 4 & 3 & 2 & 1 \\ \hline \multicolumn{8}{c}{(1, 8)\,(2, 7)\,(3, 6)\,(4, 5) = y_2^4} \end{array} \qquad (OS):\begin{array}{cccccccc} 1 & 2 & 3 & 4 & 5 & 6 & 7 & 8 \\ 6 & 5 & 4 & 3 & 2 & 1 & 8 & 7 \\ \hline \multicolumn{8}{c}{(1, 6)\,(2, 5)\,(3, 4)\,(7, 8) = y_2^4} \end{array}$$

$$(OT):\begin{array}{cccccccc} 1 & 2 & 3 & 4 & 5 & 6 & 7 & 8 \\ 4 & 3 & 2 & 1 & 8 & 7 & 6 & 5 \\ \hline \multicolumn{8}{c}{(1, 4)\,(2, 3)\,(5, 8)\,(6, 7) = y_2^4} \end{array}$$

Therefore, according to equation (1),

$$Z(A) = \frac{1}{8}\,(y_1^8 + 2y_4^2 + 5y_2^4) \tag{2}$$

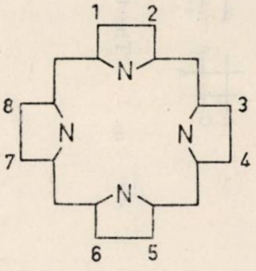

I

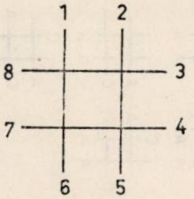

II

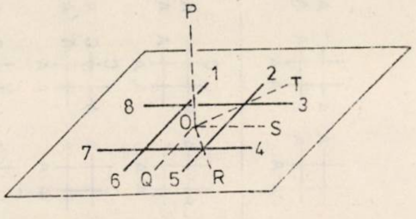

III

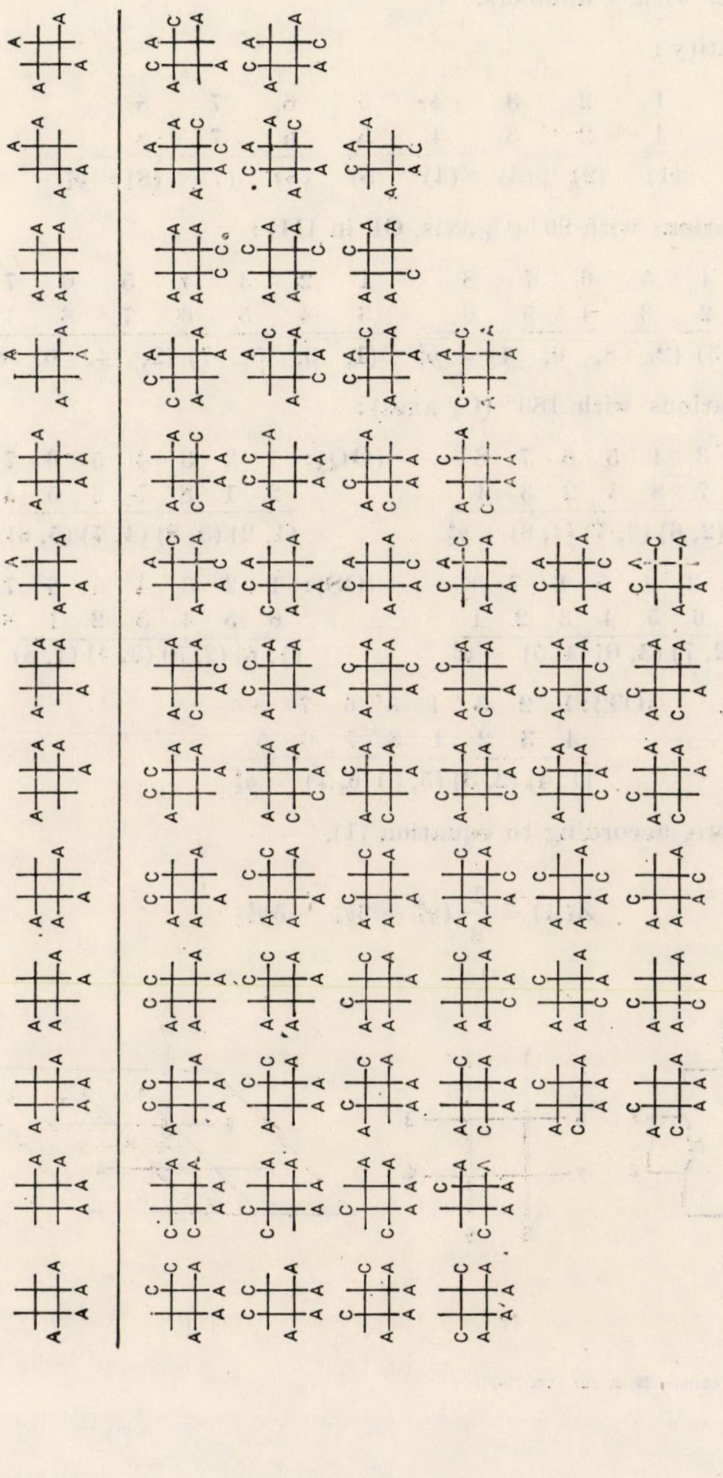

Fig. 1. — The thirteen isomers A_4B_4 (above) and the sixty isomers $A_4B_2C_2$ (below); for simplicity, letter B was omitted.

PÓLYA'S THEOREM

According to Pólya's counting theorem, the number of configurations (in our case, of isomers) results by substituting a ***figure-counting series*** $y_k(r, s, \dots)$ into the cycle index $Z(A)$. If we wish to calculate numbers of isomers for up to three types of substituents, the figure-counting series has three terms :

$$y_k = r^k + s^k + t^k \tag{3}$$

The result of this substitution is a polynomial in r, s, and t, named the *configuration-counting series*, or simply the *counting polynomial* $P(r,s,\dots)$. Pólya's theorem states that :

$$P(r, s, \dots) = Z(A, y_k(r, s, \dots)) \tag{4}$$

The coefficient of each term $r^a s^b t^c$ is the number of isomers with a substituents of type A, b substituents B, and c substituents C.

Substituting (3) into (2), we have to add terms whose exponents correspond to partitions of the total number of substituents, i. e. eight. In this case, Pólya's theorem affords :

$$P(r, s, t) = \frac{1}{8}\left[(r + s + t)^8 + 2(r^4 + s^4 + t^4)^2 + 5(r^2 + s^2 + t^2)^4\right] \tag{5}$$

The calculations are summarized in table 1.

Table 1

Coefficients of terms in the calculation of the counting polynomial $P(r,s,t)$ after formula (5)

Terms of counting polynomial	r^8	r^7s	r^6s^2	r^5s^3	r^4s^4	r^6st	r^5s^2t	$r^4s^2t^2$	r^4s^3t	$r^3s^3t^2$
$(r+s+t)^8$	1	8	28	56	70	56	168	420	280	560
$2(r^4+s^4+t^4)^2$	2	—	—	—	4	—	—	—	—	—
$5(r^2+s^2+t^2)^4$	5	—	20	—	30	—	—	60	—	—
Sum = Coefficients of 8P (r,s,t)	8	8	48	56	104	56	168	480	280	560
Coefficients of P(r,s,t)	1	1	6	7	13	7	21	60	35	70

The coefficients of the counting polynomial $P(r, s, t)$ therefore indicate that with two types of substituents, A and B, there exist one monosubstituted A_7B, six disubstituted A_6B_2, seven trisubstituted A_5B_3, and thirteen tetrasubstituted A_4B_4 isomers of the porphyrins. The latter isomers are presented in the upper part of figure 1. As seen from the coefficient of term $r^4s^2t^2$, there are 60 possible isomers with three types of substituents $A_4B_2C_2$. These are presented in the lower part of figure 1, so as to indicate on the same column which isomers become identical, when C becomes identical to B. It may be seen that when the A_4B_4 isomer has no symmetry axis, it gives rise to six $A_4B_2C_2$ isomers, when it has one C_2 axis it produces four, when it has three C_2 axes (one vertical C_{2v}, and two horizontal C_{2h}) it produces three, and when it has a C_4 axis it produces two $A_4B_2C_2$ isomers.

The procedure illustrated in the present paper may be applied to other isomer enumerations.[11-13] Thus it explains why the numbers of isomers are equal for benzene and benzprismane, leading to the historical controversy between Kekulé and Ladenburg on the benzene formula, since the cycle indices are equal; an analysis of this and other cases of "coisomeric graphs" for valence isomers of annulenes is available.[14]

Note. After the manuscript was submitted, another paper made the same correction without employing Pólya's theorem.[15]

---

[11] W. G. Klemperer, *Inorg. Chem.*, **11**, 2669 (1972).

[12] D. H. McDaniel, *Inorg. Chem.*, **11**, 2678 (1972).

[13] J. E. Leonard, *Dissert. Abstr.*, **32** B, 5659 (1972).

[14] A. T. Balaban, *Rev. Roumaine Chim.*, **19**, 1323 (1974).

[15] R. L. C. Pilgrim, *J. Chem. Educ.*, **51**, 316 (1974).

Revue Roumaine de Chimie, **20**, *2*, 233–240 (1975)

BICYCLO[2.2.2]OCTANE DERIVATIVES. I

STEREOISOMERIC 5,6,7,8-TETRACARBOMETHOXYBICYCLO[2.2.2]OCT-2-ENES

F. IORDACHE, F. CHIRALEU and MARGARETA AVRAM

Polytechnical Institute of Bucharest, Chair of Organic Chemistry.

Received June 15 1974

The base-catalysed isomerization of *all-exo*-ester **1**, and of esters **2**, **3** and **4** is described. Their structure is established by means of NMR spectroscopy. A mechanism for the isomerization of ester **1** is proposed.

There are seven possible stereoisomeric tetracarbomethoxy-bicyclo[2.2.2]oct-2-enes (**1**–**7**).

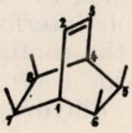

1

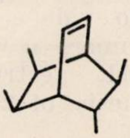

2

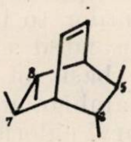

3

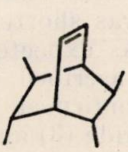

4

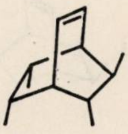

5

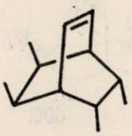

6

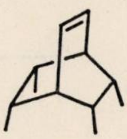

7

Only one isomer is described in the literature, obtained by Diels and Alder[1] through a "diene" reaction between dihydrophthalic anhydride (**8**) and maleic anhydride (**9**), followed by the esterification of the resulting dianhydride **10**. On the basis of the classical rule of maximum accumulation of unsaturation,[2] the configuration * of *all-exo*

---

* In the present paper prefixes *endo* and *exo* designate substituents situated below and respectively above the cyclohexane ring 1,6,5,4,8,7.

[1] O. Diels and K. Alder, *Liebigs Ann. Chem.*, **490**, 257 (1931).

[2] K. Alder and G. Stein, *Angew. Chem.*, **47**, 837 (1934); **50**, 510 (1937); K. Alder and R. Schmitz-Josten, *Liebigs Ann. Chem.*, **595**, 18 (1955).

(5, 6, 7, 8-*exo*) **1** has been ascribed to this isomer.

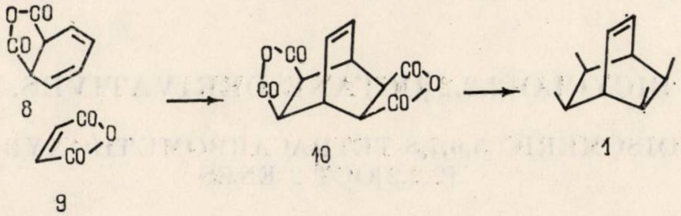

In the present paper we report the preparation of the stereoisomeric 5, 7, 8-*exo*-6-*endo* **2**, 5, 7-*exo*-6, 8-*endo* (*all-trans*) **3** and 5,8-*exo*-6,7-*endo* **4** derivatives.

On treatment with sodium methoxide in methanol *all-cis* ester **1** is readily isomerized. From the reaction mixture *all-trans* ester **3** and *trans-trans*-ester **4** were isolated and their structure was established on the basis of NMR spectra (see below).

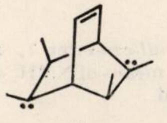
11

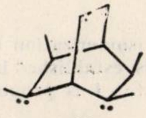
12

Assuming that the formation of esters **3** and **4** from the *all-cis* ester **1** is not a primary process (which would involve the formation of improbable dianions of type **11** and **12**) but a stepwise one, the reaction time was shortened in order to be able to evidence possible intermediates.

As expected, we isolated a new isomer, to which the configuration **2** was ascribed on the basis of its NMR spectrum. This configuration was confirmed by unambiguous synthesis of **2** from dihydrophthalic anhydride (**8**) and fumaryl chloride (**13**).

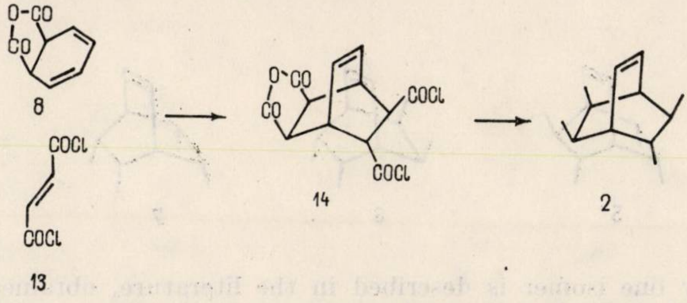

Ester **2** is formed from **1** *via* the carbanion **15** resulted from the attack of the base on any of the four equivalent hydrogens.

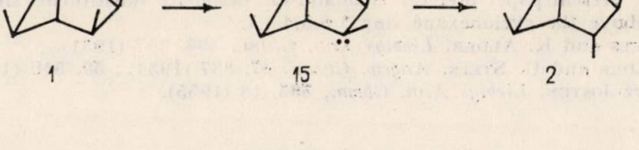

In ester **2** hydrogens are no longer sterically equivalent. We may assume that the base prefers to attack H-8 rather than H-7 which is hindered by the neighbouring *endo*-carbomethoxy group in the position 6.

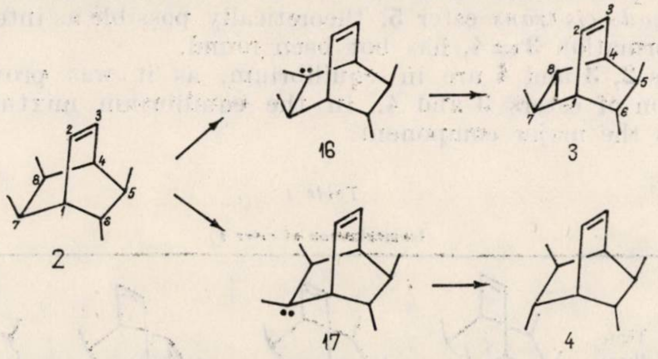

This is the reason why isomer **3** was expected to be formed preferentially, in addition to a minor proportion of isomer **4**.

The isomerization of ester **1** carried out for 4 hours, at reflux, led to a mixture of 70.04% **3**, 21.70% **4** and only 8.26% **2**; the conversion of isomer **1** is total, as the latter is absent from the final mixture. Consequently, we studied the isomerization of ester **1** at lower temperatures (0° and 10°), recording the distribution of isomers in time. The results are shown in table 1.

Data in the table indicate a rapid decrease of *all-cis* isomer **1** accompanied by the formation of *cis-trans* isomer **2**. When the latter reaches high concentrations, *all-trans* isomer **3** starts to appear as the major compound, together with minor amounts of **4**.

The behaviour of esters **3** and **4** in the presence of sodium methoxide was studied further. The results are shown in table 2. The figures indicate a relatively slow conversion of ester **3** into a mixture of **2**, **3** and **4** (in which **3** prevails); one may also notice a constant and minor concentration of **2**. Ester **4** is isomerized to a mixture of similar composition.

On the basis of the experimental results it was assumed that the isomerization of bicyclo[2.2.2]octene-tetracarboxylic esters proceeds *via* the following reactions:

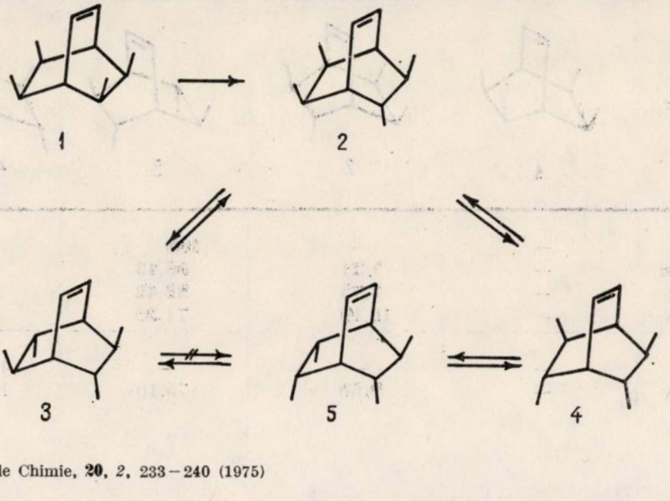

The *all-cis* ester **1** is readily and totally isomerized to **2**. The latter is converted into a mixture of **3** and **4**. The equilibration **3** ⇄ **4** cannot be a direct process and must involve ester **2** as intermediate.

The *endo-cis-trans* ester **5**, theoretically possible as intermediate in the transformation **3** ⇄ **4**, has bot been found.

Esters **2**, **3** and **4** are in equilibrium, as it was proved by the isomerization of esters **3** and **4**. In the equilibrium mixture, *all-trans* isomer 3 is the major component.

Table 1

Isomerization of ester 1

Temp. C	Time (hrs)	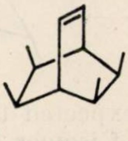 1	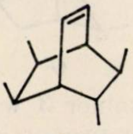 2	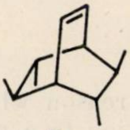 3	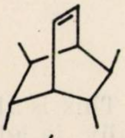 4
0	0	100	—	—	—
	0.5	73.7	26.0	0.3	—
	1	38.0	59.8	2.2	—
	3	2.5	82.8	13.2	1.5
	6	—	69.6	26.1	4.3
	12	—	45.3	47.4	7.3
	24	—	16.7	72.3	11.0
	34	—	8.2	77.6	14.2
10	0	100			—
	0.25	40.7	57.3	2.0	traces
	0.5	7.8	83.8	7.6	0.8
	1.5	—	68.7	27.3	4.0
	3	—	48.9	44.3	6.8
	6	—	19.5	68.7	11.8
	15	—	9.7	76.0	14.3

Table 2

Isomerization of esters 3 and 4 (at 25°)

Time	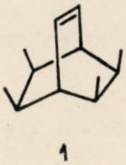 1	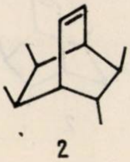 2	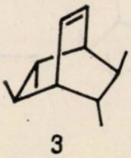 3	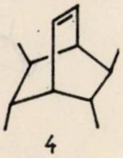 4
0	—	—	100	—
20 min	—	1.21	96.43	2.35
20 hrs	—	1.75	82.42	15.82
100 hrs	—	10.10	74.20	15.70
0	—	—	—	100
100 hrs	—	9.60	75.10	15.40

CONFIGURATION OF ESTERS 1, 2, 3 AND 4

In order to establish the configuration of these compounds we used the NMR spectra, namely the chemical shifts of protons H-5, H-6, H-7, and H-8 adjacent to carbomethoxy groups (table 3), together with those of the olefinic protons H-2 and H-3, in correlation with coupling constants (table 4).

In the NMR spectrum of the Diels-Alder adduct **1**, protons H-5, H-6, H-7, H-8 appear as a singlet at δ 3.06 ppm. Olefinic protons H-2 and H-3 (at δ 6.37 ppm) form an A_2X_2 system by coupling with the bridgehead protons H-1 and H-4 (at δ 3.31 ppm). Methyl protons from carbomethoxy groups appear as a singlet at δ 3.63 ppm (12H). The equivalence of the protons adjacent to the carbomethoxy group rules out a 5,6-endo-7,8-*exo* **6** configuration.

The chemical shift of protons H-5, H-6, H-7 and H-8, of δ 3.06 ppm, is in agreement with literature data for *endo*-oriented protons (configuration **1**) and excludes structures in which these protons would be *exo* with respect to the double bond (as in formula **7**).

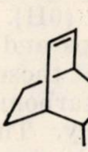

18

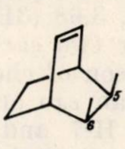

19

In the bicyclooctene system **18**, the *exo*-oriented, more shielded, proton H-6 appears at δ 2.91 ppm while the *endo*-oriented proton H-5 appears at δ 3.19 ppm.[3] In the bicyclooctene system **19** with *exo-cis*-carbomethoxy groups, similarly, to the isomer **1**, the two protons appear at δ 3.0 ppm.[3] This analogy is in good agreement with the proposed configuration **1**.

The NMR spectrum of the ester melting at 65°, to which the configuration **3** was ascribed, exhibits a doubled AB system for the protons H-5, H-6, H-7 and H-8. Olefinic protons H-2 and H-3 from δ 6.3 ppm and bridgehead protons H-1 and H-4 from δ 3.45 ppm form an A_2X_2 system. Methyl groups appear as two singlets at δ 3.70 and 3.80 ppm.

The data are in agreement with configuration **3** with *trans*-oriented carbomethoxy groups, possessing a symmetry which confers the same chemical shift to olefinic protons H-2 and H-3 as to bridgehead protons H-1 and H-4.

The *endo* orientation of protons H-5 and H-7 at δ 3.13 ppm and the *exo* orientation of protons H-6 and H-8 at δ 2.91 ppm were assigned in view of the shielding effects, mentioned in the case of ester **1**.

Configuration **6**, which should display for bridgehead and olefinic protons an A_2X_2 system also, is excluded by the chemical shifts of protons H-7, H-8 and H-5, H-6. In a configuration **6** one could expect the above protons to appear as two singlets at about δ 2.9 and 3.1 ppm, instead of the doubled AB system corresponding to the proposed *trans* configuration as in formula **3**.

---

[3] K. TORI, Y. TAKANO and K. KITAHONOKI, *Chem. Ber.*, **97**, 2798 (1964).

In the NMR spectrum of the isomer melting at 154°, to which the configuration **4** was ascribed, protons H-5, H-6, H-7 and H-8 form also a doubled AB system at δ 2.88 and 3.30 ppm. Olefinic protons H-2 and H-3 and bridgehead protons H-1 and H-4 give rise to an ABXY system. The four methyls in carbomethoxy groups appear as two singlets at δ 3.70 and 3.75 ppm. According to all these values, a *trans* orientation of carbomethoxy groups can be assumed, with a symmetry able to ensure a different shielding to the olefinic and bridgehead protons. Assignment of *endo* orientation for protons H-5, H-8 and of an *exo* one for protons H-6 and H-7 (shielded by the double bond region) has been made as shown for esters **1** and **3**.

Ester **2** exhibits in the NMR spectrum a doubled AB system at δ 2.97 and 3.18 ppm, assigned to protons H-5 and H-6, and a singlet at δ 3.13 ppm for protons H-7 and H-8. Olefinic protons H-2, H-3, and bridgehead protons H-1 and H-4 give rise, as in isomer **4**, to an ABXY system; the methyls in carbomethoxy groups have distinct signals at δ 3.77 (3H), 3.68 (3H) and 3.60 ppm (6H). These data indicate a *cis* orientation for two carbomethoxy groups and a *trans* one for the other two. Comparison of chemical shifts with those of isomers **3** and **4** allowed to assume an *exo* orientation for *3* carbomethoxy groups, with *endo* protons H-5, H-7 and H-8 respectively. The fourth carbomethoxy group is *endo* oriented and proton H-6 is *exo*, respectively, being shielded by the neighbouring double bond.

Decoupling experiments led to the coupling constants listed in table 4.

According to literature data, vicinal couplings appearing in bicyclo [2.2.2] octene systems can be treated on the basis of Karplus curve. Consequently, the coupling constants of 5.7 Hz in **3**, 6.0 Hz in **4** and 5.6

Table 3

Chemical shifts (δ, ppm))*

	H-1 H-4	H-2 H-3	H-5 H-6	H-7 H-8	$COOCH_3$
18	— —	6.21 6.38	3.19 2.91	1.20−1.60	
19	2.92	6.33	3.00		
1	3.31 m	6.37 m	← 3.06 s	→	3.63 ($4CH_3$) s
2	3.30−3.60 m	6.17 6.36	3.18 2.97 d.d. d.d.	3.13 s.	3.77; 3.68; s s 3.60 ($2\ CH_3$) s
3	3.45 m	6.30 m	3.13 2.91 d.d. d.d.	3.13 2.91 d.d. d.d.	
4	3.51−3.65 m m	6.11 6.58 octed octet	3.30 2.88 d.d. d.d	2.88 3.30. d.d d.d	3.70 ($2\ CH_3$) s 3.73 ($2CH_3$) s

* solvent: $CDCl_3$

Hz in **2**, appearing in AB patters, correspond to dihedral angles of about 120°, that is to a *trans* orientation of substituents in undistorted bicyclo [2.2.2]octene systems.

Table 4

Coupling constants (Hz)

	$J_{1.2} = J_{3.4}$	$J_{1.3} = J_{2.4}$	$J_{2.3}$	$J_{1.6}$	$J_{1.7}$	$J_{4.5}$	$J_{4.8}$	$J_{5.6}$	$J_{7.8}$
1	H-1,H-4 and H-2, H-3 A_2X_2 system			—	—	—	—	—	—
2	6.0	1.2	8.0	2.7	—	2.0	—	5.5	—
3	A_2X_2 system			2.7	2.0	2.0	2.7	5.7	5.7
4	6.0	1.2	8.0	2.5	2.5	2.0	2.0	6.0	6.0

EXPERIMENTAL

Microanalyses were performed by Miss E. Şliam and Mrs. V. Daniel. IR spectra were recorded with a double-beam UR 20 spectrophotometer. NMR spectra were determined with a Varian A-60A spectrometer using TMS as internal standard. Gas chromatography analyses were carried out on a Carlo Erba gas chromatograph by Miss L. Stănescu and Miss D. Georgescu. The columns were 3 % neopentylglycol succinate on Chromosorb W sylanized (60–80 mesh), l = 2 m, Ø = 2 mm, the column temperature was 220° (vaporizer temperature 290°); carrier gas: hydrogen, 32.2 ml/min.

5,6,7,8-*exo*-Tetracarbomethoxy-bicyclo[2.2.2]oct-2-ene (1)

This starting material was prepared after Diels and Alder, [1] in 80 % yield, and was purified by several recrystallizations from methanol until no trace of impurities were found by gas-chromatography; m.p. 131°. IR (CCl_4): ν_{CO} 1760 cm^{-1}.

Reaction of *all-exo* ester 1 with sodium methoxide

Into a solution of 0.62 g (26 mmoles) sodium in 75 ml anhydrous methanol, 10.0 g (29 mmoles) ester **1** were added, and the mixture (which becomes rapidly a solution) was boiled for 1 hr. The mixture was then poured in 25 ml cold water and the crystals which separated were filtered, yielding 6.0 g (60 %) *5,8-exo-6,7-endo-tetracarbomethoxy-bicyclo[2.2.2]oct-2-ene* (**4**), m.p. 154° (from methanol).

$C_{16}H_{20}O_8$ *Calcd.*: C, 56.47; H, 5.92
Found: C, 56.39; H, 6.05
IR (CCl_4): ν_{CO} 1745 cm^{-1}.

The filtrate was treated with hydrochloric acid until neutral and the solvent was removed *in vacuo*. The residue was extracted with anhydrous acetone, the solution was filtered and evaporated to dry in vacuum. The new residue (which contained an acid component, as shown by the IR spectrum) was treated with an excess of ethereal solution of diazomethane, yielding crude **3**, contaminated with **4**. By selective extractions with ether, *5,7-exo-6,8-endo-tetracarbomethoxy-bicyclo*[*2.2.2*]*-oct-2-ene* (**3**), m.p. 65° (from methanol), was obtained.

$C_{18}H_{20}O_8$ *Calcd.*: C, 56.47; H, 5.92
Found: C, 56.49; H, 6.19.

5,7,8-*exo*-6-*endo*-Tetracarbomethoxy-bicyclo [2.2.2]oct-2-ene (2)

a. By isomerization of ester **1**.

Into a solution of 0.25 g (10.8 mmoles) sodium in 30 ml anhydrous methanol, 5.0 g (15 mmoles) ester **1** was added, and the mixture was left at room temperature for 10 min. After evaporation of the solvent *in vacuo*, the residue was treated with water and extracted with ether, yielding 3.5 g (70 %) **2**, viscous oil with b.p. 215°/3 mm; the IR and NMR spectra are identical with those of an authentic sample (which is described below).

b. By synthesis from 1.2-dihydrophthalic anhydride (**8**) and fumaryl chloride (**13**).

A mixture of 9.0 g (60 mmoles) of dihydrophthalic anhydride (**8**) and 9.0 g (60 mmoles) fumaryl chloride (**13**) was heated, after the vigorous reaction ceased, at 70° for 2 hrs. The unreacted chloride **13** was removed *in vacuo*, at 5 mm and 60°, the residue was treated with 50 ml methanol and the mixture was boiled for 6 hrs. The solvent was removed and the new residue was dissolved in ether. The solution was washed until all hydrochloric acid was removed, then dried and evaporated. Distillation of the oily residue yielded 7.0 g (34 %) **2**, b.p. 215°/3 mm.

$C_{16}H_{20}O_8$ *Calcd.*: C, 56.47; H, 5.92.
Found: C, 56.66; H, 6.18.

IR (CCl_4): ν_{CO} 1750 cm^{-1}.

ISOMERIZATION OF ESTERS 1, 3 AND 4. GENERAL PROCEDURE

50 ml solution of sodium methoxide in methanol (0.36N) was treated with 1.00 g (3 mmoles) ester and the mixture was stirred at constant temperature. The reaction was stopped by bubbling gaseous hydrochloric acid. The solution was then evaporated *in vacuo* and the residue was extracted with dichloromethane. Sodium chloride was filtered off and the solvent was evaporated, yielding 0.90–0.95 g (90–95 %) crude product, which was analyzed by gas chromatography.

Revue Roumaine de Chimie, **20**, *2*, 241–244 (1975)

SULTAM-STEROIDE. I[*]

DIE SYNTHESE VON ESTERN EINIGER STERINE MIT SULTAMYL-N-PHENYL-CARBONSÄUREN[**]

SENOT H. DOSS[***]
Organisch-Chemisches Institut der Universität Bonn

Eingegangen am 19. September 1973

Einige Sterine und Steroide wurden mit Butansultamyl–(1,4)-N-phenyl-*m*-carbonsäurechlorid und mit Butansultamyl–(1,4)-N-phenyl-*p*-carbonsäurechlorid zu den entsprechenden Estern kondensiert.

Die Synthese von aromatischen Sultamen [1] und aliphatischen Sultamen[2] war vorher beschrieben worden. Verbindungen, die den Sultam-Ring enthalten, haben ,,manchmal Antitumor-[3] oder antiepileptische[4] Wirkung".

Die physikalischen Eigenschaften dieses Ringes haben wir veröffentlicht: Infrarot,[5] Kern Magnetic Resonance,[6] Circular Dichroismus,[7] sogar Massenspectra.[8]

Bei dieser Arbeit lassen sich zum ersten Mal Sterine und Steroide mit mindestens einer Hydroxylgruppe in Benzollösung unter Zusatz von Pyridin mit Butansultamyl-(1,4)-N-phenyl-*m*-Carbonsäure und mit Butansultamyl-(1,4)-N-phenyl-*p*-Carbonsäure zu den entsprechenden Estern kondensieren. Als Sterine – Steroide kamen zunächst Cholesterin und Cholestanol zur Verwendung (Sultamen 1, 2, 3 und 4).

---

[*] Diese Arbeit wird fortgesetzt.

[**] Meinem verehrten Lehrer Herrn Professor Dr. B. Helferich zu seinem 87. Geburtstag herzlichst gewidmet.

[***] Neue Anschrift: National Research Center, Sh. El Tahrir, Dokki, Kairo, VAR – ÄGYPTEN.

[1] B. Helferich, K. Geist und H. Plübe, *Liebigs Ann. Chem.*, **651**, 17 (1962); B. Helferich und G. Pietsch, *ibid.*, **651**, 43 (1962); B. Helferich und S. H. Doss, *ibid.*, **756**, 170 (1972).

[2] B. Helferich und S. H. Doss, *Liebigs Ann. Chem.*, **741**, 139 (1970); 107 (1971).

[3] S. Hayashi, H. Ueki, Y. Soko, T. Ashimura, K. Hayashi und K. Takase, Kumamot, *Pharm. Bull.*, **5**, 327 (1962).

[4] F. Flügel, D. Bente, T. Itil, *Dtsch. Med. Wochensch.*, **85**, 2199 (1960); B. Helferich, R. Behrisch, U.S. Pat. 2, 916, 486 (Dec. 8. 1959); B. Helferich, B. Talweg, U.S. Pat. 2, 917, 512 (Dec. 15, 1959).

[5] S. H. Doss, *Chem. & Industry*, **1971**, 961; *Acta. Chem. Acad. Sci. Hung.*, **72**, 341 (1972); *Rev. Roumaine Chim.*, **17**, 1611 (1972).

[6] S. H. Doss, *Rev. Roumaine Chim.*, **17**, 905 (1972).

[7] G. Snatzke und S. H. Doss, *Tetrahedron*, **28**, 2539 (1972); S. H. Doss und G. Snatzke (1972); S. H. Doss, *J. Chem. Educ.* (1972).

[8] H. D. Beckey, H. R. Schulten, G. Eckhardt und S. H. Doss, *Tetrahedron*, **29**, 386 (1973); H. D. Beckey, H. R. Schulten und S. H. Doss, in Vorbereitung (1974).

Da Cholesterin und Cholestanol vermutlich kaum irgendeine pharmazeutische Wirkung haben, sind diese Verbindungen pharmazeutisch wenig interessant.

Anders ist es mit 3β-Hydroxy-Androsterin 5–17-on (Verbindungen 7 und 8).

Diese können eventuell neuartige Wirkungen durch Kombination von Sterinen und Sultamylderivaten zeigen.

Das I.R. zeigt das charakteristische Sultam-Band zwischen 1291 – 1270 cm^{-1} bei allen schon erwähnten Verbindungen. Für P.M.R., C.D. und M.S. sind mehr Beispiele nötig, um eine Regel aufstellen zu können.

Folglich werden C.D., P.M.R. und M.S. später veröffentlicht.

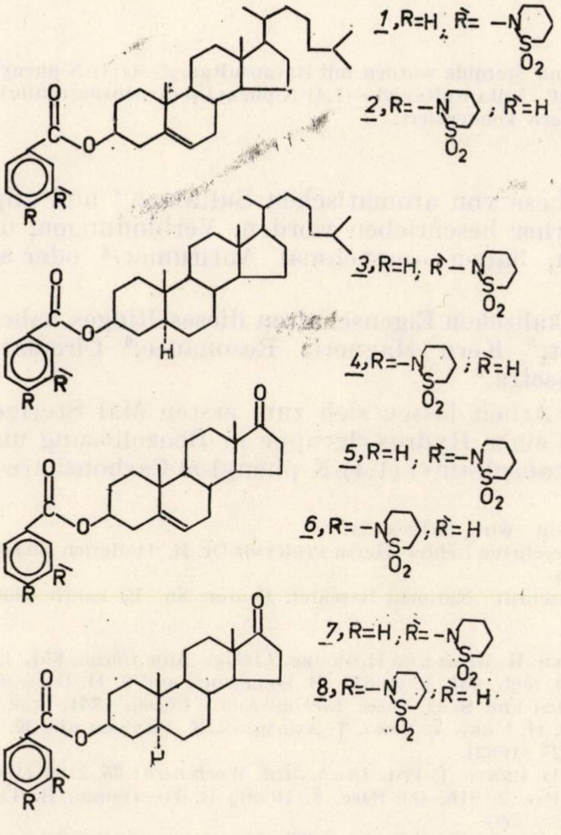

BESCHREIBUNG DER VERSUCHE. ALLGEMEINE ARBEITSVORSCHRIFT

Aequimolekulare Mengen des Sterins (Steroids) in ca. 20 Voltln. abs. Benzol und abs. Pyridin werden im Laufe von ca. 30 Min. unter Eiskühlung und Rühren mit einer Lösung des Sultamyl-N-phenylcarbonsäurechlorids in ca. 17 Voltln. abs. Benzol versetzt. Nach weiterem Rühren bei Raumtemperatur wird der entstandene Niederschlag, der etwa nach 4 Stdn. sich abzuscheiden beginnt, abgesaugt und mit Benzol ausgewaschen. Der Niederschlag besteht meist aus salzsaurem Pyridin und etwas freier Sultamyl-phenyl-carbonsäure. Die vereinigten Benzollösungen werden—eventuell mit viel Äther— verdünnt, um eine bessere Trennung zu ermöglichen, nacheinander mit 2n HCl, Wasser, $NaHCO_3$-Lösung und Wasser gewaschen, mit Na_2SO_4 getrocknet und i.V. bis zur Trocknung verdampft : Rohprodukt.

BUTANSULTAMYL-(1,4)-N-PHENYL-*m*-CARBONSÄURE-CHOLESTERIN-ESTER (1)

Das kristalline Rohprodukt aus 2,5 g Cholesterin wird nach Auswaschen mit Äther zweimal aus einem Gemisch von 41 ml Petroläther, 45 ml gew. Alkohol und 20 ml Benzol umkristallisiert. Ausbeute 1,2 g, 30 %. Schmp. *209—211°*. $[\alpha]_{\mathrm{D}}^{16} = -7{,}48^\circ$, in Chloroform.

$C_{38}H_{57}O_4NS$

Ber. C, 73,16 ; H 9,21 ; S 5,12

Gef. C, 72,53 ; H 9,15 ; 5,45 %

Die Substanz ist leicht löslich in Chloroform, Benzol, CCl_4, Dimethylformamid, schwer läslich in Dioxan, so gut wie unlöslich in Methanol, Alkohol, Acetonitril und Wasser.

BUTANSULTAMYL-(1,4)-N-PHENYL-*p*-CARBONSÄURE-CHOLESTERIN-ESTER (2)

Das Rohprodukt aus 2,5 g Cholesterin wurde mehrfach mit Äther extrahiert und der ungelöste Rückstand, 1,4 g, aus Cyclohexan umkristallisiert. Ausbeute an *2* : 0,9 g.
Schmp. *204°*. $[\alpha]_{\mathrm{D}}^{13} = +15.6^\circ$, in Chloroform, 0.03 %.

Aus der Ätherlösung ließen sich durch Eindampfen zur Trocknung 1,1 g aus 200 ml Methanol umkristallisieren und dann aus Cyclohexan noch weitere 0,2 g der etwas unreineren Substanz *2* isolieren. Gesamtausbeute ca. 1,1 g = 27 %.

$C_{38}H_{57}NO_4S$

Ber. C, 73,16 ; H 9,21 ; S 5,12

Gef. C, 72,74 ; H 9,37 ; S 5,27 %

Die Verbindung ist löslich in Dioxan, Chloroform, Aceton, Benzol, mäßig löslich in Dimethylformamid, so gut wie unlöslich in Methanol, Acetonitril, Isooctan und Wasser.

BUTANSULTAMYL-(1,4)-N-PHENYL-*m*-CARBONSÄURE-CHOLESTANOL-ESTER (3)

Das Rohprodukt aus 1,3 g Cholestanol, 2,2 g, wurde in Benzol-Äther (je 100 ml) aufgelöst. Die Lösung wurde mehrfach mit 2n HCl, Wasser und Na_2CO_3-Lösung gewaschen, mit $NaSO_4$ getrocknet und i.V. eingedämpft : 1,3 g, die nach 5-maligem Waschen mit je 50 ml Äther und Umkristallisieren aus 10 ml Alkohol + 4 ml Chloroform 0,19 g der Verbindung *3* ergaben.
Die vereinigten Äther-Auszüge ergaben nach Eindampfen und Umkristallisieren aus 100 ml Alkohol + 40 ml Chloroform dann nochmals aus 30 ml Alkohol + 12 ml Chloroform 0,3 g einer etwas unreineren Substanz *3*.

Gesamtausbeute 0.49 g = 20 %.

Schmp. *223—224°* $[\alpha]_{\mathrm{D}}^{16} = +14.40^\circ$, in Chloroform (c = 0,6 %)

Ber. C, 72, 92 ; H, 9,50 ; N, 2,24 ; S, 5,11

Gef. C, 72, 78 ; H, 9,17 ; N, 2,38 ; S, 5,12 %

Die Substanz ist löslich in Aceton, Chloroform und Benzol, mäßig löslich in Äther, unlöslich in Alkohol und Wasser.

BUTANSULTAMYL-(1,4)-N-PHENYL-*p*-CARBONSÄURE-CHOLESTANOL-ESTER (4)

Die Verbindung wurde auf die gleiche Weise wie der *m*-Ester *3* hergestellt. Ausbeute aus 1.3 g Cholestanol 0.7 g = 33 %.

Schmp. *188—189°*. $[\alpha]_{\mathrm{D}}^{12} = +15{,}9^\circ$ in Chloroform, c = 0,3 %

$C_{38}H_{59}NO_4S$
Ber. C, 72,92 ; H, 9,50 ; N, 2,24 ; S, 5,11
Gef. C, 72,76 ; H, 9,33 ; N, 2,42 ; S, 5,14%
Die Löslichkeiten der Substanz *4* sind etwa die gleichen wie die der Substanz *3.*

BUTANSULTAMYL-(1,4)-N-PHENYL-*m*-CARBONSÄURE 3 β-HYDROXY-ANDROSTEN-(5)-17-ON-ESTER (5)

Das Rohprodukt (5,3 g aus 2,88 g des Sterins) wurde viermal mit je 100 ml Äther gewaschen und der unlösliche Anteil (3,5 g) aus 280 ml Alkohol umkristallisiert. Ausbeute : 3,15 g, d.i. 60% d. Th.
Schmp. *208—210°* $[\alpha]_D^{13} = +22{,}35°$ in Chloroform.
c = ca. 0,6%.
$C_{30}H_{39}$ H O_5 S
Ber. C, 68,55 ; H, 7,48 ; N, 2,66 ; S, 6,06
Gef. C, 68,56 ; H, 7,34 ; N, 2,86 ; S, 6,26%

Der Ester ist löslich in Chloroform, Aceton, Dioxan, Benzol, Diethylformamid und Trichloraethanol, sehr wenig löslich in Alkohol und Äther, so gut wie unlöslich in Wasser, Isooctan, Cyclohexan und Acetonitril.

BUTANSULTAMYL-(1,4)-N-PHENYL-*p*-CARBONSÄURE 3 β-HYDROXY-ANDROSTEN-(5)-17-ON-ESTER (6)

Das Rohprodukt (0,5 g aus 0,96 g des Sterins, nach 14 Tage Schütteln) ergab nach sechsmaligem Waschen mit je 30 ml Äther und Umkristallisieren aus Aceton 0,3 g des Esters.
Der nach 14-tägigem Schütteln unlösliche Anteil (1,1 g) ergab nach Lösen in Benzol, Waschen dieser Lösung mit 2n HCl, Na_2CO_3-Lösung und Wasser und Umkristallisieren des Rückstande nach Verdampfen der Lösung aus 80 ml Aceton 0,8 g.
Gesamtausbeute 1,1 g = 63 %.
Schmp. *287—289°* $[\alpha]_D^{22} = +29{,}6°$ in Chloroform, c = 1,5
$C_{30}H_{39}NO_5S$
Ber. C, 68,55 ; H, 7,48 ; S, 6,06.
Gef. C, 68,18 ; H, 7,43 ; S, 6,25%

Der Ester ist löslich in Benzol, Chloroform und Dimethylformamid, mäßig löslich in Dioxan und Cyclohexan, so gut wie unlöslich in Isooctan, Aceton und Wasser.

BUTANSULTAMYL-(1,4)-N-PHENYL-*m*-CARBONSÄURE-3 β-HYDROXY-5 α-ANDROSTAN-17-ON-ESTER (7)

Das Rohprodukt aus 1,8 g Sterin, 1,8 g Säurechlorid und 0,38 g Pyridin : 4,3 g, wird nach 6-maligem Waschen mit je 60 ml Äther : 1,6 g aus 50 ml Alkohol umkristallisiert : 1,4 g = 42%.
Schmp. *180°*. $[\alpha]_D^{22} = +54.2°$ in Chloroform, c = ca. 0,49
$C_{30}H_{41}NO_5S$
Ber. C, 68,29 ; H, 7,83 ; S, 6,08
Gef. C, 67,89 ; H, 7,71 ; S, 6,14%
Die Substanz ist löslich in Benzol, Chloroform, Dioxan, Cyclohexan und Dimethylformamid, mäßig löslich in Methanol, unlöslich in Isooctan und Wasser.

BUTANSULTAMYL-(1,4)-N-*p*-PHENYLCARBONSÄURE-3 β-HYDROXY-5 α-ANDROSTAN-17-ON-ESTER (8)

Das Rohprodukt aus 0,96 g Sterin (1,2 g) ergab nach Waschen mit Äther (4-mal mit je 50 ml) 0,7 g, nach Umkristallisieren aus 50 ml Aceton 0,6 g des Esters *8.*
Schmp. *267—268°.*
$[\alpha]_D^{20} = +54{,}6°$ in Chloroform, c = 0,7%.
Ber. C, 68,29 ; H, 7,83 ; S, 6,08
Gef. C, 68,70 ; H, 7,66 ; S, 6,14 %
Die Löslichkeiten sind etwa gleich denen der *m*-Verbindung.

Der Deutschen Forschungsgemeinschaft und Herrn Professor B. Helferich danke ich für die Förderung dieser Arbeit.

Revue Roumaine de Chimie, **20**, *2*, 245–250 (1975)

CYANOETHYLATION OF KETOXIMES. I

CYANOETHYLATION OF *PARA*-SUBSTITUTED ACETOPHENONE OXIMES

P. BUCHWALD and A. KÖVENDI

Chemical-Pharmaceutical Research Institute,
Str. Fabricii 126, Cluj, Romania

Received November 30, 1973

A series of oximinoethers with general formula $p-X-C_6H_4-C(CH_3)=N-O-CH_2-CH_2-CN$ were obtained by cyanoethylation of the corresponding *para*-substituted acetophenone oximes. Conversion of the nitrile group, of obtained derivatives, into carboxyl, by alkaline and acid hydrolysis was also investigated.

1. INTRODUCTION

The reaction between acrylonitrile and an organic compound possessing labile hydrogen atoms, in the presence of alkaline catalysts, is commonly known as "cyanoethylation". In this reaction there always result molecules containing a cyanoethyl group ($-CH_2-CH_2-CN$) attached to the atom to which reactive hydrogen atom is bonded.

Thus, the cyanoethylation of a variety of organic compounds as: alcohols, mercaptans, amines, active methylene containing molecules, etc. is known.[1]

Though the literature reports that the hydroxyl group of aldoximes and ketoximes is also involved in the addition of acrylonitrile to form oximino ethers in the presence of alkaline catalysts,[2,3] only a few oximes were cyanoethylated, and a study of the reaction mechanism and stability of these compounds has not been produced yet.

In order to carry out a detailed study of the cyanoethylation of ketoximes and the hydrolysis of the nitrile group of resulting O-cyanoethyl derivatives, cyanoethylation of some *para*-substituted acetophenone oximes, according to the following reaction was performed :

---

[1] H. A. Bruson, "Organic Reactions" vol. 5., Wiley Inc., New York, 1962, p. 79.

[2] N. A. Bruson and T. W. Reiner, *J. Amer. Chem. Soc.*, **65**, 23 (1943).

[3] H. A. Bruson and T. W. Reiner, U. S. Pat. 2,352.516; *Chem. Abstr.*, **38**, 5506 (1944).

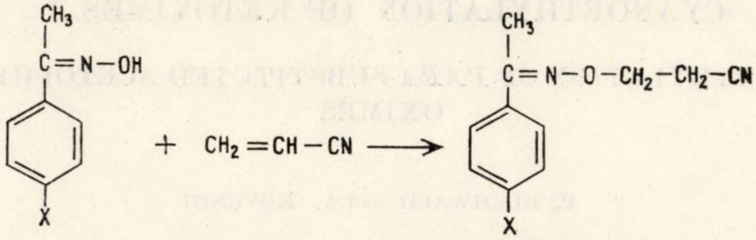

where

$X = -H(I)$; $-NO_2(II)$; $-Cl(III)$; $-Br(IV)$; $-CH_3(V)$; $-C_2H_5(VI)$; $CH_3O-(VII)$; $C_2H_5O-(VIII)$; $-NH_2(IX)$; $-NH-CO-CH_3(X)$;

where

$X = -H(XI)$; $-NO_2(XII)$; $-Cl(XIII)$; $-Br(XIV)$; $-CH_3(XV)$; $-C_2H_5(XVI)$; $CH_3O-(XVII)$; $C_2H_5O-(XVIII)$; $-NH_2(XIX)$; $-NH-CO-CH_3(XX)$.

2. RESULTS AND DISCUSSION

The hydroxyl group of these *para*-substituted acetophenone oximes adds to acrylonitrile in the presence of alkaline catalysts to form the corresponding oximino-ethers with 40–80% yield. The reactions take place at or close to room temperature and are exothermal, so that slight cooling and use of inert solvent is advisable. Benzene has been proved to be the most adequate solvent. As alkaline catalyst we successfully used the trimethyl-benzyl-ammonium-methoxide in methanolic solution (Rodionov's catalyst[4]), which has been prepared from trimethylamine, benzyl chloride and sodium methoxide.

Cyanoethylation was performed by dropping acrylonitrile under stirring in oxime and catalyst containing benzene solution, a temperature of 25–40° being maintained by slight cooling. A ratio of 2–5% catalyst to oxime weight and acrylonitrile excess 10–20% was used. When the reaction was over (after 2–5 hours), the benzene solution was washed with 10% sodium hydroxide solution, then with water, and the solvent removed by distillation. Cyanoethyl ethers derivatives of the acetophenone oximes formed crystallize after cooling. The adequate solvent for recrystallization has been proved to be isopropyl alcohol. The fine plates obtained are well crystallized and stable.

The cyanoethylated derivative of *para*-amino-acetophenoneoxime (XIX) is an oily material which decomposed under vacuum distillation at 150°/2 mm Hg, but by acetylation with acetic anhydride, it was easily converted into (XX), the same compound yielded by cyanoethylation of *para*- acetylamino-acetophenone oxime (X).

---

[4] A. P. TERENTIEV, A. N. KOST and S. M. GURVICI, *Zhur. obshchei Khim.*, **22**, 1977 (1952).

The cyanoethyl ether of acetophenone oxime (XI) was identified by its melting point (found : 44°; indicated 44°[2]); the other cyanoethyl derivatives by the data supplied by their elementary analysis, after repeted recrystallization, and their infrared spectra. The infrared spectra of these substances show extinction maximum at 2260 cm^{-1} (specific to $-\mathrm{CN}$ group) and at 1050 cm^{-1} (specific to $-\mathrm{N}-\mathrm{O}-\mathrm{C}$). The characteristic vibration frequencies of these substances are presented in table 1.

In order to obtain the carboxyethyl ethers of the corresponding acetophenone oximes from the respective cyanoethyl derivatives, we intended to convert the nitrile group into carboxyl.

However, using classical alkaline,[5] or acid[6] hydrolysis methods, we have not obtained the desired result. In alkaline media even under relatively mild conditions (10 per cent potassium hydroxide, 50–60°, after one hour), the respective acetophenone oximes were evidenced in reaction mixture, probably as a result of the decyanoethylation reaction, which is characteristic of all O-cyanoethylated derivatives.[7] In acid media (concentrated hydrochloric acid), after three hours of refluxing the respective acetophenone appears, as a result of the lability of $-\mathrm{C}=\mathrm{N}-$ bond in this medium, together with an insignificant amount of a substance having a carboxylic acid character.

Thus, for the conversion of $-\mathrm{CN}$ into $-\mathrm{COOH}$ with a good yield and without other molecule changes, we had to examine another route. This conversion, together with the study of very interesting decyanoethylation in alkaline medium, will be described in another paper.

3. EXPERIMENTAL PART

Infrared spectra were determined on a Perkin-Elmer Infracord-137-B spectrophotometer. The melting points have not been corrected.

The acetophenones used were obtained as follows :

— *para*-nitro-acetophenone was obtained by isonitrosation of *orto*- and *Para*-nitroethylbenzene mixture, according to Balog et al, [8]

— the vast majority of *para*-substituted acetophenones were prepared by acetylation of the corresponding benzene derivatives, according to the Friedel-Crafts reaction, using acetic anhydride in the presence of aluminium chloride[9]. From *para*-acetylamino-acetophenone, obtained by this method, by hydrolysis with diluted hydrochloric acid the desired *para*-amino-acetophenone was synthethized.

Acetophenones were characterized by preparing the corresponding oximes (I–X). All oximes were prepared from the appropriate ketones with hydroxylamine hydrochloride in the presence of sedium acetate in aqueous ethanol, according to classical oximation reaction[10]. The acetophenone oximes thus obtained are shown in table 2. Melting points are given in comparison with literature data.

---

[5] W. Mann, *Ber. dtsch. chem. Ges.*, **14**, 1645 1881).

[6] A. Spiegel, *Ber. dtsch. chem. Ges.*, **14**, 239 (1881).

[7] P. F. Butzkus, *Uspekhi Khim.*, **30**, 1352 (1961).

[8] A. Balog, A. Kövendi, D. Rotaru and E. Crăciunescu, Romanian Patent NC. 41.341 (1959).

[9] R. Adams and C. R. Noller, "Organic Synthesis", Coll. vol. I. J. Wiley, New York, Second Edition 1948, p. 109.

[10] A. I. Vogel, "Practical Organic Chemistry", 3rd ed., Longmans, London, 1957, p. 345.

PREPARATION OF THE ALKALINE CATALYST : TRIMETHYL-BENZYL-AMMONIUM-METHOXIDE

Add 127 g (1 mole) of benzyl chloride to 420 ml methyl alcohol solution of 66 g (1.1 moles) trimethylamine, with stirring and cooling, so that the temperature remains below 40° and keep one hour at room temperature. Distil under diminished pressure to a volume of 350 ml methanol solution of trimethyl-benzyl-ammonium-chloride. After cooling, under stirring, add a methyl alcohol solution of sodium methylat, prepared from 200 ml methanol and 23 g sodium. Filter the precipitated sodium chloride and concentrate the methanol solution until a concentration of 35—40 g/100 ml trimethyl-benzyl-ammonium-methoxide in methyl alcohol is obtained.

CYANOETHYLATION OF *PARA*-SUBSTITUTED ACETOPHENONE OXIMES

Representative experiment is described.

To a solution of 9 g *para*-nitro-acetophenone oxime (0.05 moles) in 50 ml benzene, add 0.5 ml solution of trimethyl-benzyl-ammoniummethoxide in methyl alcohol (40 g/100 ml) and drop, under stirring 4 ml acrylonitrile at 25°. Keep stirring for two hours and wash afterwards the benzene solution twice with 25 ml 10 per cent sodium hydroxide solution and with water. Remove benzene by distillation under reduced pressure. The residual yellow oil crystallizes on cooling. Recrystallize the resulted cyanoethyl derivative of *para*-nitro-acetophenone oxime (XII) from 50 ml isopropyl alcohol.

The yield of pure material; m.p. 81° is 8 g (68%) (*Found* : C, 56.86 ; H, 5.10 ; N, 18.07. *Calcd.* for $C_{11}H_{11}N_3O_2$: C,56.65 ; H,4.75 ; N, 18.02%)

The other cyanoethyl derivatives (XI and XIII—XX) were obtained under the same general conditions. Compounds, further details and analysis are given in table 3.

ACETYLATION OF (XIX)

Reflux 2 g cyanoethyl ether of *para*-amino-acetophenone oxime (XIX) (viscous yellow oil), with 5 ml acetic anhydride for 15 minutes, pour into 50 ml water under stirring. Filter the resulting crystals after one hour, wash with water and after drying recrystallize from isopropyl alcohol. The melting point of the resulting substance is 121° (without depression with (XX), resulted from cyanoethylation of (X)). (*Found* : C, 63.80 ; H,6.50 ; N, 17.30. *Calcd.* for $C_{13}H_{15}N_3O_2$: C,63.70 ; H,6.16 ; N, 17.18%)

HYDROLYSIS OF CYANOETHYL ETHER OF ACETOPHENONE OXIME (XI)

a.) *in alkaline medium* : keep one hour at 60°, with stirring the mixture of 4.7 g cyanoethyl ether of acetophenone oxime (XI) in 20 ml alcohol and 4 g sodium hydroxide in 20 ml water. After cooling and acidulation with dilute hydrochloric acid at $pH = 1$, extract with 50 ml benzene. Wash the organic layer with water and then extract with saturated sodium bicarbonate solution. The bicarbonic solution remains clear after acidulation with dilute hydrochloric acid (to $pH = 1$).

When the benzene solution is extracted with 10 per cent aqueous sodium hydroxide, from the aqueous solution after acidulation crystals with melting point 56—70° are obtained, without depression with acetophenone oxime (I).

b.) *in acid medium* : keep for 3 hours at 60—70°, under stirring, the mixture of 7 g (XI) and 20 ml concentrated hydrochloric acid. After cooling extract with 50 ml benzene, wash the benzene layer three times with water, extract twice with 50 ml saturated bicarbonic solution. After acidulation, the bicarbonic solution yielded 0.5 g crystalline material, which after recrystallization from 1 :1 aqueous acetic acid has a melting point 69—70°. According to 0.1 n NaOH titration the dosage is 98.90%, calculated on $C_6H_5-C(CH_3)=N-O-CH_2-CH_2-COOH$ (*Found* : C,64.05 ; H,6.78 ; N,6.89. *Calcd.* for $C_{11}H_{13}NO_3$: C, 63.80 ; H,6.35 ; N, 6.76%).

From the extracted benzene layer, concentrated and dried under reduced pressure, resulted an oleous material with specific acetophenone odour, which yielded by oximation acetophenone oxime with m.p. 59°.

Table 1

Characteristic vibration frequencies of the compounds XI – XVIII and XX (in cm^{-1})

Comp. XI; 2940m; 2260w; 1610w; 1440m; 1370vs; 1305s; 1205m; 1100s; 1050vs; 990s; 930m; 885vs

Comp. XII; 2900m; 2260w; 1600s; 1510s; 1380vs; 1350vs; 1200m; 1090vs; 1040vs; 1000m; 940m; 855vs

Comp. XIII; 2900m; 2260w; 1600m; 1500m; 1370s; 1320s; 1210m; 1100vs; 1045vs; 1020s; 900vs; 832vs

Comp. XIV; 2940m; 2270w; 1600m; 1490m; 1370s; 1330s; 1200m; 1090s; 1040vs; 1020s; 940m; 890s; 825s

Comp. XV; 2900m; 2260w; 1620m; 1500m; 1420m; 1370s; 1330s; 1220m; 1100s; 1055vs; 940m; 890vs; 820m

Comp. XVI; 2850s; 2260w; 1600m; 1500w;1400s; 1370s; 1320s; 1200m; 1100s; 1055vs; 935m; 890vs; 835vs

Comp. XVII; 2900m; 2260 m; 2050w; 1600s; 1500m; 1450s; 1370s; 1310vs; 1235s; 1170vs; 1030vs; 930m; 880vs; 835s

Comp. XVIII; 2930m; 2260w; 1620s 1510m; 1370s; 1310s; 1235vs; 1175s; 1045vs; 930m; 880s; 835s

Comp. XX; 3330m; 2940m; 2260w; 1670vs; 1600vs; 1500vs; 1370s; 1320vs; 1230vs; 1100m; 1045vs; 1000m; 935m; 895s: 840m

w = weak; m = medium; s = strong; vs = very strong

Table 2

The melting points of *para* $X-C_6H_4-C(CH_3)=N-OH$

Compound	X =	Melting points		References
		Experimental data	Literature data	
I	H–	58°	59–60°	11
II	$-NO_2$	175°	174–5°	11
III	Cl–	96–7°	98–9°	11
IV	Br–	129–30°	130–31° 129–30°	11 12
V	CH_3-	88°	88–9°	11
VI	C_2H_5-	84–5°	83–4°	13
VII	CH_3O-	88°	86–8° 88–9°	11 13
VIII	C_2H_5O-	122°	125°	14
IX	$-NH_2$	151°	147–8°	15
X	CH_3-CO $-NH-$	207° from	CH_3-OH*	–

* (*Found:* C, 62.20; H, 6.34; N, 14.35. *Calcd.* for $C_{10}H_{12}N_2O_2$: C, 62.60; H, 6.30; N, 14.60%).

---

[11] D. E. Pearson, J. F. Baxter and J. C. Martin, *J. Org. Chem.*, **17**, 1511 (1952).

[12] D. E. Pearson and E. D. Watts, *J. Org. Chem.*, **20**, 494 (1955).

[13] P. J. Mc Nulty and D. E. Pearson, *J. Amer. Chem. Soc.*, **81**, 612 (1959).

[14] S. Swaminathan, *Science and Culture*, **12**, 199 (1946); *Chem. Abstr.* **41**, 2402g (1947).

[15] A. B. Sen and D. D. Mukerji, *J. Indian Chem. Soc.*, **28**, 161 (1951).

Table 3

Reaction conditions and characteristics of para-$X-C_6H_4-C(CH_3)=N-O-CH_2-CH_2-CN$ compounds

Compound	X =	Temp. °C	Time. hr.	Yield %	m.p. °C	Empirical formula	C % *Calcd.* *Found*	H % *Calcd.* *Found*	N % *Calcd.* *Found*	Halogen % *Calcd.* *Found*
XI	H—	40	3	90	44°; 44[2]	$C_{11}H_{12}N_2O$	—	—	—	—
XII	$-NO_2$	25	2	68	81°	$C_{11}H_{11}N_3O_3$	56.65 56.86	4.75 5.10	18.02 18.07	— —
XIII	Cl—	25	2	50	61°	$C_{11}H_{11}ClN_2O$	59.33 60.03	4.98 5.51	12.58 12.85	15.92 15.88
XIV	Br—	25	2	79	88°	$C_{11}H_{11}BrN_2O$	49.45 50.07	4.15 4.34	10.49 10.03	29.92 29.60
XV	CH_3-	30	4	50	48—9°	$C_{12}H_{14}N_2O$	71.30 71.54	6.98 7.00	13.86 13.46	—
XVI	C_2H_5-	30	3	44	31°	$C_{13}H_{16}N_2O$	72.20 72.10	7.45 7.65	12.95 12.75	—
XVII	CH_3O-	25	5	39	75°	$C_{12}H_{14}N_2O_2$	66.04 66.29	6.47 6.80	12.84 12.65	—
XVIII	C_2H_5O-	25	4	60	81°	$C_{13}H_{16}N_2O_2$	67.22 67.16	6.94 7.48	12.06 11.78	—
XX	$-NH-CO-CH_3$	30	4	65	123°	$C_{13}H_{15}N_3O_2$	63.70 63.80	0.16 6.50	17.18 17.30	— —

Acknowledgement. We are indebted to Livia Moraru and Iolanda Mureşan for pe forming the elementary analysis.

Revue Roumaine de Chimie, **20**, *2*, 251–258 (1975)

ÉTUDE DU PARTAGE DE L'ACIDE FORMIQUE, DE L'URANIUM (VI) ET DU PLUTONIUM (IV) DANS LE SYSTÈME TRIBUTYLPHOSPHATE – DODÉCANE – ACIDE NITRIQUE – ACIDE FORMIQUE – EAU

A. ARSENE* et M. GERMAIN**

* Institut de Technologies Nucléaires, Bucarest, Roumanie
** Centre d'Etudes Nucléaires de Fontenay-aux-Roses, France

Reçu le 13 février 1974

Le travail résume les principaux résultats obtenus dans le cadre du traitement chimique des combustibles irradiés par voie aqueuse dans le système $TBP-HNO_3-HCOOH-H_2O$.

INTRODUCTION

Le traitement des combustibles irradiés est réalisé de façon quasi universelle par voie aqueuse. Par suite des conditions de dissolution, il s'effectue en milieu acide nitrique.

Le solvant le plus utilisé pour la séparation de l'uranium, d'une part du plutonium, d'autre part des produits de fission, est le tributylphosphate (TBP).

La chimie de l'extraction de ces éléments en milieu nitrique est bien connue[1–10] et quelques études relatives à leur partage en présence d'acides carboxyliques ont été publiées.[11–15]

---

[1] K. Alcock, S. S. Grimley, T. V. Healy, J. Kennedy et H. A. C. McKay, *Trans. Faraday Soc.*, **52**, 39 (1956).

[2] R. Spence et M. W. Lister, U. S. Patent 2 864 664, déc. 16 1958 ; *N.S.A.*, **1959**, 8431.

[3] W. H. Baldwin et C. E. Higgins, U. S. Patent 2 864 668, déc. 16 1958 ; *N.S.A.*, **1959**, 8435.

[4] T. Sato, *J. Inorg. Nuclear Chem.*, **6**, 334 (1958).

[5] C. M. Nicholls, I. Wells et R. Spence, U.S. Patent 2 908 547, oct. 13 1959 ; *N.S.A.*, **1960**, 7465.

[6] K. Naito et T. Suzuki, *J. Phys. Chem.*, **66**, 989 (1962).

[7] A. P. Smirnov-Averin, G. S. Kovalenko et N. N. Krot, *Zhur. neorg. Khim.*, **8**, 2400 (1963).

[8] A. Bathellier, G. Koehly, J. J. Perez et A. Chesne, *Rapport CEA–R–2594*, **1964**.

[9] A. Chesne, G. Koehly et A. Bathellier, *Nuclear Sci. Eng.*, **17**, 557 (1964).

[10] H. H. C. McKay et R. J. W. Ctreeton, *J. Inorg. Nuclear Chem.*, **27**, 879 (1955).

[11] N. M. Adamskii, S. M. Karpacheva et A. M. Rozen, „Extraktsya, Teoriya, Primenenie, Apparatura", vol. 2, Gosatomizdat, Moscou, 1962, p. 80.

[12] T. Ishimori, K. Watanbe, K. Naito et T. Suzuki, Japan Pat 1862, Mars 8 1963 ; *Chem. Abstr.*, **61**, 267 (1964).

[13] T. Ishihara et K. Owada, *J. Nuclear Sci. Technol.* (Tokyo), **3**, 67 (1966).

[14] S. Ramamoorthy et M. Santappa, *Bull. Chem. Soc. Japan*, **42**, 411 (1969).

[15] Z. I. Nagnibeda, *Radiokhimiya*, **13**, 284 (1971).

En présence d'acide formique, les études ont été réalisées en présence de trilaurylamine.[16-17] Nous nous proposons dans ce travail d'étudier le système HCOOH – HNO_3 en présence de tributylphosphate. Le pouvoir complexant de l'acide formique vis-à-vis des éléments actinides tétravalents[17,18] et en particulier de plutonium doit permettre de réaliser la réextraction d'un phase organique de TBP.

1. PARTAGE DE L'ACIDE FORMIQUE

Par sa structure et son caractère organique, le partage de l'acide formique entre la phase aqueuse et la phase solvant va jouer un rôle important dans le mécanisme des extractions.

La mesure du partage a été réalisée par extraction avec le TBP 30% dodécane, de phases aqueuses d'acide formique de titres variables.

L'isotherme d'extraction (figure 1) ne présente pas de rupture de pente et l'on peut observer la décroissance du coefficient de partage avec l'acidité extraite dans le solvant (tableau 1). L'équilibre peut s'écrire :

$$(\mathrm{TBP})_s + \mathrm{x}\,(\mathrm{HCOOH})_{aq} \rightleftarrows [\mathrm{TBP}\,(\mathrm{HCOOH})_x]_s$$

La constante d'équilibre est :

$$K = \frac{(\mathrm{TBP})_{1,s} \cdot (\mathrm{HCOOH})^x_{aq}}{[\mathrm{TBP}, (\mathrm{HCOOH})_x]_s}$$

Si l'on assimile les activités aux concentrations, et compte tenu de la relation

$$D = \frac{(\mathrm{HCOOH})_s}{(\mathrm{HCOOH})_{aq}}$$

on arrive à :

$$D = 1/K(\mathrm{TBP})_{1,s}\,(\mathrm{HCOOH})^{x-1}_{aq}$$

Dans cette relation x est inconnu ; cependant l'allure de l'isotherme indique que x est petit et vaut vraisemblablement 1.

Pour cette valeur, on aurait $D = 1/\mathrm{K}.\ (\mathrm{TBP})_{1,s}$ avec $(\mathrm{TBP})_{1,s} = (\mathrm{TBP})_1 - (\mathrm{HCOOH})_s$

---

[16] N. Souka, *Radiochim. Acta*, **13**, 71 (1970).

[17] T. S. Lobamova, K. M. Dunaeva et E. A. Ipolitova, *Vestnik Moskva Univ. Ser. II Khim.*, **12**, 229 (1971).

[18] A. G. Samartseva et Z. A. Zhurvleva, *At. Energ.* (USSR), **29**, 342 (1970).

La figure 2 montre que cette relation est vérifiée et que, en conséquence, le complexe organique formé est dans le domaine étudié (TBP, HCOOH).

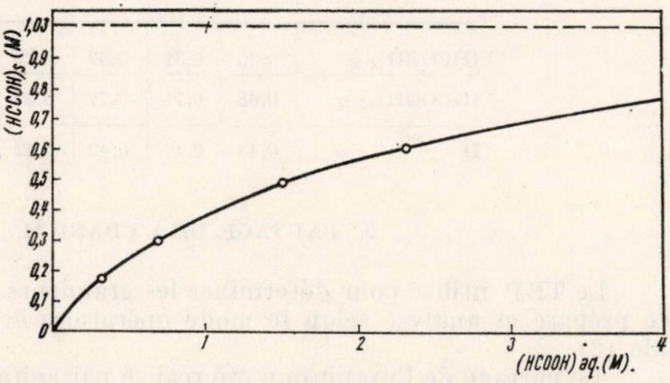

Fig. 1. — Isotherme d'extraction de HCOOH par TBP 30 % dodécane.

Tableau 1

Partage de l'acide formique

$(HCOOH)_{s_M}$	0,176	0,30	0,49	0,61
$(HCOOH)_{aq_M}$	0,325	0,68	1,5	2,34
D. HCOOH	0,50	0,44	0,33	0,26

Nous avons alors examiné l'influence de la présence d'acide nitrique sur le coefficient de partage de l'acide formique. Pour ce faire, les deux phases ont été agitées ensemble pendant 10 minutes, centrifugées, puis analysées selon le mode opératoire de la partie expérimentale (1). Les résultats rassemblés dans le tableau 2 permettent d'observer une très légère décroissance du coefficient de partage, qui s'explique par la compétition l'acide nitrique et l'acide formique à complexer le TBP en phase organique. Cette faible influence de l'acide nitrique s'explique aisément par sa faible extractibilité comparée à celle de l'acide formique.

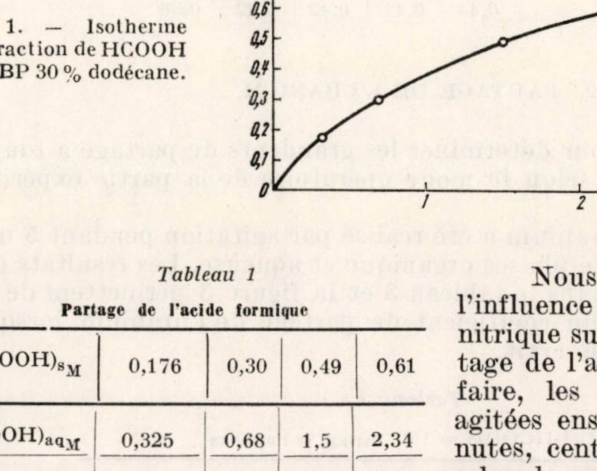

Fig. 2. — Coefficient de partage de l'acide formique.

Tableau 2

Partage de l'acide formique en présence d'acide nitrique

$(HNO_3)_{aq,initial}$	0	0,4	0,6	0,8	1
$(HCOOH)_s$ M	0,30	0,31	0,32	0,29	0,26
$(HCOOH)_{aq}$ M	0,68	0,71	0,77	0,69	0,74
D	0,44	0,44	0,42	0,42	0,36

2. PARTAGE DE L'URANIUM

Le TBP utilisé pour déterminer les grandeurs de partage a toujours été préparé et analysé selon le mode opératoire de la partie expérimentale (2).

Le partage de l'uranium a été réalisé par agitation pendant 5 minutes de volumes égaux de phases organique et aqueuse. Les résultats expérimentaux rassemblés dans le tableau 3 et la figure 3 permettent de constater l'augmentation du coefficient de partage de l'uranium, lorsque le titre en acide nitrique croît.

Tableau 3

$5 g.l^{-1}$ HCOOH = 1M **Partage de l'uranium**

HNO_3	0	0,2	0,3	0,4	0,5	0,6	0,8	1
D_U	0,31	0,42	0,73	1,1	1,2	1,7	2,6	3,6

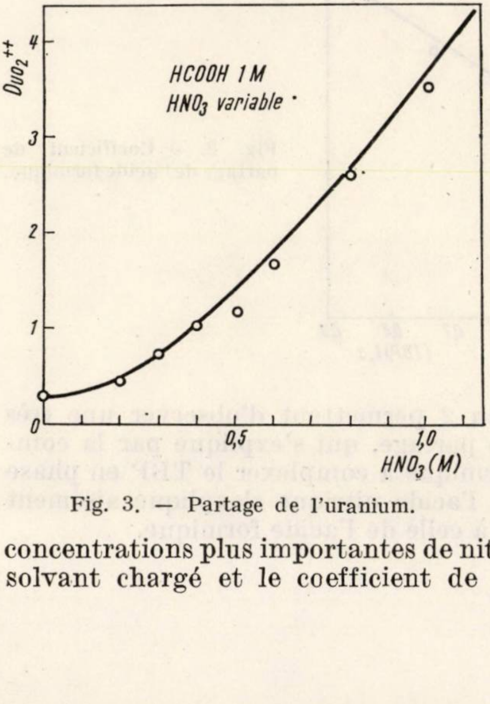

Fig. 3. — Partage de l'uranium.

Cette allure de la courbe montre le déplacement des ions formiques de leur complexe avec l'uranium, par les ions nitrate ; ceci par l'action combinée des deux mécanismes suivants :

1) un déplacement de l'équilibre de dissociation en HCOOH, dû à la présence d'un acide fort :

$$HCOOH \xrightleftharpoons{(HNO_3)} H^{\oplus} + HCOO^{\ominus}$$

2) la compétition à la complexation de l'uranium entre les ions formique et nitrique.

Le partage de l'uranium a alors été mesuré en présence de concentrations plus importantes de nitrate d'uranyle, par réextraction d'un solvant chargé et le coefficient de partage mesuré, après la deuxième réextraction, afin d'être affranchi de la présence d'acide nitrique résiduel ; de ce fait, la concentration maximale obtenue, dans le solvant après le deuxième équilibrage n'a été que de 37 g.l^{-1}.

On peut cependant remarquer (tableau 4) que :

1) Pour une même série, le coefficient de partage de l'uranium décroît avec le titre en HCOOH (complexation par les ions formiques),

2) Si l'on considère un même titre en HCOOH, $D_{U(VI)}$ croît avec la teneur en uranium en phase aqueuse (figure 3). On observe même que cette croissance est sensiblement linéaire, soit :

$$D \# \mathrm{DO} + K(\mathrm{UO}_2^{2\oplus})_{aq}$$

$$D \# \mathrm{DO} + K'(\mathrm{NO}_3^{\ominus})_{aq}\,.$$

Tableau 4

Partage de l'uranium

Série	HCOOH	0,10	0,20	0,51	1,05	2,05
Série 1	U_s	5,0	4,4	4,2	3,5	2,7
	D	0,52	0,44	0,41	0,31	0,22
Série 2	U_s	12,2	12,0	11,4	10,1	8,3
	D	0,56	0,54	0,50	0,40	0,31
Série 3	U_s	15,5	15,2	14,2	12,2	9,9
	D	0,57	0,55	0,49	0,40	0,30
Série 4	U_s	33,4	32,3	30,6	26,5	25,3
	D	0,76	0,74	0,68	0,54	0,48
Série 5	U_s	37,3	35,9	35,7	33,0	29,0
	D	0,76	0,79	0,69	0,60	0,49

U_s = uranium en phase solvant exprimé en g.l^{-1}.

Ce phénomène s'explique partiellement si l'on considère que lorsque la teneur en uranium croît, le rapport HCOOH/U décroît et ce fait les équilibres de complexation sont déplacés défavorablement si l'on considère la réextraction de l'uranium.

3. PARTAGE DU PLUTONIUM

— L'isotope 239 du plutonium a été utilisé, la solution mère ayant la composition suivante : $\mathrm{Pu^{IV}} = 1$ M, $\mathrm{HNO_3} = 5$ M.
Elle était diluée au moment de son utilisation, à des concentrations comprises entre 4.10^{-6} et 4.10^{-5} M, dans le milieu convenable.

— Le coefficient de partage est mesuré à la température ordinaire, par réextraction du solvant chargé (volume V) par la solution aqueuse (volume 2V).

— Les déterminations des concentrations en plutonium dans les phases à l'équilibre sont faites par comptage de l'activité α.

— Le partage a été mesuré dans diverses conditions d'acidités formique et nitrique.

Nous avons d'abord étudié l'évolution du coefficient de partage en fonction de la teneur en acide formique, à acidité nitrique constante.

On observe expérimentalement (figure 4, tableau 5), que le coefficient de partage décroît sensiblement lorsque le titre en HCOOH croît.

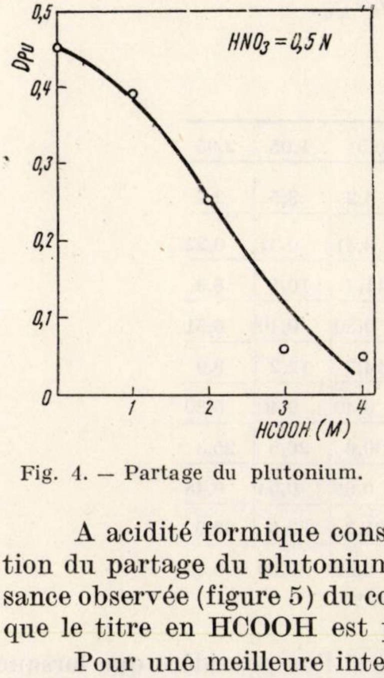

Fig. 4. — Partage du plutonium.

Tableau 5

$HNO_3 = 0{,}5$ N **Partage du plutonium**

$HCOOH_M$	0	1	2	3	4
D Pu^{IV}	0,45	0,39	0,25	0,06	0,05

A acidité formique constante (1M et 2M), nous avons suivi l'évolution du partage du plutonium avec la teneur en acide nitrique. La croissance observée (figure 5) du coefficient de partage est d'autant plus limitée que le titre en HCOOH est plus grand.

Pour une meilleure interprétation des résultats, nous avons mesuré le partage des complexes formiques du plutonium dans le TBP 30%, en l'absence d'acide nitrique. Pour ce faire, la solution de nitrate de plutonium en milieu nitrique a été précipitée à l'ammoniac, l'hydroxyde obtenu a été lavé à l'eau, puis redissous dans l'acide formique 1M. Le coefficient de partage trouvé est de 6.10^{-4}, ce qui indique la mauvaise extractibilité des complexes formiques du plutonium. Les courbes obtenues (figure 5) représentent donc sensiblement l'extraction des complexes nitriques et donnent, de ce fait, une bonne indication sur la complexation du plutonium en phase aqueuse.

Sur ces bases, si l'on admet que seul le complexe nitrique $Pu(NO_3)_4$ est extrait, et que tous les autres complexes sont inextractibles, on peut avoir une bonne idée de la complexation (tableau 6).

Dans le milieu HNO_3 0,5N, la complexation par l'acide formique ne devient prépondérante qu'en milieu formique au moins égal à 3M. Ceci semble indiquer que les constantes de complexation du plutonium sont environ 10 fois plus petites en milieu formique qu'en milieu nitrique.

Tableau 6

Complexation par l'acide formique

HNO_3 = 0,5N

$HCOOH_M$	0	1	2	3	4
DPu	0,45	0,39	0,25	0,06	0,05
% complexe extractible	100	87	55	15	10

4. SÉPARATION URANIUM–PLUTONIUM

Nous avons comparé à acidité formique constante, l'influence de la teneur en acide nitrique sur le facteur de séparation uranium-plutonium.

$$\alpha = \frac{D_{U(VI)}}{D_{Pu(IV)}}$$

Les résultats rassemblés dans le tableau 7 montrent que ce facteur α est petit et varie peu avec le titre en HNO_3.

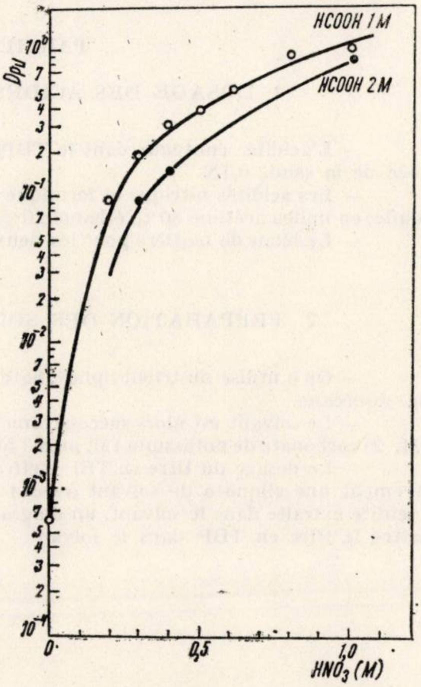

Fig. 5. — Partage du plutonium.

Tableau 7

Facteur de séparation uranium-plutonium

HCOOH = 1M

HNO_3	0,2	0,3	0,4	0,5	0,6	0,8	1
$\alpha = \frac{D_U{}^{VI}}{DPu^{IV}}$	4,4	3,8	3,5	3	3,1	2,8	3,4

CONCLUSION

Les essais réalisés dans le système TBP – HNO_3 – HCOOH ont permis de mettre en évidence les possibilités de réextraction du plutonium. Bien qu'il apparaît que les complexes formiques soient faibles, un choix convenable des concentrations de réactifs permet de réaliser une bonne réextraction du plutonium et de l'uranium.

Revue Roumaine de Chimie, **20**, *2*, 251–258 (1975)

On peut même envisager de réaliser une séparation uranium — plutonium à l'occasion de cette réextraction, toutefois il serait nécessaire d'élargir le champ des investigations faites, de façon à obtenir des facteurs de séparation plus élevés.

PARTIE EXPÉRIMENTALE

1. DOSAGE DES ACIDES NITRIQUE ET FORMIQUE

— L'acidité contenue dans le TBP(HNO_3+HCOOH) a été dosée en milieu hétérogène avec de la soude 0,1N.

— Les acidités nitrique et formique des phases aqueuses ont aussi été dosées avec de la soude, en milieu acétone 80 %, éthanol 20 %, qui permet de différencier les deux acides.

— Le bilan de matière pour les deux acides permet de connaître $(HNO_3)_s$ et $(HCOOH)_s$

2. PRÉPARATION DES SOLUTIONS DE TRIBUTYLPHOSPHATE

— On a utilisé du tributylphosphate pur (Eastman Kodak) que l'on a dilué à 30 % dans du dodécane.

— Le solvant est alors successivement lavé avec la moitié de son volume de : 1) potasse 2M, 2) carbonate de potassium 1M, puis 3 fois avec son volume d'eau distillée.

— Le dosage du titre en TBP s'effectue alors de la façon suivante : on équilibre successivement une aliquote de solvant avec 4 fois son volume d'acide nitrique 8N, puis on dose l'acidité extraite dans le solvant, un diagramme préexistant permet par simple lecture de connaître le titre en TBP dans le solvant.

Revue Roumaine de Chimie, 20, 2, 259–265 (1975)

SYNTHETIC SINGLE CRYSTAL LEAD SULPHIDE ELECTRODE. I

DIRECT POTENTIOMETRIC TITRATION OF LEAD WITH NA_2EDTA

D. C. CÖRMÖS*, IOVANCA HAIDUC* and P. STEȚIU**

*Department of Analytical Chemistry, University of Cluj,
Str. Arany Janos, 11, Cluj, Romania
**Solid State Laboratory, University of Cluj, Str. Arany
Ianos, 11, Cluj, Romania

Received December 6, 1973

The paper presents a direct potentiometric titration method of Pb^{2+} ions with sodium ethylenediaminotetraacetate (Na_2EDTA) using synthetic single crystal lead sulphide electrodes as indicating electrodes. The potential versus time dynamic response curves are given as a function of the Pb^{2+} ion concentration, as well as the electrode function at pH 2 and 10.

The influence of the concentration of the auxiliary complexing agent (Seignette salt), of the pH and of the concentration of Pb^{2+} ions upon the shape of the titration curves and the potential variation at the equivalence point, are estimated. The optimal working conditions are given and the lower limit of lead concentration at which titration is still possible was also determined.

INTRODUCTION

The titrimetric determination of cations using ion-sensitive electrodes has become in recent years a constant preoccupation of analytical chemists. This is due to the fact that the electrometric indication of the equivalence point in various types of ion-sensitive electrode titrations, is precise, and with fast response, which permits the automation of many titrations.

Among cation titrations, an important role is played by chelating agents. The different stability of the chelates formed during titration depending on the nature of the reagent and pH value, offers a large variety of titration procedures.

For the determination of lead by potentiometric titration, various types of electrodes like silver,[1,2] mercury[3,4] lead amalgam,[5,6] molybdenum

---

[1] J. P. Cummings, *Talanta*, **17**, 1013 (1970).

[2] H. Khalifa, R. Patzak and O. Doppler, *Z. analyt. Chem.*, **161**, 264 (1958).

[3] E. I. Golkina, "Materialy Nauchnoi Konferentsii Aspirantov", Rostov na Donu, Gosudarstvenii Universitet, 1967, p. 257.

[4] T. Takahashi, *Bunseki Kagaku*, **18**, 1251 (1969) ; *Chem. Abstr.*, **72**, 62472 (1970).

[5] E. S. Amanzhalova and K. A. Atchibaev, *Izv. Akad. Nauk Kaz. SSR, Ser. Khim*, **17**, 5 (1967).

[6] E. S. Amanzhalova and G. D. Protopopova, *Izv. Akad. Nauk Kaz. SSR, Ser. Khim.*, **20**, 10 (1970).

and tungsten[7] were used in the past, as were the electrodes made from various chemical compounds like manganese dioxide,[8] heavy metal synthetic sulphides, alone or in mixtures, prepared by pressing or sintering,[9-11] or from synthetic lead sulphide embedded in silicone rubber[12] or polyvinyl chloride polymer.[13] Sintered electrodes made from powders of lead selenide and telluride[14] were also used. There are some reports about the titration of lead with ion-sensitive electrodes in liquid state.[15,16]

In the present paper we report a new electrode for the chelatometric titration of lead; the electrode is made from a single crystal of lead sulphide, synthetically prepared.

EXPERIMENTAL

Electrode preparation. The electrode was prepared from a crystal of synthetic lead sulphide, grown from a melt, having the following dimensions : 1.5 × 2.0 × 2.5 mm, which provides a contact surface area of *ca.* 16 mm^2. This crystal was sealed to a copper conductor with the aid of a solid seal of silver paste and tightly sealed at the end of the glass tube, with the aid of piceine. The other end of the copper wire was sealed to the outer end of the electrode as shown in fig. 1.

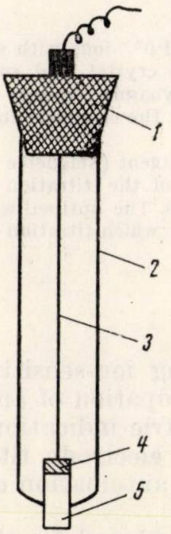

Fig. 1. — Single crystal PbS electrode.

1, metallic support; *2*, glass tube; *3*, copper wire; *4*, silver paste; *5*, PbS crystal.

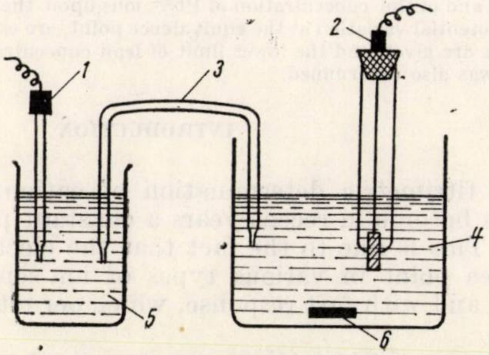

Fig. 2. — Electrolytic cell used in Pb^{2+} titration with single crystal PbS electrode.

1, CSE; *2*, single crystal PbS electrode; *3*, agar-agar in KNO_3 0.1 M; *4*, test solution *5*, KNO_3 0.1 M; *6*, magnetic stirrer.

[7] R. Geyer and N. Manfred, *Acta Chim. Acad. Sci. Hung.*, **60**, 349 (1969).

[8] T. Nomura and G. Nakagawa, *Bunseki Kagaku*, **16**, 1314 (1967); *Chem. Abstr.*, **68**, 74815 (1968).

[9] E. A. Moya and L. C. Kuang, *Analyt. Chem.*, **42**, 1669 (1970).

[10] J. Ružicka and C. G. Larum, *Analyt. Chim. Acta*, **53**, 206 (1971).

[11] M. S. Frant and J. W. Ross, *Analyt. Chem.*, **41**, 967 (1969).

[12] H. Hirata and K. Date, *Analyt. Chem.*, **43**, 279 (1971).

[13] M. Mascini and A. Liberti, *Analyt. Chim. Acta*, **60**, 405 (1972).

[14] H. Hirata and K. Higashiyama, *Analyt. Chim. Acta*, **54**, 415 (1971).

[15] S. Lal and G. D. Christian, *Analyt. Chim. Acta*, **52**, 41 (1970).

[16] Y. Ružicka and Chr. Tjell, *Analyt. Chim. Acta*, **51**, 1 (1970).

Reagent used. For titrations we used a solution of $Pb(NO_3)_2$ prepared from metallic lead of 99.99% purity and analytical grade nitric acid. The sodium salt of ethylenediaminetetraacetic acid, the Seignette salt (sodium, potassium tartrate) and the buffer solutions (pH 5.5, 8.0 and 10) have been prepared from analytical grade reagents and bidistilled water. The Na_2EDTA solution was standardized with a Zn^{2+} solution, prepared from analytical grade metallic zinc.

Apparatus and measurements. The electrolytic cell used for the determination of the electrode function for Pb^{2+} ion and for chelatometric titrations is shown in fig. 2.

The electrochemical chain on which the measurements were based was the following:

$$- \text{SCE} \;\Big|\; \begin{array}{l} Pb(NO_3)_2 \\ \text{test} \\ \text{solution} \end{array} \;\Big|\; \text{PbS electrode} \;\Big|\; Ag_2S/Ag/Cu \; +$$

The potential-time dynamic curves for solutions of concentrations between $10^{-1} - 10^{-7}$ M were recorded with a Radelkis r—OH 102 Polarograpf. The reproductibility of the readings was ± 1 mV. The electrode potential during the chelatometric titration of Pb^{2+} was measured with a Bekman pH-meter model 1019. The saturated calomel electrode (SCE) was used as a reference electrode, conected with the titrated solution with an agar-agar bridge (0.1 M in KNO_3).

RESULTS AND DISCUSSION

The response speed of the electrode. The potential-time dynamic curves of the single crystal PbS electrode, have been recorded in $Pb(NO_3)_2$ solutions of increasing concentration 10^{-7} to 10^{-1} at pH 2 (HNO_3 10^{-2} M) and at pH 10 ($NH_4OH - NH_4Cl$). The measurements were made at 22° under constant stirring performed with an electromagnetic stirrer. Response speeds are shown in fig. 3.

Figure 3 shows, that at both pH = 2 and pH = 10, the single crystal electrode PbS attains constant potential much faster in solutions of lower concentration (5 sec for 10^{-6} M Pb^{2+} and 30 – 40 sec for 10^{-1} M Pb^{2+}, both at pH = 2). This fast response of the electrode is an obvious advantage since it suggests the possibility of its use in automatic titrations. Under these working conditions, when the potential values for small concentrations of lead are established almost instantaneously (close to the equivalence point), the single crystal PbS electrode will indicate correctly the value of the equivalence volume in automatic titrations.

The electrode function for Pb^{2+}. The electrode function has been determined for Pb^{2+} at two pH values. For this purpose, the lead nitrate solution at pH = 2 and pH = 10 was used. To keep Pb^{2+} in solution at pH = =10, the ratio of Seignette salt added was 10 :1. The electrode potentials were measured in Pb^{2+} solutions in the concentration range from 10^{-1} to 10^{-7} M prepared by successive dilutions and at constant ionic strength ($J = 0.1$) achieved with KNO_3. To record $E - p\text{Pb}^{2+}$ curves the constant values of dynamic curves were used. The electrode functions are given in fig. 4.

The electrode functions do not show a Nernstian response; they exhibit a slope with continuous variation.

The chelatometric titration of Pb^{2+}. Na_2EDTA is very often used as a titrating reagent. The chelatometric determination of lead with the use of colour indicators is not very accurate because of the lack of sharpness in the colour change of the indicator. Therefore we found most convenient to use the potentiometric chelatometric titration by emploing a single crystal PbS indicating electrode.

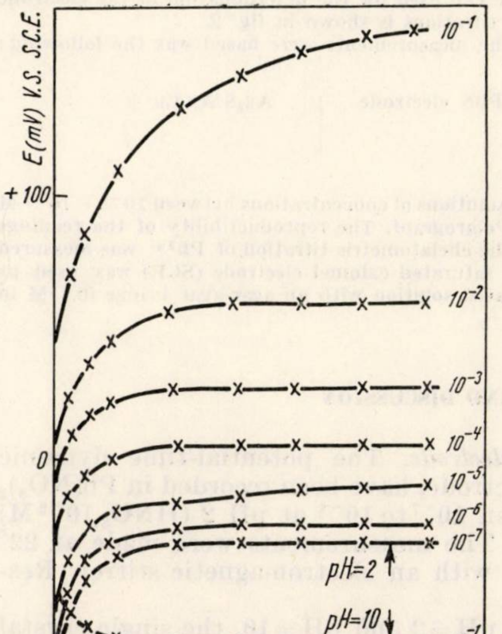

Fig. 3. — The potential-time dynamic response of PbS single crystal electrode at pH = 2 and pH = 10.

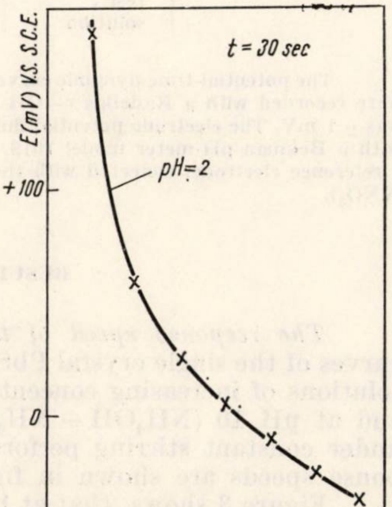

Fig. 4. — The electrode function for Pb^{2+} using PbS single crystal electrode at pH = 2 and pH = 10.

In order to establish the optimal conditions for titration, the influence of various factors was investigated : the concentration of Seignette salt, the pH of the solution and the Pb^{2+} concentration.

The influence of the Seignette salt concentration. To maintain the Pb^{2+} in solution during titration in alkaline medium (pH = 10), various molar proportion of Seignette salt in respect to lead ions were added, in order to establish the optimal ratio [Pb^{2+}]/[Seignette salt]. The titration curves of lead solution [Pb^{2+}]$=7.5\times10^{-4}$ (10 mg Pb^{2+} in 65 ml solution) in the presence of various concentrations of Seignette salt are shown in fig. 5.

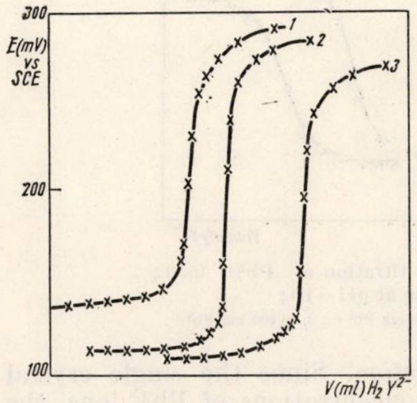

Fig. 5. — Potentiometric titration of 7.5×10^{-4} Pb^{2+} with 10^{-2} M Na_2EDTA using PbS single crystal electrode in the presence of Seignette salt.

1, [Pb^{2+}]/[Seignette salt] = $1/10^2$, $\Delta E_{\pm2\%}=45$mV
2, [Pb^{2+}]/[Seignette salt]= $4/10^1$, $\Delta E_{\pm2\%}=75$mV,
[Pb^{2+}]/ [Seignette salt] = $1/10^2$, $\Delta E_{\pm2\%}=80$mV

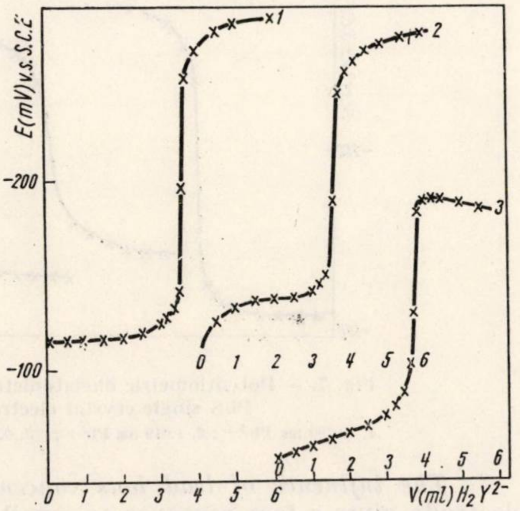

Fig. 6. — Potentiometric titration of 7.5×10^{-4} Pb^{2+} with 10^{-2} M, Na_2EDTA using PbS single crystal electrode.

1, pH = 10.0–10.2; *2*, pH=8.0–8.2; *3*, pH = 5.2–5.5.

The potential variation round the equivalence point ($\Delta E_{+2\%}$, table 1) shows that the sharpness index increases with the decrease of the Seignette salt concentration. The molar optimal ratio between Seignette salt and lead ions is 10 :1. After the decrease of the Seignette salt concentration below this value, no sensible improvement is observed in the potential jump and there appears a danger of precipitation of Pb^{2+} ions.

The influence of pH. Since the stability of lead complexonate is strongly influenced by hydrogen ion concentration in the solution to be titrated, several titrations were performed at pH = 5.5, pH = 8 and pH =10, in order to establish the range in which the direct titration of lead with Na_2EDTA is possible. For titration a 0.01 M solution of Na_2 EDTA was used. Titration curves at various pH value are shown in fig. 6.

The most symmetrical titration curve is obtained at pH = 10 (fig. 6, curve *1*). The potential jump for ±2% error is about 80 mV. The titration curve at pH = 5.5 exhibits for the same stages of titration, a potential jump of 90 mV., thus electrode sensitivity is improved; the electrode potentials show higher positive values, as expected on the basis of the electrode function determined in acid medium (-55 mV *vs.* SCE at pH $= 5.5$ and -120 mV at pH $= 10$). Therefore the titration of lead by chelatometric potentiometry can be satisfactorily performed in the range of 5.5 to 10.

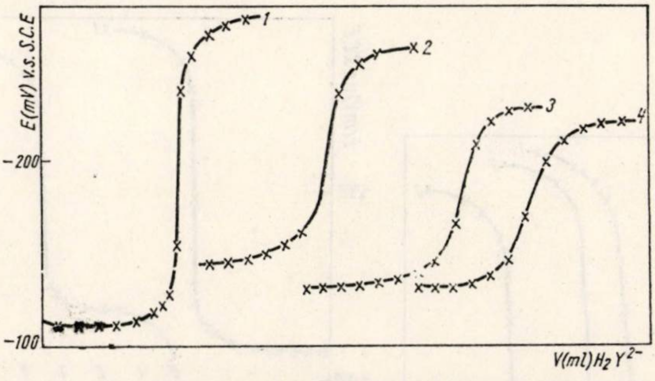

Fig. 7. — Potentiometric chelatometric titration of Pb^{2+} using PbS single crystal electrode at pH=10;
1, 10.190 mg Pb^{2+}; *2*, 1.019 mg Pb^{2+}; *3*, 0.218 mg Pb^{2+}; *4*, 0.109 mg Pb^{2+}.

The influence of lead ions concentration. Since the single crystal electrode gives a fast response to small concentrations of Pb^{2+} ions, the minimal amount of Pb^{2+} which can be titrated was determined. For this purpose Pb^{2+} ion titration was performed at the following concentrations: 7.5×10^{-4}, 7.5×10^{-5}, 3.5×10^{-5} and 1.5×10^{-5} M. Titrations, were performed at pH $= 10$ with Na_2EDTA 2×10^{-2}, 1×10^{-2} and 5×10^{-3} M. Titration curves are shown in fig. 7.

Figure 7 shows that a 1.5×10^{-5} M Pb^{2+} solution can be titrated with Na_2EDTA 5×10^{-3}M with a potential jump around the equivalence point of *ca.* 40 mV (fig. 7, curve 4).

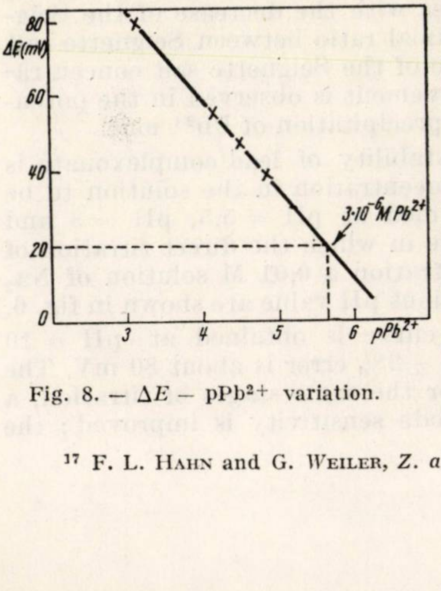

Fig. 8. — ΔE — pPb^{2+} variation.

The results of titrations are summarized in table 1. The amount of lead found was determined from the inflexion points calculated according to the Hahn—Weiller method.[17]

If the value of potential jumps $\Delta E_{\pm 2\%}$ (table 1, column 5) are plotted against lead concentration, the curve shown in fig. 8 is obtained. It can be used to establish the limit concentration of lead ions which can be determined by chelatometric titration with a single crystal lead sulfide electrode.

Taking into account that a jump of 20 mV around the equivalence point for $e = \pm 2\%$ can easily be detected allowing for exact determinations, the extrapolation of $\Delta E_{\pm 2\%}$ *vs.* pPb^{2+} for 20 mV gives a concentration of $3.5 \times 10^{-6} Pb^{2+}$ which can be precisely determined by titration. (corresponding to 0.2 mg Pb^{2+} in 50 ml solution).

---

[17] F. L. Hahn and G. Weiler, *Z. analyt. Chem.*, **69**, 417 (1927).

Table 1

Potentiometric chelatometric titration of Pb^{2+} with PbS single crystal electrode*

Pb^{2+} taken mg	Pb^{2+} found mg	ΔG mg	$\Delta E \pm 2\%$ mV	pH of titrated solution
10.912	10.936	+0.024	80	10.0
10.912	10.903	−0.009	80	10.0
10.912	10.892	−0.030	80	10.0
1.091	1.063	−0.028	55	10.0
0.545	0.611	+0.065	45	10.0
0.218	0.231	+0.013	40	10.0
10.912	10.933	+0.021	70	8.0
10.912	10.952	+0.040	90	5.5

* Pb^{2+} : Seignette salt molar ratio 1:10 in all cases.

CONCLUSIONS

The single crystal lead sulphide electrode prepared from a synthetic material can be succesfully used in the chelatometric potentiometric titration of lead. Titrations are reproducible and the electrode potential is established rapidly. The minimum amount of Pb^{2+} titrated with an error of +6% was 0.218 mg. The minimum amount of Pb^{2+} which can be titrated with a potential variation $\Delta E_{\pm 2\%} = 20$ mV is of *ca.* 2.5×10^{-6}M. The optimal pH range for the titration is 5.5 to 10. With titration at pH = = 10, the optimal molar ratio between the auxiliary complexing agent and Pb^{2+} is 10 :1.

Revue Roumaine de Chimie, **20**, *2*, 267–273 (1975)

ÉTUDE SPECTROPHOTOMÉTRIQUE DE LA RÉACTION DU WOLFRAM (VI) AVEC LE SOLOCHROME VIOLET RS

MARIA PLENICEANU et OLIMPIA RUSU
Université de Craiova, Faculté de Chimie, 165, Calea Bucureşti

Reçu le 29 décembre 1973

On présente une étude spectrophotométrique du système W (VI)-solochrome violet RS et on propose l'institution d'une méthode de détermination spectrophotométrique du W (VI) avec ce réactif. De l'étude de la dépendance de l'extinction en fonction du pH on a conclu qu'il se forme une seule combinaison complexe, au pH = 2. Le nouveau composé correspond au rapport molaire W (VI)/solochrome = 1/2 et présente une constante d'instabilité exprimée par $\overline{\text{pK}} = 7{,}91 \pm 0.033$. Par cette méthode spectrophotométrique on peut déterminer W (VI) avec solochrome violet RS entre les limites de concentration : 4,41 – 88,2 μg W (VI)/cm³ à la longueur d'onde λ = 550 nm.

Le réactif organique utilisé, solochrome violet RS ou le sel de sodium de l'acide 2-hydroxynaphtyle-azo-1 phénol-4 sulphonique (I), présente la formule suivante :

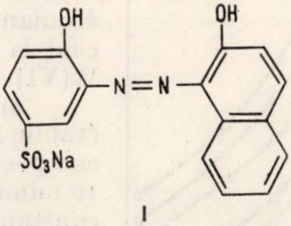

I

La littérature de spécialité indique l'utilisation de ce réactif pour la détermination spectrophotométrique des éléments suivants : molybdène (VI),[1] zirconium (IV),[2] thorium (IV),[3] chrome (III),[4] gallium (III),[5] aluminium (III),[6] indium (III),[7] uranium (VI),[8] zinc (II),[9] cadmium (II)[9] et vanadium (V).[10]

---

[1] J. Korkisch et M. Osman, *Z. analyt. Chem.*, **171**, 107 (1959).

[2] J. Korkisch et M. Osman, *Z. analyt. Chem.*, **171**, 3471 (1959).

[3] I. M. Korenman, F. R. Sheyanova et Z. M. Gurieva, *Khim. Tekhnol.*, **2**, 292 (1966).

[4] R. D. Bentley et J. P. Elder, *J. Soc. Dyers and Colouristes*, **72**, 332 (1956).

[5] V. Croitoru et G. Nicolae, *Chimie Analitică*, **1**, 155 (1971).

[6] Gr. Popa, M. Pleniceanu et V. Croitoru, *Anal. Univ. Bucureşti*, **1970**, 67.

[7] Gr. Popa et V. Croitoru, „Lucrările celei de a III-a Conferinţe Naţionale de Chimie Analitică. (Metode optice)", **3**, 65 (1971).

[8] Gr. Popa, L. Vlădescu et V. Croitoru, *Anal. Univ. Bucureşti*, **1971**, 109.

[9] V. Croitoru, A. Deac et F. Pîrlog, *Anal. Univ. Bucureşti*, **1972**, 27.

[10] I. Burnea, M. Pleniceanu et L. Burnea, *Rev. Roumaine Chim.*, **19**, 501 (1974).

Dans le travail on étudie le système W(VI)-solochrome violet RS et on propose une méthode de dosage spectrophotométrique du W(VI) avec ce réactif.

PARTIE EXPÉRIMENTALE

RÉACTIFS

- Des solutions faiblement acides de wolframate d'ammonium (Merck).
- Des solutions aqueuses de solochrome violet RS (Serva).
- Des solutions tampons d'acide chlorhydrique-acétate de sodium.[11]

APPAREILS

- Le spectrophotomètre universel Zeiss Jéna V.S.U.1.
- Le pH-mètre M.V.11 Clamann Grahnert, Dresden.

RÉSULTATS ET DISCUSSIONS

Etude spectrophotométrique des facteurs qui influencent le système W(VI)—solochrome violet RS. Comme suite de la réaction entre W(VI) et solochrome violet RS(I) on observe la formation d'un composé de couleur rouge foncé, couleur qui apparaît au froid et qui ne se modifie pas par le chauffage. En étudiant les facteurs qui influencent la formation du complexe W(VI)—I il a résulté :

a) Le temps nécessaire pour établir la coloration du nouveau composé est d'approximativement 10 minutes, après quoi celle-ci reste constante.

b) Le pH optimal de travail égal à 2 se déduit de la figure 1 qui montre la dépendance de l'extinction de pH.

Puisque la réaction de la formation de la combinaison complexe est influencée par la concentration des ions d'hydrogène, on a maintenu dans les déterminations ultérieures le même pH, tant dans l'essai à analyser que dans l'essai témoin.

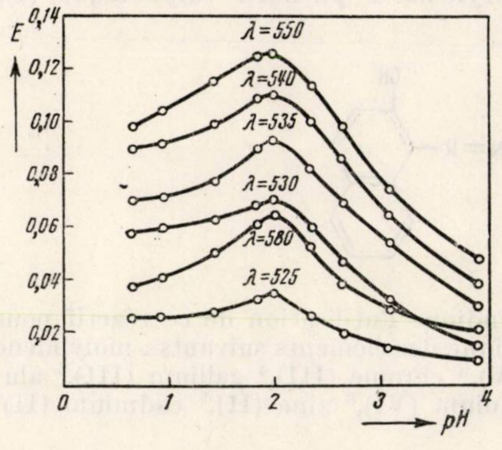

Fig. 1. — Variation de l'extinction en fonction du pH (8.10^{-5}M W (VI) + $2,4.10^{-4}$M I).

c) La longueur d'onde correspondant à l'absorption optique maximale, résulte de la figure 2, qui représente la courbe d'absorption du composé face au réactif, pour diverses valeurs de pH.

---

[11] C. Luca, „PH-ul şi aplicaţiile lui". Ed. tehnică, Bucarest, 1964, p. 57.

A la suite des données obtenues on observe que la longueur d'onde la plus favorable aux déterminations spectrophotométriques du nouveau composé formé est de 550 nm.

Tableau 1

Influence de la quantité de réactif sur l'extinction [W(VI)] = $4 \cdot 10^{-5}$ M; pH = 2; λ = 550 nm

[Solochrome] $\times 10^{-5}$M	Extinction
0,5	0,030
1,0	0,065
1,5	0,100
2,0	0,130
3,0	0,132
4,0	0,135
5,0	0,138
6,0	0,140
7,0	0,142

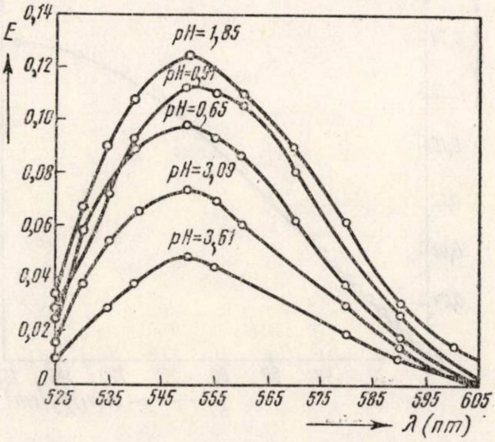

Fig. 2. — Variation de l'extinction en fonction du λ (8.10^{-5}M W (VI) + $2,4.10^{-4}$ M I.)

d) La quantité de réactif suffisante pour obtenir une extinction maximale est de 8.10^{-5} M I pour 4.10^{-5} M W (VI) au pH = 2 et λ = = 550 nm (tableau 1), mais pour favoriser le déplacement de l'équilibre de la réaction pour la formation de la combinaison complexe on a utilisé dans toutes les déterminations un excès de réactif.

Détermination spectrophotométrique du W(VI) avec solochrome violet RS. Tenant compte des résultats obtenus sur l'étude du système W(VI)—I, on a essayé d'instituer une méthode de détermination spectrophotométrique du W(VI) avec ce réactif.

Courbe d'étalonnage. Pour tracer la courbe, absorption optique-concentration de l'ion W(VI), on a utilisé des quantités variables de wolframate d'ammonium en concentrations contenues entre $0,4 . 10^{-5}$M et $8 . 10^{-5}$M, auxquelles on a ajouté une quantité constante de réactif de concentration $4,8 . 10^{-4}$M.

Les essais ont été préparés dans des ballons à mesurer de 25 cm³, étant remis au signe avec la solution tampon HCl 1N — CH_3COONa 1M, au pH = 2. Après avoir uniformisé les essais, on a fait les mesures d'extinction au spectrophotomètre, dans des cuves grosses de 1 cm, utilisant comme essai témoin une solution de réactif préparée de la même façon que les essais qui contiennent du W(VI).

Les résultats des déterminations sont représentés dans la figure 3, où l'on constate que la détermination spectrophotométrique du W(VI) avec solochrome violet RS est possible entre les limites de concentration 4,41 — 88,2 μg W(VI)/cm³.

La sensibilité de la méthode, exprimée par le coefficient molaire d'extinction (ε) est de 3500 pour la longueur d'onde $\lambda = 550$ nm.

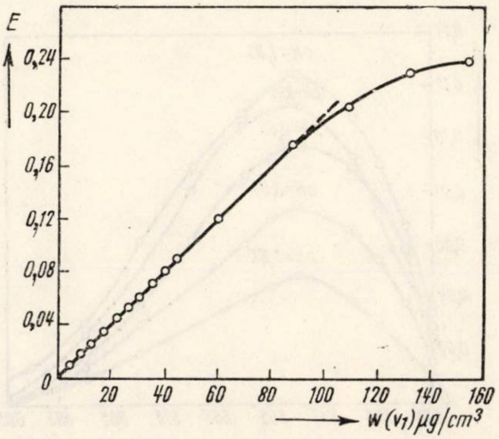

Fig. 3. — Variation de l'extinction en fonction de la concentration W(VI)($0{,}4.10^{-5}$M — 8.10^{-5}M W (VI) + $4{,}8.10^{-4}$M I).

Pour le calcul de la pente de la droite on a utilisé la méthode des moindres carrés à l'aide de laquelle on a obtenu la valeur $m = (19 \pm 0{,}13).10^{-4}$. Dans ce cas l'intervalle de sûreté a été calculé dans la distribution Student pour une probabilité de 95%, en utilisant 12 déterminations.

En étudiant la spécificité de la réaction entre le W(VI) et le solochrome violet RS on a constaté que le W(VI) peut être déterminé en présence de V(v) jusqu'au rapport W(VI)/V(v) = 1/4, en présence de Zn(II), Al(III), Ga(III), Tl(I), Tl(III), U(VI) jusqu'aux rapports suffisamment grands, grâce aux différents maxima d'absorption des complexes correspondants.

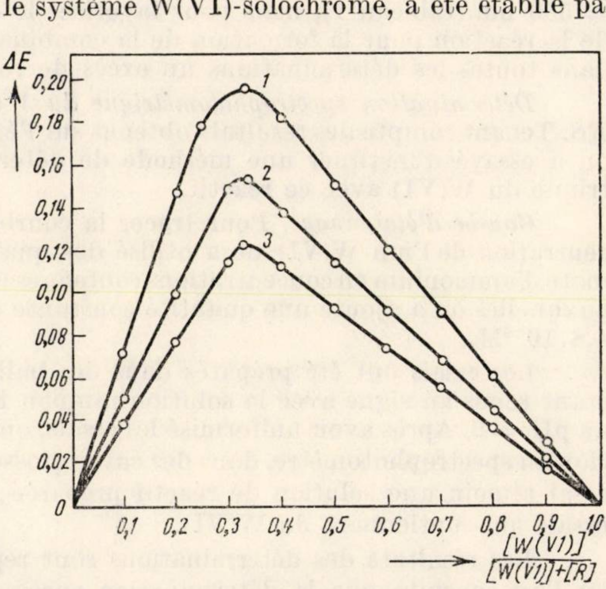

Fig. 4. — Détermination de la composition du complexe formé par la méthode des séries de solutions isomolaires :

1, solutions 1.10^{-3} M ; *2*, solutions $6{,}66.10^{-4}$ M ; *3*, solutions 5.10^{-4}M

Détermination de la composition du complexe formé. La composition du complexe obtenu dans le système W(VI)-solochrome, a été établie par la méthode des variations continues du Job, ainsi que par la méthode du rapport molaire. À la suite de l'application de la méthode des séries isomolaires de Job au pH = 2 et $\lambda = 550$ nm, ont résulté les courbes présentées dans la figure 4, où ΔE représente la valeur de l'absorption optique obtenue par la détermination de l'essai W(VI) + solochrome violet RS en rapport avec la même quantité de solochrome, et $\frac{[W(VI)]}{[W(VI)] + [R]}$ constitue la fraction molaire de la substance à analyser.

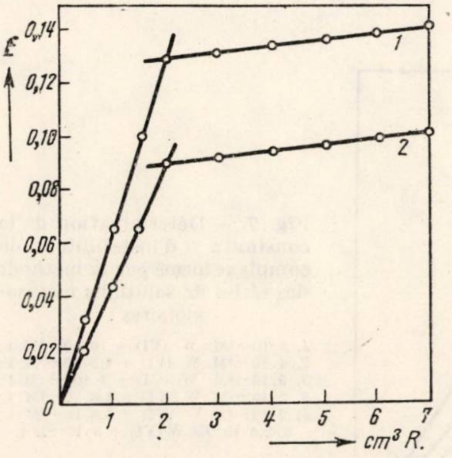

Fig. 5. — Détermination de la composition du complexe par la méthode du rapport molaire :

1, solutions 1.10^{-3}M ; 2, solutions 5.10^{-4}M.

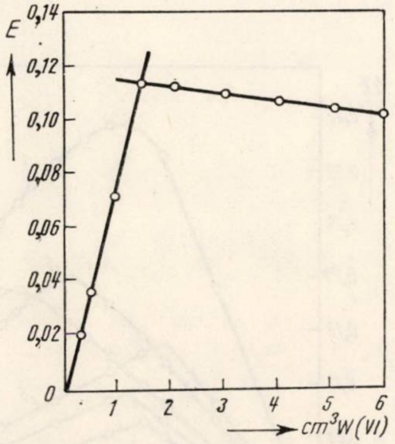

Fig. 6. — Détermination de la composition du complexe par la méthode du rapport molaire : solutions $6,66.10^{-4}$M.

Dans la figure 5, on présente les résultats obtenus pour le cas où l'on a maintenu constante la quantité de W(VI) (4.10^{-5} M pour la courbe 1 et 2.10^{-5} M pour la courbe 2), en variant la quantité de réactif entre les limites de concentration 2.10^{-5} M – $2,8.10^{-4}$ M, (courbe 1) et 1.10^{-5} M – $1,4.10^{-4}$ M (courbe 2), et dans la figure 6 on a tracé les courbes pour la situation inverse quand on a maintenu constante la quantité de réactif ($7,99.10^{-5}$ M) et on a varié la quantité de W(VI) entre les limites de concentration $6,66.10^{-6}$ M – $1,6.10^{-4}$ M.

Les deux méthodes utilisées ont conduit au même résultat, c'est-à-dire dans la réaction entre l'ion W(VI) et le solochrome violet RS se produit une combinaison complexe où le rapport stœchiométrique de combinaison des substances réagissantes est W(VI)/solochrome égal à 1/2.

Calcul de la constante d'instabilité du complexe formé. La stabilité de la combinaison complexe formée dans le système étudié est caractérisée par la constante d'instabilité, qui peut être calculée en utilisant la méthode des séries non isomolaires de Job. En ce sens, on a représenté dans la figure 7 les résultats des déterminations observées en suivant la variation de l'extinction en fonction de la fraction molaire *x* du réactif pour six séries de solutions non isomolaires.

Des courbes présentées on a déduit les fractions molaires du réactif dont l'extinction est maximale, à l'aide desquelles on a calculé les constantes d'instabilité en utilisant la relation de Job, pour le rapport de combinaison W(VI)/solochrome = 1/2 :

$$K = \frac{C^2 p[(p+2)x-2]^3}{(p-1)^2(2-3x)}$$

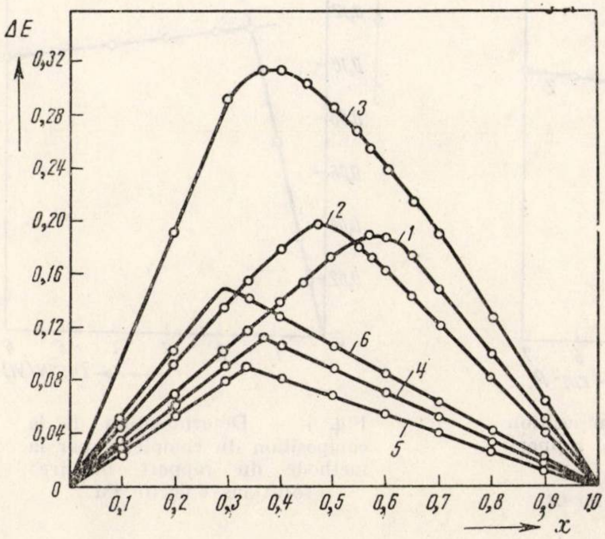

Fig. 7. — Détermination de la constante d'instabilité du complexe formé par la méthode des séries de solutions non isomolaires :

1, 5.10^{-4}M W (VI) + 10.10^{-4}M I;
2, 4.10^{-4}M W (VI) + $1,5.10^{-3}$M I;
3, 5.10^{-4}M W (VI) + 3.10^{-3} M I;
4, $2 \cdot 10^{-4}$M W (VI) + $1,3.10^{-3}$M I;
5, 2.10^{-4}M W (VI) + $1,5.10^{-3}$M I;
6, $2,5 \cdot 10^{-4}$M W (VI) + $3 \cdot 10^{-3}$M I.

où,

C = la concentration molaire du ion W(VI);
p = le rapport des concentrations molaires du réactif et de l'ion W(VI);
x = la fraction molaire du réactif dont l'extinction est maximale;
K = la constante d'instabilité.

Les valeurs des constantes d'instabilité pour les séries de solutions non isomolaires étudiées sont présentées dans le tableau 2 sous forme de $\overline{\text{pK}}$.

Tableau 2

Valeurs des constantes d'instabilité du complexe W (VI) — I

Nombre de la série non isomolaire	C	p	x	pK	$\overline{\text{pK}}$
I	5.10^{-4}	2	0,57	7,82	
II	4.10^{-4}	3,75	0,47	7,74	
III	5.10^{-4}	6	0,37	7,63	7,91 ± 0,033
IV	2.10^{-4}	6,5	0,365	8,29	
V	2.10^{-4}	7,5	0,34	8,27	
VI	$2,5.10^{-4}$	12	0,29	7,72	

L'intervalle de sûreté est donné par l'erreur moyenne carrée de la moyenne dans la distribution Student pour une probabilité de 95%, de six déterminations.

Le calcul de la propagation des erreurs montre que la dispersion des données du tableau est déterminée par des erreurs accidentelles, fait qui a conduit à la possibilité de calculer la valeur moyenne de la constante d'instabilité, exprimée par $\overline{pK}$. La valeur moyenne de la constante d'instabilité $\overline{pK}$ a été déterminée à la température de 25° et à la force ionique $\mu = 2$.

Le complexe formé dans la réaction étudiée présente une valeur moyenne de la constante d'instabilité qui indique une stabilité relativement bonne.

CONCLUSIONS

L'étude spectrophotométrique effectuée sur le système W(VI)-solochrome violet RS a conduit aux conclusions suivantes :

— Le wolfram (VI) produit avec le solochrome un composé de couleur rouge foncé, qu'on peut déterminer spectrophotométriquement dans des conditions de travail faciles à réaliser ;

— La sensibilité de la méthode exprimée par le coefficient molaire d'extinction la situe parmi les méthodes relativement bonnes de dosage du wolfram ;

— La valeur de la constante d'instabilité du composé formé est assez petite, ce qui indique sa grande stabilité.

Revue Roumaine de Chimie, 20, 2, 275–282 (1975)

SPECTROPHOTOMETRIC STUDIES OF SOME DERIVATIVES OF PHENINDIONE

I. M. ISSA, A. M. ISLAM, R. M. ISSA * and A. K. ABDELKADER

Chemistry Department, Faculty of Science, Assuit University, A. R. Egypt

Received November 7, 1973

The absorption spectra of 2-phenylindan-1 :3 dione derivatives are investigated in various media which revealed that the absorption bands are readily influenced by solvent polarity and substitution. From the uv-spectra in buffer solutions, the values of pK_a are determined and commented upon in the light of molecular structure and medium used.

INTRODUCTION

The study of indandione –1,3 derivatives has attracted a growing interest as it entails some theoretical problems of tautomerisation and reactivity. Also because it is related to the discovery of new medicinal preparations.[1–3] Thus different methods of synthesis of phenindione derivatives have been reported,[4–6] and various spectrophotometric studies dealing with structure problems were carried out.[7–10]

The present investigation includes the study of the solvent and substitution effects on the absorption spectra of some derivatives of 2-phenylindan-1 :3 dione in the uv, visible and ir-range. The spectral behaviour of some compounds in universal buffer solutions is utilised for the determination of pK_a. The molecular structure of these compounds is clarified according to the results obtained by spectrophotometric measurements.

---

* Present address : Chem. Dept. — Faculty of Science — TANTA Univ. A. R. Egypt.

[1] G. Vanages, "Cyclic β-Diketones", Latvean Acad. Sci. Publishing House, Riga, 1961.

[2] G. Vanages, *Doklady Akad. Nauk. S.S.S.R.*, **109**, 535 (1956) ; *Chem. Abstr.*, **51**, 5022 (1957).

[3] S. Eskola, *Nord-Kemistmatet. Helsingsfors*, **7**, 193 (1950).

[4] W. Borsche, K. Diacent and H. Hanov, *Ber. deutsch. chem. Ges.* **67** (B), 675 (1934).

[5] H. Zimmer and R. D. Barry, *J. Org. Chem.*, **27**, 3710 (1962).

[6] A. M. Islam and M. El-Shafie, (forthconing ; *Egypt. J. Chem.*).

[7] J. Linabergs, A. Veis and G. Vanages, *Doklady Akad. Nauk. S.S.S.R.* **154**, 1385 (1964).

[8] N. A. Broiserich and N. N. Khovratovich, *Zhur. priklad. Spektrosk.* **7**, 538 (1967).

[9] I. Smirnov, E. A. Podoral and A. E. Skaya, *Zhur. obshchei Khim.* **39**, 1373 ; 1378 (1969).

[10] D. Zacharova and P. A. Zelensky, *Coll. Czech. Chem. Comm.*, **35**, 225 (1970).

EXPERIMENTAL

1 — Preparation of 2-phenylindan-1 : 3 dione derivatives :

These derivatives were obtained by rearrangement of the respective benzalphthalides with sodium methoxide in ethanol after prolonged reaction.[6,11] The compounds prepared have the general formula :

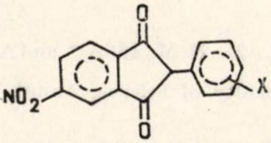

X=H (I); 4−OCH_3 (II); 2−OH (III); 2−NO_2 (IV); 3 NO_2 (V); 2−OCH_3, 4−OH (VI).

2 — Preparation of solutions :

(i) 10^{-3} M stock solutions were obtained by dissolving the accurately weighed quantity of the solid compound in the appropriate volume of the required solvent. Due to the low solubility of some phenindiones in some of the solvent used, a saturated solution was first prepared, from which the appropriate concentrations were obtained by dilution.

(ii) The solvents used were of laboratory grade and purified by recommended methods.[12]

(iii) The buffer solutions used were components of the modified universal series of Britton and, Robinson.[13]

3 — Apparatus :

The uv- and visible spectra were recorded within the wavelength range 200−500 nm, using 1 cm matched silica cells, on a Unicam SP. 8000 uv. recording spectrophotometer and BMQ_2−Zeiß type.

The ir-spectra of the compounds were obtained by a Beckman IR 4 infrared spectrophotometer.

The pH's of the buffer were checked using a Radiometer pH-meter model 28.

RESULTS AND DISCUSSION

(A) Spectra in organic solvents :

The spectra of the compound under investigation were recorded in various media which revealed that the absorption bands are readily influenced by solvent polarity and substitution (table 1, fig. 1).

The absorption bands observed are mainly three sets. The first set lies in the 214 −230 nm range which is assigned to $\pi-\pi^*$ transition of the aromatic system ($^1L_a - {}^1A$). The second located within 250 −270 nm which is ascribed to a $\pi-\pi^*$ transition of the aromatic system ($^1L_b - {}^1A$). Also some compounds show a band near 275 −290 due to the $\pi-\pi^*$ transition of the $C = 0$ conjugated with unsaturation center. This band is usually covered by the band of the aromatic system. The third band found within 330 −425 nm which is mainly ascribed to $\pi-\pi^*$ transition

---

[11] A. E. Poraikoshita and I. I. Ohizhevskaya, *Zhur. obshchei. Khim.* **26**, 842 (1956); *Chem. Abstr.*, **50**, 14720 (1956).

[12] A. I. Vogel, "Practical Organic Chemistry", 3rd Edit., Longmans, London, 1961, p. 163.

[13] H. T. S. Britton, "Hydrogen Ions", Vol. I, 2nd Edit., Chapman and Hall, New York, 1952, p. 313.

Table 1

Results obtained in organic solvents

λ_{max} (nm) ε_{max} ($cm^2\ mol^{-1} \times 10^{-3}$)

N°	Solvent	λ_{max}	ε_{max}	λ_{max}	ε_{max}	λ_{max}	ε_{max}	C.T.	
								λ_{max}	ε_{max}
I	D.M.F.			280	6.20			400	0.85
	Methanol	230	2.60	295	3.25			370	1.40
	Ethylene glycol	240	3.60	260	3.00			380	0.75
	Ether	225	—	270	—			350	—
	Acetone			275	0.53			340	0.98
	Dioxane	230	6.15	275	2.90			375	0.55
	CCl_4			270	—			350	—
II	D.M.F.			280	1.80			420	2.80
	Methanol	230	2.93	265	2.50			425	0.30
	Ethylene glycol	225	4.05	263	3.25			420	0.50
	Ether	230	—	270	—			420	—
	Acetone			275	1.00	345	1.15	420	0.70
	Dioxane	235	6.70	265	5.30			420	0.50
	CCl_4							410	—
III	D.M.F.			290	1.80			340	5.00
	Methanol	220	7.80	280	2.10			335	1.30
	Ethylene glycol	230	3.13	255	1.55			330	0.85
	Ether	215	—	250	—			335	—
	Acetone			275	1.05			340	1.70
	Dioxane	220	1.25	265	1.65			325	1.00
	CCl_4							320	—
IV	D.M.F.			280	5.40			330	4.00
	Methanol	230	1.80	260	1.25			325	0.70
	Ethylene glycol	225	2.75	250	2.03			315	0.82
	Ether	220	—	255	—			320	—
	Acetone			260	3.00			320	1.35
V	Methanol	230	4.50	265	2.85	280	2.90	370	1.20
	Ethylene glycol	225	2.25	265	1.90			360	0.65
	Ether	220	—	270	—			340	—
	Acetone			275	0.50			330	0.89
	CCl_4			295	—			330	—
VI	D.M.F.					290	8.00	425	10.00
	Ethanol	230	3.20	260	3.40	295	2.00	413	0.75
	Ethylene glycol	227	3.72	265	1.40	299	0.70	411	0.10
	Ether	220	—	255	—			410	—
	Acetone					280*	2.55	410	5.85
	Dioxane	225	4.40			290	3.30	410	5.60
	CCl_4							400	—

— saturated solution used. * broadened.

with charge transfer character. The C.T. takes place from the phenyl ring as donor while substituents with unsaturated structure essentially the NO_2 group act as acceptor.

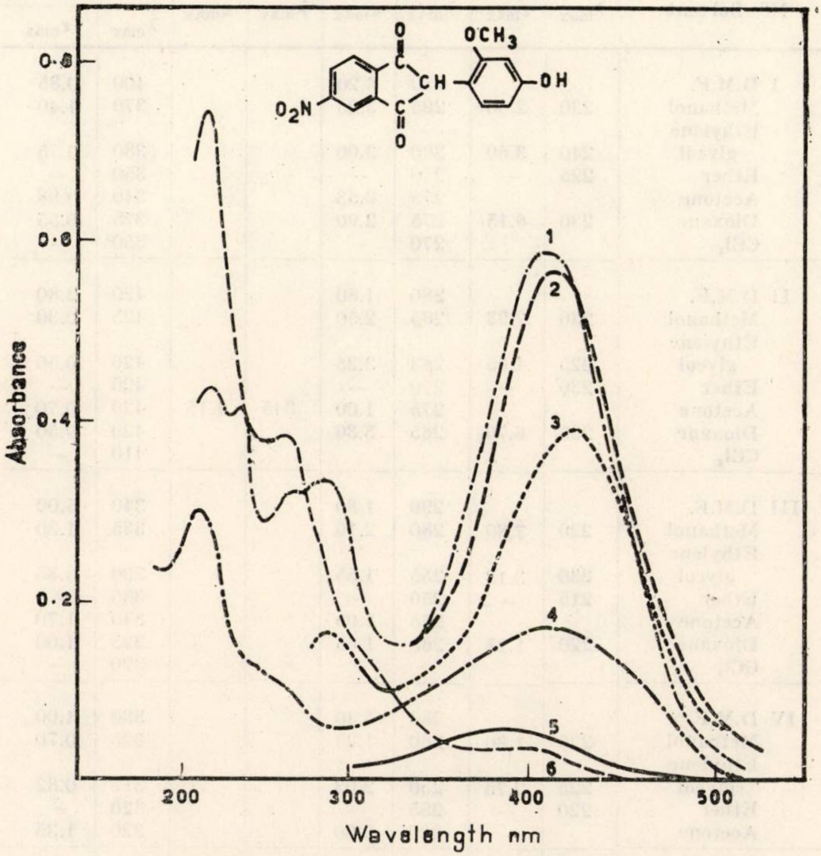

Fig. 1. — Absorption spectra of VI in organic solvents :

1, Dioxane (1×10^{-4} M) ; *4*, Ether (sat. solution) ;
2, Acetone (1×10^{-4} M) ; *5*, CCl_4 (sat. solution) ;
3, DMF (2×10^{-5} M) ; *6*, Ethylene glycol (2×10^{-4} M).

The bands due to local excitation of the aromatic system are slightly influenced by substitution or solvent polarity. The $C = 0$ band is mostly red shifted with increasing solvent polarity. This shift can be ascribed to the resultant of the polarising effect of solvent molecules which causes a polarisation red shift, and an increase of the solvation energy on excitation.

The interaction between the solute and the solvent through the formation of an intermolecular hydrogen bond, though weak, exhibits a weaker effect compared to cases where no H-bond can be formed.

Considering the molecular structure of the compounds it becomes apparent that the molecule is strongly planar. Thus it seems that the actual state of the molecule in diones would be the enolic form. The energy of this form will be lower than that of the keto form due to the higher conjugation in the enol form II.

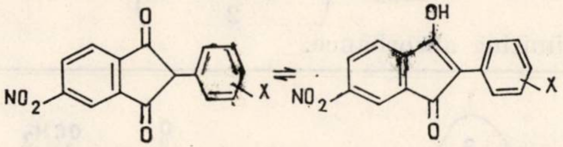

The existence of the enol form is supported by the results of the analysis of the ir-spectra given below. Also it clarifies the effect of substitution on the position of charge transfer band. The band shifts to red on introducing an electron donor substituent. However, with the o-OH group the band is blue shifted relative to the non-substituted compound. This behaviour can be explained by the steric effect of the o-substituent which causes a certain rotation of the ring from the plane defined by the rest of the molecules. The rotation increases with the size of the substituent. Thus with the o-nitro derivative the blue shift is very apparent. This large shift is due both to the steric effect of the bulky substituent and the character of its strong acceptor which largely hinders charge migration from the benzal ring to the acceptor center on the NO_2 group of the nitro phthalide part.

(B) – Spectra in universal buffer solutions :

The absorption spectra of III and VII in universal buffer solutions containing 50% by volume dioxan and 40% DMF were studied at pH's ranging from 4.5 to 11.5. The spectrum in 50% dioxan-buffer solution comprises three bands as shown in fig. (2) ranging from 215 to 420 nm. At $\lambda_{max} = 215$ and 225 in case of III and VII, respectively absorbance shows an irregular behaviour with increasing pH.

An isosbestic point is obtained at $\lambda = 215$ nm in III which represents an equilibrium between the ionic and nonionic forms whereas three ill-defined isosbestic points are obtained in case of VII at 305, 380 and 445 nm.

The absorption spectra in 40% DMF-buffer mixture comprise a single band located at 340 nm in case of III. Absorbance at λ_{max} increases with increasing pH of the solution up to pH 7.8 and then decreases till it disappears completely at pH 10.2. In case of VII, the spectrum includes the main band with $\lambda_{max} = 415$; absorbance decreases with increasing pH of the solution till it disappears above 10.3. An isosbestic point is obtained at 330 nm.

The A-pH plot at specified wavelength near the maxima, represented in fig. 3, yields more or less S-shaped curves with a single step indicating that one equilibrium dominates these compounds within the pH range investigated. The spectral data obtained from the A–pH curve can be utilised in the determination of the dissociation constant by the two methods described below :

1 – The half-height method[14]

---

[14] R. M. Issa, *Egypt J. Cehm.*, **14**, 113 (1971).

In this method pK_a is equal to the pH at half-height of the A-pH plot, $A_{1/2}$ can be determined from the relation:

$$A_{1/2} = \left(\frac{A_{\max} + A_{\min}}{2} \right)$$

where $A_{\max}$ = limiting absorbance.

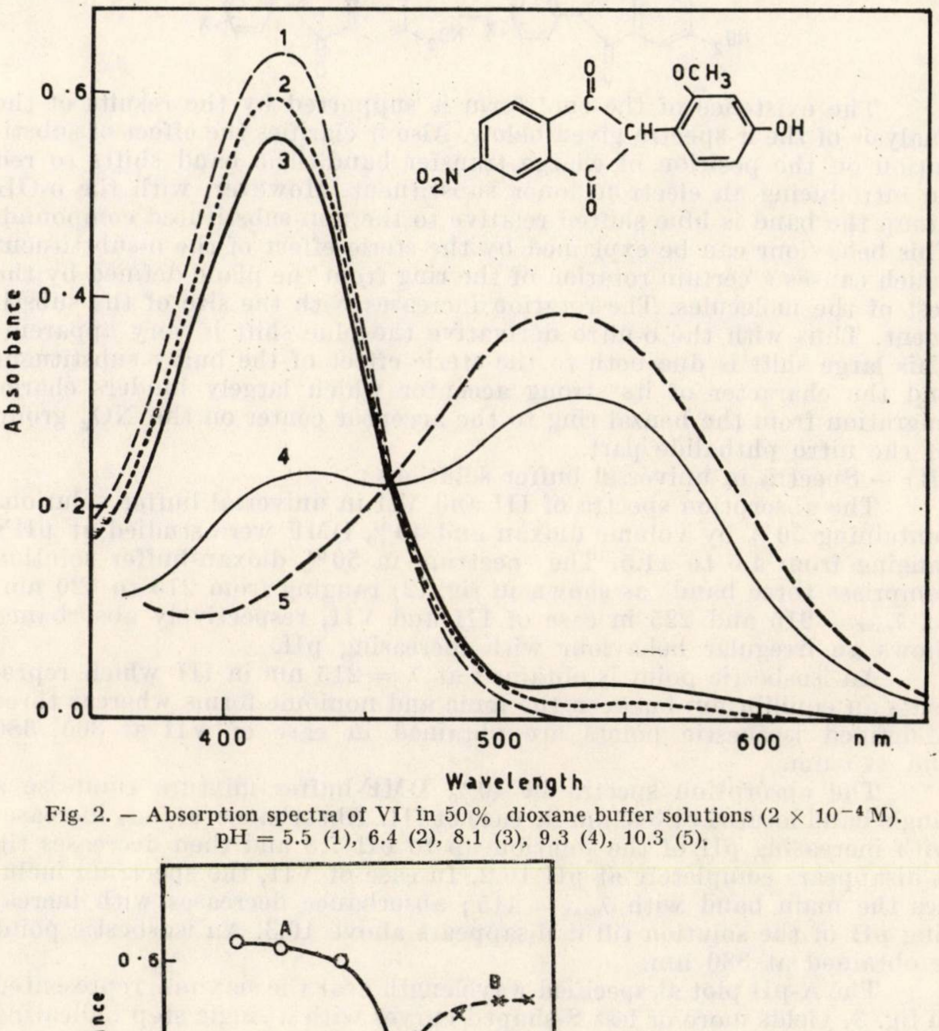

Fig. 2. — Absorption spectra of VI in 50% dioxane buffer solutions (2×10^{-4} M). pH = 5.5 (1), 6.4 (2), 8.1 (3), 9.3 (4), 10.3 (5).

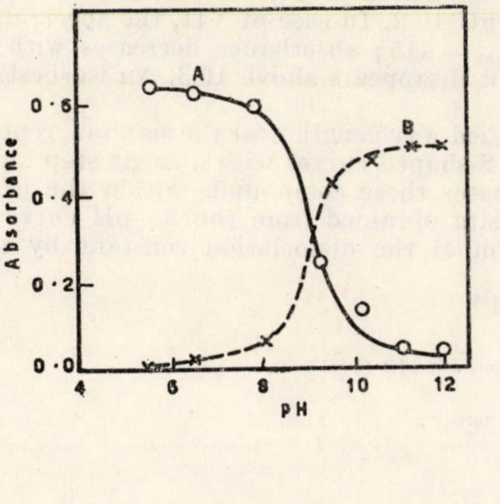

Fig. 3. — Absorbance-pH curves for VI in 50% dioxane buffer solutions λ = 420 nm (A), λ = 520 nm (B).

A_{min} = minimum absorbance value on the A-pH curve.

2 – The limiting absorbance method[14]:

This method is based on the trend observed in the relation between absorbance and pH. The equation applied has the form:

$$\text{pH} = pK_a + \log\left(\frac{A - A_{\text{min}}}{A - A}\right) + \log \gamma_{\text{BH}^-}$$

The plot of $\log\left(\frac{A + A_{\text{min}}}{A - A}\right)$ vs pH gave a straight line, from which the value of pK_a was evaluated.

The results obtained by the two methods in different media are depicted in table (2). The pK_a values of VII are higher than those of III due to the presence of the donor OCH_3 group in VII. Also pK_a values in dioxane media are higher than in dimethyl-formamide due to higher polarity and basicity of the latter solvent compared to the former.

Table 2

pK_a values of hydroxyl derivatives in different media

Method	50% dioxane		40% dimethyl-formamide	
	III	VII	III	VII
1	8.1	8.6	7.5	7.8
2	7.8	8.64	7.8	8.0
Mean	7.95	8.62	7.65	7.9
ΣG° K.cal/mole^{-1}	11.00	11.91	10.57	10.95

(C)–ir–Spectra:

The ir-spectra of phenindiones were the subject of several studies which considered the main bands.[6,8] However, it seemed of interest to reinvestigate these spectra in order to through more light in the actual structure of the molecule and the ground state.

The ir-spectrum of 2-phenyl-5-nitro-indan 1,3-dione shows a broad band at 3480 cm^{-1} which can be assigned to ν_{OH} resulting from the inolisation of one C = O group. For the 2-vanilyl derivative (VII), the OH-groups yields an assymetric band with maximum at 3460 cm^{-1} and a shoulder at 3500 cm^{-1}, denoting the possible existence of two different OH-groups. The C = O band is found at 1700 cm^{-1}, being much lower compared to those of the corresponding benzal-derivative,[15] due to the possible tautomeric shift in the dione compound.

For the C = C linkage two broad bands are observed near 1620 and 1580 cm^{-1}. The broadening of the bands and their relatively lower values compared to benzalphthalides,[15] supports the idea that the bands are involved in the tautomeric shift.

The main feature of the ir-spectra is the shift of the NO_2 bands on changing the substituents on the phenyl ring. The asymmetric band within the 1520 cm^{-1} does not show a regular behaviour, however, the symmetric band at 1345 cm^{-1} is shifted to red with donor substituents and to blue with acceptor ones. This behaviour reveals strong conjugation through the whole molecule which is influenced by intramolecular charge transfer. This would be only the case for the enolic structure. The charge transfer interaction can be formulated as follows :

---

[15] R. M. Issa, I. M. Issa, A. K. Abdelkader and M. H. Abdelkader, (under print).

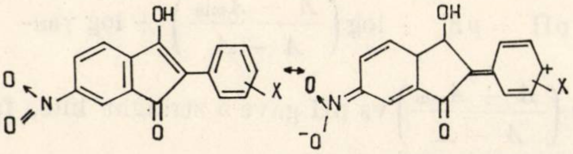

Thus donor substituents would decrease the N = O band order while acceptor ones increase the bond order though the decreased participation of the polar structure to the ground state.

The band near 1180 – 1190 cm^{-1} can be assignment to the C – N bond stretching. This band shifts to red with acceptor substituents and is but slightly blue shifted with donor ones which is in accordance with the direction of the intramolecular charge transfer effect.

Revue Roumaine de Chimie, **20**, *2*, 283–295 (1975)

CARBONIUM ION REACTIONS. XI*

BENZOBICYCLONONENE DERIVATIVES THROUGH DOUBLE BOND PARTICIPATION

ILEANA DRĂGUȚAN, C. DRĂGHICI and ECATERINA CIORĂNESCU
Organic Chemistry Centre, Bucharest, Spl. Independenței, 202 B, Romania

Received December 3, 1974

Product analysis and kinetic measurements show that acetolysis of 7-(β-tosyloxyethyl)-1,2-benzo-1,3-cycloheptadiene **(5-OTs)** proceeds with double bond participation to a greater extent than that of its lower homolog, **1-OTs**. The reaction affords 45% bicyclic compounds: 2,3-benzobicyclo[3.2.2]nonen-4-yl acetate **(10-OAc)**, a direct π-route product, and the epimeric 2,3-benzobicyclo[3.3.1]nonen-4-yl acetates **(9-OAc)**, resulting from subsequent rearrangements. The intervention of an SN2 mechanism leads to the unrearranged acetate **5-OAc**.

In a previous paper[1] we reported that the acetolysis of 7-(tosyloxymethyl)-1,2-benzo-1,3-cycloheptadiene **(1-OTs)** proceeds with both benzene ring and double bond assistance. Besides the main product **2**, with enlarged ring, significant proportions (25%) of π-route products are formed (**3** and **4** in buffered and unbuffered solution, respectively).

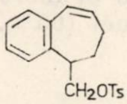

1-OTs

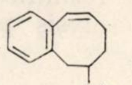

2

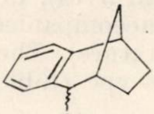

3

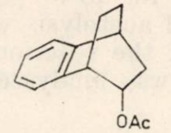

4

This result suggested the study of the solvolytic behaviour of the homologous tosylate **5-OTs**. Models show that in the most favourable

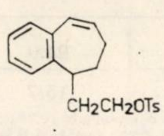

5-OTs

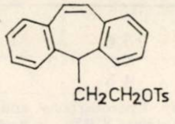

6-OTs

conformation for participation the distance between the ionizing centre and the double bond (1.7 Å) is shorter than that in tosylate **1-OTs** (2.7 Å).

---

* Part X. M. Banciu, E. Dragu, D. Georgescu and E. Ciorănescu, *Rev. Roumaine Chim.*, **19**, 1343 (1974).

[1] I. Drăguțan, C. Drăghici, A. Haneș, A. Dumitriu, E. Ciorănescu and C. D. Nenitzescu, *Rev. Roumaine Chim.*, **19**, 67 (1974).

In the solvolysis of tosylate **5-OTs** a greater double bond participation was therefore to be expected. This hypothesis was also supported by the fact that the acetolysis of the dibenzo-analog, **6-OTs,** gave rise almost exclusively to double bond participation products.[2]

We now report the results obtained from the buffered acetolysis of 7-(β-tosyloxyethyl)-1,2-benzo-1,3-cycloheptadiene **(5-OTs)**.*

RESULTS

The tosylate **5-OTs** was synthesized by lengthening the side chain of **1-OTs** using conventional methods.** Condensation of **1-OTs** with sodium cyanide in DMSO afforded a nitrile which was hydrolized to the corresponding acid (**7**). The reduction with $LiAlH_4$ of the ester of **7** yielded the alcohol **5-OH,** from which the tosylate **5-OTs** was obtained in the usual manner. The ir and nmr spectra of compounds **7, 5-OH** and **5-OTs** are in perfect agreement with the expected structures.

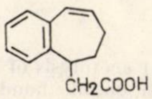

7

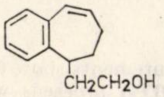

5-OH

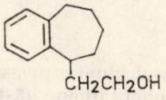

8-OH

Following a similar reaction sequence, the saturated alcohol **8-OH**[3] and its unknown tosylate, **8-OTs,** were prepared. Tosylate **8-OTs** was used as a reference compound in the kinetic measurements.

The solvolysis of tosylate **5-OTs** was carried out in acetic acid, at 110°, for 48 hr (12 half-lives), in presence of sodium acetate (the unbuffered acetolysis was accompanied by resinification of more than one third of the reaction mixture). The acetolysis product (95%, *calcd.* on **5-OTs)** was analysed by vpc (table 1).

Table 1

Acetolysis products of tosylate 5-OTs

5-OTs mol/l	AcONa mol/l	% Products				
		A *exo*-**9-OAc**	B *endo*-**9-OAc**	C **10-OAc**	**5-OAc**	Unidentified compounds
0.15	0.26	15.6	5.6	24.0	45.8	9[a]
0.15[b]	0.76	4.5	0.8	15.7	66.1	8.8[c]

[a] 15 components (8.3%), probably hydrocarbons and two components (0.7%), probably acetates. [b] The starting material contained 6% saturated tosylate **8-OTs**; in acetolysis, 4.3% acetate **8-OAc** was formed. [c] 3 components (4.8%), probably hydrocarbons and two components (4%), probably acetates.

---

* 5-(β-tosyloxyethyl)-6,7-dihydro-5*H*-benzocycloheptene, according to Chem. Abstr. nomenclature.

** Attempts to introduce directly a two-carbon side chain (by Reformatsky reaction or reaction of a Grignard compound with ethylene oxide), starting from 1,2-benzo-1,3-cycloheptadien-7-one, failed to produce the expected result.

[2] E. Ciorănescu, M. Banciu, R. Jelescu, M. Rentzea, M. Elian and C. D. Nenitzescu, *Tetrahedron Letters*, **1969**, 1871 ; *ibid.*, *Rev. Roumaine Chim.*, **14**, 911 (1969).

[3] R. C. Gilmore and W. J. Horton, *J. Amer. Chem. Soc.*, **73**, 1411 (1951).

The main reaction product (46%) was, surprisingly, the acetate **5-OAc,** corresponding to the starting material. (In a run (table 1, entry 2) in which a threefold concentration of AcONa was used, the proportion of this acetate raised to 66%.) Two more acetates, A (15.6%) and C (24%), were found in significant amounts; to a lesser extent, acetate B (5.6%) was formed. Analysis also indicated many other small components (included in the figures given in the last column) which could not be identified or separated.

The acetates **5-OAc,** A and C were separated by preparative vpc.

Acetate **5-OAc** was identified by comparison of its retention time with that of an authentic sample, prepared from alcohol **5-OH.** In addition, the ir and nmr spectra of the acetate **5-OAc** (separated from the reaction mixture) perfectly match those of the authentic sample.

STRUCTURE OF THE ACETATES 9-OAc (A, B) AND 10-OAc (C)

By comparison with **6-OTs** the acetates A–C were expected to be bicyclic, originating from double bond participation. The tosylate **5-OTs** could give rise by π-route to two benzobicyclononene systems, **10-X** and **11-X,** the former being mechanistically favoured.

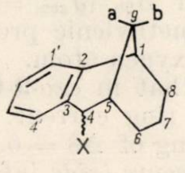

9-X

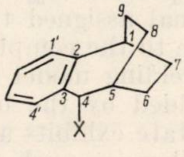

10-X

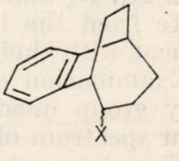

11-X

A first proof of the presence of the acetate **10-OAc** in the acetolysis mixture was found when its retention time in vpc proved to be identical with that of an authentic sample, prepared according to Chart 1. The ir and nmr spectra of the acetate **10-OAc** separated by preparative vpc and independently synthesized were in perfect agreement.

It should be mentioned that assignment of the structure **10** to the acetate C, based on its nmr spectrum alone, could not be regarded as reliable. Indeed, this spectrum indicates a bicyclic structure, with the acetoxy group located in a benzylic position: the proton H_4, adjacent to OAc, is coupled only to the bridgehead H_5 by $J_{45} = 5$ Hz; in the **10-OAc** – Eu(DPM)$_3$ spectra only $H_{4'}$, H_4 and H_5 are considerably shifted. Even in the presence of the shift reagent, the eight methylenic protons give rise but to a broad signal, so that the number of carbon atoms in the two saturated bridges of the acetate C could not be specified. The synthesis of an authentic sample of **10-OAc** was therefore necessary.

The benzylic position of the functional group in the product C (**10-OAc**) was further confirmed by the ir spectrum of the corresponding ketone, **12** ($\nu_{C=O} = 1680$ cm^{-1}). This ketone easily forms by autoxidation of the alcohol **10-OH**, merely on standing. Such autoxidation of benzylic alcohols has been previously reported.[4]

Properties and spectra of ketone **12** and alcohol **10-OH** resulting from acetolysis and independent synthesis are also identical.

The major participation product (24%) is thus the 2,3-benzobicyclo[3.2.2]nonen-4-yl acetate (**10-OAc**).*

The structure **11**, possibly arising also from participation, could be excluded for the products A (15.6%) and B (5.6%), by comparing their retention times with that of the authentic acetates **11-OAc**, prepared from the ketone **14** (Chart 3).

The nmr spectrum (fig. 1) of the acetate A, as in the case of **10-OAc**, suggests a bicyclic benzylic structure. This compound cannot therefore be a direct π-route product, but must originate from some subsequent rearrangement. Considering the reported stability of the benzobicyclo[3.3.1]nonene system,[5,6] we assumed this structure to be more probable.

In order to prove this, the epimeric 2,3-benzobicyclo[3.3.1] nonen-4-yl acetates (**9-OAc**) were synthesized, starting from the known ketone **13**[5] (Chart 2). Products A and B showed the same retention times as the authentic *exo*- and *endo*-**9-OAc**, respectively.

The nmr spectra of the complex acetate A — $Eu(DPM)_3$ (fig.1) supplied further support of its structure and configuration. Thus, with increasing amounts of $Eu(DPM)_3$, besides the expected rapid shift of the protons H_4, H_5 and $H_{4'}$, the protons H_{9a} and then H_{9b} ($J_{gem} = 13$ Hz) separate from the broad signal assigned to the methylenic protons, in agreement with their distance to the complexing oxygen atom.

Examination of the Dreiding model shows that in *exo*-**9-OAc** the acetoxy group must be shielded by the benzene ring current. Indeed, the nmr spectrum of this acetate exhibits a shielding of $\Delta\delta = 0.21$ ppm, as compared to *endo*-**9-OAc** where no such effect occurs (*vide infra*). This also confirms the established configurations of the products A and B.

SYNTHESIS OF AUTHENTIC SAMPLES

The acetate **10-OAc** was synthesized starting from the ketone **12**, obtained ** in turn by polyphosphoric acid cyclization of 4-phenylcyclohexanecarboxylic acid.[7] Sodium borohydride reduction of ketone **12**

Chart 1

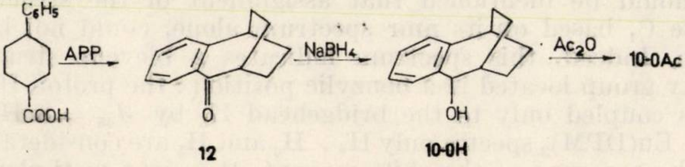

---

* Its Chem. Abstr. name would be 5,8-ethano-5*H*-benzocyclohepten-6,7,8,9-tetrahydro-9-yl acetate.

** Experimental details will be reported in a future communication.

[4] A. Le Berre, *Bull. Soc. chim. France*, **1961**, 1198.

[5] J. W. Cook and C. L. Hewett, *J. Chem. Soc.*, **1936**, 62.

[6] R. Huisgen, W. Rapp, I. Ugi, H. Walz and E. Mergenthaler, *Liebigs Ann. Chem.*, **586**, 1 (1954); W. A. Brown, G. Eglington, J. Martin, W. Parker and G. A. Sim, *Proc. Chem. Soc.*, **1964**, 57.

[7] C. D. Nenitzescu and I. G. Gavăt, *Ann.* **519**, 260 (1935); H. E. Zimmerman and H. J. Giallombardo, *J. Amer. Chem. Soc.*, **78**, 6259 (1956).

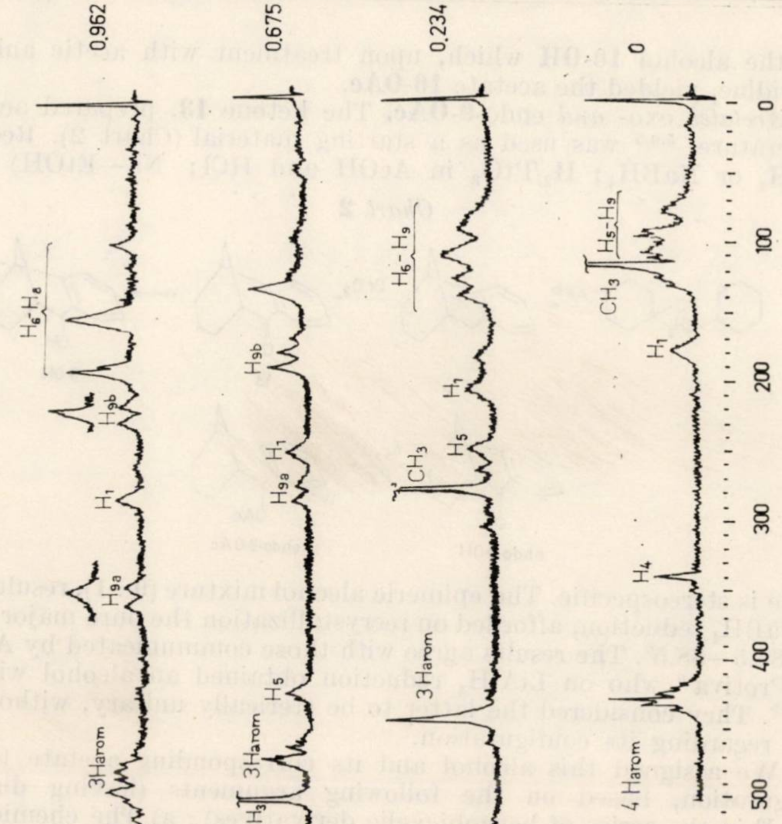

Fig. 1. — Nmr spectra of the complex acetate A — $Eu(DPM)_3$. The figures (right) indicate the molar ratio $Eu(DPM)_3$/acetate.

gave the alcohol **10-OH** which, upon treatment with acetic anhydride in pyridine, yielded the acetate **10-OAc**.

Acetates exo- *and* endo-**9-OAc.** The ketone **13**, prepared according to literature, [5,8,9] was used as a starting material (Chart 2). Reduction ($LiAlH_4$ or $NaBH_4$; H_2/PtO_2 in AcOH and HCl; Na–EtOH) of this ketone is stereospecific. The epimeric alcohol mixture (9 : 1), resulted from the $NaBH_4$ reduction, afforded on recrystallization the pure major epimer, m.p. 86.5–88.5°. The results agree with those communicated by Adlerova and Protiva [9] who on $LiAlH_4$ reduction obtained an alcohol with m.p. 86–7°. They considered the latter to be sterically unitary, without comment regarding its configuration.

Chart 2

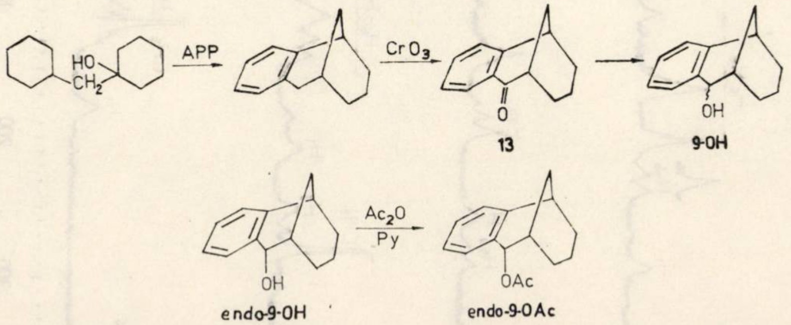

We assigned this alcohol and its corresponding acetate the *endo* configuration, based on the following arguments (having diagnostic value [10] in the series of benzobicyclic derivatives) : a) The chemical shift (4.83 ppm) of the doublet due to the proton H_4 and its large coupling to the bridgehead H_5 ($J_{45} = 6.5$ Hz), in agreement with the dihedral angle observed on the Dreiding model; b) The deshielding of the $H_{4'}$, aromatic proton by the adjacent *endo*-OH; c) The chemical shift (2.16 ppm) of the singlet assigned to the acetoxy group (*vide supra*).

The configuration of this alcohol is also supported by its mode of formation, the attack of the hydride presumably proceeding from the less hindered *exo* side.*

Reduction of the ketone **13** gave *exo*-**9-OH** only in low yield. The acetate *exo*-**9-OAc** could be obtained by epimerization of *endo*-**9-OAc,** on refluxing in buffered acetic solution. The ratio *exo*/*endo* (2.7) of the two acetates in the resulted mixture is the same after 24 or 106 hr, suggesting an equilibrium.

The doublet at 5.68 ppm ($J_{45} \simeq 1$ Hz) in the nmr spectrum of the epimeric mixture is absent from that of *endo*-**9-OAc** and perfectly superimposes the signal assigned to the proton H_4 in the spectrum of *exo*-**9-OAc** arising from acetolysis.

---

* We registered similar results on reduction of the analogous 2,3-benzobicyclo[3.2.1]-octen-4-one [1].

[8] R. Huisgen and G. Seidl, *Tetrahedron* **20**, 231 (1964); E. Adlerova and M. Protiva, *Coll. Czech. Chem. Comm.*, **32**, 3177 (1967).

[9] E. Adlerova and M. Protiva, *Coll. Czech. Chem. Comm.*, **25**, 528 (1960).

[10] W. Herz and G. Caple, *J. Amer. Chem. Soc.*, **84**, 3517 (1962).

The acetates **11-OAc** were obtained as shown in Chart 3. Ketone **14**[11] was hydrogenated to the saturated ketone **15**[11]. On subsequent reduction, **15** led to a practically 1 : 1 mixture of diastereoisomers **11-OH**, which was converted into the acetate mixture, used in vpc analysis.

Chart 3

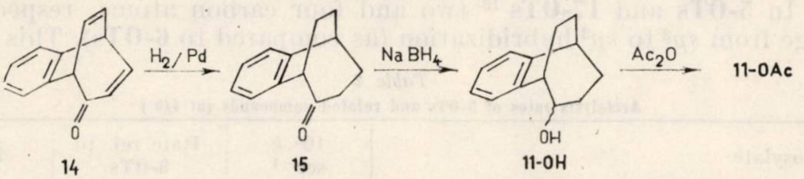

DISCUSSION

Acetolysis of tosylate **5-OTs** shows first-order kinetics (at least up to 50% reaction). The rate constant together with those of some related compounds are listed in table 2.

It must be noted that each pair of compounds indicated in table 2 have similar solvolytic reactivity. Rate comparision within these pairs demonstrates that benzene ring annelation plays but a minor part. Indeed, the rates of the saturated tosylates **8-OTs** and **16-OTs,** comparable with that of β-cycloheptylethyl tosylate, * show the expected absence of phenyl group assistance. Thus the ionization of the unsaturated analogs **5-OTs** and **6-OTs** can be considered to proceed only with double bond participation.

Models show that the unsaturated tosylates **17-OTs, 5-OTs, 6-OTs** and **18-OTs** have a conformation in which the primary carbon is located practically at the same distance (1.7—1.8 Å) from the middle of the double bond. Thus, in this series steric factors alone, namely the conformation of the seven-membered ring, can decisively influence the double-bond assistance.

In the cycloheptatriene compounds (**6-OTs, 18-OTs**) the seven-membered ring adopts a stable bath conformation, the side chain possibly being pseudo-axial or -equatorial. It is very likely that the pseudoaxial orientation is preferred.** In this conformer good conditions for the double bond participation are achieved : **6-OTs** [2] and **18-OTs** [15] solvolyze with ring closure in high yields (over 90%), at considerably greater rates than those of their saturated analogs (table 2).

---

* The solvolysis rate of cycloheptylethyl tosylate can be considered as equal to that of ethyl tosylate[14] (at 110°, $k = 2.1 \times 10^{-5}$ sec^{-1}) since rate constants for acetolysis of β-substituted ethyl arenesulphonates are markedly intensitive to steric variations in the substituent.[16]

[11] J. Ciabattoni, J. E. Crowley and A. S. Kende, *J. Amer. Chem. Soc.*, **89**, 2778 (1967).

[12] M. Voicu and F. Badea, *Rev. Roumaine Chim.*, **14**, 929 (1969).

[13] M. Voicu, Ph. D. Thesis, Organic Chemistry Center, Bucharest, 1971.

[14] S. Winstein and H. Marshall, *J. Amer. Chem. Soc.*, **74**, 1120 (1952).

[15] G. D. Sargent and T. E. McLaughlin, *Tetrahedron Letters*, **1970**, 4359.

[16] P. D. Bartlett and G. D. Sargent, *J. Amer. Chem. Soc.*, **87**, 1297 (1965); P. D. Bartlett, W. S. Trahanovsky, D. A. Bolon and G. H. Schmidt, *J. Amer. Chem. Soc.*, **87**, 1314 (1965).

In **5-OTs** and **17-OTs** [13] two and four carbon atoms, respectively, change from sp^2 to sp^3 hybridization (as compared to **6-OTs**). This results in an increase of the number of molecular conformations ; consequently, the population of the favourable conformer, hence double bond participation, diminish. In acetolysis of **5-OTs** only 45% of the products form by π-route and the k_u/k_s ratio is smaller than that of the dibenzo-analogs.

Table 2

Acetolysis rates of 5-OTs and related compounds (at 110°)

Tosylate	$10^5 . k$ sec^{-1}	Rate rel. to **8-OTs**	k_u/k_s
8-OTs 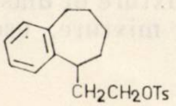	0.78	1	
16-OTs 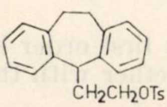	1.34^a	1.7	
17-OTs 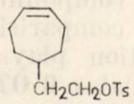	4.93^b	6.3	2.35^c
5-OTs 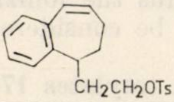	4.17^d	5.35	5.35
6-OTs 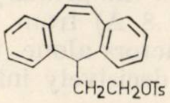	20.40^a	26.1	15.2
18-OTs 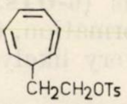	19.45^e	25.1	16.0

^{a} Ref. 12. ^{b} Ref. 13. ^{c} The rate constant of ethyl tosylate (Ref. 14) was used as k_s. ^{d} Extrapolated to zero reaction timee. ^{e} *Calcd.* from data for the nosylate (Ref.[15] with $k_{ONs}/k_{OTs} = 11.1$.

When comparing reactivities of the homologous tosylates **1-OTs** [1] and **5-OTs**, a rate ratio of 26 (at 100°) was observed ; the higher aceto-

---

** It has been demonstrated [17] that the predominant conformation of the 5-(β-hydroxyethyl)-5*H*-dibenzo[*a, d*]cycloheptene is that with a pseudo-axial 5-substituent.

[17] M. Elian, Ph. D. Thesis, Organic Chemistry Center, Bucharest, 1973.

lysis rate of **1-OTs** is due to assistance of both double bond and aromatic ring. In these two esters conformational and electronic factors have a similar influence on the nucleophilic function of the double bond π-electrons. The longer side chain in **5-OTs** brings about the observed increase of the π-route in its solvolysis.

About one half of the products arising from acetolysis of **5-OTs** are bridged compounds. Their structure as well as kinetic measurements ($k_u/k_s = 5.35$) indicate that π-route is one of the reaction paths.

The nonclassical ion **19**, generated by double bond participation, can be a first π-route intermediate. It is likely that it rapidly rearranges to ion **20**, stabilized by benzylic conjugation and, to a smaller extent, to the secondary ion **21**.

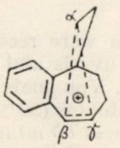

19

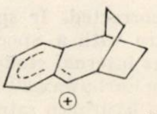

20

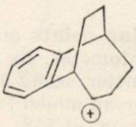

21

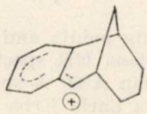

22

By solvent attack, the ion **20** leads to the major participation product, the acetate **10-OAc** (24%).

The acetates **11-OAc**, corresponding to the ion **21**, were not identified in the acetolysis mixture.

The formation of the other bicyclic products, the acetates *exo*- and *endo*-**9-OAc** (21%), implies the intervention of the benzylic ion **22**. The generation of this ion (which is not a direct π-route intermediate) could be interpreted by assuming several rearrangements. The driving force of these rearrangements is the formation of the stable benzobicyclo[3.3.1]nonene system.[5,6] In order to clarify this mechanism we undertook the study of the relations between the benzobicyclo[3.2.2]- and -[3.3.1]nonene systems, which will form the subject of a future paper.

The *exo*/*endo* ratio in which the acetates **9-OAc** are found (15.6/5.6) can be explained by the assumption of stereoelectronic factors favouring the formation of pseudo-axial over pseudo-equatorial bonds,[18] in agreement with the results obtained from reduction of the ketone **13**. The same conclusion was inferred from the epimerization *endo*-**9-OAc** → *exo*-**9-OAc**, proceeding very likely through the same intermediate, **22**; the stability of this cation accounts for the facile ionization of the acetate *endo*-**9-OAc** in buffered medium.

Acetolysis of the tosylate **5-OTs** is only partly assisted by the double bond. The major reaction product (45%) is the unrearranged acetate **5-OAc**, which could be formed either by an SN1 or an SN2 process. The increased proportion of **5-OAc** in the run where a threefold concentration of AcONa was used (table 1, entry 2) obviously shows the intervention of the bimolecular mechanism.

---

[18] S. J. Cristol, F. P. Parungo and D. E. Plorde, *J. Amer. Chem. Soc.*, **87**, 2870 (1965); S. J. Cristol, F. D. Parungo, D. E. Plorde and K. Schwarzenbach, *ibid.*, **87**, 2879 (1965).

On the other hand, if all the acetate **5-OAc** resulted from an SN2 reaction, the ratio bicyclic products/**5-OAc** ought to be 5 : 1 (in the plausible assumption that k_2 for **5-OTs** is equal to the solvolysis rate of **8-OTs** which can react only by SN2). The observed ratio (1 : 1) suggests that **5-OAc** is also, to a certain extent, a π-route product arising from attack of the acetate ion on the α-position of the nonclassical cation **19**.

As expected, double bond participation is more significant in acetolysis of **5-OTs** than in the case of its homolog **1-OTs**. The failure to obtain a higher proportion of π-route products is to be ascribed to the relative mobility of the benzocycloheptadiene system, also allowing competition of the bimolecular mechanism.

EXPERIMENTAL

Boiling points and melting points are uncorrected. Ir spectra were recorded with a Carl Zeiss Jena UR spectrophotometer, uv spectra with a Specord uv-vis and nmr spectra with a Varian A-60 A spectrometer, using TMS as internal standard. Vpc analyses were performed on a Carlo Erba Fractovap model D using Carbowax 20 M columns (20% on Chromosorb W, 30–60 mesh, 2 m × 4 mm, at 178°, with a hydrogen rate flow of 80 ml/min. Preparative vpc was carried out on a Carlo Erba model GV, with columns similarly packed, 3m × × 5 mm, at 170°, with a hydrogen rate flow of 90 ml/min. The kinetic method was the same as that described earlier.[12]

1,2-Benzo-1,3-cycloheptadien-7-yl-acetic acid (**7**). A procedure similar to that described by Johnson *et al*[19] was used. To a solution of 1.45 g (29.6 mmol) sodium cyanide in 21 ml dry DMSO, stirred at 70° under nitrogen, 4.75 g (14.5 mmol) tosylate **1-OTs** were added. The mixture was heated at 85° for 4 hr. The work-up afforded 2.4 g of a yellow oil, which was added to a solution of 2.8 g (50 mmol) of potassium hydroxide in 14 ml ethylene glycol and heated at 145° for 3.5 hr, under nitrogen and stirring. The mixture was then poured into water and extracted with ether.

The aqueous solution was acidified with concd. hydrochloric acid; extraction with ether followed by washing, drying and removal of the solvent gave 1.9 g (65%) of a brown oil which crystallized after several hours. Recrystallization from methanol-water afforded 1.6 g of white crystals, m.p. 64.5–66.5°.

Anal. Calcd. for $C_{13}H_{14}O_2$: C, 77.22; H, 6.93. *Found* : C, 76.90; H, 6.94. *Ir spectrum* (CS_2 and CCl_4; cm^{-1}) : 752 s, 787 m, 942 m, 1282 s, 1296 s, 1422 s, 1708 vs, 2300–3400 (assocd. OH). *Nmr spectrum* [$CDCl_3$; δ (ppm)] : 1.9–3.0 m (6H, H_5, H_6, H_8), 3.2–3.7 m (1H, H_7), 5.84 d (2t) (1H, H_4), 6.54 d (2t) (1H, H_3), 7.2 s (4 $H_{arom.}$), 10.9 s (COO*H*).

From the ether extracts of the alkaline solution, 0.35 g nitrile was recovered, which on subsequent hydrolysis afforded an additional 0.2 g **7** (total yield relative to **1-OTs** 68.5%).

The *methyl ester* of acid **7** was prepared by refluxing the acid in methanol saturated with hydrogen chloride. After the usual work-up the oily ester was obtained in 91.8% yield. *Ir spectrum* (CCl_4; cm^{-1}) : 1028 m, 1115 m, 1165 vs, 1200 s, 1226 m, 1263 m, 1282 s, 1308 m, 1335 m, 1355 m, 1745 vs, 2925 m, 2950 m, 3020 m, 3065 w.

7-(β-Hydroxyethyl)-1,2-benzo-1,3-cycloheptadiene (**5-OH**). A solution of 7.1 g (33 mmol) of the above ester in 50 ml ether was added dropwise to a stirred suspension of 1.5 g (39.5 mmol) $LiAlH_4$ in 50 ml ether, so as to maintain a gentle reflux. Refluxing was continued for 5 hr and the mixture was allowed to stand overnight. The excess hydride was destroyed by slow addition of 10% H_2SO_4 to the cooled reaction mixture. The ether solution was decanted, washed with water, dried over Na_2SO_4 and evaporated to give 5.7 g (92%) of a viscous oil. Vpc analysis of the crude alcohol indicated a 98% purity. *Ir spectrum* (CS_2, CCl_4; cm^{-1}) : 753 vs, 783 s, 1038 m, 1056 m, 1448 w, 1498 w, 2831 w, 2881 s, 2925 s, 3017 m, 3070 w, 3200–3550 w, 3637 m. *Nmr spectrum* [$CDCl_3$; δ(ppm)] : 1.6–2.6 m (7H, H_5, H_6, H_8 and O*H*), 2.9–3.4 m (1H, H_7), 3.58 t (2H, H_9), 5.85 d (2t) (1H, H_4), 6.4 d (2t) (1H, H_3), 7.1–7.2 m (4 $H_{arom.}$).

7-(β-Tosyloxyethyl)-1,2-benzo-1,3-cycloheptadiene (**5-OTs**). To a solution of 2.25 g (11.8 mmol) alcohol **5-OH** in 1.3 ml pyridine and 2 ml anhydrous ether, stirred in an ice-bath, 2.4 g (12.6 mmol) *p*-toluenesulphochloride was added over a 15-min. period. After stirring in the ice-bath for 30 min. the solution was placed in a refrigerator for 6 days. Water was then added to the solidified mixture and the separated oil was extracted with ether. The extracts were washed with 10% HCl and then with water, dried over $MgSO_4$ and evaporated to give 3.8 g (93%) of an oily material which did not crystallize on long standing in refrigerator.

---

[19] C. R. Johnson, J. E. Keiser and J. C. Sharp, *J. Org. Chem.*, **34**, 860 (1969).

Anal. Calcd. for $C_{20}H_{22}O_3S$: C, 70.10 ; H, 6.46 ; S, 9.36. *Found* : C, 69.70 ; H, 6.71 ; S, 9.16. *Ir spectrum* (CS_2 and CCl_4 ; cm^{-1}) : 756 vs, 773 vs, 1178 vs, 1188 vs, 1371 vs, 2832 w, 2865 w, 2926 s, 3020 m, 3068 w. *Nmr spectrum* [$CDCl_3$; δ(ppm)] : 1.5–2.5 m (6H, H_5, H_6, H_8), 2.4 s (CH_3), 2.7–3.3 m (1H, H_7), 3.95 t (d) (2H, H_9), 5.78 d (2t) (1H, H_4), 6.40 d (2t) (1H, H_3), 6.8–8.0 (8 $H_{arom.}$) ; $J_{34} = 12$ Hz, $J_{35} = 1.5$ Hz, $J_{45} = 3.8$ Hz and $J_{89} = 6.5$ Hz.

7-(β-Acetoxyethyl)-1,2-benzo-1,3-cycloheptadiene (**5-OAc**). A solution of 0.2 g (1.06 mmol), alcohol **5-OH** in 1.5 ml acetic anhydride and 0.3 ml pyridine was heated at 50° for 1 hr, then left overnight at room temperature. The solution was treated with Na_2CO_3 and extracted twice with ether. The combined extracts were successively washed with water, 10% HCl and again with water, then dried over $MgSO_4$ and evaporated to give 0.2 (82%) of a clear yellow oil.

An analytical sample of **5-OAc** was purified by preparative vpc.

Anal. Calcd. for $C_{15}H_{18}O_2$: C, 78.22; H, 7.87. *Found*: C, 78.04; H, 7.68. *Ir spectrum* (CCl_4; cm^{-1}): 1034 m, 1241 vs, 1363 m, 1385 w, 1431 w, 1742 s, 2831w, 2923 m, 2956 w, 3016 w, 3066 w. *Nmr spectrum* [CCl_4; δ(ppm)] : 1.6–2.7m (9H, H_5, H_6, H_8, CH_3), 3.0 m (1H, H_7), 3.92 t(2H, H_9), 5.8 d(2t)(1H,H_4), 6.4 d(2t)(1H,H_3), 6.8-7.3m (4$H_{arom.}$); J_{34}–12Hz, J_{35}=1.5 Hz, J_{45}=4Hz and J_{89}=6.8 Hz.

7-(β-Hydroxyethyl)-1,2-benzcycloheptene (**8-OH**). The alcohol **8-OH** was synthesized in the same manner as its unsaturated analog (**5-OH**) using 7-tosyloxymethyl-1,2-benzocycloheptene [20] as a starting material. The physical properties of the product correspond to those reported by Gilmore and Horton.[3]

The acetate **8-OAc** was prepared by treating the alcohol **8-OH** with Ac_2O and pyridine (82% yield). Purification of the crude product by column chromatography on neutral alumina eluted with a 9 : 1 light petroleum – ether mixture afforded a colourless oil. *Ir spectrum* (CS_2, CCl_4 ; cm^{-1}) : 748 s, 753 s, 1035 m, 1242 vs, 1363 m, 1448 m, 1742 vs, 2853 m, 2926 vs, 3016 w, 3061 w. *Nmr spectrum* [CCl_4 ; δ(ppm)] : 1.5–2.4 m (8H, H_4, H_5, H_6 and H_8), 1.96 s (CH_3), 2.86 m (3H, H_3, H_7), 4.03 t (2H, H_9), 6.85–7.2 (4$H_{arom.}$).

The tosylate **8-OTs** was prepared from **8-OH** as in the case of **5-OTs**. The oily products (98% yield) slowly crystallized on standing in refrigerator. Two recrystallizations from methanol (the tosylate crystallized from the dilute solution on cooling in a dry ice bath) afforded white crystals, m.p. 44.5–45.5°.

Anal. Calcd for $C_{20}H_{24}O_3S$: C, 69.76 ; H, 6.97 ; S, 9.30. *Found* : C, 69.94 ; H, 7.25 ; S, 9.51. *Ir spectrum* (CCl_4 ; cm^{-1}) : 895 m, 935 s, 970 m, 985 m, 1175 vs, 1185 vs, 1372 vs, 1448 m, 2855 m, 2925 s, 3015 w, 3035 w, 3070 w. *Nmr spectrum* [$CDCl_3$; δ(ppm)] : 1.5–3.1 m (11H, H_3–H_8), 2.4 s (CH_3), 4.0 t (2H, H_9), 6.8–6.9 (8 $H_{arom.}$).

ACETOLYSIS OF 7-(β-TOSYLOXYETHYL)-1,2-BENZO-1,3-CYCLOHEPTADIENE (5-OTs)

Reaction products and syntheses of authentic samples

A solution of 2 g (5.85 mmol) **5-OTs** and 0.85 g (10.4 mmol) anhydrous sodium acetate in 40 ml glacial acetic acid was refluxed for 48 hr. The mixture was then neutralized with $NaHCO_3$ and extracted with ether. The extracts were washed with water, dried over $MgSO_4$ and evaporated, yielding 1.3 g (96%) of a reddish oil. This material was analyzed by vpc (table **1**, entry **1**).

The same procedure was used for the run with a threefold concentration of AcONa (0.76 mol/l) (table 1, entry 2).

2,3-Benzobicyclo[3.2.2]nonen-4-ol (**10-OH**). A solution of 0.5 g (13.2 mmol) $NaBH_4$ in 3 ml water was added to a solution of 1.4 g (7.5 mmol) ketone **12** in 50 ml methanol. The mixture was allowed to stand overnight. The solvent was then removed *in vacuo* and the residue treated with water and extracted with ether. The ether solution gave on evaporation 1.3 g (91.5%) of a colourless liquid which rapidly crystallized to a white solid, m.p. 86–8°.

---

[20] R. Huisgen and G. Seidl, *Chem. Ber.*, **96**, 2740 (1963).

Ir spectrum (CCl_4 ; cm^{-1}) : 1003 s, 1365 m, 1441 m, 1474 m, 2861 s, 2941 vs, 3017 w, 3060 w, 3150−3580 (assoc. OH), 3610 m. *Nmr spectrum* [$CDCl_3$; δ(ppm)] : 1.16−2.5 m (10 H, $H_5 - H_9$, O*H*), 2.9 m (1H, H_1), 4.95 d (1H, H_4), 6.91−7.7 m (4 $H_{arom.}$) ; J_{45} = 5 Hz.

2,3-Benzobicyclo[3.2.2]nonen-4-yl acetate (**10-OAc**). A solution of 0.15 g (0.805 mmol) **10-OH** in 0.4 ml pyridine and 1.6 ml acetic anhydride was heated for 1 hr at 40°, then left overnight. The usual work-up gave 0.15 g (81 %) colourless oil.

A pure sample of **10-OAc** was separated by preparative vpc from the solvolysis product. *Anal. Calcd* for $C_{15}H_{18}O_2$: C, 78.22 ; H, 7.87. *Found* : C, 77.96 ; H, 8.13. *Ir spectrum* (CCl_4 ; cm^{-1}) : 965 m, 1019 s, 1240 vs, 1374 s, 1740 vs, 2866 m, 2937 vs, 3022 w, 3062 w. *Nmr spectrum* [CCl_4 ; δ(ppm)] : 1.1−2.16 m (8H, $H_6 - H_9$), 2.0 s (3H, CH_3), 2.31 m (1H, H_5), 2.85 m (1H, H_1), 6.05 d (1H, H_4), 6.8−7.35 (4 $H_{arom.}$) ; J_{45} = 5.5 Hz.

exo- *and* endo-*6,7-Benzobicyclo[3.2.2]nonen-4-ol* (**11-OH**). A solution of 0.1 g (2.6 mmol) $NaBH_4$ in 2 ml water was added to a solution of 0.12 g (0.645 mmol) ketone **15** [11] in 10 ml methanol and the mixture was left overnight at room temperature. The usual work-up afforded 0.1 g (80 %) of a liquid material, which on long standing crystallized as white needles, m.p. 55−9°. Vpc analysis of this solid showed that the two epimeric alcohols **11-OH** were present in practically equal proportions (50.3 % and 49.1 %).

The mixture of diastereoisomers **11-OH** was converted into the *acetate mixture* by treatment with Ac_2O and pyridine (85 % yield). Nmr spectrum [CCl_4 ; δ(ppm)] : 1.2−2.4 m (8H, H_2, H_3, H_8, H_9), 1.93 s (CH_3), 2.06 s (CH_3), 3.05 m (2H, H_1, H_5), 4.76 m (1H, H_4). The signals corresponding to the methyl protons of the two epimeric acetates have almost the same intensity.

REDUCTION OF 2,3-BENZOBICYCLO[3.3.1]NONEN-4-ONE (13)

The ketone **13** was synthesized according to literature [5,8,9].

a) A solution of 0.1 g (2.6 mmol) $NaBH_4$ in 1 ml water was added to a solution of 0.3 g (1.61 mmol) **13** in 12 ml methanol. The mixture was allowed to stand overnight, then worked-up as described above, yielding 0.25 g (82.5 %) of a white crystalline product. Vpc analysis of this material indicated two major components (80 % and 8.6 %). Recrystallization from aqueous methanol afforded white crystals, m.p. 86.5−88.5 (lit.[9] 86−7°, light-petroleum). This compound proved to be *endo*-2,3-benzobicyclo[3.3.1]nonen-4-ol (*endo*-**9-OH**). *Ir spectrum* (CCl_4 ; cm^{-1}) : 1034 s, 1380 w, 1455 m, 2858 s, 2905 s, 2930 vs, 3020 w, 3073 w, 3608 m. *Nmr spectrum* [CCl_4 ; δ(ppm)] : 0.8−2.4 m (9H, H_5, $H_6 - H_9$), 2.6 s (1H, O*H*), 2.88 m (1H, H_1), 4.83 d (1H, H_4), 6.7−7.7 m (4 $H_{arom.}$) ; J_{45} = 6.5 Hz.

b) To a stirred solution of 0.45 g (2.4 mmol) **13** in 28 ml 95 % ethanol, sodium (0.8 g, 35 mmol) was added in small portions, so as to avoid refluxing of the solvent. Stirring was continued for 45 min. The yellow solution was then poured into 50 ml dilute hydrochloric acid and ether-extracted. The combined extracts were washed with water, dried over Na_2SO_4 and evaporated to give 0.4 g of a yellow oil consisting (vpc) of 83 % ketone **13**, 7.5 % *endo*-**9-OH** and 1.5 % *exo*-**9-OH**.

c) The catalytic hydrogenation procedure described by Youssef [21] was followed, using a longer reaction time (5 hr). The work-up yielded a yellow oil which, according to ir and nmr spectra, consisted mainly of the hydrocarbon [5,8,9] corresponding to the ketone **13**; the alcohol **9-OH**, which was probably an intermediate, was found only in a low proportion.

In another experiment, 0.1 g ketone **13** in 4 ml AcOH was hydrogenated over the same catalyst, for 35 min. In the ir spectrum of the product (50 mg) the absorptions at 1700 cm^{-1} and 3608 cm^{-1} correspond to $\nu_{C=O}$ in **13** and ν_{OH} in *endo*-**9-OH**, respectively; in the nmr spectrum the doublet at δ = 4.83 ppm (J = 6.5 Hz) matched the signal of the proton H_4 in *endo*-**9-OH**.

In the experiments b) and c) the reduction of ketone **13** was not completed, but the results showed that, as in the $NaBH_4$ reduction, *endo*-**9-OH** formed in higher yield.

endo-*2,3-Benzobicyclo[3.3.1]nonen-4-yl acetate* (endo-**9-OAc**). The acetate *endo*-**9-OAc** (colourless oil) was obtained in the usual manner from the alcohol **9-OH** and Ac_2O and pyridine. *Ir spectrum* (CS_2 ; cm^{-1}) : 725 m, 738 w, 768 m, 1038 s, 1233 vs, 1368 m, 1740 vs, 2853 m, 2903 s, 2929 vs, 3020 w, 3061 w. *Nmr spectrum* [CCl_4 ; δ(ppm)] : 1.0−2.3 m (8H, $H_6 - H_9$), 2.16 s (3H, CH_3), 2.45 m (1H, H_5), 2.95 m (1H, H_1), 6.11 d (1H, H_4), 6.75−7.33 m (4$H_{arom.}$) ; J_{45} = 6.5 Hz.

---

[21] A.A. YOUSSEF, M.E. BAUM and H. M. WALBORSKY, *J.Amer.Chem.Soc.*, **81**,4709 (1959).

Epimerization of endo-**9-OAc**. A solution of 0.2 g (0.87 mmol) *endo*-**9-OAc** and 0.15 g (1.8 mmol) anhydrous sodium acetate in 6 ml AcOH was refluxed for 106 hr. The reaction mixture was worked-up as described for the acetolysis of **5-OTs**. According to the nmr spectrum and vpc analysis, the product (0.15 g; 75%) was a mixture of *exo*-**9-OAc** and *endo*-**9-OAc** (67.4% and 25.2%, respectively).

In another run, the reaction time was shortened to 24 hr. The product showed a similar composition (69.2% *exo*-**9-OAc** and 26.8% *endo*-**9-OAc**). An analytical sample of *exo*-**9-OAc** was obtained by preparative vpc.

Anal. Calcd for $C_{15}H_{18}O_2$: C, 78.22; H, 7.87. *Found* : C, 78.24; H, 8.25. *Ir spectrum* (CCl_4 ; cm^{-1}) : 960 m, 1015 m, 1240 vs, 1374 s, 1736 vs, 2867 m, 2932 vs, 3012 w, 3066 w. *Nmr spectrum* [CCl_4 ; δ(ppm)] : 0.85–2.33 m (9H, H_5, H_6-H_9), 1.95 s (3H, CH_3), 2.95 m (1H, H_1), 5.68 d (1H, H_4), 6.75–7.5 m (4 $H_{arom.}$); $J_{45} = 1$ Hz, $J_{9a9b} = 13$ Hz.

Acknowledgement. The authors are much indebted to Dr. J. Ciabattoni for a sample of ketone **14** and to Dr. F. Badea for helpful discussions.

NOTE POUR LES AUTEURS

La *Revue Roumaine de Chimie* publie des articles en anglais, français, russe, allemand ou espagnol. Les auteurs sont priés d'envoyer des articles, notes, communications et comptes rendus inédits.

Les manuscrits seront dactylographiés à deux intervalles. Les tableaux seront dactylographiés sur des feuilles séparées, de même que la légende des figures. Les diagrammes seront tracés à l'encre de Chine sur papier calque. Les tableaux et les figures seront numérotés par des chiffres arabes, en nombre strictement nécessaire. Prière de ne pas inscrire les mêmes données dans les tableaux et les figures. Les formules chimiques seront incluses dans le texte ; en outre, elles seront transcrites sur des feuilles séparées. Les auteurs sont priés d'indiquer les caractères italiques (en soulignant les lettres au crayon), ainsi que tout autre caractère spécial. L'ordre des références bibliographiques sera celui de leur mention dans le texte ; le nom de l'auteur sera précédé de l'initiale du prénom ; les publications périodiques seront présentées suivant les prescriptions internationales. Les références seront ajoutées à la fin de l'article ; elles paraîtront comme des notes, au bas de la page. Le texte sera précédé d'un résumé comprenant 15 lignes au maximum.

L'entière responsabilité du contenu des articles appartient aux auteurs. On publie des articles dus aux collaborateurs roumains ou étrangers.

PRINTED IN ROMANIA

1975 JUL 2

TRAVAUX PARUS AUX ÉDITIONS DE L'ACADÉMIE DE LA RÉPUBLIQUE SOCIALISTE DE ROUMANIE

M. AVRAM, **Antidăunători** (Pesticides), Ed. Academiei, Bucarest, 1974, 495 p., 41 lei.

I. ZUGRĂVESCU, **Chimia N-Ilidelor** (La chimie des N-Ylures), Ed. Academiei, Bucarest, 1974, 347 p., 19 lei.

CRISTOFOR SIMIONESCU, MARGARETA GRIGORAŞ, AGATA CERNĂTESCU-ASANDEI et GHEORGHE ROZMARIN, **Chimia lemnului din România — plopul şi salcia** (La chimie du bois en Roumanie — le peuplier et le saule), 1973, 228 p., 28 lei.

TIBERIU NĂSCUŢIU, **Metode radiochimice de analiză** (Méthodes radiochimiques d'analyse), 1973, 384 p., 23 lei.

MARIA FITI, **Dozimetria chimică a radiaţiilor ionizante** (La dosimétrie chimique des radiations ionisantes), 1973, 240 p., 13, 60 lei.

MIHAI FLORESCU, **Eficienţa economică a cercetării ştiinţifice** (L'efficience économique de la recherche scientifique), 1972, 115 p., 15 lei.

GEORGETA LĂZĂRESCU, **Sistematizarea informaţiilor în Chimia organică** (La systématisation des informations dans la Chimie organique), 1972, 252 p., 10,15 lei.

P. BALTĂ şi E. BALTĂ, **Introducere în chimia fizică a stării vitroase** (Introduction à la chimie physique de l'état vitreux), 1971, 240 p., 15,50 lei.

LYDIA-MARIA VAICUM, **Biodegrabilitatea detergenţilor** (La biodégrabilité des détergents), 1971, 254 p., 16 lei.

I. ZUGRĂVESCU et L. STOICESCU-CRIVETZ, **Polimeri heterociclici** (Polymères hétérocycliques), 1971, 190 p., 9,50 lei.

CRISTOFOR SIMIONESCU et C. V. UGLEA, **Fracţionarea compuşilor macromoleculari** (Fractionnement des composés macromoléculaires) 1962, 292 p., 18,50 lei.

I. MAXIM, **Materiale nucleare** (Matériaux nucléaires), 1969, 444 p., 30 lei.

CRISTOFOR SIMIONESCU et CLEOPATRA VASILIU-OPREA, **Mecanochimia compuşilor macromoleculari** (La mécanochimie des composés macromoléculaires), 1967, 344 p., 23,50 lei.

CORNEL BODEA et collab., **Tratat de biochimie vegetală**, partea I, **Fitochimie** (Traité de biochimie végétale, Ire partie, Phytochimie), Ier vol., 1964, 747 p. + 4 annexes + 2 pl., 41 lei ; IIe vol., 1965, 1262 p., 1 pl., 56 lei ; III vol., 1967, 773 p., 35 lei.

V. GHEŢIE et V. MICUŞAN, **Analiza imunochimică. Teorie şi practică** (Analyse immunochimique. Théorie et pratique), 1966, 369 p., 28 lei.

I.P.I. c. 1676

43 426

Lei 25.—

F 1103

04-001 7ut

ACADÉMIE DE LA RÉPUBLIQUE SOCIALISTE DE ROUMANIE

R

REVUE ROUMAINE DE CHIMIE

REFERÁLVA

TOME 20
N° 3
Mars 1975

RECHAX, **20**, *3*, 297–446 (1975)

EDITURA ACADEMIEI REPUBLICII SOCIALISTE ROMÂNIA

Rev. Roumaine Chim. **20**, *3*, p. 297–446 (1975), Bucarest

ACADÉMIE DE LA RÉPUBLIQUE SOCIALISTE DE ROUMANIE

COMITÉ DE RÉDACTION

Rédacteur en chef:

I. G. MURGULESCU, membre de l'Académie de la République Socialiste de Roumanie

Rédacteurs en chef adjoints:

A. T. BALABAN et V. EM. SAHINI, membres correspondants de l'Académie de la République Socialiste de Roumanie

Collège de rédaction:

EM. BRATU, ELENA CEAUŞESCU, ECATERINA CIORĂNESCU-NENITZESCU, C. DRĂGULESCU, RALUCA RIPAN, CR. SIMIONESCU, membres de l'Académie de la République Socialiste de Roumanie; P. SPACU, membre correspondant de l'Académie de la République Socialiste de Roumanie; MARGARETA AVRAM, D. I. MARCHIDAN, G. NIAC et D. SĂNDULESCU

Toute commande de l'étranger (fascicules ou abonnements) sera adressée à Intreprinderea Rompresfilatelia, Boîte Postale 2001, télex 011631, Bucarest, Roumanie

Les manuscrits, les livres et les revues proposés en échange, ainsi que toute correspondance seront envoyés à la rédaction

REVUE ROUMAINE DE CHIMIE

23, str. Dumbrava Roşie, Bucarest, Roumanie, téléphone 12 41 60

EDITURA ACADEMIEI REPUBLICII SOCIALISTE ROMÂNIA

3 bis, str. Gutenberg, Bucarest, téléphone 16 40 79

REVUE ROUMAINE
DE
CHIMIE

ORSZÁGOS MŰSZAKI KÖNYVTÁR ÉS DOKUMENTÁCIÓS KÖZPONT
1883

Tome 20, N° 3 Mars 1975

D. I. MARCHIDAN and LIANA PANDELE, Thermal properties of KCl, CsCl and binary mixture KCl + CsCl. High temperature heat content . . . 299–304

O. RADOVICI and VERONICA POPESCU-TUCSEK, An investigation of silicon-hydrofluoric acid interface by measuring its differential capacity 305–315

E. SEGAL, Certains problèmes concernant la cinétique de l'adsorption sur des surfaces hétérogènes 317–321

N. CALU et ADINA POPA-RANG, Le système nickel (II)-thiosemicarbazide 323–335

EUGENIA IVAN and P. SPACU, New compounds of yttrium and lanthanides with derivatives of anthranilic acid. II. The N-(carboxy methyl) anthranilic acid 337–344

CONSTANŢA GHEORGHIU and CRISTINETA MĂRCULESCU, Contribution to the coordination chemistry of *s*-triazines. II. Coordination compounds of copper with melamine derivatives . . . . 345–351 R

F. IORDACHE, F. CHIRALEU and MARGARET AVRAM, Bicyclo [2.2.2] octene derivatives. II. Addition of halogens to stereoisomeric 5,6,7,8-tetracarbomethoxy-bicyclo [2.2.2] oct-2-enes 353–359

D. JOULAIN et F. ROUESSAC, Dérivés du bicyclo [4.1.1] octane. II. Préparations de quelques hydrocarbures, aldéhydes et cétones 361–378

P. BUCHWALD and L. FEY, Cyanoethylation of ketoximes. II. Kinetics and mechanism of decyanoethylation of some cyanoethyl ethers of *para*-substituted acetophenone oximes 379–385

ANTOANETA SPINZI and I. V. NICOLESCU, Catalytically active iron oxides prepared by mechanotopochemical method. II. Thermal analysis of some iron hydroxides . . . . 387–396 R

I. C. POPESCU, C. LITEANU and A. MOCANU, Differential potentiometry at zero current using two membrane-electrodes with different selectivity . . . 397–406 R

A. CARPOV, DEMETRA DRĂGAN, GEORGETA MOCANU and CORNELIA LUCA, Studies on the synthesis and characterization of weakly basic anion-exchange resins. I. Amination of chloromethylated macroporous ternary styrene-divinylbenzene-acrylic monomer copolymers with dimethylamine 407–419 R

DEMETRA DRĂGAN, GEORGETA MOCANU and A. CARPOV, Studies on the synthesis and characterization of weakly basic anion-exchange resins. II. Upon the nature of the functional groups . . . . 421–433 R

DEMETRA DRĂGAN, GEORGETA MOCANU and A. CARPOV, Studies on the synthesis and characterization of weakly basic anion-exchange resins. III. Operating characteristics . . . . 435–444 R

COMPTES RENDUS 445–446

Rev. Roumaine Chim. **20**, *3*, p. 297–446 (1975), Bucarest

Revue Roumaine de Chimie, 20, 3, 299–304 (1975)

THERMAL PROPERTIES OF KCl, CsCl AND BINARY MIXTURE KCl + CsCl.[*] HIGH TEMPERATURE HEAT CONTENT

D. I. MARCHIDAN and LIANA PANDELE
Institute of Physical Chemistry
Str. Galaţi 31, Bucharest 13, Romania

Received October 1, 1974

The heat contents of pure KCl, CsCl and equimolecular mixture KCl–CsCl were determined by means of drop calorimeter (copper-block). The measurements were carried out both for solid and for liquid states. By processing the experimental data, heat capacities and heats of fusion have been evaluated. A tabulation of thermodynamic values is presented.

Heat capacities, entropies and free energy functions at high temperatures are usually derived from the experimentally determined enthalpy values. These data are required for the study of many problems in high-temperature chemistry. They constitute in particular the basic data used by the powerful tool of equilibrium thermodynamics. Determinations of the thermochemical properties of pure fused salts and of their mixtures has a theoretical importance for testing structural models, and a practical importance due to their utilization in diverse fields such as metallurgy, electrochemistry and nuclear technology.

The study of the thermochemical properties of pure salts in solid [1] and liquid state [2] has been made in this laboratory by continuous investigations over the past few years. A study on the heats of fusion of binary mixtures of fused salts which form solid solutions on cooling has also been carried out. [3]

Therefore the present investigation was undertaken in order to determine or to re-evaluate the heat contents and associated thermodynamic properties of the chlorides involved in the previous works of this laboratory. For this purpose, a copper block drop calorimeter was used. After calibration with N.B.S. synthetic sapphire, measurements were made on pure KCl, CsCl and on their equimolecular mixture for temperatures up to about 1,140 K.

---

[1] D. I. Marchidan and M. Ciopec, *Rev. Roumaine Chim.*, **15**, 1177 (1970).

[2] D. I. Marchidan and Cr. Telea, *Rev. Roumaine Chim.*, **13**, 1291 (1968); **14**, 1495 (1969); **15**, 1675 (1970).

[3] D. I. Marchidan and L. Vasu, *Rev. Roumaine Chim.*, **17**, 1649 (1972), **18**, 1295 (1973).

EXPERIMENTAL

The experimental technique has been described in detail in a previous paper,[4] and the accuracy of the measurements is considered to be within reproducibility, i. e. ± 0.4 per cent. In order to account for the heat content of the container and the heat lost during the drop, similar experiments were made with the empty container (fused silica) at the same temperatures. The essential features of the drop calorimeter consist of two main assemblies : a furnace to heat samples to the desired temperature and the isoperibolic copper-block calorimeter proper. The heating furnace was made from a Kanthal element around a steel tube. The jacket was water-cooled to maintain the furnace exterior near room temperature. The drop samples consisted of weighed quantities of the desired compounds sealed within weighed evacuated quartz capsules equipped with quartz hook. The temperature of the sample was precisely regulated by a proportional electronic controller. The temperature rise of the calorimeter proper, after the admission of the sample, was measured by means of a thermistor (CICE-France), characterized by high sensitivity and reproducibility which permitted the measurement of a small temperature variation of 0.001 K. The relationship between the thermistor output and the heat increase of the calorimeter block was determined using U.S. National Bureau of Standards synthetic sapphire.[5] The potassium chloride with a purity, "specpure" (Johnson, Matthey & Co.) and the caesium chloride (purity 99.9% British Drug Houses) were melted before use in a platinum crucible in an atmosphere of pure, dry nitrogen. After solidification, clear crystals were picked out from the samples and sealed into the containers under vacuum.

RESULTS AND DISCUSSION

ENTHALPY MEASUREMENTS ON PURE COMPOUNDS

The thermochemical properties of potassium chloride are mentioned by Douglas,[6] Markov,[7] Marchidan,[1] and Thompson[8] in their works, and the thermochemical properties of caesium chloride, by Brönsted[9] and Kaylor.[10]

POTASSIUM CHLORIDE

The heat content of pure potassium chloride has been determined in the temperature range 513–1140 K. The experimental results are listed in table 1 and plotted in figure 1.

Our data are in good agreement with the values reported in literature. For example, the value obtained for heat of fusion is 6,300 cal. mole^{-1} close to that of Dworkin and Bredig[11] (6,340 cal. mole^{-1}), of Douglas[12] (6,270 cal. mole^{-1}) and of Thompson (6,250 cal. mole^{-1}).

[4] D. I. Marchidan and M. Ciopec, *Studii şi Cercetări Chim. Acad. R. S. Romania* **17**, 737 (1969).

[5] G. Furukava, T. Douglas, R. McCoskey and D. Ginnings, *J. Research Nat. Bur. Standards*, **57**, 67 (1956).

[6] T. B. Douglas, U.S. Atom. Energy Comm. BNL 2446, 13 (1955).

[7] B. F. Markov and T. A. Tishura, *Ukrain. khim. Zhur.* **39**, 8 (1973).

[8] W. T. Thompson and S. N. Flengas, *Canad. J. Chem.* **49**, 1550 (1971).

[9] I. Brönsted, *Z. Elektrochem*, **20**, 554 (1914).

[10] C. E. Kaylor, G. E. Walden and D. F. Smith, *J. Phys. Chem.*, **64**, 276 (1960).

[11] A. S. Dworkin and M. A. Bredig, *J. Phys. Chem.*, **64**, 269 (1960).

[12] T. B. Douglas, Original communication in ref. 11.

Table 1

Experimental and calculated enthalpy increments for solid and liquid potassium chloride

T(K)	$H°(T)-H(298.15)$ exp.	cal. mole^{-1} calc.
	solid	
513.15	2,728	
597	3,807	
662.3	4,680	
685.85	4,950	
753.10	6,025	
854.95	7,403	
889.80	7,820	
950.50	8,793	
1020.20	9,885	
1040.30	10,106	
	liquid	
1050.15	16,412	16,355
1065	16,470	16,611
1076.15	16,800	16,801
1080.39	16,878	16,874
1140.50	17,891	17,910

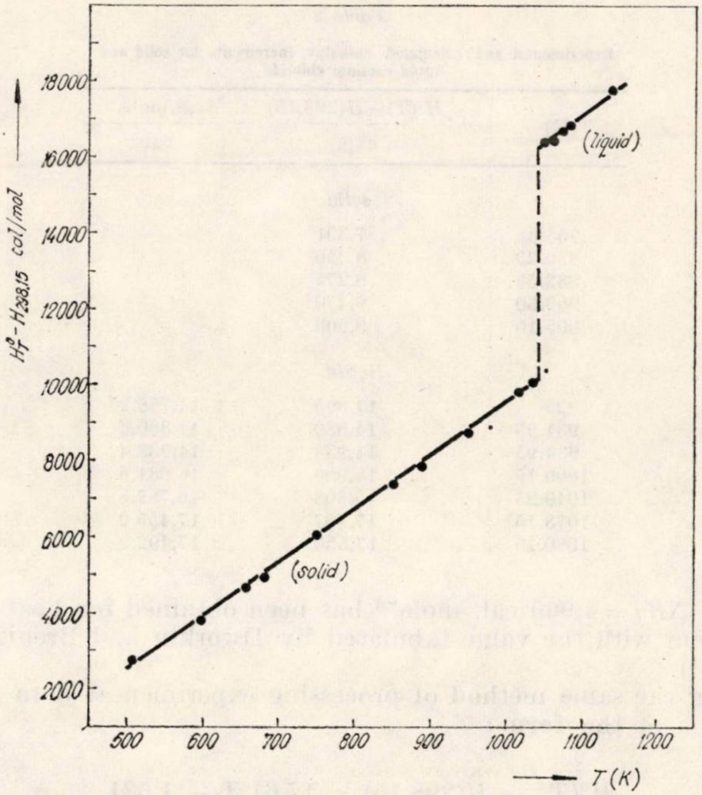

Fig. 1. — Heat content variation of pure KCl in terms of temperature.

Processing by the least squares method the experimental results recorded at temperatures beyond the fusion temperature we obtained the following equation :

$$H(\mathrm{T}) - H(298{,}15) = 17.20\ \mathrm{T} - 1{,}707 \qquad (1)$$

By deriving equation (1) in terms of absolute temperature we obtain :

$$C_p = 17.20\ \mathrm{cal.K^{-1}\ mole^{-1}}$$

This value is in agreement with the values reported by Douglas[6] 17.59 cal.K^{-1} mole^{-1}) and Markov[7] (17.77 cal.K^{-1} mole^{-1}).

CAESIUM CHLORIDE

The heat content of caesium chloride has been determined in the temperature range 765–1080 K. The experimental results are given in table 2 and plotted in figure 2 in comparison with those of Kaylor.[10]

Table 2

Experimental and calculated enthalpy increments for solid and liquid caesium chloride

T(K)	$H°(\mathrm{T})-H(298.15)$	cal.mole^{-1}
	exp.	calc.
	solid	
765.3	7,391	
830.25	8,350	
882.55	9,275	
900.30	9.470	
905.10	9,600	
	liquid	
925	14,805	14,758.25
931.95	14,880	14,880.6
934.95	14,938	14,933.4
1000.15	15,980	16,081.6
1040.25	16,808	16,787.8
1078.15	17,497	17,455.2
1080.15	17,530	17,492.2

The value $\Delta H_f = 4{,}900$ cal. mole^{-1} has been obtained for heat of fusion in agreement with the value tabulated by Dworkin and Bredig[11] (4,840 cal. mole^{-1}).

Using the same method of processing experimental data we obtain an equation of the form :

$$H°(\mathrm{T}) - H(298.15) = 17.61\ \mathrm{T} - 1{,}531 \qquad (2)$$

By deriving the equation in terms of absolute temperature we obtained :

$$C_p = 17.61 \text{ cal. K}^{-1} \text{ mole}^{-1}$$

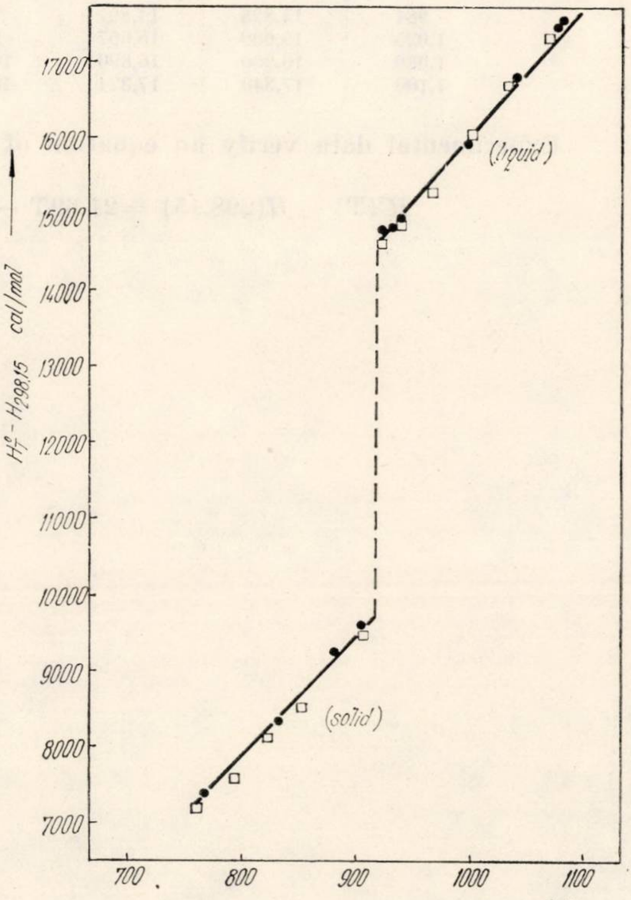

Fig. 2. — Heat content variation of pure CsCl in terms of temperature: ● the authors' results; ◻ Kaylor's results.

MEASUREMENTS OF ENTHALPY CONTENT OF MOLTEN SOLUTIONS

The KCl—CsCl system

The heat content of the equimolecular fused system KCl—CsCl has also been determined. Experimental results are given in table 3 in comparison with calculated values obtained by the method of the least squares.

Table 3

Heat content (experimental and calculated values) for equimolecular system of molten salts KCl – CsCl. Deviation of experimental data from the calculated curve

T(K)	$H^\circ(\mathrm{T})-H(298.15)$ cal. mole^{-1}			Deviation
	exp.	calc. eq.(3)	(cal/mole)	%
984	14,828	14,807	19	0.13
1,025	15,689	15,697	−8	0.05
1,080	16,900	16,890	10	0.06
1,100	17,340	17,324	16	0.09

Experimental data verify an equation of the form:

$$H^\circ(\mathrm{T}) - H(298.15) = 21.69\mathrm{T} - 6{,}535. \qquad (3)$$

Revue Roumaine de Chimie, 20, 3, 305–315 (1975)

INVESTIGATION OF SILICON-HYDROFLUORIC ACID INTERFACE BY MEASURING ITS DIFFERENTIAL CAPACITY

O. RADOVICI and VERONICA POPESCU-TUCSEK
Centre of Physical Chemistry, Str. Galaţi 31,
Bucharest, Romania

Received January 11, 1974

The differential capacity at Si/HF interface has been measured in the potential range +200 to −700 mV and the frequency range ω, $2.5\ 10^3$ to $10^6\ s^{-1}$. Equivalent circuits were selected for p Si/HF and n Si/HF interfaces.

INTRODUCTION

The field effect method allows the investigation of the surface of semiconducting materials by separating surface and volume effects. A variant of this method, the differential capacity method, is particularly suitable for the investigation of the semiconductor-electrolyte interface structure. Such measurements have been previously performed especially on germanium and information has been obtained about the surface states on the one hand,[1–3] and about the solution effect, on the other hand.[4,5]

In some previous works[6,7] we studied the n Si/HF interface, within +200 to −700 mV potential range by the differential capacity technique within 800 to 8000 c frequency range. In order to interpret the results, relatively simple equivalent circuits were used, which allowed us to emphasize the existence of the surface states and the solution contribution to the double layer as well.

In the present work the experimental investigation has been extended to p-type silicon, as well as to the effect of the carriers concentration on the interface behaviour. The measurement range has also been extended up to 150 kc so as to obtain a more detailed model of the Si/HF structure.

---

[1] K. Bohnenkamp and H. I. Engell, *Z. Elektrochem.*, **61**, 1184 (1957).
[2] E. A. Efimov and I. G. Erusalimcik, *Zhur. fiz. Khim.* **33**, 441 (1959).
[3] P. I. Boddy and W. H. Brattain, *J. Electrochem. Soc.*, **109**, 574 (1962).
[4] M. Hofman-Perez and H. Gerischer, *Z. Elektrochem*, **65**, 771 (1961).
[5] R. M. Hurd and P. T. Wrotenbery, *Ann. N. Y. Acad. Sci.*, **101**, 876 (1963).
[6] O. Radovici and V. Tucsek, *Rev. Roumaine Chim.*, **13**, 1549 (1968).
[7] O. Radovici and V. Tucsek, *Rev. Roumaine Chim.*, **15**, 325 (1971).

EXPERIMENTAL

Single crystal (1,1,1)-oriented p silicon of 200 and 110Ωcm and in silicon of 150, 100 and 17Ωcm have been used as electrodes. The working solution, an 2.5 N HF aqueous solution has been prepared from electronic grade HF. The teflon cell with cylindrical symmetry which has been used is shown in fig. 1.

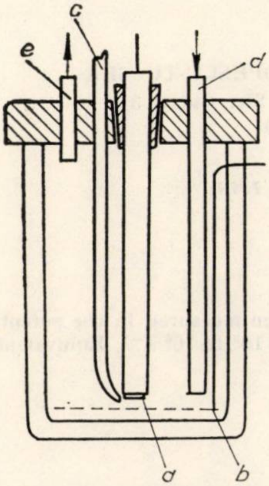

Fig. 1. — Cross-section of the teflon cell : *a*, Si electrode ; *b*, Pt counter electrode ; *c*, Luggin capillary ; *d*, gas inlet ; *e*, gas outlet.

The d.c. electric field has been applied to the surface of the silicon by polarizing the cell with a Wenking potentiostate. The electrode potential has been measured against a caloasmel electrode with an RFT 187a electronic voltmeter. The cell impedance has been meured within the frequency range $\omega = 2.5\,10^3 - 5\ 10^4\ s^{-1}$ with a Wayne Kerr B 641 audio frequency bridge, provided with fast autobalance for the interval frequency $\omega = 10^4\ s^{-1}$, and with a Wayne Kerr B 601 radio frequency bridge within the frequency range $\omega = 10^5 - 10^6\ s^{-1}$. As a signal source a Tesla RC oscillator BM 344 has been used, and a Tel—Mes TT 1302 selective voltmeter coupled with a Tel—Mes TT 1401 amplifier have ensured bridge balance detection.

The measurements have been performed starting from the rest potential, by applying potential steps of 100 mV, 200 mV etc., of various lengths, first in the cathodic range, then in the anodic one. In order to ensure fast measurements (within less than 1 sec), the output of the bridge in autobalance mode has been recorded with a Sefram GRVAC Graphispot recorder. Otherwise the measurement time for a potential step was about 1 minute.

RESULTS AND DISCUSSION

Differential capacity curves for the Si/HF interface, within the potential range +200 to −700 mV, have been recorded and compared with the theoretical curves for the space charge region $C_{sc}(V_s)$, calculated with Poisson's equation. [8]

Fig. 2 shows the differential capacity curves calculated for the space charge region, with the volume carriers concentration as a parameter, from which one may observe that : (i) the potential $V_{s\min}$ which corresponds to the capacity minimum depends on the carriers concentration, (ii) within the reverse bias potential range the curves have two branches which correspond to the existence of the inversion and depletion layers, respectively.

---

[8] A. Many, Y. Goldstein and N. B. Grover, "Semiconductor Surfaces" North-Holland, Amsterdam 1965, p. 138.

The differential capacity of the Si/HF interface measured within the frequency range w $= 2.5\ 10^3 - 10^6\ s^{-1}$, on p-type silicon of 110 Ωcm, n-type silicone of 150 Ω cm and n-type silicon of 17 Ωcm, are presented in fig. 3 and fig. 4, respectively.

From this it can be seen that the capacity curves depend strongly on frequency. The decrease of the capacity with frequency increases may be attributed to the surface states behaviour. These states are relatively slow and their participation in the charge accumulation process involved in the measurements, is reduced when the frequency increases and is completely negligible at high frequencies.

An important feature of the Si n capacity curves in the anodic range is a saturation effect which is more pronounced for higher resistivity (i. e. for lower hole concentration). The effect is enhanced at higher frequencies for which the rising branch in the anodic branch is completely missing. This is a specific behaviour for a complete depletion of the surface layer.

Further, comparing the experimental curves with the calculated C_{cs} (V_s) curves, it may be noticed that at high frequencies the curves in figs. 3 and 4 are decreasing below the level of the curves in fig. 2. This behaviour suggests the existence of a solution effect on the measurements which consists in a potential drop additional to that of the semiconductor. Moreover, it may be seen from fig. 5, that the potential of the minimum capacity does not correlate with the carriers concentration according to fig. 2 and it is within the same potential range (—100 to —300 mV) for all the silicon samples.

In other words the potential of the minimum capacity is not controlled by the space charge region, but by the solution, i. e. the measured capacity depends on the double layer in the solution.

In order to better reveal the solution effect, investigations covered the dependence of the capacity on the immersion time of the electrode into the solution and the length of the potential step (i. e. the time during which the d. c. field was applied).

In fig. 6 differential capacity curves are plotted for a 200 Ωcm p silicon at a frequency $\omega = 10^4\ s^{-1}$, for an immersion time varying from 2 hrs to 175 hrs. The measuring time was below 1 sec. The curves show that the capacity decreases with the immersion time, especially in the reverse bias range, and tends finally to saturate to a limiting value.

Fig. 7 shows the dependence of the capacity curves on the measuring time for a 150 Ωcm n silicon, at a frequency $\omega = 10^4\ s^{-1}$. One may notice that in the anodic range the minority carriers show up only in fast measurements, $t < 1$ sec. For longer measuring time saturation. appears, i. e. the limitation of the minority carrier concentration.

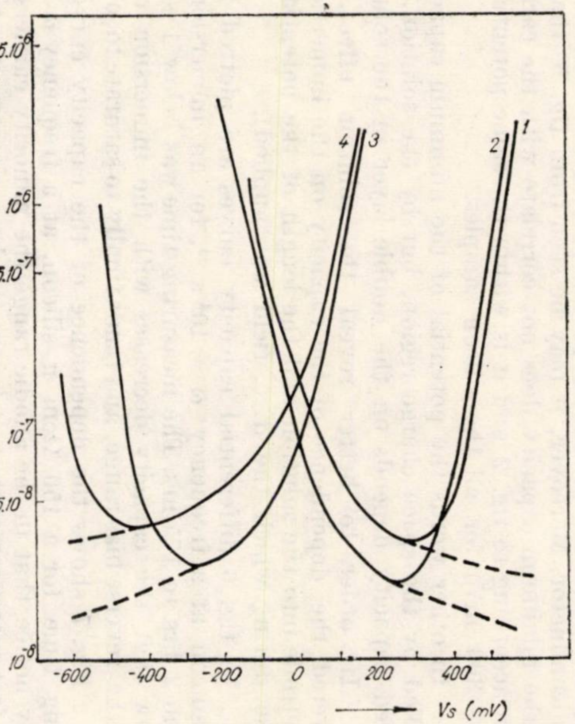

Fig. 2. — Calculated capacity of Si space-charge region : *1*, p Si 100Ωcm *2*, p S 200Ωcm ; *3*, n Si 150Ωcm ; *4*, n Si 17Ωcm.

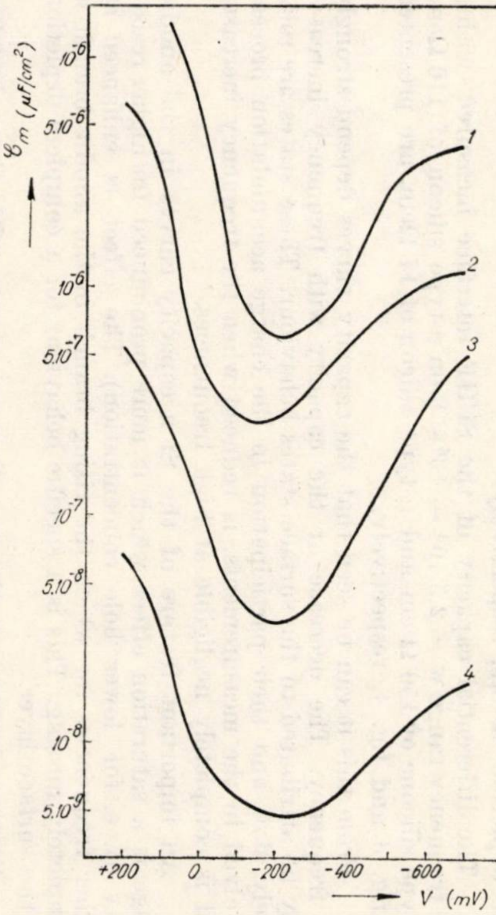

Fig. 3. — Differential capacity curves of p Si 110 Ωcm : *1*, $\omega = 2.5\ 10^3$; *2*, $\omega = 10^4$; *3*, $\omega = 2\ 10^5$; *4*, $\omega = 10^6$.

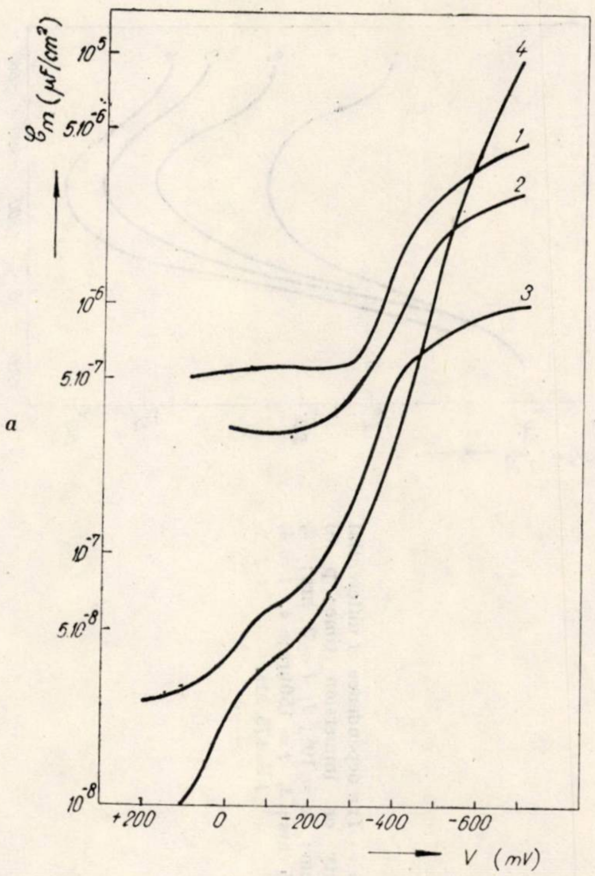

Fig. 4a. — Differential capacity curves of n Si 150Ωcm ; *1*, $\omega = 2.5 \ 10^3$; *2*, $\omega = 10^4$; *3*, $\omega = 2 \ 10^5$; *4*, $\omega = 10^6$.

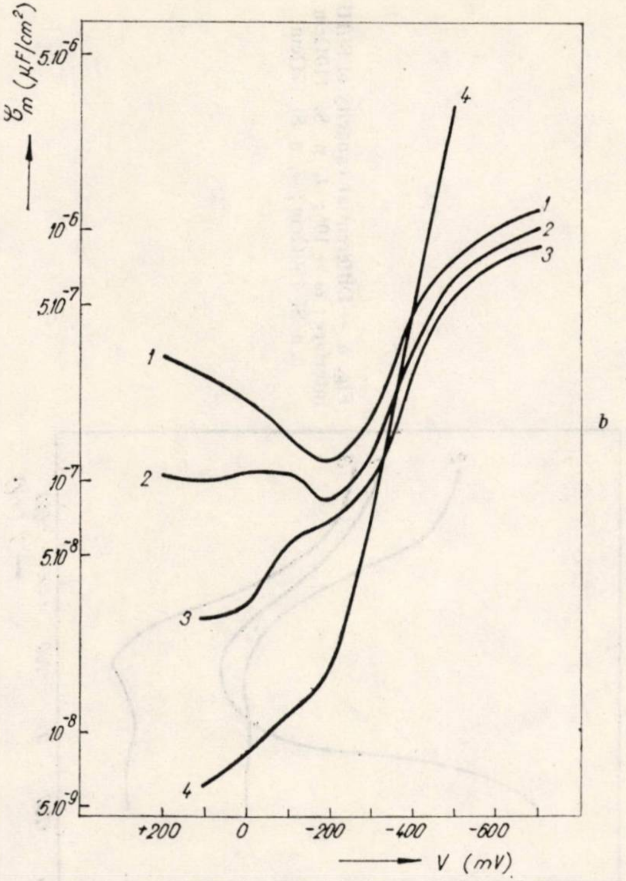

Fig. 4b. — Differential capacity curves of n Si 17Ωcm ; *1*, $\omega = 2.5 \ 10^2$; *2*, $\omega = 10^4$; *3*, $\omega = 2.5 \ 10^4$; *4*, $\omega = 10^6$.

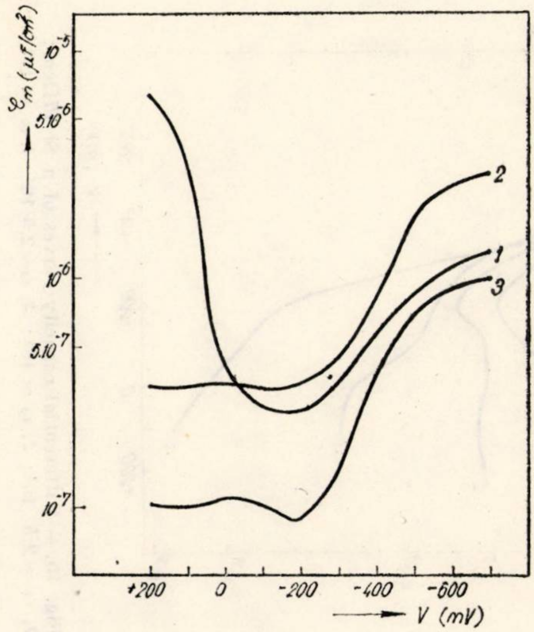

Fig. 5. — Differential capacity of Si/HF interface; $\omega = 10^4$; *1*, p Si 110Ωcm; *2*, n Si 150Ωcm; *3*, n Si 17Ωcm.

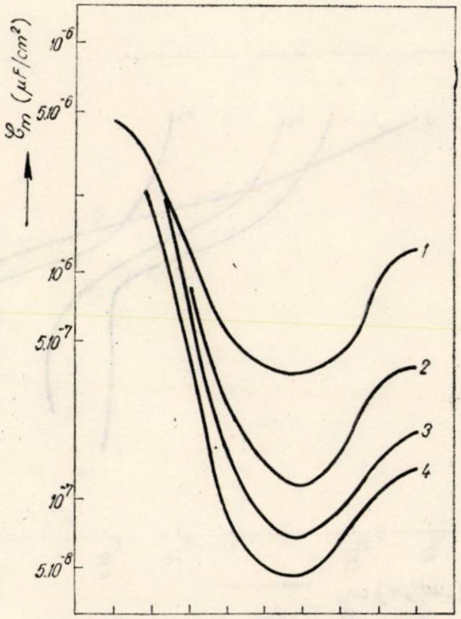

Fig. 6. — The dependence of differential capacity on immersion time; p Si 200Ωcm; $\omega = 10^4$; *1*, $t = 2$ hrs; *2*, $t = 25$ hrs; *3*, $t = 150$hrs; *4*, $t = 4$, $t = 175$ hrs.

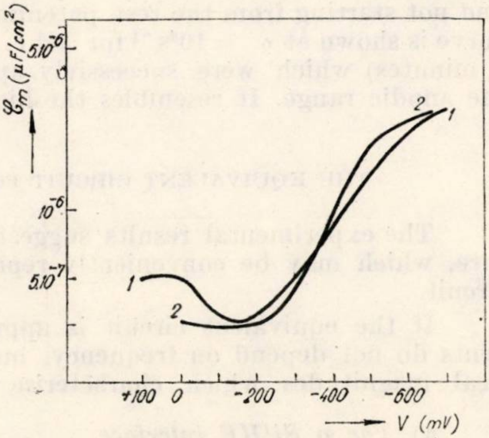

Fig. 7. — The influence of measuring time on differential capacity curves : n Si 150Ωcm ; $\omega = 10^4$; 1, $t < 1$ sec ; 2, $t \sim 1$ minute.

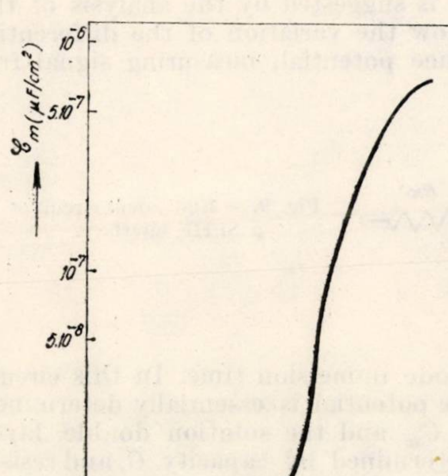

Fig. 8. — The influence of measuring conditions on differential capacity curves ; n Si 100Ωcm ; $\omega = 10^4$.

The saturation effects get even more pronounced if the measuring conditions are changed in what regards the way the continuous field is applied, i. e. if the successive potential steps are additionally applied and not starting from the rest potential. In fig. 8 a differential capacity curve is shown at $\omega = 10^4 s^{-1}$ for a d.c. bias in long potential steps (about 5 minutes) which were successivly applied from the cathodic, towards the anodic range. It resembles the high frequency curve of fig. 5.

THE EQUIVALENT CIRCUIT FOR THE Si/HF INTERFACE

The experimental results suggest a model for the interface structure, which may be conveniently represented by an equivalent electric circuit.

If the equivalent circuit is appropriately synthetised, its components do not depend on frequency, but are directly related to the physical magnitudes which characterise the surface.

a) *The p Si/HF interface*

The equivalent circuit in fig. 9 is suggested by the analysis of the curves in fig. 3 and fig. 6, which show the variation of the differential capacity of the *p* Si, with the surface potential, measuring signal frequency, carriers frequency and electrode immersion time. In this circuit the variation of the capacity with the potential is essentially determined by the space charge layer capacity C_{sc} and the solution double layer C_{sol}; the frequency dependence is determined by capacity C_s and resistance r_s associated to the surface states which have a relaxation time $\tau = r_s C_s$.

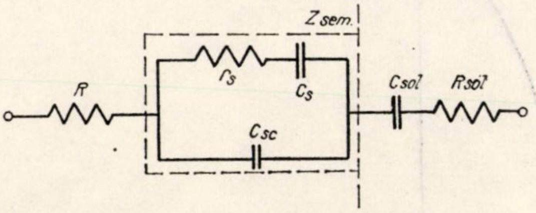

Fig. 9. — Equivalent circuit of p Si/HF interface.

The impedance of the circuit is expressed by equation,

$$Z = R + Z_{sem} + \frac{1}{j\omega C_{sol}} + R_{sol} = R_m + \frac{1}{j\omega C_m} \tag{1}$$

in which R_m and C_m are the measuring parameters and Z_{sem} is expressed according to fig. 9 by its components,

$$Z_{sem} = R_{sem} + \frac{1}{j\omega C_{sem}} \tag{2}$$

in which

$$R_{\text{sem}} = \frac{\tau C_s}{(C_s + C_{sc})^2 - \omega^2 \tau^2 C_{sc}{}^2} \tag{3}$$

$$C_{\text{sem}} = \frac{(C_{sc} + C_s)^2 - \omega^2 \tau^2 C_{sc}{}^2}{C_s + C_{sc} + \omega^2 \tau^2 C_{sc}} \tag{4}$$

Thus the impedance may be written as

$$= R + R_{\text{sol}} + R_{\text{sem}} + 1/j\omega(1/C_{\text{sem}} + 1/C_{\text{sol}}) = R_m + 1/j\omega C_m \tag{5}$$

in which R_{sem} and C_{sem} are frequency dependent due to surface states introduced through r_s and C_s.

These equations (1–5) allow the analysis of the measuring parameters R_m and C_m.

At high frequencies, $\omega\tau \gg 1$,

$$1/C_m \simeq -1/C_{sc} + 1/C_{\text{sol}} \tag{6}$$

At low frequencies, $\omega\tau \ll 1$,

$$1/C_m \simeq 1/C_{sc} + C_s) + 1/C_{\text{sol}} \tag{7}$$

Thus the proposed equivalent circuit is correctly described by the frequency variation of the measured capacity C_m. At high frequencies the contribution of the components which characterise the surface states C_s, r_s and τ is completely negligible, and the semiconductor takes part in the measurement only through the space charge region C_{sc}. At sufficiently low frequencies, the surface state contribution appears through the whole additive capacity C_s. Throughout the intermediary frequency range the parameter C_m is within the limits.

$$|C_{sc} + C_s| > |C_m(\omega)| > |C_{sc}| \tag{8}$$

b) *The n Si/HF interface*

The analysis of the curves in figs. 4a, 4b, 7 and 8 shows the saturation tendency of the capacity in the anodic range (the more so the higher the frequency) and finally reaching the characteristic values of the depleted space charge region range.

If this behaviour is correlated to the fact that the holes are consumed in the anodic range at the interface due to the d.c. field and the a. c. signal, one may assume that a delay appears in the surface, being fed with holes by the volume. At high frequencies the holes no longer reach the surface which appears as completely depleted and does not form an inversion layer.

The equivalent circuit proposed for the p Si should thus be completed with components which describe the carriers transport towards the surface.[9] Such an equivalent circuit for a reverse biased n type silicon is shown in fig. 10, in which two capacitances are associated to the space charge region: (i) C_D determined by the majority carriers (electrons) which characterise the depletion layer and (ii) C_I determined by the minority carriers (holes) which characterise the inversion layer. The inversion layer is fed with carriers through resistance R_D which limits the holes transport through the space charge region. The C_s capacitance is associated to the charge accumulated on the surface states, and resistance r_s characterises the charge exchange between the surface states and the space charge region.

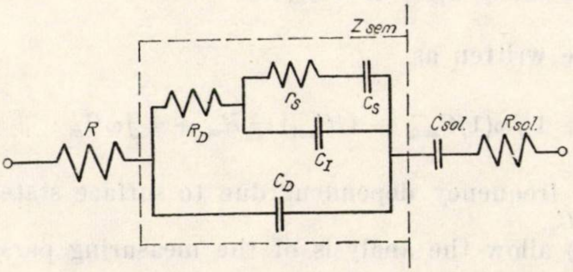

Fig. 10. — Equivalent circuit of reverse biased n Si/HF interface.

This model can also be described by eq. (5) if one takes for the $C_{\rm sem}$ the following expression

$$C_{\rm sem}=\frac{\dfrac{(C_{\rm I}+C_D+C_{\rm s})^2}{\omega^2}+\omega^2\tau^2R_D^2C_I^2C_D^2+R_{\rm D}^2C_{\rm D}^2(C_{\rm I}+C_{\rm s})^2+2\tau R_{\rm D}C_{\rm D}^2C_{\rm s}-\tau^2(C_{\rm I}+C_{\rm D})^2}{-\dfrac{C_I+C_D+C_s}{\omega^2}-\omega^2\tau^2R_D^2C_I^2C_D+R_{\rm D}^2C_D(C_{\rm I}+C_{\rm s})^2+\tau R_{\rm D}[2C_{\rm I}(C_{\rm I}+C_{\rm s}+C_{\rm D})+C_{\rm D}(2C_{\rm s}+C_{\rm I})+\tau^2(C_{\rm I}+C_{\rm D}} \tag{9}$$

The analysis of eq (9) shows that, at high frequencies $\omega\tau\gg 1$, whatever $R_{\rm D}$,

$$C_{\rm sem}\simeq -C_D \tag{10}$$

i. e. the space charge region takes part in the measurement only as completely depleted for a reverse bias.

At low frequencies $\omega\tau\ll 1$ and not a very high R_D

$$C_{\rm sem}\simeq-(C_I+C_D+C_s) \tag{11}$$

i. e. the space charge takes part in the measurement completely depleted through C_s, with the minority carriers through C_I and with the surface states through C_s.

---

[9] K. Lehovec and A. Slobodskoy, *Solid State Electronics*, **7**, 59 (1964).

At the intermediate frequencies, C_{sem} is within the upper discussed limits. It is worth mentioning here the case when there is a deficient supply of minority carriers, i. e. when R_D is high.

Under such conditions,

$$C_{\text{sem}} \simeq C_D \left[-1 + \frac{2(C_I + C_s)^2}{(C_I + C_s)^2 - \omega^2 \tau^2 C_I^2} \right] \tag{12}$$

and the semiconductor behaves in a way similar to the high frequency case, i. e. it takes part in the measurements mainly through the depleted space charge region, through C_D.

CONCLUSIONS

The proposed model which is described by equivalent circuits in figs. 9 and 10, accounts for all the experimental findings. A detailed analysis has been made on the semiconductor contribution. Further investigations are necessary to obtain more details about the solution contribution.

Revue Roumaine de Chimie, 20, 3, 305–315 (1975)

Revue Roumaine de Chimie, 20, 3, 317–321 (1975)

CERTAINS PROBLÈMES CONCERNANT LA CINÉTIQUE DE L'ADSORPTION SUR DES SURFACES HÉTÉROGÈNES

EUGEN SEGAL

Chaire de théorie cinétique de la matière
et de cinétique chimique Université de Bucarest 13, Bd. Republicii

Reçu le 14 janvier 1974

En partant d'un modèle simple et général, on analyse l'influence de la forme de la fonction de distribution des énergies d'activation des centres superficiels sur la forme des équations cinétiques de l'adsorption.

L'hétérogénéité de la surface, telle qu'elle est traitée par la théorie statistique de l'adsorption, peut être considérée du point de vue de la chaleur d'adsorption, aussi bien que de celui de l'énergie d'activation de ce phénomène.[1,2] Pour le second cas d'hétérogénéité, si on suppose que la surface adsorbante est formée par des portions dont l'énergie d'activaton a une certaine valeur E, le degré de recouvrement étant θ_E et la fonction de distribution des énergies d'activation $-\rho(E)$, le degré total de recouvrement sera exprimé par :

$$\theta = \int_{E_1}^{E_2} \theta_E \, \rho(E) \, \mathrm{d}E \tag{1}$$

où E_1 et E_2 sont les valeurs minimale et, respectivement, maximale de l'énergie d'activation.

Si on considère homogène la portion de surface pour laquelle le degré de recouvrement est égal à θ_E, la cinétique de l'adsorption sur cette portion sera décrite par la loi simple

$$\frac{\mathrm{d}\theta_E}{\mathrm{d}t} = k_E \, \mathrm{e}^{-k_E t} \tag{2}$$

où

$$k_E = k_0 \, \mathrm{e}^{-\frac{E}{RT}} \tag{3}$$

---

[1] S. Z. Roghinsky, « Adsorbtsia i kataliz na neodnorodnykh poverhnostiakh », Izdatelstvo Akademii Nauk S.S.S.R., Moscou—Leningrad, 1948.

[2] S. Z. Roghinsky et I. Zeldovitch, *Acta Phys. Chim. U.R.S.S.*, **1**, 449, 554, 595, 651 (1934); *Nature*, **134**, 935 (1934). S. I. Elovitch et G. M. Jabrova, *Zhur. fiz. khim.*, **13**, 1761, 1775 (1939).

t représentant le temps. L'équation cinétique différentielle (2) correspondant à la vitesse d'adsorption pour un certain groupe de centres a été établie sans tenir compte de l'effet de la désorption.

En supposant que les groupes de centres d'adsorption sont successivement recouverts intégralement ($\theta_E = 1$), la relation (1) devient [3,4]:

$$\theta = \int_{E_1}^{E_2} \rho(E)\, \mathrm{d}E \tag{4}$$

En introduisant dans (4) la condition

$$\rho(E) = H = \text{const.} \tag{5}$$

qui caractérise du point de vue cinétique les surfaces uniformément hétérogènes, on obtient, à la fin des calculs, l'équation cinétique intégrale

$$\theta = k \ln t + C \tag{6}$$

qui est une variante de la bien connue équation Roghinsky-Zeldovitch-Elovitch (RZE).[2] En appliquant l'équation (6), on obtient pour le moment initial une valeur infinie de la vitesse d'adsorption.

En analysant critiquement les hypothèses à partir desquelles on a établi l'équation (6), Peers, [4] basé sur les recherches de Kubokawa, [5] a considéré que l'inconsistance de cette équation est due aux approximations utilisées dans les calculs et a réexaminé le problème d'une façon plus rigoureuse. En renonçant à l'approximation $\theta_E = 1$ et en supposant la surface uniformément hétérogène du point de vue cinétique, il a obtenu une équation cinétique différentielle qui diffère de l'équation RZE mais décrit le phénomène de façon semblable.

Dans cette note, on présente un essai d'établir, à l'aide du modèle de Peers, des équations cinétiques correspondant au processus d'adsorption pour d'autres fonctions de distribution des énergies d'activation. C'est pourquoi, on considère la solution générale du problème qui doit être particularisé pour différentes formes de la fonction de distribution.

La forme la plus générale de l'équation cinétique différentielle de l'adsorption peut être obtenue en dérivant l'égalité (1) par rapport au temps

$$\frac{\mathrm{d}\theta}{\mathrm{d}t} = \int_{k_1}^{k_2} \frac{\mathrm{d}\theta_E}{\mathrm{d}t}\, \rho(E)\, \frac{\mathrm{d}E}{\mathrm{d}k_E}\, \mathrm{d}k_E \tag{7}$$

En introduisant dans l'équation (7) différentes fonctions de distribution des énergies d'activation et en supposant la surface homogène par rapport à l'entropie d'activation de l'adsorption (k_0 = constant pour toutes les

---

[3] F. S. STONE, « Chemistry of the Solid State » (W. E. Garner, ed.), Butterworths, Londres, 1955, p. 367.

[4] A. M. PEERS, *J. Catalysis*, **4**, 499 (1965).

[5] Y. KUBOKAWA, *Bull. Chem. Soc. Japan*, **33**, 734 (1960).

portions de la surface), on peut obtenir, en principe, les équations cinétiques correspondant aux différents types d'hétérogénéité.

En intégrant l'équation différentielle (7), on obtient

$$\theta = f(t, k_1, k_2) + C \tag{8}$$

où k_1 et k_2 représentent des paramètres. On déduit la constante C en tenant compte que $\theta = 0$ pour $t = 0$. Si la fonction $f(t, k_1, k_2)$ devient infinie pour $t = 0$, alors, pour déterminer la constante C, on utilisera la condition la plus désavantageuse d'après laquelle $\theta = 1$ pour $t = \infty$. Les résultats peuvent encore être simplifiés en considérant $E_2 \gg E_1$, si bien qu'on peut introduire la condition $k_2 \to 0$ dans les équations cinétiques (7) et (8).

Dans ce qui suit, on présente les équations cinétiques différentielles et intégrales obtenues pour les fonctions de distribution linéaire $\rho(E) = HE$ et exponentielle $\rho(E) = He^{\alpha E}$, où H et α sont des constantes.

$$1.\ \rho(E) = HE \tag{9}$$

$$\frac{\mathrm{d}\theta}{\mathrm{d}t} = H(RT)^2 \int_{k_1}^{k_2} e^{-k_1 t}\left(\ln \frac{k_E}{k_0}\right) \mathrm{d}k_E \tag{10}$$

$$\begin{aligned} \frac{\mathrm{d}\theta}{\mathrm{d}t} = H(RT)^2 \Bigg\{ & \frac{1}{t}\left[\left(\ln \frac{k_1}{k_0}\right) e^{-k_1 t} - \left(\ln \frac{k_2}{k_0}\right) e^{-k_2 t}\right] + \\ & + \sum_{n=2}^{\infty} (-1)^n \frac{(n-2)!}{t^n}\left[\frac{1}{k_1^{n-1}} e^{-k_1 t} - \frac{1}{k_2^{n-1}} e^{-k_2 t}\right]\Bigg\} \end{aligned} \tag{11}$$

$$\begin{aligned} \theta = H(RT)^2 \Bigg\{ & \left(\ln \frac{k_1}{k_0}\right) E_i(-k_1 t) - \left(\ln \frac{k_2}{k_0}\right) E_i(-k_2 t) + \\ & + \sum_{n=2}^{\infty} (-1)^n (n-2)\left[\frac{1}{k_1^{n-1}}\left(\frac{(-k_1)^{n-1}}{(n-1)!} E_i(-k_1 t) + \right.\right. \\ & \left. + e^{-k_1 t} \sum_{k=1}^{n-1} (-1)^k \frac{k_1^{k-1}}{\left[\prod_{k=1}^{k} (n-k)\right] t^{n-k}}\right) - \frac{1}{k_2^{n-1}}\left(\frac{(-k_2)^{n-1}}{(n-1)!} E_i(-k_2 t) + \right. \\ & \left.\left. + e^{-k_2 t} \sum_{k=1}^{n-1} (-1)^k \frac{k_2^{k-1}}{\left[\prod_{k=1}^{k} (n-k)\right] t^{n-k}}\right)\right] + \frac{1}{H(RT)^2}\Bigg\} \end{aligned} \tag{12}$$

La fonction $E_i(-x)$ est définie par la relation[6]

$$E_i(-x) = -\int_x^{\infty} y^{-1}\, \mathrm{e}^{-y}\, \mathrm{d}y.$$

L'équation cinétique différentielle (11), ainsi que celle intégrale (12), sont compliquées et ne peuvent être simplifiées pour le cas de $k_2 \to 0$, discuté antérieurement.

Pour la même fonction de distribution, en utilisant l'approximation $\theta_E = 1$, on obtient une isotherme cinétique plus simple[1]:

$$\theta^{1/2} \cong a \ln t + C \tag{13}$$

$$2.\ \rho(E) = H\, \mathrm{e}^{\alpha E} \tag{14}$$

$$\frac{\mathrm{d}\theta}{\mathrm{d}t} = -HRT \int_{k_1}^{k_2} \mathrm{e}^{\left(\alpha RT \ln \frac{k_0}{k_1} - kt\right)} \mathrm{d}k \tag{15}$$

$$\frac{\mathrm{d}\theta}{\mathrm{d}t} = HRT \left[\frac{1}{\frac{\alpha RT}{k_1} + t}\, \mathrm{e}^{\left(\alpha RT \ln \frac{k_0}{k_1} - k_1 t\right)} - \frac{1}{\frac{\alpha RT}{k_2} + t}\, \mathrm{e}^{\left(\alpha RT \ln \frac{k_0}{k_2} - k_2 t\right)} \right] \tag{16}$$

Pour $k_2 \to 0$, l'équation cinétique différentielle (16) devient

$$\frac{\mathrm{d}\theta}{\mathrm{d}t} = \frac{A\, \mathrm{e}^{-k_1 t}}{B + t} \tag{17}$$

où

$$A = HRT\, \mathrm{e}^{\ln \frac{k_0}{k_1}}$$

$$B = \frac{\alpha RT}{k_1}$$

Etant donné que, pour $x \ll 1$[6],

$$E_i(-x) \cong \ln\,(1{,}781\ x) \tag{18}$$

en supposant les valeurs de k_1, t et B encadrées dans un intervalle pour lequel la relation (18) est satisfaite, on obtiendra

$$\theta = \text{const.} \ln \frac{B + t}{B} \tag{19}$$

qui est une forme de l'équation RZE.

---

[6] J. Weber et T. Loucka, *Coll. Czech. Chem. Comm.*, **36**, 3214 (1971).

On remarque que, pour $\theta_E = 1$, l'équation cinétique intégrale résultée pour la même forme de la fonction de distribution aura la forme [1]

$$\theta \cong a\ t^{1/n} - C \tag{20}$$

La particularisation de l'équation (2) pour les premiers moments de l'adsorption sur une certaine catégorie de centres, ou bien pour des valeurs réduites de la constante k_E, nous permettra d'obtenir

$$\frac{\mathrm{d}\theta_E}{\mathrm{d}t} = k_E \tag{21}$$

$$\frac{\mathrm{d}\theta}{\mathrm{d}t} = \int_{E_1}^{E_2} k_E\, \rho(E) \frac{\mathrm{d}E}{\mathrm{d}k_E}\, \mathrm{d}k_E = k \tag{22}$$

et, par conséquent,

$$\theta = kt \tag{23}$$

L'équation (23) représente un cas particulier de l'équation de Bangham. [7]

CONCLUSIONS

En conclusion, on peut affirmer que l'équation RZE décrit de façon formelle la cinétique de l'adsorption, même pour certains cas d'hétérogénéité qui ne sont pas caractérisés par la condition (5). Il résulte que la vérification de l'équation (6) ne représente pas un indice certain sur l'hétérogénéité uniforme. De même, la vérification expérimentale, dans un grand nombre de cas, de différentes variantes de l'équation RZE, s'explique justement par le fait que celle-ci décrit de façon convenable plusieurs types d'hétérogénéité.

---

[7] D. H. Bangham et F. F. Burt, *Proc. Roy. Soc.*, **105**, 481 (1924) ; *J. Phys. Chem.*, **29**, 540 (1925).

On remarque que, pour $l_0 = 1$, l'équation cinétique intégrale [illegible] pour la même forme de la fonction de distribution que la relation

$$\vartheta = a\,t^{[illegible]} - C \qquad (20)$$

La particularisation de l'équation (?) pour les premiers moments de l'adsorption sur une certaine catégorie de centres, ou bien pour des valeurs réduites de la constante k_0, nous permettra d'obtenir

$$\frac{d\vartheta}{dt} = k_1 \qquad (21)$$

$$\frac{d\vartheta}{dt} = \int_{\varepsilon_1}^{\varepsilon_2} k_0\, c(t)\, \frac{dN}{d\varepsilon_0}\, d\varepsilon_0 = k \qquad (22)$$

et, par conséquent

$$\vartheta = kt \qquad (23)$$

L'équation (23) représente un cas particulier de l'équation de Bangham.[7]

CONCLUSIONS

En conclusion, on peut affirmer que l'équation RZE décrit de façon formelle la cinétique de l'adsorption, même pour certains cas d'hétérogénéité qui ne sont pas caractérisés par la condition (5). Il résulte que la vérification de l'équation (6) ne représente pas un indice certain sur l'hétérogénéité uniforme. De même, la vérification expérimentale, dans un grand nombre de cas, de différentes variantes de l'équation RZE, s'explique justement par le fait que celle-ci décrit de façon acceptable plusieurs types d'hétérogénéité.

---

[7] D. H. Bangham et F. P. Burt, Proc. Roy. Soc. 105, 481 (1924); J. Phys. Chem. 29, 540 (1925).

Revue Roumaine de Chimie, 20, 3, 323–335 (1975)

LE SYSTÈME NICKEL (II)-THIOSEMICARBAZIDE

N. CALU et ADINA POPA-RANG

Faculté de Chimie, Université « Al. I. Cuza », Jassy, 11, str. 23 August

Reçu le 21 avril 1973

L'ion Ni^{2+} aq forme avec la thiosemicarbazide, dans des solutions aqueuses de pH$\sim$5, plusieurs ions complexes $[NiL_n]^{2+}$, où L = la thiosemicarbazide et $n = 2, 3, 4$ et 6, le ligand fonctionnant avec 3, 2, 1, 5 (en moyenne) et, respectivement, une fonction basique comme centre de coordination. Les équilibres s'établissent à la longue. Les spectres électroniques des ions complexes mentionnés ont été interprétés à l'aide de la théorie du champ cristallin et de celle du champ des ligands. Les valeurs calculées pour D_q se situent entre 1025 et 1064 cm^{-1} et, pour β_{35}, entre 0,81–0,82. Dans ces ions complexes, la liaison métal-ligand a un caractère partiellement covalent.

Certains ions complexes du nickel (II) avec la thiosemicarbazide ont été préparés par Jensen et ses collaborateurs, [1–3] à partir de 1934.

D'après Jensen, le complexe de rapport 1 : 2, formé en milieu alcalin présente une structure de complexe interne, avec une liaison covalente... S—Ni..., et celui de rapport 1 : 3, une structure avec des liaisons coordinatives.

L'étude de ces complexes a été continuée à l'aide de méthodes comme : les spectres de rayons x,[4–7] les méthodes spectrophotométriques,[8] potentiométriques [9] et d'autres. [10,11]

Néanmoins les ions complexes du nickel (II) avec la thiosemicarbazide ne sont pas élucidés.

Dans le présent travail, on donne les résultats de certaines études spectrophotométriques sur le système Ni (II)-thiosemicarbazide en solutions aqueuses de pH ~ 5.

---

[1] K. A. Jensen et E. Randke-Madsen, *Z. anorg. Chem.*, **219**, 213 (1934).
[2] K. A. Jensen, *Z. anorg. Chem.*, **221**, 11 (1934).
[3] K. A. Jensen, *Z. anorg. Chem.*, **229**, 265 (1936).
[4] M. Nardelli et P. Boldrini, *Gazz. chim. Ital.*, **91**, 280 (1961).
[5] P. Domiano, G. Fava Gaspari et M. Nardelli, *Ricerca Sci.*, **36**, 744 (1966).
[6] R. Groenback et S. E. Rasmussen, *Acta chem. Scand.*, **14**, 782 (1960).
[7] R. Groenback, *Acta chem. Scand.*, **22**, 2171 (1968).
[8] M. K. Akhmedli et L. F. Zhirova, *Zhur. neorg. Khim.*, **5**, 2742 (1960).
[9] T. A. Preobrazhenskaia, *Sb. Aspir. Rab. Kazan Gos. Univ. Khim. Geol.*, 77 (1967); *Chem. Abstr.*, **70**, 109614 (1969).
[10] R. A. Haines et K. W. Sun Kenneth, *Canad. J. Chem.*, **46**, 3241 (1968).
[11] Jun Moon Am, *Punsok Hwahak*, **8**, 51 (1970) ; *Chem. Abstr.*, **75**, 94234 (1971).

RÉSULTATS ET DISCUSSIONS

A) LES RÉACTIFS

On a utilisé des solutions aqueuses de chlorure de nickel (M) et de thiosemicarbazide (L) de concentrations situées entre $2.10^{-2} - 5.10^{-3}$ moles/l

La structure de la thiosemicarbazide, — un dérivé de la thio-urée — peut être discutée à partir de quelques formes canoniques, structures limites, avec une conjugaison $n\pi$, à savoir :

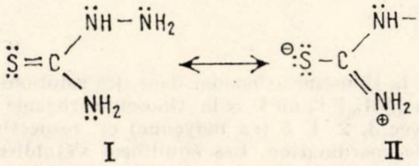

Parmi les formes tautomères possibles, nous mentionnons celle avec la structure (III) :

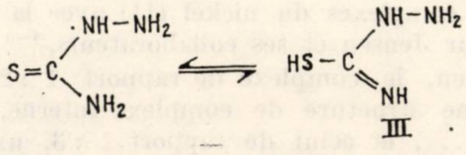

La fonction $-NH_2$ du reste $-NH-NH_2$ de la thiosemicarbazide représente probablement la partie la plus basique.

Dans la figure 1, on représente la variation du pH, au titrage de la thiosemicarbazide avec l'acide chlorhydrique et l'hydroxyde de sodium.

Sur la courbe $\Delta pH/\Delta V = f(V)$ apparaît un maximum devant 1,25 ml HCl, ce qui correspond au rapport 1,56 moles HCl : 1 mole thiosemicarbazide.

Le résultat obtenu suggère que, dans ces conditions, les molécules du ligand sont en équilibre d'après les formes (I) et (III) et qu'elles manifestent en moyenne ~1,5 fonctions$-NH_2$, titrables avec acide dans un seul palier, entre les pH-s 5,2 et 1,5. Ce comportement se reflète aussi dans la structure des complexes du nickel (II) avec la thiosemicarbazide.

Le reste des groupements basiques de la molécule du ligand sont plus faibles et pour des valeurs du pH plus petites leur neutralisation n'est pas observée sur la courbe de titrage.

La thiosemicarbazide réagit aussi avec l'hydroxyde de sodium (figure 1), processus qui implique la forme tautomère iso (III).

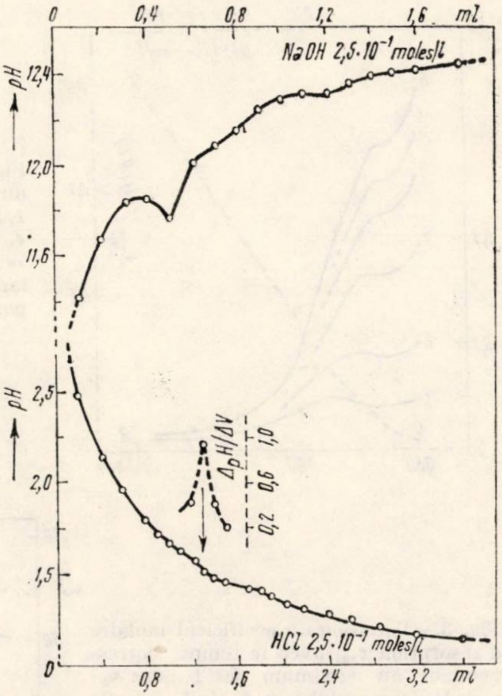

Fig. 1. — Variation du pH au titrage de la thiosemicarbazide avec du HCl et du NaOH. Thiosemicarbazide : 5 ml 4. 10^{-2} moles/l. Un équivalent d'acide (de base) : 0,8 ml HCl (NaOH) 2,5.10^{-4} moles/l.

B) COMPOSITION ET STABILITÉ DES IONS COMPLEXES DU SYSTÈME Ni(II)-THIOSEMICARBAZIDE (ML)

Dans la réaction de l'ion Ni^{2+} aq et de la thiosemicarbazide, se forment par degrés plusieurs ions complexes ; les équilibres sont influencés par le pH et la concentration de la solution et s'établissent à la longue.

Dans la figure 2, on représente quelques bandes d'absorption de ces ions complexes, obtenus en solutions aqueuses au pH ~ 5.

On observe d'importants effets hypsochromiques et hyperchromiques par rapport à la bande de l'ion $Ni^2 + $ aq, preuve de la formation de nouveaux composés dans le système ML.

Dans la figure 3, on donne une représentation

$$\varepsilon_{365} = f(t) \qquad (1)$$

où ε_{365} = le coefficient molaire d'absorption pour le maximum des bandes ν_3,

$$t = \text{le temps,}$$

qui indique quelques modifications subies à la longue par les ions complexes étudiés. Au bout de 50 heures environ, il y a une bonne ressemblance en ce qui concerne les valeurs ε_{365}, entre les composés formés pour les rapports 1 : 3 et 1 : 4.

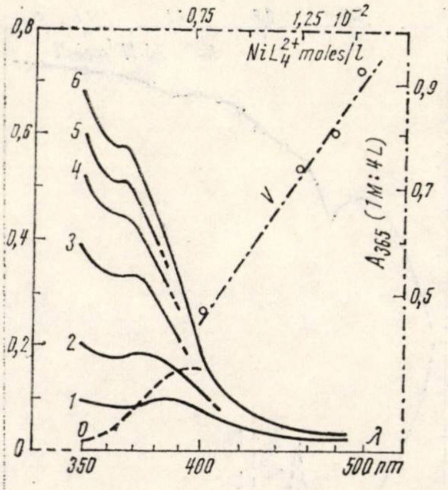

Fig. 2. — Bandes ν_3 de quelques ions complexes du système ML. Ni^{2+} aq = 1,66.10^{-2} ions-g/l; *1*, M : L = 1 :1 ; *2*, M : L = 1 : 2 ; *3*, M : L = 1 : 3 ; *4*, M : L = 1 : 4 ; *5*, M : L = 1 : 5 ; 6, M : L = = 1 : 6 ; 1 – 6. conc. du Ni^{2+} = 8,33.10^{-3} ions-g/l ; *v* — vérification de la loi de Beer pour l'ion complexe de rapport 1 : 4 $[NiL_4]^{2+}$.

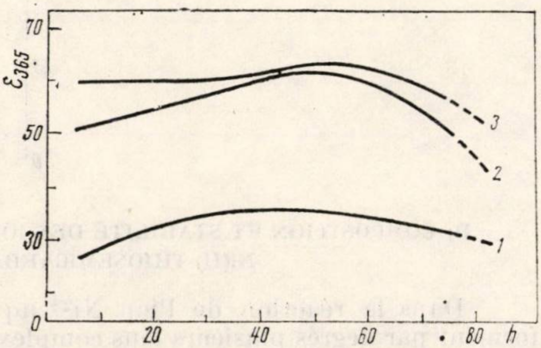

Fig. 3.— Variation du coefficient molaire d'absorption ε_{365} avec le temps, correspondant au maximum des bandes ν_3, pour les ions complexes. *1*, M : L = 1 : 2 ; *2*, M : L = 1 :3 ; *3*, M : L = 1 : 4 ; conc. du Ni^{2+} = 1,54.10^{-2} ions-g/l.

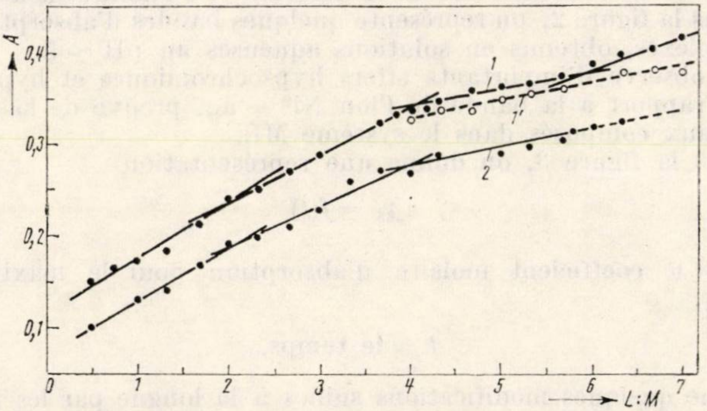

Fig. 4. — Données concernant la composition des ions complexes du système ML, par la méthode des rapports molaires. 1. λ = 345 nm ; cuve 0,5 cm ; *t* = 26 h ; 1'. λ=345 nm ; cuve 0,5 cm ; *t* = 0 ; 3. λ = 592 nm ; cuve 1 cm ; *t* = 26 h ; conc. du Ni^{2+} = 7,14.10^{-3} ions-g/l.

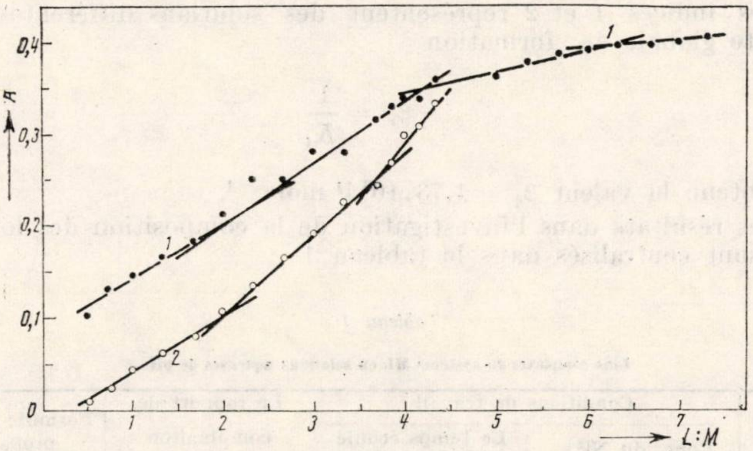

Fig. 5. — Données concernant la composition des ions complexes du système ML, par la méthode des rapports molaires. *1*, $\lambda = 345$ nm ; cuve 0,5 cm ; $t = 15$ h ; *2*, $\lambda = 345$ nm ; cuve 0,5 cm ; $t = 42$ h ; conc. du $Ni^{2+} = 8{,}33$ ions-g/l.

La composition des ions complexes du système ML au pH ~ 5 a été déterminée sur la base de l'analyse

$$A = f(L : M) \tag{2}$$

où

$A =$ l'absorbance de la solution,

au moyen de la méthode des rapports molaires.[12]

Les résultats obtenus sont représentés dans les figures 4 et 5.

La composition et la constante globale de formation de l'ion complexe, pour un excès de ligand, ont été déterminées, d'après la méthode de Edmonds et Birnbaum,[13] à l'aide de la relation

$$K_i = \frac{C_{L_1}^n \cdot C_{L_2}^n (A_1 - A_2)}{A_2\, C_{L_1}^n - A_1\, C_{L_2}^n} \tag{3}$$

où

A = l'absorbance de la solution pour $\lambda = 365$ nm,
C_L = la concentration du ligand,
n = le nombre de coordinence,
K_i = la constante d'instabilité

---

[12] J. Joe et A. Jones, *Ind. Eng. Chem. Anal. Ed.*, **16**, 11 (1944).
[13] S. Edmonds et N. Birnbaum, *J. Amer. Chem. Soc.*, **63**, 1471 (1941).

(les indices 1 et 2 représentent des solutions différentes) et la constante globale de formation

$$\beta_n = \frac{1}{K_i} \tag{4}$$

On a obtenu la valeur $\bar{\beta}_4 = 1{,}73 . 10^6 \ l^4 \ \text{mole}^{-4}$.

Les résultats dans l'investigation de la composition des ions complexes sont centralisés dans le tableau 1.

Tableau 1

Ions complexes du système ML en solutions aqueuses de pH∼5

N°	Conditions de travail		Le rapport de combinaison M : L	Formule chimique probable de l'ion complexe
	Conc. du Ni^{2+} ions-gramme/l	Le temps écoulé après la jonction des réactifs		
1	$7{,}14.10^{-3}$ et $8{,}33.10^{-3}$	0, 15, 24 et 45 heures	1 : 2	$[NiL_2]^{2+}$
2	$8{,}33.10^{-3}$	45 heures	1 : 3, 4 (. . 6)	$[NiL_3]^{2+}$
3	$7{,}14{,}10^{-3}$ et $8{,}33.10^{-3}$ 5.10^{-3}	0, 15 24 heures O heures ; en excès de ligande	1 : 4	$[NiL_4]^{2+}$
4	$7{,}14.10^{-3}$ et $8{,}33.10^{-3}$	15 et 24 heures	1 : 6	$[NiL_6]^{2+}$

C) STRUCTURE DES IONS COMPLEXES DANS LE SYSTÈME Ni(II)-THIOSEMICARBAZIDE

Puisque la thiosemicarbazide a plusieurs centres de coordination avec différentes possibilités de réaction, quelques problèmes concernant la structure de ces complexes se posent, à savoir :

— Quel est le nombre des centres de coordination, utilisés par le ligand, dans ces ions complexes de différents rapports M : L.

— Si dans les ions complexes formés en solutions aqueuses à un pH ∼ 5 apparaissent des liaisons covalentes . . . S—Ni. .

— Si les ions complexes contiennent aussi des molécules d'eau de coordinence.

En marge de ces problèmes, on fournit quelques données expérimentales :

1. Dans le cas d'une réaction

$$n \, HL' + NiCl_2 \rightleftharpoons [NiL'_n]^{(+2-n)} + n \, HCl \tag{5}$$

avec la formation des ions complexes qui contiennent des liaisons covalentes ...S—Ni... dans le système il résulte un acide fort et la concentration des ions H^+ est indiquée par la relation :

$$\text{ions-gramme } H^+ = n.\ \text{ions-gramme } [NiL'_n]^{(+2-n)} \qquad (6)$$

C'est dans ce sens qu'on a poursuivi le pH de certaines solutions de ces ions complexes, en comparaison du pH des réactifs. Les valeurs obtenues sont présentées dans la figure 6 et le tableau 2.

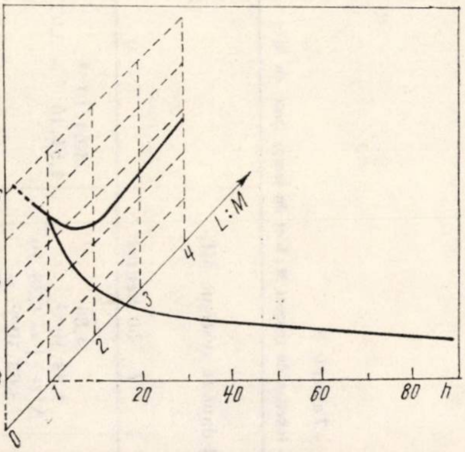

Fig. 6. — Variation du pH pour le système ML, en fonction du rapport L : M. Pour le rapport 1 : 1, on donne la variation du pH en fonction du temps.

On constate que, dans la réaction de $NiCl_2$ et de la thiosemicarbazide, il résulte une certaine quantité d'ions H^+, mais beaucoup trop petite, par exemple $0{,}68.10^{-3}$ fois plus petite que celle correspondant à la formation d'une seule liaison covalente, dans un tel complexe.

En conséquence, pratiquement, il n'y a pas de liaison covalente ...S—Ni..., dans les ions complexes du système étudié, dans des solutions aqueuses au pH ~ 5.

2. Par l'étude de la compétitition des ions Ni^{2+} et ceux H^+, envers la thiosemicarbazide, à la base d'un équilibre du type suivant :

$$[L''NH_2 \rightarrow Ni\ldots]^{2+} + H^+ \rightleftarrows Ni^{2+}\,aq + L''NH_3^+ \qquad (7)$$

on obtient des informations relatives à la coordinence de ce ligand.

Pratiquement, le processus (7) est analysé sur la base de la relation.

$$A = f(\text{HCl}) \qquad (8)$$

où

A = l'absorbance de la solution avec l'ion complexe $[NiL\ aq]^{2+}$ ou $[NiL_4]^{2+}$ pour $\lambda = 365$ nm.

Tableau 2

Variation de la concentration des ions H+ dans le système ML, en fonction du rapport M : L et du temps Conc. du Ni^{2+} : $1{,}54.10^{-2}$ ions-gramme/l

Le rapport de combinaison M : L	Le pH et la $[H^+]$ dans les solutions des réactifs		Le pH et la $[H^+]$ dans le système ML		Le rapport $[H^+]$: $[Ni^{2+}]$	
	Ni^{2+}	L	$t = 0$	$t = 50$ heures	$t = 0$	$t = 50$ heures
1 : 1	6,09	6,44 $3{,}63.10^{-7}$	5,30 $5{,}01.10^{-6}$ $\Delta[H^+] = 5{,}01.10^{-6} - 3{,}63.10^{-7} = 4{,}64.10^{-6}$	4,86 $1{,}38.10^{-5}$ $\Delta[H^+] = 1{,}38.10^{-5} - 3{,}63.10^{-7} = 1{,}34.10^{-5}$	$4{,}64.10^{-6} : 1{,}54.10^{-2} = 3{,}02.10^{-4}$	$1{,}34.10^{-5} : 1{,}54.10^{-2} = 0{,}87.10^{-3}$
1 : 2		6,23 $5{,}89.10^{-7}$	5,04 $9{,}12.10^{-6}$ $\Delta[H^+] = 8{,}53.10^{-6}$	4,89 $1{,}29.10^{-5}$ $\Delta[H^+] = 1{,}23.10^{-5}$	$5{,}54.10^{-4}$	$0{,}79.10^{-3}$
1 : 3		6,08 $8{,}32.10^{-7}$	5,09 $8{,}13.10^{-6}$ $\Delta[H^+] = 7{,}29.10^{-6}$	4,94 $1{,}15.10^{-5}$ $\Delta[H^+] = 1{,}06.10^{-5}$	$4{,}73.10^{-4}$	$0{,}68.10^{-3}$
1 : 4		5,88 $1{,}32.10^{-6}$	5,10 $7{,}94.10^{-6}$ $\Delta[H^+] = 6{,}62.10^{-6}$	4,85 $1{,}41.10^{-5}$ $\Delta[H^+] = 1{,}27.10^{-5}$	$4{,}29.10^{-4}$	$0{,}82.10^{-3}$

HCl = la quantité d'acide ajoutée par degrés à la solution de l'ion complexe.

Les résultats obtenus sont présentés dans les figures 7 et 8.

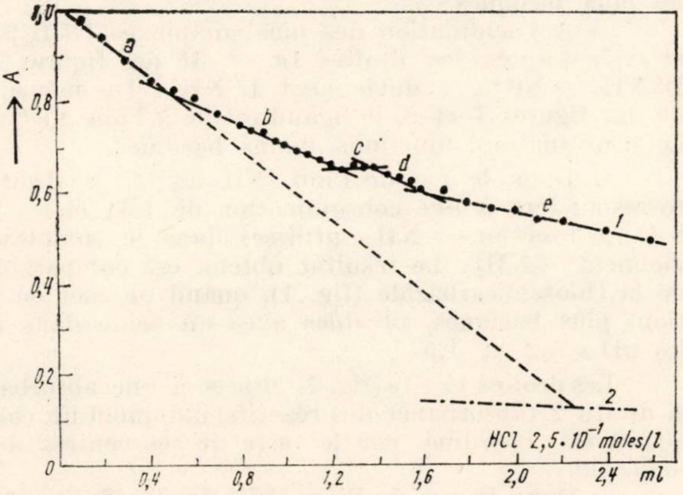

Fig. 7. — *1 a—e*. Variation de l'absorbance d'une solution de l'ion complexe $[NiL\ aq]^{2+}$ à l'addition de HCl ; 5 ml solution de l'ion complexe de conc. 4.10^{-2} ions-g/l ; l'équivalent d'acide = 0,8 ml HCl $2,5.10^{-1}$ moles/l ; $\lambda = 365$ nm ; cuve 2 cm. *2*, Absorbance des réactifs.

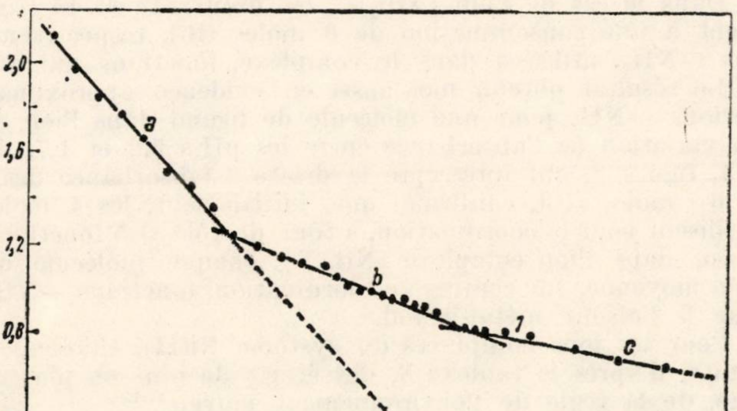

Fig. 8. — 1 *a— c*, Variation de l'absorbance d'une solution de l'ion complexe $[NiL_4]^{2+}$ à l'addition de HCl ; 5 ml solution de l'ion complexe de conc. $1,5.10^{-2}$ ions-g/l ; *1*, équivalent acide = 0,32 ml HCl $2,5.10^{-1}$ moles/l ; $\lambda = 365$ nm, cuve 2 cm. *2*, Absorbance des réactifs.

Les données expérimentales concernant le processus (7) permettent certaines remarques sur la coordinence de la thiosemicarbazide autour de l'ion Ni^{2+}, à savoir :

— Le nombre des centres de coordination utilisés par ce ligand dans l'ion complexe dépend, parmi d'autres facteurs, du rapport L : M.

Ainsi, dans la série des ions complexes des rapports L : M de 1—4, le nombre de ces centres pour une molécule de ligand baisse graduellement.

— La coordinence du ligand commence surtout par ses centres les plus basiques.

— A l'acidulation des ions complexes $[NiL_n]^{2+}$, entre les pH-s 5,2 et 1,7, d'après les droites 1*a* et 1*b* des figures 7 et 8, les fonctions $L''NH_2 \rightarrow Ni^{2+}$ ... deviennent $L''NH_3^+$. De même, à partir des droites 1*b* des figures 7 et 8, le ligand est lié à l'ion Ni^{2+} par les autres centres de coordination, fonctions moins basiques.

— Dans le cas de l'ion $[NiL\ aq]^{2+}$, les droites 1*a* et 1*b* (fig. 7) correspondent à une consommation de 1,54 moles HCl, respectivement, à ~ 1,5 fonctions $-NH_2$, utilisées dans le complexe, fonctions qui deviennent $-NH_3^+$. Le résultat obtenu est comparable à celui du titrage de la thiosemicarbazide (fig. 1), quand on met en évidence ~1,5 fonctions plus basiques, titrables avec un acide dans un seul palier, entre les pH-s 5,2 et 1,5.

Les droites 1*b*—1*e* (fig. 7) situées à une absorbance plus grande que la droite 2 (absorbance des réactifs) indiquent un complexe dans lequel le ligand est coordiné par le reste de ses centres de coordination de la molécule.

— Dans le cas de l'ion $[NiL_4]^{2+}$, les droites 1*a* et 1*b* (fig. 8) correspondent à une consommation de 6 moles HCl, respectivement, à 6 fonctions $-NH_2$, utilisées dans le complexe, fonctions qui deviennent $-NH_3^+$. Le résultat obtenu met aussi en évidence approximativement 1,5 fonctions $-NH_2$ pour une molécule de ligand dans l'ion complexe.

La variation de l'absorbance entre les pH-s 5,2 et 1,7, d'après la droite 1*a*, figure 8, qui intercepte la droite 2 (absorbance des réactifs) devant 6 moles HCl, confirme que, initialement, les 4 molécules de ligand utilisent pour la coordination, à tour de rôle, 1,5 fonctions $-NH_2$.

Ainsi, dans l'ion complexe $[NiL_4]^{2+}$, chaque molécule de ligand utilise, en moyenne, 1,5 centres de coordination, fonctions $-NH_2$, quand on réalise 6 liaisons métal-ligand.

3. Pour les ions complexes du système Ni(II). thiosemicarbazide, on constate, d'après le tableau 3, des écarts de plus en plus grands, à la longue, de la règle de l'environnement moyen[14,15] :

$$\bar{\nu}\ ML_nL'_{6-n} \simeq \frac{n}{6}\bar{\nu}_{ML_6} + \frac{6-n}{6}\bar{\nu}_{ML'_6} \qquad (9)$$

où

$ML_6 = Ni^{2+}$ aq,
$ML'_6 = NiL_4^{2+}$,
n = le nombre de coordinence du métal,
$ML_nL'_{6-n}$ = les éventuels ions complexes intermédiaires formés avec l'eau et la thiosemicarbazide.

---

[14] R. Tsuchida, *Bull. Chem. Soc. Japan*, **13**, 436 (1938).

[15] C. K. Jorgensen, « Absorbtion Spectra and Chemical Bonding in complexes », Pergamon Press, Oxford, 1962.

Tableau 3

Données relatives à la règle de l'environnement moyen pour les ions complexes du système ML

Le rapport de combinaison $Ni^{2+}:L$	$t = 0$ heures			$t = 50$ heures		
	$\bar{\nu}$ calculée d'après la relation (9) cm^{-1}	$\bar{\nu}$ expérimentale cm^{-1}	$\Delta\bar{\nu}$ cm^{-1}	$\bar{\nu}$ calculée d'après la relation (9) cm^{-1}	$\bar{\nu}$ expérimentale cm^{-1}	$\Delta\bar{\nu}$ cm^{-1}
Ni^{2+} aq	—	25.325	—	—	25.325	—
1 : 1	25.835	26.277	442	25.853	26.385	532
1 : 2	26.345	26.892	547	26.381	27.375	994
1 : 3	26.855	27.141	286	26.909	27.328	419
$[NiL_4]^{2+}$	—	27.365	—	—	27.438	—

Il est possible que le ligand éloigne, à la longue, complètement les molécules d'eau de coordination du complexe et qu'il utilise en plus grand nombre ses centres de coordination.

En conclusion, on admet que, dans les ions complexes $[NiL_n]^{2+}$, où $n = 2$, 3, 4 et 6, en solutions aqueuses de pH ~ 5, la thiosemicarbazide fonctionne avec 3, 2, $1 \sim 5$ (en moyenne) et, respectivement, un centre de coordination. Les ions complexes ont le nombre de coordinence 6 et la microsymétrie proche de O_h.

D) SPECTRES CHAMP CRISTALLIN DE QUELQUES IONS COMPLEXES DU SYSTÈME Ni(II)-THIOSEMICARBAZIDE

Une partie des spectres électroniques de quelques ions complexes du système étudié, en solutions aqueuses de pH ~ 5, sont représentés dans la figure 9 et dans le tableau 4 on trouve quelques données caractéristiques.

Tableau 4

Données relatives aux spectres d'absorption de certains ions complexes du système ML en solutions fraîches

Ion complexe	ν_1 $^3T_{2g} \leftarrow {^3A_{2g}}$		ν_2 $^3T_{1g(F)} \leftarrow {^3A_{2g}}$		ν_3 $^3T_{1g(P)} \leftarrow {^3A_{2g}}$	
	λ_{max} cm^{-1}	ε $l.cm^{-1}.mole^{-1}$	λ_{max} cm^{-1}	ε $l.cm^{-1}.mole^{-1}$	λ_{max} cm^{-1}	ε $l.cm^{-1}.mole^{-1}$
$[NiL_2]^{2+}$	10.250	20,78	16.662	13,31	26.892	28,57
$[NiL_4]^{2+}$	10.500	28,89	16.898	25,97	27.365	59,74
$[NiL_4]^{2+}$ en excès de ligand	10.638	34,4	17.000	30,00	27.569	78,00

Les spectres présentés, qui sont du type champ cristallin, sont interprétés sur la base du diagramme des niveaux énergétiques propres au cas d8, la symétrie O_h (fig. 10).

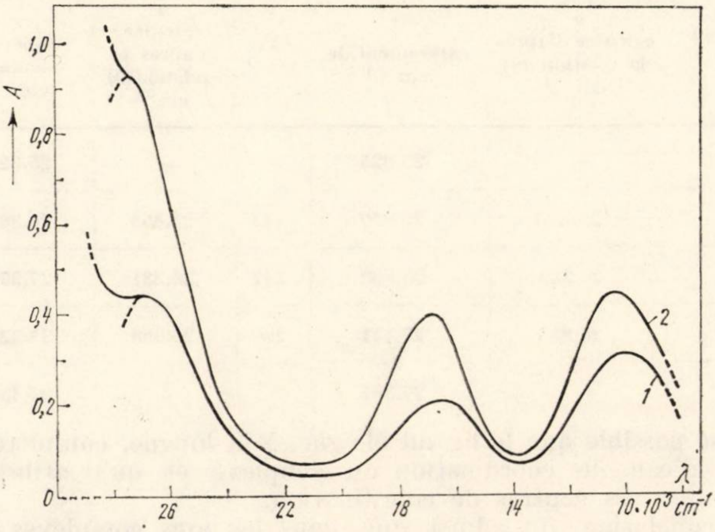

Fig. 9. — Spectres champ cristallin de quelques ions complexes du système ML ; 1. $[NiL_2]^{2+}$; conc. $1{,}54.10^{-2}$ ions-g/l ; $t = 0$; cuve 1 cm. 2. $[NiL_4]^{2+}$; conc. $1{,}54.10^{-2}$ ions-g/l ; $t=0$; cuve 1 cm.

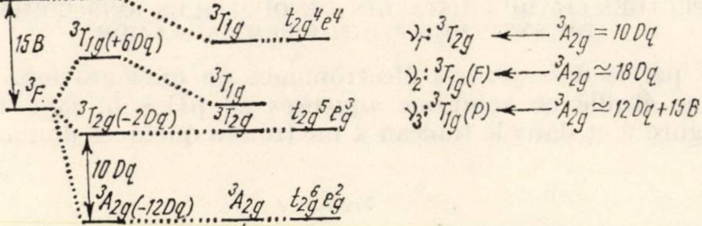
³P
³T1g
15B
³T1g(+6Dq)
³F
³T2g(-2Dq)
10 Dq
³A2g(-12Dq)
a
³T1g
³T1g
³T2g
³A2g
b
t2g⁴e⁴
t2g⁵eg³
t2g⁶eg²
ν1: ³T2g ← ³A2g = 10 Dq
ν2: ³T1g(F) ← ³A2g ≃ 18 Dq
ν3: ³T1g(P) ← ³A2g ≃ 12 Dq + 15 B

Fig. 10. — Termes spin triplet pour un ion d^8 dans la symétrie O_h.
a — champ faible ; *b* — champ élevé.

Le paramètre champ cristallin 10 D_q et celui néphélauxétique β_{35} ont été déterminés par une méthode graphique,[16] sur la base de quelques représentations

$$\nu_m/\nu_n = f(D_q/B) \tag{10}$$

où

$$m = 2{,}3 \text{ et } n = 1{,}2.$$

---

[16] A. B. P. Lever, « Inorganic Electronic Spectroscopy », Elsevier, Amsterdam — Londres — New York, 1968, p. 216 ; 392—400.

Les données sont enregistrées dans le tableau 5.

Tableau 5

Paramètres champ cristallin et néphélauxétique des ions complexes du système ML

Ion complexe	D_q	β_{35}	Observation
$[NiL_2]^{2+}$	1025	0,82	Pour calculer ces paramètres on a utilisé les rapports :
$[NiL_4]^{2+}$	1050	0,82	ν_2/ν_1, ν_3/ν_1, ν_3/ν_2
$[NiL_4]^{2+}$ en excès de ligand	1064	0,81	et $(\nu_2+\nu_3-3\nu_1)/15$

Les valeurs pour les deux paramètres $D_q = 1025-1064$ cm^{-1} et $\beta_{35} = 0{,}81-0{,}82$, distribuées dans un intervalle étroit, sont en accord avec la structure ressemblante des ions complexes du système ML. Le paramètre β_{35} indique des liaisons métal-ligand avec un caractère partiellement covalent.

CONCLUSIONS

— Dans le système Ni (II)-thiosemicarbazide, en solutions aqueuses de pH $\sim$ 5, on a identifié les ions complexes $[NiL_n]^{2+}$ où $n = 2, 3, 4$ et 6.

— Les équilibres s'établissent à la longue.

— La stabilité de l'ion complexe $[NiL_4]^{2+}$, obtenu en excès de ligand, en solutions fraîches, est $\beta_4 = 1{,}73 . 10^6$ l^4 mole^{-4}.

— Les ions complexes $[NiL_n]^{2+}$ des solutions aqueuses au pH $\sim$ 5 ne contiennent pas de liaisons covalentes ...S—Ni... Le nombre de coordinence est 6 et la microsymétrie O_h et le ligand fonctionne avec $3, 2, 1 \sim 5$ (en moyenne) et, respectivement, 1 fonction basique de coordination pour les valeurs $n = 2$, 3, 4 et 6.

— Les spectres électroniques de certains de ces ions complexes, dans des solutions fraîches ont été interprétés sur la base de la théorie du champ cristallin et de celle du champ des ligands. Le paramètre champ cristallin D_q a des valeurs entre 1025—1064 cm^{-1} et celui néphélauxétique de 0,81—0,82. Dans ces complexes, la liaison métal-ligand présente donc un caractère partiellement covalent.

Revue Roumaine de Chimie, 20, 3, 337 – 344 (1975)

NEW COMPOUNDS OF YTTRIUM AND LANTHANIDES WITH DERIVATIVES OF ANTHRANILIC ACID. II.[1,2]

N-(CARBOXY METHYL) ANTHRANILIC ACID

EUGENIA IVAN and P. SPACU
Research Center of Physical Chemistry
Str. Dumbrava Roşie 23, Bucharest, Romania

Received January, 22 1974

Some new complexes of certain lanthanides with N-carboxy methyl anthranilic acid abbreviated as [Ph—gl *o—C*] (phenyl-glycine *ortho*-carboxylic acid) have been isolated. IR and electronic spectral data have been recorded and discussed in connection with the molecular structure of the mentioned compounds. The hydroxo complexes were also prepared and characterized.

INTRODUCTION

As an extension to our previous papers [1,2] on the lanthanide coms plexes with derivatives of anthranilic acid, the present paper studie- some N-carboxy methyl anthranilic acid compounds of certain lanthanides.

Complexes with the same ligand with Fe(III) have already been investigated. [3] Recently, the acid-basic properties of both carboxy methyl derivatives of anthranilic acid, abbreviated as [ANDA] and [Ph—gl *o*—C] were studied and also their ability to form complexes with Fe(III) and Cr(III). [4] Complexes of trivalent metal ions of Al, Sc and Ga [5] with [Ph—gl *o*—C] were studied in solution within 1—14 pH.

EXPERIMENTAL

CHEMICALS

The lanthanide chlorides were prepared from the oxide Johnson Mathey of 99.9% purity, except Eu_2O_3 of 98% purity.

The N-(carboxy methyl) anthranilic acid or *phenyl-glycine ortho-carboxylic acid* [Ph—gl *o—C*] was prepared by the reaction of anthranilic acid in excess with monochloroacetic acid.

---

[1] P. Spacu and E. Ivan, *Rev. Roumaine Chim.*, **18**, 405 (1973).

[2] P. Spacu and E. Ivan, *Rev. Roumaine Chim.*, **18**, 589 (1973).

[3] I. V. Dubski, E. Tesalik, St. Rusnak and V. Sindelar, *Chem. listy*, **33**, 346 (1939).

[4] C. Drăgulescu, R. Pomoje, I. Menessy, M. Pîrlea and C. Mihăescu, *Rev. Roumaine Chim.*, **14**, 1595 (1969).

[5] C. Drăgulescu, R. Pomoje, I. Menessy and M. Pîrlea, *Rev. Roumaine Chim.*, **16**, 1329 (1971).

This reaction was studied by Philips [6] and Haller.[7] The product recrystallised from water, melts at 215–216° and is highly soluble in organic solvents, but in water it is soluble only by boiling.

PREPARATION OF COMPLEXES

All normal complexes were prepared by the same procedure. They precipitated from a mixture of ammonia solution of acid in water (pH = 4.5–5) with a solution of lanthanide chlorides at a molar ratio of about 3 : 2. The product was filtered off, washed with a small amount of water, ethyl alcohol and finally dried in vacuo over P_4O_{10}.

The hydroxocompounds were obtained when pH of the reaction medium was over 6 or by refluxing the normal complex with an ammonia solution with pH 8–9 on a boiling water bath for about one hour.

ANALYSIS

Lanthanides were estimated as their oxides by direct combustion of the compounds. Carbon, hydrogen and nitrogen were determined by microanalysis. The results of the chemical analyses are given in tables 1 and 2.

Table 1

The results of chemical analysis for: Ln_2 (Ph–gl *o*–C)$_3$. $3H_2O$

Ln	Ln %		N %		C %		H %	
	Calc.	Found	Calc.	Found	Calc.	Found	Calc.	Found
Pr	30.79	30.72	4.59	4.54	35.43	34.98	2.97	3.40
Nd	31.29	31.49	4.55	4.61	35.17	35.11	2.95	3.20
Sm	32.19	32.13	4.50	4.31	34.71	34.16	2.91	3.10
Eu	32.42	31.95	4.48	4.54	34.59	34.25	2.90	3.10
Gd	33.17	33.40	4.43	4.61	34.20	33.98	2.87	3.12
Tb	33.41	33.40	4.41	4.68	34.08	33.79	2.86	3.11
Dy	33.91	33.97	4.38	4.50	33.83	33.50	2.84	3.06
Ho	34.24	34.44	4.36	3.97	33.66	33.59	2.82	3.00

Table 2

The results of chemical analysis for the hydroxocompounds: Ln (Ph–gl *o*–C)OH.nH_2O

Ln.nH_2O	Ln %		N %		C %		N%	
	Calc.	Found	Calc.	Found	Calc.	Found	Calc.	Found
Pr.$3H_2O$	34.78	34.53	3.45	3.74	36.68	27.09	3.48	3.39
Nd.$3H_2O$	35.31	35.26	3.42	3.21	26.46	26.05	3.45	3.70
Gd.$4H_2O$	35.79	35.25	3.19	3.47	24.60	24.79	3.67	3.99
Er.$4H_2O$	37.21	37.00	3.11	3.50	24.05	23.80	3.59	3.36
Yb.$4H_2O$	38.01	38.47	3.08	3.01	23.75	23.66	3.54	3.56
Y.$4H_2O$	23.96	24.22	3.77	3.85	29.14	28.89	4.35	4.51

MEASUREMENTS

The reflectance spectra were measured in UV on the pellets in 1 : 10 dilutions with MgO and in the visible range on the substance itself using MgO as standard.

The measurements were carried out by means of a Carl Zeiss VSU–1 spectrophotometer.

---

[6] M. PHILIPS, *J. Ind. Eng. Chem.*, **13**, 759 (1921).

[7] H. L. HALLER, *J. Ind. Eng. Chem.*, **14**, 1040 (1922).

The absorption spectra were also measured for the 10^{-4} M solutions in methanol, ethanol and water at various pH's. These measurements were carried out with a Carl Zeiss VSU–2 spectrophotometer.

The infrared spectra were recorded at a UR–10 spectrometer on KBr pellets in the range 400–4000 cm^{-1}.

RESULTS AND DISCUSSION

Based on the chemical analysis, it was established that the composition of compounds of the first series (table 1) is suitable for one and a half molecule of ligand to be attached to a metal atom. Such a composition is possible only if the compounds have a dimeric structure: $Ln_2[Ph-gl\ o-C]_3$.

For hydroxocompounds, the general formula was established: $Ln[Ph-gl\ o-C]\ OH$ (table 2).

All compounds of both series are solvated and contain 3–4 molecules of water. As to the colour, it is cream for $Tb_2[Ph-gl\ o-C]_3$, cream-green for $Pr_2[Ph-gl\ o-C]_3$, cream-lavender for $Nd_2[Ph-gl\ o-C]_3$ and gray-blue for all the other compounds with darker shades for hydroxocompounds. They are stable in time, do not melt up to 300° and are not soluble in common organic solvents nor even in N-methyl pyrolidon.

The halo-shape of the diffraction effects appearing in the debyegrams recorded for certain compounds shows the amorphous and polymeric structure of the compounds of $Ln_2[Ph-gl\ o-C]_3$ type. The polymeric structure may be due to the steric hindrance of the chelate groups, which easily explains the composition, the high thermal stabilities and the insolubility of the compounds in organic solvents.

For the free ligand $[Ph-gl\ o-C]$ the absorption spectra in solutions with pH 1–10,[8] the reflectance spectra in the solid state in UV have already been studied and also the IR spectra.[6]

The reflectance spectra of all synthetized compounds of both series are similar, both in shape and intensity. Fig. 1 shows the reflectance spectra of the free ligand and of certain compounds.

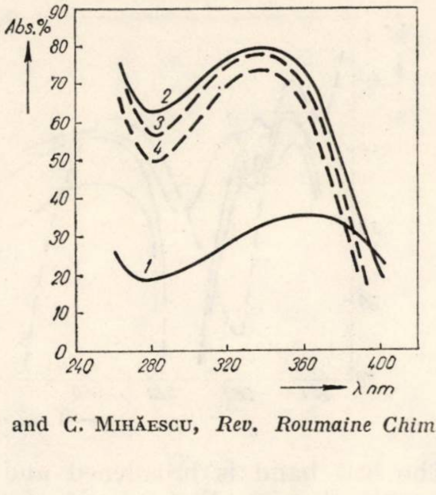

Fig. 1. — Reflectance spectra in UV in 1 : 10 dilutions with MgO for: *1*, $[Ph-gl\ o-C]$; *2*, $Nd_2\ [Ph-gl\ o-C]_3.3H_2O$; *3*, $Pr\ [Ph-gl\ o-C]\ OH.3H_2O$; 4–$Er[Ph-gl\ o-C]\ OH.4H_2O$.

---

[8] C. Drăgulescu, R. Pomoje, I. Menessy and C. Mihăescu, *Rev. Roumaine Chim.*, **12**, 553 (1967).

As may be seen in fig. 1, the absorption maxima of the coordinated ligand are shifted towards higher wave numbers. These shifts could be ascribed to the interruption of the "π" conjugation between the carboxylic group and the phenyl ring, as a consequence of nonplanarity between them, caused by coordination requirements.

The above assumption agrees with the chemical properties and the X-ray data which would indicate a polymeric structure.

In solution, it was possible to study the influence of various solvents on the UV absorption spectra for the free ligand, but for compounds only absorption spectra in ethanol could be recorded.

The absorption curve of solutions of the free ligand in methanol, ethanol and water with $pH < 4$ presented maxima at about the same wave lengths :

$\lambda_1 = 255$ nm	— in ethanol —	$\lambda_2 = 350$ nm
$\lambda_1 = 253$ nm	— in methanol —	$\lambda_2 = 346$ nm
$\lambda_1 = 251-52$ nm	— in water, $pH < 4$	$\lambda_2 = 345$ nm,

while in the absorption spectrum of water solution with $pH > 6$ (in the presence of NH_4OH) two maxima are also observed, but the second maximum is shifted, $\lambda_2 = 330$ nm.

Fig. 2 presents the absorption spectra in ethanol solutions for the compounds: $\mathrm{Pr_2[Ph{-}gl,\ \mathit{o}{-}C]_3}$, $\mathrm{Nd_2[Ph{-}gl\ \mathit{o}{-}C]_3}$ and $\mathrm{Pr[Ph{-}gl\ \mathit{o}{-}C]OH}$ compared with the free ligand. The absorption maxima for compounds are the following :

$\mathrm{Pr_2[Ph{-}gl\ \mathit{o}{-}C]_3}$	$\mathrm{Nd_2[Ph{-}gl\ \mathit{o}{-}C]_3}$	$\mathrm{Pr[Ph{-}gl\ \mathit{o}{-}C]OH}$
$\lambda_1 = 254$ nm	$\lambda_1 = 255$ nm	$\lambda_1 = 251-52$ nm
$\lambda_2 = 269$ nm	$\lambda_2 = 269$ nm	$\lambda_2 = 268$ nm
$\lambda_3 = 278$ nm	—	$\lambda_3 = 277$ nm
$\lambda_4 = 354-360$ nm	$\lambda_4 = 362-368$ nm	$\lambda_4 = 354-356$ nm

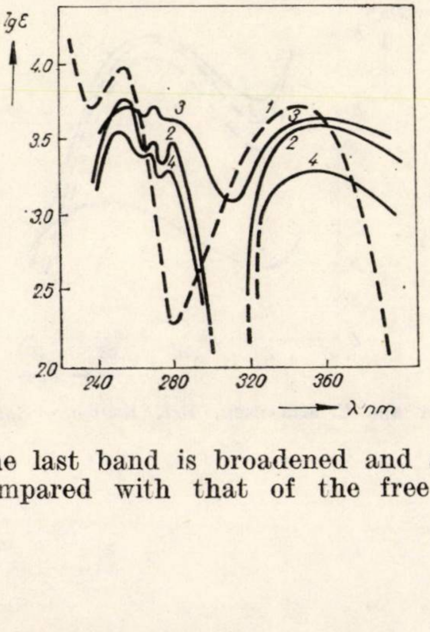

Fig. 2. — Absorption spectra in UV for ethanol solutions of : *1*, $\mathrm{[Ph{-}gl\ \mathit{o}{-}C]}$; *2*, $\mathrm{Pr_2[Ph{-}gl\ \mathit{o}{-}C]_3}$; *3*, $\mathrm{Nd_2[Ph{-}gl\ \mathit{o}{-}C]_3}$; *4*, $\mathrm{Pr[Ph{-}gl\ \mathit{o}{-}C]OH}$.

The last band is broadened and shifted towards higher wave lengths compared with that of the free ligand.

The presence of the bands in the range 270—280 nm in the spectra of the studied compounds, is an indication that the nitrogen atom becomes tetracoordinated by its coordination to the lanthanide ion.

The reflectance spectra for the compounds of Pr, Nd, Er were also recorded in the visible range. The absorption maxima in spectra of both types of compounds appear at the same wave lengths as in the corresponding nitrates. For this reason, the δ parameter, usually taken as a measure of the mean covalency degree, could not be calculated. This fact indicates that the chemical bonds through the oxygen atoms of the carboxylic groups are practically the same as those through the water oxygen atoms; the contribution of the nitrogen atom to the bond covalency being thereby insignificant.

The peaks corresponding to the different vibrations in IR spectra of [Ph—gl *o*—C] and compounds Ln_2[Ph—gl *o*—C]$_3$ and hydroxocompound Pr[Ph—gl *o*—C]OH are summarized in table 3.

The assignments were made according to the related literature. [4,9]

For the stretching vibration $\nu_{C=C}$ from the *ortho*-substituted benzene ring, the main absorption bands were already assigned. [10]

The changes of the characteristic vibrations of the COOH and CN groups going from the free ligand to the coordinate one, constitute an obvious indication of complex formation. The absorption frequency characteristic of the non-ionized carbonyl, appearing in the free ligand at 1725 cm^{-1} is not to be found in the compounds, which tells us that all carboxylic groups of the ligand in the compounds participate in the coordination. By comparing the frequency intensities in the spectra of the compounds within 1700—1600 cm^{-1} to those of the ligand, one notices that the chelation effect appears markedly in the complexes by a strong intensification of the absorption bands.

On the other hand, the bands found in the region 1300—1100 cm^{-1} possibly due to the C—N stretching,[11] are modified in their intensity. Thus, the frequency of the aliphatic ν_{CN} (1140 cm^{-1}) is markedly decreased in intensity, while the ν_{CN} for nitrogen bound to the ring (1400 cm^{-1}) is not modified in intensity. This should be an indication of the nitrogen participation in coordination with the lanthanide ion.

The vibration characteristic of the NH group appears as a narrow and intense band at 3375 cm^{-1} in the free ligand and broadened in the coordination compounds at 3500—3200 cm^{-1}, due probably to the polymeric associations through intermolecular hydrogen bonds.

As for the three water molecules, they can be considered as crystallization water to which the broad band in 3500—3200 cm^{-1} range is also ascribed as the OH stretching.[12]

---

[9] L. J. Bellamy, *The Infrared Spectra of Complex Molecules*, London Methuen & Co. Ltd., New York, John Wiley & Sons INC, 1959.

[10] A. R. Katritzky and R. A. Jones, *J. Chem. Soc.*, **1959**, 3670.

[11] B. das Sarma and J. C. Bailar, *J. Amer. Chem. Soc.*, **77**, 5476 (1955).

[12] D. Scargil, *J. Chem. Soc.*, **1961**, 4444.

Table 3

IR spectra

[Ph−gl *o*−C]		Pr_2[Ph−gl *o*−C]$_3$		Pr[Ph−gl *o*−C]OH		Eu_2[Ph−gl *o*−C]$_3$		HO_2[Ph−gl *o*−C]$_3$		Assignment
$\overline{\nu}$ cm^{-1}	intens.	$\overline{\nu}$ cm^{-1}	intens.	$\overline{\nu}$ cm^{-1}	intens.	$\overline{\nu}$ cm^{-1}	intens.	$\overline{\nu}$ cm^{-1}	intens.	
3380	s	3380−60	s	3460−20	s	3390−70	s	3400−3370	s	ν_{N-H}; ν_{O-H}
3180	s	—		—		—		—		ν_{N-H}
3020	m	3080	w	3080	vw	3090	w	3100	w	
2930	w	2930	w	2930	w	—		2950	vw	$\nu_{(C-H)}$
2830	vw									
2650−40	vw									$\nu_{(OH)}$ of COOH arom.
2530	w									$\nu_{(OH)}$ of COOH aliph.
2460−40	w									
1990 1940	w									
1725	vs	—		—		—		—		$\nu_{(-COOH)}$
1660	vs	—		—		—		—		$\nu\left(-\mathrm{C}\genfrac{}{}{0pt}{}{\diagup \mathrm{O-H-}}{\diagdown\!\!\diagdown \mathrm{O}}\right)$
1605	w	1615	vs	1615−10	vs	1630−20	vs	1625	vs	
1575	vs	1580−60	vs	1570	s	1605−1595	vs	1600−1590	vs	$\nu_{(COO)}$
						1580	s	1570	s	asym.
1520	s	1520−05	s	1520	s	1530	s	1530	s	$\delta_{OH} + \delta_{C=O}$ } $\nu_{C=C}$
										aryl group
1460	m	1460	m	1460	m	1470	m	1470	m	$\delta_{OH} + \delta_{C=O}$ (alkyl group)
1435	s	—				—		—		
1395	s	1410−00	vs	1405−00	s	1420	vs	1420	vs	$\nu_{s(COO^-)}$, $\nu_{(CN)}$
1315	w	1295	s	1295	s	1305	s	1305	s	
1225	vs	1260−40	w	1270−40	w	1270−1250	w	1270−50	w	$\delta_{OH} + \delta_{C=O}$ (aryl group)
1180	s	1165	s	1165	s	1175	s	1175	s	$\delta_{OH} + \delta_{C=O}$ (alkyl group)
1170										$\nu_{(CCN)}$
1140	s	1140−20	vw	1140−20	w	1140	w	1140	w	asym.
1075	m	1080	vw	1080	w	1090	vw	1090	vw	$\nu_{C=C}$
1045	m	1050	w	1050	w	1060	w	1060	w	
1000	w	1005	w	1005	vw	1015	w	1010	w	$\nu_{C=C}$

960	vw	960–40	w	960–50	w	965	w	970–60	w	
925	m									δ_{OH}
860	w	865	m	870–50	m	880	m	880	m	$\nu_{(COO^-)}$; $\nu_{s(CCN)}$
850										
805	m	805	w	805	w	820	w	820	w	
790	m									
780	s	780	m–s	780	m	760	m–s	760	m–s	
750	w	755	m							$\nu_{C=C}$
710	s	710	m	710	m	715	m	715	m	
675	m	665	m	665	m	665	m	665	m	$\rho_w(COO^-)$
590	w									
580	m									
525	m	535–30	w	530–25	w	535	w	530	w	$\rho_r(COO^-)$

vs – very strong; s – strong; m – medium; w – weak; vw – very weak.

The observed broadening and marked intensification (fig. 3) also in this region of hydroxocompounds spectra could be explained as being due to the presence of the OH group directly attached to the central lanthanide ion.

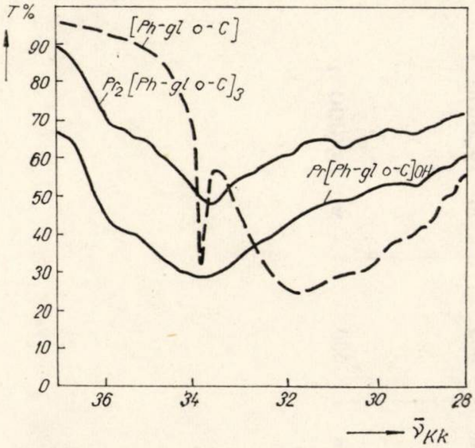

Fig. 3. — IR spectra in 3600—2800 cm^{-1} range for: *1*, [Ph—gl *o*—C]; *2*, Pr_2[Ph—gl *o*—C]$_3$; *3*, Pr[Ph—gl *o*—C]OH.

Revue Roumaine de Chimie, 20, 3, 345–351 (1975)

CONTRIBUTION TO THE COORDINATION CHEMISTRY OF *S*-TRIAZINES. II[1]

COORDINATION COMPOUNDS OF COPPER WITH MELAMINE DERIVATIVES

CONSTANȚA GHEORGHIU* and CRISTINETA MĂRCULESCU**

* Department of Inorganic Chemistry, University of Bucharest
** Centre of Physical Chemistry, Str. Dumbrava Roșie 23, Bucharest, Romania

Received January 26, 1974

In this paper, some copper coordination compounds of the general formula $CuLX_2$ (L = 2,4-diphenylamino-6-amino-*s*-triazine, X=Cl, Br, I) are presented. They are characterized by chemical reactions, electrical conductivities and magnetic measurements, u. v. and visible reflectance spectra, as well as i. r. vibration spectra.

The tendency of NH_2-substituted *s*-triazine derivatives to form coordination compounds, was poorly studied. Only few coordination compounds, formed by transition metals with diamino- and triamino-*s*-triazine (melamine) were mentioned in the literature.

Thus, Meloan and Butel [2] tried to obtain coordination compounds of 2,4-diamino-6-phenyl-*s*-triazine with different metals, in solution, in order to establish some analytical methods. Only the copper (II) compound is a stable one, with the stability constant of $2,5.10^{-5}$, the other metals give unstable coordination compounds.

Some amino-derivatives of *s*-triazine, in which NH_2-groups are in the 1,3,5- or 2,4,6-positions respectively, are presented in other papers.[3,4] Only in the second case mentione is made that a blue compound had been obtained with $CuSO_4$, but nothing is specified about the constitution and properties of the compound formed.

Taking into account the most interesting problem of the *s*-triazine, in general, and of the triamino derivatives (melamine), in particular we intended, in the present paper, to obtain coordination compounds of copper with 2,4-diphenylmelamine (ME), to characterize these compounds as well as to elucidate the nature of copper-ligand bond.

---

[1] C. Gheorghiu and C. Mărculescu, *Anal. Univ. Buc.*, **23** (1974) under Press.

[2] C. E. Meloan and J. Butel, *Analyt. Chem.*, **35**, 768 (1963).

[3] G. D'Alelio, U.S.Pat. 3 700 671, 24 Oct. 1972; *Chem. Abstr.*, **78**, 59021 (1973).

[4] G. D'Alelio, U.S.Pat 3 669 964, 13 Jun. 1972, *Chem. Abstr.*, **74**, 165266 (1972).

— c.1750

EXPERIMENTAL

In order to obtain some coordination compounds of copper with melamine derivatives (2, 4, 6-triamino-*s*-triazine), 2,4-diphenylmelamine was used as ligand.

The ligand 2, 4-diphenylmelamine (ME) ($C_{15}H_4N_6$) was synthesized by us, according to literature indications,[5] by carrying out the reaction of 1-phenylbiguanide with phenylisothiocyanate, in DMF medium, at room temperature. By isolating the final products in acid medium, a concomitant elimination of hydrogen sulphid and ammonia takes place and 1, 4-diphenyl-2-thioammeline and 2, 4-diphenylmelamine were obtained. In a higher temperature range, hydrogen sulphide is preferentially released so that the melamine derivative tends to become the main product, the yield increasing in time. The separation of the two products was realized by fractionated crystallization.

Reflectance spectra were drawn on a VSU-1 Zeiss-Jena spectrophotometer within a 260—1100 nm range, using MgO as standard.

I. R. spectra were recorded in KBr pellets on a UR-20 Zeiss-Jena spectrophotometer.

Molar electrical conductivities were determined in a DMF solution, at 25°, by means of a OK 102/1 Radelkis conductometer with a 0,1 μ s—0,5 s measuring range. The Gouy method was applied for the determination of magnetic susceptibility.

PREPARATION OF COMPOUNDS OF THE $CuMEX_2$ TYPE (X=Cl, Br, I)

Chloride and bromide can be obtained:

a) In a DMF (dimethylformamide) concentrated solution of ME, copper chloride or bromide is added in a 1 : 1 molar ratio; the brown solution obtained is treated, on ice, with anhydrous ether, the operation being repeated by decantation. The initially obtained glue changes, over time, into a microcrystalline product, when DMF is drawn out with anhydrous ether. The khaky precipitate is filtered off, washed with ether and air-dried.

b) Chloride can also be obtained in methanol solution:

In a ME suspension in methanol, $CuCl_2.2H_2O$ is added (1 : 1 molar ratio) under vigorous stirring and slight heating. The resulting yellow greenish crystals are filtered after cooling, washed with some methanol and air-dried.

c) Bromide and iodide were synthesized through a metathethical reaction, starting from $CuMECl_2$ and KX (Br, I) in a DMF concetrated solution and a 1 : 2 molar ratio, at room temperature. After cooling, the potassium chloride formed is filtered off and the solution is treated with ethyl ether in excess, vigorously stirred and kept on ice. The resulted product is filtered off, washed with ether and dried in vacuum.

PREPARATION OF COMPOUNDS OF Cu_2MEX_2 TYPE (X = Br, I)

These compounds are obtained by refluxing in water bath, a suspension of $CuMECl_2$ in ethanol together with KX (X = Br, I), in a 1 : 2 molar ratio. The yellow products resulted are filtered off, washed with CCl_4, ethanol and ethyl ether.

RESULTS AND DISCUSSION

The experimental data show that copper (II) ion reacts with 2,4-diphenylmelamine (ME) in a 1 : 1 molar ratio, in methanol solution, on heating and in DMF concentrated solution at room temperature, followed by anhydrous ether extraction, leading to microcrystalline products. These deep coloured compounds, from yellow-greenish to khaky, are air-stable in solid state.

The analytical data (table 1) lead us to the assumption that the obtained products have the following formulation: $CuMEX_2$ (X = Cl, Br, I) which is confirmed by chemical reactions, magnetic and spectral data.

In substitution reactions (molar ratio 1 : 2), in DMF and in anhydrous conditions, the compound $CuMECl_2$ reacts with potassium or ammonium halides and pseudohalides yielding products of the form $CuMEX_2$ (X = Br, I, SCN, SeCN, NO_3).

---

[5] P. Spacu and C. Mărculescu, *Rev. Roumaine Chim.*, **16**, 513 (1971).

Table 1

Analytical data

Nr.	Compounds		Colour	Found (calculated)			Conductivity ohm^{-1} cm^2 mol^{-1}
				Cu %	N %	C %	
I	ME	$C_{15}H_{14}N_6$	white	—	30.02 (30.21)	64.36 (64.75)	—
II	$CuMECl_2$	$C_{15}H_{14}N_6Cl_2Cu$	khaky	15.27 (15.39)	20.23 (20.36)	43.45 (43.63)	27.04
III	$CuMEBr_2$	$C_{15}H_{14}N_6Br_2Cu$	green-yellow	12.58 (12.66)	16.51 (16.75)	36.02 (35.89)	56.16
IV	$CuMEI_2$	$C_{15}H_{14}N_6I_2Cu$	brown-green	10.36 (10.66)	14.21 (14.10)	30.56 (30.22)	48.15
V	Cu_2MEBr_2	$C_{15}H_{14}N_6Br_2Cu_2$	yellow-green	22.26 (22.48)	14.99 (14.87)	31.55 (31.87)	55.08

The electrical conductivities, measured in a DMF solution, at 25°, display values between 26 and 56 ohm^{-1} cm^2 mol^{-1} (table 1) assuming values which correspond to non-electrolyte type compounds.

Magnetic moments present values ranging between 1.79–1.82 M.B. which indicates a paramagnetism that corresponds to the valence state two of copper (d^9) in these compounds.

All these compounds are insoluble in ethyl ether and water, sparingly soluble in methanol and ethanol, easily soluble in DMF and DMSO.

On heating, the solutions of bromide and iodide in DMF, as well as the suspensions in ethanol, deposit off, over time, microcrystalline yellow powders. These yellow products are air-stable in solid state, sparingly soluble in water, ethanol, ethyl ether, partially soluble in DMF.

The electrical conductivities, determined in DMF solution, present values around 57 ohm^{-1} cm^2 mol^{-1}, thereby proving that these products are non-electrolytes.

The diamagnetism found in these compounds prompts us to consider the valence state of copper (I), (d^{10}), respectively.

Based on analytical data, on electrical conductivities and on magnetic data, the following formulation Cu_2MEX_2 (X = Br, I) may be attributed to the yellow products.

In order to confirm the formulation proposed for these two series of compounds, electronic and i. r. spectra were performed.

ELECTRONIC SPECTRA

The reflectance spectrum of the ligand, 2,4-diphenylmelamine (ME) used by us shows one absorption band at 300 nm (33.330 cm^{-1}). The literature[6] reports that both spectra of melamine and of all their derivatives show a maximum at 280—340 nm (35.710—29.410 cm^{-1}) and for 2,4-diphenylmelamine at 270 nm (37.040 cm^{-1}). These values refer to spectra in solution. As can be seen, the u.v. band presents a hypsochrome shift in the solution spectra, due to the influence of the solvent. This band, richer in energy, is a $\pi \rightarrow \pi^*$ transition band of the ligand. Compared to the spectrum of 1,3,5-triazine, the melamine (2,4,6-triamino-*s*-triazine) spectra present important modifications due to amino-exocyclic groups, since the electron pair of the nitrogen atom comes into conjugation with the electron π-system of the triazine ring, itself isoelectronic with benzene.

Table 2

Reflectance spectra

Nr.	Compound	$\pi \rightarrow \pi^*$		ΔE_{xz}		ΔE_{xy}	
		λnm	$\nu_{cm}{}^{-1}$	λnm	$\nu_{cm}{}^{-1}$	λnm	$\nu_{cm}{}^{-1}$
I	ME	300	33330	—	—	—	—
II	$CuMECl_2$	270	37040	430	23260	860	11630
III	$CuMEBr_2$	265	37740	405	24690	850	11760
IV	$CuMEI_2$	290	34480	360	27780	730	13700
V	Cu_2MEBr_2	355	28170	—	—	—	—

While melamine shows only low-intensity absorption in the 280—340 nm. range, phenylmelamine has a high-intensity peak at 264 nm. The absorption curve of 2,4-diphenylmelamine resembled that of the monosubstituted analogue, except for the slightly higher intensity and small bathochrome displacement (to 270 nm) of the absorption maximum. This high intensity absorption of phenyl derivatives is ascribed to the conjugation of the aromatic substituent with the triazine nucleus.

In the spectrum of 2,4-diphenylmelamine, the literature[7] also reports a weak band at 232 nm (43.100 cm^{-1}) due to a symmetry-forbidden-π-electron transition. The low sensitivity of our apparatus, under 240 nm, did not permit an easy evidence.

As far as the reflectance spectra of the compounds formed by ME with Cu (II) of $CuMEX_2$ type, are concerned, they reveal in the u.v. range the same band as in the ligand ME, shifted towards shorter wavelenghts probably, as a consequence of coordination. Thus the absorption band at 300 nm in the ligand ME has shifted to 265—270 nm (37.740—37.040 cm^{-1}) in chloride and bromide, and at 290 nm (34.480 cm^{-1}) in iodide.

---

[6] F. Kurzer and E. D. Pitchforck, *J. Chem. Soc.* (*C*), **1967**, 6296.

[7] F. Kurzer and E. D. Pitchforck, *J. Chem. Soc.*, **1964**, 3459.

The electronic spectra of these coordination compounds show two visible bands at around 400 nm (25.000 cm^{-1}) and at 800—900 nm (12.500—11.110 cm^{-1}). The former, more intense in chloride (430 nm, 23.260 cm^{-1}) and iodide (360 nm, 27. 780 cm^{-1}) and weaker in bromide (405 nm, 24.690 cm^{-1}), may be assigned to metal-ligand charge transfer, while the latter broader band would correspond to a d-d transition of the metal.

These data enable us to assign most likely a distorted tetrahedron symmetry to compounds $CuMEX_2$ (X = Cl, Br, I) obtained by us.

Reflectance spectra of the type Cu_2MECl_2 compounds (X = Br, I) show one single band at 350—355 nm (28.570 —28.170 cm^{-1}). The presence of a maximum in the u.v. range only, the aspect of the curve and the absence of an absorption band in visible range proves the existence of copper in a configuration d^{10} for which the theory of the crystalline field fails to report visible absorption bands.

INFRARED SPECTRA

The i. r. spectrum of 2,4-diphenylmelamine (ME) is shown in table 3, and will be discussed by comparing it to spectra of 2,4,6-triamino-*s*-triazine (melamine)[8] and 2,4,6-triamino-hexahydrotriazine,[9] mentioned in the literature.

In the 400—800 cm^{-1} range, the spectrum of ME exhibits 6 bands — 480, 510, 570, 610, 748, 820 cm^{-1} characteristic of the melamine cycle, respectively δ_{C-N}, δ_{cycle}, and γ_{NH_2}, slightly shifted, relative to the bands from the i. r. spectrum of unsubstituted melamine (468, 518, 576—81, 619,733 and 814 cm^{-1}).

Other absorption bands appearing in the ME spectrum at 1405, 1520 and 1645 cm^{-1} are slightly shifted (1408, 1515—35 and 1653 cm^{-1}) being characteristic of all triamino-*s*-triazine. [8]

The presence of substituents in the nitrogen ring or in the exocyclic amino groups, determines important changes in the i. r. spectra. Thus the absorption band at 695 cm^{-1} in the ME spectrum, as well as that at 1150 cm^{-1} assigned to the ρ_{NH_2} frequency and that at 1250 cm^{-1} to vibration frequency $C-NH-C_6H_5$ are found in the 2,4,6-triphenylamino hexahydrotriazine spectrum.

The absorption bands at 1610 and 1645 cm^{-1} in the spectrum of ME, assigned to the stretching vibration δ_{NH_2} are shifted relative to the bands at 1610 and 1680 cm^{-1} characteristic of all diamino-*s*-triazine [10] due probably to the overlapping of the vibration frequency of the aromatic structure .[11]

---

[8] W. Sawodny, K. Niedenzu and J. W. Dawson, *J. Chem. Phys.*, **45**, 3155 (1966).

[9] C. N. Rao, "Chemical Applications of Infrared Spectroscopy", Academic Press, New York, 1963.

[10] R. Bacaloglu, F. Neamţu, I. Bacaloglu and G. Ostrogovich, *Rev. Roumaine Chim.*, **17**, 747 (1972).

[11] J. Bellamy, "The Infrared Spectra of Complex Molecules", Methuen, London, 1962.

Tabel 3

Infrared spectra

2,4-diphenyl-melamine ME cm^{-1}	$CuMECl_2$ cm^{-1}	Triphenylamino-hexahydro *s*-triazine	2,4,6-triamino *s*-triazine (melamine)	Assignments
480	—	—	468	δ_{C-N}
510	—	—	518	δ_{C-N}
570	—	—	581−76	δ cycle
610	—	—	619	γ_{-NH_2}
695	—	690	—	ρ_{NH_2}
748	—	752	733	δ-cycle melamine
820	—	835	814	δ-cycle
1010	1010red.	1010−37	1028	C−N in cycle
1090	1120	1130	—	hexahydro *s*-triazine
1150	—	1163	1178	$\rho-NH_2$
1190	—	1203	1194	
1250	1240	1229	—	$-C-NH-C_6H_5$
1405	1410	1337−89	1408	symmetrical substituted ring
1450	—	1445	1448	ν CYCLE
1520	—	—	1515−35	ν MELAMINE RING
1610	—	1600	1627	$\delta-NH_2$
1645	1640	—	1653	

The i. r. spectra of coordination compounds of the type $CuMEX_2$ (X = Cl, Br, I) show bands characteristic of ligand ME. Thus in the 900−1300 cm^{-1} range, some bands are shifted or reduced in intensity, due to the perturbed cycle frequency, ρ_{NH_2} frequency and to $C-NH-C_6H_5$ group. In a similar manner, two very sharp bands appear, in the $CuMECl_2$ spectrum, one at 1410 cm^{-1}, assigned to the vibration frequency of melamine cycle, which is split at ME (1405, 1415 cm^{-1}) and the second at 1640 cm^{-1} ascribed to the δ_{NH_2} frequency, overlapping the vibration frequency C = N in unconjugated cyclic system.[11]

In addition to this, some characteristic bands in the ME spectrum disappear totally in the $CuMECl_2$ spectrum: the vibration modes proper to the melamine cycle at 480 and 723 cm^{-1}, as well as, those assigned to the vibration frequency γ_{NH_2} at 610−625 cm^{-1} and at 820 cm^{-1}, due to the coupling vibration of *s*-triazine ring and $C-NH_2$ group.

The i. r. spectra of $CuMEX_2$ ($X = Cl, Br, I$) type coordination compounds compared to the i. r. spectrum of the 2,4-diphenylmelamine ligand reveal the strongest perturbation in the vibration frequencies of simple or substituted exocycle $C=NH$ groups, as well as in $C=N$ group of unconjugated cyclic system; the vibration frequencies characteristic of melamine cycle are affected to a lesser degree.

Taking into account these spectral data and also the chemical and physico-chemical properties of the compounds formed by Cu(II) with ME, of the $CuMEX_2$ type, we assume, by comparison with the similar Cu(II) coordination compound with 2,4-biphenylthioammeline,[1] that the copper atom is bound to 2,4-diphenylmelamine through the two exocycle nitrogen atoms.

Investigations into this field with other s-triazine derivatives and various transition metals are in progress.

Revue Roumaine de Chimie, **20**, *3*, 345 – 351 (1975)

Revue Roumaine de Chimie, **20**, *3*, 353–359 (1975)

BICYCLO [2.2.2] OCTENE DERIVATIVES. II[1]

ADDITION OF HALOGENS TO STEREOISOMERIC 5,6,7,8-TETRACARBOMETHOXY-BICYCLO [2.2.2] OCT-2-ENES

F. IORDACHE, F. CHIRALEU and MARGARET AVRAM
Polytechnical Institute Bucharest, Chair of
Organic Chemistry

Received June 15, 1974

The results of halogen addition to previously described[1] esters **1**–**4** are presented. A mechanism is proposed for these reactions.

Furthermore, our interest in steric shielding effects and in the participation of remote groups in the course of addition reactions to polycyclic systems,[2,3] the behaviour of stereoisomeric bicyclo [2.2.2] oct-2-ene tetracarboxylic esters (**1**–**4**) was investigated.

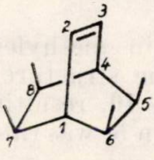

1

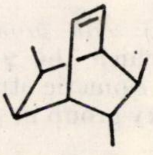

2

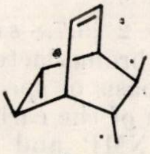

3

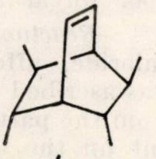

4

The various orientations of carbomethoxy groups in these compounds facilitated the study of steric hindrance of the double bond in the attack of electrophilic species. We report here the results of bromine addition to compounds **1**–**4**.

Reaction of ester **1** (5,6,7,8-*exo*, *all-exo*) *with bromine.* It was observed that ester **1** does not discolour the aqueous bromine solution and does not react instantly with a solution of 1 mole bromine per mole of substrate, in methylene chloride or carbon tetrachloride, neither in daylight nor on UV illumination. However, a reaction was noticed on a prolonged stay (24 hrs) with an excess of at least 1 mole bromine in the same solvents.

---

[1] Part I: F. Iordache, F. Chiraleu and M. Avram, *Rev. Roumaine Chim.*, **20**, (in press).

[2] M. Avram, G. D. Mateescu and C. D. Nenitzescu, *Liebigs Ann. Chem.*, **636**, 174 (1960).

[3] M. Avram, I. G. Dinulescu, F. Chiraleu and C. D. Nenitzescu, *Rev. Roumaine Chim.*, **18**, 863 (1973).

Under the latter conditions ester **1** yielded a compound the elemental analysis of which corresponded to a bromo-γ-lactone. Using NMR and IR data, the product was assigned the structure of a γ-lactone **5**.

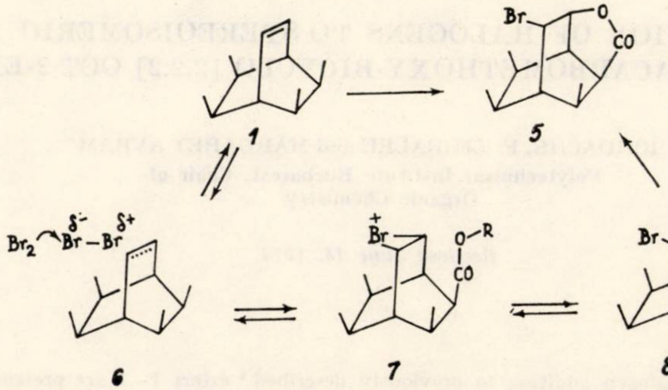

The low reactivity of ester **1** in the addition of bromine can be attributed to a steric effect, the carbomethoxy groups hindering the access of bromine to the double bond. Most probably, the excess of bromine is necessary for the formation of the bromonium ion **7** from the π complex **6**. The intervention of a second bromine molecule was also observed in bromine additions to alkenes in concentrated solutions, using poor solvating solvents.[4-7]

Reaction of ester **2** (5,7,8-*exo*-6-*endo*) *with bromine*, in methylene chloride, afforded a bromo-lactone to which the γ-lactone structure **9** was ascribed on the basis of spectra. An isomeric structure **10**, resulting from the participation of the carbomethoxy group in position 5, was ruled out on the basis of NMR and IR data.

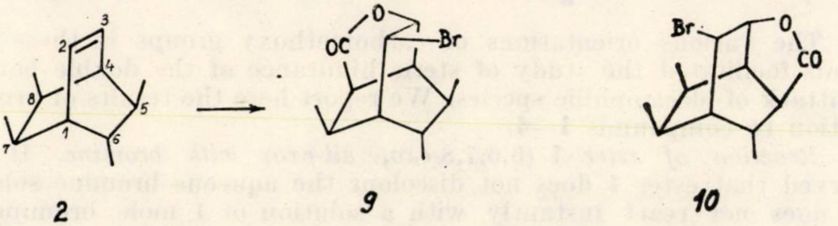

In ester **2** the *endo* orientation of the carbometoxy-group in the 6 position favours the attack of bromine on carbon-2 of the double bond.

---

[4] F. Badea, ,,Mecanisme de reacţie în chimia organică," Ed. II, Ed. ştiinţifică, Bucharest, 1973, p. 518.

[5] P. B. D. de la Mare, *Quart. Rev.*, **3**, 126 (1949)

[6] J. H. Pincock and K. Yates, *J. Amer. Chem. Soc.*, **90**, 5643 (1948).

[7] J. H. Rolston and K. Yates, *J. Amer. Chem. Soc.*, **91**, 1483 (1969).

Ion **11** or bromonium ion **12** react intramolecularly with the carbomethoxy group yielding, through the acylonium ion **13**, bromo-lactone **9**. The absence of bromo-lactone **10** illustrates the shielding effect of carbomethoxy groups on the double bond.

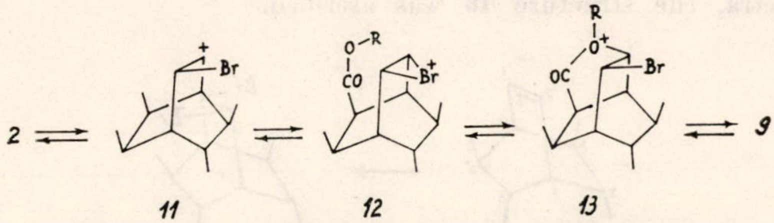

Reaction of ester **3** (5,7-*exo*-6,8-*endo*, *all-trans*) *with bromine* displayed the following features. As expected, treatment of **3** with bromine in methylene chloride yielded the dibromo-derivative **14**. In ester **3**, because of the *trans* orientation of carbomethoxy groups, the double bond is accessible to the attack of bromine from two equivalent sterically free sides (C_6 or C_8).

Bromonium ion **16** (formulated for the bromine addition from the direction of the 6 position) can follow two reaction pathways : an intramolecular attack of carbomethoxy group in the 7 position, which would yield bromo-lactone **17**, or an attack of bromide anion on the opposite side of the bromonium ring, sterically free due to the *endo* orientation of the carbomethoxy group in position 8.

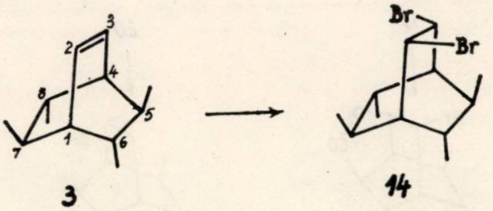

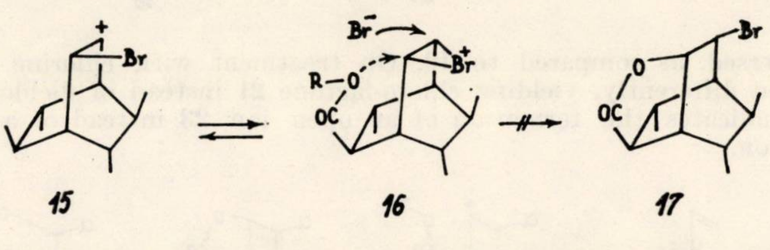

The formation of the dibromo-derivative **14** illustrated the stability of the bromonium ion **16** which is able to discern between a reaction with bromide anion or a reaction with the neighbouring carbomethoxy group. The higher nucleophilicity of the bromide anion, as compared to the ester group oxygen, is responsible for the formation of dibromide **14**.

Reaction of ester **4** (5,8-*exo*-6,7-*endo*) *with bromine* in methylene chloride yielded a dibromo-derivative to which, on the basis of NMR and IR spectra, the structure **18** was ascribed.

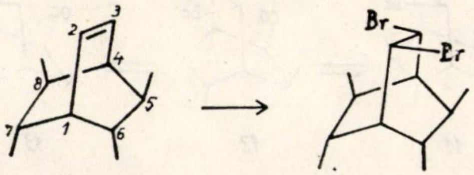

4 **18**

In ester **4**, the *endo* orientation of carbomethoxy groups in positions 6 and 7 facilitates bromine attack on the atom 2 of olefin bridge, which leads to ion **19** or bromonium ion **20** and finally to product **18**. In this interpretation, the configuration of bromine in position 2 should

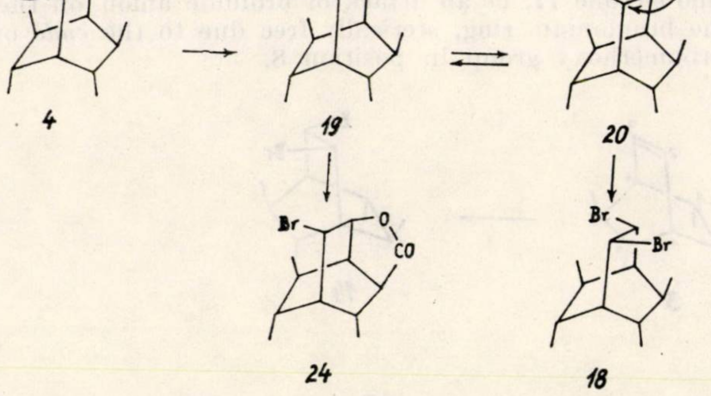

4 **19** **20** **24** **18**

be reversed, as compared to **19**. On treatment with chlorine ester **4** behaved differently, yielding chloro-lactone **21** instead of dichloride **22**. This indicates the formation of an open ion **23** instead of a chloronium ion.

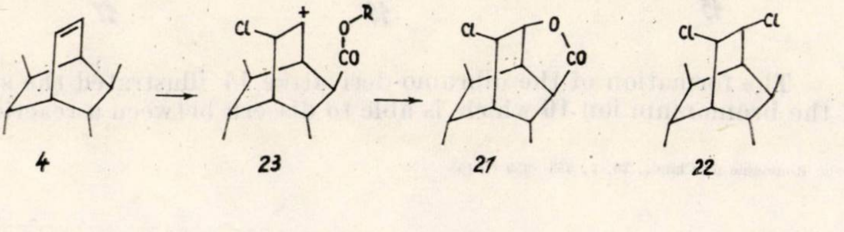

4 **23** **21** **22**

Addition of bromine to ester **4** in a polar solvent in which the equilibrium between the open ion **19** and bromonium ion **20** should favour the former species, yielded as expected bromo-lactone **24**.

It was also expected that the greater stability of iodonium ion **25**, together with the lower nucleophilicity of chloride ion with respect to bromide ion, would favour an intramolecular iodo-lactone product. Confirming these predictions, the treatment of ester **4** with chlorine-iodine in methylene chloride yielded iodo-lactone **26** and not a chloro-iodo-derivative **27**.

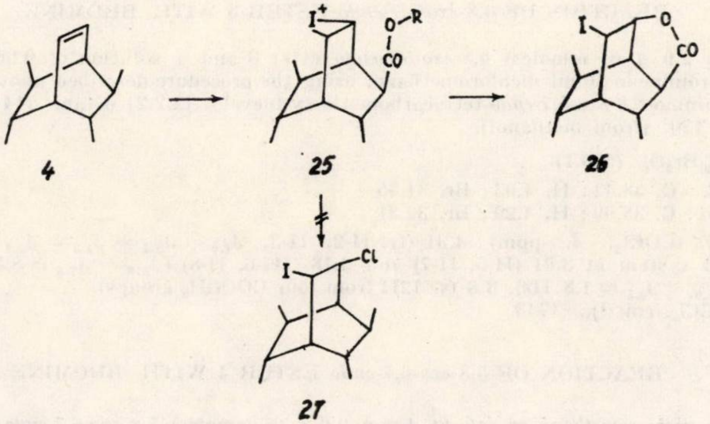

4 **25** **26** **27**

EXPERIMENTAL

Microanalyses were performed by Miss E. Şliam and Mrs. V. Daniel. IR spectra were recorded with a double beam UR 20 spectrophotometer. NMR spectra were determined with a Varian A-60A spectrometer.

REACTION OF *all-exo* ESTER 1 WITH BROMINE

A solution of 2.0 g (6 mmoles) ester *all-exo* **1** in 10 ml dichloromethane was treated with a solution of 1.92 g (0.61 ml, 12 mmoles) bromine in 30 ml dichloromethane, and the mixture was left at room temperature for 24 hours. After evaporation of the solvent, the residue was purified by recrystallization from ethanol, yielding 1.5 g (62%) bromo-lactone **5**, m.p. 190°.

$C_{15}H_{18}BrO_8$ (406.2)

Calcd. : C, 44.35 ; H, 4.46 ; Br, 19.67

Found. : C, 44.49 ; H, 4.44 ; Br, 20.16

NMR ($CDCl_3$, δ, ppm) : 4.73 (q, H-2, $J_{1,2} = 4.5$ Hz, $J_{2,3} = 6.5$ Hz), 4.96 (d, H-3, $J_{2,3} = 6.5$ Hz), 3.71, 3.73 and 3.75 (s, 9H from 3 carbomethoxy groups), 2.95–3.20 (complex m) and 3.5 (broad s, H-1, H-4, H-5, H-6, H-7, H-8).

IR (CH_2Cl_2, cm^{-1}) : 1793, 1743.

REACTION OF 5,7,8-*exo*-6-*endo* ESTER 2 WITH BROMINE

A solution of 4.0 g (12 mmoles 5,7,8-*exo*-6-*endo* ester **2** in 10 ml dichloromethane was treated with a solution of 1.92 g (0.61 ml, 12 mmoles) bromine in 30 ml dichloromethane, and the mixture was left at room temperature for 24 hours. After evaporation of the solvent, the residue was recrystallized from ethanol, yielding 3.5 g (70%) bromo-lactone **9**, m. p. 145°.

$C_{15}H_{18}BrO_8$ (406.2)
Calcd. : C, 44.35 ; H, 4.46 ; Br, 19.67
Found : C, 44.76 ; H, 4.22 ; Br, 19.42

NMR ($CDCl_3$, δ, ppm) : 4.93 (d, 2H, H-2 and H-3, $J_{1.2} = J_{3.4} = 4$ Hz), 3.74 (s, 3H from $COOCH_3$ group), 3.80 (s, 6H from two $COOCH_3$ groups), 3.82 (broad, H-6), 3.60 (broad s, H-4), 2.85–3.25 (unresolved m, H-5, H-7, H-8), 2.85 (broad s, H-1).
IR (CH_2Cl_2, cm^{-1}) : 1786, 1735.

REACTION OF 6,8-*exo*-5,7-*endo* ESTER 3 WITH BROMINE

From 2.0 g (6 mmoles) 6,8-*exo*-5,7-*endo* ester **3** and a solution of 0.96 g (0.30 ml, 6 mmoles) bromine in 30 ml dichloromethane, using the procedure described above, 2.g (66%) 2,3-*trans*-dibromo-6,8-*exo*-5,7-*endo*-tetracarbomethoxy-bicyclo [2.2.2] octane (**14**) were obtained ; m. p. 120° (from methanol).

$C_{16}H_{20}Br_2O_8$ (500.1)
Calcd. : C, 38.42 ; H, 4.03 ; Br, 31.95
Found : C, 38.69 ; H, 4.29 ; Br, 32.21

NMR ($CDCl_3$, δ, ppm) : 4.31 (tr, H-2, H-3, $J_{1.2} = J_{3.4} = J_{1.3} = J_{2.4} = 1$ Hz), a doubled AB system at 3.61 (H-5, H-7) and 3.18 (H-6, H-8) ($J_{5.6} = J_{7.8} = 8.5$ Hz, $J_{1.6} = J_{7.8} = J_{1.9} = J_{4.5} = 1.8$ Hz), 3.8 (s, 12H from four $COOCH_3$ groups).
IR (CCl_4, cm^{-1}) : 1743.

REACTION OF 5,8-*exo*-6,7-*endo* ESTER 4 WITH BROMINE

a. *In dichloromethane as solvent.* From 2.0 g (6 mmoles) 5,8-*exo*-6,7-*endo* ester **4** and a solution of 0.96 g (0.30 ml, 6 mmoles) bromine in 30 ml dichloromethane, after working as above, 2.0 g (66%) 2,3-*trans*-dibromo-5,8-*exo*-6,7-*endo*-tetracarbomethoxy-bicyclo [2.2.2] octane (**18**) were obtained ; m.p. 126° (from methanol).

$C_{16}H_{20}Br_2O_8$ (500.1)
Calcd. : C, 38.42 ; H, 4.03 ; Br, 31.95
Found : C, 38.86 ; H, 4.27 ; Br, 32.09

NMR ($CDCl_3$, δ, ppm) : 4.45 (dd, J = 2 and 6 Hz) and 4.20 (dtr, J = 1.5 and 6 Hz) (an AB system for H-2 and H-3), 3.81, 3.79, 3.71, 3.69 (s, 12H from four $COOCH_3$ groups), 3.20–3.75 (complex system for H-1, H-4, H-5, H-6, H-7, H-8).
IR (CCl_4, cm^{-1}) : 1740.

b. *In acetic acid as solvent.* Working as above, from 4.0 g (12 mmoles) ester **4** and a solution of 1.92 g (0.61 ml, 12 mmoles) bromine in 30 ml anhydrous acetic acid, 3.5 g (70%) bromo-lactone **24** were obtained ; m.p. 138° (from ethanol).

$C_{15}H_{18}BrO_8$ (406.2)
Calcd. : C, 44.35 ; H, 4.46 ; Br, 19.67
Found : C, 44.47 ; H, 5.12 ; Br, 19.45

NMR ($CDCl_3$, δ, ppm) : 4.81 (q, H-3, J = 2.5 and 3.5 Hz), 4.29 (d, H-2, J = 3.5Hz), 3.69, 3.73, 3.80 (s, 9H from 3 $COOCH_3$ groups), 3.85 (broad s, H-7), 3.60 (broad s, H-4), 3.18 (broad s, H-5, H-6, H-8), 2.88 (broad s, H-1).
IR (CCl_4, cm^{-1}) : 1780, 1725.

REACTION OF 5,8-*exo*-6,7-*endo* ESTER 4 WITH CHLORINE

A solution of 1.0 g (3 mmoles) 5,8-*exo*-6,7-*endo* ester **4** in 10 ml dichloromethane was treated with a solution of 0.318 g (4.5 mmoles) chlorine in 10 ml dichloromethane, and the solution was left for 24 hours at room temperature. The solvent was removed *in vacue* and the residue was recrystallized from methanol yielding 1.0 g (93%) chloro-lactone **21**, m.p 131°.

$C_{15}H_{18}ClO_8$ (361.7)
Calcd. : C, 49.80 ; H, 5.01 ; Cl, 9.80
Found : C, 49.77 ; H, 4.75 ; Cl, 9.83

NMR ($CDCl_3$, δ, ppm) : 4.67 (tr, H-3, J = 3 Hz), 4.21 (d, H-2, J = 3.2 Hz), 3.80, 3.73, 3.70 (s, 9H from 3 $COOCH_3$ groups), 3.18 (broad s, H-5, H-6, H-8), 2.80 (broad s, H−1).

IR (CCl_4, cm $^{-1}$) : 1805, 1746.

REACTION OF 5,8-*exo*-6,7-*endo* ESTER 4 WITH CHLORINE-IODINE

A solution of 1.0 g (3 mmoles) 5,8-*exo*-6,7-*endo* ester **4** in 10 ml dichloromethane was treated with a solution of 0.5 g (3.07 mmoles) chlorine-iodine in 30 ml dichloromethane, and the mixture was left at room temperature for 24 hours. After evaporation of the solvent, the residue which contained small quantities of iodine was treated with 50 ml carbon tetrachloride, which were evaporated *in vacuo* in order to remove the traces of iodine. The new residue (free of iodine) was recrystallized from methanol, yielding 0.5 g (36%) iodo-lactone **26**, m.p. 165°.

$C_{15}H_{18}IO_8$ (453.21)
Calcd. : C, 39.75 ; H, 4.00 ; I, 28.00
Found : C, 39.81 ; H, 4.00 ; I, 27.77

NMR ($CDCl_3$, δ, ppm) : 4.55 (broad s, H-2, H-3), 3.77 (s, 3H from a $COOCH_3$ group), 3.68 (s, 6H from two $COOCH_3$ groups), 3.60−3.00 (m, 6H, H-1, H-4, H-5, H-6, H-7, H-8).

IR (CH_2Cl_2, cm $^{-1}$) : 1794, 1740.

Revue Roumaine de Chimie, 20, 3, 361–378 (1975)

DÉRIVÉS DU BICYCLO [4.1.1] OCTANE. II[1]

PRÉPARATIONS DE QUELQUES HYDROCARBURES, ALDÉHYDES ET CÉTONES

DANIEL JOULAIN et FRANCIS ROUESSAC
Laboratoire de Synthèse Organique, Centre Universitaire du Mans, Route de Laval,
72 000 Le Mans

Reçu le 4 juin 1974

Un certain nombre d'hydrocarbures (8, 9, 11, 12, 24) de cétones saturées (16, 20, 21, 22, 23, 27, 28) ou éthyléniques (13, 26) et enfin d'aldéhydes (18, 19) ayant un squelette bicyclo [4.1.1] octanique sont obtenus par des réactions simples d'hydrogénolyse, d'oxydation, d'hydroboration-oxydation et d'alcoylation à partir des produits d'addition du dichlorocarbène sur l'α-pinène et l'orthodène. Certaines réactions et les données spectrales de ces composés nouveaux permettent d'en définir les conformations privilégiées.

L'addition, vers – 15°, du dichlorocarbène sur l'α-pinène ou l'orthodène, suivie de la réduction des dérivés gemdichlorocyclopropaniques obtenus, constitue une voie d'accès aux deux couples d'halogénures vinyliques **1** et **2** d'une part et **3** et **4** d'autre part.[1]

Dans le présent travail, on décrit la préparation de quelques oléfines ou composés carbonylés, appartenant à la série du bicyclo [4.1.1] octane issus de **1**, **3** ou **5**

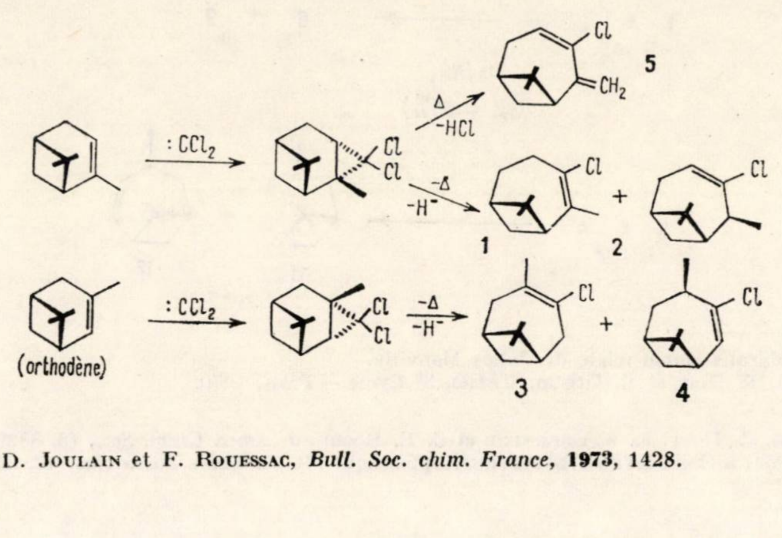

---

[1] D. Joulain et F. Rouessac, *Bull. Soc. chim. France*, **1973**, 1428.

HYDROGÉNOLYSE

Toutes les tentatives effectuées pour substituer l'atome de chlore présent dans **5** par un atome d'hydrogène ou un groupement hydroxyle en vue d'obtenir **6** ou **7** ayant échoué (par ex : action de l'hydrogène en présence de catalyseur (PtO_2 ou Pd/C) ou action de $LiAlH_4$ 92 heures à 120°[1]) **5** a été traité par le sodium dissous dans l'ammoniac liquide.[2] Dans ces conditions, on aboutit aux trois oléfines **8**, **9** et **10** dont la séparation en CPV, difficile, a été rendue possible par l'emploi d'une phase stationnaire (LAC 296) adsorbée sur Chromosorb G.[3]*

Les structures de **8**, **9** et **10** sont aisément déduites de leurs spectres de RMN ; en particulier, **9** présente un effet stérique important entre les méthyles 10 et 11, qui se manifeste par le déplacement des signaux correspondants vers les champs faibles. Par ailleurs, ces caractéristiques spectrales présentent une analogie avec celles de dérivés appartenant à la série bicyclo [3.1.1] heptanique étudiée par Bras et Grison. **

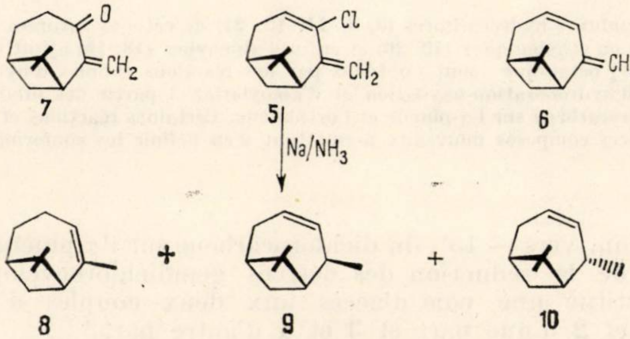

Afin de disposer d'une plus grande quantité de l'homologue **8** de l'α-pinène et de l«*homo*-orthodène» **11**, nous avons répété cette dernière réaction d'hydrogénolyse au départ de mélanges riches soit en **1** soit en **3** :

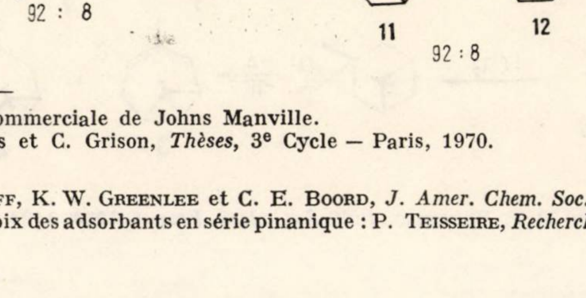

---

* Marque commerciale de Johns Manville.

** J. P. Bras et C. Grison, *Thèses*, 3e Cycle — Paris, 1970.

[2] M. C. Hoff, K. W. Greenlee et C. E. Boord, *J. Amer. Chem. Soc.*, **73**, 3329 (1951).

[3] Pour le choix des adsorbants en série pinanique : P. Teisseire, *Recherches*, **17**, 37 (1969).

Les couples d'oléfines **8** + **9** d'une part, **11** + **12** d'autre part peuvent être résolus par CPV (*vide supra*), cependant ces deux mélanges sont utilisés tels quels dans les réactions ci-après :

OXYDATION ALLYLIQUE DE 8 + 9

1-*t*-BuOOH

Appliquée au mélange **8** + **9** l'oxydation par *t*-BuOOH conduit à un mélange complexe dans lequel on trouve trois constituants principaux : l'homoverbénone **13**, l'homoverbénol **14**, ainsi qu'un alcool III^{re} vraisemblablement de structure **15** (RMN).

Ces structures sont attribuées par analogie avec les produits obtenus avec ce réactif au départ de l'α-pinène.[4]

Le mélange brut obtenu, soumis à l'oxydation chromique en milieu acide (0°—6 h) est constitué par **13** (80%) accompagné d'un reste des hydrocarbures **8** et **9** de départ. (Ces derniers peuvent être éliminés par chromatographie sur alumine neutre.) L'alcool **15** conduit à **13** par réarrangement allylique suivi d'oxydation[5]

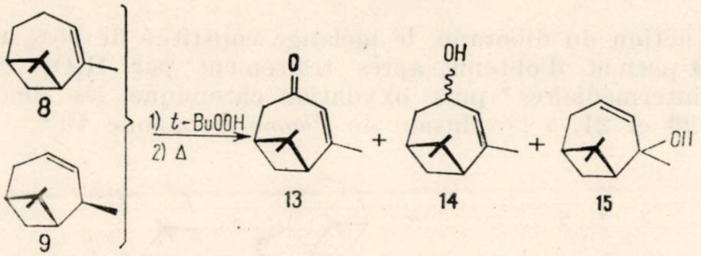

Par hydrogénation catalytique (C/Pd 5%), on obtient l'homoverbanone **16** dans laquelle le CH_3 en 11 est en *cis* par rapport au pont gem-diméthylé

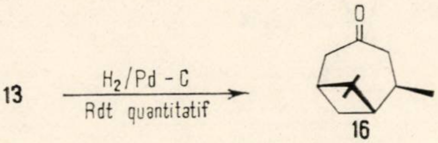

2-SeO_2

Le mélange **8** + **9** a été soumis à l'action du dioxyde de sélénium dont la réaction connue sur l'α-pinène permet la préparation du myrténal avec un rendement voisin de 55%.[6] Le mode d'action, longtemps controversé, de ce réactif,[7] a récemment été interprété [8].

---

[4] Y. Bessiere-Chretien et J. P. Montheard, *Bull. Soc. chim. France*, **1967**, 1185.

[5] a) A. F. Thomas et W. Pawlak, *Helv. Chim. Acta*, **54**, 1822 (1971) ; b) P. A. Grieco, *J. Org. Chem.*, **37**, 2363 (1972).

Dans ces conditions, on observe l'apparition d'au moins 9 constituants (CPV sur colonne Reoplex 400 à 135°). Le composé principal (70% du mélange), après séparation, a des caractéristiques spectrales en accord avec la structure **18***. L'*homo*myrténal **19** constitue 15% du produit total de réaction. Sa structure est déterminée par les méthodes spectrales habituelles (voir partie expérimentale). La présence de **18** peut s'expliquer par une double réaction d'oxydation et de déshydrogénation provoquée par SeO_2 mais l'étude de cette réaction n'a pas été plus approfondie

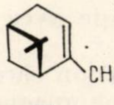

17

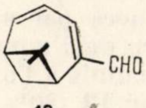

18

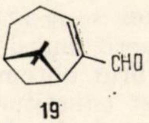

19

SYNTHÈSE DE BYCYCLO [4.4.1] OCTANONES PAR HYDROBORATION-OXYDATION

1 — OLÉFINES 8 ET 9

Par action du diborane, le mélange constitué de 90% de **8** et de 10% de **9** permet d'obtenir, après traitement par H_2O_2—NaOH des boranes intermédiaires [9] puis oxydation chromique, les deux cétones épimères **20** et **21**, à l'exclusion de l'*homo*-verbanone **16**[10]

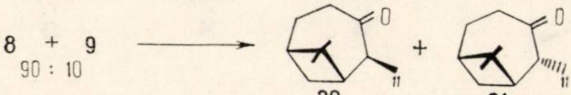

20 **21**

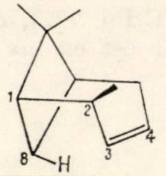

9

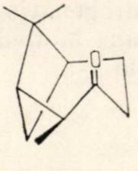

20

---

* En spectroscopie ultra-violette, l'existence d'une forte conjugaison est confirmée par la valeur élevée de $\lambda_{max} = 321$ nm (éthanol) ; par ailleurs, la valeur relativement faible de ε (7500) est compatible avec un système diénique *homo*-annulaire.

[6] a) G. Vavon, R. Dulou et N. Lozac'h, « Manipulations de Chimie Organique », Masson Paris, 1946, p. 67 ; b) J. A. Retamar, *Bull. Soc. chim. France*, **1966**, 1227.

[7] E. N. Trachtenberg, « Oxidation », Ier vol., R. L. Augustine editor, M. Dekker, New York, 1969.

[8] a) K. B. Sharpless et R. F. Lauer, *J. Amer. Chem. Soc.*, **94**, 7154 (1972) ; b) D. Arigoni, A. Vasella, K. Sharpless et H. Jensen, *J. Amer. Chem. Soc.*, **95**, 7917 (1973).

[9] G. Zweifel et H. C. Brown, *Org. Reactions*, **13**, 1 (1964).

[10] D. Joulain et F. Rouessac, *Compt. rend.*, **273** (C), 561 (1971).

La non-réactivité de **9** (récupéré inchangé après le traitement indiqué (cf. partie expérimentale) laisse supposer que cette oléfine doit être dans une conformation telle que l'approche de la double liaison par le diborane est gênée à la fois en « *endo* » et en « *exo* » (méthyle sur le C 2 ou H sur le C 8).

Cette réaction constitue donc un moyen indirect pour obtenir **9** pur, après chromatographie sur alumine du produit d'hydroboration de **8** + **9**. Une analyse RMN très soignée des épimères **20** et **21** formés indique que les signaux correspondant aux méthyles 9 et 11 sont confondus dans le tétrachlorure de carbone comme solvant, mais distincts dans le benzène. Seul, le singulet du méthyle 10 permet de connaître la composition du mélange.

Le rapport **20** : **21** dépend des conditions opératoires de l'oxydation chromique. A 0°, on obtient des mélanges très riches en cétone **20** (95%) plus stable que **21**, la molécule adoptant une des conformations chaise-croisée rendant le méthyle-11 pseudo-équatorial. Par analogie avec le cycloheptane non substitué [11] une telle conformation doit correspondre à un minimum énergétique (voir figure).

2 – OLÉFINES 11 ET 12

Soumises à l'action d'un excès de diborane dans le THF à 0°, pendant 6 heures, les deux oléfines **11** et **12** conduisent, après oxydation, au mélange des deux cétones **21** et **23** normalement attendues dans ce cas

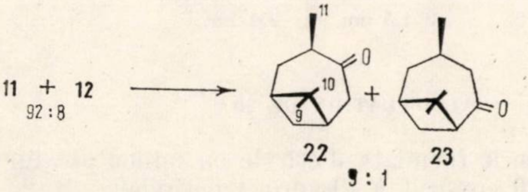

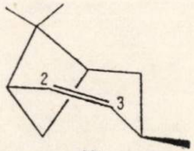

12

Par distillation du produit brut de réaction correspondant à une hydroboration par défaut, on recueille une fraction (Eb_{15} : 65°) constituée de **11** n'ayant pas réagi. La réactivité moins grande de cette oléfine **11** vis-à-vis de **12** corrobore la remarque concernant la non-réactivité de l'oléfine **9** : les oléfines en 2 seraient dans une conformation permettant une approche du diborane plus aisée que dans le cas des oléfines en 3 (voir figure).

L'hydrogénation catalytique rend compte également du rôle important joué par les conformations dans lesquelles se trouvent ces oléfines : il est possible d'hydrogéner facilement (Pd—C, température ambiante) le mélange **8** + **9** en un hydrocarbure saturé unique **24**; Par contre, au départ du mélange **11** + **12** (ou **11** seul) on n'observe jamais d'hydrogénation mais une simple isomérisation de **12** en **11** quelle que soit la nature du solvant ou du catalyseur – insoluble ou soluble –), (cf. pour des réactions semblables [12] :

---

[11] J. B. Hendrickson, *J. Amer. Chem. Soc.*, **89**, 7043, 7047 (1967).

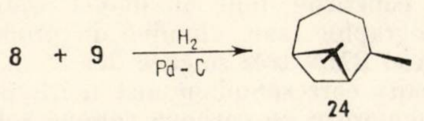

24

Les données spectrales de **22** et **23** sont en accord avec les structures déduites de la stéréochimie de la réaction d'hydroboration sur les oléfines étudiées : Par application de la règle semi-empirique de Maroni [13]

$$\lambda_{max} = (272 + \Delta\lambda)\text{nm (ethanol)},$$

le calcul de $\Delta\lambda$ conduit à un bon accord entre les maxima calculés et observés.

Spectres UV des cétones isomères 22 et 23

	λ_{max} calculé	λ_{max} mesuré
22	280,5 nm	279 nm
23	291,5 nm	291 nm

ALCOYLATION DE 20

Par traitement avec le formiate d'éthyle en milieu alcalin (NaH – C_6H_6), la cyclanone **20** conduit à l'hydroxyméthylène-cétone correspondante **25** avec un rendement de 72% ; cette transformation est accompagnée d'une épimérisation au niveau du méthyle 11. Les deux composés **25** *cis* et *trans* (rapport 35 : 65) sont séparés par CPV sur colonne polaire (S.A.I.B.) et identifiés par l'examen de leurs spectres

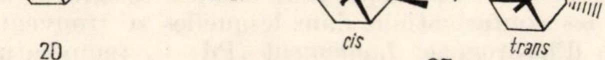

20 **25**

---

[12] a) F. Richter et W. Wolff, *Ber. dtsch. chem. Ges.*, **59**, 1733 (1926) ; b) K. Takeda, H. Minato et S. Nosaka, *Tetrahedron*, **13**, 308 (1961) ; c) A. Van Der Gen, L. M. Van der Linde et J. G. Witteveen, *Rec. Trav. chim.*, **91**, 1433 (1972).

[13] P. Maroni, *Ann. Chim.* (*Ital.*), **2**, 757 (1957).

L'hydroxyméthylène **25** peut être représentée par plusieurs formes tautomères, en particulier *Ia* ou *Ib*. Cependant, **25** se trouve presque exclusivement sous la forme *Ia*, ce qui est tout à fait exceptionnel d'après les travaux de Garbisch[14*]. En effet, par examen du spectre de RMN de **25** (isomère *cis* ou *trans*), on note l'absence de tout proton éthylénique du type Hb dans la région de 5 à 8 ppm (unités δ). Par contre, la présence de deux singulets à 9,15 et 15,3 ppm, d'égale intensité (proton aldéhydique et proton énolique) est en faveur de la forme *Ia*

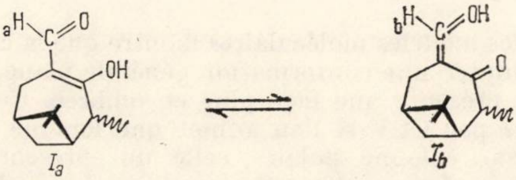

En appliquant la méthode de Garbisch,[14] il est possible de calculer les pourcentages à l'équilibre des deux formes *Ia* et *Ib*, en comparant le déplacement chimique observé ($\delta_0 = 9{,}15$ ppm pour H_a et H_b) avec ceux de l'hydroxyméthylène camphre (un proton type H_b à $\delta = 6{,}71$ ppm) et de l'aldéhyde salicylique (un proton type H_a à $\delta = 9{,}21$ ppm)

$$\% \text{ de } I_b = \frac{0{,}06}{2{,}50} \times 100 \text{ soit } 3\,\%$$

Mis dans les conditions de la réaction de Manson et Wood,[16] **25** conduit à un produit brut constitué (CPV) d'environ 30% d'α-méthylène-cétones **26** (*cis* et *trans*) et 70% d'énols de départ **25** (*cis* et *trans*) inchangés. Les deux composés épimères **26** (*cis* et *trans*) n'ont pu cependant être séparés

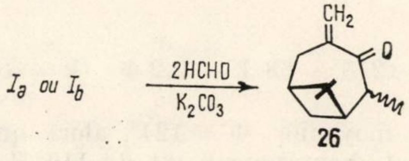

Le mélange des deux méthylène-cétones épimères **26** séparé du produit de départ **25** par distillation fractionnée est utilisé tel quel pour aboutir par hydrogénation catalytique (Pd/C, CH_3OH — Rdt quantitatif) aux deux cyclanones **27** et **28**, facilement séparables par CPV (Carbowax 20 M)

---

* En série bicyclo [3.1.1] heptanique, on admet que l'on n'observe pratiquement jamais de forme homologue de *Ia*.[15]

[14] E. W. Garbisch, *J. Amer. Chem. Soc.*, **85**, 1696 (1963).

[15] Y. Bessiere-Chretien et C. Grison, *Bull. Soc. chim. France*, **1970**, 3103.

[16] A. J. Manson et D. Wood, *J. Org. Chem.*, **32**, 3434 (1967).

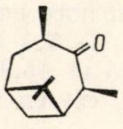
27

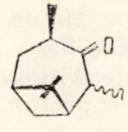
28

L'examen des modèles moléculaires montre que la cétone diméthylée *cis-cis* **27** doit adopter une conformation générale plane, contrairement à l'isomère **28**, qui présente une face plus encombrée. Ceci permet de les identifier *a priori* par CPV si l'on admet que lorsque deux cyclanones sont séparables sur colonne polaire, celle qui présente une face plus encombrée est éluée plus rapidement, car moins bien adsorbée.[17] Le rapport **27** : **28** est sensiblement égal à 1.

L'identification de ces isomères s'appuie également sur l'analogie des spectres UV de **27** et **28** avec les spectres correspondants des *cis-* et *trans-* diméthyl -2,6 cyclohexanones.[18]

Les quantités trop faibles des isomères **27** et **28** obtenus par CPV n'ont pas permis d'étudier leurs stabilités relatives en milieu alcalin.

CARACTÉRISTIQUES SPECTRALES DES COMPOSÉS CARBONYLES PRÉPARÉS

INFRA-ROUGE

Les fréquences d'absorption correspondant à la vibration d'étirement du carbonyle des bicyclo [4.1.1] octanones-3 **16**, **20**, **21**, **22**, **27**, **28** et **29*** sont comparables à ce que l'on observe pour une cycloheptanone sans tension particulière (valeurs comprises entre 1696 et 1700 $cm^{-1} \pm 2\ cm^{-1}$)[19]**. L'angle de valence Φ évalué à l'aide des formules empiriques [20] telle :

$$\nu_{C=O} = 1278 + 68\ k - 2{,}2\ \Phi \quad (k = 10,\ 24),$$

conduit à la valeur moyenne $\Phi = 124°$, alors que l'angle Φ adopté pour une bicyclo [3.1.1] heptanone-3 est de 116°.[21]

---

* Les auteurs remercient MM. Tubiana et Waegell pour un échantillon de cétone *29*.

** Pour des échantillons à l'état de film liquide (Appareil Perkin Elmer 257).

[17] J. M. Conia et F. Rouessac, *Tetrahedron*, **16**, 45 (1961).

[18] R. L. Alumbaugh, G. O. Pritchard et B. Rickborn, *J. Phys. Chem.*, **69**, 3225 (1965).

[19] R. Zbinden et H. K. Hall, *J. Amer. Chem. Soc.*, **82**, 1215 (1960).

[20] a) J. O. Halford, *J. Phys. Chem.*, **24**, 830 (1961) ; b) P. Von R. Schleyer et R. D. Nicholas, *J. Amer. Chem. Soc.*, **83**, 182 (1961) ; c) S. Bank, N. D. Closson et L. T. Hodgins, *Tetrahedron*, **24**, 381 (1968).

[21] F. V. Brutcher et W. Bauer, *J. Amer. Chem. Soc.*, **84**, 2236 (1962).

Par contre, la bicyclo [4.1.1] octanone-2 **23**, comparée aux cétones précédentes, présente un effet bathochrome de 18 cm^{-1} ($\nu_{C=O} = 1682 \pm cm^{-1}$). Ce résultat pourrait provenir d'une interaction d'origine électronique entre le carbonyle et le cyclobutane. De même, l'homoverbénone **13** présente un $\nu_{C=O}$ de 1650 cm^{-1}, valeur plus faible d'environ 20 cm^{-1} que celle attendue pour une cétone α, β-insaturée. Ces données qui traduisent un effet de « conjugaison » sont à rapprocher des caractéristiques de la caranone-5 **30**[22] pour laquelle on note un effet bathochrome de 40 cm^{-1}

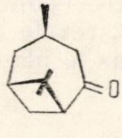

23

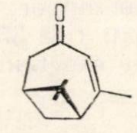

13

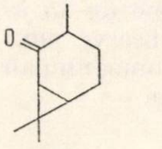

30

ULTRA-VIOLET

Il est intéressant de comparer les fréquences de transition ($\pi \rightarrow \pi^*$) du carbonyle des composés nouveaux **13, 18** et **19** dont nous disposions avec celles d'autres composés connus (tableau 1).

Tableau 1

Comparaison des spectres UV des corps 13, 18, 19 et des composés carbonylés connus

	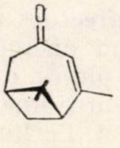 13	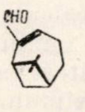 19	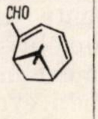 18	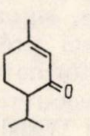 31	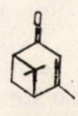 32	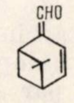 33	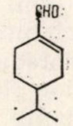 34	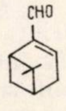 17
λ_{max}^{EtOH} (nm)	253	235	321	235	253	245	228	247
ε	10300	8600	7500	17800	6840	7200	18600	8900

Ainsi, **13** présente par rapport à la pipéritone **31**, ou encore par rapport à la valeur calculée (Woodward),[23] un effet bathochrome de 18 nm. La même anomalie est connue en série bicyclo [3.1.1] heptanique, pour la verbénone **32**, le myrténal **17**[24,25] et la thioverbénone.[26] Divers auteurs,

---

[22] M. L. Josien et N. Fuson, *Bull. Soc. chim. France*, **1952**, 389.

[23] R. B. Woodward, *J. Amer. Chem. Soc.*, **63**, 1123 (1941) ; **64**, 72, 76 (1942).

[24] R. Moore et G. Fisher, *J. Amer. Chem. Soc.*, **78**, 4362 (1956).

[25] P. Teisseire, P. Rouillier et A. Gelfre, *Recherches*, **16**, 68 (1967).

[26] P. Metzner et J. Vialle, *Bull. Soc. chim. France*, **1972**, 3138.

Moore et Fisher,[24] Teisseire[25] ont formulé des hypothèses faisant intervenir soit des tensions inhérentes au système bicyclo [3.1.1] heptanique, soit des hybridations d'orbitales, pour expliquer les effets bathochromes observés pour **32** et **17** par exemple.

L'examen du tableau 1 montre cependant que **13** et **32** présentent des effets bathochromes et hypochromes identiques, alors que la tension du système bicyclo [3.1.1] heptanique est très différente de celle du bicyclo [4.1.1] octane. La seule particularité commune à ces deux composés étant la situation du chromophore en α du cyclobutane.

L'examen du modèle moléculaire de **18**, qui présente un effet bathochrome de 15 à 17 nm, par rapport aux règles énoncées par Woodward ou observé pour des diénals tels **35** ou **36**, révèle que le système diénique homoannulaire est situé exactement dans le plan bissecteur du cyclobutane

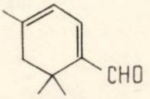

35

λ_{max}^{hexane} 308 nm
ε = 8800[27]

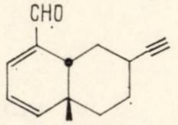

36

$\lambda_{max}^{CH_3OH}$ 305 nm
ε = 7500[28]

Cette particularité, que l'on retrouve pour le myrténal **17** n'existe plus pour l'*homo*myrténal **19**, probablement parce que dans ce dernier exemple les plans définis par la double liaison et le cyclobutane sont orientés différemment entr'eux. (L'examen du modèle moléculaire de **19** fait apparaître un angle voisin de 25°.)

A l'appui de ces conclusions, signalons les calculs effectués sur le cation cyclobutylcarbinyle. Celui-ci présente un minimum énergétique très net lorsqu'il adopte la conformation bissectée (a) plutôt que la conformation (b)[29] par suite du recouvrement maximum entre une orbitale non liante dégénérée de type Walsh du cyclobutane et l'orbitale *p* du cation cyclobutylcarbinyle *

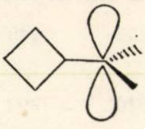

a

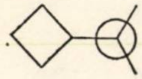

b

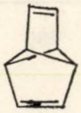

37

---

* Une telle interaction existe de façon très évidente dans le tricyclo [3.3.0.$0^{2,6}$] octadiène **37** pour lequel les deux systèmes π perpendiculaires et les quatre orbitales de Walsh du cyclobutane sont disposés de façon idéale pour qu'une interaction ait lieu. Pour ce composé, qui n'est formellement qu'un *diène non conjugué*, le spectre électronique présente une absorption exceptionnelle commençant vers 300 nm (ε = 190), et qui est la preuve directe de l'existence de cette interaction.[30]

[27] E. A. Braude et E. A. Evans, *J. Chem. Soc.*, **1939**, 55.

[28] T. Asao, S. Ibe, K. Takase, Y. S. Cheng et T. Nozoe, *Tetrahedron Letters*, **1968**, 3639.

[29] R. Hoffmann et R. B. Devidson, *J. Amer. Chem. Soc.*, **93**, 5699 (1971).

[30] R. Gleiter et T. Kobayashi, *Helv. Chim. Acta*, **54**, 1081 (1971).

Bien qu'aucun calcul n'ait été effectué jusqu'à ce jour sur des énones *conjuguées* avec un cyclobutane (telles **13**, **32** et **33**), il semble probable que l'effet bathochrome observé pour ces énones puisse être associé avec une certaine interaction entre un niveau π de l'énone et les orbitales de Walsh du cyclobutane.[31] Pour tous ces composés, la spectroscopie photo-électronique apportera probablement beaucoup d'informations sur ces phénomènes.[32]

RÉSONANCE MAGNÉTIQUE NUCLÉAIRE

Plusieurs conformations limites du système bicyclo [4.1.1] octanique étudié peuvent être envisagées : ce sont les deux formes chaises-croisées (a), chaise (b) et bateau (c)

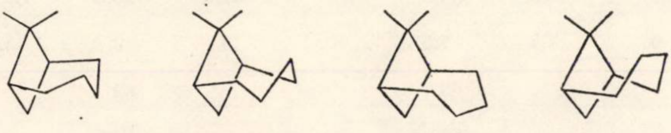

L'examen du modèle moléculaire montre que la conformation bateau (c) est très improbable du fait de l'interaction stérique sévère entre le méthyle-10 et les méthylènes en 3 et 4.

Une analyse conformationnelle *sommaire* peut être réalisée en RMN au moyen de la méthode ASIS * en utilisant la règle empirique du plan de Connolly—Mc Grindle,[33] ou encore, de façon assez peu rigoureuse, en utilisant les déplacements chimiques induits par les réactifs de pseudocontact.[34]

Si on représente par $\Delta_{C_6H_6}^{CCl_4}$ la différence des déplacements chimiques (unités δ) d'un proton d'une cétone dans deux solvants tels CCl_4 et C_6H_6, la valeur et le signe de Δ permettent de définir son orientation par rapport au plan du carbonyle.

Nous avons enregistré les spectres des cétones **16**, **20** à **23** et **27** à **29** dans CCl_4 et C_6H_6 et nous avons noté les déplacements chimiques des différents groupes méthyles pour ces deux solvants (tableau 2).

Ainsi, les valeurs négatives observées pour les méthyles 11 β ou 12 β des cétones **20**, **22**, **27** et **28** sont en faveur d'une conformation chaise-croisée schématisée ci-dessous, conformation pour laquelle la

---

* Aromatic Solvent Induced Shift.

[31] R. Hoffmann, *Communication personnelle.*

[32] R. Gleiter et D. Joulain, *Résultats non publiés.*

[33] J. Connolly et R. Mc Grindle, *Chemistry and Industry*, **1965**, 1379.

[34] D. Joulain, *Travaux non publiés.*

Tableau 2

Effets de solvants, en RMN de ^1H, sur les cétones dérivées du squelette bicyclo [4.1.1] octanique

	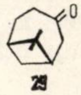 19	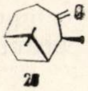 20	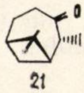 21	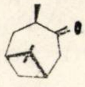 22	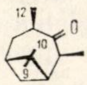 27	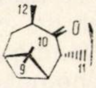 28	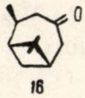 16	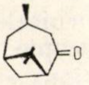 23
δ_1 (9)	77	77,5	77,5	76,5	76	76	80,5	81
δ_2 (9)	62	65	75	64	65,5	76	66,5	64
$\Delta_2^1\delta(9)$	15	12,5	2,5	12,5	10,5	0	14	17
$\delta_1(10)$	46	43,5	47	42	40,5	41	70	60
$\delta_2(10)$	37	40,5	39,5	37	37,5	38,5	64,5	46
$\Delta_2^1\delta(10)$	9	3,5	7,5	5	3	2,5	5,5	14
$\delta_1(11\alpha)$			63			62		
$\delta_2(11\alpha)$			55			54,5		
$\Delta_2^1\delta(11\alpha)$			8			7,5		
$\delta_1(11\beta)$		63		63	64		65,5	61
$\delta_2(11\beta)$		67,5		67	67,5		51,5	43,5
$\Delta_2^1\delta(11\beta)$		−4,5		−4	−3,5		14	17,5
$\delta_1(12\beta)$					63,5	61,5		
$\delta_2(12\beta)$					67,5	66,5		
$\Delta_2^1\delta(12\beta)$					−4	−5		

Afin de rendre le tableau plus homogène, nous n'avons pas toujours respecté les configurations absolues des cyclanones.

Les indices 1 et 2 correspondent respectivement au tétrachlorure de carbone et au benzène; les déplacements chimiques sont donnés en hertz.

On définit par α ou β tout substituant qui est *trans* ou *cis* par rapport au pont *gem*-diméthylé.

tension entre les méthylènes en 4 et 5 et le méthyle 10 est minimale. Cette conformation est *probablement* la même pour les autres cétones

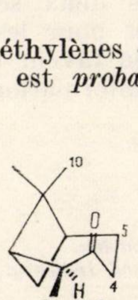

20

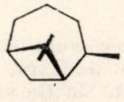

24

Ces résultats complètent ceux qui ont été obtenus par Zschunke et coll., qui avaient mis pour la première fois en évidence la conformation chaise-croisée des alcoylcycloheptanones par la méthode ASIS.[35]

Cette exploitation directe de la règle du plan de Connolly n'est cependant pas toujours aussi facile, car on constate souvent un Δ non nul pour les hydrocarbures saturés correspondant aux cétones étudiées.[36] Pour le seul hydrocarbure saturé **24** dont nous disposions, $\Delta = 0 \pm 1$ Hz.

CONCLUSION

Nous avons développé une méthode permettant un accès facile à de nombreux dérivés du bicyclo [4.1.1] octane, classe de composés dont on ne connaît que peu de représentants. Leur étude physico-chimique a permis de consolider l'argumentation déjà existante en faveur de la possibilité d'une *conjugaison* entre un système insaturé et un cyclobutane. Dans cette perspective, d'autres études physico-chimiques et photochimiques doivent être réalisées au départ de l'*homo*verbénone et des bicyclo [4.1.1] octanones-2.[34]

PARTIE EXPÉRIMENTALE

Les conditions expérimentales générales ont déjà été données.[1]

Les *chromatographies gaz-liquide*, analytiques ou préparatives ont été effectuées avec un appareil Varian-Aerograph 90 P (gaz vecteur : hélium), au moyen des colonnes d'acier inoxydable suivantes : *Colonne 1*, 3 m × 0,25 in. garnie de 20% de Carbowax 20 M sur Chromosorb P, AW, DMCS, 45–60 mesh ; *Colonne 2*, 4 m × 0,25 in. garnie de 18% de S.A.I.B. sur Chromosorb P, AW, 45–60 mesh ; *Colonne 3*, 3 m × 0,25 in. garnie de 14% de squalane sur Chromosorb W, AW, 60–80 mesh ; *Colonne 4*, 3 m × 0,25 in. garnie de 3,5% de Reoplex 400 sur Chromosorb G, AW, 30–60 mesh ; *Colonne 5*, 3,5 m × 0,25 in. garnie de 4% de N.P.G.S. sur Chromosorb G, AW, 30–60 mesh ; *Colonne 6*, 4 m × 0,25 in. garnie de 17% de LAC 1 – R 296 sur Chromosorb W, AW, DMCS, 60–80 mesh ; *Colonne 7*, 4 m × 0,25 in. garnie de 20% de silicone QF-1 sur Chromosorb P, AW, 45–60 mesh.

HYDROGÉNOLYSE DU MÉLANGE **1** + **2** : OBTENTION DES OLÉFINES **8** ET **9**

Dans un réacteur, on prépare à –50° une solution de 23 g de sodium (1 atome-g, ≃ 6 équivalents) dans 400 cm³ d'ammoniac fraîchement distillé sur sodium. A la solution agitée mécaniquement, on ajoute goutte à goutte une solution de 30,0 g (0,163 mole) du mélange des halogénures vinyliques **1** et **2** dans 200 cm³ d'éther anhydre, puis on agite pendant 2 heures à –33°. On ajoute goutte à goutte une solution saturée de NH_4Cl jusqu'à disparition totale du sodium dissous. La phase éthérée est séparée puis lavée successivement à l'eau (3 fois 50 cm³), à HCl 10%, avec une solution de $NaHCO_3$ à 5%, et enfin à l'eau jusqu'à neutralité. Après séchage ($MgSO_4$) et élimination du solvant, il reste un liquide mobile et incolore que l'on distille : on obtient 20,7 g (85%) du mélange des deux oléfines **8** et **9** incolores. Eb_{20} : 72°.

---

[35] A. Zschunke, F. J. Struber et R. Borsdorf, *J. prakt. Chem.*, **311**, 296 (1969).

[36] C. Grison, *Thèse de 3ème Cycle*, Paris, 1970.

CPV : a) *Colonne 3*, 145°, débit He : 55 cm^3/mn
8 et **9** ont le même temps de rétention de 44 mn.
b) *Colonne 4*, 105°, débit He : 40 cm^3/mn
8 et **9** ont des temps de rétention légèrement différents (21 et 22 mn respectivement) mais insuffisants pour permettre une séparation à l'échelle préparative. Les proportions estimées d'après cette analyse et d'après l'intégration en RMN sont de 90 % en **8** et 10 % en **9**.

HYDROGÉNOLYSE DE L'HALOGÉNURE DIÉNIQUE 5

Même mode opératoire que ci-dessus : une solution de 18,2 g de l'halogénure diénique **5** (0,10 mole) dans 100 cm^3 d'éther anhydre est ajoutée à une solution de 13,5 g de sodium dans 300 cm^3 d'ammoniac liquide. Après traitement habituel, on obtient après distillation 12,3 g (82 %) du mélange des trois oléfines **8**, **9** et **10**.

Caractéristiques des isomères **8**, **9** et **10** séparés par CPV (colonne 6, 95°) :

TRIMÉTHYL-2,7,7 BICYCLO[4.1.1]OCTÈNE-2 8

Spectre IR(cm^{-1}) : 1655 (faible) et 800.
Spectre de RMN : (CCl_4), deux singulets à 0,82 et 1,28 (*gem*-diméthyle), un multiplet centré à 1,60 (CH_3—11), un multiplet centré à 5,32 (H-3).

Cis-TRIMÉTHYL-2,7,7 BICYCLO[4.1.1]OCTÈNE-3 9

Spectre IR (cm^{-1}) : 1660 (très faible), 738 et 695.
Spectre de RMN : (CCl_4), deux singulets à 0,96 et 1,23 (*gem*-diméthyle), un doublet centré à 1,06 (J = 7,5 Hz, CH_3—11), un multiplet centré à 5,38 (2 protons vinyliques H-3 et H-4).

Trans-TRIMÉTYL-2,7,7 BICYCLO[4.1.1] OCTÉNE-3 10

Spectre IR (cm^{-1}) : 1655 (très faible), 740 et 700.
Spectre de RMN : (CCl_4), deux singulets à 0,86 et 1,21 (*gem*-diméthyle), un doublet centré à 0,93 (J = 7 Hz, CH_3—11), un multiplet centré à 5,31 (2 protons vinyliques H-3 et H-4).

HYDROGÉNOLYSE DU MÉLANGE 3 + 4 : Obtention des oléfines 11 et 12

14,30 g du mélange des deux halogénures vinyliques **3** et **4** (0,077 mole), en solution dans 65 cm^3 de diméthoxy-1, 2 éthane anhydre, sont ajoutés à une solution de 11 g de sodium dans 180 cm^3 d'ammoniac liquide, à −50°. Après deux heures d'agitation à cette température, on traite le mélange réactionnel comme ci-dessus, et on obtient après distillation 9,0 g (78 %) du mélange des deux oléfines **11** et **12**. Eb_{15} : 58°.

TRIMÉTHYL-3,7,7 BICYCLO[4.1.1] OCTÈNE-3 11 (*homo*-orthodène)

503 mg du mélange des oléfines **11** et **12** (3,35 mmoles), en solution dans 30 cm^3 de méthanol absolu contenant en suspension 50 mg de palladium à 5 % sur charbon de bois, sont soumis à l'hydrogénation catalytique (1 atm, température ambiante, 6 heures). Après filtration du catalyseur et élimination du solvant, il reste 500 mg de produit brut, homogène en C C M, correspondant à l'oléfine **11** pure, non hydrogénée. Rdt ≃ 100 %.

$[\alpha]_D^{22} = +3{,}6°$ (C = 26,4 cyclohexane)
Spectre IR (cm^{-1}) : 1655 ($\nu_{C=C}$) très faible ; 860 (γ_{C-H}).
Spectre de RMN : (CCl_4), deux singulets à 0,83 et 1,21 (*gem*-diméthyle), un multiplet centré à 1,70 ($CH_3-\underset{|}{C}=C$), un multiplet centré à 2,1 (4 protons allyliques), un multiplet large centré à 5,25 (proton vinylique).
Spectre de masse : pics principaux : m/e (%) : M^+ 150 (20), 135 (15), 95 (85), 79 (100), 41 (95).

TRIMÉTHYL-2,7,7 BICYCLO[4.1.1] OCTÈNE-2 ONE-4 (*homo*verbénone) 13

A 45,7 g (0,305 mole) du mélange des deux oléfines **8** et **9** et 1,25 g d'iodure cuivreux, on ajoute goutte à goutte 58 g d'hydroperoxyde de *tertio*-butyle (à 79 % dans le *t*-butanol), de façon que la température reste comprise entre 65° et 70°. On agite le mélange à 80° pendant 6 à 8 jours, jusqu'à disparition de la bande O-O en IR (ou absence de peroxydes — test au NaI). On dilue le mélange avec 400 cm^3 d'éther et on lave avec plusieurs portions de 30 cm^3 d'HCl N pour éliminer les sels de cuivre. Après traitement habituel, il reste une huile brune et mobile que l'on distille : on recueille la fraction passant entre 45 et 65° (0,3 mm Hg) soit 32,5 g, constituée d'*homo*-verbénone **13**, d'*homo*-verbénol **14**, de l'alcool tertiaire **15** et aussi d'hydrocarbures de départ.

Le mélange est mis en solution dans 150 cm^3 d'éther et soumis à l'oxydation chromique (10 g de $Na_2Cr_2O_7$ et 7,5 cm^3 H_2SO_4 dilués avec 42 cm^3 H_2O) pendant 6 heures à 5°. Après extraction et traitement habituel, on isole 27,0 g d'un liquide jaune pâle, constitué d'*homo*-verbénone **13** qui peut être purifiée par chromatographie sur 250 g d'alumine neutre. Une première élution avec 800 cm^3 d'hexane permet d'éliminer 5,72 g du mélange des hydrocarbures **8** et **9** n'ayant pas réagi, accompagnés d'hydrocarbures non identifiés. Une deuxième élution avec 600 cm^3 d'acétate d'éthyle conduit à 18,65 g d'une huile jaune pâle que l'on distille soigneusement pour obtenir finalement 16,57 g d'*homo*-verbénone **13** (pureté 98 %, C P V, colonne 2, 200°). Eb$_{0,15}$: 62°. Rdt : 32 %, 20 % par rapport à l'α-pinène.

CPV analytique : Colonne 2, 200°, débit He : 45 cm^3/mn.
13 a un temps de rétention de 47 mn.

CCM : Gel de silice, éluant : benzène-acétate d'éthyle, 93/7, Rf : 0,42.

Un échantillon analytique présente :
$[\alpha]_D^{20} = -33°$ (C = 3,4 cyclohexane)

Spectre UV

$\lambda_{max} = 253$ nm, $\varepsilon = 10300$ et $\lambda_{max} = 317{,}5$ (inflexion), $\varepsilon = 75$ (éthanol)
$\lambda_{max} = 243$ nm, $\varepsilon = 11200$ et $\lambda_{max} = 337$, $\varepsilon = 50$ (cyclohexane)

Spectre IR (cm^{-1}) : bandes très fortes à 1650 (C=O) et 1628 (C=C).

Spectre de RMN : (CCl_4), deux singulets à 0,93 et 1,40 (*gem*-diméthyle), un méthyle doublet centré à 1,93 (J = 1,7 Hz), un doublet centré à 2,55 (J = 3,5 Hz, $-CH_2-$ $-CO-$), un multiplet centré à 5,86 (H-3).

Dinitro-2, 4 phénylhydrazone F : 208° (tube scellé, éthanol)

Spectre UV : $\lambda_{max} = 375$ nm, $\varepsilon = 27\,800$ (éthanol)

Spectre de RMN : (CCl_4 70 %, C_6D_6 30 %), deux singulets à 0,80 et 1,30 (*gem*-diméthyle), une méthyle doublet centré à 1,90 (J = 1,7 Hz).

Cis-TRIMÉTHYL-2,7,7 BICYCLO[4.1.1] OCTANONE-4 **16**

2,30 g (14 mmoles) d'*homo*-verbénone **13**, en solution dans 30 cm^3 d'éthanol absolu sont hydrogénés à température ambiante (pression : 2 bars) en présence de 80 mg de charbon palladié à 5 %. Après deux heures d'agitation, on filtre le catalyseur et on élimine le solvant. La distillation fournit 2,10 g (90 %) de cétone **16**. Eb$_{0,2}$: 47°.

CPV : Colonne 6, 170°, débit He : 60 cm^3/mn, temps de rétention correspondant au pic unique : 52 mn.

Spectre UV : $\lambda_{max} = 282$ nm, $\varepsilon = 28$ (éthanol)

Spectre IR (cm^{-1}) : 1700 ($\nu_{C=O}$)

Spectre de RMN : (CCl_4), deux singulets à 1,17 et 1,33 (*gem*-diméthyle), un méthyle doublet centré à 1,09 (J = 6,5 Hz).

Spectre de masse : pics principaux, m/e (%) : M$^+$ 166 (10), 97 (40), 83 (67), 69 (73), 55 (67), 41 (100).

Dinitro-2,4 phénylhydrazone F : 161° (éthanol)

Semi-carbazone : F : 234–235° (EtOH) (tube scellé)

Analyse	Calculé %	C	64,54	H	9,48	N	18,81
	Trouvé %		64,47		9,76		19,0

FORMYL-2 DIMÉTHYL-7,7 BICYCLO[4.1.1] HEPTADIÈNE 2,4 **18**

10,8 g du mélange des deux oléfines **8** et **9** (0,072 mole) en solution dans 70 cm^3 d'éthanol anhydre sont portés à reflux avec agitation magnétique et on ajoute goutte à goutte une solution de 9,50 g d'anhydride sélénieux dans 80 cm^3 d'éthanol absolu. Le mélange est agité à reflux pendant 18 heures. Après refroidissement, on filtre le sélénium et on évapore le solvant. Il reste 12,5 g d'une huile brune qui est distillée sous pression réduite. $Eb_{0,3}$: 40—75° (6,6 g). Par CPV préparative (colonne 3, 135°), on isole les deux aldéhydes insaturés **18** et **19**.

Spectre UV : $\lambda_{max} = 321$ nm, $\varepsilon = 7500$ (éthanol)
$\lambda_{max} = 314$ nm, $\varepsilon = 5500$ (n-hexane)

Spectre IR (cm^{-1}) : 2720 (ν_{C-H} aldéhyde), 1672 ($\nu_{C=O}$ forte), 1630 ($\nu_{C=C}$ faible), 1575 ($\nu_{C=C}$ très forte), 730 (γ_{C-H} très forte).

Spectre de RMN : (CCl_4), deux singulets à 0,67 et 1,38 (*gem*-diméthyle), un multiplet de 6 à 6,75 (3 protons éthyléniques), un singulet à 9,37 (—C*H*O).

FORMYL-2 DIMÉTHYL-7,7 BICYCLO[4.1.1] HEPTÈNE-2 **19**

Séparé par chromatographie en phase vapeur préparative (colonne 3, 135°).

Spectre UV : λ_{max} 235 nm, $\varepsilon = 8600$ (éthanol)

Spectre IR (cm^{-1}) : 2715 (ν_{C-H} aldéhyde), 1685 ($\nu_{C=O}$), 1640 ($\nu_{C=C}$)

Spectre de RMN : (CCl_4), un multiplet centré à 6,72 (H vinylique) et un singulet à 9,35 (-C*HO*) deux singulets à 0,94 et 1,39 (*gem*-diméthyle).

TRIMÉTHYL-2,7,7 BICYCLO[4.1.1] OCTANONE-3 **20**

9,35 g (62,3 mmoles) du mélange des deux oléfines **8** et **9**, en solution dans 100 cm^3 de THF anhydre à 0°, sont traités par un courant de diborane résultant de la réaction de 14g de BF_3-Et_2O sur 2,50 g de borohydrure de sodium dans le THF à reflux. On maintien l'agitation pendant 15 heures à température ambiante, puis la température du milieu réactionnel est ramenée à 0° (glace-sel). On additionne une solution de 13,7 g de bichromate de sodium dans 10 cm^3 d'H_2SO_4 à 96 % dilué dans 65 cm^3 d'eau, goutte à goutte de façon que la température ne dépasse jamais 5°. Après 3 heures d'agitation à 5°, in extrait à l'éther et on lave les phases organiques au bicarbonate puis à l'eau jusqu'à neutralité. Après séchage ($MgSO_4$) et élimination des solvants, le résidu incolore obtenu est distillé sous pression réduite et donne 7,85 g de cyclanone **20** incolore (76 %). $Eb_{0,3}$: 57°.

CPV analytique : Colonnes 2 et 7, température 205°, débit hélium 40 cm^3/mn. Pour **20** : $t_R = 23$ mn (colonne 2).

$[\alpha]_D^{20} = -44°$ (C = 3,6 cyclohexane)

Spectre IR (cm^{-1}) : 1702.

Spectre de RMN : (CCl_4), deux singulets à 0,72 et 1,29 (*gem*-diméthyle), un doublet centré à 1,05 ($^3J = 7$ Hz, méthyle-11).

Spectre de masse : pics principaux, m/e (%) : M^+ : 166 (11), 111 (29), 83 (93), 69 (82) 55 (100), 41 (82).

Dinitro-2,4 phénylhydrazone F : 192—194° (éthanol, tube scellé)

Analyse				
	Calculé	C 58,94	H 6,40	N 16,17%
	Trouvé	58,51	6,14	16,16 %

HYDROBORATION-OXYDATION DU MÉLANGE **11** + **12**

Dans un tricol de 500 cm^3, équipé d'un thermomètre plongeant, d'un réfrigérant et d'une ampoule à brome, on place 5,0 g du mélange des deux oléfines **11** et **12** (33,3 mmoles) (composition : 92 de 11 et 8 % de 12), 465 mg de $NaBH_4$ et 80 cm^3 de THF anhydre. Le mélange est refroidi à —10° avec agitation magnétique et sous azote. On ajoute goutte à goutte en 4 heures une solution de 2,40 g de BF_3, Et_2O (fraîchement distillé) dans 40 cm^3 de THF anhydre. Puis, le mélange est agité pendant 15 heures à température ambiante.

On refroidit à nouveau à—10° et on ajoute successivement 4,1cm^3 d'une solution d soude 3N et goutte à goutte, 4,1 cm^3 de peroxyde d'hydrogène (à 130 volumes, diluée de moitié). On abandonne le mélange à température ambiante, avec agitation, pendant une dizaine d'heures. La majorité du THF est éliminée sous pression réduite et on extrait à l'éther. Les phases éthérées réunies sont lavées avec une solution de sulfate ferreux, puis traitées de la manière habituelle. On isole 5,50 g d'une huile incolore constituée des alcools bruts ne présentant toutefois qu'un pic unique en CPV analytique (colonne 5, 180°), et qui est utilisé sans autre purification.

Le mélange ainsi obtenu, en solution dans 35 cm^3 de benzène est refroidi à 5° et on ajoute, en deux heures, et en agitant fortement, une solution de 7,95 g de bichromate de sodium dihydraté, 33 cm^3 d'eau, 10,8 cm^3 d'acide sulfurique concentré et 3,5 cm^3 d'acide acétique glacial, de façon que la température soit constamment maintenue au-dessous de 10°. Après extraction à l'éther et traitement habituel, on isole après distillation 4,50 g (81 %) de liquide incolore. $Eb_{0,4}$: 50−51°.

Par CPV préparative (colonne 5, 170°), on isole les deux cétones isomères **22** et **23** (rapport 91 : 9).

TRIMÉTHYL-4,7,7 BICYCLO[4.1.1] OCTANONE-3 **22**

Temps de rétention : 23 mn

$[\alpha]_D^{22} = -13°$ (C = 4,1 cyclohexane)

Spectre UV : $\lambda_{max} = 278$ nm, $\varepsilon = 77$ (hexane)
$\lambda_{max} = 279$ nm, $\varepsilon = 27$ (éthanol)

Spectre IR (cm^{-1}) : 1696 ($\nu_{C=O}$).

Spectre de RMN : (CCl_4), deux singulets à 0,70 et 1,27 (*gem*-diméthyle), un doublet centré à 1,05 ($^3J = 6,5$ Hz, méthyle-11).

Spectre de masse : pics principaux, m/e (%) : M^+ : 166 (10), 151, 127 (15), 97 (50), 69 (100), 55 (40), 41 (81).

TRIMÉTHYL-4,7,7 BICYCLO[4.1.1] OCTANONE-2 **23**

Temps de rétention : 33 mn.

$[\alpha]_{22}^{D} = +125°$ (C = 1,6 cyclohexane).

Spectre UV : $\lambda_{max} = 280$ nm, $\varepsilon = 68$ (hexane).
$\lambda_{max} = 291$ nm, $\varepsilon = 32$ (éthanol).

Spectre IR (cm^{-1}) : 1682 ($\nu_{C=O}$).

Spectre de RMN : (CCl_4), deux singulets 1,0 et 1,35 (*gem*-diméthyle), un doublet centré à 1,02 ($^3J = 6$ Hz, méthyle-11).

Spectre de masse : pics principaux, m/e (%) : M^+ 166 (7), 151 (7), 124 (15), 96 (90), 83 (100), 69 (55), 55 (65), 41 (100).

Semi-carbazone : F : 183°, tube scellé (méthanol)

TRIMÉTHYL-2,7,7 BICYCLO[4.1.1] OCTANE **24**

Le mélange des deux oléfines **8** et **9** (1,05 g, 7 mmoles) en solution dans 20 cm^3 de méthanol contenant 2 % d'eau est hydrogéné à température ambiante, en présence de charbon palladié à 5 % (25 mg). On obtient 1,00 g (94 %) d'hydrocarbure **24** incolore.

CPV : Colonne 3, 145°, débit He : 55 cm^3/mn, temps de rétention : 53 mn (pic unique).

Spectre de RMN : (CCl_4), deux singulets à 1,03 et 1,26 (*gem*-diméthyle), un doublet centré à 0,96 (J = 7 Hz, méthyle-11).

HYDROXY-3 FORMYL-4 TRIMÉTHYL-2,7,7 BICYCLO[4.1.1] OCTÈNE-3 **25**

A une suspension, agitée magnétiquement, de 2,60 g de NaH (dispersion 50 % dans l'huile) dans 25 cm^3 de benzène anhydre, on ajoute goutte à goutte à 5°, 8,7 cm^3 de formiate d'éthyle et on agite pendant 15 minutes. Toujours à 5°, on ajoute une solution de 3,90 g de **20** (23,5 mmoles) dans 40 cm^3 de benzène sec, et on agite le mélange à température ambiante pendant 15 heures. On hydrolyse avec 30 cm^3 d'eau et on sépare la phase aqueuse. La phase benzénique est extraite avec une solution de soude à 15 %. Les phases aqueuses sont réunies et acidifiées à pH 5 (HCl 2 N). Après extraction à l'éther, séchage ($MgSO_4$) et élimination du solvant, il reste 3,26 g d'une huile jaune vif. Par distillation, $Eb_{0,2}$: 72−74°, on recueille

2,94 g d'un liquide jaune constitué du mélange des aldéhydes **25** *cis* et *trans*, séparables par CPV préparative (colonne, 2, 210°, débit : 60 cm^3/mn). Rdt : 64 %.

a) ALDEHYDE **25** *trans* : temps de rétention : 29 mn

$[\alpha]_D^{22} = -13°$ (C = 6,8 cyclohexane).

Spectre UV : $\lambda_{max} = 314$ nm, $\varepsilon = 7400$ (éthanol).

Spectre IR (cm^{-1}) : 1630, 1585, 900 et 790.

Spectre de RMN : (CCl_4), deux singulets à 0,88 et 1,25 (*gem*-diméthyle), un méthyle doublet centré à 1,20 ($^3J = 7$ Hz), un singulet à 9,15 (proton aldéhydique), un singulet large à 15,3 (proton énolique).

b) ALDEHYDE **25** *cis* : temps de rétention : 34 mn

Spectre UV : $\lambda_{max} = 315$ nm, $\varepsilon = 5700$ (éthanol).

Spectre IR (cm^{-1}) : 1630, 1585, 900 et 790.

Spectre de RMN : (CCl_4), deux singulets à 0,98 et 1,28 (*gem*-diméthyle), un méthyle doublet centré à 1,30 ($^3J = 7$ Hz), un singulet à 9,20 (proton aldéhydique), un singulet à 15,3 (proton énolique).

MÉTHYLÈNE-4 TRIMÉTHYL-2,7,7 BICYCLO[4.1.1] OCTANONE-3 **26**

A 2,79 g du mélange des deux β-hydroxy-aldéhydes **25** (*cis* et *trans*) (14,5 mmoles) dissous dans 50 cm^3 d'éther, on ajoute 9,75 g de carbonate de potassium et 10 cm^3 d'une solution aqueuse de formaldéhyde à 30 %. On agite à température ambiante pendant 40 mn, puis on ajoute le minimum d'eau pour dissoudre le carbonate. La phase éthérée est séparée et lavée à l'eau jusqu'à neutralité.Après traitement habituel, on distille 760 mg de liquide jaune, $Eb_{0,5}$: 66° (30 %). Le résidu est constitué du produit de départ inchangé. Les deux épimères **26** (*cis* et *trans*) ne peuvent être séparés par chromatographie.

Spectre UV

$\lambda_{max} = 224$ nm, $\varepsilon = 1530$; $\lambda_{max} = 307$ nm, $\varepsilon = 160$ (éthanol).

Spectre IR (cm^{-1}) : 1685 ($\nu_{C=O}$), 1620 ($\nu_{C=C}$) et 940.

Spectre de RMN : (CCl_4), les deux épimères **26** (*cis* et *trans*) présentent tous deux, deux multiplets à 5,05 et 5,31 (largeur à mi-hauteur : 5 Hz) correspondant au méthylène *exo*.

TÉTRAMÉTHYL-2,4,7,7 BICYCLO[4.1.1] OCTANONE-3 **27** et **28**

108 mg du mélange des deux cétones α, β-instaurées **26** (*cis* et *trans*), en solution dans 10 ml de méthanol absolu, sont hydrogénés à température ambiante en présence de 30 mg de charbon palladié à 5 %. Après filtration et élimination du solvant, il reste 105 mg (96 %) de produit incolore.

CPV : Colonne 1, 165°, débit He : 100 cm^3/mn. **28** (≃50 %) a un temps de rétention de 19 mn et **27** (≃50 %), de 21 mn.

a) CÉTONE DIMÉTHYLÉE *cis-cis* **27**

Spectre UV : $\lambda_{max} = 290$ nm, $\varepsilon = 80$ (éthanol).

Spectre IR (cm^{-1}) : 1700 ($\nu_{C=O}$).

Spectre de RMN : (CCl_4), deux singulets à 0,62 et 1,09 (*gem*-diméthyle), deux méthyles doublets centrés à 1,06 ($^3J = 6{,}5$ Hz) et 1,08 ($^3J = 6{,}5$ Hz).

b) CÉTONE DIMÉTHYLÉE *cis-trans* **28**

Spectre UV : $\lambda_{max} = 297$ nm, $\varepsilon = 96$ (éthanol).

Spectre IR (cm^{-1}) : 1700.

Spectre de RMN : (CCl_4), deux singulets à 0,69 et 1,27 (*gem*-diméthyle), deux méthyles doublets confondus, centrés à 1,04 ($^3J = 7$ Hz et 6,5 Hz).

Revue Roumaine de Chimie, **20**, *3*, 379–385 (1975)

CYANOETHYLATION OF KETOXIMES. II[1]

KINETICS AND MECHANISM OF DECYANOETHYLATION OF SOME CYANOETHYL ETHERS OF *PARA*-SUBSTITUTED ACETOPHENONE OXIMES

P. BUCHWALD and L. FEY

Chemical-Pharmaceutical Research Institute
str. Fabricii 126, Cluj, Romania

Received January 17, 1974

The kinetics and mechanism of the decyanoethylation reaction of the compounds having the general formula *para*-X-$C_6H_4-C(CH_3)=N-O-CH_2-CH_2-CN$ (A) were studied by means of a convenient spectrophotometric method. The reaction is of first order both in (A) and the sodium hydroxide used, the overall order of the reaction being 2. The first step of the reaction is carbanion formation on the α carbon activated by CN group. This is followed by a slower, rate-determining step : the simultaneous elimination of an acrylonitrile molecule and the formation of the *para*-substituted acetophenone oxime anion. The effect of *para*-substituents on the rate of the reaction fits excellently the Hammett equation.

INTRODUCTION

In the previous paper [1] we described the preparation of compounds having the general formula :

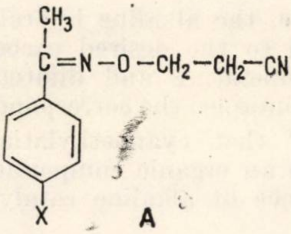

A

where X = *H* (*I*) ; NO_2(II) ; Cl (III) ; Br (IV) ; CH_3 (V) ; CH_3O (VI) ; and $NH-CO-CH_3$ (VII)

---

[1] P. Buchwald and A. Kövendi, *Rev. Roumaine Chim.*, **19**, (1974).

They were obtained by the cyanoethylation of the appropriate *para*-substituted acetophenone oximes.

It was mentioned, in a recently published patent,[2] that the compounds having the general formula :

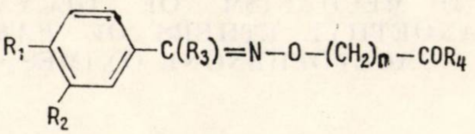

where : $R_1\ R_2 = H, \mathrm{Cl}$; $R_3 = H, \mathrm{CH_3}$; $R_4 = \mathrm{OH}, \mathrm{OCH_3}, \mathrm{NH_2}, \mathrm{NH{-}NH_2}$
$n = 1{-}3$

obtained by coupling Na or K salts of the corresponding acetophenone oximes with ω-halo-acids, present a pronounced anti-inflammatory and analgesic effect. Therefore, we intended to synthesize similar derivatives, converting the —CN group of the cyanoethyl derivatives (A) into —COOH group, according to the reaction :

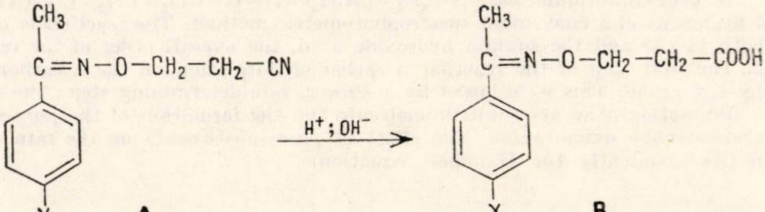 (1)

Using the classical acid [3] and alkaline [4] hydrolysis method, we have not obtained the desired result. Thus, for the preparation of *para*-substituted (benzylidene-aminoxy)-propionic acids (B) we chose another, indirect way : through iminoethers. The results of this conversion form the subject of another paper.

As mentioned above, the alkaline hydrolysis of (A), according to reaction (1) did not lead to the desired carboxilic acids (B). Even in mild conditions (low temperature and diluted sodium hydroxide) the reaction mixture always contained the corresponding acetophenone oximes.

It is well known[5] that cyanoethylation, namely, the reaction between acrylonitrile and an organic compound possessing labile hydrogen atoms, in the presence of alkaline catalysts, is reversible.

---

[2] J. VAN DIJK, J. M. A. ZWAGEMAKERS and V. CLASSEN (to N. V. Philips' Gloeilamphenfabrieken) *Ger. offen*, 1960910 ; *Chem. Abstr.*, **73**, 76833 (1970).

[3] A. SPIEGEL, *Ber. dtsch. chem. Ges.*, **14**, 239 (1881).

[4] W. MANN, *Ber. dtsch. chem. Ges.*, **14**, 1645 (1881).

[5] P. F. BUTZKUS, *Uspekhi Khim.*, **30**, 1352 (1961).

We supposed that the failure of —CN into —COOH conversion was due to decyanoethylation reaction, according to the following scheme :

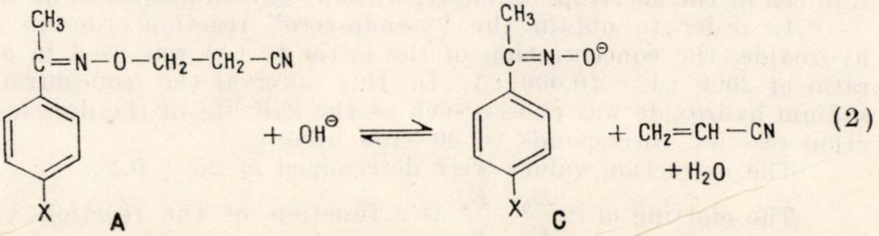

The decyanoethylation of ketoximes has not been studied yet.

As the cyanoethyl derivatives (A) obtained by us form an adequate series for studying the effects of *para*-substituents on the reaction rate, we performed a kinetic study in order to elucidate the fine reaction mechanism of this reaction. (2).

RESULTS AND DISCUSSION

It was proved that the most convenient method for the kinetic study of alkaline decyanoethylation reaction (2) was the spectrophotometric determination of the (A)/(C) ratio.

According to the literature data [6] the U.V. spectra of ionized and undissociated forms of the substituted acetophenone oximes are different.

Since, the π electronic system of the cyanoethyl derivatives of substituted acetophenone oximes (A) is similar to that of the undissociated forms of the corresponding acetophenone oximes, and the reaction product of alkaline decyanoethylation is the very ionized form of these oximes, we supposed that the reaction course would involve corresponding changes in the absorption values of the different spectral regions.

As a result of some preliminary tests, it has been stated that good kinetic determinations could be ensured by choosing a wave length at which the difference between the absorption values of (A) and (C) was the greatest and the spectral curves presented moderate slopes. The searched wavelengths were found to be $\lambda = 280-300$ nm, where the ionized *para*-substituted acetophenone oximes, except for the *para*-nitroderivative (II) present their extinction maximum. The measurments, even by decyanoethylation of (II) were carried out at $\lambda = 300$ nm, in which case, a decrease of the extinction values was observed, as at this wavelength the undissociated *para*-nitro-acetophenone oxime has its extinction maximum, the extinction maximum of the ionized form being shifted bathochromic toward $\lambda = 360$ nm.

---

[6] N. Bodor, L. Fey and A. Kövendi, *Rev. Roumaine Chim.*, **11**, 421 (1966).

The concentration of cyanoethyl derivatives being chosen round 5×10^{-5} mole/l, the extinction values obtained enabled carrying out alkaline decyanoethylation reactions in the thermostated quartz absorption cell of the spectrophotometer, without any additional dilution.

In order to obtain the "pseudo-zero" reaction order in sodium hydroxide, the concentration of the latter to (A) was used in a molar ratio of 2000 : 1 — 10.000 : 1. In this interval the concentration of sodium hydroxide was chosen such as the half life of the decyanoethylation reaction corresponds to 20—100 minutes.

The extinction values were determined at 25 ± 0.1°.

The plotting of $\ln \frac{E_0 - E_\infty}{E_t - E_\infty}$ as a function of the reaction time (t) (fig. 1) gave well correlated straight lines, which confirmed the first order of the reaction in *para*-substituted cyanoethylethers of acetophenone oximes.

The proportional dependence of the slopes of lines on the sodium hydroxide concentration confirmed that the partial order of the reaction for sodium hydroxide is also 1. Thus, the overall reaction order is 2.

The E_∞ values were determined by two different methods:

a) the extinction values of pure *para*-substituted acetophenone oximes were determined under same conditions as for the decyanoethylation reaction

b) the decyanoethylation reactions of (A) were accelerated by heating the reaction mixture at 50—60° for 3—4 hours.

The fact that in both cases identical E_∞ values have been obtained means that there are no secondary reactions involving the resulted *para*-substituted acetophenone oxime. This also proves that the chosen spectrophotometric method is suitable to kinetic studies.

Extinction values were determined every 6—20 minutes (6 minutes at the beginning of the reaction, spaced out at greater intervals later).

Reaction constants (table 1) were calculated from extinction values according to equation:

$$k = 1/t \ \ln \frac{E_0 - E_\infty}{E_t - E_\infty}$$

Table 1

The reaction constants of decyanoethylation reaction (2)

X =	C_{NaOH} mol/l	$k' \times 10^2$ min^{-1}	$k \times 10^2$ min^{-1}	$s \times 10^2$	$s.t_{99} \times 10^2$	d.f.
CH_3O	0.50	2.81	5.62	0.08	0.2	6
CH_3O	0.25	1.38	5.53	0.1	0.3	6
CH_3	0.10	0.705	7.05	0.03	0.08	8
$CH_3-CO-NH$	0.40	3.52	8.80	0.03	0.1	5
$CH_3-CO-NH$	0.20	1.78	8.90	0.08	0.2	9
H	0.10	0.92	9.20	0.03	0.1	12
Cl	0.10	1.19	11.90	0.04	0.1	7
Br	0.10	1.18	11.80	0.2	0.6	8
NO_2	0.10	2.98	29.80	0.07	0.2	9

x: *para*-substituent; C_{NaOH} sodium hydroxide concentration in mol/l k': rate constant for the reaction of pseudo-first order to C_{NaOH}; k: rate constant for the decyanoethylation reaction with reaction order 2; s: standard deviation; $s.t_{99}$: confidence interval at t_{99} (Student); d.f.: degrees of freedom

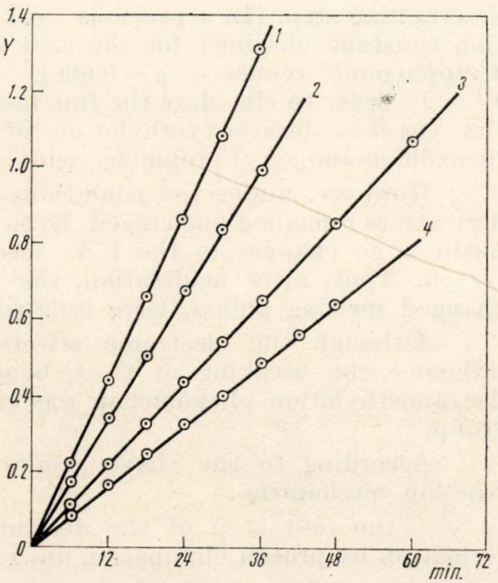

Fig. 1. — Correlation of $Y = ln \frac{E_0 - E_\infty}{E_t - E_\infty}$ with time: *1*, $X = CH_3 - CO - NH$, $C_{NaOH} = 0.40$ mol/l; *2*, $X = CH_3O$, $C_{NaOH} = 0.50$ mole/l. *3*, $X = CH_3-CO-$ $-NH$, $C_{NaOH} = 0.20$ mol/l; *4*, $X = CH_3O$, $C_{NaOH} = 0.25$ mole/l.

The dependence of *k* values on *para*-substituent (X) confirmed transmission of electronic effects from substituent X to the reaction centre through the benzene nucleus — double bond — p electron pair of oxygen conjugated system. The susceptibility of the reaction to the influence of the substituents confirmed that the breaking of the $O-CH_2$ bonding in the rate-determining step of the decyanoethylation.

Plotting log *k* values as a function of the substituent constants (σ) gave a perfectly correlated straight line ($r = 0.989$) (see fig. 2).

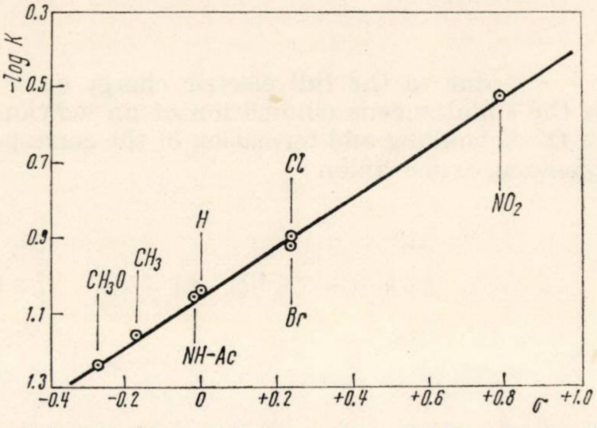

Fig. 2. — Hammett plot for decyanoethylation of (A) series: $r = 0.989$; $s = 0.03$; $\rho = 0.664$ (Substituent constants tabulated by Mc Daniel and Brown[7] were used).

The validity of Hammett's equation and the value of the obtained reaction constant ($\rho = 0.664$) confirmed the proposed reaction mechanism according to which the breaking of $O-C$ bonding is the rate-determining step. (In a previous work [6] we have reported that the reaction constant obtained for the acid dissociation of some *p*-substituted acetophenone oximes is $\rho = 0.666$).

---

[7] D. H. Mc Daniel and H. C. Brown, *J. Org. Chem.*, **23**, 420 (1958).

In order to elucidate the fine mechanism of this decyanoethylation, the possible decarboxyethylation of the corresponding *p*-substituted (benziliden-aminoxy)-propionic acids (B) was also studied.

However, under the conditions used for decyanoethylation, these derivatives remained unchanged. Even after prolonged heating in alkaline medium no changes in the U.V. spectra of these derivatives were observed. Thus, after acidulation, the initial carboxylic acids, with unchanged melting points, were isolated from the reaction mixture.

Although the electronic effects of —CN group cannot directly influence the breaking of O—C bonding, this result implies that the decyanoethylation phenomenon was conditioned by the presence of this group.

According to the above results we have proposed the following reaction mechanism:

— the first step of the decyanoethylation reaction is carbanion formation by proton elimination on α carbon activated by —CN group:

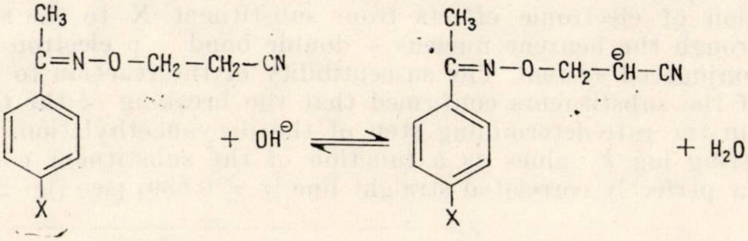

— due to the full electric charge on α carbon, the following step is the simultaneous elimination of an acrylonitrile molecule by breaking of O—C bonding and formation of the corresponding *p*-substituted acetophenone oxime anion:

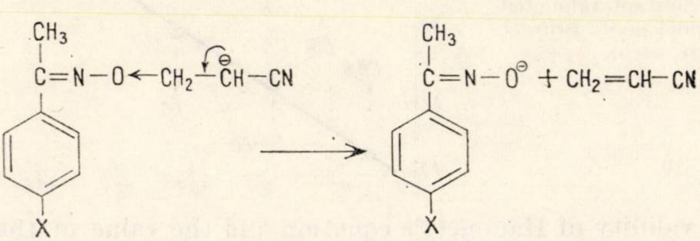

The marked susceptibility of the reaction to the influence of the *para*-substituents indicates that this is the slower rate-determining step of the reaction.

The suggested ElcB type elimination reaction mechanism [8] is in good agreement with the results obtained.

The *p*-substituted acetophenone oximes obtained from the decyanoethylation reaction were isolated by filtration after acidulation of the reaction mixture. The presence of the acrylonitrile cannot be revealed in the reaction mixture, probably because of its polymerisation or a secondary reaction between acrylonitrile and water.

EXPERIMENTAL

Compounds used: The compounds described in our previous paper.[1]

Kinetic determinations: The decyanoethylation reaction of (A) series was carried out in the thermostated quartz absorption cell of a "Zeiss V.S.U.-1" ultraviolet spectrophotometer at 25 ± 0.1°.

An illustrative experiment: the decyanoethylation of (I) (MW: 118,23) is described: 0.0667 g (3.54×10^{-4} mole) weighed (I) were dissolved in 50 ml of methanol. To 100 ml of this solution (7.08×10^{-6} mole) are added 10 ml NaOH 1 N and water (7.08×10^{-5} mole/l) to make up 100 ml. (All reagents were previously stored at 25°).

A portion of this solution was introduced in the thermostated quartz absorption cele (1 cm layer) of the spectrophotometer. The extinction values were determined at an interval of 6 minute at $\lambda = 280$ nm ($t = 0$ was considered the moment of the first reading. As reference solution we used 1 ml methanol with addition of NaOH 0.1 N up to 100 ml.

Determination of E_∞:

a) 0.0500 g pure acetophenone oxime (m. p. 59°) were dissolved in 50 ml methanol. To 1.00 ml of this solution was added 10 ml NaOH 1 N and water to 100 ml. The extinction value of this solution was determined at $\lambda = 280$ nm at 25°: $E_{\text{ox}} = 0.544$

E_∞ was calculated by means of equation:

$$E_\infty = E_{ox} \frac{MW_{ox} \cdot 0.0667}{MW_{CN} \cdot 0.0500} = 0.521$$

where MW_{ox} is the molecular weight of the acetophenone oxime (135.16); and MW_{CN} is the molecular weight of (I), respectively.

b.) 50 ml solution of (I), prepared as above, was maintained at 60° for 3 hrs. After cooling, the extinction value was determined at $\lambda = 280$ nm: $E = 520$. After additional heating, the extinction value was determined again. Since the value was unchanged it was considered as E_∞.

The E_t values obtained and the calculated k_t values are given in table 2:

Table 2

E_t and k_t values obtained for decyanoethylation of (I)

t minutes	E_t	$k_t \times 10^2$ min^{-1}
0	0.093	—
6	0.116	8.86
12	0.139	9.23
18	0.1585	9.09
24	0.178	9.14
30	0.198	9.29
36	0.215	9.23
42	0.232	9.29
48	0.248	9.29
54	0.262	9.23
60	0.278	9.04
72	0.304	9.39
84	0.328	9.44
100	0.355	8.95

---

[8] C. K. Ingold, "Structure and Mechanism in Organic Chemistry", Cornell University Press, Ithaca, N.Y., 1953, Sec. 30 a.

Revue Roumaine de Chimie, 20, 3, 379–385 (1975)

Revue Roumaine de Chimie, **20**, *3*, 387–396 (1975)

CATALYTICALLY ACTIVE IRON OXIDES PREPARED BY MECHANOTOPOCHEMICAL METHOD. II[1]

THERMAL ANALYSIS OF SOME IRON HYDROXIDES

ANTOANETA SPINZI* and I. V. NICOLESCU**
* Institute of Physical Chemistry str. Dumbrava Roşie 23, Bucharest, Romania
**Faculty of Chemistry, University of Bucharest,
Spl. Independenţei 89, Bucharest, Romania

Received April 19, 1974

The paper presents the results obtained from the thermal analysis of four iron hydroxides of different origins. It has been found that the determining role in the process of thermal formation of the crystalline iron oxide α-Fe_2O_3 is played by the nature of the initial iron salt and not by the working procedure. DTG and TG data were used for the evaluation of the kinetic parameters of two consecutive dehydration steps, distinct in the case of FTS sample.

A previous paper[1] presented some data on the preparation and structural-textural characterization of some iron hydroxides obtained by the mechanotopochemical method versus that of precipitation in solution. Along this line, a thermographic study of iron hydroxide samples was carried out, to specify the characteristic phase-transformation thermal steps in correlation with the parameters involved in preparation.

A series of papers [2–7] have focussed on the thermal behaviour of iron hydroxides since this working procedure is adequate for investigation into this system. However, some aspects are still obscure owing to the structural variety of possible terms and compounds.

---

[1] I. V. Nicolescu, A. Spinzi, Z. Toma and G. Galaţchi, *Rev. Roumaine Chim.*, **20**, 61 (1975).

[2] "Differential Thermal Analysis", ed. R. C. Mackenzie, Academic Press, London, 1970, vol. I, chp. 9.

[3] N. F. Ermolenko and M. D. Erros, "Reguliarovanye poristoi struktury okisnykh adsorbentov i katalizatorov", Izd. Nauka i tehnika, Minsk, 1971, p. 160.

[4] L. P. Ni, M. M. Goldman, T. V. Solenko, L. V. Bunchiuk and O. B. Haliapina, "Okisly zheleza i proizvodstvo glinozenia", Izd. Nauka Kazanskoi S.S.S.R., Alma-Ata, 1971, p.7.

[5] W. F. Wilburn, J. R. Hesford and J. R. Flower, *Analyt. Chem.*, **40**, 777, (1968).

[6] E. P. Tzimbal, S. I. Sinyshleaev and L. M. Dvornikova, *Zhur. neorg. Khim.*, **12**, 3175 (1970).

[7] J. Babcan and J. Kristin, *J. Therm. Anal.*, **3**, 307 (1971).

Table 1

Variants of iron hydroxides studied

Symbol	Raw material	Method of preparation	Chemical composition	Structural composition		
				80°	300°	400 – 800°
FTS	$FeSO_4 . 7H_2O + (NH_4)_2CO_3$	mechanotopo-chemical	$Fe_2O_3 . 1.18H_2O$	$\alpha - FeOOH$ $\delta - FeOOH$ $\alpha - Fe_2O_3$	$\alpha - Fe_2O_3$	$\alpha - Fe_2O_3$ Fe_3O_4
FTSB	$FeSO_4 . 7H_2O + NH_4HCO_3$	–,,–	$Fe_2O_3 . 1.19H_2O$	$\alpha - FeOOH$ $\alpha - Fe_2O_3$ $\delta - FeOOH$	$\alpha - Fe_2O_3$	$\alpha - Fe_2O_3$ Fe_3O_4
FTA	$Fe(NO_3)_3 . 9H_2O + (NH_4)_2CO_3$	–,,–	$Fe_2O_3 . 1.17H_2O$	$Fe_2O_3 . H_2O$ amorphous	$\alpha - Fe_2O_3$	$\alpha - Fe_2O_3$ Fe_3O_4
FP	$FeSO_4 . 7H_2O + (NH_4)_2CO_3$	precipitation from solution	$Fe_2O_3 . H_2O$	$\alpha - FeOOH$ $\delta - FeOOH$	$\alpha - Fe_2O_3$	$\alpha - Fe_2O_3$ Fe_3O_4

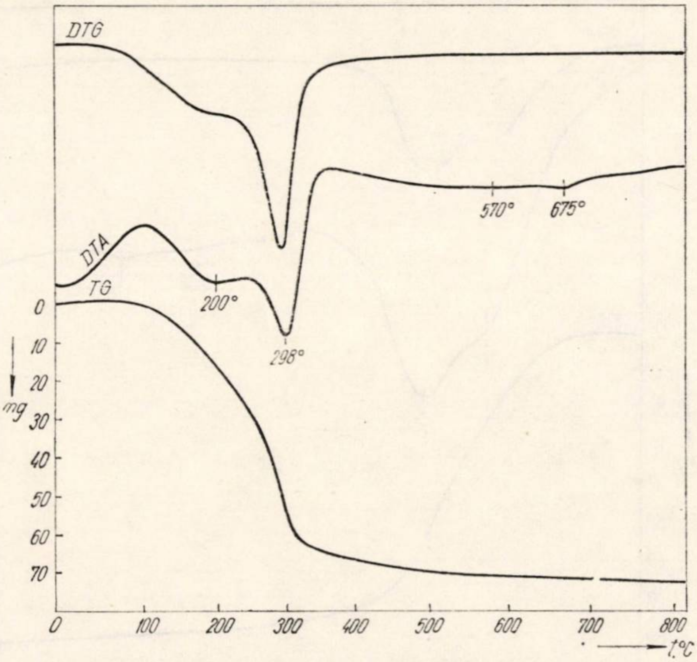

Fig. 1. — Thermogram of sample FTS; $G = 0.562$ g.

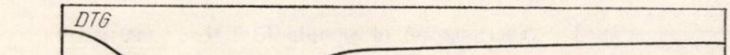

Fig. 2. — Thermogram of sample FTSB; $G = 0.575$ g.

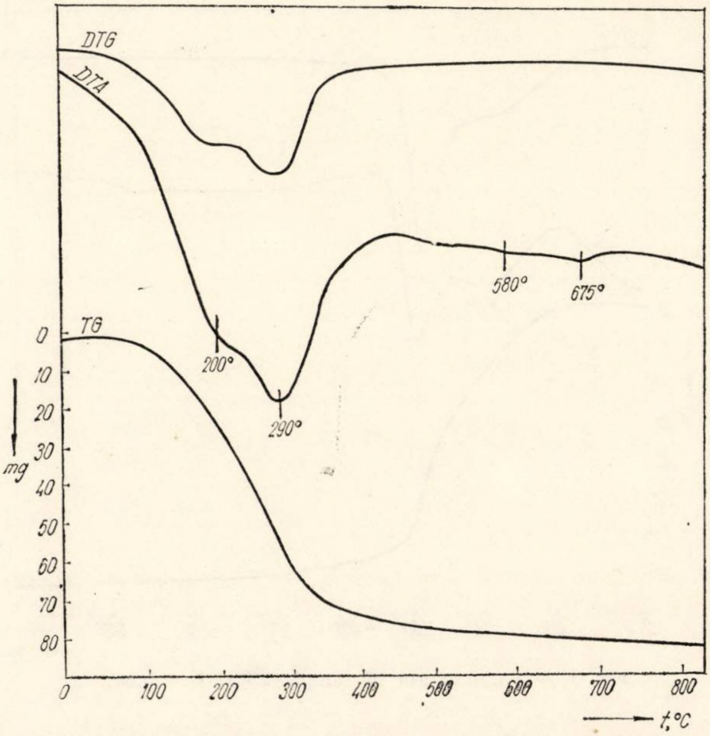

Fig. 3. — Thermogram of sample FP; $G = 0.690$ g.

This paper described the thermal analysis performed in the case of four samples of pure iron hydroxide, after drying, to a constant weight of 80°. The origin and phase-composition of the studied samples is presented in table 1.

The thermal analysis was carried out on a Paulyk-Paulyk-Erdey-type MOM derivatograph, in a chamotte crucible using the following parameters: a) temperature 1200°; b) inert substance $\alpha-Al_2O_3$; c) heating rate $= 10°/\text{min}$; d) DTA and DTG sensitivity $= 1/5$. Figure 1 shows the thermograms of the products resulting from $FeSO_4$.

These reveal remarkable similarities from the point of view of their aspect and transition points. The first section of the thermograms reveals two endothermal heat effects accompanied on the DTG curve by analogous effects with loss in weight. The first effect extends over a large domain ranging between 80—240°, the second presents a sharp peak at ~298°. The effects are clear and distinct from each other only in the case of FTS sample.

These effects are assigned to a two-step dehydration process of initial hydroxides. The calculation of loss in weight according to curve TG confirms the elimination of ~1 mole H_2O for the FP sample and of 1.14 mole for the FTS and FTSB samples, in the 80—350° interval, which verifies the global formula of iron monohydrate simple or hydrated, established by chemical analysis.[1] For products FTSB and FP, the curves showing the loss in weight TG have a mild slope indicating the continuity between the two dehydration steps ; in product FTS these steps are distinct.

In general, the occurrence of low-temperature endothermal peaks (140—180°) is attributed to the loss of adsorption water contained in the capillaries and between the layers, whereas the endothermal effect at 300° is correlated with goethite dehydration (α-FeOOH) and formation of iron oxide. For component δ—FeOOH one mentions the existence of a low-temperature endothermal effect and of two small endothermal peaks at 275° and 320°, presumably due to an exothermal peak overlapping.

In the present case, the coexistence of relatively small amounts in phase δ—FeOOH compared to α-FeOOH cannot be perceived on the thermogram because its thermal effects may be completely masked by those of the main component.

The dehydration process in two steps is recorded on the thermogram for the sample FP too, which contains only structural water. Similarly, samples FTS and FTSB eliminate, up to the temperature of the first thermal effect, more than the quantity contained as adsorption water. It has been found that about half of the total water contained in the initial samples is lost up to ~240°. For this reason, we considered the loss of structural water to occur in two steps, being also associated, at lower temperature, with the loss of adsorption water.

It is mentioned that by thermal decomposition α-FeOOH changes first into amorphous Fe_2O_3 which subsequently becomes crystalline.[3] The latter process is marked by an exothermal effect at 300° on the DTA curve which may be totally excluded by the endothermal component owing to the simultaneity of dehydration and crystallization processes. Another interpretation considers that continuous diffusion of molecular water from the structure leaves a residue which rapidly nucleates into α-Fe_2O_3 prior to the occurrence of the exothermal peak which represents the final development of α-Fe_2O_3 from the already existing „protohematite".[2]

In our case, a weak exothermal effect is reported to appear at ~340° only in the case of FTSB sample. Conversely, the X-ray diffraction analysis of all samples calcined at 300° prove the exclusive existence of crystallized α-Fe_2O_3. For this reason, if the effect represented a true exothermal peak and was not due to sample contraction or to factors partaining to the apparatus [5] it would probably correspond to the development of a better crystallized α-Fe_2O_3. The absence of an exothermal effect in FTS and EP samples seems not to be due to the masking effect, but to the transformation goethite → hematite, directly into the crystalline form.

The thermogram of the FTA sample prepared of ferric nitrate is differentiated from that of samples prepared of iron (II) sulphate precisely by the clear detection of the strong exothermal effect at 300°. It is preceded by two endothermal effects : the first, a sharp peak at 203°, the second, a weak one, due to its being masked by the exothermal component (fig. 4).

The calculation of weight losses corresponding to the first endothermal effect (80–200°) is equivalent with 0.55 mole H_2O of the total of 1.14 mole H_2O eliminated between 80–350°. In this case, too, the loss of the adsorption water takes place simultaneously with that of the weaker bound structural water, the thermal effect being slightly shifted towards higher temperatures.

Since X-ray diffraction of sample FTA obtained after drying at 80° indicates the exclusive existence of amorphous iron hydroxide and that of the sample calcined at 300° indicates the complete change into α-Fe_2O_3, the exothermal peak may be interpreted in terms of converting "protohematite" into well-crystallized α-Fe_2O_3.

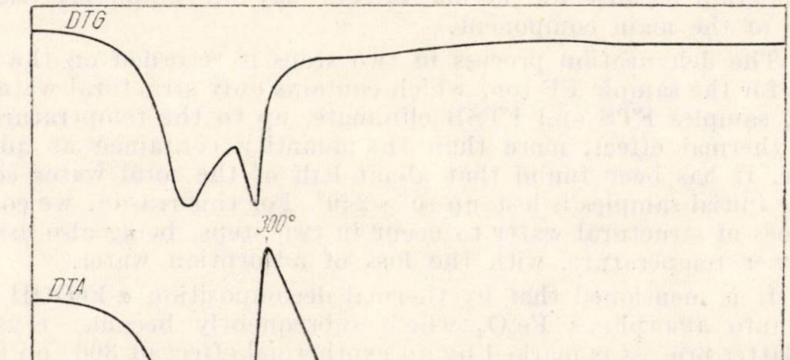

Fig. 4. – Thermogram of sample FTA; $G = 0.730$ g.

The appearance of the α-Fe_2O_3 form, a thermally stable oxidic phase, is maintained without major modifications throughout the investigated temperature interval. The X-ray analysis indicates the appearence of Fe_3O_4 (belong 10%) as low as 400° for all investigated samples. Yet, this slight reduction fails to explain the loss in weight (1–2.5%) recorded on the TG curve between 300–900° which would be due to the appearence of some suprastoichiometric iron ions in the oxidic lattice, too.

Furthermore, all thermograms indicate an endothermal effect at 675° which is certainly due to the variation of magnetic properties of α-Fe_2O_3 and may represent the sum of two transitions – Curie point and Neel point. In the case of some Fe_2O_3–Fe_3O_4 (>10%) mixtures, the appearence of an additional effect at 570° is possible and would represent the same transitions for magnetite. This effect is perceived on the thermograms of products FTS, FTSB and FP.

Based on the thermograms obtained, attempts were made at giving a quantitative interpretation of data expressed as apparent kinetic parameters (reaction order, activation energy, pre-exponential factor) of the two consecutive dehydration processes of iron hydroxides. This was possible only in the case of sample FTS where the corresponding thermal and thermogravimetric effects were clearer. In the case of the other samples, owing to the continuity between processes, the effects are overlapping and do not permit an evaluation of kinetic parameters.

It is known that the heating rate of the investigated product may have a decisive influence on the nature of its thermal decomposition. Therefore, the formation kinetics of FTS oxide was deduced on the basis of a thermogram run at a rate of 2.5°/min. It does not differ from the thermogram presented in fig. 1 as it does not record either additional splitting effects from the DTA curve or displacements of characteristic temperatures.

The kinetic parameters were evaluated by both the differential method suggested by Freeman and Carroll and the integral method of Coats and Redfern.[8,9] The application of these methods consists in plotting equations :

$$\frac{\Delta \log \dfrac{dW}{dT}}{\Delta \log W_r} = -\frac{E}{2.3R} \cdot \frac{\Delta(1/T)}{\Delta \log W_r} - n \qquad (1)$$

and

$$\log\left[\frac{1-(1-\alpha)^{1-n}}{T^2(1-n)}\right]_{n\neq 1} = \log\left[\frac{Z_\alpha P}{\beta E}\left(1-\frac{2RT}{E}\right)\right] - \frac{E}{2.3R}\cdot\frac{1}{T} \qquad (2)$$

in which :

$$\alpha = W/W_\infty$$

---

[8] E. S. Freeman and B. Carroll, *J. Phys. Chem.*, **62**, 394 (1958).

[9] A. W. Coats and P. J. Redfern, *Nature*, **21**, 68 (1964).

and W = amount of eliminated volatile product (g);
W_r = amount of residual volatile product (g);
W_∞ = total amount of volatile compound (g);
E = activation energy of reaction (kcal/mole);
n = reaction order;
Z_W = pre-exponential factor of eqn. (1) ($g^{1-n}.s^{-1}$);
Z_α = pre-exponential factor of eqn. (2) (s^{-1});
β = heating rate (C/min).

Since magnitudes Z_W and Z_α differ from a dimensional standpoint, their numerical values were compared by the following conversion formula :

$$Z_W = Z_\alpha \, W^{1-n} \tag{3}$$

Associating the two calculation procedures provided the advantage that, based on the reaction order determined by the analysis of thermographic data according to the Freeman-Carroll method, the subsequent application of the Coats-Redfern method is much facilitated.[10]

The kinetics of the I-st dehydration stage was calculated by applying the two associated calculation procedures. Processing of the obtained experimental data leads to the verification of the two equations for $n = 2$ (fig. 5).

In the case of the II-nd stage of dehydration it was not possible to use the Freeman-Carroll equation because as it uses the results of a differential curve (DTG), it is much more liable to errors, particularly in the case of some consecutive processes. For this reason, the calculation resorted to the method of successive approximations of the Coats-Redfern equation which removes this drawback by using the integral curve TG. The results obtained demonstrate the verification of this equation for $n = 1.5$ (fig. 6).

Evaluation of the kinetic parameters presented in table 2 leads to a satisfactory agreement of stage I activation energies calculated by means of these two methods. The relatively low values obtained indicate the existence of a weak bond of water in the product at the lower limit of the chemical bond. This accounts for the elimination of this structural water fraction at lower temperatures.

Table 2

Kinetic parameters of dehydration reactions of FTS oxihydroxide

Reaction	Freeman-Caroll method			Coats-Redfern method			
	n	E kcal/mole	Z_W $g^{1-n}.s^{-1}$	n	E kcal/mole	Z_α s^{-1}	Z_W $g^{1-n}.s^{-1}$
Ist stage of dehydration	2	12.60	5.10^5	2	11.10	$2.1..10^5$	$1.9.10^5$
IInd stage of dehydration	—	—	—	1.5	18.75	$5.5.10^5$	$3.7.10^5$

---

[10] I. G. Murgulescu, E. Segal and D. Fătu, *Rev. Roumaine Chim.*, **11**, 291 (1966).

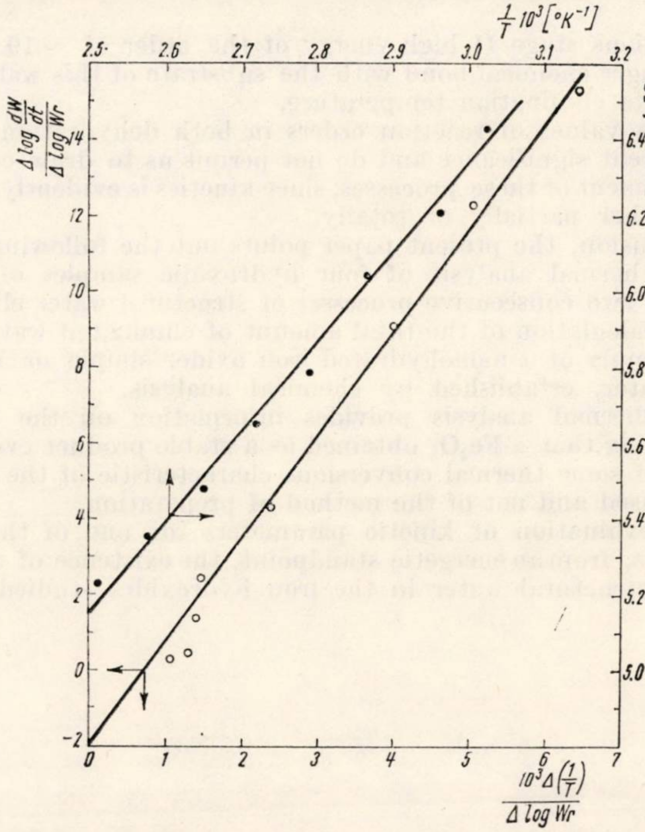

Fig. 5. — Verification of Freeman-Carroll and Coats-Redfern equations for the first dehydration stage of FTS oxihydrate.

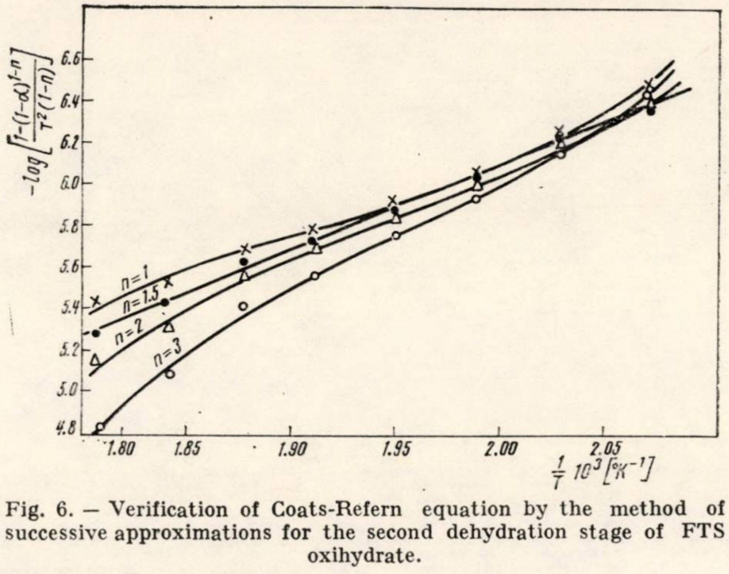

Fig. 6. — Verification of Coats-Refern equation by the method of successive approximations for the second dehydration stage of FTS oxihydrate.

The obvious stage II high energy of the order of ~ 19 kcal/mole attests a stronger chemical bond with the substrate of this water, a fact which raises its elimination temperature.

The high values of reaction orders in both dehydration processes have an apparent significance and do not permit us to draw conclusions on the development of these processes, since kinetics is evidently diffusion-controlled, either partially or totally.

In conclusion, the present paper points out the following :

1) The thermal analysis of four hydroxidic samples of different origins attests two consecutive processes of structural water elimination.

2) The calculation of the total amount of eliminated water verifies the global formula of a monohydrated iron oxide, simple or with some adsorption water, established by chemical analysis.

3) The thermal analysis provides information on the structural analysis, showing that α-Fe_2O_3 obtained as a stable product even at 300° is the result of some thermal conversions characteristic of the nature of the iron salt used and not of the method of preparation.

4) The evaluation of kinetic parameters for one of the samples (FTS) confirms, from an energetic standpoint, the existence of two bonding types of structural water in the iron hydroxides studied.

Revue Roumaine de Chimie, 20, 3, 397–406 (1975)

DIFFERENTIAL POTENTIOMETRY AT ZERO CURRENT USING TWO MEMBRANE-ELECTRODES WITH DIFFERENT SELECTIVITY

I. C. POPESCU, C. LITEANU and A. MOCANU
"Babeş-Bolyai" University, Cluj-Napoca
Department of Analytical Chemistry, str. Arany Janoş 11, Cluj-Napoca

Received January 17, 1974

The paper describes a new technique of differential potentiometric titration at zero current, based on the utilization of two membrane-electrodes with different selectivity to the titrated ion. The method is exemplified in the case of KCN titration with $AgNO_3$ using the indicator couple membrane-electrode of $AgI-Ag_2S$/membrane-electrode of Ag_2S. A first or second order differential signal appears at equivalence on the corresponding titration curves.

It is known that the following situations may arise from the standpoint of the behaviour of the electrode couple necessary for conducting a potentiometric titration:

1. An indicator electrode $\left(\frac{\mathrm{d}E_i}{\mathrm{d}V} \neq 0\right)$ associated with a reference electrode $\left(\frac{\mathrm{d}E_r}{\mathrm{d}V} = 0\right)$, *potentiometric titration.*

2. Two indicator electrodes $\left[\left(\frac{\mathrm{d}E_i}{\mathrm{d}V}\right)_{1,2} \neq 0\right]$, *differential potentiometric titration.*

On the other hand, when applying the various known techniques of potentiometric titration at zero current belonging to the two abovementioned cases one may use either conventional electrodes (electrodes of type I, II, III and redox) or membrane-electrodes. Thus, potentiometric titrations at zero current conducted by means of conventional electrodes have long been known. Similarly, potentiometric titrations at null current, achieved with a membrane-electrode employed as an indicator electrode are widely used at present.

The present paper introduces a new technique of differential potentiometric titration at zero current, based on the use of two membrane-electrodes with different selectivity to the titrated ion.[1] The method is exemplified in the case of KCN titration with $AgNO_3$, using the indicator couple membrane-electrode formed of Ag_2S[2] / membrane-electrode formed of $AgI-Ag_2S$.[3]

---

[1] I. C. Popescu, C. Liteanu and A. Mocanu, *IUPAC International Symposium Selective Ion-Sensitive Electrodes*, Cardiff, 1973, paper 50.

[2] I. C. Popescu, C. Liteanu and L. Savici, *Rev. Roumaine Chim.*, **18**, 1451 (1973).

[3] C. Liteanu, I. C. Popescu and A. Mocanu, *Rev. Roumaine Chim.*, **18**, 1467 (1973).

EXPERIMENTAL

Apparatus and reagents. All emf measurements were made by a pH-meter (Radelkis OP-401/1). Cyanide standard solutions were prepared by dilution from a KCN 1 M stock solution obtained by weighing. Solutions of the other employed reagents were obtained by weighing from substances of *p. a.* purity.

Working procedure. The potential of both membrane-electrodes was measured during KCN titration with $AgNO_3$ versus a calomel-saturated electrode, as well as the potential difference between them. To do this, the emf of the following cells was evaluated:

SCE ‖ test solution ‖ salt bridge KNO_3 0.1 M agar-agar | membrane-electrode of AgI-Ag_2S (1)

SCE ‖ test solution ‖ salt bridge KNO_3 0.1 M agar-agar | membrane-electrode of Ag_2S (2)

Membrane-electrode Ag_2S | test solution | membrane-electrode AgI$-Ag_2S$ (3)

The test solutions were magnetically stirred. All measurements were performed at room temperature.

EXPERIMENTAL RESULTS

The electrode functions of the two utilized ion-selective membrane-electrodes are illustrated in figure 1.

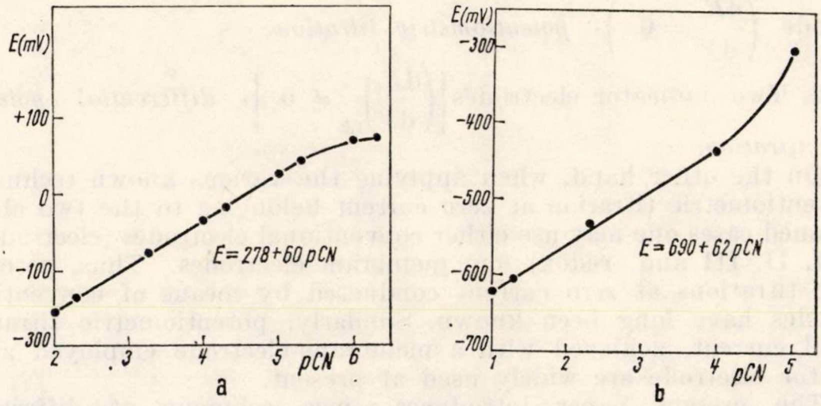

Fig. 1. — E$-$pCN electrode function (pH = 13); a) electrode of AgI$-Ag_2S$; b) electrode of Ag_2S

The integral and the differential titration curves (fig. 2a, curve 1 and 2 and fig. 2b, respectively) were traced by measuring during KCN 10^{-2} M titration with $AgNO_3$ 5×10^{-2}M both the potential of the membrane-electrode formed of AgI$-Ag_2S$ and that of the membrane electrode formed of Ag_2S, respectively, relative to SCE and the potential difference between them.

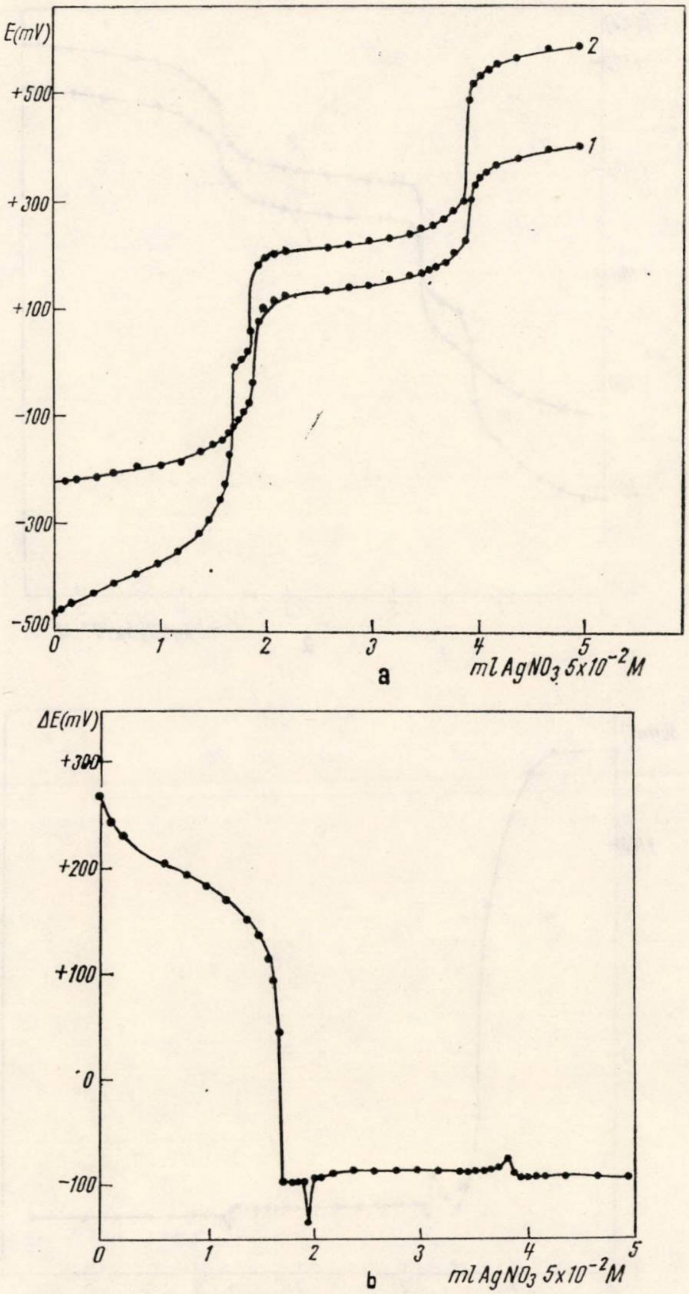

Fig. 2. — KCN 10^{-2} M titration with $AgNO_3$ 5×10^{-2} M ; a) with the membrane-electrode of $AgI-Ag_2S$ (1) and with the membrane-electrode of Ag_2S (2) b) with the membrane-electrode of $AgI-Ag_2S$/membrane electrode of Ag_2S couple.

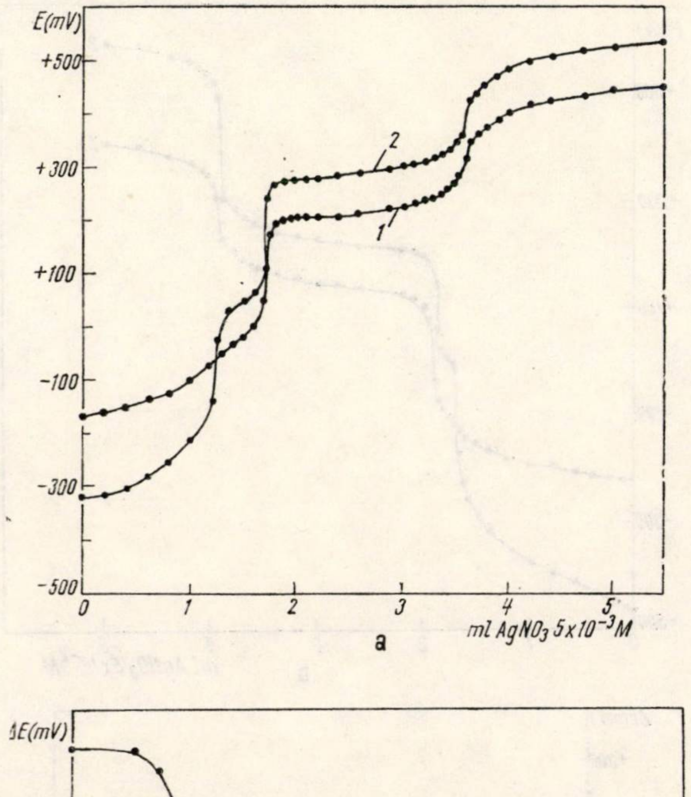

Fig. 3. — KCN 10^{-3} M titration with $AgNO_3$ 5×10^{-3} M ; a) with the membrane-electrode of $AgI-Ag_2S$ (1) and with the membrane-electrode of Ag_2S (2) ; b) with the membrane-electrode of $AgI-Ag_2S$/membrane-electrode of Ag_2S couple.

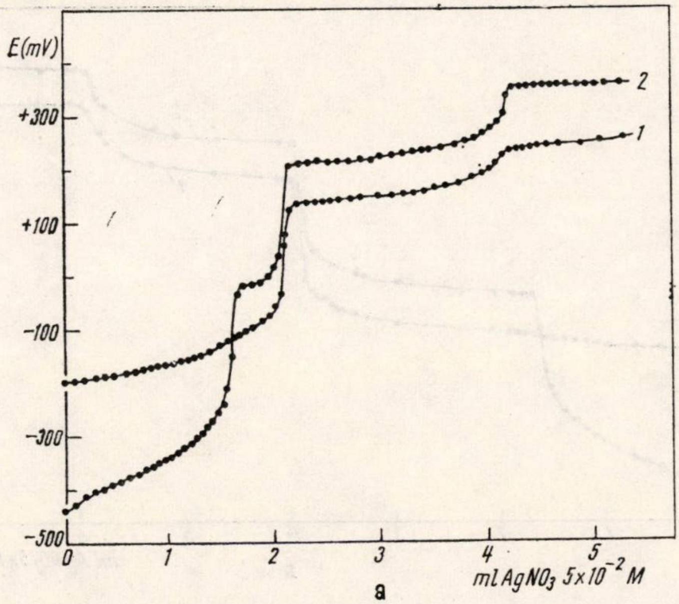

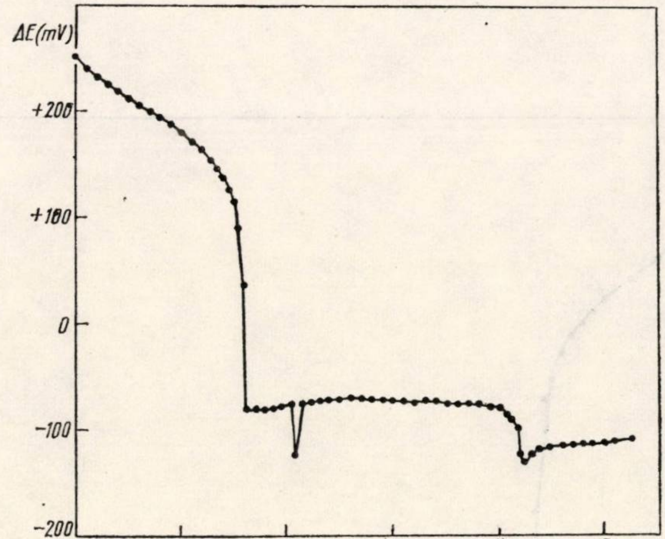

Fig. 4. — KCN 10^{-2} M titration with $AgNO_3$ 5×10^{-2} M in the presence of NaOH 10^{-2} M; a) with the membrane-electrode of $AgI-Ag_2S$ (1) and with the membrane-electrode of Ag_2S (2); b) with the membrane-electrode of $AgI-Ag_2S$/membrane electrode of Ag_2S couple.

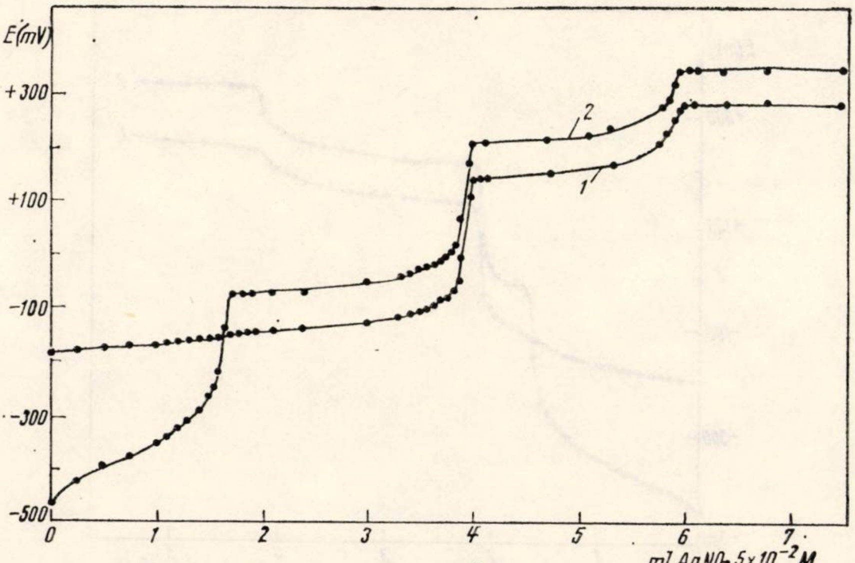

a

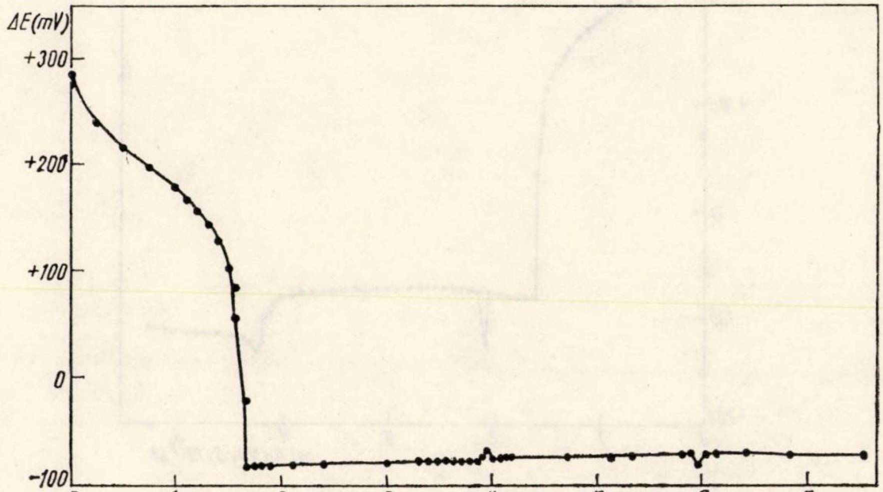

b

Fig. 5. — Titration of a mixture of KCN 10^{-2}M and KI 5.10^{-3} M with $AgNO_3$ $5 \times \times 10^{-2}$ M; a) with the membrane-electrode of $AgI-Ag_2S$ (1) and with the membrane-electrode of Ag_2S (2); b) with the membrane-electrode of $AgI-Ag_2S$/membrane-electrode of Ag_2S couple.

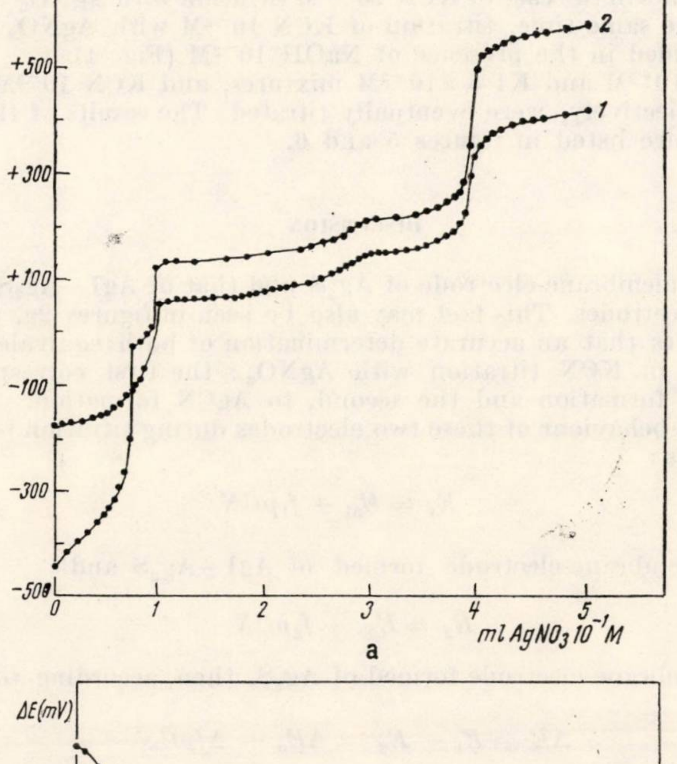

Fig. 6. — Titration of a mixture of KCN 10^{-2} M and KBr 10^{-2}M with $AgNO_3$ 10^{-2}M ; a) with the membrane-electrode of AgI — —Ag_2S (1) and with the membrane-electrode of Ag_2S (2) ; b) with the membrane electrode of AgI—Ag_2S/membrane electrode of Ag_2S couple.

Results shown in figure 3 were obtained by performing the same measurements in the case of KCN 10^{-3} M titration with $AgNO_3$ 5×10^{-3}M.

At the same time, titration of KCN 10^{-2}M with $AgNO_3$ 5×10^{-2}M was performed in the presence of NaOH 10^{-2}M (Fig. 4).

KCN10^{-2}M and KI 5×10^{-3}M mixtures, and KCN 10^{-2}M and KBr 10^{-2}M, respectively, were eventually titrated. The results of these determinations are listed in figures 5 and 6.

DISCUSSION

Both membrane-electrode of Ag_2S and that of $AgI-Ag_2S$ are CN^--sensitive electrodes. This fact may also be seen in figures 2a, 3a and 4a, which proves that an accurate determination of both equivalence points is possible in KCN titration with $AgNO_3$: the first corresponding to $[Ag(CN)_2]^-$ formation and the second, to AgCN formation.

If the behaviour of these two electrodes during titration is described by relations:

$$E_1 = E_{01} + f_1 pCN \tag{4}$$

for the membrane-electrode formed of $AgI-Ag_2S$ and

$$E_2 = E_{02} + f_2 pCN \tag{5}$$

for the membrane-electrode formed of Ag_2S, then, according to relation:

$$\Delta E = E_1 - E_2 = \Delta E_0 + \Delta f pCN \tag{6}$$

assuming that $\Delta f \neq 0$, the emf of the cell (3) should depend from a logarithmic standpoint on the titrant volume throughout the titration. However, it can be observed from figure *2b* that the $\Delta E - V$ dependence has an aspect which fits relation (6) only in the first segment of the titration curve. Then, the potential difference between the two membrane electrodes becomes almost constant and it is only in the positions corresponding to each of the two equivalence points, present on the curves in figure *2a*, that a marked peak appears (Ist-order differential signal).

A similar behaviour was also found in the case of KCN 10^{-3} M titration with $AgNO_3$ 5×10^{-3}M, the only difference being a IInd-order differential signal which appears on the titration curve (fig. *3b*).

By performing KCN titration with $AgNO_3$ in the presence of NaOH, one obtains a differential titration curve, similar to the previous ones, yet better outlined (fig. *4b*).

To understand the behaviour of the couple of indicator electrodes used during KCN titration with $AgNO_3$, a fact revealed by a close inspection of the titration curve of KCN with $AgNO_3$ traced by means of the membrane-electrode of Ag_2S is of prime importance. Thus, it may be observed that both in non-alkalized solutions (figs. *2a* and *3a*) and in alkalized solutions (fig. *4a*) a small plateau appears on this curve shortly before the equivalence point corresponding to $[Ag(CN)_2]^-$ formation (curves 2 in figs. 2*a*, 3*a* and 4*a*). In order to establish whether this plateau is real or it is the result of an experimental error (for instance, non-equilibrium potentials) titrations were repeated several times, the following being found:

1. In the case of non-alkalized solutions, the width of the plateau is smaller than in the case of alkalized solutions.

2. The plateau may always appear around a certain potential value of the membrane-electrode.

Based on these observations and knowing, on the one hand, that the potential of the membrane-electrode formed of Ag_2S corresponding to the onset of I^- precipitation is around zero value (relative to SCE)[2] and, on the other hand, that AgI of the electrode-membrane based on $AgI-Ag_2S$ may possibly be dissolved in cyanide solution[4-9] it was concluded that this plateau corresponded to the precipitation of I^- present in the solution. This hypothesis can be supported by the finding that the length of the plateau is not constant even with cyanide solutions of similar concentration, obviously due to the different exposure time of the electrode to the action of the cyanide solution. Finally, the hypothesis was totally confirmed by the titration of a mixture of KCN 10^{-2}M and KI 5.10^{-3}M when a broadening of the plateau was found as expected (over a distance of 2 ml titrant, as seen in fig. 5*a*, curve 2).

Secondly, it is known [3] that the membrane-electrode formed of $AgI-Ag_2S$ practically fails to differentiate I^- ions from CN^- ones (curves 1 in figs. 2*a*, 3*a* and 4*a*).

Knowing all these facts, the behaviour of the indicator in the first segment of the titration curve becomes explicable. Thus, although the variation in the slopes of the two CN^--sensitive membrane-electrodes is practically insignificantly different from zero, yet, due to the occurrence of ion I^- in the titrate solution and to the clearly different selectivity of the two membrane-electrodes against it, relation (3) will describe the difference $E-V$ until ion I^- has disappeared from the system.

On the other hand, it is highly probable that the appearance of differential signals with a relatively reduced amplitude but perfectly distinct and precisely localized at the equivalence is due to the different "selectivity" of the two membrane-electrodes used. Caused by the different response mechanisms of the two electrodes [4-9,10] this difference in "selec-

---

[4] E. PUNGOR, *Analyt. Chem.*, **39** (13), 29A (1967).

[5] J. W. ROSS, JR., *Ion Selective Electrodes*, R. A. Durst ed., N.B.S.Spec. Publ. No. 314, Washington, 1969, p. 84.

[6] K. TOTH and E. PUNGOR, *Analyt. Chim. Acta*, **51**, 221 (1970).

[7] B. FLEET and H. VON STROP, *Analyt. Chem.*, **43**, 1575 (1971).

[8] D. H. EVANS, *Analyt. Chem.*, **44**, 875 (1972).

[9] G. P. BOUND, B. FLEET, H. VON STROP and D. H. EVANS, *Analyt. Chem.*, **45**(4), 788 (1973).

[10] J. W. ROSS, JR., *Ion Selective Electrodes*, R. A. Durst ed, N.B.S. Spec. Publ. No. 314, Washington, 1969, p. 77.

tivity" is materialized in the electrode functions, various selectivities and response rates. In the equivalence region, these differences are more markedly manifest bringing about the observed phenomena.

In conclusion, although the experimental investigations have not been extended to alternate types of possible titrations with these two electrodes, except for the titration of the KCN and KBr mixture (fig. 6), it may be stated that the differential potentiometric titration at zero current with two ion-selective membrane-electrodes with a different selectivity against the titrated ion is recommended for indicating the end point of certain titrations, as it is a simple, precise and unbiased method.

Revue Roumaine de Chimie, 20, 3, 407–419 (1975)

STUDIES ON THE SYNTHESIS AND CHARACTERIZATION OF WEAKLY BASIC ANION-EXCHANGE RESINS. I

AMINATION OF CHLOROMETHYLATED MACROPOROUS TERNARY STYRENE-DIVINYLBENZENE-ACRYLIC MONOMER COPOLYMERS WITH DIMETHYLAMINE

A. CARPOV, DEMETRA DRĂGAN, GEORGETA MOCANU and CORNELIA LUCA
"Petru Poni" Institute of Macromolecular Chemistry,
Aleea Grigore Ghica Vodă, 41 A, Jassy, Romania

Received June 4, 1974

The amination conditions with dimethylamine of chloromethylated macroporous ternary styrene-divinylbenzene-acrylic monomer copolymers, depending on the nature of the solvent, the ternary copolymer porosity and the nature of the acrylic comonomer, were studied. It was found that the acrylonitrile present in the ternary copolymer favours the amination reaction to a greater extent than the same methyl-methacrylate amount. According to their favourable action on the amination reaction with dimethylamine, the following order of the investigated solvents has been established: N,N-dimethylformamide $\gg$ acetonitrile $>$ benzene $>$ methanol $>$ water.

With a view to preparing practically homofunctional macroporous weakly basic anion-exchange resins, several amination methods using secondary aliphatic amines, either anhydrous or in aqueous solution, of some copolymers based on halomethylated mono- and bifunctional vinyl-aromatic monomers, with or without small ratios of acrylic monomers, have been studied and improved.[1–7]

In the present paper, we are dealing with the conditions of obtaining a weakly basic anion-exchange resin, essentially homofunctional,

---

[1] H. Corte and A. Meyer (to Bayer A.G.) Ger. Pat. 1 045 102, 30 Jan. 1964.

[2] W. Busse and E. Schmidt (to Permutit A.G.) Ger. Pat. 1 569 285, 6 May 1970; *Chem. Abstr.*, **73**, 26244 (1970).

[3] J. A. Oline (to Rohm and Haas Co.) U.S. Pat. 3 367 889, 6 Feb. 1968; *Chem. Abstr.* **68**, 87 890 (1968).

[4] R. Bachmann, U. Krauss and H. Reuter (to VEB Farbenfabriken Wolfen) Ger. Pat. 1 184 959, 07 Jan. 1965; *Chem. Abstr.* **62**, 7954 (1965).

[5] H. Seifert, W. Richter and M. Quaedvlieg (to Bayer A.G.) Brit. Pat. 1 133 920, 20 Nov. 1968; *Chem. Abstr.* **70**, 48215 (1969).

[6] J. Cleij (to Akzo N.V.) Ger. Offen. 2 121 448, 11 Nov. 1971; *Chem. Abstr.* **76**, 86581 (1972).

[7] J. D. Nolan (to Permutit Co. Ltd.) Brit. Pat. 1 026 838, 25 March 1964; *Chem. Abstr.* **65**, 10759 (1966).

by reacting chloromethylated macroporous ternary styrene-divinylbenzene-acrylic monomer copolymers with dimethylamine. Emphasis is placed on the influence of different solvents on the amination reaction and the nature of the third comonomer. By these studies we also intend to assess the development of this reaction in aqueous medium.

Weakly basic anion-exchange resins are commonly used in the treatment of industrial waters or other effluents in order to remove strong acids, in preference to strongly basic ones, since they are more readily regenerated when exhausted.

Usually, in the production of industrial waters for thermal power stations, the weakly basic anion-exchange resin is inserted between a cation- and a strongly basic anion-exchange resin.

Recently, weakly basic anion-exchange resins have found new applications due to their properties revealed by some studies of their thermal regeneration.[8]

In the opinion of R. Kunin, their systematic study has not gone too far in the last 15 years; consequently, there is a major need for additional efforts in this field to complete the data on the structure and behaviour of this type of anion-exchangers.[9]

Therefore, we intend to study some other aspects of this subject, e.g. the functional character, ion-exchange performances, the physical and chemical resistance of resin beads to the osmotic shock in connection with their synthesis conditions.

MATERIALS AND METHODS

— Dimethylamine (DMA), reagent grade (Gas-chromatographic analysis did not reveal the presence of tertiary amines).

— Benzene, N, N-dimethylformamide (DMF), methanol (MA), acetonitrile (ACN), analytical grade.

— Macroporous ternary copolymers [10,11] whose characteristics are summarized in table 1.

— Chloromethylation of the macroporous ternary copolymers was carried out with monochlorodimethylether (MCDE) in the presence of $ZnCl_2$, at a molar ratio copolymer $/MCDE/ZnCl_2 = 1/10/0.4$, 8 h, at 58°. The chlorine content of the chloromethylated macroporous ternary copolymers (Co—CM) was:

Chloromethylated copolymer (Co—CM)	%Cl after chloromethylation
Co—CM A	17.50
Co—CM B	14.10
Co—CM C	20.54
Co—CM D	16.40

— Chloromethylated ternary copolymer styrene-8% divinylbenzene 3.50% acrylonitrile of a gel type, having 21.00% Cl, used for comparative studies (Co—CM gel for reference).

---

[8] D. E. Weiss, B. A. Bolto, R. Mc. Neil, A. S. Macpherson, R. Siudak, E. A. Swinton and D. Willis, *Austral. J. Chem.*, **19**, 561 (1966).

[9] R. Kunin "Ion Exchange in the Process Industries" — Papers of Conference held in London, July 1969, London, Society of Chemical Industry, 1970, 446.

[10] I. Poinescu, S. Drăgan, S. Maxim and M. Dima, *Rev. Roumaine Chim.* (in press).

[11] I. Poinescu, S. Drăgan and M. Dima, *Rev. Roumaine Chim.* (in press).

Table 1

Physico-chemical characteristics of the macroporous ternary copolymers studied

Copolymer	Code	Inert phase at copolymerization	Methanol coefficient	Toluene coefficient	Apparent density (ρ_a)	Specific density (ρ_s)	Porosity P^* (%)
styrene-15 % divinylbenzene-3.03 % acrylonitrile	A	polystyrene	0.33	0.65	0.7979	1.0668	25.21
styrene-15 % divinylbenzene-3.00 %methylmethacrylate	B	polystyrene	0.36	0.68	0.8045	1.0392	22.59
styrene-10 % divinylbenzene-3.20 % acrylonitrile	C	polystyrene	0.37	0.795	0.869	1.0480	17.08
styrene-15 % divinylbenzene 4.40 %acrylonitrile	D	benzine	0.55	1.38	0.6788	1.1211	39.46

*) Calculated by the formula : $P = \left(1 - \frac{\rho_a}{\rho_r}\right) \times 100$ where ρ_r is the real density. [12]

— Amination by DMA of the macroporous and gel-type chloromethylated ternary copolymers was carried out by using either aminic solutions in the above mentioned organic solvents or aqueous solutions with or without a polar organic co-solvent. The DMA solution was added, under constant stirring, to the chloromethylated copolymer in the reaction vessel provided with condenser, stirrer and thermometer. For thermostating the reaction vessels, a water bath with continuous circulation of the cooling water, at 22°, was used.

— The amination degree of the chloromethylated ternary copolymers was expressed by their total exchange capacity (meq/g of dry resin), estimated from the aminic nitrogen content of the samples and from its direct determinations[13,14].

Nitrogen analyses were carried out by the semimicroanalytical Kjeldahl method on the free base form of the respectiv samples.

— Determination of the functional character and the examination of the ion-exchange particularities of the weakly basic anion exchangers synthesized according to the conditions discussed under "Results and Discussion" are presented in other papers of this journal.[13,14]

RESULTS AND DISCUSSION

Kinetic studies regarding the influence of the different parameters on the amination reaction with DMA of chloromethylated ternary copolymers were chiefly centered around Co—CM A and Co—CM B (table 1).

In a series of preliminary attempts it was established that the molar ratio Co—CM/DMA = 1/3 represents the maximum value for which, under any given reaction conditions, the increase in the amination degree is insignificant (figure 1). For this reason, in every experiment carried out in order to establish the influence of the other parameters on the amination degree, we exclusively used this value for the molar ratio Co$-$CM/DMA.

---

[12] R. Kunin, F. E. Meitzner, A. J. Cline, S. Fischer and N. Frisch, *Ind. Eng. Chem. Res. Develop.*, **1**, 140 (1967).

[13] D. Drăgan, G. Mocanu and A. Carpov, *Rev. Roumaine Chim.*, **20**, 431 (1975).

[14] D. Drăgan, G. Mocanu and A. Carpov, *Rev. Roumaine Chim.*, **20**, 445 (1975).

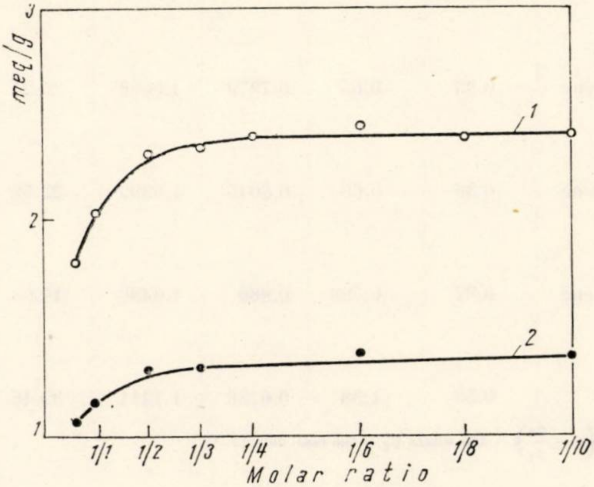

Fig. 1. — Variation of the exchange capacity versus molar ratio Co$-$CM/DMA, aqueous solution of 4.42 g DMA/100 ml, 22°, 24 hrs; *1*, Co$-$CM A; *2*, Co$-$CM B.

It is well known that small quantities up to 5% of an acrylic comonomer (acrylonitrile, methyl-methacrylate) in the chloromethylated ternary copolymer have a positive influence on amination with aliphatic amines of the chloromethylated styrenic groups and, at the same time, confer the ensuing weakly basic anion-exchange resin a higher craze resistance in comparison with binary styrene-divinylbenzene copolymers.[15,16]

In order to establish the influence of the nature of the third comonomer on the reaction rate, we performed comparative kinetic studies by DMA amination of the copolymers Co$-$CM A and Co$-$CM B. These two copolymers have the same cross-linking degree and about the same content of acrylonitrile or methyl-methacrylate, respectively (see table 1); the latter shows different concentration as against the whole amount of the chloromethylated styrenic units in the copolymers. For this purpose, we studied the amination reaction with DMA using aqueous DMA solutions of different concentrations (figures 2 and 3).

From figures 2 and 3 it results that with all the four selected concentrations and especially with short reaction times, the DMA amination reaction takes place at a higher rate with Co$-$CM A containing acrylonitrile as the third comonomer.

---

[15] S. Maxim, I. Poinescu, S. Drăgan and M. Dima, *Rev. Roumaine Chim.*, **17**, 1447 (1972).

[16] H. Morawetz "Chemical Reactions of Polymers", Ed. E. M. Fettes, Interscience Publishers, New York, 1964, p. 10.

If the cross-linking degree is not too high, as in the present case, the tridimensional macromolecular network of the ternary copolymer is still sufficiently elastic to permit a favourable influence of the acrylonitrile units in the copolymer to be exerted on the transition state of amination of a neighbouring chloromethylated styrenic unit.

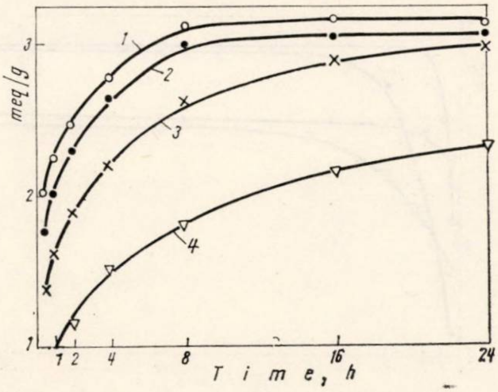

Fig. 2.—Variation of the exchange capacity versus time, Co — CM A, aqueous solution of DMA, 22°, molar ratio Co—CM A/DMA = 1/3 : *1*, solution of 31.80 g DMA/100 ml; *2*, solution of 27.54 g DMA/100 ml; *3*, solution of 19.34 g DMA/100 ml; *4*, solution of 4.42 g DMA/100 ml.

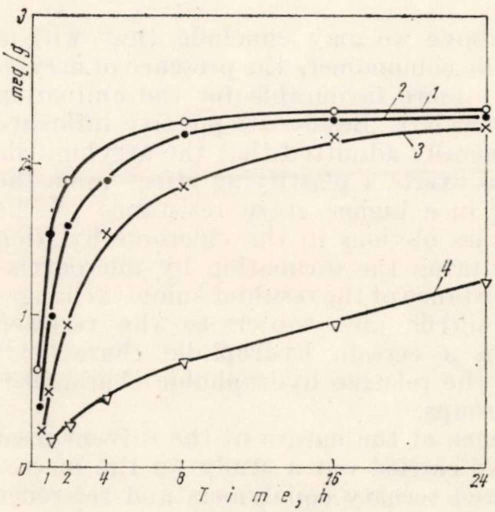

Fig. 3.—Variation of the exchange capacity versus time, Co—CM B, aqueous solutions of DMA, 22°, molar ratio Co—CM B/DMA = 1/3 : *1*, solution of 31.80 g DMA/100 ml; 2, solution of 27.54 g DMA/100 ml; *3*, solution of 19.34 g DMA/100 ml; *4*, solution of 4.42 g DMA/100 ml.

This positive influence of the acrylonitrile present in the ternary copolymer on the amination reaction with DMA is also revealed by the data in figure 4 which presents the comparative values of the exchange capacity versus time for Co—CM A and Co—CM C in aqueous and benzenic solutions.

From the data in figure 4 it also results that for both DMA solutions, especially with short reaction times, the amination reaction of Co—CM A with DMA is faster. This experimental result can be explained by the higher concentration of the acrylonitrile units as against the total amount of the chloromethylated styrenic units in the Co—CM A having a higher crosslinking degree. It may also be a consequence of a greater porosity of Co—CM A due to the different contents of the crosslinking agent in these two copolymers, the higher the crosslinking degree, the greater the porosity of the copolymer (see also table 1).

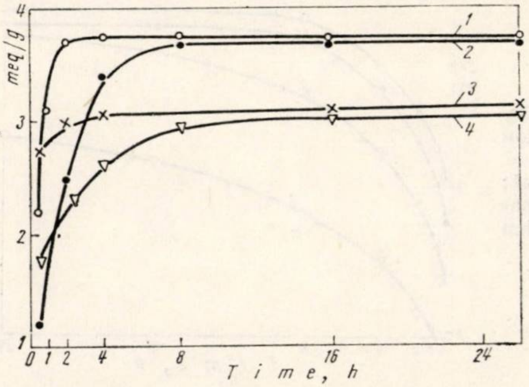

Fig. 4. — Variation of the exchange capacity versus time, Co — CM A and Co—CM C, DMA in aqueous and benzenic media : *1*, Co—CM C, benzenic solution of 20.52 g DMA/100 ml ; *2*, Co—CM C, aqueous solution of 27.54g DMA/100 ml ; *3*, Co—CM A, benzenic solution of 20.52 g DMA/100 ml ; *4*, Co — CM A, aqueous solution of 27.54 g DMA/100 ml.

From the data mentioned above we may conclude that with a rather similar content of either acrylic comonomer, the presence of acrylonitrile in the ternary copolymer is more favourable for the amination reaction compared to methyl-methacrylate. Besides its positive influence on the amination reaction, it is generally admitted that the acrylonitrile present in a ternary copolymer also exerts a plastifying effect upon the macromolecular network, resulting in a higher craze resistance of the copolymer beads. This effect becomes obvious in the chloromethylation and amination stages, as well as during the estimation by microcyclation of the physical and chemical resistance of the resulted anion-exchanger beads.[14] At the same time, acrylonitrile also confers to the resulted weakly basic anion-exchange resin a certain hydrophilic character [17] that may partially counterbalance the relative hydrophobic character [18] of the functional dimethylaminogroups.

In order to specify the influence of the nature of the solvent used in the DMA amination reaction, we carried out a study on the macroporous and gel-type chloromethylated ternary copolymers and reference Co—CM A, Co—CM B and Co—CM gel using solutions of DMA of close concentrations in water and in different organic solvents (figures 5, 6 and 7).

For all the three chloromethylated ternary copolymers under investigation, one observes quite a superposition of the curves in which the variation of the exchange capacity versus time during amination with DMA in benzene, DMF or ACN media is plotted.

---

[17] G. P. Ziemba, "Encyclopedia of Polymer Science and Technology", **7**, Ed. H. F. Mark, N. G. Gaylord and N. M. Bikales, Interscience Publishers, New York, 1964, p. 425, 431.

[18] I. M. Abrams and L. Benezsa, "Encyclopedia of Polymer Science and Technology", **1**, Ed. H. F. Mark, N. G. Gaylord and N. M. Bikales, 1967, p. 706.

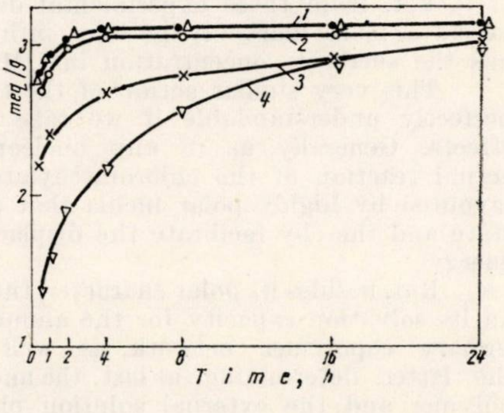

Fig. 5. — Influence of the solvent upon variation of the exchange capacity versus time, Co—CM A, molar ratio Co — CM A/DMA = 1/3, 22° : *1* —○— ACN solution of 18.65 g DMA/100 ml ; — Δ — DMF solution of 14.00g DMA/100 ml ; *2*, benzenic solution of 20.52 g DMA/100 ml ; *3*, MA solution of 18.33 g DMA/100 ml ; *4*, aqueous solution of 19.34 g DMA/100 ml.

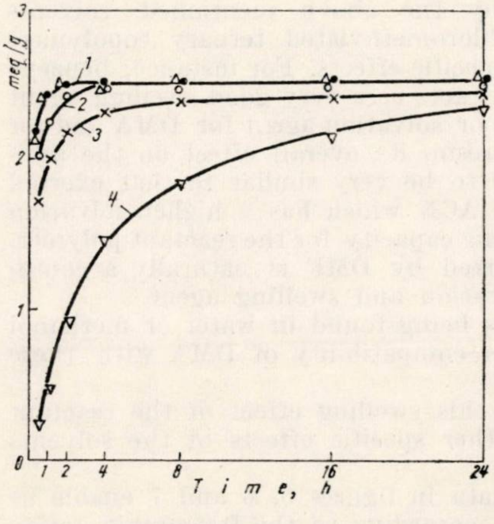

Fig. 6. — Influence of the solvent upon variation of the exchange capacity versus time, Co—CM B, molar ratio Co—CM B/DMA = 1/3, 22° : The symbols : —●—, —Δ—, —○—, —x—, —∇— have the same significance as in fig. 5.

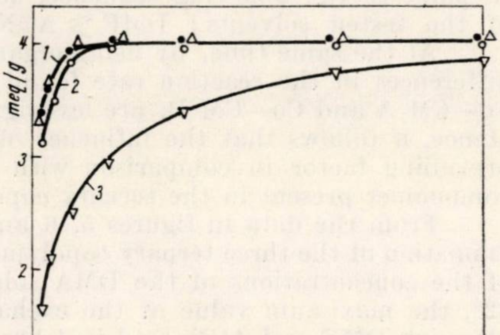

Fig. 7. — Influence of the solvent upon variation of the exchange capacity versus time, Co—CM gel, molar ratio Co — CM gel/DMA = 1/3, 22°; the symbols : —●— —Δ—, —○— and —∇— have the same significance as in figs. 5 and 6 ; for —●—, —○—, —∇— Co—CM gel was previously swollen in benzene and for —Δ— in DMF, respectively.

Yet, from these experimental data, we may conclude that DMF exerts a more markedly positive influence, as this DMA solution also has the smallest concentration in DMA, namely 14.00 g DMA/100 ml.

This very similar action of the three solvents mentioned above is perfectly understandable if we take into consideration their specific effects. Generally, as in any nucleophilic displacement reaction, the actual reaction of the chloromethylated styrenic groups with DMA is favoured by highly polar media that stabilize the semi-ionic transition state and thereby facilitate the displacement by reducing its activation energy.

But, besides its polar character, the action of the solvent also depends on its solvation capacity for the aminic groups already linked with the ternary copolymer network, as well as on its swelling capacity for the latter, determining, at last, the nucleophile partitioning between the polymer and the external solution phase.[19]

The overall action exerted by the above mentioned solvents during amination with DMA of chloromethylated ternary copolymers is probably a consequence of these specific effects. For instance, benzene is a non-polar solvent but because it acts as a very good swelling agent for the polymer network and as a poor solvation agent for DMA and for the tertiary aminic groups in the resin, its overall effect on the amination reaction with DMA appears to be very similar to that exerted by a polar aprotic solvent such as ACN which has a higher solvation capacity for DMA but a lower swelling capacity for the reactant polymer. The highest positive influence exerted by DMF is naturally a consequence of its best qualities as solvation and swelling agent.

The much lower reaction rates being found in water or methanol media are probably due to a higher compatibility of DMA with these polar protic solvents.[19]

For macroporous copolymers, this swelling effect of the reactant polymer is insignificant and the other specific effects of the solvents become prevalents.

Therefore, the experimental data in figures 5, 6 and 7 enable us to point to the following sequence, according to the favourable action of the tested solvents : DMF $\geqslant$ ACN $>$ benzene $>$ MA $>$ water.

At the same time, by using organic solvents as reaction media the differences in the reaction rate found during amination by DMA with Co—CM A and Co—CM B, are less significant than in aqueous solution. Hence, it follows that the influence of the nature of the solvent is the prevailing factor in comparison with that of the nature of the third comonomer present in the ternary copolymers under investigation.

From the data in figures 5, 6 and 7, it also results that by DMA amination of the three ternary copolymers studied, at relative low values of the concentrations of the DMA solutions (ca. 20 g DMA/100 ml) at 22°, the maximum value of the exchange capacity is reached in 2 hrs by using DMF and ACN, and in 4 hrs by using benzene.[20]

---

[19] W. G. Lloyd and T. E. Durocher, *J. Appl. Polymer Sci.*, **7**, 2025 (1963).

[20] A. Carpov, D. Drăgan, G. Mocanu, I. Petrariu and I. Poinescu (Institutul de Chimie Macromoleculară "P. Poni", Iași, R. S. Romania, Rom. Pat. 72 550, 18 Oct. 1972.

The concentration of DMA in solutions of more volatile organic solvents (benzene, ACN) is practically limited to values up to 20–25 g DMA/100 ml, because higher concentration values make them very unstable for handling.

Moreover, when we use organic solvents of low solvation capacity for DMA (benzene), an increase in the amine concentration beyond the limits pointed to in the present paper has a negative influence upon the functional character of the ensuing weakly basic anion-exchange resin, by increasing the probability of side crosslinking reactions during amination.[13]

The successful utilization of a polar organic co-solvent in the nucleophilic displacements on chloromethylated polystyrene, by using different nucleophiles in aqueous solutions, is also well known.[19,21] Essentially, the functions of a polar organic co-solvent may be two-fold : a) to make the polymer network more accessible by its swelling and b) to carry the nucleophile to the polymer network.

Consequently, the favourable influence of a given polar co-solvent on the DMA transfer rate from the external solution to the polymer phase and, thereby, on the overally reaction rate depends on its polar character, its solvation capacity for DMA and for the aminic groups already linked with the polymer network, as well as on the co-solvent/water ratios.

To exemplify such an effect exerted by a polar organic co-solvent added to the aqueous DMA solution, kinetic studies of amination with DMA were carried out with the macroporous and gel-type copolymers Co–CM A, Co–CM B and Co–CM gel, using aqueous DMA solutions having 5–15% (v/v) DMF[20] (figures 8, 9 and 10).

From the data in figures 8, 9 and 10, it comes out that in all the three investigated cases, the addition of DMF to the aqueous DMA solutions results in an increased reaction rate.

The DMA amination of chloromethylated ternary copolymers is also favoured by a higher DMA concentration of the reaction medium; for a constant Co–CM/DMA molar ratio, such an increased aminic concentration corresponds to a simultaneously decreased gravimetric Co–CM/(liquid phase) ratio (g/g).

DMA amination of Co–CM A and Co–CM B with aqueous DMA solutions of different concentrations (figure 11) renders obvious that for a reaction time of 8 hrs at higher DMA concentrations, such as 30g DMA/100 ml, the exchange capacity increase becomes insignificant.

A similar conclusion arises for Co–CM gel on examining the data in figure 12.

In very similar reaction conditions, for a given reaction time, the degree of amination with DMA also depends on the ternary copolymer porosity.

The exchange capacity values for DMA aminated Co–CM A and Co–CM D, having a similar chemical composition but

[21] A. Carpov, D. Drăgan and I. Petrariu, *Rev. Roumaine Chim.*, **17**, 1923 (1972).

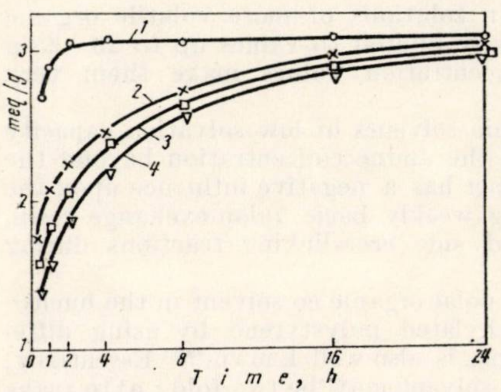

Fig. 8.—Variation of the exchange capacity versus time, Co—CM A, DMA in DMF and aqueous solution of 5—15 % DMF (v/v), molar ratio Co—CM A/DMA = 1/3, 22°: *1*, DMF solution of 14.00 g DMA/100 ml; *2*, aqueous solution with 15 % DMF, of 18.90 g DMA/100 ml; *3*, aqueous solution with 5 % DMF, of 18.68 g DMA/100 ml; *4*, aqueous solution of 19.34g DMA/100 ml.

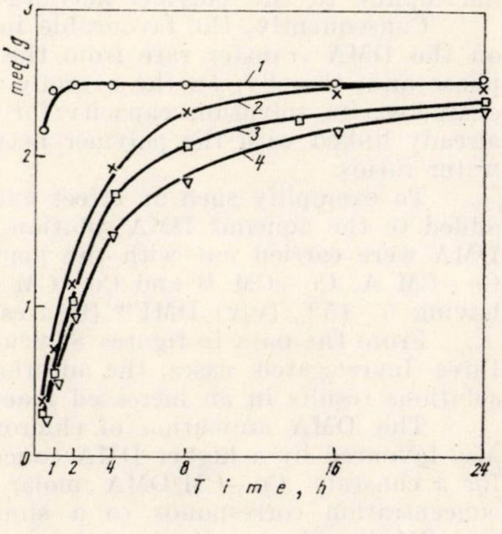

Fig. 9.—Variation of the exchange capacity versus time, Co — CM B, DMA in DMF and aqueous solutions of 5—15 % DMF (v/v), molar ratio Co—CM B/DMA = 1/3, 22°; the symbols: —○—, —x—, —□— and —▽— have the same significance as in fig. 8.

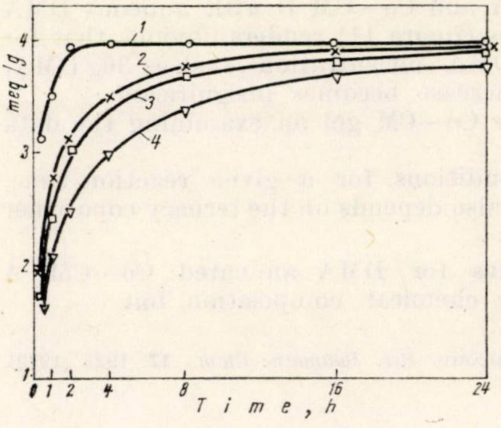

Fig. 10.—Variation of the exchange capacity versus time, Co—CM gel, DMA in DMF and aqueous solution of 5—15 % DMF (v/v), molar ratio Co—CM gel/DMA = 1/3, 22°; the symbols: —○—, —x—, —□— and —▽— have the same significance as in Figs. 8 and 9. For —x—, —□—, —▽— Co—CM gel was previously swollen in benzene and in DMF for —○—, respectively.

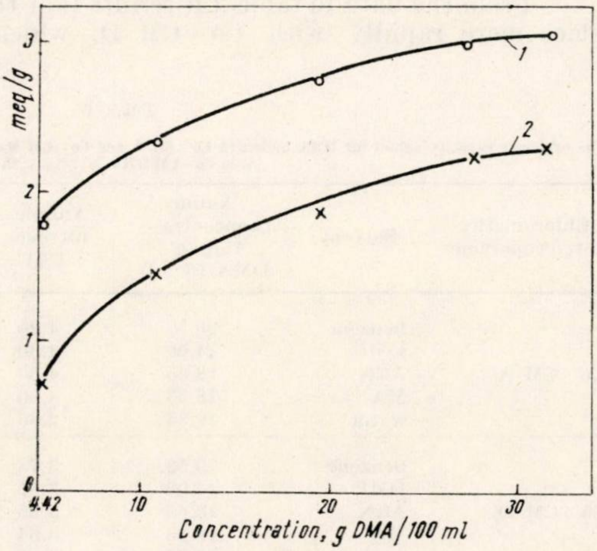

Fig. 11. — Variation of the exchange capacity versus aqueous solution concentration of DMA, molar ratio Co—CM/DMA = 1/3, 22°, 8 hrs : 1 —O— Co — CM A; 2 —x— Co—CM B.

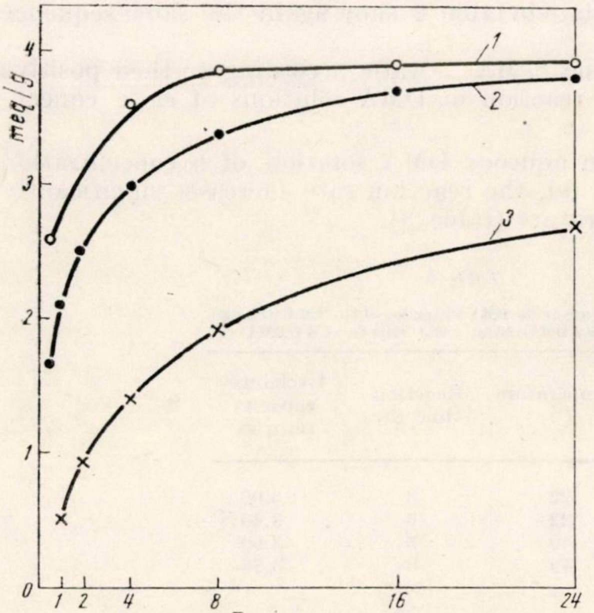

Fig. 12. — Variation of the exchange capacity versus time, Co—CM gel, previously swollen in benzene, aqueous solution of DMA, 22°, molar ratio Co—CM gel/DMA = 1/3 : *1*, solution of 31.80 g DMA/100 ml; *2*, solution of 19.34 g DMA/100 ml; *3*, solution of 4.42 g DMA/100 ml.

different porosities (see table 1) are summarized in table 2. The same DMA solutions as those specified in the plots 5, 6 and 7 are used.

From the data in table 2 it results that the amination reaction takes place more rapidly with Co−CM D, which has a higher porosity.

Table 2

The exchange capacity values for DMA aminated Co−CM A and Co−CM D by using different solvents for DMA, molar ratio Co−CM/DMA = 1/3,22°,2h

Chloromethylated copolymer	Solvent	Amine concentration (g DMA/100ml)	Aminic nitrogen (%)	Exchange capacity (meq/g)	Fraction from the maximum exchange capacity* (%)
Co−CM A	benzene	20.52	4.20	3.00	96.77
	DMF	14.00	4.30	3.05	98.39
	ACN	18.65	4.30	3.05	98.39
	MA	18.33	3.50	2.50	80.64
	water	19.34	2.66	1.90	61.29
Co−CM D	benzene	20.52	3.78	2.75	98.21
	DMF	14.00	3.90	2.78	99.28
	ACN	18.65	3.85	2.75	98.21
	MA	18.33	3.34	2.40	85.75
	water	19.34	3.08	2.20	78.57

*) The maximum exchange capacity is 3.10 for Co−CM A and 2,80 for Co−CM D, respectively.

At the same time, the data in table 2 show again the same sequence of solvents :

DMF $\geqslant$ ACN $>$ benzene $>$ MA $>$ water according to their positive influence on the amination reaction in DMA solutions of close concentration values.

By DMA amination in aqueous DMA solution of a concentration value of ca. 30 g DMA/100 ml, the reaction rate increases significantly with the increase of temperature (table 3).

Table 3

Influence of temperature on the DMA amination of Co−CM C with aqueous solution of 31.80 g DMA/100 ml, molar ratio Co−CM C/DMA = 1/3

Sample	Temperature (°)	Reaction time (h)	Exchange capacity (meq/g)
1	22	3	3.00
2	22	6	3.40
3	40	3	3.60
4	40	6	3.80

Therefore, according to the data in table 3, by raising the temperature from 22° to 40°, the reaction time necessary to reach the maximum amination degree is reduced by over 50%.

CONCLUSIONS

The kinetic studies by DMA amination of chloromethylated macroporous ternary copolymers suggest that the acrylonitrile present in the tridimensional polymer network has a more positive influence on the amination reaction than the same amount of methylmethacrylate.

The following sequence of solvents, according to their favourable action on the amination reaction rate, was found:

DMF $\geqslant$ ACN $>$ benzene $>$ MA $>$ water.

At room temperature (22°), the maximum amination degree (the maximum exchange capacity of the resin) is reached in 8 hrs or 2 – 4hrs if aqueous solutions of ca. 30 g DMA/100 ml or DMF, ACN and benzenic solutions of ca. 20 g DMA/100 ml concentrations, are used.

The addition of a polar organic co-solvent (DMF) to the aqueous DMA solution also increases the reaction rate.

Revue Roumaine de Chimie, **20**, *3*, 407 – 419 (1975)

Revue Roumaine de Chimie, **20**, *3*, 421–433 (1975)

STUDIES ON THE SYNTHESIS AND CHARACTERIZATION OF WEAKLY BASIC ANION-EXCHANGE RESINS. II[1]

ON THE NATURE OF THE FUNCTIONAL GROUPS

DEMETRA DRĂGAN, GEORGETA MOCANU and A. CARPOV
"Petru Poni" Institute of Macromolecular Chemistry
Aleea Grigore Ghica Vodă 41 A, Jassy, Romania

Received October 11, 1973

The influence of the synthesis conditions upon the nature of the functional groups in a weakly basic anion-exchange resin prepared by amination with dimethylamine of a chloromethylated ternary macroporous copolymer was studied. It was established that at higher temperature, the decreased polar character of the solvent used as reaction medium, as well as the small values of the chloromethylated copolymer/dimethylamine molar ratio favour the formation of the strongly basic groups.

In another paper [1] the study of the influence exerted by different parameters on the amination reaction with dimethylamine of some chloromethylated ternary macroporous styrene-divinylbenzene-acrylic monomer copolymers is reported.

In order to efficiently put into operation the weakly basic anion-exchange resins it is particularly important to know exactly the nature of the functional groups linked with the macromolecular network, that is, the degree of their homo- or heterofunctionality.

It is well known that by reacting chloromethylated polystyrene or styrene-divinylbenzene copolymers with primary, secondary or di-tertiary aliphatic amines, intra- and inter-chain side reactions between the non-reacted chloromethyl groups and the aminic groups already linked with the macromolecular network are possible. By these side reactions functional groups of different basicity are built up.[2,3]

When chloromethylated crosslinked styrenic copolymers react with a secondary aliphatic amine, alongside with the tertiary aminic groups, quaternary ammonium groups resulting from the additional crosslinking reactions may also appear.

---

[1] A. Carpov, D. Drăgan, G. Mocanu and C. Luca, *Rev. Roumaine Chim.* **20**, 417 (1975).

[2] R. M. Wheaton and M. J. Hatch "Ion-Exchange", **2**, Edit. J. A. Marinsky, Marcel Dekker, New York, 1968, chap. 6, p. 313.

[3] H. Kawabe and M. Yanagita, Bull. Chem. Soc. Japan, **4**, 1518 (1968).

Thus, the purpose of the present work is to establish whether during amination with dimethylamine of the chloromethylated crosslinked styrene copolymers, quaternary ammonium groups really appear and to what extent their appearance is influenced by the synthesis conditions used.

MATERIALS AND METHODS

Weakly basic anion-exchange resins prepared from the chloromethylated copolymer Co—CM C, based on the ternary macroporous styrene-10% divinylbenzene-3.20% acrylonitrile copolymer, having 20.54% Cl, used in the synthesis studies with dimethylamine[1] (see also tables 1 and 2).

Reference weakly basic anion-exchange resins, Duolite A-305, Amberlite IRA-93, Relite 4MS having benzyldimethylamino functional groups and Lewatit MP-64 containing tertiary aminic and ca. 10% of strongly basic functional groups, according to the manufacturers.

Homofunctional strongly basic anion-exchange resin of type I (CT) prepared from the chloromethylated copolymer Co—CM C with trimethylamine having a 3.40 meq/g exchange capacity, also used for comparative studies.

Sodium chloride, hydrochloric acid, analytical grade.

N,N-dimethylformamide (DMF), acetonitrile (ACN), benzene, analytical grade.

The values of the total exchange capacity (in meq/g dry resin) of the studied anion-exchange resins, in their free-base form, were obtained as follows:

— indirectly, from the aminic nitrogen content of samples, determined by means of the semi-microanalytical Kjeldahl method;

— directly, from the acid consumption, using the batch method, determined by the alkalimetric titration of the remaining acid after the weakly basic anion-exchange resin was equilibrated with an excess amount of 0.1 N HCl solution.

— directly, by pH-metric titration.

The pH-metric titration of the studied anion-exchange resins was also carried out by means of the batch method, as follows: A 0.5 g amount of the respective resin was introduced into each of twenty 100 ml capacity flasks fitted with a gas-tight stopper and a device for nitrogen circulation, taking into account the previously determined humidity. A 50 ml total volume of a mixture of 0.1 N HCl solution and water or 0.1 M and 1M aqueous solution of a neutral electrolyte (NaCl) respectively, in different ratios, was added into each flask. At the same time, in one of the flasks the equilibration of the anion-exchange resin was achieved only with water or NaCl solution.

The flasks were kept in a thermostat at 20°, their content being shaken from time to time. The pH-values of the solution in equilibrium with the anion-exchange resin were read at time intervals of 24—48 hrs, till their stabilization was observed.

A 22-type pH-meter Radiometer Copenhagen and a GK-2025C type of a combined electrode of glass and calomel were used.

The strong base exchange capacity (in meq/g dry resin), that is, the content in quaternary ammonium groups of the respective resins, was measured by equilibrating the samples in their free-base form with a neutral 1M NaCl solution, and then by estimating the value of the ion-exchange OH ⟷ Cl.[4]

The infrared spectra were recorded by using a UNICAM SP-200 infrared spectrophotometer, in potassium bromide pellets.

The thermal stability of the studied samples was estimated by thermogravimetric analysis, in air, using a F. Paulik, J. Paulik and L. Erdey Derivatograph, for a heating rate of 9.8°/minute.

The water regain was measured by centrifuging the previously swollen samples, in their free-base form.[5]

---

[4] D. Drăgan, A. Carpov and I. Petrariu, *Ion Exchange and Membranes* **1**, 215 (1974).

[5] K. W. Pepper, D. Reichenberg and D. K. Hale, *J. Chem. Soc.*, **1952**, 3129.

RESULTS AND DISCUSSION

The additional crosslinking side reactions as a result of which quaternary ammonium groups are formed during the amination with DMA of the structural chloromethylated styrenic units, are essentially influenced by :

— The accessibility of DMA to the three-dimensional macromolecular network of the copolymer and the mutual position of the groups able to act upon each other that is, by the crosslinking divinylbenzene degree and the composition of the chloromethylated copolymers used.

— The nature of the solvent used as reaction medium which, through its specific effects,[1] determines the amination reaction rate and also the solvation degree of the aminic functional groups already linked with the polymer network and, hence, their ability to react with the neighbouring chloromethyl groups.

— The value of the molar ratio of the reactants.

The extent to which these crosslinking side reactions are occurring during the synthesis of such an anion-exchange resin can be expressed by its content in quaternary ammonium groups.

Thus, the data in table 1 show these contents in quaternary ammonium groups, quoted as percentages from the respective values of the total exchange capacity, both for the anion-exchange resins prepared from Co—CM C according to the different conditions of synthesis [1] and for the weakly basic ones for reference.

From the data presented in table 1 some conclusions can be drawn :

— When the reaction with DMA is carried out in aqueous solution for a given Co—CM C/DMA molar ratio, the additional crosslinking reactions are favoured either by higher temperature (samples CS_2 and CS_3) or by a substantially increased concentration of the aqueous DMA solution (samples CS_1 and CS_2).

— ACN and DMF have nearly similar effects (samples CS_5 and CS_6).

— For the same value of the Co—CM C/DMA molar ratio ($=1/3$) and for DMA solutions in different solvents of close concentration values, the respective content in quaternary ammonium groups of the resulted anion-exchange resins increases inasmuch as the polar character of the solvent and its solvation power for DMA diminishes (samples CS_1, CS_5, CS_6 and CS_7). Thus, according to such a criterion in respect to the favouring of the additional crosslinking reactions, the studied solvents may be placed in the following order :

$$\text{Benzene} > \text{ACN} \geqslant \text{DMF} > \text{water}$$

Therefore, when the reaction with DMA is carried out in the aforesaid solvents,[1] apart from benzene, anion-exchange resins of less than 10 % of quaternary ammonium groups from their total amount of functional groups are obtained.

At the same time, using aprotic polar solvents (DMF, ACN) or aqueous DMA solutions to which polar solvents (DMF) are added, instead

Table 1

Contents in quaternary ammonium groups of the reference samples and of those obtained from Co–CM C depending on the synthesis conditions: molar ratio Co–CM C/DMA = 1/3, aminic solutions of ca. 20–30 g DMA/100 ml

Anion-exchange resin (code)	Solvent	Total exchange capacity (meq/g), determined from			Strong base exchange capacity (meq/g)	The content in quaternary ammonium groups (% from the total exchange capacity *)
		Aminic nitrogen (%)	0.1N HCl consumption (batch method)	pH-metric titration		
CS_1	water	2.70	2.72	2.66	0.053	2.07
CS_2**	water	3.70	3.60	3.60	0.20	5.55
CS_3**	water	3.85	3.80	3.80	0.40	10.52***
CS_4	water+15% (v/v)DMF	3.75	3.80	3.70	0.10	2.70
CS_5	ACN	3.90	3.75	3.80	0.31	8.15
CS_6	DMF	3.90	3.75	3.70	0.21	5.67
CS_7	Benzene	3.75	3.70	3.60	0.624	17.33
Doulite A-305	—	—	4.01	4.00	0.15	3.75
Amberlite IRA-93	—	—	4.20	4.00	0.21	5.25
Relite 4MS	—	—	3.85	3.90	0.10	2.50
Lewatit MP-64	—	—	5.60	5.60	0.543	10.62

The data in the last column are mean values of three individual determinations.

*) The total exchange capacity for reference is that obtained from pH-metric titrations.

**) The DMA solution used to synthetize the samples CS_2 and CS_3 had a concentration of ca. 10% higher than the aminic solutions used for the other samples.

***) Synthesis carried out at a temperature of 20° higher than that used for the other samples.[1]

of aqueous DMA solutions of an equal concentration, weakly basic anion-exchange resins practically homofunctional, at a higher amination reaction rate, may be obtained.

The data recorded in table 1 also show that, apart from the samples CS_3 and CS_7, the respective amounts of quaternary ammonium groups in the resins synthetized according to the given reaction conditions [1] are of the same order of magnitude as those of the reference weakly basic resins.

Otherwise, if we conventionally assume that only the weakly basic anion-exchange resins of less than 10% of quaternary ammonium groups as against their total exchange capacity should be considered as homofunctional, the sample CS_7 should be rather thought of as a bifunctional anion-exchange resin belonging to the so-called "intermediate base" anion-exchange resins.

Among the samples chosen for reference, Lewatit MP-64 holds a special place because, according to the manufacturer, it is deliberately synthetized with ca. 10% of strongly basic groups whose origin is not specified.

The additional crosslinking reactions, by which strongly basic functional groups are formed, may be practically avoided by using amounts of amine in large excess to the chloromethylated styrene units in the copolymer.[3]

For a given DMA solution the increased chloromethylated copolymer/DMA molar ratio corresponds to a simultaneously increased chloromethylated copolymer/ (liquid phase) (g/g) gravimetric ratio.

The experimental data in table 2 attest this considerable decrease of the corresponding amounts of strongly basic groups in the resulted resin inasmuch as the Co—CM C/DMA molar ratio used for the synthesis grows higher.

For example, according to the data in table 2, it becomes obvious that for the molar ratio Co—CM C/DMA $= 1/10$ and irrespective of the nature of the solvent used, weakly basic anion-exchange resins of 98—99% of a homofunctional character are obtained.

Therefore, depending on the practical aim pursued, the synthesis of an anion-exchange resin of tertiary aminic groups may be directed in such a way as to drop as much as possible its content in strongly basic groups.

The conclusions derived from the data presented in tables 1 and 2 are also supported by other experimental evidence. Next, we will restrict our discussion about the nature of the functional groups only to the variants of the sample CS_7 which highly differ from one another (see table 2).

It is to be expected that the presence of quaternary ammonium groups alongside with the tertiary ones should increase the hydrophilic character of the respective anion-exchange resin. Consequently, water regain should be increased inasmuch as the content in quaternary ammonium groups becomes greater.

Table 2

Contents in quaternary ammonium groups of the anion-exchange resins prepared from Co – CM C as against the Co – CM C/DMA molar ratio used for synthesis

Anion exchange resin (code)	Co – CM C/DMA molar ratio	Solvent	Total exchange capacity (meq/g) determined from			Strong base exchange capacity (meq/g)	The content in quaternary ammonium groups (% from the total exchange capacity *)
			Aminic nitrogen (%)	0.1N HCl consumption (batch method)	pH-metric titration		
CS_2	1/3	water	3.70	3.60	3.60	0.20	5.55
$CS_{2.1}$	1/6	water	3.75	3.80	3.80	0.112	2.94
$CS_{2.2}$	1/10	water	3.80	3.85	3.90	0.04	1.02
CS_5	1/3	ACN	3.90	3.75	3.80	0.31	8.15
$CS_{5.1}$	1/6	ACN	3.70	3.85	3.80	0.14	3.68
$CS_{5.2}$	1/10	ACN	3.90	3.80	3.90	0.05	1.28
CS_7	1/3	benzene	3.75	3.70	3.60	0.624	17.33
$CS_{7.1}$	1/6	benzene	3.85	3.70	3.80	0.246	6.47
$CS_{7.2}$	1/10	benzene	3.85	3.85	3.90	0.05	1.28

*) Total exchange capacity determined from pH-metric titration.

In table 3 the values of water regain for samples CS_7, $CS_{7.1}$ and $CS_{7.2}$ in comparison with the respective values for the weakly basic anion-exchange resins for reference are presented.

Table 3

Water regain for the anion-exchange resins CS_7, $CS_{7,1}$ and $CS_{7,2}$ and for the reference samples

Sample	Water regain g.H_2O/g dry resin	The maximum humidity g H_2O /100g wet resin
CS_7	0.494	33.11
$CS_{7.1}$	0.396	28.40
$CS_{7.2}$	0.308	23.60
Duolite A-305	0.379	27.48
Amberlite IRA-93	0.315	23.95
Relite 4 MS	0.255	20.30
Lewatit MP-64	1.086	52.05
CT	0.676*	40.35*

*) Data for C.T. correspond to its Cl form.

Estimation of the data recorded in table 3 shows that among the three samples synthetized by us, sample CS_7 having the greatest amount of quaternary ammonium groups is also the one for which the largest water regain was measured.

At the same time, the respective data for Lewatit MP-64 again indicate that this commercial resin holds a special place among the other ones. Its much greater water regain and its maximum humidity degree in comparison with the corresponding values of the other samples having benzyldimethylamino functional groups, may be interpreted as an indication that another amine than DMA was used for its synthesis. This supposition can also be supported by the much larger value of its total exchange capacity as against the other samples (table 1).

Another experimental evidence to assert the distinct difference between the samples CS_7 and $CS_{7.2}$ in respect to the nature of their functional groups is also given by their infrared spectra. In this respect, in table 4, the common characteristic infrared bands exhibited by all samples CS_1-CS_7 synthetized by us are summarized. In figure 1 the infrared spectra of samples CS_7 and $CS_{7.2}$ are also presented. Examination of the spectra in figure 1 enables us to point to the spectral alterations which are brought about by the presence of the quaternary ammonium groups.

Accordingly, some changes in the infrared spectrum of sample CS_7 (a, figure 1) may be attributed, with a considerable degree of certitude, to the presence of quaternary ammonium groups involving, in this case, nearly 1/5 from the total amount of the functional groups (table 1). Thus, the characteristic absorption band of quaternary ammonium groups ($\sim$920 cm^{-1}) is clearly outlined but, at the same time, one

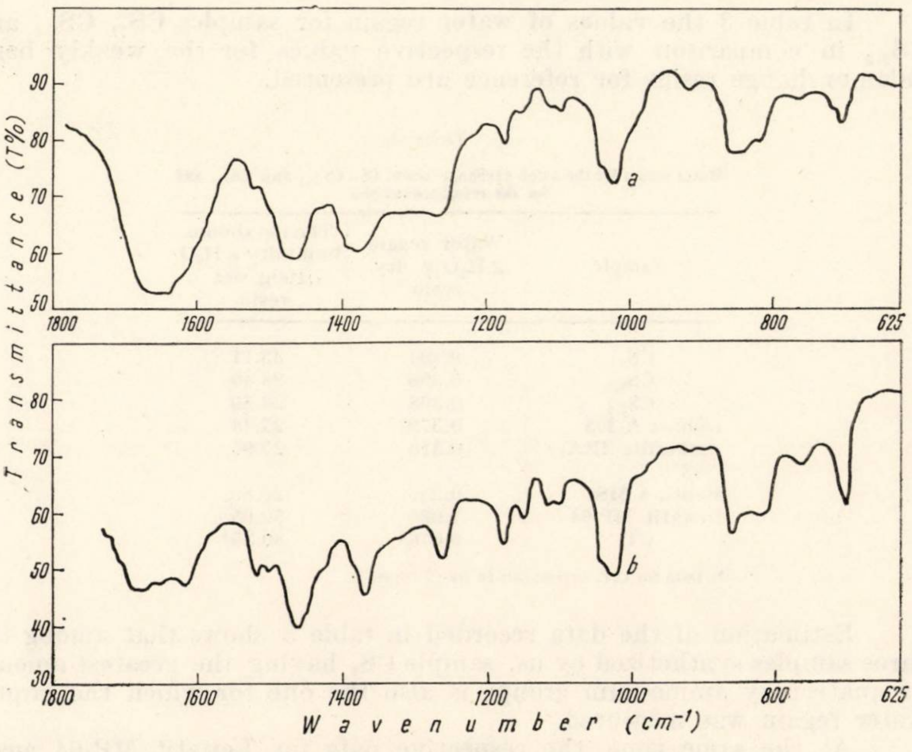

Fig. 1. — Infrared spectra : *a*, CS_7 ; *b*, $CS_{7.2}$.

Table 4

Characteristic infrared bands of the studied anion-exchange resins (in free base form)

Characteristic band	Position (cm^{-1})
ν CH (aromatic)	3 040
ν CH (CH_2, CH_3)	2 850 2 930
$\nu_{-C=C-}$ (aromatic)	1 520 1 620
$\nu_{-C\equiv N}$	2 250 770
$\delta_{CH(CH_2, CH_3)}$	1 370 1 460
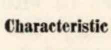 (benzyldimethylamino)	1 176 1 265 1 370 *
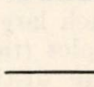	920**

*) According to Z. Vašiček and others.[6]

**) This band is not distinguishable for values of the strongly basic exchange capacity below 5% of the total exchange capacity.

can observe a certain extension, of the absorption bands at 1370 cm^{-1} and 1460 cm^{-1} which are assigned to C–H valence vibrations in $>CH_2$ and $-CH_3$ groups. This fact may be due to the additional crosslinkages, their result being the formation of dibenzyldimethylammonium functional groups. A decrease of the absorption bands at 1176 cm^{-1} and 1265 cm^{-1} which may be ascribed to the tertiary aminic groups[6] is also obvious as the concentration of the quaternary ammonium groups in the resin rises.

The differences regarding the nature of the functional groups, already discussed, are also confirmed by an examination of the pH-metric titration curves of our samples CS_7 and $CS_{7.2}$ (figure 2) and of the commercial resins, Amberlite IRA-93 and Lewatit MP-64, for reference (figure 3).

Thus, on examining the curves in figure 2 we have found that the presence of quaternary ammonium groups in a considerable amount in sample CS_7 (curve 1, figure 2) makes more visible the pH leap about the equivalence point. In the case of samples $CS_{7.2}$, practically homofunctional (curve 2, figure 2), a more monotonous variation of the pH-values with the neutralization degree expressed as HCl consumption is observed. This is also noticeable for Amberlite IRA-93 (curve 2, figure 3).

The manner in which the shape of the pH-metric titration curve of a practically homofunctional weakly basic anion-exchange resin is influenced by the concentration of the neutral electrolyte (NaCl) solution used for equilibration, is presented in figure 4 (Amberlite IRA-93). On examining the three curves in figure 4 we have also found that the pH-leap about the equivalence point becomes more visible as the concentration of the salt solution in equilibrium with the resin increases.

It is also to be expected that the presence of additional crosslinkages as quaternary ammonium groups in sample CS_7 should exert some influence on its thermal stability.

In this respect, in figure 5 and table 5, the TG curves and the correlation between certain weight losses, in percentages from the initial weight ($\%\Delta G$), and the corresponding temperatures, respectively are presented. These data concern the samples CS_7, $CS_{7.2}$ and the strongly basic anion-exchange resin CT, for reference.

The particular shape of the TG curves and also the data in table 5 point to a much greater thermal stability of the homofunctional weakly basic resin $CS_{7.2}$ than that of the strongly basic one, CT.

The experimental results of the thermogravimetric analysis presented in figure 5 and table 5 also indicate a nearly similar behaviour of samples CS_7 and $CS_{7.2}$ during their thermal decomposition up to temperatures of ca. 240°. However, one can notice a slightly decreased thermal stability of sample CS_7 in the temperature range of 80–240° where, for both samples, almost 50% of the total amount of functional groups is lost. From this fact it may be concluded that during the thermal decomposition process, the additional crosslinkages may, to some extent, exert a negative influence on the strength of CH_2-N bond in the tertiary aminic functional groups.

---

[6] Z. Vašiček, J. Klaban and J. Štamberg, *Coll. Czech. Chem. Comm.* **36**, 1825 (1971).

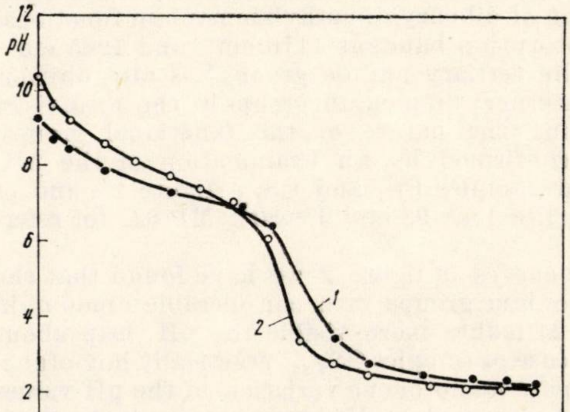

Fig. 2. — pH-metric titration curves, in 1M NaCl aqueous solution, 20° : *1*, $CS_{7.2}$; *2*, CS_7.

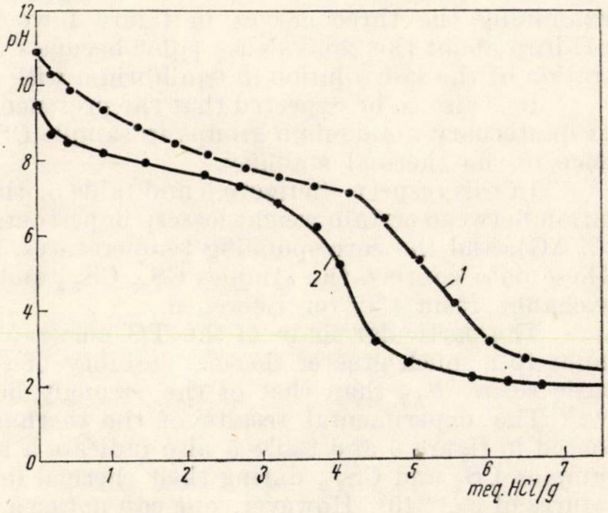

Fig. 3. — pH-metric titration curves, in 1M NaCl aqueous solution, 20° ; *1*, Lewatit MP-64 ; *2*, Amberlite IRA-93.

Other authors have also found that, for similar temperature intervals, a strongly basic resin as well as a weakly basic one become more stable as the degree of crosslinking decreased.[7] They explained this

---

[7] G. R. Hall, J. T. Klaschka, A. Nellestyn and M. Streat, "Ion Exchange in Process Industries", Papers of Conference held in London, July 1969, London, Society of Chemical Industry, 1970, p. 62.

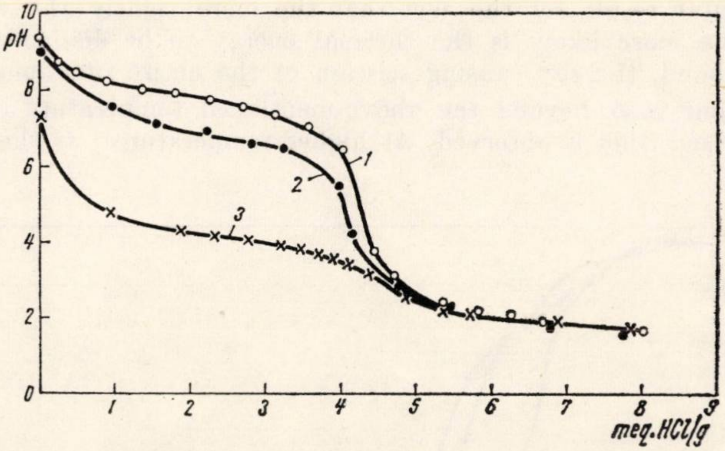

Fig. 4. — Influence of the concentration of the neutral electrolyte solution on the shape of pH-metric titration curve, Amberlite IRA-93, 20° : *1*, 1M NaCl aqueous solution ; *2*, 0.1M NaCl aqueous solution ; *3*, water.

Table 5

Correlation between weight losses and temperatures, according to the thermogravimetric analysis

Anion-exchange resin	$\Delta G(\%)$	Temperature (°)
CT*	—	78**
	10	200
	20	232
	30	260
	40	322
	50	380
	75	580
$CS_{7.2}$	—	75**
	10	260
	20	340
	30	375
	40	410
	50	460
	75	635
CS_7	—	82**
	10	240
	20	340
	30	380
	40	440
	50	550
	75	742

*) CT was analyzed in its Cl form

**) Temperature corresponding to the beginning of thermal decomposition.

Revue Roumaine de Chimie, **20**, *3*, 431−443 (1975)

experimental result by the fact that the more tightly the matrix is bound, the more likely is the thermal energy to be dissipated in the CH_2-N bond, thereby causing scission of the entire functional group.

In our case, beyond the above-mentioned temperature (ca. 240°) a reverse situation is observed. At higher temperatures, as the thermal decomposition proceeds, a nearly similar behaviour of samples $CS_{7.2}$ and CT is observed.

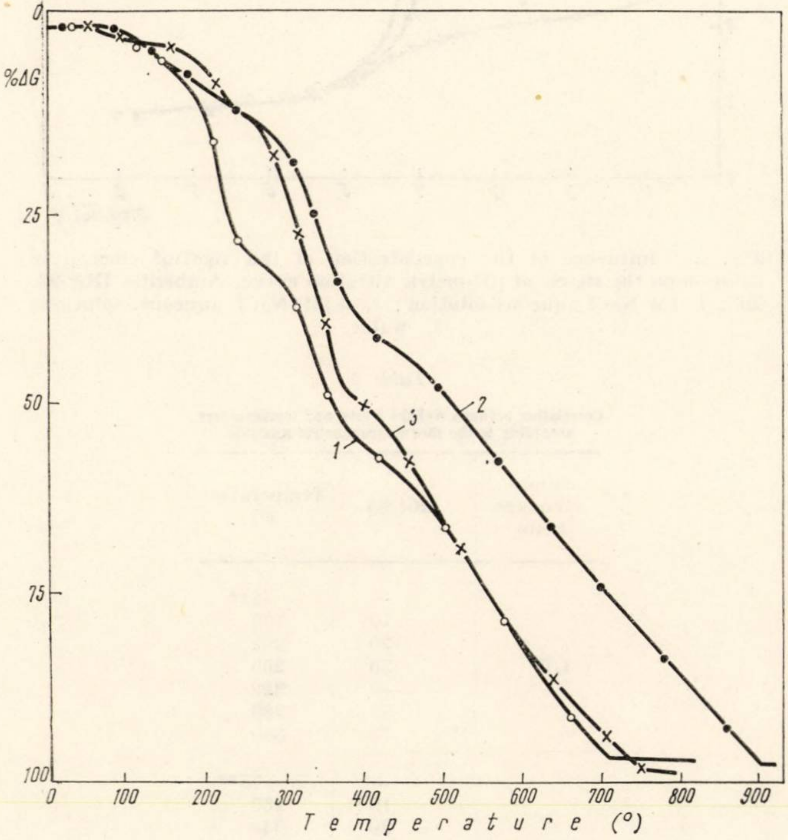

Fig. 5. — TG curves: *1*, CT; *2*, CS_7; *3*, $CS_{7.2}$.

But these experimental results suggest that we are likely to refer only to an improved thermal stability of the three-dimensional macromolecular network of the resin CS_7. This fact needs some further experimental proofs to explain it but we should consider that the additional crosslinkages, initially present in the resin, make certain contribution to this.

CONCLUSIONS

The correlation between the synthesis conditions of a weakly basic anion-exchange resin and the nature of its functional groups formed during the amination of the chloromethylated copolymer Co—CM C with dimethylamine was studied.

It was found that the additional crosslinking reactions leading to strongly basic groups are favoured by a higher temperature, a considerable increase of the amine concentration in the solution and by the decreased polar character of the solvent used as reaction medium.

By using high values of Co—CM C/DMA molar ratio the side crosslinking reactions could be, as far as possible, avoided.

By means of determination of the strongly basic exchange capacity and water regain as well as by pH-metric titrations, infrared spectra and thermogravimetric analysis the formation of quaternary ammonium groups during amination reaction was proved.

Revue Roumaine de Chimie, **20**, *3*, 435–444 (1975)

STUDIES ON THE SYNTHESIS AND CHARACTERIZATION OF WEAKLY BASIC ANION-EXCHANGE RESINS. III[1]

OPERATING CHARACTERISTICS

DEMETRA DRĂGAN, GEORGETA MOCANU and A. CARPOV
"P. Poni" Institute of Macromolecular Chemistry,
Aleea Grigore Ghica Vodă 41 A, Jassy, Romania

Received October 11, 1973

The operating performances of a practically homofunctional macroporous weakly basic anion-exchange resin with benzyldimethylamino functional groups are studied. The influence on the operating characteristics exerted by the strongly basic groups possibly present in the resin is also revealed. The physical characteristics of the resin and its regeneration and exhaustion isotherms are compared with the data on some reference resins.

Sorption operations are commonly carried out in fixed-bed columns — regeneration, rinse and exhaustion of the resin being the main steps of an ion-exchange cycle.

The performance of a fixed ion-exchange bed is governed by a combination of stoichiometric, equilibrium and rate relationships between the exchanging ion-species. Accordingly, apart from the concentration of the feeding solutions and of their flow rates, the ion-exchange operations essentially depend on the nature of the resin, that is, on the characteristics of the macromolecular matrix and the type of the functional groups.

In two other papers [1,2] the study concerning the influence exerted by different parameters on the course of the amination reaction with dimethylamine of some chloromethylated macroporous ternary styrene-divinylbenzene-acrylic monomer copolymers and on the nature of the functional groups in the resulted anion-exchangers is reported.

The aim of the present work is to study the operating performances of the resins we have synthetized, by means of the respective sorption isotherms of the regeneration and exhaustion processes.

MATERIALS AND METHODS

— Homofunctional weakly basic anion-exchange resins synthetized by amination with dimethylamine (DMA) of chloromethylated macroporous ternary copolymers (Co—CM), A, B and C noted here AS, BS and CS_1 respectively.

---

[1] A. Carpov, D. Drăgan, G. Mocanu and C. Luca, *Rev. Roumaine Chim.* **20**, 417 (1975).
[2] D. Drăgan, G. Mocanu and A. Carpov, *Rev. Roumaine Chim.* **20**, 431 (1975).

— Intermediate-base anion-exchange resin CS_2 also based on the chloromethylated copolymer Co—CM C, having benzyldimethylamino and ca. 17% quaternary ammonium functional groups according to its synthesis conditions.[2]

— Reference weakly basic anion-exchange resins Duolite A-305, Amberlite IRA-93, Relite 4MS having benzyldimethylamino functional groups and Lewatit MP-64 containing tertiary aminic and ca. 10% of strongly basic functional groups according to the manufacturers' specifications.

— Sodium hydroxide, hydrochloric and sulphuric acids, analytical grade.

The operating characteristics of the samples under investigation were analyzed at 20° using their free-base form as the reference one, on the fraction of a 0.4—0.8 mm mean diameter of the beads.

The samples were made ready for experiments by previously passing them twice, alternatively, from the HCl form into their free-base form.

The operating exchange capacities during regeneration and exhaustion were determined under flow conditions. As a term of these operating exchange capacities the values of the breakthrough capacities were used.

At the exhaustion step strong acid solutions of 0.04N HCl and mixtures of HCl and H_2SO_4 having concentrations of 0.008 N and 0.16N respectively, were used.

To regenerate the resins back to their free-base form 1M NaOH solution, at 20°, was used.

The flow rates used at the regeneration and exhaustion steps were the same as those pointed to by the practical use of the weakly basic anion-exchange resins.

The total weight and volume exchange-capacities were also determined under flow conditions by fully converting the resins into a selected ionic form which is achieved with a large excess of the appropriate analytical grade reagent.

Sorption isotherms were obtained by gradually measuring the concentration increase of the loading ionic-species in the effluent till it equaled the value in the influent.

In these diagrams the variation of the volume exchange capacity of the resin in the respective anionic form, as percentages of its total column exchange capacity, versus the ratio of the volumes of the regenerant or exhaustion solution per volume of anion exchanger (v/v) is plotted.

The osmotic shock test was carried out by subjecting the resins to alternate swelling and shrinking, using the cyclic treatment, according to the microcyclation method.[3]

The swelling degree in water and the changes in volume when the resins quantitatively passed from one ionic form to another were measured with graduated cylinders, after the resin beads had been left to settle down in water for 24 hrs.

RESULTS AND DISCUSSION

In order to estimate the attrition resistance of the resin beads, both for the reference samples and for those synthetized by us, a tentative study by means of the osmotic shock test was made (table 1).

On examining the experimental results recorded in table 1 we find that the resins AS and CS_1 with acrylonitrile as the third comonomer of their macromolecular matrix[1] have a higher attrition resistance than resin BS which contains methyl-methacrylate. In the same experimental data we also find that the attrition resistance of the beads increases inasmuch as the crosslinking divinylbenzene degree rises (samples AS and CS_1).

At the same time, the data in table 1 show that the resins AS and CS_1 have a physical and chemical stability of nearly the same magnitude order as the resin Lewatit MP-64 chosen for reference.

Next, taking into account the above mentioned conclusions concerning the osmotic shock test, we will restrict our discussion about operating performances only to the sample CS_1 whose physical and chemical characteristics are very similar to those of the reference samples.

---

[3] A. Carpov, G. Mocanu and I. Petrariu, *Materiale Plastice*, **10**, 133 (1973).

Table 1

Physical and chemical stability of the samples tested by microcyclation

Anion-exchange resin	Number of microcycles	Initial total exchange capacity * (meq/g)	Final total exchange capacity * (meq/g)	Decrease of the total exchange capacity(%)	Particle size distribution after microcyclation (mm) **			
					<0.20	0.20–0.35	0.35–0.5	>0.5
AS	1 000	2.96	2.86	3.05	traces	3.26	2.60	94.14
BS	1 000	2.52	2.44	3.18	0.42	24.32	8.53	66.73
CS_1	1 000	3.90	3.78	3.05	traces	10.20	2.20	87.60
Duolite A-305***	220	4.00	3.69	7.62	11.61	19.80	3.10	65.49
Amberlite IRA-93	1 000	4.20	4.04	3.72	7.20	55.86	6.70	30.24
Relite 4 MS	1 000	3.85	3.73	3.05	0.92	35.64	3.33	60.11
Lewatit MP–64	1 000	5.60	5.51	1.62	traces	3.30	1.40	95.30

*) The total exchange capacity was determined by using the batch method.[2]

**) Fractions of a 0.5–0.8 mm mean diameter of the beads were analysed.

***) Recently, Duolite A-305 which is no longer manufactured, was replaced by Duolite A-368.

At the same time, to point out the influence exerted by the quaternary ammonium groups which may, to some extent, be present in a weakly basic anion-exchange resin, the sample CS_2 is also comparatively studied.

Some analytical characteristics of the tested resins are listed in table 2.

Table 2

Analytical characteristics of the tested resins

Anion-exchange resin	Expansion of the resin, ΔV (%)		Total exchange capacity (flow conditions), determined by		
	by swelling in water (the free-base form)	by passing from the free-base form into HCl form	exhaustion with 0.04N HCl solution		regeneration with 1M NaOH solution
			meq/g	meq/ml	meq/ml
CS_1	20.00	8.50	3.90	1.53	1.52
CS_2	28.00	6.00	3.55	1.43	1.40
Duolite A-305	44.66	31.60	4.10	1.65	1.62
Relite 4MS	53.80	40.00	3.90	1.58	1.56
Amberlite IRA-93	14.90	29.40	4.30	1.52	1.51
Lewatit MP-64	57.00	32.00	5.60	1.53	1.52

It is to be noted that among all the resins studied, the macroporous samples CS_1 and CS_2 synthetized by us show the lowest values of contraction and expansion of the resin bed during the salt-free base ion-exchange cycle.

The characteristic elution curves of HCl during the regeneration step when the resins pass from the HCl form to their free-base form by using 1M NaOH solution are presented in figures 1 and 2. The operating exchange capacities which show their most favourable regeneration levels are also listed in table 3.

On examining these experimental data we find quite a superposition of the regeneration isotherms and very close values of the

Table 3

Regeneration step with 1 M NaOH solution, 20°. Operating exchange capacities of the tested resins

Anion-exchange resin	Breakthrough capacity *	
	(meq/ml)	% of the total volume exchange capacity
CS_1	1.39	91.32
CS_2	1.03	72.16
Duolite A-305	1.44	87.53
Relite 4MS	1.37	86.91
Amberlite IRA-93	1.27	83.70
Lewatit MP-64	1.20	78.68

*) Determined after a previous 100% exhaustion with HCl solution

breakthrough capacities of the three commercial resins (Duolite A-305, Relite 4MS, Amberlite IRA-93 (figure 1) and of the resin CS_1 synthetized by us (figure 2). This fact is perfectly understandable if we take into consideration both their practically homofunctional character [2] and their very close values of the total exchange capacity (table 2).

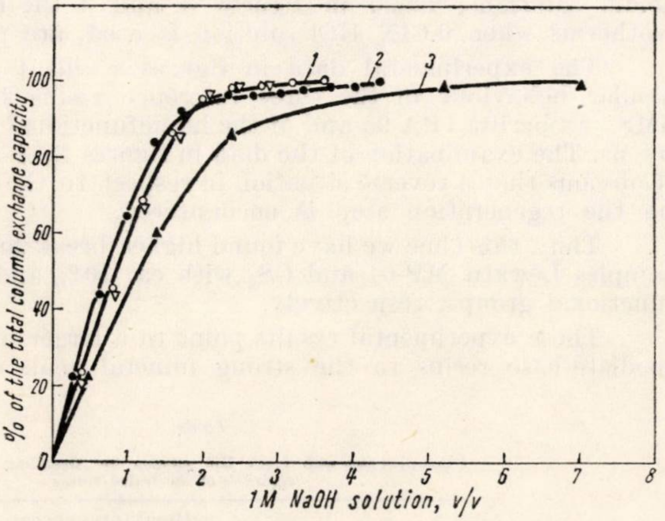

Fig. 1. — Regeneration isotherms of the reference resins, 1M NaOH regenerating solution, 20° : *1*, —○— Relite 4MS, —▽— Duolite A-305 ; *2*, Amberlite IRA-93 ; *3*, Lewatit MP-64.

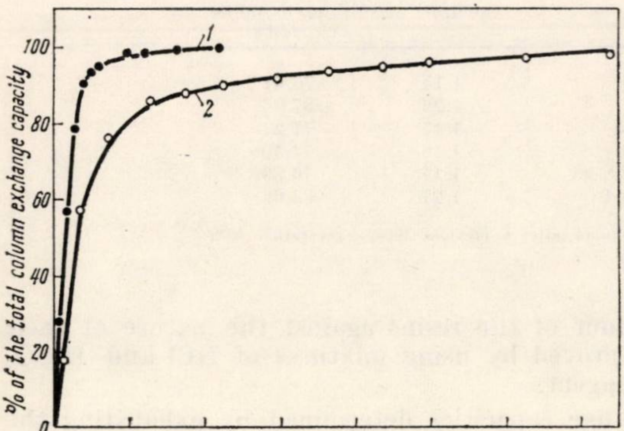

Fig. 2. — Regeneration isotherms of the resins CS_1 and CS_2, 1M NaOH regenerating solution, 20° : *1*, CS_1 ; *2*, CS_2.

In contrast with the homofunctional resins, the reference sample Lewatit MP-64 and to a much larger extent the resin CS_2, require higher consumptions of caustic soda in order to reach the same regeneration level. This effect is more marked at higher regeneration levels.

The lower regeneration efficiencies of these samples — both of them belonging to the so-called intermediate-base anion-exchange resins — are naturally a consequence of the strongly basic functional groups present in the resins.

The ability of the studied resins to remove strong mineral acids from the feeding supply is tested by using mono- and bicomponent influent acidic solutions. Thus, in figures 3 and 4 the respective exhaustion isotherms when 0.04N HCl solution is used, are presented.

The experimental data in figures 3 and 4 also point to a very similar behaviour of the three reference resins Duolite A-305, Relite 4MS, Amberlite IRA-93 and of the homofunctional resin CS_1 synthetized by us. The examination of the data in figures 3, 4 and in table 4 makes it obvious that a reverse situation in respect to that revealed by the data on the regeneration step is encountered.

Thus, this time we have found higher breakthrough capacities of the samples Lewatit MP-64 and CS_2 with ca. 10% and more strongly basic functional groups, respectively.

These experimental results point to a larger affinity of these intermediate-base resins to the strong mineral acids than to the alkalies.

Table 4

Exhaustion step with 0.04N HCl solution, 20°. Operating exchange capacities of the tested resins

Anion-exchange resin	Breakthrough capacity *	
	meq/ml	% of the total volume exchange capacity
CS_1	1.14	76.61
CS_2	1.26	87.94
Duolite A-305	1.17	71.24
Relite 4MS	1.18	74.40
Amberlite IRA-93	1.17	76.30
Lewatit MP-64	1.27	83.00

*) Determined after a previous 100% regeneration with NaOH solution.

The differing behaviour of the resins against the nature of their functional groups is also proved by using mixtures of HCl and H_2SO_4 solutions as exhausting reagent.

The operating exchange capacities determined by exhausting the resins with a 0.008N solution of an almost equal meq-g concentration in HCl and H_2SO_4 are listed in table 5.

The higher absorption capacities for strong acids which are found with the homofunctional resins (table 5) are a consequence of their larger regeneration levels previously achieved with the same quantity of the regenerating solution. In all the samples tested we have also found a very close value of the H_2SO_4/HCl (meq/meq) ratio of the absorbed acids in the resins, practically the same value as that of the influent solution.

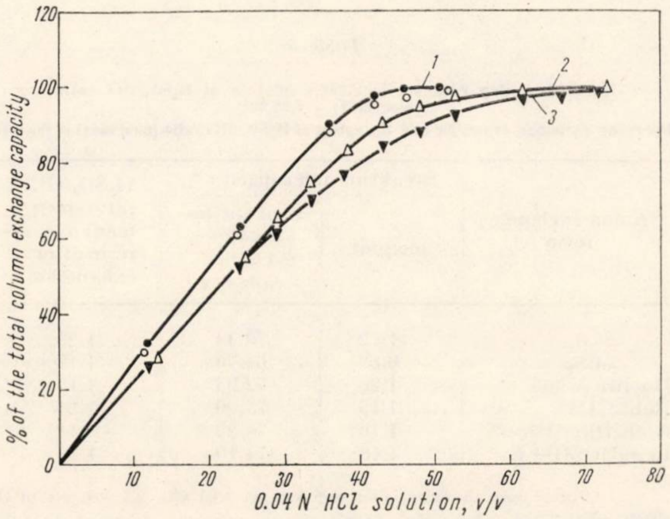

Fig. 3. — Exhaustion isotherms of the reference resins 0.04N HCl exhausting solution, 20° : *1* —●— Lewatit MP-64, —○— Amberlite IRA-93 ; *2*, Relite 4MS ; *3*, Duolite A-305.

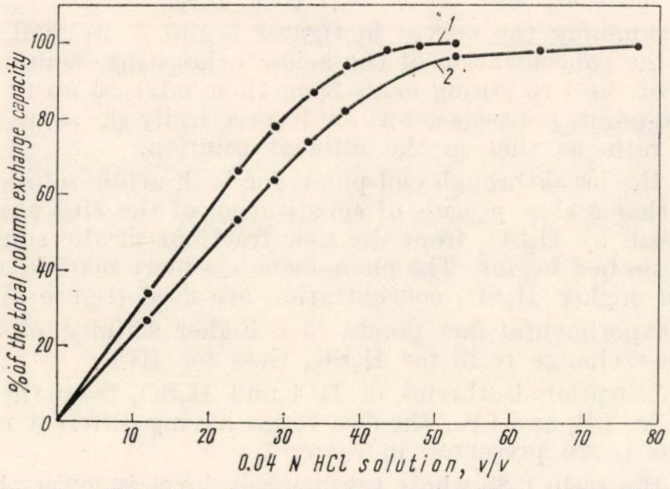

Fig. 4. — Exhaustion isotherms of the resins CS_1 and CS_2, 0.04N HCl exhausting solution, 20° : 1 CS_2 ; 2 CS_1.

Revue Roumaine de Chimie, 20, 3, 435–444 (1975)

This fact points to an equivalent absorption of the two strong acids used up to the breakthrough end-point.

Table 5

Exhausting step with acidic 0.008N solution of H_2SO_4/HCl ratio (meq/meq) = 1.16,20°

Operating exchange capacities and the values of H_2SO_4/HCl ratio (meq/meq) in the resin

Anion-exchange resin	Breakthrough capacity *		H_2SO_4/HCl ratio (meq/meq) in the resin after exhaustion
	meq/ml	% of the total volume exchange capacity	
CS_1	1.12	73.44	1.25
CS_2	0.88	61.75	1.12
Duolite A-305	1.20	72.93	1.15
Relite 4MS	1.15	73.00	1.21
Amberlite IRA-93	1.16	76.22	1.11
Lewatit MP-64	1.18	74.10	1.20

*) In all cases the regeneration step was achieved with 2.5 volumes of 1M NaOH solution per volume of the resin.

The gradual absorption of HCl and H_2SO_4 and the effect of the acidic influent concentration as well as its H_2SO_4/HCl ratio upon it are revealed by the respective absorption isotherms presented in figures 5, 6 (Amberlite IRA-93) and in figure 7 (CS_1, CS_2).

On examining the curves in figures 5 and 6 we find that, irrespective of the concentration of the acidic exhausting solution used, the absorption of the two strong acids from their mixture up to the breakthrough end-point, proceeds according to practically the same H_2SO_4/HC_1 (meq/meq) ratio as that in the influent solution.

After the breakthrough end-point, for both acidic solutions used, it is obvious that a slow process of substitution of the HCl already linked with the resin by H_2SO_4 from the new fractions of the solution which cross the resin bed begins. The phenomenon is more marked when acidic mixtures of higher H_2SO_4 concentration are used (figure 6).

This experimental fact points to a higher affinity of the weakly basic anion-exchange resin for H_2SO_4 than for HCl.

The absorption isotherms of HCl and H_2SO_4 from their mixture, with the resins CS_1 and CS_2, the two resins having different regeneration levels (table 5) are presented in figure 7.

With the resin CS_2 whose regeneration level is lower than that of the homofunctional resin CS_1, immediately after the breakthrough end-point, considerable deviations of the H_2SO_4/HCl (meq/meq) value from that of the influent are observed.

This fact is easily understandable if we take into account the quite different concentrations of HCl and of Cl^- ions initially linked with the resins CS_1 and CS_2.

Accordingly, the $H_2SO_4 \rightarrow HCl$ acidic exchange is more marked with the resin CS_2 having the lowest regeneration level.

Fig. 5.—Exhaustion isotherms of the reference resin Amberlite IRA-93, 0.008N exhausting solution of HCl and H_2SO_4, H_2SO_4/HCl (meq/meq) ratio = 1.16, 20° : —●— absorption of H_2SO_4 ; —○— absorption of HCl.

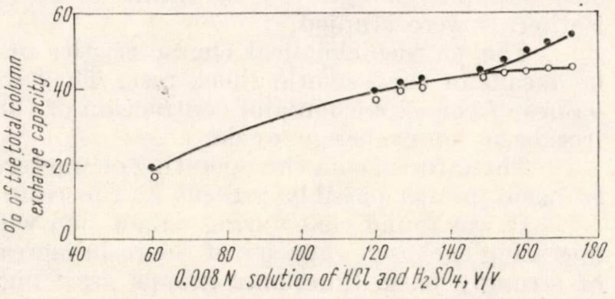

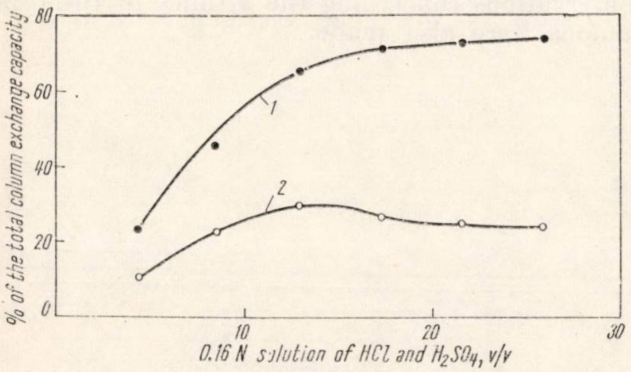

Fig. 6.—Exhaustion isotherms of the reference resin Amberlite IRA-93, 0.16N exhausting solution of HCl and H_2SO_4, H_2SO_4/HCl (meq/meq) ratio = 2.02, 20° : *1*, absorption of H_2SO_4 ; *2*, absorption of HCl.

Fig. 7. — Exhaustion isotherms of the resins CS_1 and CS_2 having different regeneration levels, 0.008 N exhausting solution of HCl and H_2SO_4, H_2SO_4/HCl (meq/meq) ratio = 1.16, 20° : 1 — ↕ — absorption of H_2SO_4, resin CS_1 ; —●— absorption of H_2SO_4, resin CS_2 ; *2*, absorption of HCl, resin CS_1 ; *3*, absorption of HCl, resin CS_2.

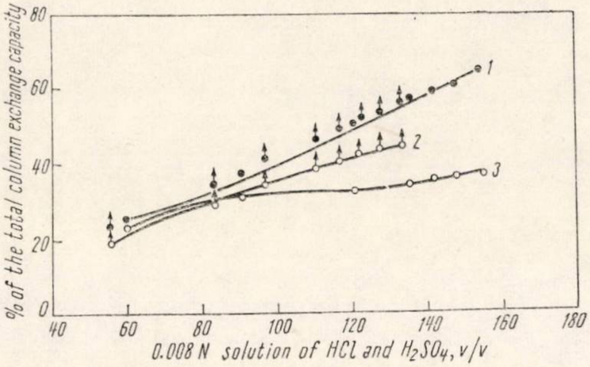

At the same time, the experimental data presented in figure 7 once again confirm the higher affinity for H_2SO_4 of both resins.

CONCLUSIONS

The operating performances of a practically homofunctional weakly basic anion-exchange resin by means of its regeneration and exhaustion isotherms were studied.

The physico-chemical characteristics of the resin were determined by means of the osmotic shock test. They were also determined by the values of the expansion and contraction of the resin bed during the salt-free base ion-exchange cycle.

The influence on the operating characteristics exerted by the strongly basic groups possibly present in the resin was also studied.

It was found that during exhaustion with mineral strong acids the operating exchange capacity of the resin increased inasmuch as its content of strongly basic functional groups grew bigger. But, with higher contents of strongly basic groups in the resin larger consumptions of the alkaline regenerant were spotted.

Some qualitative observations concerning the affinity of the resin for uni- and bivalent anions were also made.

Revue Roumaine de Chimie, **20**, *3*, 445–446 (1975)

COMPTES RENDUS

B. VOLLMERT, *Polymer Chemistry*, Springer, Berlin-Heidelberg-New York, 1973, 652 pages.

This recently published volume is, in broad lines, the translation from German of the book "Grundriess der makromoleculären Chemie", which is well-known in our country and was issued in 1962 by the same Publishing House. Considering that it first appeared over ten years ago, and that new data have been gathered since then, which are reflected in the coverage of many rewritten chapters, and that several generations of specialists have been formed in the meantime, a new presentation of this volume seems to be useful.

Emphasis must be laid from the very beginning, on the special character of the book, both in point of contents and format. It is much more comprehensive than ordinary books on polymer chemistry in that it includes for instance, biopolymers (nucleic acids, proteins, polysaccharides) and their enzymatic synthesis or the latest breakthroughs in the field of polymer crystallization and deformation. A large number of tables, figures and diagrams concentrate a wealth of data used by the author to explain the occurrence of certain processes or of certain special features in polymers. The classical approach of treatises has been replaced by a lively, instructive and educational presentation concerned with the elucidation of more complicated phenomena even if this requires certain detours. The exposition is generally ordered in an unanimously accepted way, being, however, interspersed with many intellectual excursions meant to elucidate some subtleties that have been investigated by the author. Such an approach has resulted, as expected, in an inequal handling — from the point of view of dimensions and of thoroughness — of problems such as the description of the main processes for obtaining polymers or of the properties of various classes of macromolecules. Yet, the theory and the experiment have been equally considered. In general, it may be stated that the author showed a preference for handling the issues and the problems so as to confer a deeper insight into the book. The text often refers to various sections of chapters which help the reader to build up a most comprehensive image of the problem under study by establishing the necessary connections.

The book includes 4 chapters. The first one reviews the structure of polymer chains• In the English version, some elements of primary, secondary and tertiary structures were added. The second chapter describes the main types of syntheses resulting in long macromolecular chains formed of small monomer molecules. Particular attention has been paid to the ordering of structural units in the chain, depending on the nature of the monomer and on synthesis conditions. As a result, the author discusses the problems related to the synthesis of carbochain macromolecules through radicalic, ionic polymerization and with complex catalytic systems and also the synthesis of heterochain macromolecules through polycondensation and polyaddition. The section devoted to enzymatic synthesis seems to be a new approach. The problem of the ordering of structural units in the chain also covers polymers chemical transformations with or without chain-splitting. The next chapter is devoted to factors referring to the chain as a whole : chain size, molecular weight determinations and their distribution ; the shape and the sizes of the macromolecule (spatial ordering) under the conditions of free movement in very diluted solutions. The last chapter discusses the shape of macromolecules in various states of aggregation : concentrated solutions, gels, rubbers, solid states (glass and crystals) and also the possible coexistence of such states.

Compared to the German version, the volume follows in broad lines both the conception of the whole and the classification into chapters. It includes a number of new elements such as those referring to the primary, secondary and tertiary structures (page 30) ; polymerization by hidride transfer (page 179), development of enzymatic synthesis (pages 258—277) synthesis of proteins (page 281) as well as numerous new data added to various sub-chapters. If the absence of a table listing the commercial names of the main macromolecular substances, their constitution, manufacturing firms and major uses may pass unnoticed, this is certainly not the case with references to the principal sources of documentation which help the reader in consulting an additional bibliography on a specific subject. The German version lists in detail the main additional documentation sources, ordered in chapters, including encyclopaediae, treatises, books, comprehensive articles and even original articles which cover almost all the aspects — including the technical ones — related to polymers. An updating of these bibliographical indications would have actually benefited the reader.

Mention should be made of the excellent graphical conditions under which the book was printed as well as of the very readable English translation. The few typing errors found now and then can be easily corrected. Like in the German version, tables and figures are numbered according to a simple, new and very convenient system. Each table or figure has been given the number of the page on which it appears so that it can be readily retrieved without one's having to skim through a large number of pages to locate it, as is the case with other books.

The purpose of the book is instructive and educative. It provides a comprehensive insight into polymers for those who being contingent with the subject, want to find the basic principles of the methods for the study and the investigation into polymer structure, in an accessible form. For certain topics, the contents compensate even for the absence of some monographs and enable those familiar with polymers to refresh their knowledge. The students and the teaching staff will find therein models of scientific topics and problems rigorously debated in that different opinions and theories on the same problem are presented. This draws the reader into the analysis of the subject and helps him find througher explanations. Owing to the special format of the book, its reading may captivate even a specialist who will find many appealing problems approached in a highly original manner.

F. Cuiban

D. HELLWINKEL, *Die systematische Nomenklatur der organischen Chemie*, Springer-Verlag, Berlin-Heidelberg-New York, 1974 (Heidelberger Taschenbücher, **135**).

In a relatively small number of pages (170), the author succeeds in presenting a clear and well-documented account of the main IUPAC rules for the organic-chemical nomenclature. The book is richly illustrated with chemical formulas, and the writing is concise. In several instances, the author mentions cases when nomenclature rules are inconsistent : on p. 12, footnote 2 and p. 26, why should not cyclobutabenzene be a better name than benzocyclobutene? ; mixing of Greek and Latin numerals in naming bridged polycyclic systems (p. 25, footnote 6). In other cases, the IUPAC rules are not precise enough (p. 48, footnote 11 ; p. 53, footnote 15), and the author devises outlets from this situation by recourse to the Ring Index and Chemical Abstracts nomenclature systems. When there is no consensus on details, as for instance whether Roman or italicized letters are to be used in denoting positions of condensation in fused polycyclic systems, this is explicitly pointed out (p. 18, Anmerkung).

One critical comment of the reviewer concerns the formulas of pyrimidinic and purinic bases on p. 149 : because they are listed under the heading "Phenols and other heterocyclic derivatives" adenine is missing, and false tautomeric forms are presented in all four cases (uracil, thymine, cytosine, guanine).

The book has two annexes. The first contains the table of trivial and semitrivial names to be conserved in the IUPAC nomenclature. It remains to be seen whether the recent initiative of Chemical Abstracts to curtail drastically the list of trivial names will be adopted by IUPAC. Unlike the author (cf. his proposal on p. 126 to expand the list of trivial names), the reviewer feels that trivial names multiply too rapidly, as we witness for the valence isomers of annulenes. The second annex is a brief presentation of the Wisweser line notation system. A subject index concludes the book.

There are a few literature quotations and a few examples left as exercises (p. 116). The book is meant as a practical introductory guide for chemists, biologists, pharmacists and physicians, and its moderate price (paperback, 14.80 DM) makes is accessible.

A. T. Balaban

NOTE POUR LES AUTEURS

La *Revue Roumaine de Chimie* publie des articles en anglais, français, russe, allemand ou espagnol. Les auteurs sont priès d'envoyer des articles, notes, communications et comptes rendus inédits.

Les manuscrits seront dactylographiés à deux intervalles. Les tableaux seront dactylographiés sur des feuilles séparées, de même que la légende des figures. Les diagrammes seront tracés à l'encre de Chine sur papier calque. Les tableaux et les figures seront numérotés par des chiffres arabes, en nombre strictement nécessaire. Prière de ne pas inscrire les mêmes données dans les tableaux et les figures. Les formules chimiques seront incluses dans le texte ; en outre, elles seront transcrites sur des feuilles séparées. Les auteurs sont priés d'indiquer les caractères italiques (en soulignant les lettres au crayon), ainsi que tout autre caractère spécial. L'ordre des références bibliographiques sera celui de leur mention dans le texte ; le nom de l'auteur sera précédé de l'initiale du prénom ; les publications périodiques seront présentées suivant les prescriptions internationales. Les références seront ajoutées à la fin de l'article ; elles paraîtront comme des notes, au bas de la page. Le texte sera précédé d'un résumé comprenant 15 lignes au maximum.

L'entière responsabilité du contenu des articles appartient aux auteurs. On publie des articles dus aux collaborateurs roumains ou étrangers.

PRINTED IN ROMANIA

1975 JUL 16

TRAVAUX PARUS AUX ÉDITIONS DE L'ACADÉMIE DE LA RÉPUBLIQUE SOCIALISTE DE ROUMANIE

I. ZUGRĂVESCU, MAGDA PETROVEANU, **Chimia *N*-Ilidelor** (Le chimie des N-Ylures), 1974, 347 p., 19 lei.

MARGARETA AVRAM, **Antidăunători** (Pesticides), 1974, 494 p., 41 lei.

CR. SIMIONESCU, VIORICA RUSAN et V. POPA, **Chimia algelor marine** (Le Chimie des algues marines), 1974, 211 p., 18 lei.

CRISTOFOR SIMIONESCU, MARGARETA GRIGORAȘ, AGATA CERNĂTESCU-ASANDEI et GHEORGHE ROZMARIN, **Chimia lemnului din România — plopul și salcia** (La chimie du bois en Roumanie — le peuplier et le saule), 1973, 228 p., 28 lei.

TIBERIU NĂȘCUȚIU, **Metode radiochimice de analiză** (Méthodes radiochimiques d'analyse), 1973, 384 p., 23 lei.

MARIA FITI, **Dozimetria chimică a radiațiilor ionizante** (La dosimétrie chimique des radiations ionisantes), 1973, 240 p., 13,60 lei.

MIHAI FLORESCU, **Eficiența economică a cercetării științifice** (L'efficience économique de la recherche scientifique), 1972, 115 p., 15 lei.

GEORGETA LĂZĂRESCU, **Sistematizarea informațiilor în Chimia organică** (La systématisation des informations dans la Chimie organique), 1972, 252 p., 10,15 lei.

P. BALTĂ și E. BALTĂ, **Introducere în chimia fizică a stării vitroase** (Introduction à la chimie physique de l'état vitreux), 1971, 240 p., 15,50 lei.

LYDIA-MARIA VAICUM, **Biodegrabilitatea detergenților** (La biodégrabilité des détergents), 1971, 254 p., 16 lei.

I. ZUGRĂVESCU et L. STOICESCU-CRIVETZ, **Polimeri heterociclici** (Polymères hétérocycliques), 1971, 190 p., 9,50 lei.

CRISTOFOR SIMIONESCU et C. V. UGLEA, **Fracționarea compușilor macromoleculari** (Fractionnement des composés macromoléculaires), 1962, 292 p., 18,50 lei.

I. MAXIM, **Materiale nucleare** (Matériaux nucléaires), 1969, 444 p., 30 lei.

CRISTOFOR SIMIONESCU et CLEOPATRA VASILIU-OPREA, **Mecanochimia compușilor macromoleculari** (La mécanochimie des composés macromoléculaires), 1967, 344 p., 23,50 lei.

CORNEL BODEA et collab., **Tratat de biochimie vegetală**, partea I, **Fitochimie** (Traité de biochimie végétale, Ire partie, Phytochimie), Ier vol., 1964, 747 p. + 4 annexes + 2 pl., 41 lei ; IIe vol., 1965, 1262 p., 1 pl., 56 lei ; IIIe vol., 1967, 773 p., 35 lei.

I. P. I. – c 1750

43 426

Lei 25. –

F 1103

7J

ACADÉMIE DE LA RÉPUBLIQUE SOCIALISTE DE ROUMANIE

REFERÁLVA

REVUE ROUMAINE DE CHIMIE

TOME 20

N° 4

AVRIL 1975

RECHAX, 20, 4, 447 – 588 (1975)

EDITURA ACADEMIEI REPUBLICII SOCIALISTE ROMÂNIA

Rev. Roumaine Chim. 20, 4, p. 447 – 588 (1975), Bucarest

ACADÉMIE DE LA RÉPUBLIQUE SOCIALISTE DE ROUMANIE

COMITÉ DE RÉDACTION

Rédacteur en chef:

I. G. MURGULESCU, membre de l'Académie de la République Socialiste de Roumanie

Rédacteurs en chef adjoints:

A. T. BALABAN et V. EM. SAHINI, membres correspondants de l'Académie de la République Socialiste de Roumanie.

Collège de rédaction:

EM. BRATU, ELENA CEAUŞESCU, ECATERINA CIORĂNESCU-NENITZESCU, C. DRĂGULESCU, RALUCA RIPAN, CR. SIMIONESCU, membres de l'Académie de la République Socialiste de Roumanie ; P. SPACU, membre correspondant de l'Académie de la République Socialiste de Roumanie ; MARGARETA AVRAM, D. I. MARCHIDAN, G. NIAC et D. SĂNDULESCU

La Revue Roumaine de Chimie paraît 10 fois par an. Toute commande de l'étranger pour les travaux parus aux Editions de l'Académie de la République Socialiste de Roumanie sera adressée à ILEXIM, Serviciul Export—Import Carte/Serviciul Export—Import Presă, POBOX 2001, Calea Griviţei n° 64—66, Bucarest, Oficiul Poştal 12, Roumanie

Les manuscrits, les livres et les revues proposés en échange, ainsi que toute correspondance seront envoyés à la rédaction

REVUE ROUMAINE DE CHIMIE

23, str. Dumbrava Roşie, Bucarest, Roumanie, téléphone 12 41 60

EDITURA ACADEMIEI REPUBLICII SOCIALISTE ROMÂNIA

Calea Victoriei, n° 125, téléphone 13 94 40

REVUE ROUMAINE DE CHIMIE

ORSZÁGOS MŰSZAKI KÖNYVTÁR ÉS DOKUMENTÁCIÓS KÖZPONT

Tome 20, N° 4 Avril 1975

ŞTEFANIA ZUCA and M. OLTEANU, Electrical conductivity of certain charge-unsymmetrical fused chloride systems KCl$-$CaCl$_2$, KCl$-$SrCl$_2$, KCl$-$BaCl$_2$ . . . 449–458

V. DANĚK and K. MATIAŠOVKSÝ, Interaction of ions in molten binary LiF $-$ AlF$_3$ mixtures . . . 459–464 R

S. STERNBERG and LUCIA BEJAN, Thermodynamic properties of molten salt binary mixture AgI + CdI$_2$ and reciprocal mixture AgI + CdCl$_2$ . . . 465–471

SESTA BIANCA, Solvent interaction with alkyl-trimethylammonium halides. II. Conductance in acetonitrile, acetone and methyl ethyl ketone at 25° . . . 473–480

O. MATEIOVICI, Behaviour of activated carbon electrode in electrolyte solutions . . . 481–485

ECATERINA VASILESCU, The behaviour of nickel in chloride ions-containing media . . . 487–491 R

I. A. ATANASIU et MARIA NEAŢĂ BĂLESCU, L'étude du système rédox $\mathrm{Fe(CN)_6^{3-}/Fe(CN)_6^{4-}}$ sur l'électrode de graphite . . . 493–500

I. SOLACOLU, MARIA MAVRODIN–TĂRĂBÎC et IOANA ONACA, L'étude de la réaction d'oxydation de l'hydrogène dans les électrodes poreuses en nickel. II. La détermination des paramètres d'obtention des électrodes . . . 501–513

D. H. BROWN and P. G. PERKINS, The electronic structure and spectra of the di-μ-sulphido-bis-[oxo-(L-cysteinato) molybdate (V)]$^{2-}$ ion . . . 515–521

RALUCA RIPAN and MARIA VÁRHELYI, Synthesis of the bromo-*m*-xylidine-bis-ethylenediamine-cobalt (III) complex and its aquation kinetics in acid solutions . . . 523–530

MARIA BREZEANU and IOANA JITARU, Coordination compounds with choline acetate . . . 531–538

ELISE AVRAM, F. CHIRALEU, I. G. DINULESCU and MARGARET AVRAM, Reactions of acetylenes with transition metals. III. Structure of the complex obtained from t-butyl-acetylene and bis-benzonitrile-palladium chloride . . . 539–545

CH. P. IVANOV and D. M. MONDESHKA, Preparation, spectral properties and electron structure of 4H-cyclopenta(b) thiophene-4-one derivatives . . . 547–560

Rev. Roumaine Chim. **20**, *4*, p. 447–588 (1975), Bucarest

I. PETRARIU, DEMETRA DRĂGAN, PAMFILIA PETRARIU et FL. POPESCU, Contribution à la synthèse des échangeurs d'ions faibles et fortement basiques, de type gel en partant des amino-alcools . . . . 561–573 R

C. N. CAŞCAVAL and I. A. SCHNEIDER, Characterization of copolymers by pyrolysis-chromatography. I. Copolymers of acrylonitrile with vinyl acetate and α-methylstyrene . . . . 575–579 R

MIHAELA HILLEBRAND, M. RĂILEANU and V. E. SAHINI, Radical-ions. III. Halogen-phenothiazone radical-ions 581–585

COMPTE RENDU 587

Revue Roumaine de Chimie, **20**, *4*, 449–458 (1975)

ELECTRICAL CONDUCTIVITY OF CERTAIN CHARGE-UNSYMMETRICAL FUSED CHLORIDE SYSTEMS

KCl–CaCl$_2$, KCl–SrCl$_2$, KCl–BaCl$_2$

ŞTEFANIA ZUCA and M. OLTEANU

Institute of Physical Chemistry, str. Galaţi 31, Bucharest, Romania

Received April 13, 1974

The specific electrical conductivities and densities in fused KCl–CaCl$_2$, KCl–SrCl$_2$ and KCl–BaCl$_2$ systems have been investigated as a function of composition and temperature. The obtained molar volume and molar electrical conductivity isotherms were explained in terms of the ionic interactions on mixing, and quantitative relationships between $\Delta\lambda$ and ionic parameters (size and polarizability) have been established.

Our previous results [1,2] on charge – symmetrical fused halide systems have proved the usefulness of a systematic investigation of electrical conductivity as a function of ionic parameters. The electrical conductivity deviations from additivity could be expressed in terms of the interionic distances and polarizability.

In order to establish the influence of ionic charge on electrical conductivity, several charge-asymmetrical fused chloride systems have also been investigated. We report here the results obtained in KCl–MCl$_2$ fused systems (M = Ca, Sr, Ba).

EXPERIMENTAL RESULTS

Both density, d, and specific conductivity, k, of pure salts and their mixtures were measured over a temperature range of about 200°. For each system the whole concentration range from pure KCl to pure alkaline earth chloride was covered. The experimental set up for the density and conductivity measurements was similar to the one previously employed[1].

All salts were *p. a.* reagent grade, twice recrystallized from water, dried for 24 hrs at 150° and melted by a technique previously described[3], in order to remove any trace of water. They were tested for neutrality with phenolphtalein both before and after each run and were consistently neutral.

---

[1] S. Zuca and M. Olteanu, *Rev. Roumaine Chim.*, 15, 307, 1508 (1970).

[2] S. Zuca and M. Olteanu, *Rev. Roumaine Chim.*, in press.

[3] S. Zuca and R. Costin, *Rev. Roumaine Chim.*, 15, 1831 (1970).

Considerable care was taken to keep the samples anhydrous. Their handling took place in a dry box. After weighing and transferring the sample into the U silica conductivity cell, or into the density crucible, it was remelted in vacuum by slowly increasing the temperature of the furnace. During the experiment a dry argon atmosphere was secured.

For each studied system the density data were fitted by the following linear equation:

$$d = a - bt \tag{1}$$

A summary of the constants *a* and *b* as determined by the least squares method is given in table 1 together with the density standard deviations and experimental temperature ranges over which the data were obtained.

Table 1

Values of *a* and *b* constants in density equation (1)

System	X_{KCl}	a	$b \times 10^3$	Standard deviations	Temperature range, °C
$CaCl_2-KCl$	0	2.3790	0.4088	±0.0021	785–1010
	0.25	2.1911	0.3868	±0.0023	790–1015
	0.31	2.2032	0.4322	±0.0011	790– 970
	0.50	2.1597	0.4940	±0.0010	780– 975
	0.75	2.0562	0.5307	±0.0008	780– 980
$SrCl_2-KCl$	0	3.1880	0.5657	±0.0003	880–1035
	0.30	2.7891	0.5698	±0.0006	790–1025
	0.50	2.5812	0.5792	±0.0020	790–1005
	0.60	2.4661	0.5935	±0.0025	795– 990
	0.75	2.3397	0.6308	±0.0014	795–1025
$BaCl_2-KCl$	0	3.7784	0.6558	±0.0010	980–1060
	0.30	3.3782	0.7590	±0.0012	890–1025
	0.50	3.0403	0.7008	±0.0024	815– 980
	0.65	2.7561	0.6789	±0.0015	890–1010
	0.77	2.5091	0.6568	±0.0014	800– 990
	0.81	2.4314	0.6384	±0.0003	780– 785

Figure 1 shows the specific conductivities of the pure alkaline earth chlorides together with the more recent literature data.

As seen in fig. 1 there is a poor agreement between our data and those reported by Janz et al.[4] in the National Bureau of Standards Circular. The deviations are of – 2.5 to – 5.2% for $CaCl_2$, – 5% for $SrCl_2$ and –2% for $BaCl_2$. However, the agreement is very good (less than 0.5%) with the latest data, (i.e. Emons et al.[5] for $CaCl_2$, $SrCl_2$ and $BaCl_2$ and

---

[4] G. J. JANZ, F. W. DAMPIER, G. R. LANKSHMINARAYANAN, P. K. LORENZ and R.P. T. TOMKINS, "Molten Salts", vol. 1, NSRBS -NBS Wash., 1968.

[5] H. H. EMONS, G. BRÄUTIGAM and H. VOGT, *Z. anorg. Chem.*, **394**, 263 (1972).

Grjotheim et al.[6] for $CaCl_2$), except for the values indicated by Smirnov and Khokhlov [7] for $BaCl_2$, which are higher by about 1.3% than ours. The present results for fused KCl are in very good agreement with our earlier data.[8]

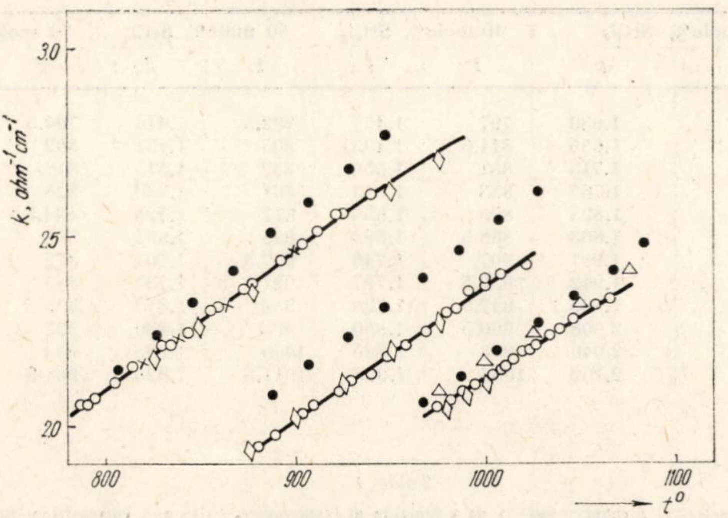

Fig. 1. — Specific conductivity k, vs. temperature in molten $CaCl_2$, $SrCl_2$ and $BaCl_2$: ○ present results, ● ref. 4 ; ◇ ref. 5 ; × ref. 6 ; △ ref. 7.

The specific conductivity for KCl – (Ca, Sr, Ba) Cl_2 mixtures as a function of temperature and composition are given in tables 2–4.

Table 2

Specific conductivity, *k* (ohm⁻¹ cm⁻¹) as a function of temperature *t*(°C) and composition for $CaCl_2$ – KCl system

25 mole % $CaCl_2$		50 mole % $CaCl_2$		69 mole % $CaCl_2$		71 mole % $CaCl_2$	
t	*k*	*t*	*k*	*t*	*k*	*t*	*k*
775	1.552	773.5	1.313	782	1.473	778	1.523
792.5	1.613	798	1.380	789	1.495	795	1.576
807.5	1.662	817.5	1.435	802	1.541	807.5	1.616
827.5	1.708	839	1.497	810	1.566	820	1.645
841	1.746	854	1.539	820	1.598	833	1.692
854	1.782	877.5	1.605	832	1.638	856.5	1.762
871	1.828	891.5	1.652	851.5	1.694	888	1.841
881.5	1.855	901	1.673	864.5	1.734	902	1.888
894.5	1.890	914.5	1.704	879.5	1.779	921	1.940
906.5	1.922	930	1.755	902	1.845	937	1.984
916	1.947	941	1.786	916.5	1.884	952	2.013
925	1.974	958	1.845	930	1.924	967.5	2.051

---

[6] K. Grjotheim, R. Nicolic and H. A. Øye, *Acta Chem. Scand.*, **24**, 489 (1970).

[7] M. V. Smirnov and V. A. Khokhlov, *Akad. Nauk SSSR, Uralskii Filial Trudi Inst. Elektrokhim*, **12**, 29 (1969).

[8] S. Zuca and L. Ionescu-Vasu, *Rev. Roumaine Chim.*, **12**, 1285 (1967).

Table 3

Specific conductivity, k(ohm^{-1} cm^{-1}) as a function of temperature t(°C) and composition for $SrCl_2$ – KCl system

25 mole% $SrCl_2$		40 mole% $SrCl_2$		50 mole% $SrCl_2$		70 mole% $SrCl_2$	
t	k	t	k	t	k	t	k
796	1.630	797	1.457	792.5	1.416	794.5	1.450
815	1.655	811.5	1.493	805	1.431	802	1.468
840	1.713	831	1.550	839	1.515	819	1.510
858	1.767	853	1.613	861	1.580	828	1.548
884	1.823	873	1.655	877	1.623	844.5	1.600
898	1.863	888.5	1.693	895	1.681	858	1.632
917.5	1.901	907	1.740	907.5	1.704	875	1.670
932	1.942	932.5	1.797	921.5	1.737	885	1.706
945.5	1.965	947.5	1.828	955	1.815	896.5	1.738
965	2.008	960.5	1.850	971	1.830	912	1.774
982	2.046	976	1.885	1000	1.895	944	1.853
1006	2.102	1005	1.955	1011.5	1.926	964.5	1.905

Table 4

Specific conductivity, k (ohm^{-1} cm^{-1}) as a function of temperature, t (°C) and composition for $BaCl_2$–KCl system

19 mole% $BaCl_2$		23 mole% $BaCl_2$		35 mole% $BaCl_2$		50 mole% $BaCl_2$		70 mole% $BaCl_2$	
t	k	t	k	t	k	t	k	t	k
790	1.772	803	1.744	803.5	1.587	827.5	1.545	790	1.772
815	1.842	824.5	1.801	821	1.633	851	1.607	815	1.842
839	1.904	849.5	1.868	839	1.680	864	1.644	839	1.904
858	1.948	878	1.928	855.5	1.722	874.5	1.674	852	1.937
869	1.976	892	1.957	880.5	1.784	885	1.703	869	1.976
883	2.008	905	1.988	894	1.817	908	1.765	874	1.989
895	2.032	921	2.022	902.5	1.839	918	1.788	895	2.032
917	2.084	938	2.055	912	1.874	944.5	1.845	917	2.084
936.5	2.122	948	2.080	943	1.927	958.5	1.981	936.5	2.122
962	2.173	965	2.113	961.5	1.970	975	1.918	962	2.173
977	2.205	979	2.134	982	2.021	992.5	1.957	977	2.205
1000.5	2.245	987	2.159	999.5	2.067	1005	1.990	1000.5	2.245

As for pure salts, there is a very good agreement with recent data[9] for the systems studied.

The data in tables 1 – 4 were used for the subsequent calculations of molar volume V_m and molar conductivity λ.

The values obtained for λ were fitted to the Arrhenius equation, $\lambda = Ae^{-E_\lambda/RT}$, by means of a least squares calculation. The pre-exponential factor A and the activation energy of electrical conductivity E_λ are summarized in table 5.

---

[9] H. Vogt, Thesis, Mersseburg, 1971.

Table 5

Pre-exponential factor A, and activation energy $E\lambda$, for $KCl-MCl_2$ mixtures

System	X_{KCl}	$A \times 10^{-2}$	$E\lambda$ kcal/mol	Standard deviations for $E\lambda$	Temperature range, °C
$CaCl_2-KCl$	0	9.97	4.63	0.014	785– 940
	0.25	8.31	4.84	0.034	775– 970
	0.31	8.96	5.12	0.051	780– 930
	0.50	9.18	5.40	0.013	770– 960
	0.75	7.75	4.75	0.021	775– 975
$SrCl_2-KCl$	0	12.31	5.45	0.041	880–1025
	0.30	9.77	5.12	0.041	790– 970
	0.50	7.24	4.74	0.077	790–1015
	0.60	6.89	4.60	0.010	795–1005
	0.75	6.08	4.19	0.021	795–1010
$BaCl_2-KCl$	0	12.21	5.44	0.033	975–1065
	0.30	9.48	5.19	0.039	885–1020
	0.50	8.00	4.80	0.018	825–1005
	0.65	6.98	4.44	0.028	800–1000
	0.77	6.09	4.02	0.016	800– 990
	0.81	6.01	3.96	0.014	790–1005

DISCUSSION

According to the phase-diagram information [10–12] in solid state, some chemical compounds are formed in the KCl — (Ca, Sr, Ba) Cl_2 systems. The presence of $(CaCl_4)^{2-}$, $(SrCl_3)^-$ and $(BaCl_3)^-$ complex ions in the corresponding melts was established by Hagiwara et al. [13] A preferred coordination of the chloride ions around the calcium ion with the formation of $(CaCl_3)^-$ groups in the $CaCl_2$ — AlKCl systems is also advanced by Roewer and Emons. [14]

Vogt [9] explained the electrical conductivity behaviour in some fused alkaline earth chlorides with alkali chlorides in terms of the "complexing" occurring in those melts on mixing. The same was suggested by the thermodynamic study carried out by Φstvold. [15]

Therefore we expect the results in presently investigated systems to point out these facts as well. Fig. 2 shows the results on molar volumes plotted against composition.

As seen in the figure the common feature of these plots is their appreciable departure from linearity. As a rule, for each system the calculated excess volumes are going beyond $+2\%$.

---

[10] H. J. Seifert and U. Langgenbach, *Z. anorg. Chem.*, **368**, 36 (1969).

[11] F. A. Bukhalova and V. M. Burlakova, *Zhur. neorg. Khim.*, **11**, 164 (1966).

[12] C. Krohn, *Acta Chem. Scand.*, **20**, 255 (1966).

[13] H. Hagiwara, R. Oyomoda and S. Fukushima, *J. Electrochem. Soc. Japan*, **36**, 35 (1968).

[14] G. Roewer and H.H. Emons, *Z. anorg. Chem.*, **370**, 128 (1969).

[15] T. Φstvold, *J. Phys. Chem.*, **76**, 1629 (1972).

As for molar conductivity vs. composition curves, figs. 3–5, they are marked by very pronounced minima within the equimolecular concentration range.

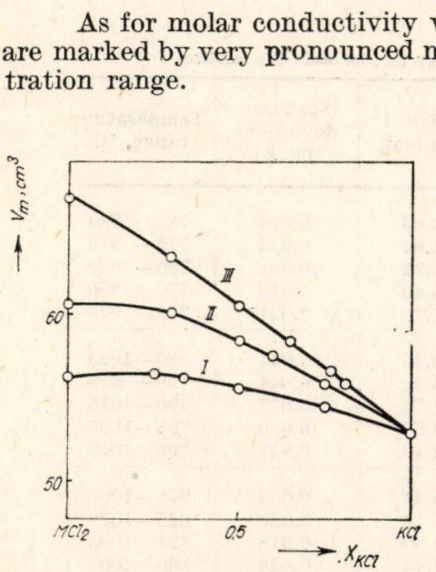

Fig. 2. — The molar volume isotherms at 1000° in KCl–(Ca, Sr, Ba) Cl_2 systems: I KCl–$CaCl_2$, II KCl–$SrCl_2$, III KCl–$BaCl_2$.

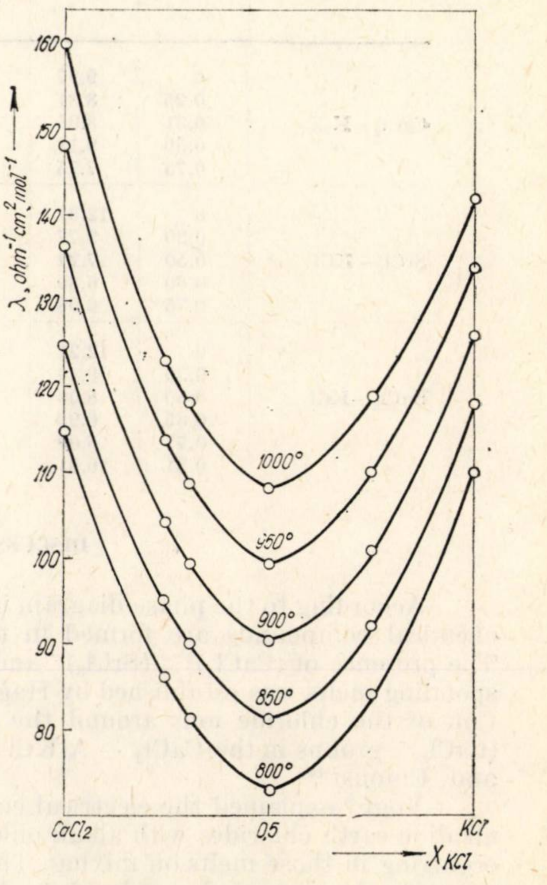

Fig. 3. — The molar electrical conductivity isotherms in fused KCl–$CaCl_2$ mixtures.

Both above-mentioned behaviours can be explained by the formation of the co-ordinated ionic groups which will cause a weakening of ionic packing and will reduce the number of effective current carriers. The significant changes in the cation-anion bonding energy on mixing are equally well proved by the large positive excess activation energy which characterizes each investigated system (fig. 6).

If we consider now the deviation of electrical conductivity from additivity, some of the regularities previously established for binary alkali halide systems [1,2] are again found in KCl – (Ca, Sr, Ba)Cl_2 mixtures:

— the excess conductivity, Δλ, in the series is higher, the larger the difference in size between the two cations in the mixture. Fig. 7 illustrates the results for 1000°.

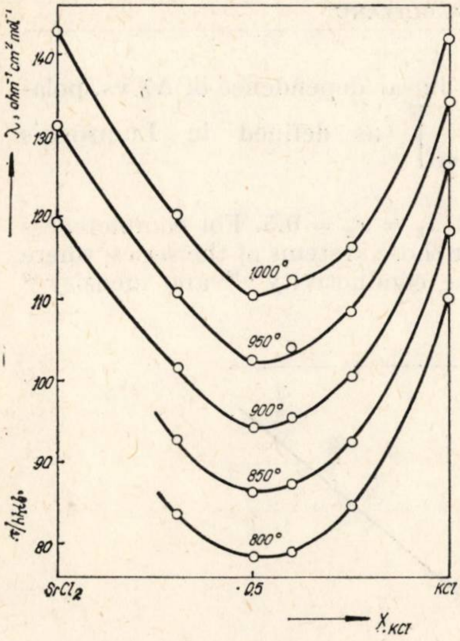

Fig. 4. — The molar electrical conductivity isotherms in fused KCl$-$SrCl$_2$ mixtures.

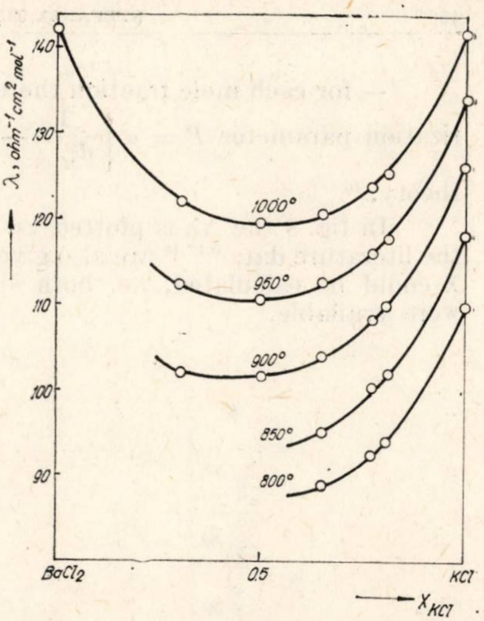

Fig. 5. — The molar electrical conductivity isotherms in fused KCl$-$BaCl$_2$ mixtures.

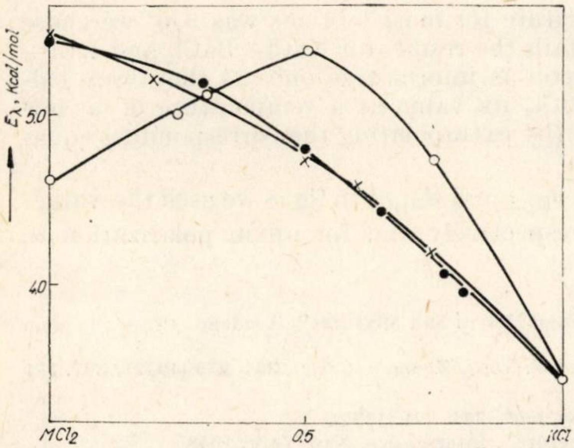

Fig. 6. — E$_\lambda$ vs. composition in fused KCl$-$(Ca, Sr, Ba)Cl$_2$ systems : ○ KCl$-$CaCl$_2$, × KCl$-$SrCl$_2$, ● KCl$-$BaCl$_2$.

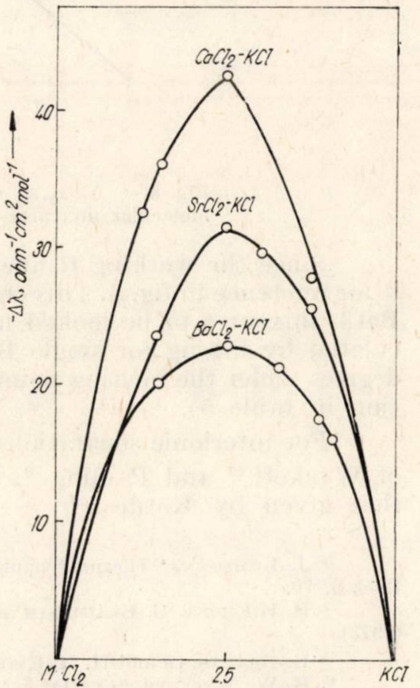

Fig. 7. — Δλ vs. composition in fused KCl$-$(Ca, Sr, Ba) Cl$_2$ systems.

— for each mole fraction there is a linear dependence of $\Delta\lambda$ vs. polarization parameter $P = \alpha \left[\frac{1}{d^2_{M_I\text{Cl}}} - \frac{2}{d^2_{M_{II}\text{Cl}}} \right]^2$ as defined in Lumsden's theory.[16]

In fig. 8 the $\Delta\lambda$ is plotted vs. P at $x_1 = x_2 = 0.5$. For completeness the literature data [5,17,18] are also given for those systems of the series where λ could be calculated, i.e. both specific conductivity [5,16] and density [17] were available.

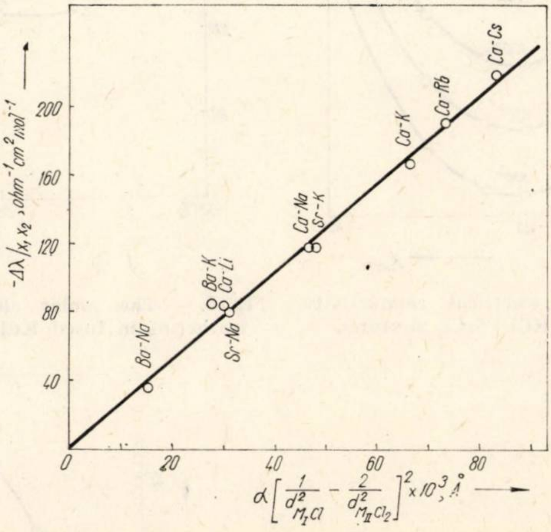

Fig. 8. — $\Delta\lambda/x_1, x_2$ vs. polarization parameter in equimolecular mixtures of alkali-alkaline earth chlorides.

Since the working temperature for most systems was 950° we chose it for reference in fig. 8. This entails the results for $NaCl-BaCl_2$ and $KCl-BaCl_2$ mixtures to be looked upon as informative only as they were calculated by taking for single $BaCl_2$ its value at a temperature of a few degrees under the melting point (by extrapolating the corresponding equation in table 5).

For interionic separations $d_{M_I\text{Cl}}$ and $d_{M_{II}\text{Cl}_2}$ in fig. 8 we used the values of Wyckoff[19] and Pauling[20], respectively and for anion polarization α, that given by Kordes.[21]

---

[16] J. Lumsden, "Thermodynamics of Molten Salt Mixtures", Academic Press, London 1966, p. 70.

[17] H. H. Emons, G. Bräutigam and H. Vogt, *Z. anorg. Chem.*, **394**, 279 (1972); 397, 131 (1973).

[18] G. Bräutigam and H. H. Emons, *ibid.*, **394**, 271 (1972).

[19] R. W. Wyckoff, "Crystal Structure", Interscience, New York, 1948.

[20] L. Pauling, "The Nature of the Chemical Bond", Cornell University Press, New York 1963, p. 505.

[21] E. Kordes, *Z. Electrochem.*, **59**, 551 (1955).

Three important features with this plot should be noted : 1) Δλ is increasing as the difference in the polarizing strength of ions (Z/r^2) is larger ; 2) Δλ's are equal with each other within experimental error, for the mixtures with similar energy of polarization regardless of the uncommon cations involved in the mixture, 3) Δλ is zero when the substituting cations have a similar polarizing strength, and the system is expected to behave ideally. All these facts can be satisfactorily explained by Lumsden's anion polarization model.[1,2]

A different correlation with distance parameter was proposed by Davis. [22,23] He developed a theory of mixing for charge-unsymmetrical molten salts based on the conformal solution theory of Reiss, Katz and Kleppa. [24] The results of this theory were quite useful in comparing the enthalpies of mixing for alkali-alkaline earth halide systems.[15] In the latest version [23] developed for constant temperature and pressure (the usual way the experiments are conducted) the thermodynamic quantities of mixing are shown to be a linear function of the difference between interionic separation of the two salts, $d_1 - d_2$ as long as one salt is kept as a common salt. Comparison among series where the common component or the anions are different is difficult since the pair correlation functions and their implicit dependence on ionic polarization are not available for molten salts and their mixtures.

An attempt is made, as seen in fig. 9, to extend the Davis plot for the excess conductivity data.

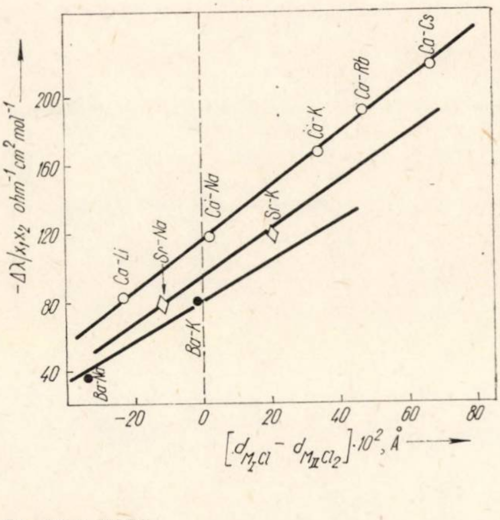

Fig. 9. — $\Delta\lambda/x_1, x_2$ vs. distance parameter in equimolecular mixtures of alkali-alkaline earth chlorides.

---

[22] H.T. Davis, *J. Chem. Phys.*, **41**, 2761 (1964).

[23] H.T. Davis, *J. Phys. Chem.*, **76**, 1629 (1972).

[24] H. Reiss, J. L. Katz and O. J. Kleppa, *J. Chem. Phys.*, **36**, 144 (1962).

As it is evident from figure, $\Delta\lambda$ is a linear function of $(d_{M_I Cl} - d_{M_{II} Cl_2})$ for each series with a common salt. Unfortunately, except for $CaCl_2$ — AlkCl series, there are too few experimental data for the other systems, so that we shall not try to advance any detailed analysis. We only note the trend of the Davis plot slopes to increase in the sequence Ca > Sr > Ba. A similar development was observed for the enthalpies of mixing and was extensively discussed by Østvold[15] in terms of ionic interaction changes.

If we compare now the results in fig. 8 with those in fig. 9, it is obvious that Lumsden's treatment is more comprehensive and that the common anion polarization is sufficient to account quantitatively for the change in electrical conductivity on mixing.

Revue Roumaine de Chimie, **20**, *4*, 459 – 464 (1975)

INTERACTION OF IONS IN MOLTEN BINARY $LiF-AlF_3$ MIXTURES

V. DANĚK and K. MATIAŠOVSKÝ

Institute of Inorganic Chemistry of the Slovak Academy of Sciences, 809 34
Bratislava, Czechoslovakia

Received February 18, 1974

On the basis of the experimentally determined values of the specific electrical conductivity and of the density of molten binary $LiF - AlF_3$ mixtures, the equivalent conductivities of the individual ions and the degree of interaction of the Li^+ and F^- ions in the above system at 1000 °C were calculated. The determined values were used in the calculation of the transport numbers of Li^+ and F^- ions in molten LiF and Li_3AlF_6. The results are discussed with respect to the recent hypotheses on the ionic composition of molten salts.

INTRODUCTION

From a comparison of the values of the equivalent conductivity of various molten salts determined on the basis of the experimental values of the specific conductivity with those calculated from the diffusion data by means of the Nernst — Einstein relation it may be seen that in all cases the calculated values are higher than the experimental ones.[1] This discrepancy was explained by the authors of the above paper by different mechanisms of the transport of the structural particles of the melt in the diffusion and in the charge transfer, this being coherent with the ionic composition of the melt. The values of the equivalent conductivities of molten NaCl and $NaNO_3$ calculated from the diffusion data using the Nernst — Einstein relation agree with the experimental data only under the presumption that a part of the mass transfer in the diffusion could be attributed to the neutral particles. According to this concept, e.g. in molten NaCl beside the simple individual ions Na^+ and Cl^-, there are also associates present which statistically correspond to the $Na^+ Cl^-$ ionic pairs. In the diffusion it makes no difference whether there are free or associated particles, since in the determination of diffusion coefficients all particles take part in the transport, whilst in the charge transfer evidently only free ions participate and the associated ions (ionic pairs) diffuse independently on the gradient of the external electric field via the complex cation-anionic vacancies and do not take part in the transport of the current. This hypothesis is consistent with the results presented by Seitz [2] and Dienes[3] who found that the activation energy of the dual diffusion was smaller than the activation energy of the individual ionic diffusion stipulated by simple vacancies, as it would agree with the mechanism of the electrical conductance. Borucka et al. [1] assume the formation of associated particles to be a common phenomenon in molten salts.

---

[1] A. Z. Borucka, J. O' M. Bockris and J. A. Kitchener, *Proc. Roy. Soc. London*, **241**, 554 (1957).

Generally, the hypothesis of association of ions in molten salts makes it possible to explain some apparent discrepancies, e.g. the irregularity in the equivalent conductivities in the series of alkali halides, or the differences between the experimentally determined values of the equivalent conductivity and the values calculated from the diffusivity data. It should be stressed that these discrepancies can not result from the experimental errors in the course of the measurement of the electrical conductivity and density, or of the diffusion coefficients of the respective molten mixtures and of their components.

On the basis of this hypothesis, Frank and Foster [4] proposed a method for the calculation of the degree of interaction of the Na^+ and F^- ions in the molten $NaF-AlF_3$ mixtures. In this calculation, the experimental values of the specific electrical conductivity and density of the above mixtures were used and the component AlF_3 is considered only with respect to the activity of NaF and to the concentration of conducting particles. In the $NaF-AlF_3$ mixtures sodium cryolite, Na_3AlF_6, is formed which partially dissociates according to the molecular scheme

$$Na_3AlF_6 \rightleftarrows 2NaF + NaAlF_4 \qquad (1)$$

The calculation was carried out under the following simplifying assumptions :

— the activities of the components are identical with the concentrations,

— the ratio of the equivalent conductivities of the individual ions is inversely proportional to the ratio of the respective ionic radii,

— the equivalent conductivities of the sodium and fluoride ions do not depend on the concentration of the remaining components of the electrolyte.

In this calculation, evidently, the contribution of the voluminous AlF_6^{3-} and AlF_4^- complex ions to the conductivity is neglected. Hence it follows that there will be a certain error in the calculated values which, however, can not affect the results essentially.

In this work, the results of the calculation of the degree of interaction of the Li^+ and F^- ions in the molten $LiF-AlF_3$ mixtures in the concentration area corresponding to the subsystem $LiF-LiAlF_4$ by the method proposed by Frank and Foster [4] are presented.

---

[2] F. SEITZ, *Rev. Mod. Phys.*, **18**, 384 (1946).

[3] G. J. DIENES, *J. Chem. Phys.*, *16*, 620 (1948).

[4] W. B. FRANK and L. M. FOSTER, *J. Phys. Chem.*, **64**, 310 (1960).

PROCEDURE AND DISCUSSION OF RESULTS

Considering the analogy between Li_3AlF_6 and Na_3AlF_6, in the calculation of the degree of interaction of the Li^+ and F^- ions in the molten $LiF-AlF_3$ mixtures, it has been assumed that lithium cryolite entirely dissociates according to the scheme

$$Li_3AlF_6 \rightleftharpoons 3Li^+ + AlF_6^{3-} \qquad (2)$$

and the newly formed AlF_6^{3-} complex anions partially dissociate :

$$AlF_6^{3-} \rightleftharpoons AlF_4^- + 2F^- \qquad (3)$$

Briefly, equations (2) and (3) are identical with the dissociation scheme (1). In agreement with the above concept on the interaction of ions, in the melt there are the complex ions AlF_6^{3-} and AlF_4^- and the simple Li^+ and F^- ions which are partially associated in the Li^+F^- ionic pairs. The degree of interaction k, which characterizes the process of association, is defined as the ratio of the associated and of the free fluoride ions both in pure LiF and in the molten $LiF-AlF_3$ mixtures where the dissociation described by schemes (2) and (3) takes place simultaneously. In the melts of the subsystem $LiF-LiAlF_4$ there is an excess of lithium ions with respect to the stoichiometric composition corresponding to LiF and the superfluous Li^+ ions evidently affect the value of the degree of interaction k.

In the calculation, the values of the specific conductivity of molten $LiF-AlF_3$ mixtures determined in our previous work [5] were used, whilst for the density of the respective mixtures and for the corresponding equilibrium concentrations of Li_3AlF_6, $LiAlF_4$ and LiF the values determined by Paučírová[6] and for the ionic radii the data presented by Waddington[7] were accepted.

The determined value of the degree of interaction of the Li^+ and F^- ions in pure LiF at 1000°C is $k_0 = 0.2$ and the corresponding values of ionic equivalent conductivities are $\lambda_{Li^+} = 111$ ohm^{-1}. cm^2 and $\lambda_{F^-} = 63$ ohm^{-1}. cm^2 (table 1).

Table 1

The degree of interaction and the equivalent conductivity of the Li^+ and F^- ions in the molten $LiF-AlF_3$ mixtures at 1000°C

Composition/mol. % AlF_3/	k_0	λ_{Li^+}	λ_{F^-}	k
5	0.21	113	62	0.22
10	0.21	113	61	0.23
15	0.20	111	62	0.24
20	0.20	110	62	0.25
25	0.20	110	64	0.26
30	0.20	110	62	0.26
35	0.20	109	63	0.25
40	0.20	109	66	0.24
Mean value	0.20	111	63	

Considering the ionic composition of the molten $LiF-AlF_3$ mixtures it can be assumed that, owing to the relative increase in the concentration of Li^+ ions in the concentration area corresponding to the subsystem $LiF-Li_3AlF_6$,with increasing concentration of AlF_3, the equilibrium of the reaction

---

[5] K. MATIAŠOVKÝ, M. MALINOVSKÝ and V. DANĚK, *Electrochim. Acta*, **15**, 25 (1970).

[6] M. PAUČÍROVÁ, CSc. Thesis, Institute of Inorganic Chemistry, Slovak Academy of Sciences, Bratislava 1969.

[7] T. C. WADDINGTON, *Trans. Faraday Soc.*, **62**, 1482 (1966).

$$Li^+ + F^- \rightleftarrows Li^+F^- \tag{4}$$

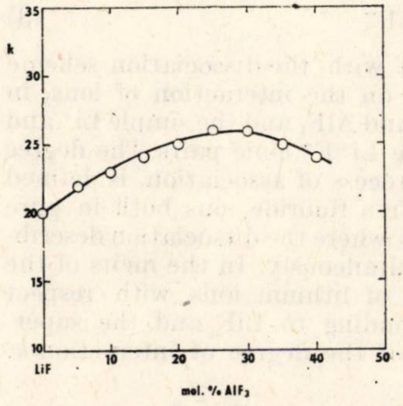

Fig. 1.—The degree of interaction *k* *vs* the composition in molten $LiF-AlF_3$ mixtures.

will be shifted in the direction of the formation of the associated particles. This assumption was confirmed also by calculation. In fig. 1, the dependence of the degree of interaction of Li^+ and F^- ions on the composition of the binary system $LiF-AlF_3$ at 1000°C is presented. The determined value of the degree of interaction of Li^+ and F^- ions in molten lithium cryolite, Li_3AlF_6, is $k=0.26$ at this temperature. On the basis of the determined values of the degree of interaction and of the equivalent conductivities of the lithium and fluoride ions, the equivalent conductivity of lithium cryolite can be calculated by means of the equation

$$\lambda = \left(1 - \frac{2}{3}\,\alpha_k \cdot k\right) \cdot \lambda_+ + \frac{2}{3}\alpha_k(1-k)\cdot\lambda_- \tag{5}$$

where the term $\left(1 - \frac{2}{3}\,\alpha_k \cdot k\right)$ represents the share of the free lithium ions and the term $\frac{2}{3}\,\alpha_k(1-k)$ the share of free fluoride ions which take part in the charge transfer. The value of the equivalent conductivity of lithium cryolite, $\lambda = 114\ \text{ohm}^{-1}.\ \text{cm}^2$, calculated on the basis of the determined degree of interaction of the Li^+ and F^- ions in lithium cryolite and of the degree of dissociation of the AlF_6^{3-} complex anion $\alpha_k = 0.3$ presented by Paučírová, [6] is practically identical with the value $\lambda = 114.4\ \text{ohm}^{-1}\cdot\text{cm}^2$ calculated from the experimental specific conductivity and density data.

On the basis of the values of the equivalent conductivity of the individual ions, the transport numbers of the respective ions in molten LiF can be calculated using the relations

$$t_+ = \frac{\lambda_+}{\lambda_+ + \lambda_-} \quad \text{(6a)}; \quad t_- = \frac{\lambda_-}{\lambda_+ + \lambda_-} \tag{6b}$$

For molten lithium fluoride at 1000°C the following values were determined : $t_{Li^+} + = 0.64$ and $t_{F^-} = 0.36$.

The calculation of the transport numbers t_{Li^+} and t_{F^-} in molten lithium cryolite was based upon the following assumption : if we attribute to the lithium ion an arbitrary conductance then the conductance of the fluoride ion will be by λ_-/λ_+ — times smaller. According to equation (5), the share of the lithium ions which take part in the charge transfer equals $\left(1 - \frac{2}{3}\right.$ $\left.\alpha_k \cdot k\right)$ and the corresponding share of the fluoride ions is given by the term $\frac{2}{3}\,\alpha_k(1 - k)$. Hence, the contribution of the F^- ions to the charge transfer will be given by the expression $\frac{2}{3}\,\alpha_k(1 - k)\,\frac{\lambda_-}{\lambda_+}$. Then, the transport number of the cation can be calculated by means of equation

$$t_+ = \frac{1 - \frac{2}{3}\,\alpha_k \cdot \mathrm{k}}{1 - \frac{2}{3}\,\alpha_k \cdot k + \frac{2}{3}\,\alpha_k(1 - k)\frac{\lambda_-}{\lambda_+}}. \qquad (7)$$

In this way, the values of the transport numbers of Li^+ and F^- ions in molten lithium cryolite at 1000°C, $t_{Li^+} = 0.92$ and $t_{F^-} = 0.08$, were determined. Here, also, the contribution of the large complex anions AlF_6^{3-} and AlF_4^- to the charge transfer was considered to be negligible.

The equivalent conductivity of a molten electrolyte of the type MX is proportional to the sum of the equivalent conductivities of individual ions. Considering the definition of the degree of interaction, the relation is valid :

$$\lambda = /1 - k_0//\lambda_+ + \lambda_-/ \qquad (8)$$

where k_0 is the degree of interaction of the M^+ and X^- ions. Introducing the corresponding values of the ionic equivalent conductivities and of the degree of interaction into equation (8), the value of the equivalent conductivity of lithium fluoride, $\lambda_{LiF} = 139$ ohm^{-1}. cm^2, is obtained, this being in a good agreement with the value 137.5 ohm^{-1}. cm^2 calculated on the basis of the experimentally determined specific conductivity and density data.

The determined values of the degree of interaction and of the ionic equivalent conductivities in molten LiF are consistent with the corresponding values determined by Frank and Foster[4] for molten NaF at 1000°C : $k_0 = 0.32$, $\lambda_{Na^+} = 96.4$ ohm^{-1}.cm^2 and $\lambda_{F^-} = 67.5$ ohm^{-1}. cm^2. (It should be mentioned that in the cited paper the interaction of Na^+ and F^- ions in molten NaF and in the NaF$-$AlF$_3$ mixtures was characterized formally by means of the degree of ionization and the $Na^+ F^-$ ionic pairs were considered to be unionized particles.) From a comparison of the determined values it follows that the degree of interaction of ions in molten LiF is smaller than that in molten NaF, though, with regard to the ionic radii and the polarizing ability of the respective cations, just the opposite should be expected. This apparent disagreement is most probably due to the relative overheating of the melt. The comparative temperature (1000°C) is only by few degrees higher than the M.P. of NaF (995°C) whilst at the same temperature LiF is strongly overheated (by appr. 150°C), which counteracts the interaction of the Li^+ and F^- ions.

On the other hand, the value of the equivalent conductivity of the sodium cation determined by Frank and Foster,[4] $\lambda_{Na^+} = 96.4\ ohm^{-1}.\ cm^2$, seems to be too high with respect to the corresponding value for the lithium ion with regard to the values of the ionic radii of both cations. It can be assumed that this discrepancy results either from the fact that in the above work unlikely high values of the specific conductivity of the $NaF - AlF_3$ mixtures were used in the calculation, or that incorrect value of the ionic radii of Na^+ ion proposed by Pauling was used, this being by appr. 6% smaller than the value determined by Waddington.[7]

It is evident that with respect to the restricted number of the reliable experimental data and to the unadequate theoretic analysis of these data, the proposed proceeding represents an approximation to the solution of the problem under investigation. Nevertheless, the determined values give some information on the ionic composition of the melt and on the basis of this some apparent discrepancies between the values determined by the various experimental methods may be accounted for.

Revue Roumaine de Chimie, **20**, *4*, 465–471 (1975)

THERMODYNAMIC PROPERTIES OF MOLTEN SALT BINARY MIXTURE $AgI + CdI_2$ AND RECIPROCAL MIXTURE $AgI + CdCl_2$

S. STERNBERG and LUCIA BEJAN

Institute of Physical Chemistry,
Str. Galaţi 31, Bucharest, Romania

Received February 1, 1974

E.m.f. measurements of formation cells with fused salt binary mixture $AgI+CdI_2$ and reciprocal mixture $AgI+CdCl_2$ were carried out. Thermodynamic functions of silver iodide (a_{AgI}, γ_{AgI}, μ^E_{AgI}, S^E_{AgI} and H^E_{AgI}) in the mixture were calculated.

INTRODUCTION

In previous papers[1-4] a thermodynamic study of reciprocal fused salt mixtures (Ag^+, M^+, I^-, X^-) where M = K, Rb, Cs and $X = Cl^-$, Br^- was presented.

The present work deals with the binary mixture $AgI + CdI_2$ and the reciprocal mixture $AgI + CdCl_2$, the study being based on e.m.f. measurements of formation cells :

$$Ag(s) \,\|\, AgI(l, x_1) + CdI_2(l, x_2) \,\|\, I_2(g, 1\ \text{atm.})\ \text{graphite}$$

and

$$Ag(s) \,\|\, AgI(l, x_1) + CdCl_2(l, x_2) \,\|\, I_2(g, 1\ \text{atm.})\ \text{graphite}$$

Iodine electrode cells were used for both systems.

Details on the cell and procedure of obtaining iodine reversible electrode were given elsewhere.[1,5,6] The e.m.f.' s of formation cells were measured within ± 1 mV with a digital voltmeter VN–4B type. To obtain a reproducible e.m.f. a previous processing of graphite electrode was necessary. Following 15–16 hours of bubbling with iodine a constant and reproducible value of e.m.f. was obtained. The electrodes were so prepared as to yield reproducible values within ± 1.5 mV 30–50 minutes after beginning the runs.

---

[1] S. Sternberg and L. Bejan, *Rev. Roumaine Chim.*, **14**, 303 (1969).
[2] S. Sternberg and L. Bejan, *J. Chem. Thermodynamics*, **2**, 341 (1970).
[3] S. Sternberg and L. Bejan, *Rev. Roumaine Chim.*, **16**, 175 (1971).
[4] S. Sternberg and L. Bejan, *Rev. Roumaine Chim.*, **18**, 11 (1973).
[5] S. Sternberg, I. Adorian and I. Galasiu, *J. Chim, phys.*, **62**, 63 (1965).
[6] S. Sternberg, I. Adorian and I. Galasiu, *Rev. Roumaine Chim.*, **11** 581 (1966).

Chemically pure grade reagents were used. AgI, CdI_2 and $CdCl_2$ were dried then melted and purified by bubbling with acids.

RESULTS AND DISCUSSION

The e.m.f. values for various compositions are given, versus temperature, in table 1 for AgI + CdI_2 and in table 2 for AgI + $CdCl_2$.

From e.m.f.'s, thermodynamic activities and excess partial molar thermodynamic functions of AgI in the two mixtures were calculated.

The following equation was used for activity of AgI :

$$\ln a_1 = -\frac{n\mathcal{F}}{RT}(E_1 - E_0) \tag{1}$$

where E_0 stands for the cell with single AgI and E_1 for that with mixture.

For the activity coefficient use has been made of equation :

$$\gamma_1 = \frac{a_1}{x_1} \tag{2}$$

where x_1 is the mole fraction of AgI and a_1, its activity in the mixture.

The molar chemical potential of AgI was calculated by equation :

$$\Delta\mu_1 = -\mathcal{F}(E_1 - E_0). \tag{3}$$

The partial molar entropy by :

$$\Delta S_1 = \mathcal{F}\left[\left(\frac{\partial E_1}{\partial T}\right)_P - \left(\frac{\partial E_0}{\partial T}\right)_P\right] \tag{4}$$

and partial molar heat of mixing by :

$$\Delta H_1 = \Delta\mu_1 + T\Delta S_1. \tag{5}$$

For the excess partial molar functions the following equations have been employed :

$$\mu_1^E = \Delta\mu_1 - \Delta\mu_1^{id} \tag{6}$$

$$S_1^E = \Delta S_1 - \Delta S_1^{id} \tag{7}$$

where

$$\left.\begin{aligned} \Delta\mu_1^{id} &= RT \ln x_1 \\ \Delta S_1^{id} &= -R \ln x_1 \end{aligned}\right. \tag{8}$$

the heat of mixing being given by equation :

$$H_1^E = \mu_1^E + TS_1^E. \tag{9}$$

a. BINARY MIXTURE AgI + CdI_2

The values of excess partial molar thermodynamic functions are listed in table 1 at 873 K.

Table 1

Experimental equations of e.m.f. variation with temperature. Thermodynamic functions of AgI in AgI + $CdCl_2$ mixture at 873 K. x_1 – mole fraction of AgI

x_1	$\frac{E}{V}$	$\Delta\mu_1$	ΔS_1	μ_1^E	S_1^E	H_1^E
		cal. mole^{-1}	cal.K^{-1}. mole^{-1}	cal. mole^{-1}	cal.K^{-1}. mole^{-1}	cal.mole^{-1}
1	$0.5510-0.272\times10^{-3}(T-873)$	—	—	—	—	—
0.8	$0.5572-0.262\times10^{-3}(T-873)$	−143	0.231	244	−0.212	+ 59
0.75	$0.5620-0.252\times10^{-3}(T-873)$	−254	0.461	245	−0.111	+148
0.66	$0.5654-0.225\times10^{-3}(T-873)$	−332	1.084	373	+0.276	+614
0.6	$0.5686-0.220\times10^{-3}(T-873)$	−406	1.199	480	+0.184	+641
0.5	$0.5816-0.223\times10^{-3}(T-873)$	−706	1.130	497	−0.248	+280
0.3	$0.6058-0.224\times10^{-3}(T-873)$	−1264	1.107	825	−1.286	−298

On figures 1 and 2 are plotted the activity of silver iodide and its activity coefficient versus mole fraction of $CdI_2(x_{CdI_2} = x_2)$ respectively. Both magnitudes give positive deviation from ideality.

The excess chemical potential of AgI versus x_2 is shown on figure 3 : μ_1^E is positive.

Figure 4 presents the excess entropy of AgI versus x_2; for $x_2 = 0.2 -$ $- 0.5$ the entropy shows small deviations from ideality while at $x_2 = 0.7$ higher and negative deviations are found out. It is also evident that a maximum is present at $x_2 = 0.33$, $S_1^E = 0.276$ cal.K^{-1}.mole^{-1}.

Finally figure 5 presents the excess partial molar enthalpy of AgI versus x_2. H_1^E is positive and has a maximum at $x_2 = 0.36 - 0.38$ which stems from the entropy effect.

b. THE RECIPROCAL MIXTURE AgI + $CdCl_2$

In the reciprocal fused salt mixtures (Ag^+, Cd^{2+}, I^-, Cl^-) the reciprocal reaction is present :

$$_2AgI(l) + CdCl_2(l) \rightleftarrows {}_2AgCl(l) + CdI_2(l).$$

The phase diagrams [7] of these mixtures indicate that AgI + $CdCl_2$ is the stable pair while AgCl + CdI_2 is the unstable pair of salts; our measurements were then carried out on the stable pair.

---

[7] H. K. Voskresenskaia, N.N. Evseeva, S.I. Berul and I. P. Vereschetina in "Spravochnik po plovkosti sistem izbezvodnykh neorganicheskikh solei", tome II, Izdatelstvo Akademii Nauk U.R.S.S., Moscow, Leningrad, 1961, p. 159, 176, 146, 141.

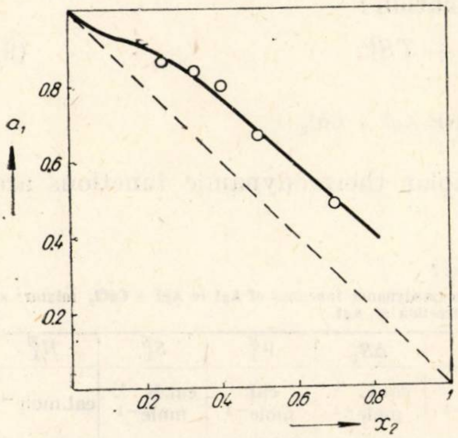

Fig. 1. — Thermodynamic activity of AgI in binary mixture AgI $+CdI_2$.

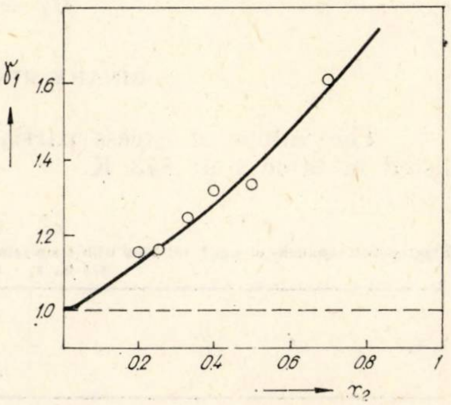

Fig. 2. — Activity coefficient of AgI in binary mixture AgI $+$ CdI_2.

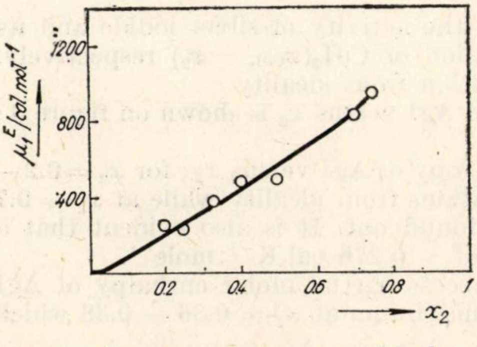

Fig. 3. — Experimental excess partial molar chemical potential for AgI in AgI $+$ CdI_2 mixture.

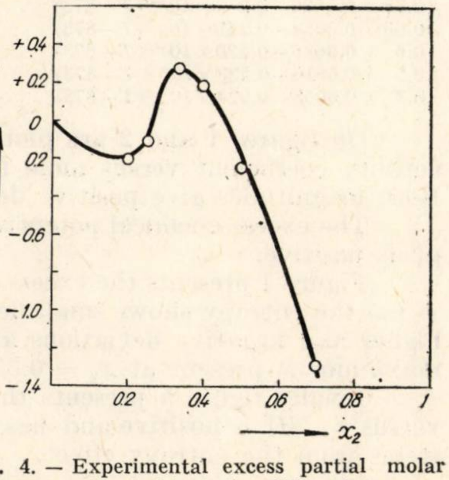

Fig. 4. — Experimental excess partial molar entropy for AgI in AgI $+$ CdI_2 mixture.

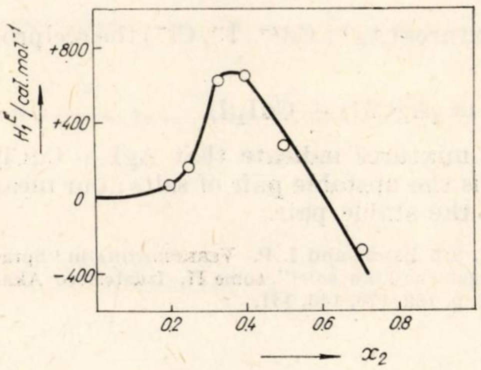

Fig. 5. — Experimental excess partial molar free enthalpy for AgI in AgI $+$ CdI_2 mixture.

The e.m.f.'s *versus* temperature as well as the partial molar and excess thermodynamic functions of AgI in the mixture at 873 K are given in table 2.

Table 2

Experimental equations of e.m.f. variation with temperature. Thermodynamic functions of AgI + $CdCl_2$ mixture at 873 K
x_1 – mole fraction of AgI

x_1	$\frac{E}{V}$	$\Delta\mu_1$ cal. mole^{-1}	ΔS_1 cal. K^{-1}. mole^{-1}	μ_1^E cal. mole^{-1}	S_1^E cal. K^{-1}. mole^{-1}	H_1^E cal. mole^{-1}
1	$0.5510 - 0.272 \times 10^{-3}(T-873)$	—	—	—	—	—
0.75	$0.5731 - 0.238 \times 10^{-3}(T-873)$	− 510	0.784	− 11	0.212	174
0.66	$0.5697 - 0.194 \times 10^{-3}(T-873)$	− 431	1.799	+ 274	0.991	1139
0.6	$0.5705 - 0.171 \times 10^{-3}(T-873)$	− 450	2.329	+ 436	1.314	1583
0.5	$0.5815 - 0.116 \times 10^{-3}(T-9873)$	− 703	3.598	+ 500	2.216	2435
0.4	$0.5815 - 0.077 \times 10^{-3}(T-873)$	− 703	4.497	+ 887	2.676	3223
0.3	$0.5904 - 0.133 \times 10^{-3}(T-873)$	− 909	3.206	+1180	0.813	1890
0.2	$0.6103 - 0.115 \times 10^{-3}(T-873)$	−1368	3.621	+1424	0.420	1792

Figure 6 represents the activity of AgI and figure 7 its activity coefficient versus $x_2 (x_2 = x_{CdCl_2})$. Positive and higher deviations from ideality than in AgI + CdI_2 system are found out.

The excess chemical potential of AgI versus x_2 in AgI + $CdCl_2$ system is plotted on figure 8; it is positive and slightly higher than μ_1^E from AgI + CdI_2 binary mixture.

On figure 9 the excess partial molar entropy of AgI versus x_2 in AgI + $CdCl_2$ mixture is plotted; the deviations from additivity are higher than in the binary mixture. S_1^E has a maximum at $x_2 \simeq 0.6$.

Finally, figure 10 shows the variation of excess partial molar enthalpy of AgI with x_2 in the mixture AgI + $CdCl_2$; one can observe that H_1^E is positive and has a maximum at $x_2 = 0.6$.

The behaviour of the two systems AgI + CdI_2 and AgI + $CdCl_2$ studied by e.m.f. measurements of formation cells may be interpreted as follows:

The appreciable positive values of excess chemical potential (μ_{AgI}^E) may be explained by the fact that fused cadmium halides are associated; that is why the mole fraction of AgI in mixture is higher than the real one, the excess entropy being predominantly negative $(S_{AgI}^E < 0)$.

On the other hand the ionic radii of silver and cadmium being very close to each other ($r_{Ag^+} = 1.13$ Å and $r_{Cd^{2+}} = 1.03$ Å) one can expect that the excess enthalpy should be relatively low in this mixture and consequently the relation:

$$\mu_{AgI}^E = H_{AgI}^E - TS_{AgI}^E \tag{9'}$$

leads to

$$\mu_{AgI}^E > 0.$$

In the reciprocal mixture AgI + $CdCl_2$ (fig. 9) the excess entropy is positive, but *a* has an evident maximum at $x_{AgI} = 0.4 (x_{CdCl_2} = 0.6)$. This

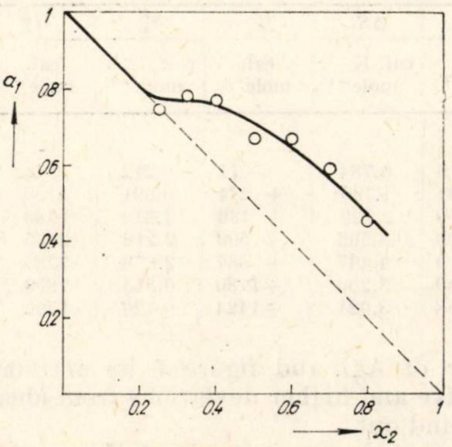

Fig. 6. — Thermodynamic activity of AgI in reciprocal mixture AgI + $CdCl_2$.

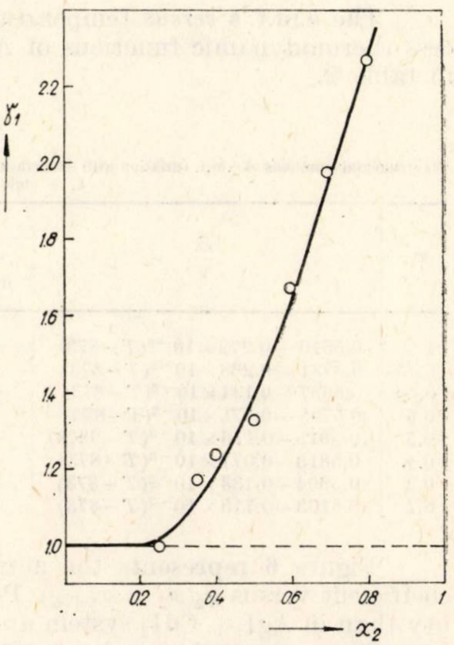

Fig. 7. — Activity coefficient of AgI in reciprocal mixture AgI + $CdCl_2$.

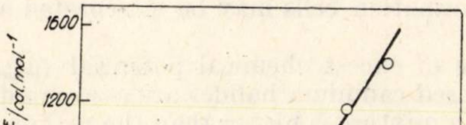

Fig. 8. — Experimental excess partial molar chemical for AgI in reciprocal mixture AgI + $CdCl_2$.

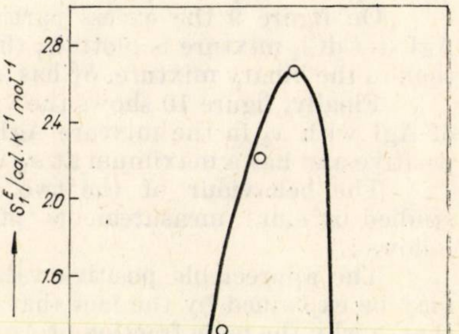

Fig. 9. — Experimental excess partial molar entropy for AgI in reciprocal mixture AgI + $CdCl_2$.

shape of the curve may be obtained by summing up the negative S^E (dissociation of $CdCl_2$) with the always positive S^E (Temkin).

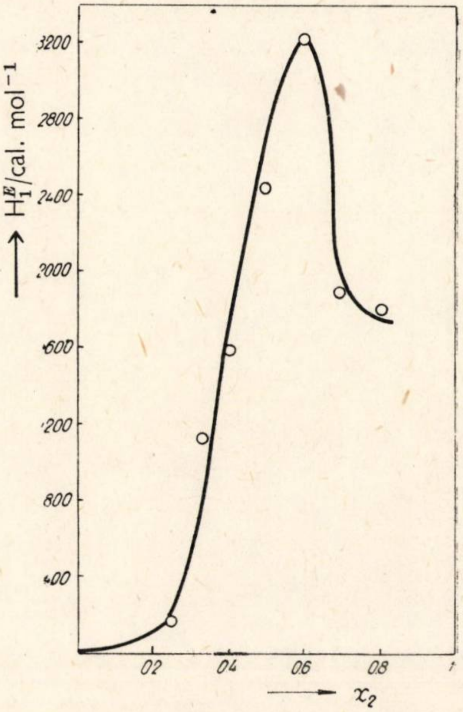

Fig. 10. — Experimental excess partial molar free enthalpy for AgI in reciprocal mixture AgI + $CdCl_2$.

As to the positive values of excess enthalpy; they may be explained by the contribution of exchange reaction :

$${}_2AgI + CdCl_2 \rightleftarrows {}_2AgCl + CdI_2$$

whose heat calculated from thermochemical data [8,9] is $\Delta H = +10310$ cal. The chemical potential is also positive.

In conclusion the behaviour of AgI + $CdCl_2$ is determined by the following main factors : the dissociation of cadmium salt (which is present in both binary and reciprocal systems), Temkin effect and exchange reactions ; the last two effects being typical for reciprocal salt mixtures.

---

[8] O. Kubashewski, E. L.L. Evans and C. Alcock, in "Metallurgical Thermochemistry", Pergamon Press, London, 1967, p. 303.

[9] G. J. Janz in "Molten Salts Handbook", Academic Press, New York, London, 1967, p. 187.

Revue Roumaine de Chimie, **20**, *4*, 473–480 (1975)

SOLVENT INTERACTION WITH ALKYL-TRIMETHYL-AMMONIUM HALIDES. II[1]

CONDUCTANCE IN ACETONITRILE, ACETONE AND METHYL ETHYL KETONE AT 25°

SESTA BIANCA

Laboratorio di Chimica Fisica ed Elettrochimica,
Istituto di Chimica dell'Universitá di Roma, Rome, Italy

Received March, 1, 1974

Conductance measurements are reported for *n*-butyl-, *n*-hexyl and *n*-octyl-trimethylammonium bromides in acetone, acetonitrile and methyl ethyl ketone or 2-butanone at 25°. The limiting conductance, Λ_0, conforming to the theoretical previsions, decreases with increasing cationic size in each solvent and with the increasing solvent viscosity for each bromide. In the absence of any appreciable ion-solvent interaction, the slight differences between the K_A and a_K values of the three bromides in each solvent may be once more explained by the spacial asymmetry of the cations. The closest approach distance, *a*, and the Zwanzig radii of the three bromides are lower than the actual size of the ions. Owing to the dielectric relaxation effect, the $\Lambda_0^+\eta$ products for the bromides decrease with the increasing dielectric constants of the aprotic solvents.

INTRODUCTION

A previous conductometric study [1] of dilute solutions of alkyl-trimethylammonium bromides in methanol, ethanol and *n*-propanol at 25° reported deviations from the expected behaviour of these electrolytes.

The deviations were attributed partly to the strong interaction between ions and polar hydrogen bonded solvent molecules, and partly to the asymmetric shape of cations, that is, to their non-conformity to the ideal spherical solute postulated by Fuoss [2] and Zwanzig.[3]

The express purpose of the present study is the investigation of the cation shape effect on the transport processes of *n*-butyl-, *n*-hexyl-and *n*-octyl-trimethylammonium bromides in weakly solvating, aprotic solvent-like acetonitrile, acetone and 2-butanone, in which the marked interferences of the solvent are obviated. These particular solvents were selected because their dielectric constants fall in the same range of values of the alcohols above mentioned.

---

[1] B. Sesta and G. Goratti, *Rev. Roumaine Chim.*, in press.

[2] R. M. Fuoss and L. Onsager, *J. Phys. Chem.*, **61**, 668 (1957).

[3] R. Zwanzig, *J. Phys. Chem.*, **68**, 1603 (1963).

EXPERIMENTAL TECHNIQUE

A description of the preparation and purification of the salts has been presented in the previous paper.[1] Cells, electrical equipment and experimental techniques have also been described[4].

Acetonitrile (Merck product) was purified by the procedure reported by Coetzee[5] and, in addition, by fractional distillation under nitrogen in the presence of calcium hydride.[6] Acetonitrile was delivered directly to the cell from the distillation receiver. Acetone (Merck product) was dried as reported by Riddick and Burger.[7] Before transferring acetone to the conductance cell, to avoid water contamination of the liquid, the cell was dried in vacuum.[8] 2-Butanone (methyl ethyl ketone) (Merck product) was dried by the same procedure used for acetone.

The densities (gm/cm^3) and conductivities (ohm^{-1}/cm) are found to be : 0.7869 and 3.10^{-8} for acetone, 0.7845 and $2\ 10^{-8}$ for acetonitrile, 0.7996 and $2\ 10^{-8}$ for 2-butanone, in good agreement with the other authors' data.[9-13]

RESULTS

The measured equivalent conductance Λ, (ohm^{-1} cm^2 equiv^{-1}) at various concentration c (equiv/liter) are given in table 1 for *n*-butyl-trimetylammonium bromide ($n-\mathrm{Bu(CH_3)_3NBr}$), for *n*-hexyl-trimethylammonium bromide ($n-\mathrm{Hex(CH_3)_3NBr}$) and for *n*-octyl-trimethylammonium bromide (n-$\mathrm{Oct(CH_3)_3NBr}$) in acetonitrile (AN), acetone (AC) and 2-butanone (MEK) at 25°.

DISCUSSION

In order to obtain Λ_0, the limiting conductance, K_A, the association constant and a_L, the closest approach distance between anion and cation, the experimental data were analysed by equation[14] :

$$\Lambda = \Lambda_0 - S\sqrt{c\gamma} + E'c\gamma\ln(6E_1'c\gamma) + Lc\gamma - K_A c\gamma f^2 \Lambda \qquad (1)$$

(S, E', E_1' and L are theoretical coefficients deriving from the long range interactions and depending on the physical properties of solutions). The following dielectric constants and viscosities (poise) are used : 36.02 and 0.003448 for acetonitrile,[6] 20.7 and 0.00303 for acetone,[8] 18.014 and 0.003774 for 2-butanone.[13]

---

[4] B. Sesta, *Ann. Chim.*, **57**, 129 (1967).

[5] J. F. Coetzee, G. P. Cunningham, D. K. McGuire and G. R. Padmanabhan, *Anal. Chem.*, **34**, 1139 (1962).

[6] D. F. Evans, C. Zawoyski and R. L. Kay, *J. Phys. Chem.*, **69**, 3878 (1965).

[7] J. A. Riddick and W. B. Bunger, "Organic Solvents", Wiley Interscience, New York, 1974.

[8] D. F. Evans, J. Thomas, J. A. Nadas and M. A. Matesich, *J. Phys. Chem.*, **75**, 1714 (1971).

[9] C. H. Springer, J. F. Coetzee and R. L. Kay, *J. Phys. Chem.*, **73**, 471 (1969).

[10] M. B. Reynolds and C. A. Kraus, *J. Amer. Chem. Soc.*, **70**, 1709 (1948).

[11] G. Pistoia and G. Pecci, *J. Phys. Chem.*, **74**, 1450 (1970).

[12] F. M. Sacks and R. M. Fuoss, *J. Amer. Chem. Soc.*, **75**, 5172 (1953).

[13] S.R.C. Hughes and D. H. Price, *J. Chem. Soc.* (*A*), **1967**, 1093.

[14] R. M. Fuoss, L. Onsager and J. F. Skinner, *J. Phys. Chem.*, **69**, 2581 (1965).

Table 1

Equivalent conductances in acetonitrile, acetone and 2-butanone

Acetonitrile

$n-Bu(CH_3)_3NBr$		$n-hex(CH_3)_3NBr$		$n-oct(CH_3)_3NBr$	
10^4c	Λ	10^4c	Λ	10^4c	Λ
4.8989	174.403	4.0171	168.143	5.1197	161.762
9.1082	169.740	6.3286	165.353	7.4599	159.250
12.5627	166.620	9.7590	161.975	11.6449	155.468
19.2592	161.597	13.1857	159.123	16.5807	151.793
22.6681	159.390	15.6983	157.280	28.1764	144.979
25.7256	157.578				

Acetone

$n-Bu(CH_3)_3NBr$		$n-hex(CH_3)_3NBr$		$n-oct(CH_3)_3NBr$	
10^4c	Λ	10^4c	Λ	10^4c	Λ
6.1195	140.216	1.8870	166.088	2.4913	155.467
10.5014	123.632	3.6302	150.646	4.4929	140.911
13.6096	115.568	5.9455	137.048	6.4389	131.000
17.1155	108.500	7.7083	129.429	9.2563	120.584
21.2770	101.958	9.6535	122.703	11.6056	113.987
24.9472	97.260	11.2156	118.185		

2-Butanone

$n-Bu(CH_3)_3NBr$		$n-hex(CH_3)_3NBr$		$n-Oct(CH_3)_3NBr$	
10^4c	Λ	10^4c	Λ	10^4c	Λ
3.3005	94.8641	1.8527	105.893	1.4771	107.087
10.5293	67.5104	3.8697	96.073	3.6520	87.562
13.9644	61.3569	4.2155	87.115	5.9577	76.444
16.5787	57.7921	5.5769	80.535	8.6675	68.139
20.7145	53.3486	6.9838	75.333	14.4532	57.446
		9.6611	68.017		

The results are given in table 2 in which are also included the standard deviations σ_Λ, where

$$\sigma_\Lambda^2 = (\Lambda_{calc.} - \Lambda_{exp.})^2/(n - 3).$$

All calculations are made by a UNIVAC 1108 computer unit.

The K_A values of these electrolytes in MEK are in order of $3 \cdot 10^3$. In this case the $K_A c\gamma f^2 \Lambda$ term of the equation (1) is much larger than the combined $E'c\gamma \ln(6E'_1 c\gamma) + Lc\gamma$ terms and the program computation fails to converge. For the purpose of obtaining a better agreement between the

Table 2

Conductance parameters for acetonitrile, acetone and 2-butanone solutions at 25°

Salts	Λ_0	K_A	a_L	σ_Λ
Acetonitrile				
$n-Bu(CH_3)_3NBr$	185.21 ± 0.02	32 ± 1	2.6 ± 0.1	0.006
$n-Hex(CH_3)_3NBr$	177.51 ± 0.02	34 ± 1	3.8 ± 0.3	0.006
$n-Oct(CH_3)_3NBr$	172.29 ± 0.03	29 ± 1	2.4 ± 0.2	0.01
Acetone				
$n-Bu(CH_3)_3NBr$	206.35 ± 0.19	1094 ± 5	3.5 ± 0.2	0.02
$n-Hex(CH_3)_3NBr$	199.95 ± 0.04	1077 ± 3	3.6 ± 0.1	0.01
$n-Oct(CH_3)_3NBr$	194.32 ± 0.07	1074 ± 4	3.8 ± 0.1	0.01
2-Butanone				
$n-Bu(CH_3)_3NBr$	152.47 ± 0.17	2983 ± 13	2.5 ± 0.1	0.03
$n-Hex(CH_3)_3NBr$	148.77 ± 0.11	2940 ± 12	2.5 ± 0.1	0.02
$n-Oct(CH_3)_3NBr$	143.85 ± 0.15	2910 ± 15	2.4 ± 0.1	0.05

experimental and the calculated Λ values, the MEK data were analysed using the Fuoss-Kraus equation [15]:

$$\Lambda = \gamma(\Lambda_0 - S\sqrt{c\gamma}) \tag{2}$$

however, the effect of disregarding the higher terms of Eq. (1) resulted in unrealistically high Λ_0 and K_A values.

From the equivalent conductances given in table 2 and using $\Lambda_{0\,Br^-} = 100.7\ \text{ohm}^{-1}\,\text{cm}^2\,\text{equiv}^{-1}$ in acetonitrile,[9] $\Lambda_{0\,Br^-} = 118.94\ \text{ohm}^{-1}\,\text{cm}^2\,\text{equiv}^{-1}$ in acetone [8] and $\Lambda_{0\,Br^-} = 86.85\ \text{ohm}^{-1}\,\text{cm}^2\,\text{equiv}^{-1}$ in 2-butanone, [13] the cationic mobilities listed in table 3 are obtained. These values are in good agreement with the cationic mobilities previously obtained from alkyltrimethylammonium iodides. [16]

Examining the results given in table 3, it is noted that the K_A of each of the bromides increases with the decreasing dielectric constant, conforming to the equation [17]:

$$K_A = \frac{4\pi\, Na^3}{3\,000} \exp\,(\varepsilon^2/aDkT) \tag{3}$$

---

[15] R. M. Fuoss and C.A. Kraus, *J. Amer. Chem. Soc.*, **55**, 476 (1933).

[16] B. Sesta and M. Battistini, *Ann. Chim.*, **63**, 163 (1973).

[17] R. M. Fuoss, *J. Amer. Chem. Soc.*, **80**, 5059 (1958).

On the other hand, the K'_As of the three bromides in each of the solvents assume nearly the same values, in contrast to the predicted K_A dependance on the a parameter.

An analogous behaviour of the same alkyl-trimethylammonium halides in methanol, ethanol and propanol in the previous study was accounted for by the asymmetrical shape of the cations,[1] postulating that a more likely approach of the halide anions to the alkyl-trimethylammonium cations exists in the direction of the three methyl groups. The same interpretation may be formulated for the presently reported results.

Table 3

Cationic mobilities Λ_0^+, Walden product Λ_0^+3 and L* function for acetonitrile, acetone 2-butanone solutions

Solvent	ion	Λ_0^+	Λ_0^+	L*
Acetonitrile	$n-Bu(CH_3)_3N^+$	84.51	0.291	0.533
	$n-Hex(CH_3)_3N^+$	76.81	0.265	0.584
	$n-Oct(CH_3)_3N^+$	71.59	0.247	0.627
Acetone	$n-Bu(CH_3)_3N^+$	87.42	0.265	0.585
	$n-Hex(CH_3)_3N^+$	81.01	0.246	0.630
	$n-Oct(CH_3)_3N^+$	75.39	0.228	0.685
2-Butanone	$n-Bu(CH_3)_3N^+$	65.62	0.246	0.628
	$n-Hex(CH_3)_3N^+$	61.91	0.233	0.665
	$n-Oct(CH_3)_3N^+$	57.00	0.215	0.722

Obviously, a_K, the closest approach distance obtained from the K_A parameter, shows no appreciable relationship with the ionic size, and it averages about 3.1 Å in acetonitrile, 3.2 Å in acetone and 2.7 Å in 2-butanone. These values agree with the a values calculated from L parameter of equation (1) and listed in table 4. However, they are too low taking into account the interatomic distances of the ions, even admitting that the ion pairs are formed along the short radius of the cations, namely, in the direction of the three methyl groups of the cations. The author of this paper agrees with Hughes interpretation,[13] that small halogenic ions as bromides can penetrate between the hydrocarbonic chains of alkylammonium cations, thereby approaching the central atomic charge and reducing the center-to-center ionic distance.

In fig. 1 $\log K_A$ are plotted against 100/dielectric constant of solvents, The values of iodides in the same acetonitrile, acetone and 2-butanone, and the values of iodides and of bromides in methanol, ethanol and propanol are plotted in the same fig. 1.

The curve of bromides in aprotic solvents lies above the curve of iodides, which proves the existence of the higher electrostatic attraction of the small bromide ion over the iodide ones. For the same electrolytes in alcohols, the solvent molecules solvate and shield the cations and anions, reducing their attraction and thus inverting the K_A order.

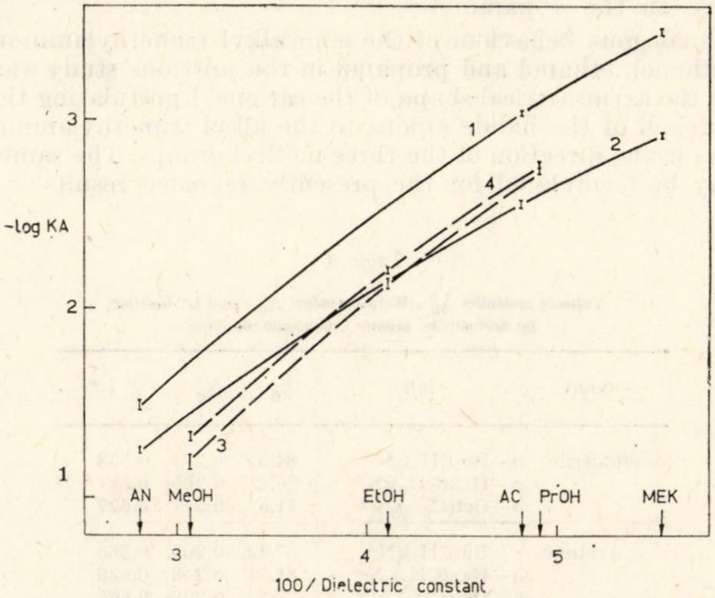

Fig. 1. – Log K_A of alkyl-trimethylammonium bromides : 1, and iodides ; 2, in acetonitrile (AN), acetone (AC) and 2-butanone (MEK) as a function of 100/dielectric constant. Dashed curves relate to alkyl-trimethylammonium bromides ; 3, and iodides ; 4, in methanol (MeOH), ethanol (EtOH) and *n*-propanol (PrOH).

For aprotic solvents, a good approach to hydrodynamic radii may be achieved by using Zwanzig equation [3] :

$$\Lambda_0^+ = \frac{F^2}{N\left[6\pi\,\eta r + \frac{2\,\tau e^2}{3r^3}\left(\frac{\varepsilon_0 - \varepsilon_\infty}{\varepsilon_0^2}\right)\right]} \tag{4}$$

where F is the Faraday, N the Avogadro number, τ the dielectric relaxation time, ε_0 the static permittivity, ε_∞ the permitivity at infinite frequency and r the hydrodynamic radius.

Equation (4) can be rearranged [18] to give :

$$\frac{F^2}{N\eta\Lambda_0^+} = 6\pi r + \frac{2\,e^2}{3\,r^3}\left[\frac{\tau}{\eta}\left(\frac{\varepsilon_0 - \varepsilon_\infty}{\varepsilon_0^2}\right)\right] \tag{5}$$

In fig. 2 $L^* = F^2/N\eta\Lambda_0^+$ are plotted against $R^* = (\tau/\eta)\ (\varepsilon_0 - \varepsilon_\infty/\varepsilon_0^2)$ for $n-$bu $(CH_3)_3N^+$, for $n-$Hex $(CH_3)_3N^+$ and for $n-$Oct $(CH_3)_3N^+$ ions. The values of r_s from the slope, and r_i from the intercept, are in table 4. They are quite satisfactory if compared with the closest approach calculated from K_A and L parameters.

[18] G. Atkinson and Y. Mori, *J. Phys. Chem.*, **71**, 3523 (1967).

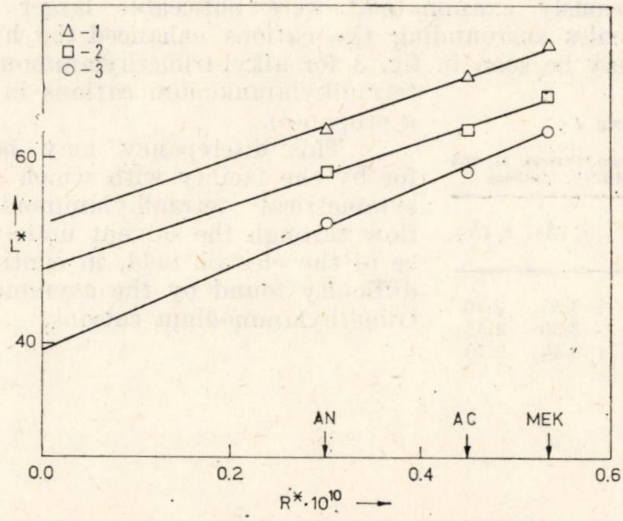

Fig. 2. — The plots of L* vs. R* for *n*-butyltrimethylammonium :

1, *n*-hexyltrimethylammonium; 2, and *n*-octyltrimethylammonium; 3. ions in acetonitrile (AN), acetone (AC) and 2-butanone (MEK).

The $\Lambda_0^+\eta$ products decrease with the increasing cationic weight faster than reported by Kay[6], Evans,[8] and Hughes[13] for symmetrical tetraalkylammonium cations (the difference of mobilities for alcoholic

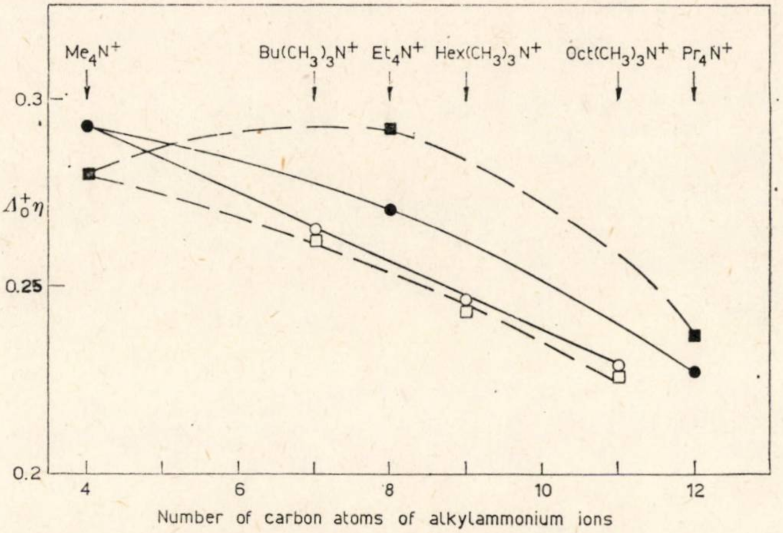

Fig. 3. — The $\Lambda_0^+\eta$ products of alkylammonium ions in acetone as a function of the number of carbon atoms. Dashed lines relate to alkylammonium ions in *n*-propanol.

solutions previously examinated,[1] were noticeable larger because the solvent molecules surrounding the cations enhanced the hydrodynamic friction, as may be seen in fig. 3 for alkyl-trimethylammonium and for tetraalkylammonium cations in acetone and *n*-propanol).

This discrepancy may be accounted for by the facility with which the spacially symmetrical tetraalkylammonium cations flow through the solvent under the influence of the electric field, in contrast with the difficulty found by the asymmetrical alkyl-trimethylammonium cations.

Table 4

Hydrodynamic radii from intercept, $\mathbf{r}_i$, and from slope, $\mathbf{r}_s$ of L*(R* functions

Cations	r_i (Å)	r_s (Å)
$n-Bu(CH_3)_3N^+$	3.55	2.20
$n-Hex(CH_3)_3N^+$	3.50	2.55
$n-Oct(CH_3)_3N^+$	3.40	2.70

Revue Roumaine de Chimie, **20**, *4*, 481–485 (1975)

BEHAVIOUR OF ACTIVATED CARBON ELECTRODE IN ELECTROLYTE SOLUTIONS

OVIDIU MATEIOVICI

Institute for Nuclear Technology, Bucharest-Măgurele

Received February 19, 1974

Investigations concerning the activated carbon electrode pointed out that it could be only partially classified as a gas electrode. The potential of the activated carbon electrode in electrolyte solutions depends on the electrochemical configuration of the chemisorbed oxygen, and does not depend on the existence of other gases on the electrode surface. From the fact that there is no relation between the presence of other chemisorbed gases on its surface and the electrode potential, one may regard the activated carbon electrode as a gas "degenerated" electrode.

At the separation limit between the activated carbon surface and an electrolyte solution a difference of potential is established.

The expression of this potential lies in the existence of electrochemical active carbon-oxygen compounds. The investigations in the activated carbon electrode in electrolyte solutions led Frumkin and Ponomarenko[1] to the conclusion that its potential depends on the absorbed gases, chemical potential and the pH value of the solution.

Garten and Weiss[2] explain the phenomena which appear on the activated carbon electrode surface taking into account the fact that functional groups take part in the adsorption of electrolytes which change their structure by means of oxidation or reduction.

Oxygen ionization on the activated carbon surface which implies the bonding of two or four electrons leads to the adsorption of the acids from their water solution.

Frumkin's discovery of the partial equivalence of the mineral acids adsorption from their diluted solutions and the chemisorbed oxygen concentration, in connection with the electrode potential, confirms the assumption of Garten and Weiss.

If one proceeds to the exhaustive desorption of the oxygen from the activated carbon surface, the latter adsorbs neither anions, nor cations, and the electrode potential becomes the zero charge potential.[3] By gradual admission of oxygen in the system Ponomarenko, Frumkin and Burstein[3] discovered that the activated carbon electrode potential shifts to more positive values.

---

[1] A. N. Frumkin and E. A. Ponomarenko, *Doklady Akad. Nauk S.S.S.R.*, **149**, 1123 (1963).

[2] S. Garten and W. Weiss, *Rev. Pure Appl. Chem. (Australia)*, **7**, 69 (1957).

[3] E. A. Ponomarenko, A. N. Frumkin and I. Burstein, *Izvest. Akad. Nauk S.S.S.R., Otdel. khim. Nauk*, **9**, 1549 (1963).

EXPERIMENTAL

Investigations regarding the activated carbon electrode potential have been carried out on the electrode with a normal composition of oxides, that is, with the superficial compounds formed by activation. In the present work an active carbon electrode made of wood char has been used. The wood char has been strongly activated by means of steam and burned gases at the temperature of 900—950° for 6—7 hours. The electrolysis cell shown in figure 1 has been closed and thermostated. The activated carbon electrode had a weight of 1.5mg and a surface area of 1.04 m^2.

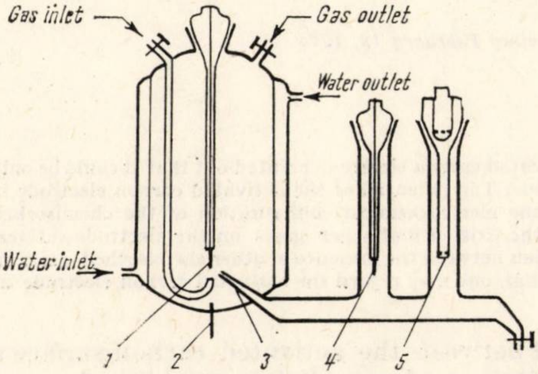

Fig. 1. — Electrolysis cell.

1, activated carbon electrode; 2, platinum electrode; 3, Luggin capillary; 4, additional activated carbon electrode; 5, calomel electrode.

The surface area has been determined according to Rubinstein and Afanasiev's method by benzene vapours adsorption.[4]

As control electrode, the saturated calomel electrode was used and the potentials reported to the normal hydrogen electrode. Also, for the preparation of the solution twice distilled water was used.

EXPERIMENTAL RESULTS

By immersing in a 0.02 M. H_2SO_4 solution, the activated carbon electrode shows an instantaneous positive potential of about 250 to 350 m volts at 25°. Afterwards, the electrode potential shifts to more positive values and reaches 640—650 m volts after 6—20 hours.

The periodical control has proved that the potential changes its value with no more than a few milivolts within six months.

This extremely constant potential has been defined as steady potential.

The polarization of the electrode by means of a weak current which varies from 1×10^{-9} amp to 3×10^{-6} amp leads to the deviation of the electrode potential from the value of the steady potential according to current polarity. The potential is established at a value which lasts as long as the electrode is polarized, provided that the current is constant and maintained within these limits.

This potential has been called dynamic potential.

---

[4] M. Rubinstein and I. Afanasyev, *Izvest. Akad. Nauk S.S.S.R., Otdel. khim. Nauk*, **11**, 1294 (1956).

By interrupting the polarization current, the dynamic potential fades away while the steady potential is re-established.

The steady potential is the same as before polarization and does not depend on the value of the previous dynamic potential.

DEPENDENCE OF ELECTRODE POTENTIAL ON THE NATURE OF THE ADSORBED GAS

This study has been carried out both on an electrode having a steady potential and on an electrode having an arbitrary value of the dynamic potential.

If the oxygen is removed from solution by means of argon or hydrogen, no sensible variation of the electrode potential is registered. Neither CO nor CO_2 influence the dynamic or steady potentials. If the electrode is saturated with AsH_3 or H_2S, the steady and dynamic potentials remain unchanged, as well.

A remarkable fact is the impossibility to obtain the theoretical hydrogen or oxygen potential on the activated carbon surface.

In order to obtain the reversible theoretical hydrogen potential, the electrode has been long-time polarized from the steady potential to zero potential using a weak current of 3 μamp.

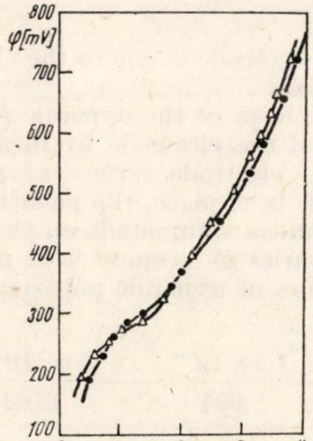

Fig. 2. — Relation between electrode polarization and the logarithm of current i, in μamp. in the case of hydrogen evolution for AsH_3 free-electrode (curve with triangles) and for the AsH_3 chemisorbed electrode (curve with full rings) in 0.02 M. H_2SO_4 solution at the temperature of 25°.

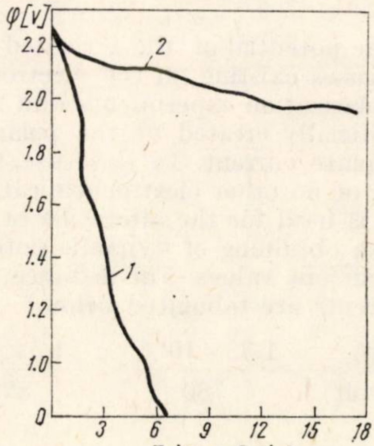

Fig. 3. — Dependence of activated carbon electrode potential on time at the open circuit for a short time anodic polarization (30 sec.) (curve *1*) and for a long time anodic polarization (24 hours) (curve *2*) in 0.02 M. H_2SO_4 solution at the temperature of 25°.

Throughout the experiment, the electrode was saturated with hydrogen.

When the current was interrupted, the electrode potential was re-established at the steady potential value.

Other gases existing on the electrode surface have not influenced the electrode potential, even in the conditions of gas release (i.e. hydrogen). A plot of electrode potential vs. the logarithm of the current intensity is illustrated in figure 2 (for the case of the hydrogen released). The curve with triangles refers to the free AsH_3 electrode, while that with the full rings reports to the same electrode which chemisorbed AsH_3. A good coincidence has been achieved in this case.

In order to investigate the electrochemical configuration, the electrode was polarized with a weak current i.e. 3 μamp for a long time (some days); then, another electrode was polarized with a stronger current i.e. 100μ amp within some minutes.

A plot of potential vs. the time on open circuit is shown in figure 3. Another experiment refers to the plotting of the discharging curve in the case of the electrode polarized with a strong current (100 μamp) for a short time (some minutes), as compared to an unpolarized electrode. As we can see from figure 4, a good coincidence of the curves appears, as well.

DISCUSSION

The potential of the activated carbon electrode is due to the chemisorbed gases existing on the electrode surface.

Polarization experiments lead to the concept of the dynamic potential, artificially created by the polarization of the electrode by means of an adequate current. In this case, if on the electrode surface no gas is released or no other electrochemical reactions take place, the polarization current is used for the alteration of the chemical compounds on the surface. The obtaining of dynamic potentials varies in keeping with polarization current values. For instance, the values of dynamic potentials vs. the currents are tabulated below:

i(amp)	1.32×10^{-8}	1.5×10^{-7}	1.5×10^{-6}	3×10^{-6}
φ(m volt)	780	822	994	1182

At weak and prolonged currents, the potential changes slowly and is finally stabilized at the value given by the current, while in the case of the strong current, i.e. about 100 μamp the potential swiftly changes and in short time (some minutes) the reactions lead to gas release.

The two values of the polarization current correspond to two different states of the surface; in one case, new superficial compounds are formed, in the other the superficial compounds have not formed yet.

From the fact that in the case of the weak and prolonged current the potential variation on the open circuit is different from another electrode, which was polarized for a short time by means of a strong current, we reach the conclusion that two different superficial states are formed.

On the other hand, a good coincidence of the curves (figure 4) proves the electrical identity of the surfaces on the investigated electrodes. The fact that other gases existing on the surface of the electrode do not influence its potential proves that the gas, which confers electrochemical activity (i.e. oxygen) is strongly bounded with the electrochemical centres.

Although one of the investigated gases, i.e. AsH_3, is chemisorbed on the surface of the electrode, the phenomenon does not interfere with the surface fraction assigned to the electrochemical processes.[5]

Hence, one may assume that the activated carbon electrode presents a double functional surface : a chemical and an electrochemical one. Also, the electrode potential is insensitive to the partial pressure of the oxygen showing that on its surface no dynamic equilibrium is established similar to that of hydrogen or oxygen on platinum.

The activated carbon electrode may be defined as a gas "degenerated" electrode.

The characteristics of the activated carbon electrode indicate that the electrochemical centres are grouped in an electrochemical configuration, probably varying from one activated carbon type to another, invariably the same for a given variety of activated carbon.

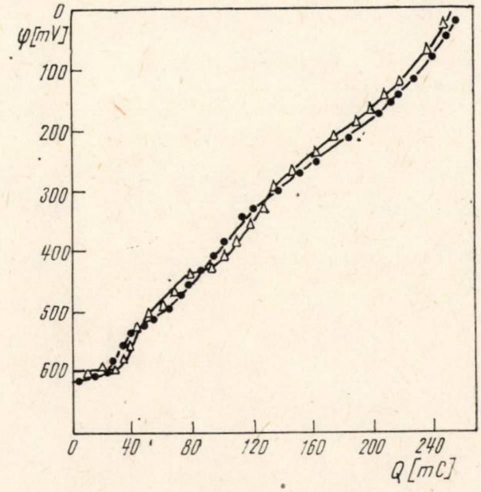

Fig. 4. — Discharge curves for a polarized electrode with a strong current (100 μamp) for a short time (30 sec) (curve with triangles) in comparison with unpolarized electrode (curve with full rings) in 0.02 M. H_2SO_4 solution at the temperature of 25°.

The rest of chemisorbed gas, which is electrochemically inert constitutes a new configuration named chemical configuration.

The fraction of the area occupied by the electrochemical configuration is small (about 5%).

The electrochemical configuration is stable and is not disturbed by the presence on the electrode of other chemisorbed gases ; it is influenced only by the temperature and polarization current.

The recurrence of the dynamic potential to the steady potential does not depend on the dynamic potential value, polarization time and polarization current, thus pointing out the rigidity of the electrochemical configuration.

---

[5] Ov. Mateiovici, Unpublished results.

Revue Roumaine de Chimie, **20**, *4*, 487–491 (1975)

THE BEHAVIOUR OF NICKEL IN CHLORIDE IONS-CONTAINING MEDIA

ECATERINA VASILESCU

Institute of Physical Chemistry, str. Galaţi 31, Bucharest, Romania

Received February 18, 1974

Data with regard to the variations of the critical pitting potential and the potential of pits repassivation with the concentration of chloride ions and pH, are reported. It is shown that both these parameters are independent characteristics of the pitting process.

Nickel is one of the main components of stainless steels, its presence bringing about remarkable improvements in the pitting corrosion of ferrous alloys.

The addition of nickel to steels, promotes the austenitic structure formation so that the resulting steels have higher corrosion resistance and better mechanical properties.[1–3]

But nickel, like stainless steels, undergoes pitting corrosion in chloride ions containing electrolytes so that it is of practical and theoretical interest to study the behavior of nickel against pitting corrosion and to assess its contribution to stainless steel behavior.

The object of this research is to determine the effect of the medium factors changes on the electrochemical parameters of pitting corrosion for pure nickel.

EXPERIMENTAL

Experimental measurements were carried out on pure nickel strips, cut down in parallelipipedic electrodes, provided with a lead for electrical contact and fixing in glass holder assembly.

After mechanical polishing on emery paper, the specimens were fixed with ARALDIT resin in the glass holder, degreased with boiling benzene, chemically polished with 15% HNO_3 at 25° for 10 minutes and then thoroughly rinsed with tap water and double-distilled water.

All electrolytes were prepared from reagent grade chemicals and double-distilled water.

Some of the measurements were made in argon deaerated electrolytes. The deaeration gas was purified by passing it over hot copper turnings at 250°.

Large quantities of electrolytes were deaerated in separated vessels and then under argon pressure, the necessary quantity of solution for an electrochemical measurement was transferred in the polarization cell.

---

[1] Raport, *Anticorrosion*, **18**, 15 (1971).
[2] T. Desestret, *Corrosion et Anticorr.*, **15**, 281 (1967).
[3] N.D. Greene and M. G. Fontana, *Corrosion*, **15**, 39 t (1959).

Additional 1 hour deaeration was accomplished before every measurement.

The electrochemical polarization glass cell was provided with a central room for the electrode assembly, two equidistant platinum counter electrodes, a Luggin probe connected with a saturated calomel reference electrode and inlets for electrolyte and deaeration gas supply.

The electrochemical measurements were made by using the potentiostatic step-by-step technique. Steps of 50 mV/5 min., were applied from a Wenking potentiostate and the resulting currents were recorded on an output instrument.

The cyclic anodic curves obtained were used to establish the values of the critical pitting potential (E_{cp}) and of the potential of pits repassivation (E_{rp}). Knowing the dependence of E_{rp} on the experimental procedure used,[4−8] the backward anodic curve was recorded after a current density of about 500 μA/cm² was reached.[4]

RESULTS

THE EFFECT OF CHLORIDE IONS CONCENTRATION

The electrochemical measurements were made using aerated solution of 0.01 – 2 M KCl.

The cyclic potential-current curves recorded for different potassium chloride concentrations permitted to determine the variation of the electrochemical pitting characteristics function of the aggressive ions content of the electrolyte.

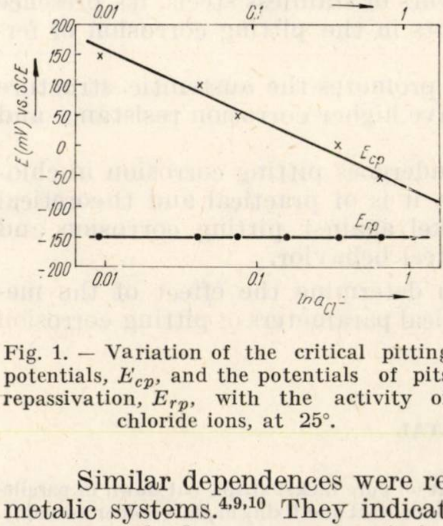

Fig. 1. — Variation of the critical pitting potentials, E_{cp}, and the potentials of pits repassivation, E_{rp}, with the activity of chloride ions, at 25°.

The obtained results for pure nickel are illustrated in figure 1.

The experimental results show that:

1. The critical pitting potential of nickel varies linearly with the logarithm of chloride ions activities, according to the equation:

$$E_{cp} = 0.220 - 0.110 \log a_{Cl^-}$$

The constant 0.220 was obtained by extrapolating to the value of the potential of pits repassivation.

Similar dependences were reported by the literature for some other metalic systems.[4,9,10] They indicate that the tendency toward pitting increases with the content in pitting ions. In case of nickel, for instance, a ten-fold increase in the chloride ions concentration, involves a decrease of 110 mV in the critical pitting potential.

2. The potential of pits repassivation is independent of the concentration of chloride ions.

---

[4] S. Ciolac and E. Vasilescu, *Rev. Roumaine Chim.*, **20**, in press.
[5] S. Ciolac and E. Vasilescu, *Rev. Roumaine Chim.*, **20**, in press.
[6] B. E. Wilde and E. Williams, *Electrochim. Acta*, **16**, 1971 (1971).
[7] V. Hospadaruk and J. V. Petrocelli, *J. Electrochem. Soc.*, **113**, 878 (1966).
[8] E. D. Vernik Jr. and M. Pourbaix, *Corrosion*, **27**, 495 (1971).
[9] T. Suzuki and Y. Kitamura, *Corrosion*, **28**, 1 (1972).
[10] H. P. Leckie and H.H. Uhlig, *J. Electrochem. Soc.*, **113**, 1262 (1966).

THE EFFECT OF THE pH

The variation of the pitting potentials, E_{cp} and E_{rp}, was studied in deaerated 0.1 M KCl whose pH was adjusted with HCl, H_2SO_4, HNO_3 and KOH.

In the acidulated 0.1 M KCl, nickel presents active-passive transition curves with narrow ranges of passivity.

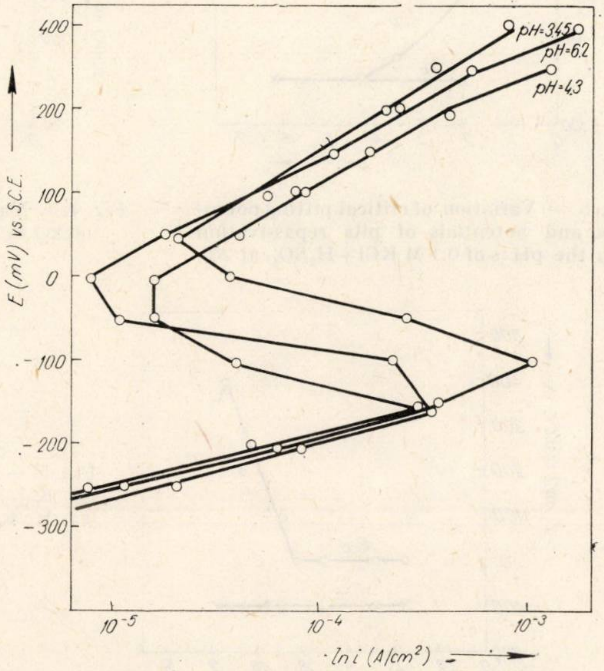

Fig. 2. — The effect of H_2SO_4 pH adjustment on nickel corrosion in 0.1 M KCl, at 25°.

So in figure 2 the anodic curves obtained for potassium chloride adjusted with H_2SO_4 at pH = 3.4 ; 4.3 and 6.2 are presented.

It can be observed that in acid solutions the passive current decreases and the region of passivity becomes larger with increasing pH.

The same results are observed with HCl and HNO_3 adjustment.

In the neutral potassium chloride (no pH adjustment) the polarization curves do not show any active-passive transition.

The width of the passive region is more pronounced with increasing pH, so that in KOH alkalized solutions the range of passivity covers approximately 600 mV, and the passive current decreases with about one order of magnitude.

Our results are in good agreement with the Pourbaix thermodynamic diagrams predictions,[11] that evidence the increase in the passivity degree with pH.

---

[11] M. POURBAIX, ,,Atlas d'Equilibre Electrochimiques'', Gauthier-Villars & Cie.. Editeur — Imprimeur — Libraire, Paris, 1963, p. 336.

The capacity of Ni to passivate, involves developments of pits on its surface in the presence of chloride ions.

The breakdown potentials of the passive films (the critical pitting potential) are affected by the pH changes.

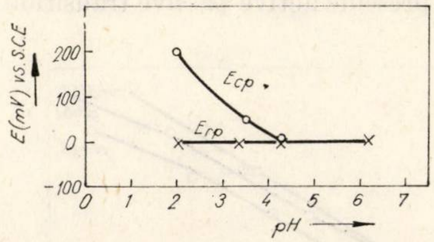

Fig. 3. — Variation of critical pitting potentials and potentials of pits repassivation with the pH:s of 0.1 M KCl+H_2SO_4, at 25°.

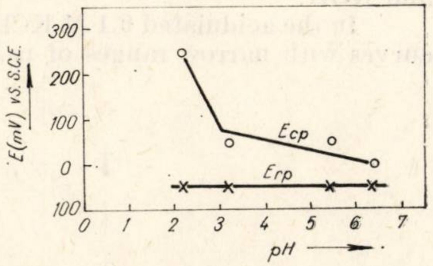

Fig. 4. — Variation of E_{cp}, $E_{rp} = f$ (pH) of nickel in 0.1 M KCl + HNO_3, at 25°.

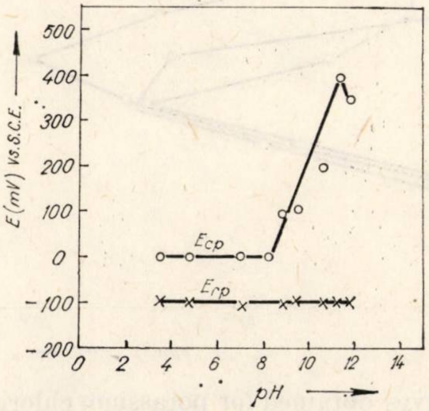

Fig. 5. — Variation diagram of E_{cp}, $E_{rp} = f$(pH) in 0.1 M KCl+HCl, KOH, at 25°.

The type of its variation is influenced by the nature of the agent used in pH adjustment, as can be seen from the comparative study of figures 3, 4 and 5.

At the same time, it can be observed that the potentials of pits repassivation are unaffected by the pH and only a little influenced by the nature of the reagent used in the pH adjustment.

From all the acids used for pH changes, nitric acid seems to be the most effective in pitting resistance improvement and especially at lower pH:s. Identical E_{cp} and E_{rp} values are found in case of H_2SO_4 adjustment (pH >4). This is not the case for nitric acid and less for hydrochloric acid adjustment.

The higher values of the critical pitting potential resulting at lower pH:s after H_2SO_4 and HNO_3 acidulation may be explained by the inhibitive action of SO_4^{2-} and NO_3^- ions on the initiation of the pitting process.

Increasing the pH, hence decreasing the content of inhibitive ions is accompanied by a reduction in the value of the critical pitting potentials (figures 3 and 4).

Remarkable increases of E_{cp} are, however, observed for higher pH:s (pH >8), a maximum value being registered at pH = 10.5 (fig. 5).

This behaviour may also be explained by the fact that OH^- ions act as inhibitors, their effect being stronger as their content is higher (hence for higher pH:s).

At the same time, this pH range corresponds to that predicted by the Pourbaix diagrams for the highest degree of stability of the passive film, i.e. the highest resistance to the destructive action of chloride ions.

There are, thus, two ways to justify the observed increments in the value of the critical pitting potential.

CONCLUSIONS

The comparative examination of the obtained results, presented in table 1, shows, that E_{cp} and E_{rp} parameters are independent characteristics of the pitting process.

So, while the critical pitting potential has a linear dependence on the logarithm of chloride ions activities, the potential of pits repassivation is independent of the chloride ions content of the electrolyte.

The existing difference between the two electrochemical pitting potentials appears more clearly from the results of the pH effect. In acidic potassium chloride solutions the variation of E_{cp} values are determined by the nature of the reagent used for pH adjustment, and is the most affected by HNO_3 acidulation. The alkaline media are, however, more effective in pitting inhibition.

Table 1

The dependence of electrochemical pitting characteristics on the changes in the medium parameters

The changed parameter		The dependence	
		E_{cp}	E_{rp}
Cl^- ions concentration		$0.220-0.110 \log a_{Cl^-}$	independent
pH adjusted with	HCl	0 mV/pH unit	independent (= −100 mV)
	H_2SO_4	86.9 mV/pH unit	independent (=0mV)
	HNO_3	107.4 mV/pH unit	independent (= −50 mV)
	KOH	129 mV/pH unit	independent (= −100 mV)

The electrolyte composition affects to a little extent the value of the potential E_{rp}. For every studied system (KCl + reagent of pH adjustment) the potential of pits repassivation is found to be independent of the value of the pH.

The different behaviours of the two electrochemical potentials characterizing the pitting process, could be considered to prove the fact that these parameters belong to different stages of pitting development.

The obtained results, supported by some of the published data, allow to appreciate that the critical pitting potential characterizes the initiation stage of the pitting process (affected by the conditions of the electrolytic medium) and the potential of pits repassivation characterizes the stage of pits propagation (less affected by the electrolytic medium, but functioning on the basis of some specific conditions created inside the pits).

Revue Roumaine de Chimie, 20, 4, 487 – 491 (1975)

Revue Roumaine de Chimie, **20**, *4*, 493–500 (1975)

L'ÉTUDE DU SYSTÈME RÉDOX $Fe(CN)_6^{3-}/Fe(CN)_6^{4-}$ SUR L'ÉLECTRODE DE GRAPHITE

I.A. ATANASIU et MARIA NEATĂ BĂLESCU

Laboratoire d'Electrochimie, Institut Polytechnique, 1, str. Polizu, Bucarest, Roumanie

Reçu le 4 mars 1974

En utilisant les courbes courant-potentiel réalisées par la technique potentiostatique ont été déterminés les paramètres cinétiques α et i_0, et la constante de vitesse k_s du système rédox $Fe\ (CN)_6^{3-}/Fe\ (CN)_6^{4-}$ sur l'électrode de graphite spectral.

Le système $Fe(CN)_6^{3-}/Fe\ (CN)_6^{4-}$, thermodynamique réversible, a été étudié jusqu'à présent par plusieurs auteurs sur des électrodes de nature et formes différentes. Ainsi, les études effectuées par Eisenberg et collab.[1] sur l'électrode rotative de Ni indiquent l'effet insignifiant de la polarisation électrochimique, l'étape déterminante de la réaction étant le transfert de substance.

Nicholson [2] recommande le système comme « standard » dans ses études sur la théorie de la diffusion pour les électrodes cylindriques stationnaires.

Gorbatschev et Gourinov [3] étudiant l'influence de la vitesse de circulation de l'électrolyte et de la température sur la cinétique du système $K_3Fe(CN)_6/K_4Fe(CN)_6$ sur l'électrode de Pt trouvent que ce système est influencé en premier lieu par la polarisation de diffusion, la polarisation électrochimique étant pratiquement nulle.

Sur une électrode disque rotatif de Ni, Holpatov et Gorbatschev [4] montrent qu'aux potentiels élevés la polarisation a le caractère de diffusion ; également, les solutions de faible concentration en espèces réactantes donnent avec priorité cette forme de surtension.

Les résultats de Morris et Schemph [5] sur l'électrode de graphite imprégnée de cérésine indiquent aussi que le système $Fe\ (CN)_6^{3-}/Fe(CN)_6^{4-}$ est thermodynamiquement réversible, l'effet de la polarisation électrochimique étant négligeable.

---

[1] N. Eisenberg, C. W. Tobias et C. R. Wilke, *J. Electrochem. Soc.*, **101**, 109 (1954).

[2] J. Nicholson, *J. Amer. Chem. Soc.*, **6**, 2559 (1954).

[3] S. V. Gorbatschev et J. S. Gourinov, *Zhur. fiz. Khim.*, **7**, 1712 (1965).

[4] L. P. Holpatov et S. V. Gorbatschev, *Zhur. fiz. Khim.*, **38**, 3020, 3024 (1964).

[5] J. B. Morris et J. H. Schemph, *Analyt. Chem.*, **31**, 286 (1959).

Les mêmes conclusions sont relatées aussi par Sharma et Jatinder[6] sur l'électrode tubulaire de graphite dans des conditions hydrodynamiques (vitesses variables de la circulation de l'électrolyte).

Le système $Fe(CN)_6^{3-}/Fe(CN)_6^{4-}$ a été aussi étudié, sur graphite, par Regner et Balej[7] en régime laminaire de la circulation de l'électrolyte. Ils trouvent que le système est contrôlé en même temps par les deux formes de polarisation.

Sur les électrodes Na-W, le système est contrôlé par le transfert d'électron, sur un domaine étendu de concentrations[8].

L'étude cinétique du système $Fe(CN)_6^{3-}/Fe(CN)_6^{4-}$ a été effectuée par diverses méthodes; ainsi les déterminations de polarisation effectuées par Esin[9] et Petrocelli-Paoulucci,[10] en courant continu, relèvent que le processus est dominé, en spécial, par la surtension de diffusion.

Les déterminations de Delahay et Mattax[11] dans des conditions galvanostatiques, sur l'électrode de Hg, indiquent aussi la prépondérance de la surtension de diffusion.

Les études de Randles et Somerton,[12] effectuées en courant alternatif, plaident pour l'existence de la polarisation de transfert de charge associée à celle de diffusion.

D'autres études cinétiques sur divers métaux[13-14] montrent l'influence à divers degrés de la polarisation.

Nous présentons plus loin les résultats expérimentaux sur l'étude du système $Fe(CN)_6^{3-}/Fe(CN)_6^{4-}$ sur l'électrode de graphite spectral.

TECHNIQUE EXPÉRIMENTALE

Les recherches ont été effectuées sur la base de déterminations de polarisation, réalisée en technique potentiostatique soit avec la variation du potentiel par étapes soit en régime continu, avec un potentiostat PS 2.

La cellule de polarisation, avec la séparation des espaces cathodique et anodique, est constituée par deux parties distinctes : le corps et le couvercle (fig. 1). Le corps d'une forme cylindrique ($H = 15$ cm, $\Phi = 5$ cm) a été muni d'un système de barbotage pour azote, fixé sous l'électrode de travail. Ainsi, l'électrode a été balayée par un courant d'azote pendant l'élimination de l'air.

Dans le couvercle de la cellule ont été fixés : la contre-électrode et le capillaire Luggin, qui a réalisé le contact entre l'électrode de travail et l'électrode de référence (E.C.S.). Le couvercle a été aussi muni d'un orifice central pour l'introduction de l'électrode de graphite. Cette électrode a été fixée par pression dans un support cylindrique en teflon fixé par vissage dans un autre corps de teflon (fig. 1). Le contact électrique à cette électrode a été réalisé par un fil de Pt.

Les recherches ont été effectuées sur des électrodes cylindriques de graphite de pureté spectrale, avec la hauteur de 3,5 cm et la section de 0,3 cm^2 ; cette section a constitué la surface de travail, qui a subi un polissage extrafin avec papier d'émeri, et après avec papier de filtre. Après ces opérations les électrodes ont été soumises à l'ébulition répétée en HCl conc., jusqu'à décoloration complète, suivie d' un lavage à l'ébullition dans l'eau doublement distillée.

---

[6] L. R. Sharma et Dutt Jatinder, *Indian J. Chem.*, **18**, 170 (1970).

[7] A. Regner et J. Balej, *Coll. Czech. Chem. Comm.*, **26**, 237 (1961).

[8] M. V. Vojnovič et D. B. Sěpa, *J. Chem. Phys.*, **12**, 5344 (1969).

[9] O. Esin, in « Electrochemische Kinetik », K. Vetter, Berlin, 1961, p. 391.

[10] J. P. Petrocelli et A. A. Paoulucci, *J. Electrochem. Soc.*, **98**, 291 (1951).

[11] P. Delahay et C.C. Mattax, *J. Amer. Chem. Soc.*, **76**, 876 (1954).

[12] I. E. B. Randles et K. W. Somerton, *Trans. Faraday Soc.*, **48**, 937 (1952).

[13] V. J. Kravtzov et B. V. Simacov, *Electrokhimiya*, **4**, 406 (1966).

[14] R. H. Baum et S. C. Enke, *Analyt. Chem.*, **41**, 655 (1969).

La contre-électrode a été constituée de Pt brilliante (s = 2 cm^2) fixée en verre. La préparation de cette électrode a été effectuée par dégraissage en Na_2CO_3 et lavage à l'eau doublement distillée.

Les solutions utilisées ont été préparées avec des substances *p.a.*, dans l'eau bidistillée.

Avant la réalisation des courbes de polarisation, les solutions ont été désaérées par le passage d'un courant l'azote purifié, pendant 3 heures. La purification de l'azote a été effectuées par son passage dans : H_2SO_4 conc., NaOH granulé, cuivre chauffé à 350°, silicagel, charbon activ et ouate de verre.

La température de travail : $25 \pm 1°$.

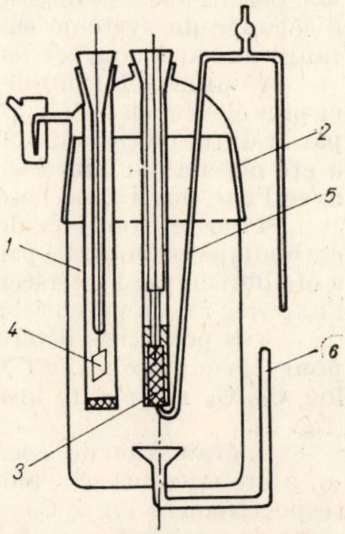

Fig. 1. — Cellule de polarisation: *1*, corps ; *2*, couvercle ; *3*, électrode de travail (graphite) ; *4*, contre-électrode (Pt) ; *5*, capillaire Luggin ; *6*, barbotage de l'azote.

RÉSULTATS ET DISCUSSIONS

Les études cinétiques du système $Fe(CN)_6^{3-}/Fe(CN)_6^{4-}$ sur l'électrode de graphite spectral ont été effectuées sur la base de variations courant-potentiel, selon la technique potentiostatique.

On a utilisé la variation du potentiel par étapes de 10 mV et l'enregistrement du courant à 1,2 et 3 minutes.

L'enregistrement à 3 minutes correspond à la réalisation de l'état stationnaire à l'électrode. Ces déterminations ont été utilisées pour le calcul des paramètres cinétiques de la réaction étudiée : le coefficient de transfert, α, et le courant d'échange, i_0, et aussi pour la détermination de la constante apparente de vitesse, k_s.

Comme solutions d'étude ont été employées des solutions de $K_3Fe(CN)_6$ *p.a.* et de $K_4Fe\,(CN)_6$ *p.a.*, en milieu sulfurique (10^{-1} mole/l) (tableau 1).

Tableau 1

Composition des solutions utilisées

Conc. $K_3Fe(CN)_6$ mole/l	Conc. $K_4Fe(CN)_6$ mole/l	C_{Ox}/C_R
5.10^{-2}	5.10^{-2}	1
10^{-1}	10^{-1}	1
10^{-2}	10^{-1}	10^{-1}
10^{-3}	10^{-1}	10^{-2}
10^{-1}	10^{-2}	10
10^{-1}	10^{-3}	10^2

Les déterminations ont permis l'étude de l'influence de quelques paramètres de travail (la concentration des espèces réactantes, respectivement le rapport des concentrations, le régime d'enregistrement et l'agitation de l'électrolyte) sur les caractéristiques de polarisation et des paramètres cinétiques.

Les courbes de polarisation *E* — log *i* montrent l'influence des concentrations des espèces sur la réaction. Ainsi, l'oxydation : $Fe(CN)_6^{4-} \rightarrow Fe\,(CN)_6^{3-} + e^-$ est influencée exclusivement par la concentration de $K_4Fe(CN)_6$ et la réduction : $Fe(CN)_6^{3-} + e^- \rightarrow Fe(CN)_6^{4-}$ par la concentration de $K_3Fe(CN)_6$. On constate la proportionnalité du courant limite anodique avec la concentration de $K_4Fe(CN)_6$ (fig. 2) et la proportionnalité du courant limite cathodique — de la concentration de $K_3Fe(CN)_6$ (fig. 3).

Les courbes des figures 2 et 3 effectuées en conditions stationnaires ont permis aussi la détermination des potentiels réversibles et du courant d'échange du système en utilisant la méthode usuelle d'intersection des tangentes aux courbes (en détail fig. 3*a*).

Pour les solutions de faible concentration en $Fe(CN)_6^{4-}$ ($<10^{-2}$ mole/l) et plus élevées en $Fe(CN)_6^{3-}$ parce qu'il y a le contrôle du processus anodique par la diffusion (le courant limite est réalisé plus vite) le courant d'échange a été obtenu par l'intersection de la pente Tafel de la courbe cathodique avec l'axe «log *i* », au potentiel réversible[8] (fig. 2).

Pour les solutions de faible concentration en $Fe(CN)_6^{3-}$, le processus cathodique est contrôlé par la diffusion et pour celui-ci le courant d'échange a été obtenu par l'intersection de la pente Tafel de la courbe anodique avec l'axe «log *i* », au potentiel réversible (fig. 3).

Les potentiels déterminés sont en accord avec l'équation de Nernst pour l'équilibre : $Fe(CN)_6^{3-} + e^- \rightleftharpoons Fe(CN)_6^{4-}$ la dépendance E — $\log C_{Ox}/C_R$ représente une droite avec la pente $\Delta E/\Delta \log C_{Ox}/C_R \simeq 60$ mV (fig. 4).

L'évaluation des coefficients de transfert anodique, α_a, et cathodique, α_c, a été effectuées à l'aide des représentations $\log i_0/C_{Ox} - \log C_R/C_{Ox}$, et respectivement $\log i_0/C_R - \log C_{Ox}/C_R$. La pente représente même le coefficient de transfert ($\alpha = \Delta \log i_0/\Delta \log C$; la valeur de ce coefficient pour la réaction cathodique et anodique est de 0,5 (fig. 5).

Il a été aussi possible de déterminer la constante apparente de vitesse, k_s, en utilisant l'équation Delahay-Berzins : $k_s = i_0/zF.C_{Ox}^{\alpha} \cdot C_R^{1-\alpha}$[15], après l'évaluation préalable de i_0 et α.

Dans le tableau 2 se trouvent les valeurs des paramètres cinétiques du système $Fe(CN)_6^{3-}/Fe(CN)_6^{4-}$ obtenus pour quelques solutions étudiées, sur l'électrode de graphite spectral.

Les paramètres cinétiques du tableau 2 sont calculés sur la surface géométrique des électrodes de graphite. En réalité, cette surface est dix fois plus grande, et, en conséquence, les valeurs de i_0 et k_s sont diminuées. On constate aussi que les paramètres i_0 et k_s pour le système $Fe(CN)_6^{3-}/Fe(CN)_6^{4-}$ sur l'électrode de graphite sont plus petits que ceux déterminés sur Pt, mais on trouve une bonne concordance pour les coefficients de transfert[16]. Les valeurs des paramètres cinétiques déterminés ici indiquent la contribution du transfert de charge dans le processus $Fe(CN)_6^{3-} + e^- \rightleftharpoons Fe(CN)_6^{4-}$ sur l'électrode de graphite.

Mais l'influence du régime de variation du potentiel (fig. 6) et l'agitation d'électrolyte (fig. 7) sur les courants limites relève aussi le rôle de la diffusion.

Ainsi, on observe l'augmentation du courant pour les solutions agitées et pour les vitesses rapides d'enregistrement des courbes.

Dans l'ensemble, les valeurs des paramètres cinétiques associées à l'influence des paramètres de travail relèvent que le système $Fe(CN)_6^{3-}/Fe(CN)_6^{4-}$ sur l'électrode de graphite spectral présente un contrôle mixt : transfert de charge et diffusion.

---

[15] P. Delahay et P. Berzins, *J. Amer. Chem. Soc.*, **77**, 6448 (1955).

[16] D. H. Angell et T. Dickinson, *J. Electroanalyt. Chem.*, **35**, 55 (1972).

Fig. 2. — La dépendance courant-potentiel pour le système : $Fe(CN)_6^{3-}/Fe(CN)_6^{4-}$ sur l'électrode de graphite.

Concentration de $K_4Fe(CN)_6$ $1-10^{-3}$; $2-10^{-2}$; $3-10^{-1}$ mole/l. Concentration de $K_3Fe(CN)_6 - 10^{-1}$ mole/l. Temps d'enregistrement : 3 minutes.

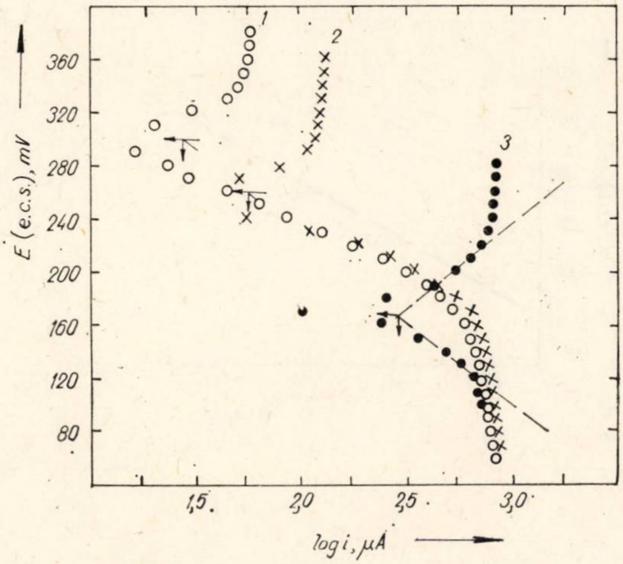

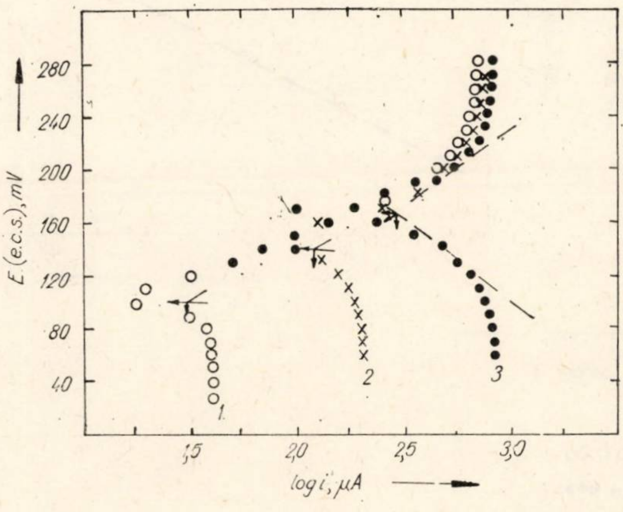

Fig. 3. — La dépendance courant-potentiel pour le système $Fe(CN)_6^{3-}/Fe(CN)_6^{4-}$ sur l'électrode de graphite.

Concentration de $K_3Fe(CN)_6$: $1-10^{-3}$; $2-10^{-2}$; $3-10^{-1}$ mole/l. Concentration de $K_4Fe(CN)_6 - 10^{-1}$ mole/l. Temps d'enregistrement : 3 minutes.

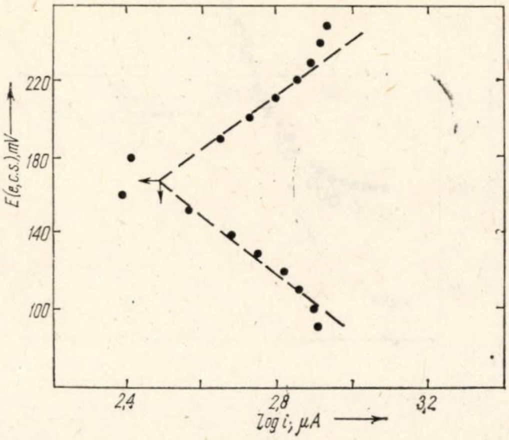

Fig. 3*a*. — Les pentes Tafel pour le système $Fe(CN)_6^{3-}/Fe(CN)_6^{4-}$ sur l'électrode de graphite.

Solution : 0,1 mole/l $K_3Fe(CN)_6$ + 0,1mole/l $K_4Fe(CN)_6$. Temps d'enregistrement : 3 minutes.

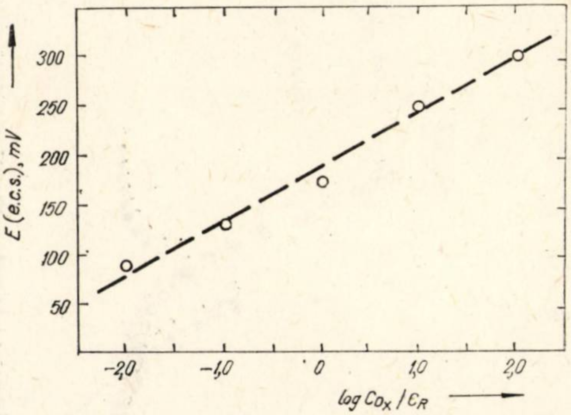

Fig. 4. — La dépendance E — — log C_{Ox}/C_R pour le système $Fe(CN)_6^{3-}/Fe(CN)_6^{4-}$ sur l'électrode de graphite.

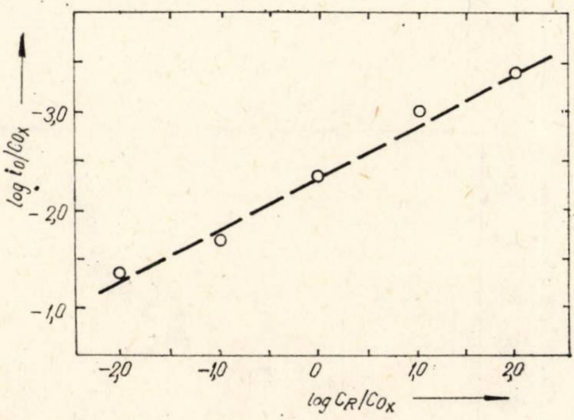

Fig. 5. — La dépendance log $i_0/$ C_{Ox} — log C_R/C_{Ox} pour le système $Fe(CN)_6^{3-}/Fe(CN)_6^{4-}$ sur l'électrode de graphite.

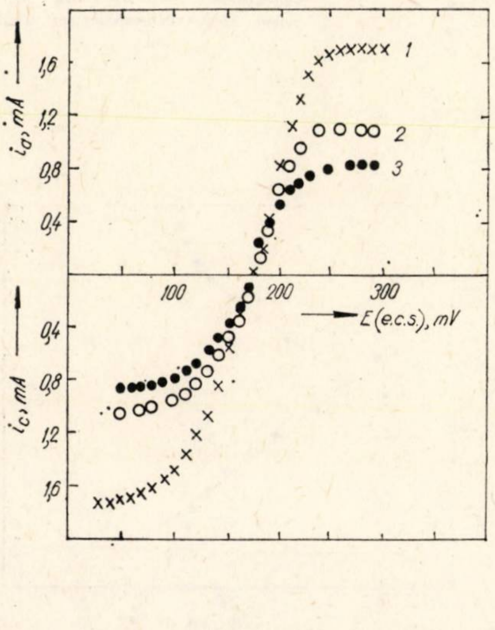

Fig. 6. — Influence du régime de variation du potentiel sur les courbes courant-potentiel pour le système $Fe(CN)_6^{3-}/$ $Fe(CN)_6^{4-}$.

Solution :0.1 mole/l $K_3Fe(CN)_6$ + 0,1 mole/l $K_4Fe(CN)_6$. Temps d'enregistrement : *1* — 1 minute ; *2* — 3 minutes ; *3* — 3 minutes.

Tableau 2

Valeurs des paramètres cinétiques pour le système $Fe(CN)_6^{3-}$/$Fe(CN)_6^{4-}$ sur l'électrode de graphite

Conc. $Fe(CN)_6^{3-}$ mole/l	Conc. $Fe(CN)_6^{4-}$ mole/l	$\log C_{Ox}/C_R$	E_{rev}, mV E.C.S.	i_0, A/cm²	$k_s \cdot 10^5$ cm/s
5.10^{-2}	5.10^{-2}	0	170	$2{,}8 \cdot 10^{-4}$	5,7
10^{-1}	10^{-1}	0	170	$4{,}7 \cdot 10^{-4}$	4,9
10^{-2}	10^{-1}	−1	130	$2{,}1 \cdot 10^{-4}$	7,0
10^{-3}	10^{-1}	−2	90	$4{,}7 \cdot 10^{-5}$	4,9
10^{-1}	10^{-2}	+1	250	$9{,}4 \cdot 10^{-5}$	3,1
10^{-1}	10^{-3}	+2	300	$4{,}4 \cdot 10^{-5}$	4,6

$\alpha_a = \alpha_c = 0{,}5$.

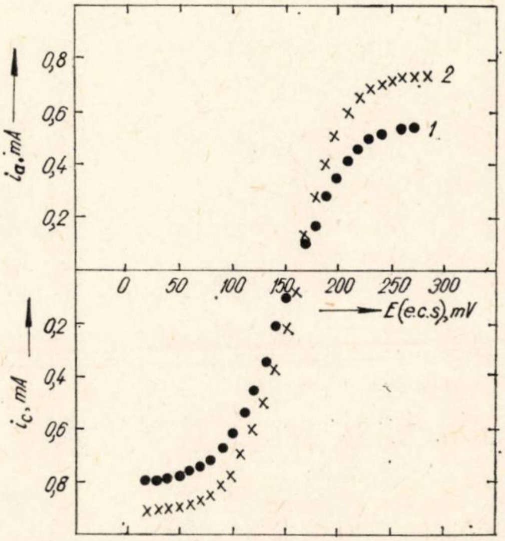

Fig. 7. — Influence de l'agitation de l'électrolyse sur les courbes courant-potentiel pour le système $Fe(CN)_6^{3-}$/$Fe(CN)_6^{4-}$.

Solution : 0,05 mole/l $K_3Fe(CN)_6$ + 0,05 mole/l $K_4Fe(CN)_6$. *1*, Sans agitation ; *2*, avec agitation. Temps d'enregistrement : 2 minutes.

CONCLUSIONS

Les données expérimentales sur la cinétique du système rédox $Fe(CN)_6^{3-}$/$Fe(CN)_6^{4-}$ sur l'électrode de graphite spectral rélèvent :

1. Le processus d'oxydation $Fe(CN)_6^{4-} \rightarrow Fe(CN)_6^{3-} + e^-$ correspond à des potentiels plus électronégatifs que le dégagement de l'oxygène, tandis que la réduction : $Fe(CN)_6^{3-} + e^- \rightarrow Fe(CN)_6^{4-}$ à des potentiels plus électropositifs que le dégagement de l'hydrogène. L'électrode de graphite se comporte, donc, comme «inerte », n'étant pas détruit lors de l'étude de ce système par l'oxygène.

2. La réaction cathodique dépend exclusivement de la concentration de $K_3Fe(CN)_6$, tandis que la réaction anodique est fonction de la concentration de $K_4Fe(CN)_6$.

3. Les valeurs des paramètres : $i_0=10^{-4}-10^{-5}$ A/cm^2 ; $\alpha_a=\alpha_c=0{,}5$ et $k_s\simeq10^{-5}$cm/s montrent aussi que le système $Fe(CN)_6^{3-}/Fe(CN)_6^{4-}$ sur graphite est contrôlé par le transfert de charge. L'influence des diverses paramètres de travail (concentration des espèces réactantes, régime de variation du potentiel, agitation de l'électrolyte) sur le processus, indique en même temps un contrôle par la diffusion.

4. Les valeurs des paramètres i_0 et k_s plus faibles sur l'électrode de graphite que sur le Pt indiquent le caractère quasi réversible du système $Fe(CN)_6^{3-}/Fe(CN)_6^{4-}$ sur l'électrode de graphite. Ce comportement est expliqué par les phénomènes de diffusion plus complexes dans l'électrode de graphite à cause de sa porosité.

Revue Roumaine de Chimie, **20**, *4*, 501–513 (1975)

L'ÉTUDE DE LA RÉACTION D'OXYDATION DE L'HYDROGÈNE DANS LES ÉLECTRODES POREUSES EN NICKEL. II[1]

LA DÉTERMINATION DES PARAMÈTRES D'OBTENTION DES ÉLECTRODES

I. SOLACOLU, MARIA MAVRODIN-TĂRĂBÎC et IOANA ONACA

Centre de Chimie Physique, Bucarest, 31, str. Galaţi

Reçu le 25 janvier 1974

On a réalisé, dans notre laboratoire, une série d'électrodes à gaz en nickel caractérisées par une structure bidispersée du type DSK (« Doppel Skelet Katalyst ») et par une structure du type double couche (électrodes avec une couche barrière), en comprimant et en frittant des mélanges homogènes qui contiennent du nickel, du carbonate de nickel et de l'acide oxalique. Les électrodes ont été comprimées à différentes pressions comprises entre 2,9. 10^8 N/m^2 et 5,4. 10^8 N/m^2 et frittées, en atmosphère d'hydrogène, à des températures comprises entre 600 et 750°. Les électrodes ont été caractérisées du point de vue structural en déterminant la porosité totale et par examen microscopique. L'étude de la réaction d'oxydation de l'hydrogène a été effectuée en déterminant les courbes de polarisation η-i, à différentes surpressions de l'hydrogène, en utilisant la technique potentiostatique. Les données expérimentales obtenues nous ont permis d'établir l'effet des paramètres d'obtention des électrodes (la pression et la température) sur leurs performances électrochimiques.

Dans un travail antérieur [1] on a établi que l'acide oxalique (particules 20–40 microns) est un poroformateur efficient qui permet la réalisation des électrodes à gaz en nickel du type DSK avec des performances supérieures. Dans ce travail nous nous sommes proposé d'étudier l'influence des paramètres de réalisation des électrodes à gaz (la pression à laquelle ont été comprimées les électrodes et la température de frittage) sur leurs performances électrochimiques dans la réaction d'oxydation de l'hydrogène.

Tracy et Williams[2,3] ont étudié, par la méthode des rayons X, les poudres de nickel frittées et ont établi la corrélation qui existe entre les paramètres de réalisation, d'une part, et la structure et la composition des masses frittées obtenues — facteurs déterminants pour les performances des électrodes, d'autre part.

La littérature de spécialité indique, en fonction du système choisi (structure de résistance, masse catalytique active, poroformateur), des valeurs différentes pour les paramètres de réalisation des électrodes.

---

[1] M. Mavrodin-Tărăbîc, I. Onaca et I. Solacolu, *Rev. Roumaine Chim.*, **18**, 1121 (1973).

[2] V. A. Tracy, *Powder Met.*, **8**, 241 (1965).

[3] V. A. Tracy et N. J. Williams, *Electrochem. Technol.*, **3**, 17 (1965).

La plupart des données concernant ce domaine se trouvent dans la littérature de patents.[4-9] L'analyse de ces travaux nous a permis d'établir les limites du domaine de notre étude (pour la pression, les valeurs de 2,9 — 5,4. 10^8 N/m^2 et pour la température, 600—750°).

1. PARTIE EXPÉRIMENTALE

1.1. RÉALISATION DES ÉLECTRODES

Les électrodes caractérisées par une structure bidispersée (du type DSK) ont été obtenues en comprimant, dans des matrices d'acier, à des pressions comprises entre 2,9.10^8 N/m^2 et 5,4 10^8. N/m^2 et par frittage en atmosphère d'hydrogène, à des températures comprises entre 600 et 750°, des mélanges homogènes qui contiennent : 25% nickel ex nickel carbonyle, 50% carbonate de nickel et 25% acide oxalique (les dimensions des particules sont situées au-dessous de 3 microns, au-dessous de 5 microns et, respectivement, d'environ 20—40 microns).

Les électrodes caractérisées par une structure du type double couche (électrode avec une couche barrière) ont été réalisées dans les mêmes conditions, en comprimant deux couches surposées : la couche A (barrière) qui contient 50% nickel ex nickel carbonyle et 50% carbonate de nickel et la couche B, avec une composition identique à celle des électrodes du type DSK.

On a utilisé des substances de pureté *p.a.*

Les électrodes obtenues présentent une forme cylindrique, avec un diamètre de 10 mm et une épaisseur de 3 mm.

Le frittage a été effectué dans un four cylindrique horizontal, le régime thermique étant le suivant : le chauffage — avec une vitesse de 2,5 degrés/mn, avec des paliers de 60 mn pour chaque 100 degrés ; le temps de frittage — 30 mn ; le refroidissement — avec une vitesse de 3 degrés/mn, avec des paliers de 30 mn pour chaque 100 degrés.

1.2. L'ÉTUDE DE LA STRUCTURE DES ÉLECTRODES

L'étude du degré de frittage des électrodes et de la répartition des pores dans la masse du matériel a été effectuée à l'aide d'un microscope métallographique du type MIM—7 (500X).

La porosité totale des électrodes a été déterminée en pesant les électrodes avant et après leur imprégnation en toluène.

Les compositions des mélanges, les conditions de réalisation et les porosités totales des électrodes sont présentées dans le tableau 1.

1.3. LES DÉTERMINATIONS ÉLECTROCHIMIQUES

L'étude de la réaction d'oxydation de l'hydrogène a été effectuée par la technique potentiostatique à l'aide d'un montage classique, en utilisant un potentiostat du type CCF (précision ± 1 mV), un milliampèremètre (classe de précision 0,5), un millivoltmètre électronique du type Radiometer 22 (précision ± 1 mV). L'électrode de référence a été une électrode de calomel saturé. L'électrode auxiliaire — une spirale de nickel de pureté 99,9%. On a appliqué des niveaux de potentiel de 10 à 50 mV, à un intervalle de temps de 5 minutes.

[4] SCHEIBE, Ger. Pat. (Est) 47 212, 5 avril 1966 ; *Chem. Abstr.*, **64**, 11771b (1966).

[5] H. OSWIN, U.S. Pat. 3 323 915, 6 juin 1967 ; *Chem. Abstr.*, **66**, 34274v (1967).

[6] G. SANDSTEDE, U.S. Pat. 3 382 067, 7 mai 1968 ; *Chem. Abstr.*, **69**, 32525r (1968).

[7] D. POULI et T. L. LARSON, Ger. Pat. 1 812 736, 21 août 1969 ; *Chem. Abstr.*, **71**, 87181x (1969).

[8] BROWN BOVERI, A.—G., Fr. Pat. 1 553 750, 5 janvier 1969 ; *Chem. Abstr.*, **72**, 17904g (1970).

[9] M. LANG et R. PASQUALE, Ger. Pat. 1 942 111, 26 fevrier 1970 ; *Chem. Abstr.*, **73**, 51648g (1971).

Tableau 1

Composition, conditions conditions et porosités des électrodes à gaz en nickel

Type de l'électrode		Composition du mélange Ni	NiCO$_3$	H$_2$C$_2$O$_4$	Pression	Température de frittage	Porosité totale	Symbole
		%	%	%	10^8 N.m^{-2}	°C	%	
DSK		25	50	25	2,9	600	69,8	E$_1$
						650	66,9	E$_2$
						700	64,1	E$_3$
						750	60,1	E$_4$
					3,3	600	67,4	E$_5$
						650	65,6	E$_6$
						750	61,9	E$_7$
					3,75	600	65,5	E$_8$
						650	63,4	E$_9$
						700	60,8	E$_{10}$
						750	59,9	E$_{11}$
					4,6	600	60,7	E$_{12}$
						650	60,1	E$_{13}$
						700	59,2	E$_{14}$
						750	57,0	E$_{15}$
					5,4	600	58,2	E$_{16}$
						650	55,0	E$_{17}$
						700	53,9	E$_{18}$
						750	54,5	E$_{19}$
à double couche	couche				4,6	650	51,2	ED$_1$
	A	50	50			700	48,4	ED$_2$
	B	25	50	25		750	46,7	ED$_3$
					5,4	600	49,6	ED$_4$
						650	47,2	ED$_5$
						700	45,1	ED$_6$
						750	42,6	ED$_7$

Comme électrolyte on a utilisé une solution de KOH 5N ; la température a été de 25 ± ±0,1°.

La cellule de travail a été confectionnée en polystyrène (120 × 72 × 56 mm).

L'alimentation des électrodes avec de l'hydrogène, à des surpressions constantes (50 à 250 mm Hg), a été réalisée à l'aide d'une installation présentée dans un travail antérieur[10].

RÉSULTATS ET DISCUSSION

Les électrodes E$_1$, E$_2$, E$_5$, E$_6$, E$_3$ et E$_9$ ont présenté un degré réduit de frittage et n'ont pas la résistance mécanique nécessaire pour leur étude électrochimique.

Des courbes de polarisation η — i, déterminées pour chaque électrode à différentes surpressions de l'hydrogène, nous avons extrait les valeurs des surtensions à différentes densités de courant, rapportées à la surface extérieure de l'électrode (tableau 2).

---

[10] O. Radovici, M. Mavrodin-Tărăbîc, I. Onaca et I. Solacolu, *Rev. Roumaine Chim.*, **17**, 1153 (1972).

Tableau 2

Valeurs de la surtension caractéristiques des électrodes à gaz en nickel, à différentes densités de courant

Electrode	Surpression de l'hydrogène	Surtension, à une densité de courant de			
		20 mA/cm²	50 mA/cm²	70 mA/cm²	100 mA/cm²
	mm Hg	mV	mV	mV	mV
E_3	100	640	780	800	850
	150	700	770	805	860
E_4	100	630	735	740	775
	150	600	740	750	765
E_7	100	620	710	730	750
	150	680	720	735	755
E_{10}	100	580	730	740	790
	150	570	640	750	800
E_{11}	100	590	700	720	750
	150	640	695	730	760
E_{12}	100	540	565	580	650
	150	525	560	570	620
	200	510	565	600	630
	250	550	590	610	655
E_{13}	100	510	540	550	585
	150	500	550	550	560
	200	520	550	565	580
	250	530	580	590	610
E_{14}	100	520	575	600	650
	150	440	540	590	630
	200	460	540	580	615
	250	500	570	605	640
E_{15}	100	560	710	730	750
	150	550	700	745	770
	200	520	620	670	740
	250	530	660	690	760
E_{16}	100	470	500	515	530
	150	480	510	530	545
	200	500	525	540	570
	250	515	540	560	580
E_{17}	100	540	570	590	620
	150	520	550	570	600
	200	530	580	600	640
	250	545	610	640	
E_{18}	100	550	700	740	820
	150	525	630	695	760
	200	540	660	780	
	250	560	635	710	
E_{19}	100	630	800	850	890
	150	620	710	720	740
	200	600	680	800	
	250	605	690	750	
ED_1	50	580	600	610	635
	100	520	570	580	610
	150	590	615	630	650
ED_2	50	400	470	485	500
	100	350	460	470	500
	150	370	495	510	530
ED_3	50	420	495	510	535
	100	355	465	480	510
	150	430	530	525	540

Tableau 2 (*suite*)

Electrode	Surpression de l'hydrogène	Surtension, à une densité de courant de			
		20 mA/cm²	50 mA/cm²	70 mA/cm²	100 mA/cm²
	mm Hg	mV	mV	mV	mV
ED_4	50	520	550	565	590
	100	470	505	525	550
	150	495	525	540	570
ED_5	50	440	480	500	520
	100	435	460	480	500
	150	470	495	510	535
ED_6	50	500	530	550	580
	100	450	475	490	510
	150	475	505	515	545
ED_7	50	520	550	590	620
	100	470	490	500	560
	150	485	510	525	570

2.1. L'EFFET DE LA PRESSION

2.1.1. Modifications structurales

L'effet de la variation de la pression entre les limites de 2,9 et 5,4. 10^8 N/m² sur la structure des électrodes est illustré par les microphotographies présentées dans la figure 1 (on a choisi seulement les microphotographies qui représentent les modifications structurales les plus évidentes).

De l'examen comparatif des microphotographies présentées dans la figure 1, il résulte que, dans le cas des électrodes frittées à 700°, l'augmentation de la pression, de la valeur de $3{,}75.10^8$ N/m² (a) à $4{,}6.10^8$ N/m² (b) conduit à un degré de frittage évidemment plus avancé. Ainsi, dans la figure 1 *b* on constate la disparition des zones partiellement frittées, visibles dans la figure 1 *a*. On constate le même phénomène en examinant les figures 1 *c* et 1 *d*, caractéristiques des électrodes frittées à 750°, les différences structurales étant moins évidentes, à cause du fait que le degré de frittage des deux électrodes (E_{11} et E_{15}) est relativement plus avancé.

2.1.2. Polarisation des électrodes

Les données de polarisation présentées dans le tableau 2 nous ont permis de tracer les courbes qui représentent la variation de la surtension des électrodes (du type DSK) en fonction de la pression à laquelle elles ont été réalisées (la figure 2, pour les électrodes frittées à 700° et la figure 3, pour les électrodes frittées à 750°), pour différentes densités de courant et différentes surpressions de l'hydrogène.

De l'examen des courbes $\eta = f(p)$, présentées dans la figure 2, il résulte que, pour les électrodes caractérisées par une structure du type DSK (frittées à 700°), la valeur minimale de la surtension correspond à la pression de $4{,}6.10^8$ N/m², à toutes les surpressions de l'hydrogène et densités de courant considérées.

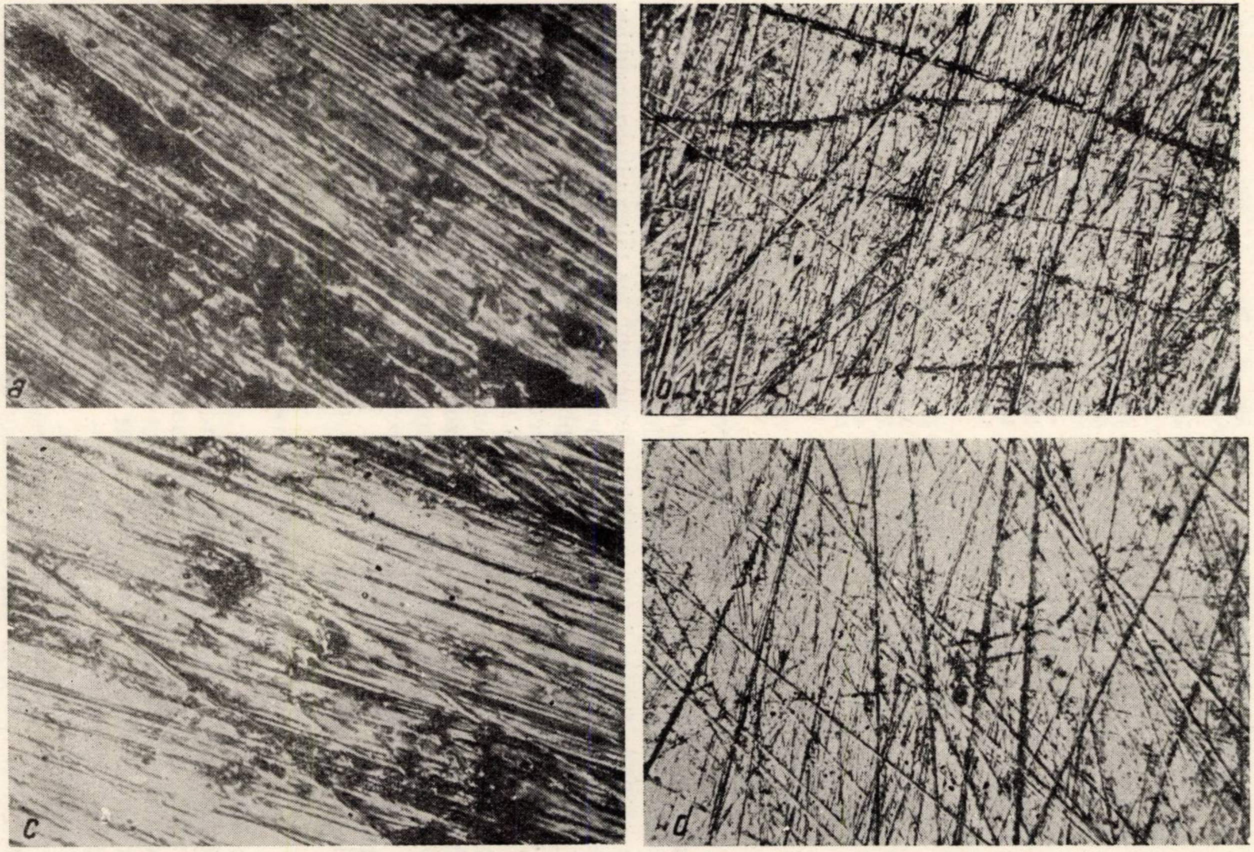

Fig. 1. — Influence de la pression sur la structure des électrodes de type DSK.

a, électrode E_{10} (3,75.10^8 N. m^{-2} 700°), *b* – électrode E_{14} (4,6.10^8 N. m^{-2}; 700°), *c*, électrode E_{11} (3,75.10^8 N.m.$^{-2}$; 750°), *d*, électrode E_{15} (4,6.10^8 N. m^{-2}; 750° (Microphotographies, 500 X)

L'examen des courbes $\eta = f(p)$ (fig. 2), dans le cas des électrodes frittées à 750°, nous a permis de tirer les conclusions suivantes :

— pour les petites densités de courant (jusqu'à 20 mA/cm^2), à toutes les valeurs de la surpression de l'hydrogène, la surtension minimale correspond aux électrodes comprimées à 4,6.10^8 N/m^2 ;

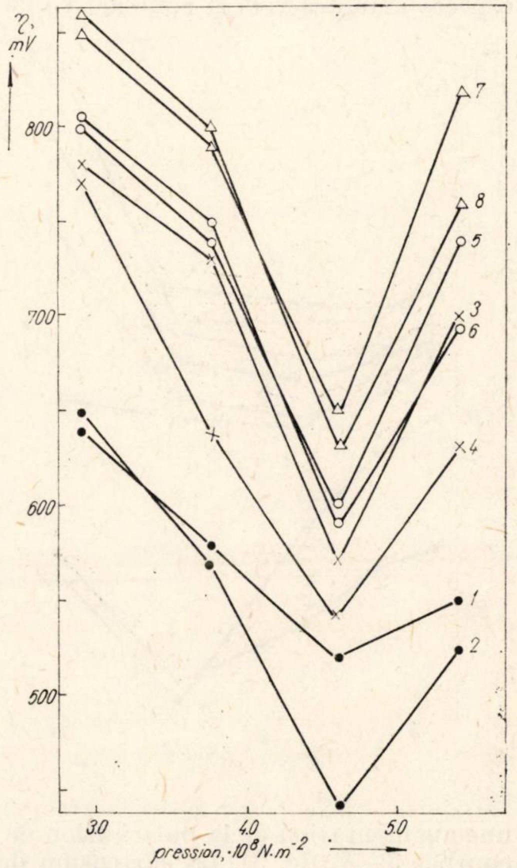

Fig. 2. — Influence de la pression sur la polarisation des électrodes de type DSK frittées à 700°.
1 – 20 mA/cm^2, 100mm Hg; *2* – 20 mA/cm^2, 150 mm Hg; *3* – 50 mA/cm^2, 100 mm Hg; *4* – 50 mA/cm^2, 150 mm Hg; *5* – 70 mA/cm^2, 100 mmHg; *6* – 70 mA/cm^2, 150 mm Hg; *7* – 100 mA/cm^2, 100mm Hg; *8* – 100 mA/cm^2, 150 mm Hg.

— pour de plus grandes densités de courant (50–100 mA/cm^2), à toutes les valeurs de la surpression de l'hydrogène, la surtension minimale correspond aux électrodes comprimées à 3,75. 10^8 N/m^2.

Cette différence entre le comportement des électrodes E_{11} et E_{15} s'explique par le fait que, dans un système poreux considéré, à de petites densités de courant prédomine la polarisation d'activation, tandis que, à de grandes densités de courant prédomine la polarisation de diffusion. Dans le cas des électrodes considérées, la diminution du diamètre des pores, effet de l'augmentation de la pression à laquelle ont été comprimées les électrodes frittées à la même température, produit, à de petites densités de courant, une diminution de la surtension des électrodes (le frittage plus avancé des électrodes conduit à la diminution du diamètre des pores et, par conséquent, à l'augmentation du rapport qui existe entre la surface intérieure électrocatalytique active et la surface extérieure à laquelle sont rapportés les courants mesurés) ; à des plus grandes densités de courant, la diminution du diamètre des pores rend plus difficile la diffusion des espèces ioniques vers la zone active de réaction, ce qui a comme résultat une augmentation de la polarisation de diffusion, illustrée par l'aspect des courbes *3*—*8* (fig. 3). La surtension des électrodes augmente avec l'augmentation de la pression dans l'intervalle 3,75—4,6.10 ^{8} N/m^2.

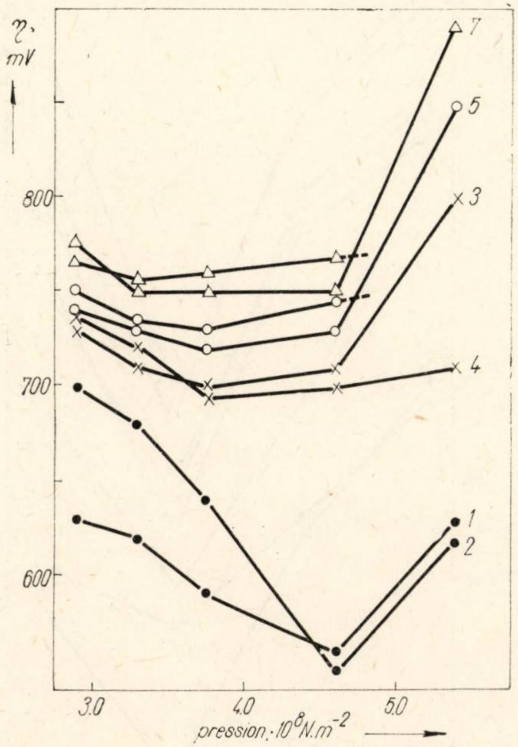

Fig. 3. — Influence de la pression sur la polarisation des électrodes de type DSK frittées à 750°.
1 — 20 mA/cm^2; 100 mm Hg; *2* — 20 mA/cm^2, 150 mm Hg; *3* — 50 mA/cm^2, 100 mm Hg; *4* — 50 mA/cm^2, 150 mm Hg; *5* — 70 mA/cm^2, 100 mmHg; *6* — 70 mA/cm^2, 150 mm Hg; *7* — 100 mA/cm^2, 100 mm Hg; *8* — 100 mA/cm^2, 150 mm Hg.

Tel qu'on le voit, à des densités de courant plus grandes (50—100 mA/cm^2), l'effet favorisant de l'augmentation de la surface intérieure active, au-dessus d'une certaine valeur, ne se reflète pas dans les performances des électrodes, à cause de l'augmentation de la polarisation de diffusion.

2.2. L'EFFET DE LA TEMPÉRATURE DE FRITTAGE

2.2.1. **Modifications structurales**

L'effet de la variation de la température de frittage (dans l'intervalle 600—750°) sur la structure des électrodes est illustré par les microphotographies présentées dans la figure 4.

De l'examen comparatif des microphotographies 4 *a*, 4 *b*, 1*b* et 1 *d*, caractéristiques des électrodes comprimées à $4{,}6.10^8$ N/m^2 on constate que les zones partiellement frittées à 600° (4 *a*) se réduisent dans le cas du frittage de l'électrode à 650° (4 b) et disparaissent dans le cas de l'électrode E_{14} frittée à 700° (1 b). A une température de frittage de 750° le numéro et le diamètre des pores se réduisent sensiblement (1 d).

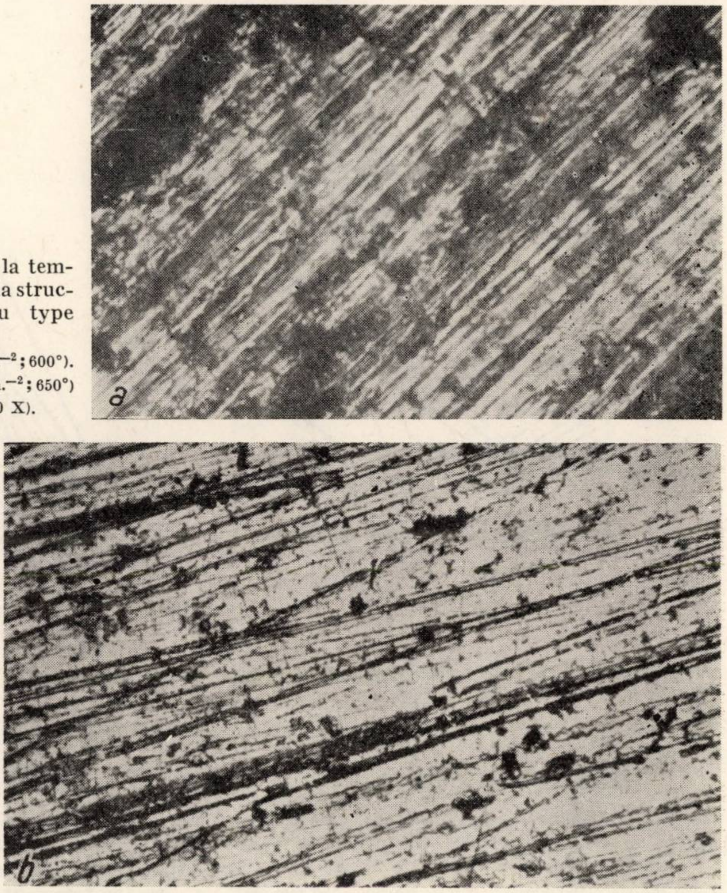

Fig. 4. — Influence de la température de frittage sur la structure des électrodes du type DSK.
a – électrode $E_{12}(4{,}6.10^8\ N.m^{-2};\ 600°)$.
b – électrode $E_{13}(4{,}6.10^8\ N.m.^{-2};\ 650°)$
(Microphotographies, 500 X).

2.2.2. Polarisation des électrodes

En utilisant les données de polarisation présentées dans le tableau 2, on a tracé les courbes qui représentent la variation de la surtension des électrodes caractérisées par une structure bidispersée (du type DSK) en fonction de la température de frittage (fig. 5, pour les électrodes comprimées à $4{,}6.10\ ^8$N/m^2 et fig. 6, pour les électrodes comprimées à $5{,}4.10\ ^8$N/m^2), pour différentes densités de courant et surpressions de l'hydrogène.

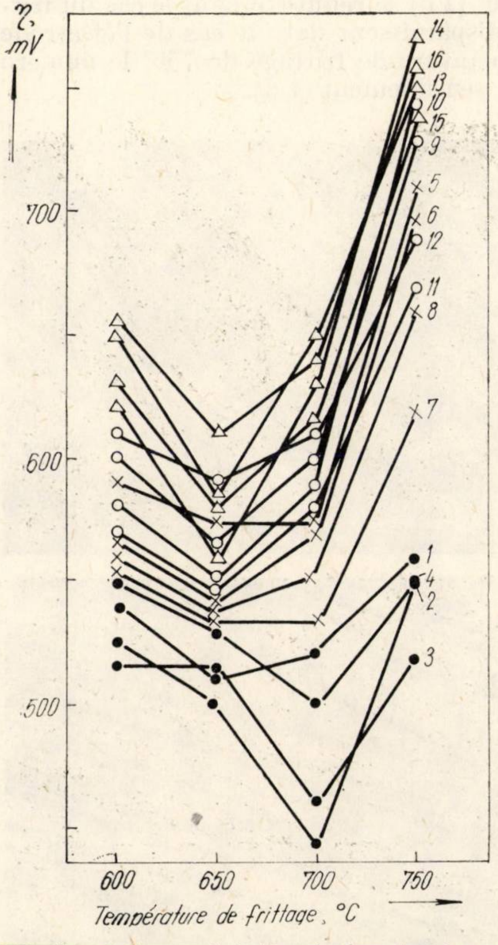

Fig. 5. — Influence de la température de frittage sur la polarisation des électrodes du type DSK comprimées à 4,6.10^8 N.m^{-2}.

1—20 mA/cm^2, 100 mmHg; *2* — 20 mA/cm^2, 150 mm Hg; *3*—20 mA/cm^2, 200 mm Hg; *4*—20 mA/cm^2, 250 mm Hg; *5*—50 mA/cm^2, 100 mm Hg. *6*—50 mA/cm^2, 150 mm Hg; *7*—50 mA/cm^2, 200 mm Hg; *8*—50 mA/cm^2, 250 mmHg; *9*—70 mA/cm^2, 100 mm Hg; *10*—70 mA/cm^2, 150 mm Hg; *11*—70 mA/cm^2, 200 mm Hg; *12*—70 mA/cm^2, 250 mm Hg; *13*—100 mA/cm^2, 100 mmHg; *14*—100 mA/cm^2, 150 mm Hg; *15* —100 mA/cm^2, 200 mm Hg; 16 — 100 mA/cm^2, 250 mm Hg.

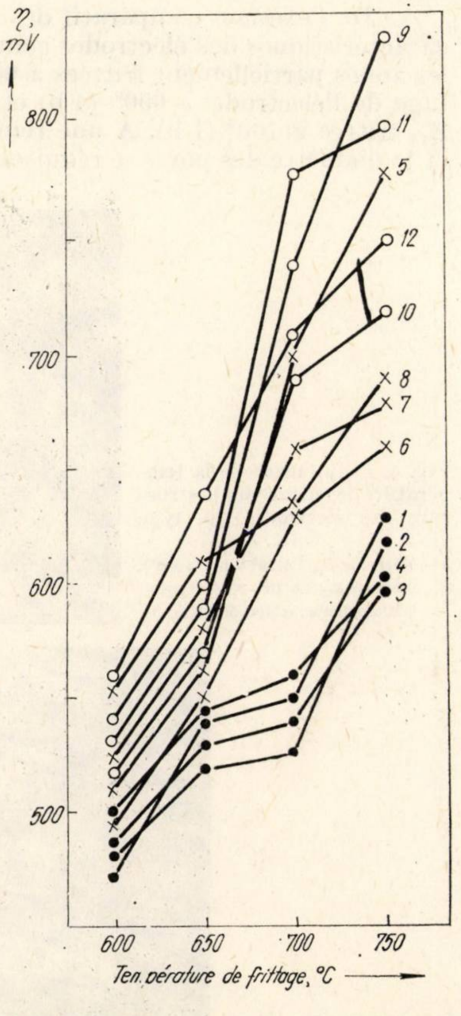

Fig. 6. — Influence de la température de frittage sur la polarisation des électrodes du type DSK comprimées à 5,4.10^8 N.m^{-2}.

1 — 20mA/cm^2, 100 mm Hg; *2* —20mA/cm^2, 150mm Hg; *3* — 20mA/cm^2, 200mmHg; *4* — 20mA/cm^2, 250 mm Hg; *5* — 50 mA/cm^2, 100 mm Hg; *6* — 50 mA/cm^2, 150 mm Hg; *7* — 50 mA/cm^2, 200 mm Hg; *8* — 50 mA/cm^2, 250 mm Hg; *9* — 70 mA/cm^2, 100 mm Hg; *10*—70 mA/cm^2, 150 mmHg; *11*—70 mA/cm^2, 200 mmHg; *12*—70 mA/cm^2, 250 mm Hg.

De l'examen des courbes $\eta = f(t)$ (présentées dans la figure 5), caractéristiques des électrodes à gaz comprimées à 4,6.10^8 N/m^2, on peut tirer les conclusions suivantes :

— à de petites densités de courant (20 mA/cm^2), les électrodes frittées à 700° présentent des surtensions minimales à des surpressions de l'hydrogène comprises entre 150 et 250 mm Hg ; pour une surpression de l'hydrogène de 100 mm Hg, les surtensions minimales ont été présentées par les électrodes frittées à 650°, ce qui s'explique par la corrélation directe qui existe entre la surpression du gaz et le diamètre des pores ($\Delta P = 2\sigma/\mathrm{r}$) ;

— à de densités de courant moyennes (50 $\mathrm{mA/cm^2}$), les valeurs minimales de la surtension ont été enregistrées pour les électrodes frittées à 650° (courbes *5* et *6*) à des valeurs de la surpression de l'hydrogène de 100 et, respectivement, de 150 mm Hg et pour les électrodes frittées à 700° (courbes *6* et *7*) à des valeurs de 200 et de 250 mm Hg ;

— à des densités de courant plus grandes (70—100 $\mathrm{mA/cm^2}$), la valeur minimale de la surtension s'enregistre, pour les électrodes frittées à 650°, à toutes les valeurs de la surpression de l'hydrogène.

Le déplacement de la température optimale de frittage, de la valeur de 700° à 650°, à mesure que la densité de courant augmente, s'explique, ainsi qu'on a démontré à 2.1.2., par l'augmentation de la contribution de la polarisation de diffusion à la polarisation totale de l'électrode à gaz. La diminution du diamètre de pores, effet de l'augmentation de la température de frittage de l'électrode, conduit à la diminution de la surtension de l'électrode dans le cas de petites densités de courant (à cause de l'augmentation de la surface de la zone active de réaction) et, au contraire, à l'augmentation de la surtension de l'électrode, dans le cas de grandes densités de courant (dans les pores à petit diamètre la diffusion est plus difficile).

De l'examen des courbes $\eta = \mathrm{f(t)}$ (fig. 6), caractéristiques des électrodes comprimées à $5{,}4.10^8\ \mathrm{N/m^2}$, il résulte que la température de frittage à laquelle les électrodes présentent des surtensions minimales est déplacée vers 600°, à toutes les densités de courant et surpressions de l'hydrogène, comme résultat de l'augmentation de la pression à laquelle ont été réalisées les électrodes de la valeur de $4{,}6 \cdot 10^8\ \mathrm{N/m^2}$ à $5{,}4 \cdot 10^8\ \mathrm{N/m^2}$. Ce comportement est explicable vu la dépendance inverse qui existe entre ces deux principaux paramètres d'obtention des électrodes à gaz.

2.3. MODIFICATIONS DES PARAMÈTRES OPTIMAUX EN FONCTION DU TYPE DE STRUCTURE

Les courbes qui représentent la variation de la surtension des électrodes à gaz caractérisées par une structure du type double couche (avec une couche barrière), en fonction de la température de frittage, sont présentées dans la figure 7 (pour les électrodes comprimées à $4{,}6 \cdot 10^8\ \mathrm{N/m^2}$) et dans la figure 8 (pour les électrodes comprimées à $5{,}4 \cdot 10^8\ \mathrm{N/m^2}$).

De l'examen des courbes $\eta = f(t)$ (fig. 7) on constate que, à toutes les valeurs des densités de courant et des surpressions de l'hydrogène, la température de frittage à laquelle les électrodes présentent des surtensions minimales est de 700°.

Les courbes de la figure 8 révèlent que la température de frittage des électrodes caractérisées par une structure du type double couche, comprimées à $5{,}4.10 \cdot \mathrm{N/m^2}$, est de 650°.

Si on compare les valeurs des températeurs de frittage établies pour les électrodes à gaz du type DSK (650°, pour les électrodes comprimées à $4{,}6\cdot 10^8$ N/m², à des densités de courant moyennes et grandes et 600°, pour les électrodes comprimées à $5{,}4\cdot 10^8$ N/m², à toutes les valeurs des densités de courant) avec celles caractéristiques des électrodes à double couche (700° et, respectivement, 650°), on constate une augmentation de

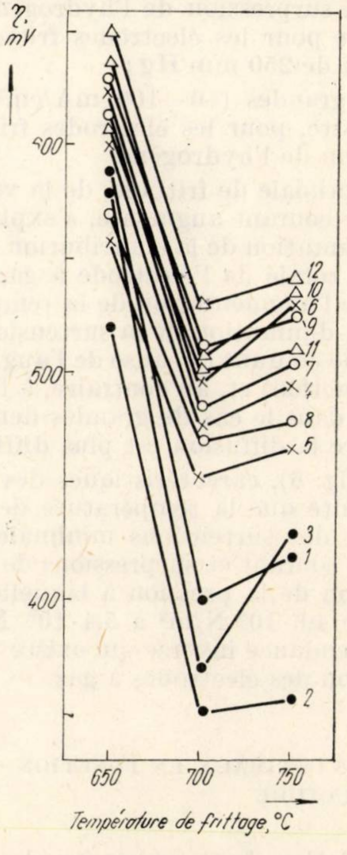

Fig. 7. — Influence de la température de frittage sur la polarisation des électrodes à double couche, comprimées à $4{,}6\cdot 10^8$ N.m^{-2}.

1 — 20 mA/cm², 50 mm Hg; 2 — 20 mA/cm², 100 mm Hg; 3 — 20 mA/cm², 150 mm Hg; 4 — 50 mA/cm², 50 mm Hg; 5 — 50 mA/cm², 100 mm Hg; 6 — 50 mA/cm², 150 mm Hg; 7 — 70 mA/cm², 50 mm Hg; 8 — 70 mA/cm², 100 mm Hg; 9 — 70 mA/cm², 150 mmHg; 10 — 100 mA/cm², 50 mm Hg; 11 — 100 mA/cm², 100 mmHg; 12 — 100 mA/cm², 150 mm Hg.

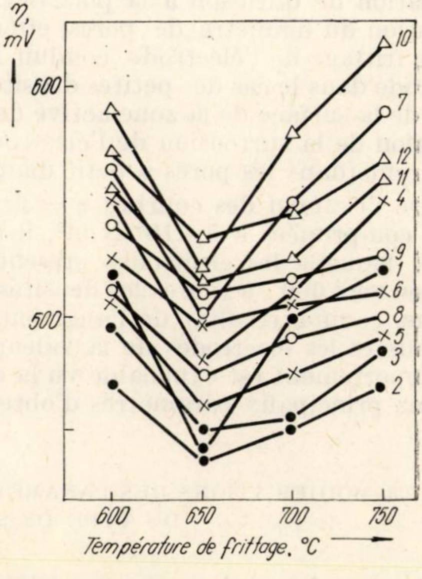

Fig. 8. — Influence de la température de frittage sur la polarisation des électrodes à double couche, comprimées à $5{,}4\cdot 10^8$ N.m.$^{-2}$.

1 — 20 mA/cm², 50 mm Hg; 2 — 20 mA/cm², 100 mm Hg; 3 — 20 mA/cm², 150 mm Hg; 4 — 50 mA/cm², 50 mm Hg; 5 — 50 mA/cm², 100 mm Hg; 6 — 50 mA/cm², 150 mm Hg; 7 — 70 mA/cm², 50mm Hg; 8 — 70 mA/cm², 100 mm Hg; 9 — 70mA/cm², 150 mm Hg; 10 — 100 mA/cm², 50 mm Hg; 11 — 100 mA/cm², 100 mm Hg; 12 — 100 mA/cm² ,150 mm Hg.

la température d'environ 50°. Etant donné que la couche B des électrodes du type barrière présente une structure identique à celle des électrodes du type DSK, cette différence de comportement s'explique par les particularités structurales de la couche A. (Dans ce cas, la pression aux points de contact des granules est plus réduite.) Il est évident que, étant donné la dépendance inverse des valeurs des paramètres de réalisations des électrodes à gaz (pression et température), la température de frittage, à laquelle les électrodes à gaz présentent des surtensions minimales, a une valeur relativement plus élevée dans le cas des électrodes caractérisées par une structure du type double couche.

3. CONCLUSIONS

1. La valeur à laquelle doivent être comprimées les électrodes est de $4,6 \cdot 10^8$ N/m², à toutes les surpressions de l'hydrogène et densités de courant, pour les électrodes du type DSK, obtenues par compression et frittage à 700° d'un mélange homogène qui contient 25 % nickel ex nickel carbonyle, 50% carbonate de nickel et 25% acide oxalique.

2. Dans le cas des électrodes du même type, frittées à 750°, le système poreux favorable au fonctionnement à de petites densités de courant (jusqu'à 20 mA/cm²) s'obtient par compression des mélanges homogènes à $4,6 \cdot 10^8$ N/m², tandis que, pour le fonctionnement à des densités de courant plus grandes (50—100 mA/cm²), le système poreux adéquat s'obtient par compression à $3,75 \cdot 10^8$ N/m². Cette différence de comportement s'explique par la différente contribution de la polarisation de diffusion à la polarisation totale des électrodes : les densités de courant supérieures réclament des systèmes poreux aux pores relativement plus grands.

3. Pour les électrodes caractérisées par une structure bidispersée (du type DSK), comprimées à $4,6 \cdot 10^8$ N/m², la valeur de la température de frittage, à laquelle les électrodes présentent des surtensions minimales, est de 700°, dans le cas du fonctionnement des électrodes à des densités de courant jusqu'à 20 mA/cm² et de 650°, dans le cas du fonctionnement à des densités de courant situées dans le domaine de 50—100 mA/cm².

4. Pour les électrodes à gaz caractérisées par une structure du type DSK, comprimées à $5,4 \cdot 10^8$ N/m², la température adéquate de frittage est de 600°.

5. Dans le cas des électrodes à gaz du type double couche (réalisées par la compression des deux couches surposées : la couche A — barrière, avec la composition 50% poudre de nickel et 50% carbonate de nickel et la couche B, avec une composition identique à celle des électrodes du type DSK) les valeurs adéquates de la température de frittage, auxquelles les électrodes étudiées présentent des surtensions minimales dans la réaction d'oxydation de l'hydrogène, sont : 700°, pour les électrodes comprimées à $4,6 \cdot 10^8$ N/m² et 650°, pour les électrodes comprimées à $5,4 \cdot 10^8$ N/m².

Revue Roumaine de Chimie, 20, 4, 501—513 (1975)

Revue Roumaine de Chimie, **20**, *4*, 515–521 (1975)

THE ELECTRONIC STRUCTURE AND SPECTRA OF THE Di-μ-SULPHIDO-BIS-[OXO-(L-CYSTEINATO)MOLYBDATE (V)]$^{2-}$ ION

D.H. BROWN and P.G. PERKINS

Department of Pure and Applied Chemistry, University of Strathclyde,
Glasgow Gl 1XL, Scotland

Received *February 13, 1974*

Compounds of molybdenum (V) react with cysteine in dilute acid solution to give the di-μ-oxo-bis (oxo-(L-cysteinato) molybdate (V)) ion. In the presence of sulphide, the corresponding sulphur-bridged compound is obtained. In this work, a theoretical study of the ground-state of the sulphur-bridged ion involving the all-valence-electron SCMO method has been carried out. It is found that there are strong bonding interactions in the bridge system. The interaction between the bridging sulphur atoms and those of the cysteine moieties, though small, is significant and could in part explain the fact that cysteine is one of the few ligands which can stabilise a sulphur bridge with respect to an oxygen bridge in aqueous solution. In separate calculations, the lower excited states were calculated, including configuration interaction : the results are in reasonable agreement with the experimental data obtained from ultraviolet and optical rotatory dispersion measurements.

INTRODUCTION

Molybdenum occurs naturally in a number of enzyme systems in an environment said to involve at least one sulphur atom. The structures of a number of complexes of molybdenum have been described with sulphur-containing ligands such as xanthates.[1] However, only a limited number[2,3] with nonligand sulphur bound to the molybdenum have been prepared although, in the absence of other ligands, sulphur can replace oxygen stepwise in the tetrahedral molybdate ion. In the presence of some organic ligands, sulphide ion reduces molybdenum (VI) to (V), with the complication that the reduced species sometimes contain sulphide ion. One of these reduced species containing sulphide ion, the complex Na_2 $[Mo_2O_2S_2$ $(SCH_2$ CH (NH_2) $CO_2)_2]$ $2H_2O$, has been previously prepared[4] and its electronic and optical rotatory dispersion spectra[5] described. A structural determination[3] has shown that the dimeric ion contains bridging sulphur, a terminal

[1] A. B. Blake, F. A. Cotton, and J.S. Wood, *J. Amer. Chem. Soc.*, **86**, 3024 (1964).

[2] M.C.B. Drew and A. Kay, *J. Chem. Soc.*, (*A*), **1971**, 1851. B. Spivac and Z. Dori, *J. Chem. Soc.*, (*Dalton*), **1973**, 1173.

[3] D. H. Brown and J.A.D. Jeffreys, *J. Chem. Soc.* (*Dalton*), **1973**, 732.

[4] A. Kay and P.C.H. Mitchell, *J. Chem. Soc.* (*A*) **1970**, 2421.

[5] D. H. Brown and J. MacPherson, *J. Inorg. Nuclear Chem.*, **34**, 1705 (1972).

oxygen atom, and a cysteine residue attached to each molybdenum. The aim of the calculations described in this paper was, first of all, to explain the nature of the electronic transitions observed both in the ultraviolet spectra and, since the complex was optically active, in the o.r.d. spectra. The second purpose was to try and determine why the di-sulphur-bridged system is stable only with a limited number of ligands — so far only with L-cysteine and its esters, L-histidine and ethylenediamine tetra-acetic acid. With other ligands such as α-hydroxycarboxylic acids, polyhydroxyalcohols and sugars, the di-oxo-bridge molybdenum (V) species are the dominant species in aqueous solution in the presence of sulphide ion.

Previous calculations on the di-oxo-bridge system[6] showed that the five highest filled and five lowest virtual orbitals were associated mainly with the Mo-Mo bonding system. In the case of the di-sulphur-bridged ion, it is necessary to consider the *d* orbitals of sulphur since previous calculations have shown that they are particularly important, both in the mutual interaction of the bridging sulphurs and with the other ligands attached to molybdenum. Thus, the calculations reported here include the formally empty *d*-orbitals situated on the sulphur atoms. Unfortunately, the complex we wish to study contains too many atoms for self-consistent field calculations of ground and excited states with configuration interaction to be readily carried out. Hence, a model system in which one cysteine ligand was replaced by an SH, an OH, and an NH_3 group, was studied, with the sulphur, oxygen, and nitrogen atoms occupying the sites corresponding to a cysteine ligand.

The calculational methods used throughout were identical to those previously described.[6]

RESULTS AND DISCUSSION

(i) REDUCTION OF MOLYBDENUM (VI) IN THE PRESENCE OF SULPHIDE ION

Molybdenum (VI) is reduced by sulphide ion (pH 4.0 and room temperature) to give the corresponding molybdenum (V) complex in the presence of the ligands, D-tartaric, L-malic, D-gluconic and L-aspartic acids, L-serine, L-threonine, L-cysteine and L-histidine. Of these complexes, the latter two ligands afford sulphur-bridged species.[4] Reduction does not take place in the presence of L-mandelic, L-lactic, D-glyceric acids, and D-glucose, D-talose, and D-mannitol, although all the latter ligands are known to form both molybdenum (V) and (VI) complexes in solution.[7] In studying the above systems, the species present were identified from their o.r.d. spectra by comparison with previous result.[5,7] The reason for the lack of reduction is, presumably, that these ligands cannot complex with the potentially oxidising molybdenum (VI)-oxide-sulphide ion.

The nature of the reduced species in solution varies. In the case of the L-cysteine and L-histidine complexes, the ultraviolet reflectance spectra of the sulphur-bridged solid complexes were the same as those of the corresponding solutions, suggesting that the species in solution were mainly the sulphur-bridged complexes. The o.r.d. of the oxygen-bridged and sulphur-bridged complexes in solution were appreciably different (table II and ref. 6). With the other ligands which gave reduction no solids containing significant amounts of sulphur were obtained, although, with D-tartaric acid, solutions were obtained which gave slightly different o.r.d. curves from the corresponding oxygen-bridged complexes (Cotton Effects at $-24.5, +30.0, -33.5, +37.5$ as compared to $-25.0, +28.5, -32.0, +35.0$). Solids were obtained from the tartaric acid solutions containing small amounts of sulphur but, on recrystallisation, only the dioxo-bridged tartrate complex $Na_4(Mo_2O_4(C_4O_6H_4)_2)\,4H_2O$ was obtained. These results suggest that reduction in tartrate solution with sulphide ion gives a mixture of species with the oxygen-bridged complex being the major product, whereas with other ligands such as L-cysteine and L-histidine : the sulphur-bridged dimer is the stable product. Since the complex for which a model is discussed in this paper, *ie*, $Na_2\,[Mo_2O_2S_2\,(SCH_2CH\,(NH_2)\,CO_2)_2]\,2H_2O$ can be prepared from the dioxo-bridged molybdenum (V)-cysteine complex on the addition of sulphide ion, it would suggest that the sulphur-and oxygen-bridged species are in equilibrium with the attached ligands.

---

[6] D. H. Brown, P.G. Perkins and J.J. Stewart, *J. Chem. Soc.*, (*Dalton*), **1972**, 1105; **1972**, 2243.

[7] D. H. Brown and J. MacPherson, *J. Inorg. Nuclear Chem.*, **32**, 3309 (1970) and **33**, 4203 (1971).

(ii) ORBITAL LEVELS AND CHARGE DISTRIBUTION

Owing to lack of symmetry of the ion examined, every molecular orbital will contain contributions from all the atomic orbitals of the basis set. Furthermore, as before, some molecular orbitals are localised on particular groups of atoms so that they alone describe the bonding approximately in certain isolated parts of the ion. In table I are listed the energies of the five filled orbitals of highest energy and the five virtual orbitals of lowest energy, together with the chief associated atomic orbitals. Because the species studied is an ion, the bound eigenvalues are positive in the scale. Superimposition of the appropriate cationic charge would exert a crystal-field effect and lower these linearly. The highest filled molecular orbital is localised in molybdenum-molybdenum bonding. This, is, as one

Table 1

Energies and character of highest bonding and lowest virtual orbitals, ψ_n

$\pm n$	E_n	
1	7.52	Mo-Mo bonding with trace on S (bridge).
2	5.67	S bridge and Mo-Mo
3	4.98	S brioge, Mo-Mo and O terminal
4	4.34	Mo-Mo, S bridge and S of cysteine
4	4.12	Diffuse over bridge system.
−1	16.35	Mo-Mo and some S bridge
−2	17.54	Mo-Mo and some S bridge
−3	17.59	Mo-Mo and Mo = O
−4	17.94	Mo-Mo
−5	18.42	Mo-Mo and Mo = O

would expect since the complex, although nominally involving molybdenum (V), is diamagnetic. All ten orbitals given in the table are associated mainly with the bridging system and the terminal oxygens. This means that the cysteine ligand perturbs them very little. Thus, one would expect the histidine complex, which has a similar bridging skeleton, to exhibit similar electronic and o.r.d. spectra. This, as is clear from table II, is found experimentally. The cysteine methyl-ester complex, which involves the Mo-Mo bond and is six coordinate with the same bridging skeleton [2] also affords a similar ultraviolet spectrum[4] (table II).

The bond orders and atomic charges are shown in figure I (*a*) and it is interesting that there are significant Mo-Mo and S—S interactions in the bridging moiety. Moreover, the limited but significant bonding between the bridging sulphur atoms with the sulphur atom of the cysteine and the terminal oxygen atoms is noteworthy (figure I (*b*)). The interaction of these sulphurs with the nitrogen and oxygen atoms of the cysteine ligand is considerably less evident. This is a consequence of *d*-orbital participation, since when *d* orbitals on the sulphurs were omitted from the calculation, it was found that the sulphur-sulphur and sulphur-terminal oxygen bond indices fell to less than 0.1. The bond distances S (br)-S (br). 0.366nm, S (br)-S (cyst), 0.324 nm, are close to the Pauling values for van der Waal's radii (0.370 nm). However, S-S bonding forces operate over large distances, *eg*, in S_4N_4 and Cs_2S_6, which have S—S distances of 0.258 nm[8] and 0.340 nm[9], respectively. This effect stems mainly from the diffuseness of sulphur *d* orbitals in an environment of atoms of low electronegativity. The radial maximum for a Slater orbital in this situation is between 0.16 nm and 0.19 nm, hence good overlap can clearly be expected between S atoms separated by <0.4 nm. In the compound studied here, the S—S bonds are mainly *d—p* and *d—s* in character.

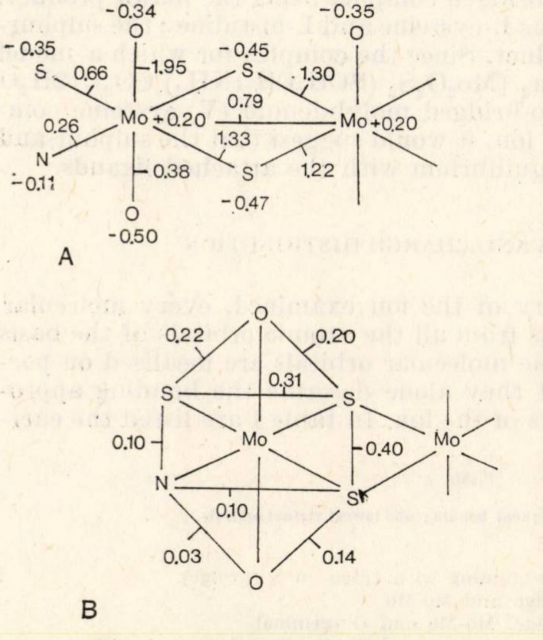

Fig. 1. — Charge distribution.

As mentioned above, only four sulphur-bridged compounds of this type have so far been isolated : this is striking when it is considered how many similar oxygen-bridged species exist. It is of interest to see to what extent our calculations throw light on this situation. Clearly the thermo-

---

[8] D. CLARK, *J. Chem. Soc.*, **1952**, 1615.

[9] S. C. ABRAHAMS and E. GRISON, *Acta Cryst.*, **6**, 206 (1953).

Table 2

Electronic spectra and cotton effects

Calculated states			Experimental kK				
			L-cysteine complex		L-histidine complex		Cysteine methyl ester
Main contributing configurations *m n*	Energy kK	Oscillator strength × 10 3	Electronic spectra	Cotton effects	Electronic spectra	Cotton effects	Electronic spectra
n *m*			13.0 (sh)				
1 1 → −1	21.60	0.6	23.2	+24.5	21.7	+23.5	22.3
2 1 → −3 1 → −2	29.40	0.6	28.6	−27.7	29.0	−27.5	27.8
3 1 −4	31.20	2.8					
4 1 → −2 1 → −3 2 → −1	32.16	124.7					
5 1 → −2 1 → −3 2 → −1	32.74	192.2	— 36.0	+31.3 −36.0	33.5 —	+30.5 −34.0	— 36.2
6 1 → −5 1 → −2 1 → −3	34.56	156.6					
7 3 → −1 2 → −2 4 → −1	36.12	10.6					
8 3 → −2 2 → −2 3 → −3	42.42	11.7					
9 2 → −3 2 → −2 3 → −2	42.56	7.9					
10 2 → −3 3 → −2 3 → −4	42.18	11.7	44.1		43.2		45.2
11 5 → −1 4 → −1 2 → −4	42.43	11.5					
12 4 → −1 2 → −4 2 → −3	43.62	5.8					
13 2 → −4 5 → −1 4 → −1	44.12	3.4					

dynamic stabilities of sulphur- and oxygen-bridged species are delicately balanced (as witnessed by the way in which S can replace 0 stepwise in the molybdate ion) and it is likely that kinetic factors will sway any particular situation. Having said this, we must consider what are likely to be the important factors here.

Since HS^-, $S^=$, H_2O, and OH^- are all nucleophilic, then they will attack the molybdenum centre since this is the only one which is formally positively charged. Hence, the higher this positive charge in any particular species, the more favoured will be the associated transition state for substitution. This essentially reduces the activation energy for the substitution process. In order to become attached to the molybdenum atom, however, the attacking species must penetrate the repulsive screen of electron density which surrounds the centre of the octahedron. Thus, the more sparse this density becomes, the more kinetically favoured will the reaction be.

We can see how these two factors are likely to operate in the present situation by studying the charge distribution throughout the sulphur-bridged cysteine and related complexes. In the former, the molybdenum atom carries a low formal charge and, moreover, the ligand-ligand interaction over the outer faces of the octahedron forms a screen of electron density in which the only weak point is an S-N-O face. This electron cloud should be effective in repelling nucleophiles and even if attack took place at the known point of weakness, it would not disturb the sulphur bridge. Hence the kinetic stability of the sulphur-bridged complex when cysteine is the ligand is explained. When we consider the analogous di-oxo-bridged cysteine complex, we find that the formal charge on molybdenum is considerably higher than it is in the sulphur-bridged species.[6] Hence, we would expect attack by HS^- to replace the oxygen bridges and form a kinetically stable ion. This is as observed.

When tartaric acid is the ligand, the compound formed possesses a di-oxo bridge. In this case the detailed structure is, unfortunately, not known but one might reasonably expect the tartaric acid to act as a polydentate ligand through the oxygen atoms. Such an environment would cause the central molybdenum to assume a rather higher positive charge than it does with sulphur atoms attached, hence when sulphur bridges form they would be more easily replaceable under attack by OH^- or H_2O. The reduction of Mo (VI) to Mo (V) by sulphide in the presence of tartaric acid will almost certainly occur *via* the formation of 1 or 2 sulphur bridges and the equilibrium between the two types of bridge is probably finely balanced.

With mandelic acid, the above reduction does not occur and this implies that the Mo-S bonds are readily broken by attacking OH^- or H_2O. This correlates with what can be surmised regarding the electronic structure of a complex of this ligand. Mandelic acid is potentially bidentate and a 1 :1 (mandelic acid : molybdenum) complex would leave at least two positions on the octahedron free for OH groups or terminal oxygens. These remove charge from molybdenum very effectively and hence we would expect the latter atom to be highly positively charged, as compared with the tartrate complex where the ligand may be quadridentate. (the oxalato- and edta complexes are a similar pair and bear out this argument[6]). In addition, electronic screening around the octahedron is poorly effected by oxygen atoms. Hence, overall we would expect the system Mo (VI)/ /mandelic acid to be unaffected by sulphide ion.

In the histidine complex, where the disulphur bridge is known, the ligand is tridentate, the donor atoms being an oxygen (of COO^-) and two nitrogens (from -NH_2 and the imidazole ring). In this complex the electronic screening will be less effective than in the cysteine adduct but the molybdenum will acquire only a low formal charge, as nitrogen atoms are less effective than oxygens in removing electrons. In the sulphur-bridged edta complex [2] the ligand acts as an additional bridge. This situation is, however, outside the scope of the present work.

It seems, therefore, that the stabilities of these complexes can be rationalised on the above basis. Clearly, however, the factors are finely balanced in individual cases.

(iii) EXCITED STATES

The results of the excited-state calculation and configuration interaction treatment are given in table II. Since the experimental data (ultraviolet and o.r.d. spectra) are not available for the regions above 45,000 and 40,000 cm^{-1}, only calculated states up to 45,000 cm^{-1} are recorded. The experimental ultraviolet spectra of both the L-cysteine and L-histidine complexes show peaks at about 36,000cm^{-1}, and 44,000cm^{-1} together with shoulders at 23, 000 cm^{-1} and 28,000 cm^{-1}. A shoulder at 13,000 cm^{-1} has also been reported[4] but in several samples we prepared, this shoulder was not reproducible and it could, perhaps, arise from traces of 'molybdenum blue' stemming from incomplete reduction of molybdenum (VI). Otherwise, the observed and calculated results are in reasonable agreement with two weak peaks in the region 20,000 – 30,000 cm^{-1}, followed by strong absorption around 33,000 cm^{-1} and a further region of absorption over 40,000cm^{-1}. It should be noted that, *eg*, in the latter region, the six calculated states have an energy spread of ~2kK. Hence, the natural line width for absorption to each state will ensure that these states will merge in the experimental spectrum, giving one observable band. Without further information on the individual band contours, closer comparison is not possible. The o.r.d. spectra show four Cotton Effects between 20,000 cm^{-1} and 36,000 cm^{-1}, and indicate the presence of at least one other electronic transition in this region.

Revue Roumaine de Chimie, **20**, *4*, 523–530 (1975)

SYNTHESIS OF THE BROMO-*m*-XYLIDINE-bis-ETHYLENEDIAMINE-COBALT(III) COMPLEX AND ITS AQUATION KINETICS IN ACID SOLUTIONS

RALUCA RIPAN and MARIA VÁRHELYI *

Chair of Inorganic Chemistry, Faculty of Chemistry, Babeş-Bolyai University, Str. Arany János 11, Cluj-Napoca, Romania

Received June, 2 1974

The complex $[Co(en)_2\ Br\ (m\text{-xylidine})]\ (NO_3)_2$ has been synthesized and its geometric configuration has been proved on the basis of i.r. spectra. The aquation kinetics of the complex ion has been studied at six temperatures in the presence of various amounts of perchloric acid. The complex ion participates in a protolytic equilibrium : $[Co\ (en)_2\ Br\ (amH)]^{2+}(I) \rightleftarrows [Co\ (en)_2\ Br\ (am)]^{+}(II) + H^{+}$. Both forms (I) and (II) participate in aquation reactions. For the amino-form (I) an activation enthalpy of $\Delta H^{\ddagger} = 24.9 \pm 0.6$ kcal/mole and for the amido-form $\Delta H^{\ddagger} = 21.2 \pm 1.2$ kcal/mole have been found. These data are compared to the kinetic parameters of the aquation reactions of analogous complexes, and they are discussed, by presuming a S_N1 mechanism.

The $[Co(en)_2Cl_2]^+$ and $[Co\ (en)_2Br_2]^+$ complexes react easily with primary and tertiary aliphatic, as well as with aromatic and heterocyclic amines or phosphines. This nucleophilic substitution reaction has been studied from point of view of preparation first by Meisenheimer and Kiderlen.[1] Ablov's investigations [2] have shown the formation of $[Co\ (en)_2\ Cl\ (amine)]^{+2}$ and $[Co\ (en)_2\ Br\ (amine)]^{2+}$ respectively, from the dihalogeno-derivatives under the action of aromatic amines, if the pK_b value of the amine is between 9–11. If the amine is a weaker base, only a geometric isomeric rearrangement occurs or $[Co\ (en)_2X\ (H_2O)]^{2+}$ is formed. In the course of this synthesis the formation of $[Co(en)_3]^{3+}$ was observed, too. Bailar and Clapp[3] showed the complexity of this reaction and the impossibility to find a relationship between the basicity (pK) of the amines and the nature of the products obtained. Bromo-amine-derivatives of this type were described and characterized with heterocyclic amines and with aniline, m- and p-toluidine.

In this paper a new compound $[Co(en)_2\ Br\ (m\text{-xylidine})]\ (NO_3)_2$ is reported and its aquation kinetics is studied.

---

* Part of Ph. D. thesis.

[1] H. MEISENHEIMER and E. KIDERLEN, *Liebigs Ann. Chem.*, **438**, 217 (1924).

[2] A. V. ABLOV, *Bull. Soc. chim. France*, **4**, 1783 (1937).

[3] J. C. BAILAR and L. B. CLAPP, *J. Amer. Chem. Soc.*, **67**, 171 (1945).

The bivalent complex cation has been obtained by the following ligand exchange reaction :

$$trans\text{-}[Co(en)_2Br_2]^+ + m\text{-xylidine} = cis\text{-}[Co(en)_2Br(m\text{-xylidine})]^{2+} + Br^- \quad (1)$$

The geometric configuration of the new complex was proved by i.r. spectral investigation.

The i.r. spectrum of the above mentioned compound is presented in fig. 1.

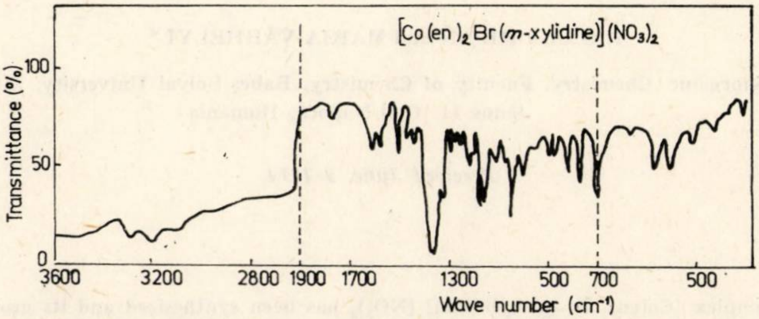

Fig. 1. — IR spectrum of $[Co\ (en)_2\ Br\ (m\text{-xylidine})]\ (NO_3)_2$.

The 510 cm^{-1}(m) and 460 cm^{-1}(m) absorption bands, which were found by Block[4] in the spectrum of $[Co\ (NH_3)_6]\ Cl_3$, too, can be assigned probably to the Co-N stretch frequencies, and this is consistent with the covalent character of the Co-N bond. The position of the ${}^{\nu}N-H$ stretch frequencies (3280 $cm^{-1}(m)$, 3200 cm^{-1} and 3090$-$3120 $cm^{-1}(m)$) pleads also for the strong covalent character of the Co$-$N bond. The shifts to lower frequencies are 200$-$250 cm^{-1} towards the free, non-coordinated amines. Amine deformation frequencies were found at the following wave numbers : ${}^{\delta s}NH_2$: 1610 $cm^{-1}(m)$, ${}^{\delta as}NH_2$: 1380 cm^{-1} (s) and ${}^{\gamma}NH_2$: 830 cm^{-1} (m) and 850 $cm^{-1}(m)$.

The i.r. spectrum enables us to make a choice between the *cis*- and *trans*-configurations, on the basis of the CH_2-rocking frequencies of the cobalt-ethylenediamine rings. These frequencies are presented in table 1 for the complex studied in comparison with some $[Co\ (en)_2\ XY]$ derivatives examined by Baldwin.[5]

Table 1

CH_2 – rocking frequencies (cm^{-1}) in the infrared spectra of some $[Co(en_2)\ XY]$ type complexes

Formula	Frequency	Reference
trans-$[Co(en)_2Cl_2]NO_3$	888	5
trans-$[Co(en)_2Br_2]NO_3$	890	this paper
trans-$[Co(en)_2Cl(NH_3)](NO_3)_2$	888	5
cis-$[Co(en)_2Cl(NH_3)](NO_3)_2$	900, 883	5
cis-$[Co(en)_2Cl(\beta\text{-picoline})]\cdot(NO_3)_2$	900, 882	9
cis-$[Co(en)_2Br(m\text{-xylidine})]\cdot(NO_3)_2$	898 870	this paper

---

[4] H. Block, *Trans. Faraday Soc.*, **55**, 867 (1959).

[5] M. E. Baldwin, *J. Chem. Soc.*, **1960**, 4369.

Since in the 870–900 cm^{-1} region two rocking frequencies appear, the studied complex must be of the *cis-* configuration.

The complex salts of this type undergo an aquation process leading to the release of halide ions.

$$[Co(en)_2X\,(amine)]^{2+} + H_2O = [Co(en)_2(H_2O)(amine)]^{3+} + X^- \qquad (2)$$

Aquation kinetics of some derivatives has been studied by Tobe,[6] Chan et al.,[7] Panasyuk et al.[8] and Zsakó et al.[9]

The aquation process of the chloro-pentamine type series with amine = NH_3 or aliphatic amines (methylamine, ethylamine, allylamine, etc.) was studied thouroughly. As compared to the analogous chloro-derivatives, the bromo-pentamines were little studied. Chan et al.[10] have found the aquation rate of the $[Co(en)_2Br\ (amine)]^{2+}$ derivatives to be 2.6–4.7 times larger than the rate of the analogous chloro-derivatives (amine = = aliphatic and heterocyclic amines). These authors carried out their kinetic measurements in neutral solutions, where the basic hydrolysis is not entirely hindered and experimental results do not allow to derive reliable activation parameters.

In a previous paper[11] the influence of the hydrogen ion concentration upon the aquation rate of the *cis*-$[Co(en)_2\ Br\text{-(benzylamine)}]^{2+}$ was studied. In the case of benzylamine and some heterocyclic amine derivatives [12] the decrease of the aquation rate with increasing hydrogen ion concentration to pH 2.5–3.0 is observed. By further acidification the rate constant remains practically constant. In the case of analogous complexes with aromatic amines in the inner co-ordination sphere the kinetic behaviour in acid medium differs substantially. In this case the aquation rate of the complexes decreases with the increase of the acidity even in more acid solutions than pH = 2.5. This observation was made in the case of $[Co\ (en)_2Cl\text{–(aniline)}]^{2+}$, $[Co(en)_2Cl(m\text{-toluidine})]^{2+}$ and $[Co(en)_2Cl\ (p\text{-toluidine})]^{2+}$ [13]

The influence of the hydrogen ion concentration upon the aquation rate can be explained by means of a protolytic equilibrium :

$$\underset{(I)}{[Co\ (en)_2X\,(amH)]^{2+}} \rightleftarrows \underset{(II)}{[Co(en)_2\,X\,(am)]^+} + H^+ \qquad (3)$$

---

[6] M. L. Tobe, *J. Chem. Soc.*, **1959**, 3776.

[7] S. C. Chan and F. Leh, *J. Chem. Soc.* (*A*), **1966**, 129, 137 ; **1967**, 288, 573, 908, 1730, 2010.

[8] V. D. Panasyuk and L. G. Reiter, *Zhur. neorg. Khim.*, **8**, 1131 (1963) ; **11**, 607 (1966) ; **12**, 2434 (1967).

[9] J. Zsakó, Cs. Várhelyi and D. Dobocan, *J. Inorg. Nuclear Chem.*, **31**, 1459 (1969).

[10] S. C. Chan and O. W. Lau, *Austral. J. Chem.*, **22**, 1851 (1969).

[11] R. Ripan and M. Várhelyi, *Stud. Univ Babeş-Bolyai, Chem.*, in press.

[12] Cs. Várhelyi, J. Zsakó and A. Ionuţ, *Monatsh,*, **104**, 1231 (1973).

[13] R. K. Nanda and R. N. Nanda, *Inorg. Chem.*, **8**, 104 (1969).

Both (I) and (II) forms participate in aquation reactions. The aquation of the amino-form (I) takes place according to the equation:

$$[Co(en)_2X\ (amH)]^{2+} + H_2O \xrightarrow{k_1} [Co(en)_2(H_2O)\ (amH)]^{3+} + X^- \quad (4)$$

The halogen exchange from the amido-form (II) occurs simultaneously:

$$[Co(en)_2X\ (am)]^{+} + H_2O \xrightarrow{k_2} [Co(en)_2(H_2O)\ (am)]^{2+} + X^- \quad (5)$$

Reaction (5) is faster than reaction (4), which makes the pH dependence on the overall rate constant quite understandable.

The overall rate constant (k_{exp}) of the aquation can be written as follows:

$$k_{exp} = k_1 + (k_2 - k_1)\frac{K}{K+[H^+]} \quad (6)$$

In this equation K stands for the equilibrium constant of reaction (3), and k_1 and k_2 stand for the rate constants of reaction (4) and (5), respectively.

In strong acid solutions the following conditions can be assumed:

$$k_2 \gg k_1 \text{ and } [H^+] \gg K$$

and therefore equation (6) may be expressed in the simplified form:

$$k_{exp} \approx k_1 + \frac{k_2 \cdot K}{[H^+]} \quad (7)$$

During the kinetic runs of the aquation of *cis*-$[Co(en)_2\ Br$-(*m*-xylidine)] $(NO_3)_2$ the release of Br^- ion has been followed titrimerically, by means of silver nitrate solution. All the kinetic runs were carried out at a constant ionic strength of $\mu = 0.1$ M, and at various $[H^+]$ concentrations.

The plot of log c_0/c versus time showed good linearity, which enabled us to derive apparent first order rate constants (k_{exp}).

In all cases positive deviations could be observed at higher temperatures as well as at lower ones when the concentration of the complex was comparable with that of the acid. The increase of the aquation rate in such conditions is probably due to the exchange of amine ligands with solvent molecules.

$$[Co(en)_2Br(Am)]^{+} + 2H_2O = [Co(en)_2Br(H_2O)]^{2+} + amH + OH^- \quad (8)$$

(amH stands for a *m*-xylidine molecule) The latter process makes the solution alkaline. Analogous processes with reaction (8) were observed in the case of $[Co(en)_2\ Cl\ (aniline)]^{2+}$.[13]

Several kinetic curves obtained at 50° and with various perchloric acid concentrations are given in fig. 2.

From the slopes and zero time tangencies of these straight lines the overall rate constants (k_{exp}) could be calculated.

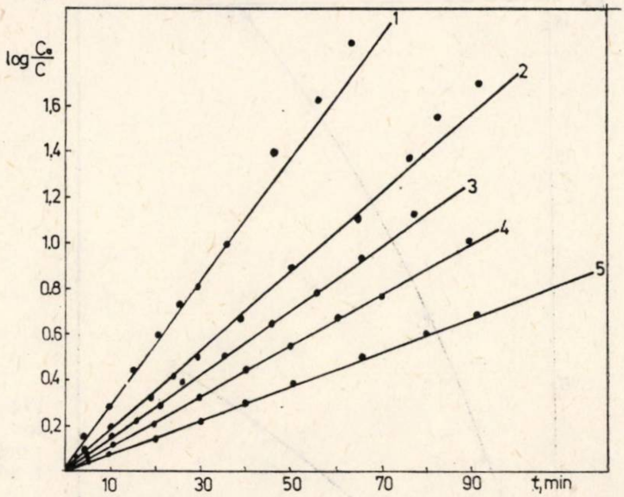

Fig. 2. — Determination of the overall rate constants (k_{exp}) at 51° and various perchloric acid concentrations : 1, 2.10^{-3} m ; 2, 3.10_{-}^{3}, 3. 4.10^{-3}, 4. 10.10^{-3} m, 5. 15.10^{-3} m.

The k_{exp} values for various $HClO_4$ concentrations and for different temperatures are given in table 2.

Table 2

First order overall rate constants of the aquation k_{exp} 10^4, s^{-1}

$[H^+]$ 10^3 mole/l	40°	45°	51°	57°	62°	68°
2	0.449	1.01	1.79	6.62	—	—
3	0.343	0.749	1.37	5.33	9.33	18.3
4	—	—	1.17	—	—	—
5	0.252	0.560	—	3.98	7.14	14.2
7	—	0.464	—	3.21	5.73	11.6
10	0.176	0.382	0.698	2.60	4.64	—
15	—	0.317	0.590	—	3.68	—
20	—	0.282	0.534	1.75	3.17	—

At higher hydrogen ion concentrations the aquation process can be described by (7) instead of equation (6).

The plot of k_{exp} versus $1/[H^+]$, gives directly the k_1 values after extrapolation to $1/[H^+] = 0$. This procedure is illustrated in fig. 3. No straight lines are obtained indicating that equation (7) is not valid in the whole pH interval.

The k_1 values obtained are given in table 3.

For the determination of k_2 and K values equation (7) is given in the form :

$$\frac{1}{k_{exp} - k_1} = \frac{1}{k_2 - k_1} + \frac{1}{K(k_2 - k_1)} \cdot [H^+] \qquad (9)$$

The plot of the left part of equation (9) *versus* $[H^+]$ yields straight lines indicating the correctness of the above scheme based on equilibrium (3).

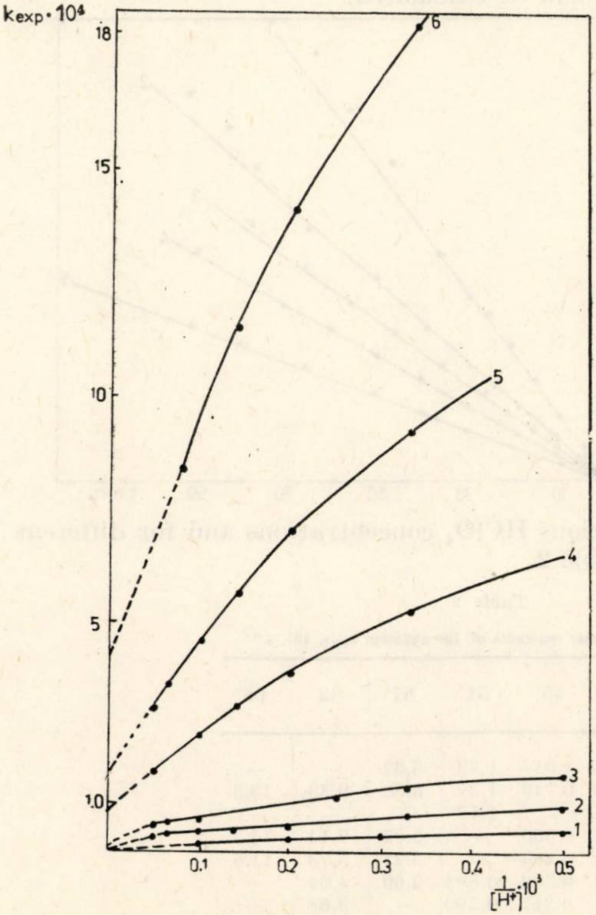

Fig. 3. – Determination of the rate constants k_1 by means of extrapolation. *1*, 40° ; *2*, 45° ; *3*, 51°, *4*, 57° ; *5*, 62° ; *6*, 68°.

The parameters of these straight lines allowed us to calculate the k_2 and K values, which are also given in table 3.

Table 3

k_1, k_2, and k values

t°	40°	45°	51°	57°	62°	68°
$k_1 \cdot 10^4$, s^{-1}	0.095	0.180	0.358	0.760	1.41	2.74
$k_2 \cdot 10^4$, s^{-1}	2.21	3.94	7.23	13.7	22.6	39.4
$K \cdot 10^3$	0.40	0.56	0.50	1.65	1.81	2.25

The activation enthalpy and entropy values of reaction (4) and (5) were obtained plotting $-\log k_1/T$ and $-\log k_2/T$, respectively, versus $1/T$. (see table 4)

Table 4

Activation parameters of the aquation reactions

Complex ion	$\Delta H^{\pm}$ (kcal/mole	$\Delta S^{\pm}$ (e.u.)
cis$-[Co(en)_2Br(amH)]^{2+}$	24.9 ± 0.6	-2.1 ± 2.7
cis-$[Co(en)_2Br(am)]^{2+}$	21.2 ± 1.2	-7.6 ± 5.2

amH = *m*-xylidine

The activation enthalpy values are higher than those of the analogous $[Co(en)_2Br(\text{benzylamine})]^{2+}$ [11] $[Co(en)_2Br(\text{pyridine})]^{2+}$ and $[Co(en)_2Br(\beta\text{-picoline})^{2+}$ [9] complexes.

This result agrees well with the decrease of the nucleophilic character of these ligands from the benzylamine and pyridine bases to the aromatic amines. The *m*-xylidine is a weaker base than both benzylamine and the above-mentioned heterocyclic bases, therefore the Co-N bond is weaker and longer in the *m*-xylidine derivative than in the above mentioned complexes. This phenomenon allows the stabilization of the ligands in cis position.

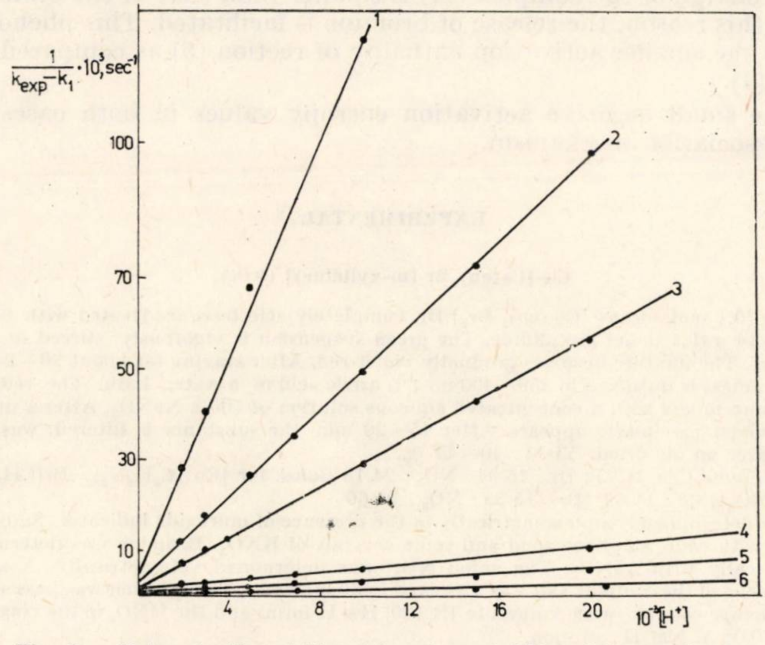

Fig. 4. — Determination of K and k_2 values at different temperatures : *1*, 40° ; *2*, 45° ; *3*, 51° ; *4*, 57° ; *5*, 62° ; *6*, 68°.

If reaction (4) takes place according to a dissociation mechanism, this stabilization corresponds to the increase of the activation enthalpy.

The strengthening of the Co—N bond in the case of the conjugated base (II) occurs owing to the possibility of π-bond formation. The octahedral structure of (II) is extended and the Co—N bond is weakened. The positive charge of the complex (II) is smaller than that of the amino-form (I). For this reason, the release of bromine is facilitated. This phenomenon explains the smaller activation enthalpy of rection (5) as compared to the process (4).

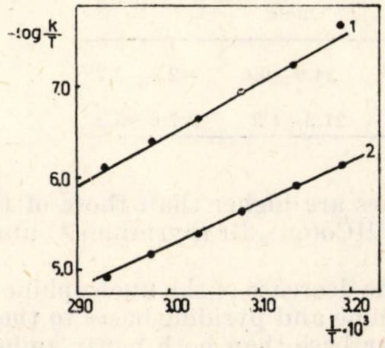

Fig. 5. — Determination of the activation enthalpy and entropy of reaction (4) [1] and (5) [2] in acid solutions.

The small negative activation entropy values in both cases plead for a dissociation mechanism.

EXPERIMENTAL

Cis-[Co(en)$_2$Br (m-xylidine)] (NO$_3$)$_2$

42 g (0.1 mole) *trans*-[Co (en)$_2$ Br$_2$] Br, completely acid free, are treated with 60—80 ml water and 14 g (0.1 mole) *m*-xylidine. The green suspension is vigorously stirred in a mortar for 6—8 hrs. The mixture becomes gradually violet-red. After staying for about 20—24 hrs, the microcryst. mass is dissolved in 350—400 ml 1% nitric acid in a water bath. The red solution is filtered and mixed with a concentrated aqueous solution of 100 g $NaNO_3$. After a short time, a reddish-violet precipitate appears. After 15—20 min the substance is filtered, washed with ice-cold water an air dried. Yield : 40—45 %.

Analysis : *Found* Co : 11.75 ; Br : 15.94 ; NO_3 ; 24.18 *Calcd.* for [Co $(C_2H_8N_2)_2$ Br$(CH_3)_2C_6H_3$—NH_2)] $(NO_3)_2$ Co : 11.69 ; Br : 15.85 ; NO_3 : 24.60

Cobalt was determined complexometrically in the presence of murexide indicator. Samples were destroyed with conc. sulphuric acid and some crystals of KNO_3. Bromine was determined potentiometrically with $AgNO_3$. The anion NO_3 was determined volumetrically. A sample of 0.400—0.600 g of the complex salt was dissolved in 50 ml water. The solution was passed through an ion exchange column (with Amberlite IR 120, R—H form) and the HNO_3 in the eluant titrated with a 0.05 M NaOH solution.

Kinetic measurements. The weighed samples of the complex salt (4.10^{-3}M) were dissolved at the desired temperature in distilled water, and the acidity and ionic strength adjusted with $HClO_4$ and $NaNO_3$ solutions (all preheated at the temperature of the experiment). Aliquot parts of the solution (5—10 ml) were cooled quickly to 0°, 20 ml 0.1 M HNO_3 was added, cooled to 0°, too, and the bromide ion was titrated with 0.01 M $AgNO_3$ solution, using a silver wire as indicator electrode.

The i.r. spectrum was obtained using a "UR—20 Carl Zeiss Jena" spectrophotometer. Measurements were made on the potassium bromide pellet of the complex.

Revue Roumaine de Chimie, **20**, *4*, 531–538 (1975)

COORDINATION COMPOUNDS WITH CHOLINE ACETATE

MARIA BREZEANU and IOANA JITARU

Inorganic Chemistry Laboratory, University of Bucharest, Splaiul Independenţei 87, Bucharest, Romania

Received April 29, 1974

A series of complex acetates of some 3d metals with choline acetate have been obtained, belonging to the following general types : $[ML(CH_3COO)_2]_2(M^{II} = Mn, Co, Ni, Cu, Zn$; $L = (CH_3)_3{}^+N-C_2H_4-O^-)$ and $[ML_4^+(CH_3COO)_2](CH_3COO)_4(M^{II} = Co, Ni ; L^+ = (CH_3)_3^+ N-C_2H_4-OH)$ in which choline behaves as a cationic ligand. The compounds obtained were characterized by elemental chemical analysis, molecular weight determinations, molecular electrical conductivity, electronic and vibrational spectra. The probable structure of these compounds and the coordination manner of choline (L+) and of the acetate ion have been established on the basis of the data obtained.

In a previous paper[1] we showed the results obtained in the synthesis and the characterization of complex compounds of some 3d metals with choline perchlorate.

This paper reports the results obtained in the study of choline coordination capacity in the presence of the acetate ion.

On this occasion, complex compounds of some 3d metals with choline acetate, belonging to the following general types were obtained and characterized : $[ML(CH_3COO)_2]_2(M^{II} = Mn, Co, Ni, Cu, Zn$; $L = (CH_3)_3{}^+ N-C_2H_4-O^-)$ and $[ML_4^+(CH_3COO)_2](CH_3COO)_4(M^{II} = Co, Ni$; $L^+ = (CH_3)_3^+ N-C_2H_4-OH)$.

These compounds were characterized by elemental chemical analysis, electronic and vibrational spectra, molecular electrical conductivity and molecular weight determinations.

RESULTS AND DISCUSSION

The acetates of some 3d divalent metals (Mn, Co, Ni, Cu and Zn) react in alcoholic solution with choline acetate leading to compounds which correspond to the minimal formula $ML(CH_3COO)_2$.

Under more drastic experimental conditions (prolonged refluxing at temperatures ranging between 70 and 80°), complex compounds of the type $[ML_4^+(CH_3COO)_2]$ $(CH_3COO)_4$ are obtained.

---

[1] M. BREZEANU and I. JITARU, *Rev. Roumaine Chim.*, in press.

The synthesis of both types of compounds was achieved at a 1 :4 M^{II} : choline ratio. It should be mentioned that the M^{II} : choline ratio does not seem to influence the nature of the obtained species.

Based on molecular weight determinations, the complex compounds belonging to the first type were formulated as dimers, choline behaving as a neutral ligand, which is coordinated by the oxygen of the deprotonated alcohol group.

In compounds belonging to the second type, monomers based on molecular weight determinations, choline behaves like a cationic ligand with the oxygen of the hydroxyl group as a donor atom.

It should be mentioned that such complex compounds could be obtained only in the case in which Co(II) and Ni(II) behaved like a central metalic ion.

From IR spectral data, it is not possible to precisely establish the nature of the bridged group (choline or acetate) in compounds formulated as dimers. More rigorous structural determinations are necessary in order to solve this problem.

All compounds obtained are characterized by relatively high thermal stability.

Compounds of type $[ML(CH_3COO)_2]_2$ are practically insoluble in most organic solvents (ethyl alcohol, methyl alcohol, isopropyl alcohol, ethyl ether, petroleum ether, acetone, carbon tetrachloride, chloroform) and decompose in water. In some solvents with high dielectric constant (for instance dimethylformamide or acetonitrile), these compounds are relatively easily dissolved without any colour change.

Compounds of the type $[ML_4^+(CH_3COO)_2](CH_3COO)_4$ are also practically insoluble in most organic solvents and dissolve with decomposition or solvation in solvents with good donor properties (water, dimethylformamide, dimethylsulphoxide). In acetonitrile, such compounds are relatively readily dissolved, maintaining the coordination sphere unaltered, at least in part.

Electronic spectra. In order to obtain some information on the stereochemistry of the compounds investigated, particularly those involving Co (II), Ni(II) and Cu (II), their electronic spectra were recorded.

A comparative examination of absorption spectra of dimer compounds $[ML(CH_3COO)_2]_2(M^{II} = Co, Ni)$ and of monomer compounds $[ML_4^+(CH_3COO)_2](CH_3COO)_4$ $(M^{II} = Co, Ni)$, reveals clear differences with regard to the position, intensity and structure of the bands (figs. 1 and 2).

Spectra of the former compounds may be interpreted in terms of a tetrahedral environment of the metallic ion, whereas those of monomer compounds indicate an octahedral configuration.

Thus, the spectrum of compound $[CoL(CH_3COO)_2]_2$ shows two bands, one at 630 nm, broad, rather intense, structured, with a shoulder towards higher frequencies ($\sim$590nm) and the second, in the near IR range (1100—1300 nm), very weak and large. The first band was assigned to $^4T_1(P) \leftarrow {}^4A_2(\nu_3)$ transition and the second, to $^4T_1(F) \leftarrow {}^4A_2(\nu_2)$ transition for an ion d^7 in a tetrahedral symmetry field.[2]

---

[2] Y. Tanabe and S. Sugano, *J. Phys. Soc. Japan*, **1954**, 457.

The spectrum of compound $[CoL_4^+(CH_3COO)_2]$ $(CH_3COO)_4$ may be satisfactorily interpreted in terms of an octahedral structure.[3]

Thus, the band appearing in the visible range (525 nm), large and having a relatively low intensity, may be assigned to $^4T_{1g}(P) \leftarrow {}^4T_{1g}$ whereas the band appearing in the near IR (1 100 nm) of a somewhat lower intensity, is attributed to transition $^4T_{2g} \leftarrow {}^4T_{1g}$.

Fig. 1.— Electronic spectra of complexes : *1.* $[CoL_4^+(CH_3COO)_2]$ $(CH_3COO)_4$ and *2.* $[CoL(CH_3COO)_2]_2$.

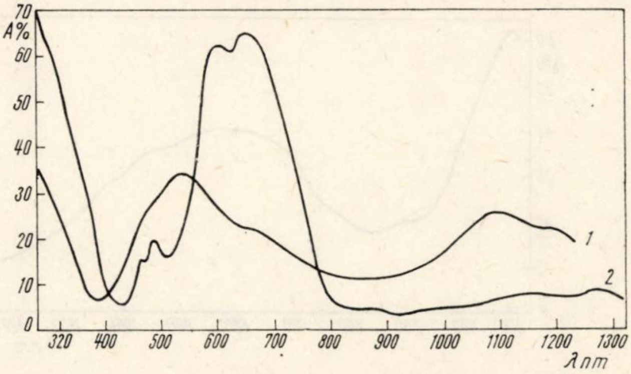

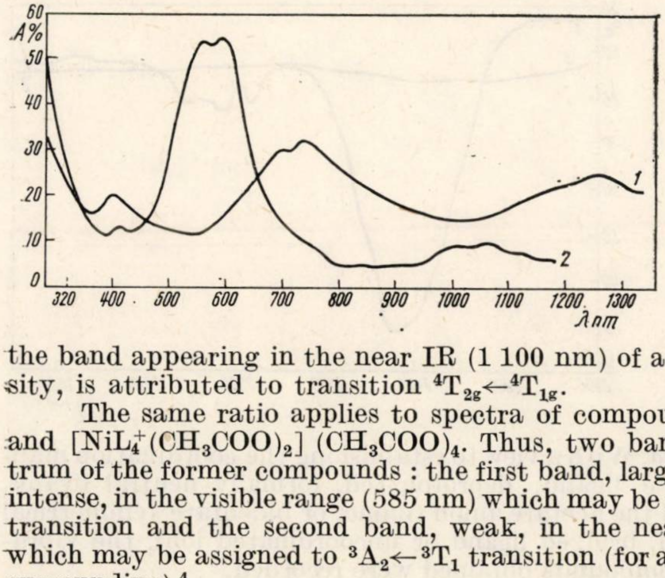

Fig. 2.— Electronic spectra of complexes : *1.* $[NiL_4^+$ $(CH_3COO)_2]$ $(CH_3COO)_4$ and *2.* $[NiL(CH_3COO)_2]_2$.

The same ratio applies to spectra of compounds $[NiL\ (CH_3COO)_2]_2$ and $[NiL_4^+(CH_3COO)_2]$ $(CH_3COO)_4$. Thus, two bands appear in the spectrum of the former compounds : the first band, large, structured, relatively intense, in the visible range (585 nm) which may be assigned to $^3T_1\ (P) \leftarrow {}^3T_1$ transition and the second band, weak, in the near IR range (1050 nm) which may be assigned to $^3A_2 \leftarrow {}^3T_1$ transition (for an ion d^8 in a tetrahedral surrounding).[4]

The spectrum of compound $[NiL_4^+(CH_3COO)_2](CH_3COO)_4$ also reveals two absorption bands : one, in the visible range (435 nm) which may be assigned to $^3T_{1g}(F) \leftarrow {}^3A_{2g}$ transition (the shoulder in the domain of higher frequencies, 405 nm, being attributed to $^3T_{1g}(P) \leftarrow {}^3A_{2g}$ transition ; the second band in the near IR (1220 nm) may be attributed to $^3T_{2g} \leftarrow {}^3A_{2g}$ transition for an ion d^8 in an octahedral surrounding.[5]

---

[3] A. B. P. Lever, "Inorganic Electronic Spectroscopy", New York, 1968, p. 318.

[4] A. B. P. Lever, "Inorganic Electronic Spectroscopy", New York, 1968, p. 365.

[5] A. B. P. Lever, "Inorganic Electronic Spectroscopy", New York, 1968, p. 333.

The spectrum of compound $[CuL(CH_3COO)_2]_2$ which presents a large absorption band of a relatively low intensity, structured in the 700—1100 nm range, may be interpreted in terms of a tetrahedral, strongly distorted configuration[6] (fig. 3).

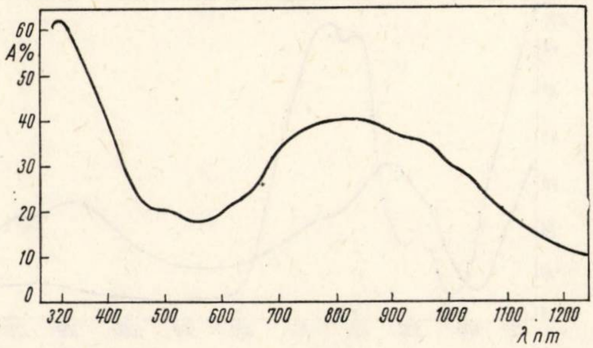

Fig. 3. — Electronic spectrum of complex $[CuL(CH_3COO)_2]_2$.

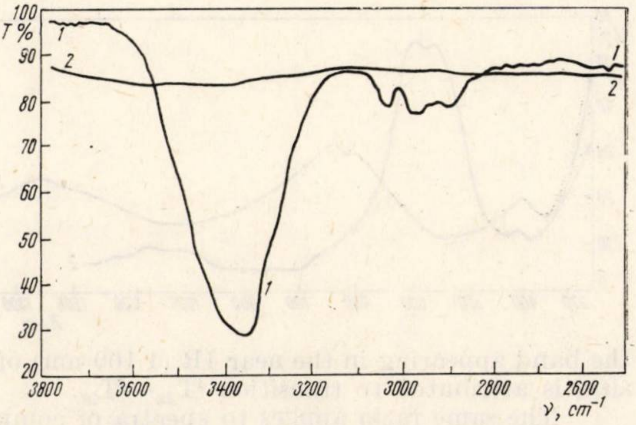

Fig. 4. — Region of ν_{OH} stretching vibration in spectra of complexes : *1.* $[CoL_4^+(CH_3COO)_2](CH_3COO)_4$ and *2.* $[CoL(CH_3COO)_2]_2$.

Vibrational spectra. With a view to establishing the coordination manner of choline (cationic ligand, deprotonated, formally neutral ligand, uncoordinated ion) and the acetate anion (mono, or bidentate symmetrical or asymmetrical ligand, bridged ligand or uncoordinated ion), the vibrational spectra of the compounds obtained were recorded.

Since the symmetry of cation $(CH_3)_3^+N-C_2H_4-OH$ does not seem to be significantly affected by coordination, no important changes appear in the vibrational spectrum of the coordinated choline, compared to the spectrum of the free choline.

However, it may be expected that the OH stretching vibration frequency (ν_{OH}) may provide useful information concerning the coordination manner of choline.[7,8]

---

[6] L. Sacconi and M. Ciampolini, *J. Chem. Soc.*, **1964**, 276.

[7] L. J. Bellamy, "The Infrared Spectra of Complex Molecules", London, New York, 1958, p. 108

[8] K. Nakamoto, "Infrared Spectra of Inorganic Coordination Compounds", London, New York, 1963, p. 159.

Thus, in the spectra of dimeric compounds $[ML(CH_3COO)_2]_2$, the frequency of the OH stretching vibration disappears, which shows that choline behaves as a deprotonated ligand in these compounds.

In the spectra of compounds $ML_4^+(CH_3COO)_6$ the frequency of the OH stretching vibration is shifted towards lower values (3340 cm^{-1} against 3450 cm^{-1} in free choline) which indicates choline coordination in these compounds by the oxygen of the alcohol group (Fig. 4).

Additional information on the choline coordination manner could be obtained from low frequency IR spectra (below 400 cm^{-1}) a domain in which the frequency of the M—O stretching vibration appears.

An examination of the IR spectrum in the region of the acetate anion vibration modes permits to establish its coordination manner.[9,10]

For this purpose, the region of the asymmetrical stretching vibration of the carboxyl group was considered ($\nu_{as(OCO)}$). Some frequencies of choline (ν_{C-H}, ν_{N-C}) also appear in the region assigned to the symmetrical stretching vibration of the carboxyl group ($\nu_{s(OCO)}$), which makes extremely difficult an assignment of acetate function. Similarly, it seems that in compounds of the type $[ML(CH_3COO)_2]_2$ and also in compounds $ML_4^+(CH_3COO)_6$, not all acetate groups are of the same nature, a fact which renders much more difficult an exact assignment of their function.

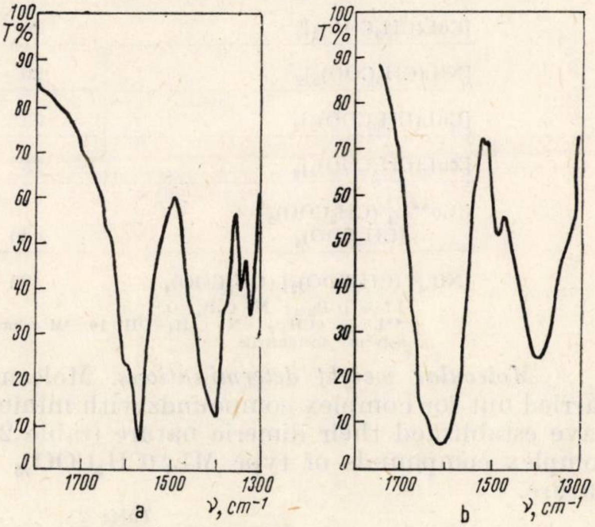

Fig. 5.— Region of $\nu_{as(OCO)}$ and $\nu_{s(OCO)}$ in spectra of complexes *1.* $[CoL_4^+(CH_3COO)_2](CH_3COO)_4$ and *2.* $[CoL(CH_3COO)_2]_2$.

Nevertheless, it can be observed that in the IR spectra of dimeric acetates $[ML(CH_3COO)_2]_2$ the ν_{as}(OCO) frequency appears as a sharp, intense, well-defined band at 1610 cm^{-1}, indicating the coordination of the acetate ion, whereas in IR spectra of compounds $ML_4^+(CH_3COO)_6$ the frequency $\nu_{as(OCO)}$ appears at 1570 cm^{-1}, a characteristic value of the free acetate ion. For illustration, fig. 5 presents the region in which absorption

---

[9] N. F. Curtis, *Bull. Chem. Soc. Japan*, **31**, 303 (1958).

[10] N. F. Curtis, *J. Chem. Soc.*, **1968**, 1579.

is assigned to the symmetrical and asymmetrical stretching vibration of the carboxyl group, $\nu_{as(OCO)}$ and $\nu_{s(OCO)}$, in the two types of Co(II) compounds.

Molecular electrical conductivity determinations. The formulation assigned to the two types of studied compounds was confirmed by determining their molecular electrical conductivity. The values obtained for the solutions of dimeric complex compounds in dimethylformamide and acetonitrile indicate a weak electric conductivity (below that of a 1 :1 electrolyte). These values were attributed to a solvation equilibrium rather than to an electrolyte character.

The data obtained for the molecular conductivity of acetonitrile solutions of the second type of compounds confirm the formulation $[ML_4^+(CH_3COO)_2](CH_3COO)_4$ (table 1).

Table 1

Molecular electrical conductivities of choline complexes in acetonitrile solution

Complex compound	Molecular electrical conductivity ($\Omega^{-1}cm^2mol^{-1}$)	Type of electrolyte
$[MnL^*(CH_3COO)_2]_2$	25	nonelectrolyte
$[CoL(CH_3COO)_2]_2$	30	nonelectrolyte
$[NiL(CH_3COO)_2]_2$	20	nonelectrolyte
$[CuL(CH_3COO)_2]_2$	22	nonelectrolyte
$[ZnL(CH_3COO)_2]_2$	25	nonelectrolyte
$[(Co^{**}L_4^+(CH_3COO)_2]$ $(CH_3COO)_4$	480	1 :4
$[NiL_4^+(CH_3COO)_2](CH_3COO)_4$	485	1 :4

$L^* = (CH_3)_3{+}\,N-C_2H_4-O-$
$^{**}L+ = (CH_3)_3\ {+}N-C_2H_4-OH$; $10-{}^3M$ sslution; t $-$ 25°;
solvent $-$ acetonitrile.

Molecular weight determinations. Molecular weight determinations carried out for complex compounds with minimal formula $ML(CH_3COO)_2$ have established their dimeric nature (table 2). The values obtained for complex compounds of type $ML_4^+(CH_3COO)_6$ indicate their monomeric nature.

Table 2

Molecular weights of the choline complexes

Complex compound	Melting point (°C)	Molecular weight	
		calcd.	found
$[MnL(CH_3COO)_2]_2$	250	552.36	565.10
$[CoL(CH_3COO)_2]_2$	220	560.36	570.20
$[NiL(CH_3COO)_2]_2$	225	559.90	565.30
$[CuL(CH_3COO)_2]_2$	200	569.56	575.40
$[ZnL(CH_3COO)_2]_2$	235	573.24	580.10
$[CoL_4^+(CH_3COO)_2](CH_3COO)_4$	210	829.82	841.20
$[NiL_4^+(CH_3COO)_2](CH_3COO)_4$	210	840.50	840.00

EXPERIMENTAL

I. SYNTHESIS OF COMPLEXES

1. $[ML(CH_3COO)_2]_2$ (M^{II} = Mn,Co,Ni,Cu,Zn ; L = $(CH_3)_3^+N-C_2H_4-O^-$)

Complex compounds of this type were obtained by mixing concentrated ethanol solutions (or methanol solutions) of metal acetates with an ethanol (or methanol) solution of choline acetate in M^{II} : choline = 1 :4 molar ratio.

Finely crystallized compounds separated on cooling from the reaction mixture, were white-pink for Mn (II), green-khaki for Co(II) light-green for Ni (II), light-blue for Cu (II) and white for Zn (II). They were filtered, repeatedly washed with ethanol or methanol and air-dried.

The same type of compounds is also obtained with M^{II} : choline = 1 :2 or 1 :6 molar ratios.

2. $[ML_4^+(CH_3COO_2)](CH_3COO)_4$ (M^{II} = Co, Ni ; L^+ = $(CH_3)_3^+N-C_2H_4-OH$)

Complex compounds of this type were obtained by prolonged contact (refluxing at a temperature of about 80° for approx. 10 hours) of diluted methanol solutions of Co (II) and Ni(II) acetates and of choline acetate, in a M^{II} : choline = 1 :5 molar ratio. Solutions obtained under reflux are concentrated on a water bath at 70—80°, when extremely fine crystalline compounds appear, their colour being pink for Co(II) and light-blue for Ni(II). These compounds are filtered, repeatedly washed with methanol and air-dried.

A similar type of compounds may also be obtained for a M^{II} : choline molar ratio higher than 1 : 5.

Attempts to obtain complex compounds of Cr(III) and Fe(III) acetates with choline acetate failed.

The data of the elemental chemical analysis are presented in table 3.

Table 3

Data on the elemental chemical analysis

Complex compunds	M %		C %		N %	
	calcd.	found	calcd.	found	calcd.	found
$[MnL(CH_3COO)_2]_2$	19.89	19.95	39.10	39.30	5.70	5.90
$[CoL(CH_3COO)_2]_2$	21.03	21.10	38.57	38.70	4.90	5.10
$[NiL(CH_3COO)_2]_2$	20.96	21.10	38.60	38.75	5.00	5.25
$[CuL(CH_3COO)_2]_2$	22.31	22.45	37.98	38.15	4.91	5.15
$[ZnL(CH_3COO)_2]_2$	22.81	22.95	37.64	37.84	4.88	4.97
$[CoL^+(CH_3COO)_2](CH_3COO)_4$	7.12	7.25	45.10	45.45	6.74	6.90
$[NiL_4(CH_3COO)_2](CH_3COO)_4$	7.07	7.15	45.12	45.60	6.74	6.90

II. MOLECULAR WEIGHTS

Molecular weights of synthesized complex compounds were determined by means of the Rast micromethod, using camphor as solvent.

III. MOLECULAR CONDUCTIVITIES

Molecular electrical conductivity measurements were made at 25° on freshly prepared solutions using Conductometer II (Czechoslovakia) with a unit cell with $K = 0.52$. The solvent used was acetonitrile.

IV. ELECTRONIC SPECTRA

Electronic spectra in the 320 – 1 300 nm region were recorded at room temperature using a VSU_1 spectrophotometer C. Zeiss, Jena and magnesium oxide as reference material.

V. VIBRATIONAL SPECTRA

IR spectra in the 400 – 3600 cm^{-1} region were measured on a UR 20 spectrophotometer C. Zeiss, Jena, using KBr disks technique.

Revue Roumaine de Chimie, **20**, *4*, 539 – 545 (1975)

REACTIONS OF ACETYLENES WITH TRANSITION METALS. III[1]

STRUCTURE OF THE COMPLEX OBTAINED FROM t-BUTYL-ACETYLENE AND BIS-BENZONITRILE-PALLADIUM CHLORIDE

ELISE AVRAM, F. CHIRALEU, I.G. DINULESCU and MARGARET AVRAM

Institute of Organic Chemistry, Spl. Independenţei 202B, Bucharest, Romania

Received June 15, 1974

From the substituted 1,2-dihydrofulvene **3** and Na_2PdCl_4, the π-allyl-Pd-Cl complex **2** is obtained, identical to that obtained from t-butyl-acetylene and $(C_6H_5CN)_2 . PdCl_2$. Treatment of **2** with HCl yields the π-complex of the substituted fulvene (**18**).

It was earlier shown[2] that treatment of t-butyl-acetylene (**1**) with bis-benzonitrile-$PdCl_2$ in benzene yields a complex with the molecular formula $C_{18}H_{30}PdCl_2$ (**2**), which on reductive decomposition yields the chloro-dihydrofulvene **3**

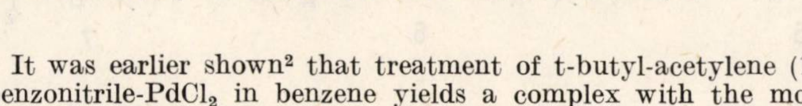

1 2 3

In the present paper we report proofs for a structure of π-allyl complex with 6-chloro-1,3,6-tri-t-butyl-1,2-dihydrofulvene skeleton for complex **2***, the previously proposed bicyclic [3] and acyclic[4] formulas being thus excluded.

* *Note added in proof.* A recent paper by Professor Maitlis *et al.* (Chem. Comm., **1974**, 567), reported for this complex two interconverting isomers, deduced from ^{13}C and ^{1}H NMR spectra at low temperature. The complex **13** with triphenylphosphine presents only a single form, as resulted from X-ray analyses.

[1] Part II : M. Avram, E. Avram, I. G. Dinulescu, N. Ştefan, F. Chiraleu, M. Elian and C. D. Nenitzescu, *Chem. Ber.*, **105**, 2375 (1972).

[2] M. Avram, E. Avram, M. Elian, F. Chiraleu, I. G. Dinulescu and C. D. Nenitzescu, *Chem. Ber.*, **104**, 3486 (1971).

[3] M. Avram, E. Avram, C. D. Mateescu, I. G. Dinulescu, F. Chiraleu and C. D. Nenitzescu, *Chem. Ber.*, **102**., 3996 (1969).

[4] K. L. Kaiser and P. M. Maitlis, *Chem. Comm.*, **1970**, 942.

On heating chloro-dihydrofulvene **3** with sodium palladite in acetic acid buffered with sodium acetate, a complex **4** was obtained containing an excess of palladium chloride. The excess of palladium chloride was removed by dissolving **4** in dimethylformamide and precipitating with water, which finally afforded a yellow complex **2**, identical to that obtained from t-butylacetylene and bis-benzonitrile · $PdCl_2$ [2,3]

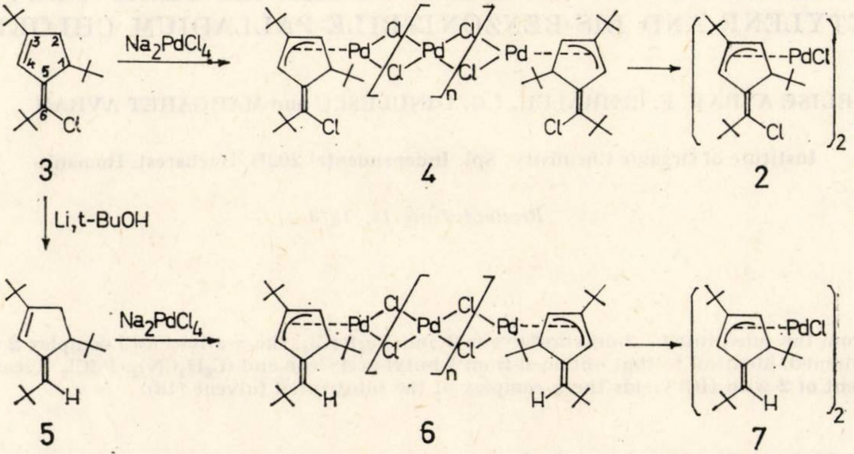

Following the same procedure, 1,2-dihydrofulvene [2] **5** yielded a raw complex with excess of $PdCl_2$. By removing the latter, a yellow dimer complex of 1,3,5-tri-t-butyl-1,2-dihydrofulvene (**7**) was obtained.

The formation of complexes with $PdCl_2$ within bridges is frequently encountered in the cyclobutenyl complex series.[5-9] It is less frequent with π-allyl complexes having simpler structures,[10] but it appears again in the case of more complicated hydrocarbons from the $(CH)_n$ series.[11]

We show below some reactions of the complex **2** which support the structure of π-allyl-complex type.

The chlorine atom from the Pd-Cl bridge in **2** can be substituted by other anions. Thus, on its treatment with silver acetate, in anhydrous benzene, the chloro-acetoxy-derivative **8** was obtained. The latter, on

---

[5] P. M. Maitlis, „The Organic Chemistry of Palladium", vol. 1, Academic Press, New York, 1971, p. 155.

[6] P. M. Maitlis, D. F. Pollock, M. L. Games and W. J. Pryde, *Can. J. Chem.*, **43**, 470 (1965).

[7] R. Hüttel and H. J. Neugebauer, *Tetrahedron Letters*, **1969**, 3541.

[8] M. Avram, I. G. Dinulescu, G. D. Mateescu, E. Avram, C. D. Nenitzescu, *Rev. Roumaine Chim.*, **14**, 1181 (1969).

[9] T. Hosokawa and J. Moritani, *Tetrahedron Letters*, **1969**, 3021.

[10] P. M. Maitlis, „The Organic Chemistry of Palladium", vol. 2, Academic Press, New York, 1971, p. 51 ; I.A. Zakharova and I.I. Moisev, *Izvest. Akad. Nauk S.S.S.R.*, **1964**, 1826 ; M. Donati and F. Conti, *Inorg. Nucl. Chem. Lett.*, **2**, 343 (1966).

[11] M. Banciu, M. Elian, C. Drăghici and E. Ciorănescu, *Rev. Roumaine Chim.*, **19**, 1179 (1974).

treatment with lithium bromide in ether, gave the complex **9**, identical to the previously described one [2,3] obtained from **2** and KBr.

The heating of **8** in acetone-water yielded compound **10**

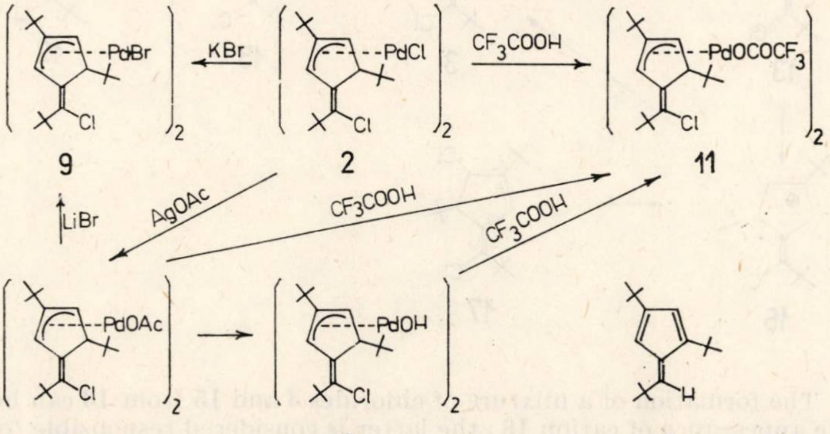
PdBr
KBr
PdCl
CF_3COOH
$PdOCOCF_3$
Cl
2
9
2
11
LiBr
AgOAc
CF_3COOH
CF_3COOH
PdOAc
PdOH
H
8
10
12

It was observed, by NMR spectroscopy, that dissolving the complexes **2**, **8** and **10** in trifluoro-acetic acid yielded, together with the fulvene **12**, a complex, the spectrum of which corresponded to a trifluoroacetoxy-derivative, but which could not be isolated; on dilution with water, the only product isolated was fulvene **12**.

Treatment of **2** with triphenylphosphine afforded the complex **13**, the molecular weight of which corresponded to a monomeric structure.

Under the same conditions compound **7** gave **14**.

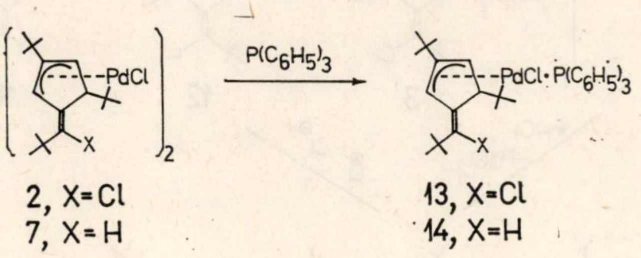
PdCl
X
2
$P(C_6H_5)_3$
$PdCl \cdot P(C_6H_5)_3$
2, X=Cl
7, X=H
13, X=Cl
14, X=H

On reductive removal of palladium from complex **13** with sodium borohydride a mixture of chlorides **3** (48%) and **15** (38%), together with about 15% fulvene **12** resulted.

Similarly treated, **2** gave only the chloride **3** together with 5% fulvene (based on v.p.c.)

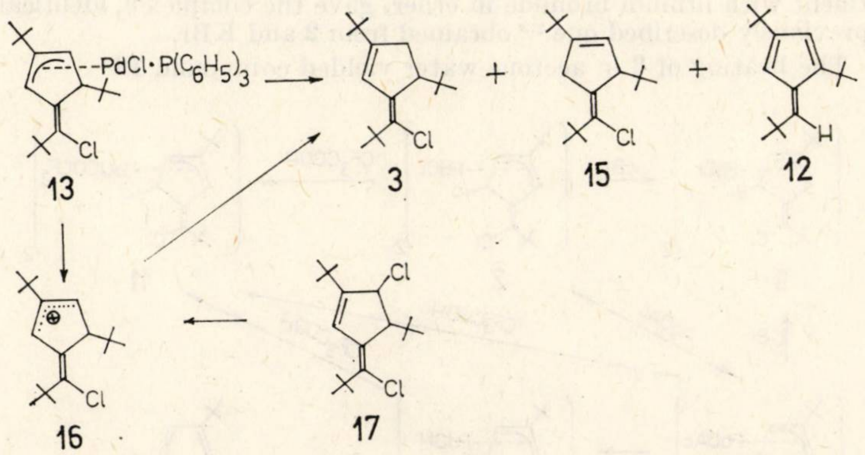
-PdCl·P(C6H5)3
Cl
13
Cl
3
+
Cl
15
+
H
12
⊕
Cl
16
Cl
Cl
17

The formation of a mixture of chlorides **3** and **15** from **13** can be due to the appearance of cation **16**; the latter is considered responsible for the formation of the same mixture, on reduction of **17** with $LiAlH_4$.[2]

Furthermore, treatment of complex **2** with dry hydrochloric acid in methylene chloride gave the palladium chloride complex of fulvene, **18**. Similarly, **13** gave fulvene **12**, together with the palladium chloride complex of triphenylphosphine.

The mechanism of transformation of π-allyl-PdCl complexes into π-$PdCl_2$ ones has been investigated and discussed in many cases.[12]

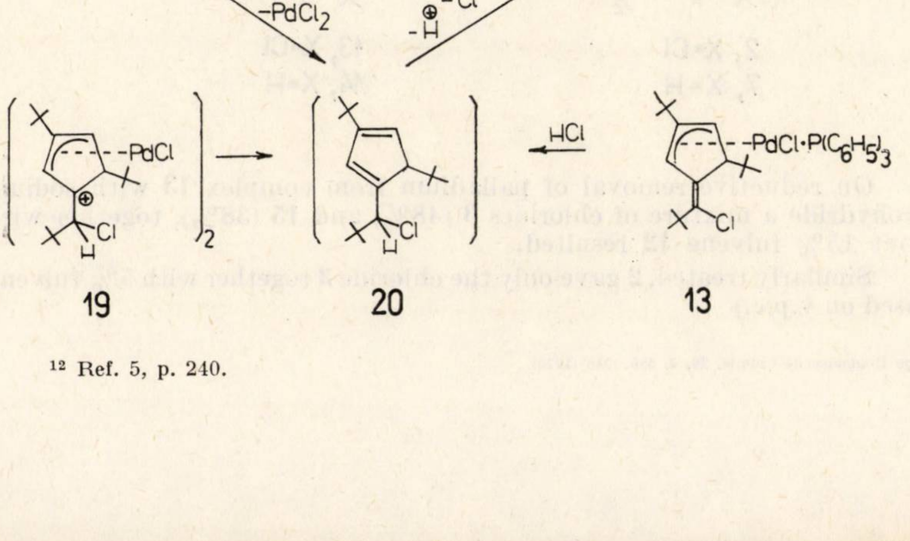
-PdCl
Cl
2
2
+ HCl
- PdCl2
Cl
3
+H⊕
H
12
PdCl2
-PdCl2
H
18
+HCl
-PdCl2
⊕
-H
-Cl⊖
-PdCl
⊕
Cl
H
2
19
Cl
H
20
HCl
-PdCl·P(C6H5)3
Cl
13

---

[12] Ref. 5, p. 240.

Transformation of π-allyl-complexes **2** and **13** into fulvene (**12**) and into its complex (**18**) respectively, involves the elimination of a vinylic chloride from the ligand molecule. Decomposition of the complexes by the direct attack of HCl, with the initial formation of a chloro-dihydrofulvene **3**, seems improbable in view of the lack of affinity of Pd-Cl bond to hydrochloric acid.[13] (According to the mechanism previously presented[2] the protonation of the exocyclic carbon in the presence of $PdCl_2$ would give fulvene **12**, or its complex **18**, respectively).

A direct protonation of complex **2** or **13** at the exocyclic carbon of the ligand, giving rise to **19**, seems more likely. The latter, through the diene intermediate **20** or its complex, and ionisation of allylic chloride, could yield fulvene **12**. In the presence of palladium chloride (formed from **2**) **12** gives **18**.

The lack of reactivity of the stable complex of triphenylphosphine with $PdCl_2$ formed, together with fulvene, from **13**, explains the isolation in this case of the free fulvene **12**.

Acknowledgement. We express our gratitude to Professor Maitlis for his kindness to inform us, prior to publication about his work regarding structural elucidation of the complex **2** and **13**.

EXPERIMENTAL

Microanalyses were performed by Miss E. Şliam and Mrs. V. Daniel. IR spectra were recorded on a double beam UR-20 spectrophotometer. NMR spectra were recorded on a Varian A-60A spectrometer, using TMS as internal standard.

REACTION OF 3 WITH SODIUM PALLADITE. COMPLEXES 2 AND 4

A solution of sodium palladite was prepared,[14] by heating at 85°, under vigorous stirring, of a mixture of 0.5 g (2.82 mmoles) palladium chloride and 0.33 g (5.6 mmoles) sodium chloride in 50 ml acetic acid. To this solution, 0.30 g (3.65 mmoles) anhydrous sodium acetate was added, then a solution of 0.64 g (2.26 mmoles) **3** in 5 ml acetic acid was dropped slowly. The mixture was then heated at 85° with stirring for 12 hours. After cooling, the sodium chloride which separated was filtered off and the solvent was removed *in vacuo*; water was added and the mixture was extracted with dichloromethane. The organic layer was washed with water, then with 5% sodium bicarbonate (until neutral) and finally dried. After evaporation of the solvent, the oily residue was triturated with petroleum ether, yielding 0.35 g **4**, yellow crystals, m.p. 185°, which was analysed as a crude product.

Found: C, 43.26; H, 6.21; Cl, 19.21; Pd, 31.51

NMR ($CDCl_3$, δ, ppm): 1.05, 1.19 and 1.35 (s, 27H, t-butyl groups), 3.76 (broad s of 5 Hz, 1H), 5.40 (broad s of 6 Hz, 1H), 6.26 (broad s of 6.5 Hz, 1H).

The petroleum ether solution (from which **4** was filtered off) was concentrated, and the oily residue was chromatographied on aluminium oxide column with petroleum ether — diethyl ether (3 :2), yielding 0.33 g **2**, identical (m.p., IR and NMR spectra) with the previously obtained compound.[2,3]

Complex **2** (0.23 g) was also obtained by dissolving **4** (0.35 g) in dimethylformamide and adding water.

The overall yield of **2** was 0.56 g (58%).

---

[13] T. Hosokawa and P. M. Maitlis, *J. Amer. Chem. Soc.*, **94**, 3238 (1972).

[14] H. C. Volger, *Rec. Trav. chim.*, **87**, 225 (1968).

$C_{18}H_{30}Cl_2Pd$ (423.7)
Calcd. : C, 51.02 ; H, 7.14 ; Cl, 16.73 ; Pd, 25.11.
Found : C, 51.65 ; H, 7.43 ; Cl, 15.59 ; Pd, 25.83
NMR (CCl_4, δ, ppm) : 1.03, 1.28 and 1.39 (s, 27H, t-butyl groups), 3.62 (broad s of 12 Hz, 1H), 5.36 (broad s of 30 Hz), 6.12 (broad s of 25 Hz, 1H).

REACTION OF **5** WITH SODIUM PALLADITE. COMPLEXES **6** AND **7**

Into a buffered solution of sodium palladite (prepared as above from 0.5 g (2.82 mmoles) palladium chloride, 0.33 g (5.6 mmoles) sodium chloride, 50 ml acetic acid and 0.30 g (3.65 mmoles) anhydrous sodium acetate) a solution of 0.6 g (2.41 mmoles) dihydrofulvene **5** in 10 ml acetic acid was added, at 80°, under vigorous stirring. The mixture was further heated for 1 hour then was left overnight at room temperature. The crystals which separated were filtered, yielding 1.0 g crude **6**, which was purified by dissolving it in dichloromethane and filtration.
Found : C, 45.86 ; H, 6.46 ; Cl, 16.10 ; Pd, 31.68
NMR ($CDCl_3$, δ, ppm) : 1.04 (s, 9H) and 1.21 (s, 18H) (*t*-butyl groups), 3.13 (broad s of 4.5 Hz, 1H), 4.96 (broad s of 4 Hz, 1H), 5.35 (broad s of 5 Hz, 1H), 6.20 (broad s of 7 Hz, 1H).

A solution of **6** in acetone was chromatographied on aluminium oxide with ether, yielding 0.50 g (53.2 %) **7**, yellow crystals, m.p. 166°.
$C_{18}H_{31}ClPd$ (389.3)
Calcd. : C, 55.53 ; H, 8.03 ; Cl, 9.11 ; Pd, 27.33
Found : C, 55.69 ; H, 8.27 ; Cl, 8.94 ; Pd, 26.85
NMR ($CDCl_3$, δ, ppm) : 0.98, 1.20 and 1.23 (s, 27H, t-butyl groups), 3.03 (broad s of 8 Hz, 1H), 5.00 (broad s of 6 Hz, 1H), 5.30 (broad s of 12 Hz, 1H), 6.10 (broad s of 14 Hz, 1H).

Acetoxy-complex **8**

A suspension of 0.42 g (1 mmole) **2** and 0.90 g (5.4 mmoles) silver acetate in 50 ml benzene was stirred at room temperature for 4 hours. The mixture was filtered and the solvent was removed *in vacuo*, yielding 0.43 g (96 %) **8**, yellow crystals with m.p. 126°.
$C_{20}H_{33}ClO_2Pd$ (447.3)
Calcd. : C, 53.70 ; H, 7.44 ; Cl, 7.93. Mol. weight for dimer, 894.6
Found : C, 54.15 ; H, 7.69 ; Cl, 7.51, Mol. weight, 964 (cryoscopy in benzene).
NMR (CCl_4, δ, ppm) : 1.11, 1.20 and 1.34 (s, 27H, t-butyl groups), 1.81 (s, 3H, $COOCH_3$), 3.73 (broad s of 4 Hz, 1H), 5.13 (broad s of 4 Hz, 1H), 6.21 (broad s of 5 Hz, 1H).
IR (nujol, cm^{-1}) : 1600 w, 1218 w (characteristic for Pd-OAc).

8 is unstable ; in $CDCl_3$ solution or during chromatography it decomposes.

Hydroxy-complex **10**

A solution of 0.23 g (0.5 mmoles) **8** in 2 ml acetone was treated with 15 ml water and the mixture was heated for 2 hours at 60°. After working up 0.17 g (81 %) **10** was obtained.
$C_{18}H_{31}ClOPd$ (405.3)
Calcd. : C, 53.34 ; H, 7.71 ; Cl, 8.75
Found : C, 54.01 ; H, 7.62 ; Cl, 8.79

Complex **9**

An ethereal solution of **8** was treated with lithium bromide and the mixture was stirred for 8 hours. After working up complex **9** was obtained, identical (m. p., IR and NMR spectra) with the previously obtained[2] compound from **2** and potassium bromide.

THE BEHAVIOUR OF COMPLEXES **2**, **8**, AND **10** in TRIFLUOROACETIC ACID

Solutions of **2**, **8** or **10** in trifluoroacetic acid show the same NMR spectrum, which was ascribed to a trifluoroacetoxy complex **11**.
NMR (CCl_4, δ, ppm) : 1.11, 1.21 and 1.38 (s, 27H, t-butyl groups), 3.82 (broad s of 3.5 Hz, 1H), 5.68 (broad s of 3.5 Hz, 1H), 6.43 (broad s of 5.5 Hz, 1H).

By diluting with water, only fulvene **12** was isolated (identified by m.p. and IR and NMR spectra).

REACTION OF COMPLEX **2** WITH TRIPHENYLPHOSPHINE. COMPLEX **13**

A solution of 3.4 g (8 mmoles) **2** in 30 ml dichloromethane was treated with a solution of 2.4 g (9 mmoles) triphenylphosphine in 20 ml dichloromethane, and the mixture was left at room temperature for 24 hours. After evaporation of the solvent *in vacuo*, the crystalline residue was purified by chromatography (petroleum ether /Al_2O_3), affording 4.2 g (76%) **13**, yellow crystals, m.p. 204°.

$C_{36}H_{45}Cl_2PPd$ (686.1)

Calcd. : C, 63.03 ; H, 6.61 ; Cl, 10.34. Mol. weight, 686.1

Found : C, 63.13 ; H, 6.74 ; Cl, 10.11. Mol. weight, 684 (osmometry in benzene)

NMR (CCl_4, δ, ppm) : 0.65, 1.20 and 1.52 (s, 27H, t-butyl groups), 2.90 (1H, H_A), 3.42 (1H, H_M), 6.83 (1H, H_X) (from and AMX system), 7.20—7.90 (m, 15H).

IR (CS_2 and CCl_4, cm^{-1}) : ν_{C-P} 498 w, ν_{C-Pd} 517 w, 534 w, ν_{C-Cl} 595 w, 642 w.

REACTION OF COMPLEX 7 WITH TRIPHENYLPHOSPHINE. COMPLEX 14

Into a solution of 0.15 g (0.38 mmoles) **7** in 10 ml dichloromethane, a solution of 0.09 g (0.34 mmoles) triphenylphosphine in 10 ml dichloromethane was added, and the mixture was left at room temperature for 12 hours. The solvent was evaporated and the residue was chromatographied with ether on Al_2O_3, yielding yellow crystals of **14**, m.p. 120° (desc.)

$C_{36}H_{46}ClPPd$ (651.6)

Calcd. : C, 66.36 ; H, 7.12

Found : C, 66.84 ; H, 7.49

NMR ($CDCl_3$, δ, ppm) : 0.58, 1.23 and 1.31 (s, 27H, t-butyl groups), 2.25 (1H, H_A), 3.80 (1H, H_M), 6.69 (1H, H_X) (from an AMX system), 5.33 (d, 1H, H-6), 7.30—8.00 (m, 15H).

IR (CS_2 and CCl_4, cm^{-1}) : ν_{C-Pd} 515 m, 530 m.

REDUCTION OF COMPLEX 13 WITH SODIUM BOROHYDRIDE

Into a suspension of 3.5 g (5.1 mmoles) **13** in 20 ml methanol was dropped a solution of 2.0 g (52 mmoles) sodium borohydride in 100 ml aqueous methanol (50%) and the mixture was further stirred for 1 hour. The palladium was filtered off, and the clear liquid was extracted with petroleum ether. The solution was washed with water, dried, the solvent was removed *in vacuo* and the residue (1.3 g) was analysed by means of gas-chromatography. The reaction mixture was found to contain 47.7% 6-chloro-1,3,6-tri-t-butyl-1,2-dihydrofulvene (**3**), 33.8% 6-chloro-1,3,6-tri-t-butyl-1,4-dihydrofulvene (**15**), 11.6% 1,3,6-tri-t-butylfulvene (**12**), together with 6.9% unidentified products.

REDUCTION OF COMPLEX 2 WITH SODIUM BOROHYDRIDE

By treating as above a solution of 5.0 g (11.8 mmoles) **2** in 30 ml methanol with a solution of 4.0 g (106 mmoles) sodium borohydride in 50 ml 50% aqueous methanol and working up as usually, 3.1 g oily product were obtained. Gas-chromatography analysis indicated a content of 86.6% **3** and 5.9% **12**, together with 7.5% unidentified products.

REACTION OF COMPLEX 2 WITH HYDROCHLORIC ACID

Into a solution of 1.5 g (3.5 mmoles) **2** in 50 ml dichloromethane a stream of hydrogen chloride was bubbled for 4 hours. The red solution was washed with water and with 5% sodium carbonate solution in order to remove the hydrogen chloride. After drying and evaporation of the solvent, a crystalline residue (1.3 g) was obtained, which was purified by recrystallization from methanol, yielding 1.04 g (70%) **18**, red crystals, m.p. 203°. This product was found to be identical (m.p., IR and NMR spectra) with a previously obtained [2] sample.

$C_{18}H_{30}Cl_2Pd$ (423.7)

Calcd. : C, 51.02 ; H, 7.14 ; Cl, 16.73 ; Pd, 25.11

Found : C, 50.82 ; H, 7.10 ; Cl, 16.37 ; Pd, 25.18

By treating a solution of **18** (0.10 g, 0.23 mmoles) in 5 ml dichloromethane with a solution of triphenylphosphine (0.12 g, 0.46 mmoles) in 5 ml dichloromethane, fulvene **12** resulted after working up, in quantitative yield.

room temperature for 24 hours. After evaporation of the solvent in vacuo, the crystalline residue was [illegible] by chromatography [illegible]

[illegible]

REACTION OF COMPLEX [illegible] COMPLEX 14

[illegible] dichloromethane, a solution of [illegible] and the mixture [illegible] for 12 hours. The solvent was evaporated and the residue [illegible] yellow crystals of 14 [illegible]

[illegible]

REDUCTION OF COMPLEX [illegible] ALUMINUM HYDRIDE

[illegible] was dropped a solution of [illegible] and the mixture [illegible] filtered off and the [illegible] was washed with water, dried, the solvent was [illegible] by preparative gas chromatography. [illegible]

REDUCTION OF COMPLEX 2 WITH SODIUM BOROHYDRIDE

[illegible] of complex 2 in 10 ml methanol with [illegible]

REACTION OF COMPLEX 2 WITH HYDROCHLORIC ACID

[illegible] complex 2 in 20 ml dichloromethane a stream of hydrogen chloride was introduced for 4 hours. The [illegible] solution was washed with water and with [illegible] sodium carbonate solution in order to remove the hydrogen chloride. After drying and evaporation [illegible] was obtained, which was purified by [illegible] the product was found to be identical [illegible] with the previously obtained sample.

[illegible]

By treatment of [illegible] dichloromethane with a solution of [illegible] complex [illegible] after working up in quantitative yield.

[illegible]

Revue Roumaine de Chimie, 20, 4, 547–560 (1975)

PREPARATION, SPECTRAL PROPERTIES AND ELECTRON STRUCTURE OF 4H-CYCLOPENTA(b) THIOPHENE-4-ONE DERIVATIVES

CH. P. IVANOV and D. M. MONDESHKA

Department of Organic Chemistry,
Higher Institute of Chemical Technology,
Sofia 56, Bulgaria

Received January 13, 1974

The cyclisation reaction of sevaral 3-(2'-thienyl)-substituted 3-hydroxy acids by conc. sulphuric acid or acetic anhydride in the presence of different Lewis acids has been investigated with the purpose to obtain derivatives of 4H-cyclopenta(b) thiophene-4-one. It has been shown that this system can be formed using only strong Lewis acids. It has been established that $AlCl_3$ favours a cyclisation with the thiophene 3-carbon atom even when a phenyl substituent is available in a β-position of the initial hydroxy acid and an attempt to clarify this fact has been made. On the basis of the UV, IR and NMR spectra of the compounds obtained, their electronic structure is discussed and compared with that of the related indene-1-one system.

In a previous paper we reported that under the action of concentrated sulphuric acid an intramolecular cyclisation of 2-phenyl-3-(2′-thienyl)-3-hydroxybutanoic acid **1a** and 2,3-diphenyl-3-(2′-thienyl)-3-hydroxypropanoic acid **1b** with a thiophene β-carbon atom took place, leading to derivatives of 4H-cyclopenta (b) thiophene-4-one **2a,b**[1] unlike 3-(2′-thienyl)-substituted propanoic and butanoic acids which under the same conditions do not afford the corresponding 5,6-dihydro-4H-cyclopenta (b) thiophene-4-ones.[2,3] However, in the presence of a phenyl substituent in a β-position of the initial hydroxy acid (as in **1b**) cyclisation took place predominantly with phenyl leading to the corresponding indene-1-one **3b**. On the other hand, we established that by dehydration of these and other 3-(2′-thienyl)-substituted 3-hydroxy acids after a method for preparation of cyclic ketones[4] (with acetic anhydride and anhydrous $ZnCl_2$) cyclisation with the thiophene ring does not occur at all, a reaction leading to the formation of α, β-unsaturated-4-(2′-thienyl)-substituted methyl ketones[4] taking place.[5]

---

[1] Ch. P. Ivanov and D. M. Mondeshka, *Compt. rend. Acad. bulg. Sci.*, **21**, 343 (1968).

[2] J. Sam and A. Thompson, *J. Pharm. Sci.*, **53**, 535 (1964).

[3] O. Meth-Cohn and S. Gronowitz, *Acta Chem. Scand.*, **20**, 1577 (1966).

[4] W. Johnson and J. Goldman, *J. Amer. Chem. Soc.*, **67**, 430 (1945).

[5] Ch. P. Ivanov and D. M. Mondeshka, *Compt. rend. Acad. bulg. Sci.*, **20**, 1287 (1967); *J. prakt. Chem.*, **315**, 993 (1973).

The purpose of the investigations reported in the present paper was to study dehydration by means of conc. sulphuric acid of other thienyl-substituted hydroxy acids, including those having two 2-thienyl groups in a β-position as well as to search some other methods for realizing an intramolecular cyclisation of the hydroxy acids with a thiophene 3-carbon atom, especially when a phenyl substituent is available at a β-position in the hydroxy acid. Bearing in mind that the derivatives of 4H-cyclopenta (b) thiophene-4-one can be considered as thiophene analogues of indene-1-ones it would be also of interest to establish the stability difference between these two bicyclic systems, one of which contains two condensed five-atomic rings. That is why we set ourselves also the task to investigate the electron structure of these compounds on the basis of their spectral behaviour and to compare it with that of the corresponding indene-1-ones. In the present paper, the dehydration by concentrated sulphuric acid of 2-phenyl-3-(2′-thienyl)-3-hydroxypentanoic **1c** and 2-phenyl-3, 3-(2′,2″-dithienyl)-3-hydroxypropanoic **1d** acids was studied as well as the dehydration of **1a**-**d** in acetic anhydride under the action of some Lewis acids : $TiCl_4$, $SnCI_4$, BF_3-etherate and $AlCI_3$.

The dehydration of **1c** and **1d** by 96.5% sulphuric acid was carried out for 1.5—2.5 min and the obtained reaction mixtures were treated as described previously[1]. The reaction proceeds similarly to the dehydration of **1a** : the quantities of the neutral products reached 40—42% and monosulphonic acids of the cyclic ketones were formed in trace amounts unlike the corresponding indene-1-ones which were considerably sulphonated on preparation by the above method.[1,6,7] By preparative TLC from the mixtures of neutral products we isolated thienyl-substituted stilbenes, small quantities of colourless compounds with the probable structure of γ-lactones, and intensely coloured carbonyl compounds (yield 14.2—14.6%) with m.p. 53—54° (from **1c**) and 129.5—131° (from **1d**). The deeper colour, the specific coloration with conc. sulphuric acid, the IR and NMR spectra of these substances confirm their structures as 5-phenyl-6-ethyl-4H-cyclopenta (b) thiophene-4-one **2c** and 5-phenyl-6-(2′-thienyl)-4H-cyclopenta (b) thiophene-4-one **2d**.

It can be seen that cyclisation with a thiophene 3-carbon atom proceeds with these acids also but the yields of cyclic ketones as in the case of **1a, b** [1] are very low compared to these of the corresponding indene-1-ones. It is known that the dehydration of substituted hydroxy acids by 45—77% sulphuric acid runs through a carbonium ion after an E_1 mechanism with the formation predominantly of the thermodynamically more stable isomer of the corresponding unsaturated acid. [8] In the conditions of cyclisation (97% sulphuric acid) a protonisation of the carboxyl group takes place probably after which the carbonium ion formed attacks the aromatic ring at β-position with closure of a five-membered ring. One of the reasons for the low yields of **2a**-**d** might be due to the formation

---

[6] Ch. P. Ivanov, *Compt. rend. Acad. bulg. Sci.*, **6**, 21 (1953) ; **7**, 29 (1954).

[7] Ch. P. Ivanov and L. Mladenova-Orlinova, *Compt. rend. Acad. bulg. Sci.*, **6**, 33 (1953).

[8] D. Noyce and Ch. Lane, *J. Amer. Chem. Soc.*, **84**, 1635 (1962) ; D. Noyce, R. King, Ch. Lane and W. Reed, *Ibid.*, **84**, 1638 (1962).

mainly of that isomer of the unsaturated acid which is not able to close a cycle, respectively from **1b** the isomer with the phenyl and carboxyl groups in *cis*-position. By means of this, however, the low yield of **2d** cannot be explained as in the initial hydroxy acid there are two equivalent thiophene rings equally accessible to cyclisation. More important reasons in that case should be looked for in the smaller reaction ability of the thiophene 3-carbon atoms for electrophilic substitutions and mainly in the more difficult formation of the bicyclic system consisting of two condensed five-membered rings.

In view of the comparatively low yields in which **2a-d** were obtained by cyclisation of **1a-d** with conc. sulphuric acid, especially in the presence of a phenyl substituent in β-position, [1] we tried some other cyclising agents. The preliminary experiments carried out with polyphosphoric acid showed that cyclisation with the thiophene ring takes place at a small degree and also that under the reaction conditions a considerable part of **1a-d** yields tar. As in a medium of acetic anhydride in the presence of $ZnCI_2$ only cyclisation with phenyl occurs, leading to the corresponding indene-1-ones, we carried out experiments under the action of stronger Lewis acids. The experiments in acetic anhydride in the presence of $TiCI_4$, $SnCI_4$ and BF_3-etherate showed that under these conditions a cyclisation with thiophene ring does not occur. Mainly thienyl-substituted stilbenes and small amounts of α, β-unsaturated methyl ketones of type **4**, the main product of the reaction in the presence of $ZnCI_2$, [5] were obtained. These catalysts proved also to be inappropriate for preparative work as they caused tar formation and decomposition of a large part of **1a-d** into the initial ketone and phenylacetic acid.

The dehydration of **1a-d** in the presence of $AICI_3$ proceeds vigorously but only traces of tar were formed. That is probably due to the quick running of reactions leading to substances stable towards $AICI_3$. The composition of the neutral products obtained under these conditions proved to be rather different from that obtained under the action of weaker Friedel-Crafts catalysts : $AICI_3$ causes cyclisation with the thiophene 3-carbon atoms, **2a-b** being obtained in an yield of 18—29% of the theoretical. The two isomeric cyclic ketones **2b** and **3b** were formed from **1b** but while by dehydration with sulphuric acid mainly **3b** was formed [1] here a higher degree of cyclisation to 5,6-diphenyl-4H-cyclopenta (b) thiophene-4-one **2b** occurred. In all experiments carried out the quantity of thienyl-substituted stilbenes was considerable (12—20%), while the unsaturated ketones **4** were obtained in trace amounts only in some of the cases. An undesirable side reaction in this case is also the decomposition of the hydroxy acids, especially of the triaryl-substituted ones. For that reason the isolation of the cyclic ketones from the complex reaction mixture even by preparative TLC is very difficult all the more so as the latter have R_f values very close to those of the corresponding 2-thienyl ketones.

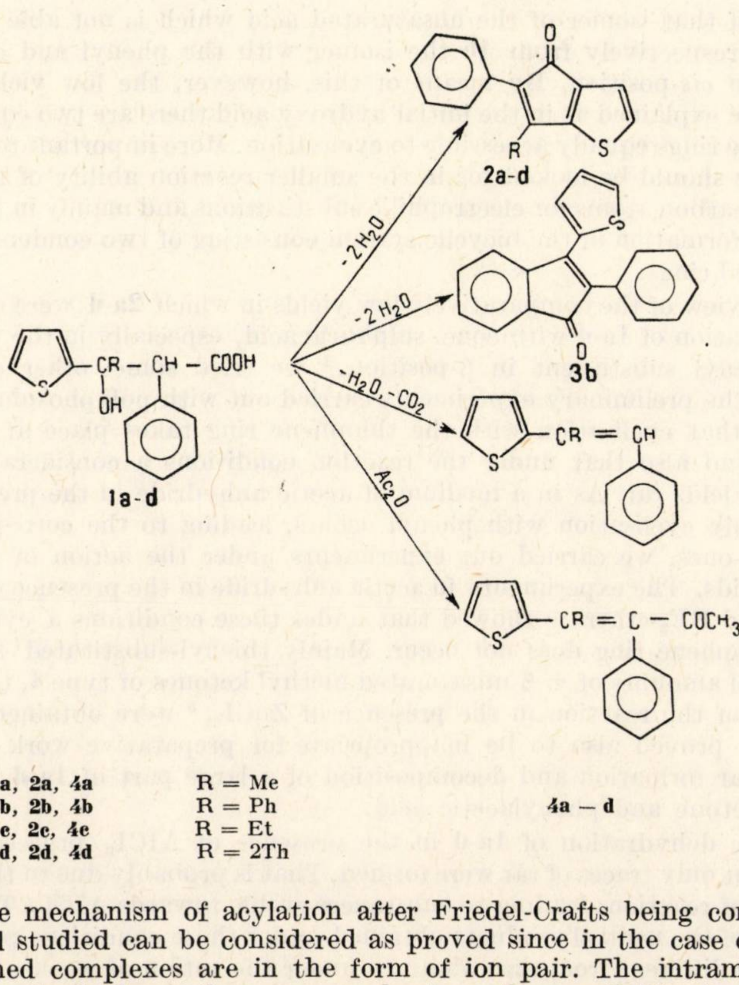

1a, 2a, 4a R = Me
1b, 2b, 4b R = Ph
1c, 2c, 4c R = Et
1d, 2d, 4d R = 2Th

The mechanism of acylation after Friedel-Crafts being comparatively well studied can be considered as proved since in the case of $AlCl_3$ the formed complexes are in the form of ion pair. The intramolecular acylation should have the same mechanism, the possibility for running either inter- or intramolecular reaction being dependent on the electrophilicity of the carbon atoms of the corresponding aromatic nucleus and on the nucleophilic ability of the reagent. Our results showed that the polarity of the complexes formed with weaker Lewis acids such as $ZnCl_2$, $TiCl_4$ and $SnCl_4$ is not sufficient for attacking the thiophene 3-carbon atoms. Nevertheless, this cannot be the only reason as the chlorides of 3- and 4-(2′-thienyl)-substituted butanoic and propanoic acids cyclize to 6- and 7-atomic cyclic ketones.[9] All these facts support the above-stated suggestion that the main reason for the low yields of **2a-d** should be searched in the difficult formation of this new bicyclic system. There are no data in the literature about a preferred cyclisation with thiophene nucleus under the action of $AlCl_3$. We assume that the reason for that must be the formation

[9] P. Cagnient and D. Cagnient, *Bull. Soc. chim. France*, **1953**, 62; **1954**, 1349; **1955**, 680; **1956**, 1152.

of complexes between the thiophene ring and $AICI_3$. It is known that many thiophene derivatives form such complexes and that thus a second acetyl group may enter the nucleus at 3-position, [10] due to reducing the influence of the electron-attracting group as well as of the α-orientation effect of the heteroatom. The acids **1a-d** form in the cold intensely coloured complexes with $AICI_3$ which are not obtained from analogous hydroxy acids unsubstituted with thiophene. Most probably, too, complexes of the type **5a, b** are formed, in which the reaction ability of the thiophene β-carbon atoms becomes higher than that of the phenyl *ortho*-carbon atoms. The

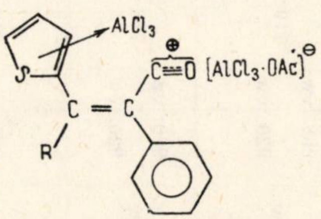

5a

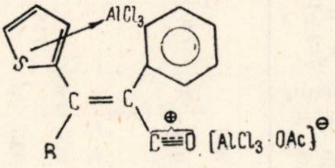

5b

5a, 5b R = Me, Et, Ph, 2-Th

difficult formation of the bicyclic system as well as the spectra of **2a-d** show that full delocalization of the π-electrons is not realized here and that the molecule of 4H-cyclopenta(b)thiophene-4-one cannot be considered as an aromatic system.

In the IR-spectra (table 1) carbonyl stretching vibrations are observed above 1700 cm^{-1} (1716 ± 2 cm^{-1}) e.g. in the region of the conjugated five-membered cyclic ketones but only by 3–5 cm^{-1} lower than that of the corresponding indene-1-ones. [11] That goes to show that conjugation in the two bicyclic systems does not differ considerably and that the carbonyl group is slightly conjugated with the thiophene nucleus. The frequency of the phenyl absorption lying in the range of 700 ± 10 cm^{-1}, assigned to the phenyl C–H out-of-plane deformation vibrations, [12] appears at 700 ± 2 cm^{-1} e.g. shifted by 4–5 cm^{-1} to higher frequencies as compared to the corresponding indene-1-ones. [13] As shown, this frequency decreases when the π-electron density of the monosubstituted benzene rings increases.[13,14] Taking into account also that this frequency is not variable one should conclude that the average π-electron density of the substituent at 5-position in the molecule of 4H-cyclopenta(b)thiophene-4-one is lower than that of the corresponding 2-position in the indenone-1-molecule.

---

[10] Ja. Goldfarb, A. Jakubov and L. Belenkyi, *Doklady Akad. Nauk S.S.S.R.*, **185**, 91 (1969).

[11] Ch. P. Ivanov and I. Yukhnovsky, "Yearbook of the Higher Institute of Chemical Technology—Sofia", **11**, 1 (1964).

[12] "Chemical Applications of Spectroscopy", Editor: W. West (Edited by "Inlit"), Moscow, 1959, p. 316.

[13] Ch. P. Ivanov and I. Yukhnovsky, "Yearbook of the Higher Institute of Chemical Technology—Sofia", **12**, 71 (1965).

[14] R. Kross, D. Fassel and A. Margoshes, *J. Amer. Chem. Soc.*, **78**, 1332 (1956).

Table 1

IR spectra (specific bands) of the derivatives of 4H-cyclopenta (b) thiophene-4-one (in CCl_4) $(\bar{\nu}\ \mathrm{cm}^{-1})$

COMPOUND	ν_{C-C} ν_{C-S} 1525±5	Intensity	ν_{C-C} ν_{C-S} 1415±8	Intensity	ν_{C-C} ν_{C-S} 1384±4	Intensity	ν_{C-C} ν_{C-S} 1227±2	Intensity	β_{C-H} 1082±2	Intensity	β_{C-H} 960±7 925±3	Intensity	β_{C-H} 719±1	Intensity	672±2	Intensity	$\nu_{C=O}$	Intensity
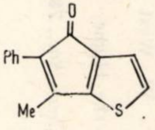 2a	1532	vw*	1408	vw	1388	m	1225	m	1080	w	963 918	vw	720	s	670	m	1718	vs
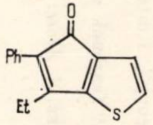 2c	1535	w	1410	vw	1387	m	1226	m	1082	w	963 925	vw vw	718	vs	674	m	1718	vs
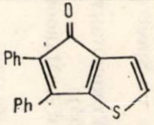 2b	1528	vw	1420	vw	1382	m	1228	m	1085	w	968 920	vw vw	719	s	670	m	1715	vs
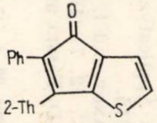 2d	1525	w	1418	w	1384	m	1229	m	1084	w	960 925	vw vw	718	s	670	m	1713	vs
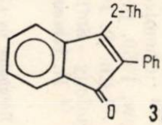 3b	1522	m	1422	m	1380 1360	vw w	1230	vw	1083	m	925	m	710	m	675	vw	1715	vs

*Abbreviations : vs – very strong ; s – strong ; m – medium ; w – weak ; vw – very weak

The spectra reveal also some specific bands, convenient for the identification of the condensed thiophene ring in this system. In the range 1400—1200 cm^{-1} two bands appear with an intensity above average. The first one, 1385 ± 3 cm^{-1} is shifted to higher frequencies with regard to the specific indenone absorption in the same region (assigned to complex joined vibrations of the CO group and of the atoms connected to it [15]) as well as to the thiophene ring symmetric stretching vibrations at 1361 ± 2 cm^{-1}. This is probably the same vibration but of decreased intensity and shifted to higher frequency, due to the weaker conjugation of the thienyl with a carbonyl in 3-position. At 1228 ± 2 cm^{-1} one observes an absorption which in the thienyl-substituted indene-1-one **3b** is of low intensity and in the other indene-1-ones is not revealed at all. The intensity of this absorption, attributed to the thiophene ring asymmetric stretching vibrations [16] is considerably higher in comparison with the 2-substituted thiophenes, where it is not always observed.

All substances **2a-d** exhibit an intensive absorption at 719 ± 2cm^{-1} and a less intensive one at 665 ± 3 cm^{-1}. Thiophene and the monosubstituted thiophenes either absorb weakly or do not absorb in this range at all. These bands are most probably due to out-of-plane deformation vibrations of the C—H bonds of the thiophene ring condensed and conjugated with the CO group. Most of the other bands related to different vibrations of the atoms and the bonds of the thiophene ring are in this case not convenient for identification since these regions absorb also monosubstituted benzenes and indene-1-ones.

In the UV spectra of **2a-d** (Table 2) are observed two maxima in the region where also indenones-1 exhibit absorption : at about 208 nm ($\varepsilon = 12000 - 13\,000$) and 260 nm ($\varepsilon = 23000 - 26000$). The presence of alkyl substituents gives rise to bathochromic shift of the longwave maximum of **2a-d** with 4—5 nm with respect to the corresponding indene-1-ones. In the visible region there appears a less intensive absorption ($\varepsilon = 2\,000 - 4\,000$) at 482—520 nm but of considerable bathochromic shift when compared to indenones. The presence of two aryl substituents increases the intensity as well as the shift of the maximum towards the longwave region. The stronger bathochromic effect of the thienyl substituent on the colour of organic substances in comparison with phenyl has been observed also in open conjugated systems, being of the order of 15—20 nm. [17,18] In this condensed system, however, the bathochromic shift reaches 60—70 nm. It can be seen that the conjugation between the two five-membered rings is stronger here than in the indenone molecule and that the influence of thienyl is considerably greater as compared to the open conjugated systems.

---

[15] Ch. P. Ivanov and I. Yukhnovsky, "Yearbook of the Higher Institute of Chemical Technology-Sofia", **12**, 81 (1965).

[16] A. Katritzky and R. Boulton, *J. Chem. Soc.*, **1959**. 3500.

[17] V. F. Lavrushin, S. V. Zuckerman and J. Sirovatka, *Zhur. obshchei Khim.*, **31**, 1275 (1961).

[18] S. V. Zuckerman, L. Kutulja and V. M. Nikitshenko, *Zhur. obshchei Khim.*, **32**, 2677 (1962).

Table 2

UV – and visible spectra of the derivatives of 4H-cyclopenta (b) thiophene-4-one and some indene-1-ones ($2.0-3.0\times 10^{-5}$g and $6.0-7.0\times 10^{-6}$g EtOH)

COMPOUND	λ_{max}	ε	λ_{max}	ε	λ_{max}	ε
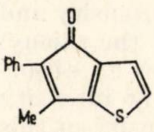 2a	208	12070	255	22700	482	2150
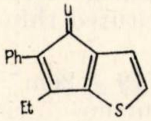 2c	208	12240	258	23200	486	2040
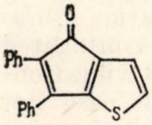 2b	207	12810	261	25240	508	2900
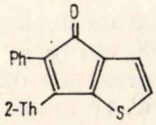 2d	206	13100	266	26500	520	4240
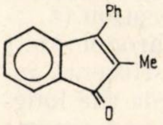	208	6210	242	16500	408	1890
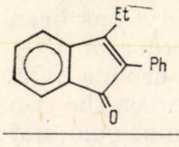	216	10700	255	26900	424	2450
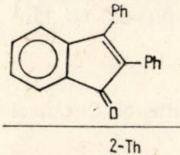	211	15500	260	38300	438	3800
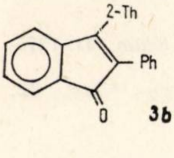 3b	214	14100	264	27100	450	5460

In the NMR spectra of these substances[19] (table 3) the thiophene protons form a typical pair of doublets with a small chemical shift difference. This shows that annelation with the cyclopentadiene ring affects almost equally the electron density of the thiophene carbon atoms. An interaction between the two rings is, however, evident as the presence of alkyl substituents in the 6-position causes a shift of about 0.15—0.20 ppm to higher field and an increase in the chemical shift difference of the two thiophene protons as compared to the unsubstituted thiophene. On the other hand, the aryl substituents decrease this difference, respectively the thiophene ring electron density.

The signal for the five protons of the monosubstituted benzene ring in the 5-position appears as a sharp singlet at 7.30—7.40 ppm i.e. at lower field than in the indenones. This fact is in accordance with the data from the IR spectra and indicates that the average π-electron density of the substituent at 5-position is lower as compared to the corresponding 2-position of the indenone molecule. On the other hand, the signal for 5-Ph is with 0.20 ppm at a higher field than that for 6-Ph. From these facts it may be concluded that in this system, analogously to the indenone-1-one[13] the average π-electron density of the substituent in 6-position is less than that of the substituent in 5-position.

The above mentioned spectral data are in agreement with some preliminary results about the behaviour of the molecule during electrophilic substitutions. Monosulphonic acid was not obtained appreciably with any of the substances **2a-d** in contrast to the indenones which are easily sulphonated in the 2-phenyl residue at *para*-position. Even on treatment with 99% sulphuric acid the aryl-alkyl substituted substances cannot be sulphonated while the diaryl-substituted derivatives lose their colour probably due to decomposition of the conjugated bicyclic system. A decomposition takes also place on attempting to brominate the molecule under considerably milder conditions than those used for indenones. All these facts are in agreement with the more difficult formation of **2a-d** and with the lower stability of this system.

It can be seen from the above results that the electron structure of 4 H-cyclopenta(b)thiophene-4-one is close to that of indene-1-one. The dipolar resonance structure **6** participates to a very small extent, and

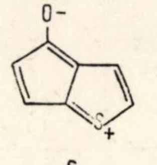

6

it could be neglected in most cases. On the other hand, this bicyclic system proved to be formed with difficulty being unstable during chemical interactions.

---

[19] S. L. Spassov, D. M. Mondeshka and Ch. P. Ivanov, *Compt. rend. Acad. bulg. Sci.*, **21**, 351 (1968).

Table 3

NMR – parameters of the derivatives of 4H-cyclopenta

Compound	ABCD	6C=Me 3C=Me	6C=Et	5C=Ph 2C=Ph	6 – Ph 3 – Ph
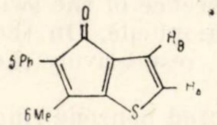 ++ **2a**	–	2.18 s, 3H	–	7.30 s, 5H	–
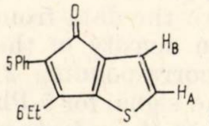 **2c**	–	–	1.28 tr, 3H 2.63 q,2H	7.31 s, 5H	–
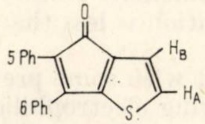 **2b**	–	–	–	7.38 s, 5H	7.53 m, 5H
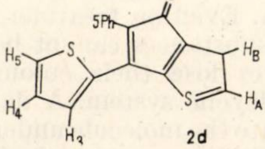 **2d**	–	–	–	7.40 s, 5H	–
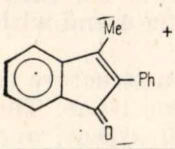 ++	7.1 – 7.6 m, 4H	2.27 s, 3H	–	7.46 s, 5H	–
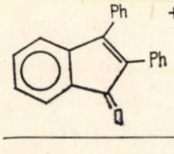 ++	7.0 – 7.7 m ,4H		–	7.22 s, 5H	7.36 s, 5H
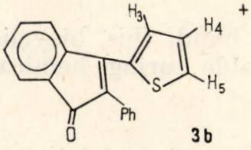 ++ **3b**	7.3 – 7.4 m, 4H		–	7.25 s, 5H	

+ s – singlet; d – doublet; tr – triplet; q – quartet; m – multiplet. + + Ref. [19]

(b) thiophene-4-one and some indene-1-ones (in $CDCl_3$) (δ, ppm)+

AB	H_3	H_4	H_5	J_{AB}	$J_{4,5}$	$J_{3,4}$	$J_{3,5}$	J_{CH_3,CH_2}
6.92 and 7.22 2d, 2H	—	—	—	4.8	—	—	—	—
7.01 and 7.22 2d, 2H	—	—	—	5.0	—	—	—	7.2
7.13 and 7.30 2d, 2H	—	—	—	4.6	—	—	—	—
7.20 and 7.36 2d, 2H	7.60 q, 1H	7.02 q,1H	7.14 q, 1H	5.1	5.0	3.9	1.8	—
—	—	—	—	—	—	—	—	—
—	—	—	—	—	—	—	—	—
—	7.50 q, 1H	6.98 q, 1H	7.12 q, 1H	—	4.8	4.0	2.2	—

EXPERIMENTAL

The IR spectra were recorded on a UR=10-Zeiss, (1958) spectrometer. Solutions of the substances in CCl_4 (1% w/v) in a 1mm NaCl cell were used.

The UV= and visible spectra were taken on a Perkin-Elmer, Model UV=137, selfrecording spectrophotometer. Solutions of the samples in EtOH ($2.0-3.0 \times 10^{-5}$ g and $6.0-7.0 \times 10^{-6}$ g) were used.

The NMR spectra were taken on a JNM=C=60=S, JEOL and on a HA=100=Varian spectrometers operating at frequencies of 60, resp. of 100 MHz. Solutions of the substances in $CDCl_3$ (10% w/v) containing 1% TMS as internal standard were used. The chemical shift values are given in ppm (δ-units).

1. DEHYDRATION BY MEANS OF CONC. SULPHURIC ACID

A. Dehydration of 2-phenyl-3-(2′-thienyl)-3-hydroxypentanoic acid 1c

10 ml of concentrated sulphuric acid (97%) were added to 1.115 g of the hydroxy acid and the mixture was vigourously shaken for 3 min. The intensively red solution was poured into 100 ml of water and extracted with ether. The ether solution was washed with water (to extract the monosulphonic acid but the water solution remained colourless), with saturated natrium carbonate solution (until complete extraction of the carboxylic acids), with water to neutral reaction and then dried (Na_2SO_4). The residue after distillation of the ether, a red coloured non-crystalline mixture of neutral products weighs 0.456 g (41% towards the initial hydroxy acid). By means of preparative TLC* (solvent system light petroleum : benzene = 3 : 1) 0.196 g thienyl-substituted stilbenes, 0.141 g (14.6%) dark red non-crystalline substance and a complex mixture of more polar products were isolated. After cooling for a long time at −12° in ethanol solution the red compound crystallized. Dark-red crystals with m.p. 53−54°** (from ethanol) which gave an intensively blue coloration with conc. sulphuric acid 2c.

IR-spectrum ν_{CO}: 1719 cm^{-1} (vs); CH_3 and CH_2: 2980 cm^{-1} (m), 2938 cm^{-1} (m), 2858 cm^{-1} (w), 2830 cm^{-1} (w), 1465 cm^{-1} (m) and 1378 cm^{-1} (w); benzene ring: 3062 cm^{-1} (w), 3036 cm^{-1} (w), 3022 cm^{-1} (w), 1603 cm^{-1} (w), 1498 cm^{-1} (w), 1447 cm^{-1} (m) and 699 cm^{-1} (s); thiophene ring: 1528 cm^{-1} (w), 1385 cm^{-1} (m), 1226 cm^{-1} (m), 718 cm^{-1} (s), 675 cm^{-1} (m).

UV = and visible spectra :

λ_{max}at 207 nm($\mathcal{E} = 12800$), 261 nm ($\mathcal{E} = 25240$) and 486 nm ($\mathcal{E} = 2040$)

NMR-spectrum : C_2H_5 : 1.28 ppm (tr, 3H) and 2.63 ppm (q, 2H); Th : 7.03 ppm and 7.17 ppm (2d, 2H); Ph : 7.37 ppm (s, 5H).

Semicarbazone — obtained after the ordinary method — red needlelike crystals with m.p. 170−171° (from ethanol).

Found : N, 13.99 ; S, 10.87 %

Calculated for $C_{16}H_{15}N_3OS$: N, 14.15 ; S, 10.77%

B. Dehydration of 2-phenyl-3,3-(2′,2″-dithienyl)-3-hydroxypropanoic acid 1d

5 ml of conc. sulphuric acid were added to 0.530 g of hydroxy acid, the mixture was shaken vigourously and after 2 min poured into 100 ml of water. The violet solution containing a violet precipitate was extracted with ether and the ether solution was treated as in 1A. From the violet coloured mixture of neutral products (0.232 g) by means of preparative TLC (solvent system, light petroleum : benzene = 2.6 : 1), thienyl-substituted stilbenes (0.084 g), violet crystals (0.067 g; 14.3%) and a complex mixture of more polar products (0.089 g) were isolated. The violet substance **2d** melts at 129.5−131° (from ethanol) and gives an intensive red coloration with concentrated sulphuric acid.

IR-spectrum : ν_{CO}: 1713cm^1 (vs); benzene ring : 3090 cm^{-1}(m), 3068 cm^{-1} (w), 3030 cm^{-1} (w), 1600 cm^{-1}(w), 1498 cm^{-1} (w), 1448cm^{-1} (m) and 699 cm^{-1}(s); thiophene ring : 1525 cm^{-1} (w), 1384 cm^{-1}(m), 1229 cm^{-1} (m), 718 cm^{-1} (s) and 670 cm^{-1} (m).

---

* For TLC Silica Gel Merck (type 60) was used.

** All melting point (uncorrected) were taken on a Koffler apparatus.

UV — and visible spectra : λ_{max} at 206 nm ($\varepsilon = 13100$), 266 nm ($\varepsilon = 26500$) and 519 nm ($\varepsilon = 4240$).

NMR-spectrum : Th : 7.27 ppm and 7.38 ppm(2d, 2H), 7.02 ppm(q, 1H), 7.14 ppm (q, 1H) and 7.60 ppm (q, 1H); Ph : 7.40 ppm (s, 5H).

Found : S, 20.49

Calculated for $C_{17}H_{10}OS_2$: S, 20.65%

2. DEHYDRATION IN ACETIC ANHYDRIDE IN THE PRESENCE OF ANHYDROUS ALUMINIUM CHLORIDE

A. Dehydration of 2-phenyl-3-(2′-thienyl)-3-hydroxybutanoic acid 1a

a. 1.112 g hydroxy acid was heated in 8 ml Ac_2O for 5 hrs at 60—65°. Then 0.4 g anhydrous $AlCl_3$ was added and the temperature was increased up to the b.p. of of the reaction mixture which become red-brown in colour. Diluted HCl was then added and the organic products were extracted with ether. The ether solution was treated with Na_2CO_3 aq. (to extract the carboxylic acids), washed with water and dried (Na_2SO_4). After distillation of the ether, 0.788 g mixture of neutral products was obtained. Preparative TLC (solvent system, light petroleum : benzene : acetone = 50 : 15 : 2.5) yielded 0.231 g of thienyl-substitutes stilbenes, 0.189 g (19.4%) of 5-phenyl-6-methyl-4H-cyclopenta (b) thiophene-4-one **2a**, 0.63 g (4.3%) of 3-phenyl-4-(2′-thienyl)-pent-3-ene-2-one **4a**[5] and complex mixture of other substances.

b. 0.490 g hydroxy acid was heated in 10 ml 1 : 1 mixture of Ac_2O and glacial AcOH and 0.25 g anhydrous $AlCl_3$ for 15 min at 136°. After hydrolysis the reaction mixture was treated as described in 2Aa. The obtained 0.338 g mixture of neutral products when subjected to preparative TLC under the above conditions gave 0.081 g thienyl-substituted stilbenes, 0.087g (20.2%) of **2a** and complex mixture of other products.

B. Dehydration of 2,3-diphenyl-3-(2′-thienyl)-hydroxypropanoic acid 1b

a. 1.075 g hydroxy acid was dehydrated according to 2Aa. The obtained 0.699 g mixture of neutral products was subjected to preparative TLC(solvent system, light petroleum : benzene : acetone = 50 : 12.5 : 2.5) yielding : 0.070 g thienyl-substituted stilbenes 0.531 g mixture of orange, violet and some colourless crystals and 0.035 g phenyl-2-thienyl ketone. The mixture was again subjected to preparative TLC (light petroleum : benzene : acetone = 50 : 6 : 2). Isolated were 0.049 g phenyl-2-thienyl ketone, 0.203 g of orange crystals and 0.294 g of violet crystals, both containing trace amounts of phenyl-2-thienyl ketone. After rechormatography (light petroleum : acetone = 50 : 1.8) 0.258 g (27%) violet crystals with m. p. 164—165° (from ethanol) and 0.187 g (19.6%) orange crystals with m.p. 124° (from ethanol) were obtained. The m.p., IR and NMR spectra of these compounds coincide with the m.p. and spectra of 5,6-diphenyl-4H-cyclopenta (b) thiophene-4-one **2b** and of 2-phenyl-3-(2′-thienyl)-indene-1-one **3b**, respectively.

b. Procedure 2Ab was followed. From 0.981 g hydroxy acid a mixture of 0.706 g of neutral products was obtained which after TLC under the above conditions gave 0.056 g thienyl-substituted stilbene, 0.245 g (28%) of **2b**, 0.184 g (21%) of **3b** and 0.127 g phenyl-2-thienyl ketone.

C. Dehydration of 2-phenyl-3-(2′-thienyl)-3-hydroxypentanoic acid 1c

According to 2Aa, 0.507 g hydroxy acid yielded 0.355 g red coloured mixture of neutral products. By preparative TLC (solvent system, light petroleum : benzene : acetone = 50 : 2.5 : 1.8) were isolated : 0.078 g thienyl-substituted stilbenes, 0.105 g (24%) of red substance (after prolonged cooling crystallized and melted at 53—54° from ethanol **2c**), 0.028 g (4.5%) of 3-phenyl-4-(2′-thienyl)-hexa-3-ene-2-one **4c**[5] and 0.071 g of a mixture of products.

D. Dehydration of 2-phenyl-3, 3-(2′,2″-dithienyl)-3-hydroxypropanoic acid 1d

According to procedure 2 Aa from 0.503 g hydroxy acid 0.346 g violet coloured mixture of neutral products was obtained which when subjected to preparative TLC (solvent system light petroleum : benzene : acetone = 50 : 7 : 2.5) gave 0.055 g thienyl-substituted stilbene,0.109 g violet crystals mixed with colourless ones, 0.118g 2,2-dithienylketone and 0.058 g of a complex mixture of other products. The violet mixture after rechromatography (light petroleum : acetone = 50 : 2.2) gave 0.089 g (20%) dark-violet crystals with m.p. 129.5—131° (from ethanol) **2d** and 0.030 g 2,2-dithienyl ketone.

Acknowledgement. The authors wish to thank Dr. A.U. Stepanyants of the Laboratory of NMR spectroscopy, Institute of Chemical Physics, USSR Academy of Sciences for recording some of the NMR-spectra.

Revue Roumaine de Chimie, **20**, *4*, 561–573 (1975)

CONTRIBUTION À LA SYNTHÈSE DES ÉCHANGEURS D'IONS FAIBLES ET FORTEMENT BASIQUES, DE TYPE GEL EN PARTANT DES AMINO-ALCOOLS

I. PETRARIU, DEMETRA DRĂGAN, PAMFILIA PETRARIU et FL. POPESCU

Institut de Chimie macromoléculaire « Petru Poni », 41 A,
Aleea Gr. Ghica Vodă, Jassy

Reçu le 16 février 1974

On a établi les meilleures conditions de synthèse pour certains échangeurs d'anions type gel, de faible et forte basicité en partant des amino-alcools. On a étudié l'effet de la modification des différents paramètres sur le degré de transformation, respectivement sur la capacité d'échange des échangeurs d'anions. On a cherché à établir la liaison existante entre les conditions de synthèse et la structure des anionites obtenus en mettant en évidence le changement de la nature de la basicité de l'anionite Co—CM—TEA dans des conditions plus sévères de synthèse. Les échangeurs d'ions synthétisés ont été caractérisés par des études en infrarouge, par analyse élémentaire, thermogravimétrique, thermodifférentielle et titrage pH-métrique des groupes ionogènes fixés sur la chaîne.

Actuellement dans le domaine de la synthèse des échangeurs d'ions on cherche à trouver de nouvelles structures, ayant de multiples possibilités applicatives.

Les caractéristiques physico-chimiques spécifiques des différents types des échangeurs d'anions dépendent de la nature du copolymère réticulé, des groupements ionogènes et de leur disposition sur la chaîne macromoléculaire.

Le type de l'amine qui se trouve sur la chaîne macromoléculaire détermine la nature des groupements ionogènes et joue le rôle le plus important parmi les facteurs qui décident les caractéristiques physico-chimiques des échangeurs anioniques.

On trouve dans la littérature de spécialité des travaux concernant la synthèse des échangeurs d'anions de faible et forte basicité par la réaction de l'amination des copolymères styrènedivinylbenzène chlorométhylés de type gel, avec des mono-, di- ou trialkylamines ou avec des alkylènepolyamines dans des solutions aqueuses, alcooliques ou dans des hydrocarbures aliphatiques chlorurés.[1-6] A côté des procédés indiqués plus haut sont mentionnées les possibilités de polymérisation des sels quaternaires d'ammonium non saturés[7-16] et aussi la nitration suivie de la réduction des copolymères styrène-divinylbenzène ainsi modifiés.[17-18]

L'introduction des échangeurs d'anions ayant des performances supérieures, dans les technologies modernes qui utilisent l'échange ionique, a déterminé sur le plan mondial une consommation accrue des divers types d'échangeurs d'anions avec des caractéristiques physico-chimiques améliorées. On connaît quelques travaux publiés[6,19-20] qui abordent une série des réactions polymère analogues, dans lesquelles le copolymère aminé avec des amino-alcools est utilisé seulement comme intermédiaire pour certaines synthèses ultérieures. On n'a pas effectué des études concernant la synthèse et la caractérisation des échangeurs d'anions en partant des amino-alcools.

Dans un travail antérieur, [21] on a précisé quelques détails sur la synthèse d'un échangeur d'anions de type gel en partant de la triéthanolamine.

[1] G. D. Jones, *Ind. Eng. Chem.*, **44**, 2686 (1952).

[2] K. W. Pepper, H. M. Paisley et M. A. Young, *J. Chem. Soc.*, **1953**, 4097.

[3] G. S. Solt, (Permutit Co. Ltd.), Brit. Pat. 728.508 (1955) ; *Chem. Abstr.*, **49**, 13. 557 (1955).

[4] S. Sekino et T. Hiraga (Asahi Glass Co.) Jap. Pat. 645 (1959) ; *Chem. Abstr.*, **53**, 10595, (1959).

[5] Y. Tsunoda et M. Seko (Asahi Chemical Industries Co.), Jap. Pat. 1240 (1958) ; *Chem, Abstr.*, **53**, 9522 (1959).

[6] E. B. Trostianskaia, S. B. Makarova et A. S. Tevlina, *Vysokomol. Soedimeniya*, **3**, 1358 (1961).

[7] G. B. Butler et R. L. Bunch, *J. Amer. Chem. Soc.*, **71**, 3120 (1949).

[8] G. B. Butler et F. L. Ingley, *J. Amer. Chem. Soc.*, **73**, 895 (1951).

[9] G. B. Butler et R. L. Goette. *J. Amer. Chem. Soc.*, **73**, 1939 (1951).

[10] G. B. Butler, R. L. Bunch et F. L. Ingley, *J. Amer. Chem. Soc.*, **74**, 2543 (1952).

[11] G. B. Butler et R. L. Bunch, *J. Amer. Chem. Soc.*, **74**, 3453 (1952).

[12] G. B. Butler et R. A. Johnson, *J. Amer. Chem. Soc.*, **76**, 713 (1954).

[13] G. B. Butler et R. L. Goette, *J. Amer. Chem. Soc.*, **76**, 2418 (1954).

[14] G. B. Butler et R. J. Angelo, *J. Amer. Chem. Soc.*, **78**, 4797 (1956).

[15] G. B. Butler et R. J. Angelo, *J. Amer. Chem. Soc.*, **79**, 3128, (1957).

[16] A. L. Clingman, J. R. Parrish et R. Stevenson, *J. Appl. Chem.* **13**, 1 (1963).

[17] G. F. D'Alelio, U.S. Pat. 2. 366.008 (1944).

[18] R. H. Boundy et R. F. Boyer, « Styrene, its Polymers, Copolymers and Derivatives », Reinhold Publ. Corp., New York 1952, p. 674—691.

[19] E. B. Trostianskaia et G. Z. Nefedova, *Vysokomol. Soedineniya*, **5**, 49 (1963).

[20] J. Szántó et J. Mikes, *Kolorisztikai Ertesitő*, **1964**, 239.

[21] I. Petrariu, P. Petrariu, Ig. Poinescu et D. Drăgan, *Materiale Plastice*, **9**, 8 (1972).

Les réactions peuvent être représentées schématiquement ainsi :

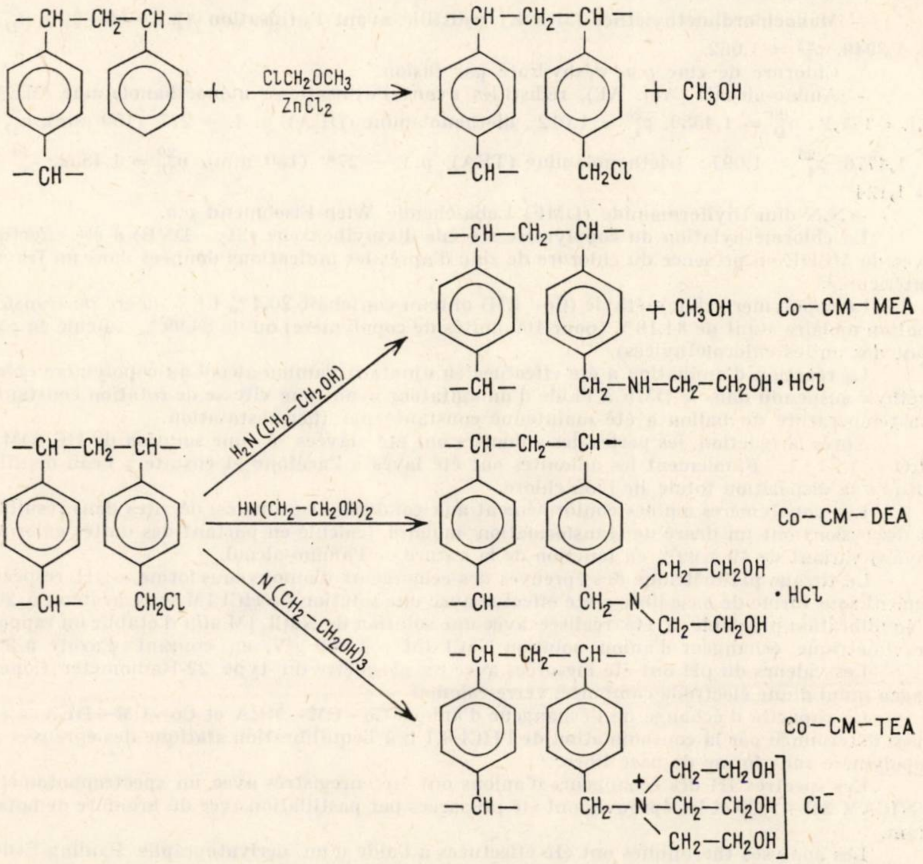
ClCH₂OCH₃
ZnCl₂
+ CH₃OH
CH₂Cl
H₂N(CH₂–CH₂OH)
+ CH₃OH Co–CM–MEA
CH₂–NH–CH₂–CH₂OH • HCl
HN(CH₂–CH₂OH)₂
Co–CM–DEA
CH₂–CH₂OH
CH₂–N
CH₂–CH₂OH
• HCl
N(CH₂–CH₂OH)₃
Co–CM–TEA
CH₂–CH₂OH
CH₂–N–CH₂–CH₂OH Cl⁻
CH₂–CH₂OH

Les échangeurs d'anions obtenus par la réaction du copolymère chlorméthylé, avec des amino-alcools primaires ou secondaires, se présentent, en principal, sous forme de base libre. En fait, la structure des groupes fonctionnels n'est pas parfaitement unitaire, pendant la synthèse étant possibles aussi des réactions de réticulation supplémentaire qui conduisent à l'apparition des groupes actifs ayant des forces basiques différentes, la probabilité des réactions secondaires étant plus grande si on utilise des amino-alcools primaires.

MATÉRIAUX ET MÉTHODES

On a utilisé les substances suivantes :

— Copolymère styrène — 8 % divinylbenzène. La copolymérisation a été réalisée en suspension.[22] Après la copolymérisation, les perles obtenues ont été triées, pour séparer la fraction comprise entre 0,4—0,8 mm, qui a été ensuite utilisée dans les réactions ultérieures de chlorméthylation et d'amination.

---

[22] I. Petrariu et J. Stamberg, *Coll. Czech. Chem. Comm.*, **32**, 798 (1967).

— Monochlordiméthyléther (MCDE) redistillé avant l'utilisation (p.f. = 56—60°), n_D^{25} = = 1,3949, ρ_4^{25} = 1,062.

— Chlorure de zinc *p.a.* déshydraté par fusion.

— Amino-alcools (Am. Al.), redistillés avant l'utilisation : monoéthanolamine (MEA), p.f. = 171,1°, n_D^{20} = 1,4539, ρ_4^{25} = 1,012 ; diéthanolamine (DEA), p. f. = 217° (150 mm), n_D^{20} = = 1,4776, ρ_4^{20} = 1,097 ; triéthanolamine (TEA), p. f. = 278° (150 mm), n_D^{20} = 1,4852, ρ_4^{20} = = 1,124.

—N,N-diméthylformamide (DMF) Loba-chemie Wien-Fischmend *p.a.*

La chlorméthylation du copolymère styrène-divinylbenzène (Sty—DVB) a été effectuée avec du MCDE en présence du chlorure de zinc d'après les indications données dans un travail antérieur.[23]

Le copolymère chlorméthylé (Co—CM) obtenu contenait 20,4% Cl, le degré de transformation molaire étant de 84,18% (pour 100 unités de copolymère) ou de 89,99% (calculé en partant des unités chlorméthylées).

La réaction d'amination a été effectuée en ajoutant l'amino-alcool au copolymère chlorméthylé suspendu dans le DMF à l'aide d'un agitateur ayant une vitesse de rotation constante. La température du ballon a été maintenue constante par thermostatation.

Après la réaction, les perles des anionites ont été lavées à une solution de HCl/DMF/H_2O = 1 : 1 : 1. Finalement les anionites ont été lavés à l'acétone et ensuite à l'eau distillée jusqu'à la disparition totale de l'ion chlore.

Les copolymères aminés conformément aux conditions optimales, décrites dans résultats et discussions ont un degré de transformation molaire (calculé en partant des unités chlorméthylés) variant de 49 à 99% en fonction de la nature de l'amino-alcool.

Le titrage pH-métrique des épreuves des échangeurs d'anions sous forme —OH, respectivement sous forme de base libre a été effectué avec une solution de HCl 1M sous azote et à 20°. L'équilibration préalable a été réalisée avec une solution de NaCl 1M afin d'établir un rapport gravimétrique, échangeur d'anions-solution NaCl 1M = 1/100 g/V, en courant d'azote à 20°.

Les valeurs du pH ont été mesurées avec un pH-mètre du type 22-Radiometer Copenhagen muni d'une électrode combinée, verre-calomel.

La capacité d'échange de l'échangeur d'anions Co—CM—MEA et Co—CM—DEA a été aussi déterminée par la consommation de l'HCl 0,1 n à l'équilibration statique des épreuves de copolymère sous forme de base libre.

Les spectres IR des échangeurs d'anions ont été enregistrés avec un spectrophotomètre UNICAM SP—1000 et les épreuves ont été préparées par pastillation avec du bromure de potassium.

Les analyses thermiques ont été effectuées à l'aide d'un dérivatographe Pauling-Erdey en présence de l'air et à une vitesse d'échauffement de 9,8°/min.

RÉSULTATS ET DISCUSSIONS

Dans une série d'expériences préliminaires on a établi que la durée de réaction — 10 heures — représente une valeur pour laquelle on obtient des degrés de transformation importantes (Co—CM—MEA = 47,5%, Co—CM—DEA = 56,5%, Co—CM—TEA = 27%) et en conséquence cette valeur a été maintenue constante pendant les expériences suivantes. Ainsi les réactions d'amination ont été effectuées dans la majorité des cas à 50° pour prévenir la possibilité de la dégradation des échangeurs d'anions formés sous l'influence d'une température plus grande.

Dans une autre série d'expériences on a cherché à déterminer le meilleur rapport molaire du Co—CM/Am.Al.

Les données présentées dans la figure 1 permettent de constater qu'à un rapport molaire Co—CM/Am.Al = 1/3 on obtient le meilleur degré de transformation et que par l'agrandissement de la quantité d'amino-alcools, le degré de transformation, respectivement la capacité d'échange des échangeurs d'anions, enregistre des croissances non significatives. En conséquence, dans toutes les expériences effectuées pour établir l'influence de ces facteurs sur le degré d'amination, on a utilisé la valeur indiquée pour le rapport molaire Co—CM/Am.Al.

---

[23] A. Carpov, D. Drăgan et I. Petrariu, *Rev. Roumaine Chim.*, **17**, 1923 (1972).

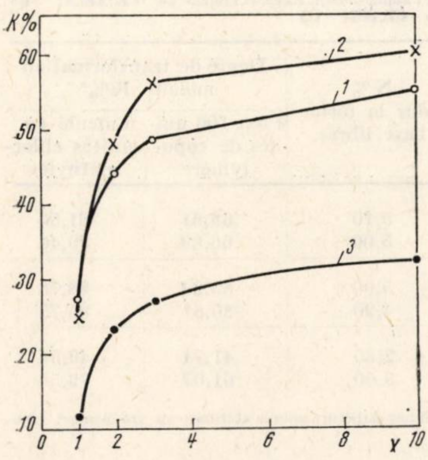

Fig. 1. — Variation du degré de transformation en fonction du rapport molaire Co—CM/Am. Al ; X = moles d'amino-alcools pour un mole de Co—CM. Conditions de réaction : t° = 50°, durée de la réaction 10 heures ; milieu de la réaction DMF ; rapport Co—CM/DMF= 1/3 (en poids). *1,* MEA ; *2,* DEA ; *3,* TEA.

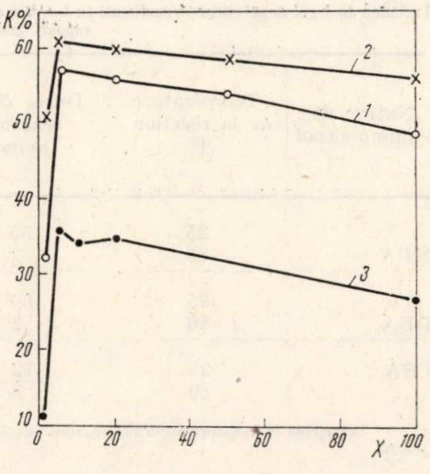

Fig. 2. — Influence de la quantité du solvant DMF sur le degré de transformation. 1 g Co—CM/X g DMF. Conditions de réaction : t° = 50°, durée de la réaction 10 h. ; rapport molaire Co — CM/Am. Al. = 1/3 ; *1,* MEA ; *2,* DEA ; *3,* TEA.

Vu que la quantité du solvant, respectivement du DMF joue un rôle important dans la réaction de l'amination du Co—CM avec des amino-alcools, on a étudié la variation du degré de transformation, en fonction du rapport gravimétrique Co—CM/DMF (g/g).

Comme on peut constater des données présentées dans la figure 2 un degré d'amination maximale est obtenu à un rapport gravimétrique Co—CM/DMF = 1/5.

En effectuant la réaction d'amination dans un milieu plus dilué, respectivement en utilisant des quantités plus grandes de DMF, la vitesse de réaction baisse.

Le tableau 1 permet d'apprécier les conditions de réaction nécessaires pour réaliser un degré d'amination maximale du Co—CM avec des amino-alcools.

On constate que dans les conditions de réaction mentionnées dans le tableau 1, la réactivité des amino-alcools utilisés pour l'amination du Co—CM, croît dans l'ordre suivant : DEA $>$ MEA $>$ TEA.

On constate aussi que, dans le cas de l'utilisation de MEA et DEA, les valeurs du degré de transformation molaire du Co—CM sont relativement approchées, chose qui indique la possibilité d'effectuer l'amination soit à 25°, la durée de la réaction étant relativement longue, soit à 80° pendant un temps plus court.

Tableau 1

Variation du degré de substitution maximale en fonction de la nature de l'amino-alcool Rapport molaire Co – CM/Am.Al. = 1/3, rapport gravimétrique Co – CM/DMF = 1/5

Nature de l'amino-alcool	Température de la réaction t°	Durée de la réaction jours	N% (pour la forme base libre)	Degré de transformation molaire K%*	
				Pour 100 unités de copolymère	Calculé en unités chlorméthylés
MEA	25	55	5,10	68,61	81,50
	80	2	5,00	66,89	79,46
DEA	25	60	5,00	83,24	98,76
	80	2	4,90	80,61	95,75
TEA	25	72	2,80	41,74	49,58
	80	2	3,60	61,07	72,54

* Les degrés de transformation molaire sont calculés en partant d'une structure unique attribuée au groupement fonctionnel.

D'ailleurs, dans le cas de la réaction du Co—CM avec MEA, il est possible d'obtenir des degrés de transformation plus petits que dans la réaction avec DEA à cause des réactions secondaires, leur probabilité étant accrue dans le cas d'une amine primaire.

Dans le cas TEA, la valeur du degré de transformation molaire à 25° est beaucoup plus petite par rapport à la valeur obtenue à 80°. Ce fait peut être attribué dans une certaine mesure à la stabilité chimique de l'anionite obtenu (Co—CM—TEA), qui peut se dégrader partiellement, en modifiant le rapport entre les groupes de faible ou forte basicité. Le calcul du degré de transformation ne tient pas compte de ce fait. Cette constatation ressort plus évidemment après l'étude des données présentées dans le tableau 2.

Tableau 2

Variation de la capacité d'échange de l'échangeur d'anions Co – CM – TEA en fonction des conditions de la réaction, pour un rapport molaire Co – CM/Am.Al. = 1/3, rapport Co – CM/DMF = 1/5 (en poids)

Température de la réaction t°	Durée de la réaction jours	Capacité d'échange totale (Ct) mech/g	Capacité d'échange fortement basique		Capacité d'échange faiblement basique	
			mech/g	%du Ct	mech/g	% du Ct
25	72	2,00	1,67	83,5	0,33	16,5
80	2	2,50	1,50	60,0	1,00	40,0

On constate qu'à 80°, la capacité d'échange fortement basique devient plus petite, pendant que la capacité d'échange attribuée aux groupes faiblement basiques croît.

Pour la détermination exacte de la capacité d'échange totale, ainsi que pour l'estimation de la fonctionnalité des échangeurs d'anions synthétisés en partant des amino-alcools, on a tracé les courbes de titrage pH-métriques de ceux-ci. Les courbes de titrage pH-métrique (fig. 3 et 4) montrent que dans le cas de l'anionite fortement basique Co—CM—TEA synthé-

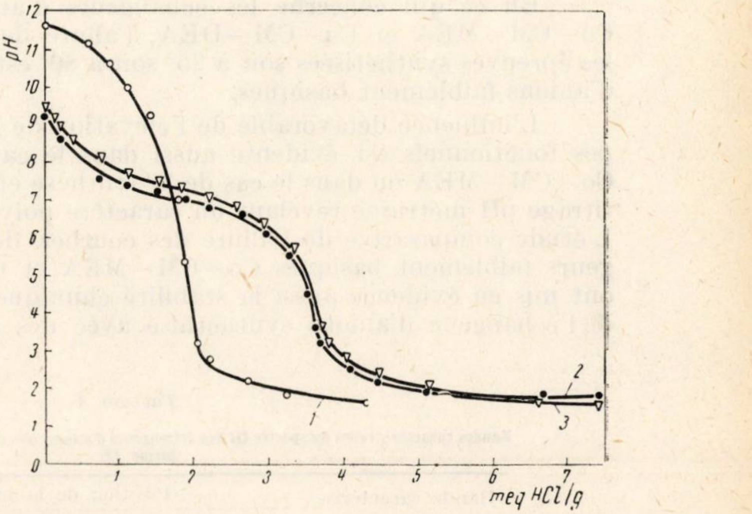

Fig. 3. — Courbes de titrage pH-métrique des anionites obtenus en partant des amino-alcools. Conditions de synthèse : t° = = 25° ; durée de la réaction : *1* — 72 jours Co—CM—TEA ; *2* — 60 jours Co—CM—DEA ; *3* — 45 jours Co—CM/Am. Al. = 1/3 ; rapport molaire Co—CM/Am. Al. = 1/3 ; rapport Co—CM/DMF = 1/5 (en poids).

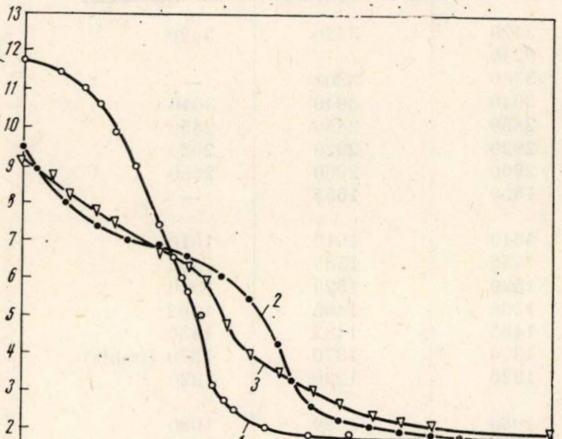

Fig. 4. — Courbes de titrage pH-métrique des anionites obtenus en partant des amino-alcools. Conditions de synthèse : t° = 80° ; durée de la réaction 48 h. ; rapport molaire Co—CM/Am. Al. = 1/3 ; rapport Co—CM/DMF = 1/5 (en poids) ; *1* — Co—CM—TEA ; *2* — Co—CM—DEA ; *3* — Co—CM—MEA.

tisé à 25° l'allure de la courbe est plus prononcée en comparaison du même anionite synthétisé à 80°, ce qui confirme aussi le changement du rapport entre les groupes de faible ou de forte basicité qui a lieu à 80°, ayant comme conséquence la formation d'un anionite qui présente un caractère polyfonctionnel plus prononcé, ayant des groupes fortement basiques en proportion de 60% et des groupes faiblement basiques en proportion de 40%. En conséquence, pour obtenir un échangeur d'anions fortement basique prédominant monofonctionnel en partant de TEA, on doit utiliser des conditions douces de réaction.

En ce qui concerne les échangeurs d'anions faiblement basiques, Co—CM—MEA et Co—CM—DEA, l'allure des courbes de titrage pour les épreuves synthétisées soit à 25° soit à 80° est spécifique des échangeurs d'anions faiblement basiques.

L'influence défavorable de l'élévation de la température sur les groupes fonctionnels est évidente aussi dans le cas des échangeurs d'anions Co—CM—MEA ou dans le cas de la synthèse effectuée à 80°, la courbe de titrage pH-métrique révélant un caractère polyfonctionnel plus prononcé. L'étude comparative de l'allure des courbes de titrage pour les échangeurs faiblement basiques Co—CM—MEA et Co—CM—DEA (fig. 3 et 4) ont mis en évidence aussi la stabilité chimique et thermique plus élevée de l'échangeur d'anions synthéthisé avec des amino-alcools secondaires.

Tableau 3

Bandes caractéristiques du spectre IR des échangeurs d'anions obtenus en partant des amino-alcools (forme Cl)

Bande caractéristique	Position de la bande (cm $^{-1}$)		
	Co—CM—MEA	Co—CM—DEA	Co—CM—TEA
νOH	3420	3420	3420
νNH	3240		
	3360	3300	—
νCH(aromatique)	3040	3040	3040
$\nu CH(CH_2.CH_3)$	2850	2850	2850
	2920	2920	2920
	2960	2960	2960
δ NH	1650	1655	—
ν—C=C(aromatique)	1610	1610	1610
	1585	1585	1585
	1520	1520	1520
$\delta\ CH_3-CH_2$	1460	1465	1462
	1435	1432	1430
$\delta\ CH_3$	1370	1370	1370 (faible)
	1220	1220	1220
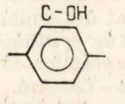	1080	1080	1080
	835	835	835

L'étude du spectre IR, des échangeurs d'anions sous forme chlorhydrate a relevé quelques bandes caractéristiques des échangeurs d'anions faiblement basiques (Co—CM—MEA et Co—CM—DEA) et aussi des échangeurs d'anions fortement basiques (Co—CM—TEA).

Ainsi qu'il résulte des données du tableau 3, les bandes caractéristiques des trois types d'anionites présentés sont semblables, à l'exception de la bande 1080 cm^{-1} qui est plus intense pour l'anionite Co—CM—TEA comparativement aux autres deux anionites, bande qui est caractéristique de l'hydroxyde lié par covalence et appartenant au groupement CH_2CH_2OH.

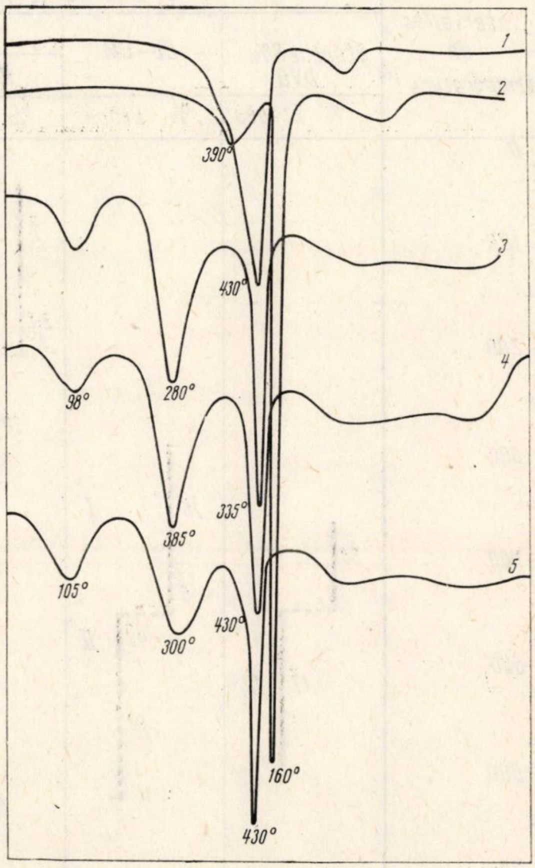

Fig. 5.— Dérivée de la courbe thermogravimétrique (DTG) des copolymères aminés comparativement au DTG des copolymères Sty-8% DVB et Co—CM.
1, Copolymères Sty-8% DVB ; *2,* Co—CM ; *3,* Co—CM—TEA ; *4,* Co—CM—DEA ; *5,* Co—CM—MEA.

Les copolymères modifiés ont été soumis à l'analyse thermique différentielle pour établir la nature des phénomènes (endo- ou exothermiques) et aussi à une étude thermogravimétrique. Les résultats de l'étude thermogravimétrique, exprimés en pertes en poids correspondant à des intervalles de température, ont été indiqués dans le tableau 4.

Les modifications de la dérivée de la courbe thermogravimétrique (DTG) en fonction de la température et de la nature du copolymère aminé, sont répresentées dans la figure 5.

L'étude du comportement thermique du copolymère chlorméthylé, modifié par le TEA, DEA et MEA, comparativement au copolymère Sty-

Tableau 4

La perte en poids pour des intervalles de température du copolymère styrène – 8% divinylbenzène chlorméthylé, modifié par mono, di et triéthanolamine

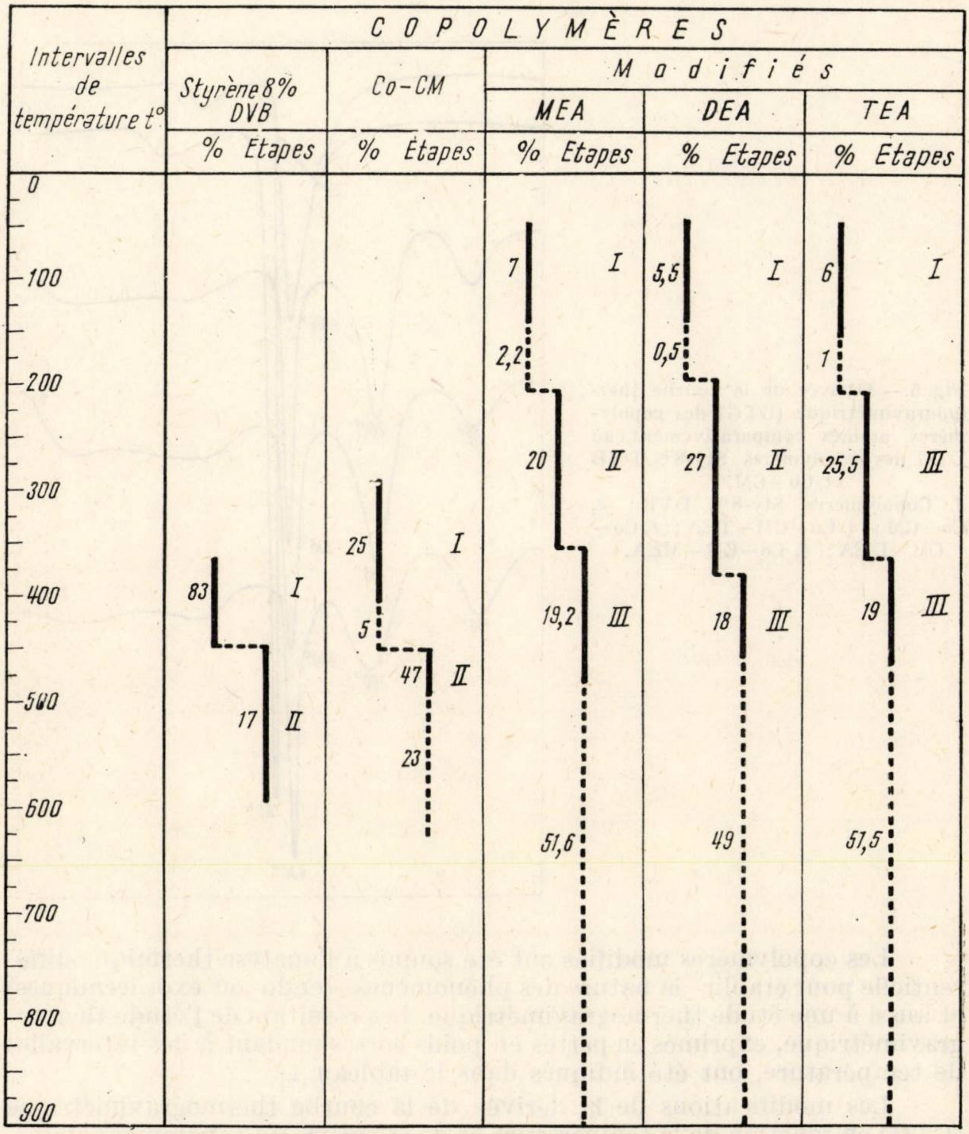

– étapes de transformation correspondant aux modifications mises en évidence par les diagrammes D.T.G. et commentés dans le texte.

··· autres intervalles de température correspondant à certaines pertes en poids du copolymère.

8%DVB a conduit aux conclusions suivantes :

— Le copolymère Sty—8%DVB perd 83% de son poids dans l'intervalle 360 à 450°. La vitesse de décomposition croît vers la fin de l'intervalle et atteint son maximum à 430°. Au-dessus de 450° la décomposition est lente. A 590° la décomposition est totale (tableau 4). Les phénomènes sont exothermes, à l'exception de l'intervalle 480 à 520° quand probablement un réarrangement a lieu dans la molécule.

— Le copolymère Co—CM présente deux intervalles de décomposition rapide, séparés par un palier (280 à 410° et 460 à 490°). Le maximum de vitesse de décomposition est situé dans le deuxième intervalle à 460° et est approximativement 2,7 fois plus rapide que dans le cas du copolymère non modifié, étant déplacé de 30°, par rapport au cas précédent, à cause du chlore présent dans la molécule (fig. 5).

— Les copolymères modifiés par l'introduction des groupes TEA, DEA et MEA présentent trois étapes principales de décomposition (I, II, III) dans lesquelles les phénomènes de transformation chimique se développent avec une vitesse appréciable, la vitesse croissant dans l'ordre I, II, III (fig. 5).

Etape I : Les copolymères perdent approximativement 5—7% en poids (fig. 5 et tableau 4) le phénomène est endothermique et peut être attribué à des réactions ayant lieu entre les groupes aminiques de la chaîne et les groupes — CH_2Cl résiduels, avec élimination de HCl.

Etape II (de décomposition) : Elle est située dans les limites (80° à 370°). La vitesse la plus grande est située à 280° pour les produits modifiés par TEA, à 285° pour ceux modifiés par DEA et à 300° pour les produits modifiés par MEA.

La perte en poids est de 20 à 27% (tableau 4). Vu que cette décomposition précède la zone de décomposition indiquée pour la chaîne de Styrène-DVB non modifiée et aussi celle établie pour Co—CM, il résulte que les groupes aminiques fixés sont responsables de la modification de la stabilité des composés étudiés.

L'étape III coïncide avec le domaine indiqué pour la dégradation du témoin Sty—8% DVB (fig. 5). La chaîne des copolymères aminés se dégrade dans un intervalle plus grand que celle du copolymère non modifié à cause de la présence de l'azote dans la molécule (370 à 900°).

La plus grande vitesse de dégradation est située à 430—435° et coïncide par sa position avec la plus grande vitesse enregistrée pour le témoin. Ses valeurs oscillent autour de la valeur obtenue pour le copolymère non modifié (0,9—1,1), rapportée à la valeur enrègistrée pour le témoin, indiquant que la nature du phénomène dans la première partie de l'intervalle est la même : la scission des liaisons C—C par oxydation.

L'analyse thermo-différentielle a confirmé la similitude du processus.

L'analyse des données fournies par l'étude thermogravimétrique (TG, tableau 4) conduit à la conclusion que la thermostabilité définie comme la température la plus basse à laquelle on constate une perte en poids, est de 230° plus basse dans le cas des composés modifiés par le TEA, DEA et MEA.

Avec la croissance de la température et à une durée de l'analyse plus prolongée, les pertes en poids deviennent plus réduites que dans le cas du témoin. À 560° le témoin se décompose totalement, tandis que les produits modifiés perdent en poids seulement 60 à 65%.

Les caractéristiques physico-chimiques des échangeurs d'anions obtenus en partant des amino-alcools sont présentées dans le tableau 5.

Tableau 5

Caractéristiques physico-chimiques des échangeurs d'anions de type faibles et fortement basiques obtenus en partant des amino-alcools (forme Cl)

Dénomination de la caractéristique	Unité de mesure	Valeur		
		Co—CM aminé avec :		
		MEA	DEA	TEA
Granulation	mm.	0,4—0,18	0,4—0,8	0,4—0,6
Poids volumétrique	kg/1	0,723	0,712	0,695
Humidité	%	14,3	10,3	4,6
Contenu de l'azote déterminé par analyse élémentaire	%N	5,10* 5,00**	5,18*** 4,90**	2,8**** 3,6**
Capacité totale d'échange calculée du contenu d'azote	mech/g	3,64* 3,57**	3,70*** 3,50**	2,0**** 2,57**
Capacité totale d'échange déterminée par la méthode statique	mech/g	3,70* 3,50**	3,62*** 3,51**	— —
Capacité totale d'échange déterminée par titrage pH-métrique	mech/g	3,65* 3,60**	3,65*** 3,55**	2,0**** 2,50**
Domaine de pH	pH	0—10	0—10	0—12
Température maximale d'utilisation	°C	60	60	50

* = synthèse effectuée à 25°, durée de la réaction = 55 jours

** = synthèse effectuée à 80°, durée de la réaction = 2 jours.

*** = synthèse effectuée à 25°, durée de la réaction = 60 jours.

**** = synthèse effectuée à 25°, durée de la réaction = 72 jours.

CONCLUSIONS

On a étudié les meilleurs conditions de synthèse pour certains échangeurs d'anions faibles et fortement basiques de type gel en partant des amino-alcools.

— À un rapport molaire Co—CM/Am.Al constant, l'agrandissement de la durée de la réaction, associée à la réduction du rapport gravimétrique Co—CM/DMF, a un effet favorable sur la vitesse de réaction.

Les échangeurs d'anions synthétisés conformément aux meilleures conditions établies ont été caractérisés par titrage pH-métrique, spectrophotométrie IR et analyse thermique (TG, ATD et DTG).

L'échangeur d'anions fortement basique Co—CM—TEA, obtenu dans des conditions de réaction plus sévères (durée de réaction 48 heures et température 80°) modifie son caractère fonctionnel en faveur des groupements de force basique plus réduite qui ont la composition suivante : 60 % groupes fortement basiques et 40 % groupes faiblement basiques. Ainsi l'échangeur d'anions synthétisé avec MEA à 80° présente un caractère polyfonctionnel plus prononcé que celui de l'échangeur synthétisé à la température ambiante. Il est moins résistant chimiquement et sa résistance thermique est aussi plus petite comparativement à l'échangeur d'ions synthétisés en partant de DEA.

On a établi aussi que les échangeurs d'anions synthétisés dans les meilleures conditions indiquées présentent des caractéristiques physicochimiques bonnes, comparables à celles des échangeurs d'anions connus et déjà exploités dans les installations industrielles.

Revue Roumaine de Chimie, **20**, *4*, 575–579 (1975)

CHARACTERIZATION OF COPOLYMERS BY PYROLYSIS-CHROMATOGRAPHY. I.

COPOLYMERS OF ACRYLONITRILE WITH VINYL ACETATE AND α-METHYLSTYRENE

C. N. CAŞCAVAL and I.A. SCHNEIDER

"P. Poni" Institute of Macromolecular Chemistry, Aleea Gr. Ghica Vodă, 41A, Iassy,

Received June 22, 1974

The paper discusses the applications of pyrolysis-chromatography in the study of some acrylonitrile copolymers. Using the ratios of characteristic peaks, acrylonitrile (AN)/acetic acid for AN-vinyl acetate (VA) copolymers and α-methylstyrene (α-MST)/AN in the case of AN-α-MST copolymers, it is shown that pyrolysis -chromatography can be used to analyse the composition of AN-VA copolymers, but this method was unsuccessful in determining the composition of AN-α-MST copolymers. It is assumed that AN units take part in the interruption of the depolymerisation process of α-MST units, this effect influencing the degradation of AN-α-MST copolymers.

INTRODUCTION

The pyrolysis technique used in conjunction with gas chromatography has in recent years gained an increased importance for the elucidation of macromolecular structure.[1] The application of pyrolysis-chromatography as a characterization technique in the case of copolymers gives some information both on the chemical composition and on some finer aspects, such as sequences distribution, configuration and conformation of molecules. However, if the method had spectacular results in many cases, the analysis of complex mixtures is troublesome and sure conclusions are not obtained without using additional identification methods (such as mass spectrometry, infrared spectrometry, a.s.o.).

In the case of copolymers, for analytical reasons some characteristic peaks on the chromatograms are sufficient for identification. When sequence and structure are followed, identification of all pyrolysis products is absolutely necessary. The problem becomes still more complicated when one intends to characterize three-component systems.

Since in the literature there are very few data regarding the use of pyrolysis-chromatography in the analysis of AN-VA copolymers[2] and no data on the study of AN-α-MST copolymers, in this paper we shall discuss only the analytical aspects concerning the possibility of pyrolysis-chromatography for the purpose of establishing the composition of AN-α-MST and AN-VA copolymers.

---

[1] C. N. CAŞCAVAL, *Studii şi Cercetări Chim., Acad. R.S. România*, **19**, 987 (1971).

[2] C. C. LIN and J. YANG, *Bulletin of the College of Eng., Natl. Taiwan University, Taipei, Taiwan*, **14**, 116 (1970) ; cited in *Chem. Abstr.*, **78**, 58930 (1973).

EXPERIMENTAL

The analysis of copolymers decomposition products was carried out with the Siemens I— 400 gas chromatograph provided with flame ionisation detector and a pyrolysis unit made in our laboratory.[3] To prevent secondary reactions to form a very small volume of the pyrolysis chamber was used. The kanthal heating coil of about 0.2 Ω was heated by using an electric power at 15 V (~ 635°). The polymer samples weighed in the small platinum boats were introduced in the heating coil. In order to avoid the condensation of pyrolysis products (especially those with low volatility) on the walls of the pyrolysis chamber, the pyrolysis unit was incorporated into the chromatograph and kept together with the detector at a temperature of 125°.

The gas chromatographic analysis was carried out under the following conditions : the chromatographic column of 3 m length and 4 mm inner diameter was packed with Chromosorb W (70—80 mesh) silanized, coated with 15% Ethyleneglycol Succinate ; the column temperature was maintained constant at 110° ; argon was used as carrier gas with a flow rate of 35ml/min.

RESULTS AND DISCUSSION

The pyrolytic study was made upon suspension binary copolymers obtained from initial mixtures with 5, 10 and 15% VA and 5, 10, 15, 20, 25, 30, 35 and 40% α-MST, respectively. At the beginning, pyrograms of homopolymers were recorded in the same conditions and the characteristic peaks of each homopolymer were identified.

The pyrogram of polyvinyl acetate with $\overline{M}_n = 170{,}000$ is presented in figure 1.

An identification of all the chromatographic peaks was not effected but by following the pyrograms obtained at various temperatures. It was observed that this polymer could be characterized by peak 7, which coresponded to acetic acid.

Figure 2 shows the polyacrylonitrile pyrogram ($\eta_{rel} = 1.38$).

Analysis of the pyrograms effected in different conditions of time and temperature shows that this polymer can be characterized by peak 2, which in accordance with the retention time corresponds to AN.

Poly-α-methylstyrene pyrolised in the same conditions gives only one single chromatographic peak with the retention time situated between AN and acetic acid. This peak is α-MST.

Pyrograms of the binary copolymers AN-VA and AN-α-MST are shown in figure 3, a and b, respectively.

The studies carried out with binary copolymers AN-VA, using samples of increasing weights (0.2, 0.4, 0.6 and 0.8 mg) and different sensitivities of the detector unit, shown a direct relationship between the height of the characteristic acetic acid peak and the amount of the sample used. In figure 4 the variation of the height of the acetic acid peak is presented as a function of the amount of the sample.

---

[3] C. N. Caşcaval, H. Oleinek, I. Zugrăvescu and I. A. Schneider, *Macromol. Chem.* **169**, 129 (1973).

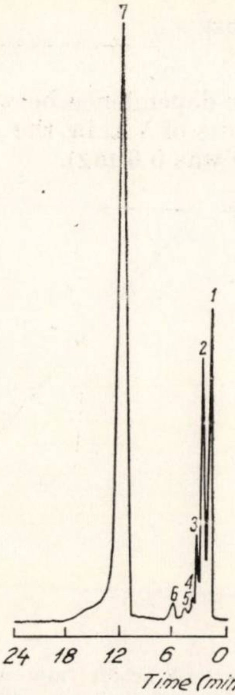

Fig. 1. — Pyrogram of polyvinyl acetate.

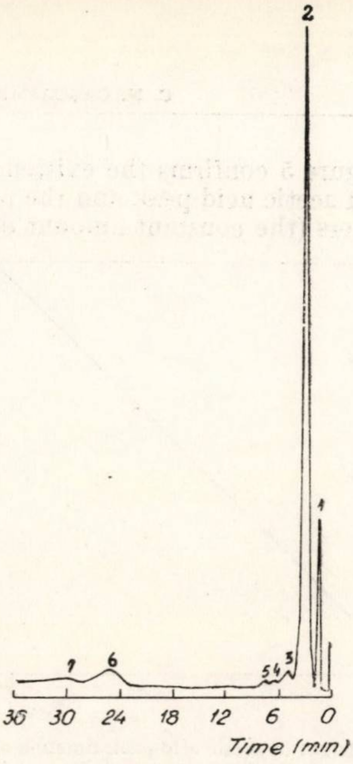

Fig. 2. — Pyrogram of polyacrylonitrile.

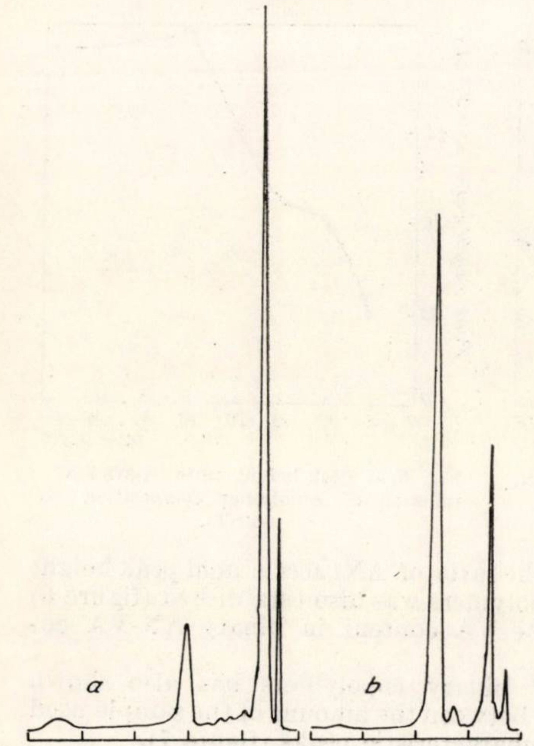

Fig. 3 a and b. — Pyrograms of binary copolymers, AN-VA (a) and AN-α-MST (b).

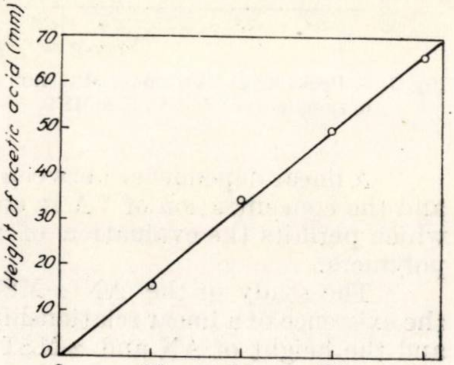

Fig. 4. — Height of acetic acid peak function of sample size.

Figure 5 confirms the existence of a linear dependence between the height of acetic acid peak and the percent contents of VA in the AN-VA copolymers (the constant amount of the sample was 0.6 mg).

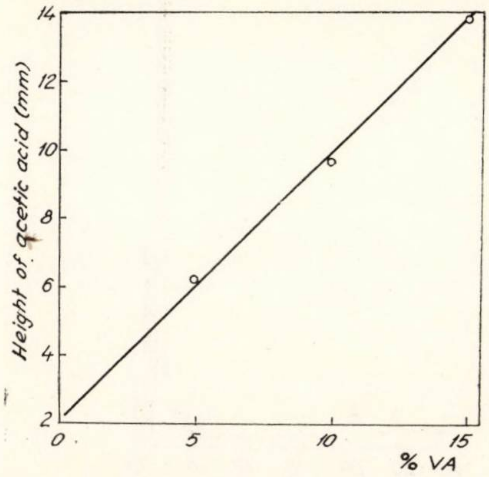

Fig. 5. — Height of acetic acid peak function of copolymer composition (% VA).

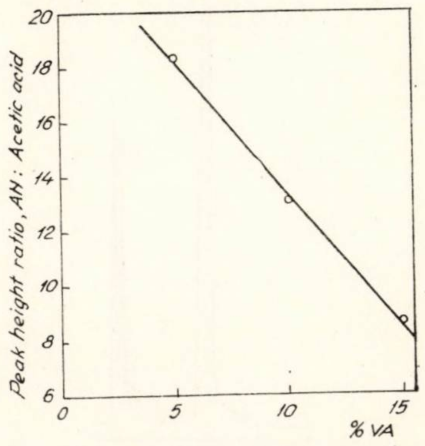

Fig. 6. — Peak height ratio AN/acetic acid function of copolymer composition (%VA).

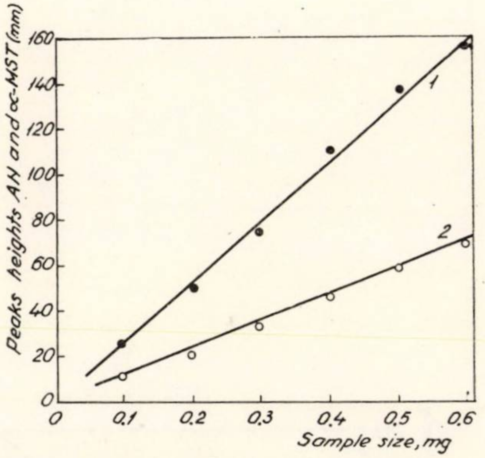

Fig. 7. — Peaks height AN and α-MST function of sample size : *1*, AN ; *2*, α-MST.

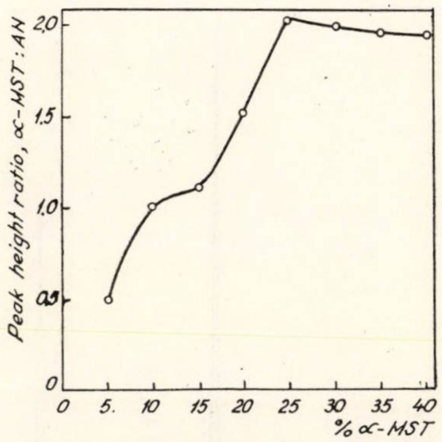

Fig. 8. — Peak height ratio, α-MST/AN function of copolymer composition (% α-MST).

A linear dependence between the ratio of AN/ acetic acid peak height and the concentration of VA in copolymers was also established (figure 6) which permits the evaluation of the VA content in binary AN-VA copolymers.

The study of the AN-α-MST binary copolymers has also shown the existence of a linear relationship between the amount of the sample used and the height of AN and α-MST characteristic peaks (figure 7).

Since the α-MST-AN copolymers are less thermally stable (especially when the α-MST content is higher than 20%) smaller amounts of samples (0.1 mg) were used in the next experiments. Unfortunately, a linear dependence was not obtained between the height of the characteristic peaks and the amount of α-MST in copolymers. This fact may be explained, in our opinion, by the extremely different degradation mechanism of the two constituent homopolymers. Therefore, the calibration curve of α-MST/AN ratio is not linear as can be seen in figure 8, showing a maximum for a content of about 25% α-MST in copolymer.

In accordance with the above results one can suppose that in the case of α-MST-AN copolymers, because of the different mechanism of degradation in comparison with the first case when both polyvinyl acetate and polyacrylonitrile degrade after a similar mechanism by the elimination reaction of small molecules with non-chain scission, unzipping of type-one sequence unit is stopped by the presence of the second one. This hypothesis was confirmed by the pyrolysis results regarding physical mixtures of homopolymers, polyacrylonitrile and poly-α-methylstyrene (of similar composition as those of the copolymers), when a concordance was found between the ratios of α-MST and AN peaks as a function of the mixtures composition. The observed behaviour is similar to that of the other AN copolymers, such as AN-styrene copolymers,[4] where the AN yield decreases with increasing AN concentration in the copolymer. In these cases information on the copolymer microstructure can be obtained by measurements of the monomer yield. But, at the same time, it seems that in such a situation the pyrolysis-chromatographic method cannot be used for the analytical determination of the composition of α-MST-AN copolymers. This conclusion was confirmed as we tried to analyse some AN-α-MST-VA ternary copolymers.

---

[4] H. KAMBE and Y. SHYBAZAKI, *Kobunshi Kagaku*, **21**, 71 (1964); cited in *Chem. Abstr.*, **61**, 3219 (1964).

Revue Roumaine de Chimie, **20**, *4*, 581–585 (1975)

RADICAL-IONS. III[1]

HALOGEN-PHENOTHIAZONE RADICAL-IONS

MIHAELA HILLEBRAND*, M. RĂILEANU** and V.E. SAHINI*

* Department of Physical Chemistry, Bucharest, Polytechnic Institute,
B-dul Republicii 13, Romania

** Department of Organic Chemistry, University of Craiova, Str. Alex. I. Cuza 13,
Romania

Received November 20, 1974

The assignment of the hyperfine splitting constants in the phenothiazone anion-radical made by the analysis of the ESR spectra of some halogenated derivatives is reported. The experimental results are compared with Mc Lachlan spin densities.

INTRODUCTION

Although there are many data concerning the physico-chemical properties of phenothiazone and its substituted derivatives, no studies had previously been made on the corresponding anion-radicals. However, differing from phenothiazine, for which only the substitution with strong electron acceptors allows the formation of negative ion-radicals, phenothiazone is easily reducible by chemical and electrochemical methods.

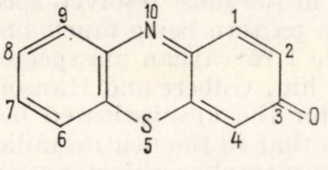

In this paper, we report the hyperfine splitting constants of the phenothiazone anion-radical, the assignment being made by the analysis of the ESR spectra of some halogenated derivatives, found suitable for this purpose.

---

[1] M. Hillebrand and M. Răileanu, *Rev. Roumaine Chim.*, **19**, 1227 (1974).

EXPERIMENTAL

The anion-radicals of phenothiazone[2] and its following substituted derivatives: 1-chloro-,[3] 7-chloro,[4] 2,4-dichloro-,[3] 2,7-dichloro[5]-,4,7-dibromo-,[5] 1,2,4,7,9-pentabromo-,[6] 1,2,4,7,8,9-hexabromo-,[6] and 4-nitro-phenothiazone[7] were electrochemically generated inside the cavity of the ESR spectrograph. The cell was equipped with platinum electrodes and tetraethylammonium chloride in dimethylformide (DMF) was used as supporting electrolyte.

Whenever the ESR spectrum was of poor quality or there were some doubts about its analysis, the radicals were also prepared by sodium reduction in the same solvent. The only difference between the two methods was observed for the 4, 7-bromophenothiazone-anion-radical. When this radical was electrochemically prepared, the spectrum changed fast in time, while in the presence of sodium, the stability was greatly increased.

The ESR spectra were taken on a JES-3B spectrograph in the X band frequency. The *g* factors were measured using peroxylaminodisulphonate as standard ($g = 2.0056$). The spectra were simulated using the QCPE-83 simulation program adapted for an IBM-360 computer.

RESULTS AND DISCUSSION

The ESR spectrum of the phenothiazone anion-radical (fig. 1) is explained by the hyperfine interaction of the unpaired electron with the heterocyclic nitrogen and seven ring protons, whose splittings are given in table 1.

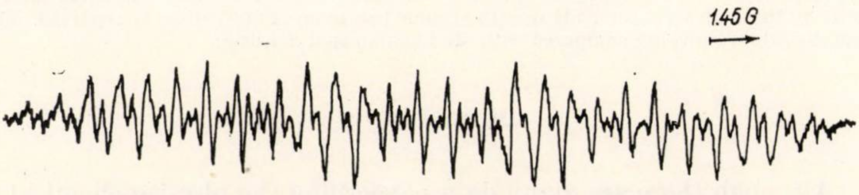

Fig. 1. — The ESR spectrum of the phenothiazone anion-radical

The assignment of the proton splittings round the ring positions was made by a comparative analysis of the ESR spectra of some halogenated derivatives, as it was found that besides a small decrease in the nitrogen splitting, the halogen substitution does not perturb the spin density distribution. Secondly, even in the most resolved spectra the halogen splitting was not measurable, the pattern being much simplified.

Inspection of table 1 reveals an unexpected ressemblance with the splittings reported by Chiu, Gilbert and Hanson[8] for the phenothiazinyl free radical, especially for the unsubstituted benzene ring. The nitrogen splitting is smaller than that in the neutral radical, but much more different than its value in the nitrophenothiazine negative ions. As for phenothiazone, the monoelectronic reduction is expected to occur at the carbonyl position, this behaviour accounts for a large contribution to the electronic structure of the anion, of a semiquinonic type formula II. The possibility of such a π electron delocalisation explains the difference as against the nitrophenothiazone negative ions, for which the unpaired electron is mainly localised on the nitro groups, and the heterocyclic nitrogen splitting does not exceed 2G.

---

[2] C. Bodea and M. Răileanu. *Studii și Cercetări Chim. Fil. Cluj*, **11**, 325 (1960).

[3] M. Terdic and C. Bodea, *Rev. Roumaine Chim.*, **13**, 833 (1968).

[4] C. Bodea and M. Răileanu, *Liebigs Ann. Chem.*, **614**, 171 (1958).

[5] M. Terdic and C. Bodea, *Rev Roumaine Chim.*, **13**, 1241 (1968).

[6] C. Bodea and M. Terdic, *Liebigs Ann. Chem.*, **698**, 186 (1966).

[7] C. Bodea, M. Terdic and E. Broser, *Liebigs Ann. Chem.*, **715**, 122 (1968).

[8] M. F. Chiu, B. C. Gilbert and P. Hanson, *J. Chem. Soc.*, B. **1970** (1700).

Table 1

Experimental ESR parameters

Anion -radical	Line-width (Ga ss)	Hyperfine splittings (Gauss)								g
		a_N	a_1	a_2	a_4	a_6	a_7	a_8	a_9	
Phenothiazone	0.10	6.40	1.80	1.80	0.30	0.90	2.55	0.90	3.10	2.0044
1-Chlorophenothiazone	0.65	6.30	—	1.80	<0.65	1.05	2.55	1.05	3.00	2.0045
7-Chlorophenothiazone	0.22	6.10	1.80	1.80	0.40	0.90	—	0.90	3.00	2.0046
2,4-Dichlorophenothiazone	0.18	6.20	1.99	—	—	0.89	2.44	0.89	2.96	2.0046
2,7-Dichlorophenothiazone	0.55	6.16	1.84	—	< 0.55	1.01	—	1.01	2.80	2.0049
4,7-Dibromophenothiazone	0.30	6.03	1.89	1.89	—	1.02	—	1.02	2.80	2.0054
1, 2, 4, 7, 9-Pentabromophenothiazone	0.33	5.40	—	—	—	0.90	—	0.90	—	2.0072
1, 2, 4, 7, 8, 9-Hexabromophenothiazone	0.52	5.25	—	—	—	0.82	—	—	—	2.0073
4-Nitrophenothiazone	0.12	6.51	1.18	0.89	—	0.89	2.59	0.89	3.18	2.0044

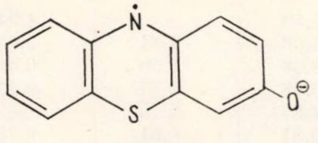

In the quinone-iminic cycle the spin distribution is determined by both carbonyl and sulphur effects. Thus, as the spin densities for the positions ortho to the carbonyl are usually the greatest, this fact is found in our case only for position 2. The other ortho position (4), the most influenced by the sulphur atom, is characterised by the smallest spin density. This assignment is also supported by the spectrum of 4-nitrophenothiazone anion-radical (fig. 2), in which the nitro group splitting is small and thus not measurable. Although the anion-radicals of nitrocompounds usually present some specific features, especially in the presence of an alkali metal, this spectrum maintains the general pattern of all phenothiazone radicals. The splittings in the benzene ring are unaffected by the nitro group presence but the spin densities in the carbonylic ring are decreased, the assignment between positions 1 and 2 being no longer conclusive.

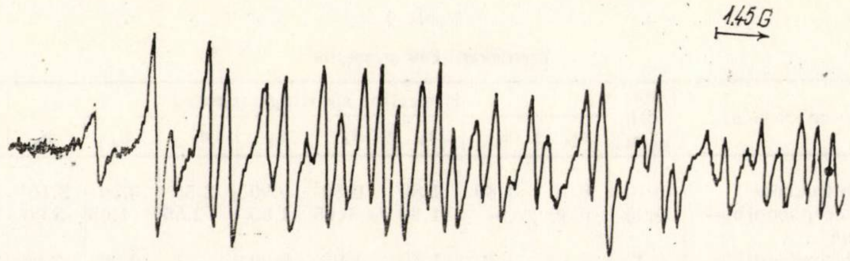

Fig. 2. — The low field side of the ESR spectrum of the 4-nitrophenothiazone anion-radical.

The g factors also collected in table 1 increase with the halogen substitution, the effect being more pronounced for the bromoderivatives. The same effect produced by the large spin-orbit coupling constant of bromine was previously mentioned for phenothiazine radicals.[9]

M.O. CALCULATIONS

As the experimental results allowed for an unambiguous assignment of the hyperfine splittings, we found interesting to compare them with theoretical spin densities. Hückel and Mc.Lachlan spin densities were calculated starting with the usually recommended parameters for nitrogen, sulphur and carbonyl group. A slight variation around these values was also performed, but the relative order of the spin densities was not modified. The results are given in table 2, together with the heteroatom parameters.

Table 2

Theoretical hyperfine splittings

Position	Phenothiazone		$\overset{*}{a}_{calc}$ (Chlorosubstituted phenothiazones)			
	a_{exp} (Gauss)	$\overset{*}{a}_{calc}$ (Gauss	1-Chloro	7-Chloro	2,4-Dichloro	2,7-Dichloro
1	1.80	1.89	—	1.94	1.67	1.64
2	1.80	2.08	1.81	2.02	—	—
4	0.30	0.38	0.30	0.41	—	0.38
6	0.90	0.68	0.67	0.73	0.65	0.70
7	2.55	2.67	2.70	—	2.62	—
8	0.90	0.81	0.81	0.76	0.78	0.76
9	3.10	2.99	3.05	3.02	2.94	2.97
N	6.40	6.39	6.46	6.44	6.22	6.42

* $h_N = 0.70$; $h_S = 1.00$; $h_O = 1.30$; $h_{Cl} = 2.000$; $k_{CS} = 0.57$; $k_{CO} = 1.56$; $k_{CCl} = 0.40$; $k_{CN} = 1.10$;

$a_H = /27/f_c^{\pi}$

$a_N = 19.1\rho_N^{\pi} + 9.1 \sum_i \rho_{ci}^{\pi}$

---

[9] C. Bodea and I. Silberg, *Rev. Roumaine Chim.*, **10**, 9 (1965).

It may be seen that the agreement with both the experimental assignment and the experimental proton splittings is very good.

Considering for the nitrogen atom a Mc. Connell type formula with $Q = 16.5$ G as derived by Chiu, Gilbert and Hanson for related systems, the calculated value is smaller than the experimental one. A good agreement is obtained using the two parameter formula given by Henning[10] with $Q_N = 19.1$ G and $Q_{CN} = 9.1$ G, and these values are presented in table 2.

As concerns the halogenated derivatives, the m.o. calculations must account for the slight decrease of the nitrogen splitting and the lack of perturbation produced on the ring proton splittings.

The spin density calculations on the chloroderivatives were performed in the frame of an inductive ($h_{\mathrm{C-Cl}} = 1.2$) and a conjugative ($h_{\mathrm{Cl}} = 2.0$, $k_{\mathrm{CCl}} = 0.4$) model. The results obtained by the inductive model are completely different from the experimental ones, and point out that, if the halogen effect were inductive, its position in the molecule would be important and the splitting constants very different from one compound to another. Secondly, the nitrogen splitting would be strongly decreased from 6.4 to 2G.

The mesomeric model leads to reasonable splittings very close to those obtained for the phenothiazone anion, accounting for the experimental data.

---

[10] J. C. M Henning, *J. Chem. Phys.*, **44**, 2139 (1966).

COMPTE RENDU

K.W. BENTLEY and G. W. KIRBY, "Elucidation of Organic Structures by Physical and Chemical Methods". Part II, Second Ed., Wiley-Interscience, New York, 1973, xvi, 561 p.

The book is in fact volume IV of "Technique of Chemistry Series", succesor of the "Technique of Organic Chemistry Series" and its companion, "Technique of Inorganic Chemistry".

The synthesis of some new derivatives and the elucidation of their structure are among the main aims of organic chemistry. The understanding of the atoms arrangement in molecule, the formation of chemical bonds between atoms, the transformation of functional groups and the application of the obtained products are principally the object of organic chemistry. Elucidation of the unknown structures of some organic compounds usually requires their transformation into known derivatives and this fact may be achieved either by synthesis or by degradation.

In preparing the second edition of the present book almost the whole work has been rewritten by a new team of contributors, thus ensuring properly structured up-to-date surveys of fields that have changed markedly since the book has been originally published, i.e. more than eight years ago. In this new edition emphasis is placed on results and interpretation rather than on physical principles and working techniques, as these are more fully dealt with in other volumes of "Technique of Chemistry Series". Some topics of the first edition are no longer included and the subjects of other chapters have, in some cases, been combined to achieve a more rational and uniform treatment. However, no details essential to an understanding of the main text have been omitted.

The second part of the "Elucidation of Organic Structures by Physical and Chemical Methods" comprises chapters X to XVIII, with the following topics : chapter X deals with dehydrogenation and zinc dust distillation. Different dehydrogenation techniques; e.g. catalytic dehydrogenation, dehydrogenation with sulfur and selenium, etc., isolation of products and behaviour of C—H bonds in dehydrogenation and disproportionation are briefly discussed. The behaviour of C—O bonds in primary, secondary and tertiary alcohol carbonyl compounds as aldehydes and ketones, carboxylic acids and their derivatives and furan rings as well as the behaviour of C—C bonds in elimination or migration reactions of alkyl groups or in expansion, contraction, cleavage of rings and the behaviour of C—N bonds in simple compounds and alkaloids are also treated. The chapter ends with discussions on the application of zinc dust distillation of phenols, quinoles, alkaloides and some carbocyclic compounds and of side reactions which occur in severe reaction conditions when, besides dehydrogenation processes, degradation of aliphatic side groups takes place. The next chapter deals with reduction processes. A series of reduction methods, e.g. hydrogenation using hydride reagents, dissolving metals and hydrazine and fission reactions are concisely treated, but the main subject is catalytic hydrogenation : heterogenous systems using Pt, Pd, Rh, Ni, etc., their model mechanism the stereochemistry and selectivity of the process, hydrogenolysis, chromatography and homogeneous catalytic hydrogenation. This chapter ends with selected examples of structural determination by reduction techniques of different derivatives, e.g. organometalic complexes, antibiotics, ergot alkaloides and structure-activity relationships in t-RNA. The fission of carbon-carbon bonds and carbon-nitrogen and carbon oxygen bonds is discussed at large in chapters XII and XIII, respectively. The next chapters deal with alkaly fusion in which the compound submitted to degradation is a liquid at reaction temperature but a solid at room temperature (chapter XIV) and degradation of polysaccharides (chapter XV), polypeptides and proteins (chapetr XVI).

All in all there are 2364 papers cited the book concluding with a subject index.

The authors and editors hope that readers will find the book useful and the reviewer highly recommends it to graduate students and chemists dealing with organic syntheses.

Received April 15, 1974

Ioan Petrariu

NOTE POUR LES AUTEURS

La *Revue Roumaine de Chimie* publie des articles en anglais, français, russe, allemand ou espagnol. Les auteurs sont priés d'envoyer des articles, notes, communications et comptes rendus inédits.

Les manuscrits seront dactylographiés à deux intervalles. Les tableaux seront dactylographiés sur des feuilles séparées, de même que la légende des figures. Les diagrammes seront tracés à l'encre de Chine sur papier calque. Les tableaux et les figures seront numérotés par des chifres arabes, en nombre strictement nécessaire. Priére de ne pas inscrire les mêmes données dans les tableaux et les figures. Les formules chimiques seront incluses dans le texte; en outre, elles seront transcrites sur des feuilles séparées. Les auteurs sont priés d'indiquer les caractéres italiques (en soulignant les lettres au crayon), ainsi que tout autre caractére spécial. L'ordre des références bibliographiques sera celui de leur mention dans le texte; le nom de l'auter sera précédé de l'initiale du prénom; les publications périodiques seront présenteés suivant les prescriptions internationales. Le réferences seront ajouteés à la fin de l'article; elles paraîtront, comme des notes, au bas de la page. Le texte sera précédé d'un rézumé comprenant 15 lignes au maximum.

L'éntiere responsabilité du contenu des articles appartient aux auteurs. On publie des articles du aux collaborateurs roumains ou étrangers.

PRINTED IN ROMANIA

1975 JUL 2

TRAVAUX PARUS AUX ÉDITIONS DE L'ACADÉMIE DE LA RÉPUBLIQUE SOCIALISTE DE ROUMANIE

I. ZUGRĂVESCU et MAGDA PETROVANU, **Chimia N-Ilidelor** (La chimie des N-Ylures), 1974, 347p., 19 lei.

MARGARETA AVRAM, **Antidăunători** (Pesticides), 1974, 494 p., 41 lei.

CR. SIMIONESCU, VIORICA RUSAN et N. POPA, **Chimia algelor marine** (La Chimie des algues marines), 1974, 211 p., 18 lei.

TIBERIU NĂŞCUŢIU, **Metode radiochimice de analiză** (Méthodes radiochimiques d'analyse), 1973, 384 p., 23 lei.

MARIA FITI, **Dozimetria chimică a radiaţiilor ionizante** (La dosimétrie chimique des radiations ionisantes), 1973, 240 p., 13,50 lei.

MIHAI FLORESCU, **Eficienţa economică a cercetării ştiinţifice** (L'efficience économique de la recherche scientifique), 1972, 115 p., 15 lei.

GEORGETA LĂZĂRESCU, **Sistematizarea informaţiilor în Chimia organică** (La systématisation des informations dans la chimie organique), 1972, 252 p., 10,50 lei.

P. BALTĂ et E. BALTĂ, **Introducere în chimia fizică a stării vitroase** (Introduction à la chimie physique de l'état vitreux), 1971, 240, 15,50 lei.

LYDIA-MARIA VAICUM, **Biodegrabilitatea detergenţilor** (La biodégrabilité des détergents), 1971, 254 p., 16 lei.

TIBERIU NĂŞCUŢIU, **Metode radiometrice de analiză** (Méthodes radiométriques d'analyse), 1971, 346 p., 19,50 lei.

I. ZUGRĂVESCU et L. STOICESCU-CRIVETZ, **Polimeri heterociclici** (Polymères hétérocycliques), 1971, 190 p., 9,50 lei.

CRISTOFOR SIMIONESCU et C. V. UGLEA, **Fracţionarea compuşilor macromoleculari** (Fractionnement des composés macromoléculaires), 1962, 292 p., 18,50 lei.

I. MAXIM, **Materiale nucleare** (Matériaux nucléaires), 1969, 444 p., 30 lei.

CRISTOFOR SIMIONESCU et CLEOPATRA VASILIU-OPREA, **Mecanochimia compuşilor macromoleculari** (La mécanochimie des composés macromoléculaires), 1967, 344 p., 23,50 lei.

CORNEL BODEA et collab., **Tratat de biochimie vegetală,** partea I, **Fitochimie** (Traité de biochimie végétale, 1re partie, Phytochimie), Ier vol., 1964, 747 p. + 4 annexes + 2 pl., 31 lei; IIe vol., 1965, 1262 p., 1 pl., 56 lei; IIIe vol., 1967, 773 p., 35 lei.

I. P. I — c 20

43 426

Lei 25.—

F 1103

REFERÁLVA

70

ACADÉMIE DE LA RÉPUBLIQUE SOCIALISTE DE ROUMANIE

REVUE ROUMAINE DE CHIMIE

TOME 20
N° 5
Mai 1975

RECHAX, 20, 5, 589–724 (1975)

EDITURA ACADEMIEI REPUBLICII SOCIALISTE ROMÂNIA

Rev. Roumaine Chim. 20, 5, p. 589–724 (1975), Bucarest

ACADÉMIE DE LA RÉPUBLIQUE SOCIALISTE DE ROUMANIE

COMITÉ DE RÉDACTION

Rédacteur en chef:

I. G. MURGULESCU, membre de l'Académie de la République Socialiste de Roumanie

Rédacteurs en chef adjoints:

A. T. BALABAN et V. EM. SAHINI, membres correspondants de l'Académie de la République Socialiste de Roumanie

Collège de rédaction:

EM. BRATU, ELENA CEAUŞESCU, ECATERINA CIORĂNESCU-NENITZESCU, C. DRĂGULESCU, RALUCA RIPAN, CR. SIMIONESCU, membres de l'Académie de la République Socialiste de Roumanie; P. SPACU, membre correspondant de l'Académie de la République Socialiste de Roumanie; MARGARETA AVRAM, D. I. MARCHIDAN, G. NIAC et D. SĂNDULESCU

Toute commande de l'étranger pour les travaux parus aux Editions de l'Académie de la République Socialiste de Roumanie sera adressée à ILEXIM Serviciul Export-Import Carte/Serviciul Export-Import Presă, P.O. BOX 2001, Calea Griviţei, n°s 64–66, Bucarest, 12, Roumanie

Les manuscrits, les livres et les revues proposés en échange, ainsi que toute correspondance seront envoyés à la rédaction

REVUE ROUMAINE DE CHIMIE

23, str. Dumbrava Roşie, Bucarest, Roumanie, téléphone 12 41 60

EDITURA ACADEMIEI REPUBLICII SOCIALISTE ROMÂNIA

Calea Victoriei, 125, Bucarest, téléphone 13 94 40

ORSZÁGOS MŰSZAKI KÖNYVTÁR ÉS DOKUMENTÁCIÓS KÖZPONT
33887

REVUE ROUMAINE DE CHIMIE

Tome 20, Nº 5 Mai 1975

I. G. MURGULESCU and MARILENA ȘERBAN, On the viscosity of molten metals. III. Activation energy . . . . 591–596 R

B. F. MARKOV, T. A. TISHURA and A. N. BUDARINA, Thermochemical study of binary salt systems 597–602

RODICA VÎLCU and B. COMAN, Determination of heat capacities of some alcohols and ketones in vapour phase 603–609

IOANA ONACA, MARIA MAVRODIN-TĂRĂBÎC et I. SOLACOLU, L'étude de la réaction d'oxydation de l'hydrogène sur les électrodes poreuses en nickel. III. La détermination des paramètres de fonctionnement 611–618

B. BREZMES, J. CASADO y F. MATA, Influencia de la acidez del medio sobre la reacción entre las aminas primarias alifáticas y el ácido nitroso 619–625

G. BOURCEANU, V. ABABI, GH. POPA and M. SANDULOVICIU, Transformation of the toluene-water mixture in the frequency discharge plasma. II. Influence of the power and residence time 627–632

E. PETROVICI, C. CSUNDERLIK, A. FERENCZ and C. DRĂGULESCU, New complexone type ligands. I. *meso*-2,3-diaminosuccinic-N,N′-diacetic acid (DSDA) and its salts 633–636

ELIZA AVRAM, I. G. DINULESCU, F. CHIRALEU, ELVIRA ȘLIAM and MARGARET AVRAM, Reaction of acetylenes with transition metals. V. β-cleavage in σ,π-alkyl-palladium complexes 637–641

CLARA MAKKAY, LEONTINA HIDIȘAN-TĂUȚEAN and MARIA IONESCU, Formation and behaviour of 4-oxazolidones. XII. An advantageous method for obtaining 2,5-diaryloxazoles 643–649

ELENA CATRINA, Z. SIMON and GH. CATRINA, Structure of thiazolidinic compounds by the del Ré method 651–655

CS. VÁRHELYI, J. ZSAKÓ and MÁRTA BOÁRIU-FARKAS, Kinetic analysis of thermogravimetric data. VIII. Thermal decomposition kinetics of some [Cobalt(II)X_2(amine)$_2$] type complexes 657–663

I.I. DRAGOTĂ, L. V. FEYNS and I. NICULESCU-DUVĂZ, Potential anticancer agents. IX. Synthesis of new urethane type nitrogen mustards from benzo- and naphtho-pyrans . . . . 665–675 R

Rev. Roumaine Chim. **20**, *5*, p. 589–724 (1975), Bucarest

MARGARETA TOMESCU et KALMAN PUSZTAI, Recherches dans le domaine de la copolymérisation multicomposante en utilisant un ordinateur . . . . 677–685 R

GH. DRĂGAN, Amorphous-crystalline coupling in polyethylene. II. DTA study of the crystalline morphology in chlorinated polyethylene 687–698

FL. POPESCU, I. PETRARIU et SIMONA PERCEC, Le comportement thermique des copolymères styrène-divinylbenzène chlorométhylés contenant des groupes quaternaires d'ammonium . . . . 699–719 R

ANA UNGUREANU and CANDIN LITEANU, A new method for the synthesis of triacetyl phosphate . . . . 721–722 R

COMPTES RENDUS 723–724

Revue Roumaine de Chimie, 20, 5, 591 – 596 (1975)

ON THE VISCOSITY OF MOLTEN METALS. III[1]

ACTIVATION ENERGY

I. G. MURGULESCU and MARILENA ŞERBAN
Department of Physical Chemistry, University of Bucharest, Bd. Republicii 13,
Bucharest, Romania

Received December 6, 1974

The present paper elucidates the problem of evaluating the activation energy of the viscous flow of metallic melts by means of the available physical data. In metals with normal behaviour it is a simple melting temperature function ; in metals with abnormal behaviour it also depends on the association degree. By solving this problem, the equation proposed in the previous note contains no adjustable parameter.

In a previous paper[1] we have shown that starting from equation :

$$\eta = h \frac{\lambda_1}{\lambda_2 \lambda_3 \lambda^2} \frac{F}{\overset{*}{F}} e^{E/RT}$$

deduced by Eyring[2] for the η viscosity coefficient by means of the transition state theory, the following equation may be obtained :

$$\eta = A \rho T e^{E/RT} \tag{1}$$

For normal metals constant A assumes the expression :

$$A = 3.57 \times 10^{-13} \frac{R V_m^{1/3}}{M^{1/2} T_m^{1/2}} \tag{2}$$

in which M represents the atomic weight of the metal and V_m, its atomic volume at the melting temperature. The expression of the preexponential constant of metals with abnormal behaviour also includes the melting heat L and the packing factor γ :

$$A' = 3.57 \times 10^{-13} \frac{R V_m^{1/3}}{\gamma M^{1/2} T_m^{1/2}} e^{L/3RT_m} \tag{3}$$

---

[1] Part II : I. G. Murgulescu and M. Şerban, *Rev. Roumaine Chim.*, **19**, 1417 (1974).

[2] S. Glasstone, K. J. Laidler and H. Eyring, "The Theory of Rate Processes", New York, London, 1941, p. 483.

Since the preexponential constant A may be evaluated from known physical magnitudes, equation (1) contains only one adjustable parameter : the activation energy E. The present paper undertakes to investigate the possibility of developing a method for deducing the activation energy from the available physical data thus removing the last adjustable parameter from equation (1).

Equation (1) is based on the assumption that the particles of the metallic liquid are assimilable with harmonic oscillators. We shall demonstrate that although the vibratory movement of the particles is inharmonic, their energy does not significantly differ from the energy of harmonic oscillators, at temperatures which do not exceed too much the melting point. Indeed, for the energy of an inharmonic oscillator we may write the equation : [3]

$$\varepsilon = \frac{p^2}{2m} + \frac{k}{2} q^2 + a q^3 \tag{4}$$

in which a is the deviation from inharmonicity. By removing the linear moment p we obtain :

$$p = \sqrt{2m\varepsilon}\,\sqrt{1 - \frac{k}{2\varepsilon} q^2}\,\sqrt{1 - \frac{\frac{a}{\varepsilon} q^3}{1 - \frac{k}{2\varepsilon} q^2}}\,.$$

By serially developing the last radical and by keeping the first three terms there results :

$$p = \sqrt{2m\varepsilon}\left[\sqrt{1 - \frac{k}{2\varepsilon} q^2} - \frac{a}{2\varepsilon}\,\frac{q^3}{\sqrt{1 - \frac{k}{2\varepsilon} q^2}} - \frac{a^2}{8\varepsilon^2}\,\frac{q^6}{\left(1 - \frac{k}{2\varepsilon} q^2\right)^{3/2}}\right]$$

By substituting $\sqrt{k/2\varepsilon}.q = x$, forming the phase integral $\oint p\,dq = n_s h$ and performing it, we obtain :

$$\frac{n_s h}{\sqrt{2m\varepsilon}} = \pi\sqrt{\frac{2\varepsilon}{k}} + \frac{15}{4}\pi\cdot\frac{a^2\varepsilon}{k^3}\sqrt{\frac{2\varepsilon}{k}}$$

Hence :

$$n_s h = 2\pi\sqrt{\frac{m}{k}}\,\varepsilon\left(1 + \frac{15}{4}\,\frac{a^2\varepsilon}{k^3}\right)$$

As $2\pi\nu_0 = \sqrt{k/m}$, ν_0 being the specific frequency of the linear harmonic oscillator,

---

[3] C. SCHAEFER, "Einführung in die theoretische Physik", III/2, Berlin, 1951, p. 180.

$$n_s h\,\nu_0 = \varepsilon\left(1 + \frac{15}{4}\frac{a^2\varepsilon}{k^3}\right) \quad \text{or} \quad \varepsilon_0 = \varepsilon\left(1 + \frac{15}{4}\frac{a^2\varepsilon}{k^3}\right)$$

ε_0 being the energy of the linear harmonic oscillator. Hence :

$$\varepsilon = \frac{\varepsilon_0}{1 + \frac{15}{4}\frac{a^2\varepsilon}{k^3}}$$

As this is a correction, energy ε of the second term in the denominator may be replaced by ε_0. At the same time $k = 2\varepsilon_0/A^2$, A being the vibration amplitude. Finally, one obtains for energy ε :

$$\varepsilon = \frac{\varepsilon_0}{1 + \frac{15}{32}\frac{a^2A^6}{\varepsilon_0^{\,2}}} \tag{5}$$

In the case of metallic melts, the second term of the denominator is negligible, so that :

$$\varepsilon \sim \varepsilon_0 \tag{6}$$

the energy of the system equals the energy of the harmonic oscillator.

In the lattice of the metallic liquid, the particle motion has three free movement directions and is therefore assimilable with the motion of three harmonic oscillators. Since the temperature of the liquid is high, energy ε may be approximated by applying the principle of energy equipartition :

$$\varepsilon = 3kT$$

In order to participate in the viscous flow, the particle must have a minimum energy :

$$\varepsilon_{\text{visc}} = 3kT_m$$

T_m being the melting temperature. For a gram-atom of metallic liquid it results :

$$E = 3NkT_m = 3RT_m \tag{7}$$

This must be the value of the activation energy for the viscous flow of normal molten metals.

An identical expression of the activation energy of the viscosity of liquid metals was deduced by Hrbek, [4] defining a reduced activation energy. Similar expressions were suggested by Fürth, [5] by Bockris and co-workers, [6–8] based on the theory of vacancies.

---

[4] A. Hrbek, *Hutnicke Listy*, **11**, 164 (1956) ; *Z. Metallkde.*, **48**, 134 (1957).

Let us also observe that, at the boiling temperature, when the vibration movement of particles evolves towards translation, $A \to \infty$ and ε

Table 1

Activation energies for the viscosity of normal liquid metals

Element	T_m, K	ΔT, K	E^*, cal/g atom	
			Exp.	Calcd.-ec(7)
Li	453.7	456–559	2,290	2,690
Na	371	376–644 371–628	2,280 2,320	2,200
K	336.6	342–440 337–449	2,050 1,790	2,000
Rb	312	311–493	1,870	1,850
Cs	301.8	301–484	1,800	1,790
Cu	1356.2	1356–1573	6,740 10,440	8,060
Ag	1234	1273–1523 1233–1573	7,300 7,000 6,960	7,330
Au	1336.2	1336–1573	6,850	7,940
Mg	924.2	923–1173 925– 998	7,250 6,920 9,410	5,490
Al	933.3	931–1173	4,770 4,170	5,540
Pb+	600.6	623– 873 600–1173 600– 873	3,690 3,250 3,240	3,570
Fe	1809	1809–2023 1823–1923 1805–1973	9,790 13,640 13,960	10,740
Co	1765	1768–2023 1773–1973	11,520 13,320	10,480
Ni	1726	1728–1973 1773–1923 1728–1923	11,020 11,330 11,300	10,350

---

[5] R. FÜRTH, *Proc. Camb. Phil. Soc.*, **37**, 281(1941).

[6] J.O'M. BOCKRIS and G. W. HOOPER, *Discuss. Faraday Soc.*, **32**, 218(1961).

[7] L. NANIS and J.O'M. BOCKRIS, *J. Phys. Chem.*, **67**, 2865(1963).

[8] J.O'M. BOCKRIS and S. R. RICHARDS, *J. Phys. Chem.*, **69**, 671(1975).

becomes zero ; therefore, the activation energy of the viscosity of metallic vapours is null, in a perfect agreement with the experiments and with the theory of gas viscosity.

In abnormal liquid metals we shall admit that apart from simple atoms there exist dimer associated particles. Noting by x the association degree, we may write :

$$E = \left[6(1 - x)\,N + 10x\,\frac{N}{2}\right]\frac{kT_m}{2} = \left(3 - \frac{x}{2}\right)RT_m \qquad (8)$$

For associated particles, two additional freedom degrees were added to the above six freedom degrees for the internal vibration within the dimer and two freedom degrees for its rotation.

Table 1 affords a comparison between the activation energies of the viscous flow in normal liquid metals and those calculated by equation (7) ; the former were calculated from the slope of the line obtained by plotting log $\eta/\rho\ T$ versus $1/T$. In order to obey the theoretical premises, temperature intervals ΔT in the vicinity of the fusion point were considered.

An inspection of the table shows a good agreement between experimental and calculated values in the metals Na, K, Rb, Cs, Ag, Pb. In copper, the mean of the experimental results also compares well with the calculated figure. An acceptable agreement is also found in Li, Au, Fe, Co, Ni. In the case of Mg and Al melts, however, the difference between experimental and calculated values is large. The disagreement might also arise from errors which may affect experimental viscosity measurements.

Table 2 exhibits the activation energies of the viscosity of abnormal liquid metals, both those deduced from experimental viscosity values and

Table 2

Activation energies for the viscosity of abnormal liquid metals

Element	T_m, K	ΔT, K	x	E^*, cal/g atom	
				Exp.	Calcd.-ec(8)
Zn+	692.7	723– 823 692– 973	0.125	4,290 3,810	4,030
Cd	594.2	623– 873	0.126	3,120	3,450
		595– 725	0.160+ +	3,230+ +	3,430
Hg+	234.3	253– 313	0.325+	1,160	1,320
Ga	303.0	325– 432	0.980	1,500	1,510
Sn	505.1	505– 623	0.910	2,510	2,540
Sb+	903.7	903–1023 975–1173	0.853	4,460 4,840	4,600
Bi+	544.2	544– 753 577– 673	0.665	2,770 2,570	2,870

* The last figure has been rounded.

+ Recalculated values compared to part II.

+ + Values obtained by data from ; A. F. Crawley, *Trans. Met. Soc. AIME*, **242**, 2237(1968) ; A. F. Crawley and H. R. Thresh, *ibid.*, **245**, 424(1969).

those calculated by equation (8). The values of the association coefficient were taken from one of our previous papers [9]. The temperature intervals ΔT corresponding to the viscosity coefficients used in the graphical evaluation of the activation energy were also maintained near the melting temperature.

The agreement between experimental and calculated values is particularly good in Ga, Sn, Sb. For the other metals, the agreement is satisfactory.

Based on these results, for normal liquid metals, equation (1) takes the form :

$$\eta = A\ \rho\ T\ e^{3T_m/T} \tag{9}$$

in which constant A assumes the expression (2). For liquids resulting from abnormal metals, we obtain :

$$\eta = A'\ \rho\ T\ e^{(3-x/2)T_m/T} \tag{10}$$

Constant A' is now given by expression (3).

From equations (9) and (2) it results that the viscosity coefficient of normal liquid metals may be calculated at temperatures which do not exceed too much the melting temperature, if we know the liquid densities as a function of temperature and the fusion temperatures in addition to the atomic weights ; the atomic volumes V_m may be obtained in the manner described in the previous paper.[9] Table 3 shows such calculation for liquid silver. The values calculated by equations (2) and (7) were used both for the preexponential constant and for the activation energy.

Table 3

Viscosity coefficient of liquid silver calculated by equation (I)

$A_{\text{calcd.}} = 1.804 \times 10^{-7}$ (cm^2 s^{-1} grad^{-1})
$E_{\text{calcd.}} = 7{,}330$ (cal/g atom)
$M = 107.87$; $T_m = 1234$ K ; $V_m = 10.90$ (cm^3/g atom)

T K	ρ, g/cm^3	$\eta \times 10^2$, Poise	
		Exp.	Calcd.
1273.1	9.26	3.89	3.86
1323.1	9.22	3.62	3.58
1373.1	9.18	3.39	3.34
1423.1	9.135	3.18	3.14
1473.1	9.09	2.99	2.96
1523.1	9.05	2.83	2.80

The agreement between the experimental and the calculated values of the viscosity coefficient is extremely good.

In order to perform the same calculation for abnormal liquid metals it is necessary to know the melting heat, the packing factor and the association coefficient, too.

In conclusion we mention that the experimental values of the activation energy of abnormal liquid metals, corresponding to the temperature ranges which are beyond, are close to the values calculated by equation (7), hence, by equation (8) in which x has become zero.

We also mention the need to re-discuss expression (3), since it has been obtained by using Lindemann and Mott's relations. Yet these relations hold only when the liquid particles exist in a monomer state and when the melting is accompanied by a volume increase respectively.

---

[9] I. G. Murgulescu and M. Şerban, *Rev. Roumaine Chim.*, **17**, 431(1972).

Revue Roumaine de Chimie, 20, 5, 597–602 (1975)

THERMOCHEMICAL STUDY OF BINARY SALT SYSTEMS

B. F. MARKOV, T. A. TISHURA and A. N. BUDARINA
Institute of General and Inorganic Chemistry, Ukrainian SSR Academy of Sciences,
Kiev, USSR

Received September, 1974

The enthalpy of the systems $KCl-LiCl$, $KCl-CaCl_2$, $KCl-MgCl_2$ has been measured over a wide temperature range. The composition dependence of the enthalpy of the systems $CaCl_2-KCl$ and $MgCl_2-KCl$, in which the congruently melting compounds $KCaCl_3$ and $KMgCl_3$ are formed, confirms the thesis that there is no structural fit between the solid and the molten states. The compound $KCaCl_3$ which is stable in the crystalline state undergoes a strong thermal dissociation into components during fusion, whereas the compound K_2MgCl_4 which is, according to some of its physiochemical properties, stable in the molten state decomposes into $KMgCl_3$ and KCl during crystallization.

It is known that the results of thermal analysis of binary salt systems allow an unequivocal conclusion to be drawn on the formation of the chemical compounds of their components in the solid phase. As to the stability of a complex compound and especially its "structure" in the molten state, the thermal analysis is able to estimate them only tentatively. The study of the thermochemical parameters of salt systems in a wide temperature range provides definite information on the stability of complex compounds in the molten state.

It should be noted that in some cases there is a discrepancy between inferences as to the structural units of a system from the results of thermal analysis and from the results of a study of some physiochemical properties of a system in the molten state. A congruently melting compound is sometimes not detectable at all by the properties of melts due to its strong thermal dissociation, whereas spectrally detectable compounds in a melt prove to be quite unstable in the solid state. The results of a study of binary systems comprising calcium, magnesium and potassium chlorides given below illustrate this point.

The thermochemical study of salt systems involves, in general, measurement of the enthalpy (heat content) of samples over a wide temperature range ($H_T - H_{298}$) with, say, a drop calorimeter, determination of the heats of formation of compounds at standard temperature from measurements of the heat of solution of components and mixtures (ΔH^0), and direct calorimetric determination of the heats of mixing of the components in the molten state (ΔH_T^M).

Given all these parameters it is possible to check their interconsistency using the following equation of thermochemical cycle, e.g., for the system $M_{II}X_2-M_IX$ of equimolar composition :

$$\Delta H^0_{MII}X_2+M_IX=(H_T-H_{298})\,M_{II}\,X_2+(H_T-H_{298})\,M_IX+2\Delta H^M$$
$$(0.5\ M_{II}X_2+0.5\ M_IX)-2\,(H_T-H_{298})\,(0.5\ M_{II}X_2+0.5\ M_IX)$$

If the standard heat of formation (ΔH^0) or the heat of mixing (ΔH^M_T) is unknown, it can easily be determined from the equation of the thermochemical cycle.

When the standard heat of formation of, say, the complex compound $M_IM_{II}X_3$ or $[M_I]_2M_{II}X_4$ has been found, then the heat of formation is calculated in the same way for other temperatures, i.e., the temperature dependence of this parameter for the solid state is derived. This dependence has been found to be specific for each particular compound.

We shall, now, consider some salt systems with a different manner of interaction between components, studied by us before.

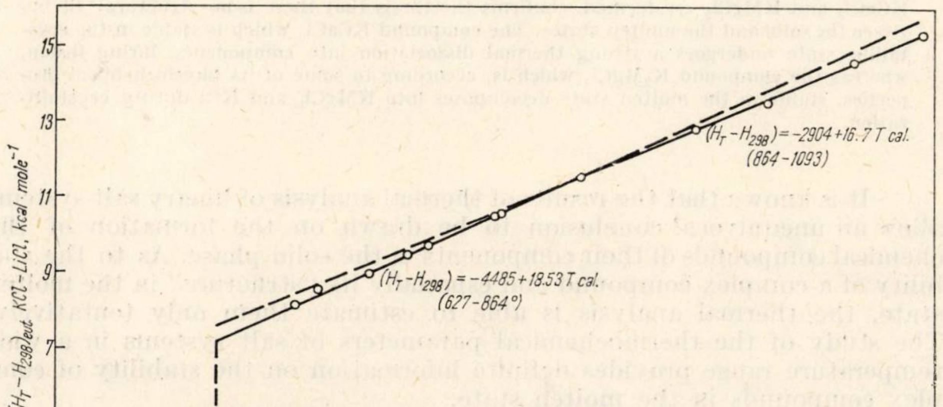

Fig. 1. — Plot of the enthalpy of the eutectic mixture KCl—LiCl against temperature.

The system KCl-LiCl is of the simple eutectic type ; the components in the solid state are not mutually soluble. Measurements of the enthalpy of the eutectic mixture (0.58 LiCl + 0.42 KCl) had been made earlier.[1] Figure 1 shows a plot of the enthalpy of the eutectic against temperature. The heat of fusion of the eutectic was found to be 2.95 kcal, while according to measurements by Solomons et al.[2] it is 3.2 ± 0.2 kcal. The inconsistency of the heat capacity of the molten eutectic is worth special notice.

---

[1] B. F. Markov, T. A. Tishura, A. N. Budarina and A. Saparov, *Ukrain. khim. Zhur.*, **39**, 84 (1973).

[2] C. Solomons, I. Goodkin, H. J. Gardner and G. J. Janz, *J. Phys. Chem.*, **62**, 248 (1958).

The dependence of the enthalpy of the molten eutectic on temperature is represented by two straight lines intersecting at about 600°, i.e., close to the melting point of the lower melting component. The heat capacity in this case naturally changes abruptly. Whereas for temperatures above 600°, the heat capacity is almost additive (experimental value 16.7 cal/g mole, additive value 16.2 cal/g mole), and has a much higher value (18.53 cal/g mole) in the range from 600° to the melting point of the eutectic. Such a change in the heat capacity is undoubtedly associated with a considerable rearrangement of the "structure" of the melt : the microheterogeneity of the melt increases as the temperature approaches the temperature of eutectic crystallization. As found before, this process affects the temperature dependence of the electrical conductivity of eutectic melts.[3]

Figure 2 shows an enthalpy curve of this system at 1043°K, which was plotted using heats of mixing measured by Hersh and Kleppa.[4] The measured heat of mixing for the eutectic melt is —1.06 kcal, whereas the heat of mixing calculated from the enthalpy found by us is —0.96 kcal.

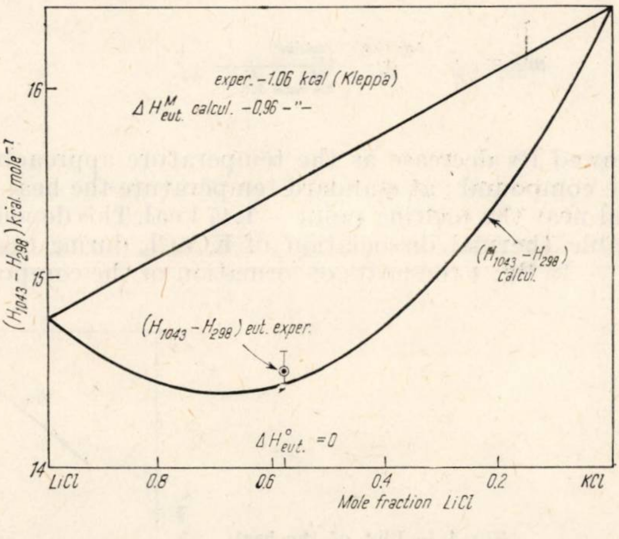

Fig. 2. — Enthalpy of the system KCl—LiCl in terms of composition.

As has been shown, [1] using only thermochemical quantities, the heat of formation of a molten eutectic may be divided into entropy component and excess free energy of mixing in the way described earlier.[5] In this case, the entropy part accounts for 40% of the thermal effect of mixing.

The system $CaCl_2$—KCl pertains to the class of systems with congruently melting compound (fig. 3). In addition to the measurement of the enthalpy of the components and the compound $KCaCl_3$,[6] the standard

[3] B. F. Markov and A. M. Tarasenko, *Zhur fiz. Khim.* **32**, 1333 (1958).

[4] L. S. Hersh and O. J. Kleppa, *J. Chem. Phys.*, **42**, 1309 (1965).

[5] B. F. Markov, *Ukrain. khim. Zhur.*, **39**, 827 (1973).

[6] B. F. Markov and T. A. Tishura, *Ukrain. khim. Zhur.*, **39**, 757 (1973).

heat of formation of $KCaCl_3$ was estimated from measurements of heats of solution (−3.0 kcal). The heat of mixing of the liquid components at 1073°K evaluated from the equation of thermochemical cycle is −2.12 kcal/mole and that determined directly by Østvold[7] is −2.19 kcal/mole. The calculation of the heat of formation of $KCaCl_3$ at other temperatures showed its decrease as the temperature approached the melting point of the compound : at standard temperature the heat of formation is −3 kcal and near the melting point −1.47 kcal. This dependence suggests a considerable thermal dissociation of $KCaCl_3$ during fusion.

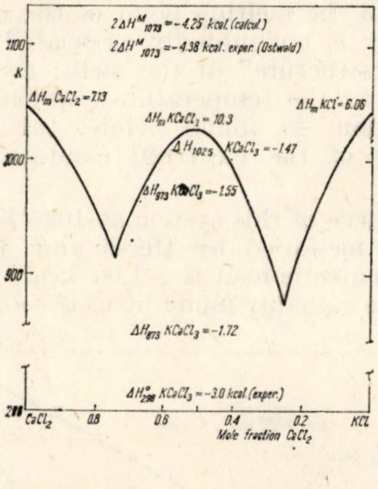

Fig. 3. – Thermochemical parameters of the compound $KCaCl_3$.

In fig. 4 the heats of formation of the compounds $KCaCl_3$, $RbCaCl_3$,[8]

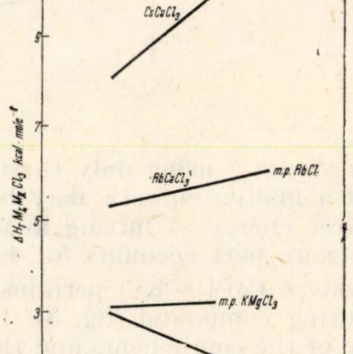

Fig. 4. – Plot of the heat of formation of $KCaCl_3$, $KMgCl_3$, $RbCaCl_3$ and $CsCaCl_3$ against temperature.

---

[7] T. Østvold, "A Thermodynamic Study of Some Fused Salt Mixtures Containing Alkali and Alkali Earth Chlorides, Bromides and Iodides", Topic Norway, 1971.

[8] B. F. Markov, T. A. Tishura and A. N. Budarina, *Ukrain. khim. Zhur.*, **38**, 823 (1972).

$CsCaCl_3$,[9] and $KMgCl_3$ as a function of temperature are comparatively presented. In contrast to $KCaCl_3$, all of the other compounds exhibit an increase in the heat of formation with temperature.

The commercially important system $MgCl_2-KCl$ is characterized by the congruently melting compound $KMgCl_3$ and the unstable compound

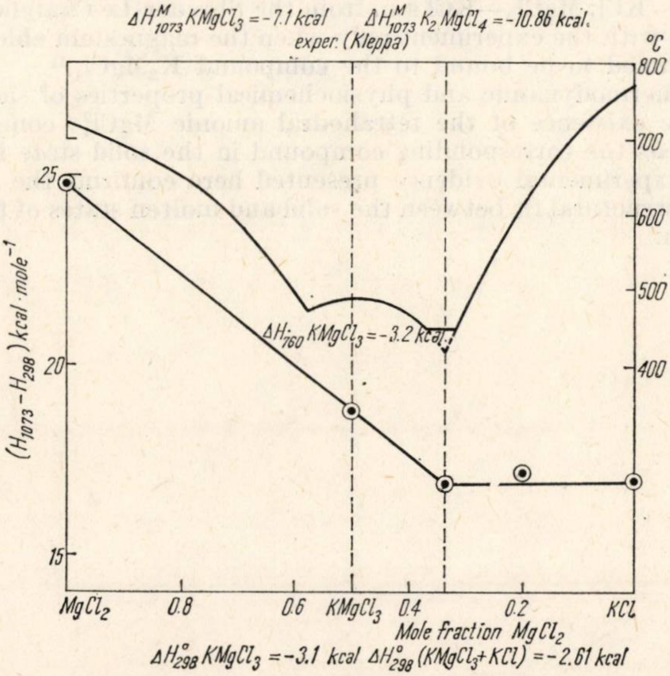

Fig. 5. — Enthalpy of the system $KCl-MgCl_2$ in terms of composition.

K_2MgCl_4 which decomposes by the decrease of temperature. Besides the enthalpy of the components, we have measured the enthalpy of mixtures with the component ratios 1 : 1 and 1 : 2. Figure 5 shows the enthalpy of molten mixtures at 1073°K as a function of composition. The enthalpy decreases linearly from the pure magnesium chloride to the ratio 1 : 2 and then does not practically change. This behaviour may be accounted for by the continuous energy release on addition of potassium chloride to the magnesium chloride until the component ratio required by the K_2MgCl_4 compound has been reached.

Using the heats of mixing of potassium and magnesium chlorides measured by Kleppa and McCarty[10] to calculate the standard heats of formation of $KMgCl_3$ and K_2MgCl_4 from the corresponding equations of thermochemical cycle, one obtains for the former compound −3.1 kcal and for the latter −2.61 kcal. This result is not unexpected since the K_2MgCl_4 compound undergoes eutectoid decomposition near the melting point and, consequently, the standard heat of formation of the mixture 2 KCl + $MgCl_2$ must be close to that of $KMgCl_3$.

---

[9] B. F. Markov, T. A. Tishura and A. N. Budarina, *Ukrain. khim. Zhur.*, **40**, 242 (1974).

[10] O. J. Kleppa and F. G. McCarty, *J. Phys. Chem.*, **70**, 1249 (1966).

The calculation of the liquids of potassium chloride in the systems $CaCl_2$—KCl, $MgCl_2$—KCl a.o. from the Shreder-Le Chatelier equation fully agrees with the experiment only when the magnesium chloride in the melt is assumed to be bound to the compound K_2MgCl_4.[11]

The thermodynamic and physiochemical properties of such systems indicate the existence of the tetrahedral anionic $MgCl_4^{2-}$ complex in the melt, whereas the corresponding compound in the solid state is unstable.

The experimental evidence presented here confirms the thesis that there is no structural fit between the solid and molten states of the systems in question.

---

[11] H. Flood und S. Urnes, *Z. Elektrochem.*, **59**, 834 (1955).

Revue Roumaine de Chimie, 20, 5, 603-609 (1975)

DETERMINATION OF HEAT CAPACITIES OF SOME ALCOHOLS AND KETONES IN VAPOUR PHASE

RODICA VÎLCU and B. COMAN

University of Bucharest, Department of Chemical Thermodynamics, Electrochemistry and Macromolecules
Bd. Republicii, Bucharest, Romania

Received February 6, 1974

The heat capacity of cyclopentanol, cyclohexanol, propanone, butanone and 3-pentanone in vapour phase was determined at temperatures ranging between the normal boiling point of liquids and 500 K. Measurements were performed by a flow calorimeter. Experimental data compare satisfactorily with the data calculated from statistical equations.

INTRODUCTION

The present paper is part of an extensive program of measuring heat capacities in some vapours generated by organic liquids in a pure state and in mixtures. The selected working domains range from the normal boiling points of liquids to round 500 K.

The physico-chemical interest in the modification of molecular interactions in vapour mixtures compared to interactions in monocomponent systems requires, in a first stage, a thermodynamic characterization of pure phases followed by a study of binary mixtures.

In the latter case, excess thermodynamic functions will illustrate the deviation of systems from an ideal behaviour, a reflection of molecular interactions.

In addition to the intrinsic value of heat capacities, as directly usuable magnitudes, heat capacities of mixtures provide additional information on the behaviour of systems.

Heat capacities determined for the above-mentioned substances in vapour phase, at normal pressure belong to the first part of the studies.

The experimental device used for measurements is a flow calorimeter, original construction of ours. Its complete description and measurement performances were presented in detail in a previous paper.[1]

---

[1] R. Vîlcu and B. Coman, *Rev. Roumaine Chim.*, **18**, 1301 (1973).

It must be mentioned that determinations were conducted from the normal boiling points of liquids to round 480 K.

EXPERIMENTAL

Heat capacities of cyclopentanol, cyclohexanol, propanone, butanone and 3-pentanone vapours were experimentally determined by measuring, at normal pressure, the amount of condensate and implicitly the volume of vapours (V) passed through a calorimeter.

The heat capacity C_p was obtained by measuring the constant K of the calorimeter, the thermal effect Q and the temperature variation ΔT, and by the well-known equation :

$$C_p = Q/(\Delta T) - K \tag{1}$$

The experimental values of molar heat capacities were listed in tables 1—5 for the alcohols and ketones under study together with the values calculated by processing statistical equations according to Bennewitz and Rossner,[2] modified by Dobratz [3] :

Table 1

Heat capacity of cyclopentanol

T K	C_v^0 J. mol K^{-1} calculated	C_p^0 J.mol K^{-1} calculated	C_p J. mol K^{-1} experimental	$C_p - C_p^0$ J. mol^{-1}K^{-1}
420	157.5	165.8	168.1±0.8	2.2
430	160.5	168.9	169.2±1.2	0.3
440	163.5	171.9	172.3±1.6	0.4
450	166.6	174.9	175.4±1.6	0.5
460	169.5	177.9	178.4±2.0	0.5
470	172.4	180.7	181.5±2.5	0.8
480	175.3	183.6	184.6±2.9	1.0

Table 2

Heat capacity of cyclohexanol

T K	C_v^0 J.mol^{-1} K^{-1} calculated	C_p^0 J. mol^{-1}K^{-1} calculated	C_p J.mol^{-1}K^{-1} experimental	$C_p - C_p^0$ J.mol^{-1}K^{-1}
433	172.5	181.0	187.8±1.2	6.8
440	175.3	183.8	186.5±1.2	2.7
450	179.1	187.6	188.2±1.6	0.6
460	182.9	191.4	192.4±1.8	1.0
470	186.6	195.2	196.3±2.0	1.1
480	190.3	198.9	200.1±2.9	1.2

---

[2] K. Bennewitz and W. Rossner, *Z. phys. Chem.*, **39 B**, 126 (1938).

[3] C. J. Dobratz, *Ind. Eng. Chem.*, **33**, 759 (1941).

Table 3

Heat capacity of propanone

T K	C_v^0 J. mol^{-1}K^{-1} calculated	C_p^0 J. mol^{-1}K^{-1} calculated	C_p J.mol^{-1}K^{-1} experimental	$C_p - C_p^0$ J. mol^{-1}K^{-1}
330	73.8	84.0	84.4±1.2	0.4
341	75.7	85.6	87.2±1.2	1.6
350	77.3	87.0	89.0±1.6	2.0
360	79.0	88.6	90.8±1.6	2.2
376	81.7	91.1	93.0±1.6	1.9
380	82.4	91.7	93.6±1.8	1.9
390	84.1	93.3	94.9±2.0	1.6
400	85.7	94.9	96.5±2.0	1.6
410	87.3	96.5	97.8±2.5	1.3
420	89.0	98.1	99.2±2.9	1.1

Table 4

Heat capacity of butanone

T K	C_v^0 J. mol^{-1}K^{-1} calculated	C_p^0 J. mol^{-1}K^{-1} calculated	C_p J. mol^{-1}K^{-1} experimental	$C_p - C_p^0$ J. mol^{-1}K^{-1}
353	96.1	106.2	106.7±0.8	0.5
360	97.5	107.5	108.7±1.2	1.2
370	99.5	109.0	110.8±1.6	1.8
380	101.5	111.2	112.6±1.6	1.4
390	103.4	113.0	114.3±1.6	1.3
400	105.3	114.8	116.0±1.8	1.2
410	107.2	116.6	117.8±1.8	1.2
420	109.1	118.5	119.3±2.0	0.8
430	111.0	120.1	121.0±2.5	0.9

Table 5

Heat capacity of 3 pentanone

T K	C_v^0 J. mol^{-1}K^{-1} calculated	C_p^0 J.mol^{-1}K^{-1} calculated	C_p J.mol^{-1}K^{-1} experimental	$C_p - C_p^0$ J.mol^{-1}K^{-1}
376	134.3	144.4	145.4±0.8	1.0
380	136.1	146.2	147.6±0.8	1.4
385	137.2	147.2	150.1±1.2	2.9
390	138.8	148.7	152.0±1.6	3.3
395	140.3	151.2	153.5±1.6	2.3
400	141.9	151.7	155.1±2.0	3.4
410	145.4	154.8	157.8±2.0	3.0
420	147.9	157.6	160.4±2.5	2.8
425	149.3	158.8	161.6±2.5	2.8

Revue Roumaine de Chimie, 20, 5, 603–609 (1975)

$$(C_v)_{p=0} = 3R + aR/2 + \Sigma q_i C_{\nu_i} + [(3n-6-a-\Sigma q_i).\ \Sigma q_i\ C_{\delta i}]/\Sigma q_j \qquad (2)$$

in which : n represents the number of atoms in the molecule, q_i, the number of type i bending valencies, C_{ν_i} and $C_{\delta i}$ — the Einstein functions characteristic of frequencies ν_i and δ_i, a — the number of bonds permitting the free rotation C—C and C—O.

Frequencies ν were evaluated from the Raman data and frequencies δ were empirically determined from previously obtained experimental data.[2]

Equation (2) represents a statistical formulation processed by addition of some empirical corrections; the experimental element was overlapped against a rigorously statistical background in which the vibration contribution to heat capacity was calculated by means of the Einstein functions, introducing valency-bending frequencies evaluated from the Raman spectra and the stretching frequency from experimental data.

The results obtained by calculations made on the basis of this equation perfectly support its validity.

It has been observed that equation (2) calculates the heat capacity of vapours at constant volume; the value of heat capacity at constant pressure was found by means of Berthelot's equation. By comparing the values calculated by this equation with experimental values the coincidence between the two series of data was considered to be satisfactory.

Berthelot's equation can be favourably applied to oxygen-containing organic compounds :

$$(C_p)_{p=p} = (C_v)_{p=0} + R\ [1 + 81\,\mathrm{P}/32\ Pc\ (Tc/T)^3] \qquad (3)$$

A combination of equation (2) with (3) leads to an equation for calculating heat capacities at constant pressure, which meets the most demanding calculation requirements for such magnitudes and compares well with experimental data.

Some of our data could be compared to the experimental values obtained by Pitzer.[4]

It has been found that the introduction of the internal relation in calculations (eqn. 2) has favourable effects, approximating the results obtained by experimental data.

Structural data necessary for statistical calculations extracted from the available references [5] are given in table 6.

In order to conveniently apply equation (2) to various temperatures, it was reformulated as a polynomial in T its constants being determined from structural data [5]:

$$C_v = a + bT + cT^2 \qquad (4)$$

---

[4] K. S. Pitzer, *J. Chem. Phys.*, 5, 473 (1937).

[5] Landolt-Börnstein, Physikalisch-Chemische Tabellen, vol. II, p. 1252, Julius Springer, Berlin, 1936.

Table 6

Bending frequency and constants evaluated from the Einstein functions

Bonding	freq. cm^{-1}	a J. $grd.^{-1}$ mol^{-1}	$b.10^3$ $J.mol^{-1}$ grd^{-2}	$c.10^6$ J. $grd.^{-3}$ mol^{-1}	$freq.cm^{-1}$	a J. $grd.^{-1}$ mol^{-1}	$b.10^3$ J. mol^{-1} grd^{-2}	$c.10^6$ $J.grd.^{-3}mol^{-1}$
C−C	990	−4.560	25.104	−14.397	390	3.054	14.284	−10.782
C−H	2920	0.958	−5.101	6.937	1320	−3.924	16.917	−5.614
C−O	1030	−7.418	25.656	−14.874	205	6.112	6.832	−5.916
C=O	1700	−1.355	−3.029	5.472	390	3.054	14.284	−11.782
C=C	1620	−1.807	5.158	3.912	845	−4.769	30.350	−20.652

The values of constants *a*, *b* and *c* in the suggested formula are given in table 7.

Table 7

Value of constants *a*, *b* **and** *c*

Substance	a J./mol.grd	b J./mol	c J.grd/mol
Cyclopentanol	−7.275	$477.741.10^{-3}$	$-200.493.10^{-6}$
Cyclohexanol	−48.153	$627.625.10^{-3}$	$-\ 24.472.10^{-6}$
Propanone	7.744	$225.977.10^{-3}$	$-\ 77.111.10^{-6}$
Butanone	13.031	$270.134.10^{-3}$	$-\ 97.445.10^{-6}$
3-Pentanone	−5.267	$428.654.10^{-3}$	$-151.925.10^{-6}$

The variation of heat capacities with temperature is plotted for each separate substance in figs. 1−5.

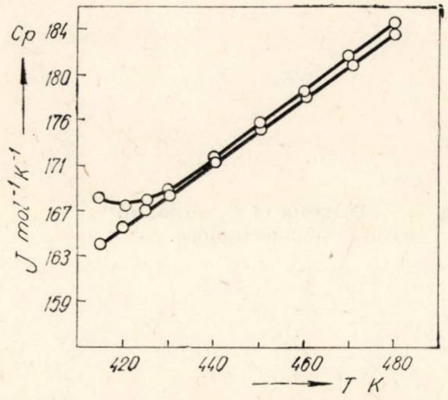

Fig. 1. — Diagram of C_p variation with T of cyclopentanol.

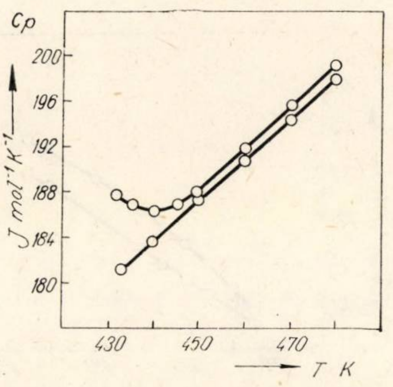

Fig. 2.—Diagram of C_p variation with T of cyclohexanol.

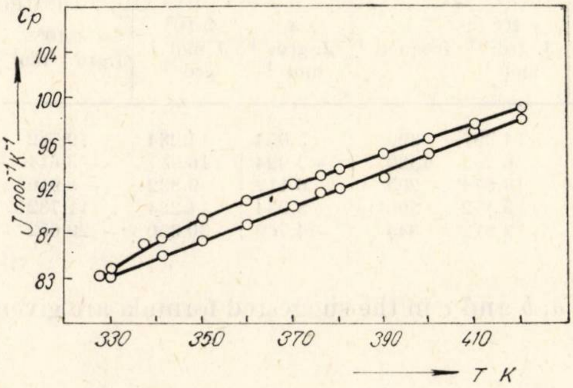

Fig. 3. — Diagram of C_p variation with T of propanone.

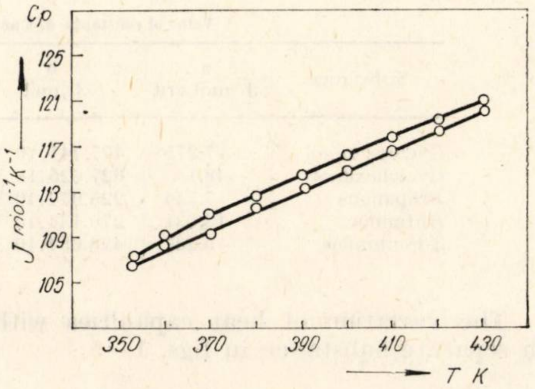

Fig. 4.—Diagram of C_p variation with T of butanone.

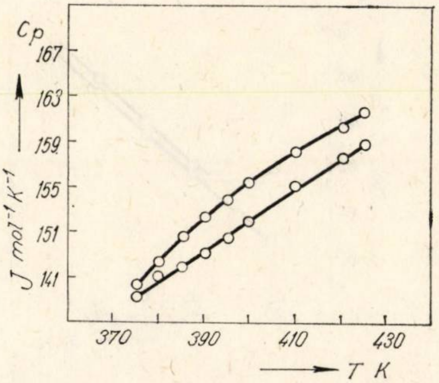

Fig. 5. — Diagram of C_p variation with T of 3-pentanone.

The diagrams provide a clear image of the behaviour of each substance under study; the heat capacity of cyclopentanol and of cyclohexanol varies with temperature as shown by the curve with the convexity oriented towards the axis of abscissae.

A comparison between the experimental values and the values calculated by eqn. (3) reveals in the case of cyclopentanol a 0.2% difference at temperatures ranging from 440 K to 460 K whereas for cyclohexanol the difference is of 0.3%. The calculated error for experimental data over the interval 420 K – 480 K does not exceed the ± 2.9 J. mol^{-1}. grd^{-1}. In the case of ketones, the variations of heat capacities with temperature are reflected in curves with the concavity towards the axis of abscissae, the difference being : 2.4% in propanone, 1.6% in butanone and 2.2% in 3-pentanone over a temperature ranging between 350 K and 380 K. The average error of experimental data lies around ± 1.6 J. mol^{-1} grd^{-1}.

In the case of 3-pentanone, the diagram shows a more significant curve at temperatures ranging from 375 K to 425 K. A similar, yet less pronounced tendency, is seen in the case of propanone while butanone obeys the equation of a straight line in the studied domain approximating an ideal behaviour although the very manner of approaching the systems by applying Berthelot's equation rules out the possibility of ideal vapours.

These deviations from linearity in the interval ranging from the normal boiling point of liquids to approx. 30–40 K may be attributed to the interaction factors between molecules a phenomenon which explains the approximation of variation C_p to linearity without reaching an ideal state.

The experimental data reveal in all cases a moderate increase of heat capacities at constant pressure with temperature : for instance in the case of 3-pentanone, in the 375–425 K range, therefore over a 50 K interval, C_p increases by some 12.5 J. mol^{-1}. degree^{-1} which amounts to an increase of about 0.25 J. mol^{-1}. degree^{-2}. In the case of the other two ketones, these increases are less significant.

For this reason the hypothesis of a constancy of heat capacities over relatively restricted intervals is justified in ordinary calculations.

The accurate C_p determination of some organic substances in vapour phase was made with a view to applying these data to the study of vapour mixtures, with important implications in the characterization of state equations, in close connection with the non-ideality degree of systems.

The diagrams plotted give a clear image of the behaviour of each substance under study; the heat capacity of cyclopentanol and of cyclohexanol varies with temperature as shown by the curves [illegible], with the convexity towards the axis of abscissae.

A comparison between the experimental values and the values calculated with (2) reveals in the case of cyclopentanol a 0.2% difference at temperatures ranging from 410 K to 460 K whereas for cyclohexanol the difference is of 0.1%. The calculated error for experimental data over the interval 420 K – 480 K does not exceed the ± 2.0 J mol^{-1} grd^{-1}. In the case of ketones, the variation of heat capacities with temperature is reflected in curves with the convexity towards the axis of abscissae, the deviations being 2.4% in propanone, 1.0% in butanone and 3.2% in pentanone over a temperature ranging between 320 K and 380 K. The average error of experimental data lies around ± 1.6 J mol^{-1} grd^{-1}.

In the case of 3-pentanone, the diagram shows a more significant curve at temperatures ranging from 375 K to 425 K. A similar, yet less pronounced tendency is seen in the case of propanone, while butanone shows the variation of a straight line to the studied interval approximating an ideal behaviour although the very manner of approaching the system by applying Berthelot's equation rules out the possibility of ideal vapours.

These deviations from linearity in the interval ranging from the normal boiling point of liquids to approx. 30–40 K may be attributed to the interaction forces between molecules, a phenomenon which explains the approximation of variation C_p to linearity without reaching an ideal state.

The experimental data reveal in all cases a moderate increase of heat capacities at constant pressure with temperature; for instance in the case of 3-pentanone, in the 375–425 K range, therefore over a 50 K interval, C_p increases by some 12.5 J mol^{-1} degree^{-1} which amounts to an increase of about 0.25 J mol^{-1} degree^{-1}. In the case of the other two ketones, these increases are less significant.

For this reason the hypothesis of a constancy of heat capacities over relatively restricted intervals is justified in ordinary calculations.

The accurate C_p determination of some organic substances in vapour phase was made with a view to applying these data to the study of vapour mixtures, with important implications in the characterization of state equations, in close connection with the non-ideality degree of systems.

Revue Roumaine de Chimie, **20**, *5*, 611 – 618 (1975)

L'ÉTUDE DE LA RÉACTION D'OXYDATION DE L'HYDROGÈNE SUR LES ÉLECTRODES POREUSES EN NICKEL. III[1]

LA DÉTERMINATION DES PARAMÈTRES DE FONCTIONNEMENT

IOANA ONACA, MARIA MAVRODIN-TĂRĂBÎC et I. SOLACOLU
Centre de Chimie Physique, Bucarest, 31, str. Galaţi

Reçu le 25 janvier 1974

On a étudié l'influence de la température et de la concentration de l'électrolyte (solution KOH) sur les performances électrochimiques des électrodes à gaz en nickel dans la réaction d'oxydation de l'hydrogène. Les électrodes étudiées se caractérisent par une structure du type DSK («Doppel Skelet Katalyst») ou par une structure du type double couche (couche barrière) et ont été obtenues par compression, à $4,6.10^8$ N/m² et $5,4.10^8$ N/m², et frittage à 700°, en atmosphère d'hydrogène. On a établi les paramètres de fonctionnement des électrodes pour lesquels les polarisations sont minimales (anodes pour les piles à combustible du type hydrogène-oxygène), en fonction de la densité de courant débitée dans le circuit extérieur.

Dans un travail antérieur[1] on a étudié l'effet des paramètres de réalisation des électrodes à gaz en nickel (la pression à laquelle ont été comprimées les électrodes et la température de frittage) sur les performances électrochimiques et on a établi les paramètres de réalisation d'un système poreux capable de performances supérieures. Dans ce travail nous nous sommes proposé d'étudier l'effet des paramètres de fonctionnement (la surpression de l'hydrogène, la température et la concentration de l'électrolyte) sur leurs performances électrochimiques dans la réaction d'oxydation de l'hydrogène.

Evidemment que la relation qui existe entre les paramètres mentionnés et les performances des électrodes à gaz en nickel, utilisées comme anodes dans les piles du type hydrogène-oxygène, dépend de la nature et de la structure de l'électrode considérée. Ces valeurs et leur dépendance du régime de fonctionnement préconisé (la valeur de la tension électrique et de l'intensité du courant) varient en fonction du type de la structure de l'électrode à gaz.

---

[1] IIe partie : I. Solacolu, M. Mavrodin-Tărăbîc et I. Onaca, *Rev. Roumaine Chim.*, sous presse.

1. PARTIE EXPÉRIMENTALE

1.1. RÉALISATION DES ÉLECTRODES

Les électrodes à gaz en nickel ont été réalisées par la compression (à $4,6.10^{8}$ N/m^{2} et à $5,4.10^{8}$ N/m^{2}) et le frittage, en atmosphère d'hydrogène, à 700°, des mélanges homogènes qui contiennent du nickel ex nickel crabonyle, du carbonate de nickel et de l'acide oxalique. Les compositions des mélanges et les caractéristiques structurales des électrodes ont été présentées dans une publication antérieure.[1]

Les électrodes sont notées par :

— E_{I}, électrode caractérisée par une structure bidispersée (du type DSK), comprimée à $4.6.10^{8}$ N/m^{2} et frittée à 700° ;

E_{II}, électrode caractérisée par une structure bidispersée, comprimée à $5.4.10^{8}$ N/m^{2} et frittée à 700° ;

— E_{III}, électrode caractérisée par une structure du type double couche (avec couche barrière), comprimée à $4,6.10^{8}$ N/m^{2} et frittée à 700°.

1.2. DÉTERMINATIONS ÉLECTROCHIMIQUES

L'étude de l'effet de la surpression de l'hydrogène, de la température et de la concentration de l'électrolyte sur les performances électrochimiques des électrodes à gaz en nickel a été effectuée par technique potentiostatique. Le montage et les conditions de travail ont été décrits dans un travail antérieur.[2]

Les électrodes à gaz en nickel ont été alimentées avec de l'hydrogène à surpression constante (100 et 200 mm Hg) à l'aide d'une installation décrite antérieurement.[3]

La concentration de l'électrolyte (KOH) a été variée entre 9 et 4N. La température de travail a été variée entre 25 et 60° et maintenue constante (± 0,1°) à l'aide d'un ultrathermostat de type U-10.

2. RÉSULTATS ET DISCUSSIONS

Des courbes de polarisation η — i, tracées pour chaque électrode, à différentes surpressions de l'hydrogène, températures et concentrations de l'électrolyte, on a extrait les valeurs des surtensions caractéristiques pour les différentes densités de courant (rapportées à la surface extérieure de l'électrode), en vue de la détermination de l'influence des paramètres de fonctionnement.

2.1. EFFET DE LA TEMPÉRATURE DE L'ÉLECTROLYTE

L'influence de la température de l'électrolyte (KOH 5N) sur les performances de l'électrode E_{I}, dans l'intervalle 25—60°, à des surpressions de l'hydrogène de 100 et de 200 mm Hg, est illustrée par les courbes $\eta = f(t)$, à différentes densités de courant comprises entre 30 et 170mA/cm^{2} (fig. 1 et, respectivement, fig. 2).

De l'examen des courbes $\eta = f(t)$ (fig. 1) on constate que, dans le cas de l'alimentation de l'électrode E_{I} avec de l'hydrogène à une surpression de 100 mm Hg, à des densités de courant jusqu'à 100 mA/cm², la polarisation de l'électrode diminue continuellement avec l'augmentation de la température de l'électrolyte dans tout l'intervalle considéré, cette diminution étant plus prononcée à des densités de courant plus réduites et à des températures plus élevées. A des densités de courant plus grandes que 100 mA/cm², l'aspect des courbes se modifie et dans l'intervalle 25—50° on n'enregistre pas une variation significative de la polarisation des électrodes ; à des températures plus grandes que 50° on enregistre une augmentation de la polarisation de l'électrode à gaz, plus prononcée à des densités de courant et à des températures plus élevées.

---

[2] M. Mavrodin-Tărăbîc, I. Onaca et I. Solacolu, *Rev. Roumaine Chim.*, **18**, 1121 (1973)

[3] O. Radovici, M. Mavrodin-Tărăbîc, I. Onaca et I. Solacolu, *Rev. Roumaine Chem.*, **17**, 1153 (1972).

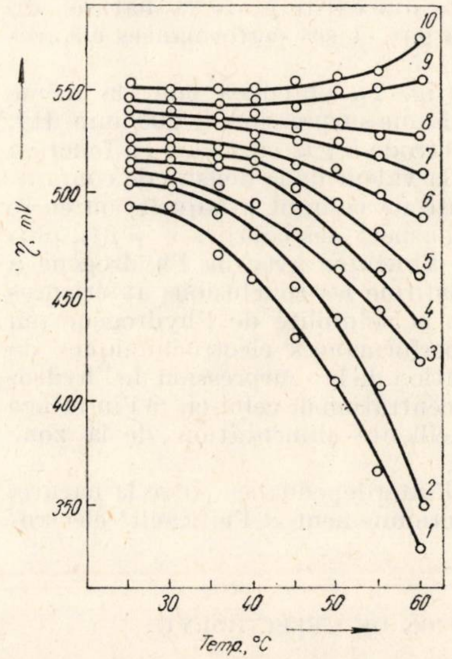

Fig. 1. — Influence de la température de l'électrolyte sur la polarisation de l'électrode E_I, à différentes densités de courant.

ΔP_{H_2} = 100 mm Hg. *1* – 30 mA/cm²; *2* – 40 mA/cm²; *3* – 50 mA/cm²; *4* – 60 mA/cm²; *5* – 70 mA/cm²; *6* – 80 mA/cm²; *7* – 90 mA/cm²; *8* – 100 mA/cm²; 9 – 110 mA/cm²; *10* – 120 mA/cm².

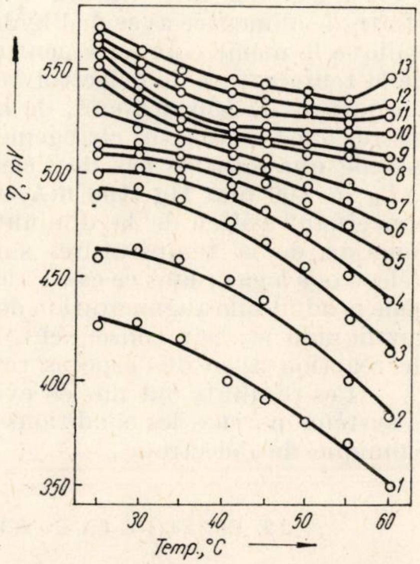

Fig. 2. — Influence de la température de l'électrolyte sur la polarisation de l'électrode E_I, à différentes densités de courant.

ΔP_{H_2} = 200 mmHg. *1* – 30 mA/cm²; *2* – 40 mA/cm²; *3* – 50 mA/cm²; *4* – 60 mA/cm²; *5* – 70 mA/cm²; *6* – 80 mA/cm²; *7* – 90 mA/cm²; *8* – 100 mA/cm²; *9* – 110 mA/cm²; *10* – 130 mA/cm²; *11* – 140 mA/cm²; *12* – 150 mA/cm²; *13* – 170 mA/cm².

Ce comportement différent de l'électrode, en fonction de la densité de courant considérée et de la température de travail s'explique par l'effet différent de la température de l'électrolyte sur la solubilité de l'hydrogène et sur les polarisations d'activation et de diffusion. Tandis que, dans l'intervalle considéré, la vitesse de réaction et de diffusion augmente avec l'augmentation de la température, la solubilité de l'hydrogène diminue. Ce dernier effet devient prédominant à des densités de courant plus grandes, ce qui se reflète dans le changement de l'aspect des courbes $\eta = f(t)$.

La comparaison de ces résultats avec ceux obtenus par Lucesoli[4] sur des électrodes à gaz en charbon, activées avec du Pt ou Pd (une diminution continuelle de la polarisation de l'électrode alimentée avec de l'hydrogène, entre −20 et 80°, à toutes les valeurs de la densité de courant) a mis en évidence la corrélation étroite qui existe entre la nature du catalyseur, la structure de l'électrode à gaz et ses performances électrochimiques.

L'examen des courbes $\eta = f(t)$ (fig. 2), obtenues pour la même électrode alimentée avec de l'hydrogène à une surpression de 200 mm Hg, indique le même comportement de l'électrode à gaz en nickel en fonction de la température de l'électrolyte et de la valeur de la densité de courant. La valeur, de 130 mA/cm², de la densité de courant à laquelle on enregistre, dans ce cas, un changement de l'aspect des courbes $\eta = f(t)$, plus grande que dans le cas de l'électrode alimentée avec de l'hydrogène à $\Delta P_{H_2} = 100$ mm Hg (100 mA/cm²), confirme les conclusions antérieures concernant l'effet de la diminution de la solubilité de l'hydrogène (en fonction de la température) sur les performances électrochimiques de l'électrode à gaz (dans ce cas, l'augmentation de la surpression de l'hydrogène produit une augmentation de la concentration de celui-ci, à l'interface gaz-liquide et, par conséquent, une meilleure alimentation de la zone de réaction avec des espèces réactives.)

Ces résultats ont mis en évidence l'interdépendance entre la nature, le système poreux, les conditions de fonctionnement et l'efficacité électrochimique de l'électrode.

2.2. EFFET DE LA CONCENTRATION DE L'ÉLECTROLYTE

En utilisant les données du tableau 2, on a tracé les courbes $\eta = f(c)$, qui caractérisent la variation de la surtension des électrodes en fonction de la concentration de l'électrolyte, dans l'intervalle 4−9N, à différentes valeurs de la densité de courant comprises entre 15 et 140 mA/cm². (Température de l'électrolyte, 25°.)

Dans les figures 3 et 4 sont représentées les courbes $\eta = f(c)$, pour l'électrode E_I alimentée avec de l'hydrogène à 100 et, respectivement, 200 mm Hg.

De l'examen de ces courbes il résulte que, à de petites densités de courant, la polarisation de l'électrode diminue continuellement (dans l'intervalle considéré) avec l'augmentation de la concentration de l'électrolyte. À de plus grandes densités de courant, on constate un changement du comportement de l'électrode, la polarisation minimale s'enregistrant dans le cas de l'électrolyte de concentration 7N.

L'augmentation de la concentration de l'électrolyte a un effet défavorable sur la solubilité de l'hydrogène et, en même temps, un effet favorable sur la diffusion des espèces réactives dans l'électrolyte. A de petites densités de courant, tel qu'il résulte de l'aspect des courbes $\eta = f(c)$ (fig. 3 et 4), c'est le deuxième effet qui prédomine, tandis que, à des densités de courant plus élevées, la polarisation de l'électrode augmente, à cause de l'insuffisante alimentation de la zone de réaction, avec de l'hydrogène, à des concentrations plus grandes que 7N. Ces conclusions sont aussi confirmées par les valeurs différentes de la densité de courant qui caractérisent le changement de l'aspect des courbes $\eta = f(c)$: 40mA/cm² à $\Delta P_{H_2} = 100$ mm Hg et 90 mA/cm² à $\Delta P_{H_2} = 200$ mm Hg ; cette augmentation de la valeur de la densité de courant s'explique aussi par la meilleure alimentation de la zone réactive, avec du réactant.

---

[4] D. B. LUCESOLI, Thèse, Université de Paris, 1971.

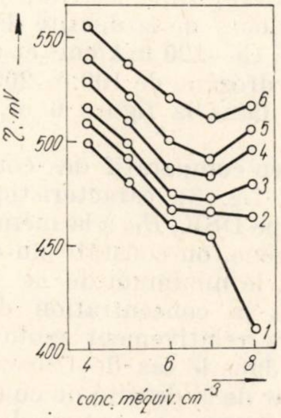

Fig. 3. — Influence de la concentration de l'électrolyte sur la polarisation de l'électrode E_I, à différentes densités de courant.

ΔP_{H_2} = 100 mm Hg. *1* – 30 mA/cm² ; *2* – 40 mA/cm² ; *3* – 50 mA/cm² ; *4* – 70 mA/cm² ; *5* – 90 mA/cm² ; *6* – 120 mA/cm².

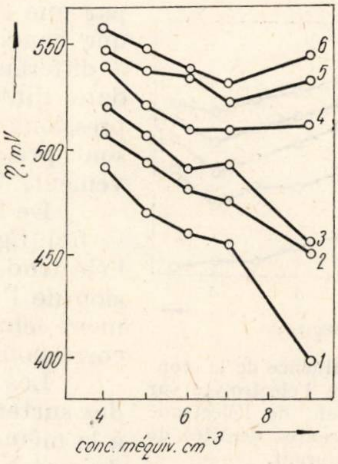

Fig. 4. — Influence de la concentration de l'électrolyte sur la polarisation de l'électrode E_I, à différentes densités de courant.

ΔP_{H_2} = 200 mm Hg. *1* – 30 mA/cm² ; *2* – 50 mA/cm² ; *3* – 70 mA/cm² ; 4 – 90 mA/cm² ; *5* – 120 mA/cm² ; *6* – 140 mA/cm².

L'influence du système poreux de l'électrode sur ses paramètres de fonctionnement est illustrée par l'aspect des courbes $\eta = f(c)$ (fig. 5), caractéristiques pour l'électrode E_{II}, alimentée d'hydrogène, à une surpression de 200 mm Hg.

On peut constater que la modification de la structure, à la suite de l'augmentation de la valeur de la pression à laquelle ont été comprimées les électrodes (5,4.10⁸ N/m², dans le cas de l'électrode E_{II}, en comparaison de 4,6.10⁸ N/m², dans le cas de l'électrode E_I), change la valeur de la concentration de l'électrolyte, à laquelle les polarisations sont réduites, de 7N à 8N. Ce comportement est explicable parce que, à la même valeur de la surpression de l'hydrogène, la position de la zone triphasique de réaction dans l'électrode E_{II} est relativement déplacée vers la surface alimentée avec le gaz (par rapport à l'électrode E_I) et, par conséquent, la diffusion des espèces réactives vers la zone triphasique de réaction joue un rôle plus important dans le développement global des processus d'électrode.

Les valeurs plus réduites de la surtension de l'électrode E_{II}, à la même valeur de la surpression de l'hydrogène et de la densité de courant, conduisent à la conclusion que cette structure est plus favorable.

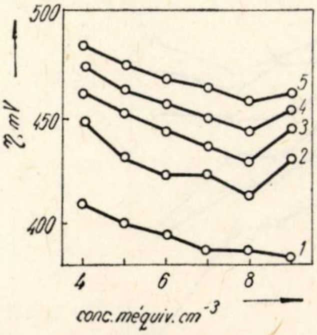

Fig. 5. — **Influence de la concentration de l'électrolyte sur la polarisation de l'électrode E_{II}, à différentes densités de courant.**

ΔP_{H_2} = 200 mm Hg. *1* – 15 mA/cm²; *2* – 30 mA/cm²; *3* – 50 mA/cm²; *4* – 70 mA/cm²; *5* – 90 mA/cm².

Dans le cas des électrodes caractérisées par une structure du type double couche (avec une couche barrière) E_{III}, les courbes $\eta = f(c)$, à différentes valeurs de la densité de courant, dans l'intervalle 15–120 mA/cm² et à des surpressions de l'hydrogène de 100 et 200 mm Hg, sont présentées dans la figure 6 et, respectivement, 7.

De l'examen comparatif des courbes $\eta = f(c)$ (fig. 6 et fig. 3), caractéristiques pour l'électrode du type DSK, E_I, à la même surpression de l'hydrogène, on constate un comportement semblable, le minimum de la surtension correspondant à la concentration de 7N.

Les valeurs relativement moins grandes des surtensions dans le cas de l'électrode E_{III}, à la même valeur de la densité de courant, conduisent à la conclusion que ce type de structure favorise la réaction.

En comparant les courbes présentées dans la figure 7 avec celles de la figure 4, on peut constater que, dans les mêmes conditions de surpression de l'hydrogène

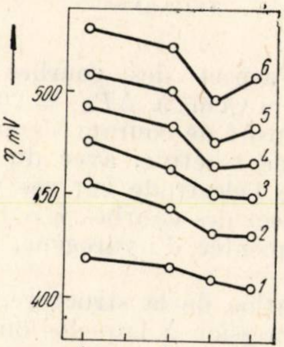

Fig. 6. — **Influence de la concentration de l'électrolyte sur la polarisation de l'électrode E_{III}, à différentes densités de courant.**

Δ P_{H_2} = 100 mm Hg. *1* – 15 mA/cm²; *2* – 30 mA/cm²; *3* – 50 mA/cm²; *4* – 70 mA/cm²; *5* – 90 mA/cm²; *6* – 120 mA/cm².

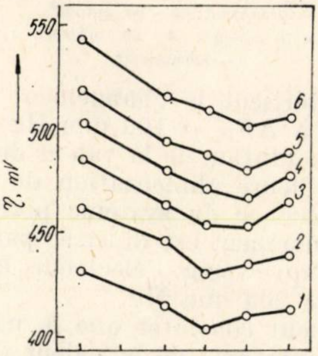

Fig. 7. — **Influence de la concentration de l'électrolyte sur la polarisation de l'électrode E_{III}, à différentes densités de courant.**

ΔP_{H_2} = 200 mm Hg. *1* – 15 mA/cm²; *2* – 30 mA/cm²; *3* – 50 mA/cm²; *4* – 70 mA/cm²; *5* – 90 mA/cm²; *6* – 120 mA/cm².

et de densité de courant, la concentration de l'électrolyte, à laquelle les polarisations sont réduites, se déplace de la valeur de 7N à 8N (pour des densités de courant plus grandes que 50 mA/cm^2), comme résultat des particularités de fonctionnement de la couche barrière.

Dans le cas de l'alimentation avec de l'hydrogène à une surpression de 100 mm Hg (fig. 6), l'électrode E_{III} fonctionne, à de grandes densités de courant, sous le contrôle de l'alimentation avec de l'hydrogène, tandis que, à une surpression de 200 mm Hg, l'alimentation avec de l'hydrogène de la zone triphasique de réaction est améliorée, cas où il est mis en évidence l'effet de la couche barrière : l'augmentation de la contribution de la polarisation de diffusion à la polarisation totale de l'électrode à gaz. (Cet effet est illustré par le changement de la valeur de la concentration de la valeur de 7N à 8N.)

*

L'étude que nous avons effectuée sur l'influence des principaux paramètres de fonctionnement (température et concentration de l'électrolyte) sur les performances réalisées par une série d'électrodes à gaz en nickel avec différentes structures, dans la réaction d'oxydation de l'hydrogène, a mis en évidence le fait qu'un facteur important qui doit être pris en considération lorsqu'on établit les valeurs de ces paramètres (auxquelles on obtient des performances maximales) est l'intensité du courant débité par la pile à combustible dans le circuit extérieur.

Etant donné que les valeurs des paramètres de fonctionnement dépendent de la densité de courant à laquelle les électrodes à gaz fonctionnent et que, pour chaque système de pile à combustible, il existe une certaine valeur du courant à laquelle la puissance débitée dans le circuit extérieur est maximale,[5] à l'établissement du régime de fonctionnement d'une pile à combustible (pertes minimales par polarisation), il faut tenir compte de l'interdépendance d'un grand nombre de facteurs de nature différente : la nature et le système poreux des électrodes à gaz, la valeur de la surpression du gaz, les valeurs de la tension électrique et de l'intensité du courant.

3. CONCLUSIONS

1. Les performances des électrodes à gaz en nickel du type DSK, dans la réaction d'oxydation de l'hydrogène, s'améliorent continuellement, à mesure que la température augmente (l'intervalle étudié 25—60°), à des densités de courant au-dessous de 100 mA/cm^2, dans le cas de l'alimentation avec de l'hydrogène, à une surpression de 100 mm Hg et de 130 mA/cm^2, dans le cas de l'alimentation avec de l'hydrogène à 200 mm Hg. A des densités de courant plus élevées, on constate une augmentation de la polarisation des électrodes à des températures supérieures à la valeur de 40° et, respectivement, de 55°.

---

[5] J. J. Gilvarry et J. Slaughter, *Electrochim. Acta*, **8**, 711 (1963).

2. La polarisation des électrodes du même type baisse continuellement à mesure que la concentration de l'électrolyte augmente (dans l'intervalle 4N—9N), à des densités de courant au-dessous de 40 mA/cm², dans le cas de l'électrode E_{I}, alimentée avec de l'hydrogène à une surpression de 100 mm Hg, de 90 mA/cm²; dans le cas de la même électrode alimentée avec de l'hydrogène à 200 mm Hg et de 15 mA/cm², dans le cas de l'électrode E_{II}, alimentée avec de l'hydrogène à 200 mm Hg. À des densités de courant plus élevées, les valeurs optimales de la concentration de l'électrolyte sont : 7N, pour les électrodes du type E_{I} et 8N, pour les électrodes du type E_{II}.

3. Les valeurs de la concentration de l'électrolyte, auxquelles les polarisations sont réduites, dans le cas des électrodes E_{III} du type double couche (à couche barrière), sont de 7N, dans le cas de l'alimentation avec de l'hydrogène à une surpression de 100 mm Hg et de 8N, dans le cas de l'alimentation avec de l'hydrogène à une surpression de 200 mm Hg.

Revue Roumaine de Chimie, **20**, *5*, 619–625 (1975)

INFLUENCIA DE LA ACIDEZ DEL MEDIO SOBRE LA REACCIÓN ENTRE LAS AMINAS PRIMARIAS ALIFÁTICAS Y EL ÁCIDO NITROSO

B. BREZMES, J. CASADO y F. MATA
Departamento de Investigaciones Quimicas, CSIC
Sección de Quimica-Física, Universidad de Valladolid, España

6 feb. 1974

Se ha estudiado la influencia de la acidez del medio sobre la cinética y mecanismo de las reacciones entre metil, etil, *n*-propil y *n*-butil amina y ácido nitroso. Se ha empleado una técnica fotocolorimétrica que permite la evaluación de parámetros cinéticos y termodinámicos en función de la acidez del medio, observandose que en las proximidades de pH = 3 la velocidad especifica de reacción se hace máxima presentando un minimo los valores de la energía de activación experimental. Se ha llevado a cabo un estudio espectrofotométrico de la reacción en la región UV. Los resultados obtenidos, acordes con los alcanzados en etapas previas de la investigación emprendida, han permitido una interpretación de la influencia de la acidez del medio sobre las reacciones estudiadas.

Aunque en trabajos anteriores se han abordado diversos aspectos cinéticos y mecanicistas de las reacciones entre las aminas primarias alifáticas y el ácido nitroso, no se había estudiado con detenimiento el papel de la acidez del medio en el mecanicismo de reacción, papel al que se han referido algunos autores.[1–3]

A) PARTE EXPERIMENTAL

Se ha utilizado una técnica fotocolorimétrica puesta a punto con anterioridad,[1,4]a aunque con ligeras modificaciones de matiz para adaptarla a las condiciones de acidez actuales[8] Se centra esencialmente en el seguimiento temporal de las variaciones de concentración de uno de los reactivos, ácido nitroso, mediante análisis espectrofotométrico en $\lambda = 470$ nm donde absorbe el colorante que se engendra al congelar la reacción mediante un rápido proceso de zocopulación.

De forma simultánea a las determinaciones fotocolorimétricas, se seguía la evolución de la acidez del medio.

[1] S. Senent y J. Casado, *Anales real Soc. españ. Fis. Quim.*, **63 B**, 495 (1967).
[2] R. H. Sahasrabudhey, *J. Indian Chem. Soc.*, **27**, 515 (1950).
[3] R. H. Sahasrabudhey, Comunicación Personal.
[4] J. Casado y P. M. Vicario, *Anales real Soc. espan. Fis. Quim.*, **62 B**, 87 (1966).
[5] S. Senent, J. Casado, y A. De Diego, *Ibid.*, **64**, 219 (1968).
[6] J. Casado y T. Ramos, *Ibid.*, **64**, 1017 (1968).
[7] J. Casado y A, Arrizabalaga, *Ibid.*, **67**, 1027 (1968).
[8] J. Casado y L. Ferrari, *Ibid.*, **67**, 1133 (1971).

Las medidas fotocolorimétricas se realizaron con un equipo Spectronic 20. Las potentiométricas con un pH-metro Radiometer 26, calibrado en el intervalo de trabajo. La constancia en la temperatura, en el intervalo 26—34°, se mantenia con un termostato convencional que garantiza con un error de ± 0,05°, es a magnitud.

Las disoluciones de las aminas empleadas se prepararon por pesada directa de las especies en forma de hidrocloruro. La metil, etil, y *n*-butil amina eran de la casa Suchardt mientras que la *n*-propil amina procedia de Fluka. El nitrito sódico empleado fue Merck p.a. ; se preparaba asi mismo por pesada directa, renovando con frecuencia las disoluciones y conservándolo en frascos de color topacio.Las disoluciones de ácidos acético y propiónico se preparaban a partir de las especies puras (acético glacial Panreac y propiónico Merck). A continuación se procedía a la medida directa de su pH. El acetato sódico empleado fue Panreac.

B) ESTUDIO CINÉTICO

Se trabajó siempre en condiciones de equimolecularidad (4.10^{-3}M) para ambos reactivos. El pH de trabajo (tanto en medio acético como propionico) estuvo comprendido entre 2 y 6.

Todos los experimentos realizados pusieron de manifiesto la existencia de una relación lineal entre los valores de log D_{470}(D = densidad óptica) y los del tiempo de reacción, lo que traduce un orden cinético uno respecto a la especie analizada. La linealidad es notablemente buena según reflejan los coeficientes de correlación lineal que se reseñan en cada caso.

La Tabla 1 da cuenta de los resultados obtenidos al analizar la influencia de la acidez del medio sobre la velocidad específica de reacción cuando se trabaja en medio acético. Puede observarse la aparición de un máximo en el entorno de pH = 3.

Se estudió seguidamente la influencia de la temperatura, observándose un satisfactorio cumplimiento de la ecuación de Arrhenius a diferentes valores del pH. Se calculó en cada caso el valor de la energía de activación experimental encontrando como se desprende de la Tabla 2, un mínimo para E_a en el mismo entorno de pH = 3.

Se comprobó asi mismo un cumplimiento satisfactorio de las previsiones derivadas de la teoría del complejo activado, encontrando valores de $\Delta H^{\neq}$ y $\Delta S^{\neq}$ totalmente en linea con los calculados en étapas anteriores de este trabajo (loc. cit.). Merece indicarse que, cuando se trabaja en medio propiónico, el valor absoluto de la energía de activación para la reacción etil amina — ácido nitroso es anormalmente alto.

C) ESTUDIO ESPECTROFOTOMETRICO

Como ya se ha indicado la concentración de especie nitrosa reactiva se ha analizado fotocolorimetricamente trabajando a una longitud de onda de λ = 470 nm.

Al representar frente al pH los valores del cociente de las densidades ópticas (λ = 470 nm) a tiempos 40 y 20 mins., se obtuvieron, en todos los casos, curvas campaniformes con un mínimo situado en el entorno de pH = 3, como ilustra la Fig. 1 correspondiente a la reacción *n*-própil amina / ácido nitroso, en medio acético. Se han utilizado los valores de la

Tabla 1

Influencia de la acidez del medio en la constante de velocidad* Temperatura 30°

pH	k.10³ mins⁻¹			
	Metil amina	Etil amina	*n*-Propil amina	*n*-Butil amina
2,0	1,82 (0,9990)	1,16 (0,9917)	1,22 (0,9977)	1,36 (0,9947)
2,1		1,22 (0,9983)		
2,2			1,97 (0,9974)	1,89 (0,9986)
2,3	2,47 (0,9980)	2,04 (0,9988)	2,30 (0,9983)	
2,4			2,47 (0,9986)	2,25 (0,9957)
2,5		2,50 (0,9998)		2,56 (0,9965)
2,6	2,98 (0,9991)		2,62 (0,9959)	
2,7				2,79 (0,9938)
2,8	3,11 (0,9985)			
2,9			2,97 (0,9990)	2,93 (0,9979)
3,0	3,15 (0,9959)	3,08 (0,9998)		
3,1				2,73 (0,9996)
3,2			2,79 (1,0062)	
3,3			2,75 (0,9921)	
3,4		2,55 (0,9990)	2,62 (0,9948)	2,36 (0,9998)
3,5	2,60 (0,9960)		2,40 (0,9996)	
3,6		2,33 (0,9982)		
3,7				1,82 (0,9933)
3,8				
3,9			1,80 (0,9982)	
4,0				
4,1		1,63 (0,9998)		
4,2	1,23 (0,9977)			0,92 (0,9996)
4,3	0,83 (0,9997)		1,17 (0,9917)	
4,4	0,65 (0,9953)		1,00 (0,9939)	
4,5				0,52 (0,9984)
4,6		0,93 (0,9997)		
4,7			0,48 (0,9910)	
4,8		0,62 (0,9929)		
4,9		0,59 (0,9984)		

* Los números entre paréntesis se refieren a los coeficientes de correlación lineal.

Tabla 2

Energía de activación experimental*

pH	E_a, kJ mol⁻¹			
	Metil amina	Etil amina	*n*-Propil amina	*n*-Butil amina
a) *Medio acético*				
2,0	77,5 (0,9980)	85,2 (0,9987)	74,9 (0,9973)	77,5 (0,9967)
2,4			69,9 (0,9997)	
2,5	75,4 (0,9980)	77,7 (0,9898)		72,1 (0,9981)
2,8			63,7 (0,9998)	
3,0	75,3 (0,9997)	69,7 (0,9975)		63,6 (0,9898)
3,5	75,7 (0,9956)			73,6 (0,9992)
3,6		75,2 (0,9989)	70,8 (0,9956)	
4,0	76,5 (0,9984)		76,6 (0,9997)	78,2 (0,9969)
4,2		79,3 (0,9959)		
b) *Medio propiónico*				
2,4	79,8 (0,9938)		68,8 (0,9987)	
2,5		126,4 (0,9986)		87,4 (0,9984)
2,9			66,5 (0.9991)	77,7 (0,9993)
3,0	64,6 (0,9992)	98,6 (0,9993)		
3,5	74,3 (0,9968)			79,5 (0,9979)
3,6		160,6 (0,9987)	76,3 (0,9976)	
4,0	78,1 (0,9984)	195,4 (0,9983)		
4,2			79,6 (0,9986)	89,1 (0,9932)

* Los números entre paréntesis se refieren a los coeficientes de correlación lineal.

densidad óptica relativa, en lugar de la absoluta, por haberse observado una reproducibilidad notablemente superior.

Estos resultados parecen traducir la existencia de una concentración mínima de especie nitrosa reactiva a pH = 3.

A continuación se llevó a cabo una serie de experimentos en condiciones idénticas a las reseñadas en B). En ellas se realizaba un análisis espectrofotométrico, en la región UV, para cada valor del pH de trabajo. En todos los casos, y tanto en medio acético como propiónico, se observó la aparición de una intensa y afilada banda a una longitud de onda de 242 nm, (en el caso del ácido propiónico Kozlov y Belov, [9] hablan de una banda a 258 nm, banda que nosotros no hemos observado), típica de los compuestos de nitrosilo. También se observaron otras bandas, ahora débiles a las siguientes longitudes de onda : 345—347, 358—360, 370—372, y 385 nm, atribuidas al ácido nitroso (loc. cit.).

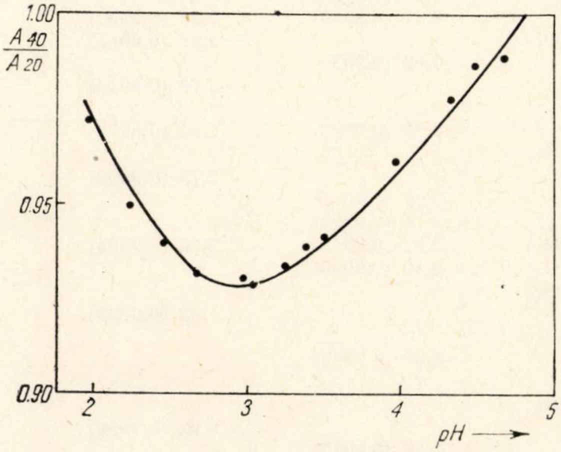

Fig. 1. — Cociente de densidades ópticas (λ = 470 nm) a tiempos 40 y 20 mins frente al pH de trabajo, para *n*-propil amina en medio de ácido acetico.

Al representar los valores de D_{242} en función del pH, se obtuvieron los resultados que refleja la Fig. 2. De ella se desprende la existencia de un mínimo a pH = 3, aunque también se observan diferencias de matiz al comparar los resultados obtenidos en medio acético y en medio propiónico (en este último aparece una rama horizontal a la derecha de la curva, rama que no se ve en medio acético).

D) DISCUSIÓN DE LOS RESULTADOS

Trabajos anteriores (loc. cits.) han puesto de manifiesto que las reacciones entre aminas primarias alifáticas y ácido nitroso parecen transcurrir a través de la formación de complejos intermedios entre especies de distinta carga iónica. Esta idea, en la línea del mecanismo propuesto por Senent y Casado [1] es también coherente con el pensamiento de Sahasrabudhey [2] quien, en el caso de la reacción metil amina/ácido nitroso

---

[9] V. V. Kozlov y B. I. Belov, *Zhur. obshchei. Khim.*, **33**, 1951 (1963)

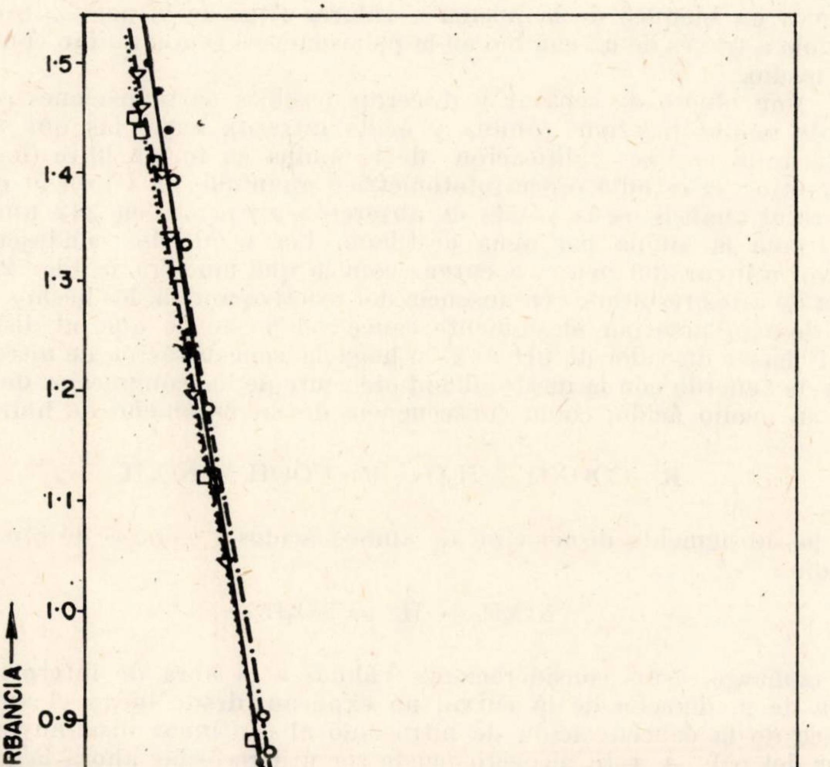

Fig. 2. — Densidad óptica (λ = 242 nm) frente al pH, para todas las aminas investigadas.

observa un bloqueo de la misma a valores altos de la acidez, interpretándolo a través de un cambio en la polaridad del grupo amino con el pH del medio.

Con objeto de separar y discernir posibles participaciones conjuntas de ambos reactivos (amina y ácido nitroso), entre las que merece destacar la posible salificación de la amina en forma libre (loc. cit.) se repitió el estudio espectrofotométrico apuntado en C) en lo que se refiere al análisis de la banda de absorción aparecida en 242 nm, pero sustituida la amina por agua destilada. Los resultados condujeron de nuevo, e invariablemente, a curvas com la que muestra la Fig. 2. A la vista de estos resultados en ausencia del reactivo amina, los hechos pudieran desarrollarse por el siguiente cauce : el hecho de que, al disminuir el pH hasta un valor de pH = 3, lo haga la concentración de nitrosonio, está de acuerdo con la inestabilidad creciente de los compuestos de nitrosilo en medio ácido, como consecuencia de un fenómeno de hidrólisis :

$$\mathrm{R{-}COONO + H_2O \rightleftharpoons R{-}COOH + NO_2H} \qquad (1)$$

con la subsiguiente disociación de ambos ácidos y génesis de ión nitrosacidio :

$$\mathrm{NO_2H + H^+ \rightleftharpoons NO_2H_2^+} \qquad (2)$$

Sin embargo, estas consideraciones válidas a la hora de interpretar la rama de la derecha de la curva, no explican, desde luego el aumento brusco de la concentración de nitrosonio al continuar disminuyendo el valor del pH. A este respecto puede ser útil recordar ahora la investigación de Polydoropoulos y Pipinis[10] quienes, al estudiar la reacción entre ácido nitroso e hiponitroso en disoluciones reguladoras acético/acetato, admiten la formación rápida de sexquióxido de nitrógeno a través del esquema siguiente :

$$\mathrm{NO_2H_2^+ + NO_2^- \rightleftharpoons N_2O_4H_2^*} \qquad (3)$$

$$\mathrm{N_2O_4H_2^* \rightarrow N_2O_3 + H_2O} \qquad (4)$$

Si a esto añadimos que el grupo NO es estraordinariamente versátil en lo que se refiere a su capacidad para perder o ganar electrones[11] (recuerdese que el potencial de ionización del NO es relativamente bajo), podría admitirse que, en disolución :

$$\mathrm{N_2O_3 \rightarrow NO^+ + NO_2^-} \qquad (5)$$

lo cual significaria, en última instancia, la aparición de iones nitrosonio cuya concentración, creciente, iría acompañada de un aumento de la absorbancia a 242 nm, cosa que se ha observado experimentalmente.

Pasemos a considerar la naturaleza del complejo amina / ión positivo. Como se ha indicado, existe una doble vía de formación : amina/nitrosacidio y amino / nitrosonio. La formación del primer tipo se comprende inmediatamente sin más que pensar, por un lado, en el carácter básico de la amina y, por otro, en la aparición del ión nitrosacidio según el proceso que se expresa en la ecuación (2).

---

[10] C. N. Polydoropoulos y M. Pipinis, *Chimika Chronika*, **30** A, 43 (1965).

[11] C. C. Addiso y J. Lewis, *Quart. Rev.*, **9**, 115 (1955).

En cuanto a la segunda posibilidad no supone, esencialmente, un cambio en el mecanismo de formación del complejo intermedio, aunque si resulte conveniente analizar la posible estructura de tal complejo. En efecto, se conoce que la estructura de los haluros de nitrosilo puede considerarse covalente pero con una participación no despreciable de formas iónicas ; así, la distancia X-N en el cloruro de nitrosilo es de 0,195 ± ± 0,001 nm y en el bromuro de nitrosilo de 0,214 ± 0,002 nm, mientras que las respectivas sumas de los radios covalentes normales son 0,171 y 0,184 nm.[12, 13] Estas longitudes de enlace han sido explicadas[14] haciendo intervenir un fenómeno de resonancia entre las formas $X^-N = O^+$ y $X-N = O$. Así mismo el cálculo de momentos dipolares arroja, para las moléculas de cloruro y bromuro de nitrosilo, los valores de $1{,}0.10^{-30}$ y $1{,}5.10^{-30}$ C.m., mientras que las correspondientes magnitudes experimentales son $6.1.10^{-30}$ y $6{,}2.10^{-30}$ C.m. lo que incide de nuevo sobre el importante papel desempeñado por las formas iónicas en tales compuestos de nitrosilo.

Pues bien, si generalizamos cualitativamente las ideas anteriores al acetato y propionato de nitrosilo, resulta lo siguiente : Según se ha visto, a uno y otro lado del mínimo situado a pH = 3 va aumentando la concentración de nitrosonio, ión que, debido a su carga positiva y poco volumen buscará, mediante acercamiento electrófilo, la carga negativa de la amina dando lugar a complejos amina/nitrosonio que, logicamente, se presentan como más estables que los correspondientes amina/nitrosacidio (simples consideraciones estéricas apoyan esta idea que aún podría verse reforzada por la aparición de un enlace de hidrógeno intramolecular). Además, dada la naturaleza semicovalente del enlace que liga al grupo NO con el anión ácido, cabría pensar también que la ligadura del ión nitrosonio con la amina pudiera ser, en cierto modo, covalente (recuerdese la versatilidad del grupo NO) dando lugar a un enlace más fuerte que el aparecido en los complejos amina/nitrosacidio. De este modo, al ir aumentaar la concentración de complejos amina/nitrosonio, deberá disminuir la de los complejos amina/nitrosacidio. Y, como la étapa cinética es la descomposición lenta y monomolecular del complejo intermedio, al disminuir la concentración de los complejos tipo amina/nitrosacidio y aumentaar consiguientemente la de los del tipo amina/nitrosonio, deberá disminuir la velocidad específica de reacción, como realmente se ha observado. Resulta así que puede hablarse, en cierto modo, de un papel inhibidor del ión nitrosonio sobre estas reacciones.

---

[12] J. A. A. Ketelaar y K. J. Palmer, *J. Amer. Chem. Soc.*, **59**, 2629 (1937).

[13] W. G. Burns y H. J. Bernstein, *J. Chem. Phys.*, **18**, 1969 (1950).

[14] J. A. A. Ketelaar, *Rec. Trav. chim.*, **62**, 289 (1943).

Revue Roumaine de Chimie, **20**, *5*, 627 – 632 (1975)

TRANSFORMATION OF THE TOLUENE-WATER MIXTURE IN THE FREQUENCY DISCHARGE PLASMA. II[1]

INFLUENCE OF THE POWER AND RESIDENCE TIME

G. BOURCEANU, V. ABABI, GH. POPA and M. SANDULOVICIU
Laboratory of Chemical Technology, "Al. I. Cuza" University, Jassy, Calea 23 August n° 11, Romania

Received January 3, 1974

In the first part of this paper, working at the same power, we checked whether we had obtained in each case the same products and in the same proportion. We have studied here the influence of the power of the high frequency generator and of the reactants residence time in the discharge zone upon the transformation efficiency of toluene ; we have also studied whether the same products have been obtained for each case under discussion.

The transformation of the organic compounds has been increasingly studied at present, even with high molecules, in plasma of low temperature (luminescence discharge, high frequency, microwaves, etc.).[2, 3]

In all investigations performed until now, optimum conditions were chosen so as to obtain reaction products from reactants that would not react under classical conditions.[4]

EXPERIMENTAL PROCEDURE

The discharge was obtained in a high frequency electromagnetic field using a Jena glass tube with a cross-section of 5.3 cm², the volume of the discharge zone being 530 cm³. We worked at variable powers of the generator, the field frequency being 30 MHz. The reaction mixture toluene-water in a $\simeq 1/1$ molar ratio was in a continuous flow.

The flow rates were measured by means of two silicone oil flowmeters. The pressure of the gaseous mixture in the discharge zone was measured by means of a silicone oil differential manometer. The condensable product under the above mentioned temperature and pressure conditions, was captured in cool traps with liquid nitrogen. With the molar flow we worked, which ranged from 0.058 to 0.21 mol/h we got different residence times varying from 5.04 to 0.72 sec. The residence time was found according to relation[5]

$$t = \frac{PV}{n_0 RT} \tag{1}$$

---

[1] G. Bourceanu, Gh. Popa, M. Sanduloviciu and V. Ababi, *Rev. Roumaine Chim.*, **19**, *2*, 207 (1974).

[2] D. D. Neiswender, *Adv. Chem. Ser.*, **80**, 338 (1969).

[3] S. Pfan and A. Rutscher, *Ann. Phys.*. **25**, 321 (1970).

[4] H. Sabadil and H. Deutsch, "Eleventh International Conference on Phenomena in Ionized Gases", Prague, Czechoslovakia, September, 10–14, 1973.

[5] * * * – "Noţiuni de cinetică chimică", Ed. tehnică, Bucharest, 1963, p. 54.

where P is the working pressure, torr, V is the discharge zone volume, cm^3, n_0 is the number of initial moles/h, and T is the temperature in K of the gaseous mixture in plasma.

The pressure of the gaseous mixture in the discharge zone varied from 3.2 to 2.1 torr.

RESULTS AND DISCUSSION

Reaction products. The mixture made up of the liquid products at normal temperature and pressure obtained from reaction as well as the gaseous mixture in normal conditions have been analysed using the gas chromatography. The chromatograph has a chatarometer as detector. Carbowax 20 M was used as stationary phase and hydrogen was used as carrier-gas. The experiments have been carried out in programmed temperature range from 120 to 220°. On the basis of analytical investigation, benzene, ethylbenzene, benzyl alcohol, phenol, diphenylmethane and diphenylethane were found in the liquid mixture in each case. Ethane, ethylene and acetylene were found in the gaseous mixture. We also found a polymer on the discharge tube. The analysis of the gaseous mixture was carried out in order to see whether the reaction follows the mechanism proposed in the first part.[1] We could not measure what weight proportion of the initial toluene turns into polymers and what proportion turns into gases. On the basis of analyses we could determine how much turned into the liquid products mentioned above. Knowing the initial quantity of toluene and the quantity of liquid products we could draw the conclusions with a view to finding the transformation degree of toluene.

In figure 1 we have drawn the variation of the relative concentration of the liquid products *versus* the residence time in the discharge zone, at a power of the generator of 240 W.

As easily observed at this power of the generator the concentrations of the products obtained from reaction follow the succession : benzene > ethylbenzene >dibenzyl >diphenylmethane >benzyl alcohol >phenol. We can notice that the concentration of each product is not maximum for the minimum flow rate, i.e. 0.058 mol/h, but at this flow rate the highest transformation degree of toluene is obtained, as we can also see in figure 2 where the logarithm of the relative conversion rises with the increase of the residence time, i.e. with the decrease of the flow rate. With the increase of the residence time more electronic-molecular collisions will occur and, consequently, the quantity of transformed toluene will be higher. The fact that the concentration of the liquid products is not maximum at the highest conversion of toluene can be explained as follows :

At the minimum flow rate of 0.058 mol/h the mean free path of the electrons is large which induces in electrons a fairly high energy between two collisions and, consequently, besides the break of the $C-C$ bond from $\gg C-CH_3$ or of the $C-H$ bond from the methyl group, the break of the $C\cdots\cdots C$ bond from the benzenic ring occurs as well. The mean energy of the electrons in plasma measured by means of a triple probe[6] was found to be $\simeq 3.5$ eV, therefore part of the electrons will have the energy to break the 5.1 eV C·····C bond from the benzenic ring.[7, 8] As the flow rate rises the percentage of products rises as well. Thus, the energy

---

[6] Sin-Li Chem and T. Sekiguchi, *J. Appl. Phys.*, **36**, 2363 (1965).

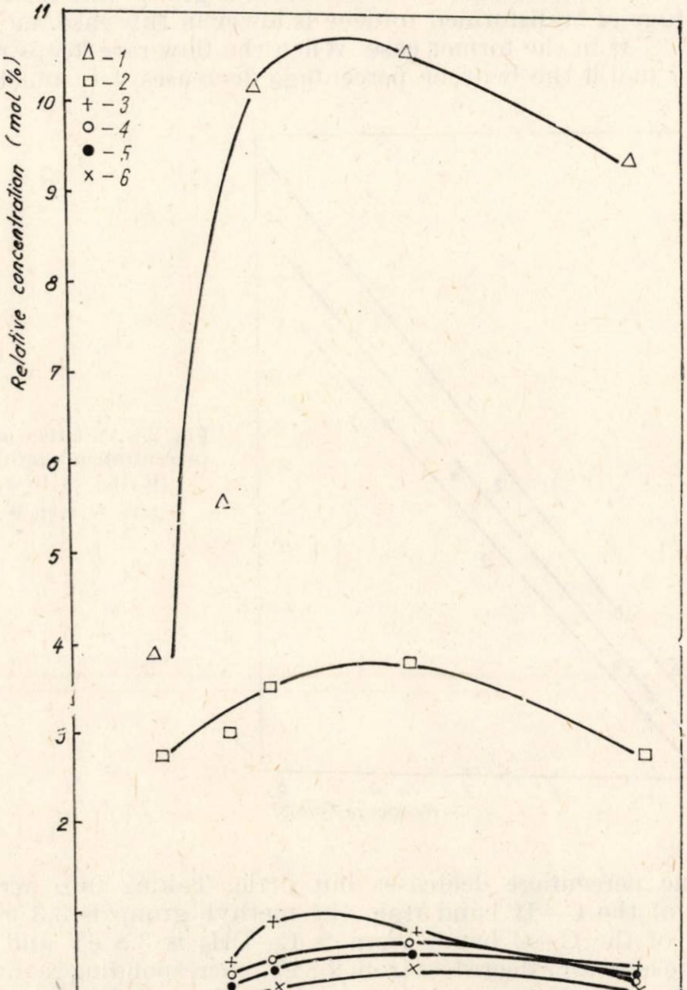

Fig. 1.—Variation of the relative concentration of reaction products as function of the residence time for a 240 Watts generator power. *1*, [Benzene]/[Toluene]$_0$; *2*, [Ethylbenzene] / [Toluene]$_0$; *3*, [Dibenzyl]/[Toluene]$_0$; *4*, [Diphenylmethan] / [Toluene]$_0$; *5*, [Benzyl alcohol] / [Toluene]$_0$; *6*, [Phenol]/[Toluene]$_0$.

---

[7] Lo H. Donald and M. A. Whitehead, *Canad. J. Chem.*, **46**, 2027 (1968).

[8] V. I. Vedeneyev, L. V. Gurvich, V. N. Kondratyev, V. A. Medvedev and Ye. L. Frankevich, "Bond Energies Ionisation Potentials and Electron Affinities", Edward Arnold (Publishers) Ltd., London, 1966, p. 56.

gained by the electrons between two collisions is weaker, of $\simeq 3.1$ eV, found by means of the same method and, thereby, the C$-$C bonds from $\gg$C$-$CH$_3$ and C$-$H bonds from the methyl group will break although the percentage of transformed toluene is lower in this case, i.e. 61% compared to 77% as in the former case. When the flow rate keeps rising, from 0.15 to 0.17 mol/h the benzene percentage decreases very much while the ethylbenzene percentage decreases but little. Taking into account that the energy of the C$-$H bond from the methyl group is 3.3 eV[9,10] while the energy of the C$-$C bonds from $\gg$ C$-$CH$_3$ is 3.8 eV and the mean energy of the electrons decreases from 2.8 eV, corresponding to the 0.15 molh flow rate, to 2.5 eV corresponding to the 0.17 mol/h flow rate, the experimental data are explained in that the proportion in which the C$-$H bond breaks decreases very little whereas the proportion in which the C$-$C bond breaks from $\gg$ C$-$CH$_3$ decreases very much. In favour of this explanation we shall notice that the maximum value of the concentration of diphenylethane corresponds to a flow rate of 0.15 mol/h while the maximum concentration of benzene, diphenylmethane and phenol corresponds to a flow of 0.089 mol/h.

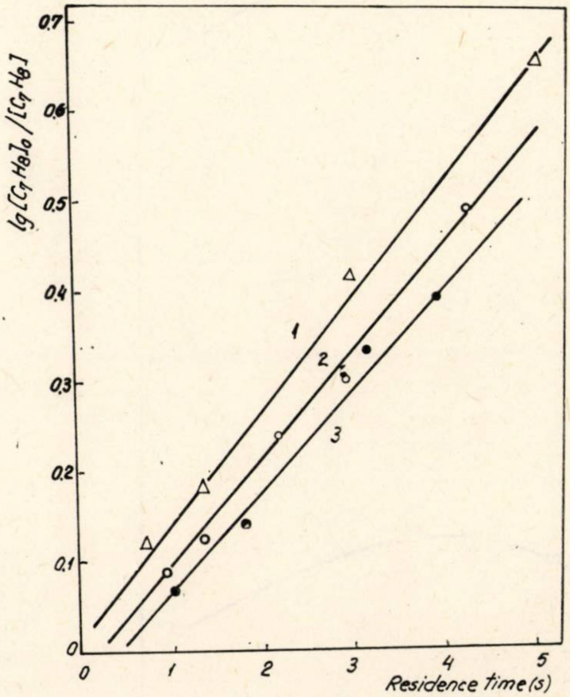

Fig. 2.—Variation of the relative concentration logarithm lg$[C_7H_8]_0$/ /$[C_7H_8]$ as time function.

1, 240 W; *2*, 210 W; *3*, 200 W.

The quantities of phenol and benzyl alcohol obtained from the reaction are small because the mean energy of the electrons in plasma

---

[9] M. Szwan, *J. Chem. Phys.*, **16**, 128 (1948).

[10] D. O. Schissler and D. P. Stevensons, *J. Chem. Phys.*, **22**, 151 (1954).

is in all cases weaker than the energy developed by the H—O bond, when breaking from the water molecule which is 4.7 eV.[11]

The transfer mechanism of the electron energy towards toluene is similar to that considered in the first part of this study.

Rate of disappearance of toluene. From the graphical representation of lg $[C_7H_8]_0/[C_7H_8]$ against residence time, where $[C_7H_8]_0$ and $[C_7H_8]$ are the concentrations of toluene at zero and t time, respectively, we get straight lines for the three generator powers we have worked at. Therefore, we may conclude that the disappearance rate of toluene follows first-order kinetics rather precisely.

The first-order rate expression for the disappearance of toluene may be written as :

$$\frac{-\mathrm{d}[C_7H_8]}{\mathrm{d}t} = k[C_7H_8] \tag{2}$$

where $[C_7H_8]$ is the concentration of toluene at time t, and k is the rate coefficient for the first-order disappearance of toluene.

After integrating equation (2) and introducing common logarithms, we get :

$$\lg \frac{[C_7H_8]_0}{[C_7H_8]} = \frac{k}{2{,}303} t \tag{3}$$

The rate coefficients corresponding to the reaction at various incident powers obtained from figure 2 are listed in table 1.

It is evident, from table 1, that the first-order rate coefficient, k is a function of the incident power, w.

When logarithm of k was plotted against incident power (w), a linear relationship was obtained as shown in figure 3.

In this case, an empirical relationship may be expressed as :

$$k = K. \mathrm{e}^{Aw} \tag{4}$$

Table 1

Rate constant for different generator powers

Incident power (Watts)	Rate constant, k (s^{-1})
200	0.23
210	0.25
240	0.29

where A is the slope and K is equal to exp (intercept in figure 3).

$$\lg k = \lg K + \frac{A}{2.303} w \tag{5}$$

From the graphical presentation it results that

$$K = 0.167\ s^{-1},$$

and

$$A = 6.21 \cdot 10^{-3} w^{-1}$$

---

[11] L. Pauling, "The Nature of Chemical Bond" (3rd edition), Cornell, Ithaca, 1960, p. 262.

therefore, the expression of k becomes

$$k = 0.167 \cdot e^{6.21 \cdot 10^{-3} w}$$

that is, the rate of disappearance of toluene rises exponentially, with power.

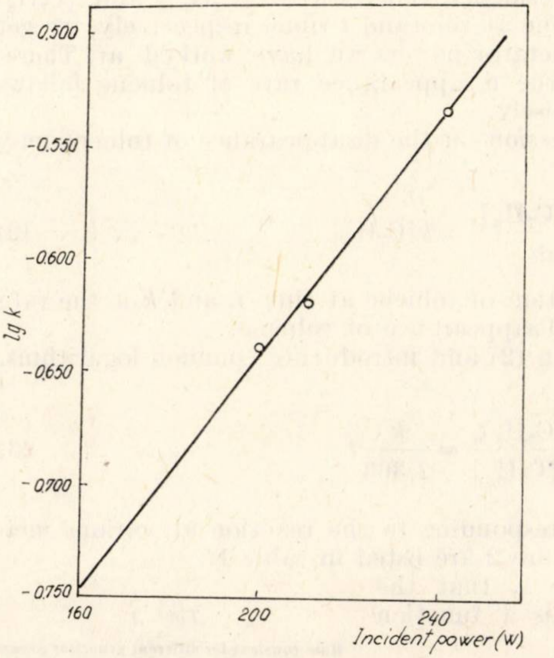

Fig. 3.— Variation of the rate constant logarithm (lg k) as a function of incident power (W).

As the kinetics is of the first-order we can certainly affirm that the electrons play the most important role in the transformation of toluene. This may be also concluded from the rise of the rate of the disappearance of toluene with the generator power since, with its rise both a rise in the energy of the electrons and in their concentration take place.[12]

CONCLUSIONS

Based on the experimental data the following conclusions result :

1. The rate of toluene disappearance rises with the increase in the power of the generator and of the residence time of the reactants in the discharge zone.

2. The electrons have a significant influence on the transformations which take place in high frequency discharge plasma, the proof of this being the fact that the reaction follows a first order kinetics.

3. The change in the working conditions (power or flows) has no influence upon the nature of the products ; it has an influence only upon their proportion in the mixture.

---

[12] I. A. Ivanov, L. S. Polak and D. I. Slovetskii, *Khim. vysokih Energhii*, **5**, 5, 382 (1972).

Revue Roumaine de Chimie, **20**, 5, 633–636 (1975)

NEW COMPLEXONE TYPE LIGANDS. I

meso-2,3-DIAMINOSUCCINIC-N,N′-DIACETIC ACID (DSDA) AND ITS SALTS

E. PETROVICI, C. CSUNDERLIK, A. FERENCZ and C. DRĂGULESCU

Department of Inorganic, General and Analytical Chemistry, Faculty of Industrial Chemistry, Polytechnic Institute of Timişoara, str. Bocşei 6, Romania

Received March 4, 1974

Pure *meso*-2,3-diaminosuccinic-N,N′-diacetic acid has been prepared. Its disodic and tetrasodic salts have been separated. Characterizations by melting point, elementary analysis, ionizable hydrogen titration and IR spectra have been carried out. Impure *meso*-2,3-diaminosuccinic-monoacetic acid has been separated as well.

In search of some ligands able to offer interesting problems of conformation and hence of coordination about a metallic ion and proceeding with our studies on the 2,3-disubstituted derivatives of the succinic acid,[1–3] we dealt with the carboxymethylic derivatives of *meso*-2,3-diaminosuccinic acid.

In 1958 Podgornaia and Postovskii[4] reported the preparation of 2,3-diaminosuccinic-N,N,N′,N′-tetraacetic acid,

$$(HOOCH_2C)N-CHCOOH-CHCOOH-N(CH_2COOH)_2$$

by condensation of diaminosuccinic acid with chloroacetic acid under alkaline conditions. No data are given about the separation of *meso*- and *d, l*-stereoisomers, or for the characterization of the free acid. Our studies concerning these substances are since about the same period. But we first focused our attention to obtain and characterize the pure *meso*- and *d, l*-diastereoisomers of 2,3-diaminosuccinic acid,[2] respectively to point out the influence of ligand configuration on the complexing properties of the *meso*- and *d, l*-2, 3-diaminosuccinic acids.[3] Our attempts in condensing the *meso*- and *d, l*-2,3-diaminosuccinic acids with chloro-

---

[1] E. Petrovici, A. Ferencz and C. Drăgulescu, unpublished data, reported at the Third Republican Conference on Chemistry Timişoara, *Abstracts*, **1966**, 52.

[2] E. Petrovici, A. Ferencz, M. Bîrzescu and C. Drăgănescu, *Buletinul Ştiinific şi Tehnic al Institutului Politehnic Timişoara*, **14**, 111 (1969).

[3] E. Petrovici, A. Ferencz and C. Drăgănescu, *Rev. Roumaine Chim.*, **16**, 663 (1971).

[4] I. V. Podgornaia and I. Ia. Postovskii, "Komplexony. Synthez, svoistova, primenenie v biol. i med.", Sverdlovsk, 1958, p. 32–39.

and iodoactic acid, did not lead to 2,3-diaminosuccinic-N,N,N′,N′-tetraacetic acid. As a first step in getting the N,N′-carboxymethyl derivatives of the diaminosuccinic acid, pure *meso*-2,3-diaminosuccinic-N, N′-diacetic acid (DSDA) has been obtained.

EXPERIMENTAL

DSDA has been obtained by the condensation of *meso*-2,3-diaminosuccinic acid (purified by repeated recrystallization at $pH = 2^2$) with chloroacetic and iodoacetic acids in alkaline solution following the Michaelis and Schubert[5] method. We have obtained DSDA also by a variant of the Strecker method suggested by Bersworth *et al.*[6] for the direct synthesis of ethylenediaminetetraacetic acid from ethylenediamine, formaldehyde and potassium cyanide in alkaline solutions.

Disodic salt and pure acid have been separated. Purification was obtained through repeated recrystallization from water. In order to characterize the acid, its tetrasodic salt was separated as well. Characterizations were made by melting point, elementary analysis, ionizable hydrogen titration and IR spectra.

The infrared spectra were recorded in KBr disks, employing a Carl-Zeiss UR 10 infrared spectrophotometer. For acidity titration a precision pH-meter MV 85 CLAMANN & GRAHNERT Dersda was used, with a glass electrode and Ag/AgCl, Cl^- as a reference electrode.

meso-2,3-diaminosuccinic-monoacetic acid (DSMA), impurified with diacetic acid, has also been separated.

Synthesis of *d*, *l*-2, 3-diaminosuccinic-N,N,N′,N′-tetraacetic acid, -N,N′-diacetic respectively, was attempted too. However, their great solubility in water makes it difficult to obtain them in pure state.

RESULTS AND DISCUSSIONS

DSDA : white rhombohedral crystals (from water), m.p. 202—213°C decomp. (warming rate 4—5°/min). *Found* for DSDA : C 36.6 ; H 4.8 ; N 10.5 ; 3COOH (titrable) 50.5 ; equiv. wt. (by titration) 89.4. *Calcd.* for $C_8H_{12}N_2O_8$: C 36.4 ; H 4.5 ; N 10.6 ; 3COOH 51.1 ; equiv. wt. 88.

$Na_2DSDA.2H_2O$: white prisms (from water), m.p. 219—223°C decomp (warming rate 4—5°/min). *Found* for $Na_2DSDA.2H_2O$: C 27.3 ; H 4.2 ; N 8.5 ; 1 COOH (titrable) 13.1 ; Na 13.0 ; equiv wt. (by titration) 342.1. *Calcd.* for $C_8H_{10}N_2O_8Va_2.\ 2H_2O$: C 27.9 ; H 4.1 ; N 8.1 ; 1 COOH 13.1 ; Na 13.4 ; equiv. wt. 344.

Found for DSMA : N 12.8 ; 1 COOH 19.0 ; 2COOH (titrable) 39.7. $C_2H_{10}N_2O_6$ requires : N 13.6 ; 1 COOH 21.8 ; 2 COOH 43.7.

It is quite clear that the monoacetic product is impurified with the diacetic one. Their separation by differences in solubility, or by precipitation at different pH values could not be carried out.

Frequencies of characteristic IR absorption bands (in cm^{-1}) for DSDA, $Na_2DSDA.2H_2O$ and $Na_4DSDA.nH_2O$ and their assignments are given below [7-9] :

---

[5] L. Michaelis and M. P. Schubert, *J. Biol. Chem.*, **106**, 331 (1934).

[6] R. Smith, J. L. Bullock, F. C. Bersworth and A. E. Martell, *J. Org. Chem.*, **14**, 355 (1949).

[7] N. B. Colthup, L. H. Daly and S. E. Wiberley, "Introduction to Infrared and Raman Spectroscopy", Academic Press, New York and London, 1964, p. 258.

[8] D. T. Sawyer and P. J. Paulsen, *J. Amer. Chem. Soc.*, **80**, 1597 (1958).

[9] S. Laitinen and T. Nortia, *Suomen Kem. B*, **43**, 61 (1970).

	H_4DSDA	$Na_2H_2DSDA.2H_2O$	$Na_4DSDA.nH_2O$
$\nu(OH)$ in H_2O		3465 i b	3420 m b
$\nu(NH)$			3300 m sh
$\nu_a(CH, CH_2)$	2965 m	3015 m	2945 w
		2990 m	2910 w
$\nu s_s(NH_2^+)$	3045 m	3115 i b	
	2850 i sh b	2830 m sh	
$\nu(OH)$ in COOH	2820 i b		
	2740 i sh b		
$\nu(NH_2^+)$ (combination band)	2550 m		
$\nu(C=O)$ in COOH	1735 i		
$\nu_a(C=O)$ in COO^-	1630 i	1660 i	1580 i
		1630 i sh	
$\delta(HOH)$		1640 i sh	1630 i sh (?)
$\delta_a(NH_2^+)$	1560 i	1525 i	
$\delta(OH)$ in COOH	1490 i		
$\delta_a(CH_2)$	1450 i sh	1430 i sh	1450 i sh
$\nu_s(C=O)$ in COO^-	1428 i	1425 i	1430 i sh
	1400 i	1410 i	1405 i
$\delta_s(NH_2^+)$	1370 i	1380 i	
$\rho_w(CH_2)$	1350 i sh	1350 i	1320 m sh
		1330 i	1305 m
$\delta_t(CH_2)$	1278 i	1270 m	1255 w sh (?)
	1260 i sh	1250 m	
$\nu(C=O)$ in COOH	1240 i		
$\nu(CN)$	1210 i	1205 i	1215 w sh (?)
$\delta(COO^-)$	995 w	995 w	950 w sh
	945 w	948 w	
$\delta_r(CH_2)$	770 w	780 m	780 w
$\gamma(C=O)$ in COO^-	655 m	677 m	670 w
		650 m	660 w sh
		625 m	

(i — intensive; m — medium; w — weak; sh — shoulder; b — broad)

On the basis of these data, we suppose that the above mentioned compounds exist in the form of :

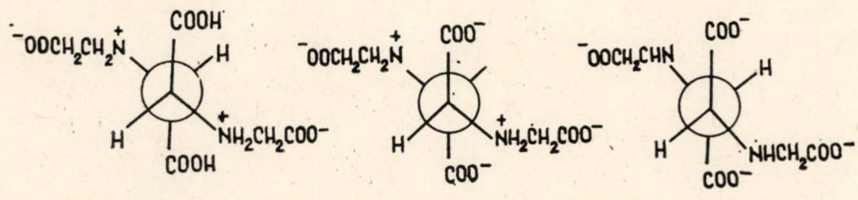

H_4DSDA (localization of nonionized COOH being unsure) Na_2H_2DSDA Na_4DSDA

We consider that our attempt to obtain the *meso*-2,3-diaminosuccinic-N,N,N′,N′-tetraacetic acid by the methods used was not successful as the loss of a proton from the nitrogen atom does not take place even during the substitution in strongly alkaline medium. This behaviour can be accounted for by intramolecular hydrogen bonds established between NH groups and the succinic carboxyl groups :

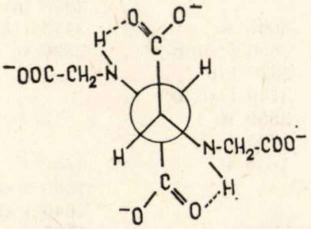

No such steric effect takes place in the case of *meso-* and *d, l*-2, 3-diaminobutane-N,N,N′,N′-tetraacetic acid obtained from 2,3-diaminobutane where four carboxymethyl groups can be introduced easily enough.[10,11] It is possible that this impediment could be eliminated using another way of synthesis. These problems are going to be studied in our further investigations.

---

[10] R. Belcher, W. Hoyle and T. S. West, *Talanta*, **3**, 201 (1959).
[11] H. M. N. H. Irving and R. Parkins, *J. Inorg. Nuclear Chem.*, **28**, 1629 (1966).

Revue Roumaine de Chimie, 20, 5, 637–641 (1975)

REACTION OF ACETYLENES WITH TRANSITION METALS. V[1]

β-CLEAVAGE IN σ,π-ALKYL-PALLADIUM COMPLEXES

ELIZA AVRAM, I. G. DINULESCU, F. CHIRALEU, ELVIRA ŞLIAM
and MARGARET AVRAM

Institute of Organic Chemistry, Splaiul Independenţei 202 B, Bucharest, Romania

Received July 25, 1974

Treatment of complex 1 with hydrochloric acid yields chloride 4. The reactions and the mechanism of formation of chloride 4 are described.

The σ,π-alkyl-palladium structure of the complex obtained from 2,5,5-trimethyl-hex-3-in-2-ol and bis-benzonitrile·$PdCl_2$ has been recently established.[1] Previous works [2] have shown that reductive decomposition with hydride of this complex yields 4,4,6-trimethyl-1,3-di-t-butyl-5,6-dihydro-*4H*-cyclopenta [*c*] furan (**2**), while on treatment with carbon monoxide,[1] ester **3** is formed.

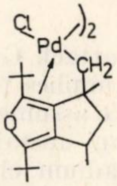

1

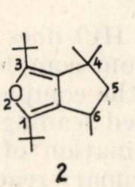

2

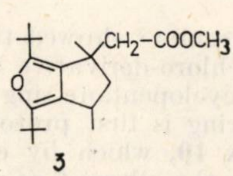

3

Our interest in this field led us to investigate the behaviour of σ,π-Pd-C complex **1** towards acids. The present paper reports these results.

By introducing gaseous hydrogen chloride into a methylene chloride solution of complex **1** and working up the mixture after 1–2 hrs stay at room temperature, a colourless oil was obtained which could not be purified; its elemental analysis corresponded to the formula $C_{18}H_{31}OCl$ (A). The NMR spectrum of the raw product A indicated the presence of a major product, to which the structure of chloro-dimethyl-butyl-furan **4** was ascribed.

---

[1] Part IV. M. Avram, E. Avram, F. Chiraleu and C.D. Nenitzescu, *Chem. Ber.*, in press.

[2] M. Avram, E. Avram, I. G. Dinulescu, N. Ştefan, F. Chiraleu, M. Elian and C.D. Nenitzescu, *Chem. Ber.*, **105**, 2375 (1972).

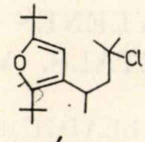

4

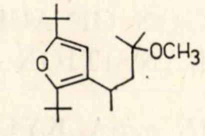

5

Heating the raw product A with a solution of potassium hydroxide in methanol led to a methoxy-derivative **5** together with a mixture of alkenes from which, by means of v.p.c., **6**, **7** and **8** were separated and identified

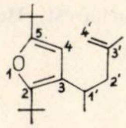

6

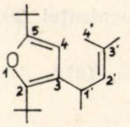

7

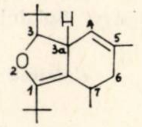

8

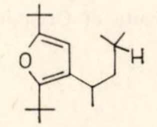

9

A mixture of alkenes **6**–**8** was also formed by the chromatography on basic alumina of the raw chloride A.

The alkenes **6** and **7** gave on hydrogenation the same saturated compound **9**.

It was noticed that on prolonged standing (24 or 48 hrs) the methylene chloride solution of complex **1** saturated with hydrogen chloride afforded cyclopentafuran **2** as the main reaction product, together with variable amounts of chloride **4** and alkenes **6** and **7**.

DISCUSSION

MECHANISM

Recent results[3] showed that HCl does not attack C-Pd bond. The formation of chloro-derivative **4** from complex **1** implies the cleavage of a bond in the cyclopentane ring of the complex. We assume that the complexed furan ring is first protonated leading to an unstable σ,π-alkyl$\cdot$PdCl$_2$ complex **10**, which by elimination of palladium chloride and β-cleavage yields the alkene **6** as a primary reaction product.

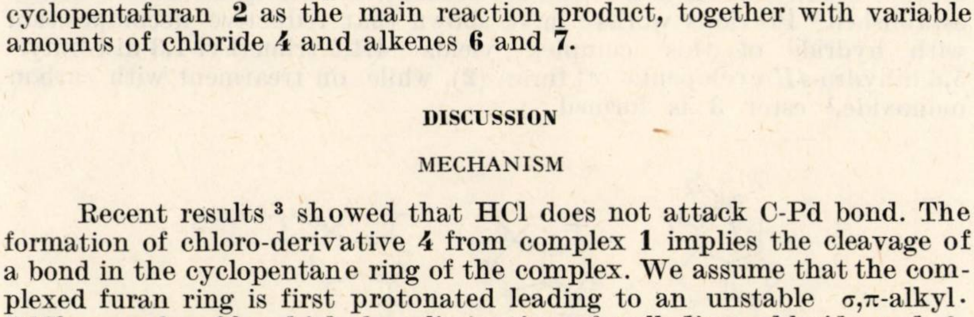

10

6

---

[3] T. Hosokawa and P. M. Maitlis, *J. Amer. Chem. Soc.*, 94, 3238 (1972).

β-Cleavage in σ,π-alkyl-palladium complexes has been observed by Maitilis [4] in other cases and seems to be a characteristic reaction of these compounds.

In the next step of the reaction, alkene **6** in the presence of excess $HCl/PdCl_2$ undergoes HCl addition to the methylene bond yielding, through cation **11**, the chloride **4** which was actually isolated in the experiments with a short reaction time.

It is probable that chloride **12**, precursor of the alkene **8** experimentally isolated after elimination, arises from **6** by a less favourable parallel reaction. Protonation of the furan ring gives rise to a conjugated cation **13** (very similar to that previously observed [2] on dissolving cyclopentafuran **2** in trifluoroacetic acid). This cation acts as an electrophilic reagent towards the double bond in the dimethylbutenyl chain, giving rise to the cyclic cation **14**. The latter may subsequently yield chloride **12**, or, by proton elimination the alkene **8**.

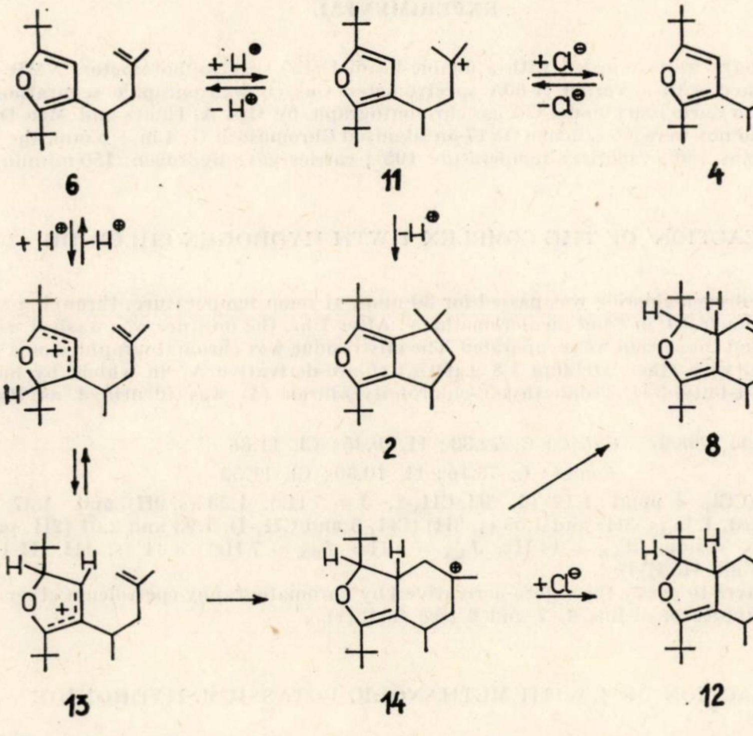

Formation of cyclopentafuran **2** at a longer reaction time represents in fact an intramolecular alkylation of the furan ring in cation **11**. The latter results by ionization of the tertiary chloride atom in chloride **4**, isolated at shorter reaction time.

---

[4] P. M. MAITLIS, „The Organic Chemistry of Palladium'', Vol. 1, Academic Press, New York, 1971, p. 93.

In order to substantiate the above mechanism, chloride **4** was treated with $AlCl_3$ in methylene chloride. After 12 hrs, at room temperature, cyclopentafuran **2** was quantitatively isolated. The same result was obtained by treating the mixture of alkenes **6** and **7** with $AlCl_3$.

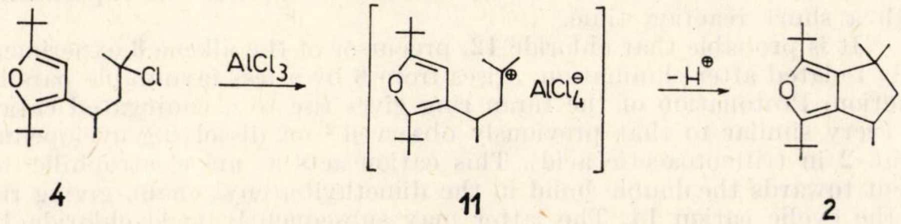

EXPERIMENTAL

IR spectra were recorded with a double-beam UR20 spectrophotometer. NMR spectra were determined with a Varian A-60A spectrometer. Gas chromatographic separations were carried out on a Carlo Erba model GV gas chromatograph, by Mrs. A. Haneş and Miss D. Georgescu. The columns were 5 % silicone OV17 on silanized Chromosorb G, 4 m × 5 mm, the column temperature was 130°, vaporizer temperature 195°; carrier gas: hydrogen, 150 ml/min.

REACTION OF THE COMPLEX 1 WTH HYDROGEN CHLORIDE

Dry hydrogen chloride was passed for 30 min., at room temperature, through a solution of 2.7 g (6.6 mmoles) **1** in 20 ml dichloromethane. After 1 hr, the mixture was washed with cold water, dried and the solvent was evaporated. The oily residue was chromatographied on a column of 1 cm Al_2O_3 with ether, yielding 1.8 g (90 %) chloro-derivative A, in which, by means of NMR, 2,5-di-t-butyl-3-(1′,3′-dimethyl-3′-chlorobutyl)-furan (**4**) was identified as the main product.

$C_{18}H_{31}clo$ (298.9) *Calcd.*: C, 72.33; H, 10.45; Cl, 11.86
Found: C, 73.16; H, 10.50; Cl, 11.52

NMR (CCl_4, δ, ppm): 1.17 (d, 3H, CH_3-1, J = 7 Hz), 1.23 (s, 9H) and 1.37 (s, 9H) (t-butyl groups), 1.43 (s, 3H) and 1.55 (s, 3H) (CH_3-3 and CH_3-4), 1.93 and 2.01 (2H, part AB from an ABX system, $J_{AB} = 14$ Hz, $J_{AX} = 5$ Hz, $J_{BX} = 7$ Hz), 3.34 (s, 1H, H-1′) and 5.63 (s, 1 olefinic H, H-4).

Tentatives to purify the chloro-derivative **4** by chromatography (petroleum ether, Al_2O_3) afforded a mixture of olefins **6**, **7** and **8** (see further).

REACTION OF 4 WITH METHANOLIC POTASSIUM HYDROXIDE

A solution of 4.0 g (71 mmoles) potassium hydroxide in 1 ml water and 20 ml methanol and 1.6 g (5.4 mmoles) chloro-derivative A was refluxed for 9 hours. Water was added, the product was extracted with dichloromethane and the organic layer washed with water. After drying and evaporation of the solvent, the liquid residue (1.3 g) was chromatographied on aluminimum oxide column and eluted with petroleum ether.

From the first runs a mixture (0.90 g, 64 %) of olefins **6**, **7** and **8** was obtained.

From the last runs 0.1 g (6.3 %) *2,5-di-t-butyl-3-(1′,3′-dimethyl-3′-methoxybutyl)-furan* (**5**) was obtained.

$C_{19}H_{34}O_2$ (294.5) *Calcd.*: C, 77.50; H, 11.64
Found: C, 77.27; H, 11.80

NMR (CCl_4, δ, ppm) : 1.02 (s, 3H), 1.08 (s, 3H) (CH_3-3′ and CH_3-4′), 1.11 (d, 3H, CH_3-1′), 1.21 (s, 9H) and 1.31 (s, 9H) (t-butyl groups), 1.63 (m, 2H, CH_2-2′), 3.16 (s, 1H, H-1′), 3.08 (s, 3H, OCH_3-3′), 5.65 (s, 1H, H-4).

The separation of the three olefins (from the first fraction) was carried out by preparative gas-chromatography.

2,5-Di-t-butyl-3-(1′,3′-dimethyl-but-3′-enyl)-furan (**6**), colourless oil.

$C_{18}H_{30}O$ (262.4) *Calcd.* : C, 82.38 ; H, 11.52
Found : C, 82.57 ; H, 11.57

NMR (CCl_4, δ, ppm) : 1.06 (d, 3H, CH_3-1′, J = 6.5 Hz), 1.22 (s, 9H) and 1.30 (s, 9H) (t-butyl groups), 1.68 (broad s, 3H, CH_3-3′), 1.90–2.35 (m, 2H from 2′), 3.08 (m, 1H, H-1′, $J_{1'.CH_3} = 6.5$ Hz, $J_{1'.2'} = 5.5$ Hz, $J_{1'.2'} = 8.5$ Hz), 4.67 (broad s, 2H, $=CH_2$ from 4′), 5.66, (s, 1H, H-4).

IR (CCl_4, cm^{-1}) : 1648 w, 1605 w, 1569 w, 1475 m, 1460 m, 1390 m, 1373 m.

2,5-Di-t-butyl-3-(1′,3′-dimethyl-but-2′-enyl)-furan (**7**), colourless oil.

$C_{18}H_{30}O$ (262.4) *Calcd.* : C, 82.38 ; H, 11.52
Found : C, 82.04 ; H, 11.76

NMR (CCl_4, δ, ppm) : 1.12 (d, 3H, CH_3-1′, $J_{1'.CH_3} = 7$ Hz), 1.24 (s, 9H) and 1.31 (s, 9H) (t-butyl groups), 1.65 (broad s, 6H, CH_3-3′ and CH_3-4′), 3.74 (quintet, 1H, H-1′, $J_{1'.2'} = 9.5$ Hz, $J_{1'.CH_3} = 7$ Hz), 5.20 (d, 1H, H-2′, $J_{1'.2'} = 9.5$ Hz, $J_{2'.CH_3\text{-}3'}$ and $J_{2'.CH_3\text{-}4'} < 1$ Hz), 5.69 (s, 1H, H-4).

IR (CCl_4, cm^{-1}) : 1668 w, 1602 w, 1570 w, 1475 m, 1458 m, 1390 i, 1372 m, 1360 m.

5,7-Dimethyl-1,3-di-t-butyl-3,3a,6,7-tetrahydrociclohexa[c]furan (**8**), colourless oil.

$C_{18}H_{30}O$ (262.4) *Calcd.* : C, 82.38 ; H, 11.52
Found : C, 82.32 ; H, 11.69

NMR (CCl_4, δ, ppm) : 0.87 (s, 9H, t-butyl-3), 1.16 (s, 9H, t-butyl-1), 1.04 (d, 3H, CH_3-7, J = 7 Hz), 1.64 (broad s, 3H, CH_3-5), 1.90 (broad d, 2H, H-6), 2.80 (quintet, 1H, H-7), 3.16 (very broad, 1H, H-3a), 3.55 (d, 1H, H-3, J = 6.5 Hz), 5.25 (very broad, 1H, H-4, J = 4.5 Hz).

IR (CCl_4, cm^{-1}) : 1677 m, 3090 w.

2,5-DI-t-BUTYL-3-(1′,3′-DIMETHYLBUTYL)-FURAN (**9**).

A solution of 0.47 g (1.8 mmoles) mixture of olefins **6** and **7** was treated with hydrogen in the presence of Pd/C. After working up, 0.235 g (49 %) practically pure **9** was obtained, which was further purified to a colourless oil, by preparative gas-chromatography.

$C_{18}H_{32}O$ (264.5) *Calcd.* : C, 81.75 ; H, 12.20
Found : C, 81.81 ; H, 12.42

NMR (CCl_4, δ, ppm) : 0.87 (d, 6H, CH_3-3′ and CH_3-4′), 1.06 (d, 3H, CH_3-1′), 1.22 (s, 9H) and 1.31 (s, 9H) (t-butyl groups), 1.20–1.75 (m, 3H, 2H-2′ and 1H-3′), 2.95 (sextet, 1H, H-1′), 5.61 (s, 1H, H-4).

IR (CCl_4, cm^{-1}) : 1577 w, 1466 m, 1381 w, 1362 m.

REACTION OF CHLORO-DERIVATIVE 4 WITH ALUMINIUM CHLORIDE

Into a solution of 0.60 g (2 mmoles) **4** in 20 ml dichloromethane, 0.4 g (3 mmoles) anhydrous aluminium chloride were added, and the mixture was left at room temperature. After 24 hours water was added and the organic layer washed until neutral. After drying and evaporation of the solvent, cyclopentafuran **2** was obtained in practically quantitative yield. (IR and NMR spectra were identical with those of an authentic sample).

REACTION OF OLEFINS 6 AND 7 WITH ALUMINIUM CHLORIDE

A solution of 0.50 g (2 mmoles) mixture of olefins **6** and **7** in 20 ml dichloromethane was treated with 0.4 g (3 mmoles) moist aluminium chloride, and the mixture was left at room temperature. After working up, cyclopentafuran **2** was obtained (identified by comparison with an authentic sample).

Revue Roumaine de Chimie, **20**, *5*, 643–649 (1975)

FORMATION AND BEHAVIOUR OF 4-OXAZOLIDONES. XII[1]

AN ADVANTAGEOUS METHOD FOR OBTAINING 2,5-DIARYLOXAZOLES

CLARA MAKKAY, LEONTINA HIDIŞAN-TĂUŢEAN and MARIA IONESCU
Faculty of Chemistry, Babeş-Bolyai University, str. Arany János 11, Cluj-Napoca, Romania

Received December 10, 1973

Isonitrosoacetophenone was condensed at 0° under the action of gaseous hydrochloric acid, with benzaldehyde, *o*-, *m*-, *p*-chloro-benzaldehyde and *o*-, *m*-, *p*-nitrobenzaldehyde, obtaining the hydrochloride of the corresponding oxazole N-oxides (I, IV, V, VI, VII, VIII, IX). Hydrochlorides turn into free N→O by aqueous hydrolysis (II, X, XI, XII, XIII, XIV, XV). The N-oxide of 2,5-diphenyloxazole, of 2-(*o*-, *m*-, *p*-chlorophenyl)-5 phenyloxazoles is reduced by metallic zinc in glacial acetic acid to the corresponding 2,5-disubstituted oxazoles (III, XVI, XVII, XVIII). The selective reduction of 2-(*o*-, *m*-, *p*-nitrophenyl)-5-phenyloxazole-N-oxides to the corresponding oxazoles (XXI, XXII, XXIII) is achieved with PCl_3 by boiling in chloroform solution. The structure of these substances was elucidated by means of the elemental analysis, the analysis of IR vibration spectra and also by identification with substances obtained through condensation of corresponding aldehydes with benzaldehyde cyanohydrin. *o*- and *p*-chlorobenzaldehydes also form oxazolidones XIX, XX during this condensation process.

The synthesis of 2,5-diaryloxazoles using benzaldehyde-cyanohydrin as a basic component [2-4] presents a series of drawbacks and this prompted us to resort to the Allan et al.[5] method for the preparation of these oxazoles.

By condensing at 0° in an anhydrous medium isonitrosoacetophenone [6] with benzaldehyde in the presence of gaseous hydrochloric acid we obtained 2,5-diphenyloxazole-N-oxide hydrochloride with a maximum yield; this passes into free N-oxide (II) through alcohol-aqueous hydrolysis. By heating with zinc in glacial acetc acid, the latter is quantitatively reduced to 2,5-diphenyloxazole (III):

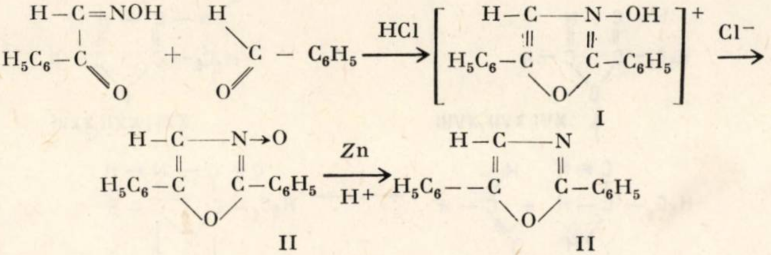

---

[1] C. Makkay, M. Nagy and M. Ionescu, *Stud. Univ. Babeş-Bolyai, Chem.*, **1974** (in print).

[2] M. Ionescu and C. Makkay, *Stud. Univ. Babeş-Bolyai, Chem.*, (fasc. 1) **1963**, 115.

[3] E. Fischer, *Ber. dtsch. chem. Ges.*, **29**, 205 (1896).

[4] S. Minovici, *Ber. dtsch. chem. Ges.*, **29**, 2097 (1896).

[5] A. W. Allan and B. H. Walter, *J. Chem. Soc. C.*, **1968**, 1397.

[6] L. Claisen, *Ber. dtsch. chem. Ges.*, **20**, 656 (1887).

Therefore isonitrosoacetophenone has an undeniable advantage over benzaldehyde-cyanohydrin in oxazole synthesis, i.e. no variable amounts of oxazolidones-4 will occur as by-product dependent on the working conditions.[2–4]

Condensation of isonitrosoacetophenone with *o*-, *m*-, *p*-chloro- and *o*-, *m*-, *p*-nitrobenzaldehyde, respectively, under analogous conditions also takes place with a good yield leading to N-oxide hydrochlorides (IV, V, VI, VII, VIII, IX) which hydrolyse in a basic medium (ethyl alcohol-diluted sol. of Na_2CO_3) into free N-oxides (X, XI, XII, XIII, XIV, XV).

The N-oxides of 2-(*o*-, *m*-, *p*-chlorophenyl)-5-phenyloxazole are reduced to the corresponding oxazoles (XVI, XVII, XVIII) by boiling with metallic zinc in glacial acetic acid. To identify these oxazoles, *o*-, *m*-, *p*-chlorobenzaldehydes were also condensed with benzaldehyde-cyanohydrin at 0° in gaseous hydrochloric acid yielding the same oxazoles (XVI, XVII, XVIII) alongside with oxazolidones (XIX and XX). We mention that 2-(*m*-chlorophenyl)-5-phenyloxazolidone has not been obtained under such conditions.

In order to avoid reduction of nitro functions, the N-oxides of 2-(*o*-, *m*-, *p*-nitrophenyl)-5-phenyloxazole (XIII, XIV, XV) were reduced by heating with PCl_3 in chloroform, to 2-(*o*-, *m*-, *p*-nitrophenyl)-5-phenyloxazoles (XXI, XXII, XXIII), identical with those prepared by condensation of nitrobenzaldehydes with benzaldehyde-cyanohydrin [2]

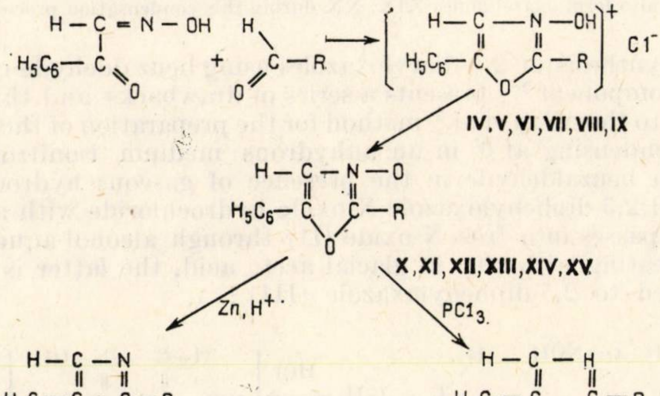

R = IV, X, XVI, XIX : o-C_6H_4Cl
V, XI, XVII : m-C_6H_4Cl
VI, XII, XVIII, XX : p-C_6H_4Cl

VII, XIII, XXI : $o\text{-}C_6H_4NO_2$
VIII, XIV, XXII : $m\text{-}C_6H_4NO_2$
IX, XV, XXIII : $p\text{-}C_6H_4NO_2$

In order to elucidate the structure of these substances and particularly the binding of hydrochloric acid in the molecule of hydrochloride-N-oxides of 2,5-disubstituted oxazoles, we studied the vibration spectra of these substances. IR spectra were recorded on a UR-20 (Zeiss Jena) model double beam spectrophotometer on solid state substances under the form of KBr pellets. Results of IR vibration spectra analyses are listed in table 1.

Table 1

Results of IR vibration spectra analyses

Substance	$\nu N^+ -OH$	$\nu N\rightarrow O$	νN^+	Disubst. benzene	Ether bond	Mono-subst. benzene	νHalogen	νNO_2	
								sym.	assym.
2,5-diphenyloxazole-hydrochloride N→O I.	3078	1270	1420–1640	—	1020	780	—	—	—
2,5-diphenyloxazole N→O II.	—	1255 1295	1408 1442	—	1020	780	—	—	—
2,5-diphenyloxazole III.	—	—	—	—	1020	772	—	—	—
2-(*o*-chlorophenyl)-5-phenyloxazole-hydrochloride N→O IV.	3070	1200	1580 1600	830	1020	730	790	—	—
2-(*o*-chlorophenyl)-5-phenyloxazole N→O X.	—	1220	1580–1602 1634	828	1020	732	790	—	—
2-(*o*-chlorophenyl)-5-phenyloxazole XVI.	—	—	—	828	1020	730	790	—	—
2-(*m*-chlorophenyl)-5-phenyloxazole hydrochloride N→O V.	3060–64	1192 1210	1580–1660	828	1023	728	842	—	—
2-(*m*-chlorophenyl)-5-phenyloxazole N→O XI.	—	1140 1160	1590 1620	828	1020	725	838	—	—
2-(*m*-chlorophenyl)-5-phenyloxazole XVII.	—	—	—	810	1022	728	838	—	—

Table 1 *(continued)*

Substance	νN+–OH	νN→O	νN+	Disubst. benzene	Ether bond	Mono-subst. benzene	νHalogen	ν NO_2	
								sym.	assym.
2-(*p*-chlorophenyl)-5-phenyloxazole-hydrochloride N→O VI.	3062	1180	1600–60	818	1020	732	840	—	—
2-(*p*-chlorophenyl)-5-phenyloxazole N→O XII.	—	1180	1600–50	815	1030	732	840	—	—
2-(*p*-chlorophenyl)-5-phenyloxazole XVIII.	—	—	—	828	1020	738	840	—	—
2-(*o*-nitrophenyl)-5-phenyloxazole hydrochloride N→O VII.	3067	1200	1460 1490	854	1023	740	—	1360	1538
2-(*o*-nitrophenyl)-5-phenyloxazole N→O XIII.	—	1208	1528	860	1020	740	—	1360	1538
2-(*o*-nitrophenyl)-5-phenyloxazole XXI.	—	—	—	860	1025	740	—	1375	1545
2-(*m*-nitrophenyl)-5-phenyloxazole hydrochloride N→O VIII.	3045	1200	1490	828	1020	735	—	1350	1545
2-(*m*-nitrophenyl)-5-phenyloxazole N→O XIV.	—	1200	1480	822	1020	740	—	1350	1542
2-(*m*-nitrophenyl)-5-phenyloxazole XXII.	—	—	—	820	1025	738	—	1355	1525
2-(*p*-nitrophenyl)-5-phenyloxazole hydrochloride N→O IX.	3040	1200	1458	858	1020	720	—	1348	1530
2-(*p*-nitrophenyl)-5-phenyloxazole N→O XV.	—	1200	1458	858	1020	720	—	1340	1528
2-(*p*-nitrophenyl)-5-phenyloxazole XXIII.	—	—	—	860	1020	722	—	1345	1525

It results from the table that all hydrochlorides show a strong absorption between 3070–3040 cm^{-1} which is absent with N-oxides and oxazoles and this is indicative of the fact that this absorption is due to the N^+- $-$ OH bond.

At the same time, IR spectra indicate absorption vibrations for $N \rightarrow O$ bonds and also for $-\underset{|}{N}=^{+}$ which proves that the proton belongs to the oxygen coordinately bound to the heterocyclic nitrogen and no oxonium salt is formed with the heterocyclic oxygen.

Evidence in support of this fact are the characteristic vibrations obtained for the ether group in the 1020 – 1023 cm^{-1} range.

IR spectra indicate the vibrations characteristic of the monosubstituted benzen (phenyl attached to C_5 of the heterocycle) at 720 – – 780 cm^{-1} and also of disubstituted benzene (substituted phenyl attached to C_2 of the heterocycle) in the 810 – 860 cm^{-1} range as well as of the respective halogen group NO_2 attached to the benzene nucleus bound to C_2 of the oxazole heterocycle.

EXPERIMENTAL

1. 2,5-diphenyloxazole N-oxide-hydrochloride I. 2 g isonitrosoacetophenone and 1.6 g benzaldehyde (1.5 ml) are dissolved in 50 ml anhydrous ether. Dry gaseous hydrochloric acid is bubbled through the solution for 2 hours at 0°. The solution is allowed to stand in a closed vessel in the cold (about 0°) until next day. The solid substance is then filtered and washed with anhydrous ether. It is air-dried. M.p. 156°. Yield 3.6 g (98.1%).

$C_{15}H_{12}NO_2Cl$ *Calculated*: Cl 12.95 *Found*: Cl 13.22%.

2. 2,5-diphenyloxazole N-oxide II. 3 g I are boiled in 25 ml aqueous ethanol (1 : 1) for 10 minutes. A white fluffy precipitate will deposit on cooling, which is then filtered and recrystallized from aqueous acetic acid (1 : 1). M.p. 110° (net). Yield 2.5 g (96.15%).

$C_{15}H_{11}NO_2$ *Calculated*: N 5.91 *Found*: N 5.75

3. 2,5-diphenyloxazole III. 0.5 g II are heated for 1.5 hr in 20 ml glacial acetic acid in the presence of 1 g zinc powder. The hot solution is filtered, diluted with cold water until the solid substance precipitates. M.p. 70° (ethanol). Yield, 0.5 g. It behaves identically with 2,5-diphenyloxazole.[2–4]

4. Hydrocloride of 2-(o-chlorophenyl)-5-phenyloxazole-N-oxide IV. 2 g isonitrosoacetophenone and 3 g *o*-chlorobenzaldehyde are dissolved in 100 ml anhydrous ether. The solution is treated at 0° with a HCl current for 2 hours. After standing for 24 hrs at 0° in a closed vessel, it is filtered, the precipitate washed with anhydrous ether and air-dried. White acicular crystals. M.p.150°. Yield, 3 g (72%).

$C_{15}H_{10}NO_2Cl$ *Calculated*: N 23.01 *Found*: N 22.78.

5. 2-(-o-chlorophenyl)-5-phenyloxazole-N-oxide X. 3 g IV are boiled in a water bath in 50 ml aqueous ethyl alcohol (1 : 1) and the hot solution is then filtered. Yellow acicular crystals would deposit in the cold. M.p. 107°, yield, 2.3 g (92,7%). (From ethanol).

$C_{15}H_{10}NO_2Cl$ *Calculated*: Cl 13.05 *Found*: Cl 13.60

6. 2-(o-chlorophenyl)-5-phenyloxazole XVI. a. 0.5 g X are boiled in 50 ml glacial acetic acid with 0.12 g zinc powder for 3 hrs. After filtration of the hot solution it would precipitate with cold water. White crystals. M.p. 90° (ethanol). Yield 0.35 g (72.6%).

$C_{15}H_{10}NOCl$ *Calculated*: Cl 13.87% *Found*: Cl 14.04

b. 2.4 ml *o*-chlorobenzaldehyde and 2.2 ml benzaldehyde-cyanohydrin are handled in 50 ml anhydrous ether with dry gaseous HCl at 0° for 3.5 hours. After 24 hours of standing at 0° in a closed vessel, the precipitated substance is filtered and washed with anhydrous ether. M.p. 89° (ethanol). Yield, 4 g (73.4%).

7. 2-(m-chlorophenyl)-5-phenyloxazole-N-oxide-hydrochloride V. 2 g isonitrosoacetophenone and 1.5 ml *m*-chlorobenzaldehyde are soluted in 70 ml anhydrous ether. One proceeds similar to point 4. M.p. 156°. Yield, 3.1 g (75,1%).

$C_{15}H_{11}NO_2Cl_2$ *Calculated*: Cl 23.01 *Found*: Cl 22.99

8. 2-(m-chlorophenyl)-5-phenyloxazole-N-oxide XI. By boiling 1 g substance V in aqueous ethyl alcohol (1 : 1) for 30 min. one obtains 0.8 g (90.9 %) white substance with m.p. 122°.

$C_{15}H_{10}NO_2Cl$ *Calculated* : Cl 13.05 ; *Found* : Cl 13.29

9. 2-(m-chlorophenyl)5-phenyloxazole XVII. a. 0.5 g XI are boiled for 3 hours with 0.2 g zinc powder in 50 ml glacial acetic acid. The substance is diluted with 200 ml water. The white crystalline substance is filtered. M.p. 104° (aqueous ethanol, 1 : 1). Yield, 0.4 g (85.1 %).

$C_{15}H_{10}NOCl$ *Calculated* : Cl 13.87 ; *Found* : Cl 14.15

b. 2.24 ml (2.8 g) *m*-chlorobenzaldehyde and 2.4 ml (2.68 g) benzaldehyde-cyanohydrin are treated in 50 ml anhydrous ether at 0° with dry gaseous hydrochloric acid for 2 hours. The solution is allowed to stand for 24 hrs in a closed vessel at 0°, filtered and the precipitate recrystallized from aqueous ethyl alcohol (1 : 1). M.p. 105°. Yield 4.5 g (65.8 %).

10. 2-(p-chlorophenyl)-5-phenyloxazole-N-oxide hydrochloride VI. 2 g isonitrosoacetophenone and 1.88 g *p*-chlorobenzaldehyde are dissolved in 100 ml anhydrous ether and treated similarly to point 4. M.p. 152°. Yield, 3.6 g (87.2 %).

$C_{15}H_{10}NO_2Cl_2$ *Calculated* : Cl 23.01 ; *Found* : Cl 22.75

11. 2-(p-chlorophenyl)-5-phenyloxazole-N-oxide XII. 0.5 g VI are boiled in aqueous ethyl alcohol (1 : 1) for 30 min. 0.14 g white crystals will deposit in the cold. M.p. 135° (diluted ethanol).

$C_{15}H_{10}NO_2Cl$ *Calculated* : Cl 13.05 ; *Found* : Cl 12.88

12. 2-(p-chlorophenyl)-5-phenyloxazole XVIII. a. 0.5 g XII are boiled with 0.2 g zinc powder in 30 ml glacial acetic acid for 3 hours. The hot solution is filtered and then diluted with 100 ml water. White crystals are filtered. M.p. 116°. Yield, 0.4 g (85.1 %).

$C_{15}H_{10}NOCl$ *Calculated* : Cl 13 87 ; *Found:* Cl 13.84

b. 2 g *p*-chlorobenzaldehyde and 1.2 ml benzaldehyde-cyanohydrin are soluted in 50 ml anhydrous ether and then treated at 0° for 2 hours with dry gaseous hydrochloric acid. After 24 hours of standing in a closed vessel at 0° the white crystalline precipitate is filtered and washed with anhydrous ether. M.p. 116°. Yield, 3.5 g (90.1 %).

13. 2-(o-chlorophenyl)-5-phenyloxazolidone XIX. Through evaporation of the ether filtrate at point 6 b, a solid substance which melts at 160° after recrystallizing three times from ethyl alcohol (with active coal) is obtained. Yield 0.5 g white acicular crystals.

$C_{15}H_{12}NO_2Cl$ *Calculated* : Cl 12.96 ; *Found* : Cl 13.12

14. 2-(p-chlorophenyl)-5-phenyloxazolidone XX. The ether filtrate at point 12 b is handled similarly to point 13. M.p. 182°. Yield 0.3 g (ethyl alcohol).

$C_{15}H_{12}NO_2Cl$ *Calculated* : Cl 12.96 ; *Found* : Cl 12.82

15. 2-(nitrophenyl)-5-phenyloxazole-N-oxide hydrochloride VII. 1.6 g *o*-nitrobenzaldehyde and 1.6 g isonitrosoacetophenone are dissolved in 100 ml anhydrous ether and treated with dry gaseous hydrochloric acid at 0° for 3 hrs. After 48 hrs of standing at 0° in a closed vessel, the white crystals are filtered and washed with anhydrous ether. M.p. 170° (with decomposition). Yield, 3 g (87.7 %).

$C_{15}H_{11}N_2O_4Cl$ *Calculated* : Cl 11.12 ; *Found* : Cl 10.86

16. 2-(o-nitrophenyl)-5-phenyloxazole-N-oxide XIII. 1 g VII is boiled for 30 min in aqueous methyl alcohol (1 : 1) and filtered thereafter in the cold. Pale yellow crystals with m.p. 134° (aqueous ethanol). Yield, 0.6 g (68 %).

$C_{15}H_{10}N_2O_4$ *Calculated* : N 9.92 ; *Found* : N 9.27

17. 2-(o-nitrophenyl)-5-phenyloxazole XXI. a. 0.3 g XIII are soluted in 15 ml chloroform and 0.3 ml PCl_3 are added thereafter. The solution is boiled for one hour. It is filtered hot and chloroform is evaporated to dryness. The residue is recrystallized twice from methyl alcohol. M.p. 112°. Yield 0.2 g (71,4 %) identical with the product prepared at point b.

b. according to the literature.[2]

18. 2-(m-nitrophenyl)-5-phenyloxazole-N-oxide hydrochloride VIII. 3 g *m*-nitrobenzaldehyde and 3 g isonitrosoacetophenone are soluted in 50 ml anhydrous ether and handled similarly to point 15. Yield, 5 g (78 %), m.p. 174°.

$C_{15}H_{10}N_2O_4Cl$ *Calculated* : Cl 11.12 ; *Found* : Cl 10.80

19. 2-(m-nitrophenyl)-5-phenyloxazole-N-oxide XIV. 1 g VIII is handled similarly to point 16. M.p. 134°. Yield, 0.5 g (56.8 %).

$C_{15}H_{10}N_2O_4$ *Calculated* : N 9.92 ; *Found* : N 9.71

20. 2-(m-nitrophenyl)-5-phenyloxazole XXII. a. 0.5 g XIV and 0.5 ml PCl_3 are soluted in 20 ml chloroform. The solution is boiled for one hour and handled similarly to point 17. Yield, 0.3 g (63.8 %). M.p. 128° (aqueous methanol). The product prepared at point b does not produce a lowering of the m.p. in the mixture.
b. according to the literature.[2]

21. 2-(p-nitrophenyl)-5-phenyloxazole-N-oxide hydrochloride IX. 1.6 g *p*-nitrobenzaldehyde and 1.6 g isonitrosoacetophenone are soluted in 100 ml anhydrous ether and treated with dry gaseous hydrochloric acid at 0° for 3 hours. It is handled similarly to point 15. M.p. 168°. Yield, 3 g (87.7 %).
$C_{15}H_{11}N_2O_4Cl$ *Calculated* : Cl 11.12 ; *Found* : Cl 10.92
22. 2-(p-nitrophenyl)-5-phenyloxazole-N-oxide XV. 1 g IX is handled similarly to point 16. M.p. 147° (aqueous methyl alcohol). Yield, 0.55 g (62.5 %).
$C_{15}H_{10}N_2O_4$ *Calculated* : N 9.92 ; *Found* : N 9.80
23. 2-(p-nitrophenyl)-5-phenyloxazole XXIII. a. 0.1 g XV and 0.1 ml PCl_3 are soluted in 10 ml chloroform and handled similarly to point 17. M.p. 204.5° does not produce lowering of the melting point in a mixture with the product prepared at point b.
b. according to the literature.[2]

Revue Roumaine de Chimie, 20, 5, 651–655 (1975)

STRUCTURE OF THIAZOLIDINIC COMPOUNDS BY THE DEL RÉ METHOD

ELENA CATRINA,* Z. SIMON,** and GH. CATRINA*

* Agricultural Institute, Department of Chemistry, Spl. T. Vladimirescu 14-a,
Timişoara, Romania

** University of Timişoara, Department of Chemistry, Bd. V. Pârvan 4, Timişoara,
Romania

Received November 6, 1973

This study of the distribution of electronic charges within substituted thiazolidinic acids was performed in relation with the synthesis of chelate compounds in this class. The effective charges of the coordinating centers are thus obtained, as well as the influence of the substituent on these charges, in relation with the nature and position of the substituents. The unsubstituted thiazolidine-4-carboxylic acid and the pyrrolidine-4-carboxylic acid (proline) are taken as reference in our study.

METHOD

The Del Ré method[1] is used in this work for saturated cycles characterised by σ-bonds.

The thiazolidinic nucleus is a pentaheterocycle with two heteroatoms and bond angles of nearly 108°; our molecules must be almost planar. [2] The distribution of atomic charges in the molecules was calculated for systems of σ-bonds.

The effective atomic electronegativities ϑ_i in the substituted thiazolidinic acids with formulas (I, II, III, IV);

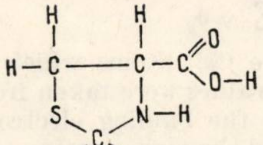

I

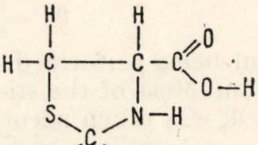

II

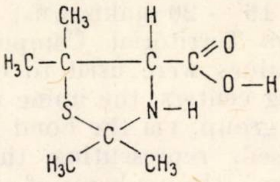

III

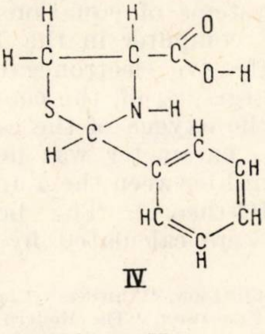

IV

---

[1] G. Del Ré, *J. Chem. Soc.*, **1958**, 4031.

[2] A. Julg, "Chimie quantique", Dunod, Paris, 1967, p. 57.

and in the reference substances with formulas (V, VI);

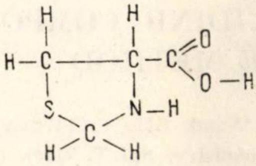

V

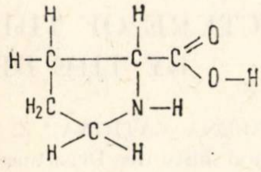

VI

were calculated, using the standard atomic electronegativities ϑ_x^0 and the $\eta_{x(y)}$ factors, representing the polarisation of atom "x" by atom "y", as given in table 1.

Table 1

Standard values ϑ_x^0, $\eta_{x(y)}$ and $\varepsilon_{\mu\nu}$ according to the Del Ré

ϑ_x^0	$\eta_{x(y)}$		$\varepsilon_{\mu\nu}$	
ϑ_H^0 0.00	$\eta_{H(O)}$	0.4	ε_{C-H}	1.00
	$\eta_{C(H)}$	0.3	ε_{C-C}	1.00
ϑ_C^0 0.07	$\eta_{O(C)}$	0.1	ε_{C-N}	1.00
	$\eta_{C(O)}$	0.1	ε_{C-S}	0.70
ϑ_N^0 0.30	$\eta_{C(C)}$	0.1	ε_{C-O}	0.95
	$\eta_{C(N)}$	0.1	ε_{N-N}	0.45
ϑ_{-O-}^0 0.40	$\eta_{C(S)}$	0.2	ε_{O-H}	0.45
$\vartheta_{=O}^0$ 0.28	$\eta_{H(C)}$	0.4		
ϑ_S^0 0.10	$\eta_{N(C)}$	0.1		

The equations are, for each atom, of the type;

$$\vartheta_x = \vartheta_x^0 + \sum \eta_{x(y)} \vartheta_y$$

the summation being performed over the "y" atoms which are adjacent to the "x" atom. Most of the standard values were taken from 1. For the sulphur atom ϑ_S^0 was taken according to the Pauling electronegativities[3]; $\vartheta_S^0 = 0.25(x_S - x_H)$ and ε_{C-S} so as to yield the correct value for the dipole-moment of the C—S bond (Volkenstein[4]). The $\eta_{S(y)}$ and $\eta_{y(S)}$ parameters were taken equal to the $\eta_{Cl(y)}$ and $\eta_{y(Cl)}$ parameters of Del Ré.

The systems of equations (with 16 — 20 unknowns) were solved on an IRIS computer in the Timişoara Territorial Computing Center.

The effective electronegativity values were used to calculate the effective charges ρ_μ of the coordinating centers, the imine nitrogen and the hydroxylic oxygen of the carboxyl group, via the bond polarisations $Q_{\mu\nu}$. The $\varepsilon_{\mu\nu}$ parameter was hereby used, representing the resonance energy integral between the μ and ν atoms (the analogue of the β-integral in the HMO-theory). The bond polarisations $Q\,\mu\nu$ and the atomic charges ρ_μ were calculated by relations:

---

[3] C. A. Coulson, "Valence", Clarendon Press, Oxford, 1953, p. 242.

[4] L. N. Ferguson, "The Modern Structural Theory of Organic Chemistry", Prentince Hall, New Jersey, 1964, p. 200.

$$Q_{\mu\nu} = \frac{\vartheta_\nu - \vartheta_\mu}{2\,\varepsilon_{\mu\nu}} \qquad \rho_\mu = \sum_{\substack{\nu \\ \nu(\text{adjacent})}} Q_{\mu\nu}$$

where $Q_{\mu\nu}$ — bond polarisation
ϑ_ν — effective electronegativity of the ν atom
ϑ_μ — effective electronegativity of the μ atom
ρ_μ — effective charge of the μ atom
$\varepsilon_{\mu\nu}$ — resonance energy integral between the μ and ν atoms.

The effective charges for the oxygen, nitrogen, sulphur and carbon atoms at which substitutions take place are listed in table 2.

RESULTS AND DISCUSSION

Analysis of table 2 gives the following results.

The electronegativity of the nitrogen and oxygen atoms is high in comparison with that of the other atoms; that of the sulphur atom is rather low. As compared to the unsubstituted molecule with $\rho_S = -0.032$, the effective electronegativity increases with substitutions in the 2 and 5 — positions, the more so in the case of methyl ($\rho_S = -0.114$) than of phenyl substitution. The low and negative charge ($\rho_{C_2} = -0.018$) of the C_2 atom in the unsubstituted thiazolidine-4-carboxylic acid is also remarkable as compared to the rather high negative charge ($\rho_{C_5} = -0.168$) of the C_5 — atom, difference due to the influence of the carboxyl group and of the sulphur atom. In the pyrrolidine-4-carboxylic acid, the charge of the C_2-atom is almost zero ($\rho_{C_2} = -0.0007$), that of the C_5-atom is also much lowered ($\rho_{C_5} = -0.065$).

The charge of the C_5-atom in the thiazolidine-4-carboxylic acid is lowered by methyl and phenyl substitution in position 2, with a resulting ρ_{C_5} between -0.085 and -0.076 e.u. Methyl substitution in both positions 2 and 5 decreases ρ_{C_8} to -0.011 e.u. This demonstrates the electron repelling character of the methyl groups, which in the 2,2′, 5,5′ tetramethylic derivative increase also the charge of the sulphur atom to -0.075 e.u. as compared to -0.032 e.u. in the unsubstituted acid.

Methyl and phenyl substitutions in position 2 increase the positive charge of the C_2 atom, ρ_{C_2} is -0.018 e.u. in the unsubstituted acid $+0.102$ e.u. in the 2-methyl derivative, $+0.144$ e.u. in the 2,2′dimethylated one, but only $+0.042$ e.u. in the 2-phenyl derivative. The negative charge of the adjacent sulphur atom increases to -0.114 e.u. by methyl substitution but only to -0.041 e.u. by phenyl substitution. These atomic charge variations agree with the idea that, in inductive interactions, the phenyl group is less electron repelling than the methyl group. This idea is confirmed also by the charge of these groups, more positive for methyl (ρ_{CH_3} is $+0.036$ e.u. in position 5 and $+0.024$ e.u. in position 2) than for phenyl ($\rho_{C_6H_5}$ in position 2 is $+0.0101$. e.u.). Concerning the electronic

Table 2

Effective charges of the C, N, O atoms and of the methyl and phenyl groups in the thiazolidine-4-carboxylic acids

Substances	Atomic charges in e.u.							
	ρ_N	ρ_O	ρ_S	ρ_{C_2}	ρ_{C_5}	$\rho_{CH_3(C_2)}$	$\rho_{CH_3(C_5)}$	$\rho_{C_6H_5(C_2)}$
2 methyl-thiazolidine-4-carboxylic acid.	−0.466	−0.478	−0.114	+0.144	−0.076	+0.023	—	—
2,2 dimethyl-thiazolidine-4-carboxylic acid.	−0.464	−0.490	−0.095	+0.102	−0.087	+0.021	—	—
2,2′, 5,5′ tetramethyl tiazolidine-4-carboxylic acid	−0.464	−0.479	−0.075	+0.091	−0.011	+0.021	+0.0036	
2 phenyl-thiazolidine-4-carboxylic acid.	−0.460	−0.479	−0.041	+0.042	−0.085	—	—	+0.0101
pyrolidine-4-carboxylic acid.	−0.471	−0.505	—	+0.0007	−0.065	—	—	—
thiazolidine-4-carboxylic acid.	−0.462	−0.481	−0.032	−0.018	−0.168	—	—	—

charges of the chelating groups, the following remarks can be made. The electronic charge of the iminic nitrogen and the hydroxyl oxygen are higher in the pyrolidine-4-carboxylic acid (−0.471 e.u. and 0.505 e.u., respectively) than in the unsubstituted thiazolidine-4-carboxylic acid (−0.462 e.u. and 0.481 e.u., respectively). The basicity of these atoms and their proton retention capacity is therefore higher in the pyrolidine-4-carboxylic acid than in the thiazolidine-4-carboxylic acid. This explains the higher pK_1 value (1.99) of the carboxyl group in the first compound, as compared to 1.77 in the second one[5], demonstrating the electron attraction inductive effect (−I) of the sulphur atom, transmitted via an alifatic carbon to the nitrogen atom.

Methyl and phenyl substitution in the thiazolidine-4-carboxylic acids increase the negative charge of the nitrogen atom. Two methyl groups substituted at the C_2- atom produce the highest increase, while two methyl groups at the more distant C_5- atom do not further increase the nitrogen charge. A phenyl group at C_2 decreases the negative charge ($\rho_N = -0.460$ e.u. and $\rho_0 = -0.479$ e.u.) and hence the basicity of the chelating atoms. The phenyl group has a weak + I effect in this case.

CONCLUSIONS

In order to obtain some information on the effective atomic charge in the thiazolidine carboxylic acid and its methyl and phenyl substitution derivatives, calculations by the Del Ré method were performed for these compounds. Methyl substitutions produce an increase in the effective electronegativity and thus in the basicity of the chelating nitrogen and hydroxylic oxygen atoms by an inductive (−I) effect. Phenyl substitution has a lower inductive effect. Most electronegative and, thus, best donors for chelation in our compounds are the oxygen atom of the carboxylic OH group and the iminic nitrogen atom.

---

[5] H. T. Clarke and J. R. Johnson, "The Chemistry of Penicillin", Princ. University Press, New Jersey, 1949, cap. III.

Revue Roumaine de Chimie, **20**, 5, 657 – 663 (1975)

KINETIC ANALYSIS OF THERMOGRAVIMETRIC DATA. VIII[*]

THERMAL DECOMPOSITION KINETICS OF SOME [Cobalt (II)X_2 (amine)$_2$] TYPE COMPLEXES

CS. VÁRHELYI, J. ZSAKÓ and MÁRTA BOÁRIU-FARKAS
Faculty of Chemistry, Chair of Physical Chemistry, Babeş-Bolyai University,
str. Arany János 11, Cluj-Napoca, Romania

Received February 1, 1974

Twelve new [CoX_2 (amine)$_2$] type complexes have been synthesized. The thermal decomposition leads presumably to the formation of a [CoX_2 (amine)$_{2/3}$] type relatively stable intermediate. This is formed directly if X = Cl and in two successive stages if X = Br or I. Apparent reaction order, activation energy and pre-exponential factor values have been derived for 10 compounds by means of a Coats-Redfern's method. The influence of the halogen is discussed. The validity of a linear kinetic compensation law is observed, i.r. spectra of several new compounds are discussed.

The pseudo-halides (NCO^-, NCS^- and $NCSe^-$) of cobalt (II) give even in aqueous or alcoholo-aqueous solutions [Co(amine)$_n$ X_2] type (n= 2 or 4) characteristic crystalline blue or pink products with heterocyclic or aromatic amines. Some of these products are used also for analytical purposes, e.g. [Co(pyridine)$_4$(NCS)$_2$] for the gravimetric determination of this metal. [1]

The halide ions, for which the π-bond formation with Co (II) is not characteristic, do not give similar products in aqueous or alcoholo-aqueous solutions [$CoCl_2$(amine)$_2$], [$CoBr_2$(amine)$_2$] and [CoI_2(amine)$_2$] type derivatives of aliphatic, aromatic and heterocyclic amines are formed in nonaqueous solutions only. To this end absolute alcohol, higher alcohols, acetone, etc., can be used. [2-4]

As far as the thermal behaviour of these complexes is concerned, release of amine can be observed by heating. A black resinic mass is obtained, which, at higher temperatures, transforms into cobalt anhydrous halides or even into oxydes. Thermal decomposition of a large number of analogous complexes, derivatives of Ni(II), Co(II), Mn(II), Cu(II) and

---

[*] Part VII. J. Zsakó and E. H. Arz, *J. Thermal Anal.*, in press.

[1] G. Spacu and P. Dick, *Z. analyt. Chem.*, **71**, 97 (1927).

[2] E. Lippmann and G. Vortmann, *Ber. dtsch. chem. Ges.*, **11**, 1068 (1878); **12**, 79 (1879).

[3] W. Hieber and F. Mühlbauer, *Z. anorg. Chem.*, **186**, 97 (1930).

[4] W. Hieber and E. Lory, *Z. Elektrochem.*, **39**, 26 (1933).

Cd(II) has been studied by Fătu and al.[5-10] and the formation of a $[MeX_2(amine)_{2/3}]$ type stable intermediate has been frequently stated.[5]

In our previous paper[11] on the kinetics of thermal decomposition of $[CoBr_2(m\text{-toluidine})_2]$ in dynamic temperature conditions, the influence of procedural variables, viz, of sample weight and heating rate, was studied. The position of the first weight loss stop has been observed to depend on sample weight, namely, the smaller the sample, the more amine released during the first stage, but the amount of amine released is lower than 1 molecule amine per 1 molecule complex. Kinetic analysis of the first stoichiometric stage (I).showed it to consist of two distinct kinetic stages, the first (I/1) requiring a lower activation energy than the second (I/2). Kinetic parameters have been observed to show a systematic variation with both sample weight and heating rate.

In the present paper a number of 12 new $[CoCl_2(amine)_2]$, $[CoBr_2(amine)_2]$ and $[COI_2(amine)_2]$ type complexes are described, derivatives of *m*-xylidine, *p*-ethylaniline, *o*-ethylaniline, 2-amino-5-chloro-ethylbenzene and 2-amino-5-bromo-ethylbenzene, as well as some known compounds, derivatives of aniline, *o*-, *m*- and *p*- toluidine. Characterization of these

Table 1

Some new $[Co_2\ (amine)_2]$ type compounds

N°	Formula	Mol. weight calcd.	Yield (%)	Aspect	Analysis		
					Calcd.		*Found*
1	$[CoCl_2\ (o\text{-ethyl-aniline})_2]$			Brilliant blue	Co	15.83	16.00
		372.2	40	thin plates	Cl	19.05	18.90
2	$[CoCl_2\ (p\text{-ethyl-aniline})_2]$			Brilliant blue	Co	15.83	15.70
		372.2	45	thin plates	Cl	19.05	19.22
3	$[CoBr_2\ (o\text{-ethyl-aniline})_2]$			Brilliant blue	Co	12.78	12.70
		461.1	40	thin plates	Br	34.67	34.50
4	$[CoBr_2\ (p\text{-ethyl-aniline})_2]$			Brilliant blue	Co	12.78	12.66
		461.1	50	thin plates	Br	34.67	34.80
5	$[CoI_2\ (o\text{-ethyl-aniline})_2]$			Sparkling green	Co	10.62	10.50
		555.1	40	thin plates	I	45.73	45.05
6	$[CoCl_2$ (2-amino-5-			Brilliant blue	Co	13.36	13.25
	Cl-ethylbenzene$)_2]$	441.1	45	thin plates	Cl^-	16.07	16.20
7	$[CoBr_2$ (2-amino-5-			Brilliant blue	Co	11.12	11.30
	Cl-ethylbenzene$)_2]$	530.0	50	thin plates	Br	30.16	30.25
8	$[CoI_2$ (2-amino-5-			Sparkling green	Co	9.44	9.50
	Cl-ethylbenzene$)_2]$	623.9	30	thin plates	I	40.58	40.40
9	$[CoCl_2$(2-amino-5-			Brilliant blue	Co	11.12	10.90
	Br-ethylbenzene$)_2]$	530.0	40	thin plates	Cl^-	12.38	13.50
10	$[CoBr_2$(2-amino-5-			Brilliant blue			
	Br-ethylbenzene$)_2]$	618.9	45	thin plates	Co	9.52	9.43
11	$[CoCl_2\ (\alpha\text{-naphtyl-amine})_2]$			Light blue	Co	14.16	14.25
		416.2	70	cryst. powder	Cl	17.04	17.16
12	$[CoBr_2\ (\alpha\text{-naphtyl-amine})_2]$			Light blue	Co	11.66	11.59
		505.1	65	cryst. powder	Br	31.64	31.40

---

[5] I. G. Murgulescu, E. Segal and D. Fătu, *J. Inorg. Nuclear Chem.*, **27**, 2677 (1965); *Rev. Roumaine Chim.*, **11**, 291 (1966).

[6] E. Schönberger, D. Fătu and E. Segal, *Rev. Roumaine Chim.*, **12**, 1205 (1967).

[7] D. Fătu and E. Segal, *Anal. Univ. Bucureşti, Chimie*, **2**, 49 (1968).

[8] D. Fătu and E. Segal, *Rev. Roumaine Chim.*, **14**, 709 (1969).

[9] D. Fătu, S. Fătu and E. Segal, *Rev. Roumaine Chim.*, **14**, 1107 (1969).

[10] D. Fătu, S. Fătu, A. Teodorescu and E. Segal, *Rev. Roumaine Chim.*, **15**, 855 (1970).

[11] J. Zsakó, E. Kékedy and Cs. Várhelyi, *Proc. 3rd Inter. Conf. Therm. Anal.* (Davos, Schwitzerland), Vol. *2*, p. 487 (1971).

compounds is given in table 1, their synthesis, yields (% to CoX_2), analysis and i.r. spectral characteristics are presented in the experimental part.

The thermal decomposition of the complexes has been studied under dynamic temperature conditions, using a thermobalance constructed on the basis of literature data, [12] a heating rate of 10°/ min and samples of 100 mg. Two typical TG curves are given in fig. 1.

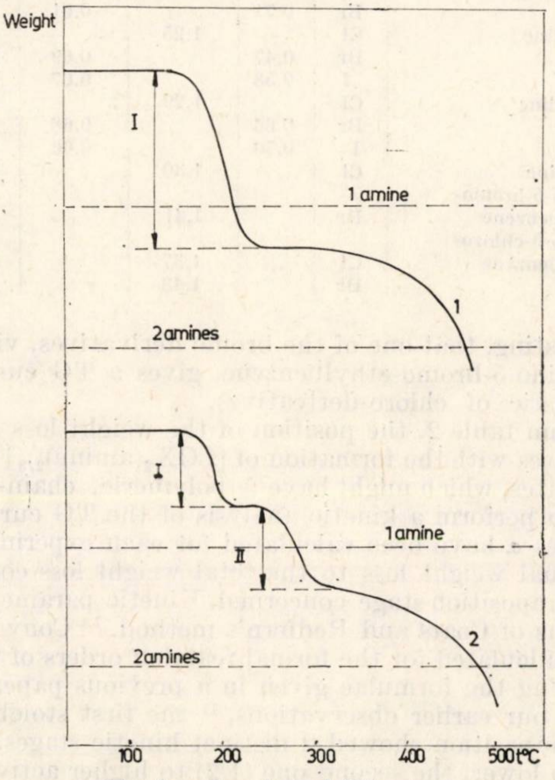

Fig. 1. — Two typical TG curves.
1 – [$CoCl_2$ (*m*-xylidine)$_2$]; *2* – [$CoBr_2$ (*m*-toluidine)$_2$]

The first type is characteristic of the chloro-derivatives. During the first stage (I) more than 1 mole of amine is released and at higher temperatures the amine is further released. In the case of bromo- and iodo-derivatives one more stage is observed. Here, only the two first stages lead to the release of as much amine as in the first stage of thermal decomposition of chloro-derivatives. Further, no weight loss stop is observed when all the amine is released. In the third stage of the decomposition, sometimes halogen is also lost and cobalt oxide is formed. The amount of amine lost during the first or the first two stages of thermal decomposition, are presented in table 2.

---

[12] L. Erdey and P. Paulik, *Magy. Tud. Akad. Kém. Osztály Közl.*, **5**, 461 (1955); L. Kékedy, P. Kröbl, A. Szurkos and E. Kékedy, *Stud. Univ. Babeş-Bolyai, Chem.*, **3**, 99 (1958).

Table 2

Number of amine molecules lost in the first two stages of thermal decomposition of $[CoX_2(amine)_2]$ type complexes

amine	X	moles of amine/1 mole complex			
		stage I	stage II		total
o-ethylaniline	Cl		1.32		1.32
	Br	0.71		0.61	1.32
p-toluidine	Cl		1.25		1.25
	Br	0.47		0.69	1.16
	I	0.58		0.67	1.15
m-toluidine	Cl		1.29		1.29
	Br	0.66		0.68	1.34
	I	0.70		0.66	1.36
m-xylidine	Cl		1.30		1.30
2-amino-5-bromo-ethylbenzene	Br		1.41		1.41
2-amino-5-chloro-ethylbenzene	Cl		1.37		1.37
	Br		1.43		1.43

It is interesting, that one of the bromo derivatives, viz, the complex containing 2-amino-5-bromo-ethylbenzene, gives a TG curve of the first type, characteristic of chloro-derivatives.

As seen from table 2, the position of the weight loss stops is consistent in all the cases with the formation of $[COX_2(amine)_{2/3}]$ type relatively stable intermediates, which might have a polymeric, chain-like structure.

In order to perform a kinetic analysis of the TG curves, the transformation degrees α have been calculated for each experimental point as the ratio of actual weight loss to the total weight loss corresponding to the thermal decomposition stage concerned. Kinetic parameters have been derived by means of Coats and Redfern's method.[13] Conversion integrals $g(\alpha)$ have been calculated for the formal reaction orders of $n = 0.1/3, 1/2, 2/3$, 1 and 2, using the formulae given in a previous paper.[14]

Similar to our earlier observations,[11] the first stoichiometric stage of thermal decomposition showed 2 distinct kinetic stages, the first (I/1) corresponding to lower, the second one (I/2) to higher activation energies. Presumably, during the first kinetic stage, decomposition is limited to the surface of the crystals and in the second stage it occurs mainly in deeper layers. Examples of graphical plot of $\log g(\alpha)/T^2$ vs. $1/T$ are given in fig. 2.

Fig. 2a shows a decomposition stage with two kinetic stages. It is apparent that only the formal reaction order $n = 2/3$ ensures good linearity. In fig. 2b a single kinetic stage is observed, and a linearisation is obtained for $n = 1$.

Apparent activation energy values have been derived from the slope of the above straight lines. Pre-exponential factors of Arrhenius' equation have been calculated by means of the following relation :[14]

$$\log Z = \log g(\alpha) - \log p(x) + \log Rq - \log E_a \tag{1}$$

---

[13] H. W. Coats and J. P. Redfern, *Nature*, **201**, 68 (1964).

[14] J. Zsakó, *J. Phys. Chem.*, **72**, 2406 (1968).

where $g(\alpha)$ stands for the conversion integral, $p(x)$ — for the exponential integral tabulated in, [14] x — for E_a/RT, E_a — for the apparent activation energy, q — for the heating rate in Ks^{-1}.

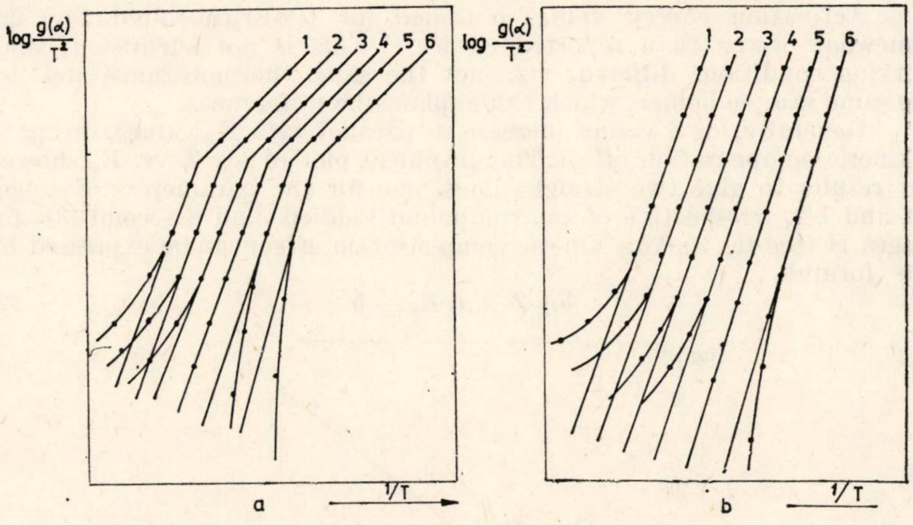

Fig. 2. — Coats-Redfern linearizations.

a — [$CoBr_2$ (*p*-toluidine)$_2$] *1* — $n = 0$; *2* — $n = 1/3$; *3* — $n = 1/2$; *4* — $n = 2/3$; *5* — $n = 1$; *6* — $n = 2$
b — [CoI_2 (*p*-toluidine)$_2$] *1* — $n = 0$; *2* — $n = 1/3$;
3 — $n = 1/2$; *4* — $n = 2/3$; *5* — $n = 1$, *6* — $n = 2$.

Kinetic parameters derived are presented in table 3.

Table 3

Kinetic parameters derived for different stages (I and II) of the thermal decomposition of [CoX_2(amine)$_2$] type complexes

amine	X	n		E_a			log Z		
		I	II	I/1	I/2	II	I/1	I/2	II
p-toluidine	Cl	0	—	12.6	25.3	—	2.8	9.3	—
	Br	2/3		12.9	30.7	—	3.3	12.4	—
	I	1	1	—	32.3	34.8	—	13.5	10.9
m-toluidine	Cl	0	—	9.5	20.3	—	1.4	7.1	—
	Br	1/3	2/3	16.1	26.8	36.2	4.7	10.2	11.4
	I	1	—	—	39.7	—	—	18.1	—
o-ethyl-aniline	Cl	0	—	—	18.2	—	—	6.4	—
	Br	2/3	1	—	23.6	84.1	—	9.3	31.7
m-xylidine	Cl	0	—	—	20.4	—	—	7.1	—
2-amino-5-chlor-ethyl-benzene	Cl	1	—	—	35.0	—	—	14.5	—

If the first stoichiometric stage consisted of a single kinetic stage, the corresponding kinetic parameters were taken for the parameters of stage I/2. Some systematic variations of kinetic parameters can be observed. Thus, for a given substance, the activation energy generally increases in the sequential stage I/1 < I/2 < II. In the case of the derivatives of the same amine, both reaction order and activation energy values increase in the following order : Cl < Br < I.

Activation energy values obtained for [$CoBr_2$(m-toluidine)$_2$] are somewhat lower than reported earlier.[14] This is not surprising, since working conditions differed, viz, not the same thermobalance and not the same sample holder, which can explain the differences.

Generally, log Z values increase in parallel with E_a values, owing to a kinetic compensation effect. The graphical plot of log Z vs. E_a showed our results to give two straight lines, one for the parameters of stages I/1 and I/2, irrespective of the compound studied, and a second one for stages II (see fig. 3). This kinetic compensation effect can be expressed by the formula

$$\log Z = a\,E_a + b \tag{2}$$

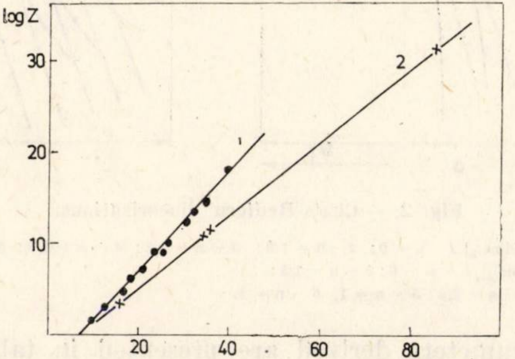

Fig. 3. — Kinetic compensation effect.
1 — stages I/1 and I/2 ; *2* — stage II.

Parameters *a* and *b*, derived by means of the least square method, are presented in table 4. Errors have been calculated in the common, statistical way.

Table 4

Kinetic compensation parameters for different stages of the thermal decomposition of [CoX_2 (amine)$_2$] type complexes

Stage	a	b
I/1 and I/2	0.534±0.020	−3.75±0.52
II	0.416±0.026	−3.47±1.16

The compensation parameters *a* and *b* are close to those reported earlier for [$CoBr_2\cdot$(*m*-toluidine)$_2$][11] and for [Co(dioxime)$_2$ (amine)$_2$]X type complexes,[15] but different from the analogous parameters derived for the decomposition of carbonates.[16,17]

---

[15] J. Zsakó and M. Lungu, *J. Thermal Anal.*, in press

[16] M. M. Pavlyuchenko, G. A. Prodan and S. A. Slyshkina, *Doklady Akad. Nauk S.S.S.R.*, **181**, 1174 (1968).

[17] J. Zsakó and H. E. Arz, *J. Thermal Anal.*, in press.

EXPERIMENTAL

Synthesis of [CoX_2 *(amine)*$_2$] *type complexes.* Since the compounds of this type are easily decomposed by water, the synthesis is performed generally in anhydrous ethanol, or in other nonaqueous media. To this end we used n-buthylalcohol, because it dissolves well both the cobalt halides and the amines.

0.02 moles of $CoCl_2$ ($CoBr_2$ or CoI_2) are dissolved in 35—50 ml n-butanol under heating. After the solution is cooled, 0.4 moles of amine are added, dissolved in 20 ml n-butanol. From the dark blue solution, brilliant blue or green products are separated within 1/2—3 hours. These are filtered, washed with a small amount of n-butanol, then 5—6 times with ether and dried in vacuum. The products must be kept in well-closed vessels, since by standing in the air the colour of most of them turns violet, indicating slow decomposition. The $CoBr_2$ and CoI_2 needed were obtained from $CoCO_3$, with an excess of 40% HBr and 40% HI, respectively, by evaporation to dy and elimination of the remaining water (120—140°).

Analysis. The cobalt content was determined complexometrically in the presence of murexid. The weighed samples were dissolved in water. The amines separated, if forming a suspension, were filtered before titration. Halogens were determined by means of potentiometric titration with $AgNO_3$.

I. R. spectra of the compounds studied have been recorded by means of an UR 20 Carl Zeiss Jena UR spectrophotometer in KBr pellets, in the range of 400 to 4000 cm^{-1}.

The symmetrical and asymmetrical ν_{N-H} valence vibrations, the δ_{NH_3} deformation vibrations and the ν_{Co-N} valence vibration are most characteristic of co-ordinated and free amines and of the Co—N bond. In table 5, data concerning the characteristic IR absorption bands of some compounds of the type studied are presented.

Table 5

Characteristic i.r. spectral data of some [CoX_2 (amine)$_2$] type compounds

Formula	ν_{N-H}	δNH_2 s	ν_{C-N}	γ_{NH_2}	ν_{Co-N}
[$CoCl_2$ (*m*-toluidine)$_2$]	3280 (s) 3240 (m)	1620 (m) 1600 (m)	1275 (m)	870 (m) 830 (w)	535(m)
[CoI_2 (*p*-toluidine)$_2$]	3290 (s) 3240 (s)	1580 (s)	1260 (w)	820 (s)	522 (s)
[$CoCl_2$ (*p*-toluidine)$_2$]	3290 (s) 3245 (s)	1618 (w) 1520 (s)	1245 (m)	830 (s)	526 (s)
[CoI_2 (aniline)$_2$]	3278 (s) 3225 (s)	1608 (s) 1570 (s)	1220 (m)	860 (m) 830 (m)	525 (m)
[$CoCl_2$ (α-naphtylamine)$_2$]	3280 (s) 3230 (s)	1640 (m) 1580 (s)	1270 (m) 1220 (m)	855 (s) 820 (s)	525 (m)
[$CoBr_2$ (α-naphtylamine)$_2$]	3280 (s) 3220 (s)	1640 (m) 1570 (s)	1220 (m)	855 (s) 815 (m)	522 (m)
[$Co(en)_2Cl$ (benzylamine)] $(NO_3)_2$	3170 (s) 3095 (s)				503 (m)

The ν_{N-H} valence vibrations are shifted towards lower frequencies, with 100—150 cm^{-1}, as compared to their position with free amines. This is consistent with the covalent character of the CO—N. bond. If these spectra are compared to the IR spectra of [$Co(en)_2$ (m-toluidine)Cl] $(NO_3)_2$, [$Co(en)_2$ (benzyl-amine)Cl] $(NO_3)_2$ or [$Co(DH)_2$ (m-toluidine)$_2$]NO_3, one can see the shift to be smaller in the case of the complexes studied in this paper, than for the other ones, where the shift can attain 250—300 cm^{-1}. This shows the covalent character of the Co-amine bond to increase in the order Co(II)→Co(III).

The ν_{Co-N} valence vibrations appear at 520—530 cm^{-1}. For the same vibration in [$Co(NH_3)_6$] Cl_3 Block [18] has calculated and observed 480—500 cm^{-1}. Taking into account that, in this case, the N atom is linked only with hydrogen atoms, this is not inconsistent with the above statement concerning the covalent character of Co(II)—N and Co (III)-N bonds.

As regards the effect of the halogen atom on the base of our IR spectra, no clear evidence has been obtained because the shifts of the characteristic vibrations are insignificant.

---

[18] H. Block, *Trans. Faraday Soc.*, **55**, 867 (1959).

Revue Roumaine de Chimie, **20**, *5*, 657—663 (1975)

Revue Roumaine de Chimie, **20**, *5*, 665–675 (1975)

POTENTIAL ANTICANCER AGENTS. IX*

SYNTHESIS OF NEW URETHANE TYPE NITROGEN MUSTARDS FROM BENZO- AND NAPHTHOPYRANS

I. I. DRAGOTĂ, L. V. FEYNS and I. NICULESCU-DUVĂZ

Oncological Institute, Bd. 1 Mai 11, Bucharest,
Romania

Received February 23, 1974

Fourteen new urethane-type nitrogen mustards derived from chromanes, benzochromanes and coumarins were synthesized and studied. The assigned structures were in good agreement with the n.m.r., i.r. and u.v. data. The new compounds seem to be devoid of anticancer activity.

The study of alkaloids offers extremely interesting possibilities to find new structures with anticancer properties. Thus, acronycine (I) extracted from Acronicia Baueri[1] exhibited a broad antitumor spectrum, proving to be active against leukemia C–1498, myeloma X–5563 and androgen-dependent carcinoma Shionogi 115.[2-5] The structure of this alkaloid was established and a number of approaches for its total synthesis developed.[6-10]

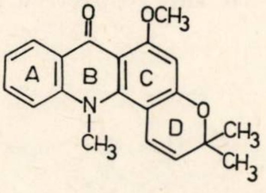

I

---

* Part VIII, I. Niculescu-Duvăz, M. Rotaru, V. Feyns and O. Maior, *Rev. Roumaine Chim.*, **18**, 1617 (1973).

[1] F. N. Lahey and W. C. Thomas, *Austral. J. Sci. Res.* (*A*), **1949**, 4213.

[2] G. H. Svoboda, G. A. Poore, P. J. Simpson and G. B. Boder, *J. Pharm. Sci.*, *55*, 758 (1966).

[3] G. H. Svoboda, *Lloydis*, **29**, 206 (1966).

[4] J. Schneider, E. L. Evans, E. Grunberg and R. Ian Fryer, *J. Medicin. Pharmaceut. Chem.*, **15**, 266 (1972).

[5] G. H. Svoboda, M. J. Sweeney and W. D. Walkling : *J. Pharm. Sci.*, **60**, 333 (1971).

[6] L. J. Drummond and F. N. Lahey, *Aust. J. Sci. Res.* (*A*), **1949**, 630.

[7] P. L. Macdonald and A. V. Robertson, *Austral. J. Chem.*, **19**, 275 (1966).

[8] J. Hlubucek, E. Ritchie and W. C. Taylor, *Chem. and Ind.*, **1969**, 1809.

[9] J. Hlubucek, E. Ritchie and W. C. Taylor, *Austral J. Chem.*, **23**, 1881, (1970).

[10] J. R. Beck, R. Kwok, R. N. Boocher, A. C. Brown, L. E. Patterson, P. Pranc, B. Rockey and A. Pholand, *J. Amer. Chem. Soc.*, **90**, 4706, 1968.

In order to establish the structural elements responsible for the antiblastic activity of this alkaloid, the study of benzopyranic C—D system has been initiated. For this purpose, in a preliminary approach, a series of urethane-type nitrogen mustards from benzo- and naphthopyranes were prepared and the biological properties were investigated.

Aliphatic[11] and aromatic nitrogen mustards[12,13] coupled with coumarin residues as carrier moieties are known, but in these compounds the alkylating group is not directly bound to the coumarinic system. Mention should be made that some hydroxylated 3-arylcoumarins were tested as potential anticancer and antiviral agents[14].

1. *Synthesis.* 2,2-Dimethyl-*n*-hydroxy-chromane-4-ones were synthesized by condensation of di- or triphenols with 1,1-dimethyl acrylic acid in the presence of $ZnCl_2$ at 175° [15,16] or $ZnCl_2$-$POCl_3$ at room temperature.[17]

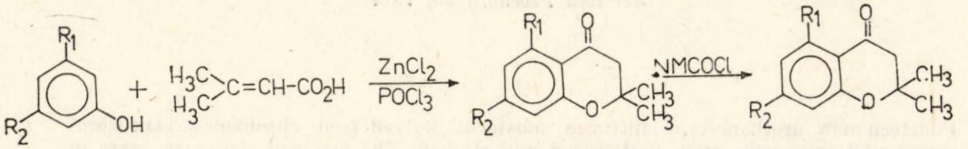

$R_1,R_2 = H, CH_3, OH$

IV

V

	R_1	R_2
a:	OH	OH
b:	H	OH
c:	CH_3	OH

	R_1	R_2
a:	OCONM	OCONM
b:	H	OCONM
c:	CH_3	OCONM

$-OCONM = -OCON(CH_2CH_2Cl)_2$

Similarly 1,3- and 2,7-dihydroxy-naphthalenes condensed with 1,1-dimethyl-acrylic acid led to the respective new benzochromane-4-ones (VI and VII).

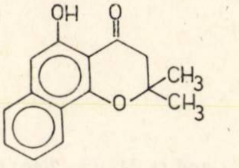

VI

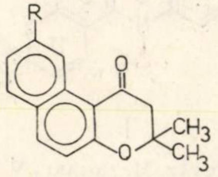

VII

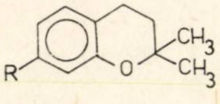

VIII

The structure assignments for these two derivatives are based on n.m.r. spectra.

---

[11] R. C. ELDERFIELD and A. C. METHA, *J. Medicin. Pharmaceut. Chem.* **10**, 921 (1967).

[12] R. C. ELDERFIELD and J. ROY, *J. Medicin. Pharmaceut. Chem.*, **10**, 918 (1967).

[13] F. D. POPP, *J. Medicin. Pharmaceut. Chem.*, **5**, 627 (1962).

[14] NG. PH. BUU-HOI, B. BKERT and R. ROYER, *J. Org. Chem.*, **19**, 1548 (1954).

[15] M. MIYANO and M. MATSUI, *Bull. Chem. Soc. Japan*, **31**, 397, (1958).

[16] W. BRIDGE, A. J. CROEKER, T. CUBIN and A. ROBERTSON, *J. Chem. Soc.* **1937**, 1530.

[17] P. R. IYER and G. D. SHAH, *Indian J. Appl. Chem.*, **6**, 227 (1968).

Clemmensen reduction of chromane-4-ones [18-21] was successful only for 2,2-dimethyl-7-hydroxy-chromane-4-one when the corresponding chromane (VIII) was obtained. The failure of the reduction of 7,8-dihydroxy-2,2-dimethyl chromane-4-one by Clemmensen procedure is already reported. [22]

Treatment of hydroxy-chromanes with N,N-bis-(2-chloroethyl) carbamoyl chloride in dry pyridine [23] afforded a good yield (aprox. 75%) of the corresponding N,N-bis- (2-chloroethyl) carbamoyl derivatives. The analytical data of these new urethane type nitrogen mustards are given in table 1.

By the same method a number of N,N-bis-(2-chloroethyl)carbamoyl-coumarins (X) was prepared with an yield of about 85%.

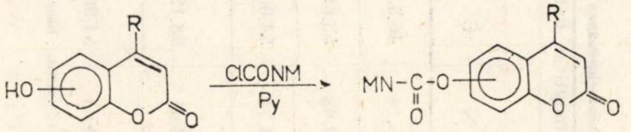

IX X

-OCONM = -OCON(CH$_2$CH$_2$Cl)$_2$

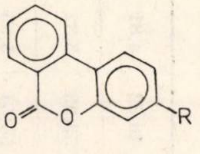

XI

R = OH, OCONM

The hydroxy-coumarins were prepared by condensation of di- or tri-phenols either with acetyl-acetic ester [24,25] (for the 4-methyl-derivatives) or with malic acid. [26]

Similarly (XI, R = OH) [27] was converted into the corresponding carbamoyl derivative (XI, R = OCONM). The new urethane-type nitrogen mustards thus obtained are summarized in table 2.

[18] W. Bridge, R. G. Heyenes and A. Robertson, *J. Chem. Soc.*, **1937**, 279.

[19] A. O. Fitton and G. R. Ramage, *J. Chem. Soc.*, **1963**, 5426.

[20] P. Naylor, G. R. Ramage and F. Schofield, *J. Chem. Soc.*, **1958**, 1190.

[21] H. B. Bhat and K. Venkataraman, *Tetrahedron*, **1973**, 77.

[22] J. H. Richards, A. Robertson and J. Ward, *J. Chem. Soc.*, **1948**, 1610.

[23] T. Nogrady, M. K. Vagi and V. W. Adamkiewicz, *Canad. J. Chem.*, **40**, 2126 (1962).

[24] L. Reichel and N. Hampel, *Liebigs Ann. Chem.*, **733**, 1 (1970).

[25] W. Borche, *Berdtsch. Chem. Ges*, **40**, 2731 (1907).

[26] S. Sethna and R. Phadke, *Organic Reactions*, **7**, 1 (1953).

[27] W. R. Hurtley, *J. Chem. Soc.*, **1929**, 1870.

Table 1

Urethane-type nitrogen mustards from chromanes and benzochromanes

Compound N°		m.p.[a] °C	Formula	Analytical data								R_f[b]
				Calculated				*Found*				
				C	H	Cl	N	C	H	Cl	N	
V	**a**	oil	$C_{21}H_{26}Cl_4N_2O_6$	46.32	4.81	26.10	5.14	46.05	4.90	26.51	5.29	0.54
	b	78	$C_{16}H_{19}Cl_2NO_4$	53.33	5.32	19.72	3.88	53.68	5.59	20.10	3.89	0.72
	c	88	$C_{17}H_{21}Cl_2NO_4$	54.54	5.65	18.98	3.74	54.00	5.90	19.35	3.69	0.78
VII	R = OCONM	113	$C_{20}H_{21}Cl_2NO_4$	58.53	5.12	17.32	3.41	58.12	5.54	17.80	3.65	0.79
VIII	R = OCONM	oil	$C_{16}H_{21}Cl_2NO_3$	55.48	6.07	20.52	4.04	54.90	5.95	20.55	4.08	0.96

[a] recryst. from ethanol. [b] T.L.C. on Merck Silicagel G; solvent system: cyclohexane: tetrahydrofuran: benzene 2:1:1.

2. *Spectral data.* The new urethane type nitrogen mustards as well as the precursors have been studied by i.r., u.v. and n.m.r. spectra.

Infrared spectra. A detailed discussion of the i.r. spectra of the new derivatives will be published elsewhere. The $\nu_{C=O}$ frequency in the carbamoyl moiety, well separated, especially in $CHCl_3$ solution, was found in the usual range (1709–1742 cm^{-1}) for aryl N,N-disubstituted urethanes.[28,29]

Ultraviolet spectra. The near u.v.spectra of coumarins are characterized by a system of two absorption bands, located at 260–290 nm (K band) and 300–330 nm (B band), respectively.[30] These absorptions were associated to transitions on excited levels, characterized by important contributions of resonance hybrids with polar structures. Accordingly, the substitution with hydroxyl groups at positions (5,7) where conjugation with the lactonic carbonyl can occur, cause important changes in the u.v. spectra.[31] The 310 nm band of the unsubstituted coumarin is bathochromically and hiperchromically displaced, while the 275 nm band is transformed in one or more inflexions of much lower intensity as against the initial band. Other authors[30] consider that the new intense band of lower frequency results from K and B bands overlapping. Additional inflexions (even a maxima for the 5-substituted derivatives) appear in the range 240–260 nm.[30–32]

In the 6-hydroxy-derivatives, the "coumarinic" aspect of the spectra is preserved, with strong bathochromic effects, especially on E and B bands.

Conversion of the hydroxy-coumarins into carbamates with the subsequent interruption of the conjugation, results in a return to coumarin-type spectra, with two absorption bands in the above-mentioned regions and with a reversal of the relative intensities (see table 3).

In the spectra of 4-chromanone (in 3-methylpentane), the 312 nm (I) and 246 and 252 nm (II) bands were assigned to $^1L_b \leftarrow {}^1A$ and $^1L_a \leftarrow {}^1A$ benzene-type transitions.[33] The bands are bathochromically displaced and intensified due to benzene ring conjugation with the coplanar carbonyl and to the interaction with the pyran oxygen atom, which causes additional shift and intensification as against α-tetralone.

Hydroxyl substitution at 5- or 7-positions, where conjugation with the carbonyl group can take place results in important bathochromic shifts, especially of band II. As in the case of coumarin derivatives, on carbamoylation a return to spectra, similar — in wavelength and intensity of the bands — with that of the unsubstituted chromanone, was observed (see table 4).

As expected, the 7-substituted chromanes (VIII) show little displacements as against 2,2-dimethyl-chromane (λ_{max} nm : 268·5 infl. 277 and 284),[34] but the fine structure is lost.

---

[28] F. Chiraleu, *Rev. Roumaine Chim.*, **11**, 999 (1966).

[29] I. Niculescu-Duvăz, Ph. D. Thesis, Timişoara, 1973.

[30] K. Sen and P. Bagghi, *J. Org. Chem.*, **24**, 314 (1959).

[31] A. Mangini and R. Paserini, *Gazz. chim. Ital.*, **87**, 243 (1957).

[32] F. Eiden and P. Meins, *Arch. Pharm.*, **305**, 124 (1972).

[33] P. J. Griffiths and G. P. Ellis, *Spectrochim. Acta*, **28 A**, 707, 1972.

[34] J. Burgidou, H. Christol and N. Mousseron, *Compt. rend.*, **256**, 3149 (1963).

Table

Urethane-type nitrogen mustards

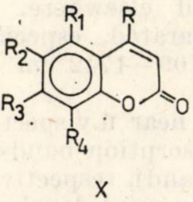

X

Compound	R	R_1	R_2	R_3	R_4	m.p.[a] °C	Formula
X A	CH_3	H	H	OCONM	H	105	$C_{15}H_{15}Cl_2NO_4$
X B	CH_3	OCONM	H	CH_3	H	106,5	$C_{16}H_{17}Cl_2NO_4$
X C	CH_3	OCONM	H	OCONM	H	115	$C_{20}H_{22}Cl_4N_2O_6$
X D	CH_3	H	OCONM	OCONM	H	103	$C_{21}H_{22}Cl_4N_2O_6$
X E	CH_3	H	H	OCONM	OCONM	182	$C_{20}H_{22}Cl_4N_2O_6$
X F	CH_3	H	OCONM	H	H	119	$C_{15}H_{15}Cl_2NO_4$
X G	H	H	H	OCONM	H	125	$C_{14}H_{13}Cl_2NO_4$
X H	H	CH_3	H	OCONM	H	110	$C_{15}H_{15}Cl_2NO_4$
X I	R = OCONM					136	$C_{18}H_{15}Cl_2NO_4$

[a] recryst. from methylene chloride: petroleum ether (30–60).

[b] TLC on silicagel Merck F 254 – solvent system (exceptions were otherwise noted): Cyclohexane: Tetrahydrofuran – benzene: methanol (2: 1: 1: 1).

The n.m.r. spectra were used for structural assignments in the new compounds. The results are given in table 5.

a) *Chromane-4-ones*. The signals arising from the pyrane ring namely the C–3 protons ($\tau = 7.22 - 7.32$) and those belonging to the C_2 – gem CH_3 groups ($\tau = 8.49 - 8.57$) are diagnostic for these protons in all examples previously reported.[35–37] The C_5 and C_7 positions in a

---

[35] W. E. Parham and L. D. Huestis, *J. Amer. Chem. Soc.*, **84**, 813 (1962).

[36] N. I. Bruckner and N. L. Bauld, *J. Org. Chem.*, **37**, 2359 (1972).

[37] A. C. Waiss and J. Corse, *J. Amer. Chem. Soc.*, **87**, 2068 (1965).

2

from coumarin derivatives

Analytical data								
Calculated				*Found*				R_f[b]
C	H	Cl	N	C	H	Cl	N	
52.32	4.30	20.64	4.07	52.62	4.60	20.60	4.10	0.53[c]
53.63	4.75	19.83	3.92	54.02	4.86	20.18	4.02	0.48[c]
45.45	4.17	26.89	5.30	45.60	4.56	26.60	5.23	0.49[c]
45.45	4.17	26.89	5.30	45.67	4.50	26.63	5.40	0.85
45.45	4.17	26.89	5.30	45.07	4.01	26.90	5.22	0.86
52.32	4.30	20.64	4.07	52.55	4.15	20.85	4.21	0.84[d]
50.90	3.90	21.52	4.24	51.00	4.37	21.90	4.37	0.82
52.32	4.36	20.64	4.07	51.94	4.40	21.10	4.30	0.74
56.89	3.94	18.68	3.68	57.79	4.32	18.60	4.01	0.80

[c] Solvent system: Cyclohexane: tetrahydrofuran: benzene (2: 1: 1).

[d] Solvent system: Toluene: ethylacetate: methanol: acetic acid (20: 5: 5: 1).

chromane derivative are conjugated to a far greater extent with the γ-pyrone carbonyl group than the other positions, so that the signals arising from the protons at these positions are expected to be located in the weaker field ($\tau_{C5} < \tau_{C7}$). These reasons and the fact the C_8 position is characterized by the highest electron density in the ring, allowed us to assign the positions of the aromatic protons (see table 4). These assignments are in good agreement with previously reported data.[38-39]

---

[38] M. M. Badawi and M. B. E. Fayez, *Indian J. Appl. Chem.*, **5**, 93 (1967).

[39] S. Masamune and N. Castelucci, *J. Amer. Chem. Soc.*, **84**, 2452 (1962).

Table 3

Ultraviolet spectra of coumarin derivatives

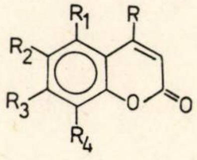

X

R	R_1	R_2	R_3	R_4			K Band		B Band	
					λmax, nm	log ε	λmax nm	log ε	λ max nm	log ε
H	H	H	H	H[a]	—	—	275 248sh	4.02 3.96	310	3.73
CH_3	H	H	H	H[a]	—	—	272 280sh	4.02 3.95	310	3.77
H	H	H	OH	H[b]	246sh 256sh	3.61 3.55	—	—	332	4.07
CH_3	H	OH	H	H[c]	—	—	280	4.06[d]	350	3.74
CH_3	H	H	OH	H[e]	253sh	3.41	290infl	3.73	328	4.14
CH_3	OH	H	CH_3	H	250infl 258	3.82 3.88	—	—	303	4.07
CH_3	OH	H	OH	H[f]	250infl 259	3.75 3.80	—	—	330	4.11
CH_3	H	OH	OH	H	254sh	3.65	298	3.75	353	4.06
CH_3	H	H	OH	OH	264	3.96	—	—	328	4.10
H	CH_3	H	OH	H	246sh	(3.76)	337	4.16	257 sh	3.70
H	H	H	OCONM	H	—	—	288	4.06	318	4.08
CH_3	H	OCONM	H	H	—	—	272 280infl	4.04 3.98	320	3.74
CH_3	H	H	OCONM	H	—	—	278	4.06	314	4.05
CH_3	OCONM	H	CH_3	H	—	—	286	4.02	312infl	3.80
CH_3	OCONM	H	OCONM	H	—	—	282	4.13	308sh	3.99
CH_3	H	OCONM	OCONM	H	—	—	271	4.13	315	4.07
CH_3	H	H	OCONM	OCONM	—	—	280	4.09	3.08	3.95
H	CH_3	H	OCONM	H	—	—	298	4.07	319	3.97

[a] according to[31]; [b] lit: 240 (infl); 325 (4.15)[31]; [c] lit: 227 (4.56); 275 (4.15) 346 (3.7)[31]; [d] E band: 228 (4.34); [e] lit: 240 infl ; 323 (4.1)[30]; [f] lit: 250 infl (3.73); 258 (3.78); 326 (4.09); [g] Compound XI, R=OCONM, λmax(log ε): 266 (4.18), 274(4.23), 292 (3.93), 304 (4.03), 322 (3.97).

Table 4

Ultraviolet spectra of chromane derivatives

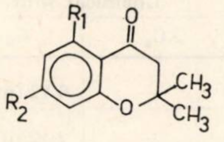

IV

R_1	R_2	Band II		Band I	
		$\lambda_{max,nm}$	log ε	$\lambda_{max,nm}$	log ε
H	H	246[a] 252	4.00 3.92	312	3.58
H	OH	276	—	315	—
CH_3	OH	282[b]	4.12	317	3.77
OH	OH	294[c]	4.15	326 sh	3.81
Compound VIII,	R = OH	286	—	—	—
H	OCONM	260	4.05	320	3.66
CH_3	OCONM	265	4.09	323	3.62
OCONM	OCONM	262	3.93	320	3.57
Compound VIII, R = OCONM		282	—	—	—
Compound VII, R = OCONM		262 infl.	4.04	314 350 360 sh	4.00 3.8 3.81

[a] according to [33] [b] λ_{max}nm (logε) – 233 (4.01); [c]lit λ_{max}nm (log ε): 290 (4.22); 325 sh.

b) *Coumarins*. Characteristic of these compounds is the signal arising from the C_3-protons ($\tau = 3.72 - 3.80$) belonging to the α-pyrone ring.[40-41]

The aromatic protons giving signals at lower values than those of the corresponding protons in chromane-4-ones, reflected the influence of the α-location of the electron-withdrawing carbonyl group. In such compounds the highest electron density is found at C_6. Accordingly, the signal arising at weakest field was assigned to the C_8-proton. These assignments are in good agreement with other data in the literature. [40]

The eight protons belonging to the N,N-bis- (2-chloroethyl) carbamoyl moiety gave a signal as an unresolved multiplet in the range $\tau = 6.08 - 6.24$.

---

[40] M. W. Jarvis and A. G. Moritz, *Austral. J. Chem.*, **21**, 2445 (1968).
[41] E. A. Abu-Mustafa and M. B. E. Fayez, *Canad. J. Chem.*, **45**, 325 (1967).

Table 5

NMR spectral data for the new benzo- and naphthopyran derivatives

Compound	Chemical shift, τ (ppm)[a]						
	C_2 [b]	C_3	C_4	C_5	C_6	C_7 [c]	C_8
V A	8.51 (s)	7.32 (s)	—	6.12 (m) [c]	3.27	6.24 (m)	3.41
V B	8.50(s)	7.29 (s)	—	2.12 (d)	3.24 (m)	6.22 (m)	3.26 (d)
V C	8.57 (m)	7.31 (s)	—	7.31 (s) [d]	3.42	6.25 (m)	3.45
VIII[e]	8.49 (s)	7.22 (s)	—	—	—	6.22 (m)	—
X A	—	3.76 (m)	7.54 (m)[f]	2.40 (d)	2.90 (m)	6.21 (m)	2.80 (m)
X B	—	3.80 (m)	7.54 (m)[f]	6.20 (m)	3.28 (m)	7.54[f]	2.92 (m)
X C	—	3.76 (m)	7.52 (m)[f]	6.22 (m)[c]	3.07	6.25 (m)	2.94
X D	—	3.72 (m)	7.55 (m)[f]	2.56	6.24 (m)[c]	6.24 (m)	2.75
X E	—	3.72 (m)	7.52 (d)[f]	2.47 (d)	2.80 (d)	6.20 (m)	6.08 (m)[c]

[a] Internal standard – tetramethylsilane ; [b] gem-CH_3 (6H) ; [c] $(ClCH_2CH_2)_2NCO_2-C_n$ (8 H) n = 5, 6, 7, 8 ; [d] C5 – CH_3 (arom) (3H) ; [e] assignments of chemical shift for the aromatic protons are uncertain ; [f] C_4-CH_3 (3H).

Table 6

Test results [a]

Compound	Doses [b]		Survival	W_t [c]	T/C [d]
	N°	mg/kg		T – C	
	2	400	3/3	1.0	90
NSC 196219	2	200	3/3	0.3	87
	2	100	3/3	0.0	90
(XA)	2	50.0	3/3	0.5	90
	2	25.0	3/3	0.4	90
	2	400	3/3	–1.6	103
NSC 196220	2	200	3/3	0.0	90
	2	100	3/3	1.0	97
(XE)	2	50.0	3/3	0.2	94
	2	25.0	3/3	–1.0	90
	2	400	3/3	–1.3	90
NSC 196221	2	200	3/3	1.0	97
	2	100	3/3	–0.8	94
(VA)	2	50.0	3/3	–0.6	113
	2	25.0	3/3	0.4	94

[a] These compounds were screened under the auspices of NCII against lymphoid leukemia L1210 in the mouse according to the protocol given in *Cancer Chemother. Rep.*, **3**, *2*, 7 (1972) ; [b] 2 doses administered intraperitoneally at 4 days interval beginning on 2nd day ; [c] Average weight difference between treated (T) andc ontrol (C) animals ; [d] the numerical results are ratios (T/C) of survival times of treated over control mice expressed in per cent ; values ⩾ 125% are positive, denoting activity.

3. *Biological data.* None of the new urethane-type nitrogen mustards showed any significant antitumor activity against Walker 256 carcinosarcoma. It is probable that in the case of this type of derivatives no *in vivo* enzymatic hydrolysis of the carbamoyl moieties occurs (see table 6).

EXPERIMENTAL PART

The m.p. were taken on a Franz Küster — Dresden apparatus and are uncorrected.

The purity of the hydroxy-chromanes and coumarines was checked by elementary analysis and melting points (which agreed with literature data).

1. *2,2-dimethyl-4'-hydroxy-benzo-5,6-chromane-4-one* (*VII*). A mixture of 5 g (0.03 moles) of dry 2,7-dihydroxy-naphthalene, 3.12 g (0.03 moles) 1,1-dimethyl acrylic acid, 25 g freshly melted $ZnCl_2$ and 70 ml $POCl_3$ was allowed to stand for 24 hours at room temperature under occasional stirring. The reaction mixture was poured on crushed ice, the resulting solid was filtered, washed with water and recrystallized from ethanol yielding 3.5 g (70%) (VII).
m.p. 206° Anal. $C_{15}H_{14}O_3$; *Calcd*: C, 74.38; H, 5.78%; *Found*: C, 74.72; H, 6.09%.
I.R. (cm^{-1}); $\nu_{C=O}$: 1643 (KBr, $CHCl_3$); ν_{OH}: 3170 (KBr) 3220 ($CHCl_3$)
U.V. λ_{max} nm (logε): 277 (3.92), 359 (4.03).
T.LC on silicagel Merck F_{254}. Solvent system cyclohexane : tetrahydrofuran : benzene 2 : 1 : 1, R_f=0.63.(VI) was prepared by the same method, with an 66% yield m.p. 232° (ethanol-water).
Anal. $C_{15}H_{14}O_3$; *Calcd*: C, 74.38; H, 5.78%; *Found*: C,74·10; H, 5.90.%
I.R. (cm^{-1}): $\nu_{C=O}$; 1635 (KBr), 1658 ($CHCl_3$); ν_{OH}: 3230 ($CHCl_3$).
U.V. λ_{max} nm (log ε); 254 (4.33), 316 (3.99), 350 (3.99), 364 (4.01); 382 (sh).
T.LC on silicagel Merck F_{254}. Solvent system :cyclohexane :tetrahydrofuran : benzene 2 : 1 : 1, R_f = 0.71.

2. *Mono- and di-N,N-bis-*(*2-chloroethyl*) *carbamoyl derivatives.* V, VII (R = OCONM), VIII (R = OCONM), X, XI (R = OCONM) were prepared by condensation of the respective hydroxy-derivative with N,N-bis-(2-chloroethyl)-carbamoyl chloride[42] in the usual manner.[43]

The carbamoyl derivatives were purified by recrystallization from appropriate solvents (usually ethanol) or by chromatography on Al_2O_3 column. The analytical and spectral data are given in tables 1—5.

3. The u.v. spectra were determined with a CF4 Optica Milano spectrophotometer in ethanol solutions.

4. The i.r. spectra were run on a U.R. 10 Carl Zeiss Jena spectrophotometer.

5. The n.m.r. spectra were run on a Tesla B487 B 80 MHz spectrometer in $CDCl_3$ solution.

ACKNOWLEDGEMENTS. We are indebted to Dr. A. Goldin (NCI) who facilitated the screening of our compounds. We thank Mrs. A. Vasilescu for the n.m.r. data and Mrs. V. Zamfir for technical assistance.

---

[42] A. F. Chilos, L. J. Goldworthy, C. F. Harding, F. E. King, A. W. Nineham, W. I. Noris, S. G. Plant, B. Selton and A. L. C. Tompsett, *J. Chem. Soc.*, **1948**, 2174.

[43] I. Niculescu-Duvăz, V. Feyns and E. Grant, *Canad. J. Chem.*, **44** 1102 (1966).

Revue Roumaine de Chimie, **20**, *5*, 677—685 (1975)

RECHERCHES DANS LE DOMAINE DE LA COPOLYMÉRISATION MULTICOMPOSANTE EN UTILISANT UN ORDINATEUR

MARGARETA TOMESCU et KALMAN PUSZTAI
Institut Polytechnique, Bucarest, 1—3, str. Polizu

Reçu le 25 janvier 1974

Ce travail présente un programme de calcul qui décrit la copolymérisation multicomposante des systèmes de monomères obéissant au modèle cinétique terminal. On a calculé la variation de la composition du mélange des monomères et de la composition instantanée et moyenne du copolymère en fonction de la conversion et les paramètres d'hétérogénéité. La composition théorique correspond aux résultats expérimentaux.

1. INTRODUCTION

Bien que dernièrement de nombreux brevets $^{1-6}$ proposent à côté des terpolymères, des copolymères à chaîne formée de plus de trois composantes, le processus de copolymérisation multicomposante radicalaire est encore très peu connu.

A cause des difficultés expérimentales et de calcul qui augmentent en même temps que le nombre de composantes du système, il existe dans ce domaine, même avec les moyens offerts par l'ordinateur, un nombre réduit et insuffisamment vérifié expérimentalement de publications.$^{7-13}$

Ce travail présente un programme simulant le processus de la copolymérisation multicomposante, en calculant avec des équations de composition simplifiées, spécialement modifiées, la composition du mélange de monomères, la composition instantanée et moyenne des copolymères à différents taux de conversion et les paramètres d'hétérogénéité.

---

[1] K. Gulbinsk, Ger. Offen 2.058.773, 31 mai 1972 ; *Chem. Abstr.*, **77**, 8940 (1972).

[2] T. Ohfuka, Y. Ichikawa et Y. Kantani, Japan Pat. 6 142 051, 13 décembre 1971 ; *Chem. Abstr.*, **77**, 115860 (1972).

[3] T. Ohfuka, Y. Ichikawa et N. Kanamori, Japan Pat. 7 205 447, 16 février 1972 ; *Chem. Abstr.*, **77**, 141312 (1972).

[4] D. R. St. Cyr, Ger. Offen 2 126 225, 13 janvier, 1972 ; *Chem. Abstr.* **76**, 22 (1972).

[5] E. S.Barabaș et M. M. Fein, Ger. Offen 2 103 898, 12 août 1971 ; *Chem. Abstr.*, **75**, 152537 (1971).

[6] H. Kitawa et I. Isao, Japan Pat. 7 142 332, 14 décembre 1971 ; *Chem. Abstr.*, **77**, 115869 (1972).

[7] C. Walling et E. R. Briggs, *J. Amer. Chem. Soc.*, **67**, 1774 (1945).

[8] R. C. Chapin, G. E. Ham, et R. G. Fordyce, *J. Amer. Chem. Soc.*, **70**, 538 (1948).

[9] A. Valvassori et G. Sartori, *Rend. Inst. Lombardo Sci. Lettere A.*, **96**, 107 (1962).

[10] G. E. Ham, *J. Polymer. Sci. A.*, **1964**, 2735.

[11] E. Friedman, *J. Polymer. Sci. C—3*, **1965**, 815.

[12] J. Seiner, *Polymer. Sci. A*, **3**, 2401 (1965).

[13] H. J. Kantow et O. Fuchs, *Makromol. Chem.*, **83**, 244 (1965).

2. RELATIONS DE CALCUL

La littérature nous offre des relations de calcul décrivant la copolymérisation multicomposante : les équations différentielles de composition de Walling-Briggs,[7] les équations de Chapin, Ham et Fordyce [8] et les équations simplifiées établies par Valvassori et Sartori [9] et séparément par Ham.[10]

Les conclusions d'un travail antérieur [14] nous ont confirmé, en comparant avec d'autres équations connues, les avantages des équations simplifiées, à savoir : des résultats formulés mathématiquement d'une manière simple et précise, ce qui explique leur choix pour la simulation mathématique du processus de la copolymérisation.

Les équations simplifiées de composition, ainsi que les équations de Walling-Briggs deviennent indéterminées quand il y a, dans le système, des monomères à vitesses de réactions d'autopropagation négligeables, introduisant la valeur zéro pour certains rapports de réactivité.

L'élaboration d'un programme résolvant n'importe quel système, indifféremment du nombre de composantes et de la présence et du nombre de monomères incapables d'homopolymérisation radicalaire, exige l'emploi d'équations simplifiées de composition, modifiées par nous dans un travail antérieur, [14] sous une forme qui est aussi valable pour ce cas-ci :

$$
\begin{aligned}
\mathrm{d}[M_1] : \mathrm{d}[M_2] : \ldots : \mathrm{d}[M_n] = m_1 : m_2 : \ldots : m_n : \\
[M_1] \sum_{i=1}^{n} \frac{[M_i]}{r_{1i}} : \\
: \frac{[M_2]}{r_{12}} \sum_{i=1}^{n} [M_i] \frac{r_{21}}{r_{2i}} : \\
\cdots\cdots\cdots\cdots \\
: \frac{[M_{h_1}]}{r_{1h_1}} \sum_{i=1}^{n} [M_i] R_{h_1 1i} : \\
\cdots\cdots\cdots\cdots \qquad (1) \\
: \frac{[M_{h_k}]}{r_{1h_k}} \sum_{i=1}^{n} [M_i] R_{h_k 1i} : \\
\cdots\cdots\cdots\cdots \\
: \frac{[M_2]}{r_{12}} \sum_{i=1}^{n} [M_i] \frac{r_{z1}}{r_{zi}} : \\
\cdots\cdots\cdots\cdots \\
: \frac{[M_n]}{r_{ln}} \sum_{i=1}^{n} [M_i] \frac{r_{n1}}{r_{ni}} :
\end{aligned}
$$

---

[14] Cr. Simionescu et M. Tomescu, données non publiées.

Dans le système d'équations (1), z prend toutes les valeurs, excepté $h_1, \ldots h_k$.

Le système d'équations différentielles (1) décrit la composition molaire instantanée des copolymères (m) en fonction de la composition molaire du mélange de monomères $[M]$, des rapports de réactivité binaire r et des rapports de réactivité multicomposante R.

$M_{h_1}, \ldots, M_{h_k}$ représentent les k monomères incapables d'homopolymériser radicalairement.

La valeur des constantes $R_{zhi} = r_{zh}/r_{zi} = k_{zi}/k_{zh}$ peut être établie en partant des expériences de copolymérisation multicomposante, ou peut être prévue par calcul à l'aide du schéma Q-e d'Alfrey et Price.[15] On a noté par k_{zi} les constantes de vitesse des réactions de propagation, qui caractérisent l'attaque d'un monomère i par un radical z.

Lorsque toutes les composantes du système homopolymérisent, les équations (1) gardent la même forme que les équations simplifiées.

Pour établir la loi de variation de la composition instantanée du copolymère en fonction du taux de conversion pour un mélange de monomères initial donné, c'est-à-dire pour intégrer les équations différentielles, nous avons appliqué une méthode numérique de calcul en étapes successives. On considère que sur un petit intervalle de conversion $\Delta\alpha$, la composition du copolymère se maintient constante. Le choix de l'incrément de conversion a été discuté dans les publications.[11,16] On a constaté que la réduction de l'incrément sous 1% n'augmente pas sensiblement la précision des résultats.

La composition molaire instantanée du copolymère à l'étape du calcul «*t*» a été calculée par la relation [14] :

$$m_z = \frac{[M_z]\dfrac{r_{z1}}{r_{1z}} \sum\limits_{i=1}^{n} [M_i]\, r_{zi}^{-1}}{\sum\limits_{\substack{i=1\\ j=1}}^{n} [M_j]\dfrac{r_{j1}}{r_{1j}} \left([M_i]\, r_{ji}^{-1}\right)} \tag{2}$$

$z = 1, 2, \ldots, n.$

Les équations (2) représentent une forme modifiée des équations simplifiées, plus utile pour le calcul numérique.

La composition molaire du mélange des monomères, non réagis à l'étape de calcul « *t* » qui est utilisé comme mélange initial dans l'étape suivante de calcul, est décrite par l'expression [12] :

$$[M_z]_t = ([M_z]_0 - [m_z^*]_t\, \alpha_t)/(1 - \alpha_t) \tag{3}$$

où

$[M_z]_0$ et $[M_z]_t$ — représente la fraction molaire du monomère z dans le mélange initial, et respectivement à l'étape de calcul « *t* »,

---

[15] T. Alfrey et C. C. Price, *J. Polymer. Sci.*, **3**, 772 (1948).

[16] K. R. Chan et E. V. Meyer, *J. Polymer. Sci. C.*, **25**, 11 (1968).

$[m_z^*]_t = \sum_{i=1}^{t} [m_z]_t$ — est la fraction molaire moyenne de la composante z dans le copolymère cumulé à l'étape « t » et $\alpha_t = t\Delta\alpha$—est la conversion molaire à l'étape de calcul « t ».

Pour l'étude des propriétés physiques et chimiques et pour les calculs d'optimisation de la composition des copolymères, il est nécessaire de connaître l'écart de la composition des copolymères de l'homogénéité parfaite, exprimée par l'égalité $[m_i] = [M_i]$. En vue de la technique de calcul appliquée à l'élaboration du programme, il est aisé d'employer le facteur d'hétérogénéité d_M déduit par Seiner[17] et modifié par nous dans les termes des rapports de réactivité dans un travail antérieur[14] :

$$\mathrm{d}_M = \sum_{j=1}^{n} [M_j]\,\mathrm{d}_j \tag{4}$$

dans lequel :

$$\mathrm{d}_j = \left| 1 - \frac{\dfrac{r_{j1}}{r_{1j}} \sum\limits_{i=1}^{n} [M_i]\, r_{ji}^{-1}}{\sum\limits_{\substack{i=1\\j=1}}^{n} [M_j] \dfrac{r_{ji}}{r_{ij}} \left([M_i]\, r_{ji}^{-1}\right)} \right| \tag{5}$$

La valeur zéro pour le paramètre d_M indique un copolymère ayant une composition parfaitement homogène, correspondant à la composition azéotrope.

3. DESCRIPTION DU PROGRAMME

La manière de calcul décrite a été utilisée pour l'élaboration d'un programme fournissant des informations sur la copolymérisation des systèmes de monomères obéissant au modèle cinétique terminal. Le programme calcule sur la base molaire et du poids, pour chaque série de données initiales, jusqu'à la conversion finale spécifiée, en pas de conversion de 1 %, la composition instantanée et moyenne des copolymères, la composition du mélange de monomères non réagis et les paramètres d'hétérogénéité d_M. En pratique, le programme peut calculer tous les systèmes de monomères, indifféremment du nombre de composantes et de la présence et du nombre de monomères incapables d'homopolymériser de manière radicalaire.

Le premier numéro du programme introduit représente l'ordre du système, après quoi on introduit les données initiales M_0, W, r_{ij}. On a exprimé par W les poids moléculaires de monomères.

Le calcul finit, soit en arrivant à la conversion finale établie, soit par l'annulation de n—1 des composantes.

---

[17] J. Seiner, *J. Polymer. Sci.* *A.* **3**, 3025 (1965).

Avec ce programme on peut calculer consécutivement plusieurs systèmes, le JOB prenant fin par l'introduction d'une carte de données vide ($n = 0$).

Les résultats du programme (m, m^*, p, M, P, α_g, d_M) sont marqués sur la bande imprimée à chaque intervalle de calcul, ou à chaque autre intervalle en fonction des options.

Les résultats peuvent être interprétés sous forme de diagrammes de variation à l'aide du plotter.

Le programme a été écrit en FORTRAN IV, contient 82 instructions et a été exécuté sur un ordinateur IBM 360.

TEXTE DU PROGRAMME FORTRAN

```
// FOR
* IOCS (CARD, 1403 PRINTER)
* LIST ALL
*ONE WORD INTEGERS
*EXTENDED PRECISION
      DIMENSION R (50, 50), W (50), CM (2,50), A (3,50), K (50), P (2, 50)
    4 READ (2, 101) N
      IF (N) 900, 2, 900
  900 READ (2, 100) ((R (I, J), J = 1, N) I = 1, N) (W (I), I = 1, N), (CM) (I, J) J = 1,N)
  100 FORMAT (10 FB8.4)
  101 FORMAT (I2)
      ALP = 0.
      DO 303 IJ = 1, N
      IF (R (1J, IJ)-10. ** (-6)) 303, 300, 303
  300 DO 225 IL = 1, N
  225 R (IJ, IL))= 1./R (IJ, IL)
  303 CONTINUE
      DO 200 I = 1, N
  200 A (3, I) = 1.
      WRIIE (5,50)
   50 FORMAT ('1', T32, 'ECUAŢII DE COMPOZIŢIE'/T26, 'PENTRU COPOLIMERI-
      ZAREA 'QUATERNARA'///T4, 'DATE INIŢIALE')
      WRITE (5, 98) ((R (I,J), J = 1, N), I = 1, N)
   98 FORMAT ('MATRICEA R (I, J)', // 2X, 10 (F9.4,2 X))
      WRITE (5, 198) (W(I), I = 1, N)
  198 FORMAT ('MATRICEA W(I)' //2X, 10 (F9.4,2X))
      WRITE (5, 298) (CM(I, J), J=1, N)
  298 FORMAT ('MATRICEA MO (I)' //2X, 10 (F9.4,2X))
      DO 201 I = 1, N
      K(I) = 0
  201 CM (2, I) = CM(1, I)
      PPP = 0.
      DO 202 L = 1, N
  202 PPP = PPP + CM (2, L) * W (L)
      P10 = CM (2,1)* W (1)/PPP
  901 DO 204 J = 1, N
      A (1, J) = 0.
      DO 205 L = 1, N
  205 A (1, J) = A (1, J) + CM (2, L)/R (J, L)
  204 A (1, J))= CM (2, J) *A (I, J) *R (J, 1)/R (I, J,
      A (1, N + 1) = 0.
      DO 206 L = 1, N
  206 A (1, N + 1) = A (I, N+1) + A (1, L)
      DO 208 L = 1, N
    A (2, L) = A (1, L)/A (1, J)
208 A(3, L) = (A(3, L)* (1—I) + A (2, L))/I
    PN = 0.
    DO 209 L = 1, N
209 PN = PN + A (3, L)* W (L)
    DO 210 L = 1, N
210 P (1, L) = A (3, L) * W (L)/PN
    ALP = ALP + 0.01
    CNUM = 1. — ALP
    DO 211 L = 1, N
    IF (CM (2, L)) 80, 211, 301
301 CM (2, L) = (CM (1, L) — A (3, L) * ALP)/CNUM
211 CONTINUE
    PPNUM = 0.
    DO 212 L = 1, N
212 PPNUM = PPNUM + CM (2, L) * W (L)
    DO 213 L = 1, N
213 P (2, L) = (CM (2, L) * W (L)/PPNUM
    BALP = ALP*A  (3,1)* P10/(CM(1,1) * P (1,1))
    WRITE  (5,20) ALP, (A  (2, J), J = 1, N), BALP
 20 FORMAT  (6 (3X, E16 .9))
801 FORMAT (6 (3X, E16.9))
    WRITE  (5,801) (A (3, J), J = 1, N), ((P (L, J), J = 1, N), L = 1, 2), (CM (2, M),
    M = 1, N)
    DO 214 L = 1, N
    IF (CM (2, L)) 302, 302, 214
302 CM (2, L) = 0.
    K (L) = 1
214 CONTINUE
    KO = 0.
    DO 215 L = 1, N
215 KO = KO + K (L)
    IF (KO—N + 1) 800, 4, 4
800 IF (ALP—0.1) 901, 4, 4
 80 WRITE (5, 99)
 99 FORMAT ('EROARE IN PROGRAM')
 2  CALL EXIT
    END
```

4. EXEMPLE DE CALCUL

Pour illustrer ces affirmations nous avons choisi comme exemple la copolymérisation quaternaire de l'acrylonitrile, de l'acide méthacrylique, du styrène et du chlorure de vinylidène, menée jusqu'à la conversion finale. Les constantes de copolymérisation utilisées dans le calcul ont été prises dans la littérature.[18,19]

Les diagrammes des figures 1 et 2 décrivant la variation de la composition molaire du mélange de monomères, respectivement de la composition instantanée du copolymère avec la conversion, ont été tracés à l'aide du plotter 1627 par des points de deux en deux pas, l'ordonnée et l'abscisse de chaque courbe étant identifiée avec les notations utilisées dans le texte.

---

[18] L. J. Young, *J. Polymer. Sci.*, 54, 411 (1961).

[19] Cr. Simionescu, N. Asandei et A. Liga, *Makromol. Chem.*, **110**, 278 (1967).

L'analyse des figures 1 et 2 nous donne des informations utiles sur la composition des monomères dans le processus de copolymérisation, mettant en évidence les changements qui apparaissent dans la composition du mélange de monomères, comme conséquence de leur réactivité diffé-

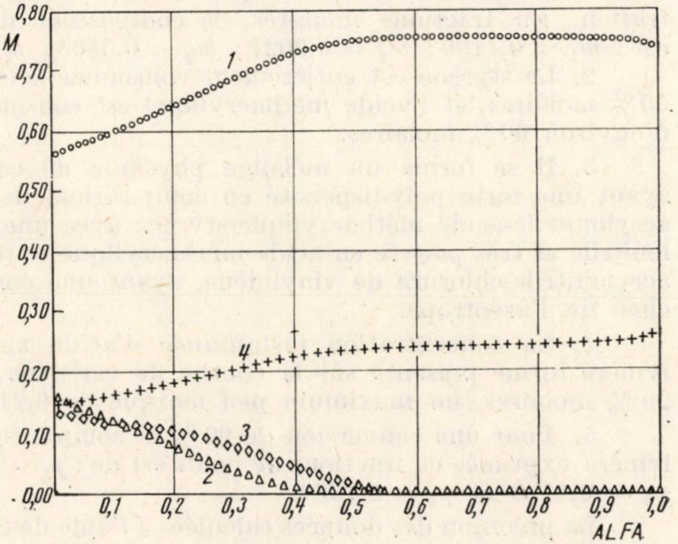

Fig. 1. — Variation de la composition du mélange de monomères avec la conversion. Système : acrylonitrile-acide méthachrylique-styrène-chlorure de vinylidène.
$/M_1/ = 0,7000$; $/M_2/_0 = 0,1000$; $/M_3/_0 = 0,1000$; $/M_4/_0 = 0,1000$, fractions de poids ; $r_{12} = 0,10$; $r_{13} = 0,04$; $r_{14} = 0,91$; $r_{21} = 2,75$; $r_{23} = 0,70$; $r_{24} = 3,00$; $r_{31} = 0,41$; $r_{34} = 2,00$; $r_{41} = 0,37$; $r_{42} = 0,15$; $r_{43} = 0,14$; $r_{32} = 0,15$.

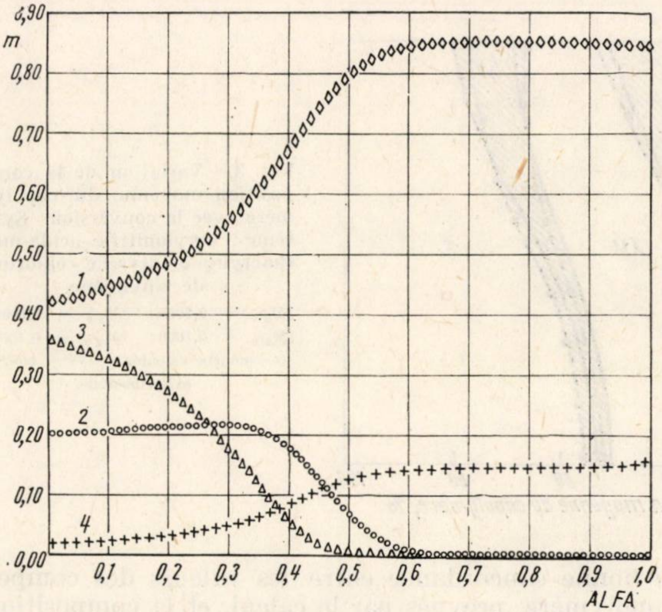

Fig. 2. — Variation de la composition instantanée du copolymère avec la conversion. Système : acrylonitrile-acide méthachrylique - styrène - chlorure de vinylidène.
$/M_1/_0 = 0,7000$; $/M_2/_0 = 0,1000$; $/M_3/_0 = 0,1000$; $/M_4/_0 = 0,1000$.

rente et qui sont visibles dans les caractéristiques de la distribution des compositions au sein de copolymères. Les calculs indiquent les particularités suivantes:

1. L'acrylonitrile et le chlorure de vinylidène entrent dans le copolymère à une moindre concentration que dans le mélange, pendant que le styrène et l'acide méthacrylique entrent à une plus grande concentration. En fractions molaires, la composition du copolymère obtenu est : $m_1 = 0{,}4190$; $m_2 = 0{,}2027$; $m_3 = 0{,}3593$; $m_4 = 0{,}0190$.

2. Le styrène est entièrement consommé à la conversion d'environ 50 % molaires, et l'acide méthacrylique est consommé à une conversion d'environ 60 % molaires.

3. Il se forme un mélange physique de copolymère quaternaire ayant une forte polydispersité en composition, de copolymère ternaire : acrylonitrile-acide méthacrylique-styrène avec une teneur riche en acrylonitrile et très pauvre en acide méthacrylique et de copolymère binaire : acrylonitrile-chlorure de vinylidène, ayant une composition très rapprochée de l'azéotrope.

4. La concentration instantanée d'acide méthacrylique du copolymère formé présente sur la courbe de variation, à une conversion de 29 % molaires, un maximum peu marqué de 0,2175 fractions molaires.

5. Pour une conversion de 90 % la composition moyenne, du copolymère exprimée en fractions de poids est de : $p_1 = 0{,}5471$; $p_2 = 0{,}1423$; $p_3 = 0{,}1723$ et $p_4 = 0{,}1383$.

La précision des données calculées à l'aide de ce programme apparaît clairement dans la figure 3, en les comparant aux données expérimentales obtenues dans un travail [14] précédent.

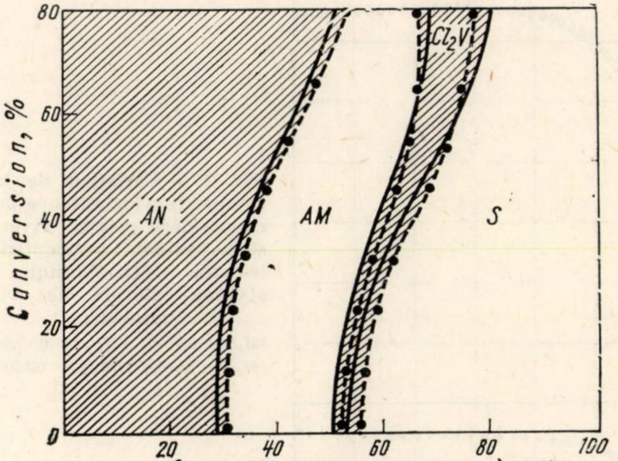

Fig. 3. — Variation de la composition moyenne du copolymère avec la conversion. Système : acrylonitrile-acide-méthacrylique - styrène - chlorure de vinylidène.
$/M_1/_0 = 0.7000$; $/M_2/_0 = 0.1000$; $/M_3/_0 = 0.1000$; $/M_4/_0 = 0.1000$.
—— courbe calculée ; — — — courbe expérimentale.

On constate une bonne concordance entre les valeurs des compositions moyennes du copolymère prévues par le calcul, et la composition des copolymères déterminée expérimentalement. Cette concordance confirme la validité et la précision obtenues par la technique de calcul discutée

Il résulte que la simulation du processus de copolymérisation multicomposante décrite par le modèle cinétique terminal offre une image complexe et assez proche de l'image réelle. On est arrivé à la même conclusion dans le cas du système quaternaire : acrylonitrile-acrylate de butyle-styrène-chlorure de vinylydène. Les diagrammes de la figure 4 mettent en évidence le comportement particulier de l'acrylonitrile, dont la concentration dans le polymère reste pratiquement constante et égale à celle du mélange initial de monomères. La courbe théorique et la courbe expérimentale de variation avec la conversion de la concentration moyenne d'acrylonitrile dans la chaîne macromoléculaire ont la même allure, et leur décalage est explicable compte tenu de la précision de la valeur des rapports de réactivité utilisés dans les calculs, des erreurs expérimentales et des limites des équations de la composition.

En conclusion, nous pouvons affirmer que les données calculées avec ce programme donnent une bonne image du comportement des monomères dans le processus de copolymérisation radicalaire. Les auteurs se sont proposés de les utiliser pour ajuster la distribution de la composition des copolymères par l'addition incrémentaire du monomère actif du système et aussi dans des calculs de sélection de la composition du copolymère selon des critères d'homogénéité.

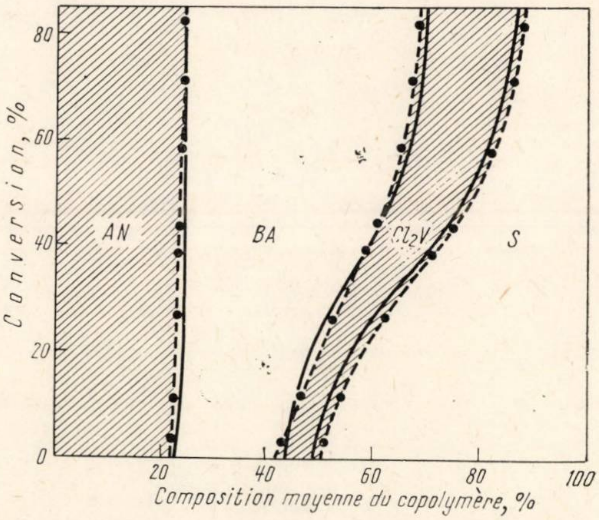

Fig. 4. — Variation de la composition moyenne du copolymère avec la conversion. Système : acrylonitrile-butylacrylate-styrène-chlorure de vinylidène. $/M_1/_0 = 0{,}4000$; $/M_2/_0 = 0{,}3000$; $/M_3/_0 = 0{,}2000$; $/M_4/_0 = 0{,}1000$. $r_{12} = 1{,}003$; $r_{13} = 0{,}91$; $r_{14} = 0{,}04$; $r_{21} = 1{,}005$; $r_{23} = 0{,}83$; $r_{24} = 0{,}15$; $r_{31} = 0{,}37$; $r_{32} = 0{,}88$; $r_{34} = 0{,}14$; $r_{41} = 0{,}41$; $r_{42} = 0{,}76$; $r_{43} = 2{,}00$. —— courbe calculée ; – – – courbe expérimentale.

Ce travail a été présenté au Congrès sur l'Emploi des Calculateurs Electroniques en Génie Chimique organisé par la Société de Chimie Industrielle, à Paris, avril 1973.

Revue Roumaine de Chimie, 20, 5, 687–698 (1975)

AMORPHOUS-CRYSTALLINE COUPLING IN POLYETHYLENE. II[1]

DTA STUDY OF THE CRYSTALLINE MORPHOLOGY IN CHLORINATED POLYETHYLENE

GH. DRĂGAN
Institute of Chemical Research, ICECHIM, Spl. Independenţei 202, Bucharest, Romania

Received January 4, 1974

The melting process of high-density polyethylene (PE) and of chlorinated samples in suspension has been investigated by thermodifferential analysis (DTA). The occurrence of endotherm T_m^1 in samples annealed at 125° for 1 hr is interpreted as a separation of amorphous areas to which chlorine atoms have been preferentially attached, from lamellar areas. Changes observed in melting endotherms and also in IR spectrum have been discussed, considering both observations made by other authors and previous conclusions regarding the general separation conditions for the separation of amorphous and crystalline substructures existing in PE. The amorphous-crystalline coupling observed in annealed chlorinated samples is discussed in terms of the thermodynamics of order-disorder transitions.

Semicrystalline polymers, like most solid-crystalline substances, in fact, have a mesophasic structure [2] in which the ordered, purely crystalline areas alternate with disordered areas. In parallel with the development of experimental procedures for the study of crystalline morphologies, the thermal, mechanical and chemical treatments were found to induce specific changes of these two phases, in the materials. The materials resulted from the treatment will have the two phases more clearly separated relative to the initial one.[1] The separation degree expressed by the induced morphological changes may be correlated with the extension of the applied treatments, thus deducing structural information on the material itself. With polymers, this information is expressed in terms of molecular configuration and conformation.[1]

Chemical treatments provide the advantage of non-uniformly inducing molecular configuration transitions in the two phases and their separation as a result of these changes is much more distinct than with alternate treatments. This kind of studies are intensively carried out, particularly on polyethylene (PE). Among the frequently met chemical treatments, we may list : oxidative degradation,[3,4] chlorination, [5-10] bromination, [7,8], γ-irradiation, [11,13] and various combined treatments (such as γ-irradiation and styrene-based treatment [13]). In all these studies, the separation of the crystalline (lamellar) phase from the amorphous one is expressed by the unitary model, suggestively termed as "shish kebab".[8] This model proposes a reordering of already existing lamellae in the block-mosaic [13-15] structure of the initial polymer, by achieving a relative spatial equidistance. This *interlamellar order* [1] is a result of the chemical attack during the period of treatment, preferentially of interlamellar disordered areas.[3,4,11,12] By their nature, these amorphous areas admit a usually uniform chemical attack (grafting, degradation by rupture of chains, degradation-reticulation, etc.). In this manner, the dimensions and the differences in molecular configuration of interlamellar areas impose a clear separation of the two phases.

---

[1] Part I. GH. DRĂGAN, *Materiale Plastice*, **10**, 87 (1973).

[2] H. MARK and V. A. TOBOLSKY, "Physical Chemistry of High Polymers", chap. VII, Wiley, New York, 1955.

The separation of the amorphous phase from the crystalline phase in the particular case of PE is the subject of this series of papers. In the first paper [1] it was concluded that this separation phenomenon is common for thermal, mechanical and chemical treatments. On the other hand, the extension of this separation was found to depend on the conformation and the configuration of the material. Therefore, a combination of these treatments may provide information on the molecular conformation and configuration of the polymer. The problem may also be considered the other way, i.e.by knowing the separation of the two phases (suggestively termed "amorphous-crystalline coupling") deduced by means of the structural method we may reconstitute the thermal, mechanical and chemical history of the material.

Hosemann and co-workers [15] developed the small-angle X-ray scattering method for the study of the correlation of the amorphous-crystalline coupling in PE, applying thermomechanical [15] and mechano-chemical [13] treatments. On the other hand, adiabatic calorimetry [1,16] is also largely used in the study of this coupling both in the case of PE [1] and in the case of micromolecular substances defined as "glassy-crystals" [16]. Although the study of these methods is in an early stage, both seem to be exclusive, no other experimental methods being approached for further information.

---

[3] R. P. Palmer and A. J. Cobbold, *Makromol. Chem.*, **74**, 174 (1964).

[4] A. Peterlin and G. Meinel, *J. Polymer Sci.*, **B3**, 1059 (1965).

[5] A. Keller, W. Matreyek and F. H. Winslow, *ibidem*, *A*2, **10**, 937 (1972).

[6] V. Era and J. J. Lindberg, *ibidem*, **62**, 691 (1962).

[7] T. Nagakawa and S. Yamada, *J. Appl. Polymer Sci.*, **16**, 1997 (1972).

[8] I. R. Harrison and E. Baer, *J. Polymer Sci.*, **B9**, 843 (1971).

[9] V. A. Era, *Makromol. Chem.*, **167** , 321 (1973).

[10] A. V. Era and L. L. Chapoy, *Acta Chem. Scand.*, **27**, 722 (1973).

[11] N. Kusumoto, T. Yamamoto and M. Takayanagi, *J. Polymer Sci.*, *A2*, **9**, 1273 (1971).

[12] W. Glenz, A. Peterlin and W. Wilke, *ibidem*, *A2*, **9**, 1243 (1971).

[13] H. Cackovic, R. Hosemann, and J. Loboda-Cackovic, *Kolloid — Z. Z. Polymere*, **247**, 830 (1971).

[14] R. Hosemann, *J. Appl. Phys.*, **34**, 25 (1963).

[15] J. Loboda-Cackovic, R. Hosemann and H. Cackovic, *Kolloid — Z. Z. Polymere*, **247**, 824 (1971).

[16] See for example K. Adachi, H. Suga and S. Seki, *Bull. Chem. Soc. Japan*, **45**, 1960 (1972).

As has been seen,[1,16] the differential thermal analysis (DTA) roughly reproduces the more precise results of adiabatic calorimetry. However, DTA is a largely applied method for the time being due to convenience of manipulation and rapidity in obtaining results. Compared to the above mentioned methods, it is not basically an absolute method, hence it is not purely quantitative and the results obtained are of an estimative and orientative nature. This is how the present paper considers and applies this method. The conclusions on the amorphous-crystalline coupling found in samples of initial and chlorinated PE are supplemented by specific changes observed in the IR spectrum. In this way,the results of other authors, obtained on similarly treated samples are confirmed, and so are the previously advanced hypotheses.[1]

EXPERIMENTAL

Preparation of samples. The sample of initial polyethylene identified as PEL 3 belonging to the homologous series consisting of 3 types, was selected as an initial polymer proposed for chlorination.[17] All these types were polymerized under similar stereospecific conditions, resulting in basically linear molecular species. Table 1 gives the more significant characteristics of these initial polyethylenes. The IR spectrum reveals a weak presence of the band at 1320—1350 cm^{-1}, which is a characteristic band of branched species.[18] The relative height of the 1350 cm^{-1} band against 721 cm^{-1} band is a measure of the density of conformational defects (table 1).

Table 1

Data on PE linear species designated as PEL

PEL	M_η x 10^{-5}	ρ g/cm^3	Q^a %	ΔH^b_m 95/3 arb. unit.	ΔH^b_m 125/1 arb. unit.	$I_{721}{}^c$ / I_{1350}
LPE 1	0.8	0.965	67	55	112	8.00
LPE 2	1.0	0.955	60	42	97	7.60
LPE 3	1.5	0.955	62.8	46.7	115	9.66

[a] Crystallinity degree of the untreated polymer obtained from the X-ray photometry curve.

[b] Melting enthalpy reported to the mass of the sample, obtained by planimetry of melting endotherm.

[c] Ratio of the amplitude of bands 721 and 1350 cm^{-1} of the IR spectrum.

Chlorination in suspension of type PEL 3[17] led to samples with a 36, 36.5, 37, 41.6 and 55.2% chlorine content (expressed in percentages by weight). The resulted samples and initial polymer were annealed in two distinct conditions. One group of samples was annealed at 95° for 3 hours (95/3) to eliminate the parasite thermal effects of the possible PVC-type ordered areas [19] in chlorinated samples. This group was repeated under conditions of slow cooling (during

---

[17] C. Trifănescu, unpublished data.

[18] G. Zerbi, L. Piseri and F. Cabassi, *Mol. Phys.*, **22**, 241 (1971).

[19] Endothermic effects to PVC annealed samples was observed initially by P. V. Mc Kinney and C. P. Foltz (*J. Appl. Polymer Sci.*, **11**, 1189 (1967)). In their theories of glass transition, many authors (see for example S. M. Wolpert, W. Wetz and B. Wunderlich, *J. Polymer Sci.*, *A2*, 9,1887 (1971)) consider that these effects proceed from enthalpy relaxation processes rather than from ordered regions.

6 hours) and rapid cooling, respectively, in an ice-water mixture. The second group was annealed at 125° for one hour (125/1), rapidly cooling the samples in an ice-water, thereafter. In both cases, annealing took place in a mineral oil bath. Samples were placed in test glass tubes having a 10 mm diameter and being, in turn, immersed in an oil bath. Samples of chlorinated PE (CPE) were checked on indicators in order to verify chlorine release during annealing.

Samples were analysed by DTA at a rate of 4°/min for 95/3 annealed samples, and 6°/min, respectively, for the other, expecting to have an optimum resolution of thermal effects associated with structural transformation processes.

The DTA apparatus was constructed in the laboratory. Figure 1a represents a cross-section of it. Containers with the sample and with the reference material are of the Pyrex glass. The joints of the cromel-kopel differential thermocouple are placed each in a Pyrex glass tube having an approx. 1–5 mm exterior diameter (fig. 1b). For an optimum sample-thermocouple heat transfer, the thermocouple is introduced into compressed γ-alumina powder.

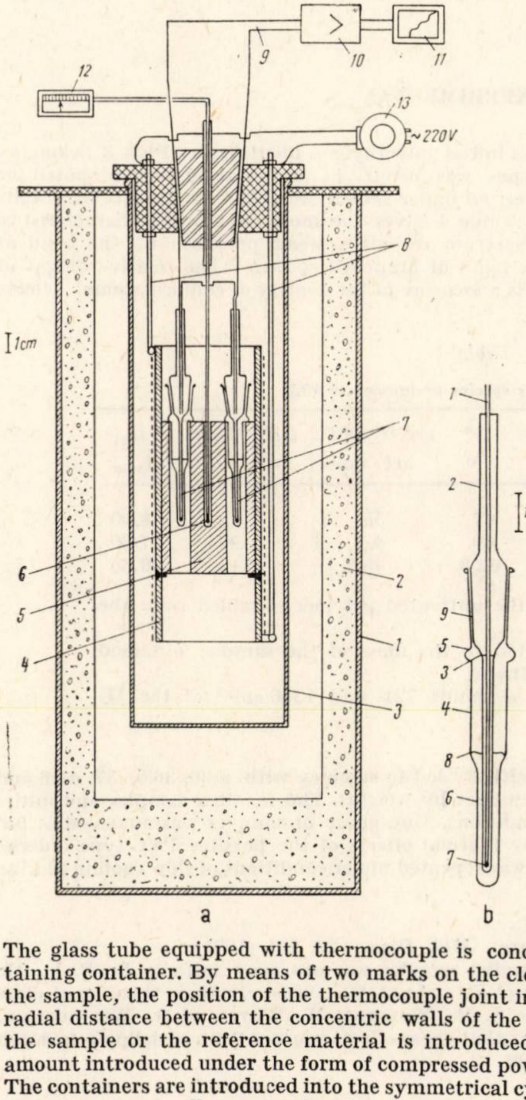

Fig. 1. — a. Cross-section in the DTA apparatus.

1, Outer metallic holder; *2*, thermoinsulating material; *3*, inner metallic holder; *4*, metallic support of heating resistance; *5*, cylindrical brass block; *6*. iron-constantan thermocouple; *7*, sample and reference material holders; *8*, supporting and terminal metallic rod of heating; *9*, terminals of differential thermocouple (cromel-kopel); *10*, Amplispot d.c. amplifiier (SEFRAM); *11*, recorder (Graphispot); *12*, temperature indicator; *13*, voltage divider.

b. Cross-section in sample holder.

1, terminals of cromel-kopel joint; *2*. support of thermocouple joint; *3*, level of α-alumina in support of the thermocouple joint; *4*, guide wall of holder in the orifice of the metallic block; *5*, degassing orifice; *6*, wall of actual holder; *7*, thermocouple joint; *8*, level of the sample or the reference powder in sample holder; *9*, closing grounded neck and stopper of the holder.

The glass tube equipped with thermocouple is concentrically introduced into the sample containing container. By means of two marks on the closing ground stopper of the container with the sample, the position of the thermocouple joint in the container is constantly the same. The radial distance between the concentric walls of the two glass tubes along the section in which the sample or the reference material is introduced (fig. 1b) is approx. 2 mm. The sample amount introduced under the form of compressed powder in this section is approx. 150–200 mg. The containers are introduced into the symmetrical cylindrical orifices of a brass block-container. Heat transfer at cells was produced by a 3 mm thick air layer. The kanthal resistance is directly heated from a voltage divider. The supply voltage also establishes the heating rate so that heating curves for the heating rates used have a ± 0.05°/min reproducibility. In the studied temperature range this dependence is practically linear. Since it is not possible to fix in the rods of the joints of the differential thermocouple another thermocouple for reading the temperature of the sample, the reference temperature is considered to be the temperature of the metallic block measured by means of an iron-constantan thermocouple. In this sense the temperature scale was calibrated based on the melting points of some standard substances of 95—99% chromatographic purity (naphthalene 80°, stearic acid 70—71°, phenathrene 100.3°, γ-hexachlorocyclohexane 112—113°, benzoic acid 121°, anthracene 217°). However, the accuracy in measurement and manual recording of the reference temperature during DTA round does not permit to discern samples according to the melting points. A 1—5% accuracy was determined in the melting enthalpy in standard substances (indium and benzoic acid with 7 cal/g and 35 cal/g, respectively). By using equal amounts of substances it was found that the shape of melting endotherms is perfectly reproduced in practice, errors being considered to mainly result from integration by planimetry. In order to obtain high-quality results, an Amplispot (SEFRAM) type amplifier was inserted for e.m.f. of the differential thermocouple. In this way, the gauge is capable of discerning thermal effects of an order of 10 μcal/sec for the samples used, maintaining the base line.

RESULTS

As was expected, the melting endotherms of samples annealed below 110° for less than 10^4 minutes[15] fail to indicate perceptible changes of the lamellar structure also in DTA results. Values listed in table 1 support this fact with regard to the initial polymer.

Figure 2 reproduces the endotherms of samples annealed at 125/1. The initial polymer (fig. 2a) presents a premelting area formed of a slight

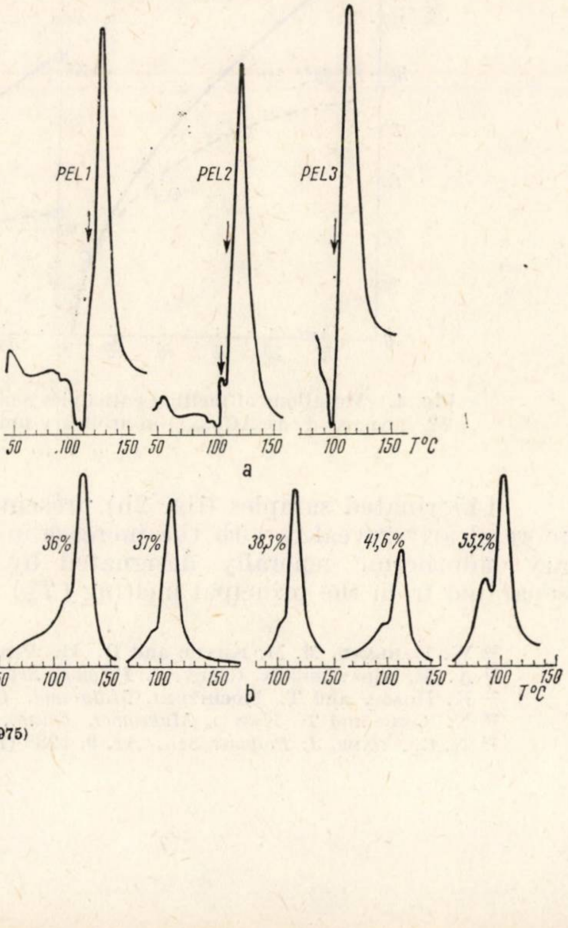

Fig. 2. — Melting endotherms of the sample annealed at 125° for 1 hour (125/1). a. Initial samples: the arrows indicate the premelting area. b. PEL 3 chlorinated samples. The endotherm of the sample with 55.2% Cl is amplified by a 4.4. factor.

crystallization exotherm followed by another premelting process vaguely detached from the principal melting. The fact that type PEL 3 of a larger molecular weight will exceed the crystallinity degree of the type involving smaller molecular weight, after this treatment (table 1), is an indication — according to the results obtained by Harland *et al* [20] on similar samples — to the effect that the molecular weight distribution is large in the considered series (M_w/M_n approx. 10).

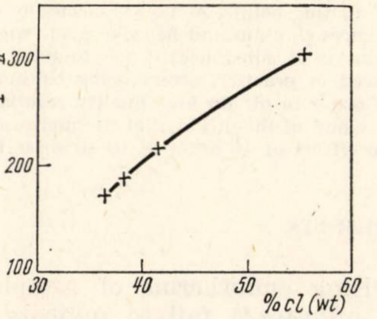

Fig. 3.— Relative increase of endotherm T^1_m (against T^0_m) with chlorine content for annealed samples at 125/1.

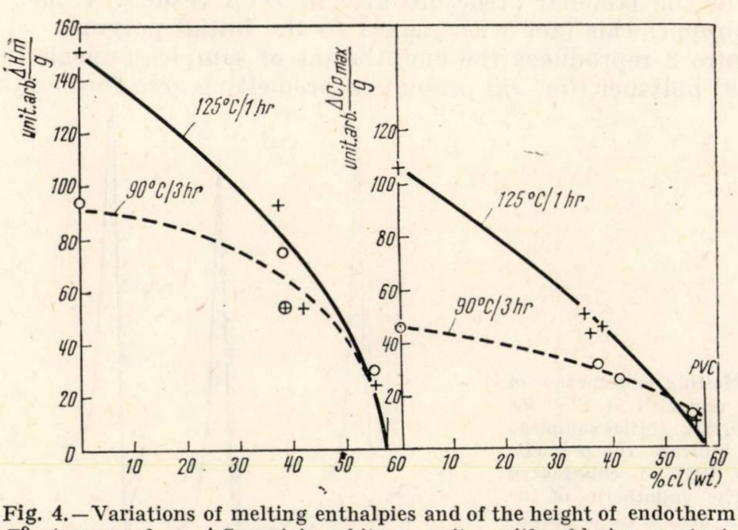

Fig. 4.—Variations of melting enthalpies and of the height of endotherm T^0_m (expressed as $\Delta C_{p\max}$) in arbitrary units, with chlorine content. (0— — —95/3, + ——125/1).

Chlorinated samples (fig. 2b) present a premelting area more and more clearly revealed with the increase in chlorine content. This secondary endotherm, generally designated by T^1_m [1, 21–24] appears distinctly separated from the principal melting (T^0_m) and with a much better resolution on the temperature scale, treatment- or configuration-wise, on the $C_p(T)$ thermogram resulted from the flash adiabatic calorimetry.[1] In the thermograms obtained by DTA the separation power of the two thermal effects is conditioned by the sample-heating source transfer function in the circuit of the caloric flow.[25]

---

[20] W. Harland, M. M. Khadr and R. H. Peters, *Polymer Eng. Sci.*, **13**, 13 (1972).

[21] A. P. Gray and K. Casey, *J. Polymer Sci., B*, 1964, 2381.

[22] K. Hoashi and T. Mochizuki, *Makromol. Chem.*, **100**, 78 (1967).

[23] N. Okui and T. Kawai, *Makromol. Chem.*, **154**, 161 (1972).

[24] G. C. Adams, *J. Polymer Sci.*, *A2*, **9**, 1235 (1971).

The effectiveness of annealing at 125/1 has also been reported by other authors [11, 21, 22, 26] and may be tentatively expressed in DTA results by the relative dependence of height h_{II} of endotherm T_m^1 against h_I (T_m^0)[26]

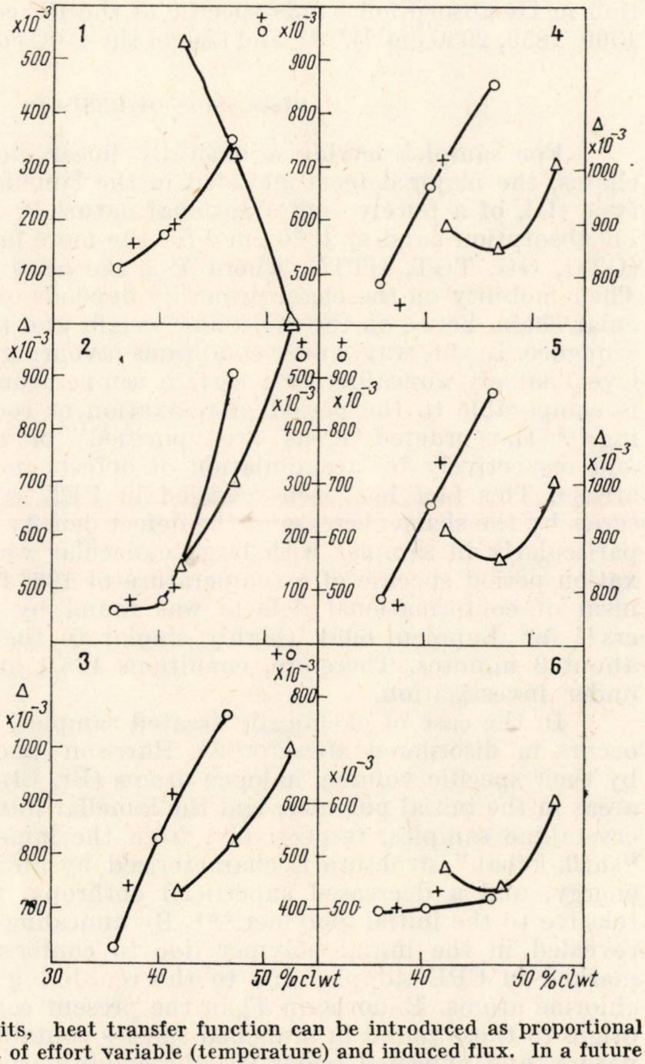

Fig. 5. — Relative variations of the main IR absorption bands with chlorine content (o insoluble segments, + initial polymer, Δ soluble segments). 1. $I_{1350}/(I_{721}+I_{1350})$; 2. $I_{1060}/(I_{721}+I_{1060})$; 3. $I_{1270}/(I_{1270}+I_{721})$; 4. $I_{2853}/(I_{721}+I_{2853})$; 5. $I_{2926}/(I_{721}+I_{2926})$; 6. $I_{2926}/(I_{2926}+I_{2853})$.

---

[25] Like in electric circuits, heat transfer function can be introduced as proportional instant value between gradient of effort variable (temperature) and induced flux. In a future paper it would demonstrate that the heat transfer function in DTA is equivalent with that from conduction calorimeter.

[26] B. SEE and T. G. SMITH, *European Polymer J.*, **7**, 727 (1971).

(fig. 3). Diagrams of figure 4 plot the dependence of total melting enthalpies (melting T_m^1 + melting T_m^0) and the height of endotherm T_m^0, estimated from the thermograms of the samples annealed under the two conditions, with chlorine content.

In view of a better separation of changes specific of the two phases of CPE samples, thermograms and certain more significant bands in the IR spectrum were compared for the tetrahydrofuran soluble and insoluble segments, respectively, separated by refluxing.

Figure 5 groups together the relative changes occurred by chlorination in IR absorption bands specific of the PE configuration (721, 1270—1300, 2850, 2930 cm^{-1}),[18,27] and also of the PVC configuration (1060 cm^{-1})[7].

DISCUSSION OF RESULTS

For samples having a basically linear conformation of molecular chains, the major defects included in the lamellar areas are of a Gauche type (G), of a purely conformational nature [28]. Zerbi *et al* [18] suggest the IR absorption band at 1350 cm^{-1} for the more important defect sequences (GTG, GG, TGT, GTTG, where T is the *trans* segment of the chain). Their mobility on the chain primarily depends on the length of the molecular chain, hence on the molecular weight and then on the nature of the sequence. In this way, under conditions favouring reorderings at a lamellar level, namely annealing at a certain temperature for a time span which is comparable to the period of relaxation, or recrystallization from melting [1,15] the ordered areas are "purified" or restored, by migration [29] and respectively by accumulation of defects in interlamellar disordered areas [1]. This fact has been revealed in PEL samples of the mentioned series by the sharp decrease of the defect density after annealing at 125/1, particularly in samples with large molecular weight (table 1). The relaxation period specific of a temperature of 126° for the migration mechanism of conformational defects was found by Hosemann and co-workers [13] for Lupolen 6001 (highly similar to the present samples) to be about 3 minutes. Therefore, conditions 125/1 are optimum for the case under investigation.

In the case of chemically treated samples, the attack preferentially occurs in disordered areas.[3,5,11,12] Harrison and Baer [8] conclude that by their specific volume, halogen atoms (Br, Cl) separate the amorphous areas in the initial polymer, and the lamellar interface areas in the monocrystalline samples, respectively, from the lamellar ordered areas. This "shish-kebab" structure is characterized by an increased superficial free energy, and a decreased superficial enthropy, respectively, of lamellae relative to the initial polymer.[6,8,9] By annealing at 125/1, the separation revealed in the initial polymer due to conformational defects is more marked in CPE samples due to the reordering of sequences containing chlorine atoms. Endotherm T_m^1 in the present case (fig. 2b) has a similar origin to those found in branched species containing groups of a different nature, and annealed under specific conditions.

---

[27] K. Nimbu, *J. Appl. Polymer Sci.*, **4**, 69 (1960).

[28] W. Pechold, S. Plasenbery and S. Woerner, *Kolloid — Z. Z. Polymere*, **189**, 14 (1963).

Regardless of the nature of the radical, i.e. $-CH_3$,[1,21,22] $-COOCH_3$,[23] $-C_6H_5$[13] etc., it was found that by maintaining material at a temperature below T_m^0 for a specific interval of time, a relative ordering of crystalline lamellae results along some preferential directions.[15] These directions are established by the lamellar surface tensions induced in mechanical[13,15,24] or chemical[3-12] treatment. The development of a theoretical and experimental base of small angle X-ray scattering technique by the team headed by Hosemann,[13,15] made it possible to precisely visualize the interlamellar ordering induced for instance by plastic distortion. It clearly results from values provided[15] (table 1) that the interlamellar reordering process achieved by annealing at 126° is a relaxation process, similar to diffusion process. More specifically, as previously mentioned,[1] all structural parameters in the mentioned paper,[15] namely H (lamellar length along the fibril), β (which is a measure of lamellar translation throughout the treatment), D (halfwidth of the distribution of amorphous areas) and *P* (the long order period), present a variation in time proper of an activated irreversible process (rate process) according to the Eyring's concept. Activated energy of this process is deduced from their results, to be approx. 35 kcal/mole.

In this context, endotherms T_m^1 observed in the present samples will reveal the very interlamellar ordering achieved by annealing at 125/1. The fact that the magnitude of these reorderings is proportional to the chlorine content (fig. 3) accounts once more for the fact that the chemical attack occurs particularly in the amorphous areas which become thus responsible for these interlamellar processes. Yet, as has been noticed with monocrystalline samples,[8] the attack will also affect the lamellae with a higher chlorine content. This may be observed both in the discontinuity of the chlorination process (sudden decrease of the reaction rate relative to a time which is proportional to the crystallinity degree of the initial polymer)[17] and in the fact that chlorine release observed throughout annealing is not proportional to the chlorine content of the sample.

DTA results of Era and Lindberg[6] obtained on PE samples similarly chlorinated in suspension indicate that the value of the melting enthalpy extrapolated to a zero crystallinity corresponds to the chlorine content of PVC species (56%). Figure 4 represents the dependences of the melting enthalpy for the two groups of samples and also the dependences of the maximum in the melting endotherm T_m^0 on chlorine content. In both cases the group of samples annealed at 125/1 has been observed to be closer to the ideal case (when chlorinated areas represent PVC species) than that incompletely annealed at 95/3. The differences observed in the two groups, due to the dependences of magnitudes characterizing the lamellar segments, represent precisely the coupling of the two phases achieved by chemical and thermal treatment.

With regard to the initial polymer used by Era and Lindberg,[6] we may further mention that it was either kept for a long time at ambient temperature under chlorinated form, or else the species of the initial polymer was of a branched type. From the data reported by these authors it results that the melting enthalpy is about 29 cal/g with a zero chlorine content. This corresponds to a crystallinity of about 40 %, which certainly represents a low density PE, having therefore a high degree of branching. Branchings represent configurational defects which contribute by their high density and volume to an effective and uniform attack of lamellae themselves. Interlamellar reorderings are possible for this case within a short while and at room temperature. It is worth mentioning that these authors fail to report the appearance of the second endotherm. This leads to the conclusion that the mobility of initial adjacent groups (primarily $-CH_3$) and their high density cause the lamellar areas to be practically independent of each other and hence the amorphous-crystalline coupling to be practically null for the separation capability of the device.

Changes shown by IR spectra, with regard to tetrahydrofurane soluble and insoluble segments respectively, and to the initial samples (fig. 5), complete the image of the interlamellar reordering mechanism. Diagrams in figure 5.1 show that chlorination also induces structural defects in the areas under attack. These defects are removed by solubilization and the recrystallization from solution to dryness restored lamellar segments with densities with such defects which become more reduced with the increase in the chlorine content on the chain. It is to be mentioned that the crystallinity percentage for soluble segments was found by DTA to be comparable to that of insoluble segments. However, lamellae restored in this way no longer have clear separation plane surfaces, neither do they have their initial dimensions so that the X-ray radial photometry perceives no orientation maximum.

The band at 1060 cm^{-1} (fig. 5.2) is specific of PVC configuration.[7] Similar to DTA magnitudes (fig. 4), the samples behaviour (particularly of the soluble segments) asymptotically tends toward that of PVC with the increase in chlorine content.

The stretching vibrations outside the chain plane, δCH_2w and δCH_2t (1270 cm^{-1}, fig. 5.3) appear like an active band in PVC species as well (like a rocking band $\gamma\, CH_2\, r^7$). The amplitudes of these vibrations are practically null for methylene groups in the frame of lamellar areas. Their increase in amplitude with chlorine content is observed both for the initial CPE samples and the insoluble segments and for the soluble ones. The latter present this dependence similar to those of the band at 1060 cm^{-1}.

The stretching vibrations νCH_2sym (2853 cm^{-1}) and νCH_2asym (2926 cm^{-1}) respectively are also restricted (they have, in particular a small halfwidth) for groups CH_2 in the lamellar areas. Diagrams 4 and 5 (fig. 5). indicate an increase in the amplitude of these vibrations with the density of chlorine content. Diagrams in graph 6 (fig. 5) support the view that by their specific volume, chlorine atoms "break up" the mosaic structure, as the amplitude of asymmetric stretching vibrations increase compared to the symmetrical ones.

CONCLUSIONS

Structural changes in PE by chemical treatment, particularly by chlorination are characterized by separation of ordered areas from the disordered ones. This separation is reflected in a sharper delimitation of those areas due to the preferential attack of amorphous areas. From a thermodynamic (energetic) standpoint, lamellae become more isolated with an increase surface energy compared to the untreated initial polymer. In this manner, the attachment of chlorine atoms on chains will induce mechanical strengths which will represent localized dislocations especially at the lamellar interface, in the block-mosaic structure. Their mobility depends on temperature and obeys an Arrhenius type law over a temperature range up to T_m^0. In the case of mechanical and chemical treatment of PE [13,15] this law is observed to become more complicated, viz., an irreversible process is reported, according to Eyring law. Indeed, in addition to the mobility of interlamellar defects, it will be necessary to keep into account intralamellar defects as well. Both the results of the present paper and those obtained by other authors prompt us to state that the annealing of a sample after treatment in general, or chlorination in particular, at a temperature below T_m^0 is characterized by:

— migration of dislocations towards disordered regions along preferential directions,[29]

— cooperation of tension fields of dislocations, and

— orientation of crystalline regions (lamellae) in this field.

Separation of the two phases in the case of PE depends therefore on the configuration of the molecular species and on the magnitude of annealing. The latter represents the coordinate of the annealing "reaction" and is time itself.

The amorphous-crystalline coupling observed in PE after various treatments was also studied by means of other methods. The latest ones, i.e. mechanical relaxations,[30] nuclear magnetic resonance,[31] and low-temperature thermoconductivity studies,[32] indicated the presence and the mobility of configuration and conformation defects in the block-mosaic structure. These studies may better complete the image of structural changes occurred throughout treatment. The relaxation processes which can be investigated by these methods may provide information with regard to the kinetics of the annealing process. However, calorimetric methods [1,16] are more direct, since they reveal the thermal effects associated with these changes. It is important to emphasize that these methods enable the study, from a thermodynamic standpoint, of structural transitions generally observed in solid-crystalline materials. As was concluded in the previous work [1] the separation of the two phases will mainly result in revealing two thermal effects, both by DTA analysis and by flash adiabatic calorimetry. These effects represent the energy absorption in the order-disorder transition at an interlamellar level (T_m^1) and a lamellar one (T_m^0), respectively.

Adiabatic calorimetry studies on materials manifesting such transitions led to the conclusion that the response function (in general C_p or C_v) shows around a certain temperature a discontinuity which may be even infinite in certain cases.[33] This makes it possible to separate two distinct behaviours of this response function over the temperature range of order-disorder transition [34]: a transition with finite latent transition enthalpy in which the variation of the response function is extended (diffuse) over a large temperature range and lambda punctual transition in which the response function has an infinite variation over a practically punctual temperature range. In the first class of materials we find alloys such as CuAu, Cu_3Au, CoPt, MgCd etc., and the class of substances defined as glassy-crystals.[16] The second class includes materials representing orderings of magnetic systems, supraconductive systems, suprafluid systems, high purity salt and alloys having a small concentration of defects, etc. At present, the difference between these two behaviours appears very clearly. As Domb also considered,[34] if the ordered "substructure" suffering the transition has a negligible coupling to the rest of the structure, then the transition will practically occur at a temperature point with an infinite variation of the specific heat of the system. This is the case, for instance, of transitions of magnetic systems, or of supraconductive systems. The spin order coupling with the rest of the lattice (here spin order represents a substructure), and of atomic clusters, respectively, in suprafluids (an other example of substructure), is far too small to be visualized. Conversely, for instance, in substances of glassy-crystal types,[16] where the molecule itself has a distribution of possible conformations at an equilibrium temperature, the various orderings achieved by various thermal treatments have a readily visualized coupling. It must be stressed that Suga and co-workers [16] have used large amounts of substance which cause the caloric pulses to be higher. The future calorimetric studies will have to consider the importance of the magnitude of caloric pulses in the separation power of the two effects involved in the amorphous-crystalline coupling.

---

[29] D. H. Reneker, *J. Polymer Sci.*, **59S**, 39 (1962).

[30] Y. S. Papir and E. Baer, *J. Appl. Phys.*, **42**, 4667 (1971).

[31] H. G. Olf and A. Peterlin, *J. Polymer Sci.*, *A2*, **8**, 771 (1970).

[32] T. A. Scott, J. de Bruin, M. M. Giles and C. Terry, *J. Appl. Phys.*, **44**, 3(1972).

Acknowledgements. The author wishes to thank Mrs. Constanța Trifănescu for CPE samples, Mrs. Viorica Dobrescu for having supplied the extracted samples. Mrs. Grațiela Stănescu and Mr. I. Rolea for the IR spectra, Mr. Radovici for providing indications of crystallinity through X-ray diffraction, and Mr. R. Aslan for his kindness in allowing the access of the author to IR apparatus.

---

[33] H. E. STANLEY, "Introduction to Phase Transitions and Critical Phenomena", chap. 2, Clarendon Press, Oxford, 1971.

[34] C. DOMB, *Proc. Phys. Soc.*, **88**, 1260 (1966).

Revue Roumaine de Chimie, 20, 5, 699–719 (1975)

LE COMPORTEMENT THERMIQUE DES COPOLYMÈRES STYRÈNE-DIVINYLBENZÈNE CHLOROMÉTHYLÉS CONTENANT DES GROUPES QUATERNAIRES D'AMMONIUM

FL. POPESCU, I. PETRARIU et SIMONA PERCEC
Institut de Chimie Macromoléculaire « Petru Poni », 41A, Jassy, Aleea Gr. Ghica Vodă

Reçu le 25 février 1974

L'étude du comportement thermique des copolymères styrène — 8 % divinylbenzène chlorométhylés et aminés, contenant des groupes quaternaires d'ammonium est mise en corrélation avec l'analyse IR et l'analyse élémentaire. Les produits chauffés à diverses températures sont comparés avec les produits initiaux non dégradés. On obtient ainsi des informations concernant l'énergie de réaction, l'élimination de chlore, la variation de la teneur en azote et la modification des bandes d'absorption du spectre IR.

L'intérêt porté aux copolymères contenant des groupes quaternaires d'ammonium est dû, en premier lieu, à leur utilisation comme échangeurs d'ions.

En fonction de la nature des groupes ionogènes substitués sur la chaîne, le type, et respectivement les propriétés de l'anionite changent, fait qui permet une diversification de leur emploi dans les technologies modernes [1–3].

Les anionites polystyréniques fortement basiques sont obtenus par l'action des amines tertiaires (triméthylamine, diméthylétanolamine, triéthylamine, etc.) sur le dérivé chlorométhylé du copolymère styrène-divinylbenzène.[1, 2, 4]

Tels produits ont été déjà utilisés [4] industriellement ces dernières années sous la dénomination de : Amberlite IRA 400, Amberlite IRA 410, Dowex 1, Dowex 2, Wofatit SBW, etc.

L'emploi des échangeurs contenant des groupes quaternaires d'ammonium présente certaines limites, les produits ayant une stabilité limitée en milieux agressifs (acides, oxydants...).

Dans les travaux antérieurs on a étudié le comportement dans les milieux oxydants des échangeurs d'ions aminés.[5, 6] Les résultats obtenus

---

[1] Z. Vasicek, Thèse présentée à l'Académie Tchéchoslovaque des Sciences, Prague (1968).

[2] H. V. Bicikov, A. I. Kasperovici et B. S. Roginskaia, *Zhur. fiz. Khim.*, **43**, 2522 (1969).

[3] I. Petrariu et J. Stamberg, *Coll. Czech. Chem. Comm.*, **32**, 798 (1967).

[4] J. Lindemann, *Zeszyty Naukowe Politechniki Wroclawskiej-Chemia*, **22**, 204 (1969).

[5] I. Petrariu, P. Petrariu, Fl. Popescu et C. Luca, *Rev. Roumaine Chim.* (à paraître).

[6] I. Petrariu, P. Petrariu, Fl. Popescu et S. Drăgan, *Rev. Roumaine Chim.* (à paraître).

ont montré la nécessité d'une étude de la dégradation thermique des copolymères styréniques aminés, dans le but de compléter les données connues pour le comportement des produits secs, à l'action de la chaleur jusqu'à leur complète destruction.

Ces dernières années un accent tout particulier a été mis sur les recherches concernant le comportement thermique des échangeurs d'ions.[7,8]

Dans le présent travail on a utilisé une série d'échangeurs d'ions qui diffèrent par la nature du radical attaché à l'atome d'azote.

Les groupes quaternaires d'ammonium ont été fixés sur le copolymère styrène 8 % divinylbenzène gel chlorométhylé. Séparément on a aminé le copolymère indiqué, en attachant des groupes $-NH_2$ au $-CH_2-$ fixé au noyau benzénique.

Dans le tableau 1 sont indiqués la nature des groupes substitués, l'analyse élémentaire et le degré de conversion des produits étudiés. Les synthèses ont été réalisées selon Vasicek [1] Bilcikov et collab.[2] et Petrariu et collab.[3]

Du tableau 1 on constate,en tenant compte de la nature des groupes substitués, que le degré de transformation est suffisamment avancé, permettant de mettre en évidence les modifications résultées pendant l'analyse thermique.

La quantité de chlore en pour cent du tableau 1 représente la somme du chlore ionique du groupement substitué et du chlore covalent des fractions chlorométhylés restées non transformées.

Séparément on a chlorométhylé et ensuite aminé le diphényle pour des études comparatives.

Le diphénylchlorométhylé a présenté une teneur en chlore de 23,02 % (valeur théorique 28 %). Le diphényle aminé après chlorométhylation contenant des groupes $-NH_2$ a présenté des valeurs en azote de 9,70 % (valeur théorique 13,20 %).

On a choisi comme substance de comparaison le diphényle qui ne contient pas de fragments de chaîne aliphatique, qui, par dégradation thermique, puissent modifier les thermogrammes en dénaturant les interprétations.

Ainsi, la molécule du produit aminé est suffisamment grande pour que sur les courbes de perte en poids le processus de scission de la molécule soit bien précisé, les variations de poids à cause de la volatilisation du composé étudié n'étant pas possibles.

Le fait que, tel qu'il résulte de l'analyse, le diphényle aminé est un mélange de produits mono et disubstitués (d'ailleurs difficiles à séparer) n'empiète pas sur l'interprétation qualitative des thermogrammes et des spectres IR, la nature des liaisons dans les deux cas étant la même.

L'analyse thermique a été effectuée en présence de l'air à l'aide d'un dérivatographe Paulik-Paulik-Erdey avec enregistrement photographique.

Des données fournies par les courbes de perte en poids (TG), par les dérivées de ces courbes (DTG) et par l'analyse thermique différentielle (ADT), il a résulté que, en général, les polymères étudiés présentent trois

---

[7] Ju. A. Leikin, A. V. Smirnov, A. B. Davankov et V. V. Korshak, *Vysokomol. Soedinenya*, **10**, 157 (1968).

[8] I. B. Ianovici, J. F. Gleim et V. S. Soldatov, *Vestnik Akad. Nauk. Belorussii S.S.S.R.* **1968**, 29.

étapes de transformation situées dans des domaines de températures ayant les valeurs moyennes de 200°, 300°, 440°.

Afin d'élucider ces processus, les polymères ont été chauffés pendant 15 mn en présence de l'air, à 200°, 300° et 440°.

Tableau 1

Nature des groupes fixés au copolymère styrène 8% divinylbenzène chlorométhylé et l'analyse élémentaire

Groupe fixé par l'intermédiaire du $-CH_2-$ au noyau	C%	H%	Cl%	N%	Degré de transformation
Copolymère chlorométhylé	71,76	6,24	22	—	97,6
$-NH_2$	75,73	6,98	12,17	4,6	53,53
$-N(CH_3)_3^+Cl^-$	68,73	7,89	17,22	4,5	69,91
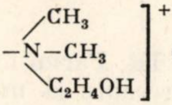 $[-N(CH_3)_2(C_2H_4OH)]^+ Cl^-$	69,93	7,51	13,55	3,37	44,53
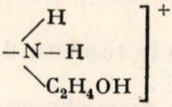 $[-NH_2(C_2H_4OH)]^+ Cl^-$	67,59	7,35	13,61	4,53	54,84
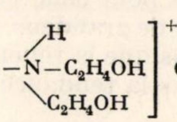 $[-NH(C_2H_4OH)_2]^+ Cl^-$	62,10	7,49	13,49	4,63	77,26
$-N(C_2H_4OH)_3{}^+Cl^-$	62,34	7,62	12,08	3,78	67,96
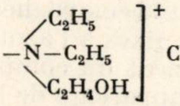 $[-N(C_2H_5)_2(C_2H_4OH)]^+ Cl^-$	68,37	7,72	11,75	3,15	46,57
$-N(C_2H_5)_3^+Cl^-$	70,91	7,68	17,71	2,71	37,59
$-N(C_4H_9)_3^+Cl^-$	72,95	8,54	16,21	2,30	35,99
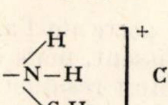 $[-NH_2(C_6H_5)]^+ Cl^-$	72,71	6,36	15,23	4,31	65,78
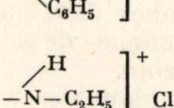 $[-NH(C_2H_5)(C_6H_5)]^+ Cl^-$	77,24	7,10	10,69	4,47	78,93

Tableau 1 (suite)

Groupe fixé par l'intermédiaire du $-CH_2-$ au noyau	C %	H %	Cl %	N %	Degré de transformation
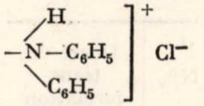	74,95	6,07	16,00	2,38	36,37
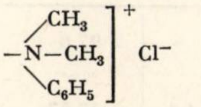	72,82	6,65	17,31	2,72	38,73
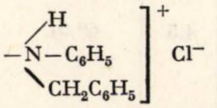	76,19	6,34	14,20	2,91	49,49

Ensuite, on a effectué l'analyse et les études IR. Parmi les données de l'analyse élémentaire le plus grand intérêt présente la modification de la teneur en chlore et en azote à diverses températures, qui est indiquée dans le tableau 2.

La décomposition totale (non indiquée dans le tableau 2) des composés étudiés est située dans l'intervalle 720 à 780°.

Aux composés considérés, les pertes en poids pour chacune des trois températures (200°, 300°, 440°) sont du même ordre de grandeur.

La teneur en chlore baisse rapidement, tandis que la teneur en azote subit de petites variations, ayant dans certains cas la tendance de croître avec l'élévation de la température (tabl. 2).

Le phénomène s'explique par le fait que les pertes de substance peuvent avoir lieu tout aussi bien aux radicaux liés à l'azote qu'à la chaîne. La perte en poids due à l'élimination de l'azote est accompagnée aussi par la perte en poids due à l'élimination des radicaux fixés à l'azote. L'azote en pour cent baisse évidemment. La perte seulement du composé micromoléculaire lié à l'azote conduit à une croissance apparente de la quantité d'azote. Dans les deux cas, le chlore ioniquement lié est éliminé et son contenu en pour cent décroît considérablement , dû à son poids de beaucoup supérieur à celui de l'azote (2,43 fois plus grand) ou à celui du carbone (2,95 fois plus grand).

Enfin la rupture de la chaîne conduit à la perte de l'azote et du chlore liés aux fragments de la chaîne qui disparaissent, mais cette perte n'est pas reflétée par l'analyse élémentaire du produit résiduel.

En conclusion, les valeurs en azote obtenues dans les produits résiduels à diverses températures indiquent la tendance de scission prioritaire des radicaux micromoléculaires liés à l'azote.

Le fait est confirmé aussi par l'analyse thermique des copolymères aminés comparativement à l'analyse thermique du diphényle aminé.

Dans la figure 1 sont données les courbes de perte en poids pour les copolymères styrène 8 % divinylbenzène chlorométhylés contenant

Tableau 2

Pertes en poids et teneur en chlore et en azote des composés chlorométylés et aminés chauffés 15 mn à 200°, 300°, et 440°

Groupe fixé par l'intermédiaire du $-CH_2-$ au noyau	200°			300°			440°		
	Pertes en poids (%)	Cl %	N %	Pertes en poids (%)	Cl %	N %	Pertes en poids (%)	Cl %	N %
$-NH_2$	4	9,07	2,47	11	5,70	1,90	51,5	1,00	2,27
$-N(CH_3)_3^+Cl^-$	9	16,00	4,29	34	5,30	4,19	54	3,24	2,80
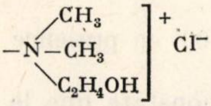 $\left.-N\begin{matrix}CH_3\\CH_3\\C_2H_4OH\end{matrix}\right]^+Cl^-$	6	12,00	3,19	28	3,35	2,18	49	2,73	1,95
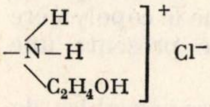 $\left.-N\begin{matrix}H\\H\\C_2H_4OH\end{matrix}\right]^+Cl^-$	7	11,70	4,25	18	4,68	4,18	40	0,77	3,62
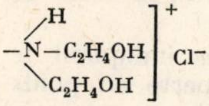 $\left.-N\begin{matrix}H\\C_2H_4OH\\C_2H_4OH\end{matrix}\right]^+Cl^-$	4	12,95	4,22	22,5	3,93	4,31	47	1,04	3,88
$-N(C_2H_4OH)_3^+Cl^-$	5	11,80	3,64	23	3,11	3,67	46,5	1,29	3,75
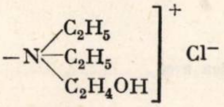 $\left.-N\begin{matrix}C_2H_5\\C_2H_5\\C_2H_4OH\end{matrix}\right]^+Cl^-$	8	11,06	3,07	25	7,39	3,39	51	1,45	2,42
$-N(C_2H_5)_3{}^+Cl^-$	7	13,00	2,20	20	6,19	2,14	48	1,24	1,78
$-N(C_4H_9)_3{}^+Cl^-$	11	12,95	2,05	29	8,27	2,03	54	1,26	1,93
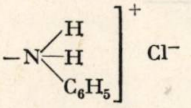 $\left.-N\begin{matrix}H\\H\\C_6H_5\end{matrix}\right]^+Cl^-$	4	14,00	3,81	6	5,52	3,87	25	1,43	3,02
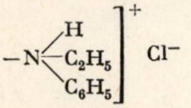 $\left.-N\begin{matrix}H\\C_2H_5\\C_6H_5\end{matrix}\right]^+Cl^-$	12	8,99	3,85	20,5	2,40	3,50	42	1,05	3,22
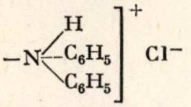 $\left.-N\begin{matrix}H\\C_6H_5\\C_6H_5\end{matrix}\right]^+Cl^-$	1	16,00	1,74	5	9,21	1,80	37	0,764	1,76
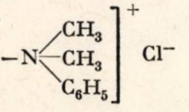 $\left.-N\begin{matrix}CH_3\\CH_3\\C_6H_5\end{matrix}\right]^+Cl^-$	6	10,62	2,30	12	2,74	2,17	23	1,27	2,51
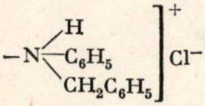 $\left.-N\begin{matrix}H\\C_6H_5\\CH_2C_6H_5\end{matrix}\right]^+Cl^-$	5	9,00	2,53	17	2,35	2,72	36	1,25	3,30

les groupes $-NH_2$ (courbe *2*, fig. 1), 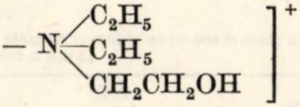 $\left[-N\begin{array}{l}C_2H_5\\C_2H_5\\CH_2CH_2OH\end{array}\right]^+$ Cl^- et aussi pour le diphényle aminé (groupes $-NH_2$) après la chlorométhylation.

Dans la figure 2 sont données comparativement les courbes de perte en poids pour le copolymère chlorométhylé contenant le groupement quaternaire d'ammonium 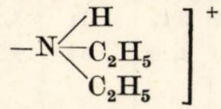 $\left[-N\begin{array}{l}H\\C_2H_5\\C_2H_5\end{array}\right]^+$ Cl^- non chauffé (courbe *1*, fig. 2) et après une période de chauffage de 80 minutes à 200° en présence de l'air.

En comparant les courbes des figures 1 et 2, on constate que le diphényle présente la meilleure stabilité thermique, tandis que le copolymère à substituents alyphatiques ou aryliques fixés à l'atome présente une stabilité thermique plus basse.

On peut apprécier que les radicaux attachés sont responsables de cette faible stabilité.

On constate aussi que les températures différentes indiquant le commencement des processus de transformation avec perte en poids sont déterminées par la nature du produit étudié (tabl. 3).

Tableau 3

Températures indiquant le commencement du processus de transformation avec perte en poids

Nature du produit	Température (t°)			
Diphényle contenant le groupe $-CH_2NH_2$			340°	
Copolymère chlorométhylé contenant le groupe :				
$-NH_2$		200°		420°
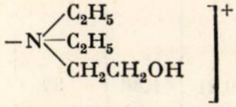 $\left[-N\begin{array}{l}C_2H_5\\C_2H_5\\CH_2CH_2OH\end{array}\right]^+$ Cl^-	60°	180°	300°	420°
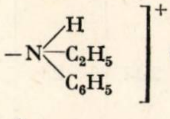 $\left[-N\begin{array}{l}H\\C_2H_5\\C_6H_5\end{array}\right]^+$ Cl^-		150°	300°	440°
* 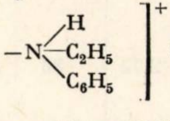 $\left[-N\begin{array}{l}H\\C_2H_5\\C_6H_5\end{array}\right]^+$ Cl^-			300°	440°

* Le même produit soumis initialement à une température constante de 200° pendant 80 mn.

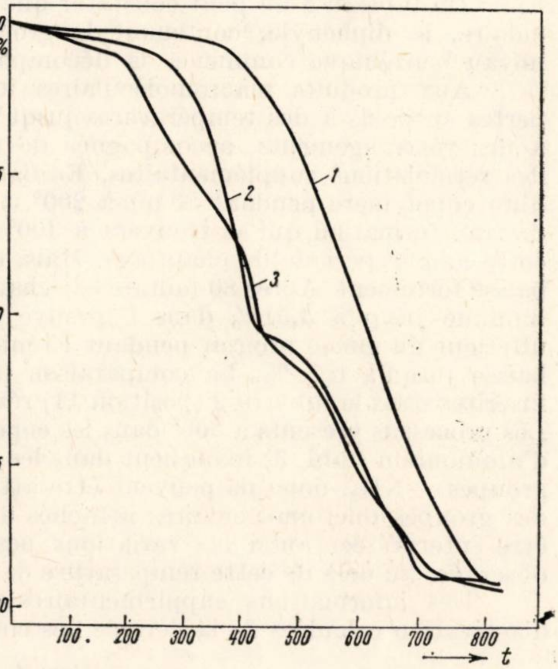

Fig. 1. — Courbe de perte en poids (TG) du diphényle aminé après chlorométhylation ($-CH_2NH_2$) (*1*) et les courbes de perte en poids (TG) des copolymères styrène-8 % divinylbenzène contenant les groupes $-CH_2NH_2$ (*2*) et $-CH_2N(C_2H_5)_2CH_2CH_2OH$ (*3*).

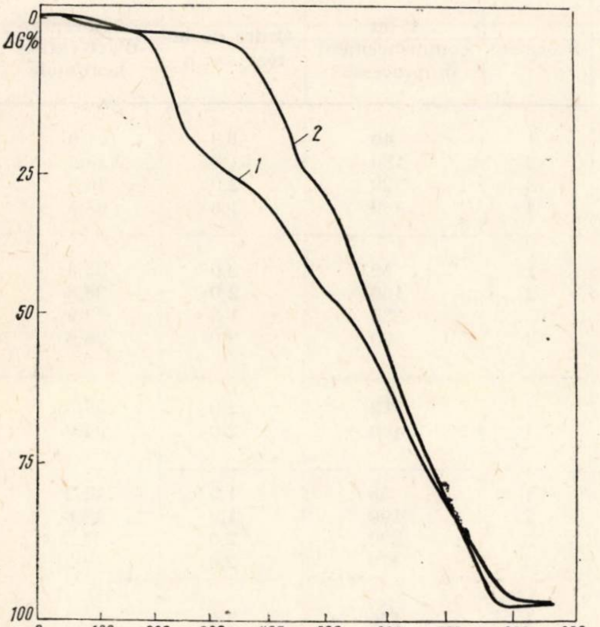

Fig. 2. — Courbes de perte en poids (TG) tracées avant (*1*) et après (*2*) que le copolymère styrène — 8 % divinylebenzène chlorométhylé, contenant le groupe $\left[-CH_2N\begin{matrix}H\\C_2H_5\\C_6H_5\end{matrix}\right]^+ Cl^-$ soit chauffé pendant 80 minutes à 200°.

Du tableau 3 on peut constater que le produit de petit poids moléculaire, le diphényle, contenant le groupement $-CH_2NH_2$ attaché au noyau benzénique commence la décomposition à 340°.

Aux produits macromoléculaires indiqués dans le tableau 3 les pertes en poids à des températures jusqu'à 200°, peuvent être attribuées à des réarrangements, accompagnés de pertes en chlore, conduisant à des réticulations supplémentaires. Edifiant dans ce cas est le chauffage d'un copolymère pendant 80 mn à 200° (tabl. 3). Le début des processus de transformation qui se trouvent à 300° et 440° ne se modifie pas après cette longue période de chauffage. Mais, en échange, la teneur en chlore baisse fortement. Après 80 minutes de chauffage à 200°, la teneur en chlore diminue jusqu'à 3,51% dans l'épreuve considérée. Après le chauffage ultérieur du même produit pendant 15 minutes à 300° la teneur en chlore baisse jusqu'à 0,78%. La comparaison de ces valeurs avec les valeurs inscrites dans le tableau 2 (position 11) révèle des différences importantes. Les processus présents à 300° dans les copolymères à groupes quaternaires d'ammonium (tabl. 3) manquent dans les composés aminés contenant des groupes $-NH_2$, donc ils peuvent être attribués, en principal, aux pertes des groupes micromoléculaires attachés à l'azote. Dans ce sens peuvent être interprétées aussi les variations positives de la teneur en azote observées au delà de cette température dans certains cas (tabl. 2).

Des informations supplémentaires sont fournies par les énergies d'activation calculées de la dérivée des courbes de perte en poids (DTG).

Tableau 4

Energies d'activation

Nº	Groupe fixé par l'intermédiaire du $-CH_2-$ du noyau	Processus	t° du commencement du processus	Ordre de la réaction n	Energie d'activation kcal/mole
1	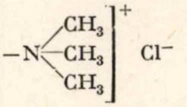 $[-N(CH_3)_3]^+\ Cl^-$	1 2 3 4	40 180 320 440	1,8 1,8 2,0 1,6	11,9 29,2 40,3 68,5
2	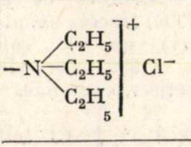 $[-N(C_2H_5)_3]^+\ Cl^-$	1 2 3 4	52 160 335 490	2,0 2,0 1,5 2,0	33,4 38,8 43,9 36,6
3	Le produit nº 2 chauffé à 200° pendant 80 mn	3 4	312 460	2,0 2,0	57,5 54,9
4	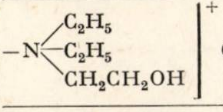 $[-N(C_2H_5)_2(CH_2CH_2OH)]^+\ Cl^-$	1 2 3 4	58 190 320 470	1,5 1,9 2,0 2,0	14,2 19,6 68,5 39,2
5	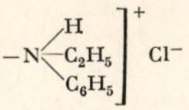 $[-NH(C_2H_5)(C_6H_5)]^+\ Cl^-$	1 2 3	130 328 470	2,0 2,0 2,0	22,7 41,2 38,7

Dans le tableau 4 sont données les énergies d'activation calculées d'après la méthode de Freeman-Carroll[9] pour quatre des produits étudiés dans le présent travail. On a calculé ainsi les énergies d'activation pour deux produits contenant seulement des substituents aliphatiques à l'atome d'azote (n°s 1 et 2, tabl. 4), un produit au groupe $-C_2H_4OH$ attaché à l'atome d'azote (n° 4, tabl.4) et un produit, à un cycle aromatique attaché à l'azote (n° 5, tabl. 4).

L'ordre de la réaction est fractionnaire en 8 cas des 18 calculés. L'ordre de la réaction résulté par l'interprétation mathématique de la courbe TG est fractionnaire, la courbe étant modifiée par la diffusion de la composante volatile dans l'épreuve soumise au chauffage.

L'énergie d'activation correspondant à des processus distincts et mesurée à l'aide des courbes DTG croît régulièrement du processus 1 au processus 4 dans un seul cas (n° 1, tabl. 4).

Dans tous les autres cas le dernier processus présente une valeur plus petite que l'avant-dernier.

On peut supposer, en tenant compte de la présence de l'azote lié par le $-CH_2-$, du copolymère, que le dernier processus découle autocatalytiquement.

L'étude des spectres IR des produits chauffés à 200°, 300° et 440° comparativement aux spectres initiaux a mis en évidence les modifications survenues dans les bandes d'absorptions en fonction de la température.

Le tableau 5 donne les absorptions IR des copolymères contenant des groupes quaternaires d'ammonium ou le groupe $-NH_2$. La nature des absorptions est indiquée en comparaison des indications de la littérature[4,10-14] et par rapport aux quatre produits de référence : diphényle, diphényle chlorométhylé, diphényle aminé et copolymère styrène 8% divinylbenzène chlorométhylé. L'enregistrement a eu lieu à 20°.

Dans le choix des substances de référence, ainsi que nous avons déjà indiqué, le diphényle a présenté l'avantage de n'avoir d'autres groupes attachés au noyau benzénique hormis le $-CH_2Cl$ et le $-CH_2NH_2$.

L'étude de la nature des absorptions initiales (tableau 5) a révélé que :

L'absorption due à la vibration ν C—Cl du domaine 650 à 680 cm^{-1} est visible dans presque tous les cas, mais dans quelques cas, couvre ou est recouverte par la bande d'absorption située à 720 cm^{-1}.

Ce phénomène s'explique par le fait que la bande 720 cm^{-1} attribuée en principal au φ C—C est en réalité complexe, provenant des restes phényle monosubstitués et des fragments du 1,3 divinylbenzène et 1,3 éthylstyrène incorporés dans la chaîne, fait qui peut engendrer des modifications de la largeur et de l'intensité de la bande d'absorption. (Le 1,3

---

[9] E. S. Freeman et B. Carroll, *J. Phys. Chem.*, **62**, 394 (1958).

[10] D. Whittington et J. R. Millar, *J. Appl. Chem.*, **18**, 122 (1968).

[11] V. N. Verma et D. K. Rai, *Appl. Spectroscopy*, **24**, 445 (1970).

[12] P. J. Krueger et J. Jan, *Canad. J. Chem.*, **48**, 3229 (1970).

[13] J. Klaban et Vl. Radl, *Chem. prumysl*, **21/46**, 445 (1971).

[14] G. Gamer et H. Wolff, *Spectrochim. Acta*, **29**, 129 (1973).

Tableau

Absorptions IR pour les copolymères styrène 8% divinyl benzène chlorométhylés

Le composé ou le groupe	Positions des bandes										
Domaines d'absorption indiqués par la littérature	C–Cl 600–800	ΦC–C 700–720	γC–H 640–745	νC–H 800	Phenylé disubstitué en para 815–830	νC–C 840–848	γC–H 860–876	γ C–H 907–923	γ C–H 962–970	C–C–C 1010–1030	νC–N 1028–1190	β C–H 1110±20
Diphényle		700	745					910				
Diphényle chlorométhylé	688	745				840		910		1010		1110
Diphényle chlorométhylé et aminé	690					840		900			1050	1100
Copolymère styrène 8% divinylbenzène chlorométhylé	680	710	745	800		845		910	950	1020		1120
Copolymère chlorométhyé contenant les groupes :												
$-\mathrm{NH_2}$	680	700	745	805				902	975	1020		1100
$-\mathrm{N(CH_3)_3}\ {}^+\mathrm{Cl^-}$		720	770	800		840	870	900	974		1050	
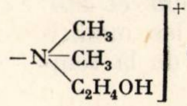 $\left[-\mathrm{N}\begin{smallmatrix}\mathrm{CH_3}\\ \mathrm{CH_3}\\ \mathrm{C_2H_4OH}\end{smallmatrix}\right]^+\mathrm{Cl^-}$	660	700			825		860	902	980	1015	1050	1095
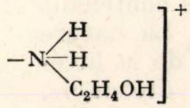 $\left[-\mathrm{N}\begin{smallmatrix}\mathrm{H}\\ \mathrm{H}\\ \mathrm{C_2H_4OH}\end{smallmatrix}\right]^+\mathrm{Cl^-}$	650	700			830					1020	1080	
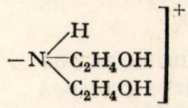 $\left[-\mathrm{N}\begin{smallmatrix}\mathrm{H}\\ \mathrm{C_2H_4OH}\\ \mathrm{C_2H_4OH}\end{smallmatrix}\right]^+\mathrm{Cl^-}$	670					850		920	960	1050	1080	
$-\mathrm{N(C_2H_4OH)_3^+\ Cl^-}$	670				830		860			1020	1090	
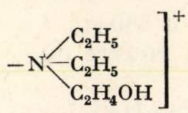 $\left[-\mathrm{N}\begin{smallmatrix}\mathrm{C_2H_5}\\ \mathrm{C_2H_5}\\ \mathrm{C_2H_4OH}\end{smallmatrix}\right]^+\mathrm{Cl^-}$	680	710		800	830			930		1030	1090	
$-\mathrm{N(C_2H_5)_3^+Cl^-}$	670	700		790	830			910		1020		
$-\mathrm{N(C_4H_9)_3^+\ Cl^-}$	680	710				850	870				1070	1120
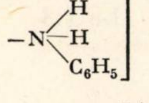 $\left[-\mathrm{N}\begin{smallmatrix}\mathrm{H}\\ \mathrm{H}\\ \mathrm{C_6H_5}\end{smallmatrix}\right]^+\mathrm{Cl^-}$			745	810		855				1010		1110
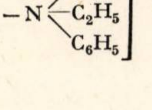 $\left[-\mathrm{N}\begin{smallmatrix}\mathrm{H}\\ \mathrm{C_2H_5}\\ \mathrm{C_6H_5}\end{smallmatrix}\right]^+\mathrm{Cl^-}$	680		805					923	970	1010	1070	1105

5

et aminés comparées avec les composés de référence et les données de la littérature[9, 10–15]

d'absorption (cm⁻1)

$\beta-CH_2$ para 1190 ± 10	Domaines superposés C−N divers et β C−H 1180−1360			νC−C 1390−1402	νC−C du cycle ou de la chaîne 1450−1470	νC=C du cycle 1495−1500	νC=C du cycle 1590−1630	β N−H 1650−1660	νC−H de la chaîne 2860−3015		νC−H cycle 3000−3100	Domaines superposés N−H et O−H divers 3380−3430	N−H divers 3450−3760
					1450	1495							
1190	1222			1400	1420	1490	1600				3000		
	1222		1272	1400	1450	1490	1610				3050		3450
1190	1220			1370	1450	1520	1620		2850	2940	3035		
1180			1360		1450	1495	1590			2940	3050		3450
		1245			1460	1500	1620		2860	2920	3030		3450
		1240											
	1210			1380	1475		1600			2900		3400	
	1210				1450	1510	1608			2900		3400	
	1210				1450	1510	1600	1640		2900		3400	
	1210	1260	1320		1430	1509	1610	1645		2900		3380	
		1220	1270		1460		1620			2940	3400		
		1260	1305		1450	1600		1682		2900		3400	
		1230	1270		1478						3000		
1180				1380		1495	1590	1655		2930			3450
1180	1225	1250	1360			1495	1590	1670		2930			3450

---

[15] M. Avram, « Spectroscopia în infraroşu. Aplicaţii în Chimia organică », Ed. tehnică, Bucarest, 1966, p. 191−206, 266−284, 299, 376−384.

Tableau 5

Le composé ou le groupe											Positions des bandes
Domaines d'absorption indiqués par la littérature	C−Cl 600−800	φC−C 700−720	γC−H 640−745	νC−H 800	Phenyle disubstitué en para 815−830	ν C−C 840−848	γC−H 860−876	γC−H 907−923	γC−H 962−970	C−C−C 1010−1030	νC−N 1028−1190	βC−H 1110±20
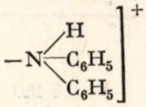 Cl^-	670	700	750		820					1000		1108
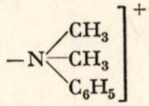 Cl^-	680	700	750		830					1020		1110
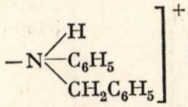 Cl^-	680	720	740	810				920	958	1010		

divinylbenzène et le 1,3 éthylstyrène se trouvent mélangés avec le 1,4 divinylbenzène utilisé comme agent de réticulation.)

La bande γ O−H du domaine 690 à 724 cm^{-1} n'a pu être mise en évidence étant recouverte par la bande à 720 cm^{-1}.

La présence des bandes situées à approximativement 840 cm^{-1} confirme le fait que les groupes actifs des anionites polystyréniques se trouvent dans la position 1−4 par rapport à la chaîne principale.

Les bandes du domaine 900 à 930 cm^{-1} apparaissent dans le spectre des anionites comme la conséquence de la superposition des bandes résultées des oscillations γ C−H.

Dans l'intervalle 1000 à 1200 cm^{-1} apparaissent les bandes caractéristiques du cycle aromatique, mais la mise en ordre de ces bandes est beaucoup plus difficile qu'au cas des bandes correspondant à l'intervalle 650 à 1000 cm^{-1}, leur provenance n'étant pas définitivement élucidée. En conséquence, les valeurs indiquées dans le tableau 5 pour ce domaine sont attribuées sous réserve, par comparaison avec les substances de référence et avec les données de la littérature [10,11] (tabl. 5).

Dans le domaine 1700 à 2043 cm^{-1} on trouve des absorptions dues à des sommes de vibrations (non indiquées dans le tableau 5).

Les valeurs et leurs positions sont fortement modifiées, après le chauffage des épreuves, ayant la tendance de s'atténuer jusqu'à leur disparition.

Les intensités des bandes d'absorption ne sont pas données dans le tableau 5 où sont indiqués seulement les produits dont le degré de substitution au noyau peut varier selon le cas, ce qui a comme conséquence des modifications de l'intensité des absorptions du spectre IR.

(*suite*)

d'absorption (cm^{-1})

$\beta C-CH_2$ para 1190±10	Domaines superposés C—N diverss et $\beta C-H$ 1180—1360		ν C—C 1390—1402	νC—C du cycle ou de la chaîne 1450—1470	ν C=C du cycle 1495—1500	ν C=C du cycle 1590—1630	β N—H 1650—1660	νC—H de la chaîne 2860—3015		νC—H cycle 3000—3100	Domaines superposés—N—H et—O—H divers 3380—3430	N—H divers 3450—3760
	1260	1360		1442	1498	1582	1690		2900	3025		3500
1210	1260		1380	1450	1510	1600			2920			3450
1210	1250	1320		1420	1490	1580	1670	2890	2920		3400	

De même, les absorptions de faible ou de très faible intensité n'ont pas été indiquées dans le tableau 5, leurs modifications à diverses températures étant incertaines.

En général, les absorptions attribuées aux vibrations de déformation γ C—H du domaine 850 à 970 cm^{-1} ont des valeurs moyennes. Les absorptions attribuées aux vibrations ν C—C du cycle ou de la chaîne (1420—1470 cm^{-1}) présentent des intensités moyennes ou très intenses, tandis que les absorptions ν C=C du cycle (1475—1500, 1590—1670 cm^{-1}) sont intenses ou très intenses.

On peut observer dans la figure 3 le mode dont sont modifiées les absorptions du point de vue de l'intensité, de la position et du nombre des bandes visibles, dans le cas du composé contenant le groupement substitué au noyau : $-CH_2-N(C_2H_5)_3{}^+Cl^-$, en fonction de la température à laquelle il a été chauffé.

Dans le cas présenté dans la figure 3 on constate que l'élévation de la température conduit à la croissance intense des bandes du domaine 1320 à 1480 cm^{-1} et à l'amincissement jusqu'à la disparition des autres bandes excepté les absorptions du domaine 1580 à 1640 cm^{-1} qui se maintiennent sous une forme atténuée.

Dans les tableaux 6—8 sont données les absorptions pour chacun des produits étudiés, après leur chauffage pendant 15 minutes à 200°, 300°, et 440°. Les attributions pour une certaine vibration est incertaine à cause de la fréquence des superpositions et des déplacements.

Tableau

Les absorptions IR résultées après chauffage des

Le composé ou le groupe	Positions des bandes												
Diphényle chlorométhylé	670				820					1020	1110		1205
Diphényle chlorométhylé et aminé	670				820					1010	1100		
Copolymère styrène 8% divinylbenzène chlorométhylé	680	700		765			918	970		1025	1118		
Copolymère chlorométhylé contenant les groupes :													
$-NH_2$		700		760	830					1020			
$-N(CH_3)_3{}^+Cl^-)$	660	700			820			950		1020	1080		1205
$\left[-N\begin{matrix}CH_3\\CH_3\\C_2H_4OH\end{matrix}\right]^+Cl^-$	660	700			820	860	900	950	980	1010	1080		1205
$\left[-N\begin{matrix}H\\H\\C_2H_4OH\end{matrix}\right]^+Cl^-$	670				830					1020	1080		1215
$\left[-N\begin{matrix}H\\C_2H_4OH\\C_2H_4OH\end{matrix}\right]^+Cl^-$					820	850	910	950			1080		1200
$-N(C_2H_4OH)_3{}^+Cl^-$	665				820		918			1030	1090		1205
$\left[-N\begin{matrix}C_2H_5\\C_2H_5\\C_2H_4OH\end{matrix}\right]^+Cl^-$	670	700			835					1030	1100		1220
$-N(C_2H_5)_3{}^+Cl^-$	665	700		760	830					1020	1070	1170	1210
$-N(C_4H_9)_3{}^+Cl^-$	660	690	740		835		910			1020	1100	1170	1200
$\left[-N\begin{matrix}H\\H\\C_6H_5\end{matrix}\right]^+Cl^-$	670	690	730		830								
$\left[-N\begin{matrix}H\\C_2H_5\\C_6H_5\end{matrix}\right]^+Cl^-$	660	695	750		820		905	970		1010	1105		
$\left[-N\begin{matrix}H\\C_6H_5\\C_6H_5\end{matrix}\right]^+Cl^-$	660		740		820		910			1050	1100		
$\left[-N\begin{matrix}CH_3\\CH_3\\C_6H_5\end{matrix}\right]^+Cl^-$	670	690	750		825		929			1020	1110		1210
$\left[-N\begin{matrix}H\\C_6H_5\\CH_2-C_6H_5\end{matrix}\right]^+Cl^-$	670	695	730	760	830			960		1020		1160	1220

6

copolymères aminés et des composés de référence, à 200° pendant 15 mn

d'absorption (cm^{-1})

		1435		1485 1490		1595 1600	1670	1683 1680			2380 2400	2880 2900	2980	3380 3410
1262		1420	1455	1500	1518	1600		1700				2910	3030	3450
1260		1420		1490		1600						2900	3000	3400
1255		1420		1500		1600						2900		3400
1250	1375	1420	1470	1500		1600						2900		3400
			1470		1520	1620						2900		3450
					1518	1620						2900		3420
1255						1610						2900		3390
1270		1430			1520	1600		1700				2900		3450
1260	1355	1420		1500		1600		1680	1890	2300	2450	2880		3380
1260	1368		1440	1510		1600		1680				2900		3400
					1520	1600		1700					2950	3480
1250			1443	1505		1600						2900	3000	3400
1250	1360	1420	1440	1490		1580		1690	1890		2400	2880	3000	
1260	1365	1420	1450	1510		1593	1680	1693			2400	2900	3000	3420
1260	1390	1420	1460		1515	1600		1690				2900		

Tableau

Les absorptions IR résultées après chauffage des copolymères aminés

Le composé ou le groupe	Positions des bandes									
Diphényle chlorométhylé et aminé	670		740	770		840	910		1010	1110	1178
Copolymère chlorométhylé contenant les groupes :											
$-NH_2$		700		760	825		910	970	1020		
$-N(CH_3)_3{+}Cl^-$	680		750		820			960	1010	1100	
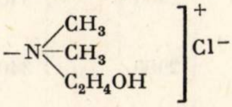 $\left[-N(CH_3)_2(C_2H_4OH)\right]^+Cl^-$	690		750		810		900	960	1010	1100	
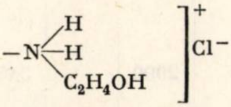 $\left[-N(H)_2(C_2H_4OH)\right]^+Cl^-$	660	700			820			960	1020	1100	1170
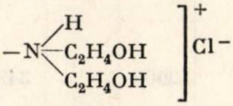 $\left[-N(H)(C_2H_4OH)_2\right]^+Cl^-$		700			820				1020	1100	
$-N(C_2H_4OH)_3{+}Cl^-$	660	690			810		890	960	1010	1100	1170
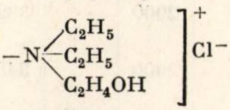 $\left[-N(C_2H_5)_2(C_2H_4OH)\right]^+Cl^-$	690				818				1060	1100	
$-N(C_2H_5)_3{+}Cl^-$	670	700			820		910	970	1020	1100	
$-N(C_4H_9)_3{+}Cl^-$	690		750		820			960	1080	1100	
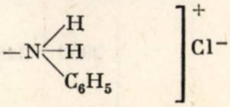 $\left[-N(H)_2(C_6H_5)\right]^+Cl^-$	660	695	740		820				1050	1100	1160
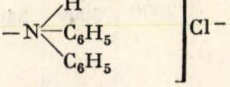 $\left[-N(H)(C_6H_5)_2\right]^+Cl^-$		690	750		830				1020	1100	1170
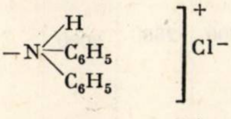 $\left[-N(H)(C_6H_5)_2\right]^+Cl^-$	690		750		820				1018	1100	1160
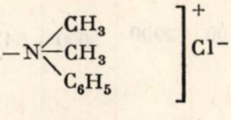 $\left[-N(CH_3)_2(C_6H_5)\right]^+Cl^-$	690		740		820				1010		1160
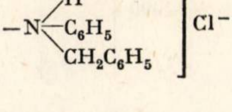 $\left[-N(H)(C_6H_5)(CH_2C_6H_5)\right]^+Cl^-$	660	680	740		820			960	1030	1100	1170

7

et des composés de références, à 300° pendant 15 mn

d'absorption (cm^{-1})																
	1280					1480	1600		1720	1760		2250	2400	2900		3420
					1450	1490	1600					2250		2910	3020	3450
				1410	1440	1510	1600		1690					2900	3000	3400
				1410	1440	1510	1600		1690					2900	3000	3400
1200	1255			1418	1440	1510	1600	1668					2800	2900	3000	3400
						1500	1600							2900		3400
	1259			1400		1500	1590	1670			1870			2850		3420
				1420	1450	1550	1600		1690					2850		3420
1200	1260	1310		1400	1450	1510	1600		1690		1890			2900	3000	3130
1200	1250			1420	1440	1520	1600		1690					2900		
1200	1220	1300		1398		1490	1590		1690	1750			2350		3000	
	1240			1370		1500	1600		1700					2920	3010	3420
	1240	1300	1360		1430	1490	1590		1690	1750				2900	3000	3400
	1250		1360	1410	1440	1500	1590		1690					2900	3050	3420
	1250	1300	1360	1418	1440	1490	1590		1690	1760				2900	3000	3400

Tableau 8

Les absorptions IR résultées après chauffage des copolymères aminés et des composés de référence, à 440° pendant 15 mn

Le composé ou le groupe	Positions des bandes d'absorption (cm $^{-1}$)																		
Diphényle chlorométhylé et aminé				770	830	900							1600	1710	2250	2400	2920		3450
Copolymère chlorométhylé contenant les groupes :																			
$-NH_2$	665	690	750		820	880	1090						1590	1690		2375		3010	3430
$-N(CH_3)_3{}^+Cl^-$													1600				2950		3500
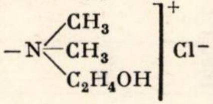 $\left[-N\begin{matrix}\diagup CH_3\\ -CH_3\\ \diagdown C_2H_4OH\end{matrix}\right]^+Cl^-$													1600				2950		3500
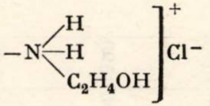 $\left[-N\begin{matrix}\diagup H\\ -H\\ \diagdown C_2H_4OH\end{matrix}\right]^+Cl^-$	660				810	883							1600				2950		3500
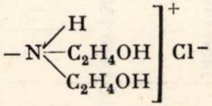 $\left[-N\begin{matrix}\diagup H\\ -C_2H_4OH\\ \diagdown C_2H_4OH\end{matrix}\right]^+Cl^-$					820						1460		1600				2950		3450
$-N(C_2H_4OH)_3{}^+Cl^-$	663		740		820					1393			1580	1680		2350		3090	
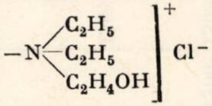 $\left[-N\begin{matrix}\diagup C_2H_5\\ -C_2H_5\\ \diagdown C_2H_4OH\end{matrix}\right]^+Cl^-$					820					1393			1580	1680		2350		3090	
$-N(C_2H_5)_3{}^+Cl^-$			750		820					1400			1600					3000	
$-N(C_4H_9)_3{}^+Cl^-$													1590				2900		3450
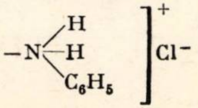 $\left[-N\begin{matrix}\diagup H\\ -H\\ \diagdown C_6H_5\end{matrix}\right]^+Cl^-$	663				810	880				1400			1600					3100	

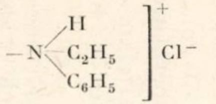 $\left[-N(H)(C_2H_5)(C_6H_5)\right]^+ Cl^-$	670		750		820						1440		1593	1700			2950		3450
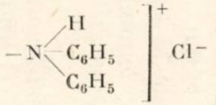 $\left[-N(H)(C_6H_5)(C_6H_5)\right]^+ Cl^-$											1450		1610				2900		3500
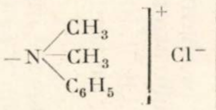 $\left[-N(CH_3)(CH_3)(C_6H_5)\right]^+ Cl^-$								1170					1590				2900		3450
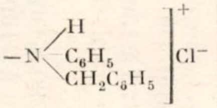 $\left[-N(H)(C_6H_5)(CH_2C_6H_5)\right]^+ Cl^-$	670	690	740		820	880	1020	1160	1235			1550	1640	1690		2400	2900	3010	3420

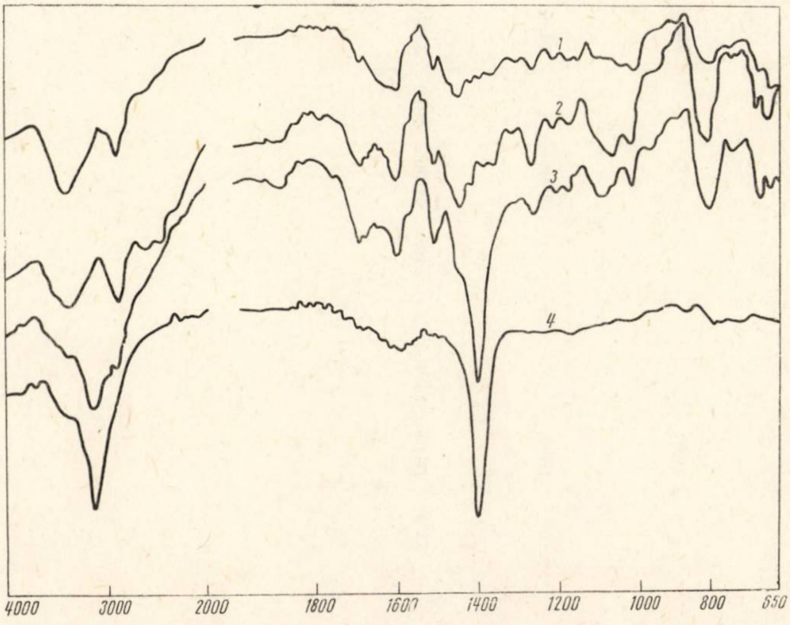

Fig. 3. — Modification des absorptions IR du copolymère chlorométhylé contenant des groupes $-CH_2N(C_2H_5)_3^+$ Cl^- en fonction de la température de chauffage. *1*, Copolymère, non modifié ; *2*, après chauffage pendant 15′ à 200° ; *3*, après chauffage pendant 15′ à 300° ; *4*, après chauffage pendant 15′ à 440°.

En comparant les données de ces tableaux avec les absorptions initiales, il résulte, qu'à la croissance de la température a lieu :

— L'abbaissement jusqu'à la disparition (dans certains cas) des bandes attribuées à la vibration ν C—Cl et son déplacement avec approximativement 10 cm^{-1}, vers des longueurs d'onde plus petites ;

— La bande 700 cm^{-1} devient plus visible dans certains cas à cause de la forte diminution de la teneur en chlore ;

— Les bandes γ C—H des domaines 705 à 765 cm^{-1} et 800 à 962 cm^{-1} tendent à s'intensifier à 200° (effet probablement dû à la baisse de la teneur en chlore). Elles maintiennent leur intensité à 300°. À des températures plus élevées elles subissent une forte diminution.

La bande ν C—N (1028—1190 cm^{-1}) se maintient à 200° et est moins visible à 440°.

Les absorptions ν C—C du cycle ou de la chaîne (1420—1470 cm^{-1}) ne sont pas visibles à tous les produits à l'élévation de la température.

Les absorptions du domaine 1475 à 1500 cm^{-1}, initialement attribuées au ν C=C du cycle ou de la chaîne (tabl. 5), ne sont plus visibles à 440° (tableau 8).

Les absorptions du domaine 1590 à 1670 cm^{-1} initialement attribuées au ν C=C ainsi que le domaine 2920 à 3100 cm^{-1} (ν C—H du cycle et des chaînes) se maintiennent à presque tous les produits. Leur intensité varie : moyenne ou de forte intensité.

Dans le présent travail (tabl. 1 et 2) sont présentés les composés auxquels le volume des radicaux attachés à l'azote croît progressivement avec un groupe $-CH_2-$ (par exemple $-H$, $-CH_3$, $-C_2H_5$, $-C_4H_9$) ou par un groupe $-C_2H_4OH$.

À cause du degré de transformation qui diffère selon le cas on n'a pu faire une corrélation directe entre les pertes en poids et la grandeur du substituent.

Au cas où il existe à l'atome d'azote seulement des substituents aliphatiques ou aromatiques, la vitesse maximale du premier processus est située entre 200—300°.

Pour les composés chlorométhylés contenant des groupes $-NH(C_6H_5)_2^+Cl^-$ et $NH_2(C_6H_5)^+Cl^-$ la vitesse maximale du premier processus est déplacée à 350° dans le premier cas et respectivement à 380, dans le deuxième cas(valeurs données par les courbes DTG des composés étudiés).

CONCLUSIONS

Dans le présent travail on a étudié le comportement thermique de certains copolymères styrène 8 % divinylbenzène contenant des groupes quaternaires d'ammonium ou le groupe $-NH_2$ fixés au noyau aromatique par l'intermédiaire du groupe $-CH_2-$.

L'étude vient compléter les travaux antérieurs avec de nouvelles données montrant que, à l'encontre des dégradations dans des milieux agressifs, quand l'azote attaché au groupement $-CH_2-$ du noyau benzénique de la chaîne est plus facilement éliminé, pendant l'élévation de la température à laquelle sont soumis les produits secs, les radicaux liés à l'azote sont éliminés avec priorité.

On relève aussi l'existence probable de certaines réactions autocatalytiques dans le dernier processus de transformation thermique, nécessitant une énergie d'activation plus faible.

L'étude IR effectuée à diverses températures, permet, par comparaison, de suivre les modifications de l'intensité et de la position des bandes d'absorption du spectre des substances étudiées.

Revue Roumaine de Chimie, **20**, *5*, 721–722 (1975)

A NEW METHOD FOR THE SYNTHESIS OF TRIACETYL PHOSPHATE

ANA UNGUREANU* and CANDIN LITEANU**
* Institute of Chemistry, Cluj-Napoca, Romania
**Department of Analytical Chemistry, Babeş-Bolyai University, Cluj-Napoca, Romania

Received April 11, 1974

A new method for the preparation of triacetyl phosphate (TAP) in 85–92% yield, by direct acetylation of the phosphoric acid with gaseous ketene is described.

Triacetyl phosphate was prepared for the first time in 1940 by Lynen[1] from silver phosphate and acetyl chloride (30–31% yield)

$$Ag_3PO_4 + 3CH_3COCl \longrightarrow (CH_3COO)_3PO + 3AgCl$$

In the present work the synthesis of TAP was carired out by direct acetylation of phosphoric acid with gaseous ketene in ethereal solution.

The absorbtion of ketene by phosphoric acid was observed as early as 1932 by Hurd and Dull.[2] Later, in 1948, Bentley [3] re-investigated this reaction aiming at preparing monoacetylphosphoric acid. This compound was indeed obtained by partial acetylation of phosphoric acid with ketene.

However, no attempt was recorded at effecting complete acetylation of phosphoric acid under the action of ketene. It is the purpose of this paper to report that complete acetylation is also possible and that TAP is formed, as depicted by the following equation :

$$H_3PO_4 + H_2C=C=O \longrightarrow (CH_3COO)_3PO$$

Obviously, acetylation takes place stepwise under initial formation of mono-, and diacetylphosphoric acid.

The formation of TAP by direct acetylation was also pointed out by Grunze and Thilo, [4] who investigated the action of acetic anhydride and of acetyl chloride on phosphoric acid. These authors obtained in both cases a mixture of acetylated polyphosphoric acids as a final product. The formation of some TAP crystals during the experiments with Ac_2O was observed but no attempt was made to turn it into a preparative method.

---

[1] F. Lynen, *Chem. Ber.*, **73**, 367 (1940).

[2] C.D. Hurd and M.F. Dull, *J.Amer. Chem. Soc.*, **54**, 3427 (1932).

[3] R. Bentley, *J.Amer. Chem. Soc.*, **70**, 2183 (1948).

[4] I. Grunze, E. Thilo and H. Grunze, *Chem. Ber.*, **93**, 2631 (1960).

EXPERIMENTAL

Materials. In the synthesis of TAP crystalline phosphoric acid was used. Anhydrous ethyl ether served as a solvent. Ketene was obtained by pyrolysis of acetone in an apparatus similar to that described by Wiliams and Hurd.[5] The flow of ketene (8 g/h) was determined by acetanilide method.[6]

Procedure. An ethereal solution of phosphoric acid (5g H_3PO_4 cryst dissolved in 100 ml of anh. ether) was introduced into a flask provided with a gas inlet, thermometer and gas outlet, then brought to -10 $-15°$ by external cooling (ice and salt). Ketene was bubbled into the reaction mixture. Efficient cooling is necessary throughout bubbling in order to avoid local overheating (the reaction is exothermal) which can cause the appearance of phosphoric polymers.

After approx. 1 hour, abundant separation of TAP in the form of white, well-formed crystals was noted. The bubbling of ketene was interrupted and the crystals were filtered off and washed with 100 ml cold anhydrous ether.

Considering the fact that TAP is an extremely hygroscopic compound and tends to turn rapidly by hydrolysis into di-, and monoacetylphosphoric acid, the filtration and washings must be carried out as rapidly as possible. The washing with larger amounts of ether or insufficient cooling of the latter causes a decrease of yield, as part of TAP is dissolved.

After filtration, the product is dried under reduced pressure at room temperature; 9–11 g TAP (mp=59–61°) were thus obtained (85–92% yield).

Analyses. For analysis the product was hydrolysed by dissolving it in water, when acetic acid and phosphoric acid were formed. The content of the acetyl group was determined by treating the aqueous solution with H_2SO_4 ($d = 1.5$) followed by steam distillation of the resulting acetic acid. Phosphorus was determined by titration of the acidity with 0.1 N NaOH solution (using bromocresol blue as a PH indicator, from yellow to blue), after removing acetic acid by boiling the solution. (Found: CH_3CO, 56.9; P, 13.4. $C_6H_9O_7P$ requires: CH_3CO, 57.5; P, 13.8%).

The NMR spectrum of freshly prepared solution in $HCCl_3$ shows a narrow singlet at δ 2.22 ppm, as expected for the equivalence of the nine protons of the molecule. It is of interest to note that the chemical shifts of CH_3 groups in TAP and acetic anhydride ($\delta = 2.20$ ppm) are almost the same. More detailed investigations of the NMR spectra of acetylated phosphoric acids will be reported elsewhere.

CONCLUSIONS

The method described above permits the preparation of TAP in a simple way and with a high yield (85–92%). The product needs no subsequent purifications.

We wish to stress especially the instability of TAP; kept in sealed tubes at temperatures above 3–5°, it begins to develop a dark colour, and at room temperature separation in two phases is observed. The bottom layer is a viscous mass consisting of acetylated polyphosphoric acids. The upper layer is fluid and consists of acetic anhydride, saturated with acetylated products from the viscous phase. The investigation of these two phases will form the object of a future work.

---

[5] J.W. Wiliams and C.D. Hurd, *J. Org. Chem.*, 5, 122 (1940).

[6] H. Gilman, "Organic Syntheses", vol. I, ed. 2, Wiley, New York, 1948, p.332.

Revue Roumaine de Chimie, 20, 5, 723—724 (1975)

COMPTES RENDUS

W. OLDEKOP ,,Druckwasserreaktoren für Kernkraftwerke'', Verlag Karl Thiemig, München 1974, XII + 336 S.

Wieder einmal bringen die bekannten Thiemig Taschenbücher ein sehr aktuelles Problem zum Vorschein : das Bauprinzip und die Anwendung von Druckwasserreaktoren für Kernkraftwerke.

Die mit Leichtwasser moderierten und gekühlten Druckwasserreaktoren, bilden heute zusammen mit den Siedewasserreaktoren die Basis für die Nützung der Kernenergie zur Energieversorgung. Da sich international gesehen sämtliche Druckwasserreaktoren-Baulinien einander nähern, wurde das vorliegende Buch nach Fachgebieten aufgegliedert, wobei häufig das Kernkraftwerk Biblis als Beispiel dient. Die Fachgebiete umfassen die reaktorphysikalische Auslegung, die Kreisläufe, kerntechnische Anlagen, Instrumentierung, Regelung, Sicherheitsfragen, Betriebserfahrungen und Entwicklungstendenzen. Jedes Fachgebiet wurde von einem selbst in der Entwicklung tätigen Experten dargestellt. Darum besteht das Buch aus 14 selbständigen Abschnitten.

Nach einer kurzen Einleitung in der die allgemeinen Merkmale von Kernkraftwerken mit Druckwasserreaktoren und die wichtigsten Baulinien skizziert werden, wird die physikalische Kernauslegung und die Wärme und strömungstechnische Auslegung besprochen. In diesen zwei Abschnitten stellen die Autoren, W. Böhm und G. Ulrych, die Grundbegriffe der Kernreaktionen und die Strömungsführung des Kühlmittels in der Anlage dar.

In den nächsten zwei Abschnitten besprechen R. Holzer und G. Bartholomé die eigentliche Konstruktion des Reaktorkerns und die Fertigung der Primärkreiskomponenten. Im Mittelpunkt der Betrachtungen steht der eigentliche Druckwasserreaktor. Die enge Verflechtung der verschiedenen Fachsysteme eines Kernkraftwerks macht es jedoch erforderlich auch andere Anlageteile zu behandeln und den Reaktor als Teil des Gesamtsystems zu sehen. Mit dem Titel des Buches ,,Druckwasserreaktoren für Kernkraftwerke'', sollte dieser Standpunkt hervorgehoben werden. Druckwasserreaktoren für Schiffsantriebe und andere Zwecke werden daher nicht behandelt. Auch beschränken sich die Ausführungen auf mit Wasser moderierte und gekühlte Reaktoren, also auf Druckwasserreaktoren im heute üblichen Sinne.

Die Autoren der nächsten drei Abschnitte, W. Debray, P. Schmiedel, E. Schwarz und J. A. Kausz, beschreiben die Werkstoffe des Primärkreises, den Brennstoffkreislauf und die kernverfahrentechnischen Anlagen. Die wichtigsten Probleme die in diesen Abschnitten eingehend besprochen werden sind : die Reaktoren-Werkstoffe, die Brennstoff-Hüllrohre, das Brennelement-Skelett, das Kerngerüst, die Beschreibung des Druckgefäßes und anderer drucktragenden Komponenten, die Aufzählung der verschiedenen eingesetzten Anlagen wie zum Beispiel die lufttechnischen Anlagen und die Abwassersysteme.

In den letzten Abschnitten werden folgende Probleme behandelt : Instrumentierung, Regelung und Betriebsverhalten, Störfallverhalten und Reaktorschutz, sicherheitstechnische Gesichtspunkte beim Kernkraftwerk, Betriebserfahrungen mit Druckwasserreaktoren in Kernkraftwerken, die Beschreibung der Reaktorstation in Biblis als Beispiel für die Anwendung moderner Kraftwerkstechnik in Kernkraftwerken mit Druckwasserreaktoren, die Entwicklungstendenzen und Zukunftsaussichten. Diese Abschnitte wurden von folgenden Spezialisten geschrieben : W. Aleite, G. Frei, E. Schomer, H. Schenk, G. Putschögel und A. Martin.

Das Buch stellt die weitgehend abgeschlossene, ausgereifteste Technik eines Reaktor-Typs dar, der im nächsten Jahrzehnt einen wesentlichen Anteil zur Lösung des Energiemangels beizutragen und eine neue, umfangreiche Industrie zu beschäftigen hat. Das Buch ist in erster Linie für Leser gedacht, die bereits über Vorkenntnisse auf dem Gebiet der Reaktortechnik verfügen und sich über die besonderen Belange von Druckwasserreaktoren informieren wollen. Es werden jedoch nur wenige Grundbegriffe als bekannt vorausgesetzt, so daß der Inhalt größtenteils auch für solche Interessenten verständlich sein sollte, die sich mit der Reaktortechnik noch nicht näher befaßt haben.

Al. Fruma

G. SCHNELL „Magnete; Grundlagen, Aufbau, Anwendungen", Verlag Karl Thiemig, München 1973, XII + 230 S.

Ausführliche Arbeiten über Magnete, über ihren Aufbau und ihre Anwendung, gibt es eine ganze Menge; viel seltener sind aber die Arbeiten die in einem kurz gefaßten Band die wichtigsten Probleme über Magnete besprechen. Aus diesem Grunde wurde dieser 49. Band der Thiemig Taschenbücher von Spezialisten und Studenten sehr gut empfangen. Magnete spielen in der Technik und Forschung eine große Rolle. In der Technik haben gut konstruierte Magnete und Werkstoffe mit richtig angepaßten magnetischen Eigenschaften einen entscheidenden Einfluß auf die Wirtschaftlichkeit, in der Forschung auf den erzielbaren wissenschaftlichen Fortschritt. Der Autor dieses Buches, Dr. G. Schnell, hat im europäischen Kernforschungszentrum CERN beim Bau großer und komplizierter Magnete verschiedener Art reichhaltige Erfahrungen sammeln können, die sich in dem Taschenbuch niederschlagen.

Das Buch besteht aus 5 Teilen und einem Sachverzeichnis. Zunächst werden die Grundlagen für die Berechnung magnetischer Felder mit zahlreichen Anwendungsbeispielen auch für schwierige Fälle, Wirbelströme, Abschirmprobleme und Verwendung von Supraleitern behandelt. Einen gebührenden Raum nehmen die bei der Erzeugung magnetischer Felder benutzten Werkstoffe ein, die elektrischen Leiter einschließlich Supraleitern, Isolierstroffe und vor allem die magnetischen Werkstoffe, die Technologie der Spulen und die Messung magnetischer Felder. Zwischen den theoretischen Problemen die in dem ersten Teil vorkommen sind folgende aufzuzählen: die Maxwellgleichungen, die Feldberechnung mittels Durchflutungsgesetzes, die Feldberechnung mittels des Biot-Savart-Gesetzes, die Potentiale, die Spiegelung, die graphische Bestimmung des Magnetfeldes, das Analogverfahren, die Feldberechnung mit dem Computer, die Bestimmung der Wirbelströme, die Abschirmung und die Theorie der Supraleitung.

Im zweiten Teil der Arbeit werden die Werkstoffe behandelt. Von diesen sind die wichtigsten Kupfer und Aluminium, dann die technischen Supraleiter wie Niobium-Titan, Niobium-Zinn, Vanadium-Gallium und verdrillte Supraleiter, und schließlich die am heufigsten gebrauchten Isolierstoffe. Im selben Teil werden auch die mechanischen Kennwerte der Spulenwerkstoffe (Siliziumeisen, Nickeleisen, Kobalteisen, Ferrite, weich- und hartmagnetische Werkstoffe) besprochen. Am Ende werden noch die Halbleiter für Hallsonden aufgezählt.

Im dritten Teil werden die verschiedenen Techniken behandelt. Dieser Teil besteht aus drei Abschnitten und zwar die Technologie der Spulen, die Messung magnetischer Felder und die Kryotechnik.

Der Schwerpunkt der Ausführungen liegt auf den Teilen vier und fünf, wo die Magnete ohne und mit Eisen besprochen werden. Hier findet der Leser eine Fülle von wichtigen Beispielen und aktuellen Anwendungen: eisenlose Magnete für die Erzeugung homogener und inhomogener Felder wie Solenoide verschiedener Form, Bitterspulen, supraleitende Magnete, Stellaratoren, magnetische Spiegel, mit ihren Anwendungen in der Elektronen-Mikroskopie und Plasmaphysik; Magnete mit Eisen zur Erzeugung homogener Felder, Führungs- und Ablenkmagnete für Beschleuniger, Magnete mit inhomogenen Feldern wie Quadrupolmagnete für Teilchenoptik; die in vielen Zweigen der Technik benutzten Dauermagnete. Außer diesen mehr praktischen Problemen, werden auch einige theoretische Prinzipien bekanntgemacht. Zwischen diesen zählen wir folgende auf: Theorie des Schwingkreises, Hysteresisschleife und Entmagnetisierung, Strombelag auf Eisen, ideales Feld und Ablenkwinkel, Induktivität und gespeicherte Energie, Matrizendarstellung der Quadrupole und Ablenkmagnete, magnetische Halterung und Schwebung.

Trotz der jeden Satz auf Kürze abwägenden Darstellung gelang es nicht, alle Gebiete der Magnettechnik im gegebenen Rahmen gebührend zu behandeln. Anderweitig ausführlich behandelte Gebiete (Arbeitsmagnete, Speichermagnete, Tonköpfe usw.) mußten sogar ganz zurücktreten. Die Abschnitte haben jeweils eigene Zeichungsnummern, auf die im eigenen Abschnitt ohne Abschnittbuchstaben, von Teil zu Teil aber mit Abschnittkennzeichnung referiert wird. Auch besitzt nicht jede Gleichung eine Gleichungsnummer, sondern nur diejenige, die im Text nochmals erwähnt wird. Auf diesem Wege erzielte der Verfasser eine leichte Lesbarkeit. Literaturangaben wurden der Zugriffsschwierigkeiten wegen vom Verfasser nur auf leicht zugängliche Werke beschränkt, mit Ausnahme einiger weniger Originalarbeiten. Dieses Taschenbuch dürfte hinsichtlich seines Inhalts und der Art der Darstellung einzigartig sein und eine wirkliche Lücke im Schrifttum ausfüllen. Das hohe wissenschaftliche Niveau der Arbeit setzt besondere mathematische Kentnisse voraus. Sie wird daher nur einem geringen Kreis von Spezialisten empfohlen.

Al. Fruma

NOTE POUR LES AUTEURS

La *Revue Roumaine de Chimie* publie des articles en anglais, français, russe, allemand ou espagnol. Les auteurs sont priés d'envoyer des articles, notes, communications et comptes rendus inédits.

Les manuscrits seront dactylographiés à deux intervalles. Les tableaux seront dactylographiés sur feuilles séparées, de même que la légende des figures. Les diagrammes seront tracés à l'encre de Chine sur papier calque. Les tableaux et les figures seront numérotés par des chiffres arabes, en nombre strictement nécessaire. Prière de ne pas inscrire les mêmes données dans les tableaux et les figures. Les formules chimiques seront incluses dans le texte ; en outre, elles seront transcrites sur des feuilles séparées. Les auteurs sont priés d'indiquer les caractères italiques (en soulignant les lettres au crayon), ainsi que tout autre caractère spécial. L'ordre des références bibliographiques sera celui de leur mention dans le texte ; le nom de l'auteur sera précédé de l'initiale du prénom ; les publications périodiques seront présentées suivant les prescriptions internationales. Les références seront ajoutées à la fin de l'article ; elles paraîtront comme des notes, au bas de la page. Le texte sera précédé d'un résumé comprenant 15 lignes au maximum.

L'entière responsabilité du contenu des articles appartient aux auteurs. On publie des articles dus aux collaborateurs roumains ou étrangers.

PRINTED IN ROMANIA

1975 SEP 17

TRAVAUX PARUS AUX ÉDITIONS DE L'ACADÉMIE DE LA RÉPUBLIQUE SOCIALISTE DE ROUMANIE

I. ZUGRĂVESCU, MAGDA PETROVANU, **Chimia N-Ilidelor** (La Chimie des N-Ilures), 1974, 347 p., 19 lei.

MARGARETA AVRAM, **Antidăunători** (Pesticides), 1974, 494 p., 41 lei.

CR. SIMIONESCU, VIORICA RUSAN, N. POPA, **Chimia algelor marine** (La Chimie des algues marines), 1974, 211 p., 18 lei.

CRISTOFOR SIMIONESCU, MARGARETA GRIGORAŞ, AGATA CERNĂTESCU-ASANDEI et GHEORGHE ROZMARIN, **Chimia lemnului din România — plopul şi salcia** (La chimie du bois en Roumanie — le peuplier et le saule), 1973, 228 p., 28 lei.

TIBERIU NĂŞCUŢIU, **Metode radiochimice de analiză** (Méthodes radiochimiques d'analyse), 1973, 384 p., 23 lei.

MARIA FITI, **Dozimetria chimică a radiaţiilor ionizante** (La dosimétrie chimique des radiations ionisantes), 1973, 240 p., 13,50 lei.

MIHAI FLORESCU, **Eficienţa economică a cercetării ştiinţifice** (L'efficience économique de la recherche scientifique), 1972, 115 p., 15 lei.

GEORGETA LĂZĂRESCU, **Sistematizarea informaţiilor în chimia organică** (La systématisation des informations dans la chimie organique), 1972, 242 p., 10,50 lei.

P. BALTĂ şi E. BALTĂ, **Introducere în chimia fizică a stării vitroase** (Introduction à la chimie physique de l'état vitreux), 1971, 240 p., 15,50 lei.

LYDIA-MARIA VAICUM, **Biodegrabilitatea detergenţilor** (La biodégrabilité des détergents), 1971, 346 p., 19,50 lei.

I. ZUGRĂVESCU et L. STOICESCU-CRIVETZ, **Polimeri heterociclici** (Polymères hétérocycliques), 1971, 190 p., 9,50 lei.

I. V. MAXIM, **Materiale nucleare** (Matériaux nucléaires), 1969, 444 p., 30 lei.

CORNEL BODEA, et collab., **Tratat de biochimie vegetală**, partea I, **Fitochimie** (Traité de biochimie végétale, Ire partie, Phytochimie), Ier vol., 1964 747 p. + 4 annexes + 2 pl., 41 lei ; IIe vol., 1965, 1962 p., 1 pl., 56 lei ; IIIe vol., 1967, 773 p., 35 lei.

CRISTOFOR SIMIONESCU et CLEOPATRA VASILIU-OPREA, **Mecanochimia compuşilor macromoleculari** (La méchanochimie des composés macromoléculaires), 1967, 344 p., 23,50 lei.

I.P.I. c. 73

43 426

Lei 25.—

F 1103

ACADÉMIE DE LA RÉPUBLIQUE SOCIALISTE DE ROUMANIE

REVUE ROUMAINE DE CHIMIE

REFERÁLVA

TOME 20
N° 6
JUIN 1975

RECHAX, **20**, *6*, 725 – 870 (1975)

EDITURA ACADEMIEI REPUBLICII SOCIALISTE ROMÂNIA

Rev. Roumaine Chim. **20**, *6*, p. 725 – 870 (1975), Bucarest

ACADÉMIE DE LA RÉPUBLIQUE SOCIALISTE DE ROUMANIE

COMITÉ DE RÉDACTION

Rédacteur en chef:

I. G. MURGULESCU, membre de l'Académie de la République Socialiste de Roumanie

Rédacteurs en chef adjoints:

A. T. BALABAN et V. EM. SAHINI, membres correspondants de l'Académie de la République Socialiste de Roumanie

Collège de rédaction:

EM. BRATU, ELENA CEAUŞESCU, ECATERINA CIORĂNESCU-NENITZESCU, C. DRĂGULESCU, RALUCA RIPAN, CR. SIMIONESCU, membres de l'Académie de la République Socialiste de Roumanie ; P. SPACU, membre correspondant de l'Académie de la République Socialiste de Roumanie ; MARGARETA AVRAM, D. I. MARCHIDAN, G. NIAC et D. SĂNDULESCU

La Revue Roumaine de Chimie paraît 10 fois par an. Toute commande de l'étranger pour les travaux parus aux Editions de l'Académie de la République Socialiste de Roumanie sera adressée à ILEXIM, Serviciul Export—Import Carte/Serviciul Export—Import Presă, P.O. BOX 2001, Calea Griviţei, 64—66, Bucarest 12, Roumanie

Les manuscrits, les livres et les revues proposés en échange, ainsi que toute correspondance seront envoyés à la rédaction

REVUE ROUMAINE DE CHIMIE

23, str. Dumbrava Roşie, Bucarest, Roumanie, téléphone 12 41 60

EDITURA ACADEMIEI REPUBLICII SOCIALISTE ROMÂNIA
Calea Victoriei, 125, Bucarest, Roumanie, téléphone 13 94 40

REVUE ROUMAINE
DE
CHIMIE

ORSZ. MŰSZAKI KÖNYVTÁR ÉS DOKUMENTÁCIÓS KÖZPONT

Tome 20, N° 6 **Juin, 1975**

RODICA VÎLCU and B. COMAN, Excess heat capacities of some binary systems in vapour mixture 727–732

D. TOPOR and VERONICA LĂCĂTUȘU, Alkali metal $-XO_3$ (X = N, Cl, Br, I) vapour composition by mass-spectrometry 733–737

SULTANA CIOLAC and ECATERINA VASILESCU, The electrochemical behaviour of stainless steels and their main metallic components in chloride ions containing media. I. The effect of chloride ions concentration and temperature 739–747

R SULTANA CIOLAC and ECATERINA VASILESCU, The electrochemical behaviour of stainless steels and their main metallic components in chloride ions containing media. II. Effect of pH 749–754

N. S. BIRADAR and S. D. ANGADI, Oxovanadium (IV) complexes with aldoximes 755–759

I. I. BĂDILESCU, Heterocyclic compounds. III. Cyclization of ring-substituted γ-phenoxybutyric acids by PPA to 2,3-dihydro-1-benzoxepin-6(*4H*)-ones 761–774

ELISE AVRAM and MARGARET AVRAM, Reactions of acetylenes with transition metals. VI. Reaction of the π-allyl complex of 6-chloro-1,3,6-tri-t-butyl-1,2-dihydrofulvene with carbon monoxide 775–779

A. C. RĂZUȘ, F. CHIRALEU und ALICE MARIE GLATZ, Aluminiumchlorid-katalysierte Reaktionen ungesättigter Säuren. VII. Reaktion der 1-Indenyliden- und 3-Indenylessigsäuren 781–790

R F. URSEANU, C. TĂRĂBĂȘANU-MIHĂILĂ, LEONTINA NEGOIȚĂ and VERONICA ZDRENȚU, New syntheses of anthraquinone dyes, derivatives of bromamine acid 791–799

A. M. EL-ABBADY, A. H. MOUSTAFA and S. A. EL-ABBADY, Geometrical orientation of Stobbe condensation involving dimethyl α, α-dimethylsuccinate with carbonyl compounds 801–811

ECATERINA TUDOR and M. IOVU, Gas chromatographic separation and identification of benzene cyclohexylation products 813–830

R MARGARETA TOMESCU and CRISTOFOR SIMIONESCU, Calculation of the multicomponent copolymer composition at high conversions 831–837

Rev. Roumaine de Chimie **20**, *6*, p. 725–870 (1975), Bucarest

I. PETRARIU, PAMFILIA PETRARIU, FL. POPESCU et CORNELIA LUCA, La dégradation des échangeurs d'anions dans des milieux agressifs. I. L'action de l'eau oxygénée en présence du $CuSO_4$ sur les échangeurs d'anions fortement basiques de type I 839–854

L. CAMPANELLA, P. L. CIGNINI and F. CROCE, Polarographic and oscillopolarographic behaviour of quinolinic acid 855–862

R

ELENA HOPÎRTEAN and EUGENIA ŞTEFĂNIGĂ, Membrane-electrodes of the metallic wire-plastic membrane type. II. Ammonium selective membrane-electrode 863–869

Revue Roumaine de Chimie, 20, 6, 727 – 732 (1975)

EXCESS HEAT CAPACITIES OF SOME BINARY SYSTEMS IN VAPOUR MIXTURE

RODICA VÎLCU and BENONE COMAN

University of Bucharest, Department of Chemical Thermodynamics, Electrochemistry and Macromolecules

Received April 11, 1974

Excess heat capacity of binary systems carbon tetrachloride-benzene, methyl alcohol-carbon tetrachloride and ethyl alcohol-carbon tetrachloride has been determined in vapour phase at temperatures ranging from 349 K to 370 K, using an adiabatic calorimeter which eliminates errors introduced by pressure gradients, owing to the operating manner of the experimental device.

INTRODUCTION

The present paper continues investigations of heat capacities of organic compounds in vapour phase.[1]

This article presents the values of mixing and excess heat capacities, of the above-mentioned binary systems with a view to focus on the changes in these magnitudes as a result of molecular interactions in the vapour mixture. In order to experimentally determine the excess heat capacity (C_p^E) it is necessary to know the mixing heat capacity (C_p^M) as a function of the molar fractions of components:

$$C_p^M = C_p - (x_1 C_{p_1} + x_2 C_{p_2}) \tag{1}$$

and

$$C_p = x_1 \bar{C}_{p_1} + x_2 \bar{C}_{p_2} \tag{2}$$

where x_1 and x_2 are the molar fractions of the components, C_{p_1} and C_{p_2} are the molar heat capacities of the components in the pure state, $\bar{C}_{p_1}$ and $\bar{C}_{p_2}$ represent partial molar heat capacities and C_p, the molar heat capacity of the solution.

The excess molar heat capacity is defined by the equation:

$$C_p^E = C_p^M - (x_1 C_{p_1}^0 + x_2 C_{p_2}^0) \tag{3}$$

$C_{p_1}^0$ and $C_{p_2}^0$ are ideal heat capacities of pure components at the normal pressure, calculated by statistical methods.

---

[1] R. Vîlcu and B. Coman, *Rev. Roumaine Chim.*, **18**, 1301 (1973).

EXPERIMENTAL

The calorimetric installation for the heat capacity measurements of pure compounds at a normal pressure, was described in a previous paper.[1] To measure the heat capacity in mixtures we used a calorimetric installation composed of a cell (*C*) (fig. 1a), manufactured of pyrex glass, a preheater (*P*) fitted with a coiled resistance (R_1) connected to an adjustable voltage source, a capacitive transducer (*S*) used for measuring and controlling the pressure inside the vessel, a heater R_2 (manufactured of Pt wire with a 6 – 8 Ω total resistance) connected to a stabilized adjustable source (*T*) of direct current, a battery of 6 thermocouples, (*Th*) differentially connected to a thermoregulator,[2] used as a zero instrument with the possibility of equilibrating the temperature of vapours in the calorimeter with that of the thermostating liquid, a magnetic stirrer (*B*) and a Beckmann thermometer used for the temperature difference (ΔT) measurements.

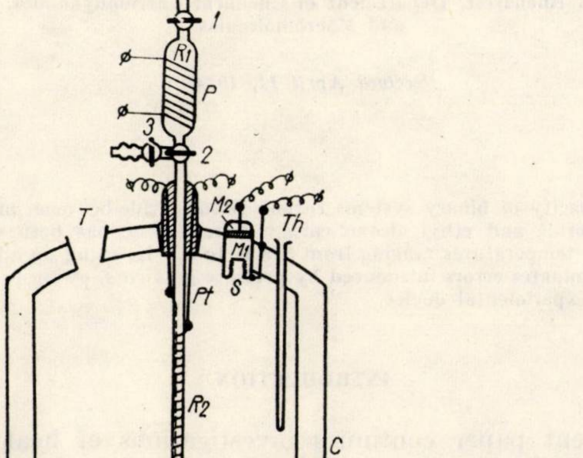

Fig. 1.a — Operating diagram of the calorimeter;
b. — Operating diagram of the capacitive transducer.

$$C_p = Q/\Delta T \tag{4}$$

---

[2] R. Vîlcu and B. Coman, *Rev. Chim.* (*Bucureşti*), **25**, 1 (1974).

The capacitive transducer system (S) is manufactured of a pyrex glass tube having a 25–30 mm diameter (fig. 1b) equipped at the bottom end by an elastic metallic membrane (M_1) under the form of a bladder which constitutes one of the transducer's armatures; the second armature is formed by the metallic ring (M_2) fixed at the upper section of the tube.

The bladder volume may vary between 2–6 cm³, providing an equilibrium between the vapour pressure and the atmospheric pressure with a difference of a few torrs.

The armatures of the capacitive transducer are connected to the resonant circuit L_1L_2 of an oscillator coupled to a phase-discriminating stage according to the block diagram (fig. 2).

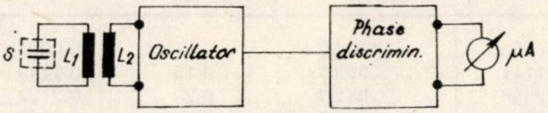

Fig. 2. — Block diagram of the electronic assembly.

The variations of the transducer capacity as a result of pressure variations are revealed by a micro-amperometer (μA).

The calorimeter was introduced into a type U_{10} ultrathermostat, whose temperature variation during the measurement period was ± 0.001 K.

Temperature variations (ΔT) were measured with a ± 0.001 K precision on a Beckmann thermometer.

The procedure was the following: after washing the installation we gauged and determined the calorimeter constant (K) at the working temperature of the system.

Constant (K) was electrically determined using distilled water as a standard:

$$K_T = C_{p_{\text{tot.}}} - C_{p_{\text{water}}} \tag{5}$$

After determining the calorimeter constant the installation was washed and desaerated.

The liquid sample of the mixture was injected in the preheater (P), after levelling off the temperature, tap 2 was turned on, the heated sample being adsorbed in the calorimeter.

We waited until vapours had the temperature of the vessel, then we provided an amount of heat Q in time τ, reading ΔT thereafter.

The sample purity was found by gas-liquid chromatography, as follows: methanol 99.90% moles; ethanol 99.94% moles; benzene 99.96% moles and carbon tetrachloride 99.95% moles

RESULTS AND DISCUSSION

The results of the measurements involving the three systems are presented in tables 1 and 2.

The variation of the excess molar heat capacity with temperature and composition is illustrated in figures 3–5.

For the carbon tetrachloride – benzene system, the C_p determinations were made at a temperature of 358 K and 370 K. Plots reflect the dependence between the excess molar heat capacity and the temperature and concentration.

It has been observed (table 2) that as the concentration increases the mixing heat capacity decreases, except for the ethanol-carbon tetrachloride system where C_p^M reaches a minimum of 72.20 J. mole^{-1} degree^{-1} for the molar fraction x_1 of 0.7052 after which C_p^M increases again reaching the value 76.15 J·mole^{-1}·degree^{-1} for $x_1 = 0.9091$. This C_p^M variation

Table 1

Mixing and excess heat capacities of the binary system carbon tetrachloride + benzene at 358 K and 370 K

Carbon tetrachloride + benzene at 754 Torr and 358 K			Carbon tetrachloride + benzene at 754 Torr and 370 K		
x_1	C_p^M J · mol^{-1} · degree^{-1}	C_p^E J · mol^{-1} · degree^{-1}	x_1	C_p^M J · mol^{-1} · degree^{-1}	C_p^E J · mol^{-1} · degree^{-1}
0.0000	100.37	—	0.0000	136.39	—
0.1141	99.69	0.15	0.1149	131.06	0.13
0.2099	98.24	0.23	0.2129	126.50	0.21
0.3201	97.07	0.29	0.3128	121.82	0.27
0.4218	95.93	0.33	0.4226	116.65	0.30
0.5068	95.01	0.33	0.5068	112.66	0.31
0.6077	93.86	0.31	0.6077	107.86	0.29
0.7010	92.79	0.28	0.7011	103.41	0.26
0.8259	91.31	0.21	0.8259	97.42	0.19
0.9086	90.33	0.15	0.9086	93.44	0.13
1.0000	89.16	—	1.0000	88.99	—

Table 2

Mixing and excess heat capacities of the binary systems methanol + carbon tetrachloride and ethanol + carbon tetra chloride at 349 K and 353 K

Methanol + carbon tetrachloride at 754 Torr, and 349 K			Ethanol + carbon tetrachloride at 754 Torr and 353 K		
x_1	C_p^M J mol^{-1} · degree^{-1}	C_p^E J · mol^{-1} · degree^{-1}	x_1	C_p^M J · mol^{-1} · degree^{-1}	C_p^E J mol^{-1} · degree^{-1}
0.0000	87.73	—	0.0000	91.21	—
0.1011	83.34	−0.60	0.1014	87.33	− 2.91
0.2014	79.09	−1.10	0.2011	83.39	− 5.90
0.3002	73.88	−2.61	0.3018	79.12	− 9.22
0.4012	67.60	−3.52	0.4010	76.24	−11.15
0.5011	64.08	−3.90	0.5004	74.24	−12.20
0.6001	61.86	−3.42	0.6011	73.68	−12.81
0.7501	57.34	−2.33	0.7052	72.20	−12.30
0.8014	56.64	−1.11	0.8010	74.07	− 9.52
0.9016	53.58	−0.62	0.9091	76.15	− 6.42
			0.9501	79.28	− 2.90
1.0000	50.33	—	1.0000	81.71	—

may be attributed to association phenomena revealed by Weltner and Pitzer [3] and Counsell and Leis, [4] as well as by other researchers. [5–7]

In fig. 3 we observe the C_p^E variation of the carbon tetrachloride — benzene system as a function of the molar fraction x_1 illustrated by the

---

[3] W. Weltner and K. S. Pitzer, *J. Amer. Chem. Soc.*, **73**, 2606 (1951).

[4] J. F. Counsell, J. O. Fenwick and E. B. Lees, *J. Chem. Thermodynamics*, **2**, 367(1970).

[5] E. G. Teicker, S. B. Farnham and S. D. Christian, *J. Phys. Chem.*, **73**, 3820 (1969).

[6] V. Cheam, S. B. Farnham and S. D. Christian, *J. Phys. Chem.*, **74**, 4157 (1970).

[7] A. N. Fletcher, *J. Phys. Chem.*, **75**, 1808 (1971).

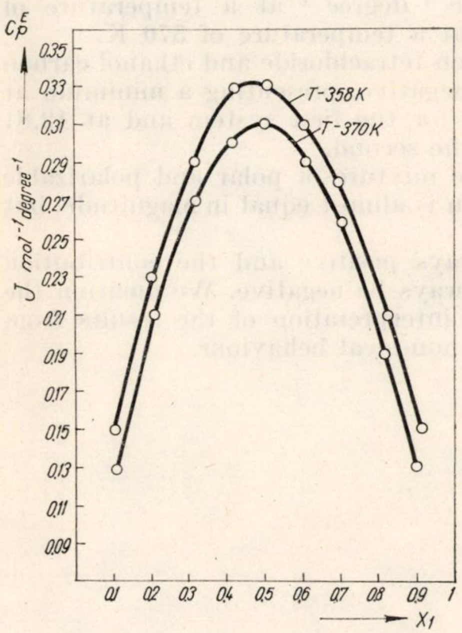

Fig. 3. – C_p^E variation with concentration of the carbon tetrachloride – benzene system at temperatures of 358 K and 370 K.

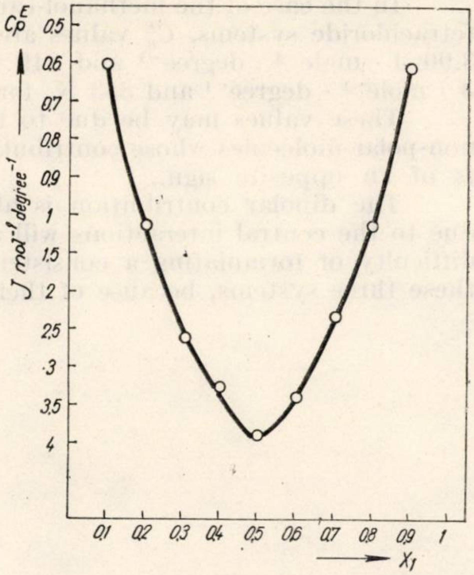

Fig. 4. – C_p^E variation with concentration of the methanol – carbon tetrachloride system at a temperature of 349 K.

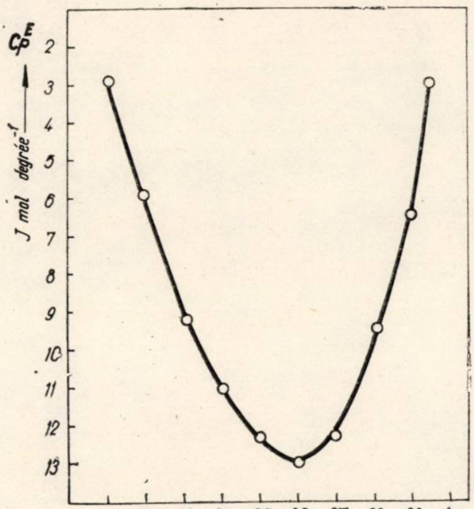

Fig. 5. – C_p^E variation with concentration of the ethanol + carbon tetrachloride system at a temperature of 353 K.

curve whose maximum is 0.33 J$\cdot$mole$^{-1}\cdot$degree^{-1} at a temperature of 358 K and 0.31 J$\cdot$mole$^{-1}\cdot$ degree^{-1}, at a temperature of 370 K.

In the case of the methanol-carbon tetrachloride and ethanol carbon tetrachloride systems, C_p^E values are negative, presenting a minimum at 3.90 J $\cdot$ mole^{-1} $\cdot$ degree^{-1} and 349 K for the first system and at 12.81 J $\cdot$ mole^{-1} $\cdot$ degree^{-1} and 353 K, for the second.

These values may be due to the mixture of polar and polarizable non-polar molecules whose contribution is almost equal in magnitude, but is of an opposite sign.

The dipolar contribution is always positive and the contribution due to the central interactions will always be negative. We mention the difficulty of formulating a consistent interpretation of the results from these three systems, because of their non-ideal behaviour.

Revue Roumaine de Chimie, **20**, *6*, 733–737 (1975)

ALKALI METAL–XO_3 (X = N, Cl, Br, I) VAPOUR COMPOSITION BY MASS-SPECTROMETRY

DUMITRU TOPOR and VERONICA LĂCĂTUŞU

Centre of Physical Chemistry
Str. Galaţi 31, Bucharest, Romania

Received March 15, 1974

The composition of alkali nitrate, chlorate, bromate and iodate vapours was established by mass-spectrometric analysis of the vapours obtained by evaporation under Langmuir conditions and ionised on a wolfram strip. Trimer, dimer, and monomer species have been evidenced in Li, Na and K nitrate vapours, but for the remaining salts there was a simple vapour phase because of strong thermal decomposition.

INTRODUCTION

The complex composition of the vapours of some inorganic salts (especially, halides) at high temperatures, was found on the basis of the information supplied by mass spectrometry, a very useful tool in the thermodynamic and structural caracterization of the vapours of these substances. [1,2]

The molecular species in vapours of alkali nitrates, chlorates, bromates and iodates at temperatures ranging between 400 and 800 K have been scarcely studied and identified, [3] except for Li, Na and Cs, as monomers and dimers.

Among the other monovalent nitrates, only $TlNO_3$ was mass spectrometrically studied by Cubicciotti[4] and Bagaratyan, Ilin and Nikitin. [5]

For obtaining direct information on the vapour composition of these compounds, use was made of a mass-spectrometer equipped with a surface ionization ion source combined with a Langmuir vapour source.

EXPERIMENTAL

The vapour source was obtained by vaporizing in the vacuum created in the mass spectrometer tube of some 2 mg alkali compound previously deposited on the hot junction zone of a Pt–PtRh 10% thermocouple placed at about 2 mm from the wolfram strip of

---

[1] J. Drowart and P. Goldfinger, *Angew. Chem.*, **6**, 581 (1967).

[2] J. Drowart, "Proceedings of the International School of Mass-Spectrometry" Ljubljana, 1969, p. 187.

[3] A. Buchler and J. Stauffer, *J. Phys. Chem.*, **70**, 4092 (1966); L. Ames, J. Wang and J. Margrave, *Inorg. Nucl. Chem. Lett.*, **9**, 1243 (1973).

[4] D. Cubicciotti, *High. Temp. Sci.*, **2**, 131 (1970).

[5] N. Bagaratyan, M. Ilin and O. Nikitin, *Vestnik. Moscov. Univ.*, **14**, 554 (1973).

the surface ionization ion source. The wolfram strip was heated to 1200–1600 K to produce constant surface ionization of the vapours it was in contact with at a certain moment. Because of thermal radiation of the strip, the thermocouple hot junction and therefore the alkali salt has reached temperatures of 400–700 K which permitted the study of vapour composition in terms of temperature.

The hot junction zone of the thermocouple was spherical, having Ø = 0.1 cm and the surface available for vaporization 0.05 cm^2.

The electromotive force of the thermocouple was measured with a milivoltmeter to within 10^{-5}V.

The measurement of ion currents was performed with a Soviet-made 60° magnetic sector mass spectrometer of MI–1305 type, equipped with a surface ionization ion source. Surface ionization has occurred only on the wolfram surface whose emissivity was estimated by the ion beam produced by the halide of an alkali metal heavier than that contained in the nitrate on the Pt–PtRh thermocouple (e.g. $LiNO_3$ on the thermocouple – NaCl on the wolfram strip). Pt and PtRh alloy were used for the vapour source due both to the absence of their chemical interaction with alkali metal $-XO_3$ compounds at high temperature and to the absence of ion emission on surface ionization.[6]

The recording of mass spectrum was performed only for the ions of molecules formed from the most abundant isotopes (^7Li, ^{14}N, ^{16}O, ^{23}Na, ^{39}K, ^{85}Rb and ^{133}Cs).

Fast recording was carried out, for each salt, in order to identify the species present in vapours, and afterwards, multiple ion current intensity recordings were made at several temperatures under stable emission conditions. At the same time, the intensity of alkali emitted by the halide on the wolfram strip was recorded, too.

RESULTS AND DISCUSSION

LITHIUM NITRATE (fig. 1)

The mass spectrum of lithium nitrate exhibits three peaks located at the masses 69, 76 and 145 corresponding to the chemical formulae of the following ions: $(LiNO_3)^+$, $(Li_2NO_3)^+$ and $(Li_3(NO_3)_2)^+$ respectively.

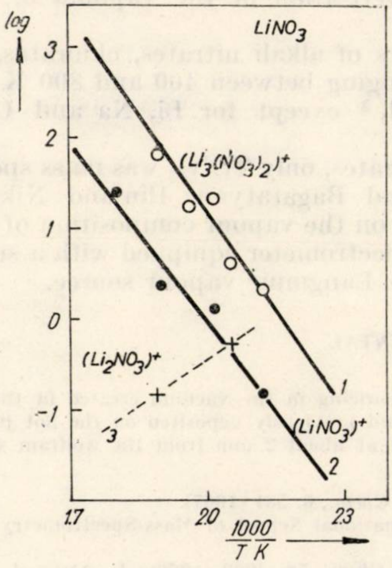

Fig. 1. – Variation of log I^+ versus 1/T for the molecular species present in lithium nitrate vapours.

---

[6] K. R. Wilson and R. J. Ivanetich, Report UCRL 11606, Univ. Calif., Berkeley, aug. 1964.

The appearance of these ions is enabled both by a dissociative ionization mechanism typical of polymer molecules which make up the vapours of simple inorganic salts[7] and by ion-molecule reactions.[8]

Lithium nitrate is characterized by the predominant part played by $Li_3(NO_3)_3$ trimer in vapour phase together with about 10 times less monomer and very little dimer.

This finding can be explained by the high stability of a symmetrical trimer molecule which is formed of the highly polarizing Li^+ ion and the planar NO_3 anion (disk).[9]

SODIUM NITRATE (fig. 2)

The mass spectrum of sodium nitrate presents two molecular ions, those of the monomer and dimer and Na^+ ion. The absence of the trimer is in agreement with the decreasing polarizing power of the cation.

The number of associated species decreases, in alkali nitrates as well as in halides, with the increasing mass and size of the alkali cation.

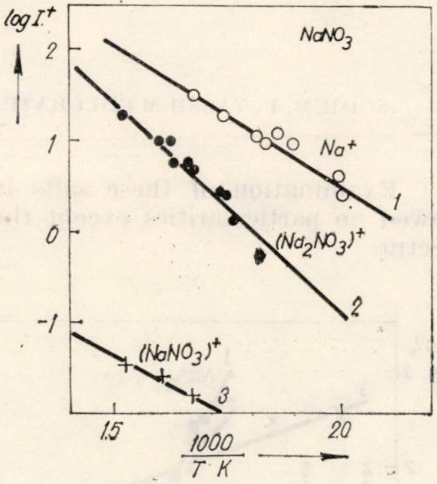

Fig. 2. – Variation of log I^+ versus 1/T for the molecular species present in sodium nitrate vapours.

POTASSIUM NITRATE. RUBIDIUM NITRATE (figs 3 and 4)

In potassium nitrate, besides K^+ ion, only the monomer ion is detectable, while in rubidium nitrate, the only identified ionic species is Rb^+ ion.

---

[7] E. Ya. Zandberg and N. I. Ionov, *Uspekhi Fiz. Nauk*, **67**, 255 (1959).
[8] T. A. Milne, *J. Chem. Phys.*, **32**, 1275 (1960).
[9] G. Pollard, N. Smyrl and J. P. Delvin, *J. Phys. Chem.*, **76**, 1826, 3093 (1972).

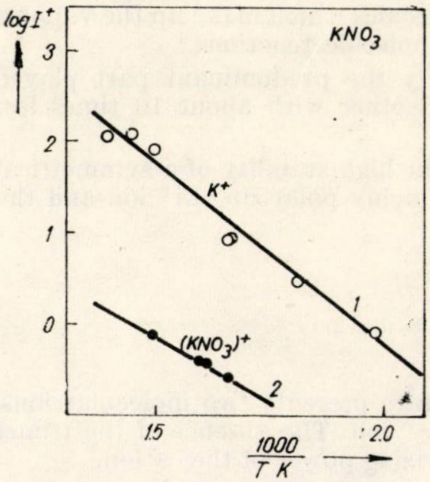

Fig. 3. — Variation of log I⁺ versus 1/T for the molecular species present in potassium nitrate vapours.

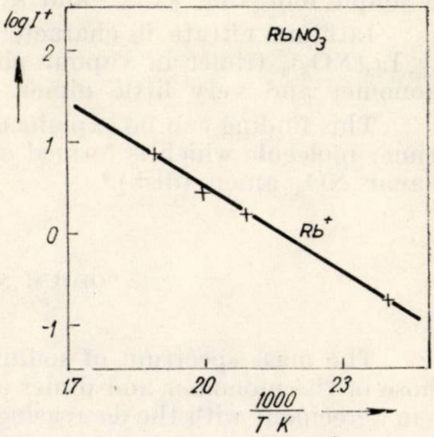

Fig. 4. — Variation of log I⁺ versus 1/T for the molecular species present in rubidium nitrate vapours.

SODIUM, POTASSIUM CHLORATES, BROMATES AND IODATES (fig. 5)

Examination of these salts in the same experiments as nitrates showed no particularities except the presence of alkali ions in the mass spectra.

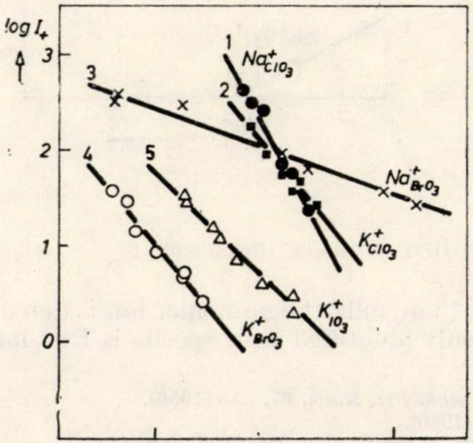

Fig. 5. — Variation of log I⁺ versus 1/T for the ionic species present in alkali chlorates, bromates and iodates. 1. Na⁺ in $NaClO_3$; 2. K⁺ in $KClO_3$; 3. Na⁺ in $NaBrO_3$; 4. K⁺ in $KBrO_3$; 5. K⁺ in KIO_3.

The data for lithium, sodium and potassium nitrate support a complex vaporization mechanism with the formation of monomer and polymer molecules in vapour phase. We can observe these species by low energy ionization condition favourable to a good conservation of 5, 10 or even 15 atom clusters. In the corresponding condensed phases, clusters of the same type are of certain significance for the structural and physico-chemical characterization, particularly for the mass and electric transport phenomena which have recently been reported by Speedding [10] and Woodcook. [11]

---

[10] P. Speeding, *J. Phys. Chem.*, **86**, 1348 (1972).

[11] L. Woodcook, *Proc. Roy. Soc.*, **328 B**, 83 (1972).

Revue Roumaine de Chimie, **20**, *6*, 739–747 (1975)

THE ELECTROCHEMICAL BEHAVIOUR OF STAINLESS STEELS AND THEIR MAIN METALLIC COMPONENTS IN CHLORIDE IONS CONTAINING MEDIA. I

THE EFFECT OF CHLORIDE IONS CONCENTRATION AND TEMPERATURE

SULTANA CIOLAC and ECATERINA VASILESCU

Str. Galaţi 31, Bucharest, Romania

Received February 25, 1974

The study of pure metals (Cr, Ni and Mo) in comparison with stainless steels, in chloride ions containing media shows that nickel is imparting its own electrochemical characteristics to the steels. Conclusive proofs are given showing that the critical pitting potential and the potential of pits repassivation are independent characteristics of pitting process development.

The presence of chloride ions in the electrolyte solutions does affect the development of the corrosion processes by changing the kinetic parameters of the electrochemical reactions both for generalized and especially for localized attack.

The degree of pitting attack, for instance, is strongly affected by the changes in chloride ion concentration. The type of variation in the critical pitting potential, induction time and number of pits with chloride ions content are already known.[1–3]

Only scarce information is available regarding the dependence of the potential of pits repassivation with such important factors as chloride ions content, temperature or pH.

It was established until now that, the critical pitting potential and the induction time characterize the initiation stage of the pitting process and that the potential of pits repassivation refers to its second stage, the pits propagation.[4–6]

---

[1] H. P. Leckie and H. H. Uhlig, *J. Electrochem. Soc.*, **113**, 1262 (1966).

[2] N. D. Stolica, *Corrosion Sci.*, **9**, 205 (1969).

[3] M. A. Streicher, *J. Electrochem. Soc.*, **103**, 375 (1956).

[4] Z. Szlarska-Smialowska, *Corrosion Sci.*, **11**, 901 (1971).

[5] B. E. Wilde, *Corrosion*, **18**, 283 (1972).

[6] B. E. Wilde and E. Williams, *J. Electrochem. Soc.*, **118**, 1057 (1971).

However, because of too little reported data, a nonunitary conception about the existence of the two potentials characterizing the process of pitting is present. [7,8]

This study gives experimental proofs concerning the variations of the critical pitting potential (E_{cp}) and the potential of pits repassivation (E_{rp}) with chloride ions concentration and temperature.

The comparative study of four stainless steels and Cr, Ni, Mo, has evidenced the contribution of the main metallic components to the behaviour of steels.

The characteristics E_{cp} and E_{rp} can be easily determined by using the electrochemical potentiostatic technique.

On a cyclic anodic polarization curve (figure 1) defining the regions of pits formation (above BC), pits propagation (BCDE) and protection (DEF) one considers as :

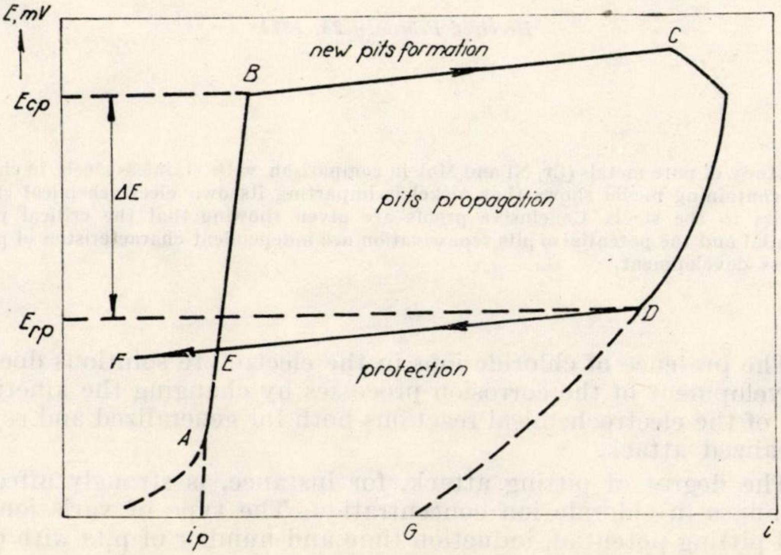

Fig. 1. — The schematic diagram of a cyclic anodic potentiostatic curve, in the case of pitting corrosion.

— the critical pitting potential, the last value of potential recorded in the passive range (AB), before a sharp increase in current (BC) occurs by applying a new step of potential.

— the potential of pits repassivation, the last value of potential for which the recorded current is bigger than the passive current i_p.

The data to be reported were obtained by using the cyclic anodic curves ($E-i$), supplemented by the variations potential-time ($E-t$) from intensiostatic polarization.

---

[7] Z. Szlarska-Smialowska, *Corrosion*, **27**, 223 (1971).
[8] Tsuguo Suzuki and Yoshiharu Kitamura, *Corrosion*, **28**, 1 (1972).

PROCEDURE

The chemical compositions of the materials tested in this investigation are shown in table 1.

Table 1

The chemical compositions of stainless steels

N°	C	S	P	Si	Mn	Cr	Ni	Ti	Mo	Fe
1	0.04	0.016	N.D.	N.D.	0.71	13.95	—	—	—	balance
2	0.04	0.012	0.01	0.64	0.71	19.43	8.09	—	0.016	”
3	0.05	0.007	0.03	0.4	1.34	17.76	8.79	0.52	0.07	”
4	0.08	0.01	0.02	0.09	1.82	16.90	11.90	0.7	2.36	”

N.D. – not determined.

All materials were machined in a convenient form to be fixed in the electrochemical cell.

Molybdenum and stainless steels were used as cylindrical electrodes, nickel as cutting strips and chromium as granules.

Before every measurement, the samples were abraded on emery paper, then mounted in glass holders even with ARALDIT resin or by fixing in a Stern-Makrides mount system.[9]

After 5 minutes of degrease in boiling benzene, the electrodes were chemically polished as follows :

Ni in 15% HNO$_3$ for 10 minutes at 25°
Mo in conc. HNO$_3$ for 1 minute at 25°
Cr in HNO$_3$ + HF + H$_2$O for 10 minutes at 25°
stainless steels in HNO$_3$ + HF + H$_2$O for 5 minutes at 90°
Then they were thoroughly rinsed with tap and distilled water.

The polarization measurements were conducted in a conventional glass cell equipped with inlets for electrolyte supply, entrance and deaeration gas exit.

All electrolytes were prepared from reagent chemicals and double-distilled water.

The measurements concerned with the effect of temperature were carried out in deaerated electrolytes. Deaeration of big quantities of solution was accomplished by the use of pure argon, which was passed over hot copper turnings. The necessary quantity for every measurement was then passed in the electrochemicall cell, under argon pressure and supplementary deaerated for 1 hour.

The solution temperatures were controlled thermostatically with ± 0.2° accuracy.

The cyclic polarization curves were obtained applying potential steps of 50mV every 5 minutes, resulting currents being registered on a chart SEFRAM recorder.

In the intensiostatic measurements, current densities of about 100 μA/cm^2 were applied.

All potentials were measured relative to a saturated calomel reference electrode, connected to the cell with a Luggin probe.

It should be pointed out that the data reported for chromium have only a qualitative value, the surface could not be accurately calculated because of the particular form of granules

RESULTS

THE EFFECT OF CHLORIDE IONS CONCENTRATION

The anodic polarization curves obtained for Cr, Mo and Ni in aerated 0.1 mol KCl are presented in figure 2.

---

[9] M. Stern and A. C. Makrides, *J. Electrochem. Soc.*, **107**, 282 (1960).

Revue Roumaine de Chimie, **20**, *6*, 739–747 (1975)

The three studied metals show different behaviours in chloride containing media. Chromium has a high degree of resistance, molybdenum is generally corroded and nickel undergoes pitting.

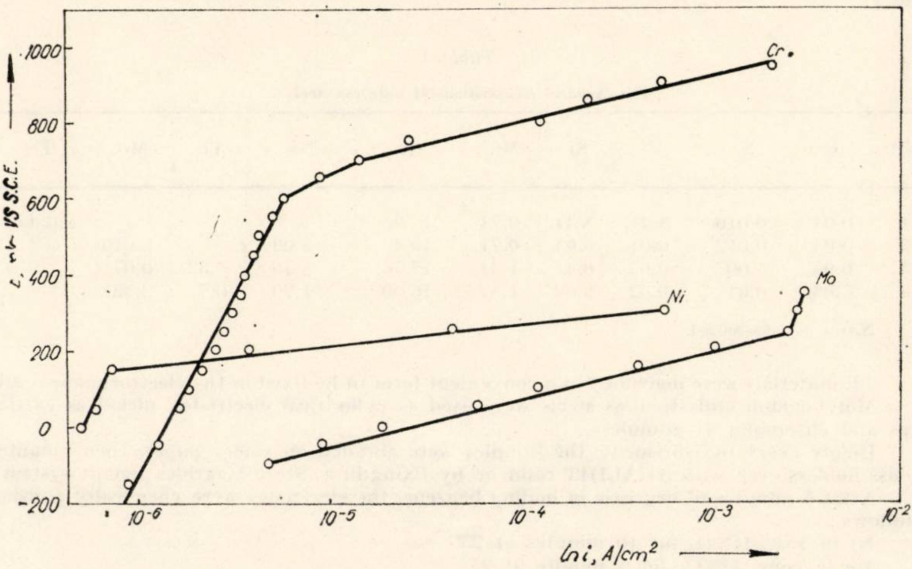

Fig. 2. — The anodic polarization curves of Cr, Ni and Mo in aerated 0.1 mol KCl.

The variation of chloride ions content over a large range of concentrations (0.01—2 mol KCl) does not bring any significant changes in the polarization curves parameters, in the case of chromium and molybdenum, but affects the resistance of nickel toward pitting.

The critical pitting potential of nickel varies with chloride ions contents according to the equation :

$$E_{cp} = -0.075 - 0.110 \log a_{Cl^-}$$

where : a_{Cl^-} is the activity of chloride ions.

No changes in the potential of pits repassivation were observed in the studied range of chloride ions concentration. [10]

Similar results were obtained for stainless steels.

As can be seen from figure 3, the critical pitting potential and the potential of pits repassivation behave differently to chloride ion concentration changes.

Our observations have proved that a certain condition, however, should be respected to get reproducible E_{rp} results, namely to reverse the potential of polarization (branch CDEF) after the current in point *C* reaches approximately the same value (see figure 1).

---

[10] E. Vasilescu, *Rev. Roumaine Chim.*, **20**, 487 (1975).

Similar observations got by some other investigators showed that the value of the potential of pits repassivation depends on the experimental conditions, more exactly on the amount of pits propagation. [5,11]

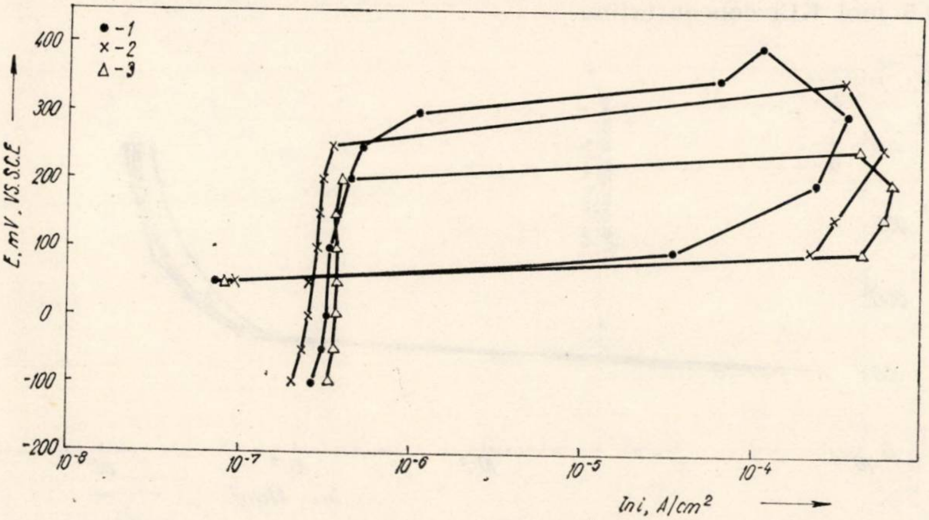

Fig. 3. — The cyclic anodic curves of 18-8-Ti-Mo stainless steel (N° 4 composition) in different concentrations of potassium chloride.

1, 0.5 mol KCl *2*, 1 mol KCl *3*, 2 mol KCl

The higher the currents in point *C* the more progressive the pitting process is, the lower (more active) the E_{rp} is.

Since the potential of pits repassivation is dependent on the applied steps $\Delta E/\Delta t$ (ΔE = variable, Δt = const.), [12,13] additional measurements were made to know the effect of the time transient (ΔE = const., Δt = variable) on the value of E_{rp}.

For this purpose, 18-8-Ti stainless steel (N° 3 composition) was polarized for 80 minutes at a potential above the critical pitting potential and then the reverse potentiostatic curves were recorded, by changing the 50 mV steps at 5, 10, 20 and 30 minutes intervals.

The obtained results in aerated 0.1 mol KCl at 25° are illustrated in figure 4.

As can be observed from this figure, for the same amount of propagation, the value Δt does not affect the value of E_{rp}. However, because of the small current densities reached after 80 minutes of anodic polarization (30—70 μA/cm^2) a little nobler values of E_{rp} result (E_{rp} = 150 mV) than earlier reported (E_{rp} = 100 mV).

---

[11] B. E. Wilde and E. Williams, *Electrochem. Acta*, **16**, 1971 (1971).

[12] V. Hospadaruk and J. V. Petrocelli, *J. Electrochem. Soc.*, **113**, 878 (1966).

[13] E. D. Vernik Jr., and M. Pourbaix, *Corrosion*, **27**, 495 (1971).

The width of hysteresis loop of anodic polarization curves depends on the metallic composition, leading to different E_{rp} values.

Cyclic anodic polarization curves ABCDG (from figure 1) were obtained for 18-8-stainless steels (N° 2 composition) in/and more than 0.5 mol KCl concentration.

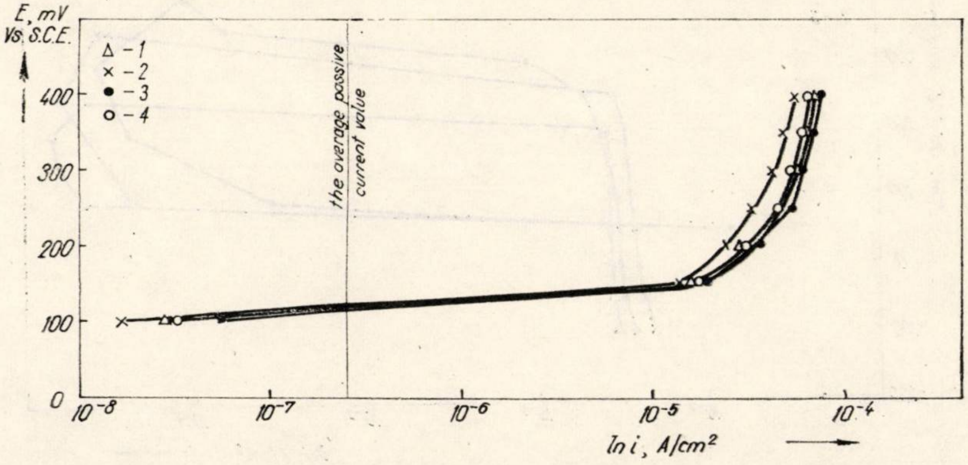

Fig. 4. — The effect of time transient on the reverse anodic curve of N° 4 stainless steel. Δt = *1*, 5 min, *2*, 10 min, *3*, 20 min, *4*, 30 min.

Very reproducible values of the potential of pits repassivation were obtained for titanium stabilized stainless steels (N° 3 and N° 4 compositions) while the unstabilized steel (N° 2 composition) showed a certain degree of scattering.

On the other hand, the dependence of the critical pitting potential on the tested composition and chloride ions content causes the difference $\Delta E = E_{cp} - E_{rp}$, to be dependent on both these parameters.

The electrochemical tests carried out on stainless steels led to the known dependences of the critical pitting potential on the chloride ions content.

Similar diagrams showing a linear dependence of E_{cp} on the logarithm of chloride ions activities were obtained in all cases studied (figure 5) and the following equations were established:

$$E_{cp} = 0.001 - 0.218 \log a_{Cl^-} \quad \text{for 18-8 steel}$$

$$E_{cp} = 0.200 - 0.140 \log a_{Cl^-} \quad \text{for 18-8-Ti steel}$$

$$E_{cp} = 0.200 - 0.130 \log a_{Cl^-} \quad \text{for 18-8-Ti-Mo steel}$$

These results prove the conception of increasing tendency toward pitting with every increase in chloride ions content and the benefit of molybdenum presence in the stainless steels composition.

At the same time, stainless steels like nickel show that the potential of pits repassivation is independent of chloride ions content.

The effect of temperature on the electrochemical pitting characteristics was pursued only on stainless steels, the variations of E_{cp}, $E_{rp} = f(°T)$ being examined in deaerated 0.1 mol KCl for a temperature range of 1 – 80°.

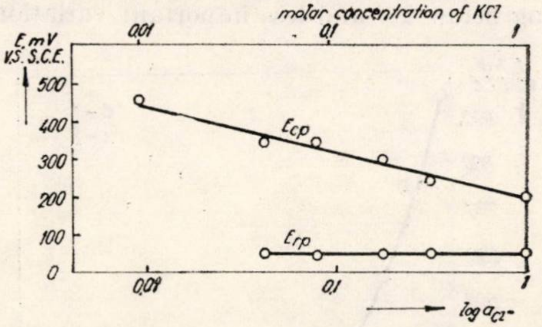

Fig. 5. – The variation of E_{cp}, $E_{rp} = f(a_{Cl^-})$ for N° 4 stainless steel at 25°.

All compositions show similar dependences, both the critical pitting potentials and the potentials of pits repassivation decreasing exponentially with the temperature increase.

For purposes of comparison besides the potentiostatic experiments, potential-time curves were recorded after intentiostatic polarization with a current density of about 100 μA/cm².

On the intensiostatic curves (figure 6), the region having approximately the same potential was considered to correspond to the repassivation process, being characterized by a certain value of E_{rp}.

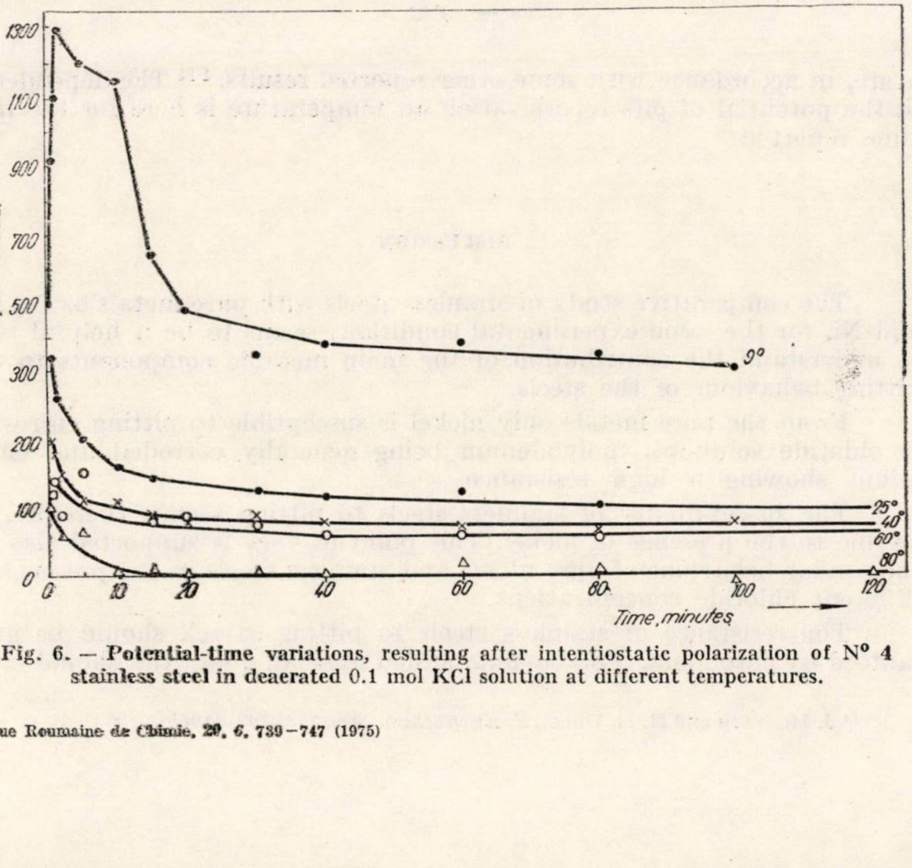

Fig. 6. – Potential-time variations, resulting after intentiostatic polarization of N° 4 stainless steel in deaerated 0.1 mol KCl solution at different temperatures.

The potentiostatic and intensiostatic techniques give comparable results of E_{rp}, as can be observed from the next diagram.

These data illustrate a strong increase in the resistance toward pitting below 25° and less important variations of E_{cp} above this temperature, in accordance with some other reported results.[1,14] The dependence of the potential of pits repassivation on temperature is here for the first time reported.

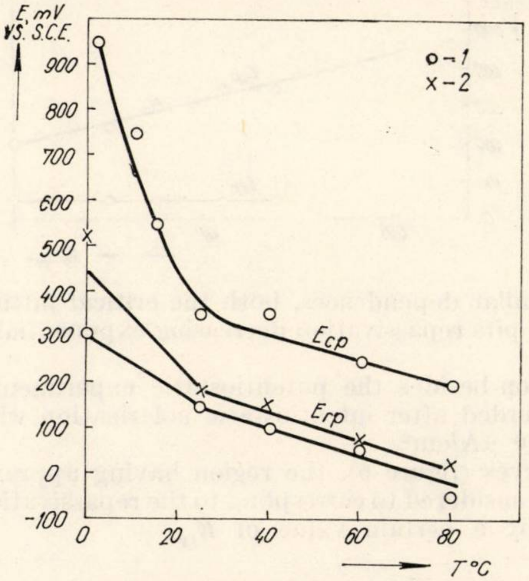

Fig. 7. – A representative type of E_{cp}, $E_{rp} = f(°T)$ variations, obtained on N° 3 stainless steel in deaerated 0.1 mol KCl by: *1*, potentiostatic or *2*, intensiostatic method.

DISCUSSION

The comparative study of stainless steels with pure metals as Cr, Mo and Ni, for the same experimental conditions seems to be a helpful way to understand the contribution of the main metallic components to the pitting behaviour of the steels.

From the pure metals only nickel is susceptible to pitting corrosion in chloride solutions, molybdenum being generally corroded and chromium showing a high resistance.

The susceptibility of stainless steels to pitting seems, therefore, to be due to the presence of nickel. This point of view is supported also by the similar behaviour of pure nickel and stainless steels in the presence of different chloride concentrations.

The resistance of stainless steels to pitting attack should be guaranteed by chromium. Molybdenum added in small quantities should have

---

[14] J. Horvath and H. H. Uhlig, *J. Electrochem. Soc.*, **115**, 792 (1968).

a stabilizing role of metallic structure.[15-17] Its contribution to the pitting behaviour of stainless steels needs further studies.

From the study of the effect of chloride ions on the pitting of nickel and stainless steels results other important conclusions.

There are two independent potentials that characterize the process of pitting:

— the critical pitting potential, that is in a linear dependence on the logarithm of chloride ions activities and

— the potential of pits repassivation, that is independent of the chloride ions content.

These very different behaviours on the same parameter show that the two potentials belong to the different stages of pitting attack.

The independence of the potential of pits repassivation to the electrochemical composition indicates that once started the pitting process develops in some special and very aggressive conditions created inside the pits. This potential refers, therefore, to the propagation stage of the pitting process.

Our observations are supported by data of some other authors regarding the aggressivity of pits anolyte.[11,18-22]

Meanwhile the dependences $E_{cp} = f(°T)$ have been explained by the changes in the double layer structure, the similar variations observed for E_{rp} could be justified by the changes in the hydrolitic equilibrium of the corrosion products and of the pH inside the pits.

---

[15] A. P. Bond and E. A. Lizlovs, *J. Electrochem. Soc.*, **115**, 1130 (1968).

[16] E. A. Lizlovs and A. P. Bond, *J. Electrochem. Soc.*, **118**, 22 (1971).

[17] E. A. Lizlovs and A. P. Bond, *J. Electrochem. Soc.*, **116**, 574 (1969).

[18] Tsuguo Suzuki, Minoru Yamabe and Yoshiharu Kitamura, *Corrosion*, **29**, 18 (1973).

[19] Ya. Kolotirkin, *Corrosion*, **19**, 261 t (1963).

[20] B. A. Brown, *Corrosion*, **26**, 249 (1970).

[21] N. D. Green and M. G. Fontana, *Corrosion*, **15**, 39t (1959).

[22] I. L. Rosenfeld, "4th European Coal and Steel Community" 1968, p. 3.

[illegible] metallic [illegible] [illegible] Lat [illegible] pitting behaviour of stainless steels needs further study.

From the study of the effect of chloride ions on the [illegible] and stainless steels [illegible] other important [illegible].

Thus the two independent potentials that characterize the [illegible] of pitting:

— the critical pitting potential, [illegible] linear [illegible] of chloride [illegible];

— the potential of [illegible] [illegible] independent [illegible] ions content.

[illegible] different behaviours on the same parameter [illegible] that the two potentials belong [illegible] different stages of pitting [illegible].

The [illegible] dependence of the potential of [illegible] concentration to the electrochemical composition [illegible] that once [illegible] the pitting process [illegible] some [illegible] and [illegible] aggressive conditions [illegible] the pits. This potential [illegible] the [illegible] stage of the pitting process.

Our observations are supported by data of some other authors regarding the aggressivity of pits [illegible].

Meanwhile the dependence of E_p [illegible] have been explained by the changes in the double layer [illegible], the similar [illegible] observed for [illegible] could be [illegible] by the changes in the [illegible] of the corrosion products and of the pH [illegible] the pits.

[illegible]

[illegible]

Revue Roumaine de Chimie, **20**, *6*, 749 – 754 (1975)

THE ELECTROCHEMICAL BEHAVIOUR OF STAINLESS STEELS AND THEIR MAIN METALLIC COMPONENTS IN CHLORIDE IONS CONTAINING MEDIA. II *

EFFECT OF pH

SULTANA CIOLAC and ECATERINA VASILESCU

Institute of Physical Chemistry,
Str. Galaţi 31, Bucharest, Romania

Received February 25, 1974

The effect of pH on the electrochemical behaviour of Cr, Ni, Mo and satinless steels in 0.1 mol. KCl is examined. The variation of the critical pitting potential function on the pH (adjusted with HCl, H_2SO_4 and KOH) is presented. It is shown that the potential of pits repassivation is independent of the pH and practically unaffected by the nature of the reagent used in pH adjustment. The similar behaviour of nickel and stainless steels proves the contribution of this metal to the behaviour of stainless steels.

It is generally known that the pH has a great influence on the electrochemical behaviour of the alloyed and pure metals, equally affecting the anodic and cathodic processes.

The electrochemical parameters like the rest potential, corrosion current, passivation potential and even the type of attack are influenced by the pH of the electrolyte.

The pH influences also localized corrosion (pitting, crevice, stress corrosion cracking) particularly affecting its initiation stage.

A rather small number of published data concerning the variation of pitting corrosion resistance with the pH are available. Most of them refer only to the variation of the critical pitting potential with the electrolytic pH and especially for acidic electrolytes. [1,2] Very little informations is provided on the variation of the potential of pits repassivation with the pH. [3]

The object of this research is to provide new data on the effect of pH on the pitting corrosion of stainless steels and to establish the contribution of Cr, Ni and Mo to their behaviour.

The chemical compositions of the studied stainless steels are listed in table 1.

---

* For the first part see ref. 4.

[1] H. P. Lekie and H. H. Uhlig, *J. Electrochem. Soc.*, **113**, 1262 (1966).

[2] V. Hospadaruk and J. V. Petrocelli, *J. Electrochem. Soc.*, **113**, 878 (1966).

[3] Tsuguo Suzuki and Yoshiharu Kitamura, *Corrosion*, **28**, 1 (1972).

The experimental procedure used has been presented elsewhere.[4]

The present observations were carried out in deaerated 0.1 mol. KCl at 25°, whose pH was adjusted with HCl and H_2SO_4 for the acid range and with KOH for the alkaline range.

Tabel 1

The chemical compositions of stainless steels

N°	C	S	P	Si	Mn	Cr	Ni	Ti	Mo	Fe
1	0.04	0.016	N.D.	N.D.	0.71	13.95	—	—	—	balance
2	0.04	0.012	0.01	0.64	0.71	19.43	8.09	—	0.016	”
3	0.05	0.007	0.03	0.4	1.34	17.76	8.79	0.52	0.07	”
4	0.08	0.01	0.02	0.09	1.82	16.90	11.90	0.7	2.36	”

N.D. — not determined.

RESULTS

The cyclic anodic potentiostatic curves were recorded to determine the critical pitting potentials and the potentials of pits repassivation. Their variations as a function of pH (HCl, KOH adjusted) are represented in figure 1.

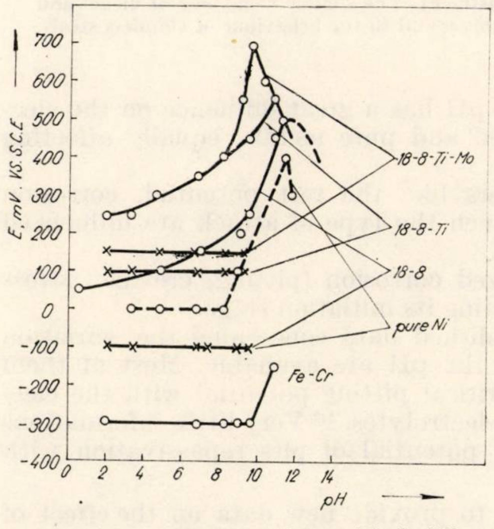

Fig. 1. — The dependence of the critical pitting potential (○ — E_{cp}) and the potential of pits repassivation (× — E_{rp}) on pH(HCl, KOH adjusted).

It appears from this figure that the critical pitting potential E_{cp} is strongly affected by the pH, especially in the alkaline range.

Depending on the metallic composition, E_{cp} varies in the acid range for a pH unit with :

0 mV for Fe—Cr steel (N° 1 composition)

19.05 mV for 18—8 stainless steel (N° 2 composition)

33 mV for 18—8—Ti stainless steel (N° 3 composition)

37 mV for 18—8—Ti—Mo stainless steel (N° 4 composition)

In the alkaline range, maximum values of E_{cp} are found, for all stainless steels, at aproximately 9—10 units of pH.

No data are reported for Fe—Cr ferritic steel at pH >10, because it dissolves strongly by chromates formation.

---

[4] S. Ciolac and E. Vasilescu, *Rev. Roumaine Chim.*, **20**, 739 (1975).

The maximum E_{cp} values of :

500 mV for 18–8 stainless steel (N° 2)
550 mV for 18–8–Ti stainless steel (N° 3)
700 mV for 18–8–Ti–Mo stainless steel (N° 4)

were found.

It results, therefore, that molybdenum-containing stainless steel is most affected by pH changes.

The potentials of pits repassivation measured for all compositions appear to be independent of the pH, at least for the studied range (pH = 2–10).

Anodic polarization curves were recorded for pure Cr, Ni and Mo in the same experimental conditions.

It was observed that the resitance of *chromium* increases with increasing pH, until pH = 10 is reached; above this value the metal is generally corroded by chromates formation. This results are in agreement with the thermodynamic data for the $Cr-H_2O-Cl^-$ system. [5]

In the case of *molybdenum*, potential -pH thermodynamic diagram predicts that molybdenum is passive only in a narrow pH range (pH = 6–9). [6] The electrochemical measurements carried out on molybdenum (figure 2) showed that in the acidic and alkalized potassium chlor-

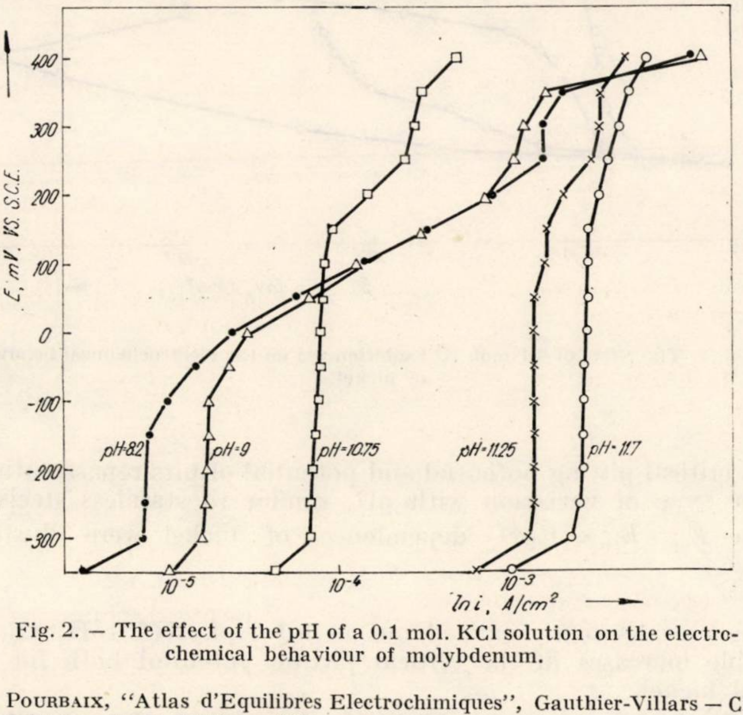

Fig. 2. – The effect of the pH of a 0.1 mol. KCl solution on the electrochemical behaviour of molybdenum.

---

[5] M. POURBAIX, "Atlas d'Equilibres Electrochimiques", Gauthier-Villars – Cie Editeur-Imprimeur-Libraire, Paris, 1963, p. 265.

[6] M. POURBAIX, "Atlas d'Equilibres Electrochimiques", Gauthier-Villars – Cie Editeur-Imprimer-Libraire, Paris, 1963, p. 272.

ide, molybdenum dissolves strongly and presents a certain degree of passivity only for pH = 8–9.

The electrochemical behaviour of *nickel* is very much influenced by the pH.

As can be seen from figure 3 the degree of nickel passivity increases from the acid to the alkaline range of pH. The regions of passivity become larger and the passive current decreases with increasing pH.

In these chloride ions-containing solutions, nickel undergoes a pitting attack.

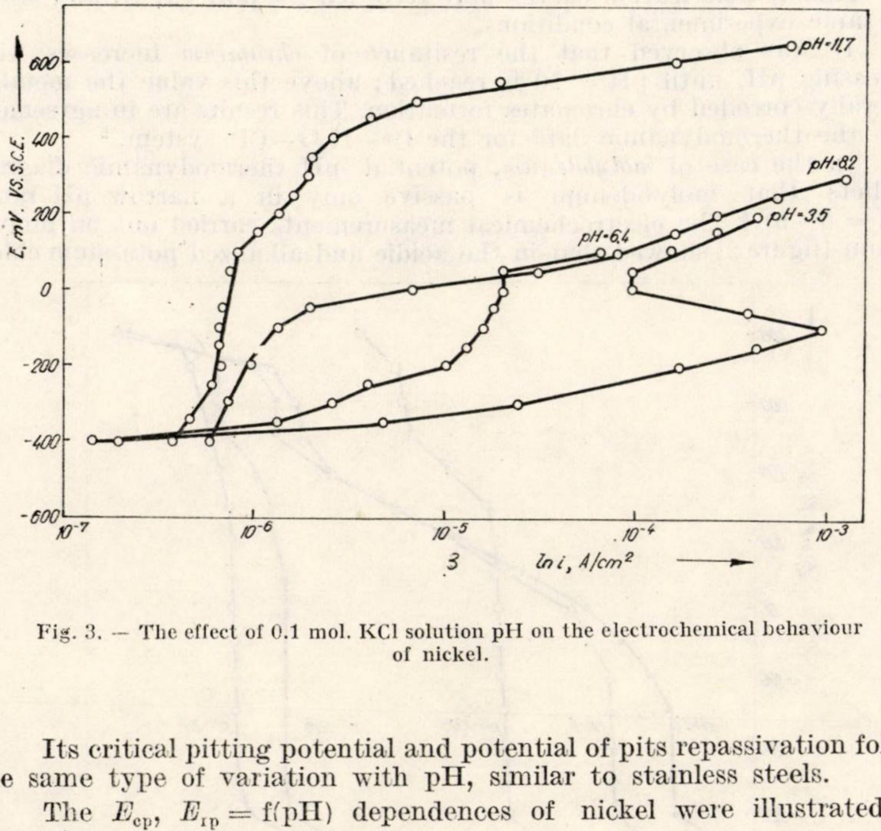

Fig. 3. – The effect of 0.1 mol. KCl solution pH on the electrochemical behaviour of nickel.

Its critical pitting potential and potential of pits repassivation follow the same type of variation with pH, similar to stainless steels.

The E_{cp}, E_{rp} = f(pH) dependences of nickel were illustrated in figure 1.

The measurements carried out in 0.1 mol. KCl + H_2SO_4, showed remarkable increases in the critical pitting potential both for stainless steel and nickel.

As in the previous case (HCl pH adjustment), the potential of pits repassivation is found to be independent of the pH.

Unlike E_{cp}, the potential of pits repassivation is practically unaffected by the nature of the acid used in pH adjustment.

It follows, therefore, that the critical pitting potential and the potential of pits repassivation behave very differently in comparison with the same parameter.

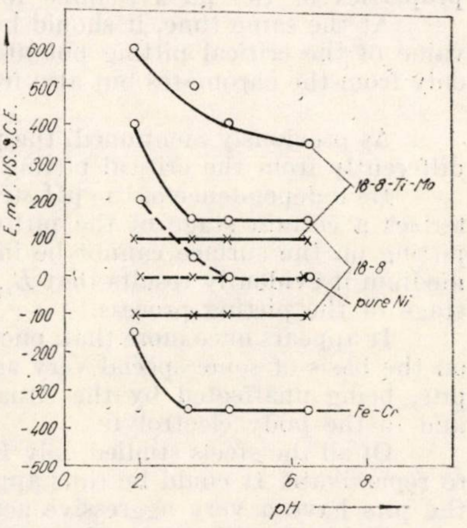

Fig. 4. — The effect of the H_2SO_4 pH adjustment of 0.1 mol. KCl on the critical pitting potential (○ $-E_{cp}$) and the potential of pits repassivation (× $-E_{rp}$).

DISCUSSION

Similar E_{cp}—pH dependences were reported by some other investigators. [2,7,8]

The small variations of the critical pitting potential found in the acidic solutions were explained either by a reduced adsorption of hydrogen ions on the metallic surface[1] or by the fact that low pH-s in the body electrolyte facilitate an earlier pH decrease inside the pits cavities.[9] The increase in E_{cp} by alkalinization was considered to be due to the inhibitive action of OH^- on the corrosion process. [1,7,8]

Our results provide another way for explaining E_{cp} —pH dependences.

The maximum values of E_{cp} were found in the range of the pH where both chromium ($pH \approx 8-9$), nickel ($pH > 9$) and molybdenum ($pH = 8-9$) possess their highest degree of passivity.

In these conditions the passive film formed on the metallic surface must have its maximum stability and thus a minimum susceptibility toward pitting. The stabilizing effect of the passive film could be equally induced by chromium, nickel and molybdenum. However, the similar behaviour of nickel and stainless steel proves that this metal would mainly contribute to the passive film stabilization and thus to the pitting behaviour.

---

[7] Z. Szlarska-Smialowska, *Corrosion*, **27**, 223 (1971).
[8] W. Schwenk, *Corrosion*, **20**, 129t (1964).
[9] T. Desestret, *Corr. et Anticorr.*, **15**, 281 (1967).

The lower degree of passivity of chromium, nickel and molybdenum in the acid range of the pH, can be a reason for the increased tendency toward pitting shown by all stainless steels, due to the less protective properties of the passive films formed on their surfaces.

At the same time, it should be pointed out that the decrease in the value of the critical pitting potential at higher pH-s seems to come not only from the chromates but also from nickel hydroxides formation.

As previously mentioned, the potential of pits repassivation behaves differently from the critical pitting potential.

Its independence of the pH strongly supports the idea that it characterizes a certain stage of the pitting process. As the initiation stage of pitting on the surface cannot be independent of the composition, of the medium it evidently results that E_{rp} is a characteristic of the propagation stage of the pitting process.

It appears once more that, once started, the pitting process developes on the basis of some special very aggressive conditions created inside the pits, being unaffected by the situation existing on the metallic surface and in the body electrolyte.

Of all the steels studied only Fe—Cr steel did not show the capacity to repassivate. It could be thus appreciated that Cr^{3+} ions present inside the pits have a very aggressive action.

Unlike ferritic steel, the austenitic stainless steels have a characteristic E_{cp} value. It follows, therefore, that the nickel present in the metallic composition should be responsible for the differences existing between the two types of steels.

It seems then reasonable to suppose that Ni^{2+} ions, present inside the pits, play an important role in pits chemistry.

Our observations led to the conclusion that the methods of protection against pitting corrosion should interfere in the first stage of pitting development. These methods should be based on a judicious selection of the metallic composition or the use of inhibitors like hydroxides or sulphates (in acid media).

Revue Roumaine de Chimie, **20**, *6*, 755–759 (1975)

OXOVANADIUM(IV) COMPLEXES WITH ALDOXIMES

N. S. BIRADAR* and S. D. ANGADI

Department of Chemistry, Karnatak University, Dharwar–580003, India

Received April 9, 1974

The complexes of oxovanadium (IV) with aldoximes have been prepared in aqueous alcohol medium. The elemental analysis show that they have 1:2 stoichiometry. Magnetic and spectral studies suggest that these complexes have coordination number five and appear to have square pyramidal structures.

INTRODUCTION

In our previous papers on oxovanadium (V) and oxovanadium (IV) complexes with Schiff bases and benzimidazoles, we have shown that oxovanadium (V) forms complexes of coordination number six with Schiff bases,[1] whereas oxovanadium (IV) forms complexes of coordination number five with benzimidazoles.[2] Now we wish to report the complexes of oxovanadium (IV) with aldoximes. It is apparent from the literature that there are quite a few scattered examples of oxovanadium (IV) complexes with aldoximes including both spectrophotometric and gravimetric studies.[3]

This paper describes the synthesis and spectral studies of oxovanadium (IV) complexes with the aldoximes shown below.

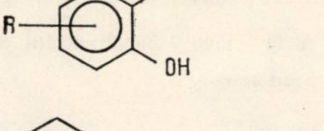

	R
I	H
II	3.Me
III	4.Me
IV	5.Me
V	5.Cl

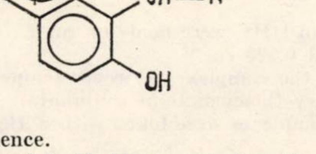

VI

---

* For correspondence.

[1] N. S. Biradar and V. H. Kulkarni, *Rev. Roumaine Chim.*, **16**, 1203 (1971); **17**, 481 (1972); **18**, 63 (1973).

[2] N. S. Biradar, S. Devale and V. H. Kulkarni, *Curr, Sci.*, **42**, 125 (1973).

[3a] H. J. Bielig and H. Möllinger, *Liebigs Ann. Chem.*, **605**, 117 (1957). *Chem. Abstr.*, **51**, 15323 (1958).

[b] H. J. Hoenes and K. G. Stone, *Talanta*, **4**, 250 (1960).

EXPERIMENTAL

MATERIALS AND METHOD

Salicylaldehyde used for the reaction was of Bush make. The substituted aldehydes were prepared according to the known method.[4] Hydroxylamine hydrochloride was of reagent grade and oxovanadium (IV) chloride was of B.D.H. make.

The aldoximes, (I–VI), were prepared according to the method reported elsewhere.[5]

PREPARATION OF THE COMPLEXES

Oxovanadium (IV) chloride (10 m.mole) in alcohol was treated with (22 m.mole) aldoxime in the same solvent and refluxed for a while. The complex from the brown reaction mixture was precipitated by adding (22 m.mole) of sodium acetate in minimum amount of distilled water and left aside to settle. The complex was filtered, washed several times with distilled water then with alcohol and finally dried in vacuum over P_2O_5.

ELEMENTAL ANALYSIS

Vanadium in the complexes was estimated by the volumetric method,[1] and nitrogen was determined by Kjeldahl method. Carbon and hydrogen were analysed by the microanalytical section of the Osmania University, Hyderabad, India.

The elemental analysis of the complexes is shown in table 1.

Table 1

Elemental analysis of oxovanadium (IV) aldoxime complexes

S.N°	Complex	V %		N %		C %		H %		Magnetic moment B.M.
		Found.	Calcd.	Found.	Calcd.	Found.	Calcd.	Found.	Calcd.	
1	$VO(Saldox)_2$	14.92	15.04	8.06	8.26	49.83	49.56	3.60	3.51	1.71
2	$VO(3\text{-}Me\text{-}Saldox)_2$	14.20	13.90	7.58	7.63	52.80	52.04	4.43	4.33	1.82
3	$VO(4\text{-}Me\text{-}Saldox)_2$	14.12	13.90	7.60	7.63	53.00	52.04	4.45	4.33	1.79
4	$VO(5\text{-}Me\text{-}Saldox)_2$	14.18	13.90	7.58	7.63	52.50	52.04	4.50	4.33	1.85
5	$VO(5\text{-}c1\text{-}Saldox)_2$	12.73	12.53	6.68	6.88	40.50	41.17	2.52	2.45	1.80
6	$VO(2\text{-}OH\text{-}Naphthaldox)_2$	11.96	11.67	6.32	6.40	59.92	60.13	3.70	3.64	1.85

Saldox = Salicylaldoxime. Naphthaldox = Naphthaldoxime.

PHYSICAL MEASUREMENTS

The conductance measurements in DMF were made on an ELICO conductivity bridge CM–82 with a cell having cell constant 0.829 cm^{-1}.

The magnetic susceptibilities of the complexes at room temperature were determined on a Gouy Balance using cobalt mercury thiocyanate as calibrant.

The electronic spectra of these complexes were taken with a Beckman DK 2A spectrophotometer.

The infrared spectra of the ligands and the complexes in nujol mull were recorded on a Perkin Elmer 337 spectrometer in the region 4000–400 cm^{-1}.

---

[4] J. C. Duff, *J. Chem. Soc.*, **1941**, 547.

[5] N. S. Biradar and V. B. Mahale, *J. Less-Common Metals*, **31**, 159 (1973).

RESULTS AND DISCUSSION

PHYSICAL PROPERTIES AND STOICHIOMETRY

These complexes are dark coloured amorphous substances soluble to some extent in DMF, DMSO and pyridine. The insolubility of these complexes in common organic solvents thwarted the determination of molecular weights.

The results of the elemental analysis shown in table 1 agree well with 1 :2 stoichiometry. Oxovanadium (IV) chloride loses two of its chloride ions in the course of the reaction with aldoximes (I—VI).

MOLAR CONDUCTANCE

The molar conductance values in DMF at 10^{-3}M are in the region 0—1 ohm^{-1} cm^2/mole. This value is too small to account for any dissociation of the complex in that solvent.

MAGNETIC PROPERTIES

The magnetic moments of the complexes at room temperature are given in table 1. The μ_{eff} values for the present complexes (table 1) closely agree with the spin only value of oxovanadium (IV) complexes hitherto reported.[6] This makes us suggest that oxovanadium (IV) was not oxidized to the 5th oxidation state in the course of reaction.

ELECTRONIC SPECTRA

Although the electronic spectra of oxovanadium (IV) complexes have been discussed in quite a large number of papers, yet the assignment of the observed bands in the complexes is a matter of controversy.[7-11] The discussions[12] made in terms of C_{4v} symmetry theoretically allow three transitions for this d^1 oxovanadium system. The lowering of the symmetry to C_{2V} results in the removal of the degeneracy in the d-orbitals, thus allowing four transitions.

The electronic spectra of these complexes taken in chloroform in the region 350—900 nm are all similar which indicates that they all have the same geometry. The third band, which forms the tail of the high intensity charge transfer band, may be attributed to $d_{xy} \rightarrow d_{z^2}$ transition and the band in the region 580−590 nm assigned to $d_{xy} \rightarrow d_{x^2-y^2}$ transition. The remaining bands are not, however, well resolved and the bands are often broad and exibit shoulders. In pyridine, these become broader and show distinct shifts. The band around 585 nm in chloroform shifts to 540 nm in pyridine. This shift may be interpreted assuming a square-pyramidal geometry for these complexes. The solvent pyridine adds to the sixth axial open site of the metal ion and can disturb the symmetry of the complexes. Similar observations have also been made by previous workers.[13,14]

---

[6] V. V. Savant and C. C. Patel, *J. Inorg. Nuclear Chem.*, **31**, 231 (1969).

[7] C. J. Ballhausen and H. B. Gray, *Inorg. Chem.*, **1**, 111 (1962).

[8] C. K. Jorgensen, *Acta Chem. Scand.*, **11**, 73 (1957).

[9] T. R. Ortolano, J. Selbin and S. P. McGlynn, *J. Chem. Phys.*, **41**, 262 (1964).

[10] R. A. D. Wentworth and T. S. Piper, *J. Chem. Phys.*, **41**, 3884 (1964).

[11] C. J. Ballhausen, B. F. Djurinskij and K. J. Watson, *J. Amer. Chem. Soc.*, **90**, 3305 (1968).

[12] K. Dey and K. K. Chatterjee, *Z. anorg. Chem.*, **383**, 199 (1971).

INFRARED SPECTRA

The important infrared frequencies of the complexes are listed in table 2.

Table 2

Infrared frequencies (in cm $^{-1}$) of oxovanadium (IV) aldoxime complexes and their assignments

N° 1	2	3	4	5	6	Assignments
3200−3300 m.br.	3150−3250 m.br.	3280−3180 w.br.	3250−3180 m.br.	3260−3190 m.br.	3260−3180 m.br.	Intermolecular H bonded −OH stretch
1535 m	1552 m	1548 s	1545 s	1550 s	1550 s	C=N stretch
1282 s	1275 s	1280 s	1275 m	1280 s	1284 s	C−H + Phenolic C−O + N−O vibrations
1196	1160−1130 b	1255 s	1190 s	1192 s	1194 s	N−O vibrations
1065−995 s. br.	985 s	984 s	988 s	985 s	986 s	V=O stretch
575−545 w.sh.	543 m	560−520 sh	575 sh 535 w.br.	550 m	545 m	V−N stretch
455 v.w.	470 m.w.	472 w	485 sh	475 m	480 m	V−O stretch

1−6 S. Nos. of the complexes as listed in table 1.

The broad medium intensity band around 3340 cm^{-1} and a weak broad band around 3200 cm^{-1} of the ligands are assigned to the intermolecular and intramolecular hydrogen bonded OH, respectively in view of the previous assignments.[15] In the complexes, the band at 3200 cm^{-1} vanishes and the other band appears slightly at lower frequency as a broad band of medium intensity (table 2). This band is inferred to be due to the intermolecular hydrogen bonded OH of the N−OH group in analogy with our previous observations.[5]

---

[13] J. Selbin, *Chem. Rev.*, **65**, 153 (1965).

[14] R. L. Dutta and G. P. Sengupta, *J. Indian Chem. Soc.*, **48**, 33 (1971).

[15] K. K. Ramaswamy, C. I. Jose and D. N. Sen, *Indian J. Chem.*, **5**, 156 (1967).

The high intensity band around 1570 cm^{-1} in the ligand assignable to the C=N stretch[15] is observed around 1550 cm^{-1} in the complexes.

A strong intense band due to V=O is observed around 990 cm^{-1} for all these complexes indicating the high π-bond order of vanadium to the oxygen bond of VO^{2+} and the presence of monomeric oxovanadium species.[16,17]

The band around 1280 cm^{-1} of the ligand having medium intensity shows an unusual increase in the intensity and becomes broad in the complexes. This may be ascribed to a mixture of $\nu(C-O) + \delta(C-H) + + \nu(N-O)$ vibrations. The strong bands in the region 1235–1190 and 960–950 cm^{-1} are attributed to the N–O stretch.

The broad band of medium intensity observed in the region 560–530 cm^{-1} is attributed to the $\nu(V-N)$ in view of the previous assignments.[18] The presence of only one band in these complexes suggests that the complexes exist in the *trans* form.

In the light of the data available on the pure $\nu(M-O)$ vibrations,[19] we have assigned the band in the region 460–450 cm^{-1} to the $\nu(V-O)$ vibration. Clark,[20] has demonstrated that the $\nu(M-O)$ vibrations are sensitive to the oxidation state and coordination number of the metal ion. The observed consistancy in the $\nu(V-O)$ vibration makes us conclude that the oxidation state and the coordination number of oxovanadium remains the same in all the complexes.

All these observations make us regard these complexes as having coordination number five. Generally, five coordinate oxovanadium (IV) complexes have square pyramidal structures.[21]

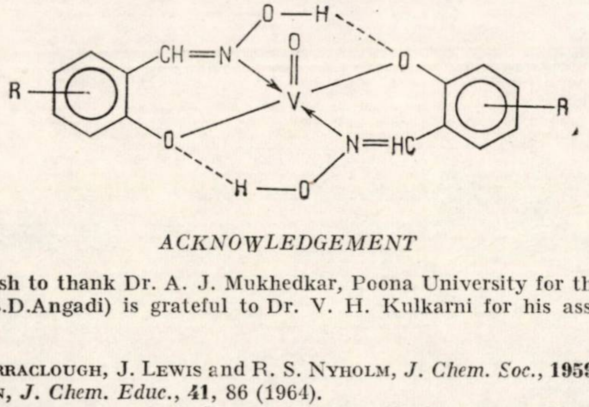

ACKNOWLEDGEMENT

Authors wish to thank Dr. A. J. Mukhedkar, Poona University for the i.r. spectra. One of the authors (S.D.Angadi) is grateful to Dr. V. H. Kulkarni for his assistance in writing this paper.

[16] C. G. Barraclough, J. Lewis and R. S. Nyholm, *J. Chem. Soc.*, **1959**, 3552.

[17] J. Selbin, *J. Chem. Educ.*, **41**, 86 (1964).

[18a] C. P. Prabhakaran, C. C. Patel, *J. Inorg. Nuclear. Chem.* **31**, 3316 (1969).

[b] B. C. Sharma and C. C. Patel, *Indian J. Chem.*, **8**, 747 (1970).

[c] N. S. Biradar and V. H. Kulkarni, *J. Inorg. Nuclear Chem.*, **33**, 3847 (1971); *Z. anorg. Chem.*, **387**, 275 (1972).

[19a] G.T. Behnke, and K.Nakamoto, *Inorg.Chem.*, **6**, 433 (1967).

[b] C. Djordjevic, *Spectrochim.Acta*, **17**, 448 (1961).

[c] R.C.Fay and T.J.Pinnavaia, *Inorg.Chem.*, **7**, 508 (1968).

[d] K. Nakamoto, P. J. McCarthy (eds), "Spectroscopy and Structure of Metal Chelate Compounds", Wiley-Interscience, New York, 1968.

[20] R. J. H. Clark, *Spectrochim. Acta*, **21**, 955 (1965).

[21] D. N. Sathyanarayana and C. C. Patel, *J. Inorg. Nuclear Chem.*, **28**, 2277 (1966); *Sci. Ind. Res.*, **27**, 348 (1968).

Revue Roumaine de Chimie, **20**, *6*, 755–759 (1975)

Revue Roumaine de Chimie, 20, 6, 761 – 774 (1975)

HETEROCYCLIC COMPOUNDS. III *

CYCLIZATION OF RING-SUBSTITUTED γ-PHENOXYBUTYRIC ACIDS BY PPA TO 2,3-DIHYDRO-1-BENZOXEPIN-5(4*H*)-ONES

ILIE I. BĂDILESCU

Department of Chemistry, Pedagogical Institute, Str. Gh. Doja 41, Pitești, Romania

Received April 2, 1974

The cyclization reaction of several γ-phenoxybutyric acids (I), in the presence of PPA, leads to the corresponding 2,3-dihydro-1-benzoxepin-5(4*H*)-ones (II), in variable yields, depending on the experimental conditions. The yields are also influenced by the substitution in the phenyl ring of I, and both electronic and steric effects were found to be effective in the reactions studied. Structural assignments were made on the basis of elemental analysis, infrared and nuclear magnetic resonance spectra of II, as well as by preparation and characterization of the ketoximes V and 2,4-DNPH derivatives VI.

INTRODUCTION

Although two homochromanone (2,3-dihydro-1-benzoxepin-5 (4*H*)-one) derivatives were reported in 1931 by Powell and Anderson, [1] the chemistry of this seven-membered heterocyclic system lay dormant until 1954. At that time, Dann and Arndt reported [2] the successful preparation of the parent 2,3-dihydro-1-benzoxepin-5(4*H*)-one, (IIa), and some other substituted compounds, by cyclodehydrating the corresponding (ring-substituted) γ-phenoxybutyric acids (I), by polyphosphoric acid, (PPA). Further studies in this field were carried out by Fontaine, [3–5] and a few

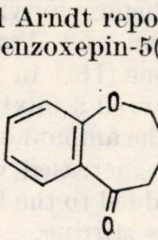

IIa

---

* Part II., I. I. Bădilescu, *Tetrahedron*, **26**, 4207 (1970).

[1] S. G. Powell and L. Anderson, *J. Amer. Chem. Soc.*, **53**, 811 (1931).

[2] O. Dann, W.-D. Arndt, *Liebigs Ann. Chem.*, **587**, 38 (1954).

[3] G. Fontaine, P. Maitte, *Compt. rend.*, **258**, 4583 (1964).

[4] G. Fontaine, *Ann. Chim. (France)*, [14], **3**, 179 (1968).

[5] G. Fontaine, *Ann. Chim. (France)*, [14], **3**, 469 (1968).

data on this heterocyclic system were reported in other papers. [6-12]

The interest for this class of compounds arises from the observation of Dann and Arndt [2] that some chemical properties of this seven-membered ring system are different in comparison with those exhibited by the six-membered heterocyclic analogs, *i.e.*, 4-chromanones.

In a paper published in this journal some years ago, [13] we noted that the cyclization of some γ-phenoxybutyric acids (I) afforded, with PPA, the corresponding cyclic ketones II, in good yields, except the chloro-substituted acids, which are easily cleaved by PPA. Now, we wish to report the results obtained by the cyclization of some γ-phenoxybutyric acids (I) to the corresponding 2,3-dihydro-1-benzoxepin-5(4*H*)-ones (II), together with the experimental procedures and the spectroscopic investigation of the compounds obtained.

RESULTS AND DISCUSSION

The starting materials for the synthesis of II, were ring-substituted γ-phenoxybutyric acids (I), which are available by the reaction of the corresponding sodium phenoxide and γ-butyrolactone, in anhydrous conditions. [13-16] Several γ-phenoxybutyric acids (I) used in this work were previously reported, [17] and some other acids were prepared as described. Two acids, Ie and If, were converted into their corresponding ethyl ester IIIe and IIIf, with a saturated solution of anhydrous hydrochloric acid in absolute ethyl alcohol. Infrared and nuclear magnetic resonance spectra of these compounds are in agreement with the structure of the compounds thus obtained.

The cyclization of the γ-phenoxybutyric acid (Ia) in the presence of PPA, by the method of Dann and Arndt [2] (procedure A) afforded 2,3-dihydro-1-benzoxepin-5(4*H*)-one (IIa) in moderate yields. As reported by Dann and Arndt, we also observed a mixture of *para*-polycondensation products and, in some instances, the amount of polymeric material exceeded 20 per cent. However, the yields increased when a larger excess of PPA was used and the molten Ia was added to the PPA preheated (at 100 – 110°) for over an hour, under vigorous stirring.

---

[6] D. Lamparsky and R. Böhm, Ger. Pat. 1,037,465, 28 Aug. 1958.

[7] H. Hofmann, *Angew. Chem.*, **77**, 864 (1965).

[8] H. Hofmann, *Chem. Ber.*, **102**, 205 (1969).

[9] H. Hofmann, H. Westernacher, H.-J. Haberstroh, *Chem. Ber.*, **102**, 2595 (1969).

[10] I. M. Lockhart and M. Wright, *J. Chem. Soc., C*, **1971**, 3182.

[11] M. Weissenfels, H. Schurig and G. Huhsam, *Z. Chem.*, **6**, 471 (1966).

[12] J. H. P. Tyman, and R. Pickles *Tetrahedron Letters*, 1966, 4993.

[13] I. I. Bădilescu, *Rev. Roumaine Chim.*, **14**, 1585 (1969).

[14] W. Reppe u. Mitarb., *Liebigs Ann. Chem.*, **596**, 190 (1955).

[15] N. N. Melnikov and S. S. Kukalenko, *Zhur. obshchei Khim.*, **29**, 3744 (1959).

[16] I. I. Bădilescu, *Rev. Chim. (București)*, **20**, 11 (1969).

[17] D. Huckle, I. M. Lockhart and N. E. Webb, *J. Chem. Soc., C*, **1971**, 2252.

CHART 1

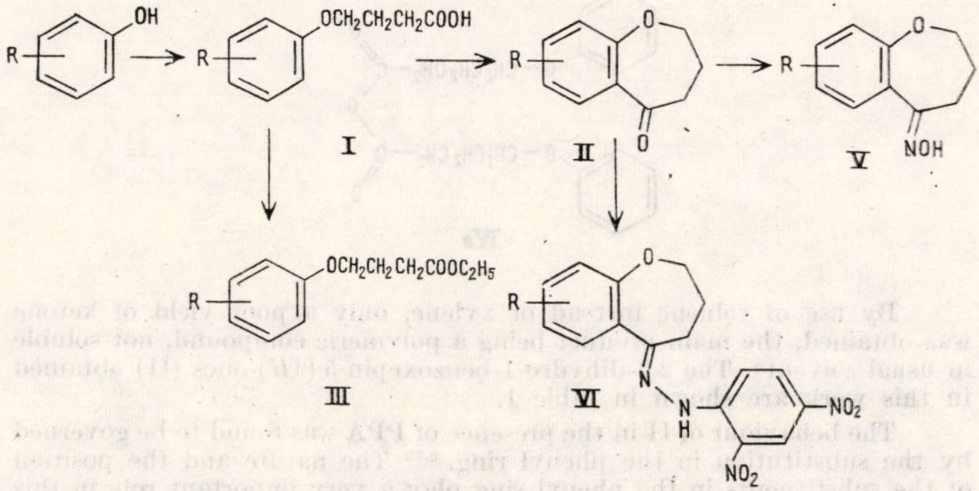
OH
R
$OCH_2CH_2CH_2COOH$
R
R
O
O
R
O
NOH
I
II
V
$OCH_2CH_2CH_2COOC_2H_5$
R
III
R
O
N
N
H
NO_2
NO_2
VI

Ia,	R = H	IIa, Va, VIa,	R = H
Ib,	R = 3−CH_3	IIb, Vb, VIb,	R = 8−CH_3
Ic,	R = 4−CH_3	IIc, Vc, VIc,	R = 7−CH_3
Id,	R = 4−F	IId, VId,	R = 7−F
Ie, IIIe,	R = 3,5−$(CH_3)_2$	IIe, Ve, VIe,	R = 6,8−$(CH_3)_2$
If, IIIf,	R = 3,4−$(CH_3)_2$	IIf, Vf, VIf,	R = 7,8−$(CH_3)_2$
Ig,	R = 3−CH_3−4−Cl	IIg,	R = 7−Cl−8−CH_3
		IIh, Vh, VIh,	R = 4−$(CH_2)_4$−4

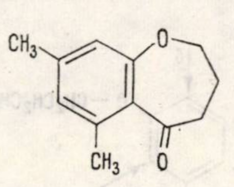

IIe

By using xylene as solvent (procedure B), the results were very close to those reported by Fontaine, [3,4] including the isolation of a compound boiling at 160−170°/7 mmHg (which proved to be the anhydride of γ-phenoxybutyric acid, IVa).

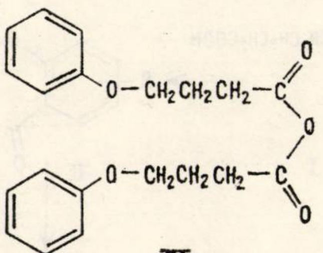

IVa

By use of toluene instead of xylene, only a poor yield of ketone was obtained, the main product being a polymeric compound, not soluble in usual solvents. The 2,3-dihydro-1-benzoxepin-5 (4*H*)-ones (II) obtained in this work are shown in table 1.

The behaviour of II in the presence of PPA was found to be governed by the substitution in the phenyl ring. [2,13] The nature and the position of the substituents in the phenyl ring play a very important role in this reaction, but it does not seems as important as that of the steric factors.

Thus, by cyclization of Ic and If, the corresponding 7-methyl-II (IIc) and 7,8-dimethyl-2,3-dihydro-1-benzoxepin-5 (4*H*)-one, (IIf) were obtained in good yields, and this fact may be explained by the presence of a methyl group in the position 4 of both Ic and If, thus precluding any *para*-polycondensation reactions. [2-4] However, the absence of 6,7-dimethyl-II in the reaction mixture resulted from the cyclization of γ-(3,4-dimethylphenoxy)butyric acid (If), cannot be explained in terms of purely electronic effects. Indeed, although the electronic effects of the substituents in If favour cyclization in both 2 and 6 positions, the sole cyclic ketone isolated from the reaction mixture was IIf, corresponding to a cyclization in position 6. This behaviour of If, in the presence of PPA, suggests that the reaction is under steric control of the *meta* substituent. This assumption was supported by the behaviour of γ-(3-methylphenoxy) butyric acid (Ib)

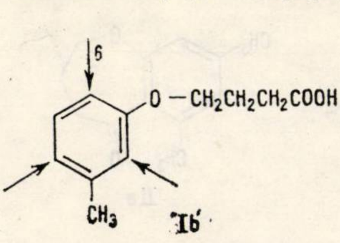

Ib′

in the presence of PPA; for this compound three reaction sites might be effective, (as indicated by the arrows, in formula Ib′), but in the presence of PPA, it undergoes ring closure solely in position *ortho*-6, to give pure 8-methyl-II, (IIb), in high yield. Thus, it seems that the presence of a *meta*-substitution results in the same effect as a *para*-substitution, *i.e.*, the absence of any polycondensation reaction.

Table 1

2,3-Dihydro-1-benzoxepin-5(4H)-ones (II)

N°	Substituent	Procedure	Yield %	M.p., °C (recryst. solvent)	B.p. °C/mmHg	n_D^{20}	Lit. b.p., °C	n_D^{20}	Ref.
IIa	None	A	31	—			$100-130/_4$	1.564	2
		B	70–80		$102/_2$	1.5665	$106/_2$	1.5650	3,4
IIb	$8-CH_3$	A	49	—	$116-120/_2$	1.5633	—	—	—
IIc	$7-CH_3$ *	A	49	—	$118-120/_1$	1.5640	$114-116/_{0.9}$	1.560	2
IId	7–F	A	75	46–47 (*n*-heptane)	$115-117/_{11}$	1.5410	—	—	—
IIe	$6,8-(CH_3)_2$*	B	75	—	$128/_4$	—	—	—	—
IIf	$7,8-(CH_3)_2$	A, B	70, 74	61 ** (ligroin)	136–140/1	—	$130-145/_{0.1}$	—	2
IIg	$7-Cl-8-CH_3$	A	15	64–65 (*n*-pentane-benzene)	$130-132/_1$	—	—	—	—
IIh	$4-(CH_2)_4-4$	C	50 ***	—	$132/_2$	1.5625	—	—	—

* Prepared by Huckle et al.[17] but not purified. **Lit.[2] m.p. 61.5–62°. *** Estimated yield (see experimental).

The importance of the steric effect is strongly evidenced by the absence of polycondensation products in the cyclization of γ-(3,5-dimethylphenoxy)butyric acid, (Ie) to 6,8-dimethyl-II (IIe).

The cyclic ketones II, obtained by the cyclization of I, are presented in table 1.

The unreported 2,3-dihydro-1-benzoxepin-5-on-4-spiro-cyclopentane (IIh) was obtained by the elegant route described by Mousseron et al.[18,19] (and successfully used by Conley and Frainier[20] to prepare several 2,2-disubstituted 1-indanones and related compounds). The starting material was the parent heterocyclic ketone Ia, which was treated with t-BuOK in anhydrous benzene, then the solution was heated at reflux for several hours and the mixture worked up. In another work,[21] we showed that, in the presence of t-BuOK, the spiro-ketone IIh undergoes cleavage, with subsequent formation of salicylic acid. A possible mechanism of the fragmentation reaction was already reported[21] and, in this paper, the experimental procedures are given in the experimental section.

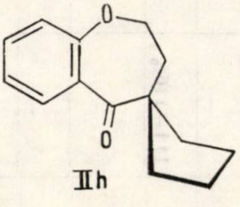
IIh

Table 2

2,3-Dihydro-1-benzoxepin-5(4H)-one ketoximes V

N°	R	Procedure	Yield %	M.p. * °C	Lit. m.p. °C	Ref.
Va	H	A, B	90, 84.5	99 – 100[a)]	99	1
Vb	$8-CH_3$	A, B	89, 75	113 – 114[a)]	—	—
Vc	$7-CH_3$	B	78	73.5 – 74.5[a)]	71.5 – 72.5[b)]	2
Ve	$6,8-(CH_3)_2$	A, B	68	137 – 138.5[a)]	—	—
Vf	$7,8-(CH_3)_2$	A, B	79, 74.5	111.5 – 112.5[c)]	109 – 110[b)]	2
Vh	$4-(CH_2)_4-4$	B	68	143 – 146[d)]	—	—

* Recrystallization solvent; a) benzene – petroleum ether; b) benzene – light petroleum; c) benzene – ligroine; d) cyclohexane.

The structure of the heterocyclic ketones II is supported by elemental analysis, spectral data and by the preparation and characterization of some derivatives.

---

[18] M. Mousseron, R. Jacquier and M. Christol, *Compt. rend.*, **239**, 1805 (1954).

[19] M. Mousseron, R. Jacquier and M. Christol, *Bull. Soc. chim. France*, **1957**, 346.

[20] R. T. Conley and L. J. Frainier, *J. Org. Chem.*, **27**, 3844 (1962).

[21] I. I. Badilescu, Tetrahedron Letters, **1974**, 1969.

The ketones IIa—IIh were converted into the corresponding oximes V (by heating ketone II with hydroxylamine in aqueous ethanol or by the hydroxylamine—pyridine—ethyl alcohol procedure). [22] The ketoximes V are recorded in table 2.

The 2,4—DNPH derivatives (VI) were obtained by treating (without heating), a solution of II in ethyl alcohol, with the reagent prepared from 2,4-dinitrophenyl-hydrazine, 85 per cent phosphoric acid and ethyl alcohol. [23] The compounds thus obtained are given in table 3.

Table 3

2,4-DNPH Derivatives of II

N°	R	M.p. °C	Colour	Molecular formula	M. W.	Analyse, N %	
						Calculated	Found
VIa	H	242$^{a,b)}$	orange	$C_{16}H_{14}N_4O_5$	342.31	16.37	16.77
VIb	$8-CH_3$	181$^{b)}$	orange	$C_{17}H_{16}N_4O_5$	356.34	15.73	15.95
VIc	$7-CH_3$	228$^{b)}$	red	$C_{17}H_{16}N_4O_5$	356.34	15.73	16.05
VId	7—F	247$^{b)}$	yellow-orange	$C_{17}H_{15}FN_4O_5$	360.30	15.55	15.48
VIe	$6,8-(CH_3)_2$	199$^{c)}$	yellow	$C_{18}H_{18}N_4O_5$	370.37	15.12$^{d)}$	14.95$^{d)}$
VIf	$7,8-(CH_3)_2$	223$^{c)}$	yellow-orange	$C_{17}H_{15}N_4O_5$	370.37	15.12	15.04
VIh	$4-(CH_2)_4-4$	189$^{c)}$	yellow	$C_{20}H_{20}N_4O_5$	396.41	14.13	14.50

a) Lit. [3,4] m.p. 242°. b) Recrystallized from benzene. c) Recrystallized from benzene — ethanol. d) *Found*; C, 57.80, H, 4.97; *calculated*; C, 58.37, H, 4.89%

In the conditions of the Fischer synthesis of indoles, from 7-methyl-2,3-dihydro-1-benzoxepin-5 (4*H*)-one (IIc) and 4-methylphenylhydrazine hydrochloride, the unreported 2,9-dimethyl-12*H*-6,7-dihydro-benz[2′, 3′] oxepino [4,5-*b*)indole, (VII) was obtained. Structure VII, assigned to the compound thus obtained, is supported by infrared and nuclear magnetic resonance spectra. Some related compounds were reported in a recent paper. [24]

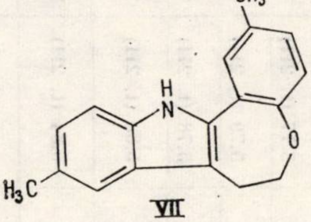

VII

The infrared absorption spectra of 2,3-dihydro-1-benzoxepin-5(4*H*)-ones II are in agreement with the structures assigned. Thus, the

---

[22] W. E. Bachmann and M. X. Barton, *J. Org. Chem.*, **3**, 307 (1938).

[23] G. D. Johnson, *J. Amer. Chem. Soc.*, **73**, 5888 (1951).

[24] L. M. Sharkova, L. A. Aksanna and N. F. Kucherova, *Khim. Geterotsikl. Soed.*, **7**, 65 (1971).

Table 4

N.m.r. spectral data of 2,3-dihydro -1- benzoxepin-5(4*H*)-ones II

N°	R	Chemical shifts (τ values)					
		$O-CH_2-$	$O-C-CH_2-$	$-CH_2-CO-$	aromatic	$-CH_3$	$\rangle C \frown (CH_2)_4$
IIa	H	5.77 (t, 2H)	7.83 (m, 2H)	7.12 (m, 2H)	3.10–2.14 (m, 4H)	—	—
IIb	$8-CH_3$	5.79 (t, 2H)	7.85 (m, 2H)*	7.10 (m, 2H)	3.10–2.35 (m, 3H)	7.59 (s, 3H)*	—
IIc	$7-CH_3$	5.78 (t, 2H)	7.85 (m, 2H)*	7.10 (m, 2H)	3.10–2.35 (m, 3H)	7.68 (s, 3H)*	—
IIe	$6,8-(CH_3)_2$	5.83 (t, 2H)	7.80 (m, 2H)*	7.20 (m, 2H)	3.23 (s, 2H)	7.58 (s, 3H)* 7.70 (s, 3H)*	—
IIf	$7,8-(CH_3)_2$	5.84 (t, 2H)	7.86 (m, 2H)*	7.22 (m, 2H)	3.23 (s, 1H) 2.55 (d, 1H)	7.92 (s, 6H)*	—
IIg	$7-Cl-8-CH_3$	5.75 (t, 2H)	7.83 (m, 2H)*	7.11 (m, 2H)	3.00 (s, 1H) 2.23 (s, 1H)	7.63 (s, 3H)*	—
IIh	$4-(CH_2)_4-4$	5.78 (t, 2H)	7.88 (m, 4H)**	—	3.17–2.30 (m, 4H)	—	8.45 (m, 6H)**

* Estimated from the integral of the multiplet centered at some 7.77 τ; ** With two protons from (spiro) cyclopentane ring.

stretching frequency of C=O bond appears between 1681–1691 cm^{-1}, which are normal values for aryl-alkyl-ketones.[25] A weak absorption band, near 3350 cm^{-1}, was present in all spectra, irrespective of the structure of II or sample purity, and it was assigned to an overtone of the $\nu_{C=O}$ band.

The nuclear magnetic resonance spectral data for these compounds are recorded in tables 4 and 5. In order to differentiate between the $C_{(3)}$ and $C_{(4)}$ methylene protons, the comparison of n.m.r. spectra of ketones II and of their corresponding oximes (V) was conclusive. Indeed, while the signals near $\tau = 7.8$ p.p.m. in the n.m.r. spectra of ketones remained unchanged in the spectra of the corresponding ketoximes, the signals at *ca.*, 7.2 τ are shifted after oximation of ketones, to lower fields, which indicates the close proximity of an isonitroso group. In the ketones, the signals corresponding to the protons at the $C_{(3)}$ are separated by *ca.* 38 c.p.s. from those corresponding to the protons at $C_{(4)}$ but, in the spectra of ketoximes, the chemical shifts are separated by *ca.* 58 c.p.s.

Table 5

N.m.r. spectral data of the ketoximes V

N°	R	Chemical shifts (τ values)					
		OH	aromatic	$-CH_2-$	$-CO_2-OC-$	$-O-C-CH_2-$	$-CH_3$
Va	H	0.13 s	2.30–3.10 m	5.80 t	7.02 q	7.97 cv	—
Vb	$8-CH_3$	0.32 s	2.57 d 3.14 d	5.83 t	7.05 q	7.99 m	7.68 s
Vc	$7-CH_3$	0.38 s	2.65–3.19 m	5.85 t	7.05 q	8.00 m	7.68 s
Ve	$6,8-(CH_3)_2$	0.55 s	3.20 (s, 1H) 3.30 (s, 1H)	5.92 t	7.20 m	8.08 m	7.63 (s, 3H) 7.72 (s, 3H)
Vf	$7,8-(CH_3)_2$	0.77 s	2.70 (s, 1H) 3.17 (s, 1H)	5.81 t	7.05 q	7.91 m	7.70 s
Vh	$4-(CH_2)_4-4$	1.00 s	2.45–3.14 m	5.78 t	—	8.02 (m, 4H)* 8.33 (m, 6H)*	—

* Together with the protons of (spiro) cyclopentane methylens.

Very conclusive was the disappearance of the signals near $\tau = 7.2$ p.p.m. after deuterium exchange, in the spectra of IIa′ and IIe′, and the absence of the corresponding signals (near 7.05 τ) in the n.m.r. spectra of their ketoximes (Va′ and Ve′).

Some chemical and stereochemical peculiarities of ketoximes V and 2,4-DNPH derivatives VI, encountered in this work, shall be reported in another paper, in preparation.

---

[25] M. Avram and Gh. D. Mateescu, "Spectroscopia în infraroșu, Aplicații în chimia organică", Ed. tehnică, Bucharest, 1966, p. 416.

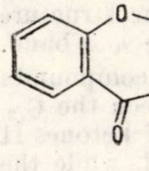

IIa′

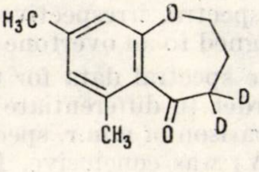

IIe′

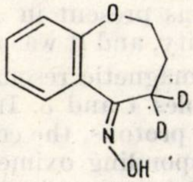

Va′

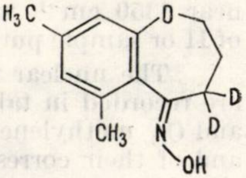

Va′

EXPERIMENTAL

All melting points were determined in capillary tubes and are uncorrected.

N.m.r. spectra were taken in $CDCl_3$ solution containing TMS as internal standard, using a Varian A-60A spectrometer.

Infrared spectra were recorded on an UR-10 Carl Zeiss — Jena and/or a Perkin-Elmer, Model 621, double beam spectrophotometers.

Ultraviolet spectra were recorded with an Unicam SP 800 spectrophotometer, in EtOH solution.

Unless otherwise stated, solutions were dried over anhydrous magnesium sulphate. The most γ-phenoxybutyric acids used in this work were already reported and obtained as described.[16]

γ-(4-Fluorophenoxy)butyric acid (Id)

Anhydrous sodium *p*-fluorophenoxide (0.04 moles) was heated at 200—205° with γ-butyrolactone (0.1 mole) for three hours. The excess γ-butyrolactone was removed by distillation at reduced pressure, the solid residue dissolved in 100 ml of water and the solution treated with hydrochloric acid solution to give 5.85 g crude Id. By recrystallization from n-hexane, 4.9 g (62%) of pure γ-(4-fluorophenoxy)-butyric acid (Id) was obtained as colourless crystals, melting at 104—106° (lit.[26] m.p. 106—107°).

γ-(3,5-Dimethylphenoxy)butyric acid (Ie)

A solution of 220 g (1.8 moles) 3,5-dimethylphenol in 200 ml absolute ethyl alcohol is treated with 1.8 moles of sodium ethoxide (obtained from 41.4 g sodium and 600 ml absolute ethyl alcohol) and then ethyl alcohol is removed by distillation at reduced pressure. The solid residue is treated with 344 g (4 moles) freshly vacuum-distilled γ-butyrolactone, the residual ethyl alcohol removed and the mixture heated for an hour at the reflux temperature of γ-butyrolactone, and then the excess γ-butyrolactone is removed by distillation. The mixture was cooled to *ca.* 80°, the solid product was dissolved in 1000 ml water and the solution cooled to room temperature and treated with a concentrated aqueous solution of hydrochloric acid. The crude precipitate was filtered off, washed with cold water, dried in air and recrystallized from ethanol to yield 300 g (80%) γ-(3,5-dimethylphenoxy) butyric acid, (Ie), melting at 68—70°. A colourless analytical sample, m.p. 69—70°, was obtained by further purification from benzene — petroleum ether.

Found: C, 69.55, H, 7.60; $C_{12}H_{10}O_3$ *requires*: C, 69.21, H, 7.76%

Ethyl γ-(3,4-dimethylphenoxy)butyrate (IIIf)

A solution of 14.6 g (0.07 moles) of If in 50 ml of ethyl alcohol saturated with anhydrous hydrochloric acid, was heated at reflux for three hours and then the reaction mixture worked up. The crude ester, (13 g, 79%), is a colourless liquid with agreeable odor, boiling at

---

[26] N.N. MELNIKOV, *Zhur. obshchei Khim.*, **29**, 3708 (1959).

146–148°/3 mm Hg. A pure sample of ethyl γ-(3,4-dimethylphenoxy)butyrate, (IIIf) was obtained by redistillation, (b.p. 141°/2 mm Hg; $d_4^{20} = 1.032$; $n_D^{20} = 1.5648$). I.r. spectrum: $\nu_{C=O}$ 1726 cm^{-1}.

Found: C, 70.95, H, 8.80; $C_{14}H_{20}O_3$ *requires*: C, 71.16, H, 8.53%.

Ethyl γ-(3,5-dimethylphenoxy)butyrate, (IIIe)

The procedure used was the same as described above. Yield 13.3 g (80%) ethyl γ-(3,5-dimethylphenoxy)butyrate, (IIIe), liquid with agreeable odor, b.p. 138–140°/3 mm Hg.

The structure IIIe was proved by spectral data: infrared: $\nu_{C=O}$1718 cm^{-1}; n.m.r. spectrum: $\tau = 3.55$ (3, s, aromatic), 5.99 (4, m, $O-CH_2$), 7.42–8.17 (10, m, $2CH_2 + 2CH_3$) and 8.77 (3, t, CH_3).

2,3-Dihydro-1-benzoxepin-5(4H)-one (IIa)

Procedure A

To 1000 g of PPA, heated at 110°, 36 g (0.2 moles) of molten γ-phenoxybutyric acid (Ia) was added dropwise for over an hour, under stirring. The reaction mixture was stirred at 105–110° for further two hours and then poured onto 3000 g crushed ice and extracted with benzene (2 × 200 ml). The organic layer was separated and washed with an aqueous $NaHCO_3$ solution, then with 10 per cent aqueous NaOH solution and finally with water. The organic solution was dried, the benzene removed and the residue was distilled at reduced pressure to yield 20.7 g (64 %) of almost pure IIa, b.p. 120 - 130°/4 mm Hg . Redistillation of this product afforded a pure sample of IIa, b.p. 109°/3 mm Hg ; $n_D^{20} = 1.5665$, (lit. [2–4] b.p. 100-130°/4 mm Hg , 106°/ 2 mm Hg, $n_D^{20} = 1.564$ and 1.650).

Procedure B

a) *With xylene.* γ-Phenoxybutyric acid (144 g, 0.8 moles) was added portionwise to a stirred mixture of PPA (1100 g) and xylene (500 ml) heated on a water-bath. The reaction mixture was stirred vigorously for another two hours at 94–96° and then poured onto chrushed ice (3000 g) and extracted with xylene (1000 ml). The organic layer was separated, washed thoroughly with aqueous $NaHCO_3$ and NaOH solutions, with water and dried. The solvent was removed and the residue was fractionated under reduced pressure to give *i*) – 30.3 g (31%) of IIa (b.p. 108–110°/7 mm Hg) and *ii*) – 27 g of an oily compound (b.p. 160–170°/ 7 mm Hg) which solidifies on standing. The latter product proved to be anhydride of the acid Ia (IVa).

When the reaction mixture was stirred for an hour at *ca.* 85°, then for another hour without heating, the cyclic ketone IIa was obtained in 70% yield, and only a poor quantity of IVa appeared in the reaction mixture.

b) *With toluene.* A mixture of 500 g of PPA and 100 ml of toluene was stirred on the water-bath and 60 g (0.333 moles) of Ia was portionwise added to the mixture, over 45 minutes. After two hours of stirring at 90–95°, the reaction mixture was worked up as in the preceding case (solvent–toluene). A large amount of polymeric material was separated; however, from the reaction organic solution 25 g (50%) IIa was obtained.

The infrared spectrum of IIa, (neat film, KBr windows) shows the following absorption bands: (3345), 3068, 2965, 2930, 2875, 1685, 1569, 1478, 1450, 1380, 1319, 1288, 1222, 1169, 1151, 1109, 1075, 1058, 1030, 985, 880, 809, 800, 782, 760, 730, 583, 547 and 536 cm^{-1}.

The ultraviolet spectrum shows the following maxima: λ_{max}^{EtOH}: 208.5, 245.5 and 301.6 nm; (ε_{max}: 18,240, 8,420 and 2,710, respectively).

The n.m.r. spectrum (table 4) also supports structure IIa for this compound.

8-Methyl-2,3-dihydro-1-benzoxepin-5(4H)-one (IIb)

The heterocyclic ketone IIb was obtained by using procedure A. Yield 49% of an oily liquid, boiling at 116–120°/2 mm Hg, $n_D^{20} = 1.5633$.

Found: C, 74.88, H, 7.10; $C_{11}H_{12}O_2$ *requires*: C, 74.98, H. 6.88%

The infrared spectrum of IIb shows the following maxima, (neat liquid on KBr windows): (3350), 3070, 3035, 2970, 2955, 2930, 2889, 2869, 1690, 1620, 1570, 1500, 1475, 1459, 1440, 1425, 1382, 1360, 1329, 1292, 1285, 1242, 1220, 1160, 1131, 1080, 1065, 1018, 990, 958, 920 880, 838, 812 and 723 cm^{-1}.

7-Methyl-2,3-dihydro-1-benzoxepin-5(4H)-one[2] (IIc)

This compound was obtained by procedure A, the results being summarized in tables 2 and 4.

7-Fluoro-2,3-dihydro-1-benzoxepin-5(4H)-one (IId)

To 20 g of PPA (preheated at 120°), 1.98 g (0.01 mole) of γ-(4-fluorophenoxy)butyric acid (Id) was added under stirring, and the mixture stirred for an hour at 120—125°. The cold mixture was treated with 100 g of ice-water, the solution extracted with ethyl ether (2 × 100 ml), washed with a 10 per cent aqueous $NaHCO_3$ solution and then with water. The ethereal solution was dried and the solvent removed. The residue was vacuum-distilled to give 1.55 g (86%) of an oil (b.p. 115—117°/11 mm Hg, $n_D^{20} = 1.5410$). A concentrated solution of this oily product, in n-heptane, afforded by cooling 1.35 g of pure IId, as colourless crystals, melting at 46—47°.

Found: C, 66.59, H, 4.90; $C_{10}H_9FO_2$ *requires*: C, 66.66, H, 5.03%

6,8-Dimethyl-2,3-dihydro-1-benzoxepin-5(4H)-one (IIe)

From 52 g (0.25 moles) Ie, by using procedure B, (1000 g PPA and 300 ml xylene), 35.6 g (75%) of almost pure 6,8-dimethyl-2,3-dihydro-1-benzoxepin-5(*4H*)-one, (IIe), was obtained, as almost colourless liquid, b.p. 134—138°/5 mmHg. By redistillation, pure IIe was obtained, as colourless oily liquid, boiling at 128°/4 mm Hg.

Found: C, 76.01, H, 7.40; $C_{12}H_{14}O_2$ *requires*: C, 75.76, H, 7.42%

7,8-Dimethyl-2,3-dihydro-1-benzoxepin-5(4H)-one [2](IIf)

The compound was prepared by procedure A, and the results summarized in tables 2 and 4.

7-Chloro-8-methyl-2,3-dihydro-1-benzoxepin-5(4H)-one (IIg)

To 250 g PPA, heated at 85—90°, 9.15 g (0.04 moles) γ-(3-methyl-4-chlorophenoxy)butyric acid, (IIg) was added during an hour, with stirring. The reaction mixture was stirred for another hour, with heating on the water-bath, then the mixture worked up. The crude product (6 g) melting at 58—63°, was purified by distillation (b.p. 130—132°/1 mm Hg) and was recrystallized from n-pentane — benzene, to give 3.15 g (15%) 7-cloro-8-methyl-2,3-dihydro-1-benzoxepin-5(*4H*)-one, (IIg) as bulky crystals, m.p. 64—65°.

Found: C, 62.93, H, 5.58; $C_{11}H_{11}ClO_2$ *requires*: C, 62.71, H, 5.26%

The infrared spectrum of IIg shows the following maxima: ν_{max}^{Nujol}: 3265, 1685, 1610, 1558, 1480, 1455, 1410, 1380, (1370), 1310, 1284, 1245, 1215, 1165, 1090, 1060, 1032, 1015, 960, 935, 910, 880, 795, 780, 730, 675, 580, 553, 510, 455 and 427 cm^{-1}.

2,3-Dihydro-1-benzoxepin-5-on-4-spirocyclopentane (IIh)

To 300 ml freshly prepared solution of t—BuOK (obtained from 8 g potassium and 190 ml t—BuOH) in benzene, 13 g (0.08 moles) 2,3-dihydro-1-benzoxepin-5(*4H*)-one, (IIa) was added with stirring, and, after ten minutes, 42.6 g (0.3 moles) 1,4-dibromobutane was added with vigorous stirring for over one hour. The reaction mixture was heated at reflux over six hours and, after cooling, the mixture was treated with 150 ml of a 15 per cent aqueous solution of hydrochloric acid. The organic layer was decanted and the aqueous layer extracted with 100 ml of diethyl ether. The combined organic solutions are dried and the solvents removed. The residue was vacuum-distilled (110—200°/3 mm Hg) and the crude product thus obtained was redistilled. Two fractions were isolated : 5.2 g of a liquid boiling at 110−125°/3 mm Hg and 3.5 g of a liquid b.p. 125−135°/3 mm Hg. These two fractions were further redistilled to give (*i*) − 4.2 g (24%) of a light yellow liquid, b.p. 118−125°/3 mm Hg, $n_D^{20} = 1.5622$, and (*ii*) − 2.8 g (16%) of almost colourless liquid (b.p. 132°/3 mm Hg; $n_D^{20} = 1.5625$) which was analysed.

Found : C, 77.46, H, 7.49 ; $C_{14}H_{10}O_2$ (IIh) *requires* : C, 77.74, H, 7.46%

The structure IIh of this compound was also supported by its n.m.r. and i.r. spectra. Thus, in the infrared spectrum (neat liquid) the following maxima appeared : (3340), 3070, 3035, 2960, 2920^{sh}, 2875, 1681, 1605, 1573, 1481, 1460^{sh}, 1450, 1384, 1317, 1286, 1229, 1215, 1193, 1153, 1101, 1053, 1017, 999, 990^{sh}, 811, 784, 760, 711, 640, 580, 545 and 525 cm^{-1}.

On standing, from the first fraction (b.p. 118−125°/3 mm) a small quantity of a crystalline compound was separated. After several recrystallizations from petroleum ether, the compound melted at 158.5°. The n.m.r. spectrum (a singlet at −0.50 τ and a multiplet between 1.93−3.17 τ, with a proton ratio 1 : 2, and no signals in the methylene region), suggested that the crystalline product may be salicylic acid. This assumption was supported by the positive test with $FeCl_3$ and proved unambiguously when comparing this compound with an authentic sample of salicylic acid : the mixture melting point was the same (without depression) and infrared spectra were superposable.

Attempted fragmentation of IIa in the presence of t−BuOK

A solution of 2 g 2,3-dihydro-1-benzoxepin-5(4*H*)-one (IIa), and 1 g t−BuOK in 50 ml anhydrous benzene was heated at the temperature of the reflux of the solvent for six hours, and the reaction mixture worked up. The IIa was nearly quantitatively recovered, and no trace of salicylic acid was found in the product thus obtained.

Fragmentation of the spiro-ketone IIh by t−BuOK

A solution of 0.5 g 2,3-dihydro-1-benzoxepin-5-on-4-spirocyclopentane (IIh), and 0.5 g t−BuOK in 50 ml anhydrous benzene was refluxed for six hours. After the reaction mixture was worked up, a crude product was obtained, which was mainly salicylic acid, as shown by the positive test with $FeCl_3$ and the infrared spectrum.

The ketoximes II obtained are recorded in table 2 ; their n.m.r. spectra are shown in table 5. Only an example of preparation is given here.

2,3-Dihydro-1-benzoxepin-5-on-4-spirocyclopentane oxime (Vh)

The spiro-ketone IIh was refluxed with a large excess of hydroxylamine hydrochloride, pyridine and ethyl alcohol. The reaction was completed in about twenty hours. The crude product was recrystallized from aqueous ethanol and then from cyclohexane, to give colourless crystals, m.p. 145−146°.

Found : C, 73.20, H, 7.83, N, 6.00 ; $C_{14}H_{17}NO_2$ *requires* : C, 72.70, H, 7.41, N, 6.06%.

Although the result of the elemental analysis was not entirely satisfactory, the correctness of the Vh structure of this compound was supported by infrared and nuclear magnetic resonance spectra.

The 2,4-dinitrophenylhydrazones VI obtained are presented in table 3.

2,9-Dimethyl-12H-6,7-dihydro-benz [2′, 3′] oxepino [4,5-b] -indole (VII)

A mixture of 3.53 g (0.02 moles) 7-methyl-2,3-dihydro-1-benzoxepin-5(4*H*)-one (IIc) and 3.33 g (0.022 moles) *p*-methyl-phenylhydrazine hydrochloride is treated with a saturated solution of hydrochloric acid in absolute ethyl alcohol. The reaction mixture was concentrated by removing ethyl alcohol (and HCl) by distillation. The residue is treated with a concentrated solution of $NaHCO_3$, extracted with ether (2 × 100 ml) and the solvent removed. The residue is triturated with water, filtered off, and the solid dried in air. The crude product thus obtained is recrystallized from aqueous ethyl alcohol (80 per cent) to give 2.83 g colourless crystals m.p. 135–137°. By further recrystallization from ethyl alcohol, an analytical sample, m.p. 138.5°, is obtained.

Found: N, 4.98; $C_{18}H_{17}NO$ *requires*: N, 5.32%

Infrared absorption spectrum of the compound (KBr pellet) shows the following bands: 3430, 3405, 3015, 2960, 2880, 1610, 1575, 1498, 1485, 1433, 1391, 1373, 1340, 1317, 1297, 1264, 1240, 1221, 1204, 1196, 1141, 1112, 1072, 1044, 1026,^{sh} 1018, 933, 880, 872, 869, 811, 792, 772^{sh}, 752, 747, 725, 664, 613, 591, 570, 529, 510, 483 and 456 cm^{-1}.

The n.m.r. spectrum of VII: 1.93 (1, s(broad), N*H*), 2.60–3.10 (6, m, aromatic), 5.60 (2, t, $O-CH_2$), 6.75 (2, t, $O-C-CH_2$), 7.53 (3, s, CH_3) and 7.65 τ (3, s, CH_3).

Acknowledgements. The author is grateful to Professor emeritus Giorgio Ostrogovich and Professor Alexadru T. Balaban for advice and encouragement. Thanks are also due to Dr. Mihai Elian and Mr Constantin Drăghici for n.m.r. spectra, Mrs. Simona Bădilescu for infrared spectra and Miss Elvira Sliam, Miss Letiţia Doşa and Mrs. Maria Roman, for elemental analysis.

Revue Roumaine de Chimie, 20, 6, 775–779 (1975)

REACTIONS OF ACETYLENES WITH TRANSITION METALS. VI [1]

REACTION OF THE π-ALLYL COMPLEX OF 6-CHLORO-1,3,6-TRI-t-BUTYL-1,2-DIHYDROFULVENE WITH CARBON MONOXIDE

ELISE AVRAM and MARGARET AVRAM
Institute of Organic Chemistry, Spl. Independenţei 202B, Bucharest, Romania

Received November 29, 1974

Treatment of the π-allyl complex of 6-chloro-1,3,6-tri-t-butyl-1,2-dihydrofulvene with carbon monoxide yields two carbomethoxy compounds, **2** and **3**. The mechanism of their formation is discussed.

A π-allylic structure was recently established for the complex obtained by trimerisation of t-butylacetylene in the presence of bis-benzonitrile·$PdCl_2$[2,3] and a dihydrofulvene skeleton[4] for the organic ligand. The existence of this complex in two π-allylic forms, **1a** ⇄ **1b**, an exocyclic and an endocyclic one, which interconvert, was elegantly demonstrated by means of ^1H and ^{13}C NMR spectra at very low temperature, as well as by an X-ray analysis, by Maitlis and his coworkers.[3]

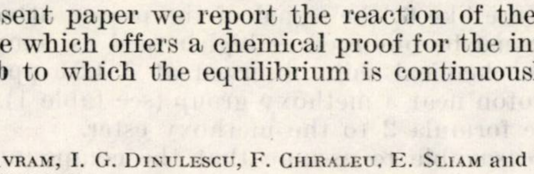

1a 1b

In the present paper we report the reaction of the complex **1** with carbon monoxide which offers a chemical proof for the intervention of the isomeric form **1b** to which the equilibrium is continuously shifted during some reactions.

---

[1] Part V. E. Avram, I. G. Dinulescu, F. Chiraleu, E. Sliam and M. Avram, *Rev. Roumaine Chim.*, **20**, 637 (1975).

[2] E. Avram, F. Chiraleu, I. G. Dinulescu and M. Avram, *Rev. Roumaine Chim.*, **20**, 543 (1975).

[3] P. M. Bailey, B. E. Mann, A. Segnitz, K. L. Kaiser and P. M. Maitlis, *J. Chem. Soc.*, (D), **1974**, 567.

[4] M. Avram, E. Avram, M. Elian, F. Chiraleu, I. G. Dinulescu and C. D. Nenitzescu, *Chem. Ber.*, **104**, 3486 (1971).

By treatment of complex **1** in methanol with carbon monoxide, at 70° and 40 atm, a mixture of two compounds, namely 6-carbomethoxy-2-methoxy-1,3,6-tri-t-butyl-1,2-dihydrofulvene (**2**) (43%) and 2,6-dicarbomethoxy-1,3,6-tri-t-butyl-1,2-dihydrofulvene (**3**) (4.7%) were isolated.

The NMR spectrum of diester **3** presents beside the three singlets due to the three t-butyl groups, other three singlets: one corresponding to a saturated proton at δ 2.80 ppm, another for an olefinic proton at δ 6.46 ppm and at δ 3.28 ppm for the proton attached to the carbon bearing the carbomethoxy group.

Among the possible isomeric structures for the diester **3**, the formula **4** was eliminated on the basis of NMR data, as there is no coupling constant between the protons H-1—H-2, as we reported in another similar structure. [4] Its UV spectrum (λ_{max} 262.0 nm, lg ε 4.15), with an extinction coefficient too large for a *cis*-diene system, [5] eliminated the formulas **4** and **5** (see table 1).

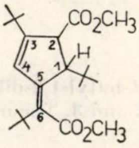

3

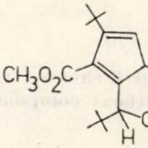

4

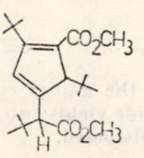

5

All physical measurements have supported a *trans*-diene structure, [6] with a dihydrofulvene skeleton. Consequently, formula **3** was ascribed to the diester.

The same considerations have determined the attribution of *trans*-diene skeleton to the second product, the methoxyester. Among the two possible formulas, **2** and **6**, the latter was excluded on the basis of NMR data. In a structure like **6**, the signal of the proton attached to a carbomethoxy group must be observed at higher field as compared with those of diester **3**. The chemical shift observed at δ 4.21 ppm had a normal value [4,7] for a proton near a methoxy group (see table 1). We have therefore ascribed the formula **2** to the methoxy ester.

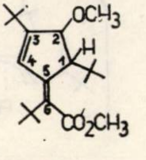

2

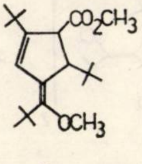

6

It seems reasonable to assume that the compounds **2** and **3** arise from the isomer **1b**. The carbon monoxide would thus attack the Pd-C

---

[5] D. Peters, *J. Chem. Soc.*, **1960**, 1832.

[6] D. M. Lemal and K. S. Shim, *Tetrahedron Letters*, **1964**, 3231; T. C. Shields, W. E. Billups, A. F. Lepley, *J. Amer. Chem. Soc.*, **90**, 4749 (1968).

[7] R. M. Silverstein and G. Clayton Bessler, „Spectrometric Identification of Organic Compounds", Second Edition, John Wiley & Sons, Inc., New York, 1968, p. 142.

Table 1

Spectral parameters for some *trans-* and *cis-*dienes

Compounds		UV		NMR
		λ_{max}, nm	lgε	H-2, δ, ppm
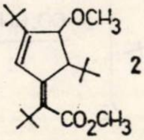	2	253	4.33	4.21
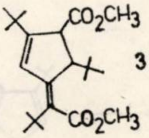	3	262	4.15	3.28
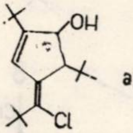	a)	263	4.15	4.26
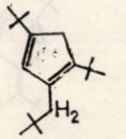	a)	260	3.71	2.86
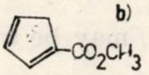	b)	274	3.71	

a) Reference [4] ; b) Reference [5] .

bond [8] leading, after the elimination of metallic palladium, to the two carbomethoxy compounds.

As intermediates for these reactions it can be assumed the existence of the ester **7** and the cation **8**, resulted by chlorine ionization. The latter can explain both the formula **2** and **3**, by the reaction with methanol or with another molecule of carbon monoxide. The nucleophilicity of carbon monoxide toward organic cations was previously established in other cases. [9]

---

[8] P. M. Maitlis, ,,The Organic Chemistry of Palladium'', vol. II, Academic Press, 1971, p. 18–33.

[9] A. T. Balaban and C. D. Nenitzescu, *Liebigs Ann. Chem.*, **625**, 66 (1959).

We can not rule out as intermediate, at least in the case of the reaction with CO, the π-allylic complex (**9**). A very small quantity of a complex with a carbomethoxy group in molecule ($\nu_{CO} = 1710$ cm^{-1}) which, by reductive decomposition with $NaHB_4$, gave a compound for which

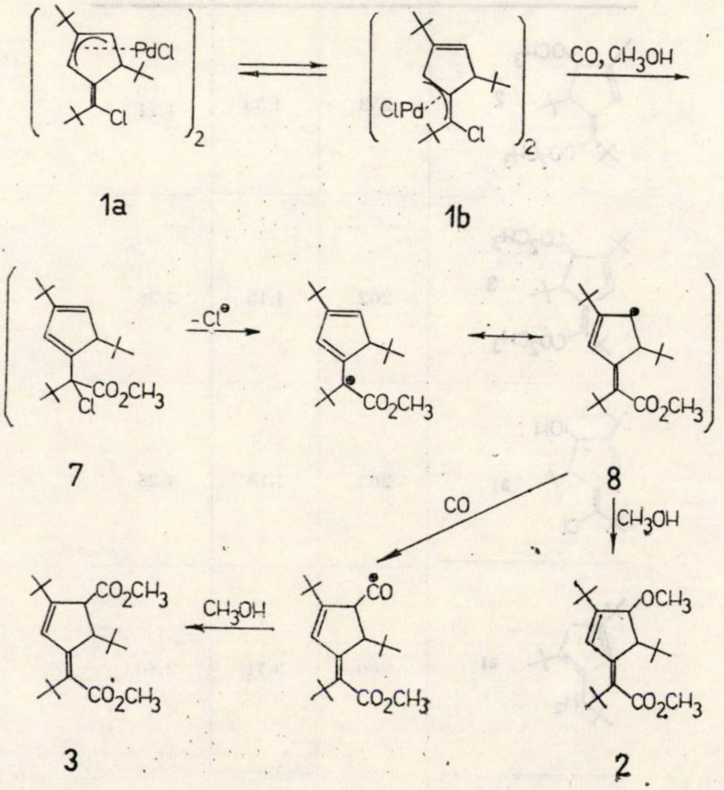
PdCl
2
1a
ClPd
Cl
2
1b
CO, CH$_3$OH
CO$_2$CH$_3$
Cl
−Cl$^⊖$
CO$_2$CH$_3$
CO$_2$CH$_3$
7
8
CO
CH$_3$OH
CO$_2$CH$_3$
CH$_3$OH
CO
CO$_2$CH$_3$
CO$_2$CH$_3$
OCH$_3$
CO$_2$CH$_3$
3
2

the formula **10** was ascribed by spectral data, may be a support for the last assignments.

It must be mentioned that under the same conditions the complex obtained by reaction of triphenylphosphine with complex **1** [2,4] (for which the structure **11** was recently established [3]), failed to react.

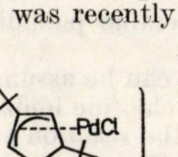
PdCl
CO$_2$CH$_3$
2

9

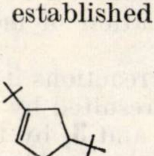

10

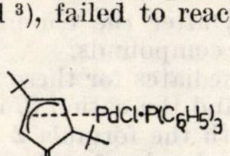
PdCl·P(C$_6$H$_5$)$_3$
Cl

11

In an earlier work [4] we have presented other reactions which could be explained only by the form **1a**.

EXPERIMENTAL

Microanalyses were performed by Miss E. Sliam and Mrs. V. Daniel. IR spectra were recorded on a double beam UR-20 spectrophotometer. NMR spectra were recorded on a Varian A-60A spectrometer, using TMS as internal standard.

REACTION OF COMPLEX 1 WITH CARBON MONOXIDE

a) A suspension of 5 g (1.17 mmoles) **1** in 150 ml methanol was introduced into an autoclave, in which was subsequently introduced at 40 atm carbon monoxide. The well-stirred mixture was heated to 60–70° for 4 hours, until the absorption of CO ceased. The metallic palladium was filtered off from the cold solution. The filtrate was concentrated, extracted with methlylene chloride, washed with water and 5% $NaHCO_3$ solution to neutral and dried. After evaporation *in vacuo* of the solvent, the oily product (2.7 g) was purified by chromatography on aluminium oxide.

On elution with petroleum ether and 20% diethyl ether 1.9 g 6-carbomethoxy-2-methoxy-1,3,6-tri-t-butyl-1,2-dihydrofulvene (**2**) was obtained as a colourless oil.

$C_{21}H_{36}O_3$ (336.5) *Calcd.* : C, 74.95 H, 10.78
Found : C, 75.19 H, 10.81

NMR (CCl_4, δ, ppm) : 0.78 (s, 9H, t-Bu-C_1), 1.16 and 1.25 (s, 18H, t-Bu groups attached to C_3 and C_6), 2.70 (s, 1H, H-1), 3.15 (s, 3H, OCH_3), 3.65 (s, 3H, $COOCH_3$), 4.21 (s, 1H, H-2), 6.58 (s, 1H, H-4).

IR (CCl_4, cm^{-1}) : 1712 s, 1608 w.

UV (cyclohexane) : λ_{max} 253 nm (lgε 4.33), 320 (sh).

The second fraction obtained on elution with 1 :1 petroleum ether and diethylether yielded **3** together with **2** (0.4 g). This mixture was again chromatographied on aluminium oxide, affording 0.2 g of 2,6-dicarbomethoxy-1,3,6-tri-t-butyl-1,2-dihydrofulvene (**3**) colourless crystals, m.p. 62°.

$C_{22}H_{36}O_4$ (364.5) *Calcd.* : C, 72.49 H, 9.95
Found : C, 73.05 H, 10.19

NMR (CCl_4, δ, ppm) : 0.78 (s, 9H, t-Bu-C_1), 1.12 and 1.25 (s, 18H, t-Bu groups attached to C_3 and C_6), 2.80 (s, 1H, H-1), 3.28 (s, 1H, H-2), 3.60 (s, 6H, two carbomethoxy groups), 6.46 (s, 1H, H-4).

IR (CCl_4, cm^{-1}) : 1712 s, 1730 (sh), 1608 w.

UV (cyclohexane) : λ_{max} 262 nm (lgε 4.157).

On elution with $CHCl_3$ it was obtained 0.15 g of a reddish complex with m.p. 93°. This complex, presenting a ν_{CO} 1710 cm^{-1} in IR spectrum, was reduced with $NaBH_4$ in methanol solution. The oily product obtained, with probably structure **10**, was analysed only by NMR and IR spectra.

NMR (CCl_4, δ, ppm) : 0.71 (s, 9H, t-Bu-C_1), 1.13 and 1.20 (s, 18H, 2 t-Bu groups), 2.30 (m, 2H), 2.82 (q, 1H, H-1), 3.60 (s, 3H, $COOCH_3$), 6.28 (pseudotriplet, 1H, H-4).

IR (CCl_4, cm^{-1}) : 1710 s, 1605 m.

b) The carbonylation carried out at room temperature and normal pressure yielded after 9 hours, less than 10% **2** and 75% unreacted starting material.

REACTION OF COMPLEX 10 WITH CARBON MONOXIDE

In the same conditions of the point *a*, 5.1 g (7.4 mmoles) complex **10**, after 7 hours was recovered unchanged.

Revue Roumaine de Chimie, 20, 6, 781 – 790 (1975)

ALUMINIUMCHLORID-KATALYSIERTE REAKTIONEN UNGESÄTTIGTER SÄUREN. VII[1]

REAKTION DER 1-INDENYLIDEN- UND 3-INDENYLESSIGSÄUREN

ALEXANDRU C. RĂZUŞ, FILIP CHIRALEU und ALICE MARIE GLATZ
Institut für Organische Chemie, Bukarest, Splaiul Independenţei 202-B

Eingegangen am 25. Juli 1974

In der aluminiumchlorid-katalysierten Reaktion der 1-Indenyliden- oder 3-Indenylessigsäuren (**1** bzw. **2**) mit Benzol wurden die 1-Indan-(**3**) *cis*- und *trans*-2-Phenylindan-(*cis* **4** und *trans* **4**), *cis*- und *trans*-3-Phenylindan- (*cis* **5** und *trans* **5**), und 3-Phenyl-1-indenyl- (**6**) -essigsäuren als Reaktionsprodukte ermittelt. Die verschiedenen Verhältnisse in denen diese Säuren gebildet werden, hängen von der Ausgangssäure und Reaktionszeit ab. In den Reaktionsgemischen wurden verschiedene Mengen der 1-Indenyliden- und 3-Indenylessigsäuren gefunden. Untersucht wurde weiterhin das Einstellen des Gleichgewichtes zwischen den Reaktionsprodukten bei längerer Reaktionsdauer. Ein Reaktionsmechanismus wird vorgeschlagen.

In der aluminiumchlorid-katalysierten Reaktion einiger offenkettigen und alicyclischen,[1-5] ungesättigten Säuren, unter milden Temperaturbedingungen (bis 50°) werden isomere, gesättigte phenylierte Säuren gebildet. Die seit bereits längerer Zeit vorgeschlagene Bildungsweise dieser Säuren, beruht auf einer Protonanlagerung an die Doppelbindung die von intramolekularer Hydridverschiebung und elektrophilem Angriff des Benzols von den so gebildeten Carbokationen gefolgt wird.

Wie erwiesen, kommt der intermolekularen Hydridverschiebung im Falle der Cyclobutylidenessigsäure und Sorbinsäure[4,5] eine bedeutende Rolle zu, festgelegt durch das Vorfinden von Indenderivaten und gesättigten Verbindungen (Wasserstoffakzeptoren) im Reaktionsgemisch. Da wie bewiesen, Indanverbindungen gute Hydriddonoren sind[2], promoviert ihre intermediäre Bildung die Hydridverschiebung, wodurch diese in Indenverbindungen übergehen und demzufolge einigermaßen den Lauf der Reaktion ändern.

---

[1] VI TEIL. A. M. Glatz, V. Wertheimer und F. Badea, *Rev. Roumaine Chim.*, **19**, 87 (1974).

[2] A. M. Glatz, *Rev. Roumaine Chim.*, **19**, 455 (1974).

[3] A. M. Glatz, A. C. Răzuş, F. Badea und C. D. Nenitzescu, *Rev. Roumaine Chim.*, **16**, 1567 (1971).

[4] A. M. Glatz, A. C. Răzuş, M. Elian und C. D. Nenitzescu, *Rev. Roumaine Chim.*, **19**, 1579 (1971).

[5] A. M. Glatz, F. Badea, C. Arvay, F. Chiraleu, V. Drăguţan und A. C. Răzuş, *Rev. Roumaine Chim.*, **18**, 2087 (1973).

Zieht man in Betracht, daß einerseits das Indansystem ein guter Hydriddonor ist und andererseits, daß fünfgliedrige cyclische, ungesättigte Säuren stereoselektiv mit Benzol reagieren[3], liegt die Zweckmäßigkeit der vorliegenden Untersuchung der 1-Indenyliden- und 3-Indenylessigsäuren (**1** und **2**) an der Hand.

Die Reaktionen wurden unter den Temperaturbedingungen der vorgehenden Arbeiten[3,4] ausgeführt, wobei dieselben Molarenverhältnisse verwendet wurden (ungesättigte Säure : Aluminiumchlorid : Benzol = = 1 :1,5 :20). Um zusätzlichen Einblick in den Verlauf der Reaktion zu gewinnen wurde außer bei der üblichen Reaktionsdauer (4 h) auch bei anderen Zeiten gearbeitet (10 Minuten, bzw. 30 Stunden).

1. ALUMINIUMCHLORID KATALYSIERTE REAKTION DER 1-INDENYLIDEN- UND 3-INDENYL-ESSIGSÄUREN (1 UND 2), MIT BENZOL

Sowohl die Säure **1** als auch **2** führt nach 10 Minuten Reaktionsdauer zu denselben Reaktionsprodukten, wobei aber die Produktverteilung jeweils verschieden ist. Die Reaktion wird nicht von Verharzung begleitet. Die gaschromatographische Analyse der entsprechenden Methylester führte zur Identifizierung folgender Säuren (wobei diese 90% der gesamten saueren Fraktion darstellen): 1-Indenyliden- und 3-Indenylessigsäuren (**1** und **2**), *cis-* und *trans-* 3-Phenylindanylessigsäuren (*cis* und *trans* **5**) und der 3-Phenyl-indenylessigsäure (**6**) (Tab. 1).

Nebenbei führt die Reaktion zur Bildung kleiner Mengen neutraler Produkte (unter denen die Gaschromatographie das Vorhandensein von den bereits in anderen Fällen beobachteten Methylphenylindenen[5] festlegte).

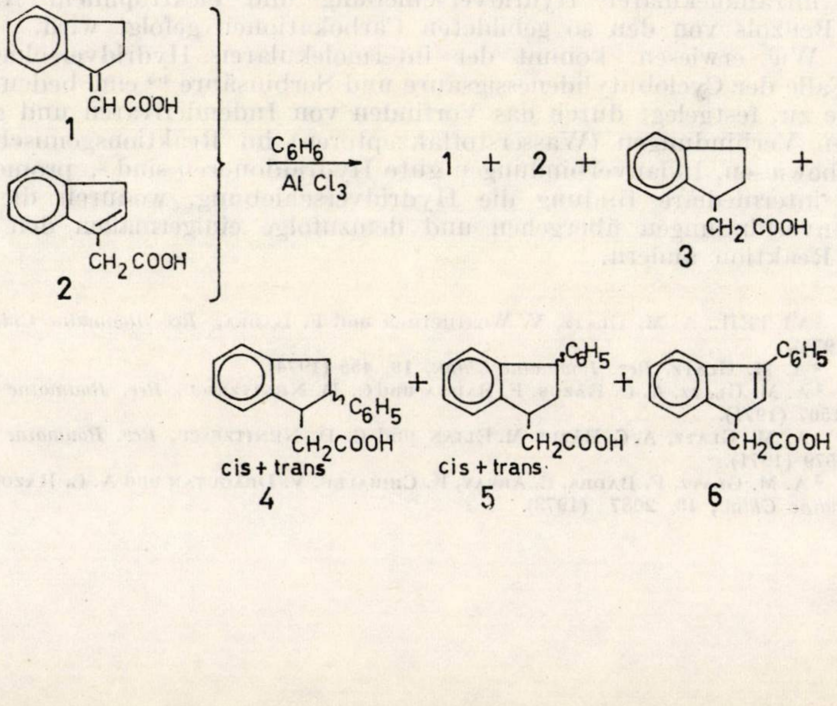

Aus der Betrachtung der Tabelle 1 ergibt sich, daß das Verhältnis in dem die Säure **1** an den zwei Ausgangsäuren gebildet wird, 52,5 beträgt, dasjenige der 3-ständig phenylierten Säuren (*cis*- und *trans*- **5** und **6**) ist 0,72, und schließlich dasjenige der 2-ständig phenylierten Säuren (*cis*- und *trans*-**4**) 3,55 ist.

Um diesen unterschiedlichen Reaktionsgang zu erklären wird folgendes Reaktionsschema geboten.

Schema 1

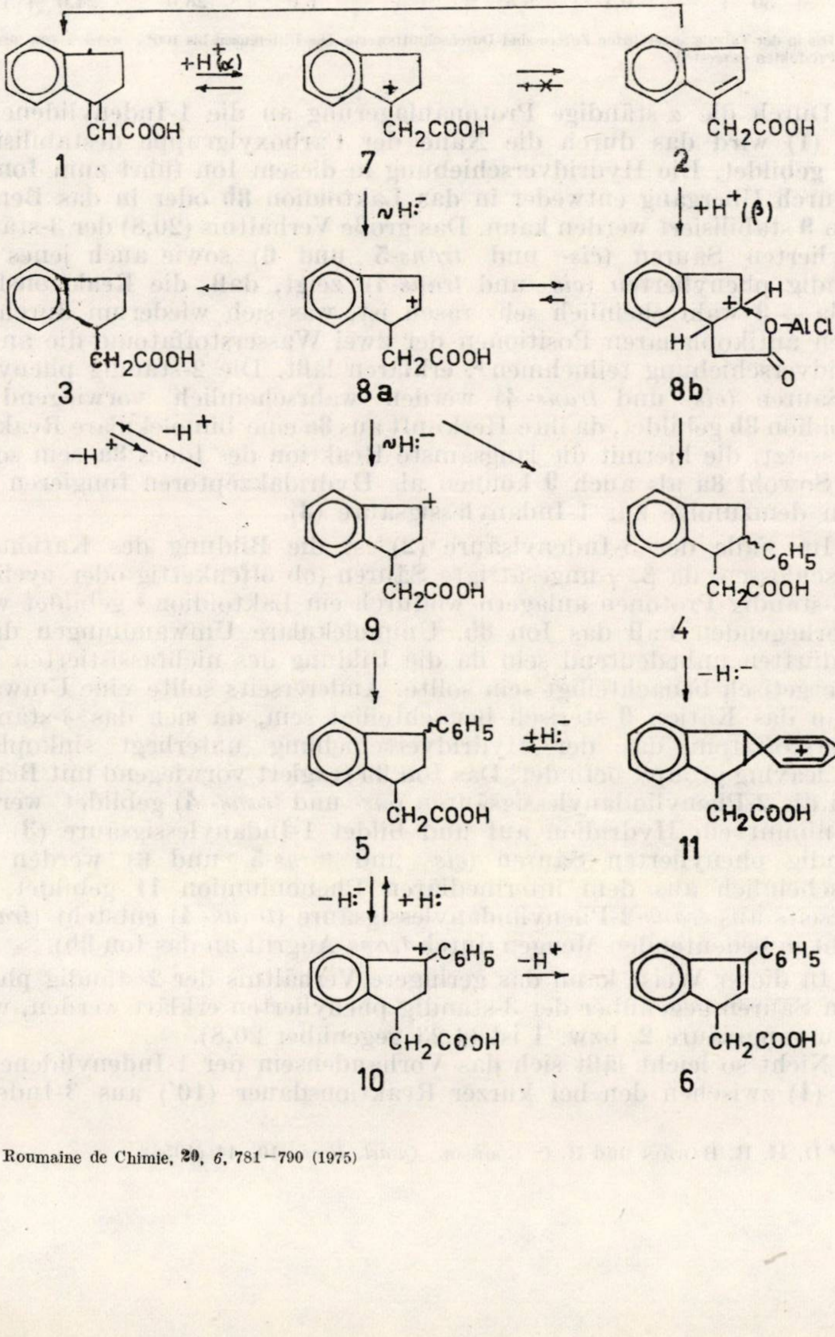
+H⁺(α)
CHCOOH
1
CH₂COOH
7
CH₂COOH
2
~H:
+H⁺(β)
CH₂COOH
3
CH₂COOH
8a
H
O-AlCl₂
O
8b
-H⁺
-H⁺
~H:⁻
CH₂COOH
9
C₆H₅
CH₂COOH
4
-H:⁻
C₆H₅
CH₂COOH
5
±H:⁻
CH₂COOH
11
-H:⁻
+H:⁻
C₆H₅
CH₂COOH
10
-H⁺
C₆H₅
CH₂COOH
6

Tabelle 1

Reaktionsprodukte der Säuren 1 und 2

Reaktant	Dauer Stdn.	Produkte[a], % Mol							
		1	**2**	**3**	*cis*-**4**	*trans*-**4**	*cis*-**5**	*trans*-**5**	**6**
1	1/6	0,2	0,2	18,0	0,1	3,0	16,5	13,5	34,5
2	1/6	10,5	1,5	24,0	3,5	7,5	10,5	11,5	24,5
	4	0,2	0,2	20,0	0,2	4,1	32,0	26,5	11,5
	30	—	0,1	9,5	0,3	6,0	28,0	24,0	19,5

[a] Die in der Tabelle angeführten Ziffern sind Durchschnittswerte. Die Differenzen bis 100% werden von unidentifizierten Produkten dargestellt.

Durch die α-ständige Protonanlagerung an die 1-Indenylidenessigsäure (**1**) wird das durch die Nähe der Carboxylgruppe destabilisierte Ion **7** gebildet. Die Hydridverschiebung in diesem Ion führt zum Ion **8a**, das durch Übergang entweder in das Laktoidion **8b** oder in das Benzylkation **9** stabilisiert werden kann. Das große Verhältnis (20,8) der 3-ständig phenylierten Säuren (*cis*- und *trans*-**5** und **6**) sowie auch jenes der 2-ständig phenylierten (*cis*- und *trans*-**4**) zeigt, daß die Reaktionsfolge **7** → **8a** → **9** wahrscheinlich sehr rasch ist, was sich wiederum durch die axialen antikoplanaren Positionen der zwei Wasserstoffatome die an der Hydridverschiebung teilnehmen [6], erklären läßt. Die 2-ständig phenylierten Säuren (*cis*- und *trans*- **4**) werden wahrscheinlich vorwiegend *via* Laktoidion **8b** gebildet, da ihre Herkunft aus **8a** eine bimolekulare Reaktion voraussetzt, die hiermit die langsamste Reaktion des Iones **8a** sein sollte.

Sowohl **8a** als auch **9** können als Hydridakzeptoren fungieren und führen demzufolge zur 1-Indanylessigsäure (**3**).

Im Falle der 3-Indenylsäure (**2**) ist die Bildung des Kationes **7** ausgeschlossen, da β, γ-ungesättigte Säuren (ob offenkettig oder cyclisch) nur β-ständig Protonen anlagern wodurch ein Laktoidion [2] gebildet wird, im vorliegenden Fall das Ion **8b**. Unimolekulare Umwandlungen dieses Ions dürften unbedeutend sein da die Bildung des nichtassistierten Ions **8a** energetisch benachteiligt sein sollte. Andererseits sollte eine Umwandlung in das Kation **9** sterisch benachteiligt sein, da sich das δ-ständige Wasserstoffatom das der Hydridverschiebung unterliegt sinkoplanar zum „leaving group“ befindet. Das Ion **8b** reagiert vorwiegend mit Benzol, wobei die 2-Phenylindanylessigsäuren (*cis*- und *trans*- **4**) gebildet werden, oder nimmt ein Hydridion auf und bildet 1-Indanylessigsäure (**3**). Die 3-ständig phenylierten Säuren (*cis*- und *trans*-**5** und **6**) werden sehr wahrscheinlich aus dem intermediären Phenoniumion **11** gebildet, das seinerseits aus *trans*-2-Phenylindanylessigsäure (*trans*- **4**) entsteht (*trans*-**4** ensteht in bedeutenden Mengen durch *trans*-Angriff an das Ion **8b**).

In dieser Weise kann das geringere Verhältnis der 2-ständig phenylierten Säuren gegenüber der 3-ständig phenylierten erklärt werden, wenn die Ausgangssäure **2**, bzw. **1** ist (4,23 gegenüber 20,8).

Nicht so leicht läßt sich das Vorhandensein der 1-Indenylidenessigsäure (**1**) zwischen den bei kurzer Reaktionsdauer (10′) aus 3-Indenylessigsäure erhaltenen Produkte erklären. Da das Kation **7** nicht als Zwischenstufe in der Umwandlung von **2** in **1** auftreten kann, sollte der Vorgänger der Säure **1** ebenfalls das Laktoidion **8b** sein. Dieses dürfte stabil genug sein und demzufolge in beträchtlicher Konzentration im Reaktiongemisch bis zum vollständigen Verbrauch der Säure **2** vorhanden sein (Schema 2). Als eher ungewöhnlich erscheint die Umwandlung von **8b** in **1**, die auf die verstärkte Azidität des α-ständigen Wasserstoffes zurückzuführen ist. Dieses Proton kann leicht abgespaltet werden, gleichzeitig mit, oder gefolgt von der schnellen Bildung der α,β Doppelbindung, Öffnung des Laktoidions und Hydridverschiebung von C_1 zu C_2 :

---

[6] D. H. R. Barton und R. C. Cookson, *Quart. Revs.*, **10**, 44 (1956).

Schema 2

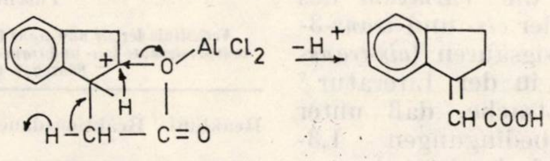

8a **1**

Eine **2** → **1** Isomerisierung wurde auch anderwärtig festgestellt: wird in eine Suspension von Aluminiumchlorid in Schwefelkohlenstoff die Säure **2** eingetragen, so geht diese binnen vier Stunden 60−70%-ig in die Säure **1** über.

Schließlich ist die Bildung der 3-Phenylindenylessigsäure (**6**) in den Reaktionen der Säuren **1** und **2** auf die Umwandlungen der 3-Phenylindanessigsäuren (*cis*- und *trans*-**5**) durch das intermediäre Benzylkation **10** zurückzuführen. Dieses Kation ist stabil und wird leicht durch Hydridabspaltung des doppelt benzylständigen Wasserstoffs gebildet. Die darauffolgende Protonabspaltung vom benachbarten Kohlenstoffatom ergibt die Säure **6**.

2. GLEICHGEWICHT DER REAKTIONSPRODUKTE

Die in den 10 Minuten Reaktion erhaltenen Ergebnisse spiegeln eine intermediäre Phase wider, die sich zwischen der Bildung der Produkte kinetischer und thermodynamischer Kontrolle befinden dürfte. Um einige Aspekte der Equilibrierung der Reaktionsprodukte eingehender zu beleuchten wurde sowohl der Effekt längerer Reaktionsdauer, als auch das Verhalten individueller Produkte studiert. Jedoch erschwert die Komplexität der Prozesse die bei längerer Reaktionsdauer stattfinden und die Bildung von Nebenprodukten höheren Molgewichts (deren Menge mit der Zunahme der Dauer wächst) die Aufklärung aller Vorgänge.

Die Analyse der Daten der Tabelle 1 ergibt aber, daß eine längere Reaktionszeit nahezu zum Verschwinden der ungesättigten, nichtsubstituierten Säuren (**1** und **2**) führt. Ebenfalls vermindert sich der Anteil der 3-Phenylindenylessigsäure (**6**) an den Produkten. Beides ist auf die Reaktivität der Doppelbindungen zurückzuführen.

Nur Säure **2** wurde längerer Reaktionsdauer unterworfen, da das Verhältnis der Reaktionsprodukte nur so lange bedeutungsvoll ist, als **1** oder **2** in beträchtlicher Menge unter den Produkten zu finden ist.

Mit der Zeit nimmt die Menge der 1-Indanessigsäure ab (siehe Tabelle 1). Diese Abnahme kann auf eine Hydridabgabe an einen vorhandenen Akzeptor zurückgeführt werden, wobei das Kation **9** entsteht, der Vorgänger der 3-Phenylindanessigsäuren (*cis*- und *trans*- **5**). Hiermit ist die Erklärung der beobachteten Zunahme des Anteils dieser phenylierten Säuren an den Reaktionsprodukten geliefert.

Ein zusätzlichens Augenmerk verdient die Variation des Verhältnisses der *cis*- und *trans*-3-Phenylindanessigsäuren (*cis*-*trans*-**5**). Vermerkt in der Literatur [7] wurde die Tatsache, daß unter Gleichgewichtsbedingungen 1,3-disubstituierte Indanderivate vorwiegend in *cis* Form vorliegen. Der Tabelle 2 ist zu entnehmen, daß sich das Gleichgewicht zwischen *cis* und *trans*-**5** schneller als 4 Stunden einstellt.

Tabelle 2

Verhältnis der *cis* und *trans* Isomeren der 3-Phenylindanessigsäure (*cis*- und *trans*- 5) in der Reaktion der Säuren 1 und 2

Reaktant	Reaktionsdauer	Verhältnis *cis*-**5** : *trans*-**5**
1	1/6 Stdn.	1,25
2	1/6	0,92
2	4	1,18
2	30	1,18

Das 1,18 Verhältnis zwischen *cis*-**5** und *trans*-**5** liegt sehr nahe an das in Falle der 1,3-Dimethylindane gefundene Verhältnis [7].

Obwohl die Reaktionsbedingungen der Isomerisierung einigermaßen von denen der eigentlichen Reaktion abweichen, wurden auch Isomerisierungen einiger Produkte durchgeführt um einige Aspekte besser zu erfassen.

Die Isomerisierungen wurden 4 Stunden lang in Schwefelkohlenstoff, bei Rückfluß durchgeführt; die Ergebnisse sind in Tabelle 3 eingetragen.

Tabelle 3

Aluminiumchlorid-katalysierte Isomerisierung der Phenylindanessigsäuren

Reaktant	Produkte, % Mol							
	1	**2**	**3**	*cis*-**4**	*trans*-**4**	*cis*-**5**	*trans*-**5**	**6**
cis-**4**	—	—	—	100	—	—	—	—
cis-**5**	—	—	13	—	0,3	39,5	31,5	9,5

Es wurde nur mit *cis*-**5** gearbeitet, da *trans*-**5** mit größter Wahrscheinlichkeit dieselben Gleichgewichtsprodukte liefert. Die durch präparative Chromatographie erhaltene Menge an *trans*-**4** war zu klein um auch dessen Isomerisierung vornehmen zu können.

Im Falle der *cis*-3-Phenylindanessigsäure (*cis*-**5**) bemerkt man leicht dessen Tendenz sich mit dem *trans*-**5** Isomeren zu equilibrieren.

---

[7] R. N. Volcov und T. A. Fedorova, *Zhur. org. Khim.*, **8**, 1929 (1972).

Auch entsteht dabei **3** durch Entphenylierung und **6** durch intermolekulare Hyidridverschiebung.

Die *cis*-2-Phenylindanessigsäure (*cis*-**4**) weist ein besonderes Verhalten auf: nach 4 Stunden wird sie praktisch unverändert zurückgewonnen. Die Bildung eines Benzylkations **12** mit Carboxylbeteiligung, infolge einer Hydridabspaltung, könnte dafür ein glaubhafter Grund sein. Ein Hydridangriff an das Ion **12** kann nur von rückwärts erfolgen, wobei **4** wiedererhalten wird.

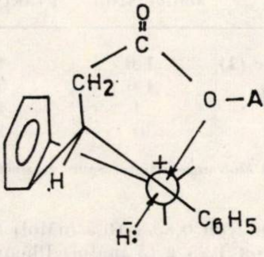

12

Sowohl die Abspaltung des β-ständigen Wasserstoffs als Hydridion aus **4** (wodurch ein Phenonium gebildet wurde), als auch die intramolekulare Hydridverschiebung in **12** wird von der sterisch ungüngstigen Lage der Substituenten erschwert.

EXPERIMENTELLER TEIL

Die Elementaranalysen wurden von E. Sliam und V. Daniel durchgeführt. Schmelzpunkte wurden nicht korrigiert. Kernresonanzspektren wurden auf einem Varian A 60A Spektrometer aufgenommen (δ in ppm, Lösungsmittel Deuterochloroform, TMS als innerer Standard). Infrarotspektren wurden auf einem UR 10 Spektrophotometer aufgenommen. Die gaschromatographischen Analysen wurden von L. Stănescu auf einem Carlo Erba Modell D Apparat durchgeführt, mit Flammionisierungsdetektor. Es wurde auf einer 2000 × 2 mm Säule mit 10% Polyäthylenglicol 20 M auf Chromosorb K (60–80 mesh), mit Temperaturprogrammierung von 170–190° gearbeitet; Trägergas: Stickstoff 40 cm^3/Minute.

Reaktion der 1-Indenylidenessigsäure (1) und der 3-Indenylessigsäure (2) mit Benzol

Zu einer gerührten Suspension von 4,8 g (0,036 Mol) Aluminiumchlorid in 21,5 ml (0,25 Mol) Benzol, wurde bei 45–50°, in 3–5 Minuten eine Lösung von 4,2 g (0,024 Mol) ungesättigte Säure (**1** oder **2**) in 21,5 ml (0,24 Mol) Benzol zugegeben. Während der Reaktionsdauer (10′, 4 oder 30 h) wurde bei 45–50° gerührt. Anschließend wurde das Reaktiongemisch mit 10%-iger eisgekühlter Salzsäure zersetzt. Die Benzolschicht wurde abgetrennt und alkalisch extrahiert. Aus der alkalinen Lösung wurde nach Ansäuern und der üblichen Aufarbeitung die sauere Fraktion gewonnen. Die nach der alkalischen Extraktion gebliebene Benzolschicht lieferte nach Aufarbeiten in üblicher Weise die neutrale Fraktion. Tabelle 4 gibt die mit Säure **1** und **2** bei verschiedener Reaktionsdauer erhaltenen Ergebnisse an.

Die sauere Fraktion wurde mit ätherischer Diazomethanlösung behandelt, das Estergemisch gaschromatographisch analysiert, wobei die Retentionszeiten der Komponenten jeweils mit denen von Vergleichspräparaten verglichen wurden. Die Ergebnisse sind in Tabelle 1 zu finden.

In der neutralen Fraktion wurde das Vorhandensein des 3-Methyl-1-phenylindens festgelegt.

Isomerisierung der Phenylindanylessigsäuren

Tabelle 4

Ergebnisse der Reaktion der Säuren **1** und **2** mit Benzol

Reaktant [a)]	Reaktionsdauer Stdn	Sauere Fraktion g	Neutrale Fraktion
1-Indenylidenessigsäure (**1**)	1/6	4,5	Spuren
3-Indenylessigsäure (**2**)	1/6	5,3	Spuren
	4	4,4	0,5
	30	4,2	0,6

a) Es wurde mit 4,2 g (0,024 Mol) ungesättigter Säure gearbeitet.

Zu einer gerührten Suspension von 0,85 g (6,5 mMol) Aluminiumchlorid in 10 ml CS_2 bei Rückfluß, wurde eine Lösung von 1,25 g (5 mMol) Phenylindanylessigsäure in 5 ml CS_2 hinzugegeben und anschließend 4 Stunden bei Rückfluß gerührt. Das Reaktionsgemisch wurde wie im Falle der oben beschriebenen Reaktion aufgearbeitet. Das Säuregemisch wurde mit Diazomethan verestert und gaschromatographisch untersucht. Die Ergebnisse sind in Tabelle 3 zu finden.

Synthese der Rohstoffe und der gaschromatographischen Vergleichssubstanzen

1-Indenylidenessigsäure (**1**) wurde durch Reformatsky Reaktion aus Indan-1-on nach Cristol und Plenat [8] hergestellt. Die Verseifung des rohen Hydroxyesters ergab die Säure mit Schmp. 196° (Benzol) (Lit.[8] 196°). Der entsprechende gaschromatographisch reine Methylester wurde mit Diazomethan erhalten, $Sdp_{1-1,5}$ 140°.

NMR ($(CD_3)_2SO$, δ, ppm) : H_7 7,76 (m) ; 3 aromatische Protonen und COOH 7,60–7,20 (m) ; H_α 6,35 (t, $J = 2,4$ Hz), 4 Protonen (H_2 und H_3) 3,40–2,90 (m).

IR (CH_2Cl_2, cm^{-1}) : $\nu_{C=C}$ 1626 (i), $\nu_{C=O}$ 1676 (i), ν_{OH} assoziert 2400–3400, ν_{OH} 3512.

3-Indenylessigsäure (2)

Die in der oben beschriebenen Reformatsky Reaktion erhaltene Benzolschicht wurde mit Wasser gewaschen, auf $MgSO_4$ getrocknet und anschließend mit katalytischen Mengen *p*-Toluensulfonsäure behandelt und der Hydroxyester durch azeotrope Destillation dehydratiert. Nach dem Entfernen des Lösungsmittels wurde durch Destillation ein Estergemisch der Säuren **1** und **2** erhalten.

Die in der Literatur beschriebenen Verseifungsmethoden in der Indanreihe [8–10] führten mit 75–80% Ausbeute zu 3-Indenylessigsäure (**2**), Schmp. 94–96° (Wasser) (Lit. [9] 95–96°).

NMR : 4 aromatische Protonen 7,50–7,10 (m), H_2 6,45 (breites s). Ein Olefinproton und die dem H_2 Proton des Indens ähnliche chemische Verschiebung [11] (6,50) zeigt das Vorhandensein einer 3-ständigen Essigsäuregruppierung 2 H_α 3,60 (m), 2 H_1 3,35 (m) ; COOH 11,38 (s).

IR (CCl_4, ν, cm^{-1}) : 1707 (i), 1752 (s) und die für an einen gesättigten Kohlenstoffatom gebundene Carboxylgruppe charakteristische weite Bande 2500–3400.

---

[8] H. Cristol und F. Plenant, *Bull. Soc. chim. France*, **1962**, 1325.

[9] H. Takamautsu, S. Umemoto, T. Shimizu und A. Kagemoto, *Yakugaku Zasshi*, **85**, 975 (1965) ; *Chem. Abstr.*, **64**, 5016 a (1966).

[10] D. A. H. Taylor, *J. Chem. Soc.*, **1960**, 2805.

[11] NMR Spectra Catalog, Varian Associates, Palo Alto, California, 1962.

Der mit Diazomethan erhaltene Methylester, Sdp_1 125° war gaschromatographisch rein.

1-Indanylessigsäure (**3**) wurde aus 3-Indenylessigsäure (**2**) durch Hydrierung bei Raumtemperatur mit 5% Pd/Al_2O_3 erhalten; Schmp. 62° (Lit.[12] 59–60°).

NMR: 4 aromatische Protonen 7,15 (breites s); H_1 3,58 (q); 4 Protonen H_2 und H_3 und zwei H_α Protonen 3,10–1,50; COOH 1,60 (s).

Der entsprechende gaschromatographisch einheitliche Methylester wurde mit Diazomethan hergestellt.

2-Phenyl-3-indenylessigsäure wurde aus 2-Phenylindan-1-on durch Reformatsky Reaktion[13] erhalten, Schmp. 108° (Essigsäure) (Lit.[13] 108°). Gaschromatographisch reiner Methylester mit Diazomethan.

cis-2-Phenyl-1-indanylessigsäure (*cis*-**4**) wurde aus 2-Phenyl-3-indenylessigsäure[13] durch Hydrierung bei Raumtemperatur und Normaldruck erhalten; Katalysator: 5% Pd/Al_2O_3; Schmp. 149–150° (Essigsäure).

(Gef.: C, 80.81; H, 6.53. Ber. für $C_{17}H_{16}O_2$: C, 80.92; H, 6.36%).

Der aus dieser Säure gewonnene Methylester war gaschromatographisch einheitlich.

Die 9 aromatischen Protonen weisen im NMR Spektrum ein charakteristisches Multiplet auf, 7,40–6,80. Bei 7,10 kann ein Singlet unterschieden werden. Bei $\delta = 3{,}85$ erscheint das den zwei H_1 und H_2 Protonen entsprechende, unvollständig aufgelöste Multiplet. Die zwei H_α Protonen weisen ein Multiplet bei 3,17 auf. Bei 2,23 und 2,03 weisen die zwei AB Protonen ($J_{AB} = 16{,}5$ Hz) ein vom H_2 Proton gespaltenes Signal auf ($J_{2,3a} = J_{2,3e} = 7$ Hz, wobei sich die Bezeichnungen *a* und *e* auf die pseudoaxiale bzw. pseudoequatoriale Lage der C_3 Protonen beziehen). Die 7 Hz Koppelungskonstante des H_2 Protons mit den zwei H_3 Protonen deutet auf die pseudoequatoriale Position des Phenyls an C_2, in Übereinstimmung mit den Dreidingmodellen. Da die Hydrierung der 2-Phenyl-3-indenylessigsäure das *cis*-Isomer ergeben sollte, folgt daß die C-1 ständige Essigsäuregruppierung pseudoaxial liegen muß.

Das COOH Proton der Säure erscheint bei 10,26.

Das NMR Spektrum des Methylesters weist zusätzlich die esterische Methylgruppe bei 3,45 auf.

trans-2-Phenyl-1-indanylessigsäure (*trans*-4)

Der Methylester wurde durch präparative Gaschromatographie erhalten.

(Gef.: C, 81.19; H, 6.98. Ber. für $C_{18}H_{18}O_2$: C, 81.17; H. 6.81%).

NMR: 9 aromatische Protonen 7,11 (breites s), $COOCH_3$ 3,42 (s); das bei 3,03–2,35 erschienene Multiplet, entspricht 6 Protonen (deutlich tritt ein Dublet bei 2,90 hervor) wurde den α-ständigen CH_2 Protonen zugeschrieben. Die exocyclische Position dieser Protonen wurde durch das Europiumkomplexspektrum bestätigt: das Signal bleibt unverändert, zunehmende Mengen Tris-dipivaloilmethanato-Eur (III) verschieben es zu tieferen Feldern.

3-Phenyl-1-indenylidenessigsäure und 3-Phenyl-1-indanylessigsäure (**6**), wurden in der Reformatsky Reaktion des 3-Phenyl-indan-1-ons erhalten. In der Literatur[14] wird das Rohgemisch als solches zu 3-Phenyl-1-indanylessigsäure (**6**) hydriert. In der vorliegenden Arbeit wurde von 0,03 Mol 3-Phenyl-indan-1-on ausgegangen. Das erhaltene Produkt wurde alkalisch verseift und die alkalische Lösung mit Benzol extrahiert. Nach Einengen der Benzollösung wurde der Rückstand auf neutralem Aluminiumoxyd chromatographiert; Elutionsmittel: Benzol-Chloroform. Erhalten wurden 1 g *1-Phenyl-3-methylinden* mit Schmp. 60° (Lit.[15] 59°).

NMR: 9 aromatische Protonen 7,40–6,90 (m) olefinisches H_2 6,20 (m); H_1 4,48 (m); 3-ständiges CH_3 2,16 (t, J = 2 Hz und J = 1,8 Hz).

Die alkaline Lösung wurde mit Salzsäure angesäuert und mit Äther extrahiert. Nach der Extraktion verblieb ein Niederschlag, unlöslich in üblichen Lösungsmitteln. Dieser wurde filtriert und in alkalischer Lösung wiederaufgenommen, mit Aktivkohle behandelt und mit Salzsäure niedergeschlagen. Erhalten wurden 1,5 g kristalline Substanz, Schmp. 215°. (Gef.: C, 81.71; H, 5.90. Ber. für $C_{17}H_{14}O_2$: C, 81.57; H, 5.64).

---

[12] A. G. ANDESON, JR., R. H. WADE, *J. Amer. Chem. Soc.*, **74**, 2274 (1952).

[13] B. B. DATTA und J. C. BARDHAN, *J. Chem. Soc.*, **1962**, 3974.

[14] D. A. CULLISON und R. K. HILL, *Tetrahedron Letters*, **1972**, 3745.

[15] H. A. UEBERWASSER (CIBA), U.S. 2.798.888, Juli, 9, 1957; *Chem. Abstr.*, **52**, 1261i (1958).

Revue Roumaine de Chimie, **20**, *6*, 781–790 (1975)

Das in $(CD_3)_2SO$ aufgenommene NMR Spektrum weist ein Multiplet bei 7,83 auf, das H_7 entspricht. Eine ähnliche chemische Verschiebung die das H_7 Proton getrennt von den drei anderen aromatischen Protonen erscheinen läßt, ist auch im Falle der 1-Indenylidenessigsäure (**1**) festzustellen. Diese Verschiebung wird der Nachbarwirkung der Doppelbindung zugeschrieben. Zwischen 7,40—7,00 erscheint ein, 9 Protonen entsprechendes Multiplet, wobei ein Proton der CO_2H Gruppe gehört. Eine ähnliche Verschiebung des Carboxylprotons in die Region der aromatischen Protonen war auch bei **1** festzustellen. Bei 6,40 erscheint das Triplet des α-ständigen Protons (J = 2,5 Hz). In der gesättigten Region weist das Spektrum ein ABM System auf: bei 4,53 H_M (entsprechend H_3), Quartett ($J_{AM}=8$ Hz und $J_{BM} = 4$ Hz) und die AB Protonen (zwei H_2) bei δ_A 3,73 und δ_B 3,10 ($J_{AB} = 8$ Hz).

Das IR Spektrum (CH_2Cl_2, cm^{-1}) weist auf das Vorhandensein einer mit Doppelbindung konjugierter Carboxylgruppe: $\nu_{C=C}$ 1630 (i), $\nu_{C=O}$ 1681 (s), 1702 (Schulter), $\nu_{OH\ \text{assoziert}} = 2500-3400$, ν_{OH} 3515.

Gemäß den analytischen Befunden wurde dieser Säure die Struktur der 3-Phenyl-1-indenylidenessigsäure zugeschrieben.

Die getrocknete ätherische Lösung wurde eingeengt wobei 7,3 g zähflüssiges Produkt blieb, das nur sehr langsam kristallisierte. Das reine Isomer wurde durch Chromatographie auf Silicagel gewonnen; Elutionsmittel Äther.

Der so gewonnene Stoff wurde aus Cyclohexan umkristallisiert. Erhalten wurde eine Substanz mit Schmp. 97,5—99,5. (Gef.: C, 81.79; H, 5.78. Ber. für. $C_{17}H_{14}O_2$: C, 81.57; H, 5.64%).

NMR: 9 aromatische Protonen 7,70—7,10 (m); H_2 6,58 (d, J=2 Hz); die gesättigten Protonen bilden ein ABM System: H_1 (H_M) $\delta_M = 3,95$ (m), 2 H_α (AB) $\delta_A = 2,90$ und $\delta_B = 2,50$ ($J_{AB}= 16$ Hz, $J_{AM}= 6$ Hz, $J_{BM}= 9,5$ Hz), CO_2H 11,6 (s).

Die Herstellungsweise der Säure **6** kann auch zur 1-Phenyl-3-indenylessigsäure führen. Die großen Kopplungswerte für J_{AM} und J_{BM} beweisen, daß sich 1-ständig ein gesättigtes Kohlenstoffatom befindet, wodurch die Doppelbindung zwischen C-2 und C-3 festgelegt wird. Wenn man annimmt, daß das Produkt die Struktur der 1-Phenyl-3-indenylessigsäure besitzt, so sollte das 1-ständige Proton (das allyl- und doppeltbenzyl-ständig ist), eine chemische Verschiebung aufweisen, das sowohl jener des H_3 Protons der 3-Phenyl-1-indenylidenessigsäure (4,53), als auch jener des H_1 Protons des 1-Phenyl-3-methyl-indens (4,48) nahekommen sollte. Der Methylester weist das CH_3-Singlet bei 3,70 auf; im übrigen sieht das Spektrum jenem der Säure ähnlich aus.

Die Diazomethan-Veresterung führt zu einem Ester der gaschromatographisch einen Peak aufweist; eine leichte Inflexion des Peaks deutet jedoch auf das Vorhandensein einer kleinen Menge von 1-Phenyl-3-indenylessigsäuremethylester, der im NMR Spektrum nicht faßbar ist.

cis- und *trans*-3-Phenylindanylessigsäure (*cis*- und *trans*-5)

Die mit 5% Pd/Al_2O_3 durchgeführte Hydrierung von **6** ergab (bei Raumtemperatur und Normaldruck) ein Produkt, das nach Trituration mit Chloroform filtrierbare Kristalle liefert. Das nicht umkristallisierte Produkte hat Schmp. 110°.

(Gef.: C, 81.21; H, 6.37. Ber. für $C_{17}H_{26}O_2$: C, 80.92; H, 6.36%). Die Behandlung mit Diazomethan führt zu zwei Estern (86% und 9,8% bzw., gaschromatographisch).

Die Kristalle wurden über Silicagel mit Chloroform chromatographiert und der Rückstand aus Hexan-Benzol umkristallisiert, Schmp. 137° (Lit. [14] 134° aus CH_2Cl_2). (*Gef.*: C, 80.41; H, 6.63. *Ber. für* $C_{17}H_{26}O_2$: C, 80.92; H, 6.36%). Die Veresterung mit Diazomethan führte zu denselben zwei Estern (wobei die Produkte in jeweils 92,5 und 5,0%-iger Menge gebildet wurden). Das den 92,5% entsprechende Isomer ist *cis*-3-Phenyl-1-indanylessigsäure (*cis*-**5**). Die *cis*-Struktur wurde durch NMR bestätigt. Das Spektrum zeigt bei 7,50—6,90 ein den 9 aromatischen Protonen entsprechendes Multiplet. H_3 gibt ein Quartett bei 4,30 (J=7.5 Hz). Zwischen 4,50 und 2,20 erscheint ein ABM System das einem Proton überlagert ist: $H_1\delta_M = 3,63$ (m), $\delta_A = 3,05$ ($J_{AB}= 16$ Hz). Das AB System wird den zwei H Protonen zugeschrieben. Bei 1,75 erscheint ein Sextett das de m2-ständigen pseudoaxialen Proton entspricht ($H_{2\alpha}$) ($J_{1,2} = 10$ Hz). Die Kopplungskonstanten bestätigen die pseudoaxiale Lage der zwei Protonen H_1 und H_3 und implizit die pseudoequatoriale Lage des Phenyls und der Essigsäuregruppe, woher die *cis*-Konfiguration der Säure abgeleitet wurde. CO_2H tritt bei 9,90 auf.

Das den 9,8 bzw. 5% entsprehende Isomer ist *trans*-**5**.

Revue Roumaine de Chimie, **20**, *6*, 791–799 (1975)

NEW SYNTHESES OF ANTHRAQUINONE DYES, DERIVATIVES OF BROMAMINE ACID

F. URSEANU, C. TĂRĂBĂŞANU-MIHĂILĂ, LEONTINA NEGOIŢĂ
and VERONICA ZDRENŢU
Laboratory of Chemistry and Technology of Aromatic Intermediates and Dyes
Polytechnic Institute, Bucharest, Calea Victoriei 149, Romania

Received May 2, 1974

Syntheses for the preparation of new dyes with anthraquinone structure, on the basis of bromamine acid condensed with various aminoheterocycles.

1. INTRODUCTION

1-Amino-4-bromanthraquinone-2-sulphonic acid I (bromamine acid [1]) represents a very good intermediate for the preparation of many anthraquinone dyes [2]; the great number of dyes deriving from bromamine acid is explained by the relatively easy substitution of bromine on treating it with various amines, under the conditions of the Ullmann reaction [3–5] (due to the activating effect of the neighbouring carbonyl and sulphonic acid group) and then to the different possibilities of replacing the sulphonic group. [6]

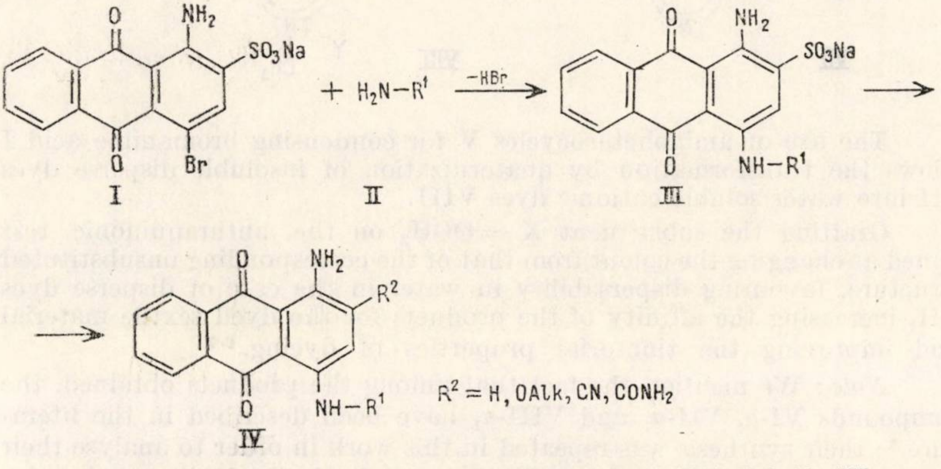

---

[1] Badische Anilin und Sodafabrik, Ger. Pat. 263 395, Ian. 13, 1911; *Frd.*, **11**, 555.

[2] L. Floru and F. Urseanu, REV. ROUMAINE CHIM., under print.

[3] F. Ullmann, *Ber. dtsch. chem. Ges.*, **43**, 536 (1910).

[4] F. Ullmann and M. Sonne, *Liebigs Ann. Chem.*, **380**, 336 (1911).

[5] F. Ullmann and P. Ochsner, *Liebigs Ann. Chem.*, **381**, 1 (1911).

[6] J. Reichel, "Tehnologia coloranţilor antrachinonici", Ed. Academiei, (Bucureşti), 1961, p. 148, 118, 233, 108.

An important advantage presented by bromamine acid is its solubility in water, hence its condensation with various amines II is carried out in aqueous solutions.

The condensation products III are acid dyes (soluble in water), used to dye wool, natural silk, leather and polyamide fibres; the products IV (insoluble in water), obtained by replacing the sulphonic group, are vat dyes used for cotton or dispersion dyes for synthetic fibres.

In the present work we undertook the synthesis of new acid dyes VI, by condensing bromamine acid I with various amino-heterocycles V, disperse dyes VII by replacing the solubilized sulphonic group of compounds VI and cationic dyes VII by methylation at the tertiary nitrogen in the heterocyclic rest of compounds VII (see table 1).

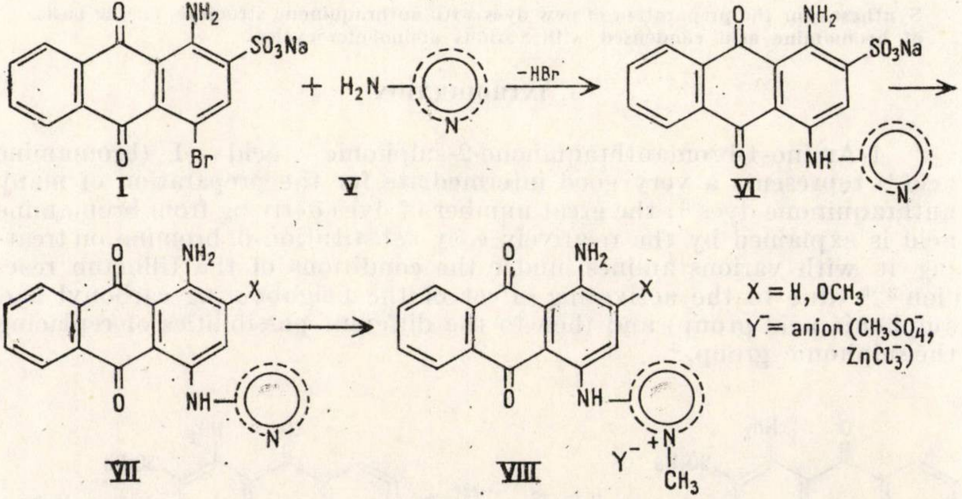

$X = H, OCH_3$

$Y^- = $ anion ($CH_3SO_4^-$, $ZnCl_3^-$)

The use of aminoheterocycles V for condensing bromamine acid I allows the transformation by quaternization of insoluble disperse dyes VII into water soluble cationic dyes VIII.

Grafting the substituent $X = OCH_3$ on the anthraquinonic rest aimed at changing the colour from that of the corresponding unsubstituted structure, favouring dispersability in water in the case of disperse dyes VII, increasing the affinity of the products for the dyed textile material and improving the tinctorial properties of dyeing.[6, 7]

Note: We mention the fact that among the products obtained, the compounds VI-*a*, VII-a_1 and VIII-a_1 have been described in the literature[8]; their synthesis was repeated in this work in order to analyse their spectral characteristics and use them as standards for dyeing wool, polyamide fibres, polyester fibres and polyacrilonitrile fibres, respectively.

---

[7] C. CĂLIN, *Bul. Inform. Laborat. Centr. Coloristic*, **7**, 23 (1967).

[8] H. SANIELEVICI, F. BRODMANN, S. ROSENBERG and C. STULEANU, Brit. Pat. 1 104 053, Feb. 13, 1967; *Chem. Abstr.*, **68**, 106 077 (1968).

Table 1

Anthraquinone dyes, derivatives of bromamine acid

Heterocycle V	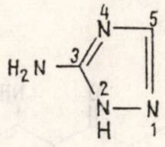 V-a	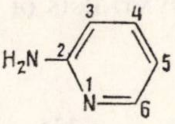 V-b	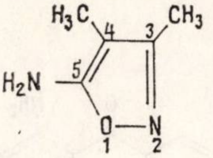 V-c
Acid dye VI	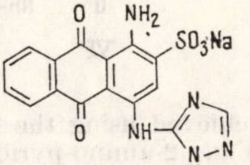 VI-a	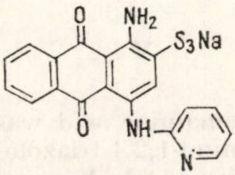 VI-b	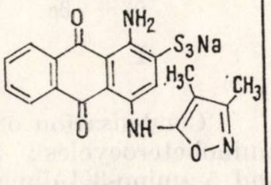 VI-c
Disperse dye VII	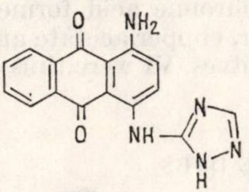 VII-a$_1$	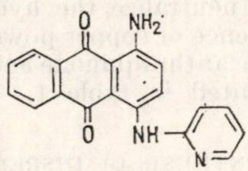 VII-b$_1$	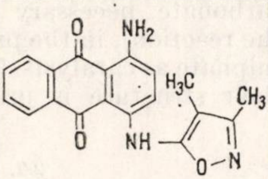 VII-c$_1$
	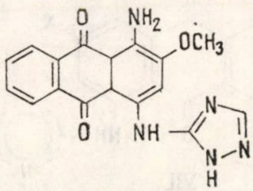 VII-a$_2$	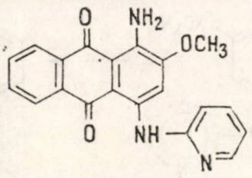 VII-b$_2$	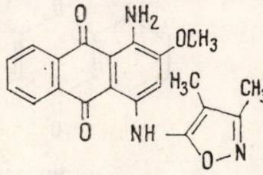 VII-c$_2$
Cationic dye VIII	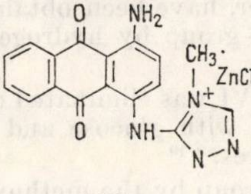 VIII-a$_1$	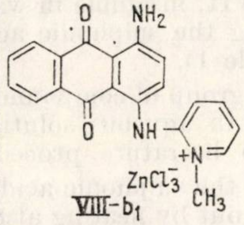 VIII-b$_1$	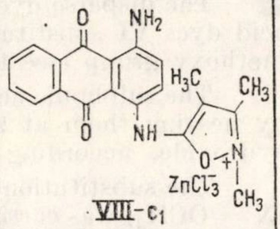 VIII-c$_1$
	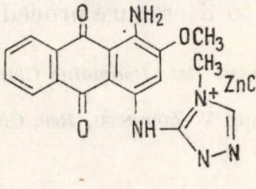 VIII-a$_2$	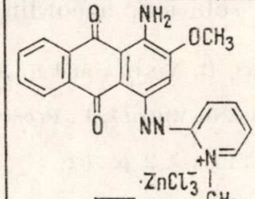 VIII-b$_2$	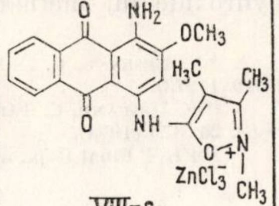 VIII-c$_2$

2. SYNTHESIS OF ANTHRAQUINONE DYES, DERIVATIVES OF BROMAMINE ACID

2.1. SYNTHESIS OF ACID DYES

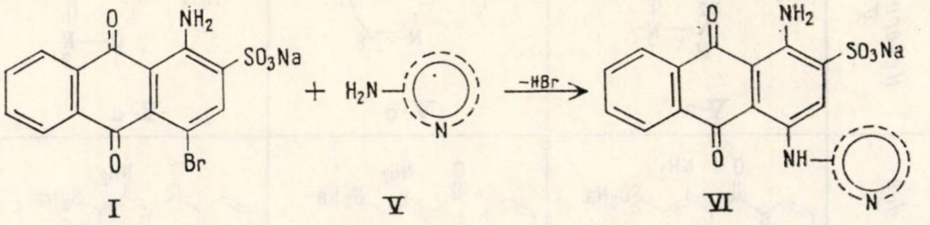

Condensation of bromamine acid was achieved using the following aminoheterocycles : 3-amino-1,2,4-triazole V-*a*, 2-amino-pyridine V-*b* and 5-amino-3,4-dimethylisoxazole V-*c*, under the conditions of the Ullmann reaction, [3-5] heating at 95−98° in aqueous alkaline solution (kalium carbonate, necessary to neutralize the hydrobromic acid formed during the reaction), in the presence of copper powder, copper acetate and copper sulphate as catalysts. The anthraquinone acid dyes VI were thus obtained ; their structure is presented in table 1.

2.2. SYNTHESIS OF DISPERSE DYES

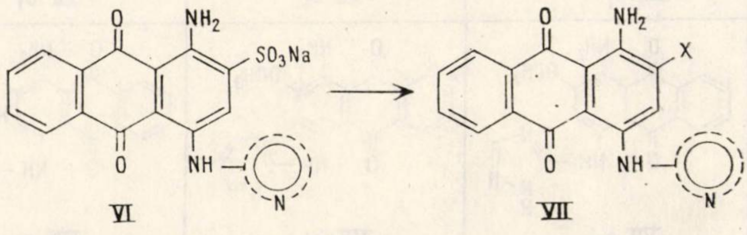

The disperse dyes VII, insoluble in water, have been obtained from acid dyes VI substituting the sulphonic acid group by hydrogen or the methoxy group (see table 1).

The sulphonic acid group of compounds VI was eliminated ($X = H$) by heating them at 95° in aqueous solution with glucose and natrium hydroxide, according to literature procedures. [9,10]

The substitution of the sulphonic acid group by the methoxy group ($X = OCH_3$) was carried out by heating at 80° compounds VI in a kalium hydroxide in, methanol solution, according to literature procedures. [9-11]

---

[9] F. URSEANU, C. DRĂGHICI, R. VINTILĂ and E. SLIAM, *Rev. Roumaine Chim.*, **18** (6), 1 019 (1973).

[10] F. URSEANU, C. TĂRĂBĂŞANU-MIHĂILĂ, L. FLORU and V. ZDRENŢU, *Rev. Chim.* (*Bucureşti*), **25**, 873 (1974).

[11] FIAT Final Rep., nr. 1 313, vol. 2, p. 202.

2.3. SYNTHESIS OF CATIONIC DYES

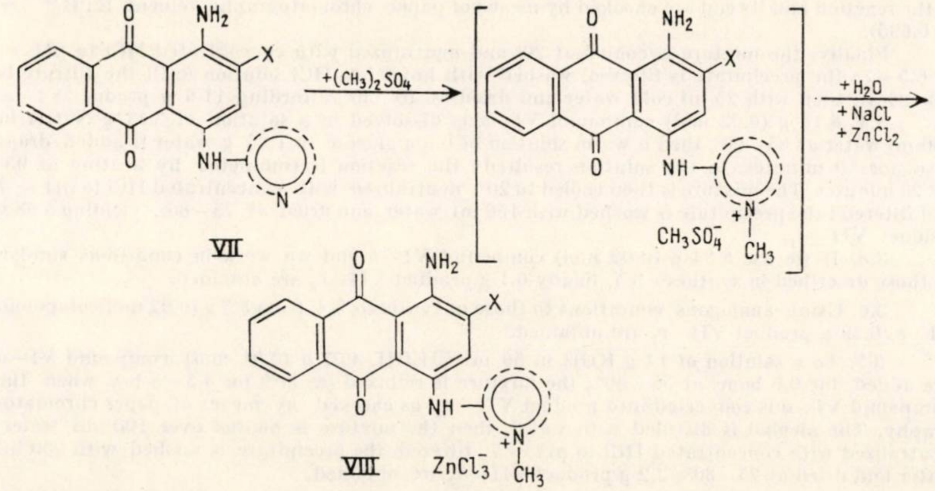

VII

VIII

Cationic dyes VIII have been obtained by quaternization of compounds VII in dimethylsulphate at 110°, followed by heating at 80° in water to hydrolise the excess of dimethylsulphate and precipitation in the form of chlorozincates by adding sodium chloride and zinc chloride, according to literature procedures.[12]

3. EXPERIMENTAL

3.1. A mixture of 12.12 g (0.03 mol) bromamine acid (I), 12.42 g K_2CO_3, 0.2 g copper powder, 0.2 g $(CH_3COO)_2Cu \cdot H_2O$ and 0.2 g $CuSO_4 \cdot 5\,H_2O$ in 200 ml water is heated at 90° until bromamine acid is completely dissolved; 10.08 g (0.12 mol) 3-amino-1,2,4-triazole (V–*a*) are then added, the temperature being raised to 95–98° and maintained there for 10 hrs.

Note: The conversion of compound I to product VI–*a* is controlled by means of Whatman N° 3 paper chromatography, in ascendent system, using an eluent (E) made up of 100 vol. *n*-butanol + 20 vol. ethanol + 44 vol. water and 1 vol. 25 % NH_3. (After an elution for 0.5 hour: $R_f^{I} = 0.797$, $R_f^{VI\text{-}a} = 0.538$).

Finally, the mixture is cooled at 20° and 18.5 ml 36 % HCl are added, then it is heated at 80° for 0.5 hour; the precipitate formed is filtered, washed with hot 0.5 % HCl solution until the filtrate is colourless, then with 25 ml cold water and dried at 75–80°, affording 10.5 g product VI–*a*.

3.2. A mixture of 12.12 g (0.03 mol) bromamine acid (I), 12.42 g K_2CO_3, 0.1 g copper powder, 0.1 g $(CH_3COO)_2Cu \cdot H_2O$ and 0.4 g $CuSO_4 \cdot 5\,H_2O$ in 200 ml water is heated at 90° to dissolve compound I; 5.64 g (0.06 mol) 2-aminopyridine (V–*b*) are then added, the temperature is raised to 95–98° and maintained then for 6 hrs when the reaction is terminated and determined by means of paper chromatography (eluent E; $R_f^{VI\text{-}b} = 0.582$).

Finally, the mixture is cooled at 20°, neutralized with concentrated HCl to pH = 6.5–7 and filtered; the precipitate is washed with hot 0.5 % HCl solution until the filtrate is colourless, then with 25 ml cold water and dried at 75–80°. 11.5 g product VI–*b* are obtained.

3.3. A mixture of 12.12 g (0.03 mol) bromamine acid (I), 12.42 g K_2CO_3, 0.4 g copper powder, 0.1 g $(CH_3COO)_2Cu \cdot H_2O$ and 0.1 g $CuSO_4 \cdot 5\,H_2O$ in 200 ml water is heated at 90°

---

[12] F. Urseanu and L. Floru, *Rev. Chim. (Bucharest)*, under print.

until compound I is dissolved, 5.04 g (0.045 mol) 5-amino-3,4-dimethylisoxazole (V$-c$) are then added, the temperature is raised to 95$-$98° and maintained there for 5 hrs; the evolution of the reaction and its end are checked by means of paper chromatography (eluent E; $R_f^{VI\text{-}c} = 0.695$).

Finally, the mixture is cooled at 20° and neutralized with concentrated HCl to pH = 6.5$-$7; the precipitate is filtered, washed with hot 0.5% HCl solution until the filtrate is colourless, then with 25 ml cold water and dried at 40$-$50°, affording 11.6 g product VI$-c$.

3.4. 8.14 g (0.02 mol) compound VI$-a$ is dissolved in a solution of 3.11 g NaOH in 100 ml water at 85$-$90°, then a warm solution of 6.6 g glucose in 13.5 g water is added dropwise, for 10 minutes, to the solution resulted; the reaction is completed by heating at 95° for 20 minutes. The mixture is then cooled to 20°, neutralized with concentrated HCl to pH = 7 and filtered; the precipitate is washed with 150 ml water and dried at 75$-$80°, yielding 5.98 g product VII$-a_1$.

3.5. If we use 8.34 g (0.02 mol) compound VI$-b$ and we work in conditions similar to those described in synthesis 3.4, finally 6.1 g product VII$-b_1$ are obtained.

3.6. Using analogous conditions to those of synthesis 3.4, from 8.7 g (0.02 mol)compound VI$-c$, 6.39 g product VII$-c_1$ are obtained.

3.7. To a solution of 14 g KOH in 50 ml CH_3OH, 4.07 g (0.01 mol) compound VI$-a$ are added, for 0.5 hour, at 50$-$60°; the mixture is refluxed ($\approx$ 80°) for 4.5$-$5 hrs, when the compound VI$-a$ is converted into product VII$-a_2$, as checked by means of paper chromatography. The alcohol is distilled with water, then the mixture is poured over 100 ml water, neutralized with concentrated HCl to pH = 7, filtered, the precipitate is washed with 250 ml water and dried at 75$-$80°; 3.2 g product VII$-a_2$ are obtained.

3.8. Working in the conditions described in synthesis 3.7, from 4.17 g (0.01 mol) compound VI$-b$, 3.17 g product VII$-b_2$ are obtained.

3.9. Similarly, from 4.35 g (0.01 mol) of compound VI$-c$, 3.54 g product VII$-c_2$ are obtained.

Syntheses of cationic dyes VIII are carried out by a common method described below:

A mixture of 0.01 mol compound VII in 40 ml dimethylsulphate is heated at 110° until a sample is soluble in water. The reaction mass is cooled at 20°, 100 ml water are added, the temperature is raised to 80° and maintained there for 15$-$30 minutes to hydrolyse the excess of dimethylsulphate, then filtered; NaCl and 50% $ZnCl_2$ are added to the filtrate to completely precipitate cationic dyes VIII. The product is filtered, washed with 15% NaCl, dried at 30$-$40° and p = 10 mm Hg.

Note: Each cationic dye obtained includes a quantity of natrium chloride from its precipitation in the form of chlorozincate.

4. ANALYSES

The analyzed compounds were previously purified.

Disperse dyes VII were recrystallized from the appropriate solvent (methanol or N.N-dimethylformamide) and the characteristic melting points were determined; the N% was determined by the micro-Dumas method (see table 2).

Cationic dyes VIII were purified by dissolution in methanol and precipitation with ether.

The purified compounds were subjected to chromatographic, spectral and tinctorial analyses.

4.1 CHROMATOGRAPHY

Chromatographic elutions were carried out on Whatman paper N° 3, in ascendent system, at 25°, for 0.5 hour, in order to check the purity

Table 2

Characteristics of the newly prepared compounds

Compound	Empirical formula	Solvent for recrystallization	MP °C	N% Calculated Found
VII $-a_1$	$C_{16}H_{11}O_2N_5$	methanol	300	22,95 22,65
VII $-a_2$	$C_{17}H_{13}O_3N_5$	methanol	242	20,89 20,59
VII $-b_1$	$C_{19}H_{13}O_2N_3$	methanol	184	13,33 13,44
VII $-b_2$	$C_{20}H_{15}O_3N_2$	methanol	235 (dec.)	12,17 11,92
VII $-c_1$	$C_{19}H_{15}O_3N_3$	DMF	169	12,61 12,30
VII $-c_2$	$C_{20}H_{17}O_4N_3$	DMF	152	11,57 11,24

DMF = N,N-dimethylformamide.

of the analyzed compounds and calculate their characteristic R_f — values The results are presented in table 3.

4.2 SPECTRAL ANALYSIS

Ultraviolet and visible spectra of the products were recorded with a "Pye Unicam SP 1800" apparatus. The determinations were carried out in N.N-dimethylformamide and the extinction coefficients ε calculated. The characteristic absorbtion maxima λ_{max} and lg ε_{max} are presented in table 3.

4.3 TINCTORIAL ANALYSIS

The compounds synthesized were used as disperse dyes for "Terom" polyester fibres, while compounds VIII were used as cationic dyes for polyacrylonitrile fibres.

The results of determinations with dyed fibres an presented in table 4. The colours were defined according to C.I. Hue Chart.[13]

Generally, the dyeings obtained are distinguished by very good fastness especially fastness to light, washing and perspiration.

The tinctorial analysis shows that products VII$-a_2$, VII$-b_1$, VII$-b_2$ and VII$-c_2$ are best suited for dying polyester fibres whereas compounds VIII$-a_1$, VIII$-b_1$ and VIII$-c_1$ for polyacrylonitrile fibres.

---

[13] C. I. Hue Indication Chart, American Association of Textile Chemists and Colourists, Lowell Institute, Lowell Massachusetts, USA.

Table 3

Paper chromatography and absorbtion maxima in ultraviolet and visible

Compound	Paper chromatography			Absorption maxima	
	Solvent	Eluent	R_f	$\lambda_{max.}$ [nm]	$\lg\varepsilon_{max.}$
VII$-a_1$	DMF	E^1	0.694	372 390 472 500	3.799 3.748 3.770 3.813
VII$-a_2$	DMF	E^1	0.780	270 318 368 460 486	4.023 3.565 3.649 3.796 3.880
VII$-b_1$	DMF	E^1	0.686	270 492	3.519 3.212
VII$-b_2$	DMF	E^2	0.750	290 266 512	3.627 3.851 3.760
VII$-c_1$	DMF	E^1	0.714	266 472	3.816 3.528
VII$-c_2$	DMF	E^2	0.804	264 548	3.846 3.598
VIII$-a_1$	CH_3COOH 10%	E^3	0.882	446 508 538	3.079 3.556 3.591
VIII$-a_2$	CH_3COOH 10%	E^3	0.875	262 342 486 520	4.018 4.404 3.554 3.535
VIII$-b_1$	CH_3COOH 10%	E^3	0.785	220–240 502	4.108 3.667
VIII$-b_2$	CH_3COOH 10%	E^3	0.765	228 232 500	4.102 4.102 3.656
VIII$-c_1$	CH_3COOH 10%	E^3	0.788	220 248 500	4.303 4.242 3.654
VIII$-c_2$	CH_3COOH 10%	E^3	0.767	218 254 518	4.186 3.772 4.042

DMF = N.N-dimethylformamide; E^1 = CH_3COOH 80%; E^2 = $CHCl_3$; CH_3COOH; H_2O = 47 : 47 : 6 (in volumes); E^3 = CH_3COOH 60%.
In case of E and E^2 eluents, the paper chromatography were impregnated with a 10% solution of 1-bromonaphthalene in ethanol.

Table 4

Determinations with dyed fibres

Compound	Dyed fibres	Colour	Fastness					
			Light	Cold water	Washing 40°	Perspiration		Rubbing
						acid pH = 5.5	alkaline pH = 8.4	
VII$-a_1$	PE	yellowish-orange 5	4–5	5/4–5/4–5	5/4–5/4–5	5/4–5/4–5	5/4–5/5	3–4
VII$-a_2$	PE	yellowish-red (bright) 7	4	5/4/4–5	5/4–5/5	5/4–5/4–5	5/4–5/4–5	4
VII$-b_1$	PE	bordeaux 34–35	4–5	5/4–4/5	5/5/5	5/4/4–5	5/4/4–5	4
VII$-b_2$	PE	reddish-violet (bright) 10	4–5	5/3–4/3–4	5/5/4–5	5/4/4	5/4/4	4
VII$-c_1$	PE	bluish-red 9–27	4–5	5/4/4	5/3–4/3	5/4/4–5	5/4/4–5	4–5
VII$-c_2$	PE	reddish-violet (bright) 10–11	4–5	5/4–5/5	5/5/4–5	5/4–5/4–5	5/5/5	4
VIII$-a_1$	PNA	reddish-violet 10–51	4	5/4–5/5	5/4–5/5	5/4–5/5	5/4–5/5	4–5
VIII$-a_2$	PNA	red 9	3–4	4–5/3–4/3	4–5/3–4/4	4–5/3–4/3	4–5/4/3–4	3–4
VIII$-b_1$	PNA	bluish-pink 50	4–5	5/4/4–5	4–5/3–4/3	5/3/4	5/3–4/4–5	3–4
VIII$-b_2$	PNA	pink 49	4–5	5/4/4–5	5/3–4/4	5/3/4–5	5/3–4/4–5	4–5
VIII$-c_1$	PNA	violet 36	4–5	4–5/4/4	4–5/4–5/4	4–5/3–4/4	4–5/4/3–4	3–4
VIII$-c_2$	PNA	violet 11	4–5	4–5/4/4–5	4–5/4–5/4	4–5/4/4	4–5/4/4–5	4

PE = polyester fibres. PNA = polyacrylonitrile fibres.

Revue Roumaine de Chimie, **20**, *6*, 801–811 (1975)

GEOMETRICAL ORIENTATION OF STOBBE CONDENSATION INVOLVING DIMETHYL α,α-DIMETHYLSUCCINATE WITH CARBONYL COMPOUNDS

A.M. EL-ABBADY *, A. H. MOUSTAFA and S. A. EL-ABBADY
Chemistry Department, University College for Women
Ain Shams University Cairo, Egypt

Received 2 March 1974

Benzaldehyde, *o*-methoxy, *p*-methoxy and *p*-chlorobenzaldehyde condense with dimethyl α,α-dimethylsuccinate in the presence of potassium *tert*-butoxide to give corresponding *cis*(Ar/$COOCH_3$)-β-half-esters as the sole product except in case of *p*-chlorobenzaldehyde where the *trans*-β-isomer is also obtained. Alkaline hydrolysis of the β-half-esters gives the corresponding dibasic acids which are converted to their anhydrides then to the α-half-esters by methanolysis. The olefinic double bond in the half-esters is easily reduced using sodium and ethanol. Cyclisation of the dibasic acids and their anhydrides is achieved giving the corresponding 2-indonyl dimethyl-acetic acids. The structure of the products obtained is verified from their analytical and spectral data. It is found that dimethyl α,α-dimethylsuccinate fails to condense with diferent types of ketones.

Ludec and Carrie[1] reported that benzaldehyde was condensed with dimethyl α, α-dimethylsuccinate in the presence of potassium *tert*-butoxide (Stobbe condition) to give the corresponding *cis*(Ar/$COOCH_3$)-half-esters (I, $R_1 = R_2 = H$). They also found that acetone failed to condense under these conditions.

Such a type of condensation is reinvestigated and extended in this work to other aromatic aldehydes (namely *o*-methoxy, *p*-methoxy and *p*-chlorobenzaldehydes) and different ketones (namely, acetophenone, cyclohexanone and cyclopentanone).

Benzaldehyde, *o*-methoxybenzaldehyde and *p*-methoxy-benzaldehyde were found to give the corresponding *cis*(Ar/$COOCH_3$) β-half-esters (I) as the sole product in each case.

However, in case of *p*-chlorobenzaldehyde, two stereoisomeric β-half-esters (I, $R_1 = H$, $R_2 = Cl$ and VIII) were obtained in crystalline forms (Chart I).

---

* Present address : Chemistry Department, Faculty of Science, Tanta University, Tanta, Egypt.

[1] J. Le Ludec and R. Carrie, *Compt. rend.*, **257**, 3935 (1963).

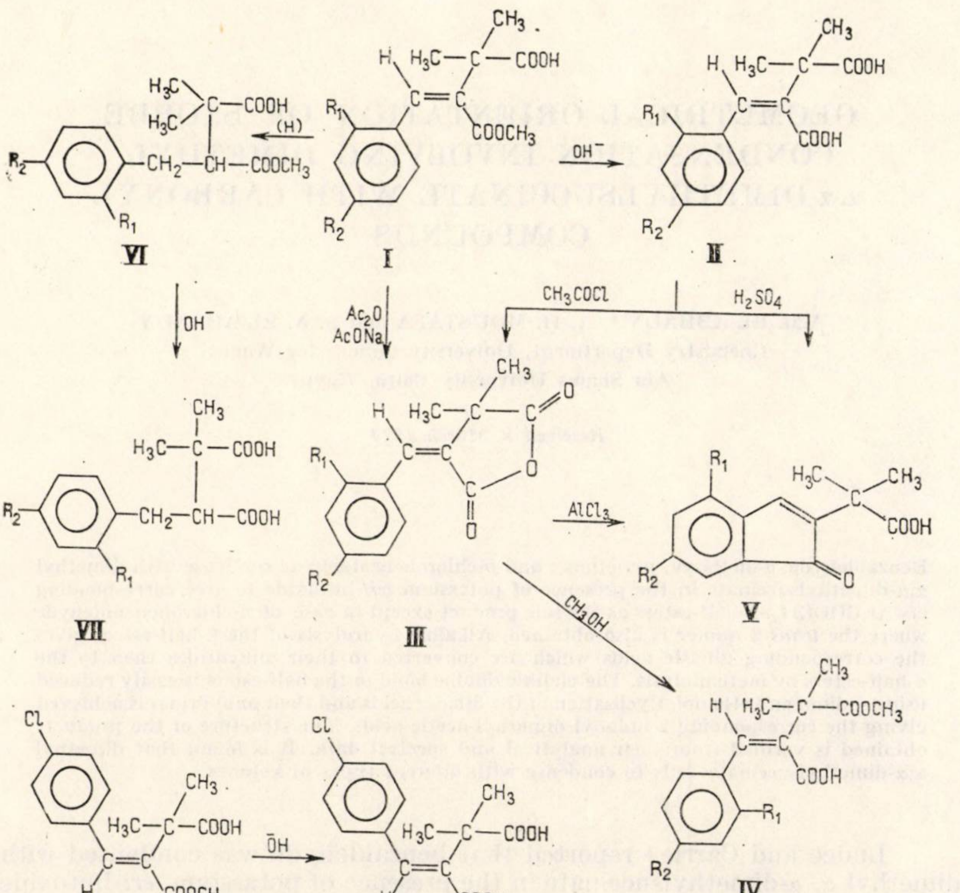
VI
I
II
(H)
OH⁻
OH⁻
Ac₂O
AcONa
CH₃COCl
H₂SO₄
VII
III
V
AlCl₃
CH₃OH
IV
VIII
IX
ŌH
CH₃OH
Al₂O
AcONa
AlCl₃
AcCl
X

Acetone, acetophenone, cyclohexanone and cyclopentanone failed to condense with dimethyl α, α-dimethylsuccinate in the presence of potassium *tert*-butoxide or sodium hydride.

The structure and *cis*(Ar/$COOCH_3$)-configuration of the produced β-half-esters was substantiated from the following evidence: (i) their analytical data; (ii) their infrared spectra which showed strong absorption bands at 3400—2400 (br.), 1730—1720, 1700—1690 (shoulder) cm^{-1}, characteristic of νOH for dimeric carboxyl groups and νC=O for nonconjugated acids and α, β-unsaturated esters.[2] (iii); the electronic spectrum (in ethanol) of Ib showed maximum absorption at 220 and 275 nm (ε max 13750 and 15100). That of I*d* showed maximum absorption at 283 and 297 nm (ε max 11800 and 11600); (iv) chemical reduction of the olefinic double bond to give β-arylmethyl α, α-dimethylsuccinic half-esters (VI); (v) cyclisation of the corresponding dibasic acids (II) and their anhydrides (III) to give the corresponding 2-indonyl dimethylacetic acids (V).

The structure and *trans*(Ar/COOCH$_3$)-configuration of the *p*-chloro-half-ester (VIII) was assigned mainly in the light of its chemical reactions besides its analytical data, i.r. spectrum, which showed similar absorption bands as the *cis*-isomer, and u.v. spectrum (in ethanol) which showed λ_{max} at 280 and 310 nm (ε max 12600 and 12250).

SAPONIFICATION OF THE β-HALF-ESTERS (I)

All β-half-esters (I and VIII) on alkaline hydrolysis gave the corresponding dibasic acids (II and IX) in excellent yield, except in case of (I, R_1 = H, R_2 = OCH$_3$) where the produced crude dibasic acid changed spontaneously on crystallisation to its anhydride as shown later on.

The structure of these diacids was supported by: (i) their analytical data; (ii) their infrared spectra which showed absorption bands at 3400—2300 (br.), 1710 and 1690 cm^{-1} characteristic of νOH for dimeric carboxylic acids and νCO for nonconjugated and conjugated acids, respectively.

REDUCTION OF THE *CIS*(ArCOOCH$_3$)-β-HALF-ESTERS (I)

Chemical reduction of the *cis*(Ar/COOCH$_3$)-β-half-esters using sodium metal and absolute ethanol afforded the corresponding reduced β-half-esters (VI) in fairly good yields. These on alkaline hydrolysis yielded the corresponding reduced dibasic acids (VII). The structure of these products was inferred from their analytical data and infrared spectra(nujol) which showed absorption bands at 3300—2500 (br.) and 1720—1700 cm^{-1} characteristic of νOH for bonded carboxyl groups and νC = O for nonconjugated carboxyl groups.

ANHYDRIDES OF THE DIBASIC ACIDS AND THEIR STABILITY

The anhydrides (III and X) were successfully obtained by treating the corresponding dibasic acids (II and IX) with acetyl chloride. The structure of these anhydrides was inferred from their analytical data and infrared spectra which showed the carbonyl doublet at 1840 and 1760 cm^{-1} characteristic of antisymmetrical and symmetrical vibrations of conjugated five-membered ring anhydrides. The ease of the anhydride formation may be due to the presence of the *gem*-dimethyl group. The *gem*-dimethyl effect was found to be fairly magnified only in the case of *p*-methoxy benzylidene dibasic acid (II, $R_1 = H$, $R_2 = OCH_3$) which could not be obtained in a pure state due to its direct conversion to its anhydride (III, $R_1 = H$, $R_2 = OCH_3$) during storage or crystallization. This may be due to the strong electron releasing effect of *p*-methoxy group which enabled the lone pair of electrons of the hydroxyl oxygen of the conjugated carboxyl group to better attack the electron deficient carbon of the nonconjugated carboxyl group.

---

[2] L. J. BELLAMY, ,,The Infrared Spectra of Complex Molecules'' John Wiley and Sons, Inc. New York, 1958, p. 125.

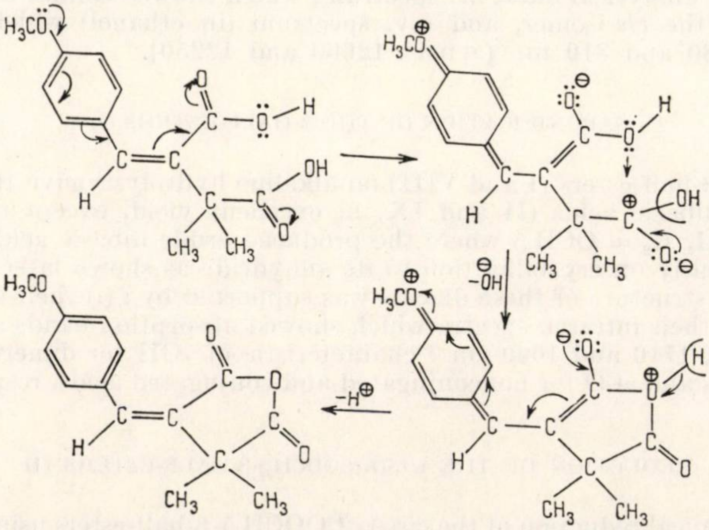

The stability of the anhydride rings was investigated by methanolysis. It was found that all *cis*-anhydrides (except III, $R_1 = H$, $R_2 = OCH_3$) were cleaved by methanol giving the corresponding isomeric α-half-esters (IV). In case of *cis-p*-chloro-anhydride (III, $R_1 = H$, $R_2 = Cl$) a small amount of the β-half-ester was isolated as well. This may be due to the lowering of the electron density on the olefinic double bond by the *p*-chlorophenyl group which makes the attack of the methanol molecule on the second carbonyl carbon possible.

In case of *cis*-β-(*p*-methoxybenzylidene) dimethyl-succinic anhydride (III, $R_1 = H$, $R_2 = OCH_3$) it was found that the anhydride ring had a marked stability towards ring fission even after long reflux with methanol.

This is expected, as such a type of compounds was found to be formed from its dibasic acid spontaneously as shown before. However, methanolysis was carried out successfully in this case, when traces of a mineral acid as hydrochloric acid was added. The products of the acid methanolysis were found to be a mixture of both α- and β-half-esters. This result is probably due to the following mechanism.

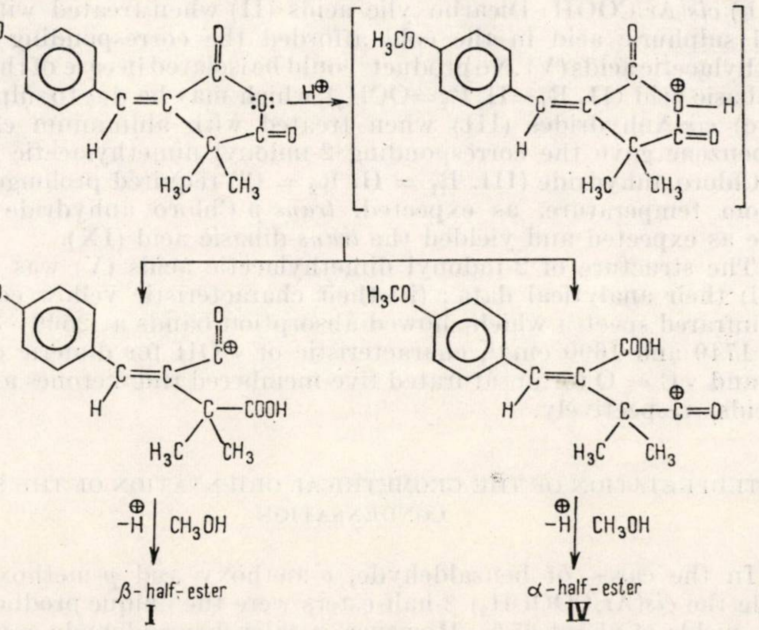

In the case of *trans-p*-chloro anhydride (X), only the *trans*-β-half-ester (VIII) was obtained. This may be explained on the assumption that the *p*-chlorophenyl group being sterically not coplanar with the five-membered anhydride ring and in turn with the olefinic double bond, makes the electrons of the aryl group unavailable at the *trans*-carbonyl carbon. This facilitates the attack of the methanol molecule on this carbon and results in the formation of *trans*- β-half-ester (VIII).

The constitution of the α-half-esters was established from their analytical data and infrared spectra which showed bands at 3300—2500 cm^{-1} (br.) characteristic of ν OH group for dimeric carboxyl group, 1720 cm^{-1} characteristic of ν $C=O$ of both nonconjugated ester group and conjugated carboxyl group.

CYCLISATION OF β-HALF-ESTERS, DIBASIC ACIDS AND ANHYDRIDES

a) β-Half-esters (I or VIII), when treated with acetic anhydride and sodium acetate, [3,4] gave only the corresponding anhydrides (III and X) inferred from their melting point and mixed melting point experiments with authentic specimens prepared by treatment of the diacids (II and IX) with acetyl chloride.

[3] W. Borsche, S. Kettner, M. Gillies, H. Kuhn, and R. Manteuffel *Liebigs Ann. Chem*; **526**, 1 (1936).

[4] A. M. El-Abbady, and L. S. El-Assal, *J. Chem. Soc.*, **1959**, 1024.

b) *cis*(Ar/COOH)-Dicarboxylic acids (II) when treated with concentrated sulphuric acid in the cold afforded the corresponding 2-indonyl dimethylacetic acids (V). No products could be isolated in case of the *p*-methoxydibasic acid (II, $R_1=H, R_2=OCH_3$), which may be due to sulphonation.

c) *cis*-Anhydrides (III) when treated with aluminium chloride in nitrobenzene gave the corresponding 2-indonyl dimethylacetic acids (V). *cis-p*-Chloro anhydride (III, $R_1 = H$, $R_2 = Cl$) required prolonged stirring at room temperature, as expected. *trans-p*-Chloro anhydride failed to cyclise as expected and yielded the *trans*-dibasic acid (IX).

The structure of 2-indonyl dimethylacetic acids (V) was supported by: (i) their analytical data; (ii) their characteristic yellow colour; (iii) their infrared spectra which showed absorption bands at 2500—3500 cm^{-1} (br.), 1740 and 1690 cm^{-1}, characteristic of ν OH for dimeric carboxylic acids and ν $C = O$ for unsaturated five-membered ring ketones and aliphatic acids, respectively.

INTERPRETATION OF THE GEOMETRICAL ORIENTATION OF THE STOBBE CONDENSATION

In the cases of benzaldehyde, *o*-methoxy and *p*-methoxy benzaldehyde the *cis*($Ar/COOCH_3$)-β-half-esters were the unique products obtained in yields of about 65%. However, *p*-chlorobenzaldehyde gave *cis*- and *trans*-($Ar/COOCH_3$)-half-esters in nearly equal proportion with total yield 66%.

Taking into consideration the Stobbe condensation mechanism, [4,5] then using Newmann's projections, the four coformers a_1, a_2, b_1 and b_2 of the two diastereomers (a and b) of the intermediate paraconic ester are possible (Chart II). Examination of the Dreiding-stereo-models showed that: (i) the substituents on Cβ and Cγ in the paraconic ester (d) are in the pseudoeclipsed conformation; (ii) the racemate (a) is the more stable (because the substituents Ar and COOR are not in a pseudoeclipsed position) and should be formed in preference to (b); (iii) the conformer (a_1) is the most stable because the groups Ar and CH_3, which are *cis* to each other, occupy pseudo-equatorial positions thus minimising the interaction between the substituents on the Cα and Cγ of the paraconic ester; (iv) conformers (a_2 and b_2) are the most suitable for anti elimination.

If we consider that the formation of the half-ester results from the concerted E_2-mechanism as in the case of unsubstituted succinic esters, then the elimination should start from the conformer (a_2) which is in equilibrium with (a_1) and we shall obtain the *trans*-half-ester (f_1) as the main product which is not the case. The formation of the *cis*-half-ester (f_2) should occur from (b_2) and epimerisation of the paraconic ester is necessary. This epimerisation in a basic medium implies the breaking of the C—O bond first. Using the theory of the variable E_2-transition state [6] we may suggest that the transition state in this reaction is located in the

---

[5] W. S. JOHNSON, and G. H. DAUB "Organic Reactions" Vol. VI John Wiley and Sons, Inc., New York, 1951, p. 2.

[6] W. S. JOHNSON, A. L. MECLOSKEY, and D. A., DUNNIGAN, *J. Amer. Chem. Soc.*, **72**, 514 (1950).

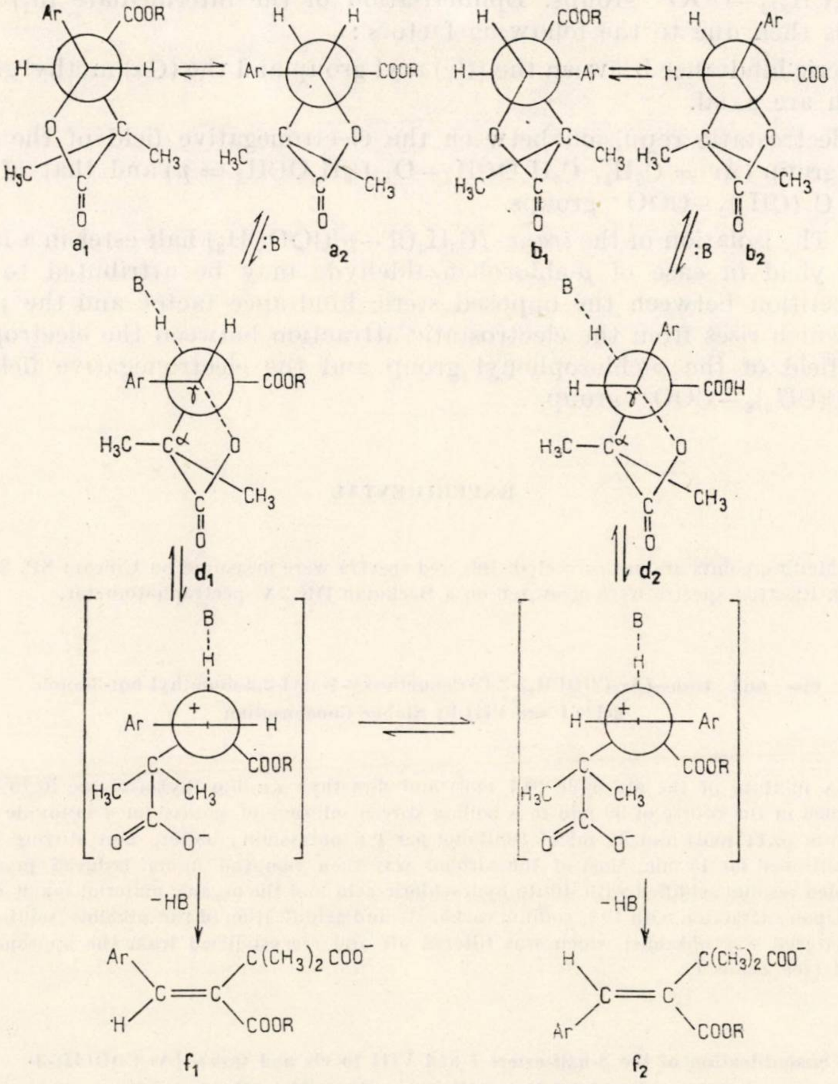

continuum near the paenecarbonium extreme as the two electron-repelling methyl substituents oppose the development ofC β-carbanion character. This would easily allow epimerisation of the paraconic ester. The geometrical orientation of the reaction is then the result of the steric and/or polar interactions [7–9] between the aromatic nucleus and the –COOR

---

[7] J. F. Bunnet, "Survey of Progress in Chemistry, ,,Vol. 5, Academic Press, New York, 1969, p. 53–93.

[8] W. I. Awad, F. G., Baddar, F. A. Fouli, S. M. Omran, and M. I. B. Selim, *J. Chem. Soc. C*, 507 (1968).

[9] F. G. Baddar, M. F. El-Neweihy and R. O. Loutfy, *J. Chem. Soc. C*, **1970**, 620.

or $C(CH_3)_2-COO^-$ groups. Epimerisation of the intermediate (d_1) into (d_2) is then due to the following factors:

a) Steric hindrance between the ($C\gamma$) aryl group and the ($C\alpha$) methyl group which are axial.

b) Electrostatic repulsion between the electronegative field of the ($C\gamma$) aryl group ($Ar = C_6H_5$, $C_6H_4OCH_3-O$, $C_6H_4OCH_3 = p$) and that of the ($C\beta$) $C(CH_3)_2-COO^-$ groups.

The isolation of the *trans*- ($C_6H_4Cl-p/COOCH_3$) half-ester in a fairly good yield in case of *p*-chlorobenzaldehyde may be attributed to the competition between the opposed steric hindrance factor and the polar one which rises from the electrostatic attraction between the electropositive field of the *p*-chlorophenyl group and the electronegative field of the $C(CH_3)_2-COO^-$ group.

EXPERIMENTAL

Melting points are not corrected. Infrared spectra were measured on Unicam SP. 200 G (Nujol). Electron spectra were measured on a Beckman DK.2A spectrophotometer.

cis- and trans-($Ar/COOCH_3$)-3-Carbomethoxy-4-aryl-2,2-dimethyl-but-3-enoic acids I and VIII by Stobbe Condensation

A mixture of the aldehyde (0.1 mol) and dimethyl α,α-dimethylsuccinate (0.15 mol) was added in the course of 30 min to a boiling stirred solution of potassium *t*-butoxide from potassium (0.11 mol) and 35 ml of *t*-butanol per 1 g potassium; boiling and stirring being then continued for 45 min. Most of the alcohol was then removed under reduced pressure, the cooled residue acidified with dilute hydrochloric acid and the organic material taken up in ether. Upon extraction with 10 % sodium carbonate and acidification of the alkaline solution, a solid material was obtained which was filtered off and recrystallised from the appropriate solvent (see table 1).

Saponification of the β-half-esters I and VIII to cis and trans- (Ar/COOCH)-3-carboxy-4-aryl-2,2-dimethylbut-3-enoic acids (II and IX)

The half-esters I and VIII were refluxed with 10 % aqueous sodium hydroxide (10 ml per 1 g half-ester) for 3 hrs. (cf. Table 1).

Conversion of the dibasic acids II and IX to the corresponding anhydrides cis- and trans-arylidene α,α-dimethyl succinic anhydrides (III and X)

This was carried out by 3 hrs refluxing of the dibasic acid II with acetyl chloride (10 ml per 1 g acid) (for details see table 2.)

Table 1

Melting points, yields and analytical data of the β-half-esters and their dicarboxylic acids

Compound			m.p. °C solv. of cryst.	yield %	Formula	Found			Requires		
N°	R_1	R_2				C	H	Cl	C	H	Cl
I_a^*	H	H	147–148 aqMeOH	65	$C_{14}H_{16}O_4$	—	—	—	—	—	—
I_b	OCH_3	H	100–101 Bz–L.P.40	65	$C_{15}H_{18}O_5$	64.60	6.30	—	64.74	6.47	—
I_c	H	OCH_3	108–109 L.P.80	66	$C_{15}H_{18}O_5$	64.70	6.30	—	64.74	6.47	—
I_d	H	Cl	131–132 L.P.80	29	$C_{14}H_{15}ClO_4$	59.50	5.40	12.60	59.46	5.30	12.56
VIII	—	—	139–140 Bz	36	$C_{14}H_{15}ClO_4$	59.40	5.20	12.46	59.46	5.30	12.56
II_a^*	H	H	196–197 aq.EtOH	quant.	$C_{13}H_{14}O_4$	—	—	—	—	—	—
II_b	OCH_3	H	164–165 water	66	$C_{14}H_{16}O_5$	63.60	6.00	—	63.63	6.06	—
$II_c^\dagger$	H	OCH_3	118–130	—	—	—	—	—	—	—	—
II_d	H	Cl	121–123 Bz	quant.	$C_{13}H_{13}ClO_4$	58.60	4.80	13.80	58.14	4.80	13.12
IX	—	—	195 Bz	90	$C_{13}H_{13}ClO_4$	58.25	4.50	13.54	58.14	4.80	13.12

* previously reported. Ref. [1]

† converted into its anhydride during crystallisation.

Bz = Benzene, L.P. 40 = Light petroleum (b.p. 40–60°), L.P. 80 = Light petroleum (b.p. 80–100°).

Conversion of the anhydrides (III) to the α-half-esters cis($Ar/COOCH_3$) methyl 3-carboxy-4-aryl-2,2-dimethyl-but-3-enoates (IV)

The anhydride was refluxed for 6 hrs with excess of absolute methanol (30 ml per 1 g anhydride) (cf. table 2).

In case of III*c* the anhydride ring did not cleave unless the traces of hydrochloric acid were added, where beside the α-half-ester IV*c*, small amount of the original β-half-ester I*c* was obtained.

The β-half-ester I *d* was isolated also beside the α-half-ester IV*d* in case of III*d*.

Cyclisation of dibasic acids (II) and anhydrides (III) to give 2-indonyl dimethyl acetic acids (V)

a) A mixture of *cis*-(Ar/COOH)-4-aryl-2,2-dimethyl-3-carboxy-but-3-enoic acid (1 g) and concentrated sulphuric acid (20 ml.) was kept for half an hour.

b) A mixture of the anhydride (1 mol) in nitrobenzene (10 ml/per 1 g anhydride) and powdered aluminium chloride (1 mol) was stirred for 6 hrs (see table 3).

When *trans-p*-chlorobenzylidene-α,α-dimethylsuccinic anhydride (X) was treated with aluminium chloride in nitrobenzene, *p*-chlorobenzylidene-α,α-dimethylsuccinic acid (IX) was isolated (from melting point and mixed melting point experiment 195°).

Table 2

Melting points, yields and analytical data of the anhydrides and α-half-esters

Compound			m.p. °C solv. of cryst.	yield %	Formula	Found			Requires		
N°	R_1	R_2				C	H	Cl	C	H	Cl
III_a^*	H	H	90—91 L.P.60	quant.	$C_{13}H_{12}O_3$	—	—	—	—	—	—
III_b	OCH_3	H	99—100 Bz—L.P.40	quant.	$C_{14}H_{14}O_4$	68.10	5.50	—	68.29	5.69	—
III_c	H	OCH_3	114—115 Bz—L.p.60	quant.	$C_{14}H_{14}O_4$	68.20	5.70	—	68.29	5.69	—
$III_d^†$	H	Cl	101—102 L.p.80	67	$C_{13}H_{11}ClO_3$	62.20	4.30	14.70	62.27	4.39	14.11
$X^†$	—	—	139—140 L.p.80	77	$C_{13}H_{11}ClO_3$	62.50	4.10	15.00	62.27	4.39	14.11
IV_b	OCH_3	H	135—136 Bz—L.p.60	quant.	$C_{15}H_{18}O_5$	64.50	6.70	—	64.74	6.47	—
IV_c	H	OCH_3	139—140 Bz—L.P.60	55	$C_{15}H_{18}O_5$	64.65	6.65	—	64.74	6.47	—
IV_d	H	Cl	79—80 L.P.40	60	$C_{14}H_{15}ClO_4$	59.50	5.30	12.6	59.46	5.3	12.65

* previously reported Ref. 1. † yellow crystals.

Reduction of β-half-esters to the corresponding 3-carbo-methoxy-4-aryl-2,2-dimethyl butanoic acids (VI)

Sodium metal (1.25 g) was added in small portions to a solution of the β-half-ester (0.5 g) in 10 ml. absolute ethanol (see table 3).

Saponification of the reduced half-esters to the corresponding dibasic acids 3-carboxy-4-aryl-2,2-dimethyl butanoic acids (VII)

The reduced half-ester (VI) was refluxed with 10% aqueous sodium hydroxide (10 ml per 1 g ester) for 3 hrs (see table 3).

Table 3

Melting points, yields and analytical data of the indonyl compounds, the reduced β-half-esters and the reduced dibasic acids.

Compound			m.p. °C solv. of cryst.	Yield %	Formula	Found		Requires	
N°	R_1	R_2				C	H	C	H
V_a*	H	H	204 aq. EtOH	—	$C_{13}H_{12}O_3$	—	—	—	—
V_b	OCH_3	H	266–267 Bz–MeOH	50	$C_{14}H_{14}O_4$	67.99	5.90	68.20	5.68
Vc **	H	OCH_3	221–222 Bz	55	$C_{14}H_{14}O_4$	68.14	5.82	68.20	5.68
V_d **	H	Cl	170–171 L.P.40	50	$C_{13}H_{11}ClO_3$	62.55	4.50	62.30	4.39
VI_b	OCH_3	H	130 Bz–MeOH	70	$C_{15}H_{20}O_5$	64.15	7.05	64.28	7.14
VI_c	H	OCH_3	116–117 Bz	63	$C_{15}H_{20}O_5$	64.25	6.90	64.28	7.14
VII_b	OCH_3	H	141 Bz–MeOH	60	$C_{14}H_{18}O_5$	62.8	6.9	63.15	6.76
VII_c	H	OCH_3	179–180 Bz	70	$C_{14}H_{18}O_5$	63.35	6.54	63.15	6.76
$VII_d^{\dagger}$	H	Cl	160–162 EtOH	quant.	$C_{13}H_{15}ClO_4$	57.85	5.23	57.67	5.54

* previously reported. Ref. 1. ** Cyclised by the Friedel Crafts method only.

* This compound was prepared by catalytic hydrogenation of *cis*-(C_6H_5 Cl-*p*/COOH) dibasic acid (IId) in dioxane (H_2/Raney nickel) for 6 hrs at room temperature and normal pressure.

Revue Roumaine de Chimie, **20**, *6*, 813–830 (1975)

GAS CHROMATOGRAPHIC SEPARATION AND IDENTIFICATION OF BENZENE CYCLOHEXYLATION PRODUCTS

ECATERINA TUDOR and M. IOVU
University of Bucharest, Faculty of Chemistry
Bd. Republicii 13, Bucharest, Romania

Received May 25, 1973

The presence of C_{12} hydrocarbons was emphasized in samples with a high content of cyclohexylbenzene : cycloalkylbenzenes with a five-membered ring, bicycloalkyls and cycloalkyl-cycloalkenes, resulted as by-products during the catalytic cyclohexylation reactions of benzene. The peaks obtained by gas chromatographic separation on four different stationary phases were identified by using the structural information deduced from the retention indices and known synthesis approaches to products used as standards.

INTRODUCTION

In connection with a study performed [1] on the catalytic cyclohexylation of benzene, attempts have been made to reveal the presence of C_{12} hydrocarbons : cycloalkylbenzenes with a five membered ring, bicycloalkyls and cycloalkyl-cycloalkenes, in samples with more than 95 % cyclohexylbenzene.

Not only is there a lack of concrete gas chromatographic data in the literature, but also a scarcity of general information about the physico-chemical properties of this kind of compounds.

Considering the multitude of possible isomers as a result of the reciprocal position of the substituents, of the special geometry of five- and six-membered rings, and for cycloalkyl-cycloalkenes of the additional complexity introduced by the double bond, we have not undertaken to exhaust in this work the subject of the separation and identification of all individual isomers, but rather to assign the chromatographic peaks to classes of hydrocarbons, in order to answer the purpose of the report. [1] This was accomplished as a result of the information deduced from our experimental data, on the basis of the Kováts retention index system [2-6] and of some syntheses made with a view to obtaining the compounds involved.

---

[1] M. Iovu and E. Tudor, *Rev. Roumaine Chim.*, **19**, 1207 (1974).

[2] E. Kováts, "Advances in Chromatography", vol, 1, J. C. Giddings and R.A.Keller, Eds., M. Dekker, New York, 1965, p. 229–247.

[3] E. Kováts, *Ber. Bunsengesellschaft Phys. Chem.*, **69**, 812 (1965).

[4] E. Kováts, *Chimia (Aarau)*, **22**, 459 (1968).

[5] L. S. Ettre, *Anal. Chem.*, **36**, 31A (1964).

[6] A. B. Littlewood, "Gas Chromatography", 2nd ed., Academic Press, New York, 1970, p. 81–95, 105–111.

EXPERIMENTAL

The chromatographic unit used was a Carlo Erba GT–200 instrument with dual column-dual thermal conductivity detector, fitted with a Speedomax W recorder 2.5 mv.

Four stainless steel chromatographic columns 2.5 m long, with a 2 mm internal diameter and the following fillings were used for measurements :

1) Carbowax 20 M (polyethyleneglycol with molecular weight about 20,000), 20% on Chromosorb W 60–80 mesh (CW 20 M);

2) Apiezon L (a mixture of high molecular weight aliphatic hydrocarbons), 10% on Chromosorb W 60–80 mesh (Ap L);

3) a mixture, 1 :1 parts by weight, Bentone 34-Silicone Oil DC 710 (dimethyldioctadecylammonium bentonite-phenyl-methyl-silicone oil), 10% on Chromosorb P 60–80 mesh (B 34–DC 710,1 :1);

4) a mixture, 3 :7 parts by weight, Bentone 34-Silicone Oil DC 710, 10% on Chromosorb P 60–80 mesh (B 34–DC 710,3 :7).

The columns were conditioned for 24 hours at 180° prior to use and they presented an efficiency of about 1600 theoretical plates as against cyclohexylbenzene (0.2 µl)

The operating conditions were :

— column oven temperature : 150° (measured with a mercury thermometer)
— vaporizer and detector temperature : 230° ;
— current in the thermal conductivity detector bridge : 180 mA ;
— the outlet flow of carrier gas, hydrogen, 30–40 cm^3/min ;
— 0.5–1 µl sample.

The substances used for identification were :

a) benzene, cyclohexane, cyclohexanol, cyclohexanone, biphenyl, *n*-alkanes C_6–C_{16} (commercial analytical grade)

b) cyclohexene, cyclohexylchloride, cyclopentylbenzene-synthesised in our laboratory, with a purity of over 95%, as tested by gas chromatography ;

c) the products of syntheses summarized in table 1.

Syntheses 1–5 give non-ambiguous information concerning retention data for bicyclohexyl, 1-methyl-1-phenyl-cyclopentane and cyclopentyl-phenyl-methane; in synthesis 4, besides the expected 1-methyl-1-phenyl-cyclopentane, which is the major component, one finds also their isomers and by-products revealed by such reactions. [1]

Syntheses 6–8 were rather indirectly useful for identification, their products being complex hydrocarbon mixtures when we expected, with great probability, the existence of certain compounds. An argument with Kováts' retention index system accounts for their presence and allows also the determination of the ratios specified in table 1.

Each separate sample was analysed in parallel on the four columns, as were the appropriate mixtures of n-alkanes C_6–C_{16} used as reference substances for expressing the retention data in the retention index system.

The retention index of a component *i*, on the stationary phase X, at column temperature *T*, was obtained by equation [6] :

$$I_T^X(i) = \mathrm{n}\cdot 100\,\frac{\lg d'_R(\mathrm{i}) - \lg d'_R(P_z)}{\lg d'_R(P_{z+n}) - \lg d'_R(P_z)} + 100\,z \tag{1}$$

Where : $d'_R(i)$, $d'_R(P_z)$, $d'_R(P_{z+n})$ are the adjusted retention distances (in mm, measured from the air peak) of the component *i* and of the reference n-alkanes with *z* and *z* + *n* carbon atoms, which frame it.

Table 1

Syntheses for obtaining some substances useful to identification

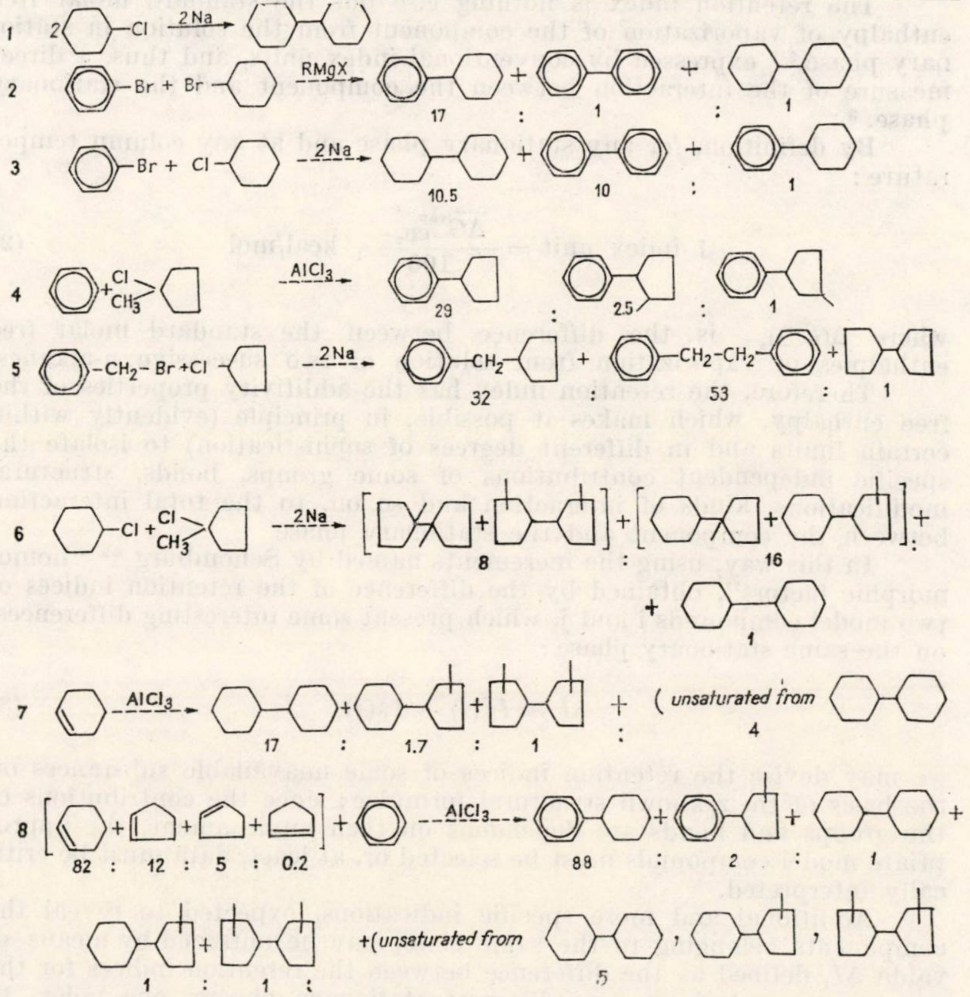
1
2 Cl
2Na
2
Br
Br
RMgX
17 : 1 : 1
3
Br
Cl
2Na
10.5 : 10 : 1
4
Cl
CH3
AlCl3
29 : 25 : 1
5
CH2
Br
Cl
2Na
CH2
CH2–CH2
32 : 53 : 1
6
Cl
Cl
CH3
2Na
8
16
1
7
AlCl3
(unsaturated from
17 : 1.7 : 1 : 4
8
82 : 12 : 5 : 0.2
AlCl3
88 : 2 : 1
+(unsaturated from
1 : 1 : 5

The reliability of the qualitative assignements as well as the follow-up of retention modifications when passing from one stationary phase to another, were tested and confirmed by the compatibility of the quantitative data, as area %, on the four columns.

USE OF RETENTION INDICES

The retention values expressed by the retention index system, ensure data generalization and the relationships between retention and the molecular structure, particularly useful to the identification of the peaks in gas chromatography.

The retention index is nothing else but the standard molar free enthalpy of vaporization of the component from the solution in stationary phase [3,7] expressed by conventional index units, and thus, a direct measure of the interaction between the component and the stationary phase. [3]

By definition, for any stationary phase and at any column temperature:

$$1 \text{ index unit} = \frac{\overline{\Delta G^{\text{vap}}_{-\text{CH}_2-}}}{100}, \text{ kcal/mol} \tag{2}$$

where $\overline{\Delta G^{\text{vap}}_{-\text{CH}_2-}}$ is the difference between the standard molar free enthalpies of vaporization from solution of two successive n-alkanes.

Therefore, the retention index has the additivity properties of the free enthalpy, which makes it possible, in principle (evidently within certain limits and in different degrees of sophistication) to isolate the specific independent contributions of some groups, bonds, structural modifications, kinds of interaction and so on, to the total interaction between the component and the stationary phase.

In this way, using the increments named by Schomburg [8,9] "homomorphic factors", obtained by the difference of the retention indices of two model compounds i and j, which present some interesting differences, on the same stationary phase:

$$\delta I = I_T^X(i) - I_T^X(j) \tag{3}$$

we may devise the retention indices of some unavailable substances on the basis of their known structural formulae; since the contributions of the groups and bonds are dependent on their environment, the appropriate model compounds must be selected or, at least, data must be critically interpreted.

Additional and more specific indications, expected to reveal the components belonging to the same class, may be obtained by means of value ΔI, defined as the difference between the retention indices for the same compound, i, on two different stationary phases, one polar, P, another non-polar (paraffinic), N:

$$\Delta I_N^P(i) = I_T^P(i) - I_T^N(i) \tag{4}$$

ΔI is a measure of all the additional interactions between i and P, as against the dispersion interaction between i and N, and is an additive value.

ΔI is higher, the more polar the component and the stationary phase P.

---

[7] L. ROHRSCHNEIDER, *J. Chromatog.*, **22**, 6 (1966).

[8] G. SCHOMBURG, *J. Chromatog.*, **23**, 1 (1966).

[9] G. SCHOMBURG, *J. Chromatog.*, **23**, 18, (1966).

ΔI is a characteristic value for a class of substances; however, within a class, there are slight differences due to the particular structure of its members.

We will refer below only to systems in which there are no donor-acceptor interactions.

The presence of a double bond and of an aromatic ring in one molecule will introduce increments at ΔI owing to the induction interaction of the π-electrons with a polar stationary phase.

It is interesting that the contributions to ΔI introduced by the five- and six-membered saturated rings are of the same order as those of a double bond; Schomburg explain this[9] by the ring strain, responsible for a raised and variable polarisability of the molecule.

Thus, for our components, we expect the order:

$$\Delta I\,(\text{cycloalkylbenzenes}) > \Delta I(\text{cycloalkyl-cycloalkenes}) > \Delta I\,(\text{bicycloalkyls})$$

and a sufficient difference in magnitude to permit a non-ambiguous assignment.

RESULTS AND DISCUSSION

Table 2 contains the values I and ΔI on the four columns at 150° for the components available as pure standards and for those which can be certainly assigned on the basis of the analysis of the products resulted from the syntheses summarized in table 1.

Thus, bicyclohexyl was the major component from synthesis 1 present in the products of syntheses 2 and 3; cyclopentyl-phenyl-methane was the only of the three main components of synthesis 5 in the retention range of cyclohexylbenzene; 1-methyl-1-phenyl-cyclopentane was the highest (60%) of the almost 30 components of synthesis 4, having concentrations between 0.5 and 5%.

The reliability limits of the means are also specified with a 95% statistical probability.

Below are given, in turn, the classes of C_{12} hydrocarbons.

Cycloalkylbenzenes $C_{12}H_{16}$

We deal with the five-membered ring isomers of cyclohexylbenzene, namely with the (methyl-cyclopentyl)-benzenes and with cyclopentyl-phenyl-methane.

Since the (methyl-cyclopentyl)-benzenes are disubstituted derivatives of cyclopentane, they may exhibit, besides the isomerism determined by the reciprocal position of substituents, the *cis/trans* isomerism as against the five-membered ring; thus, we have five isomers: 1-methyl-1-phenyl-, *cis*- and *trans*-1-methyl-2-phenyl- and *cis*- and *trans*-1-methyl-3-phenyl-cyclopentanes.

Table 2

Retention indices I and index differences $\Delta I = I^{X} - I^{ApL}$ of the standards used for identification; column temperature: 150°

	CW 20M		B 34–DC 710 1:1		B 34–DC 710 3:7		ApL
	I	Δ*I*	*I*	Δ*I*	*I*	Δ*I*	*I*
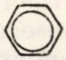	997±5	302	800	105	798±3	103	695±4
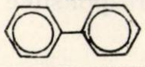	2040±5	620	1660±10	240	1618	198	1420±8
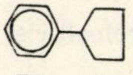	1602±3	338	1365±5	101	1362±4	98	1264±4
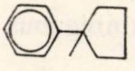	1626±2	324	1396±2	94	1397±2	95	1302±2
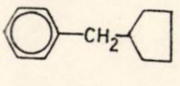	1660±3	329	1432±3	101	1430±2	99	1331±2
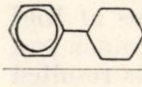	1694±5	334	1456±8	96	1459±8	99	1360±3
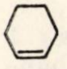	822* (856)	129* (142)	706*	13*	713*	20*	693* (714)
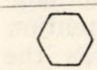	737* (756)	66*(56)	678*	7*	684*	13*	671* (700)
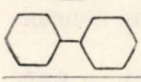	1483±3	120	1374±7	11	1376±6	13	1363
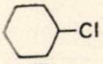	1200±6	270	1021±9	91	1016±6	86	930±5
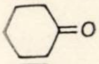	1354±5	454					900
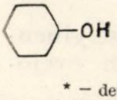	1403±4	513					890

* – determined at 50°; in parantheses the values extrapolated to 150° according to the experimental data in the range of 50–80°.

We do not know to what extent their physico-chemical properties differ. It is known that Δ*I* values for cyclopentane and cyclohexane[9] are practically identical and decrease with the methyl-substituted compounds, due to ring shielding.

We expect this shielding to increase with the number and volume of the substituents and to depend on the general geometry of the molecule.

It may be assumed that ΔI for cycloalkylbenzenes consists of the positive contributions of :

1) the induction interaction of the aromatic ring with polar stationary phase, $\delta(\Delta I)_{\text{arom}}$.

2) an excess of interaction of the saturated five- and six-membered rings, $\delta(\Delta I)_{\text{sat. ring}}$

3) dipolar interactions due to small dipol moments strongly dependent on the molecular geometry, and

4) negative contributions of the steric hindrances in the interaction of the two rings with the stationary phase.

We note the contributions 3) and 4) which cannot be discriminated on the basis of our experimental data, with $\delta(\Delta I)_{\text{geom}}$; the differentiation between isomers results just from the difference in these effects. In this way :

$$\Delta I(\text{cycloalkylbenzene}) = \delta(\Delta I)_{\text{arom}} + \delta(\Delta I)_{\text{sat. ring}} + \delta(\Delta I)_{\text{geom}} \qquad (5)$$

The same contribution $[\delta(\Delta I)_{\text{arom}} + \delta(\Delta I)_{\text{sat. ring}}]$ is valid for all isomers ; $\delta(\Delta I)_{\text{arom}}$ and $\delta(\Delta I)_{\text{sat. ring}}$ may be obtained experimentally, as shown in table 3.

Table 3

Basic contributions to ΔI

Contribution and its experimental determination	CW 20M	B 34–DC 710 1 : 1	B 34–DC 710 3 : 7
$\delta(\Delta I)$ arom = $0.5[\Delta I(\text{benzene}) + 0.5\Delta I\,(\text{biphenyl})]$	306	112	101
$\delta(\Delta I)$ sat. ring = $0.5[\Delta I\,(\text{cyclohexane}) + 0.5\Delta I\,(\text{bicyclohexyl})]$	58	6	10
$\delta(\Delta I)$olef = ΔI(cyclohexene)-ΔI (cyclohexane)	86	6*	7*

* – determined at 50°.

Thus, $\delta(\Delta I)_{\text{geom.}}$ may be estimated as a sum total, by the difference against ΔI (cycloalkylbenzene) serving as a guide to the degree of shielding, necessary in our assignments (table 4).

Despite the fact that the slight differences between the geometrical effects are close enough taking into account the magnitude of the experimental errors, table 4 clearly reflects the conclusion that, among the introduced standards, the greatest steric hindrance of the interaction belongs, as expected, to 1-methyl-1-phenyl-cyclopentane.

$\delta(\Delta I)_{\text{arom}}$ has by far the greatest weight in ΔI (tables 2–4), so that we can further predict the behaviour of unknown isomers, mainly from the point of view of aromatic ring shielding.

Our samples and the products of syntheses 4 and 8, in the range of ΔI values of cycloalkylbenzenes (see further table 8) contained for all the columns used, besides the components listed in table 2, also the com-

Table 4

Contributions of $[\delta(\Delta I)_{arom} + \delta(\Delta I)_{sat.ring}]$ and $\delta(\Delta I)_{geom}$ to cycloalkylbenzenes $C_{12}H_{16}$

	CW 20M	B 34–DC 710, 1 : 1	B 34–DC 710, 3 : 7
$\delta(\Delta I)_{arom} + \delta(\Delta I)_{sat \cdot ring}$	364	118	111
		$\delta(\Delta I)_{geom}$	
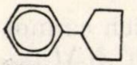	−26	−17	−13
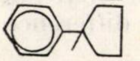	−40	−24	−16
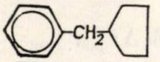	−35	−17	−12
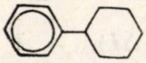	−30	−22	−12

ponents noted as A and B, whose values I, ΔI and $\delta(\Delta I)_{geom}$ are summarized in table 5.

Component A, as shown by its retention index, occurs prior to 1-methyl-1-phenyl-cyclopentane and exhibits the greatest value $\delta(\Delta I)_{geom}$ on all columns; the only isomer which may have a higher shielding of the interaction between the aromatic ring and the stationary phase than 1-methyl-1-phenyl-cyclopentane, is *cis*-1-methyl-2-phenyl-cyclopentane.

Table 5

I, ΔI and $\delta(\Delta I)_{geom}$ for the unknown components, assumed to be cycloalkylbenzenes $C_{12}H_{16}$

Possible assignment	CW 20 M			B 34–DC 710,1 : 1			B 34–DC 710, 3 : 7			Ap L
	I	ΔI	$\delta(\Delta I)_{geom}$	I	ΔI	$\delta(\Delta I)_{geom}$	I	ΔI	$\delta(\Delta I)_{geom}$	I
A 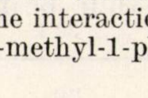	1587±3	310	−54	1372±3	95	−23	1369±2	92	−19	1277±2
B 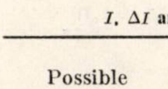	1637±8	327	−37	1405±4	95	−23	1406±4	96	−15	1310±2

1-methyl-1-phenyl-cyclopentane is practically superposed, upon component B which arises only as a distortion of this peak in certain samples.

Bearing in mind that the methyl group is rather apart from the aromatic ring in 1-methyl-3-phenyl-cyclopentane, we may expect that its *cis*- and *trans*- isomers are not separated under our conditions of resolution. In any case, compared to 1-methyl-1-phenyl-cyclopentane, they are less sterically hindered at the aromatic ring and more hindered at the cyclopentane ring, so that we expect them to have a more reduced value $\delta(\Delta I)_{geom}$ than that of 1-methyl-1-phenyl-cyclopentane; this corresponds the data in tables 4 and 5.

On the other hand, for the same reasons, we expect them to have a slightly higher boiling point.

Thus, we think that component B represents the 1-methyl-3-phenyl-cyclopentanes, unseparated from 1-methyl-1-phenyl-cyclopentane and probably, from *trans*-1-methyl-2-phenyl-cyclopentane, either.

Bicycloalkyls $C_{12}H_{22}$

These components, resulting as by-products in some cyclohexylations of benzene (with cyclohexene and cyclohexanol) are: bicyclohexyl and its isomers with one or two five-membered rings.

On the basis of some considerations concerning the volatility of branched compounds relative to non-branched compounds with the same carbon number and of experimental indications concerning the substituted cyclanes,[9] the elution order on any stationary phase may be expected to be: bi-(methyl-cyclopentyl)s, methyl-cyclohexyl-cyclopentanes, bicyclohexyl.

Among the stationary phases used, the only one permitting a separation into the saturated/ olefinic/ aromatic hydrocarbon classes, was CW 20 M.

The mixed stationary phases with B 34—DC 710 and the non-polar Ap L, are not selective in this respect and the retention change of the low and numerous peaks passing from one column to another, is difficult to be followed. For this reasons, for bicycloalkyls and cycloalkyl-cycloalkenes we used in the first place the homomorphic factors, δI and not ΔI; nevertheless, for shielding considerations, we expect:

ΔI [bi(methyl-cyclopentyl)s] $<$ ΔI (methyl-cyclopentyl-cyclopentanes) $<$ ΔI (bicyclohexyl)

Bicyclohexyl

We may see from tables 2 and 5, on the basis of I values, that bicyclohexyl is well separated from the cycloalkylbenzenes on CW 20 M, superposed with cyclohexylbenzene on ApL and placed between (methyl-cyclopentyl)-benzenes, without being well separated on columns with B 34—DC 710.

Methyl-cyclohexyl-cyclopentanes and cyclohexyl-cyclopentyl-methane

The possible isomers: 1-methyl-1-cyclohexyl-cydclopentane, *cis*- and *trans*-1-methyl-2-cyclohexyl-cyclopentanes, *cis*- and *trans*-1-methyl-3-cyclohexyl-cyclopentanes were not available as pure standards, but one or several of them may be expected among the numerous components resulted from reactions 6, 7, 8-table 1. Moreover, in samples of cyclohexylbenzene containing bicyclohexyl, this was accompanied by peaks (up to 0.2 %) which might belong to this type (table 6).

The retention indices of the hydrocarbons involved may be obtained by means of those of the corresponding cycloalkylbenzenes and of retention index increment δI_{arom} :

$$I(\text{methyl-cyclohexyl-cyclopentane}) = I(\text{cycloalkylbenzene}) - \delta I_{\mathrm{arom}} \qquad (6)$$

δI_{arom} (table 6) was obtained with the only available model compounds :

$$\delta I_{\mathrm{arom}} = I\ (\text{cyclohexylbenzene}) - I\ (\text{bicyclohexyl}) \qquad (7)$$

For the other isomers, we expect this increment to be lower than or equal to that from equation 7, because of the steric hindrances ; in this way, the following values will result from equation 6 :

$$I_{\mathrm{predicted}} \leqslant I_{\mathrm{actual}} \qquad (8)$$

The retention indices predicted according to equations 6–7 and those determined experimentally for our samples are summarized in table 6.

Table 6

Retention indices for the bicycloalkyls $C_{12}H_{22}$, predicted cf. eq. 6–7 and found experimentally in analysed mixtures

	CW 20M		B 34–DC 710 1 : 1		B 34–DC 710 3 : 7		Ap L	
δI_{arom}	211		82		83		–3	
	$I_{\mathrm{pred.}}$	$I_{\mathrm{exp.}}$	$I_{\mathrm{pred.}}$	$I_{\mathrm{exp.}}$	$I_{\mathrm{pred.}}$	$I_{\mathrm{exp.}}$	$I_{\mathrm{pred.}}$	$I_{\mathrm{exp.}}$
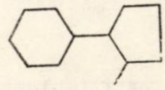	1376	1365 1377 1392	1290	1245 1298	1286	1280 1298	1280	1272 1286
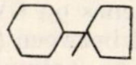	1415	1423	1314	1321	1314	1305	1305	1299
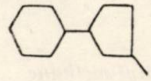	1426	1430	1323	1336	1323	1328	1313	1318
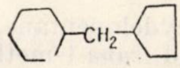	1449	1456	1350	1358	1347	1348	1334	1331

The presence of these substances in the analyzed mixtures is confirmed in this manner, yet the conformation of the isomers could not le stated precisely. Nevertheless, 1-methyl-1-cyclohexyl-cyclopentane is mainly expected to result from synthesis 6 table 1 and this is confirmed by the retention index information obtained as above.

Bi-(methyl-cyclopentyl)s

Bearing in mind their very low concentration in the cyclohexylbenzene samples (overall value up to 0.02 – 0.03 %) and the very large number of possible isomers, there is no question of identifying them individually. We have assigned to this class the peaks with lower retention indices than those of methyl-cyclohexyl-cyclopentanes, resulted from the product of synthesis 6 table 1, namely on columns :

CW 20 M-about 11 peaks with retention indices between 1100 – 1365,

B 34 – DC 710,1 :1 and B 34 – DC 710,3 :7, about 8 peaks with retention indices between 1088 – 1245 and 1100 – 1265, respectively.

Ap L-superposed with the other components.

Cycloalkyl-cycloalkenes $C_{12}H_{20}$

These components were not available either, but their presence was expected in the dimerisation products of the cyclohexene and methylcyclopentenes (syntheses 7 and 8, table 1) and in some of the samples of cyclohexylbenzene derived from cyclohexene and cyclohexanol (table 7).

The presence of double bond increases the number of isomers.

On polar columns, such as CW 20 M, these compounds are retained more than the corresponding saturated hydrocarbons; we will limit our discussion to this stationary phase, since the others are not selective in this respect.

If we define δI_{olef} and $\delta(\Delta I)_{\text{olef}}$ of a cycloalkene as against the cycloalkane with the same skeleton,

$$\delta I_{\text{olef}}\,(\text{cycloalkene}) = I(\text{cycloalkene}) - I(\text{cycloalkane}) \qquad (9)$$

$$\delta(\Delta I)_{\text{olef}}\,(\text{cycloalkene}) = \Delta I(\text{cycloalkene}) - \Delta I(\text{cycloalkane}) \qquad (10)$$

this excludes the interaction of the saturated ring (inclusively its steric effects) with the stationary phase.

Generally, we have :

$$\delta I_{\text{olef}}(\text{cycloalkene}) = \delta I_{\text{d.b. nonshielded}} + \delta I_{\text{d.b. electronic effects}} + \delta I_{\text{d.b. geometrical effects}} \quad (11)$$

where d.b. = double bond ; the geometrical effects are negative, the electronic effects are positive.

The same kind of relation exists for $\delta(\Delta I)_{\text{olef}}$.

The only model compounds available to us were cyclohexene and cyclohexane. To estimate the actual situation with our cycloalkyl-cycloalkenes compounds, it is useful to review some of Schomburg's conclusions [9] concerning the behaviour of the five- and six-membered cycloalkanes on the stationary phase Emulphor O, having the same kind of polarity as CW 20 M.

So, $I_{70^\circ}^{\text{Emulphor O}}$ for cyclopentenes and cyclohexenes were:
1-methyl-cyclopentene (57) >methylene-cyclopentane (53) >cyclopentene (20) >4-methyl-cyclopentene (10) >3-methyl-cyclopentene (7);
1-methyl-cyclohexene (86) >methylene-cyclohexane, cyclohexene (53) > 4-methyl-cyclohexene (49) >3-methyl-cyclohexene (46).

Thus, we expect that, in the case of cycloalkyt-cycloalkenes derived from bicyclohexyl, where the second ring acts as a bulky substituent as against the double bond of the first ring, and where we do not expect remarkable electronic effects,

$$\delta I_{\text{olef}}\,(\text{cycloalkyl-cyclohexenes}) \leqslant \delta I_{\text{olef}}\,(\text{cyclohexene})$$

For unsaturated hydrocarbons, derived from the bicycloalkyls with one or two five-membered rings, we expect both (negative) steric effects produced by the second ring and methyl group and (positive) electronic effects produced by a methyl substituent at the double bond; considering the above values on Emulphor O, particularly for 1-methyl-cyclopentene compared to cyclohexene, and the bulkiness of the second ring, we can state in general:

$$\delta I_{\text{olef}}\,(\text{cycloalkyl-cycloalkenes}) \leqslant \delta I_{\text{olef}}(\text{cyclohexene}) \qquad (12)$$

The same applies to $\delta(\Delta I)_{\text{olef}}$.

For CW 20 M, we have experimentally $\delta I_{\text{olef}}(\text{cyclohexene}) = 100$, so that,

$$\delta I_{\text{olef}}^{\text{CW 20 M}}(\text{cycloalkyl-cycloalkenes}) \leqslant 100 \qquad (13)$$

We can establish now the retention ranges of these compounds according to equations 9 and 13, by:

$$I^{\text{CW 20 M}}(\text{cycloalkyl-cycloalkene}) \leqslant I^{\text{CW 20 M}}(\text{bicycloalkyl}) + 100 \qquad (14)$$

Table 7 comprises the retention index ranges predicted in this manner on the basis of the data from table 6 (the extension toward the inferior limit is represented by points), and the retention indices found experimentally and assigned as such.

Concerning the value ΔI for cycloalkyl-cycloalkenes, the following results from the above considerations:

$$\Delta I(\text{cycloalkyl-cycloalkene}) \leqslant [\Delta I\ (\text{bicyclohexyl}) + \delta\,(\Delta I)_{\text{olef}}\,(\text{cyclohexene})] \qquad (15)$$

To emphasize that the identification with ΔI values (used for cycloalkylbenzenes, components A and B) is meaningful, in the sense that the three classes of hydrocarbons are clearly distinct on all the stationary

Table 7

Retention indices for the cycloalkyl-cycloalkenes 5 $C_{12}H_{20}$ on CW 20 M, predicted cf. eq. 14 and found experimentally in the products of syntheses 7 and 8 table I and in some of the cyclohexylbenzene samples

cycloalkyl-cycloalkenes derived from :	The range of I predicted	I found experimentally
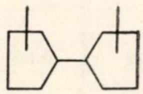	(1100...1365) + 100 = = ...1200...1465	numerous low peaks, difficult to discern from others
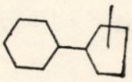	(1365...1430) + 100 = = ...1465...1530	1465, 1487
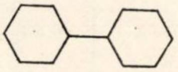	1483 + 100 = ...1583	1513, 1540, 1560, 1570

phases used, the ΔI values are summarized in table 8 ; ΔI for cycloalkylbenzenes is the average value for all isomers, the ΔI for cycloalkyl-cycloalkenes was obtained from equation 15, and the ΔI value of bicyclohexyl was taken as illustrative for bicycloalkyls.

Table 8

The order of magnitude of ΔI values for hydrocarbon classes

	CW 20 M	B 34–DC 710, 1 : 1	B 34–DC 710, 3 : 7
cycloalkylbenzenes	327	97	96
cycloalkyl-cycloalkenes	206	17	20
bicycloalkyls	120	11	13

The use of several stationary phases increase the confidence in assignment. As an example, in table 9 are summarized the quantitative results for the analysis of the same sample on the four columns used ; these are very similar, in spite of the difference in the sequence of elution or even of the superposition of some components. The averages include also the quantities, derived by difference, yielded by the superposed components.

Fig. 1, contains some examples of chromatograms on CW 20 M. Fig. 1a represents a model mixture prepared with available standards. Fig. 1b, represents a typical case of cyclohexylbenzenes analysed samples,

Table 9

Comparison of some quantitative results on the four columns used. Cyclohexylbenzene resulted from the cyclohexylation of benzene with cyclohexene with $AlCl_3 . H_2O$ as catalyst at 25°

	area %				
	CW 20M	B 34-DC 710,1:1	B 34-DC 710,3:7	ApL	average value
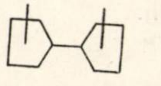	0.02	0.03	0.02	0.05	0.03
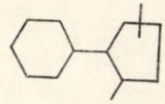	0.06	0.06	0.05	0.17*	0.06
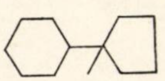	0.04	0.04	0.03	0.03	0.04
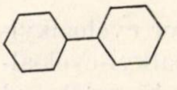	0.48	0.64	0.60	**	0.48
cis- 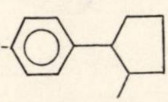	0.14			*	0.13***
trans- 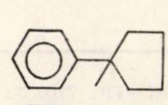	0.29	0.23	0.30	0.26	0.27
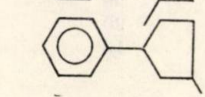	0.05	0.03	0.03	0.04	0.04
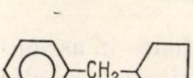	98.92	98.97	98.96	99.45**	98.95***

* 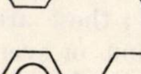 superposed with cis- 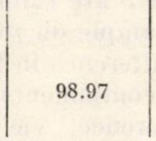

** 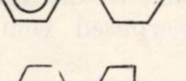 superposed with 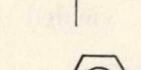

*** — the average value involve also the quantities, derived by difference, yielded by the superposed components.

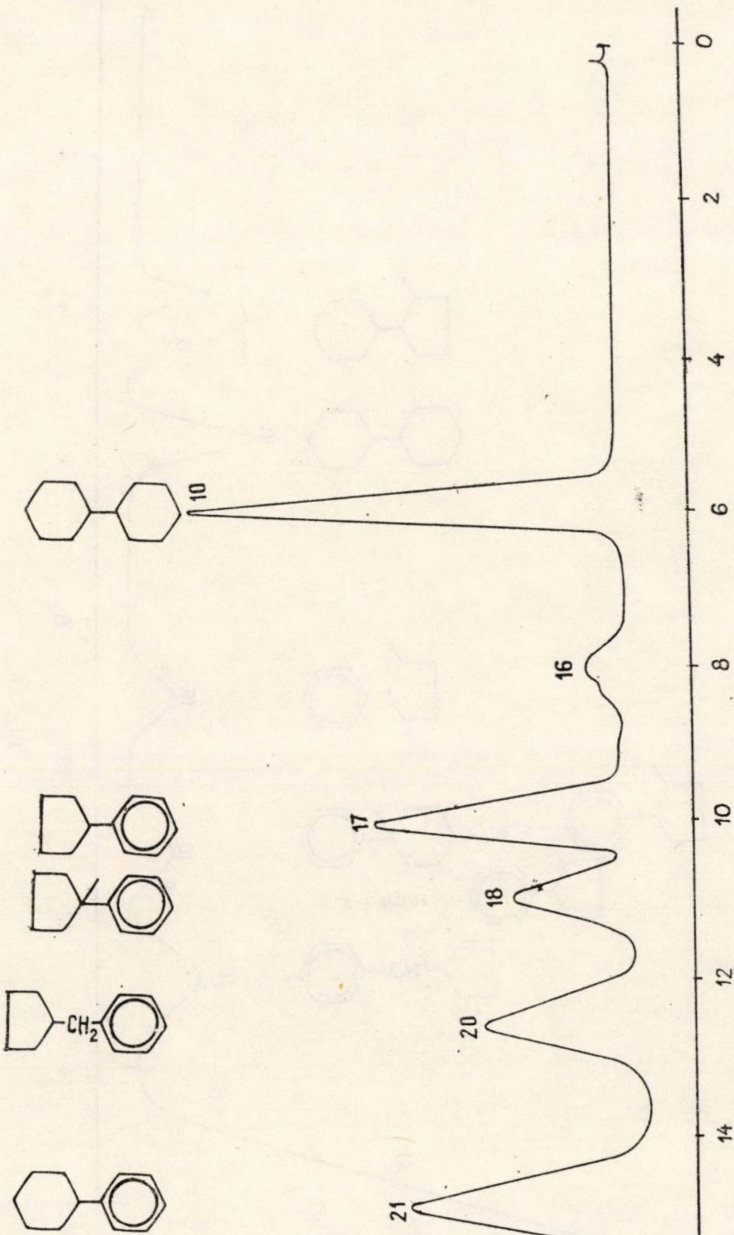

Fig. 1a.

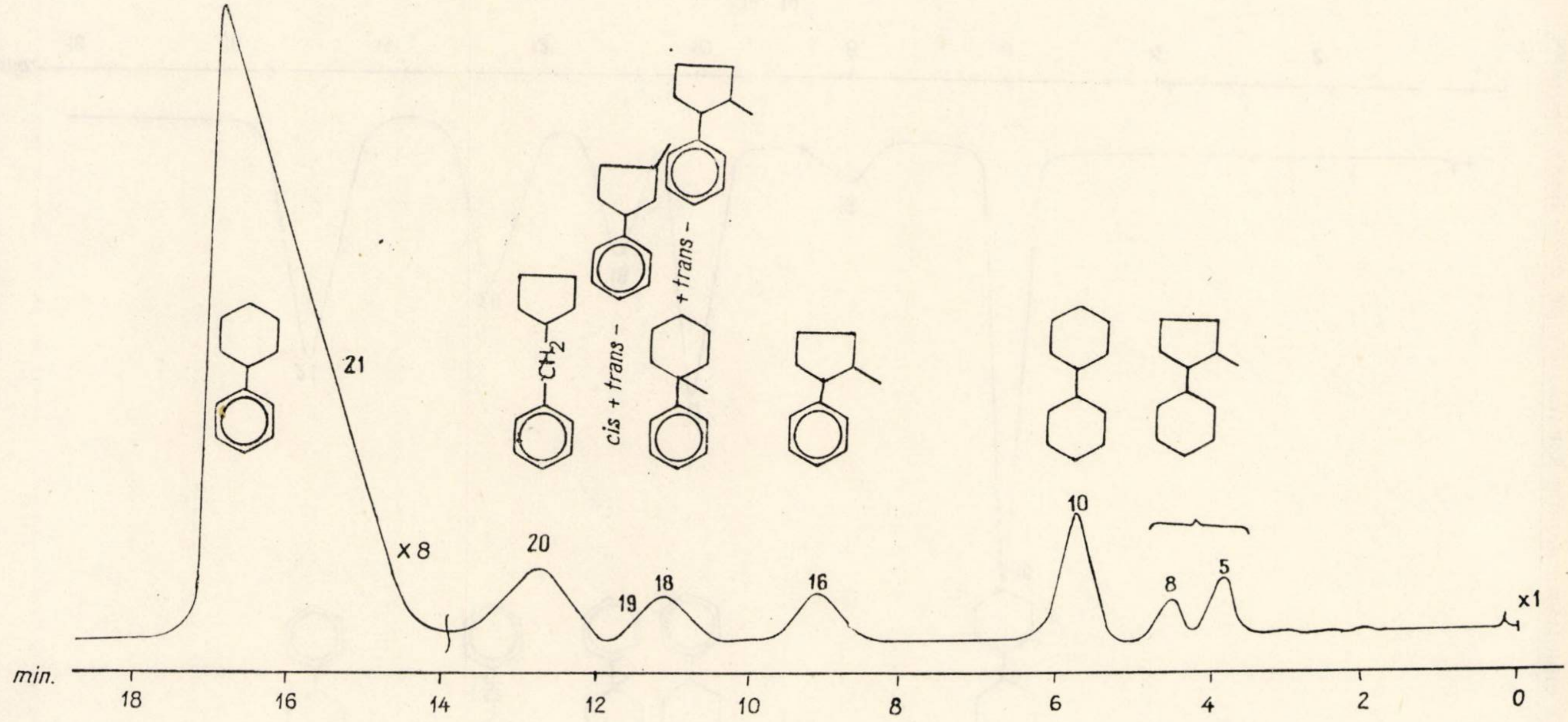
21
X 8
20
CH2
cis + trans -
+ trans -
19
18
16
10
8
5
x1
min.
18
16
14
12
10
8
6
4
2
0

Fig. 1b.

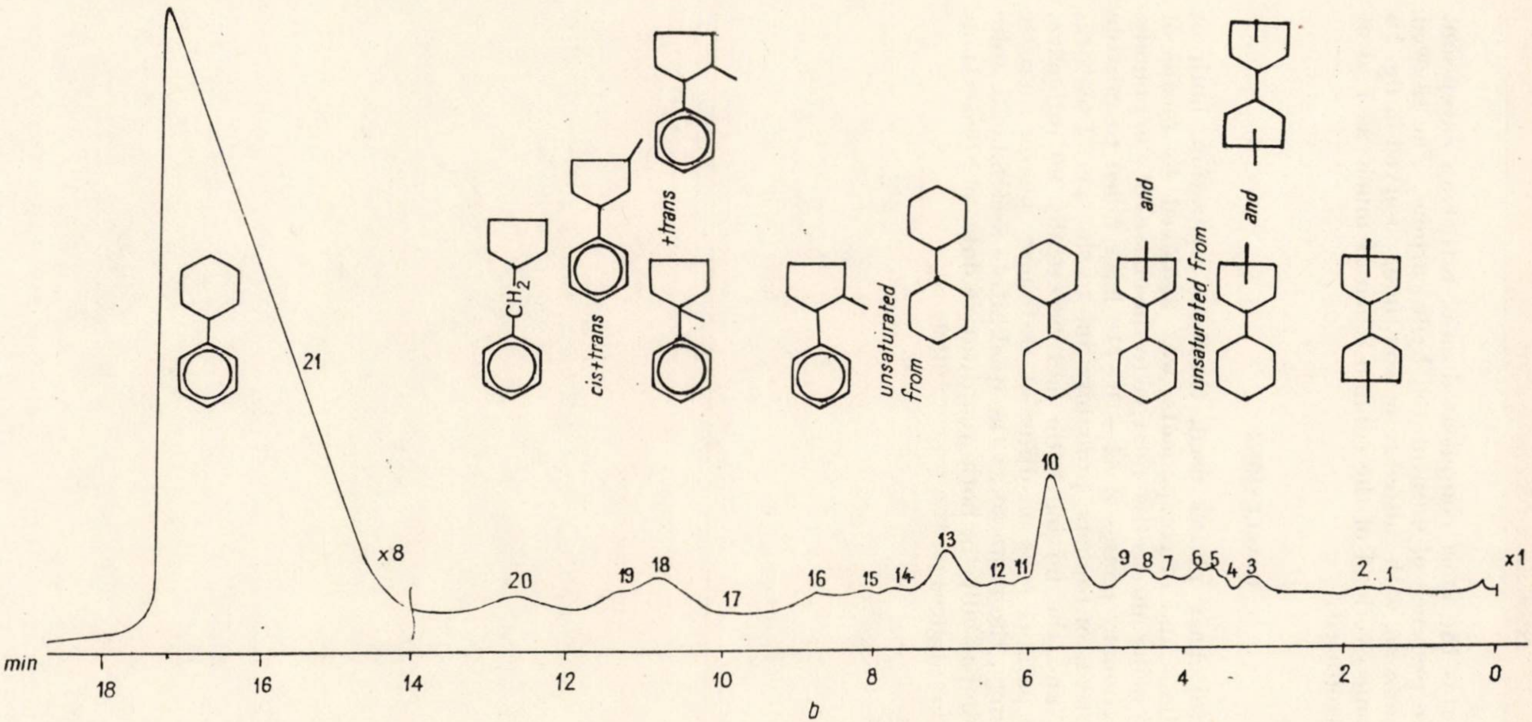

Fig. 1. — Examples of chromatograms obtained on the colum with Carbowax 20 M (see Exeprimental) :

a) model mixture prepared with available standards ; b) and c) ; 1 µl cyclohexylbenzene derived from the alkylation of benzene with cyclohexene in the presence of catalysts ; $AlCl_3$ at 80° (b) and H_2SO_4 at 25° (c). Assignment of GC peaks in the limits specified above ; *1, 2*, bi-(methyl-cyclopentyl)s ; *3, 4, 6, 7, 9*, unsaturated derived from methyl-cyclohexyl-cyclopentanes and bi-(methyl-cyclopentyl)s ; *5, 8*, methyl-cyclohexyl-cyclopentanes ; *10*, bicyclohexyl ; *11 – 15*, unsaturated derived from bicyclohexyl ; *16*, *cis* 2-methyl-cyclopentylbenzene ; *17*, cyclopentylbenzene ; *18*, 1-methyl-cyclopentylbenzene and *trans*-2-methyl-cyclopentylbenzene ; *19*, 3-methyl-cyclopentylbenzene ; *20*, cyclopentyl-phenyl-methane ; *21*, cyclohexylbenzene.

while fig. 1c illustrates the most complicated case, rather an exception, characterized by the presence of unsaturated hydrocarbons. The skewed peak of cyclohexylbenzene, with shifted retention time, observed in fig. 1b and 1c, is due to some overload of the column when as much as 1 μl of pure product is introduced.

CONCLUSIONS

Among the stationary phases used, the best separation, both of classes of hydrocarbons and of components, was achieved by means of CW 20 M, the others being unselective relative to the classes of compounds.

The mixed stationary phases B 34—DC 710 have failed to provide the expected separations of isomers, probabily due to the special features of saturated rings, and the mixing ratio had practically no influence.

However, the parallel runs on different stationary phases increase the degree of certainty, the more so as the qualitative assignments were confirmed by the compatibility of both quantitative data and deductions based on the retention indices on the four columns.

Revue Roumaine de Chimie, **20**, *6*, 831–837 (1975)

CALCULATION OF THE MULTICOMPONENT COPOLYMER COMPOSITION AT HIGH CONVERSIONS

MARGARETA TOMESCU * and CRISTOFOR SIMIONESCU **
* Polytechnic Institute, str Polizu 1, Bucharest, Romania
** "P. Poni" Institute of Macromolecular Chemistry, Aleea Gr. Ghica Vodă 41 A, Iassy, Romania

Received May 22, 1974

The paper describes the mathematical model of free radical multicomponent copolymerization at high conversions. Simplified composition equations have been used, modified in a more convenient form which takes into account the existence in the system of monomers incapable of free radical homopolymerization or of copolymerisation with all the present monomers. Calculated composition data agree with the experimentally determined ones.

1. INTRODUCTION

The possibility for assessing by calculation the copolymer composition has a significant theoretical and practical importance.

Most publications in this field are concerned with binary and ternary copolymerization and a very few refer to copolymerization of systems formed of more than three components. The explanation must be sought in the experimental and calculation difficulties which increase with the rise in the number of components in the system.

If, until recently the number of copolymers formed of more than three components (obtained by synthesis) was restricted to one single quaternary copolymer synthesized in 1945 by Walling and Briggs,[1] numerous patents have lately proposed syntheses of multicomponent copolymers with applications in various fields such as that of synthetic fibres, press sensitive adhesives, synthetic lubricants.

Under these conditions, a critical examination of the existing theoretical data becomes imperative as well as the development of a simple computing model capable of simulating as faithfully as possible the general case of *n* component copolymerization, an objective that we undertake to solve in this note.

---

[1] C. Walling nad E. R. Briggs, *J. Amer. Chem. Soc.*, *67*, 1774 (1945).

2. LOW CONVERSION COPOLYMERIZATION

Mathematical relations, deduced from the kinetic study of copolymerization, describe the dependence of copolymer composition on the composition of the monomers mixture and on their reactivities. For the general case of the copolymerization of *n* component systems, Walling-Briggs' equations [1] were established as well as Fordyce, Ham and Chapin's equations [2] and also the simplified ones deduced by Valvassori and Sartori [3] and separately by Ham. [4] Their experimental verification was achieved on ternary systems and on one single quaternary system of monomers.

We shall try to experimentally verify the validity and the accuracy of composition equations listed for the quaternary copolymerization of mixtures formed of acrylonitrile (AN), methacrylic acid (AM), styrene (S), vinylidene chloride (CV) and acrylonitrile, butyl acrylate (BA), styrene, vinylidene chloride.

The reactivity ratios and the Q—e parameters [5] used in calculations were taken from the literature. [6,7] Calculations were performed for various compositions of the monomer feed. The calculated average compositions of the respective copolymers were compared in table 1 with the experimental data taken from a previous paper. [8] A good agreement was found when using Walling-Briggs' equations and simplified composition equations. Larger deviations of the calculated compositions from the experimental data were observed when applying Fordyce, Chapin and Ham's equations explainable by the semiempirical character of the Q—e scheme and its limited accuracy because it neglects the steric effect.

Taking into account some computing difficulties existing in the copolymer composition calculations by applying Walling-Briggs' equations and the accuracy flaws caused by Fordyce, Ham and Chapin's equations, we consider the use of simplified equations to be more profitable under both aspects.

The simplified composition equations become undetermined when the system includes monomers with negligible rates of self-propagation reactions. In such cases, some of the reactivity ratios approach zero value. To solve these cases one can apply the special equations established by us in a previous note. [9] These equations are valid for any monomer system regardless of the number of components and of the presence and the number of monomers incapable of free radicalic homopolymerization, such as

---

[2] E. C. Chapin, G. E. Ham and R. G. Fordyce, *J. Amer. Chem. Soc.*, **70**, 538 (1948).

[3] A. Valvassori and G. Sartori, *Rend. Inst. Lombardo Sci.* **A 96**, 107 (1962).

[4] G. E. Ham, *J. Polymer Sci.*, **A 2**, 2735 (1964).

[5] T. Alfrey and C. C. Price, *J. Polymer Sci.*, 3, 772 (1948).

[6] L. J. Young, *J. Polymer Sci.*, **54**, 411 (1961).

[7] Cr. Simionescu, N. Asandei and A. Liga, *Makromol. Chem.*, **110**, 278 (1967).

[8] Cr. Simionescu and M. Tomescu, *Makromol. Chem.*, **175**, 000 (1975).

[9] M. Tomescu and Cr. Simionescu, *European Polymer J.*, in press.

Table 1

Experimental verification of copolymer composition differential equations for n component system

Monomers system	Monomer feed mole fraction	Conversion %	Initial copolymer composition, mole fraction			
			Calcd. by Walling-Briggs' eqn.[1]	Cald. by simplified eqn.	Calcd. by Fordyce, Ham, Chapin's eqn.[2]	Experimental
AN	0.7000	2.23	0.4131	0.4180	0.4068	0.4369
AM	0.1000		0.2198	0.2027	0.2502	0.2172
S	0.1000		0.3389	0.3593	0.3160	0.3242
CV	0.1000		0.0282	0.0200	0.0270	0.0217
AN	0.6000	5.03	0.3723	0.3649	0.3604	0.3612
AM	0.1000		0.1621	0.2052	0.2162	0.1818
S	0.2000		0.4512	0.4167	0.4019	0.4403
CV	0.1000		0.0144	0.0132	0.0215	0.0167
AN	0.4000	2.70	0.3653	0.3722	0.3356	0.3568
BA	0.3000		0.1532	0.1368	0.2054	0.1500
S	0.1000		0.4133	0.4387	0.3924	0.4280
CV	0.2000		0.0772	0.0523	0.0666	0.0652
AN	0.2000	3.62	0.2297	0.2546	0.2108	0.2412
BA	0.3000		0.2087	0.1831	0.2556	0.2120
S	0.1000		0.4496	0.4422	0.3778	0.4168
CV	0.4000		0.1120	0.1201	0.1558	0.1300
AN	0.3000	3.90	0.3322	0.3239	0.2863	0.3433
BA	0.3000		0.1810	0.1538	0.2334	0.1413
S	0.1000		0.4226	0.4391	0.3725	0.4130
CV	0.3000		0.0642	0.0832	0.1078	0.1024

$M_{h_1} \ldots M_{h_k}$ or of monomers incapable of participating in copolymerization reactions with all the other monomers in the system, such as $M_{j_1} \ldots M_{j_s}$:

$$\begin{aligned}
d[M_1] : d[M_2] : \ldots : d[M_n] = [m_1] : [m_2] : \ldots : [m_n] = & \\
& [M_1] \sum_{i=1}^{n} \frac{[M_i]}{r_{1i}} : \\
& : \frac{[M_2]}{r_{12}} \sum_{i=1}^{n} [M_i] \frac{r_{21}}{r_{2i}} : \\
& \ldots\ldots\ldots\ldots \\
& : \frac{[M_{h_1}]}{r_{1h_1}} \sum_{i=1}^{n} [M_i] R_{h_1 1i} : \\
& \ldots\ldots\ldots\ldots \\
& : \frac{[M_{h_k}]}{r_{1h_k}} \sum_{i=1}^{n} [M_i] R_{h_k 1i} : \\
& \ldots\ldots\ldots\ldots \qquad (1)
\end{aligned}$$

$$: [M_{j_1}] \sum_{\substack{i=1 \\ i \neq j_1, \ldots, j_s}}^{n} \frac{[M_i]}{r_{1i}} \cdot \frac{r_{i1}}{r_{ij_1}} :$$

$$\cdots\cdots\cdots\cdots$$

$$: [M_{j_s}] \sum_{\substack{i=1 \\ i \neq j_1, \ldots, j_s}}^{n} \frac{[M_i]}{r_{1i}} \cdot \frac{r_{i1}}{r_{ij_s}} :$$

$$\cdots\cdots\cdots\cdots$$

$$: \frac{[M_n]}{r_{1n}} \sum_{i=1}^{n} [M_i] \frac{r_{n1}}{r_{ni}}$$

In equations (1) we noted by $[m]$ the instantaneous copolymer composition in molar fractions, by $[M]$ the monomer mixture composition in molar fractions, by r_{ij} the binary reactivity ratios. The multicomponent copolymerization constants $R_{h1i} = r_{h1}/r_{hi} = k_{hi}/k_{h1}$ may be determined from multicomponent copolymerization data or can be estimated from Q—e value.[10] Rate constants of the macromolecular chain growth reactions were noted by k.

3. HIGH CONVERSION COPOLYMERIZATION

Differential composition equations may be applied only for the initial copolymerization step for conversions below 3—5% when the copolymer composition may be practically considered unvariable.

At higher conversions, due to the different monomer reactivities, modifications appear in the composition of the monomer mixture which determine changes in the copolymer composition.

The dependence of the copolymer composition on conversion may be evaluated by the integration of composition differential equations. The literature has postulated analytical, graphical and numerical integration methods,[1,11–18] the latter being widely used in parallel with the introduction of computers in chemical research.

In this note we propose the integration of composition simplified equations rewritten so as to be more convenient for a numerical calculation in successive steps.

To illustrate the method we consider a system in which all the reactivity ratios are non—zero.

[10] G. E. Ham, *J. Polymer Sci.*, **A 2**, 4191 (1964).

[11] A. Kumar, *J. Appl. Polymer Sci.*, **12**, 1853 (1968).

[12] V. E. Meyer and G. G. Lowry, *J. Polymer Sci.*, **A 3**, 2843 (1965).

[13] I. Skeist, *J. Amer. Chem. Soc.*, **68**, 1781 (1946).

[14] J. Crescentini, G. Gechele and A. Zanello, *Appl. Polymer Sci.*, **9**, 1323 (1965).

[15] E. Friedman, *J. Polymer Sci.*, **C 3**, 815 (1965).

[16] K. R. Chan and E. V. Meyer, *J. Polymer Sci.*, **C 25**, 11 (1968).

[17] J. A. Seiner, *J. Polymer Sci.*, **A 3**, 2401 (1965).

[18] P. Wittmer, F. Haffner and H. Gerrens, *Makromol. Chem.*, **104**, 101 (1967).

If we consider relation :

$$m_z = \mathrm{d}[M_z]/\mathrm{d}\left(\sum_{i=1}^{n} \mathrm{d}[M_i]\right) \tag{2}$$

which defines the instantaneous polymer mole fraction M_z as the ratio between the consumption rate of M_1 and the consumption rate of all n monomers in the system, and apply it to simplified composition equations we obtain :

$$m_z = \frac{[M_z]\dfrac{r_{z1}}{r_{1z}}\sum\limits_{i=1}^{n}[M_i]r_{zi}^{-1}}{\sum\limits_{\substack{i=1\\ j=1}}^{n}[M_j]\dfrac{r_{ji}}{r_{ij}}\left([M_i]r_{ji}^{-1}\right)} \tag{3}$$

$z = 1, 2, \ldots, n$

The set of equations (3) which describes the instantaneous copolymer composition $[m_z]$ during polymerization of a n component system provides the advantage of a simple mathematical formulation accessible to timely numerical calculation.

It is assumed that over a very low conversion interval $\Delta\alpha$, the copolymer composition does not vary. The accuracy of calculation depends on the size of the incremental conversion.[15,16] It has been found that the use of 1 % mole incremental conversion does not introduce significant errors in the results obtained and the reduction of the increment below 1 % mole will not significantly increase the accuracy of results.

The composition of the unreacted monomers mixture at a calculation step "t" is described by the relation suggested by Seiner[17] :

$$[M_z]_t = [M_z]_0 - [m_z^*]_t \alpha_t/(1 - \alpha_t) \tag{4}$$

The zero indices correspond to the initial state and indices "t" correspond to the respective calculation step.

We noted by $[m_z^*]_t$ the average mole fraction of monomer z in the copolymer cumulated to the calculation step "t" and by $\alpha = t\Delta\alpha$ the molar conversion.

The calculation is repeated until the specified final conversion has been obtained, thus establishing the dependence between conversion and instantaneous copolymer composition, respectively average composition of the copolymer or of the monomers mixture.

Compared to toilsome methods of numerical integration such as the Runge-Kutta method advanced by some publications[16,18] for copolymer composition calculations at high conversions, the proposed numerical method is simple and adequate to a rapid calculation, even if it cannot be computerized.

The above-formulated calculation hypotheses were experimentally verified for the systems acrylonitrile-methacrylic acid-styrene-vinylidene chloride and acrylonitrile-butyl acrylate-styrene-vinylidene chloride. Experimental composition data obtained in the previous work were used. [8] The reactivity ratios used in the calculation were taken from the literature. [6] Calculations were performed on an IBM 360 computer by programming the mathematical relations in a FORTRAN IV language.

Table 2

Comparison between the average composition of quaternary copolymers established experimentally and by calculation

Monomers system	Monomer feed mole fraction	Conversion %	Copolymer composition, %							
			experimental				calculated			
			AN	M*	S	CV	AN	M*	S	CV
AN AM S CV	0.7 0.1 0.1 0.1	2.85	30.10	24.10	43.45	2.35	28.26	22.13	47.24	2.37
		11.53	31.00	22.07	43.33	3.60	29.19	22.46	45.71	2.64
		32.90	34.70	22.10	37.90	5.30	32.36	23.61	40.37	3.66
		46.01	37.80	24.60	31.70	5.90	36.63	24.20	33.80	5.37
		55.14	42.52	21.98	27.50	8.00	40.82	23.01	28.93	7.24
		66.00	47.70	18.20	25.78	8.32	46.65	19.61	23.78	9.96
		79.80	53.80	13.56	22.14	10.50	51.05	16.69	20.21	12.05
AN AM S CV	0.6 0.1 0.2 0.1	5.02	23.48	19.10	55.52	1.90	24.29	16.97	56.99	1.75
		11.00	23.70	19.30	54.49	2.51	24.59	16.96	56.62	1.83
		21.38	26.40	17.10	53.75	2.75	25.21	16.96	55.83	2.00
		31.47	27.00	17.37	51.78	3.85	25.95	17.02	54.82	2.21
		48.32	28.30	17.30	48.78	5.62	27.69	17.32	52.13	3.86
		62.61	32.40	18.40	43.19	6.01	30.98	17.85	46.66	4.51
		78.55	36.70	15.30	40.50	7.50	38.10	15.48	37.51	8.91
AN BA S CV	0.4 0.3 0.2 0.1	2.70	21.24	21.70	49.86	7.20	22.78	19.73	51.57	5.92
		10.73	21.50	23.13	46.96	8.41	22.91	21.51	48.98	6.60
		26.63	22.57	28.60	37.49	11.34	23.40	27.68	39.86	9.06
		38.99	23.66	34.40	28.95	12.99	23.93	34.22	30.01	11.84
		58.79	23.66	41.28	18.52	16.54	24.39	40.61	19.84	15.16
		71.87	23.88	44.00	14.87	17.25	24.44	42.59	16.23	16.74
		82.67	24.35	45.12	12.37	18.16	24.40	43.49	14.06	18.05
AN BA S CV	0.3 0.3 0.1 0.3	3.90	20.02	19.81	49.24	10.93	18.93	22.31	49.56	9.20
		9.01	19.13	22.40	46.95	11.52	18.90	23.45	47.87	9.78
		15.52	19.13	24.84	43.73	12.30	18.86	25.46	44.85	10.83
		31.79	18.54	31.04	35.67	14.75	18.78	32.52	34.00	14.70
		45.12	18.94	36.46	24.67	19.93	18.70	38.15	24.92	18.23
		66.50	18.62	41.11	16.44	23.83	18.43	42.49	16.64	22.44
		74.50	18.39	43.31	13.30	25.00	18.28	43.07	14.85	23.80

M*, AM or BA

Table 2 which comparatively presents the values found by calculation and experimental composition data shows a good agreement.

The conclusion must be accepted that the developed calculation model describes with an acceptable accuracy the composition of multicomponent copolymers which obey the classical terminal kinetic scheme of free radicalic copolymerization.

The accuracy of theoretical data assessed by the above calculation relations depends on a judicious selection of the most accurate values for the reactivity ratios, on the choice of the method of chemical analysis and on a careful examination for each studied system of simplifying hypotheses that had been adopted by the classical kinetic scheme of copolymerization.

Considering these observations it results that the calculation relations presented provide the possibility for predicting the monomers behaviour in multicomponent polymerization, supplying information on the compositional modifications which take place in the copolymer chain.

Revue Roumaine de Chimie, **20**, *6*, 831–837 (1975)

Revue Roumaine de Chimie, **20**, *6*, 839–854 (1975)

LA DÉGRADATION DES ÉCHANGEURS D'ANIONS DANS DES MILIEUX AGRESSIFS. I

L'ACTION DE L'EAU OXYGÉNÉE EN PRÉSENCE DU $CuSO_4$ SUR LES ÉCHANGEURS D'ANIONS FORTEMENT BASIQUES DE TYPE I

I. PETRARIU, PAMFILIA PETRARIU, FL. POPESCU et CORNELIA LUCA
Institut de Chimie Macromoléculaire » Petru Poni » Jassy, 41 A,
Aleea Gr. Ghica Vodă

Reçu le 4 mars 1974

On a étudié l'influence de la température, de la concentration de l'eau oxygénée, du temps de contact entre l'agent oxydant et l'échangeur d'anions, de sa forme ionique et aussi de la présence du $CuSO_4$, sur la stabilité chimique d'un anionite fortement basique de type I, le chlorure de poly(vinylbenzyltriméthylammonium). On a mis en évidence aussi la corrélation des conditions de dégradation avec la structure des groupes fonctionnels, ainsi que le changement du rapport entre les groupes faiblement et fortement basiques pendant la dégradation. Les caractéristiques physico-chimiques de l'échangeur d'anions dégradé de type I ont été estimées par la capacité d'échange, les spectres IR et les analyses thermiques.

Le développement à grande échelle de la production des échangeurs d'anions fortement basiques pour une série d'industries, ainsi que leur emploi de plus en plus fréquent dans des buts analytiques ou scientifiques ont posé le problème de connaître leur stabilité chimique dans différents milieux agressifs : acides, oxydants, réducteurs, etc.

La littérature de spécialité indique certaines solutions oxydantes, par exemple l'hypochlorite de sodium [1-2] pour l'élution plus avancée des matières organiques retenues sur un échangeur d'anions, l'eau oxygénée pour l'élution du germanium, du titanium et du molybdène, [3] les solutions d'acide azotique avec addition de perbromate de potassium pour la désorption du neptunium, [4] les solutions d'acide perchlorique pour l'élution du sodium et du potassium, [5-6] etc.

---

[1] R. V. Skold et J. F. Wilkes, *Ind. Eng. Chem.*, **47**, 90 (1955).

[2] S. Iwashina, T. Miyao et T. Asami, *Proc. Research Soc. Jap. Sugar Ref. Technol.*, **6**, 23 (1957).

[3] T. N. E. Strelow, *Anal. Chim.*, **35**, 1297 (1963).

[4] E. N. Kazantev, P. I. Condrasov, B. S. Calinichenco et A.A. Galman, *Radiokhimiya*, **4**, 81 (1962).

[5] K. A. Kraus, F. Nelson et G. W. Smith, *J. Phys. Chem.*, **58**, 11 (1954).

[6] I. Danon, *J. Amer. Chem. Soc.*, **78**, 5953 (1956).

Ces oxydants provoquent aussi des effets secondaires de dégradation chimique qui modifient dans une certaine mesure la structure des groupes basiques des échangeurs d'anions. Ainsi, à des concentrations plus grandes ils peuvent produire des transformations même au niveau du réseau macromoléculaire.

Dans la littérature sont données une série d'informations sur la stabilité des échangeurs d'anions fortement basiques de type I dans des milieux oxydants [7-12] ou sous l'influence de l'oxygène dissous dans l'eau [13] ou de l'oxygène de l'air [14] sur ceux-ci.

L'existence en petites quantités de certains métaux comme le fer, le cobalt, le cuivre, etc. englobés dans la matrice des échangeurs d'anions, consécutivement au processus de fabrication, ainsi que leur présence dans différents milieux agressifs dans lesquels ces échangeurs fonctionnent, provoquent un puissant effet catalytique de dégradation.

Le présent travail étudie les transformations chimiques qui ont lieu dans la structure d'un échangeur d'anions fortement basique de type I, dégradé dans l'eau oxygénée, en présence et en l'absence du $CuSO_4$.

Les conditions pour la synthèse de l'échangeur d'anions fortement basique, gel, de type I, sont données dans des travaux antérieurs. [15-16]

MÉTHODES D'EXPÉRIMENTATION

Les perles d'anionite ont été tamisées. On a utilisé la fraction comprise entre 0,4—0,8 mm. Pour éliminer les traces d'impuretés englobées dans l'anionite, celui-ci a été introduit dans une colonne d'échange ionique et traité successivement à l'HCl 4%, lavé à de l'eau distillée, lavé ensuite au NaOH 4% et finalement de nouveau à de l'eau distillée exempte de CO_2, jusqu'à la réaction neutre à la phénolphtaléine. [17]

L'anionite ainsi préparé a été séché dans un exsiccateur en présence de $CaCl_2$ anhydre et de KOH jusqu'au poids constant. Une autre quantité d'anionite a été transformée sous forme de Cl^- avec de l'HCl 4% et lavé à de l'eau distillée jusqu'à la disparition de l'ion chlore de l'élué. L'épreuve a été séchée dans l'air jusqu'au poids constant.

De chaque épreuve ainsi préparée on a prélevé un gramme d'anionite qui a été introduit dans un ballon de 50 millilitres, prévu d'un réfrigérant ascendant. On a ensuite ajouté 10 ml d'eau oxygénée d'une concentration variant de 10 à 30%.

D'autres épreuves ont été dégradées dans un milieu agressif formé de 10 ml de H_2O_2 30% et 0,0188 g de $CuSO_4 \cdot 5H_2O$. La dégradation a eu lieu soit à la température ambiante et dans l'obscurité soit à la lumière, à 40—80°, dans un intervalle de temps compris entre 10 à 432 heures.

[7] A. C. Reents et F. H. Kahler, *Ind. Eng. Chem.*, **47**, 75 (1955).

[8] E. I. Kozantsev, *Zhur. priklad. Khim.*, **35**, 2567 (1962).

[9] A. S. Konishcheva, N. M. Morozov et K. M. Olishanova, Sb. « Sintez i Svoistva Ionoobmennykh Materialov », Moscou, 1968, S. 115.

[10] H. V. Bichikov, A. I. Kasperovichi et B. S. Roginskaia, *Zhur. fiz. Khim.*, **43**, 2522 (1969).

[11] I. Petrariu, O. Petreuş, A. Carpov, C. Luca et M. Dima, *Rev. Chim.* (Bucureşti), **22**, 177 (1971).

[12] V. M. Vinogradov, E. I. Kazantev et O. N. Chupakhin, *Zhur. priklad. Khim.*, **45**, 1042 (1972).

[13] R. Kunin et N. W. Frisch, *Ind. Eng. Chem.*, **49**, 1365 (1957).

[14] Z. Vasicek, J. Stamberg et O. Dufka, *Coll. Czech. Chem. Comm.*, **36**, 1817 (1971).

[15] I. Petrariu et J. Stamberg, *Coll. Czech. Chem. Comm.*, **32**, 798 (1967).

[16] I. Petrariu, P. Petrariu et C. Luca, *Materiale Plastice*, **7**, 71 (1970).

[17] I. Petrariu, « Thèse », Académie Tchécoslovaque des Sciences, Prague 1964.

Après réaction, les perles d'anionite ont été introduites dans des colonnettes prévues de frittes, lavées à de l'eau distillée et ensuite transformées en cycle chlore avec de l'HCl 4% et de nouveau lavées à du méthanol jusqu'à neutralité. En final, on a déterminé la capacité d'échange fortement basique (C_{pb}) et faiblement basique (C_{sb}).[18] Leur somme a donné la capacité totale (C_t).

Le coefficient de basicité K_b a été défini comme le rapport entre la capacité fortement basique et la capacité totale (C_{pb}/C_t).

Le coefficient K_b' représente le rapport entre la capacité fortement basique obtenue après la dégradation de l'anionite à un certain moment (C_{pb}) et la capacité fortement basique initiale (C_{pbi}) et est défini par le rapport C_{pb}/C_{pbi}.

Les pertes de la capacité d'échange dues à la réaction de désalcoylation ont été calculées de la croissance de la capacité d'échange faiblement basique. Les pertes de la capacité d'échange dues à la réaction de désamination ont été calculées en utilisant les différences entre les pertes de capacité dues aux groupes fortement basiques et la croissance de la capacité due aux groupes faiblement basiques.

Ainsi, on a fait des considérations sur les transformations chimiques subies par les anionites pendant la dégradation, à l'aide de l'analyse des spectres IR effectuée avec un spectrophotomètre SP 200. La préparation des épreuves pour l'analyse a été faite par pastillage avec du bromure de potassium.

L'analyse thermogravimétrique a été réalisée avec un dérivatographe Paulik-Paulik-Erdey, en présence de l'air, avec une vitesse d'échauffement de 9,8°/mn.

Les caractéristiques physico-chimiques de l'échangeur d'anions fortement basique de type I soumis à la dégradation sont données dans le tableau 1.

Tableau 1

Caractéristiques physico-chimiques de l'échangeur d'anions fortement basique de type I

Caractéristiques	Unité de mesure	Valeur
Groupe fonctionnel	$-N(CH_3)_3^+$	
Support polymérique	styrène-divinylbenzène	
Forme ionique d'expérimentation	Cl et OH	
Poids volumétrique (humidité 14,5%)	Kg/m³	710
Granulation	mm	0,4–0,8
Domaine de pH	–	0 – 14
Teneur totale en azote déterminée par analyse élémentaire	%N	5,2
Capacité d'échange totale calculée d'après la teneur en azote	méq/g	3,71
Capacité d'échange totale déterminée par la méthode dynamique	méq/g	3,62
a. Capacité d'échange fortement basique	méq/g	3,25
b. Capacité d'échange faiblement basique	méq/g	0,37
Température maximale d'utilisation	°C	50

---

[13] J. Stamberg et F. Yurachica, *Zhur. priklad. Khim.*, **35**, 2295 (1962).

RÉSULTATS ET DISCUSSIONS

Les échangeurs d'anions fortement basiques utilisés dans des différentes installations industrielles perdent graduellement leur capacité d'échange, soit à cause de certaines rétentions de substances organiques soit à cause de certaines dégradations chimiques. Dans des travaux antérieurs [11,15,16] on a montré que, consécutivement à l'interaction de l'agent agressif et des échangeurs d'anions, fonction des conditions de dégradation trois processus importants sont possibles :

1. Une réaction de désamination qui conduit à la scission du groupe $-N(CH_3)_3$, sur le squelette macromoléculaire résultant de l'alcool benzylique qui ne participe pas à l'échange ionique.

2. Une réaction de désalcoylation qui conduit à la scission à l'azote quaternaire, d'un groupement alcoyle sous forme d'halogénure de méthyle ou d'alcool méthylique.

Le groupement fonctionnel fortement basique se transforme dans un groupement faiblement basique et en conséquence la capacité fortement basique (C_{pb}) s'amincie, tandis que celle faiblement basique (C_{sb}) s'accroît.

3. Une réaction de dégradation du réseau macromoléculaire qui conduit à l'abaissement du degré de réticulation du polymère. Dans des conditions plus sévères le polyélectrolyte réticulé peut se détruire jusqu'à sa totale dissolution dans le milieu de la réaction.

Le processus de dégradation indiqué plus haut devient plus compliqué, en présence de l'eau oxygénée, résultant une série de produits d'oxydation (mis en évidence par l'analyse IR) parmi lesquels nous mentionnons l'alcool polyvinylbenzylique, ou le polyvinylbenzaldéhyde qui forment des segments de chaîne sans capacité d'échange ionique.

Il se forme aussi une quantité réduite de groupes faiblement acides à côté de ceux faiblement ou fortement basiques et le caractère du produit devient amphotère.

En analysant la solution d'eau oxygénée qui a servi comme milieu de dégradation pour l'anionite, on a trouvé des quantités plus réduites de triméthylamine que celles qui doivent résulter des pertes de capacité déterminées sur l'anionite. Cela montre qu'une grande quantité de $-N(CH_3)_3$ résultée de la dégradation a été oxydée. On a identifié aussi du formaldéhyde résulté de l'oxydation du méthanol scindé par la réaction de désalcoylation. Ce mécanisme de dégradation confirme celui indiqué par Vašiček et collab., [14] qui ont dégradé en milieu de NaOH et atmosphère d'oxygène l'hydroxyde d'isopropylbenzyltriméthylammonium et l'hydroxyde de benzyltriméthylammonium.

Le processus de dégradation en présence de l'eau oxygénée peut être représenté ainsi :

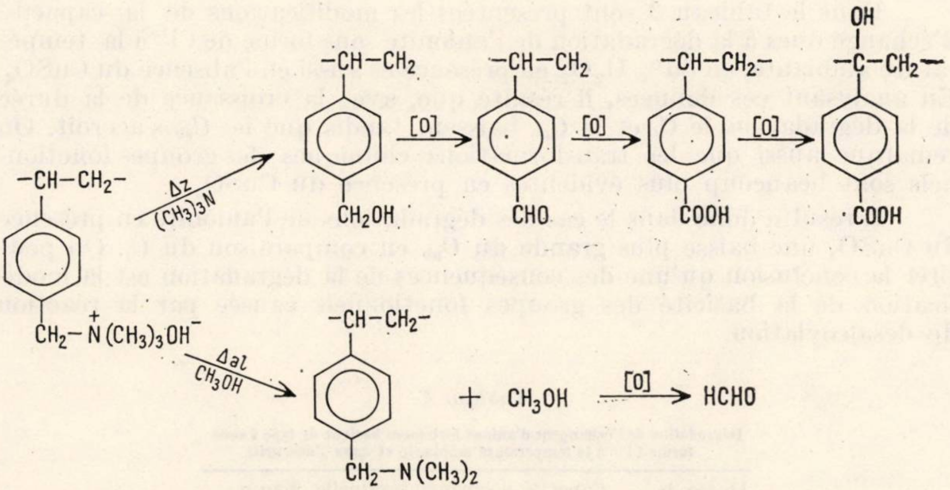

L'interaction de l'eau oxygénée et des échangeurs d'anions fortement basiques de type I donnent lieu à trois processus principaux[10] :

1. L'absorption de l'eau oxygénée par les anionites.
2. La décomposition de l'anionite sous l'action de l'eau oxygénée.
3. La décomposition catalytique de l'eau oxygénée.

Dans le présent travail on a constaté que la dégradation des groupes actifs et du squelette macromoléculaire croît considérablement avec la croissance de la température de dégradation, la concentration en eau oxygénée et l'addition du $CuSO_4$.

Des données présentées au tableau 2, il résulte qu'avec la croissance de la concentration en eau oxygénée, la durée de dégradation et l'addition du $CuSO_4$ la stabilité chimique de l'anionité décroît. Parmi ces trois facteurs qui contribuent à la dégradation, la présence du $CuSO_4$ dans le milieu de réaction joue un rôle des plus importants, activant catalytiquement la décomposition de l'eau oxygénée, respectivement accélérant le processus de dégradation.

Tableau 2

Dégradation de l'échangeur d'anions fortement basique de type I, forme Cl−, à la lumière et à la température ambiante, en H_2O_2 en présence et en l'absence du $CuSO_4$

Concentration en H_2O_2 %	Durée de la dégradation heures	K % en l'absence du $CuSO_4$	K % en présence du $CuSO_4$
10	24	0,29	—
20	24	1,14	9,69
20	48	1,43	11,01
20	72	3,42	—
20	120	7,69	—
30	24	3,15	17,38

Dans le tableau 3 sont présentées les modifications de la capacité d'échange dues à la dégradation de l'anionite sous forme de Cl^- à la température ambiante, en 30 % H_2O_2, en présence et aussi en l'absence du $CuSO_4$. En analysant ces données, il résulte que, avec la croissance de la durée de la dégradation, le C_t et le C_{pb} baissent tandis que le C_{sb} s'accroît. On remarque aussi que les transformations chimiques des groupes fonctionnels sont beaucoup plus évidentes en présence du $CuSO_4$.

Il résulte donc dans le cas des dégradations de l'anionite en présence du $CuSO_4$ une baisse plus grande du C_{pb} en comparaison du C_t. On peut tirer la conclusion qu'une des conséquences de la dégradation est la modification de la basicité des groupes fonctionnels causée par la réaction de désalcoylation.

Tableau 3

Dégradation de l'échangeur d'anions fortement basique de type I sous forme Cl− à la température ambiante et dans l'obscurité

Durée de la dégradation jours	Capacité d'échange résiduelle méq/g					
	En H_2O_2 30 %			En H_2O_2 30 % + $CuSO_4$		
	C_{sb}	C_{pb}	C_t	C_{sb}	C_{pb}	C_i
—	0,37*	3,25*	3,62*	0,37*	3,25*	3,62*
2	0,36	3,17	3,53	0,73	2,42	3,15
8	0,40	3,15	3,45	0,92	0,76	1,68
18	0,38	3,14	3,52	0,89	0,07	0,96

* Valeurs de la capacité d'échange initiale de l'anionite non dégradé.

Si on représente les pertes de la capacité d'échange dues à la réaction de désamination ou de désalcoylation on constate que la dégradation de l'anionite par les deux processus est aussi beaucoup plus accusée en présence du $CuSO_4$ (fig. 1).

Le processus de désamination présente un grand intérêt parce que, avec l'élimination de $-N(CH_3)_3$, les chaînes macromoléculaires en perdant leurs groupes ionogènes deviennent inertes, fait mis en évidence par la baisse rapide du C_{pb}, respectivement du C_t. Dans le cas de la dégradation de l'anionite dans le H_2O_2 et en l'absence du $CuSO_4$, les pertes de la capacité d'échange dues à la réaction de désamination sont relativement petites. Celles qui proviennent de la réaction de désalcoylation sont insignifiantes.

Les coefficients de basicité K_b et K_b' (fig. 2) varient entre des limites relativement restreintes pour les dégradations effectuées dans le H_2O_2 30 %. La croissance du temps de dégradation a aussi un effet très limité sur la modification de ces coefficients (fig. 2, courbes *1* et *2*).

Si la dégradation a lieu dans l' H_2O_2 30 % et en présence du $CuSO_4$, les valeurs des coefficients de basicité baissent sensiblement (fig. 2, courbes *3* et *4*), indiquant ainsi des modifications importantes dans la nature des groupes basiques.

Dans une autre série d'expérimentations, on a étudié les pertes dans la capacité d'échange en fonction de la température de dégradation et de la forme ionique des anionites.

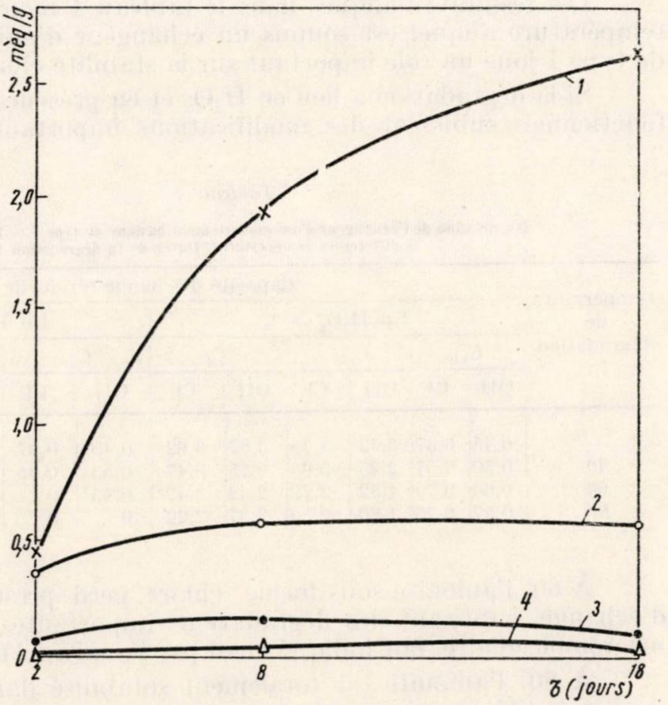

Fig. 1. — Variation de la capacité d'échange dans le processus de dégradation de l'anionite.

Conditions de dégradation ; 30% H_2O_2 avec ou sans $CuSO_4$, dans l'obscurité et à la température ambiante. Variations dues ; *1*, à la réaction de désamination dans le mélange H_2O_2 30% + $CuSO_4$; *2*, à la réaction de désalcoylation dans le mélange H_2O_2 30% + $CuSO_4$; *3*, à la réaction de désamination en H_2O_2 30% ; *4*, à la réaction de désalcoylation en H_2O_2 30%.

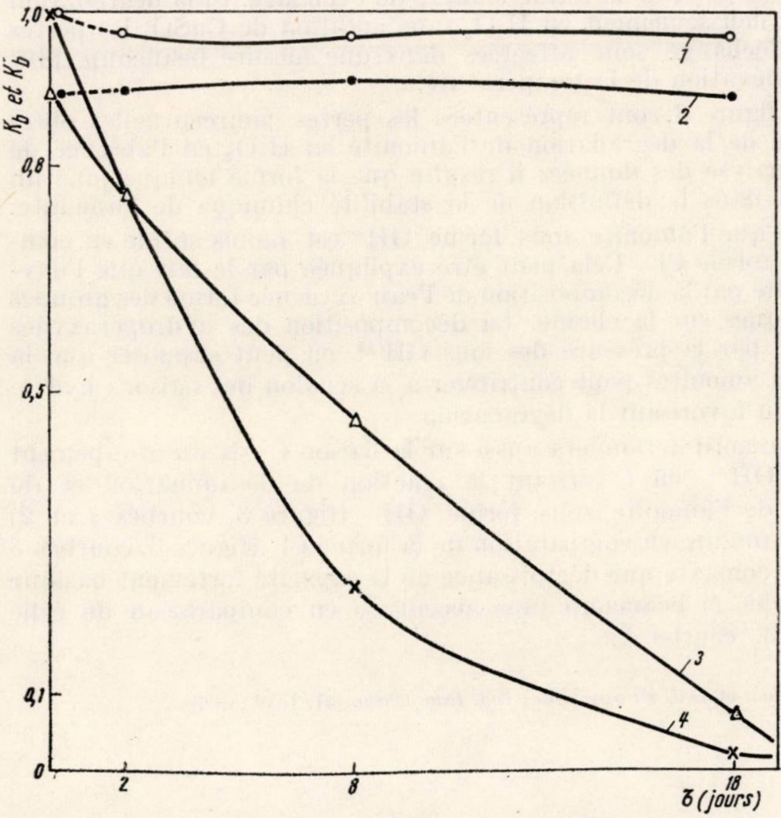

Fig. 2. — Variation des coefficients de basicité K_b et K'_b en fonction de la durée de dégradation.

Conditions de dégradation ; température ambiante et obscurité.

1 et *4* = K_b ; *2* et *3* = K'_b

1 et *2* = H_2O_2 30% ; *3* et *4* = H_2O_2 30% + $CuSO_4$

Les résultats indiqués dans le tableau 4 montrent que le régime de température auquel est soumis un échangeur d'anions fortement basique de type I joue un rôle important sur la stabilité chimique de celui-ci.

Si la dégradation a lieu en H_2O_2 et en présence du $CuSO_4$ les groupes fonctionnels subissent des modifications importantes même à 40°.

Tableau 4

Dégradation de l'échangeur d'anions fortement basique de type I – forme OH^- et Cl^-, à différentes températures. Durée de la dégradation 10 h

Température de dégradation t°	Capacité d'échange résiduelle méq/g											
	En H_2O_2 30 %						En H_2O_2 30 % + $CuSO_4$					
	C_{sb}		C_{pb}		C_t		C_{sb}		C_{pb}		C_t	
	OH	Cl	OH	Cl	OH	Cl	OH	Cl	OH	Cl	OH	Cl
—	0,45	0,37	3,42	3,25	3,87	3,62	0,45	0,37	3,42	3,25	3,87	3,62
40	0,50	0,57	2,25	2,90	2,75	3,47	0,53	0,95	2,09	1,60	2,62	2,55
60	0,60	0,70	1,82	2,72	2,42	3,42	0,45	0	0,60	0	1,05	0
80	0,57	0,70	1,80	2,50	2,37	3,20	0	0	0	0	0	0

À 60° l'anionite sous forme chlore perd presque toute sa capacité d'échange, subissant des dégradations importantes même dans le réseau macromoléculaire, fait indiqué aussi par l'analyse IR du tableau 5.

À 80° l'anionite est totalement solubilisé dans le milieu de dégradation, indifféremment de la forme ionique de l'échange. Si la dégradation de l'anionite a lieu seulement en H_2O_2 sans addition de $CuSO_4$ les pertes de capacités d'échange sont affectées dans une mesure beaucoup plus réduite, par l'élévation de la température.

Dans la figure 3 sont représentées les pertes pourcentuelles obtenues à la suite de la dégradation de l'anionite en H_2O_2 en l'absence de $CuSO_4$. De l'analyse des données il résulte que la forme ionique joue un rôle important dans la définition de la stabilité chimique de l'anionite.

Il résulte que l'anionite sous forme OH^- est moins stable en comparaison de la forme Cl^-. Cela peut être expliquée par le fait que l'oxygène actif résulté par la décomposition de l'eau oxygénée forme des groupes hydroperoxydiques sur la chaîne. La décomposition des hydroperoxydes étant accélérée par la présence des ions OH [19], on peut supposer que la forme OH^- des anionites peut contribuer à la scission des liaisons hydroperoxydiques en favorisant la dégradation.

L'oxygène actif actionnera aussi sur la liaison C—N du groupement $-CH_2N(CH_3)_3^+OH^-$, en favorisant la réaction de désamination et de désalcoylation de l'anionite sous forme OH^- (figure 3, courbes *1* et *2*) en plus grande mesure en comparaison de la forme Cl^- (figure 3, courbes *3* et *4*). Ainsi, on constate une décroissance de la capacité fortement basique (figure 3, courbe *1*) beaucoup plus accentuée en comparaison de celle totale (figure 3, courbe *2*).

---

[19] K. U. Ingold et I. E. Puddington, *Ind. Eng. Chem.*, **51**, 1319 (1959).

Les mêmes constatations sont valables pour l'anionite sous forme de Cl^- (à comparer la courbe *3* avec la courbe *4* de la figure 3).

Dans la figure 4 est indiqué le degré de transformation K de l'anionite par le système H_2O_2 30% + $CuSO_4$, en fonction de la température.

On remarque dans ce cas que l'anionite sous forme OH^- est plus stable que celui sous forme Cl^-.

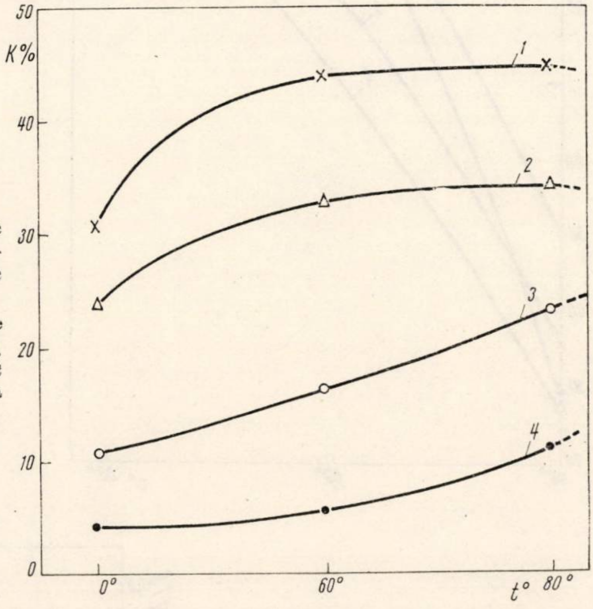

Fig. 3. — Dépendance des pertes de la capacité d'échange de la température de dégradation et de la forme ionique.

Conditions de dégradation ; H_2O_2 30%, durée de dégradation 10 heures. *1*, pertes en C_{pb}, l'anionite étant en forme OH^- . *2*, pertes en Ct pour la forme OH^-, *3*, Pertes C_{pb} pour la forme Cl^- ; *4* pertes C_t pour la forme Cl^-.

Ainsi, la présence du $CuSO_4$ dans le milieu de dégradation influence radicalement la cinétique de décomposition. C'est pourquoi les pertes C_t de l'anionite sous forme OH^-, dégradé en H_2O_2 à 60° sont en proportion de 33,15% seulement (figure 3, courbe *2*). Quand la dégradation a lieu en présence d'un métal (figure 4, courbe *4*), les pertes C_t sont de 71%.

En partant du fait que la dégradation des groupes fortement basiques de l'anionite a lieu par les deux mécanismes, dans la figure 5 ont été présentées les pertes C_{pb}, en fonction de la forme ionique de l'anionite par la réaction de désamination et la réaction de désalcoylation pour le cas où la dégradation a été réalisée seulement avec de l'H_2O_2 30%.

On constate que les pertes de la capacité d'échange, fortement basiques, sont beaucoup plus grandes quand l'anionite se trouve sous forme OH^- (figure 5, courbe *1*) par rapport à la forme Cl^- (figure 5, courbe *2*). Ainsi quand l'anionite se trouve sous forme OH^-, les pertes de la capacité d'échange par le mécanisme de désamination (figure 5, courbe *3*) donnent des valeurs beaucoup plus élevées, en comparaison des pertes de capacité réalisées par le mécanisme de désalcoylation (figure 5, courbe *5*). Pour la forme Cl^-, l'anionite subit des pertes dans sa capacité d'échange, par les deux mécanismes indiqués plus haut, leurs valeurs n'étant pas trop différentes entre elles (figure 5, courbes *4* et *6*).

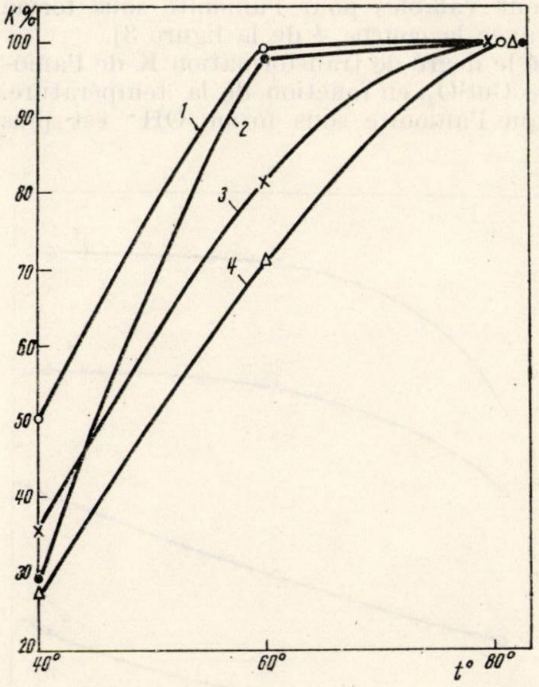

Fig. 4. — Dépendance du degré de transformation *K* des groupes basiques de l'anionite en fonction de la température et de la forme ionique

Conditions de dégradation ; H_2O_2 30% + $CuSO_4$; durée de dégradation 10 heures. *1*, pertes en C_{pb} pour la forme Cl^- ; *2*, pertes en C_t pour la forme Cl^- ; *3*, pertes en C_{pb} pour la forme OH^- ; *4*, pertes C_t pour la forme OH^-.

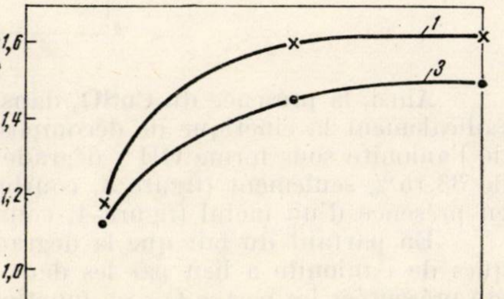

Fig. 5. — Pertes C_{pb}, fonction de la forme ionique de l'anionite et de la température, exprimées par la réaction de désamination (Δz) et de désalcoylation (Δal).

Conditions de dégradation ; 30% H_2O_2, durée de dégradation 10 heures. *1*, C_{pb} pour la forme OH^- ; *2*, C_{pb} pour la forme Cl^- ; *3*, Δz pour la forme OH^- ; *4*, Δt pour la forme Cl^- ; *5*, Δal pour la forme OH^- ; *6*, Δal pour la forme Cl^-.

Le coefficient de basicité (figure 6) indique que l'effet thermique joue un rôle important dans le changement de la nature des groupes basiques, en spécial quand la dégradation a lieu avec de l'H_2O_2 30 % en présence du $CuSO_4$ (figure 6, courbes *3* et *4*). En l'absence du $CuSO_4$, la modification de la basicité de l'anionite est moins importante (figure 6, courbes *1* et *2*).

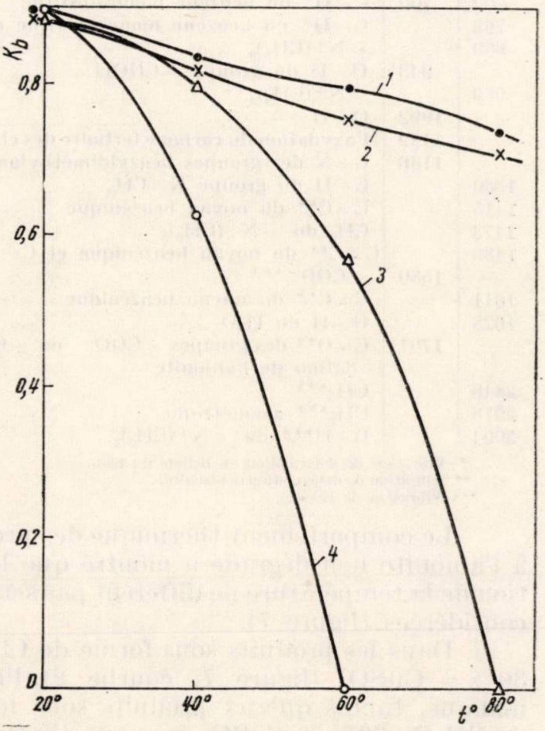

Fig. 6. — Variation du coefficient de basicité K_b en fonction de la température et de la forme ionique de l'anionite. Conditions de dégradation ; *1* et *2* = H_2O_2 30 % ; *3* et *4* = H_2O_2 30 % + $CuSO_4$. Durée de la dégradation 10 heures (1 et 4 forme Cl^-, 2 et 3 forme OH^-).

En étudiant les spectres IR on a obtenu les informations indiquées dans le tableau 5. Pour élucider les modifications constatées dans les spectres IR, les bandes d'absorption caractéristiques de l'anionite initial (I) ont été comparées à celles citées dans la littérature [20-23] et les nouvelles bandes d'absorptions parues à la suite de la dégradation ont été comparées avec celles indiquées par Vašiček et collab. [23]

On a analysé seulement les épreuves dégradées en H_2O_2 30 % et en présence du $CuSO_4$ à 40°. À des températures plus grandes, en partant de 60°, le réseau macromoléculaire et les groupes fortement basiques sont tellement modifiés que les superpositions complexes résultées sont difficilement interprétables.

[20] A. Strasheim et K. Buijs, *Spectrochim. Acta*, **17**, 388 (1961).
[21] D. Whittington et J. R. Millar, *J. Appl. Chem.*, **18**, 122 (1968).
[22] J. Klaban et V. Radl, *Chem. průmysl.*, **21**, 445 (1971).
[23] Z. Vašiček, J. Klaban et J. Stamberg, *Coll. Czech. Chem. Comm.*, **36**, 1825 (1971).

Tableau 5

Les positions des bandes d'absorptions, par l'échangeur d'anions fortement basique de type I non dégradé (A) et dégradé avec de l'H_2O_2 30% + $CuSO_4$ à 40°

A	B	Attribution des bandes d'absorption	Littérature
702	702	C—H* du benzène monosubstitué	20
763		C—H* du benzène monosubstitué et *o*-disubstitué	20
889		$-N^+(CH_3)_3$	20
	943	O—H du groupe —COOH	23
989		$-N^+(CH_3)_3$	23
	1092	O—H	
	1139	l'oxydation du carbone tertiaire des chaînes latérales de polyvinyle	23
	1186	C—N des groupes benzyldiméthylamine	23
1380		C—H du groupe $N-CH_3$	20
1415		C=C** du noyau benzénique	20
1473		CH_3 du $-N^+(CH_3)_3$	23
1485		C=C** du noyau benzénique et C—H* des groupes CH_2 et CH_3	20,23
	1580	$-COO^-$***	
1611		C=C** du noyau benzénique	20,21,23
1628		O—H du H_2O	20
	1701	C=O** des groupes $-COO^-$ ou —CHO formés à la suite de l'oxydation de l'anionite	23
2848		CH_2***	20,23
2918		CH_2*** asymétrique	20,23
3004		C—H*** du $-N^+(CH_3)_3$	20,23

* Vibration de déformation en dehors du plan.
** Vibration de déformation coplanaire.
*** Vibration de valence.

Le comportement thermique des produits dégradés comparativement à l'anionite non dégradé a montré que les pertes en poids dues à l'élévation de la température ne diffèrent pas sensiblement dans le cas des épreuves considérées (figure 7).

Dans les produits sous forme de Cl^-, dégradés en présence de l'H_2O_2 30% + $CuSO_4$ (figure 7, courbe *2*), l'inflexion du domaine 420—440° manque, tandis qu'aux produits sous forme OH^-, dégradés en présence de l'H_2O_2 30% + $CuSO_4$, manque l'inflexion du domaine 290—320° (fig. 7, courbe *3*).

Des informations plus intéressantes sont données par la dérivée de la courbe thermogravimétrique (DTG).

Dans les figures 8 et 9 sont données les courbes DTG pour les épreuves non dégradées et dégradées, sous formes de Cl^- et OH^-.

On constate la modification de la vitesse de réaction pour les processus 2 et 3 dans tous les cas présentés.

Pour la forme Cl^-, non dégradée, le processus 2 présente la vitesse la plus élevée, la vitesse maximale étant située à 280° (fig. 8 courbe 1).

Les modifications les plus importantes sont enregistrées pour la forme Cl^- dégradée en présence du catalyseur $CuSO_4$. La vitesse du processus II baisse fortement, tout en restant supérieure aux processus I, III, IV, tandis que le maximum est déplacé vers 260°.

Dans le cas de la dégradation du même produit en l'absence du catalyseur, mais en présence de l'eau oxygénée, on constate que dans le domaine initialement attribué au processus 2 (fig. 8 courbe *3*) sont visibles deux amplitudes, la plus intense étant située toujours à 280° comme dans le cas

Fig. 7. — Courbes TG.

1, L'anionite forme Cl^- non dégradé ; *2*, L'anionite forme Cl^- dégradé à 40° (H_2O_2 30% + $CuSO_4$) ; *3*, L'anionite forme OH^- dégradé à 80° (H_2O_2 30% + $CuSO_4$).

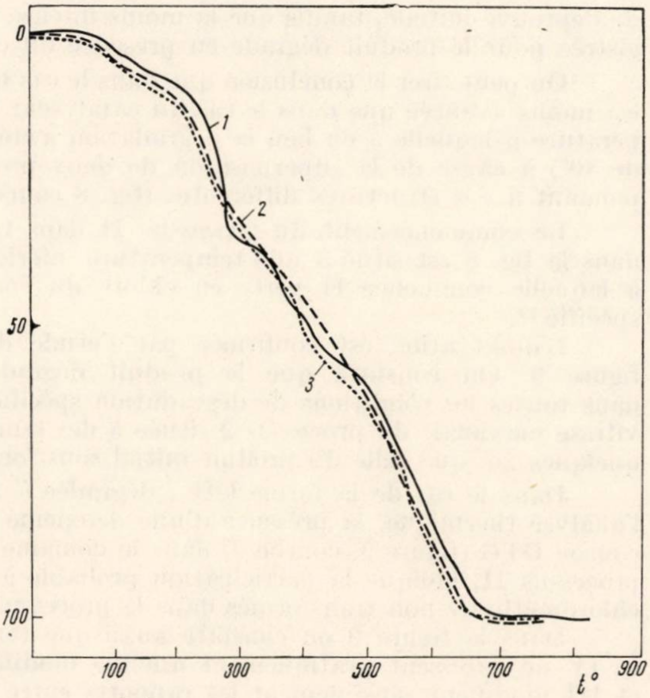

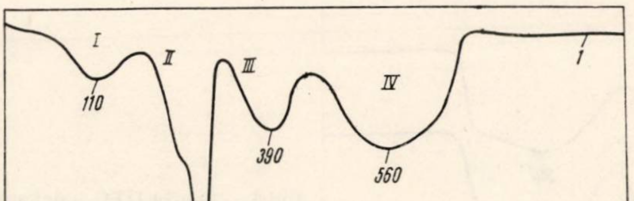

Fig. 8. — Courbe DTG pour l'anionite forme Cl^-.

1, non dégradé ; *2*, dégradé à 40° (H_2O_2 30% + $CuSO_4$) ; *3*, dégradé à 80° (H_2O_2 30%).

I, II, III, IV, processus indiqués sur la courbe DTG.

de l'épreuve initiale, tandis que la moins intense coïncide avec celle enregistrée pour le produit dégradé en présence du catalyseur (260°).

On peut tirer la conclusion que dans le cas mentionné la dégradation est moins avancée que dans le cas du catalyseur $CuSO_4$, bien que la température à laquelle a eu lieu la dégradation a été plus haute (80° au lieu de 40°) à cause de la superposition de deux processus différents correspondant à des structures différentes (fig. 8 courbe *3*).

Le commencement du processus II dans tous les trois cas donnés dans la fig. 8 est situé à une température inférieure à 200°, température à laquelle commence la perte en chlore du composé macromoléculaire spécifié [24].

L'observation est confirmée par l'étude des courbes DTG de la figure 9. On constate que le produit dégradé forme OH^- présente dans toutes les conditions de dégradation spécifiées dans la figure 9 une vitesse maximale du processus 2 située à des températures plus basses de quelques 20° que celle du produit initial sous forme Cl^-.

Dans le cas de la forme OH^-, dégradée à 20° et ensuite soumise à l'analyse thermique, la présence d'une deuxième amplitude à 290° sur la courbe DTG (figure 9, courbe *1*) dans le domaine attribué initialement au processus II, indique la participation probable à la réaction des groupes chlorométhylés non transformés dans le processus de l'amination.

Dans la figure 9 on constate aussi que tandis que les processus I et IV ne subissent pratiquement aucune modification, les processus II et III modifient sensiblement les rapports entre les vitesses de réaction.

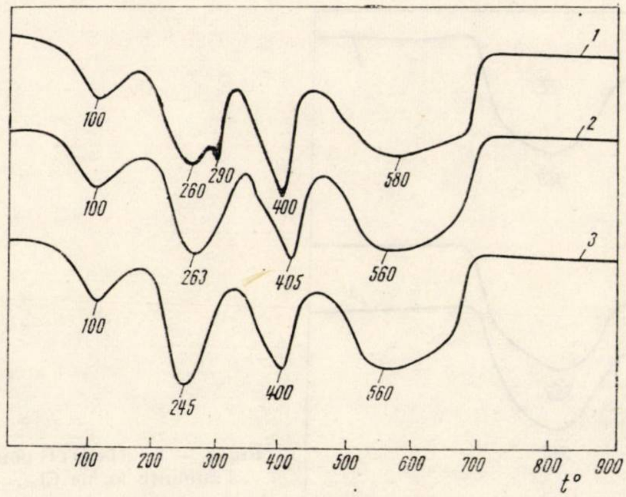

Fig.9. — Courbe DTG pour l'anionite forme OH^- dégradé par le H_2O_2 30 % + $CuSO_4$.
1, dégradé à 40° ; *2*, Dégradé à 60° ; *3*, dégradé à 80°. I, II, III, IV, processus indiqués sur la courbe DTG.

Dans le tableau 6 est présentée l'énergie d'activation. On constate que l'énergie d'activation du processus II est plus petite dans le cas des produits dégradés que dans les produits initiaux.

---

[24] Fl. Popescu, I. Petrariu et S. Percec, *Rev. Roumaine Chim.*, **20** (*1*), 711 (1975).

Tableau 6

Energies d'activation

N°	Type I	Processus	Ordre de réaction n	Energies d'activation kcal/mol
1	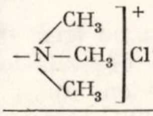 $\left[-\overset{\displaystyle CH_3}{N}(CH_3)_2\right]^+ Cl^-$	1	1,8	11,9
		2	1,8	29,2
		3	2,0	40,3
		4	1,6	68,5
2	La même forme Cl^- dégradée à 80° en H_2O_2 30%	1	1,5	19,1
		2	1	20,7
		3	2	48,5
		4	2	50,8
3	La même forme OH^- dégradée à 60° en H_2O_2 30% + $CuSO_4$	1	2	15,1
		2	2	27,4
		3	1,5	28,8
		4	2	42,0

L'analyse thermodifférentielle a montré que les processus III et IV sont fortement exothermes. Mise en corrélation avec les pertes en poids des courbes TG (figure 7) pour les mêmes températures, elle indique des réactions d'oxydation avec élimination des produits micromoléculaires.

CONCLUSIONS

On a étudié les transformations chimiques d'un anionite fortement basique de type I, dégradé dans l'eau oxygéné, en présence et aussi en l'absence du $CuSO_4$.

Dans ce but l'attention des auteurs a porté sur l'influence de la concentration de l'eau oxygénée, du $CuSO_4$, de la durée de dégradation, de la température de dégradation et de la forme ionique de l'anionite, sur la stabilité dynamique de l'anionite.

On a mis en évidence le mécanisme de dégradation de l'échangeur d'anions fortement basique de type I, dans l'eau oxygénée.

À l'aide de la spectroscopie IR, on a identifié les produits qui résultent de la dégradation et aussi les échanges qui ont lieu dans la structure macromoléculaire de l'échangeur d'anions.

Si la dégradation a lieu dans H_2O_2 30%, à des températures diverses, on constate que la forme Cl^- de l'anionite est plus stable que la forme OH^-. En présence du $CuSO_4$ la forme OH^- devient plus stable.

Les pertes en C_{pb} sont beaucoup plus grandes en comparaison du C_t indifféremment de la forme ionique de l'anionite ou des conditions de la dégradation.

Le régime de température auquel est soumis un échangeur d'anions joue un rôle important sur la stabilité dynamique de celui-ci, en spécial quand dans le milieu de dégradation se trouve aussi le $CuSO_4$. A 40° (température à laquelle tous les échangeurs d'anions obtenus en partant des polymères organiques sont stables) dans l'H_2O_2 30% et en présence du $CuSO_4$, le C_t baisse en fonction de la forme ionique de 27 à 30% et le C_{pb} baisse jusqu'à 36–50%.

Les courbes DTG ont montré des modifications très importantes dues en principal aux pertes en chlore pendant la dégradation dans les milieux agressifs étudiés. L'énergie d'activation devient aussi plus petite pour le deuxième processus indiqué sur les courbes DTG à cause des pertes en chlore dans les produits dégradés.

Revue Roumaine de Chimie, **20**, *6*, 855–862 (1975)

POLAROGRAPHIC AND OSCILLOPOLAROGRAPHIC BEHAVIOUR OF QUINOLINIC ACID

LUIGI CAMPANELLA, PIER LUIGI CIGNINI and FAUSTO CROCE
Institute of Analytical Chemistry, University of Rome—Italy
Italian National Researches Council (C.N.R.)

Received March 11, 1974

The polarographic and oscillopolarographic behaviour of quinolinic acid was studied in aqueous media at $(25.0 \pm 0.5)°$. Four polarographic waves and three oscillopolarographic peaks were evidenced. By their analysis (existence field, influence of concentration, pH and addition of surface active agents on the characteristic values of potential and current) it can be concluded that the first (at less negative potentials) and the third processes are of mixed nature, involving the discharge of hydrogen catalyzed by adsorbed species of the acid; the second is a reduction process of the acid with hydrogenation in the ring, differently diffusion controlled according to the pH value; the fourth is a simple catalytic hydrogen discharge. The Ilkovich and Randles-Sevcik equations are generally followed, ensuring the possibility for quantitatively determining the acid by the polarographic method, the analysis appearing particularly advantageous in the pH range 5.5÷6.5.

INTRODUCTION

In previous papers [1–5] we studied the polarographic behaviour of some mono and dicarboxilic acids of pyridine. These heterocyclic compounds show both normal and catalytic reduction processes. Recently our attention has been focussing on quinolinic acid (or 2.3 pyridinedicarboxylic acid) melting point 190–5°, dissociation constants $pK_1 = 2.43$, $pK_2 = 5.06$, [6] and $pK_1 = 2.406$, $pK_2 = 5.047$, [7] as this acid is of great biological and pharmaceutical interest.

The polarographic data reported in the literature are limited to the half wave potential in Et_4NI 0.1 M [8] and to the apparent dissociation constants. [9]

The study was performed in 1.0 M $NaClO_4$ as supporting electrolyte and 0.02 M citric buffer as buffering agent.

RESULTS

The reduction of quinolinic acid at D.M.E. shows four waves differently evidenced depending on pH (fig. 1). Only for $pH \ll 2.3$ all the four

---

[1] L. Campanella, G. De Angelis, *Rev. Roumaine Chim.*, **16**, 545 (1971).

[2] L. Campanella, E. Chiacchierini and M. Palchetti, *Rev. Roumaine Chim.*, **17**, 647 (1972).

[3] L. Campanella, G. De Angelis, *Rev. Roumaine Chim.*, **17**, 1087 (1972).

[4] L. Campanella, P. L. Cignini and G. De Angelis, *Rev. Roumaine Chim.*, **18**, 1269 (1973).

[5] L. Campanella, P. L. Cignini and G. De Angelis, *Rev. Roumaine Chim.*, **18**, 1649 (1973).

[6] A. M. Leko, R. P. Saper, *Glasnik Hem. Drstva*, **25–26**, 267 (1960–61).

[7] V. D. Canic, *Ber. dtsch. chem. Ges.*, **20**, 29 (1957).

[8] A. G. Pozdeeva, E. G. Novikov, *Zhur. priklad. Khim.*, **40**, 213 (1967).

[9] J. Volke, *Chem. listy*, **49**, 1236 (1955).

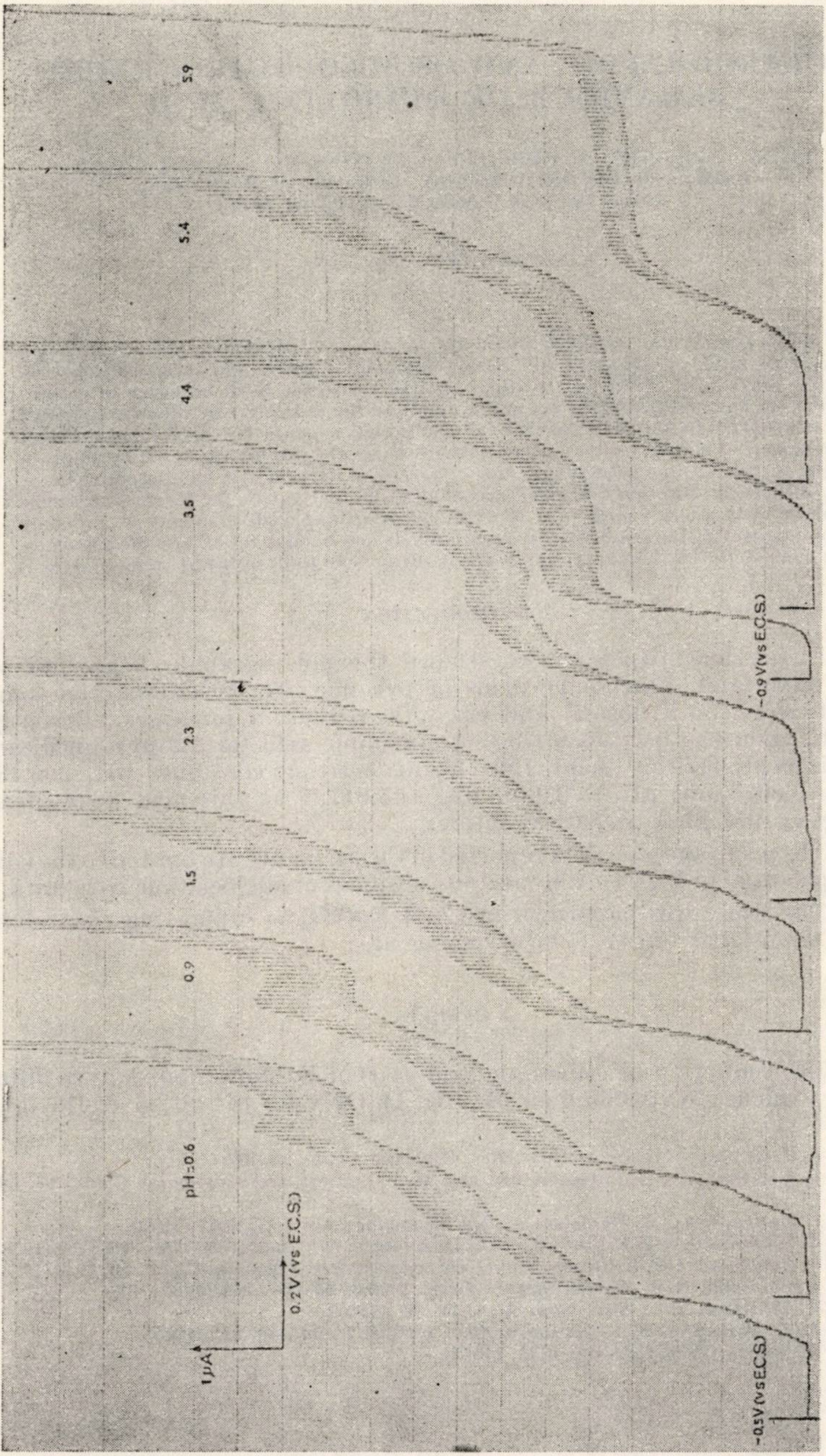

Fig. 1. — Polarographic behaviour of 10^{-3} M quinolinic acid at various pH.

waves can be observed at the same time, above pH 7 no polarographic activity is observed.

For the first, the third and the fourth wave $E_{1/2}$ is a linear function of pH in the whole explored range, the second wave shows a breakpoint near pH 4.5 (fig. 2).

First and third waves do not follow the Ilkovick equation, while for the second and fourth ones, proportionality between current and concentration is observed.

The influence of the mercury column height on the value of the limiting current was studied by the Kheifets curves (i.e. log i_d vs log h_{Hg}) : straight lines were obtained with slope 1 for the 1st and 3rd wave and 0.8 for the 2nd and 4th one.

The variation of the ionic strength has different effects depending on pH value. In very acid medium we note a slight lowering of the limiting current while $E_{1/2}$ remains constant ; on the contrary, in sub-acidic medium the second wave seems to change into two waves, while its $E_{1/2}$ becomes more negative and the limiting current decreases rapidly with the increase of the ionic strength.

In addition, we have studied the behaviour in the field of very high acidities, in order to evaluate the protonation constant of the quinolinic acid, found to be pK = 0.4 (fig. 3).

The oscillopolarographic method evidenced three peaks (fig. 4) corresponding to the 2nd, 3rd and 4th polarographic waves, respectively

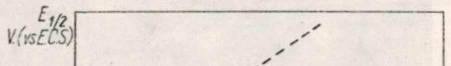

Fig. 2. — Half wave potential of the four waves as function of pH.

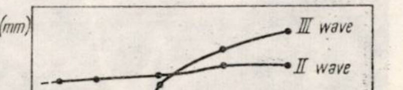

Fig. 3. — Limiting current values of the four waves vs[H+] concentration.

the peak currents, like polarographic waves, are depending on the pH value of the solution.

The first peak is the best formed and thus suitable for the study, while the second and the third peaks suffer reciprocal interference and the discharge of the supporting electrolyte.

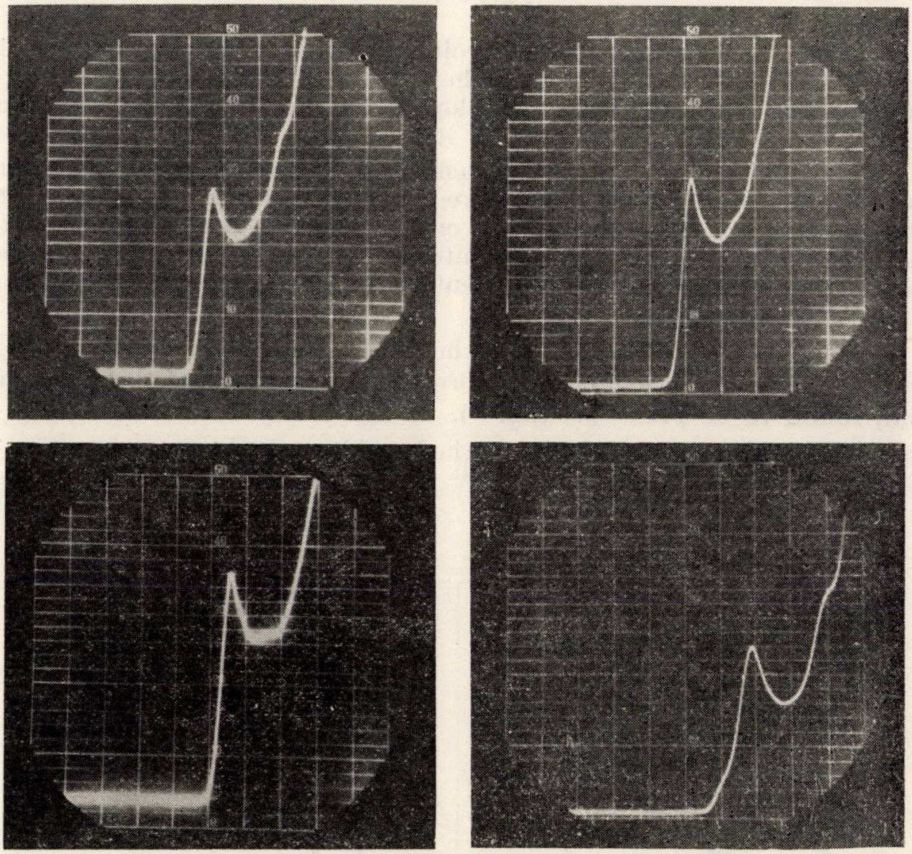

Fig. 4. — Oscillopolarographic direct curves of quinolinic acid at different pH, from left to right and up downwards pH = 2.0; 3.0; 4.0; 5.6.

The effect of concentration variation of quinolinic acid on the height of the oscillopolarographic peaks (fig. 5) is helpful in comprehending the described phenomenon with regard to the variation of ionic strength in polarography. Moreover, the height of the first and the third peaks follows the Randles-Sevcik equation at low pH (fig. 6).

By the oscillopolarographic method, too, the protonation constant of the acid can be evaluated with the increase of the free acidity degree of the analysed solutions: first, the second peak grows, then it remains constant, the inflexion point occurring at about pH 0.3.

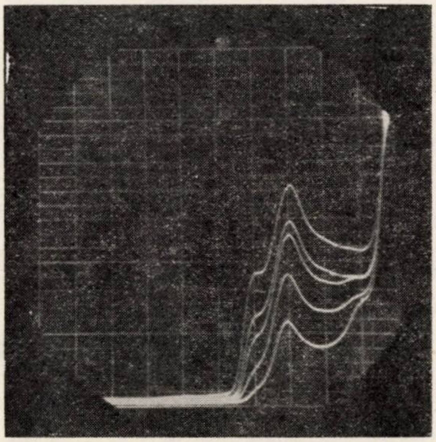

Fig. 5. — Oscillopolarographic behaviour of quinolinic acid as function of concentration, down upwards C = 1.00 ; 1.34 ; 1.66 ; 2.26 ; 2.76 ; $3.22 \cdot 10^{-3}$ M pH = 5.6

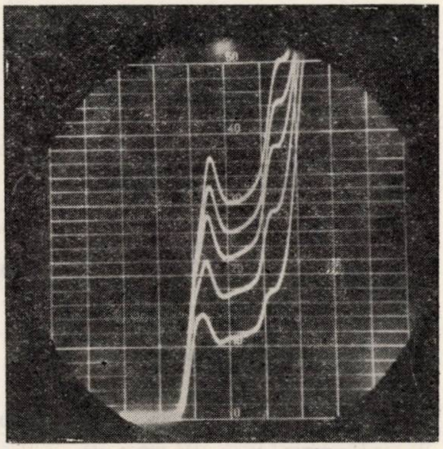

Fig. 6. — Oscillopolarographic behaviour of quinolinic acid as function of concentration, down upwards C = 1.00 ; 1.34 ; 1.66 ; 2.26 ; 2.76 ; $3.22 \cdot 10^{-3}$ M pH = 1.0

DISCUSSION

As observed in previous papers, consideration of the equilibria among the species of quinolinic acid in aqueous solution is the first step to the interpretation of the experimental results (fig. 7). On the basis of the value of the quinolinic acid dissociation constants and of the absence of polarographic steps for solutions at pH$\gg$ 7, any polarographic activity for the bivalent anionic completely deprotonated species can be excluded. The presence of four waves and three peaks at lower pH values suggests that also for quinolinic acid, as for other pyridinecarboxylic acids the protonated cationic species can be reduced at the dropping mercury electrode both directly and through a kinetic process of equilibrium with the other species of the acid and with hydrogen ions :

$$H_2PC + H^+ \rightleftarrows H_3PC^+$$

$$HPC^- + 2H^+ \rightleftarrows H_3PC^+$$

where H_2PC and HPC^- represent the species of the quinolinic acid at the protonation level 0 and -1.

On the basis of the described results regarding the number of electrons involved in the reduction processes, $\Delta E_{1/2}/\Delta$pH values for the different waves, existence of fields of the four evidenced reduction processes,

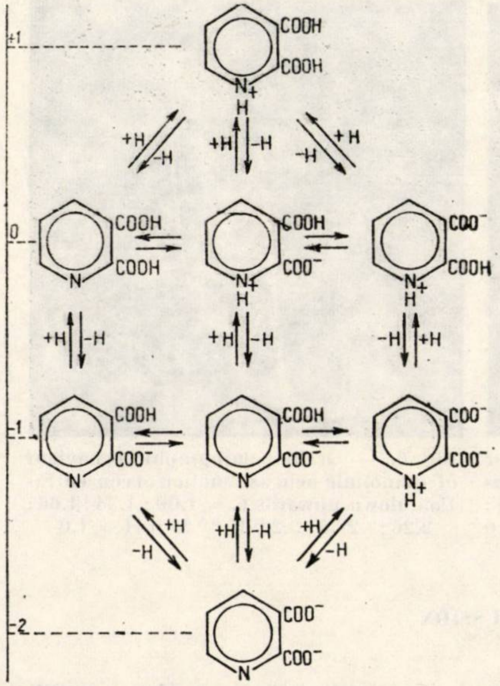

Fig. 7. — Equilibria of quinolinic acid in aqueous solution.

effects of prolonged electrolysis in polarographic conditions, we can postulate the following electrode processes:

1st wave $(H_3PC^+)_{ads.} + 3H^+ + 3e \rightarrow 3/2\ H_2 + H_3PC^+$

2nd wave $H_3PC^+ + 2H^+ + 2e \rightarrow H_3PC^+(H_2)$

$$H_{-}PC + 2H^+ + 2e \rightarrow H_2PC(H_2) \qquad \uparrow [H^+]$$

$$HPC^- + (HPC^-)_{ads.} + 4H^+ + 2\ e \rightarrow H_2PC(H_2) + H_2PC$$

3rd wave $(H_3PC^+)_{ads.} + H^+ + 2e \rightarrow H_2PC + H_2$

$$(H_2PC)_{ads.} + H^+ + 1e \rightarrow H_2PC + \frac{1}{2} H_2 \qquad \uparrow [H^+]$$

4th wave $H_3PC^+ + H^+ + 1e \rightarrow \frac{1}{2} H_2 + H_3PC^+$

$$H_2PC + H^+ \rightleftarrows H_3PC^+ + 1e \rightarrow \frac{1}{2} H_2 + H_2PC \qquad \uparrow [H^+]$$

$$HPC^- + 2H^+ \rightleftarrows H_3PC^+ + 1e \rightarrow H_2 + HPC^-$$

where with $X(H_2)$ a species reduced in the ring (dihydroderivative) is indicated.

While the first and the third processes are of a mixed nature involving hydrogen discharge catalyzed by species of the acid adsorbed on D.M.E., the second one is a reduction in the ring of the quinolinic acid and the fourth is a simple catalytic discharge of hydrogen. The hypothesis is substantiated by the following experimental results :

1) As described above, prolonged electrolysis of the solution involved a decrease of the limiting current of the second wave (fig. 8), the only one which involves a reduction in the ring and not only a catalytic discharge of hydrogen. This wave is also complicated by the latent presence of an adsorption pre-wave, so well evidenced in the pH range 4.5 ÷ 5, that a doubling of the wave in two is observed by lowering of the second wave anyway both with the increase of the ionic strength and with addition of gelatine to the solution ; decrease of the current of the second wave is recorded even if doubling is not evidenced. This adsorption pre-wave might correspond to the shoulder appearing before the first peak, in the oscillopolarographic analysis, provided that suitable pH and concentration values are adopted (Fig. 5).

2) By adding gelatine, the first and the third waves disappear, because they are due to the adsorption of one or more electroactive species of the acid. On the basis of electrocapillary curves, recorded in the presence or not of the organic acid, the adsorption of a cationic protonated species can be foreseen.

3) The temperature coefficent (6 %) of the fourth wave is a clear indication of its catalytic character, while the first and the third waves are of a mixed type (catalysis and adsorption), the second one being diffusive.

4) The Kheifets slope for the first and the third wave is 1, that is the theoretical value for adsorption waves ; for the second one, it is in the range 0.5 (theoretical value for diffusion processes) — 1 (probably due to the mentioned adsorption pre-wave).

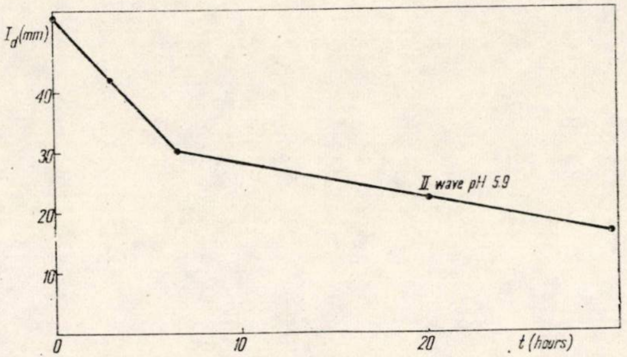

Fig. 8. — Limiting current values of the second wave at pH 5.9, after prolonged electrolysis under polarographic conditions.

5) All the waves, except the first one, are characterised by a value of the irreversibility degree near to that typical of the catalytic hydrogen discharge.

An objection can be advanced on the proposed mechanism for the third and the fourth waves since for the same process we have hypothetized two different values of $E_{1/2}$: firstly, the third wave involves adsorption phenomena with the increase of the electroactive species concentration at the mercury electrode surface, thus favouring the electrochemical reduction ; secondly, at the potential values of the third wave gaseous hydrogen is formed on the dropping mercury electrode that becomes polarized, so requiring an excess of voltage to be applied for the maintenance of the same process.

Finally, regarding the analytical aspect, it may be generally said that the polarographic quantitative determination of the quinolinic acid can be performed in the whole studied range of pH, but in the interval 5.5 ÷ 6.5, where only one wave of height proportional to concentration is present, the quantitative determination is particularly advantageous.

Revue Roumaine de Chimie, **20**, *6*, 863–869 (1975)

MEMBRANE-ELECTRODES OF THE METALLIC WIRE-PLASTIC MEMBRANE TYPE. II*

AMMONIUM-SELECTIVE MEMBRANE-ELECTRODE

ELENA HOPÎRTEAN and EUGENIA ŞTEFĂNIGĂ
"Babeş-Bolyai" University Cluj-Napoca, Department of Analytical Chemistry
str. Arany János 11, Cluj-Napoca

Received March 4, 1974

The paper studies the NH_4^+-selective electrode of the type platinum wire coated by a plastic membrane obtained from PVC, dibutylphthalate and tetraphenylborate. The electrode functions of ammonium have been established both in the absence and in the presence of some interfering ions (Na^+, Ca^{2+}, Mg^{2+}), with electrodes formed of tetraphenylborate included under the form of sodium, ammonium or potassium salt. Ammonium-sodium, ammonium-calcium and ammonium-magnesium selectivity constants have also been calculated. The electrodes obtained are used for analytical purposes in the determination of NH_4^+ by potentiometric titration with sodium or calcium tetraphenylborate.

1. INTRODUCTION

The need for determining ammonium in its various compounds has promoted investigations obtaining NH_4^+-selective membrane-electrodes. As a result of the development of the cation-selective glass-electrode, [1] ammonium determination was possible both in aqueous solutions [2–6] and in non-aqueous media. [7,8] Modified NH_4^+-sensitive glass-electrodes [9,10] are also known, and have been obtained by covering the H^+-selective glass-electrode by an ammonia-permeable membrane. Similarly,

---

* Part I: E. Hopîrtean, C. Liteanu and E. Ştefănigă, *Rev. Roumaine Chim.*, **19**, 1651 (1974).

[1] G. Eisenman, D. O. Rudin and J. U. Casby, *Science*, **126**, 831 (1957).

[2] G. A. Rechnitz, S. B. Zamochnick and M. Katz, *Analyt. Chem.*, **35**, 1322 (1963).

[3] K. Camman, *Beckman Rep.*, 1966 (2), 13; *Chem. Abstr.*, **69**, 8228 (1969).

[4] G. I. Goodfellov and H. M. Welber, *Analyst*, **97** (115), 95 (1972).

[5] J. M. Bremner and M. A. Tabatabai, *Commun. Soil. Sci. Plant. Anal.*, **3**, 159 (1972); *Chem. Abstr.*, **77**, 47157 (1972).

[6] F. R. Thomas and L. R. Broth, *Environ Sci. Technol.*, **7**, 523 (1973); *Chem. Abstr.*, **79**, 23362 (1973).

[7] R. A. Shuirba and L. W. Jolly, *J. Amer. Chem. Soc.*, **90**, 5289 (1968).

[8] W. M. Baumann and W. Simon, *Helv. Chim. Acta*, **52**, 2054 (1969).

[9] G. J. Montalvo and G. G. Guilbault, *Analyt. Chem.*, **41**, 1897 (1969).

[10] H. C. Beebe and A. Strickler, German patent, 2 009 937, 10 Sept. 1970–3 May 1969; *Chem. Abstr.*, **73**, 137109 (1970).

NH_4^+-selective electrodes were developed, based on ion-exchange resins[11] or on sequestering neutral agents.[12-15]

Among the classical methods for determining the NH_4^+ ion reported in the literature, worth mentioning are the methods based on the use of sodium tetraphenylborate reagent for gravimetric[16] or turbidimetric[17] determination. By developing a membrane-electrode for ammonium with tetraphenylborate as active component it becomes possible to determine NH_4^+ by a far simpler and more rapid approach than the classical methods mentioned.

A previous paper[18] was concerned with the development and the study of the K^+-selective electrode with $K[B(C_6H_5)_4]$ as active component distributed in a plastic membrane coming into direct contact with the platinum wire.

In this paper, investigations concerning membrane-electrodes of the Pt wire-plastic membrane type have been extended, with a view to developing the NH_4^+-selective electrode. Studies were made on the electrodic behaviour to ammonium of the membrane containing as an active component a tetraphenylborate ion under the form of sodium, ammonium or potassium salt, dispersed in the dibutylphthalate plastified PVC. Electrode functions were established for ammonium both in the absence and in the presence of some interfering ions (Na^+, Ca^{2+}, Mg^{2+}). Selectivity constants relative to Na^+, Ca^{2+} and Mg^{2+} ions were also determined. The electrodes were used in the determination of NH_4^+ by potentiometric titration with sodium or calcium tetraphenylborate.

2. EXPERIMENTAL

2.1. OBTAINMENT OF THE ELECTRODE

Membrane-electrodes of the type platinum wire-plastic membrane with active electrode component : $Na[B(C_6H_5)_4]$, $NH_4[B(C_6H_5)_4]$ and $K[B(C_6H_5)_4]$ were obtained according to the method described in the previous paper.[18] The plasticizer used was dibutylphthalate. The membranes achieved contain 3% active component, 35% PVC and 62% dibutylphthalate. The diagram of these electrodes is presented in fig. 1.

2.2. RESULTS AND DISCUSSION

2.2.1. E-pNH_4 electrodic functions. In order to establish the electrode functions, the e.m.f. of the following electrolytic chain was measured :

Pt | membrane | test solution | salt bridge | reference electrode (Ag/AgCl)

---

[11] M. Adhikari, M. Paul and D. Gangopadhyay, *Indian J. Chem.*, **8**, 79 (1970) ; *Chem Abstr.*, **72**, 83503 (1970).

[12] R. P. Scholer and W. Simon, *Chimia*, **24**, 372 (1970) ; *Chem. Abstr.*, **74**, 8974 (1971).

[13] R. E. Cosgrove, I. H. Krull and C. A. Mask, German patent, 2 132 333, 13 Jan. 1972—29 June 1970 ; *Chem. Abstr.*, **76**, 94275 (1972).

[14] G. A. Rechnitz and E. Eyal, *Analyt. Chem.*, **44**, 370 (1972).

[15] J. Mertens, P. Van dem Winkel and D. L. Massart, *Analyt. Lett.*, **6**, 81 (1973) ; *Chem. Abstr.*, **78**, 88433 (1973).

[16] F. E. Crane jr. and E. A. Smith, *Chemist Analyst*, **49**, 38 (1960).

[17] Z. Gregorowicz and F. Buhl, *Z. analyt. Chem.*, **223**, 42 (1966).

[18] E. Hopîrtean, C. Liteanu and E. Ştefănigă, *Rev. Roumaine Chim.*, **19**, 1651 (1974).

Potential measurements were made at room temperature without stirring, using a MV—11 pH-meter with a ± 1 mV precision. A salt-bridge of 10^{-1}M $NaNO_3$ with 1% agar-agar was used so as to avoid the contamination of the test solution with K^+ ions of the reference electrode.

The results obtained are presented in figures 2, 3 and 4 and also in table 1.

In NH_4Cl solutions, in the absence of interfering ions, the three electrodes have a similar behaviour (slope 54 mV). Among the tested interfering ions, the influence of sodium is more pronounced. The slope of the electrode function and the concentration range of the linear response are not significantly affected by the presence of Ca^{2+} and Mg^{2+} ions, respectively.

2.2.2. Selectivity. Ammonium-sodium ($K_{NH_4,Na}$), ammonium-calcium ($K_{NH_4,Ca}$) and ammonium-magnesium ($K_{NH_4,Mg}$) selectivity constants were calculated by the method suggested by Srinivasan and Rechnitz [19] (activity ratio of primary and interfering ion which determine the same electrode potential). The electrode functions obtained against a constant background of interfering ions ($a_i = 10^{-2}$M) were used for the graphical evaluation of NH_4^+ ion activity, corresponding to the lower response limit of the electrode. In the case in which the interfering ion did not restrict the linearity domain of the electrode function, selectivity constants were evaluated from the electrode functions established in the separate solutions of the two ions.[19] The values of the obtained selectivity constants are listed in table 2.

The data given in table 2 reveal that the best ammonium-sodium selectivity is obtained in the case of the electrode with $K[B(C_6H_5)_4]$. Since the solubility of potassium tetraphenylborate [20] ($S_{K[B(C_6H_5)_4]} = 2 \cdot 25 \times 10^{-8}$) is lower than that of ammonium tetraphenylborate [21] ($S_{NH_4[B(C_6H_5)_4]} = 8 \cdot 29 \times 10^{-8}$), it can be stated that the lower the solubility product of the membrane active electrode component, the weaker the interference of the Na^+ ion. Na^+ ion affects the electrode potential generated by the ion exchange equilibrium :

$$M[B(C_6H_5)_4] + NH_4^+ \rightleftharpoons NH_4[B(C_6H_5)_4] + M^+, \qquad (1)$$

by the appearance of the competitive equilibrium :

$$M[B(C_6H_5)_4] + Na^+ \rightleftharpoons Na[B(C_6H_5)_4] + M^+ \qquad (2)$$

which is obviously favoured because the solubility of the active electrode component is higher.

Concerning the ammonium-calcium selectivity, electrodes with $Na[B(C_6H_5)_4]$ and with $K[B(C_6H_5)_4]$ respectively, behave similarly. The higher ammonium-calcium and ammonium-magnesium selectivity respectively, of the three electrodes compared to the ammonium-sodium selectivity shows that these divalent cations participate to a much lesser extent than the sodium ion in the ion-exchange process with the membrane

---

[19] K. Srinivasan and G. A. Rechnitz, *Analyt. Chem.*, **41**, 1203 (1969).

[20] W. Geibmann and W. Gebauhr, *Z. analyt. Chem.*, **139**, 161 (1953).

[21] C. L. Howick and R. T. Pflaum, *Analyt. Chim. Acta*, **19**, 342 (1958).

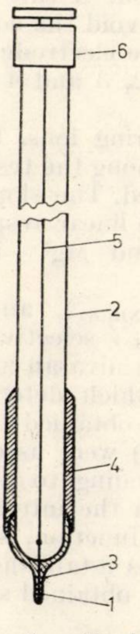

Fig. 1. — Membrane-electrode.

1, Pt wire; *2*, glass tube; *3*, membrane; *4*, paraffin layer; *5*, copper wire; *6*, terminal contact.

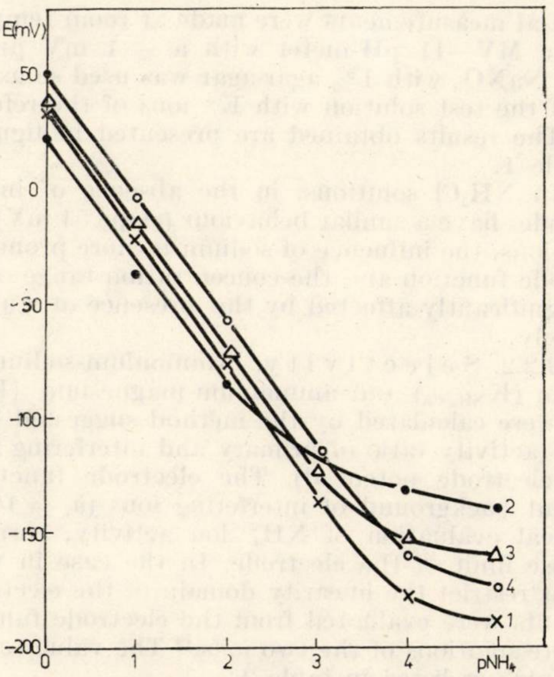

Fig. 2. — E-pNH_4 electrode functions. Electrode: $Na[B(C_6H_5)_4]$ + dibutylphthalate + PVC.

1, without interfering ions; *2*, background $10^{-2}M$ NaCl; *3*, background $10^{-2}M$ $CaCl_2$; *4*, background $10^{-2}M$ $MgCl_2$.

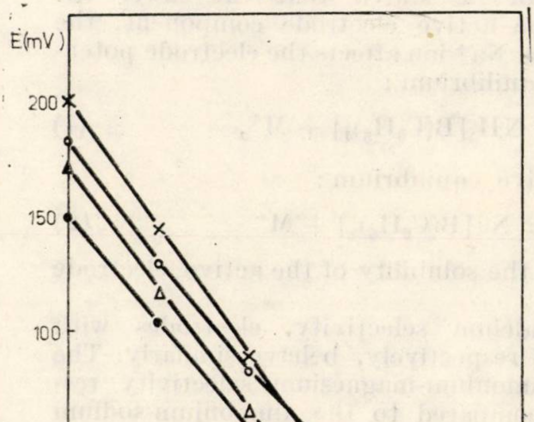

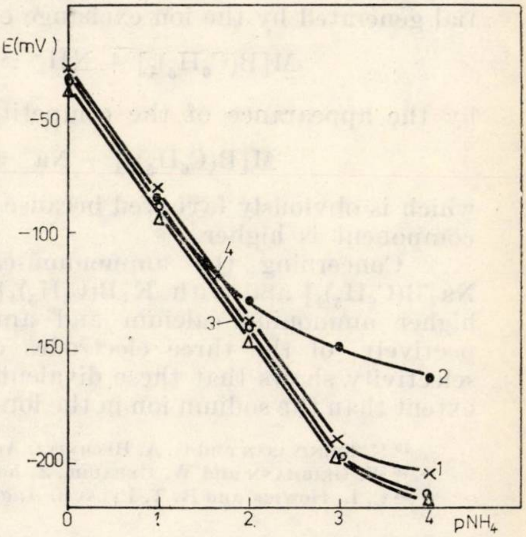

Fig. 3. — E-pNH_4 electrode functions. Electrode: $NH_4[B(C_6H_5)_4]$ + dibutylphthalate + PVC.

1, without interfering ions; *2*, background $10^{-2}M$ NaCl; *3*, background $10^{-2}M$ $CaCl_2$; *4*, background $10^{-2}M$ $MgCl_2$.

Fig. 4. — E-pNH_4 electrode functions. Electrode: $K[B(C_6H_5)_4]$ + dibutylphthalate + PVC.

1, without interfering ions; *2*, background $10^{-2}M$ NaCl; *3*, background 10^{-2} M $CaCl_2$; *4*, background $10^{-2}M$ $MgCl_2$.

Table 1

Electrode behaviour

Electrode	Interfering ion	Concentration of interfering ion	Concentration range (pNH_4)	Slope ($\Delta E/\Delta pNH_4$)
$Na[B(C_6H_5)_4]$ + dibutylphthalate + + PVC	—	—	$0-3.8$	54
	Na^+	$10^{-2}M$	$0-2.0$	53
	Ca^{2+}	$10^{-2}M$	$0-3.3$	53
	Mg^{2+}	$10^{-2}M$	$0-3.8$	54
$NH_4[B(C_6H_5)_4]$ + dibutylphthalate + PVC	—	—	$0-3.5$	54
	Na^+	$10^{-2}M$	$0-2.0$	47
	Ca^{2+}	$10^{-2}M$	$0-3.0$	52.5
	Mg^{2+}	$10^{-2}M$	$0-2.5$	50
$K[B(C_6H_5)_4]$ + dibutylphthalate + + PVC	—	—	$0-3.2$	54
	Na^+	$10^{-2}M$	$0-2.0$	50
	Ca^{2+}	$10^{-2}M$	$0-3.0$	54
	Mg^{2+}	$10^{-2}M$	$0-3.2$	55

Table 2

Selectivity constants

Electrode	Selectivity constant		
	$K_{NH_4,Na}$	$K_{NH_4,Ca}$	$K_{NH_4,Mg}$
$Na[B(C_6H_5)_4]$ + + dibutylphthalate + PVC	5×10^{-1}	2.3×10^{-3}	$<10^{-3}$
$NH_4[B(C_6H_5)_4]$ + + dibutylphthalate + PVC	3.8×10^{-1}	2×10^{-3}	1.5×10^{-2}
$K[B(C_6H_5)_4]$ + + dibutylphthalate + PVC	3.1×10^{-1}	1.2×10^{-3}	$<10^{-3}$

active component. At the same time, we must admit that the ion-exchange equilibrium is also conditioned by the membrane permeability to the two (primary and interfering) ions. The results obtained support this statement. In conclusions, the selective diffusion of ions present in solution across the membrane may constitute an important source in selectivity.

2.3. ANALYTICAL USE

Titration curves of ammonium obtained by using sodium tetraphenylborate as a titrant are presented in fig. 5 and those obtained with calcium tetraphenylborate are exhibited in fig. 6. It results from fig. 5 that the electrode with sodium tetraphenylborate cannot be used in ammonium determination with sodium tetraphenylborate titrant. When using calcium tetraphenylborate as a titrant (fig. 6), good results are obtained with each electrode regardless of its active component. In this case, a somewhat

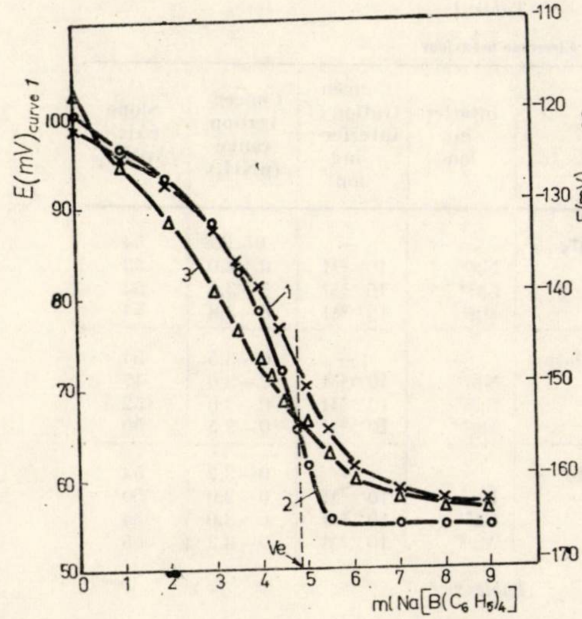

Fig. 5.– Titration of 10^{-2}M NH_4Cl with $\sim 5 \times 10^{-2}$ M $Na[B(C_6H_5)_4]$. *1*, electrode; $NH_4[B(C_6H_5)_4]$ — dibutylphthalate + PVC; *2*, electrode; $K[B(C_6H_5)_4]$ + dibutylphthalate + PVC; *3*, electrode: $Na[B(C_6H_5)_4]$ + dibutylphthalate + PVC

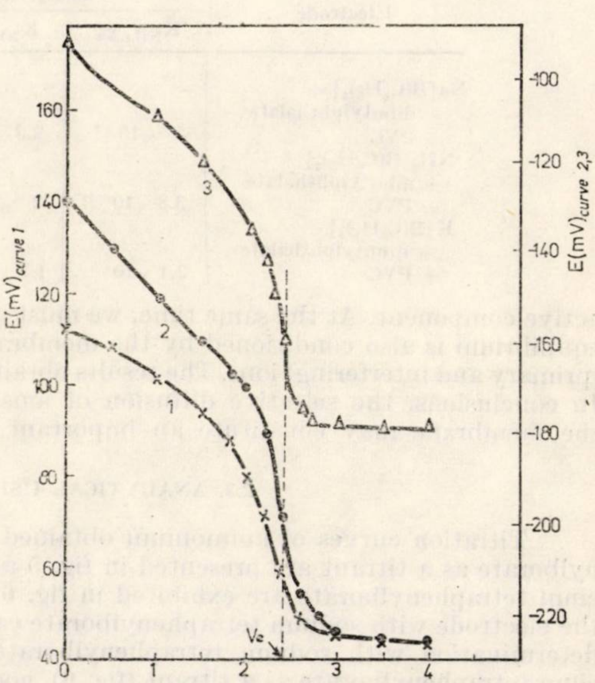

Fig. 6.—Titration of 10^{-2}M NH_4Cl with $\sim 10^{-1}$M $Ca[B(C_6H_5)_4]_2$. *1*, electrode; $NH_4[B(C_6H_5)_4]$ + dibutylphthalate + PVC; *2*, electrode; $K[B(C_6H_5)_4]$ + dibutylphthalate + PVC; *3*, electrode; $Na[B(C_6H_5)_4]$ + dibutylphthalate + PVC.

weaker behaviour of the electrode with ammonium tetraphenylborate as active component has been found (fig. 6, curve 1). This fact is in agreement with the previously presented selectivity constants.

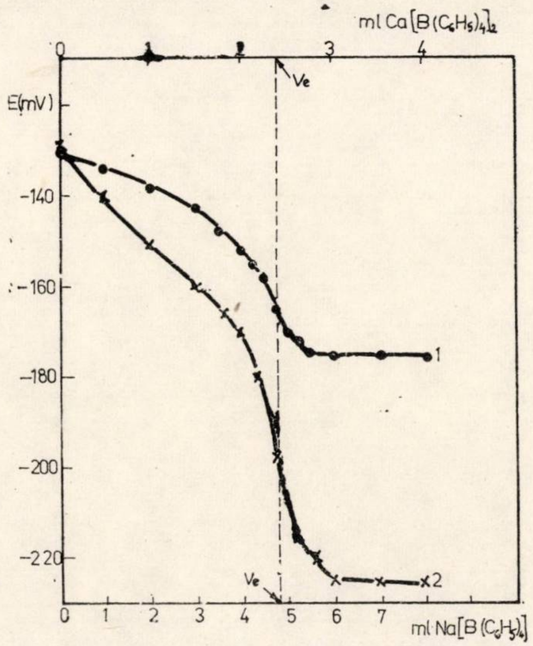

Fig. 7. — Titration of 10^{-2} M NH_4Cl with $\sim 5 \times 10^{-2}$ M $Na[B(C_6H_5)_4]$ (curve *1*) and with $\sim 10^{-1}$M $Ca[B(C_6H_5)_4]_2$ (curve *2*), respectively. Electrode : $K[B(C_6H_5)_4]$ + dibutylphthalate + PVC.

With regard to the potential jump around the equivalence point this is incomparably clearer when using calcium tetraphenylborate as a titrant (fig. 7, curve 1) rather than sodium tetraphenylborate as a titrant (fig. 7, curve 2).

CONCLUSIONS

The paper presents the obtainment of a NH_4^+-selective electrode of the type platinum wire coated by a plastic membrane obtained of PVC, dibutylphthalate and an active component-sodium, ammonium and potassium tetraphenylborate. An analysis of the behaviour of these electrodes results in the following :

— the electrode functions for NH_4^+ obtained in the absence of interfering ions are practically identical, regardless of the nature of the cation of the active electrode component.

— the presence of sodium ion significantly restricts the concentration range of the linear response domain of electrodes.

— the linear response domain of electrodes with active component $Na[B(C_6H_5)_4]$ and $K[B(C_6H_5)_4]$ respectively, is practically unaffected by the presence of Ca^{2+} and Mg^{2+} ions.

The electrodes obtained and studied may be used with good results in the determination of NH_4^+ ion both by direct potentiometry and by potentiometric titration, particularly with calcium tetraphenylborate.

weaker behaviour of the electrode with aluminium tetraphenylborate as active component has been found (fig. 6, curve 1). This fact is in agreement with the previously presented selectivity constants.

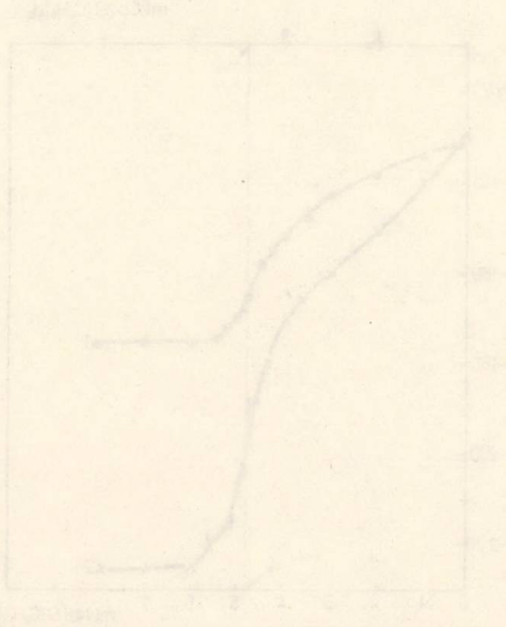

Fig. 7. — Titration of [illegible] with [illegible]

With regard to the potential jump around the equivalence point this is more clearly visible when using calcium tetraphenylborate as a titrant (fig. 7, curve 1) rather than sodium tetraphenylborate as a titrant (fig. 7, curve 2).

CONCLUSIONS

The paper presents the obtainment of a NH_4^+ selective electrode of the type platinum coated by a plastic membrane obtained of PVC, dibutylphthalate and an active component sodium, aluminium and magnesium tetraphenylborate. An analysis of the behaviour of these electrodes results in the following:

— the electrode functions for NH_4^+ obtained in the absence of interfering ions are practically identical regardless of the nature of the cation of the active electrode component.

— the presence of sodium ion significantly restricts the concentration range of the linear response domain of electrodes.

— the linear response domain of electrodes with active component $Na[B(C_6H_5)_4]$ and $K[B(C_6H_5)_4]$ respectively, is practically unaffected by the presence of Ca^{2+} and Mg^{2+} ions.

The electrodes obtained and studied may be used with good results in the determination of NH_4^+ ion both by direct potentiometry and by potentiometric titration, particularly with calcium tetraphenylborate.

NOTE POUR LES AUTEURS

La *Revue Roumaine de Chimie* publie des articles en anglais, français, russe, allemand ou espagnol. Les auteurs sont priés d'envoyer des articles, notes, communications et comptes rendus inédits.

Les manuscrits seront dactylographiés à deux intervalles. Les tableaux seront dactylographiés sur des feuilles séparées, de même que la légende des figures. Les diagrammes seront tracés à l'encre de Chine sur papier calque. Les tableaux et les figures seront numérotés par des chiffres arabes, en nombre strictement nécessaire. Prière de ne pas inscrire les mêmes données dans les tableaux et les figures. Les formules chimiques seront incluses dans le texte ; en outre, elles seront transcrites sur des feuilles séparées. Les auteurs sont priés d'indiquer les caractères italiques (en soulignant les lettres au crayon), ainsi que tout autre caractère spécial. L'ordre des références bibliographiques sera celui de leur mention dans le texte ; le nom de l'auteur sera précédé de l'initiale du prénom ; les publications périodiques seront présentées suivant les prescriptions internationales. Les références seront ajoutées à la fin de l'article ; elles paraîtront comme des notes, au bas de la page. Le texte sera précédé d'un résumé comprenant 15 lignes au maximum.

L'entière responsabilité du contenu des articles appartient aux auteurs. On publie des articles dus aux collaborateurs roumains ou étrangers.

PRINTED IN ROMANIA

NOTE POUR LE LECTEUR

Le Recueil [illegible] 1958 [illegible] d'envoyer des [illegible] autres [illegible].

[illegible]

[illegible] maximum.

[illegible] ou étrangers.

PRINTED IN ROMANIA

1975 OKT 1 6

TRAVAUX PARUS AUX ÉDITIONS DE L'ACADÉMIE DE LA RÉPUBLIQUE SOCIALISTE DE ROUMANIE

I. ZUGRĂVESCU et MAGDA PETROVANU, **Chimia N-Ilidelor** (La chimie des N-Ylures), 1974, 347p., 19 lei.

MARGARETA AVRAM, **Antidăunători** (Pesticides), 1974, 494 p., 41 lei.

CR. SIMIONESCU, VIORICA RUSAN et N. POPA, **Chimia algelor marine** (La Chimie des algues marines), 1974, 211 p., 18 lei.

TIBERIU NĂŞCUŢIU, **Metode radiochimice de analiză** (Méthodes radiochimiques d'analyse), 1973, 384 p., 23 lei.

MARIA FITI, **Dozimetria chimică a radiaţiilor ionizante** (La dosimétrie chimique des radiations ionisantes), 1973, 240 p., 13,60 lei.

MIHAI FLORESCU, **Eficienţa economică a cercetării ştiinţifice** (L'efficience économique de la recherche scientifique), 1972, 115 p., 15 lei.

GEORGETA LĂZĂRESCU, **Sistematizarea informaţiilor în chimia organică** (La systématisation des informations dans la Chimie organique), 1972, 252 p., 10,50 lei.

P. BALTĂ et E. BALTĂ, **Introducere în chimia fizică a stării vitroase** (Introduction à la chimie physique de l'état vitreux), 1971, 15,50 lei.

LYDIA-MARIA VAICUM, **Biodegrabilitatea detergenţilor** (La biodégrabilité des détergents), 1971, 254 p., 16 lei.

I. ZUGRĂVESCU et L. STOICESCU-CRIVETZ, **Polimeri heterociclici** (Polymères hétérocycliques), 1971, 190 p., 9,50 lei.

I. MAXIM, **Materiale nucleare** (Matériaux nucléaires), 1969, 444 p., 30 lei.

CRISTOFOR SIMIONESCU et CLEOPATRA VASILIU-OPREA, **Mecanochimia compuşilor macromoleculari** (La mécanochimie des composés macromoléculaires), 1967, 344 p., 23,50 lei.

CORNEL BODEA et collab., **Tratat de biochimie vegetală**, partea I, **Fitochimie** (Traité de biochimie végétale, Ire partie, Phytochimie), Ier vol., 1964, 747 p. + 4 annexes + 2 pl., 41 lei; IIe vol., 1965, 1262 p., 1 pl., 56 lei; IIIe vol., 1967, 773 p., 35 lei.

I. P. I. — c. 189

43 426

Lei 25. —

F 1103

ACADÉMIE DE LA RÉPUBLIQUE SOCIALISTE DE ROUMANIE

REVUE ROUMAINE DE CHIMIE

R

TOME 20
N° 7
Juillet 1975

RECHAX, 20, 7, 871–1026 (1975)

EDITURA ACADEMIEI REPUBLICII SOCIALISTE ROMÂNIA
Rev. Roumaine Chim. 20, 7, p. 871–1026 (1975), Bucarest

ACADÉMIE DE LA RÉPUBLIQUE SOCIALISTE DE ROUMANIE

COMITÉ DE RÉDACTION

Rédacteur en chef:

I. G. MURGULESCU, membre de l'Académie de la République Socialiste de Roumanie

Rédacteurs en chef adjoints:

A. T. BALABAN et V. EM. SAHINI, membres correspondants de l'Académie de la République Socialiste de Roumanie

Collège de rédaction:

EM. BRATU, ELENA CEAUŞESCU, ECATERINA CIORĂNESCU-NENITZESCU, C. DRĂGULESCU, RALUCA RIPAN, CR. SIMIONESCU, membres de l'Académie de la République Socialiste de Roumanie; P. SPACU, membre correspondant de l'Académie de la République Socialiste de Roumanie; MARGARETA AVRAM, D. I. MARCHIDAN, I. MOLDOVAN, G. NIAC et D. SĂNDULESCU

Toute commande de l'étranger pour les travaux parus aux Editions de l'Académie de la République Socialiste de Roumanie sera adressée à ILEXIM, Serviciul Export-Import Carte/Serviciul Export-Import Presă, P.O. BOX 2001, 64–66, Calea Griviţei, Bucarest, 12, Roumanie

Les manuscrits, les livres et les revues proposés en échange, ainsi que toute correspondance seront envoyés à la rédaction:

REVUE ROUMAINE DE CHIMIE

23, str. Dumbrava Roşie, Bucarest, Roumanie, téléphone 12 41 60

EDITURA ACADEMIEI REPUBLICII SOCIALISTE ROMÂNIA

125, Calea Victoriei, Bucarest, téléphone 50 27 25

REVUE ROUMAINE DE CHIMIE

ORSZÁGOS

Tome 20, Nº 7 Juillet, 1975

Page

MARIANA CIUREANU and V. E. SAHINI, Infrared spectra of benzene halogen complexes 873–881

D. R. ARMSTRONG, The electronic structure of 1,5-dicarba-*closo*-pentaborane (5) and 1,6-dicarba-*closo*-hexaborane(6) 883–888

RODICA VÎLCU and AL. BÎRHALĂ, Second virial coefficient of organic vapours. I. Apparatus 889–899

RODICA VÎLCU and MIHAELA OLTEANU, The surface charge of aluminosilicates in aqueous solutions 901–910

MIHAELA CONSTANTINESCU, E. SEGAL and M. VASS, Thermoelectric power variation during oxygen adsorption on zinc oxide thin films 911–914

MARIA MAVRODIN-TĂRĂBÎC, IOANA ONACA et I. SOLACOLU, Contribution à l'étude de la source chimique de courant Zn/MeOH/O_2. II. L'effet de la variation des paramètres de fonctionnement sur les performances d'une pile à cathode en argent 915–923

I. TEOREANU, MARCELA MUNTEAN and I. DRAGNEA, On the formation of $3(CaO.Al_2O_3).CaSO_4$ in the $CaCO_3-Al_2O_3-FeSO_4$ system 925–928

AMALIA CRUSOS et CR. SIMIONESCU, Greffage mécano-chimique des polyoxyméthylènes. IV. Influence de la température sur la destruction par broyage vibratoire 929–937

CR. I. SIMIONESCU, SVETLANA DUMITRESCU, I. DIACONU and L. GORAŞ, Study of organic polymers with special electrophysical properties. I. On the electric conductivity of diethynylbenzene–2–methylpentinol copolymer films 939–943

N. VOICULESCU, LUCIA ROMAN and I. POPESCU, Reactions of coordinated ligands. VII. Zinc-organic compounds of salicylaldoxime coordinated with Ni(II), Pd(II) and Cu(II) 945–949

ALICE VASILESCU, Dynamics of the ligand exchange in uranyl bis-chelated complexes. I. Fast exchange between bis-(acetylacetonato)-uranyl and acetylacetone studied by NMR 951–955

L. ENESCU, F. CHIRALEU and MARGARETA AVRAM, Investigation in the cyclobutane series. XXXVI. Rearrangement of 8-diazo-*endo*-benzo[*c*]-tricyclo[4.2.1.$0^{2,5}$]non-3-en-7-one on photolysis and in acid media. . . . 957–964

Rev. Roumaine Chim. **20**, 7, p. 871–1026 (1975), Bucarest

A. M. EL-ABBADY and M. A. OMARA, Further studies on the Stobbe condensation of *p*-chlorobenzophenone with dimethyl succinate 965–971

I. DRIMUŞ et L. PAPAHAGI, Oxydation du *n*-dodécane en phase liquide par l'oxygène moléculaire en présence des catalyseurs métalliques pseudohomogènes. II. L'effet des naphténates des métaux lourds 973–980

B. V. BADAMI and G. S. PURANIK, Reactions of sydnones. II. Benzylsydnone and its derivatives 981–984

CECILIA CONSTANTINESCU and LUCIA ANTONESCU, Separation by extraction and spectrophotometric determination of In(III) with triphenylmethane basic dyes 985–991

I. C. POPESCU, ELENA HOPÎRTEAN, L. SAVICI and RODICA VLAD, Characterization of ceramic ion-selective membrane-electrodes. IX. Hg^{2+}-sensitive membrane-electrode 993–999

L. BADEA, Modelling the material balances of chemical flowsheets 1001–1011

S. STERNBERG and MARIANA TERZI, Surface tension of fused ternary mixtures: $NaCl+KCl+AgCl$ and $NaCl+RbCl+AgCl$ 1013–1026

Revue Roumaine de Chimie, **20**, **7**, 873–881 (1975)

INFRARED SPECTRA OF BENZENE HALOGEN COMPLEXES

MARIANA CIUREANU and V.E. SAHINI
Physical Chemistry Laboratory,
University of Bucharest, Bd. Republicii 13, Bucharest, Romania

Received November 19, 1974

An extension of the vibronic formalism proposed by Friedrich and Person [1] is used to explain the intensity enhancement of the infrared bands in donor-acceptor complexes in terms of the present authors' previous results on the ground state structure.[2] The vibrational transition moments are calculated both for the donor and the acceptor bands in benzene-halogen complexes; the results indicate the importance of the resonance integrals changes during the vibration, as well as the necessity of taking into account the contribution of the upper CT states.

1. INTRODUCTION

Studies of changes occurring in the vibrational spectra of donor (D) and acceptor (A) molecules when they combine to form a molecular complex (DA) revealed : a) a characteristic shift of the vibrational frequencies belonging to the D and A molecules [3]; b) a considerable change in the intensity of the bands, as well as the appearance of absorption bands of D and A in the complex that are forbidden in the free molecules [4]; c) the appearance of new low frequency intermolecular bands.[5] Most of the theoretical studies of the IR spectra of the complexes were devoted to the second effect. Thus, Ferguson and Matsen [6] used Mulliken's "resonance model" and pointed out that a possible explanation for the infrared changes observed on complex formation was that they were due to a change in the electron affinity of the acceptor (or ionization potential of the donor) with the vibration coordinates. Friedrich and Person [1,7] described this mechanism in a vibronic interaction formalism and calculated the transition moment for the stretching vibrations of halogens complexed with benzene. Ratajczak and Orville-Thomas [8] used the vibronic formalism to derive a relation between the infrared intensity enhancement and the enthalpy of formation of iodine-base complexes. The possible role of the overlap change during the vibration was stressed by Ferguson[9a] and Szczepaniak.[9b] A comment of the possible role of these terms in the case of weak and strong complexes was made by Shmite and Silins. [10] The theories aiming at demonstrating the non-negligible role of electrostatic interactions in determining infrared spectral changes have a rather contradictory character : in treating benzene-halogen complexes Hanna [11] considers that they are mainly due to quadrupole-induced-dipole interactions ; Mantione [12] demonstrates that for a trigonally hybridized carbon atom the quadrupole moment of the $2p_z$ orbital is completely cancelled by the quadrupole moment due to the other three sp^2 electrons.

---

[1] H. B. Friedrich and W. B. Person, *J. Chem. Phys.*, **44**, 2161 (1966).

[2] a) M. Dobrescu, *Rev. Roumaine Chim.*, **16**, 1825 (1971); b) *ibid.*, **16**, 1841 (1971); M. Dobrescu-Ciureanu and V. E. Sahini, *Rev. Roumaine Chim.*, **18**, 921 (1973).

[3] a) W. B. Person, R. E. Humphrey and W. A. Deskin, *J. Amer. Chem. Soc.*, **80**, 2049 (1958); *ibid.*, **81**, 273 (1959).

[4] a) H. Yada, J. Tanaka and S. Nagakura, *J. Mol. Spectr.*, **9**, 461 (1962) : b) Y. Yarwood, *Trans. Faraday Soc.*, **65**, 934 (1969); c) W. B. Person, C. F. Cook and H. B. Friedrichs, *J. Chem. Phys.*, **46**, 2521 (1967).

[5] a) J. Yarwood, *Spectrochim. Acta*, **26**, 2099 (1970); b) R. F. Lake and H. W. Thompson, *Spectrochim. Acta*, **24-A**, 1321 (1968); c) J. Yarwood and W. B. Person, *J. Amer. Chem. Soc.*, **90**, 3930 (1968).

[6] a) E. E. Ferguson and F. A. Matsen, *J. Chem. Phys.*, **29**, 105 (1958); b) ibid., *J. Amer. Chem. Soc.*, **82**, 3268 (1960).

The purpose of the present paper is to re-examine the problem of infrared spectra of donor-acceptor complexes using Person and Friedrich's formalism in terms of our previous results on the electronic structure of molecular complexes. [2] The discussion is extended to the main spectral changes observed for benzene-halogen complexes.

2. GENERAL SECTION

The intensity of a vibrational transition between two states l and s in the K electronic state is determined by the transition moment vector $M_{k_l k_s}$:

$$M_{k_l k_s} = \iint \Omega_{K_l}(q, Q)\, \mu \Omega_{K_s}(q, Q)\, \mathrm{d}q\, \mathrm{d}Q \tag{1}$$

where Person's [1] notations are used. In the vibronic interaction formalism Ω_{K_l} is given by the product between the vibrational function $\Phi_l^K(Q)$ (depending only on vibrational coordinates Q) and the electronic wave function $\Xi_K(q, Q)$ (depending both on electronic and vibrational coordinates).

---

[7] R. S. Mulliken and W. B. Person, "Molecular Complexes", Willey Intersci. Publ. New York, 1969.

[8] H. Ratajczak and W. J. Orville-Thomas, *J. Mol. Struct.*, **14**, 155 (1972).

[9] a) E. E. Ferguson, *J. Chim. phys.*, **61**, 257 (1964). b) K. Szczepaniak and A. Tramer, *J. Phys. Chem.*, **71**, 3035 (1967).

[10] J. Shmite and E. Silins, *Latv. P.S.R. Zinat. Akad. Vestis. Fiz. Tehn. Zinat. Ser.*, **6**, 45 (1968).

[11] M. W. Hanna and D. E. Williams, *J. Amer. Chem. Soc.*, **90**, 5358 (1968).

[12] M. J. Mantione, *Internat. J. Quant. Chem.*, **3**, 185 (1969).

The electronic wave function in the ground state of a DA complex is given by :

$$\Xi_{\mathcal{N}_0} = \Psi_{N_0}(D, A) + \sum_i a_{E_i} \Psi_{E_i}(D^+A^-) + \sum_j \xi_{N_j} \Psi_{N_j}(DA^*) + \\ + \sum_n \eta_{N_n} \Psi_{N_n}(D^*A) + \cdots \tag{2}$$

The coefficients η_{N_n} and ξ_{N_j} are generally small and will be neglected below. The basic idea of the vibronic interaction formalism is that the dependence of the electronic wave function on the vibronic coordinates can be expressed by expanding $\Xi_{\mathcal{N}_0}$ in a Taylor's series in Q ; therefore, $M_{\mathcal{N}_l\mathcal{N}_s}$ will be given by :

$$M_{\mathcal{N}_l\mathcal{N}_s} = \left\{ \left(\frac{\partial \mu}{\partial Q_l} \right)_0 + 2 \sum_i a^0_{E_i} \mu_{ii} \left(\frac{\partial a_{E_i}}{\partial Q_l} \right)_0 + 2 \sum_i \mu_{0i} \left(\frac{\partial a_{E_i}}{\partial Q_l} \right)_0 + \right. \\ \left. + 2 \sum_{i,j} a^0_{E_i} \mu_{ij} \left(\frac{\partial a_{E_j}}{\partial Q_l} \right)_0 \right\} \times \int \Phi^N_l(Q_l)\, Q_l\, \Phi^N_s(Q_l)\, \mathrm{d}Q_l = \\ = M_{\mathrm{del}} \int \Phi^N_l(Q_l)\, Q_l\, \Phi^N_s(Q_l)\, \mathrm{d}Q_l \tag{3}$$

where the dative coefficients a_{E_i} are approximatively given by :

$$a_{E_i} \cong - \frac{\int \Psi_{N_0} H \Psi_{E_i}\, \mathrm{d}\tau}{W_{E_i} - W_{N_0}} = - \frac{H_{0i}}{\Delta W_i} \cong - \frac{H_{0i}}{\varepsilon_{i_d} - \varepsilon_{j'_a} - C} \tag{4}$$

where W_{E_i} is the energy of the first CT state and W_{N_0} the energy of the ground state ; C contains first and second order energy terms depending mainly on the repulsion integrals $(\delta\delta \mid \rho\rho)$ which are known to vary very slowly with the nuclear coordinates. If E_i is the first CT state, ε_{i_d} and $\varepsilon_{j'_a}$ will be given by the first ionization potential of the donor and, respectively, the electron affinity of the acceptor. If the CT state is obtained by promoting an electron from one of the donor's inner orbitals, the appropriate ionization potential should be taken into account.

H_{0i} is given in a first approximation by :

$$H_{0i} \cong \sqrt{2} \sum_{\delta,\rho} C^{\delta}_{i_d} C^{\rho}_{j'_a} \beta_{\delta\rho} \tag{5}$$

Differentiating eq. (4) one obtains :

$$\left(\frac{\partial a_{E_i}}{\partial Q_l} \right)_0 = - \frac{1}{\Delta W_i} \left(\frac{\partial H_{0i}}{\partial Q_l} \right)_0 - \frac{a_{E_i}}{\Delta W_i} \left(\frac{\partial \Delta W_i}{\partial Q_l} \right)_0 \tag{6}$$

Thus, the change in the a_{E_i} is due both to the changes in ΔW_i and in the resonance integral $\beta_{\delta\rho}$ with the vibrational coordinate.

As readily seen, the present treatment is an extension of Friedrich and Person's [1] theory, with several important changes which will be summarized in the following :

i) The above mentioned authors take into account only the mixing between the ground and the first CT state ; they approximate ΔW_i in eqs.(4), (6) by the CT transition energy $h\nu_{\mathrm{CT}}$ and correlate μ_{0i} with the transition moment of the CT band μ_{EN} ; however, in our previous papers[2] we have shown that the highest occupied orbital of the donor and the lowest energy empty orbital of the electron acceptor are neither the only, nor necessarily the most important contributors to the ground state properties. Ground state properties like dipole moment and stabilization energy are determined to a non-negligible extent by the mixing with the upper CT states ; therefore, it seems reasonable that the latter should be also considered in this case. Besides, in many cases (as for example in the case studied here – the benzene-halogen complexes), the mixing between the ground and first CT state is symmetry forbidden in the equilibrium geometrical configuration. Thus, as a rule, the infrared intensity enhancement cannot be correlated with the transition energy and transition moment of the CT electronic band.

ii) In calculating $(\partial a_{E_i}/\partial Q_l)_0$ Friedrich and Person neglected the first term in (6). In this case, the enhancement of vibrations which do not change ΔW_i (as for example the benzene e_{1g} vibration in benzene-halogen complexes) cannot be explained.

iii) Finally, we note that Friedrich and Person neglected the last two terms in M_{del} which in some cases provide the only possible explanation for the infrared intensity enhancement.

3. APPLICATION TO BENZENE-HALOGEN COMPLEXES

The appearance in the benzene-halogen spectra of several infrared bands which are known to be forbidden in the free molecules will be discussed [7] :

a) the halogen-halogen stretching vibration $\nu\,(X-X)$

b) the out-of-plane hydrogen bending mode (ω_{10})* and the totally symmetrical breathing mode of the benzene ring (ω_1).

The electronic wave function of the complex in the ground state is given by :

$$\Xi_{\mathcal{N}_0}(q, Q) \cong \Psi_{N_0}\;(q, 0) + a_1^0\,\Psi_1(q, 0) + a_2^0\,\Psi_2(q, 0) + a_3^0\,\Psi_3(q, 0) + \tag{7}$$

$$+ \Psi_1(q, 0)\left(\frac{\partial a_1}{\partial Q_l}\right)_0 Q_l + \Psi_2(q, 0)\left(\frac{\partial a_2}{\partial Q_l}\right)_0 Q_l + \Psi_3(q, Q)\left(\frac{\partial a_3}{\partial Q_l}\right)_0 Q_l$$

---

* The numbering of benzene vibrations follows Wilson's notation.[13]

[13] E. B. Wilson, J. C. Decius and P. C. Cross, "Molecular Vibrations. The Theory of Infrared and Raman Vibrational Spectra", McGraw Hill, London, 1955.

where Ψ_1 and Ψ_2 denote the degenerated E_1 states, which are responsible for the charge transfer transition, and Ψ_3 is the upper CT state; Ψ_1 and Ψ_2 arise by promotion of an electron from the degenerated E_{1g} orbitals of benzene (φ_1 and φ_2*) to the empty $5p\sigma_u$ orbital of the halogen; thus, in the geometrical equilibrium configuration (fig. 1) these states are of E_1 symmetry and cannot mix with the $\Psi_{N_0}: a_1^0 = a_2^0 = 0$. However, if the axial geometry of the complex is not preserved during the vibration, Ψ_1 and Ψ_2 may mix with Ψ_{N_0} in a less symmetrical configuration, that is, a_1 and a_2 could have non-equilibrium values different from zero. In other words, vibrations which change the symmetry of the complex might be expected to have nonzero values for $\left(\frac{\partial a_1}{\partial Q_l}\right)_0$ or $\left(\frac{\partial a_2}{\partial Q_l}\right)_0$. Therefore, the delocalization moment is given by:

$$M_{\text{del}} = \left\{\left(\frac{\partial \mu}{\partial Q_l}\right)_0 + 2a_3\,\mu_{33}\left(\frac{\partial a_3}{\partial Q_l}\right)_0 + 2\mu_{01}\left(\frac{\partial a_1}{\partial Q_l}\right)_0 + \right.$$
$$\left. + 2\mu_{02}\left(\frac{\partial a_2}{\partial Q_l}\right)_0 + 2\mu_{03}\left(\frac{\partial a_3}{\partial Q_l}\right)_0 + 2a_3\left[\mu_{13}\left(\frac{\partial a_1}{\partial Q_l}\right)_0 + \mu_{23}\left(\frac{\partial a_2}{\partial Q_l}\right)_0\right]\right\} \tag{8}$$

3.1. CHOICE OF PARAMETERS

All complexes studied here were supposed to have an axial geometry. The main equilibrium geometrical data are those recommended in [2b].

The resonance integrals $\beta_{\delta\rho}$ were calculated by formula:

$$\beta_{\delta\rho} = 0.5\,\mathrm{K}\,S_{\delta\rho}\,(I_\delta + I_\rho) \tag{9}$$

where I_δ and I_ρ are the valence state ionization potentials.

To calculate the overlap integrals $S_{\delta\rho}$ the atomic orbitals of the basic system were decomposed into a σ and a π part and the contributions were estimated separately (fig. 1).

We considered that the vibrations of either the donor or acceptor did not change the distance between the mass centres of the molecules (R); however, they change the interatomic distances $r_{\delta\rho}$, thus producing a change in the resonance integrals $\beta_{\delta\rho}$. Therefore, in order to evaluate the $(\partial H_{0i}/\partial Q_l)_0$

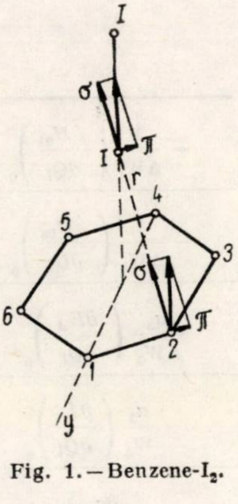

Fig. 1. – Benzene-I_2.

---

* The occupied orbitals of bezene are:

$$\varphi_1 = \frac{1}{\sqrt{2}}(\chi_2 + \chi_3 - \chi_5 - \chi_6)\,(E_{1g})\,;\; \varphi_2 = \frac{1}{\sqrt{12}}(2\chi_1 + \chi_2 - \chi_3 - 2\chi_4 - \chi_5 + \chi_6)\,(E_{1g})$$
$$\varphi_3 = \frac{1}{\sqrt{6}}(\chi_1 + \chi_2 + \chi_3 + \chi_4 + \chi_5 + \chi_6)\,(A_{1u})$$

we have calculated for each vibration several values for H_{0i}, which were plotted *versus* Q_l; the derivative $(\partial H_{0i}/\partial Q_l)_0$ is easily seen to be the slope of this curve at the equilibrium value of Q_l.

The $(\partial E_A/\partial Q_l)_0$ values used in our calculations were those estimated by Person.[14]

The value of $(\partial I_D/\partial Q_l)_0$ for the a_{1g} vibration in benzene was calculated, by formula:

$$\left(\frac{\partial I_D}{\partial Q_l}\right)_0 = K'(Q_0 - Q_0') \tag{9'}$$

where K' and Q' are the force constant and the equilibrium coordinate for the positive ion. Both K' and Q' were estimated by the method proposed by Ferguson[6a] using vibrational analysis data in the vacuum UV spectrum of benzene.

The ΔW_i values used in our calculations were those previously estimated in paper II.

3.2. ENHANCEMENT OF THE HALOGEN STRETCHING VIBRATION

The delocalization moment for the halogen stretching vibration was calculated for several benzene-halogen complexes.

Table 1

Calculated values of $\left(\frac{\partial a_i}{\partial Q_1}\right)_0$

	Halogen stretching vibration			Benzene (C−C) stretching vibration (ω_1)	Benzene C−H bending vibration (ω_{10})
	ν(I − 1)	ν(Br − Br)	ν(Cl − Cl)		
$-\frac{1}{\Delta W_1}\left(\frac{\partial H_{01}}{\partial Q_l}\right)_0$	0	0	0	0	0.0679
$-\frac{1}{\Delta W_3}\left(\frac{\partial H_{03}}{\partial Q_l}\right)_0$	0.0175	0.0220	0.0224	−0.0186	0
$\frac{a_3}{\Delta W_3}\left(\frac{\partial E_A}{\partial Q_l}\right)_0$	0.0119	0.0176	0.0171	—	—
$-\frac{a_3}{W_3}\left(\frac{\partial I_D}{\partial Q_l}\right)_0$	—	—	—	−0.0109	0
$\left(\frac{\partial a_1}{\partial Q_l}\right)_0$	0	0	0	0	0.0679
$\left(\frac{\partial a_3}{\partial Q_l}\right)_0$	0.0294	0.0396	0.0395	−0.0295	0

---

[14] W. B. PERSON, *J. Chem. Phys.*, **38**, 109 (1963).

As the halogen stretching vibration does not change the axial symmetry of the complex, the terms in $(\partial a_1/\partial Q_i)_0$ and $(\partial a_2/\partial Q_i)_0$ vanish and eq. (8) reduces to :

$$M_{\text{del}} = 2\,(a_3\,\mu_{33} + \mu_{13})\left[\frac{a_3}{\Delta W_3}\left(\frac{\partial E_A}{\partial Q_1}\right)_0 - \frac{1}{\Delta W_3}\left(\frac{\partial H_{03}}{\partial Q_i}\right)_0\right]. \tag{10}$$

The values of $\left(\dfrac{\partial a_3}{\partial Q_i}\right)_0$ computed by eq. (6) are listed in table 1 for the complexes under consideration. As seen from this table, the major part of $\left(\dfrac{\partial a_3}{\partial Q_i}\right)_0$ is yielded by the change in H_{03} during the vibration, that is, by a term which was neglected by Friedrich and Person. The calculated values of M_{del} as well as the experimental results are shown in table 2.

Table 2

Experimental and calculated M_{del}

	Halogen stretching vibration			Benzene vibrations in benzene I_2 complex	
	ν(I − I)	ν(Br − Br)	ν(Cl − Cl)	ω_1	ω_{10}
M_{del} (calc)[a]	0.26	0.31	0.19	0.26	0.15
M_e (calc)[a]	0.09	0.11	0.07	0.09	—
M_{del} (exp)[a]	0.19[b]	0.31[b]	0.19[b]	0.21[c]	0.27[c]

a) Values expressed in $D/$ Å uam$^{1/2}$

b) See reference.[7]

c) Experimental values calculated as ;

$M = 1.1936 \quad [A_i/g_i]^{1/2}/N^{1/2}\, 10^{10}\, D/\text{Å}$

where A_i – is the intensity of the band in cm/m. mols in an inert solvent and g_i – is the degeneracy of the vibration The A_i were taken from reference.[15]

3.3. ENHANCEMENT OF THE C–C STRETCHING VIBRATION OF THE BENZENE RING (ω_1)

The normal coordinate Q for the symmetrical stretching mode of the benzene ring is given by :

$$Q = (m/6)^{1/2}\,\Sigma_i\,\delta R_i \tag{11}$$

where m is the carbon mass and δR_i is the length change of the i-th C-C bond.

The delocalization moment for the C-C stretching vibration in benzene complexed with iodine can be calculated by eq. (8). Again, the terms in $\left(\dfrac{\partial a_1}{\partial Q_i}\right)_0$ and $\left(\dfrac{\partial a_2}{\partial Q_i}\right)_0$ will vanish as the overall symmetry of the complex is preserved during the vibration. Thus,

---

[15] E. E. Ferguson and I. Y. Chang, *J. Chem. Phys.*, **34**, 628 (1961).

$$M_{\mathrm{del}} = 2(a_3\,\mu_{33} + \mu_{13})\left[-\frac{1}{\Delta W_3}\left(\frac{\partial H_{03}}{\partial Q_l}\right)_0 - \frac{a_3}{\Delta W_3}\left(\frac{\partial I_D}{\partial Q_l}\right)_0\right] \tag{12}$$

where I_D — is the second ionization potential of the molecule. As seen from table 1 the term in $\left(\frac{\partial H_{03}}{\partial Q_l}\right)_0$ plays a non-negligible part in determining the change of the mixing coefficient $\left(\frac{\partial a_3}{\partial Q_l}\right)_0$.

The calculated value of M_{del} is presented in table 2 together with the available experimental data.

3.4. ENHANCEMENT OF BENZENE E$_{1g}$ VIBRATION (ω_{10})

The e_{1g} mode is an out-of-plane bending of the hydrogen atoms but, as Ferguson [8] pointed out, the C plane has to move in order to preserve the angular momentum; therefore, the vibration has the character of a non-planar rotation — the benzene plane oscillates about the y axis. The normal coordinate for this motion in the complex is, according to Wilson: [13]

$$Q = I_y^{1/2}\,\alpha \tag{13}$$

in which I_y is the moment of inertia of the benzene molecule about the y axis and α is the angle of rotation from the equilibrium position.

As Ferguson [9a] pointed out, in this case $\left(\frac{\partial I_D}{\partial Q_l}\right)_0$ vanishes, because $I_D(+Q_l) = I_D(-Q_l)$; our results show that the same happens with $\left(\frac{\partial H_{03}}{\partial Q_l}\right)_0$, as $H_{03}(Q_l) = H_{03}(-Q_l)$. Therefore, the terms in $\left(\frac{\partial a_3}{\partial Q_l}\right)_0$ are zero in Q (8).

Finally, we must note that during the vibration the symmetry of the complex is lowered from C_{6v} to C_s; therefore, for the nonequilibrium positions of the benzene plane, the degeneracy of the first two CT states disappears and Ψ_1 can mix with the ground state of the complex; thus, $\left(\frac{\partial a_1}{\partial Q_l}\right)_0$ is different from zero in this case and eq. (8) becomes:

$$M_{\mathrm{del}} = -\frac{1}{\Delta W_1}\left\{(2\mu_{01} + 2a_3\,\mu_{13})\left(\frac{\partial H_{01}}{\partial Q_l}\right)_0\right\}. \tag{14}$$

A rigorous treatment of such a motion requires two coordinate systems: i) a space fixed XYZ system with the Z axis along the iodine molecule in its equilibrium position, and ii) a rotating benzene-fixed axis system xyz.

The components of the delocalization moment in the *XYZ* system will be given by :

$$M_X^{\mathrm{del}} = -\frac{2}{I_v^{1/2}\,\Delta W_1}\left(\frac{\partial H_{01}}{\partial \alpha}\right)_0 \{[a_3\,\mu_{13}^x + \mu_{01}^x]\cos\alpha + [a_3\,\mu_{13}^z + \mu_{01}^z]\sin\alpha\} \tag{15}$$

$$M_Z^{\mathrm{del}} = -\frac{2}{I_v^{1/2}\,\Delta W_1}\left(\frac{\partial H_{01}}{\partial \alpha}\right)_0 \{[a_3\,\mu_{13}^x + \mu_{01}^x]\sin\alpha - [a_3\,\mu_{13}^z + \mu_{01}^z]\cos\alpha\}. \tag{16}$$

In both (15) and (16) the second term in paranthesis vanishes, as μ_{13} and μ_{01} have no components along the z axis.

The calculated and experimental values of M_{del} are shown in table 2.

4. DISCUSSION

As seen from table 2, the agreement between the calculated and experimental values of M_{del} is very good in all cases, considering the approximations required in evaluating the parameters. This agreement supports our basic idea (also formulated in ref. 7)) that at least the major part of the observed infrared intensities can be accounted for by the "vibronic interaction" formalism. The differencies between calculated and experimental data can be assigned to the neglect of electrostatic contributions.

We note that in all cases the greatest part of the calculated M_{del} is due to the terms in $\left(\frac{\partial H_{0i}}{\partial Q_l}\right)_0$ wich were neglected until now : in fact, in order to point out their importance, the calculated values of the term $M_e = -\frac{2a_3^2\,\mu_{33}}{\Delta W_3}\left(\frac{\partial \Delta W_3}{\partial Q_l}\right)_0$ (which was the only one considered by Friedrich and Person in calculating $\nu(X - X)$) were listed in table 2. Besides, it has to be noted that, except for the benzene ω_{10} vibration, we have calculated the change in the mixing coefficient of an upper CT state; the first CT states (which are responsible for the CT electronic band) have in these cases no contribution to the infrared enhancement.

An interesting result of the present calculation was the possibility to evaluate M_{del} for the ω_{10} vibration; though the calculated value is smaller than the experimental data, it has been proved that CT states which do not mix with the ground state in the equilibrium configuration may have a non-zero contribution to the delocalization moment (Ferguson [9a] discarded such a possibility).

As for this vibration the ionization potential of the donor has no reason to change, the M_{del} is entirely due to the resonance integral change, thus demonstrating again the necessity of taking into account the first term in (6).

The components of the delocalization moment in the XYZ system will be given by:

$$M_X^{gk} = \frac{2}{R^2 \Delta W_1} \left(\frac{\partial W_{01}}{\partial Q_k} \right)_0 \{ [a_1 \mu_1^X + \mu_{01}^X] \cos\chi + [a_1 \mu_1^Y + \mu_{01}^Y] \sin\chi \} \quad (15)$$

$$M_Y^{gk} = -\frac{2}{R^2 \Delta W_1} \left(\frac{\partial W_{01}}{\partial Q_k} \right)_0 \{ [a_1 \mu_1^X + \mu_{01}^X] \sin\chi - [a_1 \mu_1^Y + \mu_{01}^Y] \cos\chi \} \quad (16)$$

In both (15) and (16) the second term in parenthesis vanishes, as μ_1 and μ_{01} have no components along the z axis.

The calculated and experimental values of M_{gk} are shown in table 2.

4. DISCUSSION

As seen from table 2, the agreement between the calculated and experimental values of M_{gk} is very good in all cases, considering the approximations required in evaluating the parameters. This agreement supports our basic idea (also formulated in ref. 7) that at least the major part of the observed infrared intensities can be accounted for by the "vibronic interaction" formalism. The differences between calculated and experimental data can be assigned to the neglect of electrostatic contributions.

We note that in all cases the greatest part of the calculated M_{gk} is due to the terms in $\left(\frac{\partial W_{01}}{\partial Q_k} \right)_0$ which were neglected until now; in fact, in order to point out their importance, the calculated values of the term $M_k = -\frac{2 a_1 \mu_{01}}{\Delta W_1} \left(\frac{\partial \Delta W_1}{\partial Q_k} \right)_0$ which was the only one considered by Friedrich and Person in calculating $(X - I)$, were listed in table 2. Besides, it has to be noted that, except for the benzene ν_{18} vibration, we have calculated the change in the mixing coefficient of an upper CT state; the first CT states (which are responsible for the CT electronic band) have in these cases no contribution to the infrared enhancement.

An interesting result of the present calculation was the possibility to evaluate M_{gk} for the ν_{18} vibration: though the calculated value is smaller than the experimental data, it has been proved that CT states which do not mix with the ground state in the equilibrium configuration may have a non zero contribution to the delocalization moment (Ferguson discarded such a possibility).

As for this vibration the ionization potential of the donor has no reason to change, the M_{gk} is entirely due to the resonance integral change, thus demonstrating again the necessity of taking into account the first term in (9).

Revue Roumaine de Chimie, **20**, 7, 883–888 (1975)

THE ELECTRONIC STRUCTURE OF 1,5-DICARBA-*CLOSO*-PENTABORANE(5) AND 1,6-DICARBA-*CLOSO*-HEXABORANE(6)

D. R. ARMSTRONG

Department of Pure and Applied Chemistry,
University of Strathclyde, Glasgow Gl,
Scotland

Received April 19, 1974

The electronic structures of 1,5-dicarba-*closo*-pentaborane and 1,6-dicarba-*closo*-hexaborane have been calculated by *ab initio* techniques. Overlap populations and electron density contour plots reveal that the bonding situation is different in the two carboranes. The framework of 1,5-$B_3C_2H_5$ is composed of boron-carbon interactions, while 1,6-$B_4C_2H_6$ is constructed from boron-carbon and boron-boron bonds. In both molecules there is an electron drift from the hydrogen atoms to the carbon atoms.

INTRODUCTION

In a recent publication, [1] the gas-phase electron diffraction patterns of 1,5-dicarba-*closo*-pentaborane (1,5-$B_3C_2H_5$) and 1,6-dicarba-*closo*-hexaborane (1,6-$B_4C_2H_6$) were reported. The carbon atoms are located at apical positions and may be considered as bonded to a planar girdle of three and four boron atoms, respectively. Although they are the smallest members of the *closo*-carborane series, the molecules possess differing structural features. The B–C bond is shorter and the B–B bond is much longer in 1,5-$B_3C_2H_5$ than in 1,6-$B_4C_2H_6$. This suggests that 1,5-$B_3C_2H_5$ may be viewed as a classically bonded structure in which the trigonal bipyramid is composed of C–B–C bonds and involves weak B–B overlap. It was also postulated that in both carboranes the more electronegative carbon atoms could drain electron density from the boron atoms, resulting in a reduction of the boron-boron bonding. A related point of interest concerns the electron density distribution within the polyhedra. Recent calculations [2] on the $B_6H_6^{2-}$ species revealed that the electronic charge is concentrated both at the centre of the cage and at the centre of the trigonal face. It was uncertain how the presence of apical carbon atoms would alter the charge distribution. Therefore, it was of considerable interest to calculate the electronic structure of these molecules.

---

[1] E. A. McNeill, K. L. Gallaher, F. R. Scholer, and S. H. Bauer, *Inorg. Chem.*, **12**, 2108 (1973).

[2] D. R. Armstrong, P. G. Perkins, and J. J. P. Stewart, *J. Chem. Soc., Dalton*, **1973**, 628.

RESULTS AND DISCUSSION

The calculations were performed within the usual LCAO-MO-SCF procedure.[3] The atomic orbitals were represented by four Gaussian functions,[4] so contracted[5] that they simulated the best atomic Slater functions of Clementi and Raimondi.[6] The exponent for the hydrogen 1*s* orbital was taken to be 1.3. The structural parameters of the molecules were extracted from reference 1 and the cartesian *z* axis was made coincidental with the C_3 and C_4 rotational axis of 1,5-$B_3C_2H_5$ and 1,6-$B_4C_2H_6$, respectively.

Table 1

The orbital energies (in au) of 1,5-$B_3C_2H_5$ and 1,6-$B_4C_2H_6$

	1,5-$B_3C_2H_5$		1,6-$B_4C_2H_6$	
vacant orbitals	0.289	$1a_2'$	0.187	$1b_{1u}$
	0.111	$4e'$	0.149	$4e_u$
filled orbitals	− 0.462	$1e''$	− 0.400	$1b_{1g}$
	− 0.504	$3e'$	− 0.501	$1e_g$
	− 0.580	$3a_2''$	− 0.527	$3e_u$
	− 0.605	$5a_1'$	− 0.575	$2b_{2g}$
	− 0.699	$2e'$	− 0.582	$3a_{2u}$
	− 0.728	$4a_1'$	− 0.615	$5a_{1g}$
	− 0.925	$2a_2''$	− 0.749	$4a_{1g}$
	− 1.208	$3a_1'$	− 0.785	$2e_u$
	− 7.734	$2a_1'$	− 0.954	$2a_{2u}$
	− 7.734	$1e'$	− 1.281	$3a_{1g}$
	−11.319	$1a_1'$	− 7.731	$1b_{2g}$
	−11.319	$1a_2''$	− 7.732	$1e_u$
			− 7.732	$2a_{1g}$
			−11.376	$1a_{1g}$
			−11.376	$1a_{2u}$

The energy levels of the two carboranes are presented in Table 1. The figures show that, overall, the filled molecular orbitals of the two compounds have comparable energies. The most noticeable exception is the highest filled orbital, where the eigenvalue of 1,5-$B_3C_2H_5$ is more stable by 162.7 kJ mol^{-1}. The highest filled orbital of 1,5-$B_3C_2H_5$ is largely composed of boron p_z orbitals and carbon p_x and p_y orbitals, while the corresponding orbital of 1,6-$B_4C_2H_6$ is a linear combination of the boron orbitals involved in the B_4 framework. Hence, the mode of electrophilic attack, if it involves the highest filled molecular orbital, will differ for the two carboranes. The CBB triangles will be the likely place for attack for

---

[3] V. R. Saunders, "Atmol2 Computer Programs", Atlas Computing Laboratory, Didcot, England.

[4] S. F. Boys, *Proc. Roy. Soc. A.*, **200**, 542 (1950).

[5] R. F. Stewart, *J. Chem. Phys.*, **52**, 431 (1970).

[6] E. Clementi and D. L. Raimondi, *J. Chem. Phys.*, **38**, 2686 (1963).

$1,5\text{-}B_3C_2H_5$, while for $1,6\text{-}B_4C_2H_6$ the reaction will occur at the boron framework. The lowest empty orbital of both carboranes is mainly comprised of the p_x and p_y orbitals of the boron atoms which are not directed towards other boron atoms. Therefore, nucleophilic attack involving the first virtual orbital will occur at the central zone of boron atoms.

Table 2

The gross atomic and overlap populations of $1,5\text{-}B_3C_2H_5$ and $1,6\text{-}B_4C_2H_6$

		$1,5\text{-}B_3C_2H_5$	$1,6\text{-}B_4C_2H_6$
Atomic populations			
Carbon	s	3.282	3.306
	p_x p_y	2.042	1.932
	p_z	1.186	1.178
	total	6.510	6.416
Boron	s	2.908	2.912
	p_x p_y	1.275	1.620
	p_z	0.752	0.535
	total	4.935	5.067
Hydrogen_B	s	0.877	0.848
Hydrogen_C	s	0.773	0.753
Overlap populations			
	$B-H_B$	0.423	0.418
	$B-B$	−0.118	0.209(*cis*) −0.295(*trans*)
	$B-C$	0.361	0.263
	$C-H_C$	0.414	0.404
	$C-C$	−0.176	−0.246

The gross atomic and overlap populations are presented in table 2. Inspection of the contributions for $1,5\text{-}B_3C_2H_5$ shows that both sets of hydrogen atoms bear a positive charge, with the hydrogens bonded to the carbon atoms donating more electron density than those attached to boron. This released electronic charge finds residence on the carbon atoms, while the borons possess a small positive charge. The overlap populations reveal that the B-B and C-C bonds are antibonding and it is the B-C bonds which are responsible for the stability of the molecule.

Examination of the corresponding figures for $1,6\text{-}B_4C_2H_5$ reveals that the charge on the hydrogens is more positive than on the hydrogen atoms of the dicarbapentaborane. As the boron atoms in $1,6\text{-}B_4C_2H_6$ have a small negative charge, the excess electron density on the carbon atoms is not as large as in $1,5\text{-}B_3C_2H_5$. The overlap population values indicate that there is bonding between *cis*-boron atoms but interactions between *trans*-boron atoms are antibonding. Boron-carbon bonding is present in $1,6\text{-}B_4C_2H_6$ but it is not as strong as in $1,5\text{-}B_3C_2H_5$.

The electronic distribution was subjected to further examination by means of electron density plots of various regions of the carboranes. Figure 1 shows the total electron density contours of $1,5\text{-}B_3C_2H_5$ through

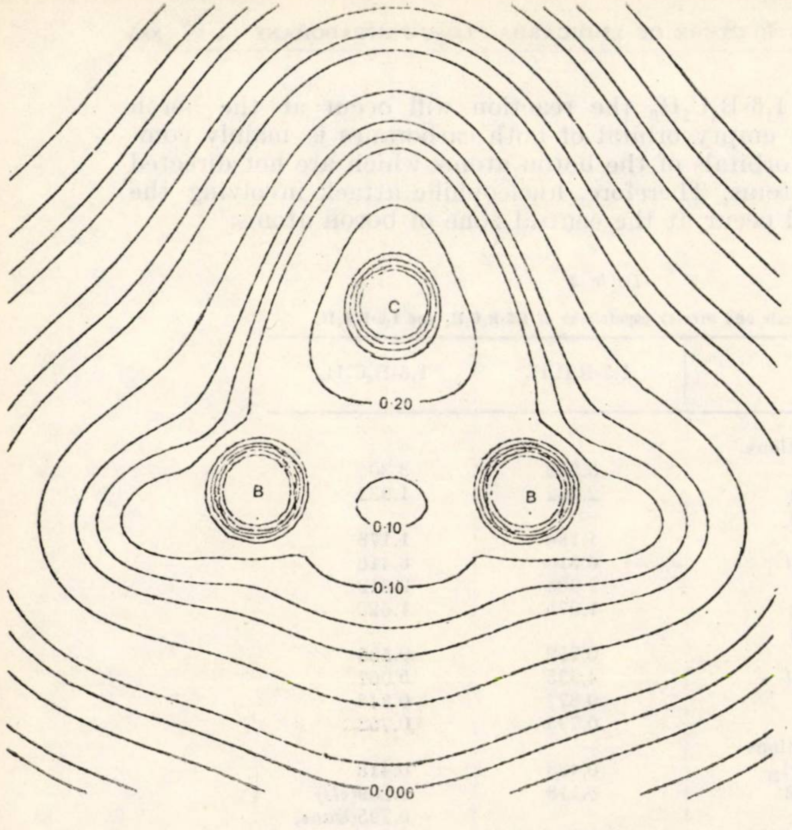

Fig. 1. — Electron density contours for 1,5-$B_3C_2H_5$, a section containing a CBB triangular face.

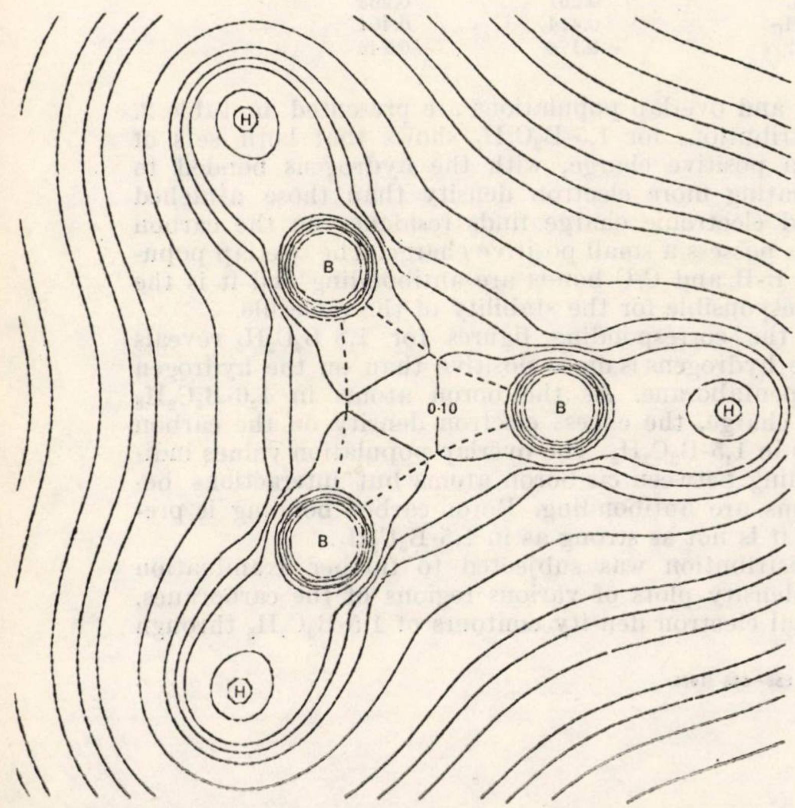

Fig. 2. — Electron density contours for 1,5—$B_3C_2H_5$, a section containing the BBB triangle.

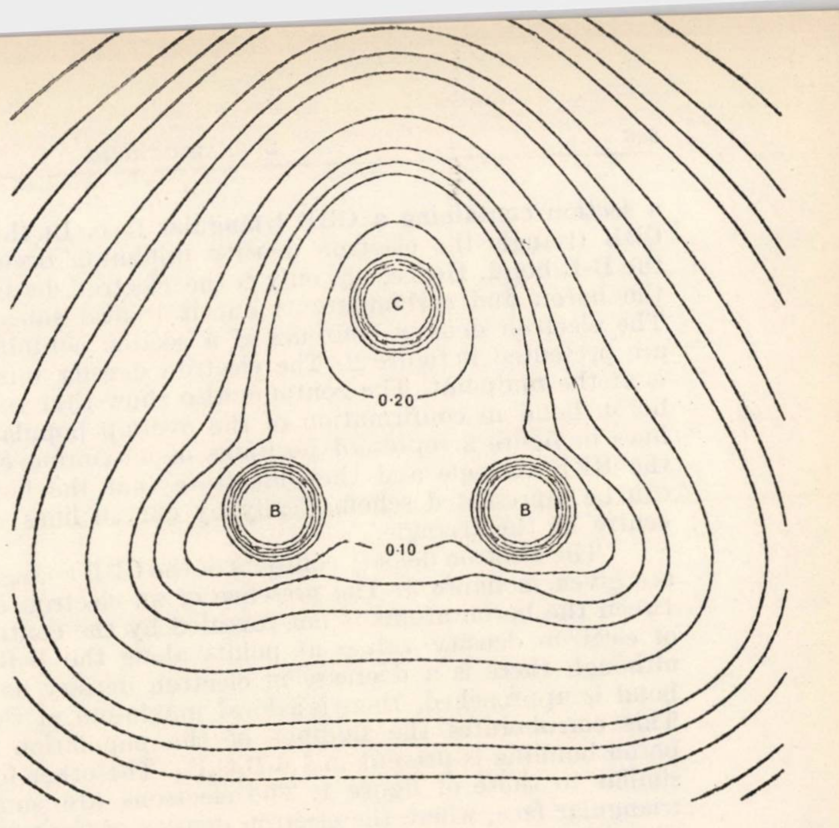

Fig. 3. — Electron density contours for 1,6-$B_4C_2H_6$, a section containing a CBB triangular face.

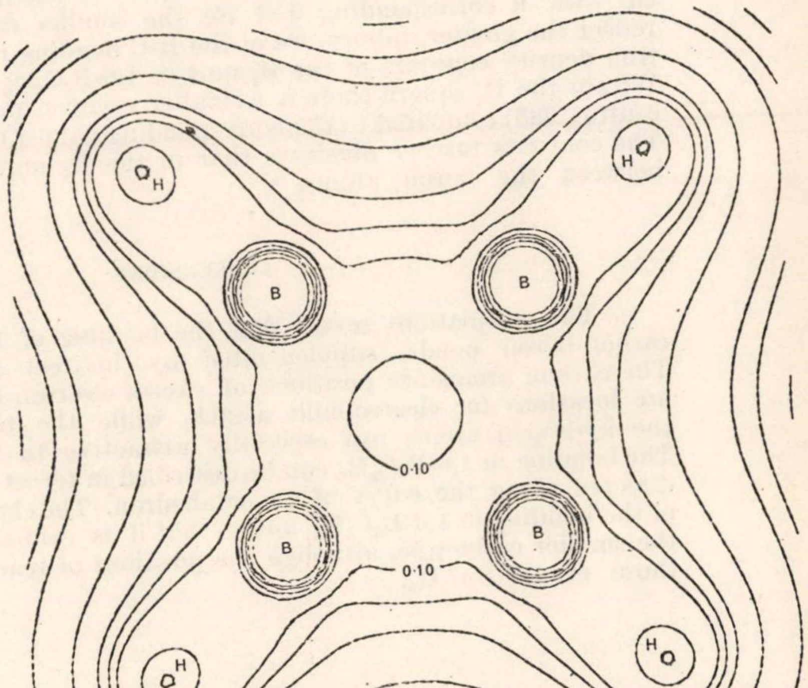
H
H
B
B
0·10
B
B
0·10
H
H

Fig. 4. — Electron density contours for 1,6-$B_4C_2H_6$, a section containing the B_4 square.

a section containing a CBB triangular face. In the area enclosed by the CBB triangle the electron density minimum occurs at the midpoint of the B-B bond. Hence, not only is the electron density distributed between the boron and carbon atoms but it is also smeared over the triangle. The electron density contours of a section containing the BBB triangle are presented in figure 2. The electron density minimum of the triangle is at the midpoint. The contours also show that there is no direct boron-boron bond in confirmation of the overlap population data. The dotted lines in figure 2 represent positions of maximum electron density within the BBB triangle and they illustrate that the boron-boron interactions can be represented schematically by curved lines which arc towards the centre of the triangle.

The electron density contours of the CBB triangular face of 1,6-$B_4C_2H_6$ are given in figure 3. The presence of an electron density minimum between the boron atoms is not revealed by the contours. Closer inspection of electron density values at points along the B-B bond discloses that, although there is a decrease in electron density as the midpoint of the bond is approached, there is a local maximum at the centre of the bond. This corroborates the findings of the population analysis that boron-boron bonding is present in 1,6-$B_4C_2H_6$. The other features of the plot are similar to those of figure 1. The electrons are smeared over the CBB triangular face, where the electron density of the midpoint is 0.19 compared with a corresponding 0.21 for the smaller carborane. These values reflect the greater importance of the B-C bonding in 1,5-$B_3C_2H_5$. The electron density contours of the B_4 unit of 1,6-$B_4C_2H_6$ are shown in figure 4. Within the B_4 square there is a smaller electron density minimum in the centre (.085) compared to the corresponding value (.094) for the B_3 triangle. The contours further illustrate that in the B_4 unit, electron density lies between the boron atoms.

CONCLUSIONS

The calculations reveal that the bonding of 1,5-$B_3C_2H_5$ consists of carbon-boron bonds, supplemented by indirect boron-boron bonding. The carbon atoms are positions of excess electron density and therefore are locations for electrophilic attack, while the boron-boron bond and the hydrogen atoms are especially attractive to nucleophilic reagents. The bonding in 1,6-$B_4C_2H_6$ can be described in terms of B-C and C-C bonds directed along the edges of an octahedron. The homogeneous character of the bonding in 1,6-$B_4C_2H_6$ means that it is probably less reactive than the smaller carborane, although the positions of reactivity are the same as those of 1,5-$B_3C_2H_5$.

Revue Roumaine de Chimie, 20, 7, 889-899 (1975)

SECOND VIRIAL COEFFICIENT OF ORGANIC VAPOURS. I

APPARATUS

RODICA VÎLCU and AL. BÎRHALĂ

Institute of Physical Chemistry, str. Galaţi 31, Bucharest, Romania

Received April 5, 1974

The experimental device employed in the second virial coefficient determinations in organic vapours, by a differential compressibility method, is described. The apparatus was checked up on vapours of *n*-hexane and benzene at temperatures between 313 and 338 K. The second virial coefficient of methylene chloride vapours within 303 – 348 K was also determined.

INTRODUCTION

Several equations of state have been advanced which correlate P, V, T values of real gases and vapours. From them the only one that has a rigorous theoretical foundation is the virial eqaution of state. It is an expansion in power series of compressibility factor PV/RT in terms of volume (density) or pressure:

$$PV/RT = 1 + B/V + C/V^2 + D/V^3 + \ldots \tag{1}$$

or

$$PV/RT = 1 + B'P + C'P^2 + D'P^3 \ldots \tag{2}$$

where P stands for pressure, V for molar volume, R for gas constant, T for temperature and B, C, D,... for virial coefficients. The latter are connected to B', C', D', ...by equations:

$$B = RTB'$$

$$C = (RT)^2 (C' + B'^2) \tag{3}$$

$$D = (RT)^3 (D' + 3B'C + B'^3).$$

At low pressure the virial series may be truncated at the second term so that it is just the second virial coefficient that has to be known. At higher pressure, higher order virial coefficients are considered.

In pure substances the virial coefficients depend only on the temperature and the nature of the substance. In mixtures, the virial equation takes the same form as in pure gases, the virial coefficients of the mixture being expressed in terms of those of pure components and their mole fractions, y :

$$B_{am} = \Sigma\, y_i\, y_j\, B_{ij} \tag{4}$$

where B_{am} is the second virial coefficient of the mixture, B_{ii} and B_{jj}, the virial coefficients of pure components and B_{ij}, the interaction virial coefficient.

In particular for a binary mixture (components 1 and 2), B_{am} is given by :

$$B_{am} = y_1^2\, B_{11} + 2y_1y_2\, B_{12} + y_{22}^2 B_{22}\,. \tag{5}$$

It is well known that the second virial coefficients of pure substances as well as those of interaction are important for the study of various intermolecular potentials and for the determination of thermodynamic properties of real gas mixtures. [1-5]

The connection between the interaction virial coefficients and intermolecular potentials is given by equations of statistical mechanics.

Thus, for molecules interacting according to a $\varphi_{12}(r)$ potential which depends only on the intermolecular distance r, B_{12} is expressed by:

$$B_{12} = -\,2\pi N \int_0^{\infty} \{\exp\ [-\ \varphi_{12}(r)/kT] - 1\}\, r^2 \mathrm{d}r \tag{6}$$

where N is Avogadro's number, and k Boltzmann's constant.

For molecules interacting according to an angle dependent potential $\varphi_{12}(r,\ \theta_1,\ \theta_2,\ \varnothing_2 - \varnothing_1)$, B_{12} is given by :

$$B_{12} = -\,\frac{1}{4}\, N \int_0^{\infty}\int_0^{2\pi}\int_0^{\pi}\int_0^{\pi} \{\exp\ [-\varphi_{12}(r,\ \theta_1,\ \theta_2, \varnothing_2 - \varnothing_1/kT] - 1\} \times$$

$$\times \sin\theta_1\, \mathrm{d}\theta_1 \sin\theta_2\, \mathrm{d}\theta_2\, \mathrm{d}(\varnothing_2 - \varnothing_1)\, r^2\, \mathrm{d}r \tag{7}$$

where θ_1, θ_2, $\varnothing_2 - \varnothing_1$, are the angle coordinates of molecules.

The second interaction virial coefficient may be calculated theoretically if the exact expression of interaction potential is known.

Since establishing the analytical form of potential has not been done so far, the practical calculations make use of empirical and semiempirical potentials of which the most frequently used are Lennard — Jones (6 — 12) (for non-polar molecules) and Stockmayer (6 — 12) (for polar ones).

---

[1] J. O. HIRSCHFELDER. C. F. CURTISS and R. B. BIRD, "Molecular Theory of Gases and Liquids", Wiley, New York, 1954.

[2] R. C. REID and T. K. SHERWOOD, "The Properties of Gases and Liquids", Mc Graw-Hill, New York, 1966, chap. 3 and 7.

[3] E. A. MASON and T. H. SPURLING, "The Virial Equation of State", Pergamon Press, Oxford, 1969.

[4] AL. BÎRHALĂ, *Studii şi Cercetări Chim. Acad. R.S.R.*, **21**, 215 (1973)

[5] AL. BÎRHALĂ, *Studii şi Cercetări Chim. Acad. R.S.R.*, in press.

In mixtures, the potential parameters are determined with the help of combinational rules which have also an empirical character.

On the other hand, the experimental virial coefficients may serve to determining the force constants of potentials which describe the molecular interaction.[3]

In order to characterize thermodynamically the mixtures of organic vapours, we have started a systematic study of the second interaction virial coefficient of such systems at low pressure (under 1 atm.).

A differential compressibility method based upon compression of vapours and a reference gas, whose virial coefficient is precisely known, was chosen. Nitrogen has been used as reference gas.

PRINCIPLE OF THE METHOD

The differential compressibility method has been used in two alternatives : measuring either the volume difference at constant pressure [6-12] or the pressure difference at constant volume,[13-18] both occurring on isothermal compression of the two gases.

We have chosen the second variant, the compression of gas taking place in precisely calibrated pipettes of identical volume. The pressure difference is related to the second virial coefficient.

Such an alternative bears advantage over the direct methods of measuring the second virial coefficient in that the precision of measurements depends on the accuracy of measuring pressure differences of some cm of Hg.

EXPERIMENTAL

The device we have used (fig. 1) is similar to that described by Mc Glashan *et al*[16-18] and consists of the following parts :

1. differential piezometer
2. vapour feed line

---

[6] C. G. Addingley and R. Whytlaw – Gray, *Trans Faraday Soc.*, **24**, 378 (1928).

[7] G. A. Bottomley, D. S. Massie and R. Whytlaw – Gray, *Proc. Roy. Soc.* **A 200**, 201 (1950).

[8] G. A. Bottomley and C. G. Reeves, *Proc. Roy Soc.*, A **246**, 504 (1958).

[9] G. A. Bottomley and T. H. Spurling, *Austral J. Chem.*, **16**, 1 (1963) **17**, 501 (1964).

[10] W. Kappallo, W. N. Lund and K. Schäfer, *Z. phys. Chem. (Frankfurt)*, **37**, 196 (1963).

[11] R. N. Lichtenthaler, B-Schramm and K. Schäfer, *Ber. Bunsengesellschaft Phys. Chem.*, **73**, 36 (1969).

[12] R. N. Lichtenthaler and K. Schäfer, *Ber. Bunsengesellschaft Phys. Chem.*, **73**, 42 (1969).

[13] S. D. Hamann and J. F. Pearse, *Trans. Faraday Soc.*, **48**, 101 (1952), **49**, 351 (1953).

[14] A. Perez Masiá and M. Diaz Peña, *Anales real Soc. españ. Fis. Quim.*, **54**, 661 (1958). **60**, 229 (1964).

[15] M. Rätzch and H. J. Bittrich, *Z. phys Chem (Leipzig)*, **227**, 121 (1964).

[16] M. L. Mc Glashan and D. J. B. Potter, *Proc. Roy Soc.*, **A 267**, 478 (1962).

[17] M. L. Mc Glashan and C. J. Wormald, *Trans. Faraday. Soc.*, **60**, 66 (1964).

[18] P. G. Francis, M. L. Mc Glashan and C. J. Wormald, *J. Chem. Thermodynamics*, **1**, 441 (1969).

3. nitrogen feed line

This was the device we have used in determinations on pure substances.

1. *Differential piezometer* (fig. 2) consists of two Pyrex glass pipettes, each made up of three bulbs, the adjacent bulbs of the two pipettes having about the same volume (72cm^3 the bottom pair, 24 cm^3 the middle one and 36 cm^3 the top one). The two pipettes are connected by a differential manometer *D*.

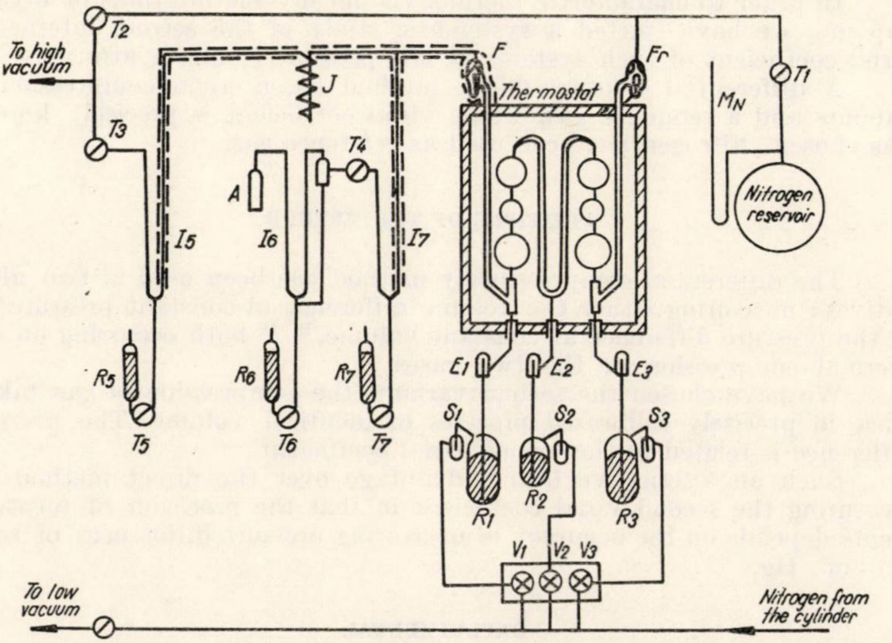

Fig. 1. — Apparatus for the second virial coefficient measurement.

The volumes were so chosen as to give successive compressions of two and three times the initial pressure.

In the left arm of the piezometer one introduces the gas under study while in the right one, denoted by *r*, the reference gas. The gases are compressed by the mercury introduced through the bottom capillaries.

The manometers *M*, *Mr* and *D* were made of Pyrex glass of 10 mm internal diameter which has allowed to avoid capillarity effects at mercury menisci readings.

On each pippete and the differential manometer reference marks were etched at positions 1, 2, ... 5 and *r*1, *r*2, ... *r*5, respectively. On the marks tungsten wire rings (Ø = = 0.02 mm) were glued which allowed a fairly good positioning of menisci at volume delimitation.

Before assembling as in fig. 2 each pipette was volumetrically calibrated. Volumes were determined with mercury by weighing.

The following volumes were defined: V_1 between marks 1 and 5, V_2 between marks 2 and 5, V_3 between marks 3 and 5, and V_{r1}, V_{r2} and V_{r3} similarly defined for the reference pipette.

In calculation only the volume ratios V_2/V_1, V_3/V_1, V_{r2}/V_{r1} and V_{r3}/V_{r1} are required.

For each pipette the volumes defined above were measured 4 times and results averaged to get the final one.

The gravimetric calibration with mercury was checked up by differential compressibility measurments with nitrogen in both pipettes.

A good agreement of volume ratios obtained by the two methods was attained.

2. *Vapour feed line* comprises :

a) the evaporation ampoule *A* (fig. 3) which serves to storing liquids and degasing them by reiterated boiling and freezing prior to evaporation.

b) mercury cut-offs I_5, I_6 and I_7 together with mercury reservoirs R_5, R_6 and R_7 and taps T_5, T_6 and T_7, which isolate the vapours from greased taps before they are introduced in the pipette *P*.

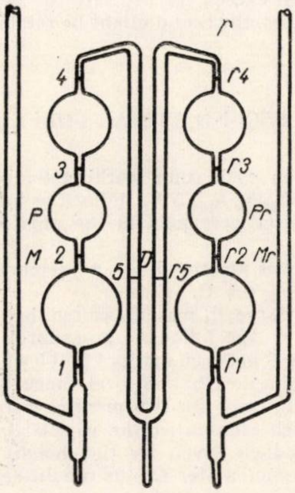

Fig. 2. — Differential piezometer.

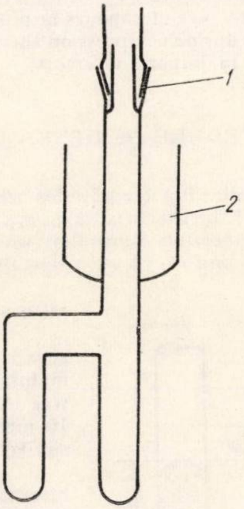

Fig. 3. — The evaporation ampoule *A* : *1*, conical joint ; *2*, cooling jacket.

The part of device surrounded in fig. 1 by dotted lines has been electrically heated during runs to prevent vapour condensing on their passing to pipette *P*.

c) cold finger *J*, which serves to condense parts of the liquid from ampoule *A* before it was vaporized and introduced in *P*.

3. *Nitrogen feed line,* consists of a purifying device (not shown in figure), the reservoir of purified nitrogen and manometer M_N on which its pressure is read.

The differential piezometer was introduced in a thermostat with glass window to facilitate measurements.

The thermostat was filled up with paraffin oil which permits raising the temperature up to 150 – 200 °C within ± 0.1 °C.

The gas introduced into piezometer is compressed by mercury which is risen or lowered from/into reservoirs R_1, R_2 and R_3 by either nitrogen pressure (from the cylinder) or pumping. Rising or lowering of the mercury is carried out by fine valves V_1, V_2 and V_3.

Traps E_1, E_2 and E_3 serve to catch air bubbles from mercury, while S_1, S_2, S_3 protect V_1, V_2, V_3.

Floating valves *F* and *Fr* located above the thermostat on *M* and *Mr* limbs of the piezometer separate the mercury from the rest of the device, whenever gas compression is too high.

T_1, T_2, T_3 and T_4 are vacuum taps ; T_4 is a three way teflon tap which allows both passing of vapours from ampoule *A* (without vacuum grease contamination) and opening the device to the atmosphere.

PROCEDURE

The whole apparatus is connected by T_2 and T_3 taps to high vacuum device and evacuated for 3 – 4 hours.

The mercury is risen into the differential manometer and nitrogen introduced from the resevoir into pipette *Pr* and the latter confined by rising mercury into *Mr*.

Part of the degased liquid from ampoule *A* was evaporated and the frozen on trap *J*. After handling I_5 and I_3 mercury cut-offs, the liquid condensed on *J* is evaporated in pipette *P* and confined by rising mercury into *M*. Then the device is pumped again.

The pressure of vapours in pipette *P* must not exceed the pressure of dew point of the substance. If during compression the vapour condenses, the liquid might be retained by mercury which leads to important errors.

PROCEDURE OF DETERMINING THE SECOND VIRIAL COEFFICIENT

The following magnitudes were measured on each run : working temperature, initial pressure P_1 of the gas, heights $h_1, h_{r1}, \Delta h_1, h_2, h_{r2}, \Delta h_2, h_3, h_{r3}, \Delta h_3$, defined as in figure 4.

The subscripts show that the mercury menisci were held in the pipette *P* and P_r at marks 1, 2, 3 and *r*1, *r*2, *r*3, respectively.

Temperature was measured by a mercury thermometer with an accuracy of ± 0.1 °C.

The initial pressure P_1 was measured by nitrogen pressure in P_r according to the following procedure : Vapours were maintained in pipette *P* between marks 1 and 5 while the mercury was maintained in pipette P_r under *r*1 mark in the tube of 10 mm diameter ; this way the two menisci were in tubes of similar diameter which eliminated the capillarity effects.

Pressure P_1 is then given by the height difference of mercury columns of manometer *D* plus the difference of P_r and M_r mercury columns.

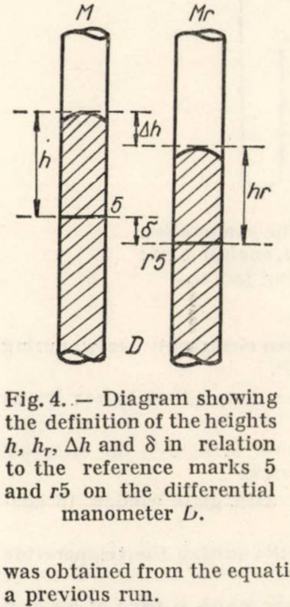

Fig. 4. – Diagram showing the definition of the heights h, h_r, Δh and δ in relation to the reference marks 5 and *r*5 on the differential manometer *D*.

MEASUREMENT OF HEIGHTS h, h_r AND Δh

To calculate the second virial coefficient one needs the following magnitudes : Δh_1 at $h_1 = 0$, Δh_2 at $h_2 = 0$, Δh_3 at $h_3 = 0$, h_{r1} at $h_1 = 0$, h_{r2} at $h_2 = 0$ and h_{r3} at $h_3 = 0$. In figure 4 one can see that $h + \delta = h_r + \Delta h$, where δ is the distance between marks 5 and *r*5 resulting from glassware assembling.

The magnitudes mentioned above were measured as follows : with mercury at marks 1 and *r*1, Δh_1 was measured on the differential manometer *D* for 8 – 10 values of *h*, within the range $h_1 = \pm 3 - 4$ cm. The value of Δh_1 at $h_1 = 0$ was interpolated from a graphic Δh_1 *vs* h_1. The value of h_{r1} at $h_1 = 0$ was obtained from the equation : $h_{r1}(h_1 = 0) = \delta - \Delta h_1 \, (h_1 = 0)$, the value of δ was taken from a previous run.

The values Δh_2 at $h_2 = 0$, Δh_3 at $h_3 = 0$, h_{r2} at $h_2 = 0$ and h_{r3} at $h_3 = 0$ were measured the same way with mercury at marks 2 and *r*2, 3 and *r*3.

This procedure has led to more exact values than those obtained from only one measurement of $\Delta h_1, \Delta h_2$ and Δh_3 on the differential manometer.

The height differences were measured with a cathetometer.

REAGENTS

High purity substances were used : nitrogen was over 99.8 % purity while the others were spectroscopically pure grade.

To remove oxygen and water traces from nitrogen it was passed through a column containing pellets of Cu-Ni catalyst deposited on kieselguhr, then through two columns of silicagel.

Organic liquids were degassed several times directly into the working ampoule prior to vaporizing.

CALCULATION OF THE SECOND VIRIAL COEFFICIENT

Starting with the virial equation of state truncated after the second term, one obtains three similar equations corresponding to the three steps of compression :

$$P_i V_i = n\,R\,T(1 + n\,B/V_i) \qquad (i = 1,2,3) \tag{8}$$

From these equations one obtains independent equations for B in terms of unknowns B and n. The pair of equations $i = 1$, $i = 2$ gives the value of B, B_{12}, while $i = 1$, $i = 3$ pair, gives B_{13}.

A calculation which eliminates n from the two pairs of equations leads to the following values of B_{12} and B_{13}.

$$-B_{12} = RT\frac{V_1V_2(V_1 - V_2)(P_1V_1 - P_2V_2)}{(P_1V_1^2 - P_2V_2^2)^2},$$

$$-B_{13} = RT\frac{V_1V_3(V_1 - V_3)(P_1V_1 - P_3V_3)}{(P_1V_1^2 - P_3V_3^2)^2} \tag{9}$$

which are simplified if one uses the volume ratios :

$$-B_{12} = RT\frac{V_2/V_1(1 - V_2/V_1)(P_1 - P_2V_2/V_1)}{[P_1 - P_2(V_2/V_1)^2]^2},$$

$$-B_{13} = RT\frac{V_3/V_1(1 - V_3/V_1)(P_1 - P_3V_3/V_1}{[P_1 - P_3(V_3/V_1)^2]^2}. \tag{10}$$

In these equations we know : the volume ratios (determined by volumetric calibration of pipettes), temperature and initial pressure P_1. The only unknowns are P_2 and P_3 which were determined by measurements of Δh and h_r as follows :

Pressures P_1, P_2, P_3 of the gas in pipette P are connected to P_{r1}, P_{r2}, P_{r3} of nitrogen in pipette P_r by the relations :

$$P_1 = P_{r1} + \Delta P_1,\; P_2 = P_{r2} + \Delta P_2,\; P_3 = P_{r3} + \Delta P_3 \tag{11}$$

where $\Delta P'\,s$ are defined by : $\Delta P_i = \rho g\,\Delta h_i$ with ρ standing for mercury density at working temperature, g for acceleration of gravity (in Bucharest,[19] 980.54 cm S^{-2}) and Δh_i for heights read on the differential manometer.

---

[19] N. Bărbulescu, "Fizică moleculară şi căldură", Ed.didactică şi pedagogică, Bucharest, 1970.

Pressures P_{r_2} and P_{r_3} of nitrogen may be connected to P_{r1}, by its equation of state.[16]

$$\begin{aligned} P_{r2} &= P_{r1}(V_{r1}/V_{r2})\,[1 - P_{r1}(V_{r1}/V_{r2} - 1)\ B_N/RT] \\ P_{r3} &= P_{r1}(V_{r1}/V_{r3})[1 - P_{r1}(V_{r1}/V_{r3} - 1)\ B_N RT] \end{aligned} \qquad (12)$$

where B_N is the second virial coefficient of nitrogen at the working temperature. The values of B_N were calculated according to the equation :

$$B_N = 274.2 - 227.1\ \text{exp.}\ (61.40/T) \qquad (13)$$

The ratios V_{r1}/V_{r2} and V_{r1}/V_{r3} were supplied by the results of pipette calibration and the values of h_{r1}, h_{r2} and h_{r3} determined as indicated above.

If one replaces (12) in (11) one ends up with P_2 and P_3 in terms of the measured magnitudes :

$$\begin{aligned} P_2 &= (P_1 - \Delta P_1)\,(V_{r1}/V_{r2})[1 - (P_1 - \Delta P_1)\,(V_{r1}/V_{r2} - 1)\ B_N/RT + \Delta P_2] \\ &\hfill (14) \\ P_3 &= (P_1 - \Delta P_1)(V_{r1}/V_{r3})\ [1 - (P_1 - \Delta P_1)\,(V_{r1}/V_{r3} - 1)\ B_N/RT + \Delta P_3]. \end{aligned}$$

Thus the direct measuring of P_2 and P_3 was avoided, as a measurement would have required a manometer 3 times longer than M, whose accomodation in a thermostat provided with a window would have been an outstandingly difficult problem.

By introducing P_2 and P_3 given by (14) in (10) one obtains the equations which were used in calculating the second virial coefficient for the two compressions (B_{12} and B_{13}). The final value of the second virial coefficient was obtained by averaging:

$$B = 1/3\ (B_{12} + 2\ B_{13}) \qquad (15)$$

since the error in B_{12} determination is twice larger than in B_{13}, s.

RESULTS AND DISCUSSION

The device built up by us was checked up with determinations of the second virial coefficient of *n*-hexane and benzene vapours at three temperatures ranging between 313 and 338 K.

The results are listed in tables 1 and 2 together with data available in literature.

cm^3/mole was maintained as unit for B as it is of general use (conversion into S.I. units would be a senseless problem).

Although we have not found comparison data at all temperatures for which the device was checked up, one can see that our results fit well the values of other workers on a wider temperature range.

After the device was verified we have determined the second virial coefficient of methylene chloride (CH_2Cl_2) vapours within the 303 – 348 K temperature range.

The results are given in table 3 compared to other authors' and to those calculated.

Table 1

Second virial coefficient of *n*-hexane vapours at different temperatures

Temp K	$-B/cm^3\ mol^{-1}$					
	This paper	a	b	c	d	e
313	—	1676	1620	—	—	1750
315	—	—	—	1750	—	—
318	1668	1637	—	—	—	—
320	—	—	—	—	1560	—
322	—	—	—	—	1500	—
323	—	—	—	1590	—	—
324	—	1496	—	—	—	—
328	1490	—	1406	—	—	1550
332	—	1419	—	—	—	—
335	—	—	—	1450	1265	—
338	1350	1326	—	—	—	—

[a] M. L. MC GLASHAN and D. J. B. POTTER, *Proc. Roy. Soc.* **A 267**, 478 (1962).

[b] G. A. BOTTOMLEY and C. G. REEVES, *J. Chem Soc*, **1958**, 3794.

[c] R. F. HAJJAR, W. B. KAY and G. F. LEVERETT, *J. Chem. Eng. Data*, **14**, 377 (1969).

[d] J. D. LAMBERT, G. A. H. ROBERTS, J. S. ROWLINSON and V. J. WILKINSON, *Proc. Roy. Soc.* **A 196**, 113 (1949).

[e] M. L. MARTIN and P. J. DUNLOP, *J. Chem Educ.*, **46**, 615 (1969).

Table 2

Second virial coefficient of benzene vapours at dfferent temperatures

Temp K	$-B/cm^3\ mol^{-1}$					
	This paper	a	b	c	d	e
313	—	—	1565	—	—	—
316	—	1300	—	—	—	—
318	1325	—	—	—	—	—
323	1240	—	1215	—	—	—
325	—	1137	—	—	—	—
329	—	—	—	—	—	1143
331	—	—	1150	1123	1125	1124
333	1136	1064	—	—	1117	1114

[a] P. G. FRANCIS, L. M. MC GLASHAN, S. D. HAMANN and W. J. MCMANOMEY, *J. Chem. Phys.*, **20**, 1341 (1952).

[b] R. F. HAJJAR, W. B. KAY and G. F. LEVERETT, *J. Chem. Eng. Data*, **14**, 377 (1969).

[c] G. A. BOTTOMLEY and T. H. SPURLING, *Austral J. Chem.*, **19**, 1331 (1966).

[d] F. G. WAELBROEK, *J. Chem Phys.*, **23**, 749 (1955); **54**, 710 (1957).

[e] P. G. FRANCIS, M. L. GLAHAN and C. J. WORMALD, *J. Chem Thermodynamics* **1**, 441 (1969).

Both these data as well as those in table 3 represent the average over three measurements whose maximum deviation does not exceed 2 %.

The experimental values and those calculated by using the parameters of the Stockmayer potential functions, from Polak and Lu's paper[20] and table II-A of reference 1, are compared. There is a good agreement between these values, the percentage deviation being of about 5 %.

Table 3

Seecond virial coefficient of CH_2Cl_2 vapours at different temperatures

Temp. K	$-B/cm^3\ mol^{-1}$			
	This paper	a	b	c
303	802	810	—	805
313	770	777	—	729
323	681	—	675	655
348	555	—	544	540

[a] M. RÄTZSCH, *Z. phys. Chem.*, *(Leipzig)*, **238**, 321 (1968).

[b] A. PEREZ MASIÁ and M. DIAZ PEÑA, *Anales real. Soc. españ. Fis. Quim.*, **54**, 661 (1958).

[c] Calculated using Stockmayer potential function.

DISCUSSION OF ERRORS

The compressibility method is affected by a series of errors of which the most important are due to the adsorption of vapours on glass, on mercury surface or vacuum grease.

Bottomley *et al.*, [21-24] have shown that errors due to vapour adsorption on glass become important at low temperatures. They are of the order ± 30 — 100 cm³/mole.

It is also Bottomley *et al.* [25] who have shown that adsorption of vapours on mercury surface increases with pressure.

To minimize the errors mentioned above, all piezometer feed line was "washed" with vapours 2 — 3 times prior to feeding of vapours into pipette *P*.

Contamination of vapours with vacuum grease was avoided by employing mercury cut-offs and the teflon tap.

The errors which affect the determination of the second virial coefficient are firstly due to errors in determining the pressure difference ΔP and initial pressure P_1.

---

[20] J. Polak and B. C. Y. Lu, *Canad. J. Chem. Eng.*, **50**, 553 (1972).

[21] G. A. Bottomley and C. G. Reeves, *Trans Faraday Soc.*, **53**, 1455 (1957).

[22] G. A. Bottomley, I. H. Coopes, G. L. Nyberg and T. H. Spurling *Austral. J. Chem.*, **15**, 1105 (1965).

[23] R. Whutlow-Gray and G. A. Bottomley, *Nature*, **180**, 1252 (1957) ; **181**, 1004 (1958).

[24] G. A. Bottomley, T. A. Remington and R. Whutlaw-Gray *Proc. Roy. Soc.* **A**, **246**, 514 (1958).

[25] G. A. Bottomley, C. G. Reeves and R. Whytlaw—Gray, *Proc. Roy. Soc.* **A**, **246**, 504 (1958).

This is evident if in the equations used for the calculation of B_{12} and B_{13} the following approximations are made :

(I) $B_N = 0$, (II) $V_2/V_1 = V_{r2}/V_{r1} = 1/2$ and $V_3/V_1 = V_{r3}/V_{r1} = 1/3$ and (III) $2 \Delta P_1 - \Delta P_2$ and $3 \Delta P_1 - \Delta P_3$ are neglected against P_1.

Then one obtains :

$$B_{12} = -RT\frac{2 \Delta P_1 - \Delta P_2}{2P_1^2}, \quad B_{13} = -RT\frac{3 \Delta P_1 - \Delta P_3}{6 P_1^2}. \qquad (16)$$

The probable error in B_{12} and B_{13} determination is given by :

$$|\delta B_{12}| = (RT/2P_1^2) \quad [4(\delta\Delta P_1)^2 + (\delta\Delta P_2)^2]^{1/2}$$

$$|\delta B_{13}| = (RT/6P_1^2) [9(\delta \Delta P_1)^2 + (\delta \Delta P_3)^2]^{1/2} \qquad (17)$$

In our runs $|\delta B_{12}|$ and $|\delta B_{13}|$ did not exceed ± 20 cm³/mole.

Revue Roumaine de Chimie, **20**, 7, 901–910 (1975)

THE SURFACE CHARGE OF ALUMINOSILICATES IN AQUEOUS SOLUTIONS

RODICA VÎLCU and MIHAELA OLTEANU

Bucharest University, Department of Physical Chemistry, Bd. Republicii 13, Romania

Received April 20, 1974

The surface charge densities ($\sigma_0^{\pm}$) as a function of pH and ionic strength in KNO_3 solutions, and the point of zero charge (p.z.c.), have been determined for a natural (kaolin) and a synthetic aluminosilicate (silico-alumina catalyst). In the same conditions, the isoelectric point (i.e.p.) has been determined by electrophoresis. There are differences between the p.z.c. measured for fast primary equilibrium of the oxide surface with the potential-determining ions (H^+ and OH^-), and the p.z.c. measured for slow equilibrium. For kaolin the differences between p.z.c. value for fast (pH 4) and slow (pH 3.3) equilibrium, were explained in terms of the specific adsorption of some ions on the surface. For silica-alumina catalyst the differences between p.z.c. value for fast (pH 4.8) and slow (pH 6) equilibrium were explained as a result of approaching to the equivalent point (pH 6.2) of the hydroxy complexes of aluminium, $Al(OH)^{2+}$ and $Al(OH)_4^-$.

INTRODUCTION

The oxide-solution interfacial phenomena are of great significance in many fields : geochemical processes, flotation, water pollution, agriculture, painting, etc. The nature and the number of the electric charges on the oxide solution interfaces determine a typical structure of the electrical double layer and they control the interfacial processes.

Insoluble oxides in aqueous suspensions carry surface charges because of hydroxylation of the interface.[1–4] Acidic dissociation of the surface hydroxyl groups can account for the negative surface charge :

$$M(OH)_{surf} + H_2O \rightleftharpoons MO^- + H_3O^+ \qquad (1)$$

The adsorption of H^+ on the neutral surface can account for the positive surface charge :

$$M(OH)_{surf} + H_3O^+ \rightleftharpoons M(OH_2)^+ + H_2O \qquad (2)$$

---

[1] L. A. Wood, *J. Amer. Chem. Soc.*, **68**, 437 (1966).

[2] G. A. Parks, *Chem. Rev.* **65**, 177 (1965) ; *Adv. Chemist. Ser.*, **67**, 125 (1967).

[3] P. H. Tewari and A. W. Mc Lean, *J. Colloid Interface Sci.*, **40**, 267 (1972).

[4] R. K. Iler, *J. Collloid Interface Sci.*, **21**, 569 (1966).

Parks and de Bruyn[5] have postulated a different mechanism for the charging of oxide surfaces, involving partial dissolution of the oxide and formation of hydroxyl complexes in solution, followed by adsorption of these complexes.

The H^+ and OH^- are the potential determining ions and so the pH controls the surface charge of oxides. The pH value for which $\sigma_0 = 0$ is called zero point of charge (p.z.c.).

The "isoelectric point" (i.e.p.) is the pH where the electrokinetic potential (ξ) is zero, identical to the pH value where the diffuse double-layer charge σ_d is zero. P.z.c. and i.e.p. are identical only in the absence of specific adsorption. Some authors erroneously call the pH where $\xi = 0$, as the point of zero charge. [2] Somasundaran [6] has suggested that the conditions under which the zeta potential is zero be called "zero-zeta point" in order to avoid confusion.

Experimentally the p.z.c. on an oxide can be evaluated by a number of methods including titration, maximum coagulation, the addition of dry powder to solutions and pH-drift. [7]

There are discrepancies between p.z.c. data obtained by different methods and for different samples of the same oxide.[2,7] A few researchers have begun to attempt to delineate factors that might be responsible for variations in the behaviour of mineral oxides in aqueous solutions the effects of impurities, [2] crystal structure,[8] micropores,[9] stoichiometry,[10] surface dehydration.[11] Important effects were found to result from the way in which the oxides were prepared and the time of contact between oxide and solution. [3,12,13] Attempts have been made to predict the p.z.c. of oxides [2,14] but such predictions are of little significance as long as we still are unable to explain the wide deviations experimentally obtained.

In this paper, the p.z.c., the surface charge densities ($\sigma_0^{\pm}$) and the i.e.p. have been determined for a natural (kaolin) and a synthetic aluminosilicate (silica-alumina catalyst). These oxides have large practical uses, the kaolin is excellent resin filler from the viewpoint of inertness, economy and pigmentary quality. In our laboratory, these oxides were used for the adsorption studies of some surface active substances.

EXPERIMENTAL

MATERIALS

The chemical composition of the colloidal kaolin appears in table 1. The water content was 0.5%.

---

[5] G. A. Parks and P. L. De Bruyn, *J. Phys. Chem.*, **66**, 967 (1962).

[6] P. Somasundaran, *J. Colloid Interface Sci.*, **27**, 659 (1968).

[7] D. W. Fuerstenau, *Pure Appl. Chem.*, **24**, 135 (1970).

[8] T. W. Healy, A. P. Herring and D. W. Fuerstenau, *J. Colloid Interface Sci.*, **21**, 435 (1966).

[9] J. Lyklema, *J. Electroanalyt. Chem.*, **18**, 341 (1968).

[10] V. Pravdiç and S. Sotman, *Croat. Chem. Acta.*, **35**, 247 (1963).

[11] D. J. O'Connor, P. G. Johansen and A. S. Buchanan, *Trans. Faraday Soc.*, **52**, 229 (1956).

[12] R. F. Conley and A. C. Althoff, *J. Colloid Interface Sci.*, **37**, 186 (1971).

[13] L. C. Bell, A. M. Posner and J. P. Quirk, *J. Colloid Interface Sci.*, **42**, 250 (1973).

[14] T. W. Healy and D. W. Fuerstenau, *J. Colloid Interface Sci.*, **20**, 376 (1965).

The specific surface area, as determined by the standard nitrogen adsorption (B.E.T. method) was 35 m^2/g and 34.2 m^2/g by a Griffin porosimeter. The sedimentometric analysis has been made with an automatic Sartorius 4600 balance and the results are shown in table 2.

Table 1

Chemical composition of the kaolin sample

Substance	Weight (%)
SiO_2	46.2
Al_2O_3	38.5
Fe_2O_3	0.56
TiO_2	0.06
CaO	0.12
MgO	0.1
K_2O	1.01
Na_2O	0.22

The silica-alumina (S.A.) cracking catalyst was a sample produced by Hydrocarbons Comp. It contains 24 %, Al_2O_3 by weight, 20% water and has a surface area of 268 m^2/g (B.E.T. method). Particle size analyses are shown in table 3. For microelectrophoretic measurements, the fraction containing particles with maximum diameter of 1 μm has been separated by the pipette method.

Table 2

Particle size distribution of kaolin

Fraction %	Average diameter (μm)
7	7.3
10	2
83	0.57

Table 3

Particle size distribution of silica-alumina

Fraction %	Diameter (μm)
70	120–170
10	50–100
5	1–50
15	<1

METHODS

Potentiometric titration. Titrations were conducted with a MV-11 type pH meter (Clammann and Grahnert, Dresden), using a GA5O type glass electrode and a calomel electrode. Concentrations of 0.1, 0.01 and 0.001 M KNO_3 *p.a.* solutions have been used as inert electrolyte.

KOH 0.1 M and HNO_3 0.1 M were used to adjust the pH. During the measurements, the calomel electrode is separated from the KNO_3 solutions by means of an agar bridge filled with KNO_3 5% solution in order to prevent the contamination of the experimental solution with Cl^-.

Two titration techniques were used. The first one is the fast continuous titration.[5,15] To a suspension of 0.1 g powder in 20 ml of KNO_3 solution having a certain ionic strength is added a known quantity of acid and it is titrated with alkali from a microbiurette, or *vice-versa*. One can cover in this manner the pH range between 2.5 and 11.5. The titratable surface charge $\sigma_0^\pm$ is defined through

$$\sigma_0 = F(\Gamma_{H^+} - \Gamma_{OH^-}) \tag{3}$$

where F is the Faraday constant and Γ_{H^+} and Γ_{OH^-} are the analytical surface excesses for H^+ and OH^- ions, respectively, in mole per cm^2.[16] Blank titrations were carried out on the appropriate electrolyte and the uptake of H^+ or OH^- by the solid was found by subtracting the titre values of the blank from that of the suspension of various pH values.

When the solid is suspended in an indifferent electrolyte of sufficiently high ionic strength, the potential determining ions can all be assigned to the solid side of the interface. The p.z.c. follows from the intersection point of σ_0-pH curves at different electrolyte concentrations. The time for establishing the adsorption equilibrium is not the same throughout the pH range; near the neutrality point and p.z.c. longer time has been necessary. By adding the oxide to the solution, the adsorption process may occur in two periods: a fast one, of $\sim 5 \div 6$ minutes and a slow one, which may last for days and weeks. The primary equilibrium of the surface with the potential-determining ions (H^+ and OH^-) is known to be complete within the first period.[3] The slow oxide-solution equilibrium is usually only 10% from the total pH variation. However, the time of attaining the equilibrium in the fast period can vary for different pH ranges, this process altering the reproducibility and the reversibility of the adsorption curves throughout the pH range.

The "point to point titration" or "batch method" is the second technique.[13,17,18] Known quantities of powder are added to KNO_3 solutions, initially adjusted to various pH values. The pH variation is followed for a total period of about 10 minutes after the oxide was added to the solution. Calibrations of pH against the molar concentration of HNO_3 and KOH were obtained by potentiometric titrations and were used in calculating the $\sigma_0^\pm$.

This method can be used to determine the p.z.c. for slow equilibrium, but not in calculating the $\sigma_0^\pm$ values which were found to be much higher than the theoretically expected values.[5,17,19] On the addition of oxides to solutions of greater pH than their respective p.z.c., a decrease on pH occurred and vice-versa, and at the p.z.c., the pH remained unchanged (the oxide surface has an equal number of positive and negative charges). The pH measurements were reproducible near the p.z.c. and at the extreme limits of pH within ± 5% and ± 2% for intermediate ranges.

Microelectrophoresis. This method has been applied only for fractions containing particles of maximum 1 μm diameter. The cell (Thomas Phila U.S.A.) had plane parallel walls separated by a distance of 0.53 mm. The measurements were carried out at a constant electric field strength of 1.8 V/cm by applying 22 V to the Zn electrodes (in 0.1 M $ZnSO_4$ solution). Calibration of the cell was carried out with a quadrant electrometer (fig. 1).

The distance between the platinum electrodes was 3 cm. For this operation, the cell was filled with 0.85 M NaCl solutions. The velocity of the particles was observed at the stationary lower level using the micrometer scale (1 division = 6.6 μm) of a Zeiss ultramicroscope (x 10 eyepiece and x 20 objective). The electrophoretic mobility U is given by relation,

$$U = \frac{S \cdot 10^{-4}}{t} \cdot \frac{l}{P} \tag{4}$$

---

[15] R. J. Atkinson, A. M. Posner and J. P. Quirk, *J. Phys. Chem.*, **71**, 550 (1967).
[16] H. R. Kruyt, "Colloid Science", vol. 1, Elsevier Amsterdam, 1952.
[17] S. M. Ahmed and D. Maksimov, *J. Colloid Interface Sci.*, **29**, 97 (1969).
[18] Y. G. Berube, P. L. De Bruyn, *J. Colloid Interface Sci.*, **27**, 305 (1968).
[19] R. S. Alwitt, *J. Colloid Interface Sci.*, **40**, 195 (1972).

where S is the distance in µm covered by a particle in time t (sec) for a potential drop P (5.4 V) between platinum electrodes separated by a distance l(3 cm).

The ξ potentials (in V) can be obtained from the relation

$$\xi = \frac{4\pi\eta}{\varepsilon} \cdot U\,(300)^2 \qquad (5)$$

where η is the solvent viscosity and ε the dielectric constant of the medium.

For our systems, with relative coarse particles, Smoluchowski's equation (5) can be used irrespective of particle shape and neglecting the relaxation correction.[16]

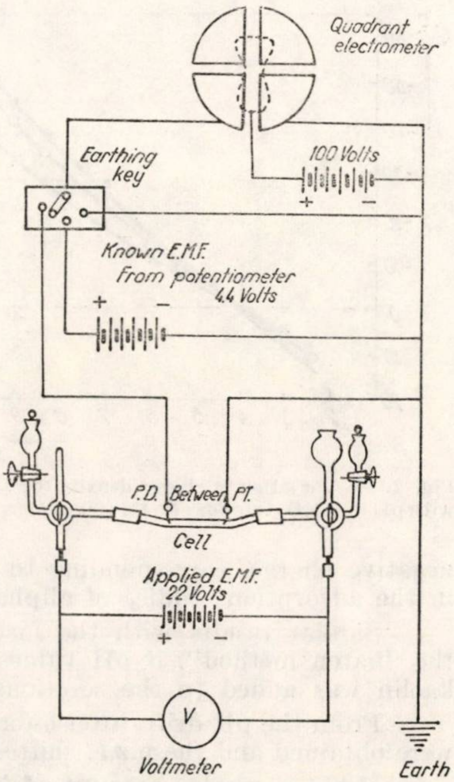

Fig. 1. — Arrangement for calibration of microelectrophoresis cell.

RESULTS AND DISCUSSION

Colloidal kaolin. The intersection of the potentiometric titration curves indicates that the pH at the p.z.c. for kaolin is 4(fig. 2). For a pH range lower than p.z.c., the kaolin surface acquires low positive surface charge due to H^+ adsorption, and for pH range greater than p.z.c., the surface acquires negative charge as a result of acidic dissociation of the surface $-OH$ groups. The maximum value of the negative surface charge density σ_0^- at pH 10 in 0.1 M KNO_3 solution is $56 \times 10^{-6}\,C/cm^2$ corresponding to 34.8×10^{13} ions/cm^2 ($\Gamma_{OH^-} = 58 \times 10^{-11}$ moles/cm^2).

For a uniform distribution of the surface charges, a surface of 28Å^2 is attributed to a single negative charge. The maximum value of σ_-^0 at pH 10 in 0.001 M KNO_3 solution is $43 \times 10^{-6}\,C/cm^2$, corresponding to 26.73×10^{13} ions/cm^2 ($\Gamma_{OH^-} = 44.55 \times 10^{-11}$ moles/cm^2) and a surface of 37.4 Å^2/ion.

The acidic character of kaolin has been a phenomenon observed for a long time. Previous studies [20,21] have demonstrated the source of acidity to be terminated bonds and structural coordination across the edge faces of kaolinite (the 010, $\bar{1}10$, and 110 surfaces). Amine adsorption experiments[21,22] serve to evaluate quantitatively the acid sites, and show excellent correlations with observed edge areas. A unit cell face of 64Å^2 consisting of two terminated silica tetrahedra and two alumina octahedra adsorbs two aliphatic amine groups independent of crystallinity. The

---

[20] M. K. Lloyd and R. F. Conley, *Clays Clay Miner.*, **18**, 37 (1970).
[21] H. A. Benesi, *J. Phys. Chem.*, **61**, 970 (1957).
[22] R. F. Conley and M. K. Lloyd, *Clays Clay Miner.*, **19**, 5 (1971).

character of the acid sites is different as they derive from the silanol groups arising from broken -O-Si-O-Si networks (Brönsted acidity or are generated from the strained gibbsite layer octahedra (Lewis acidity). To add to the complexity, acid kaolin formulated by ion exchange reactions is labile, undergoing surface alterations and forming ionic and exchangeable aluminium which may catalyze other reactions (the degeneration of polyphosphates). Further, the acidity changes unpredictably with temperature and dehydration of the surface. The natural kaolin may be considered having p.z.c. at pH 4.5 and an ion exchange capacity of 5 — 60 μmoles/g. [12]

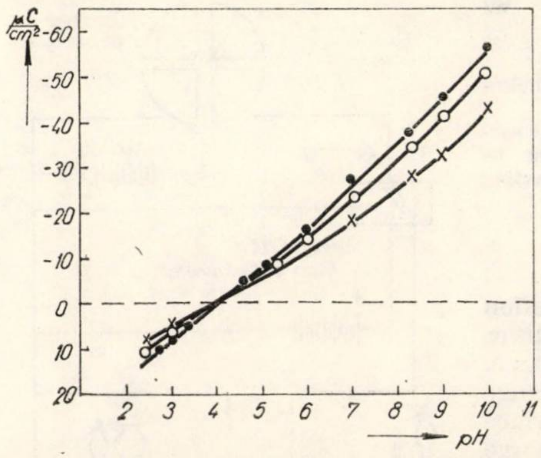

Fig. 2. — Variation in charge density ($\sigma_0^{\pm}$) on kaolin with pH in KNO_3 solutions (0.1M ; 00.01 M ; x 0.001 M)

The maximum values of σ_0^- obtained for the studied kaolin lead to 28 and 37.4Å² for the surfaces of negative charge, corresponding to the surface occupied by an acid center in the adsorption studies of aliphatic amines.

Similar results with the fast titration method were obtained by the "batch method", if pH values were measured 10 minutes after the kaolin was added to the solutions.

From the pH drift, after 6-days equilibration time, very high values were obtained and the p.z.c. shifted to pH 3.3 (fig. 3).

Using a greater amount of kaolin (0.4 in 20 ml solution), after 6 days, the same final pH values was found for all samples initially adjusted to various pH values.

This final pH value coincides with the p.z.c. for slow equilibrium.

When a sparingly soluble oxide is added to an electrolyte solution, the following reactions will occur[5,15,17,18] : a) hydrolysis and complex formation of the surface atoms and dissociation of the surface groups as a primary step accompanied by b) dissolution of the oxide leading to secondary reactions, such as hydrolysis, complex formation, dissociation of the dissolved complexes, adsorption of the dissolved complexes on the surface and precipitation in colloidal form. The primary equilibrium of the surface (type a) with the potential determining ions (H^+ and OH^-) is complete within a few minutes, the secondary reactions (type b) arising from the solubility of the material are very slow and may last for days and weeks. The primary equilibrium (a) depends on the dissociation constants of the surface -OH groups in contact with the electrolyte solutions and the slow equilibrium (b) is determined by the dissociation constants of the complexes dissolved in solution. For these two equilibrium conditions, the point of zero charge of the oxide-solution interface may be different.

No matter the way of appearence of the simple or complex ions in solution, specific adsorption of these ions at the p.z.c. leads to a shift of this quantity, depending on the charge and nature of ions. The shift observed in the p.z.c. of kaolin from pH 4 to pH 3.3 indicates specific adsorption of some cations proceeding from type b reactions. It is known from the theories of the electrical double layer that if cations are specifically adsorbed (in the inner Helmholtz layer), on the surface at the p.z.c., the p.z.c. itself would shift towards lower pH values, whereas specific adsorption at pH values greater than z.p.c., leads to an obvious high negative charge.[17,23] The kaolin contains bi — and trivalent metal oxides (table 1) which provide cations from type b reactions. These cations can be specifically adsorbed on the surface. [23,24] This assumption is consistent with the variation of electrophoretic mobility *vs* pH values (table 4), or the variation of electrokinetic potential ξ (fig. 4), which indicates an isoelectric point at pH 4.2. Due to specific adsorption z.p.c. and i.e.p. are shifted in different directions,[23] so that it is expected to find an i.e.p. higher than z.p.c. for kaolin.

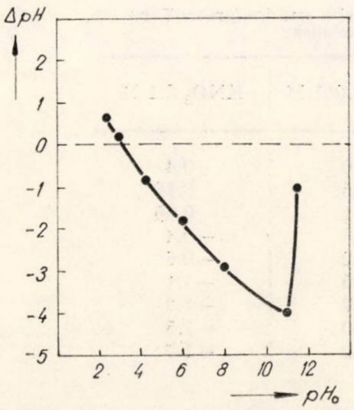

Fig. 3. — Variation in pH 6-days after addition of kaolin, with initial pH_0 of solutions (0.2 g kaolin in 25 ml 0.1 M KNO_3 solution).

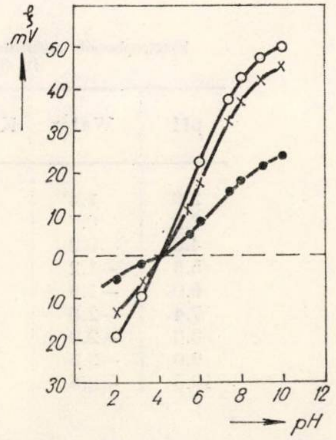

Fig. 4. — Zeta potential of kaolin as a function of pH in different solutions (o water ; x 0.001 MKNO_3 ; .0.1 MKNO_3).

Silica-alumina. The intersection of the fast potentiometric titration curves indicates that the pH at the p.z.c. is 4.8 (fig. 5).
The maximum σ_0^- values at pH 9 in 0.1 M KNO_3 is 31.45×10^{-6} C/cm² ($\Gamma_{OH^-} = 3.26 \times 10^{-10}$ moles/cm²) and in 0.001 M KNO_3 is 25.57×10^{-6} C/cm² ($\Gamma_{OH^-} = 2.65 \times 10^{-10}$ moles/cm²). For a uniform distribution of the surface charges these values lead to a specific ionic surface of 49 Å² and, respectively, 62.8 Å².

---

[23] A. BREEUWSMA and J. LYKLEMA, *J. Colloid Interface Sci.*, **43**, 437 (1973).

[24] A. BREEUWSMA and J. LYKLEMA, *Disc. Faraday Soc.*, **52**, 324 (1971).

The surface acidity of hydrated silica-alumina is due to isomorphic substitution of Al^{3+} for Si^{4+} in the silica tetrahedra. It was found that synthetic silica-alumina with 33.2% Al_2O_3 shows the maximum exchange capacity of 1.08 mequiv/g ($\Gamma = 4.67 \times 10^{-10}$ moles/cm² $\sigma = 45 \times 10^{-6}$ C/cm²), minimum specific surface, 231 m²/g and 23.5 % water [25-27].

Table 4

Electrophoretic mobilities of kaolin particles (μm/sec/V/cm) in different solutions

pH	Water	KNO_3 0.001 M	KNO_3 0.1 M
2.0	1.4	1.0	0.4
3.2	0.7	0.5	0.18
4.0	0.2	0.1	0.05
5.3	−1.2	−0.8	−0.4
6.0	−1.6	−1.2	−0.6
7.4	−2.6	−2.5	−1.1
8.0	−2.9	−2 7	−1.3
9.0	−3.3	−3.0	−1.5
10.0	−3.5	−3.2	−1.7

Adsorption studies on synthetic SA catalysts have indicated both Lewis and Brönsted type acid sites on the surface. The conversion of the Lewis sites to Brönsted sites by the adsorbed water molecules was confirmed by titration [28] and infrared spectrum of adsorbed ammonia. [29] The literature data show different values for the number of Lewis and Brönsted sites.

For an SA with 24% Al_2O_3 content, similar to that we have studied, the same number of Lewis and Brönsted sites has been found by adsorbed pyridine,[30,31] up to 5.6×10^{13} OH/cm² ($\sigma = 8.96 \times 10^{-6}$C/cm²); Mac Iver [27,31] pointed out a value of 1.24×10^{14} OH/cm² ($\sigma = 19.84 \times 10^{-6}$ C/cm²) for total acidity, and Hall [32] a value of 12×10^{13} OH/cm² ($\sigma = 19.2 \times 10^{-6}$ C/cm²) from which only 25% (3×10^{13}/cm²) as Brönsted type.

By titrating butylamine by the Jonson method, [33] it was found for SA with 23% Al_2O_3 only 4.2×10^{13} sites/cm² from which 90% are very strong. [21] Ammonia adsorption on SA (33.2 % Al_2O_3) have indicated a value of 4.16×10^{14} molecules/cm² irreversible adsorbed and respectively 2.88×10^{14} molecules/cm² reversible adsorbed. [25]

---

[25] J. J. Fripiat, A. Leonard and J. B. Uytterhoeven, *J. Phys. Chem.*, **69**, 3274 (1965).

[26] A. Leonard, S. Suzuki, J. J. Fripiat and C. De Kimpe, *J. Phys. Chem.*, **68**, 2608 (1964).

[27] Kozo Tanabe "Solid Acids and Bases" Kodansha, Tokyo, Academic Press, New York, 1970, p. 58.

[28] Y. Trambauze, *J. Chem. Phys.*, **21**, 723 (1954).

[29] M. R. Basila and R. T. Kantner, *J. Phys. Chem.*, **71**, 467 (1967).

[30] M. R. Basila, *J. Chem. Phys.*, **35**, 1151 (1961).

[31] M. R. Basila, T. R. Kantner and K. H. Rhec, *J. Phys. Chem.*, **68**, 3197 (1964).

[32] W. K. Hall, H. P. Leftin, F. J. Cheselske and D. E. O'Reilly, *J. Catalysis*, **2**, 506 (1963).

[33] O. Jonson, *J. Phys. Chem.*, **59**, 1827 (1955).

The surface acidity of SA is very dependent on the method of preparation, Al_2O_3 content, temperature of dehydration of SA and experimental method of investigation.

Our reported values for the surface density of charges are situated between the value of maximum total acidity determined by chemisorption and the maximum value found for the ionic exchange capacity in solution.[25] The water content found for the studied SA (by thermogravimetric analysis) is in agreement with available data.[26]

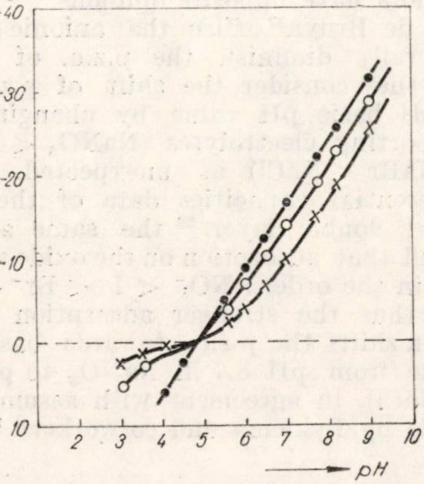

Fig. 5. — Variation in charge density ($\sigma_0^{\pm}$) on silica-alumina with pH in KNO_3 solutions (0.1 M; 00.01M; x 0.001 M).

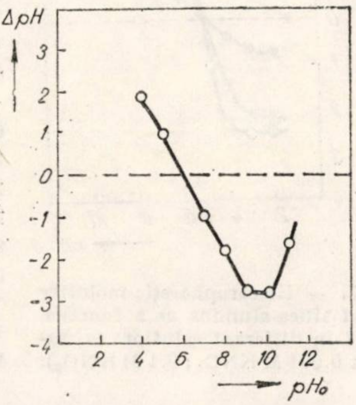

Fig. 6. — Variation in pH 6-days after addition of silica-alumina with initial pH_0 of solutions (0.1 g S.A. in 25 ml. 0.001 M KNO_3 solution).

The p.z.c. of SA for slow adsorption equilibrium was obtained at pH 6 (fig. 6). The shift in the p.z.c. towards a more basic value should be attributed to specific adsorption of some anions. Having the catalyst purity in view, the only anionic species could proceed from the hydrolysis of some Al atoms passed in solution. The equivalency point between $Al(OH)^{2+}$ (in acid media) and $Al(OH)_4^-$ (in alkaline media) was established at pH 6.2.[4,34] The existence of this equilibrium as well as of other complexes[35] of $Al_x(OH)_y$ type (for instance $Al_8(OH)^{4+}$ and $Al_8(OH)_{22}^{2+}$) complicates very much the determination of the p.z.c. of compounds containing Al_2O_3 and can explain the wide variation in the observed p.z.c. by different workers.[19] The presence of hydrated aluminium ions is also confirmed by the i.e.p. hysteresis found in the case of aluminosilicates, due to removal of all surface aluminium ions by acid leaching.[36]

---

[34] S. R. Chen, J. N. Buttler and W. Stumm, *J, Colloid Interface Sci.*, **43**, 421 (1973).

[35] E. Matijeviç, K. G. Mathai, R. H. Ottewill and M. Kerker, *J. Phys. Chem.*, **65**, 826 (1961).

[36] T. J. Smolik, D. Harman and D. W. Fuerstenau, *Trans. AIME*, 235, 367 (1966)

Microelectrophoretic measurements gave p.z.c. value of pH 5 (fig. 7).

There are opposite points of view in the literature concerning the influence of specific adsorption of anions and cations on the p.z.c. and i.e.p. shift. Some authors consider the shift of the p.z.c. towards basic pH values due to specific adsorption of cations[19] and the shift towards acid pH values due to specific adsorption of anions,[13,17] and other authors have opposite opinions.[17,23,24] Blok and de Bruyn[37] affirm that anionic species generally diminish the p.z.c. of oxides and they consider the shift of p.z.c. towards basic pH value by changing the supporting electrolytes ($NaNO_3 < NaI < NaBr < NaCl$) as unexpected. From differential capacities data of the electrical double layer,[38] the same authors found that adsorption on the oxide surface fall in the order : $NO_3^- < I^- < Br^- < Cl^-$, and thus the stronger adsorption of Cl^- anion shifts the p.z.c. towards basic pH value (from pH 8.7 in $NaNO_3$ to pH 9.2 in NaCl), in agreement with assumptions made by Lyklema and co-workers.[23,24]

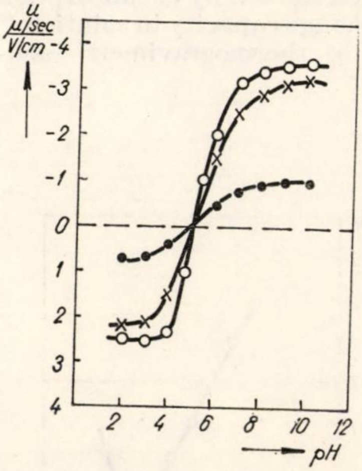

Fig. 7. — Electrophoretic mobility (u) of silica-alumina as a function of pH in different solutions (o water; x 0.001 M KNO_3; 0.1 M KNO_3).

---

[37] L. Blok and P. L. De Bruyn, *J. Colloid Interface Sci.*, **32**, 518 (1970).

[38] L. Blok and P. L. De Bruyn, *J. Colloid Interface Sci.*, **32**, 533 (1970).

Revue Roumaine de Chimie, 20, 7, 911–914 (1975)

THERMOELECTRIC POWER VARIATION DURING OXYGEN ADSORPTION ON ZINC OXIDE THIN FILMS

MIHAELA CONSTANTINESCU, E. SEGAL and M. VASS

Institute of Physical Chemistry Bucureşti, str. Dumbrava Roşie 23, Romania

Received April 22, 1974

The influence of oxygen adsorption on the thermoelectric power (TEP) of zinc oxide thin films was studied. TEP decreases when the film in high vacuum is subsequently exposed to oxygen and air, respectively. One can explain the results obtained by taking into account the shift of the Fermi level produced by surface states which are a result of adsorption.

The study of TEP is beneficial in obtaining valuable information about semiconductor properties[1]: the conduction mechanism, the nature of the majority carriers (*n* or *p* type of semiconductibility), sometimes even the position of Fermi level, the numbers of carriers, the width of the forbidden band, etc.

The temperature gradient for substances having a high surface/volume ratio, for powders and thin films, may be macroscopically uniform but depends on the thermal conduction mechanism.[2] At high temperatures, radiation is an important conduction mechanism, and may lower the high thermal impedance of the narrow necks, so that nearly all of the temperature gradient occurs in the crystallites. In this case the TEP would be characteristic of the bulk material within the crystallites. A gas atmosphere might also have the same effect.

In vacuum and at lower or medium temperature, a large fraction of the total temperature drop through the sample might be localized at the necks, so that the measured TEP will supply information about the surface properties of the substance and, at the same time, it will be sensitive to surface conditions.

In the present paper the results of a study on TEP variation of zinc oxide polycrystalline films at medium temperatures are given.

EXPERIMENTAL

The experimental design is similar to the one previously described.[3] The temperature gradient between the ends of the film was measured with a differential chromel alumel thermocouple, attached with silver contacts to the circulating water pipes.

---

[1] C. Gleitzer, *Rev. Chim. minerale*, 6, 475 (1969).

[2] A. R. Hutson, "Semiconductors", ed. N. Hannay, Reinhold Publishing Corporation, New York, 1959, p. 546.

[3] D. Cismaru, E. Segal and S. Fătu, *Rev. Roumaine Chim.*, 2, 163 (1970).

Zinc oxide film was prepared by depositing zinc metallic film in vacuum ($P = 10^{-5}$ torr), onto an optically polished glass support, and then it was oxidized in air for 24 hours at 450°. Another chromel alumel thermocouple was placed in the middle of the support to measure the average temperature.

Electrical ohmic contacts for the zinc oxide film were made by covering the platinum embedded wire with silver.

TEP was directly recorded on a Philips 8100 recorder. A compensation circuit[4] was also used and identical results were obtained.

RESULTS

The experiments were carried out on zinc oxide films of different thicknesses (2000 – 5000Å).

Zinc oxide films, outgassed in vacuum at 450° for five hours, were brought then to room temperature. The temperature gradient was established step by step from 0 to 40°, and the variation of the thermoelectric voltage was recorded. A plot of thermoelectric voltage *versus* thermal gradient for a fresh zinc oxide film outgassed in vacuum ($P = 5.10^{-8}$ torr) is a straight line, shown in figure 1(*a*).

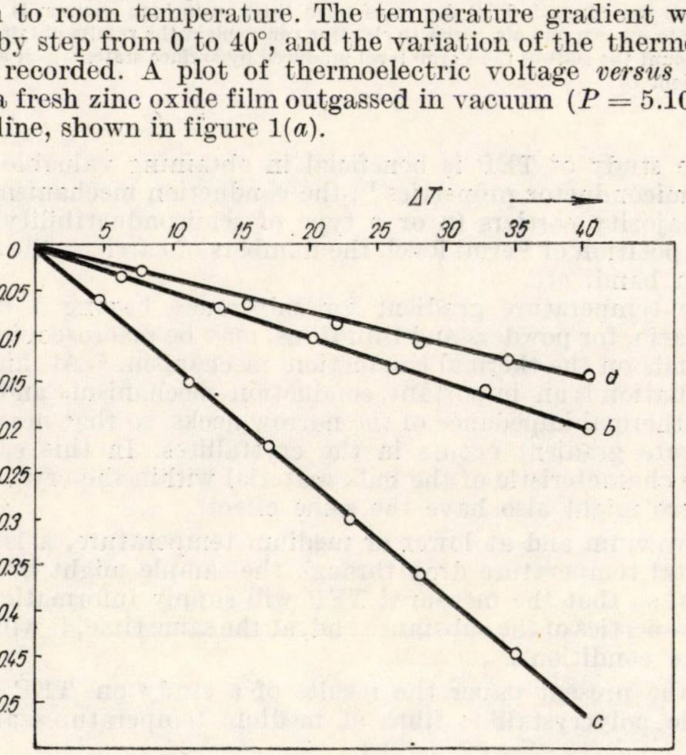

Fig. 1. — Thermoelectric voltage variation *versus* temperature gradient for a zinc oxide film : *a*, fresh outgassed ; *b*, with oxygen adsorbed on the surface ; *c*, in air.

The TEP was calculated from the slope of the straight line, according to :

$$Q = \Delta V / \Delta T \tag{1}$$

---

[4] S. FĂTU, Thesis, 1971, Institute of Physical Chemistry, Bucharest.

where : ΔV is the thermoelectric voltage variation corresponding to the temperature gradient ΔT.

For the outgassed zinc oxide film TEP was : $Q_v = -3.3\mu\text{V/deg}$.

Oxygen adsorption on zinc oxide film leads to the increase of the absolute value of thermoelectric voltage. The saturation value is obtained about three minutes after the introduction of gas. The plot of thermoelectric voltage change for the zinc oxide film with adsorbed oxygen ($P = 10^{-4}$ torr) is also given in figure 1 (*b*). The corresponding TEP is : $Q_0 = -4.9\mu\text{V/deg}$.

If the same film is left in air for 24 hours and the thermoelectric voltage is measured again for different gradients, a third straight line is obtained (figure 1, *c*). The TEP is : $Q_a = -12\mu\text{V/deg}$.

Experimentally, the following relation was established :

$$|Q_a| > |Q_0| > |Q_v| \tag{2}$$

where the sign | | denotes absolute values.

The sign of TEP is always negative showing an *n* type semiconductor. This result is in agreement with the literature about zinc oxide powders, [5] single crystals[6] and alumina-supported[7] zinc oxide catalyst.

DISCUSSION

The results can be understood if we take into account the single band conductivity mechanism, which was present in the given experimental conditions. Charge carriers are electrons from the conduction band produced by the complete ionization of zinc atoms in the interstitial position (ionization energy for Zn^+ is 0.04eV[8]). In this case the formula for TEP[9] is :

$$Q = \frac{k}{e}\left[\frac{E_c - E_F}{kT} + A_c\right] \tag{3}$$

where : $(E_c - E_F)$ shows the position of Fermi level relative to the bottom of the conduction band, T — temperature, k — Bolzman constant, e — electronic charge, A_c — a temperature independent term connected to charge carrier distribution in the conduction band.

Oxygen adsorption on a clean zinc oxide film produces an increase in electrical resistance.[10] This effect is due to the decrease of the number of charge carriers and the appearance of surface states (O^- or O_2^-) which in turn leads to a new potential barrier of the surface.

---

[5] H. Heinrich, *Z. Naturforsch.*, **20**, 99 (1965).

[6] A. R. Hutson, *J. Appl. Physics*, **32**, 2287 (1961).

[7] I. Ursu, F. Puskas and V. Cristea, *Rev. Roumaine Phys.*, **10**, 65 (1965).

[8] S. R. Morrison, *Adv. Catalysis*, **7**, 259 (1955).

[9] H. Fritzche, *Solid State Comm.*, **9**, 1813 (1971).

[10] M. Constantinescu and E. Segal, *Rev Roumaine Chim.*, **12**, 75 (1967).

Appearance of the surface barrier is accompanied by an upward bending of the conduction band; accordingly the difference ($E_c - E_F$) increases; hence, the absolute value of TEP should be higher. This can explain the relation found in our experiments : $|Q_0| > |Q_v|$.

The difference ($E_c - E_F$) is higher in air due to the bigger number of the surface states induced; correspondingly higher TEP's are obtained : $|Q_a| > |Q_0|$.

There is no hole contribution to conductivity in thin zinc oxide films and no inversion layer at the surface as in some powders.[11] Lander[12] has shown that even with strong lithium doped zinc oxide single cristals, a p contribution to conduction is impossible at normal oxygen pressure.

A quantitative comparison between the data obtained for sintered powders, single crystals and thin films is difficult. For example,[13] in single crystals there is a strong phonon drag component (Q_p) in TEP even at room temperature. At 25°, $Q_p = Q_e$, where Q_e is electronic component. Is it obvious that if Q_m is the measured TEP then :

$$Q_m = Q_p + Q_e. \tag{4}$$

For thin films Q_p is negligible [14] since it is directly proportional to mean free phonon path and is limited by phonon-phonon collisions, depending on the sample size. Moreover, the surface scattering due to small thickness can also explain low values of TEP for thin zinc oxide films. For our films TEP increases as the thickness increases, which is in agreement with other results obtained with metal thin films,[5] and polycrystalline semiconductor thin films.[15]

CONCLUSSIONS

1. Thermoelectric voltage variation was measured as a function of different temperature gradients for zinc oxide thin films in different conditions. The TEP may be evaluated from the straight line obtained.

2. TEP decreases when oxygen is adsorbed. Surfaces states induced increase the n type character of the surface. The following relations were found experimentally :

$$|Q_a| > |Q_o| > |Q_v|$$

3. TEP is proportional to the thickness of the films.

---

[11] A. Cimino, E. Molinari and F. Cramarossa, *J. Catalysis*, **2**, 315 (1963).

[12] J. J. Lander, *J. Phys. and Chem. Solids*, **15**, 324 (1960).

[13] A. R. Hutson, *J. Phys. and Chem. Solids*, **8**, 467 (1959).

[14] V. S. Sardaryan and K. T. Ermaganbetov, *Nizktemp. Termoelek. Mater.*, **138**, 43 (1970).

[15] A. K. Dua and R. P. Agrawala, *Thin Solid Films*, **15**, 3 (1973).

Revue Roumaine de Chimie, 20, 7, 915–923 (1975)

CONTRIBUTION À L'ÉTUDE DE LA SOURCE CHIMIQUE DE COURANT $Zn/MeOH/O_2$. II[1]

L'EFFET DE LA VARIATION DES PARAMÈTRES DE FONCTIONNEMENT SUR LES PERFORMANCES D'UNE PILE À CATHODE EN ARGENT

MARIA MAVRODIN-TĂRĂBÎC, IOANA ONACA et I. SOLACOLU
Centre de Chimie Physique, Bucarest, 31, str. Galaţi

Reçu le 23 avril 1974

On a réalisé, dans le laboratoire, une source chimique de courant $Zn/KOH/O_2(Ag)$ à cathode en argent (électrode à gaz du type DSK). On a étudié l'effet de la variation de la concentation (2N—7N) et de la température (20—70°) de l'électrolyte, ainsi que de la surpression d'alimentation avec de l'oxygène (300—600 mm Hg), sur les caractéristiques électriques et sur les rendements de conversion de l'énergie. On a constaté qu'à la concentration de KOH 6N, la variation de la température, entre 20 et 70°, présente un effet favorable dans tout le domaine étudié. La variation de la concentration de l'électrolyte (à la température de 60°) a démontré que les performances les plus élevées correspondent à une concentration d'approximativement 6N, tandis que la variation de la surpression, dans le domaine 300 — 600 mm Hg, a comme effet l'amélioration des performances de la source chimique de courant dans tout l'intervalle étudié.

Les sources chimiques de courant du type métal-air se caractérisent, ainsi que les piles à combustible, par les rendements élevés réalisés dans la conversion, en énergie électrique, de l'énergie dégagée dans la réaction d'électro-oxydation du métal. La valeur de ce rendement de conversion dépend tant du rendement thermodynamique de la réaction qui est à la base de l'obtention du courant électrique [2]

$$Zn + \frac{1}{2}O_2 + 2OH^- \rightleftarrows ZnO_2^{2-} + H_2O$$

dans les conditions pratiques de fonctionnement, que du rendement électrique de la pile, dont la valeur varie selon la grandeur des pertes énergétiques irréversibles (polarisation de transfert de charge, de concentration, de résistance ohmique, pertes ohmiques dans les conducteurs, etc.[3]).

---

[1] O. Radovici, M. Mavrodin-Tărăbîc, I. Onaca et I. Solacolu, *Rev. Roumaine Chim.* **18**, 767 (1973).

[2] J. P. G. Farr et N. A. Hampson, *J. Electroanalyt. Chem.*, **13**, 433 (1967).

[3] M. Mavrodin-Tărăbîc, I. Onaca et I. Solacolu, *Studii şi Cercetări Chim., Bucureşti*, **21**, 335 (1973).

Evidemment, le rendement de conversion et les performances réalisées varient selon la valeur des paramètres de fonctionnement (concentration, température, etc.) et les études concernant la détermination des valeurs optimales de ces paramètres (valeurs auxquelles les pertes irréversibles sont minimales) sont très utiles.

Parmi les cathodes utilisées dans les piles de ce type, ce sont les électrodes à gaz en argent[1,4–8] qui se remarquent par leur polarisation réduite, leur efficience élevée, les conditions commodes d'exploitation, leur résistance à la corrosion dans le milieu agressif de KOH, etc.

Dans ce travail nous nous sommes proposé d'étudier l'effet de la variation des principaux paramètres de fonctionnement (la concentration et la température de l'électrolyte, la surpression d'alimentation avec de l'oxygène) sur les performances d'une pile Zn-oxygène à cathode en argent, en vue de déterminer les conditions optimales de fonctionnement. Les mesures électriques nécessaires ont été effectuées en déchargeant la pile, sur une résistance variable, et les valeurs des tensions électriques et des densités apparentes de courant correspondantes ont permis le calcul des caractéristiques de la pile par une méthode présentée dans un travail antérieur.[1]

1. PARTIE EXPÉRIMENTALE

On a réalisé, dans le laboratoire, une source chimique de courant du type

$$(-)\ \mathrm{Zn/KOH/O_2(Ag)}\ (+)$$

à cathode en argent (électrode à gaz du type DSK) et anode de zinc de pureté 99,9%. Les électrodes à gaz en argent ont été obtenues par la compression et le frittage en atmosphère d'hydrogène et à 375°, des mélanges homogènes qui contiennent 81,25% carbonate d'argent et 18,75% bicarbonate d'ammonium. Les électrodes obtenues se caractérisent par une répartition uniforme des pores (établie par l'examen microscopique) et par une porosité moyenne totale de 30,5% (déterminée en pesant les échantillons avant et après l'immersion dans du toluène).

La concentration de l'électrolyte a été variée entre 2N et 7N (niveaux de concentration de 1 équiv.cm^{-3}), en maintenant la température à la valeur de 60° et la surpression de l'oxygène à 400 mm Hg; la température a été variée entre 20 et 70° (niveaux de température de 10°), en maintenant la concentration de KOH à la valeur de 6N et la surpression de l'oxygène à 400 mm Hg. Les électrodes ont été alimentées avec de l'oxygène à des surpressions comprises entre 300 et 600 mm Hg (niveaux de surpression de 100 mm Hg), en maintenant la concentration de l'électrolyte à la valeur de 5N et la température à 60°. Les paramètres de fonctionnement de la pile ont été maintenus constants dans les limites : $\pm$ 0,005 équiv. cm^{-3}, $\pm$ 0,1° et, respectivement, $\pm$ 2 mm Hg.

On a tracé les courbes de décharge $E - i$ sur une résistance variable, à l'aide d'un montage, décrit dans une autre étude,[1] en utilisant un milliampèremètre de type DU 20 (précision $\pm$ 1%), un millivoltmètre de type Universal-Röhrenvoltmeter 187a (précision $\pm$ 2 mV) et une boîte à résistances de type VEB Messtechnik (précision $\pm$ 0,1Ω).

---

[4] J. Jausta, *Coll. Czech. Chem. Comm.*, **33**, 160 (1968).

[5] I. Lindholm, *J. Electrochem. Soc.*, **116**, 1150 (1969).

[6] Ling-Ying Ku et V. S. Bagotskii, *Electrokhimiya*, **3**, 1279 (1967).

[7] J. Mrha et J. Jindra, *Coll. Czech. Chem. Comm.*, **34**, 2465 (1969).

[8] O. Radovici, M. Mavrodin-Tărăbîc, I. Onaca et I. Solacolu, *Rev. Roumaine Chim.*, **17**, 1153 (1972).

2. RÉSULTATS ET DISCUSSIONS

La méthode d'interprétation des courbes de décharge $E - i$, tracées pour différentes conditions de concentration, de température et de surpression d'alimentation avec du gaz, a été présentée en détail dans un travail antérieur.[1] Pour élaborer les tableaux qui illustrent l'effet de la variation de chaque paramètre de fonctionnement sur les performances de la source chimique de courant étudiée on a utilisé les formules et les symboles suivants :

— *tension totale* $E_t = \Delta H/zF$

— *perte thermodynamique* $\Delta E_u = -T \Delta S/zF$

— *tension idéale* $E_i = -\Delta G/zF$

— *rendement thermodynamique* $\eta_T = \Delta G/\Delta H$

— *tension réelle*, E_r— l'ordonnée à l'origine des courbes de décharge, dans la zone d'exploitation (la zone des grandes densités apparentes de courant)

— *rendement électrique maximal* $\varepsilon_{max} = E_r/E_i$

— *pertes par polarisation* $\sigma = (E_i - E_r)/E_t$

— *la pente de la zone de fonctionnement* R — déterminée par voie graphique

— *rendement maximal de conversion* $\eta_{max} = \eta_T . \varepsilon_{max}$

— *densité apparente maximale de courant* $i_{max} = \varepsilon_{max} . E_i/R$

— *densité apparente moyenne de courant* $i_{moyenne} = \dfrac{1}{2}\, i_{max}$

— *puissance maximale* $P_{max} = R \cdot i_{moyenne}$

— *tension moyenne* $E_{moyenne} = E_r - R \cdot i_{moyenne}$

— *rendement réel de conversion* $\eta_{réel} = \eta_{max} - R \cdot i_{moeynne}/E_t$.

2.1. EFFET DE LA VARIATION DE LA CONCENTRATION DE L'ÉLECTROLYTE

Pour la détermination de l'effet de la variation de la concentration de l'électrolyte sur les caractéristiques électriques et sur le rendement de conversion réalisé par la source chimique de courant étudiée, on a tracé les courbes de décharge $E - i$, sur résistance variable, à différentes concentrations comprises entre 2N et 7N ($\Delta P_{O_2} = 400$ mm Hg, température 60°). Les résultats obtenus par l'interprétation de ces courbes sont présentés dans le tableau 1.

Tableau 1

Effet de la variation de la concentration de l'électrolyte sur les caractéristiques de la pile du type Zn-oxygène (température 60°; ΔP_{O_2} = 400 mm Hg; $\Delta H = -390.800$ j/mole; $\Delta G = -326.400$ j/mole; $T\Delta S = 64.400$ j/mole; $E_t = 2{,}025$ V; $\Delta E_u = 0{,}325$ V; $E_i = 1{,}700$ V; $\eta_T = 0{,}8325$)

Conc. équiv. cm^{-3}	E_r V	ε_{max}	σ	R ohm	η_{max}	i_{max} mA/cm^2	$i_{moyenne}$ mA/cm^2	P_{max} mW/cm^2	$E_{moyenne}$ V	η_{moyen}
2	1,410	0,8294	0,1432	3,70	0,6905	381,08	190,54	134,33	0,705	0,3424
	1,405	0,8264	0,1457	3,64	0,6902	385,96	192,98	135,57	0,702	0,3433
3	1,400	0,8235	0,1481	3,48	0,6878	402,28	201,14	140,79	0,700	0,3421
	1,390	0,8176	0,1531	3,37	0,6829	412,44	206,22	143,31	0,695	0,3397
4	1,415	0,8323	0,1407	3,50	0,6951	404,26	202,13	143,00	0,707	0,3458
	1,410	0,8294	0,1432	3,46	0,6927	407,51	203,76	143,65	0,705	0,3446
5	1,455	0,8559	0,1210	3,56	0,7148	408,71	204,36	148,68	0,727	0,3556
	1,460	0,8588	0,1185	3,54	0,7173	412,42	206,21	150,53	0,730	0,3568
6	1,490	0,8765	0,1037	3,63	0,7321	410,46	205,23	152,89	0,745	0,3642
	1,480	0,8706	0,1086	3,57	0,7221	414,56	207,28	153,38	0,740	0,3617
7	1,445	0,8500	0,1259	3,60	0,7151	401,39	200,70	145,00	0,722	0,3583
	1,460	0,8588	0,1185	3,61	0,7144	404,42	202,21	147,61	0,730	0,3539

Des données présentées dans le tableau 1 on constate que les performances maximales de la pile correspondent à une concentration d'approximativement 6N. L'augmentation de la concentration de l'électrolyte à partir de la valeur de 2N jusqu'à 6N a comme effet l'augmentation de la tension réelle, de la valeur d'approximativement 1,40 jusqu'à 1,49 V, l'amélioration du rendement électrique maximal de la valeur de 82 jusqu'à 87%, du rendement maximal de conversion de la valeur de 69 jusqu'à 73%, ainsi que la réduction des pertes par polarisation, de la valeur de 14 jusqu'à 10%. Les performances de la source chimique de courant (dans les conditions qui correspondent à une puissance maximale dans le circuit extérieur) s'améliorent avec l'augmentation de la concentration de l'électrolyte : la tension moyenne augmente à partir de la valeur de 0,7 jusqu'à 0,74 V, la densité apparente de courant de la valeur de 190 jusqu'à 207 mA/cm^2, la puissance maximale de la valeur de 134 jusqu'à 153 mW/cm^2, le rendement réel de conversion, en énergie électrique, de l'énergie chimique dégagée dans la réaction, de la valeur de 34 jusqu'à 36%. À la suite de l'augmentation de la concentration de l'électrolyte à partir de la valeur de 6N jusqu'à 7N, on constate un abaissement des performances de la source chimique Zn-oxygène à cathode en argent : la tension réelle baisse à partir de 1,49 jusqu'à 1,45 V, le rendement électrique maximal, de la valeur de 87 jusqu'à 85%, les pertes par polarisation augmentent à partir de 10 jusqu'à 12%, le rendement maximal de conversion baisse, de la valeur de 73 jusqu'à 71%, la densité apparente de courant, de la valeur de 207 jusqu'à 201 mA/cm^2, la tension moyenne, de la valeur de 0,74 jusqu'à 0,725V, la puissance maximale, de la valeur de 153 jusqu'à 146 mW/cm^2, le rendement réel de conversion de l'énergie, de la valeur de 36 jusqu'à 35%.

L'effet de la variation de la concentration de l'électrolyte sur les performances de la source chimique de courant étudiée s'explique par son influence sur la solubilité de l'oxygène, sur la dissolution anodique du zinc, sur la conductibilité de l'électrolyte et il est en concordance avec nos études antérieures concernant le comportement des électrodes à gaz en argent.[9] Étant donné que la dissolution anodique du zinc n'est pas influencée par la variation de la concentration dans le domaine étudié (on considère qu'à des valeurs de pH > 12 la solubilité du zinc, en milieu de KOH est maximale [10]), on peut admettre que ces effets sur les performances de la pile sont provoqués par les processus cathodiques et par la modification de la conductibilité de l'électrolyte : la solubilité de l'oxygène en milieu de KOH baisse avec l'augmentation de la concentration, [11] mais cet effet négatif est compensé par l'augmentation de la conductibilité de l'électrolyte,[12] qui présente un maximum à la concentration d'approximativement 6N. [13] Ce comportement de la source chimique de courant Zn-oxygène est en concordance avec la variation des valeurs des énergies apparentes d'activation, caractéristiques pour la réaction de réduction de l'oxygène sur les électrodes à gaz en argent, en milieu de KOH, déterminées dans un travail antérieur.[14] (Ces énergies présentent des valeurs minimales dans le domaine de concentration de 5N — 6N.)

2.2. EFFET DE LA VARIATION DE LA TEMPÉRATURE DE L'ÉLECTROLYTE

En vue de déterminer l'effet de la variation de la température de l'électrolyte sur les caractéristiques électriques et sur les performances réalisées par la source chimique de courant Zn-oxygène à cathode en argent, on a tracé les courbes de décharge sur résistance variable $E - i$, à différentes températures comprises entre 20 et 70° ($\Delta P_{O_2} = 400$ mm Hg, la concentration de KOH 6N). Les résultats obtenus par l'interprétation des courbes sont présentés dans le tableau 2.

De l'examen des données du tableau 2 on constate que les performances de la source chimique de courant augmentent continuellement dans tout le domaine de température considéré. Ainsi, par l'augmentation de la température à partir de la valeur de 20 jusqu'à 70°, la tension réelle augmente à partir de la valeur de 1,40 jusqu'à 1,52 V, le rendement électrique maximal de la valeur de 84 jusqu'à 89%, les pertes par polarisation baissent de la valeur de 13 jusqu'à 9%, le rendement maximal de conversion augmente de la valeur de 71 jusqu'à 74%. Dans les conditions correspondant à une puissance maximale dans le circuit extérieur, l'augmentation de la température de l'électrolyte conduit à l'amélioration des performances : la tension électrique moyenne augmente à partir de la valeur de 0,70 jusqu'à 0,76 V, la densité apparente de courant, de la valeur de 82 jusqu'à 209 mA/cm², la puissance maximale, de la valeur de 57 jusqu'à

---

[9] M. Mavrodin-Tărăbîc, I. Onaca et I. Solacolu, *Rev. Roumaine Chim.*, (sous presse).

[10] B. E. Roetheli, G. L. Cox et W. B. Littreal, *Metals and Alloys*, **3**, 73 (1932).

[11] A. Seidell, « Solubilities of Inorganic and Metal Organic Compounds », Ier vol., Van Nostrand Co., New York, 1953, p. 1352.

[12] E. L. Simons, D. W. McKee et E. J. Cairns, « Comptes rendus des troisièmes journées d'étude des piles à combustible », Presses Académiques Européennes, Bruxelles, 1969, p. 132.

[13] D. B. Lucesoli, Thèse, Univ. Paris, 1971.

[14] I. Onaca, M. Mavrodin-Tărăbîc et I. Solacolu, *Rev. Roumaine Chim.*, (sous presse).

Tableau 2

Effet de la variation de la température de l'électrolyte sur les caractéristiques électriques de la pile du type Zn-oxygène (concentration de l'électrolyte 6N, $\Delta P_{O_2} = 400$ mm Hg)

Température	ΔH	ΔG	$T\Delta S$	E_t	ΔE_u	E_i	η_T	E_r	ε_{max}	σ	R	η_{max}	i_{max}	i_{moyenne}	P_{max}	E_{moyenne}	η_{moyen}
°C	j. mole^{-1}	j. mole^{-1}	j. mole^{-1}	V	V	V		V			ohm		mA/cm^2	mA/cm^2	mW/cm^2	V	
20	−375380	−318720	−56660	1,945	0,285	1,660	0,8490	1,400	0,8433	0,1337	8,51	0,7160	164,50	82,25	57,57	0,700	0,3561
								1,420	0,8554	0,1234	8,82	0,7262	160,99	80,50	57,16	0,710	0,3612
30	−379240	−320640	−58600	1,965	0,295	1,670	0,8455	1,460	0,8743	0,1069	7,02	0,7392	207,99	103,00	75,19	0,730	0,3677
								1,465	0,8772	1,1043	6,75	0,7416	217,03	108,52	79,49	0,732	0,3689
40	−383090	−322560	−60530	1,985	0,305	1,680	0,8420	1,465	0,8720	0,1083	5,36	0,7342	273,31	136,66	100,10	0,732	0,3652
								1,465	0,8720	0,1083	5,32	0,7342	275,37	137,69	100,86	0,732	0,3652
50	−386950	−324480	−62470	2,005	0,315	1,690	0,8386	1,475	0,8728	0,1072	4,48	0,7319	329,25	164,63	121,41	0,737	0,3641
								1,485	0,8786	0,1022	4,47	0,7368	332,18	166,09	123,32	0,742	0,3665
60	−390800	−326400	−64400	2,025	0,325	1,700	0,8352	1,490	0,8765	0,1037	3,63	0,7321	410,46	205,23	152,89	0,745	0,3642
								1,480	0,8706	0,1086	3,57	0,7271	414,56	207,28	153,38	0,740	0,3617
70	−394650	−328320	−66330	2,045	0,335	1,710	0,8319	1,500	0,8772	0,1027	3,58	0,7297	419,00	209,50	157,12	0,750	0,3630
								1,525	0,8918	0,0905	3,68	0,7419	414,40	207,20	157,99	0,762	0,3681

158 mW/cm^2, le rendement réel de conversion de l'énergie chimique en énergie électrique de la valeur de 35 jusqu'à 37%.

L'amélioration des performances de la source chimique de courant, comme résultat de l'augmentation de la température de l'électrolyte, s'explique par l'effet favorable de l'augmentation de la température sur la conductibilité de l'électrolyte [12] et sur le développement des processus anodiques et cathodiques, qui compense l'effet défavorable sur la solubilité de l'oxygène.[11] L'augmentation de la température favorise la dissolution de l'anode, la vitesse de la réaction cathodique, la diffusion des espèces réactives et des produits de réaction vers et à partir de la zone de réaction. Les résultats obtenus sont en concordance avec des études antérieures[14] et avec les données présentées dans la littérature de spécialité.[4,13,15]

En comparant les données présentées dans les tableaux 1 et 2 on constate que l'effet de la variation de la température de l'électrolyte est plus prononcé que l'effet de la variation de la concentration. Cette conclusion est en concordance avec les résultats de l'étude de l'effet de la variation de ces paramètres sur la polarisation des électrodes à oxygène.[9,14] Les données du tableau 2 recommandent, en vue de l'optimisation du processus (l'établissement des valeurs des paramètres de fonctionnement pour lesquelles la source chimique de courant présente des performances maximales), l'exploration du domaine de température supérieur à la valeur de 70° ; évidemment, il faut tenir compte des effets négatifs de l'augmentation de la température au-dessus d'une certaine valeur, tels que : l'augmentation de la pression de vapeurs de l'électrolyte, la corrosion avancée de l'installation, les pertes de chaleur qui influencent le bilan énergétique de l'installation, l'abaissement de la puissance et de l'énergie spécifique (comme résultat de l'augmentation du gabarit de l'installation), les difficultés d'exploitation, etc.

2.3. EFFET DE LA VARIATION DE LA SURPRESSION D'ALIMENTATION AVEC DE L'OXYGÈNE

On a tracé les courbes de décharge, sur résistance variable, $(E - i)$, de la source chimique de courant étudiée (concentration de l'électrolyte 5N, température 60°), en variant la surpression d'alimentation avec de l'oxygène, entre 300 et 600 mm Hg. L'interprétation des courbes obtenues nous a permis d'obtenir les données présentées dans le tableau 3.

À la suite de l'augmentation de la surpression de l'oxygène à partir de la valeur de 300 jusqu'à 600 mm Hg, on constate une amélioration des performances de la pile Zn-oxygène : la tension électrique réelle augmente à partir de la valeur de 1,46 jusqu'à 1,51 V, le rendement électrique maximal, de la valeur de 86 jusqu'à 89%, les pertes par polarisation baissent à partir de la valeur de 12 jusqu'à 9%, le rendement maximal de conversion augmente de la valeur de 71 jusqu'à 74%, la densité apparente de courant

---

[15] M. Marinescu, S. Doboş et I. Minea, *Studii şi Cercetări Energetică Electrotehnică*, **19**, 427 (1969).

Tableau 3

Effet de la variation de la surpression de l'oxygène sur les caractéristiques de la pile du type Zn-oxygène (concentration de l'électrolyte 5 N; température 60°; $\Delta H = -390.800$ j/mole; $\Delta G = -326.400$ j/mole; $T\Delta S = 64.400$ j/mole; $E_t = 2{,}025$ V; $\Delta E_u = 0{,}325$ V; $E_i = 1{,}700$ V; $\eta_T = 0{,}8325$)

ΔPo_2 mm Hg	E_r V	ε_{max}	σ	R ohm	η_{max}	i_{max} mA/cm²	$i_{moyenne}$ mA/cm²	P_{max} mW/cm²	$E_{moyenne}$ V	η_{moyen}
300	1,460	0,8588	0,1185	3,79	0,7150	385,22	192,61	140,60	0,730	0,3546
	1,470	0,8647	0,1136	3,86	0,7198	380,83	190,42	139,96	0,735	0,3568
400	1,455	0,8559	0,1210	3,56	0,7148	408,71	204,36	148,68	0,727	0,3556
	1,460	0,8588	0,1185	3,54	0,7173	412,42	206,21	150,53	0,730	0,3568
500	1,465	0,8618	0,1160	3,69	0,7198	397,02	198,51	145,41	0,732	0,3581
	1,470	0,8647	0,1136	3,65	0,7222	402,74	201,37	148,01	0,735	0,3593
600	1,500	0,8823	0,0988	3,80	0,7345	394,71	197,36	148,02	0,750	0,3608
	1,520	0,8941	0,0889	3,82	0,7443	397,91	198,96	151,20	0,760	0,3690

moyenne (fournie par la pile dans les conditions correspondantes à une puissance maximale dans le circuit extérieur) augmente à partir de la valeur de 191 jusqu'à 198 mA/cm², la tension électrique moyenne, de la valeur de 0,73 jusqu'à 0,76 V, la puissance maximale, de la valeur de 140 jusqu'à 151 mW/cm², le rendement réel de conversion de l'énergie, de la valeur de 35 jusqu'à 36%.

En comparant les données des tableaux 1 —3, il résulte que l'effet de la variation de la surpression d'alimentation avec de l'oxygène sur les performances de la source chimique de courant étudiée est moins prononcé que l'effet de la variation de la concentration et de la température de l'électrolyte, ce qui confirme nos résultats antérieurs concernant le comportement des électrodes à gaz en argent.[16] L'amélioration des performances de la pile Zn-oxygène s'explique par l'effet favorable de l'augmentation de la surpression du gaz sur la solubilité de l'oxygène et sur l'étendue de la zone triphasique de réaction de la cathode ; l'augmentation de la surpression vers la limite supérieure du domaine étudié conduit au bullage de l'oxygène dans les pores les plus grands, phénomène qui a des effets favorables sur les performances de la pile, grâce à l'agitation de l'électrolyte qui améliore la diffusion des espèces réactives et des produits de réaction. L'agitation de l'électrolyte empêche la passivation de l'anode de zinc par la formation des pellicules de zincate et c'est ainsi qu'on peut expliquer l'effet favorable, plus prononcé, de l'augmentation de la surpression dans le cas de la source chimique Zn-oxygène que dans le cas des électrodes à oxygène en argent.[16]

L'étude de la variation des paramètres de fonctionnement (la concentration et la température de l'électrolyte, la surpression d'alimentation avec du gaz) sur les performances d'une source chimique de courant de type Zn-oxygène à cathode en argent a mis en évidence l'effet favorable de l'augmentation de la concentration jusqu'à 6N, de l'augmentation de la température et de la surpression jusqu'à la limite supérieure du domaine étudié (70° et, respectivement, 600 mm Hg). Les données obtenues démontrent la complexité de cet effet et le caractère interdépendant des effets singuliers. Evidemment, en vue de la détermination des valeurs optimales des paramètres de fonctionnement, auxquelles la source chimique de courant présente des performances maximales, il est nécessaire d'effectuer une étude détaillée d'optimisation, par l'exploration de la zone définie par les valeurs 5N – 7N, 60 – 70° et 400 – 600 mm Hg.

---

[16] I. Solacolu, M. Mavrodin-Tărăbîc et I. Onaca, *Rev. Roumaine Chim.* (sous presse).

3. CONCLUSIONS

1. L'étude de l'influence de la variation de la concentration de l'électrolyte (dans le domaine 2N – 7N) sur les performances de la source chimique de courant Zn-oxygène à cathode en argent (température 60°, $\Delta P_{O_2} = 400$ mm Hg) a mis en évidence l'effet favorable de l'augmentation de la concentration jusqu'à 6N.

2. L'augmentation de la température de fonctionnement, dans le domaine 20 – 70° (concentration de KOH, 6N, $\Delta P_{O_2} = 400$ mm Hg) présente un effet favorable sur les performances réalisées, dans tout l'intervalle étudié.

3. La variation de la surpression d'alimentation avec de l'oxygène, à partir de la valeur de 300 mm Hg jusqu'à 600 mm Hg (concentration de KOH, 5N, température 60°) a comme résultat l'amélioration des performances de la source chimique de courant Zn-oxygène, dans tout le domaine étudié.

Revue Roumaine de Chimie, **20**, 7, 925–928 (1975)

ON THE FORMATION OF $3(CaO.Al_2O_3).CaSO_4$ IN THE $CaCO_3-Al_2O_3-FeSO_4$ SYSTEM

I. TEOREANU, MARCELA MUNTEAN and I. DRAGNEA
Polytechnic Institute, Str. Polizu No 1,
Bucharest, Romania

Received June 7, 1974

The formation of the compound $3(CaO.Al_2O_3).CaSO_4$ in the $CaO(CaCO_3)-Al_2O_3-FeSO_4$ system is studied. Some conclusions are drawn regarding the mechanism of the processes. Chemical analysis (free lime and SO_3 content) and roentgenographic analysis were utilized.

1. The formation of $3(CaO.Al_2O_3).CaSO_4$ in the system $CaO(CaCO_3)-Al_2O_3-CaSO_4$ has been evidenced. The formula for the calcium aluminosulphate as it is accepted today in the literature, was first conventionally suggested by Rogozina,[1] and was then established by Okorokov *et al*[2,3] and by Fukunda.[4,5]

The formation, the stability and the properties of $3(CaO.Al_2O_3).CaSO_4$ have also been studied by other workers. In a previous paper[6] we also studied these problems; a special attention was given to the formation of the calcium aluminosulphate from stoichiometric mixtures.*

The finding that ferrosulphate has a mineralizing action[7,8] suggested the possible formation of a compound of the type $3(CaO.Al_2O_3).MSO_4$. The present paper examines the nature, the mechanism of formation and the stability of such a compound in mixtures of $CaCO_3$, Al_2O_3 and $FeSO_4$.

2. For this purpose stoichiometric mixtures of reactants corresponding to the hypothetical compound "$3(CaO.Al_2O_3)$. $FeSO_4$" were prepared. Chemical grade reactants were used. The mixtures were pressed and burnt at 800°, 1000°, 1200°, 1250°, 1300°, 1380° and 1450° in an electric furnace. The samples were maintained for 1 hour at the maximum temperature and were then quenched in the air.

---

* In what follows : $CaO = C$, $Al_2O_3 = A$, $Fe_2O_3 = F$, $SO_3 = S$, M = metallic cation, $R = (Al, Fe)$.

[1] A. T. Rogozina, *Zhur. priklad. Khim.*, **30**, 1742 (1957).

[2] S. D. Okorokov, S. L. Golynko-Vol'fson, G. N. Jarkina and R. A. Czepik, *Zhur. priklad. Khim.*, **35**, 256 (1962).

[3] S. D. Okorokov, S. L. Golynko-Vol'fson, G. N. Jarkina and R. A. Czepik, *Zhur. priklad. Khim.*, **35**, 2354 (1962).

[4] N. Fukada, *Sement Gijusto Nenpo*, **15**, 26 (1961).

[5] N. Fukada, *Bull. Chem. Soc. Japan*, **34**, 138 (1961).

[6] I. Teoreanu and M. Muntean, *Rev. Roumaine Chim.*, **19**, 1483 (1974).

[7] B. V. Volkonski, P. E. Konovalov and S. D. Makaşev, "Mineralizatory v tsementnoi promyshlenosti", Stroiizdat, Moskva, 1961, p. 163.

[8] S. D. Okorokov, S. L. Golynko-Vol'fson and V. I. Korneev, *Tr. Leningr. Technol. Inst. im. Lensoveta*, **56**, 93 (1960).

In parallel, a synthesis at 1300° with a 4 hours constant temperature period followed by cooling in the furnace down to 800° and then by air quenching was performed; the magnitude of the constant temperature period and the way in which the samples were cooled have not significantly influenced the free lime content as well as the mineralogical composition of the synthetized samples.

The synthetized masses were then analysed. Chemical and roentgenographic analyses were performed.

Fig. 1 represents the diffractogram of the sample synthetized at 1300°. The existence of calcium aluminosulphate, of C_2A and of CA (in fact solid solutions with iron) is evident. The results of the impulse measurements, with a TUR-M-62 diffractometer, are represented in fig. 2 (the impulse measurements have not revealed the presence of other compounds). The chemical analyses performed which refer to the content of iron and its valence show the complete finding of iron introduced in initial mixture as well as quasitotally converting of Fe^{2+} into Fe^{3+}. The results regarding free lime and SO_3 content are presented in table 1.

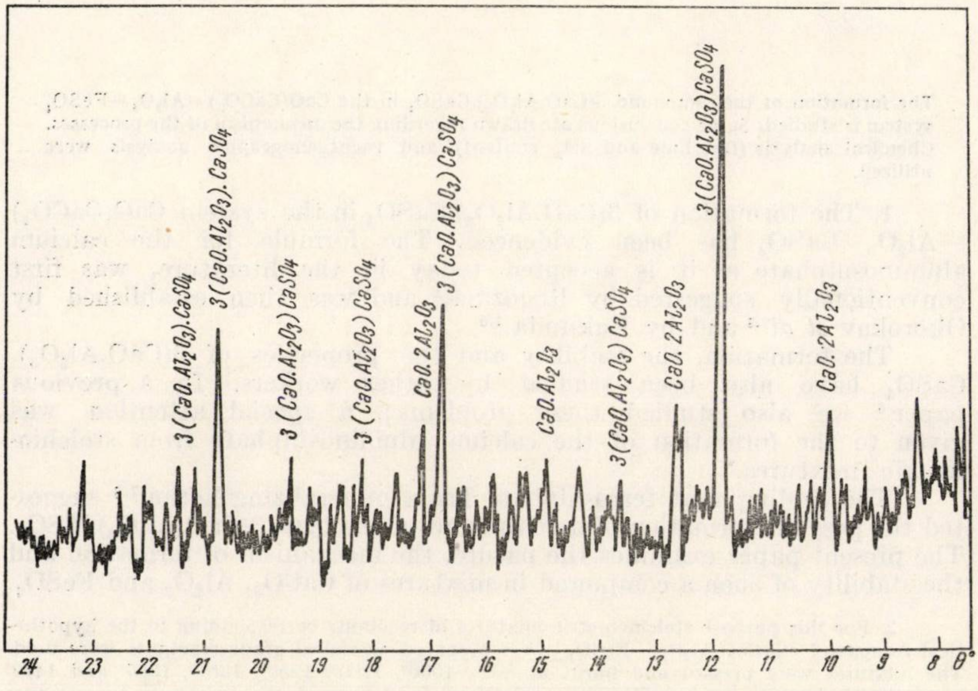

Fig. 1.—The roentgenogram for the sample burnt at 1300°.

3. The present results show the formation of an aluminosulphate compound of type $C_4A_3\overline{S}$; this compound is characterized by absolutely similar diffraction lines as those evidenced when its synthesis is conducted in the system $CaO(CaCO_3)-Al_2O_3-CaSO_4$ (see [6, 9, 10]). The presence of

---

[9] P. P. Budnikov and I. P. Kuznețova, *Cement-Wapno-Gips*, **20/32**, 153 (1965).

[10] P. P. Budnikov, I. P. Kuznețov and V. G. Savielev, *Silikatechnik*, **16**, 414 (1965).

$C_4A_3\overline{S}$ is evident in the samples synthetized at temperatures over 1100°; around 1300° the rate of formation has a maximum and, after that, its rate of decomposition becomes preponderant.

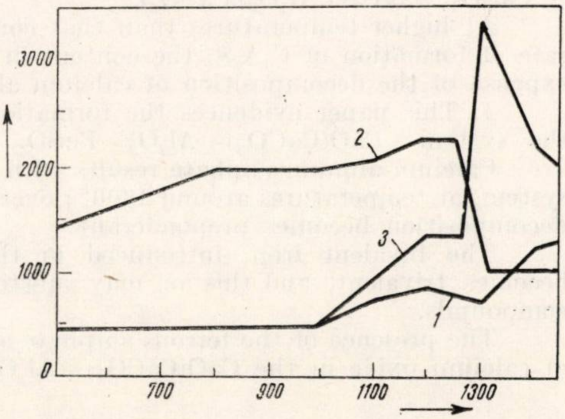

Fig. 2. – The variation of the principal diffraction lines for $CaO.Al_2O_3$, $CaO.2Al_2O_3$ and $3(CaO.Al_2O_3)CaSO_4$.
1. $CaO.Al_2O_3$; 2. $CaO.2Al_2O_3$;
3. $3(CaO.Al_2O_3)CaSO_4$.

The calcium aluminates (solid solutions with iron) are present beginning with the samples synthetized at 800°; between 800° and 1000° only the presence of CA_2 is evidenced. At 1100° and over, CA also appears. CA_2 is preponderant in every sample synthetized at temperatures $\theta<1300°$. This fact has to be correlated with the SO_3 contents of the synthetized samples and with the rate of formation of $C_4A_3.\overline{S}A$ big loss of SO_3 is possible, at lower burning temperatures, maintaining a level of this temperature for 1 hour, due to a reduced reaction rate of SO_3 (resulted from $FeSO_4$ decomposition) with $CaO(CaCO_3)$. The rate of the mentioned reaction becomes important at higher temperatures and, therefore, the content in SO_3 of the synthetized samples is bigger (see the synthetized sample at 1200° in comparison with the synthetized sample at 800°). The blocking of some part of CaO at $CaSO_4$ leads to the diminution of the CaO/Al_2O_3 ratio; this diminution is the more important the greater is the amount of $CaSO_4$ formed in the system. In these conditions CA_2 is preponderant; this diminution is accentuated by the fact that Fe^{3+} ion partially substitutes Al^{3+} ion in aluminated compounds. Before that calcium sulphate be blocked with an important rate in $C_4A_3\overline{S}$, over 1200 – 1250°, a sensible increasing

Table 1

Free lime and SO_3 content of the synthetized samples (%)

Compound	The values for the samples synthetized at:							
	800°	1000°	1100°	1200°	1250°	1300°	1380°	1450°
Free lime	—	3.14	1.12	0.79	0.31	0	0.25	0.68
SO_3	7.59	—	—	8.96	—	4.53	3.27	1.97

of the decomposition rate of the $CaSO_4$ formed is possible. In this way, the diminution of the SO_3 content of the synthetized samples at 1300° and, consequently, of the content in CA_2 may be explained (as a result of the reactions : $CaO.2Al_2O_3 + CaO \rightarrow 2CaO.Al_2O_3$; $3(CaO.Al_2O_3) + CaSO_4 \rightarrow 3(CaO.Al_2O_3).CaSO_4$).

At higher temperatures than that corresponding to the maximum rate of formation of $C_4A_3\bar{S}$, the content in CA begins to increase at the expense of the decomposition of calcium aluminosulphate.

4. This paper evidences the formation of the compound $C_4A_3\bar{S}$ in the system : $CaO(CaCO_3)-Al_2O_3-FeSO_4$.

Calcium aluminosulphate results with maximum rate in the present system, at temperatures around 1300° ; over these temperatures its rate of decomposition becomes preponderant.

The bivalent iron, introduced in the system as ferrosulphate, becomes trivalent, and this ion may substitute the Al^{3+} ion in aluminate compounds.

The presence of the ferrous sulphate accelerates the binding process of calcium oxide in the $CaO(CaCO_3)-Al_2O_3$ system.

Revue Roumaine de Chimie, **20**, 7, 929–937 (1975)

GREFFAGE MÉCANO-CHIMIQUE DES POLYOXYMÉTHYLÈNES. IV[*]

INFLUENCE DE LA TEMPÉRATURE SUR LA DESTRUCTION PAR BROYAGE VIBRATOIRE

AMALIA CRUSOS et CR. SIMIONESCU
Institut de Chimie macromoléculaire « P. Poni, » Jassy, 41 A,
Aleea Gr. Ghica Vodă

Reçu le 28 mai 1974

Les auteurs étudient la dégradation par broyage vibratoire d'un polymère oxyméthylénique dans un domaine large de température compris entre −55 et +95°, mettant en évidence l'influence du facteur thermique dans les processus mécano-chimiques. Pour certaines conditions de dégradation vibratoire il y a une interférence entre la destruction mécanique et thermique.

I. INTRODUCTION

On peut mentionner le fait qu'au broyage vibratoire des polyoxyméthylènes l'influence d'un facteur important comme la température est abordée dans un nombre réduit de travaux.

Dès les premières recherches appartenant à Hess et Steurer[1,2] qui signalent l'influence de la température dans la destruction mécanochimique, la littérature est très pauvre en données concernant ce thème.

Les études effectuées par Grohn et collab.[3,4] révèlent le comportement du polyméthylmétacrylate dans le broyage vibratoire, dans le domaine de températures comprises entre −75° et +140°.

Baramboin et collab.[5-9] étudient l'influence du facteur thermique sur la destruction de quelques élastomères et plastomères dans un domaine plus large d'investigation, tant des polymères à l'état de haute élasticité, que des polymères à l'état de vitrification, et établissent que pendant le broyage vibratoire sous la température de vitrification on assiste à l'accroissement de la surface spécifique, S_p, et à la diminution du poids moléculaire, M, remarquant la relation, $M = f(S_p)$.

---

[*] IIIe partie: Cr. Simionescu, A. Crusos et D. Feldman, *Rev. Roumaine Chim.*, **16**, 585 (1971).

[1] K. Hess et E. Steurer, *Kolloid-Z.*, **98**, 148, 290 (1942).
[2] K. Hess et E. Steurer, *Z. phys. Chem.* (*Leipzig*), **193**, 234 (1944).
[3] H. Grohn et K. Bischof, *Plaste u. Kautschuk*, **8**, 311 (1961).
[4] H. Grohn, K. Bischof, M. Losche et K. Mockel, *Plaste u. Kautschuk*, **8**, 593 (1961).
[5] N. Baramboim, *Doklady Akad. Nauk. S.S.S.R.*, **114**, 568 (1967).
[6] N. Baramboim, *Zhur. fiz. Khim.*, **32**, 433, 806, 1049 (1958).
[7] N. Baramboim et V. Gordilov, *Vysokomol. Soedineniys*, **2**, 197 (1960).
[8] L. L. Polukhina et N. Baramboim, *Vysokomol. Soedineniya*, **6**, 441 (1969).
[9] N. Baramboim, « Mekanochimia visokomolekularinykh, soedinenii », Moscou, 1971, p. 8

Les surfaces de scission apparaissent aux endroits de certains défauts présents dans le polymère initial ou résultés sous l'action des forces mécaniques. D'après quelques travaux,[10,11] le champ des forces près des scissions est plan et la vitesse d'augmentation de ces scissions est proportionnelle à la vitesse de diffusion des ondes longitudinales sonores dans le polymère, $C_e = (E/\rho)^{1/2}$.

Baramboim et collab.[8] démontrent que pendant la mouture vibratoire des polymères à l'état de vitrification la constante de la vitesse de destruction mécanique représente une fonction linéaire de la vitesse de propagation des ondes sonores élastiques.

Les données de la littérature mentionnée permettent une conclusion unitaire en ce qui concerne la liaison entre la cinétique, l'efficacité de l'énergie mécanique fournie, etc., et l'état physique du polymère, les lois de la mécanodestruction étant différentes pour les divers états physiques du produit macromoléculaire.

Les polymères amorphes linéaires, en fonction de la température, peuvent se trouver dans les trois états bien délimités l'un de l'autre. Les températures caractéristiques des transformations de l'état, T_v (la température de vitrification) et $T_{éc.}$ (la température d'écoulement) sont mises en évidence par les courbes thermomécaniques caractéristiques de chaque polymère.

Un produit macromoléculaire qui se trouve dans un des trois états se caractérise par un mécanisme spécifique de déformation et relaxation, par un certain ordre de grandeur du module d'élasticité, etc. Tous ces facteurs décident la résistance du polymère sur l'action des forces mécaniques. Le degré de destruction, la cinétique des procesus de dégradation sont déterminés dans un mode prépondérent par l'interdépendance entre la température et les propriétés physico-mécaniques.

II. DONNÉES EXPÉRIMENTALES

La destruction mécano-chimique a été effectuée dans un vibrateur du type LS-60 (Veb-Kefama-Katzhütte), avec des vases en acier V_2A ayant une capacité de 4 litres, munis d'un manteau pour la thermostabilité et des soupapes pour l'évacuation des gaz. On a utilisé comme corps de broyage des boulets confectionnés en acier V_2A d'un diamètre de 20 mm.

Pour réaliser une destruction optimale on a imposé les conditions mécaniques suivantes: le rapport de remplissage 0,4%, l'amplitude des oscillations 2 mm et le nombre de tours 1450 tours/mn.

Le broyage vibratoire a été réalisé en air aux températures : $-55°$; $+20°$; $+95°$. Les températures basses ont été obtenues avec une installation du type T.T. Medingen-Dresden effectuant le refroidissement en deux étapes: 1 — mélange de neige carbonique et d'acétone 2— azote liquide.

La durée de l'action mécano-chimique a été variée de 3 à 15 heures.

Pour les expérimentations on a utilisé Delrin-500 (D-500), fourni par Du Pont de Nemours[12] dont on a écarté au préalable les stabilisateurs en deux étapes : le polymère sous forme

---

[10] N. Mott, *Ingineering*, **165**, 16 (1948).

[11] S. Bateson, *Phys. Amer. Chem. Glass.*, 1, 139 (1960).

[12] Du Pont de Nemours, « Le Delrin, le moulage de la résine acétal Delrin », Du Pont de Nemours, International, S. A. Genève, 1960, p. 11.

de granules (2 — 2,5 mm) a été dissous en diméthylformamide à 145° et reprécipité de la solution, filtré et séché à 60° ; la poudre de polymère obtenue (0,2 — 0,8 mm) a été soumise à des extractions successives en Soxhlet pendant 12 heures avec du chloroforme, du méthanol et de l'acétone, selon une méthode indiquée par Schröder et Hagen.[13] Le séchage final du produit a été perfectionné sous vide avec du pentoxyde de phosphore.

III. RÉSULTATS ET DISCUSSIONS

Dans des notes antérieures [14,16] nous avons prouvé par l'analyse thermogravimétrique que, au fur et à mesure de l'augmentation de la durée de destruction mécano-chimique, on modifie la thermostabilité des produits et les résultats montrent une diminution prononcée tant en milieu inerte qu'en présence d'accepteurs des radicaux.

On peut signaler un nouvel aspect qui dans nos recherches effectuées jusqu'à présent, en ce qui concerne l'interdépendance température-mécanodestruction, n'a pas été pris en considération et qui a un rôle très important sur l'effet final de la dégradation mécano-chimique.

La modification de la thermostabilité du polymère, pendant le traitement mécanique, crée la possibilité de l'apparition d'une dégradation thermique à côté de la dégradation mécanique. Cette dégradation thermique contribue cumulativement à la valeur finale atteinte par le degré de la destruction du polymère pendant le processus mécano-destructif. On peut donc considérer, que à un certain stade de la destruction mécano-chimique et pour une certaine température, à cause de la modification de la thermostabilité (sa diminution), il peut intervenir à côté de la destruction mécanique, à proprement parler, une thermo-destruction, la dégradation finale étant la résultante de deux processus parallèles de destruction : mécanique et thermique.

Nous nous sommes proposé de suivre l'influence de la température sur la destruction mécano-chimique des polyoxyméthylènes, les modifications de la thermostabilité qui ont lieu et les conséquences sur le degré de la destruction.

La littérature relève que la thermostabilité des polymères oxyméthyléniques est influencée par deux facteurs principaux : l'agrandissement du poids moléculaire et la nature des groupes finals.[17,20] Dans les processus mécano-chimiques ce sont surtout les deux caractéristiques qui subissent d'importantes modifications ce qui évidemment aura des répercussions sur la stabilité des produits dégradés.

Le broyage vibratoire des polyoxyméthylènes conduit à la rupture des chaînes macromoléculaires et à l'apparition de groupes finals radicaliques. Ceux-ci déterminent la libération progressive du formaldéhyde conformément au mécanisme :

---

[13] E. Schroder, E. Hagen et M. Helmsted, *Plaste u. Kautschuk*, **8**, 560 (1967).

[14] A. Crusos, D. Feldman et Cr. Simionescu, *Rev. Roumaine Chim.*, **13**, 1489 (1968).

[15] Cr. Simionescu, D. Feldman et A. Crusos, *Bull. Soc. chim. France*, **1968**, 1525.

[16] J. Furukawa et T. Saegusa, « Polymerization of aldehydes and oxides », Interscience Publishers, New York, 1963, p. 260.

[17] N. Grassie et R. Roche, *Makromol. Chem.*, **112**, 16 (1968).

[18] J. Sedlařc et M. Kucera, *Makromol. Chem.*, **102**, 245 (1967).

[19] W. Kern et H. Cherdron, *Makromol. Chem.*, **101**, 23 (1960).

[20] H. Cherdron, L. Hohr et W. Kern, *Makromol. Chem.*, **52**, 48 (1962).

$$1)\sim CH_2-O-CH_2-O-CH_2-O-CH_2-O-CH_2-O-CH_2-O-CH_2-O\sim \xrightarrow[\text{mécano-chimique}]{\text{destruction}}$$

$$2)\sim CH_2-O-CH_2-O-CH_2O.+\cdot CH_2-O-CH_2-O-CH_2-O-CH_2\sim$$

$$3)\sim CH_2-O-CH_2-O-CH_2-O-CH_2-O-CH_2-O-CH_2-.O\rightarrow$$

$$\rightarrow\sim CH_2-O-CH_2-O-CH_2-O\cdot+CH_2O$$

La quantité d'aldéhyde formique libérée croît au fur et à mesure de l'augmentation de la durée de la destruction.

Le broyage vibratoire du D-500 a été conduit comme il a été déjà mentionné, dans un large intervalle de température. Dans ce mode on peut suivre le comportement du polymère aux températures qui incluent le point de vitrification, compris d'après la littérature, [21] entre —40 et 60° ; le domaine se caractérise par un empaquetage serré des macromolécules et une rigidité prononcée. On a passé ensuite dans la zone de haute élasticité (+20°), dans laquelle la flexibilité augmentée détermine un autre mécanisme de déformation.

Enfin, on a poursuivi la destruction à 95°, la température à laquelle, conformément aux données d'analyse thermogravimétrique, commence la dégradation thermique du produit moulu.

Tableau 1

La perte en poids des produits moulus, à l'analyse thermogravimétrique effectuée entre 95 et 140°

Epreuve	Perte en poids, %		
	Température, °C		
	95°	120°	140°
D—500 produit initial	0	0	0
D—500 moulu 3h à 20°	0	0,51	1,03
D—500 moulu 9h à 20°	0	1,03	1,54
D—500 moulu 15 h à 20°	0	1,03	2,06
D—500 moulu 3h à —55°	0,51	1,02	2,04
D—500 moulu 9h à —55°	1,03	1,54	2,06
D—500 moulu 15h à —55°	1,09	2,08	2,60
D—500 moulu 3h à 95°	1,57	2,10	3,15
D—500 moulu 9h à 95°	2,10	2,10	4,20
D—500 moulu 15h à 95°	2,60	4,68	7,80

Du tableau 1 et des figures 1 — 4 qui présentent les résultats de la thermoanalyse on remarque, que tandis que D-500, le produit initial, non dégradé mécano-chimique est thermostable jusqu'à la température au-dessus de 200°, les produits moulus commencent à se décomposer à la température d'environ 90°, quand en fonction des conditions de la mouture (température et durée), la perte en poids a des valeurs comprises entre 0,5 et 2,6 % (tableau 1). Cette observation est très importante : il résulte qu'aux températures de mouture supérieures à celle de 90°, on peut parler tant d'une activation mécanique de la dégradation thermique, que d'une activation thermique de la dégradation mécanique.

---

[21] N. Gaylord, « Polyethers », Interscience Publishers, New York, 1963, p. 47.

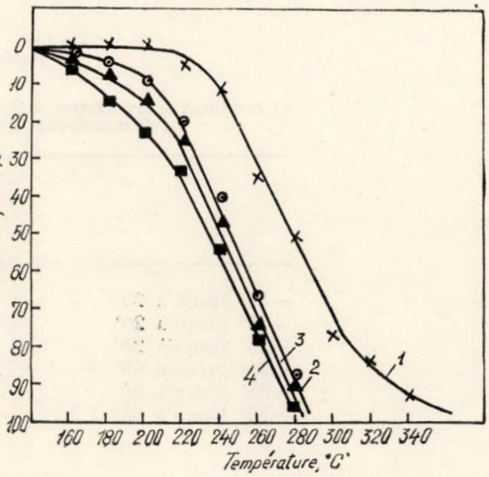

Fig. 1. — Données de l'analyse thermogravimétrique. Température de la destruction mécano-chimique —55°

1) D-500 produit initial; 2) D-500 dégradé 3 h; 3) D-500 dégradé 9 h; 4) D-500 dégradé 15 h.

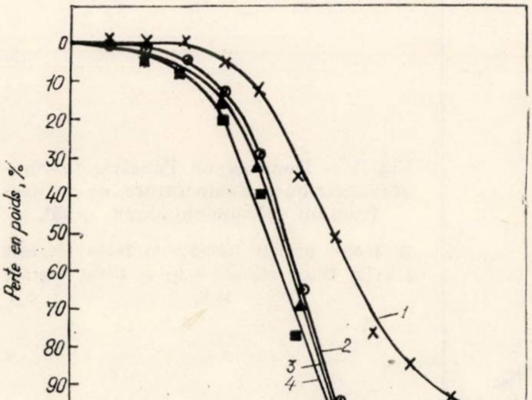

Fig. 2. — Données de l'analyse thermogravimétrique. Température de la destruction mécano-chimique + 20°.

1) D-500 produit initial ; 2) D-500 dégradé 3 h; 3) D-500 dégradé 9 h; 4) D-500 dégradé 15 h.

La confirmation de cette conclusion est donnée par les valeurs du coefficient de température $d(d\eta/dt/d\rho)$ où $[\eta]$ = la viscosité intrinsèque, t = la durée d'action mécano-chimique, ρ = la température dans le domaine — 55° jusqu'à 95° et qui sont en accord avec les résultats obtenus par Baramboim [9] et Grohn.[4] Dans le domaine de la haute élasticité (de —55° jusqu'à + 20°), le coefficient de température est négatif (tableau 2), tandis qu'aux température élevées (de 20° à 95°) où adjacent au processus de la destruction mécanique il intervient aussi la destruction thermique, le coefficient de température a des valeurs positives. Son signe se change conformément à la modification du mécanisme de la destruction prédominant : mécanique ou thermique.

Tableau 2

Le coefficient de température, d $(d[\eta]/dt/d\rho)$, à différents intervalles de températures et durées de mouture

°C	dt heures	$\dfrac{d\left(\dfrac{d[\eta]}{dt}\right)}{d\rho}$
−55° jusqu'à 20°	3	−0,00141
−55° jusqu'à 20°	9	−0,000148
−55° jusqu'à 20°	15	−0,000150
−55° jusqu'à 95°	3	+0,000266
−55° jusqu'à 95°	9	+0,000502
−55° jusqu'à 95°	15	+0,000577

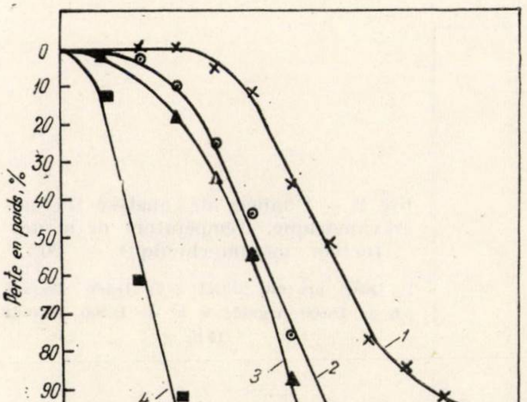

Fig. 3. — Données de l'analyse thermogravimétrique. Température de la destruction mécano-chimique +95°.

1) D-500 produit initial; 2) D-500 dégradé 3 h; 3) D-500 dégradé 9 h; 4) D-500 dégradé 15 h.

Les investigations sur d'autres effets qui retiennent la destruction du polymère en fonction de la température soutiennent les observations de plus haut. Ainsi, en même temps que la diminution de la thermostabilité des produits, au fur et au mesure que la durée de mouture croît (fig. 1 — 3), on modifie aussi la thermostabilité en fonction de la température à laquelle a été effectuée la destruction mécanique (fig. 4). Les épreuves moulues à 95°, où intervient dans le processus mécano-chimique aussi

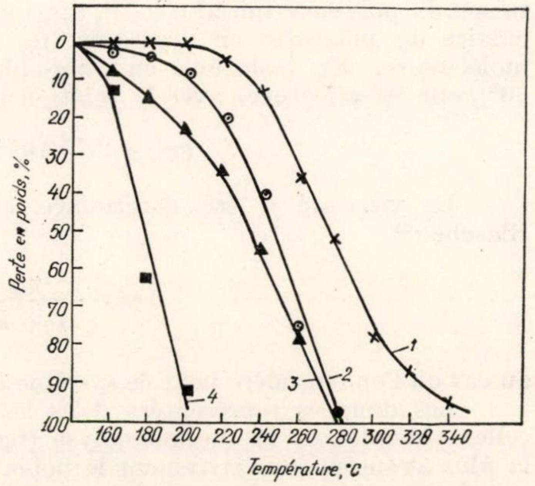

Fig. 4. — Données de l'analyse thermogravimétrique. Durée de la destruction mécano-chimique 15h ;

1) D-500 produit initial ; 2) D-500 dégradé mécano-chimique à la température de + 20° ; 3) D-500 dégradé mécano-chimique à la température de − 55° ; 4) D-500 dégradé mécano-chimique à la température de + 95°.

une dégradation thermique enregistrent la plus basse stabilité (fig. 4, courbe 4). Aux températures du domaine de la haute élasticité (+20°), où, à cause de la flexibilité augmentée des macromolécules, la destruction mécanique est moindre, et où la destruction thermique n'intervient pas, les épreuves moulues présentent la thermostabilité la plus élevée. Les produits qui ont subi la dégradation mécanique aux températures basses, (−55°), favorables à la destruction mécanique présentent la modification de la thermostabilité (fig. 4, courbe 3).

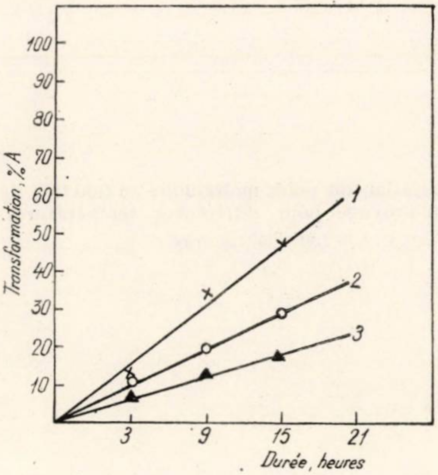

Fig. 5. — Variation de la destruction en fonction de la température.

1) +95° ; 2) −55° ; 3) +20°.

En fonction de la température de la mouture, la destruction est représentée, de même, par la transformation totale, %A, qui représente la variation de la viscosité intrinsèque des épreuves dégradées en comparaison du polymère initial (fig. 5), ainsi que la modification du poids moléculaire du polymère en processus (fig. 6). Les déterminations du poids moléculaire, $\bar{M}_n$ (solutions en *para*-chlore-phénol avec 2 % α-pinènes à 60°), ont été effectuées avec la relation indiquée par la littérature :[22, 23, 24]

$$[\eta] = 2{,}75.10^{-4} \cdot \bar{M}_n^{0.8}$$

La viscosité a été déterminée en utilisant la relation Schulz-Blasche :[21]

$$[\eta] = \frac{\eta_{sp}/c}{1 + k\eta_{sp}}$$

au cas où l'on considère pour ce système $k = 0{,}23$.[18, 20]

Les données représentées dans les figures 5 et 6 concordent avec celles obtenues de la thermoanalyse (fig. 4), c'est-à-dire la destruction la plus avancée, respectivement le poids moléculaire le plus bas est enregistré soit aux températures élevées (95°), où a lieu aussi une destruction thermique, soit aux températures basses (−55°), où la destruction mécanique est favorisée par la flexibilité réduite des macromolécules.

La plus basse destruction mécanique (les valeurs les plus élevées pour le poids moléculaire des épreuves dégradées) est obtenue aux températures situées dans le domaine d'élasticité élevée (+20°), où la mobilité des macromolécules permet leurs soustractions de l'action mécanique et où on ne peut parler aussi d'une destruction thermique (fig. 5, courbe 3 ; fig. 6, courbe 1).

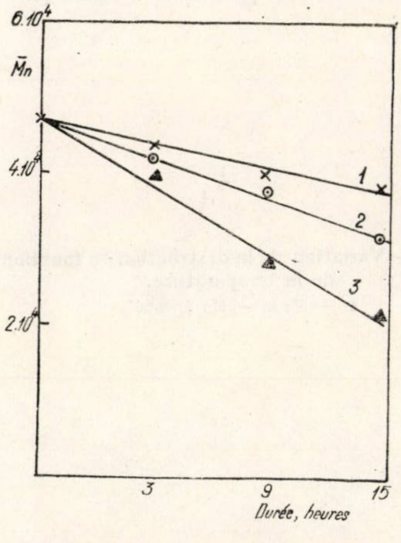

Fig.6. — Variation du poids moléculaire en fonction de la durée du broyage pour différentes températures. 1) +20° ; 2) −55° ; 3) +95°.

---

[22] W. Thummler, *Plaste u. Kautschuk*, **10**, 582 (1965).

[23] W. Thummler et G. Hantzsch, *Plaste u. Kautschuk*, **14**, 881 (1967).

[24] J. Mayer, *Makromol. Chem.*, **82**, 169 (1965).

IV. CONCLUSIONS

1. La destruction par broyage vibratoire du D-500 dans le domaine des températures −55° jusqu'à 95° et durée de 3 — 15 heures met en évidence l'influence du facteur thermique dans les processus mécano-chimiques.

2. Comme résultat de la destruction mécano-chimique on modifie la thermostabilité des polymères oxyméthyléniques qui présente des abaissements sensibles tant avec la durée de mouture que surtout en fonction de la température de destruction mécanique.

3. L'apparition de la destruction thermique dans le processus est confirmée par les données d'analyse thermogravimétrique et les valeurs du coefficient de la température.

4. Le degré de destruction, le poids moléculaire du polymère sont évidemment nettement affectés par la température. L'augmentation de la température du broyage vibratoire au-dessus de 90°, produit de façon concomitante avec la destruction mécanique aussi une décomposition thermique qui détermine une diminution prononcée du poids moléculaire. C'est le domaine dans lequel, on peut considérer l'influence réciproque des deux facteurs de destruction : mécanique et thermique.

Revue Roumaine de Chimie, **20**, 7, 939–943 (1975)

STUDY OF ORGANIC POLYMERS WITH SPECIAL ELECTROPHYSICAL PROPERTIES. I

ON THE ELECTRIC CONDUCTIVITY OF DIETHYNYLBENZENE–2–METHYLPENTINOL COPOLYMER FILMS*

CR. I. SIMIONESCU, SVETLANA DUMITRESCU, I. DIACONU and L. GORAŞ
"P. Poni" Institute of Macromolecular Chemistry, Aleea Gr. Ghica Vodă No 41 A
Jassy, Romania

Received September 6, 1974

The results of the d.c. intensity measurements on the diethynylbenzene–2–methylpentinol (DEB – 2MP) copolymer films obtained in solution as a function of time (*t*), temperature (*T*), voltage (*U*) and pressure (*p*) are better explained by the electronic nature of the charge carriers. Optical activation energy (E_{op}=1.91 eV), calculated using the spectral dependence of the optical absorption constant on copolymer film is greater than intrinsic thermal activation energy of the electrical conductivity (ΔE_2 = 1.67 eV). This is better explained by means of the hopping model than by the band or tunneling model.

INTRODUCTION

Until late, the deviations from Ohm's law, in the case of the electric conductivity measurements on the organic polymers, were attributed to experimental errors. Now, this phenomenon is considered as a specific characteristic of many organic substances with high electric resistivity.[1-10] In this case the intensity-voltage ($I - U$) characteristic becomes nonlinear at high electric fields when the injected charge density exceeds the quilibrium charge density at $U = 0$.

The electrode thermal emission,[5,7] the space charge,[1,4,7] the Schottky[1,9] and Poole-Frenkel [8,10] effects (the last two effects appear at very high

---

[*] Presented at the "Polymer' 73" Symposium, Varna, 1973.

[1] M. Kryszewski and A. Szymanski, *J. Macromol. Sci.*, *D*, **4**, 245 (1970).

[2] M. Kryszewski, P. Wojciechowski and S. Sapieha, *Discuss. Faraday Soc.*, **1971**, 144.

[3] M. Kryszewski, N. Kasica, J. Patora and J. Piotrowski, *J. Polymer Sci.*, *C*, **30**, 343 (1971).

[4] A. Szymanski and M. Kryszewski, *J. Polymer Sci.*, *C*, **22**, 867 (1969).

[5] R. P. Bugers, *J. Polymer Sci.*, *C*, **17**, 51 (1967).

[6] D. D. Eley, *J. Polymer Sci.*, **17**, 73 (1967).

[7] F. Gutmann and L. E. Lyons, "Organic Semiconductors", Willey, New York, 1967, chap. 10.

[8] L. F. Babcock and R. W. Christy, *J. Appl. Phys.*, **43**, 4 (1972).

[9] C. M. Vodenicharov, M. B. Vodenicharova and I. D. Shopov, *Doklady Acad. Nauk S.S.S.R.*, **24**, 10 (1971).

[10] R. W. Christy, *J. Appl. Phys.*, **35**, 2179 (1964).

electric fields) are the main causes of this phenomenon. The nonohmic behaviour takes place when n from relation $I \sim U^n$ differs from unit. If the electrical conductivity is electronic in nature, n may be either $n < 1$ or $n > 1$, but in the case of ionic conductivity $I = f(U)$ is a hyperbolic sine relationship.[11]

The study of the variation of the electrical conductivity (σ) with pressure at a constant temperature was used by many workers[12–16] as an experimental method for elucidating the nature of the charge carriers; ionic for $d\sigma/dp < 0$ and electronic for $d\sigma/dp > 0$.

The aim of this report was to establish the nature and the transport model of the charge carriers in diethylbenzene—2—methylpentynol copolymer films, using electrical conductivity measurements as a function of temperature, time, pressure and d.c. voltage as well as the optical absorption constant (α).

EXPERIMENTAL

Investigations were made on copolymer samples having a molecular weight of about 600, a crystallinity degree of about 23% and the ratio between the monomers 2MP/DEB = = 10. The copolymer films of about 0.8 μm thickness were obtained by evaporation of the copolymer solution and the rectangular silver electrodes of about 0.6 cm^2 were deposed under vacuum of 10^{-4} torr. A PM 2436 Philips DC—Microvoltmeter was used for the d.c. dark current measurements, and a Philips X — Y Recorder was coupled to map out the $I = f(t)$ characteristics. The temperature was electronically stabilized with a precision of 0.2°. The measurements were made in the air.

The pressure measurements of the electrical resistivity were made using a pressure cell as shown in fig.1 .

The absorption and reflexion spectra of the films, used to determine the values of the optical absorption constant, were recorded on a SP 800 B.U.V. spectrograph.

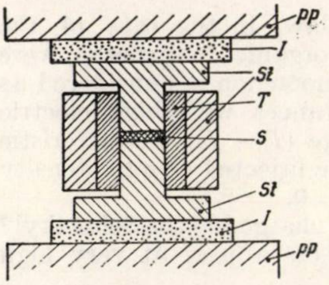

Fig.1.—Pressure cell : PP — Press Plates ; I—Insulation ; St— Steel ; T — Teflon ; S — Sample.

RESULTS AND DISCUSSIONS

When d.c. voltage was applied, the current through the sample decreased and attained a steady-state in about 30s (Fig.2).

When the d.c. supply was shorted out, a fairly large back current was observed, which decreased rapidly to a zero value. The rather high values of the charge and discharge current can be explained as being due to the dipolar effect in electric field and the injected space charge near the electrodes. These rapid current variations as well as the constancy of the equilibrium current suggest an electronic nature for the charge carriers.

---

[11] L. E. Amborski, *J. Polymer Sci.*, **62**, 331 (1962).

[12] R. Somoano, S.P.S. Yen and A. Rembaum, *J. Polymer Sci.*, *B*, **8**, 467 (1970).

[13] H. Sasabe, K. Sawamura, S. Saito and K. Yoda, *Polymer J.*, **2**, 518 (1971).

[14] H. A. Pohl, A. Rembaum and A. W. Henry, *J. Amer. Chem. Soc.*, **84**, 2699 (1962).

[15] D. D. Eley, G. D. Parfit and D. H. Paysum, *Trans. Faraday Soc.*, **49**, 79 (1953).

[16] H. Inokuchi, *Bull. Chem. Soc. Japan*, **23**, 570 (1955).

The log $I = f$ (log U) curve was plotted for different temperatures in the range $40 - 80°$ (Fig. 3).

Ohm's law is obeyed up to an electric field of about 6×10^{5} Vcm^{-1} and then the current rises supralinearly with the voltage owing to the trapped space charge from the sample.[1,4,7] On the basis of the experimental data, there was found that for electromagnetic fields greater than 6×10^{5} V/cm exponent n from $I = BU^{n}$ relation, where B is a constant, is 1.15. The trapping centers can be structural defects of the copolymer as well as ionized or nonionized impurities, from the synthesis process itself.

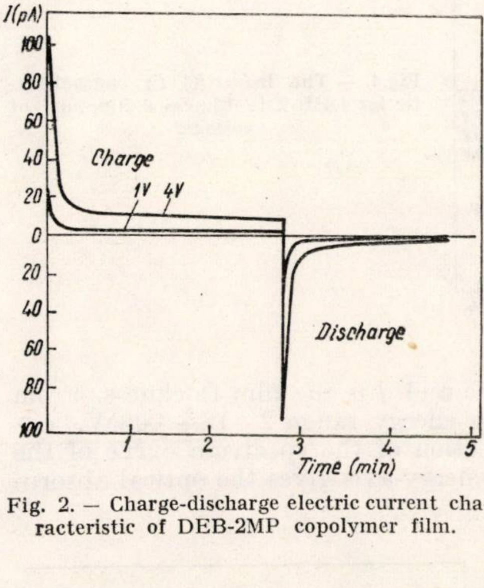

Fig. 2. — Charge-discharge electric current characteristic of DEB-2MP copolymer film.

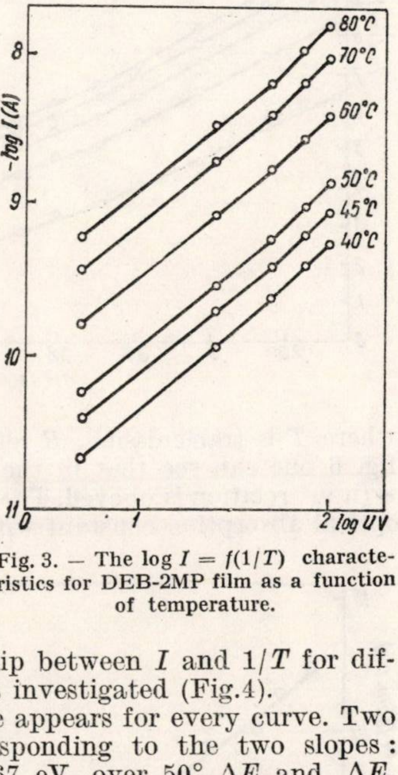

Fig. 3. — The log $I = f(1/T)$ characteristics for DEB-2MP film as a function of temperature.

For the same samples, the relationship between I and $1/T$ for different voltages in the range $5 - 100$V was investigated (Fig.4).

At a temperature of about 50° a knee appears for every curve. Two activation energies were calculated corresponding to the two slopes: $\Delta E_1 = 1.21$ eV up to 50° and $\Delta E_2 = 1.67$ eV over 50°. ΔE_1 and ΔE_2 were calculated by means of relation $I = I_0 \exp(-\Delta E/2kT)$ resulted from relation $\sigma = \sigma_0 \exp(-\Delta E/2\,kT)$, were $I_0 = US/d$; S is the surface of the sample between electrodes, d is the thickness of the copolymer films and U is d.c. voltage applied on the electrodes. The change of the slope may be attributed to an impurity extrinsic — intrinsic transition.

At the room temperature the copolymer has a not too high negative piezo-resistive coefficient (Fig.5).

Although our experimental conditions did not allow pressure measurements of resistivity over 15,000 bars, however, the decrease of resistivity with one order in magnitude, when the pressure increases from zero to 12,000 bars can be explained rather by electronic conductivity than by ionic one.

The curves of optical absorption constant *vs* the photon energy were used to determine the optical activation energy.[17] (Fig. 6).

The optical absorption constant was calculated using the formula[18] :

$$T = (1 - R)^2 \exp\ (-\alpha d)$$

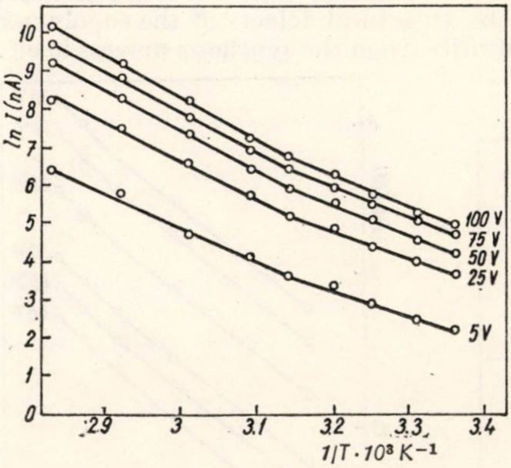

Fig.4. — The $\ln I = f(1/T)$ characteristic for DEB-2MP film as a function of voltage.

where T is transmission, R reflectance and d is the film thickness. From fig. 6 one can see that in the photon energy range 2−17−3.00eV, $\alpha \sim \sim (h\nu)^2$ relation is obeyed. The intersection of the spectrum curve of the optical absorption constant with the energy-axis gives the optical absorption threshold ($E_{op} = 1.91$ eV) which is greater than the intrinsic thermal activation energy of the electrical conductivity ($\Delta E_2 = 1.67$ eV). As $\Delta E_2 < < E_{op}$ the hopping model explains the experimental data better than the

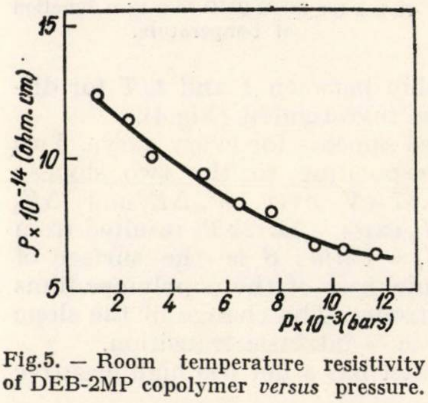

Fig.5. — Room temperature resistivity of DEB-2MP copolymer *versus* pressure.

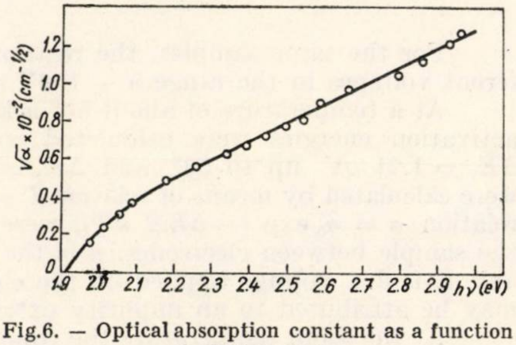

Fig.6. — Optical absorption constant as a function of photon energy.

[17] R. H. Colburn and R. W. Christy, *J. Appl. Phys.*, **40**, 3958 (1969).

[18] S. Couve, L. Gouskov and L. Szeoessy, *Thin Solid Films*, **15**, 223 (1973).

band or tunneling model. This model was often assumed for polymers with semiconductive properties. [19,21]

Certainly, one needs more experimental proofs to establish the exact transport model, mainly the current carrier mobility determinations and its temperature dependence.

In conclusion, the rapid current variations when the voltage is applied and shortened out, its keeping at constant values for a long while the shape of the curves from fig.3, and the negative piezo-resistive coefficient are some experimental proofs which permit to admit the electronic nature of the current carriers in the case of copolypmer DEB-2MP.

---

[19] I. D. Schpov and C. Vodenicharov, *J. Macromol. Sci.*, **44**, 1627 (1970).

[20] R. M. Voitenko and E. M. Raskina, *Doklady Acad. Nauk. S.S.S.R.*, **136**, 1137 (1961)

[21] A. Lipinski, J. Kondrasiuk and A. Szymanski, *Mol. Cryst.*, **13**, 381 (1971).

Revue Roumaine de Chimie, **20**, 7, 945–949 (1975)

REACTIONS OF COORDINATED LIGANDS. VII[1] ZINC-ORGANIC COMPOUNDS OF SALICYLALDOXIME COORDINATED WITH Ni(II), Pd(II) AND Cu(II)

N. VOICULESCU, LUCIA ROMAN and I. POPESCU
"P. Poni" Institute of Macromolecular Chemistry,
Aleea Grigore Ghica Vodă 41-A, Iassy, Romania

Received April 15, 1974

Zinc-organic compounds of salicylaldoxime coordinated with Ni(II), Pd(II) and Cu(II) ions have been synthesized by the reaction of salicylaldoximates of the respective ions with $Zn(C_6H_5)_2$. The compounds resulted are formed by replacing the OH. . .O hydrogen bonds from chelates with $-ZnC_6H_5$ groups. The synthesized compounds were isolated as amorphous solid powders and characterized by chemical analyses, IR absorption spectra, X-ray diffraction spectra and magnetic measurements.

INTRODUCTION

The reaction of zinc-organic derivatives with compounds containing active hydrogen atoms [2,3] has been known for over one hundred years. However, the systematic study of the reactivity of zinc-organic compounds towards inorganic compounds is quite recent. [4-6]

Depending on the reactivity of the partner and also on the reaction conditions, zinc-organic derivatives undergo partial or total substitution reactions with a series of organic ligands [4-6] resulting in associated compounds in the form of dimers, trimers or tetramers.[5-7] Most compounds obtained by substitution or addition reactions are represented by cyclic formulae, in which the zinc atom has usually the coordination number 4. A feature of the compounds obtained in this manner is their ability to form addition compounds with mono- or bidentate ligands containing donor elements (N, P, O). Although diphenylzinc is less reactive than alkyl derivatives, it produces substitution reactions with active hydrogen-containing compounds.[8-10]

No reports on the chemical interaction between zinc-organic derivatives and the compounds of transition metals have so far been found in the literature.

---

[1] N. Voiculescu, *Rev. Roumaine Chim.*, **18**, 1919 (1973).

[2] A. M. Butlerow, *Jahresber.*, **1864**, 467.

[3] E. Frankland, *Jahresber.*, **1857**, 418.

[4] G. E. Coates and D. Ridley, *J. Chem. Soc.* (*A*), **1966**, 1064.

[5] J. G. Noltes and J. Boersma, *J. Organometal. Chem.*, **12**, 425 (1968).

[6] J. Boersma and J. G. Noltes, *J. Organometal. Chem.*, **13**, 291 (1968).

[7] G. E. Coates and D. Ridley, *J. Chem. Soc.*, **1965**, 1870.

[8] S. Fişel, L. Roman, I. Popescu and M. Poni, *Rev. Roumaine Chim.*, **12**, 511 (1967).

[9] A. Ciobanu, L. Roman, M. Bostan, N. Voiculescu and D. Giurgiu, *Rev. Roumaine Chim.*, **15**, 783, (1970).

[10] D. Giurgiu, L. Roman, I. Popescu and A. Ciobanu, *Rev. Roumaine Chim.*, **16**, 1217(1971).

In this paper we report some compounds resulted from the reaction of Ni(II), Pd (II) and Cu (II) bis-salicylaldoximates with $Zn(C_6H_5)_2$ and the characteristic features of the newly synthesized compounds, resulted from IR absorption spectra, X-ray diffraction spectra and from magnetic measurements.

EXPERIMENTAL

Diphenylzinc was synthetized according to the Krause and von Grosse[11] method, from diphenylmercury and zinc splinter.

Ni(II), Pd(II) and Cu(II) bis-salicylaldoximates were prepared according to methods given in the literature.[12, 13]

The solvents used were purified by distillation on metallic sodium in the presence of benzophenone as dehydration indicator.

The reaction between $Zn(C_6H_5)_2$ and Ni(II), Pd(II) and Cu(II) bis-salicylaldoximates and also the handling of the new products was carried out in Schlenk vessels in an inert atmosphere (nitrogen or argon).

Reaction of $Zn(C_6H_5)_2$ with Ni(II), Pd(II) and Cu(II) bis-salicylaldoximates

To the $Zn(C_6H_5)_2$ solution in benzene, filtered through a G-4 frit, in a Schlenk vessel, a suspension of the metal salicylaldoximate in benzene at a 2 :1 molar ratio was added. A change in colour and a slight heating of the reaction vessel took place immediately after mixing the reagents. The mixture was vigorously stirred for a couple of hours at room temperature until complete consumption of bis-salicyl-aldoximate occurred. The solution was concentrated in vacuum. The resulted solid product was separated from the liquid fraction by decanting, washed 3 — 4 times with anhydrous ethyl ether and vacuum-dried.

Adducts with amines of zinc-organic derivatives of salicyl-aldoxime coordinated with Ni(II), Pd(II) and Cu(II) ions were obtained by adding amine in excess to the solution of $M(II)(C_7H_5O_2N)_2Zn_2(C_6H_5)_2$ derivative in benzene. The adducts were separated from the excess amine by precipitation with ethyl ether. The product was allowed to deposit and the clear solution was decanted. It was washed several times with ethyl ether and vacuum-dried.

Among the adducts with amines, only those with pyridine were characterized.

The analyses and characteristics of the synthesized products are given in table 1.

Table 1

Analyses and properties of the synthetized products

Compound	Colour	Magnetic characteristics	Analyses				
			C Calc. Found %	H Calc. Found %	Zn Calc. Found %	N Calc. Found %	M Calc. Found %
$Ni(C_7H_5O_2N)_2Zn_2(C_6H_5)_2$	grey violet	diamagnetic	50.89	3.26	21.33	4.56	9.62
			50.50	3.20	21.19	4.50	9.60
$Pd(C_7H_5O_2N)_2Zn_2(C_6H_5)_2$	brown	diamagnetic	47.20	3.02	19.66	4.23	16.03
			47.00	3.00	19.40	4.10	16.29
$Cu(C_7H_5O_2N)_2Zn_2(C_6H_5)_2$	green	paramagnetic	50.48	3.23	21.19	4.53	10.35
			50.40	3.00	21.33	4.40	10.30
$Ni(C_7H_5O_2N)_2Zn_2(C_6H_5)_2Py_2$	brown	diamagnetic	56.03	3.89	16.99	7.26	7.65
			56.00	3.60	16.80	7.10	7.60
$Pd(C_7H_5O_2N)_2Zn_2(C_6H_5)_2Py_2$	brown	diamagnetic	52.75	3.66	15.98	6.83	12.94
			52.70	3.60	15.75	6.70	13.00
$Cu(C_7H_5O_2N)_2Zn_2(C_6H_5)_2Py_2$	green	diamagnetic	55.70	3.86	16.88	7.21	8.24
			55.60	3.80	16.95	7.10	8.00

---

[11] E. KRAUSE and A. von GROSSE, "Die Chemie der metallorganischen Verbindungen" Verlag Gebrüder Borntraeger, Berlin, 1937, p. 118.

[12] F. EPHRAIM, *Ber. dtsch. chem. Ges.*, **64**, 1210, 1215 (1931).

[13] E. G. COX, F. W. WARDLAW and K. O. WEBSTER, *J. Chem. Soc.*, **1935**, 459.

IR absorption spectra of compounds were recorded on a Unicam SP-200 apparatus, using KBr pellets.

X-ray diffraction spectra were obtained by the powder method with the help of a TUR M-60 apparatus using CuK α radiation and nickel filter. Samples were exposed in Lindemann glass capillaries at 40 kV and 12 mA for 8 hrs.

Magnetic measurements were made on a Gouy balance in a nonhomogeneous magnetic field.

RESULTS AND DISCUSSION

The formation reaction of zinc-organic compounds of salicyl-aldoxime coordinated with Ni(II), Pd (II) and Cu(II) ions can be written as follows :

$$\mathrm{M(II)\,(C_7H_6O_2N)_2 + 2Zn(C_6H_5)_2 \rightarrow M\,(II)\,(C_7H_5O_2N)_2\,Zn_2\,(C_6H_5)_2 + 2C_6H_6}$$

The ratio between chelate and zinc-organic derivative is dictated by the number of the hydrogen bonds present in the chelate.

Diphenylzinc as well as triphenylaluminium[14] in reaction with Ni(II), Pd(II) and Cu(II) bis-salicylaldoximates were found to replace the intramolecular hydrogen[15,16] bonds occurring in the chelate, by the $-\mathrm{ZnC_6H_5}$ group.

We consider that the substitution mechanism of hydrogen bonds, OH ... O, by O–Zn–O bridges may be illustrated by a successive two-step reaction, as in the case of the reaction of Ni(II), Pd(II) and Cu(II) bis-salicylaldoximates[14] with $\mathrm{AlR_3}$. In the first step, an unstable addition compound is probably formed between a chelate molecule and two diphenylzinc molecules, through two dative bonds Zn←O. The elimination of two benzene molecules and the formation of substitution compounds corresponding to formula 1 takes place in the second step.

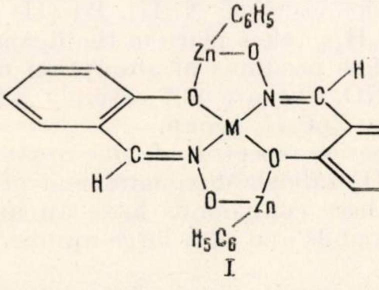

I

The chemical analyses of compounds (table 1) are in agreement with the proposed formula.

Zinc-organic compounds of salicylaldoxime coordinated with Ni(II), Pd(II) and Cu(II) ions are solid, coloured substances, insoluble in common organic solvents and sensitive to air and moisture. These substances are readily decomposed by water and alcohols with recovery of parent chelates.

---

[14] N. Voiculescu, I. Popescu and N. Luchian, *Rev. Roumaine Chim.*, **18**, 1601 (1973).

[15] L. L. Merritt Jr., C. Guare and A. E. Lessor, *Acta Cryst.*, **9**, 253 (1956).

[16] M. A. Jarski and E. C. Lingafelter, *Acta Cryst.*, **17**, 1109 (1964).

Structural changes resulting from the substitution of hydrogen bonds, OH...O in the chelates by O—Zn—O bridges were revealed by IR absorption spectra in a spectral region ranging between 1650—700 cm^{-1} (table 2).

Table 2

IR absorption spectra of M (II) $(C_7H_5O_2N_2)_2Zn_2(C_6H_5)_2$ (values in cm^{-1})

Ni	Pd	Cu	Assigned to
1 600	1 600	1 598	C=N
1 557	1 560	1 555	C=N and C=C
1 480	1 490	1 480	
			Ortho
1 445	1 450	1 443	
1 340	—	—	
1 290	1 290	1 290	C—H in the plane
1 248	—	—	
1 200	1 200	1 200	N—O
1 155	1 160	1 175	
			Benzene ring vibration
1 125	1 130	1 123	
1 020	1 020	1 018	C—O
920	925	920	N—O
820	820	855	
758	775	820	C—H out of plane
		760	

As a result of this substitution, absorption bands characteristic of the OH group in chelates are absent in zinc-organic compounds of salicylaldoxime coordinated with Ni(I), Pd (II) and Cu (II). This absence is the only proof indicating that the reaction between Ni(II), Pd (II) and Cu(II) bis-salicylaldoximates and $Zn(C_6H_5)_2$ takes place in the ligand rather than in the central metallic atoms. The positions of absorption maxima of the main ligand : C=O, C = N, NO, ring are not severely affected after substituting hydrogen by the $-ZnC_6H_5$ group.

From X-ray diffraction spectra of zinc-organic derivatives with Ni(II), Pd (II) and Cu(II) salicylaldoximates and of their adducts with amines it follows that these compounds have an amorphous structure, typical of polymer compounds and of a large number fof organo-metallic compounds.[9,10,14]

One of the important results obtained by determining the magnetic properties is the paramagnetism of the zinc-organic derivative of copper salicylaldoximate, proving that the copper atom is found in oxidation state two. Another important result, equally obtained from these measurements, is the diamagnetism of the adducts with amines, particularly in the case of the nickel derivative.

Adducts with amines (pyridine, lutidine, picoline, etc.) of zinc-organic derivatives of salicylaldoxime coordinated with Ni(II), Pd(II) and Cu(II) ions are formed according to reaction :

$$M(II)\ (C_7H_5O_2N)_2Zn_2(C_6H_5)_2 + 2L \rightarrow M(II)\ (C_7H_5O_2N)_2Zn_2(C_6H_5)_2L_2$$

$$M(II) = Ni, Pd, Cu$$

$$L = \text{pyridine, lutidine, etc.}$$

This reaction is vigorous, probably owing to the passage of the zinc atom from the unstable three-coordinated state to a stable state in which the zinc atom has the coordination number four (formula II). The high chemical stability of the adducts, compared to that of parent zinc-organic derivatives, is probably explained in this manner. The diamagnetism of adducts suggests that the ligand is bound to the zinc atom, rather than to the central atom (formula II).

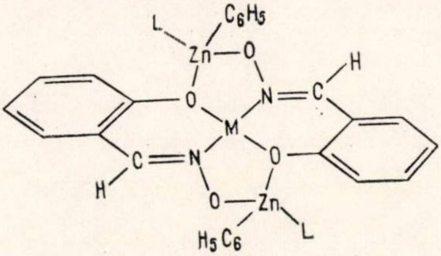

II

Revue Roumaine de Chimie, 20, 7, 951–955 (1975)

DYNAMICS OF THE LIGAND EXCHANGE IN URANYL BIS-CHELATED COMPLEXES. I

FAST EXCHANGE BETWEEN BIS-(ACETYLACETONATO)-URANYL AND ACETYLACETONE STUDIED BY NMR

ALICE VASILESCU
Laboratory of Organic Labelled Compounds
Institute for Atomic Physics, P.O.Box 35, Bucharest, Romania

Received April 22, 1974

The temperature dependence of the NMR spectrum of bis-(acetylacetonato)-uranyl and of the free ligand in acetonitrile solution is presented. Rate constants at different temperatures were determined and an Arrhenius activation energy of 13.6 ± 1.0 kcal/mole was found. The experimental data suggest a mechanism consisting of two processes: a unimolecular and a bimolecular one.

I. INTRODUCTION

The first data concerning the lability of the metal-donor bond in bis-(acetylacetonato)-uranyl were reported by Starke[1] in his attempt at preparing radioisotopes of high specific activity by the Szilard-Chalmers method.

As far as we are aware, kinetic studies of the ligand exchange between coordinated β-diketones in uranyl complexes and their free enolic tautomer have not been published. We observed that bis-(2 ^{14}C-acetylacetonato)-uranyl lost almost instantly its radioactivity after reacting with inactive acetylacetone at room temperature. The rate of exchange is within the range of high-resolution NMR kinetic technique.

II. EXPERIMENTAL

Bis-(acetylacetonato)-uranyl was prepared according to Comnys et al.[2] The structure of the complex was checked by its infrared spectrum.

Kinetic measurements were performed with the thermal probe of the Tesla NMR spectrometer operating at 80 MHz, with a temperature accuracy of ± 1°.

For every temperature were measured sets of samples differing by the concentration of a single reactant. The samples were prepared by introducing a weighed amount of the complex and the necessary volume of the free ligand up to a constant volume of solution. The best solvent for our purposes was found to be anhydrous acetonitrile.

The NMR spectra of the pure complex and the free ligand were recorded before and after the exchange experiment. This procedure ruled out any error due to the change in the homogeneity of the magnetic field. The temperature scale was calibrated using the manufacturer's recommended procedure. The spectra were recorded twice generally considering the average values of several measurements.

---

[1] H. Starke, *Naturwiss.*, **30**, 107, 577 (1942).

[2] A. E. Comnys, B. M. Gatehouse and E. Wait, *J. Chem. Soc.*, **1958**, 4662.

III. RESULTS AND DISCUSSION

The temperature-dependent broadening of the resonance signals corresponding to the methinic hydrogens in coordinated and free enolic ligand was observed. The mean lifetimes τ were determined by the Clatux computer program. [3] The input consisted of: relative chemical shifts of the observed hydrogens, their spin-spin relaxation times, their populations and the hypothetic values of τ. The output gave the theoretical shapes of considered signals.

The agreement of the experimental spectra with the theoretical ones is presented for 1 : 1 molar ratio within 25 − 90° in figure 1.

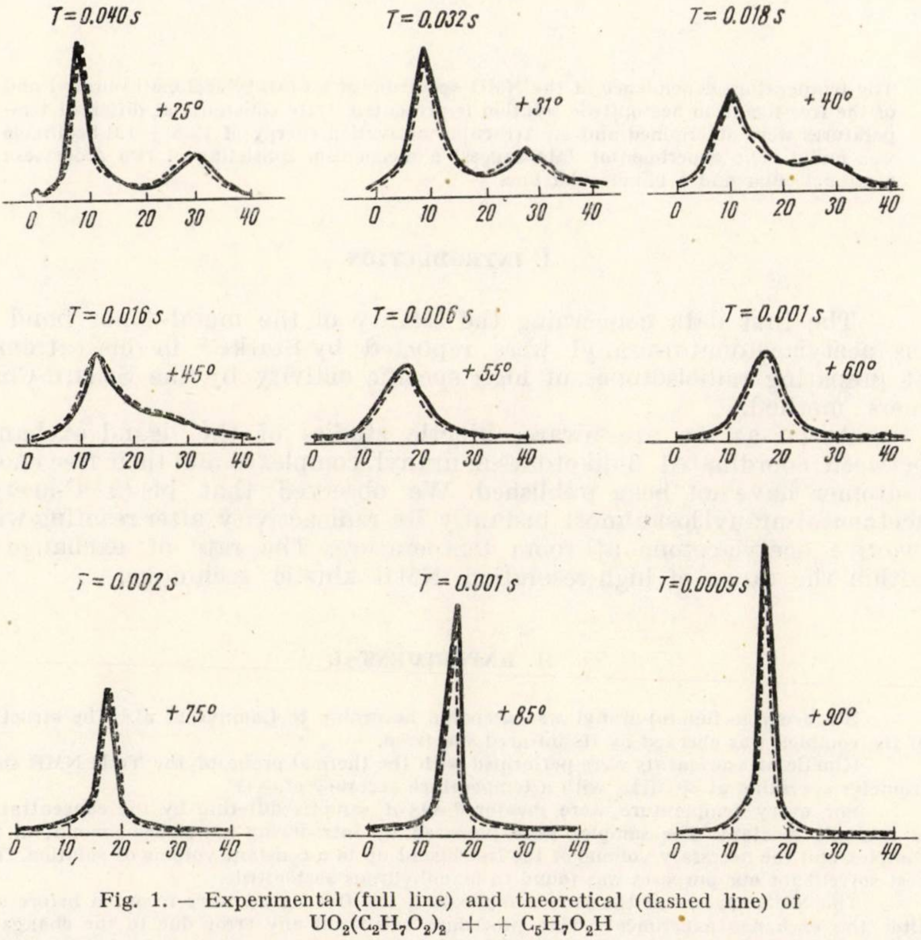

Fig. 1. — Experimental (full line) and theoretical (dashed line) of $UO_2(C_2H_7O_2)_2 + + C_5H_7O_2H$

The τ values corresponding to different molar ratios between reactants and temperatures ranging from 25 to 90° are listed in table 1.

---

[3] G. Binsch, *J. Amer. Chem. Soc.*, **91**, 1304 (1969).

Table 1

τ values (s) for different molar ratios between reactants

t° / [ML]/[L]	25	31	40	45	50	55	60	65	70	75	80	85	90
1 : 1	0.0440	0.0320	0.0018	0.0160	0.0070	0.0060	0.0040	0.0033	0.0028	0.0020	0.0014	0.0010	0.0006
1 : 2	0.0460	0.0400	0.0200	0.0150	0.0100	—	0.0090	—	0.0050	—	0.0040	—	—
1 : 3	0.0344	0.0246	0.0168	0.0135	0.0100	—	0.0050	—	0.0016	—	0.0012	—	—
1 : 6	0.0240	0.0220	0.0150	—	—	0.0080	0.0060	—	—	0.0040	—	—	—
1 : 8	0.0340	0.0200	0.0100	—	—	0.0080	0.0060	—	—	0.0040	—	—	—
1 :10	0.0300	—	—	—	—	—	—	—	—	—	—	—	—

Table 2

Kinetic data on the exchange of acetylacetone in bis-(acetylacetono)-uranyl

$\frac{[ML]}{[L]}$	[ML] [M]	[L] [M]	25°			31°			40°			45°		
			$\tau_{ML}(s)\cdot 10^{-2}$	$\tau_L(s)\cdot 10^{-2}$	R (M.s^{-1})	$\tau_{ML}(s)\cdot 10^{-2}$	$\tau_L(s)\cdot 10^{-2}$	R (M.s^{-1})	$\tau_{ML}(s)\cdot 10^{-2}$	$\tau_L(s)\cdot 10^{-2}$	R (M.s^{-1})	$\tau_{ML}(s)$ 10^{-2}	$\tau_L(s)$ 10^{-2}	R (M.s^{-1})
1 : 1	0.168	0.168	12.00	6.00	2.79	9.60	4.80	3.50	5.40	2.70	6.26	4.80	2.40	6.93
1 : 2	0.110	0.220	9.20	9.20	2.39	8.00	8.00	2.75	4.00	4.00	5.50	3.00	3.00	7.33
1 : 3	0.168	0.504	5.60	8.50	5.94	4.10	6.10	8.21	2.70	4.20	11.99	2.00	3.40	14.82
1 : 6	0.110	0.660	3.20	9.60	6.87	2.90	8.80	7.49	1.60	4.80	13.74	—	—	—
1 : 8	0.110	0.880	4.20	17.00	5.17	2.50	10.00	8.80	1.20	5.00	17.60	1.00	4.00	22.00
1 :10	0.110	1.110	3.60	18.00	6.16	—	—	—	—	—	—	—	—	—
	$k_1(s)$		12.31±0.21			6.56±0.19			5.84 ± 1.62			3.78±1.91		
	$k_2(M^{-1}. s^{-1})$		39.77±0.30			86.46±0.37			182.7±2.94			212.92±3.56		

To estimate the exchange rates the following equations were considered[4]:

$$R = k\,[M\ L_2]^{\mu}\cdot\ [L]^{\nu} = \tau_{ML}^{-1}\cdot 2[ML_2] = \tau_L^{-1}\cdot[L] \qquad (1)$$

where R is the exchange rate, k – the rate constant, $[ML_2]$ and $[L]$ the molar concentrations of the metal chelate and enol tautomer of the free ligand. The mean lifetimes τ_{ML} and τ_L for the exchanging nuclei in coordinated and free ligand are related to τ, by definition:

$$\tau^{-1} = \tau_{ML}^{-1} + \tau_L^{-1}$$

The orders of exchange with respect to ML_2 and L are μ, respectively ν. The order of exchange is obtained from the slope of the straight line formed by plotting $\log \tau_{ML_2}^{-1}$ or $\log \tau_L^{-1}$ versus $\log[L]$ or $\log[ML_2]$. In both cases the slopes obtained are approximately 1. The rate equation consistent with the experimental data, as shown in table 2, is:

$$R = k_1[ML_2] + k_2[ML_2].[L] \qquad (2)$$

The eq. (2) assumes two parallel processes: a unimolecular reaction and a bimolecular one. This may be explained by the frequently considered pattern[5-9] implying a rapid one-ended dissociation of the chelated complex as a first step of exchange (Fig. 2).

The one-end dissociated chelate II has two possibilities for reaction: a) a heterolytic dissociation with the formation of the charged species, IV, followed by the addition of a neutral molecule of the ligand (first-order process) and b) an addition of a free monodentate ligand yielding III, which is equivalent with III′ through the exchange of a hydrogen atom; the further loss of a molecule of the ligand leads to the exchanged final complex V. (second-order processs).

As indicated in table 2 the second-order term in the rate equation is major at 25° for a ligand concentration over 0.3M. At higher temperatures a much lower ligand concentration is needed for achieving a pure bimolecular reaction.

The thermal coefficient of the exchange rate is assured by the strong increase of the second-order constants k_2 with the temperature. An Arrhenius plot of the overall rate constant versus $1/T$ gives an activation energy of 13.6 ± 1.0 kcal/mole. The decrease of the first-order rate constant k_1 with the temperature is explained by that the stationary concentration of the intermediate II, responsible for both processes, is preferentially consumed by the second-order reaction as the temperature is raised.

---

[4] A. Loewenstein and T. M. Connor, *Ber. Bunsenges. Phys. Chem.*, **67**, 286 (1963).

[5] A. C. Adams and E. M. Larsen, *Inorg. Chem.*, **5**, 814 (1966).

[6] R. G. Pearson and M. Anderson, *Angew. Chem.*, **77**, 361 (1965).

[7] R. C. Fay and T. S. Piper, *Inorg. Chem.*, **3**, 348 (1964).

[8] K. Saito and T. Masuda, *Bull. Chem. Soc. Japan*, **41**, 348 (1968).

[9] A. Barabas., *Inorg. Nuclear Chem. Letters*, **6**, 775 (1970).

Finally, in the particular case of uranium, it is reasonable to include in a general mechanism the possibility for an intermediate VI, with an increased coordination number.[10] A further breaking of a metal-oxygen bond (VII) and a rapid rearrangement to the initial geometry of the complex (III) would complete this pattern.

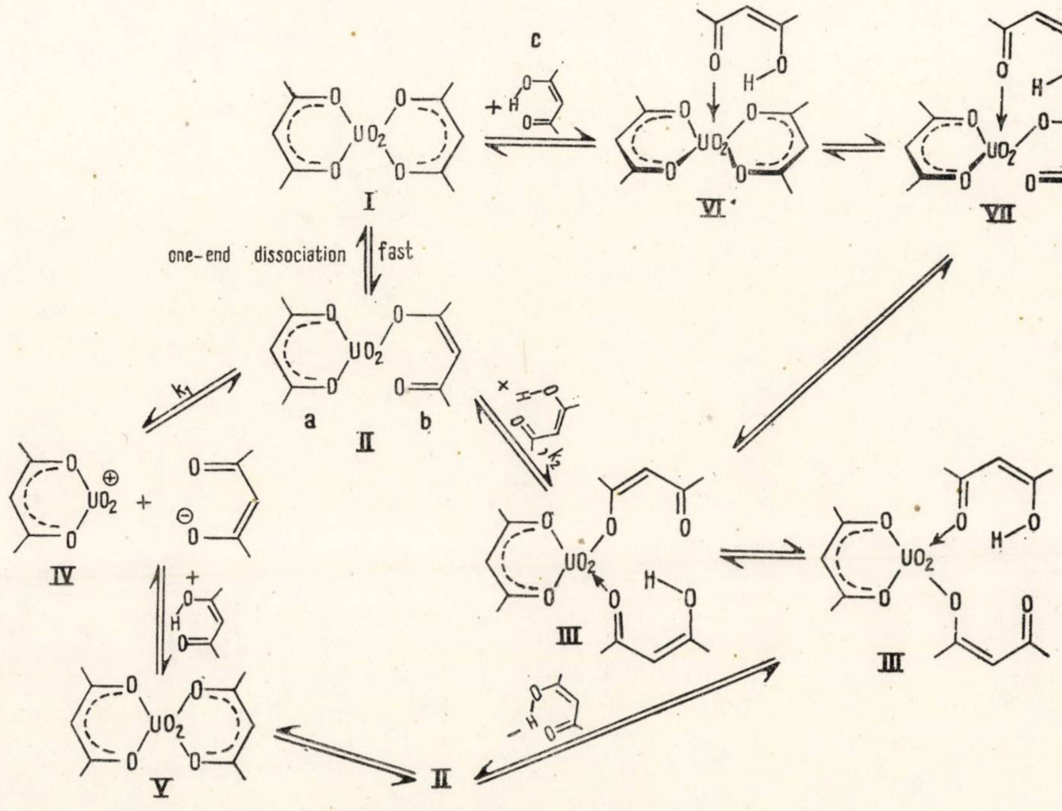

Fig. 2. — The general mechanism of ligand exchange in chelate complexes.

The study of the influence of the solvation and steric factors on ligand exchange in bis-chelated uranyl complex is in progress.

Acknowledgement. Thanks are due to Mr. Mircea Gheorghiu for providing the computer program.

---

[10] P. Hurwitz and K. Kustin, *J. Phys. Chem.*, **71**, 324 (1967).

Revue Roumaine de Chimie, 20, 7, 957–964 (1975)

INVESTIGATION IN THE CYCLOBUTANE SERIES. XXXVI[1]

REARRANGEMENT OF 8-DIAZO-*endo*-BENZO[*c*]TRICYCLO [4.2.1.$0^{2,5}$] NON-3-EN-7-ONE ON PHOTOLYSIS AND IN ACID MEDIA

L. ENESCU, F. CHIRALEU and MARGARETA AVRAM
Department of Organic Chemistry, Polytechnic Institute, Bucharest, Romania

Received September 24, 1974

The synthesis of diazo-ketone **3** is presented. The photolysis of **3** in dioxane-water led to a mixture of two acids (**7a** and **8a**) and to a neutral fraction containing mainly the ketol **9a**. A mixture of **8a**, **9a** and the acetate **9b** was obtained by treatment of **3** with acetic acid. The mechanism of these reactions is discussed.

In an earlier paper [2] we reported the behaviour on photolysis of 8-diazo-*syn*-9-bromo-*exo*-benzo[*c*]tricyclo [4.2.1.$0^{2,5}$] non-3-en-7-one (**1**), leading to ring contraction products, namely the epimeric *syn*-8-bromo-*exo*-benzo[*c*]tricyclo [4.1.1.$0^{2,5}$] oct-3-ene-7-carboxylates (**2**).

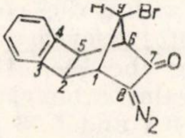

1

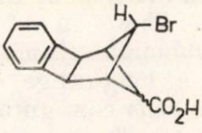

2

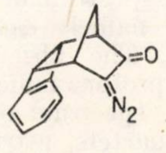

3

As a continuation of these investigations, we describe here the synthesis and behaviour on photolysis, as well as the acid-catalyzed rearrangement of 8-diazo-*endo*-benzo[*c*] tricyclo [4.2.1.$0^{2,5}$] non-3-en-7-one (**3**).

The synthesis of **3** was achieved starting from *endo*-benzo [*c*]tricyclo [4.2.1.$0^{2,5}$] non-3-en-7-one (**4**)[3,4].

On treatment with selenium dioxide in boiling dichloro-benzene, **4** led to the diketone **5**. The monotosylhydrazone **6**, generated by treatment of **5** with one mole of tosylhydrazone yielded, after chromatography on basic alumina, the diazoketone **3**.

---

[1] Part XXXV : I. G. Dinulescu, F. Chiraleu, M. S. Pop and M. Avram, *Rev. Roumaine Chim.*, **20**, 85 (1975).

[2] M. Avram, L. Enescu, I. G. Dinulescu, F. Chiraleu and C. D. Nenitzescu, *Rev. Roumaine Chim.*, **16**, 1783 (1971).

[3] M. Avram, I. Pogany, I. G. Dinulescu, F. Chiraleu and C. D. Nenitzescu, *Rev. Roumaine Chim.*, **15**, 1207 (1970).

[4] M. Avram, I. Pogany, F. Badea, I. G. Dinulescu and C. D. Nenitzescu, *Tetrahedron Letters*, **1969**, 3851.

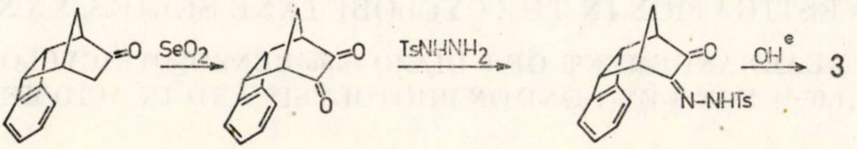

4 5 6

The irradiation of **3** in a mixture of dioxane-water gave a mixture of an acidic fraction and a neutral one, in almost equal quantities.

From the acidic fraction, after treatment with diazomethane, the esters **7b** (12.8%) and **8b** (28.0%) was isolated; from the neutral fraction as main product the ketol **9a** (27.5%) was separated.

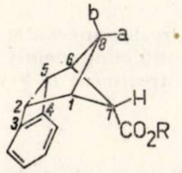

7 a) R=H

b) R=CH$_3$

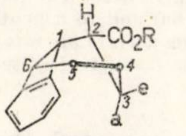

8 a) R=H

b) R=CH$_3$

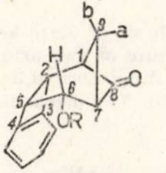

9 a) R=H

b) R=COCH$_3$

The structure and configuration of the reaction products were assigned mainly on the basis of an analysis of NMR and IR spectral data.

The spectrum of the ester **7b** was in agreement with a ring contraction product,[2] namely *endo*-7-carbomethoxy-*endo*-benzo[*c*] tricyclo $[4.1.1.0^{2,5}]$ oct-3-ene. The absence of a long-range coupling between the H-8b and H-7 protons indicates an *endo* configuration for the carboxylate group.

The spectrum of the ester **8b** presents at δ 6.1 and 5.73 ppm two double quartets, attributed to the protons H-5 and H-4. A doublet of triplets for the H-2 proton together with the multiplet of the protons H-1 and H-6 are in agreement with the *cis* orientation of the carboxylate group with respect to the benzocyclobutene ring.

Due to the conformational flexibility of the cyclohexene ring of the ester **8b**, two *cis* conformers are to be considered, one with an equatorially-oriented carboxylate group, **A**, and the other with an axial carboxylate group, **B**.

The complexation of the ester group with Eu(DPM)$_3$ led to a larger shift in the NMR spectrum for the H-2 proton adjacent to the carboxylate group, as well as for one proton of the cyclobutene ring (H-1) and one proton of the benzene ring. Only the conformer **A** with *cis*, equatorially-oriented carboxylate group in the vicinity of the benzocyclobutene ring is in agreement with these spectral data. The *trans* conformers **C** and **D**, represent probably the ester described in literature[5] resulting from solvolytic reactions.

In the IR spectrum, the ν_{CO} frequency of an ester group, of 1741 cm^{-1}, different from that of the ester described by Baker[5], at 1729 cm^{-1}, supports the proposed structure.

---

[5] R. Baker and J. C. Salter, *J. Chem. Soc.*, **1973**, 150; R. Baker, T. J. Mason and J. C. Salter, *Chem. Com.* **1970**, 509.

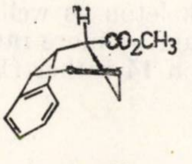

A = 8b

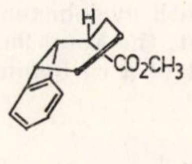

B

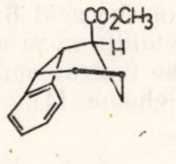

C

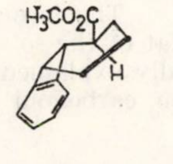

D

For the ketol **9a**, the NMR spectrum is in agreement with the proposed structure, as it shows a double triplet for H-9a and H-9b, a triplet for H-2 and a multiplet for H-7. The IR frequency of the carbonyl group, $\nu_{CO} = 1788\ cm^{-1}$, indicates the strained cyclobutanone skeleton.[6] The high value of the coupling constant for the proton H-6 ($J_{5\text{-}6} = 9.0$ and $J_{6\text{-}7} = 4.0$ Hz) supports the *endo* orientation of the hydroxy group. The *endo-cis* orientation of the benzocyclobutene ring with respect to the carbonyl group is supported also by the chemical shift of the CH_2 bridge which presents signals at δ 2.13 (H-9a) and 1.50 ppm (H-9b). An *exo* orientation of the benzocyclobutene ring would show a difference between the signals of these protons of approx. 1.5 ppm, much greater than the 0.63 ppm, value actually recorded.

In accordance with the accepted mechanism for the ring contraction of diazoketones during photolysis, we assumed the intervention of the carbenoid **10** as an intermediate (Scheme I). This can rearrange, by participation of the $C_6 - C_7$ bond, to the ketene **11**,[7] which by further reaction with water leads to the normal ring-contraction product, the acid **7a**, with bicyclo[2.1.1]hexane skeleton.

Scheme I

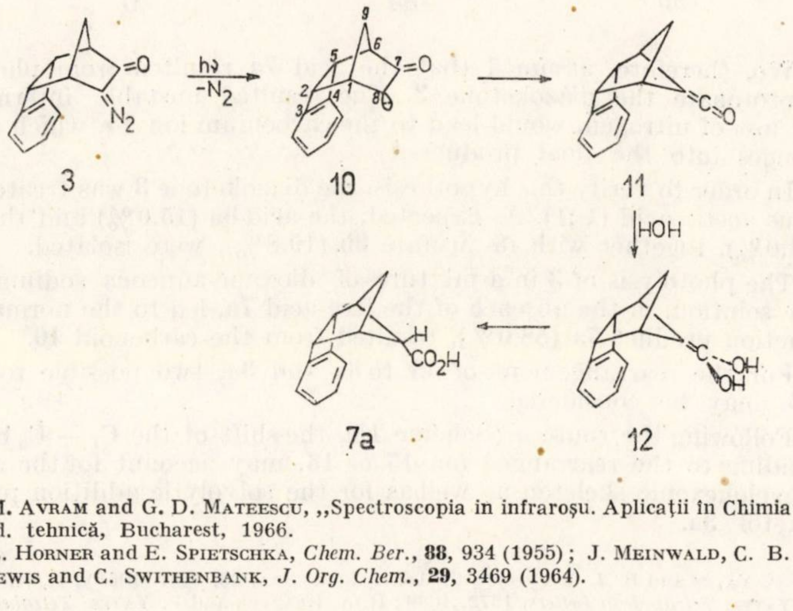

---

[6] M. Avram and G. D. Mateescu, „Spectroscopia in infraroşu. Aplicaţii în Chimia Organică'', Ed. tehnică, Bucharest, 1966.

[7] L. Horner and E. Spietschka, *Chem. Ber.*, **88**, 934 (1955); J. Meinwald, C. B. Jensen, A. Lewis and C. Swithenbank, *J. Org. Chem.*, **29**, 3469 (1964).

The formation of the acid **8a** with cyclohexenic skeleton as well as that of the solvolytic addition product, the ketol **9a**, could be more rationally explained by the rearrangement of a carbenium ion **14** rather than the carbenoid **10** (Scheme II).

Scheme II

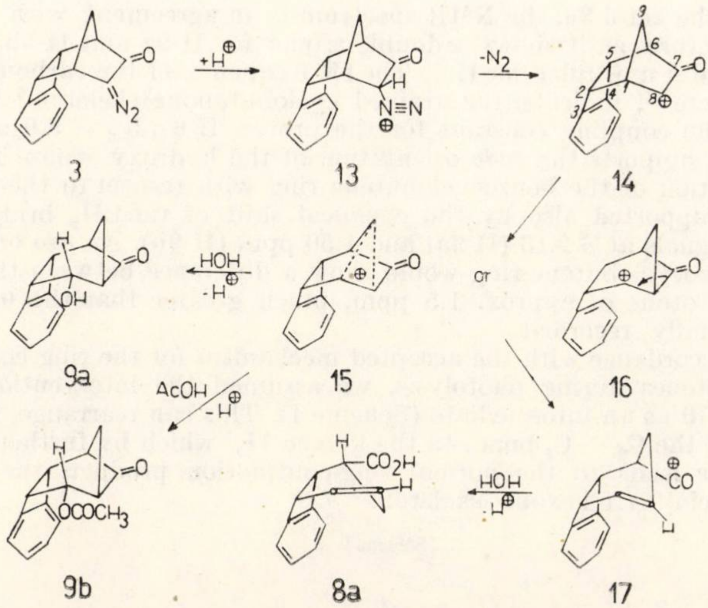

We, therefore, assumed that the acid **7a** resulted from photolysis may protonate the diazoketone **3**. The resulted unstable intermediate **13**, by loss of nitrogen, would lead to the carbenium ion **14**, which in turn rearranges into the final products.[8]

In order to verify this hypothesis, the diazoketone **3** was treated with aqueous acetic acid (1 :1). As expected, the acid **8a** (15.0 %) and the ketol **9a** (24.0 %), together with its acetate **9b** (19.8 %), were isolated.

The photolysis of **3** in a mixture of dioxane-aqueous sodium bicarbonate solution, in the absence of the free acid **7a**, led to the normal ring-contraction product **7a** (58.0 %), resulted from the carbenoid **10**.

For the rearrangement of **14** to **8a** and **9a**, two possible routes, *a* and *b*, may be considered.

Following the route *a* (Scheme II), the shift of the $C_1 - C_9$ bond in **14**, leading to the rearranged ion **15** or **16**, may account for the acid **8a** with cyclohexenic skeleton as well as for the solvolytic addition product, the ketol **9a**.

---

[8] P. Yates and R. I. Crawford, *J. Amer. Chem. Soc.*, **88**, 1561 (1966) ; R. A. Blattel and P. Yates, *Tetrahedron Letters*, **1972**, 1069 ; R. A. Blattel and P. Yates, *Tetrahedron Letters*, **1972**, 1073.

The structure of the ion **15** would also explain the predominance of the ketol with the *endo*-oriented hydroxy group.

The other possible route (*b*), which cannot be ruled out off-hand, involves the $C_1 - C_2$ bond delocalization. The intermediate ion **18** or **19** could also explain the formation of the acid **8a**.

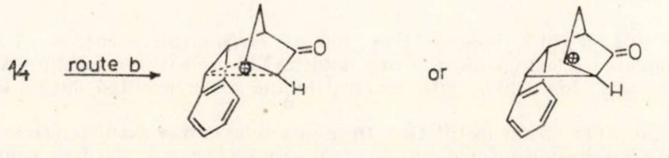

18 19

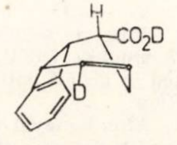

20

In order to distinguish between the two routes, photolysis of the diazoketone **3** was carried out in a mixture of dioxane/D_2O. The acids **21a**, **22a** and the ketol **23a** were isolated. The 4-position of the deuterium on the cyclohexene ring of acid **22a** is in agreement with the intervention of an ion **15** or **16**. An isomeric acid with the deuterium at C_5 (**20**), which would form by route *b*, was not isolated.

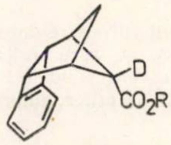

21 a) R=D
b) R=CH$_3$

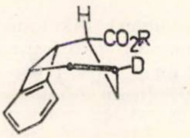

22 a) R=D
b) R=CH$_3$

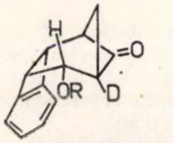

23 a) R=D
b) R=COCH$_3$

When the NMR spectrum of the deuterated ester **22b** is compared with that of the undeuterated ester **8b**, one may notice the disappearance of the signal at δ 5.73, attributed, on the basis of decoupling experiments, to the proton H-4. Using the technique of the proton-shift induced by complexation with $Eu(DPM)_3$, a significant shift is observed for the proton H-1; by coupling with H-5 and H-1, the proton H-6 gives rise to a triplet. In a deuterated acid like **20** with the deuterium at carbon C_5, a doublet resulting from coupling between H-5 and H-6 would be expected.

The presence of the deuterium at C_7 in **23a** is evident from the NMR spectrum, as compared with the spectrum of the ketol **9a**. The signal of H-7 (at δ 3,15 ppm in **9a**) is absent and the quartet of H-6 of **9a** is transformed into a doublet ($J = 9.0$ Hz), together with the exchange of the doublet of triplets of the bridge CH_2 which gives a double doublet.

Acknowledgement. The authors wish to thank Mr. T.V. Constantinescu for helpful comments and suggestions.

EXPERIMENTAL

Microanalyses were performed by Miss E. Sliam and Mrs. C. Daniel. IR spectra were run on a double-beam UR 20 spectrophotometer. NMR spectra were determined with a Varian A—60A spectrometer.

endo-Benzo[*c*]tricyclo [4.2.1.$0^{2,5}$] non-3-en-7,8-dione (5)

Into a solution of 10.2 g (54.4 mmoles) **4** in 100 ml *ortho*-dichlorobenzene, 7.3 g (66.7 mmoles) freshly sublimated selenium dioxide were added. The well-stirred mixture was heated in an oil bath (160—185°) for 6 hrs., with removal of the water resulted during the reaction.

After removal of the solvent by steam distillation, the aqueous layer was extracted several times with dichloromethane. After drying and evaporation of the solvent *in vacuo*, the dark coloured residue was chromatographed on neutral alumina with a mixture of petroleum ether-dichloromethane (20 : 3) as eluent; 8 g (73.0%) **5**, yellow crystals with m.p. 129.5° (from petroleum ether) were obtained.

$C_{13}H_{10}O_2$ (198.2)

Calcd. : C, 78.77 ; H, 5.08

Found : C, 78.17 ; H, 5.43

IR (CCl_4, cm^{-1}) : ν_{CO} 1760, 1779.

NMR ($CDCl_3$, δ, ppm) : 6.9—7.2 (m, 4H, aromatic), 4.35 (m, 2H, H-2 and H-5), 3.33 (m, 2H, H-1 and H-6), 2.33 and 2.63 (AB system for H-9a and H-9b, $J_{AB} = 12.0$ Hz).

endo-Benzo[*c*]tricyclo [4.2.1.$0^{2,5}$] non-3-en-8-one-7-tosylhydrazone (6)

Into a solution of 6.0 g (3.1 mmoles) diketone **5** in 48 ml anhydrous chloroform, 1 g anhydrous magnesium sulphate and 5.64 g (3.1 mmoles) tosylhydrazine were added and the mixture was left in the refrigerator for 48 hrs. Evaporation of the solvent yielded 10.85 g (97.6%) **6**, white crystals, m.p. 200—201° (from ethanol), almost insoluble in ether, chloroform or dichloromethane.

$C_{20}H_{18}O_3N_2S$ (366.4)

Calcd : C, 65.55 ; H, 4.95 ; N, 7.64 ; S, 8.75

Found : C, 66.07 ; H, 5.28 ; N, 7.79 ; S, 7.90

IR (KBr, cm^{-1}) : ν_{CO} 1754, $\nu_{C=N}$ =1645, ν_{NH} 3218, $\nu_{SO_2\text{-sym}}$ 1170, $\nu_{SO_2\text{-asym}}$ 1348.

7-Diazo-*endo*-benzo[*c*]tricyclo[4.2.1.$0^{2,5}$]non-3-en-8-one (3)

3.78 g (1.03 mmoles) **6** well mixed with basic alumina (Merck), were chromatographied on a basic alumina column (240/30 mm), with dichloromethane as eluent. The evaporation of the solvent yielded 2.1 g (98.5%) diazoketone **3**, as a yellow crystalline residue, m.p. 104—105° (decomp.), which could be recrystallized from petroleum-ether.

$C_{13}H_{10}ON_2$ (210.2) : *Calcd.* : N, 13.32. *Found* : N, 12.61.

IR (CCl_4, cm^{-1}) : ν_{CO} 1701, $\nu_{N\equiv N}$ 2085, 1362.

Photolysis of 3 in dioxane-H_2O

A solution of 4.2 g (20 mmoles) diazoketone **3** in a mixture of 72 ml dioxane and 27 ml water was irradiated with a mercury high-pressure lamp (Hanau 75 W) for 60 hrs, until the evolution of nitrogen ceased and the $\nu_{N\equiv N}$ band disappeared. The solution was then concentrated *in vacuo* to 15 ml, 20 ml dichloromethane were added, and the organic layer was vigourously shaken with 25 ml 2% aqueous sodium bicarbonate solution.

a. *Acid fraction.* The basic aqueous layer was carefully acidified with diluted hydrochloric acid and finally extracted with ether. Removal of the solvent *in vacuo* yielded 2.0 g crude acidic fraction, m.p. 95—100°.

2.0 g crude acid in 30 ml ether was treated with an ethereal solution of diazomethane. After evaporation of the solvent, 2.0 g oily residue was obtained. The gas-chromatography analysis showed a content of 62.4% **8b**, 27.7% **7b**, together with some impurities totalling 9.9%.

By chromarography on neutral alumina with a mixture of petroleum ether-ether (1 : 1) as eluent, 1.2 g (28.0%, calcd. from **3**) *endo*-2-carbomethoxy-*endo*-benzo [*g*] bicyclo [4.2.0] octa-4,7-diene (**8b**), as a colourless oil, was obtained.

$C_{14}H_{14}O_2$ (214.3) : *Calcd.* : C, 78.48 ; H, 6.58
Found : C, 78.80 ; H, 6.52

IR (CCl_4, cm^{-1}) : ν_{CO} 1741, ν_{COC} 1205

NMR (CCl_4, δ, ppm) : 6.7–7.2 (m, 4H, aromatics), 6.1 (d. quartet, 1H, H-5, $J_{4.5}$ = = 10,0, $J_{5.6}$ = 5.0, $J_{3e.5}$ = 2.5 Hz), 5,73 (d. quartet, 1H, H-4, $J_{4.5}$ = 10,0, $J_{4.6}$ = 3.0 $J_{3e.4}$ = 6.0 Hz), 4.05 (m, 2H, H-1 and H-6), 2.63 (dt, 1H, H-2, $J_{2.3a}$ = 12.0, $J_{1.2}$ = $J_{2.3e}$= = 4.5 Hz), 1.5–2.5 (m, 2H, H-3e and H-3a), 2.92 (s, 3H, CH_3 from ester group).

0.103 g (0.48 mmoles) ester **8b** were boiled for 7 hrs with a solution of 0.52 g sodium hydroxide in 0.5 ml methanol and 2 ml water. After solvent evaporation *in vacuo*, water was added. The en-8-one (**9a**), white crystals with m.p. 107–108° (petroleum ether), were obtained.

$C_{13}H_{12}O_2$ (200.2) *Calcd.* : C, 78.01 ; H, 6.04
Found : C, 77.58 ; H, 6.12

IR (CCl_4, cm^{-1}) : ν_{CO} 1788, ν_{OH} 3586 and 3200–3560.

NMR ($CDCl_3$, δ, ppm) : 7.0 – 7.3 (m, 4H, aromatics), 4.64 (quartet, 1H, H-6, $J_{5.6}$ =9.0, $J_{6.7}$= 4.0Hz), 4.43 (t, 1H, H-2, $J_{2.5}$ = 4.7Hz), 4.14 (quartet, 1H, H-5, $J_{5.6}$=9.0, $J_{2.5}$ = 4.7 Hz), 3.53 (m, 1H, H-1), 3.15 (m, 1H, H-7), 2.13 (dt, 1H, H-9a, $J_{1.9a}$=$J_{7.9a}$=6.2, $J_{9a.9b}$=10.0 Hz), 1.50 (dt, 1H, H-9b, $J_{1.9b}$= $J_{7.9b}$= 1.7, $J_{9a.9b}$= 10.0 Hz).

endo-6-Acetoxy-*endo*-benzo[*c*]tricylo[5.1.1.$0^{2,5}$]non-3-en-8-one (9b).

A solution of 0.12 g (0.6 mmoles) **9a**, 10 ml acetic anhydride and two drops of pyridine were left at room temperature for 24 hrs. After working up, the resulted crude acetate was chromatographied on neutral alumina with dichloromethane-petroleum ether (1 :5) as eluent. Evaporation of the solvent afforded 0.13 g (92.5%) acetate **9b**, m.p.116°.

$C_{15}H_{14}O_3$(242.3) *Calcd.* : C, 74.36 ; H, 5.82
Found : C, 74.15 ; H, 6.02

IR (CCl_4, cm^{-1}) : ν_{CO} 1791, ν_{COOR} 1743 and 1240.

NMR ($CDCl_3$, δ, ppm) : 6.9–7.4 (m, 4H, aromatics), 5.61 (q, 1H, H-6, $J_{5.6}$=9.0, $J_{6.7}$= = 4.0Hz), 4.46 (t, 1H, H-2, J = 4.5 Hz), 4.23 (q, 1H, H-5, $J_{5.6}$=9.0, $J_{2.5}$ = 5.0 Hz), 3.6 (m, 1H, H-1), 3.2 (m, 1H, H-7), 2.2 (dt, 1H, H-9a), 1.6 (dt, 1H, H-9b, $J_{1.90}$=$J_{7.9b}$=1.7, $J_{9a.9b}$= = 10.0 Hz), 2.13 (s, 3H, CH_3COO).

Photolysis of 3 in dioxane-D_2O

A solution of 1.0 g (4.76 mmoles) diazoketone **3** in 19 ml dioxane and 5.0 ml D_2O was irradiated under the same conditions as in the procedure described above. After working up in the same manner, 0.45 g acidic fraction and 0.45 g neutral fraction were obtained.

By treating the crude acidic mixture with an ethereal solution of diazomethane and chromatography on neutral alumina, the deuterio-esters **21b** and **22b** were isolated.

From the neutral fraction, after chromatography on alumina (dichloromethane as eluent), the deuterio-ketol **23a** was obtained.

The products were characterized by their NMR spectra, which were identical with those of the parent compounds **7b**, **8b** and **9a**, except for the signals due to the deuterated positions, which were absent.

Photolysis of 3 in dioxane/aqueos sodium bicarbonate solution

A solution of 0.49 g (2.33 mmoles) diazoketone **3** in a mixture of 50 ml dioxane, 20 ml water and 0.2 g sodium bicarbonate was irradiated with a mercury high-pressure lamp (Hanau 75W) for 67 hrs, until the evolution of nitrogen ceased and the $\nu_{N\equiv N}$ band disappeared. The solution was then concentrated *in vacuo*,10ml dichloromethane were added, and the aqueous sodium bicarbonate layer was separated. The organic layer was shaken with 20 ml saturated sodium bicarbonate solution. The basic aqueous layer was carefully acidified with diluted hydrochloric acid and finally extracted with ether. Removal of the solvent *in vacuo* yielded 0.27 g (58%) *endo*-7-carboxy-*endo*-benzo[*c*]tricyclo[4.1.1.$0^{2,5}$)]oct-3-ene **(7a)** white crystals with m.p. 118° (petroleum ether).

$C_{13}H_{12}O_2$(200.2) : *Calcd* : C, 78.01 ; H, 6.02
Found : C, 77.51 ; H, 6.11

IR (CCl_4, cm^{-1}) : ν_{CO} 1705.

NMR ($CDCl_3$, δ, ppm) : 6.98 (m, 4H, aromatics), 3.76 (m, 2H, H-2 and H-5), 3.11 (m, 2H H-1 and H-6), 2.43 (t, 1H, H-7, J = 3.0 Hz), 1.81 (dt, H-8a, $J_{8a.8b}$ = 6.8, $J_{1.8a}$ = $J_{6.8a}$ = 2.5, Hz), 1.16 (dd, 1H, H-8b, $J_{8a.8b}$ = 6.8, $J_{7.8b}$ = 1.5 Hz), 8.7 (broad s, 1H, CO_2H).

The neutral fraction, still uninvestigated, did not show the IR absorption characteristic of the ketol **9a** (ν_{CO} = 1788 cm^{-1}).

Reaction of 3 in aqueous acetic acid

Into a mixture of 80 ml acetic acid and 80 ml water, 0.7 g (3.33 mmoles) diazoketone **3** were added. After the nitrogen evolution subsided (5 hrs), the mixture was concentrated *in vacuo*. The residue was extracted with 20 ml dichloromethane and the organic layer was washed with two portions of 10 ml water, and finally extracted four times with 20 ml portions of saturated bicarbonate solution. The aqueous solution was acidified with diluted hydrochloric acid and the organic acid was extracted with ether. Evaporation of the solvent *in vacuo* yielded 0.1 g (15.0%) white crystals of **8a**, m.p. 142° (petroleum ether).

The dichloromethane solution (containing the neutral fraction), after evaporation *in vacuo*, afforded 0.4 g dark coloured oil. Gas-chromatography analysis (using a 1.5 m x 2 mm diameter column filled with 10% Neopenthyl-glycol succinate on Chemosorb W 60-80 mesh, at 250° and 40 ml/min. hydrogen as carrier gas), shows a content of 42.3% ketol **9a**, 40.6% acetate **9b**, together with some impurities totalling 17.1%.

By chromatography on neutral alumina with petroleum ether as eluent, 0.16 g (19.8%) white crystals of **9b** were isolated; a further elution with dichloromethane afforded 0.16 g (24.0%) ketol **9a**.

The compounds which were isolated were characterized by their NMR and IR spectra, which were identical with those of the parent compounds **8a**, **9a** and **9b**.

Revue Roumaine de Chimie, **20**, 7, 965–971 (1975)

FURTHER STUDIES ON THE STOBBE CONDENSATION OF *p*-CHLOROBENZOPHENONE WITH DIMETHYL SUCCINATE

A. M. EL-ABBADY and M. A. OMARA
Chemistry Department, Faculty of Science, Tanta University
TANTA, EGYPT

Received November 30, 1973

p-Chlorobenzophenone is condensed with dimethyl-succinate to give the two isomeric half-esters (I_a and I_b) as a semisolid mixture. These are separated as diesters (II_a and II_b). The diesters are hydrolysed to the corresponding dicarboxylic acids (III_a and III_b) which on cyclisation with concentrated sulphuric acid (III_a) give 6-chloro-1-oxo-3-phenyl-2-indenylacetic acid (IV_a) while (III_b) give 3-*p*-chlorophenyl-1-oxo-2-indenylacetic acid (IV_b). However, on treating the acids (III_a and III_b) separately with thionyl chloride followed by aluminium chloride, one and the same product was yielded. (IV_b). The diesters (II_a and II_b) are further condensed with several aryl aldehydes to give 1,1,4-triarylbuta-1,3-diene-2,3-dicarboxylic acids (V_a and V_b), respectively. On treating V with acetyl chloride they gave the corresponding anhydride (VI) cyclised by sunlight or just by heating above their melting points or heating in nitrobenzene to 1,4-diarylnaphthalene-2,3-dicarboxylic anhydrides (VII). In all cases each pair of isomeric anhydrides (VI) yields one product of (VII) in which the *p*-chlorophenyl group is free, i.e. not involved in the naphthalene ring.

Recently Baddar et al.[1] reported the condensation of *p*-chlorobenzophenone with diethyl and dimethyl succinate in the presence of potassium *t*-butoxide and the isolation of a small amount of only one pure half-ester namely *cis*- or *trans*-($C_6H_5/COOCH_3$)-4-*p*-chlorophenyl-3-methoxycarbonyl-4-phenylbut-3-enoic acid (I_a or I_b). In this work the reaction was reinvestigated and further studied. The expected two isomeric Stobbe condensation products were successfuly isolated and separated as diesters (II_a and II_b). The structure of these compounds was established from: (i) their different melting points; (ii) their analytical data; (iii) their i.r. and electronic absorption spectra (table 1).

The *cis*-($C_6H_5/COOCH_3$)-and *trans*-($C_6H_5/COOCH_3$)-forms were assigned to the compounds (II_a and II_b), respectively on the fact that, the cyclisation of the dicarboxylic acids (III_a and III_b) using concentrated sulphuric acid at 0° gave 6-chloro-1-oxo-3-phenyl-2-indenylacetic acid (IV_a) and 3-*p*-chlorophenyl-1-oxo-2-indenylacetic acid[1](IV_b), respectively. The structure of the dicarboxylic acids (III_a and III_b) and that of the indenyl acids (IV_a and IV_b) was established from their analytical data and their i.r. and electronic absorption spectra (table 1).

---

[1] F. G. Baddar, V. B. Baghos and A. Habachi, *J. Chem. Soc., C*, **1966**, 603.

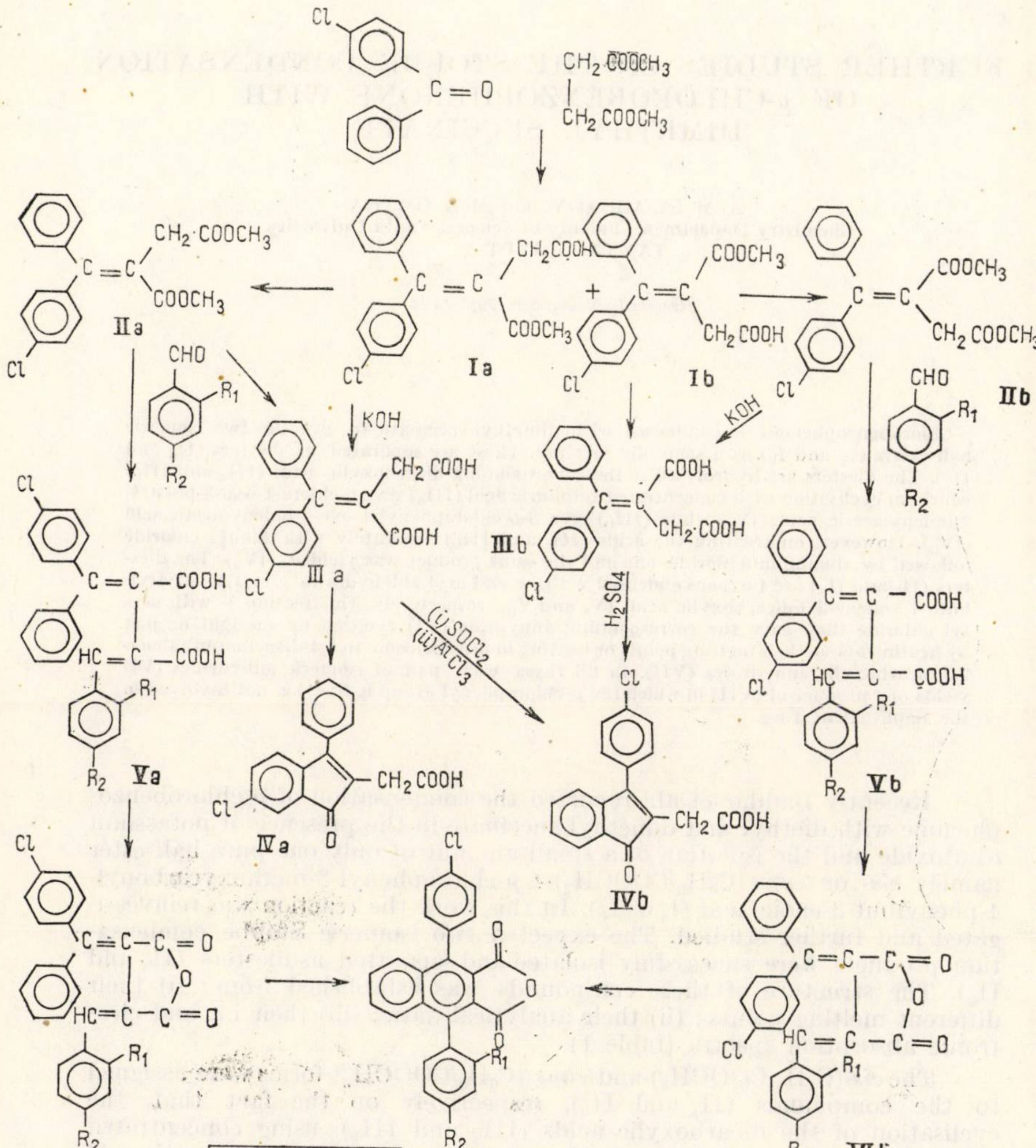
Cl
CH_2COOCH_3
C=O
CH_2COOCH_3
$CH_2 \cdot COOCH_3$
C=C
$COOCH_3$
IIa
Cl
CH_2COOH
C=C
$COOCH_3$
Ia
Cl
+
$COOCH_3$
C=C
CH_2COOH
Ib
Cl
$COOCH_3$
C=C
CH_2COOCH_3
IIb
Cl
CHO
R_1
R_2
KOH
CH_2COOH
C=C
COOH
IIIa
Cl
KOH
COOH
C=C
$CH_2 \cdot COOH$
IIIb
Cl
H_2SO_4
(i) $SOCl_2$
(ii) $AlCl_3$
Cl
C=C—COOH
HC=C—COOH
R_1
R_2
Va
Cl
CH_2COOH
O
IVa
Cl
CH_2COOH
O
IVb
C=C—COOH
HC=C—COOH
R_1
R_2
Vb
Cl
C=C—C=O
O
HC=C—C=O
R_1
R_2
VIa
Cl
O
O
R_1
R_2
VII
C=C—C=O
O
Cl
HC=C—C=O
R_1
R_2
VIb

R_1	R_2
H	OCH_3
H	Cl
OCH_3	H
H	NO_2

Table 1

Infrared and electronic spectra of compounds II, III and IV

Compd.	Infrared spectra			Electronic spectra	
	$\nu C = O (cm^{-1})$ sat. acid or ester	$\nu C = O (cm^{-1})$ unsat. acid or ester	γ-C-H(cm^{-1}) aromatic	λ_{max} (nm)	ε_{max}
II$_a$	1740	1705	770, 710	232 261	19114 11557
II$_b$	1730	1720	760, 710	232 261	20432 12389
III$_a$	1712	1681	744, 700	235 265	13398 8283
III$_b$	1695	1681	743, 700	235 265	16421 10947
IV$_a$	1735	1725	760, 715	248 288	35917 7468
IV$_b$	—	1725	755, —	245.5 287	45191 9957

However, on treating each of the acids (III$_a$ and III$_b$) by thionyl chloride followed by refluxing with aluminium chloride in acetylenetetrachloride they gave one and the same product namely 3-*p*-chlorophenyl-1-oxo-2-indenylacetic acid (IV$_b$). This result may be due to isomerisation prior to cyclisation.

In another trial to establish the structure of the diesters (II) they were further condensed with several substituted benzaldehydes. The resulted 1,1,4-triarylbuta-1,3-diene-2,3-dicarboxylic acids (V) were given the assigned structure from their analytical data and characteristic infrared and electronic absorption spectra[2] (table 2).

However, on treating 1,1,4-triarylbuta-1,3-diene-2,3-dicarboxylic acids (V) with acetyl chloride they were converted into the corresponding 1,1,4-triarylbuta-1,3-diene-2,3-dicarboxylic anhydrides (VI).
The structure of these anhydrides was confirmed by : (i), their deep red colour ; (ii) their analytical data ; (iii) their infrared absorption spectra[2] (table 3).

The anhydrides (VI) were converted into 1,4-diarylnaphthalene-2,3-dicarboxylic anhydrides (VII) by the following methods : (1) heating just above their melting points ;[3] (2) heating under reflux in nitrobenzene ; (3) irradiation of their benzene solution by u.v.radiations.[4]

In this investigation it was found that each pair of isomeric anhydrides (VI$_a$ and VI$_b$) gave one and the same product indicating that isomerisation had occurred during cyclisation. The structure of the products in each pair was established by the identity of their infrared absorption spectra and mixed melting points. It was also concluded that the unsubstituted phenyl group is engaged in the naphthalene nucleus of the products (VII), by the absence of the out-of-plane bending band at 690 – 710 cm^{-1} region [5] in their infrared absorption spectra (table 4).

---

[2] W. I. Awad, F. G. Baddar, M. A. Omara and (in part) S.M.A. Omran. *J. Chem. Soc., C*, **1971**, 3721.

[3] F. G. Baddar, L. S. El-Assal, N. A. Doss and A. H. Shehab, *J. Chem. Soc.*, **1955**, 1016.

[4] H. Stobbe, *Ber. dtsch. Chem. Ges.*, **39**, 3681 (1906).

Table 2

1,1,4-Triarylbuta-1,3-diene-2,3-dicarboxylic acids

Compd.	R_1	R_2	m.p. (°C)	Infrared spectra		Electronic	
				$\nu C = O$ acid (cm^{-1})	$\gamma - C - H$ arom. (cm^{-1})	spectra $\varepsilon_{max.}$ (nm)	$\varepsilon_{max.}$
V_a	H	OCH_3	205-6	1680, 1600	770, 700	213	32835
						231	26865
						271	19104
						310	16417
V_a	H	Cl	245	1695, 1678	743, 700	—	—
V_a	OCH_3	H	198	1690, 1670	743, 700	—	—
V_b	H	OCH_3	235	1685, 1600	777, 700	213	28305
						231	26087
						273	17971
						310	15651
V_b	H	Cl	253 – 4	1685, 1615	770, 700	213	31250
						229	25825
						265	19375
						300	13125
V_b	OCH_3	H	204 – 5	1690, 1675	770, 700	—	—

Table 3

1,1,4-Triarylbuta-1,3-diene-2,3-dicarboxylic anhydrides

Compd. (VI)	R_1	R_2	m.p. (°C)	Infrared spectra (cm^{-1})		
				$\nu - CO -$	$- O - CO -$	$\gamma - C - H$ aromatic
a	H	OCH_3	170	1810	1760	770, 700
a	H	Cl	219	1810	1770	770, 700
a	OCH_3	H	185	1820	1780	770, 710
a	H	NO_2	159 – 60	1825	1775	760, 700
b	H	OCH_3	168	1825	1775	760, 700
b	H	Cl	225	1810	1770	770, 700
b	OCH_3	H	194	1808	1745	750, 701
b	H	NO_2	217	1825	1775	750, 700

The structure of 1,4-diarylnaphthalene-2,3-dicarboxylic anhydrides (VII) was further established from their analytical data and characteristic infrared absorption spectra (table 4).

The cyclisation of the anhydrides (VI) to (VII) was again carried out by using sunlight to avoid any vigorous conditions which may lead to isomerisation, but results yielded were the same.

---

[5] J. R. Dayer "Applications of Absorption Spectroscopy of Organic Compounds" Prentice-Hall of India, New Delhi, 1971, p. 33.

Table 4

1,4-Diarylnaphthalene-2,3-dicarboxylic anhydrides

Compd.	R_1	R_2	m.p. (°C)	Infrared spectra (cm^{-1})		
				ν−CO−	O−CO−	γ−C−H aromatic
VII	H	OCH_3	290	1803	1757	755
VII	H	Cl	300	1808	1740	752
VII	H	NO_2	305	1805	1754	750

EXPERIMENTAL

Infrared spectra were measured on Beckmann spectrophotometer IR4 (KBr discs). Electronic spectra were performed on Unicam SP800 in ethanol.

Analysis were carried out by El-Naser Company for pharmaceuticals and chemicals.

cis- and *trans-*(C_6H_5/$COOCH_3$)*-Methyl 4-(p-chlorophenyl)-3-methoxy-carbonyl-4-phenylbuta-3-enoates* (II_a and II_b) :

p-Chlorobenzophenone (25 g, 1 mole) dissolved in dry benzene (80 ml), dimethyl succinate (22.5 g, 1.5 mole) and a solution of potassium-*t*-butoxide (from 6 g potassium and 120 ml *t*-butanol) were heated under reflux for 45 minutes and the mixture was worked up as usual.[6] The oily product (31.5 g, 77 % yield) was dissolved in methanol (100 ml) and treated with concentrated sulphuric acid (10 ml). The reaction mixture was either left at room temperature for 2 days or heated in a boiling water-bath for 10 hours, then cooled whereupon *cis*-(C_6H_5/$COOCH_3$) -methyl 4-(*p*-chlorophenyl)-3-methoxycarbonyl-4-phenylbut-3-enoate (II_b) separated (10.6 g). This solid product was dissolved in ether and washed with sodium carbonate solution then with water. The ether layer was dried (Na_2SO_4) and the ether was removed by evaporation. The solid thus obtained was crystallised from petroleum ether (b.p.40 − 60°) as colourless crystals, m.p. 102°.

Found: C, 65.97 ; H, 4.94 $C_{19}H_{17}O_4Cl$ requires : C, 66.18 ; H, 4.93 %.

The mother liquor was heated in a boiling water-bath for 3 hours. The reaction mixture was cooled and poured on water and extracted with ether. The ethereal layer was washed with sodium carbonate solution then with water. The ether was dried (Na_2SO_4), removed by evaporation whereupon a semisolid was obtained which was crystallised from petroleum ether (b.p. 40 − 60°) to give colourless crystals of *trans*-(C_6H_5/$COOCH_3$)-methyl 4-*p*-chlorophenyl-3-methoxycarbonyl-4-phenyl-but-3-enoate (II_a), m.p.80°. Yield 20 g.

Found : C, 66.16 ; H, 4.94 $C_{19}H_{17}O_4Cl$ requires C, 66.18 ; H, 4.93 %.

trans-(C_6H_5/COOH)*-3-Carboxy-4-p-chlorophenyl-4-phenylbut-3-enoic acid* (III_a) :

The diester II_a (1.5 g, 0.0043 mole) was hydrolysed with 10 % ethanolic potassium hydroxide solution (10ml). The *trans*-dicarboxylic acid III_a (1.3 g, 90 %) was crystallised from benzene/ethanol as colourless crystals, m.p. 181°. Found : C, 65.05 ; H, 4.1 ; Cl, 10.9 $C_{17}H_{13}O_4Cl$ requires C, 64.5 ; H, 4.1 ; Cl, 11.2 %.

cis-(C_6H_5/COOH)*-3-Carboxy-4-p-chlorophenyl-4-phenylbut-3-enoic acid* (III_b) :

The diester II_b (2 g, 0.006 mole) was hydrolysed with 10 % ethanolic potassium hydroxide solution (10 ml). The *cis*-dicarboxylic acid was crystallised from benzene/ethanol as colourless crystals, m.p. 162° (mixed melting point with III_a 157°). Yield 1.8 g (100 %). Found : C, 63.9 ; H, 4.6 ; Cl, 10.9 $C_{17}H_{13}O_4Cl$ requires C, 64.5 ; H, 4.1 ; Cl, 11.2 %.

Cyclisation of the dicarboxylic acids (III_a and III_b) :

(a) *By the Friedel-Crafts reaction* :

The *trans*-acid III_a (1.5 g, 0.005 mole) was refluxed with thionyl chloride (30 ml) for 3 hours, then the excess thionyl chloride was distilled off. The remaining oil was dissolved in acetylene-tetrachloride (10 ml) then treated with anhydrous aluminium chloride (3g). The reaction mixture was heated in a water-bath, for 2 hours, then worked up as usual. The solid product was crystallised from benzene to give 3-*p*-chlorophenyl-1-oxo-2-indenylacetic acid (IV_b)

---

[6] W. S. Johnson, J. W. Petersen and W. P. Schneider, *J. Amer. Chem. Soc.*, **69**, 74 (1947).

m.p. 179 — 80°. Yield 1.1 g (79%). Found : C, 69.1 ; H, 4.0 ; Cl, 11.6 $C_{17}H_{11}O_3$ Cl requires C, 68.4 ; H, 3.7 ; Cl, 11.8%.

Using the same procedure, the *cis*-acid III_b (0.G, 0.001 mole) gave 0.3g (80%) of 3-*p*-chlorophenyl-1-oxo-2-indenylacetic acid (IV_b) (identified by melting and mixed melting points).

(b) *Using concentrated sulphuric acid* :

The solution of the *trans*-acid III_b (1 g, 0.003 mole) in glacial acetic acid (2 ml) was treated portionwise with concentrated sulphuric acid (10 ml) at 0° during 30 minutes then worked up as usual. The product obtained (IV_a) was crystallised from benzene as orange crystals, m.p. 150°. Yield 0.8 g(89%). Found : C, 68.8 ; H, 4.2 ; Cl, 11.3 $C_{17}H_{11}O_3Cl$ requires C, 68.4 ; H, 3.7 ; Cl, 11.8%.

Using the same procedure, the *cis*-acid III_b (1.2 g ; 0.0039 mole) gave 3-*p*-chlorophenyl-1-oxo-2-indenylacetic acid (IV_b). Yield 0.8 g(71%). (melting and mixed melting point with that obtained by the Friedel-Crafts reaction).

1,1,4-*Triarylbuta-1,3-diene-2,3-dicarboxylic acids* (*V*) :

General procedure :

A solution of ice-cold potassium *t*-butoxide (0.04 mole, from 1.56 g potassium and 22 ml *t*-butanol) was treated with a mixture of the dimethyl ester II(3.75 g, 0.01 mole) and the arylaldehyde (0.01 mole) in the least amount (100 ml) of dry ether. The reaction mixture was left in ice for 3 hours after which it was heated on a boiling water-bath for another 3 hours. The reaction mixture was diluted with water and the organic solvents were removed by distillation. The reaction mixture was cooled and acidified, the solid thus obtained was filtered off and crystallised from the suitable solvent.

1-*p*-*Chlorophenyl*-4-*p*-*methoxyphenyl*-1-*phenylbuta*-1,3-*diene*-2,3-*dicarboxylic acid* (V_a, $R_1 = H$, $R_2 = OCH_3$):

The yellow solid thus obtained was crystallised from dilute acetic acid, m.p. 205—6°. Yield 4.3 g(93%). Found : C, 69.17 ; H, 4.5 ; $C_{25}H_{19}O_5Cl$ requires C, 69.04 ; H, 4.37%.

1-*p*-*Chlorophenyl*-4-*p*-*methoxyphenyl*-1-*phenylbuta*-1,3-*diene*-2,3-*dicarboxylic acid* (V_b, $R_1 = H$, $R_2 = OCH_3$) :

The yellow solid thus obtained was crystallised from dilute acetic acid, m.p. 235 — 36°. Yield 4 g (90%). Found : C, 68.98 ; H, 4.6 $C_{25}H_{19}O_5Cl$ requires C, 69.0 ; H, 4.37%.

1,4-*Di*-(*p*-*chlorophenyl*)-1-*phenylbuta*-1,3-*diene*-2,3-*dicarboxylic acid* (V_a, $R_1 = H$, $R_2 = Cl$) :

The solid product thus obtained was crystallised from acetic acid as yellow crystals, m.p. 245°. Yield 3.6 g (70%). Found : C, 65.4 ; H, 3.97 $C_{24}H_{16}O_4Cl_2$ requires C, 65.6 ; H, 3.64%.

1,4-*Di*-(*p*-*chlorophenyl*)-1-*phenylbuta*-1,3-*diene*-2,3-*dicarboxylic acid* (V_b, $R_1 = H$, $R_2 = Cl$) :

The solid product thus obtained was crystallised from acetic acid to give yellow crystals, m.p. 253—4°. Yield 3.2 g (70%). Found : C, 65.4 ; H, 3.9 ; Cl, 16.4 $C_{24}H_{16}O_4Cl_2$ requires C, 65.6, H, 3.6 ; Cl, 16.17%.

1-*p*-*Chlorophenyl*-4-*o*-*methoxyphenyl*-1-*phenylbuta*-1,3-*diene*-2,3-*dicarboxylic acid* (V_a, $R_1 = OCH_3$, $R_2 = H$) :

The solid product thus obtained was crystallised from acetic acid to give yellow crystals, m.p. 204—5°. Yield 4.2 g(90%).

Found : Cl, 7.3 $C_{25}H_{19}O_5Cl$ requires Cl, 8.1%.

1,1,4-*Triarylbuta-1,3-diene-2,3-dicarboxylic anhydrides* :

General procedure :

The dicarboxylic acid V (1.g, 0.0034 mole) was treated with acetyl chloride (30 ml), then heated to dissolution. The solvent was then removed by slow evaporation. The red solid thus obtained was crystallised from the suitable solvent.

1-*p*-*Chlorophenyl*-4-*p*-*methoxyphenyl*-1-*phenylbuta*-1,3-*diene*-2,3-*dicarboxylic anhydride* (VI_a, $R_1 = H$, $R_2 = OCH_3$) :

The red solid thus obtained was crystallised from benzene/petrolleum ether (b.p.60 — 80°), m.p. 170°. Yield 1 :2 g (84%). Found : C, 71.66 ; H, 4.24 $C_{25}H_{17}O_4Cl$ requires C, 72.02 ; H, 4.56%.

1-*p*-*Chlorophenyl*-4-*p*-*methoxyphenyl*-1-*phenylbuta*-1,3-*diene*-2,3-*dicarboxylic anhydride* (VI_b, $R_1 = H$, $R_2 = OCH_3$) :

The solid product obtained was crystallised from benzene/petroleum ether (b. p. 60 — 80°) to give deep red crystals, m.p. 168°. Yield 1.2 g(84%). Found : C, 72.38 ; H, 4.0 $C_{25}H_{17}O_4Cl$ requires C, 72.02 ; H, 4.56%.

1,4-*Di*-(*p*-*chlorophenyl*)-1-*phenylbuta*-1,3-*diene*-2,3-*dicarboxylic anhydride* (VI_a, $R_1 = H$; $R_2 = Cl$) :

The red solid thus obtained was crystallised from benzene/petroleum ether (b.p. 60 — 80°) to give deep red crystals, m.p. 219°.

Yield 1 g (70 %). Found C, 69.0 : H, 3.5 $C_{24}H_{14}O_3Cl_2$ requires C, 68.4, H, 3.3 %.

1,4-*Di-(p-chlorophenyl)-1-phenylbuta-1,3-diene-2,3-dicarboxylic anhydride* (VI_b, $R_1 = H$, $R_2 = Cl$) :

The red product thus obtained was crystallised from benzene/petroleum ether (b.p. 40 – 60°), m.p. 225°. Yield 1.1 g(76 %).

Found : C, 69.05 ; H, 3.5 ; Cl, 16.6 $C_{24}H_{14}O_3Cl_2$ requires C, 68.4 ; H, 3.3 ; Cl, 16.8 %.

1-*p-Chlorophenyl-4-o-methoxyphenyl-1-phenylbuta-1,3-diene-2,3-dicarboxylic anhydride* (VI_a, $R_1 = OCH_3$, $R_2 = H$) :

The red solid so obtained was crystallised from benzene/petroleum ether (b.p. 60 – 80°), m.p. 185° Yield 1.2 g(82 %). Found : C, 72.6 ; H, 4.48 ; Cl, 8.1 $C_{25}H_{17}O_4Cl$ requires C, 72.0 ; H, 4.08 ; Cl, 8.5 %.

1-*p-Chlorophenyl-4-o-methoxyphenyl-1-phenylbuta-1,3-diene-2,3-dicarboxylic anhydride* (VI_b, $R_1 = OCH_3$, $R_2 = H$) :

The red solid so obtained was crystallised from benzene/petroleum ether (b.p. 60 – 80°), m.p. 194°. Yield. 1.2 g(82 %). Found : C, 72.05 ; H, 4.26 ; Cl, 8.4 $C_{25}H_{17}O_4Cl$ requires C, 72.0 ; H, 4.08 ; Cl, 8.5 %.

1-*p-Chlorophenyl-4-p-nitrophenyl-1-phenylbuta-1,3-diene-2,3-dicarboxylic anhydride* (VI_a, $R_1 = H$, $R_2 = NO_2$) :

The solid obtained was crystallised from benzene to give deep red crystals, m.p. 150 – 60°. Yield 1 g(70 %). Found : C, 67.03 ; H, 3.6 $C_{24}H_{14}O_5NCl$ requires C, 66.94 ; H, 3.24 %.

1-*p-Chlorophenyl-4-p-nitrophenyl-1-phenylbuta-1,3-diene-2,3-dicarboxylic anhydride* (VI_b, $R_1 = H$, $R_2 = NO_2$) ;

The solid product thus obtained was crystallised from benzene to give deep red crystals, m.p. 217°. Yield 1 g (70 %). Found : C, 67.0 ; H, 3.4 $C_{24}H_{14}O_5NCl$ requires C, 66.94 ; H, 3.24 %.

1,4-*Diarylnaphthalene-2,3-dicarboxylic anhydrides* :

General procedure :

These compounds were prepared from the anhydrides (VI_a or VI_b) by : (a) heating just above their melting points for 3 hours, (b) irradiation of their benzene solution in the presence of iodine by u.v. radiations for 20 hours or left for one weak in sunlight (June in Tanta-Egypt), (c) heating their solutions in nitrobenzene under reflux for 3 hours. The solutions were charcoalized, filtered off, concentrated by evaporation and cooled whereupon the anhydrides (VII) precipitated in quantitative yields and crystallised from the suitable solvents.

1-*p-Chlorophenyl-4-p-methoxyphenylnaphthalene-2,3-dicarboxylic anhydride* (VII, $R_1 = H, R_2 = OCH_3$) :

The solid product obtained from the anhydrides (VI_aor VI_b, $R_1 = H$, $R_2 = OCH_3$, 0.82 g, 0.002 mole) was crystallised from benzene to give pale yellow crystals, m.p. 290°. Yield 0.8g (95 %). Found : C, 72.7 ; H, 3.8 ; Cl, 8.5 $C_{25}H_{15}O_4Cl$ requires C, 72.27 ; H, 3.6 ; Cl, 8.54 %.

1,4-*Di-(p-chlorophenyl)naphthalene-2,3-dicarboxylic anhydrides* (VII, $R_1 = H$, $R_2 = Cl$) :

The solid product obtained from the anhydrides (VI_a or VI_b, $R_1 = H$, $R_2 = Cl$, 0.84 g, 0.002 mole) was crystallised from benzene to give colourless crystals, m.p. 300°. Yield 0.75 g(90 %).

Found : C, 68.83 ; H, 3.09 ; Cl, 16.9 $C_{24}H_{12}O_3Cl_2$ requires C, 68.7 ; H, 2.86 ; Cl, 16.9 %.

1-*p-Chlorophenyl-4-p-nitrophenylnaphthalene-2,3-dicarboxylic anhydride* (VII, $R_1 = H, R_2 = NO_2$) :

The solid product obtained from the anhydrides (VI_a or VI_b, $R_1 = H$, $R_2 = NO_2$, 0.86 g, 0.002 mole) was crystallised from benzene as colourless crystals, m.p. above 305°. Yield 0.72g (85 %). Found : C, 66.98 ; H, 3.0 ; Cl, 7.8 $C_{24}H_{12}O_5NCl$ requires C, 67.05 ; H, 2.8 ; Cl, 8.2 %.

Revue Roumaine de Chimie, 20, 7, 973–980 (1975)

OXYDATION DU *n*-DODÉCANE EN PHASE LIQUIDE PAR L'OXYGÈNE MOLÉCULAIRE EN PRÉSENCE DES CATALYSEURS MÉTALLIQUES PSEUDO-HOMOGÈNES. II[1]

L'EFFET DES NAPHTÉNATES DES MÉTAUX LOURDS

IOSIF DRIMUŞ et LAMBRACHE PAPAHAGI

Faculté de Chimie Industrielle de l'Institut Polytechnique de Bucarest, Chaire de Technologie Chimique Organique, 149, Calea Victoriei, Bucarest

Reçu le 22 avril 1974

On a étudié l'influence des naphténates des métaux lourds (y compris l'aluminium) : Cu, Ag, Zn, Cd, Hg, Al, Sn, Pb, Cr, Mn, Fe, Co et Ni sur l'oxydation du *n*-dodécane en phase liquide par l'oxygène moléculaire, l'influence de ces catalyseurs pseudo-homogènes sur l'initiation de la réaction, l'accumulation de peroxydes et d'acides par rapport au temps. On a également réalisé la chromatographie des esters méthyliques des acides gras obtenus par l'oxydation, afin de pouvoir conclure sur la nature de ces acides.

INTRODUCTION

Au cours du processus d'oxydation des *n*-alcanes par l'oxygène moléculaire se produit une série de nombreuses réactions consécutives parallèles, induites, etc., qui conduisent à la formation de nombreux isomères et homologues (peroxydes, acides monocarboxyliques et dicarboxyliques, esters, alcools, cétones, aldéhydes, etc.).

L'utilisation des catalyseurs permet au processus d'oxydation de se développer dans des conditions moins dures, à une température moins élevée, ce qui détermine la diminution de la quantité des produits secondaires de dégradation, caractéristiques d'une oxydation plus avancée.

La littérature de chimie montre que, en général, pour l'oxydation des hydrocarbures en phase liquide on utilise, comme catalyseurs les sels de cobalt, manganèse, fer, chrome, plomb, nickel, etc. des différents acides organiques, qui forment, en présence des hydrocarbures, des solutions colloïdales. Ces catalyseurs occupent une position intermédiaire entre les catalyseurs homogènes et ceux hétérogènes, ce qui explique leur nom de catalyseurs pseudo-homogènes (ou pseudo-hétérogènes).[2]

---

[1] I. Drimuş et A. Lupu, *Rev. Roumaine Chim.*, **17**, 8 (1972).

[2] E. T. Denisov et N. M. Emanuel, *Uspekhi Khim.*, **29**, 1409 (1960).

Ces catalyseurs s'utilisent à grande échelle non seulement dans les laboratoires, mais aussi dans l'industrie pour la réalisation de certains processus technologiques.

L'oxydation non catalytique des hydrocarbures se caractérise par une période d'induction. Les catalyseurs, d'habitude, diminuent la période d'induction et accélèrent l'oxydation. Par exemple, les naphténates de cobalt, chrome, manganèse diminuent la période d'induction de l'oxydation du cyclohexane [3] et l'acetate de cobalt raccourcit la période d'induction de l'oxydation de la tétraline.[4] L'action d'accélération des catalyseurs est liée à leur capacité de réagir avec formation de radicaux libres. Pour la participation directe des catalyseurs à l'initiation de la chaîne des réactions plaident les expériences dans lesquelles le catalyseur a été éloigné de la zone de réaction.[5]

Le rôle des catalyseurs dans l'apparition de la chaîne des réactions a été démontré à l'aide de la méthode des inhibiteurs appliquée au cas de l'oxydation de l'huile lubrifiante en présence des stéarates de fer et cuivre[6] ou bien au cas de l'oxydation du cyclohexane en présence du stéarate de cobalt.[7]

Les déterminations effectuées démontrent clairement que l'initiation de la chaîne par les sels des métaux à valence variable est liée à la modification de la valence du métal. L'oxydation du cobalt et du manganèse bivalent s'observe aisément par la modification de la couleur des solutions. La solution de stéarate ou naphténate de cobalt bivalent dans un hydrocarbure a une légère couleur violette. Dans l'hydrocarbure oxydé le cobalt devient trivalent et la solution prend une couleur verte intense. [5,8–10]

La solution du sel de manganèse dans l'hydrocarbure est incolore ; au cours de l'oxydation elle prend la couleur brune-rouge qui caractérise le manganèse de valence supérieure. [8,10–12,13]

L'oxydation du cobalt et du manganèse (de bivalents à trivalents) est confirmée aussi par l'analyse spectrale.[9,10]

En étudiant la cinétique de l'accumulation du cobalt trivalent au cours de la réaction d'oxydation du cyclohéxane, on a constaté que le cobalt ne passait pas totalement à l'état trivalent.[11] La concentration du cobalt trivalent s'élève jusqu'à un maximum et ensuite diminue.

L'étude cinétique de l'accumulation du manganèse trivalent au cours de l'oxydation du *n*-décane [13] montre que la concentration du manganèse trivalent passe par un maximum qui représente 20 – 30% de la concentration totale du manganèse.

---

[3] N. Ota et T. Tesuka, *J. Chem. Soc. Japan, Ind. Chem. Sect.*, **57**, 641 (1954).

[4] A. E. Woodward et R. B. Mesrobian, *J. Amer. Chem. Soc.*, **75**, 6189 (1953).

[5] E. T. Denisov et N. M. Emanuel, *Zhur. fiz. Khim.*, **30**, 2327 (1956).

[6] J. Book et J. Matthews, *Disc. Faraday Soc.*, **10**, 298 (1951).

[7] B. V. Erofeev et N. M. Ushkina, *Sbornyi naucynykh robot AN URSS*, **8**, 161 (1960).

[8] G. A. Knorre, Z. K. Maizis et N. M. Emanuel, *Zhur. fiz. Khim.*, **29**, 710 (1955).

[9] R. Lombard et L. Rommert, *Bull. Soc. Chim. France*, **1956**, 36.

[10] B. G. Freidin. *Zhur. priklad. Khimii*, **30**, 768 (1957).

[11] E. T. Denisov et N. M. Emanuel, *Zhur. fiz. Khim.*, **30**, 2499 (1956).

[12] V. K. Tyskovski et A. N. Kiseleva, *Zhur. priklad. Khim.*, **23**, 1001 (1950).

[13] G. D. Knorre, Z. K. Maizis, M. I. Marki et N. M. Emanuel, *Zhur. fiz. Khim.*, **33**, 213 (1959).

Dans le présent ouvrage on a étudié l'influence des métaux suivants : cuivre, argent, zinc, cadmium, mercure, aluminium, étain, plomb, chrome, manganèse, fer, cobalt et nickel (sous forme de naphténates) sur l'oxydation du *n*-dodécane par l'oxygène moléculaire, en poursuivant la vitesse du processus d'oxydation par la variation des indices d'acidité et de peroxyde, ainsi que la nature des acides formés.

PARTIE EXPÉRIMENTALE

Préparation des catalyseurs. Ainsi qu'on a déjà mentionné dans le présent ouvrage, on a utilisé, comme catalyseurs, des sels d'acides naphténiques. Les acides naphténiques de provenance indigène ont les caractéristiques suivantes :

- masse moléculaire 217
- indice d'acidité 258 mg KOH/g
- non saponifiables 3 %
- couleur : jaune clair
- d_4^{20} 0,970 g/cm³

Les naphténates utilisés comme catalyseurs ont été obtenus par des réactions de double échange entre un naphténate soluble dans l'eau (naphténate de sodium) et un sel du métal dont on veut préparer le naphténate. Par exemple, dans le cas d'un métal bivalent, la réaction est la suivante :

$$2\,RCOONa + MSO_4 \rightarrow (RCOO)_2M + Na_2SO_4$$

Les naphténates des métaux utilisés sont insolubles dans l'eau, mais solubles dans le dodécane à chaud et en partie à froid.

Réalisation de l'oxydation. L'oxydation a été réalisée dans un réacteur en verre, capacité 80 ml, chauffé électriquement et thermoréglé à 140°, dans lequel on a introduit 40 g de *n*-dodécane. Par une plaque poreuse en verre (G_3) 5 litres d'oxygène furent barbotés par heure.

Le catalyseur est utilisé de sorte que la solution contienne pour 100 molécules de *n*-dodécane une molécule de catalyseur.

Analyses. A chaque 30 mn on détermine dans la masse de réaction l'indice d'acidité et l'indice de peroxyde. A la fin de l'oxydation (indice d'acidité environ 40 mg KOH/g) on détermine aussi dans la masse de réaction l'indice de carbonyle, l'indice d'hydroxyle, l'indice de saponification.

On sépare de la masse de réaction les acides gras et on les transforme en esters à l'aide d'une solution de trifluorure de bore en alcool méthylique. On chromatographie les esters méthyliques ainsi obtenus.

RÉSULTATS

En comparant les valeurs concernant l'accumulation de l'acidité (fig. 1 et 2), on observe que la même valeur de l'indice d'acidité (40 mg KOH/g) a été obtenue plus vite dans le cas de l'utilisation comme catalyseurs des naphténates de zinc, cadmium, cobalt ou fer.

On obtient aussi de bonnes vitesses d'accumulation des acides dans le cas des naphténates de chrome, aluminium, nickel et manganèse. Dans le cas des naphténates d'argent, de mercure et de plomb on constate une vitesse lente d'accumulation de l'acidité.

A ce propos, une constatation importante est le fait suivant : les naphténates de cuivre et d'étain inhibent la réaction d'oxydation des

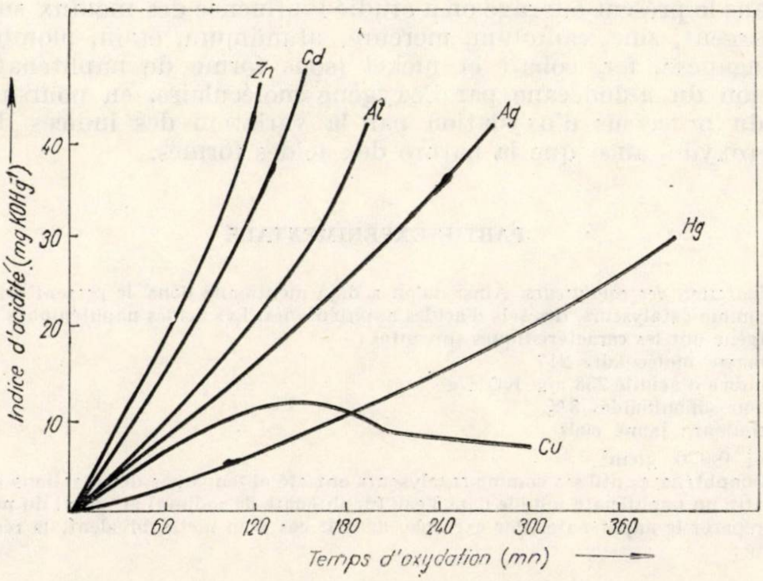

Fig. 1. — Variation de l'indice d'acidité en fonction du temps au cours de l'oxydation du *n*-dodécane par l'oxygène moléculaire, à 140°, en présence des naphténates de : cuivre, argent, zinc, cadmium, mercure et aluminium.

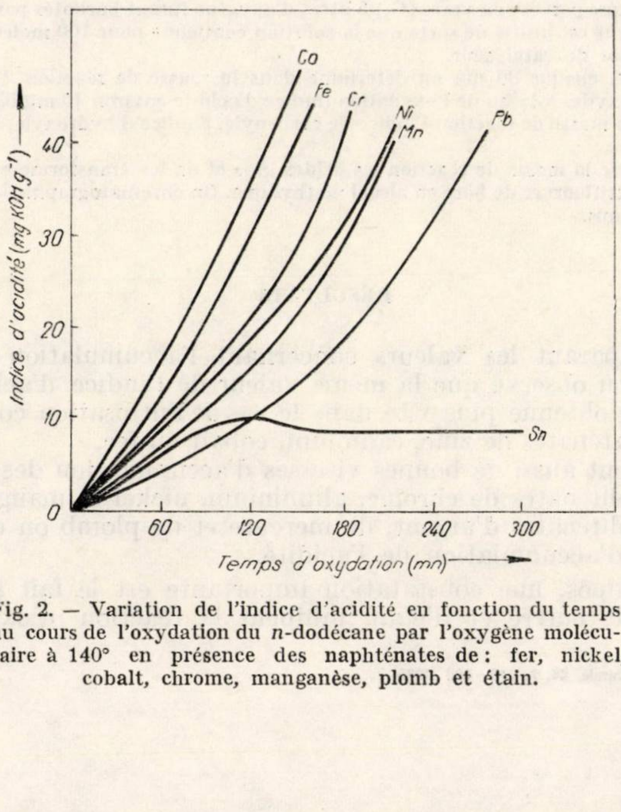

Fig. 2. — Variation de l'indice d'acidité en fonction du temps au cours de l'oxydation du *n*-dodécane par l'oxygène moléculaire à 140° en présence des naphténates de : fer, nickel, cobalt, chrome, manganèse, plomb et étain.

hydrocarbures paraffiniques, l'accumulation d'acides dans le cas de ces catalyseurs étant très réduite.

L'indice de peroxyde (fig. 3 et 4) a une valeur moindre de 1 mg O/g, indépendante de la nature du catalyseur utilisé.

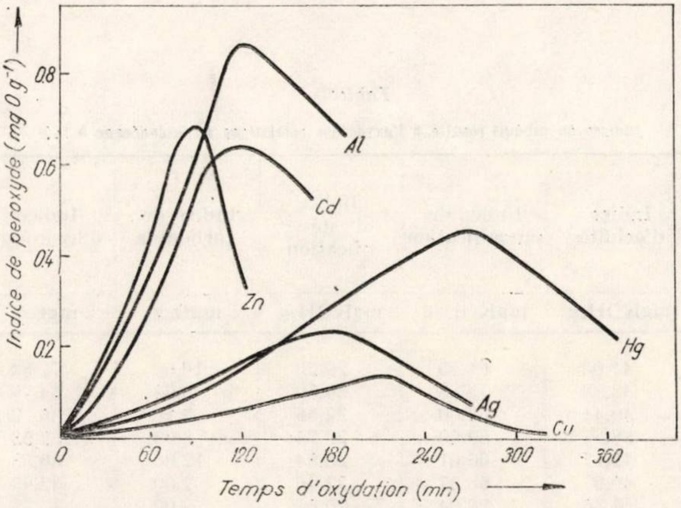

Fig. 3. — Variation de l'indice de peroxyde en fonction du temps au cours de l'oxydation du n-dodécane par l'oxygène moléculaire à 140° en présence des naphténates de : cuivre, argent, zinc, cadmium, mercure et aluminium.

Fig. 4. — Variation de l'indice de peroxyde en fonction du temps au cours de l'oxydation du n-dodécane par l'oxygène moléculaire à 140° en présence des naphténates de : fer, cobalt, nickel, chrome, manganèse, plomb et étain.

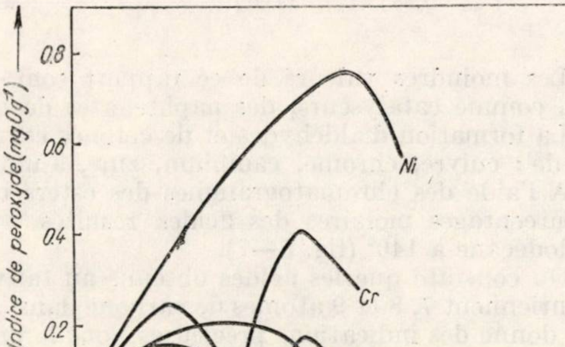

On constate une accumulation importante de peroxydes quand on utilise comme catalyseurs les naphténates d'aluminium, nickel, zinc, cadmium, mercure et chrome.

Le naphténate de cuivre, de même que dans le cas de l'acidité, conduit à des valeurs minimales pour l'accumulation des peroxydes.

Des valeurs du rapport indice d'acidité/indice d'estérification (tabl. 1) on constate que pour obtenir des acides les catalyseurs les plus indiqués sont les naphténates de nickel, le manganèse, le fer, le chrome, le cadmium et le cobalt.

Tableau 1

Indices du produit résulté à l'oxydation catalytique du *n*-dodécane à 140°

Catalyseur	Indice d'acidité	Indice de saponification	Indice d'estérification	Indice de carbonyle	Indice d'hydroxyle	Indice d'acidité / Indice d'estérification
Naphténate	mgKOH/g	mgKOH/g	mgKOH/g	mgO/g	mgO/g	
nickel	41,05	61,25	20,20	10,00	72,84	2,34
cobalt	48,38	78,88	30,50	8,00	64,79	1,58
fer	40.44	63,00	22,56	7,10	36,72	1,79
manganèse	38,87	59,60	20,73	8,00	32,53	1,87
chrome	42.77	66,61	23,84	12,00	30,53	1,79
plomb	40,97	68,37	27,40	7,00	32,93	1,49
étain	7,36	28,04	20,68	8,00	17,85	0,35
aluminium	38,11	66.61	28,50	10,00	38,10	1,33
mercure	29,13	72,92	43,79	6,00	17,02	0,66
cadmium	46,20	73,60	27,40	11,00	63,40	1,68
zinc	42,35	72,20	29,85	11,00	42,10	1,41
argent	40,90	68,00	27,10	11,00	31,20	1,50
cuivre	7,58	35,00	27,42	21,00	25,99	0,27

Les moindres valeurs de ce rapport sont obtenues lors de l'utilisation, comme catalyseurs, des naphténates de cuivre, étain et mercure.

La formation d'aldéhydes et de cétones est favorisée par les naphténates de : cuivre, chrome, cadmium, zinc, aluminium, argent et nickel.

A l'aide des chromatogrammes des esters méthyliques on a calculé les pourcentages molaires des acides résultés au cours de l'oxydation du *n*-dodécane à 140° (fig. 5—7).

On constate que les acides obtenus au taux le plus élevé sont ceux qui contiennent 7, 8 et 9 atomes de carbone dans la molécule. Cette constatation donne des indications précieuses pour le problème du lieu d'attaque de l'oxygène sur la chaîne de l'hydrocarbure.

CONCLUSIONS

Dans le cas de l'oxydation du *n*-dodécane par l'oxygène moléculaire à 140°, en présence des naphténates des métaux lourds on observe que :

1. On obtient de bonnes vitesses d'accumulation des acides dans le cas des naphténates de : zinc, cadmium, cobalt, fer, chrome, aluminium, nickel et manganèse.

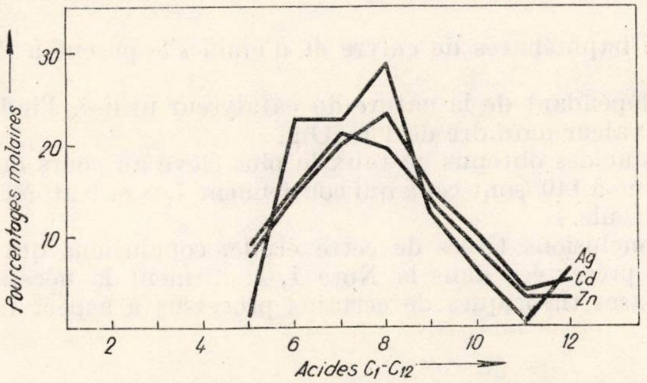

Fig. 5. — Répartition des acides obtenus au cours de l'oxydation du n-dodécane à 140° en présence des naphténates d'argent, de cadmium et de zinc.

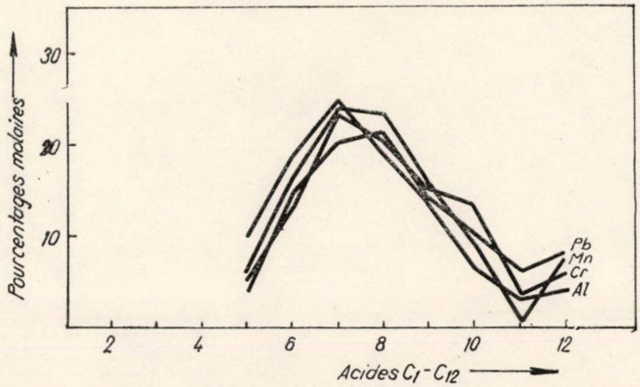

Fig. 6.—Répartition des acides obtenus au cours de l'oxydation du n-dodécane à 140° en présence des naphténates de : aluminium, plomb, chrome et manganèse.

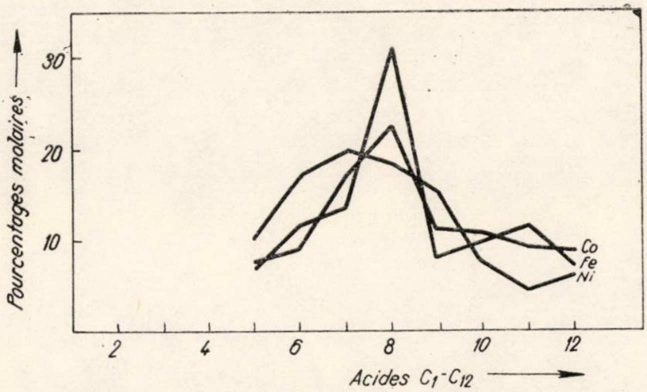

Fig. 7.—Répartition des acides obtenus au cours de l'oxydation du n-dodécane à 140° en présence des naphténates de fer, cobalt et nickel.

2. Les naphténates de cuivre et d'étain s'opposent à l'initiation de la réaction.

3. Indépendant de la nature du catalyseur utilisé, l'indice de peroxyde a une valeur moindre de 1 mgO/g.

4. Les acides obtenus au taux le plus élevé au cours de l'oxydation du *n*-dodécane à 140° sont ceux qui contiennent 7, 8 et 9 atomes de carbone dans la molécule.

Les conclusions tirées de cette étude, conclusions qui complètent les données présentées dans la Note I, confirment la nécessité d'approfondir les bases théoriques de certains processus à aspect technologique prononcé.

Revue Roumaine de Chimie, 20, 7, 981–984 (1975)

REACTIONS OF SYDNONES. II[1]

BENZYLSYDNONE AND ITS DERIVATIVES

B.V. BADAMI and G. S. PURANIK

Department of Chemistry, Karnatak University, Dharwar-580003,
INDIA

Received April 15, 1974

3-Benzylsydnone is chlorinated and the 4-halogeno-3-benzylsydnones are subjected to 1,3-dipolar addition to give the corresponding 5-halogeno-substituted 1-benzylpyrazoles.

In Part I[1] of this series, the easy synthesis of 5-substituted pyrazoles through sydnones, with phenyl and substituted phenyl groups in the 3-position was described. But the sydnone with benzyl group in 3-position which possesses no aromatic nucleus directly attached to the sydnone ring has also been found to be aromatic and stable. 3-Benzylsydnone undergoes electrophilic substitution to give the 4-bromo-3-benzylsydnone.[2] So the stability of the sydnone ring does not depend to any extent on the nature of the substituent in the 3-position.

However, chlorination of 3-benzylsydnone has not been attempted. Introduction of chlorine in any position in the sydnone molecule results in enhancing the antimalarial properties.[3]

Unsubstituted sydnones, especially having the structure similar to 3-benzylsydnone, exhibit a varied biological activity. They are given in table 1.

With the general programme of preparing substituted pyrazoles via sydnones in this laboratory, through 1,3-dipolar addition, 4-chloro-3-benzylsydnone was subjected to 1,3-dipolar addition with dimethyl acetylene dicarboxylate to yield 5-chloro-1-benzylpyrazole.

4-Bromo-3-benzylsydnone was treated similarly to give 5-bromo-1-benzyl-pyrazole.

3-Benzylsydnone and 4-bromo-3-benzylsydnone were prepared according to literature methods.[2,4] Chlorination was tried with chlorine in acetic anhydride as well as with N-chlorosuccinimide. The latter proved to be a better chlorinating agent.

---

[1] B. V. Badami and G. S. Puranik, Indian J. Chem. (accepted for publication).

[2] S. A. Zotova and V. G. Yashunskii, *Zhur. organ. Khim.*, **1**, 2218 (1965).

[3] L. B. Kier and E. B. Roche, *J. Pharm. Sci.*, **56**, 149 (1967).

[4] W. Baker, W. D. Ollis and V. D. Poole, *J. Chem. Soc.*, **1949**, 307.

Table 1

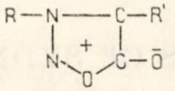

R	R′	Biological activity	Reference
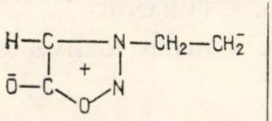	H	Anticancer.	5
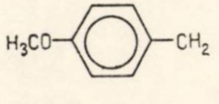	H	Anticancer.	6
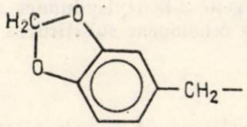	H	Antimalarial	7
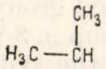 $H_3C-CH(CH_3)$	H	Diuretic and hypotensive	8,9
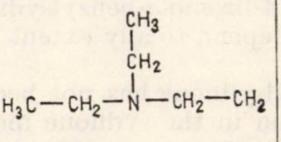 $H_3C-CH_2-N(CH_2CH_3)-CH_2-CH_2$	CH_3	Analgesic	10
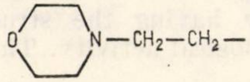	H		
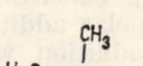 $H_3C-CH(CH_3)-$	H	CNS Stimulants	11,12
$H_3C-CH_2-CH_2-$	CH_3		

[5] H. U. Daeniker and J. Druey, *Helv. Chim. Acta.*, **40**, 918 (1957).

[6] C. V. Greco, W. H. Nyberg and C. C. Cheng, *J. Med. Pharm. Chem.*, **5**, 861 (1962).

[7] W. H. Nyberg and C. C. Cheng, *J. Med. Chem.*, **8**, 531 (1965).

[8] M. J. Fregly, L. B. Kier and D. Dhawan, *Toxicol. Appl. Pharmacol.*, **6**, 529 (1964).

[9] L. B. Kier, D. Dhawan and M. J. Fregly, *J. Pharm. Sci.*, **53**, 677 (1964).

[10] L. B. Kier and D. Dhawan, *J. Pharm. Sci.*, **51**, 1058 (1962).

[11] L. B. Kier, L. E. Fox, D. Dhawan and I. W. Waters, *Nature*, **195**, 817 (1962).

[12] D. Dhawan and L. B. Kier, *J. Pharm. Sci.*, **53**, 83 (1964).

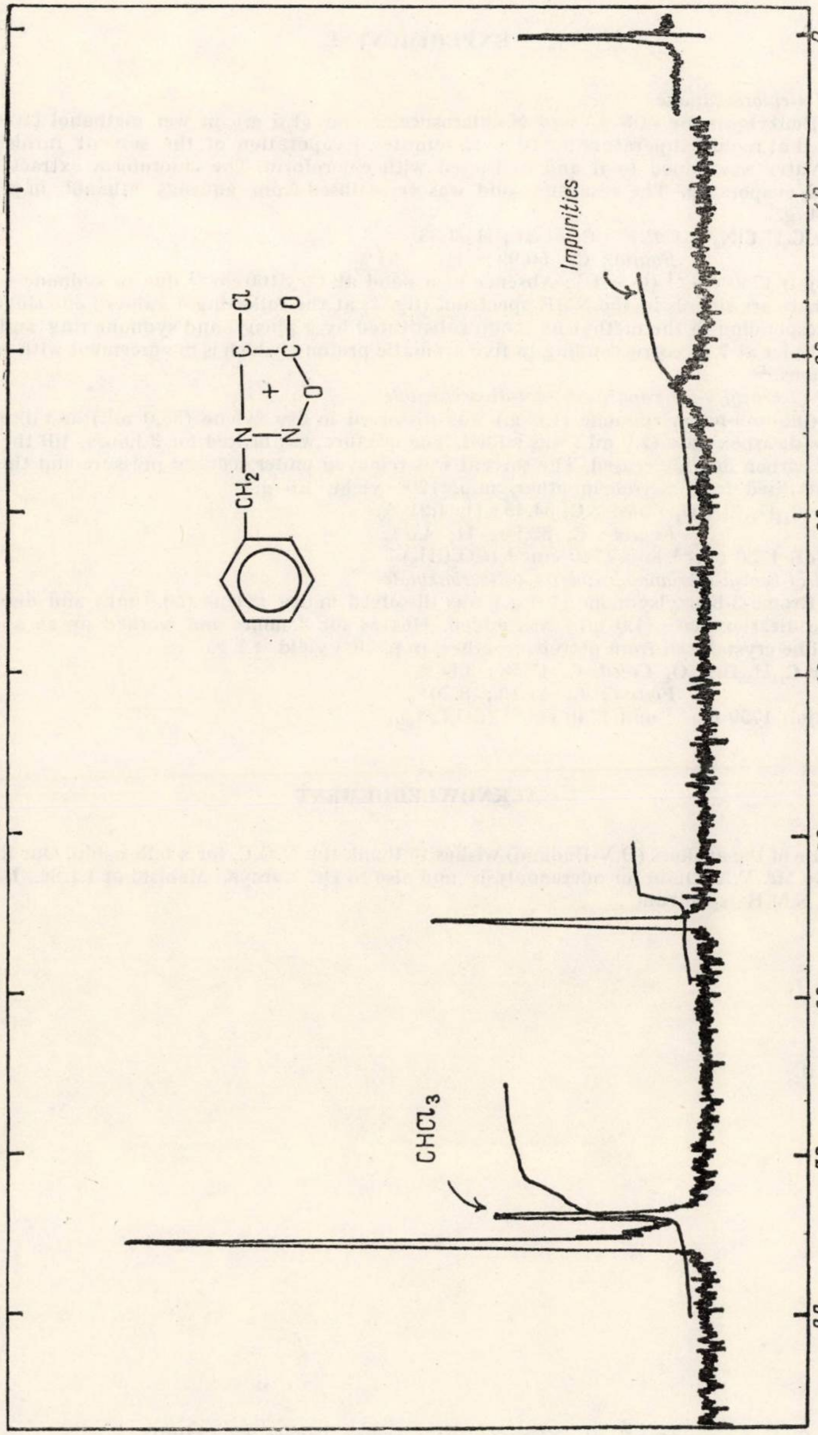

Fig.1 – NMR spectrum of 3-benzyl-4-chlorosydnone.

EXPERIMENTAL

3-Benzyl-4-chlorosydnone :

3-Benzylsydnone (1.8 g.) and N-chlorosuccinimide (1.5 g.) in wet methanol (100 ml.) was stirred at room temperature for 10 — 15 minutes. Evaporation of the solvent furnished a slurry. Water was added to it and extracted with chloroform. The chloroform extracts were dried and evaporated. The resulting solid was crystallised from aqueous ethanol, m.p. 72°; yield, 1.4 g.

Anal. for $C_9H_7ClN_2O_2$ *Calcd* : C, 51.31 ; H, 3.38.
Found : C, 50.99 ; H, 3.41 %.

I.R. (Nujol) 1750 cm^{-1} (C = O) ; Absence of a band at *Ca* 3100 cm^{-1} due to sydnone — CH.

There are signals in the NMR spectrum (fig. 1) at the following δ values : one singlet at 5.45 corresponding to the methylene group substituted by a phenyl and sydnone ring and another multiplet at 7.45 corresponding to five aromatic protons, which is in agreement with earlier observations. [13]

Dimethyl-(1-benzyl-5-chloropyrazole)-3,4-dicarboxylate

4-Chloro-3-benzylsydnone (1.0 g.) was dissolved in dry xylene (50.0 ml.) and dimethyl acetylene dicarboxylate (1.0 ml.) was added. The mixture was heated for 3 hours, till the evolution of carbon dioxide ceased. The solvent was removed under reduced pressure and the residue crystallised from petroleum-ether, m.p. 120°, yield, 1.0 g.

Anal. for $C_{14}H_{13}ClN_2O_4$ *Calcd.* : C, 54.45 ; H, 4.21 %
Found : C, 53.90 ; H, 4.0 %

I.R.(Nujol) 1750 cm^{-1} and 1740 cm^{-1} (CO_2CH_3).

Dimethyl-(1-benzyl-5-bromopyrazole)-3,4-dicarboxylate

4-Bromo-3-benzylsydnone (1.0 g.) was dissolved in dry xylene (50.0 ml.) and dimethyl acetylene dicarboxylate (1.0 ml.) was added. Heated for 3 hours and worked up as above. The residue crystallised from petroleum-ether, m.p. 70° ; yield, 1.1 g.

Anal. for $C_{14}H_{13}BrN_2O_4$ *Calcd.* C, 47.58 ; 3.68 %
Found : C, 47.13 ; 3.70 %

I.R. (Nujol) 1750 cm^{-1} and 1740 cm^{-1} (CO_2CH_3).

ACKNOWLEDGEMENT

One of the authors (B.V-Badami) wishes to thank the U.G.C. for a fellowship. Our thanks are due to Mr. V.A. Desai for microanalysis and also to Dr. Narayan Mahishi of I.I.Sc., Bangalore for N.M.R. spectrum .

---

[13] C. V. Greco and B. P. O'Reilly, *Tetrahedron Letters* 3057 (1971).

Revue Roumaine de Chimie, 20, 7, 985–991 (1975)

SEPARATION BY EXTRACTION AND SPECTROPHOTOMETRIC DETERMINATION OF In(III) WITH TRIPHENYLMETHANE BASIC DYES

CECILIA CONSTANTINESCU and LUCIA ANTONESCU

Institute of Petroleum and Gas, Ploiești

Received July 8, 1974

The paper reports the result of the investigations on the reactions, with formation of ionic associations, between the complex anion In Br_4^- with the cations of basic dyes: Victoria Blue compared to Victoria Pure Blue BO, and also some properties of these compounds. The organic extracts were studied spectrophotometrically, and the interferences due to extraneous ions were also followed.

The reactions between the cations of basic dyes and the complex metal anions, with the formation of ionic association-type compounds[1] are known from the literature. Such reactions occur in acid solutions and as the compounds formed are water-insoluble, they may be separated by means of organic solvents.

Triphenylmethane basic dyes commercially labelled as Victoria Blue (I) and Victoria Pure Blue BO (II) (C.I.42595) have the following structures:

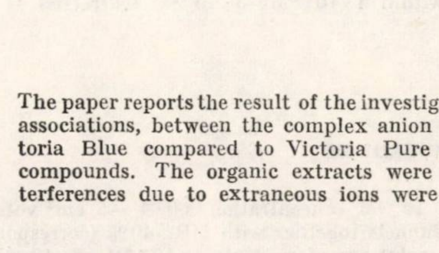

I

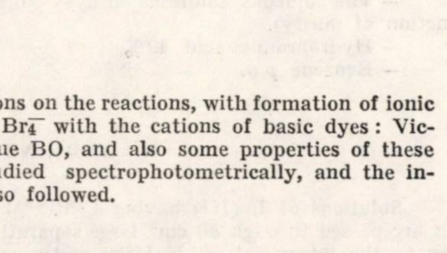

II

Their purification took place by repeated dissolutions in ethyl alcohol, filtrations and reprecipitations.[2]

In aqueous solution, both dyes are dark blue while the colour turns yellowish-brown in a strongly acidic medium (1-4N).

---

[1] I. A. Blüm and L. I. Oparina, *Zavodskaya Lab.*, **8**, 36, 897 (1970).

[2] R. P. Lestonschi and I. I. Vainstein, "Analiza tehnică în industria produselor interne", Moscova, 1958.

According to structures (I) and (II), the reagents used by us contain a naphthalene nucleus with delocalized electrons, a fact which supposes good reaction properties. They have been previously studied[3-5] in reactions with $AuCl_4^-$, $TlBr_4^-$ and $GaCl_4^-$.

In the case of In(III) spectrophotometric determinations were made with a mixture of Victoria Blue B and R dyes (in an unspecified proportion).[6]

REAGENTS

— The In (III) aqueous solution was obtained by treating pure spectral metal in an as reduced amount of HBr as possible. Solutions $1 \cdot 10^{-3}M-5 \cdot 10^{-5}M$ were prepared by adequate dilutions.

— The aqueous solutions of dyes range within $1 \cdot 10^{-3}M-5 \cdot 10^{-5}M$ (corrected as a function of purity).

— Hydrobromic acid 40%

— Benzene *p.a.*

WORKING PROCEDURE

Solutions of In (III) having $1 \cdot 10^{-3}M-5 \cdot 10^{-5}M$ concentration in $0 \cdot 1 - 5$ cm^3 volumes are passed through 50 cm^3 large separation funnels together with HBr 40% (corresponding to the interval 1—2 N HBr) and aqueous solutions of reagents $1 \cdot 10^{-3}M-5 \cdot 10^{-5}M$ so that the total aqueous volume be 10 cm^3. Samples are stirred for two minutes with 10 cm^3 benzene. The reference samples, used for measuring the absorbance of organic extracts of the complexes at the corresponding wavelengths, are prepared in an analogous manner.

RESULTS AND DISCUSSION

The formation equilibrium was studied in solution as well as the factors influencing it : solvent, acidity, reagent concentration. On the other hand, these compounds were characterized from the point of view of the composition, of the formation constant and of the applicability domain of the Bouguer Lambert-Beer law.

Selection of the solvent. The complex compounds resulted from the In Br_4^- reaction and the mentioned basic dyes are insoluble in water and soluble in organic solvents. Experiments involved solvents such as benzene, chloroform, cyclohexanol, benzene in a mixture with small amounts of acetone or methylethyl ketone. Our investigations made use of benzene for both complexes, this being a solvent which provides a good extractibility.

Visible absorption spectra. By determining the absorption spectra of aqueous solutions of Victoria Blue dyes, respectively Victoria Pure Blue BO and also those of complex benzene extracts, an absorption maximum of 610 — 615 nm was found for pure dyes (I and II), respectively 620 —

---

[3] C. Constantinescu, *Rev. chim. (București)*, **24**, 565 (1973).

[4] C. Costinescu and C. Constantinescu, *Rev. chim. (București)*, **24**, 740 (1973).

[5] Gh. Constantinescu, *Rev. chim. (București)* (under press).

[6] Gr. Popa and C. Pătroescu, *Analele Univ. București, seria St. naturii, chimie XV*, **1**, 51 (1966).

630 nm for their compounds with In (III) (fig. 1). A bathochromic effect of the complex absorption maxima was found relative to reagents, which was to be expected in the charge-transfer complex formation.

Acidity of the aqueous solution. Reactions between In(III) and the mentioned reagents take place in a HBr medium. Fig. 2 shows that when using HBr, the complex extractibility attains a maximum with an acidity of approx. 1 — 2 N HBr for complex In(III) with Victoria Blue and respectively 1.5 N HBr for complex In(III) with Victoria Pure Blue BO.

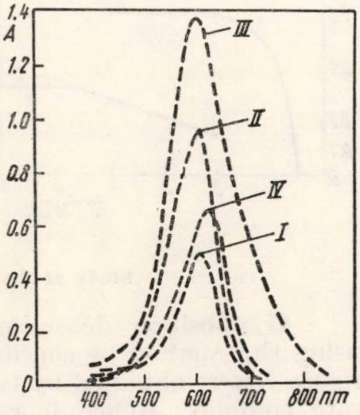

Fig. 1. — Electronic absorption spectra : I — spectrum of Victoria Blue dye : II — spectrum of Victoria Pure Blue BO dye, III — spectrum of the complex In (III) — Victoria Blue IV — spectrum of the complex In (III) — Victoria Pure Blue BO.

It has been found that a large amount of free dye is extracted at small acidities whereas a little amount of dye, if any, is extracted at high acidities.

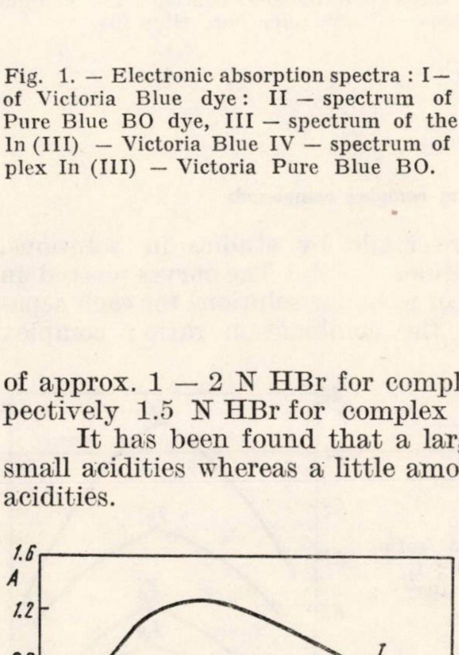

Fig. 2. — Influence of the solution acidity : I — In (III) — Victoria Blue ; II — In (III) — Victoria Pure Blue BO.

Excess of reagents. The minimum reagent concentrations for which extractibility is maximum were followed in the reaction with In(III) and the excess of reagent was established for the shift towards the right of the equilibrium or reaction $InBr_4^-$ with the reactants used (fig. 3).

$$InBr_3 + HBr \rightarrow \overset{+}{H}\,[InBr_4]^-$$

$$H^+[InBr_4]^- + R^+Cl^- \rightarrow \overset{+}{R}\,[InBr_4]^-$$

It has been found that the formed complex presents a maximum absorbance at a 2.10^{-3} M concentration of Victoria Blue dye, compared to Victoria Pure Blue BO for which a maximum absorbance is obtained at a concentration of 5.10^{-3} M. There also results an increased sensitivity of the $InBr_4^-$ reaction with the former dye compared to the latter.

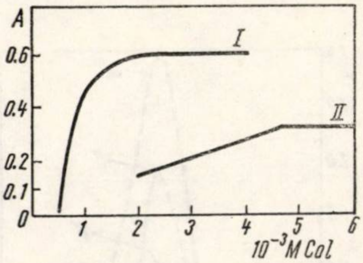

Fig. 3. — Influence of the concentration : I — Victoria Blue, II — Victoria Pure Blue BO.

Study of the composition of complex compounds

Composition determinations were made by studies in solutions, using the method of continuous variations — Job.[7] The curves plotted in figure 4 were obtained by taking pairs of isomolar solutions for each separate complex. Hence it results that the combination ratio : complex anion — dye in the case of both reagents is 1 :1. It has been concluded that in the case of the dyes used by us, one single amino group functions cationically and the structure of ionic association type compounds is the following :

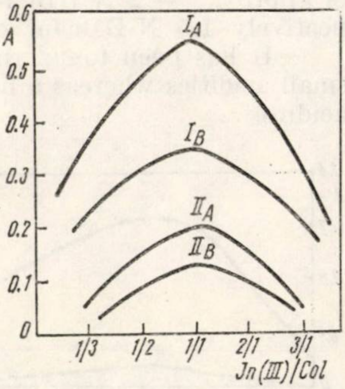

Fig. 4. — Determination of the combination ratio. Job method : I — In(III)—VB : $I_A = 1 \cdot 10^{-4}$ M ; $I_B = 5 \cdot 10^{-5}$M ; II — In (III)—VB—BO : $II_A = 5 \cdot 10^{-4}$M ; $II_B = 1 \cdot 10^{-4}$M.

$$[R_1]^+ [InBr_4]^- ; \quad [R_2]^+ \quad [InBr_4]^-$$

in which R_1^+ and R_2^+ are the cations of dyes corresponding to formulas I and II.

---

[7] P. Job, *Ann. Chim.* (*France*), **9**, 113 (1928).

Apparent formation constant of the complexes. Pairs of non-isomolar solutions were used in view of approximating the instability constants of those compounds, using the Job method applied to diphase systems.[8] The results obtained experimentally are listed in figure 5 and x values resulted from the graphs of this figure were introduced into the relation :

$$K_i = \frac{G[(1+p)x-1]^2}{(p-1)(1-2x)}$$

in which x is the point of intersection of the straight lines, corresponding to pairs of nonisomolar solutions (fig. 5) and p is :

$$p = \frac{G'(\text{molar conc. of dye})}{G(\text{molar conc. of metal})}$$

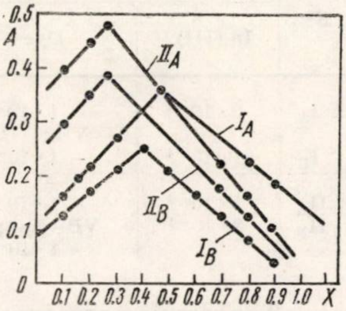

Fig. 5. — Instability constant. Job method : I — In (III) — VB : I_A : In = $2 \cdot 10^{-5}$M ; Col = $1 \cdot 10^{-3}$M I_B : Im = = $1 \cdot 10^{-5}$M ; Col = $1 \cdot 10^{-3}$ M ; II — In (III) — VB — BO : II_A : In = $2 \cdot 10^{-4}$M ; Col = $1 \cdot 10^{-3}$M ; II_B : In = $1 \cdot 10^{-4}$; Col = $1 \cdot 10^{-3}$M.

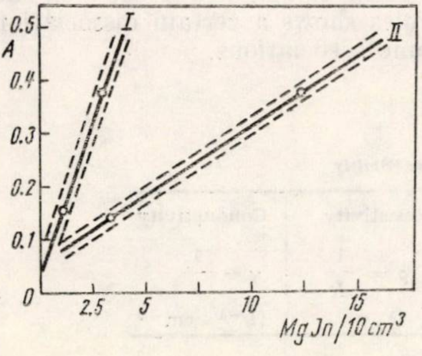

Fig. 6. — Calibration line : I) In(III) — Victoria Blue, and II) In(III) — Victoria Pure Blue BO.

Table 1 gives the values of the instability constants. A good stability of complexes In(III) has been found with Victoria Pure Blue BO.

Conductometric determinations. Determinations were made on extracts[9] of the complexes, compared to the reference sample and to pure benzene. A Tetralin Statron type Megaohmmetre apparatus (GDR) was used applying relations :

---

[8] J. H. Joe and A. E. Harney, *J. Amer. Chem. Soc.*, **70**, 648 (1948).

[9] J. D. Phielipa, *J. Amer. Chem. Soc.*, **83**, 3370, 1806 (1961).

$$U_K = U_M \cdot R_N \cdot k \cdot \text{scale } (\Omega)$$

$$\rho = U_K . 0.75 \ (\Omega . \text{cm}), \text{ where } 0.75 \text{ is the cell constant}$$

$$\gamma = \frac{1}{\rho} \ (\Omega^{-1} \cdot \text{cm}^{-1})$$

Table 1

Approximation of the instability constant

Nº	Molar concentration		$p = \frac{G'}{G}$	$X_{\max}$	K_i mean	$K_f = \frac{1}{K_i}$
	In (III)	Dye				
I_A	$2 \cdot 10^{-4}$	$-1 \cdot 10^{-3}$ VB :	5	0.4	$1 \cdot 10^{-4}$	10^4
I_B	$1 \cdot 10^{-4}$	$-1 \cdot 10^{-3}$	10	0.45		
II_A	$1 \cdot 10^{-4}$	$-1 \cdot 10^{-3}$	10	0.26	$5.75 \cdot 10^{-5}$	$1.7 \cdot 10^6$
II_B	$2 \cdot 10^{-4}$	VB−BO ; $-1 \cdot 10^{-3}$	5	0.28		

The results are presented in table 2.

The conductivity difference by one order of magnitude between the analysed samples and the reference samples shows a certain dissociation of complexes due to the formation of ionic associations.

Table 2

Determination of conductibility

Compound	U_K Ω	Resistivity $\rho = \frac{1}{R}$ Ω. cm	Conductivity $\gamma = \frac{1}{\rho}$ Ω^{-1} . cm^{-1}
Pure benzene	$0.1 \cdot 10^{12}$	$0.85 \cdot 10^{11}$	$1.2 \cdot 10^{-11}$
Reference	$0.4 \cdot 10^{8}$	$0.30 \cdot 10^{8}$	$3.0 \cdot 10^{-8}$
$[R_1]^+$; $[InBr_4]^-$	$0.45 \cdot 10^{7}$	$0.338 \cdot 10^{7}$	$3.0 \cdot 10^{-7}$
$[R_1]^+$; $[InBr_4]^-$	$0.34 \cdot 10^{7}$	$0.255 \cdot 10^{7}$	$3.9 \cdot 10^{-7}$

Calibration graph. Studies were made on the sensitivity and the selectivity of the reactions between $InBr_4^-$ and Victoria Blue and Victoria Pure Blue BO dyes.

The study concerning the variation of the absorbant with indium (III) concentration showed that the Bouguer Lambert-Beer law is verified in the domain : (I) 0.3 – 3.7 μg In/cm^3 (curve I, fig. 6) and (II) 0.4 – – 16 μg In/cm^3 (curve II, fig. 6).

The mean calibration staight line was determined by the method of discontinuous means [10] and the reliability interval was calculated from product $t.s_x$ in which $t = 4.30$ at a 95% probability and $s_x = 0.0564$. The reliability interval $t.s_x = 0.22$ for the first reaction and 0.3 respectively for the second reaction.

The sensitivity of the reaction was found at 0.3 μg In/cm^3 in the case of reaction In(III) with Victoria Blue and 0.4 μg In/cm^3 in the case of reaction In(III) with Victoria Pure Blue BO.

The absorption molar coefficients are : $\varepsilon_1 = 120{,}000$ for reaction In(III) with Victoria Blue and $\varepsilon_2 = 29{,}500$ for reaction In(III) with Victoria Pure Blue BO.

As seen from the values of absorption molar coefficients, ε is larger in the case of the reaction of ion $InBr_4^-$ with Victoria Blue and smaller in the case of the reaction with Victoria Pure Blue BO, which again confirms the higher sensitivity of the first reaction.

The complex compounds formed are stable for 48 hrs.

The order in which reagents were added was established by following the logical action of each one and was then checked by tests. The tetrabromoindic ion forms first and the reaction with the dye folows next. The order of reagents is therefore : In (III) solution, HBr, dye, benzene.

Interference of extraneous ions

The interference of ions which induce compounds similar to indium or which usually accompany indium in various materials was verified.

Reactions are disturbed by the increased absorbance of the following ions :

$$Tl > Au$$

and are not disturbed by moderate amounts of : V(V) ; Sb(III) ; Fe(III) ; Ge(IV) ; Zn(IV) ; Pb(II) ; Cd(II) ; Co(II) ; Ni(II) and Ti(IV).

CONCLUSIONS

The reaction of the tetrabromoindic complex anion with Victoria Blue dye is more sensitive than with Victoria Pure Blue BO ($\varepsilon_1 = 120{,}000$ respectively $\varepsilon_2 = 29{,}500$). Compounds are extracted in benzene; they obey Lambert-Beer's law within the limits :
(I) 0.3 – 3.7 μg In/cm^3 and (II) 0.4 – 16 μg In/cm^3.

These differences in reactivity are considered to be due to the influence of aryl or alkyl substituents in nitrogen atoms and the steric factors.

By elimination of the observed interferences, the mentioned reagents may be used as analytical reagents for the determination of small amounts of indium in various materials.

---

[10] C. LITEANU, "Analiza chimică cantitativă– Volumetrie", Ed. V, Ed. didactică şi pedagogică, Bucharest, 1973.

Revue Roumaine de Chimie, 20, 7, 990–991 (1975)

in the domain (I) 0.3 – 3.7 μg In/cm³ (curve I, fig. 6) and (II) 0.4 – 16 μg In/cm³ (curve II, fig. 6).

The exact calibration straight line was determined by the method of discontinuous means[8] and the reliability interval was calculated from product ts, in which t = 4.30 at a 95% probability and s = 0.0054. The reliability interval ts_x = 0.022 for the first reaction and 0.8 respectively for the second reaction.

The sensitivity of the reaction was found at 0.3 μg In/cm³ in the case of reaction In(III) with Victoria Blue and 0.4 μg In/cm³ in the case of reaction In(III) with Victoria Pure Blue BO.

The absorption molar coefficients are ε_1 = 120,000 for reaction In(III) with Victoria Blue and ε_2 = 38,500 for reaction In(III) with Victoria Pure Blue BO.

As seen from the values of absorption molar coefficients, ε is larger in the case of the reaction of In(III) with Victoria Blue and smaller in the case of the reaction with Victoria Pure Blue BO which again, confirms the higher sensitivity of the first reaction.

The complex compounds formed are stable for 48 hrs.

The ways in which complex [illegible] was established by following the [illegible] action of each [illegible] and was then changed [illegible]. The [illegible] bromoindic ion forms first and [illegible] reaction with the dye [illegible] forms [illegible]. The order of reagents is therefore: In(III) + water, HBr, dye, benzene.

INTERFERENCE OF EXTRANEOUS IONS

The interference of ions which might form complexes similar to indium or which usually accompany indium in various materials was studied.

These ions are determined by the increase of absorbance and the following ions

Tl > Au

and are not disturbed by moderate amounts of: Al(III); Sb(III); Fe(III); Ge(IV); Zn(II); Pb(II); Cd(II); Cu(II); Ni(II) and Co(II).

CONCLUSIONS

The reaction of the tetrabromoindic complex anion with Victoria Blue dye is more sensitive than with Victoria Pure Blue BO: ε_1 = 120,000 respectively ε_2 = 38,500. The compounds are extracted in benzene; they obey Lambert-Beer's law within the limits:

(I) 0.3 – 3.7 μg In/cm³ and (II) 0.4 – 16 μg In/cm³.

These differences in sensitivity are considered to be due to the influence of methyl and ethyl substituents in the amino groups and the steric factors.

By elimination of the observed interferences, the mentioned reagents may be used as analytical reagents for the determination of small amounts of indium in various materials.

[8] [illegible], Analiza chimică cantitativă – Volumetrie, Ed. [illegible] pedagogică, Bucureşti 19[illegible].

Revue Roumaine de Chimie, **20**, 7, 993–999 (1975)

CHARACTERIZATION OF CERAMIC ION-SELECTIVE MEMBRANE-ELECTRODES. IX. * Hg^{2+}-SENSITIVE MEMBRANE-ELECTRODE

I. C. POPESCU*, ELENA HOPÎRTEAN*, L. SAVICI** and RODICA VLAD*

*Department of Analytical Chemistry, "Babeş-Bolyai" University
Cluj-Napoca, str. Arany János 11, Romania

**Institute of Chemistry, Str. Donath 59, Cluj-Napoca, Romania

Received April 29, 1974

The paper describes the influence of the composition and the preconditioning of $AgI-Ag_2S$ mixture on the E-pHg electrode function of Hg^{2+}-sentitive electrodes having a membrane of $AgI-Ag_2S$. It also presents some data regarding the influence of the pH on the E-pHg electrode function, data which discuss the operating mechanism attributed at present to this type of electrode. The Hg^{2+}-sensitive membrane-electrodes obtained were used with good results in the Hg^{2+} complexometric tiration. The use of sodium chloride as titrant enables the determination of Hg^{2+} alongside with Cu^{2+} or Ni^{2+}.

Obviuosly, Hg^{2+} titrimetric determination, using ion-selective membrane-electrodes can be performed, in principle, in two manners: employing a titrant-sensitive indicating electrode or a Hg^{2+}-sensitive indicating electrode. The former approach was made for the determination of Hg^{2+} in radioactive solutions,[1] by titration with potassium iodide in the presence of a I^--selective electrode.[2] The latter approach has become accessible by establishing [3] that the I^--selective membrame-electrode[2] presents a Nernstian response relative to Hg^{2+} ion (slope 59 mV) in the $10^{-1}-5\times10^{-8}$M concentration range.

Knowing this fact and possessing an I^--selective electrode of original make, [4] an attempt has been undertaken at establishing the optimum parameters for the obtention and operation of the above-mentioned electrode with a view to using it as a Hg^{2+}-sensitive electrode in the Hg^{2+} complexometric determination.

---

* Part VIII: C. Liteanu, I. C. Popescu and V. Ciovîrnache, *Stud. Univ. Babeş-Bolyai, Chem.*, **18**, 53 (1973).

[1] R. F. Overman, *Analyt. Chem.*, **43**, 616 (1971).

[2] "Guide to Specific Ion Electrodes and Instrumentation", Orion Research Inc., Cambridge, USA.

[3] Orion Research Inc., *Newsletter*, **2**, 41 (1970).

[4] I. C. Popescu and M. Hălălău, *Rev. Roum. Chimie*, in press.

EXPERIMENTAL AND RESULTS

APPARATUS AND REAGENTS

E.m.f. measurements were performed at room temperature in magnetically stirred solutions, using an electronic pH-meter (type MV–11). The electrode potential was identified by e.m.f. of the following electrochemical cell;

$$\text{ESC} \left\| \begin{array}{l} \text{salt bridge} \\ KNO_3\ 10^{-1}M \text{ agar-agar} \end{array} \right\| \begin{array}{l} \text{test} \\ \text{solution} \end{array} \left| \begin{array}{l} Hg^{2+}\text{-sensitive} \\ \text{membrane-electrode} \end{array} \right. \qquad (1)$$

All reagents used were of p.a. purity.

Obtention of Hg^{2+}-sensitive membrane-electrode

Hg^{2+}-sensitive membranes used in the construction of the electrodes studied were achieved by pressing an AgI and Ag_2S mixture obtained by precipitation of S^{2-} and I^- ions from a solution of sodium sulphide and potassium iodide, with a silver nitrate solution. The precipitate obtained was purified by washing with distilled water, overdried at 120° and pressed ($p = 16$ tf/cm^2) in the form of pellets ($\varnothing = 10$ mm, $h = 1-4$ mm). The membranes thus obtained were fixed by an adequate adhesive at the end of the electrode body described in a previous paper.[5]

Electrode functions, E-pHg

Influence of the conditions for obtaining the electrodic material. Membranes of various compositions were prepared in order to establish the influence of the AgI/Ag_2S ratio on the E-pHg electrodic function. By using the electrodes obtained in this manner it was possible to establish the electrode functions E-pHg in the concentration range $5 \times 10^{-2}-10^{-6}$ M at $pH = 2$ and constant ionic strength ($J = 0.11$ M) achieved with $10^{-2}M$ HNO_3, respectively with $10^{-1}M$ KNO_3. The Hg^{2+} standard solutions used were obtained from a $10^{-1}M$ $Hg(NO_3)_2$ stock solution by successive dilutions with a solution containing $10^{-1}M$ KNO_3 and $10^{-2}M$ HNO_3. The results obtained, averaged from four determinations, were processed by the method of the least squares; the parameters of the calculated E-pHg electrodic functions are listed in table 1.

Table 1

Influence of membrane composition on the E-pHg electrode function

Membrane composition (molar % AgI)	Slope of electrode function E-pHg (mV)	E_0 (mV)	Correlation coefficient r_{xy}
100	43.0	587	−0.993
90	40.0	554	−0.989
80	39.3	572	−0.991
70	37.7	546	−0.984
64	34.2	548	−0.994
55	31.0	531	−0.990
40	31.4	514	−0.997
30	33.1	544	−0.994
20	31.6	547	−0.993
10	34.1	569	−0.981
0	29.8	614	−0.977

The influence of preconditioning the precipitates used for obtaining the membrane on the E-pHg electrodic function was then investigated. To this end, three samples were taken from a freshly obtained AgI charge and conditioned for 12 hours in a different manner maintaining them in the following solutions : 10^{-1}M $AgNO_3$, 10^{-1}M KI, 25 % NH_4OH. The E-pHg electrode functions obtained, averaged from two determinations, are listed in table 2 together with their statistically estimated parameters.

---

[5] I. C. POPESCU and C. LITEANU, *Rev. Roumaine Chim.*, **17**, 1635 (1972).

Table 2

Influence of the preconditioning of AgI on the E-pHg electrode function (pH = 2)

pHg	E(mV)			
	AgI untreated	AgI treated by $AgNO_3$	AgI treated by KI	AgI treated by NH_4OH
1.3	545	546	549	551
2	523	523	528	531
3	481	480	481	486
4	432	427	426	430
5	374	370	370	370
6	330	332	330	322
Slope (mV)	47.3	47.3	48.6	50.5
E_0 (mV)	614.5	614.5	620.0	627.5

Influence of pH. Fig. 1 presents the E-pHg electrode functions obtained for the electrode whose membrane contains 40 % molar AgI at constant ionic strength (J = = 0.11 M) and pH = 2 (curve 1), respectively in a solution of constant ionic strength (0.1 M KNO_3) without pH adjustment (curve 2).

ANALYTICAL APPLICATIONS

Three of the electrodes yielded were used in the determination of Hg^{2+} by complexometric titration. The titration curves obtained for Hg^{2+} of $\sim 4 \times 10^{-3}$M concentration and Hg^{2+} of $\sim 4 \times 10^{-4}$M concentration are plotted in figs. 2 and 3, respectively.

Experiments were performed at pH = 6 (urotropine). The results concerning the accuracy of determinations, expressed by the error calculated relative to the equivalence volume obtained

Table 3

Result of Hg^{2+} complexometric titrations

Membrane composition (molar % AgI)	Hg^{2+} concentration	H_2Y^{2-} concentration	V_e(ml)		Error (%)	$\Delta E_{\pm 2\%}$
			Indicator	Membrane		
55	$\sim 4 \times 10^{-3}$M	2×10^{-2} M	5.15	5.12	−0.5	40
75				5.16	+0.2	58
100				5.13	−0.3	42
55	$\sim 4 \times 10^{-4}$ M	2×10^{-3} M	4.85	4.87	+0.4	10
75				4.84	−0.2	10
100				4.87	+0.4	13

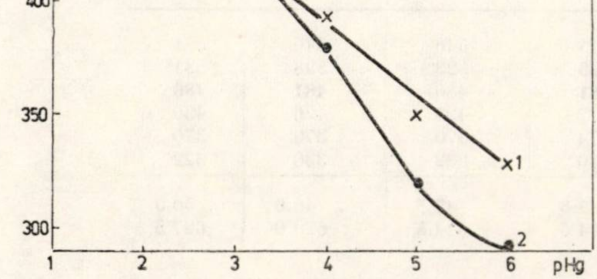

Fig. 1.—E-pHg electrode functions corresponding to the electrode whose membrane contains 40 % AgI. 1 — pH = 2, J = 0.11 M ; 2 — J = = 0.1 M.

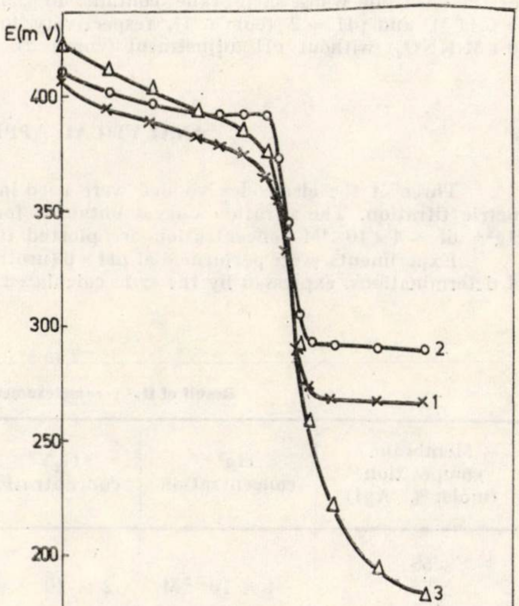

Fig. 2.— Titration of ~4 × 10^{-3} M Hg^{2+} with 2 × 10^{-2} M EDTA-solution. 1 — membrane of AgI ; 2 — membrane with 75 % AgI ; 3 — membrane with 55 % AgI.

in titration with chemical indication (xylenolorange) as well as the potential variation around the equivalence point for a $\pm 2\%$ error are listed in table 3.

In the case of instrumental titrations the equivalence volume was calculated by the Hahn-Weiler interpolation method.[6]

Another titrant used for Hg^{2+} was sodium chloride which enables a selective determination of Hg^{2+} alongside with some cations to which the chloride ion fails to react. The titration curves obtained for Hg^{2+} found alone in solution or together with Cu^{2+}, Ni^{2+}, respectively, using the electrode whose membrane contains 75% AgI and NaCl as titrant, are presented in fig. 4.

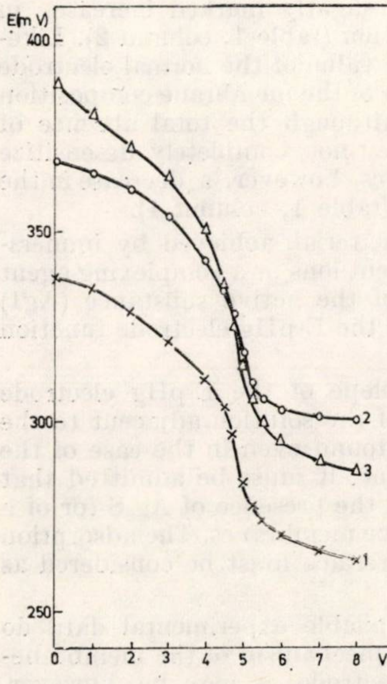

Fig. 3. — Titration of $\sim 4 \times 10^{-4}$ M Hg^{2+} with 2×10^{-3} M EDTA-solution. 1 — membrane of AgI; 2 — membrane with 75% AgI; 3 — membrane with 55% AgI.

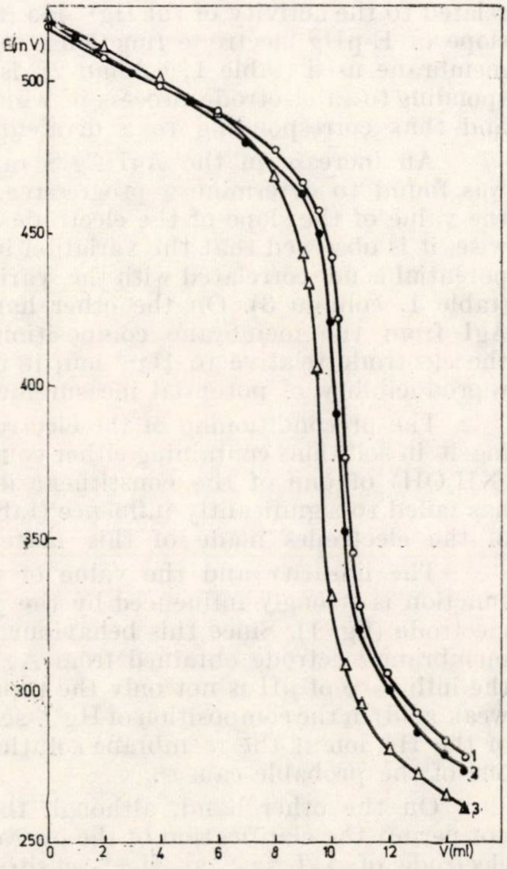

Fig. 4. — Titration of $\sim 4 \times 10^{-3}$M Hg^{2+} with 2×10^{-2}M NaCl. 1 — in the absence of other cations of heavy metals; 2 — in the presence of $\sim 4 \times 10^{-3}$M Ni^{2+}; 3 — in the presence of $\sim 4 \times 10^{-3}$M Cu^{2+}.

---

[6] F. L. Hahn and G. Weiler, *Z. analyt. Chem.*, **69**, 417 (1926).

DISCUSSION

Using the experimental results obtained, it is possible to state that Hg^{2+}-sensitive membranes are obtained by pressing an AgI-Ag_2S mixture. In the concentration domain $5 \times 10^{-2} - 10^{-6}$ M, the membrane-electrodes obtained in this manner develop an electrode potential which is closely related to the activity of the Hg^{2+} ion (table 1, column 4). The value of the slope of E-pHg electrode functions, regardless of the composition of the membrane used (table 1, column 2), is intermediate between that corresponding to an electrode process in which a monovalent cation is involved and that corresponding to a divalent cation.

An increase in the AgI/Ag_2S ratio in the membrane composition was found to determine a progressive, yet slightly marked increase in the value of the slope of the electrode function (table 1, column 2). Likewise, it is observed that the variation in the value of the normal electrode potential is not correlated with the variation of the membrane composition (table 1, column 3). On the other hand, although the total absence of AgI from the membrane composition does not completely desensitize the electrode relative to Hg^{2+} ion, it induces, however, a decrease in the reproducibility of potential measurements (table 1, column 4).

The preconditioning of the electrode material, achieved by immersing it in solutions containing either constituent ions or a complexing agent (NH_4OH) of one of the constituent ions of the active substance (AgI) has failed to significantly influence (table 2) the E-pHg electrode function of the electrodes made of this material.

The linearity and the value of the slope of the E-pHg electrode function is strongly influenced by the pH of the solution adjacent to the electrode (fig. 1). Since this behaviour was found even in the case of the membrane-electrode obtained from AgI alone, it must be admitted that the influence of pH is not only the result of the presence of Ag_2S (or of a weak acid) in the composition of Hg^{2+}-sensitive membranes. The adsorption of the H^+ ion at the membrane-solution interface must be considered as one of the probable causes.

On the other hand, although the available experimental data do not permit the clarification of the operating mechanism of the membrane-electrode of AgI-Ag_2S as Hg^{2+}-sensitive electrode, it may be, however, concluded from the above, that reaction :[3]

$$AgI + Hg^{2+} \rightleftharpoons HgI^+ + Ag^+ \qquad (2)$$

assumed to be a determining reaction of the electrode potential is actually not the only one involved. Thus, reaction (2) provides no explanation for either the value of the pH-dependence of the value of the slope of the E-pHg electrode function.

From the point of view of the use of an AgI-Ag_2S mixture to obtain a Hg^{2+}-sensitive membrane-electrode useful for indicating the end point of Hg^{2+} complexometric titration, it can be assessed that any of the studied compositions is appropriate. Yet, in order to achieve an as sensitive electrode as possible, AgI must prevail in the membrane composition, as it results from the data presented in table 1.

With regard to the Hg^{2+} complexometric determinations made, they have been found satisfactory in point of accuracy even at a concentration of 4×10^{-4} M. It is possible to further lower this value by using special techniques for the localization of the equivalence point. Thus, some preliminary investigations have shown that the titration of Hg^{2+} in a concentration of 4×10^{-5} M can be achieved by using the Gran method.[7]

In conclusion, the membrane-electrode of $AgI-Ag_2S$ displays an adequate sensitivity relative to Hg^{2+} ion, meaning that it may serve as indicating electrode in the complexometric determination of the latter.

---

[7] Orion Research Inc., *Newsletter*, **2**, 49 (1970).

electrode as possible. AgI must prevail in the membrane composition, as it results from the data presented in table I.

With regard to the Hg^{2+} complexometric determinations made, they have been found satisfactory in point of accuracy, even at a concentration of 4×10^{-4} M. It is possible to further lower this value by using special techniques for the localization of the equivalence point. Thus, some preliminary investigations have shown that the titration of Hg^{2+} in a concentration of 4×10^{-5} M can be achieved by using the Gran method.[7]

In conclusion, the membrane electrode of AgI – Ag_2S displays an adequate sensitivity relative to Hg^{2+} ion, meaning that it may serve as indicating electrode in the complexometric determination of the latter.

---

[7] Orion Research Ions. Newsletter, 2, 49 (1970).

Revue Roumaine de Chimie, 20, 7, 1001–1011 (1975)

MODELLING THE MATERIAL BALANCES OF CHEMICAL FLOWSHEETS*

L. BADEA

Ministry of Chemical Industry – Technical Department
Splaiul Independenţei 202, Bucharest, Romania

Received September 6, 1974

The material balance model for chemical flowsheets was established on the basis of the equations for a transformation stage and for a separation stage, which are fed with raw materials and intermediate products consisting of a multitude of components. The stage was divided into substages specific to each component participating in its feeding. The separation substage was considered as a particular case of the transformation stage.

When modelling the material balance of a chemical process, the process is usually represented by a flowsheet consisting of its chemical reaction (transformation) stages.

In the practice of material balance modelling, cases where the separate evidence of the other flowsheet stages is necessary, often appear.

In these cases, otherwise representing the general case of the material balance modelling, the stages can represent, according to the type of flowsheet, process phases, operations, equipment, parts of equipment or abstract divisions of the respective process.

To establish a mathematical model, allowing the flowsheet material balance calculation, a j stage (j being any stage) of a flowsheet consisting of a number m of stages ($j = 1, 2, 3, \ldots, \mathrm{m}$), is considered (figure 1).

The j stage can be fed with mixtures of i components ($i = 1, 2, 3, \ldots, \mathrm{n}$, being any component) constituting fresh raw materials ($f_{i(0j)}$), intermediate products resulting from another j' stage (j' being any stage) ($b_{i(j'j)}$ $g_{i(j'j)}$) and recycled products ($g_{i(jj)}$).

From the j stage there can result mixtures of i components constituting intermediate products feeding j' stage ($b_{i(jj')} g_{i(jj')}$), recycled products, products used in secondary processes or considered losses ($g_{i(j0)}$, ($1 - b_{i(jj')}$) $g_{i(jj')}$) and mixtures of $i + i'$ components ($i' = n + 1, n + 2, \ldots, n'$, being any component resulting by the transformation of i component) constituting finite products ($\Sigma\, p_{i,i'(j)}$).

---

* **Paper presented to the Fourth Republican Conference on Physical General and Applied Chemistry, Bucarest, September 2–5, 1974.**

To simplify, we consider from the viewpoint of the flowsheet material balance modelling, that the flow sheets are composed only of two types of stages, namely;

— the transformation stages and

— the separation and/or mixings stages (designated "separation" stages).

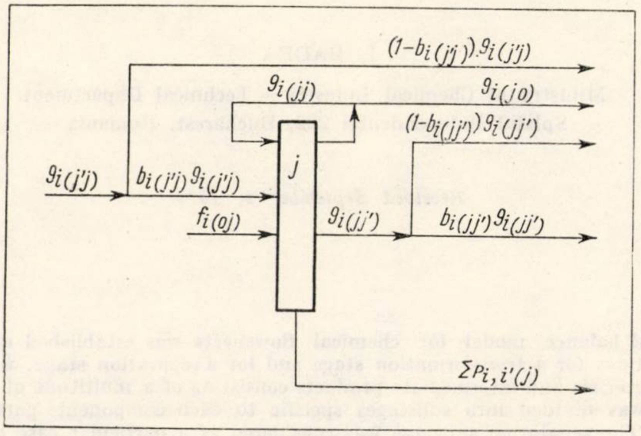

Fig. 1. — The *j* stage of a chemical flowsheet composed of *m* stages.

In the transformation stage, a (partial or total) transformation of *i* component into *i'* component and a distribution of $i + i'$ components in the products resulting from it are carried out.

In the separation stage a distribution of *i* components in the products resulting from it is carried out.

Considering the *j* stage as a transformation stage, the variation of *i* component amount after *N* passes ($N = 1, 2, 3, \ldots, N$) through *j* stage, at steady state conditions of the process, according to the recycling theory,[1] is:

$$dG(1)_{i(j)} = f_{i(0j)}\,dt + \Sigma b_{i(j'j)}\,g_{i(j'j)}\,dt \tag{1.1.1)T}$$

$$\begin{aligned} dG(2)_{i(j)} &= dG(1)_{i(j)} + b_{i(jj)}\,c^{+}_{i(jj)}\,(dG(1)_{i(j)} \\ &\quad -(1 - a_{i(j)})\,dG(1)_{i(j)}) - (1 - a_{i(j)})\,dG(1)_{i(j)} \\ &= a_{i(j)}\,dG(1)_{i(j)} + a_{i(j)}\,b_{i(jj)}\,c^{+}_{i(jj)}\,dG(1)_{i(j)} \end{aligned} \tag{1.1.2)T}$$

$$\begin{aligned} dG(3)_{i(j)} &= dG(1)_{i(j)} + b_{i(jj)}\,c^{+}_{i(jj)}\,dG(2)_{i(j)} \\ &\quad -(1 - a_{i(j)})\,dG(1)_{i(j)} \\ &= a_{i(j)}\,dG(1)_{i(j)} + b_{i(jj)}\,c^{+}_{i(jj)}\,dG(2)_{i(j)} \end{aligned} \tag{1.1.3)T}$$

. . . .

---

[1] M. F. Nagiev, "Uchenie o retsirkulatsionykh protsesakh v khimicheskoi tekhnologii", Azerbaidzkhanskoe Gosudarstvenoe Izdatelstvo, Baku, 1965.

$$dG(N)_{i(j)} = dG(1)_{i(j)} + b_{i(jj)}\, c^{+}_{i(jj)}\, dG\,(N-1)_{i(j)}$$

$$-\,(1 - a_{i(j)})\, dG(1)_{i(j)}$$

$$= a_{i(j)}\, dG(1)_{i(j)} + b_{i(jj)}\, c^{+}_{i(jj)}\, dG(N-1)_{i(j)} \qquad (1.1.N)\mathrm{T}$$

where $f_{i(0j)}$ is the flow rate of i component constituting the fresh raw material feeding j stage;
$g_{i(j'j)}$ — the sum of i component flow rates resulting from j' stage which is feeding j stage and used in a secondary process;
$b_{i(j'j)}$ — the distribution rate of i component resulting from j' stage to j stage;
$c^{+}_{i(jj)}$ — the transformation rate of i component feeding j stage in i component maximum possible to be recycled;
$b_{i(jj)}$ — the recycling yield of i component resulting from j stage;
$a_{i(j)}$ — the recovery yield of i component feeding j stage, in the finite product;
t — the time.

The constants $b_{i(j'j)}$, $c^{+}_{i(jj)}$, $b_{i(jj)}$ and $a_{i(j)}$ are referring to one pass and together with the flow rates $f_{i(0j)}$ and $g_{i(j'j)}$, are considered to remain constant in the interval of $N = 1, 2, \ldots, N$ passes, at steady state conditions of the process.

Consecutively, eliminating the variables $G(1)_{i(j)}, G(2)_{i(j)}, \ldots, G(N)_{i(j)}$ from eqs.(1.1.1)T –(1.1.N)T, we get

$$dG(1)_{i(j)} = (f_{i(0j)} + \sum b_{i(j'j)}\, g_{i(j'j)})\, \mathrm{d}t \qquad (1.2.1)\mathrm{T}$$

$$dG(2)_{i(j)} = a_{i(j)}\,(f_{i(0j)} + \sum b_{i(j'j)}\, g_{i(j'j)})\,(1 + b_{i(jj)}\, c^{+}_{i(jj)})\; dt \qquad (1.2.2)\mathrm{T}$$

$$dG(3)_{i(j)} = a_{i(j)}\,(f_{i(0j)} + \sum b_{i(j'j)}\, g_{i(j'j)})$$

$$(1 + b_{i(jj)}\, c^{+}_{i(jj)} + b^{2}_{i(jj)}\, c^{+2}_{i(jj)})\; dt \qquad (1.2.3)\mathrm{T}$$

. . . .

$$dG(N)_{i(j)} = a_{i(j)}(f_{i(0j)} + \sum b_{i(j'j)}\, g_{i(j'j)})$$

$$(1 + b_{i(jj)}\, c^{+}_{i(jj)} + b^{2}_{i(jj)}\, c^{+2}_{i(jj)} + \ldots + b^{N-1}_{i(jj)}\, c^{+N-1}_{i(jj)})\; dt \qquad (1.2.N)\mathrm{T}$$

Multiplication and division of eq. (1.2.N)T by $(1 - b_{i(jj)})c^{+}_{i(jj)}$, gives

$$dG(N)_{i(j)} = \frac{a_{i(j)}\,(f_{i(0j)} + \sum b_{i(j'j)}\, g_{i(j'j)})(1 - b^{N}_{i(jj)}\, c^{+N}_{i(jj)})\; dt}{1 - b_{i(jj)}\, c^{+}_{i(jj)}} \qquad (1.3)\mathrm{T}$$

By integrating eq. (1.3)T, we get

$$G(N)_{i(j)} = \frac{a_{i(j)}\,(f_{i(0j)} + \sum b_{i(j'j)}\, g_{i(j'j)})(1 - b^{N}_{i(jj)}\, c^{+N}_{i(jj)})}{1 - b_{i(jj)}\, c^{+}_{i(jj)}}\, t + C \qquad (1.4)\mathrm{T}$$

where C is an integration constant.

At $t = 0$, $G(N)_{i(j)} = 0$ and $C = 0$; consequently eq. (1.4)T becomes

$$G(N)_{i(j)} = \frac{a_{i(j)}\,(f_{i(0j)} + \sum b_{i(j'j)}\, g_{i(j'j)})(1 - b^{N}_{i(jj)}\, c^{+N}_{i(jj)})}{1 - b_{i(jj)}\, c^{+}_{i(jj)}}\, t \qquad (1.5)\mathrm{T}$$

Because always $c^{+}_{i(jj)} < 1$, and, at steady state conditions of the process, $N = +\infty$

$$\lim_{N \to +\infty} b^{N}_{i(jj)}\, c^{+N}_{i(jj)} = 0$$

and eq. (1.5)T reduces to

$$G(N)_{i(j)} = \frac{a_{i(j)}\,(f_{i(0j)} + \sum b_{i(j'j)}\, g_{i(j'j)})}{1 - b_{i(jj)}\, c^{+}_{i(jj)}}\, t \qquad (1.6)\mathrm{T}$$

When the material balance calculations are made on the basis of amounts per time unit and the conditions of the process are considered steady state ones, instead of eqs. (1.1.1)T–(1.1.N)T the following linear equations can be written

$$g(1)_{i(j)} = f_{i(0j)} + \sum b_{i(j'j)}\, g_{i(j'j)} \qquad (1.7.1)\mathrm{T}$$

$$g(2)_{i(j)} = a_{i(j)}\, g(1)_{i(j)} + a_{i(j)}\, b_{i(jj)}\, c^{+}_{i(jj)}\, g(1)_{i(j)} \qquad (1.7.2)\mathrm{T}$$

$$g(3)_{i(j)} = a_{i(j)}\, g(1)_{i(j)} + b_{i(jj)}\, c^{+}_{i(jj)}\, g(2)_{i(j)} \qquad (1.7.3)\mathrm{T}$$

. . . .

$$g(N)_{i(j)} = a_{i(j)}\, g(1)_{i(j)} + b_{i(jj)}\, c^{+}_{i(jj)}\, g(N-1)_{i(j)} \qquad (1.7.\mathrm{N})\mathrm{T}$$

where $g(N)_{i(j)} = \dfrac{G(N)_{i(j)}}{t}$ is the sum of i component flow rates feeding j stage, at pass N.

Dividing eq.(1.6)T by $t(f_{i(0j)} + \sum b_{i(j'j)}\, g_{i(j'j)})$ we get

$$\frac{g(N)_{i(j)}}{f_{i(0j)} + \sum b_{i(j'j)}\, g_{i(j'j)}} = \frac{a_{i(j)}}{1 - b_{i(jj)}\, c^{+}_{i(jj)}} = k_{i(j)} \qquad (1.8)\mathrm{T}$$

where $k_{i(j)}$ is the recycling constant of i component to j stage.

Equation (1.8)T gives

$$g(N)_{i(j)} = k_{i(j)} (f_{i(0j)} + \sum b_{i(j'j)} g_{i(j'j)}) \tag{1.9)T}$$

Since at steady state conditions of the process, $N = + \infty$, we can consider $g_i(N)_{i(j)} = g(N - 1)_{i(j)}$ and eq. (1.7.N)T becomes

$$g(N)_{i(j)} = a_{i(j)} g(1)_{i(j)} + b_{i(jj)} c^+_{i(jj)} g(N)_{i(j)} \tag{1.9.1)T}$$

or

$$g(N)_{i(j)} = g(1)_{i(j)} - (1 - a_{i(j)}) g(1)_{i(j)} + b_{i(jj)} c^+_{i(jj)} g(N)_{i(j)}$$

and also, by expressing $g(1)_{i(i)}$ according to eq. (1.7.1)T

$$\begin{aligned} g(N)_{i(j)} = f_{i(0j)} + \sum b_{i(j'j)} g_{i(j'j)} - (1 - a_{i(j)}) (f_{i(0j)} + \\ + \sum b_{i(j'j)} g_{i(j'j)}) + b_{i(jj)} c^+_{i(jj)} g(N)_{i(j)} \end{aligned} \tag{1.9.2)T}$$

From eq.(1.9.2)T we get the flow rate of i component recycled to j stage

$$\begin{aligned} g(N)_{i(jj)} &= g(N)_{i(j)} - (f_{i(0j)} + \sum b_{i(j'j)} g_{i(j'j)}) \\ &= b_{i(jj)} c^+_{i(jj)} g(N)_{i(j)} - (1 - a_{i(j)})(f_{i(0j)} + \sum b_{i(j'j)} g_{i(j'j)}) \end{aligned} \tag{1.10)T}$$

The flow rate of i component resulting from j stage, liable to being recycled, but used in a secondary process, can be deduced from the relationship defining the constant $b_{i(jj)}$

$$g(N)_{i(j0)} = \frac{g(N)_{i(jj)} (1 - b_{i(jj)}) + (1 - a_{i(j)}) (f_{i(0j)} + \sum b_{i(j'j)} g_{i(j'j)})(1 - b_{i(jj)})}{b_{i(jj)}} \tag{1.10.1)T.}$$

Substituting the expression for $g(N)_{i(jj)}$ given in eq. (1.10)T into eq. (1.10.1)T gives

$$g(N)_{i(j0)} = (1 - b_{i(jj)}) c^+_{i(jj)} g(N)_{i(j)} \tag{1.11)T}$$

Supposing the accumulation in the process is equal to zero and using eq. (1.9)T, the sum of i component flow rates resulting from j stage which is feeding j' stage and which is used in a secondary process, is given by

$$\begin{aligned} g(N)_{i(jj')} &= b_{i(jj')} g(N)_{i(jj')} + (1 - b_{i(jj')}) g(N)_{i(jj')} \\ &= k_{i(j)} (f_{i(0j)} + \sum b_{i(j'j)} g_{i(j'j)}) c^+_{i(jj')} \\ &= c^+_{i(jj)j} g(N)_{i(j)} \end{aligned} \tag{1.12)T}$$

where $b_{i(,j')}$ is the distribution rate of i component resulting from j stage to j' stage;

$c^{+}_{i(jj')}$ – the transformation rate of i component feeding j stage in i component feeding j' stage.

The flow rate of i component resulting from j stage and contained in the finite product can be expressed by

$$p(N)_{i(j)} = (1 - a_{i(j)})(f_{i(0j)} + \sum b_{i(j'j)}\, g_{i(j'j)}) \tag*{(1.12.1)T}$$

The flow rate of i' component resulting from j stage and constituting the pure finite product is

$$p(N)_{i'(j)} = k_{i(j)}\,(f_{i(0j)} + \sum b_{i(j'j)}\, g_{i(j'j)})\, c^{+}_{i'(j)} \tag*{(1.12.2)T}$$

Substituting into eq. (1.12.2)T the expression for $k_{i(j)}(f_{i(0j)} + \sum b_{i(j'j)} g_{i(j'j)})$ according to eq. (1.9)T gives

$$p(N)_{i'(j)} = c^{+}_{i'(j)}\, g(N)_{i(j)} \tag*{(1.12.3)T}$$

where $c^{+}_{i'(j)}$ is the transformation rate of i component feeding j stage in i' component.

Defining the flow rate of the finite product as $\sum p(N)_{i,i'(j)} = p(N)_{i(j)} + \sum p(N)_{i'(j)}$ and using eqs. (1.12.1)T and (1.12.3)T we get

$$\sum p(N)_{i,i'(j)} = (1 - a_{i(j)})(f_{i(0j)} + \sum b_{i(j'j,}\, g_{i(j'j)}) + \sum c^{+}_{i'(j)}\, g(N)_{i(j)} \tag*{(1.13)T}$$

Noting $g(N)_{i(j)} = g_{i(j)},\ g(N)_{i(jj)} = g_{i(jj)},\ g(N)_{i(j0)} = g_{i(j0)},$

$$g(N)_{i(jj')} = g_{i(jj')},\ p(N)_{i(j)} = p_{i(j)},\ p(N)_{i'(j)} = p_{i'(j)},$$

$\sum p(N)_{i,i'(j)} = \sum p_{i,i'(j)}$, the eqs. (1.9)T –(1.13)T become

$$\begin{aligned} g_{i(j)} &= k_{i(j)}\,(f_{i(0j)} + \sum b_{i(j'j)}\, g_{i(j'j)}) \\ &= f_{i(0j)} + \sum b_{i(j'j)}\, g_{i(j'j)} + g_{i(jj)} \end{aligned} \tag*{(1.14.1)T}$$

$$\begin{aligned} g_{i(jj)} &= b_{i(jj)}\, c^{+}_{i(jj)}\, g_{i(j)} \\ &\quad -(1 - a_{i(j)})(f_{i(0j)} + \sum b_{i(j'j)}\, g_{i(j'j)}) \end{aligned} \tag*{(1.14.2)T}$$

$$g_{i(j0)} = (1 - b_{i(jj)})\, c^{+}_{i(jj)}\, g_{i(j)} \tag*{(1.14.3)T}$$

$$\begin{aligned} g_{i(jj')} &= b_{i(jj')}\, g_{i(jj')} + (1 - b_{i(jj')})\, g_{i(jj')} \\ &= c^{+}_{i(jj')}\, g_{i(j)} \end{aligned} \tag*{(1.14.u)T}$$

$$\sum p_{i.i'(j)} = (1 - a_{i(j)})(f_{i(0j)} + \sum b_{i(j'j)}\, g_{i(j'j)})$$

$$+ \sum c^{+}_{i'(j)}\, g_{i(j)}$$

$$= g_{i(j)} - g_{i(jj)} - g_{i(j0)} - \sum b_{i(jj')}\, g_{i(jj')}$$

$$- \sum (1 - b_{i(jj')})\, g_{i(jj')} \qquad (1.14.\mathrm{u}+1)\mathrm{T}$$

In eq. (1.14.1)T the variable $g_{i(j)}$ is also expressed by the sum of i component flow rates feeding j stage and in eq. (1.14u + 1)T, the variable $\sum p_{i,i'(j)}$ by the difference between the variable $g_{i(j)}$ and the sum of i component flow rates resulting from j stage.

Equations (1.14.1)T –(1.14.u+ 1)T are constituting the material balance mathematical model of a transformation stage fed with a single component.

When $\sum b_{i(j'j)}\, g_{i(j'j)} = 0$, the above mentioned model reduces to the case of a model for a transformation stage fed only with fresh raw material consisting of a single component.[2]

If the j stage is fed with a mixture of i components, the variables $g_{i(j)}, f_{i(0j)}$ and $p_{i(j)}$ must be substituted by their respective sums $\sum g_{i(j)}$, $\sum f_{i(0j)}$ and $\sum p_{i(j)}$.

It follows that

$$k_{i(j)} = k_{(j)} \frac{g_{i(j)} \sum (f_{i(0j)} + \sum b_{i(j'j)}\, g_{i(j'j)})}{(f_{i(0j)} + \sum b_{i(j'j)}\, g_{i(j'j)}) \sum g_{i(j)}} \qquad (2.1)\mathrm{T}$$

$$c^{+}_{i(jj)} = c_{i(jj)} \frac{\sum g_{i(j)}}{g_{i(j)}} \qquad (2.2)\mathrm{T}$$

$$c^{+}_{i(jj')} = c_{i(jj')} \frac{\sum g_{i(j)}}{g_{i(j)}} \qquad (2.3)\mathrm{T}$$

$$c^{+}_{i'(j)} = c_{i'(j)} \frac{\sum g_{i(j)}}{g_{i(j)}} \qquad (2.4)\mathrm{T}$$

$$p_{i(j)} = \sum p_{i(j)} \frac{(1 - a_{i(j)})(f_{i(0j)} + \sum b_{i(j'j)}\, g_{i(j'j)})}{\sum (1 - a_{i(j)})(f_{i(0j)} + \sum b_{i(j'j)}\, g_{j(j'j)})} \qquad (2.5)\mathrm{T}$$

where $k_{(j)}$ is the recycling constant of i components to j stage;

$c_{i(jj)}$ — the transformation rate of i components feeding j stage in i component maximum possible to be recycled;

---

[2] L. BADEA, *Rev. Chim.* (*Bucureşti*), **23**, 617 (1972).

$c_{i(jj')}$ — the transformation rate of i components feeding j stage in i component feeding j' stage;

$c_{i'(j)}$ — the transformation rate of i components feeding j stage in i' component.

Substituting into eqs. (1.14.1)T — (1.14.u + 1)T the expressions for $k_{i(j)}$, $c^{+}_{i(jj)}$, $c^{+}_{i(jj')}$, $c^{+}_{i'(j)}$ and $p_{i(j)}$ according to eqs. (2.1)T — (2.5)T, we get

$$\begin{aligned} \sum g_{i(j)} &= k_{(j)} \sum (f_{i(0j)} + \sum b_{i(j'j)}\, g_{i(j'j)}) \\ &= \sum (f_{i(0j)} + \sum b_{i(j'j)}\, g_{i(j'j)} + g_{i(jj)}) \end{aligned} \tag{2.6.1)T$$

$$g_{i(jj)} = b_{i(jj)}\, c_{i(jj)} \sum g_{i(j)} - (1 - a_{i(j)})\, (f_{i(0j)} + \sum b_{i(j'j)}\, g_{i(j'j)}) \qquad (2.6.\mathrm{s})\mathrm{T}$$

$$g_{i(j0)} = (1 - b_{i(jj)})\, c_{i(jj)} \sum g_{i(j)} \qquad (2.6.\mathrm{t})\mathrm{T}$$

$$g_{i(jj')} = b_{i(jj')}\, g_{i(jj')} + (1 - b_{i(jj')})\, g_{i(jj')} = c_{i(jj')} \sum g_{i(j)} \qquad (2.6.\mathrm{u})\mathrm{T}$$

$$\begin{aligned} \sum p_{i,i'(j)} &= \sum p_{i(j)} + \sum p_{i'(j)} \\ &= \sum (1 - a_{i(j)})(f_{i(0j)} + \sum b_{i(j'j)}\, g_{i(j'j)}) + \sum c_{i'(j)} \sum g_{i(j)} \\ &= \sum g_{i(j)} - \sum g_{i(jj)} - \sum g_{i(j0)} - \sum b_{i(jj')}\, g_{i(jj')} \\ &\quad - \sum (1 - b_{i(jj')})\, g_{i(jj')} \end{aligned} \qquad (2.6.\mathrm{v})\mathrm{T}$$

In eq. (2.6.1)T the variable $\sum g_{i(j)}$ is also expressed as a sum of i components flow rates feeding j stage and in eq. (2.6.v)T the variable $\sum p_{i,i'(j)}$ as the diference between the variable $\sum g_{i(j)}$ and the sum of the other i components flow rates resulting from j stage.

When constant ratios of i component amounts to the sum of i component amounts feeding j stage are imposed, the following relationship can be written

$$h_{i(j)} \sum g_{i(j)} = f_{i(0j)} + \sum b_{i(j'j)}\, g_{i(j'j)} + g_{i(jj)} \qquad (2.6.\mathrm{z})\mathrm{T}$$

where $h_{i(j)}$ is the ratio of i component amount to the sum of i components amounts feeding j stage.

Equations (2.6.1)T — (2.6.z)T represent the material balance model of a transformation stage fed with a mixture of i components.

Expressing the variable $\sum g_{i(j)}$ by the sum of each i component amounts feeding j stage and substituting this expression into eqs. (2.6.1)T — (2.6.z)T, we get the following equivalent model

$$\sum g_{i(j)} = g_{1(j)} + g_{2(j)} + g_{3(j)} + \cdots + g_{n(j)} \qquad (2.7.1)\mathrm{T}$$

$$g_{i(j)} = f^{i}{}_{(0j)} + \sum b_{i(j'j)}\, g_{i(j'j)} + g_{i(jj)} \qquad (2.7.\mathrm{s})\mathrm{T}$$

$$g_{i(jj)} = b_{i(jj)}\, c_{i(jj)} \sum g_{i(j)} - (1 - a_{i(j)})(f_{i(0j)} + \sum b_{i(j'j)}\, g_{i(j'j)}) \qquad (2.7.\mathrm{t})\mathrm{T}$$

$$g_{i(j0)} = (1 - b_{i(jj)})\, c_{i(jj)} \sum g_{i(j)} \tag{2.7.u)T}$$

$$g_{i(jj')} = b_{i(jj')}\, g_{i(jj')} + (1 - b_{i(jj')})\, g_{i(jj')} = c_{i(jj')} \sum g_{i(j)} \tag{2.7.v)T}$$

$$\begin{aligned} \sum p_{i,i'(j)} &= \sum (1 - a_{i(j)}) (f_{i(0j)} + \sum b_{i(j'j)}\, g_{i(j'j)}) + \sum c_{i'(j)} \sum g_{i(j)} \\ &= \sum g_{i(j)} - \sum g_{i(jj)} - \sum g_{i(j0)} - \sum b_{i(jj')}\, g_{i(jj')} \\ &\quad - \sum (1 - b_{i(jj')})\, g_{i(jj')} \end{aligned} \tag{2.7.z)T}$$

$$h_{i(j)} \sum g_{i(j)} = g_{i(j)} \tag{2.7.w)T}$$

Equations (2.7.1)T–(2.7.w)T represent the material balance model corresponding to the division of the transformation stage into "substages" specific to each component feeding it.

The system of eqs. (2.7.1)T–(2.7.w)T can be applied to the material balance simulation of chemical flowsheets composed of transformation stages as previously described.[3]

In order to establish the corresponding material balance model for a separation stage, we suggest to consider the j stage as being divided into substages specific to each component and the substage as a particular case of the transformation stage fed with a single component, where $i' = i$ and $a_{i(j)} = 1$.

Proceeding in this manner, the equations describing j stage material balance are

$$\sum g_{i(j)} = g_{1(j)} + g_{2(j)} + g_{3(j)} + \dots + g_{n(j)} \tag{3.1.1)S}$$

$$g_{i(j)} = f_{i(0j)} + \sum b_{i(j'j)}\, g_{i(j'j)} + g_{i(jj)} \tag{3.1.s)S}$$

$$g_{i(jj)} = b_{i(jj)}\, c^{+}_{i(jj)}\, g_{i(j)} \tag{3.1.t)S}$$

$$g_{i(j0)} = (1 - b_{i(jj)})\, c^{+}_{i(jj)}\, g_{i(j)} \tag{3.1.u)S}$$

$$g_{i(jj')} = b_{i(jj')}\, g_{i(jj')} + (1 - b_{i(jj')})\, g_{i(jj')} = c^{+}_{i(jj')}\, g_{i(j)} \tag{3.1.v)S}$$

$$p_{i(j)} = c^{+}_{i(j)}\, g_{i(j)} \tag{3.1.z)S}$$

When j stage is fed also with fresh raw materials, the following equations can be written

$$f_{i(0j)} = h^{+}_{i(j)}\, g_{i(j)} \tag{3.1.w)S}$$

where $h^{+}_{i(j)}$ is the ratio of i component amount constituting fresh raw material to the sum of i component amounts feeding j stage.

---

[3] L. BADEA, *Rev. Chim.* (*Bucureşti*), **25**, 491 (1974).

The flow rate of i component resulting from j stage can also be defined as a product of the respective concentration and mixture flow rate and as a difference between the variable $g_{i(j)}$ and the sum of i components flow rates resulting from j stage.

Expressing in this manner the variables $g_{i(jj)}$, $g_{i(j0)}$, $g_{i(jj')}$ and $p_{i(j)}$ into eqs. (3.1.1)T – (3.1.w)T, it follows

$$\sum g_{i(j)} = g_{1(j)} + g_{2(j)} + g_{3(j)} + \ldots + g_{n(j)} \tag*{(3.2.1)S}$$

$$g_{i(j)} = f_{i(0j)} + \sum b_{i(j'j)}\, g_{i(j'j)} + g_{i(jj)} \tag*{(3.2.s)S}$$

$$g_{i(jj)} = b_{i(jj)}\, c^{+}_{i(jj)}\, g_{i(j)} \tag*{(3.2.t.1)S}$$

$$= c'_{i(jj)} \sum g_{i(jj)} \tag*{(3.2.t.2)S}$$

$$= g_{i(j)} - \sum b_{i(jj')}\, g_{i(jj')} - \sum (1 - b_{i(jj')})\, g_{i(jj')}$$

$$- g_{i(j0)} - p_{i(j)} \tag*{(3.2.t.3)S}$$

$$g_{i(j0)} = (1 - b_{i(jj)})\, c^{+}_{i(jj)}\, g_{j(j)} \tag*{(3.2.u.1)S}$$

$$= c'_{i(jj)} \sum g_{i(j0)} \tag*{(3.2.u.2)S}$$

$$= g_{i(j)} - \sum b_{i(jj')}\, g_{i(jj')} - \sum (1 - b_{i(jj')})\, g_{i(jj')}$$

$$- g_{i(jj)} - p_{i(j)} \tag*{(3.2.u.3)S}$$

$$g_{i(jj')} = b_{i(jj')}\, g_{i(jj')} + (1 - b_{i(jj')})\, g_{i(jj')} = c^{+}_{i(jj')}\, g_{i(j)} \tag*{(3.2.v.1)S}$$

$$= c'_{i(jj')} \sum g_{i(jj')} \tag*{(3.2.v.2)S}$$

$$= g_{i(j)} - \sum b_{i(jj'')}\, g_{i(jj'')} - \sum (1 - b_{i(jj'')})\, g_{i(jj'')}$$

$$- g_{i(jj)} - g_{i(j0)} - p_{i(j)} \tag*{(3.2.v.3)S}$$

$$p_{i(j)} = c^{+}_{i(j)}\, g_{i(j)} \tag*{(3.2.z.1)S}$$

$$= c'_{i(j)} \sum p_{i(j)} \tag*{(3.2.z.2)S}$$

$$= g_{i(j)} - \sum b_{i(jj')}\, g_{i(jj')} - \sum (1 - b_{i(jj')})\, g_{i(jj')}$$

$$- g_{i(jj)} - g_{i(j0)} \tag*{(3.2.z.3)S}$$

$$f_{i(0j)} = h^{+}_{i(j)}\, g_{i(j)} \tag*{(3.2.w)S}$$

$$\sum g_{i(jj)} = \sum b_{i(jj)}\, c^{+}_{i(jj)}\, g_{i(j)} \tag*{(3.2.w+t.2)S}$$

$$\sum g_{i(j0)} = \sum (1 - b_{i(jj)})\, c^{+}_{i(jj)}\, g_{i(j)} \qquad (3.2.\mathrm{w}+\mathrm{u}.2)\mathrm{S}$$

$$\sum g_{i(jj')} = \sum c^{+}_{i(jj')}\, g_{i(j)} \qquad (3.2.\mathrm{w}+\mathrm{v}.2)\mathrm{S}$$

$$\sum p_{i(j)} = \sum c^{+}_{i(j)}\, g_{i(j)} \qquad (3.2.\mathrm{w}+\mathrm{z}.2)\mathrm{S}$$

where $c'_{i(jj)}, c'_{i(jj')}, c'_{i(jj'')}$ and $c'_{i(j)}$ are *i* component concentrations in the respective mixtures $\sum g_{i(jj)}$, $\sum g_{i(jj')}$, $\sum {}_{i(jj'')}$ and $\sum p_{i(j)}$;
j'' – any stage.

The equations (3.2.1)S – (3.2.w+ z.2)S are describing the material balance model for a separation stage.

The choice of one of equations (3.2.t.1)S, (3.2.t.2)S, (3.2.t.3)S for the variable $g_{i(jj)}$, (3.2.u.1)S, (3.2.u.2)S, (3.2.u.3)S, for the variable $g_{i(j0)}$, (3.2.v.1)S, (3.2.v.2)S, (3.2.v.3)S, for the variable $g_{i(jj')}$ and (3.2.z.1)S, (3.2.z.2)S, (3.2.z.3)S, for the variable $p_{i(j)}$ depends on the imposed purpose.

When only *i* component distribution restrictions are imposed (respectively the constants $c^{+}_{i(jj)}, c^{+}_{i(jj')}$ and $c^{+}_{i(j)}$ are known) eqs. (3.2.t.1)S, (3.2.u.1)S, (3.2.v.1)S and (3.2.z.1)S are used for $n_j - 1$ component mixtures resulting from *j* stage (n_j being the total number of component mixtures resulting from *j* stage) and one of the eqs. (3.2.t.3)S, (3.2.u.3)S, (3.2.v.3)S, (3.2.z.3)S for the remaining component mixture.

When constant composition restrictions of some component mixtures are imposed (respectively constants $c'_{i(jj)}, c'_{i(jj')}$ and $c'_{i(j)}$ are known) eqs. (3.2.t.2)S, (3.2.u.2)S, (3.2.v.2)S, (3.2.z.2)S are used for $n_j - 1$ component mixtures and one of the eqs. (3.2.t.3)S, (3.2.u.3)S, (3.2.v.3)S, (3.2.z.3)S for the remaining component mixture.

In this last case, the respective eqs. (3.2.w+t.2)S, (3.2.w+ u.2)S, (3.2.w + v.2)S and (3.2.w + z.2)S are necessary, too.

Because in the separation stage no transformation of components occurs for each *i* component the following equation must be verified :

$$g_{i(j)} = g_{i(jj)} + g_{i(j0)} + \sum b_{i(jj')}\, g_{i(jj')} + \sum (1 - b_{i(jj')})\, g_{i(jj')} + p_{i(j)} \qquad (3.3)\mathrm{S}$$

This verification is necessary in the cases where the stage initially considered as a separation stage represents a multitude of phases and operations of the process.

Based on the previous consideration whereby a chemical flowsheet is composed of a number *m* of stages which can be transformation or separation ones, we get the material balance mathematical model of the flowsheet summarising the respective (2.7.1)T –(2.7.w)T and (3.2.1)S–(3.2.w + z.2)S equations.

This model can also be used for the flowsheet material balance optimization as previously described.[4,5]

By testing the presented model on various chemical flowsheets, the calculated results (on corresponding computers) fitted well with the experimental data, even in the case of a great number of equations.

---

[4] L. Badea, *Rev. Chim.(Bucureşti)*, **25**, 207 (1974).

[5] L. Badea and I. Belcea, *Rev. Chim. (Bucureşti)*, **25**, 291 (1974).

$$\sum g_{ik} = \sum (1 - \xi_{ikl})\, c_{ikl}\, g_{il}$$

$$\sum g_{il} = \sum c'_{ikl}\, g_{il}$$

$$\sum p_{ik} = \sum c''_{ikl}\, g_{il}$$

where c_{ikl}, c'_{ikl} and c''_{ikl} are i component concentrations in the respective mixtures $\sum g_{ik}$, $\sum g_{il}$ [illegible] and $\sum p_{ik}$ [illegible] j [illegible] any stage.

The equations (3.2 [illegible]) – (3.2.w + [illegible]) are describing the material balance model for a separation stage.

The choice of one of equations [illegible], for the variable g_{ik}, [illegible], for the variable g_{il}, [illegible] for the variable w_{il} and [illegible], for the variable p_{ik} depends on the imposed purpose.

When only 1 component distribution restrictions are imposed (respectively the constants c_{ikl}, c'_{ikl} and c''_{ikl} are known) eqs. [illegible] are used for $n_j - 1$ component mixtures resulting from j stage (n_j being the total number of component mixtures resulting from j stage) and one of the eqs. [illegible] for the remaining component mixture.

When constant composition restrictions of some component mixtures are imposed (respectively constants [illegible] are known) eqs. [illegible] are used for $n - 1$ component mixtures and one of the eqs. [illegible] for the remaining component mixture.

In this last case, the respective eqs. [illegible] are necessary, too.

Because in the separation stage no transformation of components occurs for each i component the following equation must be verified:

$$g_{ik} = g_{ikl} + [illegible] + \sum w_{il}\, g_{il} + \sum (1 - \xi_{ikl})\, g_{ikl} + p_{ik}$$

This verification is necessary in the cases where the stage initially considered as a separation stage represents a multitude of phases and operations of the process.

Based on the previous consideration whereby a chemical flowsheet is composed of a number of stages which can be transformation or separation ones, we [illegible] the material balance mathematical model of the flowsheet summarising the respective [illegible] and [illegible] equations.

This model can also be used for the flowsheet material balance optimization as previously described.*

By testing the presented model on various chemical flowsheets, the calculated results (on corresponding computers) fitted well with the experimental data, even in the case of a great number of equations.

---

* L. Bozga, Rev. Chim. (Bucharest) 25, [illegible] (1974).
L. Bozga and I. Dinescu, Rev. Chim. (Bucharest) 25, [illegible] (1974).

Revue Roumaine de Chimie, 20, 7, 1013–1026 (1975)

SURFACE TENSION OF FUSED TERNARY MIXTURES: $NaCl + KCl + AgCl$ AND $NaCl + RbCl + AgCl$

S. STERNBERG and MARIANA TERZI

Institute of Physical Chemistry, str. Galaţi 31, Bucharest, Romania

Received June 1, 1974

The method of detachment of platinum pin has been used in surface tension measurements on fused ternary $NaCl + KCl + AgCl$ and $NaCl + RbCl + AgCl$ mixtures. The temperature and composition dependence of surface tension has been studied in both mixtures. Surfaces tension isotherms in several sections of ternary mixtures show negative deviations from ideality. The composition of ternary mixtures in surface layer has been determined; it is different from that of the bulk of liquid. Eberhart's equation was extended to ternary mixtures and the partial enrichment coefficients have been calculated. The possibility of evaluating surface tension of ternary mixtures from those of binary ones has been discussed. The experimental surface tension values in ternary mixtures have been compared to those calculated by modified Guggenheim equations.

Previous papers[1,2] have presented results of surface tension measurement in binary (Na, K, Rb, Cs)Cl + AgCl systems. The deviations from linearity of surface tension (δ) isotherms increase in the order $Na < K < Rb < Cs$. In the present work we have extended the study to cover ternary fused salt mixtures which contain $NaCl + KCl + AgCl$ and $NaCl + RbCl + AgCl$; such data are scarce in scientific literature.[3-5]

EXPERIMENTAL

Measurements have been carried out by detaching a pin from liquid surface.[6] The platinum pin has been calibrated at room temperature and a constant of 2.492 sec^{-2} came out. Details on equipment and procedure are given elsewhere.[1,2]

NaCl and KCl (reagent grade) and RbCl (Merck analytical grade) have been dried and then melted in dry gaseous HCl stream. AgCl was prepared from $AgNO_3$ (reagent grade) and HCl; it was premelted.

---

[1] S. Sternberg and M. Terzi, *Rev. Roumaine Chim.*, **15**, 527 (1970).

[2] S. S. Sternberg and M. Terzi, *J. Chem. Thermodynamics*, **3**, 259 (1971).

[3] G. W. Mellors and S. Semderoff, *J. Electrochem. Soc.*, **111**, 1355 (1964).

[4] J. N. Reding, *J. Chem. and Eng. Data*, 11, 239 (1966).

[5] K. Grjotheim, J. L. Holm, B. Lillebuen and H. A Øye, *Acta Chem. Scand.*, **26**, 2050 (1972).

[6] G. I. Janz and M. R. Lorenz, *Rev. Sci. Instr.*, **31**, 18 (1960).

RESULTS AND DISCUSSION

Measurements were carried out at different temperatures and compositions. Surface tension of ternary mixtures decreases with increasing temperature according to a linear equation, $\delta = a - bt$, with t the temperature in Celsius degrees. In tables 1 and 2 a and b values are listed as obtained by the least square method, together with temperature range and surface tension at 700°, for the two ternary mixtures : $NaCl + KCl + AgCl$ and $NaCl + RbCl + AgCl$.

Table 1

The change of surface tension with temperature for the ternary NaCl + KCl + AgCl mixture

$x(NaCl)$ x_1	$x(KCl)$ x_2	$x(AgCl)$ x_3	$\delta^{700°}_{exp}$ dyne cm^{-1}	a dyne cm^{-1}	$-b.10^2$ dyne cm^{-1} degree^{-1}	Range of temperature °C
$x_1' = 0.5$						
0.10	0.10	0.80	135.5	183.67	6.88	481 – 681
0.15	0.15	0.70	127.9	171.35	6.20	531 – 791
0.25	0.25	0.50	118.7	161.94	6.18	629 – 803
0.35	0.35	0.30	111.7	160.35	6.95	615 – 820
0.40	0.40	0.20	109.6	157.53	6.85	705 – 863
0.50	0.50	–	107.4	157.43	7.15	686 – 900
$x_1' = 0.7$						
0.28	0.12	0.60	126.2	172.42	6.60	605 – 821
0.42	0.18	0.40	118.0	163.19	6.46	662 – 845
0.56	0.24	0.20	114.2	164.77	7.22	721 – 915
0.70	0.30	–	110.8	162.42	7.38	731 – 920
$x_1' = 0.8$						
0.32	0.08	0.60	128.2	177.08	6.99	641 – 813
0.48	0.12	0.40	120.6	171.52	7.28	671 – 893
0.64	0.16	0.20	116.5	169.13	7.54	768 – 897
0.80	0.20	–	112.9	162.26	7.05	769 – 956

Table 2

The temperature variation of surface tension for the ternary NaCl + RbCl + AgCl mixture

$x(NaCl)$ x_1	$x(RbCl)$ x_2	$x(AgCl)$ x_3	$\delta^{700°}_{exp}$ dyne cm^{-1}	a dyne cm^{-1}	$-b.10^2$ dyne cm^{-1} degree^{-1}	Range of temperature °C
$x_1' = 0.5$						
0.1	0.1	0.8	130.4	179.21	6.97	589 – 802
0.2	0.2	0.6	116.9	165.47	6.94	650 – 853
0.3	0.3	0.4	108.8	155.43	6.66	649 – 875
0.4	0.4	0.2	104.3	153.33	7.00	673 – 921
0.5	0.5	–	100.3	146.38	6.58	683 – 913

The composition of ternary mixture was expressed by mole fractions (their ordinary meaning):

$$x_1 + x_2 + x_3 = 1 \tag{1}$$

To characterize the ratio of the two components the following relations have been introduced :

$$x'_1 = \frac{n_1}{n_1 + n_2} \qquad \text{and} \quad x'_2 = \frac{n_2}{n_1 + n_2} \tag{2}$$

For $x_3 = 0$, $x_1 = x'_1$ and $x_2 = x'_2$ evidently $x'_1/x'_2 = x_1/x_2$. The measurements were carried out for 3 sections of ternary NaCl + KCl + AgCl mixture, that is x'_1=0.8, 0.7 and 0.5 and just one section of the NaCl+RbCl + AgCl mixture, x'_1 = 0,5.

The variation with composition of surface tension of ternary mixtures at 700° is plotted as δ istoherms, in Fig. 1 for 3 sections of NaCl + KCl + + AgCl mixture and in Fig. 2 for one section of NaCl + RbCl + AgCl mixture.

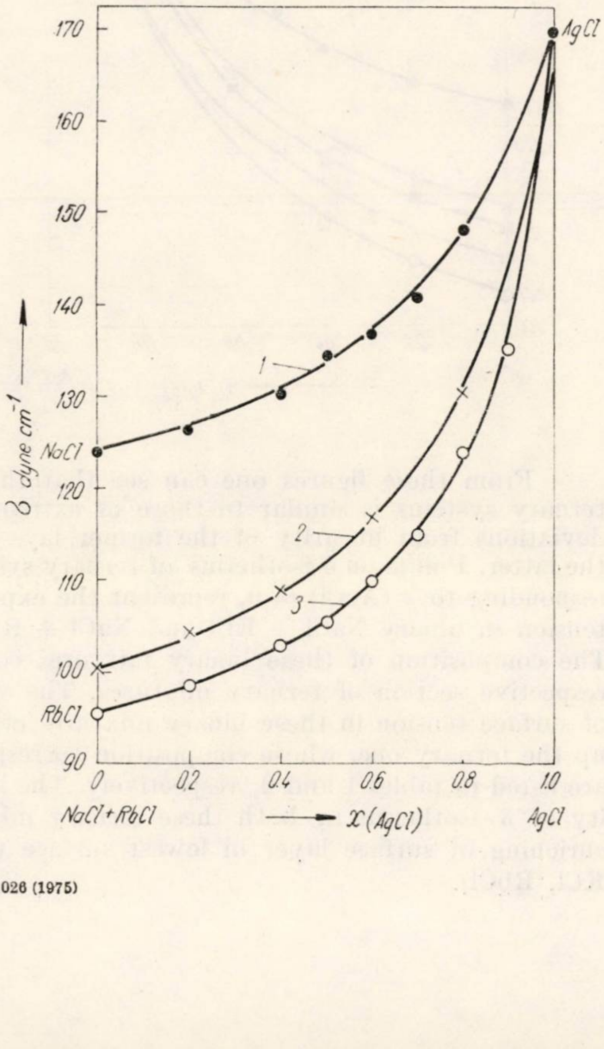

Fig. 1. — Surface tension insotherms in NaCl+AgCl, NaCl+ +KCl + AgCl and KCl+AgCl mixtures at 700°.

1, δ isotherm for NaCl + AgCl ; *2*, δ isotherm for x'_1 = 0.8 section of the ternary mixture ; *3*, δ isotherm for x'_1 = = 0.7 section of the ternary mixture ; *4*, δ isotherm for x'_1 = 0 .5 section of the ternary mixture ; 5, δ isotherm for KCl+AgCl, Curves calculated as explained herein ; points are experimental values of δ.

In both figures, data are plotted against x_3, mole fraction of AgCl, the points representing experimental data. Large negative deviations from linearity are visible for both systems. In the same figures isotherms of δ at 700° are shown, for comparison, for binary NaCl + AgCl, KCl + AgCl mixtures[1] (Fig. 1) and NaCl + AgCl, RbCl + AgCl mixtures (Fig. 2).

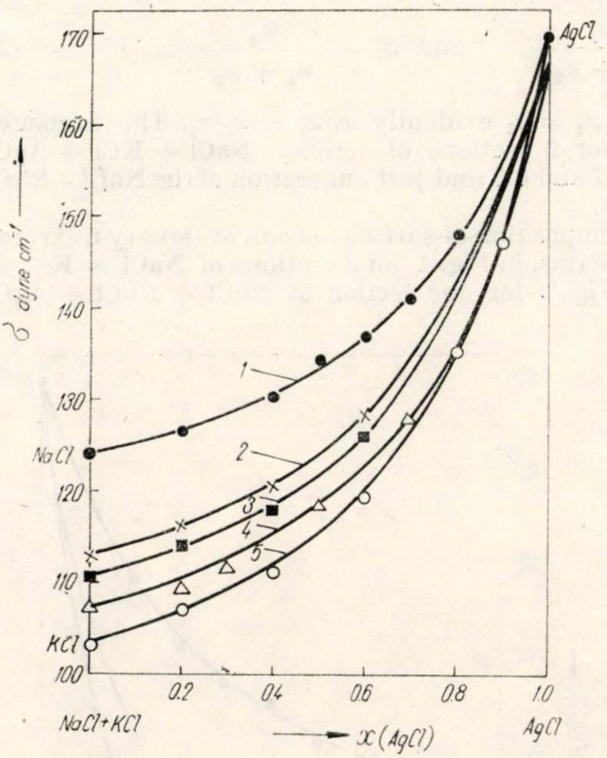

Fig. 2. — Surface tension isotherms in NaCl + AgCl, NaCl + + RbCl + AgCl and RbCl + + AgCl mixtures at 700°.

1, δ isotherm for NaCl + AgCl; *2*, δ isotherm for $x'_1 = 0.5$ section of the ternary mixture; *3*, δ isotherm for RbCl + AgCl.

From these figures one can see that the shape of δ isotherms of ternary systems is similar to those of extreme binary systems and the deviations from linearity of the former lays between the deviations of the latter. Points on δ isotherms of ternary systems (figures 1 and 2) corresponding to x (AgCl) = 0, represent the experimental values of surface tension in binary NaCl + KCl and NaCl + RbCl mixtures, respectively. The composition of these binary mixtures corresponds to x_1/x_2 of the respective section of ternary mixtures. The variation with temperature of surface tension in these binary mixtures of alkali halides which make up the ternary one, whose composition corresponds to the given section, are listed in tables 1 and 2, respectively. The large deviations from linearity of δ isotherms in both these ternary mixtures are ascribed to the enriching of surface layer in lowest surface tension components (NaCl, KCl, RbCl).

In figures 1 and 2, together with experimental points, are plotted (by solid lines) the δ isotherms calculated by Eberhart's[7] equation:

$$\delta + x_1^\delta \delta_1 + x_2^\delta \delta_2 = (sx_1\delta_1 + x_2\delta_2)/(sx_1 + x_2) \tag{3}$$

where x_1, x_2 stand for mole fractions in bulk liquid, x_1^δ, x_2^δ for the mole fractions in surface layer and s for the enrichment coefficient of surface layer in the lowest component. For binary mixtures:

$$s = \frac{x_2^\delta}{x_1^\delta} \cdot \frac{x_1}{x_2} \tag{4}$$

One finds out that for the ternary mixtures under study, which are assimilated with quasibinary ones, one may use the modified Eberhart equation, i.e.:

$$\delta = \frac{s^{12\ 3}(x_1 + x_2)\ \delta_{12} + x_3\delta_3}{s^{12\ 3}(x_1 + x_2) + x_3} \tag{5}$$

where δ_{12} is surface tension of binary mixture, made up of the two components of lower surface tension, of composition x_1'; $s^{12\ 3}$ is the enrichment coefficient of the surface layer with those compounds whose δ is smaller. This latter parameter is defined as:

$$s^{12\ 3} = \frac{(x_1^\delta + x_2^\delta)}{x_3^\delta} \cdot \frac{x_3}{(x_1 + x_2)} \tag{6}$$

In binary mixtures: NaCl + AgCl, KCl + AgCl, RbCl + AgCl, curves *1*, *5* in Fig. 1 and *1*, *3* in Fig. 2 have been calculated by eq (3) while for various sections of ternary mixtures, curves *2*, *3* and *4* of Fig. 1 and curve *2* of Fig. 2 have been plotted according to eq (5). A good agreement between experimental and calculated values is found out. The values of $s^{12\ 3}$ of ternary mixtures calculated according to Eberhart are given in table 3. In figure 3 the variation of quasibinary enrichment coefficient is plotted *vs* relative mole fraction of lowest δ (KCl, RbCl), x_2' for both

Table 3

The enrichment coefficient for the ternary mixtures at 700°

	NaCl + KCl + AgCl					NaCl + RbCl + AgCl		
x_2'	0	0.2	0.3	0.5	1.0	0	0.5	1.0
s	3.508	3.891	4.115	4.415	4.34	3.508	4.716	6.192

---

[7] J. G. Eberhart, *J. Phys. Chem.*, **70**, 1183 (1966).

ternary systems. Positive deviations from linearity are found in NaCl + + KCl + AgCl system such that at $x'(\mathrm{KCl}) = 0.5$, $s^{12\,3}$ become practically equal to that of binary mixture. This behaviour is ascribed to the tendency of the lowest δ component (KCl) to agglomerate on the surface. In the case of NaCl + RbCl + AgCl mixture the enrichment coefficient for $x'_1 = 0.5$ section is not higher than in the binary system (RbCl + AgCl),

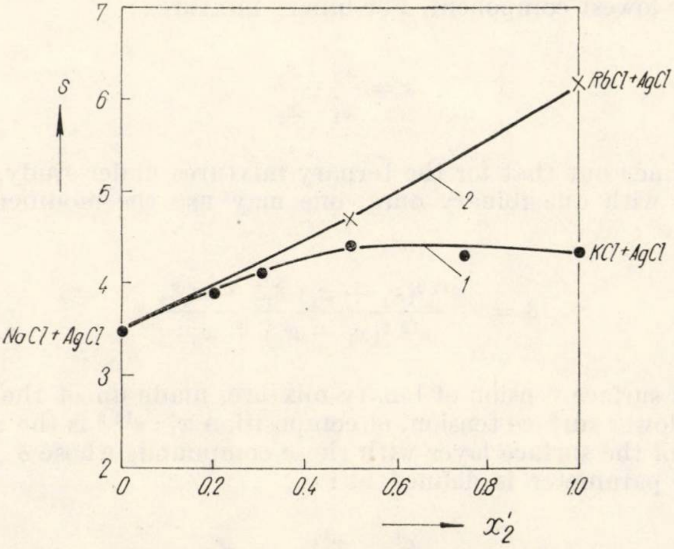

Fig. 3. – The change of enrichment coefficient with composition for NaCl + KCl + AgCl and NaCl + RbCl + AgCl ternary mixtures at 700°.
1, NaCl + KCl + AgCl; *2*, NaCl + RbCl + AgCl.

An attempt is made below to extend Eberhart equation to ternary mixtures. If one knows the values of the enrichment coefficient of ternary system $s^{12\,3}$ (defined by eq (6)) and one considers the equations :

$$x_1^\delta + x_2^\delta + x_3^\delta = 1 \tag{7}$$

$$x_1^\delta \delta_1 + x_2^\delta \delta_2 + x_3^\delta \delta_3 = \delta \tag{8}$$

mole fractions of the three components within the surface layer of liquid were calculated ; they are listed in table 4 for NaCl + KCl + AgCl mixture and in table 5 for NaCl + RbCl + AgCl mixture.

For a ternary mixture the partial enrichment coefficients were defined as :

$$s^{12} = \frac{x_2^\delta}{x_1^\delta} \cdot \frac{x_1}{x_2}; \quad s^{13} = \frac{x_1^\delta}{x_3^\delta} \cdot \frac{x_3}{x_1}; \quad s^{23} = \frac{x_2^\delta}{x_3^\delta} \cdot \frac{x_3}{x_2} \tag{9}$$

Table 4

The surface layer composition of the NaCl + KCl + AgCl mixture at 700°

x_1	x_2	x_3	x_1^δ	x_2^δ	x_3^δ	s^{12}	s^{13}	s^{23}	$\delta^{\mathrm{calcd.}}_{\mathrm{dyne\ cm^{-1}}}$	$\delta^{\mathrm{exp}}_{\mathrm{dyne\ cm^{-1}}}$
0.10	0.10	0.80	0.0934	0.4313	0.4753	4.617	1.572	7.259	135.5	135.5
0.15	0.15	0.70	0.1249	0.5293	0.3458	4.237	1.684	7.142	127.7	127.9
0.25	0.25	0.50	0.1765	0.6388	0.1847	3.619	1.911	6.917	118.1	118.7
0.35	0.35	0.30	0.1341	0.7774	0.0885	5.797	1.298	7.528	112.3	111.7
0.40	0.40	0.20	0.1455	0.8009	0.0536	5.504	1.359	7.421	110.1	109.6
$x_1' = 0.5$			average value			4.75	1.56	7.26		
0.28	0.12	0.60	0.2858	0.4471	0.2671	3.64	2.29	8.37	125.9	126.2
0.42	0.18	0.40	0.2826	0.5780	0.1394	4.76	1.93	9.21	118.5	118.0
0.56	0.24	0.20	0.3520	0.5907	0.0573	3.91	2.19	8.58	113.9	114.2
$x_1' = 0.7$			average value			4.10	2.13	8.72		
0.32	0.08	0.60	0.3485	0.3733	0.2782	4.28	2.35	10.06	128.1	128.2
0.48	0.12	0.40	0.3874	0.4663	0.1463	4.81	2.20	10.55	120.8	120.6
0.64	0.16	0.20	0.4444	0.4952	0.0604	4.45	2.29	10.24	116.1	116.3
$x_1' = 0.8$			average value			4.51	2.28	10.28		

Table 5

The surface layer composition of the NaCl + KCl + AgCl mixture at 700°

x_1	x_2	x_3	x_1^δ	x_2^δ	x_3^δ	s^{12}	s^{13}	s^{23}	$\delta^{\mathrm{calcd.}}_{\mathrm{dyne/cm}}$	$\delta^{\mathrm{exp}}_{\mathrm{dyne/cm}}$
0.1	0.1	0.8	0.0752	0.4659	0.4589	6.195	1.310	8.122	130.8	130.4
0.2	0.2	0.6	0.1482	0.6105	0.2413	4.119	1.842	7.590	118.1	116.9
0.3	0.3	0.4	0.1592	0.7170	0.1238	4.504	1.714	7.722	108.5	108.8
0.4	0.4	0.2	0.1860	0.7637	0.0503	4.106	1.826	7.591	103.7	104.3
$x_1' = 0.5$				average value		4.73	1.67	7.75		

Their values are also given in tables 4 and 5 for the two ternary mixtures.

One can see, in the first place, that these coefficients are constant over the whole concentration range encompassed by a section of ternary mixture. The average value of partial enrichment coefficient s^{12}, corresponding to the two salts, NaCl + KCl, in ternary (Na+K+Ag)Cl mixture changes slightly with the increase of the relative mole fraction of the first component ($x'_1 = 0.5$; 0.7 ; 0.8), unlike the other two coefficients s^{13} and s^{23} which increase with the same relative mole fraction ; s^{13} increases from 1.56 to 2.28 while s^{23} from 7.26 to 10.28 when x'_1 increases from 0.5 to 0.8.

Secondly, one can observe a change of partial enrichment in both ternary mixtures against enrichment coefficients of corresponding binary systems. Thus s^{12} takes an average 4.50 value, higher than the 2.31 corresponding to NaCl+KCl system, the average s^{13} being lower than 3.508 of NaCl + AgCl system and s^{23} increases in the ternary system up to a value of 10.28 against the 4.34 of KCl + AgCl system. Both KCl(RbCl) and NaCl have a share in surface layer enrichment as they both are surface active components. Yet, KCl having the lowest δ takes the largest share in enrichment as is seen from the vaule of partial enrichment coefficient s^{23} which increases in ternary against binary system. This is done on the account of NaCl whose partial enrichment coefficient is decreased and of AgCl, the highest surface tension component.

The knowledge of average partial enrichment coefficients in a ternary mixture allows calculation of its surface tension for any composition within a given section. Average s^{12}, s^{13}, s^{23} are used to recalculate the surface mole fractions which are then introduced in eq (8). The surface tensions thus calculated are compared to the experimental ones in NaCl + + KCl + AgCl (table 4) and in NaCl + RbCl + AgCl (table 5). An excellent agreement is found out.

Interesting results, mainly from practical viewpoint, are obtained if one considers the surface tension isotherms of ternary system as represented *vs* relative mole fraction, x'_1 (Fig. 4). Each isotherm corresponds to a constant AgCl composition (x_3). Experimental points on ordinate at $x'_1 = 0$ correspond to surface tensions of KCl + AgCl mixture, at several AgCl mole fractions, while those on ordinate at $x'_1 = 1$ to NaCl + AgCl mixture.

The system was assimilated with a quasibinary one and Eberhart's equations have been applied in determining the enrichment coefficient ; similar values have been obtained for the 4 isotherms. These values of enrichment coefficient (s') together with the average value are listed in table 6.

In the calculation of surface tension of ternary system use has been made of the equation :

$$\delta = \frac{\delta_{23}\, s'\, x'_2 + \delta_{13}\, x'_1}{s' x'_2 + x'_1} \tag{10}$$

where δ_{23} stands for surface tension of binary KCl + AgCl mixture at constant AgCl mole fraction, δ_{13} for NaCl + AgCl system at the same

AgCl mole fraction. Surface tension values, calculated according to eq (10), with $s' = 4.078$, are given in table 7 and compared with experimental values at 700°. The good agreement is evident.

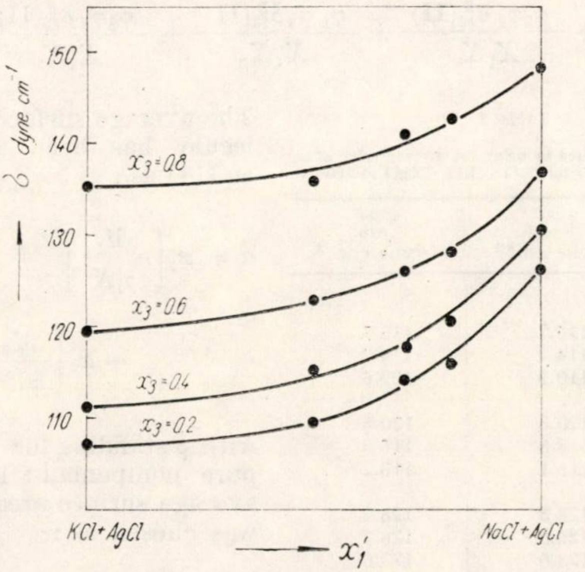

Fig. 4. — Surface tension isotherms of NaCl + KCl + AgCl ternary mixture plotted *vs* relative mole fraction of NaCl, x_1' at 700°.

Table 6

Partial enrichment coefficient, s', for NaCl + KCl + AgCl system at 700° *vs*, mole fraction of AgCl

x(AgCl)	0.2	0.4	0.6	0.8	
s'	4.176	3.704	3.968	4.464 average value	4.078

The practical interest of this finding lays in that it allows calculation of surface tension in a ternary system starting up with those of binary ones and that of a $x_3 =$ ct. section (x_3 refers to the highest surface tension component), of the ternary system under consideration.

Further, the surface tension of the two ternary mixtures has been calculated from component binary systems according to the following semiempirical equations given by Grjotheim and collab. :[5]

$$\delta_{(\mathrm{I})} = -\frac{kT}{a}\ln\left[x_1 e^{-\frac{\delta_1 a}{kT}} + x_2 e^{-\frac{\delta_2 a}{kT}} + x_3 e^{-\frac{\delta_3 a}{kT}}\right] + \frac{x_1 x_2 \delta_{12}^{E}(\mathrm{I})}{X_1 X_2} + \frac{x_1 x_3 \delta_{13}^{E}(\mathrm{I})}{X_1 X_3} + \frac{x_2 x_3 \delta_{23}^{E}(\mathrm{I})}{X_2 X_3} \qquad (11)$$

$$\delta_{(II)} = -\frac{kT}{A}\ln\left[\varphi_1 e^{-\frac{\delta_1 A}{kT}} + \varphi_2 e^{-\frac{\delta_2 A}{kT}} + \varphi_3 e^{-\frac{\delta_3 A}{kT}}\right] +$$

$$+ \frac{\varphi_1\varphi_2\,\delta_{12}^E(\mathrm{II})}{X_1X_2} + \frac{\varphi_1\,\varphi_3\,\delta_{13}^E(\mathrm{II})}{X_1X_3} + \frac{\varphi_2\varphi_3\,\delta_{23}^E(\mathrm{II})}{X_2X_3} \qquad (12)$$

Table 7

Comparison of δ calculated by using the average value of s′ with experimental δ's for NaCl + KCl + AgCl at 700°

x_1'	$\delta^{700°}_{\text{calcd.}}$ dyne cm^{-1}	$\delta^{700°}_{\text{exp}}$ dyne cm^{-1}
$x_3 = 0.2$		
0.8	116.7	116.3
0.7	114.2	114.2
0.5	110.9	109.6
$x_3 = 0.4$		
0.8	120.8	120.8
0.7	118.3	118.0
0.5	115.1	115.2
$x_3 = 0.6$		
0.8	128.3	128.2
0.7	126.0	126.2
0.5	123.0	123.0
$x_3 = 0.8$		
0.8	141.7	142.7
0.7	140.0	140.0
0.5	137.8	138.0

The average surface area per molecule has been considered in eq.(11) as:

$$a = x_1\left[\frac{M_1}{\rho_1 N}\right]^{2/3} + x_2\left[\frac{M_2}{\rho_2 N}\right]^{2/3} + x_3\left[\frac{M_3}{\rho_3 N}\right]^{2/3} \qquad (13)$$

with ρ standing for the density of pure component; in eq (12) the average surface area per molecule was chosen as:

$$A = \left[\frac{\varphi_1 V_1 + \varphi_2 V_2 + \varphi_3 V_3}{N}\right]^{2/3} \qquad (14)$$

in which V is the molar volume and φ the volume fraction:

$$\varphi_1 = \frac{x_1V_1}{x_1V_1 + x_2V_2 + x_3V_3}; \quad \varphi_2 = \frac{x_2V_2}{x_1V_1 + x_2V_2 + x_3V_3} \qquad (15)$$

$$\varphi_3 = \frac{x_3V_3}{x_1V_1 + x_2V_2 + x_3V_3}$$

$\delta_{ij}^E(\mathrm{I})$ and $\delta_{ij}^E(\mathrm{II})$ represent the excess surface tension of component binary mixtures which are obtained by subtracting from experimental δ those calculated by Guggenheim[8] equations modified by Grjotheim:[5]

$$\text{I. } e^{-\frac{\delta a}{kT}} = x_1 e^{-\frac{\delta_1 a}{kT}} + x_2 e^{-\frac{\delta_2 a}{kT}} \qquad (16)$$

where a is given by equation:

$$a = x_1\left[\frac{M_1}{\rho_1 N}\right]^{2/3} + x_2\left[\frac{M_2}{\rho_2 N}\right]^{2/3} \qquad (17)$$

---

[8] E. A. GUGGENHEIM, "Mixtures", Oxford at the Clarendon Press, London, 1952.

$$\text{II. } e^{-\frac{\delta A}{kT}} = \varphi_1 e^{-\frac{\delta_1 A}{kT}} + \varphi_2 e^{-\frac{\delta_2 A}{kT}} \tag{18}$$

in which φ_1 and φ_2 are calculated by :

$$\varphi_1 = \frac{x_1 V_1}{x_1 V_1 + x_2 V_2}; \quad \varphi_2 = \frac{x_2 V_2}{x_1 V_1 + x_2 V_2} \tag{19}$$

and A, surface area per molecule, is

$$A = \left[\frac{\varphi_1 V_1 + \varphi_2 V_2}{N} \right]^{2/3} \tag{20}$$

The values of these excess surface tensions for component binary mixtures have been evaluated graphically from figures 5 and 6.

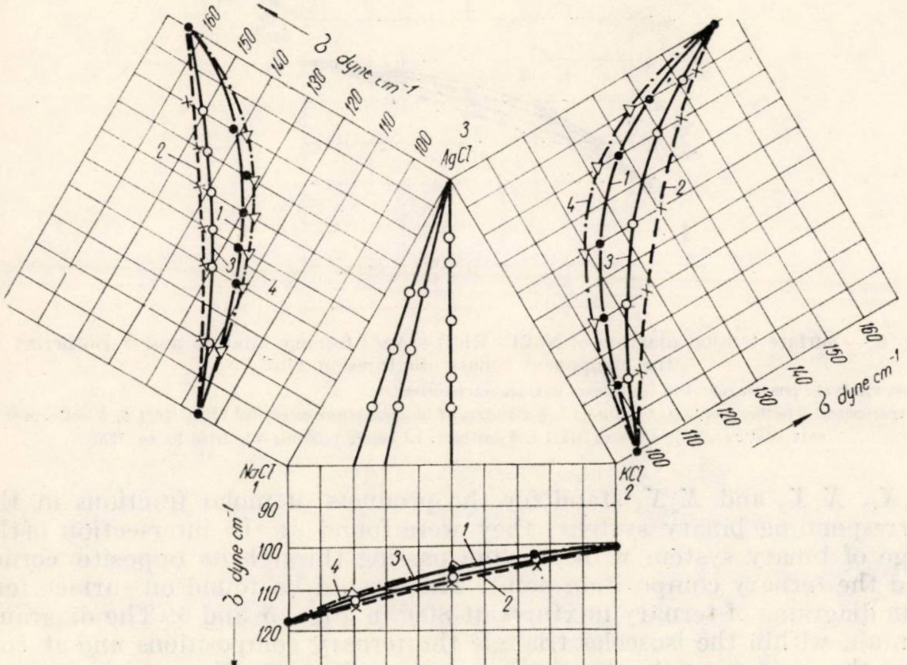

Fig. 5. — Surface tension diagram of NaCl + KCl + AgCl ternary mixture and δ isotherms of the component binary mixtures at 800°.

Points within the triangle represent the ternary mixture composition ;

***1*, experimental δ isotherm of binary mixture ; *2*, δ isotherm of binary mixture calculated by eq (16) ; *3*, δ isotherm of binary mixture calculated by eq (18) ; *4*, δ isotherm of binary mixture calculated by eq (25).**

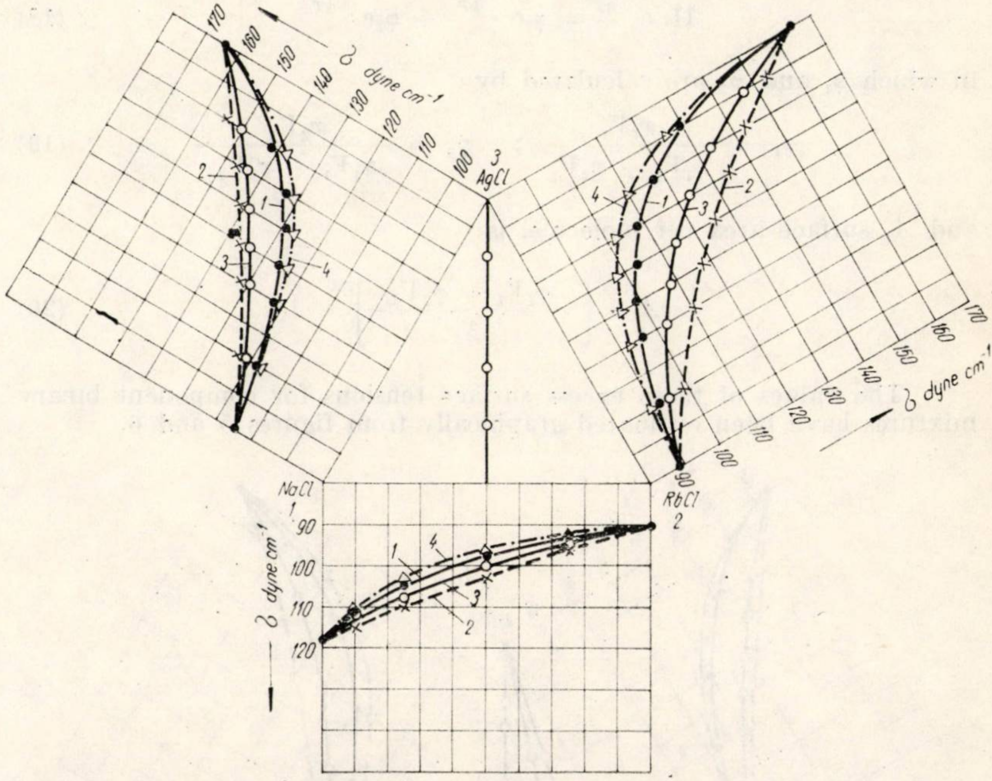

Fig. 6.— Surface tension diagram of NaCl+RbCl+AgCl ternary mixture and δ isotherms of the component binary mixtures at 800°.

Points within the triangle represent the ternary mixture composition;

1, experimental δ isotherm of binary mixture; *2*, δ isotherm of binary mixture calculated by eq (16); *3*, δ isotherm of binary mixture calculated by eq (18); *4*, δ isotherm of binary mixture calculated by eq (25).

X_1X_2, X_1X_3 and X_2X_3 stand for the products of molar fractions in the corresponding binary system; they were found at the intersection of the edge of binary system with the line passing through its opposite corner and the ternary composition point. These could be found on surface tension diagrams of ternary mixtures at 800° in Figs. 5 and 6. The diagrams contain within the isosceles triangle the ternary compositions and at corners the pure components of the ternary mixtures. The surface tension isotherms of component binary mixtures are drawn in the rectangles perpendicular on triangle sides. Curves *1* are experimental isotherms, curves *2* the ones calculated according to eq (16) and curves *3* calculated according to eq (18). The experimental surface tensions in binary NaCl + KCl and NaCl + RbCl mixtures at 800° are taken from Bertozzi's paper.[9]

The results of these calculations are listed in tables 8 and 9 for both ternary mixtures, as δ calculated by the semiempirical equations

---

[9] G. Bertozzi, *J. Phys. Chem.*, **69** 2606 (1965).

(11) and (12) and compared to experimental values. One can see the good agreement within ±4%.

If in equations (11) and (12) the last three terms of the right side are neglected (that is the contribution of δ of binary components, which is termed by Grjotheim and co-workers the interaction parameter) the following relations are obtained :

Table 8

Comparison of surface tensions calculated according to eqs. (11), (12), (21), (22) and (23) with the experimental ones for NaCl + KCl + AgC system at 800°

x_1'	x_1	$\delta_{calcd.}$ (l)	$\delta_{calcd.}$ (II)	$\delta_{calcd.}$ (III)	$\delta_{calcd.}$ (IV)	$\delta_{calcd.}$ (V)	$\delta_{exp.}$
		dyne/cm					
0.5	0.10	129.1	125.4	147.4	143.1	123.1	128.6
0.5	0.15	119.6	117.9	140.0	135.8	117.2	121.7
0.5	0.25	110.3	111.4	129.1	123.8	109.4	112.5
0.5	0.35	106.8	107.5	118.6	114.4	103.0	104.8
0.5	0.40	105.5	105.8	113.8	110.5	101.5	102.7
0.7	0.28	117.3	116.9	137.0	132.6	115.9	119.6
0.7	0.42	117.8	112.3	126.6	122.6	109.0	111.5
0.7	0.56	109.2	109.4	117.3	114.4	105.6	107.0
0.8	0.32	120.0	117.5	138.0	134.4	117.9	121.2
0.8	0.48	114.2	114.6	128.0	124.6	110.9	113.3
0.8	0.64	111.3	111.4	119.0	116.6	107.5	108.8

Table 9

Comparison of surface tensions calculated according to eqs. (11), (12), (21), (22) and (23) with the experimental ones for NaCl + RbCl + AgCl system at 800°

x_1'	x_1	$\delta_{calcd.}$ (I)	$\delta_{calcd.}$ (II)	$\delta_{calcd.}$ (III)	$\delta_{calcd.}$ (IV)	$\delta_{calcd.}$ (V)	$\delta_{exp.}$
		dyne/cm					
0.5	0.1	118.4	111.3	145.9	139.7	116.4	123.5
0.5	0.2	106.4	105.5	132.2	124.2	105.0	110.0
0.5	0.3	102.4	103.0	120.1	112.9	99.0	102.2
0.5	0.4	99.2	99.3	109.5	104.3	95.4	97.3

$$\text{III.}\quad e^{-\frac{\delta a}{kT}} = x_1 e^{-\frac{\delta_1 a}{kT}} + x_2 e^{-\frac{\delta_2 a}{kT}} + x_3 e^{-\frac{\delta_3 a}{kT}} \tag{21}$$

$$\text{IV.}\quad e^{-\frac{\delta A}{kT}} = \varphi_1 e^{-\frac{\delta_1 A}{kT}} + \varphi_2 e^{-\frac{\delta_2 A}{kT}} + \varphi_3 e^{-\frac{\delta_3 A}{kT}} \tag{22}$$

By calculating surface tension δ (III) and δ (IV) according to eq (21) and (22) much higher values than the experimental ones were obtained (tables 8 and 9). Replacing mole or volume fractions by surface fractions, one obtains :

$$\text{V.}\quad e^{-\frac{\delta a^{\delta}}{kT}} = x_1^{\delta} e^{-\frac{\delta_1 a^{\delta}}{kT}} + x_2^{\delta} e^{-\frac{\delta_2 a^{\delta}}{kT}} + x_3^{\delta} e^{-\frac{\delta_3 a^{\delta}}{kT}} \tag{23}$$

in which a^δ is the surface area per molecule and is taken as :

$$a^\delta = x_1^\delta\left[\frac{M_1}{\rho_1 N}\right]^{2/3} + x_2^\delta\left[\frac{M_2}{\rho_2 N}\right]^{2/3} + x_3^\delta\left[\frac{M_3}{\rho_3 N}\right]^{2/3} \tag{24}$$

The surface tensions of ternary mixtures calculated by eq. (23), δ (V), are also listed in tables 8 and 9 and are much closer to experimental δ than δ (III) and δ (IV).

In figures 5 and 6, curves *4* for binary mixtures represent the surface tension isotherms calculated by the following equation (similar to that for ternary mixtures but with surface fractions) :

$$e^{-\frac{\delta a^\delta}{kT}} = x_1^\delta e^{-\frac{\delta_1 a^\delta}{kT}} + x_2^\delta e^{-\frac{\delta_2 a^\delta}{kT}} \tag{25}$$

One can see that curves *4* are the closest to experimental isotherms.

In conclusion, the enrichment coefficient, s, introduced by Eberhart in binary mixtures could be extended to ternary ones as quasibinary coefficients, $s^{12,3}$ and as partial enrichment coefficients, s^{ij}.

It has also been shown that one may calculate the surface tensions for any composition of a ternary mixture from those of binary (1—3) and (2—3) mixtures and from one $x_3 = ct$ section (x_3 refers to the highest surface tension component) of the ternary one.

ACKNOWLEDGEMENT

The authors are grateful to Mr. M. Ciopec from the Institute of Physical Chemistry, Bucharest for the programming on the I.B.M. System 360/30 computer and for assistance in calculations.

COMMUNIQUÉ

VIIIe CONGRÈS INTERNATIONAL DE CYBERNÉTIQUE

Le VIIIe Congrès International de Cybernétique est organisé par l'Association Internationale de Cybernétique. Il se tiendra à Namur (Belgique) du *6 au 11 septembre 1976.* Les thèmes du Congrès sont les suivants:

1. Principes de Cybernétique et Théorie Générale des Systèmes
2. La Cybernétique dans les Systèmes Sociaux
3. La Cybernétique apliquée aux Systèmes Mécaniques
4. La Cybernétique en Biologie et en Médecine.

Le Congrès est ouvert à tous ceux qui sont intéressés par les thèmes du Congrès.

Les auteurs de communications sont priés de faire parvenir avant le 1er janvier 1976 le titre et un résumé de la communication qu'ils comptent présenter.

Toute information complémentaire peut être obtenue au Secrétariat de l'Association Internationale de Cybernétique, Palais des Expositions, Place André Rijckmans, B—5000 NAMUR (Belgique).

COMMUNIQUE

VIIIe CONGRÈS INTERNATIONAL DE CYBERNÉTIQUE

Le VIIIe Congrès International de Cybernétique est organisé par l'Association Internationale de Cybernétique. Il se tiendra à Namur (Belgique) du 6 au 11 septembre 1976. Les thèmes du Congrès sont les suivants :

1. Principes de Cybernétique et Théorie Générale des Systèmes
2. La Cybernétique dans les Systèmes Sociaux
3. La Cybernétique appliquée aux Systèmes de [illegible]
4. La Cybernétique en Biologie et en Médecine

Le Congrès est ouvert à tous ceux qui sont intéressés par les thèmes du Congrès.

Les auteurs de communications sont priés de faire parvenir avant le 1er janvier 1976 le titre et un résumé de la communication qu'ils comptent présenter.

Toute information complémentaire peut être obtenue au Secrétariat de l'Association Internationale de Cybernétique, Palais des Expositions, Place André Rijckmans, B - 5000 NAMUR (Belgique).

NOTE POUR LES AUTEURS

La *Revue Roumaine de Chimie* publie des articles en anglais, français, russe, allemand ou espagnol. Les auteurs sont priés d'envoyer des articles, notes, communications et comptes rendus inédits.

Les manuscrits seront dactylographiés à deux intervalles. Les tableaux seront dactylographiés sur des feuilles séparées, de même que la légende des figures. Les diagrammes seront tracés à l'encre de Chine sur papier calque. Les tableaux et les figures seront numérotés par des chiffres arabes, en nombre strictement nécessaire. Prière de ne pas inscrire les mêmes données dans les tableaux et les figures. Les formules chimiques seront incluses dans le texte ; en outre, elles seront transcrites sur des feuilles séparées. Les auteurs sont priés d'indiquer les caractères italiques (en soulignant les lettres au crayon), ainsi que tout autre caractère spécial. L'ordre des références bibliographiques sera celui de leur mention dans le texte ; le nom de l'auteur sera précédé de l'initiale du prénom ; les publications périodiques seront présentées suivant les prescriptions internationales. Les références seront ajoutées à la fin de l'article ; elles paraîtront comme des notes, au bas de la page. Le texte sera précédé d'un résumé comprenant 15 lignes au maximum.

L'entière responsabilité du contenu des articles appartient aux auteurs. On publie des articles dus aux collaborateurs roumains ou étrangers.

PRINTED IN ROMANIA

1975 OKT 12

TRAVAUX PARUS AUX ÉDITIONS DE L'ACADÉMIE DE LA RÉPUBLIQUE SOCIALISTE DE ROUMANIE

I. ZUGRĂVESCU, MAGDA PETROVANU, **Chimia N-Ilidelor** (La Chimie des N-Ylures), 1974, 347 p., 19 lei.

MARGARETA AVRAM, **Antidăunători** (Pesticides), 1974, 494 p., 41 lei.

CR. SIMIONESCU, VIORICA RUSAN, N. POPA, **Chimia algelor marine** (La Chimie des algues marines), 1974, 211 p., 18 lei.

MARIA FITI, **Dozimetria chimică a radiaţiilor ionizante** (La dosimétrie chimique des radiations ionisantes), 1973, 240 p., 13,60 lei.

MIHAI FLORESCU, **Eficienţa economică a cercetării ştiinţifice** (L'efficience économique de la recherche scientifique), 1972, 115 p., 15 lei.

GEORGETA LĂZĂRESCU, **Sistematizarea informaţiilor în Chimia organică** (La systématisation des informations dans la chimie organique), 1972, 252 p., 10,50 lei.

P. BALTĂ et E. BALTĂ, **Introducere în chimia fizică a stării vitroase** (Introduction à la chimie physique de l'état vitreux), 1971, 240, 15,50 lei.

LYDIA-MARIA VAICUM, **Biodegrabilitatea detergenţilor** (La biodégrabilité des détergents), 1971, 254 p., 16 lei.

TIBERIU NĂŞCUŢIU, **Metode radiometrice de analiză** (Méthodes radiométriques d'analyse), 1971, 346 p., 19,50 lei.

I. ZUGRĂVESCU et L. STOICESCU-CRIVETZ, **Polimeri heterociclici** (Polymères hétérocycliques), 1971, 190 p., 9,50 lei.

CRISTOFOR SIMIONESCU et C. V. UGLEA, **Fracţionarea compuşilor macromoleculari** (Fractionnement des composés macromoléculaires), 1962, 292 p., 18,50 lei.

I. MAXIM, **Materiale nucleare** (Matériaux nucléaires), 1969, 444 p., 30 lei.

CRISTOFOR SIMIONESCU et CLEOPATRA VASILIU-OPREA, **Mecanochimia compuşilor macromoleculari** (La mécanochimie des composés macromoléculaires), 1967, 344 p., 23,50 lei.

CORNEL BODEA et collab., **Tratat de biochimie vegetală**, partea I, **Fitochimie** (Traité de biochimie végétale, Ire partie, Phytochimie), Ier vol. 1964, 747 p. + 4 annexes + 2 pl., 41 lei ; IIe vol., 1965, 1262 p., 1 pl., 56 lei ; IIIe vol., 1967, 773 p., 35 lei.

I.P.I. c. 212

43 426

Lei 25.–

F 1103

R

REFERÁLVA

ACADÉMIE DE LA RÉPUBLIQUE SOCIALISTE DE ROUMANIE

REVUE ROUMAINE DE CHIMIE

70

TOME 20
N° 8
AOÛT 1975

RECHAX, **20**, *8*, 1027 - 1192 (1975)

EDITURA ACADEMIEI REPUBLICII SOCIALISTE ROMÂNIA

20, *8*, p. 1027—1192 (1975) Bucarest

Rev. Roumaine Chim.

ACADÉMIE DE LA RÉPUBLIQUE SOCIALISTE DE ROUMANIE

REVUE ROUMAINE DE CHIMIE

COMITÉ DE RÉDACTION

Rédacteur en chef :

I. G. MURGULESCU, membre de l'Académie de la République Socialiste de Roumanie

Rédacteurs en chef adjoints :

A. T. BALABAN et V. EM. SAHINI, membres correspondants de l'Académie de la République Socialiste de Roumanie

Collége de rédaction :

EM. BRATU, ELENA CEAUŞESCU, ECATERINA CIORĂNESCU-NENITZESCU, C. DRĂGULESCU, RALUCA RIPAN, CR. SIMIONESCU, membres de l'Académie de la République Socialiste de Roumanie : P. SPACU, membre correspondant de l'Académie de la République Socialiste de Roumanie; MARGARETA AVRAM, D. I. MARCHIDAN, G. NIAC et D. SĂNDULESCU

Toute commande de l'étranger pour les travaux parus aux Editions de l'Académie de la République Socialiste de Roumanie sera adressée à ILEXIM, Serviciul Export — Import Carte/Serviciul Export — Import Presă, P.O. BOX 2001, 64—66, Calea Griviţei, Bucarest, 12, Roumanie

Les manuscrits, les livres et les revues proposés en échange, ainsi que toute correspondance seront envoyés à la rédaction

REVUE ROUMAINE DE CHIMIE

23, str. Dumbrava Roşie, Bucarest, Roumanie, téléphone 12 41 60

EDITURA ACADEMIEI REPUBLICII SOCIALISTE ROMÂNIA
125, Calea Victoriei, Bucarest, Roumanie, téléphone 13 94 40

ORSZÁGOS MŰSZAKI KÖNYVTÁR ÉS DOKUMENTÁCIÓS KÖZPONT * 1883 *

REVUE ROUMAINE
DE
CHIMIE

Tome 20, Nº 8 Août 1975

LILIANA CIUREA, V. EM. SAHINI and ELENA VOLANSCHI, ESR spectra and electronic structure of isatin and N-methylisatin radical anions 1029–1035

MARIANA CIUREANU and V. EM. SAHINI, *n* Ionization potentials of nitrogen heterocyclic molecules 1037–1040

RODICA VÎLCU and MIHAELA OLTEANU, Adsorption of some alkyl pyridinium chlorides at the silica-alumina-water interface 1041–1050

CONSTANŢA HERDLICKA and S. STERNBERG, Interdiffusion coefficient of Tl^{+} and Cd^{2+} in fused alkali chlorides by the chronopotentiometric method 1051–1055

R SULTANA CIOLAC, The induction time for pitting corrosion 1057–1063

A V. P. KUDESIA, Kinetics of oxidation of some glycols by bromine 1065–1070

N. VOICULESCU, Reactions of coordinated ligands. VIII. Aluminium-organic derivatives of diphenylglyoxime 1071–1075

I. I. BĂDILESCU, Heterocyclic compounds. V. Beckmann rearrangement of some 2,3-dihydro-1-benzoxepin-5(4H)-one oximes to 1,5- and 1,6-benzoxazocinones 1077–1087

G. M. BENEDIKT and ANCA VOICU, An intramolecular hydrogen bridge with the double bond in spiro[cyclopropane-1,5′(2-hydroxymethyl)-[5′H] dibenzo [*a*,*d*] cycloheptene] 1089–1093

M. IOVU et S. RADU, Condensation des sels de sodium des 4-hydroxyazobenzènes substitués avec le 1,4-bis(chlorométhyl)benzène 1095–1101

R M. A. RUMBEA, G. LANCHEC et B. BLOURI, Sur l'oxydation thermique des hydrocarbures à longues chaînes en phase liquide 1103–1114

I. MOŢOC, Sur la relation algébrique entre les énantiomères de l'atome de carbone asymétrique 1115–1118

IUDITA MUREŞAN and LUCIA ZADOR, Principles and methods for the potentiometric investigation of polyacids beginning from low degrees of neutralization 1119–1132

A. SZURKOS, P. NAGY and I. GÖRBE, A polarographic study on styrylcyanines. II. Substituent effects on the polarographic reduction of 1-ethyl-2-(*p*-X-styryl) and 1-ethyl-4-(*p*-X-styryl)-pyridinium ions 1133–1140

GHEORGHIŢA I. JINESCU and CORNELIA BALABAN, Mass transfer from dispersed particles to continuous fluid media. I. Non-oscillating fluid media 1141–1156

Rev. Roumaine Chim. **20**, *8*, p. 1027–1192 (1975), Bucarest

A CR. SIMIONESCU, SVETLANA DUMITRESCU, M. DĂRÎNGĂ, MARIA GROVU, SILVIA VASILIU, I. DIACONU and M. LEANCĂ, Study on the polymerization of acetylenic derivatives. XVII. Study on electric properties of some polyphenylacetylenes 1157–1166

A I. PETRARIU, PAMFILIA PETRARIU, FL. POPESCU et STELA DRĂGAN, La dégradation des échangeurs d'anions dans des milieux agressifs. II. L'action de l'eau oxygénée en présence du $CuSO_4$ sur les échangeurs d'anions contenant des groupes quaternaires d'ammonium de type II. 1167–1182

F.A. GOTHARD, T. PÎRVUŢOIU et ELENA CONSTANTIN, La généralisation des valeurs de la volatilité relative obtenues par la méthode chromatographique 1183–1189

COMPTES RENDUS 1191

Revue Roumaine de Chimie, **20**, *8*, 1029 – 1035 (1975)

ESR SPECTRA AND ELECTRONIC STRUCTURE OF ISATIN AND N-METHYLISATIN RADICAL ANIONS

LILIANA CIUREA, V. EM. SAHINI and ELENA VOLANSCHI
Polytechnic Institute of Bucharest, Department of Physical Chemistry
and Electrochemical Technology
Bd. Republicii, 13

Received January 20, 1975

ESR and optical spectra of the anion radicals obtained by the chemical and electrochemical reduction of isatin and N-methylisatin in dimethylsulphoxide and dimethylformamide are studied. MO calculations in the frame of Hückel and McLachlan approximations were performed and the results account for the observed hyperfine splittings and electronic transitions.

The first study of the radicals derived from isatin and N-methylisatin was that reported by Russell and coworkers [1] concerning the ESR spectra of the semidione radicals, obtained by the propiophenone enolate anion addition in dimethylsulphoxide.

The object of the present paper is to investigate the anion radicals obtained by the chemical and electrochemical reduction from these compounds, correlating their ESR and optical spectra in order to provide information about their electronic structure.

EXPERIMENTAL

Isatin reagent grade was recrystallized from benzene (m.p. = 200°). *N*-methylisatin was synthetised by the methylation of isatin in alkali solution with dimethylsulphate [2] (m.p. = = 131°). The solvents, dimethylformamide (DMF) and dimethylsulphoxide (DMSO) were purified by usual methods. [3]

The anion radicals were prepared in an inert atmosphere by both the electrochemical reduction and the action of the alkali metals on the parent compounds. The electrochemical reduction was performed on a 10^{-3} M solution of the neutral molecule in DMSO or DMF, using two Pt electrodes and 0.1 M tetrabutylammonium iodide as supporting electrolyte. The potential was controlled by means of an Ag wire passed through a glass capillary and dipped into the solution till above the cathode.[4]

For the ESR study the anions were generated directly within the microwave cavity, while for the optical study an electrolytic cell with two separated compartments was used, in order to prevent the diffusion of the anodic products to the cathode.

---

[1] G. A. Russell, C. L. Myers, P. Bruni, F. A. Neugebauer and R. Blankespoor, *J. Amer. Chem. Soc.*, **92**, 2762 (1970).

[2] R. G. Ault, E. L. Hirst and R. A. Morton, *J. Chem. Soc.*, **1935**, 1653.

[3] J. B. Goldberg and A. J. Bard, *J. Phys. Chem.*, **75**, 3281 (1971).

[4] A. Bard, *Pure Appl. Chem.*, **25**, 379 (1971).

The chemical reduction was made in a cell connected both to the optical cuve and the ESR tube. The ESR spectra were recorded on a JES—3B Spectrometer in the X-band frequency and the optical ones on a Beckman DK-2 Spectrophotometer in the range 400—700 nm. The MO calculations were carried out on an IBM—360 computer at the Computer Center, Bucharest University.

RESULTS AND DISCUSSION

1. ESR SPECTRA

The comparative study of isatin and *N*-methylisatin anion radicals evidences for isatin the existence of two radicalic species, depending on the working conditions. The ESR data of the studied anion radicals are presented in Table 1 and are in good agreement with the simulated spectra.

Table 1

ESR data for anions

Radical	Method of reduction	Splitting constants in G				Total width*	g
		a^H_{ring}	a_N	a^H_{NH}	a_{CH_3}		
Isatin	Na in DMF	3.86; 3.22; 1.05; (2H)	1.05	—	—	11.2	2.0043
	K in DMF	3.98; 3.35; 1.11; (2H)	1.11	0.23	—	11.5	
	electrol. in DMSO	3.71; 3.11; 1.02; 0.94	1.09	0.19	—	—	
Isatin dianion	electrol. in DMSO	4.40; 3.56; 0.99; (2H)	0.57	—	—	10.8	2.0038
N-methylisatin	electrol. in DMSO K in DMF	3.78; 3.13; 1.02; (2H)	0.95	—	0.65	12.5	2.0043

* Measured between centers of the extreme lines.

The general pattern of the ESR spectra obtained by both chemical and electrochemical reduction is similar to that reported for the corresponding semidione radicals. [1] Therefore, the two radicalic species provided by isatin were assigned to the mono- and respectively dianion radicals. The equilibrium existent between these radicals is well evidenced in the DMSO solutions, and was found to depend on solvent, temperature, applied voltage and concentration. The spectrum *a* in figure 1 shows the presence of a mixture of the two radicalic species with slightly different *g* values. The spectrum *b* belongs to the dianion radical and it is distinguished from the spectrum assigned to the monoanion radical by a smaller nitrogen hyperfine constant and by the absence of the NH proton splitting. A similar behaviour was established in DMF, especially on cooling. As the m.p. of DMSO is 18.5°, the temperature effect in this case was studied as the change of the ESR spectrum on melting.

For N-methylisatin a single radicalic species was obtained in both chemical or electrochemical reduction. The figure 2 shows the spectrum of the N-methylisatin anion obtained with K in DMF, which was interpreted with the hyperfine constants given in Table 1. For no spectra the splitting of the alkali metal could be evidenced.

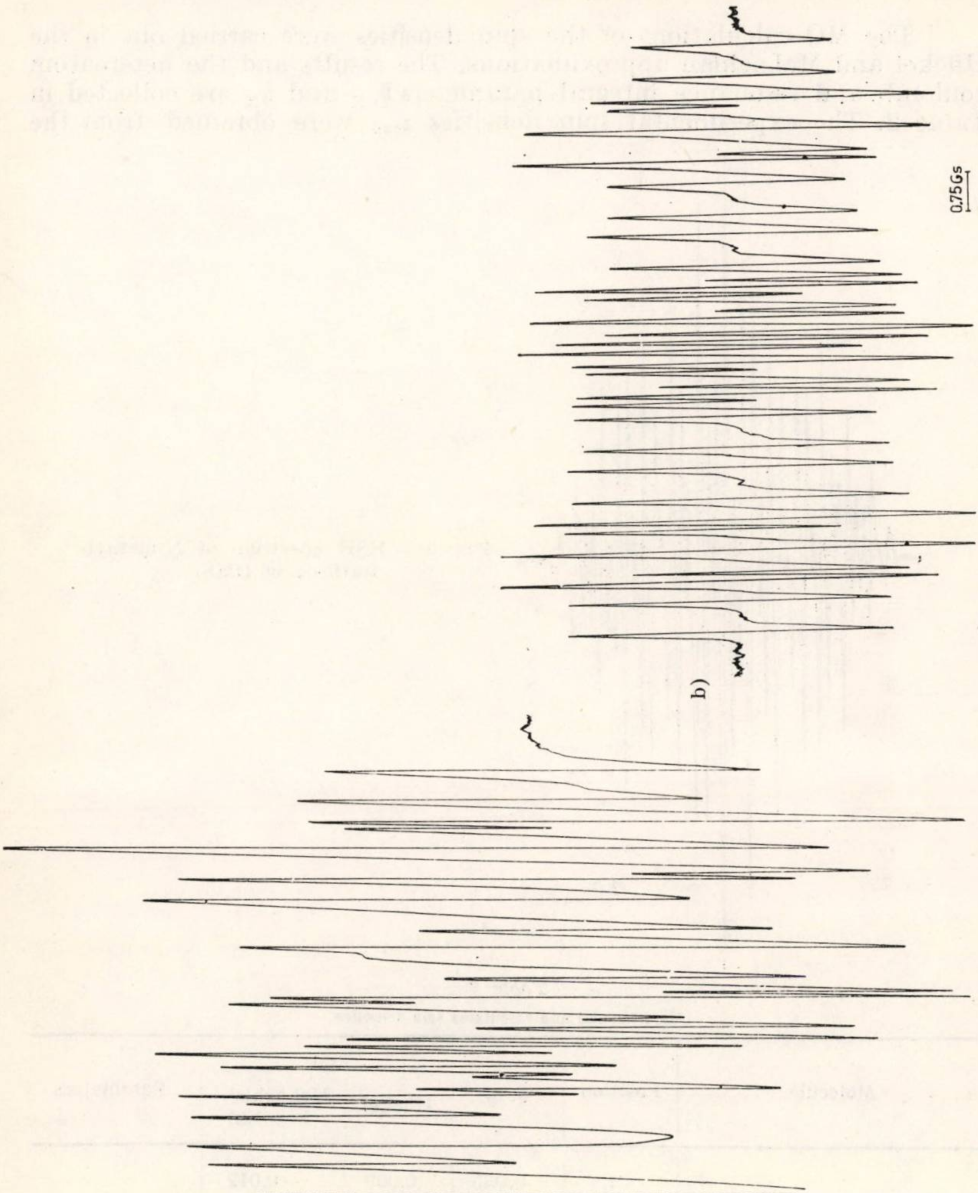

Fig. 1. — ESR spectra of the electrochemically obtained isatin anions in DMSO.

The MO calculations of the spin densities were carried out in the Hückel and McLachlan approximations. The results and the heteroatom coulomb and resonance integral parameters h_{CX} and k_X are collected in Table 2. The experimental spin densities ρ_{exp} were obtained from the

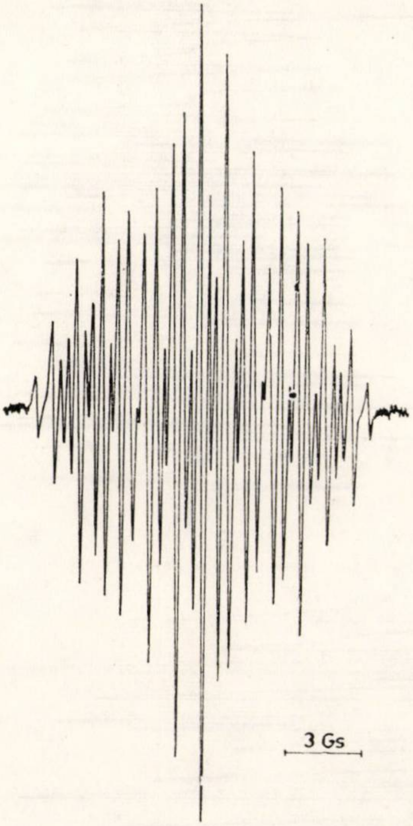

Fig. 2. — ESR spectrum of N-methylisatin-K in DMF.

Table 2

Experimental and calculated spin densities

Molecule	Position	ρ_{exp}	ρ_{calc}		Parameters
			Hückel	McLachlan ($\lambda = 1.2$)	
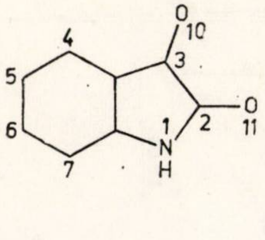 O 10 3 4 5 6 7 1 N H 2 O 11	1	0.035	0.009	−0.012	
	2	—	0.180	0.209	
	3	—	0.172	0.164	$h_O = 1.8$
	4	0.115	0.071	0.091	
	5	0.035	0.005	−0.030	$k_{CO} = 1.6$
	6	0.137	0.079	0.105	
	7	0.038	0.000	−0.041	$h_N = 1$
	10	—	0.273	0.310	
	11	—	0.114	0.109	$k_{CN} = 0.8$

splitting constants of the electrochemically generated anions using the McConnell relationship[5] and the following $\sigma-\pi$ interaction parameters : $Q_{CH}^{H} = 27$ and $Q_{N}^{N} = 30.9$ Gs. The calculated spin density pattern indicates that the protons at the 4 and 6 positions are responsible for the greatest splitting constants. About 4/5 from the unpaired electron density is localized on the carbonyl groups, which explaines the small total width of the ESR spectra. Table 2 gives a satisfactory agreement between the experimental and calculated spin densities. The difference obtained for the nitrogen spin density ρ_N is probably due to the fact that the simple McConnel formula may not be suitable for this case. The expression proposed by Karplus and Fraenkel :[6] $a_N = Q_N^N \rho_N + Q_{CN}^{C} \Sigma\rho_C$, which takes into account the spin densities on the carbon atoms (ρ_C) bonded to the nitrogen atom, gives a better agreement for the nitrogen splitting constant, that is 0.90 Gs versus the experimental value of 1.09 Gs. This fact points out a great contribution (of about two thirds) in this case from the adjacent carbon atoms. For Q_N^N and Q_{CN}^{C} we used the values 30.9 Gs and -2Gs respectively, usually applied in nitrogen heterocyclic anion radicals.[7] For N-methylisatin, a hyperconjugative model was used (parameters from the last column and methyl group parameters of Coulson and Crawford ;[8] the spin density pattern obtained is practically unmodified, in agreement with the hyperfine constants from Table 1. For the calculated a_{CH_3} a value of 0.35 Gs was found versus experimental $a_{CH_3} = 0.65$ Gs, using a McConnell type formula with $Q_{CH_3}^{C} = 27.2$ Gs.[9]

2. OPTICAL SPECTRA

The optical spectral data of the anion radicals provided by isatin and N-methylisatin are contained in Table 3 and point out comparatively to the neutral molecules the additional maxima in the range 400–600 nm.

In the case of isatin, the same equilibrium between two forms observed in the ESR spectra is evidenced by the presence of two maxima. The figures 3 and 4 present the dependence of the positions and relative intensities of the two peaks on concentration, reduction agent, temperature and solvent. It may be seen from Fig. 4, that in comparison with isatin anion, N-methylisatin anion exhibits a single sharp absorption band in the same range.

The Hückel calculated transition energies, with the parameters from the last column of Table 2, are given in Table 3. It may be seen that the calculated values are within the limits of the experimental values.

---

[5] H. M. McConnell, *J. Chem. Phys.*, **24**, 632, 764 (1956).

[6] M. Karplus and G. K. Fraenkel, *J. Chem. Phys.*, **35**, 1312 (1961).

[7] E. W. Stone and A. H. Maki, *J. Chem. Phys.*, **39**, 1635 (1963).

[8] C. A. Coulson and V. A. Crawford, *J. Chem. Soc.*, **1953**, 2052.

[9] J. M. Lhoste and F. Tonnard, *J. Chim. phys.*, **63**, 678 (1966).

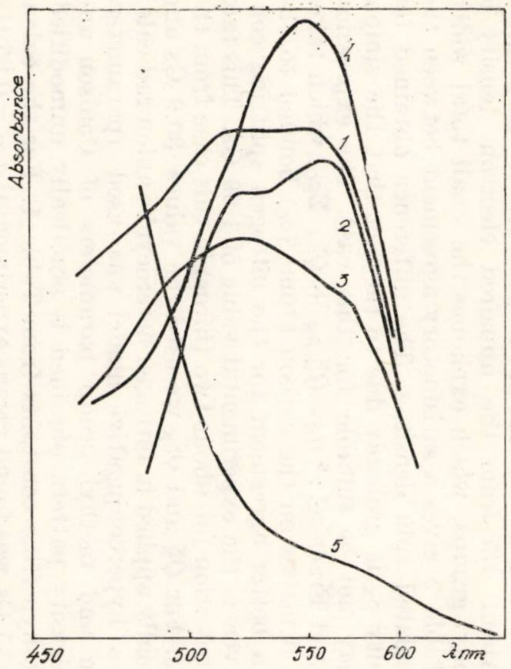

Fig. 3. — Visible spectra of isatin anions in DMSO :

1, 2 — obtained with Na, concentration of 10^{-3} M, respectively 5.10^{-4} M; *3* — effect of cooling on sample 2; *4* — obtained by electrochemical reduction; *5* — decomposed sample.

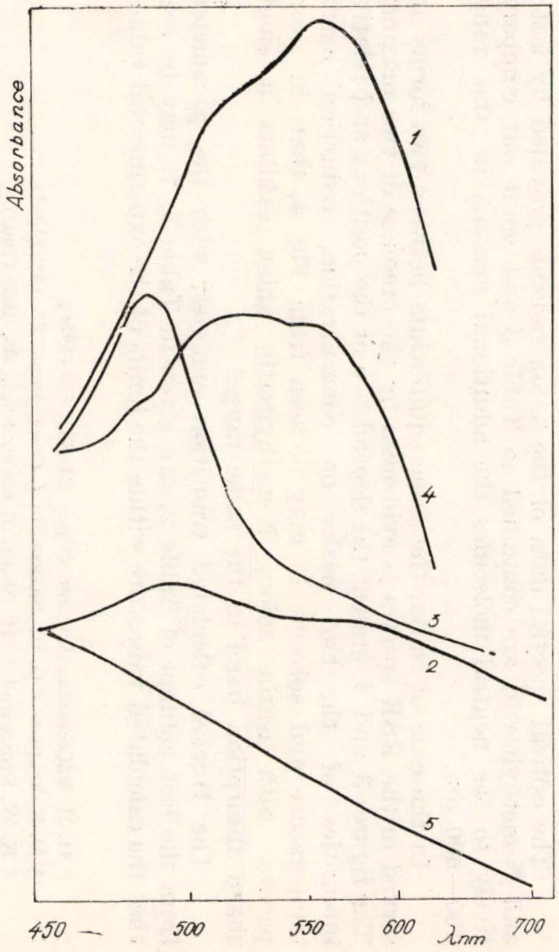

← Fig. 4. — Visible spectra of isatin and N-methylisatin anions in DMF :

1, obtained with Na; *2*, electrochemical reduction; *3*, effect of cooling on sample 1; *4*, N-methylisatin — Li anion; *5*, decomposed sample.

Table 3

Visible spectral data

Solvent	Reduction	λ_{max} in nm Isatin (N-methylisatin)			ΔE_{exp} (eV)	ΔE_{calc} (eV) $\beta = -2.8$ eV
DMF	Li	520	560	(550)	—	—
	Na	515	550	(540)	—	(2.17)
	K	510	540	—	—	—
	electrol.	520	560	—	2.38 2.21	2.18
DMSO	Li	485	550	—	—	
	Na	515	560	(530)	—	
	electrol.	515	560	—	2.40 2.21	

In conclusion, correlating the ESR data to the optical spectra, the equilibrium between the two radicalic forms of isatin could be evidenced. The MO calculations account well for the experimental spin densities and transition energies in the visible spectrum.

Revue Roumaine de Chimie, **20**, *8*, 1037 – 1040 (1975)

n IONIZATION POTENTIALS OF NITROGEN HETEROCYCLIC MOLECULES

MARIANA CIUREANU and V. EM. SAHINI
Department of Chemistry, Polytechnic
Institute of Bucharest, Bd. Republicii, 13

Received November 19, 1974

A method is given to calculate the *n* ionization potentials of nitrogen heterocyclic molecules. Calculated values show a linear correlation with the experimental pKa values.

1. INTRODUCTION

Ionization potentials of nitrogen heterocyclic molecules have been object of considerable interest both from theoretical and experimental standpoint. In fact, azines should have three different types of ionization potentials, namely n, π and σ, depending on the orbital from which the ionized electron originates. The lowest ionization potential of pyridine and picolines was assigned by Higasi [1] and coworkers to the ionization of a nonbonding electron on the nitrogen atom, that is, they considered it an n ionization potential; the same conclusion was reached by Omura [2] in the case of diazines. However, El Sayed [3] as well as El Bayoumi [4] and their coworkers have proved that the lowest I. P. of azines represents the ionization from the highest filled π orbital and that the n I. P. should have a somewhat higher value; therefore, the experimental data on the n ionization potentials of azines are very scarce.

A method to calculate the n ionization potentials of azines was proposed by Nakajima and Pullman [5,6]; it is a SCF-type method which takes into consideration the electron repulsions between the nitrogen lone pair and π electrons. The calculated values show, within the same series of bases, a satisfactory correlation with the experimental basicity data; however an unexplainable discrepancy appears between the data obtained in the case of different series [7]; for example, calculated ionization potentials in the range of 9.5–9.7 eV were found to correspond to pKa values of 6−7 for methylpyridines and of 3−4 for diazines. We considered therefore interesting to reconsider the problem of ionization potentials calculation. The method proposed by us takes into consideration the electron interactions between the lone pair and all the other valence shell electrons (π or σ) in the molecule.

---

[1] K. Higasi, I. Omura and H. Baba, *J. Chem. Phys.*, **24**, 623 (1956).

[2] I. Omura, H. Baba, K. Higasi and Y. Kanaoka, *Bull Chem. Soc. Japan*, **30**, 633 (1957).

[3] M. F. El. Sayed, M. Kasha and Y. Tanaka, *J. Chem. Phys.*, **34**, 334 (1961).

[4] M. A. El-Bayoumi and O. S. Khalil, *J. Chem. Phys.*, **47**, 4863 (1967).

[5] T. Nakajima and A. Pullman, *J. Chim. phys.*, **55**, 793 (1955).

[6] T. Nakajima and A. Pullman, *Compt. rend.*, **246**, 1047 (1958).

[7] G. Briegleb, "Elektronen Donator-Acceptor Komplexe", Springer Verlag, Berlin, 1961.

2. METHOD OF CALCULATION

Our method of n ionization potentials calculation is based on the traditional ideas of localized lone pair.*

The π and σ systems of the basic system are considered separately, making use of the PPP SCF-MO method for the former; for the latter we used Del Re's method[9] which considers the bonds to be entirely localized.

The energy of nitrogen lone pair will be calculated according to the formula:

$$-I_n = F_{nn} = U_{nn} + \left(P_{NN} - \frac{1}{2}p_{nn}\right)\gamma_{NN} + \sum_{\mathrm{B}\neq\mathrm{N}}(P_{\mathrm{BB}} - Z_{\mathrm{B}})\gamma_{\mathrm{NB}} \qquad (1)$$

where P_{BB} is the overall atomic charge density on atom B, calculated as the sum of π and σ atomic electron densities; Z_{B} is the number of valence shell electrons on atom B; p_{nn} is the n orbital charge density. The core integral U_{nn} is calculated as:

$$U_{nn} = -\frac{1}{2}(I_{\mathrm{N}} + A_{\mathrm{N}}) - \left(Z_{\mathrm{N}} - \frac{1}{2}\right)\gamma_{\mathrm{NN}} \qquad (2)$$

where I_{N} and A_{N} are the nitrogen ionization potential and electron affinity. The electron repulsion integrals γ_{NB} are calculated using Klopman's formula.[10]

3. RESULTS AND DISCUSSION

Table 1 shows the calculated ionization potentials for the nitrogen heterocyclic molecules we studied, together with the available experimental data concerning the basicity of these compounds. The SCF π

---

* Accurate *ab initio* calculations [8] on pyridine have shown that these ideas are not too much in error.

[8] E. Clementi, *J. Chem. Phys.*, **46**, 4731 (1967).

[9] G. Del Re, *J. Chem.* **1958**, 4031; G. Del Re and B. Pullman, *J. Chim. phys.*, **62**, 942 (1965).

[10] G. Klopman, *J. Amer Chem. Soc.*, **86**, 4550 (1964).

Table 1

Calculated ionization potentials

Molecule	I_D (calc)	pKa*	P^{π}_{NN}**
Pyridine	9.88	5.23	1.362
Quinoline	9.78	4.94	1.360
Acridine	9.54	5.6	1.383
Phenazine	10.64	1.23	1.246
Pyrazine	10.69	0.6	1.255
Pyridazine	10.36	2.33	1.178
Pyrimidine	10.37	1.30	1.431
Quinoxaline	10.73	0.8	1.244
Phtalazine	10.22	3.47	1.205
Quinazoline	10.08	3.51	1.456
Benzimidazole	9.67	5.53	1.390
Benzotriazole	10.91	0.4	1.096
Imidazole	9.33	7.2	1.390

* The pKa are those recommended in ref. [5,11]

** The π electronic charges are given for the most basic nitrogen in the molecule. The SCF MO calculations were performed with the same choice of parameters in all cases.

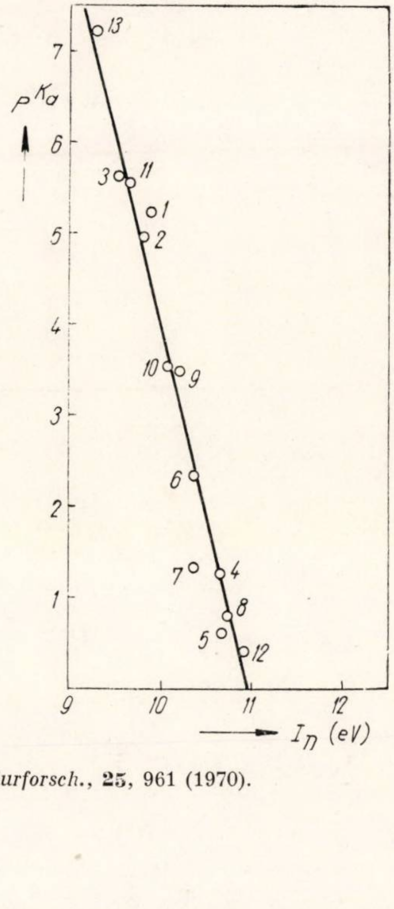

Fig. 1. — Plot of the experimental pKa values versus calculated ionization potentials.

1, Pyridine; *2*, Quinoline; *3*, Acridine; *4*, Phenazine; *5*, Pyrazine; *6*, Pyridazine; *7*, Pyrimidine; *8*, Quinoxaline; *9*, Phtalazine; *10*, Quinazoline; *11*, Benzimidazole; *12*, Benzotriazole; *13*, Imidazole.

---

[11] W. C. Aten and K. Euechel, *Z. Naturforsch.*, **25**, 961 (1970).

electronic charges of the nitrogen atoms (generally correlated with the basicity data) are also presented. As seen from this table, the experimental order of basicity shows a better agreement with the calculated *n* ionization potentials than with the π electronic charges.

In fact, Eq (1) shows that the *n* ionization potential and therefore the basicity of the nitrogen heterocycles depends on the ensemble of atomic charges and not only on the nitrogen electron density.

Figure 1 shows the linear correlation between the calculated ionization potentials and the experimental pKa values; as seen from this figure, there are no longer discrepancies between the data obtained in the case of mono and diazines.

More studies are required in order to clarify the problem of substituents role on the *n* ionization potentials of heterocycles.

Revue Roumaine de Chimie, **20**, *8*, 1041–1050 (1975)

ADSORPTION OF SOME ALKYL PYRIDINIUM CHLORIDES AT THE SILICA-ALUMINA-WATER INTERFACE

RODICA VÎLCU and MIHAELA OLTEANU
Institute of Chemistry, Department of Physical Chemistry
Bucharest, Bd. Republicii 13

Received July 19, 1974

The adsorption isotherms of the surface-active cationic substances of the type alkylpyridinium and alkyloxyethylenepyridinium chlorides have been determined at the silica-alumina water interface at pH 7 and 25°. The electrophoretic mobilities of silica-alumina particles have been determined as a function of surfactant concentration. The shape of the isotherms and of electrophoretic curves was interpreted in terms of hydrophobic bonding theory and "hemimicelle" formation. A value of $-0.7\,kT - -0.83\,kT$ for the free energy of transfer of a CH_2 group from aqueous solution at the solid-liquid interface was calculated. The oxyethylene groups occurring between the alkyl chain and ionic group produce an increase in the number of the CH_2 groups involved in the formation of hydrophobic bonds.

INTRODUCTION

Whereas there exists an extensive body of literature on the aqueous solution properties of surfactants and their behaviour at liquid-gas interface, disproportionately few works have been done on the properties of surfactants at the solid-liquid interface.

The fact that soluble surfactants concentrate at a liquid-solid interface is used widely in mineral processing (flotation), detergency and water purification industries.

From studies on the adsorption of ionic surfactants at mineral-water interfaces,[1-5] several aspects of the general adsorption at solid-liquid interfaces have been established.

The model developed by Fuerstenau and co-workers [1-3] is expressed in terms of the "hemimicelle" hypothesis; at low adsorption densities surfactant ions act as counterions in the electrical double layer at the solid-aqueous solution interface until hydrophobic bonding interactions require that surfactant alkyl (or aryl) chains be rejected from the aqueous

---

[1] D. W. Fuerstenau, *J. Phys. Chem.*, **60**, 981 (1956).

[2] P. Somasundaran, T. W. Healy and D. W. Fuerstenau, *J. Phys. Chem.* **68**, 3562, (1964).

[3] P. Somasundaran and D. W. Fuerstenau, *J. Phys. Chem.*, **70**, 90 (1966).

[4] H. Shubert and H. Baldauf, *Tenside*, **6**, 172 (1967).

[5] B. Dobiás, *Tenside*, **6**, 322 (1972).

environment. Then at higher coverages a two-dimensional aggregation process — hemimicelle formation — at the interface appears to bring surfactant ions inside the Stern layer. This is expressed in the theory as a van der Waals interaction (or hydrophobic bonding), i.e. a specific adsorption potential contribution to the adsorption free energy. The hydrophobic bonding contribution is a linear function of the number of carbon atoms in the alkyl chain with a total free energy change per CH_2 group, $\Phi_{h\,(sl)}$ from $-0.71\ kT$ to $-0.98\ kT$. [2,6,7] The critical equilibrium concentration of surfactant at which two-dimensional aggregation is observed to occur is defined as the hemimicelle concentration (H.M.C.) by analogy to critical micelle concentration (C.M.C.) in bulk solution. [8]

The theory is supported also by the electrokinetic data for mineral particles in surfactants solutions. [1,5,6]

The aim of the present study is to obtain quantitative adsorption and electrokinetic data of a series of cationic surfactants to examine the hemimicelle hypothesis for adsorption of surfactants at solid-liquid interfaces. The effect of the presence of one or two $-OCH_2CH_2-$ groups between the alkyl chain and the ionic head group on adsorption and hydrophobic bonding processes is also investigated.

Silica-alumina was selected as the solid substrate due to the possibilities of detailed characterization of SA/water interface.

EXPERIMENTAL

Materials. The surfactants used are listed in Table 1. The detailed description of these compounds, their synthesis and physical characteristics have been reported. [9] The C.M.C. values were determined from conductivity and surface tension data.[10]

The silica-alumina (S.A.) cracking catalyst was a sample from Hydrocarbons Co. with 24% Al_2O_3 and a point of zero charge (P.Z.C.) of pH 6 ± 0.2 determined for slow equilibrium by potentiometric titration. [11] The surface area was found to be 268 m^2/g by the B.E.T. method.

Methods. Adsorption isotherms were determined by equilibrating 0.1 — 0.5 g S.A. with 10—25 ml surfactant solution of different concentrations in sealed tubes for 48 h at $25 \pm 0.1°$. The analysis of aliquots taken from the stirred suspension was carried out by interferometry (type I.T.R. 2 — USSR) after centrifugation for 15 minutes. The lowest concentration that could be measured was 10^{-5} mol/l in the aqueous solution. The calibration curves were determined for each surfactant and straight lines were obtained. Adsorption of surfactants (mol/g) was calculated using the relation:

$$a = \frac{(C - C_e)\,V}{m} \tag{1}$$

where C (mole/l) is the concentration of the surfactant in solution before adding silica-alumina; C_e (mole/l) the concentration after equilibration with "m" grams of solid, and V — litres of solution used.

---

[6] T. Wakamatsu and D. W. Fuerstenau, *Adv. Chem. Ser.*, **79**, 161 (1968).

[7] I. J. Lin and P. Somasundaran, *J. Colloid Interface Sci.*, **37**, 731 (1971).

[8] K. Shinoda et al. "Colloidal Surfactans", Academic Press, New York, 1963.

[9] I. Mîndru, *Rev. Chim. (București)*, **21**, 265 (1970); *Anal. Univ. București, Ser. Chim.*, **19**, 143 (1970).

[10] I. Mîndru, *J. Colloid Interface Sci.*, **41**, 430 (1972).

[11] R. Vîlcu and M. Olteanu, *Rev. Roumaine Chim.*, **20**, 901 (1975).

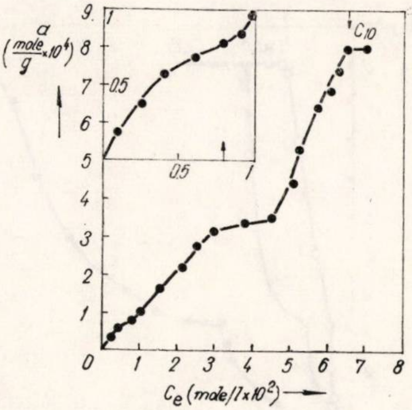

Fig. 1. — Adsorption isotherm of decylpyridinium chloride (C_{10}) on silica-alumina at pH 7 and 25° ; ↓ C.M.C. value. The insert plot shows the initial portion of the isotherm ; ↑ H.M.C. value.

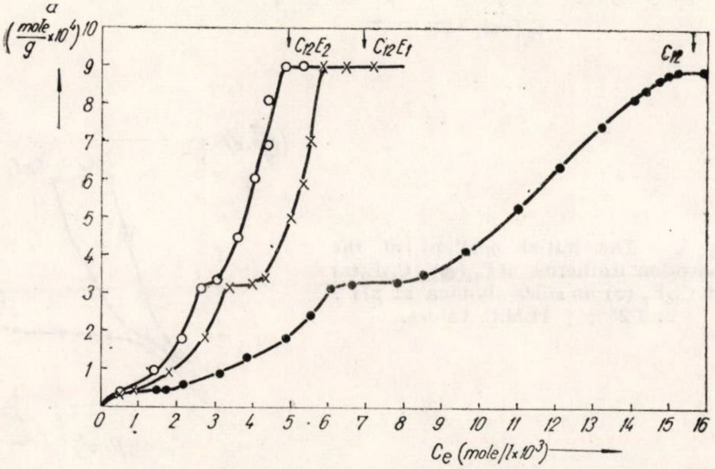

Fig. 2. — Adsorption isotherms of dodecylpyridinium (C_{12} — ●) dodecyloxyethylenepyridinium ($C_{12}E_1$ — ×) and dodecyldioxyethylenepyridinium ($C_{12}E_2$ — ○) chloride on silica-alumina at pH 7 and 25° ; ↓ C.M.C. values.

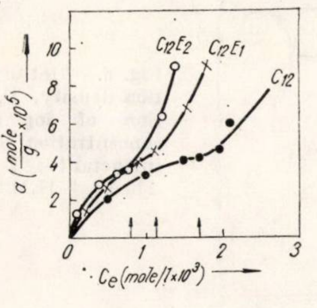

Fig. 3. — The initial portions of the adsorption isotherms of C_{12}(●), $C_{12}E_1$ (×) and $C_{12}E_2$ (○) on silica-alumina at pH 7 and 25° ; ↑ H.M.C. values.

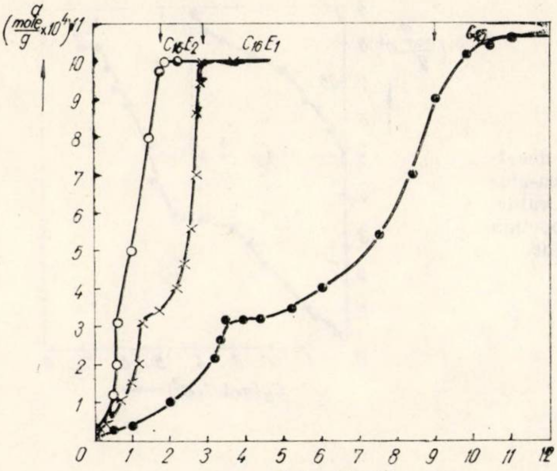

Fig. 4. — Adsorption isotherms of hexadecylpyridinium (C_{16} — ●), hexadecyloxyethylenepyridinium ($C_{16}E_1$ — ×) and hexadecyldioxyethylenepyridinium ($C_{16}E_2$ — ○) chloride on silica-alumina at pH 7 and 25°; ↓ C.M.C. values.

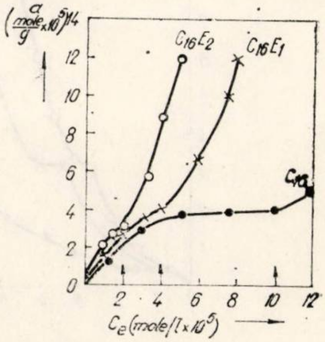

Fig. 5. — The initial portions of the adsorption isotherms of C_{16}(●), $C_{16}E_1$(×) and $C_{16}E_2$ (○) on silica-alumina at pH 7 and 25°; ↑ H.M.C. values.

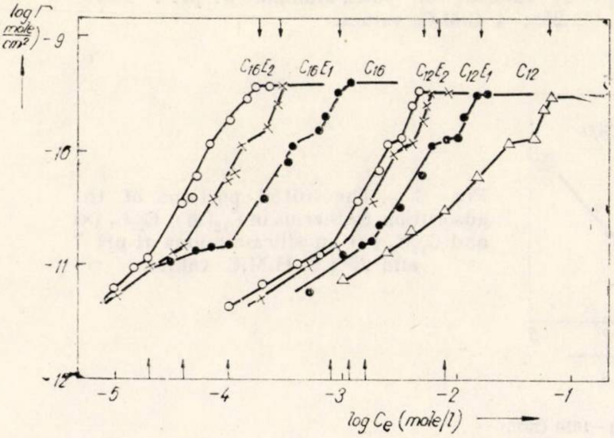

Fig. 6. — Plot of log adsorption density, Γ, as a function of log equilibrium concentration of cationic surfactants; ↓ C.M.C. values; ↑ H.M.C. values.

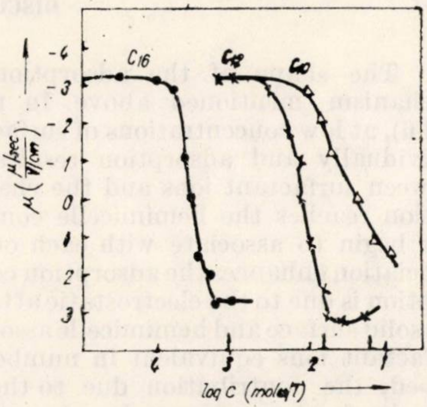

Fig. 7. — Electrophoretic mobility of silica-alumina particles as a function of log concentration of surfactants at pH 7 and 25° ; C_{10}(△), C_{12} (×), C_{16} (●) ; ↑ C.M.C. values.

The electrophoretic mobility of the S.A. particles was determined by means of a microelectrophoresis method, described in detail previously.[11] This method was necessary if the measurement of electrokinetic behaviour was to be determined with the same small particles that were used in the adsorption experiments. The microelectrophoretic cell (Thomas Phila, USA) had plane parallel walls. The velocity of the particle was observed at the stationary lower level using the micrometer scale of a Zeiss ultramicroscope (×10 eyepiece and ×20 objective). The electrophoretic mobility μ expressed in μm/v. sec is given by the relation

$$\mu = \frac{S}{t} \cdot \frac{l}{P} \tag{2}$$

where S is the distance in μm covered by a particle in time t (sec) for a potential drop P (Volts) between platinum electrodes separated by a distance l (cm).

Determinations of pH were made after the equilibrium was attained and about pH 7 value was found for all surfactants. Distilled conductivity water was used for adsorption and electrokinetic data.

RESULTS

The adsorption isotherm of alkylpyridinium and alkyloxyethylenepyridinium chlorides on silica-alumina at 25° and pH 7 are shown in Figs. 1—5. Electrophoretic mobilities of the silica-alumina under the same conditions are given in Fig. 7 for alkylpyridinium chlorides.

The adsorption isotherm for the entire concentration range consists of four regions : region 1, characterized by a low increase in adsorption with surfactant concentration ; region 2, by an abrupt increase in the slope of the isotherm ; region 3, again by a lower dependence of adsorption of surfactant concentration ; and region 4, by a new increase in the slope before the saturation is attained. The inflexion points are better shown in Fig. 6.

The electrophoretic mobility exhibits an almost negligible dependence on surfactant concentration in region 1, but it decreases abruptly through region 2. The end of region 2 is characterized by the mobility becoming zero. In region 3, the mobility is opposite in sign. At the end of region 3 and in region 4, the net electrophoretic mobility is characterized by a slow change, even a decrease in value.

DISCUSSION

The shape of the adsorption isotherm supports the adsorption mechanism mentioned above. In region 1 (insert plots in Figs. 1, 3, 5 and 6), at low concentrations of surfactants the surfactant ions are adsorbed individually and adsorption results primarily from electrostatic forces between surfactant ions and the charged solid surface. When the concentration reaches the hemimicelle concentration (the end of region 1), the ions begin to associate with each other at the solid-liquid interface. This association enhances the adsorption considerably. Thus, in region 2, the adsorption is due to the electrostatic attraction between the ions and the charged solid surface and hemimicelle association of hydrocarbon chains. When surfactant ions equivalent in number to the surface sites have been adsorbed, the contribution due to the electrostatic attraction disappears, and the further increase in adsorption will be only due to association between the hydrocarbon chains. Thus in region 3, the slope of the adsorption isotherm decreases. The reason mentioned above for the decrease in slope from region 2 to region 3 is supported by the electrophoretic mobilities curves (Fig. 7) which show that the net charge on the particles becomes close to zero at the concentration C_0, where the adsorption isotherm changes its slope. It can be seen from Fig. 6 that the adsorption density Γ, at the C_0 (point of inflexion between region 2 to 3) is constant ($1.17 \times \times 10^{-10}$ mole/cm^2), depending on the number of surface charges. For silica-alumina used, previous work[11] showed that at pH 7 the net surface charge (in 0.001 mole/l KNO_3 solution) is 1.03×10^{-10} mole OH^-/cm^2 ($\sigma = = -1 \times 10^{-5}$ coul/cm^2), and literature data [12-14] indicate values from 0.93×10^{-10} to 2.06×10^{-10} mole OH^-/cm^2. At pH 7, the silica-alumina is negatively charged because of hydroxylation of the surface and acidic dissociation of the surface hydroxyl groups. [15] The value of 1.17×10^{-10} mole/cm^2 found from adsorption data at C_0 corresponds very well with values for the negative surface charge density of S.A. particles determined by other methods.

The surfactants concentrations corresponding to the first change in slope of isotherms and mobility curves, H.M.C., as well as the surfactans concentrations corresponding to zero charge density of particles, C_0, are listed in Table 1.

In region 3, after the net charge becomes zero, the surfactant ions that associate with those ions that are already absorbed might adsorb with the polar head away from the surface, since this reduces the repulsion between the ionic heads, and the sign of the net electrical charge at the interface is reversed (Fig. 7). Over this region the surface active cation is adsorbing into a surface which has a net positive charge and hence the electrostatic contribution to the free energy of adsorption does not favour adsorption. The adsorption process in this region must be motivated

---

[12] Kozo Tanabe "Solid Acids and Bases", Kodansha, Tokyo, Academic Press, New York-London, 1970, p. 58.

[13] M. R. Basila, T. R. Kantner and K. H. Rhec, *J. Phys. Chem.*, **68**, 3197 (1964).

[14] W. K. Hall, H. P. Leftin, F. J. Cheselske and D. E. O'Reilly, *J. Catalysis*, **2**, (1963).

[15] G. A. Parks, *Chem. Rev.*, **65**, 177 (1965).

Table 1

The characteristic points of inflexion of isotherms and electrokinetic curves for adsorption of cationic surfactants on silica-alumina (pH7 and 25°)

Compund	Abbreviation	H.M.C.[a] (mole/l)		C_0^b(mole/l)	
		from isotherm	from mobilities	from isotherm	from mobilities
$C_{10}H_{21}NC_5H_5Cl$	C_{10}	8.0×10^{-2}	1.0×10^{-2}	2.95×10^{-2}	4.4×10^{-2}
$C_{12}H_{25}NC_5H_5Cl$	C_{12}	1.7×10^{-3}	3.2×10^{-3}	5.90×10^{-3}	8.0×10^{-3}
$C_{12}H_{25}OCH_2CH_2NC_5H_5Cl$	$C_{12}E_1$	1.13×10^{-3}	—	3.32×10^{-3}	—
$C_{12}H_{25}(OCH_2CH_2)_2NC_5H_5Cl$	$C_{12}E_2$	8.0×10^{-4}	—	2.64×10^{-3}	—
$C_{16}H_{33}NC_5H_5Cl$	C_{16}	1.0×10^{-4}	1.8×10^{-4}	3.50×10^{-4}	2.8×10^{-4}
$C_{16}H_{33}OCH_2CH_2NC_5H_5Cl$	$C_{16}E_1$	3.2×10^{-5}	—	1.30×10^{-4}	—
$C_{16}H_{33}(OCH_2CH_2)_2NC_5H_5Cl$	$C_{16}E_2$	2.0×10^{-5}	—	6.32×10^{-5}	—

a "Hemimicelle concentration".

b Equilibrium concentration of surfactants needed to make the net charge densites of the solid particles zero.

by the decrease in free energy occurring on removing the alkyl chain from the solution.

In region 4, as the solution critical micelle concentration (C.M.C.) of the cationic surfactants is approached, an increase in adsorption occurs, which suggests a strong association of the alkyl chains on the surface [16] or the adsorption of small aggregates resulting from dimerization or premicellization. [17,18]

For all alkylpyridinium chlorides, the saturation value of adsorption was reached at an equilibrium concentration corresponding to C.M.C. value for each surfactant. The C.M.C. values are indicated by arrows on isotherms. The same results were obtained for the adsorption of alkyltrimethylammonium chlorides on S.A.[19] This region of the isotherms is governed by the energetics that control micelle formation in solution and hemimicelle formation at the solid-liquid interface. The constant value of adsorption at the C.M.C. indicates that the micelle formation in solution is preferred.

The standard free energies of micelle (ΔG_M) and hemimicelle (ΔG_{HM}) formation can be similarly expressed as

$$\Delta G_M = \Delta G_{e(M)} + \Delta G_h \tag{3}$$

and

$$\Delta G_{HM} = \Delta G_{e(HM)} + \Delta G_h \tag{4}$$

where G_h is the standard free-energy change associated with hydrophobic interactions in the system, and $G_{e(M)}$ and $G_{e(HM)}$ are electrostatic free-energy terms associated with micelle and hemimicelle formation, respectively. The surface charge being opposite in sign to that of the surfactant ion means that $G_{e(\mathrm{HM})}$ is in fact negative whereas $G_{e(\mathrm{M})}$ positive. Since G_h is always negative,[20–22] hemimicelle formation at an interface will occur at a much lower concentration than micelle formation (Fig. 6). The total free energy over CH_2 group for transfer of the alkyl chains during hemimicelle formation $\Phi_{h(\mathrm{sl})}$, was found to be larger than the corresponding total energy obtained for the formation of micelles of ionic surfactants Φ_m.

---

[16] P. CONNOR and R. H. OTTEWILL, *J. Colloid Interface Sci.*, **37**, 642 (1971).

[17] J. S. CLUNIE, J. F. GOODMAN and P. C. SYMONS, *Trans. Faraday Soc.*, **63**, 754 (1967).

[18] P. MUKERJEE "Advances in Colloid and Interface Science", vol. **1**, Elsevier, Amsterdam, 1967, p. 241.

[19] S. TILENSCHI and M. OLTEANU, Al 39-lea Congres Internaţional de Chimie Industrială, Vol. 4, Bucharest, 1970, p. 15/29.

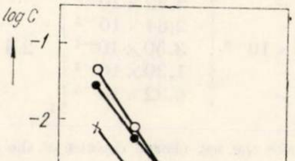

Fig. 8. — Plot of log C of alkylpyridinium chlorides as a function of the number of carbon atoms in the alkyl chain; log H.M.C. (×); log C from adsorption data (●); log C_0 from electrokinetic data (○); values for C_nE_1 compounds (□); values of C_nE_2 compounds (△).

The values for Φ were found to be in the range of $-0.71\ kT$ to $-0.98\ kT$ for hemimicellization and $-\ 0.61\ kT$ to $-0.69\ kT$ for micellization.[7] At saturation of the adsorption isotherms, the electrostatic contribution to the free energy of adsorption $G_{e(\mathrm{HM})}$ is positive, and only the G_h terms remain to decide between hemimicelle or micelle formation. The transfer energy per CH_2 group from aqueous environment to micelle, excluding the electrostatic energy term, was found to be $-1.04\ kT$ to $-\ 1.13\ kT$,[23] more negative than $\Phi_{h(\mathrm{sl})}$ (maximum $-\ 0.98\ kT$) and the transfer in micelle is favoured. This might be partly due to the possible higher restriction in the movement of the molecules in the hemimicelles than in the micelles. The larger exposure to the aqueous environment of the portions of the alkyl chains in the hemimicelle than in the micelle must also certainly be taken into account.

From the data of Table 1 it can be seen that the H.M.C. and C_0 values decrease as the alkyl chain length of the cationic compounds increases.

A plot of log H.M.C. as a function of the number of carbon atoms in the chain gives a straight line (Fig. 8).

---

[20] H. S. Frank and M. W. Evans, *J. Chem. Phys.*, **13** , 507 (1945).

[21] G. Nemethy and H. A. Scheraga, *J. Chem. Phys.*,**36**, 3401 (1962).

[22] G. Nemethy and H. A. Scheraga, *J. Phys. Chem.*, **66**, 1773 (1962); *ibid.*, **67**, 2888 (1963).

[23] K. Schinoda, *J. Phys. Chem.*, **58**, 1136 (1954); *ibid.*, **59**, 432 (1955).

The slope of this line is the free energy of cohesion per CH_2 group in the hemimicelle, in units of kT, according to the equation

$$\text{H.M.C.} = A \exp. [(W_e + n\,\Phi_{h(sl)})/kT] \qquad (5)$$

developed for hemimicelle formation by analogy to micelle formation [23]; n is the number of CH_2 groups in the chain; W_e is the electrical part of the free energy of hemimicelle formation, assumed to be independent of the chain length; A is a constant; k is the Boltzmann constant and T is the absolute temperature. Equation (5) in logarithmic form gives a slope equal to $-\Phi/2.3\,kT$.

Variation of log concentration of alkylpyridinium chlorides at zero electrophoretic mobility (or at zero surface charge density) as a function of alkyl chain length have to present the same linear trend, with the slope having the same value, as predicted by Stern-Grahame model of the electrical double layer (Fig. 8).

Grahame's treatment of the compact double layer, [24] based on Stern's original concept, [25] leads to an expression for the adsorption of positive counterions at the Stern plane * (δ) which is of the form

$$\Gamma_\delta^+ = 2rC \exp(-W_\delta/kT) \qquad (6)$$

where r is the radius of the adsorbed ion at the plane δ and W_δ is the work to bring the ion from the bulk of the solution up to the plane. The work W_δ can be divided into electrostatic $ze\,\psi_\delta$ and chemical work terms so that for cation adsorption,

$$W_\delta = z_+\, e\psi_\delta - n\Phi_{h(sl)} \qquad (7)$$

where z is the valence, e is the electronic charge and ψ_δ the potential at plane δ.

The adsorption isotherm is described by

$$\Gamma_\delta^+ = 2rC \exp(z_+\, e\,\psi_\delta - n\Phi_{h(sl)})/kT \qquad (8)$$

If after association of the alkyl chains the potential ψ_δ is reduced to zero, it follows from equation (8) that

$$\log C_0 = -\, n\,(\Phi_{h(sl)}/2.3\,kT) \qquad (9)$$

if the ratio of the adsorption density at $\psi_\delta = 0$ to the factor $2r$ is relatively independent of chain length. The linear relation between $\log C_0$

---

[24] D. C. Grahame, *Chem. Rev.*, **40**, 441 (1947).

[25] O. Stern, *Z. Elektrochem.*, **30**, 508 (1924).

* δ is the distance of closest approach of positive counterions to the negative solid surface

and n is verified in Fig. 8. A convenient measure of ψ_δ is the electrokinetic or ξ-potential who are calculated from experimental electrophoretic mobility.

The values obtained from the slopes of Fig. 8 for the free energy per CH_2 group, $\Phi_{h(sl)}$, in units of kT, for transfer of alkyl chains from aqueous solution to solid-liquid interface are given in Table 2.

Table 2

Free-energy change $\Phi_{h(sl)}$, per CH_2 groups for transfer of alkyl chains from aqueous solution to solid-liquid interface (n = number of carbon atoms in the alkyl chain)

From	$\Phi_{h(sl)}$	$\triangle G$/mole CH_2(cal/mole)
Adsorption data		
H.M.C. vs.n	-0.7 kT	-420
Co vs. n	-0.735 kT	-421
Electrokinetic data		
H.M.C. vs.n	-0.69 kT	-414
Co vs. n	-0.832 kT	-499

In order to analyse the effect of the presence of one or two $-CH_2CH_2O-$ groups between the alkyl chain and the ionic head group on the adsorption, it is necessary to compare the behaviour of the new compounds with that of simple alkylpyridinium compounds. This can be done by examining the variation of the H.M.C. values with changes in structure of the surfactant molecule. The H.M.C. values taken from Table 1 for alkyloxyethylenepyridinium compounds are included along the line of Fig. 8. In this way it is possible to assign an effective number of CH_2 groups to each C_nE_x – type surfactant, or an effective alkyl chain length. The effective alkyl chain lengths taken from Fig. 8 are listed in Table 3.

Table 3

Effective alkyl chain-lengths for alkyloxyethylenepiridinium and alkyldioxyethylenepiridinium chlorides adsorbed on silica-alumina at pH 7 and 25°

Compound	Effective alkyl chain length
$C_{12}E_1$	12.8
$C_{12}E_2$	13.2
$C_{16}E_1$	17.4
$C_{16}E_2$	18.4

Thus one can conclude that oxyethylene groups occurring between an alkyl chain and ionic group produce an increase in the number of the CH_2 – groups involved in the formation of hydrophobic bonds. This is the same conclusion deduced from C.M.C. values of these compounds .[10]

This result further establishes the basic assumption in the hemimicelle model of surfactant adsorption, viz., that hydrophobic [interactions, identical to those operative in micelle formation, control the nature of the adsorption of surfactant molecules.

Revue Roumaine de Chimie, 20, 8, 1051–1055 (1975)

INTERDIFFUSION COEFFICIENT OF Tl^+ AND Cd^{2+} IN FUSED ALKALI CHLORIDES BY THE CHRONOPOTENTIOMETRIC METHOD

CONSTANȚA HERDLICKA and S. STERNBERG
Institute of Physical Chemistry
str. Galați 31, Bucharest, Romania

Received May 13, 1974

The interdiffusion coefficients of Tl^+ in NaCl+KCl (1 : 1) and RbCl and of CD^{2+} in NaCl and KCl have been determined at several temperatures by the chronopotentiometric method. The following equations for the dependence on interdiffusion coefficients on temperature have been found : $D_{Tl^+} = (5.16 \pm 1.20)\ 10^{-3} \exp\ [-(8526 \pm 202)/RT]$ in NaCl + KCl(1 : 1); $D_{Cd^{2+}} = (2.97 \pm 2.00)\ 10^{-3} \exp\ [-(8055 \pm 617)/RT]$ in NaCl and $D_{Cd^{2+}} = (1.12 \pm 0.31)\ 10^{-3} \exp\ [-(6209 \pm 256)/RT]$ in KCl. D_{Tl^+} in RbCl is 5.25×10^{-5} at 730° and 5.74×10^{-5} cm²/sec at 750°.

INTRODUCTION

Previously published papers [1–4] have presented experimental values of interdiffusion coefficients and activation energies for diffusion of Ag^+ in nitrates[1,2] and alkali chlorides [3] and of Pb^{2+} in alkali halides [4] as determined by the chronopotentiometric method. The data have been interpreted in terms of structure parameters of both diffusing ion and the medium in which it diffuses, and have been correlated to other transport properties.

The present paper features data for Tl^+ ions in NaCl+KCl of equimolecular composition and in RbCl and Cd^{2+} in NaCl and KCl at various temperatures all determined by the chronopotentiometric method.

EXPERIMENTAL

The electrolysis cell and the device have been described elsewhere.[1–5] The working electrode was a platinum disk attached to a platinum wire ; this geometry of the electrode was preferred to a rectangular one since it allows a uniform distribution of the current over electrode surface. The effective working surface area of the electrode, consisting of the disk and 1 mm of supporting wire measured by a micrometer, was 0.60 cm².

---

[1] S. Sternberg and C. Herdlicka, *Rev. Roumaine Chim.*, **14**, 991 (1969).
[2] S. Sternberg and C. Herdlicka, *Rev. Roumaine Chim.*, **15**, 343 (1970).
[3] S. Sternberg and C. Herdlicka, *Rev. Roumaine Chim.*, **17**, 343 (1972).
[4] C. Herdlicka and S. Sternberg, *Rev. Roumaine Chim.*, **18**, 1689 (1973).
[5] S. Sternberg and C. Herdlicka, *Rev. Roumaine Chim.*, **19**, 197 (1974).

The auxiliary electrode was a platinum plate of 3 cm^2 surface area.

The reference electrode consisted of a silver wire introduced in a silica test tube containing a mixture of AgCl (0.I.M.) with the solvent in which diffusion measurements were carried out. The electric contact with the solution under study was made through the thin wall of silica test tube.

The three electrodes were kept in separate compartments.

The potential-time curves were recorded by a RFT-magneto-optic oscillograph.

The measurements were carried out for concentration of diffusing substances TlCl or $CdCl_2$ ranging between 3×10^{-5} and 7×10^{-5} mole/cm^3 and current densities of 25×10^{-3} to 12×10^{-2} A/cm^2. At constant temperature runs were conducted, for each concentration, at 5—6 current densities. At least three chronopotentiograms were recorded for each current density and the transition time was averaged.

The transition time for the concentrations and current densities selected was within 0.5—1.2 sec; thus the conditions of liniar semi-infinite diffusion were fulfilled.

The substances used in measurements have been p.a. reagent grade. Alkali chlorides have been recrystallized from aqueous solutions, dried, premelted in HCl atmosphere. To make diffusion measurement, the electrolysis cell was loaded with alkali chloride which was pumped for 2—3 hours and then melted in argon atmosphere. After melting argon has been bubbled to eliminate dissolved HCl. The purity of fused alkali chloride was checked by recording potential-time curve in the absence of the diffusing substance; the sudden increase of potential to the value of decomposing potential of alkali chloride proved the absence of any electrochemically active substance.

The diffusing substance, TlCl and $CdCl_2$-reagent grade have been melted in closed cells, then brought to boiling and the vapours caught and condensed in ampoules which were closed in flame as soon as distillation was terminated. Both salts obtained in this way were free of water and other impurities.

RESULTS AND DISCUSSION

Measurements have been performed within 100° above melting point for diffusion of Tl^+ in equimolecular NaCl+KCl mixture, at 730 and 750° for diffusion of Tl^+ in RbCl and within 80° above melting point for Cd^{2+} in NaCl and KCl.

The interdiffusion coefficient was calculated by Sand's equation:

$$\tau^2 = nF\,\pi^{1/2}\,D^{1/2}\,C/2i_0$$

where τ (sec) stands for transition time, i_0 (A/cm^2) for current density, D (cm^2/sec) for diffusion coefficient, C (mole/cm^3) for bulk concentration of electrochemically active substance, n for the number of electrons participating in electrode reaction and F (coulombs) for Faraday constant.

In Tables 1 and 2 the values of interdiffusion coefficients of Tl^+ and Cd^{2+} in the studied solvents are listed.

The working temperature for diffusion of Tl^+ has not exceeded 760° due to thermal decomposing of TlCl which boils at 806°. That is why no experiments have been carried out in single NaCl and KCl.

Figures 1, 2 and 3 show plots of the logarithm of interdiffusion coefficient of Tl^+ and Cd^{2+} vs the reciprocal of absolute temperature, together with data for diffusion of Ag^+ and Pb^{2+} previously obtained.[1–4] As illustrated by these figures the systems under study, like in the case of Ag^+ and Pb^{2+} diffusion, have an Arrhenius behaviour. The equations of lines which

Table 1

The interdiffusion coefficient of Tl^+ in molten $NaCl + KCl$ (1 : 1) and RbCl

Solvent	Temp °C	$D_{Tl^+} \times 10^5$ $cm^2\ sec^{-1}$
NaCl+KCl (1 : 1)	672	5.70
	680	5.81
	685	5.83
	693	6.05
	696	6.28
	704	6.23
	711	6.28
	713	6.48
	721	6.85
	727	7.22
	741	7.67
	752	8.19
	762	8.26
	768	8.16
RbCl	730	5.25
	750	5.74

Table 2

The interdiffusion coefficient of Cd^{2+} in molten NaCl and KCl

NaCl		KCl	
Temp. °C	$D_{Cd^{2+}} \times 10^5$ $cm^2\ sec^{-1}$	Temp. °C	$D_{Cd^{2+}} \times 10^5$ $cm^2\ sec^{-1}$
825	7.43	777	5.76
834	7.88	794	5.90
852	7.92	797	6.07
863	8.13	802	6.36
870	8.64	831	6.49
880	9.13	862	7.27

described the temperature dependence of interdiffusion coefficient obtained by the least square method are as follows :

$$TlCl + (NaCl+KCl)$$

$$D_{Tl^+} = (5.16 \pm 1.20)\, 10^{-3} \exp\left(-\frac{8526 \pm 202}{RT}\right) \quad (672 - 768°)$$

$$CdCl_2 + NaCl$$

$$D_{Cd^{2+}} = (2.97 \pm 2.00)\, 10^{-3} \exp\left(-\frac{8055 \pm 617}{RT}\right) \quad (825 - 880°)$$

$$CdCl_2 + KCl$$

$$D_{Cd^{2+}} = (1.12 \pm 0.31)\, 10^{-3} \exp\left(-\frac{6209 \pm 256}{RT}\right) \quad (777 - 862°)$$

At the same temperature, the interdiffusion coefficient of Tl^+ in $NaCl+KCl$ (1:1) is smaller than that of Ag^+ in the same solvent which was to be expected given the ionic radius, larger for Tl^+ (1.40 A°) than for Ag^+(1.26 A°) and the similar structures of fused AgCl and TlCl. The same is true for interdiffusion Tl^+ and Ag^+ in RbCl; e.g. at 750°, D_{Tl^+} is 5.74×10^{-5} while D_{Ag^+} is 6.88×10^{-5} cm^2 /sec.

Another comparison may be drawn between interdiffusion coefficient of Tl^+ in RbCl and of Rb^+ in Rb Cl.[6] Since ionic dimensions of Tl^+ and Rb^+ are similar (1.40 and 1.48 A° respectively) we would expect the two diffusion coefficients to be similar.

[6] J. O'M Bockris, S. R. Richards and L. Nanis, *J. Phys. Chem.*, **69**, 1627 (1965).

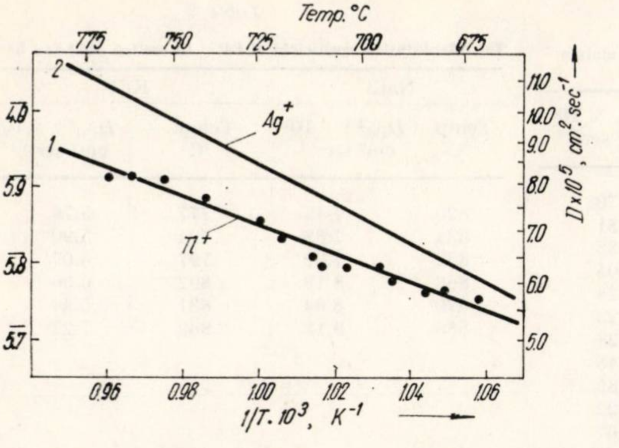

Fig. 1. – Arrhenius eq. plot for the interdiffusion coefficient of Tl^+ (1) and Ag^+ (2) in NaCl + KCl 1 :1.

1, present work; *2*, ref. [3].

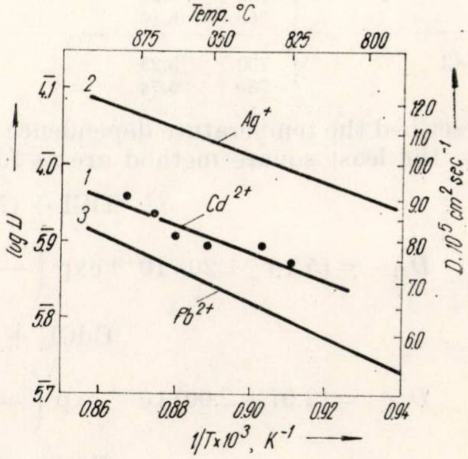

Fig. 2. – Arrhenius eq. plot for the interdiffusion coefficient of Cd^{2+} (1), Ag^+ (2) and Pb^{2+} (3) in NaCl.

1, present work; *2*, ref. [3]; *3*, ref. [4].

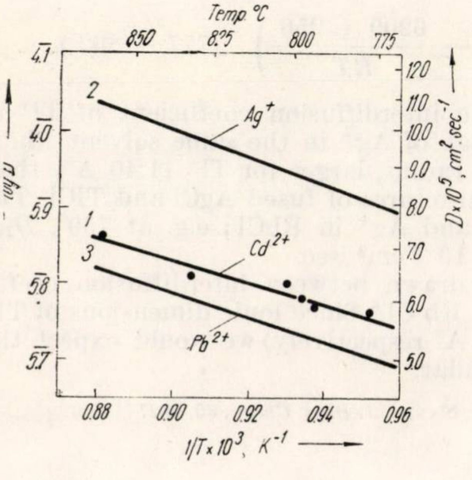

Fig. 3. – Arrhenius eq. plot for the interdiffusion coefficient of Cd^{2+} (1), Ag^+ (2) and Pb^{2+} (3) in KCl.

1, present work; *2*, ref. [3]; *3*, ref. [4].

In fact D_{Tl^+} is higher than D_{Rb^+} in RbCl (at 750° the self-diffusion coefficient of Rb^+ is 4.88×10^{-5} cm²/sec). Thus one may say that ionic radius is not the only criterion for the explanation of values of diffusion coefficient, yet one should consider the type of ionic interaction between the diffusing substance and the diffusion medium.

Figure 4 plotted the values of interdiffusion coefficients of some metallic ions in NaCl+KCl (1 : 1) available in the literature against ionic charge density.

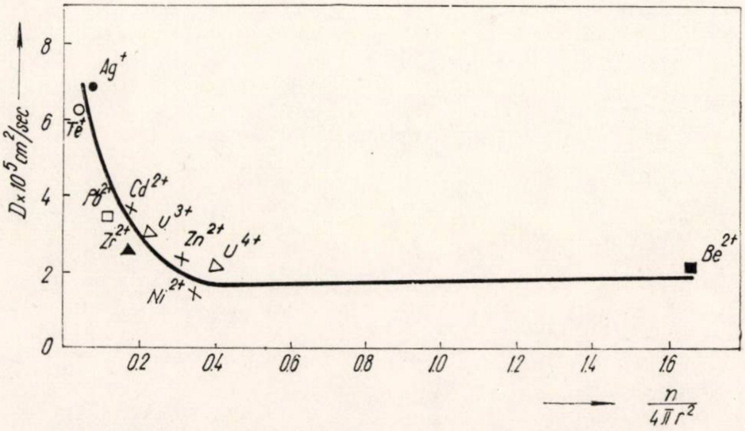

Fig. 4. — The interdiffusion coefficient of several metallic ions in NaCl + KCl (1 :1) at 710° as function of charge density of diffusing ions. ▲ — ref. [7]; ■ ref. [8]; × — ref. [9]; □ — ref. [10]; Δ — ref. [11].

The highest values are characteristic of monovalent ions whose charge density is lower than that of polyvalent ions. These latter, although of low ionic radii, are more strongly bonded to the anion and have a much lower ability to move due to their high charge density.

The interdiffusion of ions of various charges and radii into single alkali halides has scarcely been studied. Our data regarding interdiffusion of Cd^{2+} in NaCl and KCl may be compared to interdiffusion of Ag^+ and Pb^{2+}.

One can see from figures 2 and 3 that $D_{\mathrm{Cd}^{2+}}$ is smaller than D_{Ag^+} and closer to $D_{\mathrm{Pb}^{2+}}$. Although the three ions are of similar radii the diffusing mobility of bivalent ions is lower than that of Ag^+ which confirms what was said above.

---

[7] A. N. Baraboshkin, M. V. Smirnov and N. A. Saltykova, "Electrockhimia Rasplavlenikh Solevikh i Tviordkh Elektrolitov", Inst. Electrokhim. Akad. Nauk, U.R.S.S. — Uralsk Filial nº 2, 1961, p. 53.

[8] I. F. Nichkov, E. A. Novikov, E. A. Raspopin and S. P. Butorov, *Zhur. priklad. Khim.*, **42**, 2828 (1969).

[9] Y. K. Delimarskii, A. V. Gorodyskii and V. V. Kuzmovitch, *Coll. Czech. Chem. Comm.*, **25**, 3056 (1960).

[10] R. B. Stein, *J. Electrochem. Soc.*, **106**, 528 (1959).

[11] O. V. Skiba, M. V. Smirnov and T. F. Khazemova, "Electrochimistry of Molten and Solid Electrolytes", translation of Consultants Bureau, New York, Ed. by M. V. Smirnov, 1964, p. 7.

In fact D_{Ag^+} is higher than D_{Na^+} in RbCl (at 750° the self-diffusion coefficient of Rb+ is 1.8 × 10^{-5} cm²/sec). Thus one may say that ionic radius is not the only criterion for the explanation of values of diffusion coefficient, yet one should consider the type of ionic interaction between the diffusing substance and the diffusion medium.

Figure 4 plotted the values of interdiffusion coefficients of some metallic ions in NaCl + KCl (1 : 1) available in the literature against ionic charge density.

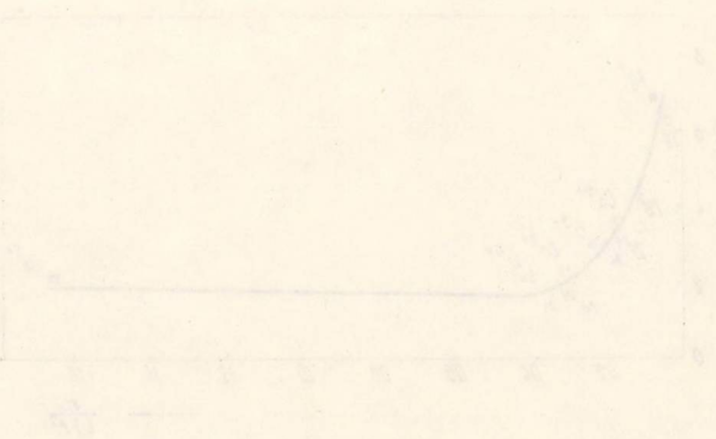

Fig. 4. – The interdiffusion coefficient of several metallic ions in NaCl + KCl (1 : 1) at 700° as function of charge density of diffusing ions.
▲ – ref. 7; ■ ref. 8; × – ref. 9; □ – ref. 10; △ – ref. 11.

The highest values are characteristic of monovalent ions whose charge density is lower than that of polyvalent ions. These latter, although of low ionic radii, are more strongly bonded to the anion and have a much lower ability to move due to their high charge density.

The interdiffusion of ions of various charges and radii into single alkali halides has scarcely been studied. Our data regarding interdiffusion of Cd2+ in NaCl and KCl may be compared to interdiffusion of Ag+ and Pb2+.

One can see from figures 2 and 3 that $D_{Cd^{2+}}$ is smaller than D_{Ag^+} and closer to $D_{Pb^{2+}}$. Although the three ions are of similar radii the diffusing mobility of bivalent ions is lower than that of Ag+ which confirms what was said above.

[7] A. N. Baraboshkin, N. V. Sumarev and N. A. Saltykova, "Elektrokhimiya Rasplavlennykh i Tverdykh Elektrolitov", Trud. Inst. Elektrokhim. Akad. Nauk. S.S.S.R. Ural. Filial 2, 1961, p. 35.

[8] I. F. Nichkov, I. A. Novikov, E. S. Filatov and S. P. Raspopin, Zhur. prikl. Khim., 42, 2258 (1969).

[9] K. Daněk, A. V. Golubkov and V. V. Kuznetsov, Coll. Czech. Chem. Comm., 34, 3565 (1969).

[10] H. Bloom, J. Electrochem. Soc., 106, 528 (1959).

[11] O. V. Lesin, H. V. Sumarev and A. N. Baraboshkin, "Electrochemistry of Molten and Solid Electrolytes", translation of Consultants Bureau, New York, Ed. by M. V. Smirnov, 1961, p. 7.

Revue Roumaine de Chimie, **20**, *8*, 1057–1063 (1975)

THE INDUCTION TIME FOR PITTING CORROSION

SULTANA CIOLAC
Institute of Physical Chemistry
Str. Galaţi 31, Bucharest, Romania

Received May 23, 1974

The induction time for pitting corrosion is determined from galvanostatic polarization, as function of temperature and pH of a 0.1 mol. KCl deaerated solution. Potential-time diagram is divided in three regions : pits initiation, reaction and protection, analogous with cyclic $E-i$ potentiostatic diagram. A comparison between galvanostatic and potentiostatic results is made.

As some other types of localized corrosion (crevice, stress corrosion cracking), pitting process develops in two stages : initiation and propagation. The differences between the different types of localized attack proceed from the initiation stage, in the second stage they acting and having very much in common.[1–9]

Starting of a local attack requires that on the metallic surface, some specific conditions to be established, which in turn suppose that a certain "induction period" to be consumed.

The induction period for pitting may be justified in two ways depending on the considered kinetic mechanism.

From the penetration theory point of view, the induction period represents the time necessary for the aggressive anions to pass across the passive film .[10–12]

The adsorption theory considers the induction period as the time required for a critical concentration of aggressive anion to be achieved on some locations of the surface, as a result of potential shift in the noble direction.[6,13]

---

[1] B. E. Wilde and E. Williams. *J. Electrochem, Soc.*, **118**, 1057 (1971).

[2] B. E. Wilde, *Corrosion*, **28**, 283 (1972).

[3] B. E. Wilde and E. Williams, *Electrochim. Acta*, **16**, 1971 (1971).

[4] B. F. Brown, *Corrosion*, **26**, 243 (1970).

[5] M. A. Streicher, *J. Electrochem. Soc.*, **103**, 375 (1956).

[6] Ya. M. Kolotirkin, *Corrosion*, **19**, 261 t (1963).

[7] I. L. Rosenfeld, "4th European Congress Coal and Steel Company", 1968, p. 3.

[8] N. D. Green and M. G. Fontana, *Corrosion*, **15**, 39t (1959).

[9] Y. Kitamura and T. Suzuki, "Proceedings to the Fourth International Congress on Metallic Corrosion", Amsterdam, 1969, p. 716.

[10] B. A. Legault and N. Walker, *Corrosion*, **20**, 282t (1964).

[11] G. M. Schimidt and M. Hackerman, *J. Electrochem. Soc.*, **108**, 741 (1961).

[12] D. A. Jones, *Corrosion*, **25**, 187 (1969).

[13] H. P. Leckie and H. H. Uhlig, *J. Electrochem. Soc.*, **118**, 1262 (1966).

The available data have evidenced that the induction period (time) for pitting depends on the potential, the surface homogeneity, presence of stirring and concentration of the aggressive anions.[3, 5, 6, 14–17]

The purpose of present work is to assess the effect of temperature and pH on the induction time for pitting produced on two austenitic stainless steels.

EXPERIMENTAL

The tested materials, having the compositions presented in table 1, have been used as cylindrical electrodes with an average surface of 6 sq. cm.

Table 1

Chemical compositions of stainless steels (%)

N°	C	S	P	Si	Mn	Cr	Ni	Ti	Mo	Fe
1	0.05	0.007	0.03	0.4	1.34	17.7	8.79	0.52	0.07	balance
2	0.08	0.01	0.21	0.09	1.82	16.9	12.23	0.7	2.23	balance

After polishing with emery paper and fixing in the holder, the electrodes were degreased in boiling benzene and then pickled for 5 minutes in a HNO_3+HF+H_2O mixture at 90°.

The measurements were taken in argon deaerated 0.1 mol. KCl at different temperatures (±0.1 accuracy) or pH-adjusted electrolyte (H_2SO_4, KOH) at 25°. The solutions were prepared from reagent grade chemicals and double-distilled water.

The determinations of the induction time were made galvanostatically, using a modified N. D. Stolica procedure.[16]

A glass polarization cell provided with a platinum electrode, Luggin capillary connected with the calomel electrode, was used.

A polarization of the tested steel in 1N H_2SO_4 at room temperature was performed, applying at first 10 mA/ sq. cm. for 5 minutes and then 1 mA/sq. cm. for 45 minutes.

Thereafter, the test was quickly washed with tap and distilled water and immersed in the electrochemical cell containing deaerated and thermostated electrolyte of interest.

The same current density of 1 mA/sq. cm. was maintained for polarization of the electrode immersed in the electrolyte containing Cl^- ions.

As a result of prepolarization, the potential of the test raises to (E_1 =) 1300–1400 mV.

The change of the potential in time was registered on a SEFRAM chart recorder of 300 mm/minute rolling speed.

Depending on the experimental conditions, a sharp decrease in the potential is observed, defining the induction time (t_i) value for pitting,

On the basis of N. D. Stolica's data and from our observations the following schematic diagram may be drawn up for $E - t$ variation :

where : E_1 — is the potential of the metal after prepolarization in $1NH_2SO_4$

AB — is the range of constant potential defining the induction period for pitting $= t_i$ (induction time)

BC — the reaction period, covering a potential region $\Delta E = E_1 - E_2$

CD — (corresponding to E_2) represents the end of the pitting process.

The completions brought in the diagram will be further discussed.

---

[14] M. Pourbaix and F. Vandervalden, *Corrosion Sci.*, **5**, 81 (1965).

[15] H. I. Engell and N. D. Stolica, *Z. phys. Chem. N. F.*, **20**, 113 (1959).

[16] N. D. Stolica, *Corrosion Sci.*, **9**, 205 (1969).

[17] Z. Sklarska-Smialowska and M. Janik-Czachor, *Corrosion Sci.*, **11**, 901 (1971).

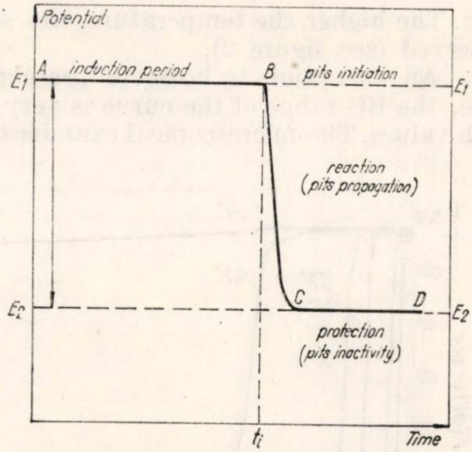

Fig. 1. — A schematic galvanostatic $E - t$ diagram for induction time of pits nucleation determination.

The results, that are going to be reported, concern both the t_i and E_2 values. The induction time, t_i, was considered as the last time for which E_1 keeps constant. The potential E_2 is measured after 5 minutes of polarization.

RESULTS

THE EFFECT OF PREPOLARIZATION TIME

Experimental observations were performed to establish the effect of the prepolarization time in 1 N. H_2SO_4, on the value of the induction time and E_2 potential, determined in 0.1 mol. KCl.

So, the prepolarization at 1 mA/sq, cm. was applied for different times and the values t_i and E_2 noted down.

The obtained results are listed in table 2, showing that both t_i and E_2 are practically unaffected by the time of prepolarization.

Table 2

The effect of prepolarization time on t_i and E_2 of № 1 stainless steel, determined at 25° in 0.1 mol. KCl

Prepolarization time minutes	t_i minutes $\times 10^{-1}$	E_2 mV/vs.s.c.e.
15	0.50	230
30	0.56	250
45	0.53	300
70	0.50	220
100	0.50	250

THE EFFECT OF TEMPERATURE

Potential-time curves recorded for both stainless steels in 0.1 mol. KCl, for most of the temperatures studied follows an ABCD type of variation. The higher the temperature, the sharper decrease in the potential is observed (see figure 2).

An exception is however present for lower temperatures. In this case, the BC range of the curve is very narrow, the potential keeping at high values. The microscopical examination of the surface after a 5 minutes polarization, evidenced the presence of a large number of pits, formed in the transpassive region of potential. The difficulty arising from BC range estimation, has determined us not to take measurements at lower temperatures.

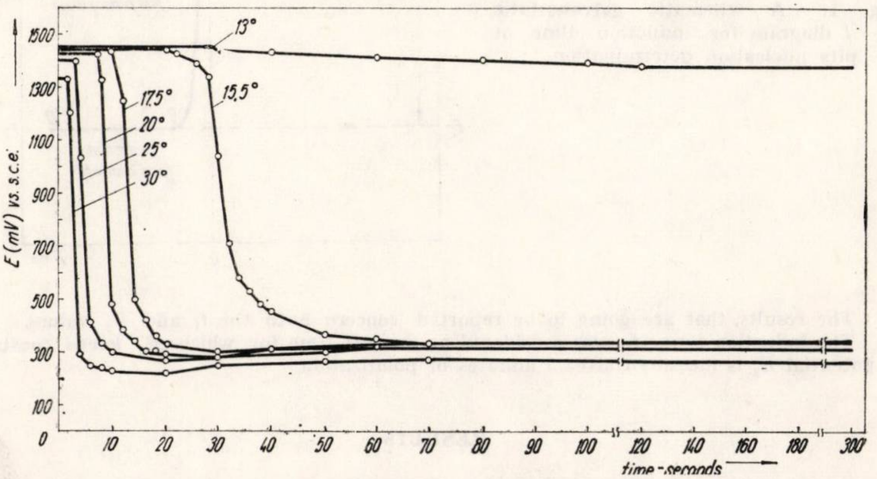

Fig. 2. — Potential-time curves for stainless steels N° 1 in 0.1 mol. KCl solution at different temperatures.

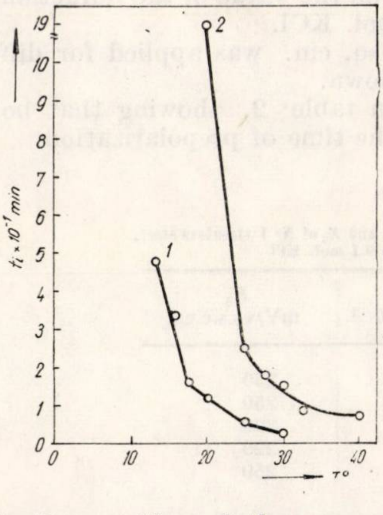

Fig. 3. — The dependence of the induction time on the temperature for both stainless steels.

The $t_i = f(^0T)$ dependences for both stainless steels in 0.1 mol. KCl solution are plotted in figure 3.

An exponential dependence of the induction time on the temperature is thus found. It evidently results from the above figure, that stainless steel N° 2 having a higher content of nickel and molybdenum (12.23 % Ni ; 2.23 % Mo) is more resistant to pitting than stainless steel N° 1 (8.79 % Ni; 0.07 % Mo) initiation.

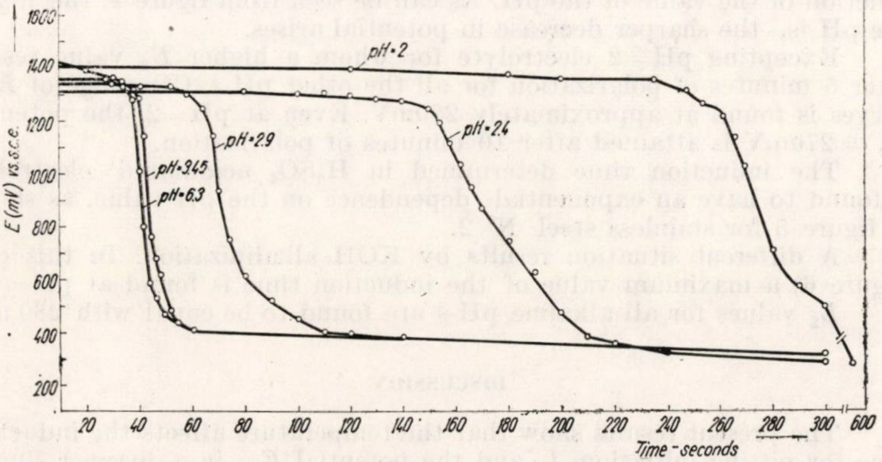

Fig. 4. — The effect of acidic pH on the $E - t$ curves of N° 2 stainless steel at 25°.

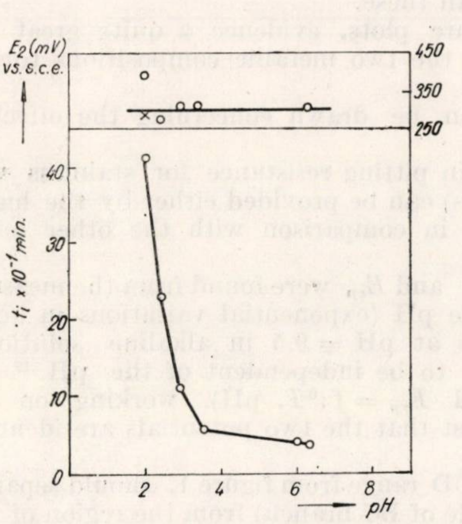

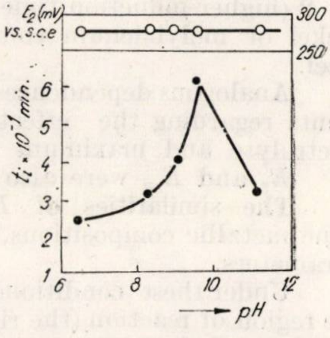

Fig. 5. — The variation of the induction time and E_2 potential of N° 2 stainless steel with the pH of 0.1 mol. KCl solution, sulphuric acid acidulated.

Fig. 6. — The dependence of the induction time and E_2 potential of N° 2 stainless steel with the alkaline pH of 0.1 mol. KCl solution.

The same exponential variation would result plotting $E_2 = f(^0T)$.

THE EFFECT OF THE pH

The effect of the pH was studied at 25° by adjusting the pH of 0.1 mol. KCl either with H_2SO_4 or KOH.

In acidic electrolyte, the shape of the potential-time curves is a function of the value of the pH. As can be seen from figure 4, the higher the pH is, the sharper decrease in potential arises.

Excepting pH=2 electrolyte for whom a higher E_2 value results after 5 minutes of polarization for all the other pH-*s*, CD range of $E-t$ curves is found at approximately 280mV. Even at pH=2, the potential $E_2 = 270$mV is attained after 10 minutes of polarization.

The induction time determined in H_2SO_4 acidulated electrolyte is found to have an exponential dependence on the pH value, as shown in figure 5 for stainless steel N° 2.

A different situation results by KOH alkalinization. In this case (figure 6) a maximum value of the induction time is found at pH=9.5.

E_2 values for all alkaline pH-s are found to be equal with 280 mV.

DISCUSSION

The present results show that the temperature affects the induction time for pitting initiation, t_i, and the potential E_2, in a manner similar to the critical pitting potential, E_{cp}, and the potential of pits repassivation, E_{rp},[18] but even stronger than these.

Induction time — temperature plots, evidence a quite great difference between the resistance of the two metallic compositions toward pitting.

However, no conclusions can be drawn concerning the effect of the metallic composition.

The improvement observed in pitting resistance for stainless steel N° 2 (higher induction time values) can be provided either by the higher nickel or molybdenum contents, in comparison with the other tested steel.

Analogous dependences of t_i and E_{cp} were found from the measurements regarding the effect of the pH (exponential variations in acidic electrolyte and maximum values at pH = 9.5 in alkaline solutions).

E_2 and E_{rp} were also found to be independent of the pH.[19]

The similarities of E_2 and $E_{rp} = f(^0T, \text{pH})$, working on the same metallic compositions, suggest that the two potentials are identical parameters.

Under these conditions, the CD range from figure 1, should separate the region of reaction (the right side of BC branch) from the region of pits inactivity (below CD).

Making a comparison with a cyclic potentiostatic diagram, the reaction period from a galvanostatic $E-t$ curve, should correspond to the region of pits propagation of the potentiostatic $E-i$ curve, and the galvanostatic region of pits inactivity should represent the corresponding region of protection defined potentiostatically.[18]

---

[18] S. Ciolac and E. Vasilescu, *Rev. Roumaine Chim.*, **19**, (1974).

[19] S. Ciolac and E. Vasilescu, *Rev. Roumaine Chim.*, **19**, (1974).

CONCLUSIONS

A comparative examination of the above data with those earlier reported is presented in table 3.

Table 3

Comparative examination of pitting characteristics function of medium parameters

Variable parameter	Type of dependence			
	E_{cp}	t_i	E_{rp}	E_2
°T	exponential (E_{cp} less sensitive than t_i)		exponential	
acidic pH ($+H_2SO_4$)	exponential (E_{cp} less sensitive than t_i)		independent $E_{rp} < E_2$	
alkaline pH (+KOH)	maximum value at pH=9.5		independent $E_{rp} < E_2$	
concentration of Cl^- ions	$E_{cp} = a + b \log a_{Cl^-}$	$1/t_i = ct. C_{Cl^-}^{16,20}$	independent[20]	

The existence of two groups of characteristics may be easily observed.

On the one hand, the critical pitting potential and the induction time are undoubtedly characteristics of pitting initiation and, on the other hand, E_{rp} and E_2 are evidently identical parameters, characterizing the propagation (reaction) stage of the pitting process.

Theoretical explanations of t_i and E_2 types of dependences function of temperature and pH should be thus the same as for E_{cp} and E_{rp}.

The apparent differences between E_{rp} and E_2 reported could proceed from the differences in the metallic surface conditions, before the exposure in chloride ions containing electrolyte (with or without prepolarization in 1N H_2SO_4).

In all studied cases E_2 is found to be higher than E_{rp} supporting the earlier concept that the protection against pitting could be realized by using those methods that interfere before or in the first stage of the pitting process development.

It appears also that the induction time for pits nucleation is more sensitive both to the medium and metallic composition changes.

It follows therefore that the determination of the induction time by galvanostatic polarization may be used as a more rapid, effective and reproducible screening tool for pitting resistance estimation than the determination of the critical pitting potential by potentiostatic polarization.

---

[20] S. Ciolac, unpublished data.

Revue Roumaine de Chimie, 20, 8, 1065—1070 (1975)

KINETICS OF OXIDATION OF SOME GLYCOLS BY BROMINE

V. P. KUDESIA*

Chemical Laboratories, D. N. College, Meerut —2, U. P. INDIA

Received May 13, 1974

The kinetics of bromine oxidation of ethane diol, propane-1,2-diol, butane-2,3-diol and pinacol has been examined. Arrhenius parameters as well as enthalpies and entropies of activation have been evaluated for various glycols. The deuterium isotope effect has also been studied and a possible mechanism involving the loss of a secondary hydrogen atom as a hydride anion in the rate determining step is suggested.

INTRODUCTION

Although several investigations have been made on the kinetics of oxidation of alcohols by aqueous bromine, no attempt has been made to investigate the kinetics of oxidation of glycols by bromine and to evaluate accurately the Arrhenius and thermodynamic activation parameters. The main aim of the study of these compounds is to know the behaviour of molecular bromine with glycols and to suggest a possible mechanism based on the experimental results.

MATERIALS AND METHOD

Diols were distilled under reduced pressure. Perchloric acid (Riedel) was used. Ionic strength was adjusted with sodium perchlorate. All other chemicals used were chemically pure.

The kinetics of bromination of glycols in 25% aqueous acetic acid was studied at different temperatures by T—60 NMR spectrometer. As the equilibrium constant for tribromide ion formation in the solvent used at 25° is 15.6[1] hence low bromine concentrations were used (The substrate concentration was $\sim .004$M and bromine $\sim 4 \times 10^{-3}$ M). The ionic strength was maintained constant at $\mu = 0.2$ by the addition of lithium perchlorate. In each experiment the concentration of sodium bromide was maintained constant at 0.1 M. to maintain the Br_3^- concentration constant throughout the reaction.

PRODUCTS ANALYSIS

The reaction of ethane diol, propane-1,2-diol, butane-2,3-diol and pinacol with aqueous bromine gave glyoxal, methyl glyoxal, acetoin and acetone respectively. The products were detected by their characteristic spot tests[2]. Acetone and α-hydroxy propionaldehyde were estimated by 2,4-dinitro phenylhydrazine method. Besides this, all the products were distilled under reduced pressure and analyzed by IR, NMR and glc techniques.

---

* This work has been done at the Laboratory of Organic Chemistry, University of Ghent, Belgium.

[1] V. P. Kudesia, *Bull. Soc. chim. belges*, **80**, 469 (1971).

[2] F. Fiegel, "Spot Tests in Organic Analysis," Elsevier Publishing Co., Amsterdam, (1956).

RESULTS AND DISCUSSION

The reaction is first order with respect to diol and first order with respect to bromine but side bromination of the products also takes place. Hence the following rate law can be proposed

$$\frac{-\,d(Br_2)}{dt} = k_1\,(Br_2)\,(\text{diol}) + k_2\,(Br_2)\,(\text{Product})$$

For getting the values of k_1 and k_2, Frost and Schwemer treatment[3] has been applied. The values (defined as A/Ao) were plotted against time. From the resulting smooth curve the amounts of the time taken by the reaction to go through various percentages of completion were determined.

The time ratios were calculated from these times for various percentages of the reaction. Now, values of $1/K$ (defined as k_1/k_2) for the reaction were obtained from these time ratios and using Frost and Schwemer tables. The average of $1/K$ values were calculated and used to obtain τ values at various given values of α. Different values of k_1 were then calculated from the formula $\tau = \mathrm{Bo}k_1 t$. The average values of $1/K$ and k_1 were used to evaluate k_2.

It was observed that the k_1 values obtained by Frost and Schwemer treatment compare well with the k_1 values calculated using ordinary second rate expression for initial percentages (25%) of reaction assuming that there was no incursion of second step.

Table 1

Rates of oxidation of some glycols at different temperatures

GLYCOL	Temp. °C	$10^2 \times k_1$ (litre mole^{-1} min^{-1})		$10^2 \times k_2$	k_1/k_2
		obs.	calc.	litre mole^{-1} min^{-1}	
Ethane diol	30	12.74	12.52	3.520	3.62
	35	15.52	16.54	5.173	3.00
	40	27.60	28.30	8.364	3.30
Propane-1,2-diol	30	18.75	19.35	3.950	4.75
	35	22.23	21.80	5.383	4.13
	40	36.05	38.80	9.389	3.84
Butane-2,3-diol	30	21.65	22.40	4.229	5.12
	35	26.20	26.80	5.610	4.67
	40	40.83	42.36	8.958	4.558
Pinacol	30	25.03	25.86	4.159	6.017
	35	33.14	34.02	6.024	5.50
	40	60.70	63.20	11.200	5.42

---

[3] A. A. Frost and W. C. Schwemer, *J. Amer. Chem. Soc.*, **74**, 1268 (1952).

The k_2 values as calculated by the above method were then checked by taking separately glycolic aldehyde, α-hydroxy propionaldehyde, acetoin and acetone. Their kinetics was studied with aqueous bromine at the same temperature and conditions which resulted that the values calculated by this procedure were about 5% higher than by the aforesaid method. This clearly exhibits that the values k_1 and k_2, as calculated by Frost and Schwemer treatment, are correct.

The second order rate constants at 30° and 35° and 40° are given in Table 1.

ACTIVATION PARAMETERS

The reactions were studied at different temperatures from 30 to 40° to evaluate the various activation parameters. The k_2 values at different temperatures have been presented in Table 1 and various activation parameters are given in Table 2. The heat of activation was calculated using the following equation :

$$\Delta H^{\neq} = E - RT$$

The entropy of activation was obtained by substituting $\Delta H^{\neq}$ in the expression

$$\Delta S^{\neq} = 2.303\, R \left[\log kr + \frac{\Delta H^{\neq}}{2.303\, RT} - \frac{\log kT}{h} \right]$$

Table 2

Thermodynamic activation parameters for the oxidation of glycols by aqueous bromine

GLYCOLS	$E \pm 0.4$ kcal/mole	$\Delta H^{\neq} \pm 0.4$ kcal/mole	$\log_{10}$ PZ	$-\Delta S^{\neq} \pm 0.9$ e.u.
Ethane diol				
I Step	11.3	10.7	7.2	25.6
II Step	11.9	11.3	7.1	25.9
Propane-1,2-diol				
I Step	11.3	10.4	7.1	25.9
II Step	11.4	10.8	6.8	26.4
Butane-2,3-diol				
I Step	10.5	9.9	6.9	27.1
II Step	10.9	10.2	6.2	29.0
Pinacol				
I Step	9.6	9.0	6.3	29.6
II Step	10.3	9.7	6.2	30.2

where kr is the rate constant, k the Boltzmann constant, and h the Planck constant. The closeness of the values of the activation energy also exhibits that the same mechanism holds good for both steps.

ISOKINETIC RELATIONSHIP

A relationship of the form $\delta \Delta H^{\neq} = \beta \delta \Delta S^{\neq}$ with $\beta \geqslant 0$ is called an isokinetic relationship.[4] A corresponding relationship between equilibrium quantities is called an isoequilibrium relationship. The parameter has the dimensions of absolute temperature and can be identified as an actual or virtual temperature at which all the differences in the rate or equilibrium constants will vanish. A plot between $\Delta H^{\neq}$ and $\Delta S^{\neq}$ is found to be nonlinear indicating that the reaction mechanism is not the same in all the cases.

EFFECT OF IONIC STRENGTH

The effect of addition of lithium perchlorate on the reaction rate has also been investigated. The results exhibited that on adding increasing quantities of the salt the k_1/k_2 ratio remains almost constant indicating that molecules are taking part in the reaction. It may be mentioned using Laidler Landskroener's[5] theory that an estimate of the dimensions of the reaction complex leads to reasonable values for the rate constants of the first and second steps of the reaction. This establishes that the mechanism in both steps is essentially the same for the three glycols but not for pinacol.

DEUTERIUM ISOTOPE EFFECT

The oxidation of various glycols by aqueous bromine has been carried out both in H_2O and D_2O at 35°.

The data given in Table 4 suggest that the mechanism of oxidation of glycols (except pinacol) with aqueous bromine is quite similar to that of alcohols and aldehydes with bromine. While studying the oxidation of isobutyraldehyde by aqueous bromine[6] the ratio of $k(H_2O)/ /k(D_2O)$ was found to be 3.6 indicating that the mechanism involves the removal of hydride ion from C(1) H of the aldehyde hydrate. Similar mechanisms have also been proposed by Kudesia in the oxidation of aliphatic[7] and aromatic alcohols[8] with aqueous bromine.

TAFT EQUATION

Application of Taft equation[9] shows that when σ values become more positive, the rate constant decreases. This trend is to be expected on the basis of polar effect of methyl group.

An examination of the data reveals that the rate of reaction increases regularly with the substitution of a methyl group for hydrogen i.e., oxidation rate of ethane diol <1,2-propane-diol < 2,3 butane diol <pinacol. This is the expected order for the electron release at the C—H bond of

---

[4] J. E. LEFFLER, *J. Org. Chem.*, **20**, 1202 (1955).

[5] K. J. LAIDLER and P. A. LANDSKROENER, *Trans. Faraday Soc.*, **52**, 200 (1956).

[6] V. P. KUDESIA, *Bull. Soc. chem. belges*, **79**, 269 (1970).

[7] V. P. KUDESIA, *Ciencia E Cultura*, **24**, 731 (1972).

[8] V. P. KUDESIA, *Ciencia E Cultura*, **24**, 61 (1972).

[9] R. W. TAFT, "Steric Effects in Organic Chemistry", John Wiley Inc., New York, 1956.

Table 3

Second order rate constants for the oxidation of ethane diol by aqueous bromine at 35°

$(NaClO_4)$	$10^2 \times k_1$	$10^2 \times k_2$	k_1/k_2
M	litre mole^{-1} min^{-1}	litre mole^{-1} min^{-1}	
0.02	15.52	5.173	3.00
0.04	15.51	5.170	3.00
0.08	15.48	5.160	3.00
0.12	15.46	5.150	3.00
0.18	15.46	5.150	3.00

Table 4

Effect of deuterium on the reaction rate at 35°

GLYCOLS	$k_1(H_2O)/k(D_2O)$ 1.mole^{-1} sec^{-1}	$k_2(H_2O)/k(D_2O)$ 1.mole^{-1} sec^{-1}
Ethane diol	4.1	3.9
Propane-1,2-diol	4.3	4.1
Butane-2,3-diol	4.2	3.8
Pinacol	4.0	3.6

Table 5

Comparison of reaction rate of different diols at 35°

DIOL	9	1.mole^{-1} min^{-1}	
	σ	$10^2 \times k_1$	$10^2 \times k_2$
Ethane diol	1.96	15.52	5.173
Propane-1,2-diol	1.47	22.23	5.383
Butane-2,3-diol	0.98	26.20	5.610
Pinacol	—	33.14	6.024

the carbinol group because of the fact that the methyl group will tend to increase the electron density at the carbon atom by their general inductive effect $CH_3^+ \rightharpoonup \underset{|}{C}HOH$.

Thus it is clear from the experimental data that the mechanism of glycols (except pinacol) with aqueous bromine should be similar to that of alcohols and aldehyde, i.e. a mechanism which involves removal of hydride ion from C(1) H with synchronous removal of proton from OH. As the pinacol does not have an $\alpha-H$ it can not yield a hydride ion as is the case with glycols. Therefore, it must have a different mechanism which is difficult to predict at this stage.

(1)

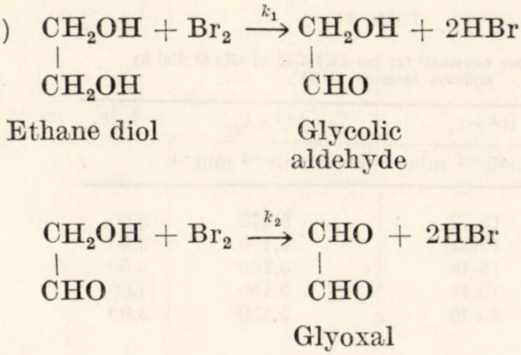

$$\begin{array}{c} CH_2OH \\ | \\ CH_2OH \end{array} + Br_2 \xrightarrow{k_1} \begin{array}{c} CH_2OH \\ | \\ CHO \end{array} + 2HBr$$

Ethane diol Glycolic aldehyde

$$\begin{array}{c} CH_2OH \\ | \\ CHO \end{array} + Br_2 \xrightarrow{k_2} \begin{array}{c} CHO \\ | \\ CHO \end{array} + 2HBr$$

Glyoxal

(2)

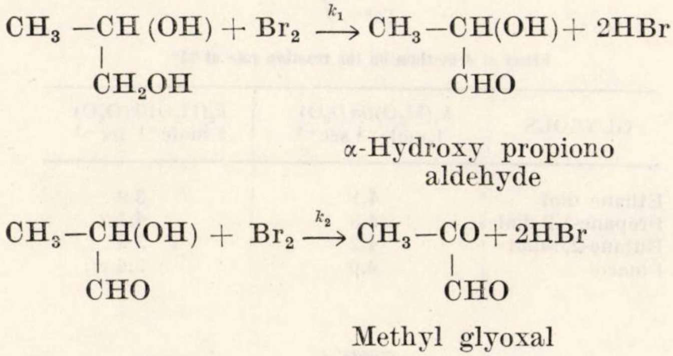

$$\begin{array}{l} CH_3-CH(OH) \\ \qquad\quad | \\ \qquad CH_2OH \end{array} + Br_2 \xrightarrow{k_1} \begin{array}{l} CH_3-CH(OH) \\ \qquad\quad | \\ \qquad CHO \end{array} + 2HBr$$

α-Hydroxy propiono aldehyde

$$\begin{array}{l} CH_3-CH(OH) \\ \qquad\quad | \\ \qquad CHO \end{array} + Br_2 \xrightarrow{k_2} \begin{array}{l} CH_3-CO \\ \qquad\ | \\ \qquad CHO \end{array} + 2HBr$$

Methyl glyoxal

(3)

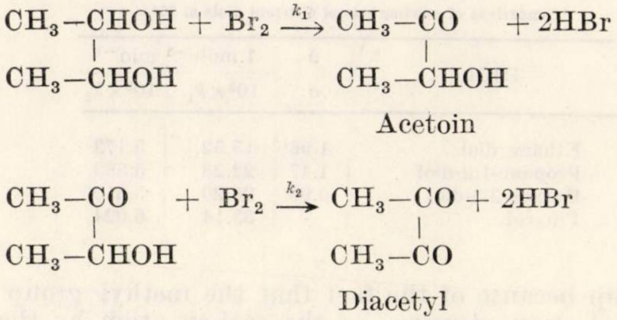

$$\begin{array}{c} CH_3-CHOH \\ | \\ CH_3-CHOH \end{array} + Br_2 \xrightarrow{k_1} \begin{array}{c} CH_3-CO \\ | \\ CH_3-CHOH \end{array} + 2HBr$$

Acetoin

$$\begin{array}{c} CH_3-CO \\ | \\ CH_3-CHOH \end{array} + Br_2 \xrightarrow{k_2} \begin{array}{c} CH_3-CO \\ | \\ CH_3-CO \end{array} + 2HBr$$

Diacetyl

Acknowledgement. The author is thankful to Ministry of Cooperation and Development Belgium for offering me postdoctoral scholarship to do this research work.

Revue Roumaine de Chimie, **20**, *8*, 1071–1075 (1975)

REACTIONS OF COORDINATED LIGANDS. VIII[1]

ALUMINIUM-ORGANIC DERIVATIVES OF DIPHENYLGLYOXIME

N. VOICULESCU

Institute of Macromolecular Chemistry "Petru Poni",
Aleea Grigore Ghica Vodă, 41–A, Jassy, Romania

Received April 15, 1974

The paper describes the compounds resulted from the reaction of tri-isobutylaluminium and triphenylaluminium with diphenylglyoxime, both free and coordinated with Ni(II) and Pd(II) ions. The compounds were separated from the reaction mixture as coloured powders and were characterized by chemical analyses, IR absorption spectra, X-ray diffraction spectra and magnetic measurements. In general, free and coordinated diphenylglyoxime behaves similarly to dimethylglyoxime, relative to the same aluminium-organic derivatives. The chemical reactivity of diphenylglyoxime towards these derivatives is, however, more reduced than in the case of dimethylglyoxime. An exception is the monomer state of diisobutylaluminium diphenylglyoximate in benzene solution.

INTRODUCTION

The action of organo-metallic compounds upon free oximes may lead to the formation of amines, [2] imines, [3] to Beckmann transposition [4,5] or to substitution of oximic hydrogens [6–9] by metallo-organic groups. Substitution products are in most cases found associated as dimers, which formed through O—Al—N bonds in the case of dioximes [9] and by Al—O—N—Al bonds in the case of monooximes. [6]

Aluminium-organic compounds of oximes coordinated with ions of transitional metals, arise by substituting intramolecular hydrogen bridges, present in these compounds, by aluminium bridges. [9–13]

---

[1] N. Voiculescu, L. Roman and I. Popescu, *Rev. Roumaine Chim.*, **20**, 945 (1975).

[2] M. S. Kharasch and O. Reimuth, "Grignard Reactions of Non-metallic Substances", Pretince-Hall, New York, 1954, p. 1217.

[3] K. N. Campbell, B. K. Campbell, L. G. Hess and I. J. Schaffner, *J. Org. Chem.*, **9**, 184 (1944).

[4] C. R. Hauser and D. S. Hoffenberg, *J. Org. Chem.*, **20**, 1482 (1955).

[5] W. Gerrard, M. F. Lappert and J. W. Wallis, *J. Chem. Soc.*, **1960**, 2141

[6] J. R. Jannings and K. Wade, *J. Chem. Soc.*, **1967**, 1333.

[7] I. Pattison and K. Wade, *J. Chem. Soc. A*, **1968**, 2618.

[8] N. Voiculescu and I. Popescu, *Rev. Roumaine Chim.*, **17**, 719 (1972).

[9] N. Voiculescu, *Rev. Roumaine Chim.*, **18**, 1919 (1973).

[10] N. Voiculescu, A. Airinei and I. Popescu, *Rev. Roumaine Chim.*, **19**, 399 (1974).

[11] N. Voiculescu, I. Popescu and L. Roman, *Rev. Roumaine Chim.*, **18**, 1595 (1973).

[12] N. Voiculescu, I. Popescu and N. Luchian, *Rev. Roumaine Chim.*, **18**, 1601 (1973).

[13] N. Voiculescu and I. Popescu, *Rev. Roumaine Chim.*, **18**, 1911 (1973).

In this paper we report aluminium-organic compounds resulted from the reaction of triisobutylaluminium and triphenylaluminium with diphenylglyoxime (further abbreviated $DPGH_2$), free and coordinated with Ni(II) and Pd(II) ions. The new compounds were isolated as solid powders and were characterized by chemical analyses, IR absorption spectra, X-ray diffraction spectra and magnetic measurements.

EXPERIMENTAL

Ni(II) and Pd(II) bis-diphenylglyoximates were obtained according to methods reported in the literature [14–16] and were recrystallized from nitrobenzene.

The working procedure for obtaining triphenylaluminium was described in previous papers. [11,12]

The reactions and handling of compounds were carried out in an inert and dry atmosphere.

Diisobutylaluminium diphenylglyoximate was obtained by mixing a triisobutylaluminium benzene solution with a suspension of diphenylglyoxime in benzene at a 2 :1 molar ratio. The reaction mixture was vigorously stirred for several hours at room temperature. The excess, unreacted diphenylglyoxime was separated from the liquid fraction by decantation . An orange powder was separated from the liquid fraction by removing benzene under vacuum.

Diphenylaluminium diphenylglyoximate was obtained by mixing triphenylaluminium with diphenylglyoxime, similar to the preparation of diisobutylaluminium diphenylglyoximate. The mixture was heated with stirring for several days until a homogeneous brown, solid compound was obtained. The solid product was separated from the liquid fraction by decantation. It was repeatedly washed with warm benzene and vacuum-dried.

$Ni(DPG)_2Al_2(i-C_4H_9)_4$ was obtained by adding a triisobutylaluminium solution in toluene to the Ni(II) $(DPGH)_2$ dried and crushed powder. The amount of chelate taken was somewhat larger than the 1 : 2 ratio required by reaction stoichiometry. The reaction mixture was heated and stirred for several days. The excess of chelate was separated by filtering on a G$-$4 frit. The solid, dark-red compound was separated from the liquid fraction by removing the solvent under vacuum.

$Pd(DPG)_2Al_2(i-C_4H_9)_4$. This product was obtained by proceeding as described above for nickel. A light green yellowish powder was eventually obtained.

$Ni(DPG)_2Al_2(C_6H_5)_4$ *and* $Pd(DPG)_2Al_2(C_6H_5)_4$ were obtained by adding triphenylaluminium solution in benzene to nickel and palladium chelate powders. Triphenylaluminium was added in excess relative to the calculated amount. In both cases the reaction mixture was stirred and heated until total disappearance of the colour characteristic of chelates. The product was precipitated with ether, it was decanted and the solid product was repeatedly washed with benzene and ether, and vacuum-dried thereafter. In the case of nickel derivative, a brown powder was obtained, whereas the powder obtained in the case of palladium derivative was grey.

The chemical analyses of synthesized compounds are given in table 1.

The molecular masses of compounds with isobutyl groups were determined by cryoscopic measurements in benzene and are presented in table 1. The molecular masses of derivatives with phenyl groups could not be determined since these compounds are not totally soluble in benzene.

X-ray diffraction spectra of compounds were obtained by the powder method on a TUR M$-$60 apparatus, using the CuK_α radiation and nickel filter. Samples were exposed in glass capillaries at 40 kV and 14 mA for 8 hours.

IR absorption spectra for the 3600$-$650 cm^{-1} range were recorded on a Unicam SP$-$200 apparatus. A Perkin-Elmer 621 apparatus was used to record the spectra in the 650$-$250 cm^{-1} range. For this range samples were exposed in Nujol, in cells with CsI windows.

Magnetic properties were determined by means of a Gouy balance in non-homogeneous magnetic field.

---

[14] L. GIUGAEV, *Z. anorg. Chem.*, **46**, 144 (1905).

[15] F. W. ATACK, *Analyst*, **38**, 316 (1913).

[16] F. W. ATACK, *J. Chem. Soc.*, **1913**, 1317.

Table 1

Analysis and molecular weights of analysed products

The compound	Molecular weight calc. found	Analyses				
		C calc. % found %	H calc. % found %	Al calc. % found %	N calc. % found %	M calc. % found %
$(DPG)Al_2(i-C_4H_9)_4$	520	69.23	8.84	10.38	5.38	—
	539	68.95	8.63	10.43	5.23	—
$(DPG)Al_2(C_6H_5)_4$	600	76.00	5.00	9.00	4.66	—
	—	75.74	4.87	9.24	4.62	—
$Ni(DPG)_2Al_2(i-C_4H_9)_4$	817	64.62	6.85	6.61	6.85	7.22
	805	64.23	6.83	6.66	6.81	7.17
$Ni(DPG)_2Al_2(C_6H_5)_4$	897	69.56	4.45	6.02	6.24	6.57
	—	69.31	4.42	6.15	6.21	6.34
$Pd(DPG)_2Al_2(i-C_4H_9)_4$	865	61.04	6.47	6.24	6.47	12.02
	856	60.84	6.45	6.26	6.43	12.13
$Pd(DPG)_2Al_2(C_6H_5)_4$	945	66.03	4.23	5.71	5.92	11.32
	—	65.94	4.21	5.82	5.88	11.18

RESULTS AND DISCUSSION

Aluminium-organic compounds of diphenylglyoxime both free and coordinated with Ni(II) and Pd(II) ions, are formed by substitution of oximic hydrogens by aluminium-organic groups, according to the reactions illustrated in the following two equations :

$$DPGH_2 + 2AlR_3 \rightarrow DPG\ (AlR_2)_2 + 2RH$$

$$M(II)\ (DPGH)_2 + 2AlR_3 \rightarrow M(II)(DPG)_2Al_2R_4 + 2RH$$

and their structures correspond to the formula I.

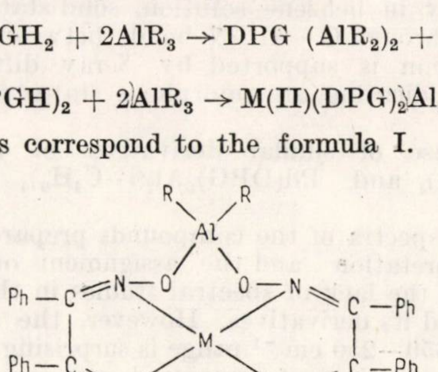

$$M(II) = Ni(II),\ Pd(II)$$

$$R = i - C_4H_9,\quad C_6H_5$$

Similar to the case of the other free and coordinated oximes, [9,11,12] this reaction involves a two-step mechanism. The first step corresponds to the formation of adducts between the free or coordinated oxime with the aluminium-organic derivative, and the second step corresponds to the elimination of two hydrocarbon molecules and the formation of the substitution derivative.

The compounds obtained by the above reactions are solid coloured substances, unstable to chemical agents like water, alcohols, acids and bases. Derivatives with $Al(i-C_4H_9)_2$ groups are soluble in organic solvents, whereas derivatives with $Al(C_6H_5)_2$ groups have a limited solubility. This fact supports the conclusion that solubility is influenced, among other factors, also by the nature of radicals left at the aluminium atom.

In practice, cooling was not necessary during the reaction and this is highly important in the case of diphenylglyoxime reaction with triisobutylaluminium. A comparison between the chemical reactivity of diphenylglyoxime and of other oximes [9] relative to aluminium organic derivatives prompt us to conclude that diphenylglyoxime has a low reactivity. We assign this behaviour to the influence exerted by the two phenyl groups in diphenylglyoxime upon the chemical reactivity of oximic groups.

The most significant observation made in the determinations of molecular masses of benzene-soluble isobutyl derivatives, is the monomer state of diisobutylaluminium diphenylglyoximate. The monomer state of this compound and probably also of the compound with $Al(C_6H_5)_2$ groups is due to the influence of phenyl groups in diphenylglyoxime which, probably due to some steric hindrances, determine diphenylglyoxime to participate in the reaction in antiform. However, it is possible that this monomer state may exist only in benzene solution, solid-state compounds being found polymerised, through $O \rightarrow Al-N$ bonds between the adjacent molecules. This supposition is supported by X-ray diffraction spectra of some compounds, indicating an amorphous state, specific to polymer compounds.

As in the case of similar derivatives of dimethylglyoxime, [8] $Ni(DPG)_2Al_2(i-C_4H_9)_4$ and $Pd(DPG)_2Al_2(i-C_4H_9)_4$ have a crystalline ordered structure.

IR absorption spectra of the compounds prepared are presented in table 2. Their interpretation and the assignment of absorption bands are difficult, due to the lack of spectral studies in this range, regarding diphenylglyoxime and its derivatives. However, the absence of absorption maxima in the $650-250$ cm $^{-1}$ range is surprising.

The magnetic behaviour of compounds was investigated, revealing their diamagnetism. Particularly the diamagnetism of aluminium-organic derivatives of the chelates reveals that the planar structure was maintained in the chelates, and the reaction occurred at the ligand rather than at the metallic central atom.

The behaviour relative to amines is similar to that found in aluminium-organic compounds of dimethylglyoxime[8,11] and of salicylaldoxime,[12,13] both free and coordinated with Ni(II)Pd(II) and Cu (II) ions. Isobutyl-derivatives are soluble in tertiary amines, with colour intensification. Nevertheless, no attempts have been made to isolate adducts with amines. In contrast,phenylaluminium derivatives are not soluble in amines.

Table 2

IR absorption spectra of the synthetized products
(Values given in cm−¹)

$M(DPG)_2Al_2(C_4H_9)_4$ and $(DPG)\ Al_2(C_4H_9)_4$			$M(DPG)_2Al_2(C_6H_5)_4$ and $(DPG)Al_2(C_6H_5)_4$		
DPG	Ni	Pd	DPG	Ni	Pd
1590 vs	1580 vs	1575 vs	1585 vs	1590 vs	1580 vs
—	1543 s	—	—	—	—
—	1493 vs	—	—	1490 s	1478 s
1460 vs	1465 s	1460 vs	1450 vs	1455 vs	1455 s
—	1442 vs	—	—	—	—
—	1365 vs	1380 s	1376 vs	1375 vs	1372 vs
1375 vs	1362 vs	1315 s	1340 vs	—	—
—	1295 vs	1240 vs	1280 s	1290 vs	1290 vs
1150 vs	1142 vs	1172 s	1140 s	1140 s	1140 s
1090 s	1068 s	1100 s	1090 s	1070 s	1070 s
—	1032 vs	1055 s	1020 s	1030 s	1030 s
990 vs	943 vs	990 s	920 s	998 s	995 s
—	915 vs	—	—	—	—
890 s	880 s	865 s	880 s	875 s	872 s
820 s	820 s	—	—	—	—
760 s	745 vs	785 vs	720 s	740 s	738 s
690 vs	695 vs	680 vs	690 vs	690 vs	685 vs

Revue Roumaine de Chimie, **20**, *8*, 1071−1075 (1975)

Revue Roumaine de Chimie, **20**, *8*, 1077 – 1087 (1975)

HETEROCYCLIC COMPOUNDS. V[1]

BECKMANN REARRANGEMENT OF SOME 2,3-DIHYDRO-1-BENZOXEPIN-5(4H)-ONE OXIMES TO 1,5- AND 1,6-BENZOXAZOCINONES

ILIE I. BĂDILESCU

Department of Chemistry, Pedagogical Institute, Str. Doja 41,
Pitești, Romania

Received April, 30, 1974

2,3-Dihydro-1-benzoxepin-5(4H)-one oximes carrying alkyl substituents in the aromatic ring have been converted by Beckmann rearrangement into 1,5- and 1,6-benzoxazocinones. The rearrangement has been found to be influenced by both electronic and steric effects. N.m.r., u.v. and i.r. spectra have been used to distinguish between the isomeric 1,5- and 1,6-benzoxazocinones. The unreported eight-membered heterocyclic 1,6-benzoxazocine (VIII) was obtained by reduction of benzolactam IIIa with $LiAlH_4$.

INTRODUCTION

As we already reported,[2,3] an attempt to synthesize an 1,6-benzoxazocin-5-one by $O^- - 8$ cyclization of 4-chloro-N-(*o*-hydroxyphenyl) butyramide failed, the reaction product was N-(*o*-hydroxyphenyl)pyrrolidin-2-one, corresponding to a $N^- - 5$ ring closure.* Our interest in developing synthetic routes for benzoxazocinones, led us to the Beckmann rearrangement of 2,3-dihydro-1-benzoxepin-5(4H)-one oximes (II). Some other results were also published.[4-9] In this paper we present the results of the Beckmann rearrangement on a variety of 2,3-dihydro-1-benzoxepin-5(4H)-one oximes (II, a—e).

---

[1] Part IV: I. I. Bădilescu, *Tetrahedron Letters*, **1974**, 1969.

[2] I. I. Bădilescu, *Tetrahedron Letters*, **1968**, 3599.

[3] I. I. Bădilescu, *Tetrahedron*, **26**, 4207 (1970).

* Notations after ref. [4]

[4] F. L. Scott, R. E. Glick and S. Winstein, *Experientia*, **13**, 183 (1957).

[5] I. I. Bădilescu, *Rev. Roumaine Chim.*, **20**, 761 (1975).

[6] D. Hukle, I. M. Lockhart and M. Wright, *J. Chem. Soc.*, **1965**, 1137.

[7] P. Ramart-Lucas, *Bull. Soc. chim. France*, [5] , **10**, 13 (1943).

[8] L. Bauer and R. E. Hewitson, *J. Org. Chem.*, **27**, 3982 (1962).

[9] M. E. Kuehne and B. F. Lambert, *J. Amer. Chem. Soc.*, **81**, 4278 (1959).

RESULTS AND DISCUSSION

The starting materials for this work were the 2,3-dihydro-1-benzoxepin-5(4H)-ones I which were converted into the corresponding ketoximes II as reported in another paper.[5] According to the n.m.r. spectra, only one isomer has always been isolated, and the stereochemistry of II was tentatively assigned *anti* geometry based on a comparison of the n.m.r. spectra of parent heterocyclic ketones I and the corresponding ketoximes II.

CHART I

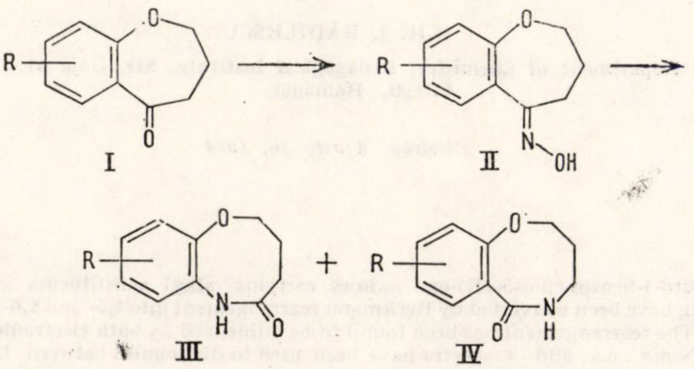

I,II	R	III,IV	R
a	H	a	H
b	8 – Me	b	9 – Me
c	7 – Me	c	8 – Me
d	7,8 – Me_2	d	8.9 – Me_2
e	6,8 – Me_2	e	7,9 – Me_2

The Beckmann rearrangements of the ketoximes IIa-IIe were carried out with PPA* (procedure A) and, in two cases (IIa and IIe), also with phosphorus pentachloride in anhydrous ethyl ether (procedure B).

In our first experiments IIa was heated with PPA at 110 – 120° for fifteen minutes and from the reaction mixture a poor yield (10%) of a compound melting at 161.5° was isolated. The elemental analysis and infrared absorption spectrum showed only that the compound obtained is a cyclic amide but these data were not sufficient to discriminate between structures IIIa and IVa, corresponding to the products arising from aryl and alkyl migration, respectively. By analogy with the course of Beckmann rearrangement of 4-chromanone oxime (V) with PPA, reported by Huckle et al.[6] to afford 2,3-dihydro-1,4-benzoxazepin-5(4H)-

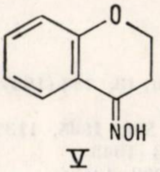

V

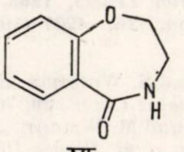

VI

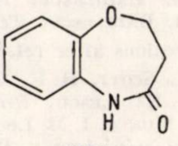

VII

---

* Polyphosphoric acid.

one (VI) by alkyl migration, one could suppose the compound m.p. 161.5° to possess structure IVa, but this is not the case. Indeed, a careful examination of the crude mixture by n.m.r. indicated the presence of another compound in minor amounts, which was then isolated from the mother liquors resulting from the recrystallization of the major product from several rearrangement reactions. The product thus obtained (m.p. 110−112.5°) had the same molecular formula as the former compound, and the i.r. spectrum indicated that this compound was a benzolactam, too.

By comparison of the infrared and ultraviolet spectra of these benzolactams with those of the seven-membered heterocyclic analogs (VI and VII) and of other compounds (table 1) it was found that the structure of the major compound (m.p. 161.5°) is IIIa, corresponding to an aryl migration, while structure IVa belongs to the minor product (m.p. 110−112.5°) which arises from an alkyl migration in the Beckmann rearrangement of IIa.

Table 1

Summary of relevant spectral data

Compound	$\nu_{c=0}$	λ_{max}^{EtOH} ($\log \varepsilon_{max}$)		Ref.
Acetanilide	1670	242 (4.16)	280 (2.70)	7,8
o-Methoxyacetanilide	1669	244 (4.02)	280 (3.66)	7
1,5-Benzoxazepin-4(5*H*)-one (VII)	1668	245 (3.90)	278[a](3.36)	b
1,6-Benzoxazocin-5(6*H*)-one (IIIa)	1678	235 (3.83)	272 (3.22)	b
Benzamide	1663	223 (4.03)	— —	9
N-Methylbenzamide	—	226 (3.99)	— —	8
1,4-Benzoxazepin-5(4*H*)-one (VI)	1652	224[a](3.81)	288 (3.14)	b
N-Methyl-1,4-benzoxazepin-5-one	1658	222[a](3.90)	282 (3.25)	b
1,5-Benzoxazocin-6(5*H*)-one (IVa)	1655	222[a](3.77)	284 (3.13)	b

[a] Shoulder.
[b] Present work.

The correctness of the structure assignments of the compounds obtained was supported by the characterization of the product resulting from reduction of benzolactam m.p. 161.5° with $LiAlH_4$, which was proved to be the unreported 6H-2,3,4,5-tetrahydro-1,6-benzoxazocine (VIII), in agreement with structure IIIa of the parent benzolactam.

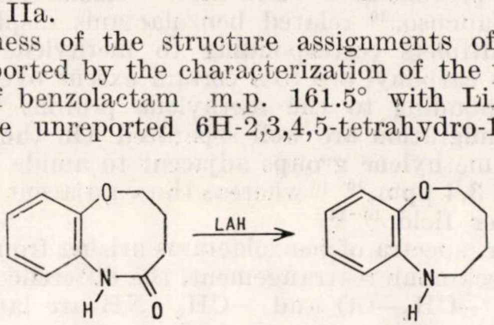

IIIa VIII

The new heterocyclic compound VIII was characterized as N-tosyl derivative IX.

Further confirmation of the structure assignment was obtained by examination of the amino acid, from hydrolysis of the benzolactam IIIa in concentrated hydrochloric acid. Thus, the solution obtained by hydrolysis was used directly for diazotization with sodium nitrite. By adding a solution of β-naphthol in sodium hydroxide to the resulting diazonium salt, a red, insoluble dye was formed. Since only the isomer with the amine group attached to the aromatic nucleus would react in the coupling reaction with β-naphthol, the position of the amino group and, therefore, the structure of lactam was established with certainty.

The Beckmann rearrangement of ketoxime IId afforded mainly benzolactam IIId by aryl migration, whose structure was proved by i.r., u.v. and n.m.r. spectra. In addition, the correctness of the structure assignment was supported by characterization of the product obtained from acid hydrolysis of IIId. By working up the reaction mixture obtained after twenty hours of heating IIId with concentrated hydrochloric acid, a compound m.p. 113° was isolated. The i.r., u.v. and n.m.r. spectra showed that the compound resulted was the unreported γ-(2-amino-4,5-dimethylphenoxy) butyric acid (X) and, implicitely, supported the structure IIId assigned to the parent benzolactam.

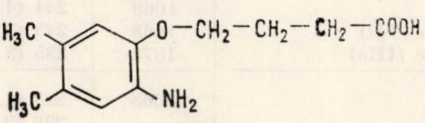

X

The Beckmann rearrangement by PPA of ketoximes IIb and IIe afforded reaction products which proved to be mixtures of lactams corresponding to both aryl and alkyl migration. In all these experiments, the ratio between benzolactams arising from aryl and alkyl migrations was estimated by means of the n.m.r. spectra of crude products. The assignment was possible thanks to the difference between chemical shifts of the methylene protons at C—4 in these benzolactams. As reported by Lansbury and Mancuso,[10] related benzolactams display n.m.r. spectra in which the multiplets corresponding to methylene protons situated α and β to amide carbonyl are to a certain extent overlapped, while the multiplets corresponding to the methylene protons in benzolactams arising by alkyl migration are well separated. On the other hand, it is well known that methylene groups adjacent to amide nitrogen generally give signals at *ca.* 3.4 ppm,[10-13] whereas those adjacent to amide carbonyl resonate at higher field.[10-14]

In the n.m.r. spectra of benzolactams arising from ketoximes IIa — — IIe, by the Beckmann rearrangement, the differences between signals corresponding to $-CH_2-CO$ and $-CH_2-NH$ are large enough (up to

---

[10] P. T. Lansbury, J. G. Colson and N. R. Mancuso, *J. Amer. Chem. Soc.*, **86**, 5225 (1964).

[11] P. T. Lansbury and N. R. Mancuso, *J. Amer. Chem. Soc.*, **88**, 1205 (1966).

[12] L. M. Jackman, "Applications of Nuclear Magnetic Resonance Spectroscopy in Organic Chemistry," Pergamon Press, New York, N. Y., 1959, p. 56.

[13] G. S. Sidhu, G. Thyagarajan and U.T. Bhalerao, *J. Chem. Soc., C*, **1966**, 969.

[14] U. T. Bhalerao and G. Thyagarajan, *Canad. J. Chem.*, **46**, 3367 (1968).

ca. 60 cps) to permit a sure characterization of the type of lactam. Thus, the n.m.r. spectrum of the crude product obtained from the Beckmann rearrangement of IIa indicated the presence of three compounds two of which are IIIa and IV a, in a ratio of 8:1 between aryl to alkyl migration (average value of three lots). The third compound was not identified. The n.m.r. spectral data of the benzolactams III and IV are presented in table 2.

Table 2

Nuclear magnetic resonance data on pure benzolactams

Compound	Chemical shifts (τ values), p.p.m.						
	NH	$O-CH_2-$	$C-CH_2-C$	$C-CH_2-CO$	aromatic	CH_3	$C-CH_2-NH$
IIIa	0.92	5.72	7.85	7.60	*ca.* 2.82	—	—
IVa	(3.00)[a]	5.67	8.02	—	*ca.* 2.70	—	6.65
IIIb	1.32	5.78	(7.60−7.80)[b]		*ca.* 3.02	7.67	—
IIId	1.07	5.82	(7.80−8.00)[b]		*ca.* 3.12	7.78	—
IIIe	1.95	5.82	(7.80−8.00)[b]		*ca.* 3.20	7.70	—

[a] This signal in the aromatic region underwent deuterium exchange with D_2O.

[b] Complex signal in this region.

Oximes II were assumed to have the sterically preferred *anti*-configuration by analogy with other related compounds[11,15−19] and we had therefore expected to obtain lactams of type III by rearrangements involving aryl migration. However, in all cases, mixtures of type III and IV of benzolactams were obtained with a predominance of compound III arising from aryl migration (table 3).

Table 3

Benzolactams obtained by the Beckmann rearrangement of II

Starting ketoxime	III/IV ratio[a]	Benzolactam (m.p., °C)			
		III		IV	
IIa	8 :1[b]	IIIa	161.5	IVa	110−112.5
IIb	5 :1	IIIb	158−160	IVb	([c])
IIc	(*d*)	IIIc	(*d*)	IVc	([d])
IId	5 :1	IIId	195−196	IVd	([c])
IIe	2 :1	IIIe[e]	212	IVe	([c])

[a] Estimated by n.m.r. in crude product.

[b] When PCl_5 was used as catalyst, the ratio was 3: 1.

[c] Pure compound was not isolated.

[d] No cyclic amides were obtained (see experimental).

[e] Lit.[30] m.p. 214−215°.

---

[15] P. A. S. Smith and E. P. Antoniades, *Tetrahedron*, **9**, 210 (1960).

[16] P. A. S. Smith, "Rearrangements Involving Migration to an Electron-Deficient Nitrogen or Oxygen", Chapter 9 in "Molecular Rearrangements", Vol. 1, P. De Mayo, Editor, Interscience Publishers, Inc., New York, 1963, p. 457.

[17] R. T. Conley and L. J. Frainier, *J. Org. Chem.*, **27**, 3844 (1962).

[18] R. Huisgen, I. Ugi, H. Brade and E. Rauenbusch, *Liebigs Ann. Chem.*, **586**, 30 (1954).

[19] E. C. Horning, V. L. Stromberg and H. A. Lloyd, *J. Amer. Chem. Soc.*, **74**, 5153 (1952).

[20] D. Huckle, I. M. Lockart and N. E. Webb, *J. Chem. Soc., C*, **1971**, 2252.

Although these apparently abnormal Beckmann rearrangements can be explained in terms of an acid-catalysed geometrical isomerization of the oximes prior to carbon migration, [21] further work necessitated an alternative explanation. Rearrangement of oximes IIa and IIe in the presence of phosphorus pentachloride in ether, which normally favours a stereospecific rearrangement, gave also mixtures of lactams arising from both aryl and alkyl migration. Moreover, the ratio aryl *vs.* alkyl migration isomers was near 2 :1 in the case of ketoxime IIe, although the stereochemistry of the parent compound favoured clearly only a IIe-(*E*) isomer. It appears that steric control due to oxime configuration is not favoured in these rearrangements and the reaction may well proceed through a non-stereoselective iminium intermediate. Group migration is then controlled by the relative stabilities of the respective transition states as in certain related oxime systems. [10, 11, 16, 22]

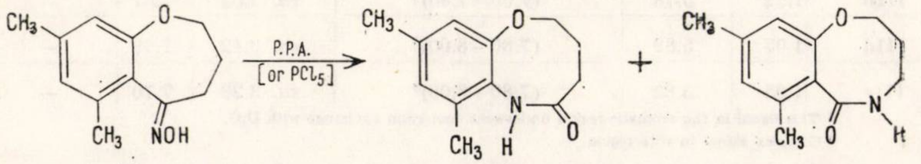

IIe IIIe IVe

It is very interesting to note here that Bhalerao and Thyagarajan[23] found only aryl migration products in the Beckmann rearrangement of 5,7-dimethyl-4-chromanone oxime (XI) and of 5,8-dimethyl-4-chromanone oxime (XII), while the seven-membered analog of XI, (IIe), in our hands, leads to a mixture of both aryl and alkyl migration products (IIIe and IVe).

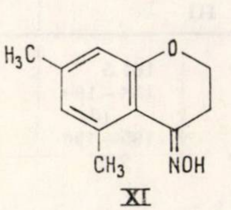

XI

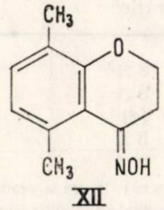

XII

In some literature data concerning the Beckmann rearrangements the *trans* migration rule is not obeyed owing to steric effects [10,11,22–24] and our results may be explained in a similar manner. Thus, the formation of the intermediate XIII required for aryl migration, to give a benzolactam of type III, is unfavoured sterically owing to the torsional strain involved, while the formation of the intermediate XIV required for alkyl migration to yield benzolactams of type IV is possible, with the azacyclopropene ring accomodated perpendicularly to the plane of the benzene ring.[16]

---

[21] J. B. Hester Jr., *J. Org. Chem.*, **32**, 3804 (1967).

[22] R. M. Pinder, *J. Chem. Soc., C*, **1969**, 1690.

[23] U. T. Bhalerao and G. Thyagarajan, *Indian J. Chem.*, **7**, 429 (1969).

[24] P. T. Lansbury and J. G. Colson, *J. Amer. Chem, Soc.*, **84**, 4167 (1962).

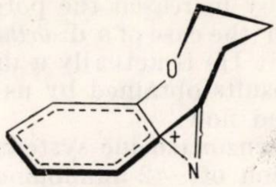

XIII

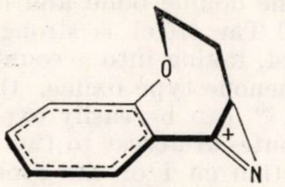

XIV

The above explanation is identical with that given by other authors for the mechanisms of the Beckmann rearrangements which were found to follow an "abnormal" course, and in which non-stereoselective iminium cations are involved.[10, 11, 17, 22, 24] However, in our case, the major product has always been a lactam of type III, and only poor yields of products corresponding to a non-stereospecific rearrangement (*i.e.* IV), were found in the reaction mixtures, a fact which may be attributed to a relatively higher flexibility of the seven-membered ring of ketoximes IIa — IIe in comparison with oximes of the related five- and six-membered benzocyclenones which, by the Beckmann rearrangement (or the Schmidt reaction on the corresponding ketones), afforded mainly lactams by alkyl migration.[10, 11, 14, 22, 25–27]

Although PPA was reported to be a medium which isomerizes geometrically ketoximes,[8, 15, 23, 25] it seems that a previous isomerization of II in the presence of PPA is not taking place or, if it does, it plays only a minor role in the generation of the lactams corresponding to alkyl migrations, as indicated by the Beckmann rearrangement of the ketoximes IIa and IIe in the presence of phosphorus pentachloride in anhydrous ethyl ether.

As noted above (see table 2), benzolactam IIIe has recently been reported[20] and it seems to be the sole compound with a 1,6-benzoxazocine system described. Since this work has been in progress, Huckle et al.[20] have reported the unattempted Beckmann rearrangement of the O-tosyl derivative of IIe in the conditions of the Neber rearrangement. This compound was found to give the benzolactam IIIe by a Beckmann rearrangement although several related O-tosylated II afforded the products expected from the Neber rearrangement.

The behaviour of tosylated IIe noticed by Huckle et al.[20] agrees with our observations on the Beckmann rearrangement of IIe by PPA or PCl_5, and with literature data on *ortho*-substituted acetophenone oxime in the Beckmann rearrangement reactions.[16, 28, 29] Indeed, *ortho*-sub-

---

[25] R. T. Conley and T. M. Tencza, *Tetrahedron Letters*, **1963**, 1781.

[26] M. Tomita, S. Minami and S. Uyeo, *J. Chem. Soc.*, *C*, **1969**, 183.

[27] A. Marsili and P. Ricci, *Ann. Chim.* (*Ital.*), **52**, 112 (1962).

[28] B. J. Gregory, R. B. Moodie and K. Schofield, *J. Chem. Soc.*, *B*, **1970**, 338.

[29] R. Huisgen, J. Witte and W. Jira, *Chem. Ber.*, **90**, 1850 (1957).

stituted acetophenone oximes rearrange more easily than *meta*- or *para*-substituted compounds and the effect was attributed to the steric influence of the substituents which reduced conjugation of the benzene ring with the oxime double bond and thereby increased the potential energy of oxime.[16, 29] The effect is stronger in the case of a di-*ortho*-substituted compound and, taking into account that IIe is actually a di-*ortho*-substituted acetophenone type oxime, the results obtained by us and those of Huckle et al.[20] can be easily explained now.

Other routes of access to the 1,6-benzoxazocine system, such as the Schmidt reaction on I or the cyclization of γ-(2-aminophenoxy)butyric acid (XV), were also attempted. The Schmidt reaction on Ia afforded only poor yields of IIIa in two trials, and this way of preparing III and IV has not been studied further. As concerns the cyclization of XV, preliminary results are not encouraging despite the positive findings of other workers with β-(2-aminophenoxy)propionic acid which afforded VII in good yields.[6,30] Our results will be reported soon.

EXPERIMENTAL

All melting points, determined in capillary tubes, are uncorrected. N.m.r. spectra were taken in $CDCl_3$ solution containing TMS as internal standard, using a Varian A–60 A spectrometer. Tests to locate N*H* or/and O*H* protons were carried out when necessary, by replacing the appropriate H atom by D.[31] I.r. spectra were recorded with a UR–10 Carl Zeiss-Jena or a Perkin Elmer (Model 621) double beam spectrophotometer, and the u.v. spectra were recorded on a Unicam SP 800 spectrophotometer, in EtOH solution. The materials used in this work were purified prior to use. Unless otherwise stated, solutions were dried on anhydrous magnesium sulphate.

Beckmann rearrangements of ketoximes IIa–IIe, by PPA (procedure A)

*2,3-Dihydro-1-benzoxepin-5(4*H*)-one oxime (IIa)*

To 250 g PPA preheated at 105°, 16 g (0.09) moles) ketoxime IIa was added under stirring. The reaction started immediately as indicated by the temperature of the mixture, which rose to 115–117°. The reaction mixture was stirred for another 15 minutes under heating (125–130°), then cooled and treated with 300 g crushed ice and 300 ml cold water. The resulted solution was extracted several times with chloroform, the combined organic solutions dried, and the chloroform removed to give a crystalline residue (2.9 g) melting at 156–159°, with softening near 153°.

The n.m.r. spectrum of the crude product indicated the presence of three main compounds in the mixture (see text). The major component of the mixture, i.e. 2,3,4,5-tetrahydro-1,6-benzoxazocin-5(6H)-one (IIIa) was obtained by several recrystallizations from benzene of the crude product. Yield 2.1 g pure IIIa as colourless needles, m.p. 161.5°.

Found : C, 67.40, H, 6.35, N, 8.20 ; $C_{10}H_{11}NO_2$ *requires* : C, 67.77 ; H, 6.26, N, 7.90 %

The infrared spectrum of IIIa (solid, KBr pellet) shows the following absorption bands : 3290, 3195, 3103, 3055, 2955, 2941, 2928, 2905, 1676, 1665, 1599, 1583, 1548, 1498, 1459, 1443, 1439,1401, 1372, 1348, 1312, 1284, 1267, 1240, 1220, 1205, 1181, 1109, 1087, 1057, 1000, 947, 941, 805, 760, 734, 670 and 630 cm^{-1}; in diluted solutions (chloroform or carbon tetrachloride) some bands are shifted: the stretching ν_{NH} band appears as a strong absorption band at 3406 cm^{-1} (free NH) and the amide carbonyl vibration $\nu_{C=O}$ as a double band at 1699 and 1685 cm^{-1}.

U.v. and n.m.r. spectra are presented in tables 1 and 2.

---

[30] G. Thyagarajan, Private communication.

[31] Ref. [12], p. 71.

By working up the mother liquors resulted from several rearrangement reactions of IIa, another compound (IVa) was obtained, crystals m.p. 110–112.5° with the same elemental composition as the major compound.

Found : C, 67.48, H, 6.20, N, 8.35 ; $C_{10}H_{11}NO_2$ *requires* : C, 67.77, H, 6.26, N, 7.90%

A mixture of 0.3 g of benzolactam m.p. 161.5° and 15 ml concentrated hydrochloric acid was heated at reflux for twenty hours. The resulted solution was cooled and treated with a stoichiometric amount of sodium nitrite in 20 ml water and then with a solution of 1 g of β-naphthol in 10 ml of 15% sodium hydroxide solution ; a red precipitate appeared.

8-Methyl-2,3-dihydro-1-benzoxepin-5(4H)-one oxime (IIb)

To 200 g PPA preheated at 110°, 10.5 g (55 mmoles) ketoxime IIb was added under stirring. The temperature of the reaction mixture rose rapidly at 155°. The mixture was stirred for another ten minutes at 135–140°, then poured onto 300 g crushed ice, and the resulted solution extracted with chloroform (3×200 ml). The organic solution was dried and the solvent removed to yield 2.85 g of a solid melting at 142–147° (with softening near 135°). The aqueous solution was neutralized, extracted with chloroform and the solvent removed to yield 0.42 g of a brown residue which was not characterized.

The n.m.r. spectrum of the first fraction showed that the major component was a benzolactame of "type III". The pure IIIb (9-methyl-2,3,4,5-tetrahydro-1,6-benzoxazocin-5 (6*H*)-one) was obtained by recrystallization of the crude product from a benzene – *n*-pentane mixture; colourless crystals m.p. 158–160°.

Found : N, 7.39 ; $C_{11}H_{13}NO_2$ *requires* : N, 7.32%

The infrared spectrum of IIIb presents the following bands : 3290, 3180, 3065, 3030, 2960, 2930, 2875, 2860, 1688 (in diluted carbon tetrachloride solution), 1675 (solid, KBr pellet), 1620, 1589, 1522, 1469, 1450, 1409, 1386, 1356, 1323, 1298, 1292, 1277, 1250, 1237, 1224, 1197, 1157, 1133, 1095, 1064, 1040, 1021, 1008, 967, 955, 934, 907, 890, 850, 823, 785, 755, 717, 676, 616, 590, 552 and 517 cm^{-1}.

Attempted rearrangement of IIc

The same procedure was employed but no exothermal reaction was observed. From 6.7 g (35 mmoles) 7-methyl-2,3-dihydro-1-benzoxepin-5(4*H*)-one oxime (IIc) and 200 g PPA, only 0.52 g of a product was obtained, whose n.m.r. spectrum indicates the absence of any cyclic amide but a preponderance of a compound which was not identified. It seems that this compound has the same structural characteristics as the impurities which were present in the crude products from the Beckmann rearrangements of all II (the "third" compound).

7,8-Dimethyl-2,3 -dihydro-1-benzoxepin-5(4H)-one oxime (IId)

The ketoxime IId (15 g) was suspended in 200 g PPA and the reaction mixture heated at 130° for 15 minutes, under stirring. The reaction mixture was poured onto 500 g ice and water, extracted with chloroform (3×200 ml) and the combined extracts dried. By removing the chloroform, 4.5 g crystalline residue resulted, which was extracted with hot benzene and the solution cooled. The resulted crystals were recrystallized from methyl alcohol to yield 1.5 g colourless crystals m.p. 193–195°. An analytical sample was obtained by sublimation at reduced pressure followed by recrystallization from methyl alcohol. The pure compund melts at 195–196°.

Found : N, 6.80 ; $C_{12}H_{15}NO_2$ *requires* : N, 6.82%

The infrared spectrum of this compound (solid, KBr pellet) was in agreement with the structure corresponding to 8,9-dimethyl-2,3,4,5-tetrahydro-1,6-benzoxazocin-5 (6*H*)-one (IIId) and showed the following absorption bands : 3298, 3183, 3070, 2966, 2940, 2882, 1679, 1577, 1516, 1460^{sh}, 1449, 1406, 1395, 1314, 1300, 1285, 1219, 1185, 1115, 1091, 1058, 1017, 1005^{sh}, 942, 910, 896, 815, 778, 711, 675, 600, 574, 540, 505, 492 and 446 cm^{-1}.

The ultraviolet spectrum, λ_{max}^{ETOH}, ($\log \varepsilon_{max}$) : 280 (3.67), 234 (3.89) and 213 nm (4.56).

Acid hydrolysis of IIId with concentrated hydrochloric acid (twenty hours at reflux) leads to a compound m.p. 113° which proved to be γ-(*2-amino 4-5-dimethylphenoxy*) *butyric acid* (X).

Found : N, 6.01 ; $C_{12}H_{17}NO_3$ *requires* : N, 6.28 %

N.m.r. spectrum : 3.42 (2, s, aromatic) 4.30 (3, broad, NH_2+OH), 5.98 (2, t, $O-CH_2$) and 7.30–8.03 τ(10, m, $2CH_3+CH_2-CH_2-C$).

The ultraviolet spectrum shows absorption bands at λ_{max}^{ETOH} 292.5 and 235 nm (log ε_{max} are 3.89 and 4.21, respectively) which are close values with those reported for the related 2-aminophenol. [32]

6,8-Dimethyl-2,3-dihydro-1-benzoxepin-5(*4*H)*-one oxime* (IIe)

To 20 g PPA preheated at 110°, 1.03 g (5 mmoles) ketoxime IIe was added under stirring and then the mixture heated at 125–130° for ten minutes. After cooling, the mixture was treated with 100 g crushed ice. The resulted solution, cooled to 0° was covered with 100 ml ethyl ether and made alkaline (pH = 10.0 – 10.5) by treating it carefully with solid KOH (pellets) at such a rate that the temperature did not rise above 20°. The organic layer was separated, the aqueous layer extracted twice with ethyl ether (100 ml each portion) and the organic solutions combined and dried. After evaporation of the solvent the crystalline residue was washed with carbon tetrachloride (50 ml) to give 0.8 g crystals m.p. 208–208.5°. By recrystallization from *n*-heptane, the compound melted at 212°.

Found : N. 6.60 ; $C_{12}H_{15}NO_2$ *requires* : N, 6.82 %

The infrared spectrum of the compound (carbon tetrachloride solution) showed the following absorption bands ; 3392, 3185, 3030, 2955, 2925, 2880, 2860, 1685^{sh}, 1680^{sh}, *1666* (C=O), 1630^{sh}, 1613, 1495, 1446, 1405, 1380, 1370, 1315, 1143 and 1072 cm^{-1}. In very diluted CCl_4 solutions, the absorption bands remained unchanged, except the amide I band (1666 cm^{-1}) which was shifted to 1683.5 cm^{-1}.

In another experiment, to 60 g PPA heated at 110°, 1.44 g IIe was added under stirring. No exothermal effect was observed. The mixture was heated and, when the temperature of the mixture reached 155°, gas bubbles evolved from the mixture. After 15 minutes at 155–165°, the reaction mixture was worked up as in the preceeding cases to yield 0.38 g viscous brown residue. The n.m.r. spectrum indicated that no trace of benzolactams were present in this product.

The spectral data of the major compound (m.p. 212°, lit. [20] m.p. 214–215°) were in agreement with the structure IIIe, *i.e.*, 7,9-dimethyl-2,3,4,5-tetrahydro-1,6-benzoxazocin-5(6H)-one.

Beckmann rearrangement of IIa and IIe, by phosphorus pentachloride in ether (*procedure B*)

2,3-Dihydro-1-benzoxepin-5(*4*H)*-one oxime* (IIa)

A solution of 3.54 g (20 mmoles) 2,3-dihydro-1-benzoxepin-5(4H)-one oxime (IIa) in 50 ml absolute ethyl ether was cooled to 0° and then to the cold solution 4 g phosphorus pentachloride was added under stirring. The mixture was stirred fifteen minutes at the same temperature then the ice bath was removed and the mixture left overnight at room temperature. The reaction mixture was treated with 40 ml ice water and the organic and aqueous layers were worked up separately. From the ethereal solution 0.91 g of a solid was obtained by removing the solvent. The crude product was checked for benzolactams by n.m.r. but no positive results were obtained. The aqueous layer was extracted with chloroform (3 × 35 ml) and worked up to give 1.67 g crystalline product, which proved to by a mixture of both IIIa and IVa, in a ratio of 3 : 1 (excluding the impurities present in the crude mixture which were near 15 %).

The mother liquor resulted after chloroform extractions was neutralized with $NaHCO_3$ and then extracted with chloroform and the solvent evaporated. A brown coloured residue (0.18 g) resulted but it was not further studied.

---

[32] J. C. Dearden and W. F. Forbes, *Canad. J. Chem.*, 37, 1294 (1959).

*6,8-Dimethyl-2,3-dihydro-1-benzoxepin-5(4*H)*-one oxime* (IIe)

The procedure used was the same as in the preceeding case. From 1.43 g (7 mmoles) IIe in 50 ml ether and 1.8 g phosphorus pentachloride, resulted 0.2 g residue (not analyzed) and 1.2 g of a solid which proved to be a mixture of IIIe and IVe in a 2 : 1 ratio (by n.m.r. measurement).

*Schmidt reaction on 2,3-dihydro-1-benzoxepin-5(4*H)*-one* (Ia)

To 5 g Ia in 150 ml anhydrous benzene, 5.6 g sodium azide was added and the mixture cooled to 0°. Then, 14 ml of concentrated sulphuric acid was added dropwise under stirring, over an hour, at such a rate that the temperature did not rise above 5°. The mixture was stirred for an hour at 0—5°, the ice bath was removed and the reaction mixture stirred for another hour and then left overnight at room temperature. By working up the reaction mixture, a very poor yield of a solid m.p. 152—156° was obtained, with an infrared spectrum identical to those of IIIa.

By repeating the reaction with the use of an excess of sulphuric acid as solvent (instead of benzene) the yield of IIIa was not improved.

6H-*2,3,4,5-Tetrahydro-1,6-benzoxazocine* (VIII)

To 80 ml anhydrous ethyl ether, 0.8 g $LiAlH_4$ was added under stirring and then, 1.0 g 2,3,4,5-tetrahydro-1,6-benzoxazocin-5(6H)-one (IIIa) was gradually added under stirring. The mixture was refluxed for three hours, then left overnight and the excess $LiAlH_4$ decomposed with wet ether and then with water. The ethereal solution was dried, the solvent removed and the residue distilled in vacuum to give 0.62 g VIII as an oily light yellow liquid, b.p. 112°/ /7 mm Hg.

Found : C, 73.00, H, 8.09 ; $C_{10}H_{13}NO$ *requires* : C, 73,59, H, 8.03 %

The infrared absorption spectrum of this compound agrees with the structure VIII and shows the following bands ; *a*) neat liquid, film on KBr windows ; 3418, 3060, 3025, 2950, 2935, 2870, 1611, 1511, 1471, 1450, 1385, 1330, 1300, 1265, 1226, 1198, 1112, 1061, 1047, 989, 796, 757 and 740 cm^{-1} ; *b*) diluted $CHCl_3$ solution, 0.27 mm NaCl cell : 3450, 3062, 3020, 2958, 2935, 2871, 2853, 1600, 1505, 1462, 1445, 1435, 1378, 1327, 1296, 1261, 1196, 1158, 1111, 1060, 1048 and 989 cm^{-1}.

The n.m.r. spectrum : 3.55—2.90 (4, m, aromatic), 5.83 (2, m, $O-CH_2$), 6.40 (2, m, $N-CH_2$), 6.48 (1, s, NH) and 8.22 τ (4, m, $C-CH_2-CH_2-C$).

*N-(p-Toluensulphonamido)-6*H-*2,3,4,5-tetrahydro-1,6-benzoxazocine* (IX)

A solution of 6H-2,3,4,5-tetrahydro-1,6-benzoxazocine (VIII) (100 mg) and triethylamine (2 ml) in 10 ml anhydrous benzene was treated with 200 mg *p*-toluenesulphochloride, under stirring. The reaction mixture was refluxed for an hour, left for half an hour and then worked up. Yield 60 mg IX, m.p. 125—126.5°.

Found : C, 64.12, H, 6.12 ; $C_{17}H_{19}NO_3S$ *requires* : C, 64.33, H, 6.03 %

N.m.r. spectrum : 2.15—2.40 (2, d, aromatic) in a complex signal between 2.05 to 2.60 (aromatic), 5.90 (2, m, $O-CH_2$), 6.40 (2, m, $N-CH_2$), 7.58 (3, s, CH_3) and 8.35 τ (4, m, $C-CH_2-CH_2-C$)

Acknowledgements. The author thanks Professor emeritus Giorgio Ostrogovich and Professor Alexandru T. Balaban for their interest in this work and for valuable discussions. Thanks are also due to Mr. F. Chiraleu and Mr. C. Drăghici for n.m.r. spectra, Mrs. Simona Bădilescu for infrared spectra, and Miss Letiţia Doşa and Mrs. Maria Roman, for elemental analysis. The author is deeply indebted to Dr. David Huckle (Parke, Davis and Co., Hounslow, England) for gifts of three benzoxazepinones.

NOTE ADDED IN PROOF ; After the work had been completed, two publications were set out on the Schmidt reaction with 2,3-dihydro-1-benzoxepin-5(6H) -one (Ia). [33,34] Both IIIa and IVa were identified in the reaction product, in a ratio of *cca.* 9 :1.

---

[33] D. Misiti, V. Rimatori and F. Gatta, *J. Heterocycl. Chem.*, **10**, 689 (1973).

[34] H. Kawamoto, T. Matsuo, S. Morosawa and A. Yokoo, *Bull. Chem., Soc. Japan*, 46, 3898 (1973).

Revue Roumaine de Chimie, **20**, *8*, 1089–1093 (1975)

AN INTRAMOLECULAR HYDROGEN BRIDGE WITH THE DOUBLE BOND IN SPIRO[CYCLOPROPANE-1,5′(2-HYDROXYMETHYL)-[5′H] DIBENZO [*a*, *d*] CYCLOHEPTENE]

G. M. BENEDIKT and ANCA VOICU

Center of Organic Chemistry, Splaiul Independenţei 202B, Bucharest,
Romania

Received October 9, 1974

Spectral evidences for the conformation of compounds 1 and 2 as well as the dramatic effect of intramolecular hydrogen bond on the NMR spectrum of compound 2 are discussed.

The possibility of IR spectroscopy to put in evidence the intramolecular hydrogen bonding in alcohols,[1] the electron donor being a heteroatom, an aromatic ring, a double or triple bond, a three-membered ring is well-known. The difference between $\nu_{\text{free}-\text{OH}}$ and $\nu_{\text{intramolecular}-\text{OH}}$ is a measure of the hydrogen bond strength in $\text{O}-\text{H}\cdots\pi$ systems[2]. Furthermore, information on the hydrogen bridges in alcohols has been obtained from their NMR spectra.[3]

The present paper deals with the comparative study of IR and NMR spectra and with the conformation of 10′,11′-dihydro-spiro[cyclopropane-1,5′(2-hydroxymethyl)-[5′H]dibenzo[*a*,*d*]cycloheptene],[4] (**1**) and spiro[cyclopropane-1,5′ (2-hydroxymethyl)-[5′H]dibenzo[a, d]cycloheptene], (**2**). The synthesis of the latter alcohol will be described elsewhere.[5]

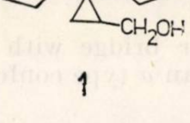
1

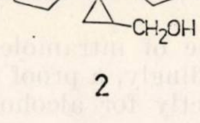
2

---

[1] M. Avram and Gh. Mateescu, "Infrared Spectroscopy Applications in Organic Chemistry", Wiley – Interscience, New York 1972, p. 252.

[2] P. R. von Schleyer, D. S. Trifan and R. Baeskai, *J. Amer. Chem. Soc.*, **80**, 6691 (1958).

[3] D. E. McGreer and M. M. Mocek, *J. Chem. Educ.*, **40**, 358 (1963).

[4] K. Smith and FRENCH LABORATRIES, Brit. Pat. 1129718, 9 oct 1968; *Chem. Abstr.*, **70**, P37560 (1969).

[5] A. Voicu and E. Ciorănescu, to be submitted.

For compounds of this type two conformations, *a* and *b*, are to be taken into account.[6] However, conformation *b* could be excluded because of the important steric hindrance between CH_2OH protons and the ortho-aromatic ones.

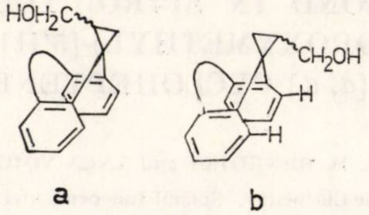

EXPERIMENTAL

The spectral study consisted in dilution experiments performed on a CCl_4 solution of alcohols **1** and **2**, starting with a 20% mol concentration and gradually adding weighed amounts of solvent, each time recording both IR and NMR spectra. IR spectra were recorded on a double beam UR 20 Carl Zeiss Jena device, and the NMR spectra on a Varian A–60A NMR Spectrometer using TMS as internal standard. The final concentration was of about 3% mol.

RESULTS AND DISCUSSION

The IR spectrum of alcohol **1** in carbon tetrachloride exhibits in the ν_{OH} streching vibration region two bands, corresponding to free OH bond (3630 cm^{-1}) and to intermolecular association (3300–3550 cm^{-1}). On dilution the latter form gradually changes, as expected, to the former.

The IR spectrum of alcohol **2** in CCl_4 exhibits in the same region three absorptions corresponding to free OH (3625 cm^{-1}), intramolecular (3575 cm^{-1}) and intermolecular association (3300–3550 cm^{-1}). We assigned the 3575 cm^{-1} vibration to the intramolecular hydrogen bridge with the double bond, excluding the possible association with one of the aromatic rings, on the basis of the absence of this band in the spectrum of compound **1**, having similar skeleton.

IR spectra of alcohol **2** at decreasing concentrations (shown in Fig. 1), qualitatively present the change of intermolecular association into the intramolecular one and by far less into that with free hydroxyl group.

The existence of intramolecular bridge with the double bond in alcohol **2** is, accordingly, a proof for an *a* type conformation of this compound and indirectly for alcohol **1**.

We further aimed at establishing the implications of the above considerations in the NMR spectra of compounds **1** and **2**.

The NMR spectrum of alcohol **1** in CCl_4 exhibits for the hydroxyl adjacent CH_2 group a signal overlapped on that of the saturated bridge between the two aromatic rings. However the doublet form of this signal ($J = 6.5$ Hz*) could be estimated at δ 3.27 ppm, the two methylene protons having the same chemical shift, in accord with the free rotation of CH_2OH group. The saturated bridge appears as a wide multiplet between δ 2.5–4 ppm due to the asymmetry induced by the same group. The three-membered ring protons appear as an overlapped multiplet too, centered at δ 1.35 ppm and the aromatic protons between δ 6.7–7.3 ppm as two apparent singlets.

---

[6] J. J. Looker, D. P. Maier and T. H. Regan, *J. Org. Chem.*, **37**, 3401 (1972).

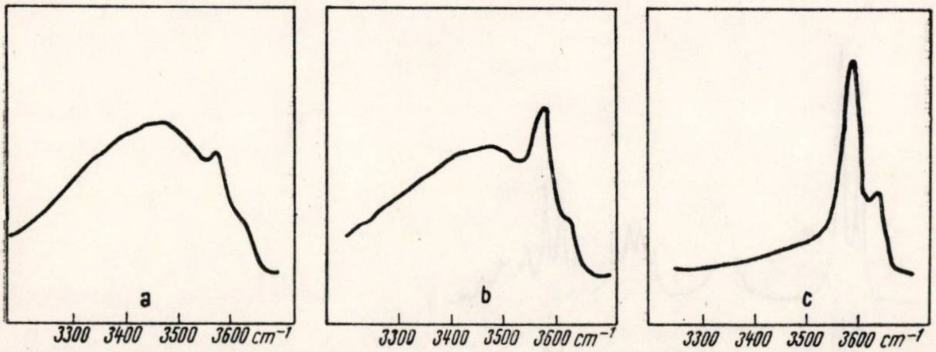

Fig. 1. – IR spectrum (ν_{OH} region) of compound **2** at different concentrations in CCl_4: (a) 15.5% mol, (b) 9.24 % mol, (c) 4.58 % mol.

By far more interesting is the NMR spectrum of alcohol **2** in CCl_4, on which the intramolecular hydrogen bonding has the dramatic effect discussed below. The saturated part between δ0.5–3.5 ppm is shown in Fig. 2, at various concentrations in CCl_4. One should note the equivalence of concentrations in Fig. 1 and Fig. 2 (see captions).

The remarkable variation in the shape of the signal corresponding to hydroxyl adjacent CH_2 group, between a doublet typical of the A_2 part in an A_2X system and the eight lines typical of the AB part in an ABX system, could be explained by the results given by IR spectra. The three forms evidenced there, are in a rapid equilibrium at the NMR time scale, but the one with intramolecular bonding is rigid. At concentrations when the latter form is prevailing the spectrum changes towards that of this one.

The chemical shifts of protons in compound **2** at two different concentrations are given in the Table 1.

The chemical shifts and the coupling constants taken at the lowest concentration (limited by the increase of noise/signal ratio) could be considered, taking in account the IR spectrum at this concentration too, as belonging to the intramolecular associated form.

---

* The coupling constant was taken from an $Eu(DPM)_3$[7] shifted spectrum in which the doublet does not overlap on any signal.

[7] a) C. C. Hinckley, *J. Amer. Chem. Soc.*, **91**, 5160 (1969); b) J. K. M. Saunders and D. H. Williams, *Chem. Comm.*, **1970**, 422.

The two vicinal coupling constants are $J_{AX} = 5.5$ Hz and $J_{BX} = 7.5$ Hz, considering H_A being the more deshielded and H_B the more shielded proton in the methylene group. The geminal coupling constant is $J_{AB} = 12$ Hz.

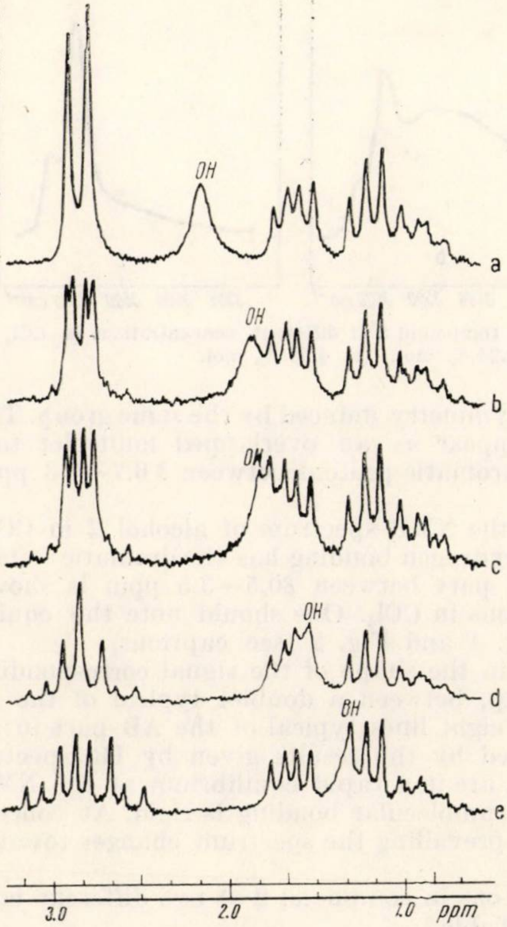

Fig. 2. — Signals of methylene, hydroxyl and 3-membered ring protons in the NMR spectrum (60 MHz) of alcohol **2**, at different concentrations in CCl_4 (in % mol) : (a) 15.5, (b) 10.5, (c) 9.24, (d) 6.77, (e) 4.58.

Table 1

Proton chemical shifts in compound 2 (in δ ppm)

Concentration	Protons							
	H_A	H_B	average H_A, H_B	double bond	3-membered ring H_X	3-membered ring H_Y	3-membered ring H_Z	aromatic
15.5 % mol	2.80	2.80	2.80	6.89	0.88	1.20	1.60	6.70 – 7.30
3.0 % mol	3.17	2.59	2.88	7.07	1	1.28	1.73	6.70 – 7.30

These vicinal coupling constants correspond on the basis of Karplus rule to dihedral angles $H_A-C-C-H_X$ of about 35–40° and $H_B-C-C-H_X$ of about 160–165°. These angles determine such positions of the methylene protons in the rigidised system, which are in agreement with a marked shielding difference between H_A and H_B. As shown in Fig. 3, H_B has to be more shielded in respect with H_A, because of both the anisotropy of benzene ring[8] and that of the three-membered ring.[9]

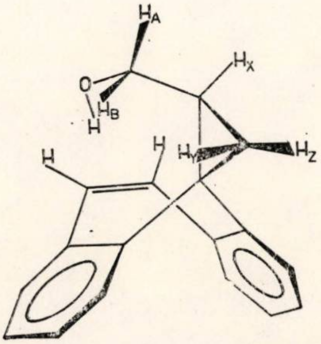

Fig. 3. — Conformation of the intramolecular associated form of alcohol **2**.

The above values of the two angles determine the C—O bond to be oriented towards the double bond, in accordance with intramolecular hydrogen bonding with this donor.

The coupling constants corresponding to the three-membered ring protons are $J_{XY} = J_{YZ} = 5$ Hz and $J_{XZ} = 9$ Hz.

In conclusion, the spectra give valuable information on the conformation of compounds **1** and **2**, and in the case of the unsaturated alcohol an unusual variation of its NMR spectrum with dilution is noted. This fact is explained through the presence in one of the three forms in rapid equilibrium, of a rigidising intramolecular hydrogen bridge with the double bond.

---

[8] C. E. Johnson and F. A. Bovey, *J. Chem. Phys.*, **29**, 1012 (1958).

[9] J. L. Pierre and P. Arnaud, *Bull. Soc. chim. France*, **1966**, 1690; T. Norin, *Acta Chem. Scand.*, **17**, 738 (1963).

Revue Roumaine de Chimie, **20**, *8*, 1095–1101 (1975)

CONDENSATION DES SELS DE SODIUM DES 4-HYDROXYAZOBENZÈNES SUBSTITUÉS AVEC LE 1,4-BIS(CHLOROMÉTHYL)BENZÈNE

M. IOVU* et S. RADU**

*Faculté de Pharmacie, 19–20, A. Sahia, Bucarest
** Faculté de Chimie, 165, Calea Bucureşti, Craiova

Reçu le 16 mai 1974

Dans ce travail nous présentons les résultats obtenus à la condensation des sels de sodium des 4-hydroxyazobenzènes substitués anhydres avec 1,4-bis(chlorométhyl)benzène. D'abord on obtient des sels de sodium des 4-hydroxyazobenzènes et des 4-hydroxyazobenzènes substitués avec du NaOH, puis on éloigne l'eau résultée, par distillation azéotrope d'un mélange azéotrope eau-éthanol-benzène. Les composés synthétisés par nous ne sont pas décrits dans la littérature. Ils sont des substances solides ayant une couleur jaune, qui contiennent au point de vue structural des fonctions éther mixtes aliphatiques-aromatiques, mises en évidence par analyse spectrale en IR. De même, sont présentés les résultats de l'analyse spectrale en IR pour les groupements azo.

Dans un article antérieur [1] nous avons analysé les résultats obtenus à la condensation du 4-4'-azobenzènedioxyde de sodium avec les dérivés monochlorométhylés du benzène ou du benzène substitué : chlorométhyl-benzène, chlorométhyl-2,5-diméthylbenzène, chlorométhyl-3,5-diméthylbenzène, chlorométhyl-2,4,6-triméthylbenzène et chlorométhyl-4-phénylbenzène.

Puisque la condensation a lieu en bonnes conditions pour tous les cas mentionnées, nous avons étudié plus loin les réactions de condensation des 4-azobenzèneoxydes de sodium avec les dérivés mono- ou bis (chlorométhylés) du benzène ou du benzène substitué.

Dans cette note nous présentons les résultats obtenus à la condensation du 1,4-bis(chlorométhyl)benzène avec les sels de sodium des 4-hydroxyazobenzènes suivants : 4-hydroxyazobenzène, 3-chlor-4-hydroxyazobenzène, 3-brom-4-hydroxyazobenzène, 4'-méthyl-4-hydroxyazobenzène, 3-méthyl-4-hydroxyazobenzènes, 2,3-diméthyl-4-hydroxyazobenzène, 3,5-diméthyl-4-hydroxyazobenzène, 2,6-diméthyl-4-hydroxyazobenzène et 2',3-diméthyl-4-hydroxyazobenzène, 2,6-diméthyl-4-hydroxyazobenzène et 2',3-diméthyl-4-hydroxyazobenzène.

Les sels de sodium des 4-hydroxyazobenzènes anhydres ont été obtenus par le traitement du 4-hydroxyazobenzène ou du 4-hydroxyazobenzène substitué avec différents substituents (—Cl, —Br, —CH_3), avec du NaOH solide, en milieu d'éthanol-benzène et l'éloignement de l'eau résultée sous forme d'un mélange azéotrope eau-éthanol-benzène.

---

[1] M. Iovu et S. Radu, *Rev. Roumaine Chim.*, **18**, 473 (1973).

Les sels de sodium des 4-hydroxyazobenzèneoxydes anhydres réagissent avec le 1,4-bis(chlorométhyl)benzène et forment un azobiséther. L'azobiséther résulte par l'action nucléophile de l'anion phénoxydique sur le dérivé bis(chlorométhylé) :

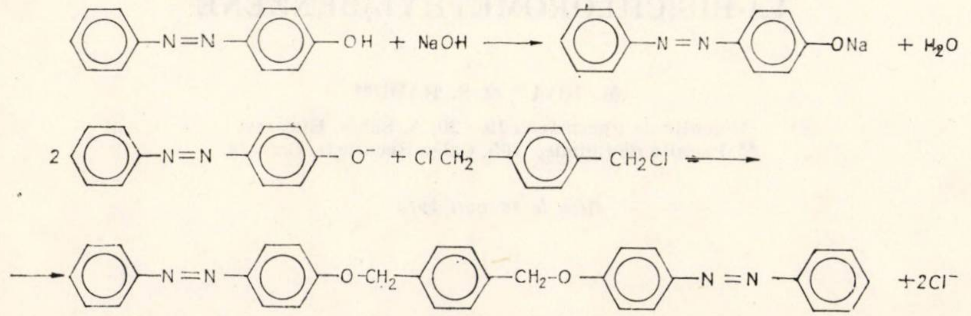

L'azobiséther précipite ensuite avec le chlorure de sodium, en milieu de réaction. Le précipité est séparé des solvants qui contiennent de petites quantités des matières premières non soumises à la réaction par filtration. Le chlorure de sodium est éloigné, en lavant le précipité sur le filtre avec de l'eau.

Pour éviter la formation des produits secondaires, les réactants ont été pris en quantités exactement stœchiométriques.

Les azobiséthers, séchés, sont récristallisés en dioxanne, benzène ou à l'aide d'un mélange d'éthanol-benzène (en différents rapports en fonction de la solubilité).

Les conditions de travail sont les mêmes pour tous les azobiséthers synthétisés, indifféremment des composés initiaux utilisés.

RÉSULTATS ET DISCUSSIONS

Dans le tableau 1 on trouve les formules structurales pour neuf azobiséthers synthétisés, les résultats de l'analyse du carbone, de l'hydrogène, du nitrogène et de l'halogène, les formules moléculaires, les températures de fusion et les rendements.

Tous les azobiséthers sont des substances solides, ayant une couleur jaune et des températures de fusion élevées, comparables à celles des produits dérivés du 4,4'-azobenzènedioxyde de sodium et les dérivés monochlorométhylés du benzène et du benzène substitué, [1] mais plus élevées comparativement aux biséthers synthétisés antérieurement, qui ne contiennent pas la fonction azo. [2–5]

---

[2] M. Iovu, *Rev. Roumaine Chim.*, **16**, 1223 (1971).

[3] M. Iovu et N. Nicolau, *Rev. Roumaine Chim.*, **16**, 1919 (1971).

[4] M. Iovu, *Rev. Roumaine Chim.*, **17**, 1261 (1972).

[5] M. Iovu, N. Miclovici et S. Creţu, *Rev. Roumaine Chim.*, **17**, 1417 (1972).

Les grandes différences qui existent entre les points de fusion de ces composés peuvent être corrélées avec la position des substituents. α,α'-bis(4'-méthyl-azobenzène-4-oxy)-*p*-xylène a la température de fusion la plus élevée, mais α,α'-bis(2,6-diméthyl-azobenzène-4-oxy)-*p*-xylène a la plus basse température de fusion.

Les rendements peuvent atteindre des valeurs élevées (90%). La différence relativement grande entre les rendements dont on obtient les azobiséthers synthétisés est plutôt due à leur solubilité différente dans le milieu de réaction (éthanol-benzène) d'où ils cristallisent. D'autre part, nous avons travaillé avec des quantités plus grandes de solvants et des quantités plus petites de matières premières, en suivant la préparation des produits d'une grande pureté.

Comme dans le cas des azobiséthers synthétisés antérieurement, [1] l'étude spectrale en IR met en évidence des bandes d'absorption dues aux vibrations caractéristiques des éthers et des azodérivés.

Tous les composés présentent une bande d'absorption à 1060 — 990 cm^{-1}, attribuée à la fréquence symétrique de la liaison C—O—C. Pour les composés dont les spectres sont représentés dans la figure 1, $\nu C-O-C_{sym}$ a les valeurs suivantes : 1016 cm^{-1} pour le α,α'-bis (azobenzène-4-oxy)-*p*-xylène, 1047 cm^{-1} pour le α,α'-bis(3-chlore-azobenzène-4-oxy)-*p*-xylène et 1053 cm^{-1} pour le α,α'-bis(3-brome-azobenzène-4-oxy)-*p*-xylène.

Aussi, les azobiséthers absorbent-ils dans la région 1150—1100 cm^{-1}, ce qu'on doit aux vibrations asymétriques de la fonction éther. Pour les composés dont les spectres sont reportés dans la figure 1, $\nu C-O-C_{asym}$ a les valeurs suivantes : 1145 cm^{-1} pour le α,α'-bis(azobenzène-4-oxy)-*p*-xylène, 1134 cm^{-1} pour le α,α'-bis (3-chlore-azobenzène-4-oxy)-*p*-xylène et 1144 cm^{-1} pour le α,α'-bis (3-brome-azobenzène -4-oxy)-*p*-xylène.

Les valeurs des longueurs d'onde où absorbent les azobiséthers synthétisés par nous, démontrent leur caractère mixte d'éther aliphatique et d'éther aromatique et se trouvent entre les valeurs caractéristiques des éthers aliphatiques et des éthers aromatiques. [1]

Bassignana et Cogrossi [6] ont attribué au groupement Ph—N une bande dans la région 1145±15 cm^{-1}. Pour les composés étudiés par nous, la bande caractéristique du groupement Ph—N se superpose à celle due à $\nu C-O-C_{sym}$.

Les spectres IR des azobiséthers synthétisés présentent aussi une bande dans la région 1425—1415 cm^{-1}, de faible intensité, et une bande dans la région 1585—1568 cm^{-1}, intense, pouvant être attribuée au groupement azo.

Les valeurs de $\nu N=N$ pour les composés dont les spectres sont présentés dans la figure 1 sont: 1418 cm^{-1} et 1580 cm^{-1} pour le α,α'-bis (azobenzène-4-oxy)-*p*-xylène, 1428 cm^{-1} et 1568 cm^{-1} pour le α,α'-bis (3-chlore-azobenzène-4-oxy)-*p*-xylène, 1421 cm^{-1} et 1570 cm^{-1} pour le α,α'-bis(3-brome-azobenzène-4-oxy)-*p*-xylène.

---

[6] P. Bassignana et C. Cogrossi, *Tetrahedron*, **20**, 2361 (1964).

Ces valeurs concordent avec de données de Fatiadi. [7] Nous précisons que la seconde bande qui, selon l'auteur mentionné, se trouve à 1580—1560 cm^{-1}, est superposée dans le cas des composés synthétisés par nous, aux bandes d'absorption caractéristiques des noyaux benzéniques de 1600 ± 25 cm^{-1} et 1580 ± 20 cm^{-1} et à la différence des autres éthers aromatiques [2,4,5] apparaît très intense.

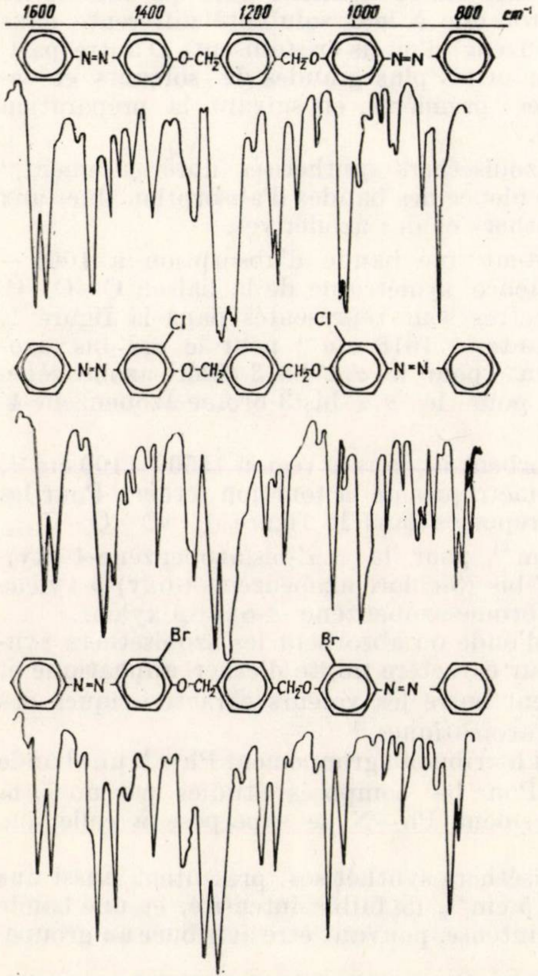

Fig. 1. — Spectres IR du α,α′-bis (azobenzène-4-oxy)-*p*-xylène, α,α′-bis (3-chlore-azobenzène-4-oxy)-*p*-xylène et du α,α′-bis(3-brome-azobenzène-4-oxy)-*p*-xylène.

PARTIE EXPÉRIMENTALE

Le 4-hydroxyazobenzène, le 3-chlore-4-hydroxyazobenzène, le 3-brome-4-hydroxyazobenzène, le 3-méthyl-4-hydroxyazobenzène, le 2,3-diméthyl-4-hydroxyazobenzène, le 2,6-diméthyl-4-hydroxyazobenzène et le 3,5-diméthyl-4-hydroxyazobenzène ont été obtenus par la diazotation de l'aniline et la copulation du sel de diazonium obtenu avec les phénols correspondants.

---

[7] A. J. Fatiadi, *J. Res. Nat. Bur. Stand.*, **71A**, 277 (1967).

Le 4'-méthyl-4-hydroxyazobenzène a été obtenu par la copulation du sel de *p*-méthylbenzènediazonium avec le phénol, mais le 2',3-diméthyl-4-hydroxyazobenzène a été synthétisé par la copulation du sel de *o*-méthylbenzènediazonium avec l'*o*-crésol.

Le 1,4-bis(chlorométhyl)benzène a été obtenu par chloration photochimique du *p*-xylène.

Les spectres IR ont été obtenus en pastilles de KBr à l'aide d'un appareil Perkin-Elmer 157.

Synthèse du α,α'-bis(azobenzène-4-oxy)-p-xylène

Dans un ballon de 100 ml à double col (avec rodage de 14,5), muni d'un réfrigérant à reflux et d'un thermomètre, nous avons introduit 2,64 g (1/75 mole) de 4-hydroxyazobenzène, 0,53 g (1/75 mole) de NaOH (excès 1/5000 mole), 20 ml d'éthanol et 20 ml de benzène.

Le contenu du ballon est chauffé à l'ébullition (65°) jusqu'à ce que le NaOH réagit avec le 4-hydroxyazobenzène, en formant le sel de sodium du 4-hydroxyazobenzène partiellement soluble dans le mélange de solvants (la durée de chauffage ~1 heure).

Puis, le réfrigérant à reflux est substitué par un réfrigérant de distillation et on distille 25 ml de mélange azéotrope eau-éthanol-benzène, pour l'éloignement de l'eau résultée de la réaction. On ajoute au sel de sodium du 4-hydroxyazobenzène anhydre, qui se trouve dans le ballon, 1,17 g (1/50 mole) de 1,4-bis(chlorométhyl)benzène (avec un petit excès) ; mais le réfrigérant de distillation est changé de nouveau par l'un de reflux, le chauffage étant fait à l'aide d'une lampe à incandescence de 25 W, à 65—67°. D'abord se dissout le 1,4-bis(chlorométhyl)benzène dans le milieu de réaction, puis a lieu la réaction du dérivé chlorométhylé de benzène avec le sel de sodium du 4-hydroxyazobenzène anhydre, en formant le chlorure de sodium qui précipite.

L'azobiséther précipite plus tard, quand la quantité formée est plus grande, la solubilité étant petite à la température de travail.

Après l'interruption du chauffage, le ballon où a eu lieu la réaction est laissé refroidir à la température ambiante, pour précipiter une quantité maximale d'azobiséther.

Le produit solide, en comprenant aussi le chlorure de sodium, est séparé de la part liquide par filtration.

Le précipité déposé sur le filtre est lavé plusieurs fois à de l'eau distillée afin d'éliminer le NaCl ; puis, on ajoute une petite quantité d'alcool (2—3 ml) sur le filtre et le produit lavé est séché dans l'étuve à 105°.

Il résulte 2,2 g. Le rendement : 66,2%.

Le α,α'-bis (azobenzène-4-oxy)-*p*-xylène a été recristallisé deux fois du benzène. La température de fusion est $T_f = 229-229{,}5°$.

La synthèse des autres produits mentionnés dans le tableau 1 a eu lieu dans des conditions identiques.

CONCLUSIONS

Dans cet article nous avons montré la possibilité de la préparation des azobisésthers, en bonnes conditions, en partant du 1,4-bis(chlorométhyl)benzène et des sels de sodium des 4-hydroxyazobenzènes. Le 4-hydroxyazobenzène et les 4-hydroxyazobenzènes substitués sont transformés en sels de sodium anhydres correspondants, en utilisant du NaOH et la distillation azéotrope pour l'éloignement de l'eau résultée.

Comme le 4,4'-azobenzènedioxyde de sodium, les sels de sodium des 4-hydroxyazobenzènes réagissent avec le 1,4-bis(chlorométhyl)benzène, en conduisant aux azobiséthers, des composés avec une couleur jaune et des températures de fusion élevées.

Les azobiséthers ont été caractérisés par l'analyse spectrale en IR.

Tableau

Azobiséthers

Azobiséthers

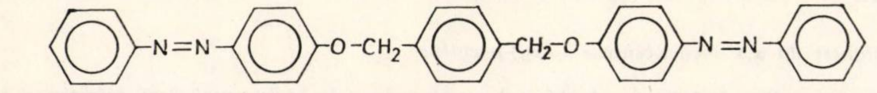

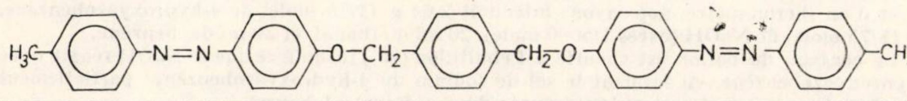

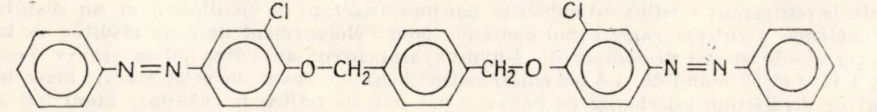

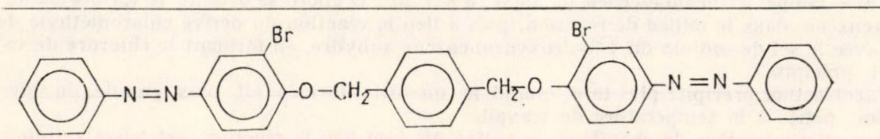

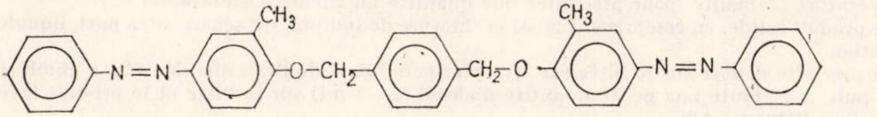

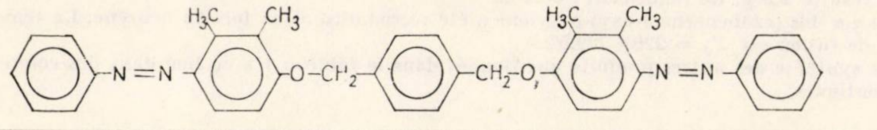

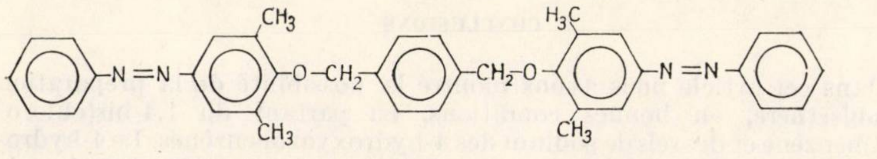

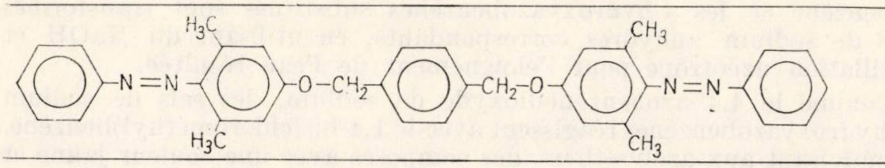

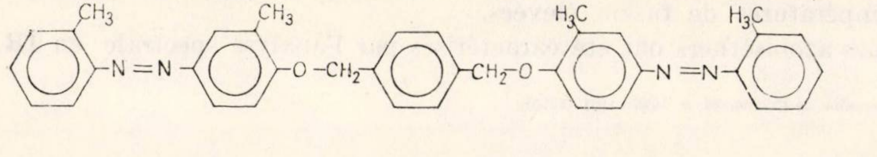

1

Formule moléculaire	C%	H%	N%	Halogène %	Point du fusion °C	Rend. %
	calculé trouvé	calculé trouvé	calculé trouvé	calculé trouvé		
$C_{32}H_{26}O_2N_4$	77,09 77,17	5,25 5,15	11,24 11,77	—	229–229,5	66,2
$C_{34}H_{30}O_2N_4$	77,54 77,01	5,74 5,55	10,64 11,44	—	243,5–245	81,8
$C_{32}H_{24}O_2N_4Cl_2$	67,73 67,14	4,26 4,03	9,87 10,07	12,49 12,55	200–200,5	66,1
$C_{32}H_{24}O_2N_4Br_2$	58,55 58,56	3,69 4,01	8,53 8,55	24,35 24,85	219,5–220	83,2
$C_{34}H_{30}O_2N_4$	77,54 77,81	5,74 5,35	10,64 10,71	—	195,5–196	83
$C_{36}G_{34}O_2N_4$	77,95 77,73	6,18 6,28	10,10 10,38	—	223,5–225	63,9
$C_{36}H_{34}O_2N_4$	77,95 77,69	6,18 6,29	10,10 10,51	—	161–161,5	75,7
$C_{36}H_{34}O_2N_4$	77,95 77,72	6,18 6,18	10,10 10,35	—	204 –205	84,4
$C_{36}H_{34}O_2N_4$	77,95 77,86	6,18 6,24	10,10 10,39	—	180,5–181,5	82

Revue Roumaine de Chimie, 20, 8, 1103–1114 (1975)

SUR L'OXYDATION THERMIQUE DES HYDROCARBURES À LONGUES CHAÎNES EN PHASE LIQUIDE

MIGUEL-ANGEL RUMBEA, GERMAIN LANCHEC et BYOUK BLOURI

Centre d'Etudes et de Recherches de Chimie Organique Appliquée, C.N.R.S.,
2 Rue Henri-Dunant, 94320–THIAIS

Reçu le 26 janvier 1974

Etude expérimentale de l'oxydation par l'air des hydrocarbures normaux de dix à seize carbones à l'état liquide. L'oxydation du décane à des températures relativement basses (entre 140 et 150°) peut aboutir à des mélanges assez riches en cétones, mais pour les hydrocarbures à chaînes plus longues, tels que le *n*-dodécane ou le *n*-hexadécane, il est plus difficile de maîtriser la réaction : on obtient peu d'alcools et de cétones mais surtout des acides et des esters.

L'oxydation en phase liquide des paraffines en alcools et acides gras de 10 à 20 carbones est exploitée industriellement en Europe occidentale et dans l'Union Soviétique.[1 à 3]

On peut extraire les hydrocarbures paraffiniques normaux des fractions du pétrole, soit par adsorption et désorption sur tamis moléculaires (C_{12} à C_{14} à partir du kérosène), soit par formation de complexes avec l'urée (C_{14} à C_{18} à partir du gas-oil, C_{20} à C_{30} à partir de coupes lubréfiantes), soit enfin en traitant par des solvants des résidus de distillation du pétrole brut. Dans ce dernier cas, la longueur de chaîne des paraffines extraites est comprise entre 26 et 50 carbones.

Dans le présent travail nous avons étudié, en fonction de la durée et de la température de réaction, les variations de la composition des produits d'oxydation du *n*-décane, du *n*-dodécane et du *n*-hexadécane.

OXYDATION D'HYDROCARBURES PARAFFINIQUES PURS

Les premières recherches dans ce domaine sont fort anciennes.

Déjà en 1935, Arditti[4] a étudié l'autoxydation de l'hexadécane en mesurant, en fonction du temps, l'absorption de l'oxygène et la formation de gaz carbonique et d'oxyde de carbone. La durée d'oxydation était très longue (700 h) et les températures basses (111 à 132°).

[1] A. N. Bashkirov, *Khim. Nauka i Prom.*, **1**, 273 (1956).

[2] Gu Bo-E et U. Chzhen-Syao, *Kim. Tekhnol. Topliv Masel.* **1960**, 21.

[3] K. H. Zieche et W. Lagodny, *Brevet RFA* 1 000 370, 1957.

[4] G. Arditti, *Compte rend.*, **201**, 398 (1935).

Larsen, Thorpe et Armfield [5] ont montré que, dans l'oxydation de l'hexadécane, du décane et du tétraisobutylène :

— pendant l'oxydation il y a déshydrogénation, rupture de liaisons carbone-carbone, formation d'hydroperoxydes, d'acides, d'esters, de cétones, d'alcools, d'anhydride carbonique et d'eau ;

— l'accroissement de la longueur de la chaîne de l'hydrocarbure augmente sa réactivité ;

— les taux d'absorption d'oxygène sont similaires pour les hydrocarbures saturés et non saturés ;

— il y a une période d'induction suivie d'un accroissement auto-catalytique de la vitesse d'oxydation jusqu'à un maximum ; celle-ci reste ensuite constante.

Kroger et Kaller, [6] en oxydant l'hexadécane par l'air entre 120 et 150°, ont montré que la formation des hydroperoxydes passe par un maximum après 8 à 12 h. A 120° la courbe d'absorption d'oxygène devient linéaire après 7 h, tandis qu'elle est linéaire dès le début à 140° et cesse de l'être à 150°.

Hass, McBee et Churchill [7] ont autoxydé l'hexadécane entre 190 et 300° sous une pression de 140 kg/cm². La durée de la réaction a varié de 0 à 15 mn. L'analyse quantitatives des produits d'oxydation formés a été faite par une mesure des indices d'acidité et de saponification pour les acides et les esters, une étude de la solubilité dans l'acide sulfurique concentré a permis de doser l'ensemble des produits oxygénés. Pour une conversion déterminée à 190 et 250°, ils ont constaté que c'est à 250° qu'on obtient le plus de produits d'oxydation partielle (alcools et cétones). Par suite des explosions et de la carbonisation de l'hydrocarbure mis en réaction, ils n'ont pas pu réaliser une oxydation contrôlée de l'hexadécane à 300°.

Bashkirov [1] a étudié l'oxydation thermique, avec de l'air et en présence de borax, de mélanges de paraffines en alcools secondaires. Le borax estérifie les alcools secondaires formés et ralentit leur oxydation en cétones ou acides.

Bashkirov et ses collaborateurs ont également étudié l'oxydation thermique, avec de l'air pur ou de l'air appauvri en oxygène, de mélanges de paraffines en vue de l'obtention de cétones à longues chaînes. [8] Pour la détermination de la composition de leurs produits d'oxydation, ils se sont surtout basés sur les indices d'acide, d'ester, d'hydroxyle et de carbonyle. Ils pensent que les cétones peuvent se former directement à partir des hydroperoxydes :

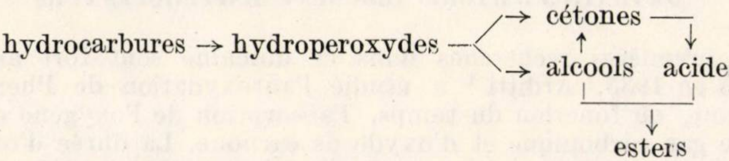

---

[5] R. C. Larsen, R. E. Thorpe et F. A. Armfield, *Ind. Eng. Chem.*, **34**, 186 (1942).

[6] C. Kroger et A. Kaller, *Öl Kohle, Brenn. Chem.*, **39**, 669 (1943).

[7] H. B. Hass E. T. McBee et J. W. Churchill, *Ind. Eng. Chem.*, **37**, 445 (1945).

[8] V. V. Kamzolkin, A. N. Bashkirov et M. M. Potain, *Doklady Akad. Nauk S.S.S.R.*, **126**, 1282 (1959).

C'est à basse température, 140°, et notamment avec de l'air dont le taux d'oxygène est abaissé à 3,5 %, qu'ils obtiennent les mélanges les plus riches en cétones.

Ils ont également constaté que l'addition d'un acide organique (formique ou acétique) ou minéral (bromhydrique ou chlorhydrique) favorisait la formation de cétones.

Bashkirov et ses collaborateurs ont également étudié l'oxydation en cétones, de mélanges d'alcools secondaires de 16 à 19 carbones.[9] Dans ce cas aussi, les taux les plus élevés en cétones sont obtenus par une oxydation avec de l'air appauvri en oxygène, à une température relativement basse : une élévation de la température favorise la formation des acides et des esters.

MÉCANISME RÉACTIONNEL

Tous les auteurs admettent l'intervention d'une chaîne de réactions radicalaires, qui peut être schématisée comme suit :[10]

Amorçage $RH \xrightarrow{O_2} R^{\cdot}+HOO^{\cdot}$ -47 kcal/mole

Propagation → $R^{\cdot}+O_2 \longrightarrow ROO^{\cdot}$ $E_A = 0$

$ROO^{\cdot}+RH \longrightarrow ROOH+R^{\cdot}$ Réaction exothermique pour la plupart des hydrocarbures

Terminaison $R^{\cdot}+R^{\cdot} \longrightarrow R-R$

$ROO^{\cdot}+R^{\cdot} \longrightarrow ROOR$

$ROO^{\cdot}+ROO^{\cdot} \rightarrow R-OH+R^1-CO-R^2+O_2$

L'hydroperoxyde ROOH est à l'origine de la formation des produits stables de la réaction : alcools, cétones, acides.

De nombreux processus chimiques ont été évoqués. Une partie de l'hydroperoxyde se décompose directement en cétone :

$$ROOH \rightarrow R^1-CO-R^2 + H_2O$$

mais une grande partie réagit avec l'hydrocarbure pour former d'autres radicaux :

$$ROOH+RH \rightarrow RO^{\cdot} + R^{\cdot} + H_2O.$$

---

[9] A. N. Bashkirov, M. M. Potain et V. V. Kamzolkin, *Doklady Akad. Nauk S.S.S.R.*, **127**, 93 (1959).

[10] N. M. Emanuel, E. T. Denisov et Z. K. Maizus, « Liquid-phase Oxidation of Hydrocarbons », Plenum Press, New York, 1967.

Le radical $RO^{\cdot}$ est transformé en alcool :

$$RO^{\cdot} + RH \rightarrow ROH + R^{\cdot}$$

et les radicaux $R^{\cdot}$ entament une nouvelle série de réactions. On a envisagé aussi des réactions de l'hydroperoxyde avec l'hydroperoxyde lui-même, avec les alcools et avec les cétones.

La formation des cétones, par exemple, peut résulter d'une réaction de l'hydroperoxyde avec un radical libre :

$$R^1-CH(OOH)-R^2 + ROO^{\cdot} \rightarrow ROOH + R^1-\dot{C}(OOH)-R^2 \rightarrow$$

$$\rightarrow R^1-CO-R^2 + \dot{O}H$$

et celle des alcools, de :

$$ROOH \rightarrow \dot{O}H + R\dot{O}$$

$$RO^{\cdot} + RH \rightarrow ROH + R^{\cdot}$$

La formation des acides s'effectuerait surtout à partir des cétones :

$$R^1-CO-CH_2-R^2 \xrightarrow{+R^{\cdot}} RH + R^1-CO-\dot{C}H-R^2 \xrightarrow{+O_2}$$

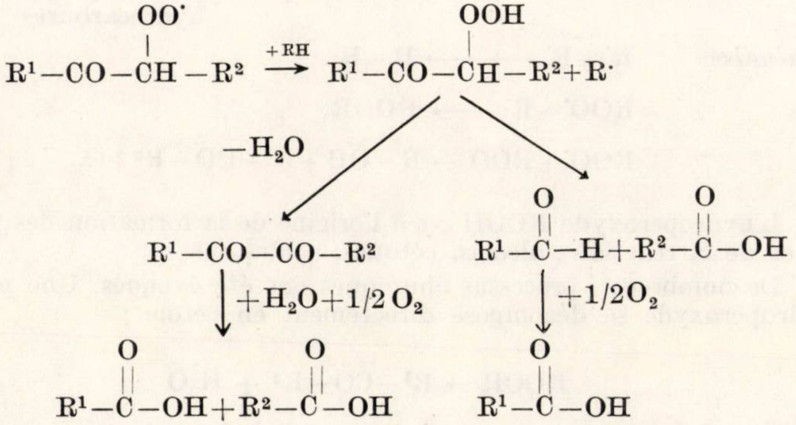

$$R^1-CO-\overset{\overset{OO^{\cdot}}{|}}{C}H-R^2 \xrightarrow{+RH} R^1-CO-\overset{\overset{OOH}{|}}{C}H-R^2 + R^{\cdot}$$

$$\xrightarrow{-H_2O} R^1-CO-CO-R^2 \xrightarrow{+H_2O+1/2\,O_2} R^1-\overset{\overset{O}{\|}}{C}-OH + R^2-\overset{\overset{O}{\|}}{C}-OH$$

$$\rightarrow R^1-\overset{\overset{O}{\|}}{C}-H + R^2-\overset{\overset{O}{\|}}{C}-OH \xrightarrow{+1/2O_2} R^1-\overset{\overset{O}{\|}}{C}-OH$$

Enfin la formation des esters résulterait d'une réaction ionique entre les alcools et les acides.

PARTIE EXPÉRIMENTALE

APPAREILLAGE

Les essais d'oxydation ont été effectués dans un appareil représenté par la figure 1.

Il se compose d'un réacteur en verre *1* de 22 mm de diamètre intérieur et 165 mm de hauteur, qui comporte une plaque en verre frittée *2* pour assurer un barbotage du mélange oxydant arrivant par un tube *3* placé en dessous. Le réacteur est relié par un rodage à une tête *4* munie d'un thermomètre *5* et d'un réservoir *6* pour recueillir les produits légers éventuellement formés dans la réaction. Ces derniers sont retenus par un condenseur à eau *7* et les gaz et vapeurs non condensés passent par un tuyau en chlorure de vinyle jusqu'à un piège *8* refroidi par de la glace, dans lequel est condensé le reste des produits légers formés. Les gaz sortants sont mesurés finalement par un gyromètre *9*.

Les débits d'air et d'azote, provenant de bouteilles en acier, sont réglés par des vannes reliées à des gyromètres *10* et *11*. Les gaz passent ensuite dans un mélangeur en U, *12*. Un manomètre *13* indique la pression et la perte de charge de l'ensemble de l'appareillage.

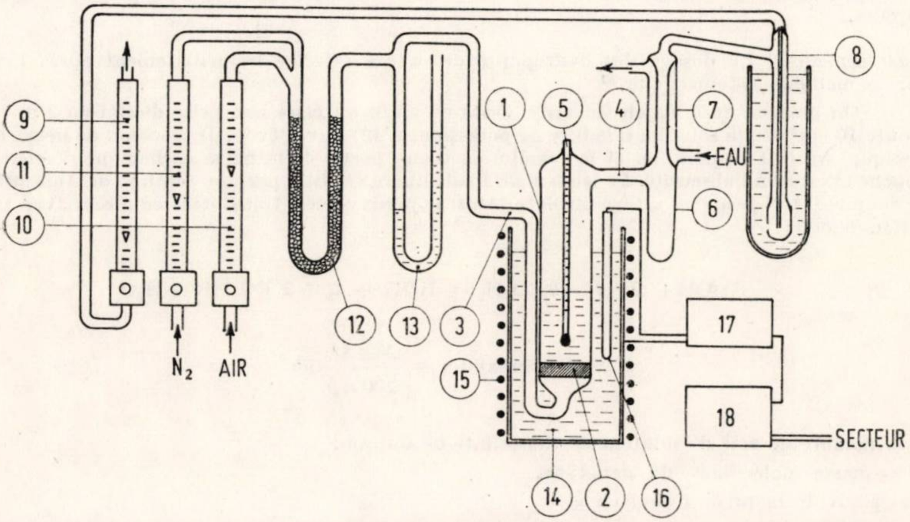

Fig. 1. — Appareillage d'oxydation.

Le chauffage du réacteur est assuré par un bain de paraffine *14* chauffé par une résistance électrique *15*. Un thermocouple *16* connecté à un régulateur de température Chauvin Arnoux *17* permet la lecture de la température et la commande de passage du courant provenant d'un autotransformateur du type ROTOTRANSFO de DEREIX *18* qui règle la puissance nécessaire pour la température d'oxydation désirée.

MODE OPÉRATOIRE

On introduit 20 cm³ d'hydrocarbure dans le réacteur, correspondant à une hauteur de 5,5 cm. On affiche la température désirée pour l'essai et on branche le réacteur jusqu'à ce que la température indiquée soit bien stable. A ce moment on fait arriver le mélange gazeux oxydant et le temps d'oxydation est compté à partir de cet instant.

Lorsque l'essai est terminé, on retire le bain de paraffine pour laisser refroidir rapidement le mélange.

Lorsque les produits d'oxydation sont suffisamment froids on prélève tout de suite des échantillons pour faire les diverses analyses.

MATIÈRES PREMIÈRES

Pour notre étude de l'oxydation des paraffines nous avons utilisé les hydrocarbures suivants : *n*-décane, *n*-dodécane, *n*-hexadécane d'une pureté de 98 à 99 % vérifiée par chromatographie en phase gazeuse.

Tous ces hydrocarbures ont été obtenus par distillation fractionnée, à l'aide d'une colonne à remplissage de 2 m de longueur pour 2 cm de diamètre intérieur, remplie avec des anneaux en acier inoxydable du type Dixon de 4 mm de diamètre, à partir de mélanges de paraffines extraites de fractions commerciales du pétrole par adsorption et désorption sur tamis moléculaire.

ANALYSE DES PRODUITS

La détermination quantitative des hydroperoxydes, acides et esters a été réalisée par voie chimique, tandis que les alcools et les cétones ont été analysés par chromotographie en phase gazeuse.

Hydroperoxydes. Le dosage des hydroperoxydes a été effectué immédiatement après l'essai par la méthode iodométrique.[11]

On procède de la façon suivante. Dans un erlen on place une prise d'essai de 2 g. On ajoute 10 cm³ d'une solution d'iodure de potassium à 40% avec un petit morceau de neige carbonique. Après l'évaporation et la dissolution d'une partie de la neige carbonique, l'erlen est bouché et laissé à l'obscurité. Le lendemain l'iode libéré est titré par une solution de thiosulfate de sodium 0,1 N jusqu'au virage incolore. Ainsi le peroxyde est transformé en alcool avec libération d'iode :

$$\mathrm{ROOH} + 2\,\mathrm{KI} + 2\,\mathrm{CO_3H_2} \rightarrow \mathrm{ROH} + \mathrm{I_2} + 2\,\mathrm{CO_3HK} + \mathrm{H_2O}$$

$$\%\ \text{de peroxydes} = \frac{N \times M}{200 \times p}\ \text{où}$$

N = nombre de cm³ de solution de thiosulfate de sodium.

M = masse moléculaire du peroxyde.

p = poids de la prise d'essai en g.

Acides. Le taux des acides des produits de réaction est déterminé par titrage avec une solution aqueuse de soude 0,1 N. L'analyse est effectuée tout de suite après l'essai. Les acides présents dans le produit d'oxydation ont une chaîne hydrocarbonée de 2 à n/2 carbones, n représentant le nombre de carbones de l'hydrocarbure de départ.

Pour le calcul du pourcentage d'acides, nous avons pris la masse moléculaire moyenne des acides formés : elle correspond à un acide ayant une chaîne de n/2 carbones.

$$\%\ \text{d'acides} = \frac{N \times M}{100 \times p}\ \text{où}$$

N = nombre de cm³ de solution de soude

M = masse moléculaire moyenne des acides formés ($C_{\frac{n}{2}-1}H_{n-1}CO_2H$).

p = poids de la prise d'essai en g.

Esters. Après le dosage des hydroperoxydes par l'iodure de potassium et des acides par la soude, le reste du produit d'oxydation est lavé à l'eau, décanté et séché sur sulfate de sodium et les esters sont dosés ensuite par saponification selon la méthode indiquée par Pesez et Poirier.[12]

On ajoute un excès de solution alcoolique de potasse 0,1 N et chauffe à douce ébullition pendant 1 h, au bain-marie, dans un ballon rodé muni d'un réfrigérant à air.

[11] V. Karnojitzki, « Les peroxydes organiques », Hermann, Paris, 1958, p. 102.

[12] M. Pesez et P. Poirier, « Méthodes et réactions de l'analyse organique », Ier vol., Masson et Cie, Paris, 1952, p. 181.

Un essai à blanc est pratiqué avec le même volume de solution alcoolique de potasse, 0,1 N, dans les mêmes conditions de chauffage.

Après refroidissement, on titre l'excès de potasse par l'acide sulfurique 0,1 N en présence de quelques gouttes de solution de phénol-phtaléine.

Soient N et n les volumes en cm^3 utilisés pour le témoin et l'essai effectué à partir de p grammes ; le pourcentage d'esters est calculé par la formule :

$$\%\ \text{d'esters} = \frac{(N-n)\times M}{100\times p} \quad \text{où}$$

M = masse moléculaire moyenne des esters formés, c'est-à-dire masse moléculaire de l'ester formé à partir de l'alcool en C_n et de l'acide en $C_{n/2}$.

Ce pourcentage d'esters ne tient pas compte du taux d'acides calculé précédemment. Pour obtenir le pourcentage réel d'esters dans le produit d'oxydation, il faut multiplier le chiffre trouvé précédemment par le facteur $\frac{100 - \%\ \text{d'acides}}{100}$.

Cétones et alcools. Un échantillon du produit brut d'oxydation est traité par de la potasse alcoolique, en excès, à chaud. Après refroidissement, on lave à l'eau, décante et sèche sur sulfate de sodium. Les hydroperoxydes sont transformés en cétones, les esters en alcools correspondants, les acides et la fraction acide des esters en sels de potassium qui sont éliminés.

Les alcools et cétones formés et l'hydrocarbure résiduel sont analysés par chromatographie en phase gazeuse dans un appareil Girdel du type 75 FD, sur une colonne à remplissage de 7 m de longueur et 3 mm de diamètre, contenant comme phase stationnaire du Versamid 900 imprégné à 5% sur du chromosorb W traité à la potasse, avec un débit d'azote de 20 cm^3/mn ; la température d'élution est différente selon l'hydrocarbure mis en réaction.

a) *n-décane.* Karpukhina et Maizus [13] avaient déjà signalé que sur une colonne de 180 cm de longueur et 6 mm de diamètre remplie avec diverses phases (triéthylèneglycol, « Polyox », ter(hydroxyméthyl)propane, etc...) on pouvait séparer au mieux 3 des 4 décanones isomères car ces composés ont des points d'ébullition voisins et élevés (210°).

Nous avons réalisé une meilleure séparation mais la décanone-5 et la décanone-4, ainsi que le décanol-5 et le décanol-4 sortent ensemble et les surfaces des pics montrent que les quatre isomères sont formés approximativement dans les mêmes proportions (figure 2).

Comme dans le cas des esters, ces pourcentages ne tiennent pas compte :

— du taux des acides et de la fraction acide des esters,

— des alcools provenant de la fraction alcool des esters,

— des cétones issues des hydroperoxydes.

Soient A, C et H les pourcentages d'alcools, de cétones et d'hydrocarbure calculés par chromatographie en phase gazeuse. Les taux réels de ces constituants sont calculés en multipliant respectivement A et C par le facteur

$$\frac{100 - (\%\ \text{d'acides} + \text{fraction acide des esters})}{100}$$

et en déduisant des chiffres trouvés pour les alcools, la fraction alcool des esters et pour les cétones, le taux d'hydroperoxyde.

L'hydrocarbure résiduel est calculé par différence.

b) *n-dodécane.* Comme dans le cas du décane, nous avons pu séparer les alcools et les cétones par familles. Avec une température d'élution de 200°, l'ordre de sortie est le suivant : *n*-dodécane, dodécanone-6 + dodécanone-5 + dodécanone-4, dodécanone-3, dodécanone-2, dodécanol-6 + dodécanol-5 + dodécanol-4, dodécanol-3, dodécanol-2.

---

[13] G. V. Karpukhina et Z. K. Maizus, *Neftekhimiya*, **6**, 901 (1962).

c) *n-hexadécane.* Avec une température d'élution de 220°, les alcools et cétones sont séparés par familles, mais les isomères en position 4, 5, 6, 7 et 8 sont élués ensemble.

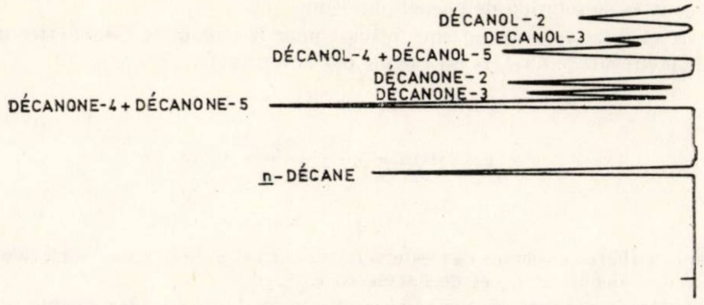

Fig. 2. — Séparation d'isomères.

RÉSULTATS

OXYDATION DU *n*-DÉCANE

Cet hydrocarbure a une chaîne relativement longue, mais ses produits d'oxydation peuvent être complètement analysés par chromatographie en phase gazeuse, notamment en ce qui concerne les mélanges d'alcools secondaires et de cétones.

Nous avons procédé à trois séries d'essais en variant la température, le temps d'oxydation et le débit d'air.

a) *Température.* Nous avons fait varier la température d'oxydation de 130 à 160° en maintenant constantes les autres conditions opératoires : débit d'air, 3,5 l/h et temps d'oxydation 4 h. La hauteur des 20 cm^3 d'hydrocarbure dans le réacteur a été, à la température ambiante, de 5,5 cm. Les résultats sont rassemblés dans le tableau 1. Il n'a pas été possible de travailler à plus de 160°, l'air entraînant l'hydrocarbure (P. E. du *n*-décane : 174°).

A 130°, le taux de conversion est très faible mais il y a un commencement de formation d'hydroperoxydes dont les taux n'augmentent d'ailleurs pas beaucoup en fonction de la température, tandis que ceux des alcools et cétones croissent régulièrement à 150 et 160°.

En ce qui concerne la composition des alcools et cétones, elle ne varie pas beaucoup en fonction de la température de réaction et les taux, des différents alcools et cétones restent pratiquement analogues entre eux, exception faite pour les isomères en position 2 favorisés par rapport à ceux en position 3. Il n'y a pas de formation d'alcool primaire (décanol-1), ni d'aldéhyde.

b) *Durée de la réaction.* A 150°, avec un débit d'air de 3,5 l/h, la durée de l'oxydation a été variée de 2 à 8 h. Les résultats sont rassemblés dans le tableau 2. Au bout de 4 h le taux d'hydroperoxydes atteint 3% et reste pratiquement constant ensuite. Les taux des acides, esters et cétones croissent régulièrement en fonction du temps, tandis que le taux des alcools libres croît d'abord et baisse ensuite.

Tableau 1

Oxydation du *n*-décane. Influence de la température

T (°C)	Composition centésimale du mélange réactionnel en g %					
	Hydro-peroxydes	Acides	Esters	Cétones	Alcools	Hydro-carbure
130	0,2	—	—	—	—	99,8
140	2,0	0,3	0,5	0,8	0,5	95,9
150	3,0	4,3	2,3	4,7	1,4	84,3
160	2,7	4,4	2,7	8,5	2,0	79,7

Composition centésimale des alcools et cétones en g%

Température (°C)	140	150	160
décanol-2	32,1	30,0	26,4
décanol-3	15,3	19,8	23,3
décanol-4 décanol-5	52,6	50,2	50,3
décanone-2	30,9	29,2	28,2
décanone-3	19,5	17,0	19,1
décanone-4 décanone-5	49,6	53,8	52,7

La prolongation du temps de réaction favorise probablement l'estérification des acides et des alcools formés au cours de l'oxydation.

c) *Débit de l'air.* 20 cm^3 de *n*-décane sont oxydés pendant 4 h à 150° avec de l'air dont le débit a varié de 1,4 à 8,0 l/h. Cela correspond à une quantité d'air allant de 96 à 548 litres par heure et par kilogramme d'hydrocarbure.

Les résultats rassemblés dans le tableau 3 montrent que, surtout du point de vue de la production de cétones, l'oxydation s'effectue le mieux avec un débit d'air optimal de l'ordre de 4 à 5 l/h. Avec un débit plus

Tableau 2

Oxydation du *n*-décane. Influence du temps de réaction

Temps (h)	Composition centésimale du mélange réactionnel en g%					
	Hydro-peroxydes	Acides	Esters	Cétones	Alcools	Hydro-carbure
2	0,4	0,5	0,3	3,8	1,0	94,0
4	3,0	4,3	2,3	4,7	1,4	84,3
6	3,1	8,8	3,0	14,0	3,3	67,8
8	3,5	14,2	4,1	16,3	0,3	61,6

Tableau 3

Oxydation du *n*-décane. Influence du débit de l'air

Débit (l/h)	Composition centésimale du mélange réactionnel en g%					
	Hydroperoxydes	Acides	Esters	Cétones	Alcools	Hydrocarbure
1,4	1,4	2,3	1,8	5,2	3,0	86,3
3,5	3,0	4,3	2,3	4,7	1,4	84,3
5,5	4,3	5,8	2,8	8,1	1,5	77,5
8,0	4,7	6,5	4,1	5,5	—	79,7

faible, le taux de transformation est très faible et avec un débit très fort de 8 l/h on abaisse également le taux de transformation. Toutes ces données sont valables pour l'appareillage que nous avons utilisé, compte tenu notamment de la nature du verre fritté (porosité 1) et de la hauteur de l'hydrocarbure à oxyder (5,5 cm). En tout cas, même avec un débit de 1,4 l/h, la totalité de l'oxygène de l'air n'est pas consommée.

OXYDATION DU *n*-DODÉCANE

Avec un débit d'air de 3,5 l/h le *n*-dodécane est oxydé pendant 4 h entre 140 et 160°. Le dernier essai est effectué à 150° pendant 8 h. La composition des mélanges de produits d'oxydation est indiquée dans le tableau 4. Pour les produits d'oxydation d'un hydrocarbure à plus de 10 carbones une séparation individuelle des différents alcools et cétones est encore plus difficile que pour ceux du décane. Mais de toute façon, nous avons vu pour le décane que la répartition de ces alcools secondaires et cétones était en rapport avec le nombre des hydrogènes susceptibles d'être substitués par un groupement hydroxyle ou carbonyle et à peu près indépendant de leur position sur un carbone secondaire.

Tableau 4

Oxydation du *n*-dodécane

T (°C)	Composition centésimale du mélange réactionnel en g %					
	Hydroperoxydes	Acides	Esters	Cétones	Alcools	Hydrocarbure
140	1,6	0,6	0,8	1,6	0,8	94,6
150	2,3	7,3	6,5	8,3	2,2	73,4
160	3,3	8,6	17,4	8,0	—	62,7
150 durée 8 h	3,0	17,8	47,6	11,7	—	19,9

En ce qui concerne la composition des produits d'oxydation, comme dans le cas du décane, il y a un accroissement, en fonction de la température et de la durée de réaction, du taux des acides et des cétones formés. Mais il se forme au contraire peu d'alcools libres. Dans l'essai à 160° et dans celui à 150° d'une durée de 8 h, la totalité de l'alcool est estérifiée.

Enfin la prolongation de l'oxydation rend l'oxydation plus complète et, avec une durée de 8 h, il ne reste que 19,9% d'hydrocarbure non transformé.

L'allongement de la chaîne hydrocarbonée favorise nettement l'oxydation en acides, ainsi que l'estérification des alcools formés.

OXYDATION DU *n*-HEXADÉCANE

Avec un débit d'air de 3,5 l/h pendant 4 h, le *n*-hexadécane a été oxydé entre 140 et 180°. Nous avons fait également deux autres essais : à 150° pendant 8 h et à 180° pendant 5 h. La composition des produits de réaction est consignée dans le tableau 5.

Tableau 5

Oxydation du *n*-hexadécane

N° de l'essai	T (°C)	Composition centésimale du mélange réactionnel en g%					
		Hydro-peroxydes	Acides	Esters	Cétones	Alcools	Hydro-carbure
1	140	1,8	0,5	4,1	1,0	—	92,6
2	150	4,4	8,6	13,4	9,9	—	63,7
3	160	2,5	11,9	19,7	11,3	—	54,6
4	180	3,0	7,3	36,8	10,8	—	42,1
5	180 durée 5 h	1,9	10,1	56,0	11,9	—	20,1
6	150 durée 8 h	1,8	17,6	67,2	11,1	—	2,3

Les résultats obtenus sont différents de ceux des produits d'oxydation du *n*-décane et du *n*-dodécane. En fonction de l'élévation de la température et surtout de la durée d'oxydation de l'hexadécane, le taux des esters croît considérablement. Dans les essais 5 et 6 ce taux atteint respectivement 56 et 67,2%. Dans ces cas le taux d'alcools libres est nul. Toutefois pour des taux de transformation aussi élevés que 97,3%, il n'est pas sûr que la longueur de chaîne moyenne des acides libres ou estérifiés soit de 8 carbones.

En effet, l'oxydation des acides étant beaucoup plus facile que celle des autres composés et notamment que celle de l'hydrocarbure initial, il est fort probable que la longueur de chaîne des acides soit raccourcie par suite d'oxydation suivant le mécanisme de β-décarboxylation des α-céto-acides.

En tout cas, les produits d'oxydation des hydrocarbures varient suivant la longueur de chaîne et si pour le décane dans des conditions opératoires relativement douces (140—150°, avec un faible débit d'air), on obtient des mélanges riches en cétones, pour les hydrocarbures à chaîne plus longue, à des températures basses la réaction d'oxydation est très peu avancée, mais avec l'élévation de la température ou la prolongation du temps d'oxydation la réaction est très poussée et on a une scission de la chaîne hydrocarbonée, qui accompagne l'oxydation et fournit surtout des mélanges d'acides et d'esters.

Nous avons oxydé des hydrocarbures purs de 10 à 16 carbones, afin de prévoir le comportement des hydrocarbures à plus longue chaîne. En effet, une analyse chromatographique précise des produits d'oxydation des hydrocarbures à plus de 16 carbones est très difficile. Comme résultat concret, on peut admettre que, dans les conditions de travail indiquées, l'oxydation des paraffines lourdes aboutira surtout à des acides et à des esters, mais très peu aux cétones que nous souhaitions obtenir.

Revue Roumaine de Chimie, **20**, *8*, 1115–1118 (1975)

SUR LA RELATION ALGÉBRIQUE ENTRE LES ÉNANTIOMÈRES DE L'ATOME DE CARBONE ASYMÉTRIQUE

IOAN MOŢOC
Département de Chimie Physique, Université de Timişoara,
Roumanie

Reçu le 25 mai 1974

On essaie la déduction de la relation algébrique entre les deux énantiomères de l'atome de carbone asymétrique.

1. INTRODUCTION

Dans un ouvrage antérieur,[1] on est arrivé, d'une manière intuitive, à formuler la relation algébrique entre les deux énantiomères de l'atome de carbone asymétrique.

Dans cet ouvrage, on obtient cette relation rigoureusement et systématiquement.

Limitant la discussion au cas de l'atome de carbone asymétrique cette chose ne se spécifiera plus par la suite.

Étant donné $c_1, c_2, \ldots, c_n, \ldots$ comme des centres asymétriques (spécifiés par les diagrammes de structure), on dénommera *représentation* un procédé par lequel on remplace un diagramme de structure c_i par un ensemble déterminé de nombres. Cet ensemble sera dénommé *représentant* de la formule de structure.*

Dans cet ouvrage nous utiliserons une représentation matricielle. Pour obtenir cette représentation, on employera le procédé proposé par Ruch et ses collaborateurs.[3,4]

Ce procédé (noté ci-dessous par α) on le suppose connu.

Soit un ligand $s_i' \in S'$.** En appliquant α à s' on obtient :

$$\alpha(s_i') = \lambda_i \in A, A \subset R \tag{1}$$

α applique bijectivement l'S' en A.

---

[1] I. Moţoc et F. Kerek, *Rev. Roumaine Chim.*, **18**, 289 (1973).

* Cette définition est similaire à celle employée dans la Mécanique quantique.[2]

[2] P. A. M. Dirac, « The Principles of Quantum Mecanics », Clarendon Press, Oxford, (1958).

[3] E. Ruch et A. Schönhofer, *Theor. Chim. Acta*, **3**, 291 (1965).

[4] E. Ruch et I. Ugi, *Theor. Chim. Acta*, **4**, 287 (1966).

** S' est l'espace fondamental des ligands.[5]

[5] I. Moţoc, *Rev. Roumaine Chim.*, **20**, (1975).

Soit aussi la multitude $\mathcal{M}$ des matrices 2×2 construites avec les éléments A. C'est-à-dire :

$$\mathcal{M} = \{ [m]_{2\times 2} / m \in A \} \tag{2}$$

Nous supposons donné le set des règles $\mathcal{L}$ qui définissent l'opérateur β, réalisant l'association de la matrice

$$[m] \in \mathcal{M} \text{ du centre } c$$

En convenant que :

$$\alpha(c_1) = (\lambda_{i1}, \lambda_{i2}, \lambda_{i3}, \lambda_{i4}) \tag{3}$$

la représentation matricielle utilisée dans cet ouvrage est définie par la relation :

$$\beta\,([\alpha(c)] = [m] \in \mathcal{M} \tag{4}$$

OBSERVATIONS

(1) Il est évident que $m = \lambda$.
(2) Comme $\mathcal{L}$ n'est pas spécifié concrètement, la forme concrète de la matrice $[m]$ n'intéresse non plus.

Soient $[m^1]$ et $[m^2]$ les représentants des deux énantiomères.

Nous nous intéresserons à la relation qui existe entre $[m^1]$ et $[m^2]$ dans le cadre de la représentation (4).

2. LA RELATION ENTRE $[m^1]$ ET $[m^2]$

Par ω_1, ω_2 on note deux pseudo-scalaires complexes (en particulier ils peuvent être réels).

Soit Y une multitude, relativement à laquelle on spécifie les choses suivantes :

$$Y \subset A, \text{ card } Y = 4 \tag{5}$$

$$m^1, m^2 \in Y \tag{6}$$

Évidemment, les relations (5) et (6) réduisent la discussion au cas de l'atome de carbone asymétrique.

Si ω_1 n'est pas conjugué de ω_2,* nous avons la suivante

---

* ω_1 et ω_2 sont conjugués si $\omega_1 = a + ib$, $\omega_2 = a - ib$; $i = \sqrt{-1}$.

Proposition. Dans la représentation (4), il y a deux nombres ω_1, ω_2 qui caractérisent l'atome de carbone asymétrique.

La démonstration aura deux parties :

A) la possibilité que deux nombres (ω_1, ω_2) caractérisent le centre asymétrique ;

B) la nécessité que ω_1 ne soit pas conjugué avec ω_2.

(A)

On déterminera ω_1, ω_2 ainsi :

soit $[m^1]$. Les valeurs propres de cette matrice sont les solutions de l'équation caractéristique :

$$\det([m^1] - \omega I) = 0 \tag{7}$$

$$\text{où } I = \begin{bmatrix} 1 & 0 \\ 0 & 1 \end{bmatrix}$$

L'équation (7) étant du deuxième degré admet les solutions ω', ω''. (7) peut être mise dans la forme équivalente :

$$\omega^2 - S\omega + P = 0 \tag{8}$$

$$\text{où } S = \omega' + \omega''; \quad P = \omega' . \omega''$$

Conformément [6] au théorème de Caylay-Hamilton, l'équation :

$$\omega^2 - S\omega + P . \mathrm{I} = [\,0\,] \tag{9}$$

où $[0] = \begin{bmatrix} 0 & 0 \\ 0 & 0 \end{bmatrix}$, est vérifiée par la matrice $[m^1]$.

L'équation (9) doit être vérifiée par les représentants des deux énantiomères, parce que les *deux* énantiomères caractérisent le centre chiral (l'atome asymétrique).

Nous observons que l'équation (9) a une infinité de solutions :

$$[m^1],\ [m^1]^{\mathrm{T}},\ C_1^{-1}[m^1]\,C_1, \ldots,\ C_n^{-1}[m^1]\,C_n, \ldots \text{où } [m^1]^{\mathrm{T}}$$

est la transposée de la matrice $[m^1]$.

C_i est une matrice insingulière, c'est-à-dire $\det C_i \neq 0$.

La matrice $[n] = C_i^{-1}[m^1]\,C$ s'appelle matrice semblable à $[m^1]$.

Les solutions qui ont la forme $C^{-1}[m^1]\,C$, avec $C \neq I$ ne conviennent pas, parce que $n \notin Y$.

---

[6] F. REZA, « Linear Spaces in Engineering », Ginn and Company, Waltham, Massachusetts, Toronto—Londres, 1971.

Il est évident que les éléments de la matrice $[m^1]^T$ sont les éléments de Y. Parce que $([m^1]^T)^2 - S\,[m^1]^T + P.I = [0]$ il en résulte que la *relation algébrique entre* $[m^1]$ *et* $[m^2]$ *est*

$$[m^1]^T = [\,m^2] \Leftrightarrow [m^1] = [m^2]^T \tag{10}$$

Mais, l'équation (9) est déterminée par la connaissance de ω' et ω''.

Il en résulte donc que nous avons aussi les relations suivantes :

$$\omega_1 = \omega' ; \quad \omega_2 = \omega'' \tag{11}$$

Par cela, (A) est démontrée.

(B)

Nous supposons que $\omega_1 = a + ib$ et $\omega_2 = a - ib$. Alors, en choisissant £ qui convient,

$$\det\,([m^1] - \omega I) = (a - \omega)^2 = b \tag{12}$$

L'équation (12) montre que dans c il y a deux ligands identiques, ce qui interdit la chiralité centrale.

Donc, pour que les solutions de l'équation (9) soient les représentants des énantiomères C, il est nécessaire que ω_1 et ω_2 ne soient pas conjuguées.

Par cela (B) est démontrée.

Autres conséquences :

D'autres conséquences de la proposition démontrée ci-dessus sont :

1) Pour toute représentation de *la forme* (4), liée à la représentation (4) par une matrice C, ω_1 et ω_2 sont les mêmes.

2) Une molécule à trois centres de chiralité peut être pseudo-chirale si elle est caractérisée seulement par deux doublets (ω_1, ω_2) différents. Elles est sûrement chirale si elle est caractérisée par trois doublets distincts.

3) Donnant une liste $s'_i \longleftrightarrow \alpha\,(s'_i)$, la proposition démontrée procure une méthode de stockage (et de retrouver) à l'ordinateur des formules c.

CONCLUSIONS

(i) on a déduit la relation algébrique entre les représentants des énantiomètres de c.

(ii) la proposition démontrée indique une méthode de stockage des formules c à l'ordinateur.

Nous remercions, à nouveau, monsieur le Professeur Zeno Simon pour les conseils et les encouragements prodigués au cours de ce travail.

Revue Roumaine de Chimie, **20**, *8*, 1119–1132 (1975)

PRINCIPLES AND METHODS FOR THE POTENTIOMETRIC INVESTIGATION OF POLYACIDS BEGINNING FROM LOW DEGREES OF NEUTRALIZATION

IUDITA MUREŞAN and LUCIA ZADOR
"Babeş-Bolyai" University, Department of Chemistry, Cluj-Napoca,
str. Arany Janos 11, Romania

Received July 3, 1974

The purpose of the paper is to find methods for extending the potentiometric investigation of polyacids to low degrees of neutralization (α) and for evaluating both the "intrinsic" dissociation constant and the deviations from the reference state behaviour. Equations free from the usual approximations, unjustified for the range of low α are proposed. By using the corrected equations the investigation of polyacrylic acid (PAA) solutions has imposed completion of the fundamental potentiometric relation of polyelectrolytes by a term ΔG_m, which reflects the nonelectrostatic deviations from the reference state. In order to determine quantitatively both the electrostatic and nonelectrostatic terms two methods, illustrated by new experimental data are proposed and discussed. One of them allows the determination of pK_0, ΔG_m and ΔG_{el} (for the desired degree of neutralization and polyacid concentration) using a reference state which may be identified with the hypothetic ideal one.

INTRODUCTION

Potentiometry proved to be an efficient method for the study of macromolecular polyacids. The investigation methods used on this purpose rely essentially on the following relations :

$$pK_c^\alpha = pK_0 + \frac{0.43}{RT}\,\Delta G_{el} \tag{1}$$

$$pK_c^\alpha = pH - \log\frac{\alpha}{1-\alpha} \tag{2}$$

The first equation[1,2] connects the apparent equilibrium constant of the ionization reaction :

$$-AH + H_2O \rightleftharpoons A^- + H_3O^+$$

---

[1] J. Th. Overbeek, *Bull. Soc. chim. belges*, **57**, 252 (1948).
[2] A. Katchalsky and J. Gillis, *Rec. Trav. chim*, **68**, 879 (1949).

with the thermodynamical ("intrinsic") one, $K_0 \cdot \Delta G_{el} = \frac{\partial \Phi_{el}}{\partial \alpha}$ is the electrostatic free enthalpy, which has to be overcome, when a mol of protons is dissociated from the chain, being yet neutralized up to degree α. Φ_{el} is the excess of the electrostatic free energy of a monomer unit in comparison with the reference state. Since in the absence of added salts ΔG_{el} depends on the concentration of the polyacid and on the degree of neutralization, the apparent equilibrium constant has been indexed with α and c to reflect these dependences.

Attempts to derive theoretical expressions for ΔG_{el}, based upon model calculations [3-6] have been successful only qualitatively, without achieving good agreement between theoretical and experimental data.

The second equation is used for experimental determination of pK_c^α.

Both equations may be easily deduced on the basis of some more or less justified approximations. Thus equation (1) ascribes all the deviations from the reference state to the electrostatic interactions. Equation (2) identifies the $\frac{c_{A^-}}{c_{AH}}$ concentration ratio with $\frac{\alpha}{1-\alpha}$ and so it excludes from the investigation range that of low α values, where the degree of ionization can be no longer confounded with the degree of neutralization. The second equation also neglects the increase in volume during neutralization.

On the other hand Katchalsky and Spitnick[7] came to the conclusion that ΔG_{el} is a linear function of $\log \frac{\alpha}{1-\alpha}$, according to

$$pK_c^\alpha = pK_s + m \log \frac{\alpha}{1-\alpha} \tag{3}$$

settled out earlier empirically by Kagawa and Tsumura[8].

Relations (2) and (3) lead to the so-called "extended Handerson-Hasselbach equation"

$$pH = pK_a + n \log \frac{\alpha}{1-\alpha} \tag{4}$$

In equations (3) and (4) $pK_a = pK_s$, $n = m + 1$ are constants for a given concentration and have to be determined empirically. According to experience, these equations, like so many other empirical ones derivable from (4) are valid only for a limited range of α values around $\alpha = 0.5$, and so they cannot describe the entire titration curve.

---

[3] J. J. Hermans and J. Th. Overbeek, *Bull. Soc. chim. belges*, **57**, 154 (1948).

[4] A. Katchalsky, N. Shavit and H. Eisenberg, *J. Polymer Sci.*, **13**, 69 (1954).

[5] Z. Alexandrowicz and A. Katchalsky, *J. Polymer Sci.*, **A — 1**, 3231 (1963).

[6] L. Kotin and M. Nagasawa, *J. Chem. Phys.*, **36**, 873 (1962).

[7] A. Katchalsky and P. Spitnick, *J. Polymer Sci.*, **2**, 432 (1947).

[8] I. Kagawa and K. Tsumura, *J. Chem. Soc. Japan, Ind. Chem. Sect.*, **67**, 437 (1944).

Thus it is evident that none of the usual relations (1) — (4) can be employed for potentiometric investigations at low degrees of neutralization, though such investigations would be very useful. They would allow, on the one hand, to put into evidence conformational transitions taking place at low α and, on the other hand, to elucidate whether the minimums — appearing at very low α on the majority of potentiometric curves[9,10,11] — plotted according to equation (2) — have any structural importance or have to be attributed to the mentioned approximations unjustified in this α range.

The purpose of the present paper was to find some new methods, free from the above specified approximations which could allow, on the one hand, the investigation at any low α, and on the other hand, the evaluation of the deviations from the reference state. With that end in view a more accurate than usual treatment of the phenomenon was carried out, and the relations obtained were compared with new experimental data regarding the potentiometric microtitration of aqueous polyacrylic acid (PAA). Although the precision of the numeric data is limited by the existence of the liquid jonction potential in the experimental cell, it may be shown that the variation of this potential during a titration may influence only the absolute values of the pK_c^{α} but not the aspect of the titration curve and the conclusions drawn from them.

EXPERIMENTAL

The electromotive forces were measured by means of an MV—11 pH-meter using a glass electrode as indicator, a calomel one as reference, separated by a saturated KCl salt bridge. The KOH solution was added with a polyethylene syringe actuated by a calibrated micrometer in portions corresponding to $\alpha = 0.02$. Constancy of temperature, inert gas atmosphere as well as continuous stirring of the solutions without solvent evaporation were assured.[12]

PRINCIPLES. COMPARISON WITH EXPERIMENTAL RESULTS

The errors deriving from ignoring the dissociation of the polyacid itself are the more significant as the degree of neutralization and the concentration is lower. In order to avoid them, the degree of neutralization α has to be replaced by the degree of ionization ν (ionicity)

$$\nu = \alpha + \alpha' = \frac{c_{A^-}}{c} \tag{5}$$

---

[9] G. Barone, V. Crescenzi, F. Quadrifoglio, and V. Vitagliano, *Ricerca sci.*, **36**, 477 (1966).

[10] T. N. Nekrasova, E. V. Anufrieva, A. M. Eliașevici and O. B. Ptițîn, *Vysokomol. Soedineniya*, **7**, 913 (1965).

[11] A. R. Mathieson and J. V. McLaren, *J. Polymer Sci.*, **A—3**, 2555 (1965).

[12] I. Mureșan and L. Zador, *Stud. Univ. Babeș Bolyai, Chem.*, **18**, 89 (1973).

where α' is the degree of dissociation of the polyacid, c the total concentration of carboxylic groups, c_{A^-} that of the ionized ones.

The correction of the usual relations regarding this sort of errors can be made by replacing the ratios $\frac{\alpha}{1-\alpha}$ by $\frac{\nu}{1-\nu} = \frac{c_{A^-}}{c_{AH}}$. At the same time the index α of the apparent dissociation constant may be replaced by ν, but not necessarily, for the value of ν is determined by the variables α and c. The ratio $\frac{c_{A^-}}{c_{AH}}$ may be calculated from potentiometric data by means of the relation

$$\frac{c_{A^-}}{c_{AH}} = \frac{c\,\alpha\,(V/V+v) + [H^+] - [OH^-]}{c(1-\alpha)\,(V/V+v) - [H^+] + [OH^-]} \tag{6}$$

where V is the volume of the initial solution, and v the added volume of the titrant.

Thus, for the evaluation of $pK_c^{\alpha}(pK_c^{\nu})$, especially for low degrees of neutralization instead of equation (2) the equation (2′) based upon equation (6) is proposed :

$$pK_c^{\nu} = pH - \log\frac{c_{A^-}}{c_{AH}} \tag{2′}$$

At the same time the more correct form of eq. (3) would be

$$pK_c^{\nu} = pK_s + m\log\frac{c_{A^-}}{c_{AH}} \tag{3′}$$

Figs. 1 and 2 illustrate the magnitude of errors introduced in the range of $\alpha < 0.2$ by applying the usual formulas (2) and (3) instead of the more correct (2′) and (3′)

On the abscissa of Fig. 1 α values are ploted and not ν for illustrating the behaviour during the neutralization, starting with the free polyacid, where $\alpha = 0$ but $\nu \neq 0$.

It can be seen that the use of corrected equations does not remove, on the contrary it emphasizes, the minimum of pK_c^{ν} curves.

Regarding the plots used in Fig. 2, it has to be mentioned that the confidence which can be reposed on eq (3′), even after correction, is limited in the range of very low α. Unlike equations (2) and (2′) referring to the calculation of pK_c^{ν}, the relations (3) and (3′) establish a linear dependence on a logarithmic term, which in principle cannot be valid down to $\alpha = 0$ (3) respectively $\nu = 0$ (3′). Thus in the range of very low α only eq. (2′) has to be used and neither (3) nor (3′).

However the fact that in investigated ν range, on the plots in Fig. 2, not simple deviations from linearity appear but minimums situated in the same range as in Fig. 1, prove that they are brought about by the same reason and are not due to the peculiarities of the logarithmical function.

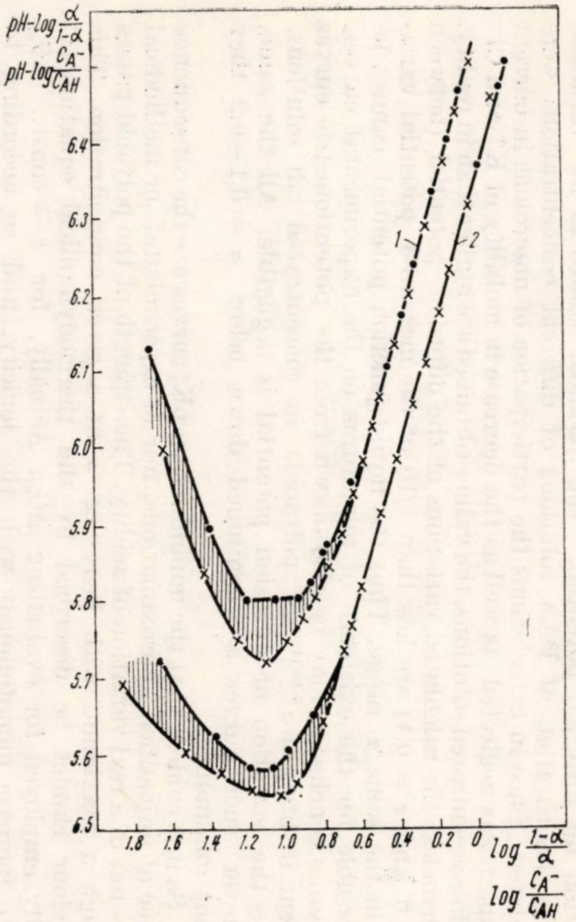

Fig. 2.—pK$_c$ plots in coordinates corresponding to equation 3( ) and 3′(×) for the same solutions as in fig. 1.

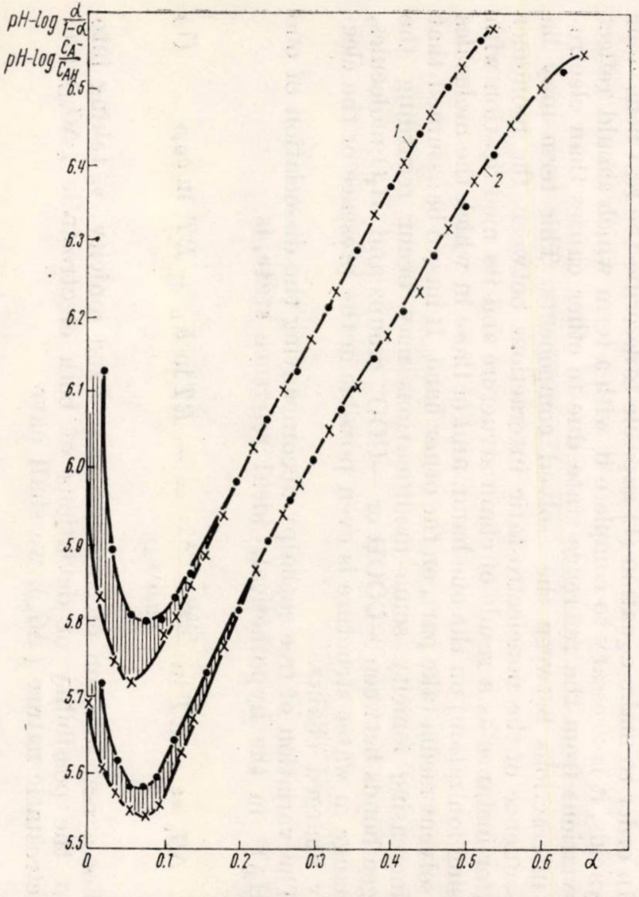

Fig. 1.—pK$_c$ values determined by means of equation 2(●) and 2′(×) for aqueous PAA solutions, with base molar concentration 0.212×10^{-2}(*1*) and 1.11×10^{-2}(*2*).

The existence of the minimums on Figs. 1 and 2 cannot be put in connection even with the jonction potential of the measuring cell. Using the Henderson equation for diffusion potential,[13] the maximal values of its variation during the titration of PAA solutions of different concentrations were calculated. Since in calculations the participation of macroions in current transport was neglected as well as the decrease in mobility of K^+ and Cl^- ions in concentrated solutions, the values obtained are higher than in reality. Nevertheless the calculated variations of the diffusion potential (between $\alpha = 0$ and $\alpha = 0.1$) are less than 1/10 of the measured potential variation in the same α range. Thus the liquid junction potential cannot be responsible for the existence of minimums on the experimental curves. The same conclusion may be also drawn from the potentiometric curves existent in literature [9,10,11] for polyacids in concentrated salt solutions, where the variation of diffusion potential is negligible. All the same, whenever such curves are continued down below $\alpha = 0.1 - 0.2$ they present minimums.

So it is evident that the minimums on $\mathrm{p}K_c^{\nu}$ curves are the consequence neither of unjustified approximations, nor of experimental or methodical errors but of a real variation of acidity. The strength of the polyacid passes through a maximum with incresing α at a given concentration. This behaviour cannot be described by the thermodynamical equation (1) usually employed for evaluating ΔG_{el}. Actually, for $c = \text{const.}$, ΔG_{el} has to increase monotonously with the ionicity, and so according to eq. (1), $\mathrm{p}K_c^{\nu}$ must have the same behaviour.

In order to make equation (1) capable to describe the real behaviour of polyacids, it is ncessary to complete it with a term which should reflect the deviations from the reference state due to other causes than electrostatic interactions between the solved components. This term may be a consequence of the nonelectrostatic interactions between the monomer units (for instance as a result of chain structure and its modification with increasing ionization) on the one hand, and of those in which the molecules of the solvent media take part, on the other hand. It has to be assumed that with increasing ionicity some modifications may occur regarding the hydrogen bonds between $-COOH$ or $-COO^-$ groups and H_2O molecules, or a change in water structure is even possible in the presence of the electrically charged chains.

The variation of free enthalpy accompanying the dissociation of one mol H_3O^+ in the hypothetical, ideal reference state, is

$$\Delta G_0 = - RT \ln \frac{c_{H_3O^+} \cdot c_{A^-}}{c_{H_2O} \cdot c_{AH}} = - RT \ln K_0 + RT \ln c_{H_2O} \qquad (7)$$

For a real solution of concentration c and ionicity ν, taking into account the possibility of deviations of both electrostatic (ΔG_{el}) and nonelectrostatic nature (ΔG_m), we shall have

$$\Delta G = \Delta G_0 + \Delta G_{el} + \Delta G_m \qquad (8)$$

---

[13] N. A. Izmailov "Elektrokhimia rastvorov", Izd. H.O.T.K.Z. Gosudarstvenovo Universiteta imeni A. M. Gorkovo, Harkov, 1959, pg. 762.

On the other hand, for real solutions ΔG_0 is defined as :

$$\Delta G_0 = -RT \ln \frac{a_{H_3O^+} \cdot a_{A^-}}{a_{H_2O} \cdot a_{AH}} \tag{9}$$

So it may be written

$$\Delta G_0 = \Delta G - RT \ln \Gamma \tag{10}$$

where

$$\Delta G = - RT \ \ln \ K_c^{\nu} + RT \ \ln \ c_{H_2O} \tag{11}$$

Let K_c^{ν} represent the apparent equilibrium constant defined as

$$K_c^{\nu} = \frac{a_{H_3O^+} \cdot c_{A^-}}{c_{AH}} \tag{12}$$

Then Γ is for the given c and ν the following ratio of activity coefficients

$$\Gamma = \frac{f_{A^-}}{f_{H_2O} \cdot f_{AH}} \tag{13}$$

From relations (8) and (10) it results that

$$\Delta G_{el} + \Delta G_m = RT \ln \Gamma \tag{14}$$

The last equation suggests to admit the possibility of the contribution of both electrostatic and nonelectrostatic effects, not only for Γ, but also for all activity coefficients included in it, according to the relations :

$$\Gamma = \Gamma_{el} \cdot \Gamma_m \qquad f = f_{el} \cdot f_m$$

On the other hand, from equations (7), (8) and (11) the correct form of equation (1) may be obtained :

$$\mathrm{pK}_c^{\nu} = \mathrm{pK}_0 + \frac{0.43}{RT} \Delta G_{el} + \frac{0.43}{RT} \Delta G_m + \log \frac{(c_{H_2O})_0}{(c_{H_2O})_c} \tag{1'}$$

The last term is negligible in diluted solutions. For more concentrated ones $(c_{H_2O})_c$ is easily evaluated, while $(c_{H_2O})_0$ may be included in K_0. Thus the proposed equation (1′) actually differs from the usual one (1) by the presence of the nonelectrostatic term. It takes into account every possible deviation from the hypothetical reference state, having by this a general validity.

Let us consider now the influence of α or ν upon the terms from the right side of equation (1′). Only the second and third term have to depend on ionicity. Theoretically a continuous increase of ΔG_{el} with α or ν may be stated as well as the identity of the electrostatic dissociation free enthalpy for the uncharged and reference state. In mathematical terms:

$$\frac{\partial \Delta G_{el}}{\partial \nu} > 0 \quad \frac{\partial \Delta G_{el}}{\partial \alpha} > 0 \tag{15}$$

$$\Delta G_{el}^{\nu=0} = 0 \tag{16}$$

It has to be noticed that $\Delta G_{el}^{\alpha=0} \neq 0$.

Thus for the uncharged state eq. (1′) turns in:

$$\mathrm{pK}_c^{\nu=0} = \mathrm{pK}_0 + \frac{0.43}{RT}\,\Delta G_m \tag{17}$$

The dependence of ΔG_m on ν cannot be foreseen theoretically. However the existence of minimums on the $\mathrm{pK}_c^{\nu} - \alpha$ plots proves that in the range of low α values

$$\frac{\partial \Delta G_m}{\partial \alpha} + \frac{\partial \Delta G_{el}}{\partial \alpha} < 0$$

and implicitely, taking into account eq. (15)

$$\frac{\partial \Delta G_m}{\partial \alpha} < 0 \tag{18}$$

Thus the experimental results demonstrate the opposite sign of the derivatives towards α of the two variable terms in eq. (1′). The minimum appears at a degree of neutralization α_{min} (or of ionization ν_{min}), for which the absolute value of the two derivatives becomes equal:

$$\left|\frac{\partial \Delta G_m}{\partial \alpha}\right| \overset{>}{\underset{<}{=}} \left|\frac{\partial \Delta G_{el}}{\partial \alpha}\right| \tag{19}$$

For $\alpha < \alpha_{min}$ the sign $>$, and for $\alpha > \alpha_{min}$ the sign $<$ has to be taken into account. Equations (15) and (18) prove that the relative significance of ΔG_m diminishes with increasing ionicity, and for sufficiently high values of the latter ($\nu \geqslant \nu_{cr}$) the ΔG_m term becomes negligible beside

ΔG_{el}. For such conditions equation (1′) may be reduced to :

$$\mathrm{pK}_c^{\nu \geqslant \nu_{\mathrm{cr}}} = \mathrm{pK}_0 + \frac{0.43}{RT}\,\Delta G_{\mathrm{el}} \tag{20}$$

So it may be concluded that the ascendent linear sections of $\mathrm{pK}_c^{\nu} - \alpha$ curves are determined by ΔG_{el}, while the initial ones by the superposition of both ΔG_m and ΔG_{el} terms.

In order to determine the individual values of the two terms the plots based upon equation (3′) cannot be used, for they do not allow extrapolation to $\nu \to 0$. For this purpose the proposed relations (1′), (17) and (20) have to be employed.

The most difficult problem of the determination is the evaluation of pK_0, since for polyelectrolytes the ideal behaviour is not approachable by dilution. In order to evaluate the free energy change of the helix-coil transition, Olander and Holtzer[14] as well as Mandel[15] determined pK_0' by extrapolating to $\alpha = 0$ the experimental pK_c^{α} data obtained for $\alpha > 0.1-$ -0.15. Though this value is useful for the followed purpose, it must not be identified with the intrinsic pK_0, for it is sensibly dependent on the concentration (see fig. 1) as well as on the ionic strength of the solution.[15] For the calculation of the termodynamical value of pK_0, Muroga and co-workers[16] proposed a method ascribing all the deviations from the standard state to the modification of $f_{\mathrm{COO^-}}$. This method cannot be used in salt free solutions.

EVALUATION OF pK_0, ΔG_m AND ΔG_{el}

Two methods are proposed for the determination of the electrostatic and nonelectrostatic terms.

1. One of them consists in evaluating only the relative significance of the two terms, avoiding the determination of pK_0. The pK_c^{ν} values have to be reported to an arbitrary but well defined reference state, unique for all concentrations. For the choice of a convenient reference state one must take in consideration that in the absence of salts pK_c^{ν} is determined by c and $\nu = \alpha + \alpha'$, where α' itself is a function of c. Thus the fundamental variables remain α and c suggesting as arbitrary reference state the one for which $\alpha = 0$ and $c = 0$. Evidently, the value of $\mathrm{pK}_{c=0}^{\nu=0}$ would be more interesting as reference value than $\mathrm{pK}_{c=0}^{\alpha=0}$, while it would correspond to the absence of electrostatic interactions. Unfortunately the last value is not approachable by direct experimental measurements (varying c, the ionicity cannot be maintained constant). The use of added salts did not seem to be indicated, for it introduces a new parameter,

---

[14] D. Olander and A. Holtzer, *J. Amer. Chem. Soc.*, **90**, 4549 (1968).

[15] M. Mandel, *European Polymer Journal*, **6**, 807 (1970).

[16] Y. Muroga, K. Suzuki, Y. Kawaguchi and M. Nagasawa, *Biopolymers*, **11**, 137 (1972).

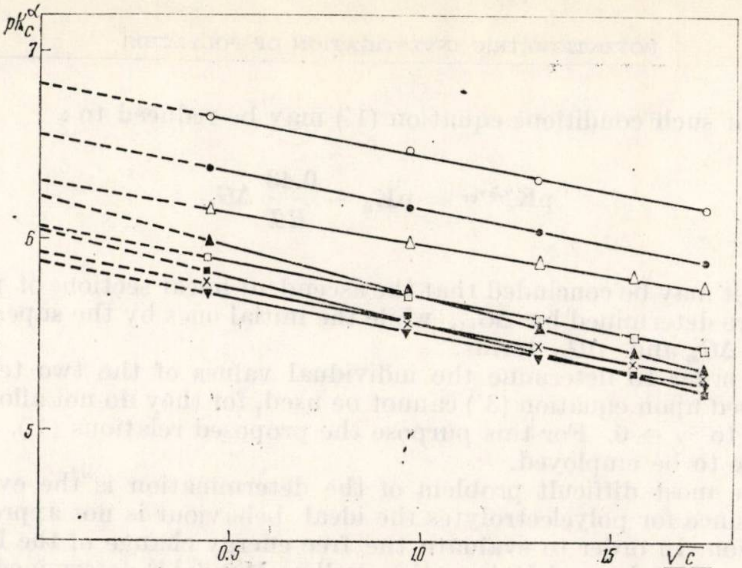

Fig. 3. — Linearization plots for the determination by extrapolation of $pK^{\alpha}_{c=0}$ values. The data were obtained for PAA solutions at different concentrations corresponding to values of α : 0.0(▲) ; 0.02(■) ; 0.06(×) ; 0.1(▼) ; 0.16(□) ; 0.3(△) ; 0.4 (●) ; 0.6(○).

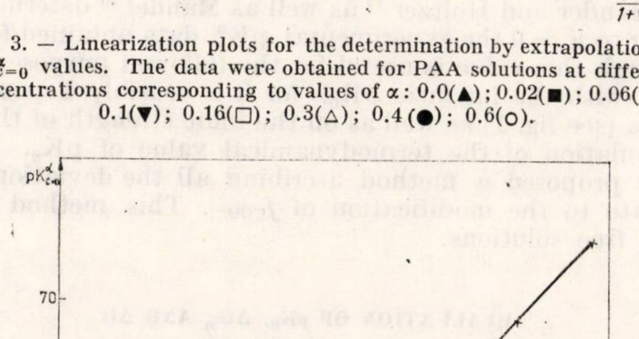

Fig. 4. — The dependence of $pK^{\alpha}_{c=0}$ on α and the evaluation of ΔG_{el} and ΔG_m (for $c = 0$ and $\alpha_1 = 0$, $\alpha_2 < \alpha_{cr}$, $\alpha_3 > \alpha_{cr}$) with assumption $pK_0'' = 5.7$ a $= \frac{0.43}{RT}\Delta G_m$, b $= \frac{0.43}{RT}(\Delta G_m + \Delta G_{el})$, d $= \frac{0.43}{RT}\Delta G_{el}$.

whereas the effect of high ionic strength is not equivalent with the absence of charge.

In order to determine $\mathrm{pK}_{c=0}^{\alpha=0}$, $\mathrm{pK}_{c}^{\alpha} - \dfrac{\sqrt{c}}{1+\sqrt{c}}$ plots are proposed (fig. 3), which allow the evaluation of $\mathrm{pK}_{c=0}^{\alpha}$ by linear extrapolation. The value of $\mathrm{pK}_{c=0}^{\alpha=0}$ obtained for PAA is 6.22.

Fig. 4 illustrates the dependence of the extrapolated $\mathrm{pK}_{c=0}^{\alpha}$ values on α.

The curve obtained makes evident that the twofold influence of α on the strength of the polyacid is also maintained at infinite (overall) dilution. From fig. 4 it also follows that the chosen reference state is not very convenient. According to it the sum of the two terms, from the right side of eq. (1′) is rendered void arbitrary for $\alpha = 0.23$, since $\mathrm{pK}_{c=0}^{\alpha=0} = \mathrm{pK}_{c=0}^{\alpha=0.23}$. It would be more convenient to adopt as a reference the value $\mathrm{pK}_0'' = 5.7$, obtained by the prolongation of the linear section to $\alpha = 0$. Fig. 4 illustrates for the last acception the evaluation of ΔG_m and ΔG_{el} for different α values on the example of $c = 0$.

2. The most interesting method would be that which allows the evaluation of pK_0 and the values of ΔG_{el} and ΔG_m in relation to the hypothetical ideal state. In order to try to find such a method, we took into consideration that such state must be characterized by a zero local concentration and by the absence of electrical charges, both conditions being experimentally unapproachable. However, the value of pK_0 would actually be determined by the extrapolation of some middle sections of the pK_c^{ν} plots against a variable reflecting the effects both of the concentration and of the ionization. The most useful plot proved to be the plots of pK_c^{ν} against $\sqrt{c_{\mathrm{A^-}}} = \sqrt{\nu c}$, illustrated in fig. 5 for PAA at different concentrations.

The values on the abscissa were calculated according to equations (5) and (6). It may be seen that starting with a certain $(c\nu)_{\mathrm{cr}}$ value of concentration of the ionized carboxylic groups, the diagrams have linear sections. The smaller the concentration of polyacid, the larger the length of these sections and the lower the value of $(c\nu)_{\mathrm{cr}}$. The prolongations of the linear parts of the plots intersect the ordinate practically in the same point situated between 4.94–4.96. This fact suggests to accept the value $\mathrm{pK}_0 = 4.95$ for PAA, the more so as it is very near to the corresponding value (4.87) for the propionic acid [17] – the low molecular representant of PAA.

Thus $\mathrm{pK}_c^{\nu} - \sqrt{\nu c}$ plots may be used for the experimental determination of pK_0. The theoretical interpretation of the method found indicates the validity of the following assumptions: a) the ascendent linear sections of these plots are due to the decrease in acidity determined by electrostatic interactions and b) the electrostatic term is a linear function of $(c\nu)^{1/2}$ also in the range where $c\nu < (c\nu)_{\mathrm{cr}}$. These assumptions are justified by the common value of the ordinates at $c\nu = 0$ of all straight lines.

---

[17] D. H. Everett, D. A. Landsman and B. R. W. Pinsent, *Proc. Roy. Soc.* (*London*), A **215**, 403 (1952).

In this way it may be written

$$B(c\nu)^{1/2} = \frac{0.43}{RT}\,\Delta G_{\text{el}} \tag{21}$$

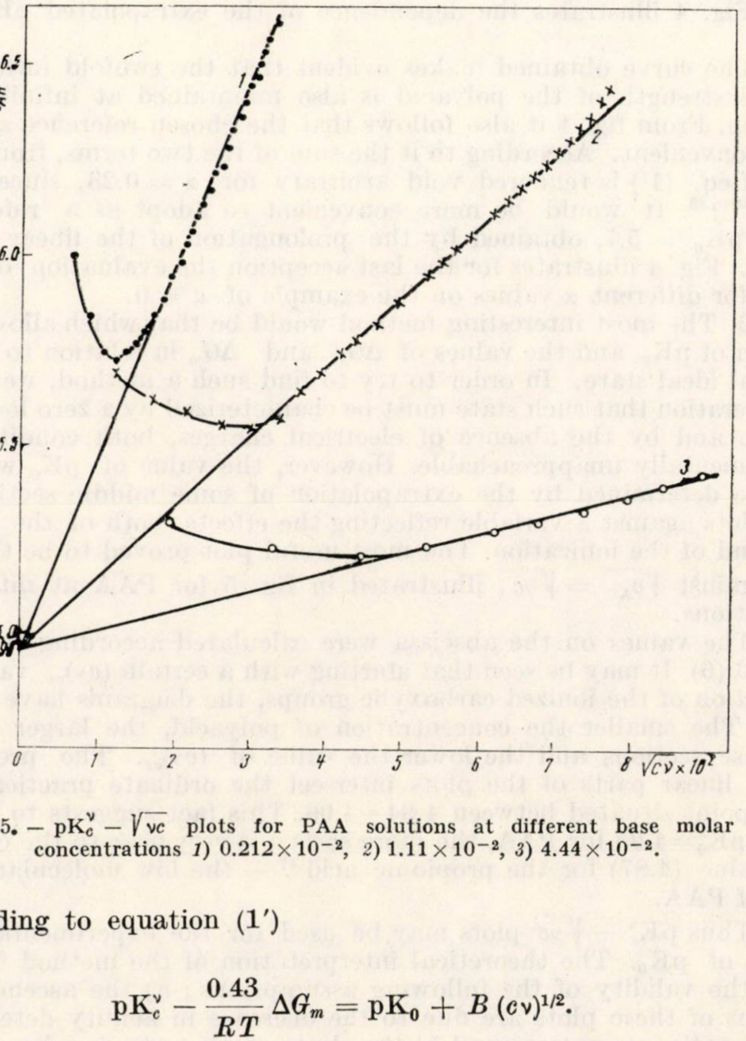

Fig. 5. — $pK_c^{\nu} - \sqrt{\nu c}$ plots for PAA solutions at different base molar concentrations *1)* 0.212×10^{-2}, *2)* 1.11×10^{-2}, *3)* 4.44×10^{-2}.

and according to equation (1′)

$$pK_c^{\nu} - \frac{0.43}{RT}\,\Delta G_m = pK_0 + B\,(c\nu)^{1/2}. \tag{22}$$

And so the ordinates of the straights characterize ΔG_{el}, while the differences between them and pK_c^{ν} are a measure for the deviations from ideality determined by other than electrostatic effects.

Fig. 6 illustrates the method proposed for the determination of the two terms ΔG_{el} and ΔG_m for the concentration and degree of neutralization desired. For this purpose equations (21) and (22) are used, which in case of the PAA may be put under the form

$$\text{for } \nu < \nu_{cr} \quad pK_c^{\nu} - 4.95 = \frac{0.43}{RT}\,(\Delta G_m + \Delta G_{el}) \qquad (23)$$

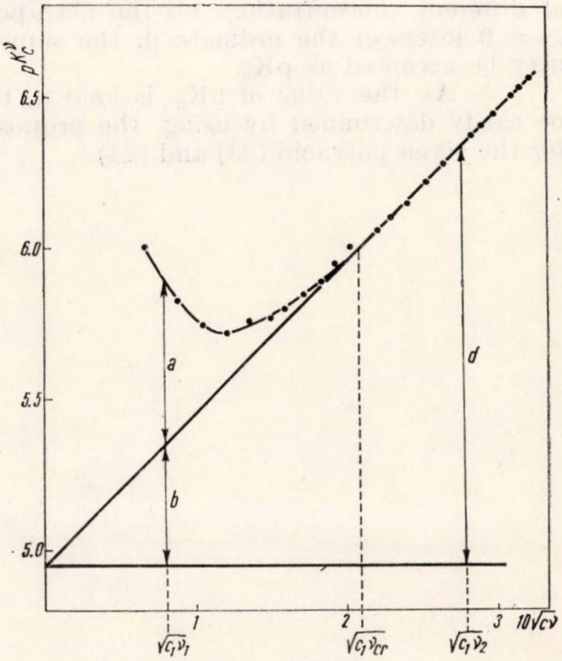

Fig. 6. — The determination of ΔG_{el} and ΔG_m for a PAA solution at 1.11×10^{-2} base molar concentration for $\nu_1 < \nu_{cr}$ and $\nu_2 > \nu_{cr}$ $a = \frac{0.43}{RT}(\Delta G_m)_c$, $b = \frac{0.43}{RT}(\Delta G_{el})_c$ $d = \frac{0.43}{RT}(\Delta G_{el})_c$.

$$\text{while for } \nu > \nu_{cr} \quad pK_c^{\nu} - 4.95 = \frac{0.43}{RT}\,(\Delta G_{el}) \qquad (24)$$

Using equations (10), (13) and (14) the results obtained may be given in terms of activity coefficient ratios.

CONCLUSIONS

1. In order to use potentiometry for the investigation of polyacids at low degrees of neutralization it is necessary to correct the usual equations. The magnitude of errors eliminated by using the corrected equations for the experimental study of the PAA solutions is significant below $\alpha = 0.2$.

2. The fundamental thermodynamic equation of potentiometry for polyacids has to be completed by a term ΔG_m which reflects the nonelectrostatic deviation from the reference state.

3. A way for evaluating the two terms ΔG_m and ΔG_{el} is to choose an arbitrary but well defined reference state. A method is given for the determination of $pK_{c=0}^{\alpha=0}$ as reference value (which for the PAA is 6.22). Another arbitrary reference value obtained by the prolongation of the linear part of $pK_{c=0}^{\alpha} - \alpha$ plots down to $\alpha = 0$, seems to be more convenient ($pK_0'' = 5.7$).

4. A second proposed way uses $pK_c^{\nu} - \sqrt{\nu c}$ plots. For PAA solutions of different concentrations all the extrapolations of the linear parts to $c\nu = 0$ intersect the ordinate in the same point 4.95, which therefore may be accepted as pK_0.

5. As the value of pK_0 is known, the terms ΔG_m and ΔG_{el} may be easily determined by using the proposed equations (21) and (22) or for the given polyacid (23) and (24).

Revue Roumaine de Chimie, **20**, *8*, 1133–1140 (1975)

A POLAROGRAPHIC STUDY ON STYRYLCYANINES. II[1]

SUBSTITUENT EFFECTS ON THE POLAROGRAPHIC REDUCTION OF 1-ETHYL-2-(p-X-STYRYL) AND 1-ETHYL-4-(p-X-STYRYL)-PYRIDINIUM IONS

A. SZURKOS, P. NAGY and I. GÖRBE

Faculty of Chemistry, Pedagogical Institute. str. Nicolae Iorga 1, Tg. Mureş, Romania

Received April 23, 1974

Studies have been made on the electronic effects of the substituents on the polarographic reduction of 1-ethyl-2-(*p*-X-styryl) and the 1-ethyl-4-(*p*-X-styryl)-pyridinium ions on the basis of linear-free-energy relationships. The σ^+ substituent constants—proposed by Brown and Okamoto — were demonstrated to be good quantitative parameters also for the polarographic reduction processes. Using Swain's and Lupton's statistical analysis of the substituent effects, the field and resonance components of the substituent effects were separated and interpreted.

In a previous note [1] it was shown that the electronic effects of the substituents on the half-wave potentials of the 1-ethyl-2-(p-X-styryl)-pyridinium ions may be described by the Brown-Okamoto equation using the σ^+ constants for the substituents. [2]

In the present paper we intend to make a comparative study of the substituent effects on the polarographic reduction of the 1-ethyl-2-(p-X-styryl) respectively 1-ethyl-4-(p-X-styryl)-pyridinium ions on the basis of the different linear-free-energy relationships. According to Zuman, these relationships have been originally introduced also for the polarographic processes.[3–6]

---

[1] A. Szurkos and P. Nagy, *Rev. Roumaine Chim.*, **15**, 607 (1970).

[2] L. P. Hammett, "Physical Organic Chemistry", Grow-Hill Book Company Inc. New York, 1940, p. 73.

[3] P. Zuman, *Coll. Czech. Chem. Comm.*, **25**, 3225 (1960).

[4] P. Zuman, *Coll. Czech. Chem. Comm.*, **27**, 630 (1962).

[5] P. Zuman, *Coll. Czech. Chem. Comm.*, **27**, 648 (1962).

[6] P. Zuman, *Coll. Czech, Chem. Comm.*, **27**, 2035 (1962).

EXPERIMENTAL

1. MATERIALS

The compounds studied have the following formula:

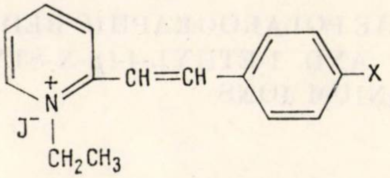

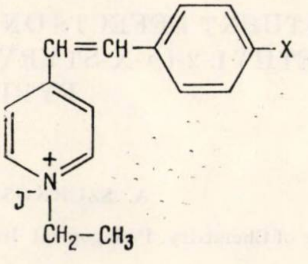

where X = OH	I	X = OH	IX
N Et_2	II	N Et_2	X
N Me_2	III	N Me_2	XI
NH_2	IV	OCH_3	XII
OCH_3	V	NHAc	XIII
NHAc	VI	H	XIV
H	VII	Cl	XV
Cl	VIII		

The compounds used were prepared by the condensation of the 2-methyl respectively 4-methyl-pyridinium ethyl iodide with the *para*-substituted benzaldehydes in the presence of pyperidine as catalyst and absolute ethanol as solvent.[7-9] Purification was achieved by recrystallization from ethanol.

2. POLAROGRAPHIC MEASUREMENTS

An LP–60 model polarograph was used to record the polarograms. The experimental conditions and the capillary characteristics were identical with those described in the previous note.[1]

RESULTS AND DISCUSSION

1. THE NATURE OF THE POLAROGRAPHIC WAVES

The polarograms obtained in the pH-interval 2.2–11.0 for the compounds (I–VIII) and (IX–XV) are given in figs. 1 and 2.

It can be observed that the shapes of the polarograms are very closely related. The nature of the polarograms and therefore the nature of the reduction processes is independent of the substituent effects and of the position of the substituted styryl-radical. The only parameter which is changed in these processes is the value of half-wave potential.

In acid media only a single wave appears, but in basic media (pH = 11.0) three well-distinguished waves can be observed.

---

[7] W. H. Mills and W. J. Pope, *J. Chem. Soc.*, **121**, 946 (1922).

[8] A. P. Phillips, *J. Org. Chem.*, **12**, 333 (1947).

[9] A. P. Phillips, *J. Org. Chem.*, **15**, 302 (1949).

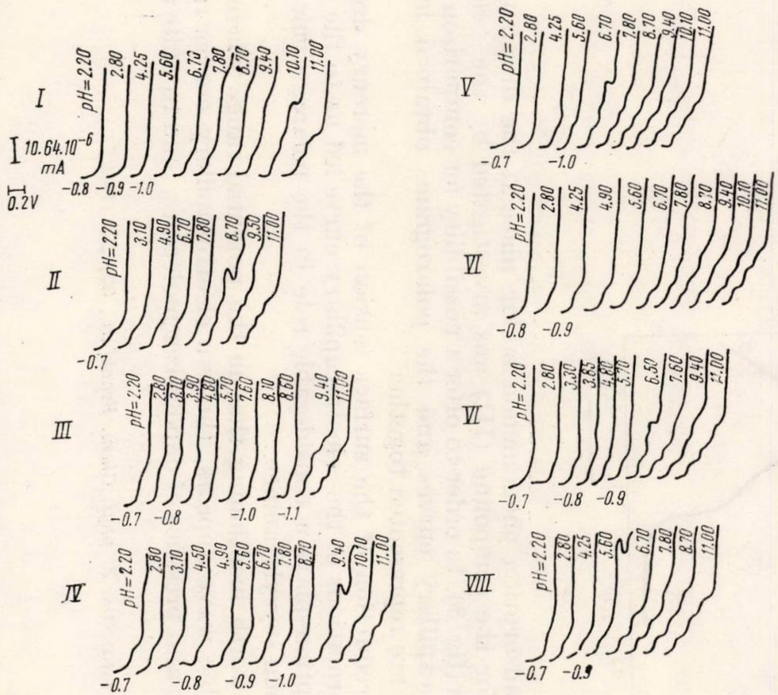

Fig. 1 — Polarographic curves of the 1-ethyl-2(*p*-X-styryl) pyridinium iodides in the 2.2—11.0 pH range.

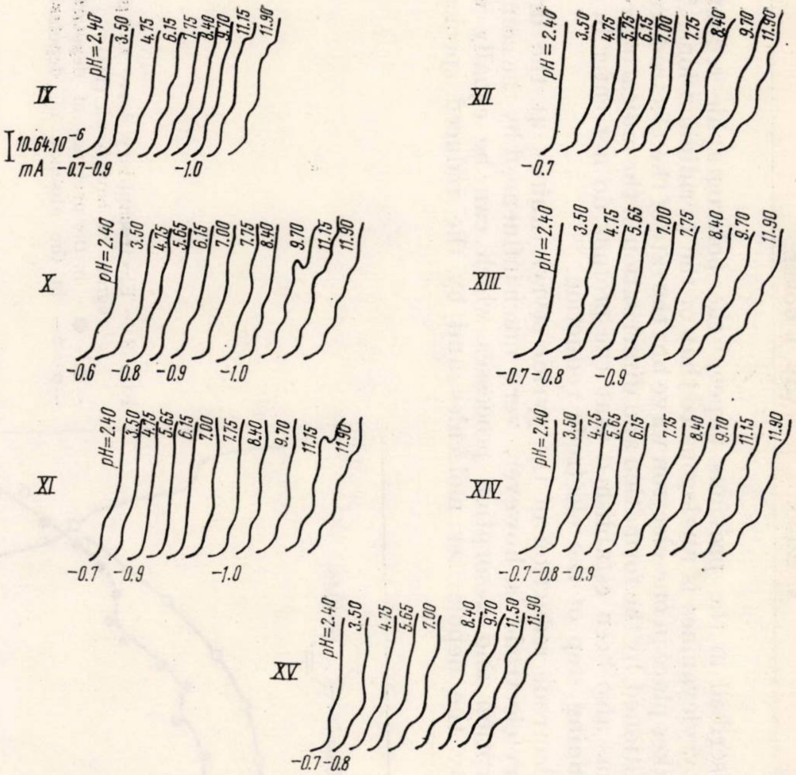

Fig. 2 — Polarographic curves of the 1-ethyl-4(*p*-X-styryl) pyridinium iodides in the 2.2—11.0 pH range.

As described in the previous paper,[1] the polarographic reduction of pyrido-styrylcyanines is analogous to that of the pyridinium ions. The reduction takes place in one-electron wave but the rate of the electrode reaction is conditioned by the formation and dimerisation of the radical intermediates. It has also been established that the protons do not enter in the rate determining step of the electrode reduction.

The electrode reduction of the pyrido-styrylcyanines at the dropping mercury electrode is, however, very much influenced by the complicated adsorption and desorption processes which can be equally well produced by the depolarizer molecules and by the reduced species.[10]

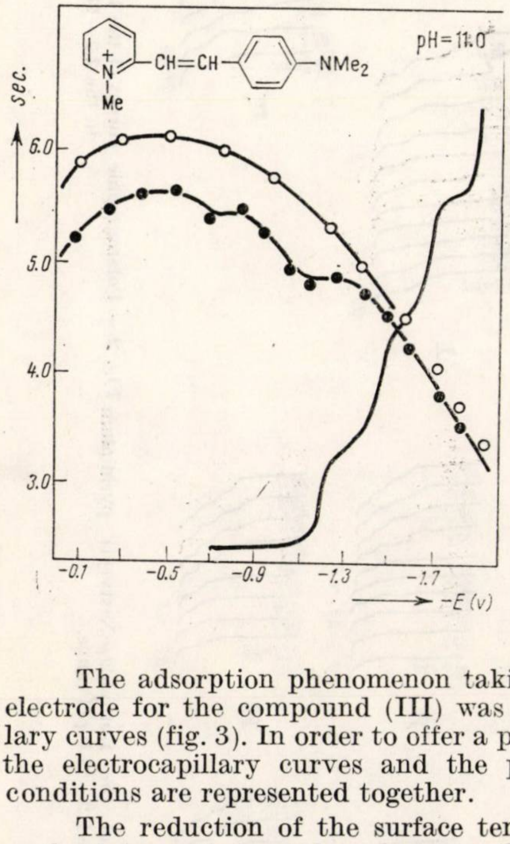

Fig. 3 — Electrocapillary curve and polarogram of compound (III)
—●—●— in the presence of depolarizer.
—○—○— in the absence of depolarizer.

The adsorption phenomenon taking place at the dropping mercury electrode for the compound (III) was investigated by the electrocapillary curves (fig. 3). In order to offer a possibility for comparison in figure 3 the electrocapillary curves and the polarograms obtained in identical conditions are represented together.

The reduction of the surface tension of the mercury drop as well as the deformations of the electrocapillary curve led us to the conclusion that adsorption plays a considerable role in the polarographic reduction of the pyrido-styrylcyanines.

It is worth mentioning that in the potential range where the third polarographic wave appears, the two electrocapillary curves recorded in the absence and presence of depolarizer molecules, tend to unite and hence, in this potential range (−1.550 V) − (−1.750 V), owing to a desorption process, the surface pressure of the mercury is not influenced by adsorption phenomena.

---

[10] A. Stanienda, *Z. phys. Chem. Frankfurt.*, **32**, 238 (1962).

It has further been established that in basic media and in the presence of ethanol, a compound with a pronounced surface activity, the first and the second waves are joined and the third wave disappears. The height of this, in fact of the single observable wave in 52% ethanol at pH = 11.0 is the sum of the heights of the first and second waves observed at the same pH value, but in the absence of ethanol. Therefore, in the presence of ethanol the adsorption of the depolariser molecules or of the reduced species does not occur and the reduction of pyridostyrylcyanines takes place in a single polarographic wave. These experimental results led us to the following conclusions with respect to the nature of the polarographic waves observed at pH = 11.0.

The first wave is a "pseudoadsorption"-wave[11] and it may be correlated with the electrode process itself, which is not hindered or is only partially hindered by adsorption. In the second wave, the main electrode process is the same as in the first, but it is hindered by the formation of an adsorption film at the dropping mercury electrode. The third wave was proved to be a desorption wave.

2. THE EFFECT OF SUBSTITUENTS

It has been observed that the electronic effects of the substituents are operating on the first polarographic wave, and in the basic media only.[1] The second and third waves are insensitive to the structural changes.

In order to describe quantitatively the effect of the substituents on the reduction potentials of the studied compounds the Hammett equation was first checked, using the classical "σ" constants. However, no linear correlation has been obtained between the σ-s and the corresponding $E_{1/2}$-s, i.e. the correlation coefficient obtained has a very low value.

Owing to the structure of the studied compounds, a positive charge in pyridine nucleus, and the + M nature of the substituents, it is logical to expect that a direct conjugation occurs between the reaction centre and the substituents. In these instances it is the Brown-Okamoto equation (using the σ^+ constants for the substituents) which describes correctly the substituent effects. The applicability of this equation in polarography was predicted by Zuman, and has the following form :

$$(E_{1/2})_x = \rho_{\pi,R}\ \sigma^+ + (E_{1/2})_0 \qquad (1)$$

If the $E_{1/2}$ values of the studied pyridostyrylcyanines are plotted against σ^+, linear correlations are obtained in both series (figs. 4 and 5).

---

[11] S. G. Mairanovskii, "Kataliticheskie i kineticheskie volny v polarografii", cap. 3, Izd. Nauka. Moscow, 1966.

The best values of $\rho_{\pi,R}$ have been calculated using the least squares method, and the equations of the regression lines are the following :

$$(E_{1/2})_{2-p-X} = (0.0104 \pm 0.01)\ \sigma^+ + 1.153 \pm 0.04 \tag{2}$$

$$r = 0.964$$

$$(E_{1/2})_{4-p-X} = (0.084 \pm 0.008)\ \sigma^+ + 1.094 \pm 0.06 \tag{3}$$

$$r = 0.986$$

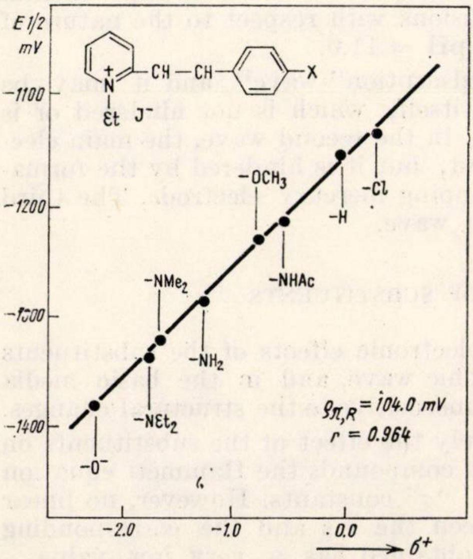

Fig. 4 — Plot of $E_{1/2}$ values of the 1-ethyl-2(*p*-X-styryl) pyridinium iodides against the σ^+ constants. pH = 11.0.

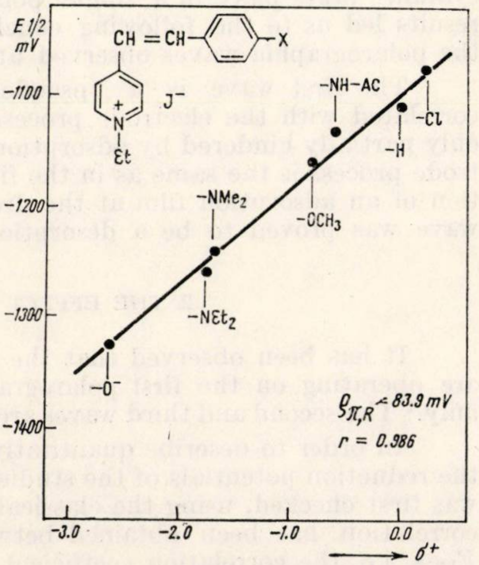

Fig. 5 — Plot of $E_{1/2}$ values of the 1-ethyl-4(*p*-X-styryl) pyridinium iodides against the σ^+ constants. pH = 11.0.

The linearity of these correlations is evident, the correlation coefficients being good (0.964) and very good (0.986). The sign of the reaction constant is positive ($\rho_{\pi,R}$). It appears that the mechanism of the potential determining step is a nucleophilic one in both cases studied. The nucleophilic agent is the electron.

There is some trouble, however, about the application of the σ^+ constants in the present reaction because these substituent constants were introduced originally for the electrophilic reactions, i.e. for the reactions with $\rho < 0$.

The applicability of the Brown-Okamoto equation can be readily explained as follows. The direct conjugation expressed by the difference $(\sigma^+ - \sigma)$ occurs in the transition state for electrophilic reactions ($\rho < 0$), while for the nucleophilic reaction ($\rho > 0$) this conjugation has to occur in the initial state.

Patai and Israeli[12] have applied in the same manner the Brown-Okamoto equation in a nucleophilic reaction, namely in the reaction of substituted benzaldehydes with malonic acid dinitrile. In the polarographic literature, however, this equation was used only for the oxidation processes.[3]

If we make a comparison between the reaction constants of the two studied reaction series, it can be seen that at 22° the sensitivity of the reduction reaction to the electronic effects of the substituents is greater for the pyrido-2-styrylcyanines ($\rho_{\pi.R} = 0.104$ V) than for the pyrido-4-styrylcyanines ($\rho_{\pi,R} = 0.084$ V).

The obtained correlations (Figs. 4 and 5) were used to establish new σ^+ constants not described in the literature for the substituents p-NEt$_2$ and p-O$^-$ pH = 11.0. These values are σ^+_{p-} NEt$_2 = -1.76$ and σ^+_{p-} O$^- = -2.23$.

3. SEPARATION OF THE FIELD AND RESONANCE EFFECTS

The σ^+ constants used in Sect. 2 to describe the substituent effect on the half-wave potentials are hybrid constants, i.e. they contain the field effects and the resonance effects of the substituents in an unknown proportion. In order to get a better understanding of the nature of the substituent effects on the polarographic reduction of the studied compounds, we have tried a separation of the field effects and the resonance effects using the Swain and Lupton[13] statistical method. We have obtained the following equations :

$$(E_{1/2})_{2-p-\mathrm{X}} = 55.7\ \mathscr{F} + 198.7\ \mathscr{R} - 1135.7 \qquad (4)$$

$$(E_{1/2})_{4-p-\mathrm{X}} = 74.1\ \mathscr{F} + 166.1\ \mathscr{R} - 1110.5 \qquad (5)$$

where $\mathscr{F}$ is the "pure" field constant of the substituent

$\mathscr{R}$ is the "pure" resonance constant of the substituent

It can be observed that the sensitivity of the reaction center with respect to the resonance effects of the substituents is much greater than that with respect to their field effects, in both reaction series studied. This result appears perfectly logical, if we bear in mind the failure of the $E_{1/2} - \sigma^+$ correlation, and the effectiveness of the $E_{1/2} - \sigma$ correlation.

If we make a comparison between the sensitivities of the reduction reactions of the pyrido-2-styrylcyanines and of the pyrido-4-styrylcyanines to the field and resonance effects of the substituents, it can be seen that the field effects are operating more effectively in the pyrido-4-styrylcyanines while the resonance effects in the pyrido-2-styrylcyanines (see equations 4 and 5). These facts, according to our assumption, can be explained by the strong interaction of the electrophilic nitrogen atom and the nucleophilic substituents which can develop only in the case of the pyrido-4-styrylcyanines, the *cis* geometrical structure being favoured in this way (fig. 6). In the series of the pyrido-2-styrylcyanines the *cis* structure is not favoured at all, owing to the steric hindrance of the free rotation of the pyridine nucleus.

---

[12] S. Patai and Y. Israei, *J. Chem. Soc.*, **1960**, 2020.

[13] G. G. Swain and E. C. Lupton Jr., *J. Amer. Chem. Soc.*, **90**, 4328 (1968).

Returning now to the pyrido-4-styrylcyanines, the *cis* structure may explain the greater sensitivity of the reaction centre to the field effects of the substituents owing to the shorter distance between them. This direct field interaction may even reduce the resonance effects of the substituents.

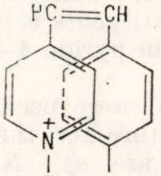

Fig. 6 — The favoured geometrical structure of the pyrido-4-styrylcyanines.

Revue Roumaine de Chimie, **20**, *8*, 1141–1156 (1975)

MASS TRANSFER FROM DISPERSED PARTICLES TO CONTINUOUS FLUID MEDIA. I. NON-OSCILLATING FLUID MEDIA

GHEORGHIȚA I. JINESCU and CORNELIA BALABAN

Polytechnic Institute of Bucharest,
Str. Polizu 1, Bucharest, Romania

Received December 6, 1974

In the introduction, a systematization of theoretical and experimental literature data on the mass transfer from dispersed particles to a continuous fluid phase is presented. An experimental method and a calculation procedure are described for obtaining the partial mass transfer coefficient for the gas bubbles-liquid system. From these determinations, relationships for the dependence of this coefficient on the magnitude and shape of the bubble were derived, for the case when the liquid is not perturbed by oscillations.

1. INTRODUCTION

Mass transfer processes may be intensified by a rational variation of the physico-chemical parameters (temperature, presence of surfactants, concentrations of the transferred substance in the two phases) and by creating favourable hydrodynamic conditions.[1,2]

In processes such as dissolution, extraction, distillation and absorption, the mass transfer takes place between a continuous liquid phase and a solid, liquid or gaseous dispersed phase (to be designated in the following by "particle", also when it is a liquid drop or a gas bubble). In practical installations, the mass transfer occurs between an ensemble of particles and a liquid phase; however, for such cases the complexity of hydrodynamic phenomena (collisions and coalescence of particles, interference of liquid films), renders the understanding and quantitative evaluation of mass transfer processes rather difficult. Therefore most studies, both theoretical and experimental, deal with the simplified case of the mass transfer from a single particle to the fluid medium.

---

[1] C. Balaban and Gh. I. Jinescu, *Rev. Chim. (București)*, **25**, 970 (1974).

[2] C. Balaban and Gh. I. Jinescu, *Rev. Chim. (București)*, **26**, 138 (1975).

Table 1 presents the significant models for mass transfer, which were devised for providing a theoretical basis for the interpretation of experimental data and for the calculation of mass transfer coefficients.[3-8]

The film-penetration model is a general one, containing as limiting cases the two-film model, the penetration model and the surface renewal model. Unlike these limiting cases, the film-penetration model eliminates the inconsistencies between the values predicted by theory for the partial transfer coefficient k, and the experimental data. In the film penetration model, k depends on the diffusivity coefficient D, following the relation :

$$k = f(D^n, \delta, \theta, s) \tag{1}$$

where n varies in the range of 0.5 – 1.0 and δ, θ and s are the film thickness, surface element contact time and surface renewal rate, respectively.

The use of the above models is limited owing to the difficulty in measuring δ, θ and s. Attempts to determine experimentally these parameters were made in isolated cases, for instance in the evaporation of liquids in wetted-wall columns.[9]

In processes where the mass transfer occurs between phases with different hydrodynamic conditions, for each phase one must apply a corresponding model (not necessarily the same one for both phases) since the choice of models depends strongly on hydrodynamic conditions.

From the models mentioned above, it results that for intensifying the mass transfer one must reduce the thickness of the limiting film and increase the renewal rate s for the fluid elements on the interface. These favourable hydrodynamic conditions may be brought about by (i) internal motions of the fluid, caused by the Marangoni effect, the presence of surfactants, or the modification of rheological properties of the fluids, or (ii) external motions such as mechanical vibrations or pulsations, introduction of sonic or ultrasonic energy.

The present survey analyzes the theoretical and experimental literature data in the case of mass transfer from disperse particles to a continuous fluid, when this fluid is not perturbed by oscillations. A forthcoming second part will analyze the case when the fluid is subjected to oscillations. Both parts will also describe original experimental data.

2. MASS TRANSFER FROM SOLID PARTICLES

The mass transfer from spherical solid particles to a fluid was studied experimentally in stationary fluids,[10] in fluids with natural[11] or forced circulation.[10, 12-16]

---

[3] W. G. Whitman, *Chem. Met. Eng.*, **29**, 147 (1923).

[4] W. K. Lewis and W. G. Whitman, *Ind. Eng. Chem.*, **16**, 1215 (1924).

[5] R. Higbie, *Trans. Am. Inst. Chem. Eng.*, **31**, 365 (1935).

[6] P. V. Danckwerts, *Ind. Eng. Chem.*, **43**, 1460 (1951).

[7] H. L. Toor and J. M. Marchello, *Amer. Inst. Chem. Engineers J.*, **4**, 97 (1958).

[8] J. M. Marchello and H. L. Toor, *Ind. Eng. Chem. Fundamentals*, **2**, 8 (1963).

[9] H. Brusset, D. Depeyre and T. Le Quang, *Chem. Eng. Sci.*, **28**, 31 (1973).

[10] F. H. Garner and R. D. Suckling, *Amer. Inst. Chem. Engineers J.*, **4**, 114 (1958).

[11] W. G. Mathers, A. J. Madden and E. L. Piret, *Ind. Eng. Chem.*, **49**, 961 (1957).

[12] S. K. Fridlander, *Amer. Inst. Chem. Engineers J.*, **7**, 347 (1961).

[13] G. L. Levich, "Physicochemical Hydrodynamics", Prentice-Hall, London, 1962, p. 80.

[14] F. H. Garner and R. W. Grafton, *Proc. Roy. Soc.*, **A 224**, 64 (1954).

[15] G. A. Hugmark, *Ing. Eng. Chem. Fundamentals*, **6**, 408 (1967).

[16] Al. Dimian and O. Muntean, *Rev. Chim. (Bucureşti)*, **23**, 369 (1972).

Table 1

Mass transfer models

Model	Characteristics of the model	Relation	Authors	References
Two-film model	Molecular diffusion in the hypothetical thin laminar film at the interface	$k_l = \frac{D}{\delta}$	Whitman, Lewis and Whitman	3 4
Penetration model	Molecular diffusion in the fresh fluid elements with fixed period of time, θ, at the interface	$k_l = 2\sqrt{\frac{D}{\pi\theta}}$	Higbie	5
Surface renewal model	Molecular diffusion in the fresh fluid elements with random age distribution, $f(\theta)$, at the interface	$k_l = \sqrt{D \cdot s}$ $f(\theta) = s e^{-s\theta}$	Danckwerts	6
Film-penetration model	Mass transfer developed in a film of thickness δ, from n fluid elements of the film constantly renewed	$k_l = \frac{D}{\delta}\left(1 - \frac{\delta^2}{3D\theta} - \frac{2\delta^2}{\pi D\theta} \cdot \sum_{n=1}^{\infty} \frac{1}{n^2} e^{-\pi^2 n^2 \frac{D\theta}{\delta^2}}\right)$	Torr and Marchello	7,8

The relationships obtained from the theoretical analysis of these experiments are presented in table 2.

It may be seen from table 2 that most relationships have the general forms :

$$Sh = A + B \cdot Re^m \cdot Sc^n \text{ (for forced circulation)} \tag{2}$$

or

$$Sh = A + B \cdot Gr^m \cdot Sc^n \text{ (for natural circulation)} \tag{3}$$

which imply a simple additivity of mass transfers achieved by molecular diffusion ($Sh = A$) and by natural ($B\,Gr^m\,Sc^n$) or forced convection ($B\ Re^m\,Sc^n$).

3. MASS TRANSFER FROM LIQUID DROPS

In systems formed from a continuous fluid (liquid or gas) and an immiscible liquid, the existence of the deformable fluid interface determines a more intense mass transfer than in systems with rigid interfaces. This is explained by the appearance of internal circulation, of continuous pulsations of the interface of proper oscillations of the drop. [1, 12, 17, 18] In the fluid interface, owing to existing or to appearing gradients of concentration or temperature, spontaneous motions appear (contractions and agitations of the drop) known as the Marangoni effect. This effect intensifies the mass transfer by improving the hydrodynamic conditions at the interface the limiting films and the zones in the immediate vicinity of the interface. [19] In mass transfer processes it is necessary to take also into account the effects occurring in the wake of the drop : strong turbulence and increase of transfer area. [16, 20] The above effects (internal circulation, proper oscillations of the drop and wake phenomena) appear above a certain value of the Reynolds number for the drop ($Re_{p,\text{crit}}$). For $Re_p < Re_{p,\text{crit}}$ liquid drops behave as solid particles whose equivalent diameter is equal to the diameter of the drop.

The intensity of the motions at the interface and of the internal circulation is considerably reduced, and sometimes cancelled, by the presence of surfactants, even when these are present only in trace amounts, as impurities. [21]

Theoretical relations for the partial mass transfer coefficient from a drop to a continuous phase were established both for the internal mass transfer within the drop $(k_d)^{22-24}$ and for the external one from the drop

---

[17] S. Hu and R. C. Kintner, *Amer. Inst. Chem. Engineers J.*, **1**, 1366 (1955).

[18] R. M. Edge and C. D. Grant, *Chem. Eng. Sci.*, **26**, 1001 (1971).

[19] D. Suciu, Thesis, Institutul Politehnic București, 1968.

[20] J. Yeheskel and E. Kehat, *Chem. Eng. Sci.*, **26**, 1223 (1971).

[21] R. M. Griffith, *Chem. Eng. Sci.*, **12**, 198 (1960).)

[22] J. Hadamard, *Compt. rend.*, **152**, 1735 (1911).

[23] A. E. Handles and T. Baron, *Amer. Inst. Chem. Engineers J.*, **3**, 127 (1957).

[24] P. M. Rose and R. C. Kintner, *Amer. Inst. Chem. Engineers J.*, **12**, 530 (1966)

Table 2

Relations for the mass transfer solid particles-fluid

Characteristics of the system	System	Relation	Region of validity	References
Solid sphere in stagnant fluids	S–L S–G	$Sh = 2$	$Re = 0, \quad Gr = 0$	10
Solid sphere in fluids in natural convection	S–L	$Sh = 2 + 0.5(\mathrm{Gr.Sc})^{0.25}$	$Re = 0$ $Gr.Sc \in [10^2 - 10^5]$	11
Solid sphere in fluids in forced convection	S–L S–G	$Sh = (0.991 \div 1.101)\ \mathrm{Pe}^{0.33}$	$Re < 1; \quad Pe \gg 1$	12
The solid sphere of naphthalene in air; $d_p \in [0.02 - 0.18]$ cm	S–G	$Sh = 2 + 0.55(\mathrm{Gr.Sc})^{0.25}$	$Sc > 1$	10
Solid sphere of naphthalene into air in forced laminar convection; $d_p \in [0.02 - 0.18]$ cm	S–G	$Sh = 2 + (0.55 \div 0.57)\mathrm{Re}^{0.5}\mathrm{Sc}^{0.33}$	$Re \in [2 - 1000]$	10
Solid sphere of adipic acid or benzoic acid in water in laminar flow; $d_p \in [0.9 - 1.8]$ cm	S–L	$Sh = 2 + 0.95\ \mathrm{Re}^{0.5}\mathrm{Sc}^{0.33}$	$Re \in [1000 - 700]$ $Sc \in [1100 - 2500]$	10
Solid sphere of potassium nitrate or potassium chloride in water in forced laminar flow	S–L	$Sh = 0.82\ \mathrm{Re}^{0.5}\mathrm{Sc}^{0.33}$	$Re \in [600 - 2600]$	10
Solid sphere in fluids in forced laminar flow	S–L	$Sh = 0.63(Re\ Sc)^{0.33}$	$Re < 2600$	13
Solid sphere in fluids in forced convection	S–L S–G	$Sh = 44 + 0.48\ Re^{0.5}Sc^{0.33}$		14
Solid sphere in liquids in forced convection	S–L	$Sh = 2 + 0.463\ Re^{0.483}\ Sc^{0.339} \cdot \left(\frac{d_p g^{1/3}}{D^{2/3}}\right)^{0.072}$	$Re > 1$	15,16
Solid sphere of benzoic acid in water in forced flow, $d_p \sim 1.5$ cm	S–L		$100 < \mathrm{Re}^{0.5}Sc^{0.33} < 300$	10
– for the front side of a sphere		$Sh = 2 + 1.08\ Re^{0.5}\ Sc^{0.33}$		
– for the inferior side ("wake") of a sphere		$Sh = 2 + 0.67\ Re^{0.5}\ Sc^{0.33}$		
– for the front stagnant side of a sphere		$Sh = 2 + 1{,}68\ Re^{0.5}\ Sc^{0.33}$		
– for the inferior stagnant side of a sphere		$Sh = 2 + 0.87\ Re^{0.5}\ Sc^{0.33}$		

Table 3

Relations for the mass transfer drops-fluid

Characteristics of the system	System	Relation	Region of validity	References
Drops with internal circulation	L−L L−G	$Sh_d = 3.75 . 10^{-3} Pe_d$; $Sh_d = \frac{k_d . d_e}{D_d}$; $Pe_d = \frac{u_p d_p}{D_d}$	$Re \sim 1000$	23
	L−L	$Sh_c = (0.6 \ldots 0.65) Pe^{1/2}$	$Re > 1,\ Sc > 1$	13,30
	L−L	$Sh_c = 1.13\, Pe^{1/2}$	$Re > 1000$	31
	L−L	$Sh_c = -\,126 + 1.8\, Re^{1/2} Sc^{0.42}$	$Re \in [18-800]$ $Sc > 1$	32
	L−L	$Sh_c = Sh_{\text{rigid}} \cdot F$ $F = 0.281 + 1.615\, Z + 3.73\, Z^2 - 1.864\, Z^3$; $Z = Re^{1/8} \left(\frac{\eta_m}{\eta_p} \right)^{1/4} \frac{\sigma_m}{\eta_p\, u_p}$		15
	L−L	$Sh_c = \left(\frac{12}{\pi} \right)^{1/2} Pe^{1/2}$		29
Drops with slow internal circulation	L−L	$Sh_c = 2 + 0.57\, Re^{1/2}\, Sc^{0.35} \left(1 + \frac{22}{13} k_v \right)$ $Sh_c = 1.13 (1 - 2.90\, Re^{-1/2})^{1/2}\, Pe^{1/2}$	$Re > 1$; $Sc > 1$	21 26

Drops with fast internal circulation	L – L	$Sh_c=2+1.13\,(Pe\,k_v)^{1/2}\ ;\ k_v=f\left(\frac{\eta_p}{\eta_m}\right)Re_m^{1/2}$	$Re>1\ ;\ Sc>1$	21
Oscillating drops	L – L	$Sh_d=\frac{4}{\pi}\left(\frac{r_p^2u_p}{D}\right)^{1/2}$		24
		$Sh_d=\frac{2}{\sqrt{\pi}}Pe_d^{1/2}$		27
		$Sh_d=0.32\ Re^{0,8}\ P^{0,1}\ \tau^{-0,14}$ $P=\frac{\rho^3\,\sigma_m}{g\eta_m}\cdot\frac{\rho_m}{\rho_p-\rho_m}\ ;\ \tau=\frac{t_sD}{r_p^2}$		28
Oscillating drops with internal circulation	L – L	$Sh_c=2+[0.65\,Re^{1/2}+0.0351\,(Re-40)^{0,935}]Sc^{1/3}$	$Re\in[40-460]$ $Sc>980$	16
		$Sh_c=50+8.5.10^{-3}\,Re\,Sc^{0.7}$	$Re\in[100-700]$ $Sc>1$	28

to the continuous phase (k_c).[25] In most cases, theoretical and experimental data were correlated by equations similar to (2). These empirical equations are presented in table 3 with their validity ranges.

It was observed for drop with internal circulation that the partial mass transfer coefficient in the continuous phase is significantly greater than for solid spheres with a diameter equal to the equivalent diameter of the drop. [15, 21, 26–32]

The differences between the experimental data of various authors, or between experimental and theoretical data, as well as the narrow validity limits of the relations are due to (i) the complex hydrodynamics of the interface, (ii) the presence of deformable transfer areas, and (iii) to the difficulty in maintaining and controlling the chemical purity of the systems.

4. MASS TRANSFER FROM GAS BUBBLES

For the mass transfer from a gas bubble to a liquid, on the basis of mass transfer theories, equations were obtained for the partial mass transfer coefficient involving bubbles of spherical shape, spherical caps and oblate spheroids. [33]

Relations for mass transfer from gas bubbles to liquids are summarized in table 4. The theoretical relations (1 through 3) indicate a dependence of the partial mass transfer coefficient on diffusivity

$$k = f(D^n) \tag{4}$$

where $n = 0.5$, so as predicted by the film-penetration model.

Relations presented in table 4 neglect the contribution to the mass transfer of the wake of the bubble, which has a very complex hydrodynamics. [5, 33–36] Theoretical attempts to include this contribution were made with the simplifying hypothesis that the rate components in the differential equation of the mass transfer were symmetrical and time-independent. [33] Assuming that the wake of the bubble was a planar interface with constant superficial concentration immersed in a semi-infinite liquid, relation (5) was obtained for the mass transfer coefficient k_w :

---

[25] E. Ruckenstein, *Int. J. Heat Mass Transfer*, **10**, 1785 (1967).

[26] A. C. Lochiel and P. H. Calderbank, *Chem. Eng. Sci.*, **19**, 471 (1964)

[27] R. J. Brunson and R. M. Wellek, *Canad. J. Chem. Eng.*, **48**, 267 (1970).

[28] A. H. P. Skelland and R. M. Wellek, *Canad. J. Chem. Eng.*, **48**, 267 (1970).

[29] E. R. Elzinga and J. T. Banchero, *Amer. Inst. Chem. Engineers J.*, **7**, 394 (1961).

[30] F. H. Garner and M. Tayeban, *Ann. Real. Soc. Espan Phys. Quim. Ser.* **56**, 479 (1960), quoted in ref. 16.

[31] J. Boussinesq, *J. Math.*, **6**, 285, 1905, citat de 16.

[32] F. H. Garner, A. Ford and M. Tayeban, *J. Appl. Chem.*, **9**, 315 (1959), quoted in ref.16.

[33] P. H. Calderbank and A. C. Lochiel, *Chem. Eng. Sci.*, **19**, 485 (1964).

[34] C. W. Bowman and A. I. Johnson, *Canad. J. Chem. Eng.*, **40**, 139 (1962).

[35] A. I. Johnson, F. Besik and A. E. Hamielec, *Canad. J. Chem. Eng.*, **47**, 559 (1969).

[36] M. H. I. Baird and J. F. Davidson, *Chem. Eng. Sci.*, **17**, 87 (1962).

$$k_w = \left(\frac{D}{\pi \tau_w} \right)^{1/2} \tag{5}$$

where τ_w is the time necessary for an elementary volume of the liquid element to traverse the distance between the centre and the outer edge of the bubble floor. The total mass transferred, calculated as the sum of transfers through the frontal surface and the wake of the bubble (in the above planar approximation), has a value which agrees with the theoretical results obtained for spherical bubbles from relation 1 (table 4), and with the experimental data.

Experimentally, mass transfer coefficients are determined by the direct or indirect measurement of the absorbed gas volume. Direct methods (photographic, cinephotographic, [37,38] X-ray cinephotographic method for non-transparent liquids) have the drawback that they yield only a projection of the gas bubble. In this case, the bubble volume is determined by Saltykov's method, [39] considering that the bubble has cylindrical symmetry. In indirect methods the amount of transferred substance is obtained by measuring the variation of the volume in a system open to the atmosphere, [35, 40] or of the pressure in a closed system. [41] By measuring the variation of the bubble volume between two level marks and the ascension, the partial mass transfer coefficient was determined experimentally using the relation : [35]

$$k_l = \frac{4(P_1 - P_2)}{4.84RTH\ \Delta\tau} \left[\frac{(PV)_1^{1/3} - (PV)_2^{1/3}}{P_1^{4/3} - P_2^{4/3}} \right] \tag{6}$$

By expressing the bubble gas volume versus the bubble excentricity $E = d_b/h$ which characterizes the shape of the bubble, equations (8) and (9) from table 4 were obtained. A striking analogy exists between relations for the mass transfer from a gas bubble to a liquid, and from liquid drops to a liquid. This is not unexpected, since in both cases the mass transfer occurs through a mobile interface with variable shape.

Experimental investigations for determining mass transfer coefficients in a gas bubble-liquid system, with or without chemical reaction, evidenced that the intensity of the mass transfer is influenced by the following factors :

—the magnitude, shape, age and ascensional velocity of the gas bubble ; [38,42]

---

[37] F. Deindoerffer and A. E. Humphrey, *Ind. Eng. Chem.*, **53**, 755 (1961).

[38] D. R. Raymond and S. A. Zieminski, *Amer. Inst. Chem. Engineers J.*, **17**, 57 (1971).

[39] S. A. Saltikov, "Proceedings of the Second International Congress for Stereology", Chicago, 1967.

[40] J. H. Leonard and G. Houghton, *Chem. Eng. Sci.*, **18**, 133 (1963).

[41] P. H. Calderbank, D. S. L. Johnson and J. Loudon, *Chem. Eng. Sci.*, **25**, 235 (1970).

[42] T. Ishii and A. I. Johnson, *Canad. J. Chem. Eng.*, **47**, 272 (1969).

Table 4

Relations for the mass transfer gas bubbles-liquid

Characteristics of the system	Relation	Observations	References
Mass transfer from spherical gas bubbles	$k_l = \left(\frac{2u_b D}{\pi R_b}\right)^{1/2}$ $k_l = 1.13\left(\frac{Du_b}{d_e}\right)^{1/2}$	Penetration theory	5,34
Mass transfer for the frontal surface of a spherical cap bubble	$k_{l,cs} = \left(\frac{4Du_b}{\pi h}\right)^{1/2}$	Penetration theory	5,35
	$k_{l,cs} = 1.32\left(\frac{u_b D}{d_e}\right)^{1/2}$ $k_{l,cs} = 1.125 g^{1/4} D^{1/2} d_e^{-1/4}$	Potential flow theory $d_e > 1.5$ cm	5,35
Mass transfer for spherical cap bubbles	$k_l = 1.13\left(\frac{u_b D}{d_e}\right)^{1/2}\left(\frac{d_e}{0.58 + 0.23 d_e}\right)^{1/2}$	Experimental data	35
	$k_l = 0.975 g^{1/4} D^{1/2} d_e^{-1/4}$	Experimental data	36
	$k_l = 1.36\left(\frac{Du_b}{d_e}\right)^{1/2}$	Experimental data	33

Mass transfer gas bubbles-liquid, in systems open to the atmosphere	$k_l = \frac{4(P_1 - P_2)}{4.84RTH}\left(\frac{(PV)_1^{1/3} - (PV)_2^{1/3}}{P_1^{1/3} - P_2^{1/3}}\right)$	Experimental data	35
Mass transfer carbon dioxide bubbles-distilled water	$k_l = \frac{D}{d_b}(2 + 0.57Re^{0.5}\,Sc^{0.35})$		41
Mass transfer from oblate spheroid gas bubbles	$\frac{Sh_{sp}}{Sh_s} = \left[\frac{2}{3}(1+k)\right]^{1/2} \cdot$ $\cdot \frac{2E^{1/3}(E^2 - 1)^{1/2}}{E(E^2 - 1)^{1/2} + \ln(E + \sqrt{E^2 - 1})}$ $E = \frac{d_b}{h}, \quad k = \text{constant}$		41
Mass transfer from gas spherical cap bubbles	$k_l = 1.79\,\frac{(3E^2 + 4)^{2/3}}{E^2 + 4}\left(\frac{Du_b}{d_b}\right)^{1/2}$	Experimental data	33
Mass transfer from carbon dioxide bubbles to alcohols	$k_l = -\ 0.126\ C_D + 0.112$ for straight chain alcohols $k_l = -\ 0.089\ C_D + 0.0903$ for branched chain alcohols $C_D = \frac{8}{3}\,\frac{gd_b}{u_b^2}$		38

— the presence or absence of proper oscillations of gas bubbles; [38, 42]
— the diffusion coefficient of gas into liquid. [43]
— the presence or absence of inert gases; [44]
— the nature and viscosity of the liquid; [41]
— the presence or absence of surfactants in the liquid [21, 38]

Results of experimental studies carried out both in stationary liquid columns [33, 35, 38, 40–44] and in columns with down-flowing liquid (in counterflow with the gas bubble) [21, 42, 45,] are not always consistent in respect to the influence of the above factors on the partial mass transfer coefficients k_l or on mass transfer rate $k_l A$.

The dependence of mass transfer on the volume of the bubble is quantitatively expressed as a function of the equivalent diameter d_e of the gas bubble. The theoretical relations 1—3 (table 4) have the form $k_l \sim d_e^{-n}$. Experimentally, for spherical caps the empirical relation [35] 4 (table 4) indicates a dependence $k_l \sim d_e^{-1/2}$, which is in fact Higbie's relationship, whereas other papers report that either for certain value ranges of the equivalent diameter, k_l does not depend on d_e, [37] or that the mass transfer rate obeys a relation $k_l A \sim d^n$ (for carbon dioxide bubbles with $d_e < 1$ cm, $n = 2$ for non-spherical bubbles [33,35]).

The variation of the partial mass transfer coefficient versus the equivalent diameter of the bubble presents maxima and minima, which are due to the occurrence of oscillations of the bubble proper. [41]

Experimental data concerning the effect of the gas bubble age on the mass transfer are contradictory. For bubbles with equivalent diameters in the range $d_e \in [0.3 - 0.8 \text{ cm}]$, the mass transfer coefficient decreases when the bubble age increases from 0.5 to 6 second. [33, 37] For bubbles with $d_e \in [0.5 - 2.65 \text{ cm}]$ the mass transfer coefficient is influenced if the gas bubble age is larger than 5 seconds. [33, 36, 46]

The mass transfer is influenced by the ascensional velocity of the gas bubble. This dependence may be expressed either directly as $k_l \simeq u_b^n$, or indirectly by means of the bubble shape and equivalent diameter, because these influence the velocity. [5,6,33,35,36]

The influence on mass transfer of the diffusion coefficient D of the gas into the liquid is reflected in theoretical and in most experimental studies by a dependence of the form $k_l \simeq D^n$, where $n = 0.5 - 1$. [9] Recently, however, for the absorption of gases into water, experimental determinations evidenced that k_l does not depend on D; [47] in this case there would be no difference between various models of mass transfer since they differ just in the value of the exponent n in the dependence $k_l \sim D^n$. To elucidate this point, it will be necessary to examine experimental data for wider ranges of the parameters.

The nature and viscosity of the liquid influence indirectly the mass transfer, since they affect the shape and ascensional velocity of bubbles.

---

[43] K. R. Weller, *Canad. J. Chem. Eng.*, **50**, 49 (1972).

[44] J. R. Laundon, P. H. Calderbank and I. Coward, *Chem. Eng. Sci.*, **21** 614 (1966).

[45] M. Moor Young, G. D. Fulford and E. W. Godsalve, *Canad. J. Chem. Eng.*, **51**, 368 (1973).

[46] D. Hammerton and F. H. Garner, *Trans. Inst. Chem. Engineers*, **32**, S 18 (1954).

[47] K. R. Weller, *Canad. J. Chem. Eng.*, **50**, 49 (1972).

On investigating the influence of inert gases in mass transfer from individual gas bubbles, it was found that the presence of inert diluents does not modify the mass transfer coefficient.[44-48]

The presence of surfactants in the liquid decreases the intensity of mass transfer: appreciably for liquid drops or for small gas bubbles ($d_e < 1.5$ cm) in liquid, and negligibly for large gas bubbles $d_e >$ > 1.5 cm).[36, 38]

These literature data evidence a wide dispersion of values, a restricted validity for their relations over narrow ranges of the parameters, and sometimes harsh contradictions in the factors which influence the mass transfer between gas bubbles and a liquid.

5. EXPERIMENTAL

The experimental set-up used in the present work was described in a previous paper.[49] Experiments studied the mass transfer by determining the amount of absorbed carbon dioxide into distilled water versus time, as a function of the bubble shape and diameter.

The initial volume of the bubble (0.02—1ml) was determined by introducing the gas from a calibrated syringe. The final volume of the bubble after rising freely between two marks on the column during a time measured with a chronometer was determined as a difference between the initial and absorbed volumes. The latter volume was measured on the basis of the displacement of the mercury level in the capillary tube, as described previously.[35,49] The bubble areas, assumed spherical, were then calculated.

6. RESULTS AND DISCUSSION

The mass transfer from individual gas bubbles rising freely in a stationary liquid column was studied in the present paper in order to obtain reference data for comparison with systems where the mass transfer was intensified by mechanical vibrations or ultrasonic energy input.

The partial mass transfer coefficient in the liquid phase k_l was calculated from the experimental data by means of the relation:

$$k_l = \frac{\Delta V}{\Delta\tau\, \bar{S}_b} \tag{7}$$

where:

$\frac{\Delta V}{\Delta\tau}$ is the ratio between the volume of absorbed carbon dioxide and the absorption time;

$\bar{S}_b$ is the average between the initial and the final area of the bubble, considered as a sphere.

---

[48] S. M. Barnett, A. E. Humphrey and M. Litt, *Amer. Inst. Chem. Engineers J.*, **12**, 253 (1966).

[49] C. Balaban, Gh. Dobraniş and R. Mihail, *Rev. Roumaine Chim.*, **18**, 1829 (1973).

Table 5 presents coefficient k_l, calculated according to relation (7). By employing more complicated relations (6) previously described, good agreement is obtained as evidenced by table 5. Therefore, the use of the simpler relation (7) is to be preferred, because it necessitates fewer parameters to be measured experimentally and taken into account. In relation (7) the variation of hydrostatic pressure, which had to be explicitly introduced into relation (6), is implicitly taken into account by the average area of the bubble.

Table 5

Values of partial mass transfer coefficient calculated with relations (6) and (7)

V_1		cm^3	0.1	0.2	0.4	0.6	0.8	1.0
d_e	cm		0.576	0.725	0.915	1.05	1.16	1.42
k_l	$\frac{cm}{s}$	relation 6	0.0159	0.02	0.0225	0.0216	0.0204	0.026
		relation 7		0.0207	0.0227	0.0217		0.026

Experimental values of the partial mass transfer coefficient k_l for various equivalent diameters of the gas bubble are presented in figure 1, together with literature values. [33] It may be seen that our values are comparable with the latter. Also, all these experimental values are well approximated by the full curves from fig. 1, corresponding to the relation (8) for mass transfer from spheres in potential flow : [31]

$$k = 1.13 \left(\frac{D\, u_b}{d_e} \right)^{1/2} \tag{8}$$

A different way of correlating our experimental data is based on a criterial equation (9), similar to literature relations : [33-36]

$$Sh = C Re_b^m Sc^{1/3} \tag{9}$$

Coefficient C and exponent m were determined from our experimental data using a program for the Felix 622 computer, leading to expression :

$$Sh = 1.138\ Re_b^{0.652}\ Sc^{1/3} \text{ for } Re_b < 1500 \tag{10}$$

We studied quantitatively the dependence of the partial mass transfer coefficient as a function of the bubble area. This area depends on the shape of the bubble. Observations on bubble shapes indicated that these can be approximated by oblate spheroids. Therefore to define the shape of the gas bubble we use the ratio (which we call eccentricity) $E = d_b/h$, where d_b is the transversal diameter of the bubble, perpendicular to the direction of its motion (major axis of the vertical elliptical section), and h is the height of the bubble, measured parallel to the direction of its motion (minor axis of the section). [33] Values of d_b and h were obtained by measuring directly the photographic images of gas bubble (fig. 2).

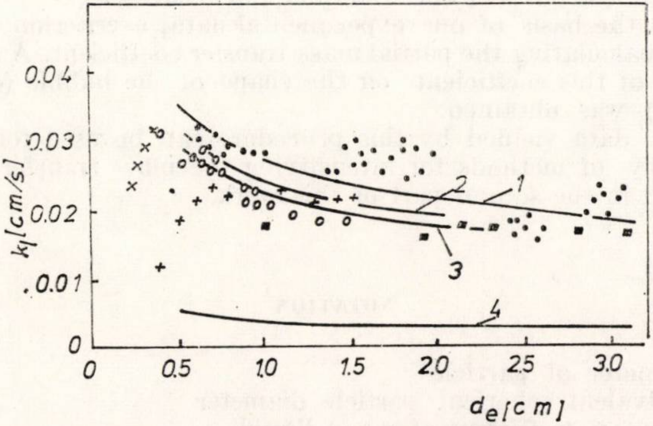

Fig. 1. – Variation of partial mass transfer coefficients, k_l, with equivalent diameters of the gas bubbles;

Curve 1 – from relation $k_l = 1.36 \left(\frac{D.u_p}{d_e}\right)^{1/2}$, curve 2 – from relation 11, table 4, for oblate spheroids; curve 3 – from relation $k_l = 1.13 \left(\frac{D u_p}{d_e}\right)^{1/2}$; curve 4 – from relation $k_l = 0.6 \frac{D}{d_e} Re_b^{1/2} \; Sc^{1/3}$; ○ – our experimental data, × – data by Hammerton, ● – data by Calderbank and Lochiel, + – data by Leonard, ■ – data by Baird.

The eccentricity has value 1 for spherical bubbles ($d_b = h$) with $d_b < 3$ mm and increases for non-spherical bubbles as seen in figure 3, up to $d_b \simeq 10$ mm. For gas bubbles with $d > 10$ mm the eccentricity remains practically constant and is equal to about 2.6.

According to the data plotted in fig. 4, the partial mass transfer coefficient depends on the eccentricity of the gas bubble obeying relation (12)

$$k_l = 3.25\, E^{-\frac{1}{2}} \tag{11}$$

Since the above observations have shown that the gas bubbles which were studied in the present paper had an appreciable departure from spherical shape as evidenced by their eccentricity of about 2.6, it was considered necessary to modify relation (7) to take into account the actual shape and area of the bubble. The resulting k_l values, calculated with the area of an oblate spheroidal bubble, are smaller than those calculated with the assumption of spherical shape, as seen in figure 5.

CONCLUSIONS

1. An experimental method for measuring the mass transfer coefficient is described as a mathematical expression for calculating this coefficient from experimental data. Compared to earlier expressions from the literature, the present one is simpler and accurate.

2. On the basis of our experimental data, a criterion relation was devised for calculating the partial mass transfer coefficient. A quantitative dependence of this coefficient on the shape of the bubble (expressed as eccentricity) was obtained.

3. The data yielded by this procedure can be used for comparing the efficiency of methods for intensifying the mass transfer, which will be described in the second part of this work.

NOTATION

d — diameter of particle
d_e — equivalent spherical particle diameter
D — diffusion coefficient of gas in liquid
E — bubble eccentricity
g — acceleration due to gravity
Gr — Grashoff number
H — Henry constant
k — partial mass transfer coefficient
P — pressure
r — radius of particle
R — gas constant
Re — Reynolds number
s — surface renewal rate
Sc — Schmidt number
Sh — Sherwood number
T — absolute temperature
u — velocity of particle
δ — film tickness
η — viscosity
σ — surface tension
θ — surface element contact time

SUBSCRIPTS

b — gas bubble
c — continuous phase
d — dispersed phase
l — liquid
m — medium
p — particle
w — wake of gas bubble

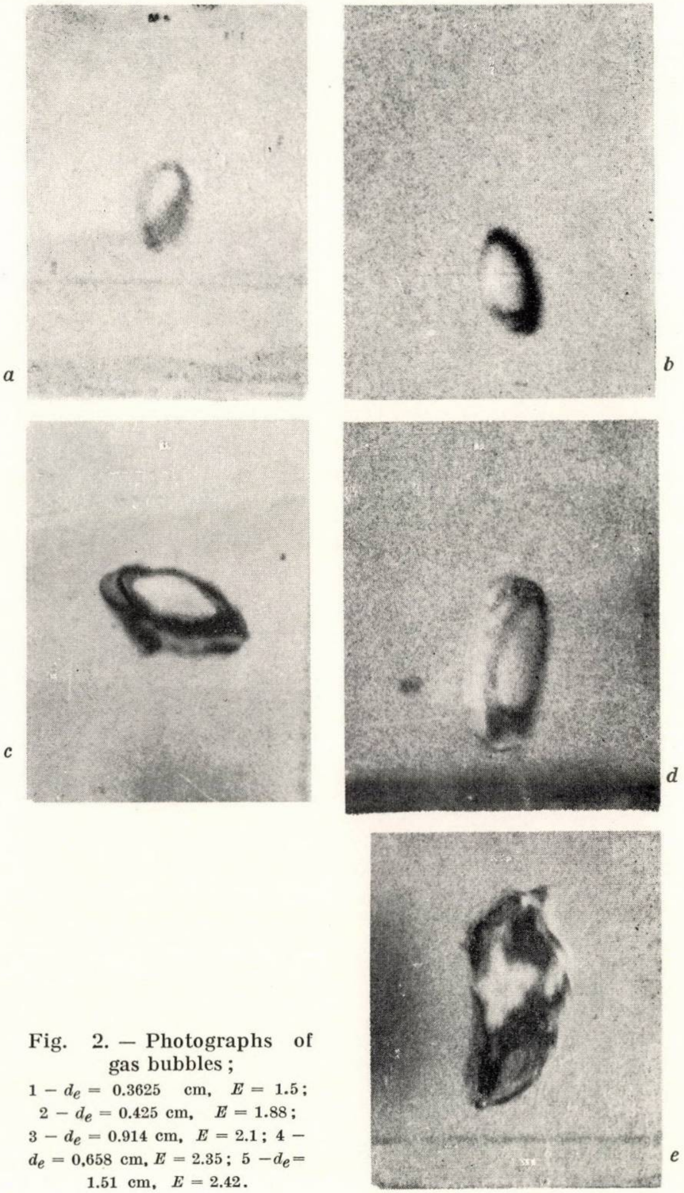

Fig. 2. — Photographs of gas bubbles ;
1 – d_e = 0.3625 cm, $E = 1.5$; 2 – d_e = 0.425 cm, $E = 1.88$; 3 – d_e = 0.914 cm, $E = 2.1$; 4 – d_e = 0,658 cm, $E = 2.35$; 5 – d_e= 1.51 cm, $E = 2.42$.

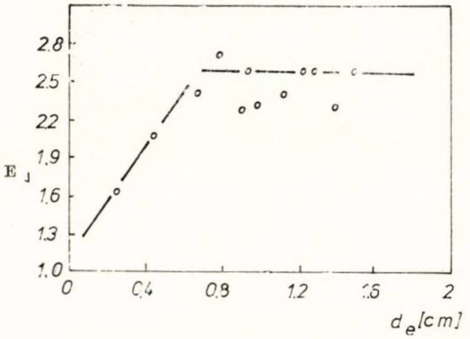

Fig. 3. — Bubble eccentricity E, versus equivalent diameter, d_e, of the gas bubbles.

Fig. 4. — Variation of partial mass transfer k_l, with bubble eccentricity E.

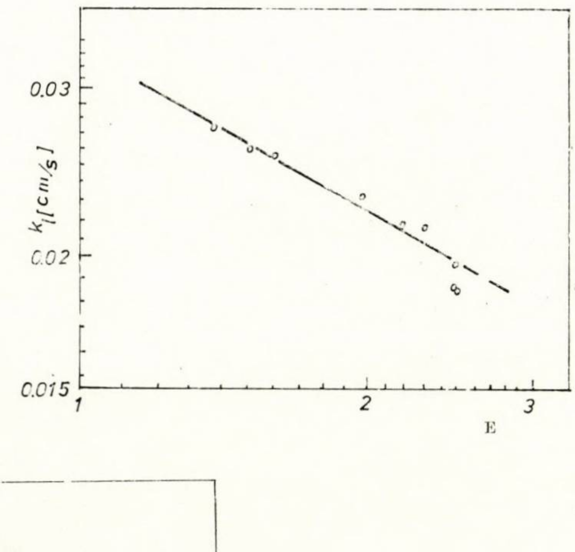

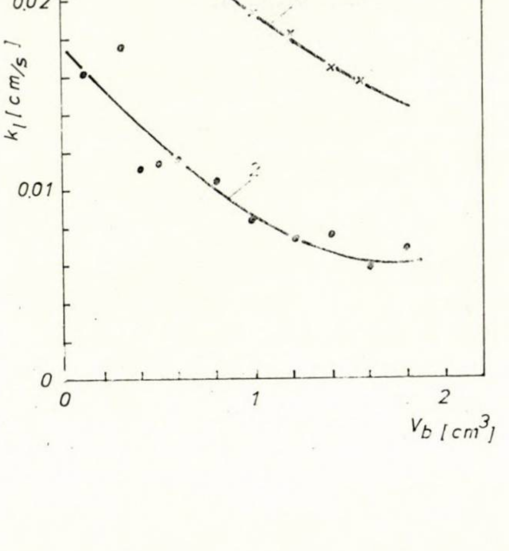

Fig. 5. — Dependence of the partial coefficient of mass transfer with the volume of the gas bubble; 1, coefficient reported to the surface of the bubble considered like sphere; 2, coefficient reported to the surface of the bubble, taken into account the real form of the bubble as spherical cap.

Revue Roumaine de Chimie, **20**, *8*, 1157–1166 (1975)

STUDY ON THE POLYMERIZATION OF ACETYLENIC DERIVATIVES. XVII*

STUDY ON ELECTRIC PROPERTIES OF SOME POLYPHENYLACETYLENES

CR. SIMIONESCU[a], SVETLANA DUMITRESCU[a], M. DĂRÎNGĂ[a],
MARIA GROVU[a], SILVIA VASILIU[a], I. DIACONU[b] and M. LEANCĂ[b]

[a] Polytechnical Institute of Jassy, Department of Macromolecular Chemistry, Str. 23 August, 11, Romania
[b] Institute of Macromolecular Chemistry "Petru Poni", Str. Grigore Ghica-Vodă, 41–A, Jassy, Romania

Received September 6, 1975

Based on electron spin resonance (ESR) measurements and on dark electric conductivity, a study of electric and magnetic properties was carried out on some polyphenylacetylenes and on their *para*-substituted derivatives with Cl, CH_3 and NO_2. This study is aimed at establishing the correlation existing between the structure of these polymers and their magnetic and electric properties.

INTRODUCTION

Though a considerable number of publications have studied electric and magnetic properties of polymers with double bonds conjugated in the main chain, few of them try to establish the correlation between structure and electrophysical properties of these polymers.[1-5] Most papers in this field aim at explaining the phenomenon of electrical conduction and the origin of paramagnetism. The different length of conjugated blocks in the macromolecular chain, the reticulation degree of linear chains as well as the degree of collectivization and delocalization of unpaired spin electrons are only a few characteristic factors. They can exert a decisive influence at a given moment, both on electric conductivity and on the form of the signal of spin electron resonance of polymers with unsaturated and conjugated chains.

---

* XVI : Cr. Simionescu, S. Dumitrescu, S. Vasiliu and V. Percec, *J. Thermal Analysis* (in press).

[1] A. V. Talroze and L. A. Blumenfeld, *Doklady Akad. Nauk S.S.S.R.*, **135**, 1450 (1960).

[2] V. A. Talroze and L. A. Blumenfeld, *Doklady Akad. Nauk S.S.S.R.*, **134**, 1123 (1960).

[3] N. N. Semenov, *J. Polymer Sci.*, **55**, 563 (1961).

[4] L. A. Blumenfeld, A. A. Berlin, A. A. Slinkin and A. E. Kalmanson, *Zhur. strukt. Khim.*, **1**, 103 (1960).

[5] A. A. Berlin, *J. Polymer Sci.*, **55**, 621 (1961).

EXPERIMENTAL

Twelve types of substituted and non-substituted polyphenylacetylenes were studied: PPhA-i.s.f. = polyphenylacetylene obtained by ionic polymerization – soluble fraction; PPhA-i.ins. f. = insoluble fraction of the same polyphenylacetylene; PPhA-p.s.f. = polyphenylacetylene obtained by photochemical polymerization – soluble fraction; PPhA-p.ins.f. = insoluble fraction of the same polymer; PPhA-c ($ZnCl_2$) = polyphenylacetylene obtained by polycondensation with $ZnCl_2$ catalyst; PPhA-c ($SnCl_2$) = polyphenylacetylene obtained by polycondensation with $SnCl_2$; PPhA-c (BF_3) = polyphenylacetylene obtained by polycondensation with BF_3; P-*p*-ClPhA-i.s.f. = poly-*p*-chlorophenylacetylene obtained by ionic polymerization – soluble fraction; P-*p*-ClPhA-i.ins.f. = insoluble fraction of the same polymer; P-*p*-MPhA-i.s.f. = poly-*p*-methylphenylacetylene obtained by ionic polymerization – soluble fraction; P-*p*-MPhA-i.ins.f. = poly-*p*-methylphenylacetylene obtained by ionic polymerization – insoluble fraction; P-*p*-NPhA-i.s.f. = poly-*p*-nitrophenylacetylene obtained by ionic polymerization – soluble fraction.

All these polymers were synthesized according to literature indications,

ESR spectra of mentioned polymers were recorded on a Varian E–12 spectrometer. Measurements were performed at room temperature with the exception of some polymers where the variation of the ESR with temperature was followed in the 130–300 K range. Polymer samples were introduced in quartz phials. To determine polymer concentration in paramagnetic particles a carbon sample was used as standard, with a spin concentration of 3×10^{15} spins/g. The concentration of impaired electrons in the analysed substance was determined using relation:

$$N_x = N_{et} \cdot \frac{Ax}{A_{et}} \tag{1}$$

where N_x and N_{et} represent the concentration of unpaired spins related to a polymer gram and standard sample, respectively; A_x and A_{et} are areas comprised between the first derivative of the ESR spectrum and the axis of the magnetic field. Recordings for polymer and sample are performed for the same value of the modulation. Areas were determined by the method of double graphic integration, using relation:

$$A = \frac{1}{2} f \,.\, h^2 \sum_{r=1}^{n} (2n - 2r + 1)\, y_r \tag{2}$$

where:

n = number of intervals in which the abscissa was divided,
h = length of every interval,
r = summation index,
f = correction factor of the amplitude,
y_r = ordinate corresponding to the r-th interval.

The width of the ESR line, ΔH_{max}, was appreciated as being equal to the distance between the maximum and the minimum of the derivated spectrum, expressed in Gauss (Gs).

In view of determining electric conductivity, powderlike polymers were turned into tablets with Ø = 13 mm and thickness $d \simeq 1$ mm. Tablet-making was carried out in the absence of air, at a pressure of 10^4 kgf/cm^2. Tablets were then metallized in vacuo ($p = 10^{-4}$ torr) with silver, resulting in circular contact areas with 8 mm diameter. Measurements were performed in air medium using a conductivity cell designed and achieved in the laboratory. Electrode pressure on the tablet was 1.5 kgf/cm^2 and it was maintained constant in all cases. Continuous electric voltage applied on the electrodes was of 500 V.

To determine the activation energy of electric conductivity, this one was measured in a certain temperature range, maintaining constant the sample cooling gradient to 1°/min. It was found that in all cases, except P-*p*-NPhA, polymers observe the exponential law of semiconductors:

$$\sigma = \sigma_0 \exp\,(-\,E_g/2KT) \tag{3}$$

where:

σ_0 = electric conductivity at infinite temperature,
K = Boltzmann constant,
T = absolute temperature,
E_g = activation energy of conductivity.

RESULTS AND DISCUSSIONS

It was established that all studied polymers evince the properties of paramagnetic substances. The characteristics of ESR spectra of soluble and insoluble fractions of substituted and nonsubstituted polyphenylacetylene are given in table 1.

Table 1

Paramagnetic properties of the polyphenylacetylene and related derivatives

Polymer	Unpaired spin concentration (spin/g)	g	ΔH_{max}· (gauss).	Line shape
PPhA-i.s.f.	2.57×10^{17}	2.0027	6.7	Narrow and Lorentzian line
PPhA-i.ins.f.	3.00×10^{16}	2.0010	16.0	,,
PPhA-p.s.f.	1.00×10^{17}	2.0070	6.7	,,
PPhA-p.ins.f.	5.00×10^{16}	2.0071	6.0	,,
PPhA-c($ZnCl_2$)	6.80×10^{19}	2.0027	8.7	,,
PPhA-c ($SnCl_2$)	9.55×10^{18}	2.0027	8.8	,,
PPhA-c (BF_3)	2.29×10^{19}	2.0027	8.8	,,
P-*p*-ClPhA-i.s.f.	—	2.2549	286.00	Wide and asymmetric line with unresolved hyperfine structure
P-*p*-ClPhA-i.ins.f.	8.7×10^{19}	—	608.00	Large line with hyperfine structure
P-*p*-NPhA-i.s.f.	—	—	476.00	Large and asymmetric line with hyperfine structure
P-*p*-MPhA-i.ins.f.	—	—	—	Very wide line with hyperfine structure
P-*p*-MPhA-i.s.f.	—	—	—	,,

In the case of non-substituted soluble and insoluble polymers (polyphenylacetylenes) obtained either by procedure of ionic or photochemical polymerization or by the polycondensation reaction, ESR spectra recorded are characterized by a single narrow symmetrical line ($\Delta H_{\max} = 6-16$ gauss), lacking hyperfine structure. An example of this type of spectrum is given in figure 1.

The values of the spectroscopic splitting factor (g), of these polymers are very close to that of free electrons ($g = 2.0023$). This type of spectrum is specific to free radicals and of most conjugated macromolecular systems, where unpaired electrons are strongly delocalized. The narrow signal is accounted for by the high degree of delocalization of unpaired electrons.

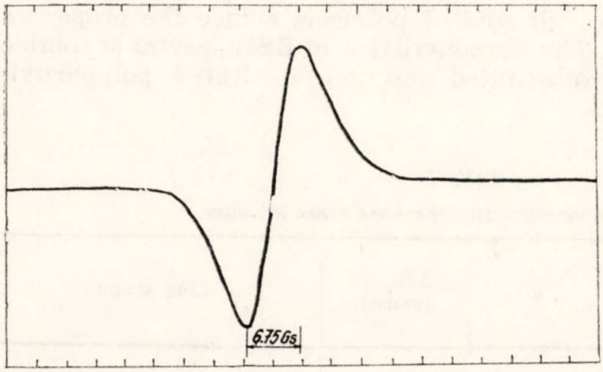

Fig. 1. – ESR signal of PPhA-i.s.f. sample.

In some authors' opinion ,[3,4] the narrow ESR signal is rather a characteristic of the macromolecule as such than of the solid polymer considered as a whole. This hypothesis was also corroborated in the case of polyphenylacetylenes. It was thus established that the ESR signal persists also in solution irrespective of its dilution.[6,7] For thermally polymerized polyphenylacetylene, Ehrlich [6,7] ascribes the ESR signal to structure defects of individual macromolecules.

It should be pointed that the method of obtaining polyphenylacetylenes does not affect polymer concentration in paramagnetic particles. It depends only on the length of the conjugated chain. Thus, polycondensation polyphenylacetylenes with mean molecular weights higher than polyphenylacetylenes obtained by polymerization are characterized by a higher content of paramagnetic particles ($\sim 10^{19}$ spins/g in the former case as compared to 10^{16} spins/g in the latter).

Between the size of the conjugated system and the width of the signal there is a relation of inverse proportionality, which is a measure of the delocalization degree of unpaired electrons.

An elementary calculation points out that in the case of studied PPhA, an unpaired electron stands for a great number of macromolecules ($\sim 4 \times 10^2$); therefore our considerations refer to the delocalization degree of the whole electronic cloud viewed as a whole.

---

[6] P. EHRLICH, *J. Macromol. Sci. Phys. B2*, **2**, 153 (1968).

[7] P. EHRLICH, R. J. KERN, E. D. PIERRON and T. PROVDER, *J. Polymer Sci. B*, **5**, 911 (1967).

All these facts underline the idea that, in the case of narrow ESR signals, the exchange of unpaired electrons among PPhA molecules occur with high frequency and that each unpaired electron is found in the same field of the nuclear spins.

It was established that for polyphenylacetylenes with narrow absorption line the shape of the ESR signal is much closer to the Lorentz type. Thus by plotting the function $\sqrt{y/I} = f(y^2)$, (where y is the distance in mm measured from the center of the signal and I the ordinate of the derived ESR spectrum), there results a straight line.[8] Such a plotting is shown in figure 2 for the case of PPhA-p. ins. f.

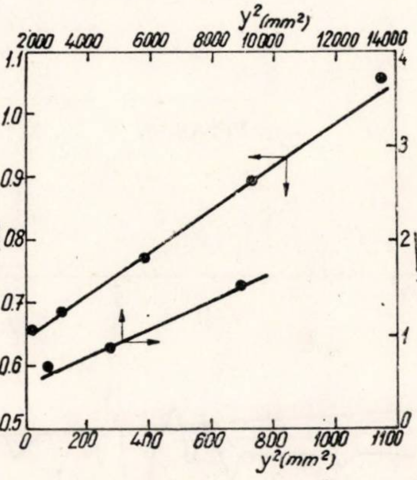

Fig. 2. — Verification of ESR signal regarding its Lorentzian shape for PPhA-p.ins.f. sample.

The Lorentz shape of the ESR signal points out that the spin-spin type interaction contributes to a greater extent to produce the relaxation phenomenon.

For two samples, viz. PPhA-p.ins. f., the variation of the concentration of paramagnetic centres with the temperature in the 130—300 K range was followed (Table 2). It was found that their number is practically constant, which proves that Curie's law is verified in these cases.

For P-*p*-NPhA-i.s.f. and P-*p*-ClPhA-i.ins.f., ESR spectra with hyperfine structure were obtained (Fig. 3), probably resulting from the interaction of unpaired electrons with the magnetic momentum of N and Cl atom nuclei.

The soluble fraction of P-*p*-ClPhA has a broad and asymmetrical signal ($\Delta H_{\max} = 286$ gauss), similar to ESR spectra of nucleic acids[9] and polydiphenyleneaminodichlorquinones.[10] Such a spectrum shows that the respective polymer has a certain structure at a supramolecular level, characterized by ordered zones (disappearing after dissolution), where unpaired and very mobile electrons strongly interact. Such macromole-

---

[8] N. A. Bax, A. V. Aannikov, A. D. Grishina, "Electroprovodnosti i paramagnetism polimer provodnikov", Ed. Nauka, Moscow, 1971.

[9] L. A. Blumenfeld, A. E. Kalmanson and Sem-;Tei-Gen, *Doklady Akad. Nauk S.S.S.R.*, **124**, 1144 (1959).

Table 2

Dependence of the unpaired spin concentration upon temperature

Polymer	Temperature °K	Unpaired spin concentration (spin/g)
PPhA-p.s.ins.	300	5.0×10^{16}
	250	5.0×10^{16}
	190	5.2×10^{16}
	150	5.3×10^{16}
	130	6.5×10^{16}
PPhA-i.s.f.	300	2.57×10^{17}
	250	2.5×10^{17}
	190	2.7×10^{17}
	150	2.7×10^{17}
	130	2.8×10^{17}

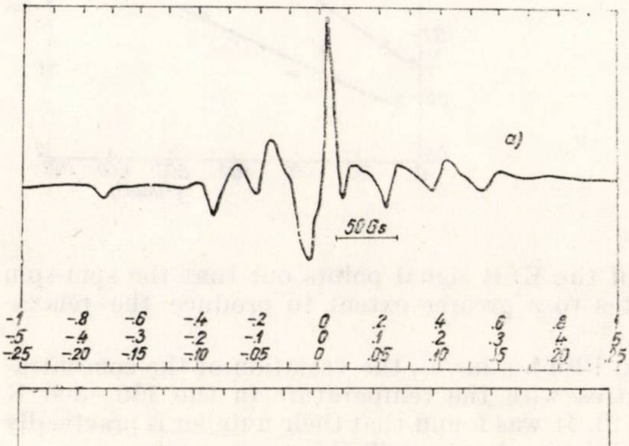

Fig. 3. — ESR signal of (a) P-*p*-NPhA-i.s.f. and (b) P-*p*-ClPhA-i.s.f.

---

[10] A. A. Berlin, *Khim. Tekhnol. Polimerov,* **7—8,** 139 (1960).

cular compounds are considered to have ferro- and antiferromagnetic properties.[9, 11–12]

Electric conductivity. Polyphenylacetylenes belong to the category of semiconductor polymers with high enough ohmic resistance. The presence of $-Cl$ and $-CH_3$ substituents in the benzene nucleus of polyphenylacetylene results in the decrease of the electric conductivity of the respective polymers, while the NO_2 substituent lends different properties from those of the other substituted polyphenylacetylenes. Thus P-*p*-PNPhA-i.s.f. is characterized by a very good electric conductivity ($\sigma_{20} = 2.9. \times 10^{-6} \text{ohm}^{-1}\ \text{cm}^{-1}$), i.e. by 12–14 orders of magnitude higher than the conductivity of other substituted polyphenylacetylenes. The values of electric conductivity at 20° range between 10^{-18} and 10^{-19} $\text{ohm}^{-1}\ \text{cm}^{-1}$ for substituted polyphenylacetylenes and between 10^{-17} and 10^{-19} $\text{ohm}^{-1}\ \text{cm}^{-1}$ for unsubstituted ones. All polycondensation polyphenylacetylenes are not soluble and at 20° evince conductivities ranging between values characteristic of polymerization polyphenylacetylenes.

Table 3

Electrical conductivity and activation energy of polyphenylacetylene and related derivatives

Polymer	Temperature range (°)	σ_0 $\text{ohm}^{-1}\cdot\text{cm}^{-1}$	σ_{20} $\text{ohm}^{-1}\cdot\text{cm}^{-1}$	E_A	
				kcal/mol	(eV)
PPhA-i.s.f.	93–138	3.4×10^{5}	1.8×10^{-18}	31.2	1.35
PPhA-i.ins.f.	66–107	8.2×10^{6}	1.9×10^{-17}	31.6	1.37
PPhA-p.s.f.	107–159	2.0	5.0×10^{-19}	24.9	1.08
PPhA-c($ZnCl_2$)	29– 86	4.9×10^{7}	3.5×10^{-17}	32.5	1.41
PPhA-c($SnCl_2$)	38–120	2.2×10^{5}	2.9×10^{-17}	29.3	1.27
PPhA-c(BF_3)	41–123	3.0×10^{3}	5.9×10^{-19}	29.1	1.26
P-*p*-ClPhA-i.s.f.	105–147	3.2×10^{8}	4.1×10^{-20}	37.4	1.62
P-*p*-ClPhA-i.ins.f.	77–118	3.0×10^{2}	2.0×10^{-18}	27.0	1.17
P-*p*-MPhA-i.s.f.	96–153	3.8×10^{5}	5.5×10^{-20}	33.2	1.44
P-*p*-MPhA-i.ins.f.	96–153	8.0×10^{4}	2.2×10^{-19}	31.6	1.37
P-*p*-NPhA-i.s.f.	23*	—	*2.9×10^{-6}	—	—

* Measured at the room temperature (23°)

Analysing the data of table 3 it appears that in all cases insoluble fractions have electric conductivities by 1–2 orders of magnitude higher than those of soluble fractions. This fact may be accounted for either by admitting the extension of conjugated spectra or by a more ordered microstructure of conjugated chains, ensuring the coplanarity of molecules on greater distances.

It should be emphasized that activation energies calculated by equation 3 are higher in the case of substituted polyphenylacetylenes than in the case of non-substituted ones.

---

[11] L. A. BLUMENFELD, *Biofizika*, **4**, 515 (1959).
[12] L. A. BLUMENFELD, *Biofizika*, **6**, 631 (1961).

All polymers, except P-*p*-NPhA, testify the exponential law of semiconductors (Fig. 4–6). As concerns variation of electric conductivity, the nitric derivative behaves analogously to metals.

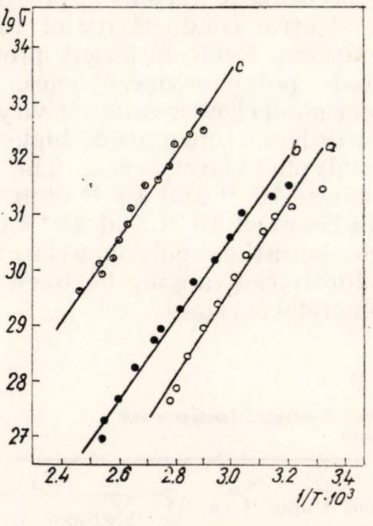

Fig. 4.— Plots of lgσ vs. $1/T$ for (a) P-*p*-ClPhA-i.ins.f., (b) P-*p*-MPhA-i.s.f., (c) P-*p*-MPhA-i.ins.f. and (d) P-*p*-ClPhA-i.s.f.

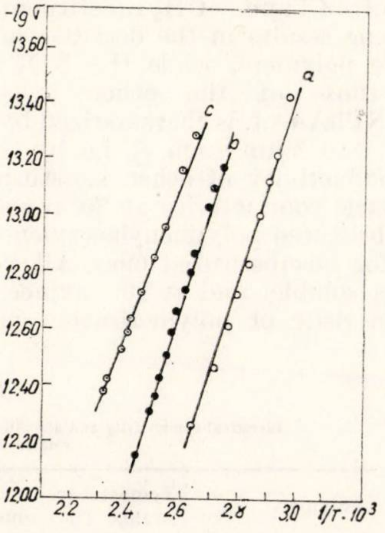

Fig. 5. — Plots of lg σ vs. $1/T$ for (a) PPhA-i.ins.f., (b) PPhA-i.s.f. and (c) PPhA-p. s.f.

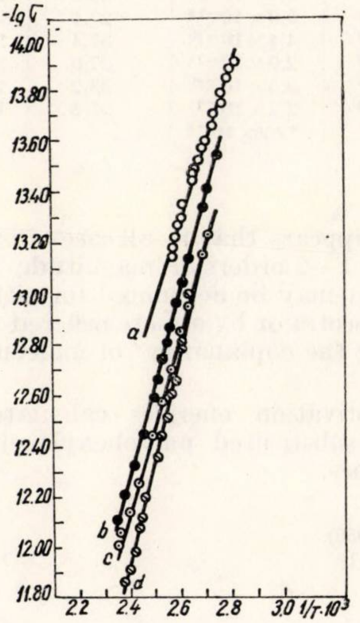

Fig. 6. — Plots of lg σ vs. $1/T$ for (a) PPhA-c. ($ZnCl_2$), (b) PPhA-c. ($SnCl_2$) and (c) PPhA-c.(BF_3).

We mention that in a previous work[13] on the polymerization of *p*-nitrophenylacetylene by the procedure of cold radiofrequency plasma, it was established that the thus obtained polymer has electrical conductivity with the same order of magnitude as that of polynitrophenylacetylene obtained by ionic polymerization. Yet, by contrast to the latter, polynitrophenylacetylene polymerized in cold plasma verifies the exponential law of semiconductors. The different behaviour of nitric polymers is not an elucidated question yet.

The inverse proportionality between electric conductivity and the activation energy is established. Numerous works in the speciality literature point to the existence of such a functional dependence between these two magnitudes, without having a universally valid character.

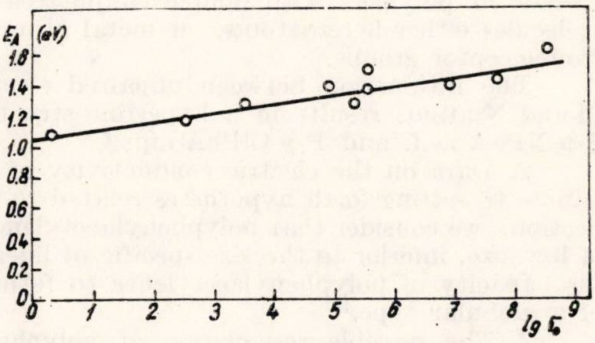

Fig. 7. — Relation between the activation energy, E_A, and log.σ_0

Talroze and Blumenfeld[1,2] studied the variation of electric conductivity with temperature for a considerable number of polymers with high ohmic resistivity. They found the so-called "compensation effect" consisting in the linear increase of the activation energy with the logarithm of the preexponential coefficient (lg σ_0). This linear dependence is expressed by equation :

$$E_A = a + b \lg \sigma_0 \, . \tag{4}$$

Figure 7 plots equation 4. Based on data obtained for the studied polymers, we may assert that polyphenylacetylenes also have a "compensation effect", with a coefficient $a = 1.25$ eV.

This phenomenon is also met with in polymers having no conjugated bonds in the main chain. The difference is that in this case coefficient a of equation (4) has higher values than in conjugated polymers.

In some authors' opinion, the compensation effect gives some indications as to the relatively reduced size of conjugated spectra.[14]

---

[13] T. Lixandru, S. Dumitrescu, F. Deneș, B. Simionescu and M. Vîță, *Revue générale des Caoutchoucs et Plastiques*, **2**, 193 (1971).

[14] * * * "Organicheskie poluprovodniki ", Ed. Nauka, Moscow, 1968.

This hypothesis seems to be corroborated by the fact that ohmic resistance — which is also a function of the size of the conjugated system, in the case of polymers with a compensation effect, is characterized by high values.

CONCLUSIONS

1. From ESR spectra of polyphenylacetylenes there appears that while the narrow signal is a characteristic of the molecule, the broad spectrum is an attribute of ordered zones whose unpaired electrons are characterized by advanced collectivization. Broad spectra are, as a rule, specific of polymers with double conjugated bonds, containing in their molecules either heteroatoms, or metal atoms, or electron-donor or electron-acceptor groups.

The interaction between unpaired electrons and the molecules of Cl and N atoms results in a hyperfine structure in the case of polymers P-*p*-NPhA-i.s.f. and P-*p*-ClPhA-i.ins.f.

2. Data on the electric conductivity of polyphenylacetylenes contribute to setting forth hypotheses related to their structure. In this connection, we consider that polyphenylacetylenes have conjugated domains of low size, inferior to the size specific of linear chains. This accounts for the capacity of polyphenylacetylenes to form supramolecular structures of a globular type.[15]

3. The possible reticulation of polyphenylacetylenes leads to the solubility loss and to the extension on the conjugated domains determining an increase of the electric conductivity.

4. The introduction of the $-CH_3$ and $-Cl$ groups in the benzene ring of polyacetylene determines a decrease of electric conductivity, while the presence of the $-NO_2$ group in the same position (*para*), results in its increase with 12—14 orders of magnitude.

---

[15] Cr. Simionescu, S. Dumitrescu, M. Leancă, M. Grovu and M. Dărîngă, *Rev. Roumaine Chim.*, **17**, 303 (1972).

Revue Roumaine de Chimie, **20**, *8*, 1167−1182 (1975)

LA DÉGRADATION DES ÉCHANGEURS D'ANIONS DANS DES MILIEUX AGRESSIFS. II *

L'ACTION DE L'EAU OXYGÉNÉE EN PRÉSENCE DU $CuSO_4$ SUR LES ÉCHANGEURS D'ANIONS CONTENANT DES GROUPES QUATERNAIRES D'AMMONIUM DE TYPE II

I. PETRARIU, PAMFILIA PETRARIU, FL. POPESCU et STELA DRĂGAN
Institut de Chimie Macromoléculaire « Petru Poni », Jassy, 41 A
Aleea Gr. Ghica Vodă

Reçu le 18 mai 1974

On a étudié la stabilité chimique d'un échangeur d'anions contenant des groupes quaternaires d'ammonium de type II-chlorure de poly(vinylbenzylediméthyle-2-hydroxyéthylammonium) forme Cl^- et OH^- dans l'eau oxygénée 30% en présence ou en l'absence du $CuSO_4$ à 20−80°. Le changement de la nature des groupes ionogènes de l'anionite, en fonction des conditions de dégradation a été étudié par l'analyse élémentaire, la variation de la capacité d'échange, l'étude des spectres IR et l'analyse thermique.

Chaque fois qu'on utilise un échangeur d'anions fortement basique, il est nécessaire que la température de travail soit plus basse que 50°. Au-dessus de cette température, la majorité des échangeurs d'anions commencent à se dégrader.

La dégradation peut être influencée par l'utilisation d'une solution alcaline concentrée ou d'une solution oxydante. Les variations brusques du pH, les absorptions irréversibles des substances organiques pendant l'utilisation et l'exploitation des échangeurs d'anions à des températures plus élevées influencent aussi la dégradation.

En fonction de la force d'action de ces facteurs, ont lieu des modifications qualitatives et quantitatives auxquelles participent les groupements fonctionnels et aussi le squelette macromoléculaire de l'échangeur d'anions.

Les données de la littérature de spécialité relatives à la stabilité chimique des échangeurs d'anions fortement basiques de type II dans des milieux oxydants ou sous l'action de l'oxygène de l'air sont peu nombreuses. [1−5]

---

* La partie antérieure est la réf. 8.

[1] L. Wirth, *Combustion*, **25**, 49 (1954).

[2] N. W. Frisch et R. Kunin, *Ind. Eng. Chem.*, **49**, 1365 (1957).

[3] L. F. Wirth, Jr. C. A. Feldt et K. Odland, *Ing. Eng. Chem.*, **53**, 638 (1961).

[4] R. Kunin et N. W. Frisch, *Ind. Eng. Chem.*, **49**, 1365 (1957).

[5] I. Petrariu, O. Petreuş, A. Carpov, C. Luca et M. Dima, *Rev. Chim. (Bucureşti)*, **22**, 177 (1971).

Dans le présent travail on expose quelques considérations sur la stabilité chimique des échangeurs d'anions gel, de type II dans l'eau oxygénée en présence ou en l'absence du $CuSO_4$.

Les conditions concernant la synthèse de l'échangeur d'anions contenant des groupes fortement basiques de type II sont données dans un travail antérieur. [6]

LA MÉTHODE D'EXPERIMENTATION

Une partie des épreuves d'anionite soumises à la dégradation a été transformée sous forme Cl et une autre partie sous forme OH.

La dégradation a été effectuée dans un ballon de 50 ml muni d'un réfrigérant ascendant dans lequel on a introduit 1 g anionite et 10 ml H_2O_2 ayant une concentration comprise entre 10–30%. La réaction de dégradation a eu lieu à la température ambiante, à la lumière ou dans l'obscurité, dans un intervalle de temps variant de 10 à 576 h. Pour un nombre restreint d'épreuves la dégradation s'est effectuée dans les mêmes conditions à la différence que le milieu agressif a été cette fois-ci le mélange H_2O_2 30%+0,0188 g $CuSO_4.5H_2O$.

La concentration des solutions de H_2O_2 a été déterminée par titrage avec du $KMnO_4$.

Dans une autre série d'expériences, la température de dégradation a oscillé de 40 à 80°, le milieu agressif étant, suivant le cas, le H_2O_2 30% ou le mélange H_2O_2 30% + 0,0188 g $CuSO_4 \cdot 5H_2O$.

Après dégradation, les perles d'anionite ont été introduites dans les colonnettes à fritte. Ici une partie des épreuves ont été transformées en forme Cl, avec de l'acide chlorhydrique 4% et ensuite lavées jusqu'à neutralité à du méthanol tandis qu'une autre partie a été convertie en forme OH^- avec du NaOH 4% et lavée jusqu'à neutralité à de l'eau distillée, soumise à l'ébullition et refroidie dans une installation protégée pour éviter l'absorption du CO_2 de l'atmosphère.

Finalement on a déterminé la capacité d'échange fortement basique (C_{pb}) et faiblement basique (C_{sb}) et de leur somme on a calculé la capacité totale résiduelle (C_t).

Les coefficients de basicité K_b et K'_b, ainsi que la perte de la capacité d'échange due à la réaction de désamination et de désalcoylation ont été calculés d'après une méthodologie indiquée dans un travail antérieur. [8]

Tableau 1

Caractéristiques physico-chimiques de l'échangeur d'anions de type II

Caractéristiques	Unité de mesure	Valeur
Groupement fonctionnel	$-N(CH_3)_2C_2H_4OH^+$	
Support polymérique	styrène-divinylbenzène gel	
Forme ionique d'expérimentation	Cl et OH	0,4–0,8
Granulation	mm	740
Poids volumétrique (humidité 12,4%)	kg/m³	0–14
Domaine de pH		
Contenu total en azote déterminé par analyse élémentaire	N%	4,7
Capacité d'échange totale calculée d'après le contenu en azote	meq/g	3,35
Capacité d'échange totale déterminée par la méthode dynamique	meq/g	3,25
a. Capacité d'échange fortement basique	meq/g	2,10
b. Capacité d'échange faiblement basique	meq/g	1,15
Température maximale d'utilisation	t^0	50

L'analyse spectrale en IR a été effectuée avec un spectrophotomètre SP-200 et l'analyse thermogravimétrique avec un dérivatographe Pauling-Erdey en présence de l'air, avec une vitesse d'échauffement de 9,8/mn.

Les caractéristiques physico-chimiques des échangeurs d'anions fortement basiques de type II soumises à la dégradation sont données dans le tableau 1.

RÉSULTATS ET DISCUSSION

On connaît que, dans la majorité des cas, les échangeurs d'anions fortement basiques de type II contiennent une quantité quelconque de groupes faiblement basiques, donc ils ne sont pas monofonctionnels. Cela signifie qu'il existe dans la structure de l'échangeur des positions plus stables (les groupes faiblement basiques) et moins stables (les groupes, fortement basiques). Vu la stabilité chimique différente de ces groupes, leur cinétique de décomposition sera différenciée, les groupes fortement basiques se dégradant au commencement du processus dans une proportion plus grande, période pendant laquelle le C_{pb} baisse et le C_{sb} croît.

On connaît aussi que les milieux oxydants sont considérés comme les plus agréssifs pour la vie d'un échangeur d'anions, en spécial quand celui-ci possède des groupes d'échange fortement basiques.

Si dans la structure des échangeurs d'anions sont englobées des traces des métaux, provenant du processus industriel de synthèse ou si ceux-ci se trouvent dans le milieu agressif dans lequel l'anionite fonctionne, la stabilité chimique des échangeurs d'anions est en grande partie affectée.[9-11]

Du fait que le milieu de dégradation utilisé par les auteurs est l'eau oxygénée, sa décomposition sera catalysée par la lumière, la température, le $CuSO_4$, la forme ionique de l'échangeur d'anions, etc. l'oxygène résulté agit tant sur le squelette macromoléculaire que sur les groupes fortement basiques. À la suite de ce processus la stabilité chimique et physique de l'échangeur d'anions baisse.

Duke et Haas [12] ont montré que les solutions aqueuses de KOH ont un rôle catalytique important dans la décomposition de l'eau oxygénée. Dans la première phase l'OH favorise la dissociation du H_2O_2 avec formation de l'ion HO_2^-. Le mécanisme de la décomposition de H_2O_2 d'après les auteurs cités et aussi d'après d'autres indications [13-14] dépend de l'interréaction de l'ion dissocié HO_2^- avec les molécules non dissociées ayant comme suite la formation d'un complexe intermédiaire $H_3O_4^-$ qui peut se décomposer avec libération d'oxygène, d'ions OH^- et de molécules d'eau.

---

[6] I. PETRARIU, C. LUCA et M. DIMA, *Rev. Chim. (București)*, **10**, 576 (1968).

[7] J. STAMBERG et F. IURACICA, *Zhur. prikland. Khim.*, **35**, 2295 (1962).

[8] I. PETRARIU, P. PETRARIU, FL. POPESCU et C. LUCA, *Rev. Roumaine Chim.*, **20**, 839 (1975).

[9] R. KUNIN et N. V. FRISCH, *Ind. Eng. Chem.*, **49**, 1365 (1957).

[10] T. MIZUNO, *Nippon Kagau Zasshi*, **69**, 1254 (1966).

[11] Z. VASICEK, Thèse Académie Tchécoslovaque des Sciences, Prague, 1968.

[12] F. R. DUKE et T. W. HAAS. *J. Phys. Chem.*, **65**, 304 (1961).

[13] E. KOUBEK, M. L. HAGGETT, C. J. BATTAGLIA, K. M. IBNE-RASA, H. Y. PYUN et J. O. EDWARDS, *J. Amer. Chem. Soc.*, **85**, 2263 (1963).

[14] R. N. SMITH, A. J. MILES et S. F. WATKINS, *Trans. Faraday Soc.*, **62**, 2553 (1966).

Schématiquement, le mécanisme proposé sera le suivant :

$$H_2O_2 + OH^- \rightarrow H_2O + HO_2^- \quad I$$

$$H_2O_2 + HO_2^- \rightarrow H_3O_4^-$$

$$H_3O_4^- \rightarrow H_2O + O_2 + OH^- \quad II$$

En partant de ces considérations, Bichikov et collab. [15] arrivent à la conclusion que la forme OH^- des anionites fortement basiques peut jouer elle-même un rôle catalytique envers la décomposition de l'eau oxygénée. On conclut donc que les échangeurs d'anions fortement basiques retiennent le H_2O_2 par un processus physique mais aussi par la voie de l'échange ionique sous forme de HO_2^-.

Bien sûr que, dans le cas de l'utilisation dans le milieu de dégradation, des sels inorganiques, comme par exemple le $CuSO_4$, ceux-ci catalyseront la décomposition du complexe $H_3O_4^-$ et accélereront la dégradation de l'anionite.

Dans quelques travaux antérieurs [5,16] on a poursuivi l'identification des produits de dégradation résultés à la suite du traitement d'un échangeur d'anions fortement basique de type II avec des milieux fortement agressifs de type NaOH et HNO_3. Dans ces conditions on a montré que, en principal, a lieu une réaction de désamination (Δz) avec scission du groupe fonctionnel par exemple de la diméthyléthanolamine. Sur la chaîne macromoléculaire restent des groupes inactifs du point de vue de l'échange ionique d'alcool polybenzylique.

Cette réaction conduit au brusque abaissement du C_{pb}, respectivement du C_t.

Simultanément une réaction de désalcoylation (Δal) a aussi lieu, à la suite de laquelle il résulte du CH_3OH et aussi du $HOCH_2CH_2OH$, sur le squelette macromoléculaire restant des groupes faiblement basiques, capables d'échange ionique de type poly(vinylbenzyldiméthylamine) ou poly(benzylméthylethanolamine).

Ces réactions conduisent à la baisse du C_{pb} simultanément avec la croissance du C_{sb}, donc à la suite de cette réaction l'anionite devient polyfonctionnel.

Le milieu oxydant utilisé, $H_2O_2 + CuSO_4$ représentant un agent fortement agressif, les produits résultés à la suite de la dégradation sont plus nombreux et leur identification est assez difficile.

Dans la majorité des cas, ces produits ont été mis en évidence par analyses IR et les résultats obtenus ont été comparés avec les bandes d'absorption obtenues par d'autres auteurs qui ont étudié les spectres IR pour les échangeurs des anions fortement basiques de type I[17–20] ou de types I et II[18-20] et aussi avec des spectres des composés organiques de petit poids moléculaire contenant des groupes semblables[19-20] avec les anionites dégradés ou non dégradés étudiés.

---

[15] H. V. Bichicov, A. I. Kasperovichi et B. G. Roginscaya, *Zhur. fiz. Khim.*, **43**, 2522 (1969).

[16] I. Petrariu, S. Drăgan et P. Petrariu, *Rev. Chim. (București)*, **21**, 207 (1970).

[17] A. Strasheim et K. Buijs, *Spectrochim. Acta*, **17**, 388 (1961).

[18] D. Whittington et J. R. Millar, *J. Appl. Chem.*, **18**, 122 (1968).

[19] Z. Vasicek, J. Klaban et J. Stamberg, *Coll. Czech. Chem. Comm.*, **36**, 1825 (1971).

[20] J. Klaban et V. Rádl, *Chem. prumysl*, **21**, 445 (1971).

En comparant les données obtenues il résulte qu'une partie des groupes CH_2OH de l'alcool polyvinylbenzylique ont été oxydés, avec formation des groupes CHO et COOH. L'édifice macromoléculaire a été affecté aussi, en spécial le carbone tertiaire de la chaîne polyvinylique, avec formation des groupes $-CH_2-\overset{|}{C}(OH)-$.

En partant des études laborieuses et de grand intêret entreprises par Vasicek et ses collaborateurs [4, 19, 21] sur des composés ayant un petit poids moleculaire et sur des anionites fortement basiques de type I dégradés dans des solutions alcalines dans une atmosphère d'oxygène, ainsi que des résultats obtenus par les auteurs du presént travail [5,16] qui ont soumis a dégradation dans des milieux alcalins et oxydants les échangeurs d'anions de type II on propose le schéma suivant:

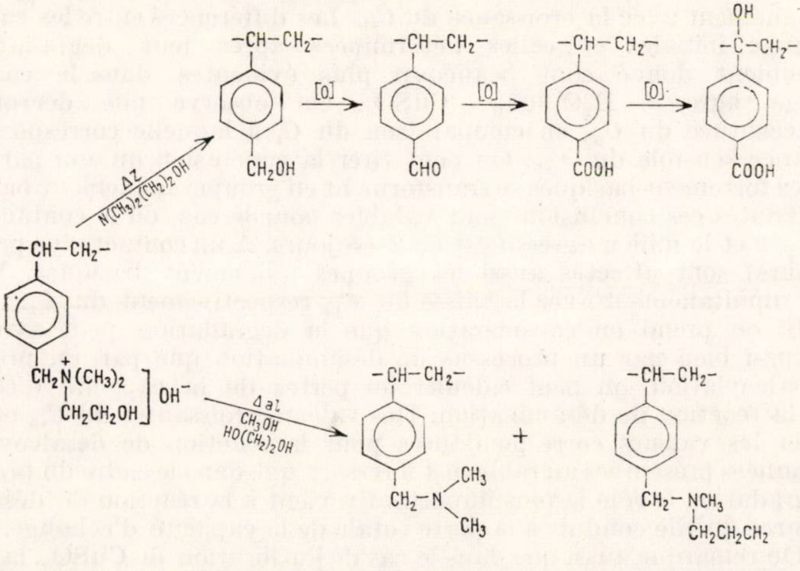

Des données présentées dans le tableau 2 on constate que l'anionite sous forme Cl^-, est suffisamment stable dans le H_2O_2 même quand sa concentration et son temps de contact prennent des valeurs relativement grandes.

On observe aussi que les valeurs qui expriment la dégradation de l'anionite en présence du $CuSO_4$ sont presque 2 fois plus grandes en comparaison de celles qui indiquent la dégradation en son absence. Ce fait dénote que le $CuSO_4$ est un catalyseur efficient pour le H_2O_2 et en conséquence, sa présence dans un milieu oxydant de type H_2O_2 dans lequel un anionite peut être obligé de fonctionner doit être évitée.

---

[21] Z. Vasicek, J. Stamberg et O. Dufka, *Coll. Czech. Chem. Comm.*, **36**, 1817 (1971).

Tableau 2

Dégradation de l'échangeur d'anions fortement basique de type II (forme Cl^-), à la lumière et à la température ambiante, en présence ou en l'absence du $CuSO_4$

Concentration H_2O_2 %	Durée de la dégradation heures	K % en l'absence du $CuSO_4$	K % en présence du $CuSO_4$
20	24	4,09	7,86
20	96	4,72	—
30	24	4,15	9,75

Dans le tableau 3 sont présentés les résultats obtenus à la suite de la dégradation de l'anionite sous forme Cl à la température ambiante et dans l'obscurité, en 30% H_2O_2 en présence, ou en l'absence du $CuSO_4$.

Des données obtenues on remarque la diminution du C_{pb} et C_t simultanément avec la croissance du C_{sb}. Les différences entre les capacités d'échange initiales et celles déterminées après leur dégradation à un moment donné sont beaucoup plus évidentes dans le cas d'un lange agressif $H_2O_2$30 % + $CuSO_4$. On observe une décroissance s accentuée du C_{pb} en comparaison du C_t à laquelle correspond une issance sensible du C_{sb}. On peut tirer la conclusion qu'une partie des upes fortement basiques se transforment en groupes faiblement basiques.

Toutes ces conclusions sont valables pour le cas où le contact entre nionite et le milieu agressif est de 2—8 jours. À un contact plus prolongé (24 jours) sont affectés aussi les groupes faiblement basiques. Le C_{sb} baisse simultanément avec la baisse du C_{pb} respectivement du C_t.

Si on prend en considération que la dégradation peut avoir lieu tout aussi bien par un processus de désamination que par un processus de désalcoylation, on peut calculer les pertes de la capacité d'échange due à la réaction de désamination. Des valeurs croissantes du C_{sb} on peut calculer les valeurs correspondantes pour la réaction de désalcoylation. Des données présentées au tableau 4 il ressort que dans le cadre du processus de dégradation le rôle le plus important revient à la réaction de désamination parce qu'elle conduit à la perte totale de la capacité d'échange.

On remarque aussi que dans le cas de l'utilisation du $CuSO_4$, la dégradation de l'anionite par le processus de désamination a lieu dans la plus grande proportion, la cinétique de la dégradation étant déterminée par le temps de contact. La réaction de désalcoylation est dans une plus petite mesure affectée par le temps de contact (jusqu'à 8 jours). En cas de l'utilisation seulement de l'eau oxygénée comme agent agressif, l'abaissement de la capacité d'échange de l'anionite causé par le désalcoylation prend des valeurs non significatives.

Dans la figure 1 sont représentées les pertes pourcentuelles de la capacité d'échange fortement basique et totale. On remarque que le temps de contact entre l'anionite et le milieu agressif joue un rôle décisif en ce qui concerne la stabilité chimique des groupes basiques.

La présence du $CuSO_4$ accélère dans une grande mesure le processus de dégradation. On observe qu'après 8 jours de contact, les valeurs C_{pb} et C_t baissent dans le cas de la dégradation de l'anionite dans H_2O_2 30%

Tableau 3

Dégradation de l'échangeur d'anions fortement basique de type II (forme Cl), à la température ambiante et à l'obscurité

Durée de la dégradation jours	Capacité d'échange résiduelle meq/g					
	en H_2O_2 30 %			en H_2O_2 30%+$CuSO_4$		
	C_{sb}	C_{pb}	C_t	C_{sb}	C_{pb}	C_t
—	1,15*	2,10*	3,25*	1,15*	2,10*	3,25*
2	1,19	2,02	3,21	1,21	1,70	2,91
8	1,20	1,95	3,15	1,38	0,34	1,72
24	0,80	1,90	2,70	0,40	0,03	0,43

* Les valeurs de la capacité d'échange initiale de l'anionite non dégradé.

Tableau 4

Dégradation de l'échangeur d'anions fortement basique de type II (forme OH), par la réaction de désamination (Δ_z) et désalcoylation (Δ_{al}).

Durée de la dégradation jours	Pertes de la capacité d'échange par rapport aux anionites initiaux ; meq/g					
	H_2O_2 30%			H_2O_2 30% + $CuSO_4$		
	C_{pb}	Δz	Δal	C_{pb}	Δz	Δal
2	0,08	0,04	0,04	0,40	0,34	0,06
8	0,15	0,10	0,05	1,76	1,53	0,23

seulement avec 3—7% (courbes *3* et *4*). L'utilisation d'un agent comme par exemple le $CuSO_4$, melangé à l'eau oxygénée, conduit dans le même intervalle de temps à une baisse prononcée aussi pour le C_{pb} (83,8% fig. 1, courbe *1*) que pour le C_t (47% fig. 1 courbe *2*).

On remarque aussi que, la cinétique de la dégradation des groupes fortement basique en présence du $CuSO_4$ est beaucoup plus accentuée les 8 premiers jours (fig. 1, courbe *1*). En prolongeant le temps de contact, l'abaissement du C_{pb} est réalisé dans une proportion beaucoup plus réduite, tandis que le C_t continue de baisser significativement (fig. 1, courbes *1* et *2*).

Compte tenu que dans le cadre du processus de dégradation ont lieu des transformations chimiques importantes au niveau des groupes basiques, la basicité de l'anionite change chaque instant à la suite de l'interréaction avec l'agent agressif.

Dans la figure 2 on a mis en évidence l'évolution des coefficients de basicité K_b et K_b' en fonction de la durée de contact. L'allure des courbes 1 et 2 révèle que les groupes basiques ne subissent pas des modifications importantes au contact avec le H_2O_2 30%. Si dans le milieu de dégradation on introduit aussi du $CuSO_4$, on constate des transformations radicales au niveau des groupes fortement basiques, par la réaction de désamination et de désalcoylation (fig. 2, courbes *3* et *4*).

On connaît que la vitesse de décomposition de l'eau oxygénée est influencée par les dimensions de la granule d'anionite, de sa forme ionique, de la concentration de l'eau oxygénée, du temps de contact entre l'agent agressif et l'anionite ainsi que par la température. [15]

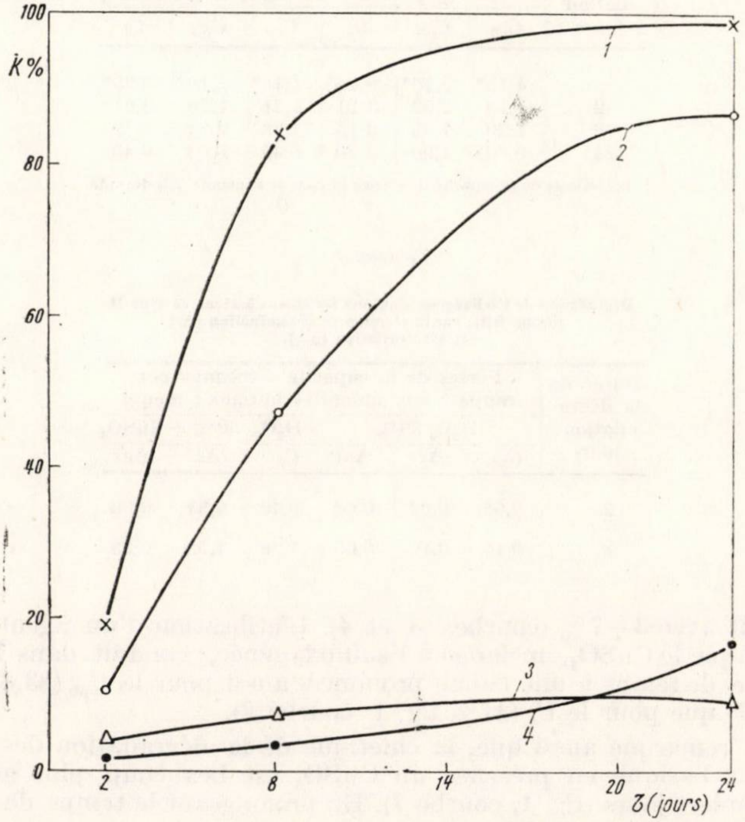

Fig. 1. — Dépendance du degré de conversion K des groupes basiques de l'anionite sous forme Cl^-, du temps de contact avec le milieu de dégradation. Conditions de la réaction : température ambiante et à l'obscurité. *1* et *3* = C_{pb} ; *2* et *4* = C_t ; *1* et *2* = H_2O_2 30% + $CuSO_4$; *3* et *4* = H_2O_2 30%.

En tenant compte de toutes ces constatations, dans une autre série d'expérimentations on a étudié les pertes de la capacité d'échange en fonction de la température de dégradation et de la forme ionique de l'anionite (tableau 5).

Des données obtenues on constate que l'effet thermique joue un rôle très important dans la définition de la stabilité chimique d'un échangeur d'anions. On constate ainsi qu'il suffit d'élever la température de dégradation à 40° (en utilisant comme milieu agressif H_2O_2 30% + $+CuSO_4$) pour que le C_{pb} baisse à environ 1/2 de sa valeur initiale. D'ici la conclusion que, la présence des métaux dans les milieux agressifs oxydants de type eau oxygénée met en danger l'activité d'un anionite même à 40°, température à laquelle n'importe quel anionite doit fonctionner avec le maximum d'efficacité.

Dans des mêmes conditions à 60° a lieu une dégradation, totale au niveau des groupes ionigènes. À 80° le réseau macromoléculaire subit des destructions profondes, l'anionite se solubilisant dans le milieu de dégradation. Si la dégradation de l'anionite se réalise seulement dans l'eau oxygénée, la baisse de la capacité d'échange en fonction de la température a lieu dans une proportion beaucoup plus petite.

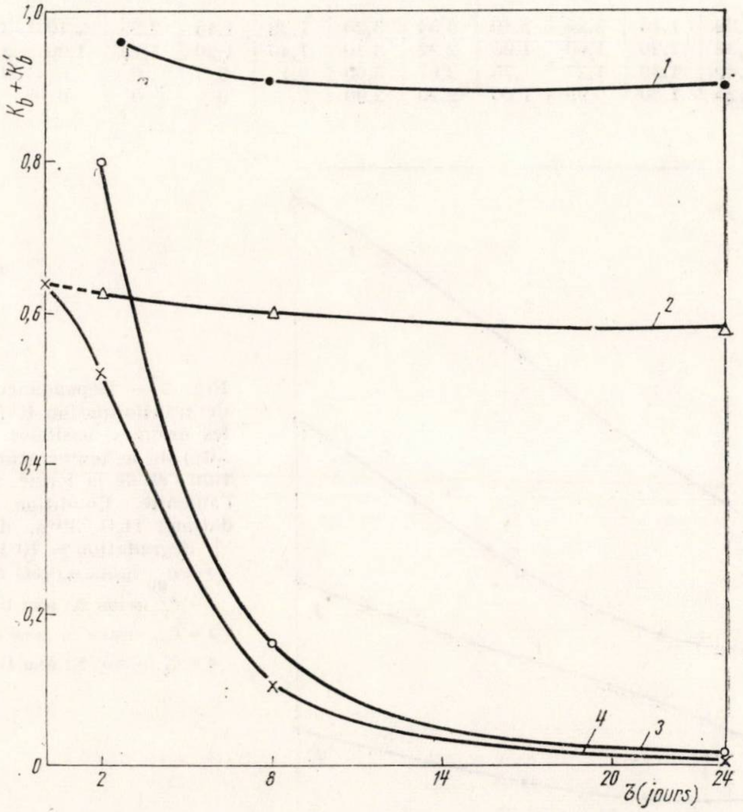

Fig. 2. — Variation des coefficients de basicité K_b et K'_b en fonction de la durée de dégradation. Conditions de la dégradation : température ambiante et à l'obscurité.

2 et 4 = K_D ; 1 et 3 = K'_D ; 1 et 2 = H_2O_2 30 % ; 3 et 4 = H_2O_2 30% + $CuSO_4$.

Pour une meilleure mise en évidence de l'influence de la forme ionique de l'échangeur d'anions sur la stabilité chimique on a représenté dans la figure 3 les valeurs pourcentuelles du degré de transformation K, en fonction de la température de dégradation pour le cas où on utilise le milieu agressif H_2O_2 30%. On observe que le C_{pb} est aussi dans ce cas le plus fortement affecté par l'effet thermique en comparaison du C_t.

Tableau 5

Dégradation des échangeurs d'anions fortement basiques de type II (forme Cl− et OH−) à différentes températures. Durée de dégradation 10 heures

Température de dégradation	Capacité d'échange résiduelle (meq/g)											
	Dans le H_2O_2 30%						Dans le H_2O_2 30% + $CuSO_4$					
	C_{sb}		C_{pb}		C_t		C_{sb}		C_{pb}		C_t	
t°	OH	Cl	OH	Cl	OH	Cl	OH	Cl	OH	Cl	OH	Cl
—	1,29	1,15	2,25	2,10	3,54	3,25	1,29	1,15	2,25	2,10	3,54	3,25
40	1,32	1,20	1,60	1,90	2,92	3,10	1,40	1,20	1,15	1,00	2,55	2,20
60	1,40	1,30	1,27	1,75	2,67	3,05	0,1	0	0	0	0,1	0
80	1,25	1,30	0,95	1,60	2,20	2,90	0	0	0	0	0	0

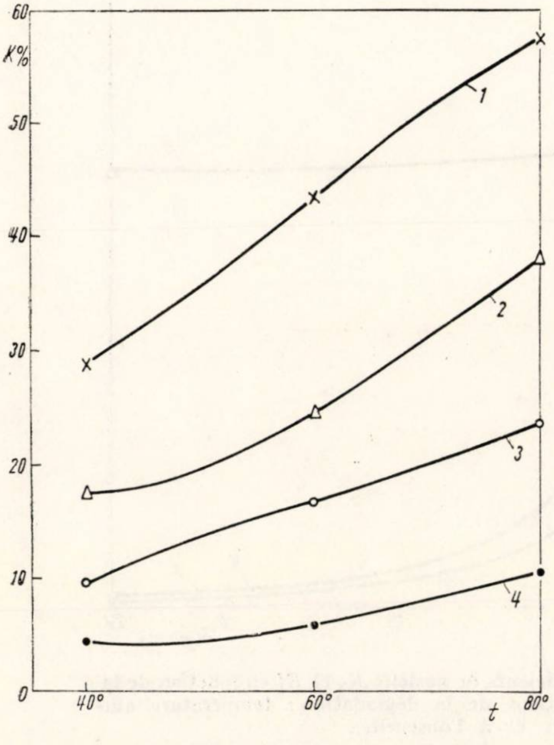

Fig. 3. — Dépendance du degré de transformation K (concernant les groupes basiques de l'anionite) de la température de réaction et de la forme ionique de l'anionite. Condition de dégradation : H_2O_2 30%, durée de la dégradation = 10 heures.

1 = C_{pb} (pertes %) pour la forme Cl−

2 = C_t (pertes %) pour la forme OH−

3 = C_{pb} (pertes %) pour la forme Cl−

4 = C_t (pertes %) pour la forme OH−

Aussi la forme ionique joue un rôle important dans la détermination de la stabilité chimique de l'anionite. Ainsi, les valeurs C_{pb} exprimées en forme Cl^- (courbe *3*) indiquent une stabilité beaucoup plus foarte en comparaison de la forme OH^- (courbe *1*). Les même notations peuvent être remarquées aussi pour le C_t (fig. 3, courbe *2* et *4*).

Ces constatations peuvent être expliquées en partant des travaux du Bichikov et collab. [15] qui ont établi que, l'eau oxygénée est absorbée par l'anionite, à la place de l'eau existante qui est éliminée. On arrive à une forte concentration en H_2O_2 dans la granule de l'anionite. Cela est possible parce que le dipôle moment du H_2O_2 (2,2 D) est plus grand que celui correspondant à la molécule d'eau (1,8 D).

En prenant aussi en considération les études entreprises par Smith et ses collaborateurs [14] qui se sont occupés de la décomposition de l'eau oxygénée dans le milieu basique, en présence du carbone on peut arriver à la conclusion que la formation du complexe $H_3O_4^-$ dans l'anionite a lieu quand on atteint une haute concentration dans l'ion HO_2^- et que la forme OH de l'anionite fortement basique décompose le complexe intermédiaire formé, beaucoup plus vite que la forme Cl^-.

Dans le tableau 6 sont présentés les résultats de la dégradation de l'anionite par les deux mécanismes possibles de désamination et de désalcoylation. On constate des différences essentielles entre les pertes de capacité dues à la réaction de désamination par rapport à la réaction de désalcoylation.

L'anionite subit des dégradations beaucoup plus prononcées à cause du mécanisme de désamination, par rapport à celui de désalcoylation.

Tableau 6

Dégradation de l'échangeur d'anions fortement basique de type II par la réaction de désamination et de désalcoylation, en fonction de la forme ionique et de la température. Durée de la dégradation : 10 heures. Milieu de dégradation H_2O_2 30%

Température de dégradation t°	Forme ionique	Pertes de la capacité d'échange par rapport à l'anionite initial (meq/g).	
		Désamination	Désalcoylation
40	OH	0,62	0,03
	Cl	0,15	0,05
60	OH	0,87	0,11
	Cl	0,20	0,15
80	OH	1,34	—
	Cl	0,35	0,15

Le coefficient de basicité de la figure 4 indique que l'effet thermique a un rôle important dans la modification de la composition des groupes basiques, la forme OH^- étant beaucoup plus exposée à ces transformations (fig. 4, courbe *2*) en comparaison de la forme Cl^- (fig. 4, courbe *1*).

En soumettant à la dégradation l'anionite fortement basique sous forme Cl^- et OH^- à différentes températures, dans un milieu agressif beaucoup plus énergique, H_2O_2 30% + $CuSO_4$) et exprimant en pour cent les valeurs du degré de conversion K, des groupes basiques, on constate des données du tableau 7 que la forme OH^- de l'anionite est plus stable, que la forme Cl^-. C'est ainsi qu'à 40° on constate une perte en C_{pb} pour la forme OH^- de 48,8%, tandis que pour la forme Cl on arrive

Tableau 7

Le degré de conversion K des groupes basiques de l'anionite fortement basique de type II en fonction de la forme ionique et de la température. Durée de la dégradation 10 heures. Milieu de dégradation : H_2O_2 30 % + $CuSO_4$

Température de dégradation $t°$	K %			
	C_{pb}		C_t	
	OH	Cl	OH	Cl
40	48,88	52,38	27,96	32,30
60	100	100	97,17	100
80	100	100	100	100

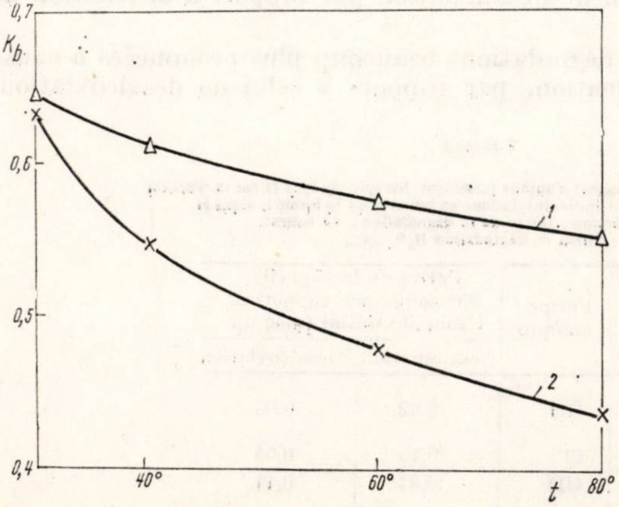

Fig. 4. — Variation du coefficient de basicité K_b en fonction de la température et de la forme ionique de l'anionite. Conditions de dégradation : H_2O_2 30 %, durée de dégradation 10 heures.

1 = anionite sous forme Cl^- ; 2 = anionite sous forme OH^-.

à une perte de 52,38 %. À 60° les groupes fortement basiques sont totalement décomposées, indifféremment de la forme ionique.

Dans le but d'obtenir des informations plus complètes concernant les transformations chimiques qui ont lieu dans les groupes basiques de l'anionite, mais aussi dans sa structure tridimensionnelle, les épreuves soumises à l'action du H_2O_2 30 % + $CuSO_4$ à 40° ont été analysées par la méthode de la spectroscopie en infrarouge. Les bandes obtenues ont été comparées avec celles indiquées par la littérature. [17-20] (tabl. 8).

L'étude du comportement thermique des produits dégradés comparativement aux produits non dégradés a indiqué que les courbes de perte en poids (TG), présentent des modifications relativement réduites (fig. 5).

La thermostabilité est plus basse aux épreuves dégradées et les inflexions des courbes subissent des déplacements vers des températures plus petites (fig. 5, courbes *2* et *3*).

Les dérivées de la courbe TG (le DTG), permettent une exploration plus complète des modifications qui ont lieu à l'élévation de la température.

Tableau 8

Positions des bandes d'absorption, pour l'échangeur d'anions fortement basique de type II, non dégradé avec du H_2O_2 30% + $CuSO_4$ à la température de 40°

A	B	Attribution des bandes d'absorption	Littérature
702	702	C–H* du benzène monosubstitué	17
763		C–H* du benzène monosubstitué et *o*-disubstitué	17
828		C–H* du benzène *p*-disubstitué	17
902		$-N^+(CH_3)_2CH_2CH_2OH$	18
	945	O–H* du groupe –COOH	
1082	1090	O–H du groupe $-N(CH_3)_2CH_2CH_2OH$	19
	1145	Oxydation du carbone tertiare des chaînes latérales de	18
		polyvinyle	19
	1186	C–N des groupes benzyldiméthylamine	19
1380		C–H du groupe $N-CH_3$	17
1425		C–H du groupement $-CH_2-$	
1448		C=C** du noyau benzénique et C–H* des groupes	17,19
		CH_2 et CH_3	17
1507		C=C** du noyau benzénique	17,19
1570		$-COO^-$	17
1608	C=C**	du noyau benzénique	17
	1698	C=O*** des groupes –COO ou –CHO formés à la suite de	
		l'oxydation de l'anionite	19
2922		C–H*** du CH_2	19
3320		O–H du groupe $-N(CH_3)_2CH_2CH_2OH$	20

* Vibration de déformation en dehors du plan.
** Vibration de déformation coplanaire.
*** Vibration de valence.

Dans les figures 6 et 7 sont donnés des exemples des courbes DTG pour la forme Cl^- (fig. 6) et la forme OH^- (fig. 7).

L'anionite de type II, forme Cl^- ou OH^-, présente sur les courbes DTG quatre processus distincts, qui sont situés autour des températures de 100° (processus I), 220–260° (processus II), 400–420° (processus III), et 540–560° (processus IV).

Dans le cas de la forme Cl^-, on constate que les processus I et IV ne subissent pas des modifications essentielles, en fonction du mode de conduite de la dégradation dans les milieux agressifs.

Le processus III présente dans le cas du composé non dégradé la vitesse de réaction la plus élevée, la vitesse de pointe étant située à 420° (fig. 6).

Pour les épreuves dégradées en présence du catalyseur et à 40°, les processus II et III indiqués sur la courbe DTG sont plus fortement modifiés, que dans le cas des dégradations effectuées en l'absence du $CuSO_4$ et à la température de 80° (fig. 6, courbe *2*).

La vitesse de processus III de l'anionite (forme Cl^- ou OH^-) décroît avec la croissance de la température de dégradation, les variations les plus grandes étant mises en évidence dans le cas de la forme Cl^- dégradée. Les vitesses deviennent plus petites que la vitesse du processus II (fig. 7, courbes *2* et *3*).

Les modifications plus petites, des courbes DTG signalées dans le cas des processus I–IV de la forme OH^-, s'expliquent par le fait que la forme Cl^- est susceptible de produire des processus plus compliqués de dégradation.

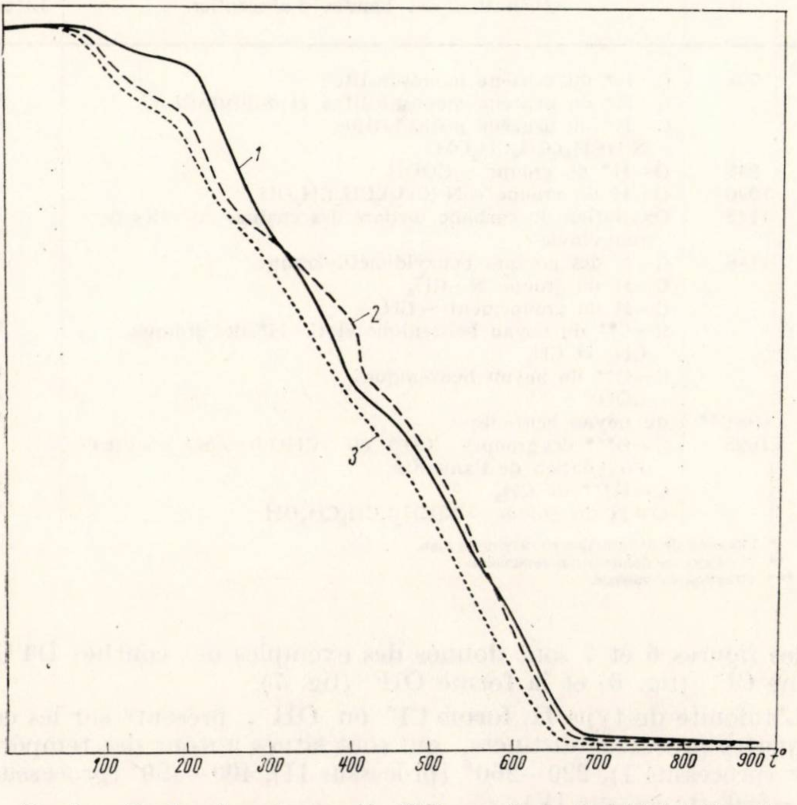

Fig. 5. — Courbes de perte en poids (TG) pour l'anionite initial et dégradé.

1, anionite initial sous forme Cl; *2*, anionite sous forme OH dégradé en présence de H_2O_2 30% + $CuSO_4$ à 40°; *3*, anionite sous forme Cl dégradé en présence de H_2O_2 30% + $CuSO_4$ à 40°.

Les processus II et III de la forme Cl^-, non dégradée sont en réalité des superpositions de deux processus distincts. Après la dégradation ces superpositions disparaissent (fig. 6).

Les énergies d'activation des processus I–IV ont été calculées des courbes DTG. On constate que (tableau 9), les énergies d'activation pour le processus IV sont plus petites que celle de processus III, fait qui permet la supposition que le processus IV a lieu autocatalytiquement, à cause des composés de l'azote, formés pendant le chauffage des produits.

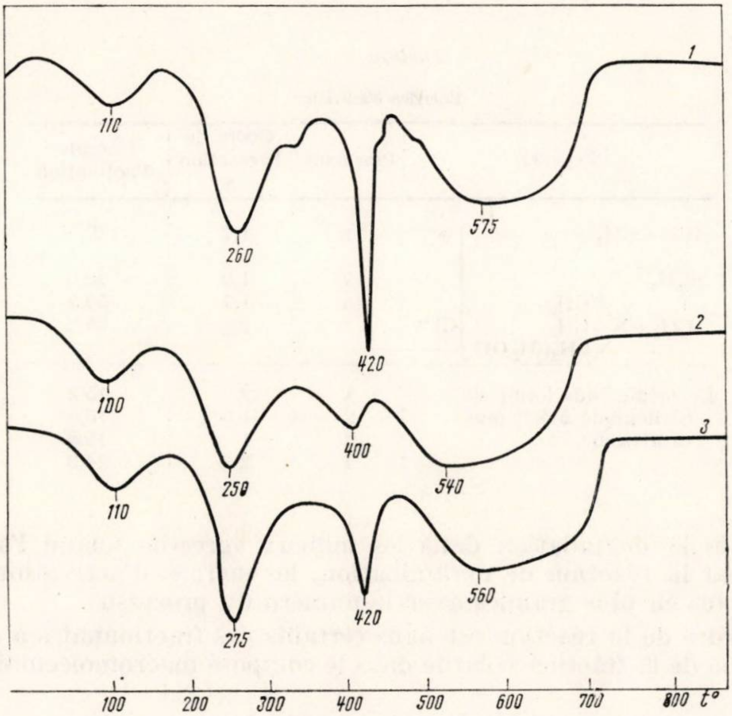

Fig. 6. — Courbes DTG pour la forme Cl de l'anionite.

1, non dégradé ; *2*, dégradé à 40° en présence de l'H_2O_2 30% + $CuSO_4$; *3*, dégradé à 80° en présence de l'H_2O_2 30%.

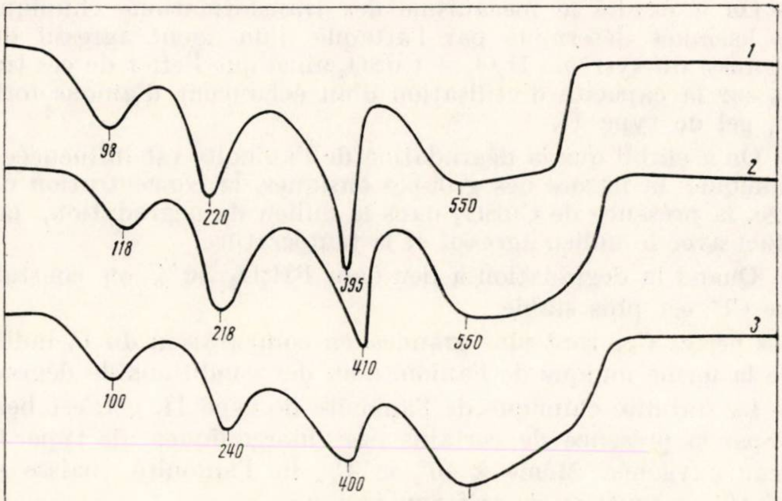

Fig. 7. — Courbes DTG, pour la forme ROH de l'anionite dégradé en présence de l'H_2O_2 30% + $CuSO_4$.

1, dégradé à 40° ; *2*, dégradé à 60° ; *3*, dégradé à 80°.

Tableau 9

Énergies d'activation

Type II	Processus	Ordre de la réaction n	Energie d'activation
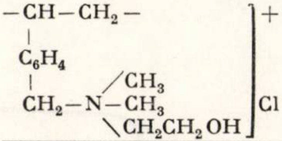 $[-CH(C_6H_4CH_2N(CH_3)_2CH_2CH_2OH)-CH_2-]^+ Cl^-$	1	1,7	140
	2	1,9	20,0
	3	1,7	50,2
	4	2	39,2
Le même sous forme de Cl dégradé à 80° sans catalyseur	1	2	15,2
	2	1,5	16,0
	3	1	18,6
	4	2	34,3

Après la dégradation dans les milieux agressifs quand l'azote est éliminé par la réaction de désamination, les énergies d'activation deviennent de plus en plus grandes avec le numéro du processus.

L'ordre de la réaction est dans certains cas fractionnaire à cause de la diffusion de la fraction volatile dans le composé macromoléculaire.

CONCLUSIONS

— On a étudié le mécanisme des transformations chimiques des groupes basiques déterminé par l'attaque d'un agent agressif de type H_2O_2 et aussi du système $H_2O_2 + CuSO_4$ ainsi que l'effet de ces transformations sur la capacité d'utilisation d'un échangeur d'anions fortement basique, gel de type II.

— On a établi que la dégradation de l'anionite est influencée par la forme ionique, la nature des groupes basiques, la concentration de l'eau oxygénée, la présence de $CuSO_4$ dans le milieu de dégradation, la durée du contact avec le milieu agressif et la température.

— Quand la dégradation a lieu dans l'H_2O_2 30% on constate que la forme Cl^- est plus stable.

Les pertes C_{pb} sont plus grandes, en comparaison du C_t indifféremment de la forme ionique de l'anionite ou des conditions de dégradation.

— La stabilité chimique de l'anionite de type II, gel, est beaucoup affectée par la présence de certains sels inorganiques de type $CuSO_4$, dans l'eau oxygénée. Même à 40°, le C_{pb} de l'anionite baisse jusqu'à 40,8–52,4% en fonction de sa forme ionique.

— L'analyse thermique a mis en évidence des modifications de la courbe DTG dues au processus de dégradation. Les produits qui ont perdu l'azote pendant le processus de dégradation présentent une croissance régulière des énergies d'activation.

Revue Roumaine de Chimie, **20**, 8, 1183–1189 (1975)

LA GÉNÉRALISATION DES VALEURS DE LA VOLATILITÉ RELATIVE OBTENUES PAR LA MÉTHODE CHROMATOGRAPHIQUE

F.A. GOTHARD, T. PÎRVUȚOIU et ELENA CONSTANTIN
Institut PETROCHIM de Ploiești, 291, Bulevardul Republicii

Reçu le 21 septembre 1973
Complété le 1er mars 1975

On présente une méthode pour généraliser la variation de la volatilité relative des constituants légers non polaires qui se trouvent dans la solution concentrée d'un solvant polaire, à partir des volatilités relatives à dilution infinie et une seule valeur à une concentration finie quelconque du solvant, obtenues par les méthodes chromatographiques. L'application de la méthode pour les systèmes formés par les hydrocarbures à cinq atomes de carbone et de la diméthylformamide, donne une bonne concordance avec les valeurs obtenues par les études d'équilibre liquide — vapeur. Les différences des paramètres, représentant les logarithmes des coefficients d'activité du solvant en dilution infinie dans les constituants plus volatils, sont proportionnelles aux différences des logarithmes des coefficients d'activité à dilution infinie des constituants plus volatils dans le solvant, propriété qui peut offrir les possibilités d'estimer les volatilités relatives en connaissant une seule valeur à concentration finie.

La méthode chromatographique pour obtenir les valeurs des volatilités relatives est appliquée fréquemment aux systèmes binaires formés par des constituants volatils en solution des solvants avec points d'ébullition plus élevés. L'intérêt particulier de cette méthode, bien connue, [1-3] s'explique par sa rapidité et la possibilité d'obtenir les données nécessaires pour la mise au point des procédés de séparation par distillation extractive, ou la sélection des solvants, simultanément pour tous les composants d'un mélange, sans leur séparation et purification.

Dans une étude antérieure [4] on avait déjà analysé les possibilités d'estimation des volatilités relatives à dilution infine à l'aide d'une méthode basée sur l'hypothèse que les paramètres des équations des coefficients d'activité de type Margules pour les systèmes solvant polaire (s) — solvé non polaire (i), sont des fonctions symétriques de la température

---

[1] M. R. Shester et S. M. Marchello, *Petrol. Refiner*, **42**, 99 (1963).

[2] P. E. Porter, C. H. Deal et F. H. Stross, *J. Amer. Chem. Soc.*, **78**, 2999 (1956).

[3] S. I. Pavlov, S. P. Pavlova, L. A. Serafimov et L. I. Kofman, *Izvest. Vys. Ucheb. Zaved Khim. i Khim. Tehnol.*, **8**, 126 (1968).

[4] D. Breban et F. Gothard, *Rev. Chim.* (*București*), **23**, 749 (1972).

absolue, donc $A_{is}(T) = A_{si}(T)$. Cette nouvelle symétrie des paramètres Margules conduit, en tenant compte de la variation des chaleurs de mélange avec la température, aux valeurs des coefficients d'activité à dilution infinie du solvant.

On présentera ci-après une autre méthode pour obtenir les coefficients d'activité et les volatilités relatives à dilutions finies, à partir de deux valeurs de la volatilité relative, l'une à dilution infinie, et l'autre à une composition quelconque.

Si la variation des coefficients d'activité avec la composition du mélange, formée par les composants i et j, plus volatils, et du solvant s, peut être décrite par les équations de type Margules, on peut écrire aussi :

$$\lg\gamma_i = x_s^2\,[A_{is} + 2x_i(A_{si} - A_{is})] \tag{1}$$

$$\lg\gamma_j = x_s^2\,[A_{js} + 2x_j(A_{sj} - A_{js})] \tag{2}$$

Pour obtenir la volatilité relative des constituants (i) et (j) à la dilution finie dans la solution du solvant (s) et à une température donnée, où les pressions de saturation des composants (i) et (j) sont P_i^s et P_j^s,

$$\alpha_{(ij)s} = \frac{P_i^s \cdot \gamma_{is}}{P_j^s \cdot \gamma_{js}}, \quad \text{c'est-à-dire } \lg\alpha_{(ij)s} = \lg\frac{P_i^s}{P_j^s} + \lg\frac{\gamma_{is}}{\gamma_{js}} \tag{3}$$

on peut substituer le lg $(\gamma_{is}/\gamma_{js})$ par la différence des équations (1) et (2). Si on néglige les effets ternaires sur la volatilité relative $\alpha_{(ij)s}$, une approximation possible au moins dans le domaine des solutions concentrées de solvant, on obtient :

$$\lg\frac{\gamma_{is}}{\gamma_{js}} = x_s^2[(A_{is} - A_{js}) + 2x_i\,(A_{si} - A_{is}) - 2x_j\,(A_{sj} - A_{js})] \tag{4}$$

Une conséquence de la même approximation est qu'on peut remplacer $x_i + x_j = 1 - x_s$, donc

$$\lg\frac{\gamma_{is}}{\gamma_{js}} = x_s^2\,\{(A_{is} - A_{js}) + 2(1 - x_2)\,[A_{si} - A_{sj} - (A_{is} - A_{js})]\} \tag{5}$$

La différence $A_{is} - A_{js}$ est exprimée par les valeurs des coefficients d'activité à dilution infinie γ_{is}^0 et γ_{js}^0 dans le solvant (s) :

$$A_{is} - A_{js} = \lg\frac{\gamma_{is}^0}{\gamma_{js}^0} \tag{6}$$

Le terme $A_{si} - A_{sj}$ peut être obtenu si on connaît le rapport des coefficients d'activité à une concentration quelconque du solvant, x_s^*, noté par $(\gamma_i/\gamma_j)_{x_s^*}$, à partir de la forme modifiée de l'équation (5) :

$$A_{si} - A_{sj} = \frac{\dfrac{\lg\left(\dfrac{\gamma_i}{\gamma_j}\right)_{x_s^*}}{x_s^{*2}} - (A_{is} - A_{js})}{2\,(1 - x)_s^*} + A_{is} - A_{js} \qquad (7)$$

En substituant la valeur $A_{si} - A_{sj}$ obtenue, dans l'équation (5), on obtient :

$$\lg \frac{\gamma_{is}}{\gamma_{js}} = x_s^2 \left\{ A_{is} - A_{js} + \frac{1 - x_s}{1 - x_s^*} \left[\frac{\left(\lg \dfrac{\gamma_i}{\gamma_j}\right)_{x_s^*}}{x_s^*} - (A_{is} - A_{js}) \right] \right\} \qquad (8)$$

L'application de la méthode proposée pour calculer la variation de la volatilité relative des hydrocarbures en solutions de solvants polaires est illustrée en utilisant les valeurs données pour les hydrocarbures à cinq atomes de carbone en solutions de diméthylformamide, par Pavlov et al.[5] Le rapport des coefficients d'activité calculé à l'aide de l'équation (8) et les valeurs publiées à dilution infinie en diméthylformamide et en solution de 75% en solvant ont été multipliés par le rapport des pressions de vapeur P_j^s / P_i^s extraites de la même publication.[5] Les valeurs obtenues sont reproduites dans le tableau 1.

Dans la figure 1 on a représenté la variation des volatilités relatives des hydrocarbures de la fraction 26—45° rapportée à la volatilité de l'isoprène, calculée par l'équation (8). Pour comparaison, on a représenté aussi les valeurs de la volatilité relative de l'isoprène et du 2-méthyl-butène-2, selon les données expérimentales de Ogorodnikov et al.,[6] en solutions de diméthylformamide. La concordance avec les valeurs obtenues à partir des données de Pavlov et al.[5] peut être considérée comme satisfaisante.

Dans le tableau 2, on a reproduit les valeurs $A_{is} - A_{js}$ et les valeurs $A_{si} - A_{sj}$ calculées à partir des volatilités relatives à dilution infinie et à la concentration de 75% diméthylformamide.

On observe une proportionnalité de ces deux différences pour tous les systèmes binaires, ainsi qu'on peut écrire les données inscrites aux tableaux 1, 2.

---

[5] S. I. Pavlov, L. A. Bolkhova, B. A. Saraev, D. A. Karpacheva et V. N. Korotkova, *Khim. Prom.*, **4**, 256 (1971).

[6] S. K. Ogorodnikov, V. V. Kogan et M. S. Nemtsov, *Zhur. priklad. Khim.*, **11**, 2441 (1961).

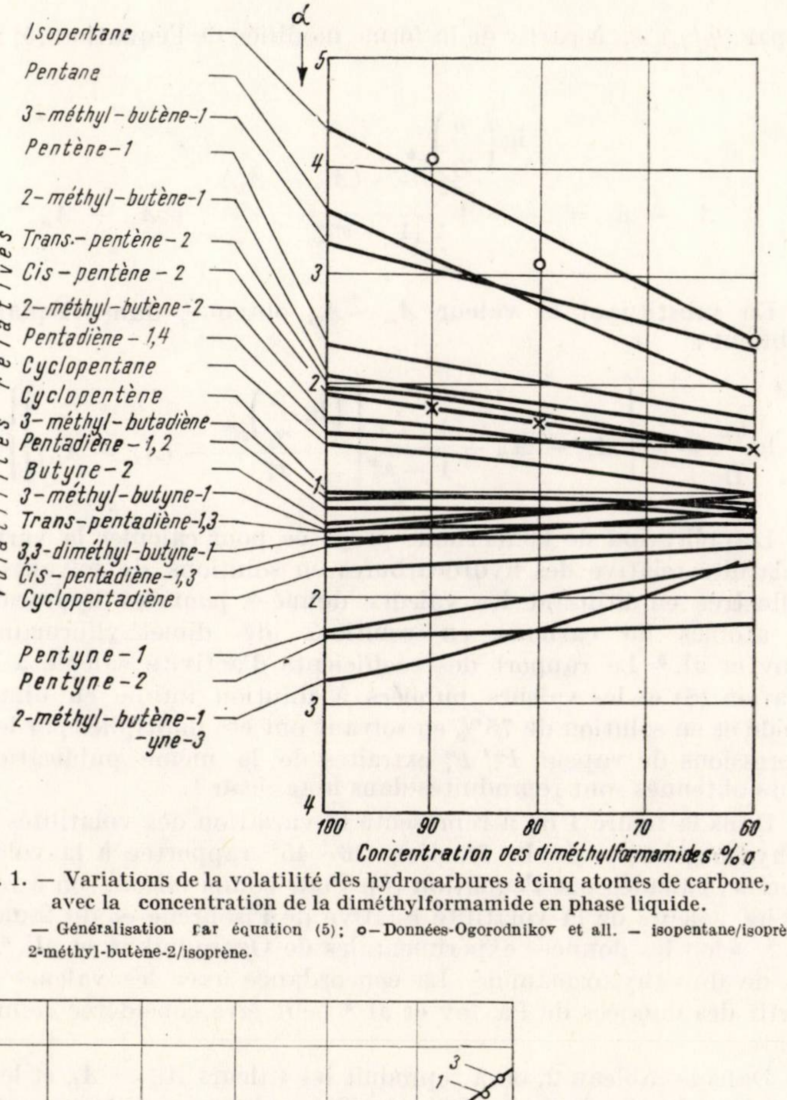

Fig. 1. — Variations de la volatilité des hydrocarbures à cinq atomes de carbone, avec la concentration de la diméthylformamide en phase liquide.

— Généralisation par équation (5); o — Données-Ogorodnikov et all. — isopentane/isoprène; × — 2-méthyl-butène-2/isoprène.

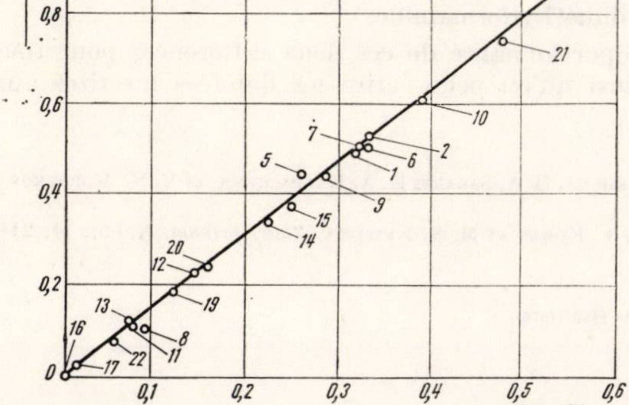

Fig. 2. — Variation des valeurs $A_{si} - A_{sj}$ avec $A_{is} - A_{js}$ pour les hydrocarbures de la fraction 26—45° en solution de diméthylformamide.

Tableau 1

Valeurs γ_{is}/γ_{js} et $\alpha_{(ij)s}$ publiées par S. I. Pavlov* et calculées par généralisation (équation(5), constituant j = isoprène)

Diméthylformamide %			100*		90		75*		60	
i	Constituant	P_i/P_j	$\frac{\gamma_{is}^0}{\gamma_{js}^0}$	$\alpha_{(ij)s}$	$\frac{\gamma_{is}}{\gamma_{js}}$	$\alpha_{(ij)s}$	$\frac{\gamma_{is}}{\gamma_{js}}$	$\alpha_{(ij)s}$	$\frac{\gamma_{is}}{\gamma_{js}}$	$\alpha_{(ij)s}$
1	Isopentane	1,200	3,700	4,440	3,524	4,229	2,594	3,113	2,001	2,401
2	3-méthyl-butène-1	1,530	2,150	3,300	1,999	3,058	1,746	2,680	1,500	2,295
3	Pentane	0,935	3,848	3,595	3,387	3,167	2,667	2,494	2,041	1,908
4	Pentène-1	1,135	2,080	2,360	1,942	2,204	1,706	1,963	1,550	1,759
5	2-méthyl-butène-1	1,100	1,830	2,070	3,354	1,924	1,585	1,746	1,407	1,547
6	*Trans*-pentène-2	0,930	2,145	1,995	1,984	1,845	1,726	1,605	1,484	1,380
7	*Cis*-pentène-2	0,913	2,091	1,910	1,952	1,782	1,714	1,565	1,481	1,352
8	Pentadiène 1,4	1,295	1,200	1,540	1,172	1,518	1,130	1,465	1,090	1,412
9	2-méthyl-butène-2	0,867	1,930	1,670	1,812	1,571	1,611	1,396	1,414	1,226
10	Cyclopentane	0,610	2,435	1,485	2,239	1,366	1,912	1,166	1,631	0,995
11	3-méthyl-butadiène-1,2	0,833	1,194	0,999	1,171	0,975	1,132	0,952	1,093	0,910
12	Cyclopentène	0,719	1,390	1,000	1,347	0,968	1,271	0,914	1,191	0,856
13	Pentadiène-1,2	0,708	1,191	0,844	1,173	0,830	1,138	0,805	1,099	0,778
j	(constituant *i* = isoprène)									
14	Butyne-2	0,775	1,667	1,290	1,583	1,228	1,445	1,120	1,305	1,011
15	3-méthyl-butyne-1	0,763	1,755	1,340	1,665	1,270	1,507	1,150	1,348	1,029
16	*Trans*-pentadiène-1,3	1,291	1,022	1,321	1,022	1,319	1,018	1,311	1,013	1,308
17	*Cis*-pentadiène-1,3	1,380	1,038	1,430	1,034	1,427	1,027	1,415	1,019	1,406
18	3,3-diméthyl-butène-1	1,069	1,330	1,418	1,295	1,384	1,230	1,312	1,162	1,242
19	Cyclopentadiène	1,250	1,442	1,780	1,391	1,738	1,302	1,605	1,211	1,514
20	Pentyne-1	1,190	1,914	2,280	1,823	2,169	1,640	1,914	1,442	1,716
21	2-méthyl-butène-1-yne-3	0,952	2,985	2,840	2,687	2,557	2,210	2,110	2,458	2,340
22	Pentyne-2	2,080	1,135	2,360	1,121	2,332	1,095	2,278	1,067	2,219

CONCLUSIONS

1. La variation de la volatilité relative pour les couples de constituants légers en fonction de la concentration d'un solvant, peut être calculée dans tout le domaine des concentrations du solvant utilisé en distillation extractive, à partir de deux valeurs de la volatilité relative, une à dilution infinie, l'autre à une concentration quelconque. L'équation proposée pour généraliser les données chromatographiques néglige les effets ternaires et ne peut rendre compte de l'influence de la compositon du mélange des hydrocarbures sur la volatilité relative.

2. On a trouvé que les différences des paramètres de l'équation Margules $A_{si} - A_{sj}$, représentant les logarithmes des coefficients d'activité du solvant en dilution infinie dans les constituants plus volatils (i) et (j), sont proportionnelles aux différences des paramètres $A_{is} - A_{js}$,

Tableau 2

Valeurs des paramètres en équation (5) pour les systèmes d'hydrocarbures à 5 atomes de carbone et diméthylformamide

i	Constituant (*j*) = isoprène	$A_{is}-A_{js}$	$A_{si}-A_{sj}$	C
1	Isopentane	0,5682	0,90368	1,59042
2	3-méthyl-butène-1	0,3324	0,5281	1,5888
3	Pentane	0,5852	0,9295	1,5884
4	Pentène-1	0,3181	0,5073	1,5948
5	2-méthyl-butène-1	0,2625	0,4488	1,7098
6	*Trans*-pentène-2	0,3314	0,5114	1,5432
7	*Cis*-pentène-2	0,3204	0,5117	1,5971
8	Pentadiène-1,4	0,0792	0,1095	1,3826
9	2-méthyl-butène-2	0,2856	0,4508	1,5784
10	Cyclopentane	0,3865	0,6144	1,589635
11	3-méthyl-butadiène-1,2	0,0770	0,1145	1,4872
12	Cyclopentène	0,1430	0,2273	1,5895
13	Pentadiène-1,2	0,0759	0,1237	1,6298
j	Constituant (*i*) = isoprène			
14	Butyne-2	0,2219	0,3465	1,5615
15	3-méthyl-butyne-1	0,2443	0,3890	1,5923
16	*Trans*-pentadiène-1,3	0,0095	0,0182	1,9158
17	*Cis*-pentadiène-1,3	0,0162	0,0249	1,5370
18	3,3-diméthyl-butyne-1	0,1248	0,1958	1,5689
19	Cyclopentadiène	0,1590	0,2485	1,5629
20	Pentyne-1	0,2819	0,4819	1,7094
21	2-méthyl-butène-1-yne-3	0,4749	0,7495	1,57822
22	Pentyne-1	0,0550	0,0851	1,5472

les logarithmes des coefficients d'activité des constituants (*i*) et (*j*) à dilution infinie dans le solvant (*s*), et que pour les hydrocarbures à cinq atomes de carbone en diméthylformamide

$$\frac{A_{si} - A_{sj}}{A_{is} - A_{js}} = 1{,}596$$

Cette propriété peut offrir une possibilité à estimer les volatilités relatives dans les systèmes formés des hydrocarbures et les solvants polaires, en connaissant les volatilités relatives à dilution infinie pour tous les constituants et encore une volatilité relative à dilution finie pour un seul constituant du mélange à séparer, nécessaire pour calculer la constante C.

$$\frac{A_{si} - A_{sj}}{A_{is} - A_{js}} = C \tag{9}$$

Par la méthode des moindres carrés on a obtenu pour la constante de proportionnalité C 1,596 avec un écart moyen carré 0,012. Ainsi cette constante peut être considérée comme une caractéristique des systèmes formés par les hydrocarbures à cinq atomes de carbone et isoprène en diméthylformamide.

NOTATIONS

A_{is}, A_{si} — Paramètres Margules ($= \lg\gamma_i^0$ et $\lg \gamma_s^0$) pour le système binaire : constituant (*i*)— solvant (*s*).
A_{js}, A_{sj} — Paramètres Margules ($= \lg\gamma_j^0$ et $\lg\gamma_s^0$) pour le système binaire : constituant (*j*) — solvant (*s*).
C — constante définie par l'équation (8).
x_i, x_j, x_s — concentrations des constituants (*i*), (*j*) et du solvant, fractions molaires.
γ_{is}, γ_{js} — coefficients d'activité des constituants (*i*) et (*j*) dans le ternaire *i, s, j*.
γ_i, γ_j — coefficients d'activité des constituants (*i*) et (*j*) dans les binaires formés avec le solvant.
$\alpha_{(ij)s}$ — volatilité relative *i*/*j* dans le ternaire.
P_i, P_j — pressions de vapeur des constituants (*i*) et (*j*), mm. Hg.
Avec ° on a noté les valeurs γ à dilution infinie.

CRISTOFOR SIMIONESCU, VIORICA RUSAN, VALENTIN POPA *"Sea weeds chemistry"*
Ed. Academiei, Bucharest, 1974

Finding new sources of raw materials and making the best use of them is a major problem of investigation the world over, today. Sea resources have always drawn the attention of researchers. Consequently, a vast programme of sub-marine studies and systematic investigations is being developed for detecting new sources of food and energy required by the steady population increase. The weeds represent one of the main inexhaustible sea sources of raw material owing to their rapid multiplication both under natural conditions and in culture media.

Formerly, Assians used weeds as food, fodder, and natural fertilizers for poor soils. Later on, weeds like Varech, Baril and Kelp were used as raw materials to extract salts containing iodine, sodium and potash.

The present botanical, chemical and biochemical investigations conducted on sea weeds established the existence of a very high polysaccharide content, based on alginic acid and its salts Agar and Carageen. These polysaccharides may be successfully used in different branches e.g chemical and food industry, cosmetics, pharmaceutics, textiles a.s.o.

The book (the first of its kind in this country) is intended to draw the attention of specialists to the possibilities of turning to account the large quantities of weeds existing in the Black Sea. With this aim in view the authors made a logical systematization and scientific presentation of a comprehensive bibliographical material in the world literature including also the authors' original investigations. The book contains six large chapters. The first chapter presents the botanics and biogeography of sea weeds, their chemical composition as well as their collection and storage. The second chapter gives a detailed description of weeds processing methods of obtaining polysaccharides. In chapter three, the structures of polyoses based on alginic acid as structural unit are critically approached and biosynthesis of polysaccharides in sea weeds discussed. Chapter four presents the properties and chemical changes of alginic polyoses. Chapter five deals with the interdependence between the structures and properties of the main polysaccharides extracted from sea weeds. The concluding chapter of the book reveals some areas in which sea weeds and their components are used as well as the part played by the weeds in sea ecology.

The material included in this book is presented in a clear and concise manner with tables and diagrams wherever necessary. Concrete and updated information, valuable for chemists, biochemists and engineers working in industrial units or research institutes as well as for professors and students of chemistry and biochemistry, is provided.

D. Ciomârtan

NOTE POUR LES AUTEURS

La *Revue Roumaine de Chimie* publie des articles en anglais, français, russe, allemand ou espagnol. Les auteurs sont priés d'envoyer des articles, notes, communications et comptes rendus inédits.

Les manuscrits seront dactylographiés à deux intervalles. Les tableaux seront dactylographiés sur feuilles séparées, de même que la légende des figures. Les diagrammes seront tracés à l'encre de Chine sur papier calque. Les tableaux et les figures seront numérotés par des chiffres arabes, en nombre strictement nécessaire. Prière de ne pas inscrire les mêmes données dans les tableaux et les figures. Les formules chimiques seront incluses dans le texte ; en outre, elles seront transcrites sur des feuilles séparées. Les auteurs sont priés d'indiquer les caractères italiques (en soulignant les lettres au crayon), ainsi que tout autre caractère spécial. L'ordre des références bibliographiques sera celui de leur mention dans le texte ; le nom de l'auteur sera précédé de l'initiale du prénom ; les publications périodiques seront présentées suivant les prescriptions internationales. Les références seront ajoutées à la fin de l'article ; elles paraîtront comme des notes, au bas de la page. Le texte sera précédé d'un résumé comprenant 15 lignes au maximum.

L'entière responsabilité du contenu des articles appartient aux auteurs. On publie des articles dus aux collaborateurs roumains ou étrangers.

PRINTED IN ROMANIA

TRAVAUX PARUS AUX ÉDITIONS DE L'ACADÉMIE DE LA RÉPUBLIQUE SOCIALISTE DE ROUMANIE

I. ZUGRĂVESCU et MAGDA PETROVANU, **Chimia N-Ilidelor** (La chimie des N-Ylures,) 1974, 347 p., 19 lei.

MARGARETA AVRAM, **Antidăunători** (Pesticides), 1974, 494 p., 41 lei.

CR. SIMIONESCU, VIORICA RUSAN et N. POPA, **Chimia algelor marine** (La chimie des algues marines), 1974, 211 p., 18 lei.

CRISTOFOR SIMIONESCU, MARGARETA GRIGORAȘ, AGATA CERNĂTESCU-ASANDEI et GHEORGHE ROZMARIN, **Chimia lemnului din România — plopul și salcia** (La chimie du bois en Roumanie — le peuplier et le saule), 1973, 228 p., 28 lei.

TIBERIU NĂȘCUȚIU, **Metode radiochimice de analiză** (Méthodes radiochimiques d'analyse), 1973, 384 p., 23 lei.

MARIA FITI, **Dozimetria chimică a radiațiilor ionizante** (La dosimétrie chimique des radiations ionisantes), 1973, 240 p., 13,60 lei.

MIHAI FLORESCU, **Eficiența economică a cercetării științifice** (L'efficience économique de la recherche scientifique), 1972, 115 p., 15 lei.

GEORGETA LĂZĂRESCU, **Sistematizarea informațiilor în Chimia organică** (La systématisation des informations dans la Chimie organique), 1972, 252 p., 10,15 lei.

P. BALTĂ et E. BALTĂ, **Introducere în chimia fizică a stării vitroase** (Introduction à la chimie physique de l'état vitreux), 1971, 240 p., 15,50 lei.

LYDIA-MARIA VAICUM, **Biodegrabilitatea detergenților** (La biodégrabilité des détergents), 1971, 254 p., 16 lei.

I. ZUGRĂVESCU et L. STOICESCU-CRIVETZ, **Polimeri heterociclici** (Polymères hétérocycliques), 1971, 190 p., 9,50 lei.

I. MAXIM, **Materiale nucleare** (Matériaux nucléaires), 1969, 444 p., 30 lei.

CRISTOFOR SIMIONESCU et CLEOPATRA VASILIU-OPREA, **Mecanochimia compușilor macromoleculari** (La mécanochimie des composés macromoléculaires), 1967, 344 p., 23,50 lei.

CORNEL BODEA et collab., **Tratat de biochimie vegetală**, partea I, **Fitochimie** (Traité de biochimie végétale, Ier partie, Phytochimie), Ier vol., 1964, 747 p. + 4 annexes + 2 pl., 41 lei ; IIe vol., 1965, 1262 p., 1 pl., 56 lei ; IIIe vol., 1967, 773 p., 35 lei.

I. P. I. – c. 287

43 426

Lei 25. –

1976 MAR 15

F 1103

R

REFERÁLVA

ACADÉMIE DE LA RÉPUBLIQUE SOCIALISTE DE ROUMANIE

REVUE ROUMAINE DE CHIMIE

TOME 20

N° 9—10

Septembre—Octobre 1975

RECHAX, **20**, 9—10, 1193 — 1356 (1975)

EDITURA ACADEMIEI REPUBLICII SOCIALISTE ROMÂNIA

Rev. Roumaine Chim. **20**, 9—10, **p. 1193 — 1356 (1975)**, Bucarest

ACADÉMIE DE LA RÉPUBLIQUE SOCIALISTE DE ROUMANIE

COMITÉ DE RÉDACTION

Rédacteur en chef:

I. G. MURGULESCU, membre de l'Académie de la République Socialiste de Roumanie

Rédacteurs en chef adjoints:

A. T. BALABAN et V. EM. SAHINI, membres correspondants de l'Académie de la République Socialiste de Roumanie

Collège de rédaction:

EM. BRATU, ELENA CEAUŞESCU, ECATERINA CIORĂNESCU-NENITZESCU, C. DRĂGULESCU, RALUCA RIPAN, CR. SIMIONESCU, membres de l'Académie de la République Socialiste de Roumanie; P. SPACU, membre correspondant de l'Académie de la République Socialiste de Roumanie; MARGARETA AVRAM, D. I. MARCHIDAN, G. NIAC et D. SĂNDULESCU

Toute commande de l'étranger pour les travaux parus aux Editions de l'Académie de la République Socialiste de Roumanie sera adressée à ILEXIM, Serviciul Export-Import Carte (livres) / Serviciul Export-Import Presă (revues), P.O. Box 2001, 64 — 66 Calea Griviței, Bucarest 12, Roumanie

Les manuscrits, les livres et les revues proposés en échange, ainsi que toute correspondance seront envoyés à la rédaction

REVUE ROUMAINE DE CHIMIE

23, str. Dumbrava Roşie, Bucarest, Roumanie, téléphone 12 41 60

EDITURA ACADEMIEI REPUBLICII SOCIALISTE ROMÂNIA

125, Calea Victoriei, Bucarest, Roumanie, téléphone 13 94 40

ORSZ. MŰSZ. KÖNYVTÁR ÉS DOKUMENTÁCIÓS KÖZPONT

REVUE ROUMAINE DE CHIMIE

Tome 20, N° 9–10 Septembre-Octobre 1975

I. G. MURGULESCU and J. PĂUN, The radiolysis of the complex oxalates in aqueous solutions. VI. Kinetics and mechanism of the radiolysis of Fe(III)-trisoxalato-complex in aqueous solution 1195–1203

MARIANA CIUREANU and V. E. SAHINI, On the electronic structure of n-σ complexes. I. Iodine complexes with heteroaromatic donors 1205–1212

LILIANA CIUREA, The ESR spectra of the acenaphthenone reduction products 1213–1217

H. CĂLDĂRARU and M. MORARU, An electron spin resonance proof of chair-boat conformation of the iminoxy radical of endo-3-carbometoxybicyclo-[3.3.1] nonan-9-one oxime 1219–1220

RODICA VÎLCU and FLORICA IRINEI, Thermodynamic excess functions in electrolyte solutions. Excess free energy of ternary solutions from interferometric measurements 1221–1225

D. I. MARCHIDAN and LIANA PANDELE, Thermal properties of $BaCl_2$ high temperature heat content 1227–1230

S. STERNBERG and VALERIA PETRESCU, The chronopotentiometric study in the molten system $AgCl + KCl +$(dissolved) Cl_2 1231–1241

W. SMITH and D.W. CLACK, Angular dependence of overlap for *s, p, d* and *f* functions 1243–1252

M. I. VASS and CR. CONȚESCU, FEM study of silver layers adsorbed on tungsten. I. Work function and surface migration 1253–1265

GH. C. CONSTANTINESCU, Die Reaktionen zwischen $H[AuCl_4]^-$ und dem in *orto*-substituierten Malachitgrün 1267–1277

LUCIA IORDĂCHESCU, N. CALU et E. NEGURĂ, Étude polarographique de quelques complexes de cobalt (III)-diméthylglyoxime 1279–1285

C. CRISTESCU, *AS*-Triazine derivatives with potential therapeutic action. XIV. A simplified synthesis of 2′, 3′, 5′-tri-O-benzoyl-β-D-ribofuranosyl-6-azauracils-5-substituted *via* 2,4-bis-(trimethylsilyloxy)-derivatives 1287–1293

S. C. BENNUR, V. B. JIGAJINNI and V. V. BADIGER, 1-substituted alkylamino-3-(4-quinazolyloxy)-2-propanol trihydrochlorides and 1-substituted alkylamino-3-(8-quinolyloxy)-2-propanol dihydrochlorides 1295–1299

T. R. BALASUBRAMANIAN and N. VENKATASUBRAMANIAN, Oxidation of alicyclic alcohols by cerium (IV) perchlorate 1301–1310

R IG. C. POINESCU, STELA DRĂGAN, STELIANA MAXIM et M. DIMA, Préparation des copolymères ternaires macroporeux 1311–1317

Rev. Roumaine Chim. **20,** *9–10*, p. 1193–1356 (1975), Bucarest

ДИМЧО И. ДИМИТРОВ, ВАСИЛ, З. АНГЕЛОВ и АНЧО Ц. БАДЕВ, Закономерности процесса жидкофазного окисления ненасыщенных соединений в присутствии борных добавок 1319–1328

EMILIA CONSTANTIN et J. CH. ABBE, Sur les réactions entre les ions CH_3^+ et CD_2H^+ avec CH_4 et CD_4 1329–1334

I. MOŢOC, Le système R/S—un point de vue mathématique. I. L'énoncé invariantif des concepts de la stéréochimie 1335–1340

I. MOŢOC, Le système R/S—un point de vue mathématique. II. Définition algébrique pour le rang d'un ligand dans une séquence 1341–1343

J. PRASHAD, Studies of the Joshi effect in pure argon in a degased quartz ozonizer : influence of the heat treatment 1345–1354

COMPTES RENDUS 1355–1356

Revue Roumaine de Chimie, **20**, *9–10*, 1195–1203 (1975)

THE RADIOLYSIS OF THE COMPLEX OXALATES IN AQUEOUS SOLUTIONS. VI[1]

KINETICS AND MECHANISM OF THE RADIOLYSIS OF Fe (III)-TRISOXALATO-COMPLEX IN AQUEOUS SOLUTION

I. G. MURGULESCU and J. PĂUN

University of Bucharest, Department of Physical
Chemistry, Radiation Chemistry Laboratory,
Bucharest, Bd. Republicii 13

Received March 18, 1975

The $\alpha-$Po and $\gamma-{}^{60}$Co radiolysis of potassium ferritrisoxalato-complex in acid and neutral, aerated and deaerated aqueous solution as well as in the presence of some scavengers has been studied. On irradiation the oxalato-complex readily decomposes, the resulted Fe^{2+} ions attaining a steady state concentration. This is determined by the two competing processes : reduction of Fe(III)-oxalato-complex ion by e_{aq}^-, H, HO_2 and oxidation of Fe(II)-oxalato-complex ion by OH, HO_2 and H_2O_2. The individual nature of ferric and ferrous oxalato-complex as well as the chemical form of the reducing and oxidizing species are strongly dependent on the p_H-value, presence or absence of air and $C_2O_4^{2-}$ ion concentration. The evidence for the reaction :

$$C_2O_4^{\cdot -} + Fe\,(C_2O_4)_3^{3-} \rightarrow Fe\,(C_2O_4)_2^{2-} + C_2O_4^{2-} + 2\,CO_2$$

is given.

The radiolysis of ferritrisoxalato-complex in aqueous solution has not been studied so far. The only information referring to this system is given by Shaghisultanova [2] who determined the rate constant for the reaction $Fe(C_2O_4)_3^{3-} + H$, as being 3.4×10^6 l.mol^{-1}s^{-1} by the method of producing atomic hydrogen in an electrodeless high frequency discharge and introducing it into the oxalato-complex solution.

EXPERIMENTAL

The ferritrisoxalato-complex was prepared by the method described in the literature. [3] For the preparation of the solutions twice distilled water has been used. The concentrations ranged from 2×10^{-4} M to 10^{-2} M. For deaeration of the solutions a pure argon stream was bubbled for 30 minutes. Due to the high photosensibility of the solution, all the operations have been conducted in a dark room.

---

[1] Part. V. : J. Păun, T. Memetea and E. Stroe, *Radiochem. Radioanal. Lett.*, in press.
[2] G. A. Shaghisultanova, *Khim. Vysokikh Energii*, **5**, 187 (1971).
[3] C. A. Parker, *Proc. Roy. Soc.*, **A 220**, 104 (1953).

The aqueous solutions of Fe(III)-trisoxalato-complex in neutral and acid medium were irradiated with α- and γ-radiations. For α-irradiations a 1 Curie ^{210}Po type PDD source from Amersham, England was used,[4] in a volume of 1.5 ml the dose rate was 2.2×10^{17} eV/ml. min in a certain irradiation geometry. A γ-radiations source of 30 Curie ^{60}Co with a high specific activity of 37 Curie/g was used; in a volume of 3.5 ml the maximum dose rate was 2.7×10^{17} eV/ml. min. The dose rate was determined by ferrous sulphate dosimeter, taking G(Fe^{3+}) as 15.6.

The radiation induced decomposition of the complex in aqueous solution has been studied spectrophotometrically by measuring the concentration of Fe^{2+} ions, resulted from irradiation, by complexing with *o*-phenoanthroline at pH 4—5 in an acetate buffer. After 30 minutes the optical density was recorded at 510 nm. Measurements were made on a SP—800 Unicam spectrophotometer.

RESULTS

On γ-irradiation at the maximum dose rate, in the absence of air, in neutral solution, the complex decomposes readily, the Fe^{2+} ions building up with the increasing dose and then rapidly attaining a steady state concentration.

In figure 1 are given the building up curves of Fe^{2+} ions during irradiation for four initial solute concentrations ranging from 2×10^{-4} M to 10^{2-} M. The decomposition degree corresponding to the steady state concentration takes values from 25% to 5% respectively.

No post irradiation effect has been observed. During irradiation no hydrogen peroxide has been identified. In the presence of air, in neutral solution almost no Fe^{2+} ions were formed. At higher doses $Fe(OH)_3$ is gradually precipitating.

On irradiation in acid solution (0.1 N H_2SO_4) in the absence of air, the Fe^{2+} ions building up curves have similar shapes but the decomposition rate is higher, as can be seen from figure 2, where the Fe^{2+} ions building up curves for 10^{-3} M initial solute concentration in acid and neutral solution are presented. In the presence of air, the solution of the complex ion decomposes at much lower extent, the Fe^{2+} ions building up curves being different from that corresponding to the absence of air. In figure 3 are given the Fe^{2+} ions building up curves for 10^{3+} M initial solute concentration in acid solution, in the absence as well as in the presence of air. The Fe^{2+} ions building up curves in the presence of air in acid and neutral solution for 10^{-3} M initial solute concentration are indicated in figure 4.

In the presence of $C_2O_4^{2-}$ ions the radiation induced decomposition rate of Fe(III)-trisoxalato-complex in solution is strongly increasing in the presence as well as in the absence of air. The decomposition degree is enhanced with the increasing $C_2O_4^{2-}$ ions concentration.

For 10^{-3} M complex concentration and 6×10^{-2} M $C_2O_4^{2-}$ ions, in the absence of air the decomposition degree increases up to 50%.

Figure 5 shows the influence of 6×10^{-2} M $C_2O_4^{2-}$ ions on the Fe^{2+} ions building up curves during irradiation, for 10^{-3} M complex concentration, in the absence of air. The influence of $C_2O_4^{2-}$ ions concentration on the Fe^{2+} ions building up curves for 10^{-3} M complex concentration in the presence of air is presented in figure 6. The accumulation of Fe^{2+} ions during irradiation, in the presence of air, for three different initial complex concentrations at 6×10^{-2} M $C_2O_4^{2-}$ can be seen from figure 7.

---

[4] I. G. Murgulescu and J. Păun, *Rev. Roumaine Chim.*, **19**, 9 (1974).

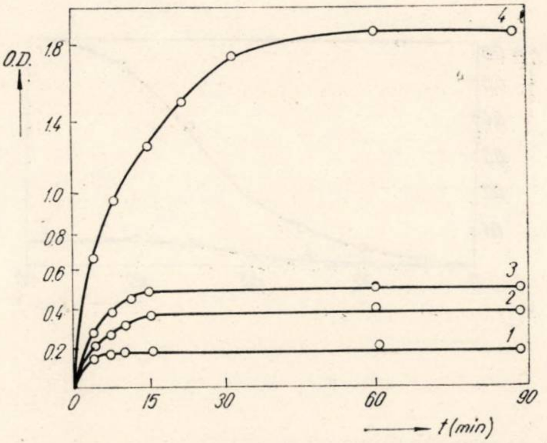

Fig. 1. — Accumulation of Fe^{2+} ions during irradiation of $K_3\,Fe\,(C_2O_4)_3$ aqueous solution in the absence of air. *1*, 2×10^{-4} M; *2*, 10^{-3} M; *3*, 2×10^{-3} M; *4*, 10^{-2} M.

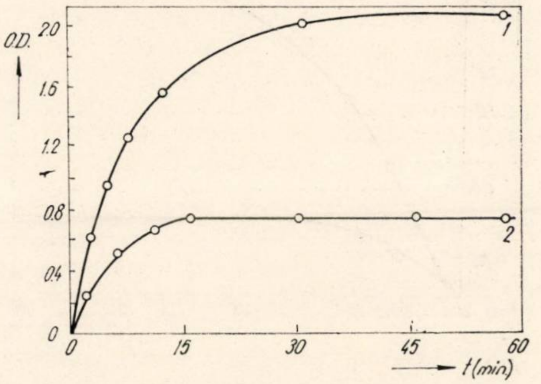

Fig. 2. — Accumulation of Fe^{2+} ions during irradiation of 10^{-3} M $K_3Fe(C_2O_4)_3$ in aqueous solution in the absence of air. *1*, acid medium; *2*, neutral medium.

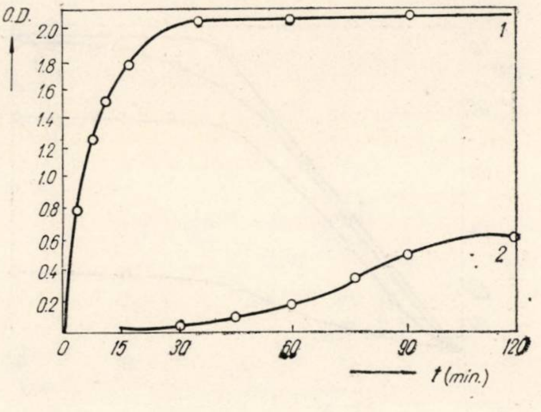

Fig. 3. — Accumulation of Fe^{2+} ions during irradiation of 10^{-3} M $K_3\,Fe\,(C_2O_4)_3$ in acid solution (0.1 N H_2SO_4). *1*, absence of air; *2*, presence of air.

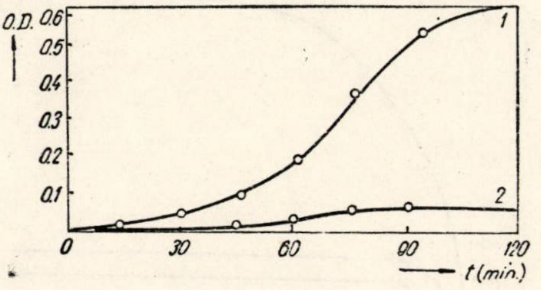

Fig. 4. — Accumulation of Fe^{2+} ions during irradiation of 10^{-3} M $K_3 Fe (C_2O_4)_3$ in the presence of air.

1, acid medium; *2*, neutral medium.

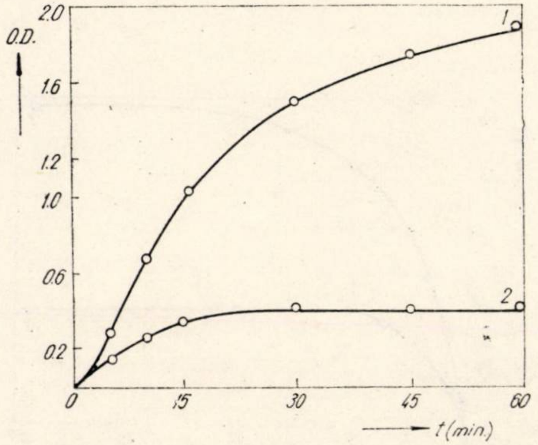

Fig. 5. — Influence of $C_2O_4^{2-}$ ions on the Fe^{2+} ions building up curves for 10^{-3} M $K_3 Fe(C_2O_4)_3$ in the absence of air.

1, 6.6×10^{-2} M $C_2O_4^{2-}$ ions added; *2*, no $C_2O_4^{2-}$ ions added.

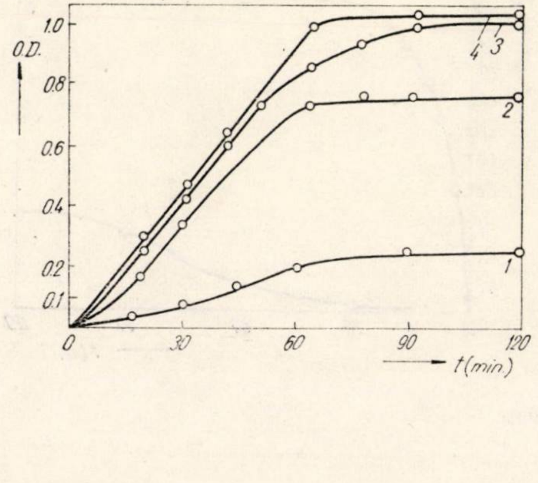

Fig. 6. — Influence of $C_2O_4^{2-}$ ions concentration on the Fe^{2+} ions building up curves for 10^{-3} M $K_3Fe(C_2O_4)_3$ in the presence of air.

1, 2×10^{-3} M; *2*, 10^{-2} M; *3*, 2×10^{-2} M; *4*, 6.6×10^{-2} M.

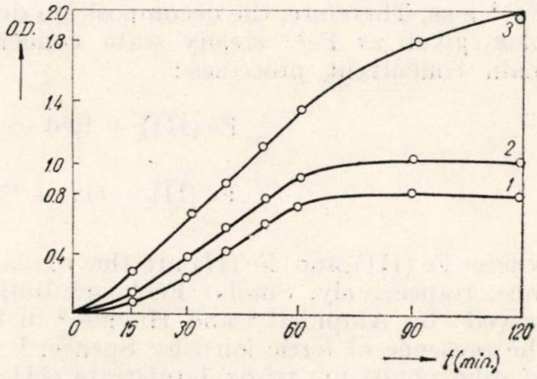

Fig. 7. — Influence of $Fe(C_2O_4)_3^{3-}$ ions concentration in 6.6×10^{-2} M $C_2O_4^{2-}$ aqueous solution in the presence of air.

1, 10^{-3} M; *2*, 2×10^{-3} M; *3*, 10^{-2} M.

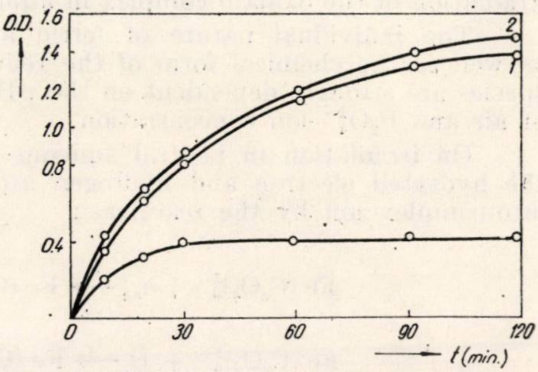

Fig. 8. — Accumulation of Fe^{2+} ions during irradiation of 10^{-3} M $K_3Fe(C_2O_4)_3$ in the absence of air, in the presence of 0.1 M OH. scavengers.

1, isopropyl alcohol; *2*, glucose; *3*, no OH scavenger added.

In the presence of some OH scavengers, such as isopropyl alcohol and glucose, the radiation induced decomposition rate is strongly increased as can be seen from figure 8.

On α-irradiation, in the absence of air, no Fe^{2+} ions could be identified. By adding *o*-phenanthroline into the complex solution before irradiation, after a very short irradiation time, a red colour appears as due to the Fe^{2+}-orthophenanthroline complex. This fact proves that the Fe^{2+} ions formed by radiolysis are immediately oxidized by hydrogen peroxide.

DISCUSSIONS

The decrease of the radiation induced decomposition rate of Fe(III) trisoxalato-complex in aqueous solution in the presence of reducing species scavengers as well as the formation of Fe^{2+} ions in irradiated oxalato-complex solution, indicates that the main process of the radiolytic decomposition is the reduction of Fe(III)-trisoxalato-complex ions by the reducing species from the radiolysis of water. The particular shape of the Fe^{2+} ions building up curves characterized by the establishment of a steady state concentration after a low absorbed radiation dose, suggests that another main process is taking place, namely the radiolytic oxidation of

Fe^{2+} ions. Therefore, the decomposition degree of Fe (III)-trisoxalato-complex, given as Fe^{2+} steady state concentration, is determined by two main concurrent processes :

$$\mathrm{Fe\,(III) + Red \rightarrow Fe\,(II)} \qquad \text{(I)}$$

$$\mathrm{Fe\,(II) + Ox \rightarrow Fe\,(III)} \qquad \text{(II)}$$

where Fe (III) and Fe (II) are the oxalato-complexes of Fe^{3+} and Fe^{2+} ions, respectively. Similar Fe^{2+} ions building up curves have been observed by Amphlett [5] and Hughes [6] in the radiolysis of ferrous ions in the presence of ferric ions, by Spencer [7] in photochemical decomposition of solid potassium trisoxalatoferrate (III) and by Margulis [8] by ultrasonic irradiation of the oxalato-complex in aqueous solution.

The individual nature of ferric and ferrous oxalato-complexes [9] as well as the chemical form of the reducing (Red) and oxidizing (Ox) species are strongly dependent on the pH value, the presence or absence of air and $C_2O_4^{2-}$ ion concentration.

On irradiation in neutral aqueous solution in the absence of air, the hydrated electron and hydrogen atoms reduce the Fe(III)-trisoxalato-complex ion by the reactions :

$$\mathrm{Fe\,(C_2O_4)_3^{3-} + e_{aq} \xrightarrow{k_1} Fe\,(C_2O_4)_2^{2-} + C_2O_4^{2-}} \qquad (1)$$

$$\mathrm{Fe\,(C_2O_4)_3^{3-} + H \xrightarrow{k_2} Fe\,(C_2O_4)_2^{2-} + HC_2O_4^{-}} \qquad (2)$$

The Fe(II)-oxalato-complex is less stable [10] than the corresponding Fe(III) oxalato-complex by a factor of 10^{13}. Therefore in the solution there are mostly Fe^{2+} ions. Due to the specific chemistry of Fe^{3+} ions in neutral aqueous solution, there is so far no precise value for the rate constant of the reaction $Fe^{3+} + e_{aq}$. Based on radiation chemistry study of Fe^{3+} ions in acid solution, Meisel and Czapski [11] calculated for the ratio of the rate constants k_a/k_b for reactions :$Fe^{3+} + e_{aq} \xrightarrow{k_a} Fe^{2+}$ and $e_{aq} + H^+ \xrightarrow{k_b} H$ a value of 0.95 which indicates that the reaction $Fe^{3+} + e_{aq}$ is fast with $k \simeq 10^{10}\ \mathrm{l \cdot mol^{-1}\ sec^{-1}}$. Therefore in the case of Fe $(C_2O_4)_3^{3-}$ complex ion considering that the $C_2O_4^{2-}$ ligand does not change much the rate constant k_1 with respect to k_a, one can assume that the reaction (1) is fast. Reaction (2) is slow, having $k_2 = 3 \cdot 4 \times \times 10^6\ \mathrm{l\,mol^{-1}\ sec^{-1}}$. This value has been experimentally determined by

---

[5] C. B. AMPHLETT, *Discuss Faraday Soc.*, **7**, 144 (1952).

[6] G. DOBSON and G. HUGHES, *Trans. Faraday Soc.*, **57**, 1117 (1961).

[7] H. E. SPENCER and M. W. SCHMIDT, *J. Phys., Chem.*, **75**, 2986 (1971).

[8] M. MARGULIS and A. MALTSEV, *Vestnik Mosk. Univ. Khim.*, **23**, 44 (1968).

[9] W. BABAERA and M. MOSYAGHINA, *Doklady Akad. Nauk. S.S.S.R.*, **64**, 823 (1949). A. BABKO and L. DUBOVENKA, *Zhur. obshchei, Khim.* **26**, 996 (1956); KH. JAKUBOV, *Doklady Akad. Nauk. Tadzh. S.S.S.R.*, **12**, 33 (1969); W. SAMUEL *Mol. Photochem.*, **3**, 387 (1972).

[10] H. STACKELBURG and H. FRAYHOLD, *T. Elektrochem.*, **46**, 120 (1940); M. BOFTELSKY, D. CHASSON and S. KLEIN, *Analyt. Chim. Acta.*, **8**, 460 (1953).

[11] G. MEISEL and G. CZAPSKI, *Internat. J. Radiat. Phys. Chem.*, **3**, 11 (1971).

Shaghisultanova [2] by the method of producing atomic hydrogen in an electrodeless high frequency discharge and introducing it into the oxalato-complex solution. As it is well known, from the radiation chemistry of Fe^{2+} ion, one can presume that the ferrous oxalato-complex ions are oxidized by OH free radicals and the hydrogen peroxide by the reactions (3) and (4):

$$Fe(C_2O_4)_2^{2-} + OH \xrightarrow[C_2O_4^{2-}]{k_3} Fe(C_2O_4)_3^{3-} + OH^- \qquad (3)$$

$$Fe(C_2O_4)_2^{2-} + H_2O_2 \xrightarrow[C_2O_4^{2-}]{k_4} Fe(C_2O_4)_3^{3-} + OH^- + OH \qquad (4)$$

The steady state concentration of ferrous ions attained after a low absorbed dose is due to the fact that the rate of $Fe(C_2O_4)_2^{2-}$ oxidation equals the rate of $Fe(C_2O_4)_3^{3-}$ reduction:

$$\frac{d\,[Fe(C_2O_4)_2^{2-}]}{dt} = \frac{d\,[Fe(C_2O_4)_3^{3-}]}{dt} \qquad (I)$$

where:

$$\frac{d\,[Fe(C_2O_4)_2^{2-}]}{dt} = (k_1\,C_{e_{aq}} + k_2\,C_H)\,C_{Fe(C_2O_4)_3^{3-}} - (k_3\,C_{OH} + k_4\,C_{H_2O_2})\,C_{Fe(C_2O_4)_2^{2-}} \qquad (II)$$

$$\frac{d\,[Fe(C_2O_4)_3^{3-}]}{dt} = k_3\,(C_{OH} + k_4\,C_{H_2O_2})\,C_{Fe(C_2O_4)_2^{2-}} - (k_1\,C_{e_{aq}} + k_2\,C_H)\,C_{Fe(C_2O_4)_3^{3-}} \qquad (III)$$

By applying the steady state kinetics to the estimation of reducing species concentrations one can calculate the equilibrium concentration for $Fe(C_2O_4)_2^{2-}$ and $Fe(C_2O_4)_3^{3-}$ ions.
Finally, for the ratio $[Fe(C_2O_4)_2^{2-}]_{eq}/[Fe(C_2O_4)_3^{3-}]_{eq}$, one obtains the relation:

$$\frac{[Fe(C_2O_4)_2^{2-}]_{eq}}{[Fe(C_2O_4)_3^{3-}]_{eq}} = \frac{(G_{e_{aq}} + G_H)\cdot I}{(k_3\,C_{OH} + k_4\cdot C_{H_2O_2})\cdot C_{Fe(C_2O_4)_3^{3-}}} \qquad (IV)$$

where I is the dose rate. The expression (IV) is in agreement with the experimental results: the Fe^{2+} ions concentration is decreasing with the increasing initial $Fe(C_2O_4)_3^{3-}$ ions concentration. In the presence of air, as it is known, the reducing species is O_2^-, which reduces the oxalato-complex ion by the reaction (5):

$$Fe(C_2O_4)_3^{3-} + O_2^- \xrightarrow{k_5} Fe(C_2O_4)_2^{2-} + C_2O_4^{2-} + O_2 \qquad (5)$$

or to a certain extent it can recombine to form hydrogen peroxide:

$$O_2^- + O_2^- \rightarrow H_2O_2 + 2OH^- + O_2. \qquad (6)$$

The low decomposition degree of the complex suggests that the reaction (5) is slow. On the other hand, H_2O_2 from reaction (6) oxidize Fe(II)-oxalato-complex by reaction (4). At high doses the uncomplexed Fe^{3+} ions will be converted to $Fe(OH)_3$.

On irradiation in acid solution in the absence of air, Fe(III) is mainly in the form[12] of $Fe\,(C_2O_4)_2^-$. Small amounts of $Fe(C_2O_4)^+$ may also be present in the absence of $C_2O_4^{2-}$ ions. The only reducing species in solution is the hydrogen atom, formed by reaction (7).

$$e_{aq} + H^+ \rightarrow H \tag{7}$$

In this case, the important radiolytic decomposition is due to reaction (8) :

$$Fe\,(C_2O_4)_2^- + H \xrightarrow{k_8} Fe\,(C_2O_4)_2^{2-} + H^+ \tag{8}$$

The reaction (8) is very probably slow with $k_8 \simeq 10^6\,l\cdot mol^{-1}\,sec^{-1}$. Reactions (3) and (4) will also contribute to the establishment of Fe^{2+} ions steady state concentration.

In the presence of air, the hydrogen atoms are totally converted to the HO_2 free radicals by the fast reaction :

$$H + O_2 \xrightarrow{k_9} HO_2 \tag{9}$$

with $k_9 = 1.2 \times 10^{10}\,l\cdot mol^{-1}\,sec^{-1}$, which will reduce the ferric oxalato-complex ions :

$$Fe\,(C_2O_4)_2^- + HO_2 \xrightarrow{k_{10}} Fe\,(C_2O_4)_2^{2-} + H^+ + O_2 \tag{10}$$

or to a certain extent it can recombine to form hydrogen peroxide :

$$HO_2 + HO_2 \rightarrow H_2O_2 + O_2 \tag{11}$$

Reaction (12) will be involved in the radiolytic oxidation of ferrous oxalato-complex together with reactions (3) and (4).

$$Fe\,(C_2O_4)_2^{2-} + HO_2 \xrightarrow[C_2O_4^{2-}]{k_{12}} Fe\,(C_2O_4)_3^{3-} + HO_2^- \tag{12}$$

$$HO_2^- + H^+ \rightleftharpoons H_2O_2 \tag{13}$$

The low Fe(II) steady state concentration is determined by the competing reactions (10) and (12), k_{12} being higher than k_{10}. From a kinetic study of the radiation chemical $Fe^{3+} - Fe^{2+}$ system, Hughes[6] calculated for the ratio $k_{Fe^{3+}HO_2}/k_{Fe^{2+}HO_2}$ a value of 3.4×10^{-3}. In our system, considering that $C_2O_4^{2-}$ ligand does not change significantly the values of the two rate constants, one can assume that the reaction (12) is faster than (10).

---

[12] G. Cooper and B. De Graff, *J. Phys. Chem.*, **75**, 2897 (1971) ; **76**, 2618 (1972).

The strong increase of the decomposition degree with the concentration of $C_2O_4^{2-}$ added ions is due to the reducing action of $C_2O_4^{\cdot -}$ formed by reaction[13] (14) :

$$C_2O_4^{2-} + OH \xrightarrow{k_{14}} C_2O_4^{\cdot -} + OH^- \tag{14}$$

with $k_{14} = 5 \times 10^6\ 1 \cdot mol^{-1} sec^{-1}$. The direct identification of $C_2O_4^{\cdot -}$ was given from E.S.R.[14] and fast[15] spectroscopy. The Fe (III)-trisoxalato-complex is reduced by reaction (15) :

$$Fe\,(C_2O_4)_3^{3-} + C_2O_4^{\cdot -} \xrightarrow{k_{15}} Fe\,(C_2O_4)_3^{4-} + 2CO_2 \tag{15}$$

At low $C_2O_4^{2-}$ excess, $Fe\,(C_2O_4)_3^{4-}$ dissociates :

$$Fe\,(C_2O_4)_3^{4-} \rightarrow Fe\,(C_2O_4)_2^{2-} + C_2O_4^{2-} \tag{16}$$

The evidence for reaction (15) has also been offered by Parker and Hatchard,[16] Cooper and De Graff[12] from flash photolysis studies of $Fe\,(C_2O_4)_3^{3-}$ ion in aqueous solution, by Pozniak[17] from photolysis of frozen aqueous solution as well as by Spencer[7] from photochemical decomposition of solid potassium trisoxalatoferrate (III).

---

[13] J. Weiss, *Discuss. Faraday Soc.*, **2**, 188 (1947).
[14] D. Ingram, W. Hodgson, C. Parker and W. Ress, *Nature*. **176**, 1227 (1955).
[15] N. Getoff et al. *J. Phys. Chem.*, **75**, 749 (1971).
[16] C. Parker and C. Hatchard, *J. Phys. Chem.*, **63**, 22 (1959).
[17] A. Pozniak, *Khim. Vysokikh Energy*, **3**, 88 (1959).

The higher [illegible] of the decomposition [illegible] copper with [illegible] the rising [illegible] due to the following action of $C_2O_4^-$ formed by [illegible]:

$$C_2O_4^- + Cu^{2+} \rightarrow [illegible] + 2CO_2 \qquad (14)$$

with [illegible]. The direct [illegible] of $C_2O_4^-$ was given from [illegible] and [illegible] spectroscopy. The Fe(III) trioxalato complex is reduced by [illegible] (15).

$$Fe(C_2O_4)_3^{3-} + [illegible] \rightarrow [illegible] \qquad (15)$$

At low $[C_2O_4^{2-}]$ [illegible], $Fe(C_2O_4)_3^{3-}$ dissociates:

$$Fe(C_2O_4)_3^{3-} \rightleftharpoons Fe(C_2O_4)_2^{-} + C_2O_4^{2-} \qquad (16)$$

The evidence for reaction (15) has also been obtained by Parker and Hatchard, [illegible] Cooper and De Graff [illegible] from flash photolysis studies of $Fe(C_2O_4)_3^{3-}$ in aqueous solution, by [illegible] of [illegible] photolysis [illegible] as well as by Spencer from photochemical decomposition of solid potassium trioxalatoferrate [illegible].

[illegible]

Revue Roumaine de Chimie, **20**, *9–10*, 1205–1212 (1975)

ON THE ELECTRONIC STRUCTURE OF n-σ COMPLEXES. I

IODINE COMPLEXES WITH HETEROAROMATIC DONORS

MARIANA CIUREANU and V. E. SAHINI
Physical Chemistry Department, Polytechnic Institute of Bucharest, Bd. Republicii 13,
Bucharest, Romania

Received April 8, 1975

The electronic structure of molecular complexes formed by iodine with heteroaromatic donors is described in terms of the variation method. The relation between the electronic structure of the donor and the charge transfer transition energy is investigated and discussed for a number of eight complexes. The transition moment of the charge transfer band, as well as the enhancement of the dipole moment are calculated for pyridine – I_2 and quinoline – I_2. A method is given to calculate the intensity enhancement of the infrared bands on complex formation.

1. INTRODUCTION

A considerable amount of effort has been devoted in the last two decades to describing the electronic structure and properties of molecular complexes formed by iodine with various heteroaromatic donors.[1–9] In spite of this effort, many questions about these complexes remain still open. In fact, according to the classical theories, a simple CI should be considered between the ground and first charge transfer (CT) state ;[3,4] such a treatment does not offer a satisfactory explanation for the abnormally high intensity of the CT band [7] as well as for the occurrence of a strong polarization of the iodine molecule in the complex.[8] Besides, there are still unanswered questions concerning the relation between the electronic structure of the heteroaromatic donor and the energy of the CT transition : according to the classical treatments[3,4] the charge transfer transition energy should depend uniquely on the ionization potentia

---

[1] Briegleb, "Elektronen Donator Acceptor Complexe" Springer Verlag, Berlin, 1961.

[2] R. S. Mulliken and W. B. Person, "Molecular Complexes", Wiley Intersci. New York, 1969.

[3] a) H. Yada, J. Tanaka, S. Nagakura, *Bull. Chem. Soc. Japan*, **33**, 1660 (1960).
b) R. S. Mulliken and W. B. Person, *Ann. Rev. Phys. Chem.*, **13**, 107 (1962).

[4] W.B.Person, *J. Chem. Phys.*, **38**, 109 (1963).

[5] G. W. Ginn and J. L. Wood, *Trans. Faraday Soc.*, **62**, 777 (1966).

[6] V. G. Krishna and B.B. Bhowmik, *J. Amer. Chem. Soc.*, **90**, 1700 (1968).

[7] R. S. Mulliken, *J. Amer. Chem. Soc.*, **91**, 1237 (1969).

[8] H. C. Fleming and M.W. Hanna, *J. Amer. Chem. Soc.*, **93**, 5030 (1971).

[9] a) H. Ratajczak and W. Orville-Thomas, *J. Mol. Struct.*, **14**, 149, 155 (1972) ;
b) H. Ratajczak, Z. Mielke and W. J. Orville-Thomas, *J. Mol. Struct.*, **14**, 165 (1972).

of the donor. This correlation was used by El-Bayoumi et al .[10] to predict the n-ionization potentials of azines ; the results thus obtained were of a qualitatively correct order of magnitude but failed to explain the observed order of basicity in a series of bases *. In fact, on the basis of the CT spectra of iodine complexes, one would expect diazines to have a lower ionization potential and therefore a higher basicity than the corresponding monoazines, which is in a complete disagreement with the experimental pk_a values.

Therefore, the purpose of this paper is to carefully reexamine the problem of the electronic structure of the n-σ complexes and to calculate several of their most important properties : the energy and transition moment of the CT band, the charge distribution and dipole moment of the complex, the intensity enhancement of the infrared bands on complex formation.

2. METHOD OF CALCULATION

The wave function of a CT complex can be described by a linear combination of ground, CT and locally excited states [2].

$$\Xi = b_0\Psi_0(D, A) + \sum_m b_m\Psi_m(D^+ - A^-) + \sum_n c_n\Psi_n(D^*, A) + \sum_p d_p\Psi_p(D, A^*). \tag{1}$$

If one assumes for the iodine-base a linear geometry (see for example fig.1 for the simplest member of the series, the pyridine $-I_2$ complex), a complete treatment will require the consideration of all the valence electrons of both molecules : n, σ and π ; therefore, eq. 1 will contain a great number of states : CT states occurring by electron transfer from the base to iodine ($n_b \rightarrow \sigma^*_{I_2}$ and $\pi_b \rightarrow \sigma^*_{I_2}$), and locally excited states of the donor ($n_b \rightarrow \pi^*_b$, $\pi_b \rightarrow \pi^*_b$) or of the acceptor ($\pi_{I_2} \rightarrow \sigma^*_{I_2}$ and $\sigma_{I_2} \rightarrow \sigma^*_{I_2}$).

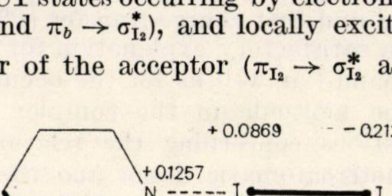

Fig. 1. — Pyridine — I_2.

Fortunately, for symmetry reasons, Ψ_0 does not mix with the greatest part of these states, so that the ground state of the complex can be described by the simpler form :

$$\Xi_N = b_{0N}\Psi_0(D, A) + b_{1N}\Psi_1(D^+ - A^-) + b_{2N}\Psi_2(D^+ - A^{-*}) + d_N\Psi_3(D, A^*) \tag{2}$$

---

* If the n donors are typical bases (H^+ acceptors) the ease of releasing an n electron (measured by the n ionization potential) will be related to the ease of accepting a proton (measured by the pk_a value of the base).

[10] M. A. El-Bayoumi and S. Khalil, *J. Chem. Phys.*, **47**, 4863 (1967).

where Ψ_1 and Ψ_2 are CT states of $(n_b \rightarrow \sigma^*_{I_2})$ type, and Ψ_3 is a $(\sigma_{I_2} \rightarrow \sigma^*_{I_2})$ locally excited state. A similar formula will hold for the first CT state Ξ_{E_1}.

The eigenvalue problem will be solved by the variation method. The following matrix elements will be used :

$$< {}^1\Psi_1(D^+ - A^-)|\mathscr{H}|\, {}^1\Psi_1(D^+ - A^-) > = I_n - E_A - \sum_{\rho} (C^{\rho}_{j'a})^2\, \gamma_{n\rho} +$$

$$+ \sum_{\delta,\rho} (C^{\rho}_{j'a})^2\, (q^{\sigma}_{\delta} + q^{\pi}_{\delta} - Z_{\delta})\, \gamma_{\delta\rho} \qquad (3)$$

$$< {}^1\Psi_3(D, A^*)|\mathscr{H}|\, {}^1\Psi_3(D, A^*) > = 6.6\mathrm{eV} \qquad (4)$$

$$< {}^1\Psi_0(D, A)|\mathscr{H}|\, {}^1\Psi_1(D^+ - A^-) > = \sqrt{2}\, \beta_{n\rho}\, C^{\rho}_{j'a} \qquad (5)$$

$$< {}^1\Psi_0(D, A)|\mathscr{H}|\, {}^1\Psi_2(D^+ - A^{-*}) > = 0 \qquad (6)$$

$$< {}^1\Psi_0(D, A)|\mathscr{H}|\, {}^1\Psi_3(D, A^*) > = \sqrt{2} \sum_{\delta,\rho} C^{\rho}_{ja}\, C^{\rho}_{j'a} (q^{\pi}_{\delta} + q^{\sigma}_{\delta} - Z_{\delta}) \gamma_{\delta\rho} \qquad (7)$$

$$< {}^1\Psi_1(D^+ - A^-)\, |\mathscr{H}|\, {}^1\Psi_2(D^+ - A^{-*}) > = \sum_{\rho} C^{\rho}_{ja}\, C^{\rho}_{j'a} \sum_{\delta} [(q^{\pi}_{\delta} +$$

$$+ q^{\sigma}_{\delta} - Z_{\delta})\, \gamma_{\delta\rho} - \gamma_{n\rho}] \qquad (8)$$

$$< {}^1\Psi_1(D^+ - A^-)\, |\mathscr{H}|\, {}^1\Psi_3(D, A^*) > = - \beta_{n\rho}\, C^{\rho}_{ja} \qquad (9)$$

$$< {}^1\Psi_2(D^+ - \overset{*}{A^-})\, |\mathscr{H}|\, {}^1\Psi_3(D, A^*) > = \beta_{n\delta} C^{\rho}_{j'a} \qquad (10)$$

where q^{π}_{δ} and q^{σ}_{δ} denote the π and σ atomic charge densities of the donor atoms ; the subscript n designates terms involving the nitrogen lone pair. All the other notations are those used in the preceding papers.[11] We note the appearance of the last term in (3) which is due to the consideration of the π and σ electrons of the donor ; this term represents the electrostatic interaction between the dipole moment of the donor and the acceptor anion in the CT state. Owing to the same reason the off-diagonal element (7) is different from zero, a fact which will be responsible for the appearance of polarization terms in the ground state properties.

We see that the main differences between the present approach and the preceding theories consist in taking into account the last two terms in (2) and in the inclusion of π and σ valence electrons of the donor molecule. Therefore, the energy of the CT state (and consequently the CT transition energy) will not depend uniquely on the ionization potential of the donor, which explains the inversions noted at the beginning.

---

* Evaluated from spectroscopic data.

[11] M. Dobrescu, *Rev. Roumaine Chim.*, **16**, 1825, 1841 (1971) ; M. Ciureanu and V.E. Sahini, *Rev. Roumaine Chim.*, **18**, 921 (1973).

3. CHOICE OF PARAMETERS

A P.P.P. SCF MO method was used to calculate the π electron densities of the donor molecules q_S^{π}; the σ atomic charges q_S^{σ} were calculated by Del Re's method.[12]

The intermolecular resonance integrals $\beta_{n\rho}$ were calculated by the Wolfsberg Helmholtz formula:

$$\beta_{n\rho} = 0.5\, K S_{n\rho} (I_\rho + I_n) \tag{11}$$

with $K = 0.5$; I_ρ and I_n are the ionization potentials of iodine and nitrogen respectively. The overlap integral $S_{n\rho}$ was estimated for a sp^2 hybridized nitrogen using the tables of Mulliken, Rieke and Orloff;[13] we note that the value calculated by us, 0.29, is in accordance with other previous estimates.[14]

The N—I distance was assumed to be 2.31 A in all cases*, so that the intermolecular resonance integral $\beta_{n\rho}$ is constant in the series of complexes under consideration.

The bielectronic repulsion integrals (both inter and intramolecular) were calculated using Klopman's[15] formula.

The ionization potentials of the donors were calculated by a method described in a preceding paper.[17]

4. RESULTS

4.1. CHARGE TRANSFER SPECTRA

The present approach was used to calculate the CT spectra for a number of eight complexes. The ionization potentials used in our calculations are shown in table 1, together with the available[18] pk_a values; as seen from this table, the calculated values vary over a range of more than 1 eV and the changes are in accordance with the basicities of the donors. The calculated CT bands evaluated on basis of these ionization potentials are in a good agreement with the experimental data. Generally the calculated values are smaller than the experimental ones, which can be explained by the neglect of the solvent effects in our calculations.

The transition moment of the CT band, M_{NE_1} was calculated for pyridine—I_2 and quinoline —I_2.

---

[12] G. Del Re, *J. Chem.*, **1958**, 4031; G. Del Re and B. Pullman, *J. Chim. Phys.*, **62**, 942 (1965).

[13] R. S. Mulliken, C. A. Rieke, D. Orloff and H. Orloff, *J. Chem. Phys.*, **17**, 1248 (1949).

[14] I. G. Arzamova, E. H. Gurianova, *Zhur. obshchei Khim.*, **36**, 1157 (1966).

* This is the value evaluated by X ray determinations for the γ picoline — I_2 complex[16].

[15] G. Klopman, *J. Amer. Chem. Soc.*, **86**, 1550 (1964).

[16] O. Hassel, Chr. Romming and T. T. Tufte, *Acta Chem. Scand.*, **15**, 967 (1961).

[17] M. Ciureanu and V. E. Sahini, *Rev. Roumaine Chim.*, **20**, 000 (1975).

[18] E. H. Gurianova, I. P. Golstein and I. P. Romm "Donorono aktseptornaya sviazi" *Izd. Khimia*, Moscva, 1973.

Table 1

Calculated and experimental CT spectra of iodine complexes with azines

Donor	I_D (eV) [a]	pk_a [a]	λ_{CT} (calc) (nm)	λ_{CT} (exp) (nm) [b]
Pyridine	9.89	5.23	233	235 (cl)
Quinoline	9.80	4.94	234	238 (h)
Phenazine	10.64	1.23	223	256 (t)
Acridine	9.54	5.6	238	253 (t)
Pyrimidine	10.37	1.30	228	237 (c)
Pyrazine	10.69	0.6	220	240 (c)
2-Cl Pyridine	10.24	—	226	230 (cl)
3-Cl Pyridine	10.37	—	226	233 (cl)

[a] reference[5,15,17].

[b] experimental CT spectra [18] in different solvents; h = heptane; cl = chloroform; t = trimethylpentane; c = cyclohexane.

Table 2

Ground and CT wave functions

Complex	Wave functions
Pyridine — I_2	$\Xi_N = 0.9274\Psi_0 + 0.3545\ \Psi_1 + 0.0148\ \Psi_2 - 0.1182\ \Psi_3$ $\Xi_{E_1} = -\ 0.3706\ \Psi_0 + 0.8294\ \Psi_1 + 0.0353\ \Psi_2 - 0.4165\ \Psi_3$
Quinoline — I_2	$\Xi_N = 0.9260\ \Psi_0 + 0.3575\ \Psi_1 + 0.0145\ \Psi_2 - 0.1208\ \Psi_3$ $\Xi_{E_1} = -\ 0.3749\ \Psi_0 + 0.8322\ \Psi_1 + 0.0366\ \Psi_2 - 0.468\ \Psi_3$

The wave functions of the ground and first excited state in these complexes are shown in table 2; with these WF the transition moment M_{NE_1} will be calculated as :

$$M_{NE_1} = b_{0N} b_{0E_1} + b_{1N} b_{1E_1} \mu_{11} + b_{2N} b_{2E_1} \mu_{22} + d_N d_{E_1} \mu_{33} + \\ + (b_{0N} d_{E_1} + b_{0E_1} d_N) \mu_{03} + (b_{1N} b_{2E_1} + b_{2E_1} b_{1N}) \mu_{22} \tag{12}$$

where μ_{ii} are the dipole moments in the Ψ_i state and μ_{ij} the overlap moments.

Our calculations show that among the terms in (12) the main role is played by the second and fifth ones. Therefore, the apparently abnormal high intensity of the CT band in $n - \sigma$ complexes can be explained by the participation of the strongly allowed transition of the iodine molecule. The calculated values of the transition moment, as well as the experimental ones are shown in table 3.

Table 3

Calculated and experimental transition moments for the CT band

Complex	M_{NE_1} (calc)	M_{NE_1} (exp)
Pyridine $- I_2$	7.67	7.48
Quinoline $- I_2$	7.87	6.49

4.2. CHARGE DISPLACEMENTS AND DIPOLE MOMENT

With the ground state wave function shown in table 2, the charge displacements occurring by complex formation on the acceptor and donor molecules are given by

$$\Delta q_{\rho} = b_{1N}^2 (C_{j'a}^{\rho})^2 + b_{2N}^2 (C_{j'a}^{\rho})^2 + 2b_{1N} b_{2N} C_{ja}^{\rho} C_{j'a}^{\rho} + + 2\sqrt{2}\, b_{0N} d_N (C_{ja}^{\rho}) (C_{j'a}^{\rho}) \tag{13}$$

$$\Delta q_n = -(b_{1N}^2 + b_{2N}^2) \tag{14}$$

The first three terms in (13) are charge transfer terms, whereas the last one is due to the reciprocal polarization of the two molecules in the ground state; owing to the non-negligible magnitude of this term, the iodine molecule will be polarized in the complex. Figure 1 shows the charge displacements occurring by complex formation on iodine atoms and on nitrogen in pyridine$-I_2$.

The dipole moment of the complex $\vec{\mu}_{complex}$ will be given by the vectorial sum of the donor dipole moment $\vec{\mu}_D$ and an increment $\Delta\vec{\mu}$ due to complex formation. The calculated values of the dipole moments as well as the experimental values are shown in table 4 for pyridine $-I_2$ and quinoline $-I_2$.

Table 4

Calculated and experimental values of dipole moments (in Debye)

	Pyridine$-I_2$			Quinoline$-I_2$		
	$\|\vec{\mu}_D\|$	$\|\Delta\vec{\mu}\|$	$\|\vec{\mu}_{complex}\|$	$\|\vec{\mu}_D\|$	$\|\Delta\vec{\mu}\|$	$\|\vec{\mu}_{complex}\|$
Calculated	2.60	4.00	6.60	2.32	4.20	6.10
Experimental	2.22	4.02	6.24	2.25	3.50	5.70

4.3. VIBRATIONAL TRANSITION MOMENTS

The observed intensity enhancement of the iodine stretching vibration on complex formation can be accounted for by a vibronic interaction formalism.[19, 20] The delocalization moment for a transition between two vibrational states l and s of the ground state will be given by :

$$\mu_{N_lN_s} = 2\sum_{i=0}^{2} b_{iN}\mu_{ii}\left(\frac{\partial b_{iN}}{\partial Q_l}\right)_0 + 2d_N\mu_{33}\left(\frac{\partial d_N}{\partial Q_l}\right)_0 + 2\sum_{i=0}^{2}\mu_{ij}\left[b_{iN}\left(\frac{\partial b_{jN}}{\partial Q_l}\right)_0 + b_{jN}\left(\frac{\partial b_{iN}}{\partial Q_l}\right)_0\right] + 2\sum_{i=0}^{2}\mu_{3i}\left[d_N\left(\frac{\partial b_{iN}}{\partial Q_l}\right)_0 + b_{iN}\left(\frac{\partial d_N}{\partial Q_l}\right)_0\right]. \tag{15}$$

The mixing coefficients change with the vibrational coordinate for any vibration which causes the matrix elements (6 — 12) to vary ; hence, for the halogen-halogen stretching vibration of the acceptor

$$c_j = f(E_A, \beta_{n\rho}) \tag{16}$$

where $c_j = b_{iN}, d_N$ $\qquad i = 0, 1, 2$

Thus, differentiating (16) we find that :

$$\left(\frac{\partial c_j}{\partial Q_l}\right)_0 = \left(\frac{\partial c_j}{\partial E_A}\right)\left(\frac{\partial E_A}{\partial Q_l}\right)_0 + \left(\frac{\partial c_j}{\partial \beta_{n\rho}}\right)\left(\frac{\partial \beta_{n\rho}}{\partial Q_l}\right)_0. \tag{17}$$

The above method was used to estimate the delocalization moment of the halogen-halogen stretching vibration in pyridine $-I_2$ complex. In order to calculate the change of the mixing coefficients with the acceptor electron affinity E_A and the resonance integral $\beta_{n\rho}$, the eigenvalue problem was solved for several values of these parameters. In order to evaluate $\left(\frac{\partial \beta_{n\rho}}{\partial Q_l}\right)_0$, several values were calculated for $\beta_{n\rho}$ which were plotted versus Q_l ; the derivative $\left(\frac{\partial \beta_{n\rho}}{\partial Q_l}\right)_0$ is easily seen to be the slope of this curve at the equilibrium value of Q_l. The $\left(\frac{\partial E_A}{\partial Q_l}\right)_0$ value used in our calculations has been estimated by Person[19].

As easily seen, there are several differences between the present approach and the method previously reported in the case of benzene-halogen complexes.[20] They consist mainly in the way of calculating the change in the mixing coefficients with the vibrational coordinates ; besides, the second and the last term in (15) account for a polarization contribution to the delocalization moment, which was neglected up to now.

---

[19] H. B. Friedrich and W. B. Person, *J. Chem. Phys.*, **44**, 2161 (1966).

[20] M. Ciureanu and V. E. Sahini, *Rev. Roumaine Chim.*, **20**,(1975).

The values of $\left(\frac{\partial c_j}{\partial Q_l}\right)_0$ computed by (17) are listed in table 5 for pyridine $-I_2$ complex. As seen from this table, the term in $\left(\frac{\partial \beta_{n\rho}}{\partial Q_l}\right)_0$ (which was neglected in the classical vibronic interaction formalism) [19] plays a non-negligible part in determining the change of the mixing coefficient with the vibrational coordinates. Eq (15) is simplified in the zero differential overlap approximation which makes the μ_{ij} vanish except for μ_{03} and μ_{12}.

Table 5

Calculated values of $\left(\frac{\partial c_i}{\partial Q_l}\right)$

c_i	$\left(\frac{\partial c_i}{\partial E_A}\right)\cdot\left(\frac{\partial E_A}{\partial Q_l}\right)_0$	$\left(\frac{\partial c_i}{\partial \beta_{n\rho}}\right)\left(\frac{\partial \beta_{n\rho}}{\partial Q_l}\right)_0$	$\left(\frac{\partial c_i}{\partial Q_l}\right)_0$
b_0	-0.0115	-0.0162	-0.0277
b_1	0.0290	0.0389	0.0679
b_2	$+0.0026$	-0.0004	0.0022
d	-0.0026	-0.0113	-0.0139

The calculated value of the delocalization moment $\mu^{N_lN_s}_{\text{calc}} = 1.11$ *D/Auam* $^1/_2$ agrees well with the experimental value

$$\mu^{N_lN_s}_{\text{exp}} = 1.2 - 1.09\,^*.$$

---

* Calculated using the triatomic molecule approximation with the interaction constant $K_{12} = 0.22 - 0.4$ mdyn/A [21]

[21] J. Yarwood and W. B. Person *J. Amer. Chem. Soc.*, **90**, 594 (1968).

Revue Roumaine de Chimie **20**, *9–10*, 1213–1217 (1975)

THE ESR SPECTRA OF THE ACENAPHTHENONE REDUCTION PRODUCTS

LILIANA CIUREA

Polytechnic Institute of Bucharest, Department of Physical
Chemistry and Electrochemical Technology
Bd. Republicii 13

Received January 20, 1975

The ESR spectra of the acenaphthenone reduction products showed that the methylene group could be oxidized to the carbonyl group during both the chemical and electrochemical reduction in the presence of trace amounts of oxygen in the system. The experimental *hfs* constants of acenaphthenone anion radical generated by the electrochemical reduction were compared with those theoretically obtained using MO calculations.

In the present paper the ESR spectra of the chemical and electrochemical products of acenaphthenone in different solvents are reported. There is no indication in literature about the spectral behaviour of the reduction products of acenaphthenone, which was generally less studied.

EXPERIMENTAL PART

Acenaphthenone, obtained by oxidizing acenaphthene,[1] was purified through repeated recrystallization from alcohol (M. P. = 121 °). The used solvents dimethoxiethane (DME), dimethylformamide (DMF) and acetonitrile (AN) were purified by refluxing and fractional distillation from Na or P_2O_5 and dimethylsulphoxide (DMSO) was distilled at reduced pressure in a current of inert gas.

The chemical reduction was made in a nitrogen atmosphere with the alkali metals in a cell connected to the ESR tube. The electrochemical reduction was performed inside the microwave cavity in a cell containing two Pt electrodes and a reference Ag electrode.[2] The supporting electrolyte was tetrabutylammonium iodide 0.1 M. The platinum cathode passed through a glass capilary was dipped into the ESR tube of the electrochemical-ESR cell, till reaching the center of the microwave cavity.

The ESR spectra were recorded on a JES — 3B Spectrometer in the X-band frequency. The calculations were carried out on an IBM-360 Computer at the Computer Center, Bucharest University.

RESULTS AND DISCUSSION

The experimental data showed that at the reduction of acenaphthenone it was possible to obtain two different kinds of spectra. One kind of the spectrum is that presented in figure 1a, which belongs to the radical obtained by the action of Na on acenaphthenone in DMSO. This spectrum resolved in 25 lines has a small total length of about 5.6 Gs. Even the ESR spectra of the radicals produced by the chemical reduction in the ethereal solvents (fig. 1b) are narrow, due to the small values of the alkali metal hyperfine splittings. The spectra like that from figure 1 interpreted as due to the interaction of the unpaired electron with three pairs of the two equivalent protons could be ascribed not to the anion radical of acenaphthenone, but to that of the corresponding quinone. Indeed, the experimental proton splitting constants presented in table 1 are very close both with those obtained from the ESR spectra of ace-

---

[1] J. Marquis, *Compt. rend.*, **182**, 1227 (1926).

[2] J. B. Goldberg and A. J. Bard, *J. Phys. Chem.*, **75**, 3281 (1971).

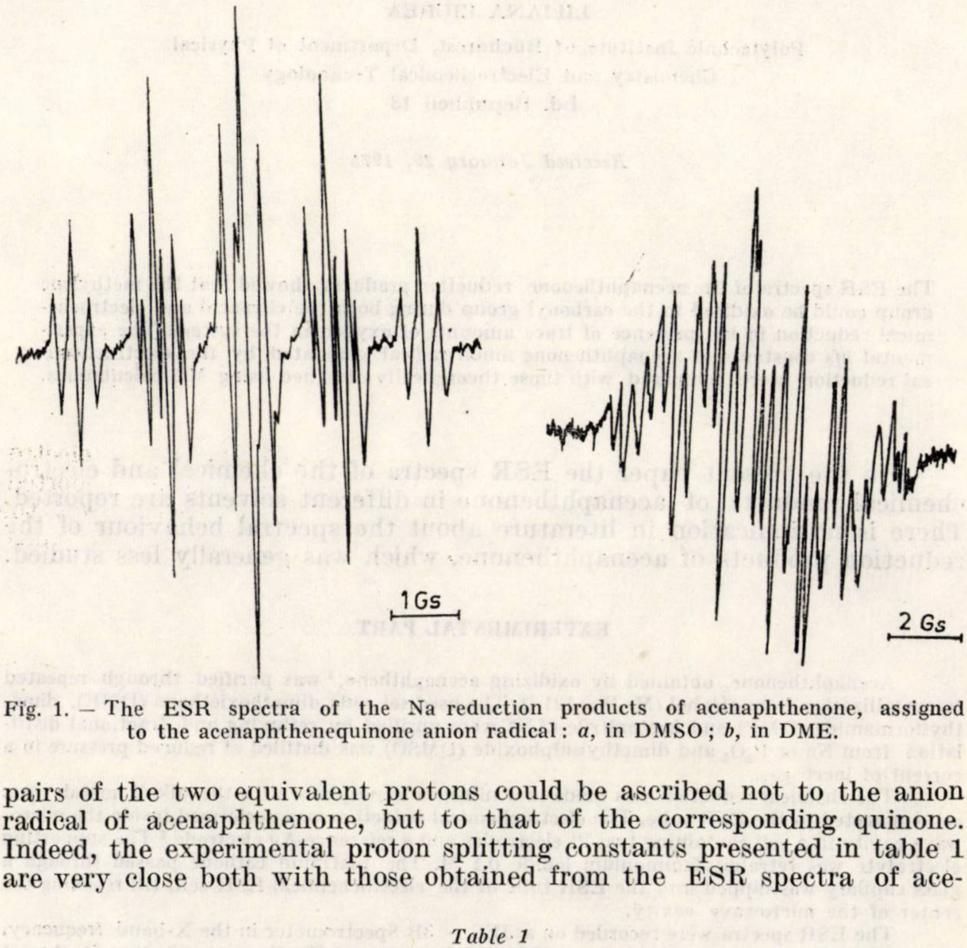

Fig. 1. – The ESR spectra of the Na reduction products of acenaphthenone, assigned to the acenaphthenequinone anion radical: *a*, in DMSO; *b*, in DME.

Table 1

Experimental splitting constants of the reduction product of acenaphthenone assigned to the anion radical of the corresponding quinone

Solvent	Reduction	a_1^{H} (2H)	a_2^{H} (2H)	a_3^{H} (2H)
DMSO	Li	1.20	0.29	1.30
	Na	1.20	0.30	1.33
	electrochem.	1.22	0.28	1.31
DMF	K	1.21	0.31	1.32
	electrochem.	1.18	0.26	1.26

naphthenequinone reduced in the same conditions and those from literature[3], characteristic to the acenaphthenequinone anion radical.

The autooxidation of acenaphthenone methylene group during the reduction due to the trace amounts of oxygen from the system was also evidenced by comparing the absorption spectra of the reduction products of acenaphthenone and acenaphthenequinone. The visible absorption spectrum of the chemical reduction products of acenaphthenone shows one maximum at about 550 nm, whose position depends on the solvent and the cation. The same band was also noticed in the absorption spectrum of the chemical reduction products of acenaphthenequinone, on whose nature the literature opinions[4–6] are contradictory.

The ESR spectra of acenaphthenone radical, electrogenerated in an inert atmosphere using as solvents DMF, a mixture of DME with DMF and AN (fig. 2), are completely different from that showed in figure 1. These spectra have a total length of about 22 Gs, intermediary between that of 45 Gs for acenaphthene anion radical[7] and of 5.6 Gs for acenaphthenequinone anion radical. The spectrum from figure 3 shows the presence of a mixture of acenaphthenone and acenaphthenequinone anion radicals.

The spectrum from figure 2 could be explained due to the interaction of the unpaired electron with the methylene group protons and five aromatic protons. The assignments of the proton hyperfine splittings were based entirely on the MO calculations. The experimental (a^H_{exp}) and the calculated (a^H_{calc}) proton hyperfine splitting constants obtained from the McConnel relation with $Q = -23.7$ Gs are compared in table 2. The spin densities were calculated with the McLachlan approximation, using two models for the methylene group, namely an inductive model (I) and hyperconjugation one (II). The used parameters are also given in table 2

Table 2

Hyperfine splitting constants of acenaphthenone anion radical

Molecule	Position	a^H_{exp}	$\vert a^H \vert_{calc}$	
			I	II
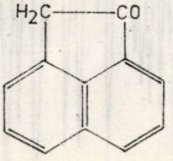	4	6.04	6.00	5.43
	5	0.53	1.37	1.36
	6	7.27	7.73	6.64
	7	2.60	2.27	2.35
	9	1.22	1.35	1.59
	CH_2	1.76	2.42	2.19

Parameters : I – $h_O = 1.65$; $K_{CO} = 1.25$; $K_{C(CO)} = 1.2$; $h_{C(CH_2)} = -0.3$
II – $h_O = 1.65$; $K_{CO} = 1.2$; $h_{H_2} = -0.5$; $h_{C(CH_2)} = -0.1$; $K_{CH_2} = 2.5$

---

[3] R. Dehl and G. K. Fraenkel, *J. Chem. Phys.*, **39**, 1793 (1963).
[4] I. M. Panayotov and I. B. Rashkov, *Compt. rend. Acad. bulg. Sci.*, **21**, 885 (1968).
[5] A. G. Evans, J. C. Evans and E. H. Godden, *J. Chem. Soc.*, (*B*), **1969**, 546.
[6] T. L. Staples and M. Szwarc, *J. Amer. Chem. Soc.*, **92**, 5022 (1970).
[7] A. M. Hermann, A. Rembaum and W. R. Carper, *J. Phys. Chem.*, **71**, 2661 (1967).

The methylene parameters were those proposed by Coulson and Crawford [8] for the methyl group.

The theoretical methylene splitting constant was calculated in the inductive model by the Whiffen relation[9] :

$$a^{\mathrm{H}}_{\mathrm{CH}_2} = 30\left\{(\mathrm{C}_{7,2}+\mathrm{C}_{7,10})^2 + \sum_{i=1}^{6}\left[(\mathrm{C}_{i,2}+\mathrm{C}_{i,10})^2-(\mathrm{C}'_{i,2}+\mathrm{C}'_{i,10})^2\right]\right\}\ \mathrm{Gs}$$

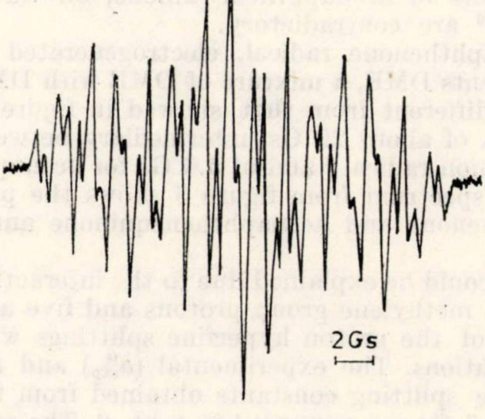

Fig. 2. — The ESR spectrum of acenaphthenone anion radical in AN.

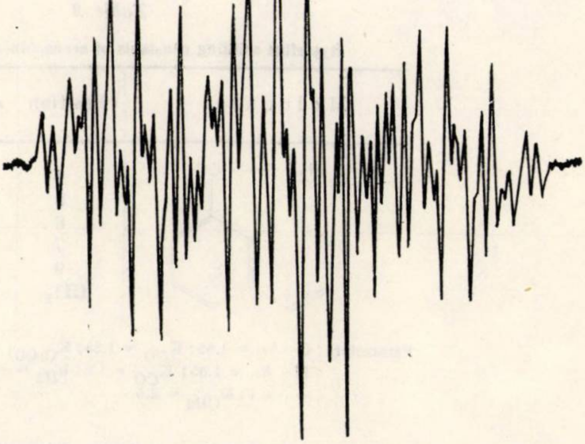

Fig. 3. — The ESR spectrum of a mixture of acenaphthenone and acenaphtenequinone anion radicals in AN.

where i refers to the appropriate molecular orbital, 2 and 10 are the carbon atoms bonded with the methylene group and C, C′ have the known sense in the McLachlan approximation.

---

[8] C. A. Coulson and V. A. Crawford, *J. Chem. Soc.*, **1953**, 2052.

[9] B. H. Whiffen, *Mol. Phys.*, **6**, 223 (1963).

Using the hyperconjugation model, the calculation of the methylene splitting constant in the Hückel approximation was carried out by this relation :

$$a^{\mathrm{H}}_{\mathrm{CH_2}} = 327\ \mathrm{C}^2_{\mathrm{H}} + 19.8\ \mathrm{C}^2_{\mathrm{C}} + 161\ \mathrm{C}_{\mathrm{C}}\mathrm{C}_{\mathrm{H}}$$

$$+ (5.95\ \mathrm{C}_{\mathrm{H}} + 1.46\ \mathrm{C}_{\mathrm{C}})(\mathrm{C}_{\mathrm{C'}} + \mathrm{C}_{\mathrm{C''}}) - 3.09\ (\mathrm{C}^2_{\mathrm{C'}} + \mathrm{C}^2_{\mathrm{C''}})\ \mathrm{Gs}$$

according to Levy [10]. In this equation the C's represent the coefficients of the atomic orbitals from the molecular orbital occupied by an odd electron, namely : C_{H} refers to the pseudo π orbital for the methylene protons while C_{C} ; $\mathrm{C}_{\mathrm{C'}}$ and $\mathrm{C}_{\mathrm{C''}}$ refer to the atomic orbitals for the methylene carbon and for the two carbons (C′ and C″) to which the methylene is attached.

The agreement between the experimental and calculated proton splitting constants of acenaphthenone anion radical is worse for the position *meta* to the carbonyl group, the same as for acenaphthene quinone anion radical [3]. From table 2 one can see that the proton hyperfine splitting constants from *para* and *ortho* position are higher than the methylene splitting constant.

---

[10] D. H. Levy, *Mol. Phys.*, **10**, 233 (1966).

Revue Roumaine de Chimie, **20**, *9–10*, 1213–1217 (1975)

Revue Roumaine de Chimie, 20, 9–10, 1219–1220 (1975)

AN ELECTRON SPIN RESONANCE PROOF OF CHAIR-BOAT CONFORMATION OF THE IMINOXY RADICAL OF ENDO-3-CARBOMETOXYBICYCLO[3.3.1]-NONAN-9-ONE OXIME

H. CĂLDĂRARU [*] and M. MORARU [**]

[*] Institute of Physical Chemistry, Bucharest 13, str. Galați, 31
[**] Department of Organic Chemistry, Polytechnical Institute of Bucharest, Spl. Independenței 78, Romania

Received April 8, 1975

ESR evidence for a chair-boat conformation of the title iminoxy radical is given.

Recent ESR studies on iminoxy radicals reported the conformational effects of 2- and 2,4- substitution in the bicyclo[3.3.1]nonane system.[1] Using as a chair-chair model the iminoxy radical I of adamantanone oxime (*hf* interaction with three protons), the molecular geometry dependence of the β-proton *hfs* [§]indicated for the iminoxy radicals II and III of exo-2-(N-morpholinyl) and exo, exo-2,4-(N-morpholinyl)phenylbicyclo[3.3.1]nonan-9-one oximes respectively a chair-boat conformation (only two interacting protons).

As a continuation of our interest in the ESR studies of conformational effects of substituents in other positions on the same framework, now we present evidence for the chair-boat conformation of the iminoxy radical IV of endo-3-carbomethoxybicyclo[3.3.1]nonan-9-oxime. The iminoxy radical IV was obtained by adding carbon disulphide to an oxime-lead tetraacetate mixture[*] in the ESR sample tube. Each line of the large nitrogen triplet ($a_N = 30.7$ G ; $g = 2.002$) shows two major *hf* splittings ($a_H = 2.5$ G ; $a_H = 2.0$ G) coming from interaction with only two protons. The absence of the third interacting proton, as compared to radical I, indicates for radical IV (as in the case of radicals II and III) a chair — boat conformation.

---

[1] H. Căldăraru and M. Moraru, *J. Amer. Chem. Soc.*, **96**, 149 (1974).

[§] A certain geometry of the·ONCCCH fragment was found to be favorable for the σ-spin density transmission. So, in the chair form only the equatorial β-proton has a significant spin density (a_H (eq) $\sim$ 2.0 G ; a_H (ax) $\sim$ 0. G), while in the boat form none of the two β-protons contributes to the *hf* interaction.[1]

[*] The oxime (m. p. 109—112°) was prepared from corresponding bicyclic ketone, having a satisfactory H, C, N analysis. The endo-3-carbomethoxybicyclo[3.3.1]nonan- 9-one was prepared as described in literature[2]

[2] J. McEuen, R. P. Nelson and R. G. Lawton, *J. Org. Chem.*, **35**, 690 (1970).

The assignment of interacting protons in radical IV follows the more generally proved assignment in similar systems [3] involving a non-flipping cyclohexane ring.

The ESR criterion, significant (~2.0 G) or close to zero value for the β-proton *hfs*, gives an unequivocal answer to the question regarding

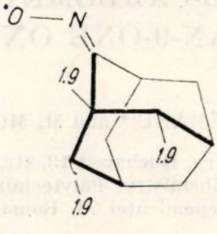

I

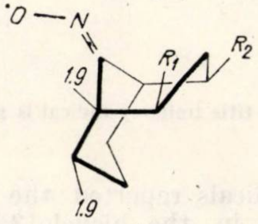

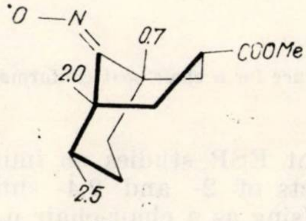

IV

II $R_1 = H$, R_2 = N-morpholinyl
III $R_1 = Ph$, R_2 = N-morpholinyl

the chair-chair or chair-boat conformation of the bicyclo [3.3.1] nonane system. Thus, the ESR method completes the set of methods used for the study of the stereochemistry of this framework.[4]

---

[3] G. A. Russell and A. Mackor, *J. Amer. Chem. Soc.*, **96**, 145 (1974).

[4] K. Kimoto, T. Imagawa and M. Kawanisi, *Bull. Chem. Soc. Japan*, **45**, 3698 (1972) and references therein.

Revue Roumaine de Chimie, **20**, *9–10*, 1221–1225 (1975)

THERMODYNAMIC EXCESS FUNCTIONS IN ELECTROLYTE SOLUTIONS

EXCESS FREE ENERGY OF TERNARY SOLUTIONS FROM INTERFEROMETRIC MEASUREMENTS

RODICA VÎLCU and FLORICA IRINEI

Chair of Chemical Thermodynamics and Electrochemistry, University of
Bucharest, Bd. Republicii 13, Romania

Received June 12, 1974

The effect of the deviation from ideality on the optical properties of the electrolyte solutions was studied. The interferometric measurements at 298 K of binary and ternary aqueous solutions of salts of univalent metals show that systems do not comply with the additivity principle as applied to the refractive indices.

INTRODUCTION

In a series of previous papers [1,2], we endeavoured to give the thermodynamic characterization of the ternary electrolyte solutions with regard to their associated binaries.

The degree of deviation from ideality of the multicomponent solutions of electrolytes was expressed by means of a function defined with regard to Gibbs's free energies of the binary systems (G_1 and G_2), as well as of the ternary system (G_{12}),resulting from the mixing of the binaries.

$$RT \ln \Delta = \frac{m_1 G_1 + m_2 G_2}{m_1 + m_2} - G_{12}. \tag{1}$$

The relation can also be written in another more useful form if Gibbs's free energies of the solutions are expressed with regard to the activity coefficients of the respective components.

We have therefore,

$$\log \Delta = \frac{m_0}{m} (m_1 \log \gamma_{01} + m_2 \log \gamma_{02} - m \log \gamma_{012}) + \\ + (m_1 \log \gamma_1 + m_2 \log \gamma_2 - m \log \gamma_{12}) \tag{2}$$

---

[1] R. VÎLCU and F. IRINEI, *Bull. Soc. chim. belges*, **81**, 479 (1972).

[2] R. VÎLCU and F. IRINEI, *Bull. Soc. chim. belges*, **79**, 3 (1970).

where

$\gamma_{01}, \gamma_{02}, \gamma_{012}$ are the activity coefficients of the solvent binary solutions [(electrolyte)$_1$ + water] and [(electrolyte)$_2$ + water] as well as in the ternary solution [(electrolyte)$_1$ + (electrolyte)$_2$ + water].

$\gamma_1, \gamma_2, \gamma_{12}$ are the activity coefficients of the electrolytes dissolved in the binary solutions and of the electrolyte mixture in the ternary solution.

m_1, m_2, m_{12} are the respective molalities, and

m_0 represents the number of moles of the solvent.

Therefore, the global function of deviation from additivity is a sum of two functions, the first being the solvent characteristic (δ_0) and the second one the dissolved components (δ_1).

$$\log \Delta = \frac{m_0}{m} \log \delta_0 + \log \delta_1$$

By establishing a series of relations, we showed that the deviation function (log Δ) representing a microscopic excess quantity, quite accurately computed with the help of cryoscopic determinations of the activity coefficients, can be correlated with Gibbs's excess free energy $\Delta m G^E$ of the mixture, that represents a macroscopic excess quantity.

On the other hand, with the help of this deviation function, we can compute Harned's coefficients, as well as the individual activity coefficients of the ternary solution components.

The above-mentioned considerations were applied to the study of some ternary systems of alkali metals halides and nitrates.

On the basis of the experimental data, we draw the conclusion that the variation of the non-optical properties of the electrolyte solutions, proceed from the ion interaction. At higher concentrations, the phenomenon of ion association appears, which is intensified as the concentration increases.

We want moreover to study here the effect of the deviation from ideality on the optical properties of the electrolyte solutions. For this end, starting from the fact that the real systems do not comply with the additivity principle as applied to the refractive indices, we can define the function.

$$\delta_n = \frac{m_1 n_1 + m_2 n_2}{m_1 + m_2} - n_{12} \qquad (3)$$

where n_1 and n_2 are the refractive indices of the binary solutions, while n_{12} is the index of the ternary solution resulted from mixing the respective binaries.

In case of the equimolecular mixtures,

$$\delta_n = \frac{1}{2} [(n_1 - n_{12}) + (n_2 - n_{12})] \qquad (4)$$

The deviation function δ_n represents an excess quantity expressed as a function of the refractive index. The deviation from the additivity of the refractive index is a particularly sensitive property to the variation of the forces acting between the considered particles as a function of the distortion of the electron layers and depends to a much higher degree on the intimate structure of the solution.

EXPERIMENTAL RESULTS

We determined with the help of the interferometric measurements, at 298 K, the differences of the refractive indices of the ternary solution and of each of the associated binary solutions for the chlorides and bromides of the alkali metals.

The experimental data results are to be found in the following tables.

Table 1

The deviation from the additivity of the refractive indices

System	Δr	$(n_1 - n_{12})/5.10^4$	$(n_2 - n_{12})/5.10^4$	$\delta n.10^4$
$(Li-Na)Cl-H_2O$	0.20	10.48	− 9.37	2.75
$(K-Cs)Cl-H_2O$	0.32	4.60	− 3.61	2.50
$(Na-K)Cl-H_2O$	0.35	5.51	− 4.20	3.37
$(Li-K)Cl-H_2O$	0.55	7.65	− 5.21	6.12
$(Li-Rb)Cl-H_2O$	0.71	11.04	− 7.42	9.05
$(K-Rb)Br-H_2O$	0.16	4.48	− 4.39	1.20
$(Li-Na)Br-H_2O$	0.20	27.69	−25.96	1.50
$(K-Cs)Br-H_2O$	0.32	20.98	−20.60	0.95
$(Na-K)Br-H_2O$	0.35	19.62	−18.67	3.30
$(Na-Rb)Br-H_2O$	0.51	23.84	−21.54	5.75
$(Li-K)Br-H_2O$	0.55	31.33	−28.90	6.05
$(Li-Rb)Br-H_2O$	0.71	37.34	−33.79	8.85

Table 2

The variation of the deviation function δn with concentration

System $(M_1-M_2)x-H_2O$	$\Delta r/r_1+r_2$	$\delta n \cdot 10^4$		
		$m=1$	$m=2$	$m = 3$
$X=Cl$				
$(Li-Na)Cl-H_2O$	0.113	1.55	2.35	2.75
$(K-Cs)Cl-H_2O$	0.107	1.32	1.48	1.57
$(Na-K)Cl-H_2O$	0.151	3.17	3.28	3.37
$(Li-K)Cl-H_2O$	0.260	5.95	6.02	6.12
$(Li-Rb)\ Cl-H_2O$	0.312	8.82	8.98	9.05
$X= Br$				
$(K-Rb)Br-H_2O$	0.058	1.13	1.17	1.20
$(Li-Na)Br-H_2O$	0.113	1.38	1.45	1.50
$(K-Cs)Br-H_2O$	0.107	0.85	0.91	0.95
$(Na-K)Br-H_2O$	0.151	0.18	0.27	3.30
$(Na-Rb)Br-H_2O$	0.206	4.58	4.95	5.75
$(Li-K)Br-H_2O$	0.260	5.12	5.70	6.05
$(Li-Rb)Br-H_2O$	3.12	8.49	8.60	8.85

In figure 1, the variation is shown of deviation function (δ_n) with regard to the differences between the radii of the ternary mixture components.

Since the measurements are made on systems with common ions, at a constant ionic strength, the observed deviation from additivity is certainly due to the interactions between ions with similar charges, as well as to the processes of formation of the nonstructures.

It results from figure 1 that the variation δ_n, as a function of the difference Δr between the ion radii of the component cations, is not linear as in the case of function log Δ.

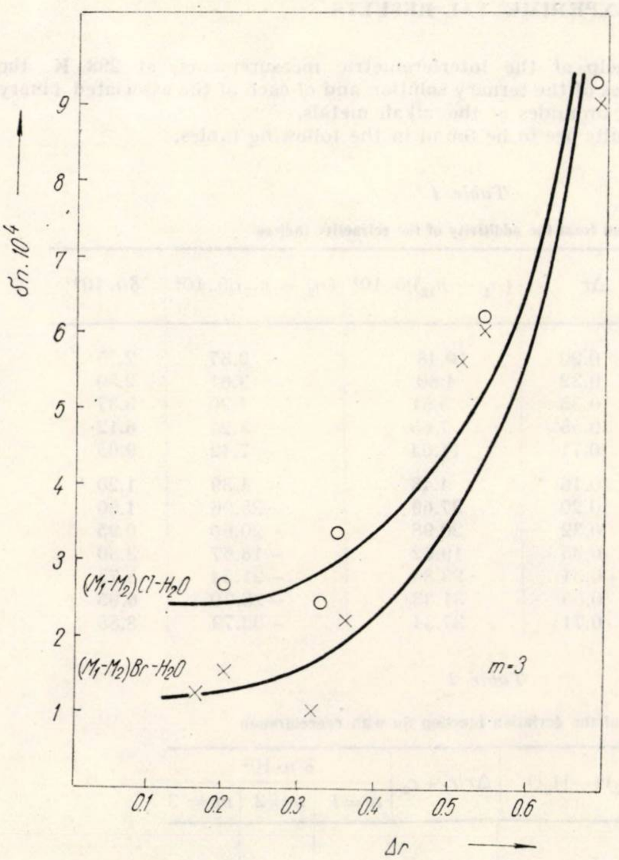

Fig. 1. — The variation of deviation function δ_n with differences between the radii of the ternary mixture components.

A linear dependence occurs only in case of the systems containing cations of various groups of hydration (Na-K; Li-K; Li-Rb).

In the case of systems containing cations belonging to the same hydration group (Li-Na; K-Rb), the influence of the hydration effect on the refractive index of the ternary solution is large enough and it is easy to bring it into relief by this method.

If δ_n is represented with regard to $\frac{\Delta r}{r_1 + r_2}$ the dependence is linear and follows a straight-line passing through the origin $\delta_n \simeq 24.80 \frac{\Delta r}{r_1 + r_2}$ for systems where $x = \mathrm{Cl}$.

This fact confirms the preponderant rôle of the polarization component in the interaction energy of the systems under consideration.

The relatively small variation with the concentration of the deviation function (δ_n) points out the rather small contribution of the interactions of a higher order in this interval of concentrations.

In figure 2, it is to be remarked that both the deviation functions studied by us ($\log \Delta$) and (δ_n) vary linearly with $\frac{\Delta r}{r_1 + r_2}$, though with different slopes.

Their interdependence (for systems ($M_1 - M_2$)$Cl-H_2O$ in the case of a 3 molar concentration) can be expressed by relations (5)

$$\log \Delta \simeq -0.018 + 0.180\,\delta_n \tag{5}$$

$$\Delta m G^E = -\frac{2.303}{4} RT \log \Delta \tag{6}$$

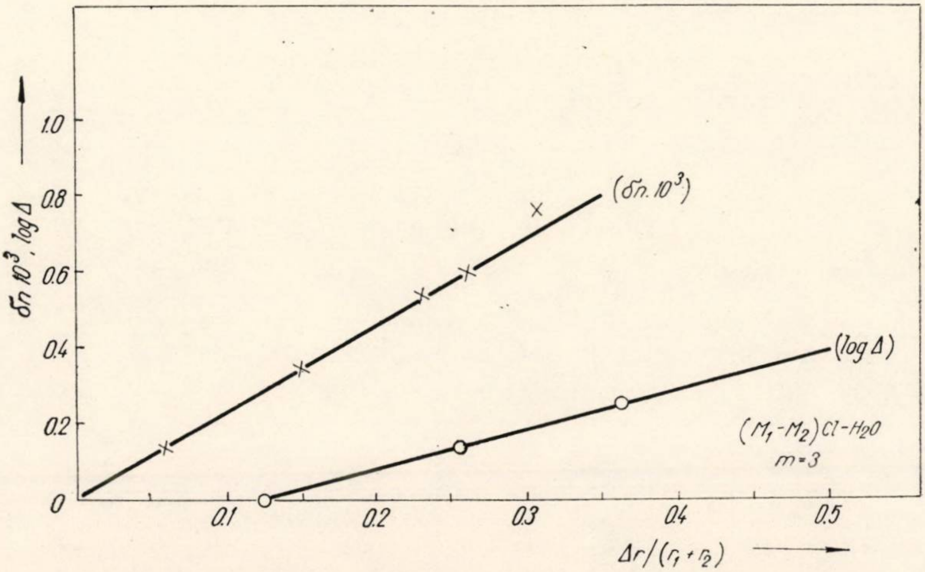

Fig. 2. — The variations of deviation functions, δ_n and $\log \Delta$ with $\Delta r/(r_1 + r_2)$.

Relation (6), deduced by us,[3] combined with equation (5) leads to equation (7) that permits to compare Gibbs's excess free energy of the ternary solutions, with the help of optical measurements

$$\Delta m G^E \simeq -\frac{2.303}{4} RT\,(-0.018 + 0.180\,\delta_n) \tag{7}$$

for systems ($M_1 - M_2$) $Cl - H_2O$ where M_1 and M_2 are Li^+, Na^+, K^+, Rb^+, Cs^+.

---

[3] R. Vîlcu and F. Irinei, *Rev. Roumaine Chim.*, **16**, 793 (1971).

Revue Roumaine de Chimie, **20**, *9–10*, 1227–1230 (1975)

THERMAL PROPERTIES OF $BaCl_2$ HIGH TEMPERATURE HEAT CONTENT

D. I. MARCHIDAN and LIANA PANDELE

Centre of Physical Chemistry
Str. Galaţi 31, Bucharest 13

Received April 3, 1975

The heat content of pure barium chloride was determined by means of the drop calorimeter. The measurements were carried out both for solid state and for liquid state. The existence of a crystalline transition from phase α to phase β was pointed out in the neighbourhood of the fusion point. By processing experimental data, heat capacities were evaluated.

Thermodynamic functions are usually derived from the experimentally determined enthalpy values. Determinations of thermal properties of fused salts have a practical importance due to their utilization in metallurgy, electrochemistry and nuclear technology and a theoretical importance for testing structural models.

Thermochemical properties of pure salts and of their mixture have been continuously investigated in this laboratory for the past few years. [1–3]

An isoperibolic drop calorimeter with copper block was used for experimental measurements.

EXPERIMENTAL PROCEDURES

The experimental technique and the installation has been described in detail in a previous paper, [4] the accuracy of the measurements is considered to be ±0.4 per cent. In order to account for the heat content for the container and the heat lost during the drop, similar experiments were made with the empty container at the same temperatures.

The essential features of the installation consist of the furnace with an inoxiterm steel core and the copper-block calorimeter proper. The temperature of the furnace was kept constant by means of a proportional thermoregulating device and was verified using a thermocouple Pt—Pt Rh (10%). The temperature variations of the calorimetric proper were measured by means of a thermistor characterised by a high sensitivity and reproducibility. The measurement of a small temperature variation of 0.001 K was possible because of the large temperature coefficient of the thermistor.

---

[1] D. I. Marchidan and Cr. Telea, *Rev. Roumaine Chim.*, **13**, 1291, (1968); **14**, 1495 (1969); **15**, 1675 (1970).

[2] D. I. Marchidan and L. Vasu, *Rev. Roumaine Chim.*, **17**, 1649 (1972).

[3] D. I. Marchidan and L. Pandele, *Rev. Roumaine Chim.*, **20**, 299 (1975).

[4] D. I. Marchidan and M. Ciopec, *Studii şi Cercetări Chim. Acad. R.S.R.*, **17**, 737 (1969).

The calibration of the calorimetric unit has been carried out both electrically and using the National Bureau of Standards synthetic saphire. [5]

Pure barium chloride, which was dried by passing a dry stream of nitrogen and hydrogen chloride for several hours was used for experimental measurements. The dried salt was handled in anhydrous medium (in dry-box) and sealed in a platinum crucible.

The thermal contributions of the container do not exceed 25% of the whole contribution, a necessary condition for obtaining more accurate results.

RESULTS AND DISCUSSIONS

Thermal properties of barium chloride were determined previously by studies on melting and premelting effects of the alkaline-earth halides.[6,7]

The heat content and the heat capacity of pure barium chloride, in the temperature range 911 − 1264 K, has been determined in our laboratory. The experimental results are listed in table 1 and plotted in figure 1.

As seen from figure 1, a steep variation of heat content values in terms of temperature takes place around 1198 K. This variation appeared due to a first order transition in solid state, from phase α to phase β, with a variation of heat $\Delta H = 17572.8$ joule/mol. This transition was also mentioned by the previously cited authors. [6,7]

Table 1

Experimental and calculated enthalpy increments for solid and liquid barium chloride

T(K)	$H_T - H_{298.15})$		Deviation	
	exp.(joul/mol	calc.(joul/mol)	(joul./mol.)	%
	Solid			
911.3	51592.9	51060.28	532.6	1.04
949.1	54011.25	54581.11	−569.86	−1.04
964.2	54756	55983.59	−1227.59	−2.18
1033.1	63647	63952.44	−305.44	−0.47
1101.6	69800.4	70437.64	637.24	0.90
1129.2	71554.34	71412.5	141.84	0.20
1158	73270.2	74026.67	−756.47	−1.04
1186.3	76449.6	76675.14	−225.54	−0.29
1195.5	77408.18	77532.03	−123.84	−0.16
	transition α−β			
1206.6	85130			
1215.9	96918			
1218.8	97357.4			
1230.9	98440.3			
	Liquid			
1243.8	116689.7	117608.5	−918.8	−0.78
1245.5	117696.9	117795.5	−99.6	−0.09
1248.8	118524.3	118158.7	365.6	0.30
1264.1	120206.3	119824.7	363.6	0,30

[5] G. Furukava, T. Douglas, R. McCoskey and D. Ginnings, *J. Res. Nat. Bur. Stand.*, **57**, 67 (1956).

[6] A. S. Dworkin and M. A. Bredig, *J. Phys. Chem.*, **64**, 269 (1960).

[7] G. I. Ianz, F. J. Kelly and J. Perano, *Trans. Faraday Soc.*, **59**, 9 (1963).

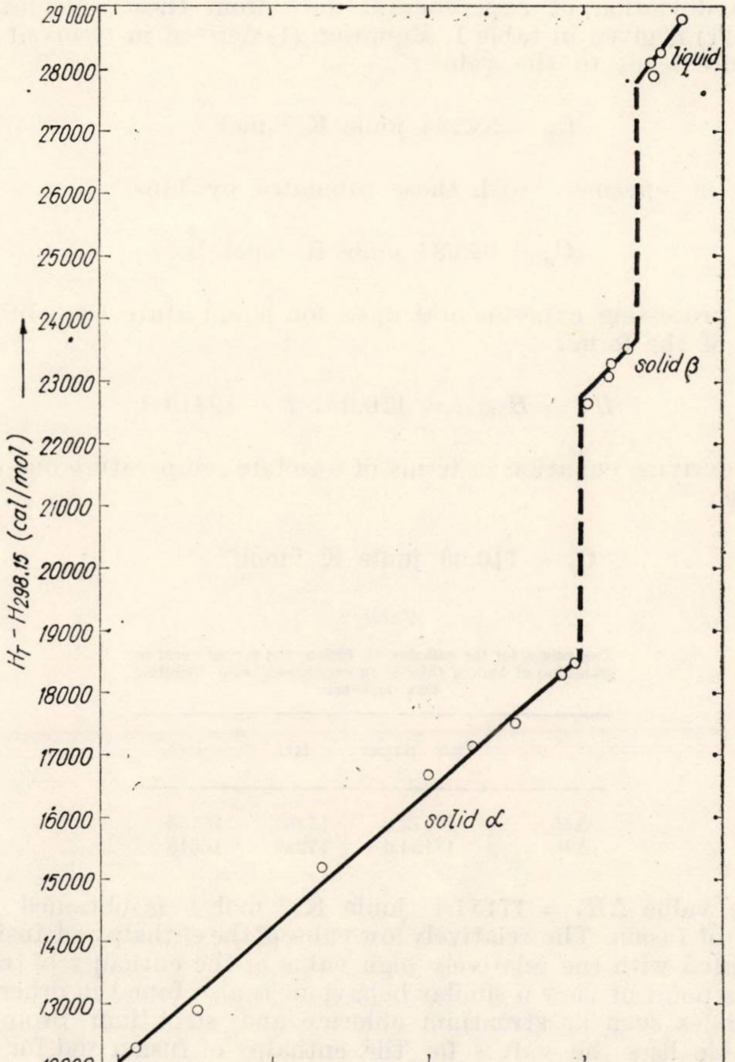

Fig. 1. – Heat content variation of barium chloride in terms of temperature.

Experimental data concerning the heat content of barium chloride for temperatures below transition temperature verify the equation below, derived by the least squares method :

$$H_T - H_{298.15} = 93.144 - 33821.78 \qquad (1)$$

The deviation of experimental data from those calculated from equation (1) is given in table 1. Equation (1) derived in terms of absolute temperature leads to the value :

$$C_p = 93.144 \text{ joule K}^{-1} \text{ mol}^{-1} \tag{2}$$

which is in agreement with those tabulated by Ianz [7]

$$(C_p = 94.684 \text{ joule K}^{-1} \text{ mol}^{-1}).$$

By processing experimental data for liquid state one obtained an equation of the form :

$$H_T - H_{298.15} = 110.081\ T - 19310.4 \tag{3}$$

By deriving equation in terms of absolute temperature one obtained the value :

$$C_p = 110.08 \text{ joule K}^{-1} \text{ mol}^{-1} \tag{4}$$

Table 2

The values for the enthalpy of fusion and for the heat of transition of barium chloride in comparison with literature data (joule/mol)

	This paper	Ref.[6]	Ref.[7]
ΔH_{tr}.	17572.8	17364	17154
ΔH_f	17154.4	17280	16318

The value $\Delta H_f = 17154.4$ joule K^{-1} mol^{-1} is obtained for the enthalpy of fusion. The relatively low value of the enthalpy of fusion could be correlated with the relatively high value of the enthalpy of transition. From this point of view a similar behaviour is also found in other alkaline earth halides such as strontium chloride and strontium bromide. The above table lists the values for the enthalpy of fusion and for the heat of transition of barium chloride in comparison with those from literature. [6,7]

Revue Roumaine de Chimie. **20**. *9–10*. 1231–1241 (1975)

THE CHRONOPOTENTIOMETRIC STUDY IN THE MOLTEN SYSTEM AgCl + KCl + (DISSOLVED) Cl_2

S. STERNBERG and VALERIA PETRESCU

Polytechnic Institute, str. Polizu 1, Bucharest

Received November 13, 1974

The chronopotentiometric method has been used to study the chlorine diffusion in the neighbourhood of a chlorine-spectral carbon electrode in the molten system AgCl + KCl at various temperatures (400°—700°). Chronopotentiometric curves were obtained over a 0.005 A—0.300 A intensity range. The intensity range in which Sand's equation holds at various temperatures has been established.

*

The present paper is concerned with the study of chlorine diffusion in the neighbourhood of a chlorine-spectral carbon electrode in the system AgCl + KCl at various temperatures (400° — 700°) by means of the chronopotentiometric method. We also want to establish the intensity range in which Sand's equation is verified for chlorine dissolved in this system. The chronopotentiometric method has also been applied for similar purposes in the molten systems $PbCl_2$ and AgCl.[1]

1. EXPERIMENTAL

The working cell is illustrated in fig. 1.

A chlorine flow is bubbled through the molten salt for four hours at a rate of approx. 10 l/h. The spectral carbon electrode C adsorbs chlorine from the molten salt and a chlorine electrode is obtained whose potential is measured in relation to a silver $(Ag)_r$ reference electrode.

The previous electrochemical formation of carbon was found to favour the potential increase of the chlorine electrode thus formed. This electrochemical formation consisted in successive anodic and cathodic polarizations under galvanostatic conditions with currents around 0.1.—0.2 A.

It must be noted that the 4-hr bubbling time before performing the chronopotentiograms is not conditioned only by reaching the reversible potential of the chlorine electrode. It has been found that the reversible potential established at a certain temperature is reached in about 1/2 h from the onset of chlorine bubbling. However, after such a time lapse the melt is not saturated with dissolved chlorine (under the conditions of the applied rate) and chronopotentiometric curves presenting a transient have been obtained only after approx. 4 hr of bubbling. Thus, fig. 2 shows a qualitative plot of chronopotentiometric curves obtained in the case of sufficient bubbling (> 4 hr), curve *a*, and of insufficient bubbling (< 4 hr), curve *b*.

---

[1] **J. D. VAN NORMAN and R. J. TIVERS, in "Molten Salts, Characterisation and analysis", Ed. G. Mamantov, Marcel Dekker, New York, 1969.**

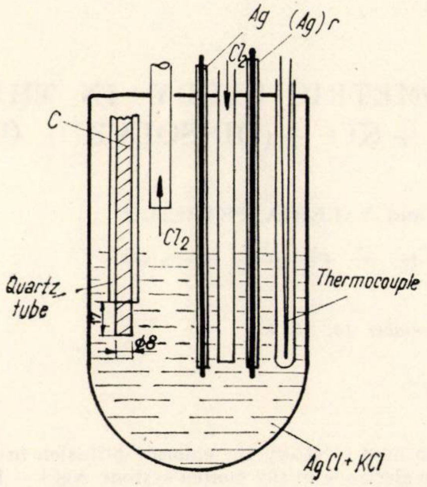

Fig. 1. – Diagram of the cell.

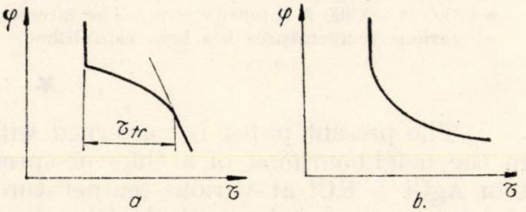

Fig. 2. – Chronopotentiometric curves obtained under different conditions of chlorine bubbling.

2. RESULTS AND DISCUSSION

The investigated current intensities range was placed between 2 mA up to 120 mA for 400°.

Extremely clear chronopotentiometric curves were obtained for intensities included in the 60 – 120 mA range at 400°, by using an oscilloscopic technique with photography, as seen in fig. 3. The transient was measured on these curves according to the procedure suggested by Reinmuth [2] and ranges within 0.53 – 2.07 seconds, as a function of the current intensity. Under such conditions, the diffusive layer is not perturbed by convection and Sand's equation is obeyed, as seen in fig. 4, which plots product $I\ \tau^{1/2}$ as a function of I.

For current intensities up to 35 mA, curves φ/τ were collected by means of an electronic voltmeter coupled between the carbon electrode and the reference electrode $(Ag)_r$. Cathodic polarization was made after saturating the melt with chlorine, by interrupting the bubbling process throughout the process. A galvanostatic circuit as seen in fig. 5 was used.

With current intensities between 2 mA and 10 mA cathodic polarization curves obtained φ/τ had a smooth slope from the beginning of the process to its end, the slope dropping towards the end of the process

---

[2] W. H. Reinmuth, *Analyt. Chem.*, **33**, 485 (1961).

(fig. 6). Such curves do not present the characteristics of transient curves. The duration of the process is long compared to the usual transients (of the order of seconds). For this reason, convection certainly occurs,

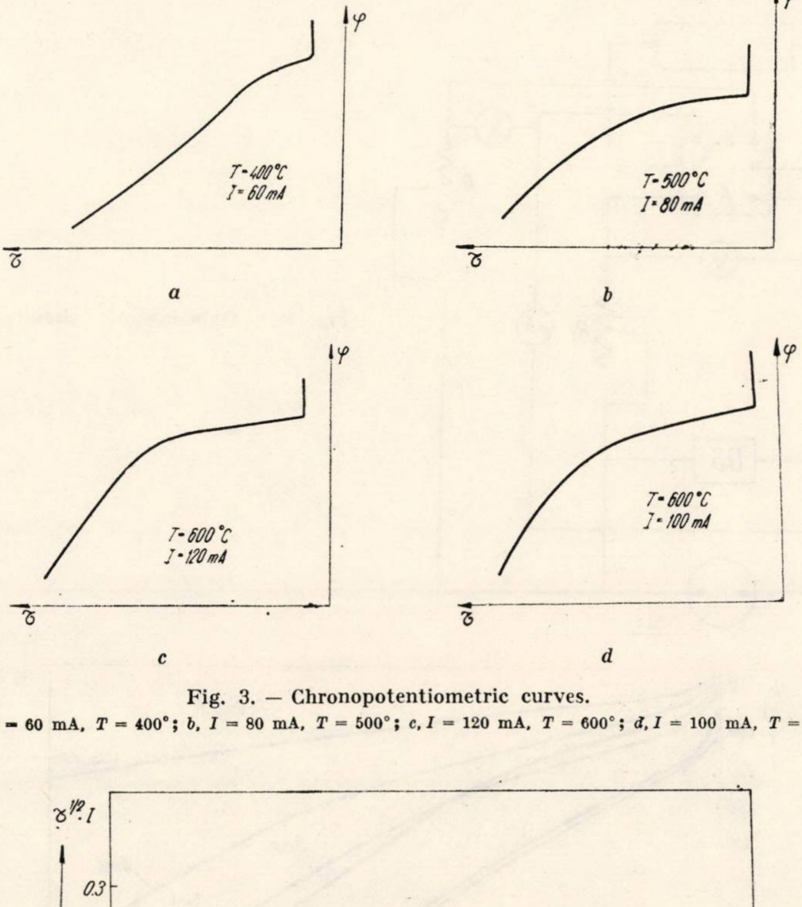

Fig. 3. — Chronopotentiometric curves.
a, $I = 60$ mA, $T = 400°$; *b*, $I = 80$ mA, $T = 500°$; *c*, $I = 120$ mA, $T = 600°$; *d*, $I = 100$ mA, $T = 60°$

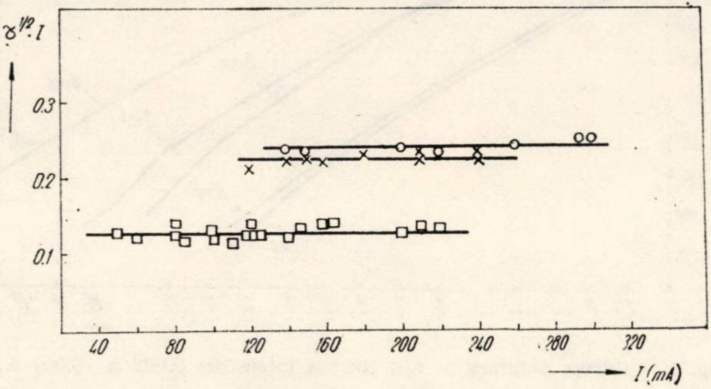

Fig. 4. — Product $I\,\tau^{\frac{1}{2}}$ as a function of I; $T = 400°$.

perturbing the conditions of chlorine diffusive transport towards the carbon/melt interface. In addition, current densities are probably smaller than the limit current density. As the electrode apparent surface is 4.77 cm^2, apparent current densities for these curves are 0.42 mA/cm^2 up to 2.1 mA/cm^2, respectively.

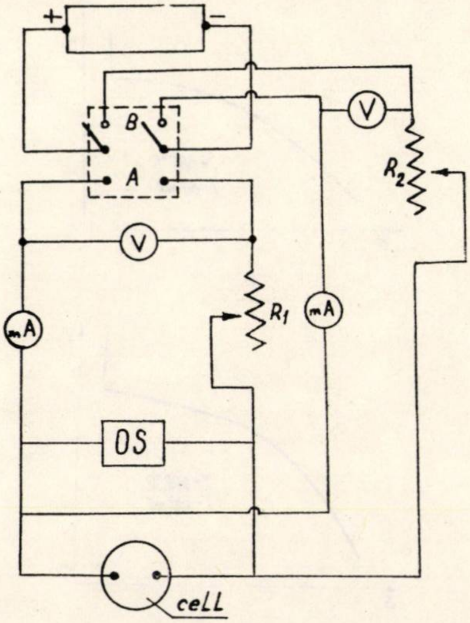

Fig. 5. — Galvanostatic circuit.

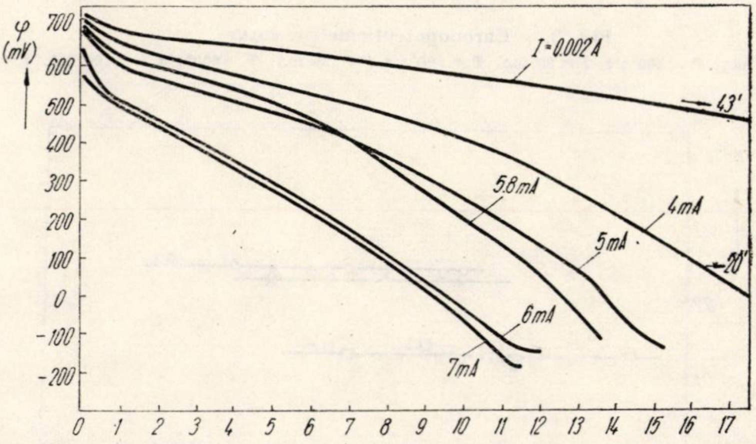

Fig. 6. — Curves obtained at low current intensities 0.002 A — 0.007 A.

Cathodic polarization curves φ/τ obtained with current intensities between 15 mA and 35 mA had a different aspect compared to the previous ones (fig. 7), i.e. a sudden potential drop appears at the beginning of the process, followed by a zone presenting a very smooth slope with a slight drop towards the end of the process.

Some of these curves (15, 20, 25 mA) present an aspect which resembles to a certain extent the transient curves, except for the fact that the slope in the final zone is too smooth. The initial dropping zone and the fact that the potential variation in the second zone ranges around 100 — — 200 mA cause these curves to look like the typical chronopotentiometric ones. The transient determination in these curves was made by the method presented by Sternberg and Vişan [3], i.e., by plotting equation :

$$t_2^{\frac{1}{2}} \cdot t_1^{\frac{1}{2}} \exp\left(-\Delta E - \frac{nF}{RT}\right) = \frac{K}{2\,i_0}\left[1-\exp\left(-E\,\frac{nF}{RT}\right)\right] \qquad (1)$$

into coordinates

$$Y = t_2^{\frac{1}{2}} - t_1^{\frac{1}{2}} \exp\left(-\Delta E\,\frac{nF}{RT}\right), \qquad X = \left[1-\exp\left(-E\,\frac{nF}{RT}\right)\right] \qquad (2)$$

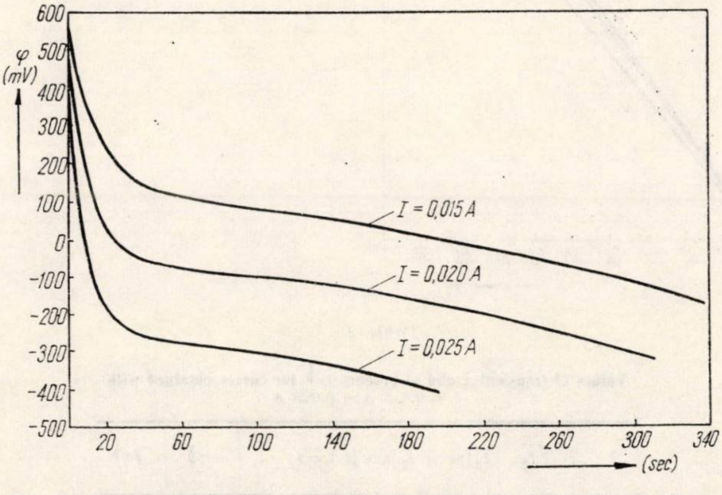

Fig. 7. Curves obtained for current intensities $I = 0.015$ A -0.025 A.

Fig. 8 shows the linear extrapolation of Yvalues for $X \to 1$.

Values obtained thus for Y corresponding to $\sqrt{t_2}$ lead to transient τ calculated in table 1 together with product $I\,\tau^{\frac{1}{2}}$. It has been found that the values of this product are increasing and therefore curves φ/τ for these current intensities fail to obey Sand's equation. This result was somehow expected, considering the fact that convection appears with long times and it perturbs the diffusive layer. Nevertheless the aspect of those curves φ/τ which differs from the previous ones resembles the aspect of transient curves obtained within a 60 — 120 mA intensity range.

---

[3] S. Sternberg and T. Vişan, *Rev. Roumaine Chim.*, **18**, 221 (1973).

Fig.4 also exhibits the values of product $I\,\tau^{\frac{1}{2}}$ obtained at 15, 20, 25 mA intensities corresponding to curves in fig. 7. These values have been found to be higher than those at which product $I\,\tau^{\frac{1}{2}}$ is constant, according to Sand's equation.

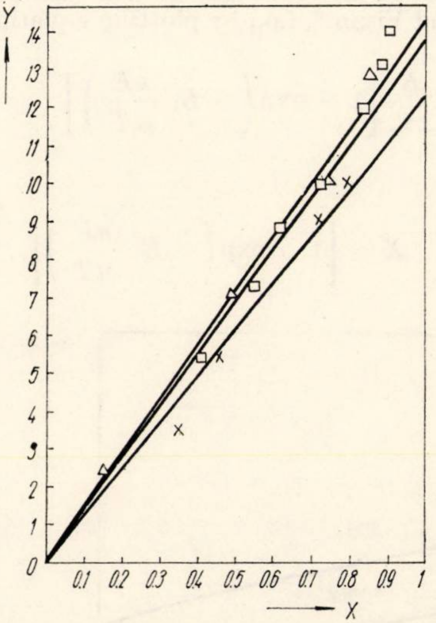

Fig. 8. — Plot of Y values for $X \rightarrow 1$.

Table 1

Values of transient τ and of product $I\tau^{\frac{1}{2}}$ for curves obtained with $I = 0.015$ A — 0.025 A

I	$\sqrt{t_2}$	t_2[sec]	t_1[sec]	$\tau = t_2 - t_1$	$\tau^{\frac{1}{2}}$	$I\tau^{\frac{1}{2}}$
0.015	14	196	60	136	11.7	0.175
0.020	14.4	208	60	148	12.2	0.244
0.025	12.5	156	40	116	10.8	0.269

The value of product $I\,\tau^{\frac{1}{2}}$ at 400° (in fig. 4) in the validity domain of Sand's equation (60 — 120 mA) was used for calculating the value which the transient should assume at a 0.02 A current

$$I_1\,\tau_1^{\frac{1}{2}} = I_2\,\tau_2^{\frac{1}{2}} = 0.075\ \text{sec}^{\frac{1}{2}} \tag{3}$$

$$\tau_2^{\frac{1}{2}} = \frac{I_1\,\tau_1^{\frac{1}{2}}}{I_2} = \frac{0.075}{0.02} = 3.75$$

Therefore

$$\tau = 10.4 \text{ sec}$$

By comparing this value (10.4 sec) to the value resulted from curve $I = 0.02$ A în fig. 7, indicated in table 1, i.e. 148 seconds, it results that experimental transients are much smaller than the theoretical ones, for a domain of low intensities (0.015 — 1 — 0.25 A). This is due to the prevailing influence exerted by convective currents on transients that are longer than a few seconds.

It results from the above that for relatively low current intensities (2 — 35 mA) the cathodic polarization curves obtained (figs. 6 and 7) correspond to the reduction process of chlorine dissolved throughout the melt mass (due to convection) rather than in a very thin diffusive layer close to the electrode, as in the case of curves with 1 — 2 sec. transient (chronopotentiometric curves). Accordingly, such curves may be used for a rough estimation of the chlorine amount dissolved in salt. Table 2 presents the durations of these processes for various current intensities and the electricity quantities corresponding to the reduction of the dissolved chlorine Q_{dis}. This quantity certainly includes also that one corresponding to the adsorbed chlorine on the electrode which is however considered to be small, since the working procedure involved a non-active carbon. The average value of Q_{dis} is 5.17 coul. It corresponds to 5.17 coul/96500 = $5.36.10^{-5}$ moles dissolved chlorine. Knowing that the molten salt volume is 65 cm^3, the chlorine solubility in the system AgCl/KCl at 400° results to be equal to $8.24.10^{-7}$ moles/cm^3. This value is highly plausible, considering the existing data in the literature [3,4] for pure component salts, i.e. $C_{\text{KCl}}^{848°} = 10.40.10^{-7}$ moles/cm ; $C_{\text{AgCl}}^{518°} = 2.31.10^{-7}$ moles/cm.

Table 2

Values of Q_{dis} for various current intensities

N° of curve	$I_d A$	t d [sec]	Q_{dis} [coul]
41	0.002	2 580	5.16
38	0.004	1 190	4.76
36	0.005	1 050	5.25
39	0.005	915	4.58
27	0.0058	820	4.77
37	0.006	710	4.26
40	0.007	690	4.83
29	0.010	663	6.65
31	0.015	385	5.77
32	0.020	310	6.20
33	0.025	190	4.75
		Total	56.98
		Average	5.17

---

[4] Y. M. Ryabukhin, *Zhur. neorg. Khim.*, **7**, 1101 (1962).

Attempts were made to evaluate the chlorine diffusion coefficient in the system AgCl + KCl by using the chlorine solubility value obtained as above and also by using the potentiometric constant $i\,\tau^{\frac{1}{2}}$ obtained with large current densities.

In Sand's equation :

$$i_0\,\tau^{\frac{1}{2}} = \frac{nF\,\pi^{\frac{1}{2}}\,D^{\frac{1}{2}}\,C}{2} \tag{4}$$

one introduces $i_0 = I/S$, where $S = \beta\,S_a$. The undulation degree was denoted by $\beta = 20$ and $S_a = 4.77$ cm² is the apparent surface of the carbon electrode

$$\frac{I\,\tau^{\frac{1}{2}}}{S} = \frac{nF\,\pi^{\frac{1}{2}}}{2}\,D^{\frac{1}{2}}\,C \tag{5}$$

The following values :

$$a = \frac{nF\,\pi^{\frac{1}{2}}}{2} = 1.71.10^5$$

$$C = 0.824.10^{-6}\ \text{moles/cm}^3$$

$$I\,\tau^{\frac{1}{2}} = 0.080\ \text{A.sec}^{\frac{1}{2}}$$

$$S = 20 \times 4.77 = 95.4\ \text{cm}^2$$

were used to determine the diffusion coefficient D

$$D^{\frac{1}{2}} = \frac{I\,\tau^{\frac{1}{2}}}{S.a.C} = \frac{0.080}{95.4 \times 1.71 \times 10^5 \times 0.824 \times 10^{-6}} = 5.94 \times 10^{-3}$$

$$D = 3.5 \times 10^{-5}\ \text{cm}^2 \times \text{sec}^{-1} \tag{6}$$

This value is comparable in terms of magnitude with the chlorine diffusion coefficients in molten halides, reported in the literature [1,5-7].

Starting from the intensity range for which Sand's equation was found to hold for the system investigated at 400°, determinations of some chronopotentiograms were made at 500, 600 and 700° applying a similar oscilloscopic technique with photography. The duration of the transient was found to increase with the rise in temperature for the same current intensity. In order to maintain the transient duration within the limits

---

[5] E. A. Ukshe, L. S. Leonova, G. N. Yavanova and G. N. Bukun, *Elektrokhimiya*, **7**, 390 (1971).

[6] Y. M. Ryabukhin, *Zhur. fiz. Khim.*, **39**, 2927 (1965).

[7] A. E. Potter and B. S. Del Duca, NASA Tech. Note N°. D-4173 (1967); *Chem. Abstr.*, **68** (1968).

of 1 – 2 seconds, the intensity domain was extended to these temperatures, being displaced towards higher intensities and reaching 700° up to 300 mA (fig. 9). The increase of product $I\tau^{\frac{1}{2}}$ with temperature was plotted in fig. 10. This increase is explained by the increase of chlorine solubility with temperature, a fact which has been reported in the literature.[4,8–12]

The literature has suggested various equations linking the chlorine solubility in molten halides to temperature [4,9,11] all of them in log form.

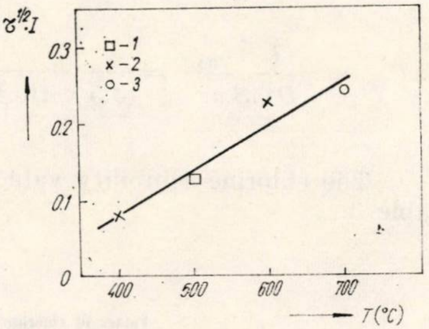

Fig. 9. – Product $I\tau^{\frac{1}{2}}$ as a function of intensity for $T = 500°$ (1) $T = 600°$ (2) ; $T = 700°$ (3).

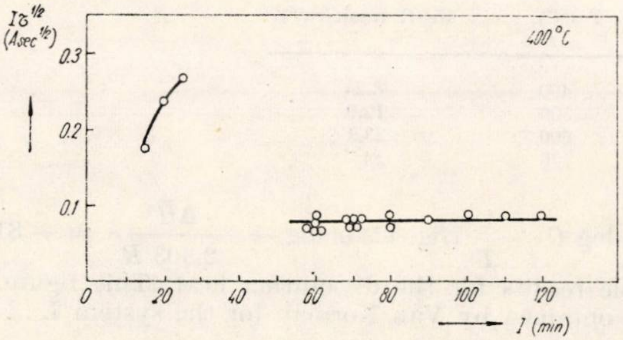

Fig. 10. – Variation of product $I\tau^{\frac{1}{2}}$ with temperature.

From the slope of line $\log C_{Cl_2} \Big/ \frac{1}{T}$ it is possible to calculate the dissolution heat $\Delta\bar{H}°$.

Attempts were made to verify whether the logarithmic relation for the link between solubility and temperature applies to the studied system AgCl + KCl.

---

[8] Y. M. Ryabukhin and N. G. Bukun, *Zhur. neorg. Khim.*, **13**, 1141 (1968).

[9] L. S. Leonova and E. A. Ukshe, *Elektrokhimiya*, **6**, 892 (1970).

[10] L. S. Leonova, Y. M. Ryabukhin and E. A. Ukshe, *Elektrokhimiya*, **5**, 464 (1969).

[11] Y. M. Ryabukhin *Zhur. neorg. Khim.*, **11**, 2415 (1966).

[12] V. Sh. Palanker and A. M. Skundin, *Novoe Proizvod. Khim. Istocinikov toka*, **3**, 65 (1967) ; *Chem. Abstr.*, **69** (1968).

To do this, Sand's equation was used (4) for calculating the chlorine solubility in an AgCl + KCl mixture at a temperature of 500 – 800°; chlorine solubility at 400° was assumed to be that calculated by means of curves in figs. 6 and 7. Considering that the diffusion coefficient varies slightly with temperature, as it results from the literature for a number of systems [9,13] a constant value of the diffusion coefficient was assumed in calculations.

Experimentally obtained values were used for $I\tau^{\frac{1}{2}}$ from figs. 4 and 9. For example, for 500°:

$$C_{500} = \frac{(I\,\tau^{\frac{1}{2}})_{500}}{D^{\frac{1}{2}}.S.a.} = \frac{0.125}{(3.5\times 10^{-5})^{\frac{1}{2}} \times 95.4 \times 1.71 \times 10^{5}} = 12.9 \times 10^{-7} \tag{7}$$

The chlorine solubility values at various temperatures are listed in table 3.

Table 3

Values of chlorine solubilities over the temperature range 400 – 700°

T (°C)	$10^7 \cdot C$ (mole/cm³)
400	8.24
500	12.9
600	23.9
700	24.7

The slope of curve log $C \Big/ \dfrac{1}{T}$ (fig. 11) being $-\dfrac{\Delta\bar{H}^\circ}{2.303\,R} = -818$, a value of 3740 cal/mole results for the dissolution heat. This figure is extremely close to that obtained by Van Norman for the system LiCl +

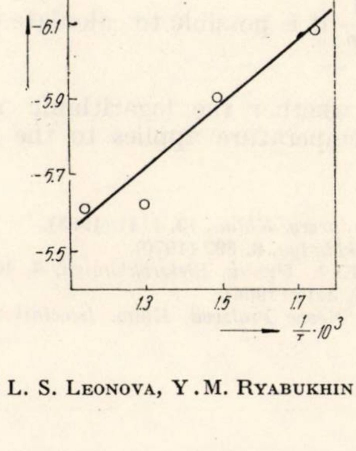

Fig. 11. – Variation of chlorine solubility with temperature.

---

[13] L. S. Leonova, Y. M. Ryabukhin and E. A. Ukshe, *Elektrokhimiya*, **5**, 210 (1969).

$+$ KCl in the temperature range 400 – 550° ($\Delta \bar{\bar{H}}^\circ = 3700$ cal/mole).

CONCLUSIONS

Three types of chronopotentiometric curves were obtained :

1. Diffusive-controlled chronopotentiograms verifying Sand's equation were obtained at large current densities, which vary between 60 mA and 310 mA as a function of temperature.

2. At very low current densities, the process is controlled by the dissolution of the whole chlorine amount in the melt.

3. At intermediate current densities, the electrode process is due both to diffusion and to convection.

Revue Roumaine de Chimie, **20**, *9–10*, 1231–1241 (1975)

[illegible] KCl in the temperature range 100 — 250° [illegible] [illegible] [illegible],

CONCLUSIONS

Three types of chronopotentiometric curves were obtained:

1. Diffusion-controlled chronopotentiograms [illegible] Sand's equation were obtained at [illegible] current densities, which [illegible] [illegible] [illegible] and [illegible] mA as a function of temperature.

2. At very low current densities, the process is controlled by the [illegible] of the whole [illegible] in the melt.

3. At intermediate current densities, the electrode process is due both to diffusion and to [illegible].

Revue Roumaine de Chimie, **20**, *9–10*, 1243–1252 (1975)

ANGULAR DEPENDENCE OF OVERLAP FOR *s*, *p*, *d* AND *f* FUNCTIONS

WILLIAM SMITH and DENIS W. CLACK
Department of Inorganic Chemistry,
University College, P.O. Box 78, Cardiff, CF1 1XL WALES (U.K.)

Received June 17, 1974

The angular behaviour of *s*, *p*, *d* and *f* type orbitals has been investigated. Formulae are derived which can be used to obtain the total overlap between any two functions of these types for any positions of the two atoms in three dimensional space.

INTRODUCTION

The first systematic theoretical study of systems containing transition metals was undertaken only eight years ago. [1] The complexes examined were highly symmetrical in structure having either a regularly octahedral, tetrahedral or square planar geometry. In view of the symmetrical nature of these systems it was only necessary to consider the overlap between orbitals of a direct type, e.g. $2s - 3d_\sigma$, $2p_\sigma - 3d_\sigma$, $2p_\pi - 3d_\pi$ etc. Since that time larger and faster computers have permitted a treatment of larger and less symmetrical molecules and for this reason it is convenient to have at hand formulae which describe the angular dependence of overlap and which are of general applicability to the evaluation of overlap integrals. These will be of use in studies of bi- and tri- nuclear metal complexes, of metal cluster systems and of complexes containing the lanthanide and actinide metals.

The angular behaviour of functions of *s*, *p*, *d* and *f* type are derived below and these are used to evaluate the gross total overlap between any two functions of these types for any direction considered.

METHOD

DESCRIPTION OF ORBITALS

The general description of an atomic orbital takes the form of a product of functions of the radial and angular coordinates, the origin of which lies at the nucleus of the atom.

$$\psi_{nlm}(r,\ \theta,\ \Phi) = R_{nl}(r)\ Y_{lm}\,(\theta,\Phi) \tag{1}$$

where the indices *n*, *l*, *m* are the principal, azimuthal and magnetic quantum numbers respectively and the symbols r, θ, Φ are the usual spherical coordinates (fig. 1). The radial function $R_{nl}(r)$ generally defies an exact analytical description. However, in view of the fact that the radial function is angularly independent it is not necessary to consider it explicitly here.

---

[1] H. Basche, A. Viste and HB. Gray. *J. Chem. Phys.*, **44**, 10 (1966).

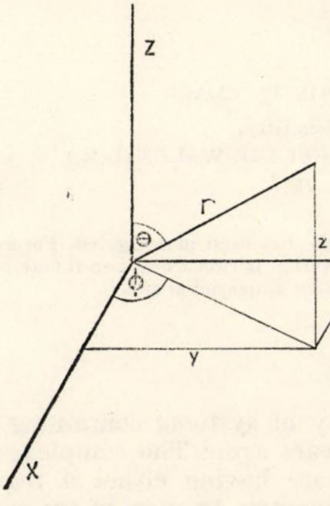

Fig. 1. — The polar coordinate system.

The angular function $Y_{lm}(\theta, \Phi)$ is a normalised spherical harmonic and has an exact analytical description. It is this function which essentially governs the "shape" of orbitals and it is according to this function that orbitals are classified as *s*, *p*, *d* or *f* etc. Since the angular properties of orbitals are governed entirely by this function it is necessary only to consider this function to determine the angular properties of overlap integrals as well.

The atomic orbitals often involve unwieldy expressions in their pure trigonometric form[2,3] (Table 1) and for this reason a more flexible representation is introduced by the use of direction cosines defined as follows :

$$\begin{aligned} i &= \sin\theta\cos\Phi \text{ or } i = x/r \\ j &= \sin\theta\sin\Phi \text{ or } j = y/r \\ k &= \cos\theta \qquad \text{ or } k = z/r \end{aligned} \tag{2}$$

The use of these parameters results in a simpler form for the orbitals (Table 1), which makes their handling somewhat easier.

THE OVERLAP INTEGRAL

In general, for two real atomic orbitals $\psi_{nlm}\ (r_A,\ \theta_A,\ \Phi_A)$ and $\psi_{n'l'm'}(r_B,\ \theta_B,\ \Phi_B)$ positioned on different atoms *A* and *B* respectively, the

---

[2] H. EYRING, J. WALTER and G. E. KIMBALL, "Quantum Chemistry", Wiley, London, 1944.

[3] H. G. FRIEDMAN, G. R. CHOPPIN and D. G. FEUERBACHER, *J. Chem. Educ.*, 41, 354 (1964).

Table 1

Angular Functions of *s*, *p*, *d* and *f* orbitals

Orbital	$Y_{lm}(\theta, \Phi)$	$Y_{lm}(i, j, k)$
s	$(1/4\pi)^{\frac{1}{2}}$	C_s
p_z	$(3/4\pi)^{\frac{1}{2}} \cos\theta$	$C_p k$
p_x	$(3/4\pi)^{\frac{1}{2}} \sin\theta \cos\Phi$	$C_p i$
p_y	$(3/4\pi)^{\frac{1}{2}} \sin\theta \sin\Phi$	$C_p j$
d_{z^2}	$(5/16\pi)^{\frac{1}{2}} (3\cos^2\theta - 1)$	$C_d(1/\sqrt{3})\ (3k^2 - 1)$
d_{xz}	$(15/4\pi)^{\frac{1}{2}} \sin\theta \cos\theta \cos\Phi$	$C_d 2\, i\, k$
d_{yz}	$(15/4\pi)^{\frac{1}{2}} \sin\theta \cos\theta \sin\Phi$	$C_d 2\, j\, k$
d_{xy}	$(15/16\pi)^{\frac{1}{2}} \sin^2\theta \sin 2\Phi$	$C_d 2\, i\, j$
$d_{x^2-y^2}$	$(15/16\pi)^{\frac{1}{2}} \sin^2\theta \cos 2\Phi$	$C_d(i^2 - j^2)$
f_{z^3}	$(7/16\pi)^{\frac{1}{2}} \cos\theta\, (5\cos^2\theta - 3)$	$C_f 2k(5k^2 - 3)$
f_{xz^2}	$(21/32\pi)^{\frac{1}{2}} \sin\theta\, (5\cos^2\theta - 1) \cos\Phi$	$C_f\sqrt{6}\, i\ (5k^2 - 1)$
f_{yz^2}	$(21/32\pi)^{\frac{1}{2}} \sin\theta\, (5\cos^2\theta - 1) \sin\Phi$	$C_f\sqrt{6}\, j\, (5k^2 - 1)$
f_{xyz}	$(105/16\pi)^{\frac{1}{2}} \sin^2\theta \cos\theta \sin 2\Phi$	$C_f 4\sqrt{15}\, i\, j\, k$
$f_{z(x^2 - y^2)}$	$(105/16\pi)^{\frac{1}{2}} \sin^2\theta \cos\theta \cos 2\Phi$	$C_f 2\sqrt{15}\, k(i^2 - j^2)$
$f_{x(x^2 - 3y^2)}$	$(35/32\pi)^{\frac{1}{2}} \sin^3\theta \cos 3\Phi$	$C_f\sqrt{10}\, i\, (i^2 - 3j^2)$
$f_{y(3x^2 - y^2)}$	$(35/32\pi)^{\frac{1}{2}} \sin^3\theta \sin 3\Phi$	$C_f\sqrt{10}\, j\, (3^2 - j^2)$

$C_s = (1/4\pi)^{\frac{1}{2}}$ $C_d = (15/16\pi)^{\frac{1}{2}}$

$C_p = (3/4\pi)^{\frac{1}{2}}$ $C_f = (7/64\pi)^{\frac{1}{2}}$

overlap integral between them is defined as :—

$$S_{AB}(nlm,\ n'\,l'\,m') = \int \psi_{nlm}(r_A,\ \theta_A, \Phi_A)\ \psi_{n'l'm'}\ (r_B,\ \theta_B,\ \Phi_B)\ \mathrm{d}\tau \tag{3}$$

The difficulty encountered in a general evaluation of equation (3) can be shown if a diatomic molecule is considered as in figure 2.

A set of immovable Cartesian axes, the molecular axes, is used to describe the positions of the atoms in a diatomic molecule. Atom *A* is positioned at the origin while atom *B* is at a distance *AB* from atom *A* in three dimensional space in the manner shown. The orbital on atom *A* is described relative to the molecular axes centred on *A* (and in polar form). The orbital on atom *B* is described relative to a set of local atomic coordinates on atom *B* whose Cartesian axes are correspondingly parallel to the molecular axes. The angles *a* and *b* are the angular coordinates of a spherical coordinate description of the position of atom *B*. This situation is completely analogous to those encountered for polyatomic molecules in general.

From figure 2 it can be seen that if angle *b* were zero the overlap between the two orbitals might be evaluated after the method of Mulliken[4] (or related methods) and moreover the overlap could be classified as a sigma (σ), pi (π) or delta (δ) overlap. It is clear, however, that when *b* is greater than zero it is not possible to evaluate an overlap integral as a pure sigma-, pi- or delta-type. However it is possible to resolve such an overlap into sigma, pi and delta components and this provides the method for the determination of overlap integrals in the general case.

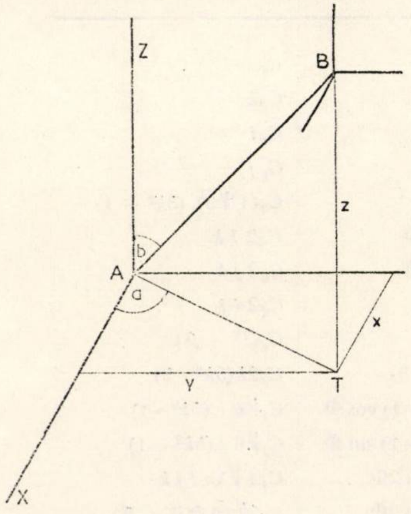

Fig. 2. — General description of the positions of two atoms *A* and *B* in three dimensional space.

RESOLUTION OF ORBITALS

In order to evaluate expression (3) it is necessary to express each orbital in terms of a set of component orbitals which would give rise to purely sigma, pi and delta overlaps along the line $A - B$. Each of these components is in fact recognisable as an orbital of the same subshell but reorientated to produce a pure overlap type and preceeded by a constant which assures that the set of components is normalised. It is, in fact, these constants which when cross multiplied with those of the adjacent atomic orbital provide a solution to the angular dependence problem.

$$\begin{bmatrix} x \\ y \\ z \end{bmatrix} = \begin{bmatrix} \cos a \cos b & -\sin a & \sin b \cos a \\ \cos b \sin a & \cos a & \sin b \sin a \\ -\sin b & 0 & \cos b \end{bmatrix} \begin{bmatrix} x' \\ y' \\ z' \end{bmatrix} \tag{4}$$

The transformation (4) expresses the original molecular coordinates (x, y, z) centred on atom *A* in terms of another set (x', y', z') whose *Z* axis is colinear with *AB* and whose *X* axis lies in the plane *ABT* (Figure 2).

---

[4] R. S. Mulliken, C. A. Rieke, D. Orloff and H. Orloff, *J. Chem. Phys.*, **17**, 1248 (1949).

Therefore by use of transformation (4) the orbital on atom A can be re-expressed in terms of this new set of axes to yield the desired set of component orbitals. Furthermore the same transformation can be applied to the local atomic coordinates of atom B to produce the counter orbitals for the overlap with those on atom A.

The resolution of an orbital is accomplished by first resolving the direction cosines i, j, and k using the matrix (4). It is clear from the definitions of the direction cosines (2) that since the radius r is always angularly independent a direct correspondence exists between i, j and k and x, y and z in this respect. The resolution is completed by substitution of the resolved direction cosines into the orbital expressions of Table 1. The resulting expressions are expanded and the terms regrouped into recognisable orbital expressions. The trigonometric constants occurring with each orbital are the parameters needed to determine the angular dependence of the overlap integral. The resolved orbitals resulting from this method are given for p, d and f orbitals in tables 2, 3 and 4 respectively.

Table 2

Resolution of p-orbitals according to fig. 2.

Original orbital	Resolved orbital		
	p_z'	p_x'	p_y'
p_z	$\cos b$	$-\sin b$	0
p_x	$\sin b \cos a$	$\cos a \cos b$	$-\sin a$
p_y	$\sin b \sin a$	$\cos b \sin a$	$\cos a$

Table 3

Resolution of d-orbitals according to fig. 2

Original orbital	Resolved orbital				
	d_{z^2}'	d_{xz}'	d_{yz}'	d_{xy}'	$d_{x^2-y^2}'$
d_{z^2}	$\frac{1}{2}(3\cos^2 b - 1)$	$-\frac{\sqrt{3}}{2}\sin 2b$	0	0	$\frac{\sqrt{3}}{2}\sin^2 b$
d_{xz}	$\frac{\sqrt{3}}{2}\cos a \sin 2b$	$\cos a \cos 2b$	$-\sin a \cos b$	$\sin a \sin b$	$-\frac{1}{2}\cos a \sin 2b$
d_{yz}	$\frac{\sqrt{3}}{2}\sin a \sin 2b$	$\sin a \cos 2b$	$\cos a \cos b$	$-\cos a \sin b$	$-\frac{1}{2}\sin a \sin 2b$
d_{xy}	$\frac{\sqrt{3}}{2}\sin 2a \sin^2 b$	$\frac{1}{2}\sin 2a \sin 2b$	$\cos 2a \sin b$	$\cos 2a \cos b$	$\frac{1}{2}\sin 2a(1 + \cos^2 b)$
$d_{x^2-y^2}$	$\frac{\sqrt{3}}{2}\cos 2a \sin^2 b$	$\frac{1}{2}\cos 2a \sin 2b$	$-\sin 2a \sin b$	$-\sin 2a \cos b$	$\frac{1}{2}\cos 2a(1 + \cos^2 b)$

Table 4

Resolution of f-orbitals according to fig. 2

Original orbital	Resolved orbital						
	f'_{z^3}	f'_{xz^2}	f'_{yz^2}	f'_{xyz}	$f'_{z(x^2-y^2)}$	$f'_{x(x^2-3y^2)}$	$f'_{y(3x^2-y^2)}$
f_{z^3}	$\frac{1}{2}\cos b\,(5\cos^2 b-3)$	$-\frac{\sqrt{6}}{4}\sin b\,(5\cos^2 b-1)$	0	0	$\frac{\sqrt{15}}{2}\cos b\,\sin^2 b$	$-\frac{\sqrt{10}}{4}\sin^3 b$	0
f_{xz^2}	$\frac{\sqrt{6}}{4}\cos a\sin b\,(5\cos^2 b-1)$	$\frac{1}{4}\cos a\cos b\,(15\cos^2 b-11)$	$\frac{1}{-4}\sin a\,(5\cos^2 b-1)$	$\frac{\sqrt{10}}{2}\sin a\,\cos b\,\sin b$	$\frac{\sqrt{10}}{4}\cos a\sin b\,(1-3\cos^2 b)$	$\frac{\sqrt{15}}{4}\cos a\cos b\,\sin^2 b$	$-\frac{\sqrt{15}}{4}\sin a\,\sin^2 b$
f_{yz^2}	$\frac{\sqrt{6}}{4}\sin a\sin b\,(5\cos^2 b-1)$	$\frac{1}{4}\sin a\cos b\,(15\cos^2 b-11)$	$\frac{1}{4}\cos a\,(5\cos^2 b-1)$	$-\frac{\sqrt{10}}{2}\cos a\,\cos b\sin b$	$\frac{\sqrt{10}}{4}\sin a\sin b\,(1-3\cos^2 b)$	$\frac{\sqrt{15}}{4}\sin a\cos b\,\sin^2 b$	$\frac{\sqrt{15}}{4}\cos a\,\sin^2 b$
f_{xyz}	$\frac{\sqrt{15}}{2}\sin 2a\,\cos b\sin^2 b$	$\frac{\sqrt{10}}{4}\sin 2a\sin b\,(3\cos^2 b-1)$	$\frac{\sqrt{10}}{4}\cos 2a\,\sin 2b$	$\cos 2a\,\cos 2b$	$\frac{1}{2}\sin 2a\cos b\,(3\cos^2 b-1)$	$-\frac{\sqrt{6}}{4}\sin 2a\sin b\,(1+\cos^2 b)$	$-\frac{\sqrt{6}}{4}\cos 2a\,\sin 2b$
$f_{z(x^2-y^2)}$	$\frac{\sqrt{15}}{2}\cos 2a\,\cos b\sin^2 b$	$\frac{\sqrt{10}}{4}\cos 2a\sin b\,(3\cos^2 b-1)$	$-\frac{\sqrt{10}}{4}\sin 2a\,\sin 2b$	$-\sin 2a\cos 2b$	$\frac{1}{2}\cos 2a\cos b\,(3\cos^2 b-1)$	$-\frac{\sqrt{6}}{4}\cos 2a\sin b\,(1+\cos^2 b)$	$\frac{\sqrt{6}}{4}\sin 2a\,\sin 2b$
$f_{x(x^2-3y^2)}$	$\frac{\sqrt{10}}{4}\cos 3a\,\sin^3 b$	$\frac{\sqrt{15}}{4}\cos 3a\,\cos b\sin^2 b$	$-\frac{\sqrt{15}}{4}\sin 3a\,\sin^2 b$	$-\frac{\sqrt{6}}{4}\sin 3a\,\sin 2b$	$\frac{\sqrt{6}}{4}\cos 3a\,\sin b\,(1+\cos^2 b)$	$\frac{1}{4}\cos 3a\,\cos b\,(3+\cos^2 b)$	$-\frac{1}{4}\sin 3a\,(1+3\cos^2 b)$
$f_{y(3x^2-y^2)}$	$\frac{\sqrt{10}}{4}\sin 3a\,\sin^3 b$	$\frac{\sqrt{15}}{4}\sin 3a\,\cos b\sin^2 b$	$\frac{\sqrt{15}}{4}\cos 3a\,\sin^2 b$	$\frac{\sqrt{6}}{4}\cos 3a\,\sin 2b$	$\frac{\sqrt{6}}{4}\sin 3a\,\sin b\,(1+\cos^2 b)$	$\frac{1}{4}\sin 3a\cos b\,(3+\cos^2 b)$	$\frac{1}{4}\cos 3a\,(1+3\cos^2 b)$

RESULTS

ANGULAR DEPENDENCE FORMULAE

The original orbitals may now be replaced by a sum of components :

$$\psi_A = \sum_{p=1}^{2l_A+1} C_{Ap}\, \psi'_{Ap} \quad \psi_A \text{ on atom } A$$
$$\psi_B = \sum_{q=1}^{2l_B+1} C_{Bq}\, \psi'_{Bq} \quad \psi_B \text{ on atom } B \tag{5}$$

where C_{Ap} and C_{Bq} are constants and ψ'_{Ap} and ψ'_{Bq} are component orbitals of the resolved parent orbital. It is to be noted that the component orbitals occurring in the summation belong to the same subshell as the parent orbital as indicated by the summation.

The overlap integral can now be written as :—

$$\int \psi_A\, \psi_B\, \mathrm{d}\tau = \sum_{p=1}^{2l_A+1} \sum_{q=1}^{2l_B+1} \int C_{Ap}\, C_{Bq}\, \psi'_{Ap}\, \psi'_{Bq}\, \mathrm{d}\tau$$
$$= \sum_{p=1}^{2l_A+1} \sum_{q=1}^{2l_B+1} C_{Ap}\, C_{Bq}\, S_{pq} \tag{6}$$

where

$$S_{pq} = \int \psi'_{Ap}\, \psi'_{Bq}\, \mathrm{d}\tau$$

It is important to note at this stage that the order of the orbitals in the parent integral is preserved in the component integrals S_{pq} also (i.e. ψ'_{Ap} preceeds ψ'_{Bq}); this is essential if the subsequent angular dependence formulae are to be unambiguous.

The expression (6) can be simplified further because some of the integrals S_{pq} evaluate to zero. This occurs whenever the Φ dependence of ψ'_{Ap} and ψ'_{Bq} is dissimilar, i.e. ψ'_{Ap} and ψ'_{Bq} are orthogonal unless they arise from the same "linear combinations" of magnetic quantum numbers. A further simplification of the formulae may also be made by the introduction of the following parameters:

$$F = \sin b \cos a$$
$$G = \sin b \sin a \tag{7}$$
$$H = \cos b$$

Table 5

Angular Dependence Formulae

$S(\mathrm{s}-\mathrm{s}) = \mathrm{S}(\sigma)$
$S(s-p_z) = H\bar{S}(\sigma)$
$S(s-p_x) = F\bar{S}(\sigma)$
$S(s-p_y) = G\bar{S}(\sigma)$

$S(s-d_{z^2}) = (3H^2-1)\, S(\sigma)/2$
$S(s-d_{xz}) = \sqrt{3}\, FH\, S(\sigma)$
$S(s-d_{yz}) = \sqrt{3}\, GH\, S(\sigma)$
$S(s-d_{xy}) = \sqrt{3}\, FG\, S(\sigma)$
$S(s-d_{x^2-y^2})) = \sqrt{3}\,(F^2-G^2) S(\sigma)/2$

$S(s-f_{z^3}) = H(5H^2-3)\, \bar{S}(\sigma)/2$
$S(s-f_{xz^2}) = \sqrt{6}\, F(5H^2-1)\, \bar{S}(\sigma)/4$
$S(s-f_{yz^2}) = \sqrt{6}\, G(5H^2-1)\, \bar{S}(\sigma)/4$
$S(s-f_{xyz}) = \sqrt{15}\, FGH\, \bar{S}(\sigma)$
$S(s-f_{z(x^2-y^2)})) = \sqrt{15}\; H(F^2-G^2)\, \bar{S}(\sigma)/2$
$S(s-f_{x(x^2-3y^2)})) = \sqrt{10}\; F(F^2-3G^2)\; \bar{S}(\sigma)/4$
$S(s-f_{y(3x^2-y^2)})) = \sqrt{10}\; G(3F^2-G^2)\; \bar{S}(\sigma)/4$

$S(p_z-p_z) = (1-H^2)\, S(\pi) + H^2\bar{S}(\sigma)$
$S(p_z-p_x) = FH(\bar{S}(\sigma) - S(\pi))$
$S(p_z-p_y) = GH(\bar{S}(\sigma) - S(\pi))$

$S(p_z-d_{z^2}) = \sqrt{3}\; H(1-H^2)\, \bar{S}(\pi) + H(3H^2-1)\, S\,(\sigma)/2$
$S(p_z-d_{xz}) = F(1-2H^2)\, \bar{S}(\pi) + \sqrt{3}\, FH^2\, S(\sigma)$
$S(p_z-d_{yz}) = G(1-2H^2)\, \bar{S}(\pi) + \sqrt{3}\, GH^2\, S(\sigma)$
$S(p_z-d_{xy}) = FGH(\sqrt{3}\; S(\sigma) - 2\bar{S}(\pi))$
$S(p_z-d_{x^2-y^2}) = H(G^2-F^2)\, \bar{S}(\pi) + \sqrt{3}\, H\,(F^2-G^2)\; S(\sigma)/2$

$S(p_z-f_{z^3}) = \sqrt{6}\,(1-H^2)\; (5H^2-1)\;\; \mathrm{S}(\pi)/4 + H^2(5H^2-3)\;\; \bar{S}(\sigma)/2$
$S(p_z-f_{xz^2}) = FH(11-15H^2)\;\; S(\pi)/4 + \sqrt{6}\, FH(5H^2-1)\;\; \bar{S}(\sigma)/4$
$S(p_z-f_{yz^2}) = GH(11-15H^2)\;\; S(\pi)/4 + \sqrt{6}\;\; GH(5H^2-1)\;\; \bar{S}(\sigma)/4$
$S(p_z-f_{xyz}) = \sqrt{10}\;\; FG(1-3H^2)\, S\,(\pi)/2 + \sqrt{15}\;\; FGH^2\; \bar{S}(\sigma)$
$S(p_z-f_{z(x^2-y^2)})) = \sqrt{10}\;\; (F^2-G^2)\; (1-3H^2)\;\; S(\pi)/4 + \sqrt{15}\;\; H^2(F^2-G^2)\, \bar{S}\;\; (\sigma)/2$
$S(p_z-f_{x(x^2-3y^2)})) = FH(F^2-3G^2)\;\; (\sqrt{10}\;\; \bar{S}(\sigma) - \sqrt{15}\;\; S(\pi)))/4$
$S(p_z-f_{y(3x^2-y^2)})) = GH(3F^2-G^2)\;\; (\sqrt{10}\;\; \bar{S}(\sigma)-\sqrt{15}\;\; S(\pi))/4$

$S(p_x-p_x) = (1-F^2)\; S\,(\pi) + F^2\bar{S}(\sigma)$
$S(p_x-p_y) = FG(\bar{S}(\sigma) - S(\pi))$

$S(p_x-d_{z^2}) = -\sqrt{3}\; FH^2\, \bar{S}(\pi) + F(3H^2-1)\;\; S(\sigma)/2$
$S(p_x-d_{xz}) = H(1-2F^2)\;\; \bar{S}(\pi) + \sqrt{3}\;\; F^2H\;\; S(\sigma)$
$S(p_x-d_{yz}) = FGH(\sqrt{3}\;\; S(\sigma) - 2\;\; \bar{S}(\pi))$
$S(p_x-d_{xy}) = G(1-2F^2)\;\; \bar{S}(\pi) + \sqrt{3}\;\; F^2\;\; GS(\sigma)$
$S(p_x-d_{x^2-y^2}) = F(1-F^2 + G^2)\;\; \bar{S}(\pi) + \sqrt{3}\;\; F(F^2-G^2)\;\; S(\sigma)/2$

Table 5 (continued)

$$S(p_x-f_{z^3}) = -\sqrt{6}\ FH(5H^2-1)\ S(\pi)/4 + FH(5H^2-3)\ \bar{S}(\sigma)/2$$
$$S(p_x-f_{xz^2}) = -(1-F^2-5H^2+15F^2H^2)\ S(\pi)/4 + \sqrt{6}\ F^2(5H^2-1)\ \bar{S}(\sigma)/4$$
$$S(p_x-f_{yz^2}) = FG(1-15H^2)\ S(\pi)/4 + \sqrt{6}\ FG(5H^2-1)\ \bar{S}(\sigma)/4$$
$$S(p_x-f_{xyz}) = \sqrt{10}\ GH(1-3F^2)\ S(\pi)/2 + \sqrt{15}\ F^2\ GH\bar{S}(\sigma)$$
$$S(p_x-f_{z(x^2-y^2)} = \sqrt{10}\ FH(2-3(F^2-G^2))\ S(\pi)/4 + \sqrt{15}\ FH(F^2-G^2)\ \bar{S}(\sigma)/2$$
$$S(p_x-f_{x(x^2-3y^2)}) = \sqrt{15}\ (F^2-G^2-F^2(F^2-3G^2))\ S(\pi)/4 + \sqrt{10}\ F^2(F^2-3G^2)\ \bar{S}(\sigma)/4$$
$$S(p_x-f_{y(3x^2-y^2)}) = \sqrt{15}\ FG(2+G^2-3F^2)\ S(\pi)/4 + \sqrt{10}\ FG(3F^2-G^2)\bar{S}(\sigma)/4$$

$$S(p_y-p_y) = (1-G^2)\ S(\pi) + G^2\bar{S}(\sigma)$$

$$S(p_y-d_{z^2}) = -\sqrt{3}\ GH^2\bar{S}(\pi) + G(3H^2-1)\ S(\sigma)/2$$
$$S(p_y-d_{xz}) = FGH(\sqrt{3}\ S(\sigma) - 2\ \bar{S}(\pi))$$
$$S(p_y-d_{yz}) = H(1-2G^2)\ \bar{S}(\pi) + \sqrt{3}G^2HS(\sigma)$$
$$S(p_y-d_{xy}) = F(1-2G^2)\ \bar{S}(\pi) + \sqrt{3}\ FG^2\ S(\sigma)$$
$$S(p_y-d_{x^2-y^2}) = G(G^2-F^2-1)\ \bar{S}(\pi) + \sqrt{3}\ G(F^2-G^2)S(\sigma)/2$$

$$S(p_y-f_{z^3}) = \sqrt{6}\ HG(1-5H^2)\ S(\pi)/4 + GH(5H^2-3)\ \bar{S}(\sigma)/2$$
$$S(p_y-f_{xz^2}) = FG(1-15H^2)\ S(\pi)/4 + \sqrt{6}\ FG(5H^2-1)\ \bar{S}(\sigma)/4$$
$$S(p_y-f_{yz^2}) = -(1-G^2-5H^2+15G^2H^2)\ S(\pi)/4 + \sqrt{6}\ G^2\ (5H^2-1)\bar{S}(\sigma)/4$$
$$S(p_y-f_{xyz}) = \sqrt{10}\ FH(1-3G^2)\ S(\pi)/2 + \sqrt{15}\ FG^2H\ \bar{S}(\sigma)$$
$$S(p_y-f_{z(x^2-y^2)}) = -\sqrt{10}\ GH(2+3(F^2-G^2))\ S(\pi)/4 + \sqrt{15}\ GH(F^2-G^2)\ \bar{S}(\sigma)/2$$
$$S(p_y-f_{x(x-3y^2)}) = -\sqrt{15}\ FG(2+F^2-3G^2)\ S(\pi)/4 + \sqrt{10}\ FG(F^2-3G^2)\ \bar{S}(\sigma)/4$$
$$S(p_y-f_{y(3x^2-y^2)}) = \sqrt{15}\ (F^2-G^2-G^2\ (3F^2-G^2))\ S(\pi)/4 + \sqrt{10}\ G^2(3F^2-G^2)\ \bar{S}(\sigma)/4$$

$$S(d_{z^2}-d_{z^2}) = 3(1-H^2)^2\ S(\delta)/4 + 3\ H^2\ (1-H^2)\ \bar{S}(\pi) + (3H^2-1)^2\ S(\sigma)/4$$
$$S(d_{z^2}-d_{xz}) = \sqrt{3}\ FH(H^2-1)\ S(\delta)/2 + \sqrt{3}\ FH(1-2H^2)\bar{S}(\pi) + \sqrt{3}\ FH(3H^2-1)\ \bar{S}(\sigma)/2$$
$$S(d_{z^2}-d_{yz}) = \sqrt{3}\ GH(H^2-1)\ S(\delta)/2 + \sqrt{3}\ GH(1-2H^2)\ \bar{S}(\pi) + \sqrt{3}\ GH(3H^2-1)\ S(\sigma)/2$$
$$S(d_{z^2}-d_{xy}) = \sqrt{3}\ FG(1+H^2)\ S(\delta)/2 - 2\sqrt{3}\ FGH^2\ \bar{S}(\pi) + \sqrt{3}\ FG(3H^2-1)\ S(\sigma)/2$$
$$S(d_{z^2}-d_{x^2-y^2}) = \sqrt{3}(F^2-G^2)(1+H^2)\ S(\delta)/4 + \sqrt{3}\ H^2(G^2-F^2)\ \bar{S}(\pi) + \sqrt{3}\ (F^2-G^2)(3H^2-1)\ S(\sigma)/4$$

$$S(d_{xz}-d_{xz}) = (G^2+F^2H^2)\ S(\delta) + (1-4F^2H^2-G^2)\ \bar{S}(\pi) + 3F^2H^2S(\sigma)$$
$$S(d_{xz}-d_{yz}) = FG(H^2-1)\ S(\delta) + FG(1-4H^2)\ \bar{S}(\pi) + 3\ FGH^2\ S(\sigma)$$
$$S(d_{xz}-d_{xy}) = GH(F^2-1)\ S(\delta) + GH\ (1-4F^2)\ \bar{S}(\pi) + 3F^2GHS(\sigma)$$
$$S(d_{xz}-d_{x^2-y^2}) = FH(F^2-G^2-2)\ S(\delta)/2 + FH(1-2F^2+2G^2)\ \bar{S}(\pi) + 3FH(F^2-G^2)S(\sigma)/2$$

$$S(d_{yz}-d_{yz}) = (F^2+G^2H^2)\ S(\delta) + (1-F^2-4G^2H^2)\ \bar{S}(\pi) + 3G^2H^2\ S(\sigma)$$
$$S(d_{yz}-d_{xy}) = FH(G^2-1)\ S(\delta) + FH(1-4G^2)\ \bar{S}(\pi) + 3\ FG^2H\ S(\sigma)$$
$$S(d_{yz}-d_{x^2-y^2}) = GH(F^2-G^2+2)\ S(\delta)/2 + GH(2G^2-2F^2-1)\ \bar{S}(\pi) + 3\ GH(F^2-G^2)\ S(\sigma)/2$$

$$S(d_{xy}-d_{xy}) = (H^2+F^2G^2)S(\delta) + (1-H^2-4F^2G^2)\ \bar{S}(\pi) + 3F^2G^2S(\sigma)$$
$$S(d_{xy}-d_{x^2-y^2}) = FG(F^2-G^2)\ S(\delta)/2 + 2\ FG(G^2-F^2)\ \bar{S}(\pi) + 3\ FG(F^2-G^2)\ S(\sigma)/2$$

$$S(d_{x^2-y^2}-d_{x^2-y^2}) = (4H^2+(F^2-G))^2)S(\delta)/4 + (1-H^2-(F^2-G^2)^2)\bar{S}(\pi) + 3(F^2-G^2)^2\ S(\sigma)/4$$

These parameters have the advantage that they may be interpreted directly in terms of the molecular coordinates of the two atoms and are thus applicable to more general cases than that given in Fig. 2, in particular to the situation in which the atom A is not at the origin of the molecular axes. For such a situation the following definitions are used :

$$\begin{aligned} F &= (X \text{ coord of } B - X \text{ coord of } A)/\text{Dist. } AB \\ G &= (Y \text{ coord of } B - Y \text{ coord of } A)/\text{Dist. } AB \\ H &= (Z \text{ coord of } B - Z \text{ coord of } A)/\text{Dist. } AB \end{aligned} \tag{8}$$

These parameters are then the direction cosines of the line AB defined relative to the molecular axes. The use of these parameters, as applied to the constants C_{Ap} C_{Bq} enables a general overlap integral such as (3) to be expressed as a sum of sigma, pi and delta components. Table (5) gives the resolved overlaps which are in common usage or likely to be of future use. The constants F, G and H are evaluated using the formulae (8). The formulae given all have the orbital of lowest l quantum number written first in the overlap integral. This does not restrict their use in practice since the overlap integral (3) is Hermitian.

Finally, in the angular dependence formulae presented certain integral types are written with a bar(-) above them. This indicates that the value of that integral as obtained by Mulliken's convention should be multiplied by (-1) before substitution of that value into the angular dependence formulae. This is necessary because Mulliken's overlap formulae are evaluated with the local atomic Z axes of atom A and B pointing towards one another, whereas the angular dependence formulae in the present work require these axes to be co-directional.

ACKNOWLEDGEMENT. One of us (W.S) thanks S.R.C. for financial support.

Revue Roumaine de Chimie, **20**, *9–10*, 1253–1265 (1975)

FEM STUDY OF SILVER LAYERS ADSORBED ON TUNGSTEN. I

WORK FUNCTION AND SURFACE MIGRATION

M. I. VASS and CR. CONȚESCU

Center of Physical Chemistry, Dumbrava Roşie 23
Bucharest 9, Romania

Received October 4, 1974

The work function variation during adsorption and growth of thin silver layers on tungsten surface has been studied by Field Emission Microscopy (FEM) method. A semiempirical procedure of calculating work function change on silver adsorption is proposed based upon structural and surface energy data and a mechanism for work function variation with increasing thickness is advanced. The position of surface energetic barriers on tungsten was specified from migration experiments.

1. INTRODUCTION

Wide interest has been shown lately in Field Emission Microscopy (FEM) studies of I – B group metals adsorption on tungsten, which could be related to possible implications in three main research fields Firstly, the study of simple adsorption systems like metal on metal could provide a theoretical insight into surface bond formation. Secondly, the emitter surface in the FEM method is suitable for nucleation and epitaxial studies. Thirdly, by the build-up of metallic epitaxial layers on the emitter surface, the FEM method became a powerful tool for the study of a large number of adsorption systems, extending practically to all metals.

The present paper is concerned with the study of the Ag – W system, with a view to later using the FEM method for adsorption and surface reactions on different planes of silver.

Nucleation and growth of silver layers on the tungsten surface have been studied by using FEM by Moazed and Pound, [1] Duell and Moss,[2] Melmed and McCarthy [3] and Gretz and Pound.[4] Sugata and Takeda's [5] data were critically examined by Jones[6–8] who thoroughly investigated the Ag — W system. Epitaxial silver layers and whiskers have been earlier mentioned by Melmed and Gomer [9,10] as potential FEM specimens for gas adsorption studies, but only recently Sachtler and co-workers have succeeded in preparing [11] and using them [12] in the study of O_2 and N_2O adsorption on silver.

---

[1] K. L. Moazed and G. M. Pound, *Trans. AIME*, **230**, 234 (1964).

[2] M. J. Duell and R. L. Moss, *Brit. J. Appl. Phys.*, **15**, 157 (1964).

[3] A. J. Melmed and R. F. Mc Carthy, *J. Chem. Phys.*, **42**, 1466 (1965).

[4] R. D. Gretz and G. M. Pound, in "Proc. Dayton Conf. on Condensation and Evaporation", Gordon and Breach, New York, 1963.

[5] E. Sugata and K. Takeda, *Phys. Status Solidi*, **38**, 549 (1970).

[6] J. P. Jones, *Surface Sci.*, **32**, 29 (1972).

[7] A. Cetronio and J. P. Jones, *Surface Sci.*, **40**, 227 (1973).

[8] A. Cetronio and J. P. Jones, *Surface Sci.*, **44**, 109 (1974).

2. EXPERIMENTAL

The measurements were carried out in a simple sealed-off FEM tube, built according to a model described by Gomer [13]. A diagram is presented in figure 1. The emitter was made of 0.07 mm tungsten wire, electrolytically etched by usual procedures [15]. Tip radii, estimated by a well-known method [14] were 1950 Å and 1200 Å. Silver vapour source was formed by melting in vacuum a specpure Johnson & Matthey silver bead on a tungsten filament.

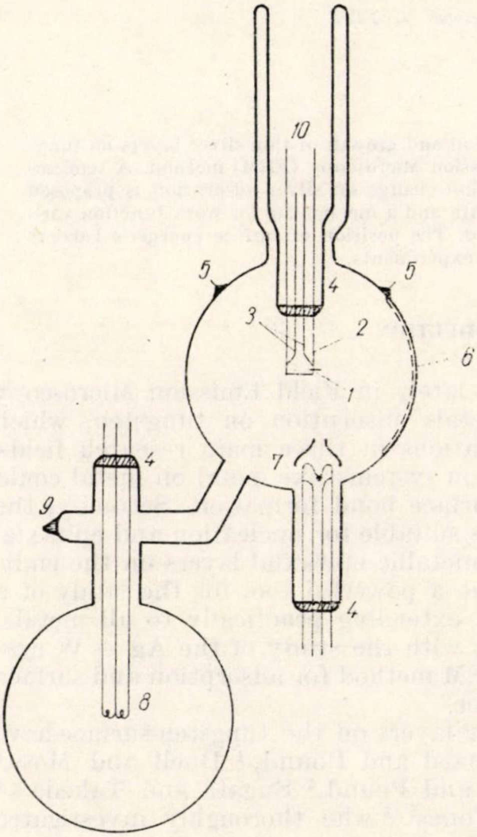

Fig. 1. — Schematic view of FEM assembly: 1 – tungsten emitter; 2 – tungsten loop; 3 – potential leads; 4 – pressed seals; 5 – anodic contacts; 6 – fluorescent screen; 7 – colimated silver source; 8 – tantalum getter; 9 – seal- off; 10 – Dewar seal.

---

[9] R. GOMER, *J. Chem. Phys.*, **28**, 457 (1958).

[10] A. J. MELMED and R. GOMER, *J. Chem. Phys.*, **34**, 1802 (1961).

[11] M. M. P. JANSSEN and J. MOOLHUYSEN, *Surface Sci.*, **42**, 86 (1973).

[12] M. M. P. JANSSEN, J. MOOLHUYSEN and W. M. H. SACHTLER, *Surface Sci.*, **33**, 624 (1972).

[13] R. GOMER, R. WORTMAN and R. LUNDY, *J. Chem. Phys.*, **26**, 1147 (1957).

[14] R. S. HANSEN and N. C. GARDNER, in "Experimental Methods in Catalytic Research", Academic Press, New York, 1968, p. 168.

[15] R. GOMER, "Field Emission and Field Ionization", Harvard University Press, Cambridge, Massachusetts, 1961.

The tube assembly was sealed-off after a standard evacuation — baking — outgasing cycle on a high vacuum installation described elsewhere. [16] Special care was given to the proper outgasing of all metallic parts inside the tube and especially to silver source. The pressure before sealing was 1.33×10^{-7}Pa. The pressure inside the tube during runs, evaluated from field emission current for a clean tip, was $\leqslant 1 \times 10^{-8}$ Pa.

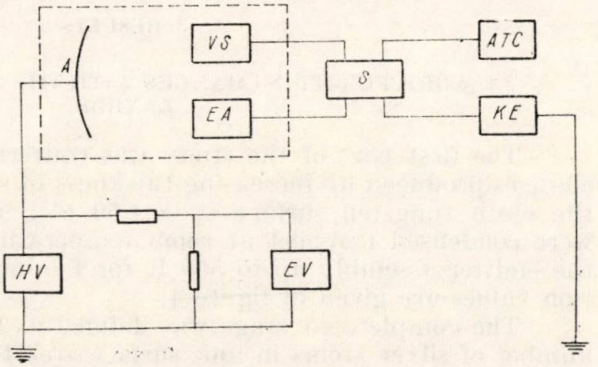

Fig. 2. — Electric equipment : A – anode ; EA – emitter assembly ; VS – vaporization silver source ; S – general switch ; ATC – automatic temperature controller ; KE – Keithley Electrometer Model 640 ; HV – High Voltage Power Supply Fluke Model 410 B ; EV – electronic voltmeter.

Block diagram of the electric equipments is given in figure 2. The high voltage was taken from a Fluke Model 410 B High Voltage Power Supply (stability ± 0.005 % per hour). The field emission current was measured with a Keithley Model 640 Electrometer. The tip and source temperature were measured by the voltage — current method, using a resistance vs. temperrature calibration curve. The temperatures of loop-emitter and source assemblies were automatically controlled by an electronic equipment built in our Institute according to a Zimmerman and Gomer [17] model, whose detailed scheme was kindly offered by the authors to one of us. Part of the experiments were carried out by manual control of temperature with a potentiometric circuit.

Use has been made of two methods of evaluating the amount of silver condensed on tip. In the first one, the flux of impinging atoms was evaluated from geometric arrangement and proper pressure data of silver at given temperature by employing the known formula : [18]

$$I = 1.\,49 \times 10^{24} \frac{PA_s}{d_0^2(MT)^{1/2}} \tag{1}$$

where : I = the flux of impinging on surface atoms per unit time (atoms/cm $^2 \cdot$ sec) ;
P = silver vapour pressure (Pa) (1 Pa = $7.\,5 \times 10^{-3}$ Torr) ;
A_s = area of vapour source slit (cm ^{2}) ;
d_0 = source to emitter distance (cm) ;
M = silver atomic mass ;
T = vaporization temperature (K).

To check the validity of the above procedure, a separate source was devised. This comprises an identical silver vapour source assembly equipped with removable thin glass slide. The distance source – slide was the same as the one between the source and tip in the tube. The microchemical quantitative analyses [19] of the silver deposits were carried out and a good agreement with the calculated values was found, which enables us to further use the formula (1).

The clean tungsten surface has been obtained by repeated flashing of the tip until a stable field emission pattern is attained. The example of clean tungsten emission image is given in figure 3 (the principal planes are also shown).

[16] I. G. Murgulescu and M. I. Vass, *Rev. Roumaine Chimie*, **11**, 266 (1966).

[17] D. Zimmerman and R. Gomer, *Rev. Sci. Instruments*, **36**, 1046 (1965).

[18] N. F. Ramsey, "Molecular Beams", Clarendon Press, Oxford, 1956.

[19] E. B. Sandell, "Colorimetric Determination of Traces of Metals", Interscience, New York, 1959.

The work function values were calculated from standard Fowler — Nordheim plots,[15] assuming a $\varphi = 4.50$ eV value for clean tungsten surface. Since in our experiments the accuracy of high voltage was better than 0.05 % and the current values in $10^{-10}-10^{-7}$ A range were measured with the medium error of 1 — 3 %, the resulting standard error in the work function was[14] $\pm$ 0.02 eV.

3. RESULTS

3.1. WORK FUNCTION CHANGES WITH THE NUMBER OF ADSORBED LAYERS

The first part of the study was concerned with the work function changes produced by increasing thickness of silver deposits. Starting from the clean tungsten surface ($\varphi = 4.50$ eV), increasing amounts of silver were condensed (support at room temperature) then spread by heating the emitter assembly up to 550 K for 1 minute. The obtained work function values are given in figure 4.

The complete coverage was defined as the ratio between the mean number of silver atoms in unit surface area to mean number of tungsten atoms in the same unit (assuming 1×10^{15} W atoms on 1 cm^2).

Unlike the frequently observed features for alkali metals adsorbed on tungsten, the bulk value of silver workfunction (4.33 eV) was observed only at coverages higher than 8 layers. It seems that all I — B group metals behave similarly.[6,20,21]. Our results are in good agreement with Jones[6] and, as can be seen from figure 4, there is a maximum in the work function (4.63 eV) at $\theta \approx 0.70$, then a minimum (4.10 eV) at $\theta \approx 6$ and finally φ reaches the bulk silver value. This behaviour is accompanied by significant changes in field emission patterns (fig. 5).

The work function maximum does not alter significantly the field emission pattern of tungsten, besides a slight increase of emission brightness from boundaries delimiting (110) and (211) planes (fig. 5, b). After the completion of the first silver layer (fig. 5, c) a new surface structure appears (fig. 5, d, e). This could be noted from the increasing emission of ⟨111⟩ zone lines and the roundness of (110) and (211) planes. Further increase of silver thickness, but before the work function minimum is reached, entails more pronounced pattern changes. The brightness of (211) and (110) increases while the (111) planes seem to be extended (fig. 5, f). The field emission pattern corresponding to minimum in the work function is very characteristic (fig. 5, g). The basic tungsten symmetry is retained but (211) planes sharply increase their emission while (110) plane is again large. On the remaining part of the curve the field emission patterns do not change significantly, even for a thickness as high as 10 layers (fig. 5, h, i).

3.2. SILVER MIGRATION ON TUNGSTEN SURFACE

Two sets of experiments were carried out in order to observe silver migration on tungsten surface. In the first experiments the tungsten support was held at room temperature.

---

[20] J. P. Jones, *Proc. Roy. Soc.*, **A 284**, 469 (1965).

[21] J. P. Jones, "Symposium on Surface Phenomena of Metals", Monograph No. 28, Soc. Chem. Ind., 1967.

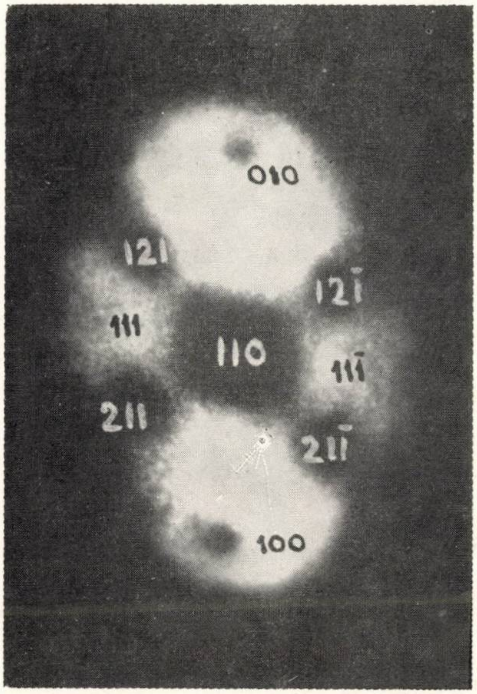
010
121
12Ī
111
110
11Ī
211
21Ī
100

Fig. 3. — Field emission pattern of clean tungsten surface. Principal crystallographic planes are shown by Miller indices.

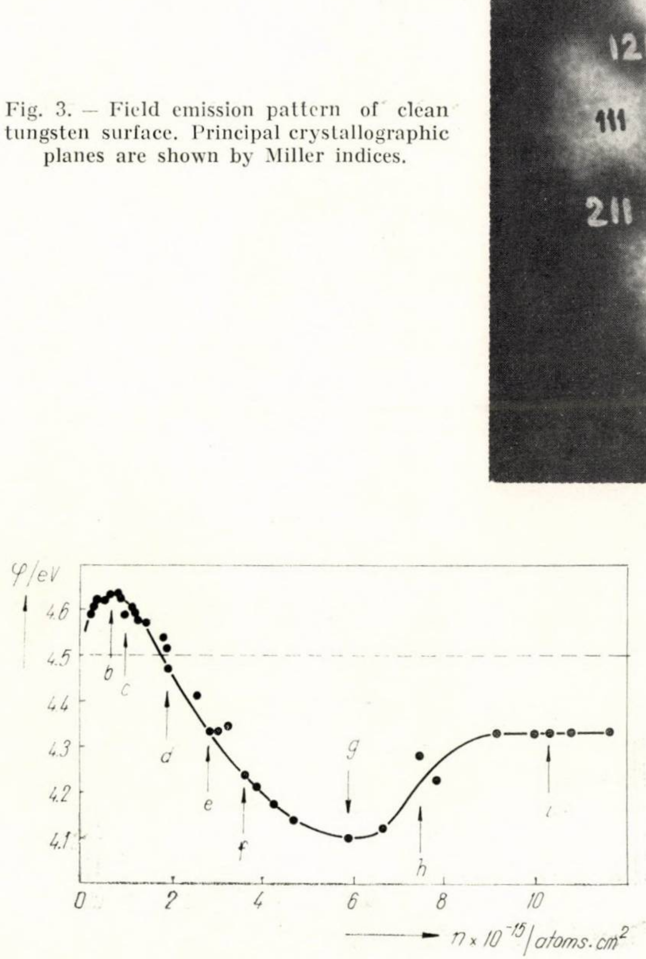

Fig. 4. — Change in work function with the amount of silver condensed at room temperature and spread at 550 K. Marked points correspond to the patterns given in fig. 5.

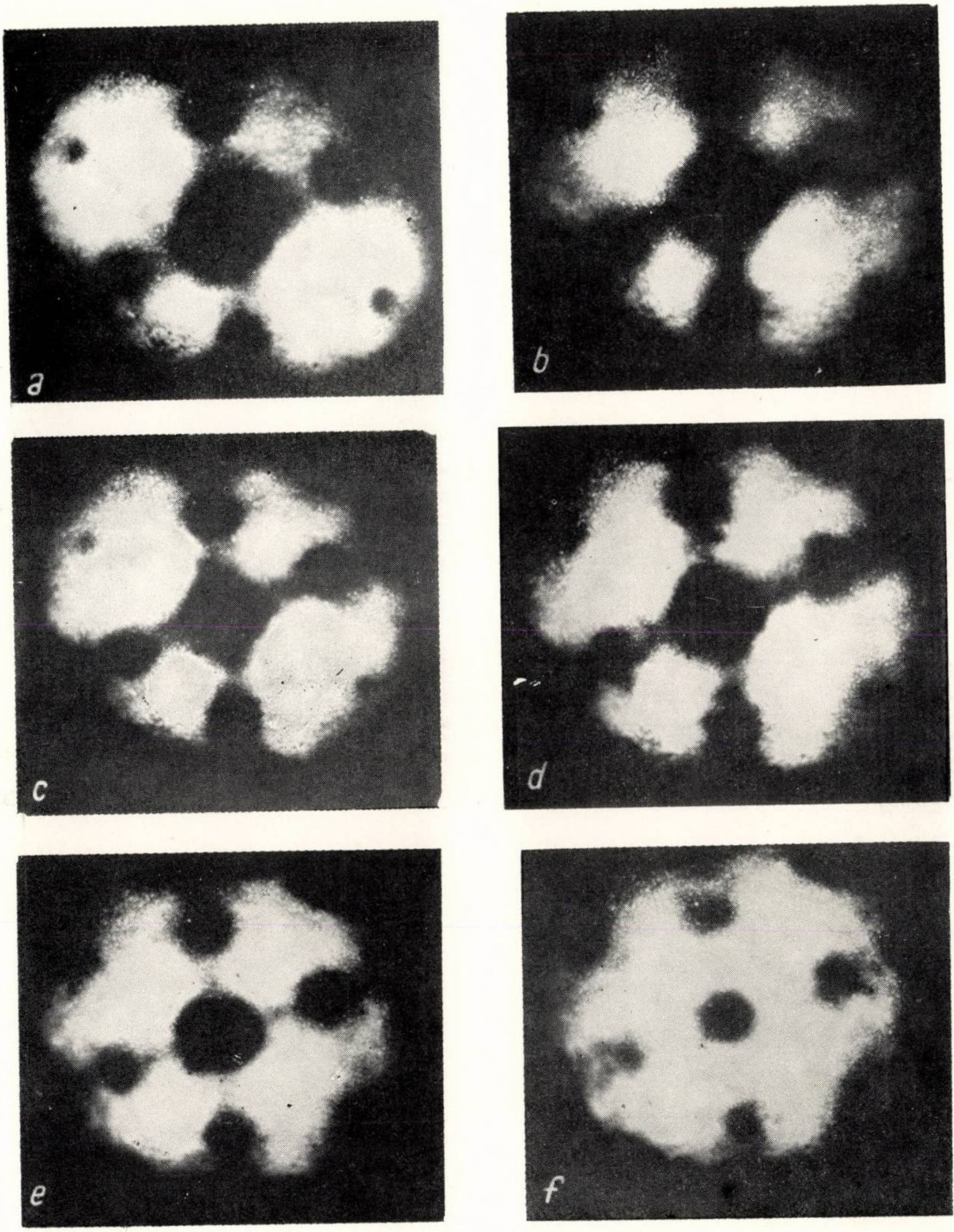
a
b
c
d
e
f

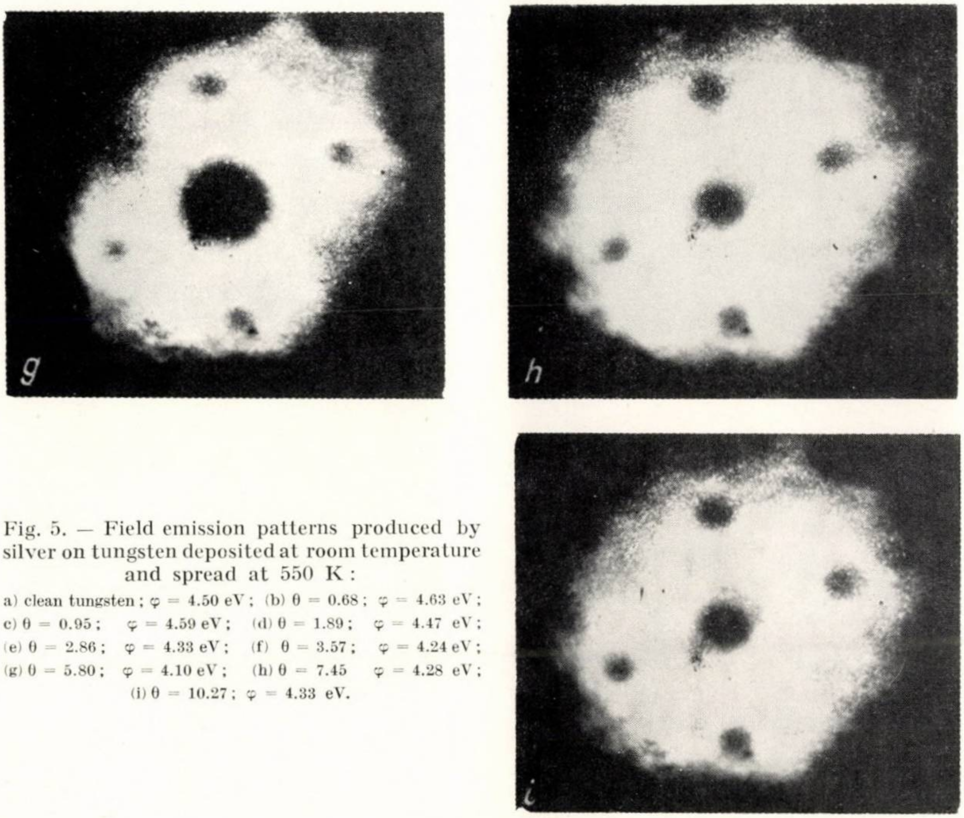

Fig. 5. — Field emission patterns produced by silver on tungsten deposited at room temperature and spread at 550 K :

a) clean tungsten ; $\varphi = 4.50$ eV ; (b) $\theta = 0.68$; $\varphi = 4.63$ eV ;
c) $\theta = 0.95$; $\varphi = 4.59$ eV ; (d) $\theta = 1.89$; $\varphi = 4.47$ eV ;
(e) $\theta = 2.86$; $\varphi = 4.33$ eV ; (f) $\theta = 3.57$; $\varphi = 4.24$ eV ;
(g) $\theta = 5.80$; $\varphi = 4.10$ eV ; (h) $\theta = 7.45$ $\varphi = 4.28$ eV ;
(i) $\theta = 10.27$; $\varphi = 4.33$ eV.

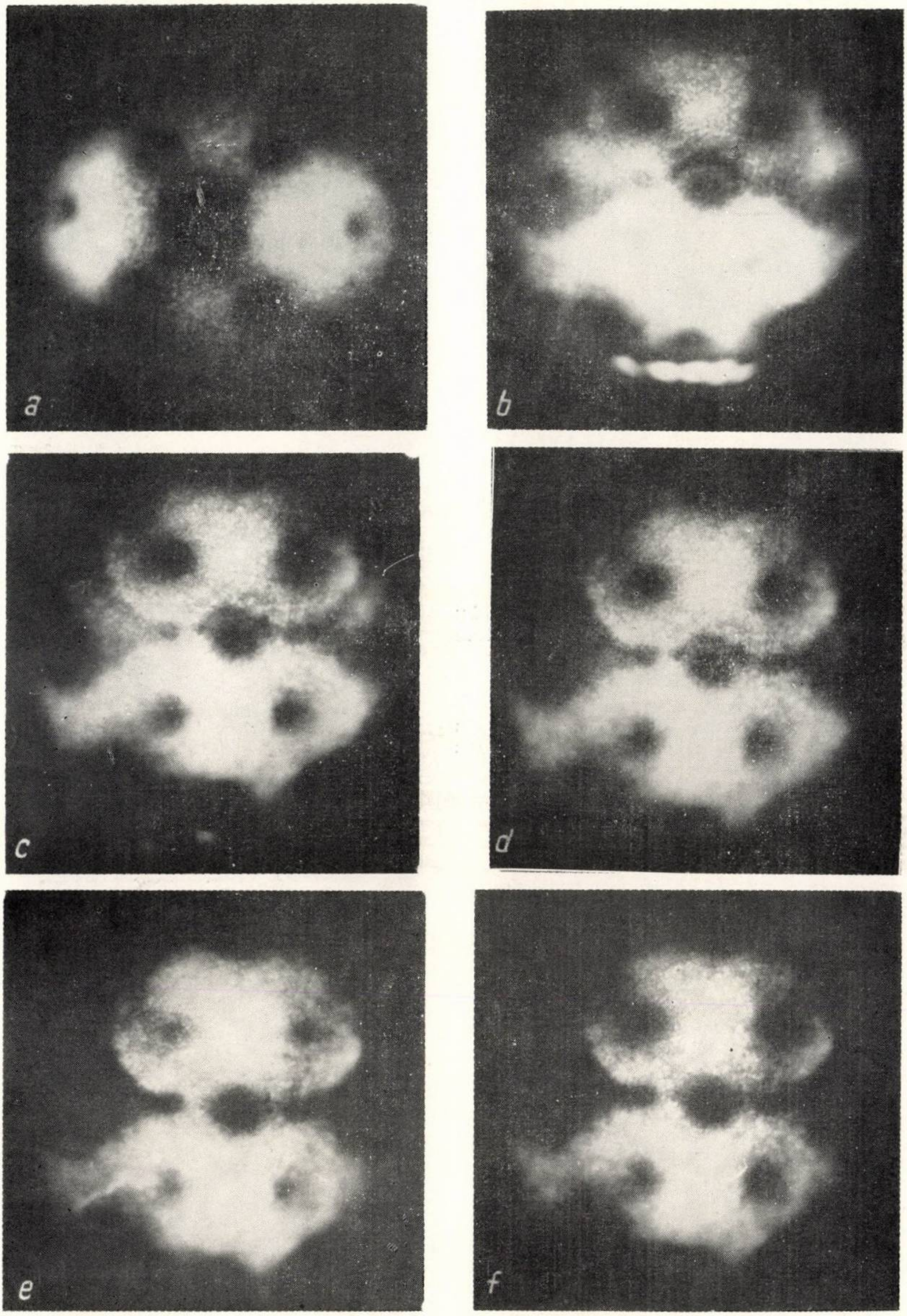

Fig. 6. — Silver migration on tungsten surface following deposition at room temperature (silver source directed upwards) :

(a) clean tungsten surface ; (b) silver deposit formed on tungsten tip at room temperature ; (c) after heating at 330 K, 1 minute ; (d) after heating at 330 K, 7 minutes ; (e) after heating at 400 K, 1 minute (f) after heating at 400 K, 7 minutes.

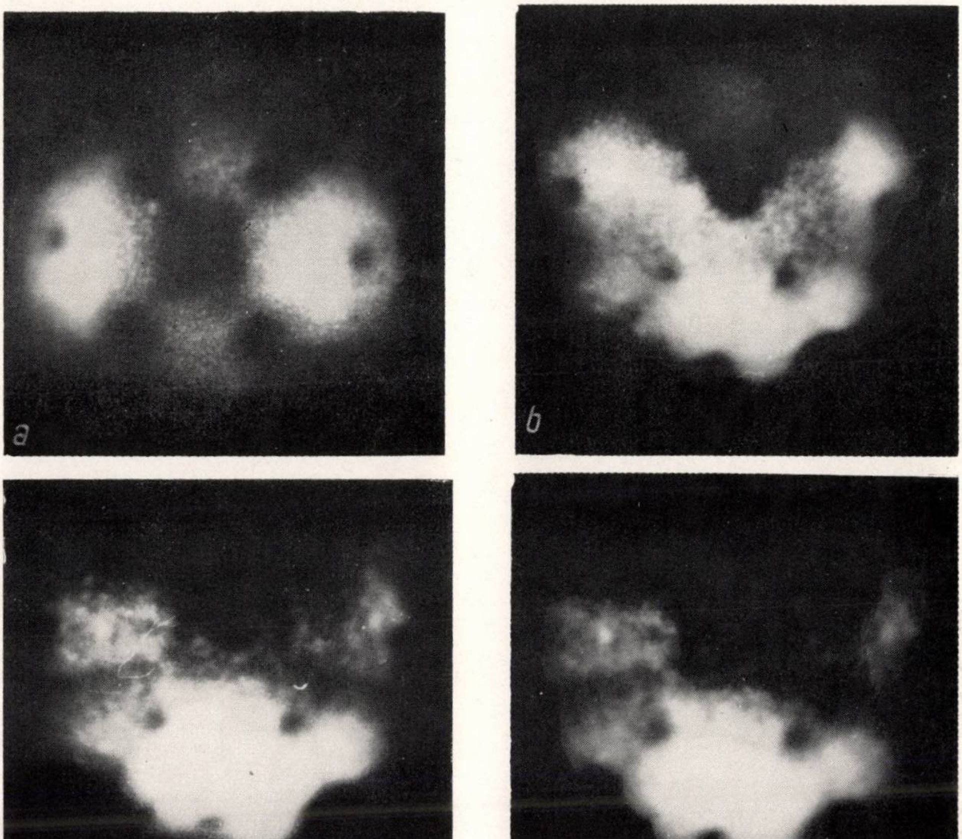

Fig. 7. Silver backward migration on tungsten surface following deposition at 78 K (silver source directed upwards):

(a) clean tungsten surface; (b) silver deposit formed on tungsten tip at 78 K; (c) after heating at 180 K, 1 minute; (d) after heating at 225 K, 1 minute; (e) after heating at 260 K, 1 minute; (f) after heating at 350 K, 6 minutes.

It is easy to see on figure 6, b that even having a thick deposit with a well-defined front determined by source position, silver is spread over the entire tungsten surface. By gentle heating (1 minute to 330 K), the silver deposit is rapidly spread which can be seen by the appearance of the almost even size of (211) planes (fig. 6, c). Continuing the heating (7 minutes to 350 K) silver is concentrated on (111) and around (211) planes and disappears from (100) environments (fig. 6, d). By the end of the heating time the field emission pattern is completely different from the initial clean tungsten one (compare fig. 6, a with figs. 6, e, f). The low emissive (111) planes on tungsten surface become bright while the emission from the rough surrounding (100) planes disappears. The dark regions around (100) planes are confined to low packed planes (301), (611), (320), which, at the same time, define the limiting barriers.

The second group of experiments was performed with tungsten support at 78 K. The silver deposit remains only on that part of the surface which is directly facing the source (fig. 7, b). Following slight heating (1 minute to 180 K) an unexpected phenomenon is observed (fig. 7, c): the backward migration of silver from barely covered planes to (111) regions where a thick silver layer already exists. Prolonged mild heating leads to further concentration of silver on (111) (down) and concomitantly silver vanishes from the (100) neighbourhood. Simultaneously, a well-defined boundary arises (figs. 7, d, e) crossing the same highly indexed planes (301), (611), (320). Finally, a very stable crystallite is built up (fig. 7, f), which cannot be removed even at 900 K.

4. DISCUSSIONS

4.1. WORK FUNCTION

The work function vs. thickness curve presented in figure 4 has features common to all I – B group metals adsorbed on tungsten.[6,20,21] Moreover, the field emission adsorption patterns are similar for these metals, retaining the initial two-fold symmetry of clean tungsten. Taking into account the shape of the curve (fig. 4) and the changes of field emission patterns, a three-step mechanism appears, most likely to explain silver layers adsorption and growth on tungsten.

(i) The initial increase in the work function could be assigned to the strong interactions of silver atoms with the clean tungsten surface; two explanations are usually given: Jones,[6] using Mignolet's [22] semiempirical relation, which takes into account the polarization of silver atoms by the tungsten surface field, calculated a 0.23 eV increase of the work function as compared to his 0.16 eV experimental value and 0.13 eV found by us. The agreement could not be considered satisfactory. Gyftopoulos and Levine's [23] approach based on the concept of surface electronegativity seems to be a better explanation since it takes into account the specific properties of the species involved. However, the calculus starting from this hypothesis is tedious without introducing new empirical variables.

---

[22] J. C. P. Mignolet, *Bull. Soc. chim. belges*, **65**, 837 (1956).

[23] E. P. Gyftopoulos and J. D. Levine, *J. Appl. Phys.*, **33**, 67 (1962).

(ii) When the surface density is larger than 1×10^{15} silver atoms/cm^2 there is a chance that silver atoms organize themselves in a new crystalline lattice. Indeed, the emission patterns (figs. 5, d, e, f) corresponding to the descending branch of the curve given in figure 4 show that the silver deposits (2 — 4 layers thick) match the tungsten surface structure. The strong interaction between the first silver layer and the tungsten substrate determines a pseudomorphic structure of the entire transition layer [24] (2 — 4 atomic rows). The existing misfit between the fcc Ag structure ($a = 4.09$ Å) and bcc W lattice ($a = 3.16$ Å) is accomodated by strong internal strains which could explain the marked work function decrease occurring on deformation of the electronic band structure within the transition layer. The stabillity of this pseudomorphic layer is ensured by the spontaneous generation of dislocations as pointed out by Frank and van der Merwe. [25,26] The process is enhanced if the substrate has different crystallographic planes as is the case of FEM sample. This does not mean that a single crystal structure and a uniform thickness should be expected. However, the crystalline structure of this transition layer is not a normal fcc silver one and could be well approximated by a W-induced bcc structure. Other supports of this hypothesis came from LEED and Auger studies [27,28]of Ag epitaxy on W (110) which proved the existence of a transition layer (whose thickness extends over several layers) of a structure completely different from that of silver bulk.

(iii) After the silver layer reaches a thickness corresponding to $\theta \approx 5-6$ the normal fcc silver structure is attained. The work function increase up to 4.33 eV (which is the general admitted value of silver work function [29,30]) proves the completion of silver bulk band structure. The corresponding field emission patterns (figs. 5, h, i) are different from clean tungsten symmetry but do not change with further increase in thickness.

The work function minimum value can be calculated from the surface energy of pseudomorphic silver layers. Recently, Missol [31] proposed a semiempirical relation between the surface energy and the work function which takes into account only the crystalline structure parameters of metals :

$$\sigma = \frac{1530}{q} \varphi \left(\frac{\gamma_s}{M} z \right)^{2/3} \tag{2}$$

---

[24] H. Mayer, in "Advances in Epitaxy and Endotaxy", VEB Deutscher Verlag für Grundstoffindustrie, Leipzig, 1971, p. 63.

[25] F. C. Frank and J. H. Van der Merwe, *Proc. Roy. Soc.*, **A 198**, 205 (1949).

[26] J. H. van Der Merwe, in "Advances in Epitaxy and Endotaxy", VEB Deutscher Verlag für Grundstoffindustrie, Leipzig, 1971, p. 129.

[27] E. Bauer and H. Poppa, *Thin Solid Films*, **12**, 167 (1972).

[28] E. Bauer and R. F. Bunshach, in "Techniques in Metal Research", vol. II 2, Interscience, New York, 1969, p. 617.

[29] E. W. J. Mitchell and J. W. Mitchell, *Proc. Roy. Soc.*, **A 210**, 70 (1951).

[30] B. J. Hopkins and J. C. Rivière, *Brit. J. Appl. Phys.*, **15**, 941 (1964).

[31] W. Missol, *Phys. Status Solidi*, **58**, 767 (1973).

where : σ = surface energy (mJ/m^2) ;
φ = work function (eV) ;
γ_s = solid density (g/cm^3) ;
M = atomic mass ;
z = effective number of electrons per atom ;
q = structural coefficient of the lattice.

The structural coefficient q is defined as the ratio of atom surface densities of liquid state (n_L) over that of solid state (n_S) of the same metal :

$$q = \frac{n_L}{n_S} \tag{3}$$

and has different values depending on the crystalline structure, e.g. :

$$q^{\text{fcc}} = 0.80 \qquad\qquad q^{\text{bcc}} = 0.93 \tag{4}$$

For polycrystalline metallic surfaces the mean surface density of atoms is calculated by weighted summation of the values corresponding to low index planes :

$$\bar{n}_S^{\text{cubic}} = \frac{1}{26}\left[6n_{(100)} + 12\, n_{(110)} + 8n_{(111)}\right] \tag{5}$$

From Eq(2) the work function can be calculated if the surface energy is known. There are several methods of evaluating the surface energy starting only from structural data. Two of them are presented and used below.

In a local configuration model, [32,33] the surface energy appears to be produced by unsatisfied bonds of surface atoms whose coordination number Z_s is smaller than Z_v corresponding to bulk value :

$$\sigma\, v_a^{2/3} = \frac{1}{2}(Z_v - Z_s)\, E_b \tag{6}$$

where : v_a = atomic volume ;
E_b = interaction energy of a pair of identical atoms.

Yatzimirskii's [34] structural model defines the surface energy for crystallographic planes of metals as :

$$\sigma = \rho_s\, \Delta h = \rho_v \frac{\Delta h}{2} \tag{7}$$

---

[32] B YA. PINES, "Otcherki po Metallofizike", Izd. Harkovskogo Universiteta, Harkov, 1961.

[33] R. FRICKE, *Kolloid Z.*, **36**, 211 (1941).

[34] V. K. YATZIMIRSKII, *Ukrain. khim. Zhur.*, **33**, 881 (1967).

where : ρ_s = energy density in surface layer ;
ρ_v = cohesion energy density ;
Δh = the inter-penetration thickness of two adjacent rows of atoms, depending upon the packing of different crystallographic planes.

ρ_v can be calculated according to :

$$\rho_v = \frac{L_s}{V_M} \tag{8}$$

where : L_s = molar heat of sublimation ;
V_M = molar volume.

To obtain the surface energy mean value for polycrystalline surfaces we proposed the following summation ;

$$\overline{\sigma}^{\text{cubic}} = \frac{24}{9}\left[\frac{1}{6}\,\sigma_{(100)} + \frac{1}{12}\,\sigma_{(110)} + \frac{1}{8}\,\sigma_{(111)}\right] \tag{9}$$

where the coefficients are the reciprocals of those employed in calculations of mean atom surface density.

Assuming that the silver layers corresponding to the observed work function minimum have a pseudomorphic structure deformed upon the tungsten bcc lattice, their surface energy and work function have been calculated.

First, Missol's and Yatzimirskii's relations (Eqs. (2) and (7 – 9)) were used to calculate the surface energy for thick silver layers. The results presented in table 1 show a good agreement with experimental data which offers additional evidence for thick silver layers (more than 8) having fcc normal structure.

Table 1

Results of surface energy calculation for thick adsorbed silver layers

Method	Parameters	$\sigma_{\text{Ag, calcd}}$ mJ/m²	$\sigma_{\text{Ag, exp}}$ mJ/m²
From work function value	$\varphi_{\text{Ag,exp}} = 4.33$ eV $q^{\text{fcc}} = 0.80$ $z = 0.5$	1 100	1100–1130
Structural model	$L_S = 2.96$ eV $V_M = 10.27$ cm³/mole	1132	

Now, since we suppose that the thin adsorbed silver layer ($\theta \approx \approx 5 - 6$) has a pseudomorphic structure, which means it approximates a bcc structure, Z_s^{bcc} coefficient should be known. In order to obtain this value for principal planes a simple model of hard spheres packed in bcc configuration was used. The mean value was obtained by a summation similar to equation (5). The surface energy of this transition layer was then evaluated by replacing Z_s^{bcc} in Eq.(6), taking for Z_v the general admitted value, 12, and for E_b the experimental[35] binding energy of silver atom pairs, 1.6 eV. The results of this calculation are presented in table 3.

Similar results for surface energy of this transition layer were obtained by using Yatzimirskii's model. The silver atoms were considered hard spheres ($r = 1.44$ Å) packed in a bcc configuration on (110), (100) and (111) tungsten planes. Instead of silver heat of sublimation we used for L_s the mean desorption energy of silver from tungsten,[6] which is more appropriate for thin silver layers. The parameters employed together with surface energy values are given in table 2.

Table 2

Parameters and surface energy values calculated in structural model for pseudomorphic silver layers

Crystal plane (hkl)	$\frac{\Delta h}{2}$	$\sigma_{\text{Ag/(W(hkl)}}$ mJ/m²	$\sigma_{\text{Ag/W}}$ mJ/m²
(100)	$r_{\text{Ag}} - 0.5(4r_{\text{Ag}}^2 - a_{\text{W}}^2/2)^{1/2}$	843	889
(110)	$r_{\text{Ag}} - 0.5(4r_{\text{Ag}}^2 - a_{\text{W}}^2/4)^{1/2}$	382	
(111)	$r_{\text{Ag}} - 0.5(4r_{\text{Ag}}^2 - 2a_{\text{W}}^2/3)^{1/2}$	1 290	

r_{Ag} = 1.44Å (silver atomic adius)
a_{W} = 3.16Å A(tungsten lattice constant)

Use has been made of both surface energy values (from local configuration and Yatzimirskii's models) in calculations of work function of this pseudomorphic layer, according to Missol's equation (2). Table 3 presents the parameters and the calculated values. The good agreement with experimentally determined values of work function minimum supports the initially advanced hypothesis of the deformed fcc structure of thin silver layers.

Table 3

Results of surface energy and corresponding work function calculation for pseudomorphic silver layers

Method	Parameters	$\sigma_{\text{Ag/W,calc.}}$ mJ/m²	$\varphi_{\text{calc.}}$ eV	$\varphi_{\text{exp.}}$ eV
Local configuration model	$Z_s^{\text{bcc}} = 7.38$ $Z_v = 12$ $v_a = 1.71 \times 10^{-23}\text{cm}^3$ $E_b = 1.6$ eV	893	4.08	4.10
Structural model	$\overline{E}_{\text{des(Ag/W)}} = 1.7$ eV $V_M = 10.27$ cm³/mole	889	4.07	

---

[35] G. Verhaegen, F. E. Stafford, P. Goldfinger and M. Ackerman, *Trans. Faraday Soc.*, **58**, 1926 (1962).

4.2. THE SILVER — TUNGSTEN SURFACE BOND

Measurements of bonding energy of Ag atoms on clean W (110) planes [28,36] and polycrystalline surfaces [6] have led to the conclusion that the first layer can accomodate two forms of adsorbed silver of bond energy decreasing from 2.86 eV to 1.79 eV [36] or 1.80 eV [6]. The outer layers are removed with an activation energy of only 1.6 eV [6]. The polarization of the first Ag layer has been invoked to account for the work function increase, but the model featuring dipoles with negatively charged silver atoms could not explain quantitatively either the work function maximum at $\theta \approx 0.7$, or the subsequent work function decrease. [6]

The experimental findings could be explained supposing that two kinds of adsorption site are available for Ag in the first monolayer, at least on some close packed W planes. The effective number of electrons participating in the adsorption bond can be evaluated from the bonding energy values, making use of the method proposed by Rhodin, Palmberg and Plummer. [37] The calculations have yielded a value close to 2 for the strong bonded form (2.86 eV up to a coverage of 6×10^{14} atoms/cm^2) and the expected value of 1 for the weak bonded form (1.79 — 1.80 eV). These electron numbers, meaning the effective surface valency [37] for the adsorbed material, could also be correlated with work function variations up to monolayer completion making use of the Gyftopoulos and Levine's[23] more general model.

It is highly probable that Ag — W bond in the first adsorbed layer has a pronounced metallic character. Indeed, the first ionization potential of the Ag atom ($I = 7.57$ eV) is larger than tungsten work function ($\varphi = 4.50$ eV), but smaller than the bottom of W conduction band ($U = 10.3$ eV). At the equilibrium separation the Ag $(5s)^1$ level will lie well below the *W* Fermi level, but still within the conduction band, forming a broad virtual bound state. The electrons from the metal (*W*) can be donated to the broad level of silver atom, filling it up to the Fermi level. The occupancy of the virtual level, depending upon its relative position within the conduction band, will generally be a fractional number.

In field emission, the metallic adsorption produces the resonance tunneling [38] of electrons which shows up as an additional peak on TED curve or as important deviations from the linearity of standard Fowler — Nordheim plots in the high field range. Our findings pointed out to such deviations of current — voltage characteristics for fields above 4.5×10^9 V/m (on the sharpest emitter) which disappeared if the silver thickness was more than one monolayer (fig. 8). Recently, the resonance tunneling was also observed in the Au — W system. [39] Both these effects prove the metallic bonding of Au and Ag adsorbed on W in the low coverage range.

In the next adsorption stages, as adsorbed atoms start to interact, a progressive change in bonding could occur, increasing the covalent character and decreasing the occupancy of the virtual bond level. This transformation could account for the observed decrease of bond energy and work function in the $\theta = 0.7 - 1.0$ coverage range.

---

[36] C.M.Lo and J. B. Hudson, *Thin Solid Films*, **12**, 261 (1972).

[37] T. N. Rhodin, P. W. Palmberg and E. W. Plummer, in "The Structure and Chemistry of Solid Surfaces", ed. G. A. Somorjai, Willey, New York, 1969, p. 22 — 1.

[38] C. B. Duke and M. E. Alferieff, *J. Chem. Phys.*, **46**, 923 (1967).

[39] P. L. Young and R. Gomer, *Surface Sci.*, **44**, 268 (1974).

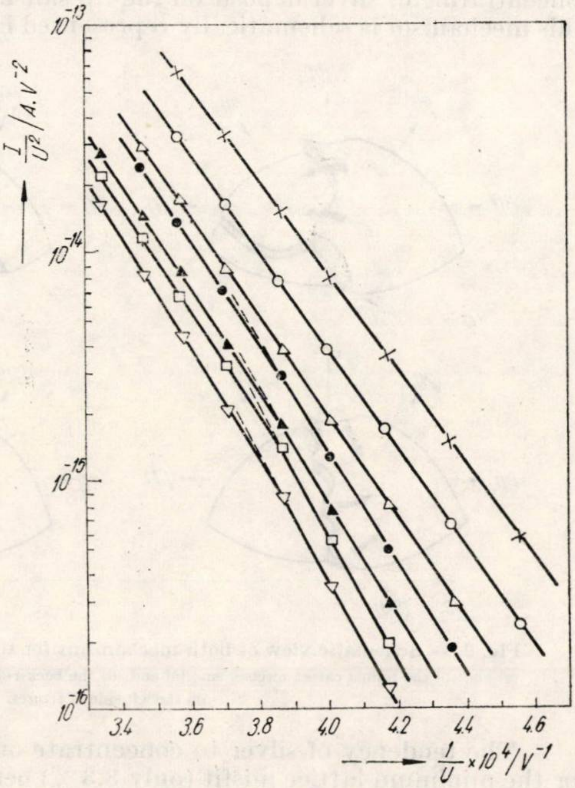

Fig. 8. — Fowler—Nordheim plots for silver layers of various thicknesses on tungsten emitter : △ clean tungsten ($\varphi = 4.50$ eV) ; silver layers showing deviations from Fowler – Nordheim linear relationship ; ▲ $\theta = 0.26$ ($\varphi = 4.59$ eV) ; ● $\theta = 0.36$ ($\varphi = 4.62$ eV) ; □ $\theta = 0.68$ ($\varphi = 4.63$ eV) ; ▽ $\theta = 1.07$ ($\varphi = 4.59$ eV) ; silver layers thicker than one monolayer, obeying Fowler – Nordheim linear relationship ; ○ $\theta = 1.87$ ($\varphi = 4.51$ eV) ; × $\theta = 2.86$ ($\varphi = 4.33$ eV).

4.3. MIGRATION OF SILVER ON TUNGSTEN

The migration experiments have proved that the process takes place in two ways, depending upon the initial silver spread and temperature range. Since the first silver layer forms strong bonds with the tungsten surface, the migration of silver over the clean tungsten requires higher energy than silver migration over an already silver-covered tungsten surface. This is exactly what we observed when the deposition was made at 78 K and at room temperature.

When the migration proceeds following deposition at room temperature, the well-known "rolling carpet" mechanism can best explain the observed patterns (fig. 6). Actually, migration of a thick silver layer over a thin one spread on the whole surface takes place (figs. 9, a, b).

The observed patterns for deposition at 78 K and slight heating (fig. 7) could be attributed to a different mechanism which we called "back-rolling carpet". Indeed, at this temperature, part of the tungsten surface remains bare and silver atoms do not receive enough energy (at the working temperature of 180 – 260 K) to conquer the rest of the surface. The only remaining possibility is the backward migration and the concentrating of silver deposit on the tip side facing the evaporation source. This mechanism is schematically represented in figure 9, c, d.

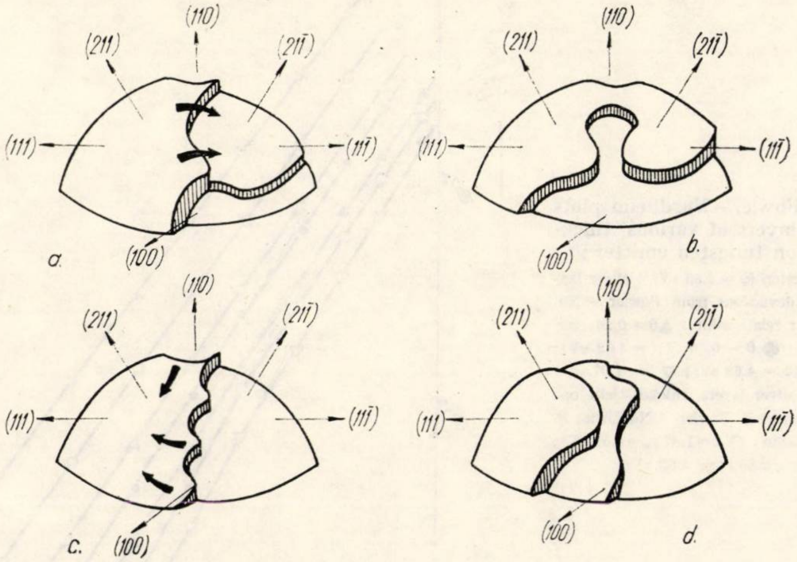

Fig. 9. – Schematic view of both mechanisms for silver migration on tungsten : (a) and (b) the rolling carpet mechanism ; (c) and (d) the back-rolling carpet mechanism. Silver source on the left side of figures.

The tendency of silver to concentrate on W (111) plane can account for the minimum lattice misfit (only 8.3%) between silver (lattice constant 4.09 Å) and tungsten (interatomic distance 4.47 Å on this plane).

5. CONCLUSIONS

The results presented above show the importance of crystallographic substrate anisotropy in the formation of thin silver layers on tungsten surfaces.

The work function variation with layer thickness, which is characteristic of all I – B group metals adsorbed on tungsten [8] indicates that layer formation passes through three stages :

(i) Up to the first monolayer completion, there are strong interactions between silver adatoms and the tungsten substrate, polarizing the adsorbed layer or leading to the formation of metallic bonds.

(ii) The growth of the next 4 or 5 layers is influenced by the atomic arrangement in the first layer. The silver fcc lattice is deformed into a pseudomorphic structure which retains much of tungsten bcc symmetry.

(iii) The normal bulk silver properties (work function 4.33 eV) can be observed only for thick (8 – 9 layers) deposits.

A semiempirical interpretation of the work function minimum observed for pseudomorphic thin layers was proposed, based on structural data and surface energy — work function correlations.

The migration experiments have shown that two surface diffusions mechanisms are possible, depending upon the initial spread of silver layer and the working temperature range. The position of surface barriers to the migration of silver on tungsten was established.

ACKNOWLEDGEMENTS. The authors would like to express their deep gratitude to Acad. Prof. I. G. Murgulescu for the interest in and continuous support to this work. One of us (M. I. Vass) is thankful to Prof. R. Gomer who taught him the FEM technique.

Revue Roumaine de Chimie, **20**, 9–10, 1267–1277 (1975)

DIE REAKTIONEN ZWISCHEN $H[AuCl]_4^-$ UND DEM IN *ORTO*-SUBSTITUIERTEN MALACHITGRÜN

GHEORGHE C. CONSTANTINESCU
Polytechnische Hochschule Bukarest, Str. Polizu 1

Eingegangen am 15. Juni 1974

In der vorliegenden Arbeit wurde die Reaktion zwischen dem Komplexanion $[AuCl_4]^-$ und dem mit $-OCH_3$, $-Cl$, $-NO_2$-Gruppen in *orto*-Stellung substituierten basischen Farbstoff Malachitgrün studiert. Die gewonnenen Farbstoffe bilden mit $[AuCl_4]^-$ in Wasser unlösliche, in organischen Lössungsmitteln aber lösliche Verbindungen, die dann in Benzol extrahiert werden. Die organischen Extrakte sind spektrophotometrisch und konduktometrisch untersucht. Außerdem wurden die Verbindungen aus Wasserlösung ausgefällt und der Elementar- bzw. IR-Spektralanalyse unterworfen. Es werden auch die Grundbedingungen für die Anwendung der Reaktionen zur Goldbestimmung festgestellt. Die studierten Reagenzien können auch für die Extraktion des Goldes aus verschiedenen Vorkommen verwendet werden.

Malachitgrün, ein Farbstoff der dyaminotriphenylmetanischen Klasse, bildet im sauren Milieu mit Einfachen- und Komplexanionen verschiedene Verbindungen vom Typ der ionischen Assoziation. Solche in Wasser unlösliche Verbindungen kristallisieren bei Zimmertemperatur. Da sie aber in organischen Lösungsmitteln leicht löslich sind und die auf diese Weise gewonnenen Extrakte bestimmte spektrophotometrische Eigenschaften besitzen, können sie zur Trennung der Metallionen und zu deren Bestimmung angewendet werden. Der Mechanismus ähnlicher Reaktionen wurde zuerst von Onishi[1] studiert und besteht in der Bildung in wäßrigen Medien der komplexen hallogeno-metallischen Säuren : H_2MX_5, HMX_4, die durch die Bindung des komplexen Anions MX^{n-}_{3+n} am Farbstoffskation gefolgt wird.

In dieser Arbeit werden die Synthesen der basischen Farbstoffe, die Ergebnisse der Forschungen bezüglich der Bildungsreaktion der ionischen Assoziationen zwischen $[AuCl_4]^-$ und der Kationen der Farbstoffe, sowie auch die Struktur und einige Eigenschaften der erhaltenen Verbindungen dargestellt.

VERSUCHSTEIL

SYNTHESE DER FARBSTOFFE

Die drei verwendeten Farbstoffe wurden durch Kondensierung von *orto*-Metoxy-, *orto*-Chlor- bzw. *orto*-Nitrobenzaldehyde mit Dimethylanilin gewonnen.[2] Die durch Erhitzung auf dem Wasserbad erhaltene dickflüssige Masse ist mit Wasserdampf angetrieben. Der zurückgebliebene Rückstand ist in Äthylalkohol aufgelöst, woraus die Leukobasis wieder ausgefällt wird. Durch Oxydation mit Bleidioxyd erhält man das entsprechende Carbinol, welches mit Chlorwasserstoff die Verbindung mit folgender Struktur bildet:

---

[1] H. Onishi und E. B. Sandell, *Analyt. Chim. Acta*, **24**, 413 (1961).

[2] H. Sanielevici und L. Floru, "Sinteza intermediarilor aromatici şi a coloranţilor" Ed. II, Ed. didactică şi pedagogică, Bukarest, 1971, S. 277.

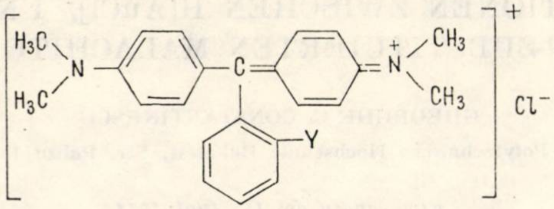

wo Y = H — Malachitgrün,
Y = Cl — Astrazonblau 5 GL,
Y = OCH_3 — *orto*-Anisgrün,
Y = NO_2 — *orto*-Nitralgrün.

Die Reinigung der Farbstoffe erfolgte durch wiederholte Umkristallisation aus Äthylalkohol wonach die Reinheit durch die Kaliumdichromatmethode bestimmt wurde.[3] Die Papierchromatorgamme mit dem Äthylalkohol Wasser 1 : 1 zeigten einheitliche Zusammensetzung.

REAGENZIEN UND LÖSUNGEN

Die wäßrige Lösung des Au(III) wurde durch die Auflösung des $H[AuCl_4]$ (Merck) unter Zuführung einer bestimmten Menge Chlorwasserstoff hergestellt. Es wird eine Eichlösung vorbereitet, die 197 μg Au/ccm enthält. Der Titer dieser Lösung wurde durch die Methode nach Chow-Beamish bestimmt.[4] Die in dieser Arbeit benutzten Lösungen sind durch angemessene Verdünnungen vorbereitet.

— Man verwendet 1.10^{-3}M Wasserlösungen bezogen auf die 100%ige Reinheit der Farbstoffe,

— 6 N Chlorwasserstofflösung

— Benzol p. a.

— Wasserlösungen verschiedener Kationen unter Form von Nitraten, Sulfaten und/oder Chloriden.

EXTRAKTION DER KOMPLEXE

Die 1.10^{-4}M Lösung von Au(III) in Volumina von 0,1—2 ccm wird in einem Scheidetrichter oder Meßkolben von 50 ccm mit 6 N-en Chlorwasserstoff (1 ccm), destilliertem Wasser und 1.10^{-3}M Reagenzlösung bis zum Volumen von 10 ccm geführt. Man fügt 10 ccm organisches Lösungsmittel hinzu und schüttelt 2 Minuten lang am Schüttelapparat. In ähnlicher Weise werden auch die Kontrollproben vorbereitet. Man mißt die Extinktionen der gefärbten organischen Phase bei den entsprechenden Wellenlängen in 1 cm dicken Küvetten.

ERGEBNISSE UND DISKUSSIONEN

DIE SYNTHESE DER KOMPLEXE

Um das Kombinationsverhältnis im festen Zustand des Gold-Komplexanions mit den untersuchten Reagenzien festzulegen, wurden 0,25 g Au(III) gelöst in 20 ccm Wasser und Chlorwasserstoff bis zu der optimalen

---

[3] R. P. Lastovski und Io. I. Vanstein, "Tehnicheskii analiz v proizvodstvo promejutochiniscкh i Crasitelei", Moskva 1958.

[4] A. Chow und F. E. Beamish, *Talanta*, **10**, 883 (1963).

Normalität (s. Tabelle 6) und mit etwa 0,50 g in 10 ccm gelösten Farbstoff gemischt. Es erscheint ein grünblauer Niederschlag, der durch Filtrierung unter Wakuum getrennt und mit Wasser gewaschen wurde, danach aus Benzol umkristallisiert. Die Verbindungen wurden bezüglich des Gehaltes an Gold,[4] an Stickstoff und an Chlor[5,6] analysiert. Die erhaltenen Ergebnisse sind in Tabelle 1 eingetragen, woraus hervorgeht, daß das molarische Kombinationsverhältnis Metall-Farbstoff 1 : 1 ist.

Tabelle 1

Die Elementaranalyse der Komplexe

Verbindung		Gold		Stickstoff		Chlor	
Name	Substituent	Berechnet %	Gefunden %	Berechnet %	Gefunden %	Berechnet %	Gefunden %
Malachitgrün	R–H	29,49	29,38	4,19	4,24	21,25	21,18
orto-Anisgrün	R–OCH_3	28,22	28,28	4,25	4,21	20,31	20,26
orto-Nitralgrün	R–NO_2	27,63	27,51	5,89	5,95	19,77	19,65
Astrazonblau 5GL	R–Cl	27,72	27,63	3,94	4,01	19,98	19,92

DIE IR-SPEKTREN

Diese Spektren werden in einem Bereich von 400 – 4000 cm^{-1} erforscht. Bei Vergleichung der IR-Spektren der freien Verbinder mit denen der entsprechenden Goldkomplexverbindungen wurde festgestellt, daß die Lagen und die Größen der Vibrationsbänder nach der Reaktion sich nicht verändert haben, ein Hinweis dafür, daß sich die Komplexe mit Ladungsübertragung bildeten. Die charakteristischen Vibrationen der Bindung C–N (1 400 cm^{-1}), C–C (1 600 cm^{-1}) (C–H (1 000 cm^{-1}) in den Spektren der Komplexe sind gewöhnlich etwas verschoben gegen kleinere Frequenzen, wegen der Ausdehnung dieser Bindungen nach der Komplexierung. Die Verbindungen mit Gold konnten nicht hervorgehoben werden, weil die betreffenden Vibrationen unter 400 cm^{-1} erscheinen und dieser Bereich mit dem verwendeten Apparat nicht erforscht wurde. Die Abbildungen 1a und 1b geben die IR-Spektren des *orto*-Anisgrüns und des damit gewonnenen Komplexes wieder.

DER THERMISCHE ABBAU

Der thermooxydative Abbau von reinen Farbstoffen und deren mit $AuCl_4^-$ hergestellten Komplexverbindungen erfolgte thermogravimetrisch[7] in einem Temperaturintervall von 20–900° mit einem Gerät von Typ

---

[5] N. H. Furman, "Standard Methods of Chemical Analysis" Ed. II. Van Nostrand' New York, 1962–1963.

[6] I. S. Lealicov, "Metode fizico-chimice de analiză" Bukarest, 1961, Kap. 19, S. 339.

[7] O. Vicol, A. Biro und I. Schneider, *Thermal Anal.*, **1**, 435 (1969).

MOM Budapest, Erwärmungsgeschwindigkeit 9°/min in 100 min. In Abbildung 2 geben wir als Beispiel die Derivatogramme vom Farbstoff *orto*-Anisgrün und dessen Komplexverbindung mit AuCl$_4^-$ wieder.

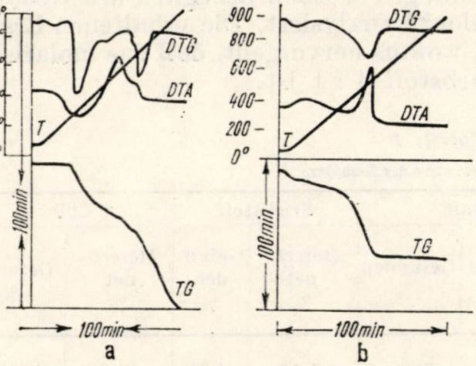

Abb.1. — Die Derivatogramme des freien Farbstoffes (1a) und des mit AuCl$_4$ gewonnenen Komplexes (1b).

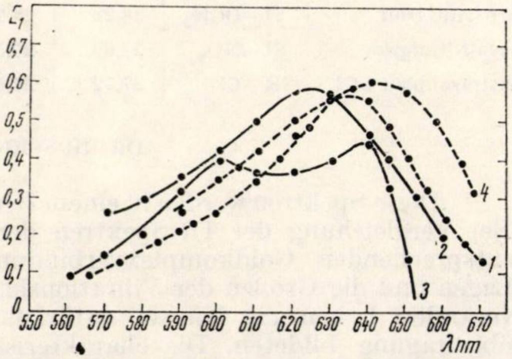

Abb. 2. — Die Absorptionsspektren im sichtbaren Bereich:

1 = Malachitgrün—AuCl$_4$, 2 = *orto*-Anisgrün—AuCl$_4$, 3 = Astrazonblau 5GL—AuCl$_4$, 4 = *orto*-Nitralgrün—AuCl$_4$.

Der Farbstoff ist bis 610° in vier Stufen abgebaut. Die DTA-Kurve gibt uns Informationen über den thermischen Effekt jeder Abbaustufe. Die ersten drei Stufen zeigen einen schwachen endothermischen Effekt und die vierte Stufe von 450—610°, einen ausgeprägten exothermischen Effekt, als Folge der Oxydation von Abbauprodukten.

Der Abbau von Komplexverbindung zeigt ein ähnliches Verhalten aber mit anderen Gewichtverlusten für jede Stufe (Abbildung 1, Tabelle 2).

Tabelle 2

Die Stufen des thermischen Abbaues

Verbindung	1. Stufe		2. Stufe		3. Stufe		4. Stufe	
	°C	Verlust Gew. %	°C	Verlust Gew. %	°C	Verlust Gew. %	°C	Verl. Gew. %
Orto-Anisgrün	45—160	3%	160—350	37%	350—620	60%	—	—
(*Orto*-Anisgrün)$^+$ (AuCl$_4$)$^-$	45—160	4%	110—350	9,5%	350—580	52,2%	580—900	1,1%

Bis 480° zeigt die Verbindung einen sehr schwachen Abbau und ab 480° zeigt die Entwicklung einen exothermischen Effekt, welcher zu Goldtrioxyd führt. Die Komplexverbindung ist temperaturbeständiger als der Farbstoff. Der Rückstand, in Gewichtsprozenten zu Einwaage, stimmt mit der berechneten Zusammensetzung der Elementaranalyse überein. Bis cca. 100° können die Verluste von 4% als Wasserverlust betrachtet werden.

DER VERTEILUNGSKOEFFIZIENT

Um den Verteilungskoeffizient des Metalls zwischen den beiden Phasen festzulegen, kam eine spektrophotometrische Methode zur Anwendung.[8] Die Komplexverbindungen wurden unter optimalischen Bedingungen hergestellt und in Benzol extrahiert. Die beiden Phasen wurden getrennt, dann jede mit konzentrierter Schwefelsäure und Wasserstoffsuperoxyd behandelt. Die auf diese Weise gelösten Goldmengen wurden in beiden Fällen durch Rodamin B in Gegenwart von Chlorwasserstoff bestimmt.[9] Die Ergebnisse sind in Tabelle 3 eingetragen.

Tabelle 3

Der Verteilungskoeffizient und die Extraktibilität der Komplexe

Reagenz	Substituent	q	E%
Malachitgrün	$-H$	5,29	84,20
Orto-Anisgrün	$-OCH_3$	8,51	89,73
Astrazonblau 5 GL	$-Cl$	8,70	90,42
Orto-Nitralgrün	$-NO_2$	11,01	98,21

Eine bessere Extraktion stellt man bei der Verwendung von *orto*-Nitralgrün gefolgt von *orto*-Anisgrün fest. Auch in dieser Beziehung ist *orto*-Nitralgrün allen anderen geprüften Farbstoffen überlegen.

DIE WAHL DES LÖSUNGSMITTELS

Es wurden folgende Lösungsmittel erprobt : Benzol, Toluol, Chloroform und Gemische von Benzol mit kleinen Mengen von Aceton, Cyklohexanon, Methyläthylceton, Alkohole oder Äther, die sich in ähnlichen Arbeiten wirksam zeigten. Die Ergebnisse sind in Tabelle 4 eingetragen. In unseren Forschungen wurde dann nur das Benzol verwendet, weil dieses Lösungsmittel keinen freien Farbstoff mitextrahiert. Die Kontrollproben waren farblos. Nur in Fall des Astrazonblau 5 GL als Lösungsmittel, wurde das Gemisch von Benzol mit Cyklohexanon gewählt.

---

[8] S. FIȘEL, "Chimie analitică cantitativă", Bukarest, 1973, S. 294.

[9] J. H. YOE und A. E. HARVEY, *J. Amer. Chem. Soc.*, **70**, 648 (1948).

Tabelle 4

Die Wahl der Lösungsmittel

Lösungsmittel	$E_{1\,max}$			
	$R-H$	$R-OCH_3$	$R-Cl$	$R-NO_2$
Benzol	0,34	0,69	0,25	0,82
Benzol-Äther 2 :1	0,14	0,16	0,10	0,08
Benzol-Methanol 2 :1	0,20	0,12	0,15	0,23
Benzol-Äthanol 2 :1	0,16	0,18	0,16	0,28
Benzol-Cyklohexanol 2 :1	0,24	0,20	0,20	0,31
Benzol-Methyläthylceton 4 :1	0,28	0,38	0,33	0,63
Benzol-Methyläthylceton 6 :1	0,35	0,52	0,40	0,70
Benzol-Methyläthylceton 8 :1	0,38	0,73	0,42	0,88
Benzol-Aceton 3 :1	0,16	0,28	0,46	0,42
Benzol-Cyklohexanon 3 :1	0,20	0,40	0,57	0,58

ABSORPTIONSSPEKTREN IM SICHTBAREN BEREICH

Bei Bestimmung der elektronischen Absorptionsspektren von wäßrigen Lösungen der Reagenzien (Tabelle 5, Abbildung 2) wird festgestellt, daß das Spektrum von Malachitgrün ein Absorptionsmaximum bei 620 nm hat. Da die Spektren von mit elektronenabstoßenden Gruppen (OCH_3) substituierten Malachitgrün ein Absorptionsmaximum bei 606 nm und die mit elektronenanziehenden Gruppen $(ClNO_2)$ Absorptionsmaxima bei 630–635 nm bzw. bei 640 nm haben, stimmten diese Tatsachen mit den von Dewar festgestellen[10,11] überein; die elektronenabstoßenden Substituenten haben einen hypsochromischen Effekt und die elektronenanziehenden Substituenten einen batochromischen Effekt zur Folge.

Tabelle 5

Absorptionsmaxima der Farbstoffe und deren mit $AuCl_4^-$ gewonnenen Komplexverbindungen

Farbstoff	Substituent	λ_{max} Wasserlösung nm	λ_{max} organische Lösung der Komplexverbindung nm
orto-Anisgrün	OCH_3	606	623
Malachitgrün	H	620	635
Astrazonblau 5GL	Cl	640	640
orto-Nitralgrün	NO_2	635	645

Die mit Au(III) in 10 ccm Benzol erhaltenen Verbindungen weisen alle auf eine batochromische Verschiebung der elektronischen Absorptionsmaxima im Vergleich zu den wäßrigen Lösungen der reinen Farbstoffe hin. Diese Verschiebung kann der Bildung von Komplexen mit Ladungsübertragung von Typ $\sigma - \pi$ zugeschrieben werden.

---

[10] M.J.S. Dewar, *J. Amer. Chem. Soc.*, **1950**, 2327, **1954**, 2134.

[11] M.J.S. Dewar, *J. Amer. Chem. Soc.*, **74**, 3341, 3357 (1952).

DIE AZIDITÄT DER LÖSUNG

Alle studierten Reaktionen laufen im Medium von Chlorwasserstoff ab. Bei 0,3 N für Malachitgrün erhält man die maximale Absorbanz. Es ist wichtig, daß alle in *orto* substituierten Farbstoffe weniger ausgeprägte Abhängigkeit von der Lösungsazidität als Malachitgrün aufweisen, d.h. man kann die Reaktion in größeren pH-Intervallen mit Behaltung der optimalischen Bedingungen ausführen. In der Abbildung 4 ist es deutlich zu ersehen.

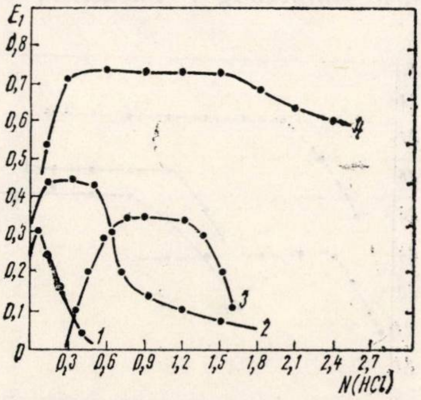

Abb. 3. – Der Einfluß der Lösungsazidität auf die Extraktibilität von Komplexen:
1 = Malachitgrün, 2 = *orto*-Anisgrün, 3 = Astrazonblau 5GL, 4 = *orto*-Nitralgrün.

Die Abhängigkeit der Komplexbildung von der Azidität der wäßrigen Phase könnte man durch das Vorhandensein von Farbstoffskation in monomerer Form erklären. Bei niedrigeren bzw. höheren pH-Werten können polymere Formen der Kationen vorhanden sein.[12] In Tabelle 6 geben wir die Abhängigkeit der Aziditätsintervalle von der Wellenlängen maximaler Absorbanz wieder:

Tabelle 6

Der Zusammenhang zwischen λ_{max} und Lösungsazidität

Reagenz	Substituent	λ_{max} [nm]	Lösungsazidität (N)	
			[min]	[max]
orto-Anisgrün	OCH_3	623	0,05	0,12
Malachitgrün	H	635	0,3	0,3
Astrazonblau 5GL	Cl	640	0,6	1,2
orto-Nitralgrün	NO_2	645	0,6	1,8

Je stärker die elektronenanziehende Kraft der Substituenten ist, desto länger ist das Intervall der Azidität wäßriger Phase, in der man optimale Reaktionsbedingungen findet und desto höher ist die optimale Azidität. Ob diese Regel verallgemeinert werden kann, ist noch durch andere Versuche festzustellen.

---

[12] O. F. Ginsburg und C. M. Zavlin, *Zhur. obschchcei Khim.*, **32**, 3559 (1962).

DIE REAGENZKONZENTRATION

Bei Veränderung der Farbstoffmenge von 0,5–5,0 ccm 1.10^{-3}M (um das eingestellte Gleichgewicht nach rechts zu verschieben) wurde eine Erhöhung der Extinktion bis zu einer bestimmten Konzentration festgestellt, nach der sie konstant bleiben. Die bestmögliche Konzentration, in Abbildung 4 ersichtlich, ist für die Komplexe mit Malachitgrün bei $1{,}6.10^{-4}$M, für die mit *orto*-Anisgrün bei 7.10^{-4}M, für die mit *orto*-Nitralgrün bei 3.10^{-4}M und für die mit Astrazonblau 5 GL bei 6.10^{-4}M zu 10 ccm wäßriger Lösung.

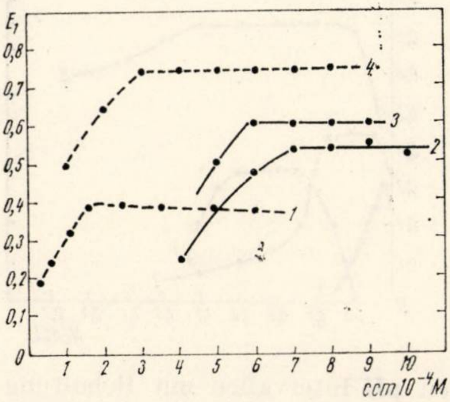

Abb. 4. – Die Reagenzkonzentration :
1 = Malachitgrün – $AuCl_4$, 2 = *orto*-Anisgrün – $AuCl_4$, 3 = Astrazonblau 5GL – $AuCl_4$, 4 = *orto*-Nitralgün – $AuCl_4$.

DIE EICHKURVEN

Das Studium der Absorptionsvariation in Abhängigkeit der Konzentration von Gold hat gezeigt, daß das Bouguer-Lambert-Beer'sche Gesetz zwischen den in der Tabelle 7 eingeordneten Grenzen als wahr erwiesen ist :

Tabelle 7

Die Grenzen des Bouguer Lambert – Beer'schen' Gesetzes

Reagenz	Substituent	µg/Au/cm³		ε
		min.	max	
Malachitgrün	$-H$	10	100	5.700
Orto-Anisgrün	$-OCH_3$	2	10	37.500
Astrazonblau 5 GL	$-Cl$	0,7	1,42	44.000
Orto-Nitralgrün	$-NO_2$	0,6	10	81.000

Die Beständigkeit der Komplexverbindungen beträgt :
– 1/2 Stunde für das Komplex mit Malachitgrün
– 3–5 Stunden für mit Astrazonblau 5 GL
– 24 Stunden für mit *orto*-Anisgrün
– 48 Stunden für mit *orto*-Nitralgrün

Die Eichungsgeraden wurden durch Verbesserung der Versuchsdaten mit Hilfe der Methode kleinster Quadrate erhalten. Durch die statistische Bearbeitung der Ergebnisse (Warscheinlichkeit 0,95) wird ersichtlich, daß die relative Abweichung zwischen ±3,2% wechselt. Die Sensibilität der Reaktion ist größer bei der Anwendung von substituiertem Malachitgrün, unabhängig von der Substituentennatur. Bei dem Vergleich der Substituenten miteinander, stellt man fest, daß die elektronenanziehenden, den elektronenabstoßenden überlegen sind. Das ist wohl durch Einfluß der Substituentenelektronen auf die Positivierung der Moleküle und auf den unterschiedlichen Einfluß des Substituenten über die Unkoplanarität der Farbstoffmolekel zurückzuführen.[13]

DAS STUDIUM DER ZUSAMMENSETZUNG DER IN ORGANISCHER LÖSUNG GEBILDETEN KOMPLEXVERBINDUNGEN

Für die Bestimmung des Kombinationsverhältnisses Metall-Farbstoff in der organischen Lösung kam die Methode Job[14] zur Anwendung. Die erhaltenen Ergebnisse sind in der Abbildung 6 dargestellt.

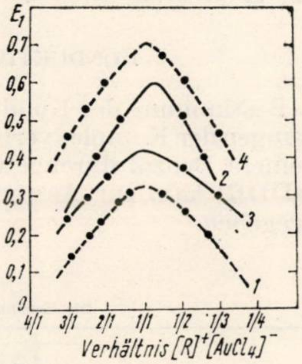

Abb. 5. — Die Zusammensetzung der gelösten Komplexverbindungen:

1 = Malachitgrün – AuCl$_4$, 2 = *orto*-Anisgrün – AuCl$_4$, 3 = Astrazonblau 5GL – AuCl$_4$, 4 = *orto*-Nitralgrün – AuCl$_4$.

Das Kombinationsverhältnis für alle vier Verbindungen ist 1 : 1. Dieses Ergebnis war allerdings zu erwarten, da die Reaktionen im pH-Bereich durchgeführt werden, in dem der Farbstoff hauptsächlich als Kation in monomerer Form vorliegt.

DIE INSTABILITÄTSKONSTANTEN

Aus den Versuchsdaten (Abbildung 6) wurden die Instabilitätskonstanten errechnet und es wurde für das zwischen Au(III) und Malachitgrün gebildete Komplex $K_i = 8{,}4 \cdot 10^{-4}$, für das mit *orto*-Anisgrün gebildete $K_i = 2{,}0 \cdot 10^{-4}$ für das mit Astrazonblau 5 GL $K_i = 6{,}7 \cdot 10^{-4}$ und für das mit *orto*-Nitralgrün gebildete $K_i = 1{,}2 \cdot 10^{-5}$ gefunden. Die erhaltenen

---

[13] S. A. Lomonosov, *Zhur. anal. Khim.*, **22**, 8, 1125 (1967).

[14] P. Job, *Ann. Chim.* (*France*), **9**, 113 (1928).

Ergebnisse zeigen, daß sich durch Fällung hauptsächlich Komplexverbindungen vom Typ ($R^+AuCl_4^-$) bildeten:

$$H[AuCl_4] + R^+Cl^- = R^+[AuCl_4]^- + HCl$$

Es ist aber möglich, daß in der Lösung auch andere in Gleichgewicht befindenden Arten existieren.

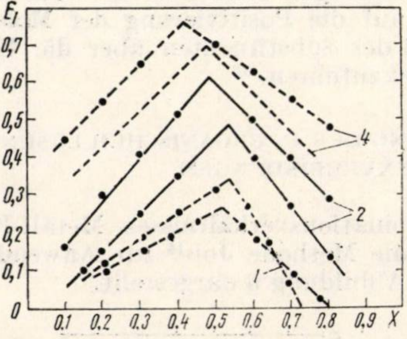

Abb. 6. — Die Instabilitätskonstanten:
1 = Malachitgrün – $AuCl_4$, 2 = *orto*-Anisgrün – $AuCl_4$, 4 = *orto*-Nitralgrün – $AuCl_4$.

KONDUKTIVITÄTSBESTIMMUNGEN

Die Bestimmung der Konduktivität wurde unter Verwendung organischer Lösungen der Komplexverbindungen im Vergleich zu der Kontrollprobe und zu reinem Benzol durchgeführt. Ein Megaohmmeter vom Typ Tetralin Statron (DDR) kam zur Anwendung. Die Ergebnisse sind in der Tabelle 8 wiedergegeben.

Tabelle 8

Die Konduktivität von Benzollösungen

	$\rho = \frac{1}{R}$ ($\Omega \cdot$cm)	$\gamma = \frac{1}{\rho}$ (Ω^{-1} cm^{-1})
Benzol	$0,82.10^{11}$	$1,22.10^{-11}$
Kontrolle	$0,33.10^{8}$	$3,0.10^{-8}$
(Malachitgrün+ $AuCl_4^-$)	$0,148.10^{7}$	$6,8.10^{-7}$
(*Orto*-OCH_3^+ $AuCl_4$)	$0,218.10^{7}$	$0,46.10^{-7}$
(*Orto*-NO_2^+ $AuCl_4^-$)	$0,338.10^{7}$	$3,0.10^{-7}$
(*Orto*-Cl+ $AuCl_4^-$)	$0,213.10^{7}$	$4,7.10^{-7}$

Der Konduktivitätsunterschied zwischen Benzol und der Kontrollprobe wird wohl der Gegenwart von in Benzol gelösten Wasser und Säuremengen, als Folge der Mischung beider Phasen zugeschrieben. Im Vergleich zur Kontrolle steigt die Konduktivität der gelösten Komplexverbindungen etwa mit einer Größenordnung, was auf eine gewisse Ionisierung hindeutet. Als Ursache vermuten wir auch das in Benzol gelöste Wasser.

DER EINFLUSS FREMDER IONEN

Es wurde die Interferenz jener Ionen geprüft, die gewöhnlich in verschiedenen Materialien Gold begleiten und ähnliche Verbindungen bilden, so wie Indium, Gallium, Eisen, Antimonium, Vanadium, Thallium, Germanium und Molibden, Cobalt, Nickel, Kupfer, Cadmium. Die Reaktionen sind in folgender Reihenfolgen von den fremden Ionen gestört:

Malachitgrün : Tl > In > Ga > Bi > Sb > Fe > Ge
Astrazonblau 5 Gl : Fe > Tl > In > Ga
orto-Anisgrün : Tl > Sb > Bi > Ga
orto-Nitralgrün : Tl > Sb > In > Ga > Bi > Fe

Die anderen geprüften Elemente stören die Reaktionen nicht.

Revue Roumaine de Chimie, 20, 9–10, 1279–1285 (1975)

ÉTUDE POLAROGRAPHIQUE DE QUELQUES COMPLEXES DE COBALT (III)-DIMÉTHYLGLYOXIME

LUCIA IORDĂCHESCU [*], NICOLAE CALU [**] et EUGEN NEGURĂ [*]

[*] Institut Pédagogique, Bacău, 157, str Mărășești
[**] L'Université de Jassy, Chaire de Chimie minérale, Calea « 23 August »

Reçu le 5 août 1974

On a étudié le processus de réduction polarographique des complexes de Co (III) -diméthylglyoxime, en fonction du pH de la solution, de la nature et de la structure des ligands, ainsi que le comportement de certains isomères de position. En ce qui concerne l'influence du pH de la solution sur le processus de réduction, on a constaté que le potentiel du demi-palier du premier échelon [Co(III) → Co(II)] est déplacé vers des valeurs plus négatives dans les milieux neutres ou basiques, tendant asymptotiquement vers −0,6V. Le potentiel de demi-palier des échelons de réduction polarographique est en quelque sorte influencé par la nature et la structure des ligands. Dans le cas des ions complexes étudiés, on peut constater par exemple que, les dérivés d'aniline augmentent la stabilité de réduction plus que la pyridine et ses dérivés (ß et γ picoline). D'autre part, les modifications de structure des ligands à cause des isomères de position n'influencent pas sensiblement la stabilité de réduction des ions complexes.

L'étude polarographique des complexes de cobalt a constitué l'objet de plusieurs recherches [1–8] où l'on a étudié l'influence de certains facteurs sur le processus de réduction, tels que : le pH de la solution, la présence des substances capillaires-actives, la substitution des ligands des ions complexes, etc.

Les complexes cobaltiques présentent deux échelons polarographiques : le premier situé à des potentiels plus bas correspond à la réduction de l'ion complexe Co(III) à Co(II) et le second, situé plus près de l'échelon de la solution fondamentale, correspond à la réduction de Co(II) à Co(0) [9,10] : On a remarqué que si le potentiel de demi-palier du premier échelon polarographique est déplacé vers des valeurs plus négatives, ce fait peut être

---

[1] S.M. Jörgensen, *J. prakt. Chem.*, **41**, 440 (1890).

[2] M. Vogel, Dissertation, Zürich, 1905, p. 10.

[3] J. B. Willis, J. A. Friend et D. P. Mellor, *J. Amer. Chem. Soc.*, **67**, 1680 (1945).

[4] H. A. Laitinen, J. C. Bailarjr, H. F. Holtzclaw et J. V. Qvagliono, *J. Amer. Chem. Soc.*, **70**, 2999 (1948).

[5] H. A. Laitinen et P. Kivalo, *J. Amer. Chem. Soc.*, **75**, 2198 (1953).

[6] H. F. Holtzclaw et D. P. Sheetz Jr., *J. Amer. Chem. Soc.*, **75**, 3053 (1953).

[7] R. Ralea, D. Giurgiu et Gh. Burlacu, *Studii și Cercetări Şti. Chim. Fil. Iași*, **14**, 75 (1963).

[8] N. Calu, C. Várhelyi, H. Kubarek, *Stud. Univ. Babeș Bolyai, Chem.*, **2**, 118 (1967).

[9] R. Ralea et A. Popa Rang, «Chimia și structura combinațiilor complexe», Ed. didactică și pedagogică, Bucarest, 1965, p. 3 — 10, 20 — 35.

[10] J. Heyrovsky, « Polarographie », Springer Verlag, Vienne, 1941, p. 85 — 175.

considéré comme un critère d'appréciation de la stabilité du complexe étudié, parce que l'énergie de réduction de l'ion à la cathode correspond à celle de la première orbitale libre du ion complexe.[11,12]

Les complexes de Co(III) — diméthylglyoxime moins étudiés jusqu'à présent sous cet aspect montrent quelques caractéristiques intéressantes qui peuvent constituer une base pour des conclusions en ce qui concerne le degré de la stabilité de la molécule de la combinaison complexe[13,14].

PARTIE EXPÉRIMENTALE

Les complexes du type $[Co(DG)_2 X_2]^+$ ont été analysés polarographiquement dans le domaine de concentration $0,6 - 4 \cdot 10^{-4}$ mole/l, en utilisant comme solution fondamentale Li Cl $5 \cdot 10^{-2}$ mole/l, associée à une solution tampon Britton-Robinson.

Les caractéristiques du tube capillaire utilisé : $m = 3,164$ mg$\cdot S^{-1}$ et $t = 2,8$ s.

Les valeurs des potentiels ont été exprimées par rapport à l'électrode de calomel saturé.

a. L'ANALYSE DES ÉCHELONS POLAROGRAPHIQUES

Dans les figures 1—2 sont présentés les échelons polarographiques qui correspondent à la réduction Co(III) à CO(II) des ions comp lexes envisagés dans cette étude.

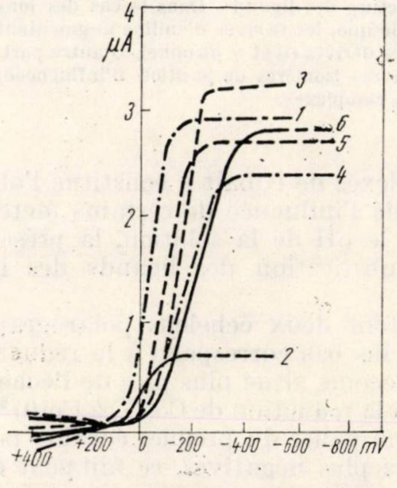

Fig. 1. — Les échelons polarographiques ($Co^{III} \rightarrow Co^{II}$) des ions :

1. $[Co(DG)_2$ (β-picoline$)_2]^+$ 2. $[Co(DG)_2$ (γ-picoline$)_2]^+$ 3. $[Co(DG)_2$ (pyridine$_2]^+$ 4. $[Co(DG)_2$ (aniline$)_2]^+$ 5. $[Co(DG)_2$ (o-toluidine$)_2]^+$ 6. $[Co(DG)_2$ (p-toluidine$)_2]^+$

Concentration en ion complexe $1,2 \cdot 10^{-4}$ mole/l

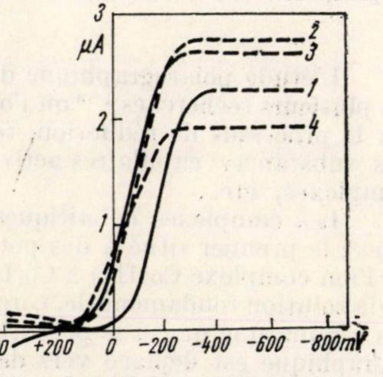

Fig. 2. — Les échelons polarographiques ($Co^{III} \rightarrow Co^{II}$) des ions :

1. $[Co(DG)_2$ (o-amino-éthyl-benzène$)_2]^+$ 2. $[Co(DG)_2$ (p-amino-éthyl-benzène$)_2]^+$ 3. $[Co(DG)_2$ (o-phénétidine$)_2]^+$ 4. $[Co(DG)_2$ (p-phénétidine$)_2]^+$

Concentration en ion complexe $1,2 \cdot 10^{-4}$ mole/l

---

[11] K. Komarek, *Coll. Czech. Chem. Comm.*, **8**, 12 (1947).

[12] A. Braley et F. B. Hobart, *J. Amer. Chem.*, **19**, 1974 (1906).

[13] L. Iordăchescu, N. Calu, E. Negură et C. Várhelyi, *Studii și Cercetări Sti. Nat. I. P. Bacău*, **2**, 17 (1972).

[14] L. Iordăchescu, N. Calu, E. Negură et C. Várhelyi, *Studii și Cercetări Ști. Nat. I. P. Bacău*, **3**, 49 (1973).

Ces échelons polarographiques ont été analysés plus loin, en suivant la dépendance du courant de diffusion par rapport à la concentration de l'ion complexe. Ainsi, les diagrammes 3—4 montrent une dépendance linéaire du courant de diffusion par rapport à la concentration des ions complexes étudiés.

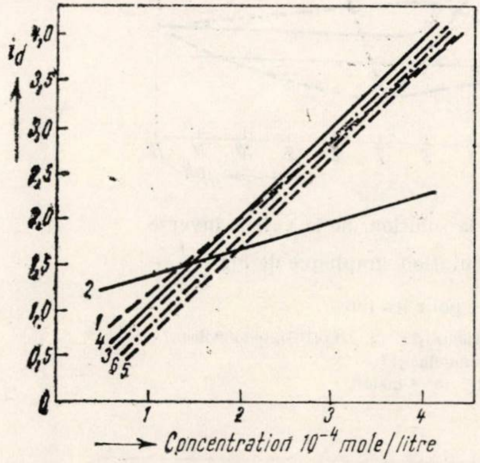

Fig. 3. — Variation du courant de diffusion (t_d) en fonction de la concentration pour les ions :

1. $[Co(DG)_2(\beta\text{-picoline})_2]^+$ 2. $[Co(DG)_2(\gamma\text{-picoline})_2]^+$ 3. $[Co(DG)_2(\text{pyridine})_2]^+$ 4. $[Co(DG)_2(\text{aniline})_2]^+$ 5. $[Co(DG)_2(o\text{-toluidine})_2]^+$ 6. $[Co(DG)_2(p\text{-toluidine})_2]^+$

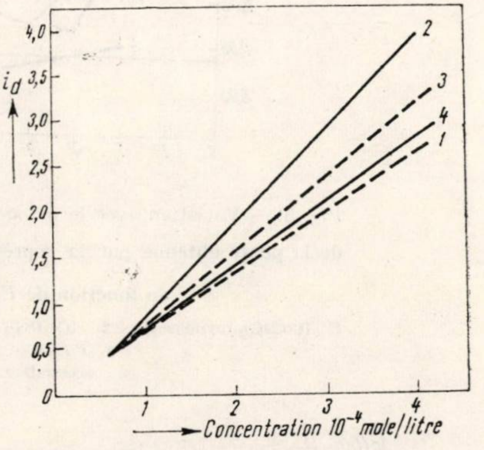

Fig. 4. — Variation du courant de diffusion (i_d) en fonction de la concentration pour les ions :

1. $[Co(DG)_2(o\text{-amino-éthyl-benzène})_2]^+$ 2. $[Co(DG)_2(p\text{-amino-éthyl-benzène})_2]^+$ 3. $[Co(DG)_2(o\text{-phénétidine})_2]^+$ 4. $[Co(DG)_2(p\text{-phénétidine})_2]^+$

On a cherché aussi d'établir le degré de la réversibilité des processus d'électrode en utilisant l'analyse logarithmique selon Tomes[15]. Dans les diagrammes 5 et 6 on représente graphiquement, en fonction du pH, la variation du rapport inverse de la pente calculée par l'analyse logarithmique des échelons polarographiques. Si on compare les données obtenues expérimentalement, on constate que, dans le milieu neutre, les processus d'électrode sont plus réversibles, la valeur du rapport inverse de la pente étant plus rapprochée de celle théorique, c'est-à-dire 0,058.

En même temps, on peut constater que, tandis que pour les combinaisons avec pyridine, aniline et *p*-phénétidine, les processus d'électrode sont plus réversibles dans les milieux basiques, pour les combinaisons avec *p*-toluidine, *o*-amino-éthyl-benzène, *p*-amino-éthyl-benzène et *o*-phénétidine, ces processus deviennent plus réversibles dans les milieux acides ; excepté le composé $[Co(DG)_2(o\text{-toluidine})_2]^+$ qui présente un certain degré d'irréversibilité dans tout milieu.

---

[15] J. Tomes, *Coll. Czech. Chem. Comm.*, **9**, 12 (1937).

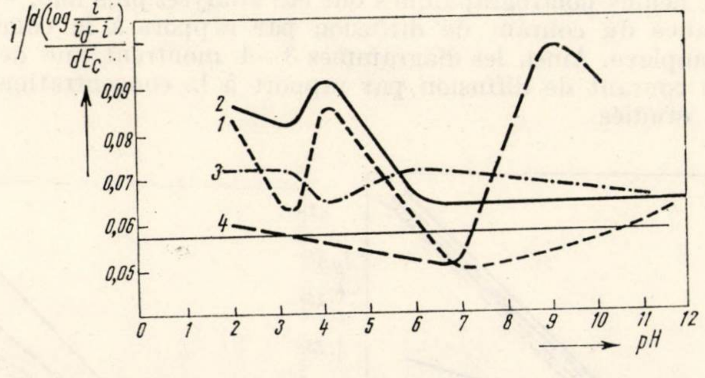

Fig. 5. — Variation avec le pH de la solution, de la valeur inverse de la pente obtenue par la représentation graphique de log $\frac{i}{i_d - i}$ en fonction de E_c, pour les ions :

1. $[Co(DG)_2\ (pyridine)_2]^+$ 2. $[Co(DG)_2\ (aniline)_2]^+$ 3. $[Co(DG)_2\ (o\text{-toluidine})_2]^+$ 4. $[Co(DG)_2\ (p\text{-toluidine})_2]^+$ en concentration $1{,}2 \cdot 10^{-4}$ mole/l

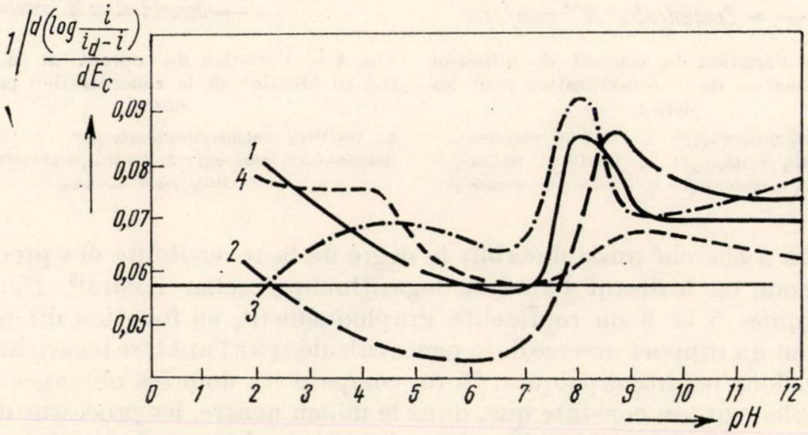

Fig. 6. — Variation avec le pH de la solution, de la valeur inverse de la pente obtenue par la représentation graphique de log $\frac{i}{i_d - i}$ pour les ions :

1. $[Co(DG)_2\ (o\text{-amino-éthyl-benzène})_2]^+$ 2. $[Co(DG)_2\ (p\text{-amino-éthyl-benz})_2]^+$ 3. $[Co(DG)_2\ (o\text{-phénétidine})_2]^+$ 4. $[Co(DG)_2\ (p\text{-phénétidine})_2]^+$ en concentration $1{,}2 \cdot 10^{-4}$ mole/l

b. INFLUENCE DU pH DE LA SOLUTION SUR LE POTENTIEL DU DEMI-PALIER

Sur les diagrammes 7—9 on représente la variation du potentiel de demi-palier dans le domaine de $pH = 2 - 12$, pour les combinaisons complexes étudiées, en concentration de $1{,}2 \cdot 10^{-4}$ mole/l. Les déterminations ont été réalisées en solution tampon Britton-Robinson.

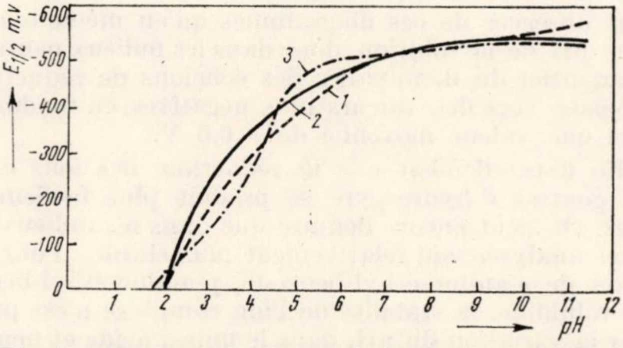

Fig. 7. — Variation du potentiel de demi-palier en fonction du pH de la solution fondamentale, pour les ions :

1. $[Co(DG)_2(\beta\text{-picoline})_2]^+$ 2. $[Co(DG)_2(\gamma\text{-picoline})_2]^+$ 3. $[Co(DG)_2(\text{pyridine})_2]^+$ en concentration $1{,}2\cdot10^{-4}$ mole/l

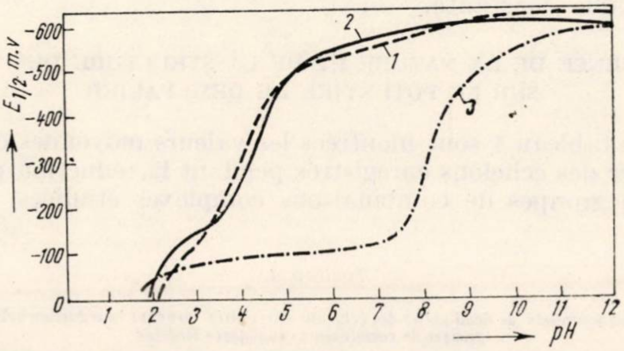

Fig. 8. — Variation du potentiel de demi-palier en fonction du pH de la solution fondamentale, pour les ions :

1. $[Co(DG)_2(\text{aniline})_2]^+$ 2. $[Co(DG)_2(o\text{-toluidine})_2]^+$ 3. $[Co(DG)_2(p\text{-toluidine})_2]^+$ en concentration $1{,}2\cdot10^{-4}$ mole/l

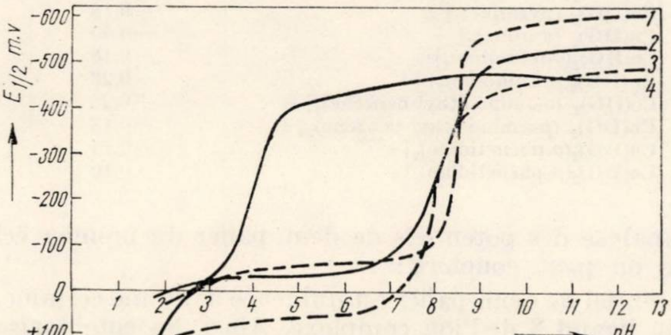

Fig. 9. — Variation du potentiel de demi-palier en fonction du pH de la solution fondamentale, pour les ions :

1. $[Co(DG)_2(o\text{-amino-éthyl-benzène})_2]^+$ 2. $[Co(DG)_2(p\text{-amino-éthyl-benzène})_2]^+$ 3. $[Co(DG)_2(o\text{-phénétidine})_2]^+$ 4. $[Co(DG)_2(p\text{-phénétidine})_2]^+$ en concentration $1{,}2\cdot10^{-4}$ mole/l

On peut observer de ces diagrammes qu'en même temps que l'augmentation du pH de la solution, donc dans les milieux neutres et pauvres alcalins, le potentiel du demi-palier des échelons de réduction Co(III) à Co(II) est déplacé vers des valeurs plus négatives, en tendant asymptotiquement vers une valeur moyenne de −0,6 V.

Il résulte naturellement que la réduction des ions complexes sur l'électrode à gouttes d'hydrargyre se produit plus facilement dans les milieux acides. On peut encore déduire que dans les milieux basiques, les ions complexes analysés sont relativement plus stables. Pour les combinaisons complexes de *o*-amino-éthyl-benzène, *p*-amino-éthyl-benzène, *o*-phénétidine et *p*-toluidine, la stabilité de l'ion complexe n'est pas tout à fait influencée par la variation du pH, dans le milieu acide et neutre, les changements plus visibles de potentiel du demi-palier ayant lieu dans le milieu basique.

La concentration de la solution tampon exerce une certaine influence sur le potentiel du demi-palier des ions complexes et c'est pourquoi elle a été maintenue constante.

c. INFLUENCE DE LA NATURE ET DE LA STRUCTURE DES LIGANDS SUR LE POTENTIEL DE DEMI-PALIER

Dans le tableau 1 sont montrées les valeurs moyennes des potentiels de demi-palier des échelons enregistrés pendant la réduction polarographique des cinq groupes de combinaisons complexes étudiées.

Tableau 1

Valeurs moyennes des potentiels de demi-palier des échelons enregistrés pendant la réduction polarographique des cinq groupes de combinaisons complexes étudiées

Le groupe	L'ion complexe	$E_{1/2}$ V Co((III)−Co(II)	$E_{1/2}$ V Co(II)−Co(0)
I	1 [Co(DG)$_2$(β-picoline)$_2$]+	−0,12	−1,21
	2 [Co(DG)$_2$ (γ-picoline)$_2$]+	−0,08	−1,20
II	1 [Co(DG)$_2$ (pyridine)$_2$]+	−0,18	−1,19
	2 [Co(DG)$_2$ (aniline)$_2$] +	−0,20	−1,27
III	1 [Co(DG)$_2$(*o*-toluidine)$_2$]+	−0,18	−1,23
	2 [Co(DG)$_2$(*p*-toluidine)$_2$]+	−0,26	−1,23
IV	1 [Co(DG)$_2$ (*o*-amino-éthyl-benzène)$_2$]+	−0,23	−1,27
	2 [Co(DG)$_2$ (*p*-amino-éthyl-benzène)$_2$]+	−0,18	−1,29
V	1 [Co(DG)$_2$(*o*-phénétidine)$_2$]+	−0,14	−1,26
	2 [Co(DG)$_2$(*p*-phénétidine)$_2$]+	−0,10	−1,22

De l'analyse des potentiels de demi-palier du premier échelon polarographique on peut conclure :

Le potentiel de demi-palier est influencé dans une certaine mesure par la nature du ligand X de l'ion complexe. Ainsi, les combinaisons des IIe, IIIe et IVe groupes présentent une stabilité un peu plus grande à la réduction, $E_{1/2}$ se trouvant dans le domaine −0,18 et −0,26 V ; les combinaisons des Ier et V^{e} groupes présentent une stabilité plus réduite, $E_{1/2}$ ayant des valeurs entre −0,08 CV et −0,14 V.

— En outre, on constate que les modifications dans la structure du ligand X, de même que dans le cas des isomères de position, exercent une influence très réduite sur la valeur du potentiel de demi-palier et en conséquence sur la stabilité de la combinaison complexe.

Si on constate certaines différences aux combinaisons étudiées, en ce qui concerne la valeur de $E_{1/2}$ pour le premier échelon de réduction, ces différences ne se maintiennent plus pour le deuxième échelon, pour lequel les valeurs de $E_{1/2}$ se groupent autour de —1,2 V jusqu'à —1,29. C'est une preuve de plus que le potentiel de demi-palier du premier échelon de réduction peut être considéré comme une mesure pour la stabilité de l'ion complexe.

CONCLUSIONS

— La réduction cathodique des ions complexes de Co(III) aux ligands hétérogènes comme diméthylglyoxime et les dérivés d'aniline et pyridine est influencée par le pH de la solution, tant pour le degré de réversibilité de la réaction de réduction, que pour la stabilité de la combinaison complexe. Ainsi, pour ces composés la réduction de la combinaison complexe se produit plus facilement dans les milieux acides.

— Le potentiel de demi-palier des échelons de réduction polarographique est influencé dans une certaine mesure par la nature et la structure du ligand. Cependant, les modifications dans la structure du ligand produites par l'emploi des isomères différents de position exercent une influence réduite sur la stabilité de l'ion complexe à la réduction, ainsi que les valeurs du potentiel de demi-palier sont rapprochées au cas de ces ligands isomères.

— Le potentiel de demi-palier du premier échelon de réduction qui présente des fluctuations d'un composé à l'autre peut constituer une mesure pour la stabilité de l'ion complexe.

Revue Roumaine de Chimie, **20**, *9–10*, 1287–1293 (1975)

AS-TRIAZINE DERIVATIVES WITH POTENTIAL THERAPEUTIC ACTION. XIV*

A SIMPLIFIED SYNTHESIS OF 2′, 3′, 5′-TRI-O-BENZOYL-β-D-RIBOFURANOSYL-6-AZAURACILS-5-SUBSTITUTED *VIA* 2,4-BIS-(TRIMETHYLSILYLOXY)-DERIVATIVES

C. CRISTESCU

Chemical and Pharmaceutical Research Institute,
Şos. Vitan 112, Bucharest 4, Romania

Received March 5, 1974

5-Substituted-6-azauracils (I) has been converted with hexamethyldisilazane in 2,4-bis (trimethylsilyloxy)-derivatives (II). These were condensed with 2,3 5-tri-O-benzoyl-D-ribofuranosyl chloride in the presence of mercuric acetate or with 1-0-acetyl-2, 3, 5-tri-O-benzoyl-D-ribofuranose in the presence of anhydrous stanic chloride to afford the corresponding 1(2′, 3′, 5′-tri-O-benzoyl-β-D-ribofuranosyl)-5-substituted-6-azauracil (III).

The interest which in recent year has been attached to the chemical synthesis of nucleosides of pyrimidine derivatives has increased by the remarkable progress of the biochemical studies on antimetabolites. By modifications in the heterocycle of the natural pyrimidine nucleosides a number of 6-aza-analogues[1−4]has resulted. These "fraudulent" nucleosides, are specific, enzymatic inhibitors, have antiviral activity and are used as anticancer agents. Examining the possible further transformation of nucleosides, it appeared of interest to prepare some compounds with similar structure of 6-azauridine.

In a previous paper of this series[5] we reported a synthetic method of 6-azauridine, starting from 2, 3, 5-tri-O-benzoyl-D-ribofuranosyl chloride and 2,4-bis (trimethylsilyloxy)-6-azauracil, at room temperature in the presence of mercuric acetate.

In the present paper, the chemical synthesis of the new series of 5-substituted-6-azauridines is described. We have investigated the synthe-

---

[*] Part. XIII, C. Cristescu and S. Sitaru, *Rev. Roumaine Chim.*, **16**, 455 (1971).

[1] T. Y. Shen, W. V. Rugle and R. L. Bugianesi, *J. Heterocyclic Chem.*, **2**, 495 (1965).

[2] G. J. Durr, F. J. Keiser and P. A. Ierardi, *J. Heterocyclic Chem.*, **4**, 291 (1967).

[3] T. Tzaczynski, J. Smejkal and F. Sorm, *Coll. Czech. Chem. Comm.*, **29**, 1736 (1964).

[4] G. J. Durr and S. Hammond, *J. Heterocyclic Chem.*, **7**, 743 (1970).

[5] C. Cristescu, *Rev. Roumaine Chim.*, **12**, 365 (1968).

sis of this nucleosides by the application of the method reported in part VI[5] and by adaptation of the recent procedure[6] of synthesis of pyrimidine nucleosides.

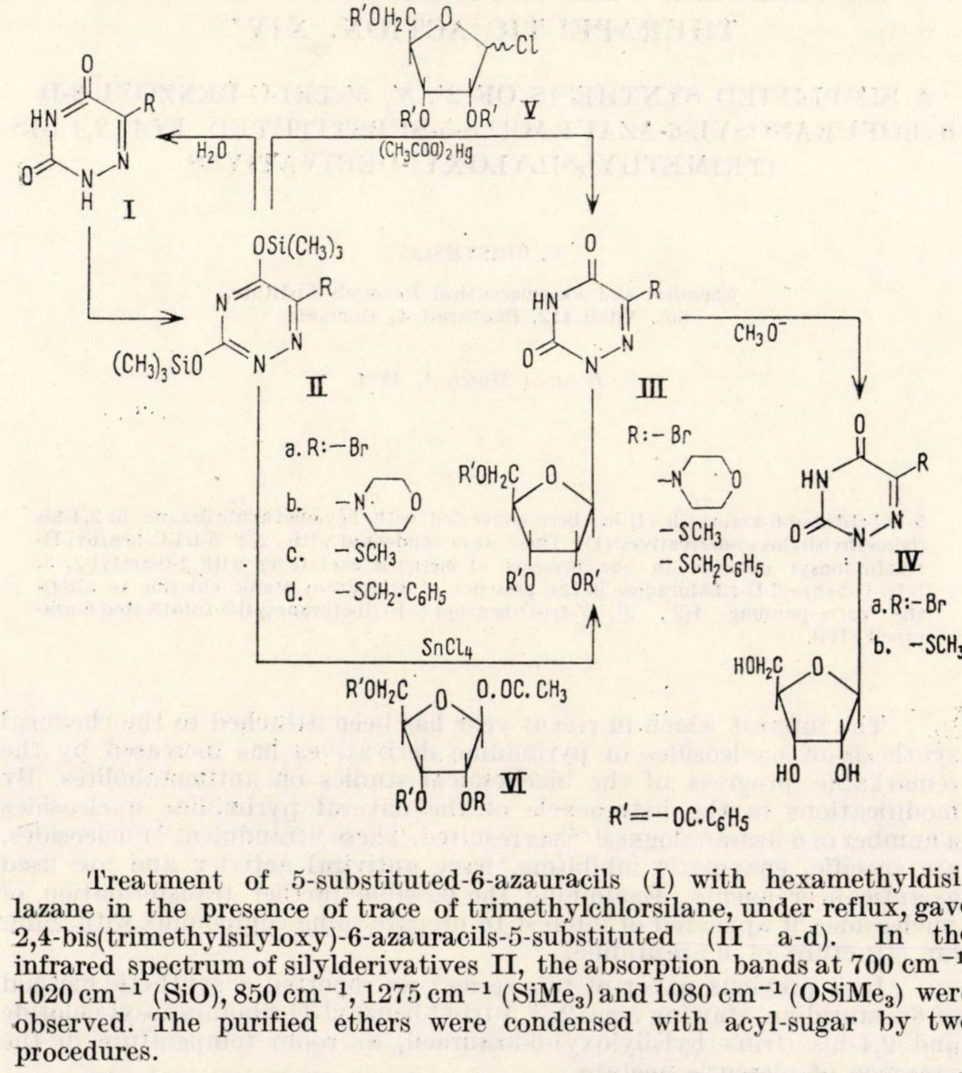
R'OH2C
O
Cl
R'O
OR'
V
H2O
(CH3COO)2Hg
I
OSi(CH3)3
(CH3)3SiO
II
III
CH3O−
a. R:—Br
b. —N O
c. —SCH3
d. —SCH2·C6H5
R:—Br
—SCH3
—SCH2C6H5
IV
a. R:—Br
b. —SCH3
SnCl4
R'OH2C
O.OC.CH3
R'O
OR
VI
HOH2C
HO
OH
R'=—OC.C6H5

Treatment of 5-substituted-6-azauracils (I) with hexamethyldisilazane in the presence of trace of trimethylchlorsilane, under reflux, gave 2,4-bis(trimethylsilyloxy)-6-azauracils-5-substituted (II a-d). In the infrared spectrum of silylderivatives II, the absorption bands at 700 cm^{-1}, 1020 cm^{-1} (SiO), 850 cm^{-1}, 1275 cm^{-1} ($SiMe_3$) and 1080 cm^{-1} ($OSiMe_3$) were observed. The purified ethers were condensed with acyl-sugar by two procedures.

The first procedure involves the condensation of II with 2, 3, 5-tri-O-benzoyl-D-ribofuranosyl chloride (V) in dry toluene, at room temperature, in the presence of anhydrous mercuric acetate as acid acceptor. Usual work-up afforded a 48—50% yield of (1(2', 3', 5'-tri-O-benzoyl-β-D-ribofuranosyl)-6-azauracils-5-substituted (III a-b).

The second procedure involves the condensation of II with 1-O-acetyl-2,3, 5-tri-O-benzoyl-D-ribofuranose (VI) in dry dichloromethane or

---

[6] U. Niedballa and H. Vorbrüggen, *Angew. Chem. Inter. Edit.*, **9**, 461 (1970).

1, 2-dichloroethane, at room temperature, in the presence of anhydrous stanic chloride, affording only N-glycosides. No O-glycosides was detected by tlc in the reaction mixture, and the optimum reaction period was 6–12 hours.

The resulting protected crystalline nucleosides (III-a, III-b) were deacylated by methoxyde catalyzed transesterification to yield the desired nucleosides (IV-a, IV-b).

The assignment of the carbohydrate moiety to the N–1 position of the 5-substituted-6-azauracil ring is based on the fact that the nucleoside (IV) exhibits a hypsochromatic shift on the absorption maximum in the ultraviolet spectrum on the change from acidic to basic conditions. This is typical of N–1 substituted 6-azauracils.[7,8]

In the infrared spectrum of the tri-O-benzoyl-derivatives (III) the intense absorption of the acyl groups overlaps a considerable number of bands of the heterocyclic and the sugar parts of the molecule. As a consequence of these overlaps the spectra seem poorer in bands. The carbonyl groups absorb in the region 1720 cm^{-1}. The absorption bands of acyl groups, linked to the ribose residue are 1272, 1318 cm^{-1} $\bar{\nu}$ (C.CO) and 1100, 1180 cm^{-1} $\bar{\nu}$ (CO.O). In spectra of all tri-O-benzoyl-derivatives, three bands regularly occurred (1099, 1128 and 1237 cm^{-1}). These bands are probably due to the strong absorption of the ribose component[9,10]. The ribose residue should exhibit absorption of the CH_2 group in the region above 1384 cm^{-1} (wagging) and 1431 cm^{-1} (scissoring).

The infrared absorption of the IV-derivatives in the carbonyl stretching region confirms the N-1 substitution of the 6-azauracil-5-substituted component since the spectra of these nucleosides are similar to that of 1-methyl-6-azauracil and different from 3-methyl-6-azauracil. Horak and col.[11] described the use of the infrared spectrum to distinguish the N–1 and N–3 substituted 6-azauracil and nucleosides.

The patterns of the anomeric protons of these nucleosides, III and IV, appear in nmr spectra as a doublet at $\delta = 5.59-6.47$ p.p.m. with a coupling constant 2.5–3,5 Hz. The position of the signal indicated that III and IV may be the β-anomer in comparison with the nmr spectra of other nucleosides of this type.[12-14]

EXPERIMENTAL

The melting points were determined on a heating microscope stage and are not corrected. Samples for analyses and spectral measurements were dried at 30°/0.1 mm Hg, for 8 hours over P_2O_5. Paper chromatography was performed by the ascending technique on paper Whatmann

---

[7] J. Johnas and J. Gut, *Coll. Czech. Chem. Comm.*, **26**, 2155 (1961).

[8] K. Y. Zee-Cheng and C. C. Cheng, *J. Org. Chem.*, **27**, 976 (1962).

[9] C. L. Ancell, *J. Chem. Soc.*, **1961**, 504.

[10] J. Pitha and J. Zemlika, *Coll. Czech. Chem. Comm.*, **29**, 410 (1964).

[11] M. Horak and J. Gut, *Coll. Czech. Chem. Comm.*, **26**, 1680 (1961).

[12] J. Beranek, *Coll. Czech. Chem. Comm.*, **34**, 618 (1969).

[13] M. P. Sweizer, E. B. Banta, J. T. Witkowsky and R. K. Robins, *J. Amer. Chem. Soc.*, **95**, 3770 (1973).

[14] D. J. Wood, F.. E. Hruska, R. Mynott and R. H. Sarma, *Canad. J. Chem.*, **51**, 2571 (1973).

Nr. 1 in the solvent systems : 1-butanol-acetic acid-water (5 : 2 : 3) A, 1-butanol-water (86 : 14) B, propane-2-ol-water-conc. ammonia (16 : 4 : 1) C. Detection of the compounds was performed visually in ultraviolet light (254 nm) after spraying with 0.1 % Rhodamine B (in ethanol). Thin-layer chromatography (tlc) was performed on precoated tlc-plates silicagel F_{254} (Merck) in the solvent systems : benzene-ethanol (9 : 1) D, benzene-ethyl acetate (7 : 3) E and benzene-methanol (1 : 1) F. Spots were detected visually in ultraviolet light (Uvitest). Preparative column chromatography was performed on a LKB 4220 column, the flow-rate 2,5 ml per min. being maintained. The fractions were collected at 10 minutes intervals (UltroRac Fraction Collector LKB 7000). Optical rotation was measured on High-Watt automatic polarimeter. Ultraviolet spectra of products were measured on a Unicam SP 1800 ultraviolet spectrophotometer. The infrared spectra were measured with an infrared spectrophotometer Zeiss-Jena UR-10. The nmr spectra were recorded at 60 MHz on a Varian 60 spectrophotometer in the indicated solvents and the chemical shifts are reported in parts per million (δ) with TMS as internal reference.

2,4-BIS(TRIMETHYLSILYLOXY)-6-AZAURACILS-5-SUBSTITUTED (II a–d)

Method 1 : 0.02 M dry powdered 5-substituted-6-azauracil, [15,16] previously dried for 2 hours at 110° , was suspended in 200 ml benzene (dried over $LiAlH_4$). The 5-substituted-derivatives were dried by azeotropical distillation of benzene (100 ml) and dried benzene (100 ml) was added. This operation was repeated twice to ensure removal of water. To azeotropically dried compound, cooled at room temperature, was added dry benzene (100 ml), 0,04 M trimethylchlorsilane and 0.04 M triethylamine (previously dried by distillation over sodium). The mixture was refluxed for 7 hours. The precipitate, a mixture of triethylamine hydrochloride and 5-substituted-6-azauracil, was filtered off and washed 3 times with benzene. The resulting clear solution was concentrated in vacuo. The viscous oily residue was distilled under reduced pressure to give a colorless oil II a-d (table 1). Due to the high reactivity of these intermediates, analysis was not attempted.

Method 2 : A mixture of 5-substituted-6-azauracil (0.025 M), hexamethyldisilazane (20 ml) and trimethylchlorsilane (1 ml) was refluxed for 2 hours, until a clear solution was obtained. The excess of hexamethyldisilazane was removed under vacuum at 15 mm and the viscous oily residue was distilled under reduced pressure to give 2,4-bis (trimethylsilyloxy)-6-azauracil-5-substituted, with the properties indicated in table 1.

Table 1

2,4-bis(trimethylsilyloxy) – 6-azauracil-5-substituted

Compd.	*R*	B.p., O (mm)	m.p.,°	Yield %
II–a	–Br	116–118 (0.4)	48–50	97
II–b	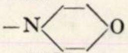	162–163 (0.4)	54–56	90
II–c	$-SCH_3$	128–130 (0.4)	75–77	92
II–d	$-SCH_2.C_6H_5$	192–193 (0.4)	90–92	92

1(2′, 3′, 5′-TRI-O-BENZOYL-β-D-RIBOFURANOSYL)-5-BROMO-6-AZAURACIL (III-a)

Method 1 : 5.67 g (0.0169 M) of II-a was dissolved in dry toluene (100 ml). To the clear solution (any cloudiness suggests hydrolysis of II-a) was added a solution of chloro-sugar (which was prepared by treating 10.35 g 1-0-acetyl-2, 3, 5-tri-O-benzoyl-ribofuranose with 250 ml dry etheral hydrogen chloride) in toluene (100 ml) and 6.48 g (0.0204 M) mercuric acetate. The suspension was stirred for 4 days at room temperature, filtered and filtercake washed with dry toluene. The filtrate and the washings were evaporated in vacuo and the residue was dissolved in chloroform (150 ml). The chloroform solution was washed with 30 % potassium iodide, then with water and, after drying (sodium sulphate), was concentrated in vacuo to a sirupy residue.

---

[15] C. Cristescu and J. Marcus, *Pharmazie*, **16**, 135 (1961).

[16] C. Cristescu and Th. Panaitescu, *Pharmazie*, **17**, 209 (1962).

The residue was dissolved in benzene and applied to a neutral alumina (150 g; Brockmann II—III) column. Elution with benzene and benzene-ethyl acetate (8 :2) provided III-a. A crude product was recrystallized from ethanol to afford 5.12 g (48 %) of III-a with m. p. 168 – 169°; $(\alpha)_D^{25}$ – 61° (Cl, 1,2-dichlorethan); Rf : 0.85 (A), 0.69 (B), 0.74 (C), 0.60 (D), 0.28 (E); $IR_{(CHCl_3)}$: 1725 $cm^{-1} \bar{\nu}$ (C=0), 1279, 1320 $cm^{-1} \bar{\nu}$ (C.CO), 1100, 1183 $cm^{-1} \bar{\nu}$ (CO.O); $UV_{(ethanol)}$: λ max 230 nm (log ε 4.63) and 275 nm (log ε 4.00); $NMR_{(CDCl_3)}$: δ 4.38–4.87 (3H, m, $H_{4'} + 2H_{5'}$), 5.79 (1H, d d., $J_{3'4'}$ = 5.5Hz, $1H_{3'}$), 5.95 (1H, d. d., $J_{2'3'}$ = 5.5 Hz, $1H_{2'}$), 6.38 (1H, d, $J_{1'2'}$ = = 3.1 Hz, $1H_{1'}$), 7.05 – 7.60 (9H, m, aromatic protons *meta* and *para* of the benzoyl groups), 7.65 – 8.07 (6H, m, aromatic protons *ortho* of the benzoyl groups), 9.7 (1H, s, NH, D_2O exchangeable).

$C_{29}H_{22}N_3O_9Br$ *Calcd.* : C, 54.72 ; H, 3.48 ; N, 6.24 ; Br, 12.55% *Found* :C, 54.60 ; H, 3.70 ; N, 6.25 ; Br, 12.65 %

Method 2 : 8.0 g (0.023 M) of II-a in dry 1.2-dichlorethan (200 ml) was added to 10.5 g (0.021 M) 1-O-acetyl-tri-O-benzoyl-D-ribofuranose, previously dissolved in 1.2-dichlorethan (200 ml). The mixture was stirred for 6 hours at room temperature in presence of anhydrous stannic chloride (1.8 ml, 0.0158 M). The solution was treated with saturated aqueous sodium hydrogen carbonate solution (200 ml) and the organic phase was filtered over Celite 533, dried with sodium sulphate and evaporated. The residue was dissolved in benzene and applied to a neutral alumina column (250 g, Brockmannn II-III). The column was washed with benzene and eluted with a mixture of benzene-ethyl acetate (8 : 2). Fractions containing the product were pooled and evaporated. The crude product was recrystallized from ethanol to afford 12.71 g (87 %) of III-a, with m. p. 168 – 169° without depression on admixture with the product prepared by method 1 ; the infrared spectra, tlc and paper chromatography of the two samples were identical.

1(2′, 3′, 5′-TRI-O-BENZOYL-β-D-RIBOFURANOSYL)-5-MORPHOLINO-6-AZAURACIL (III-b)

Method 1 : To a clear solution of 5.8 (0.0169 M) of II-b in dry toluene (100 ml) was added a solution of chloro-sugar (prepared) from 10.35 g 1-O-acetyl-2, 3, 5-tri-O-benzoyl-D-ribofuranose with dry etheral hydrogen chloride) in toluene (100 ml) and 6.48 g (0.0204 M) mercuric acetate. The suspension was stirred for 5 days at room temperature. The mixture was filtered, the filtrate evaporated under diminished pressure and the residual oil was washed with 30 % potassium iodide (3 × 100 ml) then with water, and after drying (sodium sulphate) was concentrated in vacuo to a sirupy residue. The residue was chromatographed on a column of neutral alumina (150 g; Brockmann activity II—III) with benzene and benzene-ethyl acetate (7 :3). Fractions containing the product were combined and evaporated. The crude product was recrystallized from propane-2-ol to afford 5.4 g (50 %) of III-b with m. p. 106 – 107°; $(\alpha)_D^{25}$ – 99°.8 (c l, chloroform); Rf : 0.80 (A), 0.82 (B), 0.76 (C), 0.69 (D), 0.22 (E); $IR_{(CHCl_3)}$: 1729 $cm^{-1} \bar{\nu}$ (C=0), 1279, 1320 $cm^{-1} \bar{\nu}$ (C.CO), 100, 1184 $cm^{-1} \bar{\nu}$ (CO.O) ;U. $V_{(ethanol)}$; λ max 230nm (log ε 4.66) and 279 nm (log ε 3.68); $NMR_{(CDCl_3)}$: δ 3,12 – 3.52 (4H, m, $-H_2C-N-CH_2-$ protons of morpholino group); 3.52 – 3.85 (4H, m, $-H_2C-O-CH_2-$ protons of morpholino group), 4.36 – 4.86 (3H, m, $H_{4'2'} + H_{5'}$), 5.83 (1H, d.d., $J_{3'4'}$ = 5.5 Hz, $1H_{3'}$), 6.0 (1H, d. d., $J_{2'3'}$ = 5.5 Hz, $1H_{2'}$), 6.43 (1H, d, $J_{1'2'}$ = 2.5 Hz, $1H_{1'}$), 7.05 – 7.60 (9H, m, aromatic protons meta and para of the benzoyl groups), 7.62 – 8.05 (9H, m, aromatic protons *ortho* of the benzoyl groups), 9.45 (1H, s, NH, D_2O exchangeable).

$C_{33}H_{30}N_4O_{10}$ *Calcd.* : C, 61. 47 ; H, 7.05 ; N, 8.71 % *Found* : C, 62.00 ; H, 6.90 ; N, 8.50 %

Method 2 : A solutionof 9.98 g (0.0198 M) 1-O-acetyl-tri-O-benzoyl-D-ribofuranose in dry 1,2-dichloretan (200 ml) was added to a clear solution of 7.60g (0.022 M) of II-b in 200 ml dry 1,2-dichlorethan. The mixture was kept at room temperature for 6 hours in the presence of 1.7 ml (0.0148 M) anhydrous stannic chloride. The solution was treated with saturated aqueous sodium hydrogen carbonate solution and the organic phase was filtered over Celite 535, dried (sodium sulphate) and evaporated. The residue was chromatographed on a column of neutral alumina (250 g; Brockmann activity II—III) with benzene and benzene-ethyl acetate (7 : 3).

Fractions containing the product were pooled and evaporated. The crude product was recrystallized from propane-2-ol to afford 9.42 g (71 %) of III-b with m. p. 106 — 107°, without depression on admixture with the product prepared by method 1 ; the infrared spectra, tlc and paper chromatography of the two samples were identical.

1(2′, 3′, 5′-TRI-O-BENZOYL-β-D-RIBOFURANOSYL)-5-METHYLTHIO-6-AZAURACIL (III-c)

5.0 g (0.0165 M) of II-c in dry 1,2-dichlorethan (100 ml) was added to 7.45 g (0.0148 M) 1-O-acetyl-tri-O-benzoyl-D-ribofuranose previously dissolved in dry 1,2-dichlorethan (200ml). The mixture was stirred for 8 hours at room temperature in the presence of anhydrous stannic chloride (1.5 ml, 0.0132 M). The solution was treated with saturated aqueous sodium hydrogen carbonate solution (150 ml) and the organic phase was filtered over Celite 535, dried (sodium sulphate) and evaporated. The residue was dissolved in benzene and applied to a column of neutral alumina (150 g, Brockmann activity II—III). The column was eluted with benzene and benzene-ethyl acetate (7 : 3) and the fractions containing the product were pooled and evaporated. The crude product was recrystallized from ethanol to afford 6.20 g (70 %) of III-c with m. p. 163 — 165° ; $(\alpha)_D^{25}$ $-80°.8$ (cl, chloroform) ; Rf : 0.84 (A), 0.78 (B), 0.73 (C), 0.54 (D), 0.38 (E) ; $IR_{(CHCl_3)}$: 1720 $cm^{-1}\bar{\nu}$ (C=0), 1280, 1320 $cm^{-1}\bar{\nu}$ (C.CO), 1095, 1082 $cm^{-1}\bar{\nu}$ (CO.O) ; $UV_{(ethanol)}$; λ max 230 nm (log ε 4.68) and 279 nm (log ε 3.68) ; $RMN_{(CDCl_3)}$: δ 2.37 (3 H, s, protons of the methyl group), 4.46 — 4.84 (3H, m, $H_{4'}$ + $2H_{5'}$) 5.87 (1H, d. d., $J_{3'4'}$ = 5.84 Hz, $1H_{3'}$), 6.02 (1H, d. d., $J_{2'3'}$ = 5.25 Hz, $1H_{2'}$) 6.45, (1H, d., $J_{1'2'}$ = 2.6 Hz, $1H_{1'}$), 7.05 — 7.60 (9H, m, aromatic protons meta and para of the benzoyl groups), 7.65 — 8.05 (6H, m, protons ortho of the benzoyl groups), 9.40 (1H, s, NH, D_2O exchangeable).

$C_{30}H_{25}N_3O_9S$ *Calcd.* ; C, 59.69 ; H, 4.17 ; N, 6.96 ; S, 5.31 % *Found* : C, 59.10 ; H, 4.20 ; N, 6.70 ; S, 5.20 %

1(2′, 3′, 5′-TRI-O-BENZOYL-β-D-RIBOFURANOSYL)-5-BENZYLTHIO-6-AZAURACIL (III-d)

A solution of 10.5 g (0.021 M) of 1-O-acetyl-2,3,5-tri-O-benzoyl-D-ribofuranose in dry 1,2-dichlorethane (200 ml) was added to a clear solution of 8.8 g (0.0231 M) of II-d in dry 1,2-dichlorethane (200 ml). The mixture was stirred at 25°C for 12 hours in the presence of 1.85 ml (0.0167 M) anhydrous stannic chloride. The solution was treated with saturated aqueous natrium hydrogen carbonate and the organic phase was filtered over Celite 535, dried (natrium sulphate) and evaporated. The residue was chromatographed on a column of neutral alumina (250 g ; Brockmann activity III) with benzene and benzene-ethyl acetate (7 :3). Fractions containing the product were pooled and evaporated. The crude product was recrystallized from ethanol to afford 11.80 g (82 %) of III-d with m. p. 182 — 184° ; $(\alpha)_D^{25}$ $-83°$ (cl, chloroform) ; Rf : 0.79 (A), 0.74 (B), 0.69 (C), 0.56 (D), 0.40 (E) ; $IR_{(CHCl_3)}$: 1733 $cm^{-1}\bar{\nu}$ (C=0), 1279, 1320 $cm^{-1}\bar{\nu}$ (C.CO), 1100, 1183 $cm^{-1}\bar{\nu}$ (CO.O) ; $UV_{(ethanol)}$: λ max 230 nm (log ε 4.64) and 275 nm (log ε 4.00) ; $NMR_{(CDCl_3)}$; δ 6.48 (1H, d., $J_{1'2'}$ = 2.7 Hz, $1H_{1'}$)

$C_{36}H_{29}N_3O_9S$, *Calcd.* : C, 63.61 ; H, 4.30 ; N, 6.18 ; S, 4.71 % *Found* : C, 63.70 ; H, 4.35 ; N, 6.30 ; S, 4.70 %

5-BROMO-6-AZAURIDINE (IV-a)

A mixture of 6.36 g (0.01M) of the protected nucleoside III-a, 18 ml 1 N sodium methoxyde and 250 ml dry methanol, was stirred for 3 hours at room temperature. The solvent was evaporated in vacuo at 50° ; the resulting oil was treated with 200 ml water and extracted with three portions of ethyl acetate-ether (2 : 1 v/v). The aqueous layer was treated with Dowex 50 W -x8, strongly acidic cation exchange resin, at pH 3, filtered and evaporated under diminished pressure at 50°. The residue was recrystallized from absolute ethanol yielding 3.02 g (93 %) of product IV-a with m. p. 190 — 192°. Recrystallization from absolute ethanol gave an analytical sample, m. p. 193 — 195° ; $(\alpha)_D^{25}$ $-53°$ (c 1, water) ; Rf : 0.55 (A), 0.05 (B), 0.37 (C), 0.55 (F) ; UV : λ max (0.1 N hydrochloric acid) 279 nm (log ε 3.80), λ max (0.1 N sodium hydroxide)

268 nm (log ε 3.68), $IR_{(KBr)}$: 1716 cm^{-1} $\bar{\nu}$ (C=0); $NMR_{(D_2O)}$: δ 3.6 − 3.8 (2H, m, $2H_{5'}$), 4.03 (1H, d.t., $J_{4'5'}$ = 3.3Hz, $J_{4'5''}$ = 5.25 Hz, $1H_{4'}$), 4.26 (1H, d. d., $J_{3'4'}$ = 6.0 Hz, $1H_{3'}$), 4.42 (1H, d. d., $J_{2'3'}$ = 4.7 Hz, $1H_{2'}$), 5.95 (1H, d., $J_{1'2'}$ = 2.8 Hz, $1H_{1'}$).

$C_8H_{10}N_3O_6Br$ *Calcd.*: C, 29.64; H, 3.11; N, 12.96; Br, 24.65%. *Found*: C, 29.75; H, 3.30; N, 12.86; Br, 24.75%.

5-METHYLTHIO-6-AZAURIDINE (IV-b)

A mixture of 6.03 g (0.01 M) of III-c, 18 ml 1N sodium methoxide and 250 ml dry methanol was stirred 1 hour at reflux. The solvent was evaporated in vacuo at 50° and the resulting oil was treated with 150 ml water and extracted with ethyl acetate-ether (2 : 1 v/v; 3 × 25 ml). The aqueous layer was treated with Dowex-X 8 at pH 3, filtered and evaporated in vacuo at 50°. The residue was crystallized from propane-2-ol, yielding 2.47 g (85%) of product IV-b with m. p. 171 − 172° Recrystallization from propane-2-ol gave an analytical sample, m. p. 173 − 175°; $(\alpha)_D^{25}$ −32°.2 (cl, water); Rf : 0.57 (A), 0.04 (B), 0.38 (C), 0.59 (F); UV : λ max (0.1 N hydrochloric acid) 310 nm (log ε 3.79), λ max (0.1 N sodium hydroxide) 299 nm (log ε 3.82); $IR_{(KBr)}$: 1708 cm^{-1} $\bar{\nu}$ (C=0) $NMR_{(D_2O)}$; δ 3.65 − 3.85 (2H, m, $2H_{5'}$), 4.08 (1H, d. t., $J_{4'5'}$ = = 3.28 Hz, $J_{4'5''}$ = 5.30 Hz, $1H_{4'}$), 4.28 (1H, d. d, $J_{3'4'}$ = 6.02 Hz, $1H_{3'}$), 4.46 (1H, d. d., $J_{2'3'}$ = = 4.72 Hz, $1H_{2'}$), 6.0 (1H, d., $J_{1'2'}$ = 2.82 Hz, $1H_{1'}$).

$C_9H_{13}N_3O_6S$ *Calcd.*: C, 34.10; H, 4.49; N, 14.42; S, 11.01% *Found*: C, 34.25; H, 4.53; N, 14.55; S, 11.20%

Thanks are due to Pharm. Ioan Cornelia, Department of Analytical Chemistry of this Institute for analyses, Dr. Arizan Sofia (of the same Department) for measurement of ultraviolet and infrared spectra and Dr. F. Cocu, Department of Chemistry of this Institute, for measurements of nuclear magnetic resonance spectra.

Revue Roumaine de Chimie, 20, 9–10, 1295–1299 (1975)

1-SUBSTITUTED ALKYLAMINO-3-(4-QUINAZOLYLOXY)-2-PROPANOL TRIHYDROCHLORIDES AND 1-SUBSTITUTED ALKYLAMINO-3-(8-QUINOLYLOXY)-2-PROPANOL DIHYDROCHLORIDES

S. C. BENNUR, V. B. JIGAJINNI and V. V. BADIGER

Department of Chemistry, Karnatak University, Dharwar – 580003,
India

Received April 2, 1974

"As a part of our study of structure activity relationships (SAR), we have prepared seventeen new 1-substituted alkylamino-3-(4-quinazolyloxy)-2-propanol trihydrochlorides and 1-substituted alkylamino-3-(8-quinolyloxy)-2-propanol dihyrdochlorides. The IR of the compounds and TLC are reported".

Structure activity relationships (SAR) of cardiac β-adrenergic agonists and antagonists are of great topical interest and are becoming clearer with newer understanding of the mode of action of adrenergic drugs.[1,2] As a part of the SAR programme Friedman[3] et al. reported three isomeric pyridyl isopropylamino ethanols and showed that most of these compounds possessed agonist activity in test animals. Synthesis and biological properties of aromatic and heterocyclic analogs of pronethalol were reported by Crowther et al.[4–6] in which the side chain was attached to the benzenoid part and to the heterocyclic part of the heterocyclic system.

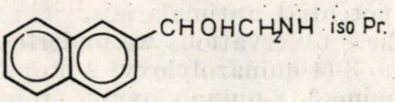

Pronethalol

---

[1] D. J. TRIGGLE, "Neurotransmitter – Receptor Interactions", Academic Press, New York, 1971, p. 217.

[2] A. BURGER, "Medicinal Chemistry", 3rd Ed., Wiley-Interscience, New York, 1971, p. 72 – 80.

[3] C. GNEWUCH and H. L. FRIEDMAN, *J. Med. Chem.*, **15**, 1321 (1972).

[4] A. F. CROWTHER and L. H. SMITH, *J. Med. Chem.*, **11**, 1009 (1968).

[5] R. HOWE B. S. RAO and M. S. CHODNEKAR, *J. Med. Chem.*, **13**, 169 (1970).

[6] M. S. CHODNEKAR, A. F. CROWTHER, W. HEPWORTH, R. HOWE, B. J. MEHOUGHLIN, A. MITCHELL, B. S. RAO, R. P. SLATENER, L. H. SMITH and M. S. STEVENS, *J. Med. Chem.*, **15**, 49 (1972).

Most of these compounds possessed β-adrenergic blocking activity similar to that of pronethalol. Nakanishi et al.[7] reported potent β-adrenergic activity in a 1-amino-3-(substituted phenoxy)-2-propanols. β-Adrenergic potency was reported in a class of N-substituted 2-amino-1-(2-thienyl) ethanols.[8] Bunalol (I) was shown to be three times more active when administered orally and 20—30 times more than propranolol (II) when administered intravenously. Shwender et al.[9,10] studied the effect of aromatic substitution on the β-adrenergic blocking activity of Bunalol and observed that aromatic substitution did not yield any β-adrenergic blocker that was superior to bunalol.

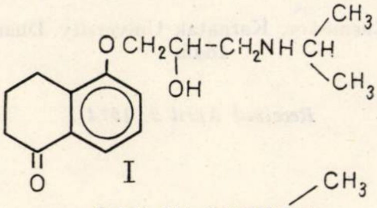

I

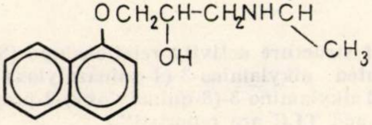

II

A number of N-alkylaminoethanols and benzothiazole derivatives of type III

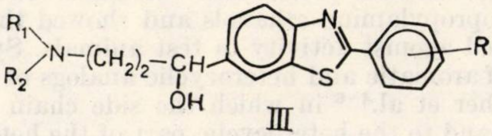

III

were investigated as potential antimalarials.[11,12]

Encouraged by these observations we undertook the preparation of 1-mono or dialkylamino-3-(4-quinazolyloxy)-2-propanol trihydrochlorides and 1-mono or -dialkylamino-3-(8-quinolyloxy)-2-propanol dihydrochlorides. The biological activity will be reported elsewhere.

The title compounds were prepared according to the scheme I.

---

[7] M. Nakanishi, T. Mura, Y. Chihara, H. Imamura and T. Nakao, *J. Med. Chem.*, **15**, 45 (1972).

[8] C. Corral, V. Davias, M. P. Fernandez — Tome, R. Madronero and J. del Rio, *J. Med. Chem.*, **16**, 882 (1973).

[9] C. F. Schwender, S. Farber, C. Blaum and J. Shavel, Jr. *J. M. Med. Chem.*, **13**, 684 (1970).

[10] C. F. Schwender, R. E. Pike and J. Shonel, Jr., *J. Med. Chem.*, **16**, 254 (1973).

[11] W. T. Colwell, V. Brown, P. Christie, J. Lange, K. Yamamoto and I. W. Henry, *J. Med. Chem.*, **15**, 771 (1972).

[12] S. N. Sawhney and J. Singh, *Indian J. Appl. Chem.*, **35**, 20 (1972).

SCHEME I

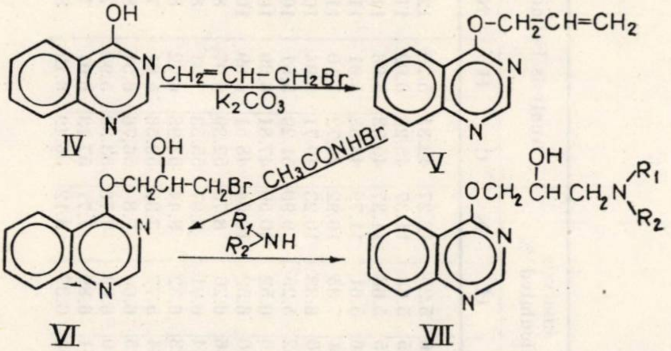

4-Hydroxyquinazoline (IV) was allowed to react with allyl bromide in the presence of anhydrous potassium carbonate to yield 4-allyloxy quinazoline (V). 4-Allyloxyquinazoline (V) was treated with N-bromo-acetamide in the presence of 1N sulphuric acid to get the bromohydrin (VI). The crude bromohydrin was condensed with different amines in absolute alcohol in basic medium to obtain free bases (VII) which were then converted to their hydrochlorides.

The method followed for the quinoline series was the same as that described above, except that 8-hydroxyquinoline was used instead of 4-hydroxyquinazoline. The IR spectra were recorded on the Perkin-Elmer Infra-red spectrophotometer. Quinazolyloxy propanol trihydrochlorides and quinolyloxy propanol dihydrochlorides showed absorption in the region of 1120—1100 cm^{-1} and 1370—1250 cm^{-1}. These were assigned to —OH deformation and C—O stretching vibrations. A strong band occurring between 1260—1250 cm^{-1} and another appearing in the region 1100—1080 cm^{-1} were assigned to ether linkage. The absorptions due to —NH— and hydrochloride were observed at 1380—12608 cm^{-1} and 3200—2500 cm^{-1}, 2050—1900 cm^{-1}[13].

The compounds were subjected to thin layer chromatography on a silica-gel plate with 5 percent acetic acid in chloroform as eluent. Only two spots were observed on developing. These spots were assumed to be due to optical isomers. No further attempt was made to isolate them.

These compounds are described in table 1.

EXPERIMENTAL[14]

4-Hydroxyquinazoline was prepared from anthranilic acid and formamide as described in the literature.[15]N-bromo-acetamide was prepared by the method reported earlier.[16]

8-Hydroxyquinoline was a BDH sample. Dimethyl-, diethyl-, and iso-propylamines, piperidine, morpholine, pyrrolidine, benzylamine and cyclohexylamine were Riedel samples. Allyl bromide was a BDH sample.

---

[13] L. J. Bellamy "The Infra-red Spectra of Complex Molecules", London, 1957.

[14] All melting points are taken in open capillary and are uncorrected.

[15] M. M. Endicott, E. Wick, M.L. Mercury and M. L. Sherrill, *J. Amer. Chem. Soc.*, **68**, 1299 (1966).

[16] E. P. Oliveto and C. Gerold, "Organic Syntheses", Coll. Vol. 4, New York, 1963, p. 104.

Table 1

$R_1-CH_2-CH(OH)-CH_2-R_2$

S.Nº	R_1	R_2	Molecular formula	Melting point	Yield %	Analysis Calculated %			Analysis Found		
						C	H	N	C	H	N
1	4-Quinazolyloxy	Methylamino-	$C_{12}H_{18}O_2N_3Cl_3$	250−253°d	30	42.06	5.25	12.27	42.31	5.29	12.19
2	”	Isopropylamino-	$C_{14}H_{21}O_2N_3Cl_3$	172−173°d	45	45.45	5.68	11.37	45.28	6.02	11.37
3	”	*n*-Butylamino−	$C_{14}H_{21}O_2N_3Cl_3$	240−241°d	39	45.45	5.68	11.37	45.53	5.98	11.12
4	”	Dimethylamino-	$C_{13}H_{20}O_2N_3Cl_3$	198−200°d	25	43.76	5.61	11.79	43.58	5.91	11.93
5	”	Diethylamino-	$C_{15}H_{24}O_2N_3Cl_3$	218−219°d	35	46.81	7.85	10.92	46.72	8.10	11.01
6	”	Cyclohexylamino-	$C_{17}H_{26}O_2N_3Cl_3$	155−156°d	40	49.40	6.33	10.23	49.71	5.94	10.35
7	”	Benzylamino-	$C_{18}H_{22}O_2N_3Cl_3$	238−239°d	50	51.62	5.25	9.90	51.29	5.51	10.37
8	”	Piperidino-	$C_{16}H_{24}O_2N_3Cl_3$	112−113°d	40	48.10	6.52	10.59	47.81	6.39	10.38
9	”	Morpholino-	$C_{15}H_{22}O_3N_3Cl_3$	212−213°d	49	48.10	6.52	10.54	48.51	6.69	10.56
10	8-Quinolyloxy	Dimethylamino-	$C_{14}H_{20}O_2N_2Cl_2$	223−224°d	35	52.66	6.26	8.78	52.39	5.97	8.91
11	”	Diethylamino-	$C_{16}H_{24}O_2N_2Cl_2$	173−174°d	30	55.34	6.91	8.07	55.53	7.31	8.21
12	”	Isopropylamino-	$C_{15}H_{21}O_2N_2Cl_2$	198−199°d	45	54.23	6.32	8.44	53.98	6.42	8.39
13	”	Benzylamino-	$C_{19}H_{22}O_2N_2Cl_2$	200−201°d	40	59.84	5.77	7.35	59.56	5.91	7.16
14	”	Piperidino-	$C_{17}H_{24}O_2N_2Cl_2$	158−159°d	35	56.45	6.68	7.8	56.76	6.51	8.13
15	”	Morpholino-	$C_{16}H_{22}O_3N_2Cl_2$	184−185°d	30	53.19	6.09	7.76	53.30	5.92	7.57
16	”	Cyclohexylamino-	$C_{18}H_{26}O_2N_2Cl_2$	101−102°d	30	57.31	6.89	7.71	57.13	6.91	7.48
17	”	Pyrrolidino-	$C_{16}H_{22}O_2N_2Cl_2$	165−166°d	38	55.65	6.37	8.12	56.49	6.12	8.59

PREPARATION OF 4-ALLYLOXYQUINAZOLINE (V)

To a mixture of 4-hydroxyquinazoline (14.6 g. 0.1 mole) and anhydrous potassium carbonate (13.8 g., 0.1 mole) in anhydrous acetone (100 ml.) was added allylbromide (12.0 g., 0.1 mole). This mixture was refluxed over a steam bath for 3 hours, under anhydrous conditions. After the reaction was over, acetone was removed under vacuum. The residue was treated with water. The reddish brown oil was extracted with ether (50 ml. × 2). The organic layer was washed with dilute sodium hydroxide solution and finally with water. The organic layer after drying over anhydrous potassium carbonate, was distilled and the oil was cooled when it solidified. This was purified by crystallizing from alcohol. Colourless needles, m.p. 62 — 63°., yield 12 g.

Anal. *calcd.*, for $C_{10}H_{10}N_2O$: C, 68.98 ; H, 5.74 ; N, 16.09%,
Found : C, 69.17 ; H, 5.90 ; N, 16.34%.

PREPARATION OF 1-ISOPROPYLAMINO-3-(4-QUINAZOLYLOXY)-2-PROPANOL TRIHYDROCHLORIDE

To 4-allyloxyquinazoline (1.7 g., 0.01 mole) in water (5 ml.) was added, with stirring, N—bromoacetamide (2.0 g. 0.015 mole). After about half an hour a white gum was formed. 1N Sulphuric acid (8 ml.) was added. The temperature of the reaction mixture rose to about 35°. After stirring for a few minutes, the pH of the reaction mixture was brought down to about 1 with the addition of more amount of 1N sulphuric acid. This was stirred for 0.5 hours, then heated to about 45° with stirring continued for further 0.5 hour. This was stirred with sodium bisulphite (0.5 g.), neutralized carefully with sodium bicarbonate and saturated with potassium carbonate. The gummy bromohydrin so obtained was extracted with dichloromethane. The extract was dried over potassium carbonate and the solvent was removed under reduced pressure.

To this crude bromhydrin (0.01 mole) in absolute alcohol (10 ml.) isopropylamine (0.015 mole) was added. Then a solution of potassium hydroxide (0.56 g., 0.01 mole) in absolute alcohol (10, ml.) was added and refluxed over a steam bath for about 5 hours. It was evaporated to dryness under reduced pressure. The residue was taken up in water and extracted with dichloromethane and washed twice with water. The organic layer was dried over anhydrous potassium carbonate and the solvent was removed. The oil which was left behind was taken in dry ether and cooled in ice-salt mixture. To this dry hydrogen chloride gas was passed. The hydrochloride separated immediately. It was filtered and washed with dry ether.

8—Allyloxyquinoline was prepared as described earlier for 4—allyloxyquinazoline. It was a pale yellow viscous oil, b.p. 185 — 186°/15 mm.

ACKNOWLEDGEMENT. We thank Prof. E.S. Jayadevappa Head, of the Chemistry Department, Karnatak University, Dharwar, for providing facilities. One of us (V.B.Jigajinni) is grateful to C.S.I.R. for financial assistance. We thank Messrs. S.B. Hinchigeri, V.H. Mulimani and V.A. Desai for recording the analytical data. Thanks are also due to Dr. P.B.Sattur, Assistant Director, Regional Research Laboratory, Hyderabad.

Revue Roumaine de Chimie, 20, *9–10*, 1301–1310 (1975)

OXIDATION OF ALICYCLIC ALCOHOLS BY CERIUM(IV) PERCHLORATE

T. R. BALASUBRAMANIAN and N. VENKATASUBRAMANIAN

Department of Chemistry, Vivekananda College, Madras 600004, INDIA

Received May 25, 1974

The kinetics of the oxidation of several alicyclic secondary alcohols by cerium (IV) perchlorate in aqueous acetic acid — perchloric acid medium has been studied. The reactions follow Michaelis-Menton type of kinetics. It is observed that the order of magnitudes of the equilibrium constant K, and the decomposition constant k_t for the oxidation of cyclanols runs counter to the *I*-strain concept. The slow rate of oxidation of *trans*-2-chlorocyclohexanol and the high rate of oxidation of *trans*-2-phenyl cyclohexanol when compared to the reactivity of cyclohexanol, have been accounted for. The thermodynamic parameters have been calculated and have been used to evaluate the isokinetic temperature.

In a recent study on the cerium (IV) oxidation of cyclanols, Hintz and Johnson[1] reported the complexing abilities and the nature of equilibria of Ce(IV) present. In continuation of our earlier studies[2-4] on the structural influences on the cerium (IV) perchlorate oxidation of aromatic primary and secondary alcohols as also aliphatic secondary alcohols, alicyclic secondary alcohols have been chosen for an investigation so that the effect of ring size on the oxidation rate and mechanism could be studied.

EXPERIMENTAL

All the liquid organic compounds which were of the extra pure variety (Fluka *AG*) were distilled from an all glass apparatus. Large head and tail fractions were rejected and the fractions distilling at temperatures correspondig to the literature values were collected. Acetic acid and conductivity water were purified by usual procedures and all the inorganic materials used were of the *AR* grade. The cerium (IV) perchlorate (G. Frederick Smith Chemical Company, U.S.A.) 0.5M solution in 6M perchloric acid was used as such and the experimental method was the same as in our earlier reports.[2-4] Though the cerium (IV) oxidation of aqueous acetic acid has been reported recently,[5] we find that under our experimental conditions, the oxidation rate of the solvent is not significant compared to the oxidation rate of cyclanols.

---

[1] H. L. Hintz and D. C. Johnson, *J. Org. Chem.*, **32**, 556 (1967).

[2] T. R. Balasubramanian and N. Venkatasubramanian, *Indian. J. Chem.*, **8**, 305 (1970).

[3] idem., *ibid.*, **9**, 36 (1971).

[4] idem., *ibid.*, **9**, 1243 (1971).

[5] R. Vasudevan and I. M. Mathai, *J. Chem. Soc., B*, **1970**, 1361.

RESULTS

The oxidation of the cyclanols — cyclopentanol, cyclohexanol, cycloheptanol, cyclooctanol, *trans*-2-chloro cyclohexanol and *trans*-2-phenyl cyclohexanol — by cerium (IV) in perchloric acid and at an ionic strength of 0.7 under pseudo unimolecular conditions were carried out in the temperature range 30—40°. The reactions are all of the first order with respect to Ce (IV) as evidenced by the first order rate profiles (Fig. 1).

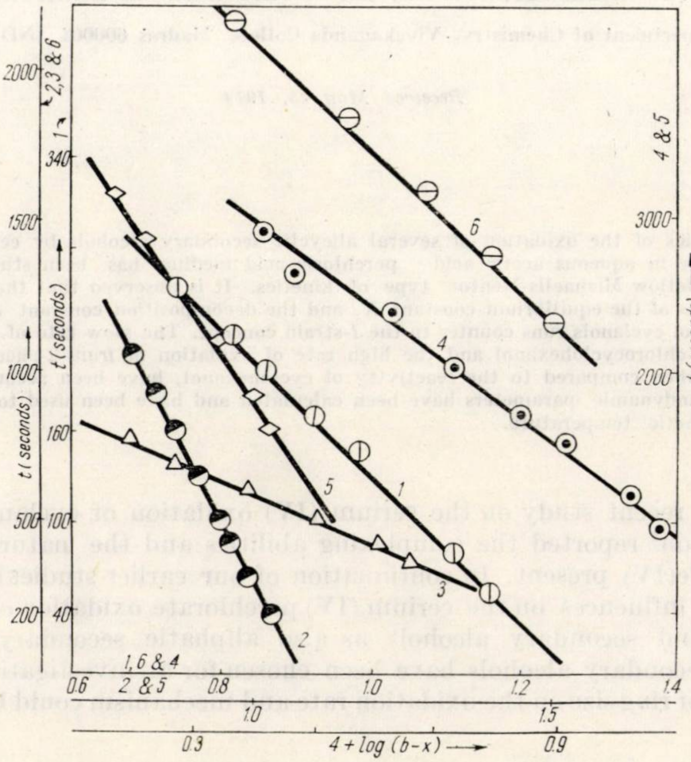

Fig. 1. — First Order Plots.

1 — Cyclopentanol (40°); 2 — Cyclohexanol (30°); 3 — *trans*-2-chloro Cyclohexanol (30°); 4 — Cycloheptanol (35°): 5-*trans*-2-phenyl Cyclohexanol (40°); 6 — Cyclooctanol (35°). Solvent: 50% HOAc; $[HClO_4]$: 0.5M.

The order with respect to the cyclanols is not simple (Table 1), The behaviour is analogous to our observation with aliphatic and aromatic secondary alcohols viz. plots of log k_{obs} versus log [alcohol] yield slopes that are less than unity. Further, the plots of $1/k_{obs}$ versus $1/[ROH]$ are linear with intercepts on the *y*-axis conforming to the Michaelis-Menton type of kinetics [6,7] (Fig. 2) which suggest a rate-law of the form

$$-\frac{d[Ce(IV)]}{dt} = k_{obs}[Ce(IV)] = \frac{k_t K[ROH][Ce(IV)]}{1 + K[ROH]}$$

---

[6] L. Michaelis and M. L. Menton, *Biochem. Z.*, **49**, 333 (1913).

[7] F. R. Duke, *J. Amer. Chem. Soc.*, **69**, 2855 (1947).

Table 1

Dependence of rate on alcohol concentration

$[HClO_4]$: 0.5M Temp. :30°
[Ce(IV)] :0.00144 OM Solvent : 50% HOAc – 50% H_2O(v/v)

Alcohol	[alcohol] M	$k_{obs} \times 10^3$ sec^{-1}
Cyclopentanol	0.01379	1.59
	0.01477	1.68
	0.01874	2.19
	0.02176	2.40
Cyclohexanol	0.01309	1.17
	0.01545	1.33
	0.01790	1.53
Cycloheptanol	0.009056	0.162
	0.01252	0.197
	0.02771	0.453
	0.04969	0.825
Cyclooctanol	0.01809	0.429
	0.02637	0.610
	0.03671	0.790
	0.04106	0.838

where K is the equilibrium constant for the alcohol-cerium (IV) complex and k_t is the disproportionation constant of the complex. The oxidation of cyclohexanol, chosen as a typical case, is acid catalysed (Table 2),

Table 2

Effect of acidity on the Ce(IV) oxidation of cyclanols

[cyclohexanol] : 0.01307M μ :0.7 Temp. : 30°
[Ce(IV)] : 0.00163M Solvent : 50% HOAc – 50 % H_2O(v/v)

$[HClO_4]$M	$k_{obs} \times 10^4$ sec^{-1}
0.125	1.65
0.300	6.88
0.600	14.5

conforming that Ce^{4+}(aq.) is the active oxidant as observed in earlier investigations.[8–12] Further, from a detailed spectrophotometric study of the system cerium (IV) perchlorate in perchloric acid, Hardwick and Robertson[13] have concluded that unhydrolysed Ce^{4+} (better represented as

---

[8] M. Ardon, *J. Chem. Soc.*, **1957**, 1811.

[9] M. Santappa and S. Venkatakrishnan, *Z. Phys. Chem.* (*Frankfurt*), **16**, 173 (1958).

[10] G. Hargreaves and L. H. Sutcliffe, *Trans. Faraday.Soc.*, **51**, 786 (1955).

[11] S. S. Muhammed and K. Vijaychander Rao, *Bull. Chem. Soc. Japan*, **36**, 943 (1963).

[12] M. Rangaswamy and M. Santappa, *Indian. J. Chem.*, **7**, 473 (1969).

[13] T. J. Hardwick and E. Robertson, *Canad. J. Chem.*, **29**, 818, 828 (1951).

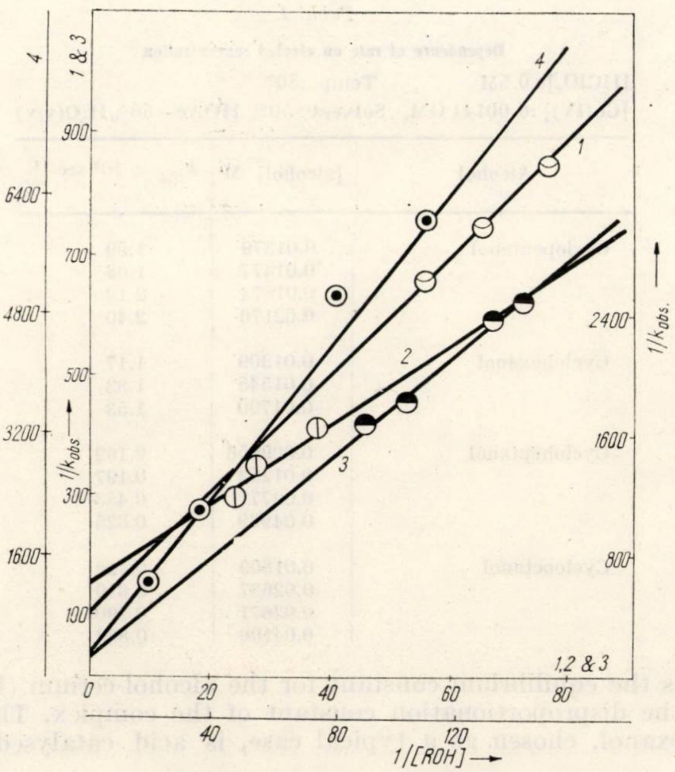

Fig. 2. — $1/k_{obs}$ versus $1/[ROH]$.
1 — Cyclohexanol; 2 — Cyclooctanol; 3 — Cyclopentanol; 4 — Cycloheptanol;
Solvent: 50% HOAc; Temp.: 30°; $[HClO_4]$: 0.5M.

$Ce(H_2O)_8^{4+}$) is the most important species at low Ce (IV) concentrations and species like $Ce^{4+}OH^-$ and $(Ce-O-Ce)^{6+}$ are not present in appreciable amounts. The increase in rate of oxidation with increasing H^+ concentration is in accordance with the equation

$$Ce^{4+} + H_2O \overset{K_h}{\rightleftharpoons} Ce^{4+}OH^- + H^+$$

The possibility of OH radicals produced by the equilibria

$$Ce^{4+} + H_2O \rightleftharpoons Ce^{3+} + H^+ + OH.$$

$$Ce^{4+}OH^- \rightleftharpoons Ce^{3+} + OH.$$

as initiators for the oxidation can be excluded on two grounds: (i) initial addition of Ce^{3+} so that $[Ce^{3+}]/[Ce^{4+}] \geqslant 2$ did not affect the rates of oxidation for all the systems studied in the present investigation and (ii) under the experimental conditions chosen, the oxidation of water by Ce^{4+} as evidenced by Ce^{4+} uptake in the absence of added organic substrate, was quite insignificant. Further, the fact that the order with respect to cerium (IV) ions was unity for all systems studied pointed to the fact that polymeric species were not present (or if present, were not active) — for were these active, higher orders in Ce^{4+} would have been observed.

However, the order with respect to $[H^+]$ is not simple. In aqueous acetic acid, the principal species of ceric ion equilibria have been shown to be the monomer (M) and a trimer (T)[13a] of which the concentration of the latter is very low. *K*, the equilibrium constant for the equilibrium

$$T \xrightleftharpoons[k_2]{k_1} 3\,\mathrm{M}$$

is known to be 7.69×10^6 litre^2 mole^{-2} at 0.1 M $[H^+]$ and therefore it has been assumed, as a first approximation, that the chief reactive species is $Ce(H_2O)_8^{4+}$ ion.

The temperature dependence of the rate of oxidation of the cyclanols was determined from $\log k_{obs}$ versus $1/T$ plots and linear relationships were observed in all cases (Fig. 3). The values of k_{obs} and the activation

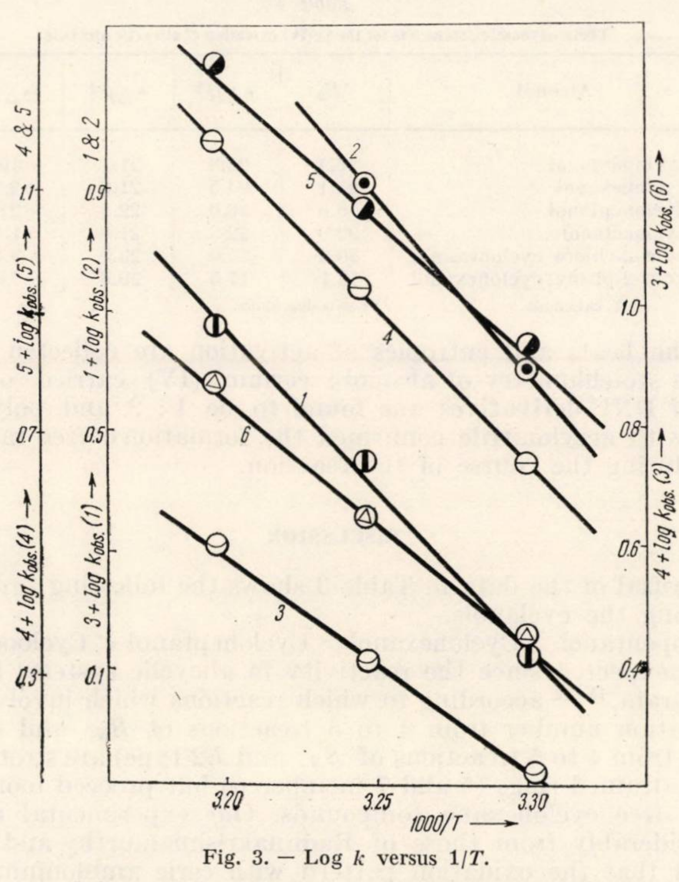

Fig. 3. – Log *k* versus $1/T$.

1 – Cyclopentanol; 2 – Cyclooctanol; 3 – Cycloheptanol; 4 – Cyclohexanol;
5 – *trans*-2-chloro-Cyclohexanol; 6 – *trans*-2-phenyl cyclohexanol
Solvent: 50% HOAc.

[13a] K. B. Wiberg and P. C. Ford, *Inorg. Chem.*, **7**, 369 (1968).

Table 3

First order rate constants for the Ce(IV) oxidation of cyclanols

[alcohol] : 0.01M [$HClO_4$] : 0.5M μ : 0.7
[Ce(IV)] : 0.001450M Solvent : 50%HOAc−50%H_2O(v/v)

Alcohol	$k_{obs} \times 10^3$ sec^{-1}		
	30°	35°	40°
Cyclopentanol	1.34	2.78	4.68
Cyclohexanol	0.443	0.864	1.53
Cycloheptanol	0.165	0.254	0.402
Cyclooctanol	0.390	0.803	. . .
trans-2-chloro cyclohexanol	0.069	0.115	0.208
trans-2-phenyl cyclohexanol	2.83	4.50	7.67

Table 4

Thermodynamic parameters for the Ce(IV) oxidation of alicyclic alcohols

Alcohol	*E_a	*$\Delta H^{\ddagger}$	*$\Delta F^{\ddagger}$	**$\Delta S^{\ddagger}$
Cyclopentanol	26.4	25.8	21.1	−15
Cyclohexanol	25.1	24.5	21.8	+9.0
Cycloheptanol	16.6	16.0	22.5	−21
Cyclooctanol	22.9	22.3	21.8	+1.5
trans-2-chloro cyclohexanol	20.6	20.0	23.0	−9.8
trans-2-phenyl cyclohexanol	18.1	17.5	20.8	−11

* k. cals/mole. ** cals/deg./mole.

energies, the heats and entropies of activation are collected in Table 3 and 4. The stoichiometry of alcohol : cerium (IV) carried out by the isolation of DNP derivatives was found to be 1 : 2 and polymerisation reactions with acrylonitrile confirmed the formation of free radical intermediates during the course of the reaction.

DISCUSSION

A perusal of the data in Table 3 shows the following order of reactivity among the cyclanols.

Cyclopentanol > Cyclohexanol > Cycloheptanol < Cyclooctanol. This order is unexpected since the reactivity in alicyclic systems is governed by the *I*-strain,[14–16] according to which reactions which involve a change of coordination number from 4 to 3 (reactions of S_{N_1} and free radical type) and from 4 to 5 (reactions of S_{N_2} and $E2$ type) are strongly favoured in the strained rings (5 and 7 membered) but proceed more slowly in the strain free cyclohexane compounds. Our experimental results also differ considerably from those of Radhnakrishnamurthy and Mahanti[16a] who found that the oxidation pattern with ceric ammonium nitrate in perchloric acid followed the *I*-strain order. It must be mentioned, how-

---

[14] H. C. Brown and M. Gerstein, *J. Amer. Chem. Soc.*, **72**, 2925 (1950).

[15] H. C. Brown, R. S. Fletcher and R. B. Johannesan, *J. Amer. Chem. Soc.*, **73**, 212 (1951).

[16] H. C. Brown, *J. Chem. Soc.*, **1956**, 7248.

[16a] P. S. Radhakrishnamurthy and M. K. Mahanti, *Indian. J. Chem.*, **9**, 957 (1971).

ever, that under their experimental conditions, there is no complex formation and the reactions follow a total second order path. The high rate with cyclopentanol is not unexpected since it exists in a semichair form. However, the increased reactivity of cyclohexanol over cycloheptanol and cyclooctanol is surprising. The mechanism of the Ce(IV) oxidation of alcohols has generally been explained on the basis of the rapid formation of 1: 1 complex and a slow subsequent decomposition of the complex to give the products.[17]

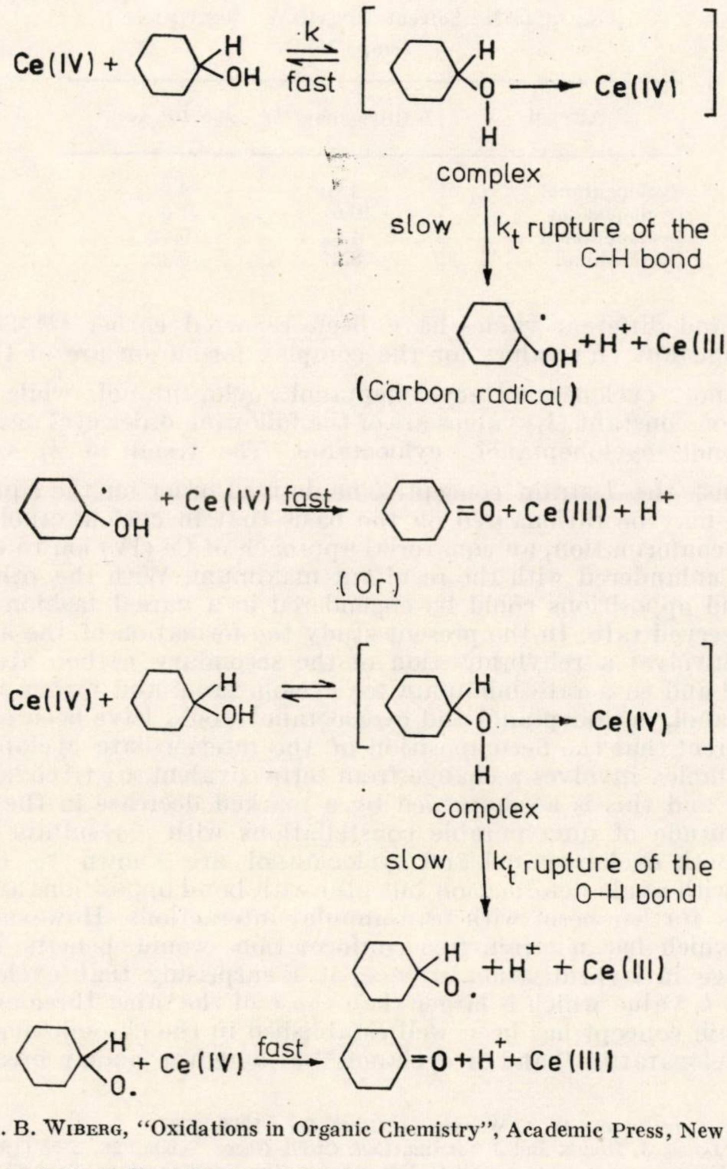
Ce(IV) +
H
OH
k
fast
H
O
Ce(IV)
H
complex
slow
k_t rupture of the C–H bond
OH
+H⁺ + Ce(III)
(Carbon radical)
OH
+ Ce(IV) fast
=0 + Ce(III) + H⁺
(Or)
Ce(IV) +
H
OH
H
O
Ce(IV)
H
complex
slow
k_t rupture of the O–H bond
H
O.
+H⁺ + Ce(III)
H
O.
+ Ce(IV) fast
=0 + H⁺ + Ce(III)

---

[17] K. B. Wiberg, "Oxidations in Organic Chemistry", Academic Press, New York, 1965.

Both the mechanisms are consistent with the stoichiometry of Ce(IV): alcohol – 2 :1 obtained in the present investigation. The values of K and k_t evaluated from the Michaelis-Menton type of plots are summarised in Table 5. It is observed that cyclohexanol has a much larger formation constant and different values have been reported earlier.[1,18] The equilibrium constant (K) values for the complex formation are of the order cyclohexanol>cyclooctanol>cycloheptanol>cylopentanol, while the decomposition constant (k_t) values are of the following order cyclopentanol> cyclohexanol>cycloheptanol> cylooctanol. The trend in k_t values is still against the *I*-strain concept. The derived order for the equilibrium constants may be rationalised on the basis that in cyclohexanol, with a strainless conformation, an equatorial approach of Ce (IV) ion to the ring, is largely unhindered with the resultant maximum. With the other three rings, bond oppositions could be engendered in a varied fashion leading to the observed rate. In the present study the formation of the activated complex involves a rehybridisation of the secondary carbon atom from sp^3 to sp^2 and so a rate minimum for cyclohexanol and higher rates for cyclopentanol, cycloheptanol and cyclooctanol would have been expected. It is apparent that the decomposition of the intermediate cyclopentanol-Ce(IV) complex involves a change from tetra covalent to a tri covalent carbon atom and this is accompanied by a marked decrease in the number and magnitude of unfavourable constellations with a resultant increase in rate. Both cycloheptanol and cyclooctanol are known to be beset not only with angle deformation but also with bond oppositions and cyclooctanol is further beset with transannular interactions. However, cyclohexanol which has a strain free conformation would benefit least by this change in hybridisation. Hence, it is surprising that cyclohexanol exhibits a k_t value which is larger than those of the other three cyclanols. The *I*-strain concept has been well established in the chromic acid oxidation of cycloparaffins[19] and of cyclanols[20] although a similar break down

Table 5

Decomposition and equilibrium constants for the Ce(IV) oxidation of alicyclic alcohols

[HClO$_4$]: 0.5M Solvent: 50 %HOAc – 50 %H$_2$O(v/v)
Temp.: 30°

Alcohol	K (litre mole^{-1})	$k_2 \times 10^2$ sec^{-1}
Cyclopentanol	3.00	4.0
Cyclohexanol	10.0	1.0
Cycloheptanol	4.32	0.42
Cyclooctanol	8.27	0.33

---

[18] J. S. Littler and W. A. Waters, *J. Chem. Soc.*, **1960**, 2767.

[19] F. Mares, J. Rocek and J. Sicher, *Coll. Czech. Chem. Comm.*, **26**, 2355 (1961).

[20] N. Venkatasubramanian and G. Srinivasan, *Proc. Indian. Acad. Sci.*, **65**, 30 (1967).

of the concept was reported in the Br_2 oxidation of cyclanols.[21] The *I*-strain concept seems to hold very well for reactions that proceed by an ionic pathway. Although a few free radical reactions of alicyclic systems have been reported to follow this theory, it seems likely that the theory is not applicable to systems that involve prior equilibria followed by a rate-determining one electron transfer. For, the conformational effects on complex formation may be quite different from the conformational effects on a subsequent abstraction of a hydrogen atom in the second step. The effects of these two factors (reflected in the k_t and K values) probably do not run parallel in the systems.

Further, it is also noticed from Table 3 that a chlorine substituent (a typical electron-withdrawing substituent) retards the rate of oxidation in *trans*-2-chloro cyclohexanol. A similar retardation of the rate was also found with the introduction of a halogen substituent in aromatic[2,3] and aliphatic alcohols.[4] A further cause for retardation with *trans*-2-chloro cyclohexanol may be the steric hindrance to attack at an axial hydrogen atom by a bulky solvated Ce (IV) ion. There is also a likelihood that complex formation with the Ce (VI) is hindered, the hydrogen of the hydroxyl being hydrogen bonded to the equatorial chlorine.[21,22] Another interesting observation (Table 3) is the increased rate of oxidation of trans-2-phenyl cyclohexanol over cyclohexanol since the phenyl ring is one carbon away from the reaction centre and is not conjugated with it, a reduced rate of oxidation would have been anticipated. However, benzylic hydrogens are known to be easily abstracted by free radicals and by one electron oxidants. Hence if the oxidation proceeds by a direct abstraction of the hydrogen atom (marked*) on C_2, the resulting radical would be a more stable resonance stabilised radical.

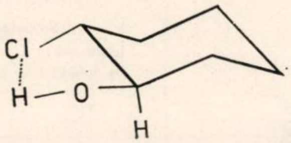

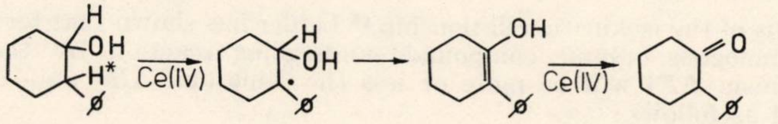

This alternate route would account for the observed increase in rate with *trans*-2-phenyl cyclohexanol. A similar observation has been made in the NBS oxidation of this alcohol[23] that the reaction proceeds not by the direct oxidation of the secondary alcoholic centre but by an initial attack at the benzylic hydrogen followed by rearrangement to the products. It should be pointed out also that Trahanovsky and Nave[24] have pointed out in the Ce(IV) oxidative cleavage of 2-aryl 1-phenyl ethanol that the position adjacent to the phenyl ring is more susceptible to attack.

---

[21] V. THIAGARAJAN, "PH. D. Thesis", University of Madras, 1968.

[22] G. G. PIMENTAL and MCCLELAN, "Hydrogen Bond", Freeman and Co., San Francisco, 1960.

[23] V. THIAGARAJAN and N. VENKATASUBRAMANIAN, *Indian. J. Chem.*, **7**, 830 (1969).

THERMODYNAMIC PARAMETERS

The values of the thermodynamic parameters summarized in Table 4 are in accordance with those that have been obtained for oxidation reactions by other oxidants involving free radicals.[1,17,25] The $\Delta F^{\ddagger}$ values for the cyclanols are more or less of the same order and may be understood

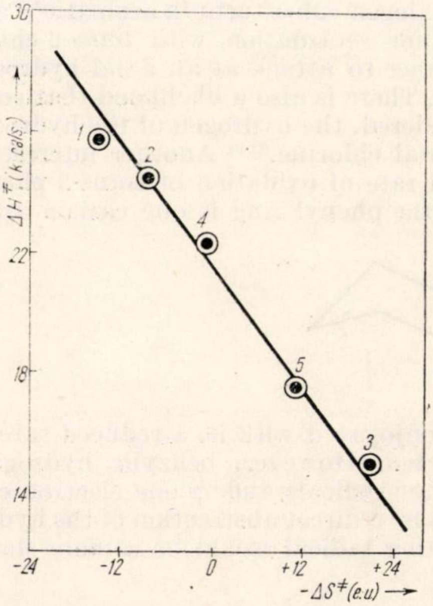

Fig. 4. – $\Delta H^{\ddagger}$ versus $\Delta S^{\ddagger}$.

1 – Cyclopentanol; 2 – Cyclohexanol; 3 – Cycloheptanol; 4 – Cyclooctanol; 5 – *trans*-2-phenyl Cyclohexanol; Solvent; 50% HOAc [$HClO_4$]; 0.5M.

in terms of the isokinetic relationship.[25] Leffler has shown that for a series of homologous organic compounds undergoing reaction by the same mechanism $\Delta F^{\ddagger}$ will be more or less the same and $\Delta H^{\ddagger}$ and $\Delta S^{\ddagger}$ are related as follows:

$$\Delta H^{\ddagger} = \Delta H_0^{\ddagger} + \beta \, \Delta S^{\ddagger}$$

where β is known as the isokinetic temperature and at this temperature all reactions obeying the same isokinetic relationship will proceed at the same rate. Figure 4 represents a least square plot of $\Delta H^{\ddagger}$ versus $-\Delta S^{\ddagger}$ and the slope β is 77°.

[24] W. S. Trahanovsky and P. M. Nave, *J. Amer. Chem. Soc.*, **90**, 4755 (1968).

[25] J. Leffler, *J. Org. Chem.*, **20**, 1212 (1955).

Revue Roumaine de Chimie, **20**, *9–10*, 1311–1317 (1975)

PRÉPARATION DES COPOLYMÈRES TERNAIRES MACROPOREUX

Ig. C. POINESCU, STELA DRĂGAN, STELIANA MAXIM et M. DIMA

Institut de Chimie Macromoléculaire « Petru Poni »
41 A, Aleea Ghica-Vodă, Jassy, Roumanie

Reçu le 16 février 1972
Complété le 6 février 1975

On présente les résultats sur l'obtention des copolymères ternaires macroporeux. On a préparé des copolymères styrène-acrylonitrile-divinylbenzène et styrène-méthacrylate d'alkyl-divinylbenzène macroporeux sous forme de perles. L'introduction d'un troisième comonomère (1 — 20%) augmente la porosité du copolymère plusieurs fois, en comparaison des copolymères macroporeux binaires styrène-divinylbenzène.

Ces dernières années les copolymères macroporeux styrène-divinylbenzène ont pris une grande importance pratique dans la synthèse des échangeurs d'ions macroporeux, en chromatographie, [1–8] etc.

Il existe une étroite interdépendance entre la porosité, le degré de réticulation et le milieu inerte. Ceci nous permet d'obtenir des copolymères ayant une structure bien établie, par le réglage de ces facteurs.

On sait que l'introduction d'un troisième comonomère améliore les propriétés physiques et chimiques des échangeurs d'ions. [9–12]

Dans cet article on étudie l'influence du troisième comonomère sur les propriétés physiques des copolymères ternaires macroporeux sous forme de perles.

[1] J. Seidl et J. Malinsky, *Fortschr. Hochpolym. -Forsch.*, **5**, 113 (1967).

[2] J. R. Millar, D. G. Smith, W. E. Morr et T. R. Kressman, *J. Chem. Soc.*, **1963**, 218, 2779 ; **1964**, 304.

[3] W. Busse et E. Schmidt, Ger. 1 569 285 (to Permutit A-9), 06 May 1970 ; *Chem. Abstr.*, **73**, 26244 (1970).

[4] H. Knall et I. Gross, *Mater. Plast.*, **5**, 182 (1968).

[5] I. M. Abrams, *Ind. Eng. Chem.*, **48**, 1469 (1956).

[6] F. Bortel, *Przemysl. Chem.*, **44**, 255 (1965).

[7] A. S. Tevlina et S. E. Sadova, *Zhur. priklad. Khim.*, **38**, 1643 (1965).

[8] Kolarz Bozena et J. Lindernann, *Chem. Stosow. A*, **14**, 265 (1970).

[9] VEB-Farbenfabrik Wolfen-Fr. 1 380 867, 4 décembre 1964 ; *Chem. Abstr.*, **62**, 10624 (1965).

[10] R. Bachmann, U. Krauss, H. Reuter, G. Schwachula, D. Warnecke, W. Wehlend et Fr. Wolf, (to Romania, Ministerul Industriei Chimice), Rom. 49 891, 6 mars 1968.

[11] Fr. Wolf, R. Bachmann, H. Reuter, G. Schwachula, D. Warnecke, W. Wehlend et U. Krauss, Brit. 1 020 907, 23 février 1966 ; *Chem.Abstr.*, **64**, 14374 (1966).

[12] G. Schwachula, « Kunstharz — Ionenaustauscher » Plenar-u. Diskussionsvortrage des vom 4 — 7 Juni 1968, in Leipzig Veranstalteten Symposiums, 30 Jahre Kunstharz. Ionenaustauscher, Akademie-Verlag, Berlin, 1970, p. 73.

PARTIE EXPÉRIMENTALE

Pour la préparation des copolymères ternaires macroporeux on a employé du : styrène, divinylbenzène (DVB), acrylonitrile, méthacrylate de méthyle, -éthyle, ou-butyle, comme le troisième comonomère et dichlorométhane, purs. La stabilisation de la suspension de monomères a été réalisée avec de la bentonite et de l'alcool polyvinylique 70/88. Comme milieu inerte on a utilisé l'essence (p. éb. 125 — 140°) et le polystyrène (M_w= 77.000), dont les quantités, rapportées au mélange de monomères ont été de 25 g de polystyrène pour 100 g de monomère et la fraction de volume $F_v = 0,40$ pour essence.

Après copolymérisation, les milieux inertes ont été extraits des perles de copolymères à l'aide de la vapeur (pour l'essence), ou du chlorure de méthylène (pour le polystyrène).

Le troisième comonomère a été varié entre 1,0 et 20,0% pour les degrés de réticulation 8,0; 12,0; 18,0; et 25,0% DVB.

L'initiation de la réaction de copolymérisation a été exécutée avec du peroxyde de benzoyle (1,5%), à 74 — 87°, et la durée de copolymérisation a été de 16 heures (milieu inerte polystyrène) ou 24 heures (milieu inerte essence).

Le contenu d'acrylonitrile des copolymères styrène-acrylo-nitrile-DVB a été calculé d'après l'analyse d'azote,[13] et celui des méthacrylates a été considéré égal à la quantité de monomères méthacryliques introduite dans la réaction.[14-15]

Les copolymères ternaires macroporeux préparés ont été caractérisés par le coefficient d'absorption d'alcool méthylique,[4] de toluène,[6] la densité et la porosité.[16]

RÉSULTATS ET DISCUSSIONS

Les résultats des déterminations physiques des copolymères ternaires macroporeux sont représentés dans les figures 1—7.

a. COPOLYMÈRES MACROPOREUX STYRÈNE-ACRYLONITRILE-DVB

Ce groupe de copolymères macroporeux a été obtenu en présence de polystyrène ou d'essence. Ainsi qu'il résulte des figures 1 et 2, on observe l'influence marquée de la quantité d'acrylonitrile introduite dans le copolymère, sur la valeur des coefficients d'absorption d'alcool méthylique et respectivement de toluène.

De même, la nature du milieu inerte, ainsi que le degré de réticulation des copolymères ternaires modifie les valeurs des coefficients d'absorption.

La nature du milieu inerte a la plus grande influence d'absorption de méthanol, ou de toluène, des copolymères obtenus en présence d'essence (fig. 1 et 2, courbes 1 et 3). La même remarque est valable si on rapporte de la même manière pour les polymères binaires (styrène—DVB).

Le degré de réticulation du copolymère influence les valeurs des coefficients d'absorption de toluène dans le sens qu'en même temps que le contenu en DVB croît, le coefficient d'absorption diminue (fig. 2). Pour la copolymérisation en présence de l'essence, cette influence disparaît. Ceci s'expliquerait par le fait que dans le cas d'absorption de toluène, les valeurs obtenues représentent la somme de deux effets : le solvatage des chaînes macromoléculaires (le gonflement des copolymères) et le remplissage des pores avec du liquide.

---

[13] T. S. Ma et G. Zauzaga, *Ind. Prod. Eng. Chem. Analyst.*, **14**, 280 (1942).

[14] G. A. Tarasov, *Vysokomol. Soedineniya*, **11**, 1601 (1960) ; **1**, 14 (1961).

[15] R. J. Solocombe, *J. Polymer. Sci.*, **26**, 9 (1957).

[16] R. Kunin, E. F. Meitzner, J. A. Oline, S. A. Fischer et N. Frisch, *Ind. and Eng. Chem.* (*Product Res. and Development*), **1**, 140 (1962).

Du point de vue du comportement des polymères vis-à-vis du toluène, une caractérisation plus exacte de la substance polymère peut se faire par la détermination du degré de gonflement en volumes (B) calculé au moyen de la relation.[1]

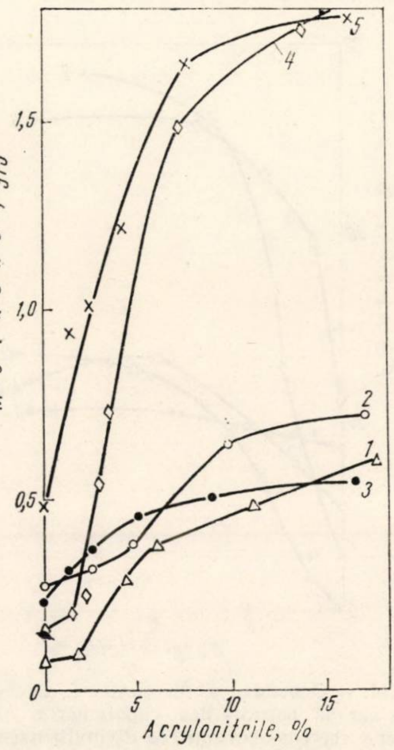

Fig. 1. — Dépendance du coefficient d'absorption de méthanol, du contenu en acrylonitrile des copolymères macroporeux styrène-acrylonitrile-divinylbenzène. Le milieu inerte, polystyrène: *1.* 8,0% DVB ; *2.* 12,0 % DVB ; *3.* 18,0% DVB. Le milieu inerte, essence 125/140 ; *4.* et *5.* 25,0% DVB.

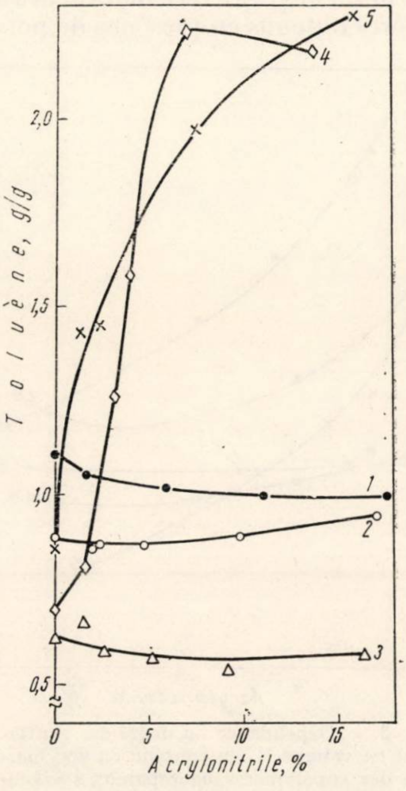

Fig. 2. — Dépendance du coefficient d'adsorption de toluène, du contenu en acrylonitrile des copolymères macroporeux styrène-acrylonitrile-divinylbenzène. Le milieu inerte, polystyrène: *1.* 8,0% DVB. *2.* 12,0 % DVB. *3.* 18,0% DVB. Le milieu inerte, essence 125/140; *4.* 18,0% DVB. *5.* 25,0% DVB.

$$B = \frac{\rho_0}{\rho_3} + (W - 1)\frac{\rho_0}{\rho_1}$$

où

ρ_0 — densité apparente du copolymère
ρ_1 — densité du solvant dans lequel on a déterminé le gonflement
ρ_3 — densité de la substance polymère en état humide
W — degré de gonflement en poids.

La dépendance du degré de gonflement en volumes de l'acrylonitrile et du degré de réticulation devient édifiante seulement au cas des copolymères obtenus en présence de polystyrène (fig. 3, courbes 1—3).

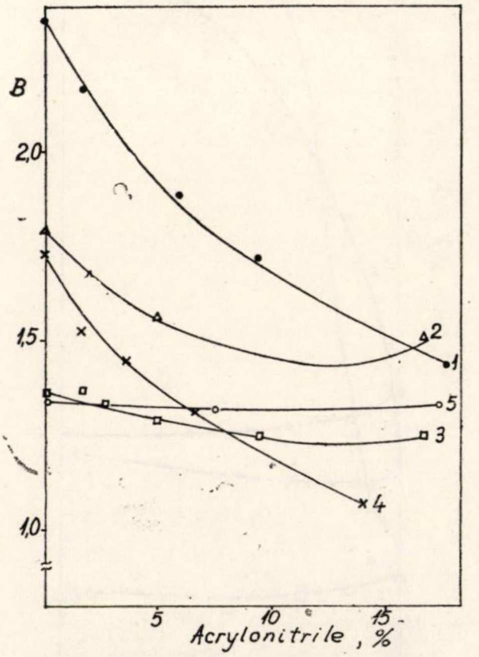

Fig. 3. — Dépendance du degré de gonflement en volume B, du contenu en acrylonitrile des copolymères macroporeux styrène-acrylonitrile-divinylbenzène. Le milieu inerte, polystyrène:
1. 8,0% DVB, *2.* 12,0 % DVB, *3.* 18,0% DVB. Le milieu inerte, essence 125/140 ; *4.* 18,0% DVB, *5.* 25,0% DVB.

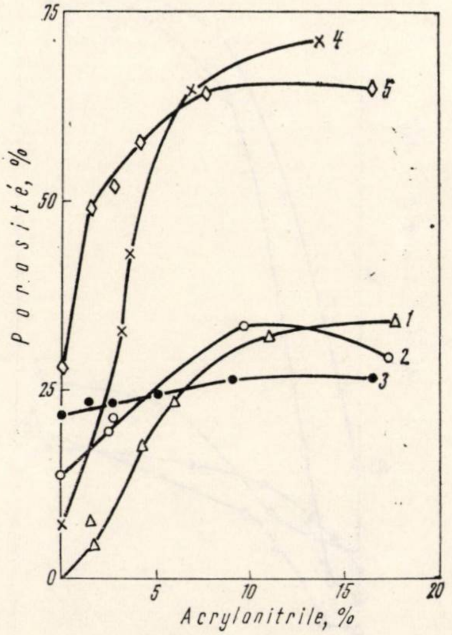

Fig. 4. — Dépendance du contenu d'acrylonitrile sur la porosité des copolymères macroporeux styrène-acrylonitrile-divinylbenzène. Le milieu inerte, polystyrène:
1. 8,0 % DVB, *2.* 12,0 % DVB, *3.* 18,0 % DVB. Le milieu inerte, essence 125/140 ; *4.* 18,0 % DVB, *5.* 25,0 % DVB.

On constate une diminution de la valeur de B, dans le cas du polystyrène, pendant que pour l'essence il existe un amoindrissement plus lent. Ce comportement de la valeur de B s'explique par la différence de porosité existante pour les deux groupes de copolymères macroporeux obtenus en présence du polystyrène ou de l'essence 125/140 (fig. 4).

Par rapport à la porosité due au gonflement, la porosité permanente des copolymères macroporeux est une caractéristique très importante, étant donné que cette valeur détermine la structure poreuse ou macroporeuse du copolymère. De même, d'après la valeur de la porosité nous pouvons nous rendre compte du volume des pores du copolymère. La valeur de la porosité, ainsi qu'il résulte de la figure 4, dépend de la nature du milieu inerte (polystyrène, courbes 1—3 ; essence, courbes 4—5) et du degré de réticulation. Dans le cas des copolymères styrène-acrylonitrile-DVB macroporeux, la porosité est aussi puissamment influencée par la quantité d'acrylonitrile contenue par le copolymère.

L'augmentation de la porosité des copolymères macroporeux par l'introduction du troisième comonomère, l'acrylonitrile, s'explique par le fait que la présence de l'acrylonitrile dans le copolymère modifie (diminue) l'action thermodynamique réciproque entre le composant inerte et les segments du réseau macromoléculaire. En même temps, l'augmentation de la différenciation dans la composition chimique des segments du réseau macromoléculaire par rapport à celle des segments du composant inerte augmente l'activité de séparation de celui-ci de la phase de polymère tridimensionnel. Il paraît que l'essence 125/140, ainsi que le polystyrène soient des agents de précipitation plus efficaces pour le copolymère avec polyacrylonitrile, que pour le polymère avec polystyrène. Ceci serait la cause qui mène à l'augmentation de la porosité des copolymères styrène-acrylonitrile-DVB en même temps que l'augmentation de la quantité d'acrylonitrile (fig. 4).

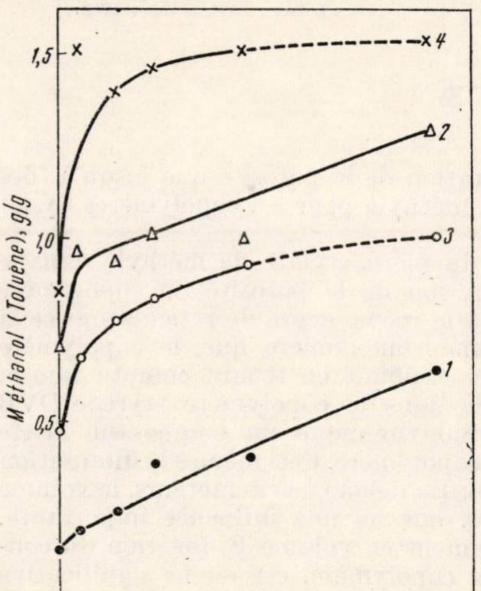

Fig. 5. — Influence du contenu de méthacrylate de méthyle sur les coefficients d'adsorption de méthanol et toluène des copolymères macroporeux styrène-méthacrylate de méthyle-divinylbenzène.

1. et *2.* 18,0 % DVB, *3.* et *4.* 25,0 % DVB. Le milieu inerte, essence 125/140.

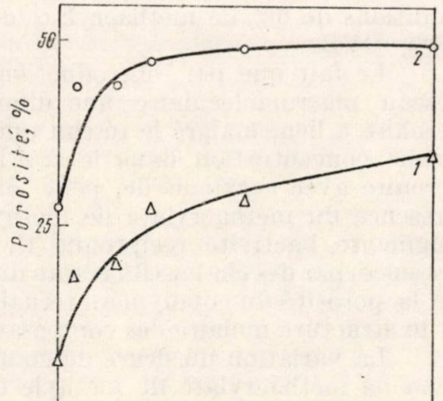

Fig. 6. — Influence du contenu de méthacrylate de méthyle sur la porosité des copolymères macroporeux styrène-méthacrylate de méthyle-divinylbenzène. Le milieu inerte, essence 125/140 :

1. 18,0% DVB, *2.* 25,0% DVB.

b. COPOLYMÈRES MACROPOREUX STYRÈNE-MÉTHACRYLATE D'ALKYL-DVB

Les coefficients d'absorption de méthanol ou toluène (fig. 5) présentent une importante augmentation en même temps que l'augmentation du contenu de méthacrylate de méthyle. Les valeurs de ceux-ci dépendent également du degré de réticulation.

En comparaison des copolymères contenant de l'acrylonitrile, les copolymères avec du méthacrylate de méthyle sont moins poreux, ce qui s'observe d'après les valeurs de la porosité (fig. 6). On n'obtient des modifications importantes dans l'augmentation de la porosité que jusqu'à des additions de 5% de méthacrylate de méthyle pour les copolymères ayant 25% DVB.

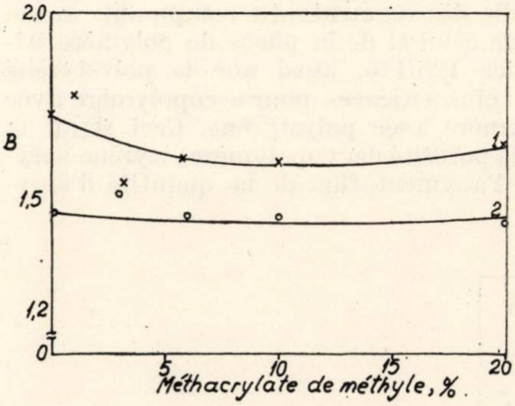

Fig. 7. — Variation du degré de gonflement en volume B, du contenu de méthacrylate de méthyle des copolymères macroporeux styrène-méthacrylate de méthyle-divinylbenzène. Le milieu inerte, essence 125/140 :

1. 18,0% DVB, *2.* 25,0% DVB.

Le fait que par l'introduction du méthacrylate de méthyle dans le réseau macromoléculaire une diminution de la porosité du copolymère ternaire a lieu, malgré le réseau qui a le même degré de réticulation et la même concentration dans le troisième comonomère que le copolymère ternaire avec acrylonitrile, peut être expliqué en tenant compte que la présence du méthacrylate de méthyle dans le copolymère styrène-DVB augmente l'activité réciproque thermodynamique du composant inerte (essence) par des chaînes du réseau du copolymère. Ceci mène à la diminution de la porosité du copolymère ternaire. En dehors de ces facteurs, le volume et la structure molaire des composants ont ici une influence importante.

La variation du degré de gonflement en volume B, fonction du contenu de méthacrylate de méthyle du copolymère, est moins significative (fig. 7). On peut expliquer ce comportement par un degré élevé de réticulation des copolymères macroporeux, fait qui détermine un accroissement de la rigidité de l'édifice macromoléculaire. Pour commencer, jusqu'à 1,0 – 2,0% de méthacrylate de méthyle, le gonflement du volume croît puissamment, pour que, ensuite, la valeur B reste approximativement constante.

Probablement que, dans ce cas, intervient le comportement différent du copolymère styrène-méthacrylate de méthyle-DVB par rapport au toluène. D'autre part, ces copolymères ont des valeurs de la porosité comprises entre celles des copolymères binaires (styrène-DVB) et ternaires (styrène-acrylonitrile-DVB).

Le volume du reste alkylique a une influence positive sur la croissance de la porosité des copolymères (tabl. 1).

Tableau 1

Dépendance des valeurs de la porosité des copolymères macroporeux de la nature (volume) du radical alkyle. (Degré de réticulation 18,0 % DVB)

Monomère méthacrylique (10,0 %)	Porosité %
Méthacrylate de méthyle	28,70
Méthacrylate d'éthyle	35,80
Méthacrylate de n-butyle	36,30

CONCLUSIONS

1. On a préparé de nouveaux copolymères macroporeux à base de styrène-acrylonitrile-divinylbenzène, styrène-méthacrylate d'alkyl-divinylbenzène, en utilisant comme milieu inerte du polystyrène ou de l'essence d'extraction (p. éb. 124—140°).

2. On a mis en évidence la dépendance existant entre la quantité d'acrylonitrile (méthacrylate de méthyle, -éthyle, -n-butyle), et les principales caractéristiques physiques des copolymères macroporeux préparés.

Revue Roumaine de Chimie, **20**, *9–10*, 1311–1317 (1975)

Revue Roumaine de Chimie, **20**, *9–10*, 1319–1328 (1975)

ЗАКОНОМЕРНОСТИ ПРОЦЕССА ЖИДКОФАЗНОГО ОКИСЛЕНИЯ НЕНАСЫЩЕННЫХ СОЕДИНЕНИЙ В ПРИСУТСТВИИ БОРНЫХ ДОБАВОК

ДИМЧО И. ДИМИТРОВ, ВАСИЛ З. АНГЕЛОВ и АНЧО Ц. БАДЕВ

Высший химикотехнологический институт, Кафедра «Основы химической технологии», София 56, Болгария

Исследовано жидкофазное окисление 20 разных по строению ненасыщенных соединений в присутствии сложных эфиров борной кислоты при следующих условиях: температура 50—170°, длительность продувания 1—9 часов, дебит воздуха 5—40 л/ч и концентрация сложного эфира бора 5 вес. % по отношению к борной кислоте. Испытана каталитическая эффективность более чем 10 нормальных и изоборатов. Прослежено изменение индукционного фактора, который характеризует величину, протекающего сопряженно с окислением, декарбоксилирования. Исследована связь «скорость реакции в условиях жидкофазного окисления — строение окисляемого олефина», а также и влияние основных кинетических факторов на рассматриваемый процесс. Установлена роль сложного эфира бора при окислении олефинов до окислов и спиртов. Идентифицированно большое число соединений и предложен механизм каталитического действия сложного эфира бора.

Окисление ненасыщенных соединений в настоящее время является перспективной дорогой к новым вариантам их технологической переработки, независимо от их широкого применения в качестве мономеров и исходного сырья в ряде процессов синтеза. Это обусловило и появление значительного числа научных сообщений, в большей части которых прослеживается кинетика накопления первичных продуктов в оксидате.

Выход гидроперекисей в зависимости от условий расматривал Бейтман [1]. По его мнению даже и в мягких условиях могут возникать некоторые вторичные продукты (альдегиды и кетоны), доминирующие однако при введении каталитических добавок. Надо отметить, что в случае олефинов добавки катализатора не изъявляются так полно, как при окислении других углеводородов (парафиновых, нафтеновых, ароматических и алкилароматических) [2]. При этом наиболее ярко выражена плохая селективность процесса, обусловленная осмолением реакционной массы, а в некоторых случаях и ее польным сгущением. Большую роль в этом отношении играют и параметры процесса: температура, дебит окислителя, природа окислителя и длительность продувания. Надежды в этом направлении часто связаны с проведением низкотемпературного окисления, с подходящих выбором каталитической добавки, с ограничением реакции взаимодействия окислов и спиртов, с протеканием термоокислительной полимеризации, с накоплением кислот, карбонильных и полифункциональных соединений.

---

[1] L. Bateman, G. Gee и A. Moris, *Discuss. Faraday Soc.*, **10**, 250 (1951).

[2] L. Bateman, *Quart. Rev.*, **3**, 1 (1949)

Из возможных продуктов жидкофазного окисления воздухом ненасыщенных соединений большой интерес вызывают ненасыщенные и насыщенные спирты и окислы, которые являются ценным сырьём в ряде химических трансформаций.

Цель настоящей работы показать некоторые закономерности процесса жидкофазного окисления ненасыщенных углеводородов, продовимого в присутствии сложных эфиров борной кислоты при изменении дебита воздуха, температуры и времени продувания. В качестве модельных соединений были использованы н-октен-1, C_{10}—C_{14} α-олефины, метил-, этил-, пропил- и бутилолеат, стирол, α-метилстирол, α-пинен, Δ^3-р-ментен, циклохексен, терпинолен и др. с чистотой выше 98% определенной газохроматографическим способом.

ЭКСПЕРИМЕНТАЛЬНАЯ ЧАСТЬ

Эксперименты проводились в периодически действующем стеклянном барботажном реакторе с диаметром 30 мм и высотой 220 мм[3,4]. Полученные до и после подходящей обработки горячей водой оксидаты были подвергнуты полному групповофункциональному анализу [5]. Отдельно были реализованы опыты для определения гидроперекисей и содержание окиси углерода в газе после выхода из реактора. В некоторых случаях использованы физические методы анализа (колонная, тонкослоевая и газовая хроматография [6], ядерный магнитный резонанс, инфракрасная спектроскопия и др.

Условия окисления были: температура 50—170°, время продувания 1—9 часов, дебит воздуха 5—40 л/ч и концентрация сложного эфира бора 5% относительно борной кислоты.

ОБСУЖДЕНИЕ РЕЗУЛЬТАТОВ

Исследования хода гидроксильного числа (Гч) показали, что после 5% нельзя достигнуть его дальнейшее повышение, напротив, стоймость его понижается. Обыкновенно при этой концентрации достигается максимум и в селективности относительно гидрооксисоединений [3,4]. При этом в зависимости от своей каталитической активности сложные эфиры бора образуют ряд: 3-н-пропил-, 3-н-бутил-, 3-i-пропил-, 3-i-бутилборат и этилборат.

Против ожиданий [7] более эффективными оказались нормальные бораты, а не изобораты.

Если для линейных олефинов и циклогексенана составить отношения между максимально достигнутыми стоймостями селективности относительно гидрооксисоединений, то получится: 3-н-пропилборат: 3-i-пропилборат: 3-i-бутилборат = 1,000:0,897:0,821.

---

[3] D. Dimitrov, V. Angelov и A. Badev, *Rev. Chim.* (*Bucureşti*), **23**, 576 (1972).

[4] D. Dimitrov, V. Angelov, A. Badev и V. Badeva, *Rev. Chim.* (*Bucureşti*), **24**, 95 (1973).

[5] M. Guglielmo, ,,Micrometodi per l'identificazione di sostanze organiche'', Rieti, Tip. Nobili, 1963.

[6] М. Видергауз, «Газовая хроматография как метод исследования нефти», Изд. Наука, Москва, 1973.

[7] А. Башкиров, П. Шимон, Compt. rend. AN SSSR, *128*, 1175 (1959).

Интересно однако проследить изменение индукционного фактора $I = \frac{CO_2}{O_2}$ т.е. отношение между объемом выделившейся двуокиси углерода и поглощенным кислородом для каждого из трех добавок в отдельности. Он характеризирует протекающиее сопряженно с окислением декарбоксилирование. Стоймость «I» растет со временем, особенно заметно это в присутствии изоборатов. После шестичасового окисления, отношение между выше упомянутыми веществами уже имеет вид: нПБ:иПБ:иББ = = 0,656:0,960:1,000. Замечателен в этом процессе более маленький или более большой прыжок в положительном направлении после четвертого часа (рис. 1). Внесение изоборатов в реакционную зону связано еще и с необходимостью достигнуть более высокую концентрацию гидроперекисей 4-5%. За исключением стирола и α-метилстирола у всех остальных олефинов полученные кривые проходят через два четко выраженных максимума. Для всех соединений в качестве каталитической добавки был использован 3-н-пропилборат.

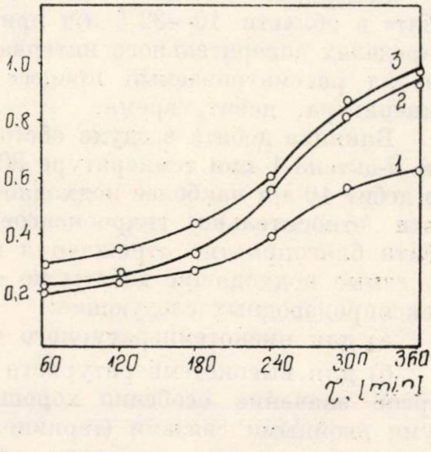

Рис. 1. — Изменение индукционного фактора «I» при окислении н-тридецена и добавлении сложного эфира бора в количестве 5 вес. % относительно H_3BO_3.
1 — нПБ, 2—i ПБ, 3—i ББ

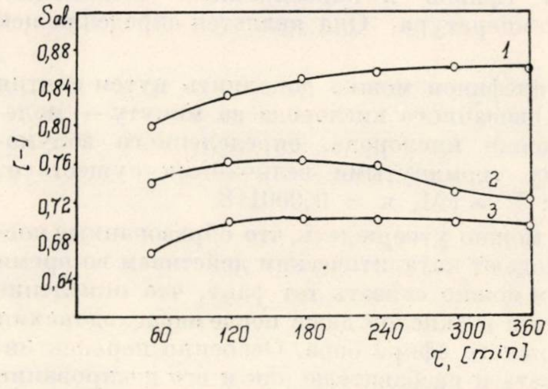

Рис. 2. — Исследование каталитической эффективности следующих борных катализаторов: нПБ, iПБ, iББ при окислении н-тридецена-1 (T = 140°, B = 25 л/ч и τ=6ч) по отношению селективности процесса относительно гидроксисоединений.
1—нПБ, 2 — iПБ, 3 — iББ.

Revue Roumaine de Chimie, 20, 9–10, 1319–1328 (1975)

На примере н-додецена-1 было подробно изучено окисление α-олефинов и было установлено, что при 140° и дебит воздуха 25 л/ч двойные связи расходуются главным образом на эпоксиды. Одновременно с ними получается и высокий выход одновалентных ненасыщенных спиртов (рис. 2). Умеренное повышение дебита воздуха и температуры (до определенного предела) содействует получению насыщенных соединений, но при этом замечается и известное ускорение окислительно-полимеризационных процессов. Методом наименьших квадратов вычислены максимальные расходы н-додецена-1 при разных температурах в исследованной области. На основании этого была определена и энергия активации по Арениусу — 55,8 кдж/моль. В ходе этих исследований установлено, что экспериментальная кривая «максимальное гидроксильное число — дебит» в области 10—32,5 л/ч при температуре 140° польностью лежит в пределах доверительного интервала, а в зависимости от степени влияния на рассматриваемый процесс изученные факторы образуют ряд: температура, дебит, время.

Влияние дебита воздуха обстоятельно было исследовано при окислении н-октена-1 при температуре 80° (рис. 3). Результаты показывают, что дебит 10 л/ч наиболее подходящий для достижения высокой селективности относительно гидрооксисоединений — 0,78. Высокие значения дебита благоприятно отражаются на расход двойных связей. Найдено, что самые подходящие дебиты по отношению к накоплению гидроокси- и оксипроизводных следующие:

а) для низкотемпературного окисления 10—15 л/ч

б) для высокотемпературного окисления 25—27,5 л/ч

Первое значение особенно хорошо потверждается для соединений с двумя двойными связами (терпинолен). Дебиты выше 15 л/ч ускоряют накопление кислот, сложных эфиров и карбонильных соединений. Почти аналогично влияет и температура. Она является определяющей и при других олефинах.

Характеристику высших олефинов можно дополнить путем снятия зависимости «процент сумарно связанного кислорода за минуту — молекулярный вес» на базе поглощения кислорода, определенного волумометрично. Найдено, что между упомянутыми величинами существует строгая линейная зависимость: $P = кM$, $к = 0{,}000118$.

Основываясь на эту связь можно утверждать, что образованные после преэтерификации бораты обладают каталитическим действием во время окислительного процесса. С этим можно связать тот факт, что окисление протекает направленно до спиртов и окислов даже после израсходования взятого в малом количестве сложного эфира бора. Особенно перспективным оказалось прибавление бората к разбавителю как и его дозирование в ходе процесса со скоростью, соответствующей накоплению окислов. Найболее подходящие в этом отношении системы: сложный эфир бора-ацетон и сложный эфир бора-нитробензол, при чем замечается и известное ингибирование термоокислительной полимеризации.

Очень интересно проводить окислительный процесс при температурах ниже 100°. Для метилолеата (модель) за время с 90—180 ^{той} минуты окисления на основании средней скорости накопления кислородосодержащих функциональных групп было найдено следующее (рис. 4):

а) до 90° группы сложных эфиров накопляются с постоянной скоростью

б) влияние температуры на расход двойных связей наиболее сильно выше 80°.

в) окислы накопляются с меньшей скоростью по сравнению со сложными эфирами, но с большей скоростью по сравнению с кислотами.

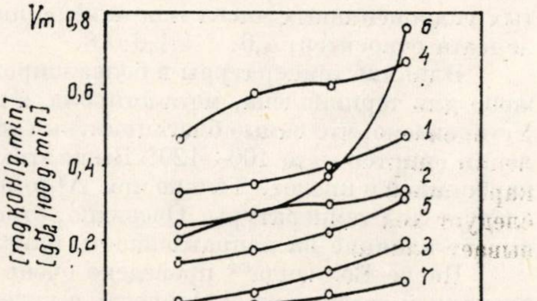

Рис. 3. — Средняя скорость накопления кислородосодержащих функциональных групп за время от начала процесса до конца первого часа при объекте н-октен-1 выраженная функцией дебита воздуха при 80°. Кр. 1, 2, 3, 4, 5, 7 — кислоты до гидролиза, оксидата, окислы, кислоты после гидролиза, спирты, эфиры и карбонилы. 6 — расход двойных связей.

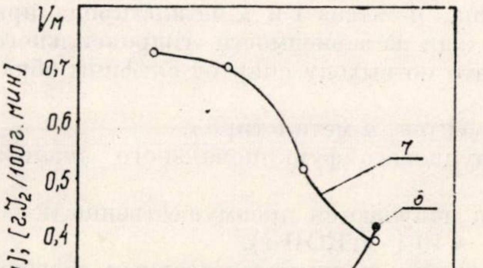

Рис. 4. — Средняя скорость накопления функциональных групп „V_m", соответственно расход двойных связей от температуры при окислении метилолеата в присутствии три-н-пропилбората.

Кривые: 1, 2, 3, 4, 5 — карбоксильные, эфирные, гидроксильные, окисные и карбонильные группы. Кр. 6—расход двойных связей. Кр. 7 — суммарная скорость накопления функциональных групп.

г) температуры 90 и 100° смещают максимум в ходе кривых Гч в интервале первого часа. При тех же температурах резко уменьшается выход карбонильных соединений.

Сопоставление кинетических данных, также как и хода кривых в интервале 90—80°, потверждает гипотезу, что совершается переход от одного механизма протекания окислительного процесса к другому. При наиболее благоприятном режиме низкотемпературного окисления, окисляемость метилолеата сравнивали с той же этил-, пропил- и бутилолеатом. Установлено, что длина эфирного остатка связанного молекулей олеиновой кислоты имеет решающее значение для накопления ряда продуктов в оксидате. С наибольшей скоростью окислы и годрооксисоединения сбразуются при метилолеате и его надо предпочесть при получении аналога касторового масла. В зависимости от сложного эфира бора можно реализировать, направление реакции до епоксидов и спиртов (нПБ, нББ) и главным образом до эпоксидов (іПБ, ЭБ). Максимальные значения достигнутых гидроксильных чисел при окислении метил-, этил-, пропил-, и бутилолеата относятся: 4,0: 1,4:1,0:0,8.

Влияние температуры в более широких границах (70—120°) прослежено для терпинолена, метилстирола, α-пинена, Δ^3-р-ментена (рис. 5—8). Установлено, что самые благоприятные температуры по отношению накопления спиртов—это 100—120°. Выше этих температур благоприятен выход карбонилей и кислот. Только при Δ^3-р-ментене ход гидроксильного числа следует ход температуры. Очевидно, строение окисляемых олефинов оказывает влияние на направленность окислительного процесса.

После Болланда[8,9] проведено очень мало экспериментов по отношению связи «реакционная скорость в условиях жидкофазного окисления—строение окисляемого ненасыщенного соединения». Данные, полученные в присутствий сложного эфира бора, в настоящее время отсутствуют. Наиболее полное сопоставление в этом вопросе можно сделать на основе циклогексена, Δ^3-р-ментена, терпинолена, н-октена-1 и α-метилстирола при дебите 10 л/ч и температуре 70°. Исходя из зависимости «гидроксильного числа-время» (рис. 7) установлено, что по выходу спиртов олефины образуют ряд:

циклогексен, терпинолен, Δ^3-р-ментен, α-метилстирол.

Если сравнить результаты группового функционального анализа можно констатировать следующее:

а) при окислении циклогексена получаются преимущественно ненасыщенные спирты (Гч = 84,7 а Окч = 10,1 мгКОН/г).

б) при тех же условиях из н-октена-1 получаются главным образом олефиновые окислы и очень мало ненасыщенных спиртов (Окч = 99,1 и Гч = 36,7 мгКОН/г).

в) наивысшая селективность относительно гидрооксисоединении в зоне оптимума наблюдается при окислении циклогексена 0,75; затем следует: н-октен-1 0,74; α-метилстирол 0,68; Δ^3-р-ментен 0,53 и терпинолен 0,51.

г) самое высокое карбонильное число (220 мгКОН/г) получается при окислении сопряженных олефинов, вследствии неустоичивости спирта, который изомеризирует еще в момент его получения. За ними следуют: терпинолен 81,1, Δ^3-р-ментен 39,0, циклогексен 29,6 и н-октен-1 15,1 мгКОН/г.

д)в наибольшем количестве окислы накопляются при сопряженных олефинах, (80—104 мгКОН/г), за ними следуют линейные олефины 20,4—64,2 мгКОН/г, в то время как циклоолефины близки по стоимостям (20,4—64,2 мгКОН/г).

---

[8] I. Bolland, *Quart. Rev.*, **8**, 147 (1954).

[9] I. Bolland, G. Gee, *Trans. Faraday Soc.*, **42**, 236, 244 (1946).

е) по глубине окисления олефины сбразуют ряд: сопряженные, циклоолефины и линейные олефины.

ж) наивысшая стоймость индукционного фактора наблюдается при терпинолене и стироле (0,22—0,30), следует Δ^3-р-ментен 0,182, н-октен—1 0,129, в то время как при циклогексене не наблюдаются протекание сопряженное с окислением декарбоксилирования.

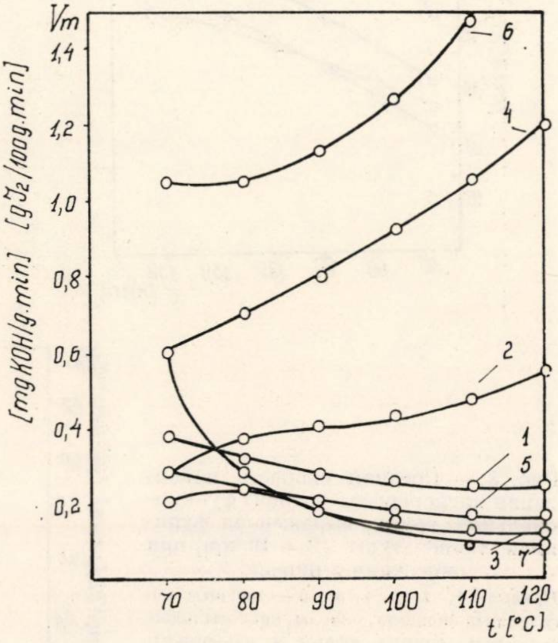

Рис. 5. — Средняя скорость накопления кислородосодержащих функциональных групп, выраженная функцией температуры при дебите 10 л/ч при окислении терпинолена (Означения кривых как на рис. 3).

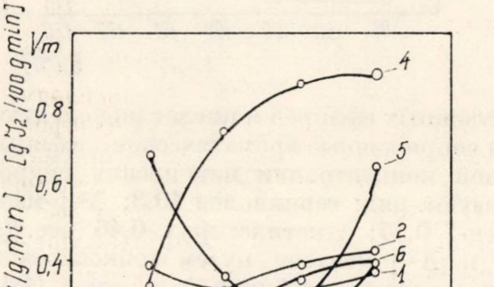

Рис. 6. — Средняя скорость накопления кислородосодержащих функциональных групп, выраженная функцией температуры при дебите воздуха 10 л/ч при окислении Δ^3-р-ментене (Означения кривых как на рис. 3).

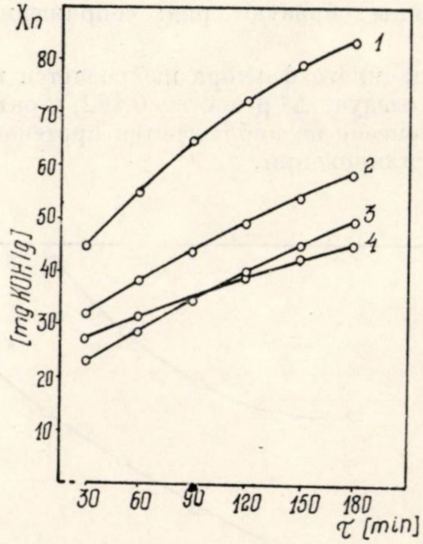

Рис. 7.— Изменение гидроксильного числа, выраженное функцией времени при окислении олефинов воздухом в присутствии три-н-пропилбората (70°,10 л/ч)

Кривые: 1, 2, 3, 4 — циклогексен, терпинолен, Δ^3-р-ментен и α-метилстирол.

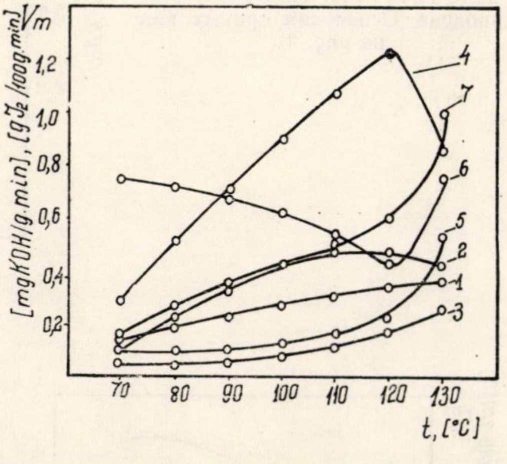

Рис. 8. — Средняя скорость накопления кислородосодержащих функциональных групп, выраженная функцией температуры (В = 10 л/ч) при окислении α-пинена.

Кривые: 1, 2, 3, 4, 5, 6 — кислоты до гидролиза оксидата, окислы, кислоты после гидролиза, спирты, сфиры и карбонилы; 7 - расход двойных связей.

з) по отношению накопления сложных эффиров и кислот ряд следующий: циклены, линейные олефины и сопряженные ароматические олефины.

и) по отношению максимальной концентрации накопления гидроперекиси, изученные олефины образуют ряд: терпинолен 10,3; Δ^3-р-ментен 4,13; циклогексен 1,6; н-октен-1 0,57; α-метилстирол 0,46 вес.%.

При α-пинене, терпинолене и Δ^3-р-ментене путем тонкослоевой хроматографии на окись алюминия в системах: эфир нефти:бензол (1:1) и бензол: этанол(98:2) или чистый бензол из оксидатов разделены и идентифицированы ряд терпеновых спиртов, карбонильных соединений и окислов [10]. Путем газовой хроматографии доказано, что наиболее широко представлены соединения с эмпирической формулой $C_{10}H_{16}O$ и $C_{10}H_{14}O$. Так в оксидатах α-пинена преобладают, в зависимости от условии, пиненовый окись, вербенол и вербенон, при окислении α-метилстирола и стирола — соответствующая окись, тропенал и фенилацетальдегид, для терпинолена основные продукты — это пиперитенол, соответствующая моноокись и пиперитенон.

---

[10] S. Hermanek, V. Schwarz, Z. Cekan, *Pharmazie*, *16*, 566 (1961).

[11] Д. Димитров, В. Ангелов, А. Бадев, Авт. св. НРБ, № 21561, 21818 (1973).

Если сопоставить окисление терпинолена и α-пинена в интервале 70—130° с дебитом 10 л/ч (рис. 5 и 8) в присутствии три-н-пропилбората можно дополнить еще следующее:

а) при 120° оба соединения дают высокий выход гидрооксисоединений.

б) температуры ниже 100° благоприятствуют в одинаковой степени накоплению карбонилей.

в) при температурах выше 130° активируются окислительнополимеризационные процессы и достигнутая селективность—очень низкая.

Так как некоторые олефины (циклогексен, стирол и др.) сравнительно легко окисляются, то сопоставление скорости поглощения кислорода и образования гидроперекисе показывает, что при цикленах и сопряженных олефинах количество гидроперекисей значительно меньше чем количество поглощенного кислорода т.е. они не единственные первичные продукты. Кинетические исследования для этих олефинов показывают, что в некоторых случаях количество перекисей на много больше количества гидроперекисей [7]. Вот почему на основе проведенных экспериментов в зависимости от строения олефинов установлены следующие два направления в механизме процесса:

а) Линейные олефины:

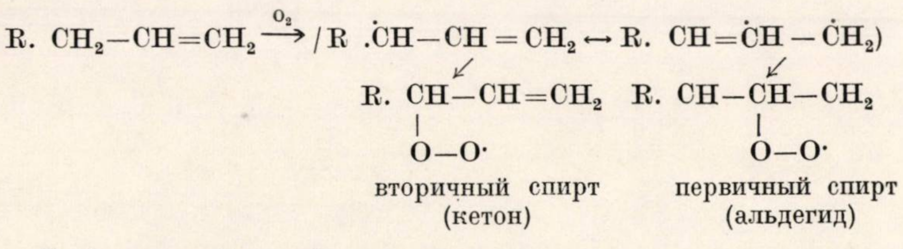

б) Сопряженные олефины и циклены

I. $RH + O_2 \rightarrow R^{\cdot} + HO_2^{\cdot}$

$R^{\cdot} + O_2 \rightarrow RO_2^{\cdot}$

II.

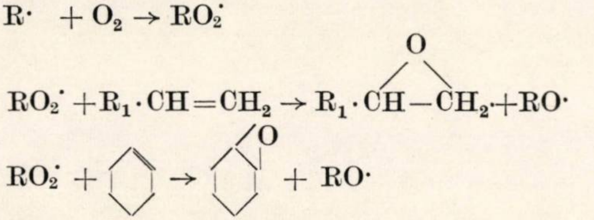

$RO_2^{\cdot} + R_1 \cdot CH{=}CH_2 \rightarrow R_1 \cdot \overset{O}{CH{-}CH_2} + RO^{\cdot}$

III. $RO^{\cdot} + RO^{\cdot} \rightarrow ROOR$

(реакция III представлена и в первом случае)

Влияние сложного эфира бора на селективность процесса относительно гидрооксисоединений объясняется ассоциацией гидроперекисей и сложного эфира бора с образованием донорно-акцепторного комплекса. Особено благоприятно для этой ассоциации начало процесса, когда количество гидроперекисей самое большое. При этом образующийся из бората алкоксильный радикал является инициатором цепной реакции.

Образование таких ассоциатов потверждается ИК-спектрами (наличием сильного валентного колебания в интервале 3300—3600 см$^{-1}$)[4,11—14]. Аналогичен случай и при окислении некоторых сопряженных олефинов и цикленов. Так как главные первичные продукты перикисей, наряду с выше упомянутым процессом, образуются и ассоциаты между перекисными радикалами и сложным эфиром бора. Образование таких ассоциатов установлено и при окисление стирола (ИК-спектры 3150—3400 см$^{-1}$ оксидата, полученного в условиях самого высокого перекисного числа). Эти сведения потверждаются анализами ядерного магнитного резонанса. Здесь надо отметить, что при некоторых олефинах (метилстиролы) в условиях самого высокого гидроксильного числа отсутствует колебание, характерное для протона свободных ОН-групп. Вероятно последние блокированны путем комплексобразования со сложным эфиром бора.

Кратко роль сложного эфира бора состоит в следующем:

а) благоприятствует образованию окислов и спиртов

б) содействует распаду гидроперекисей

в) ограничивает скорость протекающего сопряженно с окислением декарбоксилирования

г) отчасти оказывает ингибирующее влияние на полимеризационные процессы

---

[12] F. Mayo, *J. Amer. Chem. Soc.*, **80**, 2497 (1958).

[13] G. Russell, *J. Amer. Chem. Soc.*, **78**, 1017 (1956).

[14] J. Howard, K. Ingold, *Canad. J. Chem.*, **42**, 1044 (1964).

Revue Roumaine de Chimie, **20**, *9–10*, 1329–1334 (1975)

SUR LES RÉACTIONS ENTRE LES IONS CH_3^+ ET CD_2H^+ AVEC CH_4 ET CD_4

EMILIA CONSTANTIN* et JEAN CH. ABBE**

* Faculté de Physique, Cluj-Napoca, Roumanie, str. M. Kogălniceanu

** Centre de Recherches Nucléaires, Laboratoire de Chimie Nucléaire, 67, Strasbourg-3, France

Reçu le 3 août 1973
Complété le 6 février 1975

On donne les résultats concernant les réactions ion-molécule dans les systèmes $CH_3^+(CH_3D)+CH_4$et CD_2H^+ $(CHD_3, CH_2D_2)+CD_4$. La nature des ions secondaires, les sections efficaces fonction de l'énergie des ions primaires et les mécanismes de réaction sont discutés.

INTRODUCTION

L'étude des réactions ion-molécule dans le méthane protoné et les méthanes deutériés par la technique de spectrométrie de masse « à haute pression » a été l'objet de nombreux travaux.[1–6] Ces expériences ont été reprises en utilisant un spectromètre de masse à deux étages de type longitudinal.[7] Ce mémoire présente les résultats obtenus avec des ions CH_3^+ (CH_3D)* et $CD_2H^+(CH_2D_2, CHD_3)$, d'énergie comprise entre 2 et 25 eV, avec CH_4 et CD_4.

RÉSULTATS

Les spectres de masse montrent la formation des ions $C_2X_5^+$, $C_2X_3^+$, $C_2X_2^+(X = H, D)$:

1. $CH_3^+ + CH_4$ . . . . . . $C_2H_5^+$ $C_2H_3^+$ $C_2H_2^+$
2. $CD_2H^+(CHD_3)+CD_4$ . . $C_2D_5^+$ $C_2D_3^+$ $C_2D_2^+$
   $C_2D_4H^+$ $C_2D_2H^+$ C_2DH^+
3. $CD_2H^+(CH_2D_2) + CD_4$ . . $C_2D_5^+$ $C_2D_3^+$ $C_2D_2^+$
   $C_2D_4H^+$ $C_2D_2H^+$ C_2DH^+

---

* $CH_3(CH_3D)$ désigne l'ion CH_3^+ formé à partir de CH_3D.

[1] F. H. Field, J. L. Franklin et M.S.B. Munson, *J. Amer. Chem. Soc.*, **85**, 3575 (1963).

[2] S. Wexler et N. Jesse, *J. Amer. Chem. Soc.*, **84**, 3425 (1962).

[3] R. Fuchs, *Z. Naturforsch.*, **16 a**, 1026 (1961).

[4] G.A.W. Derwisch, A. Galli, A. Giardini-Guidini et G. G. Volpi, *J. Chem. Phys.*, **40**, 5 (1964).

[5] D. O. Stevenson, *J. Phys. Chem.*, **61**, 1453 (1957).

[6] L. Matus, I. Opauszky, A.J. Masson, K. Birkinshaw et M. J. Henchman, *Trans. Faraday, Soc.*, **44**, 146 (1967).

[7] J.P.L'Hote, J. Ch. Abbe, J. M. Paulus et R. Igerseim, *Int. J. Mass. Spectrom. Ion Phys.*, **7**, 309 (1971).

Les variations des sections efficaces relatives $\sigma(\sigma = kI_{sec}/I_t,\ I_t = \Sigma I_{sec}$ I_{sec} = le courant ionique pour un certain type d'ion secondaire) de formation des ions secondaires $C_2X_5^+$, $C_2X_3^+$, $C_2X_2^+$ en fonction de l'énergie des ions primaires sur les figures 1 et 2 sont représentées (pour les systèmes 1 et 2). L'examen de ces courbes montre que lorsque l'énergie de l'ion incident augmente :

— $\sigma(C_2X_5^+)$ décroît rapidement ;

— $\sigma(C_2X_3^+)$ croît rapidement et passe par un maximum ;

— $\sigma(C_2X_2^+)$ croît d'abord lentement puis plus rapidement pour atteindre une valeur maximale.

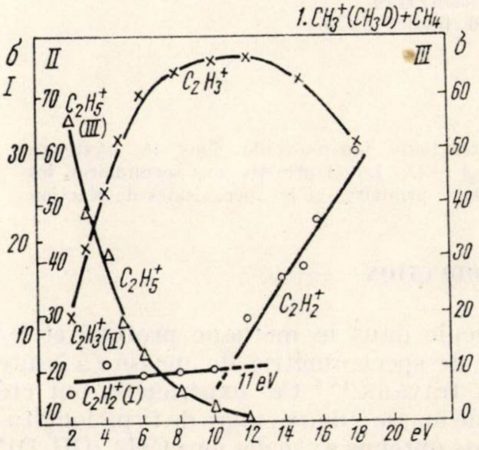

Fig. 1. — Variation des sections efficaces relatives des ions secondaires formés au cours de l'interaction entre CH_3^+ et CH_4 en fonction de l'énergie de CH_3^+.

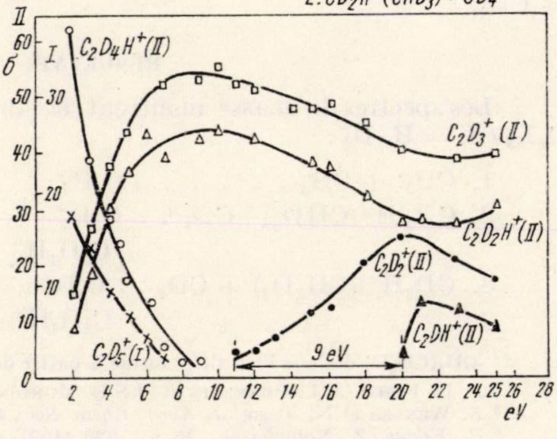

Fig. 2. — Variation des sections efficaces relatives des ions secondaires formés à partir de $CD_2H^+(CHD_3)$ et CD_4 en fonction de l'énergie.

DISCUSSION ET INTERPRÉTATION DES RÉSULTATS

Les différentes réactions possibles de formation des ions secondaires au cours de l'interaction de CH_3^+ avec CH_4 sont indiquées dans le tableau 1.

L'examen de bilans énergétiques montre que la formation de $C_2H_5^+$ est exothermique (réaction 1), alors que celle de $C_2H_3^+$ et $C_2H_2^+$ est endothermique (réactions 2–5). Ces différences suggèrent que $C_2X_5^+$ se forme aisément avec des ions primaires de faibles énergies et qu'une augmentation de l'énergie du projectile entraînera une décomposition rapide de l'ion formé et donc une diminution de σ ($C_2X_5^+$). Par contre, la formation de $C_2X_3^+$ et $C_2X_2^+$ nécessite une contribution de l'énergie cinétique du projectile. L'énergie cinétique maximale convertie en énergie interne est donnée par la formule :

Tableau 1

Valeurs de l'énergie pour différentes réactions entre CH_3^+ et CH_4

N°	Réaction	E	
		kcal	eV
1	$CH_3^+ + CH_4 \ldots C_2H_5^+ + H_2$	− 23,1	−1
2	$C_2H_3^+ + H_2 + 2H$	130,9	5,66
3	$C_2H_3^+ + 2H_2$	26,9	1,15
4	$C_2H_2^+ + H_2 + H$	126,9	5,49
5	$C_2H_2^+ + 3H$	230,9	10

$$E_L = E_R \frac{M_n + M_i}{M_n}$$

où E_L représente l'énergie du projectile, E_R l'énergie convertie, M_n et M_i la masse de la molécule et de l'ion.

La valeur 11 eV pour laquelle $\sigma(C_2H_2^+)$ croît brusquement (fig. 1) est égale à E_L calculé pour la réaction 4 (tableau 1), ainsi que l'expérience est en bon accord avec la valeur prévue. La même conclusion résulte pour les ions $C_2H_3^+$: $E_L = 2{,}2$ eV (système 1).

En ce qui concerne les réactions de CD_2H^+ (fig. 2) avec CD_4 le seuil d'apparition pour $C_2X_2^+$ doit être $E_L = 10{,}2$ eV pour la réaction 4 et 18,5 eV pour la réaction 5 (tableau 1). Il ressort de la figure 2 qu'il est difficile de définir le seuil d'apparition des ions $C_2X_2^+$. En même temps il faut noter que dans le système 3 on a trouvé des ions $C_2D_2^+$ jusqu'à $E_L = 8$eV et des ions C_2DH^+ jusqu'à $E_L = 17$ eV. La différence correspondant aux plus faibles intensités mesurées est donc 9 eV comme dans le système 2 (fig. 2).

L'apparition des ions $C_2X_2^+$ au-dessous de l'énergie relative $E_R = 5{,}49$ eV peut s'expliquer par la présence des ions primaires excités : CH_3^+ (CH_3D) et CD_2H^+ (CH_2D_2).

EFFETS ISOTOPIQUES

Pour rechercher les effets isotopiques accompagnant la formation des ions secondaires, les rapports *f* et *A* définis ci-après ont été calculés :

$$f = \frac{C_2D_5^+}{C_2D_4H^+}$$

$$A = D/H = \frac{5C_2D_5^+ + 4C_2D_4H^+}{C_2D_4H^+}$$

« *A* » représente un facteur dont la valeur indique la concentration en deutérium[8].

Dans le tableau 2 sont données les valeurs expérimentales f_e et A_e, ainsi que les valeurs calculées dans l'hypothèse que les ions CD_2H^+ et les molécules forment des complexes $C_2D_6H^+$ excités qui se dissocient en $C_2D_5^+$ et $C_2HD_4^+$:

Tableau 2

Valeurs de f et A pour les ions $C_2X_5^+$ formés à partir de CD_2H^+ et CD_4

Energie eV	f_e		A_e	
	système		système	
	2	3	2	3
2	0,27	0,36	5,37	5,79
3	0,33	0,34	5,66	5,69
4	0,35	0,35	5,76	5,78
5	0,35	0,28	5,76	5,41
6	0,35	0,20	5,70	5,00

$f_s = 0,4$ $A_s = 6$

$f_s^i = 0,56$ $A_s^i = 6,82$

$$\begin{array}{lll} CD_2H^+ + CD_4 \ldots (C_2D_6H^+)^- & \ldots & C_2D_5^+ \\ & \ldots & C_2D_4H^+ \end{array}$$

Deux valeurs f_s^i, A_s^i et f_s, A_s sont ainsi obtenues suivant que la différence des énergies de liaisons C—H et C—D est prise en considération ou non. Dans le premier cas (f_s^i, A_s^i) la rupture de D_2 est affectée du coefficient 1 et celle de DH du coefficient $\sqrt{2}$ [9,10]

Le tableau 2 montre que les valeurs f_e et A_e sont inférieures à f_s, f_s^i et A_s, A_s^i. La formation de $C_2D_5^+$ apparaît donc défavorisée par rapport à celle de $C_2D_4H^+$ et ce résultat conduit à la conclusion que la réaction s'opère par l'intermédiaire d'un complexe actif très faible ou bien par un processus direct. Les valeurs de *A* montrant des concentrations différentes en deutérium pour $C_2X_5^+$ et $C_2D_4H^+$ sont également en faveur de cette hypothèse. Ces résultats sont en bon accord avec ceux obtenus par Herman [11] : la distribution angulaire des ions $C_2H_5^+$ et $C_2D_5^+$ formés dans les réactions des CH_3^+ et CD_3^+ avec CH_4 et CD_4 montre qu'il y a une grande probabilité pour le mécanisme direct (domaine d'énergie : 1 – 10 eV).

---

[8] V. Mercea et E. Constantin « Sesiunea Univ. Babes-Bolyai Cluj », 26 — 27 V 1969.

[9] H. Von Koch, *Arkiv Fysik*, **28**, 559 (1965).

[10] A. B. Callear et R. J. Cvetanovic, *J. Chem. Phys.*, **24**, 873 (1956).

Le tableau 3 contient les rapports f, A pour les ions $C_2X_3^+$; f_s représente la valeur statistique de f pendant que A_s la valeur de D/H pour le système ion primaire + molécule. L'examen de ces valeurs aboutit à la même conclusion : les réactions donnant naissance aux ions $C_2X_3^+$ augmentent la concentration en deutérium dans les fragments neutres. La

Tableau 3

Valeurs de f et A pour les ions secondaires $C_2X_3^+$ formés à partir de CD_2H^+ et CD_4

Energie eV	f_e		A_e	
	système		système	
	2	3	2	3
2	1,66	1,28	7	5,85
3	1,40	1,43	6,15	6,30
4	1,27	1,32	5,80	5,60
5	1,22	1,23	5,67	5,70
6	1,22	1,14	5,70	5,50
7	1,26	1,18	5,80	5,56
8	1,24	1,16	5,72	5,45
9	1,23	1,18	5,62	5,63
10	1,21	1,18	5,60	5,70
12	1,21	1,22	5,60	5,70
15	1,25	1,29	5,85	5,88
17	1,30	1,33	5,90	6,00
20	1,40	1,34	6,20	6,00
25	1,33	1,62	6,00	6,90

$f_s = 1{,}33$ $A_s = 6$

$$f = \frac{C_2\,D_3^+}{C_2\,D_2\,H^+}$$

$$A = D/H = \frac{3C_2D_3^+ + 2C_2D_2H^+}{C_2D_2H^+}$$

concentration des ions $C_2X_3^+$ décroît par rapport au système ion primaire + molécule, excepté 2 et 3eV quand les ions secondaires ont une concentration plus grande que celle du système primaire.

---

[11] Z. Herman, P. Hierl, A. Lee et R. Wolfgang, *J. Chem. Phys.*, **51**, 454 (1969).

CONCLUSIONS

Les résultats obtenus montrent la formation des ions secondaires $C_2X_5^+$, $C_2X_3^+$, $C_2X_2^+$.

Le calcul des effets isotopiques indique une diminution de la concentration en deutérium des ions $C_2X_3^+$ et $C_2X_5^+$ par rapport au système ion primaire + molécule.

En ce qui concerne le mécanisme de réaction il paraît qu'il y a une préférence pour un transfert direct ou pour un complexe avec une vie plus courte que la période de la rotation moléculaire.

REMERCIEMENTS. Les auteurs remercient M. R. Keller pour sa contribution technique à la réalisation de ce travail.

Revue Roumaine de Chimie, **20**, *9–10*, 1335–1340 (1975)

LE SYSTÈME R/S–UN POINT DE VUE MATHÉMATIQUE. I

L'ÉNONCÉ INVARIANTIF DES CONCEPTS DE LA STÉRÉOCHIMIE

IOAN MOŢOC

Département de Chimie Physique Université de Timişoara, Roumanie

Reçu le 25 mai 1974

L'ouvrage propose une manière de traiter axiomatiquement les concepts de la stéréochimie. Les considérations développées sont situées dans le cadre du système R/S de Cahn, Ingold et Prelog. L'invariance des concepts de la stéréochimie à certains groupes de rotation suggère la manière de les traiter mathématiquement. La conséquence immédiate en est la possibilité de construire des algorithmes représentables sur l'ordinateur.

1. INTRODUCTION

On n'insistera pas sur les significations de certains concepts stéréochimiques. Ils sont élégamment traités dans différents livres. [1–3] Dans cet ouvrage, ainsi que dans nos prochains ouvrages, ces concepts sont supposés connus.

Compte tenu de l'ample diffusion [4,5] du système R/S, on supposera connu son contenu. Le système de nomenclature R/S a été présenté par ses auteurs Cahn, Inglod et Prelog d'une manière claire dans plusieurs ouvrages. [6–9]

2. L'AXIOME DE LA FORMULATION INVARIANTIVE

Toute discussion sur la stéréochimie emploie des termes d'un système de nomenclature. Nos ouvrages, où l'on essaie la présentation d'un point de vue mathématique sur les concepts de la stéréochimie, vont considérer les

---

[1] N. L. Allinger et E. L. Eliel, « Topics in Stereochemistry », Ier vol. 1, Interscience—Wiley, New York, 1969.

[2] K. Mislow, « Introduction to Stereochemistry », Benjamin, New York, 1965.

[3] E. L. Eliel, « Stereochemistry of Carbon Compounds », McGraw-Hill, New York, 1962.

[4] IUPAC 1957, Definitive Rules, A72 ; *J. Amer. Chem. Soc.*, **82**, 5545 (1960) ; Special Publication, No. 14, The Chemical Society, London (1960), p. 48.

[5] IUPAC ; Tentative Rules for the Nomenclature of Organic Chemistry, *J. Org. Chem.*, **35**, 2849 (1970).

[6] R. S. Cahn et C. K. Ingold, *J. Chem. Soc.*, **1951**, 612.

[7] R. S. Cahn, C. K. Ingold et V. Prelog, *Experientia*, **12**, 81 (1956).

[8] R. S. Cahn, *J. Chem. Educ.*, **41**, 116, erratum 508 (1964).

[9] R. S. Cahn, C. K. Ingold et V. Prelog, *Angew. Chem. Internat. Edn.*, **5**, 385 (1966).

concepts stéréochimiques analysés comme définis dans le cadre du système de nomenclature R/S.

On a choisi ce contexte parce qu'il présente plusieurs avantages de principe :

i) une large possibilité d'application *.

ii) le repère est la molécule analysée.

iii) la manière d'établir l'appartenance d'une caractéristique de la molécule à un certain concept stéréochimique (par exemple, les règles de chiralité par rapport auxquelles la configuration — l'une des caractéristiques de la molécule — est R ou S — le concept stéréochimique).

Le thème de cet ouvrage (et de certains ouvrages prochains) est l'essai de construire un formalisme algébrique dont les objets mathématiques permettent la description simple et *satisfaisante* des molécules organiques (avec des possibilités de généralisation aussi pour les molécules inorganiques).

Le but d'un tel formalisme est l'élaboration des algorithmes représentables sur l'ordinateur, ce qui a été déjà réalisé, [10] l'ordinateur arrivant à identifier, à l'aide d'un programme FORTRAN, la configuration d'un atome de carbone asymétrique.

Le formalisme qui sera développé a pour base :

AXIOME. Dans le cadre du système R/S, les concepts de la stéréochimie sont invariantifs à certains groupes de rotations.

OBSERVATIONS

1) Ce qu'on a affirmé ci-dessus ne nécessite pas une motivation quelconque, constituant l'axiome explicite de la théorie.

Cet axiome peut être illustré. Soit le cas de l'atome de carbone asymétrique :

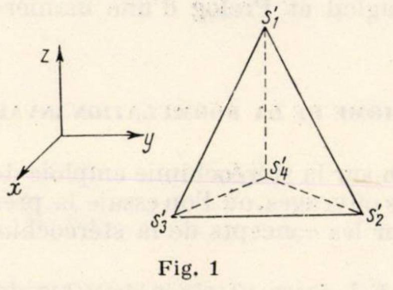

Fig. 1

où $s'_{i=1\div 4}$ sont des ligands. Les ligands sont complètement caractérisés en donnant la séquence :

$$s'_1 \succ s'_2 \succ s'_3 \succ s'_4 \tag{1}$$

($\succ$: précède)

---

* Les causes qui déterminent la large application de système R/S sont discutées, du point de vue algébrique, dans notre ouvrage.

[10] I. Moţoc, *Theor. Chim. Acta* (pris en considération).

Comme l'on sait bien, la molécule de la figure 1 a la configuration R. Conformément aux règles de chiralité, les molécules de la figure 2 ont, elles aussi, la configuration R.

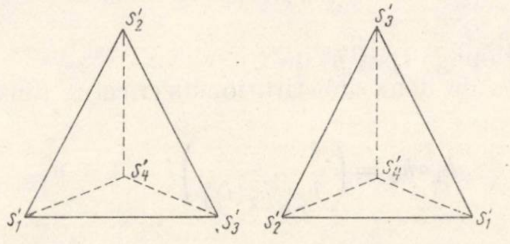

Fig. 2

Donc, la configuration n'a pas changé par rapport au groupe cyclique ponctuel C_{3x}.

Le sens de l'axiome devient clair par la spécification : du point de vue de la décision d'un observateur sur le nom de la configuration, les deux affirmations suivantes sont équivalentes :

1) le modèle moléculaire est fixe et l'observateur est mobile, ce dernier observant les ligands l'un après l'autre.

2) l'observateur est fixe et le modèle moléculaire est mobile de sorte que, par rotation, il lui présente les ligands l'un après l'autre.

L'axiome suggère les conséquences suivantes, auxquelles il est nécessaire de vérifier la théorie.

A) que les relations et les équations de la théorie ne modifient pas leur signification par rapport au groupe de rotations respectif ;

B) que les objets mathématiques de la théorie décrivent la distribution spatiale des ligands.

Nous observons ici que (A) impose naturellement (B). (B) recommande comme une possibilité commode et générale l'utilisation des *substitutions*.

Les objets mathématiques de la théorie seront donc les substitutions. Par conséquent, l'axiome accepté, ainsi que la description de la molécule à l'aide des substitutions fixent le cadre général du formalisme.

2.1. SUR LES SUBSTITUTIONS

Étant donnée une multitude $I \subset \mathbb{N}$ ($\mathbb{N}$ étant le signifiant des nombres naturel), l'application de *I en I* s'appelle *substitution*. Donc :

$$h : I \to I \tag{2}$$

Si I a n éléments, h est noté ainsi :

$$h = \begin{pmatrix} 1 & 2 & 3 \ldots & n \\ i_1 & i_2 & i_3 \ldots & i_n \end{pmatrix} \tag{3}$$

où $i_1, i_2, \ldots, i_n$ sont les n premiers nombres naturels écrits dans un certain ordre.

On a encore l'habitude de noter :

$$h = \begin{pmatrix} i \\ h\,(i) \end{pmatrix},\ i = 1 \div n \tag{4}$$

où $h(i)$ est l'image (par h) de i.

La composition, $\circ$, de deux substitutions s'effectue ainsi :

$$h_1 \circ h_2 = \begin{pmatrix} i \\ h_2\,[(h_1(i)] \end{pmatrix} i = 1 \div n \tag{5}$$

Nous observons que (5) a lieu si :

$$h_1, h_2 : I \to I \tag{6}$$

Ainsi, parce que, en général,

$$h_1 \circ h_2 \neq h_2 \circ h_1$$

l'ordre des «facteurs» n'est pas indifférent.

On peut démontrer que le groupoïde $(H = \{h\}, \circ)$ a une structure de groupe.

2.2. LA SIGNIFICATION GÉOMÉTRIQUE DES SUBSTITUTIONS

La signification géométrique des substitutions sera illustrée par l'exemple suivant :

si :

$$h_1 = \begin{pmatrix} 1 & 2 & 3 & 4 \\ 1 & 2 & 3 & 4 \end{pmatrix}$$

correspond à la situation :

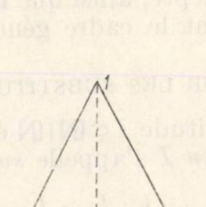

Fig. 3

alors

$$h_2 = \begin{pmatrix} 1 & 2 & 3 & 4 \\ 2 & 3 & 1 & 4 \end{pmatrix},\ \text{respectivement},\ h_3 = \begin{pmatrix} 1 & 2 & 3 & 4 \\ 4 & 1 & 2 & 3 \end{pmatrix}$$

correspondront à :

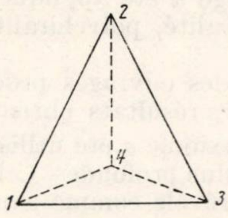

respectivement à

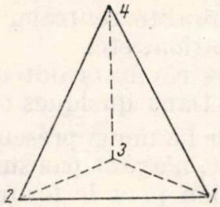

Fig. 4

C'est-à-dire, h_2 est une rotation du modèle de la figure 3, et h_3 est le reflet du modèle de la figure 3.

Les substitutions obtenues par des permutations circulaires d'une substitution donnée (par exemple h_1) représentent des rotations.

Les autres substitutions s'appellent transposées, et elles ont la signification de reflets.

Nous croyons que la possibilité d'utiliser les substitutions dans le but déclaré est devenue claire.

2.3. LA MANIÈRE DE CONSTRUCTION DES SUBSTITUTIONS

La construction des substitutions qui doit servir le but proposé est basée sur l'observation suivante : les ligands d'un modèle moléculaire sont complètement caractérisés par la spécification du rang*, conformément aux règles de succession du système R/S.

Du fait que la multitude M, dont les éléments sont les rangs des ligands, et la multitude P des positions des ligands dans le modèle moléculaire vérifient la relation :

$$\operatorname{Card} M = \operatorname{Card} P = n \qquad (8$$

on considérera comme leur représentant la multitude :

$$I = \{1, 2, \ldots, n\}$$

Dans ce cas, pour

$$h = \begin{pmatrix} i \\ h\,(i) \end{pmatrix}, \; i = 1 \div 4$$

on trouve l'interprétation suivante :

$h(i)$ est le ligand (caractérisé par le rang) qui se trouve en position i.

Évidemment, on suppose une certaine indexation numérique (implication de la relation (8) en P).

Il en résulte que les substitutions vérifient la condition 2—(B).

---

* Pour la définition axiomatique, basée sur les treillis, voir.[11]

[11] I. Moţoc, *Rev. Roumaine Chim.*, **20**, 1341 (1975).

3. DISCUSSION

i) Le formalisme développé dans cet ouvrage a été appliqué au cas de la chiralité centrale, prochiralité, pseudo- chiralité, polychiralité, à la conformation, etc.

Les résultats obtenus seront exposés dans des ouvrages prochains.*

ii) Dans quelques ouvrages antérieurs[12-15] les résultats obtenus sont basés sur l'axiome présenté dans cet ouvrage. L'axiome a été utilisé intuitivement, n'ayant pas suivi ses conséquences les plus profondes. Cela justifie l'option pour le formalisme matriciel, qui se révèle comme ayant une mise en pratique relativement limitée.

C'est une joie pour moi de remercier, à nouveau, monsieur le Professeur Zeno Simon pour les conseils et les encouragements que j'ai reçus de lui, au cours de ce travail

---

* Les ouvrages seront publiés dans cette revue.

[12] F. Kerek et I. Moțoc, *Rev. Roumaine Chim.*, **18**, 285 (1973).

[13] I. Moțoc et F. Kerek, *Rev. Roumaine Chim.*, **18**, 291 (1973).

[14] F. Kerek et I. Moțoc, *Rev. Roumaine Chim.*, **18**, 655 (1973).

[15] I. Moțoc et F. Kerek, *Rev. Roumaine Chim.*, **18**, 1419 (1973).

Revue Roumaine de Chimie, **20**, *9–10*, 1341–1343 (1975)

LE SYSTÈME R/S – UN POINT DE VUE MATHÉMATIQUE. II*

DÉFINITION ALGÉBRIQUE POUR LE RANG D'UN LIGAND DANS UNE SÉQUENCE

IOAN MOŢOC
Département de Chimie Physique
Université de Timişoara,
1900 Timişoara

Reçu le 25 mai 1974

La conséquence des résultats obtenus dans des ouvrages antérieurs c'est la possibilité d'une définition algébrique pour le rang d'un ligand quelconque, d'une séquence donnée. Interprétant la séquence des ligands comme un treillis, cet ouvrage propose une définition abstraite pour le rang d'un ligand.

1. INTRODUCTION

Soit une multitude A, sur laquelle on définit deux lois de composition**. $\triangle$ et $\triangledown$, ainsi :

$$\triangle,\ \triangledown : A \times A \to A$$

et $a \triangle b = \inf(a, b)$ — c'est-à-dire, la marge inférieure de a et b en A. $a \triangledown b = \sup\,(a, b)$ — c'est-à-dire, la marge supérieure de a et b en A.

Comme on sait,[1-3] si $\triangle$ et $\triangledown$ ont aussi les propriétés :

$$a \triangledown b = b \triangledown a\,;\ a \triangledown (b \triangledown c) = (a \triangledown b) \triangledown c\,;\ a \triangledown (a \triangle b) = a\,;$$

$$a \triangle b = b \triangle a\,;\ a \triangle (b \triangle c) = (a \triangle b) \triangle c\,;\ a \triangle (a \triangledown b) = a\,;$$

$$a \triangle a = a\,;\ a \triangledown a = a\,;\ \text{où } a, b, c \in A, \text{ alors } A \text{ est un treillis.}$$

On représente graphiquement les treillis finis à l'aide des diagrammes Haase.

Soit S' l'espace fondamental des ligands[4].

2. Chaque sous-multitude finie $S'_j \in S'$ est un treillis. De plus, S'_j sont des treillis complets. La première partie de l'affirmation ci-dessus est immédiatement démontrée par l'application du théorème [4] : « S'_j est ordonnée, inductive, filtrante à droite et à gauche. Plus encore, les majorants sont maximums, et les minimisants sont minimums ».

---

* Ière partie, I. Moţoc, *Rev. Roumaine Chim.*, **20**, 1335 (1975).
** On suit la notation de 1.

[1] A. Kaufmann et M. Precigout, « Cours de mathématiques nouvelles pour le recyclage des ingénieurs et cadres », Dunod, Paris, 1966.
[2] V. Glivenko, « Théorie générale de structures », Hermann, Paris, 1938.
[3] M. J. Weiss, « Higher Algebra for Undergraduates », Wiley, New York, 1949.
[4] I. Moţoc, *Rev. Roumaine Chim.*, **20**, 1335 (1975).

On vérifie immédiatement la deuxième partie de l'affirmation, en appliquant la définition du treillis complet : S'_j est un treillis complet si chaque $A \subset S'_j$ a sup et inf en S'_j. S' n'est pas complet parce qu'il n'a pas de marge supérieure.

Les diagrammes Haase attachés aux treillis S'_j ont la forme :

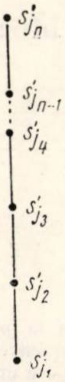

$$\text{où } s'_{j1}, s'_{j_2}, \ldots, s'_{jn} \in S'_j \qquad \text{(I)}$$

$$\text{Card } S'_j = n$$

Observation. S'_j sont les sous-treillis du treillis S'.

Ensuite, nous nous occuperons des treillis S'_j, ceux-ci étant importants dans les applications.

3. S'_j sont des treillis distributifs (donc, aussi modulaires). Un treillis est distributif s'il vérifie l'une des conditions équivalentes :

$$a \bigtriangledown (b \bigtriangleup c) = (a \bigtriangledown b) \ \bigtriangleup (a \bigtriangledown c) \qquad (1)$$

$$a \bigtriangleup (b \bigtriangledown c) = (a \bigtriangleup b) \ \bigtriangledown (a \bigtriangleup c) \qquad (2)$$

Soit $s'_{j_p}, s'_{j_q}, s'_{j_e} \in S'_j$. Conformément au diagramme de la figure 1 tous les éléments $s' \in S'_j$ sont comparables. Soit la situation suivante (pour fixer la discussion) :

$$s'_{j_p} \succ s'_{j_q} \succ s'_{jl}.$$

Nous avons :

$$s'_{j_p} \bigtriangledown (s'_{j_q} \bigtriangleup s'_{j_e}) = s'_{j_p} \bigtriangledown s'_{j_e} = s'_{j_p} \qquad \text{(1 a)}$$

$$(s'_{j_p} \bigtriangledown s'_{j_q}) \bigtriangleup (s'_{j_p} \bigtriangledown s'_{j_e}) = s'_{j_p} \bigtriangleup s'_{j_p} = s'_{j_p}. \qquad \text{(1b)}$$

De (1a) et (1b) on déduit que S'_j, $\forall j$, vérifie la condition (1). S'_j est un treillis distributif.

4. S'_j n'est pas un treillis complémentaire. Cette chose est évidente, parce que seulement s'_{j_n} a de complément :

$$s'_{j_n} \bigtriangledown s'_{j_1} = s'_{j_n}; \, s'_{j_n} \Delta s'_{j_1} = s'_{j_1} \qquad (2)$$

s'_{j_n} et s'_{j_1} sont respectivement l'élément universel et l'élément nul du treillis S'_j.

Les éléments s'_j, $1<p<n$, ne vérifient pas la relation (2).

Observation. Sur un treillis complémentaire on ne pourrait pas définir un système du type R/S de Cahn, Ingold et Prelog.

5. Soit le treillis S'(ou, pour des cas particuliers, le treillis S'_j correspondant). On notera :

$$A = \triangle(S' \times S') = \{(s'_p \triangle s'_q) / s'_p ,\ s'_q \in S'\} \tag{3a}$$

$$B = \nabla(S' \times S') = \{(s'_p \nabla s'_q) / s'_p ,\ s'_q \in S'\} \tag{3b}$$

On établira une définition pour le rang des ligands $s'_p \in S'$ à un centre asymétrique (avec du carbone).

Pour m, n, p, q différents entre eux, on définit ainsi le rang r du ligand $s'(r_{s'})$:

$$\left.\begin{aligned} r_{\nabla(B\times B)} &= 1 \\ r_{\triangle(B\times B)} &= 2 \\ r_{\nabla\, A\times A)} &= 3 \\ r_{\triangle(A\times A)} &= 4 \end{aligned}\right\} \tag{4}$$

$$\left.\begin{aligned} \text{où}\quad \nabla(B\times B) &= \{(s'_m \nabla s'_n)\ \nabla(s'_p \nabla s'_q)\} \\ \triangle(B\times B) &= \{(s'_m \nabla s'_n)\ \triangle(s'_p \nabla s'_q)\} \\ \nabla(A\times A) &= \{(s'_m \triangle s'_n)\ \nabla(s'_p \triangle s'_q)\} \\ \triangle(A\times A) &= \{(s'_m \triangle s'_n)\ \triangle(s'_p \triangle s'_q)\} \end{aligned}\right\} \tag{5}$$

Observation. « En traduisant » en langage courant le sens des opérateurs ∇ et $\triangle$, on constate facilement que la définition abstraite du rang d'un ligand — dans une séquence donnée de quatre membres — fournie par les relations (5) coïncide avec la définition intuitive du rang d'un ligand.

CONCLUSIONS

1) On a mis en évidence la structure de treillis de l'espace fondamental des ligands, S'.

2) Il est devenu possible de formuler une définition abstraite pour le rang d'un ligand $s' \in S'$.

C'est une joie pour moi de remercier, à nouveau, monsieur le Professeur Zeno Simon pour les conseils et les encouragements prodigués au cours de ce travail.

Revue Roumaine de Chimie, **20**, *9–10*, 1341–1343 (1975)

Les éléments a, $1-a$ [illegible] ne vérifient pas la relation (3).

Observation. Sur un treillis complémentaire on ne pourrait pas définir un système du type [illegible] de Cahn, Ingold et Prelog.

4. Soit le treillis $\mathscr{S}(n)$, pour des cas particuliers, le treillis $\mathscr{R}$ correspond à [illegible]. On a alors :

$$A(\nabla \mathscr{S}' \times \mathscr{S}') = [illegible] \tag{3a}$$

$$B = \nabla(\mathscr{S}' \times \mathscr{S}') = [illegible] \tag{3b}$$

On établit une définition pour le rang des ligands $\varphi \in \mathscr{S}$ à un centre asymétrique [illegible].

Pour α, β, γ différents entre eux, on définit ainsi le rang r du ligand $\varphi(1_\alpha)$:

$$
(4)\qquad
\begin{aligned}
&r_{1,\alpha} = 1\\
&r_{2,\alpha} = 2\\
&r_{3,\alpha} = 3\\
&r_{4,\alpha} = 4
\end{aligned}
$$

où $\nabla(\mathscr{B} \times \mathscr{B}) = [illegible]$

$\Delta(\mathscr{B} \times \mathscr{B}) = [illegible]$

(5)

$\nabla(A \times A) = [illegible]$

$\Delta(A \times A) = [illegible]$

Observation. « En traduisant » en langage courant le sens des opérations ∇ et Δ, on constate facilement que la définition abstraite du rang d'un ligand — dans une séquence donnée de quatre membres — fournie par les relations (5) coïncide avec la définition intuitive du rang d'un ligand.

CONCLUSIONS

1) On a mis en évidence la structure de treillis de l'espace fondamental des ligands, $\mathscr{S}$.

2) Il est devenu possible de formuler une définition abstraite pour le rang d'un ligand $\varphi \in \mathscr{S}$.

C'est une joie pour moi de remercier à nouveau monsieur le professeur [illegible] pour les conseils et les encouragements prodigués au cours de ce travail.

Revue Roumaine de Chimie, **20**, *9–10*, 1345–1354 (1975)

STUDIES OF THE JOSHI EFFECT IN PURE ARGON IN A DEGASED QUARTZ OZONIZER : INFLUENCE OF THE HEAT TREATMENT

JAGDISH PRASHAD

Chemistry Department, Meerut College, Meerut—250001, India

Received December 17, 1973

A large negative Joshi effect ($-\Delta i$) corresponding to practically a total suppression of the current (i) instantaneously on irradiation (visible) from a 200 watt bulb was observed in spectroscopically pure argon (4.5 mm, 25°) in a thoroughly degased (1000°) quartz ozonizer. $-\Delta i$ increased progressively from nil to over 96% current suppression by giving a continuous exposure to discharge (aging) at the incipient, threshold potential (V_m). A further prolonged aging, however, decreased the effect markedly. The comparative influence of aging in dark and under irradiation on the Joshi effect is studied, as well as the influence of heat treatment. The results are interpreted by considering the freezing in of the high temperature imperfections due to rapid air quenching and the adsorption of the gas under electric field on the active centres developed during heat treatment.

INTRODUCTION

An apparent anti-aging effect of the rest period, particularly after aging with enhanced frequencies of the applied field has been observed.[1] Increase of temperature may hasten the effect of rest period,[2] especially in the initial stages;[1] this might occur by deconditioning, presumably by desorption of the postulated boundary-layer formed under discharge. The influence of the heat treatment was, therefore, studied in some detail.

EXPERIMENTAL

The quartz ozonizer, $Q_6(A)$ was degased at 250°, 500°, 1000°, 500° and 250° for 10 hours at 10^{-5}mm. Spectroscopically pure argon was led through a series of traps L_1-L_4, cooled by liquid air and was admitted into $Q_6(A)$ at 4.5 mm, 25° (*cf.* Fig.1). It was then sealed off.

After the attainment of over 96% negative Joshi effect by continuous aging (*vide* Fig.4), the effect ($-\%\Delta i$) decreased progressively and rapidly due to aging until the system became almost insensitive to light within a moderate period. After resting for one week, the following series of operations (hereafter called "heat treatment" for short) were carried out.

The ozonizer was heated to, and kept for 4 hours at 150°, allowed to cool at 30° and the $(V-i)D, L$ characteristic was taken. This was repeated at temperatures of 200°, 400°, 500°, 600° (*cf.* Figs. 2 and 3).

In the next set of experiments, after giving heat treatment at 600°, $Q_6(A)$ was aged in dark near Vm (0.39 kV). Besides $(V-i)\ D, L$ characteristics, current wave forms were also recorded (cf. Fig.5).

---

[1] J. Prashad, *Rev. Roumaine Chim.*, **6**, 1074 (1973).

[2] J. Prasad, *J. Hindi Sci. Acad.*, **15**, 79 (1972).

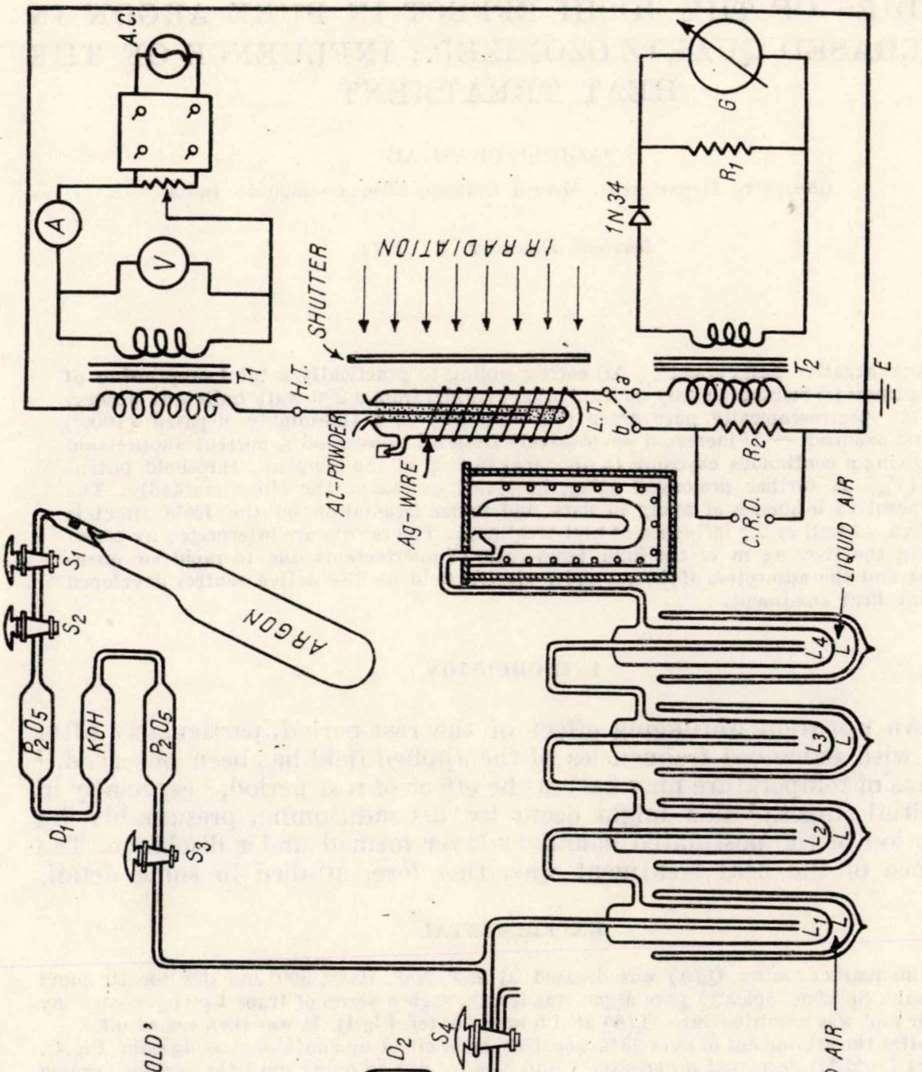
A.C.
G
R$_1$
1N 34
A
V
IR RADIATION
SHUTTER
H.T.
T$_1$
T$_2$
E
AL-POWDER
Ag-WIRE
L.T.
a
b
R$_2$
C.R.O.
LIQUID AIR
S$_1$
S$_2$
ARGON
L$_4$
L$_3$
L$_2$
L$_1$
L
P$_2$O$_5$
KOH
P$_2$O$_5$
D$_1$
S$_3$
TO LEYBOLD
D$_2$
S$_4$
KOH
P$_2$O$_5$
P$_2$O$_5$
LIQUID AIR

Fig. 1, — Degasing o Q_6 for Δi in A.

Heat treatment at 600° was then given to Q_6(A) and intermittently aged (aged for 5 – 10 minutes and rested for a similar period, reaged and so on) at Vm in dark. The $(V - i)_{D,L}$ data (*cf.* Fig.6) indicated that the discharge current under irradiation (iL) attained a steady value after a few minutes of aging and remained practically unaffected by further aging at Vm. The ozonizer, after the heat treatment at about 400°, was aged at the threshold potential, $Vm(L)$ (0.39 kV), under irradiation (as determined by the sudden increase of the corresponding discharge current (i_L), which, however, was less in magnitude than that in dark corresponding to $-\Delta i$). It was next kept exposed to light through a water cell acting as heat filter. At a series of intervals, the light was screened off momentarily and the current in dark (i_D) recorded (*vide* Figs. 7 and 8).

$(V - i)_{D,L}$ characteristics were recorded after 56, 63 and 69 weeks' rest of the ozonizer. After 69 week rest, three sleeves of bright copper wire (intersleeve distance = 10 mm) were wound tightly on the side-tube of the quartz ozonizer. Influence of aging at $2 - 8 \times V_m$, 50 c/s was studied for 272 hours.

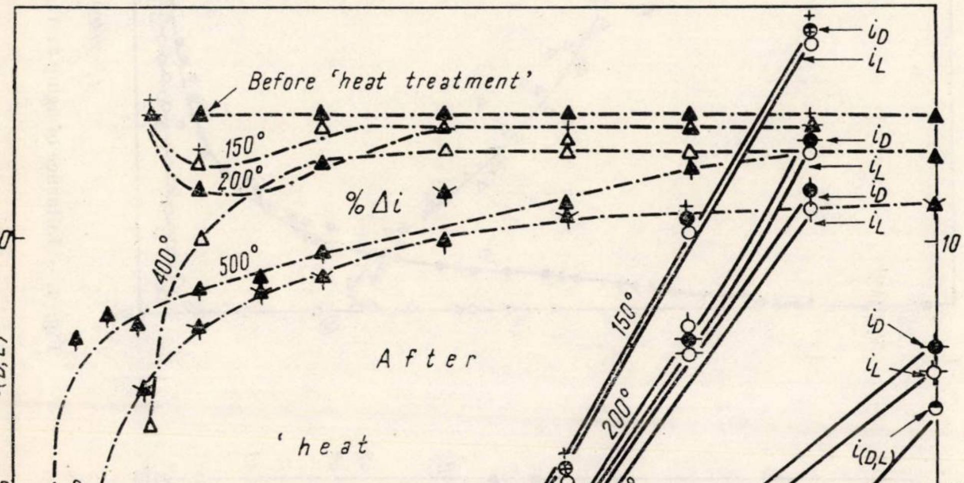

Fig. 2. – Influence of heat treatment on the Joshi effect in Q_6 (*A*).

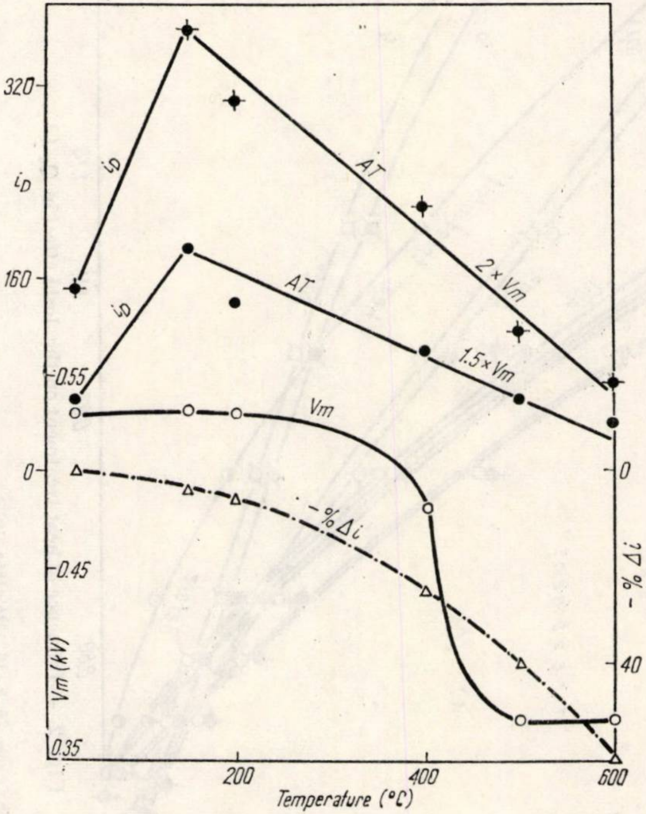

Fig. 3. — Influence of temperature of heat treatment on V_m, i_D and Δi in $Q_6(A)$.

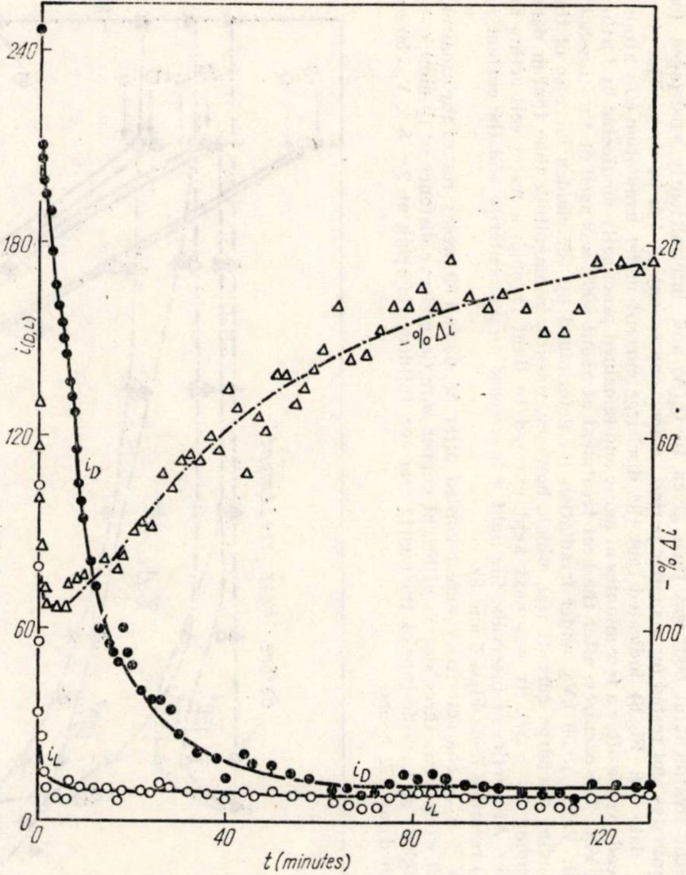

Fig. 4. — Influence of aging at $V_m(D)$ on the Joshi effect in Q_6 (A)

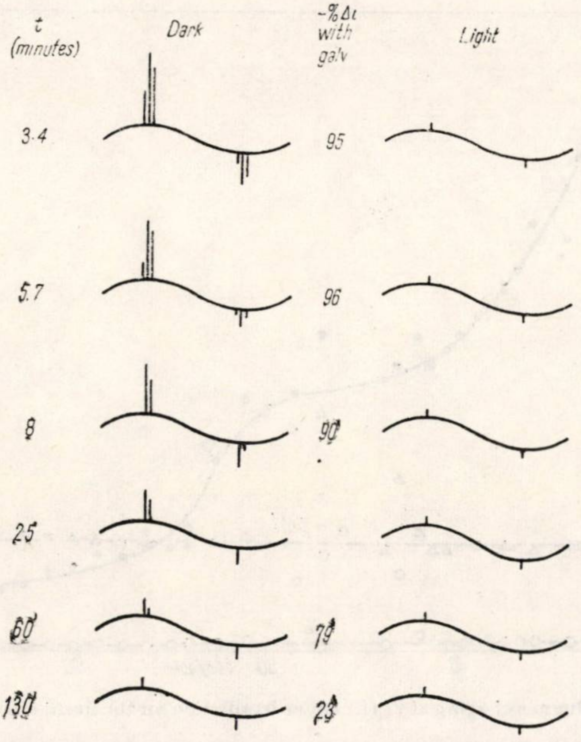

Fig. 5. — Wave form of i during aging at $V_m(D)$.

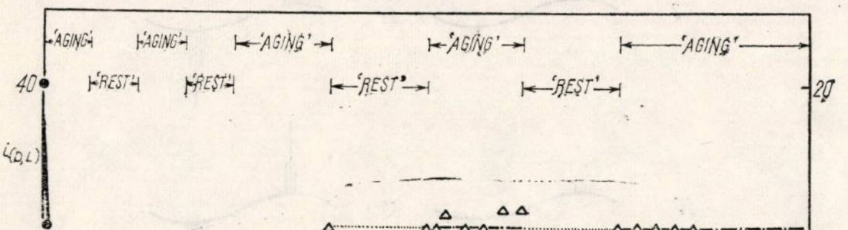

Fig. 6.— Influence of intermittent aging at V_m and rest on the Joshi effect in Q_6 (*A*).

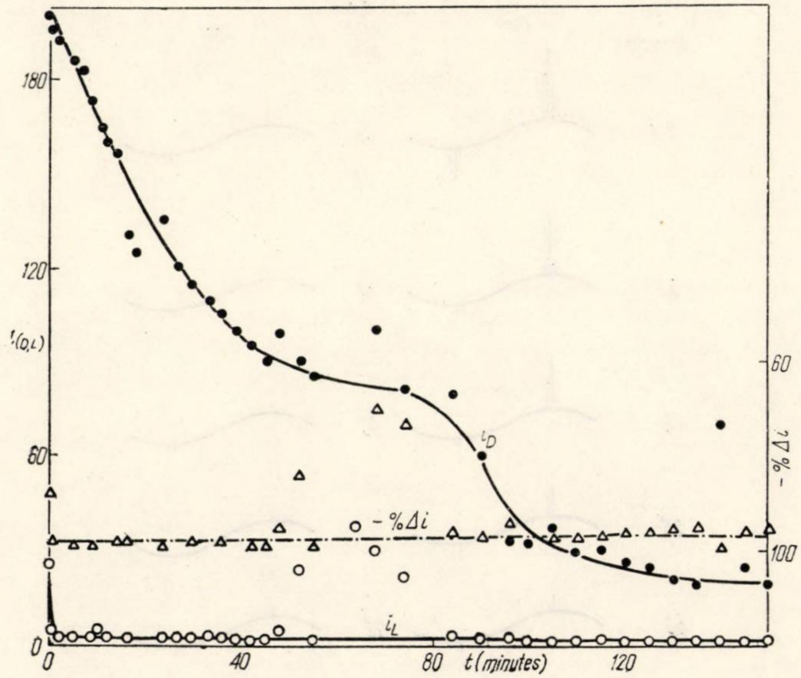

Fig. 7. — Influence of aging at $V_m(L)$ under irradiation on the Joshi effect in Q_6 (A).

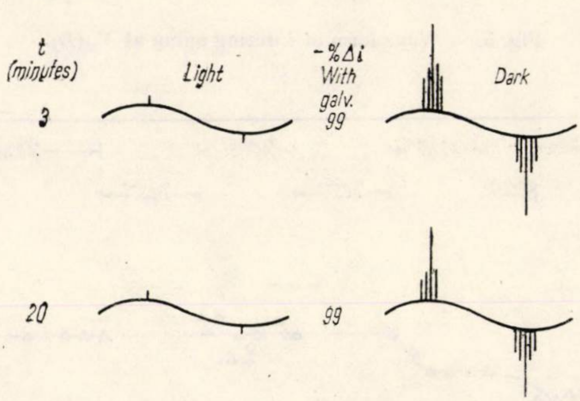
t (minutes)
Light
- % Δi With galv.
Dark
3
99
20
99
57
98
78
96
148
96

Fig. 8. — Wave form of i during aging at $V_m(L)$ under irradiation.

RESULTS AND DISCUSSION

Development of — $\triangle i$ by heat treatment. The temperature dependent properties of glasses vary not only with the chemical composition but also depend on the previous history of the glass.[3] Very slowly cooled glasses exhibit only slight anomalies or none at all; whereas on slow cooling the mutual positions of the particles (atoms, ions or molecules) forming the glass are able to change; on rapid cooling the state of affairs predominating at higher temperatures is to a certain extent frozen[4] and later unable to change further on account of the high viscosity. The freezing usually takes place at a viscosity of about 10^{13} c.g.s. units, but vitreous substances are also known which have already entered into the transformation region at $\eta = 10^{11} - 10^{1.5}$. Rapid quenching causes a freezing in of the high temperature imperfections.[5]

The imperfections or defects include holes or vacant sites, interstitial atoms or ions in a heteropolar lattice with normal position but anomalous charge, or foreign atoms in substitutional or interstitial positions. Such defects deform a region of the lattice and it is the region which should be regarded as the defect.[6] Defect or disorder may be biographical or thermal. Biographical disorder increases progressively with temperature to a maximum. After cooling, the biographical disorder (defect sites) does not recover completely to its previous extent. That is, the defect sites are frozen in. Chemisorption occurs in the region of defect sites.[7]

In an ozonizer, the electrodes being of dielectric nature, develop active centres on the surface under electrical excitation. A strain caused either by continuation of discharge or a total removal of the applied potential, as under rest, or/and any other factor will affect these spots considerably. These centres retain some residual charge after completion of a cycle, the proportion of which is conditioned by their previous history, in charge density in various centres, the expansion of active spots and the maintenance of charge in these spots. This will develop a strain which will be loosened or destrained when allowed to rest or subjected to heat treatment.

The electrical adsorption is chiefly of chemical nature and not due to mechanical driving in of the ions and molecules.[8,9] Even after the heat treatment at 150°, the walls of the ozonizer were not blank. Adsorption of the gas might have taken place before starting the electrical discharge in the system. So, an increase in i after the first heat treatment at 150° was observed (*cf.* Figs. 2 and 3). The decrease of i after further heat treatment at higher temperatures (200—600°) may be due to a pressure reduction of the system by adsorption of argon by the active centres on the container walls,[10] produced as a result of heat treatments at 200–600°.

---

[3] W. HUCKEL, "Structural Chemistry of Inorganic Compounds" Elsevier Publishing Company, New York, 1951.

[4] F. SIMON, *Naturwiss.*, **9**, 244 (1930).

[5] A. JAHODA, *Akad. Wiss. Wien II a*, **135**, 675 (1926).

[6] F. F. VOLKENSTEIN, *Zhur. fiz. Khim.*, **23**, 917 (1949).

[7] H. S. TAYLOR, *Discuss, Faraday Soc.*, **8**, 9 (1950).

[8] R. S. WILLOWS, *Proc. Phys. Soc.*, **28**, 124 (1916).

[9] S. E. HILL, *Proc. Phys. Soc.*, **25**, 35 (1912).

In certain type of systems during aging a moderate heating of the system favoured inception of $-\triangle i$[11]. These systems get also desensitized on long resting. The rest period allows an appreciable residual $-\Delta i$. The magnitude of this residual $-\triangle i$ depends as mentioned above upon the previous history of the system, the nature of the gas-solid interface, pressure of the gas, frequency and potential of a.c. supply and specially the time and manner of aging. Out of these, aging develops a strain which relaxes when allowed to rest.

Influence of aging at $Vm(D)$ in dark. The adsorbed gas at the defect sites acts as an activator. When the electric field is applied, the activator abstracts energy from the applied excitation field, stores this energy in the activator and then releases it partly by photon radiation.[12] When a part of the discharge energy is stored up on the defect sites, the discharge current should decrease and has been observed to be so. The storing up of energy is a time process; so the discharge current decreases for some time and then becomes steady.

The surface compounds formed due to chemical or valency forces are generally more resistant to temperature. But Emmett and Brunauer,[13] Trapnell[14] for nitrogen and Shukla[15] for chlorine have shown that heat of adsorption is of the order of 35, 12 and 20 k. cal per mole, which is a suggestive evidence in favour of chemisorption. Cases are known (specially in certain rare gases and nitrogen) when hours of aging are a pre-requisite for the production of $\pm\triangle i$. It has been observed in certain cases that from the crushed wall material gases are obtained, which is in accord with the above deduction of adsorption under discharge.

The process of adsorption alters the capacitance associated with the container walls and the gas phase; consequently the conductivity is altered. Associated with the instability of the formation of the adsorbed layer, there is intermittent sorption and desorption or /and the production at the surface of the walls, of unstable intermediate products of discharge reaction — all leading to a synchronous time variation in the conductivity. The production of $\triangle i$ is different from that of a change in the magnitude of i_D due to alteration in the capacitance associated with the walls and gas phase. The latter is well a time process whereas the former has been shown to be, from the measurements of time lag on the production of $\triangle i$, apparently almost an instantaneous process.[16,17] The results suggest that the boundary layer, which is a seat of $\triangle i$ in Joshi's theory,[18,19] is not formed intantaneously under discharge; but it may well be a time process. The first increase from 53 to 96 and then the decrease of $-\,\%\triangle i$ to a steady value of about 23 also suggest the formation and eventuous stabilisation of an adsorbed layer (*cf.* Figs. 4 and 5). Under aging, the excited particles may become stable or saturated, i.e., the adsorbed layer is stabilised.[16] This will increase the surface work function and hence further continuation of discharge (aging) will decrease $-\%\triangle i$.

---

[10] B. N. Prasad and V. Venkateshwarlu, *Univ. Rajasthan Studies* (*Phys. Sci.*), **2**, 56 (1953).

[11] B. N. Prasad and R. Vedantum. *Proc. Indian Sci. Cong. Part III, Phys. Sec. Abst.* 30 (1949).

[12] T. J. Gray, "The Defect Solid State", Interscience Publishers, Inc., New York, 1957.

[13] P. H. Emmett and S. Brunauer, *J. Amer. Chem. Soc.*, **56**, 35 (1934).

[14] B. M. W. Trapnell, *Trans. Faraday Soc.*, **48**, 100 (1952).

[15] B. M. Shukla, *J. Sci. Res., B.H.U.*, **5**, 28 (1954 – 55).

[16] S. S. Joshi, *Indian Sci. Cong. Presid. Add. Chem. Sec.* (1943).

[17] S. S. Joshi, *Curr. Sci.*, **13**, 253 (1944).

[18] S. S. Joshi, *Proc. Indian Sci. Cong. Part III, Phys. Sec.* Abst. 26 (1946).

[19] S. S. Joshi, *Curr. Sci.*, **16**, 19 (1947).

Photoelectric emission from the adsorption-like boundary layer is fundamental to the production of $\triangle i$.[18] Its occurrence in the above system, only after aging the ozonizer under discharge for a certain time period suggests, therefore, that the ionic bombardment of an otherwise photoelectrically inactive surface[20] may lead to the formation of the activated boundary layer responsible for the production of $\triangle i$. A specially prolonged aging, however, may lead to stabilisation and hence inactivation.

Influence of intermittent aging. During the first instalment of intermittent aging, i_D decreased to a value very near to that when the current became steady (*cf.* Fig. 6), presumably because its starting value (just after the commencement of aging) was small. Intermittent rest periods of short durations were insufficient to affect the discharge current and the associated relative Joshi effect, owing to the fact that the action of applied electric field on the adsorption of the gas on the walls is very much effective as compared with the rate of the desorption of the gas, during rest period, from the boundary layer formed under discharge.

Influence of aging at $Vm(L)$ under irradiation. The oscillograph revealed, besides the frequency of the a.c. supply, "a large number of higher frequencies of widely varying strengths; they were not transient but repeatable and characteristic constituents of the discharge current".[17,21] Moreover, under irradiation, h. fs. are suppressed and as h. fs. do not contribute much towards $-\triangle i$, their suppression under irradiation should not affect $\triangle i$ during aging under irradiation. As the discharge current under irradiation (i_L) was much smaller than that in dark, aging under irradiation means aging at a lower current value which would decrease the influence of aging— had it been carried out in dark, where the current (i_D) was greater. So the decrease in the rate of the decrease of i was observed as is indicated by the fact that the curve of I_a-t for aging in dark is more steep than the corresponding curve for aging under irradiation (*cf.* Figs. 4 and 7). This means that the rate of adsorption of argon on quartz has decreased due to aging under irradiation; i.e., h. fs. also influence the rate of reaction of the type as adsorption of argon on quartz, though the reaction is mainly due to the fundamental (lower) frequencies. The present investigation shows that during aging under irradiation, there was not much change in the wave form of i (in dark) up to about 76 minutes, except that the heights of some of the longer pulses decreased (*cf.* Fig. 8), further aging affected the number of pulses as well, whereas the pulses (under irradiation) had undergone no appreciable change. This necessitates a modification of the views of Warburg [22,23,24] and Viswanathan [25] regarding the complete ineffectiveness of the higher harmonics to bring about the chemical change.

---

[20] P. Tartakowsky, *Z. Physik*, **58**, 398 (1929).

[21] S. S. Joshi, *Nature*, **154**, 147 (1944).

Influence of aging the side-tube. During the rest period, the adsorbed layer formed under discharge is attenuated. So, the magnitude of the relative Joshi effect ($-\%\triangle i$) decreased from about 96 to 31, 29 and 17 in 56, 63 and 69 weeks rest respectively. During the excitation of the annular space of the ozonizer, a proportion of ions and excited particles might have moved to the side-tube of the ozonizer and deposited there. These have given the positive Joshi effect near V_m beyond which there was no $\pm \triangle i$. The absence of the negative Joshi effect in the side-tube before aging and the observation of an irreversible $-\%\triangle i$ after 1.5 hours aging at $2 \times V_m$ is to be marked. The development of the negative Joshi effect after 124 hours aging at $8 \times V_m$ and its increase with further aging period of 148 hours (from $+ 67$ to $- 100\%$ Δi near V_m) is due to the normal influence of aging in a major excited part of the discharge tube, *viz.*, the annular space.

ACKNOWLEDGEMENT. Grateful thanks are due to Professor S.S.Joshi, Ex-Head, Chemistry Department, Banaras Hindu University for his kind interest, valuable suggestions and providing adequate facilities for the present work.

---

[22] E. Warburg, *Jahrb. Radioakt. Electronic,* **6**, 181 (1909).
[23] E. Warburg, *Z. Tech. Physik.*, **4**, 450 (1923).
[24] E. Warburg, *Ibid.*, **6**, 625 (1925).
[25] K. S. Viswanathan, *Proc. Indian Acad. Sci.*, **27**, 300 (1948).

A. GOSSAUER, "Die Chemie der Pyrrole" (Chimia Pirolilor), Springer, Berlin, Heidelberg, 1974, 433 p.

Over 40 years have elapsed since the appearance of the classical treatise on pyrrole chemistry by H. Fisher and H. Orth. In the meanwhile this class of organic compounds has had a tremendous development. Pyrrole and its derivatives have important utilizations as basic technical products and the natural products are of a great interest. Numerous publications have appeared since then on their synthesis and in particular on their physico-chemical properties. For this reason, the author has decided to change the conception and the division of the book, compared to the known classical treatise. Using over 2,600 bibliographical references from the period 1934 to 1971—1972, the monograph gives an almost exhaustive picture of advances made in the chemistry of pyrrole derivatives except for porphyrins and of related compounds. Particular emphasis has been laid on the synthesis and the use of quantum mechanical calculation and spectroscopic methods in the chemistry of pyrrole.

The first chapter presents the quantum mechanical calculation methods applied to substantiate and interpret the properties of molecules having a pyrrolic ring. The next chapter elaborates on analytical chemical and physical research methods applied to isolate and characterize pyrrole derivatives. Details are provided on colour reactions, on chromatographic methods and on spectroscopic investigations and an impressive amount of processed data are included in tables and largely discussed in the text. The third chapter is devoted to the reactivity of pyrrole derivatives being ordered according to the reaction types. It includes substitution reactions, Diels-Alder reactions, radicalic and carbene-involving reactions, transpositions, hydrogenations, oxidations and the photochemistry of pyrrole compounds. A special chapter deals with the description of pyrrole metallic derivatives and of compounds with other elements. Natural products, which are derivatives of simple pyrroles are examined in a separate chapter which also deals with metabolites of molecules having a pyrrolic ring. Antibiotics with a pyrrolic structure and also halogenated phenyl-substituted derivatives, such as pyrrolenitrine and verrucarine *E* or pyrrole-amide derivatives and prodigiosines have been studied more thoroughly. The discussion on pyrroles contained in superior plants and in human and animal organisms focusses on the importance of porpholbilinogen for diagnostic purposes. Like in the case of other natural substances, reference is made of toxicological and pharmacological studies.

Almost half of the book is devoted to synthetic methods for the preparation and conversion of pyrrole derivatives. The pyrrolic cycle syntheses are ordered according to the manner in which smaller units adhere to each other in the heterocyclic construction. The introduction of various substituents occurs according to the nature of functional groups, which is illustrated by numerous tables. Apart from common examples meant to provide a better understanding of the text, different reactions are described in which pyrrole serves as a raw material for the preparation of other heterocyclic rings (indoles, pyrrolysines, azepines, etc.). A special care has been given to the description of reaction mechanisms.

Researchers involved in the preparatory work relative to the chemistry of pyrroles will find in this book a rigorous systematization of synthetic methods and of techniques for the investigation of their properties. For further details, they can consult the original literature indicated in the text. A rich subject index facilitates the identification of the problem of interest. The work appeals not only to chemists. It could be largely used as an auxiliary material for those dealing with the pharmaceutical aspect of pyrrole derivatives and also for those interested in the study of natural products having an indole structure.

F. Cuiban

S. HOLLY and P. SOHÁR "Absorption spectra in the infrared region. Theoretical and technical introduction", edited by L. Láng and W.H. Prichard, Akademiai Kiadó, Budapest, Hungary, 1975, 183 p.

Infrared spectroscopy is undoubtedly the most powerful physical technique available to chemists for the elucidation of molecular structure and for qualitative and quantitative measurements.

Infrared spectroscopic analyses are generally rapid, nondestructive, simple, reproducible and may be performed upon gaseous, liquid or solid phases.

"Absorption spectra in the infrared region. Theoretical and technical introduction" aims to present the basic concepts, measurements and techniques of infrared spectroscopy.

The introductory chapter is devoted to a comprehensive presentation of the vibrations of molecules and normal frequencies, the symmetry of normal vibrations and their assignment to simple molecules and their experimentally determined frequency values as well as the factors affecting the normal vibrational modes.

The second chapter deals with the infrared absorption bands of individual groups or types of compounds and the corresponding characteristic bond and group frequencies : saturated hydrocarbons, unsaturated hydrocarbons, absorption of the hydroxyl group, bands of nitrogen-hydrogen bonds, effects of association on oxygen-hydrogen and nitrogen-hydrogen stretching bands, carbonyl bands, groups containing nitrogen-oxygen bonds, multiple bond systems, the carbon-nitrogen double bond, characteristic bands of ethers, peroxides, ketals and acetals, sulphur, halogen, silicon, phosphorus and boron compounds, heterocyclic compounds and a table which contains a summary of the characteristics bands of some of the more common inorganic anions.

The last chapter provides a general view of the main features of the infrared spectrometers, principles of operation, the accessories necessary for and the techniques of obtaining an infrared spectrum. In addition, mention is made of instrument calibration and the documentation of spectra.

The book gives, in a particularly condensed mode, the theoretical background for an understanding of infrared spectroscopy, its techniques and applications. It is provided with detailed tables of spectra-structure correlations.

In conclusion, the volume is designed for students, technicians and research workers, as a reference work and as an aid to enable more effective use of infrared spectroscopy in chemistry.

Marina Olteneanu

NOTE POUR LES AUTEURS

La *Revue Roumaine de Chimie* publie des articles en anglais, français, russe, allemand ou espagnol. Les auteurs sont priés d'envoyer des articles, notes, communications et comptes rendus inédits.

Les manuscrits seront dactylographiés à deux intervalles. Les tableaux seront dactylographiés sur des feuilles séparées, de même que la légende des figures. Les diagrammes seront tracés à l'encre de Chine sur papier calque. Les tableaux et les figures seront numérotés par des chiffres arabes, en nombre strictement nécessaire. Prière de ne pas inscrire les mêmes données dans les tableaux et les figures. Les formules chimiques seront incluses dans le texte ; en outre, elles seront transcrites sur des feuilles séparées. Les auteurs sont priés d'indiquer les caractères italiques (en soulignant les lettres au crayon), ainsi que tout autre caractère spécial. L'ordre des références bibliographiques sera celui de leur mention dans le texte ; le nom de l'auteur sera précédé de l'initiale du prénom ; les publications périodiques seront présentées suivant les prescriptions internationales. Les références seront ajoutées à la fin de l'article ; elles paraîtront comme des notes, au bas de la page. Le texte sera précédé d'un résumé comprenant 15 lignes au maximum.

L'entière responsabilité du contenu des articles appartient aux auteurs. On publie des articles dus aux collaborateurs roumains ou étrangers.

PRINTED IN ROMANIA

TRAVAUX PARUS AUX ÉDITIONS DE L'ACADÉMIE DE LA RÉPUBLIQUE SOCIALISTE DE ROUMANIE

I. ZUGRĂVESCU et MAGDA PETROVEANU, **Chimia *N*-Ilidelor** (La chimie des N-Ylures), 1974, 347p., 19 lei.

MARGARETA AVRAM, **Antidăunători** (Pesticides), 1974, 494 p., 41 lei.

CR. SIMIONESCU, VIORICA RUSAN et N. POPA, **Chimia algelor marine** (La Chimie des algues marines), 1974, 211 p., 18 lei.

CRISTOFOR SIMIONESCU, MARGARETA GRIGORAŞ, AGATA CERNĂTESCU-ASANDEI et GHEORGHE ROZMARIN, **Chimia lemnului din România — plopul şi salcia** (La chimie du bois en Roumanie — le peuplier et le saule), 1973, 228 p., 28 lei.

TIBERIU NĂŞCUŢIU, **Metode radiochimice de analiză** (Méthodes radiochimiques d'analyse), 1973, 384 p., 23 lei.

MARIA FITI, **Dozimetria chimică a radiaţiilor ionizante** (La dosimétrie chimique des radiations ionisantes), 1973, 240 p., 13,60 lei.

MIHAI FLORESCU, **Eficienţa economică a cercetării ştiinţifice** (L'efficience économique de la recherche scientifique), 1972, 115 p., 15 lei.

GEORGETA LĂZĂRESCU, **Sistematizarea informaţiilor în Chimia organică** (La systématisation des informations dans la Chimie organique), 1972, 252 p., 10,50 lei.

P. BALTĂ et E. BALTĂ, **Introducere în chimia fizică a stării vitroase** (Introduction à la chimie physique de l'état vitreux), 1971, 240 p., 15,50 lei.

LYDIA-MARIA VAICUM, **Biodegradabilitatea detergenţilor** (La biodégradabilité des détergents), 1971, 254 p., 16 lei.

I. ZUGRĂVESCU et L. STOICESCU-CRIVETZ, **Polimeri heterociclici** (Polymères hétérocycliques), 1971, 190 p., 9,50 lei.

CRISTOFOR SIMIONESCU et C. UGLEA, **Fracţionarea compuşilor macromoleculari** (Fractionnement des composés macromoléculaires), 1962, 292 p., 18,50 lei.

I. MAXIM, **Materiale nucleare** (Matériaux nucléaires), 1969, 444 p., 30 lei.

CRISTOFOR SIMIONESCU et CLEOPATRA VASILIU-OPREA, **Mecanochimia compuşilor macromoleculari** (La mécanochimie des composés macromoléculaires), 1967, 344 p., 23,50 lei.

CORNEL BODEA et collab., **Tratat de biochimie vegetală**, partea I, **Fitochimie** (Traité de biochimie végétale, Ire partie, Phytochimie), Ier vol., 1964, 747 p. + 4 annexes + 2 pl., 41 lei ; IIe vol., 1965, 1262 p., 1 pl., 56 lei ; IIIe vol., 1967, 773 p., 35 lei.

I. P. I. — c. 839

43 426

Lei 25. —

1976 MAR 15

F 1103

71

ACADÉMIE DE LA RÉPUBLIQUE SOCIALISTE DE ROUMANIE

REFERÁLVA

REVUE ROUMAINE DE CHIMIE

TOME 20
Nos 11—12
Novembre—Décembre 1975

RECHAX, 20, *11—12,* 1357—1520 (1975)

EDITURA ACADEMIEI REPUBLICII SOCIALISTE ROMÂNIA

Rev. Roumaine Chim. 20, *11—12,* p. 1357—1520 (1975), Bucarest

ACADÉMIE DE LA RÉPUBLIQUE SOCIALISTE DE ROUMANIE

COMITÉ DE RÉDACTION

Rédacteur en chef:

I. G. MURGULESCU, membre de l'Académie de la République Socialiste de Roumanie

Rédacteurs en chef adjoints:

A. T. BALABAN et V. EM. SAHINI, membres correspondants de l'Académie de la République Socialiste de Roumanie

Collège de rédaction:

EM. BRATU, ELENA CEAUŞESCU, ECATERINA CIORĂNESCU-NENITZESCU, C. DRĂGULESCU, RALUCA RIPAN, CR. SIMIONESCU, membres de l'Académie de la République Socialiste de Roumanie; P. SPACU, membre correspondant de l'Académie de la République Socialiste de Roumanie; MARGARETA AVRAM, D. I. MARCHIDAN, I. MOLDOVAN, G. NIAC et D. SĂNDULESCU

Toute commande de l'étranger pour les travaux parus aux Éditions de l'Académie de la République Socialiste de Roumanie sera adressée à ILEXIM Serviciul Export-Import Carte (Livres)/Serviciul Export-Import Presă (Revues), P. O. BOX 2001, 64–66, Calea Griviţei, Bucarest 12, Roumanie

Les manuscrits, les livres et les revues proposés en échange, ainsi que toute correspondance seront envoyés à la rédaction :

REVUE ROUMAINE DE CHIMIE

23, str. Dumbrava Roşie, Bucarest, Roumanie, téléphone 12 41 60

EDITURA ACADEMIEI REPUBLICII SOCIALISTE ROMÂNIA

125, Calea Victoriei, Bucarest, Roumanie, téléphone 50 76 80

REVUE ROUMAINE
DE
CHIMIE

ORSZÁGOS MŰSZAKI KÖNYVTÁR ÉS DOKUMENTÁCIÓS KÖZPONT 1883

Tome 20, Nos 11-12 Novembre-Décembre 1975

RODICA VÎLCU and ALEXANDRINA SIMION, Thermodynamic characterization of some organic solutions from acoustical data 1359–1364

D. I. MARCHIDAN et SPERANȚA TĂNĂSESCU, Propriétés thermodynamiques des oxydes non stœchiométriques d'uranium 1365–1370

R. M. ARCHIBALD, D. R. ARMSTRONG and P. G. PERKINS, *Ab initio* calculations using spherical Gaussian orbitals on water, methane, acetylene, ethylene, ethane and diborane 1371–1411

V. MACOVEI, Spectral solvent effects in aromatic compounds solutions. I. Solvent effects on the position and intensity of the $^1A_{1g} \rightarrow {}^1B_{2u}$ benzene transition 1413–1432

SURENDER K. JAIN and HARBANS L. JINDAL, Densities and partial molar volumes in concentrated electrolyte solutions. I. Magnesium nitrate — — (Sodium, potassium) nitrate—water mixtures 1433–1436

I. TEOREANU et MARIA GEORGESCU, La réactivité de certaines compositions mélilitiques par rapport à l'eau 1437–1442

О. А. РЕУТОВ, А. С. ГУДКОВА, Перегруппировки в реакциях дезаминирования 1443–1470

IOANA BALLY and A. T. BALABAN, Synthesis of ^{14}C-labelled isotope-isomeric alkanes. II. Preparation of 2, 2, 4-trimethylpentane-$^{14}C_2$ labelled at both methyl groups of the isopropyl moiety 1471–1472

NICOLETA ȘTEFAN, I. G. DINULESCU, F. CHIRALEU and MARGARETA AVRAM, Investigations in the cyclobutane series. XXXVII. The stereochemistry of bromine addition to the angular dimer of benzocyclobutadiene 1473–1478

V. LAIBER, L. ALERGUȘ, D. DAVID and D. SĂNDULESCU, Computation of the isenthalpic expansion of ethylene at high pressure. 1479–1490

D. DONESCU, Kinetic studies on copolymerization of 1,3-dioxepane with epichlorohydrin initiated with $AlEt_3 + H_2O$. 1491–1502

COMPTES RENDUS 1503–1504

INDEX DES AUTEURS 1505 1513

INDEX DES SUJETS 1513 1520

Revue Roumaine Chim. 20, *11–12*, 1357–1520, (1975) Bucarest

Tome 24, N° 11–12 [illegible] Décembre 1979

[illegible] and [illegible] NORICA SIMION, [illegible] dynamic [illegible] of [illegible] solutions [illegible] . . . [illegible]

[illegible] STEFANIA TANASESCU, [illegible] de [illegible] . . . [illegible]

[illegible] and [illegible], [illegible] acetylene, [illegible] . . . [illegible]

[illegible] effects on the position and intensity of the [illegible] . . . [illegible]

[illegible] solutions. [illegible] magnetic [illegible] . . . [illegible]

[illegible] Le [illegible] de [illegible] . . . [illegible]

[illegible] . . . [illegible]

[illegible] labelled [illegible] labelled at both [illegible] . . . [illegible]

[illegible] and [illegible] . . . [illegible]

[illegible] . . . [illegible]

[illegible] with [illegible] . . . [illegible]

COMPTES RENDUS . . . [illegible]

INDEX [illegible] . . . [illegible]

INDEX [illegible] . . . [illegible]

Revue Roumaine de Chimie, **20**, *11-12*, 1359-1364 (1975)

THERMODYNAMIC CHARACTERIZATION OF SOME ORGANIC SOLUTIONS FROM ACOUSTICAL DATA

RODICA VÎLCU and ALEXANDRINA SIMION

University of Bucharest, Chair of Chemical Thermodynamics and Electrochemistry,
Bd. Republicii 13, Bucharest, Romania

Received May 28, 1974

The densities and the velocity of ultrasounds in the system benzene + ethyl methyl ketone were measured as well as the velocity of ultrasounds in the system benzene + toluene at temperatures from 20 to 60°. Densities were determined by the picnometer method and velocities by an interferometer with double quartz crystal, at 1 MHz frequency. The values of the velocities correlated with those of densities and surface tensions allowed to compute the adiabatic compressibility, the ratio of heat capacities and the isothermal compressibility. Moreover, the excess volumes and the excess adiabatic compressibility of the binary systems under study were computed.

INTRODUCTION

Ultrasounds are more and more applied both to science and to technique[1]. The ultrasonic velocity, correlated with various parameters of the liquid [2] and solid states, contribute to their study.

Starting from van der Waals'equation and from relation $v^2 = \partial p/\partial \rho$ Schaafs [3] found for the velocity a dependence in the form

$$v^2 = f(\gamma,\ M,\ b,\ \rho) \tag{1}$$

where

$$\gamma = C_p/C_V$$

M is the molar mass

b is the covolume

ρ is the density.

The velocity being known, the covolume can be determined and this supplies information on the molecular sizes.

Schaafs [3] found thus relation

$$b = \frac{M}{\rho}\left[1 - \frac{\gamma RT}{Mv^2} - \left(\sqrt{1 + \frac{Mv^2}{RT}} - 1\right)\right] \tag{2}$$

---

[1] "The fourth National Conference of Acoustics", May 1973, Bucharest.

[2] R. Vîlcu and A. Simion, *Rev. Roumaine Chim.* (in press).

[3] W. Schaafs, *Z. Physik*, **114**, 110 (1939); **115**, 69 (1940), *J. Phys. Chem.*, **196**, 397 (1951).

where T represents the temperature (in K) and R the universal constant of gases.

By using certain thermodynamic relations between the parameters characterizing the liquids, Kudriavtsev[4] established a relation between the ultrasonic velocity in the liquid and the surface tension of the later :

$$\sigma = \frac{1}{18.66}\left(\frac{v^2}{\gamma} - \frac{RT}{M}\right)\left(\frac{M\rho^2}{N}\right)^{1/3} \tag{3}$$

where σ is the surface tension and N Avogadro number, the meanings of the other quantities being the usual ones.

Kudriavtsev[5] pointed out that by using the data concerning the internal pressure in liquids, it is possible to compute $\int_{V_1}^{V_2} p\mathrm{d}V$ and hence ratio C_p/C_V by formula

$$C_p/C_V = C_p/\left(C_p - \int_{V_1}^{V_2} p\mathrm{d}V\right) \tag{4}$$

Between the surface tension, σ, the internal pressure, p_i, and the molecular diameter $\varnothing$, the following relation was established[6]

$$p_i = \pi\sigma/\Phi$$

In this paper, the propagation of ultrasonic waves is studied in relation with other quantities, in two different systems : the benzene + toluene system with nonpolar or slightly polar and similar molecules of the components and the benzene + ethyl methyl ketone system with nonpolar, respectively polar, and dissimilar structure molecules, but havng boiling points and molar volumes of neighbouring values.

EXPERIMENTAL

The ultrasonic velocities were measured with an interferometer built on the principle of the double crystal interferometer described in a previous paper ;[2] the maximum error was 0.3 %.

For the benzene + ethyl methyl ketone system, the densities were determined by picnometer, with a maximum error of 0.01 % ; for the benzene + toluene system, the density values were borrowed from another paper.[7]

The liquids were purified by the usual methods.[8]

In view of the mixture preparation, the components were weighed in the same flask.

---

[4] B. B. Kudriavtsev, *Akust. Zhur.*, **11**, 1, 39 (1956).

[5] B. B. Kudriavtsev, *Zhur. fiz. Khim.*, **28**, 930 (1954).

[6] N. Bărbulescu, *Bul. Soc. chim. France*, **1936**, 462.

[7] B. I. Konobeev and V. V. Liapin, *Zhur. priklad. Khim.*, **43**, 803 (1970).

[8] A. I. Vogel, "A Textbook of Practical Organic Chemistry Including Qualitative Organic Analysis", second edition, Longmans and Green, London, 1951.

RESULTS AND DISCUSSIONS

BENZENE + ETHYL METHYL KETONE SYSTEM

Table 1 gives the density values at various temperatures and table 2 the excess volume values deduced from the densities, of the benzene + + ethyl methyl ketone system.

Table 1

Densities of the benzene (1) + ethyl methyl ketone (2) system at various temperatures

x_2 / t	ρ (g/cm^3)				
	20	30	40	50	60
0.00000	0.8781	0.8674	0.8566	0.8462	0.8350
0.1998	0.8639	0.8533	0.8425	0.8327	0.8208
0.3965	0.8500	0.8396	0.8291	0.8184	0.8079
0.5999	0.8358	0.8249	0.8145	0.8037	0.7931
0.8166	0.8190	0.8085	0.7985	0.7883	0.7868
1.0000	0.8060	0.7953	0.7844	0.7736	0.7623

Table 2

Excess volumes of the benzene (1) + ethyl methyl ketone (2) system at various temperatures

x_2 / t	V^E(cm^3/mole)			
	20	30	40	50
0.0000	0.00	0.00	0.00	0.00
0.1998	−0.03	−0.04	−0.04	−0.12
0.3965	0.05	−0.09	−0.13	−0.13
0.5999	−0.07	−0.09	−0.15	−0.14
0.8166	0.02	−0.05	−0.10	−0.17
0.0000	0.00	0.00	0.00	0.00

Since the molecules of the components differ from one another by nature and form, it would be expected that their mixture should undergo a volume increase, but the negative excess volumes, though very small, show a slight decrease of volume. On the other hand, when the temperature rises they become more negative. Similar results were supplied by the benzene + acetone system. [9]

An explanation of this slight decrease of volume could be offered by the possibility of some molecules of ethyl methyl ketone to be included within the benzenic nucleus, which would mean that the decrease would be due rather to a geometric packing than to a difference between the forces of interaction (taking into account the similar values of the boiling points and the molar volumes).

Figure 1 exhibits the variation curves of the velocity of ultrasound at various temperature as a function of the mole fraction of the second

[9] R. K. Nigam, B. S. Mahl and P. P. Singh, *J. Chem. Thermodynamics*, **4**, 41 (1972).

component and table 3 contains the values of the adiabatic compressibility β_s deduced by the usual formula from the values of the densities and velocities.

Taking into account the maximum error of velocity measurement one gets a maximum error in β_s of ± 0.6 %.

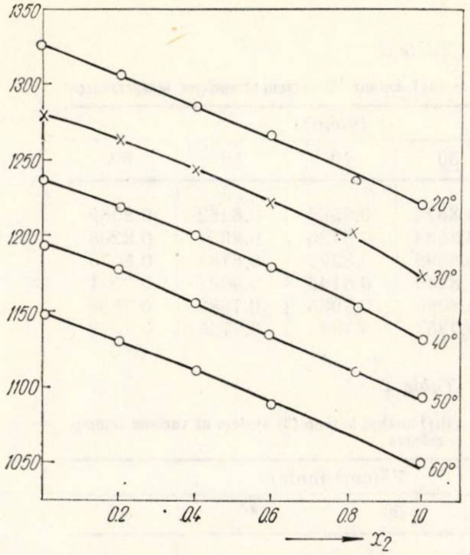

Fig. 1. — Variation of ultrasonic velocity with mole fraction of the second component and with temperature, in the benzene + ethylmethyl ketone system.

Table 3

Adiabatic compressibility of the benzene (1) + ethyl methyl ketone (2) system

x_2 / t	$10^{12}\,\beta_S$ (cm² dyne⁻¹)				
	20	30	40	50	60
0.0000	64.9	70.5	76.4	82.9	90.7
0.1998	67.8	73.4	79.9	86.5	95.4
0.3965	71.2	76.9	83.7	91.4	100.1
0.5999	74.6	81.2	88.3	96.6	106.3
0.8166	79.9	85.6	94.2	102.9	110.0
1.0000	83.1	91.1	99.6	108.6	118.9

From the standpoint of velocity too, the behaviour of the system is quasi-ideal ; the velocities vary according to straight lines situated between the values of the proper velocities in the case of pure components.

The representation of the adiabatic compressibility as a function of the mole fraction of the second component leads to parallel curves with a slight convexity toward the x axis.

The computation of the excess adiabatic compressibilities yields more negative values up to 30° which remain practically constant.

Taking into account the velocity curves, the low values of the mixing volumes and of the excess adiabatic compressibilities, the above system behaves as an ideal system, which could lead to the conclusion that the interaction forces of the components are nearly equal to one another.

BENZENE + TOLUENE SYSTEM

For this system, the ultrasonic velocities were measured at temperatures of 20, 40, 60° for which the literature supplies the values of the densities and of the surface tensions.

The ultrasonic velocities were also measured in this system at other temperatures and mole fractions.[10]

We made these measurements with the purpose of correlating the velocity with the surface tension and with the ratio of heat capacities γ according to relation (3).

The velocities in both benzene and toluene proved to be equal within the limits of our experimental errors (table 4) which shows that the increase of toluene compressibility is proportional to the decrease of the density of benzene.

Since within the interval under study the velocity is practically constant and equal to the value of that of its pure components, there results that the compressibility varies only as a function of the density variation to the exclusion of any other factor.

The values of the velocity, adiabatic compressibility and surface tension of the benzene + toluene system are given in table 4.

Table 4

Velocity of ultrasound, adiabatic compressibility and surface tension of the bezene (1) + toluene (2) system

x_1 / t	$v(ms^{-1})$		$10^{12}\beta_S$ (cm^2 $dyne^{-1}$)		$\sigma(Nm^{-1})$	
	20	60	20	60	20	60
0.000	1323	1139	66.0		285	
0.232	1323	1143	65.9		286	
0.440	1325	1143	65.5	92.1	287	238
0.638	1325	1146	65.3	91.5	288	237
0.824	1323	1147	65.2	91.1	288	237
1.000	1323	1149	64.9	90.6	289	237

It is easy to see that the variation of the adiabatic compressibility is inverse to that of surface tension which was to be expected since a higher surface tension implies stronger interaction forces between the component particles of the liquid and therefore a lower compressibility.

---

[10] K. S. Iyengar, *Proc. Indian Acad. Sci.*, **35 A**, 1193 (1952).

In table 5, the ratios of the heat capacities, γ, are given as determined by relation (3).

The values of the density and surface tension were borrowed from Liapin's paper.

Table 5

Ratios of heat capacities, γ and isothermal compressibility, for the benzene (1) + toluene (2) system

x_1 / t	γ 20	γ 60	γ (literature)	$10^{12}\beta_T$(cm^2 dyne^{-1}) 20	$10^{12}\beta_T$(cm^2 dyne^{-1}) 60	$10^{12}\beta_T$(cm^2 dyne^{-1}) (literature) 20	$10^{12}\beta_T$(cm^2 dyne^{-1}) (literature) 60
0.000	1.56			103.0			
0.232	1.53			100.7			
0.440	1.52	1.32		99.7	121.5		
0.638	1.50	1.31		97.8	120.1		
0.823	1.48	1.29	1.456 *	96.7	117.3		
1.000	1.47	1.29	1.436(27°)[11] 1.429 (30°)[11]	95.2	117.2	96[12]	129[12]

* from statistical measurements.[5]

The values of the adiabatic compressibility and of the ratios of the heat capacities permitted to compute the values of the isothermal compressibility.

The value of the isothermal compressibility of benzene at 30° thus computed concorde well enough with the experimental value directly determined.

---

[11] G. H. Findenegg and F. Kohler, *Trans. Faraday Soc.*, **63**, 870 (1967).

[12] M. Diaz Pena and B. Cavero, *Anales real Soc. espan. Fiz. Quim.*, ser B **60**, 357 (1964).

Revue Roumaine de Chimie, **20**, *11–12*, 1365–1370 (1975)

PROPRIÉTÉS THERMODYNAMIQUES DES OXYDES NON STŒCHIOMÉTRIQUES D'URANIUM

D. I. MARCHIDAN et SPERANȚA TĂNĂSESCU
Centre de Chimie physique P.O.BOX 2103, Bucarest 13, Roumanie

Reçu le 7 avril 1975

On a effectué des mesures de forces électromotrices à piles galvaniques avec un électrolyte solide pour obtenir des données thermodynamiques pour des oxydes d'uranium compris entre UO_2 et U_3O_8 dans l'intervalle de température 1073–1373 K. On a calculé les valeurs des énergies, enthalpies et entropies libres partiellement molaires et intégrales de l'oxygène, ainsi que les pressions partielles d'équilibre de l'oxygène dans les oxydes étudiés et on a déterminé la variation de ces propriétés en fonction du rapport atomique O/U et de la température. Les résultats obtenus mettent en évidence différents aspects des relations de phase entre les oxydes non stœchiométriques stables à haute température.

Le système uranium-oxygène est l'un des systèmes métal-oxygène les plus complexes. Bien que ce système ait constitué l'objet de nombreuses investigations effectuées moyennant différentes techniques et méthodes expérimentales, elles n'ont pas toutes abouti à des résultats concordants. Ainsi, les informations disponibles à l'heure actuelle ne sont ni assez précises, ni complètes pour fournir un ample set de données thermodynamiques.

La possibilité d'appliquer la méthode de mesure des forces électromotrices aux piles galvaniques à électrolyte solide aux fins de déterminer les propriétés thermodynamiques des composés d'uranium aux températures élevées a été montrée antérieurement.[1–3]

Dans notre laboratoire on a initié une étude du système uranium-oxygène compris entre UO_2 et U_3O_8 dans l'intervalle de température 1073–1373 K.

Les piles électrochimiques à électrolyte solide étaient du type :

$$\text{Fe, wüstite} \;/\; 0{,}85\ ZrO_2 + 0{,}15\ CaO \;/\; \text{oxyde d'uranium}$$

Les piles impliquent une électrode de référence en fer-wüstite avec une énergie libre, partiellement molaire relative connue de l'oxygène et avec un électrolyte solide lequel, ainsi que nous l'avons montré avant, [4]

---

[1] S. Aronson et J. Belle, *J. Chem. Phys.*, **29**, 151 (1958).

[2] K. Kiukkola, *Acta Chem. Scand.*, **16**, 327 (1962).

[3] T. L. Markin, L. E. J. Roberts et A. Walter, « Thermodynamics of nuclear materials », IAEA, Vienne, 1962, p. 693.

[4] F. Hund, *Z. phys. Chem.* (*Leipzig*), **199**, 142 (1952).

présente une conductivité anionique, due aux vacances présentes dans le réseau de l'oxygène. L'électrode droit consiste en oxyde d'uranium ayant un rapport O/U prédéterminé.

PARTIE EXPÉRIMENTALE

Les mesures FEM ont été effectuées dans une installation à vide, à une pression résiduelle du gaz d'environ $133{,}322 \times 10^{-6}$ N. m^{-2}.

L'ensemble de la cellule, formé par la tablette de l'électrolyte comprise entre les deux tablettes des électrodes, est introduit dans une cellule de quartz (figure 1) placée dans un fourneau électrique vertical.

La cellule est assemblée dans l'installation à vide.

Les mesures FEM ont été effectuées à l'aide d'un Voltmètre Digital « Solartron » ayant une grande résistance interne (10^{10} Ω), de type LM 1440,2.

Les déterminations ont été effectuées dans le domaine de température de 1073—1373 K, aux intervalles de 323 K, en attendant chaque fois, jusqu'au moment où l'on gagnait les valeurs d'équilibre.

L'installation, le procédé de travail expérimental, ainsi que la technique de préparation des tablettes ont été minutieusement décrits dans des travaux antérieurs. [5,6]

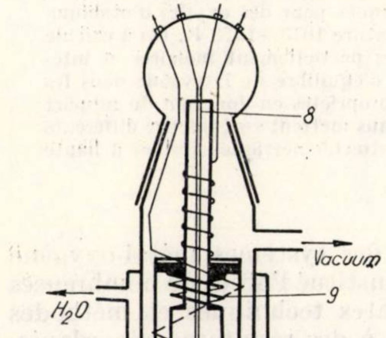

Fig. 1. — La cellule de travail.
1. Parois de la cellule de quartz; 2. tablettes des électrodes; 3. tablette de l'électrolyte; 4. disques en platine; 5—6. conducteurs en platine; 7. tube en quartz; 8. thermocouple; 9. arc.

RÉSULTATS ET DISCUSSIONS

Le but du présent travail est celui de communiquer les résultats obtenus en vue de l'étude des propriétés thermodynamiques des oxydes aux compositions non stœchiométriques $UO_{2,20}$ et $UO_{2,54}$ et de les comparer aux données obtenues par les auteurs dans des études antérieures concernant d'autres oxydes compris entre UO_2 et U_3O_8.

L'énergie libre molaire partielle de l'oxygène d'équilibre avec l'oxyde d'uranium peut être obtenue en combinant l'énergie libre standard de formation de la wüstite, connue à la suite des mesurages d'équilibre des gaz, avec la variation de l'énergie libre mesurée de la cellule, comme il résulte des équations :

$$\Delta G_{\mathrm{cel}} = -4\mathcal{F}E \tag{1}$$

$$\Delta G_{\mathrm{cel}} = 2\Delta G^0 \text{ wüstite} - \Delta\bar{G}_{O_2} \tag{2}$$

$$(\mathcal{F} = 96{,}508 \text{ KJ/volt équivalent})$$

Telle qu'elle résulte de (1) une incertitude de 0,001 V dans la FEM correspond à une incertitude de 0,386 KJ dans ΔG_{cel}.

---

[5] D. I. Marchidan et S. Matei, *Rev. Roumaine Chim.*, **15**, 1491 (1970).

[6] D. I. Marchidan et S. Matei, *Studii și Cercetări Chim.*, București, **18**, 617 (1970).

De plus, les enthalpies et les entropies libres partiellement molaires, les pressions partielles de l'oxygène en équilibre, ainsi que les quantités molaires intégrales peuvent être calculées des rapports thermodynamiques connus.[2,5]

En effectuant des déterminations sur l'oxyde caractérisé par le rapport atomique de 2,20 dans le domaine de température 1073—1373 K, on a obtenu un changement brusque dans la pente de la courbe de la FEM en fonction de la température, à 1160 K environ, ce qui indique une transition de phase à cette température : la phase homogène UO_{2+x} apparaît au-dessus de cette température, pendant qu'au-dessous de cette dernière, les phases UO_{2+x} et U_4O_{9-y} coexistent (figure 2).

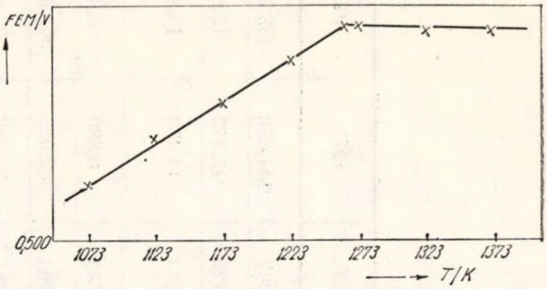

Fig. 2. — Variation de la FEM avec la température pour l'oxyde $UO_{2.20}$.

Les valeurs des énergies, enthalpies et entropies libres partiellement molaires pour des températures comprises entre 1073—1373 K sont présentées dans le tableau 1.

On doit étudier séparément la dépendance de température de $\Delta\bar{G}_{O_2}$ pour les domaines de température situés des deux côtés du point de transformation. Ainsi, pour le domaine de température où il existe une phase unique UO_{2+x} nous avons déterminé la relation :

$$\Delta\bar{G}_{O_2}/\mathrm{KJ.mol^{-1}} = 302{,}925 - 0{,}1238\ T \qquad (3)$$

tandis que pour le domaine de température où UO_{2+x} se trouve disproportionné dans $UO_{2+x} + U_4O_{9-y}$ on a établi que

$$\Delta\bar{G}_{O_2}/\mathrm{KJ.mol^{-1}} = 432{,}864 - 0{,}348\ T \qquad (4)$$

Les déterminations antérieures effectuées dans notre laboratoire[5,7] sur d'autres oxydes aux rapports atomiques rapprochés ($UO_{2.18}$, $UO_{2.19}$, $UO_{2.21}$) ont aussi indiqué des changements de phase à certaines températures.

En déterminant les équations qui montrent la variation de l'énergie libre ayant une température correspondant à chacun de ces oxydes et en les comparant avec la valeur obtenue par l'oxyde $UO_{2.20}$, on a constaté

---

[7] D. I. Marchidan et S. Matei, *Rev. Roumaine Chim.*, **17**, 1457 (1972).

Tableau 1

Données thermodynamiques pour l'oxyde $UO_{2,20}$

Temp./K	1073	1123	1173	1223	1273	1323	1373
$-\Delta\overline{G}_{O_2}$ K/J mol^{-1}	188,321	177,799	166,569	155,347	144,896	138,691	132,482
$-\Delta G$/KJ mol^{-1}	17,118	16,163	15,142	14,122	13,172	12,608	12,043
$-\Delta G \cdot n^{-1}_{UO_2}$ /KJ (g atome uranium)$^{-1}$	18,831	17,779	16,656	15,534	14,489	13,869	13,248
$-\log p_{O_2}$/N · m^{-2}	4,112	3,205	2,352	1,569	0,880	0,410	−0,026
$-\Delta\overline{H}_{O_2}$/KJ · mol^{-1}	432,864	432,864	432,864	432,864	302,925	302,925	302,925
$-\Delta H$/KJ · mol^{-1}	39,351	39,351	39,351	39,351	27,538	27,538	27,538
$-\Delta H \cdot n^{-1}_{UO_2}$ /KJ · (g atome uranium)$^{-1}$	43,286	43,286	43,286	43,286	30,292	30,292	30,292
$-\Delta\overline{S}_{O_2}$ /KJ · K^{-1} · mol^{-1}	3,489	3,489	3,489	3,489	0,1238	0,1238	0,1238
$-\Delta S$/KJ · K^{-1} · mol^{-1}	0,317	0,317	0,317	0,317	0,0112	0,0112	0,0112
$-\Delta S \cdot n^{-1}_{UO_2}$ /KJ · K^{-1} · (g atome uranium)$^{-1}$	0,348	0,348	0,348	0,348	0,0123	0,0123	0,0123

que, dans la région à deux phases, la dépendance de la température est pratiquement donnée par la même équation, en indiquant le fait que, dans la région à deux phases, $\Delta\bar{G}_{O_2}$ ne change pas, au fait, avec la composition.

De plus, les valeurs que nous avons obtenues pour cette région sont rapprochées de celles relatées par Perron [8] qui, en systématisant les données se référant à la région à deux phases $UO_{2+x}+U_4O_{9-y}$ à l'aide de l'analyse statistique élémentaire, a trouvé que :

$$\Delta\bar{G}_{O_2}/\mathrm{KJ.mol^{-1}} = -430{,}466 + 0{,}229\ T \qquad (5)$$

Dans le tableau 1 sont aussi présentées les valeurs $\Delta\bar{H}_{O_2}$ et $\Delta\bar{S}_{O_2}$ pour l'oxyde de $UO_{2.20}$. On peut constater, dans le tableau, que le passage de la région à phase unique à celle de deux phases est accompagnée d'un puissant décroissement de la chaleur partiellement molaire relative, pour la dissolution de l'oxygène dans l'oxyde d'uranium, ainsi que de la diminution de l'entropie partiellement molaire relative de l'oxygène. Cette constatation peut être interprétée comme un indice de l'accroissement continuel de l'ordonance dans le réseau de l'oxygène dans la phase UO_{2+x}.

En effet, le passage de la phase UO_{2+x} à la phase U_4O_9 a lieu par l'incorporation des ions d'oxygène dans les endroits interstitiels du réseau de la fluorite, menant à une configuration plus stable des atomes. Les interactions d'attraction entre les ions d'oxygène interstitiels produiront la diminution de l'oxygène en même temps que l'accroissement de la teneur en oxygène.

L'oxyde à composition non stœchiométrique $UO_{2.54}$ a été étudié dans le domaine de température compris entre 1123–1373 K. La dépendance de température de la FEM est présentée dans la figure 3.

Tel qu'il est présenté dans le diagramme de phase du système uranium-oxygène dans le domaine de température étudié, l'oxyde $UO_{2.54}$ fait partie de la région de deux phases $U_4O_9 + U_3O_{8-y}$. Il est prévu que, de même, dans cette région de deux phases, similaire à la région de

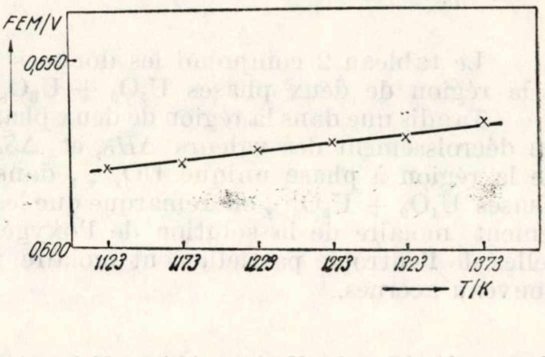

Fig. 3. — Variation de la FEM avec la température pour l'oxyde $UO_{2.54}$.

---

[8] P. O. PERRON, « Thermodynamics of Nonstoichiometric Uranium Dioxide », Chalk River, Ontario, 1968.

$UO_{2+x} + U_4O_9$, les valeurs de l'énergie libre partiellement molaire ne changent pas avec la composition. En effet, les valeurs que nous avons obtenues pour l'oxyde $UO_{2,54}$ sont pratiquement identiques à celles obtenues et communiquées dans les travaux antérieurs se référant à $UO_{2,46}$ et $UO_{2.50}$ qui font partie de la même région de phase.

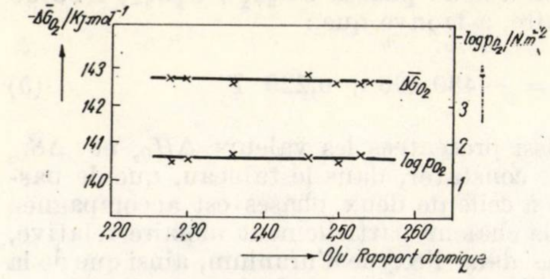

Fig. 4. – Variation de $\overline{\Delta G}_{O_2}$ et de log P_{O_2} avec la composition pour le domaine $UO_{2,25} - UO_{2,55}$ et à 1073 K.

Afin d'illustrer ceci, la figure 4 présente les valeurs de l'énergie libre partiellement molaire relative, ainsi que celles des pressions partielles de l'oxygène en équilibre, en fonction de la composition, à 1073 K.

Tableau 2

Données thermodynamiques pour la région de deux phases $U_4O_9 + U_3O_{8-y}$

Temp./K	$-\overline{\Delta G}_{O_2}$/KJ · ·mole^{-1}	$-\Delta G$/KJ ·mol^{-1}	$-\Delta G \cdot n^{-1}_{UO_2}$ /KJ · (g atome uranium)$^{-1}$	$-\log p_{O_2}$/N · m^{-2}
1123	142,670	30,331	38,520	1,570
1173	135,302	28,764	36,531	0,959
1223	127,553	27,117	34,439	0,382
1273	120,189	25,552	32,451	−0,134
1323	112,825	23,986	30,462	−0,611
1373	104,687	22,256	28,265	−1,083

$-\overline{\Delta H}_{O_2}$/KJ · mol^{-1} = 312, 641

$-\Delta H$/KJ · mol^{-1} = 66,466

$-\Delta H \cdot n^{-1}_{UO_2}$/KJ · (g atome uranium)$^{-1}$ = 84,413

$-\Delta\bar{S}_{O_2}$/KJ · mol^{-1} · K^{-1} = 0,151

$-S$/KJ · mol^{-1} · K^{-1} = 0,0321

$-S \cdot n^{-1}_{UO_2}$/KJ . (g atome uranium)$^{-1}$ = 0,0407

Le tableau 2 comprend les données thermodynamiques se référant à la région de deux phases $U_4O_9 + U_3O_{8-y}$.

Tandis que dans la région de deux phases $UO_{2+x} + U_4O_9$ on remarque un décroissement des valeurs $\Delta\bar{H}_{O_2}$ et $\Delta\bar{S}_{O_2}$ par rapport à leurs valeurs de la région à phase unique UO_{2+x}, dans la deuxième région de deux phases $U_4O_9 + U_3O_{8-y}$ on remarque que les valeurs de la chaleur partiellement molaire de la solution de l'oxygène dans l'oxyde d'uranium et celles de l'entropie partiellement molaire relative de l'oxygène sont de nouveau accrues.

---

[9] D. I. Marchidan et S. Tănăsescu, *Rev. Roumaine Chim.*, **19**, 1435 (1974).

Revue Roumaine de Chimie, 20, *11–12*, 1371–1411 (1975)

AB INITIO CALCULATIONS USING SPHERICAL GAUSSIAN ORBITALS ON WATER, METHANE, ACETYLENE, ETHYLENE, ETHANE AND DIBORANE

R. M. ARCHIBALD, D. R. ARMSTRONG, and P. G. PERKINS *
* Department of Pure and Applied Chemistry
University of Strathclyde, Glasgow G1 IXL, Scotland

Received June 22, 1974

Ab intio calculations, using a variety of basis sets of spherical 'fixed' and 'floating' gaussian orbitals on H_2O, CH_4, C_2H_2, C_2H_6, and B_2H_6, have been performed in order to test the power of the method against more conventional S.T.O.'s and G.T.O.'s. It is found that the larger basis sets are capable of achieving an energy-accuracy which is near-Hartree-Fock and comparable to that attainable only by large G.T.O. basis sets. Furthermore, the limited bases reproduce well the eigenvalues and charge distribution of the larger basis sets. The wave functions afford good agreement with secondary properties such as multipole moments and diamagnetic shielding. The basis sets also provide a simple and pleasingly comprehensible localised picture of the bonding in these molecules.

1. INTRODUCTION

In a recent publication we described the construction of basis sets of 'fixed' and 'floating' spherical gaussian orbitals for use in molecular calculations involving atoms of the first row.[1] In that paper details of the exponents and orbital ranges for all these atoms were given and it was shown by reference to NH_3 that one possible advantage of these functions over conventional G.T.O.'s would be that the time required for computations yielding results of equivalent accuracy should be reduced. We have now made an extensive study of a number of well-known molecules, the choice of which was guided by the need to test our method critically against previous high-accuracy work.

Further, we believe that a possible additional advantage of the floating gaussian basis set is its ability to yield a description of molecular bonding which correlates with the chemist's intuitive localised picture. This is valuable since, although the computational superiority of the L.C.A.O.—M.O.—S.C.F. method over the alternative V.B. method for the prediction of electron distribution in molecular species is well established, an interpretative disadvantage of the former is that the molecular orbitals (M.O.) do not, in general, correspond to localised chemical bonds, lone-pairs of electrons, etc. Hence, computed M.O. wave functions frequently appear to have little connection with the classical ideas of electronic structure theory, whereas valence-bond concepts such as hybridisation have provided an extremely useful basis for the qualitative description of chemical bonds.

---

[1] R. M. Archibald, D. R. Armstrong, and. P. G. Perkins, *J. C. S. Faraday II*, in press.

The appeal of a localised orbital model was first exploited by Lennard-Jones,[2] who demostrated that highly-localised orbitals can, in fact, be obtained from delocalised M.O. by subjecting the set of occupied M.O. to suitable linear transformations such that the total determinantal wave function remains unchanged. These localised orbitals, which can often be represented approximately as linear combinations of hybrid orbitals, are identifiable qualitatively with chemical bonds and lone-pairs of electrons in molecules. This is an intrinsic property of M.O. and is independent of the level of approximation used in their construction. Unfortunately, the particular matrix necessary to effect such a transformation to equivalent orbitals is not always obvious; however, Edmiston and Ruedenberg[3] have now developed a systematic and quantitative method for dealing with this problem.

More recently, hybridisation has been introduced into M.O. wave functions in order to accomplish a second objective, namely, to improve the accuracy of the total wave function. This method contrasts with that above in that (i) it is confined to the L.C.A.O. approximation, (ii) it does not produce an equivalent description but, rather, modifies the total wave function, (iii) it only produces a localised description in the most formal sense. The procedure essentially involves improving the basis set by incorporating atomic orbitals which normally remain formally unoccupied in the ground state of the free atom (the analogy with the configuration interaction technique is obvious). These additional basis functions then form hybrids with specific members of the original set and so polarise the electron density in a particular direction. Hopefully, this improves the L.C.A.O.M.O. description and yields a lower energy for the system. The most commonly used polarisation functions in molecular calculations are the *p* orbitals of hydrogen and the *d* orbitals of the second-and third-row atoms.

In the previous paper we suggested that, by employing an atomic basis set of S.G.T.O. within the L.C.A.O.—M.O. formalism in the manner prescribed there, we can attain the conceptual insight of the rigorous treatment of Lennard-Jones without the need for any additional mathematical manipulation. Moreover, because of the nature of the basis set, further improvement is readily brought about *via* the polarisation technique but without the involvement of higher orbitals. We now wish to illustrate, by means of a detailed and critical examination of the computed wave functions, that our method also affords an accurate quantitative description of molecular bonding and properties.

In order to assess properly the quality of the wave functions, it is necessary to calculate not only the minimum total energy but also a wide variety of expectation values and to compare these with both other-calculated, and experimentally-measured values where available. Before proceeding to this, however, it is worthwhile first to comment here on the definitions and utility of various one-electron properties and their relationship to physical observables.

---

[2] J. E. Lennard-Jones, *Proc. Roy. Soc.* (*London*), **A198**, 14 (1949).

[3] C. Edmiston and K. Ruedenberg, *Rev. Mcd. Phys.*, **35**, 457 (1963).

2. THE ONE-ELECTRON DENSITY DISTRIBUTION

One of the most convenient and useful methods of relating molecular electronic structure to a given wave function is *via* a direct analysis of the associated electron probability functions.[4,5] Because of the way in which our basis sets differ from the conventional single-centred atomic orbitals, we must discuss possible changes in the definition of the probability functions.

The probability of finding electron 1 located in the volume element $\mathrm{d}r_1$, electron 2 simultaneously in $\mathrm{d}r_2$, etc., is given by the quantity

$$P_N = \Phi^* (r_1, r_2 \ldots r_N)\, \Phi (r_1, r_2 \ldots r_N)\, \mathrm{d}r_1 \ldots \mathrm{d}r_N \tag{1}$$

where P_N is the N-electron density function. Similarly, the probability of locating one electron at the point r_1 while the others are anywhere at all is given by the one-electron density function

$$P_1(r_1) = N \int \Phi^* (r_1, r_2 \ldots r_N) \cdot \Phi (r_1, r_2 \ldots r_N)\, \mathrm{d}r_1 \ldots \mathrm{d}r_N \tag{2}$$

In this expression the indistinguishability of the electrons is properly accounted for by the factor N. It has been shown by Lowdin[4] that, for determinantal wave functions, the density function $\mathrm{P}_1(r_1)$ can be expressed as

$$P_1(r_1) = N_i \sum_{i}^{\text{occ.}} \Phi_i^* (r_1)\, \Phi (r_1) \tag{3}$$

where N_i is the occupation number of the ith orbital ($N_i = 2$ for closed-shell orbitals).

Within the L.C.A.O. approximation, with

$$\Phi_i = \sum_{p} \lambda_p C_{pi} \tag{4}$$

$P_1(r_1)$ is given in terms of real basis functions and coefficients as

$$\begin{aligned} P_1(r_1) &= N_i \sum_{i}^{\text{occ.}} \sum_{p} \sum_{q} C_{pi}\, C_{qi}\, \lambda_p (r_1)\, \lambda_q (r_1) \\ &= N_i \sum_{i} \sum_{p} (C_{pi})^2 S_{pp} \frac{\lambda_p(r_1)\, \lambda_p(r_1)}{S_{pp}} + N_i \sum_{i} \sum_{p>q} \sum C_{pi} C_{qi} S_{pq} \frac{\lambda_p(r_1)\, \lambda_q(r_1)}{S_{pq}} \end{aligned} \tag{5}$$

---

[4] P. O. Lowdin, *Phys. Rev.*, **97**, 1474 (1955).

[5] R. McWeeny, *Proc. Roy. Soc. (London)*, **A223**, 63 (1954); *ibid.*, **A232**, 114 (1955).

which now allows a formal distinction between one-centre orbital density and overlap density.

Mulliken Population Analysis. Mulliken[6] suggested a further partitioning of the density function $P_1(r_1)$, namely, that the electron distribution should be analysed in terms of the individual contributions from each atom, plus an additional contribution from both intra-atomic and inter-atomic overlap terms.

Thus, the one-electron density function can be written as

$$\begin{aligned} P_1(r_1) = \sum_R \sum_p D^R_{Tpp} P^R_{pp}(r_1) + \sum_R \sum_{pq} D^R_{Tpq} S^R_{pq} P^R_{pq}(r_1) \\ + \sum_{S \neq R} \sum_{pq} D^{RS}_{Tpq} S^{RS}_{pq} P^{RS}_{pq}(r_1) \end{aligned} \tag{6}$$

where the respective normalised orbital and overlap densities $\rho^R_{pq}(r_1)$ and $\rho^{RS}_{pq}(r_1)$ are defined as

$$\begin{gathered} \rho^R_{pq}(r_1) = \frac{\lambda^R_p(r_1)\,\lambda^R_q(r_1)}{S^R_{pq}} \\ \rho^{RS}_{pq}(r_1) = \frac{\lambda^R_p(r_1)\,\lambda^S_q(r_1)}{S^{RS}_{pq}} \end{gathered} \tag{7}$$

and the so-called density matrices D_T are defined as

$$D_{T_{pp}} = \sum_k C^*_{pk} C_{kp}, \quad D_{Tpq} = \sum_k C^*_{pk} C_{kq} \tag{8}$$

In these equations the summations involving p and q are over the subset of orbitals belonging to the atoms R and S.

From (6) we can extract three quantities which, to some extent, characterise the charge distribution in our system. These are the net atomic population of atom R, Y^R, the overlap population between atoms R and S, X^{RS}, and the gross atomic population of atom R, Z^R, these quantities being defined as

$$\begin{gathered} Y^R = \sum_p D^R_{Tpp} + \sum_{pq}{}' S^R_{pq} D^R_{Tpq} \\ X^{RS} = 2 \sum_{pq} S^{RS}_{pq} D^{RS}_{Tpq} \\ Z^R = Y^R + \sum_{\mathrm{R} > S} X^{RS} \end{gathered} \tag{9}$$

---

[6] R. S. Mulliken, *J. Chem. Phys.*, **23**, 1833 (1955).

It will be noted that in the evaluation of gross atomic charges the overlap population X^{RS} is arbitrarily apportioned equally between the atoms R and S. This is somewhat unsatisfactory and, in an attempt to partially relieve this unsatisfactory allocation, we propose to partition the components of X^{RS} in accordance with the ratio of the exponents of λ_p and λ_q, the less diffuse orbital (larger exponent) acquiring the smaller portion of overlap density, *i.e.*

$$Z^R = Y^R + \sum_{R>S} \sum_{pq} 2\left(\frac{\alpha_q}{\alpha_p + \alpha_q}\right) S_{pq}^{RS} D_{Tpq}^{RS} \qquad (10)$$

Not only should this produce a better measure of bond polarity but also, because of the involvement of further atomic parameters, it provides us with a more sensitive test of the quality of our wave function, particularly as regards the problem of attaining a well-balanced basis set.

As an alternative to the Mulliken population analysis, it is possible to evaluate directly the function $P_1(r_1)$ or its individual orbital contributions (equation (3)). The function may be plotted as a density contour map. A clearer picture of charge distribution is obtained if the free atom density functions are deducted from the molecular function before plotting takes place, so producing an electron density difference contour map.

3. ONE-ELECTRON PROPERTIES

The expectation value of the total wave function with respect to a one-electron operator $\mathbf{O}$ can be expressed as the sum of the expectation values of each constituent M.O., that is,

$$N\langle\Phi|\mathbf{O}\,\Phi\rangle = N_i \sum_i \langle\Phi_i|\mathbf{O}|\Phi_i\rangle \qquad (11)$$

This relationship allows an examination of the properties of individual electrons but, of course, there are no experimental data with which we can compare such results. Nevertheless, an investigation of this type often yields valuable information regarding the nature of the bonding present.

a Multipole Moments Any electron distribution described, for instance, by the spinless one-electron density function $P_1(r_1)$, will interact with an external electrostatic field with potential $V(r_1)$, where r_1 is measured from a fixed origin C. The energy of such an interaction can be formulated as

$$E = E' + \int \mathrm{P}_1(r_1)\, V(r_1)\, \mathrm{d}r_1$$

where E' is the energy in the absence of the external field. If the potential $V(r_1)$ is expanded as a series in powers of r_{Ci} (the components of r_1 relative to C), then we obtain the result that

$$E = E' + \int \mathrm{P}_1(r_1)\Big\{V_0 + \sum_i (\partial V/\partial r_{Ci})_0 r_{Ci} + \qquad\qquad$$

$$+ \frac{1}{2}\sum_{ij}(\partial^2 V/\partial r_{Ci}\,\partial r_{Cj})_0 r_{Ci} r_{Cj} + \tag{12}$$

$$+ \frac{1}{6}\sum_{ijk}(\partial^3 V/\partial r_{Ci}\partial r_{Cj}\,\partial r_{Ck})_0 r_{Ci} r_{Cj} r_{Ck} + \dots\Big\}\,\mathrm{d}r_1$$

where the subscript $0'$ denotes a value at C

$${}^{ie}E = E' + qV_0 - \sum_i \mu_i F_i - \frac{1}{2}\sum_{ij} Q_{ij} F'_{ij} - \frac{1}{6}\sum_{ijk} R_{ijk} F''_{ijk} - \dots \tag{13}$$

F_i and F'_{ij} are defined,

$$\begin{aligned} F_i &= -(\partial V/\partial r_{Ci})_0 \\ F'_{ij} &= -(\partial^2 V/\partial r_{Ci}\,\partial r_{Cj})_0 \end{aligned} \tag{14}$$

and are, respectively, the field strength and field gradient at C. In (13) q is the zeroth moment, μ the dipole moment, Q the second and R the third moment. These constitute the multiple moments of the electron distribution with reference to C as origin. Only the first non-vanishing multipole is independent of the choice of origin. The definition of each moment is given as

$$\begin{aligned} q &= \int P_1(r_1)\,\mathrm{d}r_1 = N\langle\Phi|\Phi\rangle = N \\ \mu_i &= \int P_1(r_1) r_{Ci}\,\mathrm{d}r_1 = N\langle\Phi| r_{Ci}|\Phi\rangle \\ Q_{ij} &= \int P_1(r_1) r_{Ci} r_{Cj}\,\mathrm{d}r_1 = N\langle\Phi| r_{Ci} r_{Cj}|\Phi\rangle \\ R_{ijk} &= \int P_1(r_1) r_{Ci} r_{Cj} r_{Ck}\,\mathrm{d}r_1 = N\langle\Phi| r_{Ci} r_{Cj} r_{Ck}|\Phi\rangle \end{aligned} \tag{15}$$

Generally, the contribution to E from the N-electron charge will be completely cancelled by the corresponding resultant nuclear charge, giving a neutral species and a total dipole moment which, if non-zero, is independent of origin. Using equation (11) and including nuclear contributions, one can re-write each of the remaining multipole moments explicitly as follows :

(i) *Dipole Moment*

$$\mu_i(C) = \sum_A Z_A(A_i - C_i) - 2\sum_n \langle \Phi_n | (r_i - C_i) | \Phi_n \rangle \tag{16}$$

All vector components are now measured with reference to the origin of the cartesian axes system and Z_A is the charge on nucleus A. With each M.O. expressed as in (4) this equation becomes

$$\mu_i(C) = \sum_A Z_A(A_i - C_i) - 2\sum_n \sum_p \sum_q C_{pn} C_{qn} \langle \lambda_p | (r_i - C_i | \lambda_q \rangle \tag{17}$$

The explicit formula for the evaluation of the matrix elements $\langle \lambda_p | (r_i - C_i) | \lambda_q \rangle$ is given in Appendix 2, equation (2.1) for the special case of a S.G.T.O. basis set.

(ii) *Second Moment*

$$Q_{ij}(C) = \sum_A Z_A(A_i - C_i)(A_j - C_j) - 2\sum_n \langle \Phi_n | (r_i - C_i)(r_j - C_j) | \Phi_n \rangle \tag{18}$$

$$= \sum_A Z_A(A_i - C_i)(A_j - C_j) - 2\sum_n \sum_p \sum_q C_{pn} C_{qn} \langle \lambda_p | (r_i - C_i)(r_j - C_j) | \lambda_q \rangle \tag{19}$$

The formula for $\langle \lambda_p | (r_i - C_i)(r_j - C_j) | \lambda_q \rangle$ is given for S.G.T.O. in Appendix 2. Buckingham [11] has defined the elements of the related quadrupole moment as

$$\theta_{ij} = \frac{1}{2}(3Q_{ij} - \sum_k Q_{kk}\delta_{ij}) \tag{20}$$

This moment is both a measure of the size and shape, or deviation from spherical symmetry, of the electron distribution whereas the second moment only provides a measure of the absolute size in each direction.

(iii) *Third Moment*

$$R_{ijk}(C) = \sum_A Z_A(A_i - C_i)(A_j - C_j)(A_k - C_k)$$
$$-2\sum_n \langle \Phi_n | (r_i - C_i)(r_j - C_j)(r_k - C_k) | \Phi_n \rangle \tag{21}$$

$$= \sum_A Z_A(A_i - C_i)(A_j - C_j)(A_k - C_k)$$
$$-2\sum_n \sum_p \sum_q C_{pn} C_{qn} \langle \lambda_p | (r_i - C_i)(r_j - C_j)(r_k - C_k) | \lambda_q \rangle \tag{22}$$

The expectation value of the tensorial operator with respect to S.G.T.O. is given in Equation (2.3), Appendix 2. The related octupole moments, as given by Buckingham, [7] are defined as

$$\Omega_{ijk} = \frac{1}{2}\left(5R_{ijk} - \sum_{l} R_{ill}\,\delta_{jk} - \sum_{l} R_{jll}\,\delta_{ik} - \sum_{l} R_{kll}\,\delta_{ij}\right) \tag{23}$$

(iv) *Magnetic Susceptibility*. This property is closely related to the second and quadrupole moments. Van Vleck [8] has shown that the average molar susceptibility of a molecule with no resultant angular momentum can be expressed as the sum of a diamagnetic term, which is a function of the ground state only, and a paramagnetic term dependent on all the molecular excited states, i.e.

$$\varkappa = \varkappa^{d} + \varkappa^{p} \tag{24}$$

This diamagnetic contribution is directly proportional to the average value of r_C^2. Specifically, the relationship is given by

$$\varkappa^{d} = (-\,\boldsymbol{e}^{2}\,N/6\,\boldsymbol{m}c^{2})\,\langle\Phi\,|\,r_C^2\,|\,\Phi\rangle \tag{25}$$

where $\boldsymbol{e}$ and $\boldsymbol{m}$ are the electronic charge and mass, respectively; N is the total number of electrons; and c is the speed of light. The whole constant has the value $0.7922765 \times 10^{-7}\,N$.

The relationship between the expectation value of r_C^2 and the principal tensorial components of the second moment is shown by the following identities:

$$\langle\Phi\,|\,r_C^2\,|\,\Phi\rangle = 2\sum_i \langle\Phi_i\,|\,(r - \mathrm{C})^2\,|\,\Phi_i\rangle$$

$$= 2\sum_i \langle\Phi_i\,|\,(x - \mathrm{C}_x)^2\,|\,\Phi_i\rangle + 2\sum_i \langle\Phi_i\,|\,(y - \mathrm{C}_y)^2\,|\,\Phi_i\rangle$$

$$+\,2\sum_i \langle\Phi_i\,|\,(z - \mathrm{C}_z)^2\,|\,\Phi_i\rangle = -\,(Q_{xx}^{E} + Q_{yy}^{E} + Q_{zz}^{E}) \tag{26}$$

The superscript E denotes the electronic contribution to the second moment.

Clearly, since the expectation value of r_C^2 is an electronic quantity, it will be less sensitive to inaccuracies in our wave function than second or quadrupole moments, which include nuclear contributions. However, experimental magnetic susceptibility data are more readily available. In fact, only the total and paramagnetic susceptibilities are available from experiment, $\varkappa^{d}$ being subsequently derived from (24).

---

[7] A. D. Buckingham, *J. Chem. Phys.*, **13**, 1580 (1958).

[8] J. H. Van Vleck, 'The Theory of Electric and Magnetic Susceptibilities', Oxford University Press (New York), 1932.

b 'Atomic' or Short-range Forces. The properties discussed in the preceding sections essentially provide criteria for ascertaining the behaviour of wave functions in the bonding and outer regions of the electron cloud. It is also instructive, however, to study those regions in the vicinity of the nuclei. Since we are using the L.C.A.O. approximation in the construction of our M.O. we expect the inner shells to be well represented, assuming, of course, that we use accurate atomic wave functions in our computational scheme. The present work, however, involves the use of S.G.T.O. which are well known to have an improper gradient at the atomic cusp. This deficiency is overcome to some extent by including a large number of highly contracted G.T.O. at the nucleus. The extent to which this measure remedies the problem can be gauged by analysing those properties associated with relatively short-range forces.

(*i*) *Potential and Diamagnetic Shielding.* An integral part of the total electronic energy of molecules originates from the interaction of nuclear charge with both electronic and other nuclear potentials, the total potential at nucleus C being given by

$$V(\mathrm{C}) = -\sum_{A}{}' Z_A(1/|A-\mathrm{C}|) + \langle\Phi|(1/|r-\mathrm{C}|)|\Phi\rangle \tag{27}$$

Experimental data on the electronic potential are available through measurements of the average diamagnetic shielding, $\sigma^d_{\mathrm{Av.}}$. The correlation between the two quantities is described by the relationship

$$\begin{aligned}\sigma^d_{\mathrm{Av.}}(\mathrm{C}) &= (\mathrm{e}^2/3\mathrm{m}c^2)\langle\Phi|(1/|r-\mathrm{C}|)|\Phi\rangle \\ &= 17\cdot74959\times10^{-6}\langle\Phi|(1/|r-\mathrm{C}|)|\Phi\rangle\end{aligned} \tag{28}$$

Within the L.C.A.O.—M.O. framework, the expectation value on the right-hand side becomes

$$\begin{aligned}\langle\Phi|(1/|r-\mathrm{C}|)|\Phi\rangle &= 2\sum_i\langle\Phi_i|(1/|r-\mathrm{C}|)|\Phi_i\rangle \\ &= 2\sum_i\sum_p\sum_q C_{pi}C_{qi}\langle\lambda_p|(1/|r-\mathrm{C}|)|\lambda_q\rangle\end{aligned} \tag{29}$$

The formula for the evaluation of these integrals over S.G.T.O. is given in equation (2.4) of Appendix 2.

Since the $1/r_C$ operator plays an important role in the determination of S.C.F. wave functions *via* the one-electron energy term, we might reasonably expect good agreement with experimental quantities. For our present purpose, however, this satisfactory agreement is not as valuable as one would like, in that it renders electronic potential a rather insensitive guide to wave function accuracy.

(*ii*) *Electric Field.* For a molecule at equilibrium geometry, the nett force on each nucleus is zero, by definition. According to the Hellman-Feynman theorem,[9] this force can be described as

$$F(C) = -\,(f(C) + \langle \Phi | \mathbf{H} | \nabla_C \Phi \rangle + \langle \nabla_C \Phi | \mathbf{H} | \Phi \rangle) = -\,(f(C) + \delta(C)) \quad (30)$$

where $f(C)$ is the Hellman-Feynman force and $S(C)$ represents all residual forces. The Hellman-Feynman force $f(C)$ arises from the interaction between nuclear charge and potential gradient, or electric field E_C, at the nucleus C, the vectorial components of the force being given by

$$\begin{aligned} f_i(C) &= Z_C E_{iC} \\ &= Z_C\Big[-\sum_A{}' Z_A\, \partial/\partial C_i (1/|A - C|) + \langle \Phi |\, \partial/\partial C_i (1/|r - C|)\, | \Phi \rangle\Big] \\ &= Z_C\Big[-\sum_A{}' Z_A (A_i - C_i)/(|A - C|)^3 \\ &\qquad + 2\sum_n \langle \Phi_n | (r_i - C_i)/|r - C|^3 | \Phi_n \rangle\Big] \\ &= Z_C\Big[-\sum_A{}' Z_A (A_i - C_i)/(|A - C|)^3 \\ &\qquad + 2\sum_n \sum_p \sum_q C_{pn} C_{qn} \langle \lambda_p | (r_i - C_i)/(|r - C|)^3 | \lambda_q \rangle \end{aligned} \quad (31)$$

The evaluation of the latter integral over S.G.T.O. is discussed in Appendix 2.

Since, for an exact wave function, the resultant forces on all nuclei are zero, the sum of the Hellman-Feynman forces is a direct measure of the total residual force and, hence, is an extremely sensitive test of the accuracy of the determinantal wave function.

(iii) *Electric Field Gradient.* Nuclei of spin greater than 1/2 possess a non-spherical charge distribution and therefore interact with the electrons within a molecule. More precisely, in the presence of an inhomogeneous electric field the nuclear quadrupole moment Q will interact with the electric field gradient q in a manner analogous to that in (13). The magnitude of such interactions is determined experimentally from measurements of the associated quadrupole coupling constants, $(\mathbf{e}Qq/h)_C$. Hence, if the nuclear quadrupole moment is known, we can ascertain the accuracy of our computed field gradient by comparing the predicted coupling constant with the experimentally determined value. Alternatively, by utilising the experimental coupling constant and our computed electric field gradient, the nuclear quadrupole moment can be estimated.

---

[9] R. P. Feynman, *Phys. Rev.*, **56**, 340 (1939).

A further experimental value with which the calculated wave function can be correlated is the asymmetry parameter η defined as

$$\eta = (q_{\alpha\alpha} - q_{\beta\beta})/q_{\gamma\gamma} \tag{32}$$

where the labels of the principal axes have been chosen such that

$$|q_{\gamma\gamma}| \geqslant |q_{\beta\beta}| \geqslant |q_{\alpha\alpha}| \tag{33}$$

In order to make the comparison, however, it is often necessary to transform the cartesian axis system into a new axis system which diagonalises the electric field gradient tensor. In the present work, this was done by first selecting one cartesian axis to coincide with one principal axis and then transforming the remaining cartesian tensorial components of q by means of the transformation

$$q_C' = \mathbf{A}\, q_C\, \mathbf{A}^T \tag{34}$$

where

$$\mathbf{A} = \begin{vmatrix} \cos\alpha & \sin\alpha \\ -\sin\alpha & \cos\alpha \end{vmatrix} \tag{35}$$

The angle α is also relatable to experiment.

The cartesian components of the field gradient tensor at the nucleus C are given by

$$q_{ij}(C) = \partial/\partial C_i\,[E_j(C)]$$

$$= -\sum_A{}' \frac{z_A(3(A_i - C_i)(A_j - C_j) - \delta_{ij}|A - C|^2)}{|A - C|^5}$$

$$+ 2\sum_n \sum_p \sum_q [C_{pn} C_{qn} \langle \lambda_p | 3(r_i - C_i)(r_j - C_j) - \delta_{ij}|r - C|^2 | \lambda_q \rangle] / |r - C|^5 \tag{36}$$

The evaluation of this latter integral is discussed in Appendix 2 for S.G.T.O. basis functions.

4. METHOD, RESULTS AND DISCUSSION

The method of calculation was fully described in the previous paper.[1] A series of basis sets of varying size and complexity were tested against the results of a number of previous calculations. All the calculations were carried out on an IBM 370/195 computer at the Rutherford High Energy Laboratory, Harwell, and the density contours were plotted automatically, using a Calcomp Graph Plotter.

We now report the relevant energies and one-electron primary properties obtained from the calculated wave functions for the molecules H_2O, CH_4, C_2H_6, C_2H_4, C_2H_2, and B_2H_6. It is not the intention to analyse here the results in detail with respect to the chemistry of the molecules but, rather, to ascertain the level of accuracy attained by each of the different basis sets. The discussion, therefore, will be mainly confined to comparisons with previous calculations and experimental data, with only cursory remarks on the chemical significance of the results. By assembling a dossier of this nature, we should be in a position to predict, with confidence, the accuracy of future calculations or, conversely, make the appropriate selection of basis set to suit the particular study on hand. Where our results are without theoretical or experimental precedent, it is expected that the values reported will provide a useful basis for further investigations.

The water molecule was chosen because of the availability of numerous previous studies, whilst the molecules CH_4, C_2H_6, C_2H_4, and C_2H_2 constitute one of the most important series of chemical entities, providing the archetypal C—H single, C—C single, C—C double, and C—C triple bond, respectively. Finally, B_2H_6 is the classical example of a molecule containing a multicentre two-electron bond.

All quantities listed in the Tables of this section are given in atomic units unless otherwise stated; in the latter case the necessary conversion factors are given in Appendix 3.

Water. The water molecule has been extensively studied by Lennard-Jones and Pople,[10–12] who developed an adequate description of the bonding in terms of an oxygen core with two localised O—H bonds and two localised 'lone-pair' orbitals tetrahedrally positioned behind the oxygen nucleus. S.G.T.O. basis sets were constructed, therefore, to approximate this bonding situation. The first trial basis set was chosen to be of the form ($s_N 4$, $s_F 2:2$, $s_F 2:2/s_N 2$), the first two equivalent sets of floating *s* orbitals being fixed at equal distances along the O—H bond while the remaining two sets, which represent the 'lone-pair' orbitals, were allowed to 'float' behind the oxygen atom. Basis I, corresponding to an inter-orbital angle of 109°28′, was used to initiate the non-linear minimisation procedure, which subsequently terminated with the selection of the basis set, denoted as III, in which the floating *s* orbitals lie directly above and below the O nucleus. The detailed energies from both these calculations, together with those of an intermediate evaluation, designated II, at the inter-orbital angle of 120°, are given in Table 1.

The relative success of these three bases in the prediction of the experimental dipole moment[13] (0.728 a.u.) substantiates the above selection of the orbital arrangement on the basis of the energy criterion alone. From Table 2 it appears that the factor controlling primarily the accuracy of the computed dipole is the 'lone pair 1*b*, orbital contribution. For basis III this contribution is zero by symmetry, whereas for both I and II it is finite and positive. This decreases the electronic moment

---

[10] J. E. LENNARD-JONES and J. A. POPLE, *Proc. Roy. Soc. (London)*, *A*202, 166 (1950).

[11] J. A. POPLE, *Proc. Roy. Soc. (London)*, **A205**, 163 (1951).

[12] J. A. POPLE, *Proc. Roy. Soc. (London)*, **A202**, 323 (1950).

[13] W. S. BENEDICT and L. D. KAPLAN, *J. Chem. Phys.*, **30**, 388 (1959).

Table 1

Total energy, energy components, and orbital energies of water at experimental geometry

Energy	Basis I	Basis II	Basis III	Bases IV, V	Basis VI	Basis VII	N.M.
Total	−75.407311	−75.408131	−75.417561	−75.744782	−75.854579	−76.014959	−76.05936
Kinetic	75·432948	75.433405	75.427368	76.330719	75.710676	75.992186	76.00938
Nuclear-electron	−197.76968	−197.77214	−197.78013	−198.91587	−198.47915	−198.94683	−199.15507
Electron-electron	37.742314	37.743497	37.748097	37.653261	37.726792	37.752577	37.84784
Nuclear-nuclear	9.187105	9.187105	9.187105	9.187105	9.187105	9.187105	9.23848
$-V/T$	1.9997	1.9997	1.9999	1.9923	2.0018	2.0003	2.0007
$E(1\,a_1)$	−20.58179	−20.58156	−20.58165	−20.60650	−20.57540	−20.56780	−20.55805
$E(2\,a_1)$	−1.33675	−1.33647	−1.33275	−1.36182	−1.34991	−1.36213	−1.35224
$E(3\,a_1)$	−0.401728	−0.401996	−0.406210	−0.524612	−0.549534	−0.568613	−0.58222
$E(1\,b_1)$	−0.472751	−0.473005	−0.476874	−0.470579	−0.487529	−0.507035	−0.50685
$E(1\,b_2)$	−0.633030	−0.632848	−0.630800	−0.675989	−0.695405	−0.718843	−0.71897

Table 2

Components of dipole moment relative to oxygen for the water molecule

	Basis I	Basis II	Basis III	Basis VII	N.M.
Total	0.8115	0.8082	0.7562	0.8166	0.785
Nuclear	2.2192	2.2192	2.2192	2.2192	2.192
Electronic	−1.4077	−1.4110	−1.4630	−1.4026	−1.407
$1\,a_1$	−0.0005	−0.0005	−0.0004	−0.0006	−0.0004
$2\,a_1$	−0.3521	−0.3515	−0.3420	−0.3509	−0.3216
$3\,a_1$	0.0854	0.0841	0.0621	0.0639	0.0858
$1\,b_1$	0.0184	0.0173	0.0	0.0	−0.0728
$1\,b_2$	−0.4551	−0.4549	−0.4512	−0.4137	−0.3949

and produces a total dipole which is too large. In contrast, Neumann and Moskowitz [14] (N.M.) predict a negative $1b$, orbital contribution, without which their estimate of the dipole would be much higher. This is a direct consequence of the inclusion of d_{xz} and p_x orbitals on oxygen and hydrogen, respectively.

The total density plot of orbitals $1b_1$ and $3a_1$ displayed in Figure 1 shows clearly how idealised is the 'lone pair' label attached to them. However, two maxima approximately at the tetrahedral angle are present and hence the general terminology seems acceptable.

Being thus satisfied of a suitable arrangement for the atomic basis functions, S.C.F. calculations on H_2O were next performed using bases IV (and V), VI, and VII of the form $[s_N 4,\ s_F 2:2,\ s_F 2:2/s_N 2]$, $(s_N 5,\ s_F 2:3,\ s_F 2:3/s_N 3)$ and $(s_N 9,\ s_F 2:5,\ s_F 2:5/s_N 5)$, respectively. In all evaluations, wave functions were computed at the equilibrium molecular geometry [15] of O−H=1.8103 a.u. and $H\hat{O}H = 104.45°$. All energies associated with these basis sets are reported in Table 1. Also tabulated are the results of an extended G.T.O. calculation, at slightly different geometry, by Neumann and Moskowitz, [14] which approaches the Hartree-Fock limit of −76.06 a.u. suggested by Ritchie and King. [16] The general observations from Table 1 are that basis VII gives a total energy 0.045 a.u. higher than the Hartree-Fock limit, while the smaller set VI yields a total energy which is slightly better than the best available minimum S.T.O. calculation [17] (−75.7684 a.u.). The contracted sets IV and V, with the coefficients from reference 1, produce identical results which are some 0.36% higher than the uncontracted set VII.

The results of the Mulliken population analysis (Table 3) indicate a gross charge on the nuclei which varies with the size of the basis set used. Moreover, the density on the hydrogen nuclei is rather low in comparison with the previous results. For example, Switkes and coworkers [18] have obtained from their minimum S.T.O. wave function (total energy = −75.7201 a.u.) a gross atomic population of 0.81 together

---

[14] D. Neumann and J. W. Moskowitz, *J. Chem. Phys.*, **49**, 2056 (1968).

[15] G. Herzberg, 'Infrared and Raman Spectra', Van Nostrand, (NEW YORK), 1945.

[16] C. D. Ritchie and H. F. King, *J. Chem. Phys.*, **47**, 564 (1967).

[17] D. Hamel, *Z. Naturforsch.*, **22a**, 176 (1967).

[18] E. Switkes, R. M. Stevens, and W. N. Lipscomb, *J. Chem. Phys.*, **51**, 5229 (1969).

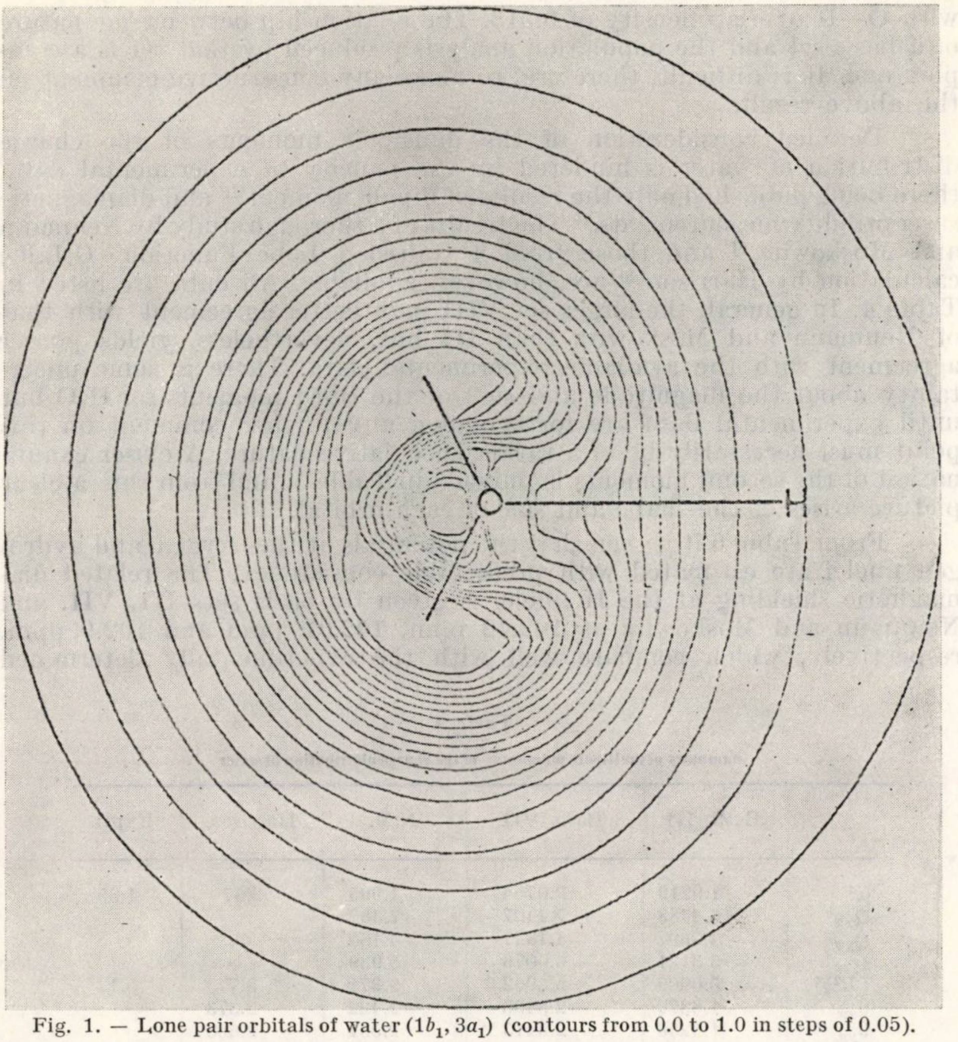

Fig. 1. — Lone pair orbitals of water ($1b_1, 3a_1$) (contours from 0.0 to 1.0 in steps of 0.05).

Table 3

Gross atomic, net atomic, and overlap populations for H_2O

	Basis I	Basis II	Basis III	Basis VI	Basis VII
Gross					
O	8.5772	8.5774	8.5846	8.7402	8.7564
H	0.7114	0.7113	0.7077	0.6299	0.6218
Net					
O	7.9363	7.9362	7.9375	8.2501	8.2327
H	0.5347	0.5345	0.5291	0.3770	0.3695
Overlap					
O−H	0.5701	0.5704	0.5745	0.5358	0.5477
H−H	−0.1460	−0.1460	−0.1447	−0.0757	−0.0671

with O—H overlap density of 0.513. The relationship between the nature of a basis set and the population analysis produced by that set is a complex one. It is difficult, therefore, to make any constructive comment on the above results.

Detailed consideration of the multipole moments of the charge distribution of water is hindered by the paucity of experimental data, there being published only the results of dipole moment [13] and diamagnetic susceptibility measurements.[19] The results of a thorough study by Neumann and Moskowitz [14] and those from a Gaussian Lobe Function (G.L.F.) calculation by Harrison [20] are, however, available. All data are listed in Table 4. In general, the larger set VIII is in better agreement with that of Neumann and Moskowitz than III but, nevertheless, yields poorer agreement with the available experimental data. There is some uncertainty about the magnitude and sign of the third moments for H_2O but until experimental data are forthcoming, any further comment on this point must necessarily be of a rather speculative nature. A closer examination of the second moments is pursued in Table 5, and from this a clear picture arises of the shape and size of each orbital.

From Table 6 it is seen that the potentials at the oxygen and hydrogen nuclei are estimated with predictable consistency. The related diamagnetic shielding at the H nuclei is given by basis sets III, VII, and Neumann and Moskowitz as 102.42 ppm, 102.01 ppm and 102.9 ppm, respectively, which compare well with the experimentally determined

Table 4

Summary of multipole moments[e] of the charge distribution of water

	Basis III	Basis VII	N.M.	Harrison	Exptl.
μ^a	1.9219	2.0754	1.995	2.57	1.85
$Q_{xx}{}^b$	−6.4788	−7.4407	−7.482		
Q_{yy}	−4.3697	−4.1827	−4.180		
Q_{zz}	−5.3121	−6.0076	−5.939		
$\langle R^2 \rangle^c$	5.0909	5.3962	5.371	5.7	5.1
θ_{xx}	−1.6379	−2.3456	−2.422	−2.373	
θ_{yy}	1.5258	2.5415	2.531	2.663	
θ_{zz}	−0.1122	−0.1959	−0.108	−2.90	
$R_{xxz}{}^d$	−0.2850	−0.0993	−0.112		
R_{yyz}	0.5210	1.1030	1.192		
R_{zzz}	−0.4717	−0.6715	0.282		
R_z	−0.2357	0.3322	1.363		
Ω_{xxz}	−0.5947	−0.4144	−0.960		
Ω_{yyz}	1.4204	2.5914	2.297		
Ω_{zzz}	−0.8257	−2.1771	−1.337		

a In Debyes.

b All second and quadrupole moments in units of 10^{-26} esu-cm^2.

c In units of 10^{-26} cm^2.

d All third and octupole moments in units of 10^{-34} esu-cm^3.

e All moments relative to centre of mass. (0.1226 a.u. from oxygen nucleus).

[19] D. Eisenberg, J. M. Pochan, and W. H. Flygare, *J. Chem. Phys.*, **43**, 4531 (1965).

[20] J. F. Harrison, *J. Chem. Phys.*, **47**, 2990 (1967).

Table 5

Components of second moment relative to centre of mass for water

	Q_{xx}		Q_{yy}		Q_{zz}		$\langle r^2 \rangle$	
	Basis VII	N.M.	Basis VII	N.M.	Basis VII	N.M.	Basis VII	N.M.
Total	−5.5325	−5.563	−3.1100	−3.108	−4.4669	−4.416		
Nuclear	0.0	0.0	4.0931	4.078	2.0685	2.015		
Electronic	−5.5325	−5.563	−7.2031	−7.186	−6.5355	−6.431	19.271	19.181
$1\,a_1$	−0.0178	−0.0177	−0.0177	−0.0177	−0.0326	−0.0327	0.0681	0.0682
$2\,a_1$	−0.4990	−0.4929	−0.7283	−0.7274	−0.6003	−0.6041	1.8276	1.8245
$3\,a_1$	−0.4772	−0.4701	−0.6550	−0.6366	−1.4708	−1.4623	2.6030	2.5690
$1\,b_1$	−1.3554	−1.3759	−0.4517	−0.4955	−0.4667	−0.4804	2.2738	2.3518
$1\,b_2$	−0.4168	−0.4249	−1.7489	−1.7259	−0.6974	−0.6362	2.8631	2.7770

value of 102.12 ppm. The derivation of this latter quantity is described by Neumann and Moskowitz.[14]

The computed electric fields (Table 7) reveal sensitively the deficiencies inherent in each basis set, the most prominent errors occurring around the O nucleus. The large difference in the residual forces produced by VII and N.M. is possibly a consequence of the slightly different molecular geometry employed in each case.

The quadrupole coupling constants of D and ^{17}O have been determined respectively by Thaddens, Krishner, and Loubser[21] and by Stevenson and Townes[22] from studies of hyperfine structure in the microwave spectrum of HD^{17}O. The theoretical values computed from our wave functions and those of Harrison[20] and Neumann and Moskowitz are compared with these experiments in Table 8. Values of 0.279×10^{-26} esu cm^2 (Ref.[23]) and 2.4×10^{-26} esu cm^2 (Ref.[24]) for the nuclear quadrupole moments of D and ^{17}O were used in the theoretical evaluations. It is obvious from Tables 9 and 10 that the calculated electric field gradients at the nuclei are too large, a defect which is clearly illuminated when the associated coupling constants are estimated. Our results for $(eQq/h)_D$ and $(eQq/h)_0$ are generally poor and lie well above the experimental values.

Methane. The electronic structure of the methane molecule can be conveniently described in terms of a carbon core and four equivalent localised C—H bond orbitals. As the initial stage in the present comparative study, therefore, a trial S.G.T.O. basis set (labelled V) of (s_N5, $s_F4:3/s_N3$) was constructed in an attempt to reproduce the essential features of this charge distribution : in this each of the equivalent sets of 'floating' *s*

---

[21] P. Thaddens, L. C. Krishner, and J. H. N. Loubser, *J. Chem. Phys.*, **40**, 257 (1964).

[22] M. J. Stevenson and C. H. Townes, *Phys. Rev.*, **107**, 635 (1957).

[23] H. Narumi and T. Watanabe, *Prog. Theoret. Phys.* (Kyoto), **35**, 1154 (1966).

[24] N. Bessis, H. Lefebvre-Brion, and C. H. Moser, *Phys. Rev.*, **128**, 213 (1962).

Table 6

Potentials at proton and oxygen in water

	V(H)			V(O)		
	Basis III	Basis VII	N.M.	Basis III	Basis VII	N.M.
Total	−1.0021	−0.9799	−1.001	−22.177	−22.327	−22.334
Nuclear	4.7683	4.7683	4.794	1.1047	1.1047	1.111
Electronic	−5.7704	−5.7482	−5.795	−23.281	−23.431	−23.145

Table 7

Electric fied at proton and oxygen in water

	E_z(O)			E_y(H)			E_z(H)		
	Basis III	Basis VII	N.M.	Basis III	Basis VII	N.M.	Basis III	Basis VII	N.M.
Total	−0.3443	−0.0348	−0.010	0.0852	0.0708	0.000	−0.0337	−0.0230	−0.002
Nuclear	−0.3740	−0.3740	−0.376	2.0508	2.0508	2.081	1.4959	1.4959	1.503
Electronic	0.0297	0.3392	0.366	−1.9656	−1.9799	−2.081	−1.4622	−1.4729	−1.505

Table 8

Quadrupole coupling constants for $HD^{17}O$

		Basis III	Basis VII	Harrison	N.M.	Exptl.
$(\boldsymbol{e}qQ/h)^a_D$	xx	−240.8	−195.1	−192.0	−194.8	−175 ± 10
$(\boldsymbol{e}qQ/h)^a_D$	$\acute{y}\acute{y}$	438.3	347.8	347.0	343.9	315 ± 7
$(\boldsymbol{e}qQ/h)^a$	$\acute{z}\acute{z}$	−197.5	−152.7	−155.0	−149.1	−140 ± 7
	η	0.0988	0.1219	0.107	0.133	0.115
	α	0.9545°	0.845°	3.1°	0.97°	1.12°
$(\boldsymbol{e}qQ/h)^b_0$	xx	12.01	18.19	11.37	10.44	6.96
$(\boldsymbol{e}qQ/h)^b_0$	yy	−10.32	−12.63	−9.97	−9.47	−9.88
$(\boldsymbol{e}qQ/h)^h_0$	zz	−1.68	−5.56	−1.40	−0.975	−2.92
	η	0.7194	0.3885	0.76	0.813	1.84

a In Kc sec^{-1}.

b In Mc sec^{-1}.

orbitals were positioned at equal distances along the C—H bonds. In order to validate this orbital arrangement, a second, non-localised model (basis IV) was constructed employing the original free-atom basis sets, *i.e.*, $(s_N 5, s_F 6 : 3/s_N 3)$. Assuming an equilibrium C—H bond distance of 2.0665 a.u. (Ref. [15]), both models were subjected to an SCF calculation, the results of which are given in Table 11. Basis V was found to be the more energetically favoured model and, hence, this orbital configuration was adopted in all subsequent SCF computations. To date, the best minimum S.T.O. energy published is that of Pitzer, [25] who reports a value of —40.12822 a.u., i.e., 0.002 a.u. below that produced by basis V.

Further SCF calculations were performed using bases I, II (and III), and VI of the form $(s_N 4, s_F 4 : 2/s_N 2)$, $[s_N 4, s_F 4 : 2/s_N 2]$, and $(s_N 9, s_F 4 : 5/s_N 5)$, respectively. The resultant SCF energies are also listed in Table 11. For comparison, we tabulate the results of a double-zeta G.L.F. [26] calculation by Rothenberg [27] (*R*) and those of an extended S.T.O. calculation at the slightly different C — H bond length of 2.067 a.u. by Arrighini [28] and his co-workers (A.G.M.M.S.). Basis VI yields 99.95% of the Hartree-Fock energy (—40.23 a.u., Ref.[16]), compares well with the A.G.M.M.S. wave function, and also represents a slight improvement on that obtained by Rothenberg. When contracted to the bases II and III, however, the resultant total energy rises by 0.09 a.u. ~ 0.22%).

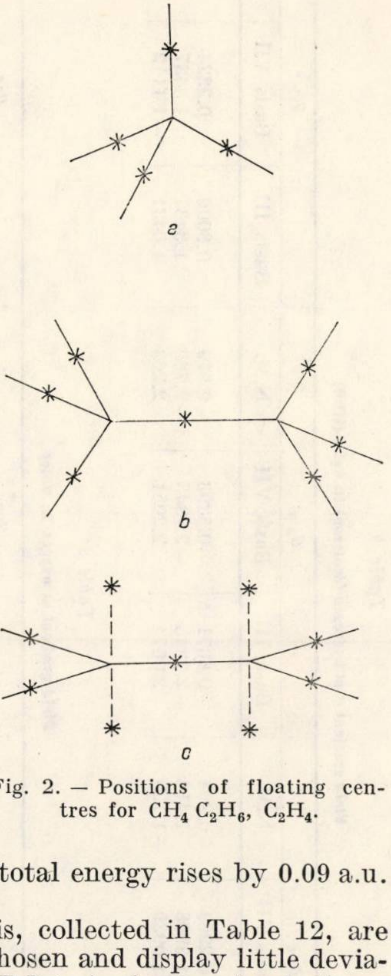

Fig. 2. — Positions of floating centres for CH_4 C_2H_6, C_2H_4.

The results of the population analysis, collected in Table 12, are fairly reproducible over the range of bases chosen and display little deviation from those of Palke and Lipscomb [29] (P.L.). A pleasing facet of our analysis is that, in the apportionment of the C—H overlap density, the greater part is donated to the hydrogen nucleus. This is satisfyingly compatible with the bond moment calculation of Moccia, [30] in which he

---

[25] R. M. Pitzer, *J. Chem. Phys.*, **46**, 4871 (1967).

[26] J. L. Whitten, *J. Chem. Phys.*, **44**, 359 (1966).

[27] S. Rothenberg, *J. Chem. Phys.*, **51**, 3389 (1969).

[28] G. P. Arrighini, C. Guidotti, M. Maestro, R. Moccia, and O. Salvetti, *J. Chem. Phys.*, **49**, 2224 (1968).

[29] W. E. Palke and W. N. Lipscomb, *J. Amer. Chem. Soc.*, **88**, 2384 (1966).

[30] R. Moccia, *J. Chem. Phys.*, **40**, 2164 (1964).

Table 9

Field gradient ^{a} at hydrogen (deuteron) in water (HDO)

	q_{xx}			$q_{y'y'}$			$q_{z'z'}$		
	Basis III	Basis VII	N.M.	Basis III	Basis VII	N.M.	Basis III	Basis VII	N.M.
Total	0.3664	0.2969	0.294	−0.6671	−0.5293	−0.519	0.3006	0.2324	0.225
Nuclear	1.3908	1.3908	1.414	−2.7345	−2.7343	−2.782	1.3437	1.3437	1.368
Electronic	−1.0244	−1.0939	−1.120	2.0674	2.2051	2.263	−1.0431	−1.1112	−1.143

Table 10

Field gradient at oxygen in water

	q_{xx}			q_{yy}			q_{zz}		
	Basis III	Basis VII	N.M.	Basis III	Basis VII	N.M.	Basis III	Basis VII	N.M.
Total	2.1291	3.2256	1.852	−1.8304	−2.2393	−1.679	−0.2988	−0.9863	−0.173
Nuclear	0.3370	0.3370	0.343	−0.2943	−0.2943	−0.304	−0.0428	−0.0428	−0.038
Electronic	1.7921	2.8886	1.509	−1.5361	−1.9451	−1.375	−0.2560	−0.9435	−0.135

Table 11

Total energy, energy components, and orbital energies of methane at experimental geometry

Energy	Basis I	Bases II, III	Basis IV	Basis V	Basis VI	R	A.G.M.M.S.
Total	−39.922836	−40.096292	−40.121735	−40.126110	−40.190172	−40.1889	−40.20452
Kinetic	39.606074	39.987133	39.972952	39.977009	40.110947	— —	— —
Nuclear-electron	−118.58252	−119.12382	−119.39324	−119.41012	−119.69601	— —	— —
Electron-electron	25.661774	25.648556	25.906717	25.915165	26.003049	— —	— —
Nuclear-nuclear	13.391840	13.391840	13.391840	13.391840	13.391840	— —	13.38589
$-V/T$	2.0078	2.0027	2.0036	2.0036	2.0019	— —	2.0002
$E(1a_1)$	−11.2737	−11.2822	−11.2267	−11.2237	−11.2133	−11.2066	−11.21478
$E(2a_1)$	0.962823	0.97053	0.948440	−0.947059	−0.944704	−0.9439	−0.93433
$E(1t_2)$	−0.529886	−0.555569	−0.543486	−0.543535	−0.543738	−0.5412	−0.53627

Table 12

Gross atomic, net atomic, and overlap populations for methane

	Basis I	Basis IV	Basis V	BasisVI	P.L.
Gross					
C	6.7512	6.5508	6.5736	6.4708	6.534
H	0.8122	0.8623	0.8566	0.8823	0.867
Net					
C	5.2877	5.3048	5.3252	5.0948	4.974
H	0.4712	0.4957	0.4863	0.5251	—
Overlap					
C−H	0.7714	0.7418	0.7506	0.7723	0.780
H−H	−0.0431	−0.0467	−0.0454	−0.0474	—

estimated a dipole of 1.52D, and the more recent evaluation of 1.792D by Arrighini and his co-workers[28] as well as the more qualitative prediction of bond polarity by Coulson.[31]

A summary of those multipole moments which characterise the charge distribution of CH_4 is presented in Table 13. In general, the computed values of $\langle r^2 \rangle$ are in good agreement with the experimental value of -33.69 ± 0.72 a.u., obtained as the difference between total[32] and paramagnetic[33] susceptibilities. The only non-vanishing component of the electric octupole moment, *xyz*, is also listed in Table 13, together with the somewhat dubious experimental value of Stogryn and Stogryn,[34] who take an average of a wide variety of theoretical and experimental estimates. A general observation, however, is that there is little discrepancy between those moments computed from our wave functions and those from the wave function of Arrighini *et al.*

Table 13

Multipole moments of the charge distribution of methane

	Basis IV	Basis V	Basis VI	A.G.M.M.S.	Exptl.
$\langle r^2 \rangle$					
Total	−35.9553	−35.9192	−36.0753	−35.3025	−33.69
$1a_1$	0.0978	0.0978	0.0978		
$2a_1$	3.5885	3.5912	3.5879		
$1t_2$	4.7638	4.7569	4.7840		
R_{xyz}					
Total	1.1074	1.1135	0.9486	1.1723	2.53
Nuclear	6.7934	6.7934	6.7934	6.8024	6.80
Electronic	−5.6860	−5.6799	−5.8448	−5.6301	4.27

---

[31] C. A. Coulson, *Trans. Farad. Soc.*, **38**, 433 (1942).

[32] C. H. Anderson and N. F. Ramsey, *Phys. Rev.*, **149**, 14 (1966).

[33] N. F. Ramsey, 'Molecular Beams', Oxford University Press, New York, 1956.

[34] D. E. Stogryn and A. P. Stogryn, *Mol. Phys.*, **11**, 371 (1966).

The potentials at the H and C nuclei (Table 14) are consistent with those of Pitzer [25] and reveal little change of any significance over the series of bases examined. The values of diamagnetic shielding as derived from bases IV, V, VI, and that of Pitzer are, respectively, 86.845, 86.875, 87.078, and 88.006 ppm. At present, however, lack of experimental data precludes evaluation of the relative accuracy of these calculations.

Table 14

Potential at proton and carbon in methane

	V(H)				V(C)			
	Basis IV	Basis V	Basis VI	Pitzer	Basis IV	Basis V	Basis VI	Pitzer
Total	−1.1003	−1.1020	−1.1134	−1.1352	−14.7013	−14.7030	−14.7431	−14.731
Nuclear	3.7925	3.7925	3.7925	3.8230	1.9357	1.9357	1.9357	1.951
Electronic	−4.8928	−4.8945	−4.9059	−4.9582	−16.6370	−16.6387	−16.6788	−16.682

The high symmetry of the methane molecule permits the existence of a finite electric field at the H nuclei only, the resulting vector being composed of three equal components directed along each of the local cartesian axes. The composition of the field along anyone of these directions is given in Table 15 in terms of the nuclear and electronic contributions. As expected, the relative accuracy of each basis, as determined by the magnitude of the residual Hellman-Feynman [9] force, increases uniformly and directly with the total energy of the system, lending support to our previous conclusions.

Table 15

Electric field at a proton in methane

	E_i(H)			
	Basis IV	Basis V	Basis VI	Pitzer
Total	0.0504	0.0479	0.0325	0.0337
Nuclear	0.9354	0.9354	0.9354	0.8232
Electronic	−0.8850	−0.8875	−0.9029	−0.7895

Values of the xy (and, by symmetry, xz and yz) component of the electric field gradient tensor at the H nuclei are reported in Table 16 together with estimates of the related quadrupole coupling constant $(\mathbf{e}Qq/h)_D$ in which Q is assumed to be 0.2796×10^{-26} esu$\cdot$ cm^2 (Ref. [23]). All computed coupling constants are similar and fall well within the experimental error associated with the rather uncertain observed result [32] of 100 ± 50 kc sec^{-1}.

Ethane. Two S.C.F. computations were performed on the staggered configuration of ethane, using the equilibrium molecular dimensions [35] C—C = = 2.9159 a.u. and C—H = 2.1154 a.u. The first wave function was expanded in terms of a small basis of free-atom S.G.T.O.,namely,$(s_N5, s_F6:3/s_N3)$.

---

[35] G. E. Hanson and D. M. Dennison, *J. Chem. Phys.*, **20**, 313 (1952).

This basis set, denoted as I, was then re-organised and distributed in a manner consistent with the nuclear geometry, as shown in Figure 2*b*. This produced the localised basis set used in the construction of wave function II. This second set is described concisely as $(s_N\,5, s_F\,1:3, s_F\,3:3/s_N 3)$, where the single set of 'floating' orbitals refers to the group of S.G.T.O. positioned on the C—C axis, while the remaining three sets are those directed along the C—H bonds. This latter orbital model was also used in a subsequent S.C.F. determination of the charge distribution in the eclipsed configuration of the molecule (basis III).

The relevant energies associated with each of the three basis sets are given in Table 14. Also quoted are the corresponding results of Fink and Allen [36] (F.A.), who employ an expanded set of the atomic G.L.F. orbitals of Whitten [26] which produce an atomic energy of double zeta Hartree-Fock accuracy. The best S.C.F. total energy published to date is that due to Veillard, [37] who reports an energy of −79.2377 a.u. for his

Table 16

Field gradient at proton and related quadrupole coupling constant in methane

	Basis IV	Basis V	Basis VI	A.G.M.M.S.	Pitzer
$\langle 3xy/r^5 \rangle$					
Total	0.16450	0.16212	0.16858	0.15803	0.16935
Nuclear	0.71893	0.71893	0.71893	0.71792	0.73643
Electronic	−0.55443	−0.55681	−0.55035	−0.55989	−0.56709
$(eqQ/h)_D$	108.09	106.53	110.77	103.84	112.

Table 17

Total energy, energy components, and orbital energies of ethane at experimental geometry

Energy	Staggered			Eclipsed	
	Basis I	Basis II	F.A.	Basis III	F.A.
Total	−79.081789	− 79.093707	− 79.14778	−79.088614	− 79.14377
Kinetic	78.759034	78.768676	78.99142	78.783810	79.00441
Nuclear-Electron	−266.76404	−266.81541	−267.2823	−266.85633	−267.3136
Electron-Electron	66.990822	67.020633	67.21208	67.044023	67.22699
Nuclear-Nuclear	41.932392	41.932392	41.93098	41.939882	41.93845
$-V/T$	2.0041	2.0041	2.0040	2.0039	2.0035
$E(1a_{1g})$	− 11.2369	− 11.2336	− 11.2313	− 11.2317	− 11.2300
$E(1a_{2u})$	− 11.2363	− 11.2330	− 11.2306	− 11.2312	− 11.2293
$E(2a_{1g})$	− 1.02547	− 1.02346	− 1.0055	− 1.02254	− 1.0052
$E(2a_{2u})$	− 0.841035	− 0.839743	− 0.83087	− 0.838854	− 0.83038
$E(3a_{1g})$	− 0.496596	− 0.497839	− 0.48879	− 0.496992	− 0.48850
$E(1e_u)$	− 0.600076	− 0.599379	− 0.59553	− 0.599742	− 0.59618
$E(1e_g)$	− 0.485260	− 0.485911	− 0.48031	− 0.483295	− 0.47873

[36] W. FINK and L. C. ALLEN, *J. Chem. Phys.*, **46**, 2261 (1967)-

[37] A. VEILLARD, *Chem. Phys. Lett.*, **3**, 128 (1969).

extended G.T.O. basis set, whereas the present best minimum S.T.O. energy of −79.09797 has been accomplished by Pitzer.[38]

From energy considerations alone, it is clear that model II provides the more favourable orbital distribution for staggered ethane, both sets achieving the level of minimum S.T.O. accuracy. All orbital energies produced by our wave functions are in excellent agreement with those of Fink and Allen, despite total energy differences of the order 0.06 a.u.

The barrier to internal rotation in ethane is of some interest and has been determined experimentally by Pitzer,[39] who recorded a barrier height of 12.03 ± 0.52 kJ mol^{-1}. By computing total energy differences between the eclipsed and staggered configurations we estimate, using the comparable bases of II and III, a potential barrier of 17.9 kJ mol^{-1} while Fink and Allen obtain the more accurate value of 10.53 kJ mol^{-1}. Even so, considering the smallness of our bases and the lack of geometrical optimisation, our calculations have proved rewarding and promote confidence for future investigations of this type.

The gross atomic, net atomic, and overlap populations of staggered and eclipsed ethane are shown in Table 18, the results for the former configuration being compared with those of Palke and Lipscomb[29] (P.L.). The only substantial dissimilarity which exists between our results and those of Palke and Lipscomb is the large discrepancy in the C−C overlap populations. The C−C bond density exhibited by our bases is much smaller than that proposed by Palke and Lipscomb, which is indicative of a freely rotating C−C axis, in accord with experiment.[39] The most significant change which occurs on rotation from the staggered to eclipsed forms is the reduction of the C−C overlap density, suggesting some weakening of the molecular structure. From considerations of the second and quadrupole moments (Table 19) it appears that internal rotation from the staggered to eclipsed configuration is accompanied by a slight elongation of the charge density along the molecular axis. The results of Sovers, Karplus and Kern[40] (S.K.K.), who used a less accurate wave function

Table 18

Gross atomic, net atomic, and overlap populations of ethane.

	Basis I	Basis II	P.L.	Basis III
Gross				
C	6.4251	6.4446	6.372	6.4497
H	0.8583	0.8518	0.876	0.8501
Net				
C	5.3682	5.3762	4.839	5.3995
H	0.4995	0.4879	—	0.4822
Overlap				
C−H	0.4628	0.4714	0.710	0.4249
C−H	0.7667	0.7704	0.785	0.7737

---

[38] R. M. Pitzer, *J. Chem. Phys.*, **47**, 965 (1967).

[39] K. S. Pitzer, *Disc. Faraday Soc.*, **10**, 66 (1961).

[40] O. J. Sovers, M. Karplus, and C. W. Kern, *J. Chem. Phys.*, **45**, 3895 (1966).

Table 19

Second and quadrupole moments[a] of the charge distribution of ethane

	Staggered			Eclipsed	
	Basis I	Basis II	S.K.K.	Basis III	S.K.K.
Q_{xx}					
Total	−15.098	−15.053	−16.820	−14.998	−16.743
Nuclear	15.526	15.526	15.526	15.526	15.526
Electronic	−30.624	−30.579	−32.346	−30.524	−32.269
Q_{zz}					
Total	−16.060	−16.002	−17.713	−16.032	−17.810
Nuclear	71.853	71.853	71.853	71.853	71.853
Electronic	−87.913	−87.855	−89.566	−87.885	−89.663
θ_{zz}					
Total	− 0.962	− 0.949	− 0.893	− 1.034	− 1.066
Nuclear	56.327	56.327	56.327	56.327	56.327
Electronic	−57.289	−57.276	−57.220	−57.361	−57.393

due to Pitzer and Lipscomb[41] (total energy = −78.5704 a.u.), support this observation, although the absolute magnitude of their moments is at variance with ours. An estimate of the (average) molecular quadrupole moment of $-0.7 \pm 0.2 \times 10^{-26}$ esu cm^2 has been obtained from microwave line-broadening studies by Hill and Smith.[42,43] The presence of a centre of symmetry in the staggered molecule precludes the existence of third moments of the charge distribution.

A comparative study of the potentials at the H and C nuclei (Tables 20, 21) in both configurations reveals little change in the local charge distribution when rotation occurs, a uniformity which is also reflected by the computed electric fields.

Ethylene and Acetylene. In both ethylene and acetylene, π orbitals are super-imposed on the electronic structure. Within the present computational framework, these π orbitals are treated in a manner completely analogous to that of Whitten,[26] each orbital being expanded in terms of antisymmetric combinations of the appropriate 'floating' *s* function on each carbon centre. The density map of the $1b_{3u}$ orbital in ethylene (obtained

Table 20

Potential at carbon and proton in ethane

	V(C)		V(H)	
	Basis II	Basis III	Basis II	Basis III
Total	−14.6915	−14.6933	−1.1087	−1.1096
Nuclear	4.2277	4.2276	5.5221	5.5246
Electronic	−18.9192	−18.9209	−6.6308	−6.6342

---

[41] R. M. Pitzer and W. N. Lipscomb, *J. Chem. Phys.*, **39**, 1995 (1963).

[42] R. M. Hill and W. V. Smith, *Phys. Rev.*, **82**, 451 (1951).

[43] W. V. Smith, *J. Chem. Phys.*, **25**, 510 (1956).

Table 21

Electric field at carbon and proton in ethane

	$E(\mathrm{C})$		$E(\mathrm{H})$	
	Basis II	Basis III	Basis II	Basis III
E_x				
Total			0.0703	0.0683
Nuclear			1.6606	1.6579
Electronic			−1.5903	−1.5896
E_z				
Total	0.0119	0.0129	0.0290	0.0300
Nuclear	0.6293	0.6293	0.8790	0.8821
Electronic	−0.6174	−0.6164	−0.8500	−0.8521

using wave function II), displayed in Figure 3, clearly illustrates that such a combination of S.G.T.O. does, in fact, afford the familiar form of a π molecular orbital.

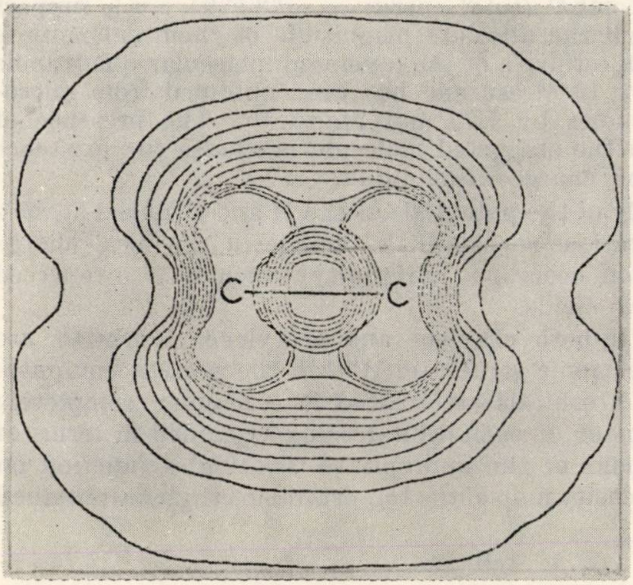

Fig. 3. — $1b_{3u}$ π orbital of ethylene (contours from 0.0 to 1.0 in steps of 0.05).

Wave functions were constructed for the two molecules, therefore, using small atomic basis sets, with free-atom exponents and distances, of the form $(s_N\,5,\ s_F\,6:3/s_N\,3)$. In order to conduct a similar investigation to that of ethane, a second S.C.F. calculation was performed for ethylene in which the positions of those carbon 'valence' orbitals lying in the molecular plane were varied so as to be situated along the lines of the nuclear force fields, as shown in Figure 2 *c*. This basis, labelled II, is described succinctly as $(s_N\,5,\ s_F\,1:3,\ s_F\,2:3,\ s_F\,2:3/s_N\,3)$, where the first two groups of 'floating' orbitals refer to those S.G.T.O. situated on the C−C and C−H bonds, respectively, and the third comprises those functions used to simulate the ethylenic π orbital. Equilibrium nuclear geometries of C−C = 2.5262 a.u., C−H = 2.0523 a.u. and $\mathrm{H\hat{C}H} = 117.3°$ for ethylene,[15] and C—C = 2.281 a.u. and C—H = 2.002 a.u. for acetylene [15] were assumed in all the calculations.

The energy components obtained for each molecule are shown in Tables 22 and 23 and are to be compared with the respective present best S.C.F. values of −78.0140 a.u. (Ref. [44]) and −76.8450 a.u. (Ref. [45]).

Table 22

Total energy, energy components, and orbital energies of ethylene at experimental geometry

Energy	Basis I	Basis II	B.P.W.I	B.P.W.II
Total	−77.896135	−77.902688	−77.9399	−78.0012
Kinetic	77.654695	77.661158		
Nuclear-electron	−247.19685	−247.22449		
Electron-electron	58.345735	58.360367		
Nuclear-nuclear	33.300281	33.300281		
$-V/T$	2.0030	2.0031	1.9876	2.0010
$E(1a_g)$	−11.2486	−11.2466	−11.3144	−11.2341
$E(1b_{1u})$	−11.2470	−11.2450	−11.3130	−11.2326
$E(2a_g)$	−1.04059	−1.03967	−1.0486	−1.0324
$E(2b_{1u})$	−0.789897	−0.789511	−0.8151	−0.7987
$E(3a_g)$	−0.582361	−0.583792	−0.6009	−0.5847
$E(1b_{2u})$	−0.643716	−0.643127	−0.6661	−0.6462
$E(1b_{3g})$	−0.501533	−0.502913	−0.5295	−0.5064
$E(1b_{3u})$	−0.376816	−0.375723	−0.4064	−0.3676

Table 23

Totalenergy, energy components, and orbital energies of acetylene at equilibrium geometry

	Present	B.P.W.I	B.P.W.II
Total	−76.696805	−76.7218	−76.7916
Kinetic	76.452487	—	—
Nuclear-electron	−227.70047	—	—
Electron-electron	49.813737	—	—
Nuclear-nuclear	24.737441	—	—
$-V/T$	2.0031	1.9747	1.9986
$E(1\,\sigma_g)$	−11.2595	−11.4141	−11.2585
$E(1\,\sigma_u)$	−11.2559	−11.4105	−11.2548
$E(2\,\sigma_g)$	−1.04096	−1.0897	−1.0406
$E(2\,\sigma_u)$	−0.761581	−0.8069	−0.7658
$E(3\,\sigma_g)$	−0.679987	−0.7309	−0.6835
$E(1\,\pi_u)$	−0.408328	−0.4761	−0.4131

---

[44] T. H. Gunning, W. J. Hunt, and W. A. Goddard, *Chem. Phys. Lett.*, **4**, 147 (1969).

[45] A. D. McLean and M. Yoshimine, *I.B.M. Journal of Res. and Devel.*, Supplement (1967).

Also included in these Tables are the energies obtained by Buenker, Peyerimhoff, and Whitten [46] using a basis of contracted gaussian lobe functions [26] (B.P.W.I.) and also those from a much more expanded version of this (B.P.W.II).

It is evident from the total S.C.F. energies (Table 22) that our localised orbital model for ethylene provides the more accurate wave function. Further evidence to support this conclusion is provided by the subsequent analysis of the residual forces for each wave function, as evaluated from the computed electric field (Table 24). Both models are consistent, however, in that they both exhibit improvements over the best minimum S.T.O. energy of −77.8343 a.u., achieved by Palke and Lipscomb, [29] and also predict orbital energies extremely close to those of B.P.W.II. Similar conclusions hold for the acetylene molecule, our wave function providing an energy 0.06 a.u. below that of the best minimum S.T.O. value of −76.6416 a.u. (Ref. [18]) and orbital energies of the same accuracy as B.P.W.II.

Table 24

Electric field at carbon and proton in ethylene

	$E_z(C)$		$E_x(H)$		$E_z(H)$	
	Basis I	Basis II	Basis I	Basis II	Basis I	Basis II
Total	0.0175	0.0165	0.0757	0.0720	0.0434	0.0414
Nuclear	0.8056	0.8056	1.4833	1.4833	1.1478	1.1478
Electronic	−0.7881	−0.7891	−1.4076	−1.4113	−1.1044	−1.1064

Electric field at proton and carbon in acetylene

$E_z(H)$			$E_z(C)$		
Total	Nuclear	Electronic	Total	Nuclear	Electronic
0.0852	1.8494	−1.7642	0.0277	0.9582	−0.9305

The results of the Mulliken population analysis are reported in Tables 25 and 26 and compared with those from the S.T.O. wave functions of Palke and Lipscomb mentioned above. The populations computed from both sources are similar and exhibit the same chemical tendencies. For instance, the difference between the C−C overlap population for bases I and II of ethylene and that of acetylene is approximately equal to 1.0, accounting for the additional π bond present in the latter. Palke and Lipscomb estimate a smaller increase of 0.7. Both sets of results also indicate that the hydrogen atoms are more positively charged in C_2H_2 than in C_2H_4, which reflects the greater acidity of the acetylene.

We computed the second and quadrupole moments (Table 27) of the respective charge distributions as well as the potentials (Table 28) and electric fields (Table 24) at each nucleus. Since most previous experi-

---

[46] R. J. Buenker, S. D. Peyerimhoff, and J. L. Whitten, *J. Chem. Phys.*, **46**, 2029 (1967).

Table 25

Gross atomic, net atomic, and overlap populations of ethylene

	Basis I	Basis II	P.L.
Gross			
C	6.3072	6.3178	6.278
H	0.8464	0.8411	0.861
Net			
C	5.2306	5.2265	4.860
H	0.4428	0.4353	— —
Overlap			
C—C	1.0501	1.0747	1.211
C—H	0.7852	0.7853	0.812

Table 26

Gross atomic, net atomic and overlap populations of acetylene

	Present	P.L.
Gross		
C	6.2438	6.188
H	0.7562	0.812
Net		
C	4.9717	4.840
H	0.3106	0.402
Overlap		
C—C	2.0117	1.875
C—H	0.7211	0.820

Table 27

Second and quadrupole moments[a] of the charge distribution of C_2H_4

	Q_{xx}	Q_{yy}	Q_{zz}	θ_{xx}	θ_{yy}	θ_{zz}	$\langle r^2\rangle^b$
Basis I	−12.2899	−15.7737	−12.2580	−1.7260	−3.4998	1.7738	23.2686
Basis II	−12.2524	−15.7815	−12.2258	−1.7513	−3.5424	1.7912	23.2557

Second and quadrupole moments[a] of the charge distribution of acetylene

Q_x	Q_{zz}	θ_{xx}	θ_{zz}	$\langle r^2\rangle^b$
−13.7338	−6.8040	−3.4649	6.9298	17.0367

a. In units of 10^{-26} esu-cm^2

b. In units of 10^{-16} cm^2

Table 28

Potential at proton and carbon in ethylene

	V(H)		V(C)	
	Basis I	Basis II	Basis I	Basis II
Total	−1.0867	−1.0880	−14.6875	−14·6894
Nuclear	5.0988	5.0988	3.3504	3.8504
Electronic	−6.1855	−6.1868	−18.5379	−18.5398

Potential at proton and carbon in acetylene

Total	V(H) Nuclear	electronic	Total	V(C) Nuclear	electronic
−1.0077	4.5570	−5.5647	−14.6842	3.3634	−18.0476

mental studies of the molecular properties of ethylene and acetylene have been concerned with the electronic spectra of the molecules, proper consideration of the calculated quantities must wait on future determination of the necessary experimental data.

Table 29

Electric field gradient and related quadrupole coupling constant at D in C_2D_2

	Present	K.K.	Exptl.
Total	0.3739	0.473	
Nuclear	1.6563	1.656	
Electronic	1.2824	1.183	
(EgQ/h)/i$^{a}_{D}$	245.7	311.	200±10

a In Kc sec^{-1}.

The quadrupole coupling constant of D in C_2D_2 was investigated theoretically by Kern and Karplus [47] (KK), who employed a minimum S.T.O. wave function previously obtained by McLean [48] (total energy = = 76.5438 a.u.). The results of this study, together with those derived from our wave function, are recorded in Table 29. Our calculation compares rather better with the experimental value of 200 ± 10 Kc sec^{-1} determined by Ramsey. [49]

Diborane. The diborane molecule is of interest because of the nature of the central bridge bonding system. The geometry of the molecule is well understood [50] and consists of four co-planar terminal hydrogen atoms (H_t) and two bridging hydrogen atoms (H_b) situated directly above and below the plane of the other six atoms. The equilibrium molecular dimensions are B$-$B $= 3.3543$ a.u., B$-$H $= 2.2602$ a.u., B$-$H $= 2.5304$ a.u., and H $\hat{\mathrm{B}}$H $= 120°$.

---

[47] C. W. Kern and M. Karplus, *J. Chem. Phys.*, **42**, 1062 (1965).

[48] A. D. McLean, *J. Chem. Phys.*, **32**, 1595 (1960).

[49] N. F. Ramsey, *Amer. Scientist*, **49**, 509 (1961).

[50] L. S Bartell and B. L. Carroll, *J. Chem. Phys.*, **42**, 1135 (1965)-

The interest in the bonding in B_2H_6 pivots around the fact that this molecule belongs to that class of electron-deficient species which possess insufficient electrons to satisfy the ideal requirement of two electrons per bond. The basic bonding scheme, [51] therefore, incorporates four two-electron $B-H_t$ bonds and two three centre two-electron $B-H_b-B$ bonds. Within the M.O. formalism, however, no preconceived notions about the strong interactions are necessary and our wave functions were evaluated without recourse to such *ad hoc* restrictions. The purpose of this study was twofold, therefore. Firstly, in common with our previous studies, we wished to investigate the effect of using a localised atomic basis set and, secondly, we attempt to justify the above assertions concerning the utility of M.O. theory.

As before, basis I comprised an assembly of free-atom S.G.T.O. and basis II represented the result of an imaginary polarisation process. To avoid any bias towards the $B-H_b$ bonds a set of S.G.T.O. was also situated along the B$-$B axis, and hence our two bases are of the form $(s_N\,5, s_F\,6:3/s_N\,3)$ and $(s_N\,5, s_F\,1:3, s_F\,2:3, s_F\,2:3/s_N\,3)$. The results of the subsequent S.C.F. energy evaluation are shown in Table 30 and, from the total energies, it is clear that basis II, by taking proper account of the molecular geometry, provides the better model. Both models, in fact, yield a total energy lower than that of the present best minimum S.T.O. [29]

Table 30

Total energy, energy components, and orbital energies of diborane at experimental geometry

	Basis I	Basis II	B.P.A.W.	B.K.
Total	-52.709666	-52.717504	-52.7551	-52.753
Kinetic	52.621613	52.626537	— —	— —
Nuclear-electron	-183.73826	-183.77423	— —	— —
Electron-electron	46.643378	46.666592	— —	— —
Nuclear-nuclear	31.763599	31.763599	— —	— —
$-V/T$	2.0017	2.0017	1.9976	— —
$E(1a_g)$	-7.64254	-7.63949	-7.6484	-7.6416
$E(1b_{1u})$	-7.64199	-7.63894	-7.6479	-7.6410
$E(2a_g)$	-0.893585	-0.892244	-0.8734	-0.8979
$E(2b_{1u})$	-0.645864	-0.644993	-0.6427	-0.6457
$E(1b_{3u})$	-0.557126	-0.557960	-0.5493	-0.5558
$E(1b_{2u})$	-0.541961	-0.541138	-0.5285	-0.5546
$E(3a_g)$	-0.521941	-0.522466	-0.5205	-0.5174
$E(b_{3g})$	-0.471412	-0.471530	-0.4744	-0.4737

---

[51] W. N. Lipscomb, 'Boron Hydrides', Benjamin (New York), 1963.

energy of −52.6782 a.u. Also included in Table 30 are the results of Buenker [52] and his associates (B.P.A.W.), who use a slightly expanded version of Whitten's gaussian lobe functions [26] and also the results of an investigation by Burnelle and Kaufman, [53] using a contracted extended G.T.O. basis of Huzinaga. [54] It will be noted that our wave functions provide energies which compare favourably with both these sets of results.

Table 31

Gross atomic, net atomic, and overlap populations of diborane

	Basis I	Basis II	P.L.	B.K.
Gross				
B	5.0480	5.0686	5.283	5.088
H_t	0.9993	0.9941	0.908	1.002
H_b	0.9534	0.9432	0.901	0.955
Net				
B	4.1331	4.1405	— —	— —
H_t	0.5450	0.5355	— —	— —
H_b	0.6732	0.6534	— —	— —
Overlap				
$B-B$	0.1840	0.2012	0.291	0.064
$B-H_t$	0.8383	0.8415	0.864	0.880
$B-H_b$	0.3293	0.3325	0.399	0.345
H_b-H_b	−0.1360	−0.1273	— —	— —

The resultant gross atomic, net atomic, and overlap populations of B_2H_6 are shown in Table 31. For comparison, we have also tabulated the results of Palke and Lipscomb [29] (best minimum S.T.O.) and Burnelle and Kaufman. [53] From the overlap population it is clear that the $B-H_t$ bonds form the strongest link, followed by the $B-H_b$, then $B-B$ and, finally, H_b-H_b. (It seems from our results that the H_b-H_b bond merits as much attention as the well-studied $B-B$ bond.) All atoms in the molecule are almost neutral, with B having a slight excess of electron density and H_b redressing the balance with a corresponding positive charge. These results are borne out by those of Burnelle and Kaufman but differ from those of Palke and Lipscomb. The latter workers obtain more highly charged atoms, with B possessing a negative charge of 0.28 and H_t and H_b having positive charges of 0.09 and 0.10, respectively. A further interesting feature of Burnelle and Kaufman's results is the very low $B-B$ charge density.

Despite numerical differences, however, all results are indicative of a weak $B-B$ bond and a much stronger three-centre $B-H_b-B$ interaction, as proposed previously. The density plot (as computed from wavefunction II) of the only out-of-plane bonding orbital ($1b_{3u}$) is shown in

---

[52] R. J. Buenker, S. D. Peyerimhoff, L. E. Auen, and J. L. Whitten, *J. Chem. Phys.*, **45**, 2835 (1966).

[53] L. Burnelle and J. J. Kaufman, *J. Chem. Phys.*, **43**, 3540 (1965).

[54] S. Huzinaga, *J. Chem. Phys.*, **42**, 1293 (1965).

Figure 4. It is evident from this that two three-centre bonds do indeed exist, with maxima situated at the centres of the $B-H_b-B$ triangles. It should be emphasised here that the above results have been obtained from a completely objective choice of orbital basis set.

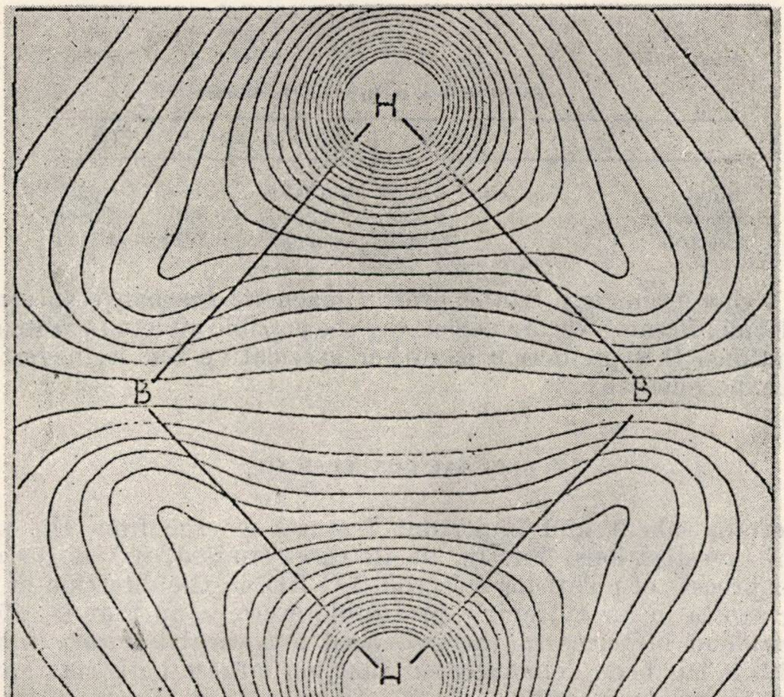

Fig. 4. — Three-centre bonds in diborane ($1b_{3u}$ orbital) (contours from 0.002 to 0.15 in steps of 0.0075).

No reliable estimates have, as yet, been published for the quadrupole moments of the diborane molecule. Nevertheless, we record our results in Table 32 in the expectation that they will provide a useful comparison for future calculations.

Finally, the potentials at B, H_t, and H_b are reported in Table 33. The values of the related average diamagnetic shielding at H_t and H_b are 95.09 and 110.25 p.p.m., respectively, which suggests that H_b will resonate

Table 32

Second and quadrupole moments[a] **of the charge distribution of diborane**

	Basis I	Basis II
Q_{xx}	-16.1662	-16.0919
Q_{yy}	-18.8113	-18.7744
Q_{zz}	-19.2094	-19.1947
θ_{xx}	2.8442	2.8927
θ_{yy}	-1.1235	-1.1311
θ_{zz}	-1.7207	-1.7616
$\langle r^2 \rangle$[b]	34.3291	34.3029

[a] In units of 10^{-26} esu-cm^2
[b] In units of 10^{-16} cm^2

Table 33

Potential at B, H_t and H_b in diborane

	$V(H_t)$	$V(H_b)$	$V(B)$
Total	-1.0339	-0.9717	-11.1575
Nuclear	4.3232	5.2396	3.5755
Electronic	-5.3571	-6.2113	-14.7330

Electric field at B, H_t and H_b in diborane

	$E_2(B)$	$E_y(H_t)$	$E(H_t)$	$E(H_b)$
Total	0.0639	0.0154	0.0399	0.0235
Nuclear	0.5296	1.0693	0.8310	1.3666
Electronic	-0.4657	-1.0539	-0.7911	-1.3431

at the higher frequency in the proton magnetic resonance spectrum of the molecule. Because we are neglecting the possible effect of paramagnetic contributions, this prediction is rather speculative but is, nevertheless, verified experimentally.[55]

GENERAL CONCLUSIONS

Certain salient and important features emerge from the present series of investigations. Firstly, in all cases studied, it was discovered that our process of polarising selected S.G.T.O. in the direction of neighbouring atoms in an extremely profitable exercise, in that it affords a large dividend in terms of the increased numerical accuracy attained. Secondly, it has been demonstrated that our largest basis sets have the capacity to produce 99.95% of the Hartree-Fock energy of systems, while the smaller sets are capable of achieving 99.7% of this limit with the same reassuring consistency. Perhaps one of the most pleasing aspects of our present analysis is the ability of the small bases to predict, with high precision, the various magnetic and spectroscopic properties studied.

We thank the S.R.C. for a Maintenance Grant (to R.M.A.)

APPENDIX 1

FORMULAE FOR INTEGRAL EVALUATION PROGRAMMES

The derivation of the one- and two-electron integrals necessary in the computation of SCF wave functions was first expounded by Boys for the case of *s*-type orbitals. The general analytic solutions relevant to orbitals of arbitrary angular momentum were then obtained by Huzinaga and the following equations are extracted from his unpublished work. After the general formulae, we list the series of special formulae employed in the present sequence of calculations.

---

[55] J. OGG, *J. Chem. Phys.*, **22**, 1933 (1954).

A. Definition of Gaussian Functions

The uncontracted, or primitive, Gaussian function, λ, on centre A, is defined as

$$\lambda\,(A,\ \alpha,\ l,\ m,\ n) = (A,\ \alpha,\ l,\ m,\ n)$$

$$= N_\alpha\,(x - A_x)^1\cdot(y - A_y)^m\cdot(z - A_z)^n\cdot\exp\,(-\,\alpha r_A^2) \tag{1.1}$$

$$= N_\alpha\, x_A^1\, y_A^m\, z_A^n \exp\,(-\,\alpha r_A^2)$$

The normalisation factor for this Gaussian orbital is

$$N_\alpha = \left(\frac{\pi}{2\alpha}\right)^{\frac{3}{2}} \left\{\frac{(2l-1)\,!\,!\,(2m-1)\,!\,!\,(2n-1)\,!\,!}{2^{2\,(l+m+n)}\,\alpha^{(l+m+n)}}\right\}^{-\frac{1}{2}} \tag{1.2}$$

When the integers l, m, and n are zero we are, in fact, dealing with the spherical s-type Gaussian, defined specifically by

$$S_A = (\mathrm{A},\ \alpha,\ 0,\ 0,\ 0) = \left\{\left(\frac{2\alpha}{\pi}\right)^{\frac{3}{4}}\right\} \exp\,(-\,\alpha\,(r - A)^2) \tag{1.3}$$

The exponent, α, is related to ρ via the relationship $\alpha = 1/\rho^2$, where ρ represents the orbital radius or that distance over which the orbital cannot be considered negligible.

B. Auxiliary Functions

In defining the integrals over Gaussian functions, the following auxiliary functions are used

$$f_j\,(l,\ m,\ a,\ b) = \sum_{i=\max\,(0,\ j-m)}^{i=\min\,(j,\ l)} \binom{l}{i}\binom{m}{j-i}\, a^{l-i}\, b^{m+i-j} \tag{1.4}$$

$$F_\nu\,(t) = \int_0^1 u^{2\nu}\,\bar{\mathrm{e}}^{tu^2}\,\mathrm{d}u \quad (t > 0\,;\ \nu = 0, 1, 2, \ldots) \tag{1.5}$$

The latter function is a form of the Incomplete Gamma Function and is evaluated in the programme, depending on the range of the argument t, by asymptotic expansions, recursion formulae or tabular interpolations. A thorough and detailed discussion of the function is given by Shavitt.[56]

---

[56] I. Shavitt, *Methods in Computational Physics*, **2**, 1 (1963).

In the formulae which follow, all coordinate systems on various centres are parallel and right-handed. Also, the convention $\overline{\mathrm{R1R2}} = \overline{\mathrm{R1}} - \overline{\mathrm{R2}}$ applies throughout.

C. The Overlap Integral

$$\langle \mathrm{A},\ \alpha_1,\ l_1,\ m_1,\ n_1 \,|\, B,\ \alpha_2,\ l_2,\ m_2,\ n_2 \rangle$$

$$= N_1 N_2 \left(\frac{\pi}{\alpha_1 + \alpha_2}\right)^{\frac{3}{2}} \cdot \exp\left(-\frac{\alpha_1 \cdot \alpha_2}{\alpha_1 + \alpha_2} \cdot \overline{AB}^2)\right) \cdot \Sigma_x \Sigma_y \Sigma_z \tag{1.6}$$

where

$$\Sigma_x = \sum_{i=0}^{\frac{1}{2}(l_1 + l_2)} f_{2i}(l_1, l_2, \overline{PA}_x, \overline{PB}_x) \cdot \frac{(2i-1)!!}{2^i \cdot (\alpha_1 + \alpha_2)^i} \tag{1.7}$$

and Σ_y, Σ_z are similarly defined in terms of the corresponding exponents and components in the y- and z- directions. The point P, appearing in (1.7) and the following formulae, is the centre of the new Gaussian function, the product of the Gaussians on A and B;

$$P_i = \frac{\alpha_1 A_i + \alpha_2 B_i}{\alpha_1 + \alpha_2}\ (i = x,\ y,\ z) \tag{1.8}$$

D. Special Formulae for the Matrix Elements of S and p Type Orbitals

In the formulae of this section, the subscripts i, j, k, and l define the axis of a p-type orbital function, and each is to be replaced with the value x or y or z as appropriate.

The Overlap Integral

$$S^{00}(a,\ b) = \langle S_a \,|\, S_b \rangle = N_1 N_2 \left(\frac{\pi}{\alpha_1 + \alpha_2}\right)^{\frac{3}{2}} \exp\left(-\frac{\alpha_1 \alpha_2}{\alpha_1 + \alpha_2} AB^2\right) \tag{1.9}$$

$$S^{i0}(a,\ b) = \langle P_{ia} \,|\, S_b \rangle = -\frac{\alpha_2}{\alpha_1 + \alpha_2} (A_i - B_i)\, S^{00}(a,\ b) \tag{1.10}$$

$$S^{0j}(a,\ b) = \langle S_a \,|\, P_{jb} \rangle = \frac{\alpha_1}{\alpha_1 + \alpha_2} (A_j - B_j)\, S^{00}(a,\ b) \tag{1.11}$$

$$S^{ij}(a,\ b) = \langle P_{ia} \,|\, P_{jb} \rangle =$$

$$= \left\{ \frac{1}{2\,(\alpha_1 + \alpha_2)}\, \delta_{ij} - \frac{\alpha_1 \alpha_2}{(\alpha_1 + \alpha_2)^2} (A_i - B_i)\,(A_j - B_j) \right\} * S^{00}(a,\ b) \tag{1.12}$$

Here, as throughout this section, δ_{ij} is the Kronecker delta.

APPENDIX 2

FORMULAE FOR MATRIX ELEMENTS OF VARIOUS ONE-ELECTRON OPERATORS WITH RESPECT TO SPHERICAL GAUSSIAN-TYPE ORBITALS

In this Appendix we catalogue those expectation values important in the evaluation of one-electron properties of molecules, restricting the list to those involving the spherical Gaussian-type orbitals (1.3) and the components of the operators r_C, r_C^2, r_C^3, $1/r_C$, $(r_i - C_i/r_C^3$ and $(3\,(r_i - C_i)(r_j - C_j) - r_C^2)/r_C^5$ only. Throughout this section we continue to use the notation developed in Appendix 1 ; in particular, r_C represents the vector operator $\bar{r} - \bar{C}$, and $(r_i - C_i) = r_{Ci}$ denotes the component of r_C along one of the principal axes, usually chosen as the x, y, z coordinate system.

A. First Moment of Electron Distribution

$$\begin{aligned}\langle S_a\,|(r_i - C_i)\,|S_b\rangle & \\ &= \langle S_a\,|(r_i - B_i) + (B_i - C_i)\,|S_b\rangle \\ &= \langle S_a\,|(r_i - B_i)\,|\,S_b\rangle + \langle S_a|S_b\rangle\,(B_i - C_i) \\ &= S^{0i}(a,\,b) + (B_i - C_i)\,S^{00}\,(a,\,b),\end{aligned} \tag{2.1}$$

where $S^{00}\,(a, b)$ and $S^{0i}\,(a, b)$ are defined as in 1.9 and 1.11.

B. Second Moment

$$\begin{aligned}\langle S_a\,|\,(r_i - C_i)\,(r_j - C_j)\,|\,S_b\rangle & \\ &= \langle S_a\,|\,\{(r_i - B_i) + (B_i - C_i)\} \ast \{(r_j - B_j) + (B_j - C_j)\}\,|\,S_b\rangle \\ &= \langle S_a\,|\,(r_i - B_i)\,(r_j - B_j)\,|S_b\rangle \\ &+ (B_i - C_i)\,\langle S_a\,|\,(r_j - B_j)\,|\,S_b\rangle \\ &+ (B_j - C_j)\,\langle S_a\,|\,(r_i - B_i)\,|\,S_b\rangle \\ &+ (B_i - C_i)\,(B_j - C_j)\,\langle S_a|S_b\rangle \\ &= \langle S_a\,|\,r_{Bi}\,r_{Bj}\;S_b\rangle + (B_i - C_i)\,S^{0j}\,(a,\,b\,) + \\ &+ (B_j - C_j)\;S^{0i}\,(a,\,b) + (B_i - C_i)\,(B_j - C_j)\,S^{00}\,(a,\,b)\end{aligned} \tag{2.2}$$

The integral $\langle S_a | r_{Bi} r_{Bj} S_b \rangle$ is computed from the general overlap equation (1.6), the function $r_{Bi} r_{Bj} S$ being regarded as a d-type orbital. For instance, if we are considering the xy component of the tensorial operator, we would require the overlap term $\langle A, \alpha_1, 0, 0, 0, | B, \alpha_2, 1, 1, 0 \rangle$.

C. Third Moment

$$\begin{aligned}
&\langle S_a | (r_i - C_i)(r_j - C_j)(r_k - C_k) | S_b \rangle \\
&\quad = \langle S_a \{(r_i - B_i) + (B_i - C_i)\} * \{(r_j - B_j) + (B_j - C_j)\} \\
&\qquad\qquad * \{(r_k - B_k) + (B_k - C_k)\} | S_b \rangle \\
&\quad = \langle S_a | r_{Bi} r_{Bj} r_{Bk} S_b \rangle + (B_i - C_i) \langle S_a | r_{Bj} r_{Bk} S_b \rangle \\
&\quad + (B_j - C_j) \langle S_a | r_{Bi} r_{Bk} S_b \rangle + (B_k - C_k) \langle S_a | r_{Bi} r_{Bj} S_b \rangle \\
&\quad + (B_i - C_i)(B_j - C_j) S^{0k}(a, b) + (B_i - C_i)(B_k - C_k) S^{0j}(a, b) \\
&\quad + (B_j - C_j)(B_k - C_k) S^{0i}(a, b) \\
&\quad + (B_i - C_i)(B_j - C_j)(R_k - C_k) S^{00}(a, b) \qquad (2.3)
\end{aligned}$$

The function $r_{Bi} r_{Bj} r_{Bk} S_b$ is treated as an f orbital and the appropriate integer values for l_2, m_2 and n_2 substituted in (1.6).

D. Electric Potential

The analytic expression for the integral $\langle S_a | 1/r_C | S_b \rangle$ describing the electric potential about the nucleus C, is given explicitly as

$$\begin{aligned}
&\langle S_a | 1/r_C | S_b \rangle \\
&= N_1 N_2 \left(\frac{2\pi}{\alpha_1 + \alpha_2} \right) \exp\left(- \frac{\alpha_1 \alpha_2}{\alpha_1 + \alpha_2} \overline{AB}^2 \right) F_0[(\alpha_1 + \alpha_2) \overline{PC}^2] \qquad (2.4)
\end{aligned}$$

E. Electric Field

In the evaluation of this integral we make use of the differential equation

$$\frac{\partial}{\partial C_i} \left(\frac{1}{r_C} \right) = \frac{(r_i - C_i)}{r_C^3} \qquad (2.5)$$

thus allowing the electric field to be re-formulated as the first derivative of the electric potential (2.4).

$$\langle S_a \,|\, (r_i - C_i)/r_C^3 \,|\, S_b \rangle = \left\langle S_a \left| \frac{\partial}{\partial C_i} (1/r_C) \right| S_b \right\rangle$$

$$= \frac{\partial}{\partial C_i} \left\{ N_1 N_2 \left(\frac{2\pi}{\alpha_1 + \alpha_2} \right) \exp \left(- \frac{\alpha_1 \alpha_2}{\alpha_1 + \alpha_2} \overline{AB}^2 \right) F_0 \, [(\alpha_1 + \alpha_2) \, \overline{PC}^2] \right\} \tag{2.6}$$

Only the Incomplete Gamma Function is dependent on C_i, via the argument $t = (\alpha_1 + \alpha_2) \overline{PC}^2$ and hence, substituting this expression for t and the value zero for the integer ν in equation (1.5) followed by differentiation with respect to C_i, we obtain the result that

$$\langle S_a \,|(r_i - C_i)/r_C^3 \,|\, S_b \rangle$$

$$= N_1 N_2 \left(\frac{2\pi}{\alpha_1 + \alpha_2} \right) \exp \left(- \frac{\alpha_1 \alpha_2}{\alpha_1 + \alpha_2} \overline{AB}^2 \right) [2\,(\alpha_1 + \alpha_2)(P_i - C_i)\, F_1\,(t)]$$

$$= 4\pi N_1 \, N_2 \,(P_i - C_i) \exp \left(- \frac{\alpha_1 \alpha_2}{\alpha_1 + \alpha_2} \overline{AB}^2 \right) F_1 \, [(\alpha_1 + \alpha_2) \, \overline{PC}^2] \tag{2.7}$$

F. Electric Field Gradient

We write the components of the electric field gradient tensor operator as

$$\frac{3\,(r_i - C_i)\,(r_j - C_j) - \delta_{ij}\, r_C^2}{r_C^5} = \frac{\partial}{\partial C_i} \frac{\partial}{\partial C_j} \left(\frac{1}{r_C} \right) + \frac{4}{3} \pi \delta\,(r_c) \tag{2.8}$$

where δ_{ij} is the Kronecker delta and the term involving the three-dimensional delta function, $\frac{4}{3} \pi\delta\,(r_C)$, is the contribution to the operator at $r_C = 0$.

$$\frac{\langle S_a \,|\, 3\,(r_i - C_i)\,(r_j - C_j) - \delta_{ij}\, r_C^2 \,|\, S_b \rangle}{r_C^5}$$

$$= \frac{\partial}{\partial C_i} \frac{\partial}{\partial C_j} \left\langle S_a \left| \frac{1}{r_C} \right| S_b \right\rangle + \frac{4}{3} \pi \,\langle S_a |\, \delta\,(r_C)\, | S_b \rangle \tag{2.9}$$

The first term in this identity is evaluated by means of the straightforward differentiation of the electric potential integral (2.4), that is,

$$\frac{\partial}{\partial C_i}\frac{\partial}{\partial C_j}\left\{N_1 N_2\left(\frac{2\pi}{\alpha_1+\alpha_2}\right)\exp\left(-\frac{\alpha_1\alpha_2}{\alpha_1+\alpha_2}\overline{AB}^2\right)F_0\left[(\alpha_1+\alpha_2)\overline{PC}^2\right]\right\}$$

$$=8\pi N_1 N_2(\alpha_1+\alpha_2)(P_i-C_i)(P_j-C_j)\exp\left(-\frac{\alpha_1\alpha_2}{\alpha_1+\alpha_2}\overline{AB}^2\right)F_2\left[(\alpha_1+\alpha_2)\overline{PC}^2\right]$$

$$-\delta_{ij}\,4\pi N_1 N_2\exp\left(-\frac{\alpha_1\alpha_2}{\alpha_1+\alpha_2}\overline{AB}^2\right)F_1\left[(\alpha_1+\alpha_2)\overline{PC}^2\right] \qquad (2.10)$$

Expanding the second integral in (2.9) explicitly, we obtain the equivalent expression

$$\frac{4}{3}\pi N_1 N_2\int\exp\left(-\alpha_1 r_A^2-\alpha_2 r_B^2\right)\delta(r_C)\,\mathrm{d}r \qquad (2.11)$$

Shavitt [56] has shown that the product of two Gaussians centred on the points A and B produces a third Gaussian, whose centre lies on the line segment $\overline{AB}$, multiplied by a constant factor. Specifically, we have the transformation

$$\exp\left(-\alpha_1 r_A^2-\alpha_2 r_B^2\right)=\exp\left(-\frac{\alpha_1\alpha_2}{\alpha_1+\alpha_2}\overline{AB}^2\right)\exp\left(-(\alpha_1+\alpha_2)\overline{PC}^2\right) \qquad (2.12)$$

which, when substituted into the expression (2.11), results in the reduction of the integral to the form

$$\frac{4}{3}\pi N_1 N_2\exp\left(-\frac{\alpha_1\alpha_2}{\alpha_1+\alpha_2}\overline{AB}^2\right)\exp\left(-(\alpha_1+\alpha_2)\overline{PC}^2\right)\int\delta(r_C)\,\mathrm{d}r$$

$$=\frac{4}{3}\pi N_1 N_2\exp\left(-\frac{\alpha_1\alpha_2}{\alpha_1+\alpha_2}\overline{AB}^2\right)\exp\left(-(\alpha_1+\alpha_2)\overline{PC}^2\right) \qquad (2.13)$$

It is useful at this stage to write the term $\exp\left(-(\alpha_1+\alpha_2)\overline{PC}^2\right)$ in terms of the Incomplete Gamma Functions $F_1\left((\alpha_1+\alpha_2)\overline{PC}^2\right)$ and $F_2\left((\alpha_1+\alpha_2)\overline{PC}^2\right)$, thus making (2.13) more compatible with (2.10) in that, together, they provide a more compact expression for the overall integral (2.9). Thus, the exponential term is now expressed in the more elaborate but nevertheless equivalent form

$$\exp\left(-(\alpha_1+\alpha_2)\overline{PC}^2\right)$$

$$=3F_1\left((\alpha_1+\alpha_2)\overline{PC}^2\right)-2(\alpha_1+\alpha_2)\overline{PC}^2F_2\left((\alpha_1+\alpha_2)\overline{PC}^2\right) \qquad (2.14)$$

This leads to the final result

$$\frac{\langle S_a \mid 3\,(r_i - C_i)\,(r_j - C_j) - \delta_{ij}\, r_C^2 \mid S_b \rangle}{r_C^5}$$

$$\begin{aligned} &= \frac{8}{3}\,\pi N_1\, N_2\,(\alpha_1 + \alpha_2)\,\{3\,(P_i - C_i)\,(P_j - C_j) - \overline{PC}^2\} \\ &* \exp\left(-\frac{\alpha_1\,\alpha_2}{\alpha_1 + \alpha_2}\,\overline{AB}^2\right) F_2\,((\alpha_1 + \alpha_2)\,\overline{PC}^2) \qquad (2.15) \\ &+ (1 - \delta_{ij})\,4\pi N_1\, N_2 \exp\left(-\frac{\alpha_1\alpha_2}{\alpha_1 + \alpha_2}\,\overline{AB}^2\right) F_1\,((\alpha_1 + \alpha_2)\,\overline{PC}^2) \end{aligned}$$

APPENDIX 3

CONVERSION FACTORS

Dipole moments :

1a.u. = 2.54154 Debye

Second moment and Quadrupole moment :

1a.u. = 1.344911×10^{-26} esu/cm^2

Third moment and Octopole moment :

1a.u. = 0.711688×10^{-34} esu/cm^3

Magnetic susceptibility :

1a.u. = 0.280016×10^{-16} cm^2

Potential :

1a.u. = 9.07618×10^{-2} esu/cm

Electric Field :

1a.u. = 0.823770×10^{-2} dynes

Field Gradient :

1a.u. = 0.324123×10^{16} esu/cm^3

Quadrupole Coupling Constants :

1a.u. = 0.235×10^{20} Mc/sec

Revue Roumaine de Chimie, **20**, *11–12*, 1371–1411 (1975)

Revue Roumaine de Chimie, **20**, *11–12*, 1413–1432 (1975)

SPECTRAL SOLVENT EFFECTS IN AROMATIC COMPOUNDS SOLUTIONS. I

SOLVENT EFFECTS ON THE POSITION AND INTENSITY OF THE $^1A_{1g} \rightarrow {}^1B_{2u}$ BENZENE TRANSITION

VASILE MACOVEI
The Physical Chemistry Laboratory, the University of Jassy, Calea 23 August, 11

Received May 28, 1974

This work deals with the benzene spectrum (the $^1A_{1g} \rightarrow {}^1B_{2u}$ band) investigated in a great number of solvents, to draw some general conclusions regarding the position and intensity of the band centered at 2550 Å, under the solvent influence.

I. INTRODUCTION

The investigation of the absorption electronic spectra in solution shows that position and intensity of the spectral bands are greatly influenced by the solvent,[1,2] as compared to their values in gas state. In the benzene case there are various opinions regarding the spectral behaviour in solution : according to some measurements,[3] the vibrational component shifts, in the $^1A_{1g} \rightarrow {}^1B_{2u}$ transition, are not constant. One considers that the first two vibrational components, on the long wave side, display small hypsochromic shifts but the other components are strongly bathochromic displaced. According to other authors,[4,5] the displacements are not constant in the same solvent, but the values do not agree with the previous data.[3] It is asserted,[6] without specifying the solvent, that the benzene band system, at 2550 Å, is displaced by 300 cm^{-1} toward the red. More recently, it was shown[7] that the principal four vibrational components, in this system, are shifted to the red, with equal amounts in the same solvent.

---

[1] S. E. Sheppard, *Rev. Mod. Phys.*, **14**, 303 (1942).
[2] O. P. Girin and N. G. Bakhshiev, *Uspekhi Fiz. Nauk*, **79**, 235 (1963).
[3] K. Lauer and R. Oda, *Ber. dtsch. chem. Ges.*, **69**, 851 (1936).
[4] N. S. Bayliss and L. Hulme, *Austral. J. Chem.*, **6** , 257 (1953).
[5] O. V. Sverdlova, *Opt. i Spektrosk.*, **6**, 349 (1959).
[6] H. Sponer, *Chem. Rev.*, **41**, 281 (1947).
[7] F. A. Trombetti and C. Zauli, *Boll. Sci. Fac. Chim., Bologna*, **21**, 202 (1963).

The explanations of the intensity changes in the benzene ${}^1A_{1g} \rightarrow {}^1B_{2u}$ transition involve especially the changes due to the appearance of the (0, 0) vibrational component, [4,8–13] without taking into account the other factors existing in solution.

To elucidate these problems, new experimental investigations are needed and the benzene spectrum is studied in a large variety of solvents.

II. RESULTS AND DISCUSSION

II.1. THE BAND POSITION

The benzene molecule is easily soluble in the majority of organic solvents, neutral and non-polar. [5] The X-ray and electronic diffraction measurements, [14] confirmed through direct observations, [15,16] show that the dipole moment imposed by the hexagonal symmetry is zero. The readily observable spectral band, [17,18] in the near ultraviolet, represents the transition from the electronic ground state, ${}^1A_{1g}$, to the electronic singlet excited state, ${}^1B_{2u}$, symmetrical relatively to the reflection plane of the benzene ring. [19–22] The principal vibrational components in the system correspond with the series [7] : $\tilde{\nu} = 38{,}089 + 520 + v.923$ cm^{-1} ($v = 0, 1, 2, \ldots$), that is the transitions from the ground state, with the zero point vibrational level, to the excited state vibrational levels with $v = 0, 1, 2, \ldots$ vibrational quanta, totally symmetrical, a_{1g}, of 920 cm^{-1}, plus a vibrational quantum of 520 cm^{-1}, e_{2g}. [22] The principal four bands, in the system at 2550 Å, are displaced with the same quantity in the same solvent, and the frequency $\tilde{\nu} = 923$ cm^{-1}, between the vibrational components in the vapour spectrum are preserved also in solution. [7] Our results validate the maintenance of constant separation between vibrational components in various solvents, within the limit of the experimental errors, and are listed in table 1. Because all of the vibrational components are displaced with the same quantity in the same direction, the examination of the most intense vibrational component will reflect the spectrum shift as a whole. The position values of this component, $\tilde{\nu}_{max}$, in vapour is different, according to various authors : some of them [23,24] give the 39,463 cm^{-1} (4.89 ev) value ; the others [7] give the position at 39,539 cm^{-1}. Considering the 39,539 cm^{-1} value as the vapour position, we find, in the majority of the solvents used, that the spectral displacement of benzene

---

[8] H. Sponer, G. Nordheim, A. L. Sklar, and E. Teller, *J. Chem. Phys.*, **7**, 207 (1939).

[9] J. S. Ham, J. R. Platt, and H. McConnell, *J. Chem. Phys.*, **19**, 1301 (1951).

[10] J. S. Ham, *J. Chem. Phys.*, **21**, 756 (1953).

[11] Y. Kanda and R. Shimada, *Spectrochim. Acta*, **17**, 7 (1961).

[12] Y. Kanda, Y. Gondo and H. Shimada, *Spectrochim. Acta*, **17**, 424 (1961).

[13] H. Tsubomura and R. P. Lang, *J. Chem. Phys.*, **36**, 2155 (1962).

[14] P. W. Alen and L. E. Sutton, *Acta Cryst.*, **3**, 46 (1950).

[15] K. B. McAlpine and C. P. Smith, *J. Amer. Chem. Soc.*, **55**, 433 (1933).

[16] L. G. Groves and S. Sugden, *J. Chem. Soc.*, **1934**, 1094.

[17] L. Skulski, *Bull. Acad. polon. Sci., Ser. Sci. Chim.*, **10**, 201 (1962).

[18] A. I. Kiss and G. Horvath, *Acta Chim. Sci. Hung.*, **39**, 39, (1963).

[19] M. G. Mayer and L. Sklar, *J. Chem. Phys.*, **6**, 645 (1938).

[20] C. C. J. Roothaan and R. S. Mulliken, *J. Chem. Phys.*, **16**, 118 (1948).

[21] C. C. J. Roothaan and R. G. Parr, *J. Chem. Phys.*, **17**, 1001 (1949).

[22] R. Pariser and R. G. Parr, *J. Chem. Phys.*, **21**, 767 (1953).

[23] H. B. Klevens and J. R. Platt, *J. Amer. Chem. Soc.*, **71**, 1714 (1949).

[24] K. Kimura, H. Tsubomura, and S. Nagakura, *Bull. Chem. Soc., Japan*, **37**,1336 (1964).

Table 1

Band positions in the benzene electronic transition $^1A_{1g} \rightarrow {}^1B_{2u}$, and separation between vibrational components in various solvents(*)

Band	v	The 0→1 series $\tilde{\nu}$ (cm^{-1})	ε (l/mol · cm^{-1})	Separation (cm^{-1})	The Ham system $\tilde{\nu}$ (cm^{-1})	ε (l/mol · cm^{-1})	Separation (cm^{-1})
1. CYCLOPENTANE $n = 1.404$; $D = 1.965$; *b.p.* = 49.30							
a		37,180	9.0				
b′				1140	—	—	
b	0	38,320	144.5				
c′				940	—	—	
c	1	39,260	215.8				
d′				920	—	—	
d	2	40,180	163.8				
e′				900	40,740	50.0	
e	3	41,080	91.6				
2. PENTANE $n = 1.357$; $D = 1.844$; *b.p.* = 36.10							
a		37,200	6.0				
b′				1140	—	—	
b	0	38,340	145.0				
c′				940	—	—	
c	1	39,280	185.0				
d′							
d	2	40,200	140.0	920	39,280	50.0	900
e′				900	40,720	44.0	
e	3	41,100	74.0				
3. CYCLOHEXANE $n = 1.426$; $D = 2.04$; *b.p.* = 80.70							
a		37,200	10.6				
b′				1120	—	—	
b	0	38,320	153.0				
c′				960	—	—	
c	1	39,280	232.0				
d′				900	39,860	71.6	
d	2	40,180	175.0				900
e′				920	40,760	65.0	
e	3	41,100	96.5				
4. HEXANE $n = 1.375$; $D = 1.890$; *b.p.* = 68.80							
a		37,120	8.8				
b′				1160	—	—	
b	0	38,340	143.4				
c′				940	—	—	
c	1	39,280	207.6				
d′				920	39,280	62.0	
d	2	40,200	163.6				940
e′				900	40,760	56.4	
e	3	41,100	88.8				

Table 1 *(continued)*

Band	v	The 0 → 1 series			The Ham system		
		$\tilde{\nu}$ (cm^{-1})	ε ($l/mol \cdot cm^{-1}$)	Separation (cm^{-1})	$\tilde{\nu}$ (cm^{-1})	ε ($l/mol \cdot cm^{-1}$)	Separation (cm^{-1})
5. HEPTANE							
$n = 1.388$; $D = 1.925$; *b.p.* $= 98.40$							
a		37,200	8.5				
b′				1120	—	—	
b	0	38,320	144.6				
c′				940	—	—	
c	1	39,260	214.6				
d′				920	39,840	68.8	
d	2	40,180	164.4				920
e′				900	40,760	58.0	
e	3	41,080	90.0				
6. OCTANE							
$n = 1.398$; $D = 1.948$; *b.p.* $= 125.65$							
a		37,200	8.5				
b′				1140	—	—	
b	0	38,340	140.0				
c′				940	—	—	
c	1	39,280	208.4				
d′				940	—	—	
d	2	40,220	163.4				
e′				880	40,800	58.0	
e	3	41,100	89.0				
7. DECANE							
$n = 1.412$; $D = 1.991$; *b.p.* $= 174.05$							
a		37,200	9.0				
b′				1120	—	—	
b	0	38,320	151.6				
c′				960	—	—	
c	1	39,280	224.2				
d′				900	—	—	
d	2	40,180	173.0				
e′				900	40,720	62.6	
e	3	41,080	96.4				
8. DODECANE							
$n = 1.422$; $D = 2.020$; *b.p.* $= 216.00$							
a		37,200	9.4				
b′				1120	—	—	
b	0	38,320	145.6				
c′				940	—	—	
c	1	39,260	218.6				
d′				920	39,840	71.4	
d	2	40,180	168.0				1120
e′				920	40,760	63.4	
e	3	41,100	94.0				

Table 1 *(continued)*

Band	v	The 0 → 1 series			The Ham system		
		$\tilde{\nu}$ (cm^{-1})	ε (l/mol·cm^{-1})	Separation (cm^{-1})	$\tilde{\nu}$ (cm^{-1})	ε (l/mol·cm^{-1})	Separation (cm^{-1})
9. METHANOL							
$n = 1.331$; $D = 33.80$; *b.p.* $= 64.60$							
a		37,240	10.6				
b′				1140	37,940	34.6	
b	0	38,380	150.6				980
c′				940	38,920	70.0	
c	1	39,320	220.0				940
d′				920	39,860	71.2	
d	2	40,240	172.6				920
e′				900	40,780	62.0	
e	3	41,140	97.4				
10. ETHANOL							
$n = 1.359$; $D = 25.80$; *b.p.* $= 78.40$							
a		37,200	11.8				
b′				1140	37,940	41.0	
b	0	38,340	159.0				840
c′				940	38,880	71.0	
c	1	39,280	236.4				920
d′				920	39,800	72.6	
d	2	40,200	194.0				1000
e′				900	40,800	70.0	
e	3	41,100	102.0				
11. 1-PROPANOL							
$n = 1.384$; $D = 21.80$; *b.p.* $= 97.20$							
a		37,180	10.0				
b′				1160	37,880	35.0	
b	0	38,340	150.6				1000
c′				940	38,880	68.0	
c	1	39,280	224.0				960
d′				920	39,840	74.0	
d	2	40,200	171.6				920
e′				900	40,760	64.0	
e	3	41,100	96.4				
12. 2-PROPANOL							
$n = 1.375$; $D = 26.00$; *b.p.* $= 82.40$							
a		37,200	10.0				
b′				1160	37,900	32.0	
b	0	38,340	156.4				880
c′				940	38,880	66.0	
c	1	39,280	235.0				980
d′				920	39,860	71.4	
d	2	40,200	178.6				900
e′				920	40,760	61.0	
e	3	41,170	99.4				

Table 1 *(continued)*

13. 1-BUTANOL

$n = 1.399$; $D = 19.20$; *b.p.* = 117.70

Band	v	The 0 → 1 series $\tilde{\nu}$ (cm^{-1})	ε (l/mol·cm^{-1})	Separation (cm^{-1})	The Ham system $\tilde{\nu}$ (cm^{-1})	ε (l/mol·cm^{-1})	Separation (cm^{-1})
a		37,180	9.4				
b′				1160	37,920	39.0	
b	0	38,340	154.0				980
c′				940	38,900	74,0	
c	1	39,280	228.4				920
d′				920	39,820	75.6	
d	2	40,200	118.0				1000
e′				900	40,820	71.6	
e	3	41,100	100.4				

14. 3-METHYL-1-BUTANOL

$n = 1.408$; $D = 15.64$; *b.p.* = 132.00

Band	v	The 0 → 1 series $\tilde{\nu}$ (cm^{-1})	ε (l/mol·cm^{-1})	Separation (cm^{-1})	The Ham system $\tilde{\nu}$ (cm^{-1})	ε (l/mol·cm^{-1})	Separation (cm^{-1})
a		31,180	8.6				
b′				1140	37,920	38.0	
b	0	38,320	153.4				900
c′				960	38,820	62.0	
c	1	39,280	229.4				980
d′				900	39,800	71.8	
d	2	40,180	176.0				920
e′				920	40,720	61.0	
e	3	41,100	98.0				

15. ETHYL ETHER

$n = 1.350$; $D = 4.335$; *b.p.* = 34.50

Band	v	The 0 → 1 series $\tilde{\nu}$ (cm^{-1})	ε (l/mol·cm^{-1})	Separation (cm^{-1})	The Ham system $\tilde{\nu}$ (cm^{-1})	ε (l/mol·cm^{-1})	Separation (cm^{-1})
a		37,220	8.4				
b′				1140	37,940	29.0	
b	0	38,360	128.6				980
c′				940	38,920	56.0	
c	1	39,300	184.4				960
d′				920	39,880	60.4	
d	2	40,220	145.6				860
e′				900	40,740	50.0	
e	3	41,120	79,6				

16. ISOAMYL ETHER

$n = 1.408$; $D = 2.82$; *b.p.* = 173.10

Band	v	The 0 → 1 series $\tilde{\nu}$ (cm^{-1})	ε (l/mol·cm^{-1})	Separation (cm^{-1})	The Ham system $\tilde{\nu}$ (cm^{-1})	ε (l/mol·cm^{-1})	Separation (cm^{-1})
a		37,120	7.2				
b′				1180	—	—	
b	0	38,300	72.4				
c′				940	—	—	
c	1	39,240	248.0				
d′				940	—	—	
d	2	40,180	264.0				
e′					—	—	
e	3	—	—				

Table 1 *(continued)*

Band	v	The 0 → 1 series $\tilde{\nu}$ (cm^{-1})	ε (l/mol·cm^{-1})	Separation (cm^{-1})	The Ham system $\tilde{\nu}$ (cm^{-1})	ε (l/mol·cm^{-1})	Separation (cm^{-1})
17. METHYLENE CHLORIDE							
$n = 1.425$; $D = 9.08$; *b.p.* = 40.60							
a		37,200	9.4				
b′				1020	37,740	32.5	
b	0	38,220	108.0				1060
c′				960	38,800	64.0	
c	1	39,180	157.0				
d′				920	—	—	
d	2	40,100	104.0				
e′				900	—	—	
e	3	41,000	72.6				
18. CHLOROFORM							
$n = 1.446$; $D = 4.806$; *b.p.* = 61.10							
a		37,180	12.0				
b′				1020	37,720	45.0	
b	0	38,200	123.4				
c′				940	—	—	
c	1	39,140	185.0				
d′				920	—	—	
d	2	40,060	148.0				
e′				900	—	—	
e	3	40,960	98.0				
19. CARBON TETRACHLORIDE							
$n = 1.460$; $D = 2.238$; *b.p.* = 76.80							
a		37,180	25.0				
b′				960	should. 37,480	67.0	
b	0	38,140	168.2				1080
c′				940	should. 38,580	140.4	
c	1	39,080	254.0				
d′					—	—	
d	2	—	—				
e′					—	—	
e	3	—	—				
20. 1,2-DICHLOROETHANE							
$n = 1.447$; $D = 10.13$; *b.p.* = 83.60							
a		37,200	13.6				
b′				1040	37,780	42.0	
b	0	38,240	130.0				1040
c′				940	38,820	77.6	
c	1	39,180	191.0				
d′				920	—	—	
d	2	40,100	159.4				
e′				920	—	—	
e	3	41,020	88.4				

Table 1 (*continued*)

Band	v	The 0 → 1 series			The Ham system		
		$\tilde{\nu}$ (cm^{-1})	ε (l/mol·cm^{1-})	Separation (cm^{-1})	$\tilde{\nu}$ (cm^{-1})	ε (l/mol·cm^{-1})	Separation (cm^{-1})

21. ACETONITRILE

$n = 1.345$; $D = 37.50$; $b.p. = 82.00$

Band	v	$\tilde{\nu}$	ε	Separation	$\tilde{\nu}$	ε	Separation
a		37,180	8.0				
b′				1180	should. 37,860	39.0	
b	0	38,360	141.4				960
c′				940	should. 38,820	70.0	
c	1	39,300	212.0				920
d′				920	should. 39,740	69.6	
d	2	40,220	163.2				940
e′				940	40,680	58.4	
e	3	41,120	91.6				

22. METHYL ACETATE

$n = 1.362$; $D = 7.08$; $b.p. = 56.90$

Band	v	$\tilde{\nu}$	ε	Separation	$\tilde{\nu}$	ε	Separation
a		37,180	8.0				
b′				1160	should. 37,840	19.0	
b	0	38,340	79.0				960
c′				940	should. 38,800	36.0	
c	1	39,280	239.2				980
d′				920	should. 39,780	38.0	
d	2	40,200	100.4				
e′					—	—	
e	3	—	—				

23. ETHYL ACETATE

$n = 1.372$; $D = 6.11$; $b.p. = 77.10$

Band	v	$\tilde{\nu}$	ε	Separation	$\tilde{\nu}$	ε	Separation
a		37,220	9.0				
b′				1140	should. 37,880	36.4	
b	0	38,360	153.0				940
c′				940	should. 38,820	66.6	
c	1	39.300	231.4				980
d′				920	should. 39,800	70.6	
d	2	40,220	186.0				
e′					—	—	
e	3	—	—				

24. BUTYL ACETATE

$n = 1.394$; $D = 5.01$; $b.p. = 126.00$

Band	v	$\tilde{\nu}$	ε	Separation	$\tilde{\nu}$	ε	Separation
a		37,200	8,4				
b′				1160	should. 37,880	35.0	
b	0	38,360	149.4				960
c′				940	should. 38,840	64.6	
c	1	39,300	224.6				1000
d′				920	should. 39,840	71.6	
d	2	40,220	179.4		—	—	
e′							
e	3	—	—				

Table 1 *(continued)*

Band	v	The 0 → 1 series $\tilde{\nu}$ (cm^{-1})	ε (l/mol · cm^{-1})	Separation (cm^{-1})	The Ham system $\tilde{\nu}$ (cm^{-1})	ε (l/mol · cm^{-1})	Separation (cm^{-1})
25. AMYL ACETATE $n = 1.402$; $D = 4.75$; $b.p. = 148.90$							
a		37,180	9.4				
b′				1160	should. 37,840	37.0	
b	0	38,340	153.0				1120
c′				940	should. 38,860	70.4	
c	1	39,280	231.2				820
d′				920	should. 39,740	70.0	
d	2	40,200	192.4				
e′					—	—	
e	3	—	—				
26.1,4-DIOXANE $n = 1.422$; $D = 2.235$; $b.p. = 148.90$							
a		37,120	10.0				
b′				1180	should. 38,020	41.0	
b	0	38,300	141.0				720
c′				940	should. 38,740	70.0	
c	1	39,240	208.6				
d′				900	—	—	
d	2	40,140	163.6				
e′				900	—	—	
e	3	41,040	94.6				
27. WATER $n = 1.333$; $D = 80.36$							
a		37,240	—				
b′				1180	37,940	—	
b	0	38,420	—				
c′				940	—	—	
c	1	39,360	—				
d′				900	—	—	
d	2	40,260	—				
e,				900	—	—	
e	3	41,160	—				

* n is the refractive index; D is the dielectric constant, and $b.p.$ the boiling point of the solvent.

in solution is around 259 ± 50 cm^{-1}, as it results from figure 1. The exceptions are the small values in water and methanol, and the high values in the halogenated solvents, isoamyl ether and 1,4-dioxane. The results disagree with the opinion[25] that the benzene absorption spectrum is very little influenced by the solvents. With the exceptions indicated, the spectral shift is approximately the same in polar and non-polar solvents.

---

[25] N. Coggeshall and E. M. Lang, *J. Amer. Chem. Soc.*, **70**, 3282 (1948).

The qualitative explanation of this behaviour may be given according to the Bayliss and McRae's [26] theory, in which, some of the solvent effects in the electronic spectra of the organic compounds are interpreted in terms of polarization, dipole-polarization, and dipole-dipole forces between solute and solvent, taking into account : 1) the transition instantaneous dipole during the absorption process ; 2) the dipole moment change of the solute in going from the ground state to the excited state, and 3) the effect of the Franck-Condon principle. On the basis of the previous results, [4,27] the authors [26] have established that the displacement toward the red is a function of the refractive index of solvent, of the transition intensity, and of solute molecular size, and have denoted it as *polarization displacement*, a denomination customarily used now. In the classical theory, the instantaneous dipole of the optical transition means the association of the light absorption with the forced oscillation of an electric dipole ; in the quantum theory, the absorbing molecule changes its charge distribution with or without the variation of the permanent dipole moment.

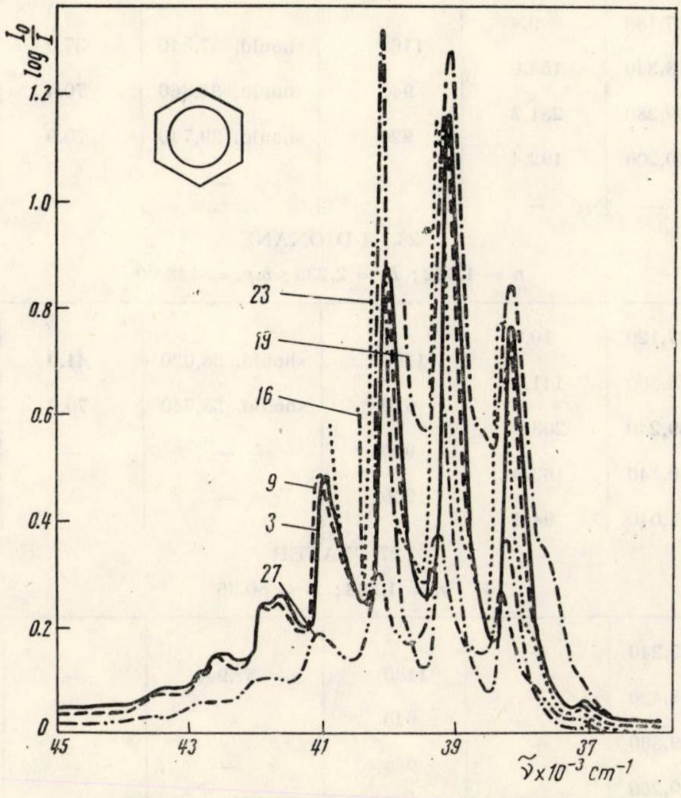

Fig. 1. — Benzene spectrum in the solvents :
3, Cyclohexane ; *9*, Methanol ; *16*, Isoamyl ether ; *19*, Carbon tetrachloride ; *23*, Ethyl acetate ; *27*, Water.

---

[26] N. S. Bayliss and E. G. McRae, *J. Chem. Phys.*, **58**, 1002 (1964).

[27] N. S. Bayliss, *J. Chem. Phys.*, **18**, 292 (1950).

The Franck-Condon principle is important in the spectral bands intensity interpretation. [26,28–30] The consequence of this principle is that the absorption process description in solution involves four energy levels: a non-equilibrium (Franck-Condon state) level and an equilibrium level for the ground and the excited states. The passing from the non-equilibrium level to the equilibrium level implies the corresponding solvation energy, in the two states. The spectral shift is correlated with the difference of the solvation energies. The equilibrium of the excited state between solute molecule and its solvent cage is reached during several molecular vibration periods ($\sim 10^{-13}$s.), and 10^{-11} s requires the readjustment of the solvent. [31] The excited state lasts 10^{-8} s, enough for the equilibrium to be established. In the non-equilibrium excited state, the excited molecule and the solvent cage are in a *strain state*, whose energy is greater than that of the equilibrium state. The strain is due to the: 1) orientation, when the solute and solvent are polar, and when solute dipole moment changes during the transition, and 2) packing when the solute molecule is much bigger in the excited state, or in complex formation. [32,33] The Franck-Condon excited state has a duration of the order of several molecular vibrations, and according to the indeterminancy principle, the vibrational quantization of the excited state will be prevented, that is the vibrational structure of the polar molecule spectra in polar solvents will be blurred or obliterated. In non-polar solutes the strain will not be present, and the vibrational structure will be preserved in polar solvents.

The benzene $^1A_{1g} \to {}^1B_{2u}$ transition is forbidden and appears only due to the vibrational induction, with a fine structure well resolved in the gas state. [7] For the weak transitions the dipole moment change is small, [34] and if the solute has no general, permanent dipole moment, one assumes that the dipole moments of the ground and excited states are zero. [35] Thus, in the excited state of benzene the polarizability [36] will increase, that is an instantaneous redistribution of the electric charge will take place. In non-polar solvents the solvation energy of the ground and excited states is determined by the dispersion forces. [37] The lack of the dipole moment of the solute explains the orientation strain absence in the excited Franck-Condon state. The benzene molecule is small, and the packing strain is not acting. The vibrational structure of the spectrum is retained, [4] the solute molecule being non-polar, and the strain in the Franck-Condon excited state being not present. The spectral shift is toward the red, and depends on the solvent refractive index. [27] In polar solvents there are not solute-solvent orientation forces, because the solute is non-polar. The orientation strain may be acting with slight effect, since the

---

[28] Y. Ooshika, *J. Phys. Soc., Japan*, **9**, 594 (1954).

[29] E. Lippert, *Z. Elektrochem.*, **61**, 562 (1957).

[30] N. G. Bakhshiev, *Opt. i Spektrosk.*, **10**, 717 (1961).

[31] D. H. Whiffen, *Quart. Rev.*, **4**, 131 (1950).

[32] R. S. Mulliken, *J. Amer. Chem. Soc.*, **72**, 600 (1950).

[33] R. S. Mulliken, *J. Amer. Chem. Soc.*, **74**, 811 (1952).

[34] D. P. Craig, *Discuss. Faraday Soc.*, **9**, 5 (1950).

[35] M. Lamotte and J. Joussot-Dubien, *J. Chim. phys.*, **66**, 161 (1969).

[36] O. Sverdlova, *Opt. i Spektrosk.*, **2**, 31 (1963).

[37] F. London, *Z. Physik*, **63**, 245 (1930).

dipolar forces between the solvent molecules themselves will tend to increase the relaxation time of the solvent cage after the transition.[38] The strain lack in the Franck-Condon state of the non-polar solute explains the vibrational structure preservation in the solution spectrum. The red polarization shift is dominant, and depends on the solvent refractive index. This spectral behaviour agrees with the cases I and II, in the theory of Bayliss and McRae.[36] Some of our results, in figure 1, confirm these interpretations and the previous investigations.[26] The numbers on the figure represent, respectively, the solvent from table 1. This notation is preserved throughout the paper.

Quantitatively, the benzene spectral shift on the solvent influence is interpreted according to McRae's[39] theory ; based on the perturbation theory, the author[39] has established, for the spectral shift in solution, a general expression from which he obtained a formula giving the spectral displacement in the microscopic terms of the solute, polarizability and dipole moment, and in the macroscopic terms of the solvent, refractive index and dielectric constant. In the case of non-polar solutes, the McRae's[39] expression reduces to :

$$\Delta\bar{\nu}_{\text{abs. (disp.)}}\ (\text{cm}^{-1}) = (A + B)[(n^2 - 1)/(2n^2 + 1)] \qquad (1)$$

where A and B are characteristic parameters of the solute molecule, and n is the refractive index of the solvent. The equation (1) shows that the spectral shift must linearly correlate with the refractive index function $f(n^2) = (n^2 - 1)/(2n^2 + 1)$. In fact, the graphical representation of our experimental data as a function of $f(n^2)$ shows, as it is seen in figure 2, that the majority of the points spreads around and in the direction of a straight line, in accordance with the other results.[4,5,35] Great deviations from the straight line display the halogenated solvents. We established the parameters sum $(A + B)$, in the equality (1) as 1432 cm^{-1}. Using this quantity the theoretical values of the spectral shifts were calculated, for comparison with the experimental data (see table 2). The graphical representation of the theoretical displacements values as a function of the $f(n^2)$ is accomplished in figure 3. The linear relations in figures 2 and 3, show that the dominant factor determining the benzene spectral displacement is made up from the dispersion forces.[37] One remarks that the straight line, in figure 3, tends to cut the ordinate axis under the origin, and this fact indicates the intervention of some subsidiary factors,[27] as : the geometry of the solute and solvent molecules ; the dimensions and the number of the solvent molecules gathered around the solute molecule, factors which are not explicitly included in McRae's[39] theory.

II.2. THE BAND INTENSITY

The spectral absorption band intensities are discussed as *molar absorptivities* (*molar extinction coefficients*), ε_ν,[40] obtainable from the *absorbance* measurement, at the corresponding wavelength, and are particularly important in the fine vibrational structure analysis of the electronic spectra. Even though the quantities ε_ν do not qualitatively correspond to the *integrated* (*absolute*) *intensities*,[41] they were determined by means of the expression :[42]

---

[38] N. S. Bayliss and A. L. G. Rees, *J. Chem. Phys.*, **8**, 377 (1940).

[39] E. G. McRae, *J. Phys. Chem.*, **61**, 562 (1957).

[40] H. H. Jaffé and M. Orchin, "Theory and Applications of Ultraviolet Spectroscopy", Wiley; New York, 1964.

$$\varepsilon_\nu = (1/l \cdot c) \cdot \log(I_0/I) \tag{2}$$

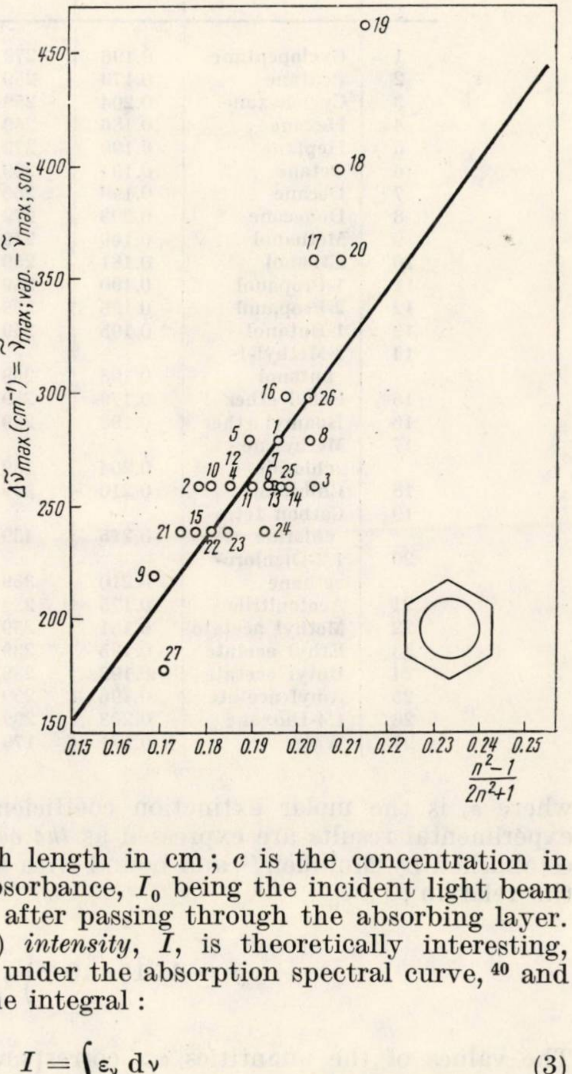

Fig. 2. — Experimental shift dependence of the benzene absorption band on the $(n^2 - 1)/(2n^2 + 1)$ function of the solvent.

where l is the absorbing path length in cm ; c is the concentration in mol/l, and log (I_0/I) is the absorbance, I_0 being the incident light beam intensity and I the intensity after passing through the absorbing layer.

The integrated (*absolute*) *intensity*, I, is theoretically interesting, rendered evident by the area under the absorption spectral curve,[40] and mathematically defined by the integral :

$$I = \int \varepsilon_\nu \, \mathrm{d}\nu \tag{3}$$

---

[41] W. M. Schubert, H. Steadly, and J. M. Craven, *J. Amer. Chem. Soc.*, **82**, 1353 (1960).

[42] H. H. Willard, L. L. Merritt, Jr., and J. A. Dean, "Instrumental Methods of Analysis", 3_{rd} ed., D. Van Nostrand, Princeton, 1960.

Table 2

The $f(n^2) = (n^2 - 1)/(2n^2 + 1)$ function of the solvent, the experimental and the theoretical displacement values, $\Delta\tilde{\nu}_{max.}$ (cm^{-1}), and the difference between them, in various solvents

N⁰	Solvent	$f(n^2)$	$\Delta\tilde{\nu}_{max.} = \tilde{\nu}_{vap.} - \tilde{\nu}_{sol.}$		Diff. $\Delta\tilde{\nu}_{exp.} - \Delta\tilde{\nu}_{calc.}$
			Exp.	Calcd.	
1	Cyclopentane	0.196	279	281	− 2
2	Pentane	0.179	259	256	+ 3
3	Cyclohexane	0.204	259	292	− 33
4	Hexane	0.186	259	266	− 7
5	Heptane	0.190	279	272	+ 7
6	Octane	0.194	259	278	− 19
7	Decane	0.199	259	285	− 26
8	Dodecane	0.203	279	291	− 12
9	Methanol	0.169	219	242	− 23
10	Ethanol	0.181	259	259	0
11	1-Propanol	0.190	259	272	− 13
12	2-Propanol	0.186	259	266	− 7
13	1-Butanol	0.195	259	279	− 20
14	3-Methyl-1-butanol	0.198	259	284	− 25
15	Ethyl ether	0.179	239	255	− 16
16	Isoamyl ether	0.198	299	284	+ 15
17	Methylene chloride	0.204	359	292	+ 67
18	Chloroform	0.210	399	301	+ 98
19	Carbon tetrachloride	0.215	459	308	+151
20	1,2-Dichloroethane	0.210	359	301	+ 58
21	Acetonitrile	0.175	239	251	− 12
22	Methyl acetate	0.181	259	259	0
23	Ethyl acetate	0.185	239	265	− 26
24	Butyl acetate	0.193	239	276	− 37
25	Amyl acetate	0.196	259	281	− 22
26	1,4-Dioxane	0.203	299	291	+ 8
27	Water	0.171	179	245	− 66

where ε_ν is the molar extinction coefficient at the ν frequency. The experimental results are expressed as *the oscillator strength*, f, a quantity established by Mulliken [43] and bound with the absolute intensity through the relation :

$$f = 4{,}315 \cdot 10^{-9} \int \varepsilon_\nu \, d\nu \qquad (4)$$

The values of the quantities ε_ν, corresponding to the $\tilde{\nu}_{max}$ frequency, and f, for the benzene are registered in table 3. The same table gives data from the previous papers, [4,7,44,45] with the references in brackets.

---

[43] R. S. Mulliken, *J. Chem. Phys.*, **7**, 14 (1939).

[44] S. Stokes, *J. Chem. Phys.*, **39**, 2309 (1950).

[45] F. Almasy and H. Laemmel, *Helv. Chim. Acta*, **34**, 462 (1951).

Assuming that $f \cdot 10^3 = 1.25$ is the best value for benzene gas spectrum,[7] our results indicate the increasing of the investigated band intensity relative to the solvents action. There is the opinion that under the perturbing effect of the solvents the vibrational components in the fine structure of the weak electronic transitions have a different intensity behaviour.[46] But the explanations of the intensity increase of the ${}^1A_{1g} \rightarrow {}^1B_{2u}$ benzene transition are referring to the changes due to the (0, 0) vibrational component appearance, which is not observed in the vapour spectrum. It is considered that its position is at 521 cm^{-1}, toward the red[47] from the prominent $0 \rightarrow 1$ component, involving the excited state, e_{2g}, and located at 38,612 cm^{-1}. The studies of benzene in condensed media, or as solid, pure, benzene have notified[8] the presence of a weak band at/or near the position of the (0, 0) component. The same findings were made in the benzene investigation in carbon tetrachloride,[9,10] and in solid hydrocarbon matrices the new band was strongly intensified by the carbon tetrachloride presence. The new band is also notified at the room temperature[4] and at low temperatures,[11-13] in carbon tetrachloride and 1,4-dioxane. The band is the first term of a progression[9,10-13] on the high frequency side, and this system is called by Platt[48] "Ham bands".

Observing the benzene spectrum in solution, on the long wavelengths side, where the spectrum is less complicated, at 20°, we noted the appearance of the new bands designated, correspondingly,[4] as b', c', d' and e', as it is seen from figure 4, for the benzene spectrum in acetonitrile.

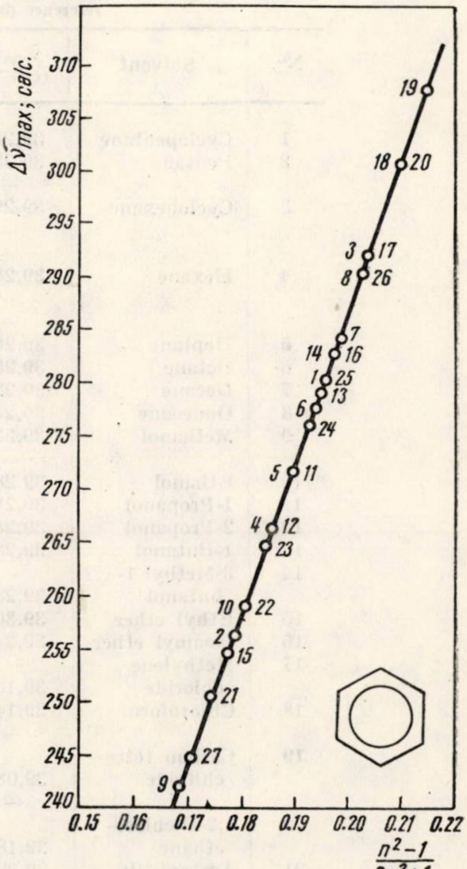

Fig. 3. — Theoretical shift dependence of the benzene absorption band on the $(n^2 - 1)/(2n^2 + 1)$ function of the solvent.

---

[46] A. Nakajima, *Bull. Chem. Soc., Japan*, **44**, 3272 (1971).

[47] F. M. Garforth and C. K. Ingold, *J. Chem. Soc.*, **1948**, 417.

[48] J. R. Platt, *J. Mol. Spectroscopy*, **9**, 288 (1962).

The a band is the $0 \rightarrow 1$ transition involving the corresponding frenquency for the ground state, e_g, of 608 cm^{-1}. According to our measurements, the mean separation between a and b vibrational components is 1132 cm^{-1} (521 + 608). The a, b, c, d, e,... components represent the $0 \rightarrow 1$ progression, involving the symmetrical frequency of 923 cm^{-1}.

Table 3

Position and intensity of benzene band at 2550 Å in various solvents, compared with reference (in brackets) results

N°.	Solvent	$\tilde{\nu}_{max.}$ (cm^{-1})	$\lambda_{max.}$ (Å)	$\varepsilon_{max.}$ (l·mol^{-1}·cm^{-1})	$f \cdot 10^3$
1	Cyclopentane	39,260	—	215.8	1.59
2	Pentane	39,280	2546	185.0	1.20
		—	—	—	1.6(44)
3	Cyclohexane	39,290	2546	232.0	1.55
		—	2549(4)	201.0(4)	1.6(4)
		—	2545(7)	—	1.78(7)
4	Hexane	39,280	2546	207.6	1.51
		—	2549(4)	206.0(4)	1.7(4,45)
		—	2544(7)	—	1.64(7)
5	Heptane	39,260	—	214.6	1.59
6	Octane	39,280	—	208.0	1.57
7	Decane	39,280	—	224.2	1.65
8	Dodecane	39,260	—	218.6	1.61
9	Methanol	39,320	2543	220.0	1.67
		—	2543(7)	—	1.77(7)
10	Ethanol	39,280	—	236.4	1.80
11	1-Propanol	39,280	—	224.0	1.66
12	2-Propanol	39,280	—	235.0	1.62
13	1-Butanol	39,280	—	228.4	1.70
14	3-Methyl-1-butanol	39,280	—	229.4	1.63
15	Ethyl ether	39,300	—	187.4	1.28
16	Isoamyl ether	39,240	—	248.0	—
17	Methylene chloride	39,180	—	157.0	—
18	Chloroform	39,140	2555	185.0	—
		—	2553(4)	192.0(4)	—
19	Carbon tetrachloride	39,080	2559	254.0	—
		—	2559(4)	222.0(4)	—
20	1,2-Dichloroethane	39,180	—	191.0	—
21	Acetonitrile	39,300	—	212.0	1.65
22	Methyl acetate	39,280	—	239.2	—
23	Ethyl acetate	39,300	—	234.4	—
24	Butyl acetate	39,300	—	246.6	—
25	Amyl acetate	39,280	—	231.2	—
26	1,4-Dioxane	39,240	—	208.6	1.77
27	Water	39,360	—	—	—

The new bands appear only as shoulders or inflections and it is difficult to establish the separation between them; however, the mean separation between b', c', d', and e' bands is ~950 cm^{-1}. In table 1 we registered some of our vibrational analysis results. It is obvious that the Ham band frequencies and the corresponding quantities are only approximate. One or two Ham terms appear in non-polar solvents (hydrocarbons), on the high wave-numbers side; four terms appear in alcohols, ethyl ether, and acetonitrile ; two terms appear in carbon tetrachloride, 1,2-dichloroethane, and 1,4-dioxane and only one term is appearing in chloroform and water, but in these last five cases on the small wave numbers side. No term is appearing in isoamyl ether. The new bands appearance causes the increase of integrated intensity and their existence in non-polar solvents, and not only in solvents with chlorine and oxygen in molecule — considered as perturbers[49] — proves that the solvent polarizability, and consequently the London[37] dispersion forces, greatly determine the existence of the new bands system. The benzene spectrum examination at various temperatures[50] leads to the same conclusion that the dispersion forces action is the principal cause of the Ham bands appearance. Using solvents with spherical molecules, Koyanagi[51] established an empirical expression between band intensity and the ratio $(\bar{\alpha}/r^6)^2$, where $\bar{\alpha}$ is the mean polarizability and r is the average intermolecular distance ; this fact is in favour of the idea that the dispersion forces cause the Ham bands appearance and the intensity increase. The hypothesis derived from the experiments at 77 K, that the solvent matrix distorts the benzene molecule from the D_{6h} symmetry to a "boat" configuration in the case of liquid solution, at 20°, seems impossible. Durocher and Sandorfy[52] obtained the intensification of the (0, 0) progression in naphthalene,[53] and consider the Ham effect as general in aromatic molecules, the principal interaction solute-solvent having the same character in all aromatic hydrocarbons ; the effect is strong for the forbidden vibrational components in the fine structure, or for the weak bands for symmetry considerations.

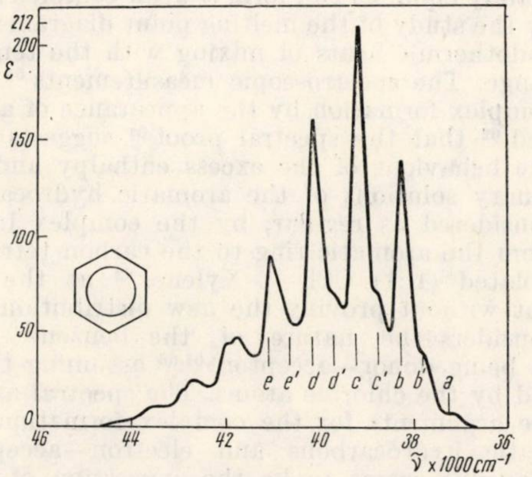

Fig. 4. — Benzene electronic spectrum in acetonitrile.

---

[49] N. S. Bayliss and N. W. Cant, *Spectrochim. Acta*, **18**, 1287 (1962).
[50] M. Koyanagi and Y. Kanda, *Spectrochim. Acta*, **20**, 993 (1964).
[51] M. Koyanagi, *J. Mol. Spectroscopy*, **25**, 273 (1968).
[52] G. Durocher and C. Sandorfy, *J. Mol. Spectroscopy*, **20**, 410 (1966).
[53] G. Durocher and C. Sandorfy, *J. Mol. Spectroscopy*, **14**, 400 (1964).

The augmented spectral shift and the remarkable intensity increase of the benzene spectral band, at 2550 Å, in carbon tetrachloride justify the assertion on the efficiency of the carbon tetrachloride as a perturber. Frequently, one considers the carbon tetrachloride as a "normal" solvent. The benzene solutions in carbon tetrachloride considered as regular [54] because they have the excess free energy and the mixing en thalpy approximately equal at 25°, form a weak complex at other temperatures, as shown by the study of the melting point diagrams [55–57] and of the increase of the endothermic heats of mixing with the temperature, [58–61] in the 25°–70° range. The spectroscopic measurements [54] support the conclusion of the complex formation by the appearance of a new spectral band. It is believed [62] that the spectral proof [54] suggests the possibility of interpreting the behaviour of the excess enthalpy and of the excess volume of the binary solutions of the aromatic hydrocarbons in carbon tetrachloride, considered as regular, by the complex formation with charge transfer from the aromatic ring to the carbon tetrachloride. A complex has been isolated (1 :1) CCl_4–p-Xylene, [63] at the liquid nitrogen temperature, but without proving the new distribution of the electronic charge. One considers the nature of the benzene – $CCl_4(CHCl_3, CH_2Cl_2)$ complex as being donor–acceptor, [64,65] assuming the benzene molecule is polarized by the chlorine atoms. The spectral and the freezing point studies [66] are arguments for the complex formations between electron-donor aromatic hydrocarbons and electron–acceptor halogenated compounds. Plausible seems to be the suggestion of π-bonding formation between benzene ring and the vacant level 3 *d* of the chlorine atom. [59] In this case, the Ham effect is observed even in the allowed bands, because the parts of the potential surface determining the various vibrations are inequally influenced by the weak complex formation,[52,53] especially if the bands have very different intensities. We may assert that the unsual benzene spectral displacement in carbon tetrachloride, toward long wavelengths is explained through the increased probability of complex formation [5] on the excitation of benzene molecule. The complex formation causes the action of the packing strain in the excited state, that is the increase of the solvation energy of this state as compared with the solvation energy of the ground state and the spectrum is red shifted. The complex formation explains also the intensity increase of spectral band, because the D_{6h} symmetry of benzene is modified and the band becomes allowed.

---

[54] R. Anderson and J. M. Prausnitz, *J. Chem. Phys.*, **39**, 1225 (1963).

[55] A. F. Kapustinskii and S. I. Drakin, *Izvest. Akad. Nauk S.S.S.R. Otdel. khim. Nauk*, **5**, 435 (1947).

[56] W. E. Wyatt, *Trans. Faraday Soc.*, **25**, 48 (1929).

[57] R. P. Rastogi and R. K. Nigam, *Trans. Faraday Soc.*, **55**, 2005 (1959).

[58] G. H. Ceeseman and A. M. B. Whitaker, *Proc. Roy. Soc. (London)*, **A 212**, 406 (1952).

[59] J. R. Goates, R. J. Sullivan, and J. B. Ott, *J. Phys. Chem.*, **63**, 589 (1954).

[60] L. A. K. Staveley, *Trans. Faraday Soc.*, **55**, 328 (1955).

[61] R. H. Noordtjitz, *Helv. Chim. Acta*, **39**, 637 (1956).

[62] R. F. Weimer and J. M. Prausnitz, *J. Chem. Phys.*, **42**, 3643 (1965).

[63] H. O. Hooper, *J. Chem. Phys.*, **41**, 599 (1964).

[64] N. S. Rao and K. K. Jatkar, *Quart. J. Ind. Inst. Sci.*, **5**, 65 (1942).

[65] N. S. Rao and K. K. Jatkar, *Quart. J. Ind. Inst. Sci.*, **6**, 1 (1943).

[66] G. Briegleb, "Elektronen–Donator–Acceptor Komplexe", Springer Verlag, Berlin, 1961.

The theoretical examination of the solvents influence on the spectral band intensities led to the establishement of some augmentation factors of the intensity increase in solution. Thus, Chako, [67] and Bakhshiev et al. [2,68,69] formulated, on classical bases, the increase factor of the spectral intensity in solution by the relation :

$$\beta = (n^2 + 2)^2/9n \tag{5}$$

and Abe [70] expresses this factor, on the quantum theory bases in the form :

$$\beta' = [9\,n^2/(2n^2 + 1)]\cdot(\tilde{\nu}_{oi}/\tilde{\nu}^{o}_{oi}) \tag{6}$$

In expressions (5) and (6) β and β' have the significance of the ratio $f_{\text{the or. sol.}}/f_{\text{the or. vap.}}$, n is the refractive index ; $\tilde{\nu}_{oi}$ and $\tilde{\nu}^{o}_{oi}$ are the transition energies of the dissolved and free molecule, in cm^{-1}, respectively. Using $f_{\text{exp. vap.}}$ [7] as 1.25 and our $f_{\text{exp. sol.}}$ values, from table 2, we listed, in table 4, the ratios $f_{\text{exp. sol.}}/f_{\text{exp. vap.}}$, β and β', for comparison. It is immediately seen that in general the solvent effect is to increase the spectral intensity and the experimental results are better reproduced by expression (5), while the increasing factor in equation (6) is everywhere greater. In this behaviour, we have an additional argument for the case of non-polar aromatic molecules, as benzene, that the spectral

Table 4

Comparison of experimental and theoretical intensites of the 2550 Å benzene band

SOLVENT	$f_{\text{exp.sol.}}/f_{\text{exp.vap.}}$	β	β'
Cyclopentane	1.272	1.248	1.419
Pentane	0.960	1.208	1.382
Cyclohexane	1.240	1.267	1.439
Hexane	1.208	1.223	1.397
Heptane	1.272	1.233	1.408
Octane	1.256	1.242	1.415
Decane	1.320	1.255	1.372
Dodecane	1.288	1.264	1.436
Methanol	1.336	1.186	1.390
Ethanol	1.440	1.211	1.385
1-Propanol	1.328	1.231	1.406
2-Propanol	1.296	1.223	1.397
1-Butanol	1.360	1.243	1.417
3-Methyl-1-butanol	1.304	1.251	1.425
Ethyl ether	1.024	1.205	1.378
Acetonitrile	1.320	1.198	1.371
1,4-Dioxane	1.416	1.264	1.433

---

[67] N. Q. Chako, *J. Chem. Phys.*, **2**, 644 (1934).
[68] N. S. Libov, N. G. Bakhshiev, and O. P. Girin, *Opt. i Spektrosk.*, **16**, 1016 (1964).
[69] N. G. Bakhshiev, *Ot. i Spektrosk.*, **24**, 896 (1968).
[70] T. Abe, *Bull. Chem. Soc., Japan*, **43**, 625 (1970).

intensity change in solution is caused by the dispersion forces, the intensity increase factor involving only the refractive index of the solvent. A comparison of vapour spectrum [7,71] with our results in solution (figure 1) shows that obliteration of the rotational structure leads, also, to the spectral intensity increase, the vibrational component in the electronic band appearing as an envelope of the rotational components. The explanation consists in the fact that the solvent molecules are closely clustered around the solute molecule, so that it has no longer a free rotation. [40]

III. EXPERIMENTAL

The purification of benzene and of solvents used is done by the known methods, [72] the purity criteria being the refractive indices, *n*, and the boiling points, *b.p.*, of which values are given in table 1, together with the dielectric constants, *D*.

The refractive index values were established with an Abbé refractometer, of the *G* type, for the yellow natrium light. The dielectric constants, *D*, were evaluated with an Oehme apparatus of the 600 RL type. The *n* and *D* constants were determined at 20° by means of an ultrathermostat of the type U 10, with adjustable temperature, at 20 ± 0.1°. The solutions were prepared in 10 ml calibrated flasks, by introduction of the necessary benzene quantity with a chromatographical syringe of 0.01 ml, and adding small portions of solvent, vigorously stirring between two portions; the concentrations ranged between 0.05 and 0.005 M. The spectra were recorded with a SPECORD UV—VIS spectrophotometer, Carl Zeiss, Jena, equipped with deuterium source, quartz prism, and a slit width system automatically adjustable so that the band width is less than 30 cm^{-1} on the whole used range. The accuracy of the band position is ± 50 cm^{-1}. The employed cells were of 0.1 and 1 cm thickness. The position of each peak and the spectral intensities are the mean of at least three measurements. The integrated intensities were evaluated by cutting up and weighing, having as integration limits the onset of the spectral band, at small wave numbers, till the deepest minimum at great wave numbers.

---

[71] R. A. Friedel and M. Orchin, "Ultraviolet Spectra of Aromatic Compounds", Wiley, New York, 1951.

[72] A. Weissberger, E. S. Proskauer, J. A. Riddick, and E. E. Toops, "Technique of Organic Chemistry", vol. VII, "Organic Solvents", 2nd ed., Interscience, New York, 1955.

Revue Roumaine de Chimie, **20**, *11–12*, 1433–1436 (1975)

DENSITIES AND PARTIAL MOLAR VOLUMES IN CONCENTRATED ELECTROLYTE SOLUTIONS. I

MAGNESIUM NITRATE – (SODIUM, POTASSIUM) NITRATE – WATER MIXTURES

SURENDER K. JAIN * and HARBANS L. JINDAL **
* Hindu College. University of Delhi. Delhi–110007, India
** Ramjas College, University of Delhi, Delhi–110007, India

Received May, 31 1974

Densities of $Mg(NO_3)-H_2O$, $Mg(NO_3)_2-NaNO_3-H_2O$ and $Mg(NO_3)_2-KNO_3-H_2O$ mixtures have been measured from 30 to 70°, by measuring the volume of a certain amount of solution in a precalibrated densitometer. Partial molar volumes ($\overline{V}_i$) of the constituents of these mixtures indicate that the principle of additivity of molar volumes does not hold good in such solutions.

In view of the fact that the progress towards understanding the behaviour of "real" electrolyte solution was more likely to result from the studies of the fused salt end of the concentration scale, than from the extension of dilute solution theories,[1,2] very recently the investigations in concentrated electrolyte solutions/hydrated melts gained considerable momentum. Braustein *et al.* [3] and Jain [4] found that the principle of additivity of equivalent volumes in the case of hydrated melts could be regarded as a useful approximation. To explore if the assumption regarding the additivity of volumes continues to be useful even in dilute solution, the results on magnesium nitrate — (sodium, potassium) nitrate — water mixtures are reported here.

EXPERIMENTAL

MATERIAL

Analar grade (BDH) $NaNO_3$, KNO_3 and LR(BDH) grade $Mg(NO_3)_2-6H_2O$ were used without further purification. Solutions of varying composition were prepared by dissolving the requisite amounts of salts in calculated amount of distilled water. Solutions with higher contents of the salts were prepared at slightly higher temperatures and then cooled slowly; thereafter, the solutions remained without crystallizing for a long period (about 10 days) even at room temperature.

---

[1] R. M. Fuoss, *Chem. Rev.*, **17**, 27 (1935).
[2] C. A. Kraus, *J. Chem. Educ.*, **35**, 324 (1958).
[3] J. Braunstein, Linda Orr and W. Mcdonald, *J. Chem. Enq. Data*, **12**, 415 (1967).
[4] S. K. Jain, *J. Chem. Eng. Data*, **18**, 397 (1973).

APPARATUS AND PROCEDURE

A manometric densitometer used by Husband [5] and Cleaver *et al.* [6] was modified to allow a direct measurement of the volume of a known amount of solution. Details regarding the design, calibration and measuring technique have been reported earlier. [4] A 10 litre liquid paraffin bath served as a constant temperature bath. The temperature was controlled and measured with a precision of ± 0.1°.

RESULTS AND DISCUSSION

Density data on various mixtures of $Mg(NO_3)_2-H_2O$, $Mg(NO_3)_2-(Na, K)NO_3-H_2O$ systems up to 70° are recorded in tables 1 and 2, respectively, in the form of least-square equations. Coefficients of expansion(α)

Table 1

Density-temperature equations and partial molar volumes for $Mg(NO_3)_2-H_2O$ mixtures

$R = \frac{n_{H_2O}}{n_{salt}}$	Molality (m)	Temperature range °C	$\rho = a - bt$ a	$b \cdot 10^4$	Standard error $\cdot 10^3$	Expansivity $(\alpha) \cdot 10^4$	$\overline{V}_{H}$ (cm³/mole) (at 70°)	$\overline{V}_{Mg}$
49.74	1.116	31−71	1.1209	5.326	0.24	4.83	15.9	55.9
24.89	2.230	33−71	1.2239	5.860	0.26	4.86	19.3	47.6
11.96	4.638	33−70	1.4015	6.887	0.26	4.98	17.2	51.5
9.98	5.563	55−70	1.4476	6.680	0.20	4.77	16.6	59.8
8.67	6.403	66−72	1.4912	5.795	0.63	3.87	16.0	69.4

Table 2

Density-temperature equations for $Mg(NO_3)_2-MNO_3-H_2O$ mixtures; (M=Na,K)

$R = \frac{n_{H_2O}}{n_{salt}}$	$\frac{n_{H_2O}}{n_{Mg}}(NO_3)_2$	$\frac{n_{H_2O}}{n_{MNO_3}}$	Temperature range (°C)	$\rho = a - bt$ a	$b \cdot 10^4$	Standard error $\cdot 10^3$	Expansivity $\cdot 10^4$ (α)
$Mg(NO_3)_2-NaNO_3-H_2O$							
6.651	9.982	19.93	62−71	1.5043	7.04	0.19	4.82
7.988	9.982	39.98	38−70	1.4758	7.13	0.20	4.92
8.911	9.982	83.10	30−70	1.4577	6.50	0.79	4.53
7.22	9.028	36.17	42−70	1.5109	7.14	0.15	4.81
12.107	18.169	36.17	38−70	1.3432	7.12	0.22	5.41
$Mg(NO_3)_2-KNO_3-H_2O$							
5.707	10.039	13.22	45−71	1.5485	7.42	0.19	4.90
6.688	10.038	20.04	37−72	1.5194	7.29	0.28	4.88
8.023	10.038	40.01	31−70	1.4765	7.11	0.40	4.88
7.186	8.987	35.78	37−71	1.5174	7.20	0.28	4.84
11.942	17.950	35.78	32−70	1.3491	6.67	0.36	5.03

---

[5] L. J. B. Husband, *J. Sci. Instrum.*, **35**, 300 (1958).

[6] B. Cleaver, E. Rhodes and A. R. Ubbelohde, *Proc. Roy. Soc.*, **A 262**, 435 (1961).

at 70°, for these solutions are also included in these tables. Consequence of stronger Coulombic interactions with the increase in the concentration of the solute, is apparent from the decrease in the magnitude of α with solute concentration.

$Mg(NO_3)_2-H_2O$ SYSTEM

Specific volumes (at 70°) were fitted by the least-square method into the equation

$$v_{70}\,(\mathrm{cm^3/gm}) = 0.5830 + 0.0144\mathrm{R} - 0.000152\mathrm{R}^2$$

Partial molar volumes of water ($\bar{V}_H$) and magnesium nitrate ($\bar{V}_{Mg}$) were computed through the use of the following relations:

$$\bar{V}_H = M_H \cdot v + [RM_H + M_{Mg}]\left(\frac{\partial v}{\partial R}\right)_{n_{Mg}} \tag{1}$$

$$\bar{V}_{Mg} = M_{Mg}\, v + \left[M_H + M_{Mg}\cdot\frac{1}{R}\right]\left(\frac{\partial v}{\partial\,(1/R)}\right)_{n_H} \tag{2}$$

The derivatives $\frac{\partial v}{\partial R}$ and $\frac{\partial v}{\partial\,(1/R)}$ were obtained by differentiating the expression in which v was expressed as a function of R and $1/R$, respectively. $\bar{V}_H$ and $\bar{V}_{Mg}$ show a maxima and a minima, respectively, near $R = 25$, however in view of computational uncertainty, no significance is attached to this composition. However, lower values of $\bar{V}_H$ are not unexpected, since most of the hydrogen bonded clusters of water molecules will have been destroyed (cf. ref. [3] and [7]). Partial molar volume of magnesium nitrate at higher salt to water ratio, approaches a value 69.4 cm^3/mole which agrees favourably with a value of 72.9 cm^3/mole for super-cooled magnesium nitrate obtained by extrapolating the eq. volume data of Cleaver *et al.*,[6] from the temperature of measurement to 70°.

$Mg(NO_3)_2-(Na, K)NO_3-H_2O$ SYSTEMS

Partial molar volumes of $NaNO_3$, KNO_3 and $Mg(NO_3)_2$ were estimated at various compositions, through the use of the following expressions:

$$\bar{V}_M = M_M v + \left[M_{Mg} + \frac{n_M}{n_{Mg}}\cdot M_M + \frac{n_H}{n_{Mg}}\cdot M_H\right]\left[\frac{\partial v}{\partial (n_M/n_{Mg})}\right]_{\frac{n_H}{n_{Mg}}} \tag{3}$$

$$\bar{V}_{Mg} = M_{Mg}\, v + \left[M_M + \frac{n_{Mg}}{n_M}\cdot M_{Mg} + \frac{n_H}{n_M}\cdot M_H\right]\left[\frac{\partial v}{\partial (n_{Mg}/n_M)}\right]_{\frac{n_H}{n_M}} \tag{4}$$

and are recorded in table 3.

---

[7] W. W. Ewing and R. J. Mikousky, *J. Amer. Chem. Soc.*, **72**, 1390 (1950).

Table 3

Partial molar volumes (at 70°) of the constituents of $Mg(NO_3)_2$-MNO_3-H_2O mixtures

$\frac{n_{H_2O}}{n_{Mg(NO_3)_2}}$	$\frac{n_{MNO_3}}{n_{Mg(NO_3)_2}}$	$\overline{V}_{MNO_3}$	$\frac{n_{H_2O}}{n_{MNO_3}}$	$\frac{n_{Mg(NO_3)_2}}{n_{MNO_3}}$	$\overline{V}_{Mg(NO_3)_2}$
		$Mg(NO_3)_2-NaNO_3-H_2O$			
9.98	0.12	41.49 *	36.17	2.0	67.24 *
	0.25	40.29		4.0	42.29
	0.50	37.93			
		$Mg(NO_3)_2-KNO_3-H_2O$			
10.03	0.25	42.52	35.78	1.99	69.70 *
	0.50	44.25		3.99	43.61
	0.76	47.29 *			

* Corresponding values extrapolated from the data of Cleaver *et al.*, are 41.0,48.9 and 72.9, cm³/mole for $\overline{V}_{Na}$ $\overline{V}_{K}$ and $\overline{V}_{Mg}$, respectively.

It is apparent from the results that $\overline{V}_i$ varies in a systematic way with the composition of the solution. $\overline{V}_{Na}$ and $\overline{V}_{Mg}$ values at lower mole ratio of the component in the mixture agree favourably with these extrapolated from the volume data of Cleaver *et al.* [6] However, a reverse trend is reflected in the values of $\overline{V}_K$; a limiting value is reached at a higher mole ratio of the component.

Dependence of $\overline{V}_i$ on the composition and the trends reflected by the $\overline{V}_i$ values suggest that the assumption of additivity of molar volumes might be a useful approximation in hydrated melts (i.e. salts mixtures containg smaller amount of water) but not for solutions containing more water than what is required to fill the first coordination.

Acknowledgements. The authors express their sincere thanks to Niraj Prakash for his help during experimentation and to the University Grants Commission, New Delhi, for financial help.

NOMENCLATURE

$\overline{V}_H$ — Partial molar volume of water.
$\overline{V}_M$ — Partial molar volume of alkali metal nitrate.
$\overline{V}_{Mg}$ — Partial molar volume of magnesium nitrate.
M_H, M_M, M_{Mg} — Molecular weight of water, alkali metal nitrate and magnesium nitrate, respectively.
v — Specific volume of the solution, cm³ per gm.
R — no. of moles of water per mole of salt.
n_i — no. of moles of component i.

Revue Roumaine de Chimie, **20**, *11–12*, 1437–1442 (1975)

LA RÉACTIVITÉ DE CERTAINES COMPOSITIONS MÉLILITIQUES PAR RAPPORT À L'EAU

I. TEOREANU et MARIA GEORGESCU
Chaire de Technologie des Silicates et des Composés Oxydiques
Institut Polytechnique, 1, str. Polizu, Bucarest

Reçu le 15 juin 1975

On étudie la capacité de certains laitiers mélilitiques d'interaction avec l'eau et les facteurs qui déterminent leur réactivité.
On a synthétisé, dans ce but, en partant d'oxydes chimiquement purs, des laitiers ayant la composition: 30% $2CaO.Al_2O_3.SiO_2$ + 70% $2CaO.MgO.2SiO_2$, 50% $2CaO.Al_2O_3.SiO_2$ + 50% $2CaO.MgO.2SiO_2$, 70% $2CaO.Al_2O_3.SiO_2$ + 30% $2CaO.MgO.2SiO_2$ et de la géhlénite – $2CaO.Al_2O_3.SiO_2$ et l'akermanite – $2CaO.MgO.2SiO_2$. Les données de conductivité et de spectroscopie en infrarouge mettent en évidence que la réactivité des mélilites par rapport à l'eau est déterminée tant par leur composition que par certains éléments structurels.

1. Les mélilites représentent la série de solutions solides ayant comme termes limite l'akermanite – $2CaO.MgO.2SiO_2$ et la géhlénite – $2CaO.Al_2O_3.SiO_2$. Elles entrent dans une proportion assez importante dans la composition des laitiers de haut fourneau utilisables comme liants, leur conférant des propriétés hydrauliques supérieures. Les recherches concernant les propriétés hydrauliques des laitiers de haut fourneau [1-6] ont relevé un bon comportement des laitiers appartenant aux sous-systèmes mélilitiques du système quaternaire $CaO - MgO - Al_2O_3 - SiO_2$ dans lequel elles s'intègrent.

Étant donné la complexité des processus physico-chimiques qui ont lieu pendant le mélange des laitiers avec l'eau, par suite de la composition minéralogique hétérogène de ceux-ci, nous avons considéré spécialement intéressante la recherche concernant le comportement des phases individuelles minéralogiques des laitiers par rapport à l'eau, ainsi que des mélilites.

[1] S. Solacolu, *Zement-Kalk-Gips*, **11**, 125 (1958).
[2] S. Solacolu et P. Baltă, *Rev. des Matér. de Constr.*, **583**, 95 (1964).
[3] S. Solacolu, « La chimie physique des silicates techniques », ed. 2-ème, Ed. Technique, Bucarest, 1967.
[4] M. Georgescu, Disertation, Bucarest, 1972.
[5] I. Teoreanu et M. Rotaru, *Rev. des Matér. de Constr.*, **608**, 202 (1964).
[6] I. Teoreanu et M. Georgescu, *Zement-Kalk-Gips*, **6**, 308 (1974).

Les résultats expérimentaux [7-10] relatifs aux propriétés hydrauilques de certains laitiers mélilitiques, ayant des compositions différentes, indiquent un meilleur comportement des mélilites à une composition plus riche en akermanite et un comportement inférieur à ceux plus riches en géhlénite. Cette différence a pu être expliquée grâce à la grande différence du comportement des composés limites de la série — géhlénite et akermanite ; tandis que l'akermanite réagit très facilement avec l'eau, en formant des produits hydratés qui durcissent après un intervalle de temps assez court, la géhlénite est un composé presque inerte. Une variation continue de la réactivité des laitiers mélilitiques par rapport à l'eau avec la composition suppose une corrélation simple entre ces deux facteurs. Les résultats expérimentaux ne mettent pas toujours en évidence une telle corrélation, ce qui impose de considérer aussi comme facteur déterminant de la réactivité en dehors de la composition des mélilites, certains éléments de structure.

Les informations données dans la littérature de chimie sur la structure de mélilites sont parfois contradictoires.

Les deux termes limites de la série de solutions solides mélilitiques — la géhlénite et l'akermanite — se caractérisent par différentes structures : la géhlénite $Ca_2Al[(Si, Al)O_7]$ est considérée [11] comme un composant du groupe des philosilicates, ayant donc un grand degré d'associations des éléments structurels, dans lesquels l'ion d'aluminium, Al^{3+} peut coordiner tant tétraédriquement qu'octaédriquement, donc il peut avoir tant le rôle de formateur, que de modificateur de structure ; l'akermanite, $Ca_2Mg[Si_2O_7]$ peut être considérée (f.v. aussi les données de spectroscopie infrarouge par Tarte [12]) ayant une structure avec un petit degré de condensation des tétraèdres $[SiO_4]^{4-}$, donc appartenant aux classes des sorosilicates. [11] Il résulte donc, que la structure décrite par Kalinichenko [13] par la formule $Ca_2[(Mg, Al)(Si, Al)_2O_7]$ — en considérant qu'elle contient des anions complexes, de forme $[Al_4Si_2O_{14}]^{8-}$ et $[Mg_2Si_4O_{14}]^{8-}$, dans lesquels Mg^{2+} et Al^{3+} coordinent seulement tétraédriquement — n'est pas possible. Aussi, est-il difficile de supposer que les mélilites—compositions intermédiaires entre la géhlénite et l'akermanite — peuvent avoir une structure isolée, ainsi que l'affirment certains chercheurs. [3] Une telle structure peut être valable seulement pour les mélilites ayant une composition plus riche en akermanite. L'augmentation de la teneur en géhlénite suppose, en même temps, l'augmentation du degré de condensation des éléments de structure. D'ailleurs, les spectres infrarouges de certains mélilites cristallisées reflètent (fig. 1 [12]) le déplacement du champ d'absorption spécifique des liaisons Si—O, centré pour akermanite à 900—950 cm^{-1}, vers des fréquences plus grandes (1100 cm^{-1}) proportion-

---

[7] Yu. M. Butt, «Practicum po technologhii vyazhushchikh veschestv i izdelii iz nikh», izd. 2e, Promstroiizdat, Moscou, 1953, p. 320.

[8] P. A. Rebinder, *Doklady Akad. Nauk S.S.S.R.*, **189**, 1314 (1969).

[9] A. V. Voljenskii, Yu. S. Burov, V. N. Vinogradov et K. V. Gladkikh, «Betony i izdeliya izshlakovykh i zolinykh tsementov", Izd. Lit. po Str., Moscou, 1969.

[10] K. Stepién, *Cement-Wapno-Gips*, **3**, 80 (1973).

[11] H. Lehmann et H. Dutz, *Tonindustrie Zeitung*, **10**, 219 (1959).

[12] P. Tarte, *Bull. Soc. franc. Ceram.*, **58**, 13 (1963).

[13] L. N. Kalenicenko, Disertation, Harkov, 1971.

nellement à l'augmentation de la géhlénite dans la composition des mélilites. D'après Launer, [14] ce déplacement du champ d'absorption IR, spécifique des liaisons Si—O des fréquences inférieures, aux fréquences supérieures ($900-950\ \text{cm}^{-1} \rightarrow 1100\ \text{cm}^{-1}$) est spécifique du changement d'une structure caractérisée par tétraèdres $[SiO_4]^{4-}$ isolée, à une structure d'un degré de condensation plus élevé ($SiO_4 \rightarrow Si_2O_7 \rightarrow [SiO_3]_\infty \rightarrow [Si_2O_5]_\infty$ $\rightarrow$ des structures tridimensionnelles).

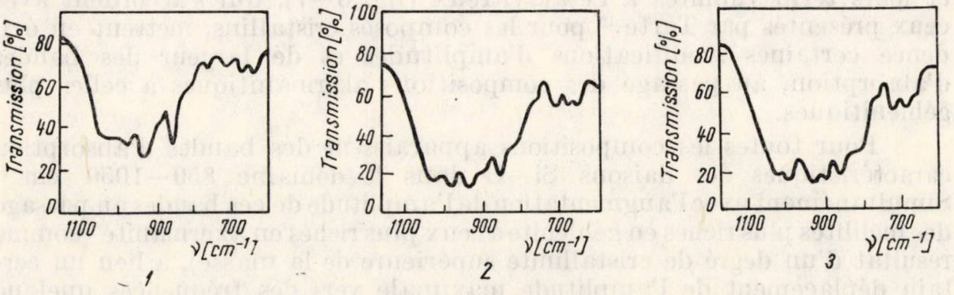

Fig. 1. — Spectres IR de certaines mélilites cristallisées.
1, 30% C_2AS+ 70% C_2MS_2; *2*, 50% C_2AS + 50% C_2MS_2; *3*, 70% C_2AS + 30% C_2MS_2.

2. Dans le présent travail on a étudié la capacité d'interaction avec l'eau de certains laitiers mélilitiques et la dépendance de celle-ci de leur composition. À cette fin, on a considéré trois compositions mélilitiques différentes : 30% $2CaO . Al_2O_3 . SiO_2$ + 70% $2CaO . MgO . 2SiO_2$, 50% $2CaO . Al_2O_3 . SiO_2$ + 50% $2CaO . MgO . 2SiO_2$, 70% $2\ CaO . Al_2O_3 . SiO_2$ + 30% $2CaO . MgO . 2SiO_2$. Les laitiers correspondant à ces compositions ont été synthétisés en partant d'oxydes chimiquement purs, par fusion dans une flamme oxyacéthylénique et refroidissement brusque dans l'eau.

En partant de la considération que les mélilites — composants des laitiers de haut fourneau — de même que les composés minéralogiques du ciment portland et alumineux — par mélange avec l'eau, durcissent comme suite des processus d'hydratation — hydrolyse, on a considéré utile pour obtenir des informations concernant la capacité d'interaction avec l'eau des laitiers mélilitiques, la méthode de conductivité électrique. [15] La conductivité électrique a été déterminée sur des suspensions à la concentration de 0,5%, le matériel solide ayant une finesse de broyage correspondant à un passage intégral par le tamis de 0,06 mm.

Les résultats de ces déterminations, présentés dans la figure 2, mettent en évidence que la réactivité des compositions mélilitiques par rapport à l'eau augmente en série * :
50% C_2AS + 50% C_2MS_2 $\rightarrow$ 70% C_2AS + 30% C_2MS_2 $\rightarrow$ 30% C_2AS + + 70% C_2MS_2.

---

* On va noter : $CaO = C$; $MgO = M$; $Al_2O_3 = A$; $SiO_2 = S$.

[14] P. J. Launer, *Amer. Mineral.*, **37**, 774 (1952).

[15] S. Solacolu, P. Baltă et C. Hofman, *Rev. Roumaine Chim.*, **11**, 481 (1966).

Il résulte que la composition des mélilites ne peut pas elle-même expliquer une telle variation de leur réactivité.

Pour obtenir quelques informations d'ordre structural on a effectué des analyses de spectroscopie en infrarouge des laitiers mélilitiques.

Les spectres d'absorption en infrarouge obtenus sur des mélilites et leurs termes limites à l'état vitreux (fig. 3—7), qui s'accordent avec ceux présentés par Tarte [12] pour les composés cristallins, mettent en évidence certaines modifications d'amplitudes et de largeur des bandes d'absorption, au passage des compositions akermanitiques à celles plus géhlénitiques.

Pour toutes les compositions apparaissent des bandes d'absorption caractéristiques des liaisons Si—O dans le domaine 850—1050 cm^{-1}. Simultanément avec l'augmentation de l'amplitude de ces bandes au passage des mélilites plus riches en géhlénite à ceux plus riches en akermanite (comme résultat d'un degré de cristallinité supérieure de la masse), a lieu un certain déplacement de l'amplitude maximale vers des fréquences quelque peu plus grandes, dans l'ordre suivant : $C_2MS_2 \rightarrow 70\%\ C_2MS_2 + 30\%\ C_2AS \rightarrow 50\%\ C_2AS + 50\%\ C_2MS_2 \rightarrow 30\%\ C_2MS_2 + 70\ C_2AS \rightarrow C_2AS$, (comme suite à l'augmentation du degré de condensation des éléments de structure).

En développant l'idée exprimée par Butt [16] sur les silicates de calcium, idée selon laquelle la réactivité des silicates augmente autant que le degré d'association du tétraèdre $[SiO_4]^{4-}$ se réduit, il faudrait que la réactivité des mélilites par rapport à l'eau augmente en série :

$$70\%C_2AS + 30\%C_2MS_2 \rightarrow 50\%C_2AS + 50\%C_2MS_2 \rightarrow$$
$$\rightarrow 30\%C_2AS + 70\%\ C_2MS_2$$

La bande d'absorption caractéristique des liaisons Mg—O, qui pour l'akermanite présente l'amplitude maximale à 500—550 cm^{-1}, apparaît pour les compositions mélilitiques plus large, centrée à 500 cm^{-1} et d'une amplitude d'autant plus petite, que les compositions mélilitiques sont plus riches en géhlénite ; pour la géhlénite elle est remplacée par une bande ayant le maximum à 420—460 cm^{-1}, caractéristique des liaisons Al—O, dans lesquelles l'ion Al^{3+} coordine octaédriquement. Pour les mélilites plus riches en géhlénite, en même temps que pour ce composé pur, les spectrogrammes mettent en évidence des bandes d'absorption de basse amplitude dans le domaine 800 cm^{-1}, caractéristiques des liaisons Al—O, dans lesquelles Al^{3+} coordine tétraédriquement.

Toutes ces modifications dans l'allure des spectres IR sont le résultat du remplacement graduel des ions Mg^{2+} et Si^{4+} par des ions Al^{3+}, en série $C_2MS_2 \rightarrow$ mélilites $\rightarrow C_2AS$.

En partant de l'akermanite vers les mélilites plus riches en géhlénite, par la substitution de Mg^{2+} et de Si^{4+} par Al^{3+} les liaisons M—O (M — cation modificateur de structure) supposent une basicité moyenne de cation métallique plus petite, tandis que les liaisons F—O (F — cation formateur de structure) doivent être considérées dans un complexe anio-

---

[16] Yu. M. Butt, *Tsement*, **10**, 19 (1971).

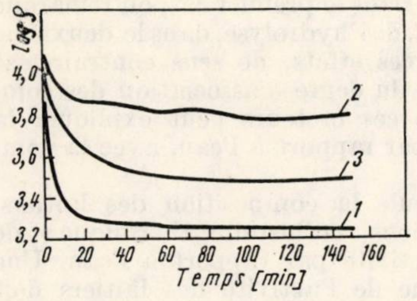

Fig. 2. — Variation du logarithme de la résistivité électrique des suspensions de certaines mélilites.

1, 30% C_2AS + 70% C_2MS_2 ; *2*, 50% C_2AS + 50% C_2MS_2 ; *3*, 70% C_2AS + 30% C_2MS_2.

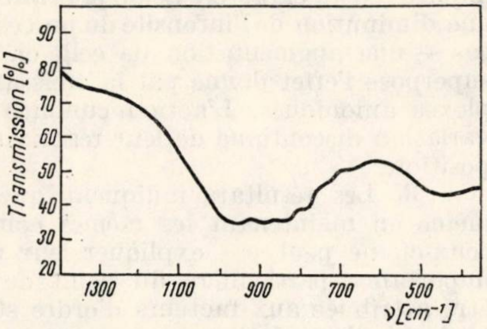

Fig. 3. — Spectre IR de la géhlénite vitreuse.

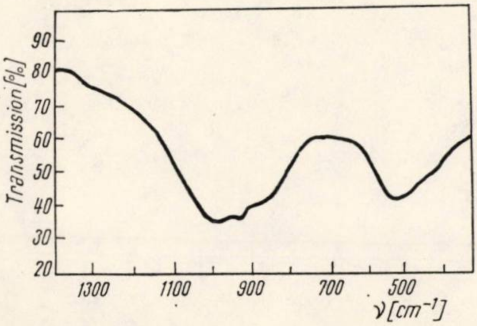

Fig. 4. — Spectre IR de la mélilite vitreuse ayant la composition 30% C_2AS + 70% C_2MS_2.

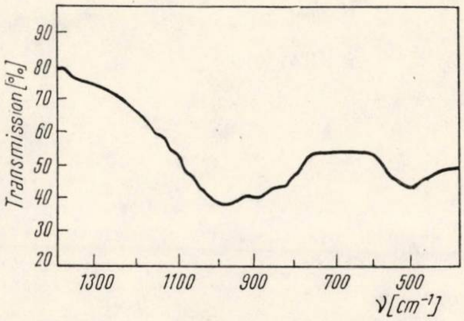

Fig. 5. — Spectre IR de la mélilite vitreuse ayant la composition 50% C_2AS + 50% C_2MS_2.

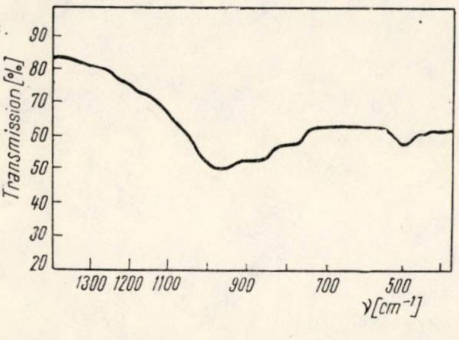

Fig. 6. — Spectre IR de la mélilite vitreuse ayant la composition 70% C_2AS + 30% C_2MS_2.

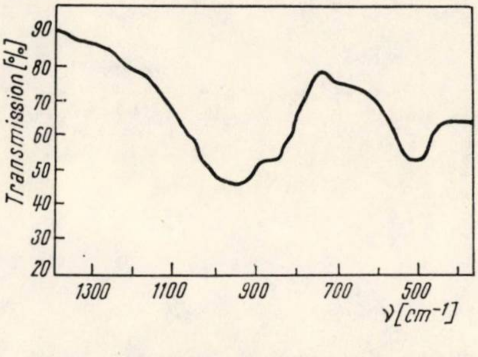

Fig. 7. — Spectre IR de l'akermanite vitreuse.

nique avec un caractère acide plus faible. Dans le premier cas, on remarque une diminution de l'intensité du processus, de l'hydrolyse, dans le deuxième cas – une augmentation de celle-ci. A ces effets, de sens contraire, se superpose l'effet donné par la croissance du degré d'association des complexes anioniques. L'action cumulée de ces facteurs peut expliquer la variation discontinue de leur réactivité par rapport à l'eau, avec la composition.

3. Les résultats indiquent que seule la composition des laitiers, même en maintenant les mêmes conditions « d'histoire thermique » de ceux-ci, ne peut pas expliquer leur réactivité par rapport à l'eau. Une importance particulière du point de vue de l'activité des laitiers doit être attribuée aux facteurs d'ordre structurel. Dans le cas des mélilites, le degré d'association des radicaux anioniques, ainsi que le rôle modificateur et formateur de structure de l'ion Al^{3+} expliquent la variation discontinue de leur réactivité par rapport à l'eau avec la composition.

Revue Roumaine de Chimie, **20**, *11–12*, 1443–1470 (1975)

ПЕРЕГРУППИРОВКИ В РЕАКЦИЯХ ДЕЗАМИНИРОВАНИЯ

О. А. РЕУТОВ, А. С. ГУДКОВА
Московский государственный университет им. М. В. Ломоносова

Получена 6 февраля 1975 г.

В данном обзоре представлен сравнительный анализ результатов исследования путей стабилизации β-галогенкарбениевых ионов алифатического, алициклического и жирно-ароматического рядов, а также β-оксипропил — и — изопропил-катионов, генерируемых в реакциях дезаминирования соответствующих β-галоген- или β-оксиалкиламинов. Состав продуктов дезаминирования β-галогенэтиламинов и γ-галогенпропиламинов исследован методом меченых атомов (^{14}C), что позволило установить наличие термонейтральных нуклеофильных перегруппировок с 1,2- (соответственно, 1,3) миграцией галогена. Результаты дезаминирования гидрогалогенидов β-галогеналкиламинов типа $RR^1CHalCH_2NH_2.HHal$ (I) и $RR^IC(NH_2.HHal)\ CH_2Hal$ (II), где R и R^I а) CH_3,H; б) CH_3,CH_3; в) RR^IC — циклогексилиден; г) C_6H_5H, а Hal — Cl или Br, исследованы методом газожидкостной хроматографии. Установлена зависимость путей стабилизации (внутренних и внешних) и, в частности, степени экзотермических и эндотермических перегруппировок с 1,2-миграцией галогена от строения первоначально и конечно образующихся карбениевых ионов, природы мигрирующей группы и условий дезаминирования (растворитель, температура). Предложен гипотетический механизм дезаминирования. В случае солей 2-хлор-2-фенилэтиламина (гидрохлорид и фосфат), а также солей β-оксипропил-и -изопропиламинов полученные результаты обсуждены с привлечением конформационного контроля.

Подробно рассмотрен метод синтеза гидрогалогенидов Iа-г и IIа-г путем нуклеофильного замещения гидроксильной группы на галоген в соответствующих аминоспиртах. Изомерная чистота объектов дезаминирования доказана методом ПМР.

В последние годы внимание исследователей привлекает химия гетерозамещенных карбокатионов, в реакционной способности которых появляются особенности, связанные с различного рода влияниями гетероатомов со свободной электронной парой. Такого рода исследования, в основном, осуществлялись на моделях алифатического ряда в реакциях сольволиза [1] и электрофильного присоединения к олефиновым системам[2].

---

[1] P. E. Peterson и др., *J. Am. Chem. Soc.*, **85**, 2865, 3608 (1963); **86**, 4503 (1964); **87**, 5163 (1965); **88**, 4990 (1966); **89**, 1283, 5902 (1967); **92**, 2834 (1970); **94**, 991, (1972); **95**, 2222 (1973). *J. Org. Chem.*, **35**, 537 (1970); **37**, 4182 (1972). *Tetr. lett.*, **1971** № 1, 13.

[2] Y. A. Olah и др., *J. Am. Chem. Soc.*, **89**, 4744 (1967); **90**, 947, 2587, 4670, 6988 (1968); **91**, 2955, 3961, 5801 (1969); **95**, 3387, 7449 (1973); **96**, 3565 (1974).

[3] П. Де Ла Мар, Р. Болтон, ,,Электрофильное присоединение к ненасыщенным системам'', Изд. ,,Мир'', Москва, 1968 г., перевод с англ., стр. 19—24,45.
И. В. Бодриков и др., *Журн. орг. химии*, **2**, 1120 (1966); **3**, 669, 775 (1967); **4**, 571, 1333 (1968); **5**, 187 (1969); **6**, 1208 (1970), **7**, 1570, 1574, 1578 (1971); **8**, 24 (1972); **9**, 535 (1973).

В наших работах проведено систематическое изучение способов стабилизации β-гетерозамещенных карбениевых ионов, генерируемых в реакциях дезаминирования и сольволиза. Особенно подробно изучено дезаминирование β-галогеналкиламинов, принадлежащих к алифатическому, жирно-алициклическому и жирно-ароматическому ряду. Как правило, нас интересовала исчерпывающая картина продуктов реакции, их отнесение к определенному типу стабилизации (внутреннему или внешнему), типу реакции (нормальное замещение без перегруппировок, элиминирование, фрагментация или перегруппировки с миграциями конкурирующих групп). Особый интерес представлял внутренний способ стабилизации, сопровождающийся миграциями углеродсодержащих остатков, гидрид-иона или соответствующего гетерозаместителя. Главным направлением при исследовании такого типа перегруппировок (нуклеофильные перегруппировки с 1, n-миграцией конкурирующих групп, где n = 2 или 3) стало выяснение влияния структурных, электронных факторов, природы заместителя, характера среды реакции, метода генерирования интермедиата на относительную миграционную способность мигрантов. Все эти вопросы решались с привлечением концепции участия соседних групп, включающей понятия о различных типах участия (p, π и δ).

В качестве модельных структур были избраны β-окси- и β-галогенкарбениевые ионы с различной степенью замещения алкильными остатками у β (α)-углеродного атома ($RR^{I}CH\underset{(OH)}{HaI}\overset{\oplus}{C}H_2$ и $RR^{I}\overset{\oplus}{C}CH_2\overset{(OH)}{HaI}$), генерируемые в реакциях дезаминирования и сольволиза. Эти два метода образования карбокатионов представляют крайние случаи образования «горячих» и «связанных» карбениевых ионов и, таким образом, имелась возможность выяснить влияние энергетического состояния образующейся частицы на её реакционную способность. Промежуточным случаем нам представляется реакция этанолиза пропиленгалогенгидринов в присутствии нитрата серебра. В данном обзоре систематически рассмотрены способы стабилизации вышеуказанных карбениевых ионов, образующихся в реакциях дезаминирования.

ДЕЗАМИНИРОВАНИЕ

Известно, что при дезаминировании первичных алифатических аминов образуются так называемые «горячие» карбокатионы (на первой стадии диазониевые ионы), наличие высокой потенциальной энергии у которых приводит к ряду особенностей в их дальнейших реакциях. Вследствие низкой избирательности образующихся интермедиатов наблюдается, как правило, большой набор продуктов реакции, которые в случае хирального β-углеродного атома могут иметь неодинаковую стереохимию. В связи с тем, что время жизни «горячих» карбениевых ионов может оказаться очень коротким по сравнению со временем оборота вокруг углерод-углеродной связи, стереоэлектронные факторы оказывают сильное влияние на характер процесса перегруппировок, что может привести к необычной миграционной способности.

1. ТЕРМОНЕЙТРАЛЬНЫЕ ПЕРЕГРУППИРОВКИ С МИГРАЦИЕЙ ГАЛОГЕНА

1.1) 1.2—Миграции галогена

Применение метода меченых атомов (C^{14}) позволило изучить реакцию дезаминирования на простейшей модели — β-галогенэтиламинах[3–6]. Радиоактивные галогенгидраты галогенэтиламинов были синтезированы на основе цианистого калия $KC^{14}N$ по следующей схеме:

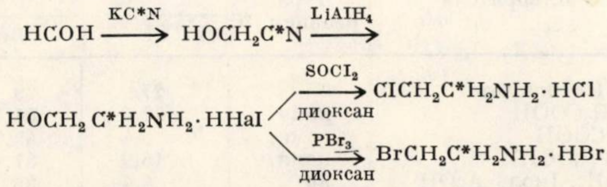

$$HCOH \xrightarrow{KC^*N} HOCH_2C^*N \xrightarrow{LiAlH_4}$$

$$HOCH_2C^*H_2NH_2\cdot HHal \begin{cases} \xrightarrow[\text{диоксан}]{SOCl_2} ClCH_2C^*H_2NH_2\cdot HCl \\ \xrightarrow[\text{диоксан}]{PBr_3} BrCH_2C^*H_2NH_2\cdot HBr \end{cases}$$

Предварительными опытами была доказана невозможность перегруппировок на каждой из применяемых стадий синтеза в указанных условиях.

Дезаминирование в различных средах (см. ниже) приводит к образованию смеси продуктов, из которой фракционной перегонкой выделяли этиленгалогенгидрины $HalCH_2CH_2OH$ или соответствующие производные $HalCH_2CH_2OCOR$ (или смесь этих соединений), которые могли оказаться как перегруппированными соединениями, так и неперегруппированными в зависимости от положения в них метки:

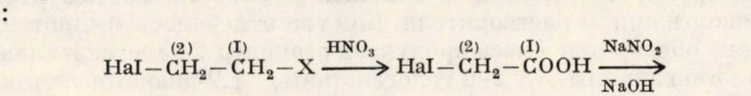

$$HalCH_2C^*H_2NH_2\cdot HHal \xrightarrow[HX]{\text{диазотирующий агент}} \begin{cases} \xrightarrow{\text{без перегр.}} HalCH_2C^*H_2X \\ \xrightarrow{1{,}2 \sim Hal} Hal\overset{*}{C}H_2-CH_2X \end{cases}$$

где $X = OH, OCOH, OCOCH_3$ или $OCOC^{14}$

Для установления положения метки (C^{14}) в выделенных соединениях был разработан метод их деструкции до нитрометана с превращением последнего в твердый ω-нитростирол, удобный для измерения радиоактивности образца:

$$Hal-\overset{(2)}{C}H_2-\overset{(1)}{C}H_2-X \xrightarrow{HNO_3} Hal-\overset{(2)}{C}H_2-\overset{(1)}{C}OOH \xrightarrow[NaOH]{NaNO_2}$$

$$\overset{(2)}{C}H_3NO_2 \xrightarrow{C_6H_5CHO} C_6H_5CH{=}CHNO_2 \quad (X{=}OH, OCOR)$$

---

[3] О. А. Реутов, Т. А. Смолина, О. Ю. Полевая, *Докл. АН СССР*, **191** (2), 366 (1970).

[4] Т. А. Смолина, А. А. Медведев, Е. Д. Гопиус, О. А. Реутов, *Докл. АН СССР*, **217** (I), 110 (1974).

[5] Т. А. Смолина, А. А. Медведев, Л. Я. Игнатов, О. А. Реутов, *Журн. орг. химии*, **10** (6), 1331 (1974).

[6] Т. А. Смолина, А. А. Медведев, Л. Н. Батюк, Л. Я. Игнатов, О. А. Реутов, *Докл. АН СССР*, **214** (5), 1091 (1974).

Полученные значения содержания C^{14} в положении (2) представлены в таблице 1.

Таблица 1

Содержание C^{14} в положении (2) продуктов деструкции в зависимости от условий дезаминирования и природы галогена в $HalCH_2CH_2NH_2 \cdot HHal$

Реагент	Растворитель	Температура реакции, °C	Содержание C^{14} в положении (2), %		Литерат. ссылка
			Cl	Br	
HNO_2	HHal-кислота	0	27	29	[3]
HNO_2	CH_3COOH	комн.	22,4	54,4	[4]
HNO_2	HCOOH	комн.	5,4	47,9	[4]
HNO_2	CF_3COOH	комн.	16,9	51,4	[4]
EtONO	C_6H_6, 1моль AcOH	80	4,4	36	[5,6]
EtONO	ТГФ, 1моль AcOH	65	3,4	25	[5,6]

Обычно за степень перегруппировки принимают мольную долю продуктов (моль. %), образовавшихся в результате смещения мигрирующей группы. Поэтому цифровые значения содержания C^{14} (табл. 1) будут совпадать со значением степени перегруппировки с 1,2-миграцией галогена лишь в тех случаях, когда соединения, подвергающиеся деструкции, являются единственными продуктами реакции. В иных случаях следует делать пересчет на полный состав продуктов реакции, причем должно быть известно отнесение каждого образующегося соединения к определенному конкурирующему процессу. Все вышесказанное сильно осложняет расчеты степени перегруппировок, а, следовательно, осуществлению корреляций между различными структурными и другими факторами, влияющими на результаты реакции. При проведении реакции в протонных средах набор продуктов реакции практически сводится к соединениям, подвергавшимся деструкции, однако, в апротонных растворителях образуется сложная смесь веществ, что приводит к заведомому завышению предполагаемой степени перегруппировки галогена. Тем не менее, совершенно очевидно, что во всех случаях степень миграции хлора меньше степени миграции брома, что связано с большей нуклеофильностью последнего. Более сложно влияние растворителя. Как уже отмечалось, в апротонных растворителях образуется смесь продуктов реакции: 2-галогенэтилацетаты-1, этиленгалогенгидрины, 1,2-дигалогенэтаны, 1,2-диацетоксиэтаны, а в случае Hal=Cl также и 2-ацетокси-1-этанол. Контрольными опытами доказано, что 2-галогенэтилацетаты-1 и этиленгалогенгидрины являются продуктами основных процессов, остальные могут быть продуктами вторичных процессов. Предполагая, что ввиду симметрии исходного объекта, содержание метки в основных продуктах отражает относительный вклад процесса перегруппировки, мы приняли это значение за степень миграции галогена.

Особенно резкое различие в степени миграции наблюдается для хлора в зависимости от дезаминирования в протонных или апротонных средах, что явно указывает на разницу в механизмах реакции. В протонных средах реакция, по-видимому, протекает через открытые β-галогенкарбениевые ионы и частично через циклические галогенониевые ионы, а в апротонных средах — частично через диазониевые катионы или через диазогидратные формы. Менее ясна закономерность для миграции брома.

При переходе от менее полярного растворителя (бензол) к более полярному апротонному растворителю (ТГФ) наблюдается тенденция к снижению степени миграции галогена (Hal=CI, Br). Для объяснения

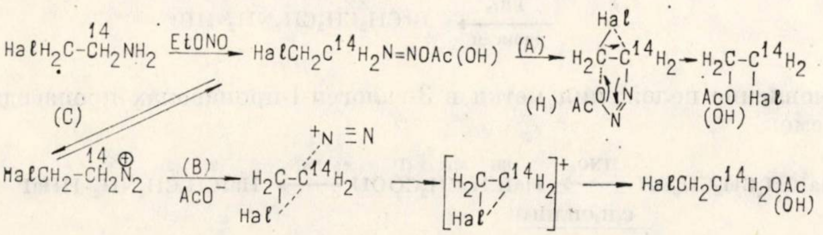

этого явления предлагается следующий возможный механизм дезаминирования. Путь «А» включает синхронный процесс 1,2-миграции галогена и атаки β-углеродного атома кислородным атомом диазоацетата или диазогидрата и приводит к перегруппированному продукту реакции. Путь « В » сводится к образованию из диазониевого катиона β-галогенкарбениевого иона, а затем галогенониевого иона, из которого возможно образование как перегруппированных, так и неперегруппированных продуктов. Соотношение перегруппированных и неперегруппированных продуктов должно зависеть от вклада путей « А » и « В ». При увеличении полярности апротонного растворителя в результате смещения равновесия « С» в сторону диазониевого катиона (большая сольватация, а следовательно большая стабильность переходного состояния) происходит увеличение вклада пути (В), что приводит к уменьшению степени перегруппировки.

То, что степень перегруппировки во всех случаях дезаминирования 2-галогенэтиламинов-1 ниже 50%, указывает на то, что во всех случаях путь « В» преобладает.

Вышеуказанные примеры перегруппировок с 1,2-миграцией галогена интересны тем, что они представляют случаи так называемых термонейтральных перегруппировок, когда энергии первоначально и конечно образующихся карбениевых ионов одинаковы. Но в данном случае это «псевдотермонейтральные» перегруппировки, поскольку движущей силой при миграции галогенов является образование циклических интермедиатов, которые всегда более стабильны по сравнению с соответствующими им открытыми формами.

1.2) 1,3-Миграции галогена

В дальнейшем было исследовано дезаминирование 3-галогенпропиламинов-I с применением метода ГЖХ и метода меченых атомов (C^{14}). Строение и чистоту исходных аминов, полученных по нижеуказанной схеме, проверяли методом ПМР-спектроскопии:

$$HOCH_2CH_2CN \xrightarrow{LiAlH_4} HOCH_2CH_2CH_2NH_2\cdot HHal \longrightarrow$$

$$\xrightarrow[\text{толуол}]{SOCl_2} ClCH_2CH_2CH_2NH_2\cdot HCl$$

$$\xrightarrow[\text{диоксан}]{PBr_3} BrCH_2CH_2CH_2NH_2\cdot HBr$$

Установление положения метки в 3-галоген-I-пропанолах производилось по схеме:

$$HalCH_2CH_2CH_2OH \xrightarrow{HNO_3} Hal\overset{(3)}{C}H_2\overset{(2)}{C}H_2\overset{(1)}{C}OOH \xrightarrow{NaN_3} Hal\overset{(3)}{C}H_2\overset{(2)}{C}H_2NH_2\cdot HHal$$

$$\downarrow C_2H_5OH, HHal$$

$$Hal\overset{(3)}{C}H_2\overset{(2)}{C}H_2\overset{(I)}{C}OOC_2H_5 \xrightarrow[-HHal]{NaOH} \overset{(3)}{C}H_2=\overset{(2)}{C}H\overset{(I)}{C}OOC_2H_5 \xrightarrow[H_2O]{O_3} HOO\overset{(2)}{C}\overset{(I)}{C}OOC_2H_5+\overset{(3)}{C}H_2O$$

При дезаминировании 3-галогенпропиламинов-1 в соответствующих галогеноводородных кислотах образуется сложная смесь продуктов реакции, состоящая приблизительно из 20 компонентов, причем многие из них являются продуктами побочных процессов — присоединение к непредельным системам, гидролиз дигалогенидов, замена гидроксила на галоген в гликолях и т.д. Оптимальные условия дезаминирования, приводящие к минимуму вторичных процессов, сводились к дезаминированию в фосфорной кислоте при 0° с эквимолярным количеством нитрита натрия. Результаты дезаминирования приведены в таблице 2.

Таблица 2

Состав продуктов дезаминирования (%) 3-галогенпропиламинов-1 ($HalCH_2CH_2CH_2NH_2\,.\,HHal$)[7]

Тип перегруппировки	Тип реакции	Продукты реакции	для амина с Hal	
			Cl	Br
без перегруппировки	S_N	$HalCH_2CH_2C^*H_2OH$	60	46,7
1,2-миграция гидрид-иона	S_N	$HalCH_2CH(OH)CH_3$ $HalCH_2CHHalCH_3$	7 23	3 —
Многократные миграции: 1,2∼H⁻ и 1,2∼Hal	S_N	$HOCH_2CHHalCH_3$		36
1,3-миграции Hal	S_N	$HalC^*H_2CH_2CH_2OH$	—	10,3
? ?	S_N E	гликоли непредельные соединения	2 8	2 2

[7] О. А. Реутов, Т. А. Смолина, О. Ю. Полевая, Е. Д. Гопиус, Л. В. Бетанели, *Докл. АН СССР*, **197** (4), 848 (1971).

Состав продуктов дезаминирования установлен методом ГЖХ, а отнесение образующегося 3-бромпропанола-1 к перегруппированному или неперегруппированному продукту — на основании опыта с меченым исходным амином. Методом деструкции установлено, что 18% C^{14} содержится в положении (3) (см. схему деструкции). Из данных ГЖХ-анализа известно, что выход 3-бром-1-пропанола составляет 57% от всех продуктов реакции. Следовательно, общий вклад процесса перегруппировки с 1,3-миграцией брома можно приблизительно рассчитать из пропорции

$$57 - 100\% \qquad (x = 10{,}3\%).$$
$$x - 18$$

Отсутствие перегруппировки с 1,2-миграцией CH_2X-группы в 3-галоген-1-пропилкатионах доказана тем, что во втором положении метка не обнаружена:

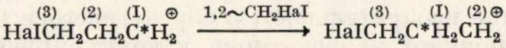

$$\overset{(3)}{\mathrm{HalCH_2}}\overset{(2)}{\mathrm{CH_2}}\overset{(I)}{\mathrm{C^*H_2}}{}^{\oplus} \xrightarrow{1,2\sim \mathrm{CH_2Hal}} \overset{(3)}{\mathrm{HalCH_2}}\overset{(I)}{\mathrm{C^*H_2}}\overset{(2)}{\mathrm{CH_2}}{}^{\oplus}$$

Таким образом, есть все основания полагать, что 1,3-миграция брома осуществляется через промежуточное образование четырехчленного галогенониевого иона 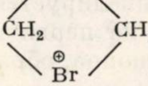. Образование четырехчленного галогенониевого иона в столь значительных количествах — явление чрезвычайно интересное. Согласно исследованиям свойств циклических галогенониевых ионов, генерерируемых в суперкислотах, известно, что их стабильность в значительной степени зависит от количества звеньев в цикле (эффект четности и не четности [8]). Все попытки получить четырехчленные галогенониевые циклы [9] приводили к перегруппировкам с образованием трехчленных галогенониевых ионов, которые непосредственно наблюдались методом двойного резонанса. Т.е. как бы происходила 1,2-миграция гидрид-иона с одновременным участием галоген-атома в образовании галогенониевых ионов:

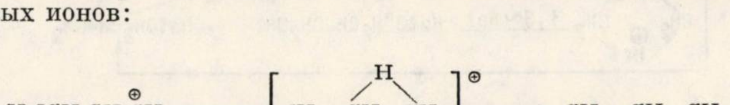

Аналогичный механизм приемлем для объяснения образования 2-бром-1-пропанола (36%) при дезаминировании 3-бромпропиламина-1, при этом становится понятным факт отсутствия аналогичного продукта с Hal = Cl. Последний не будет проявлять склонности к завязыванию связи в промежуточном соединении (или переходном состоянии) типа

---

[8] P. E. Peterson, *J. Org. Chem.*, **37**, 4180 (1972).

[9] G. A. Olah, Y. M. Bollinger, J. K. Mo, Y. M. Brinich, *J. Am. Chem. Soc.*, **94** (4), 1164 (1972).

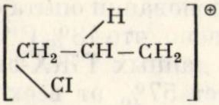

1-Галоген-2-пропанолы и 1,2-дигалогенпропанолы можно рассматривать как продукты 1,2-миграций гидрид-иона:

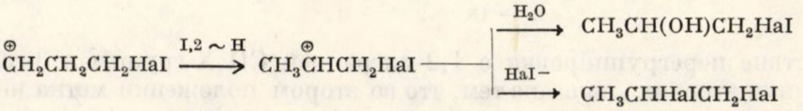

$$\overset{\oplus}{C}H_2CH_2CH_2HaI \xrightarrow{1,2\sim H} CH_3\overset{\oplus}{C}HCH_2HaI \begin{cases} \xrightarrow{H_2O} CH_3CH(OH)CH_2HaI \\ \xrightarrow{HaI^-} CH_3CHHaICH_2HaI \end{cases}$$

Из 1,2-дигалогенпропанов обнаружен лишь 1,2-дихлорпропан, что можно объяснить высокой избирательностью образующегося после 1,2-миграции гидрид-иона вторичного карбокатиона к конкурирующим нуклеофилам среды (правило Корнблюма).

Суммарная степень 1,2-миграции гидрид-иона близка как для хлор-, так и бромпропилкатионов (7 + 23 = 30% для HaI=Cl, 3 + 36 = 39% для HaI = Br). Эта разница практически нивелируется, если принять, что непредельные соединения образуются не из первичных 3-галоген-1-пропилкатионов, а из вторичных карбениевых ионов, образующихся после гидридных смещений.

Таким образом, предлагается следующая общая схема изомеризации 3-галоген-1-пропилкатионов:

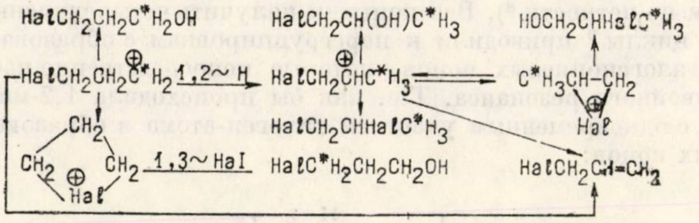

2. ЗАВИСИМОСТЬ СТЕПЕНИ ПЕРЕГРУППИРОВОК С 1,2-МИГРАЦИЕЙ ГАЛОГЕНА ОТ СТРОЕНИЯ ПЕРВОНАЧАЛЬНО И КОНЕЧНО ОБРАЗУЮЩИХСЯ КАРБЕНИЕВЫХ ИОНОВ, ПРИРОДЫ ГАЛОГЕНА И УГЛЕРОДСОДЕРЖАЩИХ ЗАМЕСТИТЕЛЕЙ У β-(α)-УГЛЕРОДНОГО АТОМА

Очень подробно исследован состав продуктов дезаминирования в протонных средах галогеналкиламинов типов $RR^ICHaICH_2NH_2 \cdot HHaI$ и $RR^IC(NH_2 \cdot HHaI)CH_2HaI$ с углеродсодержащими остатками R и R^I, принадлежащими к алифатическому, алициклицескому или ароматическому ряду. Вышеуказанные амины стабильны при нормальных условиях лишь в виде солей. Задачи, поставленные в наших работах, обусловили особые требования к изомерной чистоте исходных соединений, что, в свою очередь, вызвало необходимость тщательного исследования их методов синтеза.

2.1. Синтез объектов дезаминирования

Как правило, синтез известных в литературе β-галогеналкиламинов осуществлялся по сходным схемам, которые на последней стадии сводятся к замещению гидроксила в β-аминоспиртах на галоген:

Схема I

$$RR^{I}CO \xrightarrow{HCN} RR^{I}C(OH)CN \xrightarrow{LiAlH_4} RR^{I}C(OH)CH_2NH_2 \xrightarrow{HHal}$$

$$RR^{I}C(OH)CH_2NH_2 \cdot HHal \xrightarrow[\text{агент}]{\text{галогенирующий}} RR^{I}CHalCH_2NH_2 \cdot HHal$$

Схема II

$$RR^{I}CO \xrightarrow{NH_4CN} RR^{I}C(NH_2)COOH \xrightarrow{LiAlH_4} RR^{I}C(NH_2)CH_2OH \xrightarrow{HHal}$$

$$RR^{I}C(NH_2 \cdot HHal)CH_2OH \xrightarrow[\text{агент}]{\text{галогенирующий}} RR^{I}C(NH_2 \cdot HHal)CH_2Hal$$

Поскольку согласно литературным данным замещение окси-группы на галоген в β-аминоспиртах часто протекает с перегруппировкой, включающей 1,2-миграцию амино-группы [3,10,11], то особенно тщательно исследовалась именно эта стадия [12-15]. Изомерная чистота всех полученных соединений контролировалась методом ПМР-спектроскопии.

В ряде случаев стадия замещения гидроксила на галоген или вовсе не протекала [15] или сопровождалась образованием небольших количеств изомерного соединения. В таких случаях прибегали к другим методам синтеза. В частности, гидрогалогениды 1-галогенметил-1-аминоциклогексанов удалось получить в изомерно чистом виде лишь гетеролизом 1-азас-

---

[10] E. Schultz, J. Sprague, *J. Am. Chem. Soc.*, **70**, 48 (1948). E. Walter, P. Ofner, R. H. Thorp, *J. Chem. Soc.*, **1949**, 648. Y. Attenburrow, У. Elks, B. Hems, K. Speyer *J. Chem. Soc.*, **1949**, 511. P. Ofner *J. Chem. Soc.*, **1951**, 1803.

[11] С. Ф. Торф, Т. Ю. Столярова, *Журн. орг. химии*, **4**, 134 (1968).

[12] А. С. Гудкова, Г. М. Остапчук, И. В. Петросян, О. А. Реутов, *Докл. АН СССР* **194** (5), 1086 (1970).

[13] О. А. Реутов, А. С. Гудкова, И. В. Петросян, *Изв. АН СССР, сер. хим.*, **1972**, 213.

[14] О. А. Реутов, А. С. Гудкова, К. Утениязов, Н. А. Нарышкова, *Докл. АН СССР*, **202** (1), 101 (1972).

[15] А. С. Гудкова, К. Утениязов, С. Г. Завгородний, О. А. Реутов, *Журн. орг. химии*, **9** (8), 1651 (1973).

пиро-(2,5)-октана с помощью соответствующих галогеноводородных кислот[16]:

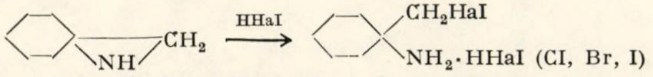

Гидрохлорид 1-аминометил-1-хлорциклогексана получен восстановлением амида α-хлорциклогексанкарбоновой кислоты с помощью гидрида алюминия[17]:

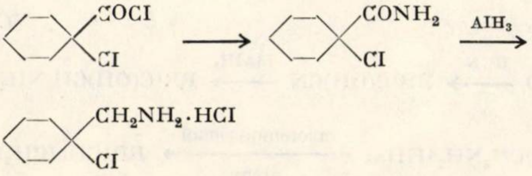

Галогеналкиламины, исследованные нами в реакции дезаминирования, представлены в таблице 3.

2.2. Дезаминирование гидрогалогенидов 2(1)-галоген 1(2)-аминоалканов

Дезаминирование гидрогалогенидов 1-амино-2-галоген- и 2-амино-1-галогеналканов осуществляли действием эквимолярных количеств нитрита натрия в соответствующей разбавленной галогеноводородной кислоте при 50°. Нами исследованы соответствующие пропильные, бутильные и изобутильные системы типов $RR^{I}CHHalCH_2NH_2 \cdot HHal$ и

$RR^{I}C(NH_2 \cdot HHal)CH_2Hal$, где а) $R=H$, $R^{I}=CH_3$, $Hal=Cl$, Br или I;

б) $R=H$, $R^{I}=C_2H_5$, $Hal=Cl$ или Br;

в) $R=R^{I}=CH_3$, $Hal=Cl$ или Br.

Состав продуктов реакции (в мольных %) устанавливался методом-газожидкостной хроматографии.

Дезаминирование гидрогалогенидов 1-амино-2-галогенпропанов $CH_3CHHalCH_2NH_2 \cdot HHal(Hal=Cl, Br, I)$ приводит к образованию смеси изомерных пропиленгалогенгидринов — 2-галоген-1-пропанолов (неперегруппированные продукты) и 1-галоген-2-пропанолов (продукты, образующиеся в результате 1,2-миграции галогенов). Степень миграции галогена зависит от природы мигрирующей руппы и отвечает ряду $Cl < Br < I$ (см. табл. 4). В случае $Hal=I$ в связи с быстрым разложе-

---

[16] О. А. Реутов, А. С. Гудкова, К. Утениязов, Н. А. Нарышкова, *Докл. АН СССР* **201** (6), 1369 (1971).

[17] А. С. Гудкова, К. Утениязов, С. Г. Завгородний, О. А. Реутов, *Докл. АН СССР* **210** (3), 595 (1973).

Таблица 3

Объекты дезаминирования

	Формула соединения	Название соединения	Лит. ссылка
1	$CH_3CHClCH_2NH_2\cdot HCl$	Гидрохлорид 1-амино-2-хлорпропана	[18]
2	$CH_3CH(NH_2\cdot HCl)CH_2Cl$	Гидрохлорид 2-амино-1-хлорпропана	—
3	$CH_3CHBrCH_2NH_2\cdot HBr$	Гидробромид 1-амино-2-бромпропана	[18]
4	$CH_3CH(NH_2\cdot HBr)CH_2Br$	Гидробромид 2-амино-1-бромпропана	—
5	$CH_3CHICH_2NH_2\cdot HI$	Гидроиодид 1-амино-2-иодпропана	[18]
6	$CH_3CH_2CHClCH_2NH_2\cdot HCl$	Гидрохлорид 1-амино-2-хлорбутана	[19]
7	$CH_3CH_2CH(NH_2\cdot HCl)CH_2Cl$	Гидрохлорид 2-амино-1-хлорбутана	[19]
8	$CH_3CH_2CHBrCH_2NH_2\cdot HBr$	Гидробромид 1-амино-2-бромбутана	[20]
9	$CH_3CH_2CH(NH_2\cdot HBr)CH_2Br$	Гидробромид 2-амино-1-бромбутана	[20]
10	$(CH_3)_2CClCH_2NH_2\cdot HCl$	Гидрохлорид 1-амино-2-хлор-2-метилпропана	[12,21]
11	$(CH_3)_2C(NH_2\cdot HCl)CH_2Cl$	Гидрохлорид 2-амино-1-хлор-2-метилпропана	[12,21]
12	$(CH_3)_2CBrCH_2NH_2\cdot HBr$	Гидробромид 1-амино-2-бром-2-метилпропана	[13,21]
13	$(CH_3)_2C(NH_2\cdot HBr)CH_2Br$	Гидробромид 2-амино-1-бром-2-метилпропана	[13,21]
14	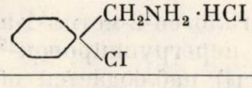	Гидрохлорид 1-аминометил-1-хлорциклогексана	[17]
15	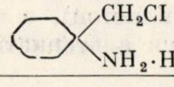	Гидрохлорид 1-хлорметил-1-аминоциклогексана	[16]
16	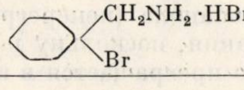	Гидробромид 1-аминометил-1-бромциклогексана	[14]
17	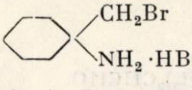	Гидробромид 1-бромметил-1-аминоциклогексана	[16]

---

[18] О. А. Реутов, А. С. Гудкова, Г. М. Остапчук, В. Г. Акимова, *Изв. АН СССР, сер. хим.*, 1922 (1968).

[19] О. А. Реутов, А. С. Гудкова, И. В. Петросян, *Докл. АН СССР*, **203** (2), 354 (1972).

[20] А. С. Гудкова, Т. Г. Мельникова, И. В. Петросян, О. А. Реутов, *Докл. АН СССР*, **203** (I), 106 (1972).

[21] В. С. Петросян, И. В. Петросян, А. С. Гудкова, О. А. Реутов, *Изв. АН СССР, сер. хим.*, **1973**, 1727.

Таблица 3

	Формула соединения	Название соединения	Лит. ссылка
18	$C_6H_5CHClCH_2NH_2 \cdot HCl$	Гидрохлорид 1-амино-2-хлор-2-фенилэтана	22
19	$C_6H_5CHClCH_2NH_2 \cdot H_3PO_4$	Фосфат-1-амино-2-хлор-2-фенилэтана	23
20	$C_6H_5CH(NH_2 \cdot HCl)CH_2Cl$	Гидрохлорид 2-хлор-1-амино-1-фенилэтана	22
21	$C_6H_5CHBrCH_2NH_2 \cdot HBr$	Гидробромид 1-амино-2-бром-2-фенилэтана	24
22	$C_6H_5CH(NH_2 \cdot HBr)CH_2Br$	Гидробромид 1-амино-2-бром-1-фенилэтана	24

нием пропилениодгидринов в условиях хроматографирования сходящихся результатов получить не удается. Во всех случаях перегруппировка сопровождается превращением первичных карбениевых ионов во вторичные[18].

При дезаминировании 1-амино-2-галогенбутанов в продуктах реакции кроме изомерных бутиленгалогенгидринов (2-галоген-1-бутанолы и 1-галоген-2-бутанолы) обнаружены также 1,2-дигалогенбутаны[19,20]). Механизм образования последних трудно трактовать однозначно, поэтому степень миграции галогена условно расчитывали по мольному содержанию 1-галоген-2-пропанолов. И в данном случае по относительной миграционной способности Br > Cl, хотя по сравнению с вышеуказанными пропильными системами степень миграции несколько снижается для одной и той же природы галогена. Следует отметить отсутствие продуктов перегруппировок с миграцией этильной группы (масляный альдегид) и гидрид-иона (метилэтилкетон).

При дезаминировании гидрогалогенидов 2-галоген-2-метил-1-аминопропанов образуются исключительно продукты перегруппировок[25]. Наряду с миграцией галогенов (основные процессы) наблюдается образование продуктов 1,2-миграции CH_3-группы (метилэтилкетон), а также изомасляного альдегида. Для последнего предлагаются альтернативные механизмы:

1) за счет разложения 2-хлор-2-метил-1-пропанола (неперегруппированный продукт) в условиях хроматографирования, поскольку последний при температуре испарителя (250°) полностью превращается в изомасляный альдегид

$$(CH_3)_2CHalC\overset{\oplus}{H_2} \longrightarrow (CH_3)_2CHalCH_2OH \xrightarrow{250^\circ} (CH_3)_2CHCHO$$

[22] А. С. Гудкова, Н. А. Нарышкова, Л. И. Матвеенко, О. А. Реутов, *Журн. орг. химии*, **10** (10), 2014 (1974).

[23] А. С. Гудкова, Н. А. Нарышкова, О. А. Реутов, *Докл. АН СССР*, **218** (3), 585 (1975).

[24] А. С. Гудкова, Н. А. Нарышкова, О. А. Реутов, *Докл. СССР* **218** (6), 1355 (1974).

[25] А. С. Гудкова, Г. М. Остапчук, И. В. Петросян, О. А. Реутов, *Докл. АН СССР* **194** (2), 335 (1970).

2) образование изомасляного альдегида путем синхронных многократных перегруппировок

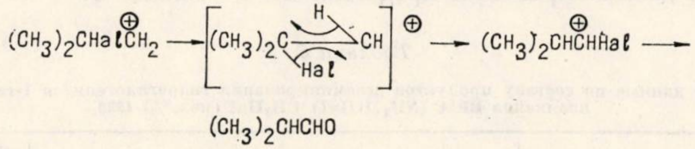
$(CH_3)_2CHalC\overset{\oplus}{H}_2$
$(CH_3)_2C$
H
Hal
CH
⊕
$(CH_3)_2CH\overset{\oplus}{C}HHal$
$(CH_3)_2CHCHO$

По относительной миграционной способности Br $>$ Cl $>$ CH_3. Таким образом, основным способом стабилизации образующегося первичного карбениевого иона $(CH_3)_2CHalC\overset{\oplus}{H}_2$ является 1,2-миграция галогена с превращением в третичный карбениевый ион $(CH_3)_2\overset{\oplus}{C}CH_2Hal$. Менее вероятна 1,2-миграция CH_3-группы, что понятно, поскольку в этом случае первичный карбениевый ион превращается не в третичный (как это имеет место при миграции галогена), а лишь во вторичный карбениевый ион $CH_3\overset{\oplus}{C}HalCH_2CH_3$, хотя и стабилизированный α-участием галогена.

В таблице 4 представлены результаты дезаминирования гидрогалогенидов 1-амино-2-галогеналканов.

Таблица 4

Сравнительные данные по составу продуктов дезаминирования гидрогалогенидов 1-амино-2-галогеналканов $RR^ICHalCH_2NH_2.NHal$ (мол. %)[19,20]

Тип перегруппировки	R	R^1	Продукты реакции	Для амина Hal = Cl	Br
1,2-миграция Hal	H	CH_3	1-галоген-2-пропанол	53	76
	H	C_2H_5	1-галоген-2-бутанол	42	55
	CH_3	CH_3	1-галоген-2-метил-2-пропанол	81	90,6
?	H	CH_3	1,2-дигалогенпропан	0	0
?	H	C_2H_5	1,2-дигалогенбутан	24	27
?	CH_3	CH_3	1,2-дигалоген-2-метил-пропан	13,3	6,2
1,2-миграция Alк	H	CH_3	пропионовый альдегид	0	0
	H	C_2H_5	масляный альдегид	0	0
	CH_3	CH_3	метилэтилкетон	3	3,2
1,2-миграция H	H	CH_3	ацетон	0	0
	H	C_2H_5	метилэтилкетон	0	0
без перегруппировки	H	CH_3	2-галоген-1-пропанол	47	24
	H	C_2H_5	2-галоген-1-бутанол	34	18
	CH_3	CH_3	изомасляный альдегид *	2,7	0

* Отнесение гипотетическое.

Для установления возможности эндотермических перегруппировок было исследовано дезаминирование β-галогеналкиламинов типа $RR^IC(NH_2 \cdot HHal)CH_2Hal$ с амино-группой у вторичного или третичного С-атома. Результаты дезаминирования представлены в таблице 5.

Таблица 5

Сравнительные данные по составу продуктов дезаминирования гидрогалогенидов 1-галоген-2-аминоалканов $RR^IC\ (NH_2 . HHal)\ CH_2Hal$ (мол. %) 1920

Тип перегруппировки		R	R^I	Продукты реакции	Для амина	
					Hal=Cl	Hal=Br
1,2-миграции галогена	$2^0 \to 1^0$	H	CH_3	2-галоген-1-пропанол	2	не иссл.
	$2^0 \to 1^0$	H	C_2H_5	2-галоген-1-бутанол	2	1,4
	$3^0 \to 1^0$	CH_3	CH_3	2-галоген-2-метил-1-пропанол	0	0
1,2-миграции гидрид-иона (из R^1)	$2^0 \to 1^0$	H	CH_3	3-галоген-1-пропанол	0	не иссл.
	$2^0 \to 2^0$	H	C_2H_5	3-галоген-1-бутанол	9,5	15
	$3^0 \to 1^0$	CH_3	CH_3	1,3-дигалогенбутан	0,7	1,4
				3-галоген-2-метил-1-пропанол	0	0
без перегруппировки		H	CH_3	1-галоген-2-пропанол	98	не иссл.
				1,2-дигалогенпропан	0	не иссл.
		H	C_2H_5	1-галоген-2-бутанол	51,8	68
				1,2-дигалогенбутан	36	14,2
		CH_3	CH_3	1-галоген-2-метил-2-пропанол	80	96,5
				1,2-дигалоген-2-метил-пропан	20	3,5

где 1^0 — первичный карбениевый ион,
2^0 — вторичный карбениевый ион,
3^0 — третичный карбениевый ион.

Из сравнительных данных таблицы 5 видно, что первоначально образующиеся вторичные, а особенно, третичные карбокатионы склонны к внешней стабилизации, т.е. образованию неперегруппированных продуктов путем взаимодействия с конкурирующими нуклеофилами среды — H_2O и Hal-анионами. Следует отметить, что в данных случаях образующиеся 1,2-дигалогеналканы более правильно отнести к неперегруппированным продуктам, хотя такое отнесение также является гипотетическим.

Наблюдается возможность термонейтральных перегруппировок с 1,2-миграцией гидрид-иона из CH_2-группы этильного остатка при дезаминировании гидрогалогенидов 1-галоген-2-аминобутанов, причем для бромзамещенных степень 1,2-миграции гидрид-иона несколько больше, чем для хлор-аналога.

Понятно полное отсутствие продуктов реакции, образующихся в результате 1,2-миграций гидрид-иона из CH_2Hal-групп, поскольку участие соответствующей σ-связи в перегруппировке затруднено отрицательным индукционным эффектом галоген-атомов. Кроме того соответствующая перегруппировка термодинамически не выгодна, поскольку при вышеуказанной миграции гидрид-иона должен образовываться первичный карбениевый ион.

Эндотермические перегруппировки протекают в незначительной степени для первоначально образующихся вторичных карбениевых ионов и вовсе не имеют места для первоначально образующихся третичных карбокатионов.

При сопоставлении данных таблиц 4 и 5 видно, что дезаминирование изомерных β-галогеналкиламинов сопровождается образованием значительных количеств 1,2-дигалогеналканов, что можно объяснить наличием некоторой избирательности у образующихся карбениевых ионов по отношению к конкурирующим нуклеофилам среды — воде и галогенанионам. Согласно правилу Корнблюма карбениевые ионы легче взаимодействуют с реагентами, обладающими большей электронной плотностью,т.е. в данном случае с галоген-анионами. Тем не менее галогенгидрины являются доминирующими продуктами в результате влияния вероятностного фактора, поскольку в изученных системах отношение концентраций конкурирующих нуклеофилов $H_2O:HHal = 100:1$. Второй особенностью состава продуктов дезаминирования является образование больших количеств дихлоридов по сравнению с дибромидами, что также согласуется с правилом Корнблюма, а именно — хлор-анион обладает большей электронной плотностью по сравнению с бром-анионом.

2.3. Дезаминирование β-галогеналкиламинов жирно-алициклического ряда

Известно, что дезаминирование β-аминоспиртов жирно-алициклического ряда типа 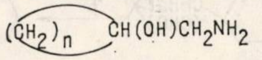

сопровождается скелетной изомеризацией с расширением цикла и образованием алициклических кетонов 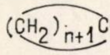

. Эта разновидность перегруппировки Демьянова получила наименование реакции Тиффно.

Интересно было выяснить влияние природы β-гетерозаместителя, содержащего p-электронную пару, на степень перегруппировки Демьянова-Тиффно или вернее на способы стабилизации образующихся интермедиатов в целом. С этой целью было исследовано дезаминирование гидрогалогенидов 1-аминометил-1-галогенциклогексанов 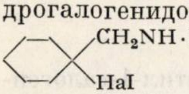

(Hal=Cl, Br) в разбавленных галогеноводородных кислотах. Чтобы проследить влияние температурных условий реакцию осуществляли при 0° и при 50°. Полученные результаты представлены в таблице 6[17,26,27].

Прежде всего следует указать на большое разнообразие продуктов дезаминирования, образующихся в результате взаимодействия с нуклеофилами среды, элиминирования, фрагментации или перегруппировок. Трактовка образования продуктов реакции однозначна во всех случаях кроме 1,2-дигалогенидов типа 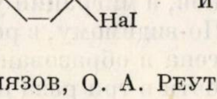

и 1-оксиметил-1-циклогек-

---

[26] А. С. Гудкова, К. Утениязов, О. А. Реутов, *Докл. АН СССР*, **214** (3), 572 (1974).

[27] А. С. Гудкова, К. Утениязов, С. Г. Завгородний, О. А. Реутов, *Докл. АН СССР*, **214** (4), 815 (1974).

сена (см. схему):

Схема

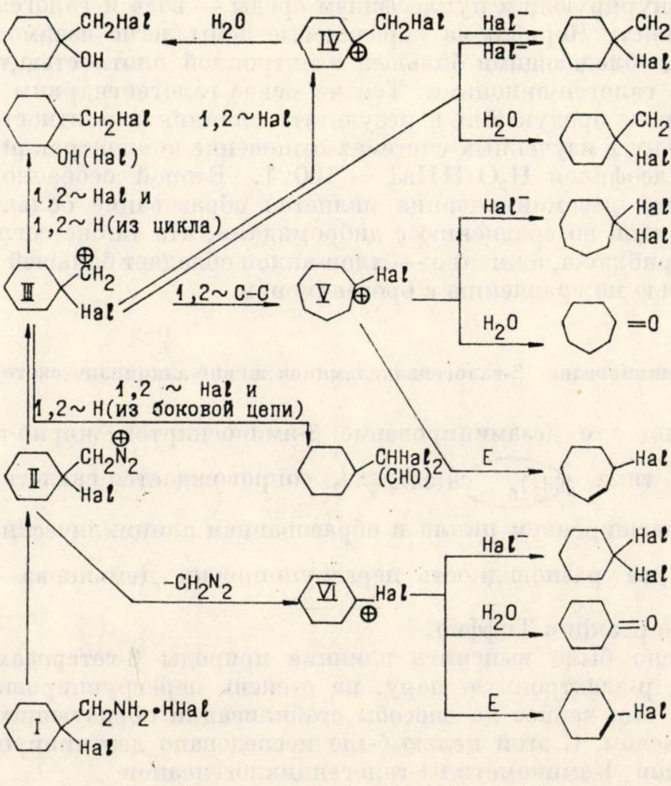
CH₂Hal
OH
H₂O
IV
CH₂Hal
Hal⁻
Hal⁻
CH₂Hal
Hal
CH₂Hal
OH(Hal)
1,2~Hal
H₂O
CH₂OH
Hal
1,2~Hal и
1,2~H(из цикла)
Hal⁻
Hal
Hal
III
CH₂
Hal
1,2~C-C
V
Hal
H₂O
=O
1,2 ~ Hal и
1,2~H(из боковой цепи)
II
CH₂N₂
Hal
CHHal₂
(CHO)
E
Hal
Hal⁻
Hal
Hal
-CH₂N₂
VI
Hal
H₂O
=O
E
Hal
I
CH₂NH₂•HHal
Hal

При дезаминировании гидрогалогенидов 1-аминометил-1-галогенциклогексанов (I) образуются диазониевые ионы (II), а затем горячие первичные карбениевые ионы (III), которые, как и следовало ожидать, проявляют склонность к стабилизации путем перегруппировок с образованием вторичных или третичных карбениевых ионов (IV—VI) в зависимости от природы мигрирующей группы. При перегруппировке иона III с 1,2-миграцией галогена образуется третичный ион IV, при перегруппировке Демьянова с расширением цикла — вторичный ион V, дополнительно стабилизированный α-участием атома галогена. Миграция галогенов протекает с участием p-электронов, а миграции углеродсодержащих остатков — с участием σ-электронов. По-видимому, в результате более легкого участия p-электронов атомов галогена в образовании переходного состояния, степень миграции галогена почти в три раза превышает степень 1,2-миграции углеродной цепи при перегруппировке Демьянова.

Как видно из схемы, продукты, образующиеся в результате различных перегруппировок и фрагментации, являются продуктами экзотермических процессов, поскольку конечно возникающие карбениевые

Таблица 6

Сравнительные данные по составу продуктов дезаминирования

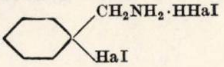

(в мол. %)

Тип перегруппировки	Продукты реакции	Для амина с Hal			
		Cl		Br	
		50°	0°	50°	0°
без перегруппировки (S_N, E и фрагментация)	1-оксиметил-1-галогенциклогексен	следы	4,8	0	0
	циклогексанон-	3	3,3	1,4	3
	1-галоген-1-циклогексан	следы	следы	1,6	0
	1,1-дигалогенциклогексен	следы	0	0	0
	Всего:	3	8,1	3	3
1,2-миграции галогена	1-галогенметил-1-циклогексанол	43	45,6	47	48,4
	1-галогенметил-1-галогенциклогексан *	11,5	6	14,4	12,2
	1-галогенметил-1-циклогексан	17,5	29,4	0	0
	(галогенметилен) циклогексан	3	3,2	1,7	0
	1-оксиметил-1-циклогексен *	следы	0	3,5	3,6
	Всего:	75	84,2	66,6	64,2
Многократные перегруппировки: 1) 1,2-миграция галогена 2) 1,2-миграция гидрида из а) боковой цепи б) цикла	а) циклогексилформальдегид	0	0	1,7	5,7
	а) (дигалогенметил) циклогексан	0	0	2,6	0
	б) 2-галогенметил-1-галоген-циклогексан	0	0	8,2	1,9**
	Всего:	0	0	12,5	7,6
перегруппировка Демьянова	циклогептанон	13	6,3	12,8	25,2
	1-галогенциклогептен	5,5	1,4	5,1	0
	1,1-дигалогенциклогептан	3,5	0	0	0
	Всего:	22	7,7	17,9	25,2

* Отнесение к типу перегруппировки гипотетическое.

** Соединению, образовавшемуся при 0°, приписано строение 1-оксиметил-2-бромциклогексана.

ионы более стабильны по сравнению с первоначальным карбокатионом III. Неясен механизм образования циклогексилформальдегида, а также 2-бромметил-1-бромциклогексана при дезаминировании гидробромида 1-аминометил-1-бромциклогексана. Для их образования можно предложить два механизма, различающиеся между собой лишь предположением о последовательности или синхронности многократных перегруппировок-1,2-миграции галогена и 1,2-миграции гидрид-иона (из боковой цепи или цикла:

Путь I (последовательные миграции)

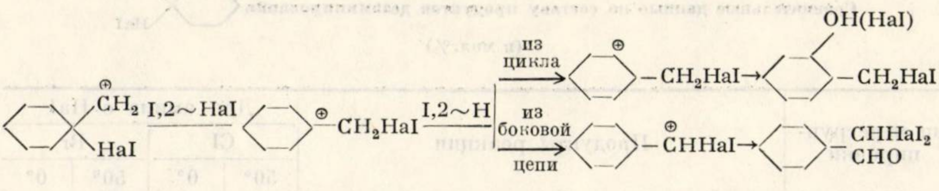

Путь II (синхронные миграции)

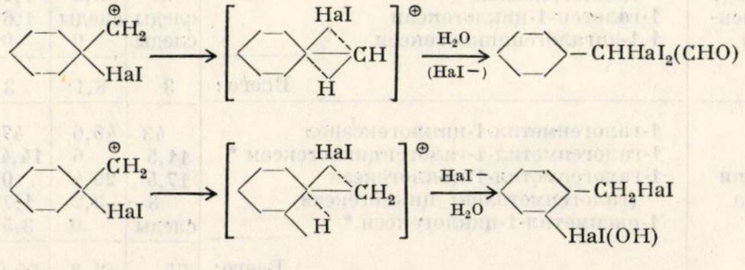

Образование 1-галогенметил-1-галогенциклогексанов можно с равной вероятностью представить как из первичного иона III, так и из третичного иона IV (см. схему). Мы обычно относили дигалогениды к карбакатиону, образующемуся в максимальной степени, т.е. в данном случае к перегруппированному иону IV.

1-Оксиметил-1-циклогексен образуется, в основном, лишь при дезаминировании соответствующего бромамина, что позволяет предположить для его образования следующую схему:

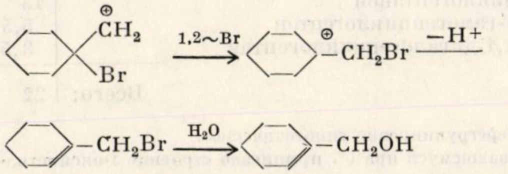

Из данных таблицы, 6 видно, что 1-хлорметил-1-циклогексен практически не гидролизуется в соответствующий спирт аллильного типа. 1-Бромметил-1-циклогексен вовсе не зафиксирован в продуктах реакции, поскольку он в условиях реакции полностью гидролизуется в 1-оксиметил-1-циклогексен.

Таким образом, для первичного 1-галоген-1-циклогексилметилкатиона 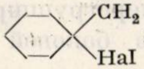 характерна внутренняя стабилизация путем нуклеофильных перегруппировок, причем перегруппировки с 1,2-миграцией галогена превалируют над процессами с расширением цикла. Общая доля перегруппированных продуктов (при 50°) не зависит от природы галогена — 97% при дезаминировании гидрохлорида 1-аминометил-1-хлорциклогексана и 97% при дезаминировании гидробромида 1-аминометил-1-бромциклогексана. При 0° для Hal = Cl доля перегруппированных продуктов на 5% меньше доли перегруппированных продуктов в случае Hal = Br, что в пределах экспериментальной ошибки отвечает количественному содержанию 1-оксиметил-1-хлорциклогексана. Это обстоятельство позволяет рассмотреть другой возможный механизм образования 1-оксиметил-1-циклогексена:

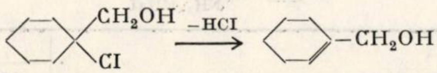

т.е. отнести его к неперегруппированным продуктам. При 50° 1-оксиметил-1-хлорциклогексан отсутствует полностью, но количество 1-оксиметил-1-циклогексена выше на 5% по сравнению с данными при 0°.

С увеличением нуклеофильного содействия галогена (Br > Cl) дезаминирование при 50° приводит к увеличению доли вторичных процессов, а при 0° также к увеличению степени перегруппировки Демьянова.

При проведении дезаминирования при 0° (по сравнению с результатами реакции при 50°) происходит некоторое уменьшение доли продуктов внешней стабилизации за счет конкурирующего нуклеофила — хлор-аниона, увеличение степени перегруппировки с 1,2-миграцией хлора и подавление перегруппировки Демьянова. В случае Hal = Br при 0° несколько подавляются вторичные процессы и несколько увеличивается степень перегруппировки с расширением цикла.

Для сравнения с другими объектами, при дезаминировании которых первоначально образуются относительно стабильные третичные β-гетерозамещенные карбокатионы, было исследовано дезаминирование гидрогалогенидов 1-галогенметил-1-аминоциклогексанов. Полученные результаты представлены в таблице 7.

Как видно из данных таблицы 7, для первоначально образующегося третичного карбокатиона 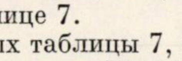 характерна внешняя стабилизация путем взаимодействия с нуклеофилами среды без перегруппировок. Однако, некоторая доля перегруппированных продуктов все же образуется. Это, в первую очередь, двукратные перегруппировки с 1,2-миграцией углеродной цепи (из цикла), что приводит к образованию производных циклогептана. По-видимому, эти многократные перегруппировки протекают синхронно, иначе трудно представить перврашение относительно стабильного третичного иона в гораздо менее стабильный первичный ион.

Для 1-бромметилциклогексилкатиона наблюдается стабилизация путем 1,2-гидридных смещений (при 50°) как из боковой цепи, так из цикла, причем миграция гидрид-иона из цикла вдвое превышает степень миграции из боковой цепи. В случае Hal = Cl миграция гидрид-иона отсутствует. Отсутствие миграции из боковой цепи можно объяснить значительным отрицательным индуктивным эффектом хлора, вследствие которого затормаживается « выталкивание » гидрид-иона. Мало понятно отсутствие миграции гидрид-иона из цикла (для Hal = Cl).

При проведении реакции при 0° (по сравнению с результатами при 50°) подавляются вторичные процессы и уменьшается вклад нуклеофильных перегруппировок.

Таблица 7

Сравнительные данные по составу продуктов дезаминирования гидрогалогенидов 1-галогенметил-1-аминоциклогексанов

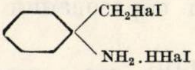

Тип перегруппировки	Продукты дезаминирования	Выход, %			
		Hal=Cl		Hal=Br	
		50°	0°	50°	0°
без перегруппировки	1-галогенметил-1-циклогексанол	58	24,8	41,2	60,8
	1-галогенметил-1-галогенциклогексан	11	3,2	4,1	8,2
	1-галогенметил-1-циклогексен	15,5	26,8	0	0
	(галогенметилен) циклогексан	15,5	18,6	9,8	17,1
	1-оксиметил-1-циклогексен	следы	0	9	12,6
	Всего:	100	73,4	64,1	98,8
1,2-миграция галогена (с фрагментац.)	циклогексанон	0	0	3,5	0,6
	1-галоген-1-циклогексен	0	0	2	0
	Всего:	0	0	5,5	0,6
двукратные перегруппировки: а) 1,2-миграция галогена б) расширение цикла		следы	14	0	0
	1,1-дигалогенциклогептан	следы	12,6	6,6	следы
	циклогептанон				
	1-галоген-циклогептен	0	0	7,1	0
	Всего:	следы	26,6	13,7	следы
1,2-миграции гидрида из а) боковой цепи б) цикла	а) циклогексилформальдегид	0	0	1,4	0,7
	(дигалогенметил) циклогексан	0	0	4,7	следы
	б) 1-галоген-2-галогенметил-циклогексан	0	0	10,6	следы
	Всего:	0	0	16,7	0,7

2.4. Дезаминирование некоторых солей β-галогеналкиламинов жирно-ароматического ряда

Удобными моделями для изучения относительной миграционной способности фенила, галогена и гидрид-иона в реакциях дезаминирования оказались гидрогалогениды 1-амино-2-галоген-2-фенил-этанов $C_6H_5CHHalCH_2NH_2 \cdot HHal$. Несмотря на то, что дезаминирование осуществляли в разбавленной фосфорной кислоте (50°), все же наблюдалось образование значительных количеств дигалогенидов в результате наличия в среде конкурирующего нуклеофила — галогенаниона[22]. В целях удаления последнего из среды было осуществлено дезаминирование фосфорнокислой соли 1-амино-2-хлор-2-фенилэтана[23]. Все полученные результаты представлены в таблице 8.

Таблица 8

Сравнительные данные по составу продуктов дезаминирования некоторых солей 1-амино-2-галоген-2-фенилэтанов (в мольн. %) $C_6H_5CHHalCH_2NH_2 . HX$

Тип перегруппировки	Продукты дезаминирования	Для исходных аминов		
		Hal = Cl X = Cl	Hal = Cl X = H_2PO_4	Hal = Br X = Br
1,2-миграция галогена	$C_6H_5CH(OH)CH_2Hal$	43,1	82,7	89,9
	$C_6H_5CHHalCH_2Hal$ *	16,5	3,3	4,8
1,2-миграция фенила	$C_6H_5CH_2CHO$	11,4	2,9	3,5
	$C_6H_5CH_2CHHal_2$	17,4	3,3	0
1,2-миграция гидрид-иона	$C_6H_5COCH_3$	5,9	2,4	1,8
без перегруппировки (включая фрагментацию)	$C_6H_5CHHal{=}CH_2$	следы	следы	0
	$C_6H_5CHHal_2$	1,7	3,1	0
	C_6H_5CHO	1,7	3,1	0

* Отнесение к типу перегруппировки гипотетическое.

Как видно из данных таблицы 8, во всех трех случаях практически отсутствуют неперегруппированные продукты. Контрольными опытами установлено, что теоретически ожидаемый неперегруппированый продукт 2-галоген-2-фенил-1-этанол в условиях дезаминирования полностью гидролизуется в стиролгликоль. Однако, последний не обнаружен в продуктах дезаминирования, что исключает образование 2-галоген-2-фенил-1-этанола в качестве промежуточного соединения. Остальные продукты реакции являются первичными продуктами и в условиях дезаминирования не изменяются. Лишь бензилиденгалогениды частично гидролизуются в бензальдегид, однако, это обстоятельство не влияет на расчет относительной миграционной способности мигрирующих групп, поскольку оба эти соединения являются продуктами фрагментации.

Уже отмечалось образование значительных количеств 1,2-дигалоген-I-фенилэтанов при дезаминировании галогеноводородных солей аминов, причем вновь дихлоридов образуется больше, чем дибромидов (правило Корнблюма). Можно предложить альтернативные пути образования 1,2-дигалоген-1-фенилэтанов — взаимодействием первоначально образующегося карбениевого иона с галогениданионом из среды (путь «а»)или в результате 1,2-миграции галогена (путь «б»):

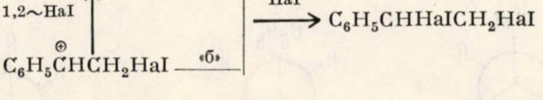
$C_6H_5CHHal\overset{\oplus}{C}H_2$
«а»
1,2∼Hal
Hal⁻
$C_6H_5CHHalCH_2Hal$
$C_6H_5\overset{\oplus}{C}HCH_2Hal$
«б»

Принимая во внимание практическое отсутствие в этих случаях неперегруппированных продуктов, мы полагаем, что более правильно рассматривать вышеуказанные дигалогениды как перегруппированные соединения.

При сравнительном анализе данных дезаминирования гидрогалогенидов 1-амино-2-галоген-2-фенилэтанов при любом из двух способов отнесения образующихся 1,2-дигалоген-1-фенилэтанов можно проследить следующие особенности:

1) Степень 1,2-миграции галогена с участием p-электронов четко преобладает над степенью миграции фенила с участием π-электронов $HaI > C_6H_5$.

2) Степень миграции бром-атома выше степени миграции хлоратома, что согласуется с соотношением их нуклеофильного содействия $Br > Cl$.

3) Наименьшая степень 1,2-миграции наблюдается у гидрид-иона. Таким образом, по относительной миграционной способности конкурирующие при нуклеофильных перегруппировках мигрирующие группы можно расположить в ряд $Br > Cl > C_6H_5 > H$. Другими словами соблюдается следующий ряд участия электронов в образовании новой связи при перегруппировках p > π > б. Этот ряд соблюдается не всегда. Например, семипинаколиновое дезаминирование β-аминоспиртов жирно-ароматического ряда $ArCH(OH)CH_2NH_2$ сопровождается не миграцией гидроксильной группы (p-участие), а, в первую очередь, арильных групп (π-участие), а иногда даже преимущественно гидрид-иона (б-участие).

К трактовке полученных данных неприменим термодинамический контроль, так как исходя из относительной стабильности первоначально и конечно образующихся карбениевых ионов следовало ожидать преимущественной миграции гидрид-иона, поскольку стабилизированный электромерным эффектом хлора бензильный вторичный карбокатион должен быть наиболее стабильным из трех возможных:

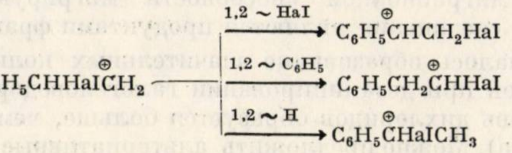

$$C_6H_5CHHalCH_2^{\oplus} \xrightarrow{1,2 \sim HaI} C_6H_5\overset{\oplus}{C}HCH_2HaI$$

$$C_6H_5CHHalCH_2^{\oplus} \xrightarrow{1,2 \sim C_6H_5} C_6H_5CH_2\overset{\oplus}{C}HHaI$$

$$C_6H_5CHHalCH_2^{\oplus} \xrightarrow{1,2 \sim H} C_6H_5\overset{\oplus}{C}HaICH_3$$

По нашему мнению, к изучаемой реакции дезаминирования применим конформационный контроль, с помощью которого легко объясняются наблюдаемые различия в количественном составе продуктов реакции, прежде всего, в зависимости от природы галогена (Cl, Br). Так в исходных 1-амино-2-галоген-2-фенилэтанах возможны три вращательных изомера:

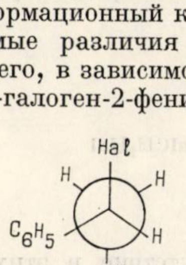

(I)

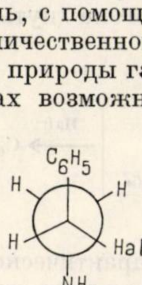

(II)

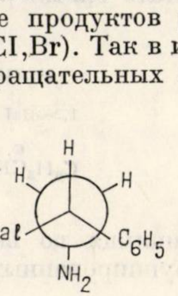

(III)

Хотя фенильное кольцо и велико по размерам, но оно может расположиться в пространстве таким образом, что о-водороды могут быть максимально удалены от близлежащей аминогруппы и тогда существенное значение может играть первичное окружение β-углеродного атома. В это первое окружение попадает либо углерод фенила и водород (I), либо атом галогена и водород (II), либо атом галогена и углерод цикла (III). Очевидно, расположение углеродного атома выгоднее по сравнению с галогеном, поэтому заселенность конформаций отвечает ряду I>II>III. Если считать, что конформационный контроль определяет образование диазониевых катионов, а затем карбениевых ионов, то наиболее вероятен ион A, определяющий миграцию галогена (с тыла), менее вероятен ион B, приводящий к миграции фенильной группы и совсем мало вероятен ион C (миграция H):

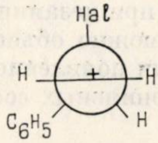

(A)

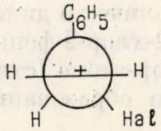

(B)

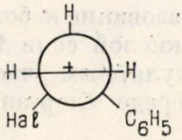

(C)

Понятно, что чем больше размер атома галогена, тем предпочтительнее конформация I, тем большую степень миграции галогена следует ожидать. Полученные данные вполне согласуются с приведенными теоретическими рассуждениями (см. табл. 8). Результаты по дезаминированию фосфорнокислой соли 1-амино-2-хлор-2-фенилэтана являются дополнительным свидетельством в пользу конформационного контроля реакции. С этой точки зрения легко объяснимо резкое увеличение степени миграции хлора и снижение степени миграции фенильной группы по сравнению с соответствующими процессами при дезаминировании солянокислой соли (см. табл. 8). Увеличение степени миграции хлора следует, по-видимому, объяснить увеличением вклада конформации I и уменьшением вклада конформаций II и III в случае фосфорнокислой соли промежуточно образующего диазониевого катиона при условии существования его в виде тесной ионной пары:

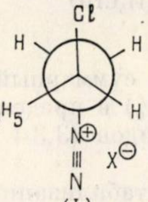

(I)

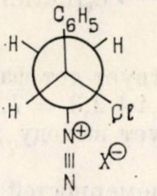

(II)

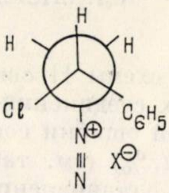

(III)

где $X = Cl^-$ или $H_2PO_4^-$.

В этом случае образование 1,2-дихлор-1-фенилэтана четко трактуется как процесс 1,2-миграции с одновременной атакой с тыла β-углеродного атома анионом хлора из тесной ионной пары:

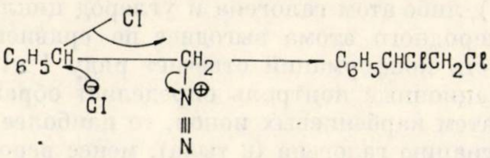

Рассмотрение моделей Стюарта-Бриглеба подтверждает наши предположения о конформационном контроле реакции.

Образование небольших количеств дихлоридов при дезаминировании фосфорнокислой соли 1-амино-2-хлор-2-фенилэтана можно объяснить или межмолекулярным участием хлор-атома (схема I) или появлением в реакционной среде хлор-аниона при образовании карбонильных соединений:

Схема I

$$C_6H_5CHHal\overset{\oplus}{C}H_2 + C_6H_5CHHalCH_2OH \longrightarrow$$

$$C_6H_5CHHalCH_2\,Hal\overset{\oplus}{C}H\,(C_6H_5)\,CH_2OH \longrightarrow$$

$$C_6H_5CHHalCH_2Hal + C_6H_5CH{=}CHOH \rightarrow C_6H_5CH_2CHO$$

Схема II

$$C_6H_5CHCl\overset{\oplus}{C}H_2 \xrightarrow{1,2\sim C_6H_5} C_6H_5CH_2\,\overset{\oplus}{C}HCl \xrightarrow[-HCl]{HO^-} C_6H_5CH_2CHO$$

$$C_6H_5CHCl\overset{\oplus}{C}H_2 \xrightarrow{1,2\sim H} C_6H_5\overset{\oplus}{C}ClCH_3 \xrightarrow[-HCl]{H_2O} C_6H_5COCH_3$$

$$C_6H_5CHClCH_2\overset{\oplus}{N_2} \xrightarrow{-CH_2N_2} C_6H_5\overset{\oplus}{C}HCl \xrightarrow[-HCl]{H_2O} C_6H_5CHO$$

В пользу схемы II свидетельствует тот факт, что суммарный выход карбонильных соединений (2,9+2,4+2,3 = 7,7 мол.%) в пределах экспериментальной ошибки соответствует выходу дихлоридов (3,3+3,3 + 3,1 = = 9,7 мол. %) (см. табл. 8).

Для установления закономерностей при стабилизации функционально замещенных бензильных катионов было исследовано дезаминирование гидрогалогенидов 1-амино-2-галоген-1-фенилэтанов (Hal = Cl, Br). Результаты представлены в таблице 9.

Как и следовало ожидать относительно устойчивый вторичный бензильный катион стабилизируется практически полностью взаимодейст-

Таблица 9

Сравнительные данные по составу продуктов дезаминирования гидрогалогенидов 1-амино-2-галоген-1-фенилэтанов $C_6H_5CH(NH_2 . HHal)\ CH_2Hal$ (в мол.%)

Тип перегруппировки	Продукты дезаминирования	Для исходных аминов	
		Hal = Cl	Hal = Br
без перегруппировки	$C_6H_5CH(OH)CH_2Hal$	89	93,4
	$C_6H_5CHHalCH_2Hal$ *	6,6	0
	$C_6H_5CH{=}CHHal$	2	1,5
1,2-миграция гидрид-иона	$C_6H_5CH_2CHO$	0,5	2,6
фрагментация	C_6H_5CHO	1,9	0

* Отнесение к типу перегруппировки гипотетическое.

вием с нуклеофилами среды без перегруппировок. 1,2-Миграция гидрид-иона протекает в незначительной степени, причем для Hal = Br несколько в большей степени, чем для Hal = Cl:

$$C_6H_5\overset{\oplus}{C}HCH_2Hal \xrightarrow{1,2\sim H} C_6H_5\ CH_2\ \overset{\oplus}{C}HHal \xrightarrow[-HHal]{H_2O} C_6H_5CH_2\ CHO$$

3. ДЕЗАМИНИРОВАНИЕ β-АМИНОСПИРТОВ

Реакция дезаминирования β-аминоспиртов под действием азотистой кислоты известна в литературе как реакция, сопровождающаяся перегруппировками пинаколинового типа. Такие перегруппировки получили название перегруппировок Тиффно. В этих случаях путь, ведущий к окончательной стабилизации первоначально образующегося карбениевого иона, существенно зависит от пространственных соотношений.

Перегруппировки при дезаминировании протекают с большой скоростью и в том направлении, при котором происходит наименьшее изменение всех участвующих заместителей, причем мигрирующая группа должна быть расположена перпендикулярно к плоскости, в которой расположен карбокатионный центр (транс-перегруппировка). Такие явления мы уже наблюдали при дезаминировании галогенаминов жирно-ароматического ряда.

Мы изучили дезаминирование β-оксиаминов, принадлежащих к жирному ряду и пространственно незатрудненных. Случаи нуклеофильных перегруппировок с 1,2-миграцией гидроксильной группы в алифатическом ряду практически не известны, хотя возможность их не отрицается при обсуждении общих схем подобных перегруппировок.

С целью выяснения возможности нуклеофильных перегруппировок с 1,2-миграцией гидроксильной группы было изучено дезаминирование гидрохлоридов этаноламина, 3-оксипропиламина-1 и 2(1)-амино-1(2)-пропанолов с помощью хлористого нитрозила.

Этаноламин-1-С^{14} дезаминировали по методу Пфистера [28] — хлористый нитрозил образовывался в реакционной среде при добавлении твердого нитрита натрия к раствору хлористого натрия в серной кислоте. В продуктах реакции обнаружен этиленгликоль и этиленхлоргидрин. Положение метки установлено методом деструкции, как указано ранее. Условия дезаминирования подобраны таким образом, что замещение окси-группы на галоген в этиленгликоле исключается. Как следует из результатов деструкции, реакция дезаминирования этаноламина хлористым нитрозилом не сопровождается нуклеофильной перегруппировкой с 1,2-миграцией окси-группы [29].

Было изучено также дезаминирование 3-оксипропиламина-1 при 0°, при этом были обнаружены лишь нормальные продукты реакции — 3-хлор-1-пропанол и триметиленгликоль [30]. При повышении температуры реакционной среды до 5° и 50° в смеси продуктов появляются пропиленгликоль, 1-хлор-2-пропанол и 2-хлор-1-пропанол. Последние, по-видимому, появляются в результате замещения гидроксила на хлор в пропиленгликоле:

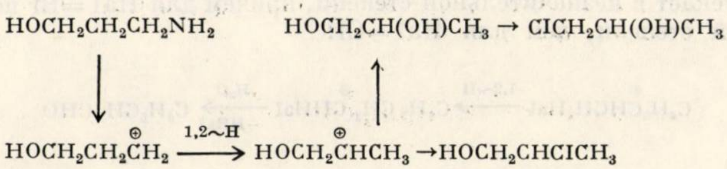

$$\begin{tikzcd}
HOCH_2CH_2CH_2NH_2 \arrow[d] & HOCH_2CH(OH)CH_3 \arrow[r] & ClCH_2CH(OH)CH_3 \\
HOCH_2CH_2\overset{\oplus}{C}H_2 \arrow[r, "1{,}2\sim H"] & HOCH_2\overset{\oplus}{C}HCH_3 \arrow[u] \arrow[r] & HOCH_2CHClCH_3
\end{tikzcd}$$

Количественные соотношения вещества, а также их отнесение к определенному процессу представлены в таблице 10 [30].

Таблица 10

Состав продуктов дезаминирования 3-оксипропиламина-1

Тип перегруппировки	Продукт реакции	Выход (%) при		
		0°	5°	50°
без перегруппировки	пропандиол-1,3	69	48	2
	3-хлор-1-пропанол	31	45	85
	аллиловый спирт	—	2	2
1,2-миграция гидрид-иона	пропиленгликоль	—	2	2
	2-хлор-1-пропанол	—	2	6
	1-хлор-2-пропанол	—	1	3

Из данных таблицы 10 видно, что с повышением температуры, во-первых появляются продукты 1,2-миграций гридрид-иона и, во-вторых, меняются количественные соотношения нормальных продуктов.

---

[28] К. Pfister, *J. Am. Chem. Soc.*, **71**, 1096 (1949).

[29] О. Ю. Полевая, ,,Изомерные превращения при синтезе и дезаминировании окси- и галоидалкиламинов'', канд. дисс., Москва, 1970 г.

[30] О. А. Реутов, Т. А. Смолина, О. Ю. Полевая, *Изв. АН СССР*, *сер. хим.*, **1970**, 1912.

Первый факт можно объяснить уменьшением избирательности «горячего» иона при повышении температуры. Чем более горячий ион, тем больше тенденция к внутренней стабилизации, тем более, что в данном случае это связано с превращением менее стабильного первичного карбениевого иона в несколько более стабильный — вторичный карбокатион. Возможен альтернативный путь — синхронное «выталкивание» гидрид-иона с участием OH-группы и образованием протонированной окиси пропилена:

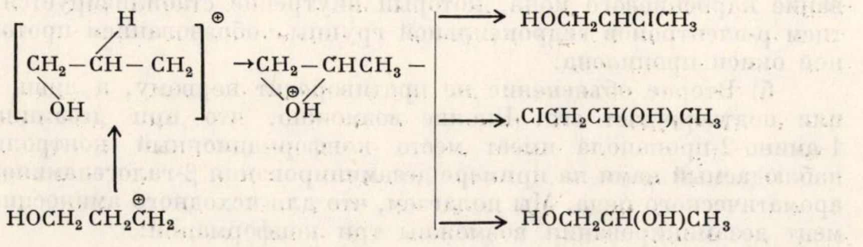

Образование в продуктах реакции больших количеств пропандиола-1,3 при низких температурах может быть объяснено конкуренцией дезаминирующих агентов — азотистой кислоты и хлористого нитрозила.

Дезаминирование *гидрохлоридов 1-амино-2-пропанола* и *2-амино-1-пропанола* осуществляли хлористым нитрозилом в среде концентрированной соляной кислоты. Реакция сопровождается перегруппировкой промежуточно образующихся карбениевых ионов с 1,2-миграцией гидроксильной группы. В результате образуется смесь изомерных пропиленхлоргидринов [31]. Дигалогенпропаны в реакционной смеси не обнаружены. Степень перегруппировки с 1,2-миграцией гидроксильной группы рассчитывали путем измерения количественных соотношений пропиленхлоргидринов методом газо-жидкостной хроматографии. Полученные результаты весьма неожиданны: степень миграции OH-группы составляет 26% для творичного 1-окси-2-пропилкатиона и лишь 3% для первичного 2-окси-1-пропилкатиона. Казалось, это противоречит общепринятым представлениям об энергетических факторах при нуклеофильных перегруппировках. В обоих случаях перегруппировка должна протекать через промежуточное образование протонированной формы окиси пропилена и дальнейший гетеролиз по S_N I или S_N 2-механизму:

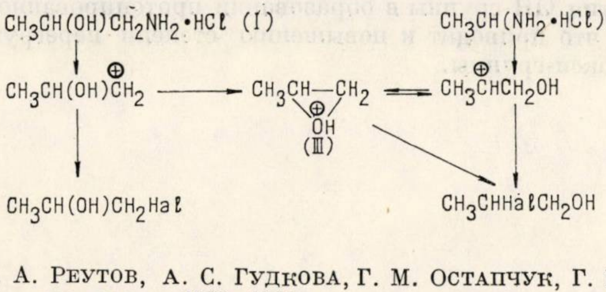

---

[31] О. А. Реутов, А. С. Гудкова, Г. М. Остапчук, Г. П. Куликова, *Изв. АН СССР.* , *сер. хим* ., **1969**, 2338.

Тот факт, что при дезаминировании 1-амино-2-пропанола протонированная форма окиси пропилена в качестве стабильного интермедиата практически не образуется можно объяснить двояко:

а) Возможно, что лимитирующей стадией реакции при дезаминировании амина 1 является образование диазониевого катиона, для которого характерно взаимодействие с нуклеофилами среды, а не внутреннее замещение с образованием интермедиата Ш. Для аминов с аминогруппой у вторичного углеродного атома должно быть характерно быстрое образование карбениевого иона, который внутренне стабилизируется с участием р-электронов гидроксильной группы и образованием протонированной окиси пропилена.

б) Второе объяснение не противоречит первому, а лишь уточняет или подтверждает его. Вполне возможно, что при дезаминировании 1-амино-2-пропанола имеет место конформационный контроль, ранее наблюдаемый нами на примере дезаминирования β-галогенаминов жирно-ароматического ряда. Мы полагаем, что для исходного аминоспирта в момент дезаминирования возможны три конформации:

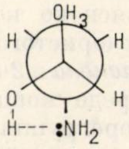

(I)

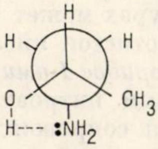

(II)

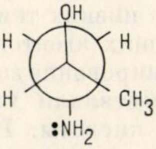

(III)

Наименее стабильной из них является конформация Ш вследствие исключения в ней возможности образования водородной связи с электронной парой аминогруппы. Эти конформации должны закрепляться при образовании соответствующих диазониевых ионов и карбокатионов вследствие большой скорости процесса. Таким образом, гидроксильная группа в конформерах с наибольшей заселенностью расположена неблагоприятно для её участия в образовании протонированной окиси пропилена, а, следовательно, и перегруппировки.

При дезаминировании 2-амино-1-пропанола конформационный контроль исключается вследствие наличия элементов симметрии у β-углеродного атома по отношению к аминогруппе и, следовательно, появляется возможность участия ОН-группы в образовании протонированной формы окиси пропилена, что приводит к повышению степени перегруппировки с 1,2-миграцией окси-группы.

Revue Roumaine de Chimie, **20**, *11–12*, 1471–1472 (1975)

SYNTHESIS OF ^{14}C-LABELLED ISOTOPE-ISOMERIC ALKANES. II[1]

PREPARATION OF 2,2,4-TRIMETHYLPENTANE-$^{14}C_2$ LABELLED AT BOTH METHYL GROUPS OF THE ISOPROPYL MOIETY

IOANA BALLY and ALEXANDRU T. BALABAN

Institute of Atomic Physics, P.O.B. 5206, Bucharest, Romania

Received May 15, 1975

The preparation of isooctane labelled with ^{14}C at both methyl groups of the isopropyl moiety is described, starting from ethyl *t*-butylacetate and ^{14}C-methylmagnesium iodide.

In the previous part, the synthesis of *n*-heptane-1-^{14}C and -2-^{14}C was reported. [1] The present paper describes the synthesis of isooctane-$^{14}C_2$ (2,2,4-trimethylpentane) labelled at the 4-methyl side chain and at the carbon 5, i.e. at both methyls of the isopropyl moiety (VII).

A previous report [2] mentioned the synthesis of singly-labelled isooctane (2,2,4-trimethylpentane-5-^{14}C) from methyl neopentyl ketone (4,4-dimethyl-2-pentanone) and $^{14}CH_3MgI$, followed by pyrolysis, preparative gas-liquid chromatographic isolation of the diisobutenes, and hydrogenation with Adams' catalyst.

Since the preparation of the above ketone from diisobutene is cumbersome, we adopted a different approach, based on the readily available *t*-butylacetic acid (3,3-dimethylbutyric acid) II, which can be prepared [3] from vinylidene dichloride (I)

$$\underset{\text{I}}{H_2C = CCl_2} + (H_3C)_3C-OH + H_2O \xrightarrow[(H_2SO_4)]{-2HCl} \underset{\text{II}}{(H_3C)_3C-CH_2-COOH} \xrightarrow{\text{EtOH}}$$

$$\rightarrow \underset{\text{III}}{(H_3C)_3C-CH_2-COOEt} \xrightarrow{2\,^{14}CH_3MgI} \underset{\text{IV}}{(H_3C)_3C-CH_2-C(^{14}CH_3)_2-OH} \xrightarrow{-H_2O}$$

$$\rightarrow \underset{\text{V}}{Me_3C-CH_2-C(^{14}CH_3) = {}^{14}CH_2} + \underset{\text{VI}}{Me_3C-CH=C(^{14}CH_3)_2} \xrightarrow{2H} \underset{\text{VII}}{Me_3C-CH_2-CH(^{14}CH_3)_2}$$

---

[1] I. Bally, E. Gârd, E. Ciornei, M. Biltz and A. T. Balaban, *J. Labelled Compounds* **11**, 63, (1975)

[2] F. R. Cannings, A. Fisher, J. F. Ford, P. D. Holmes and R. S. Smith, in "Radioisotopes in the Physical Sciences and Industry", Proc. Conf. Copenhagen, 6–17 Sept. 1960, vol. 3, p. 205.

[3] K. Bolt, *Chem. Ber.*, **100**, 978 (1967).

Reaction of ethyl *t*-butylacetate (III) with ^{14}C-labelled methylmagnesium iodide affords the tertiary carbinol IV which was not isolated, but dehydrated directly to the mixture of the two isomeric diisobutenes (V and VI). This mixture was then hydrogenated at normal pressure over platinum using the automatic hydrogenator described by Brown and Brown [4] which generates hydrogen from sodium borohydride.

This procedure has the added advantage that the specific activity of the resulted labelled isooctane VII is twice that of the starting methyl iodide. Of course at the fairly low specific activity requested for the subsequent work with our labelled isooctane, most molecules are unlabelled, some are singly-labelled and only an insignificant fraction are doubly ^{14}C-labelled; however, if need arises, the procedure described in the present paper can be adapted to afford high specific activities (if methyl iodide is replaced by methyl bromide prepared *in situ* from methanol-^{14}C).

EXPERIMENTAL

t-Butylacetic acid (*II*). [3] A mixture of 37 g anhydrous *t*-butanol and 72.5 g freshly prepared and distilled 1,1-dichloroethane (I) was introduced dropwise at 0—5° into a mixture of 184 ml 94% sulphuric acid and 16 ml boron fluoride etherate during 2 hrs. The clear solution was poured over crushed ice, the organic layer was separated and the solution was extracted twice with benzene. The combined organic layers were extracted twice with 20% aqueous sodium hydroxide. The alkaline layer was first extracted twice with benzene, then separated, acidified with sulphuric acid and extracted with benzene.

Ethyl t-butylacetate (III). The above benzenic solution of *t*-butylacetic acid was treated with 100 ml ethanol and 5 ml sulphuric acid, and refluxed with a water separator for 10 hrs. The unreacted acid and alcohol were extracted with aqueous sodium hydrogen carbonate. After drying over magnesium sulphate, the solution was fractionated under reduced pressure affording 22 g ethyl *t*-butylacetate.

Reaction with $^{14}CH_3MgI$. Into the Grignard reagent prepared from 3.25 g (0.135 gram-atoms) magnesium turnings and 19.3 g ^{14}C-methyl iodide (with total activity 10 mCi) in diethyl ether, an ethereal solution of 10 g (67.5 mmoles) of the above ester III was added dropwise, then the mixture was refluxed for one hour. After hydrolysis with ice and sulphuric acid, the ethereal layer and two extracts of the aqueous solution with ether were dried over potassium carbonate and the solvent was removed under reduced pressure.

Diisobutenes-$^{14}C_2$ (V + VI). The resulted carbinol (IV) was refluxed with iodine for one hour, then the mixture was fractionated collecting the fraction with b.p. 80—105°. The distillate was taken with ether, washed with aqueous sodium hydrogen sulphite, dried over calcium chloride and fractionated, collecting the fraction 95—105°. Yield of labelled diisobutene mixture 3.3 g, 43%. The product was controlled by GLC.

Isooctane-$^{14}C_2$ (VII). Into a small Erlenmeyer flask with magnetic stirrer, 5 ml anhydrous ethanol, 0.25 ml 0.2 M methanolic hexachloroplatinic acid, and 0.25 g animal carbon were introduced. The flask was connected to the hydrogenator, [4] and the air was flushed with nitrogen. A 1 M ethanolic solution of sodium borohydride was introduced into the buret of the hydrogenator, and 1 ml of the same solution was injected with a hypodermic syringe into the mixture. This was followed by injections of 1 ml conc. hydrochloric acid and of the above diisobutene mixture. Then the hydrogenation proceeded at room temperature and was left with magnetic stirring for one hour. The resulted solution was filtered with sucction, and poured into 20 ml of 10% aqueous calcium chloride solution. Then after three extractions with ether, the combined organic layers were dried and distilled affording the labelled 2,2,4-trimethylpentane, b.p. 99—100°, chemical yield 55% relatively to the diisobutene mixture. The radiochemical yield is practically equal to the chemical yield.

Radioactivity measurements were performed with a Packard TRI—CARB instrument.

---

[4] C. M. Brown and H. C. Brown, *J. Org. Chem.* **31**, 3989 (1966).

Revue Roumaine de Chimie, 20, *11–12*, 1473–1478 (1975)

INVESTIGATIONS IN THE CYCLOBUTANE SERIES. XXXVII[1]

THE STEREOCHEMISTRY OF BROMINE ADDITION TO THE ANGULAR DIMER OF BENZOCYCLOBUTADIENE

NICOLETA ŞTEFAN, I. G. DINULESCU, F. CHIRALEU
and MARGARETA AVRAM
Center of Organic Chemistry, Spl. Independenţei 202B, Bucharest 15, Romania

Received September 24, 1974

The reaction of the dimer of benzocyclobutadiene with bromine in polar and nonpolar media is described. The structures and the conformations of the reaction products are established by means of NMR spectroscopy and by chemical methods.

The examination of the Dreiding model of the benzocyclobutadiene dimer, [2] with dibenzo[*b*, *g*]bicyclo[4.2.0]octa-2,4,7-triene (**1**) skeleton, indicates that the double bond is sterically more accessible to electrophilic attack from the *exo* than from the *endo* side of the molecule.

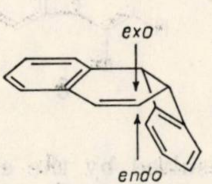

In order to elucidate the stereochemical course of bromine addition, the reaction of hydrocarbon **1** in polar and nonpolar media has been investigated.

Treatment of **1** with N-bromosuccinimide in a mixture of dioxane-water, followed by acetylation of the bromo-hydroxy-derivative **2**, yielded the bromo-acetoxy-derivative **3**. Compound **3** has also been obtained by treating **1** with N-bromosuccinimide in acetic acid.

The reaction of **1** with N-bromosuccinimide in methyl alcohol afforded the bromo-methoxy-derivative **4**.

The bromine addition in dichloromethane led to the previously described [2] dibromo-derivative **5**.

---

[1] Part XXXVI: L. Enescu, F. Chiraleu and M. Avram, *Rev. Roumaine Chim.*, **20**, 957 (1975).

[2] M. P. Cava and D. R. Napier, *J. Amer. Chem. Soc.*, **79**, 1701 (1957).

The structure of compounds **2**, **3** and **4** was determined on the basis of chemical behaviour and spectral data.

The oxidation of **2** yielded the bromoketone **6**, having the carbonyl frequency in the IR spectrum at 1720 cm^{-1}, in agreement with that of benzylic carbonyl groups in α-halo-ketones.[3]

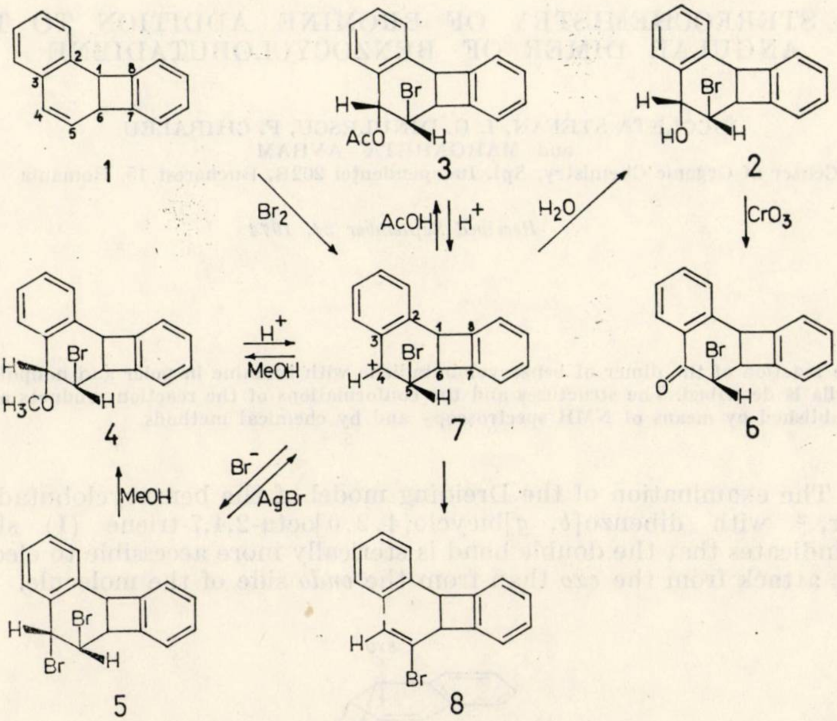

The benzylic ion **7** resulted by the electrophilic attack of Br$^+$ on 5-C, was assumed to arise intermediately in the solvolytic addition. In the case of bromine addition in nonpolar media, the ion **7** can also be taken into account, in agreement with the classical character of unsymmetrical benzylic bromonium ions.[4]

The stereochemistry of the solvolytic addition products **2**, **3** and **4**, together with that of dibromide **5**, was established by analysis of their NMR spectra.

For the bromo-derivatives **3**, **4** and **5**, the *trans* isomers *a* and *c*, resulted by *exo* or *endo* attack of the electrophile, have been considered. Both *a* and *c* could exist as two distinct conformers, $a \leftrightarrows b$ and $c \leftrightarrows d$, respectively.

---

[3] M. Avram and G. D. Mateescu, "Infrared Spectroscopy. Applications in Organic Chemistry", Wiley-Interscience, New York, 1972.

[4] F. Badea, "Mecanisme de reacţie în chimia organică", IInd Ed., Ed. ştiinţifică, Bucharest, 1973, p. 514, 519, 520; J. A. Pincock and K. Yates, *J. Amer. Chem. Soc.*, **90**, 5643 (1968); K. Yates and R. S. McDonald, *J. Org. Chem.*, **38**, 2465 (1953).

The NMR spectrum of compound **4** exhibits the signals corresponding to aromatic protons as a multiplet at δ 7.10—7.50 ppm, a doublet centered at δ 4.82 ppm assigned to proton 1-H and a multiplet between δ 4.25—4.65 ppm corresponding to three protons (4-H, 5-H and 6-H); methoxy protons appear as a singlet at 3.34 ppm.

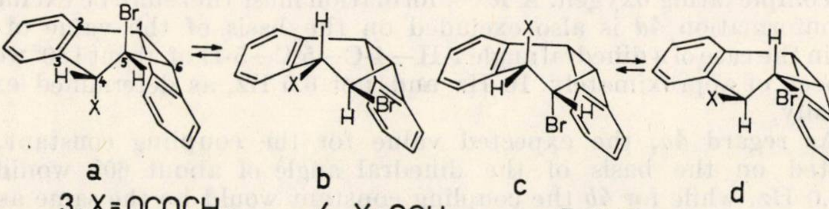

3, $X = OCOCH_3$ 4, $X = OCH_3$ 5, $X = Br$

The important shielding of the methoxy group by one of the benzene rings, which is to be expected for this *endo*-axial group, at 4-C in **4**, is a strong argument in favour of structure **4a**.

Further arguments supporting the structure **4a** have been provided by the lanthanide induced shift study, using $Eu(DPM)_3$.

Thus, with the molar ratio $Eu(DPM)_3/4 = 0.27$, the NMR spectrum displayed a doublet at δ 8.03 ppm and a multiplet between δ 7.15—7.60 ppm, corresponding to one and to seven aromatic protons, respectively, a doublet at δ 5.75 ppm corresponding to 4-H, an apparent triplet at δ 5.28 ppm (5-H), a doublet at δ 4.93 ppm (1-H), a triplet at δ 4.60 ppm (6-H) and a singlet at δ 4.53 ppm corresponding to the methoxy group. The following coupling constants could be estimated: $J_{4.5} = 6.5$ Hz, $J_{1.6} = J_{5.6} = 5.5$ Hz.

In Figure 1 the $Eu(DPM)_3$ induced shifts of protons 1-H, 4-H, 5-H are plotted *versus* the molar ratio complex/compound **4**.

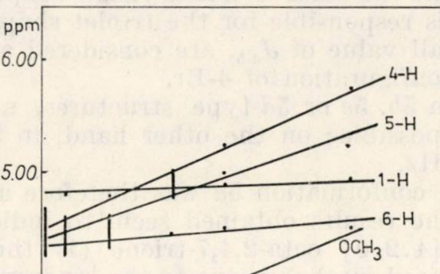

Fig. 1. — Variation of the proton chemical shifts in compound **4** at different $Eu(DPM)_3$/substrate molar ratios.

From the spectrum and from Fig. 1 it can be seen that the induced shifts of protons 1-H and 6-H are negligible with respect to that of protons 4-H, 5-H and the methoxy group.

In a *4c*-type conformation one could have expected induced shifts of approximately the same magnitude for protons 1-H, 4-H, 5-H, 6-H and for the methoxy group, because of the nearly equal distance to the complexating oxygen. A *4c* conformation must therefore be excluded. The conformation *4d* is also excluded on the basis of the value of $J_{4.5}$ which in the case of a dihedral angle 4-H—4-C—5-C—5-H of about 180° would have been of approximately 10 Hz and not 6.5 Hz, as determined experimentally.

As regard *4a*, the expected value for the coupling constant, as estimated on the basis of the dihedral angle of about 60°, would be 1.7—2.0 Hz, while for *4b* the coupling constant would be the same as for *4d* that is 10 Hz. The recorded value of 6.5 Hz can be explained by the electronegativity of the substituent;[5] therefore, it cannot be ruled out of hand that it may represent an average value determined by the equilibration between the conformers *4a* and *4b*.

The same configuration has been ascribed to compounds **2** and **3**, the latter being formed on the acetylation of **2**, and exhibiting a similar NMR spectrum.

The structure of the dibromo-derivative **5** has been established by chemical methods and by analysis of NMR spectra as well.

The fact that treatment of **5** with methyl alcohol yields **4** is an indication for the same configuration of dibromide **5** at 5-C as **4**, namely *exo*-5-bromo.

The NMR spectrum of the dibromo-derivative **5** exhibits a multiplet between δ 7.00—7.50 ppm, corresponding to aromatic protons, an apparent triplet at δ 5.51 ppm (4-H) and a triplet at δ 5.30 ppm (5-H), a doublet at δ 4.84 ppm (1-H) and a multiplet at δ 4.50 ppm (6-H). The following coupling constants could be estimated from the spectrum: $J_{1.6} = 5.5$ Hz, $J_{4.5} = J_{5.6} = 2.2$ Hz, $J_{4.6} = 1.5$ Hz.

The existence of a long-range coupling between protons 4-H—6-H, which is responsible for the triplet shape of proton 4-H, together with the small value of $J_{4.5}$, are considered as strong arguments for an *endo-axial* configuration of 4-Br.

In **5***b*, **5***c* or **5***d*-type structures, a long-range coupling 4-H—6-H is not possible; on the other hand, in **5***b* and **5***d*, $J_{4.5}$ would be nearly 8—10 Hz.

A conformation **5***a* was therefore ascribed to dibromide **5**.

The results obtained seem to indicate that for the dibenzo[*b*, *g*]-bicyclo[4.2.0] octa-2,4,7-triene (**1**) the *exo* attack of the electrophile is preferred, probably due to the hindrance of the *endo* side by the benzocyclobutene moiety.

The tendency of benzylic carbenium ion **7** to regenerate the conjugated olefinic dibenzo[*b*, *g*]bicyclo[4.2.0]octa-2,4,7-triene system was demonstrated by formation of bromo-olefine **8**, both by treatment of **3** or **4** with hydrobromic acid and by treatment of **5** with silver bromide in carbon tetrachloride.

---

[5] H. Booth, *Tetrahedron Letters*, **1965**, 411.

EXPERIMENTAL

Microanalyses were performed by Miss E. Şliam and Mrs. V. Daniel. IR spectra were recorded with a double beam UR 20 spectrophotometer. NMR spectra were determined with a Varian A–60A spectrometer.

endo-4-Hydroxy-*exo*-5-bromo-dibenzo[*b*,*g*]bicyclo[4.2.0]octa-2,7-diene (2)

A solution of 1.0 g (4.9 mmoles) **1** in 25 ml dioxane and 4 ml water was treated with 0.88 g (4.9 mmoles) N-bromosuccinimide and the mixture was left at room temperature for 24 hours. The crystalline product was filtered off and washed with water, yielding 1.35 g (92 %) **2**, m.p. 222°.

$C_{16}H_{13}BrO$ *Calcd.* : C, 63.80 ; H, 4.35 ; Br, 26.53
Found : C, 63.57 ; H, 4.42 ; Br, 26.92

endo-4-Acetoxy-*exo*-5-bromo-dibenzo[*b*,*g*]bicyclo[4.2.0]octa-2,7-diene (3)

A solution of 0.5 g (2.4 mmoles) **1** in 10 ml acetic acid was treated with 0.42 g (2.4 mmoles) N-bromosuccinimide and the mixture was left at room temperature. After 24 hours water was added, the product was extracted with dichloromethane and the organic layer washed with a 5 % sodium carbonate solution. After drying and evaporation of solvent, a crystalline residue was obtained, which was purified by recrystallization from aqueous methanol, yielding 0.16 g (19.5 %) **3**, m.p. 127°.

$C_{18}H_{15}BrO_2$ *Calcd.* : C, 62.99 ; H, 4.40 ; Br, 23.28
Found : C, 62.78 ; H, 4.52 ; Br, 22.96

NMR ($CDCl_3$, δ, ppm) : 7.10–7.50 (m, 8H, aromatics), 6.10 (dd, 1H, 4-H, $J_{4,5} = 5.2$ Hz, $J_{4,6} = 1$ Hz), 4.83 (d, 1H, 1-H, $J_{1,6} = 4.5$ Hz), 4.77 (t, 1H, 5-H, $J_{4,5} = 5.2$ Hz, $J_{5,6} = 5.2$ Hz), 4.41 (t, 1H, 6-H, $J_{1,6} = 4.5$ Hz, $J_{4,6} = 1$ Hz), 1.68 (s, 3H from a CH_3COO group).

IR (CCl_4, cm^{-1}): ν CO 1735.

The same compound was obtained in 50 % yield by acetylation of bromohydrine **2** with acetic anhydride in the presence of pyridine.

endo-4-Methoxy-*exo*-5-bromo-dibenzo[*b*, *g*]bicyclo[4.2.0]octa-2,7-diene (4)

A solution of 0.5 g (2.4 mmoles) **1** in 10 ml methanol was treated with 0.43 g (2.4 mmoles) N-bromosuccinimide and the mixture was left at room temperature for 24 hours. The crystalline product was filtered off, yielding 0.6 g (92 %) **4**, m.p. 102° (from methanol).

$C_{17}H_{15}BrO$ *Calcd.* : C, 64.77 ; H, 4.79 ; Br, 25.35
Found : C, 64.62 ; H, 4.65 ; Br, 25.02

NMR ($CDCl_3$, δ, ppm) : 7.10–7.50 (m, 8H, aromatics), 4.82 (d, 1H, 1-H, $J_{1,6} = 5.0$ Hz), 4.25–4.65 (m, 2H, 4-H, 6-H, $J_{1,6} = 5.0$ Hz), 3.34 (s, 3H from OCH_3).

NMR with $Eu(DPM)_3$ ($CDCl_3$, δ, ppm ; molar ratio $Eu(DPM)_3/\mathbf{4} = 0.27$) : 8.03 (d, 1H, aromatic, $J = 7.0$ Hz), 7.15–7.60 (m, 7H, aromatics), 5.75 (d, 1H, 4-H, $J_{4,5} = 6.5$ Hz), 5.28 (apparent t, 1H, 5-H, $J_{4,5} = 6.5$ Hz, $J_{5,6} = 5.5$ Hz), 4.93 (d, 1H, 1-H, $J_{1,6} = 5.5$ Hz), 4.60 (t, 1H, 6-H, $J_{1,6} = J_{5,6} = 5.5$ Hz), 4.53 (s, 3H from OCH_3).

exo-5-Bromo-dibenzo[*b*, *g*]bicyclo[4.2.0]octa-2,7-dien-4-one (6)

A solution of 1.0 g (3.32 mmoles) **2** in 15 ml anhydrous pyridine was added to a suspension of chromic anhydride-pyridine complex obtained from 1.0 g (10 mmoles) chromic anhydride and 10 ml pyridine. The mixture was left at room temperature for 24 hours with occasional shaking. Water was added and the product was extracted with ether. In order to remove the pyridine, the ethereal solution was washed several times with a 2% hydrochloric acid solution. After washing with water and drying, the ether was removed and the crude crystalline residue was purified by recrystallization from methanol, yielding 0.34 g (34%) **6**, m.p. 190°.

$C_{16}H_{11}BrO$	*Calcd.*	: C, 64.23 ; H, 3.70 ; Br, 26.71
	Found	: C, 64.04 ; H, 4.01 ; Br, 26.50

NMR ($CDCl_3$, δ, ppm) : 7.81 (d, 1H arom. near keto group), 6.80—7.65 (m, 7H, aromatics), 5.25 (d, 1H, 5-H, $J_{5,6} = 7$ Hz), 4.91 (d, 1H, 1-H, $J_{1,6} = 5$ Hz), 4.73 (quartet, 1H, 6-H, $J_{1,6} = 5$ Hz, $J_{5,6} = 7$ Hz).

IR (CCl_4, cm^{-1}) : ν CO 1720.

endo-4-*exo*-5-Dibromo-dibenzo[*b*, *g*]bicyclo[4.2.0]octa-2,7-diene (5)

The dibromide **5** was obtained after Cava[2] in 80% yield by treating **1** with bromine in dichloromethane solution ; m.p. 111° (from *n*-heptane).

NMR (CCl_4, δ, ppm) : 7.00—7.50 (m, 8H, aromatics), 5.51 (apparent *t*, 1H, 4-H, $J_{4,5} = 2.2$ Hz, $J_{4,6} = 1.5$ Hz), 5.30 (t, 1H, 5-H, $J_{4,5} = J_{5,6} = 2.2$ Hz), 4.84 (d, 1H, 1-H, $J_{1,6} = 5.5$ Hz), 4.50 (m, 1H, 6-H, $J_{1,6} = 5.5$ Hz, $J_{4,6} = 1.5$ Hz, $J_{5,6} = 2.2$ Hz).

Reaction of dibromo-derivative 5 with methanol

A mixture of 0.250 g (0.68 mmoles) **5**, 0.250 g anhydrous sodium hydrogen carbonate and 25 ml methanol was refluxed for 8 hours. The filtered solution was concentrated *in vacuo* and the residue (0.200 g, 92%) was found to be pure **4** (IR and NMR spectra were identical with those of an authentic sample).

5-Bromo-dibenzo[*b*,*g*]bicyclo[4.2.0]octa-2,4,7-triene (8)

a. From bromo-acetoxy-derivative **3.** A solution of 0.3 g (0.87 mmoles) **3** in 10 ml acetic acid was treated with 0.2 ml (63%) hydrobromic acid and the mixture was boiled for 8 hours. Water was added, the product was extracted with dichloromethane and the organic layer washed with 5% sodium carbonate solution until neutral. After drying and evaporation of solvent, a crystalline residue was obtained, which was purified by chromatography on aluminium oxide with diethylether, yielding 0.16 g (60%) **8**, m.p. 105°.

$C_{16}H_{11}Br$	*Calcd.*	: C, 67.87 ; H, 3.91 ; Br, 28.22
	Found	: C, 67.72 ; H, 4.02 ; Br, 28.40

NMR (CCl_4, δ, ppm) : 6.90—7.35 (m, 8H, aromatics), 6.53 (s, 1H, 4-H), 4.86 and 4.55 (m, 2H, 1-H and 6-H, AB system, $J = 6$ Hz).

b. From bromo-methoxy-derivative **4.** By boiling a solution of 0.25 g (0.8 mmoles) **4** with 0.5 ml 63% hydrobromic acid and 20 ml acetic acid, for 12 hours, and working up as above, 0.17 g (75%) **8** were obtained.

c. From dibromo-derivative **5.** The bromo-olefine **8** was also obtained in 64% yield by boiling for 16 hours a mixture of 0.2 g (0.55 mmoles) dibromo-derivative **5** in 5 ml anhydrous carbon tetrachloride with 0.2 g anhydrous silver bromide.

Revue Roumaine de Chimie, 20, *11–12*, 1479–1490 (1975)

COMPUTATION OF THE ISENTHALPIC EXPANSION OF ETHYLENE AT HIGH PRESSURE

V. LAIBER *, L. ALERGUŞ *, D. DAVID * and D. SĂNDULESCU **

* Petrochemical Group, Electronic Computer Center, Şoseaua Giurgiului, N° 127, Piteşti, Romania

** Institute of Petroleum and Gas, Bd. Bucureşti, N° 3, Ploieşti, Romania

Received November 8, 1974

A computer program, called IZENT has been written in FORTRAN IV and was run on an IBM 1800 process computer, for the computation of the integral Joule – Thomson effect of ethylene at high pressure in the gas phase ethylene polymerization plant.

The recent development of new industrial procedures in the chemical industry, on the one hand, and the progress in the study of the thermodynamical behaviour of the chemical systems, on the other hand, have stimulated and interconditioned each other in the last twenty years. The improvements of the physical and chemical research methods and the practically unlimited possibilities in data processing, due to the high-speed digital computers, enable the establishment of new laws and of some quantitative correlations which are very useful in the estimation of the thermodynamical properties of systems in such conditions which are very far from the ideal state.

This knowledge was successfully applied in the design and the improvement of new industrial procedures under very difficult operating conditions, such as high pressures.

But, efficient plant control of such plants depends more and more on the real-time control of the process variables based on mathematical models, which includes, apart from the chemical changes, described by kinetic equations, also the thermodynamic equations of chemical-physical phenomena.

This paper presents a computation of some thermodynamic properties of ethylene in the non-ideal state, as well as a computer program to estimate temperature increase, after the isenthalpic expansion of ethylene at high pressures (Joule-Thomson effect). The working conditions of the polyethylene plant correspond to the region outside the inversion parabola with the peak at 470 atm and 425 K, as calculated by the van der Waals equation. Therefore, the Joule-Thomson effect will be negative ; the free expansion leads to a heating of ethylene, which however results also from the pressure-enthalpy diagram.

This program may be used e.g. in the case of on-line computer control of a high pressure, gas-phase ethylene polymerization plant.

1. THE JOULE-THOMSON EFFECT

By taking into account the usual enthalpy function, let us consider a "free" expansion of an ideal gas. According to classical works (Joule and Kelvin) such an expansion is an isenthalpic process, that means :

$$\mathrm{d}H = \left(\frac{\partial H}{\partial T}\right)_p \cdot \mathrm{d}T + \left(\frac{\partial H}{\partial p}\right)_T \cdot \mathrm{d}p = 0 \tag{1}$$

Therefore, the Joule-Thomson coefficient can be expressed :

$$\left(\frac{\partial T}{\partial p}\right)_H = -\left(\frac{\partial H}{\partial p}\right)_T \Big| \left(\frac{\partial H}{\partial T}\right)_p \tag{2}$$

If any mathematical correlations of experimental data, such as regression equations, are available for $H = f(p, T)$, the coefficient can obviously be easily computed for limited pressure and temperature ranges.

But it can be more exactly computed, by using measurable quantities instead of enthalpy, such as the thermic expansion coefficient α, and the specific heat at constant pressure, c_p. In this case eq. (2) becomes[1]

$$\left(\frac{\partial T}{\partial p}\right)_H = -\frac{-V(1-\alpha T)}{c_p} \tag{3}$$

Of course, it is possible now to set up certain equations which will differ from each other, depending on the choice of the volume function. Providing that we use an equation of state at constant temperature, e.g. :

$$V = \frac{A}{p} + B + Cp \tag{4}$$

where A, B, C are the virial coefficients which depend only on temperature, eq. (3) may be written as follows :

$$\left(\frac{\partial T}{\partial p}\right)_H = \frac{T^2}{c_p} \cdot \frac{\mathrm{d}\,(B/T)}{\mathrm{d}T} \tag{5}$$

Expressions, such as the above mentioned series of increasing powers of p, must be considered as simplified expressions, with estimated virial coefficients and, thereby, they have a limited validity. Thus, for instance, eq. (4) is considered valid only up to 100 atm.

---

[1] E. A. GUGGENHEIM, "Thermodynamique", ed. Dunod, Paris, 1965, chap. 4.

However, high confidence level computations are actually possible by always including some correlations, to estimate experimental data.

Such correlations have been made for many gaseous systems under some, p, V, T conditions, but usually not for conditions far from the ideal state.

2. EQUATION OF STATE UNDER NON-IDEAL CONDITIONS

For the operating conditions under which radicalic polymerization of ethylene occurs, the thermodynamical values of state could not be easily estimated and for a long period of time, no equations of state have been available for pressures above 1000 atm.

Benzler proposed in 1954 such an equation [2]

$$\pi = a + b(\nu - 1) + c(\nu - 1)^2/\nu \qquad (6)$$

where π and ν are, respectively, the reduced pressure and the reduced temperature and a, b, c are characteristic volume-functions. These were correlated by Benzler from p, V, T measurements, performed by Michels, [3] in 1942 in the range 0–150° and up to 3000 atm.

Benzler has worked out some polynomial regressions for $a = f(\delta)$, $b = f(\delta)$ and $c = f(\delta)$, where δ is the reduced specific gravity ($\delta = 1/\varphi$) and φ the reduced specific volume for more ranges of δ, improving in this way the accuracy of the estimations.

These correlations were:

$$\delta < 1 : a = 1 - (1 + 0.445\ \delta)(1 - \delta)^4 \qquad (7)$$

$$b = 3.555\ (1 + 1.448\ \delta - 0.603\ \delta^2) \qquad (8)$$

$$c = -\ 6.55\ \delta^2 + 2.027\ \delta^3 \cdot (4.31 - \delta) \qquad (9)$$

$$\text{for } \delta < 0.3 : c = -\ 37.48\ \delta^3 + 71.80\ \delta^4 \qquad (10)$$

$$\delta > 1 : a = 1 + \delta^2 (\delta - 1)^4 .$$
$$[1.331 - 0.692\ (\delta - 1) + 0.126\ (\delta - 1)^2] \qquad (11)$$

$$b = 6.55 + \delta^2 (\delta - 1) \cdot [7.4 - 2.80\ (\delta - 1) +$$
$$+ 1.282\ (\delta - 1)^2 - 0.312\ (\delta - 1)^3] \qquad (12)$$

$$c = -16.65 + 30.22\ \delta - 15.01\ \delta^2 + 1.60\ \delta^3 \qquad (13)$$

---

[2] H. Benzler and A. V. Koch, *Chem. Ing. Tech.*, **27**, 71 (1955).

[3] A. Michels and M. Geldermans, *Physica*, **9**, 967 (1942).

Benzler used the integrals $\int f(\delta)\,\mathrm{d}\delta/\delta^2$ and found the critical data :

$$p_c = 51.66 \text{ atm} ; \; T_c = 282.6 \text{ K} ; \; V_c = 4.65 \text{ cm}^3/\text{g}$$

The same author proposed the following equation for enthalpy :

$$H = \left[u_0 + \int c_{v0}\,\mathrm{d}T\right] + \rho_c v_c \left[\int \frac{a}{\delta^2}\,\mathrm{d}\delta - \int \frac{b}{\delta^2}\,\mathrm{d}\delta - 2\left(1 - \frac{1}{\nu}\right)\int \frac{c}{\delta^2}\,\mathrm{d}\delta + \frac{\pi}{\delta}\right] \tag{14}$$

where u_0 was a constant term, calculated by supposing the critical enthalpy $H_c = 100$ kcal/kg. Taking into account some experimental data, the authors of the above mentioned article [2] reach the conclusion that specific heat c_{v0} (in kcal/°kmol) for the positive temperatures up to 400° can be expressed quite correctly by the relationship :

$$c_{v0} = 0.359 + 3.083(T/100) - 0.100(T/100)^2 \tag{15}$$

By using the previous eq. (6) to (15), Benzler has constructed the H_p — diagram for a temperature range from −150° to +440° and up to 10 000 atm.

3. COMPUTATION OF ETHYLENE ENTHALPY

Published relationships and some data from previous works have been completed with others. In this work we first established the integration constants for the volume functions and for the specific heat. The c_{v0} value has been related to 1 kg ethylene.

In a previous article, Steiner and Thies [4] proposed a multiple regression for the specific volume, v, (m³/kg) of ethylene ; where p and T are used in atm resp. K :

$$\frac{1}{v} = 1995.85 - 601.2 \log\left(\frac{p}{1000}\right) + 593.3 \left(\log \frac{1}{T} - \right.$$
$$\left. - 335.8\left(\log \frac{p}{1000}\right)\left(\log \frac{1}{T}\right)\right. \tag{16}$$

We prove now, that this equation does not provide high accuracy values for pressures below 1000 atm, and the enthalpy-values calculated by using eq. (16) do not agree with the Benzler-diagram at these pressures.

---

[4] R. Steiner and J. W. Thies, *Chem. Ztg.*, **92**, 665 (1968).

Consequently, we found out a similar regression for v-values for ranges below 1000 atm (in the same units as in eq. (16)).

$$\frac{1}{v} = 2041.2618 - 1205.8937 \log \frac{p}{1000} + 610.27546 \log \frac{1}{T} - 567.73609 \left(\log \frac{p}{1000}\right)\left(\log \frac{1}{T}\right) \tag{17}$$

In attempts to obtain a correlation of the best agreement with the Benzler-diagram we have performed thirty-eight regressions.

The significance of correlation coefficients and of the t and F-values has been tested by modifying an IBM standard multiple linear regression program, REGRE [5] and performing correlation analysis and analysis of variance.

The multiple nonlinear regression with the best agreement with the Benzler-diagram and of highest confidence level was the following:

$$v = a_0 + a_1 \log \frac{p}{1000} + a_2 \log \frac{1}{T} + a_3 \left(\log \frac{p}{1000}\right)^2 + a_4 \left(\log \frac{1}{T}\right)^2 + a_5 \log \frac{p}{1000} \log \frac{1}{T} + a_6 \log \frac{p}{1000} \left(\log \frac{1}{T}\right)^2$$

$$\begin{aligned} a_0 &= 0.006 \times 10^{-2} & a_4 &= 1.318 \times 10^{-2} \\ a_1 &= 4.175 \times 10^{-2} & a_5 &= 0.668 \times 10^{-2} \\ a_2 &= 6.807 \times 10^{-2} & a_6 &= -0.354 \times 10^{-2} \\ a_3 &= 0.568 \times 10^{-2} \end{aligned} \tag{18}$$

v is expressed in m^3/kg, p in atm and T in K.

Although the equation proposed is more complicated, there will be no computational difficulties, if it is used in computer programs.

The v-values obtained by eqs. (16), (17) and (18) are compared with Benzler's data and table 1 shows the results. We used the equation with the minimum variance – to – variance ratio, i.e. eq. (18), to compute enthalpy in pressure ranges below 1000 atm.

In the above mentioned article [4] the authors had also proposed a multiple regression equation to compute enthalpy values for ethylene (in kcal/kg). Temperatures are expressed in °C, and the pressure in atm:

$$H = 0.67877 \cdot 10^2 + 6.0195 \cdot 10^{-1} \cdot t + 1.0673 \cdot 10^{-2} \cdot p - 2.6559 \cdot 10^{-5} \cdot p \cdot t + 2.2411 \cdot 10^{-4} \cdot t^2 + 5.0215 \cdot 10^{-6} \cdot p^2 \tag{19}$$

---

[5] IBM Application Program H 20–0252–3.

Equations of this type are certainly useful, in approximate calculations, for limited domains, such as plant design, but they do not satisfy some requirements in theoretical or industrial applications. Hence, they do not permit computation in other domains than those for which they were worked out. If a computational method with higher accuracy is available, it is of course desirable to use it in computer on-line control programs.

The same authors[4] indicated also another equation to compute directly the Joule-Thomson effect :

$$t = 0.0375\,\Delta p + 34.7 \tag{20}$$

for $1600 < p_1 < 2800$ atm and $250 < t < 350°$.

We must take into account the remarks made above also in this case. Many industrial polymerization vessels are operated between 1100 atm and 1500 atm, due to the use of new promoters, instead of oxygen. On the other hand, if a regression formula is used for H and after that, with this H another regression formula is used for Δt, the deviations from accurate values will obviously increase.

We found also some nonlinear correlations for the current estimation of enthalpy (eqs. (21) — (23)) as it can be seen in the figure and table 1 which show the H values, and the F- and t-values for testing the variances against the variance of Benzler's data. H is expressed in kcal/kg, p in atm and T in K.

200 atm $< p <$ 1000 atm

$$H = a_0 + a_1 \log\left(\frac{p}{1000}\right) + a_2 \log\left(\frac{1}{T}\right) + a_3\left(\log\frac{p}{1000}\right)^2 + a_4\left(\log\frac{1}{T}\right)^2 + a_5 \log\left(\frac{p}{1000}\right)\cdot\log\frac{1}{T} \tag{21}$$

$a_0 = 3280.62499$ $a_3 = 81.25405$

$a_1 = 347.62462$ $a_4 = 684.94389$

$a_2 = 2980.58267$ $a_5 = 111.54545$

2000 atm $> p >$ 1000 atm

$$H = a_0 + a_1 \log\left(\frac{p}{1000}\right) + a_2 \log\left(\frac{1}{T}\right) + a_3\left(\log\frac{1}{T}\right)^2 \tag{22}$$

$a_0 = 4653.08561$

$a_1 = 93.22688$

$a_2 = 4028.85038$

$a_3 = 884.18922$

$200 \text{ atm} < p < 2000 \text{ atm}$

$$H = a_0 + a_1 \log\left(\frac{p}{1000}\right) + a_2 \log\left(\frac{1}{T}\right) + a_3 \left(\log \frac{p}{1000}\right)^2 + $$

$$+ a_4 \left(\log \frac{1}{T}\right)^2 + a_5 \log\left(\frac{p}{1000}\right) \log\left(\frac{1}{T}\right) + \tag{23}$$

$$+ a_6 \log\left(\frac{p}{1000}\right)\left(\log \frac{1}{T}\right)^2$$

$$a_0 = 3842.14861 \qquad a_4 = 770.47453$$

$$a_1 = 320.59510 \qquad a_5 = 123.39354$$

$$a_2 = 3419.52361 \qquad a_6 = 8.85064$$

$$a_3 = 85.47886$$

The temperature ranges for eqs. (21)–(23) are 300–600 K.

Every equation resulted as being the best one, from a stepwise regression analysis and all statistical tests (r, F, t) were satisfied at probability levels higher than 95%. The statistical data processing was made on more than 200 sets of data for the given ranges (Table 1).

But, in the IZENT computer program we used the method of Benzler (eqs. (6)–(15)) with the completions mentioned above, to compute enthalpy, and a high-speed convergence, iterative procedure to compute the temperature after pressure reduction.

We have also computed some multiple nonlinear regression equations to estimate directly, either the temperature t_2 (eq. (24)), or the gradient Δt (eq. (25)) of temperature increase and we compared, in turn, the results obtained, with the Benzler-data; we proved in this way, that the linear formula (eq. (20)) was anything but satisfactory for our conditions, as expected.

$$t_2 = a_0 + a_1 p_1 + a_2 t_1 + a_3 p_2 + a_4 p_2^2 \tag{24}$$

$$a_0 = 1.877 \times 10^2 \qquad a_3 = -1.362$$

$$a_1 = 5.417 \times 10^{-2} \qquad a_4 = 0.252 \times 10^{-2}$$

$$a_2 = -3.212 \times 10^{-2}$$

Table 1

Analysis of significance

Statistical values Computed property	Computational mode	Eq.	Mean	F-value	t-value	Pressure range
Specific volume (V)	Benzler diagram	—	0.00321	—	—	< 1000 atm
	Regression	(16)	0.00310	1.4493	-0.6456	
	Regression	(17)	0.00323	1.1498	0.1062	
	Regression	(18)	0.00316	1.0320	-0.2704	
	Benzler diagram	—	0.00208	—	—	$\geqslant 1000$ atm
	Regression	(16)	0.00208	1.0886	-0.1253	
	Benzler diagram	—	0.00262	—	—	200–2000 atm
	Regression	(16)	0.00259	1.37	-0.2911	
Enthalpy (H)	Benzler diagram	—	182.198	—	—	< 1000 atm
	Program by using for v	(16)	178.822	1.0328	-0.3939	
	idem	(17)	179.142	1.0349	-0.3568	
	idem	(18)	179.858	1.1109	-0.2779	
	Regression	(19)	306.68	2.5823	10.7691	
	Regression	(21)	182.174	1.0031	-0.0027	
	Benzler diagram	—	199.926	—	—	$\geqslant 1000$ atm
	Program by using for v	(16)	201.751	1.0229	0.2314	
	Regression	(22)	199.895	1.0003	-0.0039	
	Regression	(19)	922.322	14.6917	32.8981	
	Benzler diagram	—	191.500		—	200–2000 atm
	Program by	(16)				
	using for v	(17)	191.003	1.003	0.0426	
	idem	(16)				
		(18)	191.344	1.03	0.0135	
	idem	(16)	190.852	1.005	-0.0556	
	Regression	(19)	629.700	25.6	10.3179	
	Regression	(23)	191.457	1.003	-0.0036	

(t in °C and p in atm)

$$\Delta t = t_2 + a_1\,\Delta p + a_2\,\Delta p^2 + a_3\,p_1^2 + a_4\,p_2^2 + a_5\,t_1^2 \tag{25}$$

$$\Delta t = t_2 - t_1 \qquad \Delta p = p_1 - p_2$$

$$a_0 = -1.315 \times 10^2 \qquad a_3 = -0.031 \times 10^{-2}$$

$$a_1 = 0.266 \qquad a_4 = 0.171 \times 10^{-2}$$

$$a_2 = 0.029 \times 10^{-2} \qquad a_5 = -0.706 \times 10^{-2}$$

It must be emphasized that the equations (24) and (25) have been conveniently carried out, not by use of regression H-values according to eqs. (21)—(23), but by means of the mathematical iterative IZENT program described below, based upon Benzler's method. [6]

For this reason, this program was transformed into a DATA subroutine which was entered into the standard REGRE program by means of standard Fortran "CALL" statement and the regression analysis was performed for the inputs and the outputs of this subroutine, i.e. for four pressure — and temperature — values. Using the above mentioned statistical tests of significance, we chose the two equations which lead to the best agreement with Benzler's data. An approximate estimation of the Joule-Thomson temperature increasing, in the working conditions of the plant, can be made by means of extrapolated fugacity coefficients :

$$\Delta t \approx - \frac{R T_1^2 \, n \, (\gamma_1/\gamma_2)}{(c_p)_m \, (\nu_1 - \nu_2) \, T_c} \simeq - 63^\circ$$

This analytical result corresponds with our computed values, which of course are more exact.

4. PROGRAM DESCRIPTION

The computer program, called IZENT, has been written in Fortran IV and was run on an IBM 1800 process computer, non-process-wise. Input data are only the temperature at high pressure and the pressures before and after the pressure reduction, p_1 resp. p_2. Critical parameters and other data are contained in the program. The core requirement for IZENT was about 1700 words.

The after-expansion-temperature is computed by an iteration until the low-pressure enthalpy, H_2, becomes approximately equal to the high-pressure enthalpy, H_1.

We considered that a maximal accuracy of 0.99° is sufficient for t_2. But for this precision it is impossible to exactly predict at the beginning of each run, which could be the minimal error $h = H_1 - H_2$. For this reason, the algorithm successively decreased this deviation, computing an integer t_2-value with maximum accuracy for the smallest possible error, h.

Briefly, the iterative procedure can be described as follows : enthalpy H_1 for p_1 and t_1 is computed and, subsequently, it is assumed, that $t_2 = t_1$ to compute H_2, which will of course differ from H_1. The real t_2-value is computed not by increasing t_1 with constant small increments, but the iteration is conceived, as a method to decrease automatically the increments, as the H_2-value oscillates with decreasing errors around the H_1-value.

---

[6] V. Laiber and L. Alerguş, "IZENT Program de calcul al detentei etilenei" Combinatul Petrochimic Piteşti, Centrul de Calcul Electronic.

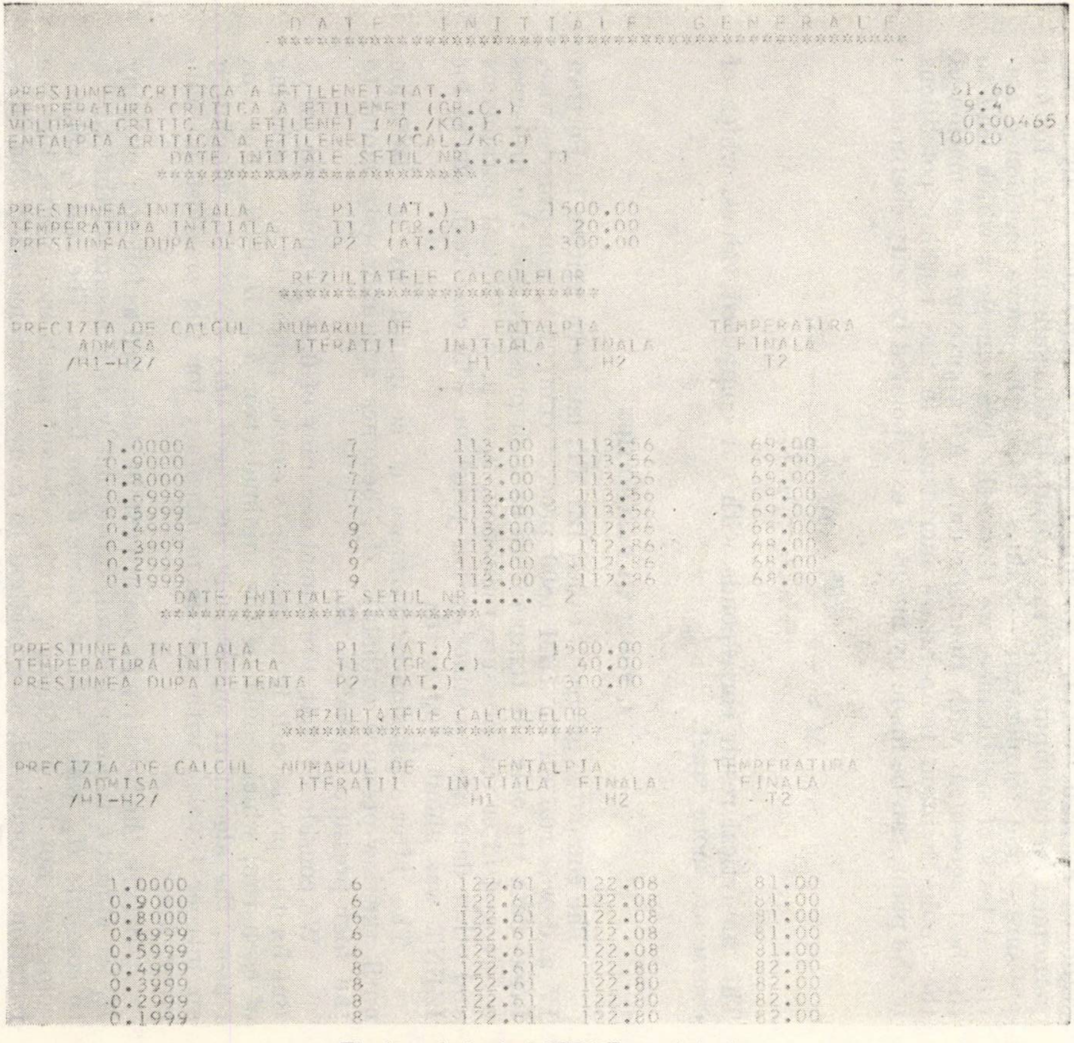

```
                    D A T E   I N I T I A L E   G E N E R A L E
                    ***********************************************

PRESIUNEA CRITICA A ETILENEI (AT.)                                          51.66
TEMPERATURA CRITICA A ETILENEI (GR.C.)                                       9.4
VOLUMUL CRITIC AL ETILENEI (MC./KG.)                                         0.00465
ENTALPIA CRITICA A ETILENEI (KCAL./KG.)                                    100.0
              DATE INITIALE SETUL NR..... 1
              ************************

PRESIUNEA INITIALA      P1  (AT.)        1500.00
TEMPERATURA INITIALA    T1  (GR.C.)        20.00
PRESIUNEA DUPA DETENTA  P2  (AT.)         300.00

                 REZULTATELE CALCULELOR
                 **********************

PRECIZIA DE CALCUL  NUMARUL DE       ENTALPIA           TEMPERATURA
     ADMISA          ITERATII    INITIALA  FINALA          FINALA
    /H1-H2/                         H1       H2              T2


     1.0000              7        113.00   113.56          69.00
     0.9000              7        113.00   113.56          69.00
     0.8000              7        113.00   113.56          69.00
     0.6999              7        113.00   113.56          69.00
     0.5999              7        113.00   113.56          69.00
     0.4999              9        113.00   112.86          68.00
     0.3999              9        113.00   112.86          68.00
     0.2999              9        113.00   112.86          68.00
     0.1999              9        113.00   112.86          68.00
              DATE INITIALE SETUL NR..... 2
              ************************

PRESIUNEA INITIALA      P1  (AT.)        1500.00
TEMPERATURA INITIALA    T1  (GR.C.)        40.00
PRESIUNEA DUPA DETENTA  P2  (AT.)         300.00

                 REZULTATELE CALCULELOR
                 **********************

PRECIZIA DE CALCUL  NUMARUL DE       ENTALPIA           TEMPERATURA
     ADMISA          ITERATII    INITIALA  FINALA          FINALA
    /H1-H2/                         H1       H2              T2


     1.0000              6        122.61   122.08          81.00
     0.9000              6        122.61   122.08          81.00
     0.8000              6        122.61   122.08          81.00
     0.6999              6        122.61   122.08          81.00
     0.5999              6        122.61   122.08          81.00
     0.4999              8        122.61   122.80          82.00
     0.3999              8        122.61   122.80          82.00
     0.2999              8        122.61   122.80          82.00
     0.1999              8        122.61   122.80          82.00
```

Fig.1. — A typical IZENT — printout.

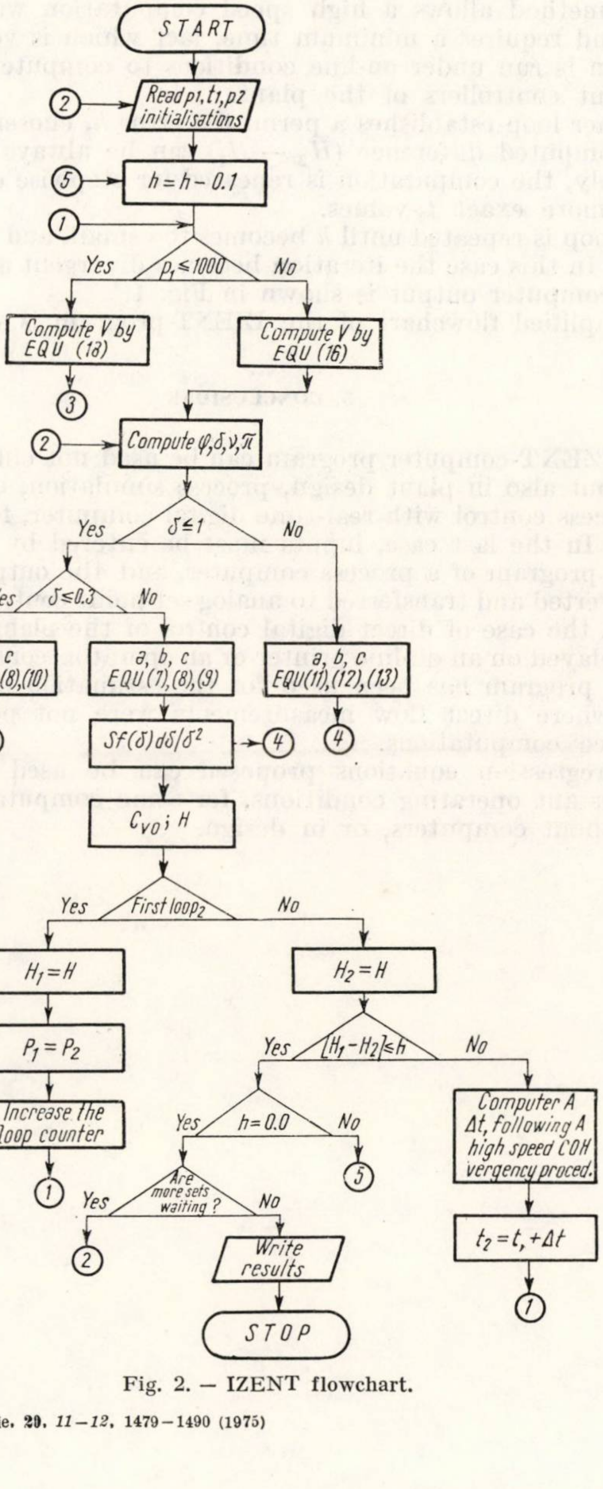
START
Read p1, t1, p2 initialisations
2
h = h – 0.1
5
1
Yes
$p_1 \leq 1000$
No
Compute V by EQU (18)
Compute V by EQU (16)
3
2
Compute φ, δ, ν, π
Yes
δ ≤ 1
No
Yes
δ ≤ 0.3
No
a, b, c EQU (7), (8), (10)
a, b, c EQU (7), (8), (9)
a, b, c EQU (11), (12), (13)
4
Sf(δ) dδ/δ²
4
4
C_{V0} ; H
Yes
First loop₂
No
$H_1 = H$
$H_2 = H$
$P_1 = P_2$
Yes
$[H_1 - H_2] \leq h$
No
Increase the loop counter
Yes
h = 0.0
No
Computer A Δt, following A high speed CON vergency proced.
1
5
Yes
Are more sets waiting ?
No
Write results
$t_2 = t_1 + \Delta t$
2
STOP
1

Fig. 2. – IZENT flowchart.

This method allows a high speed computation with a good convergency and requires a minimum time, fact which is very important if the program is run under on-line conditions to compute new targets for the set-point controllers of the plant.

Another loop establishes a permitted error h, chosen in such a way, that the computed difference $(H_2 - H_1)$ can be always smaller than h. Consecutively, the computation is repeated for stepwise decreased values, to obtain more exact t_2-values.

The loop is repeated until h becomes too small, and $H_2 - H_1$ cannot be smaller. In this case the iteration becomes divergent and it is stopped. A typical computer output is shown in Fig. 1.

A simplified flowchart of the IZENT-program is shown in Fig. 2.

5. CONCLUSIONS

The IZENT-computer program can be used not only for theoretical purposes, but also in plant design, process simulation, optimization and on-line process control with real-time digital computer, for any operating conditions. In the last case, inputs must be entered by an on-line data acquisition program of a process computer, and the outputs are automatically converted and transferred to analog set point controllers or back-up stations (in the case of direct digital control of the plant), but they can also be displayed on an on-line printer or an operator console, as operator guide. The program has been used for the estimation of some material balances (where direct flow measurements were not possible) through heat balance computations.

The regression equations proposed can be used successfully for mainly constant operating conditions, for some computations in process control without computers, or in design.

Revue Roumaine de Chimie, **20**, *11–12*, 1491–1502 (1975)

KINETIC STUDIES ON COPOLYMERIZATION OF 1,3-DIOXEPANE WITH EPICHLOROHYDRIN INITIATED WITH $AlEt_3 + H_2O$

DAN DONESCU

Institute of Macromolecular Chemistry "P. Poni", "Polymerization Process"
Department, str. Dumbrava Roşie, 18, Bucharest, Romania

Received May 28, 1974

The kinetics of copolymerization of 1,3-dioxepane (DH) with epichlorohydrin (ECH) is investigated. The kinetic relations established for the consumption rates of the two monomers show that their growth reaction occurs preponderantly by the interaction between monomers and active sites having ECH as terminal structural unit. The formation of copolymers is proved by: promoting effect exerted by ECH, decrease of the equilibrium concentration of DH below the value established for homopolymerization, IR spectra and elementary analyses of toluene-soluble and insoluble copolymer fractions. By copolymerizing DH with ECH the activation energies of the consumption reactions decrease from 25 kcal/mole to 7 kcal/mole in the case of DH and increase from 6.2 kcal/mole to 13 kcal/mole in the case of ECH, compared to those established for homopolymerization. Propylene-oxide (PO) fails to copolymerize with DH.

I. INTRODUCTION

In a previous paper we studied the homopolymerization of DH initiated with the catalytic system $AlEt_3 + H_2O$ and the promoting effect exerted by ECH on this reaction.[1]

The fact that ECH behaves as a promoter indicates that DH may polymerize through the active sites of the cyclic ether, a necessary condition for their copolymerization.

The copolymerization of DH has also been studied with different monomers such as trioxan,[2–17] formaldehyde,[18–21] trioxocan,[22] tetrahydrofuran,[23,24] ketene,[25] isobutyl-vinyl-ether,[26] isobutylene-oxide.[27]

---

[1] D. Donescu, *Makromol. Chem.*, **175**, 2355 (1974).

[2] J. Tsuji, M. Morikawa, M. Kamachi and T. Nogi, Japan Pat. 7632; *Chem. Abstr.*, **68**, 3378 (1968).

[3] J. Tsuji and T. Nogi, Japan Pat. 3033; *Chem. Abstr.*, **67**, 11 938 (1967).

[4] T. Kataoka and S. Inoue, Japan Pat. 3032; *Chem. Abstr.*, **67**, 11981 (1967).

[5] F. Hoechst A. G., Belg Pat. 618509; *Chem. Abstr.*, **58**, 14213 (1963).

[6] F. Hoechst A. G., S. African Pat. 6801978; *Chem. Abstr.*, **70**, 78803 (1969).

[7] F. Hoechst A. G., Neth. Appl. 6512699; *Chem. Abstr.*, **56**, 9109 (1966).

[8] M. Minami, Y. Tsuda, K. Sando, J. Kashiro and K. Tamura, U. S. Pat 3337505; *Chem. Abstr.*, **67**, 82718 (1967).

[9] Per G. M. Flodin, Per Kornfeld, S. Okamura and K. Hayashi, German Pat 1 256 897; *Chem. Abstr.*, **68**, 50324 (1968).

2. EXPERIMENTAL

2.1. *Materials* were conditioned according to the procedure described in the previous paper.[1]

2.2. *Copolymerization procedure.* The previously described apparatus and working procedure were used, and toluene was added to the reaction medium (0.471 mole/l) to serve as internal standard in chromatography.

The concentrations of unreacted monomers were determined chromatographically on reaction mixtures from which copolymers had been completely precipitated with *n*-hexane. The chromatographic analyses were carried out with a Perkin Elmer 452 chromatograph whose column was filled with Cromosorb P 60/80 mesh with 20% deposit of Carbowax 20 M. The working conditions were the following: column temperature 60°, injection block temperature 130°, rate of H_2, eluent gas, 100 cm^3/min.

The catalyst concentration was 0.09 mole/l.

2.3. *Analysis of copolymers.* Their composition was established by determining the chlorine content. NMR spectra were taken on copolymer solutions in benzonitrile at 60 MHz and a temperature of 70° by means of a Jeol JNM–60 HL instrument. IR spectra were taken at room temperature on a Hilger and Watts 800 spectrophotometer.

3. RESULTS

In the copolymerization of DH with ECH, monomer consumption in time is similar to the case of homopolymerization[1,28] (Fig. 1).

It has been observed that DH consumption rate is much higher than in homopolymerization, which is presumably due to a high ECH concentration. Under these conditions the initial consumption rate of DH depends on $[DH]_0$ and $[ECH]_0$ as shown in Figs. 2 and 3. Due to continuous variation in the equilibrium concentration of DH as the composition of monomer mixture changes, we may establish, for the results presented in Fig. 2, a similar relation to that in Fig. 3 only in the case in which equilibrium concentration of DH is neglected (it may vary between 0.5 mole/l and 0

[10] Deutsche Gold und Silber Scheideanstalt vorm. Roessler, Franc. Pat 1 579896; *Chem. Abstr.*, **72**, 112280 (1970).

[11] K. Weissermel, E. Fischer, K. Gutweiler and H. D. Herman, *Kunststoffe*, **54**, 410 (1964).

[12] M. Inoue, *J. Appl. Polymer Sci.*, **8**, 2225 (1964).

[13] S. Roesinger, *J. Polymer Sci.*, **5**, 183 (1967).

[14] W. Kern and V. Jaacks, U.S. Pat. 3293221; *Chem. Abstr.*, **66**, 95616 (1967).

[15] A. Hilt, F. Schmidt and E. Schwartz, Ger Offen 191 744; *Chem. Abstr.*, **74**, 54345 (1971).

[16] E. Baeder and H. Aman, Ger. Offen. 2003270; *Chem. Abstr.*, **75**, 152330 (1971).

[17] G. Sammer, E. Baeder and W. Sibenhorn, Ger. Pat. 1 720 510; *Chem. Abstr.*, **76**, 128156 (1972).

[18] F. Hoechst A. G., Neth. Appl. 6412355; *Chem. Abstr.*, **64**, 880 (1966).

[19] Kurashiki Rayon Co. Ltd., Brit. Pat. 1 087 034; *Chem. Abstr.*, **67**, 117550 (1967).

[20] Kurashiki Rayon Co. Ltd., Brit. Pat. 1 057 961; *Chem. Abstr.*, **66**, 116150 (1967).

[21] H. D. Herman and K. Weissermel, *Makromol. Chem.*, **94**, 91 (1966).

[22] K. Thinius and D. Weichart, Ger. Pat. (East) 43164; *Chem. Abstr.*, **65**, 2372 (1966).

[23] BASF, Ger. Pat. 191 106; *Chem. Abstr.*, **63**, 1903 (1965).

[24] Y. Yamashita, S. Kozawa, K. Chiba and M. Okada, *Makromol. Chem.*, **135**, 75 (1970).

[25] Wacker Chemie G.m.b.H., Franc. Pat. 1 541 871; *Chem. Abstr.*, **71**, 30837 (1969).

[26] M. Okada and Y. Yamashita, *Makromol. Chem.*, **126**, 266 (1969).

[27] Y. Yamashita, T. Inoue and K. Ito, *Makromol. Chem.*, **138**, 305 (1970).

[28] M. Dimonie and I. Gavăt, *European Polymer Journal*, **4**, 541 (1968).

under the experimental conditions used). With this approximation initial consumption rate of DH may be considered to depend on the third power of its initial concentration.

The variation in the initial consumption rate of ECH as a function of the reaction condition differs largely from that of DH. The consumption

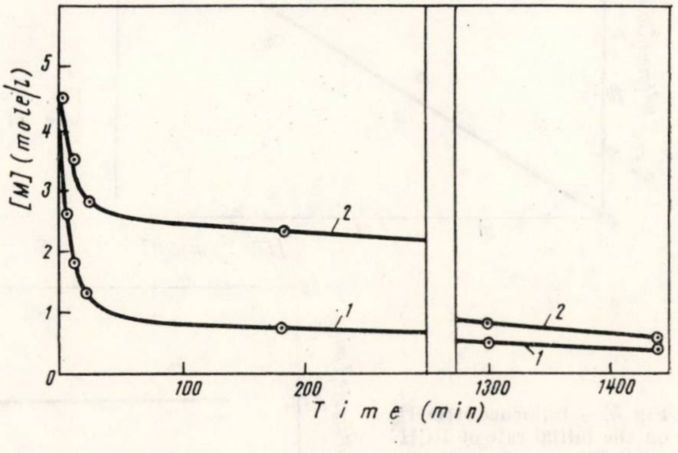

Fig. 1. — Variation of DH(*1*) and ECH(*2*) concentrations in time.

([DH]$_0$ = 4 mole/l,

[ECH]$_0$ = 4.5 mole/l)

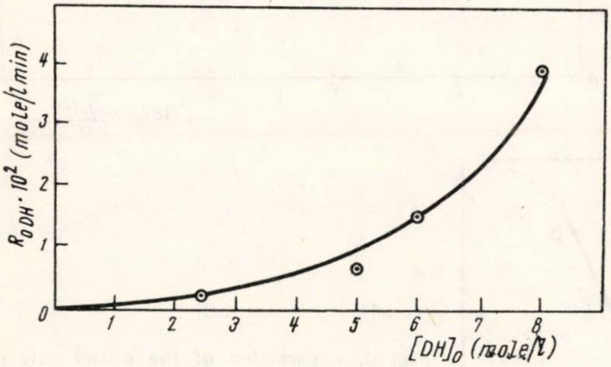

Fig. 2. — Dependence of the initial consumption rate of DH on [DH]$_0$.

(ECH]$_0$ = 0.5 mole/l)

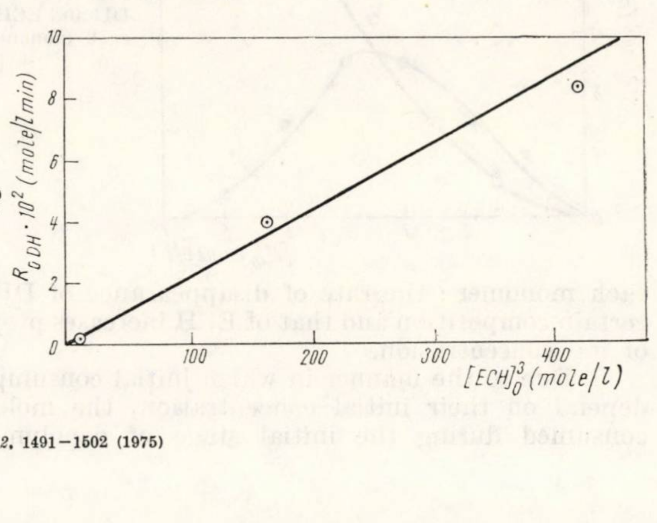

Fig. 3. — Influence of [ECH]$_0$ on DH initial rate. ([DH]$_0$ = = 1 mole/l).

rate of ECH depends on the square of its concentration and is not affected by the concentration of the formal (Figs. 4, 5).

Fig. 6 shows that for a certain total monomer concentration the individual rates depend in different ways on the initial concentration of

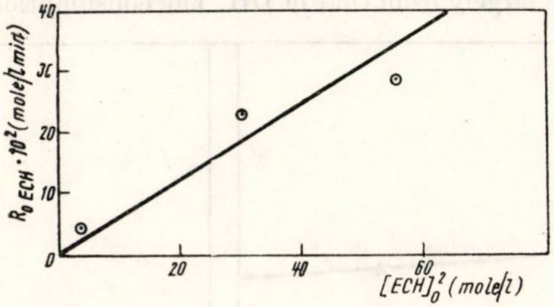

Fig. 4. — Dependence of the initial rate of ECH on $[ECH]_0$($[DH]_0$ = = 1 mole/l).

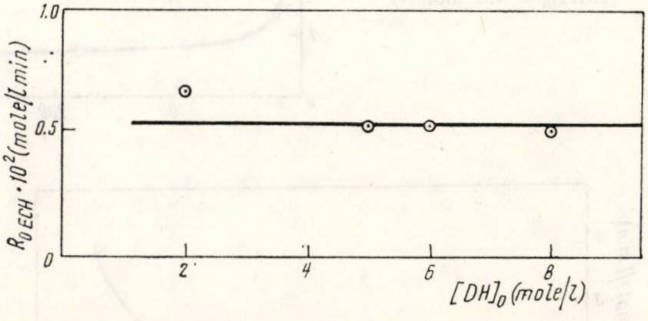

Fig. 5. — Influence of $[DH]_0$ on the initial rate of ECH. $(ECH]_0$ = 0.5 mole/l).

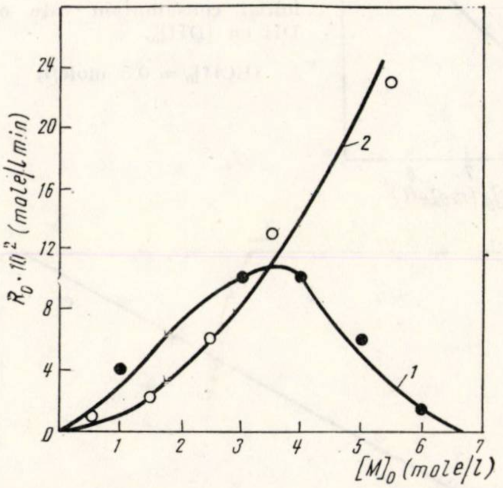

Fig. 6. — Variation of the initial rate of DH and ECH on the initial concentration of each monomer (*1*—DH, *2*—ECH, $[DH_0$ + + $[ECH]_0$ = 6.5 mole/l).

each monomer: the rate of disappearance of DH has a maximum for a certain composition and that of ECH increases proportionally to the square of its concentration.

Due to the manner in which initial consumption rates of monomers depend on their initial concentration, the mole fraction of monomers consumed during the initial stage of copolymerization are markedly influenced by the total monomer concentration. Fig. 7 outlines the fact that the relative activity of ECH decreases as the total monomer concentration increases.

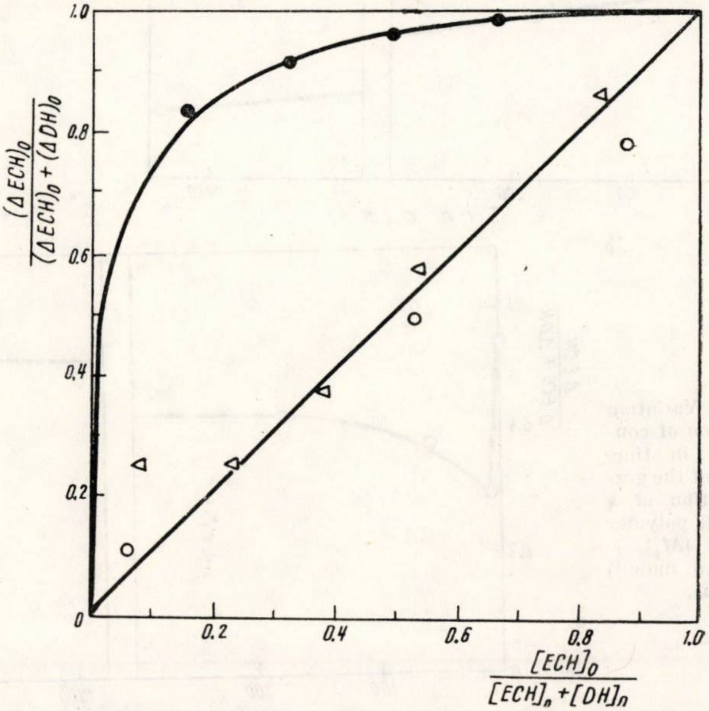

Fig. 7. —Correlation between ECH relative activity and initial monomer concentration.

(M_1 – ECH, $[M_1]_0 + [M_2]_0 = 3$(●), 6.5(△), 8.5(○)).

The difference in the behaviour of these two monomers can be seen throughout the process, not just at the beginning.

By following the variation in time of the mole fraction of consumed ECH in Fig. 8 we observe two distinct periods : an initial one in which the concentration of consumed ECH decreases, followed by a period in which there is an increase in ECH weight.

Since comonomers are consumed at different rates during the process, the products have a variable composition. In this sense, the variation in time of the weight-fraction of a toluene-soluble polymer is suggestive. Toluene is a solvent in which polydioxepane is totally soluble whereas polyepichlorohydrin is very sparsely soluble. This fraction continually decreases during the process with the increase of ECH concentration in the polymer (Fig. 8).

A particularly significant phenomenon is the fact that the ECH content in the toluene-soluble and insoluble fractions varies in time in a similar manner with the mole fraction of consumed ECH (Fig. 9).

IR spectra of those fractions are given in Fig. 10.

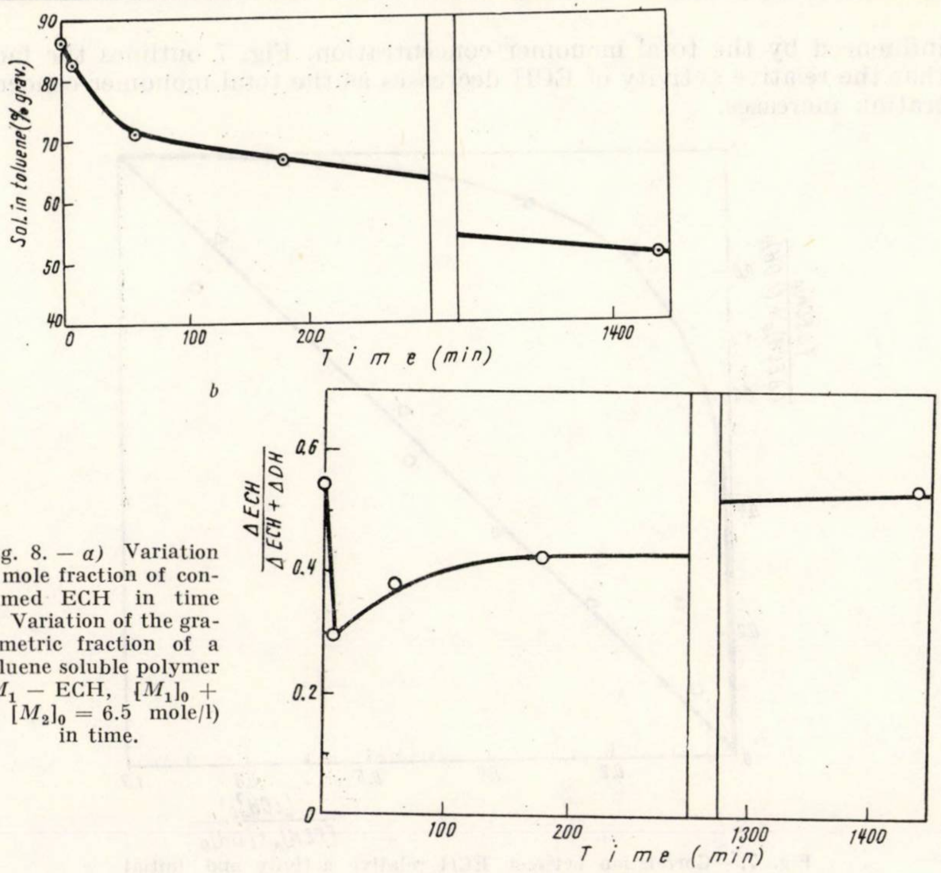

Fig. 8. — *a)* Variation of mole fraction of consumed ECH in time *b)* Variation of the gravimetric fraction of a toluene soluble polymer (M_1 — ECH, $[M_1]_0 + [M_2]_0 = 6.5$ mole/l) in time.

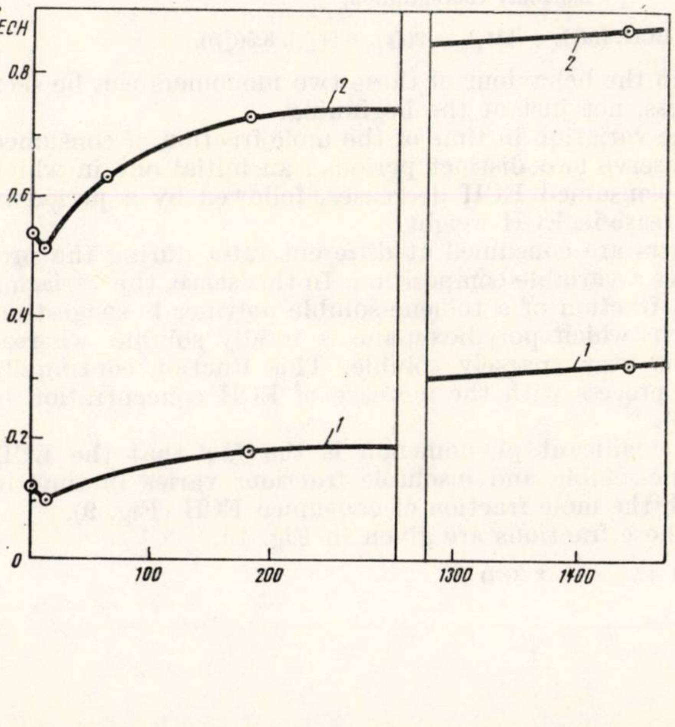

Fig. 9. — Mole fraction of ECH in the toluene-soluble (*1*) and insoluble (*2*) copolymers *vs* time (reaction conditions the same as in Fig. 8).

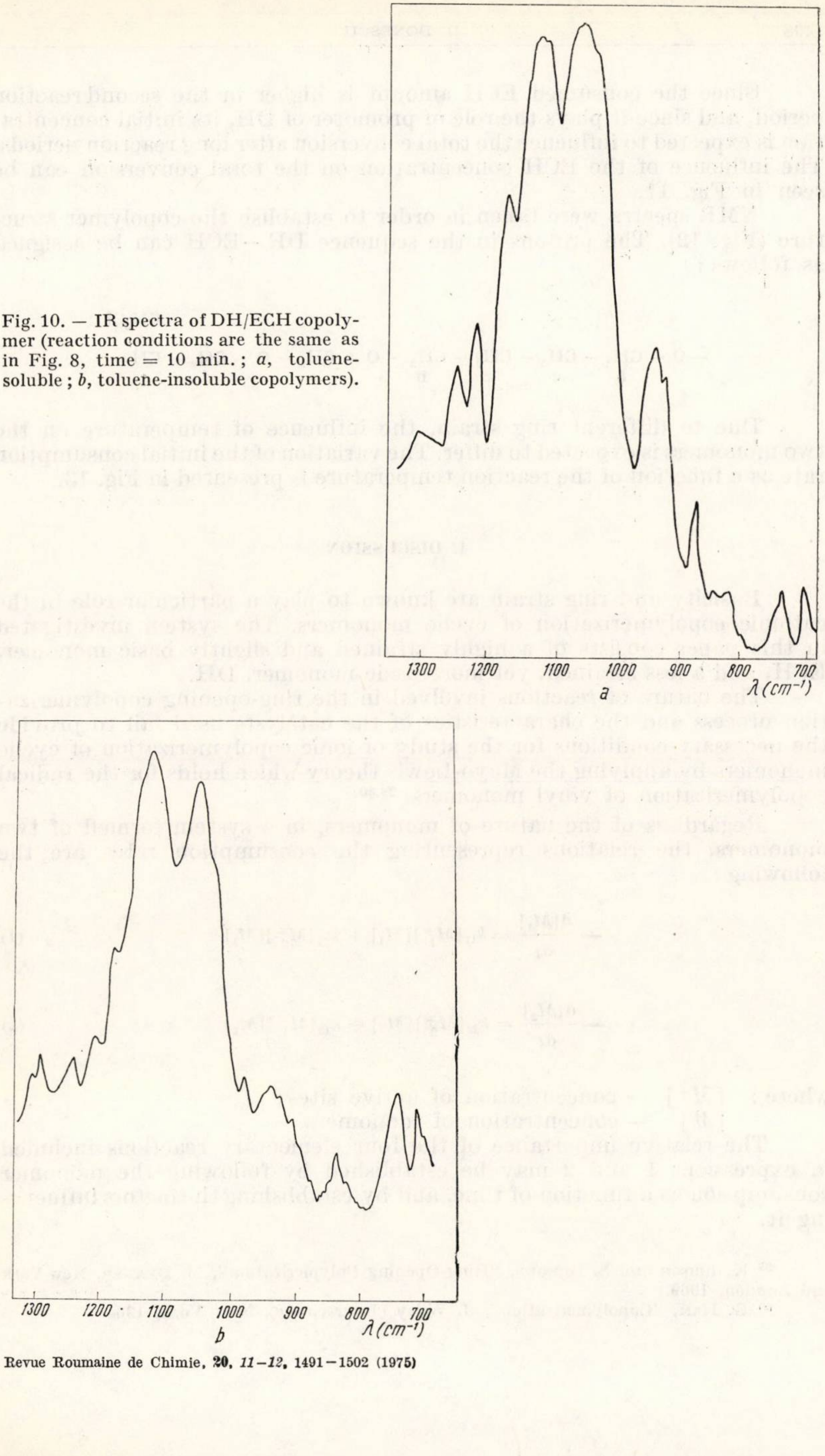

Fig. 10. — IR spectra of DH/ECH copolymer (reaction conditions are the same as in Fig. 8, time = 10 min. ; *a*, toluene-soluble ; *b*, toluene-insoluble copolymers).

Revue Roumaine de Chimie, **20**, *11–12*, 1491–1502 (1975)

Since the consumed ECH amount is higher in the second reaction period, and since it plays the role of promoter of DH, its initial concentration is expected to influence the total conversion after long reaction periods. The influence of the ECH concentration on the total conversion can be seen in Fig. 11.

NMR spectra were taken in order to establish the copolymer structure (Fig. 12). The protons in the sequence DH—ECH can be assigned as follows :

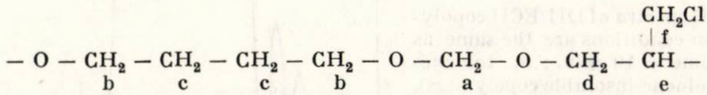

$$-O-\underset{b}{CH_2}-\underset{c}{CH_2}-\underset{c}{CH_2}-\underset{b}{CH_2}-O-\underset{a}{CH_2}-O-\underset{d}{CH_2}-\underset{e}{\overset{\overset{CH_2Cl}{|\,f}}{CH}}-$$

Due to different ring strain, the influence of temperature on the two monomers is expected to differ. The variation of the initial consumption rate as a function of the reaction temperature is presented in Fig. 13.

4. DISCUSSION

Basicity and ring strain are known to play a particular role in the cationic copolymerization of cyclic monomers. The system investigated in this paper consists of a highly strained and slightly basic monomer, ECH, and a less strained, yet more basic monomer, DH.

The nature of reactions involved in the ring-opening copolymerization process and the characteristics of the catalysts used fail to provide the necessary conditions for the study of ionic copolymerization of cyclic monomers by applying the Mayo-Lewis theory which holds for the radical copolymerization of vinyl monomers.[29,30]

Regardless of the nature of monomers, in a system formed of two monomers, the relations representing the consumption rates are the following :

$$-\frac{d[M_1]}{dt} = k_{11}[M_1^+][M_1] + k_{21}[M_2^+][M_1] \qquad (1)$$

$$-\frac{d[M_2]}{dt} = k_{22}[M_2^+][M_2] + k_{12}[M_1^+][M_2] \qquad (2)$$

where : $[M^+]$ — concentration of active sites ;
$[M]$ — concentration of monomers.

The relative importance of the four elementary reactions included in expressions 1 and 2 may be established by following the monomer consumption as a function of time, and by establishing the factors influencing it.

---

[29] K. Frisch and S. Reegen, "Ring-Opening Polymerization", M. Dekker, New York and London, 1969.

[30] G. Ham, "Copolymerization", J. Wiley (Interscience), New York, 1964.

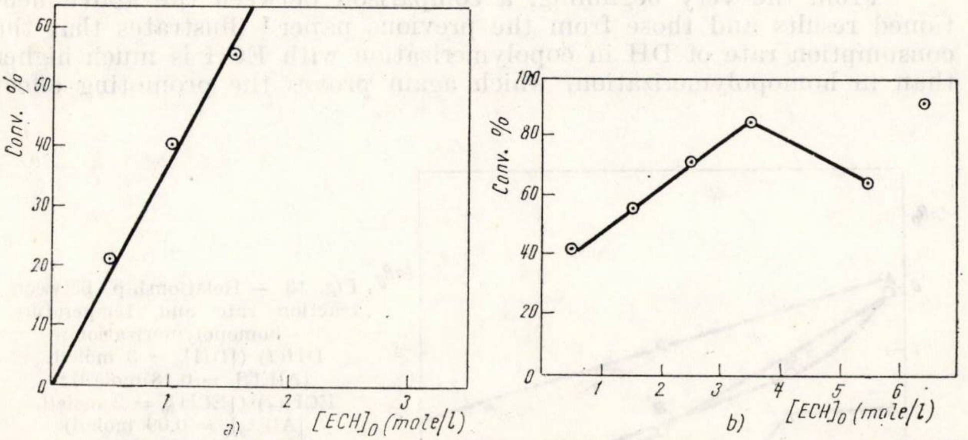

Fig. 11. — Influence of $[ECH]_0$ on total conversion. ($[DH]_0 + [ECH]_0 = 3$ (a), 6.5 (b) mole/l)

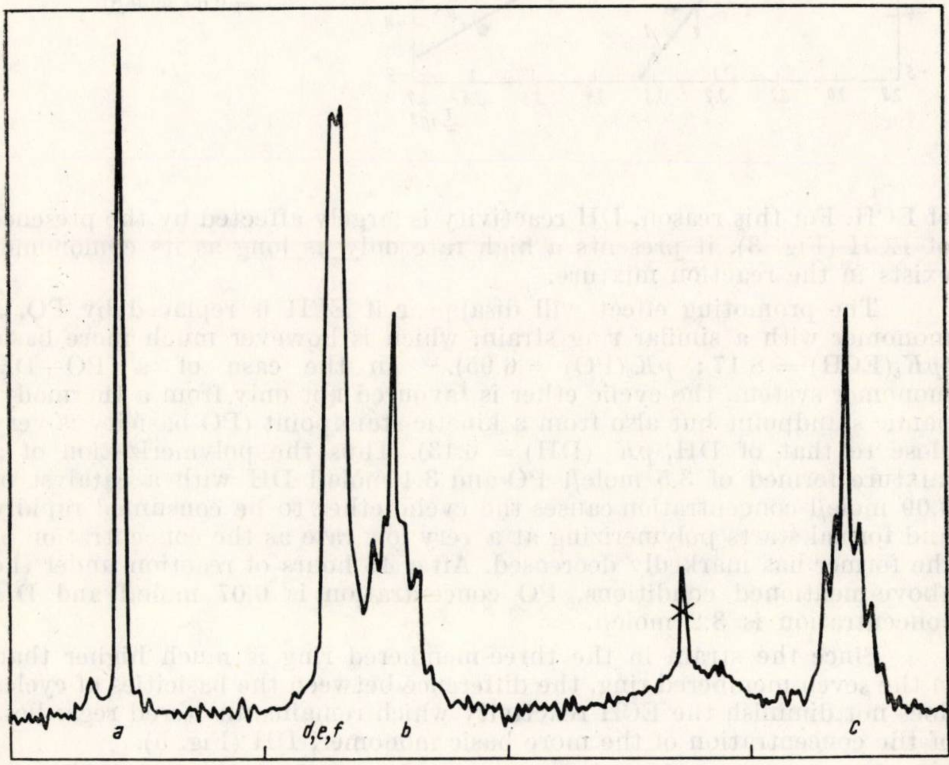

Fig. 12. — NMR spectrum of DH/ECH copolymer (reaction conditions are the same as in Fig. 1, time reaction — 24 hours).

From the very beginning, a comparison between the above-mentioned results and those from the previous paper[1] illustrates that the consumption rate of DH in copolymerization with ECH is much higher than in homopolymerization, which again proves the promoting effect of ECH. For this reason, DH reactivity is largely affected by the presence of ECH (Fig. 3), it presents a high rate only as long as its comonomer exists in the reaction mixture.

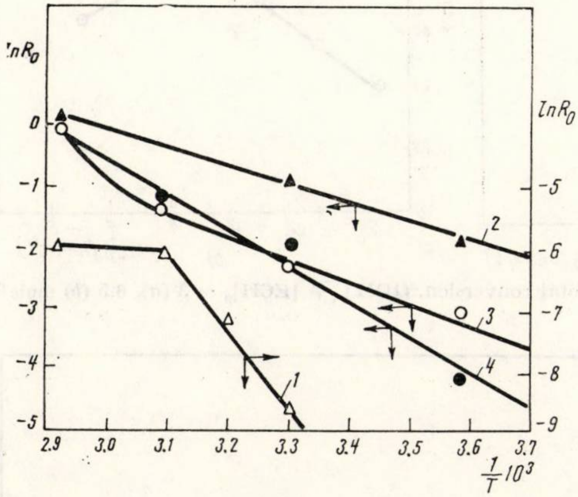

Fig. 13. — Relationship between reaction rate and temperature — homopolymerization: DH(*1*) ($[DH]_0 = 3$ mole/l, $[AlEt_3]_0 = 0.18$ mole/l); ECH(*2*) ($[ECH]_0 = 2$ mole/l, $[AlEt_3]_0 = 0.09$ mole/l) — copolymerization: DH(*3*); ECH(*4*) ($[DH]_0 = 3$ mole/l, $[ECH]_0 = 3.5$ mole/l, $[AlEt_3]_0 = 0.09$ mole/l).

The promoting effect will disappear if ECH is replaced by PO, a monomer with a similar ring strain, which is however much more basic ($pK_b(ECH) = 8.17$; $pK_b(PO) = 6.95$).[29] In the case of a PO−DH monomer system, the cyclic ether is favoured not only from a thermodynamic standpoint but also from a kinetic standpoint (PO basicity is very close to that of DH, pK_b (DH) = 6.13). Thus the polymerization of a mixture formed of 3.5 mole/l PO and 3.4 mole/l DH with a catalyst of 0.09 mole/l concentration causes the cyclic ether to be consumed rapidly and formal starts polymerizing at a very low rate as the concentration of the former has markedly decreased. After 48 hours of reaction under the above-mentioned conditions, PO concentration is 0.07 mole/l and DH concentration is 3.2 mole/l.

Since the strain in the three-membered ring is much higher than in the seven-membered ring, the difference between the basicities of cycles does not diminish the ECH reactivity which remains unaltered regardless of the concentration of the more basic monomer, DH (Fig. 5).

We showed in the previous paper that in the presence of $AlEt_3 + H_2O$ the consumption rate of DH depends on a monomer concentration power which is greater than one. In the copolymerization the initial consumption rates also depend on concentration powers of proper monomers which are greater than one (Figs. 2, 4), a fact which shows that the formation of the initial active sites occurs by a complex cationic mechanism in which monomers play an important role.[1,31,32]

Since the curve in Fig. 6 which represents the variation in the initial consumption rate of DH has a maximum at an initial monomer concentration which coincides with that of expression $[\mathrm{DH}]_0^3[\mathrm{ECH}]_0^3$ and since the curve practically passes through the origin we may write for the initial consumption rate :

$$\left\{-\frac{\mathrm{d[DH]}}{\mathrm{d}t}\right\}_0 = k_1[\mathrm{DH}]_0^3[\mathrm{ECH}]_0^3 \tag{3}$$

and for ECH (Fig. 4—6) :

$$\left\{-\frac{\mathrm{d[ECH]}}{\mathrm{d}t}\right\}_0 = k_2[\mathrm{ECH}]_0^2 \tag{4}$$

Reduction of equations 1 and 2, formed each of two terms, to equations 3 and 4 shows that two elementary reactions do not have a great importance in the copolymerization of DH with ECH.

The promoting effect exerted by ECH on the consumption reaction of DH and the fact that the DH concentration does not influence the consumption rate of ECH demonstrate that the negligible elementary reactions are those of monomer consumption through active sites which have DH as a terminal structural unit.

The dependence of initial rates on monomer concentrations as presented in relations 3 and 4 explains the fact that the mole fraction of initially consumed monomers is strongly influenced by the total concentration of monomers (Fig. 7).

The relatively different behaviour of ECH and of DH is due both to the existing kinetic causes — monomer concentrations, their basicity and to causes of a thermodynamical nature — the different ring strain. The difference in behaviour is maintained throughout the process. It may be observed from Fig. 8 that DH is more reactive than ECH in the initial stage of process. The changes in the relative reactivities of monomers in time are explained by the fact that due to the equilibrium character of the polymerization of DH,[32] its reactivity decreases with the decrease in the monomer concentration. At large conversions, the total concentration of monomers, and particularly of DH, largely decreases. For this reason, with the same mole fraction of DH in the monomer mixture, its activity is larger at the beginning of the process.

This phenomenon is not found in the case of copolymerization of ECH with a monomer that does not polymerize in equilibrium, such as PO.[33]

---

[31] P. KUBISA and ST. PENCZEK, *Makromol. Chem.*,**144**, 169 (1971).

[32] M. OKADA, S. KOZAWA and Y. YAMASHITA, *Makromol. Chem.*, **127**, 271 (1969).

[33] V. DIMONIE, D. DONESCU and I. GAVĂT, *Rev. Roumaine Chim.*, **1**, 125 (1974).

Revue Roumaine de Chimie, **20**, *11–12*, 1491–1502 (1975)

It can be seen from Fig. 8 that the composition of the product varies in time, and this non-homogeneity is also maintained in the two fractions : toluene-soluble and insoluble (Figs. 8, 9)

The occurrence of DH units in the toluene-insoluble fraction revealed both by the analysis of the composition and by IR spectra (Figs. 9, 10) is a strong argument when demonstrating the formation of copolymers.

The possibility of copolymer formation is also supported by kinetic results : the ECH promoting effect in the polymerization of DH and the decrease of the equilibrium concentration of DH below the value determined in homopolymerization.[32] Thus, in the copolymerization of a mixture in which $[ECH]_0$ and $[DH]_0$ are respectively 5.5 and 1 mole/l or 7.5 and 1 mole/l after 24 hours of reaction, DH concentrations are 0.17 and 0.05 mole/l. This fact is explained only by the modification in the nature of the structural units of the growing chain, modification which takes place by introducing ECH into the chain, hence by the appearance of copolymers.

The microstructure of copolymers, the manner in which the structural units are arranged under the form of long blocks or statistically, could not be determined by NMR spectra because of the lack of clear separation of DH peaks due copolymers, a fact also mentioned for other copolymers.[27] In addition, the ECH units in copolymer produce one single peak, impossible to analyse. An important cause of these phenomena is the high molecular mass of copolymers.

A particularly interesting result obtained in the study of DH copolymerization with ECH is the way in which the activation energy of the monomer consumption reaction is affected by temperature (Fig. 13). In the case of DH a decrease of the activation energy is observed in copolymerization compared to homopolymerization, from 25 kcal/mole to 7 kcal/mole due to the presence of much more reactive active sites of ECH and due to its pronounced basicity.

The presence of a more basic monomer having therefore a more pronounced affinity to active centers but being less tensional, hence less susceptible to ring opening reaction causes the activation energy of the ECH consumption reaction to increase from 6.2 kcal/mole in homopolymerization to 13 kcal/mole in copolymerization. Despite the large difference of activation energies in homopolymerization, the activation energies involved in copolymerization tend to get closer in this monomer system.

COMPTES RENDUS

"Topics in Carbon-13 NMR Spectroscopy", Edited by George C. Levy, John Wiley and Sons, New York, 1974, 292 p.

This is the first volume of what is evidently intended as a continuing series of reviews. The importance of ^{13}C nmr spectroscopy in solving problems of chemical and biochemical interest is evidenced by the veritable explosion of papers on this subject within the past three to four years.

According to the preface, "The explosive growth of ^{13}C nmr studies is not easily documented. *Topics in Carbon-13 NMR Spectroscopy* is intended to fill the gap between the current research literature and available ^{13}C nmr texts and reviews. All chapters are written by ^{13}C nmr experts currently doing research on the specific topics being covered. Thus, in many cases the articles are reviewing future literature !"

There are six chapters, of which four are devoted to theoretical development : Theory of ^{13}C Chemical Shifts by R. Ditchfield and P. D. Ellis ; Substituent Effects on ^{13}C Chemical Shifts by G. E. Maciel ; Carbon-13 Nuclear Spin Reaction by J. R. Lyerla and G. C. Levy ; ^{13}Carbon NMR at High Magnetic Fields by F. A. L. Anet. The literature analyses presented in these chapters are oriented toward the phenomenon of ^{13}C magnetic resonance rather than towards the application of ^{13}C nmr to the study of various classes of chemical compounds. Two chapters deal with the application of Carbon-13 nmr spectroscopy : The Carbon-13 NMR Analysis of Synthetic High Polymers by J. Schaefer ; ^{13}C NMR Studies of — Reaction Mechanisms and Reactive Intermediates by J. B. Stathers.

All the chapters on theory and applications are well written and highly specialized. It is somewhat regrettable that topics such as Fourier transformation and instrumentation are not covered. This volume provides the magnetic resonance specialist with a most useful guide to selected topics in the current research literature but is not, in general, sufficiently detailed to warrant use of the volume as an introductory text for a nonspecialist.

The editor has indicated that certain topics, such as applications in biochemistry, organometallic chemistry and experimental methods will be covered in the subsequent volume.

Cezar Ungurenaşu

O. G. KOCH and G. A. Koch-Dedic, "Traces Analysis Handbook", Publishing House, Springer, Berlin, Heidelberg, New York, 1974.

Published in two big volumes, only five years after the first edition, the book entitled "Traces Analysis Handbook" presents up-to-date information (till the middle of 1973) regarding traces analytical chemistry. The valuable works of the Romanian school of chemistry are included among the 5000 new bibliographical references added to the new edition.

The book is intended to the chemical engineers and researchers working in analytical laboratories and facing difficulties in analysing the elements appearing in concentrations under 0.01 %, in different patterns.

The handbook is divided into two parts.

The first part, the general one, having about 175 pages includes 7 chapters. It presents the principles of traces analysis, mathematical and statistic processing of the experimental data, methodic sensibility, accuracy and precision. The physico-chemical methods of traces analysis based on : spectroscopy, spectrophotometry, chlorometry, visible and Roentgen fluorescence, neutron activation, gas chromatography, as well as electrochemical, radiochemical and microbiological methods are also presented. Extraction and separation methods for the elements existing in the traces are discussed in principle, and the special working conditions required by traces analysis are finally presented : instrumentation, reagents and apparatuses employed.

The second part, the special one, containing about 1400 pages has 7 comprehensive chapters. The first three chapters largely present the problems of : analytical sample dressing, working techniques for separating the trace element, specific reagents. The fourth chapter is the most important and comprehensive one describing in detail the analysis of each element existing in different patterns (the elements are alphabetically presented, according to their chemical symbol). It deals with problems specific of element separation, the most suitable reagents and physico-chemical methods used in various analytical cases for the respective element, finally presenting the whole bibliography specific of the element analysis. Chapter five discusses the multielementary traces analysis developed for : water, organic materials, metallic alloys and other various materials. Chapter six discusses microbiological methods of traces analysis. Chapter seven, the last one, contains tables of physico-chemical constants and other important laboratory data.

Compared with other analytical handbooks the above one is more concrete, the methods are minutely described and can be readily used. The reagents list is presented before treating each problem. The special glass apparatuses are drawn in detail and standardized. The peak spectral values of the reagents are given in tables or diagrams. Sensibility and precision limits are also given in tables for the respective method. Chemical formulae are structurally written and the explanations are clear and modern, based on the present IUPAC standards.

The handbook is a valuable working instrument when used as laboratory guide.

Dan Ciomârtan

MARTIN OBERHOFER "Safe Handling of Radiation Sources", Publishing House, Karl Thieming München, 1974.

The book entitled "Safe Handling of Radiation Sources" is addressed to the specialists working with nuclear or roentgen sources in different fields of activity.

Without offering precise rules but only recommendations, the book constitutes a practical guide of protection methods and actions against radiations. The 240 pages in pocket size include 5 chapters : protection principles against radiation, work developed in radiation fields around the installation, handling of open radiation sources, handling of the screened sources as well as a chapter referring to accidents.

The numerous pictures and drawings included in the book enable a good understanding of the safe handling of the equipment and apparata with radiation sources, the reader needing no complicated explanatory notes. Complex and difficult mathematical proofs are avoided, the author insisting especially upon phenomena understanding. The book includes simple formulae useful in our daily activity as well as tables and diagrams.

Consequently a large quantity of quickly assimilable information is presented in a reduced space.

The first chapter defines the measuring units in nucleonics and radiology, radiation measuring instruments and their handling as well as the methods of reducing radiation exposure, namely : time limiting, keeping a minimum protection distance and screening.

The second chapter describes the X-ray installations working in : crystallography, chemical analysis, medicine, industrial defectoscopy, electron accelerators, nuclear reactors, insisting upon protectory architecture, general administrative measures and operational protection against irradiation risks.

Chapter 3 presents the screened sources (closed sources) their type and marking, transport, radioactivity measuring, storing and handling.

Chapter 4 refers to radioactive isotope handling. It presents the principles of building radioisotope laboratories. The necessary protective clothing, the rules for isotope handling, describing at the same time the work developed in the hot rooms and production of radioactive sources by mechanical and physico-chemical treatment. Decontamination methods and waste storage are also discussed.

Chapter 5 specifies the possible accidents when handling nuclear radiations, proposing first aid rules and presenting decontamination processes for the objects, places and waste storage.

In the end the book contains a bibliographical list including 165 references and a table of radionuclides classification according to their toxicity.

Dan Ciomârtan

Revue Roumaine de Chimie, 20, 11–12, 1505–1520 (1975)

INDEX DU TOME 20, 1975

INDEX DES AUTEURS

A

Ababi V., voir Bourceanu, G. 627
Abbe J. Ch., voir Constantin E. . . . 1329
Abdelkader A. K., voir Issa I. M. . 275
Adorian I., Molar polarization and permanent electric moment of *n*-butyl butyrate in nonpolar solvents . 51
Alerguș L., voir Laiber V. 1479
Angadi S. D., voir Biradar N. S. . . . 755
Anghelov V. Z., voir Dimitrov D. I. 1319
Antonescu L., voir Constantinescu C. 985
Archibald R. M. and D. R. Armstrong, P. G. Perkins, *Ab initio* calculations using spherical Gaussian orbitals on water, methane, acetylene, ethylene, ethane and diborane 1371
Armstrong D. R., The electronic structure of 1,5-dicarba-*closo*-pentaborane (5) and 1,6-dicarba-*closo*-hexaborane (6) 883
—, voir Archibald R. M. 1371
—and P. G. Perkins, J. J. P. Steward, The electronic structure and spectra of titanium tetrachloride and the methyltitanium chlorides 177
Arsene A. et M. Germain, Étude du partage de l'acide formique, de l'uranium (VI) et du plutonium (IV) dans le système tributyl-phosphate-dodécane-acide nitrique-acide formique-eau 251
Atanasiu I., voir T. Badea 45
— et M. Neață Bălescu, L'étude du système rédox Fe(CN$_6^3$)$^-$/Fe(CN)$_6^{4-}$ sur l'électrode de graphite 493
Avram E. and M. Avram, Reactions of acetylenes with transition metals. VI. Reaction of the π-allyl complex of 6-chloro-1,3,6-tri-t-butyl-1,2-dihydrofulvene with carbon monoxide 775
— and F. Chiraleu, I. G. Dinulescu, M. Avram, Reactions of acetylenes with transition metals. III. Structure of the complex obtained from t-butyl-acetylene and bis-benzonitrile-palladium chloride . . . 539
— and I. G. Dinulescu, F. Chiraleu, E. Șliam, M. Avram, Reaction of acetylenes with transition metals. V. β-clevage in σ, π-alkyl-palladium complexes 637
Avram M., voir Avram E. 539,637,775
—, voir Dinulescu I. G. 85
—, voir Enescu L. 957
—, voir Gheorghiu M. D. . . . 75
—, voir Iordache F. 233,353
—, voir Ștefan N. 1473

B

Badalov Iu. A., voir Naziev Ia. M. . . 55
Badami B. V. and G. S. Puranik, Reactions of sydnones, II. Benzylsydnone and its derivatives 981
Badea F., voir Banciu M. 121
Badea L., Modelling the material balances of the chemical flowsheets 1001
Badea T. and I. Atanasiu, Electrochemical behaviour of 18 Cr-10 Ni stainless steel in organic acid solutions. II. Acetic acid 45
Badev A. T., voir Dimitrov D. I. . . 1319
Badiger V. V., voir Bennur S. C. . . 1295
Bădilescu I. I., Heterocyclic compounds. III. The cyclization of ring-substituted γ-phenoxybutyric acids by PPA to 2,3-dihydro-1-benzoxepin-6 (4*H*)-ones 761
— , Heterocyclic compounds. V. Beckmann rearrangement of some 2,3-dihydro-1-benzoxepin-5(4*H*)-one oxime to 1,5- and 1,6-benzoxacinones 1077
Balaban C., voir Jinescu G. I. . . . 1141
Balaban A. T., Chemical graphs. XXV. Isomers of the porphyrins-an exercise using Pólya's counting theorem 227
—, voir Bally I. 1471
Balasubramanian T. R. and N. Venkatasubramanian, Oxidation of alicyclic alcohols by cerium(IV) perchlorate 1301
Bally I. and A. T. Balaban, Synthesis of ^{14}C-labelled isotope-isomeric alka-

nes. II. Preparation of 2,2,4-trimethyl-pentane-$^{14}C_2$ labelled at both methyl groups of the isopropyl moiety 1471

Banciu M. and F. Badea, R. Jelescu, E. Ciorănescu, Carbonium ion reactions. XII. Acetolysis of 5-(2-bromoethyl)-5H-dibenzo [*a*, *d*] cycloheptene and nitrous acid deamination of 5-(2-aminoethyl)-5H-dibenzo [*a*, *d*] cycloheptene 121

Banerji S. K., voir Prasad C.S.G. . . 115

Barb D., voir Solacolu Ş. 69

Bărbulescu E., voir Solacolu Ş. . . 69

Bejan L., voir Sternberg S. 465

Bendic C. and D. Oancea, Reactivity of benzyl halides in SN_2 reactions 195

Benedikt G. M. and A. Voicu, An intramolecular hydrogen bridge with the double bond in spiro [cyclopropane-1,5′ (2-hydroxymethyl)-[5′H] dibenzo [*a*, *d*] cycloheptene] 1089

Bennur S. C. and V. B. Jigajinni and V. V. Badiger, 1-Substituted alkylamino-3-(4-quinazolyloxy)-2-propanol trihydrochlorides and 1-substituted alkylamino-3-(8-quinolyloxy)-2-propanol dihydrochlorides 1295

Biradar N. S. and S. D. Angadi, Oxovanadium (IV) complexes with aldoximes 755

Bîrhală Al., voir Vîlcu R. 889

Blouri B., voir Rumbea M. A. 1103

Boáriu-Farkas M., voir Várhelyi Cs. 657

Bourceanu G. and V. Ababi, Gh. Popa, M. Sanduloviciu, Transformation of the toluene-water mixture in the frequency discharge plasma. II. Influence of the power and residence time 627

Brezeanu M. and I. Jitaru, Coordination compounds with choline acetate 531

Brezmes B. y J. Casado, F. Mata, Influencia de la acidez del medio sobre la reacción entre las aminas primarias alifáticas y el ácido nitroso 619

Brown D. H. and P. G. Perkins, The electronic structure and spectra of the di-μ-sulphido-bis-[oxo- L-cysteinato) molybdate (V)] $^{2-}$ ion . . 515

Buchwald P. and L. Fey, Cyanoethylation of ketoximes. II. Kinetics and mechanism of decyanoethylation of some cyanoethyl ethers of *para*-substituted acetophenone oximes 379

— and A. Kövendi, Cyanoethylation of ketoximes. I. Cyanoethylation of *para*-substituted acetophenone oximes 245

Budarina A. N., voir Markov B. F. 597

C

Căldăraru H. and M. Moraru, An electron spin resonance proof of chair-boot conformation of the iminoxy radical of endo-3-carbomethoxybicyclo [3.3.1] nonan-9-one oxime 1219

Calu N., voir Iordăchescu L. 1279
— et A. Popa-Rang, Le système nickel(II)-thiosemicarbazide . . . 323

Campanella L. and P. L. Cignini, F. Croce, Polarographic and oscillopolarographic behaviour of quinolinic acid 855

Carpov A., voir Drăgan D. 421,435
— and D. Drăgan, G. Mocanu, C. Luca, Studies on the synthesis and characterization of weakly basic anion-exchange resins. I. Amination of chloromethylated macroporous ternary styrene-divinylbenzene-acrylic monomer copolymers with dimethylamine 407

Casado J., voir Brezmes B. 619

Caşcaval C. N. and I. A. Schneider, Characterization of copolymers by pyrolysis-chromatography. I. Copolymers of acrylonitrile with vinyl acetate and α-methylstyrene . . 575

Catrina E. and Z. Simon, Gh. Catrina, Structure of thiazolidinic compounds by the del Ré method . . 651

Catrina Gh., voir Catrina E. . . . 651

Chiraleu F., voir Avram E. 539,637
— , voir Dinulescu I. G. 85
— , voir Enescu L. 957
— , voir Iordache F. 233,353
— , voir Răzuş, A. C. 781

Cignini P. L., voir Campanella L. . . 855

Ciocîrlă I,. voir Lixandru T. 129

Ciolac S., The induction time for pitting corrosion 1057
— and E. Vasilescu, The electrochemical behaviour of stainless steels and their main metallic components in chloride ions containing media. I. The effect of chloride ions concentration and temperature . . 739
— and E. Vasilescu, The electrochemical behaviour of stainless

steels and their main metallic components in chloride ions containing media. II. Effect of pH 749

Ciopec M., voir Marchidan D. I. . . . 143

Ciorănescu E., voir Banciu M. . . . 121

— , voir Drăguțan I. 283

Ciurea L., The ESR spectra of the acenaphthenone reduction products 1213

— and V. E. Sahini, E. Volanschi, ESR spectra and electronic structure of isatin and N-methylisatin radical anions 1029

Ciureanu M. and V. E. Sahini, Infrared spectra of benzene halogen complexes 873

— and V. E. Sahini, *n*-Ionization potentials of nitrogen heterocyclic molecules 1037

— and V. E. Sahini, On the electronic structure of *n*-6 complexes. I. Iodine complexes with heteroaromatic donors 1205

Clack D. W., voir Smith W. 1243

Coman B., voir Vîlcu R. 603, 727

Comptes Rendus 139, 445, 446, 587, 723, 724, 1191, 1355, 1355, 1503, 1503, 1504.

Constantin E. et J. Ch. Abbe, Sur les réactions entre les ions CH_3^+ et CD_2H^+ avec CH_4 et CD_4 . . . 1329

—, voir Gothard F. A. 1183

Constantinescu C. and L. Antonescu, Separation by extraction and spectrophotometric determination of In (III) with triphenylmethane basic dyes 985

Constantinescu Gh., Die Reaktionen zwischen $H[AuCl_4]^-$ und dem in *orto*-Substituierten Malachitgrün 1267

Constantinescu M. and E. Segal, M. Vass, Thermoelectric power variation during oxygen adsorption on zinc oxide thin film 911

Conțescu Cr., voir Vass M. I. 1253

Cőrmős D. C. and I. Haiduc, P. Stețiu, Synthetic single crystal lead sulphide electrode. I. Direct potentiometric titration of lead with Na_2 EDTA 259

Costeanu E. et Th. Deleanu, Sur le mécanisme du processus de nucléation dans les interactions oxygène-métal 29

Crișan D., voir Udrea I. 217

Cristescu C., as-Triazine derivatives with potential therapeutic action. XIV. A simplified synthesis of 2′, 3′, 5′-tri-O-benzoyl-β-D-ribofuranosyl-6-azauracils-5-substituted *via* 2,4-bis-(trimethylsilyloxy)-derivatives 1287

Croce F., voir Campanella L. 855

Crusos A. et Cr. Simionescu, Greffage mécano-chimique des polyoxyméthylènes. IV. Influence de la température sur la destruction par broyage vibratoire 929

Csunderlik C., voir Petrovici E. . . . 633

D

Daněk V. and K. Matiašovský, Interaction of ions in molten binary LiF-AlF_3 mixtures 459

Dărîngă M., voir Simionescu Cr. . . . 1157

David D., voir Laiber V. 1479

Deleanu Th., voir Costeanu E. . . . 29

Diaconu I., voir Simionescu Cr. . 939,1157

Dinulescu I. G., voir Avram E. . . 539,637

— and F. Chiraleu, M. S. Pop, M. Avram, Investigations in the cyclobutane series. XXXV. NMR spectral parameters of some compounds with different *syn*-dibenzotricyclodecadiene skeletons 85

— voir, Ștefan N. 1473

Dima M., voir Poinescu Ig. 1311

Dimitrov D. I. i V. Z. Anghelov, A. T. Badev, Zakonomernosta protsessa zhidkofaznovo okisleniya nenasyshchenykh soedinenii v prisutstvii bornykh dobavok 1319

Donescu D., Kinetic studies on copolymerization of 1,3-dioxepane with epichlorohydrin initiated with $AlEt_3 + H_2O$ 1491

Doré J. C., voir Marçot B. 91

Doss S. H., Sultam-steroide. I. Die Synthese von Estern einiger Sterine mit Sultanyl-N-phenylcarbonsäuren 241

Drăgan D., voir Carpov A. 407

— and G. Mocanu, A. Carpov, Studies on the synthesis and characterization of weakly basic anion-exchange resins. II. On the nature of the functional groups 421

— and G. Mocanu, A. Carpov, Studies on the synthesis and characterization of weaklybasic anion-exchange resins. III. Operating characteristics 435

—, voir Petrariu I. 561

Drăgan Gh., Amorphous-crystalline coupling in polyethylene. II. DTA study of the crystalline morphology in chlorinated polyethylene 687

Drăgan S., voir Petrariu I. 1167

—, voir Poinescu Ig. 1311

Drăghici C., voir Drăguţan I. 283

—, voir Urseanu F. 107

Dragnea I., voir Teoreanu I. 925

Dragotă I. I. and L. V. Feyns, I. Niculescu-Duvăz, Potential anticancer agents. IX. Synthesis of new urethane type nitrogen mustard from benzo- and naphto-pyrans . . 665

Drăgulescu C., voir Petrovici E. . . . 633

Drăguţan I. and C. Drăghici, E. Ciorănescu, Carbonium ion reactions. XII. Benzobicyclononene derivatives through double bond participation 283

Drimuş I. et L. Papahagi, Oxydation du *n*-dodécane en phase liquide par l'oxygène moléculaire en présence des catalyseurs métalliques pseudohomogènes. II. L'effet des naphténates des métaux lourds 973

Dumitrescu S., voir Simionescu Cr. 939,1157

E

El-Abbady A. M. and A. H. Moustafa, S. A. El-Abbady, Geometrical orientation of Stobbe condensation involving dimethyl α,α-dimethylsuccinate with carbonyl compounds 801

— and M. A. Omara, Further studies on the Stobbe condensation of *p*-chlorobenzophenone with dimethyl succinate 965

El-Abbady S. A., voir El-Abbady A. M. 801

Enescu L. and F. Chiraleu, M. Avram, Investigation in the cyclobutane series. XXXVI. Rearrangement of 8-diazo-*endo*-benzo [*c*] tricyclo [4.2.1.0^{2,5}] non-3-en-7-one on photolysis and in acid media 957

F

Ferencz A., voir Petrovici E. 633

Fey L., voir Buchwald P. 379

Feyns L. V., voir Dragotă I. I. 665

Floru L., voir Urseanu F. 107

G

Galaţchi G., voir Nicolescu I. V. 61

Georgescu M., voir Teoreanu I. . . 1437

Germain M., voir Arsene A. 251

Gheorghiu C. and C. Mărculescu, Contribution to the coordination chemistry of *s*-triazines. II. Coordination compounds of copper with melamine derivatives 345

Gheorghiu M. D. and F. Kerek, M. Avram, Regio- and stereospecific cycloaddition of *t*-butylcyanoketene to styrene 75

Ghirvu C. I., A rotational study of *o*-chloronitrobenzene and *o*-dinitrobenzene 203

Glatz A. M., voir Răzuş A. C. 781

Goraş L., voir Simionescu Cr. . . . 939

Goratti G., voir B. Sesta 37

Gőrbe I., voir Szurkos A. 1133

Gothard F. A. et T. Pîrvuţoiu, E. Constantin, La généralisation des valeurs de la volatilité relative obtenues par la méthode chromatographique 1183

Grovu M., voir Simionescu Cr. . . . 1157

Gudkova A. S., voir Reutov O. A. . . 1443

Guseinov K. O., voir Naziev Ia. M. . 55

H

Haiduc I., voir Cőrmős D. C. 259

Herdlicka C. and S. Sternberg, Interdiffusion coefficient of Tl$^+$ and Cd^{2+} in fused alkali chlorides by the chronopotentiometric method . . . 1051

Hidişan-Tăuţean L., voir Makkay C. 643

Hillebrand M. and M. Răileanu, V. E. Sahini, Radical-ions. III. Halogenphenothiazone radical-ions 581

Hopîrtean E., voir Popescu I. C. . . 993

— and E. Ştefănigă, Membrane-electrodes of the metallic wire-plastic membrane type. II. Ammonium selective membrane-electrode . . . 863

I

Ionescu M. voir Makkay C. 643

Iordache F. and F. Chiraleu, M. Avram, Bicyclo [2.2.2] octane derivatives. I. Stereoisomeric 5, 6, 7, 8-tetracarbomethoxy-bicyclo [2.2.2] oct-2-enes 233

— et F. Chiraleu, M. Avram, Bicyclo[2.2.2]octene derivatives. II. Addition of halogens to stereoisomeric 5, 6, 7, 8-tetracarbomethoxybicyclo[2.2.2]oct-2-enes 353

Iordăchescu L. et N. Calu, E. Negură, Étude polarographique de quelques complexes de cobalt (III) diméthylglyoxime 1279

Iovu M. et S. Radu, Condensation des sels de sodium des 4-hydroxyazo-

benzènes substitués avec le 1,4-bis (chlorométhyl) benzène 1095
—, voir Tudor E. 813
Irinei Fl., voir Vîlcu R. 1221
Islam A. M., voir Issa I. M. 275
Issa I. M. and A. M. Islam, R. M. Issa, A. K. Abdelkader, Spectrophotometric studies of some derivatives of phenindione 275
Issa R. M., voir Issa I. M. 275
Ivan E. and P. Spacu, New compounds of yttrium and lanthanides with derivatives of anthranilic acid. II. The N-(carboxy methyl) anthranilic acid 337
Ivanov Ch. P. and D. M. Mondeshka, Preparation, spectral properties and electron structure of 4H-cyclopenta (b) thiophene-4-one derivatives . . . 547

J

Jain S. K. and H. L. Jindal, Densities and partial molar volumes in concentrated electrolyte solutions: I — Magnesium nitrate (— Sodium, potassium), nitrate, water mixtures 1433
Jelescu R., voir Banciu M. 121
Jigajinni V. B., voir Bennur S. C. 1295
Jindal H. L., voir Jain S. K. 1433
Jinescu G. I. and C. Balaban, Mass transfer from dispersed particles to continuous fluid media. I. Non-oscillating fluid media 1141
Jitaru I., voir Brezeanu M. 531
Joulain D. et F. Rouessac, Dérivés du bicyclo [4.1.1] octane. II. Préparations de quelques hydrocarbures, aldéhydes et cétones . . . 361

K

Kerek F., voir Gheorghiu M. D. . . 75
Kővendi A., voir Buchwald P. . . . 245
Kudesia V. P., Kinetics of oxidation of some glycols by bromine 1065

L

Lăcătușu V., voir Topor D. 733
Laiber V. and L. Alerguș, D. David and D. Săndulescu, Computation of the isenthalpic expansion of ethylene at high pressure 1479
Lanchec G., voir Rumbea M.-A. . . . 1103
Leancă M., voir Simionescu Cr. 1157
Liteanu C., voir Popescu I. C. 397
—, voir Ungureanu A. 721
Luca C., voir Carpov A. 407
—, voir Petrariu I. 839
Lixandru T. and L. Tătaru, I. Mazilu, I. Ciocîrlă, Contribution to the polymerization of some substituted vinyl monomers 129

M

Macovei V., Spectral solvent effects in aromatic compounds solutions. I. Solvent effects on the position and intensity of the $1_{A_{1G}} \rightarrow 1_{B_{2u}}$ benzene transition 1413
Makkay C. and L. Hidișan-Tăuțean, M. Ionescu, Formation and behaviour of 4-oxazolidones. XII. An advantageous method for obtaining 2,5-diaryloxazoles 643
Marchidan D. I. and M. Ciopec, Enthalpy of non-stoichiometric uranium oxides and saphire to 1500 K by drop calorimetry 143
— and L. Pandele, Thermal properties of $BaCl_2$ high temperature heat content 1227
— and L. Pandele, Thermal properties of KCl, CsCl and binary mixture KCl + CsCL. High temperature heat content 299
— et S. Tănăsescu, Propriétés thermodynamiques des oxydes non stœchiométriques d'uranium . . . 1365
Marçot B. et J. C. Doré, S. Munavalli, C. Viel, Recherche en chimiothérapie antitumorale. VIII. Activité antitumorale *in vitro* d'acides régulateurs de la croissance végétale, d'analogues et de certains dérivés 91
Mărculescu C., voir Gheorghiu C. 345
Markov B. F. and T. A. Tishura, A. N. Budarina, Thermochemical study of binary salt systems . . 597
Mata F., voir Brezmes B. 619
Mateiovici O., Behaviour of activated carbon electrode in electrolyte solutions 481
Matiaşovský. K, voir Daněk V. . . 459
Mavrodin-Tărăbîc M., voir Onaca I. 611
— et I. Onaca, I. Solacolu, Contribution à l'étude de la source chimique de courant $Zn/MeOH/O_2$. II. L'effet de la variation des para-

mètres de fonctionnement sur les performances d'une pile à cathode en argent 915
— et I. Onaca, I. Solacolu, L'influence de la température et de la concentration de l'électrolyte sur les performances d'une pile à combustible hydrogène-oxygène . . . 209
—, voir Solacolu I. 501
Mazilu I., voir Lixandru T. 129
Maxim S., voir Poinescu Ig. 1311
Misdolea C., voir Vîlcu R. 9
Mocanu A., voir Popescu I. C. 397
Mocanu G., voir Carpov A. 407
—, voir Drăgan D. 421,435
Mondeshka D. M., voir Ivanov Ch. P. 547
Morariu M., voir Solacolu Ş. 69
Moraru M., voir Căldăraru H. . . . 1219
Moţoc I., Le système R/S — un point de vue, mathématique. I. L'énoncé invariantif des concepts de la stéréochimie 1335
— , Le système R/S — un point de vue mathématique. II. Définition algébrique pour le rang d'un ligand dans une séquence 1341
—, Sur la relation algébrique entre les énantiomères de l'atome de carbone asymétrique 1115
Moustafa A. H., voir El-Abbady . . 801
Munavalli S,. voir Marçot B 91
Muntean M,. voir Teoreanu I. 925
Mureşan I. and L. Zador, Principles and methods for the potentiometric investigation of polyacids beginning from low degrees of neutralization 1119
Murgulescu I. G. and J. Păun, The radiolysis of the complex oxalates in aqueous solutions. VI. Kinetics and mechanism of the radiolysis of Fe (III),trisoxalato-complex in aqueous solutions . . . 1195
— and M. Şerban, On the viscosity of molten metals. III. Activation energy 591

N

Nagy P., voir Szurkos A. 1133
Naziev Ya. M. i K. O. Guseinov, Yu. A. Badalov, Issledovanie dinamicheskoi viaskosti cistogo n-geptana i ego vinarnykh smesei s n-dekanom pri vysokikh davleniakh 55
Neaţa Bălescu M., voir Atanasiu I. 493
Negoiţă L., voir Urseanu F. 791
Negură E., voir Iordăchescu L. . . . 1279
Nicolescu I. V., voir Spinzi A.. . . 387
— and A. Spinzi, Z. Toma, G. Galaţkchi, Catalytically active iron oxides prepared by mechanotopochemical method. I. Preparation, structural and textural properties 61
Niculescu-Duvăz I,. voir Dragotă I.I. 665

O

Oancea D., voir Bendic C. 195
Olteanu M., voir Vîlcu R. . . . 901,1041
— , voir Zuca Şt. 449
Olteanu M., voir Sahini V. E. . . 3
Omara M. A., voir El-Abbady A. M. 965
Onaca I., voir Mavrodin Tărăbîc M. 209,915
— et M. Mavrodin-Tărăbîc, I. Solacolu, L'étude de la réaction d'oxydation de l'hydrogène sur les électrodes poreuses en nickel. III. La détermination des paramètres de fonctionnement 611
—, voir Solacolu I. 501

P

Pandele L., voir Marchidan D.I. 299,1227
Papahagi L., voir Drimuş I. . . . 973
Păun J,. voir Murgulescu I. G. . . . 1195
Percec S., voir Popescu Fl. 699
Perkins P. G., voir Archibald R. M. 1371
—, voir Armstrong. D. R. 177
— , voir Brown D. H. 515
Petrariu I. et D. Drăgan, P. Petrariu, Fl. Popescu, Contribution à la synthèse des échangeurs d'ions faibles et fortement basiques, de type gel en partant des amino-alcools . . . 561
— et P. Petrariu, Fl. Popescu, S. Drăgan, La dégradation des échangeurs d'anions dans des milieux agressifs. II. L'action de l'eau oxygénée en présence du $CuSO_4$ sur les échangeurs d'anions contenant des groupes quaternaires d'ammonium de type II 1167
— et P. Petrariu, Fl. Popescu, C. Luca, La dégradation des échangeurs d'anions dans des milieux agressifs. I. L'action de l'eau oxygénée en présence du $CuSO_4$ sur les échangeurs d'anions fortement basiques de type I 839
— , voir Popescu Fl. 699
Petrariu P., voir Petrariu I. . 561,839,1167
Petrescu V., voir Sternberg S. . . 159,1231
Petrovici E. and C. Csunderlik, A. Ferencz, C. Drăgulescu, New complexone type ligands. I. *meso*-2, 3-diaminosuccinic-N,N′-diacetic acid (DSDA) and its salts 633
Pîrvuţoiu T,. voir Gothard F. A. 1183

Pleniceanu M. et O. Rusu, Étude spectrophotométrique de la réaction du wolfram (VI) avec le solochrome violet RS 275

Poinescu Ig. et S. Drăgan, S. Maxim, M. Dima, Préparation des copolymères ternaires macroporeux . . 1311

Pop M. S., voir Chiraleu F. 85

Popa Gh., voir Bourceanu G. . . . 627

Popa-Rang A., voir Calu N. 323

Popescu Fl., voir Petrariu I. . 561,839,1167

— et I. Petrariu, S. Percec, Le comportement thermique des copolymères styrène divinylebènzene chlorométhylé, contenant des groupes quaternaires d'ammonium . . 699

Popescu I., voir Urseanu F. 107

— , voir Voiculescu N. 945

Popescu I. C. and E. Hopîrtean, L. Savici, R. Vlad, Characterization of ceramic ion-selective membrane-electrodes. IX. Hg^{2+}-sensitive membrane electrode 993

— and C. Liteanu, A. Mocanu, Differential potentiometry at zero current using two membrane-electrodes with different selectivity 397

Popescu-Tucsek V., voir Radovici O. 305

Prasad C. S. G. and A. D. Taneja, S. K. Banerji, Studies on the sodium derivatives of some 1-substituted-3-(2-pyridyl)-2-thioureas . . 115

Prashad J., Studies of the Joshi effect in pure argon in a degased quartz ozonizer: influence of the heat treatment 1345

Puranik G. S., voir Badami B. V. . 981

Pusztai K., voir Tomescu M. 677

R

Radovici O. and V. Popescu-Tucsek, An investigation of silicon-hydrofluoric acid 305

Radu S., voir Iovu M. 1095

Răileanu M., voir Hillebrand M. 581

Răzuş A. C. und F. Chiraleu, A. M. Glatz, Aluminiumchlorid katalysierte Reaktionen ungesättigter Säuren. VII. Reaktion der 1-Indenyliden- und 3-Indenylessigsäuren 781

Reutov O. A. i A. S. Gudkova, Peregrupirovki v reaktsiiakh dezaminirovaniya 1443

Ripan R. and M. Várhelyi, Synthesis of the bromo-*m*-xylidine-bis-ethylenediamine-cobalt (III) complex and its aquation kinetics in acid solutions 523

Roman L., voir Voiculescu N. 945

Rouessac F., voir Joulain D. . . . 361

Rumbea M. A. et G. Lanchec, B. Blouri, Sur l'oxydation thermique des hydrocarbures à longues chaînes en phase liquide 1103

Rusu O., voir Pleniceanu M. . 275

S

Sahini V. E., voir Ciurea L. . . . 1029,873, 1037,1205

— , voir Hillebrand M. 581

— and M. Olteneanu, Solvent effect on the infrared spectra of xylidine isomers 3

Săndulescu D., voir Laiber V. . . . 1479

Sandulovici M., voir Bourceanu G. 627

Savici L., voir Popescu I. C. 993

Schneider I. A., voir Caşcaval C. N. 575

Segal E., Certains problèmes concernant la cinétique de l'adsorption sur des surfaces hétérogenes . . 317

— , voir Constantinescu M. 911

Şerban M., voir Murgulescu I. G. 591

Sesta B., Solvent interaction with alkyl-trimethylammonium halides. II. Conductance in acetonitrile, acetone and methyl ethyl ketone at 25° 473

— and G. Goratti, Solvent interaction with alkyl-trimethylammonium halides. I. Conductance in methanol ethanol and propanol at 25°C 37

Simion A., voir Vîlcu R. 1359

Simionescu Cr., voir Crusos A. . . 929

— and S. Dumitrescu, M. Dărîngă, M. Grovu, S. Vasiliu, I. Diaconu and M. Leancă, Study on the polymerization of acetylenic derivatives. XVII. Study on electric properties of some polyphenylacetylenes 1157

— and S. Dumitrescu, I. Diaconu, L. Goraş, Study of organic polymers with special electrophysical properties. I. On the electric conductivity of diethynylbenzene-2-methylpentinol copolymer films . 939

— voir Tomescu M. 831

Simon Z., voir Catrina E. 651

Şliam E., voir Avram E. 637

Smith W. and D. W. Clack, Angular dependence of overlap for *s*, *p*, *d* and *f* functions 1243

Solacolu I., voir Mavrodin-Tărăbîc M. 209,915

— et M. Mavrodin-Tărăbîc, I. Onaca, L'étude de la réaction d'oxydation de l'hydrogène dans les élec-

trodes poreuses en nickel. II. La détermination des paramètres d'obtention des électrodes 501
— , voir ONACA I. 611
SOLACOLU Ş. and E. BĂRBULESCU, D. BARB, M. MORARIU, Polymorphic transformations in the $BaTiO_3$—$BaSnO_3$ system revealed by Mössbauer effect 69
SPACU P., voir IVAN E. 337
SPINZI A., voir NICOLESCU I. V. 61
— and I. V. NICOLESCU, Catalytically active iron oxides prepared by mechanotopochemical method. II. Thermal analysis of some iron hydroxides 387
ŞTEFAN N. and I. G. DINULESCU, M. AVRAM, Investigations in the cyclobutane series. XXXVII. The stereochemistry of bromine addition to the angular dimer of benzocyclobutadiene 1473
ŞTEFĂNIGĂ E., voir HOPÎRTEAN E. . . 863
STERNBERG S. and L. BEJAN, Thermodynamic properties of molten salt binary mixture $AgI + CdI_2$ and reciprocal mixture $AgI + CdCl_2$. 465
— , voir HERDLICA C. 1051
— and V. PETRESCU, The chronopotentiometric study in the molten system $AgCl + KCl +$ (dissolved) Cl_2 1231
— and V. PETRESCU, Overvoltage in chlorine discharge on graphite electrode in AgCl—KCl molten mixture at various temperatures (400—700°) 159
— and M. TERZI, Surface tension of fused ternary mixtures : NaCl + +KCl + AgCl and NaCl + RbCl + + AgCl 1013
— and M. TERZI, Surface tension of reciprocal fused salt pairs (Na, K ; Cl, Br) and (K, Rb ; Cl, Br) . . 17
STEŢIU P., voir CŐRMŐS D. C. 259
STEWART J. J. P., voir D. R. ARMSTRONG 177
SZURKOS A. and P. NAGY, I. GŐRBE, A polarographic study on styrylcyanines. II. Substituent effects on the polarographic reduction of 1-ethyl-2- (*p*-X-styryl) and 1-ethyl-4-(*p*-X-styryl)-pyridinium ions 1133

T

TĂNĂSESCU S., voir MARCHIDAN D. I. 1365
TANEJA A. D., voir PRASAD C. S. G. 115
TĂRĂBĂŞANU-MIHĂILĂ C., voir URSEANU F. 791
TĂTARU L., voir LIXANDRU T. 129
TEOREANU I. et M. GEORGESCU, La réactivité de certaines compositions mélilitique par rapport à l'eau . . 1437
— and M. MUNTEAN, I. DRAGNEA, On the formation of $3(CaO.Al_2O_3).CaSO_4$ in the $CaCO_3—Al_2O_3—FeSO_4$ system 925
TERZI M., voir STERNBERG S. 17,1013
TISHURA T. A., voir MARKOV B. F. . . 597
TOMA Z., voir NICOLESCU I. V.. 61
TOMESCU M. et K. PUSZTAI, Recherches dans le domaine de la copolymérisation multicomposante en utilisant un ordinateur 677
— and CR. SIMIONESCU, Calculation of the multicomponent copolymer composition at high conversions 831
TOPOR D. and V. LĂCĂTUŞU, Alkali metal-XO_3 (X = N, Cl, Br, I) vapour composition by mass-spectrometry 733
TOTIR N. and I. VARTIRES, Determination of trace quantities of zinc ion by anodic stripping voltammetry 23
TUDOR E. and M. IOVU, Gas chromatographic separation and identification of the benzene cyclohexylation products 813

U

UDREA I. and D. CRIŞAN, The catalytic system $ZnO—Al_2O_3$. I. The influence of chemical composition and crystalline structure upon the formation of the active phases in the decomposition reaction of isopropyl alcohol 217
UNGUREANU A. and C. LITEANU, New method for the synthesis of triacetyl phosphate 721
URSEANU F. and L. FLORU, I. POPESCU, C. DRĂGHICI, V. ZDRENŢU, Disperse dyes with dibenz [f, ij] isoquinoline [2, 3,-b] quinazoline -5, 10-dione structure 107
— and C. TĂRĂBĂŞANU-MIHĂILĂ, L. NEGOIŢĂ, V. ZDRENŢU, New syntheses of anthraquinone dyes, derivatives of bromamine acid . 791

V

VÁRHELYI CS. and J. ZSAKÓ, M. BOÁRIU-FARKAS, Kinetic analysis of thermogravimetric data. VIII. Thermal decomposition kinetics of some [Cobalt (II) X_2 $(amine)_2$] type complexes 657
VÁRHELYI M., voir RIPAN R. 523

Vartires I., voir Totir N. 23

Vasilescu A. Dynamics of the ligand exchange in uranyl bis-chelated complexes. I. Fast exchange between bis- (acetyl-acetano-)-uranyl and acetylacetone studied by NMR . 951

Vasilescu E., The behaviour of nickel in chloride ions-containing media 487

— , voir Ciolac S. 739,749

Vasiliu S., voir Simionescu Cr. 1157

Vass M., voir Constantinescu M. . . . 911

— and Cr. Conţescu, FEM study of silver layers adsorbed in tungsten. I. Work function and surface migration 1253

Vasu L., On the electrical conductivity of molten alkali halides 169

Venkatasubramanian N,. voir Balasubramanian T, R. 1301

Viel C,. voir Marçot B. 91

Vîlcu R. and Al. Bîrhală, Second virial coefficient of organic vapours. I. Apparatus 889

— and B. Coman, Determination of heat capacities of some alcohols and ketones in vapour phase . . . 603

— and B. Coman, Excess heat capacities of some binary systems in vapour mixture 727

— and Fl. Irinei, Thermodynamic excess functions in electrolyte solutions. Excess free energy of ternary solutions from interferometric measurements 1221

— and C. Misdolea, Significant structure theory. Heat of mixing and ternary excess enthalpy in reciprocal fused salts mixtures Na, K // Cl, Br 9

— and M. Olteanu, Adsorption of some alkyl pyridinium chlorides at the silica-alumina-water interface 1041

— and M. Olteanu, The surface charge of aluminosilicates in aqueous solutions 901

— and A. Simion, Thermodynamic characterization of some organic solutions from acoustical data . . 1359

Vlad R., voir Popescu. I. C. 993

Voicu A., voir Benedikt G. M. . . . 1089

Voiculescu N., Reactions of coordinated ligands. VIII. Aluminium-organic derivatives of diphenylglyoxime 1071

— and L. Roman, I. Popescu, Reactions of coordinated ligands. VII. Zinc-organic compounds of salicylaldoxime coordinated with Ni(II), Pd(II) and Cu(II) 945

Volanschi E., voir Ciurea L. 1029

Z

Zador L., voir Mureşan I. 1119

Zdrenţu V., voir Urseanu F. 107

— , voir Urseanu F. 791

Zsakó J,. voir Várhelyi Cs. 657

Zuca Şt. and M. Olteanu, Electrical conductivity of certain charge-unsymmetrical fused chloride systems $KCl-CaCl_2$, $KCl-SrCl_2$, $KCl-BaCl_2$ 449

INDEX DES SUJETS

A

Acenaphthenone reduction products. The ESR spectra of the —, L. Ciurea 1213

Acetylenes with transition metals. III. Structure of the complex obtained from t-butyl-acetylene and bis-benzonitrile-palladium chloride, Reactions of-, E. Avram, F. Chiraleu, I. G. Dinulescu and M. Avram, 539

Acetylenes with transition metals. V. β-cleavage in τ, π-alkyl-palladium complexes. Reaction of-, E. Avram, I. G. Dinulescu, F. Chiraleu, E. Şliam and M. Avram 637

Acetylenes with transition metals. VI. Reaction of the π-allyl complex of 6-chloro-1, 3, 6-tri-t-butyl-1, 2-dihydrofulvene with carbon monoxide , Reactions of-, E. Avram and M. Avram 775

Acetylenic derivatives. XVII. Study on electric properties of some polyphenylacetylenes, Study on the polymerization of-, Cr. Simionescu, S. Dumitrescu, M. Dărîngă, M. Grovu, S. Vasiiliu, I. Diaconu and M. Leancă 1157

Activité antitumorale *in vitro* d'acides régulateurs de la croissance végétale, d'analogues et de certains dérivés, Recherche en chimiothérapie antitumorale. VIII. —, B. Marçot, J. C. Doré, S. Munavalli et C. Viel 91

Adsorption of some alkyl pyridinium - chlorides at the silica-alumina-

water interface, R. Vîlcu and M. Olteanu 1041
Adsorption sur des surfaces hétérogènes, Certains problèmes concernant la cinétique de l'-, E. Segal . . . 317
Alicylic alcohols by cerium (IV) perchlorate, Oxidation of —, T. R. Balasubramanian and N. Venkatasubramanian 1301
Alkali metal-XO_3 (X = N, Cl, Br, I) vapour composition by mass-spectrometry, D. Topor and V. Lăcătușu 733
Alkanes. II. Preparation of 2, 2, 4-trimethylpentane-$^{14}C_2$ labelled at both methyl groups of the isopropyl moiety, Synthesis of ^{14}C-labelled isotope-isomeric-, I, Bally and A. T. Balaban 1471
Alkylamino-3-(4-quinazolyloxy)-2-propanol trihydrochlorides and 1-substituted alkylamino-3-(8-quinolyloxy)-2-propanol dihydrochlorides, 1-Substituted-, S. C. Bennur, V. B. Jigajinni and V. V. Badiger . . . 1295
Aluminiumchlorid-katalysierte Reaktionen der 1-Indenyliden-und 3-Indenylessigsäuren, A. C. Răzuș, F. Chiraleu und A. M. Glatz 781
Aluminosilicates in aqueous solutions, The surface charge of-, R. Vîlcu and M. Olteanu 901
Aminas primarias alifáticas y el ácido nitroso, Influencia de la acidez del medio sobre la reacción entre las-, B. Bretzmes, J. Casado y F. Mata 619
Angular dependence of overlap for *s*, *p*, *d* and *f* functions, W. Smith and D. W. Clack 1243
Anion-exchange resins. I. Amination of chloromethylated macroporous ternary styrene-divinylbenzene-acrylic monomer copolymers with dimethylamine, Studies on the synthesis and characterization of weakly basic-, A. Carpov, D. Drăgan, G. Mocanu and C. Luca 407
Anion-exchange resins. II. On the nature of the functional groups, Studies on the synthesis and characterization of weakly basic—, D. Drăgan, G. Mocanu and A. Carpov 421
Anion-exchange resins. III. Operating characteristics, Studies on the synthesis and characterization of weakly basic-, D. Drăgan, G. Mocanu and A. Carpov 435
Anodic stripping voltammetry, Determination of trace quantities of zinc ion by-, N. Totir and I. Vartires 23
Anthraquinone dyes, derivatives of bromamine acid, New syntheses of —, F. Urseanu, C. Tărăbășanu-Mihăilă, L. Negoiță and V. Zdrențu 791
Anticancer agents. IX. Synthesis of new urethane type nitrogen mustards from benzo- and naphtopyrans, Potential —, I. I. Dragotă, L. V. Feyns and I. Niculescu-Duvăz 665
Aromatic compounds solutions. I. Solvent effects on the position and intensity of the -l_{A1g} —l_{B2u} benzene transition, Spectral solvent effects in-, V. Macovei 1413

B

Benzene cyclohexylation products, Gas chromatographic separation and identification of-, E. Tudor and M. Iovu 813
Benzene halogen complexes, Infrared spectra of-, M. Ciureanu and V. E. Sahini 873
Benzyl halides in SN_2 reactions, Reactivity of-, G. Bendic and D. Oancea 195
Bicyclo [2.2.2] octane derivatives. I. Stereoisomeric 5, 6, 7,8-tetracarbomethoxy-bicyclo [2.2.2] oct-2-enes, F. Iordache, F. Chiraleu and M. Avram 233
Bicyclo [4.1.1]octane. II. Préparations de quelques hydrocarbures, aldéhydes et cétones, Dérivés du-, D. Joulain et F. Rouessac . . . 361
Bicyclo [2.2.2]octene derivatives. II. Addition of halogens to stereoisomeric 5, 6, 7, 8-tetracarbomethoxybicyclo [2.2.2]oct-2-enes, F. Iordache, F. Chiraleu and M. Avram . . 353
Binary salt systems, Thermochemical study of-, B. F. Markov, T. A. Tishura and A. N. Budarina 597
Binary systems in vapour mixture, Excess heat capacities of some-, R. Vîlcu and B. Coman 727

C

Carbone asymétrique, Sur la relation algébrique entre les énantiomères de l'atome de -, I. Moțoc 1115
Carbonium ion reactions. XII. Acetolysis of 5-(2-bromoethyl)-5H-dibenzo (*a*, *d*] cycloheptene and nitrous acid deamination of 5-(2-aminoethyl)-5H-dibenzo (*a*, *d*) cycloheptene, M. Banciu, F. Badea, R. Jelescu and E. Ciorănescu 121

Carbonium ion reactions. XII. Benzobicyclononene derivatives through double bond participation, I. Drăguţan, C. Drăghici and E. Ciorănescu 283

Catalytic system ZnO—Al_2O_3. I. The influence of chemical composition and crystalline structure upon the formation of the active phases in the decomposition reaction of isopropyl alcohol, The-, I. Udrea and D. Crişan 217

Catalytically active iron oxides prepared by mechanotopochemical method. I. Preparation, structural and textural properties, I. V. Nicolescu, A. Spinzi, Z. Toma and G. Galaţchi 61

Ceramic ion-selective membrane-electrodes. IX. H^{2+} -sensitive membrane electrode, Characterization of-, I. C. Popescu, E. Hopîrtean, L. Savici and R. Vlad 993

Chemical flowsheets, Modelling the material balances of the —, L. Badea 1001

Chemical graphs. XXV. Isomers of the porphyrins- an exercise using Pólya's counting theorem, A. T. Balaban 227

o-Chloronitrobenzene and *o*-dinitrobenzene, A rotational study of-, C. I. Chirvu 203

Cobalt (III) complex and its aquation kinetics in acid solutions, Synthesis of the bromo-*m*-xylidine-bis-ethylenediamine-, R. Ripan and M. Várhelyi 523

Cobalt (III) dimethylglioxime, Etude polarographique de quelques complexes de-, L. Iordăchescu, N. Calu et E. Negură 1279

Complexes, Kinetic analysis of thermogravimetric data. VIII. Thermal decomposition kinetics of some [Cobalt (II) X_2 (amine)$_2$] type-, Cs. Várhelyi, J. Zsakó and M. Boáriu -Farkas 657

n-6 Complexes. I. Iodine complexes with heteroaromatic donors, On the electronic structure of-, M. Ciureanu and V. E. Sahini 1205

Complexone type ligands. I. *meso*-2, 3-diaminosuccinic-N, N′-diacetic acid (DSDA) and its salt, New-, E. Petrovici, C. Csunderlik, A. Ferencz and C. Drăgulescu . . . 633

Comptes Rendus, 139, 445, 446, 587, 723, 724, 1191, 1355, 1355, 1503, 1503, 1504

Coordinated ligands. VII. Zinc-organic compounds of salicyl-aldoxime coordinated with Ni(II), Pd(II) and Cu (II), Reactions of-, N. Voiculescu, L. Roman and I. Popescu 945

Coordinated ligands. VIII. Aluminium-organic derivatives of diphenylglyoxime, Reaction of-, N. Voiculescu 1071

Coordination compounds with choline acetate, M. Brezeanu and I. Jitaru 531

Copolymères styrène-divinylebènzene chlorométhyles, contenant des groupes quaternaires d'ammonium, Le comportement thermique des-, Fl. Popescu, I. Petrariu et S. Percec 699

Copolymères ternaires macroporeux, Préparation des-, Ig. C. Poinescu, S. Drăgan, S. Maxim et M. Dima 1311

Copolymérisation multicomposante en utilisant un ordinateur, Recherches dans le domaine de la -, M. Tomescu et K. Pusztai 677

Copolymerization of 1,3-dioxepane with epichlorohydrin initiated with $AlEt_3$ $+H_2O$, Kinetic studies, on-, D. Donescu 1491

Copolymers by pyrolysis-chromatography. I. Copolymers of acrylonitrile with vinyl acetate and α-methylstyrene, Characterization of-, C. N. Caşcaval and I. A. Schneider . . 575

Cyanoethylation of ketoximes. I. Cyanoethylation of *para*-substituted acetophenone oximes, P. Buchwald and A. Kővendi 245

Cyanoethylation of ketoximes. II. Kinetics and mechanism of decyanoethylation of some cyanoethyl ethers of *para*-substituted acetophenone oximes, P. Buchwald and L. Fey 379

Cycloaddition of t-butylcyanoketene to styrene, Regio- and stereospecific-, M. D. Gheorghiu, F. Kerek and M. Avram 75

Cyclobutane series. XXXV. NMR spectral parameters of some compounds with different *syn*- dibenzotricyclodecadiene skeletons, Investigations in the-, I. G. Dinulescu, F. Chiraleu, M. S. Pop and M. Avram . . . 85

Cyclobutane series. XXXVI. Rearrangement of 8-diazo-*endo*-benzo [*c*] tricyclo [4.2.1.$0^{2,5}$] non-3-en-one on photolysis and in acid media, Investigation in the-, L. Enescu, F. Chiraleu and M. Avram . . . 957

Cyclobutane series. XXXVII. The stereochemistry of bromine addition to the angular dimer of benzocyclobutadiene, Investigations in the-, N. Ştefan, I. G. Dinulescu, F. Chiraleu and M. Avram 1473

D

Dezaminirovaniya, Peregrupirovki v reaktsiyakh-, O. A. Reutov i A. S. Gudkova 1443

1,5-Dicarba-*closo*-pentaborane (5) and 1,6-dicarba-*closo*-hexaborane (6), The electronic structure of-, D. R. Armstrong 883

Differential capacity, An investigation of silicon-hydrofluoric acid interface by measuring its-, O. Radovici and V. Popescu-Tucsek . . . 305

Differential potentiometry at zero current using two membrane-electrodes with different selectivity, I. C. Popescu, C. Liteanu and A. Mocanu 397

Dinamicheskoi viazkosti cistogo n-geptana i ego binarnykh smesei s n-dekanom pri vysokikh davleniakh, Issledovanie —, YA. M. Naziev, K. O. Guseinov i Yu. A. Badalov 55

Disperse dyes with dibenz [f, ij] isoquinoline [2, 3-b] quinazoline-5,10-dione structure, F. Urseanu, L. Floru, I. Popescu, C. Drăghici and V. Zdrenţu 107

n-Dodécane en phase liquide par l'oxygène moléculaire en présence des catalyseurs métalliques pseudo-homogènes. II. L'effet des naphténates des métaux lourds, Oxydation du-, I. Drimuş et L. Papahagi . . . 973

E

Echangeurs d'anions dans des milieux agressifs. I. L'action de l'eau oxygénée en présence du $CuSO_4$ sur les échangeurs d'anions fortement basiques de type I. La dégradation des-, I. Petrariu, P. Petrariu Fl. Popescu et C. Luca 839

Echangeurs d'anions dans des milieux agressifs. II. L'action de l'eau oxygénée en présence du $CuSO_4$ sur les échangeurs d'anions contenant des groupes quaternaires d'ammonium de type II., La dégradation des-, I. Petrariu, P. Petrariu, Fl. Popescu et S. Drăgan 1167

Echangeurs d'ions faibles et fortement basiques, de type gel en partant des amino-alcools, Contribution à la synthèse des-, I. Petrariu, D. Drăgan, P. Petrariu et Fl. Popescu 561

Electrical conductivity of certain charge-unsymmetrical fused chloride systems $KCl-CaCl_2$, $KCl-SrCl_2$, $KCl-BaCl_2$ Şt. Zuca and M. Olteanu 449

Electrochemical behaviour of 18 Cr-10 Ni stainless steel in organic acid solutions. II. Acetic acid, T. Badea and I. Atanasiu 45

Electrodes poreuses en nickel. II. La détermination des paramètres d'obtention des électrodes, L'étude de la réaction d'oxydation de l'hydrogène dans les-, I. Solacolu, M. Mavrodin-Tărăbîc et I. Onaca 501

Electrodes poreuses en nickel. III. La détermination des paramètres de fontionnement, L'étude de la réaction d'oxydation de l'hydrogène sur les-, I. Onaca, M. Mavrodin-Tărăbîc et I. Solacolu 611

Electrolyte solutions, Behaviour of activated carbon electrode in-, O. Mateiovici 481

Electrolyte solutions : I — Magnesium nitrate — (sodium, potassium) nitrate-water mixtures, Densities and partial volumes in concentrated-, S. K. Jain and H. L. Jindal . . . 1433

Electronic structure and spectra of the di-μ-sulphido-bis-oxo-(L-cysteinato) molybdate (V)]^2 ion, D. H. Brown and P. G. Perkins 515

Enthalpy of non-stoichiometric uranium oxides and sapphire to 1500 K by drop calorimetry, D. I. Marchidan and M. Ciopec 143

Ethylene at high pressure, Computation of the isenthalpic expansion of-, V. Laiber, L. Alerguş, D. David and D. Săndulescu 1479

F

Frequency discharge plasma. II. Influence of the power and residence time, Transformation of the toluene-water mixture in the-, G. Bourceanu, V. Ababi, Gh. Popa and M. Sandulovicu 627

Fused salt pairs (Na, K ; Cl, Br) and (K, Rb ; Cl, Br), Surface tension of reciprocal-, S. Sternberg and M. Terzi 17

Fused salts mixture Na, K // Cl, Br, Significant structure theory. Heat of mixing and ternary excess enthalpy in reciprocal-, R. Vîlcu and C. Misdolea 9

G

Glycols by bromine, Kinetics of oxidation of some—, V. P. Kudesia 1065

H

^{4}H-cyclopenta(b)thiophene-4-one derivatives, Preparation, spectral properties and electron structure of—, Ch. P. Ivanov and D.M. Mondeshka 547

Heat capacities of some alcohols and ketones in vapour phase, Determination of—, R. Vîlcu and B. Coman 603

Heterocyclic compounds. III. The cyclization of ring -substituted γ-phenoxybutyric acids by PPA to 2,3-dihydro-1-benzoxepin-6(4H)-ones, I. I. Bădilescu 761

Heterocyclic compounds. V. Beckmann rearrangement of some 2,3-dihydro-1-benzoxepin-5 (4H)-one oximes to 1,5-and 1,6-benzoxazocinones, I. I. Bădilescu 1077

Hydrocarbures à longues chaînes en phase liquide, Sur l'oxydation thermique des—, M. A. Rumbea, G. Lanchec et B. Blouri 1103

4-Hydroxyazobenzènes substitués avec le 1,4-bis (chlorométhyl) benzène, Condensation des sels de sodium des—, M. Iovu et S. Radu 1095

I

Iminoxy radical of endo-3-carbometoxybicyclo [3.3.1] nonan-9-one oxime, An electron spin resonance proof of chair-boot conformation of the—, H. Căldăraru and M. Moraru 1219

In (III) with triphenylmethane basic dyes, Separation by extraction and spectrophotometric determination of—, C. Constantinescu and L. Antonescu 985

Interdiffusion coefficient of Tl^+ and Cd^{2+} in fused alkali chlorides by the chronopotentiometric method, C. Herdlicka and S. Sternberg 1051

Ions CH_3^+ et CD_2H^+ avec CH_4 et CD_4, Sur les reactions entre les—, E. Constantin et J. Ch. Abbe 1329

Iron oxides prepared by mechano-topochemical method. II. Thermal analysis of some iron hydroxides, Catalytically active—, A. Spinzi and I. V. Nicolescu 387

Isatin and N-methylisatin radical anions, ESR spectra and electronic structure of —, L. Ciurea, V. E. Sahini and E. Volanschi 1029

J

Joshi effect in pure argon in a degased quartz ozonizer : influence of the heat treatment, Studies of the —, J. Prashad 1355

M

Malachitgrün, Die Reaktionen zwischen $H[AuCl_4]^-$ und dem in *orto*-substituierten-, Gh. C. Constantinescu 1267

Mass transfer from dispersed particles to continuous fluid media. I. Non-oscillating fluid media, G. I. Jinescu and C. Balaban 1141

Mélilitiques par rapport à l'eau, La reactivité de certaines compositions —, I. Teoreanu and M. Georgescu 1437

Membrane-electrodes of the metallic wire-plastic membrane type. II. Ammonium selective membrane-electrode, E. Hopîrtean and E. Ştefănică 863

Molar polarization and permanent electric moment of *n*-butyl butyrate in nonpolar solvents, I. Adorian 51

Molten alkali halides, On the electrical conductivity of —, L. Vasu 169

Molten binary LiF-AlF_3 mixtures, Interaction of ions in —, V. Daněk and K. Matiašovský 459

Molten metals. III. Activation energy, On the viscosity of —, I. G. Murgulescu and M. Şerban 591

Molten salt binary mixture AgI + CdI_2 and reciprocal mixture AgI + + $CdCl_2$, Thermodynamic properties of—, S. Sternberg and L. Bejan 465

Molten system AgCl + KCl + (dissolved)Cl_2, The chronopotentiometric study in the—, S. Sternberg and V. Petrescu 1231

Multicomponent copolymer composition at high conversions, Calculation of the—, M Tomescu and Cr. Simionescu 831

N

Nickel in chloride ions-containing media, The behaviour of —, E. Vasilescu 478

Nickel (II)-thiosemicarbazide, Le système—, N. Calu et A. Popa-Rang 323

Nitrogen heterocyclic molecules, *n*-Ionization potentials of —, M. Ciureanu and V. E. Sahini 1037

Nucléation dans les interactions oxygène-métal, Sur le mécanisme du processus de —, E. Costeanu et Th. Deleanu 29

O

Okisleniya nenasyshcenykh soedinenii v prisutstvii bornykh dobavok, Zakonomernosta prosessa jidkofaznovo-, D. I. Dimitrov, V. Z. Anghelov i A. T. Badev 1319

Orbitals on water, methane, acetylene, ethylene, ethane and diborane, *Ab initio* calculations using spherical Gaussian-, R. M. Archibald, D. R. Armstrong and P. G. Perkins . . 1371

Organic polymers with special electrophysical properties. I. On the electric conductivity of diethynylbenzene-2-methylpentinol copolymer films, Study of —, Cr. Simionescu, S. Dumitrescu, I. Diaconu and L. Goraş 939

Overvoltage in chlorine discharge on graphite electrode in AgCl—KCl molten mixture at various temperatures (400—700°), S. Sternberg and V. Petrescu 159

4-Oxazolidones. XII. An advantageous method for obtaining 2,5-diaryloxazoles, Formation and behaviour of—, C. Makkay, L. Hidişan-Tăuţean and M. Ionescu 643

Oxovanadium (IV) complexes with aldoximes, N. S. Biradar and S. D. Angadi 755

Oxydes non stoéchiometriques d'uranium, Propriétés thermodynamiques des—, D. I. Marchidan et S. Tănăsescu 1365

P

Phenindione, Spectrophotometric studies of some derivatives of—, I. M. Issa, A. M. Islam, R. M. Issa and A. K. Abdelkader 275

Pile à combustible hydrogène-oxygène, L'influence de la température et de la concentration de l'électrolyte sur les performances d'une —, M. Mavrodin-Tărăbîc, I. Onaca et I. Solacolu 209

Pitting corrosion, The induction time for —, S. Ciolac 1057

Polyacids beginning from low degrées of neutralization, Principles and methods for the potentiometric investigation of—, I. Mureşan and L. Zador 1119

Polyethylene. II. DTA study of the crystalline morphology in chlorinated polyethylene, Amorphous-crystalline coupling in —, Gh. Drăgan 687

Polymerization of some substituted vinyl monomers, Contribution to the —, T. Lixandru, L. Tătaru, I. Mazilu and I. Cocîrlă 129

Polymorphic transformations in the $BaTiO_3-BaSnO_3$ system revealed by Mössbauer effect, Ş. Solacolu, E. Bărbulescu, D. Barb and M. Morariu 69

Polyoxyméthylènes. IV. Influence de la témperature sur la destruction par broyage vibratoire, Greffage mécano-chimique des—, A. Crusos et Cr. Simionescu 929

Q

Quinolinic acid, Polarographic and oscillopolarographic behaviour of —, L. Campanella, P. L. Cignini and F. Croce 855

R

Radical-ions. III. Halogen-phenothiazone radical-ions, M. Hillebrand, M. Răileanu and V. E. Sahini 581

Radiolysis of the complex oxalates in aqueous solutions. VI. Kinetics and mechanism of the radiolysis of Fe(III)-trisoxalato-complex in aqueous solution, The —, I. G. Murgulescu and J. Păun 1195

S

Second virial coefficient of organic vapours. I. Apparatus, R. Vîlcu and Al. Bîrhală 889

Silver layers adsorbed in tungsten. I. Work function and surface migration, FEM study of —, M. I. Vass and Cr. Conțescu 1253

Sodium derivatives of some 1-substituted-3-(2-pyridyl)-2-thioureas, Studies on the—, C. S. G. Prasad, A. D. Taneja and S. K. Banerji . . 115

Solvent interaction with alkyl-trimethylammonium halides. I. Conductance in methanol, ethanol and propanol at 25°C, B. Sesta and G. Goratti 37

Solvent interaction with alkyl-trimethylammonium halides. II. Conductance in acetonitrile, acetone and methyl ethyl ketone at 25°, B. Sesta 473

Source chimique de courant Zn(MeOH) O_2.II. L'effet de la variation des paramètres de fonctionnement sur les performances d'une pile à cathode en argent, Contribution à l'étude de la—, M. Mavrodin-Tărăbîc, I. Onaca et I. Solacolu 915

Spiro [cyclopropane-1,5′ (2,hydroxyméthyl)-[5′H]dibenzo [*a*, *d*] cycloheptene], An intramolecular hydrogen bridge with the double bond in—, G. M. Benedikt and A. Voicu 1089

Stainless steels and their main metallic components in chloride ions containing media. I. The effect of chloride ions concentration and temperature, The electrochemical behaviour of—, S. Ciolac and E. Vasilescu 739

Stainless steels and their main metallic components in chloride ions containing media II. Effect of pH, The electrochemical behaviour of—, S. Ciolac and E. Vasilescu 749

Stobbe condensation involving dimethyl α, α-dimethylsuccinate with carbonyl compounds, Geometrical orientation of—, A. M. El-Abbady, A. H. Moustafa and S. A. El-Abbady 801

Stobbe condensation of *p*-chlorobenzophenone with dimethyl succinate, Studies on the—, A. M. El-Abbady and M. A. Omara 965

Styrylcyanines. II. Substituent effects on the polarographic reduction of 1-ethyl-2-(*p*-X-styryl) and 1-ethyl-4-(*p*-X-styryl),-pyridinium ions, A. Szurkos, P, Nagy and I. Görbe 1133

Sultam-steroide. I. Die Synthese von Estern einiger Sterine mit Sultamyl-N-phenylcarbonsäuren, S. H. Doss 241

Surface tension of fused ternary mixtures: NaCl + KCl + AgCl and NaCl + RbCl + AgCl, S. Sternberg and M. Terzi 1013

Sydnones. II. Benzylsydnone and its derivatives, Reactions of—, B. V. Badami and G. S. Puranik . . . 981

Synthetic single crystal lead sulphide electrode. I. Direct potentiometric titration of lead with Na_2EDTA, D. C. Cörmös, I. Haiduc and P. Stețiu 259

System, On the formation of 3(CaO. Al_2O_3). $CaSO_4$ in the $CaCO_3-Al_2O_3-FeSO_4$-, I. Teoreanu, M. Muntean and I. Dragnea 925

Système R/S — un point de vue mathématique. I. L'énoncé invariantif des concepts de la stéréochimie, Le—, I. Moțoc 1335

Système R/S — un point de vue mathématique. II. Définition algébrique pour le rang d'un ligand dans un séquence, Le—, I. Moțoc . . . 1341

Système rédox $Fe(CN)_6^{3-}/Fe(CN)_6^{4-}$ sur l'électrode de graphite, L'étude du—, I. A. Atanasiu et M. Neață Bălescu 493

T

Thermal properties of $BaCl_2$ high temperature heat content, D. I. Marchidan and L. Pandele . . . 1227

Thermal properties of KCl, CsCl and binary mixture KCl + CsCl. High temperature heat content, D. I. Marchidan and L. Pandele . . . 299

Thermodynamic characterization of some organic solutions from acoustical data, R. Vîlcu and A. Simion 1359

Thermodynamic excess functions in electrolyte solutions. Excess free energy of ternary solutions from interferometric measurements, R. Vîlcu and Fl. Irinei 1221

Thermoelectric power variation during oxygen adsorption on zinc oxide thin films, M. Constantinescu, E. Segal and M. Vass 911

Thiazolidinic compounds by the del Ré method, Structure of—, E. Catrina, Z. Simon and Gh. Catrina . . . 651

Triacetyl phosphate, A new method for the synthesis of—, A. Ungureanu and C. Liteanu 721

as-Triazine derivatives with potential therapeutic action. XIV. A simplifield synthesis of 2′, 3′, 5′-tri-O-benzoyl-β-D-ribofuranosyl-6-azauracils-5-substituted *via* 2,4-bis- (trimethylsilyloxy)-derivatives, C. Cristescu 1287

s-Triazines. II. Coordination compounds of copper with melamine derivatives, Contribution to the coordination chemistry of —, C. Gheorghiu and C. Mărculescu 345

Tributylphosphate-dodécane-acide nitrique-acide formique-eau, Etude du partage de l'acide formique, de l'uranium (VI) et du plutonium (IV) dans le système —, A. Arsene et M. Germain 251

Titanium tetrachloride and the methyltitanium chlorides, The electronic structure and spectra of —, D. R. Armstrong, P. G. Perkins and J. J. Stewart . . . 177

U

Uranyl bis-chelated complexed. I. Fast exchange between bis- (acetylacetonato)-)-uranyl and acetylacetone studied by NMR, Dynamics of the ligand exchange in —, A. Vasilescu 951

V

Volatilité relative obtenues par la méthode chromatographique, La généralisation des valeurs de la —, F. A. Gothard, T. Pîrvuţoiu et E. Constantin 1183

W

Wolfram (VI) avec le solochrome violet RS, Etude spectrophotométrique de la réaction du —, M. Pleniceanu et O. Rusu 267

X

Xylidine isomers, Solvent effect on the infrared spectra of — V. E. Sahini and M. Olteneanu 3

Y

Yttrium and lanthanides with derivatives of anthranilic acid. II. The N-(carboxy methyl) anthranilic acid, New compounds of —, E. Ivan and P. Spacu 337

ORSZÁGOS MŰSZAKI KÖNYVTÁR ÉS DOKUMENTÁCIÓS KÖZPONT 1883

NOTE POUR LES AUTEURS

La *Revue Roumaine de Chimie* publie des articles en anglais, français, russe, allemand ou espagnol. Les auteurs sont priés d'envoyer des articles, notes, communications et comptes rendus inédits.

Les manuscrits seront dactylographiés à deux intervalles. Les tableaux seront dactylographiés sur feuilles séparées, de même que la légende des figures. Les diagrammes seront tracés à l'encre de Chine sur papier calque. Les tableaux et les figures seront numérotés par des chiffres arabes, en nombre strictement nécessaire. Prière de ne pas inscrire les mêmes données dans les tableaux et les figures. Les formules chimiques seront incluses dans le texte; en outre, elles seront transcrites sur des feuilles séparés. Les auteurs sont priés d'indiquer les caractères italiques (en soulignant les lettres au crayon), ainsi que tout autre caractère spécial. L'ordre des références bibliographiques sera celui de leur mention dans le texte; le nom de l'auteur sera précédé de l'initiale du prénom; les publications périodiques seront présentées suivant les prescriptions internationales. Les références seront ajoutées à la fin de l'article; elles paraîtront comme des notes, au bas de la page. Le texte sera précédé d'un résumé comprenant 15 lignes au maximum.

L'entière responsabilité du contenu des articles appartient aux auteurs. On publie des articles dus aux collaborateurs roumains ou étrangers.

PRINTED IN ROMANIA

1976

TRAVAUX PARUS AUX ÉDITIONS DE L'ACADÉMIE DE LA RÉPUBLIQUE SOCIALISTE DE ROUMANIE

I. ZUGRĂVESCU, MAGDA PETROVANU, **Chimia N-Ilidelor** (La Chimie des N-Ilures), 1974, 347 p., 19 lei.

MARGARETA AVRAM, **Antidăunători** (Pesticides), 1974, 494 p., 41 lei.

CR. SIMIONESCU, VIORICA RUSAN, N. POPA, **Chimia algelor marine** (La Chimie des algues marines), 1974, 211 p., 18 lei.

CRISTOFOR SIMIONESCU, MARGARETA GRIGORAŞ, AGATA CERNĂTESCU-ASANDEI et GHEORGHE ROZMARIN, **Chimia lemnului din România — plopul şi salcia** (La chimie du bois en Roumanie — le peuplier et le saule), 1973, 228 p., 28 lei.

TIBERIU NĂŞCUŢIU, **Metode radiochimice de analiză** (Méthodes radiochimiques d'analyse), 1973, 384 p., 23 lei.

MARIA FITI, **Dozimetria chimică a radiaţiilor ionizante** (La dosimétrie chimique des radiations ionisantes), 1973, 240 p., 13,50 lei.

MIHAI FLORESCU, **Eficienţa economică a cercetării ştiinţifice** (L'efficience économique de la recherche scientifique), 1972, 115 p., 15 lei.

GEORGETA LĂZĂRESCU, **Sistematizarea informaţiilor în chimia organică** (La systématisation des informations dans la chimie organique), 1972, 242 p., 10,50 lei.

P. BALTĂ şi E. BALTĂ, **Introducere în chimia fizică a stării vitroase** (Introduction à la chimie physique de l'état vitreux), 1971, 240 p., 15,50 lei.

LYDIA-MARIA VAICUM, **Biodegrabilitatea detergenţilor** (La biodégrabilité des détergents), 1971, 346 p., 19,50 lei.

I. ZUGRĂVESCU et L. STOICESCU-CRIVETZ, **Polimeri heterociclici** (Polymères hétérocycliques), 1971, 190 p., 9,50 lei.

I. V. MAXIM, **Materiale nucleare** (Matériaux nucléaires), 1969, 444 p., 30 lei.

CORNEL BODEA, et collab., **Tratat de biochimie vegetală**, partea I, **Fitochimie** (Traité de biochimie végétale, Ire partie, Phytochimie), Ier vol., 1964 747 p. + 4 annexes + 2 pl., 41 lei; IIe vol., 1965, 1962 p., 1 pl., 56 lei; IIIe vol., 1967, 773 p., 35 lei.

CRISTOFOR SIMIONESCU et CLEOPATRA VASILIU-OPREA, **Mecanochimia compuşilor macromoleculari** (La méchanochimie des composés macromoléculaires), 1967, 344 p., 23,50 lei.

I.P.I. c. 403

43 426

Lei 25.—